OCS Study
BOEM 2022-039

Collaboration with the North Pacific Research Board, Arctic Marine Research Program

U.S. Department of the Interior
Bureau of Ocean Energy Management
BOEM Alaska Region, Anchorage, AK

BOEM
Bureau of Ocean Energy Management

OCS Study
BOEM 2022-039

Collaboration with the North Pacific Research Board, Arctic Marine Research Program

July 2022

Authors:
Danielle Dickson and Matthew Baker

Prepared under Agreement M16AC00016
By
North Pacific Research Board
1007 W. 3rd Avenue, Suite 100
Anchorage, AK 99501

U.S. Department of the Interior
Bureau of Ocean Energy Management
BOEM Alaska Region, Anchorage, AK

BOEM
Bureau of Ocean Energy Management

DISCLAIMER

Study collaboration and funding were provided by the U.S. Department of the Interior, Bureau of Ocean Energy Management (BOEM), Environmental Studies Program, Washington, DC, under Agreement Number M16AC00016. This report has been technically reviewed by BOEM, and it has been approved for publication. The views and conclusions contained in this document are those of the authors and should not be interpreted as representing the opinions or policies of BOEM, nor does mention of trade names or commercial products constitute endorsement or recommendation for use.

REPORT AVAILABILITY

To download a PDF file of this report, go to the U.S. Department of the Interior, Bureau of Ocean Energy Management Data and Information Systems webpage (http://www.boem.gov/Environmental-Studies-EnvData/), click on the link for the Environmental Studies Program Information System (ESPIS), and search on 2022-039. The report is also available at the National Technical Reports Library at https://ntrl.ntis.gov/NTRL/.

CITATION

Dickson, D.M.S. (North Pacific Research Board, Anchorage, AK). 2022. Collaboration with the North Pacific Research Board, Arctic Marine Research Program. Anchorage (AK): U.S. Department of the Interior, Bureau of Ocean Energy Management. 16 p. Report No.: OCS Study BOEM 2022-039. Contract No.: M16AC00016.

ABOUT THE COVER

Arctic Integrated Ecosystem Research Program logo/Eric Cline

ACKNOWLEDGMENTS

North Pacific Research Board expresses deep appreciation for the enthusiastic cooperation and unwavering commitment of BOEM staff to partnership with NPRB on the Arctic Integrated Ecosystem Research Program. In particular, NPRB expresses thanks to the following individuals who were BOEM staff in the early stages of development of this partnership and/or participated actively throughout 2016-2021: Dee Williams, Cathy Coon, James Kendall, Rodney Cluck, Walter Cruikshank, Guillermo Auad, Rick Raymond, Sean Burril, Lorena Edenfield, Heather Crowley, and Paula Barksdale.

Contents

List of Abbreviations and Acronyms

Arctic IES	Arctic Integrated Ecosystem Survey
ASGARD	Arctic Shelf Growth, Advection, Respiration, and Deposition Rates Study
BIA	Bureau of Indian Affairs
BOEM	Bureau of Ocean Energy Management
COVID-19	Coronavirus Disease of 2019
DataONE	Data Observation Network for Earth
DBO	Distributed Biological Observatory
IARPC	Interagency Arctic Research Policy Committee
ICC-Alaska	Inuit Circumpolar Council-Alaska
IERP	Integrated Ecosystem Research Program
IPCoMM	Indigenous People's Council for Marine Mammals
K-12	Kindergarten-12th grade
NOAA	National Oceanic & Atmospheric Administration
NPRB	North Pacific Research Board
NSF	National Science Foundation
OCS	Outer Continental Shelf
ONR	Office of Naval Research
PacMARS	Pacific Marine Arctic Regional Synthesis
PAG	Pacific Arctic Group
PI	Principal Investigator
PICES	Pacific Marine Science Organization
PLOS	Public Library of Science
RFP	Request for Proposals
SOAR	Synthesis of Arctic Research
SSC	Science Steering Committee
UAF	University of Alaska Fairbanks
USFWS	U.S. Fish & Wildlife Service

1 Introduction

North Pacific Research Board (NPRB) and the Bureau of Ocean Energy Management (BOEM) entered into this Cooperative Agreement to support the Arctic Integrated Ecosystem Research Program (Arctic IERP, www.nprb.org/arctic) in partnership during 2016-2022. NPRB provided administration of the research program under this Cooperative Agreement as detailed in this report.

The Arctic IERP involved the integration of multiple streams of marine data, from physical forcing factors to the processes driving marine ecology, human dimensions and ecosystem services. The geographic scope of the program included the northern Bering Sea, Bering Strait, Chukchi Sea and the adjacent Beaufort Sea. Research from this multilateral collaboration supported mutually-identified information needs on the physical, biological and social processes in the Arctic marine environment to improve BOEM's scientific understanding of large marine ecosystem dynamics.

The Arctic IERP was led by NPRB and included partnership with BOEM, the North Slope Borough/Shell Baseline Studies Program, and the Office of Naval Research (ONR) Marine Mammals & Biology Program. The proposals funded under the Arctic IERP brought generous in-kind support from the National Oceanic & Atmospheric Administration (NOAA), University of Alaska Fairbanks (UAF), U.S. Fish & Wildlife Service (USFWS), and National Science Foundation (NSF). The program was developed in coordination with the Interagency Arctic Research Policy Committee (IARPC) and the U.S. Arctic Research Commission (USARC).

Since 1974, the BOEM Alaska OCS Region has produced a collection of studies in the Arctic to conduct interim baseline research and monitoring in fields of interest that include: meteorology, ice dynamics and basic oceanography, benthic fauna and sedimentation, marine mammals (including whales, walrus, seals, and polar bear), fish, birds, and social systems. Most of the projects have exhibited complex, multilateral collaborations with explicit inter-disciplinary linkages between the physical and biological sciences. These types of studies have pursued multi-year data collection efforts on a regional scale, with careful attention to inter-annual variability and ecosystem processes.

NPRB staff discussed the IERP model with BOEM staff at the Alaska Region and Headquarters and expressed interest in establishing a partnership to address mutual needs for information. These conversations are described in more detail in section 2 of this report that provides a brief history of the development of the partnership that enabled this Cooperative Agreement.

BOEM and NPRB built upon synthesis projects such as the "Synthesis of Arctic Research (SOAR)" and the "Pacific Marine Arctic Regional Synthesis (PacMARS)" to examine areas where collaborative studies could enhance informed decision-making on the sustainable use of marine resources. The multiple tasks of this collaborative effort included several individual study proposal topics of high interest to BOEM, such as: the influence of sea ice dynamics and advection on biotic phenology, magnitude and location of primary and secondary production; distribution and life history of upper trophic predators in response to availability of lower trophic prey resources; and quantification of rates of consumption, growth, and reproduction of benthic and pelagic organisms.

A representative of BOEM was invited to participate in the NPRB Science Panel and Advisory Panel review of proposals that NPRB received in response to a request for proposals (RFP). The BOEM representative shared the perspectives of the agency with NPRB during NPRB's discussion of the proposals and NPRB took that information into account when making funding decisions.

The overarching research question addressed by the Arctic IERP was the following:

"How will reductions in Arctic sea ice and the associated changes in the physical environment influence the flow of energy through the ecosystem in the Chukchi Sea?"

The Arctic IERP provided funding for the following scientific research projects:

- Arctic Shelf Growth, Advection, Respiration, and Deposition Rate Experiments (ASGARD)
- Arctic Shelf Growth, Advection, Respiration, and Deposition Rate Experiments (ASGARD): Marine Mammals
- Arctic Integrated Ecosystem Study (IES): Oceanography & Lower Trophic Levels
- Arctic Integrated Ecosystem Study (IES): Upper Trophic Levels
- Chukchi Coastal Communities' Understanding of and Responses to Environmental Change

This report on the Cooperative Agreement between BOEM and NPRB for the administration of the Arctic IERP includes reports on the scientific research projects identified above as appendices.

The Arctic IERP represented a direct investment of >$18.6 million to support the five scientific research projects above. The Arctic IERP also served as a nexus to support broader collaboration during 2016-2022 and several other Arctic research projects participated, many of which were supported by BOEM. These collaborations are described in the science reports, and the significant results of some of these collaborations are published in individual chapters in the science reports or in peer-reviewed manuscripts in a series of special issue publications in *Deep-Sea Research II* organized by NPRB.

2 Partnership Development

NPRB strives to fund IERP research in partnership with other agencies and institutions. Integrated multi-disciplinary marine science programs conducted in Alaska waters are expensive and require several million dollars to support. NPRB seeks to ensure that research programs of this scale address the needs of other agencies and organizations. To facilitate partnerships and ensure that these programs reflect the insights and interests of co-funding agencies, NPRB welcomes direct engagement in establishing research priorities and in developing the RFP, the implementation plan, and outreach activities. This is intended to leverage the valuable perspectives of other institutions and ensure that the research remains relevant to the missions of other agencies and organizations.

NPRB approached partnerships with engagement from the outset. Well in advance of the research program launch, NPRB staff began discussing research priorities with a wide range of relevant agencies, regional entities, and other potential partners, including BOEM. Discussions between NPRB staff and BOEM staff were initiated in 2011, more than five years in advance of the Arctic IERP launch in 2016. NPRB staff initiated a series of meetings with BOEM staff in both the Alaska Regional Office in Anchorage and at BOEM Headquarters in Washington, D.C. NPRB staff traveled to meet in person with colleagues at BOEM Headquarters on multiple occasions and met with BOEM staff in Anchorage regularly during the five years prior to the initiation of the Arctic IERP and this Cooperative Agreement. This high level of interaction was designed to ensure that those making budget decisions at every level of the agency understood the unique value of the NPRB IERP model and how the outcomes would provide information necessary to meet the BOEM mission.

Ultimately, this collaboration led to the development of a profile for "Collaboration with North Pacific Research Board (NPRB) Arctic Marine Research Program" that was incorporated into the FY15 BOEM Alaska Annual Studies Plan. NPRB responded to this profile with the proposal that was funded under this Cooperative Agreement.

As stated in the profile objectives, NPRB successfully "buil[t] upon existing working relationships with NPRB, NOAA, USGS, AOOS, industry and others by establishing financial cooperation, coordinated Request for Proposals, data sharing agreements, and logistical support agreements"... to establish a "new collaboration [that] involve[d] established funding partners and existing research implementation strategies (e.g., IARPC, Arctic Council, Distributed Biological Observatories) to form interdependent but linked studies to examine physical, biological, and social processes".

This high level of engagement with BOEM was maintained throughout the collaboration. Prior to the solicitation of research proposals, NPRB staff shared drafts of the Request for Proposals (RFP) for the Arctic IERP with BOEM staff and welcomed input. Prior to decisions on funding, NPRB also invited a BOEM Representative to observe the proposal review discussions at the NPRB Science and Advisory Panels. A BOEM representative was also invited to join the May 2016 NPRB Board meeting and used that opportunity to comment on proposals and express the BOEM perspective about the value and relevance of the proposed research to the BOEM mission. While BOEM did not vote on funding decisions, the NPRB Board seriously considered all comments voiced by BOEM prior to determining funding. BOEM Alaska Region staff actively participated throughout the Arctic IERP 2016-2021, participating in Principal Investigator meetings, and coordinating regularly with NPRB staff to stay apprised of progress and significant emerging results.

NPRB greatly appreciates the enthusiastic cooperation and unwavering commitment of BOEM staff at all levels throughout the development and implementation of the Arctic IERP.

3 Coordination Meetings

NPRB hosted coordination meetings throughout the Arctic IERP 2016-2022 to ensure coordination among all participants. Meetings included a kickoff meeting to begin coordination among the scientists; logistics meetings prior to each field season (2017-2019); hub meetings to facilitate communication with Alaska communities; annual Principal Investigator (PI) meetings; monthly Science Steering Committee (SSC) meetings; monthly PI calls/virtual meetings; Communications Working Group meetings; and funding partner coordination meetings. More detail about each of these coordination meetings is provided below. The agendas for some of these meetings are available on the Events & Meetings section of the Arctic IERP website.

3.1 Kickoff Meeting

NPRB hosted a kickoff meeting in June 2016 shortly after announcing funding decisions to facilitate coordination among the research projects. Each of the Lead Principal Investigators (PIs) discussed the hypotheses and objectives described in their respective proposals and they worked together to identify the following overarching question that the Arctic IERP would address:

> "How will reductions in Arctic sea ice and the associated changes in the physical environment influence the flow of energy through the ecosystem in the Chukchi Sea?"

An Integrated Work Plan (Appendix A; https://www.nprb.org/assets/uploads/files/Arctic/Arctic_IERP_Integrated_Work_Plan_FINAL.pdf) was developed to articulate in a cohesive manner how each of the scientific research projects would contribute to addressing the overarching question and the broad objectives of the Arctic IERP.

Representatives of research projects not funded directly under the Arctic IERP but listed in Appendix A of the NPRB request for proposals ("Appendix A projects") were invited to share information about their research and express interest in collaboration.

Discussion was invited about gaps in the funded research program and as a result, NPRB funded some smaller-scale projects to address critical gaps. These projects included:

- Microzooplankton biomass and grazing rates
- Phytoplankton-related measurements on spring cruises (2017-2018)
- ASGARD: Productivity fractionation
- ASGARD: Fish
- Seasonal distribution and energetics of Arctic fishes in the Chukchi Sea

The results of these smaller-scale projects were included in the final reports of the five main science projects funded under the Arctic IERP.

During the kickoff meeting, NPRB staff led discussions about the roles and responsibilities of all participants to set expectations. A Science Steering Committee (SSC) was established comprised of the Lead PIs of each of the five main science projects. NPRB staff formalized plans for monthly meetings with the SSC and monthly PI meetings in which all scientists funded under the Arctic IERP were expected to participate. Conversations were also hosted about plans for outreach activities.

Staff of Axiom Data Science were invited to share information about plans for data management and the services they planned to provide under a contract established by NPRB. These services included establishing a secure Research Workspace, advising scientists on authoring metadata, archiving final datasets in national repositories (e.g., DataONE), and creating a public portal for Arctic IERP data at the conclusion of the research program.

3.2 Logistics Meetings

NPRB hosted logistics meetings to facilitate communication and coordination prior to each field season in 2017, 2018, and 2019. These meetings were hosted in person over two days in October or November. NPRB staff worked in cooperation with the SSC to organize the agendas.

During these logistics meetings, scientists discussed plans for chartering vessels for the upcoming field season, the allocation of berths, the expected dates of the vessel charters, division of the cruises into legs and identifying the Chief Scientist for each leg, ports for crew changes, needs for gear and plans for shipment of gear, chain of custody for samples and allocation of samples, and standardizing data collection protocols.

NPRB staff stressed the importance of discussing how sampling plans would be adjusted in the event that the sampling could not be carried out as planned (e.g., weather delays). Scientists were encouraged to discuss, for example, the ramifications of cutting some types of sampling versus increasing the spacing between stations and how that might affect the ability to meet the broad objectives of the Arctic IERP.

Scientists also discussed plans for communicating with coastal communities about sampling plans during the research cruises. For example, during field operations, emails were sent daily to a broad distribution list to describe where the vessel was located, where it planned to be operating in the coming 24 hours, and the types of sampling planned. The Chief Scientist also announced this information over the VHF radio at least twice daily. Scientists would change the sampling plans if notified that operations would interfere with subsistence activities.

3.3 Hub Meetings

NPRB organized meetings in the "hub" communities of Nome, Kotzebue, and Utqiagvik to engage members of Alaska communities in the Bering Strait, Northwest Arctic, and North Slope regions of Alaska in conversation about Arctic IERP research plans. NPRB cooperated with Kawerak, Inc., the Northwest Arctic Borough, and the North Slope Borough to host these meetings. Every tribal council in each region was invited to nominate a representative to participate and NPRB covered their travel expenses.

Hub meetings were held in late 2016 and early 2017 prior to Arctic IERP field operations. NPRB planned to repeat these meetings periodically throughout the five-year research program and/or at the conclusion of the program, however, challenges that included the COVID-19 pandemic prevented such meetings at later stages of the Arctic IERP.

During the hub meetings, NPRB staff and Lead PIs of the science projects introduced the research plans and welcomed dialogue with meeting participants. Community members were encouraged to share concerns about any potential conflicts of research operations with subsistence harvests. During the meeting in the Bering Strait region, concerns were raised about the potential for the ASGARD cruise planned in May to conflict with walrus harvests. As a result, the cruise was shifted to June.

Participants were also asked about any environmental concerns they might have that Arctic IERP research cruises might be able to address. Participants reaffirmed that their primary concerns centered around food security. Much of the Arctic IERP research planned was relevant to addressing food security, and Arctic IERP scientists added sampling for harmful algal blooms to their research plans to further strengthen the relevance of the science to people living in the Arctic.

3.4 Principal Investigator Meetings

NPRB organized annual PI meetings in coordination with the SSC to convene all Arctic IERP participants over a period of approximately three days to share their research findings and integrate their results. These meetings are a hallmark of NPRB's IERPs. They provide important opportunities to share information across disciplines and discuss the mechanistic linkages from physics and chemistry to biology at all trophic levels. The agendas for these meetings are available on the Events & Meetings section of the Arctic IERP website.

The social science project brought members of eight Alaska communities to the annual PI meetings to share their perspectives on the science and discuss how the environmental research was relevant to their communities. They also shared their insights about the relevance of environmental versus socio-economic factors to food security for their communities.

Scientists shared plans for manuscripts they planned to submit a series of special issues in *Deep-Sea Research II* or to other peer-reviewed journals. This coordination opportunity allowed the development of papers that were broad in scope, complementary, and interdisciplinary.

PI meetings provided opportunities for the discussion of plans for outreach that were led by the NPRB Communications and Outreach Director. Scientists were encouraged to engage in outreach activities with an emphasis on communicating about the goals and scope of the broader Arctic IERP rather than one scientist's narrow field of research.

Staff of Axiom Data Science led discussions about data management and data standardization. They were available to provide assistance to scientists in authoring metadata and formatting data to meet the standards of national data repositories.

3.5 Monthly Steering Committee Meetings

NPRB staff met monthly via Zoom with SSC members to coordinate all aspects of the research program and discuss any challenges as they arose. Conversations included developing the agendas for monthly PI calls/virtual meetings and annual in-person PI meetings.

NPRB maintained a "contingency fund" in reserve to allow flexibility to respond to challenges. Staff typically discussed the application of contingency funds with the SSC, and while staff and the NPRB Executive Committee retained decision-making power, the input of the SSC was valued.

The SSC served as the Guest Editors for the series of special issues in *Deep-Sea Research II* and the SSC meetings provided an opportunity to coordinate those publications.

3.6 Monthly Principal Investigator Calls/Virtual Meetings

NPRB staff and the SSC Chair hosted monthly calls/virtual meetings in which all Arctic IERP scientists were expected to participate. Collaborating projects listed in Appendix A of the RFP were also invited to participate, as were representatives of funding partners.

Monthly meetings provided an important opportunity to facilitate regular communication among Arctic IERP scientists between the annual in-person meetings. Monthly meetings included brief updates from each participant that allowed the sharing of information about preliminary results and planned publications, for example.

NPRB staff used these meetings as opportunities to share information related to project administration (e.g., reminders about biannual progress report deadlines) and to seek input from the scientists in the development of outreach products.

3.7 Communications Working Group Meetings

The NPRB Communications and Outreach Director organized a working group comprised of communications and outreach specialists from some participating institutions including NOAA and UAF and a selection of Arctic IERP scientists who expressed interest. The working group discussed plans for developing outreach products, including a brochure highlighting the significant results of the research, a series of brief videos, lesson plans for K-12 educators updated with information about current Arctic marine science, and a museum exhibit capable of sending remote modules to Arctic communities.

3.8 Funding Partner Coordination Meetings

NPRB staff met regularly with representatives of funding partner organizations throughout the Arctic IERP to keep them apprised of the program's progress and highlight exciting preliminary results. Staff of the BOEM Alaska Region participated in monthly PI meetings and the Chief of the Alaska Environmental Studies Program met one-on-one with the NPRB Senior Program Manager for the Arctic IERP at regular intervals.

4 Award Administration

4.1 Request for Proposals and Proposal Review

NPRB drafted a request for pre-proposals (RFP) and shared it with BOEM Alaska Region staff prior to releasing it in May 2015. After the RFP was released, NPRB staff held an informational teleconference and 127 callers participated. An audio recording of the event was made available via the NPRB website. This teleconference was hosted to ensure equal access to information and to allow participants to see who else might be interested in the opportunity to help scientists identify potential collaborators.

The Arctic IERP website provided "Resources for Investigators" to help interested parties find relevant information that NPRB and funding partners hoped would be considered as proposals were developed. Resources included reports such as the Arctic IERP Implementation Plan; the Pacific Marine Arctic Regional Synthesis final report; the IARPC Arctic Research Plan 2013-2017; a report entitled "Developing a Conceptual Model of the Arctic Marine Ecosystem" that resulted from a workshop that NPRB co-sponsored in 2013; an IARPC report on "Framing Arctic Marine Research Initiatives"; and a report on the BOEM-funded Hanna Shoal research project. The website also provided links to data archives and map servers, including the Alaska Ocean Observing System's Arctic Portal; Distributed Biological Observatory; Chukchi Sea Environmental Studies Program industry-funded data; National Science Foundation Arctic Data Center; North Slope Science Initiative Data Catalog; and the Pacific Marine Arctic Regional Synthesis Data Archive and Map Server.

Eighty pre-proposals were received in response to the RFP. Following review by the NPRB Science and Advisory Panels and the Board, a selection of the applicants was invited to submit full proposals for funding consideration.

Twenty-three full proposals underwent review by peer reviewers, the NPRB Science and Advisory Panels, the Board, and representatives of funding partner organizations. Representatives of funding partners were invited to listen to the discussion of the NPRB Science and Advisory Panels and were invited to share their perspectives during the Board meeting prior to the Board's vote to fund proposals in May 2016.

4.2 Subawards, Budgets, and Grant Compliance

Scientists were notified of funding decisions in May 2016 and NPRB staff formulated a plan to allocate the funds from various sources (three NPRB Prime Awards from NOAA, BOEM Cooperative Agreement, and North Slope Borough/Shell Baseline Studies Program) to support the institutions funded under the umbrella of the Arctic IERP.

NPRB staff worked with grants administrators at the Alaska Sea Life Center (ASLC), NPRB's fiscal agent, to establish subawards. Throughout the course of the Arctic IERP, a total of 44 subawards were issued and administered by NPRB/ASLC.

ASLC assisted NPRB in ensuring that all subawards complied with applicable federal guidelines. NPRB awards were reviewed during annual audits and no issues of concern were identified.

4.3 Review of Biannual Progress Reports from Science Projects

NPRB reviewed progress reports from each of the science projects funded under the umbrella of the Arctic IERP twice per year. Progress reports provided an opportunity for the scientists to share

preliminary results of their scientific analyses, notify NPRB of any needs for no-cost extension or rebudget of their subaward, inform NPRB of any challenges with respect to their own progress or the delay of analyses that relied on collaborators, and to document progress on their provision of data.

NPRB shared progress reports from the science projects with BOEM Alaska Region program officers. These were shared as attachments to the quarterly progress reports that NPRB provided to BOEM under this Cooperative Agreement in the quarter following NPRB's receipt of the reports.

4.4 Provision of Quarterly Progress Reports to BOEM

NPRB provided quarterly progress reports to BOEM under this Cooperative Agreement. Reports included information on administrative and outreach/engagement activities undertaken during the reporting period and progress reports from the science projects were attached twice per year.

4.5 Review of Final Reports from Science Projects

The NPRB IERP Senior Program Manager and the Science Director reviewed the final reports for each of the science projects funded under the umbrella of the Arctic IERP and shared them with staff of the BOEM Alaska Region for review during winter 2022. The reports restated the hypotheses and objectives of each project and documented progress towards addressing them. Manuscripts that were accepted or submitted for publication in peer-reviewed journals were included. The full reports are attached as appendices.

The SSC, in collaboration with NPRB staff, authored a preamble that was included in each final report that provided an overview of the Arctic IERP to acknowledge the full breadth and scope of the program. This included a summary of the field operations undertaken 2017-2019 and the goals of the social science project. It also included an introduction to the history of the development of the Arctic IERP using input from previous synthesis efforts and input from Alaska communities.

5 Publication of Special Issues

NPRB has facilitated the publication of the peer-reviewed scientific research papers that result from IERPs in special issues to showcase the results of these programs in a cohesive manner. All the IERPs to date have published Special Issue volumes in the journal *Deep-Sea Research II*. The NPRB Science Director served as the Managing Guest Editor and the members of the SSC served as the Guest Editors for the Arctic IERP special issues.

The first volume of the special issue in *Deep-Sea Research II* dedicated to the Arctic IERP was published in May 2020, with 14 manuscripts (see Baker et al., 2020 for overview). All manuscripts are available online here. Twenty-six manuscripts were submitted to the second special issue volume in early 2022, including five manuscripts from Russian scientists working in collaboration with the Arctic IERP, which complement research in U.S. waters and characterize dynamics in the western Bering and Chukchi Seas. The manuscripts cover a variety of research areas, including oceanography and plankton, benthic structure and invertebrate communities, stock structure and distribution for groundfishes and pelagic fishes, shifts in distribution of pollock and cod and marine mammal distributions.

NPRB plans to support a third volume of the Arctic IERP special issue in the future to welcome manuscripts resulting from the Arctic IERP synthesis and those that were still in development when the second volume closed for submissions in early 2022.

Additional manuscripts associated with Arctic IERP data and collaborative research have been published in other journals, including PLOS One, Progress in Oceanography, Conservation Physiology, Nature Climate Change, Polar Biology, and the Proceedings of the National Academy of Sciences.

6 Administration of Contingency Funds

NPRB established a $1M Contingency Fund for the Arctic IERP, the intent of which was to provide NPRB the ability to respond to needs as they arose to ensure the integrity of the overall research program and protect the investments of NPRB and funding partners. Staff suggested the creation of such a fund based on experience during past IERPs.

NPRB staff and the Executive Committee of the Board reviewed requests for the application of the contingency funds as they arose. Examples of applications of the funds include cost-sharing contracts for the recovery of lost moored instruments and vessel repairs when gear was tangled in the propeller of a research vessel in the Chukchi Sea during field operations. Contingency funds were also applied to support the addition of sampling to address critical gaps identified during the Arctic IERP kickoff meeting in June 2016.

7 Data Management

NPRB established a contract with Axiom Data Science, Inc. to provide data management services for the Arctic IERP. Axiom provided a password-protected Research Workspace to allow scientists to share their data and derived products throughout the course of the research program 2016-2021. At the conclusion of the Arctic IERP, finalized datasets were archived in national data repositories (e.g., DataONE).

Axiom staff attended monthly PI virtual meetings and annual in-person meetings and regularly interacted with PIs about data organization, data standardization, and metadata authorship. Axiom staff offered one-on-one assistance to PIs in authoring metadata and ensured that all datasets were ready for archive at the conclusion of the Arctic IERP.

Axiom coordinated with NPRB staff to develop a public Arctic IERP data portal at the conclusion of the research program that is accessible via the Arctic IERP website. NPRB pointed to this data portal when the request for proposals for the synthesis phase of the Arctic IERP was advertised in fall 2021.

NPRB staff met regularly with Axiom staff throughout the course of the Arctic IERP to discuss the organization of the Research Workspace, provide feedback on the development of updated tools (e.g., metadata editor), and to discuss possibilities for Axiom to produce visualizations of Arctic IERP data to facilitate interdisciplinary data exploration and/or analysis.

8 Outreach and Engagement

8.1 Hub Meetings

As discussed in more detail in section 2.3 above, NPRB organized meetings in the “hub” communities of Nome, Kotzebue, and Utqiagvik to engage members of Alaska communities in the Bering Strait, Northwest Arctic, and North Slope regions of Alaska in conversation about Arctic IERP research. NPRB cooperated with Kawerak, Inc., the Northwest Arctic Borough, and the North Slope Borough to host these

meetings. Every tribal council in each region was invited to nominate a representative to participate and NPRB covered their travel expenses.

These meetings were organized based on a model used by the Pacific Marine Arctic Regional Synthesis (PacMARS) project that served as an assessment phase for the Arctic IERP and informed NPRB's development of the Arctic IERP. During those meetings in 2013, participants expressed appreciation for the opportunity those meetings provided to share information among rural Alaska communities in each region.

During the hub meetings, NPRB staff and Lead PIs of the science projects introduced research plans and welcomed dialogue with meeting participants. Discussion included the relevance of the research to addressing issues of interest to communities and how best to avoid any potential conflict of research with subsistence activities.

8.2 Reports at Meetings of Alaska Native Organizations, National, and International Venues

8.2.1 Arctic Waterways Safety Committee

The Arctic Waterways Safety Committee was active during the period that the Arctic IERP engaged in field data collection and the NPRB Senior Program Manager for the Arctic IERP and lead PIs of the field research projects participated in these meetings regularly. Prior to each field season, draft research plans were shared with the Committee, and this provided an opportunity for the scientists to learn of concerns about the potential for conflict with Alaska Native subsistence harvests. Following each field season, the scientists shared presentations about their preliminary results.

8.2.2 Alaska Native Co-Management Organizations and Inuit Circumpolar Council-Alaska

The NPRB Senior Program Manager for the Arctic IERP, and often also the Lead PIs of the science projects that involved field operations, provided reports to Alaska Native Co-Management Organizations throughout the course of the Arctic IERP. Presentations were offered both before and after field operations in 2017, 2018, and 2019 to share information about research plans and allow dialogue about how best to avoid potential conflict with subsistence activities and to share preliminary results after the field season.

Presentations were welcomed at regular intervals by the Alaska Eskimo Whaling Commission, the Indigenous People's Council for Marine Mammals (IPCoMM, a statewide umbrella organization in which many Arctic marine mammal co-management organizations participate) and occasionally the Ice Seal Committee and Alaska Beluga Whale Committee. Although other co-management organizations could not offer us time on their agendas, they did receive the information during IPCoMM meetings. Vera Metcalf of the Eskimo Walrus Commission was a member of the NPRB Advisory Panel and heard updates on the research program twice per year in that forum.

NPRB staff also communicated with staff of the Inuit Circumpolar Council-Alaska during the early stages of the Arctic IERP to discuss synergies among our respective activities, especially with respect to a food security project led by ICC-Alaska.

8.2.3 North Slope Borough Fish & Game Management Committee

The NPRB Senior Program Manager for the Arctic IERP and the SSC Chair provided a lengthy presentation to the North Slope Borough Fish and Game Management Committee and staff of the North

Slope Borough Department of Wildlife Management in Utqiagvik when it became impossible to repeat hub meetings in the North Slope Region at later stages of the research program. Participants voiced their appreciation for the opportunity for engagement in September 2018. NPRB planned to return to present the final research results of the program in later years, however, the COVID-19 pandemic prevented travel. Instead, print materials were distributed to members of the Committee by mail in fall 2021.

8.2.4 Interagency Arctic Research Policy Committee and U.S. Arctic Research Commission

The NPRB Senior Program Manager for the Arctic IERP, Danielle Dickson, served as a Co-Lead of the Marine Ecosystems Collaboration Team (MECT) for the Interagency Arctic Research Policy Committee (IARPC) throughout the course of the Arctic IERP. (Cathy Coon of the BOEM Alaska Region also served as a Co-Lead of the MECT.) MECT's >400 members include a wide range of individuals representing federal agencies and non-federal organizations and academic scientists affiliated with universities nationwide. Regular communications were provided to the MECT to share updates on the progress of Arctic IERP research and opportunities for collaboration. Plans for research cruises were shared prior to each field season and at times scientists funded by other agencies (e.g., National Science Foundation) were able to secure berths on vessels chartered for Arctic IERP research or to secure samples collected by Arctic IERP scientists.

Arctic IERP scientists were invited to share presentations about their research results during meetings of the IARPC MECT, which typically hosted monthly webinars. Personal invitations were sent to members of the research community to notify them of discussion topics that they might find particularly relevant to their interests.

The U.S. Arctic Research Commission (USARC) holds a seat on the NPRB Board and NPRB staff occasionally provided updates during Commission meetings.

8.2.5 BIA Provider's Conference and Alaska Forum on the Environment

The NPRB Senior Program Manager for the Arctic IERP and Lead PIs of the science projects provided presentations regularly at the Bureau of Indian Affairs Provider's Conference and the Alaska Forum on the Environment in which environmental scientists from rural Alaska communities statewide participated. Presentations were offered to share the results of preliminary analyses. The COVID-19 pandemic prevented opportunities to share final results at the conclusion of the Arctic IERP as planned.

8.2.6 Arctic Icebreaker Coordinating Committee

The NPRB Senior Program Manager for the Arctic IERP regularly participated in meetings of the Arctic Icebreaker Coordinating Committee to share information about plans for Arctic IERP research, particularly for the ASGARD cruises in 2017 & 2018 that were conducted aboard the R/V *Sikuliaq*. NPRB shared plans for communication with Alaska coastal communities and Alaska Native Organizations (e.g., Alaska Eskimo Whaling Commission) during research operations.

8.2.7 International Pacific Arctic Group and Pacific Marine Science Organization (PICES)

The NPRB Senior Program Manager for the Arctic IERP regularly participated in meetings of the Pacific Arctic Group (PAG), an international body that includes participation by the U.S. Canada, Japan, South Korea, China, and Russia. The PAG is organized under the International Arctic Science Committee (IASC) and its mission is to serve as a Pacific Arctic regional partnership to plan, coordinate, and collaborate on science activities of mutual interest, including the Distributed Biological Observatory (DBO). The DBO supports the collection of time series data at a set of standardized stations in the

Northern Bering, Chukchi and Beaufort Seas. Arctic IERP scientists contributed data to the DBO. PAG meetings were typically hosted twice per year in spring and fall and during these meetings NPRB staff reported the plans for the upcoming field season and the preliminary results of the previous field season. NPRB staff also advertised the expected IERP synthesis opportunity that would follow the Arctic IERP field program beginning in 2022.

The NPRB Science Director regularly participated in meetings of the International Pacific Marine Science Organization (PICES) to facilitate coordination with international scientists. Of particular interest to NPRB was attracting the collaboration of Russian scientists who could share information about the marine ecosystem on the Russian side of the Chukchi Sea where U.S. scientists were not able to gather data. Consecutive workshops were led and facilitated by the NPRB Science Director at PICES Annual Science Meetings in San Diego in 2016 and Vladivostok in 2017 in collaboration with NOAA and Russian Federal Fisheries Research Institute (VNIRO) colleagues to explore means to promote data sharing and exchange in the eastern and western Bering Sea and eastern and western Chukchi Sea. Those discussions led to longstanding international collaborations where Russian scientists participated in Arctic IES surveys in 2017 and 2019. These collaborations resulted in five manuscripts that integrated data from Russian waters and either engaged Russian scientists in collaborative data analysis or were led by Russian scientists.

More recently, international collaborations have been suspended related to complications from the COVID-19 pandemic and the current geopolitical situation.

8.2.8 Scientific Conferences

NPRB staff and Arctic IERP scientists shared the exciting results of the Arctic IERP as they emerged at a variety of science conferences, including the annual Alaska Marine Science Symposium, the biennial Ocean Sciences conference, the Society for Marine Mammalogy biennial conference, meetings of the American Fisheries Society, the Gordon Research Conference on Polar Marine Science, Arctic Science Summit Week, Arctic Observing Network meetings, and others.

During the period that the Arctic IERP was ongoing, the Nansen Legacy program was established on the Atlantic side of the Arctic and NPRB staff seized opportunities to communicate with leaders of that effort to discuss opportunities for synergy. Individual Arctic IERP scientists formed collaborations with colleagues associated with that research program.

8.3 Outreach Products

8.3.1 Website, Blog, and Social Media

NPRB created a website (www.nprb.org/arctic-program) for the Arctic IERP where information about the program was shared publicly. NPRB expects that this website will remain publicly available in perpetuity as long as NPRB exists. The website recognizes all funding partners.

The website provides a history of the funding of the Arctic IERP, including access to the RFP and the "Resources for Investigators" page that was created to help interested parties find relevant information that NPRB and funding partners hoped would be considered as proposals were developed. Resources included reports (e.g., Arctic IERP Implementation Plan, the Pacific Marine Arctic Regional Synthesis final report, the IARPC Arctic Research Plan 2013-2017, a report entitled "Developing a Conceptual Model of the Arctic Marine Ecosystem" that resulted from a workshop that NPRB co-sponsored in 2013, an IARPC report on "Framing Arctic Marine Research Initiatives", a report on the BOEM-funded Hanna Shoal research project) and links to data archives and map servers (e.g., Alaska Ocean Observing System's Arctic Portal, Distributed Biological Observatory, Chukchi Sea Environmental Studies

Program, National Science Foundation Arctic Data Center, Pacific Marine Arctic Regional Synthesis Data Archive and Map Server).

The website also provides the Integrated Work Plan established for the Arctic IERP following the kickoff meeting in June 2016 that guided the research 2016-2021. The Events & Meetings page provides the agendas for the annual PI meetings and the logistics meetings.

During the field seasons in 2017, 2018, & 2019, a field blog and social media presence were maintained to share information in near-real time about what was happening aboard the research vessels. Some of the blogs were written by Alaska Native and early career scientists who participated in the research.

8.3.2 Brochure Highlighting Significant Results

NPRB staff and Arctic IERP scientists cooperated to author an outreach brochure highlighting the significant results of the Arctic IERP. NPRB contracted a graphic designer to assist with the layout of the brochure. The brochure is available in electronic form on the Arctic IERP website.

Hard copies were mailed to a distribution list of approximately 115 tribes and Alaska Native Organizations in the Bering Strait, Northwest Arctic, and North Slope regions of Alaska. The brochure was accompanied by a cover letter expressing regret that the COVID-19 pandemic prevented travel to rural communities to share the results in person.

8.3.3 Videos

NPRB contracted a video production team to create a series of brief videos about the Arctic IERP. NPRB staff (the Communications & Outreach Director and the Senior Program Manager for the Arctic IERP) worked closely with the production team to shape the messages that these videos will convey.

NPRB hopes the videos will appeal to a broad range of audiences, including Alaska communities, the interested public nationwide and internationally, youth, the science community, and potential funding partners of future IERP research. The videos will be available via the Arctic IERP website (in late summer or fall 2022) and they will be showcased in an exhibit at the Anchorage Museum expected in 2024.

The videos provide an introduction to the scope and goals of the Arctic IERP and the value of an integrated, multidisciplinary approach to studying a marine ecosystem. The videos feature interviews with a variety of Arctic IERP scientists and include footage filmed aboard the research vessels and discussion of results filmed at the conclusion of the research program.

The videos also feature interviews with Alaska Native participants in the research, including Billy Adams, a leader from the North Slope Borough who was a member of the social science team; Harmony Wayner, a student in the Alaska Native Science and Engineering Program at the University of Alaska who worked as a summer fellow for NOAA aboard the Arctic IES surveys in 2017; and Opik Ahkinga, a community leader from Little Diomede who participated in the ASGARD cruises in 2017 & 2018 and who is conducting science in her community to monitor for harmful algal blooms. The comments shared in these interviews highlight the relevance of Arctic IERP research to Alaska communities and the value of working with communities to conduct the research.

8.3.4 K-12 Lesson Plans

NPRB issued a contract to the Arctic Research Consortium of the U.S. (ARCUS) to update Arctic marine lesson plans for K-12 educators originally created in 2013 using updated information that resulted from the Arctic IERP. NPRB co-sponsored a workshop in Barrow, Alaska (now Utqiagvik) in 2013 to create

the original lesson plans in cooperation with the Alaska Ocean Observing System, ARCUS, and the Center for Ocean Science Education Excellence Alaska. The workshop brought K-12 educators, informal education specialists, and scientists working on Alaska research projects together to cooperate to develop the lesson plans using real data collected in Alaska waters. Staff of the North Slope Borough Department of Wildlife Management and local experts also participated.

8.3.5 Museum Exhibit with Traveling Modules for Rural Communities

NPRB is pursuing an exhibit at the Anchorage Museum to showcase the Arctic IERP. The exhibit, if realized, would be on display beginning in 2024. NPRB intends to develop smaller-scale modules that could travel to rural Alaska communities and potentially use technology like virtual reality goggles to simulate research activities. The exhibit will be co-produced with Alaska Native partners and NPRB is in the early stages of discussion with the North Slope Borough Department of Wildlife Management about their interest and capacity. BOEM communications experts will be invited to participate in the design and execution of the exhibit.

9 Conclusions

NPRB greatly appreciates the partnership provided by BOEM for the Arctic IERP under this Cooperative Agreement. BOEM partnership and the involvement of BOEM staff throughout the research program helped to ensure that Arctic IERP research was relevant to meeting the applied needs of this resource management agency and others (e.g., NOAA, USFWS).

The science conducted under the umbrella of the Arctic IERP resulted in significant results that are relevant to BOEM-Alaska. The research documented significant changes in water temperature, large shifts in the distributions of species that represent important nodes in the Arctic marine food web (e.g., Arctic cod), and changes in the distribution, abundance, and timing of subarctic species presence in the Chukchi sea (e.g., Pacific cod, walleye pollock, subarctic marine mammals). All these results are relevant to updating environmental assessments for permitting activities in the Alaska OCS region.

This Cooperative Agreement allowed BOEM to leverage NPRB's experience in administering IERPs to achieve integrated, multi-disciplinary research that provides updated information about the mechanistic processes governing how the marine ecosystem in the Chukchi Sea is structured under a changing climate. NPRB is a respected leader in facilitating integrated ecosystem research and attracted highly qualified scientists affiliated with a wide range of federal and non-federal institutions and the active participation of Alaska Native and industry partners. NPRB staff applied lessons learned through previous IERPs to strengthen the Arctic IERP, for example, requiring logistics coordination meetings prior to each field season and maintaining a contingency fund to respond nimbly to challenges as they arose.

NPRB welcomes the partnership of BOEM on future Integrated Ecosystem Research Programs and looks forward to future opportunities to cooperate. NPRB intends the next IERP to continue integrated research in the Bering and Chukchi Seas, centered on the Northern Bering Sea. Areas of interest include how shifts in environmental conditions and processes may influence species of commercial, ecological and subsistence importance, and implications for state and federal fisheries management and communities that depend on these resources.

10 References

Baker MR, Farley EV, Ladd C, Danielson SL, Stafford KM, Huntington HP, Dickson DMS. 2020. Integrated ecosystem research in the Pacific Arctic–understanding ecosystem processes, timing and change. Deep Sea Research II 177, 104850. https://doi.org/10.1016/j.dsr2.2020.104850

U.S. Department of the Interior (DOI)
DOI protects and manages the Nation's natural resources and cultural heritage; provides scientific and other information about those resources; and honors the Nation's trust responsibilities or special commitments to American Indians, Alaska Natives, and affiliated island communities.

Bureau of Ocean Energy Management (BOEM)
BOEM's mission is to manage development of U.S. Outer Continental Shelf energy and mineral resources in an environmentally and economically responsible way.

BOEM Environmental Studies Program
The mission of the Environmental Studies Program is to provide the information needed to predict, assess, and manage impacts from offshore energy and marine mineral exploration, development, and production activities on human, marine, and coastal environments. The proposal, selection, research, review, collaboration, production, and dissemination of each of BOEM's Environmental Studies follows the DOI Code of Scientific and Scholarly Conduct, in support of a culture of scientific and professional integrity, as set out in the DOI Departmental Manual (305 DM 3).

Arctic Integrated Ecosystem Research Program

Integrated Work Plan

As a changing climate and sea-ice retreat progressively expose the Chukchi Sea to a longer open water season, society will confront new resource management issues. These include the future of the cultures and subsistence lifestyles of local indigenous communities, potential impacts of industrial activities (e.g. commercial fishing, oil and gas extraction), potential changes to regional ocean carrying capacity, and resilience of the arctic marine ecosystem (NRC, 2014).

To address these issues, the North Pacific Research Board in cooperation with other organizations[1] has funded integrated ecosystem research, the Arctic Integrated Ecosystem Research Program (Arctic IERP), with the goal to better understand the mechanisms and processes that structure the ecosystem and influence the distribution, life history, and interactions of biological communities in the Chukchi Sea. The overarching question that the Arctic IERP study will address is:

How will reductions in Arctic sea ice and the associated changes in the physical environmental influence the flow of energy through the ecosystem in the Chukchi Sea? Specifically, we will examine:

- Transport, seasonal composition, distribution, and production of phytoplankton, particulate matter, zooplankton, fishes, benthic invertebrates, seabirds, and marine mammals
- Timing, magnitude and fate of the primary and secondary productivity
- Partitioning/flux of energy between pelagic and benthic realms

[1] Funding for this $16 million program is provided by the North Pacific Research Board, Collaborative Alaskan Arctic Studies Program (formerly the North Slope Borough/Shell Baseline Studies Program), Bureau of Ocean and Energy Management, and the Office of Naval Research Marine Mammals and Biology Program. Additional in kind support has been contributed by the National Oceanic and Atmospheric Administration and the University of Alaska Fairbanks.

- Distribution, condition, and standing stocks of large crustacean zooplankton that serve as the prey base for upper trophic level fishes and seabirds
- Assemblages, distributions, abundances, and condition of larval and early juvenile fishes that influence the recruitment success of later life stages
- Density of marine mammals and seabirds
- Human use of, and interaction with, the marine environment

To address the goals and overarching question, Arctic IERP scientists and scientists with collaborating projects (see Appendix A) plan a diverse set of investigations, including seasonal integrated ecosystem surveys that will sample hydrography, pelagic fishes, benthic communities, observations of seabird and mammal distributions, year-round measurements from fixed autonomous samplers, and documentation of traditional knowledge of the Chukchi Sea ecosystem and the changes it is undergoing. The Arctic IERP individual project hypotheses and objectives are listed in Appendix B. The individual project timelines are listed in Appendix C.

Background

The northern Bering and Chukchi sea continental shelves that constitute a portion of the Pacific Arctic Region (PAR; Grebmeier and Maslowski 2014) annually transmit freshwater, heat, nutrients, and carbon (dissolved, particulate, and planktonic) from the North Pacific into the Arctic (Woodgate et al., 2005; Carmack & Wassmann, 2006). Previous work during the 1982-1988 Inner Shelf Transfer and Recycling (ISHTAR) program (with field work primarily in July and August) showed that the Chukchi inflow is an important source of new nitrogen for western Arctic productivity and the Arctic carbon budget as a whole (Walsh et al., 1989). Recent estimates of net community production (NCP) by Codispoti et al. (2013) on the order of 70-100 g C m^{-2} identify the northern Bering and Chukchi shelves as the singular most productive region across the entire Arctic marine system, exceeding the NCP of the Nordic seas by a factor of 2-3 and exceeding other Arctic shelf and basin systems by factors of 6-100.

An extraordinary feature of the northern Bering and Chukchi shelves that fundamentally shape the regional ecosystem is the year-round delivery of substantial nutrient concentrations (NO_3 > 10 μM) that lies many hundreds of kilometers from the nearest continental slope (Sambrotto et al., 1984; Kinder et al., 1986; Walsh et al., 1989). Nutrient delivery to the Chirikov Basin

euphotic zone is maintained at consistently high levels by the nutrient rich Anadyr Water (AW) carried by the Anadyr Current (Figure 1) where production is estimated at 250–300 g C m^{-2} y 1988; Walsh et al., 1989). Bering Strait transport can vary by nearly a factor of two inter-annually (Woodgate et al., 2012) and nutrient concentrations vary year-to-year (Danielson et al., 2016) but nutrient flux variations into the Chukchi remain unquantified.

Primary production begins initially in early spring, leading to rich sympagic communities (Gradinger 2009). Phytoplankton growth accelerates in late spring once ice retreat and snow melt permit sufficient light penetration into the water column (Hill et al., 2005; Mundy et al., 2005). Production quickly outpaces consumption by grazers, leading to the spring bloom. With an overall thinning of sea-ice, substantial under-ice blooms may also occur (Arrigo et al. 2012, Zhang et al. 2015). As the bloom wanes, ungrazed cells age and tend to settle quickly to the shallow (< 60 m) shelf, but the degree to which sinking particles are remineralized or repackaged in the pelagic zone is unknown. Nonetheless, a large fraction of the organic matter makes it to the seafloor where it sustains a thriving benthic community (Highsmith & Coyle, 1990; Feder et al., 2007; Grebmeier & Maslowski, 2014, and references therein) that supports benthic-feeding fish and marine mammals. However, during this critical period of ice retreat, the magnitude and spatial extent of the spring bloom, phyto-and zooplankton growth rates, planktonic grazing rates, and benthic deposition rates are all poorly known, thus precluding construction of a robust carbon budget. Even later in the season when zooplankton communities support rich seabird communities (Day et al., 2013; Gall et al. submitted), rate measurements of primary and secondary production remain scarce (Nelson et al., 2014).

Historically, the food web of the Chukchi ecosystem has been based on primary production driven by under-ice algal communities. However, rising Arctic temperatures have contributed to reduction in the percentage of thick, multi-year ice and a shift to thinner, first-year ice (Comiso et al. 2008). This shift has contributed to earlier seasonal sea-ice retreat which favors open water phytoplankton primary production and benefits a pelagic ecosystem (Grebmeier et al., 2006; 2015; Moore and Stabeno, 2015). The increase in water column primary production occurs in shallower water where light levels are adequate, as long as sufficient nutrients are available. During late summer, due to nutrient exhaustion in the upper mixed layer, phytoplankton in the northeastern Chukchi are typically found below the pycnocline (subsurface; Martini et al. 2016).

Thus changes in stratification will impact primary production through the inverse relationship of light availability from the surface and nutrient availability from depth.

Restructuring in the Chukchi ecosystem is not limited to a change from a benthic to a pelagic dominated system. Physical changes (e.g., increased stratification) are expected to influence nutritional quality of the prey base via a shift in the phytoplankton community to a greater fraction of small cells (Ardyna et al. 2011, Arrigo et al. 2014, Li et al. 2009). This nutritional shift is expected to re-shape zooplankton assemblage composition (Ershova et al. 2015a, 2015b, Pinchuk and Eisner in review) and energy content, increase food chain length, and decrease the trophic transfer efficiency among food web constituents. When sea-ice structures the system, waters are nutrient-rich, prolific blooms of under-ice algae are supported, and the zooplankton community is dominated by large copepods and euphausiids that provide a lipid-rich source of energy to upper trophic levels. This food web is short and efficient, supporting large numbers of seasonally abundant fish, birds, and mammals. In contrast, under warm, stratified conditions, near-surface waters contain fewer nutrients, the phytoplankton community is dominated by picoplankton and the zooplankton community is dominated by small, lipid-poor copepods. This food web is longer, less efficient, and of relatively poor nutritional quality (Richardson 2008). These food web changes will manifest as shifts in upper trophic level species distributions, changes in species assemblages at all trophic levels, seasonal changes in timing of life-cycle events (Beaugrand et al. 2002, 2003), less efficient feeding interactions (Berchok et al. 2015, Norcross et al. 2013, Logerwell et al. 2015, Sigler et al. in review), and overall reductions in biomass.

Arctic fishes such as Arctic cod (*Boreogadus saida*) and saffron cod (*Eleginus gracilis*) are key components of the PAR food web (Lowry and Frost 1981, Welch et al. 1992) and contribute to supporting large numbers of seabirds (Matley et al. 2012) and marine mammals (Bradstreet et al. 1986; Holst et al. 2001) which migrate to the Arctic to take advantage of high seasonal production. Arctic cod are particularly abundant in the PAR (Moore et al. 2014) and along with snow crab and saffron cod, are recognized as potential target species for new fisheries in this region (Arctic Fishery Management Plan 2009). Continued loss of sea ice and warming in the PAR may restructure the food web by negatively impacting Arctic cod growth and survival (Laurel et al. 2015). For instance, age-0 Arctic cod have a low thermal tolerance (< 7°C) for

growth and survival; whereas saffron cod have a much wider tolerance and are expected to thrive at higher temperatures (Laurel et al. 2015). Age-0 Arctic cod have 2.7 times more lipid per unit body mass than Age-0 saffron cod (Ron Heintz, personal communication). Therefore continued warming along the Chukchi Sea shelf may reduce the abundance of lipid-rich prey (Arctic cod) with negative consequences to other fishes and post-breeding seabirds, similar to that experienced by walleye pollock (Heintz et al. 2013) and Pacific cod (Farley et al. 2014) in the southeastern Bering Sea during a recent warming event (see Coyle et al. 2011).

In addition, continued warming of surface temperatures could increase salmon production in the Arctic. During 2007, summer sea temperatures in the Chukchi Sea were anomalously warm (Eisner et al. 2013). Integrated ecosystem surveys conducted in the Arctic during 2007 documented relatively high abundances of juvenile pink and chum salmon in the Chukchi Sea (Moss et al. 2009b). The abundant juvenile salmon returned as adults to the coastal regions of the PAR in relatively high numbers during 2008 (pink salmon) and 2009/10 (chum salmon) as reported by subsistence users in coastal communities (Carothers et al. 2013; Taquilik Hepa, personal communication). These events (anomalously warm summer sea temperatures, historic summer sea ice minima, and highly abundant juvenile pink and chum salmon in the Chukchi Sea) were all "surprises" in that they were large variations from predicted anthropogenic effects on temperatures and sea ice loss from climate models (Overland 2011). These "surprises" could become the norm in the not too distant future and while the presence of maturing salmon in Arctic waters north of known salmon producing drainages likely reflects straying and not colonization (Stephenson 2006), continued warming in marine, terrestrial and riverine environments may make it possible for these salmon to become permanently established in the Arctic.

It is also highly likely that climate warming in the Arctic will impact the abundance and distribution of seabird species. Seabird distribution is often influenced by oceanographic characteristics that promote productivity and concentrate prey (Piatt et al. 1991; Gall et al. 2013). In the Chukchi Sea, 'hotspots' of seabird abundance varied among foraging guilds (i.e., surface or diving foragers) and between summer (breeding season) and fall (post-breeding and migration), but were often associated with persistent topographic features such as shelf breaks and underwater canyons (Kuletz et al. 2015). During 2012 and 2013 northern Bering and

Chukchi Sea surveys, the distribution of planktivorous and piscivorous seabirds reflected the distribution of their prey at broad spatial scales (see reports from the Arctic Ecosystem Integrated Survey (Arctic Eis) at: https://web.sfos.uaf.edu/wordpress/arcticeis/). Gall et al. (2016) have also shown a decadal-scale shift from a predominantly piscivorous seabird community to one dominated by planktivores. If warming seas lead to longer ice-free conditions and generally higher productivity, this trend could continue. However, an alternative hypothesis is that these conditions lead to smaller zooplankton and thus less suitable prey to support high densities of planktivorous seabirds, resulting in a shift back towards a predominantly piscivorous seabird community. Furthermore, lack of high-lipid prey (Arctic cod) near breeding colonies could result in low reproductive success and high nutritional stress (see Paredes et al. 2014).

Furthermore, a "reorganization," from benthic- to pelagic-based in the PAR, might negatively impact marine mammal species that rely on sea ice for habitat (e.g., ice seals, walrus, bowhead whales) and/or benthic infauna for food (e.g., walrus, gray whales, some ice seals) via a reduction in habitat and prey abundance (Grebmeier et al. 2006). Other species, however, such as sub-Arctic "summer whales" may benefit from increased access to northern habitat and pelagic prey species (Clarke et al. 2013). One means of assessing changes in marine ecosystems (the physical environment can be measured directly) is to examine the distribution of fauna that are directly influenced by such changes (Moore et al. 2014). As the top of short Arctic food webs, marine mammals can be considered sentinels of environmental change (Moore 2008; et al. 2014). Changes in cetacean abundance and distribution have been shown in conjunction with short and long time scale climate events in the north Pacific (Benson et al. 2002; Fiedler 2002; Croll et al. 2005) and Bering Sea (Stafford et al. 2010).

Lastly, understanding the relationships between coastal residents and the marine environment is an essential contribution to the effective management of Arctic marine resources and activities that affect those communities and resources (e.g., BOEM 2014). Year-to-year variability in subsistence harvests of many species is high (e.g., ADF&G, N.D., Noongwook et al. 2007, Huntington et al. 2013c). Much of the variability can be attributed to changes in physical conditions (e.g., Ashjian et al. 2010, Kapsch et al. 2010), affecting access as well as distribution of the species being sought. When longer term variability has been documented, it has reflected factors such as the shift from dog teams to snowmachines (Burch 1985), the imposition of the

International Whaling Commission's quota for bowhead whales (Huntington 1992), access to financial resources stemming from oil development at Prudhoe Bay (Huntington 1992), and changing tastes, for example in fur seals on St. Paul Island (Lestenkof et al. 2011, Fall et al. 2013).

Gross indicators of well-being in Arctic communities suggest improvements in recent decades (e.g., AHDR 2004, 2014). In the Chukchi region, subsistence harvests overall appear to be robust (ADF&G, N.D.), with some prominent exceptions such as poor walrus hunting years on St. Lawrence Island (due in part to sea ice conditions) or high variability in bowhead whale harvests in many communities (personal communications from community residents). These variations are likely related to environmental variability, but distinct from long-term trends. There are many assertions of negative impacts from climate change and other forms of environmental change, but few unambiguous demonstrations that the impacts are indeed negative and widespread.

Project design

Shipboard Surveys

Arctic Shelf Growth Advection Respiration Deposition Rate (ASGARD) – Spring 2017 and 2018

Berth Space: Contact the PI for berth availability discussions.

The R/V Sikuliaq, a newly-constructed ice-capable research vessel engineered to be acoustically quiet, will be used to survey the northern Bering and southern Chukchi shelf (Figure 1). The survey will consist of water-column and benthic work in open-water and in/near the ice-edge, in late May and early June 2017 and 2018. The research surveys will work south to north, occupying ten "process" stations (yellow squares in Figure 1), setting up growth rate experiments that require extended (~ 10 day) incubation times and collecting our broad suite of standard measurements (Table 1). Moorings that record year-round time-series will be serviced when the ship stops for process stations. Once all process-station experiments are running, the ship would transition to a "survey" mode of operation, rapidly working north-to-south along multi-station transects and re-occupying the process stations with a more limited sampling suite to provide information about short-term (~days) changes to the water-column and continued trawl and benthic samplings. Throughout the cruise we will collect continuous underway navigational, ocean surface, ocean profile, and meteorological data to provide additional environmental

context for subsequent analyses. In addition, measurements of microzooplankton carbon biomass and grazing rates will be conducted throughout the spring survey as well as phytoplankton-related measurements to compliment those planned on the late summer surveys. Collection of fishes will occur as part of the spring-season ASGARD expeditions on the *R/V Sikuliaq* within the northern Bering and southern Chukchi seas. Sampling will take place in open water, at the ice edge, and in the pack ice in late May through early June in 2017 and 2018. The fish stations (n = 20) will include all process stations, equidistant sampling along the Arctic Marine Biodiversity Observing Network (AMBON) and Distributed Biological Observatory (DBO) lines, the Alaska side of the Bering Strait, and across Chirikov Basin. Demersal fishes will be sampled using a 3-m plumb staff beam trawl, allowing for direct comparison with collections with past Arctic research programs and with the late summer Arctic IES cruise. Sub samples of fishes collected during the survey will be preserved on board the vessel and processed at the UAF Oceanography Laboratory following a systematic protocol that includes length, weight, removal of otoliths, stomachs, and tissues (for stable isotopes and seasonal energetics).

Arctic Integrated Ecosystem Survey (Arctic IES) – Summer 2017 and 2019

Berth Space: Contact the PI for berth availability discussions.

An integrated ecosystem survey of the Chukchi and western Beaufort seas (Figure 2) will occur during August through early October in 2017 and 2019. Operations performed at each grid station are listed in Table 2. The survey will follow the protocols developed for Arctic Eis (Arctic Ecosystem Integrated Survey 2014) and Bering Aleutian Salmon International Survey (BASIS) (Farley et al. 2005). Sampling of oceanography and lower trophic levels (LTL) and upper trophic levels (UTL) will be conducted on one vessel capable of deploying bio/physical oceanographic gear, fish trawls (pelagic/surface/midwater) and demersal trawls (3-m plumb-staff beam trawl). Acoustic measurements along survey transects (gridded regions from east to west) along with modified Marinovich midwater trawl samples targeting water column backscatter will be used to estimate the distribution and abundance of midwater young-of-the-year cods and other forage fishes in the survey area. Surface trawls (Cantrawl 400/600) will be conducted at nearshore stations to assess juvenile salmon. Demersal trawls (3-m plumb-staff beam trawl (PSBT) will be utilized along gridded stations to assess older age classes of Arctic cod and crab.

Similar to the spring survey, subsamples of fishes and jellyfish from surface, midwater, and bottom will be collected for diet, otoliths, isotopes and seasonal energetics.

Oceanography and plankton sampling will be coordinated with the Arctic Integrated Ecosystem Survey Phase II Lower Trophic Level (LTL) team. Four transects on the Chukchi shelf have been occupied previously by the Ecosystems and Fisheries Oceanography Coordinated Investigations Program (EcoFOCI) and others, and three transects sample across the Chukchi slope. Three transects across the Beaufort Slope will investigate connections between the Chukchi and Beaufort ecosystems. The Barrow Canyon transect corresponds to DBO-5; the Icy Cape and Cape Lisburne lines have been occupied annually since 2010 by EcoFOCI; the Pt. Hope line is the U.S. portion of DBO-3. Shipboard activities will include: CTD casts, paired bongo tows for zooplankton tows; and deployment of towed vehicle (Sea Sciences Inc. Acrobat). High-resolution measurements from the Acrobat will include pressure, temperature (T), salinity (S), chlorophyll a (Chla) fluorescence, oxygen, nitrate and photosynthetically active radiation. In addition measurements of microzooplankton community composition, abundance, and biomass will be conducted throughout the late summer survey and phytoplankton-related measurements to complement those collected during the spring survey.

Seabird surveys will be conducted using visual observations and standardized strip transects (Tasker et al. 1984, Kuletz et al. 2008), with adjustments used for previous Alaska surveys (USFWS 2008). Surveys will be conducted during daylight hours while transiting between sample stations. The observer records all marine bird and mammal sightings within 300m and a 90° arc forward from the 'center line' (line of travel). Standard transect width will be 300m, with individual sightings recorded in distance bins (0-50m, 50-100m, 100-200m, 200-300m, >300m), and angle from the observer in 5 degree increments. Birds in the water or actively foraging are recorded continuously, while flying birds are recorded during quick 'scans' of the transect window at intervals of approximately 1• min-1 (depending on vessel speed) to avoid overestimating. The observer records observations directly into a laptop computer using survey software DLog3 (A.G. Ford, Inc., Portland, OR), recording species, number of individuals, behavior (on water, in air, on ice, foraging), distance bin, and angle. Environmental variables such as sea state (Beaufort scale), glare, weather, and sea ice cover (proportion in tenths) are recorded at first entry and automatically thereafter unless updated as necessary.

Moorings

ASGARD

The *ASGARD* mooring array consists of three biophysical moorings south of Bering Strait, two moorings in the southern Chukchi Sea plus the NPRB Long-Term Monitoring Program NE Chukchi Sea Ecosystem Mooring located on the southern flank of Hanna Shoal near Barrow Canyon. Together, these six moorings will collect bio/physical oceanographic data to examine cross-shelf differences between the Anadyr Water (AW) and Alaska Current Water (ACW) regimes and physical and biogeochemical changes imparted as the waters flow across the shelf into the Arctic. These instruments will record year-round to reveal time histories of: a) Nutrient and phytoplankton concentrations and fluxes; b) The bifurcation of flow to either side of St. Lawrence Island and the influence of regional winds on the upstream structure and partitioning of water masses feeding Bering Strait; c) Conditions in Anadyr Strait, in the nexus of the most important zone at which subsurface nutrients are mixed to the surface as they arrive at Chirikov Basin and Bering Strait; d) AW and ACW properties and advection rates; e) Phytoplankton blooms, sinking organic matter fluxes and their relationship to advective supply, light, ice thickness and the retreating ice edge; and f) Bottom sediment resuspension with respect to water and ice motion.

In addition, data will be collected on the occurrence of vocal marine mammals as upper trophic level consumers at the top of a complex Arctic ecosystem. To do so, hydrophone packages will be added onto three proposed oceanographic moorings as part of the ASGARD program to improve our understanding of the northern Bering and Chukchi Sea ecosystem and its constituent parts, structure and functioning by examining productivity drivers, energy pathways and turnover rates, migratory and distribution patterns, and human dimensions. The hydrophone data will be used to 1) document the inter-seasonal and inter-annual presence of vocal marine mammals (Arctic and sub-Arctic) in the Bering Strait; 2) Integrate presence with co-located oceanographic data to better understand how the physical environment influences the biological inhabitants of that environment; 3) Provide data on ambient noise levels in the region to assess the impact of commercial shipping; 4) Report to local communities on the health of the ecosystem including information on new species, and residency times of Arctic species. The combination of passive acoustic and physical and biological oceanographic data sets will provide urgently required

information on how species presence varies seasonally with changes in benthic and water column prey, sea ice, currents, ocean water temperatures and freshwater flow. The proposed effort in collaboration with other ASGARD PIs will provide data on interannual variability and the bio-physical drivers of this variability. Co-located ecosystem measurements from "wind to whales" will allow for the testing of scientific hypotheses such as: how do oceanographic conditions dictate the residency of different marine mammal species? Are temperate species "invading" the Arctic and what will their influence be on Arctic species and Arctic food security?

Arctic IES

Subsurface moorings would be deployed at sites provided in Figure 2. These moorings measure current speed and direction (ADCP; RCM-9), near-bottom T and S, oxygen, nitrate, Chla fluorescence, PAR, bottom pressure and turbidity. C2 also measures ice thickness. C1, C2 and C4 moorings are presently in the water and will be redeployed in 2016 by PMEL/RUSALCA. All four moorings will be recovered and re-deployed in 2017 and in 2018 on RUSALCA or another cruise, and recovered in 2019. Data from these moorings thus constitute a valuable long-term record that allows examination of interannual variability. Also at C2, a summer, surface mooring will measure radiation (shortwave, longwave, direct/diffuse), meteorological parameters (wind speed/direction, atmospheric pressure, air temperature, relative humidity, sky camera) and oceanographic parameters (T, S, Chla fluorescence, oxygen, nitrate, PAR) at multiple depths throughout the water column. The radiometer suite will include a new-generation radiometer (SPN-1 from Delta-T Devices) that distinguishes between direct and diffuse light. Three of the moorings (C1, C4, C11) will be instrumented from 2017 to 2019 with next generation upward-looking active acoustic instrumentation (i.e., Simrad wideband autonomous transceiver; WBAT) to collect 70 kHz and/or 38/200kHz data continuously to describe abundance, distribution, and movement patterns of the dominant fish backscattering (e.g., Arctic cod) throughout the water column at different spatio-temporal scales (vertical and geographic scales over hourly to interannual periods).

<u>Autonomous Platforms</u>

Numerous new sensors and platforms are being developed at PMEL through the Innovative Technology for Arctic Exploration (ITAE) program http://www.pmel.noaa.gov/itae/technologies).

Profiling Floats: To sample ice-covered waters in spring, two types of profiling floats are under development: a pop-up float, and an ice-reinforced ARGO-like float. In collaboration with this proposal, ITAE will deploy both types of floats in spring 2017, and results from these early missions will steer future development and help guide 2019 deployment strategy. Pop-up floats reside on the bottom until scheduled release when they rise toward the surface profiling the water column. Upon reaching the ice, they continue to sample directly under the ice until it melts, at which time they transmit all data back to PMEL. A series of pop-up floats will be anchored (near C2) and programmed to sequentially release under the ice in spring, recording the evolution of water properties throughout the water column and the environment directly under the ice as it melts. Planned sensors include pressure, tilt, T, S, PAR or multi-channel irradiance, and Chla fluorescence.

Once free of ice, data from the float will be returned via satellite. Current development is for profile data to also be transmitted to a moored data recorder that would be recovered in summer/fall. These floats acquire otherwise difficult-to-obtain profiles and time series of light, Chla, warming and freshening directly under the ice. ITAE is working with MRV Systems LLC to develop ice-reinforced biogeochemical ARGO floats (Air- Launched Autonomous Micro-Observer [ALAMO]) designed for use in shallow waters. In collaboration with this proposal, ITAE plans to deploy 6 biogeochemical ALAMO floats from aircraft and/or ships of opportunity. In spring 2016, two ALAMO floats with a CTD will be deployed from a Twin Otter aircraft in open waters of the Chukchi Sea as part of a heat flux experiment. These floats are expected to provide ~100 profiles of the water column shortly after ice retreat. The development plan is to incorporate oxygen, Chla fluorescence and PAR or multi-channel irradiance sensors into ALAMO floats equipped with ice algorithms and hardened crowns for protection when encountering ice. These floats will provide numerous profiles of the water column before and after ice retreat, with potential to observe the release of ice-algae and determine sinking rates of algal mats. For more Eulerian like time series, ALAMO floats can

park on the bottom between scheduled profiles. Thus, profiles can be closely linked to other moored time series.

Profiling Gliders: In 2017, PMEL will provide a Slocum glider for measuring CTD, oxygen and nitrate through the water column. The Slocum will be deployed from the USCGC Healy during Arctic Shield (or other ship of opportunity), and recovered during the fall survey. In addition, ITAE and NOAA-OAR are currently building two variable-speed coastal gliders. This glider is designed to rapidly change buoyancy to avoid bottom, and has maximum speed of ~2 kts to allow the glider to punch through buoyant layers or escape strong coastal currents. The gliders will measure pressure, T, S, oxygen, Chla fluorescence, colored dissolved organic matter (CDOM) fluorescence, red-light backscatter (to estimate organic particle concentration), and irradiance (either PAR or multi-channel irradiance).

In addition, one glider will be equipped with a multi-wavelength Light Detection and Ranging (LIDAR) sensor. This sensor is being developed by Dalgleish and Twardowski (Harbor Branch Oceanographic Institute) with funding from NOAA-OAR. LIDAR will be used to quantify particle size and distinguish between diffuse phytoplankton blooms and sinking algal clumps associated with the ice. The second glider will be equipped with a holographic zooplankton Video Plankton Recorder (VPR). This system is currently being developed by Hare (NMFS) and Davis (Woods Hole Oceanographic Institution) in collaboration with SeaSCAN Inc. and ITAE. The system will have two prongs extending in front of the glider nose-cone that encase the camera and laser light source. The holographic camera brings into focus all particles >60 μm that pass between the prongs. An onboard classification system is designed to identify and quantify zooplankton and ichthyoplankton.

Field testing of gliders and LIDAR are planned in spring and summer 2016; the initial field program is planned for Gulf of Mexico in 2017. Incorporation of the VPR into the glider should be complete by fall 2017. In spring 2018 and 2019, ITAE will deploy these two gliders in the Chukchi Sea in collaboration with this proposal with the goal to quantify particle size, identify and quantify species of zooplankton and ichthyoplankton, distinguish between phytoplankton and ice-derived algal clumps, explore the light field, patch size, sinking rate, and duration of sinking ice-algae, and determine whether events are widespread or localized to hotspots.

Profiling Mooring: The Profiling Crawler (PRAWLER) is a programmable autonomous platform attached to the radiation buoy's mooring line. This platform uses wave energy to crawl up the mooring line, and can either crawl or free-fall back down the mooring line. Operation is controlled from shore with options for profiling frequency (~5 min per round trip) or holding at fixed depth. The instrument package includes CTD, oxygen sensor, and Chla fluorometer. Data from the PRAWLER, together with other instruments at the site, can be used to investigate internal waves and mixing processes, determine heat flux of the upper water column, and provide high-resolution sampling of oxygen and Chla biomass in the two-layer system. In summer 2015, the PRAWLER, sampled between 5 and 25 m, completing ~30,000 profiles.

Saildrone: The Saildrone is an autonomous vehicle that utilizes wind for propulsion and solar panels to power on-board systems. The Saildrone derives its speed from a 4-m wing. In heavy seas, outrigger hulls provide stability and the wing can be eased to reduce power and heeling. The payload capacity (~100 kg) is distributed among several payload bays along the 5.8-m hull. The drones autonomously sail to a series of remotely provided waypoints. Data (returned in real time) include position, atmospheric parameters (sunlight, barometric pressure, wind, air temperature and relative humidity) and oceanic parameters (T, S, Chla and CDOM fluorescence, oxygen, nitrate, red-light backscatter). ITAE will plan an oceanographic and acoustic survey in 2019 to augment the Lower Trophic Level (LTL) - Upper Trophic Level (UTL) field program in the Chukchi Sea. (In 2017, the Saildrones are obligated to a CO2 survey in the Chukchi Sea). Active acoustics will be the same instrument to be used in the UTL moorings (as described in the linked UTL proposal), either a 70 kHz splitbeam, or 38/200 kHz (38/200 split/single beam).

Arctic Communities

Literature & Archive Review: Using the results of a PI survey circulated in summer 2016 as well as the hypotheses and work plans of other Arctic IERP components, a survey of publications on LTK and subsistence harvests will be carried out, supplemented by reviewing archival materials from the Kawerak Eskimo Heritage Program, University of Alaska Fairbanks Oral History Program and Project Jukebox, and other sources. The intent is to find relevant material that has already been documented so that this existing information can be used by Arctic IERP and associated researchers to address their hypotheses and find connections between their work and LTK. This work will proceed iteratively. A first review will be done prior to the March 2017 PI

meeting, so that results can be shared at that time with other researchers. The resulting conversations, in person at the PI meeting and subsequently by email and teleconference, will point to areas where further details are desired, which will guide further review of the literature and archives. This process will continue in FY18 and FY19.

Annual Team Meetings: The LTK team, consisting of the four PIs/co-PIs, and nine residents of coastal communities in the Arctic IERP region (one each from Savoonga, Diomede, Buckland, Kotzebue, Kivalina, Point Hope, Point Lay, Wainwright, Barrow; participants will be selected for experience with scientific-LTK collaborations as well as the depth of their own LTK) will meet in conjunction with the annual PI meeting in FY17, FY18, and FY19. The group will consider the results of the literature and archive review and analyze these and other information, including personal experience and LTK, to address the hypotheses of this component of the Arctic IERP. The group will also consider the areas of focus and interest of other Arctic IERP components and associated projects and review the available information to prepare for interactions with the other Arctic IERP researchers. In FY20 and FY21, the effort will shift to writing and synthesis, and the team will be reduced to the four researchers plus one coastal resident from each of the three regions (Bering Strait, Northwest Arctic, North Slope).

The approach will be structured as follows. Prior to the annual LTK team meetings, the core research team will review the compiled information and assemble the evidence for and against each of our hypotheses. This information will be shared with our community partners prior to the meeting. At the meeting, we will review the evidence, discuss additional sources of information including the community partners' own experience and observations, and assess the hypothesis in question. This stage is the central piece of our approach, having community residents help in the analysis of available evidence rather than just serving as sources of information for others to analyze later and elsewhere. We expect the discussions to provide far greater depth and context than will be apparent from the written and recorded sources we have reviewed, few if any of which will have been targeted to our specific hypotheses. The assessment will include an appraisal of what other information would help determine whether the hypothesis is true or false, and/or help increase the confidence we have in our conclusion. We will then develop a plan for further research, with published and archival materials as well as with the personal experiences and community connections of our community research partners. The additional research will be

carried out for the following annual meeting, at which time we will repeat the compilation of evidence, discussion, and assessment. It is likely that the outcome will be a more sophisticated revision of the hypothesis statement rather than a simple true/false determination, as these topics are complex and likely to vary greatly from one community to the next.

Annual PI Meetings: The LTK team (four researchers, nine community members) will participate in the annual PI meetings in FY17, FY18, and FY19. The intent is to interact as much as possible with other researchers, to share the LTK we have gathered, to get new direction for further LTK inquiry, and to find opportunities to collaborate on analysis (teasing apart the pieces of the system that make it work) and synthesis (developing a conception of the system as a whole based on our understanding of the pieces). In FY20 and FY21, as noted above, the LTK team will be reduced from 13 to seven members, and will focus at the PI meetings on collaborative papers and other products involving other AIERP researchers.

The approach here will be similar to that for our own research team's meetings. For topics of interest to other researchers, we will lay out the findings from LTK and from scientific studies side by side and compare and contrast them in collaboration with the other PIs, looking for complementarity seeking insight into differences, and drawing greater confidence from similarities. These initial insights will be the basis for further exploration of the topic in question, which if sufficiently insightful will be developed into a collaborative paper.

During these interactions and discussions, we will apply the principles of LTK research that have proven successful. For example, we will let the coastal residents take the discussions in directions they find interesting and important, allowing them to establish chains of thought that might not occur to other researchers. We will emphasize discussion over formal presentations, and find ways to encourage informal conversations, e.g., during meals and breaks. We will recognize different communication styles, such as comfort with silence and different ways of expressing dissent, to make sure all perspectives are heard and no participants are left out.

References

ADF&G. N.D. *Community Subsistence Information System*. Juneau: Alaska Department of Fish and Game, Division of Subsistence. https://www.adfg.alaska.gov/sb/CSIS/

AHDR. 2004. *Arctic Human Development Report*. Akureyri, Iceland: Stefansson Arctic Institute.

AHDR. 2014. *Arctic Human Development Report: Regional Processes and Global Linkages*. Copenhagen: Nordic Council of Ministers.

Arctic Fishery Management Plan 2009. Fishery Management Plan for fish resources of the Arctic Management Area. North Pacific Fishery Management Council, Anchorage, Alaska. 158 Pgs.

Ardyna, M., Gosselin, M., Michel, C., Poulin, M., and Tremblay, J.E., 2011. Environmental forcing of phytoplankton community structure and function in the Canadian High Arctic: contrasting oligotrophic and eutrophic regions, Mar. Ecol. Prog. Ser., 442, 37–57, doi:10.3354/meps09378.

Arrigo, K. R., D. K. Perovich, R. S. Pickart, Z. W. Brown, G. L. van Dijken, K. E. Lowry, M. M. Mills, M. A. Palmer, W. M. Balch, N. R. Bates, C. R. Benitez-Nelson, E. Brownlee, K. E. Frey, S. R. Laney, J. Mathis, A. Matsuoka, B. Greg Mitchell, G. W. K. Moore, R. A. Reynolds, H. M. Sosik, and J. H. Swift., 2014. Phytoplankton blooms beneath the sea ice in the Chukchi Sea. Deep Sea Res. Part II, 105:1-16. DOI: 10.1016/j.dsr2.2014.03.018.

Arrigo, K.R., Perovich, D.K., Pickart, R.S., Brown, Z.W., van Dijken, G.L., Lowry, K.E., Mills, M.M., Palmer, M.A., Balch, W.M., Bahr, F., Bates, N.R., Benitez-Nelson, C., Bowler, B., Brownlee, E., Ehn, J.K., Frey, K.E., Garley, R., Laney, S.R., Lubelczyk, L., Mathis, J., Matsuoka, A., Mitchell, B.G., Moore, G.W.K., Ortega- Retuerta, E., Pal, S., Polashenski, C.M., Reynolds, R.A., Schieber, B., Sosik, H.M., Ste hens, M., Swift, J.H., 2012. Massive Phytoplankton Blooms Under Arctic Sea Ice. Science 336(6087), 1408.

Ashjian, C.J., S.R. Braund, R.G. Campbell, J.C. George, J. Kruse, W. Maslowski, S.E. Moore, C.R. Nicolson, S.R. Okkonen, B.F. Sherr, E.B. Sherr, and Y.H. Spitz. 2010. Climate variability, oceanography, bowhead whale distribution, and Iñupiat subsistence whaling near Barrow, Alaska. *Arctic* 63:179-194.

Beaugrand G., Brander K. M., Lindley J. A., Souissi S., Reid P. C. 2003. Plankton effect on cod recruitment in the North Sea. Nature. 426:661-664.

Beaugrand. G., Reid P. C., Ibañez F., Lindley J. A., Edwards M. 2002. Reorganisation of North Atlantic marine copepod biodiversity and climate. Science. 296:1692-1694.

Benson, S., D.A. Croll, B.B. Marinovic, F.P. Chavez, J.T. Harvey. 2002. Changes in the cetacean assemblage of a coastal upwelling ecosystem during El Nino 1997-98 and La Nina 1999. Progress in Oceanography 54(1-4):279-291.

Berchok, C.L., J.L. Crance, J.A. Mocklin, P.J. Stabeno, J.M. Napp, M. Wang, and C.W. Clark. 2015. Chukchi Offshore Monitoring In Drilling Area (COMIDA): Factors Affecting the Distribution and Relative Abundance of Endangered Whales. Draft Final Report, OCS Study BOEM 2015. National Marine Mammal Laboratory, Alaska Fisheries Science Center, NMFS, NOAA, 7600 Sand Point Way NE, Seattle, WA 98115-6349.

Bradstreet, M.S.W., K.J. Finley, A.D. Sekerak, W.B. Griffiths, C.R. Evans, M.F. Fabijan, and H.E. Stallard. 1986. Aspects of the biology of Arctic cod (*Boreogadus saida*) and its importance in Arctic marine food chains. Canadian Technical Report of Fisheries and Aquatic Sciences 1491. 193pgs.

Burch, E.S. Jr. 1985. *Subsistence in Kivalina: a Twenty-Year Perspective*. Technical Paper No. 128. Juneau:Alaska Department of Fish &Game, Division of Subsistence.

Carmack, E. and P. Wassmann, 2006. Food webs and physical-biological coupling on pan-Arctic shelves: unifying concepts and comprehensive perspectives, Prog. Oceanogr., 71, pp. 446–477

Carothers, C., S. Cotton, and K. Moerlein. 2013. Subsistence use and knowledge of salmon in Barrow and Nuiqsut, Alaska. Final Report to OCS study Bureau of Ocean and Energy Management 2013 – 0015. 58 pgs.

Clarke J, Stafford K, Moore SE, Rone B, Aerts L, Crance J. 2013. Subarctic Cetaceans in the Southern Chukchi Sea: Evidence of Recovery or Response to a Changing Ecosystem *Oceanography* 26(4):136–149

Codispoti, L.A., V. Kelly, A. Thessen, P. Matrai, V. Hill, M. Steele and B. Light, 2013. Synthesis of primary production in the Arctic Ocean: III. Nitrate and phosphate based estimates of net community production. Progress in Oceanography 110, 126–150.

Comiso, J.C., Parkinson, C.L., Gersten, R., Stock. L. 2008. Accelerated d cline in arctic sea ice cover. Geophysical Research Letters, 35, L01703, doi:10.1029/2007GL031972.

Coyle, K.O., L.B. Eisner, F.J. Mueter, A.I. Pinchuk, M.A. Janout, K.D. Cieciel, E.V. Farley, and A.G. Andrews. 2011. Climate change in the southeastern Bering Sea: impacts on pollock stocks and implications for the oscillating control hypothesis. Fisheries Oceanography 20(2):139-156.

Croll, D.A., B. Marinovic, S. Benson, F.P. Chavez, N. Black; et al., 2005. From wind to whales:trophic links in a coastal upwelling system. Marine Ecology Progress Series 289:117-130.

Danielson. S. L., L. Eisner, C. Ladd, C. Mordy, L. de Sousa, and T. J. Weingartner 2016. A comparison between late summer 2012 and 2013 water masses, macronutrients, and phytoplankton standing crops in the northern Bering and Chukchi Seas, Arctic Eis DSR-II Special Issue

Day, R.H., T.J. Weingartner, R.R. Hopcroft, L.A.M. Aerts, A.L. Blanchard, A.E. Gall, B.J. Gallaway, D.E. Hannay, B.A Holladay, J.T. Mathis, B.L. Norcross, J.M. Questel and S.S. Wisdom, 2013. The offshore northeastern Chukchi Sea, Alaska: a complex high-latitude ecosystem. Cont. Shelf Res. 67, 147–165, http://dx.doi. org/10.1016/j.csr.2013.02.002.

Eisner, L., N. Hillgruber, E. Martinson, and J. Maselko. 2013. Pelagic fish and zooplankton species assemblages in relation to water mass characteristics in the northern Bering and southeast Chukchi seas. Polar Biology 36:87-113.

Ershova, E., Hopcroft, R., and Kosobokova, K. 2015a. Inter-annual variability of summer mesozooplankton communities of the western Chukchi Sea: 2004-2012. Polar Biology. doi: 10.1007/s00300-015-1709-9.

Ershova, E., Hopcroft, R., Kosobokova, K., Matsuno, K., Nelson, R., Yamaguchi, A., Eisner, L. 2015b. Long- Term Changes in Summer Zooplankton Communities of the Western Chukchi Sea, 1945–2012. Oceanography 28(3):100-115, http://dx.doi.org/10.5670/oceanog.2015.60.

Fall, J.A., N.S. Braem, C.L. Brown, L. Hutchinson-Scarbrough, D.S. Koster, and T.M. Krieg, T.M. 2013. Continuity and change in subsistence harvests in five Bering Sea communities: Akutan, Emmonak, Savoonga, St. Paul, and Togiak. *Deep-Sea Research II* 94:274-291.

Farley, E.V., Jr., J.M. Murphy, B.W. Wing, J.H. Moss, and A. Middleton. 2005. Distribution, migration pathways, and size of western Alaska juvenile salmon along the eastern Bering Sea shelf. Alaska Fisheries Research Bulletin 11:15-26.

Farley, E.V., Jr., R.A. Heintz, A.G. Andrews, and T.P. Hurst. 2014. Size, diet, and condition of age-0 Pacific cod (*Gadus macrocephalus*) during warm and cool climate states in the eastern Bering Sea. Deep-Sea Research II, http://dx.doi.org/10.1016/j.dsr2.2014.12.011.

Feder H.M., S. C. Jewett and A L. Blanchard, 2007. Southeastern Chukchi Sea (Alaska) macrobenthos Polar Biology 30:261-275 doi:10.1007/s00300-006-0180-z

Fiedler, P.C. 2002. Environmental change in the eastern Tropical Pacific Ocean:Review of ENSO and decadal variability. Marine Ecology Progress Series 244:265-283.

Gall, A. E., T. C. Morgan, R. H. Day, and K. J. Kuletz. 2016. Ecological shift from piscivorous to planktivorous seabirds in the Chukchi Sea, 1975-2012. Global Change Biol.

Gall, A.E., R.H. Day, and T.J. Weingartner. 2013. Structure and variability of the marine-bird community in the northeastern Chukchi Sea. Continental Shelf Research 67:96-115.

Grebmeier, J.M., J.E. Overland, S.E. Moore, E.V. Farley, E.C. Carmack, L.W. Cooper, K.E. Frey, J.H. Helle, F.A. McLaughlin, and S.L. Mc Nutt. 2006. A major ecosystem shift in the northern Bering Sea. Science 311: 1461-1464.

Grebmeier, J.M., W. Maslowski, 2014. The Pacific Arctic region: ecosystem status and trends in a rapidly changing environment. In: Grebmeier, J.M., Maslowski, W. (Eds.), The Pacific Arctic Region: Ecosystem Status and Trends in a Rapidly Changing Environment. Springer, Dordrecht, pp. 1–16.

Grebmeier, J.A., B.A. Bluhm, L.W. Cooper, S.L. Danielson, K.R. Arrigo, A.L. Blanchard, J.T. Clarke, R.H. Day, K.E. Frey, R.R. Gradinger, M. Kedra, B. Konar, K.J. Kuletz, S.H. Lee, J.R. Lovvorn, B.L. Norcross, and S.R. Okkonen 2015. Ecosystem characteristics and processes facilitating persistent macrobenthic biomass hotspots and associated benthivory in the Pacific Arctic. Progr. Oceanogr. Synthesis of Arctic Research (SOAR) special issue 136: 92-114.

Heintz, R.A., E.C. Siddon, E.V. Farley, Jr., and J.M. Napp. 2013. Correlation between recruitment and fall condition of age-0 pollock (*Theragra chalcogramma*) from the eastern Bering Sea under varying climate conditions. Deep-Sea Research II 94:150-156.

Highsmith, R. C. and K. O. Coyle, 1990. High productivity of northern Bering Sea benthic amphipods. Nature 344(6269):862–864

Hill, V., Cota, G.F., Stockwell, D., 2005. Spring and summer phytoplankton communities in the Chukchi and Eastern Beaufort Seas. Deep Sea Research II 52, 3369-3385.

Holst, M., I. Stirling, and K.A. Hobson. 2001. Diet of ringed seals (*Phoca hispida*) on the east and west sides of the north water polynya, northern Baffin Bay. 2001. Marine Mammal Science 17(4):888-908.

Huntington, H.P. 1992. *Wildlife Management and Subsistence Hunting in Alaska*. London: Belhaven Press.

Huntington, H.P. 1998. Observations on the utility of the semi-directive interview for documenting traditional ecological knowledge. *Arctic* 51(3): 237-242.

Huntington, H.P., and the Communities of Buckland, Elim, Koyuk, Point Lay, and Shaktoolik. 1999. Traditional knowledge of the ecology of beluga whales (*Delpinapterus leucas*) in the eastern Chukchi and northern Bering seas, Alaska. *Arctic* 52(1): 49-61.

Huntington, H.P., P.K. Brown-Schwalenberg, K.J. Frost, M.E. Fernandez-Gimenez, D.W. Norton, and D.H. Rosenberg. 2002. Observations on the workshop as a means of improving communication between holders of traditional and scientific knowledge. *Environmental Management* 30(6): 778-792.

Huntington, H.P., N.M. Braem, C.L. Brown, E. Hunn, T.M. Krieg, P. Lestenkof, G. Noongwook, J. Sepez, M.F. Sigler, F.K. Wiese, and P. Zavadil. 2013a. Local and traditional knowledge regarding the Bering Sea ecosystem: selected results from five indigenous communities. *Deep-Sea Research II* 94:323-332.

Kapsch, M.-L., H. Eicken, and M. Robards. 2010. Sea ice distribution and ice use by indigenous walrus hunters on St. Lawrence Island, Alaska, in: I. Krupnik, C. Aporta, S. Gearheard, L. Kielsen Holm, and G. Laidler, eds. *SIKU – Arctic Residents Document Sea Ice and Climate Change*. Berlin: Springer. pp. 115-144.

Kinder, T.H.,D. C. Chapman and J.A. Whitehead, 1986. Westward intensification of the mean circulation on the Bering Sea Shelf. J. Phys. Oceanogr. 16, 1217-1229. 10.1175/1520-0485(1986)016<1217:wiotmc>2.0.co;2.

Kuletz, K., M. Ferguson, A. Gall, B. Hurley, E. Labunski, and T. Morgan. 2015. Seasonal Spatial Patterns in Seabird and Marine Mammal Distribution in the Eastern Chukchi and Western Beaufort Seas: Identifying Biologically Important Pelagic Areas. Progress in Oceanography 136: 175–200.

Kuletz, K.J., E.A. Labunski, M. Renner, and D. Irons. 2008. The North Pacific Pelagic Seabird Observer Program. North Pacific Research Board, Final Report, Project No. 637.

Laurel, B.J., M. Spencer, P. Iseri, L.A. Copeman. 2015. Temperature-dependent growth and behavior of juvenile Arctic cod (*Boreogadus saida*) and co-occurring North Pacific gadids. Polar Biology.

Lestenkof, P.M., P.A. Zavadil, S.M. Zacharof, and E.M. Melovidov. 2011. *Subsistence Harvest Monitoring Results from 1999 to 2010 and Local and Traditional Knowledge Interview Results for St. Paul, Alaska. A Report to the North Pacific Research Board*. St. Paul: Aleut Community of St. Paul Island, Alaska, Tribal Government Ecosystem Conservation Office.

Li, W.K.W., McLaughlin F.A., Lo ejoy C., Carmack, E.C., 2009. Smallest algae thrive as the Arctic Ocean freshens. Science, 326, 5952–539.

Logerwell, E., Busby, M., Carothers, C., Cotton, S., Duffy-Anderson, J.T., Farley, E., Heintz, R., Holladay, B., Horne, J., Johnson, S., Lauth, R., Moulton, L., Neff, D., Norcross, B., Parker-Stetter, S., Seigle, J., and Sformo, T. 2015. Fish communities across of spectrum of habitats in the western Beaufort Sea and Chukchi Sea. Progress in Oceanography. 136:115-132.

Lowry, L.F., and K.J. Frost. 1981. Distribution, growth, and foods of Arctic cod (*Boreogadus saida*) in the Bering, Chukchi, and Beaufort Seas. Canadian Field-Naturalist 95(2):186-191.

Martini, K.I., Stabeno, P., Ladd, C., Winsor, P., Weingartner, T., Mordy, C., Eisner, L., 2016. Dependence of subsurface chlorophyll on seasonal water masses in the Chukchi Sea. J. Geophys. Res. - Oceans.

Matley, J. K., A. T. Fisk, and T. A. Dick. 2012. Seabird predation on Arctic cod during summer in the Canadian Arctic. Marine Ecology Progress Series 450:210-228.

Moore, S. E. 2008. Marine mammals as ecosystem sentinels. Journal of Mammalogy **89**:534–540.

Moore, S.E., E. Logerwell, L. Eisner, E.V. Farley, Jr., L.A. Harwood, K. Kuletz, J. Lovvorn, J. M. Murphy, and L.T. Quakenbush. 2014. Marine fishes, birds and mammals as sentinels of ecosystem variability and reorganization in the Pacific Arctic Region. Pgs. 337-392 *In* J.M. Grebmeier and W. Maslowski (eds.), The Pacific Arctic Region: Ecosystem Status and Trends in a Rapidly Changing Environment, DOI 10.1007/978-94-017-8863-2_2.

Moore, S.E., and P.J. Stabeno 2015. Synthesis of Arctic Research (SOAR) in marine ecosystems of the Pacific Arctic. Progr. Oceanogr. Synthesis of Arctic Research (SOAR) special issue 136: 11.

Moss, J.H., J.M. Murphy, E.V. Farley, Jr., L.B. Eisner, and A.G. Andrews. 2009b. Juvenile pink and chum salmon distribution, diet, and growth in the northern Bering and Chukchi Seas. North Pacific Anadromous Fish Commission Bulletin 5:191-196.

Mundy, C.J., Gosselin, M., Ehn, J.K., Belzile, C., Poulin, M., Alou, E., Roy, S., Hop, H., Lessard, S.,Papakyriakou, T.N., Barber, D.G., Stewart, J., 2011. Characteristics of two distinct high-light acclimated algal communities during advanced stages of sea ice melt. Polar Biol. 34:1869–1886, doi: 10.1007/s00300-011-0998-x.

National Research Council (NRC), 2014. The Arctic in the Anthropocene, Emerging Research Questions. Committee on Emerging Research Questions in the Arctic,Polar Research Board,Division on Earth and Life Studies, H. Huntington and S. Pfirman, co-chairs, 224 pp., ISBN: 978-0-309-30183-1.

Nelson, R.J., Ashjian, C., Bluhm, B., Conlan, K., Gradinger, R., Grebmeier, J., Hill, V., Hopcroft, R., Hunt, B., Joo, H., Kirchman, D., Kosobokova, K., Lee, S., Li, W.K.W., Lovejoy, C., Poulin, M., Sherr, E., Young, K., 2014. Biodiversity and biogeography of the lower trophic taxa of the Pacific Arctic region: sensitivities to climate change. In: Grebmeier, J.M., Maslowski, W. (Eds.), The Pacific Arctic Region: Ecosystem Status and Trends in a Rapidly Changing Environment. Springer, Dordrecht, pp. 269–336.

Noongwook, G., the Native Village of Savoonga, the Native Village of Gambell, H.P. Huntington, and J.C. George. 2007. Traditional knowledge of the bowhead whale (*Balaena mysticetus*) around St. Lawrence Island, Alaska. *Arctic* 60(1):47-54.

Norcross, B., Raborn, S., Holladay, B., Gallaway, B.J., Crawford, S.T., Priest, J., Edenfield, L.E., and Meyer, R. 2013. Northeastern Chukchi Sea demersal fishes and associated environmental characteristics 2009-2010. Continental Shelf Research. 67: 77-95.

Overland, J.E. 2011. Potential Arctic change through climate amplification processes. Oceanography 24(3):176-185.

Paredes, R., R.A. Orben, R.M. Suryan, D.B. Irons, D.D. Roby, et al. 2014. Foraging Responses of Black-Legged Kittiwakes to Prolonged Food-Shortages around Colonies on the Bering Sea Shelf. PLoS ONE 9(3):e92520. doi:10.1371/journal.pone.0092520.

Piatt, J.F., J.L. Wells, A. MacCharles, and B.S. Fadely. 1991. The distribution of seabirds and fish in relation to ocean currents in the southeastern Chukchi Sea. *In*: W.A. Montevecchi and A.J. Gaston (eds), Population Biology and Conservation of Marine Birds Symposium, St. Joh's, NF. Occasional Papers of the Canadian Wildlife Service, Ottawa, ON.

Pinchuk, A., Eisner L., in review. Spatial heterogeneity in zooplankton distribution in the eastern Chukchi Sea as a result of large-scale interactions of water masses. Deep Sea Res. II, Arctic Eis Special Issue.

Richardson, A.J. 2008. In hot water: zooplankton and climate change. ICES J. Mar. Sci. 65(3): 279-295.

Sambrotto, R.N., J.J. Goering, and C.P. McRoy, 1984. Large yearly production of phytoplankton in the western Bering Strait. Science. 225:1147-1150.

Sigler, M., Mueter, F., Bluhm, B., Busby, M., Cokelet, E., Danielson, S., Robertis, A., Eisner, L., Farley, Iken, K., Kuletz, K., Lauth, R., Logerwell, L., Pinchuk, A. in review. Summer zoogeography of the northern Bering and eastern Chukchi Seas, Deep Sea Res II.

Stafford, K. M., S. E. Moore, P. J. Stabeno, D. V. Holliday, J. M. Napp, and D. K. Mellinger. 2010. Biophysical Ocean Observation in the Southeastern Bering Sea, Geophys. Res. Lett., doi:10.1029/2009GL040724.

Stephenson, S.A. 2006. A review of the occurrence of Pacific salmon (*Oncorhynchus* spp.) in the Canadian Western Arctic. Arctic 59(1):37-46.

Tasker, M.L., P.H. Jones, T. Dixon, and B.F. Blake. 1984. Counting seabirds at sea from ships: a review of methods employed and a suggestion for a standardized approach. Auk 101:567-577.

USFWS, 2008. North Pacific Pelagic Seabird Observer Program Observer's Manual, U.S. Fish and Wildlife Service, Migratory Bird Management, Anchorage, AK, 33pgs.

Walsh, J.J., C.P. McRoy, L.K. Coachman, J.J. Goering, J.J. Nihoul, T.E. Whitledge, T.H. Blackburn, P.L. Parker, C.D. Wirick, P.G. Shuert, J.M. Grebmeier, A.M. Springer, R.D. Tripp, D.A. Hansell, S. Djenidi, E. Deleersnijder, K. Henriksen, B.A. Lund, P. Andersen, F.E. Mullerkarger and K. Dean, 1989. Carbon and nitrogen cycling within the Bering Chukchi Seas - source regions for organic-matter effecting AOU demands of the Arctic Ocean. Prog. Oceanogr. 22, 277-359. 10.1016/0079-6611(89)90006-2

Welch, H.E., M.A. Bergmann, T.D. Siferd, K.A. Martin, M.F. Curtis, R.E. Crawford, R.J. Conover, and H. Hop. 1992. Energy flow through the marine ecosystem of the Lacaster Sound region, Arctic Canada. Arctic 45(4):343-357.

Woodgate, R. A., K. Aagaard, and T. J. Weingartner, 2005. Monthly temperature salinity, and transport variability of the Bering Strait throughflow, Geophys. Res. Lett., 32, L04601, doi:10.1029/2004GL021880

Woodgate, R. A., T. J. Weingartner, and R. Lindsay, 2012. Observed increases in Bering Strait oceanic fluxes from the Pacific to the Arctic from 2001 to 2011 and their impacts on the Arctic Ocean water column, Geophys. Res. Lett., 39, L24603, doi:10.1029/2012GL054092

Zhang, J., Ashjian, C., Campbell, R.G., Spitz, Y.H., Steele, M., Hill, V., 2015. The influence of sea ice and snow cover and nutrient availability on the formation of massive under-ice phytoplankton blooms in the Chukchi Sea. Deep-Sea Res. II. 118, 122-135.

Table 1. Survey Station measurements on ASGARD surveys. All measurements listed here will also be made at all Process Stations. Underway samples (Table 4) will also be collected at all stations. Abbreviations include: T=temperature, S = Salinity, Chla = cholorophyll a , ChlaF = chlorophyll a fluorescence, DO = Dissolved Oxygen, PAR = photosynthetically available radiation, CTD = conductivity temperature depth datalogger.

Measurement	Instrument	Temporal/Spatial resolution
T,S,P, ChlaF, DO, PAR, Beam Transmittance	SeaBird SBE 911 CTD	1-m ave. profiles all survey stations
Photosystem-II efficiency Photosystem-II quantum yield	CDT-mounted Chelsea FRRF	5-m ave. profiles all survey stations
NO_3, NO_2, NH_4, PO_4, SiO_4, Total size-fractioned Chla	CTD Rosette	5-10 depths per station. All survey stations
Quantity & quality of sediment organic matter, and modeled degradation rates within sediments (labile protein, chloropigments, TOC, $d^{13}C$)	Multicore	20-30 survey stations
Sediment grain size	Multicore	20-30 survey stations
Bacterial biomass in sediments (ATP)	Multicore	20-30 survey stations
Abundance, biomass and functional group analysis of benthic meio-and macro-infauna with $d^{13}C$ and $d^{14}N$ of select species	Multicore	20-30 survey stations
Metazooplankton composition, abundance, biomass	Plankton nets (150 and 505µm)	20-30 survey stations
Microzooplankton composition, abundance, biomass	CTD Rosette	20-30 survey stations
Particle size distribution (65 µm – 2.5 cm)	Underwater Vision Profiler 5	5 m depth bins All survey stations

Particle size distribution (2.5 – 500 µm)	Sequoia LISST	5 m depth bins All survey stations
Mesozooplankton abundance	Underwater Vision Profiler 5	All survey stations
Phytoplankton primary production (total and size fractionated) and taxonomic identification	CTD Rosette	6 depths per station at a subset of stations
Fatty acid analysis of seston and zooplankton	CTD Rosette Plankton nets	At a subset of stations

Table 2. Station measurements taken on the Arctic Integrated Ecosystem Survey. Abbreviations include: T=temperature, S = Salinity, Chla = cholorophyll a , ChlaF = chlorophyll a fluorescence, DO = Dissolved Oxygen, PAR = photosynthetically available radiation, CTD = conductivity temperature depth datalogger.

Measurement	Instrument	Temporal/Spatial resolution
T,S,P, ChlaF, DO, PAR, Beam Transmittance	SeaBird SBE 911 CTD	1-m ave. profiles all survey stations
NO_3, NO_2, NH_4, PO_4, SiO_4, Total size-fractioned Chla	CTD Rosette	5-10 depths per station. All survey stations
Metazooplankton and ichthyoplankton composition, abundance, biomass	Plankton nets (150 and 505µm)	All grid survey stations
Microzooplankton composition, abundance, biomass	CTD Rosette	All grid survey stations
Abundance, biomass, composition of benthic community	3 m plumb staff beam trawl	All grid survey stations

Abundance, biomass, composition of pelagic community	Acoustic – modified marinovich trawl	Continuous collection of acoustic data with trawl sampling as needed to verify acoustic targets
Abundance, biomass, composition of epi-pelagic community	Cantrawl rope trawl	All nearshore grid stations (red triangles)
Phytoplankton primary production (total and size fractionated) and taxonomic identification	CTD Rosette	6 depths per station at a subset of stations
Fatty acid analysis of seston and zooplankton	CTD Rosette Plankton nets	At a subset of stations

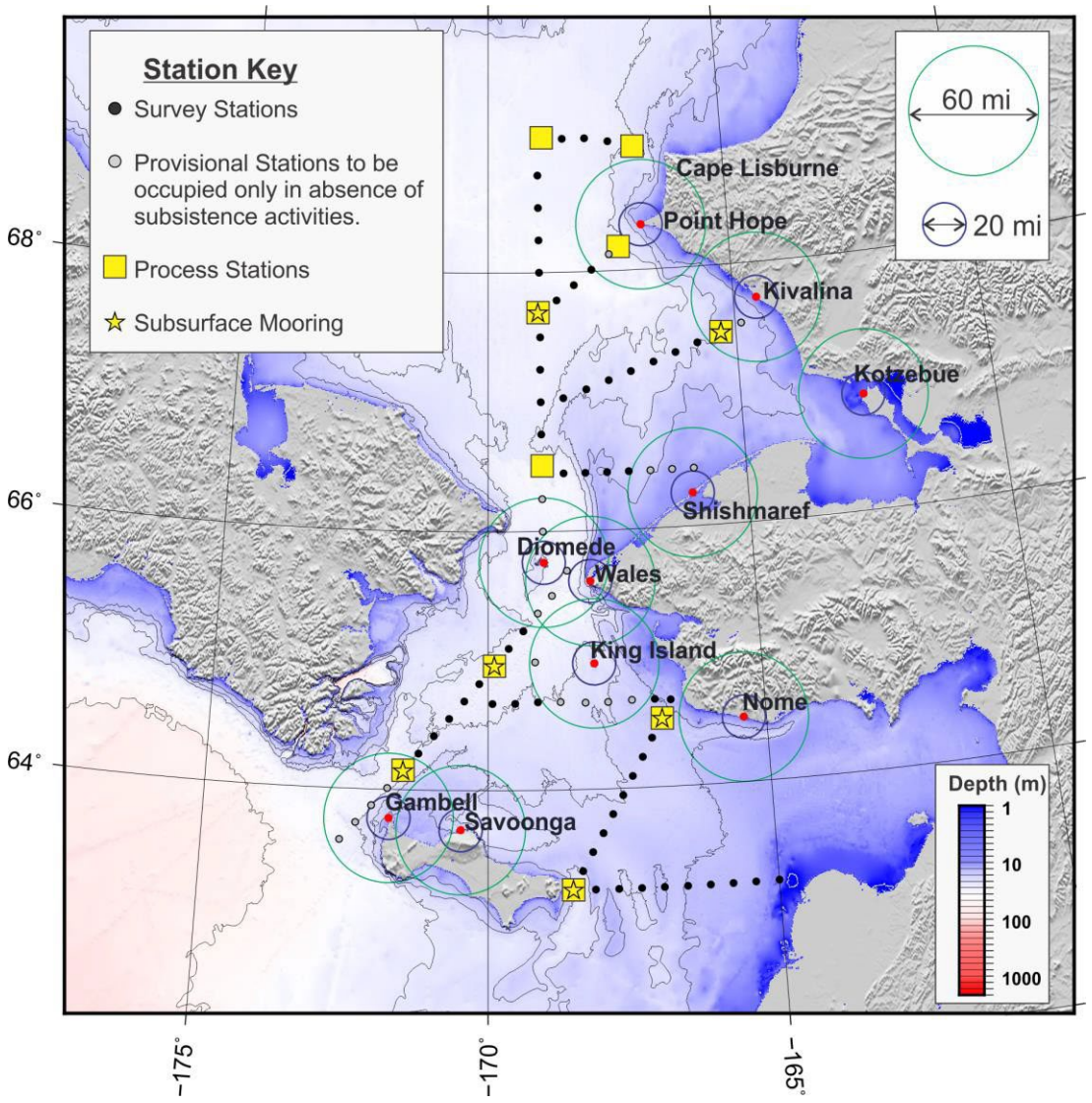

Figure 1. Proposed station and mooring locations for ASGARD during May and June 2017 and 2019. Process stations would be occupied first (from south to north), then survey stations would be occupied from north to south. Microphone icons denote locations of companion marine mammal recorders.

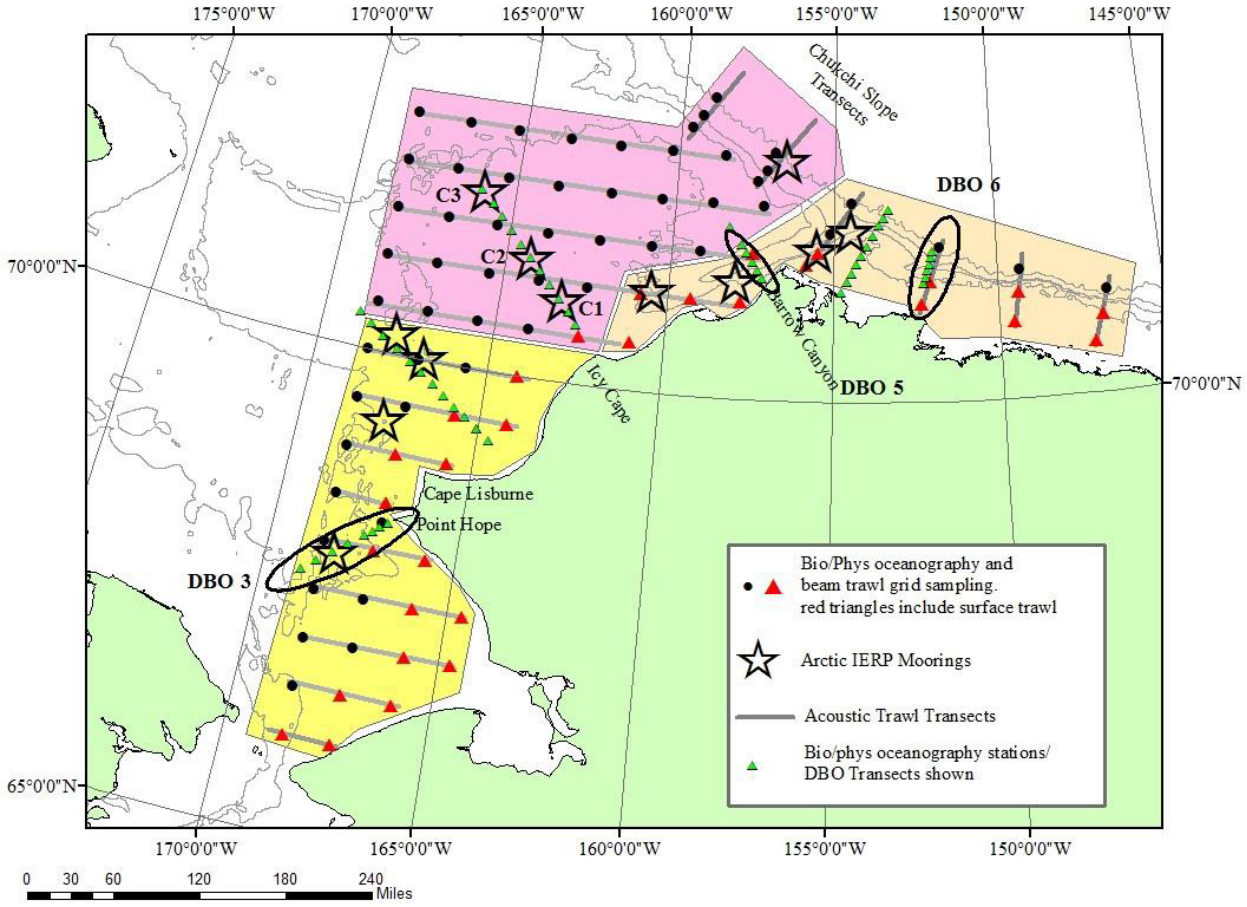

Figure 2. Proposed station (black dots, green and red triangles), mooring (black stars) locations, and acoustic trawl transects (grey lines) during Arctic Integrated Ecosystem Surveys, August to October 2017 and 2019.

Integration and Plans for Synthesis

Integration of analyses will occur throughout the Arctic IERP, and will involve collaborating Appendix A projects when feasible. To the extent that collaborating investigators are interested, joint manuscripts will be prepared that draw on data collected directly by this program and by other relevant projects. NPRB plans to organize a series of special issue publications to publish the results of this program, and papers that involve collaboration with other projects are encouraged.

Lead Principal Investigators (PIs) of other ongoing projects may elect to commit to collaboration and join the list of Appendix A collaborators at any point. The Arctic IERP expects such projects to commit to sending a representative to annual Arctic IERP PI meetings (travel expenses and salary will not be reimbursed) and to share data within a password-protected portal established for the Arctic IERP. In turn, collaborators will gain access to the Arctic IERP data and will be invited to join collaborative discussions throughout. If interested, contact the NPRB Senior Program Manager, Danielle Dickson (Danielle.Dickson@nprb.org).

NPRB intends to issue a call for proposals for a synthesis that will begin shortly after the main Arctic IERP field program concludes in fall 2021. Ideally the synthesis will include some investigators who have participated throughout and some new participants. The synthesis may emphasize modeling projects that would integrate the data collected by the field program.

Appendix A−Collaborating Projects

North Pacific Research Board is cooperating with other funding organizations to formally include the existing projects listed here in the Arctic ecosystem program. These projects will collaborate with projects funded through this call for proposals; the lead Principal Investigators will participate in annual PI meetings, share preliminary data with collaborators, and contribute intellectually to addressing the core hypotheses of the funded research program. Proposers are encouraged to describe how their research would use the data and expertise provided by existing projects. Existing projects are not intended to constrain the direction of the new research projects proposed.

Bering Strait mooring program

Funding provided by National Science Foundation

A physical oceanographic year-round mooring program has been maintained in the Bering Strait since 1990, with measurements for other disciplines being incorporated in recent years. For an overview of this prior mooring and accompanying section work, please see Woodgate, Stafford and Prahl (submitted) http://psc.apl.washington.edu/HLD/Bstrait/BStraitMooringSynthesis2015.html. Under National Science Foundation Arctic Observing Network (NSF-AON) funding, a set of 3 Bering Strait moorings will be maintained in the strait from summer 2014 to recovery in summer 2018, with annual mooring turn-around cruises, which (as time and weather allow) run accompanying CTD sections (no water samples) in the strait.

Lying all in US waters, the three mooring

- A2 (center of US channel);
- A4 (east side of US channel, measuring the Alaskan Coastal Current); and
- A3 (central to the strait about ~ 35km north of the Diomede Islands, at a site found to give a useful average of the flow through the Russian and US channels of the strait).

The data from the 3 moorings sites (combined with some satellite data) allow hourly quantification of the volume, heat and freshwater fluxes through the strait and an estimate of the physical water properties of the mean flow, of the waters in the US and Russian channels, and of

the Alaskan Coastal Current. These data are being combined with modeling results (Heimbach and Nguyen, MIT) and traditional knowledge (Raymond-Yakoubian, Kawerak, Inc) to yield a fuller understanding of the properties of the throughflow.

Each mooring carries lower level (~45m) and upper level (~17m) temperature and salinity sensors and an upward looking ADCP measuring water velocity in 2m bins to the surface, and some measure of ice thickness and ice velocity. (All instruments are internally recording, thus data are only available after recovery, and data calibration.) All calibrated data and data products are available via our website (psc.apl.washington.edu/BeringStrait.html), ACADIS and NODC. See e.g., the 2014 cruise report for full details, including mooring locations, cruise maps, and preliminary results (Woodgate et al., 2014, Bering Strait Norseman II 2014 Mooring Cruise Report, 73 pp, available at http://psc.apl.washington.edu/BeringStrait.html).
For further details (e.g., re data collaborations or possible additions to the moorings), contact Rebecca Woodgate.

Rebecca Woodgate, University of Washington, (206) 221-3268, woodgate@apl.washington.edu, psc.apl.washington.edu/BeringStrait.html

Arctic Marine Biodiversity Observing Network (AMBON)

Funding provided by Bureau of Ocean Energy Management, National Oceanic and Atmospheric Administration, and Shell

This study will build on emerging distributed biological observatories (DBOs) by developing a prototype ecosystem-based marine biodiversity network over offshore oil and gas lease areas in the Chukchi Sea, monitoring multiple trophic levels and species, and informed by historical data and past modeling efforts. Such a network will: expand upon planned and recently-launched observing sites, systems, and programs; employ innovative techniques for data discovery and methods that dynamically interrelate data sets and add value to existing monitoring data; collaborate with the U. S. Integrated Ocean Observing System (U.S. IOOS) participants and funding agencies to optimize data management and modeling capabilities.

Katrin Iken, University of Alaska Fairbanks, (907) 474-5192, kbiken@alaska.edu, https://www.sfos.uaf.edu/

Aerial Survey Arctic Marine Mammals (ASAMM)

Funding provided by Bureau of Ocean Energy Management

Bowhead whales, gray whales, beluga whales, Pacific walrus, polar bears, bearded seals, and other species of ice seals are known to seasonally occupy the Chukchi Sea. All of these species are subject to changes in environmental variables such as oceanographic currents, sea temperature, sea ice cover, prey availability, and anthropogenic impacts. Having a good understanding of the seasonal distribution, relative abundance, and habitat use of marine mammals in the Chukchi Sea is fundamentally important to evaluating the potential environmental impacts associated with oil and gas exploration and development and other anthropogenic activities. Aerial surveys of marine mammals are an efficient tool because they offer quick coverage of large marine areas. Past surveys are available for comparison with new data to assess whether changes in distribution or abundance have occurred since the earlier surveys were completed.

Megan Ferguson, National Oceanic and Atmospheric Administration, (206) 526-6274, Megan.Ferguson@noaa.gov, http://www.nmfs.noaa.gov/

Chukchi Acoustic, Oceanography and Zooplankton Study (CHAOZ)

Funding provided by Bureau of Ocean Energy Management

Baleen whales are subject to changes in environmental variables such as oceanographic currents, sea temperature, sea ice cover, prey availability, and anthropogenic impacts. Extreme ice-retreat and climate warming in the western Arctic over the last decade is anticipated to lead to changes in species composition and distribution, evidenced already through local knowledge and opportunistic observations. Hanna Shoal in the northeast Chukchi Sea is an area of special biological concern bordering the boundary between Chukchi and Arctic Ocean waters and its importance bowhead, gray and other whales, as well as walruses and ice seals, is not well known. The shallower waters of the shoal have long been known as traps for grounding of sea ice, and the creation of reoccurring polynyas. In most recent years, floating pack ice in summer persists in this area longer than elsewhere in the Chukchi, often surrounded by open water even to the north. Biological “hot spots” in the Chukchi Sea are thought to be related to coupled pelagic and benthic productivity.

Catherine Berchok, National Oceanic and Atmospheric Administration, (206) 526-6331, Catherine.Berchok@noaa.gov, http://www.nmfs.noaa.gov/

Characterization of the Circulation on the Continental Shelf Areas of the Northeast Chukchi and Western Beaufort Seas

Funding provided by Bureau of Ocean Energy Management

This study is a continuation and expansion of the existing surface circulation study within the northeast Chukchi Sea. Prior to 2009, surface current observations on the Chukchi shelf were extremely limited. Through a joint Industry/BOEM supported study, the University of Alaska Fairbanks (UAF), Coastal Marine Institute began measuring surface currents during the open water period on the Chukchi shelf beginning in September 2009 with the deployment of long range, High Frequency (HF) radar systems located at the villages of Barrow and Wainwright. In 2010, coverage was expanded to the southwest to include additional offshore lease areas. The surface current data was supplemented by water column profile data collected by Slocum Gliders. Acoustic Doppler current profilers (ADCPs) were also deployed across the Alaska Coastal Current at the head of Barrow Canyon to assess the annual flow regime, the connectivity between surface and subsurface currents during the open water season, and the changes in subsurface currents beneath the mobile pack ice and lead system during the winter months. This study will expand present efforts to improve understanding of the flow regime and shelf dynamics between the inner and outer Chukchi shelf, the exchange of waters between the Chukchi Sea and western Beaufort shelf through Barrow Canyon, and the upwelling of Atlantic Waters.

Thomas Weingartner, University of Alaska Fairbanks, (907) 474-7993, tjweingartner@alaska.edu, https://www.sfos.uaf.edu/

Distribution of Fish, Crab and Lower Trophic Communities in the Chukchi Sea Lease Area

Funding provided by Bureau of Ocean Energy Management

This study proposes to develop a broader understanding of abundance and distribution of demersal and pelagic fish, crab, and lower trophic communities needed to evaluate and mitigate the effects of offshore oil and gas development. Formerly, several BOEM funded studies have

identified temporal, seasonal, and spatial gaps in data on fish in the Chukchi Sea near the lease areas. This study is designed specifically to fill these information needs. It will build upon recent information on invertebrate communities in the Chukchi offshore lease area obtained by the 2009 study "Chukchi Sea Offshore Monitoring in Drilling Area (COMIDA): Chemistry and Benthos (CAB)." It will create a similar survey design such that data sets are compatible, comparable, and extend the time series and contribute to further knowledge of pelagic fishes in the northeast Chukchi Sea.

Franz Mueter, University of Alaska Fairbanks, (907) 796-5448, fmueter@alaska.edu, https://www.sfos.uaf.edu/

Marine Arctic Ecosystem Study (MARES)

Funding provided by Bureau of Ocean Energy Management, Office of Naval Research, Shell, U.S. Arctic Research Commission, U.S. Coast Guard, and ArcticNet

This project intends to collect additional comprehensive and integrated information in the Arctic on the spatio-temporal distribution of fundamental physical, biological and chemical variables, their associated interactions and regulating mechanisms, as well as the distribution of cultural and subsistence resources which sustain local communities. This information will be used to better understand and assess arctic ecosystem sensitivities and vulnerabilities as a function of space and time to aid decision-makers in minimizing the impact of the oil and gas industry on the Outer Continental Shelf. The resulting information will support NEPA analyses, environmental impact assessments, in validating models, as well as in Oil-Spill Risk Analysis. Additionally, these observations and improved description and understanding of biogeochemical and physical interactions will aid to improve the accuracy of model simulations and forecasts. Coordinated observational and modeling efforts will produce information that will be analyzed from different perspectives: a) ecosystem understanding and environmental protection, b) climate change and monitoring, and c) Oil-Spill Risk Analysis.

Francis Weise, Stantec Consulting, (907) 343-5276, francis.wiese@stantec.com, http://www.stantec.com/

Hanna Shoal Project

Funding provided by Bureau of Ocean Energy Management

The Hanna Shoal Project complements the earlier BOEM-supported COMIDA CAB project. Field work for the Hanna Shoal Project is complete and the PIs are synthesizing the results. Hanna Shoal is a shallow topographic feature of the northeastern Chukchi Sea that lies about 100 mi northwest of Barrow, Alaska at latitude 72° N. Water depths on various parts of the Shoal are as shallow as 20 m (60 ft), compared to 55 to 60 m (180 ft) on the surrounding seabed. The deeper flanks of the shoal are biologically rich, as reflected in the historically high concentration of walruses there in the summer that actively feed on the abundance of molluscs, crustaceans, polychaete worms, and other benthic fauna. 5

Oceanographers attribute the high productivity of Hanna Shoal, and the northeastern Chukchi Sea shelf in general, to the unique physics that steer highly productive water masses into the region, the relatively shallow average depth (42 m on the northeastern Chukchi Shelf), and weak grazing pressure from low zooplankton abundance during spring. These factors facilitate the deposition of a large proportion of pelagic primary production to the seabed, thus providing a major carbon subsidy to the benthic food web. The result is an extraordinary high diversity and biomass of benthic fauna that coincides with high water column chlorophyll a in localized "hotspots" of the Chukchi Sea. Benthic grabs revealed chlorophyll a concentrations among the highest ever reported in marine sediments (up to 665 mg m-2) and levels varied depending on the overlying water mass type. Estimates of epibenthic and infaunal organisms around Hanna Shoal, collected using plumb staff beam trawls and van Veen grabs (respectively), were enormous. Epibenthic assemblages ranged to 500 g m-2 (and thousands of individuals m-2); infaunal biomass and abundances approached 820 g m-2 and 5,500 individuals m-2, respectively. In both sampling years, the greatest biomass was not on the Shoal itself, but on its northwest and southeast flanks (or both), which receive Bering Sea water that originates in the North Pacific.

Ken Dunton, University of Texas at Austin, (361) 749-6744, ken.dunton@utexas.edu

NE Chukchi Sea Moored Ecosystem Observatory

Funding provided by Alaska Ocean Observing System, North Pacific Research Board, Olgoonik-Fairweather, University of Alaska Fairbanks, Université Laval, and University of Washington

A multi-institutional, multi-investigator partnership operates and maintains a subsurface moored observatory on the NE Chukchi shelf near 71.6N, 161.5W. The first deployment occurred in September 2014 and the mooring will be re-deployed annually through at least 2018.

The instruments record with high temporal resolution throughout the year, including the under-sampled and poorly understood seasons when sea ice typically inhibits ship-based sampling. Measurements include ice, ocean physics, nutrient and carbonate chemistry, particulate matter, phytoplankton, zooplankton, fisheries, and marine mammal datasets, thereby providing multifaceted views into the inter-trophic co-variability of the Chukchi shelf ecosystem. The scientific objectives of this monitoring effort are to:

1. Quantify hourly, daily, seasonal, annual, and inter-annual variations in selected physical, chemical, and biological measurement parameters on the shallow Chukchi Sea continental shelf.
2. Relate the timing and magnitude of fluctuations in nutrient and carbonate chemistry, particulate, and fish/zooplankton parameters to the current field and the physical hydrography, wind, light, and ice environment.

3. Provide researchers and resource managers with a broad-spectrum and multi-year set of reference observations that can be applied to evaluating and improving regional and global-scale biogeochemical, ice-ocean circulation, ecosystem, and stock-assessment models.

The observatory consortium welcomes new partners, new applications of the data already being collected, and new instrumentation that can further enhance the value of the existing efforts.

In accordance with the NPRB data policy, all data collected on this mooring are publicly available. There will be two data releases associated with each dataset. The first will come immediately after the recovery cruise and will include raw, unprocessed, data for users with time-sensitive applications. The second release includes fully processed data following requisite calibrations, application of calibration coefficients, and editing, typically within ~6 months of mooring recovery. Additional details about the mooring configuration, data policy, and the observatory consortium are available online at: http://mather.sfos.uaf.edu/~seth/CEO.

Seth Danielson, University of Alaska Fairbanks, (907) 474-7834, sldanielson@alaska.edu, http://www.sfos.uaf.edu/directory/faculty/danielson/

Northern Bering Sea bottom trawl survey

Funding provided by National Oceanic and Atmospheric Administration

Biennial northern Bering Sea (NBS) shelf surveys will start in 2017. This survey will provide long-term monitoring of bottom fishes, crabs, and other demersal macrofauna to help provide a better understanding of how biota and the ecosystem are responding to climate change and loss of sea ice. The ultimate goal is a long time-series of standardized data collections that will provide quantitative indices of abundance for determining how climate change is affecting population trends and community structure. The expanded survey data collections from the NBS will also augment those from the eastern Bering Sea (EBS) shelf and provide new insight into the spatial and temporal response of bottom fish and crab populations to highly variable interannual ice cover and summer bottom temperatures across the entire eastern Bering Sea shelf. Digital data are available online (http://www.afsc.noaa.gov/RACE/groundfish/survey_data/data.htm).

Bob Lauth, National Oceanic and Atmospheric Administration, (206) 526-4121
Bob.Lauth@noaa.gov

Northern Bering Sea BASIS (Bering-Arctic Subarctic Integrated Survey)

Funding provided by National Oceanic and Atmospheric Administration

The northern Bering Sea BASIS survey will continue in 2016 and 2018. These surveys will assess the relative abundance, size, and energetic status of late summer/early fall fish species such as western Alaska juvenile Chinook and chum salmon, capelin, herring, juvenile pollock, and saffron cod. Bio/physical oceanographic data will also be collected to assess the impact of climate change and variability on the ecosystem. When combined with the southeastern Bering Sea BASIS survey, the resulting survey effort will cover much of the eastern Bering Sea shelf. Digital data are available from the program leader Ed Farley.

Ed Farley, National Oceanic and Atmospheric Administration, (907) 789-6085,
Ed.Farley@noaa.gov

Chukchi Ecology and Seal Survey (CHESS)

Funding provided by National Oceanic and Atmospheric Administration

A comprehensive survey for the abundance and distribution of bearded and ringed seals in the Chukchi Sea will be conducted in 2016. In collaboration with the U.S. Fish and Wildlife Service, the objectives may be expanded to include polar bears. The survey will be based on coupled infrared and color imagers. Animals will be detected by infrared video and the species will be identified from high-resolution color photographs, a method demonstrated to be highly effective in recent surveys of the Bering Sea pack ice zone. Because large portions of the bearded and ringed seal populations use the Russian waters of the western Chukchi Sea, the survey will require collaboration with the Russian Federation. The Chukchi survey will complement the results of the Bering Sea survey, leaving only the Beaufort Sea as a gap in complete estimates of the breeding populations of ice seals in the seas surrounding Alaska.

Peter Boveng, National Oceanic and Atmospheric Administration, (206) 526-4244, peter.boveng@noaa.gov

Influence of sea ice on ecosystem shifts in Arctic seas

Funding provided by U.S. Geological Survey Changing Arctic Ecosystems Initiative

The decline of Arctic sea ice is predicted to promote an ecosystem shift from benthic-dominated to pelagic-dominated communities on Arctic shelves, raising concern for species like walrus and eiders that feed on benthic organisms. Sea ice dynamics are thought to support a rich benthic ecosystem by promoting the export of surface primary production to the ocean floor. As sea ice extent diminishes, more prolonged open-water phytoplankton blooms and increased zooplankton grazing may increasingly route surface primary production to pelagic consumers. The pace of declining benthic production has been difficult to quantify, leaving resource managers with much uncertainty. We propose to relate annually resolved growth increments in benthic bivalves with satellite derived sea ice records to develop a predictive relationship between sea ice and benthic production. Bivalves are a key prey item for both walrus and eiders. The relative contributions of sea ice algae and phytoplankton, the two major sources of surface primary production, will also be described for bivalves using stable isotope analysis. Changes in bivalve size will be converted to differences in caloric content available to predators. Combining these products with model projections of future sea ice cover will allow us to predict the pace of shifts in benthic

production, clarify the underlying mechanism, and enhance forecasts of the population response of Department of Interior managed species to a changing Arctic environment. (Funded FY2014-FY2019)

Vanessa von Biela, U.S. Geological Survey, Alaska Science Center, (907) 786-7073, vvonbiela@usgs.gov, USGS Changing Arctic Ecosystems Initiative

Regional Arctic System Model (RASM)

Funding provided by U.S. Office of Naval Research

The Regional Arctic System Model (RASM) has been developed to advance capability in simulating critical physical processes, feedbacks and their impact on the Arctic climate system and to reduce uncertainty in its prediction. RASM is a limited-area, fully coupled ice-ocean-atmosphere-land model that uses the Community Earth System Model (CESM) framework. It includes the Weather Research and Forecasting (WRF) model, the LANL Parallel Ocean Program (POP) and Community Ice Model (CICE) and the Variable Infiltration Capacity (VIC) land hydrology model. In addition, a streamflow routing (RVIC) model was recently implemented in RASM to transport the freshwater flux from the land surface to the Arctic Ocean. Finally, marine biogeochemistry components are currently being implemented in the ocean and sea ice components to expand RASM capability into Arctic ecosystem studies. The model domain is configured at horizontal resolution of 1/12° (or ~9km) for the ice-ocean and 50 km for the atmosphere-land model components. It covers the entire Northern Hemisphere marine cryosphere, terrestrial drainage to the Arctic Ocean and its major inflow and outflow pathways, with optimal extension into the North Pacific / Atlantic to model the passage of cyclones into the Arctic. All RASM components are coupled at high frequency to realistically represent interactions among model components at inertial and longer time scales.

Wieslaw Maslowski, Naval Postgraduate School, (831) 656-3162, maslowsk@nps.edu, http://www.oc.nps.edu/NAME/RASM.htm

Arctic Coastal Ecosystem Survey (ACES)

Funding provided by North Pacific Research Board (project 1229), Bureau of Ocean Energy Management, National Oceanic and Atmospheric Administration, and North Slope Borough/Shell Baseline Studies Program

In response to a rapidly changing Arctic, we developed a multi-faceted approach to examine variation in community structure and trophodynamics of nearshore arctic nekton during the ice-free season of 2013 and 2014. Fish samples were collected weekly via beach seine at 12 stations surrounding Pt. Barrow in three water bodies (Chukchi, Beaufort, Elson Lagoon) from ice breakup (early July) until late August in 2013 and 2014 (also planned for 2015). Juvenile and larval stages (98%) comprise the majority of catch data suggesting nearshore areas might serve as nursery habitat similar to those in similar lower latitude systems. The Elson Lagoon is dominated by euryhaline and amphidromous species, whereas the Beaufort and Chukchi Sea stations were dominated by marine species. Several species of sculpin are common but rarely abundant throughout all sites; catch data from 2007-2009 and 2012-2014 show that availability of high quality forage species (capelin and Pacific sand lance) in the nearshore is linked to fluctuations in temperature, salinity and turbulence. A laboratory study has examined the temporal scale of tissue turnover for nitrogen and carbon stable isotopes, using Arctic sculpin. Results will offer insight into the rates of change in tissue and how landfast ice breakup alter foodweb structure. These different approaches will offer a better understanding of important drivers of spatiotemporal variability in nearshore foodwebs and improve the ability to predict how these systems may shift in the face of Arctic climate change.

Coincident with biological collections was a series of meteorological and oceanographic observations within Elson Lagoon and at the interface between the lagoon and the Beaufort Sea. The primary rationale for these observations was to link the meteorological and hydrodynamic conditions to changes in the biological community. To examine temporal patterns, an ADCP was moored in the inlet between Elson Lagoon and the Beaufort Sea during ice free periods of both 2013 and 2014 (also planned for 2015). Additionally, several mobile ADCP surveys were conducted within this inlet as well as the inlet between Elson Lagoon and North Salt Lagoon near Barrow to characterize flow dynamics between adjacent water bodies. These measurements

were linked to a nearby meteorological station to examine coupling from atmospheric and oceanographic processes at local scales. Based on preliminary analyses, responses in the biological community are likely mediated by the strong dependence of physical controls, both meteorological and hydrodynamic, and suggest variation in the temporal and spatial patterns. For more information about the project, see http://boswelllab.wix.com/boswelllab#!aces-project-summary/ce65.

Kevin Boswell, Florida International University, (305) 919-4009, kmboswel@fiu.edu

Ron Heintz, National Oceanic and Atmospheric Administration, (907) 789-6058, ron.heintz@noaa.gov

Tracing sea ice algae in Arctic benthic food webs using the sea ice diatom biomarker IP25

Funding provided by North Pacific Research Board (project 1503)

Sea ice cover over the Chukchi Sea shelf is continually decreasing with a warming climate and the effects on primary production regimes, especially sea ice algal production and subsequently benthic food webs are still uncertain. Here we propose to use IP25 as an ice-algal specific tracer to reliably track sea ice algal sources in the Chukchi Sea benthic food web and to distinguish ice algae from other production sources such as pelagic phytoplankton. We will combine the IP25 tracer use with the sterol brassicasterol as a biomarker for phytoplankton to identify the relative proportions of sea ice algae (IP25) and phytoplankton (brassicasterol) in consumer diets (PIP25 ratio). Benthic bivalves and polychaetes are used as representatives of benthic food web consumers for their prominence in benthic communities and their wide variety of feeding types. We will use stable carbon isotope composition of dissolved inorganic carbon and of IP25 in sea ice algae, surface sediments and benthic consumers to ground-truth the sea ice origin of IP25 and its specificity for ice algae. This work can significantly advance our ability to project changes in the primary production regime to subsequent lower and higher trophic levels. Many of these higher trophic levels such as walrus and spectacled eiders are of subsistence interest to Alaska Native peoples, and knowledge gleaned from this project can enhance our understanding how these subsistence resources may be affected with continued climate warming.

Katrin Iken, University of Alaska Fairbanks, (907) 474-5192, kbiken@alaska.edu, https://www.sfos.uaf.edu/

Assessing the role of oceanic heat fluxes on ice ablation on the Chukchi Sea Shelf

Funding provided by North Pacific Research Board (project 1504)

This proposal seeks to understand the role of oceanic heat flux convergences in the summertime retreat of sea ice over the central Chukchi Sea. It is motivated by observations and preliminary numerical model results indicating that eddies generated along the marginal ice zone front carry substantial quantities of heat laterally beneath the ice. The lateral eddy heat flux is via intrusions of warm water into the pycnocline separating cold, dilute surface meltwaters and near-freezing, salty bottom waters. This process is potentially important in heating the underside of the ice and thus enhancing summer ice melt and retreat. In addition, the mean summer currents in the Central Channel may be thermodynamically important in the summertime retreat of sea ice directly and, indirectly, as a source of the eddies to other portions of the shelf. This project will support one graduate student and use an ocean-ice circulation model to: 1) determine the proportion of ice melt due to the vertical heat flux from the ocean with that due to the net air-sea heat flux at the ice surface; 2) evaluate the role of intra-pycnocline eddies versus the mean flow in providing this sub-surface heat flux; and 3) evaluate the role of winds in modifying the subsurface heat flux to the ice. Outreach consists of developing digital model animations (and explanations) for use in schools and communities to explain how the ocean affects sea ice melt in the Chukchi Sea. The content will be directed at junior high and high school audiences. Weingartner's role on the North Slope Borough-Shell Baseline Studies Science Steering Committee (SSC) will assist in outreach. The SSC includes representatives from six NSB villages and meets four times/year. He will use these meetings to inform the village representatives and present to the communities.

Thomas Weingartner, University of Alaska Fairbanks, (907) 474-7993, tjweingartner@alaska.edu, https://www.sfos.uaf.edu/directory/faculty/weingartner/

Growth and dispersal of early life history stages of Arctic cod and saffron cod under variable climate forcing

Funding provided by North Pacific Research Board (project 1508)

We propose to develop a biophysical transport model to simulate the dispersal of early life history stages of the two most abundant fish species, Arctic cod (*Boregadus saida*) and saffron

cod (*Eleginus gracilis*), in the Chukchi Sea and Beaufort Sea. These species form a crucial link from lower trophic levels to seabirds, marine mammals, and humans and have been recognized as potential target species for new fisheries in the Arctic. We combine observations of late larval and early juvenile stages of both species during the summer of 2012 and 2013 with laboratory-derived estimates of their temperature-dependent growth to parameterize an individual particle tracking model (TRACMASS) that includes growth and vertical movement. The model will be linked to a recently developed pan-arctic ocean circulation model (PAROMS) to test hypotheses about the origin and fate of young-of-the-year Arctic and saffron cod. Specifically, we aim to (1) identify likely spawning locations by tracking particles backward in time from known summer aggregations in the Chukchi Sea and (2) simulate pathways of dispersal from these aggregations to downstream nursery areas, which may include areas in the Beaufort Sea. Improved understanding of the growth, distribution, and movements of early life history stages of Arctic cod and saffron cod in the region, and of the connectivity between the Chukchi Sea and Beaufort Sea, has several immediate and long-term benefits. It directly addresses research priorities identified in the Arctic Fisheries Management Plan, enhances required descriptions of Essential Fish Habitat for two key prey species, and provides benchmarks against which to assess future changes to the Arctic marine ecosystem that may result from new development in the Arctic and from anthropogenic climate change.

Franz Mueter, University of Alaska Fairbanks, (907) 796-5448, fmueter@alaska.edu, https://www.sfos.uaf.edu/directory/faculty/mueter/

Glider based real-time monitoring of marine mammals in the Arctic

Funding provided by North Pacific Research Board (project 1515)

Shipboard observations of marine mammal distribution and habitat are expensive and logistically challenging to collect in Arctic waters. Port facilities are minimal and access to appropriate vessels for spending extended periods of time at sea is extremely limited. Autonomous platforms like gliders provide the capability to collect both oceanographic and passive acoustic data for far longer periods of time (weeks to months) and at significantly reduced costs than traditional shipboard or aerial surveys. We have developed a system to record, detect, classify, and remotely report Arctic and sub-Arctic marine mammal calls in real time from Slocum ocean gliders based on the digital acoustic monitoring (DMON) instrument and the low-frequency detection and

classification system (LFDCS). The system has been used several times in the northwest Atlantic Ocean and was successfully demonstrated for Arctic research during two pilot studies in the Chukchi Sea during September 2013 and 2014. Deployments to date have been short (1-3 weeks), but the capability exists for much longer missions. Our objective is to conduct an 8-10 week survey of the northeastern Chukchi Sea using a G2 Slocum glider to (1) examine the distribution, occurrence, and habitat of marine mammals using in-situ passive acoustic and oceanographic data collected by the glider, and (2) demonstrate the near real-time detection and reporting capability of the system. We hypothesize that some Arctic species associate with a front separating Bering Sea water and Alaska Coastal Current water to take advantage of aggregations of either pelagic or benthic prey. We further hypothesize that marine mammal community composition will change predictably with the strong spatial variability in oceanographic properties found in this region. We anticipate that these predictions will improve efforts to (1) mitigate impacts on marine mammals by human activities and (2) forecast changes in species distributions caused by climate change.

Peter Winsor, University of Alaska Fairbanks, (907) 474-7740, pwinsor@alaska.edu, https://www.sfos.uaf.edu/directory/faculty/winsor/

Northern Alaska Sea Ice Project Jukebox, Phase II

Funding provided by North Pacific Research Board (project 1521)

The project examines the complex interrelationship between people and their environment as it relates to nearshore and shorefast sea ice and humans having to continually adapt responses to changes in ice conditions. Also addressed is how climate change is affecting the ecosystems, which in turn affect the local people. This project tells the story of the changing Arctic through those who live within it daily.

Building upon the Northern Alaska Sea Ice Project Jukebox website (www.jukebox.uaf.edu/seaice) researchers can listen to recordings made in 1978, 2008, 2009, and 2013 with local experts in Barrow and other northern Alaska communities talking about their local traditional knowledge about and observations of changing sea ice. Conducting interviews in 2015 in Barrow will provide continuity in documentation of changing nearshore sea ice conditions and of "unusual" years. This expanding record is useful to researchers trying to

understand the ice environment as well as social scientists studying human adaptation, decision making, and risk taking behavior. Conducting similar interviews in Kotzebue will begin documentation of traditional knowledge of nearshore and shorefast sea ice there. This will serve as both a comparative dataset for a location with vastly different ice conditions than Barrow, and as the start of another longitudinal research plan in that area.

Leslie Joan McCartney, University of Alaska Fairbanks, (907) 474-7737, lmccartney@alaska.edu

NOAA Office of Exploration and Research

In FY15, NOAA Office of Exploration and Research will be supporting exploration projects in the Chukchi Borderlands. Three two-year projects are presently considered for funding. The field work for these projects is expected to take place in the August-September 2016 time frame.

For more information please contact John McDonough at john.mcdonough@noaa.gov, Jeremy Potter at jeremy.potter@noaa.gov or Nathalie Valette-Silver at Nathalie.Valette-Silver@noaa.gov.

'Pacification' of the Arctic: Climate change impacts on the eggs and larvae of Alaskan gadids

Funding provided by North Pacific Research Board (project 1403)

Both Arctic cod (*Boreogadus saida*) and saffron cod (*Eleginus gracilis)* play a crucial role in the Arctic by channeling energy between plankton and higher level marine mammals and seabird in a moderately simple pelagic, ice-dominated food web. Both cod species have physiology adapted for their cold-water environment, but may not be able to compete with other gadids invading northward i.e., Pacific cod, *Gadus macrocephalus* and walleye pollock, *Gadus chalcogramma*. For example, earlier experimental work from NPRB project #1228 indicated dramatic differences in the thermal optima within and among gadids from each region during the juvenile stage. However, the thermal sensitivity of dispersive egg and larval stages is unknown, yet could be the key component governing current and future biogeography of gadids in Alaskan waters. This project uses the multi-species broodstock program at the Alaska Fisheries Science Center's 20,000 sq. ft. cold-water laboratory at the Hatfield Marine Science Center. Gadids include

mature individuals from collections of juvenile Arctic and saffron cod (2012, 2013, 2014) and Pacific cod and walleye pollock (2005 – present). The first successful mass-scale spawning and larviculture of Arctic cod was completed during the spring of 2015. Current experiments are examining how variability in temperature and food availability influences growth, development, lipid storage and survival at these early, critical life stages in all four gadid species. Data from these common garden experiments will be used to predict future effects of warming on fish distribution and energetic impacts on food webs in the Arctic. Temperature-dependent growth and development data from these experiments are also being used to parameterize the individual particle tracking model (TRACMASS) for NPRB project #1508.

Benjamin Laurel, National Oceanic and Atmospheric Administration, (541) 867-0197, ben.laurel@noaa.gov

Sustainability of critical areas for eiders and subsistence hunters in an industrializing nearshore zone

Funding provided by National Science Foundation ArcSEES Program

Throughout the Arctic, indigenous people are faced with difficult choices between the economic benefits of industrialization versus associated threats to subsistence hunting. Evaluating alternatives is especially challenging when climate change is likely to shift the location and quality of habitats, as well as the ice conditions that govern access to those habitats by both animals and hunters. In the Chukchi Sea, anticipated infrastructure to support offshore oil wells, including a major pipeline, will be placed in a nearshore corridor used by most marine birds and mammals that migrate to the western Arctic. Such industrial development can provide employment for local residents and tax revenue for local governments, but should minimize potential impacts on subsistence species. In this research, we are modeling habitat requirements and mapping viable prey densities for commonly hunted sea ducks in the Chukchi nearshore corridor (10 to 40 m depth), and assessing long-term variations in accessibility of those feeding areas through the ice. We are supplementing these habitat maps with long-term delineations of the landfast ice edge along which much of the eider hunting occurs. In parallel with this representative study of potential shifts in habitat and hunter accessibility, we are conducting workshops based on methods of structured decision analysis in the village of Wainwright. These workshops will help create a local vision for sustainability, in terms of potential risks to

subsistence hunting and related lifestyles versus economic benefits of different development scenarios.

James Lovvorn, Southern Illinois University, (307) 399-7441, lovvorn@siu.edu

Tuula Hollmen, University of Alaska, Fairbanks, (907) 224-6323, tuulah@alaskasealife.org

Henry Huntington, Huntington Consulting, (907) 696-3564, hph@alaska.net

Appendix B. Arctic Integrated Ecosystem Research Program, individual project hypotheses and objectives.

Hypotheses and Objectives:

Communities (Huntington):

H-1: To date, the primary drivers of short-term variability in subsistence harvests have been environmental, whereas the primary drivers of long-term trends have been economic, cultural, regulatory, and technological.

H-2: Environmental variability affects food security in the short-term, but lack of economic well-being is the main long-term threat to food security.

H-3: Trends in the Chukchi marine environment (in contrast to short-term variability) have not demonstrably affected communities' overall well-being.

H-4: Chukchi coastal communities have a variety of response mechanisms for coping with marine environmental variability and shifts.

O-1:.Analyze existing information about subsistence harvests and traditional knowledge

O-2.Determine with other PIs how existing and new LTK information can inform their research & findings

O-3.Document additional information through community workshops

O- 4.Analyze existing and additional information to develop (a) summary of the Chukchi ecosystem as seen by coastal residents and (b) collaborations to connect local understanding with the results of other project components

Arctic IES: LTL (Ladd):

H-1. The source of heat to the Chukchi Sea comprises relatively even contributions from advected heat from the northern Bering Sea and local atmospheric heat fluxes. The contribution of local atmospheric fluxes is expected to increase with future reduction in sea ice.

H-2. Earlier ice retreat/melt will result in stronger stratification. The contribution of temperature to stratification is expected to increase, while the contribution of salinity to stratification is expected to decrease or remain unchanged.

H-3. In the southern Chukchi Sea, the primary source of nutrients is from Bering Strait; while in the northern Chukchi, nutrient supply is a combination of Bering Strait and upwelled Arctic basin water. Remineralization of organic matter provides a local source of ammonium, and will decrease with earlier ice retreat/melt.

H-4. Earlier ice retreat/melt will further shift the balance of spring primary production from ice-associated algae to pelagic phytoplankton, thereby reducing organic matter export to the benthos and increasing organic matter flow to pelagic zooplankton grazers early in the season.

H-5. Warming ocean temperatures will increase upper-ocean stratification and reduce vertical nutrient inputs to the mixed layer resulting in the formation of more spatially and temporally extensive subsurface phytoplankton blooms and productivity maxima.

H-6. Increased stratification will shift the phytoplankton community to a greater fraction of small cells, thus diverting more energy flow through the microzooplankton community.

H-7. Nutritional quality of phytoplankton and their zooplankton grazers will decrease with increased warming (due to increases in stratification and reductions in nutrients).

H-8. Summer zooplankton community will shift due to a) increases in the presence of Bering-Pacific fauna and a poleward retraction of arctic species, and b) changes in size structure of the copepod community to smaller-bodied microzooplankton and mesozooplankton as a consequence of the shift in size structure of phytoplankton.

H-9. Ichthyoplankton community composition will shift due to a) species-specific responses to temperature changes, and b) changes in species composition and size structure of zooplankton prey base.

O-1. Stratification (H1, H2) Quantify the strength of stratification, its temporal evolution, and the relative contribution of temperature and salinity throughout the spring ice melt/retreat. (Stabeno, Ladd, McCabe)

O-2. Circulation (H3) Quantify transport in Herald Canyon (RUSALCA) and the eastern Chukchi shelf. Identify pathways of flow and their respective heat, salt, and nutrient concentrations. (Stabeno, Ladd, McCabe, Mordy)

O-3. Heat Flux (H1, H2, H3) Estimate surface heat fluxes (summer) and compare to estimates of advective heat fluxes. (Stabeno, Ladd, McCabe)

O-4. Ice and Phytoplankton (H4) Examine the relationship among ice thickness, ice retreat, and the timing and magnitude of near-bottom chlorophyll that fuels benthic-pelagic coupling. (Stabeno, Mordy, Eisner, Lomas)

O-5. Phytoplankton Abundance (H4, H5) Quantify the relative abundance of pelagic phytoplankton species compared to sinking ice-associated algae. (Eisner, Lomas, Mordy)

O-6. Primary Production (H5, H6) Quantify spatial patterns in rates of total and new production, and phytoplankton community size structure as a function of water column physics and chemistry (nitrate and ammonium). (Eisner, Lomas, Mordy, Ladd, Stabeno)

O-7. Primary Production Model (H4, H5) Use new primary production data to validate and constrain a model of ocean primary productivity and fate (Liu et al., in press) in regions where subsurface productivity maxima are important. (Lomas)

O-8. Secondary Production (H8, H9) Quantify the distribution, size, abundance, and species composition of zooplankton and ichthyoplankton throughout the US shelf waters of the Chukchi Sea. Compare data to relative oceanographic conditions and to historical estimates as derived from AFSC sampling 2003- present. (Duffy-Anderson, Kimmel, Spear, Eisner, Stabeno)

O-9. Trophic Interactions – Hot Spots (H4, H5) Use primary production data to understand spatial variability in net community production and identify 'hot spots' of trophic connections between LTL and UTL, and how these might change in relation to other on-going projects in the region focused on detecting change (e.g., Distributed Biological Observatory [DBO]). (Lomas, Eisner, Mordy)

O-10. Trophic Interactions – Nutrition (H6, H7, H8, H9) Determine spatial and temporal relationship between phytoplankton, zooplankton and ichthyoplankton. Link observations to UTL-derived data to provide mechanistic understanding of trophic relationships. Compare fatty acid profiles of seston (primarily phytoplankton) and zooplankton to relate carbon sources to nutritional condition of key forage fish (e.g. Arctic cod). (Eisner, Lomas, Kimmel, Duffy-Anderson, Heintz (UTL))

O-11. Ecosystem Connectivity (H8, H9) Examine connectivity and exchange of lower trophic biota (zooplankton, ichthyoplankton, juvenile fish) between ecosystems (northern Bering Sea, Chukchi, Beaufort) to determine if each region acts as a source or a sink of ichthyo- and zooplankton stocks. (Duffy-Anderson, Kimmel, Spear, Eisner, Farley (UTL))

O-12. Arctic Cod and Saffron Cod (H9) Further resolve spawning and connectivity of Arctic cod and saffron cod adults, larvae and juveniles by providing new field data on late-stage larvae in summer that will be used to ground truth results from biophysical transport model efforts. (links to NPRB project 1508; Duffy-Anderson collaborator, postdoctoral co-advisor; Farley (UTL))

O-13. US/Russian Chukchi (H8, H9) Connect US Chukchi Sea IERP surveys to those planned in the Russian exclusive economic zone (EEZ; 2017, 2019; Melnikov, TINRO; Afanasyev, VNIRO). (Duffy-Anderson, Farley (UTL))

ASGARD: LTL (Danielson):

H-1. The structure (timing, magnitude and direction) of the wind field is the primary regulator of: a) variations in the partitioning of flow to either side of St. Lawrence Island, b) variations in advective pathways, sediment resuspension and sediment deposition events, c) two-way coupling of nutrient-poor coastal water masses with nutrient-rich mid-shelf water masses, d) temporally

variable advective contributions to the pre-bloom nutrient concentrations throughout the water column and to near-bottom nutrient concentrations year-round.

H-2. Near-surface stratification during the period of ice retreat regulates macronutrient availability, the depth, location, and magnitude of primary productivity, and the type (small vs. large) of phytoplankton community that subsequently dominates.

H-3. Fluxes and quality of particulate matter supplied to the benthos are tightly coupled to the phenology of sea-ice retreat and primary production. Beginning with under-ice phytoplankton blooms in the late spring and continuing through the summertime open-water season, sinking fluxes of fresh planktonic-derived organic matter provide a sustained food supply. In other times of year, supply of organic matter is small and less labile, coming primarily from resuspended, reprocessed and advective sources further south.

H-4. Although zooplankton are unable to contain the phytoplankton bloom, they are nonetheless important in both transferring some portion of this production into the metazoan planktonic food-web and efficient at repackaging material into fecal pellets for accelerated export to the benthos. The composition of the zooplankton community, and the temperatures at which they are operating, determine the efficiency of energy transfer into the zooplankton (i.e. losses to respiration versus growth and reproduction) and the rates of fecal flux. Some of these rates are consistent with emerging empirical global relationships (i.e. respiration), while others (i.e. growth rate) deviate significantly because polar data is currently underrepresented in such syntheses.

H-5. Benthic respiration, carbon biomass, production, macrofaunal community structure, functional group composition, and community-level production all vary with oceanic advection, water mass characteristics, and pelagic production regimes.

O-1. Quantify ice, water volume, heat, salt, nutrient, carbon, and planktonic fluxes at under-sampled locations and times in the northern Bering and Chukchi seas.

O-2. Assess particulate organic matter sinking and deposition rates and lower trophic level growth and respiration rates in locations and times that currently lack data.

O-3. Better quantify synoptic, seasonal, and inter-annual changes in the regional biological carbon pump dynamics and kinematics.

O-4. Collect physical, chemical, biogeochemical, and biological process rate data needed to constrain and evaluate biophysical and ecosystem models.

O-5. Help develop educational and outreach materials to communicate compelling narratives about our research to indigenous and non-indigenous local, regional, national and international audiences.

O-6. Contribute to the education and research programs of at least 6 M.S. and Ph.D. graduate students.

O-7. Support additional NPRB Arctic Program research projects with moored and ship-based measurement platforms.

O-8. Form coordinated data collection and analysis collaborations with national and international partners.

O-9. Enhance the Distributed Biological Observatory (DBO) program by occupying DBO stations at a time of year in which few samples have been collected previously.

Arctic IES: UTL (Farley):

H-1. Cods in the Arctic - Winners and Losers: Loss of sea ice and continued warming of sea temperatures during summer in the Chukchi Sea will restructure the food web, decreasing the amount of fat available to higher trophic level predators.

H-2. Cod habitat in the Arctic: The northern Chukchi serves as a nursery area for young-of- the-year Arctic cod, supplying juveniles to other areas of the Arctic.

H-3. Salmon expansion into a warming Arctic: Summer surface waters in the northeastern Bering Sea will continue to warm and be a source of heat advected to the Pacific Arctic Region, providing new marine habitat for juvenile salmon.

H-4. Seabird community structure and seabird-prey dynamics: The current predominance of planktivorous seabirds in the Arctic may shift back towards piscivorous seabirds, if warming sea temperatures restructure the food web.

O-1. (H1) Quantify the distribution, abundance, and condition of demersal fishes and shellfishes throughout the US shelf waters of the Chukchi and western Beaufort Sea.

O-2. (H1, H2, H3) Quantify the distribution, abundance, and condition of pelagic marine fishes, in particular young-of-the year Arctic gadids and other forage fishes, throughout the US shelf waters of the Chukchi and western Beaufort Sea (BOEM). Link observations with those derived from LTL component (physics, primary, secondary production) to provide mechanistic understanding of trophic relationships.

O-3. (H1, H2, H3) Combine results from previous (2003, 2007 - BASIS, 2012, 2013 - Arctic Ecosystem Integrated Survey (Arctic Eis)) and planned surveys (2017, 2019) to assess variability in pelagic and demersal fish ecology over time and relative to oceanographic conditions.

O-4. (H3) Establish the relative abundance, size, and condition of juvenile salmonids that utilize the coastal regions of the Northern Bering (NBS project), Chukchi, and western Beaufort Sea (BOEM) and determine their likely origin.

O-5. (H2) Further resolve early life history characteristics of Arctic cod and saffron cod and their behavior and connectivity between the Chukchi Sea and western Beaufort Sea using new survey results and the continuous observations from moored echosounders.

O-6. (H4) Quantify the distribution, abundance, and prey association (as a proxy for diet) of seabirds in the US shelf waters of the Chukchi and western Beaufort Sea (BOEM) in relation to oceanographic conditions, prey abundance, and feeding guilds.

O-7. (H1, H2, H3) Develop a spatially explicit bioenergetics model for Arctic cod and saffron cod as well as juvenile pink and chum salmon utilizing past and proposed integrated ecosystem data and test the impact of warming summer temperatures on their growth and distribution.

O-8. (H1, H2) Connect/collaborate US Chukchi Sea integrated ecosystem surveys to those planned in the exclusive economic zone within Russia.

ASGARD: Mammals (Stafford):

H-1. The presence of sub-Arctic marine mammals will be driven by prey availability (fish, zooplankton) that is in turn driven by water mass characteristics

H-2. The relationship between ice cover and Arctic species migration from the Bering Sea in to the Pacific Arctic can be quantitatively determined by comparing the onset of acoustic detection with ice advance (or formation) from, and retreat towards, the north (in the winter and spring, respectively).

H-3. Temperate marine mammal species will move progressively northwards as seasonal ice cover decreases and remain north of Bering Strait longer.

H-4. There will be differences in the species and seasonal occurrence of species between the eastern (eastern SLI and US Bering Strait) and western (Anadyr Strait and Russian Bering Strait) recordings. Data from the A3 climate site and the NE Chukchi Ecosystem Mooring site help establish if there are northern limits to sub-Arctic species and what the southern limits of Arctic species are.

H-5. The number of ship passages through both sides of the Bering Strait will continue to increase over time.

H-6. The northeastern Bering and southeastern Chukchi Seas are moving from a benthic ecosystem to a more pelagic-driven ecosystem similar to the northeastern Chukchi Sea

O-1. Have hydrophones deployed for two years on 3 moorings in the northern Bering and Chukchi Sea

O-2. Document the inter-seasonal and inter-annual presence of vocal marine mammals in the Pacific Arctic Region and compare of acoustic detections in the eastern, western, and central PAR

O-3. Integrate oceanographic drivers with acoustic detections to better understand how the physical environment influences the biological inhabitants of that environment.

O-4. Collaborate with other ASGARD PIs to develop an integrated understanding of the ecosystem components of the Pacific Arctic Region from physical forcing through to upper trophic level consumers.

Appendix C: Arctic Integrated Ecosystem Research Program, individual project timelines

Communities (Lead PI: Huntington)

	individual responsible for	FY16	FY17				FY18				FY19				FY20				FY21			
		July-Sept	Oct-Dec	Jan-Mar	Apr-June	July-Sept	Oct-Dec	Jan-Mar	Apr-June	July-Sept	Oct-Dec	Jan-Mar	Apr-June	July-Sept	Oct-Dec	Jan-Mar	Apr-June	July-Sept	Oct-Dec	Jan-Mar	Apr-June	July-Sept
Objective #1: Analyze existing information about subsistence harvests and traditional knowledge																						
Identify existing sources	PI, Co-PIs		x																			
Compile information from those sources	PI, Co-PIs			x	x																	
Analyze information and draft paper	PI					x																
Objective #2: Discuss with other PIs how existing information informs their research & findings																						
Meet at PIs meetings	PI, Co-PIs			x				x				x				x				x		
Follow up as appropriate	PI, Co-PIs				x	x	x		x	x	x		x	x								
Share results of Objective #1	PI					x																
Develop appropriate topics/questions for community workshops, regional meetings	PI, Co-PIs			x	x	x	x	x	x	x	x	x										
Objective #3: Document additional information through community workshops	Co-PIs																					
Hold regional meetings	Co-PIs, PI			x								x										
Choose dates, participants with communities	Co-PIs						x															
Hold workshops	Co-PIs							x														
Analyze information and prepare summaries	Co-PIs								x	x												
Objective #4: 4. Analyze existing and additional information to develop (a) summary of the Chukchi ecosystem as seen by coastal residents and (b) collaborations to connect local understanding with the results of other project																						
Prepare summary paper based on LTK	PI, Co-PIs									x	x	x	x									
Prepare collaborative papers with other PIs	PI, Co-PIs											x	x	x	x	x	x	x	x	x	x	x
Other																						
Progress report	PI		x		x		x		x		x		x		x		x		x		x	
AMSS presentation	PI			x				x				x				x				x		
PI meeting	PI, Co-PIs, regional reps			x				x				x				x				x		
Logistics planning meeting	PI		x				x															
Publication submission	PI						x						x				x				x	
Final report (due within 60 days of project end date)	PI																					x
Metadata and data submission (due within 60 days of project end date)	PI														x							

Arctic IES: Oceanography & Lower Trophic Levels (Lead PI: Ladd)

	Individual Responsible for Completion	FY16	FY17				FY18				FY19				FY20				FY21			
		July-Sept	Oct-Dec	Jan-Mar	Apr-Jun	July-Sept	Oct-Dec	Jan-Mar	Apr-Jun	July-Sept	Oct-Dec	Jan-Mar	Apr-Jun	July-Sept	Oct-Dec	Jan-Mar	Apr-Jun	July-Sept	Oct-Dec	Jan-Mar	Apr-Jun	July-Sept
Meetings, Logistics, Reports and Publications																						
Kickoff meeting	All PIs	x																				
Progress report	All PIs		x		x		x		x		x		x		x		x		x		x	
Logistics planning meeting	All PIs		x								x											
Cruise planning	All PIs	x	x	x	x	x				x	x	x	x	x								
AMSS presentation	All PIs			x				x				x				x				x		
PI meeting	All PIs			x				x				x				x				x		
Publication submission	All PIs															x	x	x	x	x	x	x
Metadata and data submission (due within 60 days of project end date)	All PIs														x	x	x	x	x	x	x	x
Final report (due within 60 days of project end date)	All PIs																	x	x	x	x	x
Data Collection (assumes field years of 2017 and 2019)																						
Moorings	Stabeno					x	x	x	x	x	x	x	x	x								
Pop-up Floats	Stabeno/Mordy	x	x	x	x	x	x	x	x	x	x	x	x	x								
ALAMO Floats	Mordy					x	x	x	x	x	x	x	x	x								
Radiation Buoy / Prawler	Stabeno/Mordy					x								x								
Profilling Gliders (Slocum in 2017, Coastal Gliders in 2019)	Stabeno/Mordy					x								x								
Hydrography/Nets/Towed Vehicle/Primary Production	All PIs					x								x								
Saildrone	Stabeno/Mordy													x								
Objectives																						
O1 STRATIFICATION																						
Data/sample processing	Stabeno/Ladd/McCabe						x	x	x						x	x	x					
Analysis	Stabeno/Ladd/McCabe						x	x	x	x	x	x			x	x	x	x	x	x		
O2 CIRCULATION																						
Data/sample processing	Stabeno/Ladd/McCabe/Mordy						x	x	x						x	x	x					
Analysis	Stabeno/Ladd/McCabe/Mordy						x	x	x	x	x	x			x	x	x	x	x	x		
O3 HEAT FLUX																						
Data/sample processing	Stabeno/Ladd/McCabe						x	x	x						x	x	x					
Analysis	Stabeno/Ladd/McCabe						x	x	x	x	x	x			x	x	x	x	x	x		
O4 ICE & PHYTOPLANKTON																						
Data/sample processing	Stabeno/Mordy/Eisner/Lomas						x	x							x	x						
Analysis	Stabeno/Mordy/Eisner/Lomas						x	x	x	x	x	x			x	x	x	x	x	x		
O5 PHYTOPLANKTON ABUNDANCE																						
Data/sample processing	Eisner/Lomas/Mordy						x	x	x	x					x	x	x	x				
Analysis	Eisner/Lomas/Mordy						x	x	x	x	x	x			x	x	x	x	x	x		
O6 PRIMARY PRODUCTION																						
Data/sample processing	Eisner/Lomas/Mordy/Ladd/Stabeno						x	x	x	x					x	x	x	x				
Analysis	Eisner/Lomas/Mordy/Ladd/Stabeno						x	x	x	x	x	x			x	x	x	x	x	x		
O7 PRIMARY PRODUCTION MODEL																						
Data Assimilation	Lomas														x	x	x	x				
Analysis	Lomas														x	x	x	x	x	x		
O8 ZOOPLANKTON/ICHTHYOPLANKTON																						
Data/sample processing	Duffy-Anderson/Spear/Kimmel/Eisner/Stabeno						x	x	x	x	x	x	x	x	x	x	x	x				
Field Analysis (zp, ichthyo)	Duffy-Anderson/Spear/Kimmel/Eisner/Stabeno										x	x	x	x	x	x	x	x	x	x	x	x
Retrospective Analysis (zp, ichthyo)	Duffy-Anderson/Spear/Kimmel/Eisner/Stabeno				x	x	x	x	x	x	x	x	x	x					x	x	x	X
O09 TROPHIC INTERACTIONS - HOT SPOTS																						
Data/sample processing	Lomas/Eisner/Mordy						x	x	x	x					x	x	x	x				
Analysis	Lomas/Eisner/Mordy						x	x	x	x	x	x			x	x	x	x	x	x		

	Individual Responsible for Completion	FY16	FY17				FY18				FY19				FY20				FY21			
		July-Sept	Oct-Dec	Jan-Mar	Apr-Jun	July-Sept	Oct-Dec	Jan-Mar	Apr-Jun	July-Sept	Oct-Dec	Jan-Mar	Apr-Jun	July-Sept	Oct-Dec	Jan-Mar	Apr-Jun	July-Sept	Oct-Dec	Jan-Mar	Apr-Jun	July-Sept
O10 TROPHIC INTERACTIONS - NUTRITION																						
Data/sample processing	Eisner/Lomas/Kimmel/Duffy-Anderson/Heintz (UTL)						x	x	x	x	x	x	x	x	x	x	x	x				
Analysis	Eisner/Lomas/Kimmel/Duffy-Anderson/Heintz (UTL)										x	x	x	x	x	x	x	x	x	x	x	x
O11 ECOSYSTEM CONNECTIVITY																						
Data/sample processing	Duffy-Anderson/Spear/Kimmel/Eisner						x	x	x	x	x	x	x	x	x	x	x	x				
Analysis	Duffy-Anderson/Spear/Kimmel/Eisner										x	x	x	x	x	x	x	x	x	x	x	x
O12 ARCTIC COD AND SAFFRON COD																						
Cruise planning/Coordination with UTL & NPRB #1508	Duffy-Anderson	x	x	x	x	x	x	x	x	x	x	x	x									
Data collection/field work/Coordination with UTL & NPRB	Duffy-Anderson					x								x								
Data/sample processing/Coordination with UTL and NPRB	Duffy-Anderson						x	x	x	x	x	x	x	x	x	x	x	x				
Analysis (retrospective)/Coordination with UTI and NPRB#1508	Duffy-Anderson				x	x	x	x	x	x	x	x	x	x					x	x	x	x
Analysis (field)/Coordination with UTL and NPRB #1508	Duffy-Anderson										x	x	x	x	x	x	x	x	x	x	x	
O13 US/RUSSIAN CHUKCHI																						
Cruise coordination/discussions	Duffy-Anderson	x	x	x	x	x	x	x	x	x	x	x	x	x								
Results sharing/feedback	Duffy-Anderson						x	x	x	x	x	x	x	x	x	x	x	x	x	x	x	x
Interpretation	Duffy-Anderson														x	x	x	x	x	x	x	x

ASGARD: (Lead PI: Danielson)

	Individual(s) responsible for completion. Multiple investigators will be responsible for various aspects of most objectives.	FY16	FY17				FY18				FY19				FY20				FY21			
		Jun-	Oct - Dec	Jan -	Apr - Jun	Jul - Sep	Oct - Dec	Jan -	Apr - Jun	Jul - Sep	Oct - Dec	Jan -	Apr - Jun	Jul - Sep	Oct - Dec	Jan -	Apr - Jun	Jul - Sep	Oct - Dec	Jan -	Apr - Jun	Jul - Sep
Objective #1	Danielson, Hopcroft, McDonnell, Stockwell																					
Data collection/field work		x	x	x	x	x	x	x	x													
Data/sample processing						x	x	x	x	x	x	x	x									
Analysis						x	x	x	x	x	x	x	x	x	x	x	x	x	x	x	x	x
Objective #2	Hardy, Hopcroft, McDonnell, Stockwell																					
Data collection/field work		x	x	x	x	x	x	x	x													
Data/sample processing						x	x	x	x	x	x	x	x									
Analysis						x	x	x	x	x	x	x	x	x	x	x	x	x	x	x	x	x
Objective #3	All ASGARD Principal Investigators																					
Data collection/field work		x	x	x	x	x	x	x	x													
Data/sample processing						x	x	x	x	x	x	x	x									
Analysis						x	x	x	x	x	x	x	x	x	x	x	x	x	x	x	x	x
Objective #4	Danielson, Hardy, Hopcroft, McDonnell, Stockwell																					
Data collection/field work		x	x	x	x	x	x	x	x													
Data/sample processing						x	x	x	x	x	x	x	x									
Provide results to modelers										x	x	x	x	x	x	x	x	x	x	x	x	x
Objective #5	All ASGARD Principal Investigators																					
Assisting outreach team			x	x	x	x	x	x	x	x	x	x	x	x	x	x	x	x	x	x	x	x
Objective #6	All ASGARD Principal Investigators																					
Student support and mentoring			x	x	x	x	x	x	x	x	x	x	x	x	x	x	x	x	x	x	x	x
Objective #7	Danielson																					
Mooring deployments		X	x	x	x	x	x	x	x													
Sikuliaq cruises					x				x													
Objective #8	All ASGARD Principal Investigators																					
Collaboration planning		X	x	x	x	x	x	x	x													
Collaborative cruises		X			x	x			x	x												
Collaborative analyses											x	x	x	x	x	x	x	x	x	x	x	x
Objective #9	All ASGARD Principal Investigators																					
Data collection/field work		x	x	x	x	x	x	x	x													
Data/sample processing						x	x	x	x	x	x	x	x									
Analysis						x	x	x	x	x	x	x	x	x	x	x	x	x	x	x	x	x
Other																						
Kickoff meeting		x																				
Progress report			x		x		x		x		x		x		x		x		x		x	

	Individual(s) responsible for completion. Multiple investigators will be responsible for various aspects of most objectives.	FY16	FY17				FY18				FY19				FY20				FY21			
		Jun-	Oct - Dec	Jan -	Apr - Jun	Jul - Sep	Oct - Dec	Jan -	Apr - Jun	Jul - Sep	Oct - Dec	Jan -	Apr - Jun	Jul - Sep	Oct - Dec	Jan -	Apr - Jun	Jul - Sep	Oct - Dec	Jan -	Apr - Jun	Jul - Sep
AMSS presentation				x				x				x				x				x		
PI meeting				x				x				x				x				x		
Logistics planning meeting			x				x															
Publication submission							x							xxx				xxxx				xxxx
Final report (due within 60 days of project end date)																						x
Final metadata and data submission (due within 60 days of project end date)																						x

Arctic IES: Upper Trophic Levels (Lead PI: Farley)

	Individual responsible for completion	FY17				FY18				FY19				FY20				FY21			
		Q 1	Q 2	Q 3	Q 4	Q 1	Q 2	Q 3	Q 4	Q 1	Q 2	Q 3	Q 4	Q 1	Q 2	Q 3	Q 4	Q 1	Q 2	Q 3	Q 4
Meetings, Logistics, Reports and Publications																					
Progress Reports	All PIs	X		X		X		X		X		X		X		X					
Logistics planning meeting	All PIs	X				X															
Cruise planning	All PIs	X	X	X	X				X	X	X	X	X								
AMSS presentation	All PIs		X				X								X						
PI meeting	All PIs		X				X								X						
Publication submission	All PIs														X	X	X	X	X	X	X
Final report (due within 60 days of project end date)	All PIs																X	X	X	X	X
Final metadata and data submission (due within 60 days of project end)	All PI's													X	X	X	X	X	X	X	X
Data collection																					
Shipboard surveys					X								X								
Upward looking sonars (moorings)					X				X				X								
Objectives																					
O-1: Demersal Fishes																					
Data/sample processing	Logerwell/Guyon					X	X	X	X					X	X	X	X				
Analyses	Logerwell/Guyon								X	X	X	X	X				X	X	X	X	X
O-2: Pelagic Fishes																					
Data/sample processing	Wilson/DeRobertis/Copeman/Heintz					X	X	X	X					X	X	X	X				
Analyses	Wilson/DeRobertis/Copeman/Heintz								X	X	X	X	X				X	X	X	X	X
O-3: Retrospective work																					
Data format and queries for BASIS & Phase 1 data	All PIs					X	X	X	X												
Data format and queries for Phase 2 data	All PIs													X	X	X	X				
Analyses	All PIs													X	X	X	X	X	X	X	X
O-4: Juvenile salmonids																					
Data/sample processing	Farley/Cieciel/Copeman/Heintz/Guyon					X	X	X	X					X	X	X	X				
Analyses	Farley/Cieciel/Copeman/Heintz/Guyon								X	X	X	X	X			X	X	X	X	X	X
O-5: Cod habitat																					
Data/samples processing	Wilson/DeRobertis/Mueter															X					
Analyses	Wilson/DeRobertis/Mueter															X	X	X			
O-6: Seabirds																					
Data/samples processing	Kuletz					X	X	X	X					X	X	X	X				
Analyses	Kuletz								X	X	X	X	X				X	X	X	X	X

	Individual responsible for completion	FY17				FY18				FY19				FY20				FY21			
		Q 1	Q 2	Q 3	Q 4	Q 1	Q 2	Q 3	Q 4	Q 1	Q 2	Q 3	Q 4	Q 1	Q 2	Q 3	Q 4	Q 1	Q 2	Q 3	Q 4
O-7: Bioenergetics/ Modeling																					
Data/sample processing	Farley/Cieciel/Copeman/Heintz					X	X	X	X					X	X	X	X				
Analyses	Farley/Cieciel/Copeman/Heintz								X	X	X	X	X			X	X	X	X	X	X
O-8: International cooperation																					
Joint survey meeting (ICC meeting)	Farley																				
Russian scientists participation on surveys	Farley				X								X								
Data sharing/interpretation	All PIs									X	X	X	X	X	X	X	X	X	X	X	X

ASGARD: Acoustics (Lead PI: Stafford)

.	individual responsible for completion	FY16	FY17				FY18				FY19				FY20				FY21			
		Jun – Sep	Oct – Dec	Jan – Mar	Apr – Jun	Jul – Sep	Oct – Dec	Jan – Mar	Apr – Jun	Jul – Sep	Oct – Dec	Jan – Mar	Apr – Jun	Jul – Sep	Oct – Dec	Jan – Mar	Apr – Jun	Jul – Sep	Oct – Dec	Jan – Mar	Apr – Jun	Jul – Sep
Objective #1 - Hydrophones deployed	KS																					
Data collection- mooring in water	KS					x	x	x	x	x	x	x	x	x								
Data/sample processing	KS									x	x	x	x	x	x	x	x	x	x	x		
Analysis	KS									x	x	x	x	x	x	x	x	x	x	x		
Objective #2 - Extract acoustic	KS																					
Data collection/field work																						
Data/sample processing	KS									x	x	x	x	x	x	x	x	x				
Analysis	KS														x	x	x	x	x	x	x	
Objective #3 - Integration with	KS																					
Data collection/field work																						
Data/sample processing	KS																					
Analysis															x	x	x	x	x	x	x	
Other																						
Kickoff meeting	KS	x																				
Progress report	KS		x		x		x		x		x		x		x		x		x		x	
AMSS presentation	KS			x				x				x				x				x		
PI meeting	KS			x				x				x				x				x		
Logistics planning meeting	KS		x				x															
Publication submission	KS													x				x				x
Final report (due within 60 days of project end date)	KS																					x
Final metadata and data submission (due within 60 days of project end date)	KS																					x

Arctic Integrated Ecosystem Research Program Final Report

ASGARD

Arctic Shelf Growth, Advection, Respiration and Deposition
Rate Experiments Project

25 June 2022

S.L. Danielson, R.R. Hopcroft, A.M.P. McDonnell, S.L. Mincks, B.L. Norcross, D.A. Stockwell, B.R. Charrier, R.E. Collins, L. Copeman, A. Deary, L. Eisner, C.E. Forster, T.D. Hennon, C. Lalande, R.M. Lekanoff, M.W. Lomas, J.M. Nielsen, S.H. O'Daly, A. Poje, and A.C. Zinkann

Table of Contents

Executive Summary

The ASGARD project

The Arctic Shelf Growth, Advection, Respiration and Deposition (ASGARD; NPRB awards A91-99a, A91-00a) Rate Experiments project and associated efforts (NPRB awards A94-00, A98-00a, A96, A97) proposed to address known information gaps that hinder a robustly comprehensive application of an ecosystem-based approach to resource management in the U.S. Pacific Arctic region. An ecosystem-based approach to resource management is needed to inform and guide policy-driven actions, but this approach requires synthesis of a detailed knowledge base that at the start of the Arctic Integrated Ecosystem Research Program (Arctic IERP) effort remained incomplete in three important ways. First, existing data were strongly biased to July through October although important ecosystem processes occur in spring, late fall and winter when access is difficult. Second, while we now understand the basic summer regional biogeography (Sigler et al., 2017), net community production (Codispoti et al., 2013), and drivers of species distributions for some taxonomic groups (Feder et al., 1994; Eisner et al. 2013; Blanchard, 2014; Grebmeier et al., 2015a; Ershova et al. 2015), we had scant information from any season about the fundamental chemical and biological rates that mediate carbon cycling and energy flows through the Northern Bering and Chukchi Sea ecosystem. Third, these knowledge gaps curtailed our ability to model the ecosystem, and our ability to make useful projections for management or policy decisions.

Accordingly, the hypotheses developed and addressed by the ASGARD project are:

H-1: *The structure (timing, magnitude and direction) of the wind field is the primary regulator of: a) variations in the partitioning of flow to either side of St. Lawrence Island, b) variations in advective pathways, sediment resuspension and sediment deposition events, c) two-way coupling of nutrient-poor coastal water masses with nutrient-rich mid-shelf water masses, d) temporally variable advective contributions to the pre-bloom nutrient concentrations throughout the water column and to near-bottom nutrient concentrations year-round.*

H-2: *Near-surface stratification during the period of ice retreat regulates macronutrient availability, the depth, location, and magnitude of primary productivity, and the type (small vs. large) of phytoplankton community that subsequently dominates.*

H-3: *Fluxes and quality of particulate matter supplied to the benthos are tightly coupled to the phenology of sea-ice retreat and primary production. Beginning with under-ice phytoplankton blooms in the late spring and continuing through the summertime open-water season, sinking fluxes of fresh planktonic-derived organic matter provide a sustained food supply. In other times of year, supply of organic matter is small and less labile, coming primarily from resuspended, reprocessed and advective sources further south.*

H-4: *Although zooplankton are unable to contain the phytoplankton bloom, they are nonetheless important in both transferring some portion of this production into the metazoan planktonic food-web and efficient at repackaging material into fecal pellets for accelerated export to the benthos. The composition of the zooplankton community, and the temperatures at which they are operating, determine the efficiency of energy transfer into the zooplankton (i.e. losses to respiration versus growth and reproduction) and the rates of fecal flux. Some of these rates*

are consistent with emerging empirical global relationships (i.e. respiration), while others (i.e. growth rate) deviate significantly because polar data is currently underrepresented in such syntheses.

H-5: *Benthic respiration, carbon biomass, production, macrofaunal community structure, functional group composition, and community-level production all vary with oceanic advection, water mass characteristics, and pelagic production regimes.*

Summary of Findings

Select key findings and descriptions of novel sample collections that target the proposed hypotheses and that are presented in the chapters of this report include the following highlights.

- Compilation and analysis of a nearly 100-year (1922-2018) historical record shows that the Bering and Chukchi continental shelves are differently impacted by climate change - including the magnitude of their warming trends. We show that the heat engines of both shelves accelerated over 2014-2018, with increased surface heat flux exchanges and increased lateral oceanic heat advection (Danielson et al., 2020).
- In contrast to prior observations that showed near-freezing waters in Anadyr Strait for many winter months, we show that 2017-2018 winter near-bottom waters advecting into Chirikov Basin were 1-2 degrees above the freezing point for all but a few weeks of time (Danielson et al., in prep.).
- We collected the first year-round northern Bering Sea set of whole water samples for major macronutrient analysis using a moored time series bag sampler. These samples are allowing us to refine our understanding of the seasonally varying heat and nutrient flux into the Arctic via the Anadyr Current (Hennon et al., in prep).
- We quantified the abundance of the *Synechococcus* and other picophytoplankton in the Northern Bering and Chukchi Seas. These observations support an increased importance of a previously marginal phytoplankton group during a warming period in the Chukchi Sea (Lomas et al., in prep.)
- We analyzed total lipids, lipid classes, fatty acids (FA) and alcohols in the dominant mesozooplankton (five taxa: euphausiids, copepods, chaetognaths, and pteropods) collected on both spring (ASGARD, 2017 and 2018) and late summer (Integrated Ecosystem Survey (IES) 2017 and 2019) Chukchi Sea research cruises. Preliminary analyses show that lipid-rich zooplankton have a high degree of reliance on diatom-sourced lipids (Eisner et al., in prep).
- We found significant seasonal differences in seston FA compositions, with diatom biomarkers more prevalent in spring, followed by a community shift to dinoflagellate and small flagellate FA biomarkers in late fall. Our analysis provide new information on FA phytoplankton dynamics and the important nutritional role of phytoplankton for higher trophic level consumers in the Northern Bering and Chukchi Sea regions (Nielson et al., in review).
- We measured sinking particulate organic carbon (POC) fluxes with drifting and moored sediment traps, as well as rates of primary production and particle-associated microbial respiration. In Bering Shelf/Anadyr Water masses, sinking POC fluxes ranged from 0.8 to 2.3 g C m^{-2} day^{-1}, making them among the highest fluxes ever documented in the global oceans. These results highlight the

extraordinary strength of the biological carbon pump on the Pacific Arctic shelf during an unusually warm and low-sea ice year (O'Daly et al., 2020).

- Fluxes of living algal cells, chlorophyll *a*, total particulate matter (TPM), POC, and zooplankton fecal pellets, along with zooplankton and meroplankton collected in the traps, were used to evaluate spatial and temporal variations in the development and composition of the phytoplankton and zooplankton communities in relation to sea ice cover and water temperature (Lalande et al., 2021).
- We present the first large-scale metabarcoding survey of 18S rRNA gene diversity in this region. Based on their biogeographical distributions, we identified exact sequence variants of *Chaetoceros*, *Pseudonitzschia*, *Micromonas*, and *Phaeocystis* as abundant taxa that may be negatively affected as the region warms (Collins et al., in review).
- We observed higher abundances of Pacific-affinity copepods (*Neocalanus* spp. and *Eucalanus bungii*) in 2017 compared to 2018. Multivariate analyses of the combined 2017 and 2018 150-µm datasets revealed five major community groupings. Euphausiids, composed of several *Thysanoessa* species, were present across the sampling domain. Amphipods, decapods, and the predatory chaetognath *Parasagitta elegans* were present in both years but did not show a particular spatial pattern. There was often a significant biomass in *Aglantha digitale* and other jellyfish and ctenophores present in the plankton nets.
- Egg production and copepodite growth rates were measured for the calanoid copepods *Pseudocalanus* spp., *Calanus marshallae/glacialis*, and *Metridia pacifica* in the northern Bering and southern Chukchi Seas during June of 2017 and 2018. Rates suggest considerable discrepancies between growth rates and egg production weights that we propose are due to differences in life history strategies. Consistent with other studies, we find that global growth models do not match our observations particularly well, likely because they are dominated by egg production estimates at lower latitudes (Poje, 2020).
- Spatial generalized additive models mapped the distribution of polar cod (also termed arctic cod by some and in some places in this report) by size class and relative to environmental variables. Seasonal differences in polar cod abundance suggest that polar cod migration may follow a classical 'migration triangle' route between nursery grounds as juveniles, feeding grounds as subadults, and spawning grounds as adults, in relation to ice cover and seasonal production in the Chukchi Sea (Forster et al., 2020).
- Polar cod (*Boreogadus saida*) and saffron cod (*Eleginus gracilis*) are ecologically important forage-fish species in the Arctic. For the first time, we were able to synthesize the seasonal distribution, abundance, and growth of two co-occurring Arctic forage fishes. Kotzebue Sound was likely a source of early-stage prctic cod and saffron cod found offshore of Point Hope / Cape Lisburne and in nearshore coastal areas to the north. However, polar cod found in the Hanna Shoal region are not likely hatched from Kotzebue Sound, but from other areas such as Bering Strait and Chukotka Peninsula. Growth rates estimated in 2017, an extremely warm year in the Arctic, were higher than in previous studies, although this should be confirmed using otolith-derived growth rates (Deary et al. 2021).
- Closed-system respirometry using non-invasive oxygen optodes was conducted using five bivalve species *(Macoma sp., Serripes groenlandicus, Astarte sp., Hiatella arctica* and *Nuculana pernula*) and one amphipod species (*Ampelisca macrocephala*). Results revealed species-specific respiration rates with high metabolic demand for *S. groenlandicus* and *A. macrocephala* compared to that of the other

species. These results suggest that observed shifts in spatial distribution of the dominant macrofaunal taxa across this region will impact carbon demand of the benthic community. Hence, ecosystem models seeking to incorporate benthic system functionality may need to differentiate between communities that exhibit different oxygen demands (Jones et al., 2021).

- Four clusters of polychaete functional guilds were identified in the northern Bering and southern Chukchi sea. Polychaete functional composition and vertical distribution reflected the quality and quantity of organic matter input and the depositional environment, with likely impacts on biogeochemical and carbon cycling within the sediment (Charrier et al., in prep).
- Meiofauna community structure largely mirrored that of polychaete communities, with similar relationships to sediment grain size and organic matter characteristics. Macrofauanl-sized nematodes represented a distinct community relative to meiofaunal nematodes, and accounted for a large portion of total macrofaunal biomass, suggesting further investigation of this neglected group is warranted (Charrier et al., in prep).
- In light of changing temperature and productivity regimes across the Pacific-Arctic domain, we measured respiration rates of sediment communities at in situ (0 ºC) (ambient) and elevated (5 ºC) temperatures. On average, sediment community oxygen demand, a proxy for organic carbon consumption, was ~30% higher in the warmer treatments (Mincks et al., in prep).
- A mass balance Chukchi Sea ecosystem model incorporated terrestrial matter as an energy source, especially for benthic consumers. This component allowed us to adjust phytoplankton biomass to better match recent empirical measurements and to update the system-wide mass-balance (Zinkann, 2020; Zinkann et al., in review).
- Iterations of the mass-balance model showed that climate-driven increased retention of phytoplankton biomass in the pelagic realm would depress biomass of most benthic-feeding organisms across several larger ecosystem groups (invertebrates, fishes, mammals). However, simulated increases in both terrestrial matter inflow and bacterial biomass have the potential to compensate for some of the reductions in the energy supply from phytoplankton to the benthic food web, as well as to diversify the supply of organic matter to the seafloor (Zinkann, 2020; Zinkann et al., in review).
- Using empirical biomass and rate measurements, we applied inverse food web modeling to in-situ phytoplankton, microzooplankton, zooplankton, sedimentation and primary production data collected from four ecosystem surveys in the Chukchi and Northern Bering seas, June (spring) 2017 and 2018, and August-September (summer) 2017 and 2019. Our results indicate variable carbon transfer efficiencies among seasons and areas of nutrient replete and nutrient deplete conditions (Nielson et al., in prep).
- Extremely warm conditions from 2017 into 2019 – including loss of ice cover across portions of the region in all three winters – were a marked change even from other recent warm years. Biological indicators suggest this state change could alter ecosystem structure and function (Huntington et al., 2020).

Acknowledgements

We thank Captain Eric Piper, the crew of R/V Sikuliaq, Seward Marine Center shore support, and the Sikuliaq technical support team of Steven Hartz, Dan Nabor and Ethan Roth for their fantastic support throughout the program. Given the size and complexity of our experiments and especially our requirements of extensive climate-controlled incubation space, we believe that no other vessel would have been able to support such a wide array of activities and generate such across-the board successes in our field work.

We thank Bill Wiseman and the National Science Foundation for the addition of funded days at sea in 2017, and UAF's Alaska Sikuliaq Program for major support of ship days in 2017 and 2018. We thank Brendan Smith for accompanying us on the ASGARD cruises and providing photo documentation of our work and we thank Danielle Dickson and Matt Baker for guidance and support of the project through all of its phases. We thank all of the Arctic IERP funders for sponsoring the program: the North Pacific Research Board (NPRB), the Collaborative Alaskan Arctic Studies Program (formerly the North Slope Borough/Shell Baseline Studies Program), the Bureau of Ocean Energy Management (BOEM), and the Office of Naval Research (ONR) Marine Mammals and Biology Program for funding the main ASGARD proposal and all associated linked studies and gap projects (grants A91-99a, A91-00a, A94-00, A98-00a, A96, A97, A99).

We acknowledge that our field work was conducted on the waters where traditional subsistence harvest activities have been conducted by Inupiaq, Siberian Yupik, and Yupik peoples, and we thank them for their continued stewardship. Out of the field, our research is also conducted at the University of Alaska Fairbanks Troth Yeddha' campus, on the customary homelands of the Lower Tanana Dene. Robert Sudyam, Craig George and the Alaska Eskimo Whaling Commission provided valuable guidance for helping us avoid conflict with subsistence harvest activities. We thank Opik Ahkinga of Little Diomede for joining both research cruises and contributing as a valued member of the benthic team and for helping us better understand perspectives of the Bering Strait region residents.

Acronyms and Abbreviations

ACCAP	Alaska Center for Climate Assessment and Policy
ACW	Alaska Coastal Water
ADFG	Alaska Department of Fish and Game
AFSC	Alaska Fisheries Science Center
AGU	American Geophysical Union
AMBON	Alaska Marine Biodiversity Observation Network
Arctic IES	Arctic Integrated Ecosystem Survey
Arctic IERP	Arctic Integrated Ecosystem Research Program
AOOS	Alaska Ocean Observing System
ASGARD	Arctic Shelf Growth, Advection, Respiration and Deposition rate experiments project
ASLO	Association for the Sciences of Limnology and Oceanography
ASP	Amnesic Shellfish Poisoning
AURAL	Autonomous Underwater Recorder for Acoustic Listening
AW	Anadyr Water
BOEM	Bureau of Ocean Energy Management
CDOM	Colored Dissolved Organic Matter
CEO	Chukchi Ecosystem Observatory
CFOS	College of Fisheries and Ocean Science
COAS	College of Earth, Ocean and Atmospheric Science
CPUE	Catch per unit effort
CTD	Conductivity-Temperature-Depth Instrument
DBO	Distributed Biological Observatory
DIC	Dissolved inorganic carbon
ECMWF	European Centre for Medium-Range Weather Forecast
EJ	Exajoules
ELHS	Early life history stages
ESV	Exact sequence variants
IARC	International Arctic Research Center
IARPC	U.S. Interagency Arctic Research Policy Committee
IES	Integrated Ecosystem Survey
IOS-DFO	Institute of Ocean Sciences, Fisheries and Oceans Canada
ISHTAR	Inner Shelf Transfer and Recycling program
JAMSTEC	Japan Agency for Marine-Earth Science and Technology
K3S	Kitikmeot Sea Science Study (Canada)
LISST	Laser In-situ Scattering and Transmissometry Instrument
LME	Large marine ecosystem
LTL	Lower Trophic Level
NCP	Net Community Production
NMFS	National Marine Fisheries Service
nMDS	Nonmetric multidimensional scaling
NOAA	National Oceanographic and Atmospheric Administration
NPRB	North Pacific Research Board
NSB-DWM	North Slope Borough Department of Wildlife Management
NSF	National Science Foundation
OBS	Optical backscatter
OMIX	Ocean mixing project (Japan)

Acronyms and Abbreviations (continued)

ONR	Office of Naval Research
OSU	Oregon State University
PACMARS	Pacific Marine Arctic Regional Synthesis
PAR	Photosynthetically Available Radiation
PI	Principal Investigator
PICES	North Pacific Marine Science Organization
PMEL	Pacific Marine Environmental Laboratory
POC	Particulate organic carbon
SEP	Weight-specific egg production
SKQ	Research Vessel Sikuliaq
SST	Sea surface temperature
TINRO	Russian Federal Research Institute of Fisheries and Oceanography
TPM	Total particulate matter
UAF	University of Alaska Fairbanks
UME	Unexplained mortality event
USARC	U.S. Arctic Research Commission
USFWS	U.S. Fish and Wildlife Service
UVP	Underwater Vision Profiler
UW	University of Washington
VNIRO	Russian Federal Research Institute of Fisheries and Oceanography
WHOI	Woods Hole Oceanographic Institute

Preamble

The Arctic Integrated Ecosystem Research Program

The Arctic Integrated Ecosystem Research Program (Arctic IERP, 2016-2021) was motivated by the rapid changes occurring in the waters of the northern Bering and Chukchi Seas. While much research has been done in the region, many important questions remain. As a cohesive research endeavor, the Arctic IERP was designed to address a single, overarching question:

How will reductions in Arctic sea ice and the associated changes in the physical environmental influence the flow of energy through the ecosystem in the Chukchi Sea?

The report you are reading now is one of five final reports from the fieldwork phase of the Arctic IERP (a synthesis phase was initiated in 2022 after the completion of the Arctic IERP field-based projects). This preamble provides a brief overview of the Arctic IERP, both to place each final report in the broader context of the whole program, and to encourage readers to examine the other final reports to learn more about the research that was done. More detailed information about the Arctic IERP can be found at https://www.nprb.org/arctic-program.

The spatial domain of interest for the Arctic IERP extended across the Chukchi Sea Large Marine Ecosystem (LME) as redefined by the Arctic Council's Protection of the Arctic Marine Environment (PAME) working group, and the northern Bering Sea (above 61.5° N) as it strongly influences dynamics in the Chukchi Sea from the upstream direction. The main focus has been on the greater Bering Strait region and the Chukchi Sea. The program included the Arctic Basin and Beaufort Sea insofar as processes in the Chukchi Sea are influenced by these adjacent areas.

Development of the Arctic IERP

Before any Arctic IERP research proposals were written, the NPRB administered an assessment program, the Pacific Marine Arctic Regional Synthesis (PACMARS; https://www.nprb.org/assets/uploads/files/Arctic/PacMARS_Final_Report_forweb.pdf), that applied $1.5M provided by Shell and ConocoPhillips to compile and synthesize existing information about the ecosystem and inform research priorities. This assessment included community meetings in 2013 in Savoonga, Gambell, Kotzebue, Nome, and Barrow (now Utqiaġvik), in which representatives from 17 communities between St. Lawrence Island in the Bering Sea and Barter Island in the Beaufort Sea participated. One major area of emphasis that emerged from these community meetings was concern about food security for the region's residents in light of the rapid environmental changes taking place. Results from the scientific assessment and input provided via the community meetings informed the creation of the Arctic IERP. The PACMARS report informed both the IERP Request for Proposals (https://www.nprb.org/arctic-program/request-for-proposals/) and the submitted proposals.

Following a proposal review process, the Arctic IERP formally began in 2016 with funding from the North Pacific Research Board (NPRB), the Collaborative Alaskan Arctic Studies Program (formerly the North Slope Borough/Shell Baseline Studies Program), the Bureau of Ocean Energy Management (BOEM), and the Office of Naval Research (ONR) Marine Mammals and Biology Program. Generous in-kind support was contributed by the National Oceanic and Atmospheric Administration (NOAA), the University of Alaska Fairbanks (UAF), the U.S. Fish & Wildlife Service (USFWS), and the National Science Foundation (NSF). This coordinated program was developed in cooperation with the Interagency Arctic Research Policy Committee (IARPC) and the U.S. Arctic Research Commission.

The Research

The Arctic Integrated Ecosystem Research Program (IERP) invested approximately $18.6 million in studying marine processes in the northern Bering and Chukchi Seas in 2017-2021, beginning in the summer of 2017. The research was divided into three main, complementary projects. The Arctic Shelf Growth, Advection, Respiration, and Deposition Rate Experiments (ASGARD) project carried out research in late spring and early summer of 2017 and 2018 aboard R/V Sikuliaq. The Arctic Integrated Ecosystem Survey (Arctic IES) conducted fieldwork aboard R/V Ocean Starr in late summer and early fall 2017 and 2019. In addition to the vessel-based surveys, sub-surface moored sensors were deployed to gather biophysical information continuously from June 2017 to September 2019.

In addition to the vessel-based work, a team of Arctic residents and social scientists, including members from eight communities in the North Slope and Northwest Arctic Boroughs and the Bering Strait region, met several times during the project to assess and analyze Indigenous observations and experiences with various types of change occurring in the region from Savoonga to Utqiaġvik. This group also compiled an annotated bibliography of Traditional Knowledge or Indigenous Knowledge (available through the data portal described below), to help researchers from other components of the Arctic IERP find information relevant to their studies.

Prior to the commencement of fieldwork, meetings were held in the three hub communities of Nome, Kotzebue, and Utqiaġvik. Scientists from the Arctic IERP and NPRB staff met with community members from each region to discuss the research purpose and plans. Research plans were also shared and discussed at meetings of the Alaska Eskimo Whaling Commission (AEWC), the Indigenous Peoples Council for Marine Mammals (IPCoMM), and with the Tribal Councils of Gambell and Savoonga on St. Lawrence Island. One result of these meetings was a shift in timing of the ASGARD cruises from May until June as well as a shift in timing and survey regions for the Arctic IES cruises, to avoid conflicts with subsistence hunting activities during what is traditionally the time for walrus hunting. Another result was the creation of communication protocols to avoid conflicts by alerting coastal communities to the presence of research vessels and adjusting the ships' routes to avoid areas where hunting was taking place. These communication protocols included regular radio broadcasts and daily emails to community members throughout the research area.

Results from the research are published in a growing list of peer-review journal articles, as well as cruise reports that provide contemporary accounts of the cruises, and many social media postings that are available through the NPRB website. Data are publicly available as described below.

Collaborations

The NPRB collaborated and coordinated with several other U.S. agencies and organizations that fund Arctic marine research. NPRB staff worked closely with the U.S. Interagency Arctic Research Policy Committee (IARPC) and the U.S. Arctic Research Commission. As the Arctic IERP was developed, the NPRB secured commitments for collaboration from 22 existing research projects that were detailed in Appendix A of the request for proposals, and made connections with new projects as they were funded.

International researchers also collaborated with the Arctic IERP via the Pacific Arctic Group (PAG), the North Pacific Marine Science Organization (PICES), and the Intergovernmental Consultative Committee (US/Russia - bilateral) as well as collaborations developed by individual investigators. PAG participants, including researchers from Canada, China, Japan, Korea, Russia, and the United States, have coordinated their cruise plans to sample standard stations in the Chukchi and Beaufort Seas termed the Distributed Biological Observatory (DBO). The Arctic IERP contributed to this effort. US-Russian data sharing initiatives were hosted in San Diego in 2016 and Vladivostok in 2017 to promote collaboration and exchange and to facilitate collaboration and synthesis of data and trends of patterns observed in the US and Russian waters in the northern Bering and Chukchi seas (PICES Press, Volume 26, Issue 1). ICC

collaborations and other connections also brought scientists from the Russian Federal Research Institute of Fisheries and Oceanography (VNIRO), the Russian Pacific Scientific Fisheries Research Center (TINRO), and Hokkaido University to the US to participate in the Arctic IES cruises and co-author results. This collaboration is expected to connect research interests within respective EEZs (Russia/US) of the Chukchi Sea.

COVID-19

While the fieldwork of the Arctic IERP was completed before the outbreak of COVID-19, the final meeting of researchers in November 2020 was changed from an in-person event to an online format. Other plans for in-person events, such as meetings in hub communities within the US Arctic region (Nome, Kotzebue, and Utqiaġvik), were cancelled. Laboratory work and some collaborations were postponed or cancelled due to COVID-related restrictions and concerns. The NPRB made supplemental funds available to assist researchers with unanticipated expenses due to the pandemic. The overall productivity of the Arctic IERP was likely not greatly reduced, due both to good fortune in the fieldwork being completed and to the collaborative relationships that had been built or strengthened during the program.

Data Portal

Axiom Data Science, Inc. provided data management support to the Arctic IERP throughout the field program. Axiom staff assisted the scientists in authoring metadata and publishing the datasets to public archives. The data collected by the Arctic IERP are publicly accessible at https://arctic-ierp.dataportal.nprb.org/

General Introduction

ASGARD Background & Scientific Rationale

As a changing climate and sea-ice retreat progressively expose the Chukchi Sea to a longer open water season, society will confront new resource management issues. These include the future of the cultures and subsistence lifestyles of local Indigenous communities, potential impacts of industrial activities (e.g. commercial fishing, oil and gas extraction), potential changes to regional ocean carrying capacity, and resilience of the Arctic marine ecosystem (NRC, 2014).

An ecosystem-based approach is needed to inform and guide policy-driven actions but this approach requires synthesis of a detailed knowledge base that at the start of the Arctic IERP remained incomplete in three important ways. First, existing data are strongly biased to July through October although important ecosystem processes occur in spring, late fall and winter when access is difficult. Second, while we now understand the basic summer regional biogeography (Sigler et al., 2017), net community production (Codispoti et al., 2013), and drivers of species distributions for some taxonomic groups (Feder et al., 1994; Eisner et al. 2013; Blanchard, 2014; Grebmeier et al., 2015a; Ershova et al. 2015), we have scant information from any season about the fundamental chemical and biological rates that mediate carbon cycling and energy flows through the Northern Bering and Chukchi Sea ecosystem. Third, these knowledge gaps curtail our ability to model the ecosystem with even a basic level of confidence – and our ability to make useful projections upon which we can base management or policy decisions.

The Arctic Shelf Growth, Advection, Respiration and Deposition Rate Experiments projects (ASGARD; NPRB awards A91-99a, A91-00a, A94-00, A98-00a) proposed to address the above limitations by:

- undertaking environmental and LTL rate and distribution measurements from spring-season expeditions to the northern Bering and southern Chukchi seas in 2017 and 2018;
- coordinating and collaborating with other ongoing projects, including participating in ship-of-opportunity sampling later in those years; and
- carrying out year-round biophysical mooring deployments.

With this approach, we gathered missing information required for next generation modeling and follow-on synthesis activities, such as sought by Gibson and Spitz (2011) and Whitehouse et al. (2014). As shown in this report, some of these synthesis analyses have already been begun in the course of our initial publication efforts. Although the Arctic IERP as whole has advanced our understanding, the analyses that we might approach today include new questions that were not well appreciated just a few years ago when the program began.

The northern Bering and Chukchi continental shelves (*Figure 1*) annually transmit freshwater, heat, nutrients, and carbon (dissolved, particulate, and planktonic) from the North Pacific into the Arctic (Woodgate et al., 2005; Carmack & Wassmann, 2006). Previous work during the 1982-1988 Inner Shelf Transfer and Recycling (ISHTAR) program (with field work primarily in July and August) showed that the Chukchi inflow is an important source of new nitrogen for western Arctic productivity and the Arctic carbon budget as a whole (Walsh et al., 1989). Recent estimates of net community production (NCP) by

Codispoti et al. (2013) on the order of 70-100 g C m^{-2} identify the northern Bering and Chukchi shelves as the singular most productive region across the entire Arctic marine system, exceeding the NCP of the Nordic seas by a factor of 2-3 and exceeding other Arctic shelf and basin systems by factors of 6-100.

A defining feature of the northern Bering and Chukchi shelf that fundamentally shapes the regional ecosystem is the year-round delivery of substantial nutrient concentrations (NO_3 > 10 µM) to a region of the shelf that lies many hundreds of kilometers from the nearest continental slope (Sambrotto et al., 1984; Kinder et al., 1986; Walsh et al., 1989). Nutrient delivery to the Chirikov Basin euphotic zone is maintained at consistently high levels by the nutrient rich Anadyr Water (AW) carried by the Anadyr Current where production is estimated at 250–300 g C m^{-2} y^{-1} (Sambrotto et al., 1984; Grebmeier et al., 1988; Springer, 1988; Walsh et al., 1989). The Bering Strait transport can vary by nearly a factor of two inter-annually (Woodgate et al., 2012) and nutrient concentrations vary year-to-year (Danielson et al., 2017) but nutrient flux variations into the Chukchi have remain unquantified until this program (Mordy, 2020; Hennon et al., in prep.).

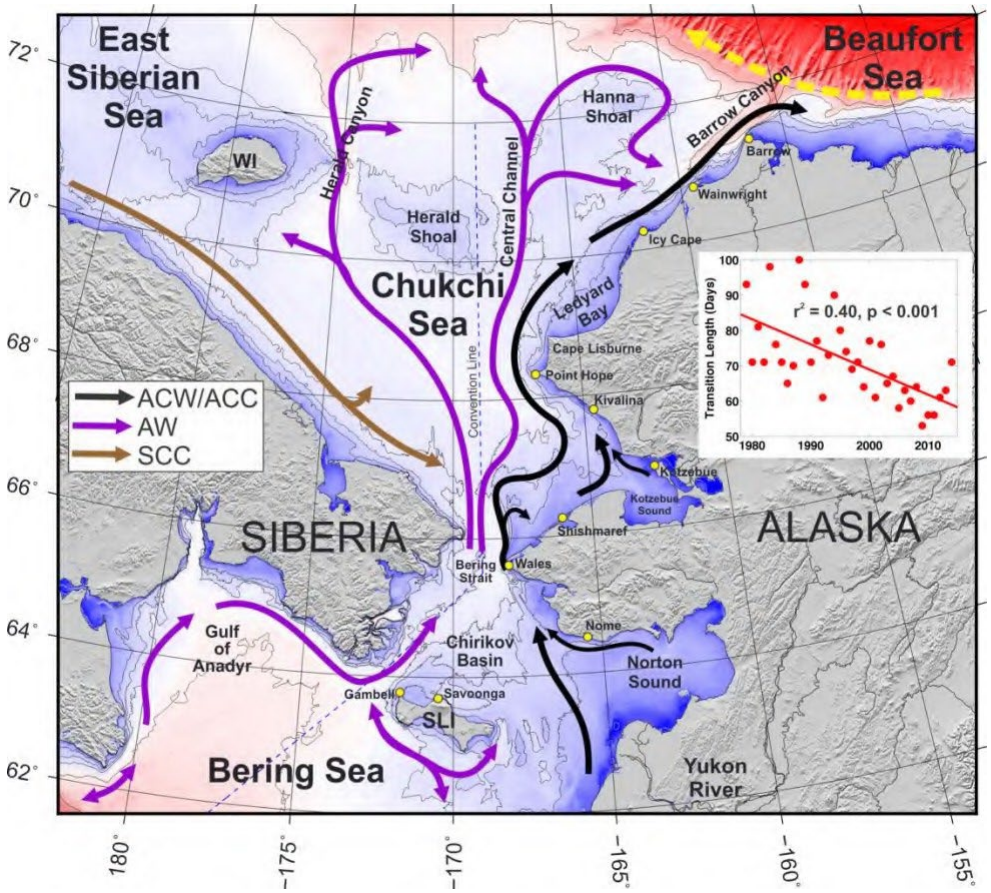

Figure 1. Map showing place names, persistent current systems, bathymetry (color shading). Inset: Decline in the regional duration of the annual spring sea-ice retreat, computed as the time between 80% and 20% ice cover.

Primary production begins initially in early spring, leading to rich sympagic communities (Gradinger, 2009). Phytoplankton growth accelerates in late spring once ice retreat and snow melt permit sufficient

light penetration into the water column (Hill et al., 2005; Mundy et al., 2005). Production quickly outpaces consumption by grazers, leading to the spring bloom. With an overall thinning of sea-ice, substantial under-ice blooms may also occur (Arrigo et al. 2012, Zhang et al. 2015). As the bloom wanes, ungrazed cells age and tend to settle quickly to the shallow (< 60 m) shelf, but the degree to which sinking particles are remineralized or repackaged in the pelagic zone is mostly unknown. Nonetheless, a large fraction of the organic matter makes it to the seafloor where it sustains a thriving benthic community (Highsmith & Coyle, 1990; Feder et al., 2007; Grebmeier & Maslowski, 2014, and references therein) that supports benthic-feeding fish and marine mammals. However, during this critical period of ice retreat, the magnitude and spatial extent of the spring bloom, phyto- and zooplankton growth rates, planktonic grazing rates, and benthic deposition rates are all poorly known, thus precluding construction of a robust carbon budget. Even later in the season when zooplankton communities support rich seabird communities (Day et al., 2013; Gall et al. submitted), rate measurements of primary and secondary production remain scarce (Nelson et al., 2014).

Substantial insight into the structure of zooplankton communities, and the physical factors that shape their distribution in the northern Bering and Chukchi Sea, have emerged in the past decade (e.g. Lane et al. 2008, Hopcroft et al. 2010, Eisner et al. 2013, Questel et al. 2013; Ershova et al. 2015). In contrast, direct measurements of process rates and carbon transfer for zooplankton are seldom determined because they are inherently more laborious. Four key vital rates of interest are intricately interconnected: growth rate is the net result of grazing rate less losses to egestion, respiration, and excretion (primarily as nitrogen compounds). With the exception of egg production studies (e.g. Plourde et al. 2005; Hopcroft & Kosobokova, 2010) that typically underestimate the (somatic) growth rates of prior life stages (Hirst and Bunker 2003), and two studies of grazing rate (Campbell et al. 2008), our knowledge of vital rates for copepods in the cold waters of the Bering and Chukchi Seas is lacking. Even globally, rate measurements are rare in water colder than 5°C (Hirst & Bunker 2003, Bunker & Hirst 2004) such as occur most of the year for the Chukchi. A rich understanding of somatic and reproductive rates of copepods is available from the Gulf of Alaska (Napp et al. 2005; Hopcroft et al. 2005; Liu & Hopcroft 2006a,b) as well as grazing rate estimates for *Neocalanus* (Liu et al 2005, 2008), but caution should be employed in applying them to the colder and more productive water of the northern Bering and Chukchi Seas (thereby stressing the need for direct measurements proposed by the ASGARD study). Simultaneous measurement of carbon flow into zooplankton growth/reproduction, grazing rate, respiration and fecal flux from the zooplankton community would establish the extent to which primary production is captured, burned off, or exported by the metazoan zooplankton versus settling to fuel the benthos.

Regardless of its form as grazed or ungrazed material, the high quantity of production reaching the seafloor sustains populations of numerous large and energy-dense prey items in “hotspot” regions, which serve as prey resources for a number of benthic feeding predators (Grebmeier et al., 2006). Hotspots of benthic biomass may be maintained by interactions of water circulation with bathymetry, resulting in locally elevated deposition of organic material (Feder et al., 2007; Blanchard & Feder, 2014; Blanchard 2015; Grebmeier et al., 2015a). Blanchard & Feder (2014) hypothesize that these variations in mechanisms delivering food to the benthos and associated indirect effects of related environmental interactions may be unrecognized sources for change in hotspot production. In addition, advection of particulate carbon northward also appears to make a significant but unquantified contribution to the annual carbon budget in the eastern Chukchi Sea (Feder et al. 1994; Dunton et al. 2005). While previous

studies in the region focused on patterns of overlying productivity and the signatures of organic matter deposition in the underlying sediments, little work has been devoted towards investigating the sizes, types, distributions, vertical fluxes, and lateral transport of water column particles that form mechanistic links between the pelagic and benthic realms. Recently-developed optical tools coupled with more traditional methods of particle collection have potential to provide new insights into the fluxes, impacts, and mechanisms of carbon cycling on the northern Bering and Chukchi Shelves.

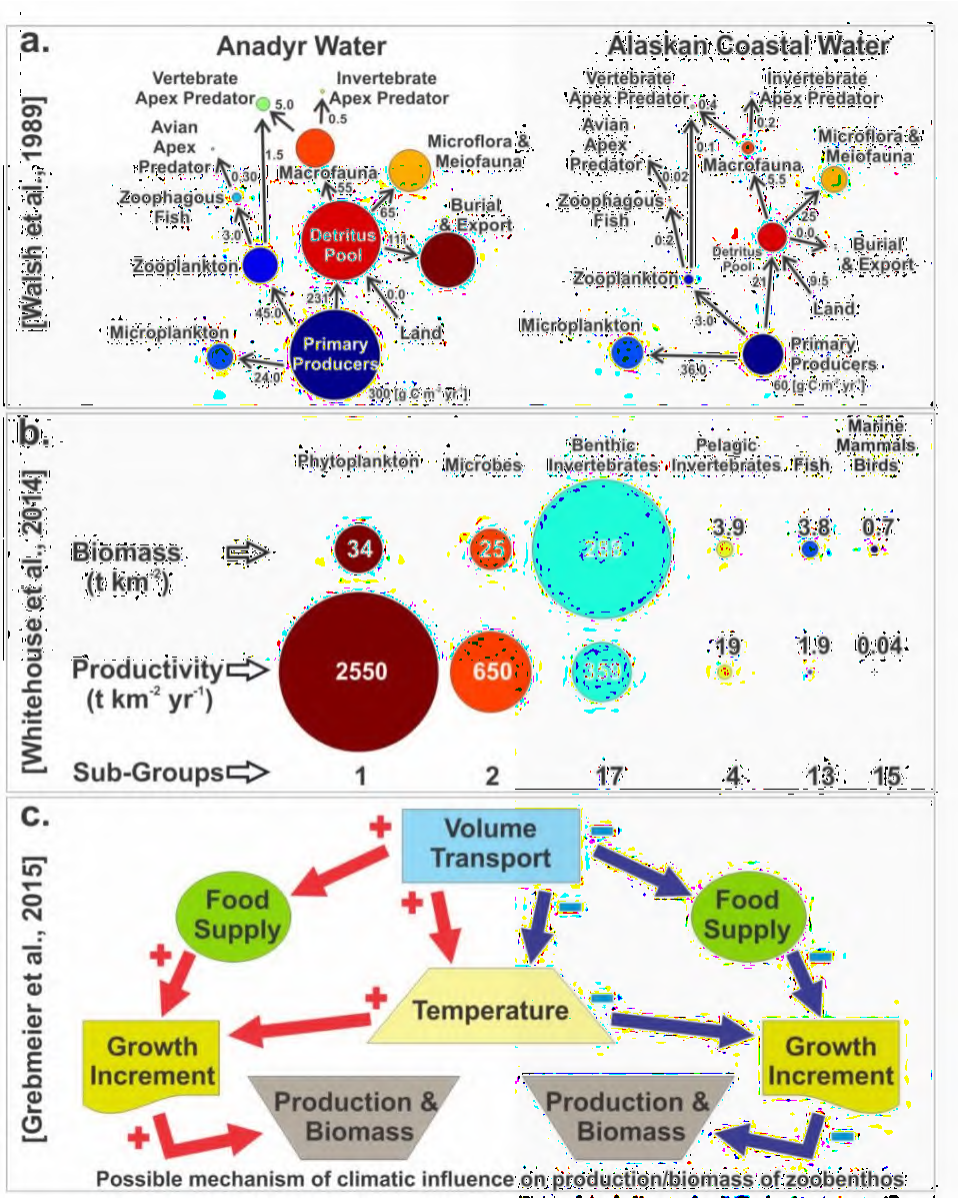

Figure 2. Three ways to consider the Pacific Arctic ecosystem. Top: Estimates of annually averaged carbon transfer rates for AW (left) and ACW (right); Middle: Biomass and productivity estimates along with number of functional subgroups per category. Bottom: Possible ramifications of a warming climate.

While macroscopic benthic communities have been relatively well-studied, the size and composition of the sediment microbial communities (bacteria, metazoan meiofauna) are largely unknown in this region,

even though these communities are most likely to show rapid responses to periodic or spatially patchy organic inputs because they are essentially non-motile and generally do not produce dispersive larval stages. Evidence from elsewhere suggests the magnitude, and perhaps quality, of particle flux influences microbial community structure, such that key ecosystem functions like remineralization rates and pathways may vary with magnitude of flux (Bienhold et al. 2012; Leduc et al. 2012). Moreover, the degradation rates of labile organic matter in sediments – crucial information in building models of energy flow for this system – have not been quantified, although they may be slower in this and other polar regions, constituting a longer-term benthic food reservoir (Mincks et al. 2005, Pirtle-Levy et al. 2009). Recent modeling attempts identify the lack of quantitative information on these key parameters describing ecosystem functioning, variability, and carbon flow in the benthos as critical data gaps (Whitehouse et al., 2014).

The ASGARD project was designed to refine existing paradigms that explain some facets of the regional ecosystem but that are otherwise known to be incomplete or outdated. Three separately published compilations that summarize many important aspects of our understanding are depicted in *Figure 2*. Together these show differences in carbon fluxes based on water mass, the importance of various functional groups to biomass and productivity, and possible ramifications of a warming climate. Inspection of each of these three cases reveals questions and information gaps that the ASGARD program addressed. For example, the seminal Walsh et al. (1989) depiction of carbon fluxes in different water masses (Figure 2a) shows microzooplankton, microflora and meiofauna as trophic dead-end carbon sinks. The Whitehouse et al. (2014) depiction (Figure 2b) provided relatively fine granularity to the upper trophic level functional groups (which account for ~1% of the biomass and 0.05% of the productivity) but does not adequately resolve the dominant contributions of the phytoplankton (1 group), microbes (2 groups), and pelagic invertebrates (4 groups). The balance described by Whitehouse et al. (2014) also utilizes many parameterizations derived from lower-latitude shelf ecosystems that may not hold for an Arctic shelf; both benthic and pelagic functional groupings require a more realistic parsing of ecological roles. Grebmeier et al. (2015b) hypothesize (Figure 2c) that warming temperatures will increase overall production and biomass, but do not explicitly include potentially important feedbacks associated with an ecosystem that is adjusting to new relations between altered timing and speed of ice retreat, spring blooms, and carbon pathways. Our proposed process studies were designed to complement – but not duplicate – the significant compilations of survey data collected in the Bering, Chukchi and Beaufort seas in recent years, positioning us to update these paradigms and write new ones.

Contemporary research programs have maintained an extensive set of summer-fall open-water Chukchi Sea observations over the last decade and more (Grebmeier & Harvey, 2005; Day et al. 2013, Pisareva et al. 2015), demonstrating that invertebrates, and to a limited degree small fishes, support the apex predators (marine mammals and seabirds) there. However, with a few notable exceptions, their cruises have sampled the Chukchi in July, August, September or October. Furthermore, many of these cruises targeted the northern Chukchi shelf or Chukchi/Beaufort slope region, far north of where much of the AW-fueled production takes place. Most of these recent Chukchi cruises were survey cruises that did not undertake the rate-process experiments that we believe hold the key to advancing our understanding of Arctic shelf carbon cycles. The 2007-2012 NSF-NPRB Bering Sea Project incorporated some valuable rate- measuring studies in multiple seasons but with a focus on the subarctic Bering shelf south of St.

Lawrence Island. Hence, our study helped fill data gaps that existed between the central and southeastern Bering Sea shelf and the northern Chukchi and Beaufort seas.

The ASGARD project was conceived as a coordinated ensemble of vessel- and mooring-based process studies consisting of physical, chemical, biological, and biogeochemical rate measurements that are designed to better constrain our knowledge of carbon and nutrient dynamics on the northern Bering and Chukchi sea continental shelves.

The fundamental science question posed in the ASGARD proposal was: **What regulates variations in carbon transfer pathways and how will the changing ice environment alter these pathways and ecosystem structure in the Pacific Arctic and beyond?**

Project Objectives

The ASGARD program was designed to address the NPRB Arctic Program's overarching questions that were outlined in their Request for Proposals (NPRB, 2015): "How do physical, biological and ecological processes in the Chukchi Sea influence the distribution, life history, and interactions of species or species guilds critical to subsistence and ecosystem function? How might those processes change in the next fifty years?". In addition to biological rate measurement studies, our research was designed to demonstrate how environmental conditions regulate flow rate variations and the associated advection of water masses, macronutrients, and particulate matter over the Northern Bering and Southern Chukchi continental shelves.

We aimed to contribute to M.S. and Ph.D. graduate student educations, including both students fully funded by the project and students not requiring financial support from ASGARD, but who participated in our cruises and collected data for use in their externally-supported research projects. We sought to strengthen existing and build new collaborations with national and international partners and scientific programs. We facilitated cruise and post-cruise involvement of outreach specialists in order to help us communicate our science and results to targeted stakeholders and the general public. We worked on strengthening our ties with coastal communities by participating in numerous co-management and other Alaskan Native Organization meetings, including Tribal Council consultations and by welcoming a Bering Strait region observer on board our research cruises as a member of the science team.

Specific objectives outlined in the ASGARD proposal are as follows:

O-1: *Quantify ice, water volume, heat, salt, nutrient, carbon, and planktonic fluxes at under-sampled locations and times in the northern Bering and Chukchi seas.*

O-2: *Assess particulate organic matter sinking and deposition rates and lower trophic level growth and respiration rates in locations and times that currently lack data.*

O-3: *Better quantify synoptic, seasonal, and inter-annual changes in the regional biological carbon pump dynamics and kinematics.*

O-4: *Collect physical, chemical, biogeochemical, and biological process rate data needed to constrain and evaluate biophysical and ecosystem models.*

O-5: *Help develop educational and outreach materials to communicate compelling narratives about our research to indigenous and non-indigenous local, regional, national and international audiences.*

O-6: *Contribute to the education and research programs of at least 6 M.S. and Ph.D. graduate students.*

O-7: *Support additional Arctic IERP research projects with moored and ship-based measurement platforms.*

O-8: *Form coordinated data collection and analysis collaborations with national and international partners.*

O-9: *Enhance the Distributed Biological Observatory (DBO) program by occupying DBO stations at a time of year in which few samples have been collected previously.*

Measurements and Approach

The ASGARD study consisted of ship-based and mooring-based studies designed to integrate with other proposed field, modeling, and human dimensions efforts. We selected the following focal measurements to help us address our main science question:

- Advective fluxes of physical, biotic and abiotic components of the water column
- Phytoplankton primary productivity
- Zooplankton growth/reproduction, respiration and fecal pellet production rates
- Particle deposition rates from the water column to the seafloor
- Quality of organic matter deposited to the seafloor
- Benthic respiration and organic matter decomposition rates
- Abundance and biomass of benthic microbial and metazoan fauna
- Distribution of fishes at different life history stages (NPRB Award A98-00a)
- Underwater sound and seasonal distributions of marine mammals (NPRB Award A94-00)

We sailed to the northern Bering and southern Chukchi shelf in 2017 and 2018 (Figure 4) on *R/V Sikuliaq*. In each year, working south to north, we first occupied ten "process" stations (yellow circles in Figure 3), setting up growth rate experiments (Table A1). that required extended (1-10 day) incubation times, along with collecting our broad suite of standard measurements (Table A2). As the ship visited the process stations, we paused to deploy and/or recover moorings (Table A3, Figure 3) that recorded year-round time-series. Following the process study phase, the ship transitioned to a "survey" mode of operation, rapidly working north-to- south along multi-station transects (Table A2, Figure 3) and re-occupying the process stations with a more limited sampling suite to provide information about short-term (~days) changes to the water-column. Along the way, we continued trawl and multi-core benthic samplings. Throughout the cruise we collected continuous underway navigational, ocean surface, ocean profile, and meteorological data (Table A4) to provide additional environmental context for subsequent analyses. The mooring array (Table A3, Figure 4) consists of four biophysical moorings south of Bering Strait, two moorings in the southern Chukchi Sea, plus the NPRB Long-Term Monitoring Program NE Chukchi Sea Ecosystem Observatory (CEO) moorings located on the southern flank of Hanna Shoal near Barrow Canyon.

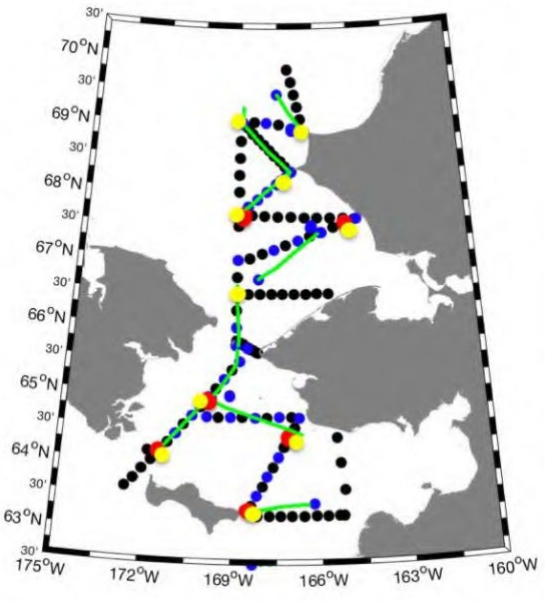

Figure 3. Location of field effort. Most 2018 stations (blue circles) were also occupied in 2017 (black circles). The Acrobat tows took place only in 2018. Some circles were shifted slightly on the map to reduce overlap.

Field Expeditions

ASGARD field efforts (Figures 3 and 4) are documented in two detailed scientific cruise reports (Danielson et al., 2017; 2018) and one community observer report (Ahkinga, 2017) that are available at the NPRB Arctic IERP website: https://www.nprb.org/arctic-program/about-the-program/. The cruises took place in June 2017 and June 2018. We joined the Arctic IES component of the IERP for final mooring recoveries in August 2019. Weather conditions and cruise timing allowed us to occupy more survey stations in 2017 than in 2018, but in 2018 we also operated a towed undulating Acrobat® sensor system that helped compensate for the reduction in occupied stations.

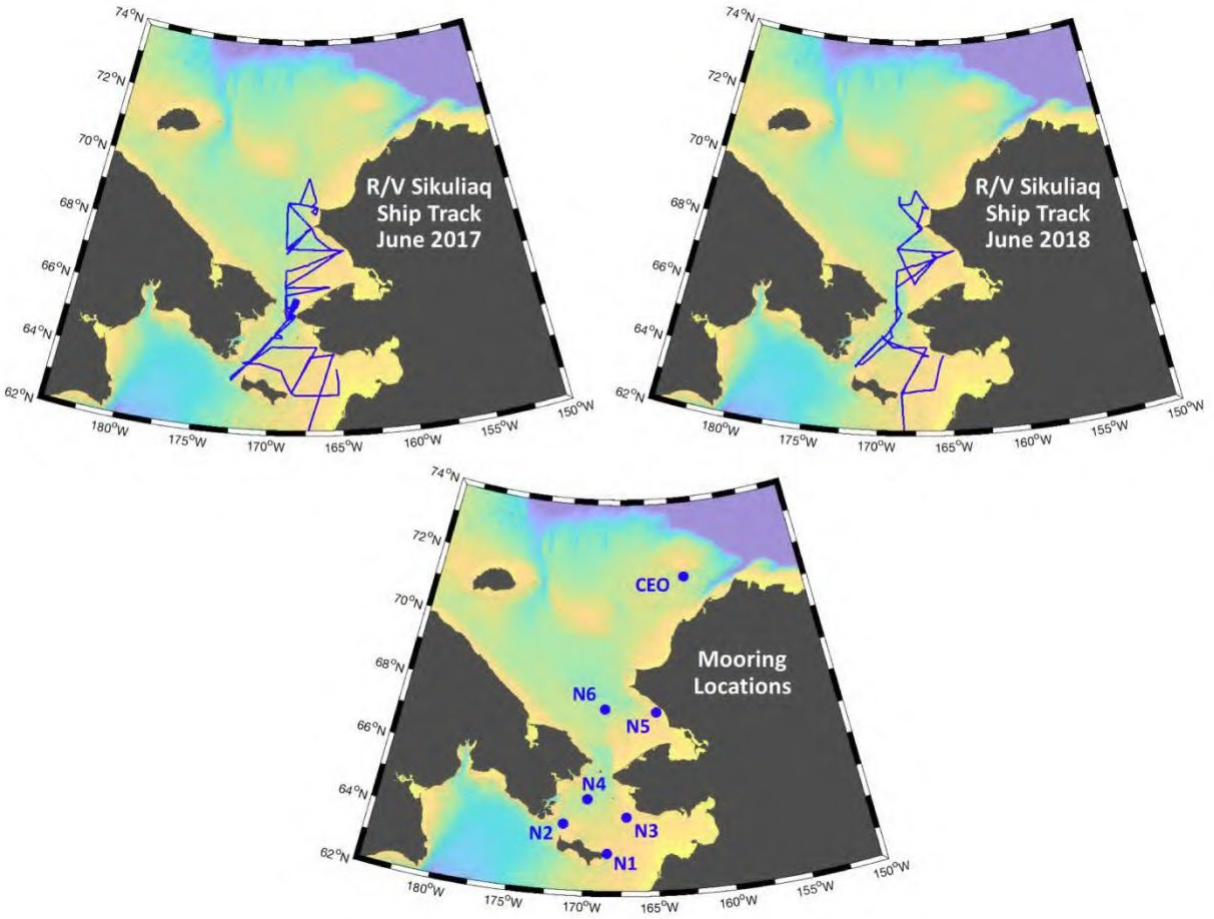

Figure 4. Vessel track lines (blue) for cruise SKQ2017-09S (June 2017, upper left), SKQ2018-13S (June 2018, upper right) and year-round mooring locations (blue circles, bottom). Identifying names for ASGARD moorings N1-N6 and the Chukchi Ecosystem Observatory (CEO) mooring cluster are labeled.

Photograph Tour: Cruise Activities

Primary Productivity Incubations

Sediment core incubations

Zooplankton artificial cohort incubations in carboys and blue fish tote incubators

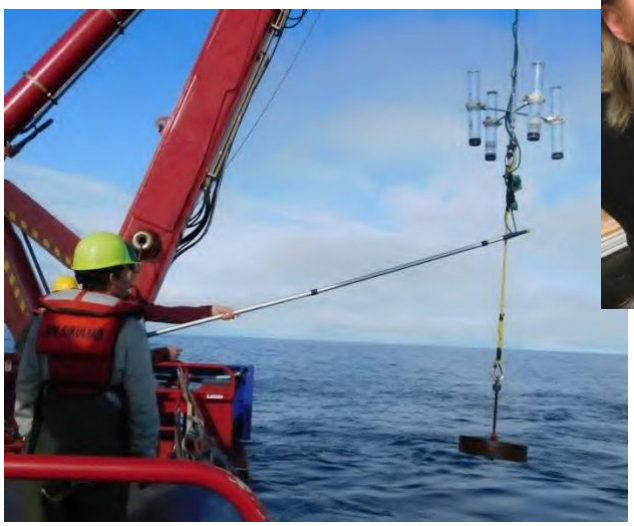

Drifting sediment traps

Zooplankton egg production incubations

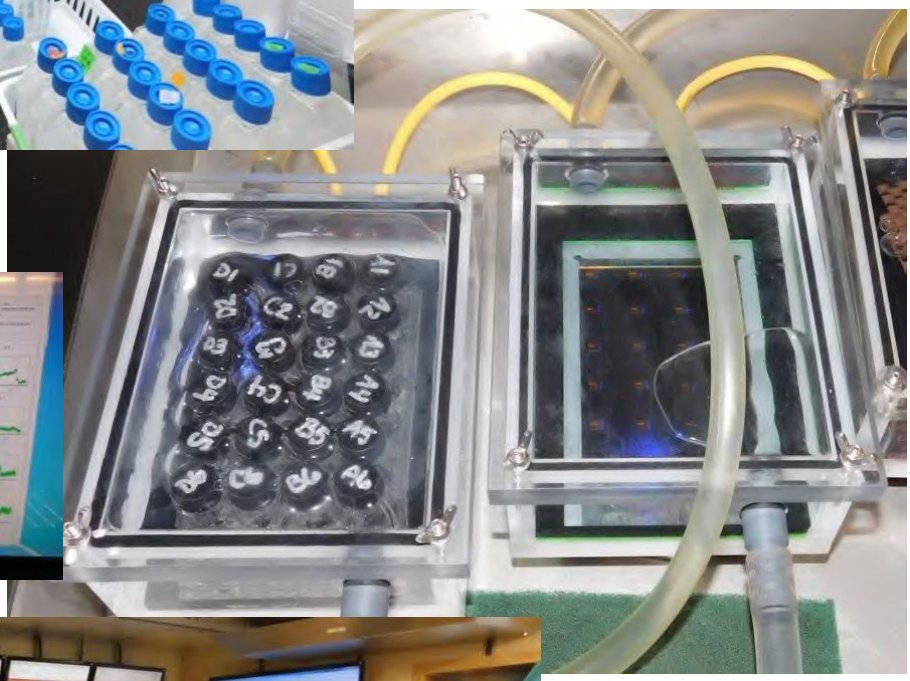

Zooplankton respirometry incubations

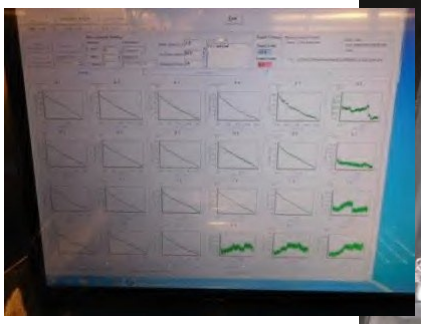

Collecting hydrographic profiles and water samples with the CTD.

Multi-core sample recovery

Zooplankton net tow sampling

Clam respirometry incubation measurements

Mooring deployment

Dense patches of *euphausiids* sampled with nets and acoustics

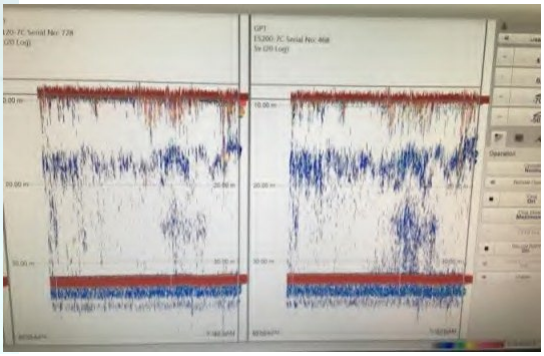

Multi-core samples

Sorting catch from a benthic-sampling beam trawl.

Project Objective Milestones

ASGARD objectives O-1 through O-4 are core scientific objectives that were achieved through collecting data and its subsequent analysis. Objectives O-5 through O-9 are programmatic objectives that are not specific to any particular disciplinary study. The objectives were addressed in the following fashion:

O-1: *Quantify ice, water volume, heat, salt, nutrient, carbon, and planktonic fluxes at under-sampled locations and times in the northern Bering and Chukchi seas.*

- Advective and state data from moorings (currents, CTD, sediment traps)
- Samples from drifting sediment traps
- Advective, station, and state data from ship-based sampling (currents, nets, acoustics)
- ASGARD Studies #1, 2, 3, 4, 5, 6, 7, 8, 12, 13, 14 (see *Results in Brief*)

O-2: *Assess particulate organic matter sinking and deposition rates and lower trophic level growth and respiration rates in locations and times that currently lack data.*

- Samples from moorings with sediment traps
- Samples from drifting sediment traps
- Data from optical sensors mounted on CTD rosette
- ASGARD Studies #8, 10, 11, 12, 13, 14, 15, 18, 19, 20 (see *Results in Brief*)

O-3: *Better quantify synoptic, seasonal, and inter-annual changes in the regional biological carbon pump dynamics and kinematics.*

- Advective and state data from moorings (currents, CTD, sediment traps)
- Samples from drifting sediment traps
- Data from ship-based sampling (nets, acoustics)
- Samples from multi-core sampler
- Data from growth and respiration incubations
- All ASGARD Studies (see *Results in Brief*)

O-4: *Collect physical, chemical, biogeochemical, and biological process rate data needed to constrain and evaluate biophysical and ecosystem models.*

- Advective flux data from moorings
- Zooplankton egg production, artificial cohort growth, and respirometery incubations
- Benthic macrofaunal incubations
- Benthic community oxygen utilization incubations
- Drifting sediment trap incubations
- All ASGARD Studies #1, 2, 3, 6, 8, 10, 12, 13, 14, 15, 18 (see *Results in Brief*)

O-5: *Help develop educational and outreach materials to communicate compelling narratives about our research to indigenous and non-indigenous local, regional, national and international audiences.*

- Contributions to the Arctic IERP informational flier
- ASGARD Synopsis products
- Numerous social media posts, blog postings, videos and other products
- Presentations delivered to scientific and public stakeholders

O-6: *Contribute to the education and research programs of at least 6 M.S. and Ph.D. graduate students.*

- All of the following graduate students participated in our cruises. Students denoted with a star (*) also analyzed samples and data collected by the ASGARD project in their thesis or dissertation:
  - Zane Chapman (UAF)*
  - Brittany Jones Charrier (UAF)*
  - Erica Escajeda (UW)*
  - Caitlin Forster (UAF)*
  - Silvana Gonzalez (UW)
  - Rachel Lekanoff (UAF)*
  - Kofan Lu (UAF)
  - Heidi Mendoza (UAF)
  - Stephanie O'Daly (UAF)*
  - Alex Poje (UAF)*
  - Jessica Pretty (UAF)
  - Sarah Seabrook (OSU)
  - Ann Zinkann (UAF)*

O-7: *Support additional Arctic IERP research projects with moored and ship-based measurement platforms.*

- We provided the ASGARD moorings as a platform for passive acoustic sensors.
- Arctic IERP scientists in the Arctic IES UTL and Arctic IES LTL projects joined the ASGARD cruises.
- Scientists with funding from NOAA, NSF, Japan, and other sources joined the ASGARD cruises.

O-8: *Form coordinated data collection and analysis collaborations with national and international partners.*

- Scientists from twelve universities, agencies, or research institute participated in the ASGARD cruises, including one from Hokkaido University in Japan.
- Scientists from at least 24 institutes in the US along with Japan, Russia, Canada and Germany participated in ASGARD PI-led manuscripts.
- ASGARD scientists participated in International symposia and data synthesis and analysis efforts.

O-9: *Enhance the Distributed Biological Observatory (DBO) program by occupying DBO stations at a time of year in which few samples have been collected previously.*

- We occupied DBO-1, DBO-2, and DBO-3 stations in June 2017 and June 2018.
- We deployed year-round moorings in the DBO-2, DBO-3, and DBO-4 regions and one mooring between DBO-1 and DBO-2.

Emerging Stories

This report documents ASGARD project activities and results through the end of the initial phase of research and analysis (2016-2021) of the Arctic IERP program. We were successful in collecting data that have been and will continue to be applied to all of our focal objectives and hypotheses, and, as shown below, we addressed each from several vantage points. The present list of ASGARD-associated publication currently numbers 55 (this number includes non-peer-reviewed cruise reports, peer-reviewed "core" ASGARD studies, studies that have leveraged data collected on ASGARD cruises, studies that leveraged ASGARD data products, and studies in which ASGARD PI participation was facilitated by participation in the Arctic IERP). At the same time, we have only begun tapping the vast suite of potential results that the rich Arctic IERP dataset may yet reveal.

The *Results in Brief* section documents experiments, observations, and analyses that use data collected in the ASGARD field effort and were written in support of helping fill the three main information gaps identified in the ASGARD proposal (i.e., seasonal data gaps, rate measurements, and model parameterization/validation data) and guiding science question (i.e., ecosystem change in the face of diminishing sea ice). These studies include graduate student theses, dissertation chapters, and peer-reviewed journal articles (published and in preparation) that were written in support of the ASGARD project proposal and the Arctic IERP Integrated Work Plan (NPRB, 2016).

ASGARD Studies are briefly summarized in the *Results in Brief* section, with titles, abstracts and one representative data figure. Studies with complete or extensive analyses correspond to Chapters bearing the same titles in the *Results in Full Section*. Studies 1-3 concentrate on environmental conditions (physics and chemistry) and their temporal and spatial variability. They examine the manifestation of climate warming, wind effects on circulation, and the Pacific-Arctic nutrient flux. Studies 4-12 focus on the pelagic realm, beginning with eukaryotic phototrophs and continuing to picocyanobacteria, phytoplankton community composition, mesozooplankton growth, reproduction, lipid composition, and respiration rates, and the spatial distributions and seasonal growth of polar cod. Studies 13 and 14 link the pelagic realm to the benthos by examining water column export fluxes of carbon. Studies 15-18 assess benthic organic matter consumption, community structure and their implications in a warming climate. Studies 19-20 apply mass balance and inverse modeling approaches, respectively, better constraining our understanding of organic matter flow through the ecosystem. Study 21 raises the question of whether this highly productive ecosystem could be in the midst of a significant ecological transformation.

Results in Brief

Study 1: Manifestation and consequences of warming and altered heat fluxes over the Bering and Chukchi Sea continental shelves

Danielson, S.L., O. Ahkinga, C. Ashjian, E. Basyuk, L.W. Cooper, L. Eisner, E. Farley, K.B. Iken, J.M. Grebmeier, L. Juranek, G. Khen, S. Jayne, T. Kikuchi, C. Ladd, K. Lu, R. McCabe, G.W.K. Moore, S. Nishino, S.R. Okkonen, F. Ozenna, R.S. Pickart, I. Polyakov, P.J. Stabeno, K. Wood, W.J. Williams, T.J. Weingartner, 2020. Manifestation and consequences of warming and altered heat fluxes over the Bering and Chukchi Sea continental shelves. *Deep-Sea Res. II: Topical Studies in Oceanogr.,* 177, 144781, https://doi.org/10.1016/j.dsr2.2020.104781

A temperature and salinity hydrographic profile climatology is assembled, evaluated for data quality, and analyzed to assess changes of the Bering and Chukchi Sea continental shelves over seasonal to century-long time scales. The climatology informs description of the spatial distribution and temporal evolution of water masses over the two shelves, and quantification of changes in the magnitude and throughput of heat and fresh water. For the Chukchi Shelf, linear trend analysis of the integrated shelf heat content over its 1922-2018 period of record finds a significant summer and fall warming of 1.4 ºC (0.14+/-0.07 ºC decade^{-1}); over 1990-2018 the warming rate tripled to 0.43 +/-0.35 ºC decade^{-1}. In contrast, the Bering Shelf's predominantly decadal-scale variability precludes detection of a water column warming trend over its 1966-2018 period of record, but sea surface temperature data show a significant warming of 0.22+/-0.10 ºC decade^{-1} over the same time frame.

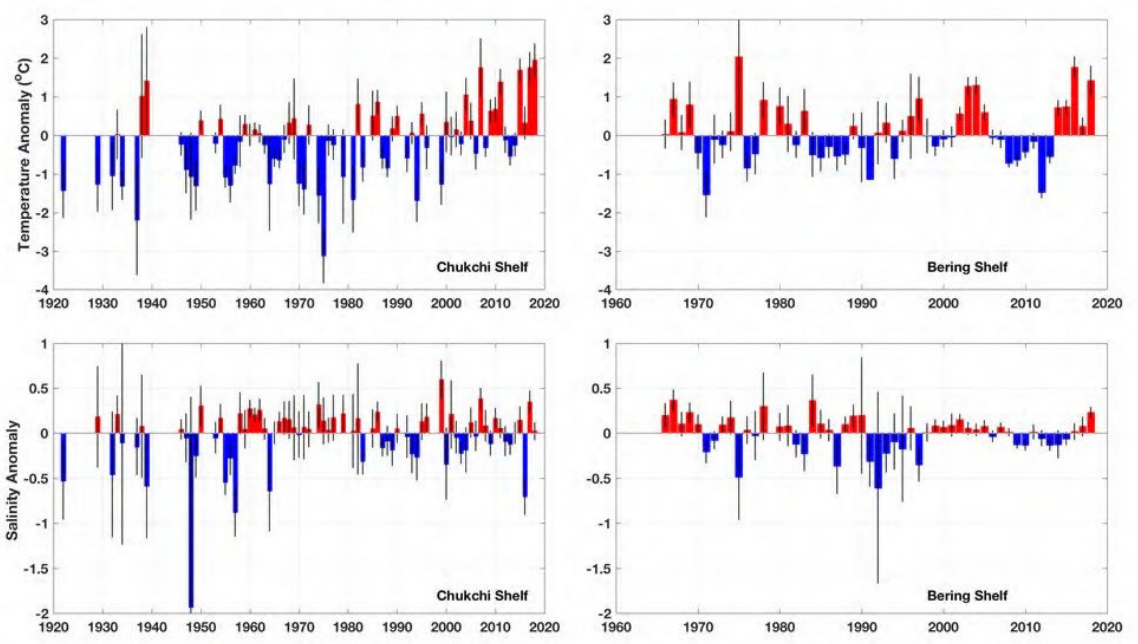

Figure 5. Annually averaged July through October thermal (top) and haline (bottom) anomalies over the Chukchi (left) and Bering (right) continental shelves. Error bar whiskers depict 95% confidence limits on the mean for each year's anomaly.

Heat fluxes over 1979-2018 computed by the European Centre for Medium-Range Weather Forecast (ECMWF) ERA5 reanalysis exhibit no record-length trend in the shelf-wide Bering surface heat fluxes, but the Chukchi Shelf cooling season (October-March) has a trend toward greater surface heat losses and its warming season (April-September) has a trend toward greater heat gains. The 2014-2018 half-decade exhibited unprecedented low winter and spring sea-ice cover in the Northern Bering and Chukchi seas, changes that coincided with reduced springtime surface albedo, increased spring absorption of solar radiation, and anomalously elevated water column heat content in summer and fall. Consequently, the warm ocean required additional time to cool to the freezing point in fall. Fall and winter ocean-to-atmosphere heat fluxes were anomalously large and associated with enhanced southerly winds and elevated surface air temperatures, which in turn promoted still lower sea-ice production, extent, and concentration anomalies.

Likely reductions in sea-ice melt were associated with positive salinity anomalies on the Southeast Bering Shelf and along the continental slope over 2014-2018. Negative salinity anomalies during 2014-2018 on the central and northern Bering Shelf may be related to a combination of 1) long-term declines in salinity, 2) an increase of ice melt, and 3) a decline of brine production. We hypothesize that freshening on the Bering Shelf and in Bering Strait since 2000 are linked to net glacial ablation in the Gulf of Alaska watershed.

We show that the heat engines of both the Bering and Chukchi shelves accelerated over 2014-2018, with increased surface heat flux exchanges and increased oceanic heat advection. During this time, the Chukchi Shelf delivered an additional 5-9 x 10^{19} J yr^{-1} (50-90 EJ yr^{-1}) into the Arctic basin and/or sea-ice melt, relative to the climatology. A similar amount of excess heat (60 EJ yr^{-1}) was delivered to the atmosphere, showing that the Chukchi Sea makes an out-sized contribution to Arctic amplification. A conceptual model that summarizes the controlling feedback loop for these Pacific Arctic changes relates heat content, sea ice, freshwater distributions, surface heat fluxes, and advective fluxes.

Study 2: Chirikov Basin Oceanography: Function, Structure, Drivers and Change (Manuscript in preparation)

Danielson, et al., In prep. Oceanography of Chirikov Basin: Function, Structure, Drivers and Change

Data from a suite of time series moorings, shipboard measurements, and numerical model integrations are assessed in order to build a better understanding of the oceanographic functioning of Chirikov Basin. We assess the regional wind forcing in order to better understand the regulation of the advective flow field over the Northern Bering and Southern Chukchi continental shelves. We show that the partitioning of flow to either side of St. Lawrence Island reflects a leaky switchyard type of balance between the central Bering Sea shelf and Chirikov Basin. Norton Sound may provide capacity to buffer a portion of and the mass transport, but sheared and bidirectional flow in Shpanberg Strait appears to be the main factor that decouples flow here from that in Anadyr Strait. Observations from outside of the Alaska Coastal Current, just downstream of Norton Sound, help show the connectivity between the two estuary and the greater shelf waters. Fluxes of heat, fresh water, ice, nutrients, and carbon are all modulated by the identified flow patterns, which reflect regionally coherent dominant patterns of flow variability. Remote sensing of sea ice presence along with optical sensors from select moorings (chlorophyll *a* fluorescence, photosynthetic available radiation and nitrate) help demonstrate how these flow patterns may influence the distribution, concentration, and productivity of phytoplankton and zooplankton here. We highlight the importance of the winter advection of oceanic heat on the regional sea ice cover and thickness, and how this is potentially affecting the local ecosystem.

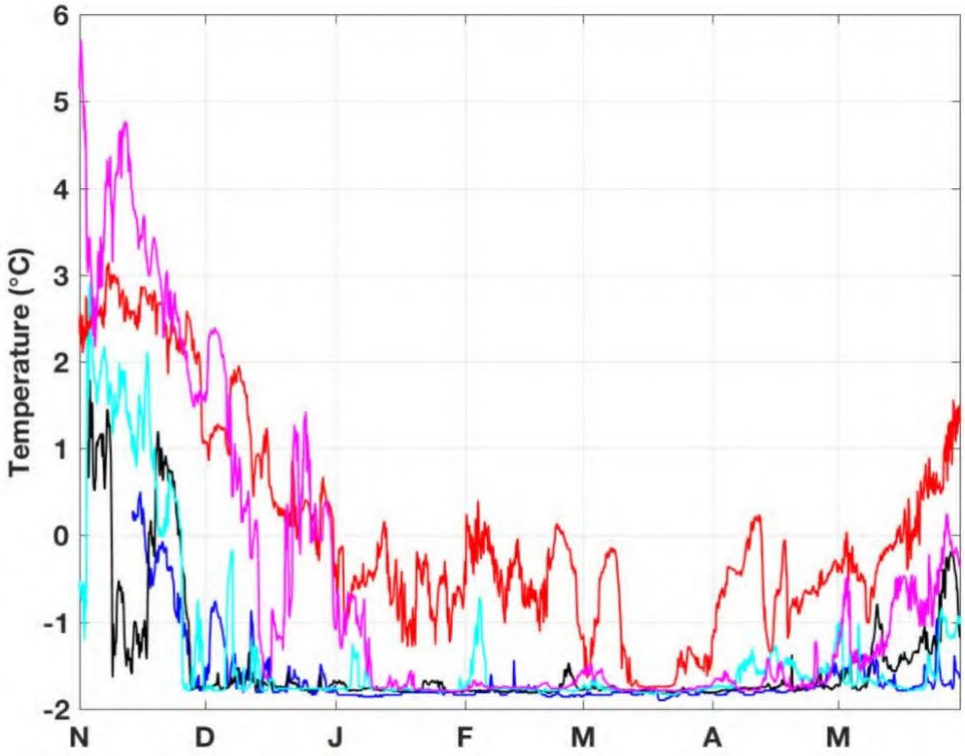

Figure 6.

Near-bottom temperature measured in Anadyr Strait from November (N) through May (M) in the winters of 1980-81 (blue), 1981-82 (black), 1984-85 (cyan), 2017-18 (red) and 2018-19 (magenta).

Study 3: Anadyr Current Contributions to the Arctic-bound Oceanic Nutrient Flux

Hennon, T.D., S.L. Danielson, C. Mordy, S. Stockwell, R. Woodgate. Anadyr Current Contributions to the Arctic-bound Oceanic Nutrient Flux. Manuscript in preparation for submission to *Geophysical Research Letters*.

Based on year-round measurements of nutrients from summer 2017-2018 from the Anadyr Strait, we use a combination of year-round mooring-based in situ measurements and salinity-nutrient relationships established at Anadyr Strait are used to estimate Pacific-to-Arctic fluxes of nitrate, phosphate, and silicate for each month spanning 1998-2018. Annually averaged fluxes are 16 ± 5, 1.6 ± 0.5, and 30 ± 10 kmol s^{-1} for nitrate, phosphate, and silicate, respectively, and inter-annual variability can reach ±30% of the means. Maximum fluxes occur in April, exceeding the annual average by ~50%, while minimum fluxes occur in December. Due to biological uptake, the seasonality of nutrient fluxes is more closely tied to nutrient concentration than transport, which peaks in June.

Our annually averaged estimates are ~ 50% higher than prior estimates, which may be rooted in methodological differences. We find significant ($p < 0.05$) increasing trends in phosphate and silicate fluxes over 1998-2018 that are associated with increasing transport. In contrast, nitrate exhibits no significant long-term trend, suggesting different nutrient composition ratios between surface and deep waters. Our data, taken from the core of the Anadyr current, will be valuable for assessing biogeochemical model performance at a globally important oceanic chokepoint and can contribute to studies that seek to understand the future trajectory of the Arctic ecosystem.

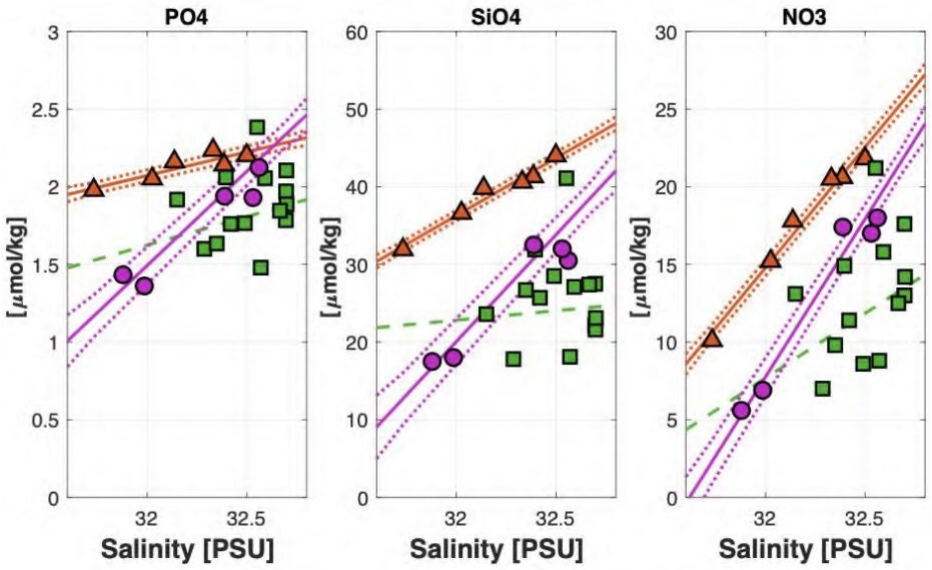

Figure 7. Seasonally-variable relationships between salinity and phosphate, silicate, and nitrate in Anadyr Strait during June 2017 to June 2018 (orange = Jan-Apr; magenta = Sep-Dec; green = May-Aug). Solid lines indicate the linear regressions to significant trends ($p<0.05$), with dotted lines indicating 95% confidence limits. The dashed green line shows the regression for May-Aug, though nutrient-salinity correlations during this time are not significant ($p>0.05$).

Study 4: Diversity and community structure of eukaryotic phototrophs in the Bering and Chukchi Seas

Collins, R.E., A. McDonnell, S. Danielson, R.M. Lekanoff, in review. Diversity and community structure of eukaryotic phototrophs in the Bering and Chukchi Seas, Submitted for review to *PlosONE*

Lekanoff, R.M., 2020. Diversity and Community Structure of Eukaryotic Phototrophs in the Bering and Chukchi Seas. University of Alaska Fairbanks. M.S. Thesis

The northern Bering and Chukchi Seas are productive high latitude ecosystems supported by tight benthic-pelagic coupling. However, warmer waters in Arctic and sub-Arctic regions are expected to alter phytoplankton community composition in the future, with unknown consequences for this critical ecosystem. Here we present the first large-scale metabarcoding survey of 18S rRNA gene diversity in this region, covering the summer 2017, the warmest on record, with sea surface temperatures rising to 10°C.

This report focuses on diatoms and "picophytoplankton" (operationally defined here as Chlorophyta, Haptophyta, and Chrysophyceae), which averaged 39% and 10% of the relative sequence abundance, respectively. In total, 201 diatom taxa and 227 picophytoplankton taxa were detected as exact sequence variants (ESVs) and categorized into 7 distinct diatom assemblages and 11 distinct picophytoplankton assemblages by hierarchical clustering.

Investigating the potential to predict phytoplankton community composition using shipboard CTD data alone, we found that predictions of individual ESV abundance were poor, but predictions of community assemblage were somewhat better, with environmental variables explaining 44% of assemblage variability for diatoms and 32% for picophytoplankton. Among diatoms, the genera *Chaetoceros* and *Thalassiosira* combined to make up 80% of the diatom relative abundance and 43% of the diatom ESVs, while among picophytoplankton the genera *Micromonas* and *Phaeocystis* combined to make up 57% of the relative abundance and 6% of the ESVs. Based on their biogeographical distributions, we identified ESVs of *Chaetoceros*, *Pseudo−nitzschia*, *Micromonas*, and *Phaeocystis* as abundant taxa that may be negatively affected as the region warms.

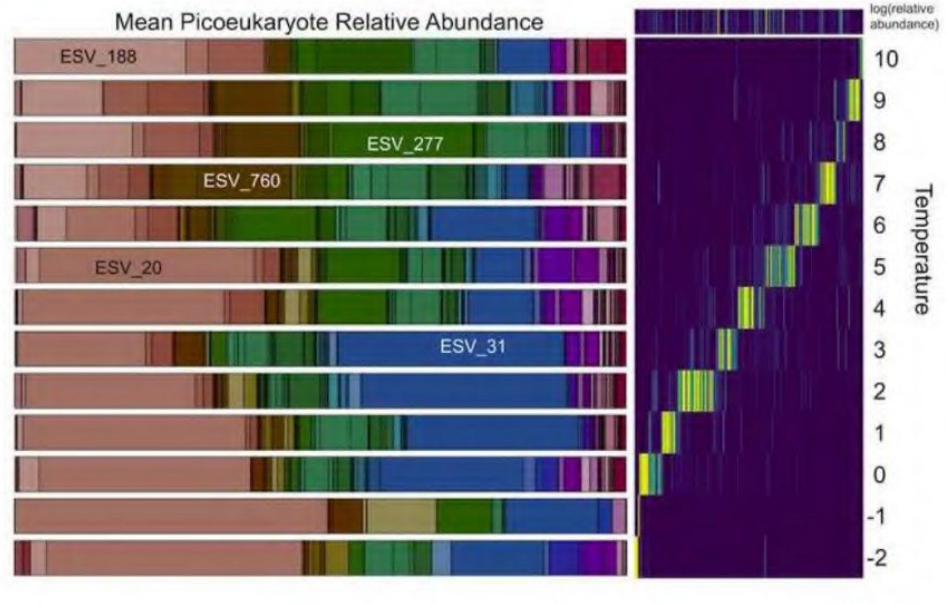

Figure 8. Mean picophytoplankton ESV relative abundance for the northern Bering and Chukchi seas cruises during 2017 after binning by temperature. ESVs are colored by genus. (right) Scaled picophytoplankton ESV relative abundance sorted by temperature at maximum relative abundance (each column is an ESV).

Study 5: Contributions of the picocyanobacteria Synechococcus to phytoplankton biomass during a period of warming in the Chukchi Sea

Lomas, M., Eisner, L., Nielsen, J., et al., In prep. Contributions of the picocyanobacteria *Synechococcus* to phytoplankton biomass during a period of warming in the Chukchi Sea.

Size structure of phytoplankton populations has been shown to be an important determinant of the flow of carbon and energy to higher trophic levels in Arctic ecosystems. Phytoplankton populations dominated by small (<10um) pico- and nanophytoplankton cells are generally dominated by eukaryotic flagellates that are tightly grazed by microzooplankton leading to increases in trophic length. General dogma suggests that the picocyanobacteria *Synechococcus* is detectable but comprises a negligible fraction of phytoplankton carbon in Arctic ecosystems.

As part of the Arctic IERP sampling program, we quantified the abundance of the *Synechococcus*, and other picophytoplankton, during the spring to fall period between 2017-2019 in the Northern Bering and Chukchi Seas. *Synechococcus* abundances increased from <500 cells/ml in spring to >50,000 cells/ml in the fall around Kotzebue Sound. Furthermore, the spatial extent of regions with elevated *Synecococcus* abundances in late summer/fall, as well as the absolute abundances, increased from 2017 to 2019, coincident with increasing late summer/fall water temperatures.

When integrated over the euphotic zone, *Synechococcus* contributed up to 40% of estimated total phytoplankton carbon during late summer/fall in Kotzebue sound and the region near Icy Cape. These observations support an increased importance of a previously marginal phytoplankton group during a warming period in the Chukchi Sea. The full implications of these changes in the phytoplankton community remain to be resolved.

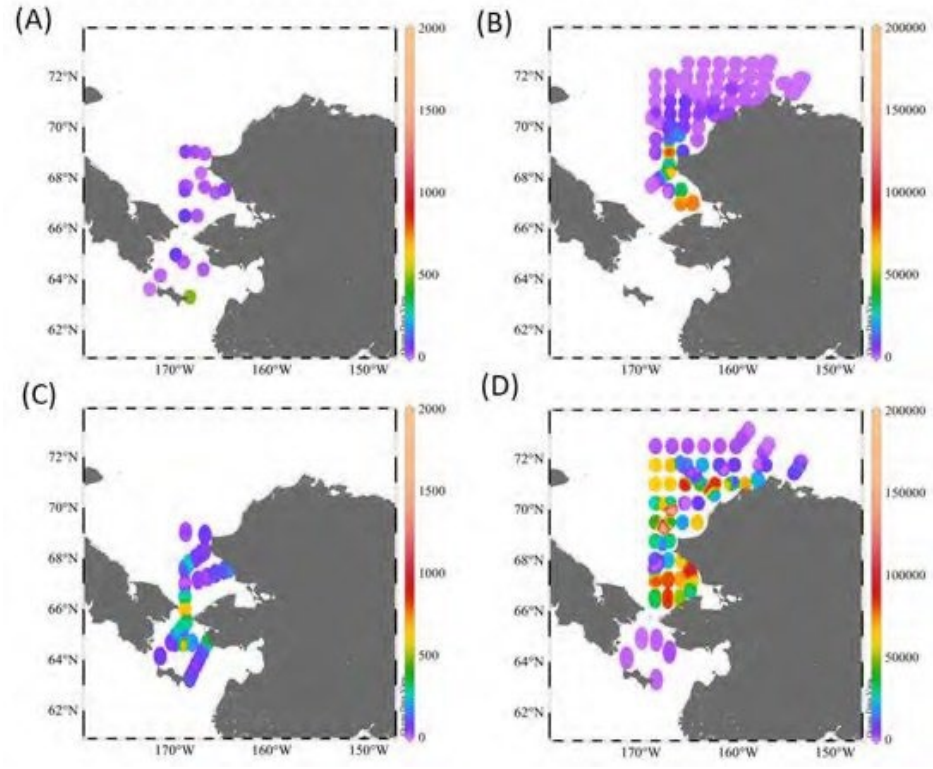

Figure 9. Spatial and seasonal distribution of *Synechococcus* abundance (cells ml^{-1}) in surface waters of the Northern Bering and Chukchi Seas. (A) Spring 2017; (B) Late Summer 2017; (C) spring 2018; (D) Late Summer 2019. Note the 100-fold difference in scales between spring and late summer.

Study 6: Variations in phytoplankton community composition, phytoplankton biomass, and primary production in a warming Arctic (Manuscript in preparation)

Eisner, Lomas, Nielsen, et al., In prep. Variations in phytoplankton community composition, phytoplankton biomass, and primary production in a warming Arctic.

Marine phytoplankton community composition, biomass and primary production are important to carbon cycling and consequently also the quality and quantity of dietary resources for higher trophic level consumers. Phytoplankton dynamics can vary considerably between spring and summer, nutrient deplete and replete water masses, and between surface and subsurface depths in Arctic seas. Phytoplankton taxonomic information, chlorophyll a biomass, and primary production data were collected during ecosystem process surveys in the Chukchi Sea in 2017 as part of Arctic ecosystem projects: Arctic Shelf Growth, Advection, Respiration & Deposition (ASGARD) and the Arctic Integrated Ecosystem Survey (Arctic IES) in June (spring) and August-September (summer), respectively. Measured primary production is compared to modelled phytoplankton growth based on equations incorporating light, temperature, and nutrient data.

Initial observational data confirm the highest chlorophyll a biomass was associated with the larger size fraction (> 5 um). As expected, diatoms were in higher abundance, primary production rates were higher although more patchy, and subsurface blooms were less prevalent in spring than in fall. Phytoplankton growth was nutrient- limited in surface waters at the majority of stations in summer. Chlorophyll biomass and production for the small (< 5 µm) size fraction, and abundance of dinoflagellates (combined autotrophic and heterotrophic) was higher in summer 2019 (the warmest year) than 2017.

These changes in phytoplankton community, in addition to reduced biomass and primary productivity, are likely to result in reduced food quality with negative ramifications for higher trophic levels.

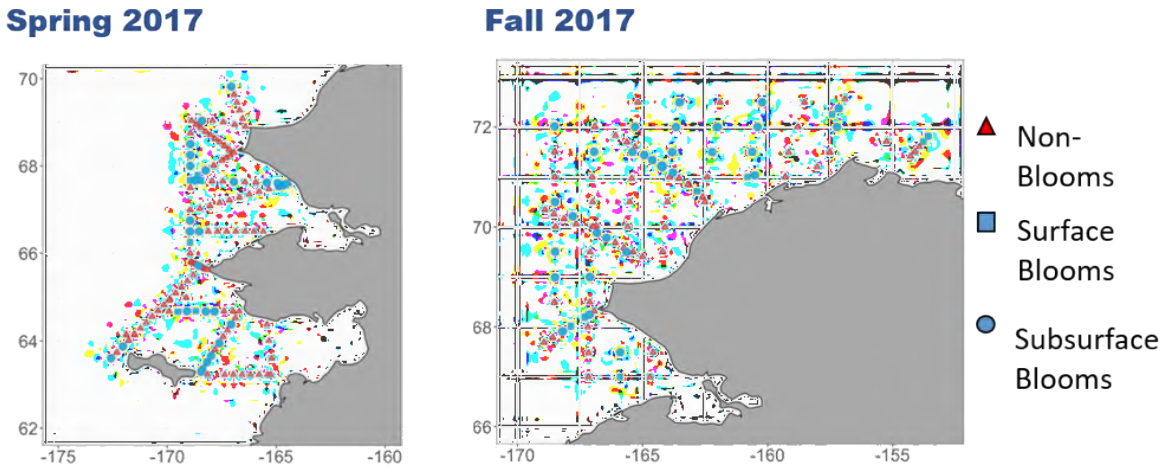

Figure 10. Phytoplankton blooms were defined as having a maximum chlorophyll a concentration >= 1 ug l^{-1} of the median for each cast. Spring: 7% surface blooms, 26% subsurface blooms, and 67% non-blooms. Fall: 8% surface blooms, 41% subsurface blooms, and 51% non-blooms. Subsurface blooms more prevalent in the fall than the spring.

Study 7: Phytoplankton and seston fatty acids dynamics in the northern Bering-Chukchi Sea region

Nielsen, J., L.A. Copeman, L.B. Eisner, K.E. Axler, C.W. Mordy, M.W. Lomas, In review, Phytoplankton and seston fatty acids dynamics in the northern Bering-Chukchi Sea region

Arctic and subarctic ecosystems are transitioning due to ocean warming, resulting in conditions that will lead to shifts in phytoplankton communities, their nutritional compositions, and production of fatty acids (FA). FA biomarkers are useful indicators of changing phytoplankton community composition and provide insight into basal resource quality for higher trophic level consumers such as zooplankton, fish, birds and marine mammals, yet phytoplankton FA information is largely lacking from the Bering and Chukchi Sea region. Therefore, we analyzed suspended particulate matter (seston) fatty acids (FA), chlorophyll-a (Chl-a) and environmental data collected from four surveys in the North Bering and Chukchi Seas, two during June of 2017 and 2018 and two during August and September of 2017 and 2019. Our objectives were to determine 1) whether, seston FA composition was correlated with phytoplankton taxonomic composition analyzed using imaging microscope (FlowCAM) techniques, 2) seasonal differences in seston FA concentrations, and 3) how FA concentrations vary with environmental parameters. We found significant seasonal differences in seston FA compositions, with diatom biomarkers more prevalent in spring, followed by a community shift to dinoflagellate and small flagellate FA biomarkers in late fall. These results were overall confirmed by FlowCAM analyses. FA seston concentrations were correlated with total and large size-fractioned Chl-a concentrations, nitrogen concentration and temperature. Lastly, we used a model framework to predict availability of the diatom-associated essential FA, eicosapentaenoic acid (EPA, 20:5n-3). Combined our analysis provide new information on FA phytoplankton dynamics and the important nutritional role of phytoplankton for higher trophic level consumers in the Northern Bering and Chukchi Sea regions.

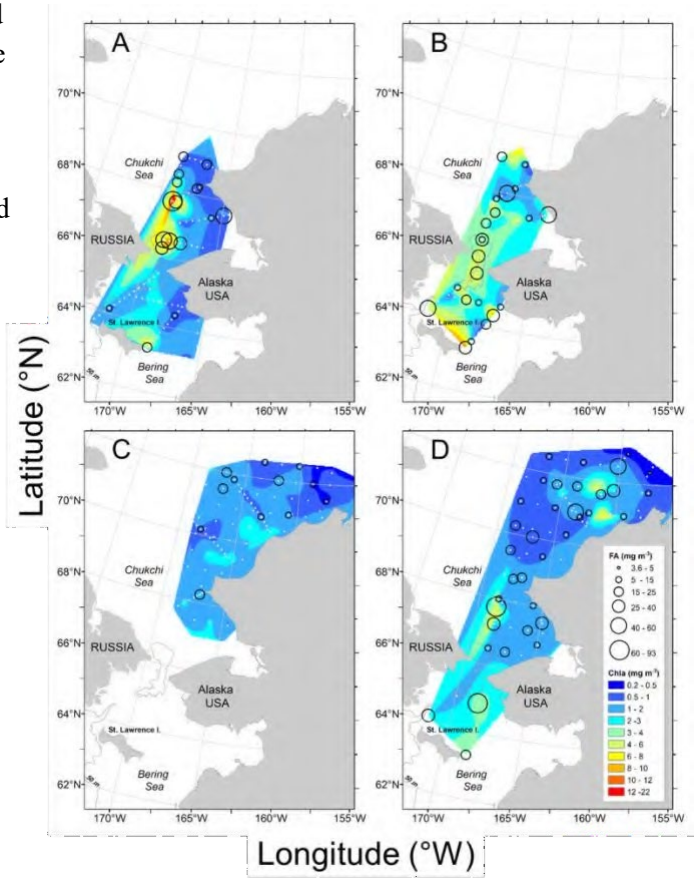

Figure 11. Mean in situ Chl-a [mg m-3] averaged from surface to 50 m and mean total FA concentrations [mg m-3] measured at each station in: A) June 2017, B) June 2018, C) Aug/Sep 2017 and D) Aug/Sep 2019 in the northern Bering and Chukchi Seas. White diamonds indicate station locations.

Study 8: Zooplankton communities of the Arctic's Bering Strait region during the spring bloom, 2017-2018 (Manuscript in preparation)

Hopcroft, R.R., C. Smoot, In prep. Zooplankton communities of the Arctic's Bering Strait region during the spring bloom, 2017-2018 (Manuscript in preparation)

Planktonic communities have been shown to serve as useful "beacons of climate change" (Richardson, 2008) due to relatively rapid response changing temperatures and their strong coupling to water mass characteristics. The Arctic Shelf Growth, Advection, Respiration and Deposition Rate Experiments (ASGARD) conducted a pair of cruises in June of 2017 and 2018 to examine the structure and function of communities during the bloom. The broad-scale survey of the zooplankton communities at those times provides context for the vital rates determined within those communities as summarized elsewhere within this report. Smaller-bodied zooplankton were collected with a vertically-hauled 60-cm diameter twin-ring net fitted with 150-µm nets pulled at ~0.5 m s^{-1}. Larger-bodied and more mobile zooplankton were targeted with an obliquely-towed 60-cm diameter Bongo net fitted with 505-µm nets pulled at ~0.5 m s^{-1}.

The zooplankton community was dominated by the copepods *Calanus marshallae/glacialis*, *Pseudocalanus* spp., *Oithona similis*, and *Metridia pacifica* that are best assessed with the 150-µm nets. These copepods were present at nearly all stations during both 2017 and 2018. The copepod *Acartia* was also present across the sampling domain in both 2017 and 2018 but had a more coastal signal. We observed higher abundances of Pacific-affinity copepods (*Neocalanus* spp. and *Eucalanus bungii*) in 2017 compared to 2018.

Multivariate analyses of the combined 2017 and 2018 150-µm datasets revealed five major community groupings. Euphausiids, composed of several *Thysanoessa* species, were present across the sampling domain in both years, with slightly higher abundances observed in 2017. The euphausiids were also primarily composed of larval calyptopsis and furcilia stages in both years. Amphipods, decapods, and the predatory chaetognath *Parasagitta elegans* were present in both years across the sampling domain but did not show a particular spatial pattern. *Aglantha digitale*, a common hydrozoan, did not display a strong spatial pattern. There was often a significant biomass in other jellyfish and ctenophores present in the plankton nets.

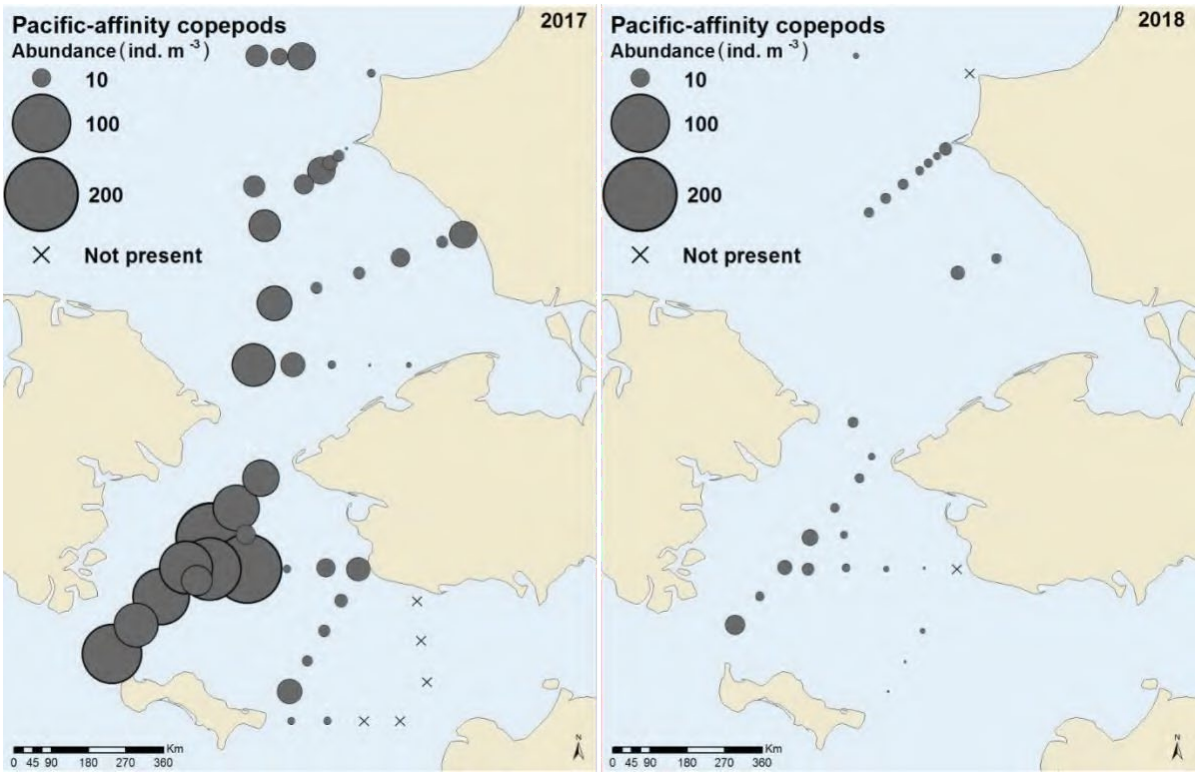

Figure 12. Abundance (ind. m^{-3}) of Pacific-affinity copepods based on the 150-µm net.

Study 9: Growth and Reproductive Rates of Calanoid Copepods in the Northern Bering and Southern Chukchi Seas

Poje, A., 2020. Growth and Reproductive Rates of Calanoid Copepods in the Northern Bering and Southern Chukchi Seas. University of Alaska Fairbanks. M.S. Thesis.

Egg production and copepodite growth rates were measured for the calanoid copepods *Pseudocalanus spp., Calanus marshallae/glacialis*, and *Metridia pacifica* in the northern Bering and southern Chukchi Seas during June of 2017 and 2018. For all taxa, instantaneous growth rates generally decreased with increasing copepodite stage, though the differences between most stages was not significant. The growth rates for *Pseudocalanus spp*. averaged 0.03 ± 0.002 day^{-1}, *Calanus spp*. 0.09 ± 0.004 day^{-1} , and *M. pacifica* 0.05 ± 0.03 day^{-1}. Egg production rates increased with prosome length for all species, but when standardized to body weight this trend reversed. All *Pseudocalanus* species had similar weight-specific egg production (SEP): 0.18 ± 0.01 for *P. acuspes*, 0.15 ± 0.00 for *P. newmani*, and 0.11 ± 0.02 *for P. minutus.* The SEP for *Calanus* was considerably lower, 0.09 ± 0.01, while for *M. pacifica* it was 0.11 ± 0.01.

These rates suggest considerable discrepancies between growth rates and egg production weights that we propose are due to differences in life history strategies. *Pseudocalanus* reproduce nearly year round, they appear to invest less in somatic growth, preferring to quickly reach their adult stage where they invest heavily into reproduction. *Calanus spp*. have 1 or possibly 2 generations per year in this region, they invest more into somatic growth in order to ensure their population is ready for a reproductive season timed to the spring phytoplankton bloom. The more omnivorous *M. pacifica* is also likely limited to 1 or 2 generations, although their ability to thrive on a wider range of food sources than *Calanus* seems to allow for relatively higher investment in reproduction and perhaps lower investment in somatic growth. Consistent with other studies, global growth models do not match our observations particularly well, likely because they are dominated by egg production estimates at lower latitudes.

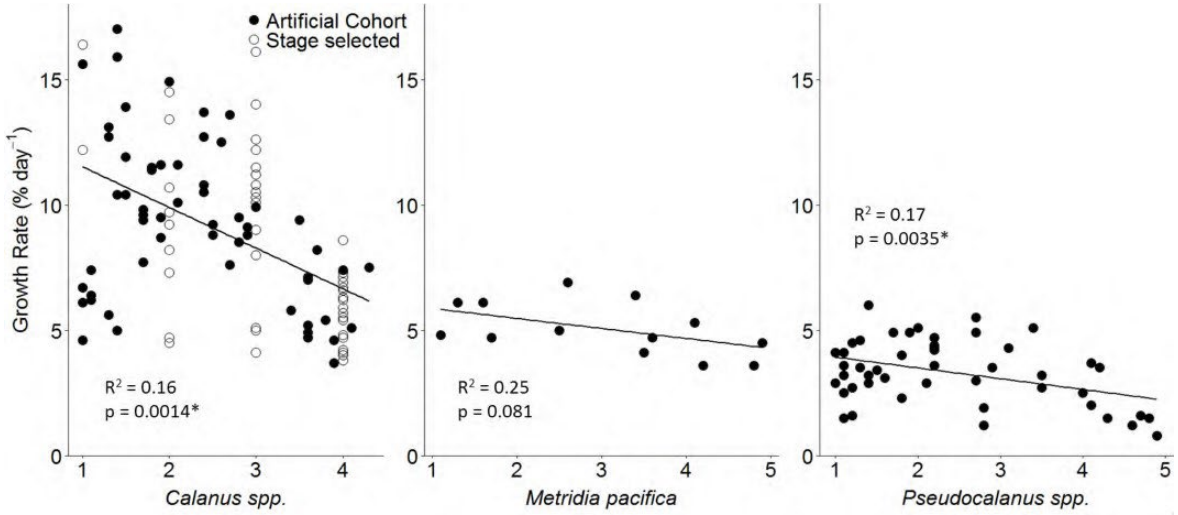

Figure 13. *Calanus spp., Metridia p*acifica, and *Pseudocalanus spp*. growth rates relative to initial copepodite stage from the artificial cohort experiments (avg. temp 4° C) during June 2017 and 2018 in the N. Bering and S. Chukchi seas.

Study 10: Seasonal and annual variation in the lipid composition of mesozooplankton from the Chukchi Sea (Manuscript in preparation)

Copeman, L., Eisner, L., Kimmel, D., Hopcroft, R. et al., In preparation and final data generation stages. Seasonal and annual variation in the lipid composition of mesozooplankton from the Chukchi Sea.

Zooplankton are major prey items for fish, seabirds and marine mammals and they also play an essential role in marine food webs where they efficiently transform energy from primary producers into lipid storage. Arctic zooplankton store particularly high levels of lipid per unit mass which is generally viewed as an adaptation to extreme seasonality in their food supply. Despite their trophic importance, we know relatively little about lipid dynamics in major zooplankton groups from the Chukchi Sea. We analyzed total lipids, lipid classes, fatty acids and alcohols in the dominant mesozooplankton (five taxa: euphausiids, copepods, chaetognaths, and pteropods) collected on both spring (ASGARD, 2017 and 2018) and late summer (IES 2017 and 2019) Chukchi Sea surveys.

Lipid-rich and abundant spring copepods included *Pseudocalanus* spp. and *Neocalanus* spp. that contained on average ~87% wax esters and only 4% triacylglycerols. Spring-collected *Pseudocalanus* spp. were the most lipid rich (308. 5 ± 42.4 mg g^{-1} WWT) compared to *Neocalanus* spp. (168.3 ± 15.3 $mg.g^{-1}$) and *Metridia* spp. (38.6 ± 3.3 $mg.g^{-1}$), but the large size of *Neocalanus* spp. resulted in much higher values per individual (579 ± 33 µg) than in other spring-collected copepods (~10 to 92 µg). Euphausiids of the species *Thysanoessa raschii* and *Thysanoessa inermis* had lipid class storage reflective of both short (16% triacylglycerols) and longer-duration (22% wax esters) energy storage. The relatively large size of *Thysanoessa* spp. combined with their elevated lipid concentrations (56.4 ± 5.0 $mg.g^{-1}$), resulted in a high value of lipids per individual, 2552 ± 299 µg. *Thysanoessa* spp. had significantly higher lipid concentrations and double the lipid per individual in spring than in fall collections. *Calanus* spp. (*C. marshallae* and *C. glacialis*) from fall surveys had total lipid per WWT of 93.1 ± 21.4 mg g^{-1} and total lipid per individual of 140.5 ± 13.9 µg. As found in other Arctic studies, *Calanus* spp. contained the majority of their lipids as wax esters (80.2 ± 1.6%).

Fatty acid biomarkers and fatty alcohols have been run on all 409 zooplankton samples. Biomarker data analyses and finalization are underway with metadata being uploaded in September 2021. Preliminary analyses show that lipid-rich zooplankton have a high degree of reliance on diatom-sourced lipids. Ongoing analyses of zooplankton fatty acids will help us understand the trophic component of spatial and annual variability in their lipid storage. Our ultimate goal is to estimate the lipid and fatty acid pools available to zooplankton predators using species-specific zooplankton lipid values coupled to zooplankton abundance data.

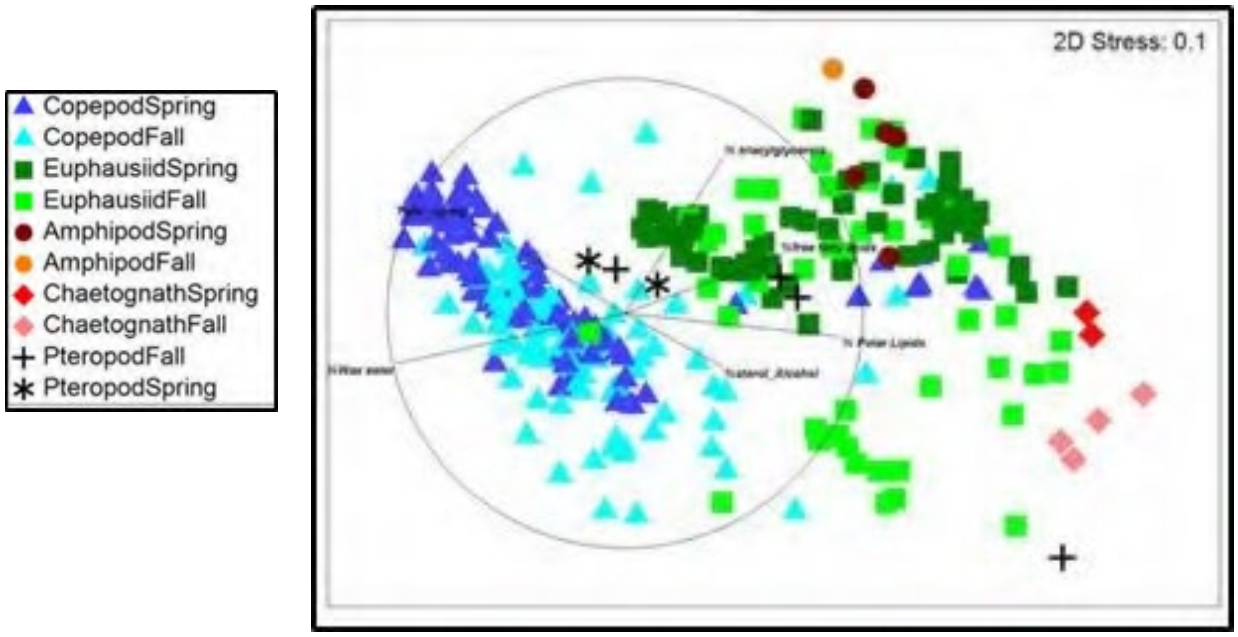

Figure 14. Nonmetric multidimensional scaling (nMDS) of major zooplankton taxa based on their lipid class composition. Zooplankton were collected on four ecosystem surveys during spring and fall of 2017 to 2019 in the Chukchi Sea. Vectors are shown for individual lipid classes.

Study 11: Respiration rates of calanoid copepods during the spring bloom for the Arctic's Bering Strait region (Manuscript in preparation)

Hopcroft, R.R., C. Smoot, In prep. Respiration Rates of calenoid copepods during the spring bloom for the Arctic's Bering Strait region

Like most living organisms, zooplankton consume oxygen. Knowing how much oxygen they consume, how much they eat, and how much they grow are important to understanding the quantity and efficiency with which they move energy through an ecosystem.

We measured the respiration of the dominate zooplankton – copepods – in the northern Bering and Southern Chukchi Seas during the ASGARD project for 2017 and 2018. Rates were determined for adult stages of four species: *Calanus glacialis*, *Metridia pacifica*, *Pseudocalanus minutus* and *Pseudocalanus acuspes*. These rates increase with increasing body mass, but weight-specific rates decline with body mass.

Rates are generally consistent with a global model proposed by Ikeda et al., but are consistently higher than those predicted. We propose this increase was a direct consequence of the either poor skill of that model for the study region or the high rates of growth and grazing occurring at the time of measurement that coincided with the region's "spring" bloom having raised overall metabolic activity.

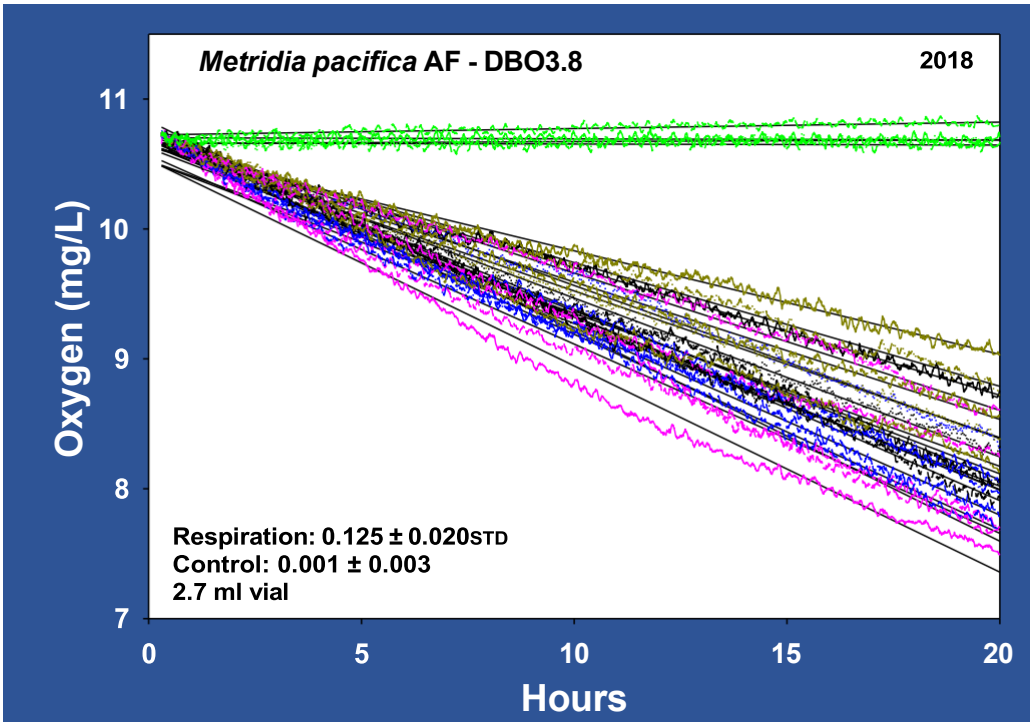

Figure 15. Example data traces from the copepod respiration incubations. Control vial (no zooplankton) measurements are shown in green.

Study 12: Spatial patterns, environmental correlates, and potential seasonal migration triangle of polar cod (*Boreogadus saida*) distribution in the Chukchi and Beaufort seas

Forster, C. E., Norcross, B. L., Mueter, F. J., Logerwell, E. A., Seitz, A. C. 2020. Spatial patterns, environmental correlates, and potential seasonal migration triangle of polar cod (Boreogadus saida) distribution in the Chukchi and Beaufort seas. Polar Biology, 43(8), 1073-1094.

Forster, C. E., 2019. Spatial patterns, environmental correlates, and potential seasonal migration triangle of Arctic cod (Boreogadus saida) distribution in the Chukchi and Beaufort seas. University of Alaska Fairbanks. M.S. Thesis.

Polar cod (*Boreogadus saida*) is a key forage fish in the Arctic marine ecosystem and provides an energetic link between lower and upper trophic levels. Despite its ecological importance, spatially explicit studies synthesizing polar cod distributions across research efforts have not previously been conducted in its Pacific range. We used spatial generalized additive models to map the distribution of polar cod by size class and relative to environmental variables. We compiled demersal trawl data from 21 cruises conducted during 2004–2017 in the Chukchi and Beaufort seas, and investigated size-specific patterns in distribution to infer movement ecology of polar cod as it develops from juvenile to adult life stages. High abundances of juvenile polar cod (≤ 70 mm) in the northeastern Chukchi Sea and western Beaufort Sea were separated from another region of high abundance in the eastern Beaufort Sea, near the US and Canadian border, suggesting possible population structure in the Pacific Arctic.

Relating environmental correlates to polar cod abundance demonstrated that temperature and salinity were related to juvenile distribution patterns, while depth was the primary correlate of adult distribution. A comparison of seasonal 2017 abundances of polar cod in the southern Chukchi Sea found low demersal abundance in the spring when compared to the summer.

Seasonal differences in polar cod abundance suggest that polar cod migration may follow a classic 'migration triangle' route between nursery grounds as juveniles, feeding grounds as subadults, and spawning grounds as adults, in relation to ice cover and seasonal production in the Chukchi Sea.

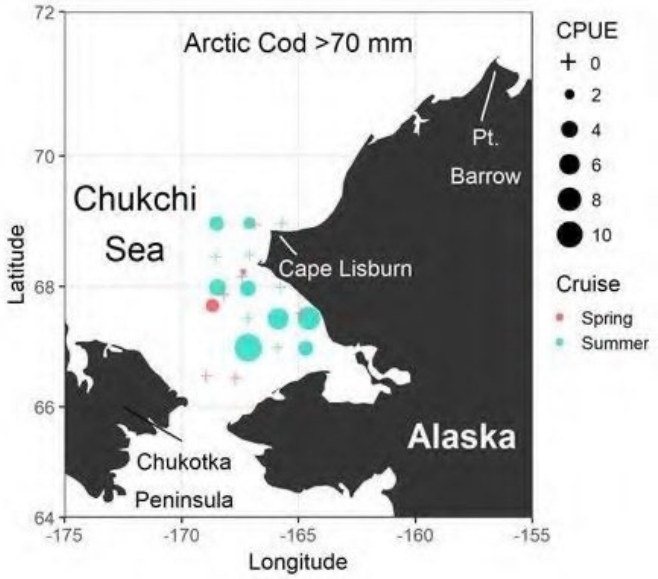

Figure 16. Distribution and length frequency of Arctic (Polar) Cod >70 mm in the Chukchi Sea in spring and summer 2017. Length frequency scaled by CPUE.

Study 13: Seasonal abundance, distribution, and growth of the early life stages of polar cod (*Boreogadus saida*) and saffron cod (*Eleginus gracilis*) in the US Arctic

Deary, A.L., Vestfals, C.D., Mueter, F.J., Logerwell, E.A., Goldstein, E.D., Stabeno, P.J., Danielson, S.L., Hopcroft, R.R. and Duffy-Anderson, J.T., 2021. Seasonal abundance, distribution, and growth of the early life stages of polar cod (*Boreogadus saida*) and saffron cod (*Eleginus gracilis*) in the US Arctic. *Polar Biology*, *44*(11), pp.2055-2076.

Polar cod and saffron cod are dominant components of the fish community in the Chukchi Sea and are ecologically important forage fishes linking plankton to upper-level consumers. In 2017, we conducted a study as part of the Arctic Integrated Ecosystem Research Program to characterize the distribution, abundance, and growth of polar cod and saffron cod early life history stages (ELHS) in late spring and late summer in the Chukchi Sea. Ship-based plankton tows showed that polar cod and saffron cod larvae were centered in Kotzebue Sound in the late spring. By late summer, polar cod juveniles were centered offshore in the northern Chukchi Sea whereas saffron cod were distributed nearshore around Cape Lisburne. Empirical fish collections were paired with an individual-based biophysical transport model to examine connectivity and relate changes in seasonal distribution to potential environmental variables. Modeled drift trajectories and growth in spring for polar cod and saffron cod matched well with empirical observations, especially along the northern coastline of Kotzebue Sound, offshore of Point Hope/Cape Lisburne. Given the coherence between modeled and observed distributions, Kotzebue Sound is likely a source of gadid ELHS in the nearshore areas of the Chukchi Sea and offshore of Cape Lisburne/Point Hope, although it is not the likely source of polar cod over Hanna Shoal in the late summer. This is the first study to examine seasonal distribution, abundance, and growth of polar cod and saffron cod in the US Arctic and provides data necessary to evaluate climate change impacts on forage fishes in the Arctic.

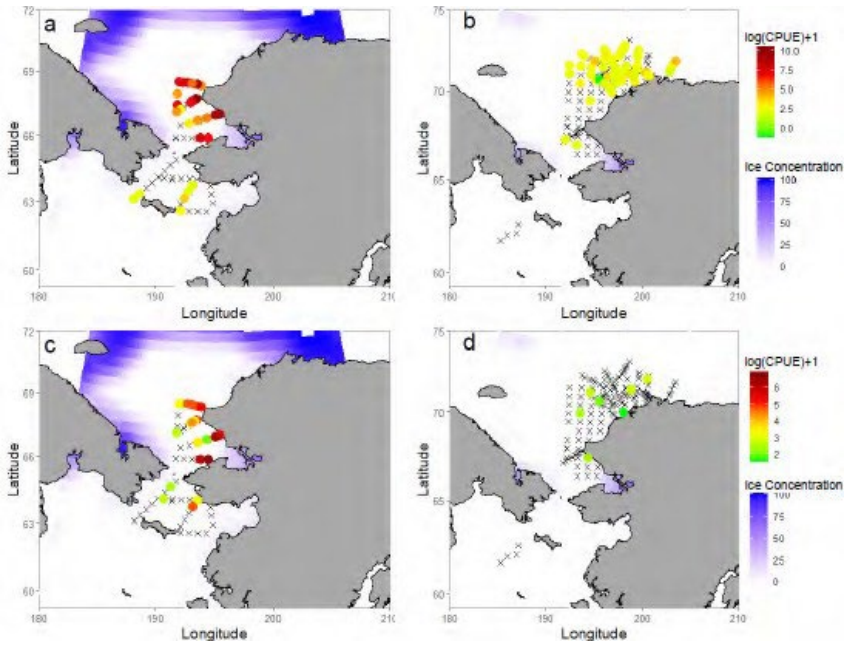

Figure 17. Distribution of polar cod (*Boreogadus saida*) (a, b) and saffron cod (*Eleginus gracilis*) (c, d) in late spring (left column; ASGARD samples) and late summer (right column) 2017 collected in the water column with the 60-cm bongo net. Catch data reported as catch-per-unit-effort (CPUE) and log(CPUE)+1 to highlight variability at low abundance. Ice concentration (% cover) is plotted in the background. Black X's denote sampled stations where polar cod and saffron cod were not caught.

Study 14: Extraordinary Carbon Fluxes on the Shallow Pacific Arctic Shelf During a Remarkably Warm and Low Sea Ice Period

O'Daly, S.H., Danielson, S.L., Hardy, S.M., Hopcroft, R.R., Lalande, C., Stockwell, D.A. and McDonnell, A.M., 2020. Extraordinary carbon fluxes on the shallow Pacific Arctic shelf during a remarkably warm and low sea ice period. *Frontiers in Marine Science*, 7, p.986.

O'Daly, S.H., 2019. Carbon flux and particle-associated microbial remineralization rates in the northern Bering and southern Chukchi seas, University of Alaska Fairbanks. M.S. Thesis.

The shallow Pacific Arctic shelf has historically acted as an effective carbon sink, characterized by tight benthic pelagic coupling. However, the strength of the biological carbon pump in the Arctic has been predicted to weaken with climate change due to increased duration of the open-water period for primary production, enhanced nutrient limitation, and increased pelagic heterotrophy. In order to gain insights into how the biological carbon pump is functioning under the recent conditions of extreme warming and sea ice loss on the Pacific Arctic shelf, we measured sinking particulate organic carbon (POC) fluxes with drifting and moored sediment traps, as well as rates of primary production and particle-associated microbial respiration during June 2018. In Bering Shelf/Anadyr Water masses, sinking POC fluxes ranged from 0.8 to 2.3 g C m^{-2} day^{-1}, making them among the highest fluxes ever documented in the global oceans. Furthermore, high export ratios averaging 82% and low rates of particle-associated microbial respiration also indicated negligible recycling of sinking POC in the water column. These results highlight the extraordinary strength of the biological carbon pump on the Pacific Arctic shelf during an unusually warm and low-sea ice year. While additional measurements and time are needed to confirm the ultimate trajectory of these fluxes in response to ongoing climate change, these results do not support the prevailing hypothesis that the strength of the biological carbon pump in the Pacific Arctic will weaken under these conditions.

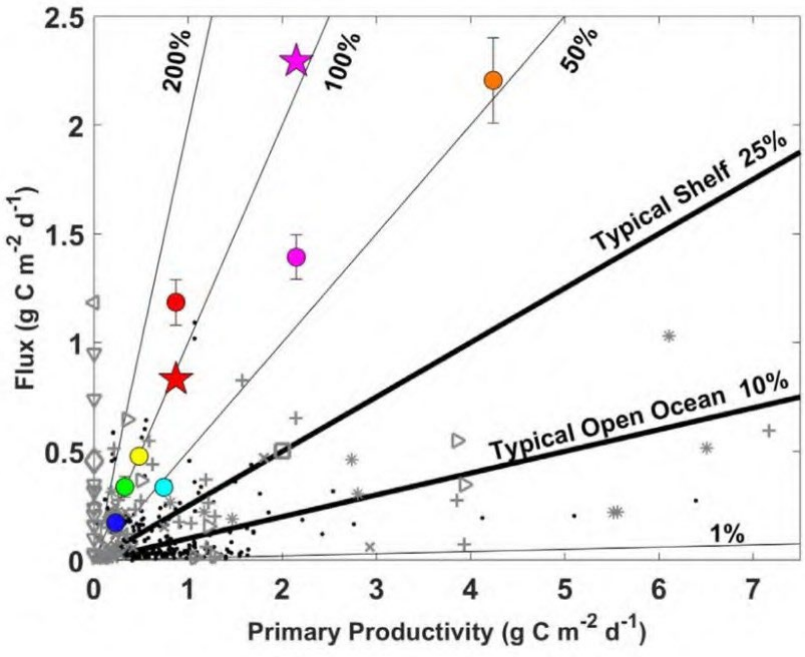

Figure 18. Sinking particulate organic carbon fluxes and primary productivity rates with contours of the export ratio between these two parameters measured during June 2018 on the Pacific Arctic shelf. Colored circles represent flux measurements from the drifting sediment trap. Colored stars represent the final flux measurement from the moored sediment traps (values plotted against the same primary productivity rates). Gray markers provide regional and black markers global context.

Study 15: Impact of a warm anomaly in the Pacific Arctic region derived from time-series export fluxes

Lalande C., Grebmeier J.M., McDonnell A.M., Hopcroft R.R., O'Daly S., Danielson S.L., 2021. Impact of a warm anomaly in the Pacific Arctic region derived from time-series export fluxes. Plos one. 2021 Aug 16;16(8):e0255837

Unusually warm conditions recently observed in the Pacific Arctic region included a dramatic loss of sea ice cover and an enhanced inflow of warmer Pacific-derived waters. Moored sediment traps deployed at three biological hotspots of the Distributed Biological Observatory (DBO) during this anomalously warm period collected sinking particles nearly continuously from June 2017 to July 2019 in the northern Bering Sea (DBO2) and in the southern Chukchi Sea (DBO3), and from August 2018 to July 2019 in the northern Chukchi Sea (DBO4).

Fluxes of living algal cells, chlorophyll *a* (chl *a*), total particulate matter (TPM), particulate organic carbon (POC), and zooplankton fecal pellets, along with zooplankton and meroplankton collected in the traps, were used to evaluate spatial and temporal variations in the development and composition of the phytoplankton and zooplankton communities in relation to sea ice cover and water temperature. The unprecedented sea ice loss of 2018 in the northern Bering Sea led to the export of a large bloom dominated by the exclusively pelagic diatoms *Chaetoceros* spp. at DBO2. Despite this intense bloom, early sea ice breakup resulted in shorter periods of enhanced chl *a* and diatom fluxes at all DBO sites, suggesting a weaker biological pump under reduced ice cover in the Pacific Arctic region, while the coincident increase or decrease in TPM and POC fluxes likely reflected variations in resuspension events. Meanwhile, the highest transport of warm Pacific waters during 2017-2018 led to a dominance of the small copepods *Pseudocalanus* at all sites.

Whereas the export of ice-associated diatoms during 2019 suggested a return to more typical conditions in the northern Bering Sea, the impact on copepods persisted under the continuously enhanced transport of warm Pacific waters. Regardless, the biological pump remained strong on the shallow Pacific Arctic shelves.

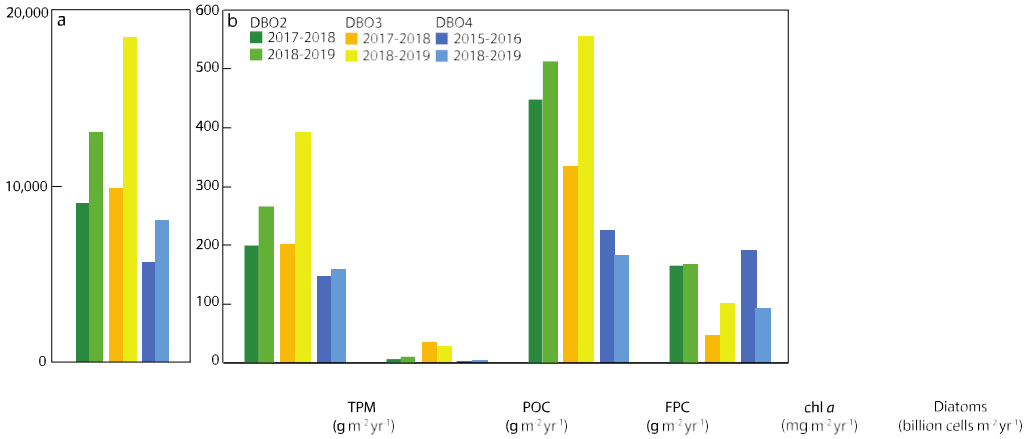

Figure 19. Annual total particulate matter (TPM) fluxes (a), and (b) annual particulate organic carbon (POC), fecal pellet carbon (FPC), chlorophyll a (chl a), andliving diatom fluxes at mooring sites N4, N6, and CEO.

Study 16: Linking polychaete functional traits and benthic ecosystem function to habitat characteristics on a shallow Arctic shelf

Charrier, B.R., T. Dorsaz, N. Matsui, and S.L. Mincks, In prep. Linking polychaete functional traits and benthic ecosystem function to habitat characteristics on a shallow Arctic shelf. Chapter 1 in University of Alaska Fairbanks Ph.D. Dissertation

Polychaetes are often numerically dominant within the macrofauna and serve essential roles in benthic ecosystem function, such as feeding and bioturbation activities. Macrofauna were collected from 12 stations in June 2017 and 11 stations in June 2018 from the northern Bering and southern Chukchi Sea continental shelves from the *R/V Sikuliaq* as part of the Arctic Shelf Growth, Advection, Respiration, and Deposition (ASGARD) project. Samples were collected using an MC-800 multi-corer with 10-cm diameter tubes. Macrofauna were counted, weighed, and identified to phylum or class level.

Polychaetes were identified to family level and assigned a functional guild based on feeding mode, motility, and feeding structures. Four clusters of polychaete functional guilds were identified. Group A was dominated by subsurface and surface/subsurface deposit feeders; had a high portion of filter feeders; and consisted of shallow, sandy stations with low amounts of low-quality food. Group B was dominated by carnivores and subsurface deposit feeders and characterized by moderate amounts of moderate-quality food. Group C was also dominated by carnivores and subsurface deposit feeders but had large amounts of high-quality food. Group C had high abundance and biomass deep within the sediment, suggesting high bioturbation activity. Group D was dominated by subsurface deposit feeders and surface/subsurface deposit feeders, with most of the abundance and biomass concentrated at the surface and mainly consisted of coastal stations. Overall, polychaete functional composition and vertical distribution reflected the quality and quantity of organic matter input, and the depositional environment as indicated by sediment grain size composition, with likely impacts on biogeochemical and carbon cycling within the sediment.

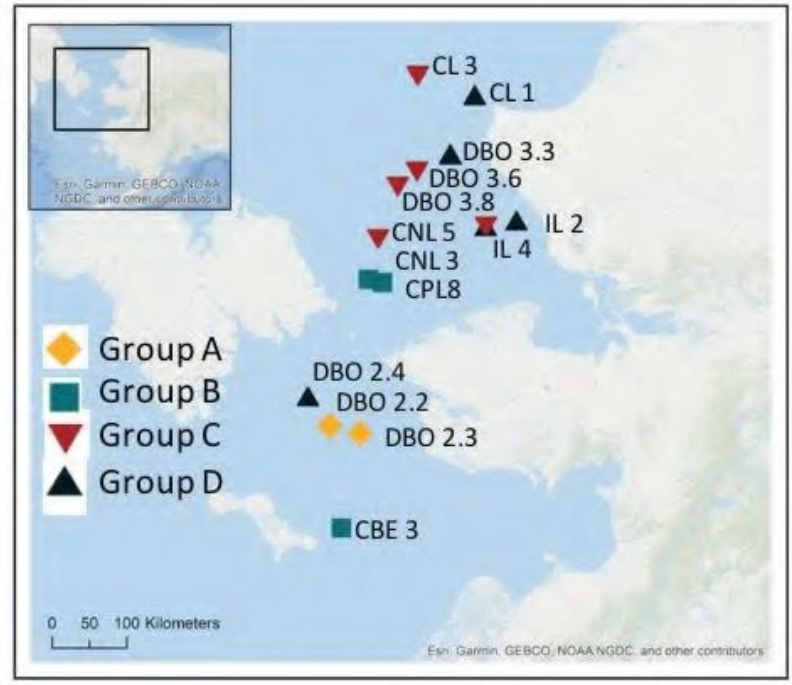

Figure 20. Macrofauna sampling locations in the northern Bering and southern Chukchi Seas in 2017 and 2018. Nine stations were sampled in both years. Symbols based on hierarchical agglomerative clustering. Station IL 4 clustered in Group D in 2017 and Group C in 2018.

Study 17: Meiofauna community structure in Pacific Arctic shelf sediments: a comparison of meiofaunal- and macrofaunal-sized nematodes and functional traits

Charrier, B.R., J. Ingels, and S.L. Mincks, In prep. Meiofauna community structure in Pacific Arctic shelf sediments: a comparison of meiofaunal- and macrofaunal-sized nematodes and functional traits. Chapter 2 in University of Alaska Fairbanks Ph.D. Dissertation

Meiofauna serve essential roles in benthic ecosystems, such as nutrient cycling and linking microbial and upper-trophic levels of the food web, and they serve as bioindicators of environmental change, particularly nematodes. However, in the rapidly changing Pacific Arctic shelf region, meiofauna remain poorly studied, and baseline data for assessing change is lacking. Sediment samples were collected at ten stations in the northern Bering and southern Chukchi Seas in June 2018 as part of the Arctic Shelf Growth, Advection, Respiration, and Deposition (ASGARD) project. We characterized meiofauna (63-500 µm) community structure and abundance at higher taxonomic levels and evaluated genus-level composition of nematodes in both meiofaunal (63-500 µm) and macrofaunal (>500 µm) size fractions. The nematodes were also classified by trophic feeding groups and life-history strategies. Total meiofauna abundance ranged from 1449 to 12875 ind. 10 cm-2 for the upper 5 cm of sediment, and the dry weight (DW) biomass of nematodes in the upper 1 cm of sediment ranged from 33 to 739 µg DW10 cm-2.

Four clusters of meiofaunal-sized nematode communities were identified occupying different regions of the Pacific Arctic shelves: the northern Bering shelf, Bering Strait region, central Chukchi Sea, and coastal Chukchi Sea. These nematodes assemblages reflected impacts of food availability and substrate type, and differences suggest these subregions should be considered separately in ecosystem modeling. Additionally, the meiofaunal- and macrofaunal-sized nematodes represented two distinct communities. The taxonomic composition and large standing stock of the macrofaunal-sized nematodes (2 - 215 µg DW 10 cm-2) suggest they are a critical component of the infauna and merit more in-depth research to consider the ecological role they play, including benthic carbon cycling and trophic dynamics. This study provides the first genus-level characterization of nematode communities in the region and among the first measurements of meiofauna standing stock. Thus, the data presented here can serve as a baseline for assessing ecosystem shifts in a rapidly changing Arctic environment.

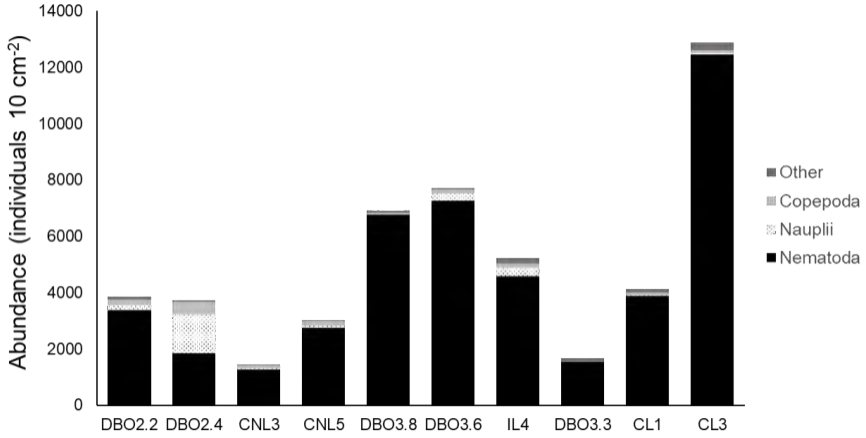

Figure 21: Meiofaunal abundance (ind. 10 cm^{-2}) in the upper 5 cm of sediment at sampling locations on the northern Bering and southern Chukchi Sea continental shelves in 2018

Study 18: Changes to benthic community structure may impact organic matter consumption on Pacific Arctic shelves

Charrier, B.R., A.L. Kelley, and S.L. Mincks, 2021. Changes to benthic community structure may impact organic matter consumption on Pacific Arctic shelves. *Conservation physiology*, *9*(1), p.coab007.

Charrier, B.R., A.L. Kelley, and S.L. Mincks, 2021. Changes to benthic community structure may impact organic matter consumption on Pacific Arctic shelves. Chapter 3 in University of Alaska Fairbanks Ph.D. Dissertation

Changes in species composition and biomass of Arctic benthic communities are predicted to occur in response to environmental changes associated with oceanic warming and sea-ice loss. Such changes will likely impact ecosystem function, including flows of energy and organic material through the Arctic marine food web. Oxygen consumption rates can be used to quantify differences in metabolic demand among species and estimate the effects of shifting community structure on benthic carbon consumption.

Closed-system respirometry using non-invasive oxygen optodes was conducted onboard the R/V Sikuliaq in June 2017 and 2018 on six dominant species of benthic macrofauna from the northern Bering and southern Chukchi Sea shelves, including five bivalve species (*Macoma sp., Serripes groenlandicus, Astarte sp., Hiatella arctica* and *Nuculana pernula*) and one amphipod species (*Ampelisca macrocephala*). Results revealed species-specific respiration rates with high metabolic demand for S. groenlandicus and A. macrocephala compared to that of the other species. For a hypothetical 0.1-g ash-free dry mass individual, the standard metabolic rate of S. groenlandicus would be 4.3 times higher than that of Astarte sp. Overall, carbon demand ranged from 8 to 475 μg C individual^{-1} day^{-1} for the species and sizes of individuals measured. The allometric scaling of respiration rate with biomass also varied among species. The scaling coefficient was similar for H. arctica, A. macrocephala and Astarte sp., while it was high for S. groenlandicus and low for Macoma sp.

These results suggest that observed shifts in spatial distribution of the dominant macrofaunal taxa across this region will impact carbon demand of the benthic community. Hence, ecosystem models seeking to incorporate benthic system functionality may need to differentiate between communities that exhibit different oxygen demands.

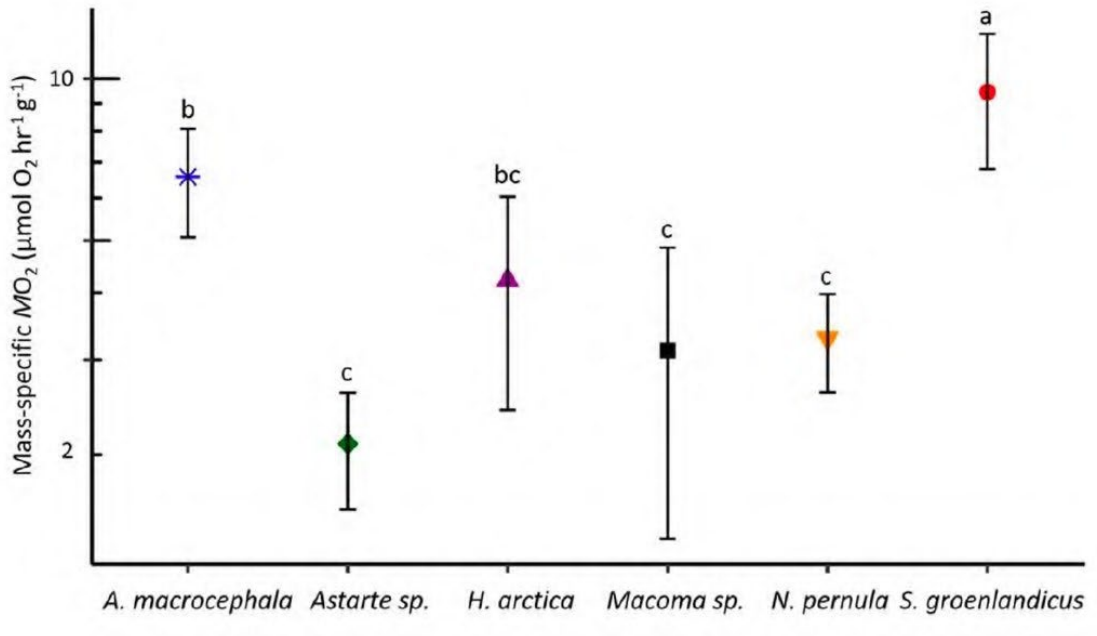

Figure 22. Average mass-specific respiration rates (µmol O_2 hr^{-1} g^{-1}) for each species with standard deviations represented by error bars.

Study 19: Spatial patterns and effects of temperature on rates of organic matter processing in sediments across the northern Bering and southern Chukchi Sea shelf (Manuscript in preparation)

Mincks, S.L., S. Seabrook, B. Charrier, A. Thurber, In prep. Spatial patterns and effects of temperature on rates of organic matter processing in sediments across the northern Bering and southern Chukchi Sea shelf

Labile organic matter deposited at the seafloor is respired by benthic organisms, and respiration rates are highly temperature dependent in both microbes and metazoan in sediments. In light of changing temperature and productivity regimes across the Pacific-Arctic domain, we measured respiration rates of sediment communities at in situ and elevated temperatures at ten locations across the N Bering and S Chukchi Seas. Intact sediment cores were incubated at 0ºC (ambient) and 5ºC (projected warming).

On average, sediment community oxygen demand, a proxy for organic carbon consumption, was ~30% higher in warmer treatments. Substrate type, productivity, and particulate flux rates varied across the study area, resulting in spatial differences in microbial and metazoan biomass. In the southeast Chukchi Sea (DBO 3 region), high biomass of large infaunal species, particularly bivalves, generated somewhat elevated oxygen demand. However, oxygen consumption rates were more consistent across the rest of the study area, with rates increasing more rapidly as a function of microbial biomass than of macrofaunal biomass.

Fluxes of dissolved inorganic carbon (DIC) were also measured in incubation experiments as an additional means of quantifying oxygen consumption due specifically to respiration of infauna. DIC fluxes were decoupled from oxygen fluxes at some locations. In some cases, DIC was taken up by sediment communities, suggesting autotrophic production which could have been producing oxygen during experiments, resulting in underestimation of respiration rates by oxygen flux measurement.

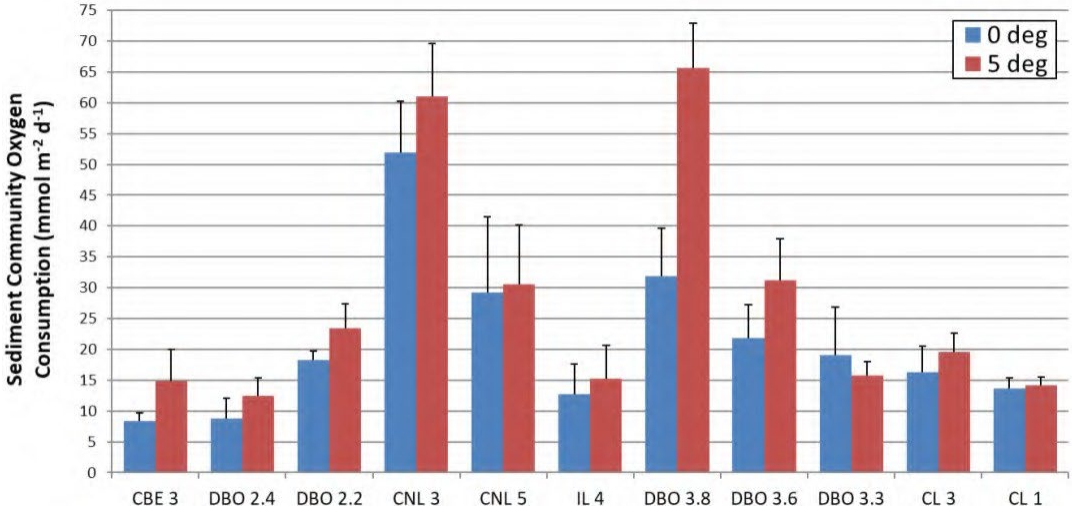

Figure 23. Sediment community oxygen consumption measured in shipboard whole-core incubations at two different temperatures during the ASGARD cruise in June 2018. Positive values indicate net flux into sediments, ±std. dev.

Study 20: The Arctic Chukchi Sea food web: simulating ecosystem impacts of future changes in organic matter flow

Zinkann, A.C., G. Gibson, K. Iken, in review. The Arctic Chukchi Sea food web: simulating ecosystem impacts of future changes in organic matter flow, submitted for review to *Ecological Modeling*

Zinkann, A.C., 2020. Chapter 3 in *Organic Matter Sources on the Chukchi Sea Shelf in a Changing Arcitc*. University of Alaska Fairbanks. Ph.D. Dissertation.

The Chukchi Sea continental shelf is a highly productive inflow shelf of the Arctic Ocean that is experiencing climate warming events and declines in seasonal sea ice cover at one of the fastest rates compared to other Arctic shelves. Climate-induced changes in phytoplankton and ice-algal primary production, inflow of terrestrial matter through riverine discharge and coastal erosion, and increases in bacterial production have previously been predicted to cause shifts in the composition and distribution of organic matter supply and energy flow in this system. The goal of this study was to examine potential shifts in the Chukchi Sea ecosystem energy flow under various future climate scenarios. To address these goals, an existing mass balance Chukchi Sea ecosystem model by was updated by incorporating terrestrial matter as an energy source, especially for benthic consumers. Incorporation of the terrestrial matter component allowed us to adjust current model phytoplankton biomass to better match recent empirical measurements and to update the system-wide mass-balance.

We also modeled potential impacts of future climate-driven alterations in the composition and flow of organic matter supply on major ecosystem groups for the 2015 – 2050 period. Iterations showed that climate-driven increased retention of phytoplankton biomass in the pelagic realm would depress biomass of most benthic-feeding organisms across several larger ecosystem groups (invertebrates, fishes, mammals). However, simulated increases in both terrestrial matter inflow and bacterial biomass have the potential to compensate for some of the reductions in the energy supply from phytoplankton to the benthic food web, as well as to diversify the supply of organic matter to the seafloor. This diversification could make the Chukchi Sea ecosystem more stable to future climate-driven changes.

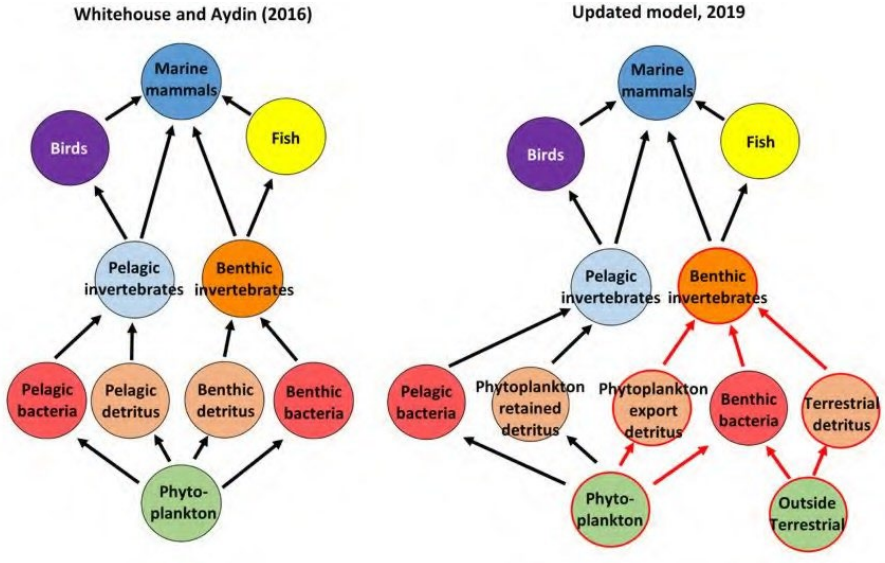

Figure 24. Comparative schematic of the original Whitehouse and Aydin (2016) and our updated mass-balanced Chukchi Sea ecosystem model. Arrows indicate feeding connections and flow of energy between larger functional groups. Red outlines and arrows indicate parameters and functional groups that reflect changes in the updated model.

Study 21: Inverse modelling of the microbial food web in the Northern Bering and Chukchi Seas in Spring and Late summer (Manuscript in preparation)

Nielsen J.M., Lomas M.W., Eisner L.B., Mordy C.W., McDonnell A., O'Daly S., Hopcroft R.R., Stockwell D., Danielson S.L., Juranek L., Cynar H., Krause J., Kimmel D., Schnetzer A., Irby M. et al., In preparation. Inverse modelling of the microbial food web in the Northern Bering and Chukchi Seas in Spring and Late summer

Resolving carbon flows in marine planktonic foodwebs is a fundamental first step for understanding the energy available for higher trophic level consumers and overall food web processes, production and function. Inverse food web modeling is a convenient data driven modeling approach for estimating carbon fluxes in marine food webs. Using empirical biomass and rate measurements, inverse food web modeling allows reconstruction of trophic flows and quantification of biological rates that are commonly challenging to measure. Here we use in-situ phytoplankton, microzooplankton, zooplankton, sedimentation and primary production data collected from 4 ecosystem surveys in the Chukchi and Northern Bering seas, June (spring) 2017 and 2018, and August-September (summer) 2017 and 2019.

Specifically, we assess 1) partitioning of energy, in terms of carbon, between the pelagic food web and deposition to the benthos, 2) how does transfer and major pathways vary between seasons (June vs August/September), and 3) how does food web carbon pathways vary between nutrient replete and deplete areas.

Initial simulations indicate seasonal differences in major carbon pathways. Higher carbon fluxes appeared to be available for benthic consumers in spring (in areas of high primary production) compared to late summer. Our initial analyses also revealed the importance of carbon uptake and transfer in microzooplankton and bacterial compartments, organisms and processes that are often underestimated on many ecosystem models. Overall, our results indicate variable carbon transfer efficiencies among seasons and areas of nutrient replete and deplete conditions, something that should be considered when evaluating larger food web processes.

Study 22: Evidence suggests potential transformation of the Pacific Arctic Ecosystem is underway

Huntington, H.P., S.L. Danielson, F.K. Wiese, M. Baker, P. Boveng, J.J. Citta, A. De Robertis, D.M. Dickson, E. Farley, J.C. George, K. Iken, D.G. Kimmel, K. Kuletz, C. Ladd, R. Levine, L. Quakenbush, P. Stabeno, K.M Stafford, D. Stockwell and C. Wilson, 2020. Evidence suggests potential transformation of the Pacific Arctic ecosystem is underway. *Nature Climate Change*, 10(4), pp.342-348

The highly productive northern Bering and Chukchi marine shelf ecosystem has long been dominated by strong seasonality in sea ice and water temperatures. Extremely warm conditions from 2017 into 2019 – including loss of ice cover across portions of the region in all three winters – were a marked change even from other recent warm years. Biological indicators suggest this state change could alter ecosystem structure and function. Here we report observations of key physical drivers, biological responses, and consequences for humans, including subsistence hunting, commercial fishing, and industrial shipping.

We consider whether observed state changes are indicative of future norms, whether an ecosystem transformation is already underway, and if so, whether shifts are synchronously functional and system-wide, or reveal a slower cascade of changes from the physical environment through the food web to human society. Understanding of this observed process of ecosystem reorganization may shed light on transformations occurring elsewhere.

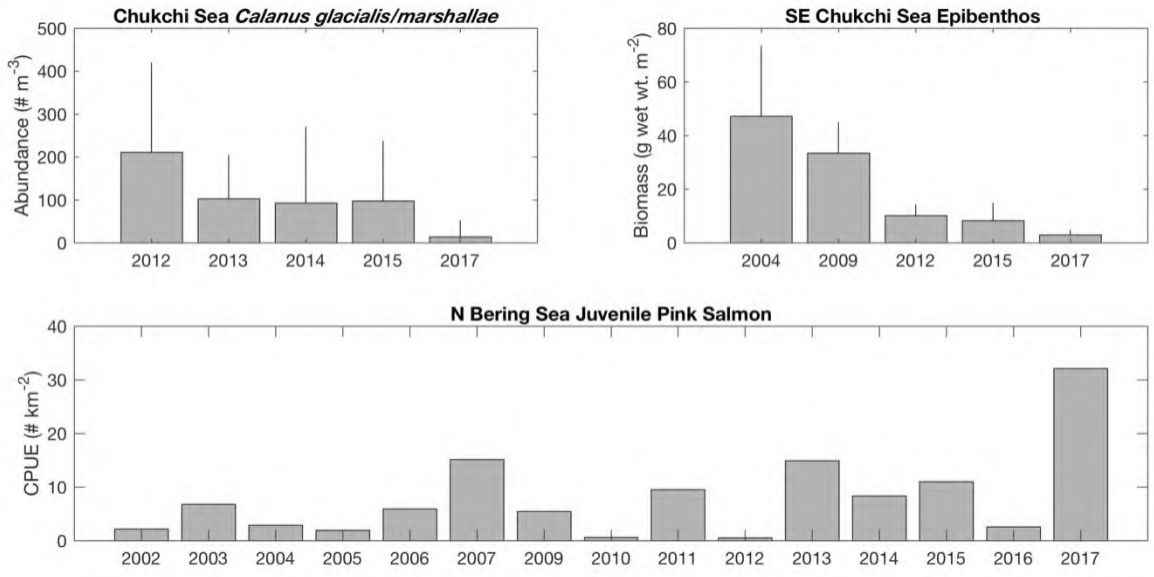

Figure 25. Observations show declines in Calanus glacialis/marshallae abundance (upper left) and epibenthic biomass (upper right) in 2017 relative to earlier years, and an increase in catch per unit effort (CPUE; bottom) for juvenile pink salmon. The upper two graphs show means and standard deviation error bars.

Additional and Leveraged Studies

In addition to the studies described in brief above, this section lists citations of other studies that leveraged ASGARD project personnel, logistics or data. These papers utilized samples collected on the ASGARD field expeditions, made use of data products compiled by the ASGARD project under the support of Arctic IERP funding, and/or ASGARD PI participation was facilitated in part by the Arctic IERP. Some of these papers are published, some are in review, and others are currently in preparation.

Anderson, D.M., Fachon, E., Pickart, R.S., Lin, P., Fischer, A.D., Richlen, M.L., Uva, V., Brosnahan, M.L., McRaven, L., Bahr, F. and Lefebvre, K., 2021. Evidence for massive and recurrent toxic blooms of Alexandrium catenella in the Alaskan Arctic. Proceedings of the National Academy of Sciences, 118(41).

Baker, M.R., Farley, E.V., Ladd, C., Danielson, S.L., Stafford, K.M., Huntington, H.P. and Dickson, D.M., 2020. Integrated ecosystem research in the Pacific Arctic–understanding ecosystem processes, timing and change. Deep-Sea Res. II, 177 (2020), p. 104850, https://doi.org/10.1016/j.dsr2.2021.104950

Chapman, Z.M., Mueter, F.J., Norcross, B.L., and D.S. Oxman. Otolith-derived hatch dates and growth rates of Arctic Cod (Boreogadus saida) support existence of several spawning populations in Alaskan waters, Deep Sea Res. II., in review

Copeman, L., M. Spencer, R. Heintz, J. Vollenweider, A. Sremba, T. Helser, L. Logerwell, L. Sousa, S.L. Danielson, A. Pinchuk and B. Laurel, 2020. Ontogenetic patterns in lipid and fatty acid biomarkers of juvenile polar cod (Boreogadus saida) and saffron cod (Eleginus gracilis) from across the Alaska Arctic. Polar Biology

Danielson, S.L., T.D. Hennon, P. Stabeno, et al., In prep. Wind-induced regulation of advective pathways and material fluxes in the Northern Bering and Southern Chukchi Sea

Danielson, S.L., T.D. Hennon, K.S. Hedstrom, A. Pnyushkov, I.V. Polyakov, E. Carmack, K. Filchuk, M.A. Janout, M. Makhotin, W.J. Williams, L. Padman, 2020. Oceanic routing of wind-sourced energy along the Arctic continental shelves, Front. Mar. Sci. – Global Change and the Future Ocean, DOI: 10.3389/fmars.2020.00509

Duffy-Anderson, et al. 2019. Responses of the northern Bering Sea and southeastern Bering Sea pelagic ecosystems following record-breaking low winter sea ice. Geophysical Research Letters, 46: 9833–9842. https://doi.org/10.1029/2019GL083396

Escajeda, E, Stafford KM, Laidre KL, Woodgate R. in prep. Characterizing spatio-temporal patterns in the acoustic presence of subarctic baleen whales in the Bering Strait in relation to environmental factors

Kimura, F., Abe, Y., Matsuno, K., Hopcroft, R.R. and Yamaguchi, A., 2020. Seasonal changes in the zooplankton community and population structure in the northern Bering Sea from June to September, 2017. Deep Sea Research Part II: Topical Studies in Oceanography, 181, p.104901.

Koch C.W., Cooper LW, Grebmeier JM, Frey K, Brown TA, 2020. Ice algae resource utilization by benthic macro- and megafaunal communities on the Pacific Arctic shelf determined through lipid biomarker analysis. Mar Ecol Prog Ser 651:23-43. https://doi.org/10.3354/meps13476

Krause, J. W., & Lomas, M. W., 2020. Understanding diatoms' past and future biogeochemical role in high-latitude seas. Geophysical Research Letters, 47, e2019GL085602. https://doi.org/10.1029/2019GL085602

Krause, J.W., Lomas, M.W. and Danielson, S.L., 2021. Diatom growth, biogenic silica production, and grazing losses to microzooplankton during spring in the northern Bering and Chukchi Seas. Deep Sea Research Part II: Topical Studies in Oceanography, p.104950.

Kuletz, KJ, Daniel Cushing, Steve Okonnen, Elizabeth Labunski. In prep. Changes in Short-tailed Shearwater distribution in Alaska and the influence of environmental conditions.

Kuletz, K., A. Prichard, D. Kimmel, A. DeRobertis, R. Levine, L. Eisner, A. Gall, others TBD. In prep. Responses of seabird foraging guilds to physical and biological changes in the Northern Bering and Chukchi Seas.

Lovvorn, J.R., Rocha, A.R., Danielson, S.L., Cooper, L.W., Grebmeier, J.M. and Hedstrom, K.S., 2020. Predicting sediment organic carbon and related food web types from a physical oceanographic model on a subarctic shelf. Marine Ecology Progress Series, 633, pp.37-54.

Mincks, S.L., A.R. Thurber, In Prep. Isotope labelling experiments reveal pathways of phytodetritus consumption by the infaunal food web in Chukchi Sea sediments.

Mincks, S.L., B.R. Jones, A.R. Thurber, In Prep. Temperature affects rates of short-term processing of a phytodetritus pulse in Chukchi Sea sediments.

Piatt, J.F., D.C. Douglas, M.L. Arimitsu, M.L. Kissling, E.N. Madison, S.K. Schoen, K.J. Kuletz, G.S. Drew. 2021. Kittlitz's Murrelet Seasonal Distribution and Post-breeding Migration from the Gulf of Alaska to the Arctic Ocean. *Arctic* 74 (4): 482-495

Romano, Marc, Heather M. Renner, Kathy J. Kuletz, Julia K. Parrish, Timothy Jones, Hillary K. Burgess, Daniel A. Cushing, Douglas Causey. 2020. Die-offs and reproductive failure of murres in the Bering and Chukchi Seas in 2018. Deep Sea Research II, vol 181-182, https://doi.org/10.1016/j.dsr2.2020.104877

Stafford, K.M., Wallace, E.E., in prep. Acoustic identity of killer whales recorded on hydrophones in Anadyr Strait

Stafford, K.M., Danielson, S.L., in prep. Seasonal and geographic variation of marine mammals in the northern Bering Sea

Stafford, K.M., Danielson, S.L., Escajeda, E., in prep. Long-term marine mammal occurrence at the Chukchi Ecosystem Observatory

Stafford K.M. et al., in prep. Shipping noise in the Bering Strait

Tian, F., Pickart, R.S., Lin, P., Pacini, A., Moore, G.W.K., Stabeno, P., Weingartner, T., Itoh, M., Kikuchi, T., Dobbins, E. and Bell, S., 2021. Mean and Seasonal Circulation of the Eastern Chukchi Sea from Moored Timeseries in 2013–2014. Journal of Geophysical Research: Oceans, 126(5), p.e2020JC016863.

Walker, A.M., M.B. Leigh, S.L. Mincks, North American Arctic benthic bacteria and archaea reflect food supply regimes and impacts of coastal and riverine inputs, in prep. for DSR II

Zinkann, A.C., 2020. Digging deep: depth distribution of organic matter sources in Arctic Chukchi Sea sediments Chapter 1 in *Organic Matter Sources on the Chukchi Sea Shelf in a Changing Arctic*. University of Alaska Fairbanks. UAF PhD Dissertation

General Discussion

Environmental Setting

The Arctic IERP proposals were written in 2016, in the midst of the well-documented North Pacific Marine Heatwave (refs; Walsh et al, 2018). Although "the Blob" of warm water was first identified in the Gulf of Alaska (Freeland et al., 2014; Bond et al., 2015) and many dramatic examples of Gulf of Alaska ecosystem impacts were evident at that time and documented in the years since (Piatt et al., 2018, Suryan et al, 2021), anomalous warmth also extended across the Pacific Arctic at this time (Danielson et al., 2020). Little did we know, however, that the Northern Bering and Chukchi seas were about to enter a period of unprecedented winter sea ice loss (Stabeno and Bell, 2018; Thoman et al., 2020) and equally as anomalous distribution shifts and changes in abundance of target commercial, non-commercial and subsistence harvest fishes and invertebrates (Huntington et al, 2020, Stevenson and Lauth, 2019).

Analysis of a nearly 100-year-long historical record (Danielson et al. 2020) shows that the Bering and Chukchi continental shelves exhibit different trends and multi-year intervals of warm and cold conditions – suggesting that while the Chukchi receives input from the Bering Sea it operates somewhat independently of the Bering's upstream heat inputs: more local processes dominate. Analyses show that the heat engines of both shelves accelerated over 2014-2018, with increased surface heat flux exchanges and increased lateral oceanic heat advection.

In retrospect, it appears that the Arctic IERP field years (2017-2019) encompassed the peak of the thermally anomalous conditions in this particular multi-year phase of regionally warm conditions; they are the only three years in the record with annual mean monthly temperature anomalies of greater than 1.5 °C (Figure 25). Given the likelihood of continued future warming, these years likely represent a preview of what may eventually be considered typical.

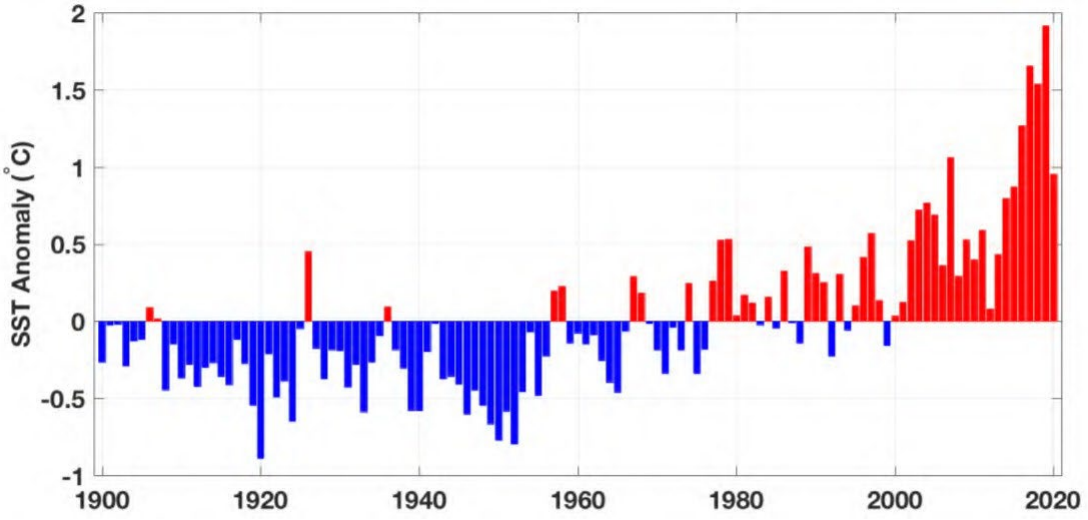

Figure 26. Sea surface temperature (SST) annual mean of all monthly anomalies over 1900-2020 from the Version 5 Extended Reconstructed SST dataset (ERSSTv5). Anomalies are computed relative to the full duration of this 1990-2020 time series. The integration region region for the data shown here extends °across the whole of the Northern Bering and Chukchi Seas (60-75 °N, 180-155 °W).

Our project collected a year-round northern Bering Sea set of whole water samples for major macronutrient analysis using a moored time series bag sampler, which was co-located with an optical SUNA sensor for hourly nitrate samples (Figure 26). This is the first year-round set of nutrient samples collected in the Pacific Arctic and represents a significant contribution to our understanding of nutrient dynamics through the months in which vessel-based samples have not been available. In particular, these data are allowing us to refine our understanding of the seasonally varying nutrient flux into the Arctic via the Anadyr Current. Using salinity as a conservative tracer, we were also able to identify an advective time scale of about two weeks for waters transiting between Anadyr Strait (mooring N2) and Bering Strait (UW mooring A3). This time scale allows us to make some rough estimates of net primary production within Chirikov Basin and thereby provide additional refinement to our estimates of nutrients entering the Arctic at Being Strait. Trend analysis of the nutrient fluxes reveal increasing concentrations of phosphate and silicate, but no trend for nitrate.

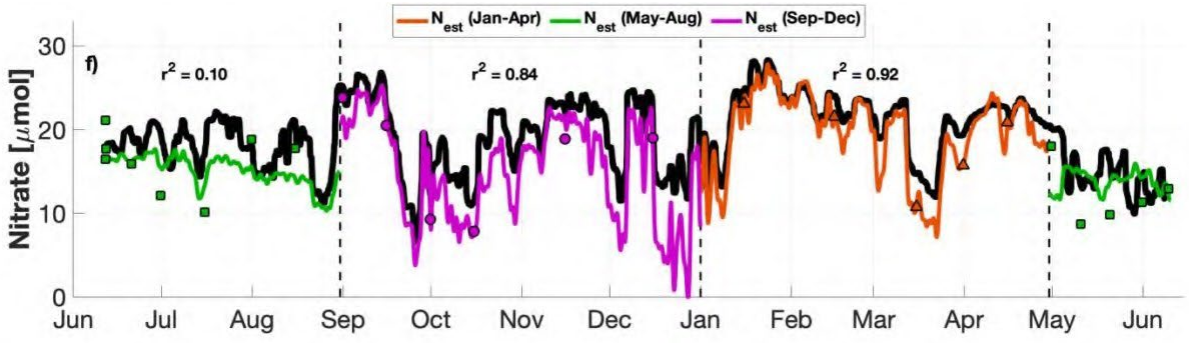

Figure 27. Colored markers show 25 nitrate/salinity pairs taken by the Green Eyes Aqua Monitor and a temperature/salinity datalogger at mooring N2, where color corresponds to the seasons denoted in the legend. SUNA nitrate (thick black) is shown in comparison to a nitrate:salinity-based regression (colored lines). Vertical dashed lines show delineations for the seasons (Jan-Apr, May-Aug, Sep-Dec).

The Pelagic Realm

As noted above, the Bering Strait region benefits from a year-round influx of high nutrient concentrations (Figure D2), helping portions of the system (e.g., Chirikov Basin and southern Hope Sea Basin) achieve relatively persistent levels of elevated productivity, although productivity exhibits a strongly patchy distribution with a regional average close to 2 gC m^{-2} day^{-1} for each of 2017 and 2018 (Figure 27). This characteristic – which is a consequence of the persistent Anadyr Current nutrient supply, the variable and energetic flow field, mixing dynamics, and variations in stratification – allows the system to initiate and/or maintain phytoplankton blooms as long as there is sufficient light to fuel primary productivity.

While large-celled diatoms are currently the most important primary producers in the Arctic, recent studies suggest that phytoplankton communities may shift towards mixotrophy (single cells capable of both photosynthesis and phagotrophy or osmotrophy) in response to climate change (Stoecker et al. 2017a; Stoecker and Lavrentyev 2018). Should these predictions prove correct, the decreased presence of diatoms could result in a reduced flux of carbon to the benthos. Other studies speculate that regional productivity could increase on the Chukchi shelf (Arrigo et al. 2008; JM Grebmeier 2012), with the potential to offset some excess CO_2 emissions. We present the first large-scale metabarcoding survey of

18S rRNA gene diversity in this region. Based on their biogeographical distributions, we identified exact sequence variants of *Chaetoceros*, *Pseudo−nitzschia*, *Micromonas*, and *Phaeocystis* as abundant taxa that may be negatively affected as the region warms.

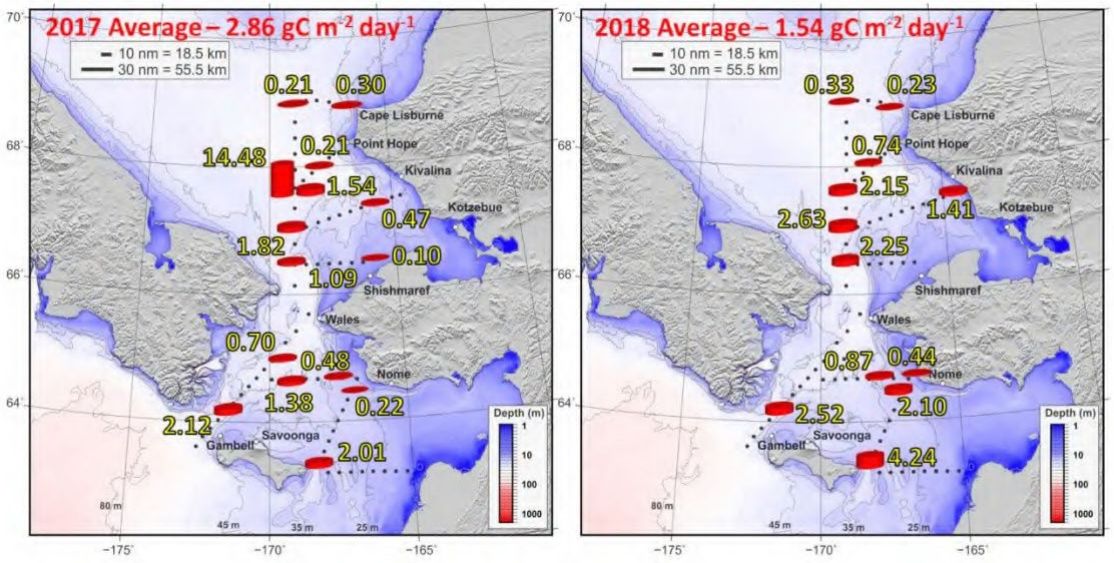

Figure 28. Primary productivity measured in June 2017 and 2018 in the ASGARD study region.

The abundance of the *Synechococcus* and other picophytoplankton was quantified across the Northern Bering and Chukchi Seas. The observations support an increased importance of a previously marginal phytoplankton group during a warming period in the Chukchi Sea. Seasonality of phytoplankton blooms, in particular the 'fall bloom' are gaining increasing recognition as being important in the trophic transfer of carbon and energy (Sigler et al., 2014). In the eastern Bering Sea shelf system, while *Synechococcus* has been observed (e.g., Liu et al., 2002; Moran et al., 2012) their abundances are generally low and represent a minor contribution to total phytoplankton carbon. The data presented by Lomas et al. [in prep.] suggest a different pattern in the Chukchi Sea, with a stronger seasonal amplitude in the abundance of *Synechococcus* and contribution to total phytoplankton carbon. Given the niche that *Synechococcus* fills globally (Flombaum et al., 2013; Visintini et al., 2021), our observations are consistent with *Synechococcus* growing into waters that are warmer and nutrient depleted.

Analyses of total lipids, lipid classes, fatty acids and alcohols in the dominant mesozooplankton (five taxa: euphausiids, copepods, chaetognaths, and pteropods) were performed on samples collected on both spring (ASGARD, 2017 and 2018) and late summer (IES 2017 and 2019) Chukchi Sea surveys. On these four cruises we also analyzed suspended particulate matter (seston) fatty acids, chlorophyll-a (Chl-a) and associated environmental data. Preliminary analyses show that lipid-rich zooplankton have a high degree of reliance on diatom-sourced lipids and our results suggest seasonality to the partitioning of the fatty acid concentrations, with diatom biomarkers more prevalent in spring, followed by a community shift to dinoflagellate and small flagellate fatty acid biomarkers in late fall. The seasonality, quality and composition of lipids and fatty acids in phytoplankton and zooplankton suggest potential ecosystem consequences under warming ocean scenarios in which the balance between nutrient concentrations and phytoplankton community assemblages shifts.

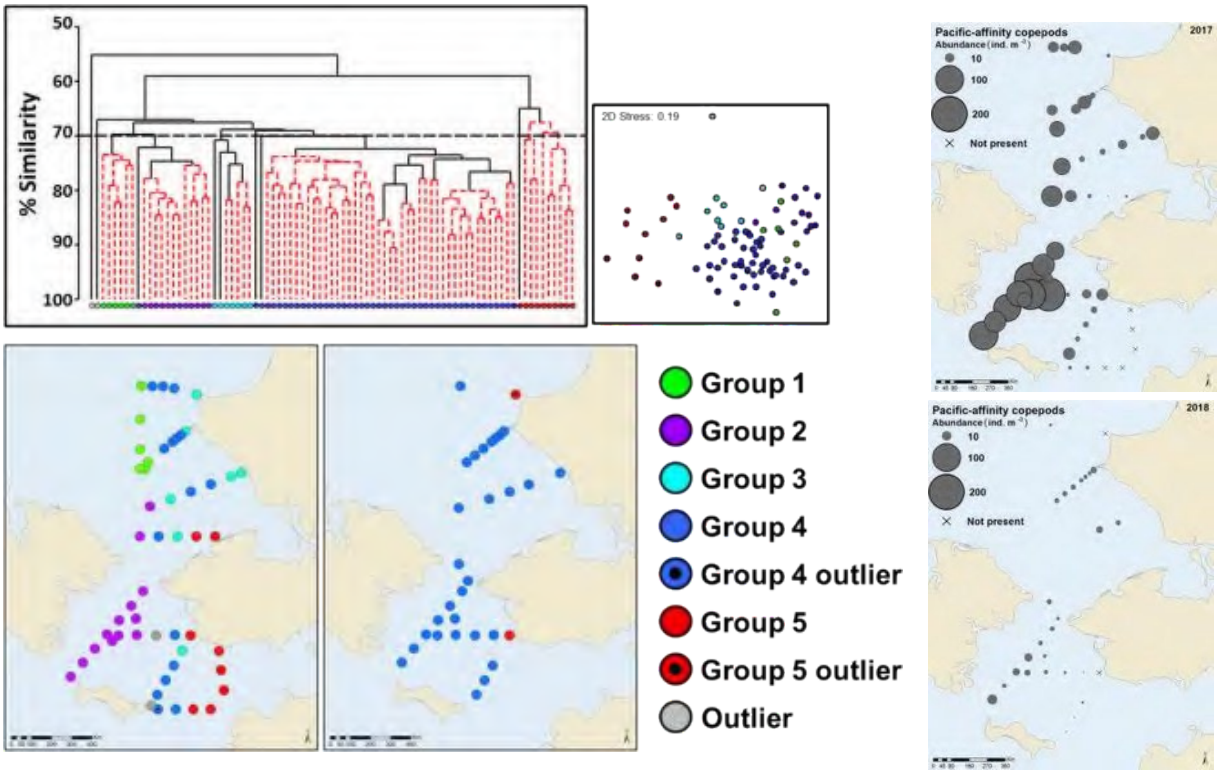

Figure 29. Non-dimensional principal component analysis shows that 2017 (bottom left and top right) and 2018 (bottom middle and bottom right) exhibited strongly contrasting mesozooplankton community structures.

Despite the similarity in the (low) prior winter ice cover, our net tows showed strongly contrasting zooplankton communities in 2017 and 2018 (Figure 28). Egg production and copepodite growth rates were measured for the calanoid copepods *Pseudocalanus* spp., *Calanus marshallae/glacialis*, and *Metridia pacifica* in the northern Bering and southern Chukchi Seas during June of 2017 and 2018. Rates suggest considerable discrepancies between growth rates and egg production weights that we propose are due to differences in life history strategies. Consistent with other studies, we find that global growth models do not match our observations particularly well, likely because they are dominated by egg production estimates at lower latitudes.

Using empirical biomass and rate measurements, we applied inverse food web modeling to in-situ phytoplankton, microzooplankton, zooplankton, sedimentation and primary production data collected from four ecosystem surveys in the Chukchi and Northern Bering seas, June (spring) 2017 and 2018, and August-September (summer) 2017 and 2019. Our results indicate variable carbon transfer efficiencies among seasons and areas of nutrient replete and nutrient deplete conditions.

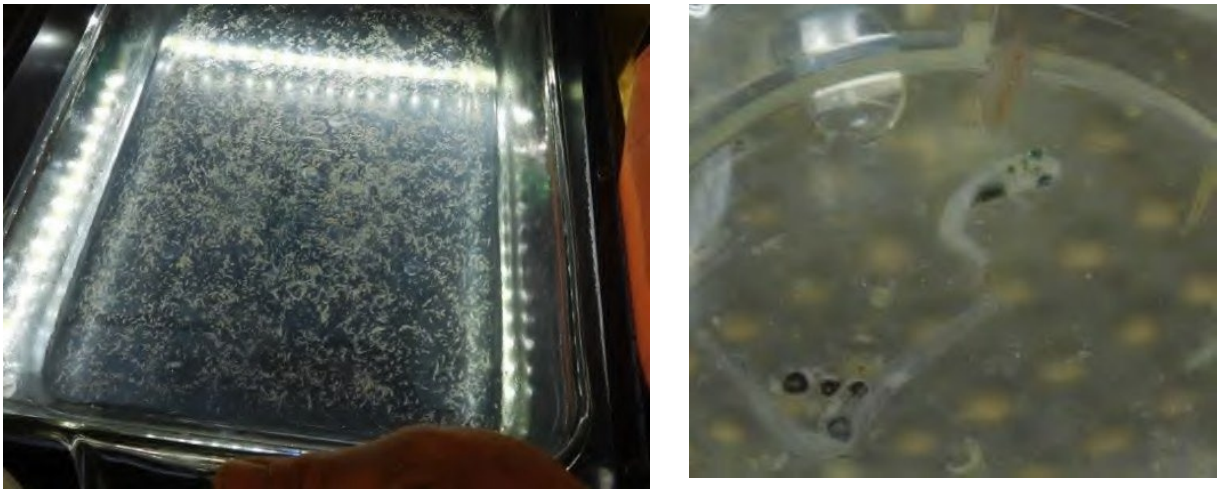

Figure 30. Larval polar cod sampled on the ASGARD SKQ201709S research cruise.

Spatial generalized additive models mapped the distribution of polar cod by size class and relative to environmental variables. Seasonal differences in polar cod abundance suggest that polar cod migration may follow a classical 'migration triangle' route between nursery grounds as juveniles, feeding grounds as subadults, and spawning grounds as adults, in relation to ice cover and seasonal production in the Chukchi Sea. High concentrations of larval polar cod sampled in coastal waters (Figure 29) having a high percentage of ice melt have allowed us to document at least one place near which these young fishes reside in at least some years (Deary et al., 2021).

Export Fluxes

We measured sinking particulate organic carbon (POC) fluxes with drifting and moored sediment traps, as well as rates of primary production and particle-associated microbial respiration. In Bering Shelf/Anadyr Water masses, sinking POC fluxes ranged from 0.8 to 2.3 g C m^{-2} day^{-1}, making them among the highest fluxes ever documented in the global oceans (O'Daly et al., 2020). These results highlight the extraordinary strength and efficiency of the biological carbon pump on the Pacific Arctic shelf during an unusually warm and low-sea ice year (Figure 30).

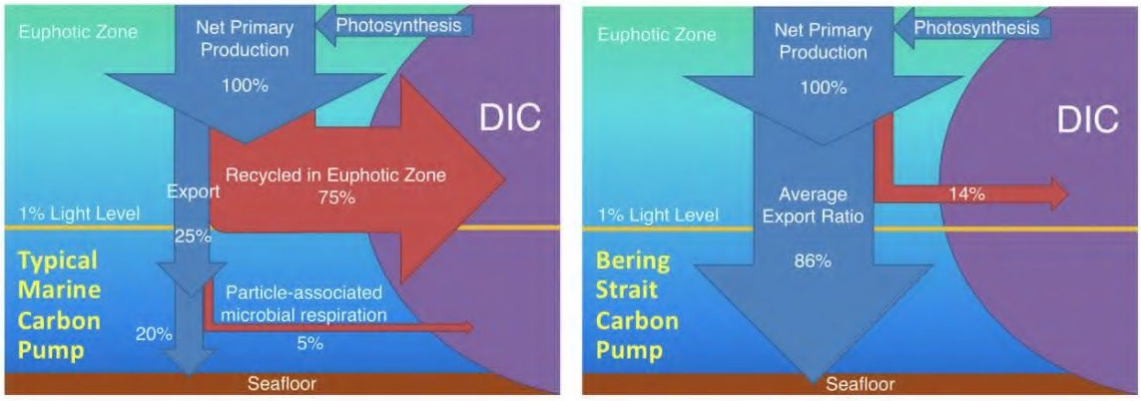

Figure 31. A typical marine carbon pump (left) and the Bering Strait region carbon pump (right), demonstrating the high export efficiency of the shallow Pacific Arctic continental shelf system.

Fluxes of living algal cells, chlorophyll *a*, total particulate matter (TPM), POC, and zooplankton fecal pellets, along with zooplankton and meroplankton collected in the traps, were used to evaluate spatial and temporal variations in the development and composition of the phytoplankton and zooplankton communities in relation to sea ice cover and water temperature.

The Benthic Realm

While most prior infaunal and benthic sediment work in the Chukchi Sea has been done with Van Veen grabs, our project used a multi-core sampler. The multi-corer allowed us to collect undisturbed samples of the seafloor/seawater interface, thereby facilitating rate-measuring incubation experiments and allowing for analysis of vertical structure of microbial and infaunal communities, including the first assessment of meiofaunal communities in this region.

The ASGARD multi-core and beam-trawl sampling provided live specimens for closed-system respirometry using non-invasive oxygen optodes to directly measure the metabolic rates of five bivalve species *(Macoma sp., Serripes groenlandicus, Astarte sp., Hiatella arctica* and *Nuculana pernula*) and one amphipod species (*Ampelisca macrocephala*). Results revealed (Figure 31) species-specific respiration rates with high metabolic demand for *S. groenlandicus* and *A. macrocephala* compared to that of the other species. These results suggest that observed shifts in spatial distribution of the dominant macrofaunal taxa across this region will impact carbon demand of the benthic community. Hence, ecosystem models seeking to incorporate benthic system functionality may need to differentiate between communities that exhibit different oxygen demands.

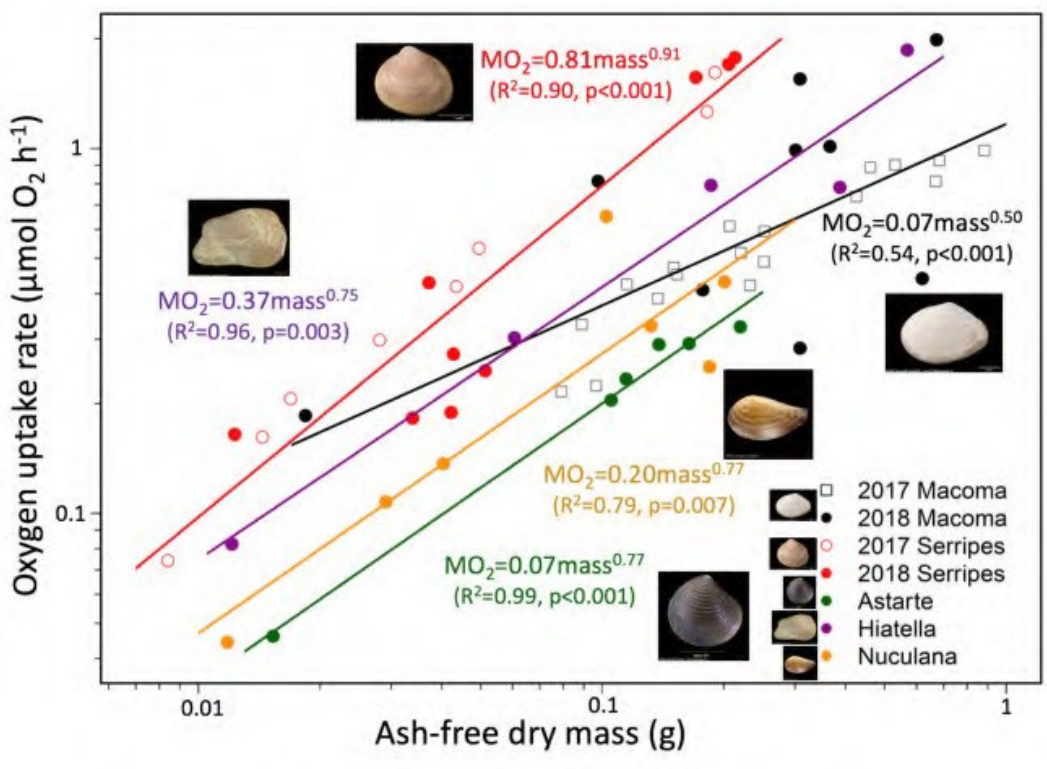

Figure 32. Species-specific respiration rates show an order-of-magnitude spread in oxygen demand amongst the various species.

In light of changing temperature and productivity regimes across the Pacific-Arctic domain, we also measured respiration rates of whole sediment communities at in situ (0 ºC) and elevated (5 ºC) temperatures. These experiments were made possible by multi-core sampling combined with *Sikuliaq's* capabilities for experimental work in temperature-controlled rooms. On average, sediment community oxygen demand, a proxy for organic carbon consumption, was ~30% higher in the warmer treatments; no differences in rates were observed between years. While locations in the "hot-spot" area in the southeast Chukchi Sea (SECS; DBO 3 region) showed markedly higher respiration rates likely due to the presence of large bivalves, all other sampled areas showed comparable rates. With the exception of the SECS sites, oxygen consumption rate showed a much stronger relationship with microbial biomass than with macro-infaunal biomass, suggesting microbial communities should not be overlooked in considering the fate of organic matter at the seafloor.

Four clusters of polychaete functional guilds were identified in the northern Bering and southern Chukchi sea. Polychaete functional composition and vertical distribution reflected the quality and quantity of organic matter input and the depositional environment, with likely impacts on biogeochemical and carbon cycling within the sediment. Meiofaunal communities similarly reflected grain size characteristics and organic matter content in sediments. Two distinct communities of nematodes were observed in the meio- and macrofaunal size fractions, with macrofaunal nematodes making up a large fraction of the total macrofaunal biomass.

A mass balance Chukchi Sea ecosystem model incorporated terrestrial matter as an energy source, especially for benthic consumers. This component allowed us to adjust phytoplankton biomass to better match recent empirical measurements and to update the system-wide mass-balance. Iterations of the mass-balance model showed that climate-driven increased retention of phytoplankton biomass in the pelagic realm would depress biomass of most benthic-feeding organisms across several larger ecosystem groups (invertebrates, fishes, mammals). However, simulated increases in both terrestrial matter inflow and bacterial biomass have the potential to compensate for some of the reductions in the energy supply from phytoplankton to the benthic food web, as well as to diversify the supply of organic matter to the seafloor.

The Over-arching Question

What regulates variations in carbon transfer pathways and how will the changing ice environment alter these pathways and ecosystem structure in the Pacific Arctic and beyond? Our observations and experiments revealed numerous insights into the character of the bottom-up forcing that helps maintain the Pacific Arctic shelf ecosystem, into how energy (carbon) is routed amongst the various marine system components, and into how it may change in a warming climate. Temperature clearly stands out as a key factor in the regulation of energy consumption and trophic transfers, but temperature alone is far from the whole answer. The aggregate combination of species abundance and distributions and environmental setting (geomorphology of the Pacific Arctic shelves, large-scale pressure gradients driving mean flows, nutrient supply, strong seasonality in light, ice, winds) combined with the ability of the Pacific Arctic ecosystem to maintain its many services ultimately sets this ecosystem's unique biological character. While this character has never been static in nature, it appears to be crossing thresholds into states that have not previously been observed (Huntington et al., 2020).

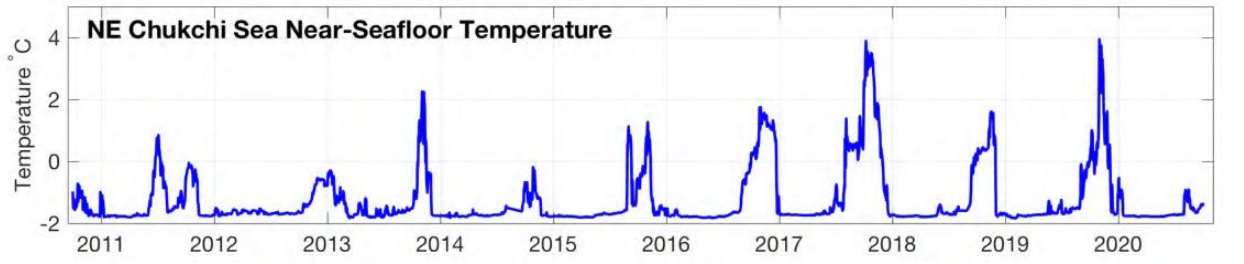

Figure 33. Near-bottom measurements of temperature in the NE Chukchi Sea at the CEO mooring site (2014-2020) and at a nearby site (2011-2014) showing an increase in the duration of waters > 0 °C over 2016-2019

Extremely warm conditions from 2017 into 2019 – including loss of ice cover across portions of the region in all three winters – were a marked change even from other recent warm years and may represent a proxy for future decade "normal" conditions. Temperature-controlled respirometry experiments show that benthic oxygen consumption increases significantly (~30%) with warming temperatures and our mooring measurements showed an extended duration of time that the seafloor water temperatures remained 2-6 degrees above the freezing point during these recent warm years (Figure 32). Biological indicators, such as these temperature-dependent benthic respiration rates, suggest that thermal state change exhibits potential to alter ecosystem structure and function (Jones et al., 2021), but our measurements also show that the system exhibits resilient capacity to buffer some of the changes from a bottom-up perspective. For example, direct measurements of upper water column export fluxes showed that even in these remarkably warm years, water column export to the benthos is extremely efficient (O'Daly et al., 2020) due to the fast sinking rates that large diatoms exhibit.

While the environmental alterations represent a bottom-up forcing, recent upper trophic level observations (Stevenson, D.E., Lauth, R.R., 2019; Huntington et. al. 2020) suggest that top-down forcing of the ecosystem will also play a key, and possibly dominant, role in determining future changes to the overall character of the Pacific Arctic ecosystem. For example, the influx of sub-Arctic Pacific Cod and Walleye Pollock exhibit potential to impart a more substantive impact on the benthic community than changes in benthic productivity due to altered pelagic realm export. Sensitivity of the local upper trophic level populations to anthropogenic disturbance (e.g. shipping traffic, noise) and intra-species competition represent other potential vulnerabilities.

In aggregate, our results have helped both define and constrain our understanding of the conditions in which the future warmer Pacific Arctic ecosystem will exist. The examples summarized here, and many others in the published manuscripts cited and reprinted in this report, directly contribute to our understanding of how energy in the marine ecosystem is routed now, and how it may change as the duration of sea ice cover continues to decline. The results of the ASGARD experiments will continue to be analyzed, synthesized, and published in coming years, each further revealing partial answers to the ASGARD and Arctic IERP over-arching question.

Relevance to Resource Management and Alaska Communities

Coastal Community Interests and Concerns

Food security is a paramount concern to residents of coastal communities that depend on a subsistence-based economy. Environmental conditions are changing rapidly and hunters find themselves dealing with a multitude of factors that can degrade hunt success (Fall et al., 2013). For example, hunters report that their ability to forecast the weather is now at times diminished, fuel costs are high; ice conditions are different and less safe, and game can be less accessible. Hunters are concerned with the impact of vessel traffic on the behavior and location of marine mammals, bycatch from commercial fisheries, and increasing rates of coastal erosion that threaten the placement of entire villages.

Practical applications of our research will directly address issues, questions and concerns posed by coastal community members (e.g., Huntington et al, 2021). These include: sea ice conditions and timing; whale, seal and walrus distributions with respect to vessel traffic noises; ramifications of changing climate conditions to the presence and success of marine mammals, clams, crabs, fish, and other animals; and toxic algae blooms that may impact whales and other marine mammals.

In particular, our research allows us to provide scientific lenses through which we can help interpret the causes and consequences of environmental change. As communities continue to adapt – as they have done for millennia – information from scientific studies and scientific observations can help inform community decisions. Such decisions now commonly deal with the practical aspects of addressing climate change impacts to the environment or location availability of subsistence food resources.

Harmful algal blooms (HAB) pose a significant potential public health risk to communities that harvest shellfish and marine mammals that consume shellfish. Recent studies have documented an increased potential for latent HAB spores to bloom from the seafloor (e.g., Anderson et al., 2021). Warmer waters also enhance the probability that a pelagic HAB boom may occur. Filter-feeding shellfish can bioaccumulate toxic plankton and pass such toxins on to marine mammals (e.g., walrus) and people. The research done in the ASGARD study is helping us understand the potential for such blooms and will help us determine future actions that can help decrease the potential for serious health impacts.

Equity in access to marine resources and economic development activities by Alaska Native communities is related to the scientific research that is conducted in the Bering and Chukchi seas because the resource management agencies consider in part the scientific data for informing their policy and management decisions. As commercially viable biomass shifts northward under a warming climate, important questions face both the coastal communities and the management of the resource. For example, in a region that has traditionally not hosted large scale commercial fisheries, what groups should be granted the right to fish: local Indigenous community members who are the sole traditional users of the local waterways, or commercial fishing entities that have no cultural or historical ties to the region? Who should economically benefit from new resources? These and many other similar questions may have once lacked immediate urgency, but we now face the reality that such decisions must be considered in the present.

Management Implications

Perhaps even sooner than many had anticipated, state and federal agencies are confronting resource management issues tied to loss of sea ice and northward-shifting distributions of sub-Arctic marine species.

The incursion of Pollock and Pacific Cod into the Bering Strait region – and farther north – demand consideration and a careful assessment of new management actions. Considerations need to include biodiversity, ecosystem structure, and ecosystem function in relation to any potential fishery harvest levels. The recent (since the start of the Arctic IERP) increase of commercial fishing in the Chukchi Sea waters of the Russian Federation suggests that despite insufficient data from the US side of the convention line in the Chukchi Sea, there likely exists significant quantities of Pollock and Pacific Cod on the US side as well. In US waters, any potential fishing activities must consider the cultures and subsistence lifestyles of local indigenous communities, potential impacts of industrial activities (e.g. commercial fishing, oil and gas extraction), potential changes to regional ocean carrying capacity, and resilience of the arctic marine ecosystem (NRC, 2014). An ecosystem-based approach to fisheries management necessitates consideration of food security of the coastal Indigenous communities, their traditional subsistence hunting activities, and conservation of endangered marine mammal and seabird species.

With carbon (or sometimes nitrogen) as the basic currency with which we describe and quantify biological and biophysical interactions - including growth, respiration, energy conversion, energy movement, energy storage and intra-trophic transfers - we need to understand the rate at which carbon is consumed, converted, stored, buried, and relocated. Biophysical numerical models require as inputs sinking rates, growth rates and respiration rates for all important species or functional groups (Stock et al., 2013). As outputs, models predict primary productivity, secondary productivity and biomass. ASGARD data provide spatially-explicit measures of the production and respiration rates for the dominant pelagic and benthic species, along with more basic information about composition, biomass and abundance. Such data will prove critical for advancing spatially and temporally explicit models of ecosystem structure, and applying them in appropriate and statistically robust to future scenario projections.

Beyond the fisheries management applications by NOAA, other federal agencies also may find the ASGARD data useful in their policy-making processes. For example, the protection of marine mammals and seabirds demands an examination of vessel regulations in locations at which there exists potential for negative interactions between species of concern and vessel traffic. Vessel routing and speed limits in Bering Strait and other shipping choke points may help decrease the probability of marine mammal strikes. Lighting protocols for vessels during the migration period for threatened seabird may reduce bird kill events. The USFWS, NOAA and USGS all must study the potential for harmful interactions relative to the species of concern that fall within their management directives. Similarly, the US Coast Guard has an opportunity to apply the environmental data assembled under the Arctic IERP program to their efforts, which include the planning for and response to oil and other contaminant spills, search and rescue missions, and fisheries enforcement activities.

Directions for Future Research

Following a concentrated effort of field work, analysis and publication, further advancements in scientific understanding relies on testable hypotheses and experimental designs that probe the edges of our knowledge base, and place our findings into a more complete ecological context. The process of analysis and interpretation of the Arctic IERP results is still ongoing, but a number of future research needs are already apparent. Below, we list a series of specific research directions that could further improve our ability to dig deeper into the ASGARD and Arctic IERP guiding questions, and could provide management agencies with actionable guidance.

Below, we identify ten study focal areas that would, if addressed, lead to a fuller understanding of the Pacific Arctic ecosystem, its drivers, and future trajectory. The ASGARD project was designed around the gaping need for more rate measurement studies, and while we have filled some needs in this realm, many still remain. Our recommendations are separated into two categories: *Rate Studies* and *Ecosystem Status and Change*. All of the below listed studies would fill information gaps and/or needs that resource management agencies could apply to their task mandates.

Biological Rate Studies and their Applications

1. **Comparison of ASGARD data to more typical years**
   Our campaign existed across the two warmest years on record for the study region and are thus not well characteristic of typical conditions found in the first two decades of the 21st century. Repeated measurements in more "normal" years would allow us to better assess our warm phase June month shipboard measurements and year-round mooring measurements.

2. **Benthic flux processes**
   Fluxes of many chemical constituents across the sediment-seawater interface are important for the Pacific Arctic ecosystem. Oxic and anoxic processes that influence sulfate reduction, denitrification, and nitrification help regulate nutrient availability and oxygen concentrations. A better understanding of the key rates and drivers of these fluxes is key to a better understanding of the future Alaskan Arctic marine realm.

3. **Species-specific biological rate measurements**
   We previously targeted a few key species for respiration and productivity rate experiments. Expanding the number of species for which we well know their biophysical models would allow future efforts to more realistically incorporate a multi-species approach to ecosystem modeling.

4. **Year-round export fluxes in the coastal realm**
   Our sediment traps were all deployed in Bering Shelf Water and Anadyr Water flow pathways. A time series sediment trap in Alaska Coastal Waters is needed to better characterize this important biophysical domain.

5. **Identifying carbon pump controls and dynamics balances**
   The microbial loop in the pelagic realm is not well described in our study region. Understanding the species and rates at which remineralization and other key processes operate is important to understanding the balance between pelagic and benthic zone carbon sources, nutrient availability, and productivity potential.

6. **Applying ASGARD measurements to ecosystem models**
   The ASGARD project was designed in part to provide data useful for the parameterization and/or validation of numerical models. The need for such modeling efforts has not diminished and we now have significant amounts of data that can help bring model studies to a more advanced stage of operation.

Ecosystem Status and Change

7. **Non-summer observations**
   The ASGARD expeditions in June provided valuable data outside of the more typical sampling months of July-September, but seasonal coverage in sampling remains heavily biased to summer and early fall months. Mooring data provided some first-ever year-round depictions of nutrient chemistry and biological observations in the study region, but these data are limited in scope by the sampling that is achievable from moored sensor packages. Shipboard biological sampling in late fall, winter and early spring could provide data that are important to our understanding during the dark and cold portion of the year.

8. **Ecosystem ramification of multiple stressors in the Pacific Arctic**
   Warming, ocean acidification, hypoxia, and increasing vessel traffic and other anthropogenic impacts present the likelihood of unanticipated outcomes due to the nature of nonlinear coupling between multiple stressors. Our ability to assess future ecosystem conditions in the study region depends on improvements in our understanding of how the system as a whole responds to such factors.

9. **Management of vessel locations and speeds in the Pacific Arctic region**
   Increasing vessel traffic poses a risk to protected marine mammal and seabird species. Modeling that assesses potential dynamic and/or adaptive management approaches would improve conservation efforts and reduce the potential for conflict. This need applies year-round due to the different migration timings of the various species of interest, and the fact that vessels are now transiting through the Bering Strait region in all months.

10. **Tracking of sub-Arctic species distribution, abundance, and biodiversity**
    Sub-Arctic species range distributions have been increasing northward in recent decades, and more recent indications show potential for displacement of endemic Arctic species as ranges over

11. **Changing phenologies**
    As the ice, temperature and light conditions change, the timing of species presence, absence, match-mismatch timing with food resources, migration considerations and human interactions all should be assessed with respect to animal behaviors and environmental conditions.

12. **Combined US and Russian sector studies**
    Many data collections end at the international dateline, but the ecosystem is not bound by national boundaries. Studies that bridge both the US and Russian Federation sectors of the Bering and Chukchi seas are needed to gain holistic understanding of the system.

Publications, Presentations, Outreach, and Collaborations

The ASGARD publications listing below includes ASGARD cruise reports, "core" ASGARD publications to date, publications in preparation, and other publications that utilize ASGARD data or the participation of an ASGARD PI was facilitated by the Arctic IERP.

Publications

1. Ahkinga, O. SKQ2017-09S ASGARD Community Observer Cruise Report, Little Diomede, AK
2. Anderson, D.M., Fachon, E., Pickart, R.S., Lin, P., Fischer, A.D., Richlen, M.L., Uva, V., Brosnahan, M.L., McRaven, L., Bahr, F. and Lefebvre, K., 2021. Evidence for massive and recurrent toxic blooms of Alexandrium catenella in the Alaskan Arctic. Proceedings of the National Academy of Sciences, 118(41).
3. Baker, M.R., Farley, E.V., Ladd, C., Danielson, S.L., Stafford, K.M., Huntington, H.P. and Dickson, D.M., 2020. Integrated ecosystem research in the Pacific Arctic–understanding ecosystem processes, timing and change. Deep-Sea Res. II, 177 (2020), p. 104850, https://doi.org/10.1016/j.dsr2.2021.104950
4. Chapman, Z.M., Mueter, F.J., Norcross, B.L., and D.S. Oxman. Otolith-derived hatch dates and growth rates of Arctic Cod (Boreogadus saida) support existence of several spawning populations in Alaskan waters, Deep Sea Res. II., in review
5. Charrier, B.R., in prep. Benthic carbon demand and community structure across the Pacific Arctic continental shelves, University of Alaska Fairbanks, Fairbanks, AK, PhD. Dissertation.
6. Charrier, B.R., T. Dorsaz, N. Matsui, and S.L. Mincks, In prep. Polychaete community and functional composition impacted by organic matter input and depositional environment on a shallow Arctic shelf, Chapter 1 in University of Alaska Fairbanks Ph.D. Dissertation
7. Charrier, B.R., J. Ingels, and S.L. Mincks, In prep. Meiofauna community structure in Pacific Arctic shelf sediments: a comparison of meiofaunal- and macrofaunal-sized nematodes and functional traits, Chapter 2 in University of Alaska Fairbanks Ph.D. Dissertation
8. Charrier, B.R., A.L. Kelley, and S.L. Mincks, 2021. Changes to benthic community structure may impact organic matter consumption on Pacific Arctic shelves. Chapter 3 in University of Alaska Fairbanks Ph.D. Dissertation
9. Collins, R.E., A. McDonnell, S. Danielson, R.M. Lekanoff, in review. Diversity and community structure of eukaryotic phototrophs in the Bering and Chukchi Seas, Submitted for review to *PlosONE*
10. Copeman, L., Eisner, L., Kimmel, D., Hopcroft, R. et al., In prep and final data generation stages. Seasonal and annual variation in the lipid composition of mesozooplankton from the Chukchi Sea.
11. Copeman, L., M. Spencer, R. Heintz, J. Vollenweider, A. Sremba, T. Helser, L. Logerwell, L. Sousa, S.L. Danielson, A. Pinchuk and B. Laurel, 2020. Ontogenetic patterns in lipid and fatty acid biomarkers of juvenile polar cod (Boreogadus saida) and saffron cod (Eleginus gracilis) from across the Alaska Arctic. Polar Biology
12. Danielson, S., O. Ahkings, L. Edenfeld, L. Eisner, C. Forster, S. Hardy, S. Hartz, B. Holladay, R. Hopcroft, B. Jones, J. Krause, K. Kuletz, R. Lekanoff, M. Lomas, K. Lu, B. Norcross, S. O'Daly, J. Pretty, C. Pham, A. Poje, E. Roth, S. Seabrook, P. Shipton, B. Smith, C. Smoot, K. Stafford, D.

Stockwell, A. Yamaguchi, and A. Zinkann, 2017. SKQ2017-09S ASGARD Cruise Report. Fairbanks, AK

13. Danielson, S., O. Ahkinga, S. Baer, Z. Chapman, E. Collins, L. Edenfeld, E. Escajeda, C.Forster, S. Gonzalez, S. Hardy, R. Hopcroft, K. Iken, B. Jones, L.Juranek, K. Kuletz, D. Naber, B. Norcross, A. McDonnell, H. Mendoza, S. O'Daly, A. Poje, E. Roth, P. Shipton, B. Smith, C. Smoot, K. Stafford, D. Stockwell, A.Thurber, 2017, SKQ2018-13S ASGARD Cruise Report. Fairbanks, AK
14. Danielson, S.L., O. Ahkinga, C. Ashjian, E. Basyuk, L.W. Cooper, L. Eisner, E. Farley, K.B. Iken, J.M. Grebmeier, L. Juranek, G. Khen, S. Jayne, T. Kikuchi, C. Ladd, K. Lu, R. McCabe, G.W.K. Moore, S. Nishino, S.R. Okkonen, F. Ozenna, R.S. Pickart, I. Polyakov, P.J. Stabeno, K. Wood, W.J. Williams, T.J. Weingartner, 2020. Manifestation and consequences of warming and altered heat fluxes over the Bering and Chukchi Sea continental shelves. *Deep-Sea Res. II: Topical Studies in Oceanogr.,* 177, 144781, https://doi.org/10.1016/j.dsr2.2020.104781
15. Danielson, S.L., T.D. Hennon, K.S. Hedstrom, A. Pnyushkov, I.V. Polyakov, E. Carmack, K. Filchuk, M.A. Janout, M. Makhotin, W.J. Williams, L. Padman, 2020. Oceanic routing of wind-sourced energy along the Arctic continental shelves, Front. Mar. Sci. – Global Change and the Future Ocean, DOI: 10.3389/fmars.2020.00509
16. Danielson, S.L., T.D. Hennon, P.S. Stabeno, et al., In prep. Wind-induced regulation of advective pathways and material fluxes in the Northern Bering and Southern Chukchi Sea
17. Deary, A.L., Vestfals, C.D., Mueter, F.J., Logerwell, E.A., Goldstein, E.D., Stabeno, P.J., Danielson, S.L., Hopcroft, R.R. and Duffy-Anderson, J.T., 2021. Seasonal abundance, distribution, and growth of the early life stages of polar cod (Boreogadus saida) and saffron cod (Eleginus gracilis) in the US Arctic. *Polar Biology*, *44*(11), pp.2055-2076.
18. Duffy-Anderson, et al. (2019). Responses of the northern Bering Sea and southeastern Bering Sea pelagic ecosystems following record-breaking low winter sea ice. Geophysical Research Letters, 46: 9833–9842. https://doi.org/10.1029/2019GL083396
19. Eisner, Lomas, Nielsen, et al., In prep. Variations in phytoplankton community composition, phytoplankton biomass, and primary production in a warming Arctic.
20. Escajeda, E, Stafford KM, Laidre KL, Woodgate R. in prep. Characterizing spatio-temporal patterns in the acoustic presence of subarctic baleen whales in the Bering Strait in relation to environmental factors
21. Forster, C. E., Norcross, B. L., Mueter, F. J., Logerwell, E. A., Seitz, A. C. 2020. Spatial patterns, environmental correlates, and potential seasonal migration triangle of polar cod (*Boreogadus saida*) distribution in the Chukchi and Beaufort seas. *Polar Biology*, 43(8), 1073-1094.
22. Forster, C. E., 2019. Spatial patterns, environmental correlates, and potential seasonal migration triangle of Arctic cod (*Boreogadus saida*) distribution in the Chukchi and Beaufort seas. University of Alaska Fairbanks. M.S. Thesis.
23. Hennon, T.D., S.L. Danielson, C. Mordy, S. Stockwell, R. Woodgate, In prep. Anadyr Current Contributions to the Arctic-bound Oceanic Nutrient Flux. In preparation for submission to *Geophysical Research Letters*.
24. Hopcroft, R.R., C. Smoot, In prep. Respiration rates of calanoid copepods during the spring bloom for the Arctic's Bering Strait region
25. Hopcroft, R.R., C. Smoot, In prep. Zooplankton communities of the Arctic's Bering Strait region during the spring bloom, 2017-2018

26. Huntington, H.P., S.L. Danielson, F.K. Wiese, M. Baker, P. Boveng, J.J. Citta, A. De Robertis, D.M. Dickson, E. Farley, J.C. George, K. Iken, D.G. Kimmel, K. Kuletz, C. Ladd, R. Levine, L. Quakenbush, P. Stabeno, K.M Stafford, D. Stockwell and C. Wilson, 2020. Evidence suggests potential transformation of the Pacific Arctic ecosystem is underway. *Nature Climate Change*, 10(4), pp.342-348
27. Jones, B.R., A.L. Kelley, and S.L. Mincks, 2021. Changes to benthic community structure may impact organic matter consumption on Pacific Arctic shelves. *Conservation physiology*, *9*(1), p.coab007
28. Kimura, F., Abe, Y., Matsuno, K., Hopcroft, R.R. and Yamaguchi, A., 2020. Seasonal changes in the zooplankton community and population structure in the northern Bering Sea from June to September, 2017. Deep Sea Research Part II: Topical Studies in Oceanography, 181, p.104901.
29. Koch C.W., Cooper LW, Grebmeier JM, Frey K, Brown TA, 2020. Ice algae resource utilization by benthic macro- and megafaunal communities on the Pacific Arctic shelf determined through lipid biomarker analysis. Mar Ecol Prog Ser 651:23-43. https://doi.org/10.3354/meps13476
30. Krause, J. W., & Lomas, M. W., 2020. Understanding diatoms' past and future biogeochemical role in high-latitude seas. Geophysical Research Letters, 47, e2019GL085602. https://doi.org/ 10.1029/2019GL085602
31. Krause, J.W., Lomas, M.W. and Danielson, S.L., 2021. Diatom growth, biogenic silica production, and grazing losses to microzooplankton during spring in the northern Bering and Chukchi Seas. Deep Sea Research Part II: Topical Studies in Oceanography, p.104950.
32. Kuletz, KJ, Daniel Cushing, Steve Okonnen, Elizabeth Labunski. In prep. Changes in Short-tailed Shearwater distribution in Alaska and the influence of environmental conditions.
33. Kuletz, Kathy., Alex Prichard, David Kimmel, Alex DeRobertis, Robert Levine, Lisa Eisner, Adrian Gall, others TBD. In prep. Responses of seabird foraging guilds to physical and biological changes in the Northern Bering and Chukchi Seas.
34. Lalande C., Grebmeier J.M., McDonnell A.M., Hopcroft R.R., O'Daly S., Danielson S.L., 2021. Impact of a warm anomaly in the Pacific Arctic region derived from time-series export fluxes. Plos one. 2021 Aug 16;16(8):e0255837
35. Lekanoff, R.M., 2020. Diversity and Community Structure of Eukaryotic Phototrophs in the Bering and Chukchi Seas. University of Alaska Fairbanks. M.S. Thesis
36. Lomas, M., Eisner, L., Nielsen, J., et al., In prep. Contributions of the picocyanobacteria *Synechococcus* to phytoplankton biomass during a period of warming in the Chukchi Sea.
37. Lovvorn, J.R., Rocha, A.R., Danielson, S.L., Cooper, L.W., Grebmeier, J.M. and Hedstrom, K.S., 2020. Predicting sediment organic carbon and related food web types from a physical oceanographic model on a subarctic shelf. Marine Ecology Progress Series, 633, pp.37-54.
38. Mincks, S.L., A.R. Thurber, In Prep. Isotope labelling experiments reveal pathways of phytodetritus consumption by the infaunal food web in Chukchi Sea sediments.
39. Mincks, S.L., B.R. Jones, A.R. Thurber, In Prep. Temperature affects rates of short-term processing of a phytodetritus pulse in Chukchi Sea sediments.
40. Mincks, S.L., S. Seabrook, B. Jones, A. Thurber, In prep. Temperature effects on sediment community oxygen consumption in the Pacific Arctic
41. Nielsen, J., L.A. Copeman, L.B. Eisner, K.E. Axler, C.W. Mordy, M.W. Lomas, In review, Phytoplankton and seston fatty acids dynamics in the northern Bering-Chukchi Sea region

42. Nielsen J.M., Lomas M.W., Eisner L.B., Mordy C.W., McDonnell A., O'Daly S., Hopcroft R.R., Stockwell D., Danielson S.L., Juranek L., Cynar H., Krause J., Kimmel D., Schnetzer A., Irby M. et al., In prep. Inverse modelling of the microbial food web in the Northern Bering and Chukchi Seas in Spring and Late summer
43. O'Daly, S.H., Danielson, S.L., Hardy, S.M., Hopcroft, R.R., Lalande, C., Stockwell, D.A. and McDonnell, A.M., 2020. Extraordinary carbon fluxes on the shallow Pacific Arctic shelf during a remarkably warm and low sea ice period. *Frontiers in Marine Science*, 7, p.986.
44. O'Daly, S.H., 2019. Carbon flux and particle-associated microbial remineralization rates in the northern Bering and southern Chukchi seas, University of Alaska Fairbanks. M.S. Thesis.
45. Piatt, J.F., D.C. Douglas, M.L. Arimitsu, M.L. Kissling, E.N. Madison, S.K. Schoen, K.J. Kuletz, G.S. Drew. 2021. Kittlitz's Murrelet Seasonal Distribution and Post-breeding Migration from the Gulf of Alaska to the Arctic Ocean. *Arctic* 74 (4): 482-495 doi.org/10.14430/arctic73992
46. Poje, A., 2020. Growth and Reproductive Rates of Calanoid Copepods in the Northern Bering and Southern Chukchi Seas. University of Alaska Fairbanks. M.S. Thesis.
47. Romano, Marc, Heather M. Renner, Kathy J. Kuletz, Julia K. Parrish, Timothy Jones, Hillary K. Burgess, Daniel A. Cushing, Douglas Causey. 2020. Die-offs and reproductive failure of murres in the Bering and Chukchi Seas in 2018. Deep Sea Research II, vol 181-182, https://doi.org/10.1016/j.dsr2.2020.104877
48. Stafford, K.M., Wallace, E.E., in prep. Acoustic identity of killer whales recorded on hydrophones in Anadyr Strait
49. Stafford, K.M., Danielson, S.L., in prep. Seasonal and geographic variation of marine mammals in the northern Bering Sea
50. Stafford, K.M., Danielson, S.L., Escajeda, E., in prep. Long-term marine mammal occurrence at the Chukchi Ecosystem Observatory
51. Stafford K.M. et al., in prep. Shipping noise in the Bering Strait
52. Tian, F., Pickart, R.S., Lin, P., Pacini, A., Moore, G.W.K., Stabeno, P., Weingartner, T., Itoh, M., Kikuchi, T., Dobbins, E. and Bell, S., 2021. Mean and Seasonal Circulation of the Eastern Chukchi Sea from Moored Timeseries in 2013–2014. Journal of Geophysical Research: Oceans, 126(5), p.e2020JC016863.
53. Walker, A.M., M.B. Leigh, S.L. Mincks, Community characterization of benthic bacteria and archaea across surface sediments of the Northern Bering and Chukchi Seas, in prep. for DSR II
54. Zinkann, A.C., G. Gibson, K. Iken, in review. The Arctic Chukchi Sea food web: simulating ecosystem impacts of future changes in organic matter flow, submitted for review to *Ecological Modeling*
55. Zinkann, A.C., 2020. Digging deep: depth distribution of organic matter sources in Arctic Chukchi Sea sediments Chapter 1 in *Organic Matter Sources on the Chukchi Sea Shelf in a Changing Arctic*. University of Alaska Fairbanks. UAF PhD Dissertation
56. Zinkann, A.C., 2020. The Arctic Chukchi Sea food web: simulating ecosystem impacts of future changes in organic matter flow. Chapter 3 in *Organic Matter Sources on the Chukchi Sea Shelf in a Changing Arcitc*. University of Alaska Fairbanks. Ph.D. Dissertation.

Presentations

2021

- Danielson, S., K. Hedstrom, T. Hennon, C. Mordy, P. Stabeno, D. Stockwell, R. Woodgate, 2021. Recent volume, heat, and nutrient fluxes on the Pacific Arctic continental shelf, Alaska Marine Science Symposium, Anchorage, AK, oral presentation
- Deary, A.L., J.T. Duffy-Anderson, F. Mueter, C.D. Vestfals, E.D. Goldstein, E.A. Logerwell, P. Stabeno, S. Danielson, R.R. Hopcroft, 2021. Seasonal abundance and distribution of larval polar cod (*Boreogadus saida*) and saffron cod (*Eleginus gracilis*) in the US Arctic, Arctic Science Summit Week International Arctic Science Committee. Lisbon, Portugal (virtual), Oral Presentation
- Gonzalez, S., J. Horne, S.L. Danielson and L. Lieber 2021, Representative Range of Acoustic Point Source Measurements in the Chukchi Sea, Alaska Marine Science Symposium, Anchorage, AK
- Lalande, C., S. Danielson, A. McDonnell,R. Hopcroft, J. Grebmeier, 2021. Time-Series Measurements of Export Fluxes across the Bering Strait, Alaska Marine Science Symposium, Anchorage, AK, poster presentation.
- Walker, A., A. Thurber, S.L. Mincks, 2021. Effects of a changing environment on microbial communities in Chukchi shelf sediments. Alaska Marine Science Symposium, Anchorage, AK, oral presentation

2020

- S. Danielson et al., 2020. Heat Over the Pacific Arctic Continental Shelves: Recent Changes in Content, Surface Fluxes and Throughput, AGU/ALSO Ocean Sciences Meeting, San Diego, CA, Poster presentation
- S. Hardy et al., 2020. Rates and pathways of sediment organic-matter processing across the northern Bering and southern Chukchi Sea shelf, AGU/ALSO Ocean Sciences Meeting, San Diego, CA
- T. Hennon et al., 2020. Linking Offshore Oceanography to Alaskan Lagoon Dynamics, AGU/ALSO Ocean Sciences Meeting, San Diego, CA
- K. Kuletz et al., 2020. Seabirds Signal Changes in the Pacific Arctic, AGU/ALSO Ocean Sciences Meeting, San Diego, CA
- K. Lu et al., 2020. Impacts of Short-Term Wind Events on Chukchi Hydrography and Sea Ice Retreat, AGU/ALSO Ocean Sciences Meeting, San Diego, CA
- A. Poje et al., 2020. Copepod Production in a High Latitude Shelf System, AGU/ALSO Ocean Sciences Meeting, San Diego, CA
- S. Danielson et al., 2020. Heat Over the Pacific Arctic Continental Shelves: Recent Changes in Content, Surface Fluxes and Throughput, Alaska Marine Science Symposium, Anchorage, AK, Poster presentation
- Farley et al., 2020. The Arctic Integrated Ecosystem Research Program: Are We Experiencing the Future Arctic?, Alaska Marine Science Symposium, Anchorage, AK, Oral Presentation
- Hennon et al., 2020. Linking Offshore Oceanography to Alaskan Lagoon Dynamics"
- Poje et al., 2020. Calanoid Copepod Egg Production and Growth Rates in the Northern Bering and Southern Chukchi Seas, Alaska Marine Science Symposium, Anchorage, AK,

- Kuletz, “Seabirds Signal Changes in the Pacific Arctic, Alaska Marine Science Symposium, Anchorage, AK,
- Axler et al., 2020. Seasonal and Annual Patterns in Fatty Acid Dynamics of Arctic Seston from the North Bering-Chukchi Sea Regions, Alaska Marine Science Symposium, Anchorage, AK,

2019

- Danielson, S. 2019. Recent surface heat fluxes and thermal and sea ice conditions of the Bering-Chukchi Continental Shelf”, Alaska Marine Science Symposium, Anchorage, AK, Oral Presentation
- Danielson, S. and IERP SSC, 2019. The Arctic Integrated Ecosystem Research Program: Observations of 2017-2018 conditions and consequences”, Alaska Marine Science Symposium, Anchorage, AK, Oral Presentation
- Deary, A.L., 2019. Ecosystem research in Alaska, Friday Harbor Laboratories, University of Washington. Friday Harbor, Washington, Oral Presentation
- Deary, A.L., 2019. Fisheries update in the northern Bering Sea and Arctic, Interagency Arctic Research Policy Committee, Washington D.C., Oral Presentation
- Deary, A.L., J.T. Duffy-Anderson, F. Mueter, C.D. Vestfals, E.D. Goldstein, E.A. Logerwell, P. Stabeno, S. Danielson, 2019. A synthesis of the early life history of two forage fishes in the US Arctic during a record sea ice minimum in 2017, Early Life History Section, American Fisheries Society, Mallorca, Spain, Oral Presentation
- Deary, A.L. and D.G. Kimmel, 2019. Fisheries research in the United States Arctic, 45th Anniversary of the American Polish Cooperation Symposium, Gdynia, Poland, Oral Presentation
- L. Eisner, M. Lomas, D. Stockwell, S. Baer, 2019. Primary production in the southern Chukchi Sea: June (ASGARD) and August/September (Arctic IES) 2017 survey results”, Alaska Marine Science Symposium, Anchorage, AK, Poster Presentation
- C. Forster, B. Norcross, F.Mueter, 2019. Spatial patterns, environmental drivers, and potential seasonal differences of Arctic Cod (Boreogadus saida) distribution in the Chukchi Sea, Alaska Marine Science Symposium, Anchorage, AK
- S. Gonzalez, J.K. Horne, S. Danielson, 2019. Temporal variability in densities and vertical distributions of pelagic fish and macrozooplankton on Hanna Shoal, Alaska Marine Science Symposium, Anchorage, AK, Poster Presentation
- B. Jones, S. Hardy, A. Thurber, A. Kelley, 2019. Benthic respiration rates across the northern Bering and southern Chukchi Sea shelf, Alaska Marine Science Symposium, Anchorage, AK, Oral presentation
- R. Lekanoff, E. Collins, A. McDonnell, 2019. Characterizing particle-associated and free-living microbes and their roles in the carbon cycle of the Bering and Chukchi seas, Alaska Marine Science Symposium, Anchorage, AK, Poster Presentation
- C. Smoot, J. Questel, A. Poje, R. Hopcroft, “Springtime zooplankton communities of the Northern Bering and Southern Chukchi Seas, Alaska Marine Science Symposium, Anchorage, AK, Poster Presentation

- S. O'Daly and A.M.P. McDonnell, 2019. Downward organic carbon flux, average particle sinking speed, and the role of particle-associated microbial respiration on the Bering and Chukchi shelf, Alaska Marine Science Symposium, Anchorage, AK, Oral presentation
- A. Poje, C. Smoot & R. Hopcroft, 2019. Growth of Calanoid Copepods on an Arctic shelf, , Alaska Marine Science Symposium, Anchorage, AK, Oral presentation

2018

- Danielson, S. and coauthors. On the Thermal and Sea Ice Conditions of the Bering-Chukchi Continental Shelf, AGU Fall Meeting, Washington DC, December 2018
- Danielson, S. and coauthors. Oral presentation, Rate Experiments of the Arctic Integrated Ecosystem Research Program, IARPC Ecosystem Collaboration Team meeting, November, 2018
- Danielson, S. Oral presentation, National Academies of Science, Engineering, and Medicine: Ocean Studies Board, Fairbanks, AK, September 2018
- B. Jones and S. Hardy, 2018. Macrofaunal respiration rates across the northern Bering and southern Chukchi Sea shelf, Alaska Marine Science Symposium, Anchorage, AK
- A. Poje, C. Smoot & R. Hopcroft, 2018. Growth of Calanoid Copepods on an Arctic shelf, Alaska Marine Science Symposium, Anchorage, AK
- S. O'Daly and A.M.P. McDonnell, 2018. Determining particle abundance, size, and composition in the North Bering and South Chukchi seas during an earlier spring melt, Alaska Marine Science Symposium, Anchorage, AK,
- R. Lekanoff, R.E. Collins, and A.M.P. McDonnell, A.M.P, 2018. Characterizing gene functions of particle-associated microbes and their role in the carbon cycle of the Bering and Chukchi Seas, Alaska Marine Science Symposium, Anchorage, AK

2017

- Danielson, S. Oral presentation, Ice floes to seals, waves to whales. Linking high latitude marine ecosystem studies and researchers through physics. Sitka Whale Fest 2017, Sitka, AK, November 2017
- Oral presentation, AIERP Update to the Pacific Arctic Group, Seattle WA, November 2017
- Danielson S. and coauthors, U.S.-Canada Northern Oil and Gas Research Forum, Anchorage, AK, October 2017
- Danielson, S. Recap of 2017 Arctic Integration Ecosystem Research Program field season to NPRB Board of Trustees, Cordova, AK, September 2017
- Danielson, S. Oral presentation, Attempting Multi-Disciplinary Measurements at Biologically & Physically Relevant Time & Length Scales, Gordon Research Conference, Ventura, CA, March 2017
- Danielson, S.L., Blanchard, A. S. Hardy, R. Hopcroft, K. Kuletz, M. Lomas, A. McDonnell, B. Norcross, K. Stafford, D. Stockwell. Tales from ASGARD: Upcoming in 2017 and 2018, Alaska Marine Science Symposium, Anchorage, AK, poster presentation

Outreach Activities and Products

Ongoing

- Danielson participates in the Ice Seal UME Investigative team, providing remotely sensed and in situ oceanographic updates to the monthly meetings.

2021

- Danielson presented at the Strait Science lecture series on January 7th.
- KNOM article High Frequency Radar Sites in Wales and Shishmaref, Could Help Track Debris and Save Lives.
- Nome Nugget article 1/14/21: High frequency radar maps ocean currents.
- O'Daly presented at the Strait Science lecture series on January 14th.
- Nome Nugget article 1/28/21: Researcher looks at sea ice carbon production reporting on O'Daly's Strait Science talk

2020

- Danielson presented a brief overview of IERP results at the July 2020 Alaska Eskimo Whaling Commission by reviewing paper titles in the AIERP DSR-II first special issue and then highlighting results of Huntington et al. 2020 and Danielson et al. 2020b.
- Danielson was a co-convener of a scientific session at the 2020 AGU/ASLO Ocean Sciences Meeting: Ecosystem Structure and Processes in a Changing Arctic, with over 50 abstract submissions. Combined, the session garnered had two sections of oral presentations and two poster sessions.
- Danielson was a co-convener of a town hall meeting at the 2020 AGU/ASLO Ocean Sciences meeting: McCammon, M., S.L. Danielson, J.M. Grebmeier, A. Holman, C. Rosa, Scientific Response to an Ever Faster Changing Arctic: Making the Most of Our Collective Research Efforts

2019

- The ASGARD project was noted in many social media and blog postings made in 2019 associated with the IERP, with R/V Sikuliaq and CFOS.

2018

- *Nome Nugget* article: 29 June 2018: "UAF Research Vessel Sikuliaq Visits Nome"
- Danielson provided an interview to KNOM for a broadcast on 27 June 2018: "Scientists studying spring transition in Bering Strait waters"
- We presented post-season ASGARD updates to the Alaska Eskimo Whaling Commission on 23 July, 2018.
- We presented post-season ASGARD updates to the Arctic Waterways Safety Committee on 18 October, 2018.
- Numerous social media postings that feature the ASGARD Sikuliaq cruise were and continue to be posted on the UAF's Sikuliaq website.

- Danielson was interviewed on KIAK and on KFBX on 21 November 2018. A link to the KFBX interview is here: http://research.cfos.uaf.edu/faculty/sldanielson/media/Danielson_KFBX_11-21-18.wav
- We presented a project update to the NPRB Board of Trustees in Cordova (September 2018).
- We presented cruise updates at the 27th Annual BIA Provider's Conference (November) and the AEWC and AWSC meetings (December).
- Numerous social media postings that feature the ASGARD Sikuliaq cruise were and continue to be posted on the UAF's Sikuliaq website.

2017

- Danielson highlighted the ArcticIERP ASGARD cruise and research questions in a presentation at the November 2017 Sitka Whale Fest.
- McDonnell, A. 2017. Video compilations featuring ASGARD/Arctic IERP activities. https://www.youtube.com/watch?v=sQDZo9Fw_hw
- Forster, C. 2017. Video compilations featuring ASGARD/Arctic IERP activities. https://www.youtube.com/watch?v=1ddMYLei9vw
- Outreach activities included NPRB-sponsored "hub" meeting in Nome.
- Media articles describing AIERP and ASGARD were published in the Nome Nugget (2 articles) and the Fairbanks Daily New Miner. The FDNM article was picked up by the Associated Press and republished in the Ketchikan Daily News and nationally in US News and World Report.
- UAF published a cruise highlight article as part of the Chancellor's "Cornerstone" weekly update.
- We gave pre-cruise and post-cruise lectures at the UAF campus in Nome as part of the "Strait Science" lecture series, hosted by UAF MAP agent Gay Sheffield. Attendance was about 35 people at each presentation.
- A. McDonnell along with students R. Lekanoff and S. O'Daly gave a public lecture in Dutch Harbor prior to sailing on the 2017 ASGARD cruise. The ship also provided tours to a limited number of community members.
- We gave a post-cruise report to the summer meeting of the Alaska Eskimo Whaling Commission on July 20th in Fairbanks.
- Hundreds of social media posts and a detailed blog were updated regularly from the research cruise. Visit https://blog.arctic.nprb.org/ for details.

2016 and early 2017

- Outreach presentations and discussions at meetings with the AEWC, IPCoMM, AWSC, the NPRB-sponsored Kotzebue "Hub meeting", the native Village of Gambell, and the Native Village of Savoonga.

Research Cruise Collaborations: Participant Home Institutions

- Bigelow Labs for Ocean Science
- BOEM
- Dauphin Island Sea Lab
- Hokkaido University

- Native Village of Diomede
- NOAA-PMEL
- NPRB
- OSU
- UAF
- USFWS
- UW-APL
- UW-Oceanography

Data Sharing and Publication Collaborations: Home Institutions

(Based on *Results* chapters' author lists and first authors of *Appendix B* publications.)

- Alaska Center for Climate Assessment and Policy
- Alaska Department of Fish and Game
- Amundsen Science
- Institute of Ocean Sciences, Fisheries and Oceans Canada (IOS-DFO) Canada
- College of Earth, Ocean and Atmospheric Science, Oregon State University
- Florida State University Coastal and Marine Laboratory
- Huntington Consulting
- International Arctic Research Center and College of Natural Science and Mathematics
- Japan Agency for Marine-Earth Science and Technology (JAMSTEC), Japan
- Native Village of Diomede
- NOAA, Alaska Fisheries Science Center, Auke Bay Lab
- NOAA, Alaska Fisheries Science Center, National Marine Fisheries Service
- NOAA, Pacific Marine Environmental Laboratory
- North Carolina State University
- North Slope Borough Department of Wildlife Management
- Russian Federal Research Institute of Fisheries and Oceanography, Pacific Branch of VINRO, TINRO, Vladivostok, Russia
- Stantec
- University of Toronto Mississauga, Mississauga, ON, Canada
- University of Manitoba, Winnipeg, Manitoba, Canada
- University of Maryland Center for Environmental Sciences, Chesapeake Biological Laboratory
- University of Washington, Applied Physics Laboratory
- University of Washington, Joint Institute for the Study of the Atmosphere and Ocean
- US Fish and Wildlife Service
- Woods Hole Oceanographic Institute

Sample Collections, Lab Analyses and Other Collaborations

(Including intra-Arctic IERP collaborations such as the NOAA-led Arctic IES projects)

- Alaska Center for Climate Assessment and Policy (weather/climate analyses)
- Alaska Ocean Observing System (AOOS) (CEO program support)

- Alaska Sea Grant (UAF Nome Campus cruise support and community liaison support)
- Amundsen Science (sediment trap samples)
- Arctic Marine Biodiversity Observation Network (AMBON) (US Arctic biodiversity)
- Bering Strait Mooring Program (APL-UW) (monitoring of Bering Strait)
- Bigelow Labs for Ocean Science (plankton samples)
- Chukchi Ecosystem Observatory (CEO) (NE Chukchi Mooring Site)
- College of Earth, Ocean and Atmospheric Science, Oregon State University (nutrient samples)
- Distributed Biological Observatory (DBO) (Bering-Chukchi-Beaufort change detect array)
- Florida State University Coastal and Marine Laboratory (benthic infauna; nematodes)
- Kitikmeot Sea Science Study (marine ecosystem study of the Northwest Passage)
- NMFS Ice Seal UME Investigation Team for UME declaration of September 2019
- NOAA, Auke Bay Laboratories (fish carcasses for energetics)
- NOAA, Crab Research Lab (measurements and samples)
- NOAA, PMEL (nutrient samples; drifter deployments)
- NOAA, AFSC, Marine Mammal Lab (mooring recovery)
- OSU, Marine Lipids Lab (plankton samples)
- Smithsonian Institute (genetic tissue samples)
- Sitka Tribe of Alaska Environmental Research Lab (ASP toxin analysis)
- UAF Fisheries, Juneau (larval gadids for aging)
- UAF Museum of the North (genetic tissue samples)
- University of Washington, Applied Physics Laboratory (mooring platform)
- Universitty of Washington, Joint Institute for the Study of the Atmosphere and Ocean (JISAO) (profiling float deployments)
- Woods Hole Oceanographic Institution (profiling float deployments)

National and International Symposia Collaborations

- 2016 – present (1-2 times per year). ASGARD representation at Distributed Biological Observatory (DBO) and the Pacific Arctic Group (PAG) collaboration meetings.
- October 2017. Participation in the 4th Pan-Arctic Synthesis: Towards a unifying pan-Arctic perspective of the contemporary and future Arctic Ocean. Workshop convened in Motovun, Croatia. Since 2002 pan-arctic integration symposia have attempted to figure out how the Arctic Ocean can be understood as an independent, mediterranean ocean and the node of the Northern Hemisphere. In order to overcome the sectorial approaches that characterize our research, the intention of the workshop was to add to the pan-arctic comprehension of the Arctic Ocean and adjacent seas. The workshop resulted in the publication of 13 peer-reviewed journal articles and one e-book compendium. Three of these manuscripts include one or two ASGARD PIs (Danielson, Hopcroft) as lead or contributing authors. https://www.frontiersin.org/research-topics/7353/towards-a-unifying-pan-arctic-perspective-of-the-contemporary-and-future-arctic-ocean
- February 2018. AGU/ALSO Ocean Sciences Meeting. Scientific session organization (with DBO and AMBON) and participation: “Linkages Between Environmental Drivers and Structure of

Arctic Ecosystems". Session Abstract: Arctic ecosystems are adjusting to rapidly warming temperatures, sea ice loss and a myriad of other factors that are changing with time. Temperature-growth relations, altered seasonality, expanded and contracted range extents, and new trophic pathways may each affect biodiversity, population status of key species, and relations between humans and marine resources. As environmental change continues, can we anticipate how future Arctic ecosystems will compare to those of yesterday and today? Will the effects of a changing climate be the same across various Arctic regions? We welcome presentations from all regions of the Arctic examining rates, processes and mechanistic controls that impart structure on any aspect of the high-latitude marine ecosystem.

- April 2019. Kitikmeot Sea Science Study (K3S) Synthesis Workshop. A results analysis and writing workshop was convened for compiling data collected in the Kitikmeot Sea region of the Canadian Arctic Archipelago's Northwest Passage in Yellowknife, Canada in March 2019. Participants included international K3S team members from Canada, Norway and the US. ASGARD project results were discussed at this workshop in the context of contrasting different Arctic marine ecosystems.
- May 2019. Japanese OMIX project (*Ocean Mixing*: http://omix.aori.u-tokyo.ac.jp/en/) is a collaborative study between physical, chemical and biological oceanography to understand turbulent vertical mixing and physical, chemical and biological oceanic processes and their relationship in the western North Pacific (2015-2019). In May 2019 OMIX hosted a penultimate international symposium and an associated session at the following Japan Geoscience Union annual meeting. Work from the ASGARD project was presented at these meetings, and the collaboration triggered additional communication between UAF and Japanese scientists, including a visit to Fairbanks by Dr. Toru Hirawake of Hokkaido University in 2020 that involved discussions of planning for future Bering Strait region data sharing collaborations.
- February 2020. AGU/ALSO Ocean Sciences Meeting. Scientific session organization (with DBO and AMBON) and participation: "Ecosystem Structure in a Changing Arctic". Session Abstract: The rate of atmospheric warming in the Arctic is outpacing that of other regions, and is associated with sea ice loss, warming ocean temperatures, changes in the hydrological cycle, and impacted ecosystems. Temperature-growth relations, nutrient cycling dynamics, altered seasonality, changing freshwater balances, expanded and contracted species range extensions, and new trophic pathways may each affect biodiversity, the population status of key species, and relations between humans and marine resources. As environmental change continues, can we anticipate how future Arctic ecosystems will compare to those of the past and present? Will the effects of a changing climate be the same across various Arctic regions? Organizers welcome presentations from all regions of the Arctic examining the drivers, rates, processes, and mechanistic controls that impart structure on any aspect of the high-latitude marine ecosystem.
- February 2020. AGU/ALSO Ocean Sciences Meeting Town Hall organization (with AOOS, USARC and DBO) and participation: "Scientific Responses to an Ever Faster Changing Arctic: Making the Most of our Collective Research Efforts". With the U.S. Arctic experiencing such unprecedented, rapid change, the objective of this town hall was to provide an opportunity for the scientific community to informally discuss causality and linkages across results from recent field work and studies, including if a "new normal" for the Arctic can be determined and what this might look like. We would also like to see proposed actions developed for moving forward with

coordinated research efforts, ideas for emerging research. And observing needs, and suggestion or how we can best oorganize ourselves to deliver the data and information products that northern communities, resource managers, industry, first responders, and other decision makers will need.

References

Arrigo, K.R., Perovich, D.K., Pickart, R.S., Brown, Z.W., van Dijken, G.L., Lowry, K.E., Mills, M.M., Palmer, M.A., Balch, W.M., Bahr, F., Bates, N.R., Benitez-Nelson, C., Bowler, B., Brownlee, E., Ehn, J.K., Frey, K.E., Garley, R., Laney, S.R., Lubelczyk, L., Mathis, J., Matsuoka, A., Mitchell, B.G., Moore, G.W.K., Ortega- Retuerta, E., Pal, S., Polashenski, C.M., Reynolds, R.A., Schieber, B., Sosik, H.M., Stephens, M., Swift, J.H., 2012. Massive Phytoplankton Blooms Under Arctic Sea Ice. Science 336(6087), 1408.

Bienhold C., A. Boetius and A. Ramette, 2012. The energy-diversity relationship of complex bacterial communities in Arctic deep-sea sediments. ISME J 6(4), 724-732.

Blanchard A.L., 2014. Variability of macrobenthic diversity and distributions in Alaskan sub-Arctic and Arctic marine systems with application to worldwide Arctic Systems Marine Biodiversity:1-15 doi:10.1007/s12526- 014-0292-6

Blanchard A.L. and H.M. Feder, 2014. Interactions of habitat complexity and environmental characteristics with macrobenthic community structure at multiple spatial scales in the northeastern Chukchi Sea Deep Sea Research Part II: Topical Studies in Oceanography 102:132-143 doi:http://dx.doi.org/10.1016/j.dsr2.2013.09.022

Bunker, A.J., Hirst, A.G., 2004. Fecundity of marine planktonic copepods: global rates and patterns in relation to chlorophyll a, temperature, and body weight. Mar. Ecol. Prog. Ser. 279, 161-781.

Campbell, R.G., Sherr, E.B., Ashjian, C.J., Sherr, B.F., Hill, V., Stockwell, D.A., 2009. Mesozooplankton prey preference and grazing impact in the Western Arctic Ocean. Deep-Sea Res. II. 56, 1274-1289.

Carmack, E. and P. Wassmann, 2006. Food webs and physical-biological coupling on pan-Arctic shelves: unifying concepts and comprehensive perspectives, Prog. Oceanogr., 71, pp. 446–477

Codispoti, L.A., V. Kelly, A. Thessen, P. Matrai, V. Hill, M. Steele and B. Light, 2013. Synthesis of primary production in the Arctic Ocean: III. Nitrate and phosphate based estimates of net community production. Progress in Oceanography 110, 126–150.

Danielson, S.L., Eisner, L., Ladd, C., Mordy, C., Sousa, L. and Weingartner, T.J., 2017. A comparison between late summer 2012 and 2013 water masses, macronutrients, and phytoplankton standing crops in the northern Bering and Chukchi Seas. Deep Sea Research Part II: Topical Studies in Oceanography, 135, pp.7-26.

Day, R.H., T.J. Weingartner, R.R. Hopcroft, L.A.M. Aerts, A.L. Blanchard, A.E. Gall, B.J. Gallaway, D.E. Hannay, B.A Holladay, J.T. Mathis, B.L. Norcross, J.M. Questel and S.S. Wisdom, 2013. The offshore northeastern Chukchi Sea, Alaska: a complex high-latitude ecosystem. Cont. Shelf Res. 67, 147–165, http://dx.doi.org/10.1016/j.csr.2013.02.002.

Dunton K.H., J.L. Goodall, S.V. Schonberg, J.M. Grebmeier, D.R. Maidment, 2005. Multi-decadal synthesis of benthic-pelagic coupling in the western arctic: role of cross-shelf advective processes Deep Sea Research Part II: Topical Studies in Oceanography 52:3462-3477 doi:10.1016/j.dsr2.2005.09.007

Eisner, L., N. Hillgruber, E. Martinson, J. Maselko, 2013. Pelagic fish and zooplankton species assemblages in relation to water mass characteristics in the northern Bering and southeast Chukchi seas Polar Biology, 36, pp. 87–113

Ershova, E. H., R.R. Hopcroft, and K.N. Kosobokova. 2015. Inter-annual variability of summer mesozooplankton communities of the western Chukchi Sea: 2004-2012. Polar Biol.: 38:1461-1481.

Feder H.M., A. S. Naidu, S. C. Jewett, J.M. Hameedi, W. R. Johnson and T. E. Whitledge, 1994. The northeastern Chukchi Sea: benthos-environmental interactions Marine Ecology Progress Series 111:171-190

Feder H.M., S. C. Jewett and A L. Blanchard, 2007. Southeastern Chukchi Sea (Alaska) macrobenthos Polar Biology 30:261-275 doi:10.1007/s00300-006-0180-z

Gall, A.E., Morgan, T.C., Day, R.H. and Kuletz, K.J., 2017. Ecological shift from piscivorous to planktivorous seabirds in the Chukchi Sea, 1975–2012. Polar Biology, 40(1), pp.61-78.

Gibson, G.A. and Y.H. Spitz, 2011. Impacts of biological parameterization, initial conditions, and environmental forcing on parameter sensitivity and uncertainty in a marine ecosystem model for the Bering Sea. Journal of Marine Systems. 88(2):214-231.

Grebmeier, J.M., C.P. McRoy, and H.M. Feder, 1988. Pelagic–benthic coupling on the shelf of the northern Bering and Chukchi Seas. I. Food supply source and benthic biomass. Marine Ecology Progress Series 48, 57– 67

Grebmeier, J.M., Harvey, H.R., 2005. The Western Arctic Shelf–Basin Interactions (SBI) project: An overview. Deep-Sea Res. II. 52, 3109-3576.

Grebmeier J.M., L. W. Cooper, H. M. Feder and B.I. Sirenko, 2006. Ecosystem dynamics of the Pacific-influenced Northern Bering and Chukchi seas in the Amerasian Arctic. Progress In Oceanography 71:331-361 doi:10.1016/j.pocean.2006.10.001

Grebmeier, J.M., W. Maslowski, 2014. The Pacific Arctic region: ecosystem status and trends in a rapidly changing environment. In: Grebmeier, J.M., Maslowski, W. (Eds.), The Pacific Arctic Region: Ecosystem Status and Trends in a Rapidly Changing Environment. Springer, Dordrecht, pp. 1–16.

Grebmeier, J.M., B. A. Bluhm, L.W. Cooper, S.L. Danielson, K.R. Arrigo, A.L. Blanchard, J. T. Clarke, R.H. Day, K.E. Frey, R.R. Gradinger, M. Kędra, B. Konar, K.J. Kuletz, S.H. Lee, J.R. Lovvorn, B.L. Norcross and S.R. Okkonen, 2015a. Ecosystem characteristics and processes facilitating persistent macrobenthic biomass hotspots and associated benthivory in the Pacific Arctic. Progress In Oceanography, 136, 92-114.

Grebmeier, J.M., B.A. Bluhm, L.W. Cooper, S. G. Denisenko, K. Iken, M. Kedra and C. Serrato, 2015b. Time- series benthic community composition and biomass and associated environmental characteristics in the Chukchi Sea during the RUSALCA 2004-2012 Program. Oceanography 28(3):116-133, http://dx.doi.org/10.5670/oceanog.2015.61

Highsmith, R. C. and K. O. Coyle, 1990. High productivity of northern Bering Sea benthic amphipods. Nature 344(6269):862–864

Hirst, A.G., Bunker, A.J., 2003. Growth of marine planktonic copepods: Global rates and patterns in relation to chlorophyll a, temperature, and body weight. Limnol. Oceanogr. 48, 1988-2010.

Hopcroft, R.R., Pinchuk, A.I., Byrd, A., Clarke, C., 2005. The paradox of Metridia spp. egg production rates: A new technique and measurements from the coastal Gulf of Alaska. Mar. Ecol. Prog. Ser. 286, 193-201.

Hopcroft, R.R., Kosobokova, K.N., Pinchuk, A.I., 2010. Zooplankton community patterns in the Chukchi Sea during summer 2004. Deep-Sea Res. II. 57, 27-39.

Lane, P.V.Z., Llinás, L., Smith, S.L., Pilz, D., 2008. Zooplankton distribution in the western Arctic during summer 2002: hydrographic habitats and implications for food chain dynamics. J. Mar. Res 70, 97-133.

Leduc D., A. A. Rowden, D.A. Bowden, P.K. Probert, C.A. Pilditch and S.D. Nodder, 2012. Unimodal relationship between biomass and species richness of deep-sea nematodes: implications for the link between productivity and diversity. Mar Ecol Prog Ser 454, 53-64.

Liu, H., Dagg, M.J., Strom, S., 2005. Grazing by the calanoid copepod Neocalanus cristatus on the microbial food web in the coastal Gulf of Alaska. J. Plankton Res. 27, 647 - 662.

Liu, H., Hopcroft, R.R., 2006a. Growth and development of Neocalanus flemingeri/plumchrus in the northern Gulf of Alaska: validation of the artificial cohort method in cold waters. J. Plankton Res. 28, 87-101.

Liu, H., Hopcroft, R.R., 2006b. Growth and development of Metridia pacifica (Copepoda: Calanoida) in the northern Gulf of Alaska. J. Plankton Res. 28, 769-781.

Liu, H., Dagg, M.J., Napp, J.M., Sato, R., 2008. Mesozooplankton grazing in the coastal Gulf of Alaska: Neocalanus spp. vs. other mesozooplankton. ICES J. Mar. Sci. 65, 351-360.

Mincks S.L., C.R. Smith and D.J. DeMaster, 2005. Persistence of labile organic matter and microbial biomass in Antarctic shelf sediments: Evidence of a sediment "food bank". Mar Ecol Prog Ser 300, 3-19.

Mordy, C.W., Bell, S., Cokelet, E.D., Ladd, C., Lebon, G., Proctor, P., Stabeno, P., Strausz, D., Wisegarver, E. and Wood, K., 2020. Seasonal and interannual variability of nitrate in the eastern Chukchi Sea: Transport and winter replenishment. Deep Sea Research Part II: Topical Studies in Oceanography, 177, p.104807.

Mundy, C.J., D.G. Barber, C. Michel, 2005. Variability of snow and ice thermal, physical and optical properties pertinent to sea-ice algae biomass during spring, Journal of Marine Systems, Volume 58, Issues 3–4, Pages 107- 120, ISSN 0924-7963, http://dx.doi.org/10.1016/j.jmarsys.2005.07.003

Napp, J.M., Hopcroft, R.R., Baier, C.T., Clarke, C., 2005. Distribution and species-specific egg production of Pseudocalanus in the Gulf of Alaska. J. Plankton Res. 27, 415-426.

National Research Council (NRC), 2014. The Arctic in the Anthropocene, Emerging Research Questions. Committee on Emerging Research Questions in the Arctic,Polar Research Board,Division on Earth and Life Studies, H. Huntington and S. Pfirman, co-chairs, 224 pp., ISBN: 978-0-309-30183-1

Nelson, R.J., Ashjian, C., Bluhm, B., Conlan, K., Gradinger, R., Grebmeier, J., Hill, V., Hopcroft, R., Hunt, B., Joo, H., Kirchman, D., Kosobokova, K., Lee, S., Li, W.K.W., Lovejoy, C., Poulin, M., Sherr, E., Young, K., 2014. Biodiversity and biogeography of the lower trophic taxa of the Pacific Arctic region: sensitivities to climate change. In: Grebmeier, J.M., Maslowski, W. (Eds.), The Pacific Arctic Region: Ecosystem Status and Trends in a Rapidly Changing Environment. Springer, Dordrecht, pp. 269–336.

Pirtle-Levy R., J.M. Grebmeier, L.W. Cooper and I.L. Larsen, 2009. Chlorophyll a in Arctic sediments implies long persistence of algal pigments. Deep-Sea Res II 56(17), 1326-1338.

Pisareva, M.N., Pickart, R.S., Iken, K., Ershova, E.A., Grebmeier, J.M., Cooper, L.W., Bluhm, B.A., Nobre, C., Hopcroft, R.R., Hu, H., Wang, J., Ashjian, C.J., Kosobokova, X.N., Whitledge, T.E., 2015. Patterns of Benthic Fauna and Zooplankton in the Chukchi Sea in Relation to the Physical Forcing. Prog. Oceanogr. 28, 68-83.

Plourde, S., Campbell, R.G., Ashjian, C.J., Stockwell, D.A., 2005. Seasonal and regional patterns in egg production of Calanus glacialis/marshallae in the Chukchi and Beaufort Seas during spring and summer, 2002. Deep-Sea Res.II. 52, 3411-3426.

Questel, J.M., Clarke, C., Hopcroft, R.R., 2013. Seasonal and interannual variation in the planktonic communities of the northeastern Chukchi Sea during the summer and early fall. Cont. Shelf Res. 67, 23-41.

Sambrotto, R.N., J.J. Goering, and C.P. McRoy, 1984. Large yearly production of phytoplankton in the western Bering Strait. Science. 225:1147-1150.

Sigler, M.F., Mueter, F.J., Bluhm, B.A., Busby, M.S., Cokelet, E.D., Danielson, S.L., De Robertis, A., Eisner, L.B., Farley, E.V., Iken, K. and Kuletz, K.J., 2017. Late summer zoogeography of the northern Bering and Chukchi seas. Deep Sea Research Part II: Topical Studies in Oceanography, 135, pp.168-189.

Springer, A.M., 1988. The paradox of pelagic food webs on the Bering–Chukchi continental shelf. Dissertation, University of Alaska Fairbanks

Stevenson, D.E., Lauth, R.R., 2019. Bottom trawl surveys in the northern Bering Sea indicate recent shifts in the distribution of marine species. *Polar Biol*. 42, 407–421. https://doi.org/10.1007/s00300-018-2431-1

Walsh, J.J., C.P. McRoy, L.K. Coachman, J.J. Goering, J.J. Nihoul, T.E. Whitledge, T.H. Blackburn, P.L. Parker, C.D. Wirick, P.G. Shuert, J.M. Grebmeier, A.M. Springer, R.D. Tripp, D.A. Hansell, S. Djenidi, E. Deleersnijder, K. Henriksen, B.A. Lund, P. Andersen, F.E. Mullerkarger and K. Dean, 1989. Carbon and nitrogen cycling within the Bering Chukchi Seas - source regions for organic-matter effecting AOU demands of the Arctic Ocean. Prog. Oceanogr. 22, 277-359. 10.1016/0079-6611(89)90006-2

Whitehouse G.A., K. Aydin T. Essington and G. Hunt Jr., 2014. A trophic mass balance model of the eastern Chukchi Sea with comparisons to other high-latitude systems Polar Biology 37:911-939 doi:10.1007/s00300- 014-1490

Woodgate, R. A., K. Aagaard, and T. J. Weingartner, 2005. Monthly temperature salinity, and transport variability of the Bering Strait throughflow, Geophys. Res. Lett., 32, L04601, doi:10.1029/2004GL021880

Zhang, J., Ashjian, C., Campbell, R.G., Spitz, Y.H., Steele, M., Hill, V., 2015. The influence of sea ice and snow cover and nutrient availability on the formation of massive under-ice phytoplankton blooms in the Chukchi Sea. Deep-Sea Res. II. 118, 122-135.

Results in Full

Chapter 1: Manifestation and consequences of warming and altered heat fluxes over the Bering and Chukchi Sea continental shelves

Chapter 2: Chirikov Basin Oceanography: Function, Structure, Drivers and Change

Chapter 3: Anadyr Current Contributions to the Arctic-bound Oceanic Nutrient Flux

Chapter 4: Diversity and community structure of eukaryotic phototrophs in the Bering and Chukchi Seas

Chapter 5: Contributions of the picocyanobacteria Synechococcus to phytoplankton biomass during a period of warming in the Chukchi Sea

Chapter 6: Phytoplankton and seston fatty acids dynamics in the northern Bering-Chukchi Sea region

Chapter 7: Zooplankton communities of the Arctic's Bering Strait region during the spring bloom, 2017-2018

Chapter 8: Growth and Reproductive Rates of Calanoid Copepods in the Northern Bering and Southern Chukchi Seas

Chapter 9: Respiration rates of calanoid copepods during the spring bloom for the Arctic's Bering Strait region

Chapter 10: Seasonal abundance, distribution, and growth of the early life stages of polar (Boreogadus saida) and saffron (Eleginus gracilis) cod in the US Arctic

Chapter 11: Spatial patterns, environmental correlates, and potential seasonal migration triangle of polar cod (*Boreogadus saida*) distribution in the Chukchi and Beaufort seas

Chapter 12: Extraordinary Carbon Fluxes on the Shallow Pacific Arctic Shelf During a Remarkably Warm and Low Sea Ice Period

Chapter 13: Impact of a warm anomaly in the Pacific Arctic region derived from time-series export fluxes

Chapter 14: Linking polychaete functional traits and benthic ecosystem function to habitat characteristics on a shallow Arctic shelf

Chapter 15: Meiofauna community structure in Pacific Arctic shelf sediments: comparison of meiofaunal and macrofaunal-sized nematodes and functional traits

Chapter 16: Changes to benthic community structure may impact organic matter consumption on Pacific Arctic shelves

Chapter 17. Spatial patterns and effects of temperature on rates of organic matter processing in sediments across the northern Bering and southern Chukchi Sea shelf

Chapter 18: The Arctic Chukchi Sea food web: simulating ecosystem impacts of future changes in organic matter flow

Chapter 19: Evidence suggests potential transformation of the Pacific Arctic Ecosystem is underway

Chapter 1: Manifestation and consequences of warming and altered heat fluxes over the Bering and Chukchi Sea continental shelves

S.L. Danielson, O. Ahkinga, C. Ashjian, E. Basyuk, L.W. Cooper, L. Eisner, E. Farley, K.B. Iken, J.M. Grebmeier, L. Juranek, G. Khen, S.R. Jayne, T. Kikuchi, C. Ladd, K. Lu, R.M. McCabe, G.W.K. Moore, S. Nishino, F. Ozenna, R.S. Pickart, I. Polyakov, P.J. Stabeno, R. Thoman, W.J. Williams, K. Wood, T.J. Weingartner. 2020. Manifestation and consequences of warming and altered heat fluxes over the Bering and Chukchi Sea continental shelves. Deep Sea Research Part II: Topical Studies in Oceanography. 177(2020):104781. doi:10.1016/j.dsr2.2020.104781.

Chirikov Basin Oceanography: Function, Structure, Drivers and Change (Manuscript in preparation)

Danielson, et al., In prep. Oceanography of Chirikov Basin: Function, Structure, Drivers and Change

Abstract

Data from a suite of time series moorings, shipboard measurements, and numerical model integrations are assessed in order to build a better understanding of the oceanographic functioning of Chirikov Basin. We assess the regional wind forcing in order to better understand the regulation of the advective flow field over the Northern Bering and Southern Chukchi continental shelves. We show that the partitioning of flow to either side of St. Lawrence Island reflects a leaky switchyard type of balance between the central Bering Sea shelf and Chirikov Basin. Norton Sound may provide capacity to buffer a portion of the mass transport, but sheared and bidirectional flow in Shpanberg Strait appears to be the main factor that decouples flow here from that in Anadyr Strait. Observations from outside of the Alaska Coastal Current - just downstream of Norton Sound - help show the connectivity between the estuary and the greater shelf waters. Fluxes of heat, fresh water, ice, nutrients, and carbon are all modulated by the identified flow patterns, which reflect regionally coherent dominant patterns of flow variability. Remote sensing of sea ice presence along with optical sensors from select moorings (chlorophyll *a* fluorescence, photosynthetic available radiation and nitrate) help demonstrate how these flow patterns may influence the distribution, concentration, and productivity of phytoplankton and zooplankton here. We highlight the importance of the winter advection of oceanic heat on the regional sea ice cover and thickness, and how this is potentially affecting the local ecosystem.

Introduction

The Bering Strait region is the single conduit for oceanic communication between the North Pacific Ocean and the Arctic Ocean and it serves many functions in its role in support of highly productive ecological systems, as a pathway for global shipping, in its regulation of the Pacific Arctic biological carbon pump, as a migratory corridor for protected marine mammal and seabird species, and as a home to numerous Indigenous Alaskan and Siberian coastal communities. This narrow oceanic corridor exerts defining control over the northern Bering and Chukchi sea ecosystems, but many aspects of its functioning remain unknown.

In this analysis, we examine some of the key behaviors that ocean waters take on as they approach and leave the Chirikov Basin region, we examine how some of the conditions have changed over time, and we relate these changes (both short and long-term) to the regional geomorphology, the wind forcing, and other factors that exert control on the circulation pathways. We use the description of the environmental conditions to help interpret the Chirikov Basin geochemical and biological character as documented in the ASGARD studies (refs).

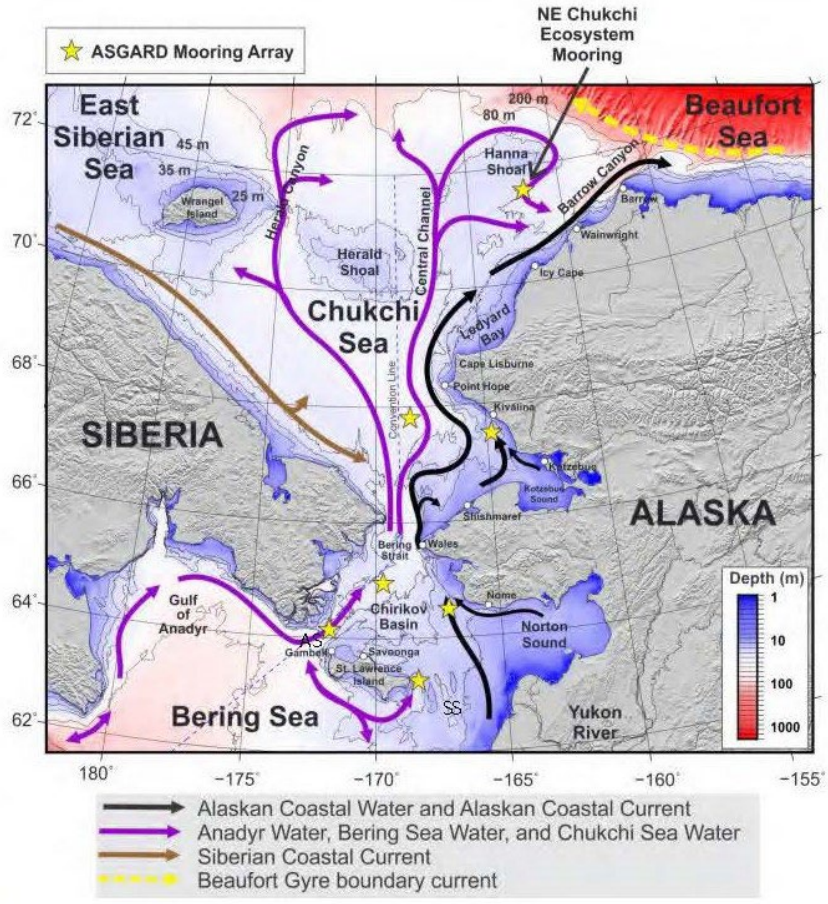

Figure 1. Map of the Bering Strait region, the location of common persistent flow fields, and moorings deployed by the ASGARD project. Abbreviations include: AS = Anadyr Strait; SS = Shpanberg Strait.

The width and depth of Anadyr, Shpanberg and Bering Straits (Figure 1) set the basic parameters of the northern Bering shelf circulation field. St. Lawrence Island separates Anadyr and Shpanberg straits on the southern side of Chirikov Basin and Bering Strait bounds Chirikov Basin to the north. Analysis of ocean circulation model results of the northern Bering Sea flow field has previously shown that the monthly-averaged flow through Anadyr and Shpanberg straits are not well coupled (Figure 1; also see discussion in Danielson et al., 2014), raising the question of how the Chirikov Basin and Norton Sound maintain mass balance and where nutrients and heat are delivered to the system. A branch of the Anadyr Current that at times extends along the southern shore of St Lawrence Island has the capacity to deliver heat and nutrient-enriched waters into Shpanberg Strait and along the east side of the St Lawrence Island, although the magnitude of the fluxes here are know well known. At the same time, structure of the flow field and its variations downstream (north) of Bering Strait are not well known, but the lateral advection of heat and nutrients and delivery to places that are biologically productive are important to reveal as we build a more complete understanding of the Pacific Arctic ecosystem.

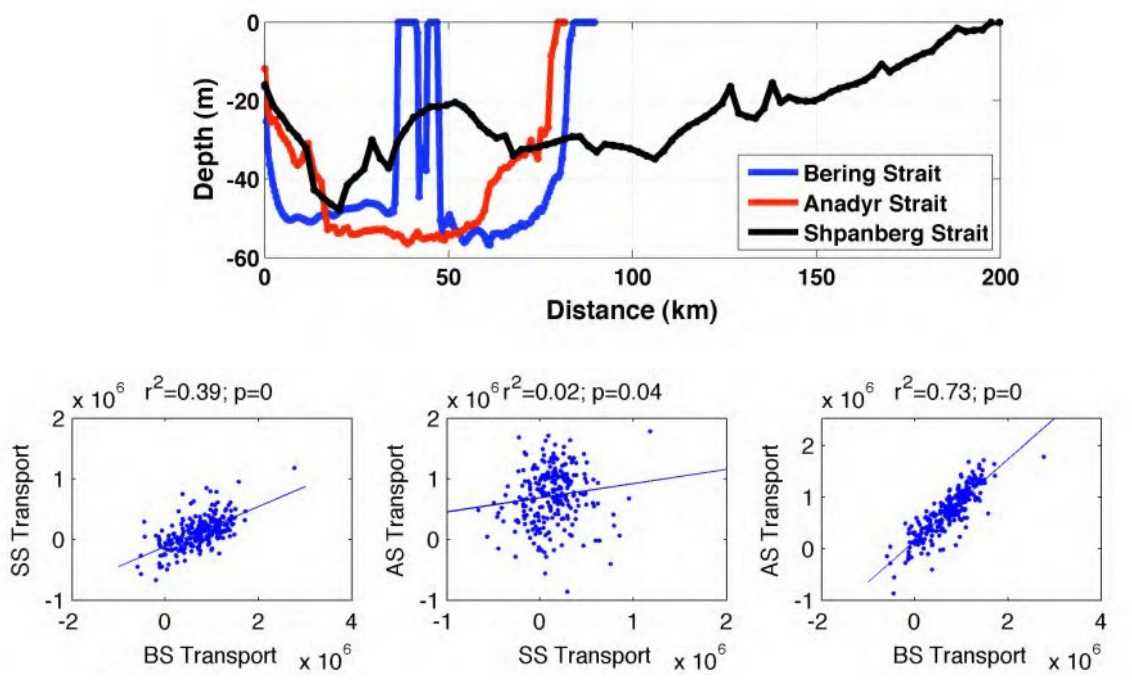

Figure 2. Top: bottom depth profiles in Anadyr (AS), Shpanberg (SS) and Bering Straits (BS). There exists little relation between the transport through Anadyr and Shpanberg straits (middle panel) even though the transport through these two straits are each significantly correlated with flow variability in Bering Strait.

Hence, in this paper we seek to analyze data and model results that will better inform our understanding of the regional flow pathways that feed Chirikov Basin, the associated heat, nutrient and carbon fluxes, and how some of these aspects have changed over time. We place the oceanographic measurements into a framework that describes linkages and co-variability between the environmental conditions, the phytoplankton, the zooplankton and fishes. The

Methods Section provides a summary of the data and numerical models used in our analyses. The Results Section examines the seasonal cycle as recorded by moored conductivity-temperature-depth (CTD) instruments. We next examine the flow field under the influence of different wind conditions, and then characterize the distributions of nutrients and full-water column conditions as measured by a suite of profiling instruments. The final Section will provide a summary and discussion of results.

Methods

Hydrography

We deployed a SeaBird 9/11 CTD at all ASGARD process and survey stations to collect water column profiles of temperature, salinity, chlorophyll-a fluorescence, dissolved oxygen, beam attenuation and photosynthetically available radiation (PAR). CTD was processed to 1- dbar pressure levels following the manufacturer's recommended automated procedures and a cast-by-cast manual inspection for removal of anomalous readings that can be caused by biofouling, deployment irregularities and various instrument problems.

We towed an undulating Acrobat ® CTD system along select transects for full water column high resolution profiles of the physical hydrography. The Acrobat ® also carried an EcoTriplett optical sensor with channels for chlorophyll a fluorescence, colored dissolved organic matter (CDOM) and optical backscatter.

Underway data

Continuously-collected underway data from the ship's science systems was archived, despiked, and compiled into 1-minute averages. These data streams include flow-through sensors connected to the seawater intake (temperature, salinity, NO_3), meteorological data streams (wind speed, wind direction, relative humidity, air temperature, surface PAR, longwave downwelling irradiance, shortwave downwelling irradiance), and ship's navigational data (heading, speed-over-ground, course-over-ground, speed- through-water, depth, latitude, longitude).

We collected and processed water column profile data from the ship's dropkeel-mounted Teledyne-RDI 300-KHz Workhorse ADCP, which provided water speed, direction, and acoustic backscatter signal strength in 4 m depth bins. The ship's EK-80 acoustic backscatter transducers and transceivers provided measurements of water column backscatter at five discrete frequencies.

Moorings

Seven bottom-anchored biophysical moorings were deployed as shown in Figure 1. All moorings had subsurface taut-wire configurations. The uppermost float on the taut-wire moorings was located at about 25 m depth to avoid drifting ice keels. All moorings had 307-KHz Teledyne-RDI Workhorse Sentinel ADCPs with bottom-tracking to measure ice motion and SeaBird SeaCat CT data-loggers with fluorometers. Including the NE Chukchi mooring at the

CEO site, select moorings were outfitted with specialized geochemical instrumentation: nitrate sensors, sediment traps, discrete water samplers, and optics (chlorophyll-a fluorescence, optical backscatter and CDOM).

We also make use of past mooring data from deployments in the 1970s and 1980s in order to help demonstrate how some aspects of the system have changed over time.

Numerical Models

We use integrations of the Alaska Region Vertically Integrated (ARVI) model, an idealized ocean circulation model that has realistic bathymetry but no density variations and forced only by wind, and the Northeast Pacific model version 6 (NEP6), a fully 3-d ice and ocean circulation model. Both models are integrated using the Regional Ocean Modeling System (ROMS) and are described, discussed and analyzed by Danielson et al. (2014) in application to the Bering-Chukchi flow field.

Results

The June 2017 to June 2018 Annual Cycle, and Comparison to the Past

Moorings N1 (east) and N2 (west) were deployed on either side of St Lawrence Island; Mooring N3 was in the Alaska Coastal Current just west of Nome, and mooring N4 was in northwestern Chirikov Basin. The annual cycle of water conditions near the seafloor at these four sites (Figure 3) helps delineate Anadyr Waters (N2 and N4: very saline) from Alaska Coastal Waters (N3: fresh) and Bering shelf waters (N1: intermediate salinity). We see that the two eastern-most moorings reached the winter freezing-point temperature in mid-January and began to warm again in mid-April. The two western moorings never stayed at the freezing point for more than a couple of weeks in a row (March) and mostly remained 1-2 degrees above the freezing point.

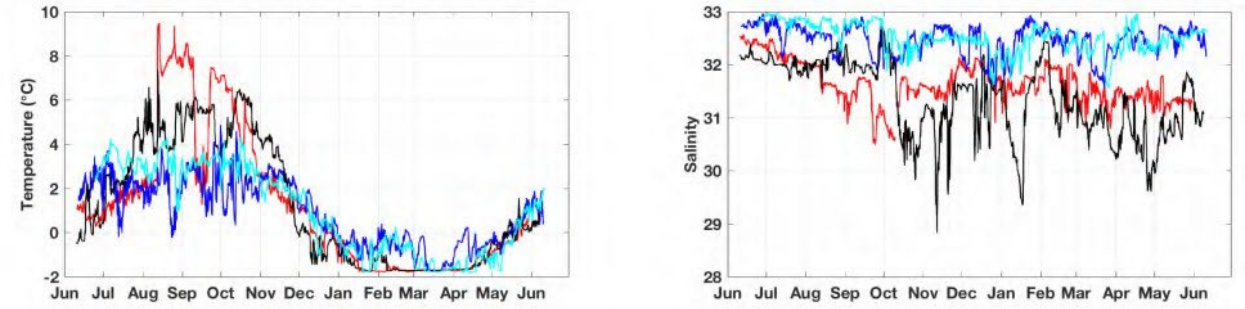

Figure 3. Near-bottom measurements from June 2017 to June 2018 at moorings N1 (red), N2 (blue), N3 (black) and N4 (cyan).

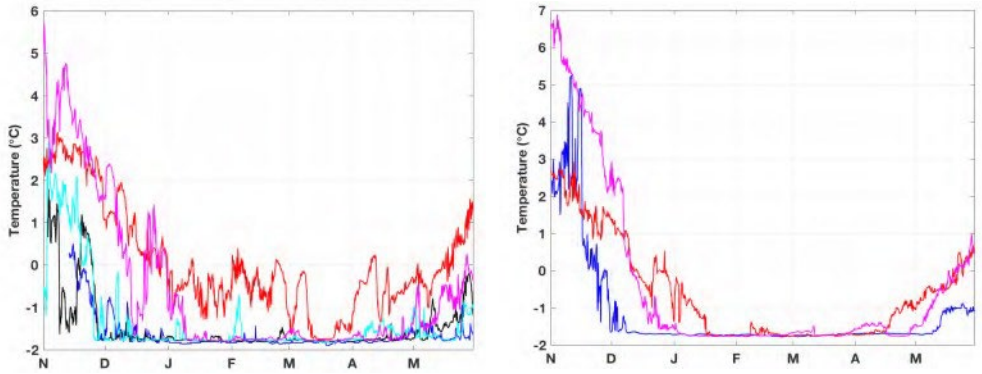

Figure 4. Left: Near-bottom temperature measured in Anadyr Strait from November (N) through May (M) in the winters of 1980-81 (blue), 1981-82 (black), 1984-85 (cyan), 2017-18 (red) and 2018-19 (magenta). Right: Near-bottom temperature measured in Shpanberg Strait from November (N) through May (M) in the winters of 1979-80 (blue), 2017-18 (red) and 2018-19 (magenta).

How has the system has changed thermally relative to past decades? Figure 4 shows fall, winter and spring temperatures measured at our mooring site N2 in Anadyr Strait (red and magenta) along with temperature records from moorings deployed in 1980, 1981 and 1984 (Schumacher et al., 1983; Muench et al. 1988). In the 1980s, the near-bottom waters had cooled to the freezing point by the end of November, and mostly remained close to freezing from mid-December until mid-May. The temperature in fall 2018 briefly cooled to near-freezing in mid-December, but did not remain near the freezing point until a week into January. Most notably, the data show that the 2017-2018 winter stands out with temperatures remaining 1-2 degrees above the freezing point for most of the winter (although March did reach the freezing point for a couple of weeks).

The Regional Flow Field

Integrations of the idealized ARVI ROMS model (Figure 3) reveal the basic change in sea level set-up and associated current fields under the conditions of 1 Sv (10^6 m3 s^{-1}) northward flow through Bering Strait for the no-wind situation (center middle panel of Figure 3) and steady, spatially invariant winds applied over the entire integration domain. We find that winds blowing to the east, southeast and south tend to enhance the eastward-flowing Anadyr Current extension on the south side of St Lawrence Island, while winds blowing to the northwest tend to reverse this flow and retard the magnitude of the Anadyr Current all along its path. We note that under all wind-forced scenarios the current velocities in Shpanberg Strait are largest near the Alaskan coastline offshore of the Yukon-Kuskokwim delta, but under the unforced wind scenario the largest currents in Shpanberg Strait are closest to the island.

Also of note is that the geochemical makeup of waters entering Chirikov Basin from the Anadyr and Shpanberg sides is not identical. Anadyr Water dominates in Anadyr Strait, while Bering

shelf water masses and even Alaskan Coastal Waters comprise those entering Chirikov Basin from Shpanberg Strait and Norton Sound.

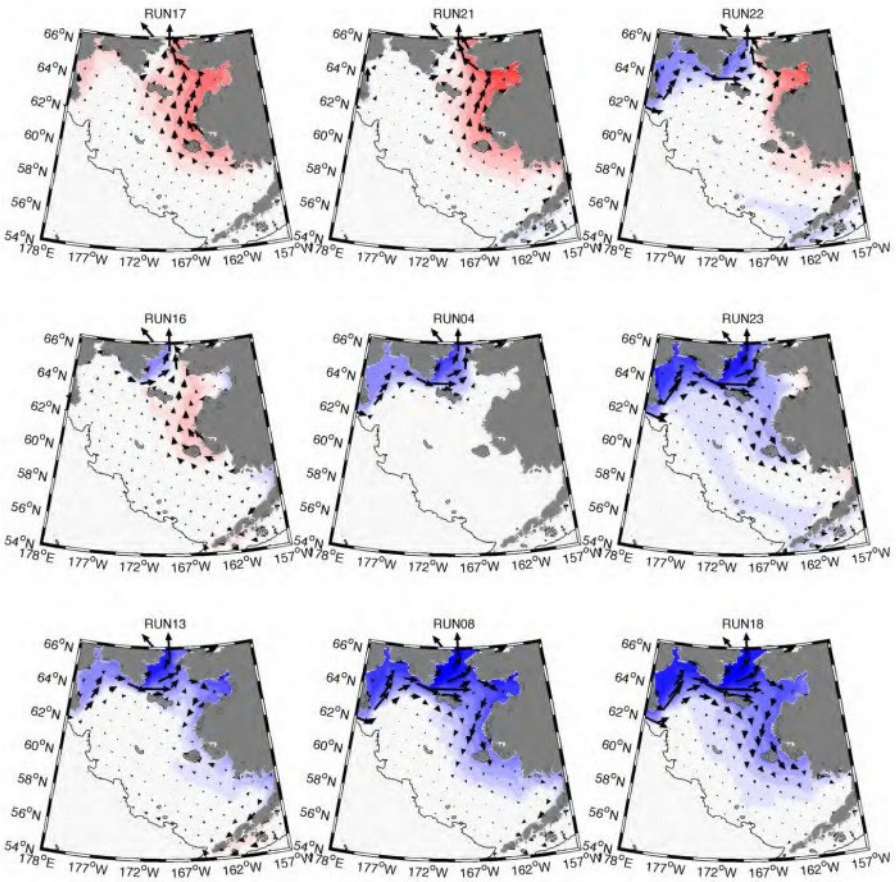

Figure 5. Steady-state circulation patterns (vectors) and associated sea surface heights (color contours) for a Bering Strait transport of 10^6 m^3 s^{-1}. Top row, left to right: wind blowing to the NW, N and NE, respectively. Middle row: wind blowing to the W, no wind, and wind blowing to the E, respectively. Bottom row: wind blowing to the SW, S and SE, respectively.

Linking physical conditions with the biogeochemistry and biology

Underway measurements of nitrate from the ASGARD cruises show that central Chirikov Basin is a zone at which high levels of NO_3 are found each time the vessel transits through. This, of course, is the signature of the Anadyr Water being mixed to the surface after its passage through Anadyr Strait, where the energetic flow is strongly turbulent. Phytoplankton productivity measurements show that Anadyr and Shpanberg Straits are regions in which the fraction of "new" nitrate fuels a large proportion of the primary productivity.

A high-resolution transect across Chirikov Basin from approximately mooring N3 to mooring N4 (Figure 7) reveals a number of key features of this region. These include the following. We note the very warm and very fresh waters adjacent to the Alaskan coast, with a strong pycnocline at less than 10 m depth. The fresh plume is associated with an elevated CDOM signal, a potential tracer of humic riverine-origin waters. The near-bottom coastal waters show the influence of the ACC, with salinities below 31. Salinities increase progressing westward, with a series of frontal systems having steeply sloping isopycnals that intersect both the surface and the bottom. In the eastern portion of the transect a subsurface chlorophyll bloom is evident but the largest bloom is

a surface-intesified peak that extends more than 20 m into the water column. Both of these chlorophyll *a* peaks are associated with dense aggregations of scatterers in the 200 kHz frequency band, a signal that was shown elsewhere on the cruise to correspond to net samples with many euphausiids.

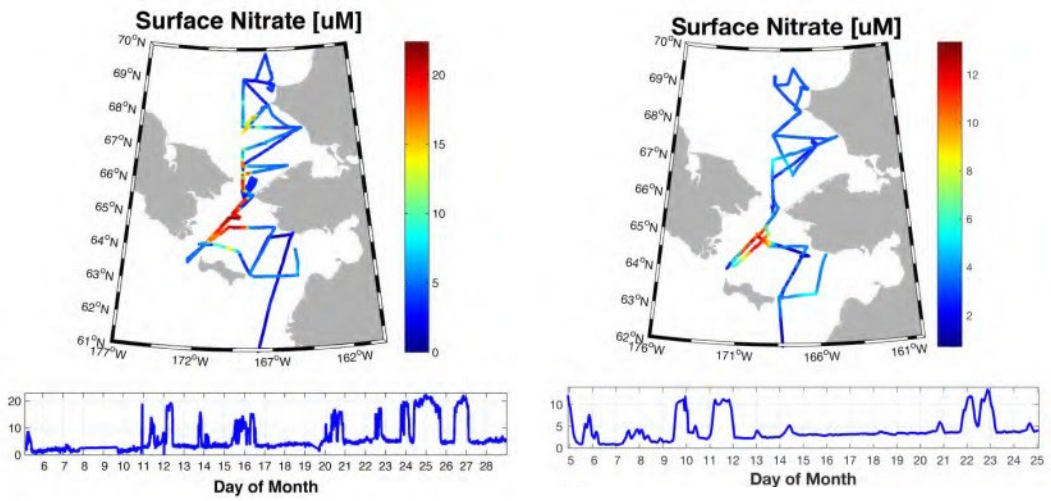

Figure 6. Underway measurements (need final calibrations) of NO_3 from the Sikuliaq's underway system in June 2017 (left) and June 2018 (right). Note elevated levels of NO_3 especially downstream of Anadyr Strait, but also north of Shpanberg Strait and Bering Strait.

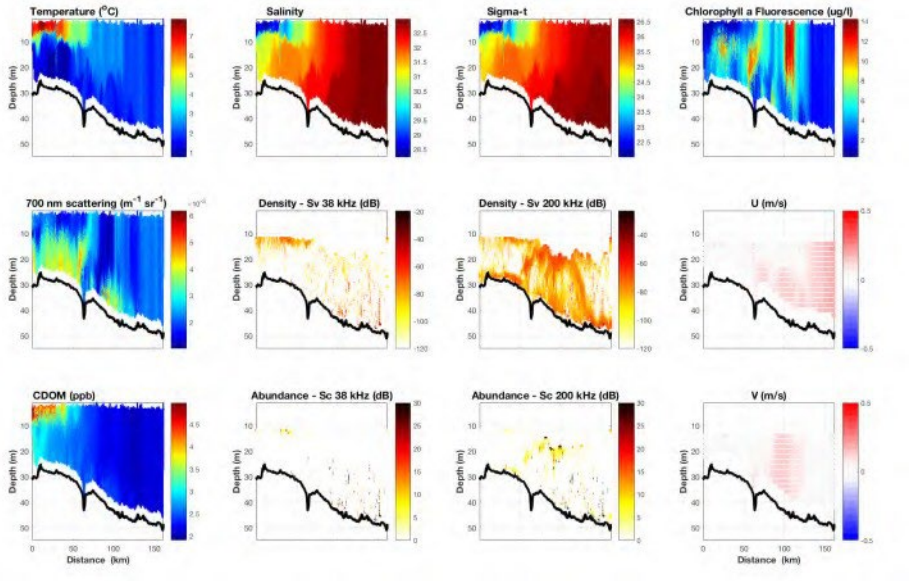

Figure 7. Water column profiles for a transect between mooring N3 (left side of panels) and N4 (right side of panels). Top row: temperature, salinity, density and chlorophyll a fluorescence. Middle row: optical backscatter, 38 kHz acoustic backscatter density, 200 kHz acoustic backscatter density, and eastward velocity. Bottom row: colored dissolved organic matter, 38 kHz acoustic abundance, 200 kHz acoustic abundance density and northward velocity.

Discussion

In contrast to prior observations that showed near-freezing waters in Anadyr Strait for many winter months, we show that 2017-2018 winter near-bottom waters advecting into Chirikov Basin were 1-2 degrees above the freezing point for all but a few weeks of time (Danielson et al., in prep.). This stark contrast in thermal flux conditions clearly was a major factor in keeping the 2017-2018 winter sea ice at such a low extent overall, and as shown by Stabeno and Bell (2019), the atmospheric conditions were favorable in this winter for maintaining these conditions.

We can identify a variety of factors that are helping set the character of the Chirikov Basin ecosystem. Chirikov Basin is a region of great ecological importance. It supports a zone massive biological productivity due to the delivery of nutrient-rich waters by the Anadyr Current, and the energetic mixing that allows this water to be brought up to the euphotic zone. This productivity feeds the seafloor community across the Chirikov Basin, but especially in the DBO-2 region. Current speeds near mooring N4 abate relative to the swifter flows found closer to shore at mooring sites N1, N2 and N3. The slower currents at N4 help allow sinking phytodetritus to reach the seafloor. Resuspension events, when they occur, are able to then deliver some of this carbon farther downstream – in the direction of the DBO-3 region that is north of Bering Strait.

Acknowledgements

To be written later.

References

Aagaard, K., A. T. Roach, and J. D. Schumacher (1985a), On the winddriven variability of the flow through Bering Strait, J. Geophys. Res., 90,
7213–7221.

Aagaard, K., Weingartner, T.J., Danielson, S.L., Woodgate, R.A., Johnson, G.C. and Whitledge, T.E., 2006. Some controls on flow and salinity in Bering Strait. Geophysical Research Letters, 33(19).

Clement, J.L., Maslowski, W., Cooper, L.W., Grebmeier, J.M. and Walczowski, W., 2005. Ocean circulation and exchanges through the northern Bering Sea—1979–2001 model results. Deep Sea Research Part II: Topical Studies in Oceanography, 52(24-26), pp.3509-3540.

Coachman, L. K., K. Aagaard, and R. B. Tripp (1975), Bering Strait: The Regional Physical Oceanography, Univ. of Wash. Press, Seattle.

Coachman, L.K., and V.V. Shigaev, 1992. Northern Bering-Chukchi Ecosystem: The Physical Basis, in: Nagel, P. (Ed.), Results of the Third Joint US-USSR Bering & Chukchi Sea Expedition (BERPAC), Summer 1988. U.S. Fish and Wildlife Service, Washington, D.C., pp. 17-27.

Danielson, S., Aagaard, K., Weingartner, T., Martin, S., Winsor, P., Gawarkiewicz, G. and Quadfasel, D., 2006. The St. Lawrence polynya and the Bering shelf circulation: New observations and a model comparison. Journal of Geophysical Research: Oceans, 111(C9).

Danielson, S., Weingartner, T., Aagaard, K., Zhang, J. and Woodgate, R., 2012a. Circulation on the central Bering Sea shelf, July 2008 to July 2010. Journal of Geophysical Research: Oceans, 117(C10).

Danielson, S., Hedstrom, K., Aagaard, K., Weingartner, T. and Curchitser, E., 2012b. Wind-induced reorganization of the Bering shelf circulation. Geophysical Research Letters, 39(8).

Danielson, S.L., Weingartner, T.J., Hedstrom, K.S., Aagaard, K., Woodgate, R., Curchitser, E. and Stabeno, P.J., 2014. Coupled wind-forced controls of the Bering–Chukchi shelf circulation and the Bering Strait throughflow: Ekman transport, continental shelf waves, and variations of the Pacific–Arctic sea surface height gradient. Progress in Oceanography, 125, pp.40-61.

Danielson, S.L., Dobbins, E.L., Jakobsson, M., Johnson, M.A., Weingartner, T.J., Williams, W.J. and Zarayskaya, Y., 2015. Sounding the northern seas. *Eos*, *96*.

Danielson, S.L., Eisner, L., Ladd, C., Mordy, C., Sousa, L. and Weingartner, T.J., 2017. A comparison between late summer 2012 and 2013 water masses, macronutrients, and phytoplankton standing crops in the northern Bering and Chukchi Seas. Deep Sea Research Part II: Topical Studies in Oceanography, 135, pp.7-26.

Frey, K.E., Moore, G.W.K., Cooper, L.W. and Grebmeier, J.M., 2015. Divergent patterns of recent sea ice cover across the Bering, Chukchi, and Beaufort seas of the Pacific Arctic Region. Progress in Oceanography, 136, pp.32-49.

Grebmeier, J.M., Bluhm, B.A., Cooper, L.W., Danielson, S.L., Arrigo, K.R., Blanchard, A.L., Clarke, J.T., Day, R.H., Frey, K.E., Gradinger, R.R. and Kędra, M., 2015. Ecosystem characteristics and processes facilitating persistent macrobenthic biomass hotspots and associated benthivory in the Pacific Arctic. Progress in Oceanography, 136, pp.92-114.

Grebmeier, J.M. and Cooper, L.W., 1995. Influence of the St. Lawrence Island polynya upon the Bering Sea benthos. Journal of Geophysical Research: Oceans, 100(C3), pp.4439-4460.

Kinder, T. H., D. C. Chapman, and J. A. Whitehead Jr. (1986), Westward intensification of the mean circulation on the Bering Sea shelf, J. Phys. Oceanogr., 16, 1217– 1229.

Martin, S., Drucker, R., Kwok, R. and Holt, B., 2004. Estimation of the thin ice thickness and heat flux for the Chukchi Sea Alaskan coast polynya from Special Sensor Microwave/Imager data, 1990–2001. Journal of Geophysical Research: Oceans, 109(C10).

Moore, S.E., Stabeno, P.J., Grebmeier, J.M. and Okkonen, S.R., 2018. The Arctic Marine Pulses Model: linking annual oceanographic processes to contiguous ecological domains in the Pacific Arctic. Deep Sea Research Part II: Topical Studies in Oceanography, 152, pp.8-21.

Mueter, F.J. and Litzow, M.A., 2008. Sea ice retreat alters the biogeography of the Bering Sea continental shelf. Ecological Applications, 18(2), pp.309-320.

Muench, R. D., J. D. Schumacher, and S. A. Salo (1988), Winter currents and hydrographic conditions on the northern central Bering Sea shelf, J. Geophys. Res., 93, 516– 526.

Overland, J. E., and A. T. Roach (1987), Northward flow in the Bering and Chukchi seas, J. Geophys. Res., 92, 7097–7105.

Overland, J.E., Wang, M., Wood, K.R., Percival, D.B. and Bond, N.A., 2012. Recent Bering Sea warm and cold events in a 95-year context. Deep Sea Research Part II: Topical Studies in Oceanography, 65, pp.6-13.

Pease, C. H. (1987), The size of wind-driven coastal polynyas, J. Geophys. Res., 92, 7049– 7059.

Roach, A. T., K. Aagaard, C. H. Pease, S. A. Salo, T. Weingartner, V. Pavlov, and M. Kulakov (1995), Direct measurements of transport and water properties through the Bering Strait, J. Geophys. Res., 100(C9), 18443-18457.

Schumacher, J. D., and T. H. Kinder (1983), Low-frequency current regimes over the Bering Sea shelf, J. Phys. Oceanogr., 13, 607– 623.

Schumacher, J. D., K. Aagaard, C. H. Pease, and R. B. Tripp (1983), Effects of a shelf polynya on flow and water properties in the northern Bering Sea, J. Geophys. Res., 88, 2723– 2732.

Stabeno, P.J. and S. W. Bell., in press. Extreme conditions in the Bering Sea (2017-2018): Record breaking low sea-ice extent, Geophys. Res. Letters.

Stigebrandt, A., 1984. The North Pacific: a global-scale estuary. Journal of Physical Oceanography, 14(2), pp.464-470.

Stroeve, J.C., Serreze, M.C., Holland, M.M., Kay, J.E., Malanik, J. and Barrett, A.P., 2012. The Arctic's rapidly shrinking sea ice cover: a research synthesis. Climatic Change, 110(3-4), pp.1005-1027.

Tachibana, Y., Komatsu, K.K., Alexeev, V.A., Cai, L. and Ando, Y., 2019. Warm hole in Pacific Arctic sea ice cover forced mid-latitude Northern Hemisphere cooling during winter 2017–18. Scientific reports, 9(1), p.5567.

Takenouti, A.Y. and Ohtani, K., 1974. Currents and water masses in the Bering Sea: A review of Japanese work. Oceanography of the Bering Sea, 2, pp.39-57.

Thoman, R.L., U.S. Bhatt, P.A. Bieniek, B.R. Brettschneider, M. Brubaker, S.L. Danielson, Z. Labe, R. Lader, W.N. Meier, G. Sheffield, J. E. Walsh, in review. The record low Bering Sea ice extent in 2018: context, impacts and an assessment of the role of anthropogenic climate change. Submitted to Bull. Am. Met. Soc. 2019

Mooring Measurements of Anadyr Current Nitrate, Phosphate, and Silicate Enable Updated Bering Strait Nutrient Flux Estimates

[1]Tyler D. Hennon, [1]Seth L. Danielson, [2]Rebecca A. Woodgate, [1]Brita Irving, [1]Dean A. Stockwell, [3,4]Calvin W. Mordy

[1]University of Alaska Fairbanks (UAF), College of Fisheries and Ocean Sciences, Fairbanks, AK, USA
[2]University of Washington (UW), Applied Physics Laboratory (APL), Seattle, WA, USA
[3]Cooperative Institute for Climate, Ocean, & Ecosystem Studies, University of Washington (UW), Seattle, WA, USA
[4]National Oceanographic and Atmospheric Administration (NOAA), Pacific Marine Environmental Laboratory (PMEL), Seattle, WA, USA

Corresponding author: Tyler Hennon (tdhennon@alaska.edu)

Key Points:

- We use in situ and salinity-based estimates of nutrient concentrations to estimate nutrient fluxes through Bering Strait.
- We estimate annually averaged fluxes of 16±6 (nitrate), 1.5±0.5 (phosphate), and 30±11 kmol/s (silicate), ~50% larger than prior studies.
- Bering Strait nutrient flux varies by season, with largest poleward fluxes occurring in April, and weakest fluxes occurring in December.

Abstract

In situ nutrient concentration data and salinity-nutrient parameterizations established at Anadyr Strait from June 2017 to June 2018 are used to estimate monthly Pacific-to-Arctic fluxes of nitrate, phosphate, and silicate through Bering Strait over 1997-2019. In most months our estimates rely on measurements made from mooring-based sensors and whole water samples, while over May-August the basis is shipboard hydrography. We find annually averaged Bering Strait fluxes of 16±6, 1.5±0.5, and 30±11 kmol/s for nitrate, phosphate, and silicate, respectively, with inter-annual variability ±30% of the mean. Maximum fluxes occur in April, exceeding the annual average by ~50%, while minimum fluxes occur in December. Annually averaged fluxes estimated here are ~50% higher than previous estimates. Significant ($p<0.05$) increasing trends in phosphate and silicate fluxes are found over 1998-2018, but not nitrate. However, it is unclear if these trend results are due to differences in draw-down or limitations of the salinity-nutrient parameterizations.

Plain Language Summary

Nutrients flowing through Bering Strait (Pacific to Arctic) regulate the growth of Arctic plankton, which form the base of the marine food web. However, because of limited nutrient data at Bering Strait, only a few studies have attempted to estimate the size of this nutrient supply. We find that nutrients and salinity are closely related at nearby Anadyr Strait. Using those relationships and long-term mooring observations of salinity and currents at Bering Strait, we are able to estimate Bering Strait nutrient concentrations and the amount carried through the strait into the Arctic. We find strong seasonal cycles as well as significant year-to-year variability. Our estimates are about 50% higher than past studies, suggesting more Pacific-Arctic nutrient delivery than previously thought.

1 Introduction

The Arctic is experiencing rapid change (Polyakov et al. 2020), including reduced sea ice extent and volume (Wang et al. 2018), and altered growing conditions for marine phytoplankton (Lewis and Arrigo 2020), affecting Arctic marine ecosystems (Huntington et al. 2020), including iconic marine mammals and seabirds, subsistence harvests vital to Indigenous communities, and biological carbon pump dynamics.

Bering Strait is the only oceanic link between the Arctic and Pacific oceans, and is relatively narrow (~85 km across) and shallow (~50 m deep) with an annual average throughflow around 1.0 Sv (10^6 m^3/s) (Woodgate 2018). The Anadyr Current (Fig. 1a) delivers approximately 80% of the Bering Strait transport through Anadyr Strait ~250 km south of the Bering Strait (Danielson et al. 2014). The advective time between them is $\geq$ 10 days (Coachman 1993). Due to typically low nutrient concentrations on the eastern Bering shelf (Danielson et al. 2011), the Anadyr Current delivers the bulk of nutrients that are advected into the Arctic through Bering Strait, supporting remarkably high levels of pelagic and benthic biological productivity in the Pacific Arctic (Grebmeier et al. 2015).

Little prior work has evaluated Arctic-bound nutrient fluxes directly at Bering Strait. Torres-Valdes et al. (2013) used a single August 2005 cross-strait transect in combination with modeled currents to estimate annually averaged fluxes into the Chukchi Sea: 9.0±0.8, 1.3±0.1, and 20.9±2.4 kmol/s for nitrate, phosphate, and silicate, respectively. Using a three-dimensional ocean-sea ice-biogeochemical model, Zhou et al. (2021) estimated an annual flux of ~10 kmol/s of nitrate. Downstream in the Chukchi Sea, Mordy et al. (2020) found inter-annual variability in winter nitrate flux of up to 10 kmol/s during 2010-2018. Here, we provide observation-based nutrient flux estimates from a year of mooring-based measurements from Anadyr Strait (2017-2018) and long term (1997-2019) mooring observations in Bering Strait.

77

78

79 **2 Data**

80 **2.1 Shipboard Hydrography**

81 Nutrient and CTD hydrographic data (>500 vertical profiles) from ship-based observation programs
82 (April-September) in the Northern Bering and Southern Chukchi seas between 2004-2018 are used to
83 characterize regional nutrient distributions (Fig. 1a, Supplementary Table S1).

84

85 **2.2 Moorings**

86 **2.2.1 Anadyr Strait Mooring**

87 Subsurface mooring N2 was deployed in 46 m of water in Anadyr Strait (Fig. 1a) from 12 June 2017 to 9
88 June 2018 at 64.1545 °N, 174.5260 °W. N2 was equipped with SeaBird conductivity-temperature-depth
89 (CTD) dataloggers, a Teledyne RDI acoustic Doppler current profiler (ADCP), a Satlantic submersible
90 ultraviolet nitrate analyzer (SUNA), and a Green Eyes LLC Aqua Monitor discrete water sampler
91 (supplementary Table A2).

92

93 Instrumentation specifics were as follows: CTDs at depths of 25 m (SBE-16, 120 minute sampling), 35 m
94 and 41 m (SBE-37s, 15 minute sampling); an upward-looking 300 kHz ADCP at 41 m depth (30 minute
95 ensembles of 1 m bins); a SUNA V2 at 35 m depth (120 minute sampling); and an Aqua Monitor at 35 m
96 depth, which over the deployment collected twenty-five 500 mL water samples in rack-mounted IV bags,
97 each primed with 400 μL of saturated mercuric chloride solution to halt microbial activity. Following
98 mooring recovery, 60 mL subsamples were filtered (0.45 mm cellulose acetate filters) and stored frozen.
99 On shore, thawed samples were analyzed for nitrate (NO_3^-), nitrite (NO_2^-), ammonium (NH_4^+), phosphate
100 (PO_4^{3-}), and silicate (H_4SiO_4) using automated continuous flow analysis (Becker et al. 2020). Quality
101 controls are described in the archived datasets. Between 30-90 minutes after deployment, the Aqua

Monitor collected four samples to estimate repeatability. Thereafter, sample spacing was between 9-31 days (more frequently in summer).

2.2.2 Bering Strait Mooring

We use monthly estimates of Bering Strait salinity and transport (Woodgate et al. 2015, Woodgate 2018) from the long-term (1997 to present) A3 mooring (Fig. 1a), which is representative of average Bering Strait through-flow properties (Woodgate 2015). These estimates do not include contributions from the Alaskan Coastal Current (ACC), which is responsible for ~10% of the net transport but is nitrate-deplete (Danielson et al. 2017).

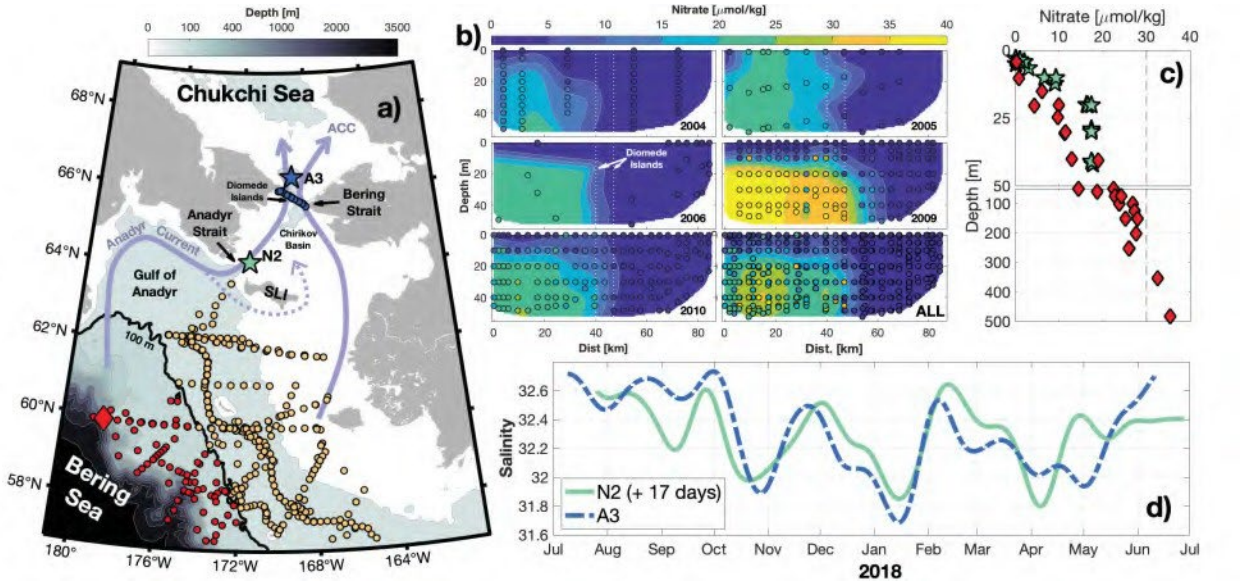

Figure 1: *a) Map of hydrography, typical flow patterns and mooring locations. Yellow/red circles are sites of hydrographic profiles collected mostly during summer from 2008-2018 (sources in Supplementary Table 1; red markers denote casts to >100 m); blue circles mark Bering Strait RUSALCA stations. Stars mark mooring sites N2 (cyan) and A3 (blue). Thick black contour is at 100 m depth. Light blue lines show nominal paths of major currents. Abbreviations: SLI=Saint Laurence Island, ACC=Alaskan Coastal*

120 *Current. b) August RUSALCA Bering Strait observations from 2004-2010. Dots mark nutrient samples,*
121 *and contours are objective maps calculated from observations. Lower right subpanel aggregates all*
122 *years. c) Nitrate profiles collected at N2 (cyan stars, June 2017) and Bering continental slope (red*
123 *diamonds, collected June, 2010). Location of continental slope observations is denoted by the large red*
124 *diamond in (a). d) Lowpass filtered (30-day cutoff period) salinity at N2 (cyan, lagged by 17 days) and*
125 *A3 (blue dashed).*
126
127

128 **3. Results**

129 **3.1 Nutrient Biases and Corrections**

130 Niskin bottle nutrient samples from the N2 mooring deployment and recovery cruises are used to correct
131 the SUNA and Aqua Monitor data for offsets and drift (e.g. Daniel et al. 2020). CTD profile and Niskin
132 samples (not shown) exhibit a well-mixed water column within ±10 m of the Aqua Monitor at
133 deployment, with average $NO3_{NIS}$=17.3±0.4, $PO4_{NIS}$=1.76±0.02, and $SiO4_{NIS}$=27.4±0.6 μmol/kg from 6
134 samples (± indicates 95% confidence interval hereinafter). The first four Aqua Monitor samples (from
135 just after deployment) had concentrations of $NO3_{AM}$=14.5±1.8, $PO4_{AM}$=1.94±0.11, and $SiO4_{AM}$=23.6±2.2
136 μmol/kg. These samples suggest initial Aqua Monitor biases of about -2.8, +0.18, and -3.8 μmol/kg, and
137 measurement uncertainties of 1.8, 0.1, and 2.2 (nitrate, phosphate, and silicate, respectively). Upon
138 recovery one year later, CTD profiles suggest a well-mixed water column within ±5 m of the Aqua
139 Monitor, with average $NO3_{NIS}$=12.9±0.2, $PO4_{NIS}$=1.75±0.04, and $SiO4_{NIS}$=26.8±0.8 μmol/kg from 5
140 samples, where a single Aqua Monitor sample measured $NO3_{AM}$=13.1, $PO4_{AM}$=1.92, $SiO4_{AM}$=23.6
141 μmol/kg. Aqua Monitor nutrient concentrations were adjusted assuming linear drift between deployment
142 and recovery during the yearlong occupation. The SUNA nitrate estimate bias was 4.0 μmol/kg on
143 deployment and 0.3 μmol/kg on recovery, and concentrations were again adjusted assuming linear drift.
144 Post-correction, the two measures of nitrate at mooring N2 (Aqua Monitor and SUNA) are strongly

145 correlated over the year-long deployment (root-mean-square-difference=2.3 μmol/kg, r=0.87 and p<0.01,
146 Fig. 2e).
147
148

149 **3.2 Salinity-Nutrient Relations**

150 Ship-based hydrography from across the northern Bering Sea shelf and continental slope exhibit a nearly
151 linear relationship between salinity (S_{HYD}) and nitrate ($NO3_{HYD}$) for measurements collected from >100 m
152 depth (Fig. 2a, dark grey dots), where S_{HYD}=33-34 and $NO3_{HYD}$=25-45 μmol/kg. Extrapolation of this
153 mixing line to full nitrate depletion at salinity ~31 PSU closely approximates the maximum observed
154 nitrate concentration at each salinity in the range of 31-34 (Fig. 2a), suggesting that in the absence of
155 biological nitrate drawdown, mixing between nitrate-rich slope waters and nitrate-deplete shelf waters
156 (upper 10-20 m across the eastern Bering shelf) primarily regulates nutrient concentration. While the
157 range of depths that the Anadyr Current draws its source waters from is not well known, near-bottom
158 observations of nitrate up to 30 μmol/kg in Anadyr Strait (Walsh et al. 1989) and typical vertical profiles
159 from the slope region (Fig. 1c) suggest that the core of the Anadyr Current must draw slope waters from
160 ≥100 m depth. This assumes no mixing between the region of upwelling and Anadyr Strait, so if Anadyr
161 Current waters mix with lower-salinity shelf waters during their transit to Anadyr Strait, the mean source
162 depth could be greater.
163

164 At N2, there is no significant relationship between nutrient (Aqua Monitor) and salinity (SBE37) *in situ*
165 measurements at 35 m depth (i.e., sub-pycnocline) when considering all samples together. However,
166 significant relationships emerge when data are partitioned seasonally (Fig. 2b-d). We divide mooring data
167 into three intervals that roughly map onto fall, winter and summer, respectively: September-December
168 (cooling, ice-free, decreasing light availability; magenta circles) and January-April (cold, ice-covered;

orange triangles); May-August (warming, ice-free or declining sea ice conditions, high light availability; green squares).

The moored S_{N2} data are strongly correlated with $NO3_{AM}$ from September-December (r=0.97, p< 0.01, N=5) and January-April (r=0.99, p<0.01, N=6), but are not well correlated for May-August (r=0.50, p=0.10, N=13). We attribute the difference between fall and winter regression lines to the fall season being at the end of the growing season after the nutrient inventory has experienced summer biological drawdown. The strong correlations show that for fall and winter (both weakly stratified), salinity provides a useful proxy for nitrate in the Anadyr Current.

Using SBE salinity (S_{N2}) and calibrated Aqua Monitor nitrate (Section 3.1) at mooring N2, we perform linear least squares regressions to parameterize nitrate concentration ($NO3_{EST,N2}$), i.e.,

$$NO3_{EST,N2} = C_1 S_{N2} + C_2 \qquad \text{Eq. 1}$$

C_1 and C_2 are coefficients calculated for each of the three seasonal intervals (Fig. 2b-d).

We find $NO3_{EST,N2}$ closely tracks both synoptic-scale and longer period signals captured by the SUNA nitrate sensor ($NO3_{SUNA,N2}$) during fall and winter intervals (Fig. 2f). Differences between $NO3_{SUNA,N2}$ and $NO3_{EST,N2}$ are not uniform from September-May (up to 10 μmol/kg in December). It is unclear why there is a consistent bias between $NO3_{SUNA,N2}$ and $NO3_{EST,N2}$ (average 2.5 μmol/kg), though it may point to limitations of our CTD calibrations, we note it is on the same scale as the Aqua Monitor precision (Section 3.1). The large deviation in December may be related to seasonally voluminous Alaskan river discharges in the eastern Bering Sea that subsequently advect westward (Danielson et al. 2006) carrying a different nitrate-salinity relation than found in the Anadyr Current.

194

195 As with nitrate, correlations with S_{N2} are significant ($p<0.05$) for $PO4_{AM}$ and $SiO4_{AM}$ for both September-
196 December ($PO4_{AM}$:0.92; $SiO4_{AM}$:0.91) and January-April ($PO4_{AM}$:0.92; $SiO4_{AM}$:0.99), but neither are
197 significantly correlated during May-August. Salinity-based estimates of phosphate ($PO4_{EST,N2}$) and silicate
198 ($SiO4_{EST,N2}$) are calculated in identical fashion to $NO3_{EST,N2}$ (Eq. 1).

199

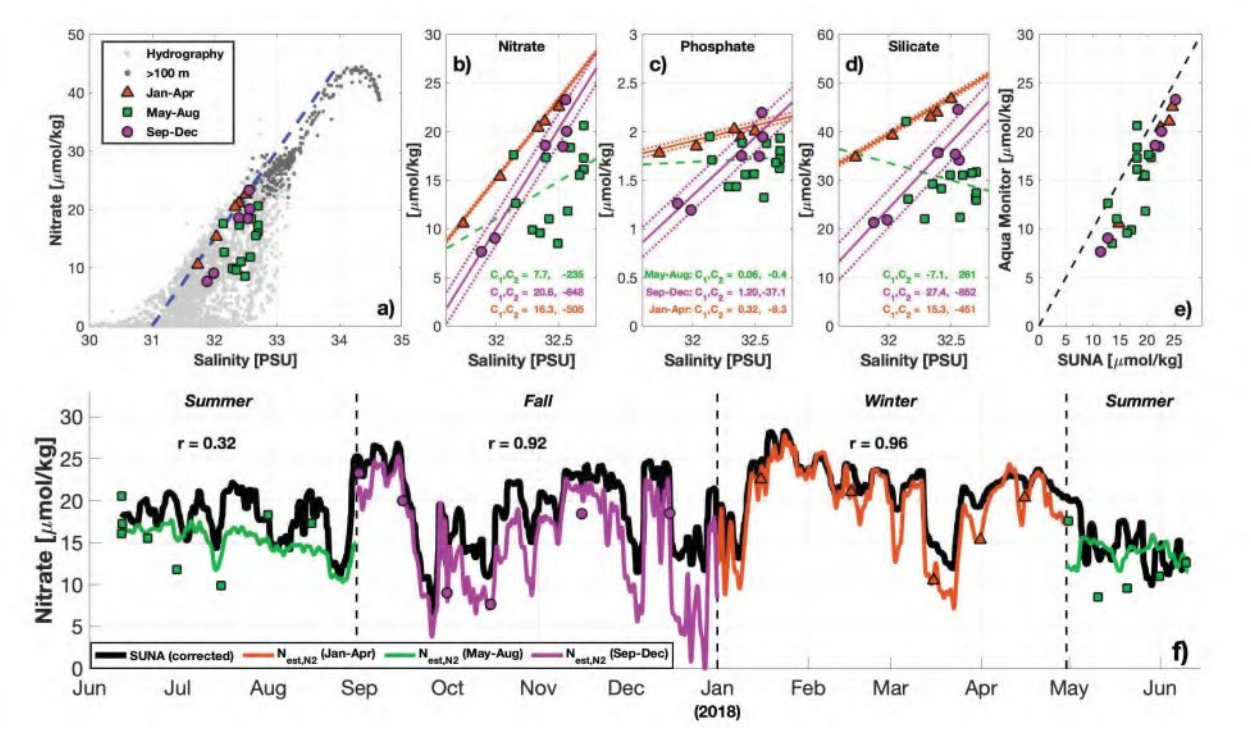

200

201 ***Figure 2.*** *a) Hydrographic samples of nitrate and salinity from across the Bering Sea in gray (see Fig.*
202 *1a). Darker markers indicate samples from ≥ 100 m depth. Colored markers show 25 nitrate/salinity*
203 *pairs taken by the moored* Aqua Monitor *and SBE at N2. Squares, circles and triangles correspond to*
204 *May-August, September-December and January-April, respectively. The dashed line shows rough mixing*
205 *line between slope and inner shelf waters. b)* $NO3_{AM}$ *vs.* S_{N2} *c)* $PO4_{AM}$ *vs.* S_{N2} *d)* $SiO4_{AM}$ *vs.* S_{N2}*. In (b)-(d),*
206 *solid lines are significant ($p<0.05$) best-fits for each season, dotted lines are 95% confidence intervals,*
207 *and dashed lines are fits where $p>0.05$. Constants from Eq. 1,* C_1 *(*[μmol/kg]/[PSU]) and C_2 *are denoted*
208 *for each season. e)* $NO3_{AM}$ *vs.* $NO3_{SUNA}$ *(dashed line is 1:1). f) Observed nitrate (*$NO3_{SUNA}$*, thick black*

209 *line) and estimated nitrate ($NO3_{EST,N2}$, colored lines); r-values show correlations between the two*
210 *seasonally. Vertical dashed lines mark seasonal delineations.*
211
212
213

214 **3.3 Nutrient Fluxes through Anadyr Strait**

215 Using velocity data from the N2 ADCP and the salinity-nutrient regressions (Section 3.2), we can
216 estimate nutrient fluxes through Anadyr Strait. Anadyr Strait is 73 km wide, has a median depth of 40 m,
217 and is approximately 2.7×10^6 m^2 in cross-sectional area. The major axis of sub-tidal barotropic currents
218 (from the ADCP on N2) is roughly normal to Anadyr Strait (oriented with through-flow). We take
219 currents along this axis as representative for the whole Anadyr Strait, and thus estimate volume transport
220 through the strait (T_{AS}). Our approach assumes the current is homogeneous across the strait, which seems
221 a reasonable first-order approximation given the prominent forcings of flow through Anadyr Strait are
222 large-scale (i.e. basin-scale pressure gradients). The average current current speed along the major axis is
223 39 cm/s for the year-long deployment, translating to 1.1 Sv of volume transport. This is similar to the A3-
224 based Bering Strait transport estimate for this timespan (1.3±0.3 Sv).
225
226 To estimate nutrient flux through Anadyr Strait, we combine the monthly salinity-based estimates of
227 nutrient concentration at N2 (Section 3.2) with the monthly mean volume transport, T_{AS}. Nitrate flux
228 ($F_{NO3,AS}$), for example, is defined as:
229

230 $$F_{N03,AS} = \pi_O \, T_{AS} \, N03_{est,N2} \qquad \text{Eq. 2}$$

231
232 where ρ_0 is the nominal density of Bering shelf water (1025 kg/m^3). Based on N2 ADCP measurements,
233 we further assume an unstratified water column from November-April such that salinity and nitrate

234 measurements at 35 m depth are representative of the full water column. For May-October, we assume
235 the water column is stratified and the upper 10 m of the water column is fully nitrate-deplete. Phosphate
236 ($F_{PO4,AS}$) and silicate ($F_{SiO4,AS}$) fluxes are calculated similarly.
237

238 From September, 2017 to April 2018 (when salinity-nutrient regressions are significant), average nitrate,
239 phosphate, and silicate fluxes are 17±4, 1.8±0.4, and 36±9 kmol/s, respectively. The flux uncertainties are
240 dominated by (and roughly scale with) the uncertainty of volume transport, here assumed to be ±20%,
241 since we lack sufficient *in situ* data to fully constrain Anadyr Strait transport. If summertime nutrient
242 depletion depths are 20 m (instead of 10 m assumed previously) this reduces our annually averaged
243 nutrient flux estimates by ~10%.
244

245 **3.4 Nutrient Fluxes Through Bering Strait**

246 Mooring data show that Anadyr and Bering Strait property variations are highly covariable due to their
247 strong advective connectivity (Fig. 1d). Specifically, at a 17-day lag, low-pass filtered (30-day cutoff
248 period) salinity measurements at N2 and A3 have a correlation coefficient of 0.70 and both records have
249 similar means and dynamic ranges. This modestly tight co-variability implies water is not strongly
250 modified in its transit between the straits, thus we employ the salinity-to-nutrient relationships of Section
251 3.2 to estimate nutrient fluxes at Bering Strait for past years. For this we use Woodgate 2018's estimates
252 of Bering Strait salinity and transport based on A3 mooring data (See Fig. 1a and Section 2.2.2).
253 Although monthly estimates of transport (T_{A3}) and salinity (S_{A3}) begin in 1990, early records are
254 intermittent so we focus on the continuous period of the record, starting in fall 1997.
255

256 For September-December and January-April we use the monthly salinity measured at A3 (S_{A3}) and the
257 salinity-nutrient regressions from N2 (i.e. Eq. 1) to estimate monthly concentrations for nitrate,
258 phosphate, and silicate at Bering Strait ($NO3_{EST,BS}$, $PO4_{EST,BS}$, and $SiO4_{EST,BS}$, respectively), assuming a

vertically unstratified regime. Using T_{A3} and these salinity-estimated nutrient concentrations, Eq. 2 provides nutrient flux estimates through Bering Strait ($F_{NO3,BS}$, $F_{PO4,BS}$, $F_{SiO4,BS}$). Since salinity and nutrients are not significantly correlated at N2 from May-August, we do not use salinity parameterization (Eq. 1) during these months. Instead, we use *in situ* observations from the Russian-American Long-Term Census of the Arctic Program (RUSALCA) (Crane and Ostrovskiy, 2015) to estimate the average nutrient concentrations within the strait. From a set of five separate cruises in August spanning 2004-2010, we select stations in close proximity to the strait to estimate the average Bering Strait nutrient cross-section for each year and nutrient parameter (See Fig. 1b for nitrate). For all nutrients, there is near-surface nutrient depletion across the whole strait, nutrient-rich subsurface waters from Anadyr Strait in the west, and nutrient-poor waters of the ACC in the east. We compute the mean concentration of each parameter over the entirety of the interpolated cross-sections and find averages of 10.9, 1.3, and 19.2 μmol/kg for nitrate ($NO3_{RUS,BS}$), phosphate ($PO4_{RUS,BS}$), and silicate ($SiO4_{RUS,BS}$), respectively. We use these as representative concentrations for Bering Strait from May-August. While we lack *in situ* Bering Strait data from May-July, SUNA data from N2 suggests this season is typically the least temporally variable (Fig. 2f), so averages from August (following most of the growing season's productivity) should provide a serviceable, perhaps conservative representation for the May-August interval. RUSALCA-based concentrations are subsequently coupled with A3 transports to estimate nutrient fluxes from May-August. By combining the RUSALCA-based (May-August) and salinity-based flux estimates (all other months) we construct a continuous monthly record of nutrient flux through Bering Strait from August 1997 to August 2019 (Supplementary Fig. S1). The period-of-record mean for nitrate, phosphate, and silicate fluxes are 16±6, 1.6±0.5, and 30±11 kmol/s, respectively.

Interannual variability (and uncertainty) is found to be 10-20 (~6), 1.0-1.9 (~0.5), and 18-36 (~11) kmol/s for nitrate, phosphate, and silicate, respectively (Fig. 3a-c). There are statistically significant ($p<0.05$) long term temporal trends for phosphate ($p<0.01$) and silicate ($p<0.02$), but not for nitrate ($p=0.16$) (See

manuscript submitted to *Geophysical Research Letters*

Discussion for possible bias here due to decreasing salinities in the Bering Strait). Sensitivity analysis,

where transport (T) and nutrient concentrations (C) are split into mean and anomaly terms ($T = \overline{T} + T'$, $C = \overline{C} + C'$, and nutrient flux is $T \bullet C$), shows that increasing transport is responsible for the increase in flux for phosphate and silicate ($|T' \bullet \overline{C}| > |\overline{T} \bullet C'|$), while for nitrate decreased concentrations offset the increased transport ($|T' \bullet \overline{C}| \approx |\overline{T} \bullet C|$). There is also considerable seasonal variability (Fig. 3d, Supplementary Table S2). Monthly average fluxes range between about 5±3 to 27±4, 0.7±0.3 to 2.1±0.3, and 12±5 to 50±7 kmol/s for nitrate, phosphate, and silicate respectively, with April maxima and December minima. This timing coincides with months of maximum and minimum salinity, consistent with our salinity-based parameterizations (Eq. 1).

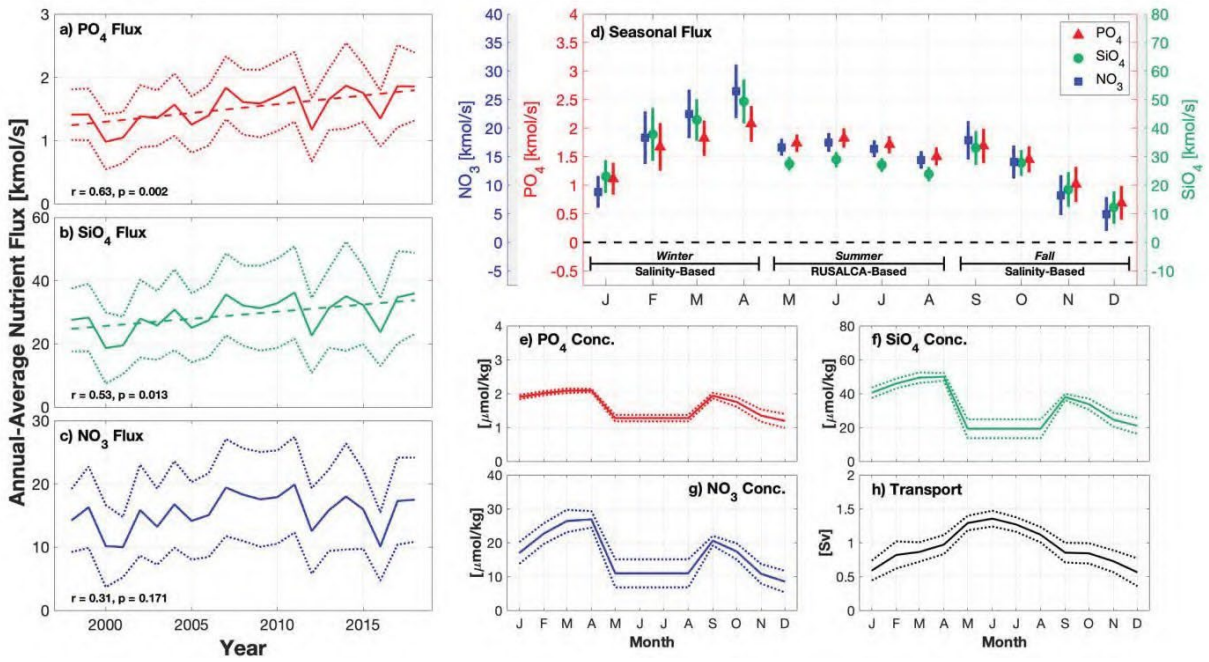

Figure 3: *a-c) Estimated annual average nutrient flux through Bering Strait from 1998-2018. Positive values represent poleward flux, dotted lines show the 95% confidence interval (CI), and dashed lines show the linear regression (only shown if significant). d) The 1997-2018 estimated monthly average nutrient flux through Bering Strait. Symbols are the mean and vertical lines show the 95% CI within each*

300 *month. e-h) The monthly averages (solid line) and standard deviation (dashed lines) of nutrient*
301 *concentrations and transport estimated at Bering Strait.*
302
303

304 **4. Discussion**

305 To sustain 50 g C $m^{-2}yr^{-1}$ of new production in the Chukchi Sea, MacDonald et al. (2010) estimate the
306 required Pacific inflow of dissolved inorganic nitrogen is 16.5 kmol/s, close to our estimate of 16±6
307 kmol/s. Our wintertime nitrate flux estimates at Bering Strait are also consistent with downstream
308 estimates at Icy Cape by Mordy et al. (2020), assuming ~40% of Bering Strait transport (Stabeno et al.
309 2018) reaches their central Chukchi mooring array (e.g. 6±2 kmol/s compared to 18±5 kmol/s found here
310 during February). However, our Bering Strait nutrient fluxes are significantly higher (~25-75%) than
311 those estimated by Torres-Valdes et al. (2013). The majority of the discrepancy is rooted in
312 methodological differences, with our single year, but year-round time series observations allowing a
313 seasonally-resolved approach. Torres-Valdes et al. (2013) use temporally static nutrient concentrations
314 based on one summer transect along with seasonally changing transport estimates. Torres-Valdes et al.
315 (2013) used a Bering Strait average nitrate concentration of 10 μmol/kg (August 2005), whereas our
316 annually averaged (for 1998-2018) concentration is ~16 μmol/kg, which is roughly the same fractional
317 difference between their nitrate flux estimate and that found here.
318

319 Recently, Zhou et al. (2021) used a three-dimensional ocean-sea ice-biogeochemical model to simulate
320 nitrate flux through Bering Strait from 1998-2015 and found values of ~12 kmol/s during February-May,
321 and ~8 kmol/s much of the remainder of the year. While that seasonality has loose qualitative agreement
322 with the monthly variability found here (Fig. 3d), their annual average of 9.63 kmol/s is lower than our
323 16±6 kmol/s, and we find greater seasonality (~5-25 kmol/s versus ~8-12 kmol/s). A possible explanation
324 for the discrepancy of the annual averages is that Zhou et al. (2021) found simulated nitrate

325 concentrations upstream of Anadyr Strait that were significantly lower (by ~5 μmol/kg) than *in situ*
326 concentrations, which may translate to lower Bering Strait nitrate fluxes.
327
328 We know of no long-term trends of deep water thermohaline and nutrient composition in the Bering Sea
329 basin, though the stability of the salinity-nutrient relationships over the multi-decadal period of record
330 (1998-2018) is a critical assumption for our methodology, given these relationships are only estimated
331 from the one yearlong N2 mooring deployment (2017-2018). The January-April salinity-nutrient
332 measurements from N2 are near the mixing line between deep nutrient-rich and shallow nutrient-poor
333 waters established from hydrographic data (Fig. 2a) collected up to 13 years before the N2 deployment,
334 possibly suggesting long-term stability. However, Woodgate (2018) observes a multi-decadal freshening
335 trend at Bering Strait, possibly due to glacier ablation in the Gulf of Alaska. Our salinity-nutrient
336 relationships are based on mixing between high-salinity high-nutrient Pacific Basin waters and low-
337 nutrient low-salinity shelf water, so changes over time to the shallow, low-salinity end member could
338 impact our estimates. If Bering Shelf water has become fresher (with constant nutrient content), we may
339 underestimate nutrient concentrations with our parameterizations (though we lack data to examine this).
340
341 Prominent discontinuities between estimated fluxes on either side of the summer season (Fig. 3d) mark
342 the changeover between salinity-based nutrient estimates and RUSALCA measurements used for May-
343 August, and demonstrate likely methodological limitations. There are different uncertainties associated
344 with each of the methods, but discontinuities may also partially reflect the seasonally varying nutrient
345 uptake cycle. Brown et al. (2011) estimate that 54% of the regional annual net primary production occurs
346 from May-July, so phytoplankton blooms during this interval draw down nutrient concentrations, thereby
347 reducing Arctic-bound nutrient fluxes. The northern Bering and southern Chukchi Seas are known for
348 high (250-300 g C m^{-2} yr^{-1}) phytoplankton productivity (Sambrotto et al. 1984, Grebmeier et al. 1988,
349 Springer 1988, Walsh et al. 1989). Though nutrient consumption during transit between Anadyr and
350 Bering Strait is unknown, we can crudely estimate this by assuming half the total production (~150 g C

351 m^{-2}) occurs evenly over the ~50 m deep shelf from May-July. The expected drawdown during the two-
352 week advective period from Anaydr to Bering Strait would be ~6 μmol N kg^{-1} (assuming a Redfield ratio
353 of 16N:106C), and the remainder of the year is ~2 μmol N kg^{-1}. Since our flux estimates only use Anadyr
354 salinity-nutrient relations from September-April, and nutrient concentrations during May-August are
355 based on late-summer RUSALCA observations directly at Bering Strait, we expect only modest error (~3
356 μmol N kg^{-1}) from biotic drawdown in Chirikov Basin.
357
358 The estimated nitrate, phosphate, and silicate flux in Anadyr Strait for the N2 mooring deployment period
359 over September 2017 - April 2018 was 17±4, 1.8±0.2, and 37±5 kmol/s, respectively (Section 3.3).
360 During the same interval at Bering Strait, fluxes are estimated to be higher, at 24±8, 2.5±0.8, and 52±16
361 kmol/s. Volume transport through Anadyr Strait is weaker than that through Bering Strait (~80%;
362 Danielson et al. 2014), but the nutrient delivery through Bering Strait is largely of Anadyr origin (e.g. Fig.
363 1), so the difference in nutrient flux is unlikely explained by volume transport alone. Though the
364 uncertainty ranges of the Anadyr and Bering Strait fluxes overlap, it is possible the larger mean values at
365 Bering Strait are partially due to the southern branch of the Anadyr Current, which on average flows
366 eastward along the south shore of St. Lawrence Island (Danielson et al. 2006). Thus, our Anadyr Strait
367 estimates could underestimate the total nutrient flux carried poleward from the Gulf of Anadyr. However,
368 we presently lack data to quantify this component or other sources and losses, such as benthic
369 remineralization and denitrification.
370
371 Estimates of volume transport through Bering Strait used here (Section 3.4, Woodgate 2018) do not
372 correct for ACC influences, an additional source of uncertainty. However, the fractional correction for
373 volume transport is ~10% (Woodgate, 2018), and ACC water is known for being nutrient deplete
374 (Danielson et al. 2017), so it is unlikely the ACC contributes a significant fraction of the overall nutrient
375 supply to the Arctic. These fluxes also do not include other forms of nitrogen (e.g., ammonium,

376 particulate organic nitrogen), that may be important for primary producers. While ammonium
377 concentrations are higher on the Bering Shelf (Mordy et al. 2008, 2010), they may be less important for
378 slope-derived water, such as the Anadyr Current.
379

380 Woodgate (2018) described a multi-year trend of increasing transport and declining salinity. For our
381 parameterizations this introduces competing effects, as increased volume transport favors increased
382 nutrient flux, while decreasing salinity translates to lower assumed nutrient concentration and fluxes (Eqs.
383 1, 2). Using salinity-nutrient parameterizations established at N2, we find silicate and phosphate fluxes
384 have likely increased significantly from 1998-2018, while nitrate has a weak, insignificant positive trend
385 ($p=0.16$). Though nitrate, phosphate, and silicate are all well correlated with salinity during non-summer
386 months ($r \geq 0.89$), changes in salinity correspond to a larger fractional change in $NO3_{EST,BS}$ than either
387 $PO4_{EST,BS}$ or $SiO4_{EST,BS}$ (Fig. 2 b-d). Thus, long term decreases in salinity at Bering Strait drive a decrease
388 in computed nitrate, which when combined with the increase in volume flux means $F_{NO3,BS}$ remains
389 relatively steady. Salinity variability causes less fractional change in $PO4_{EST,BS}$ and $SO4_{EST,BS}$, such that the
390 increased transport is the determining factor in long term changes of $F_{PO4,BS}$ and $F_{SiO4,BS}$ (Section 3.4).
391

392 **5. Conclusions**

393 Though we calculate significant decadal trends for phosphate and silicate, but not for nitrate, we caution
394 that these results are built upon the assumption that salinity-nutrient reletionships are static across years.
395 Verifying this is vital for validating our trend conclusions. Independent of potential decadal trends, we
396 also find that nutrient flux through Bering Strait is considerably higher than previous estimates. Torres-
397 Valdes et al. (2013) found that Bering Strait is a substantial source of annual nutrient supply to the
398 broader Arctic Ocean (21±4%, 35±6%, and 61±11% for nitrate, phosphate, and silicate, respectively).
399 Our analysis suggests Bering Strait may be a proportionally more significant source of Arctic nutrients
400 than previously appreciated.
401

Acknowledgements

We thank the captain and crew of R/V Sikuliaq and UAF mooring technician Pete Shipton for successful cruises. This work was funded by Arctic Integrated Ecosystem Research Program (Arctic IERP) grants A91-99a, A91-00a to the Arctic Shelf Growth, Advection, Respiration and Deposition (ASGARD) rate experiments project. CW was funded by Arctic IERP grant A92. The Arctic IERP was supported by the North Pacific Research Board, the Collaborative Alaskan Arctic Studies Program (formerly the North Slope Borough/Shell Baseline Studies Program), the Bureau of Ocean Energy Management (BOEM), and the Office of Naval Research (ONR) Marine Mammals and Biology Program. This publication is partially funded by the Cooperative Institute for Climate, Ocean, & Ecosystem Studies (CIOCES) under NOAA Cooperative Agreement NA20OAR4320271. This is NPRB publication #ArcticIERP-46, PMEL publication #5350, EcoFOCI publication #1024, and CICOES publication #2022-1177. Bering Strait moorings are funded by NSF-AON (PLR-1304052, PLR-1758565).

Open Research

CTD-corrected Aqua Monitor data can be found in Table S3. Bering Strait transport and salinity are available at http://psc.apl.washington.edu/BeringStrait.html and doi:10.18739/A2PZ51M3V. RUSALCA hydrography, Bering and Arctic IERP hydrography, and N2 mooring data is found in the supporting information file associated with this manuscript. Archiving is underway; all data will be publically available in advance of publication (using the Axiom/Alaska Ocean Observing System (AOOS) DataONE member node).

References

Becker, S., Aoyama, M., Woodward, E.M.S., Bakker, K., Coverly, S., Mahaffey, C. and Tanhua, T., 2020. GO-SHIP repeat hydrography nutrient manual: the precise and accurate determination of dissolved inorganic nutrients in seawater, using continuous flow analysis methods. *Frontiers in Marine Science*, *7*, p.908.

Brown, Z. W., Dijken, G. L. Van, & Arrigo, K. R. (2011). A reassessment of primary production and environmental change in the Bering Sea. *Journal of Geophysical Research*, *116*, C08014. https://doi.org/10.1029/2010JC006766

Coachman, L. K. (1993). On the flow field in the Chirikov Basin. *Continental Shelf Research*, *13*(5-6), 481-508. https://doi.org/10.1016/0278-4343(93)90092-C

Crane, K., and A. Ostrovskiy. 2015. Introduction to the special issue: Russian-American Long-term Census of the Arctic (RUSALCA). *Oceanography* 28(3):18-23, https://doi.org/10.5670/oceanog.2015.54.

Daniel, A,; Laes-Huon, A.; Barus,; Beaton, A.D.; Blandfort, D.; Guigues, N.; Knockaert, M.; Muraron D., Salter, I.; Woodward, E.M.S.; Greenwood N. and Achterberg E.P. (2020) Toward a Harmonization for Using in situ Nutrient Sensors in the Marine Environment. Frontiers in Marine Science, 6: 773, 22pp. DOI: 10.3389/fmars.2019.00773

Danielson, S., Aagaard, K., Weingartner, T., Martin, S., Winsor, P., Gawarkiewicz, G., & Quadfasel, D. (2006). The St. Lawrence polynya and the Bering shelf circulation: New observations and a model comparison. *Journal of Geophysical Research: Oceans*, *111*(9), 1-18. https://doi.org/10.1029/2005JC003268

Danielson, S., Curchitser, E., Hedstrom, K., Weingartner, T., & Stabeno, P. (2011). On ocean and sea ice modes of variability in the Bering Sea. *Journal of Geophysical Research: Oceans*, *116*(12), 1-24. https://doi.org/10.1029/2011JC007389

Danielson, S. L., Weingartner, T. J., Hedstrom, K. S., Aagaard, K., Woodgate, R., Curchitser, E., & Stabeno, P. J. (2014). Coupled wind-forced controls of the Bering-Chukchi shelf circulation and the Bering Strait throughflow: Ekman transport, continental shelf waves, and variations of the Pacific-Arctic sea surface height gradient. *Progress in Oceanography*, *125*, 40-61. https://doi.org/10.1016/j.pocean.2014.04.006

Danielson, S. L., Eisner, L., Ladd, C., Mordy, C., Sousa, L., & Weingartner, T. J. (2017). A comparison between late summer 2012 and 2013 water masses, macronutrients, and phytoplankton standing crops in the northern Bering and Chukchi Seas. *Deep-Sea Research Part II: Topical Studies in Oceanography*, *135*, 7-26. https://doi.org/10.1016/j.dsr2.2016.05.024

Grebmeier, J., McRoy, C., & Feder, H. (1988). Pelagic-benthic coupling on the shelf of the northern Bering and Chukchi Seas. I. Food supply source and benthic bio-mass. *Marine Ecology Progress Series*, *48*, 57-67. https://doi.org/10.3354/meps048057

Grebmeier, J., Bluhm, B. A., Cooper, L. W., Danielson, S. L., Arrigo, K. R., Blanchard, A. L., Clarke, J. T., Day, R. H., Frey, K. E., Gradinger, R. R., Kedra, M., Konar, B., Kuletz, K. J., Lee, S. H., Lovvorn, J. R., Norcross, B. L., Okkonen, S. R. (2015). Ecosystem characteristics and processes facilitating persistent macrobenthic biomass hotspots and associated benthivory in the Pacific Arctic. *Progress in Oceanography*, *136*(May), 92-114. https://doi.org/10.1016/j.pocean.2015.05.006

Huntington, H. P., Danielson, S. L., Wiese, F. K., Baker, M., Boveng, P., Citta, J. J., De Robertis, A., Dickson, D. M.S., Farley, E., George, J. C., Iken, K., Kimmel, D. G., Kuletz, K., Ladd, C., Levine, R., Quakenbush, L., Stabeno, P., Stafford, K. M., Stockwell, D., Wilson, C. (2020). Evidence suggests potential transformation of the Pacific Arctic ecosystem is underway. *Nature Climate Change*, *10*(4), 342-348. https://doi.org/10.1038/s41558-020-0695-2

Lewis, K. M., & Arrigo, K. R. (2020).Ocean color algorithms for estimating chlorophyll a, CDOM absorption, and particle backscattering in the ArcticOcean. Journal of Geophysical Research: Oceans, 125, e2019JC015706. https://doi.org/10.1029/2019JC015706

MacDonald, R.W., Anderson, L.G., Christensen, J.P., Miller, L.A., Semiletov, I.P., Stein, R., 2010. The Arctic Ocean. In: Liu, K.-K., Atkinson, L., Qui~nones, R., Talaue- McManus, L. (Eds.), Carbon and Nutrient Fluxes in Continental Margins: A Global Synthesis. Springer Berlin Heidelberg, pp. 291-303.

Mordy, C.W., Stabeno, P.J., Righi, D. and Menzia, F.A., 2008. Origins of the subsurface ammonium maximum in the southeast Bering Sea. *Deep Sea Research Part II: Topical Studies in Oceanography*, *55*(16-17), pp.1738-1744.

Mordy, C.W., Eisner, L.B., Proctor, P., Stabeno, P., Devol, A.H., Shull, D.H., Napp, J.M. and Whitledge, T., 2010. Temporary uncoupling of the marine nitrogen cycle: Accumulation of nitrite on the Bering Sea shelf. *Marine Chemistry*, *121*(1-4), pp.157-166.

Mordy, C. W., Bell, S., Cokelet, E. D., Ladd, C., Lebon, G., Stabeno, P., Strausz, D., Wisegarver, E., Wood, K. (2020). Seasonal and interannual variability of nitrate in the eastern Chukchi Sea: Transport and winter replenishment. *Deep-Sea Research Part II: Topical Studies in Oceanography*, *177*(May), 104807. https://doi.org/10.1016/j.dsr2.2020.104807

Polyakov, I. V., Rippeth, T. P., Fer, I., Alkire, M. B., Baumann, T. M., Carmack, E. C., Ingvaldsen, R., Ivanov, V. V., Janout, M., Lind, S., Padman, L., Pnyushkov, A. V., Rember, R. (2020). Weakening of cold halocline layer exposes sea ice to oceanic heat in the eastern arctic ocean. *Journal of Climate*, *33*(18), 8107-8123. https://doi.org/10.1175/JCLI-D-19-0976.1

Sambrotto, R.N., Goering, J.J., McRoy, C.P., 1984. Large yearly production of phytoplankton in the western Bering Strait. Science 225 (4667), 1147-1150. https://doi.org/10.1126/science.225.4667.1147.

524 Springer, A.M., 1988. The Paradox of Pelagic Food Webs on the Bering-Chukchi Continental Shelf
525 (Dissertation). University of Alaska Fairbanks.
526
527 Torres-Valdes, S., Tsubouchi, T., Bacon, S., Naveira-Garabato, A. C., Sanders, R., McLaughlin, F. A., .
528 Whitledge, T. E. (2013). Export of nutrients from the Arctic Ocean. *Journal of Geophysical*
529 *Research: Oceans*, *118*(4), 1625-1644. https://doi.org/10.1002/jgrc.20063
530
531 Walsh, J. J., McRoy, C. P., Coachman, L. K., Goering, J. J., Nihoul, J. J., Whitledge, T. E., Blackburn, T.
532 H., Parker, P. L., Wirick, C. D., Shuert, P. G., Grebmeier, J. M., Springer, A. M., Tripp, R. D.,
533 Hansell, D. A., Djenidi, S., Deleersnijder, E., Henriksen, K., Lund, B. A., Andersen, P., Muller-
534 Karger, F. E., Dean, K. (1989). Carbon and nitrogen cycling within the Bering/Chukchi Seas:
535 Source regions for organic matter effecting AOU demands of the Arctic Ocean. *Progress in*
536 *Oceanography*, *22*(4), 277-359. https://doi.org/10.1016/0079-6611(89)90006-2
537
538 Wang, M., Yang, Q., Overland, J. E., & Stabeno, P. (2018). Sea-ice cover timing in the Pacific Arctic :
539 The present and projections to mid-century by selected CMIP5 models. *Deep-Sea Research II*, *152*,
540 22-34. https://doi.org/10.1016/j.dsr2.2017.11.017

541 Woodgate, R. A., Stafford, K. M., & Prahl, F. G. (2015). A synthesis of year-round interdisciplinary
542 mooring measurements in the Bering Strait (1990-2014) and the RUSALCA years (2004-2011).
543 *Oceanography*, *28*(3), 46-67. https://doi.org/10.5670/oceanog.2015.57

544 Woodgate, R. A. (2018). Increases in the Pacific inflow to the Arctic from 1990 to 2015, and insights into
545 seasonal trends and driving mechanisms from year-round Bering Strait mooring data. *Progress in*
546 *Oceanography*, *160*(June 2017), 124-154. https://doi.org/10.1016/j.pocean.2017.12.007

547 Zhou, J., Luo, X., Xiao, J., Wei, H., Zhao, W., & Zheng, Z. (2021). Modeling the seasonal and
548 interannual variations in nitrate flux through Bering Strait. *Journal of Marine Systems*, *218*(June
549 2020), 103527. https://doi.org/10.1016/j.jmarsys.2021.103527
550

Figure1.

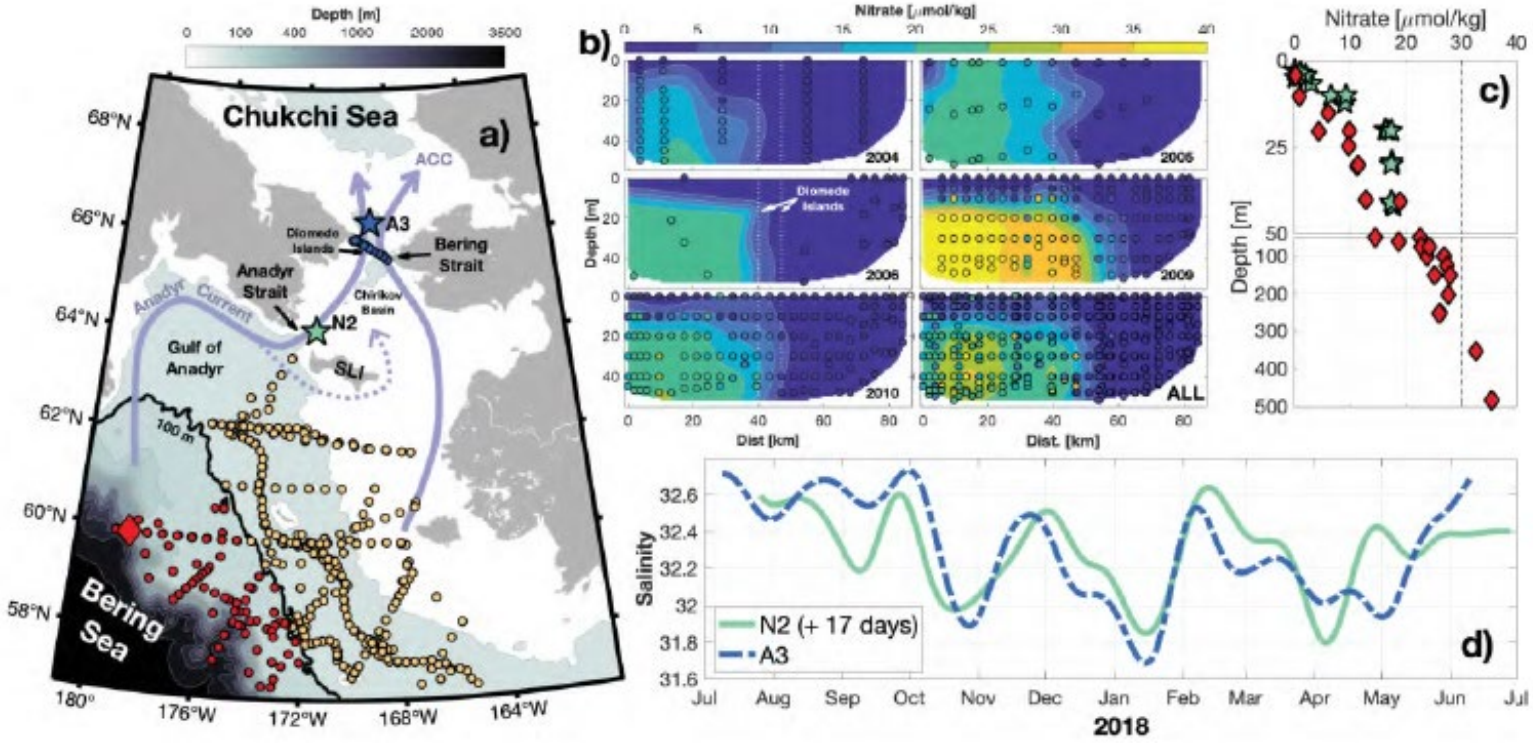
Depth [m]
0 100 400 1000 2000 3500
Chukchi Sea
a)
ACC
A3
Diomede Islands
Bering Strait
Anadyr Strait
Anadyr Current
Chirikov Basin
N2
Gulf of Anadyr
SLI
100 m
Bering Sea
68°N
66°N
64°N
62°N
60°N
58°N
180°
176°W
172°W
168°W
164°W
b)
Nitrate [μmol/kg]
0 5 10 15 20 25 30 35 40
2004
2005
2006
2009
2010
ALL
Diomede Islands
Depth [m]
Dist [km]
Dist. [km]
c)
Nitrate [μmol/kg]
0 10 20 30 40
Depth [m]
0 25 50 100 200 300 400 500
d)
Salinity
32.6 32.4 32.2 32 31.8 31.6
N2 (+ 17 days)
A3
Jul Aug Sep Oct Nov Dec Jan Feb Mar Apr May Jun Jul
2018

Figure2.

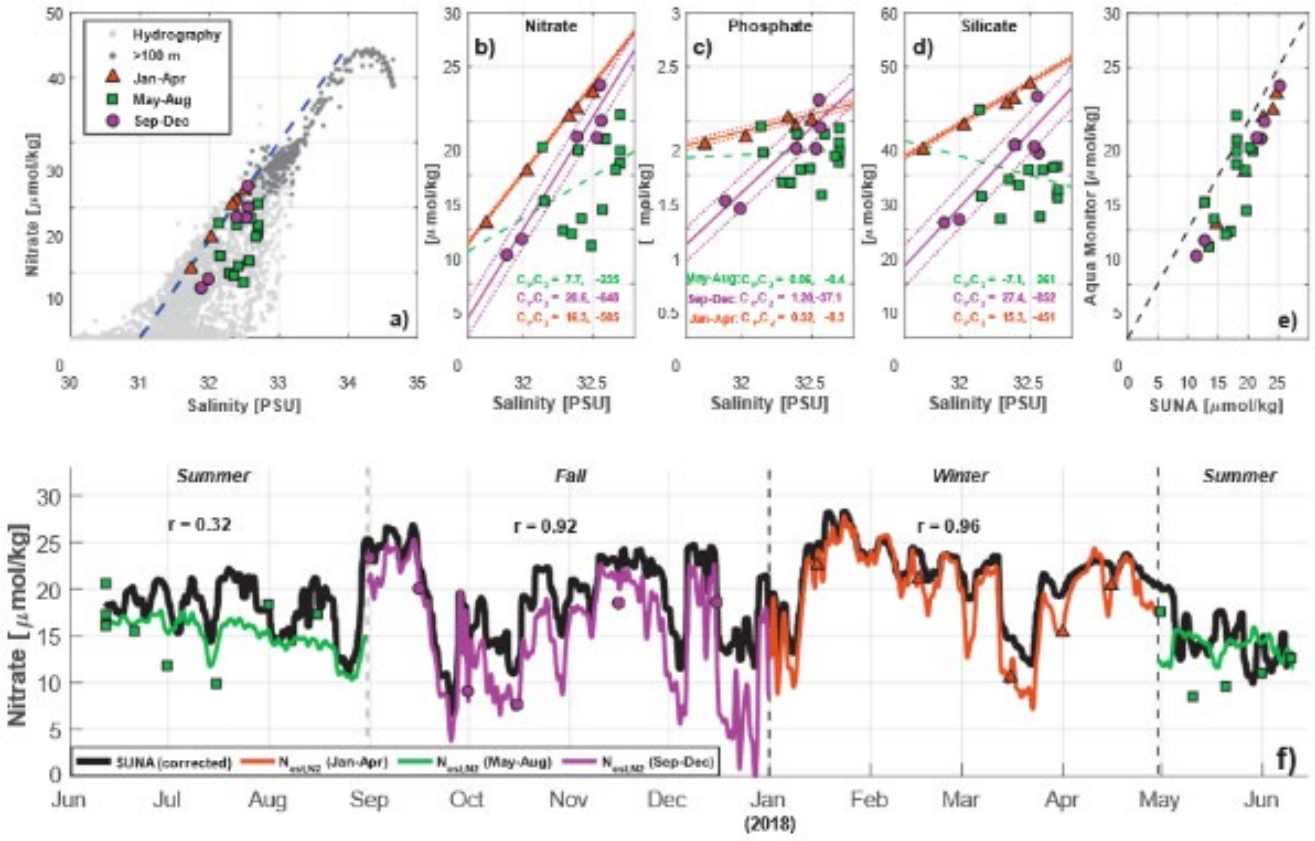
Hydrography
>100 m
Jan-Apr
May-Aug
Sep-Dec
Nitrate [μmol/kg]
Salinity [PSU]
a)
b)
Nitrate
c)
Phosphate
d)
Silicate
e)
Aqua Monitor [μmol/kg]
SUNA [μmol/kg]
Summer
Fall
Winter
Summer
r = 0.32
r = 0.92
r = 0.96
SUNA (corrected)
(Jan-Apr)
(May-Aug)
(Sep-Dec)
f)
Jun
Jul
Aug
Sep
Oct
Nov
Dec
Jan
(2018)
Feb
Mar
Apr
May
Jun

Figure3.

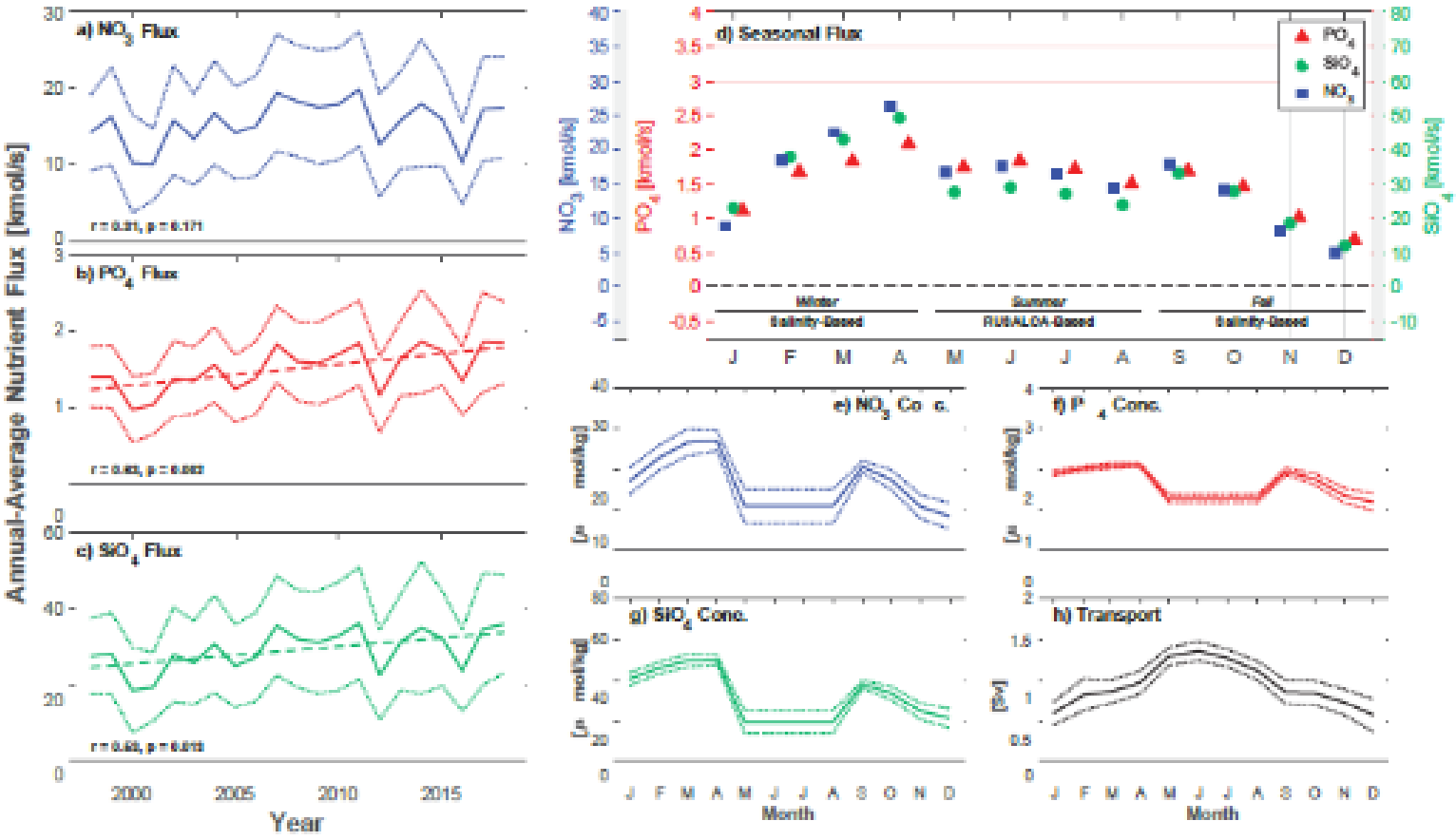
a) NO3 Flux
b) PO4 Flux
c) SiO4 Flux
Annual-Average Nutrient Flux [kmol/s]
Year
d) Seasonal Flux
PO4
SiO4
NO3
Winter
Salinity-Based
Summer
RUBALCVA-Based
Fall
Salinity-Based
e) NO3 Conc.
f) PO4 Conc.
g) SiO4 Conc.
h) Transport
Month

Full title: Diversity and community structure of eukaryotic phototrophs in the Bering and Chukchi Seas

Short title: Eukaryotic phototrophs in the Bering and Chukchi Seas

Rachel M. Lekanoff[1], Seth Danielson[1],
Andrew McDonnell[1], R. Eric Collins[2*]

[1]College of Fisheries and Ocean Sciences, University of Alaska Fairbanks, Fairbanks, Alaska, USA

[2]Centre for Earth Observation Sciences, University of Manitoba, Winnipeg, Manitoba, Canada

* Corresponding author

E-mail: eric.collins@umanitoba.ca

ABSTRACT

The northern Bering and Chukchi Seas are productive high latitude ecosystems supported by tight benthic-pelagic coupling. However, warmer waters in Arctic and sub-Arctic regions are expected to alter phytoplankton community composition in the future, with unknown consequences for this critical ecosystem. Here we present the first large-scale metabarcoding survey of 18S rRNA gene diversity in this region, covering the summer of 2017 --- the warmest on record, with sea surface temperatures rising to 10°C. This report focuses on diatoms and "picophytoplankton" (operationally defined here as Chlorophyta, Haptophyta, and Chrysophyceae), which averaged 39% and 10% of the relative sequence abundance, respectively. In total, 201 diatom taxa and 227 picophytoplankton taxa were detected as exact sequence variants (ESVs) and categorized into 7 distinct diatom assemblages and 11 distinct picophytoplankton assemblages by hierarchical clustering. Investigating the potential to predict phytoplankton community composition using shipboard CTD data alone, we found that predictions of individual ESV abundance were poor, but predictions of community assemblage were somewhat better, with environmental variables explaining 44% of assemblage variability for diatoms and 32% for picophytoplankton. Among diatoms, the genera *Chaetoceros* and *Thalassiosira* combined to make up 80% of the diatom relative abundance and 43% of the diatom ESVs, while among picophytoplankton the genera *Micromonas* and *Phaeocystis* combined to make up 57% of the relative abundance and 6% of the ESVs. Based on their biogeographical distributions, we identified ESVs of *Chaetoceros*, *Pseudo−nitzschia*, *Micromonas*, and *Phaeocystis* as abundant taxa that may be negatively affected as the region warms.

INTRODUCTION

Due to an increase in anthropogenic carbon emissions, the sub-Arctic and Arctic are warming at a fast pace (Held and Soden 2006; Zelinka and Hartmann 2011), resulting in sea ice retreat, increased areas of open water, more light, and changing patterns of productivity as the Arctic shifts from a light-limited to a nutrient-limited system (Henson et al. 2013). Presently, diatoms are the dominant primary producers in the Bering and Chukchi Seas, contributing as much as 470 g C m^{-2} $year^{-1}$ (Springer and McRoy 1993), playing an essential role in Arctic biogeochemical cycles. Diatoms in the Arctic are typically large chain-forming taxa falling within microplankton (20--200 μm) size ranges or larger, which are typically associated with food webs dominated by larger copepods and an increase in biological pump efficiency due to sedimentation (Pomeroy 1974; Azam et al. 1983; Laws et al. 2000). However, because the Arctic shelves are so shallow (the Chukchi Sea shelf has a mean depth of about 40m), the amount of carbon that reaches the seafloor leads to some of the highest densities of benthic biomass in the world.

While large-celled diatoms are currently the most important primary producers in the Arctic, recent studies suggest that phytoplankton communities may shift towards mixotrophy (single cells capable of both photosynthesis and phagotrophy or osmotrophy) in response to climate change (Stoecker et al. 2017a; Stoecker and Lavrentyev 2018). Should these predictions prove correct, the decreased presence of diatoms could result in a reduced flux of carbon to the benthos. Other studies speculate that regional productivity could increase on the Chukchi shelf (Arrigo et al. 2008; JM Grebmeier 2012), with the potential to offset some excess CO_2 emissions.

Diatoms have been the dominant phytoplankton of the Bering and Chukchi seas for millennia (Moran et al. 2012; Giesbrecht et al. 2019), as shown by the presence of diatom-dominated siliceous seafloor sediment (Ran et al. 2013) dating back to the late Quaternary, when

sea level rise flooded the area (Sancetta et al. 1984). In today's ocean, Pacific waters transported northwards into the Bering Sea from depth have relatively high nutrient concentrations (Harrison et al. 2004; Pisareva et al. 2015), spurring diatom productivity (Walsh et al. 1989; Codispoti et al. 2005). Large-celled diatom taxa like *Thalassiosira* and *Chaetoceros* bloom at retreating sea ice edges in spring and early summer (Sukhanova et al. 2009) and tend to be prominent along the coast (Hill et al. 2005). In one study on the Bering Sea shelf, microplankton-sized diatoms made up about 80% of the organic carbon (Moran et al. 2012). High diversity within *Chaetoceros spp.* has been observed in the Chukchi and Beaufort seas (Balzano et al. 2017) with four distinct genetic clades reported within *C. neogracilis* using 18S and 28S rRNA gene sequencing. *Thalassiosira* and *Pseudo−nitzschia* were also prevalent throughout that study region, although *Chaetoceros* was the dominant genus. Phytoplankton blooms have also been observed under and around sea-ice, where *Chaetoceros*, *Thalassiosira*, and *Fragilariopsis* were the dominant diatoms, forming unique seawater assemblages (Arrigo et al. 2012).

Picoplankton, typically defined as plankton between 0.2 and 2.0 μm in size, (Sieburth et al. 1978), were once thought to be exclusively bacterioplankton (Platt et al. 1983). Now, many clades of (mostly) flagellated eukaryotic protists are recognized as important members of the picoplankton (Vaulot et al. 2008), and are commonly referred to as picoeukaryotes. Picoeukaryotes may be phototrophic (i.e. picophytoplankton), heterotrophic (Worden and Not 2008), or mixotrophic (McKie-Krisberg and Sanders 2014). Picophytoplankton can account for up to 90% of primary production in other marine environments (Worden et al. 2004; Jardillier et al. 2010), but in the Arctic they currently play a smaller role (McKie-Krisberg and Sanders 2014).

Prominent picophytoplankton taxa in the Arctic belong to flagellated groups including Chrysophyta, Cryptophyta, Haptophyta (Prymnesiophyta), and Chlorophyta (Stoecker and

Lavrentyev 2018). Among chrysophytes, the genera *Ochromonas* and *Dinobryon* are common and both are known to be mixotrophic (Estep et al. 1986; Andersson et al. 1989; Keller et al. 1994; McKenzie et al. 1995). In addition, *Dinobryon* forms colonies important to particle flux (Olli et al. 2002; Stoecker and Lavrentyev 2018). Cryptophytes have been identified, e.g. in the southeastern Bering Sea (Olson and Strom 2002), but rarely down to genera and species (Stoecker and Lavrentyev 2018). An exception is *Teleaulax amphioxeia*, a mixotroph (Yoo et al. 2017). The most common haptophyte in the Arctic is *Phaeocystis* (Stoecker and Lavrentyev 2018). These colonial picophytoplankton can form massive blooms, spurring seasonal production and affecting marine carbon cycling (Smith et al. 1991). Another group that is becoming increasingly recognized as important in the Arctic are the Chlorophytes, especially the genus *Micromonas*. Once thought to comprise a single species, *Micromonas* is now known to contain a diverse array of taxa (Simon et al. 2017). Laboratory experiments have also found high rates of bacterivory by *Micromonas* under oligotrophic conditions similar to those found in polar seas in the summer (McKie-Krisberg and Sanders 2014).

This study aims to establish a robust baseline of phytoplankton community composition at the molecular level, in the midst of changing sub-Arctic and Arctic environments, with a focus on diatom and picophytoplankton communities. This study is the first molecular analysis to cover such a large area over the Bering and Chukchi seas and includes hundreds of samples collected over the course of three spring and summer months (June, August, and September). To describe latitudinal changes within these communities over the Bering and Chukchi seas, we selected sites within the Distributed Biological Observatory (DBO), an established set of monitoring stations designed to study biodiversity and productivity shifts in response to global climate change (Grebmeier et al. 2010; Grebmeier 2012). Phytoplankton size, biomass, and composition are core

standardized ship-based sampling parameters of the DBO; our study adds genetic analyses for taxonomic identification of phytoplankton over time and large environmental gradients, providing insights into fine-scale seasonal community shifts of phytoplankton that are not captured by microscopy and pigment analyses.

MATERIALS AND METHODS

Sampling Sites

Seawater samples were collected during June, August, and September 2017. June sampling took place aboard *RV Sikuliaq* as part of the Arctic Shelf Growth, Advection, Respiration and Deposition Rate Experiments (ASGARD) project. August sampling took place aboard *RV Norseman II* as part of the Arctic Marine Biodiversity Observing Network (AMBON). September sampling took place aboard *USCGC Healy* as part of the DBO-Northern Chukchi Integrated Study (DBO-NCIS). ASGARD covered transects in the northern Bering Sea, across the Bering Strait, and into the southern Chukchi Sea, AMBON covered study sites in the southern and northern Chukchi Sea, and DBO-NCIS covered sites in the Chukchi Sea (Fig 1). The DBO3 line was visited on each of the three cruises, the DBO4 line was visited by the DBO-NCIS and AMBON cruises, and lines DBO1 (DBO-NCIS), DBO2 (ASGARD), and DBO5 (DBO-NCIS) were visited on one cruise each.

Fig 1: Map of sampling sites with bathymetric lines at depths of 20, 40, and 60 meters. Stations sampled during each cruise are demarcated by symbol: ASGARD (●), AMBON (▲), and DBO-NCIS (▼). Sampling type is shown in color: Hydrographic (CTD-only; *red*), Process (size-

fractionated filtering; *green*), and Survey (0.2µm filtering only; *blue*). DBO lines 1 through 5 are shown in colored boxes.

Seawater was generally collected from a subset of standard sampling depths (e.g. surface, 10, 20, 30, 40, 50, 75, 100, 125, 150, 250, 500, 1000, 2000, 3000 m) and, if present, from oceanographic features (chlorophyll maxima, pycnocline, thermocline, halocline, etc.). A median of 3 depths were sampled per station, and the modal depths per station were 5 m, 20 m, and 40 m. Seawater was collected using Niskin bottles on a rosette with an attached Sea-Bird CTD (Sea-Bird Electronics Inc., Bellevue, WA, USA).

Nutrients and Chlorophyll

For each cruise, nutrients were collected immediately after recovering the CTD with 60 mL syringes, filtered through 0.45 µm Nuclepore filters, and kept frozen below −20 °C until processed colorimetrically by autoanalyser post-cruise (Gordon, Jennings and Krest 1993). ASGARD nutrient samples were collected June 9–28, 2017, with concentrations of nitrate, nitrite, phosphate, and silicate provided. AMBON nutrient samples were collected August 7–22, 2017. DBO-NCIS nutrient samples were collected from August 28 to September 13, 2017.

Microbe and Particle Filtration

Seawater was drained from Niskin bottles into 20 L Cubitainers and stored at 4 °C until filtration using a peristaltic pump within six hours of collection. No pre-filter was used to exclude

151 macroscopic plankton. At “Survey” stations, a single 1–5 L seawater sample per depth was filtered
152 directly onto 0.2 µm-pore size Sterivex cartridge filters to collect microbes. Seawater from selected
153 “Process” stations was sequentially filtered based on size, first through a 47 mm-diameter 20 µm-
154 pore size nylon net filter, then a 47 mm-diameter 3 µm-pore size membrane filter, and finally
155 through a 0.2 µm-pore size Sterivex cartridge filter (all filters from Millipore Sigma, Burlington,
156 MA, USA). The 20 µm and 3 µm filters were folded cells-in using forceps cleaned with ethanol
157 and then placed in 2 mL microcentrifuge tubes with approximately 1 mL of RNAlater (Life
158 Technologies Corporation, Carlsbad, CA, USA). Approximately 1 mL of RNAlater was injected
159 directly into Sterivex filters prior to sealing. Filters were stored in freezers (below −20 °C) until
160 lab processing and sequencing.

161 ***CHN and SPM Analyses***

162 Precombusted 25 mm-diameter Whatman GF/F filters were used to collect particulate
163 matter for carbon, hydrogen, nitrogen (CHN) analysis and suspended particulate matter (SPM),
164 following established methods (Knap et al. 1996; Neukermans et al. 2016). For both CHN and
165 SPM samples, 500 to 1000 mL of seawater was filtered from each target depth. After filtration,
166 CHN and SPM filters were rinsed with fresh Milli-Q water to remove salts, dried at 60 °C for 12
167 hours, and stored in petri dishes until analysis. CHN filters were acidified with 10% hydrochloric
168 acid for 6 hours to remove inorganic carbon and then exposed to a standard high temperature
169 combustion technique to determine levels of carbon, hydrogen, and nitrogen in each sample at the
170 Alaska Stable Isotope Facility at University of Alaska Fairbanks’ (UAF) Water and Environmental
171 Research Center. SPM filters were massed and the original weight of the filter was subtracted and
172 divided by the volume of seawater filtered to obtain in situ concentrations.

DNA Sequencing

DNA was extracted from filters using the DNeasy PowerWater kit (Qiagen, Hilden, Germany) following the manufacturer's instructions, with the exception that prior to extraction, RNALater was expelled from the thawed Sterivex filter cartridge and the filter was rinsed with 1 mL ultrapure water. PCR-amplification of 18S rRNA genes was used for analysis of phytoplankton communities. The KAPA HiFi HotStart PCR Kit (Kapa Biosystems, Wilmington, MA, USA) was used for PCR-amplification of 18S rRNA genes. Thermocycling parameters were: one cycle at 98 °C for 1-min, 26 cycles at 98 °C for 30 s, 55 °C for 30 s, 72 °C for 30 s, and one cycle at 72 °C for five minutes. Primers used in PCR to target the eukaryotic V4 hypervariable region were TAReuk454FWD1 5'-CCAGCASCYGCGGTAATTCC-3' and TAReukREV3_modified 5'-ACTTTCGTTCTTGATYRATGA-3' (Stoeck et al. 2010). Amplified DNA was dual-indexed using unique adapters (Glenn et al. 2016) before TruSeq library preparation and sequencing on an Illumina MiSeq in the UAF DNA Core Lab. Sample counts and mean reads per sample are shown in Supplementary Table 1. DNA sequences have been submitted to GenBank under accession number SUB8918463.

Data Analysis

Oceanographic data was visualized in Ocean Data View (Schlitzer 2016) and in R (R Core Team 2013). Water mass definitions (Pisareva et al. 2015) were used with the addition of an extra water mass extending from 6 °C to 14 °C, denoted "WACW" here for "Warm Alaska Coastal Water". For some analyses and visualizations, samples were grouped by depth, with all samples taken between 0 and 7 m considered 'surface', all samples taken within 10 m of the seafloor considered 'bottom', and samples from depths in between denoted 'midwater'.

195 Bioinformatics and statistical analyses were carried out in R. After sequencing, samples
196 were demultiplexed and primers were removed using cutadapt v2.8 (Martin 2011). Exact sequence
197 variants (ESVs) were called using DADA2 (divisive amplicon denoising algorithm 2), an open
198 source R package (Callahan et al. 2016) that performs quality control, error correction, merging,
199 chimera checks, and taxonomic classification using SILVA database v132 (Quast et al. 2012).
200 Samples with less than 3000 quality-controlled reads were omitted, resulting in the removal of
201 about 12% of samples. For taxonomic group analyses, "diatoms" were defined as all ESVs that
202 were classified to the class Diatomea, and "picophytoplankton" were operationally defined as all
203 ESVs that were classified to the groups Chlorophyta, Haptophyta, or Chrysophyceae. Open source
204 scripts implementing sequence analysis and visualization are available at
205 https://github.com/rec3141/microscape, and scripts to generate the plots and tables found in this
206 manuscript are available at https://github.com/rec3141/rml_thesis.
207 Diatom and picophytoplankton relative abundance tables were subjected to fourth-root
208 transformation before clustering (using 'ggplot2', 'gplots', and 'heatmap.plus' packages for R). A
209 table of Bray-Curtis dissimilarities was calculated from the transformed relative abundance matrix,
210 and samples were hierarchically clustered using Ward's minimum variance method.
211 Canonical Correspondence Analysis (CCA) finds response variables that are maximally
212 related to linear combinations of the explanatory variables provided. In this study we used taxa
213 relative abundances as response variables and the following metadata and environmental
214 parameters as explanatory variables: day of year, depth, bottom depth, distance to shore, latitude,
215 longitude, temperature, salinity, fluorescence, and dissolved oxygen. These parameters were
216 chosen because they can be obtained in situ via shipboard data streams and during a CTD cast.
217 Using the R package 'vegan' (Oksanen et al. 2019), CCA was performed across taxonomic subsets

of the relative abundance tables. In addition to ESVs, diatom and picophytoplankton communities were analyzed after aggregation to the taxonomic levels of genus and family to explore patterns of community composition at higher taxonomic levels.

RESULTS

Environmental Conditions

During the ASGARD expedition in June 2017, sampled surface water temperatures ranged from 1.1 °C to 10.9 °C, with the warmest water consistently above 6 °C appearing south of Nome (Fig 2). Beneath the surface, sampled water temperatures ranged from −1.4 °C to 7.3 °C. Water masses present at the time of sampling included Alaskan Coastal Water (ACW), Bering Shelf Water (BSW), and Remnant Winter Water (RWW; Fig 3). Concentrations of chlorophyll a were highest during June, with an average across sampled stations of 2.8 mg m^{-3}; surface waters averaged 2.8 mg m^{-3}, midwater depths 3.8 mg m^{-3}, and bottom depths 1.7 mg m^{-3}. The highest concentration observed was 26.2 mg m^{-3} at 3 m depth at station DBO3.6.

Fig 2: Sea surface temperature (°C) at each sampling site for each cruise in the northern Bering and Chukchi seas during the spring and summer of 2017. Values were gridded using weighted-average gridding in ODV. From left to right: ASGARD (June 9–29), AMBON (August 7–22), and DBO-NCIS (August 28–September 13)

Fig 3: Temperature-Salinity plots of water sampled in the northern Bering and Chukchi seas during the 2017 cruises overlaid with environmental metadata: (A: upper left) water mass designations; (B: upper right) total nitrate (μM; NO_3^{2-} + NO^-); (C: lower left) dissolved oxygen (μmol/kg); (D: lower right) chlorophyll fluorescence (mg m^{-3}; from the CTD fluorometer).

During the AMBON cruise in August, sampled surface seawater temperatures ranged from 3.8 °C to 10.1 °C, with subsurface temperatures ranging from −0.2 °C to 9.9 °C (Fig 2). Water masses encountered were the ACW, BSW, and RWW (Fig 3). Concentrations of chlorophyll a were lower during August sampling, averaging 1.4 mg m^{-3} across all samples and depths, 1.1 mg m^{-3} at the surface, 1.6 mg m^{-3} at midwater depths, and 1.2 mg m^{-3} at bottom depths. The highest concentration observed was 7.9 mg m^{-3} at 32 m depth at station DBO4.6.

During the DBO-NCIS cruise in late August–early September, sampled surface seawater temperatures ranged from 1.8 °C to 7.5 °C, with subsurface temperatures ranging from −1.7 °C to 8.6 °C (Fig 2). Water masses encountered included ACW, Atlantic Water (AW), ACW, BSW, Melt water/river water (MWR), RWW, and Winter water (WW; Fig 3). Across the Chukchi shelf, strong winds from the east drove upwelling through Barrow Canyon and even reversed the ACW, detectable at lines DBO3, DBO4, and DBO5. Concentrations of chlorophyll a were the lowest of the three cruises, averaging 0.8 mg m^{-3} across all samples and depths; mean values of 1.1 mg m^{-3}

were observed at the surface, 0.7 mg m^{-3} at midwater depths, and 0.9 mg m^{-3} at bottom depths. The highest concentration observed was 5.8 mg m^{-3} at 33 m depth at station W-4.

Taxonomic Diversity

Overall Structure

Eukaryotic microbial communities in the Bering Strait and Chukchi Seas during the open water season of 2017 were assigned (bootstrap support > 60%) to 35 Phyla and 58 Classes. The 7 most abundant Phyla (as classified using SILVA) made up 93% of the relative sequence abundance across all samples: Ochrophyta (39.8%, primarily Diatomea and Chrysophyta), Dinoflagellata (24.6%, mostly mixotrophic taxa), Ciliophora (8.0%), Protalveolata (6.4%, primarily Syndiniales), Chlorophyta (5.2%, primarily *Mamiella*les), Chytridiomycota (4.8%), and Prymnesiophyceae (4.4%). Overall, the groups we defined as "picophytoplankton" made up 10.0% of the relative sequence abundance across all samples.

Despite an opportunistic sampling scheme that resulted in spatiotemporal heterogeneity of sampling sites and little direct overlap among cruises, the dominance of diatoms was particularly consistent over the course of the season, with mean relative abundances of 36.0 ± 0.1% across cruises. Chlorophyta also remained fairly consistent over the summer at 4.8 ± 0.7% across cruises. Prymnesiophyceae (i.e. Haptophytes) reached maximal relative abundances in June (8.2%) but were nearly absent in September (0.5%). The dominant mixotrophs and heterotrophs (Dinoflagellata and Ciliophora, respectively) reached maximal relative abundances in August (27.6% and 11.3%, respectively). Among parasites, *Sydiniales* represented 1.0% of the mean relative abundance in June and 9.6% in September (with high spatial variability), while the Chytridiomycota exhibited the opposite pattern with maximal relative abundances in June (6.5%) and minimum in September (1.1%).

278

279 *Size Structure*

280 Picophytoplankton, generally defined as single-celled eukaryotes that are less than 2.0 μm
281 in diameter, were operationally defined here as all taxa that were classified to the taxonomic groups
282 Chlorophyta (green algae), Haptophyta, or Chrysophyceae (golden algae, with the Ochrophyta).
283 While size does not necessarily correlate with taxonomy, we found that these flagellated cells
284 generally fell into the expected size range, with the prominent exception of *Micromonas* ESV 20,
285 which was found frequently on 20 μm filters (Supp Fig 1). This abundant organism may have
286 fallen prey to larger protists that were captured on the large filter. Some picophytoplankton taxa
287 are known to be able to form colonies (e.g. *Phaeocystis*), but these taxa were quite rare on 20 μm
288 filters, suggesting they were free-living (or easily disaggregated) in the study region. The
289 remainder of this manuscript will focus only on results from the "Survey" stations, which were not
290

291 size-fractionated prior to filtration onto 0.2 μm filters.

292

Diversity within Genera

293 A significant positive correlation was observed between genus relative abundance and ESV
294 richness for diatoms ($N=25$, $p<<0.001$, Spearman correlation) but not for picophytoplankton
295 ($N=16$, $p>0.05$, Spearman correlation). In diatoms, the genera with the highest relative abundances
296 (*Chaetoceros*, *Thalassiosira*) also had the highest diversity at the ESV level (43 and 44 ESVs,
297 respectively).

298

Diatoms

Diatom taxa were classified to 5 families, 25 genera, and 201 unique ESVs, which were used as molecular proxies for species (or lower) level taxonomy (Table 2). The most prominent family was Mediophyceae (88% diatom relative abundance) with the other families contributing from <1% to 6% of the diatom relative abundance. Multiple genera represented the families Mediophyceae (9), Bacillariophyceae (9), and *Fragilaria*les (3), while only 2 genera each were found within the Melosirids and Rhizosolenids (Table 2). The distribution of diatom proportions was highly skewed, with only 14 ESVs making up 80%, 26 ESVs making up 90%, and 99 ESVs making up 99% of the cumulative relative abundance (Supp Fig 2).

Chaetoceros was the most common diatom genus across all depth bins (48–71%) followed by *Thalassiosira* (15–26%). Other genera ranged from <1–6% at all depths. Some prominent diatom ESVs were putatively identified to species using best BLAST hits, including ESV 2 (*Chaetoceros socialis* complex) and ESV 19 (*Chaetoceros diadema*).

317 Table 2: Diatom taxonomy list for the northern Bering and Chukchi seas cruises during 2017 using
318 a taxonomic bootstrap cutoff of 60%. Taxonomy follows SILVA v132.

319

Family	**Genus**	**Relative Abundance (%)**	**ESVs**	**Mean bootstrap support**
Mediophyceae	*Chaetoceros*	61.7	43	96
	Thalassiosira	18.6	44	98
	Unidentified	2.8	12	28
	Lauderia	2.1	1	92
	Arcocellulus	1.9	3	91
	Skeletonema	1.0	4	100
	Attheya	0.3	2	100
	Brockmanniella	0.1	2	100
	Cyclotella	< 0.1	1	100
	Eucampia	< 0.1	1	100
Bacillariophyceae	Unidentified	1.6	21	46
	Pseudo−nitzschia	1.5	6	94
	Fragilariopsis	1.3	2	88
	Cylindrotheca	0.5	7	93
	Nitzschia	0.3	6	82
	Navicula	0.2	4	96

	Pleurosigma	0.1	3	75
	Entomoneis	0.1	1	95
	Asterionellopsis	< 0.1	2	100
	Amphora	< 0.1	1	100
Rhizosolenids	*Rhizosolenia*	0.3	2	92
	Guinardia	0.2	3	95
	Unidentified	0.1	2	45
Fragilariales	*Thalassionema*	< 0.1	2	100
	Fragilaria	< 0.1	1	60
	Synedropsis	< 0.1	1	73
Melosirids	*Melosira*	< 0.1	1	100
	Stephanopyxis	< 0.1	1	100
Unidentified Diatoms	Unidentified	5.4	22	15

320

321 *Picophytoplankton*

322 Picophytoplankton taxa were classified to 3 kingdoms and 16 genera, with 227 unique
323 ESVs (Table 3). Multiple genera represented Chlorophyta (8) and Haptophyta (7), while only 1
324 was identified in Chrysophyceae. The most prominent ESVs (Table 3) were within the
325 Chloroplastida (52% picophytoplankton relative abundance), followed by Haptophyta (42%), and
326 Chrysophyta (6%). The distribution of picophytoplankton proportions was highly skewed, with

only 9 ESVs making up 80% of the total, 23 ESVs making up 90%, and 99 ESVs making up 99% of the cumulative relative abundance (Supp Fig 3).

Among the picophytoplankton were well-known genera like *Bathycoccus*, *Micromonas*, *Mamiella*, *Chrysochromulina*, *Phaeocystis*, and *Nannochloris* (Lovejoy et al. 2006; McKie-Krisberg and Sanders 2014). *Micromonas* was the most common genus in the picophytoplankton assemblage, comprising 36% of the picophytoplankton sequences at the surface, 36% in midwater depths, and 24% at the bottom. *Phaeocystis* was the second most common genus with 20% relative abundance at the surface, 19% at midwater depths, and 38% at the bottom, followed by *Chrysochromulina* which comprised 11%, 10%, and 8% of picophytoplankton sequences in the surface, midwater, and bottom, respectively. All other identified genera varied from <1 to 3% across all depths. Prominent picophytoplankton ESVs that were putatively identified to species level using best BLAST hits included ESV 20 (*Micromonas pusilla*), ESV 31 (*Phaeocystis pouchetii*), and ESV 188 (*Bathycoccus prasinos*).

While many of the top ESVs for diatoms and picoeukaryotes were easily identified, numerous others did not have good matches to sequences in the database used for taxonomic identification. Future studies should work to identify these sequences using cultured representatives that might also be identified in older studies based on morphological data.

349 Table 3: Diatom taxonomy list for the northern Bering and Chukchi seas cruises during 2017
350 using a taxonomic bootstrap cutoff of 60%. Taxonomy follows SILVA v132 (ref).

351

Taxonomic Group	Genus	Relative Abundance (%)	ESVs	Mean bootstrap support
Chrysophyceae	Unidentified	6.5	54	59
	Paraphysomonas	0.8	9	100
Chlorophyta	*Micromonas*	33.5	6	99
	Unidentified	14.4	34	64
	Prasinoderma	1.2	6	97
	Pyramimonas	0.8	2	94
	Mamiella	0.4	7	85
	Pterosperma	0.3	12	82
	Dolichomastix	0.2	10	87
	Cymbomonas	0.2	1	73
	Nephroselmis	0.1	1	100
Haptophyta	*Phaeocystis*	23.8	8	99

Chrysochromulina	9.9	26	89
Unidentified	6.4	32	45
Prymnesium	0.6	6	87
Braarudosphaera	0.4	2	100
Haptolina	0.3	5	95
Imantonia	0.1	1	100
OLI16029	< 0.1	5	76

Community Clustering

Diatom Assemblages

Samples were categorized into seven assemblages (D1–D7) based on hierarchical clustering of diatom community composition, with 32–140 samples per cluster (Table 4). The sample assemblages separated into two major branches, defined primarily by the relative abundance of *Chaetoceros* ESV 2, which was singularly dominant in clusters D1 and D2, while of varying importance in D3–D7 (Fig 4). Of the clusters with abundant *Chaetoceros* ESV 2, its relative abundance increased from D4 (16%) to D6 (23%) to D7 (31%) to D2 (58%) to D1 (96%). Cluster D3 was highly diverse, with no single dominant ESV. Compared to other clusters, D3 had relatively high proportions of unknown taxon ESV 56 (8%) and *Skeletonema* ESV 336 (4%).

Fig 4: Hierarchical clustering of samples based on diatom community composition from the northern Bering and Chukchi seas cruises during 2017. (a) The dendrogram shows the relationships among the clusters (D1—D7) and number of samples categorized to each. (b) Barplots show the relative abundance of the top 90% most abundant ESVs in each assemblage. (c) The color legend shows the taxonomic identification of each ESV, with numbers in brackets indicating taxonomic bootstrap support for the genus label, and numbers in parentheses indicating the mean relative abundance of that ESV across all samples in parts per thousand.

Cluster D6 was the only cluster to have a majority of *Thalassiosira*, dominated by ESV 85 (27%), unknown taxon ESV 453 (12%), and unknown taxon ESV 389 (8%). Cluster D2 had a higher proportion of *Thalassiosira* ESV 104 (16%) compared to any other cluster. Cluster D4 was distinguished by higher concentrations of unknown taxon ESV 323 (12%; tentatively assigned to *Nitzschia*) and *Chaetoceros* ESV 27 (12%) than any other cluster. Cluster D5 was characterized by high proportions of *Chaetoceros* ESV 19 (27%), which was commonly found throughout the study region, and ESV 246 (20%; tentatively assigned to *Helicotheca*), and ESV 56 (5%; tentatively assigned to *Guinardia*), which were not.

Table 4: Hierarchical clustering of samples based on diatom community composition (D1-D7) from the northern Bering and Chukchi seas cruises during 2017. Numbers of samples per cluster are shown for each cruise and depth bin. Within each cruise and depth bin, the most frequent cluster is shown in bold.

Project	Depth Bin	D1	D2	D3	D4	D5	D6	D7
ASGARD	surface	2	2	3	12	0	7	**32**
ASGARD	midwater	3	3	1	10	0	16	**32**
ASGARD	bottom	0	1	3	10	0	9	**34**
AMBON	surface	1	1	**33**	1	14	0	1
AMBON	midwater	3	4	**66**	6	18	0	17
AMBON	bottom	1	5	**22**	0	1	0	13
DBO-NCIS	surface	**11**	10	1	0	0	0	1
DBO-NCIS	midwater	47	**55**	6	2	0	0	5
DBO-NCIS	bottom	**22**	1	1	0	0	0	5

Each cluster was composed of samples originating from a range of environmental conditions, with D3 standing out as having a particularly high median temperature (7 °C), D1 having relatively high nutrient concentrations, and D4 and D5 having relatively low nutrient concentrations (Fig 5). Cluster D3 was found in the largest range of environmental conditions, from –1 to 11 °C and from salinities of 25 to 35. Cluster D6 had the lowest temperature range, from 2 °C to 5 °C.

394

395 Fig 5: Distribution of temperature (above) and silicate concentrations (below) from samples in
396 each diatom assemblage cluster (D1–D7), colored by water mass for the northern Bering and
397 Chukchi seas cruises during 2017.

398

399 D7 was the most frequently observed cluster during the ASGARD cruise (54% of samples;
400 Table 4; Fig 6), followed by D4 and D6 (18% each). D7 was prominent throughout the Bering
401 Strait region, with the exception of the DBO3 line off the coast of Point Hope, AK, where
402 *Thalassiosira*-rich cluster D6 was common. A surface bloom was apparent at the western-most
403 station of that transect, indicated by elevated chlorophyll fluorescence (>12 mg m^{-3}). D7 was again
404 common along the northernmost transect sampled during June (Fig 6), where fluorescence values
405 were lower (<3 mg m^{-3}).

406

407 Fig 6: Spatiotemporal trends in diatom community assemblages from the northern Bering and
408 Chukchi seas cruises during 2017.

409

410 D4 and D6 occurred overwhelmingly in June (87% of all occurrences) and were mostly
411 confined to the Bering Strait region (Fig 6), where chlorophyll fluorescence values were relatively
412 high; they appeared proportionally across surface, midwater, and bottom depths (Fig 6). D4
413 appeared in coastal zones both north and south of the Bering Strait, whereas D6 appeared only in
414 a patch in the central channel offshore of Point Hope (Table 4; Fig 4; Fig 6).

415 During the AMBON cruise in August, D3 was the most common cluster, occurring 58%
416 of the time (Table 4), followed by D5 (16%), and D7 (15%). Cluster D5 was observed exclusively

during the AMBON cruise, primarily in surface waters of an offshore transect crossing Hanna Shoal (Fig 6). Cluster D7 was still common, but found almost exclusively at midwater and bottom depths, potentially indicating a sinking *Chaetoceros* bloom (Table 4; Fig 5; Fig 6).

During the DBO-NCIS cruise in late August and September, clusters D1 (48%) and D2 (40%) were most prominent. Both the overall diversity and chlorophyll fluorescence values were lower during this cruise, with most samples dominated by *Chaetoceros* ESV 2 (Table 4; Fig 5; Fig 6).

Picophytoplankton Assemblages

Samples were categorized into eleven assemblages (P1–P11) based on hierarchical clustering of picophytoplankton community composition, with 16–86 samples per cluster (Table 5, Fig 7). The sample clusters split first between P1–P3 and P4–P11, followed by a second major split between P4–P7 and P8–P11; these divisions roughly reflect the seasonality/cruise schedule.

Clusters P1 and P4 were both characterized by very low diversity (Fig 7), dominated by *Micromonas* ESV 20 (78%) and *Phaeocystis* ESV 31 (81%), respectively. *Micromonas* ESV 20 also made up major portions of the picophytoplankton diversity in P2 (36%), P3 (32%), P5 (35%), P6 (15%), P7 (15%), P9 (29%), P10 (49%), and P11 (14%). *Phaeocystis* ESV 31 was also an important contributor to P5 (43%), P7 (37%), P10 (6%), and P11 (28%).

Fig 7: Hierarchical clustering of samples based on picophytoplankton community composition from the northern Bering and Chukchi seas cruises during 2017. (a) The dendrogram shows the relationships among the clusters (P1—P11) and number of samples categorized in each. (b) Barplots show the relative abundance of the top 90% most abundant ESVs in each assemblage. (c) The color legend shows the taxonomic identification of each ESV, with numbers in brackets indicating taxonomic bootstrap support for the genus label, and numbers in parentheses indicating the mean relative abundance of the ESV across all samples in parts per thousand.

Other taxa that contributed to distinguishing clusters include *Bathycoccus* ESV 188 (P8: 17%), *Nannochloris* ESV 277 (P3: 54%), *Chrysochromulina* ESV 297 (P10: 17%), *Chrysochromulina* ESV 307 (P11: 18%), ESV 659 (P9: 37%; possibly *Uroglena*), ESV 665 (P7: 15%; possibly *Chrysochromulina*), ESV 748 (P6: 19%; possibly *Chrysolepidomonas*), ESV 760 (P8: 15%; unidentified), *Chrysochromulina* ESV 840 (P9: 12%), and *Prasinoderma* ESV 1381 (P2: 23%).

Each cluster was composed of samples originating from a range of environmental conditions, with P8 standing out as having a particularly high median temperature, P2 and P6 for having relatively high nutrient concentrations, and P8 and P9 for having relatively low nutrient concentrations.

Table 5: Hierarchical clustering of samples based on picophytoplankton community composition (P1-P11) for the northern Bering and Chukchi seas cruises during 2017. Numbers of samples per cluster are shown for each cruise and depth bin. Within each cruise and depth bin, the most frequent cluster is shown in bold.

Project	Depth Bin	P1	P2	P3	P4	P5	P6	P7	P8	P9	P10	P11
ASGARD	surface	0	0	0	4	16	0	**17**	5	0	0	**17**
ASGARD	midwater	1	0	0	11	**23**	0	17	0	0	0	12
ASGARD	bottom	0	0	0	6	**18**	1	17	3	0	0	13
AMBON	surface	2	0	0	0	0	2	0	**29**	7	10	0
AMBON	midwater	3	2	1	2	2	18	5	**36**	7	20	11
AMBON	bottom	1	0	2	1	2	**19**	3	10	0	0	3
DBO-NCIS	surface	6	1	**7**	2	2	0	0	0	1	0	0
DBO-NCIS	midwater	34	13	**37**	5	7	0	1	3	1	1	1
DBO-NCIS	bottom	1	**11**	4	2	3	1	0	0	0	0	0

Picophytoplankton spatiotemporal distributions

The three primary splits in the picophytoplankton assemblage clustering roughly reflected the seasonality of the cruise that the samples were collected on (Table 5), with P1–P3 composed primarily of samples from DBO-NCIS (90%), P4–P7 mostly from ASGARD (63%), and P8–P11 mostly from AMBON. However, P6 was an exception to this trend (95% collected on AMBON), as was P11 (74% collected on ASGARD).

During the ASGARD cruise in June, *Phaeocystis*-rich clusters P4, P5, P7, and P11 occurred 94% of the time (Table 5). Cluster P11 was prominent throughout the Bering Strait, while P4 and P7 appeared more frequently at the edges of P11 along the central channel, and P5 appeared more often closer to the Alaskan coast

During the AMBON cruise in August, picophytoplankton communities were *Phaeocystis*-poor (Table 5), with diverse clusters P8 (38%) and P6 (20%) becoming common (Fig 8), along with *Micromonas*-rich P10 (15%). Clusters P8 and P10 were widely distributed across the Chukchi Shelf, and about 10 times as common at surface and midwater depths than at the bottom (Table 5; Fig 8; Fig 9). Cluster P10 was particularly prevalent in the channel between Wainwright and Hanna Shoal, and was not found at the warm, fresh coastal sites, which were primarily affiliated to P8. While cluster P6 was common across the central Chukchi Shelf, it was never observed near shore, and was found at midwater and bottom depths 94% of the time (Table 5; Fig 8; Fig 9).

Fig 8: Distribution of temperature (*above*) and phosphate concentrations (*below*) from samples in each picophytoplankton assemblage (P1–P11), colored by water mass, from the northern Bering and Chukchi seas cruises during 2017.

Fig 9: Spatiotemporal trends in picophytoplankton community assemblages for the northern Bering and Chukchi seas cruises during 2017.

During the DBO-NCIS cruise in late August and September, the *Phaeocystis*-rich clusters were again absent, as were the diverse clusters P8 and P10 (Table 5). In their place were clusters

P1 (28%, rich with *Micromonas* ESV 20), P3 (33%, rich with *Nannochloris* ESV 277), and P2 (17%), similar to P1 with the addition of *Prasinoderma* ESV 1381 (Table 5; Fig 8; Fig 9).

Environmental Drivers of Community Variability

The ability to predict microbial communities in Arctic seawater in real time while aboard ships would be a valuable tool. To test our current ability to make such predictions, we restricted the analysis of environmental drivers to those parameters that are readily available at sea, i.e. those available during a CTD cast: day of year, sampling depth, bottom depth, distance to shore, latitude, longitude, temperature, salinity, fluorescence, and dissolved oxygen. Exploratory analyses including additional explanatory variables (e.g. SPM, CHN, nutrients) did not display marked improvements in predictions (not shown).

Aggregation by Taxonomy

In general, diatom and picophytoplankton relative abundances were not easily predictable based on metadata or environmental variables available at the time of sampling (Fig 10). After aggregating at the ESV, Genus, and Family levels, no linear combination of environmental parameters explained more than 12.6% of variability within diatom communities or 19.7% in picophytoplankton (Table 6).

Fig 10: Diatom (*left*) and picophytoplankton (*right*) sample assemblages overlaid on temperature-salinity plots for the northern Bering and Chukchi seas cruises during 2017.

Table 6: Proportion of constrained variability captured by selected environmental variables for the northern Bering and Chukchi seas cruises during 2017.

	Diatoms	**Picophytoplankton**
Family	11.6%	19.7%
Genus	12.6%	14.2%
ESV	12.5%	7.4%
Cluster	43.6%	32.5%

For diatom ESVs, the first two CCA axes contributed 47% of the inertia (Supp Fig 4), driven primarily by day of year and salinity, respectively. At the genus level, the first two axes contributed 61% of the inertia, driven primarily by temperature and day of year, respectively. At the family level, the first two axes contributed 99% of the inertia, driven primarily by temperature and distance to shore, respectively.

For picophytoplankton ESVs, the first two CCA axes contributed 44% of the inertia (Supp Fig 4), driven primarily by day of year and temperature, respectively. At the genus level, the first two axes contributed 59% of the inertia, driven primarily by day of year and dissolved oxygen, respectively. At the family level, the first two axes contributed 68% of the inertia, driven primarily by day of year and distance to shore, respectively.

Analysis of variance (ANOVA) was used to determine the significance of each environmental parameter in explaining the variability in relative abundance of taxa (Supp Fig 4). For diatoms, the number of significant ($p < 0.05$) parameters decreased from ESV (9/10) to genus

(8/10) to family (5/10). For picophytoplankton, 9/10 parameters were significant at each taxonomic level.

Aggregation by Cluster

CCAs were also performed on communities that were aggregated by community assemblage. To aggregate by sample cluster (D1–D7 in diatoms, P1–P11 in picophytoplankton), the relative abundance of each taxon in each sample was replaced by the mean relative abundance of that taxon in the samples within the sample cluster prior to CCA analysis.

Significant improvements in explaining community variability were detected after aggregating by cluster: 43.6% in diatoms and 32.5% in picophytoplankton (Table 6). For diatom clusters, the first two CCA axes contributed 83% of the inertia, driven primarily by day of year and temperature, respectively. For picophytoplankton clusters, the first two axes contributed 73% of the inertia, also driven primarily by day of year and temperature, respectively. Cluster aggregation resulted in 9/10 significant parameters for both diatoms and picophytoplankton.

Temperature Effects on Community Structure

Using CCA, temperature was repeatedly identified as an important factor structuring the microbial communities in our study region. The clustering analyses (Fig 5; Fig 8; Fig 10) also suggested that a shift in community structure may have occurred around 5–7 °C, so we used Student's t-tests to identify breakpoints in ESV relative abundance as a function of temperature (Table 7).

The three most abundant diatoms (all *Chaetoceros*) showed a clear preference for waters colder than 7 °C (Table 7; Fig 11), as did the two most abundant picophytoplankton: *Micromonas*

549 ESV 20 and *Phaeocystis* ESV 31 (Table 7; Fig 12). Among diatoms, about 70% of ESVs had a
550 maximal relative abundance in waters colder than 7 °C (Fig 11); among picophytoplankton, it was
551 over 80% (Fig 12). Some taxa preferred warmer waters, however, including *Skeletonema* ESV 336
552 and *Pseudo−nitzschia* ESV 274 (Fig 13), as well as *Bathycoccus* ESV 188 and *Nannochloris* ESV
553 277.
554

555 Fig 11: (*left*) Mean diatom ESV relative abundance for the northern Bering and Chukchi seas
556 cruises during 2017 after binning by temperature; ESVs are colored by genus. (*right*) Scaled
557 diatom ESV relative abundances sorted by temperature at maximum relative abundance (each
558 column is an ESV).
559

560 Fig 12: (left) Mean picophytoplankton ESV relative abundance for the northern Bering and
561 Chukchi seas cruises during 2017 after binning by temperature; ESVs are colored by genus.
562 (right) Scaled picophytoplankton ESV relative abundance sorted by temperature at maximum
563 relative abundance (each column is an ESV).
564

565 Fig 13: The relative abundances of two ESVs corresponding to the genus *Pseudo−nitzschia* as a
566 function of temperature.

Table 7: Breakpoints in preferred water temperature identified for some abundant ESVs for the northern Bering and Chukchi seas cruises during 2017. The t-tests tested the hypothesis that the relative abundance of an ESV was significantly different (two-sided, alpha = 0.05, Bonferroni-corrected) in samples collected in warm water (> breakpoint) compared to cold water (< breakpoint). For each ESV, the test statistics were computed for every unique temperature in the dataset and breakpoints were identified as local minima of the test p-values, all of which were $p<<0.0001$.

	ESV	**Breakpoint (°C)**	**Prefers warm/cold**
Diatoms	*Chaetoceros* ESV 2	6.7	cold
	Chaetoceros ESV 19	7.0	cold
	Chaetoceros ESV 27	7.0	cold
	Skeletonema ESV 336	5.2	warm
	Pseudo−nitzschia ESV 274	4.5	warm
	Pseudo−nitzschia ESV 518	4.5	cold
	Thalassiosira ESV 104	4.2	warm
Picophytoplankton	*Micromonas* ESV 20	6.2	cold
	Phaeocystis ESV 31	6.9	cold
	Bathycoccus ESV 188	5.9	warm

	Nannochloris ESV 277	3.4	warm

574

575

DISCUSSION

This study is the first synoptic, high-throughput molecular phylogenetic investigation of phytoplankton diversity in the Bering and Chukchi Seas based on hundreds of samples collected from June to September in 2017 (Fig 1). We use this unique opportunity to describe the seasonal diversity and geographic distributions of phytoplankton communities in the Chukchi and Bering Seas using metabarcoding. We focus primarily on diatoms and picophytoplankton, both prominent primary producer groups in this region. We also highlight the diversity within these groups and explore the environmental and biological drivers of phytoplankton community structure. These results will help in determining how sub-Arctic and Arctic microbial communities might respond to changes in their environment resulting from anthropogenic global warming.

Diversity, Community Resilience, and Potential Impacts of a Warmer Arctic

The expeditions described here were conducted during the warmest temperatures on record in the Bering and Chukchi Seas, a harbinger of a "new normal" in the warmer Arctic Ocean expected in the future. Paleoecological reconstruction of marine microbial community structure during past periods of climatic change has shown that, even at the species level, communities can be resilient to large changes in environmental conditions (Moritz and Agudo 2013); here we explore the baseline variability in microbial community structure across space and time in this region. While numerous studies have characterized phytoplankton bloom timing (Kahru et al. 2011; Sigler et al. 2014), there are few studies that characterize and identify the diversity of the Bering and Chukchi Sea phytoplankton communities at the molecular level. Here we focus on the 18S rRNA gene as a marker of diversity to examine the ecological mechanisms of resilience to changes in environmental conditions in modern biological communities (Tesson et al. 2014; Sjöqvist and Kremp 2016).

Diatom and picophytoplankton assemblages each consisted of over 200 ESVs, but differed in their relative abundances, with diatoms making up a large fraction (36.0 ± 0.1% mean relative abundance across all sampling seasons), as expected to result from the influx of nutrients through Bering Strait. Among diatoms, 90% of the relative abundance was contributed by the most abundant 26 ESVs, including genera that are well known from the Pacific Arctic like *Chaetoceros*, *Fragilariopsis*, *Navicula*, *Nitzschia*, *Pseudo−nitzschia*, and *Thalassiosira* (Sakshaug 2004; von Quillfeldt 2005). Here we compared diatoms and picophytoplankton to provide baseline estimates for future comparisons to a coming "new Arctic" (Overpeck et al. 2005; Carmack et al. 2015), which is expected to feature increased temperatures and stratification levels, limiting nutrient turnover in surface waters, and possibly causing a shift towards picophytoplankton (Li et al. 2009) resulting from regenerated production (Ardyna et al. 2011). Additionally, diatoms are better adapted to lower light availability, provided nutrients are sufficient (Siemering et al. 2016), another indicator that diatoms as a whole may be negatively affected with less ice coverage throughout the year and with stratification limiting nutrient turnover.

Diatoms and picophytoplankton were sensitive to a temperature transition zone observed at around 5–7 °C (Table 7). One of these, *Chaetoceros* ESV 2, was cosmopolitan, found in nearly every sample in the study, across all seasons, temperatures, and salinities. However, this taxon reached its highest relative abundances in waters colder than 6.7 °C, and declined precipitously above that temperature. *Chaetoceros* ESV 2 was most closely related to *Chaetoceros socialis*, a species complex already known to have high intraspecific diversity (Degerlund et al. 2012; Gaonkar et al. 2017). *Skeletonema* ESV 336 was found almost exclusively in waters warmer than 5.2 °C, consistent with literature descriptions as a genus of temperate, coastal diatoms (Thornton and Thake 1998; Kooistra et al. 2008). Among the picophytoplankton, *Bathycoccus prasinos* ESV

188 appeared almost exclusively in waters warmer than 5.9 °C, while *Phaeocystis pouchetii* ESV 31 and *Micromonas pusilla* ESV 20 appeared predominantly in waters colder than 6.9 °C and 6.2°C, respectively. The clear temperature preferences for some of the most relatively abundant taxa in this region presage changes for these communities as the Arctic and sub-Arctic continue to warm.

In addition to a decline in some common diatoms, the Alaskan Arctic could see shifts in taxa related to known harmful algal bloom-forming species (HABs). *Pseudo−nitzschia* is a genus containing HAB-forming diatoms in which about 50% of species are known to produce domoic acid, a neurotoxin that has recently been identified in Alaskan waters (Lefebvre et al. 2016; Huntington et al. 2020). We found two prominent ESVs classified as *Pseudo−nitzschia* to the genus level in our dataset, with *Pseudo−nitzschia* ESV 518 predominant at lower temperatures, and *Pseudo−nitzschia* ESV 274 predominant at higher temperatures (Fig 13). While it was not possible to identify these to the species level, about 50% of *Pseudo−nitzschia* species have been shown to produce the toxin domoic acid (Bates et al. 2018); this genus may persist and increase in abundance with warming temperatures (Hallegraeff 2010). The picophytoplankter *Phaeocystis pouchetii* ESV 31, detected prominently throughout our study region but especially in early summer, is also a known toxin producer (Eilertsen and Raa 1995); however it's prominence in the Alaskan Arctic may decrease as temperatures rise (Table 7). Nonetheless, changing conditions in the Arctic are still expected to lead to increases in certain HAB-forming taxonomic groups that stand to affect higher trophic levels (Walsh et al. 2011).

These strong temperature preferences are exhibited by taxonomic groups that, combined, contributed a high proportion of the relative abundance. Climate change has occurred cyclically throughout Earth's history (Sarmiento and Bender 1994), though the current pace of

anthropogenically driven climate change is unprecedented (Jeffries et al. 2014). Despite the evidence of diatoms persisting through past climatic events, a rapidly warming Arctic today signals change for numerous prominent taxa. While salinity, nutrients, and temperature each have influence on community structure (Lozupone and Knight 2007), our results imply that temperature plays a greater role than other environmental factors in driving structural changes. This finding is in agreement with a comprehensive TARA Oceans metagenomic study (Sunagawa et al. 2015) examining prokaryotes and picoeukaryotes across temperate, tropical, and polar latitudes, which also concluded that temperature is one of the primary drivers of marine microbial community structure.

Our identification of key groups with strongly preferred temperature ranges allows us to confidently state that primary producer communities will change in the face of climate change, with ramifications felt throughout the Bering and Chukchi Sea ecosystem. Specifically, we expect to see a loss of *Chaetoceros* (especially ESV 2) and *Phaeocystis* ESV 31 (Fig 11, Fig 12). Diatoms with a preference for warmer conditions could still be outcompeted if temperature-driven stratification suppressed the upwelling of nutrients to the surface (Cermeño et al. 2012), which diatoms rely on to outgrow other phytoplankton early in the growing season (Litchman 2007). *Chaetoceros* and *Thalassiosira* both rely on high nutrient concentrations to bloom, and form large chains that contribute significantly to the carbon cycle. The combination of high nutrient requirements and strong temperature preferences of some taxa (Fig 11) could lead to a decrease in their abundance in the future, and a subsequent increase by other taxa. If the replacement taxa are smaller, solitary diatoms, or picophytoplankton like *Micromonas*, this could have significant effects on the carbon cycle, leading to a reduced flow of particulate carbon to the benthos. In the present ecosystem, this flow drives the tight benthic-pelagic coupling observed over the Bering

and Chukchi shelves (Grebmeier and Barry 1991; Dunton et al. 2005); rapid changes could cause significant stress to those animal communities.

In general, we observed a spectrum of generalist to specialist diatom ESVs: some taxa were found to thrive in a range of environmental conditions while some were found only in specific and narrow environmental conditions. The CCA analysis captured only a rough summary of this diversity, making it difficult to distinguish specialist from generalist taxonomic groups, and illustrating that this type of analysis may be more meaningful for picking informative variables to investigate than in finding the root causes of community variability (Thaler and Lovejoy 2014). To better understand how these communities change with environmental conditions, collecting samples from the same area over a long period of time may be more useful than collecting samples at sites just one time during the year. Because ship-based observations are limited in temporal scope, long-term mooring deployments like the Chukchi Ecosystem Observatory (Hauri et al. 2018) will be critical for understanding the seasonal changes in planktonic community structure, and future deployments of the Chukchi Ecosystem Observatory are expected to include sampling of microbial communities for this purpose.

Biogeography

Clustering the samples by community assemblage revealed cases where sample clusters dominated by chain-forming diatoms (e.g. *Chaetoceros* and *Thalassiosira* in clusters D1, D2, and D7) were more prevalent in midwater and bottom depth bins, suggestive of a bloom in the process of sinking as also indicated by low chlorophyll concentrations. Alternatively, these diatoms could be indicative of sustained production due to higher nutrient concentrations found deeper in the water column since the vast majority of sampling depths fell within the euphotic zone.

A similar phenomenon was observed for *Phaeocystis*, another important group in the carbon cycle. After blooming, *Phaeocystis* can aggregate, sink, and carry large quantities of organic carbon to the seafloor, supporting the benthos and potentially sequestering carbon. Two *Phaeocystis*-rich clusters, P4 and P5, were more prevalent at midwater and bottom depth bins, again suggesting a sinking bloom or sustained production at the bottom due to nutrients and suitable conditions at depth.

Similarly, clusters were also useful in identifying temperature preferences for certain taxa, allowing the prediction of certain ESVs that may be more sensitive to a warming Alaskan Arctic. Each of these putatively sinking communities (clusters D1, D2, P4, and P5) was substantially more prevalent in waters colder than 6 °C compared to waters warmer than 6 °C, suggesting that these sinking communities may indeed be negatively affected by warmer waters in the future Arctic.

We found several *Micromonas* ESVs to be prominent members of the picophytoplankton community, though the most abundant, *Micromonas* ESV 20, was most commonly found at temperatures below 6.2 °C, replaced by *Bathycoccus* ESV 188 in warmer coastal waters. Future studies could investigate the different physiologies of *Micromonas* and *Bathycoccus* to predict potential changes in biogeochemical cycling or primary or secondary productivity in the case that *Bathycoccus* expanded further into the *Micromonas* niche. While this pattern may hold at the large scale, in more localized settings, factors like currents, wind direction, advection of water from off shelf, or upwelling of nutrients may provide stronger indications of community composition due to mixing water masses, or the growth of opportunistic taxa when certain conditions are met, e.g. increased nutrient loads.

Top-Down and Bottom-Up Controls on Community Structure

Our study focused primarily on environmental variables that are bottom-up controls on primary producers. Top-down controls were not explored in this study, however grazing by heterotrophic protists has been demonstrated to impact phytoplankton community structure. Changes in phytoplankton bloom development has been shown to impact food web structure and top-down and bottom-up control of marine ecosystems in polar waters (Arrigo and van Dijken 2004). The PCR primers used in this study also amplify heterotrophic protist DNA (e.g. dinoflagellates and ciliates), but their analysis was outside of the scope of this work at this time. Future studies should include them as potential drivers of phytoplankton community composition in this region.

Top-down and bottom-up controls have long been debated in the field. Results from this study suggest that bottom-up controls may influence diversity in terms of ESVs, but do not appear to drastically reshape communities at the family level and above. We suggest that top-down controls are more likely to drive community structure in terms of broad shifts in diversity. Our results also suggest that top-down and bottom-up controls may oscillate as environmental conditions shift over time and space, a trend demonstrated in another coastal sea (Mozetič et al. 2012). If shifts in community structure are more likely, climate change may not have the detrimental effects predicted, i.e., resilience in diatoms means the efficiency of the biological carbon pump to the seafloor will be maintained. As seawater temperatures continue to rise in the Arctic, some studies have suggested that a shift to more mixotrophic plankton could also occur, altering biogeochemical cycling (Ward and Follows 2016). Common throughout temperate oceans (Hartmann et al. 2012; Flynn et al. 2013), mixotrophs are multifunctional protists that photosynthesize when nutrient concentrations are high, and assume an osmotrophic or

734 phagotrophic lifestyle in nutrient deplete conditions (Ward and Follows 2016). Diatoms, in
735 general, are relatively large and heavy, meaning they sink quickly, raising the efficiency of transfer
736 of carbon to the seafloor. In contrast, mixotrophic picophytoplankton are much smaller, and are
737 expected to increase in abundance in a warmer Arctic due to the advantages that mixotrophy brings
738 in conditions of high resource variability (Mitra et al. 2016; Stoecker et al. 2017b).

739 Hypothesized changes as a result of increased mixotrophy in the Arctic include increased
740 carbon fixation but decreased vertical carbon flux (Stoecker and Lavrentyev 2018), which would
741 be expected to increase trophic transfer, possibly raising planktonic production at higher trophic
742 levels (Mitra et al. 2014; Ward and Follows 2016). An increase in mixotroph abundance could
743 reduce carbon flux to the benthos, which could have long-lasting repercussions all the way up the
744 food web to humans. Our study observed a relatively high abundance of *Micromonas* ESV 20 (not
745 identified to species), a prominent genus of picophytoplankton found throughout the world ocean
746 that has been identified as mixotrophic. Recent studies (Lovejoy et al. 2007; McKie-Krisberg and
747 Sanders 2014) have demonstrated that this genus has dispersed widely throughout the Arctic
748 Ocean, and has been observed to be particularly sensitive to temperature (Demory et al. 2018).
749 The strain found in the Arctic differs from the clades found in other oceans by notably thriving at
750 6–8 °C due to its adaptations to cold and low-light conditions (Lovejoy et al. 2007). Our study
751 found the peak abundance of *Micromonas* ESV 20 occurred at 6.2 °C and this taxa preferred colder
752 waters (Table 7). As a mixotroph, *Micromonas* could impact production in the Arctic if it were to
753 displace phytoplankton that rely solely on photosynthesis. Combined with its strong temperature
754 preferences and numerous studies from across the global ocean, *Micromonas* is a key genus to
755 watch and monitor in the face of a changing Alaskan Arctic.

Taxonomic Resolution and Environmental Influence

Our results suggest that over broad scales (multiple sampling seasons and regional sites), taxonomic genera provide a suitable level to understand general impacts of environmental variables on community structure. However, higher taxonomic resolution is needed to observe more subtle shifts not detectable at higher taxonomic levels (e.g. *Chaetoceros* ESV 2 and different temperature preferences of *Micromonas* ESVs). Not only is high taxonomic resolution the most useful for studying community changes, it also adds to our understanding of diversity in a rapidly changing ocean environment. When possible, it is best to identify organisms to the highest taxonomic resolution possible, underscored by numerous studies demonstrating the importance of microdiversity (Allison and Martiny 2008; Needham et al. 2017; García-García et al. 2019).

In our study we used primers targeting the V4 hypervariable region of the 18S ribosomal RNA gene, which is often specific enough to identify taxa to species level but often not specific enough to identify intraspecific diversity. Because many cultured representatives of Arctic phytoplankton remain missing from sequence databases, and we did not collect morphological data, we deferred from making strong claims to species identifications and focus instead on ESVs as indicators of taxonomic diversity. Future studies should consider the use of more sensitive primers in order to quantify microdiversity within these communities. Even with these limitations, it was still possible to identify several specific ESVs that stand to be the most affected in the face of a warming Arctic, as well as build a comprehensive taxonomic dataset in conjunction with environmental data across the late spring and summer in the Bering and Chukchi Seas. We have clearly demonstrated specific taxonomic groups that stand to be most affected in a new and warming Alaskan Arctic.

Drivers of Community Structure

Statistical analyses suggested that, overall, environmental parameters measured at the time of sample collection (e.g. temperature, salinity, chlorophyll, dissolved oxygen) were not the primary drivers of phytoplankton community structure at broad spatial and temporal scales. While the composition of individual samples across all cruises were not well characterized using these measured variables, the amount of variability explained (i.e. the quality of predictions) increased somewhat when samples were clustered by community assemblage. Environmental parameters accounted for only 12.5% of variability for diatoms at the ESV level and 7.4% for picophytoplankton, but accounted for 43.6% and 32.5% of the variability across clustered sample assemblages for diatoms and picophytoplankton, respectively (Table 6). This suggests clustering samples based on similarity improves the ability to anticipate community composition from environmental data.

During the summer of 2017, environmental parameters measured at the time of sampling held little value for predicting phytoplankton community structure. Many studies have debated which parameters are most important to driving community structure (Krug et al. 2013; Sunagawa et al. 2015; Neeley et al. 2018), with a lack of clear consensus. However, our findings consider these communities at the ESV-level (genus, species, and, when possible, subspecies taxonomic resolution), while prior studies characterized to genus and species. Our higher taxonomic resolution allowed us to determine temperature as having more of a measurable effect on certain taxonomic groups, and especially those ESVs that are most prevalent (Table 7). Water mass has previously been attributed to shaping Arctic phytoplankton communities with some water masses observed to hold distinct communities—including diatoms, chlorophytes, and haptophytes—specifically within Pacific Halocline Water (originating through the Arctic Ocean) and deep

801 Atlantic Water (Fehling et al. 2012; Kalenitchenko et al. 2019). The mixing of these distinct water
802 masses, separated by global thermohaline circulation, may explain the high degree of community
803 dissimilarity observed there, whereas in our study many communities originated from closely
804 related water masses flowing northward from the Pacific Ocean and into the Bering and Chukchi
805 Seas. However, some mixing of water masses appeared to have an impact on our samples. At
806 midwater and bottom depths at AMBON's furthest northeast transect, an inflow of water through
807 Barrow Canyon, suggested by ADCP and nutrient profiles from the area, may have introduced
808 deep Arctic water onto the shelf, with its own unique community, consistent with other
809 observations of distinct communities between on- and offshore environments (Siemering et al.
810 2016). Other instances of community introduction via advection of water have been documented
811 with significant differences attributed to hydrography (Hamilton et al. 2008; Kalenitchenko et al.
812 2019).

813 While our study did not identify any diatom and picophytoplankton taxa found exclusively
814 in temperate waters, our results confirm temperature shifts are likely to affect the distribution of
815 taxa. Changes in temperature have driven poleward shifts of numerous temperate taxa, including
816 phytoplankton, across the globe (Poloczanska et al. 2013). On the Atlantic side of the Arctic, the
817 fronts of Atlantic water masses have moved further north due to sea temperature warming, bringing
818 with it phytoplankton communities characteristic of warmer Atlantic waters (Neukermans et al.
819 2018). While our study did not find strong correlations with water mass, the local trends observed
820 in combination with previous studies indicate water movement is important to communities on a
821 regional level. Highly different water masses in conjunction with increased water masses have a
822 potential to bring in their own distinct communities, creating conditions more suitable for taxa not
823 traditionally found in the Arctic. A clear understanding of the physical environment is needed to

824 understand the context of changes within communities across all oceans, and future studies could
825 usefully incorporate backtracing of water parcels using models of current flow to better predict the
826 origins of sampled water.
827

828 **CONCLUSIONS**

829 Objectives of this study were to explore the spatial and temporal distributions of eukaryotic
830 phytoplankton communities in the Pacific Ocean inflow to the Arctic, covering the Chukchi Sea
831 and Bering Strait regions. This project aimed to determine whether reproducible patterns of
832 occurrence were present within community assemblages of diatoms and picophytoplankton, and
833 the role of environmental conditions in structuring these communities. The sampling coverage
834 attained in this study in both the spatial and temporal domains was much larger than typical studies
835 of its kind, allowing for unique insights into the structuring of microorganisms at the base of the
836 Alaskan Arctic food web.
837 Overall, the low predictability of community composition based on measured
838 environmental variables suggests that more explanatory variables exist that were not considered
839 in this study. However, our most notable finding is identifying temperature as a driver for certain
840 taxa, especially ones that make up a high proportion of the primary producers (e.g. *Chaetoceros*
841 ESV 2). Other integrative, bottom-up forcing factors that could contribute to phytoplankton
842 community structure, such as historical light availability, cloud cover, weather patterns,
843 stratification levels, mixing, ice extent, and freshwater input (e.g., ice melt, precipitation, rivers,
844 runoff), were beyond the scope of this study, so we cannot comment on their utility in predicting
845 microbial community structure at this time. Future studies should incorporate remote sensing

observations or seascape predictions to include these additional parameters as explanatory variables.

Our study also captured the diversity of these communities, all the more important considering diversity is a key buffer in rapid environmental changes (especially as the Arctic warms in response to climate change). Our study identified key genera and ESVs of diatoms and picophytoplankton. While we did identify hundreds of ESVs, more work is needed to determine both abiotic and biotic drivers of community assembly, and more specific genetic studies are needed to delineate microdiversity within the primary producer communities of the Alaskan Arctic. Our work does begin to fill in the gaps, allowing us to contribute more genetic information to existing databases. Monitoring of changes in zooplankton grazer abundance and distribution (e.g. copepods, ciliates, dinoflagellates) will also be important to understand how top-down controls could change and affect the phytoplankton. However, we did reaffirm the importance of temperature in structuring many key members of the diatom and picoeukaryote communities. Connecting certain taxa with temperature allowed for some insights into the future primary producer community of the Bering and Chukchi seas.

Our study highlights the diversity of primary producers and demonstrates that these communities are driven by a variety of environmental and biological parameters that are difficult to fully quantify. We observed a weaker influence of nutrients, water mass, water depth, and geography on diatom and picophytoplankton communities as a whole compared to other phytoplankton community studies (Sunagawa et al. 2015; Neeley et al. 2018; Kalenitchenko et al. 2019). However, we have demonstrated some key taxonomic groups are sensitive to temperature and these same taxonomic groups influence the structure of the communities. The taxonomic groups' responses to temperature are consistent with predictions of shifts to smaller celled

mixotrophs and away from larger celled phytoplankton (Ward and Follows 2016). Since the biological carbon pump in the Arctic is currently driven primarily by the sinking of large (>10 μm) diatom cells and chains, we can expect to see declines in benthic-pelagic coupling and seafloor productivity and higher trophic levels. However, this is also dependent on the resilience provided by biodiversity, especially microdiversity within primary producers, an area which is in need of more study. A shift to small-celled phytoplankton in a freshening Alaskan Arctic could have disruptive implications for primary productivity that supports the seafloor (Li et al. 2009).

Our analyses, conducted on almost a thousand samples collected across four months and three cruises, has established a baseline of microbial communities in the Bering and Chukchi seas and identified prominent taxa that are the most vulnerable to climate change. Already we can see the impacts of climate change on the lowest trophic levels that support the entire Alaskan Arctic ecosystem. Long-term monitoring along our study sites, especially the DBO and Chukchi Environmental Observatory, will be imperative to continue increasing our understanding of photoautotrophs and other microbes in the warming Bering and Chukchi seas.

ACKNOWLEDGEMENTS

We gratefully acknowledge the dedication and skillfulness of the captains, crews, and chief scientists aboard the R/V Sikuliaq, CGC Healy, and R/V Norseman II, without which this work could not have been completed. Funding for this work was provided by the National Oceanic and Atmospheric Administration (NA14OAR0110266, NA15OAR0110208), and the North Pacific Research Board (1802). This work was also funded through a National Ocean Partnership Program (NOPP Grant NA14NOS0120158) by the National Oceanographic and Atmospheric

Administration (NOAA), the Bureau of Ocean Management and Shell Exploration & Production, under management of the Integrated Ocean Observing System (IOOS).

REFERENCES

Alldredge AL, Passow U, & Logan BE. (1993). The abundance and significance of a class of large, transparent organic particles in the ocean. *Deep Sea Research Part I, 40*, 1131-1140. doi:10.1016/0967-0637(93)90129-Q

Alldredge A, Passow U, & Haddock S. (1998). The characteristics and transparent exopolymer particle (TEP) content of marine snow formed from thecate dinoflagellates. *Journal of Plankton Research, 20*, 393-406.

Allison SD & Martiny JBH. (2008). Resistance, resilience, and redundancy in microbial communities. *Proceedings of the National Academy of Sciences USA, 105*, 11512–11519. doi:10.1073pnas.0801925105

Andersson A, Falk S, Samuelsson G, & Hagström A. (1989). Nutritional characteristics of a mixotrophic nanoflagellate, *Ochromonas* sp. *Microbial Ecology, 17*, 251-262. doi:10.1007/BF02012838

Ardyna M, Gosselin M, Michel C, & Tremblay J-E. (2011). Environmental forcing of phytoplankton community structure and function in the Canadian High Arctic: Contrasting oligotrophic and eutrophic regions. *Marine Ecology Progress Series, 442*, 37-57. doi:10.3354/meps09378

911 Arrigo KR, & van Dijken GL. (2004). Annual cycles of sea ice and phytoplankton in Cape Bathurst
912 polynya, southeastern Beaufort Sea, Canadian Arctic. *Geophysical Research Letters, 31*.
913 doi:10.1029/2003GL018978

914 Arrigo KR, van Dijken G, & Pabi S. (2008). Impact of a shrinking Arctic ice cover on marine
915 primary production. *Geophysical Research Letters, 35,* L19603. doi:10.1029/
916 2008GL035028

917 Arrigo KR, Perovich DK, Pickart RS, Brown ZW, van Dijken G, Lowry KE, Mills MM, Palmer
918 MA, Balch WB, Bahr F, Bates NR, Benitez-Nelson C, Bowler B, Brownlee E, Ehn JK,
919 Frey KE, Garley R, Laney SR, Lubelczyk L, Mathis J, Matsuoka A, Mitchell BG, Moore
920 GWK, Ortega-Retuerta E, Pal S, Polashenski CM, Reynolds A, Schieber B, Sosik HM,
921 Stephens M, Swift JH. (2012). Massive phytoplankton blooms under Arctic Sea ice.
922 *Science, 336*, 1408. doi:10.1126/science.1215065

923 Ashjian CJ, Campbell RG, Gelfman C, Alatalo P, & Elliott SM. (2017). Mesozooplankton
924 abundance and distribution in association with hydrography on Hanna Shoal, NE Chukchi
925 Sea, during August 2012 and 2013. *Deep Sea Research Part II, 144*, 21-36.
926 doi:10.1016/j.dsr2.2017.08.012

927 Azam F, Fenchel T, Field J, Gray J, Meyer-Reil L, & Thingstad F. (1983). The ecological role of
928 water-column microbes in the sea. *Marine Ecology Progress Series, 10*, 257-263.

929 Azam F, Smith D, & Hagström Å. (1994). Bacteria-organic matter coupling and its significance
930 for oceanic carbon cycling. *Microbial Ecology, 28*, 167-179.

931 Balzano S, Percopo I, Siano R, Gourvil P, Chanoine M, Marine D, Vaulot, Daniel, Sarno, D.
932 (2017). Morphological and genetic diversity of Beaufort Sea diatoms with high

933 contributions from the *Chaetoceros neogracilis* species complex. *Journal of Phycology,*
934 *53*, 161-187. doi:10.1111/jpy.12489

935 Burkhardt B, Watkins-Brandt K, Defforey D, Paytan A, & White A. (2014). Remineralization of
936 phytoplankton-derived organic matter by natural populations of heterotrophic bacteria.
937 *Marine Chemistry, 163*, 1-9.

938 Callahan BJ, McMurdie PJ, Rosen MJ, Han AW, Johnson AJ, & Holmes SP. (2016). DADA2:
939 High-resolution sample inference from Illumina amplicon data. *Nature Methods, 13*, 581-
940 587. doi:10.1038/nMeth.3869

941 Campbell RG, Ashjian, CJ, Sherr EB, Sherr BF, Lomas MW, Ross C, Alatalo P, Gelfman C, Van
942 Keuren D. (2016). Mesozooplankton grazing during spring sea-ice conditions in the eastern
943 Bering Sea. *Deep-Sea Research Part II: Topical Studies in Oceanography, 134*, 157-172.
944 doi:10.1016/j.dsr2.2015.11.003

945 Carmack E, Polyakov I, Padman L, Fer I, Hunke E, Hutchings J, Jackson J, Kelley D, Kwok R,
946 Layton C, Melling H, Perovich D, Persson O, Ruddick B, Timmermans M-L, Toole J, Ross
947 T, Vavrus S, Winsor, P. (2015). Toward quantifying the increasing role of oceanic heat in
948 sea ice loss in the new Arctic. *Bulletin of the American Meteorological Society, 96*, 2079-
949 2106. doi:10.1175/BAMS-D-13-00177.1

950 Carneiro FM, Bini LM, & Rodrigues LC. (2010). Influence of taxonomic and numerical resolution
951 on the analysis of temporal changes in phytoplankton communities. *Ecological Indicators,*
952 *10*, 249-255. doi:10.1016/j.ecolind.2009.05.004

953 Cermeño P, Marañón E, & Romero OE. (2012). Response of marine diatom communities to Late
954 Quaternary abrupt climate changes. *Journal of Plankton Research, 35*, 12-21.
955 doi:10.1093/plankt/fbs073

956 Codispoti L, Flagg C, Kelly V, & Swift J. (2005). Hydrographic conditions during the 2002 SBI
957 process experiments. *Deep-Sea Research II, 52*, 3199-3226.

958 Cooney R & Coyle K. (1982). Trophic implications of cross-shelf copepod distributions in the
959 Southeastern Bering Sea. *Marine Biology, 70*, 187-196. doi:10.1007/BF00397684

960 Cowen J, & Holloway C. (1996). Structural and chemical analysis of marine aggregates: In situ
961 macrophotography and laser confocal and electron microscopy. *Marine Biology, 126*, 163-
962 174. doi:10.1007/BF00347441

963 Coyle K, Bluhm B, Konar B, Blanchard A, & Highsmith R. (2007). Amphipod prey of grey whales
964 in the northern Bering Sea: changes in biomass and distribution. *Deep-Sea Research Part*
965 *II, 54*, 2906-3928. doi:10.1016/j.dsr2.2007.08.026

966 Degerlund M, Huseby S, Zingone A, Sarno D, & Landfald B. (2012). Functional diversity in
967 cryptic species of *Chaetoceros socialis* Lauder (Bacillariophyceae). *Journal of Plankton*
968 *Research, 34*, 416-431. doi:10.1093/plankt/fbs004

969 Demory D, Baudoux A-C, Monier A, Simon N, Six C, Ge P, Rigaut-Jalabert F, Marie D, Sciandra
970 A, Bernard O, & Rabouille S. (2018). Picoeukaryotes of the *Micromonas* genus: sentinels
971 of a warming ocean. *The ISME Journal, 13*, 132-146. doi:10.1038/s41396-018-0248-0

972 Dunton KH, Goodall JL, Schonberg SV, Grebmeier JM, & Maidment DR. (2005). Multi-decadal
973 synthesis of benthic-pelagic coupling in the western Arctic: Role of cross-shelf advective
974 processes. *Deep Sea Research Part II, 52*, 3462-3477. doi:10.1016/j.dsr2.2005.09.007

975 Eilertsen HC & Raa J. (1995). Toxins in seawater produced by a common phytoplankter
976 *Phaeocystis pouchetii*. *Journal of Marine Biotechnology, 3*, 115-119.

977 Estep KW, Davis PG, Keller MD, & Sieburth JMcN. (1986). How important are oceanic algal
978 nanoflagellates in bacterivory? *Limnology and Oceanography, 31*, 646-650.

979 Fehling J, Davidson K, Bolsch CJ, Brand TD, & Narayanaswamy BE. (2012). The relationship
980 between phytoplankton distribution and water column characteristics in North West
981 European Shelf sea waters. *PLoS One*. doi:10.1371/journal.pone.0034098

982 Flynn KJ, Stoecker DK, Mitra A, Raven JA, Glibert PM, Hansen PJ, Granéli E, & Burkholder, J.
983 M. (2013). Misuse of the phytoplankton-zooplankton dichotomy: the need to assign
984 organisms as mixotrophs within plankton functional types. *Journal of Plankton Research,*
985 *35*, 3-11. doi:10.1093/plankt/fbs062

986 Gaonkar CC, Kooistra WHCF, Lange CB, Montresor M, & Sarno D. (2017). Two new species in
987 the *Chaetoceros socialis* complex (Bacillariophyta): *C. sporotruncatus* and *C.*
988 *dichatoensis*, and characterization of its relatives, *C. radicans* and *C. cinctus*. *Journal of*
989 *Phycology, 53*. doi:10.1111/jpy.12554

990 García-García N, Tamames J, Linz AM, Pedrós-Alió C, & Puente-Sánchez F. (2019).
991 Microdiversity ensures the maintenance of functional microbial communities under
992 changing environmental conditions. *The ISME Journal, 13*, 2969-2983.
993 doi:10.1038/s41396-019-0487-8

994 Giesbrecht K, Varela DW, Grebmeier JM, Kelly B, & Long J. (2019). A decade of summertime
995 measurements of phytoplankton biomass productivity and assemblage composition in the

996 Pacific Arctic region from 2006 to 2016. *Deep Sea Research Part II, 162*, 93-113.
997 doi:10.1016/j.dsr2.2018.06.010

998 Glenn TC, Nilsen RA, Kieran TJ, Finger Jr JW, Pierson T W, Bentley KE, Hoffberg SL, Louha S,
999 García-De León FJ, Del Río-Portilla MA, Reed KD, Anderson JL, Meece JK, Aggrey SE,
1000 Rekaya R, Alabady M, Bélanger M, Winker K, & Faircloth BC. (2016). Adapterama I:
1001 Universal stubs and primers for 384 unique dual-indexed or 147,456 combinatorially-
1002 indexed Illumina libraries (iTru & iNext). *bioRxiv*. doi:10.1101/049114

1003 Gordon LI, Jennings JC, Ross AA, & Krest JM. (1993). *A suggested protocol for continuous flow*
1004 *automated analysis of seawater nutrients (phosphate, nitrate, nitrite, and silicic acid) in*
1005 *the WOCE Hydrographic Program and the Joint Global Ocean Fluxes Study.* WOCE
1006 Hydrographic Program Office, Methods Manual WHPO 91-1. Oregon State University,
1007 Corvalis.

1008 Grebmeier JM, & Barry JP. (1991). The influence of oceanographic processes on pelagic-benthic
1009 coupling in polar regions: A benthic perspective. *Journal of Marine Systems, 2*, 495-518.
1010 doi:10.1016/0924-7963(91)90049-Z

1011 Grebmeier JM, Moore SE, Overland, JE, Frey KE, & Gradinger R. (2010). Biological response to
1012 recent Pacific Arctic sea ice retreats. *Eos, Transactions American Geophysical Union, 91,*
1013 161-168. doi:10.1029/2010EO180001

1014 Grebmeier JM. (2012). Shifting patterns of life in the Pacific Arctic and Sub-Arctic seas. *Annual*
1015 *Review of Marine Science, 4*, 63-78. doi:10.1146/annurev-marine-120710-100926

1016 Hallegraeff GM. (2010). Ocean climate change, phytoplankton community responses, harmful
1017 algal blooms: A formidable predictive challenge. *Journal of Phycology, 46*, 220-235.
1018 doi:10.1111/j.1529-8817.2010.00815.x

1019 Hamilton A, Lovejoy C, Galand P, & Ingram R. (2008). Water masses and biogeography of
1020 picoeukaryote assemblages in a cold hydrographically complex system. *Limnology and*
1021 *Oceanography, 53*, 922-935. doi:10.4319/lo.2008.53.3.0922

1022 Harrison PJ, Whitney FA, Tsuda AS, & Tadokoro K. (2004). Nutrient and plankton dynamics in
1023 the NE and NW gyres of the Subarctic Pacific Ocean. *Journal of Oceanography, 60*, 93-
1024 117. doi:10.1023/B:JOCE.0000038321.57391.2a

1025 Hartmann M, Grob C, Tarran GA, Martin AP, Burkill PH, Scanlan DJ, & Zubkov MJ. (2012).
1026 Mixotrophic basis of Atlantic oligotrophic ecosystems. *Proceedings of the National*
1027 *Acadamy of Sciences of the United States of America, 109*, 5756-5760.
1028 doi:10.1073/pnas.1118179109

1029 Hauri C, Danielson SL, McDonnell AMP, Hopcroft RR, Winsor P, Shipton P, Lalande C, Stafford
1030 KM, Horne JK, Cooper LW, Grebmeier JM, Mahoney A, Maisch K, McCammon M,
1031 Statscewich H, Sybrandy A, Weingartner T (2018). From sea ice to seals: A moored
1032 marine ecosystem observatory in the Arctic. *Ocean Sci, 14*, 1423-1433.

1033 Held I, & Soden B. (2006). Robust responses of the hydrological cycle to global warming. *Journal*
1034 *of Climate, 19*, 5656-5699.

1035 Henson S, Cole H, Beaulieu C, & Yool A. (2013). The impact of global warming on seasonality
1036 of ocean primary production. *Biogeosciences, 10*, 4357-4369. doi:10.5194/bg-10-4357-
1037 2013

1038 Hill V, Cota G, & Stockwell D. (2005). Spring and summer phytoplankton communities in the
1039 Chukchi and Eastern Beaufort Sea. *Deep Sea Research Part II, 52*, 3369-3385.

1040 Holloway C, & Cowen J. (1997). Development of a scanning confocal laser microscopic technique
1041 to examine the structure and composition of marine snow. *Limnology and Oceanography,*
1042 *42*, 1340-1352.

1043 Hunt G, Coyle K, Eisner L, Farley E, Heintz R, Mueter F, Napp JM, Overland, JE, Ressler PH,
1044 SaloS, & Stabeno P. (2011). Climate impacts on eastern Bering Sea foodwebs: a synthesis
1045 of new data and an assessment of the Oscillating Control Hypothesis. *ICES Journal of*
1046 *Marine Science 68*, 1230–1243. doi:10.1093/icesjms/fsr036

1047 Huntington HP, Danielson SL, Wiese FK, Baker M, Boveng P, Citta JJ, De Robertis A, Dickson
1048 DMS, Farley E, George JC, Iken K, Kimmel DG, Kuletz K, Ladd C, Levine R, Quakenbush
1049 L, Stabeno P, Stafford KM, Stockwell D, & Wilson C. (2020). Evidence suggests potential
1050 transformation of the Pacific Arctic ecosystem is underway. *Nature Climate Change*.
1051 doi:10.1038/s41558-020-0695-2

1052 Jardillier L, Zubkov M, Pearman J, & Scanlan D. (2010). Significant CO_2 fixation by small
1053 prymnesiophytes in the subtropical and tropical northeast Atlantic Ocean *The ISME*
1054 *Journal, 4*, 1180-11992.

1055 Jeffries M, Richter-Menge J, & Overland J. (2014). *Arctic Report Card 2014.* Retrieved from
1056 http://www.arctic.noaa.gov/reportcard on March 25, 2020.

1057 Kahru M, Brotas V, Manzano-Sarabia M, & Mitchell BG. (2011). Are phytoplankton blooms
1058 occurring earlier in the Arctic? *Global Change Biology, 17*, 1733-1739.
1059 doi:10.1111/j.1365-2486.2010.02312.x

1060 Kalenitchenko D, Joli N, Potvin M, Tremblay J-É, & Lovejoy C. (2019). Biodiversity and species
1061 change in the Arctic Ocean: A view through the lens of Nares Strait. *Frontiers in Marine*
1062 *Science, 6*, 1-18. doi:10.3389/fmars.2019.00479

1063 Keller M, Shapiro L, Haugen E, CT, Sherr E, & Sherr B. (1994). Phagotrophy of fluorescently
1064 labeled bacteria by an oceanic phytoplankter. *Microbial Ecology, 28*, 39-52.
1065 doi:10.1007/BF00170246

1066 Kitchell JA, Clark DA, & Gombos Jr AM. (1986). Biological selectivity of extinction: A Link
1067 between background and mass extinction. *PALAIOS, 1*, 504-511. doi:10.2307/3514632

1068 Knap A, Michaels A, Close A, Ducklow A, & Dickson A. (1996). Protocols for the Joint Global
1069 Ocean Flux Study (JGOFS) core measurements, JGOFS Report Nr. 19 (Reprint of the IOC
1070 Manuals and Guides No. 29, UNESCO, Paris, 1994). 170.

1071 Kooistra WHCF, Sarno D, Balzano S, Gu H, Andersen RA, & Zingon A. (2008). Global diversity
1072 and biogeography of *Skeletonema* species (Bacillariophyta). *Protist, 159*, 177-193.

1073 Kosobokova KN, & Hopcroft RR. (2010). Diversity and vertical distribution of mesozooplankton
1074 in the Arctic's Canada Basin. *Deep Sea Research Part II, 57*, 96-110.
1075 doi:10.1016/j.dsr2.2009.08.009

1076 Krug LA, Platt T, Sathyendranath S, & Barbosa AB. (2013). Unraveling region-specific
1077 environmental drivers of phytoplankton across a complex marine domaine (off SW Iberia).
1078 *Remote Sensing of Environment, 203*, 162-184. doi:10.1016/j.rse.2017.05.029

1079 Laws EF, Smith W, Ducklow H, & McCarthy J. (2000). Temperature effects on export production
1080 in the open ocean. *Global Biogeochemical Cycles, 14*, 1231-1246.

1081 Lefebvre KA, Quakenbush L, Frame E, Huntington KB, Sheffield G, Stimmelmayr R., Bryan A,
1082 Kendrick P, Ziel H, Goldstein T, Snyder JA, Gelatt T, Gulland F, Dickerson B, & Gill, V.
1083 (2016). Prevalence of algal toxins in Alaskan marine mammals foraging in a changing
1084 arctic and subarctic environment. *Harmful Algae, 55*, 13-24. doi:10.1016/j.hal.2016.01.007

1085 Li W, McLaughlin F, Lovejoy C, & Carmack E. (2009). Smallest algae thrive as the Arctic Ocean
1086 freshens. *Science, 326*, 539. doi:10.1126/science.1179798

1087 Litchman E. (2007). Resource competition and ecological success of phytoplankton. In: Falkowski
1088 G and Knoll AH (ed.). *Evolution of Primary Producers in the Sea*, 351-375.
1089 doi:10.1016/B978-012370518-1/50017-5.

1090 Lovejoy C, Massana R, & Pedrós-Alió C. (2006). Diversity and distribution of marine microbial
1091 eukaryotes. *Applied and Environmental Microbiology, 72*, 3085-3095.
1092 doi:10.1128/AEM.72.5.3085–3095.2006

1093 Lovejoy C, Vincent WF, Bonilla S, Roy S, Martineau M- J, Terrado R, Potvin M, Massana R, &
1094 Pedrós- Alió C. (2007). Distribution, phylogeny, and growth of cold-adapted
1095 picoprasinophytes in Arctic Seas. *Journal of Phycology, 43*. doi:10.1111/j.1529-
1096 8817.2006.00310.x

1097 Lozupone C, & Knight R. (2007). Global patterns in bacterial diversity. *Proceedings of the*
1098 *National Academy of Sciences of the USA, 104*, 11436-11440.
1099 doi:10.1073/pnas.0611525104

1100 Machado KB, Borges PP, Carneiro FM, de Santana JF, Vieira LC, Huszar V.L, & Nabout JC.
1101 (2015). Using lower taxonomic resolution and ecological approaches as a surrogate for
1102 plankton species. *Hydrobiologia, 743*, 255-267. doi:10.1007/s10750-014-2042-y

1103 Martin M. (2011). Cutadapt removes adapter sequences from high-throughput sequencing reads.
1104 *EMBnet.journal, 17*, 10-12. doi:10.14806/ej.17.1.200

1105 McKenzie C, Deibel D, Paranjape M, & Thompson R. (1995). The marine mixotroph *Dinobryon*
1106 *balticum* (Chrysophyceae) – phagotrophy and survival in a cold ocean. *Journal of*
1107 *Phycology, 31*, 19-24. doi:10.1111/j.0022-3646.1995.00019.x

1108 McKie-Krisberg ZM, & Sanders RW. (2014). Phagotrophy by the picoeukaryotic green alga
1109 *Micromonas*: implications for Arctic Oceans. *The ISME Journal, 8*, 1953-1961.
1110 doi:10.1038/ismej.2014.16

1111 Mitra A, Flynn K, Burkholder J, Berge T, Calbet A, Raven J, Granéli E, Glibert PM, Hansen PJ,
1112 Stoecker DK, Thingstad F, Tillman U, Våge S, Wilken S, & Zubkov M. (2014). The role
1113 of mixotrophic protists in the biological carbon pump. *Biogeosciences, 11*, 995-1005.
1114 doi:10.5194/bg-11-995-2014

1115 Mitra A, Flynn K, Tillman U, Raven J, Caron D, Stoecker D, Not F, Hansen PJ, Hallegraeff G,
1116 Sanders R, Wilken S, McManus G, Johnson M, Pitta P, Våge S, Berge T, Calbet A,
1117 Thingstad F, Jeong HJ, Burkholder J, Glibert PM, Granéli E, & Lundgren V. (2016).
1118 Defining planktonic protist functional groups on mechanisms for energy and nutrient
1119 acquisition: Incorporation of diverse mixotrophic strategies. *Protist, 167*, 106-120.
1120 doi:10.1016/j.protis.2016.01.003

1121 Moran S, Lomas M, Kelly R, Gradinger R, Iken K, & Mathis J. (2012). Seasonal succession of net
1122 primary productivity, particulate organic carbon export, and autotrophic community
1123 composition in the eastern Bering Sea. *Deep Sea Research Part II, 65-70*, 84-97.
1124 doi:10.1016/j.dsr2.2012.02.011

Moritz C, & Agudo R. (2013). The future of species under climate change: Resilience or decline? *Science, 341*, 504-508. doi:DOI: 10.1126/science.1237190

Mozetič P, Francé J, Kogovšek T, Talaber I, & Malej A. (2012). Plankton trends and community changes in a coastal sea (northern Adriatic): Bottom-up vs. top-down control in relation to environmental drivers. *Estuarine, Coastal and Shelf Science, 115*, 138-148. doi:10.1016/j.ecss.2012.02.009

Needham DM, Sachdeva R, & Fuhrman JA. (2017). Ecological dynamics and co-occurrence among marine phytoplankton, bacteria and myoviruses shows microdiversity matters. *The ISME Journal*, 1614-1629. doi:10.1038/ismej.2017.29

Neeley A, Harris L, & Frey K. (2018). Unraveling phytoplankton community dynamics in the Northern Chukchi Sea under sea-ice covered, and sea-ice-free conditions. *Geophysical Research Letters, 45*, 7663-7671. doi:10.1029/2018GL077684

Neukermans G, Reynolds R, & Stramski D. (2016). Optical classification and characterization of marine particle assemblages within the western Arctic Ocean. *Limnology and Oceanography, 61*, 1472-1494. doi:10.1002/lno.10316

Neukermans G, Oziel L, & Babin M. (2018). Increased intrusion of warming Atlantic water leads to rapid expansion of temperate phytoplankton in the Arctic. *Global Change Biology, 24*, 2545-2553. doi:10.1111/gcb.14075f

Oksanen J, Blanchet FG, Friendly M, Kindt R, Legendre P, McGlinn D, Minchin PR, O'Hara RB, Simpson GL, Solymos P, Stevens HH, Szoecs E, & Wagner, H. (2019). vegan: Community Ecology Package. Retrieved from https://CRAN.R-project.org/package=vegan on September 1, 2019.

1147 Olli K, Riser CW, Wassmann P, Ratkova T, Arashkevich E, & Pasternak A. (2002). Seasonal
1148 variation in vertical flux of biogenic matter in the marginal ice zone and the central Barents
1149 Sea. *Journal of Marine Systems, 38*, 189-204. doi:10.1016/S0924-7963(02)00177-X

1150 Olson MB, & Strom SL. (2002). Phytoplankton growth, microzooplankton herbivory and
1151 community structure in the southeast Bering Sea: insight into the formation and temporal
1152 persistence of an *Emiliana huxleyi* bloom. *Deep Sea Research II, 49*, 5969-5990.
1153 doi:10.1016/S0967-0645(02)00329-6

1154 Overpeck NT, Sturm M, Francis JA, Perovich DK, Serreze MC, Benner R, Carmack E, Chapin
1155 III FS, Gerlach SC, Hamilton LC, Hinzman LD, Holland M, Huntington HP, Key JR, Lloyd
1156 AH, McDonald GM, McFadden J, Noone D, Prowse TD, Schlosser P, Vörösmarty C.
1157 (2005). Arctic system on trajectory to new, seasonally ice- free state. *Eos, Transactions of*
1158 *the American Geophysical Union, 86*, 309-316. doi:10.1029/2005EO340001

1159 Passow U. (2002). Transparent exopolymer particles (TEP) in aquatic environments. *Progress in*
1160 *Oceanography, 55*, 287-333.

1161 Piontek J, Lunau M, Borchard C, Wurst C, & Engle A. (2010). Acidification increases microbial
1162 polysaccharide degradation in the ocean. *Biogeosciences, 7*, 1615-1624. doi:10.5194/bg-
1163 7-1615-2010

1164 Pisareva MN, Pickart RS, Spall M, Nobre CT, Moore G, & Whitledge TE. (2015). Flow of pacific
1165 water in the western Chukchi Sea: Results from the 2009 RUSALCA expedition. *Deep-*
1166 *Sea Research I, 105*, 53-73. doi:10.1016/j.dsr.2015.08.011

1167 Platt T, Rao D, & Irwin B. (1983). Photosynthesis of picoplankton in the oligotrophic ocean.
1168 *Nature*, *301*, 702-704.

1169 Poloczanska ES, Brown CJ, Sydeman WJ, Kiessling W, Schoeman D S, Schoeman DS, Moore PJ,
1170 Brander K, Bruno JF, Buckley LB, Burrows MT, Duarte CM, Halpern BS, Holding J,
1171 Kappel CV, O'Connor MI, Pandolfi JM, Parmesan C, Schwing F, Thompson SA, &
1172 Richardson AJ. (2013). Global imprint of climate change on marine life. *Nature Climate*
1173 *Change, 3*, 919-925. doi:10.1038/NCLIMATE1958

1174 Pomeroy L. (1974). The ocean's food web, a changing paradigm. *Bioscience, 24*, 499-504.

1175 Quast C, Pruesse E, Yilmanz P, Gerken J, Schweer T, Yarza P, Peplies J, & Glöckner FO. (2012).
1176 The SILVA ribosomal RNA gene database project: improved data processing and web-
1177 based tools. *Nucleic Acids Research, 41*, D590-D596. doi:10.1093/nar/gks1219

1178 R Core Team. (2013). R: A language and environment for statistical. (R. F. Computing, Compiler)
1179 Vienna, Austria. Retrieved from http://www.R-project.org/ on September 1, 2018.

1180 Ran L, Jianfang C, Haiyan J, Hongliang L, Yong L, & Kui W. (2013). Diatom distribution of
1181 surface sediment in the Bering Sea and Chukchi Sea. *Advances in Polar Science, 24*, 1-6.
1182 doi:10.3724/SP.J.1085.2013.00000

1183 Sakshaug E. (2004). Primary and secondary production in the Arctic Seas. In Stein R and
1184 MacDonald R (eds.). *The Organic Carbon Cycle in the Arctic Ocean*. Berlin: Springer, 7-
1185 81. doi:10.1007/978-3-642-18912-8_3

1186 Sancetta C, Heuser L, Labeyrie L, Naidu A, & Robinson S. (1984). Wisconsin-Holocene
1187 paleoenvironment of the Bering Sea: Evidence from diatoms, pollen, oxygen isotopes and
1188 clay minerals. *Marine Geology, 62*, 55-68. doi:10.1016/0025-3227(84)90054-9

1189 Sarmiento JL, & Bender M. (1994). Carbon biogeochemistry and climate change. *Photosynthesis*
1190 *Research, 39*, 209-234. doi:10.1007/BF00014585

Schlitzer R. (2016). Ocean Data View. Retrieved from https://odv.awi.de on September 1, 2018.

Sieburth J, Smetacek V, & Lenz J. (1978). Pelagic ecosystem structure: heterotrophic compartments of the plankton and their relationship to plankton size fractions. *Limnology and Oceanography, 23*, 1256-1263. doi:10.4319/lo.1978.23.6.1256

Siemering B, Bresnan E, Painter SC, Daniels CJ, Inall M, & Davidson K. (2016). Phytoplankton distribution in relation to environmental drivers on the North West European Shelf Sea. *PLoS One, 11*. doi:10.1371/journal.pone.0164482

Sigler MF, Stabeno PJ, Eisner LB, Napp JM, & Mueter FJ. (2014). Spring and fall phytoplankton blooms in a productive subarctic ecosystem, the eastern Bering Sea, during 1995-2011. *Deep Sea Research Part II, 109,* 71-83. doi:10.1016/j.dsr2.2013.12.007

Simon N, Foulon E, Grulois D, Six C, Desdevises Y, Latimier M, Le Gall F, Tragin M, Houdan A, Derelle E, Jouenne F, Marie D, Le Panse S, Vaulot D, & Marin, B. (2017). Revision of the genus *Micromonas* Manton et Parke (Chlorophyta, Mamiellophyceae), of the type species *M. pusilla* (Butcher) Manton & Parke and of the species *M. commoda* van Baren, Bachy and Worden and description of two new species based on the genetic and phenotypic characterization of cultured isolates. *Protist, 168*, 612-635. doi:10.1016/j.protis.2017.09.002

Sjöqvist C, & Kremp A. (2016). Genetic diversity affects ecological performance and stress response of marine diatom populations. *The ISME Journal, 10*, 2755-2766. doi:10.1038/ismej.2016.44

1211 Smith W, Codispoti L, Nelson D, Manley T, Buskey E, Niebauer H, & Cota G. (1991). Importance
1212 of *Phaeocystis* blooms in the high-latitude ocean carbon cycle. *Nature, 352*, 514-516.
1213 doi:10.1038/352514a0

1214 Springer AM, McRoy CP, & Turco KR. (1989). The paradox of pelagic food webs in the northern
1215 Bering Sea – II. Zooplankton communities. *Continental Shelf Research, 9*, 359-386.
1216 doi:10.1016/0278-4343(89)90039-3

1217 Springer AM, & McRoy P. (1993). The paradox of pelagic food webs in the northern Bering Sea
1218 – III. Patterns of primary production. *Continental Shelf Research, 13*, 575-599.
1219 doi:10.1016/0278-4343(93)90095-F

1220 Stemman L, & Boss E. (2012). Plankton and particle size and packaging: From determining optical
1221 properties to driving the biological pump. *Annual Review of Marine Science, 4*, 263-290.

1222 Stoeck T, Bass D, Nebel M, Christen R, Jones MD, Breiner H-W, & Richards TA. (2010). Multiple
1223 marker parallel tag environmental DNA sequencing reveals a highly complex eukaryotic
1224 community in a marine anoxic water. *Molecular Ecology, 19*, 21-31. doi:10.1111/j.1365-
1225 294X.2009.04480.x

1226 Stoecker DK, Hansen PJ, Caron DA, & Mitra A. (2017a). Mixotrophy in the marine plankton.
1227 *Annual Review of Marine Science, 9*, 311-335. doi:10.1146/annurev-marine-010816-
1228 060617

1229 Stoecker D, Hansen P, Caron D, & Mitra A. (2017b). Mixotrophy in aquatic protists. *Annual*
1230 *Review of Marine Science, 9*, 311-335. doi:10.3354/meps338061

1231 Stoecker DK, & Lavrentyev PJ. (2018). Mixotrophic plankton in the polar seas: A pan-Arctic
1232 review. *Frontiers in Marine Science, 5*. doi:10.3389/fmars.2018.00292

1233 Sukhanova I, Flint M, Pautova L, Stockwell D, Grebmeier JM, & Sergeeva V. (2009).
1234 Phytoplankton of the western Arctic in the spring and summer of 2002: Structure and
1235 seasonal changes. *Deep Sea Research II, 56*, 1223-1236. doi:10.1016/j.dsr2.2008.12.030

1236 Sunagawa S, Coelho LP, Chaffron S, Kultima JR, Labadie K, Salazar G, Djanschiri B, Zeller G,
1237 Mende DR, Alberti A, Cornejo-Castillo, FM, Costea PI, Cruaud C, D'Ovidio F, Englen S,
1238 Ferrera I, Gasol JM, Guidi L, Hildebrand F, Kokoszka F, Lepoivre C, Lima-Mendez G,
1239 Poulain J, Poulos BT, Royo-Llonch M, Sarmento H, Vieira-Silva S, Dimier C, Picheral M,
1240 Searson S, Kandels-Lewis S, Tara Oceans coordinators, Bowler C, de Vargas C, Gorsky
1241 G, Grimsley N, Hingamp P, Iudicone D, Jaillon O, Not F, Ogata H, Pesant S, Speich S,
1242 Stemmann L, Sullivan MB, Weissenbach J, Wincker P, Karsenti E, Raes J, Acinas SG, &
1243 Bork P. (2015). Structure and function of the global ocean microbiome. *Science, 348*.
1244 doi:10.1126/science.1261359

1245 Tesson SVM, Montressor M, Procaccini G, & Kooistra WHCF. (2014). Temporal changes in
1246 population structure of a marine planktonic diatom. *PLoS One, 9*, 1-23.
1247 doi:10.1073/pnas.1400909111

1248 Thaler M, & Lovejoy C. (2014). Environmental selection of marine stramenopile clades in the
1249 Arctic Ocean and coastal waters. *Polar Biology, 37*, 347-357. doi:10.1007/s00300-013-
1250 1435-0

1251 Thierstein H. (1982). Terminal Cretaceous plankton extinctions: A critical assessment. (LT Silver,
1252 & PH Schultz, Eds.) *Geological Society of America Special Paper 190*, 385-399.

Thornton D, & Thake B. (1998). Effect of temperature on the aggregation of *Skeletonema costatum* (Bacillariophyceae) and the implication for carbon flux in coastal waters. *Marine Ecology Progress Series, 174*, 223-237.

Vaulot D, Eikrem W, Viprey M, & Moreau H. (2008). The diversity of small eukaryotic phytoplankton (≤3 μm) in marine ecosystems. *FEMS Microbiology Reviews, 32*, 795-820.

von Quillfeldt C. (2005). Identification of some easily confused common diatom species in Arctic spring blooms. *Botanica Marina, 44*, 375-389. doi:10.1515/BOT.2001.048

Walsh JJ, McRoy CP, Coachman LK, Goering JJ, Nihoul JJ, Whitledge TE, Blackburn TH, Parker PL, Wirick CD, Shuert PG, Grebmeier JM, Springer AM, Tripp RD, Hansell DA, Djenidi S, Deleersnijder E, Henriksen K, Lund BA, Andersen P, Müller-Karger FE, & Dean K. (1989). Carbon and nitrogen cycling within the Bering/Chukchi Seas: source regions for organic matter effecting AOU demands of the Arctic Ocean. *Progress in Oceanography, 22*, 277-359. doi.org/10.1016/0079-6611(89)90006-2

Walsh JJ, Dieterle DA, Chen RF, Lenes JM, Maslowski W, Cassan JJ, Whitledge TE, Stockwell D, Flint M, Sukhanova IN, & Christensen J. (2011). Trophic cascades and future harmful algal blooms within ice-free Arctic Seas north of the Bering Strait: A simulation analysis. *Progress in Oceanography, 91*, 312-343. doi:10.1016/j.pocean.2011.02.001

Ward BA, & Follows MJ. (2016). Marine mixotrophy increases trophic transfer efficiency, mean organism size and vertical carbon flux. *Proceedings of the National Academy of Sciences, 113*, 2958-2963. doi:10.1073/pnas.1517118113

Willhelm S, & Suttle C. (1999). Viruses and nutrient cycles in the sea: viruses play critical roles in the structure and function of aquatic food webs. *BioScience, 49*, 781-788.

1275 Worden AZ, Nolan JK, & Palenik B. (2004). Assessing the dynamics and ecology of marine
1276 picophytoplankton: The importance of the eukaryotic component. *Limnology and*
1277 *Oceanography, 49*, 168-179.

1278 Worden AZ, & Not F. (2008). Ecology and diversity of picoeukaryotes. In: Kirchman DL (ed.).
1279 *Microbial Ecology of the Oceans* (2nd ed). Hoboken: John Wiley & Sons, Inc, 159-196.

1280 Yoo Y, Seong K, Jeong H, Yih W, Rho J, Nam S, & Kim H. (2017). Mixotrophy in the marine
1281 red-tide cryptophyte *Teleaulax amphioxeia* and ingestion and grazing impact of
1282 cryptophytes on natural populations of bacteria in Korean coastal waters. *Harmful Algae,*
1283 *68*, 105-117. doi:10.1016/j.hal.2017.07.012

1284 Zelinka M, & Hartmann D. (2011). Climate feedback and their implications for poleward energy
1285 flux changes in a warming climate. *Journal of Climate, 25*, 608-624.

1286 Zhang J. (2005). Warming of the arctic ice-ocean system is faster than the global average since the
1287 1960s. *Geophysical Research Letters, 32*. doi:10.1029/2005GL024216

1288

Figure;Fig1

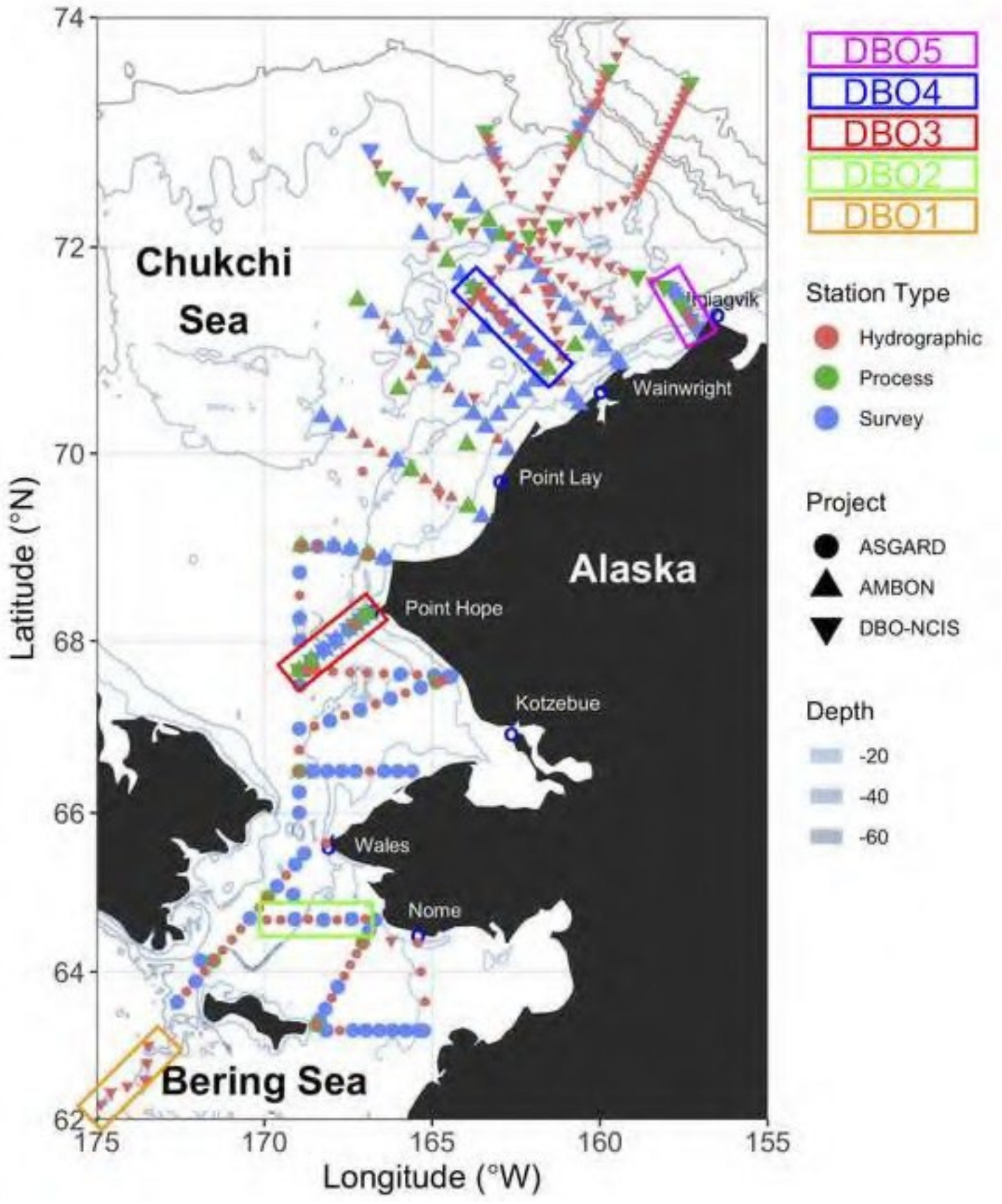
DBO5
DBO4
DBO3
DBO2
DBO1
Station Type
Hydrographic
Process
Survey
Project
ASGARD
AMBON
DBO-NCIS
Depth
-20
-40
-60
Chukchi Sea
Alaska
Bering Sea
Wainwright
Point Lay
Point Hope
Kotzebue
Wales
Nome
Latitude (°N)
Longitude (°W)
74
72
70
68
66
64
62
175
170
165
160
155

Figure;Fig2

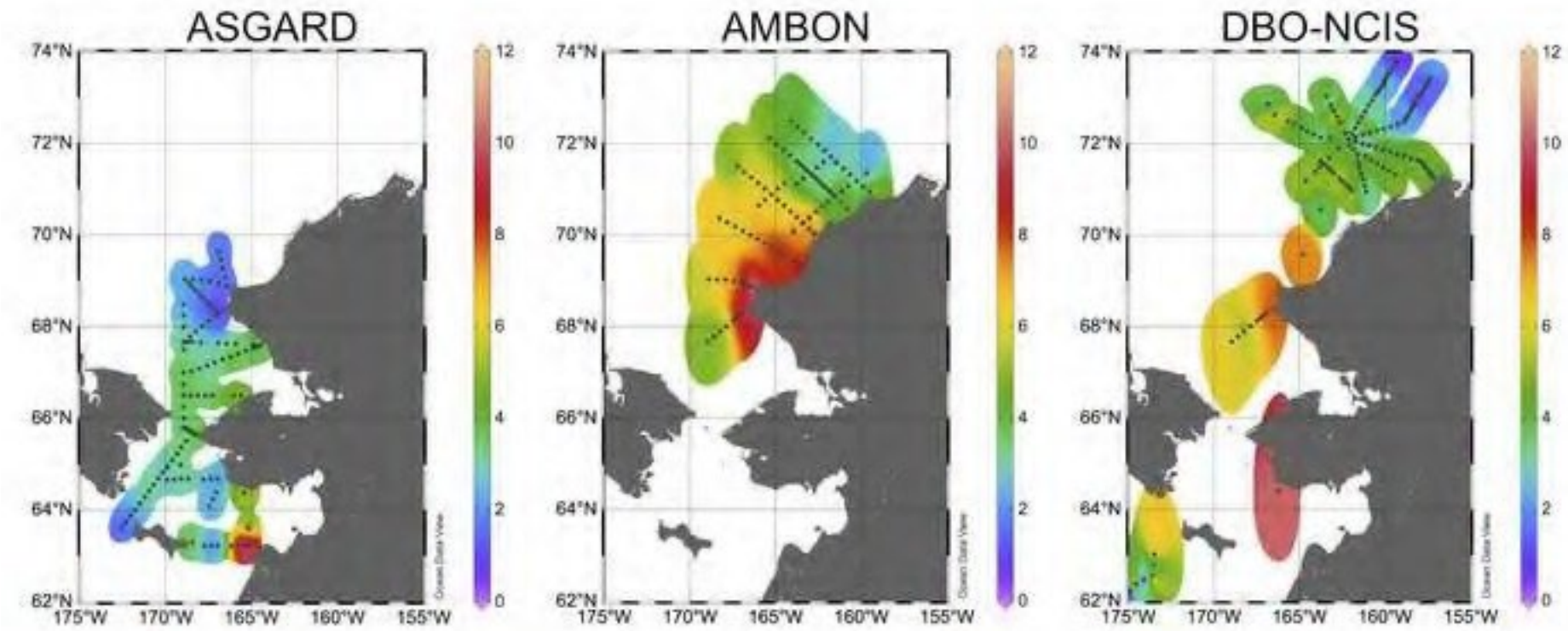
ASGARD
AMBON
DBO-NCIS
74°N
72°N
70°N
68°N
66°N
64°N
62°N
175°W
170°W
165°W
160°W
155°W
12
10
8
6
4
2
0

Figure;Fig3

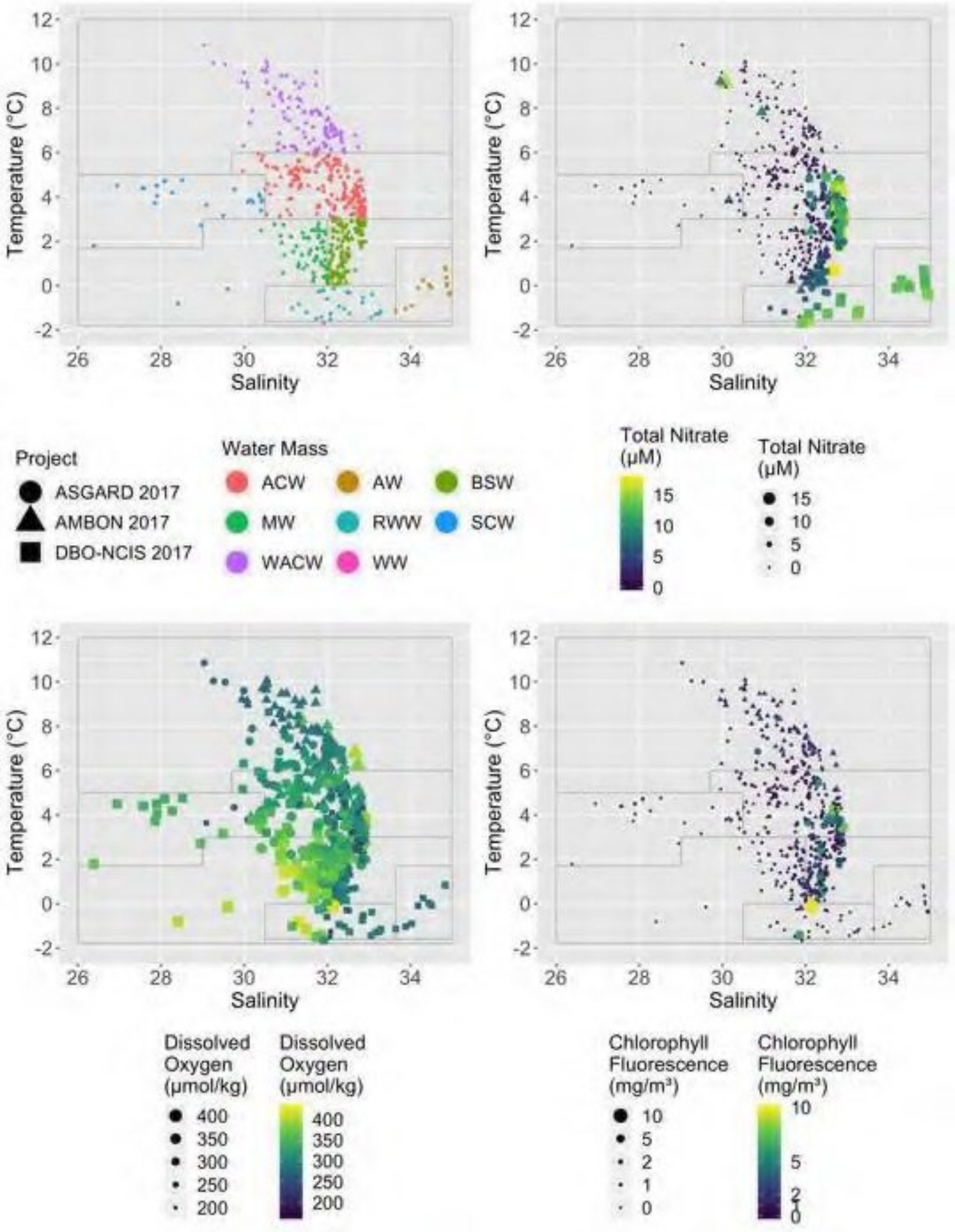
Temperature (°C)
Salinity
Project
ASGARD 2017
AMBON 2017
DBO-NCIS 2017
Water Mass
ACW
AW
BSW
MW
RWW
SCW
WACW
WW
Total Nitrate (µM)
Dissolved Oxygen (µmol/kg)
Chlorophyll Fluorescence (mg/m³)

Figure;Fig4

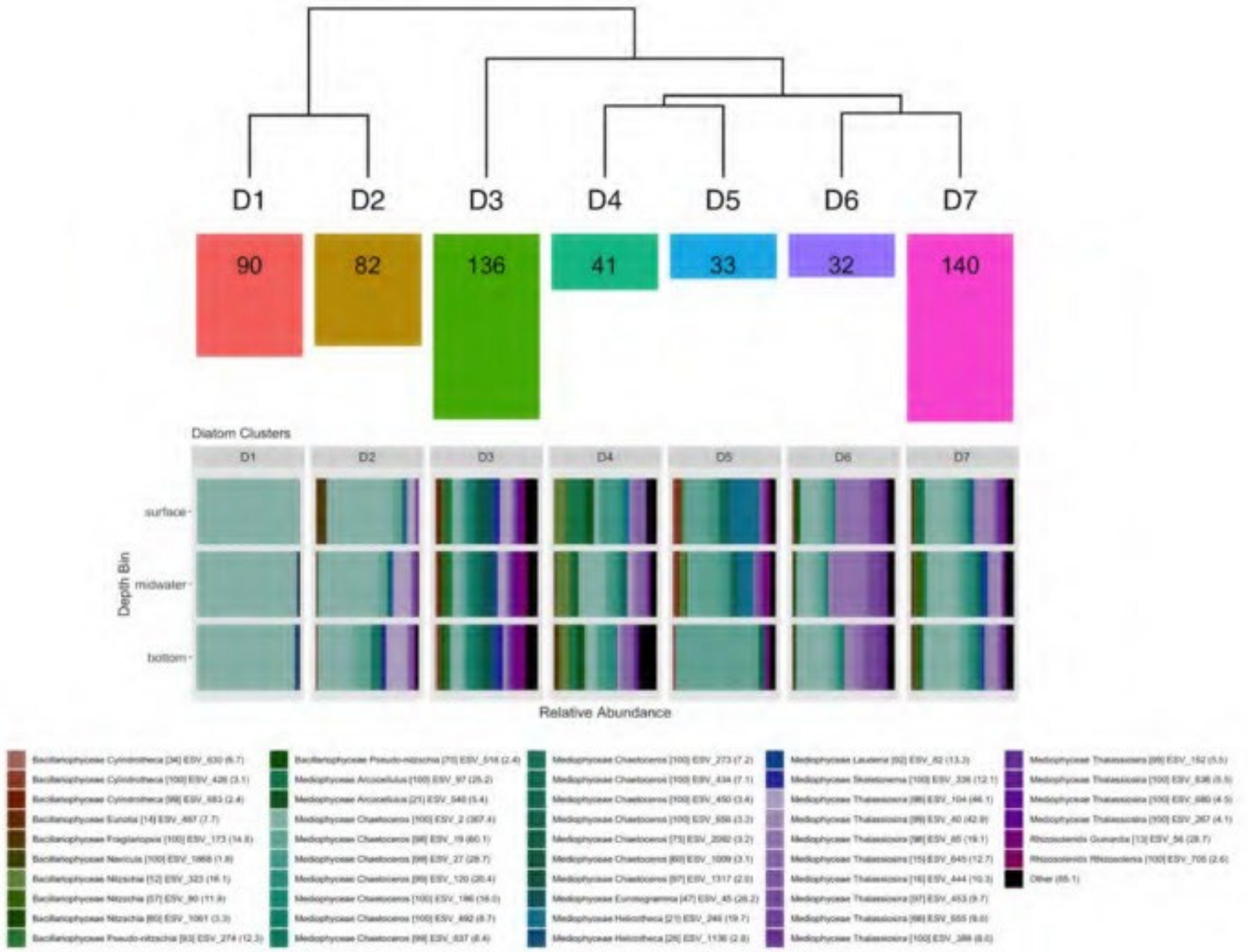
D1
D2
D3
D4
D5
D6
D7
90
82
136
41
33
32
140
Diatom Clusters
surface
midwater
bottom
Depth Bin
Relative Abundance

Figure;Fig5

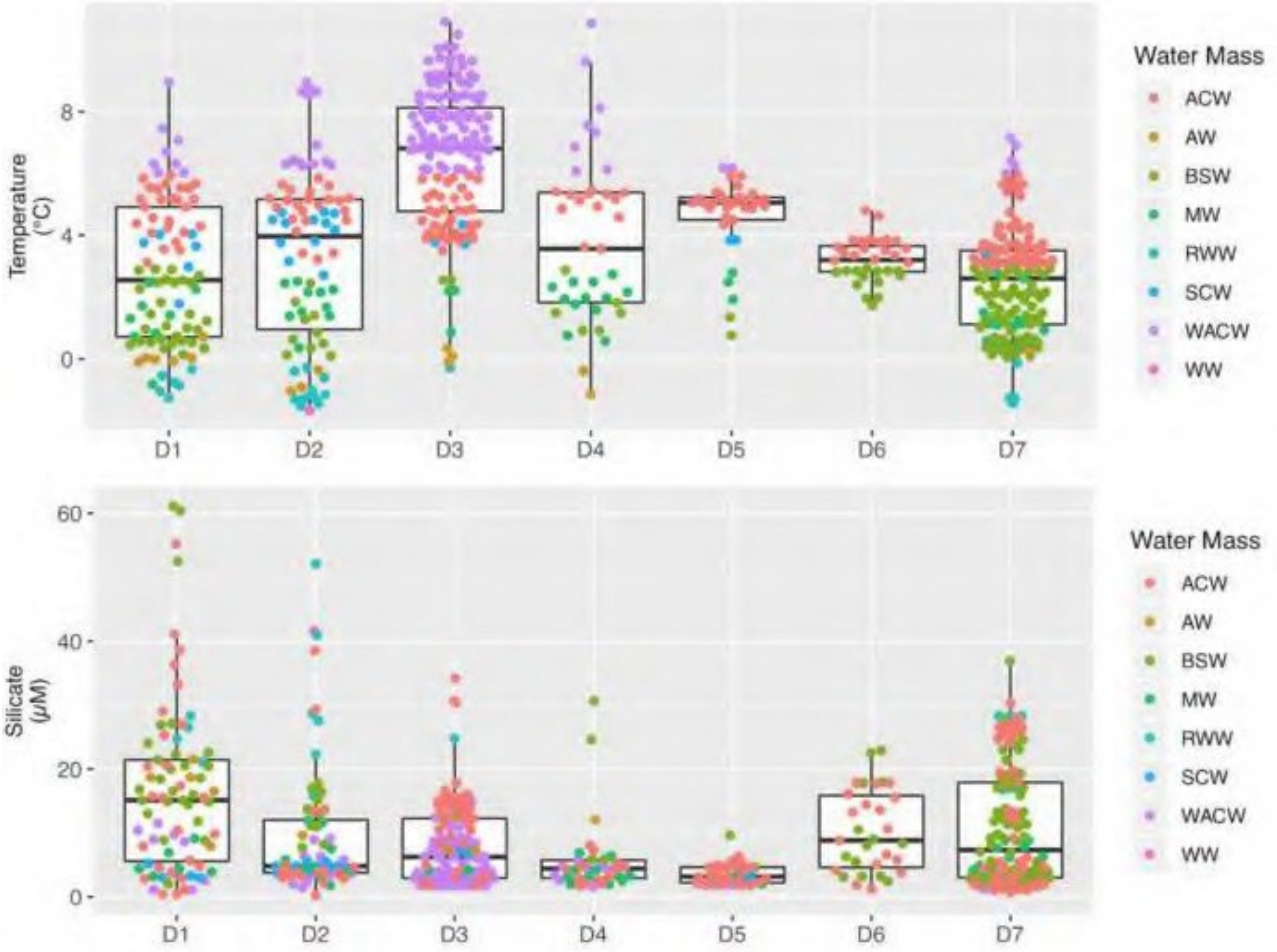
Temperature (°C)
8
4
0
D1
D2
D3
D4
D5
D6
D7
Water Mass
ACW
AW
BSW
MW
RWW
SCW
WACW
WW
Silicate (μM)
60
40
20
0
D1
D2
D3
D4
D5
D6
D7
Water Mass
ACW
AW
BSW
MW
RWW
SCW
WACW
WW

Figure;Fig6

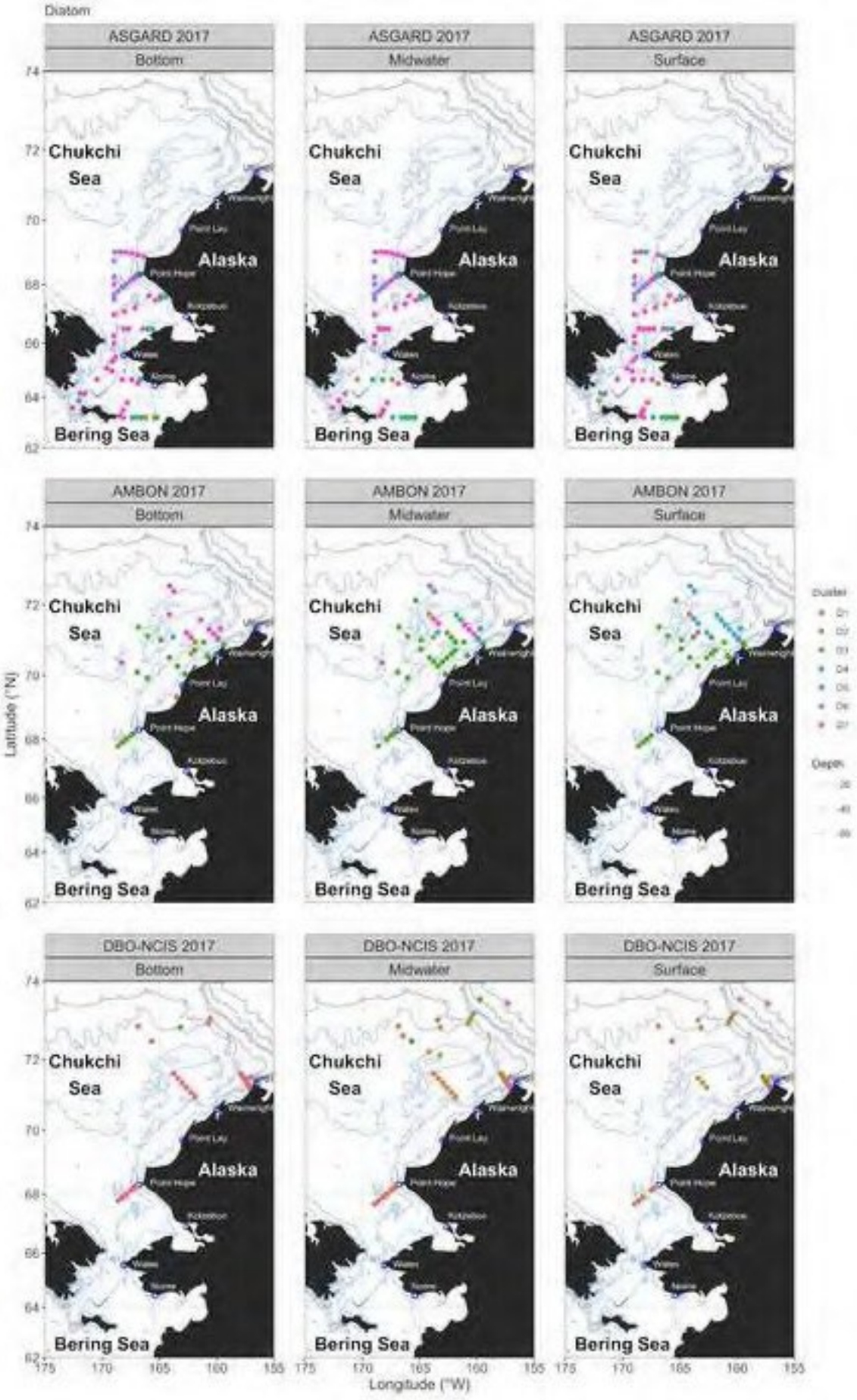
Diatom
ASGARD 2017
Bottom
ASGARD 2017
Midwater
ASGARD 2017
Surface
AMBON 2017
Bottom
AMBON 2017
Midwater
AMBON 2017
Surface
DBO-NCIS 2017
Bottom
DBO-NCIS 2017
Midwater
DBO-NCIS 2017
Surface
Chukchi Sea
Alaska
Bering Sea
Point Lay
Point Hope
Kotzebue
Wales
Nome
Latitude (°N)
Longitude (°W)
Cluster
Depth

Figure;Fig7.png

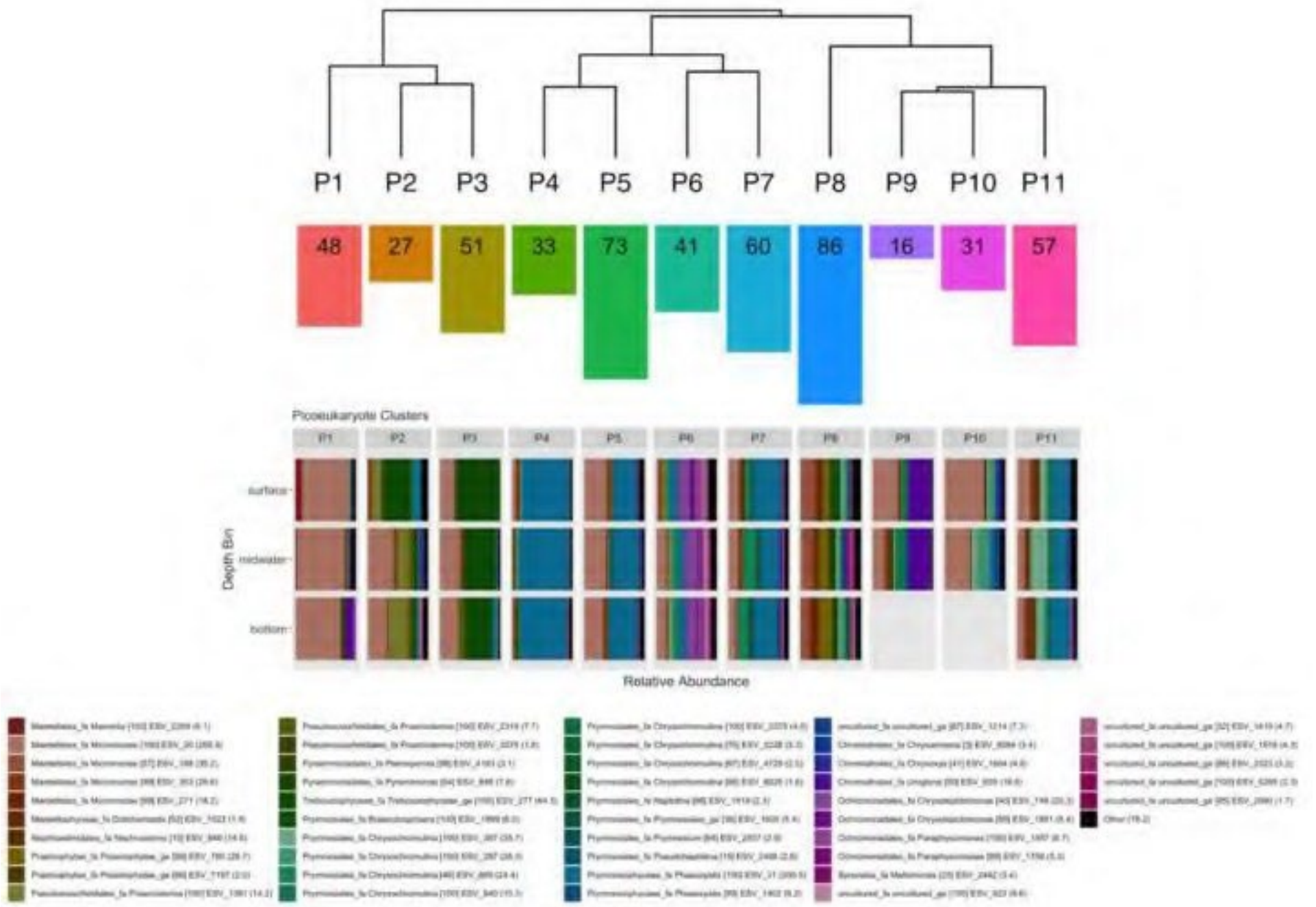

Figure;Fig8

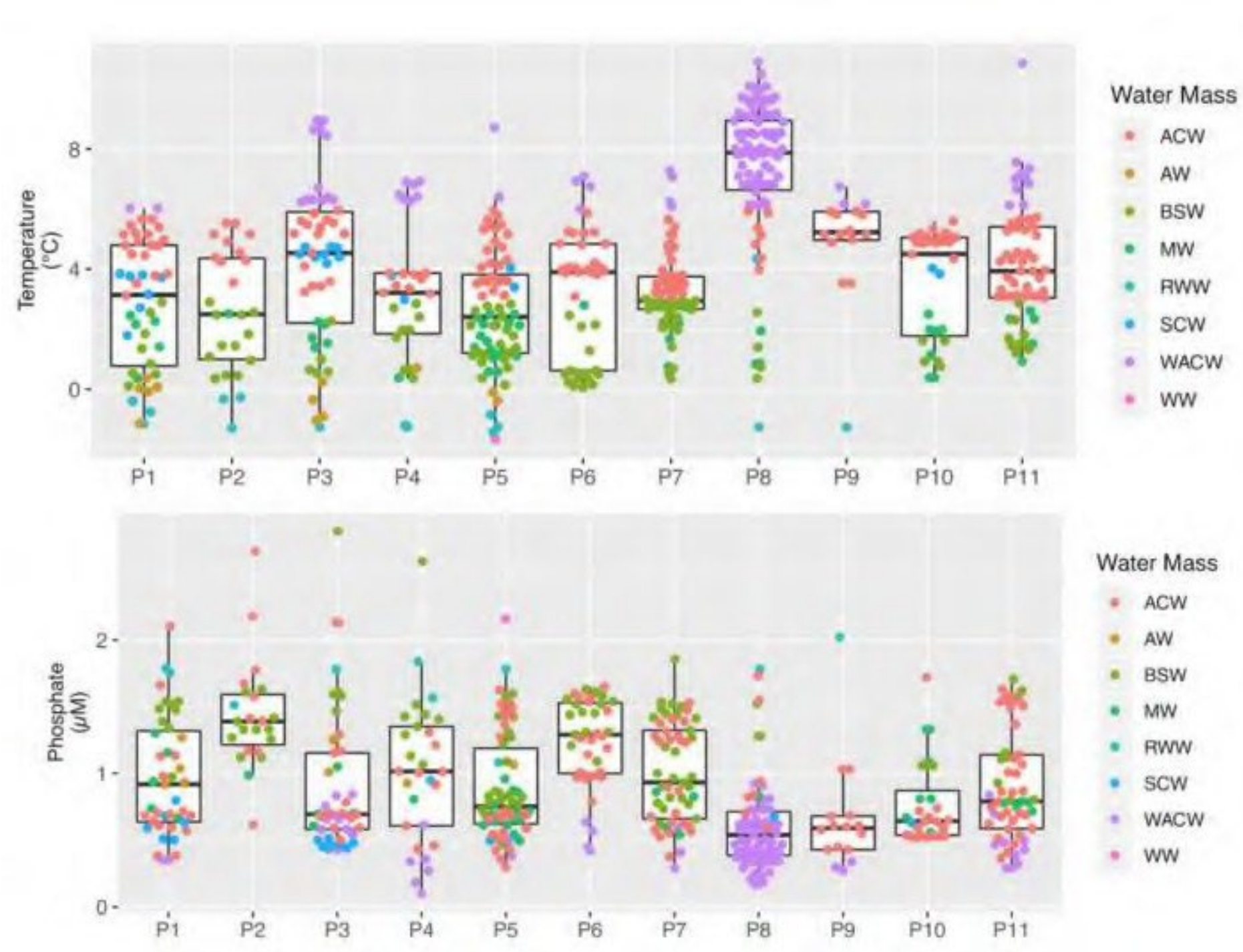
Temperature (°C)
8
4
0
P1
P2
P3
P4
P5
P6
P7
P8
P9
P10
P11
Water Mass
ACW
AW
BSW
MW
RWW
SCW
WACW
WW
Phosphate (μM)
2
1
0
P1
P2
P3
P4
P5
P6
P7
P8
P9
P10
P11
Water Mass
ACW
AW
BSW
MW
RWW
SCW
WACW
WW

Figure;Fig9

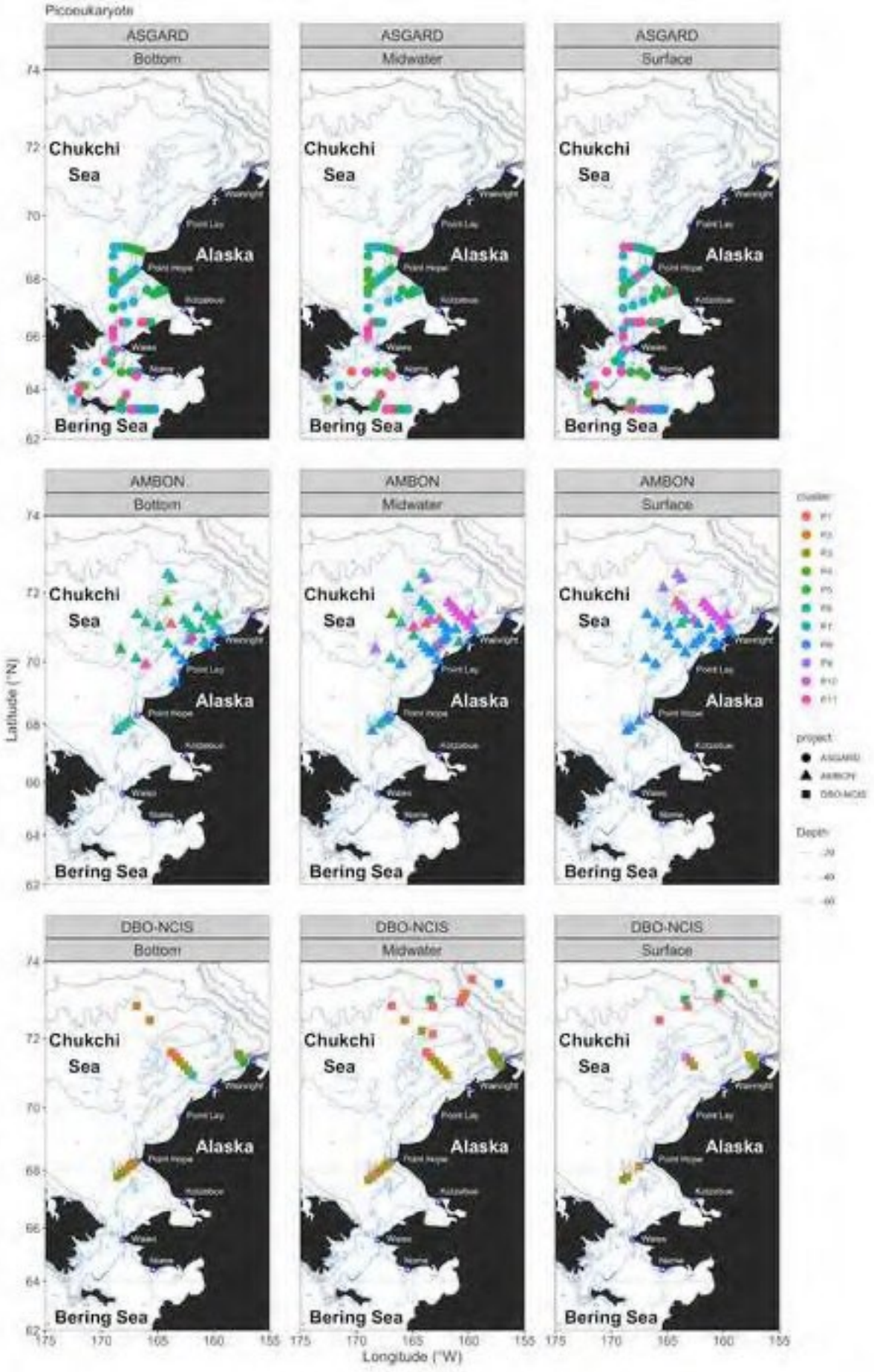
Picoeukaryote
ASGARD
Bottom
ASGARD
Midwater
ASGARD
Surface
AMBON
Bottom
AMBON
Midwater
AMBON
Surface
DBO-NCIS
Bottom
DBO-NCIS
Midwater
DBO-NCIS
Surface
Chukchi Sea
Alaska
Bering Sea
Point Lay
Point Hope
Kotzebue
Wales
Nome
Latitude (°N)
Longitude (°W)
cluster
project
Depth

Figure;Fig10

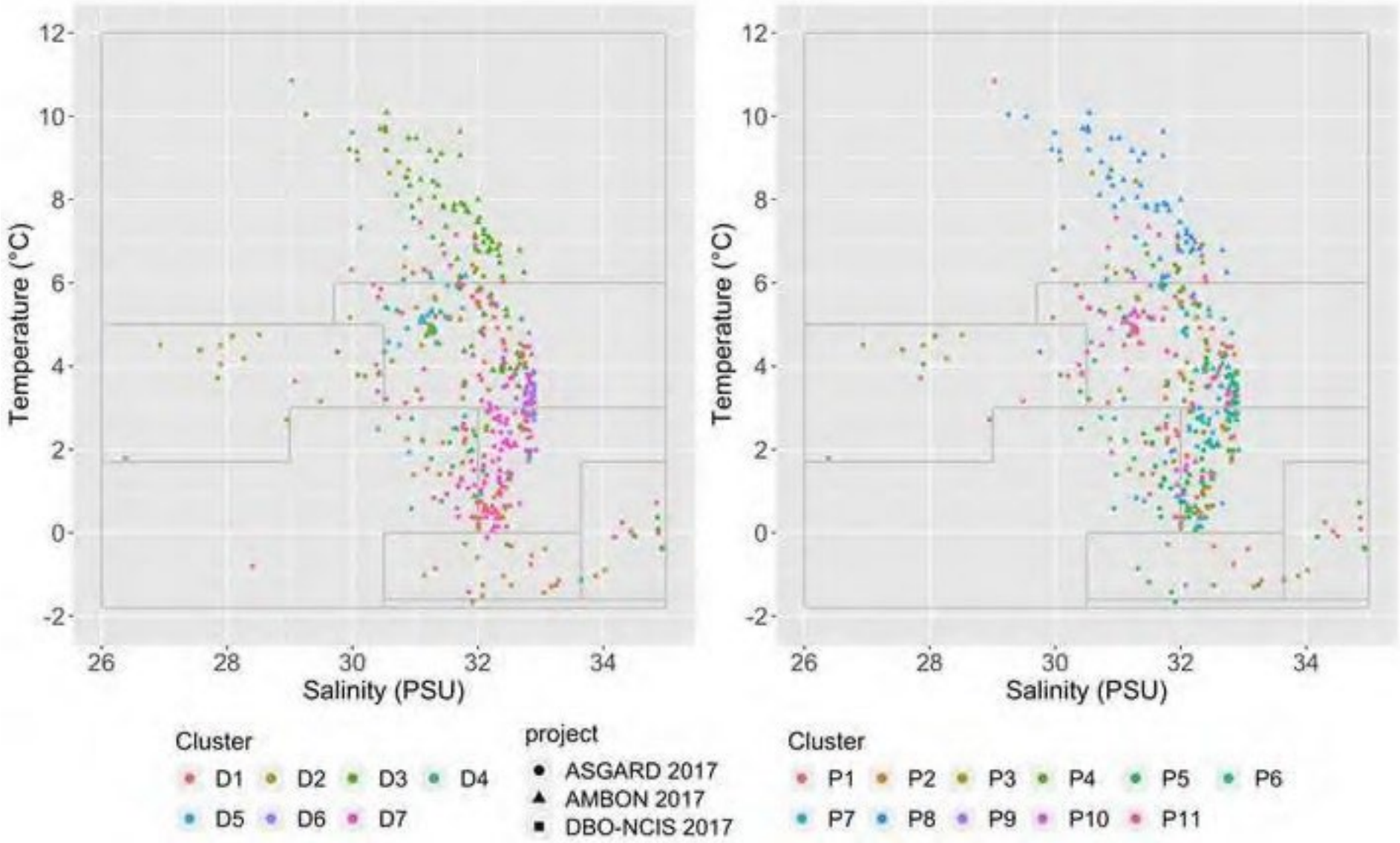

Figure;Fig11

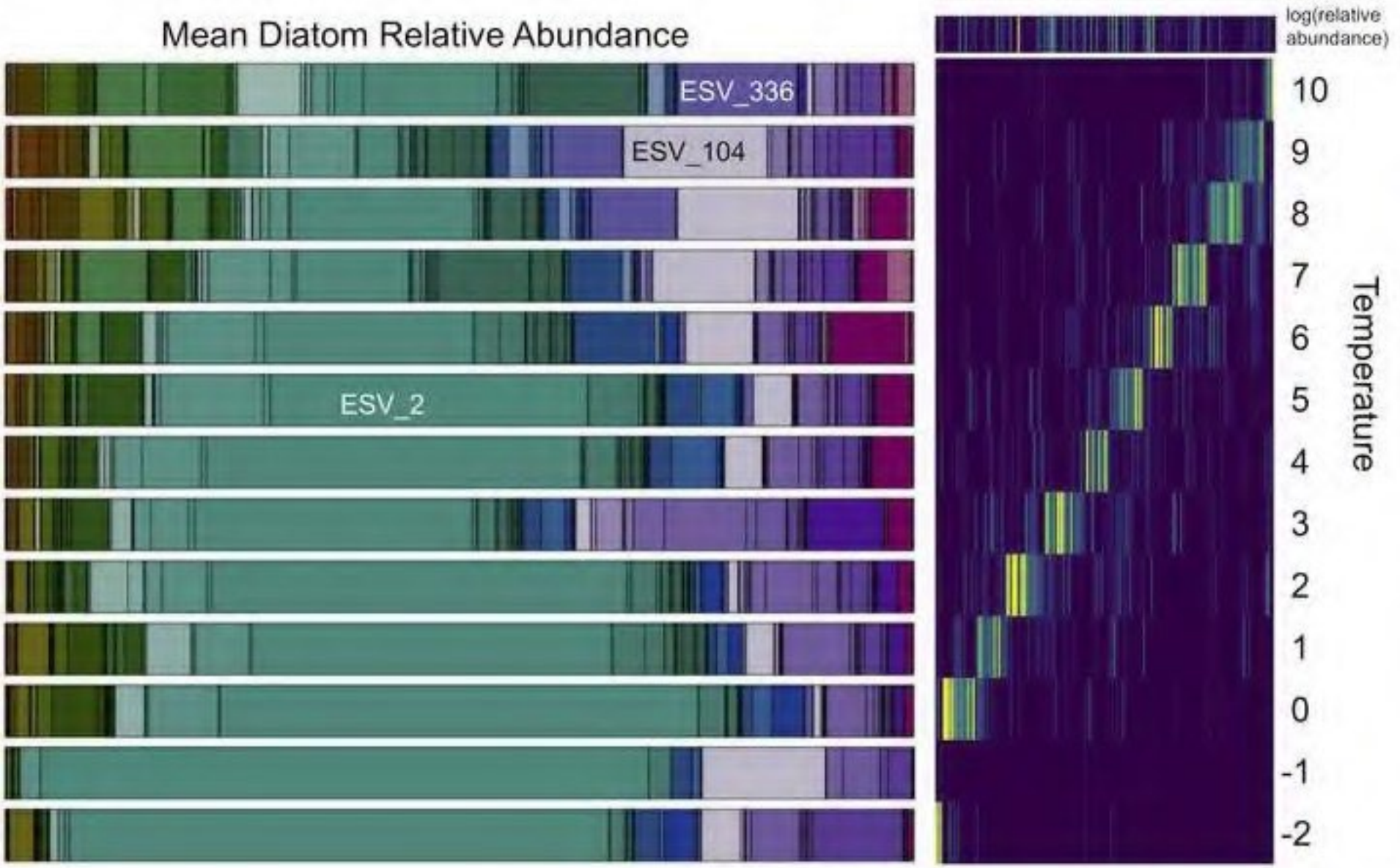

Figure;Fig12

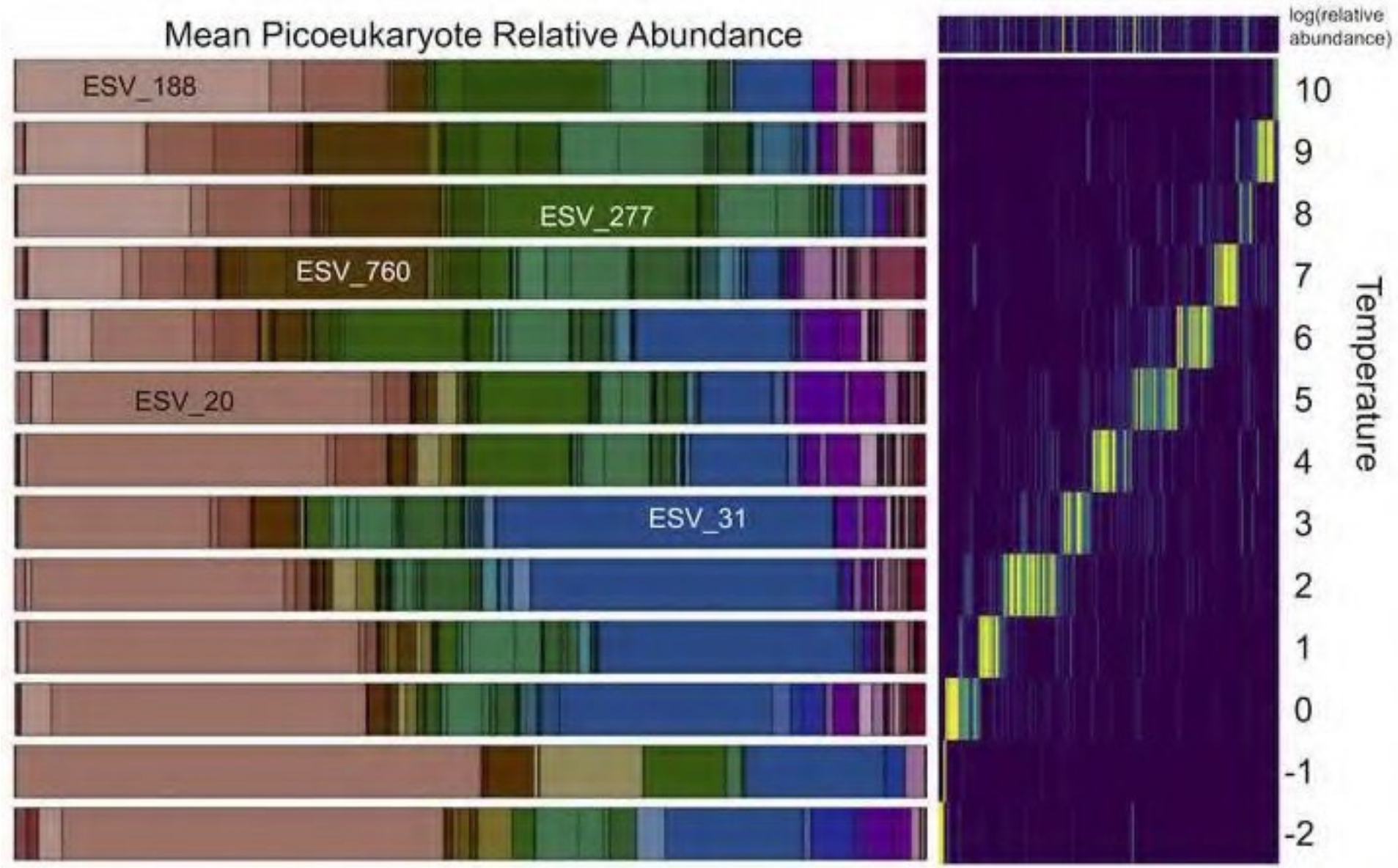

Figure;Fig13

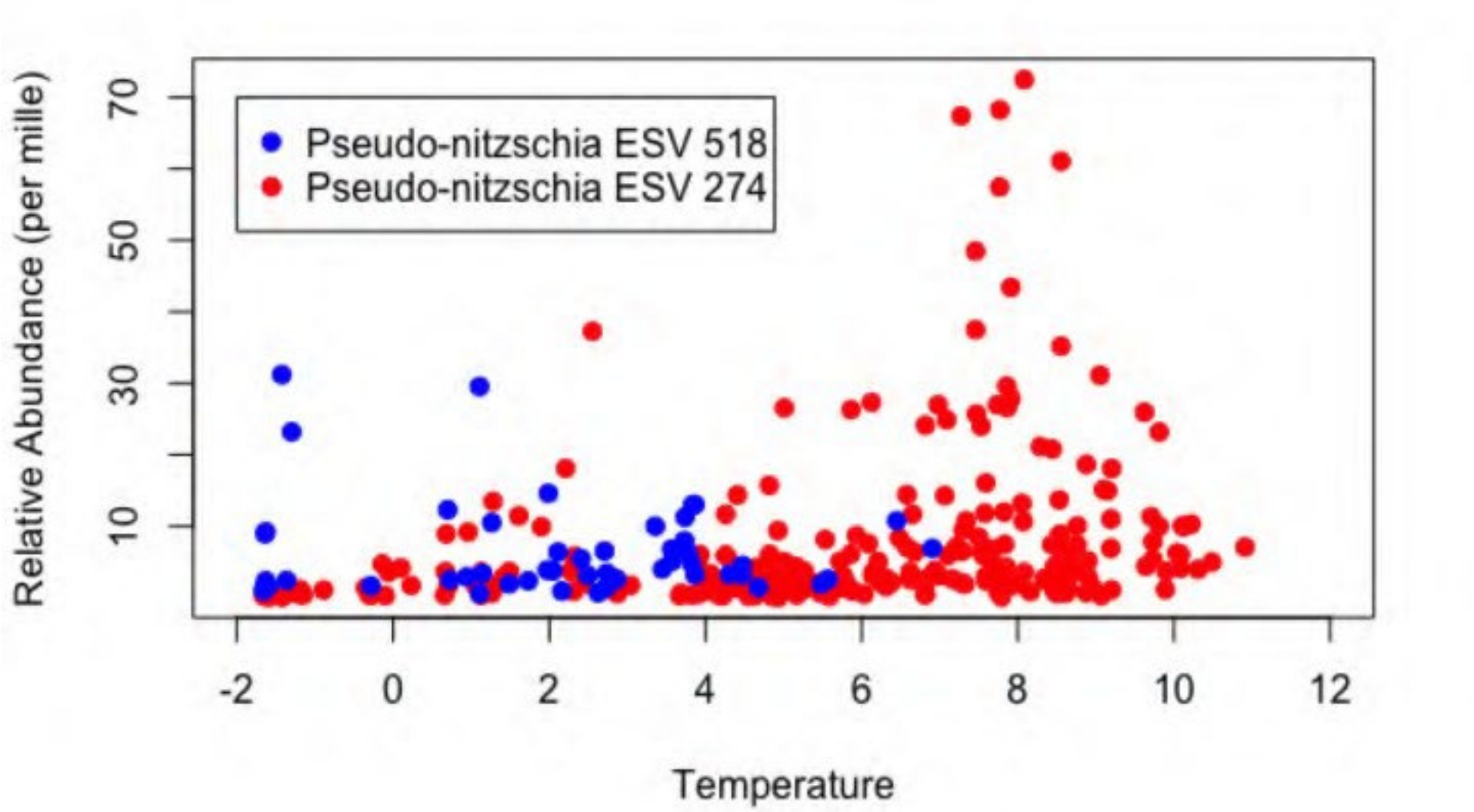

Synechococcus abundance and biomass in the Northern Bering and Chukchi seas.

Lomas, M.W.[1], Eisner, L.E.[2,3], Nielsen, J.[4], Danielson, S.[5], Mordy, C.W.[4,6] Stabeno, P.J.[6], Laney, S.R.[7]

[1] Bigelow Laboratory for Ocean Sciences, East Boothbay, ME 04544, USA

[2] NOAA Alaska Fisheries Science Center, Seattle, WA 98115, USA

[3] NOAA Alaska Fisheries Science Center, Auke Bay Laboratories, Juneau, AK 99801, USA

[4] Cooperative Institute for Climate, Ocean, and Ecosystem Studies, University of Washington, Seattle, WA 98115, USA

[5] College of Fisheries and Ocean Science, University of Alaska Fairbanks, Fairbanks, AK 99775, USA

[6] NOAA Pacific Marine Environmental Laboratory, Seattle, WA 98115, USA

[7] Woods Hole Oceanographic Institution, Woods Hole, MA 02543, USA

Key words: Phytoplankton, Bering Sea, Chukchi Sea, Synechococcus

Intended Journal: Oceans

Abstract:

Size structure of phytoplankton populations has been shown to be an important determinant of the flow of carbon and energy to higher trophic levels in Arctic ecosystems. Phytoplankton populations dominated by small (<10um) pico- and nanophytoplankton cells are generally dominated by eukaryotic flagellates that are tightly grazed by microzooplankton leading to increases in trophic length. General dogma suggests that the picocyanobacteria *Synechococcus* is detectable but comprises a negligible fraction of phytoplankton carbon in Arctic ecosystems. As part of the Arctic IERP sampling program, we quantified the abundance of the *Synechococcus*, and other picophytoplankton, during the spring to fall period between 2017-2019 in the Northern Bering and Chukchi Seas. *Synechococcus* abundances increased from <500 cells/ml in spring to >50,000 cells/ml in the fall around Kotzebue Sound. Furthermore, the spatial extent of regions with elevated *Synecococcus* abundances in late summer/fall, as well as the absolute abundances, increased from 2017 to 2019, coincident with increasing late summer/fall water temperatures. When integrated over the euphotic zone, *Synechococcus* contributed up to 40% of estimated total phytoplankton carbon during late summer/fall in Kotzebue sound and the region near Icy Cape. These observations support an increased importance of a previously marginal phytoplankton group during a warming period in the Chukchi Sea. The full implications of these changes in the phytoplankton community remain to be resolved.

Introduction:

Arctic and subarctic seas are facing many stressors that may lead to significant changes in its function in the future (IPCC 2021). An important change is sea ice loss that when coupled with intensification of the hydrological cycle (Peterson et al., 202; Serreze et al., 2006) will likely lead to increases in stratification in near shore shelf systems, a key controlling factor of the productivity, through negative impacts on nutrient inputs, and structure of marine ecosystems of the Arctic Ocean (Carmack et al., 2006, Carmack 2007). The impact(s) of these changes on phytoplankton at the base of marine food chains is not completely resolved, particularly changes in phytoplankton community size structure (Tremblay and Gagnon, 2009).

Globally picophytoplankton (<2um) are well known and dominate in the major oligotrophic ocean gyres, but dogma is that they are not quantitatively important in the sub/arctic systems (Buitenhuis et al. 2011, Flombaum et al. 2013). In contrast, numerous measurements of size-fractionated chlorophyll have shown that the picoplankton size fraction can dominate phytoplankton biomass in sub/arctic systems during oligotrophic periods (e.g., summer) and regions (e.g., off-shelf) (e.g., Booth and Horner, 1997; Brugel et al., 2009; Legendre et al., 1993; Li et al., 2009; Odate, 1996). Given that picophytoplankton have a much higher carbon to chlorophyll ratio than microphytoplankton, it is likely that their importance to both carbon cycling and quality as a food source has been further underestimated (Lee et al., 2013). Within the picophytoplankton size class there is a wide diversity of both eukaryotic (e.g., prasinophytes and cryptophytes, Lovejoy et al., 2007; Sergeeva et al., 2010) and prokaryotic (e.g., Cottrell and Kirchman, 2009; Not et al., 2005) organisms. More recent studies have used flow cytometry as a more efficient tool to numerically quantify these <2um cells into operational categories (i.e., pico- and nanophytoplankton; Laney and Sosik, 2014), although some organisms do contain unique pigment signatures that allow them to be distinguished from other similar cells. For example, *Synechoccocus* and cryptophytes both contain

the orange pigment phytoerythrin, and thus can be identified as specific groups within the pico- and nanophytoplankton.

In the region between the eastern Beaufort Sea and Baffin Bay picophytoplankton numerically dominate in deeper water stations off shelf, and particularly in the SCM (e.g., Ardyna et al., 2011, Schlooss et al. 2008). In the Chukchi and western Beaufort Seas, it has also been shown that small prasinophytes, other flagellates (e.g., cryptophytes) and non-colonial phaeocystis (<5um) dominated in the deeper basin sites during summer and fall, while diatoms dominated on the shallow shelf (Gosselin et al 1997, Booth and Horner, 1997; Hill et al., 2005; Sergeeva et al., 2010; Sherr et al., 2003). Based upon a few stations in the southern Bering Sea, Liu et al. (2002) observed that picophytoplankton abundance, both *Synechococcus* and eukaryotes decreased from the basin to the shelf. Some eukaryotic picophytoplankton strains have been shown to persist through the winter maintaining growth rates that exceed grazing losses, and have been suggested to represent unique temperature controlled biogeographical clades (Lovejoy et al., 2007). Representatives of this eukaryotic psycrophillic clade are pan-Arctic, with some representatives having maximum growth temperatures of ~12.5ºC, so there may be problems in the future, and could cause disruptions in the food web. In contrast, the picocyanobacteria *Synechococcus,* has been found to be associated with slightly warmer and saltier water than eukaryotic picoplankton (Cottrell and Kirchman, 2009; Not et al., 2005; Tremblay and Gagnon, 2009, Waleron et al., 2007, Gradinger and Lenz 1989). Interestingly, Waleron et al. (2007), using eDNA analysis, identified 6 OTUs similar to *Synechoococcus* from the Mackenzie River system. These OTUs were linked to freshwater *Synechococcus* and it was concluded that they flushed into the system and implied they survived but were not actively growing.

The distributions of picophytoplankton around the sub/Arctic are important to understand, in particularly their contributions to total biomass (not just numbers), as well as the environmental variables that they correlate with to understand the niches that they currently occupy and when those niche boundaries might be exceeded. In this study we address the following questions. 1) what are the large spatial (i.e., cross shelf) and seasonal patterns of *Synechococcus* abundance and biomass in the Northern Bering and Chukchi Seas; 2) what are the environmental parameters associated with patterns in *Synecococcus* biomass; and 3) is there evidence of long term trends in *Synechococcus* biomass.

Methods:

Sample collection: Physical, chemical and biological measurements were made as part of the Arctic Integrated Ecosystem Research Program (AIERP, 4 cruises, and one cruise of opportunity) within the Northern Bering and Chukchi Sea region (Table 1, Figure 1). Samples were collected in clean Niskin bottle at roughly 10m spacing throughout the water column. At each station and depth a range of discrete phytoplankton samples were collected including size-fractionated chlorophyll a (Chl-a), picoplankton and nanoplankton counts by quantitative flow cytometry (e.g., Lomas et al., 2010), microplankton counts by inverted microscopy and FlowCAM, and seston particulate organic carbon (POC). Only flow cytometry data data are reported in this study.

Phytoplankton cell counts and carbon biomass estimates: Samples for picoplankton enumeration were generally collected at four to seven depths throughout and just below the euphotic zone, fixed with paraformaldehyde (0.5% final concentration), stored at ~4ºC for 1-2 h, before long-term storage at -80ºC.

Samples were analyzed on a Becton Dickinson (formerly Cytopeia Inc.) Influx or Jazz cytometer using a 488 nm blue excitation laser, appropriate Chl-*a* (692 ± 20 nm) and phycoerythrin (580 ± 15 nm) bandpass filters, and was calibrated daily with 0.53-µm and 3.0-µm fluorescent microbeads (Spherotech Inc. Libertyville, Illinois, USA). Each sample was run for 4-6 min (~0.3-0.5 mL total volume analyzed), with log-amplified Chl-*a* and phycoerythrin fluorescence, and forward and right-angle scatter signals recorded. Data files were analyzed from two-dimensional scatter plots based on Chl.-*a* or phycoerythrin fluorescence and characteristic light scattering properties (e.g., DuRand and Olson, 1996) using FCS Express 3.0 (DeNovo Software Inc. Los Angeles, California, USA) or SortWare (Becton Dickenson, East Rutherford, New Jersey, USA). Picophytoplankton, operationally defined as cells <3.0-um, were identified as *Synechococcus* cells based upon cell size and the presence of phycoerythrin. Based upon these gating criteria, the number of cells in each identified population was enumerated and converted to cell abundances by the volume-analyzed method (Sieracki et al., 1993). Precision of triplicate samples was <10% for cell concentrations >200 cells mL^{-1}. Carbon per cell was estimated for flow cytometrically identified phytoplankton using a calibration curve that related cellular particulate organic carbon (POC) to normalized geometric mean cellular forward scatter (proxy for cell size) (e.g., DuRand et al., 2001, Casey et al. 2013, data specific to the flow cytometer used in this study). Carbon content of each identified population was estimated by multiplying volumetric cell abundance and POC per cell derived from the calibration curve.

Chlorophyll: Sample volumes varied depending upon the cruise, but ranged from 0.1 - 1L, and in all cases were gently vacuum filtered (≤5 mm Hg) for total chlorophyll (Chl-a) analysis onto Whatman GFF (or equivalent) filters (nominal 0.7 µm pore size). At selected stations, size-fractionated chlorophyll concentrations were estimated by filtered paired samples sequentially through a 5 µm Whatman Track Etch polycarbonate filters and then a Whatman GFF filter. After filtration, samples were stored frozen at -80°C until extraction and analysis. For analysis, samples were extracted in 5 ml of 90% acetone for 24 h at -20°C. Samples were analyzed on a calibrated fluorometer, either Turner Designs TD-700 or 10-AU, with day-to-day performance of the fluorometer tracked using a commercially available solid standard. Fluorescence readings were taken before and after the addition of 75 µl of 1.2M HCl and concentrations calculated using standard equations (Parsons et al., 1984).

Table 1. Summary details associated with cruises included in this analysis.

Cruise ID	**Dates**	**Latitude (°N) (min-max)**	**Longitude (°W) (min-max)**	**Stations (>/< 50m)**
SKQ-2017-09S	5th June – 26th June 2017	56.4 to 69	-172.6 to -169	
OS-1701	6th Aug – 27th Sept 2017	67.0 to 72.5	-169.0 to -152.3	
SKQ-2018-13S	7th June – 23rd June 2018	63.3 to 69	-171.5 to -164.4	
HLY-1801	8th Aug – 23rd Aug 2018	64.7 to 71.8	-170.0 to -153.8	
OS-1901	1st Aug – 2nd Oct. 2019			

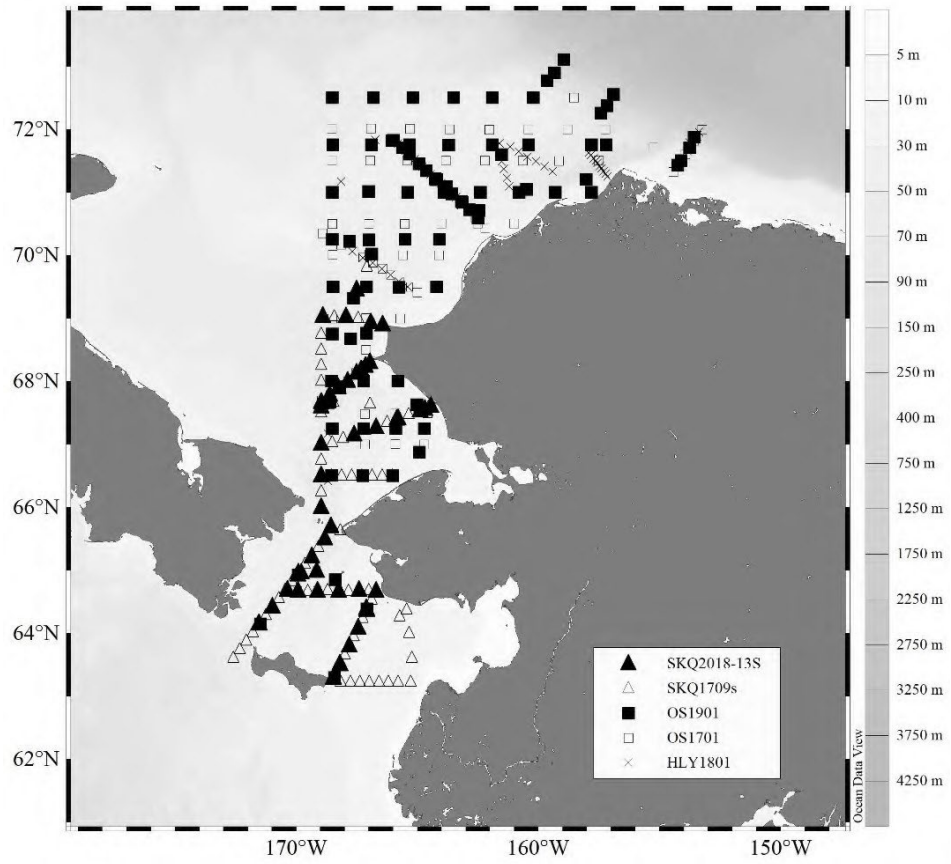

Figure 1. Map of station locations included in this analysis. There are a total of 494 discrete stations, although some are sampled multiple times over multiple cruises within the same program.

Dissolved nutrients: Samples for nutrient analysis were collected at the same depths as Chl-a and rate process incubation samples. Samples were syringe filtered using 0.45µm cellulose acetate membranes, and collected in 30ml acid washed, high-density polyethylene bottles after three rinses. On the BASIS and EcoFOCI cruises, samples were stored frozen at -80ºC and analyzed later at the shore-based facility, while samples from the BEST cruises were stored at 4ºC until analysis at sea, usually within 12 hrs of collection. Phosphate, nitrate, nitrite, and ammonium concentrations were determined using a combination of analytical components from Alpkem, Perstorp and Technicon. WOCE-JGOFS standardization and analysis procedures (Gordon et al., 1993) were closely followed including reagent preparation, calibration of lab glassware, preparation of primary and secondary standards, and corrections for blanks and refractive index. Nutrient data from the Bering Sea program cruises were accessed from the Bering Sea Project Data Archive (Stabeno et al., 2013a, b), and data from the BASIS and EcoFOCI cruises were provided by co-author CWM.

POC analysis: [to be written]

Data analysis: [to be written]

Results:

Spatial and temporal distribution of Synechococcus. *Synechococcus* cell abundance showed a clear seasonal variation in each major region (Figure 2). Cell abundance in the spring period were generally low (<1000 cells/ml), with the highest concentrations in the Northern Bering Sea/Bering Strait region. In stark contrast, in late summer/early fall, cell abundances could exceed 100,000 cells/ml. In summer/fall periods highest abundances were in Kotzebue Sound, although between years in the study the spatial extent of high cell abundances increased substantially.

Synechococcus abundances were found to have a seasonal vertical distribution pattern (Figure 3). During spring periods (e.g., June 2018), *Synechococcus* abundances were greater at depth, whereas in late summer/early fall (e.g., Aug/Sept. 2019), greatest *Synechococcus* abundances were restricted to the upper 20m of the water column over the broader spatial range where they were observed.

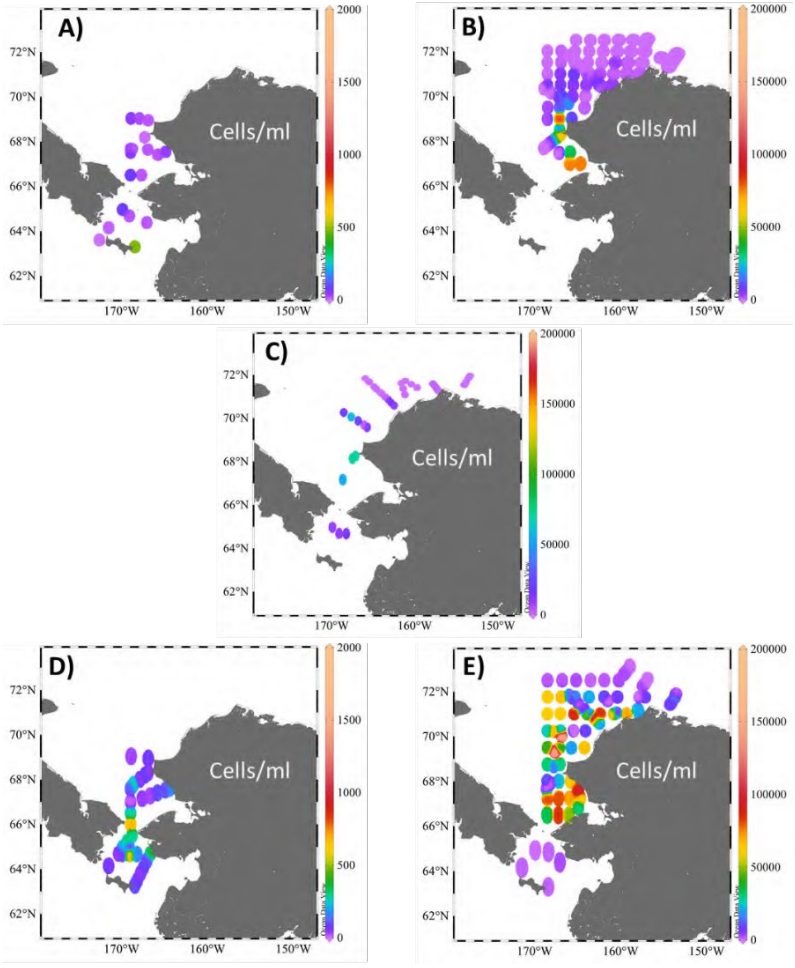

Figure 2. Seasonal patterns of *Synechococcus* abundance in the Northern Bering and Chukchi Seas. A) spring 2017 (SKQ-2017-09S), B) late summer/early fall 2017 (OS1701), C) summer 2018 (HLY1801), D) spring 2018 (SKQ-2018-13S), and E) late summer/early fall 2019 (OS1901). Note the 100x different in scales between the spring and late summer/early fall cruises.

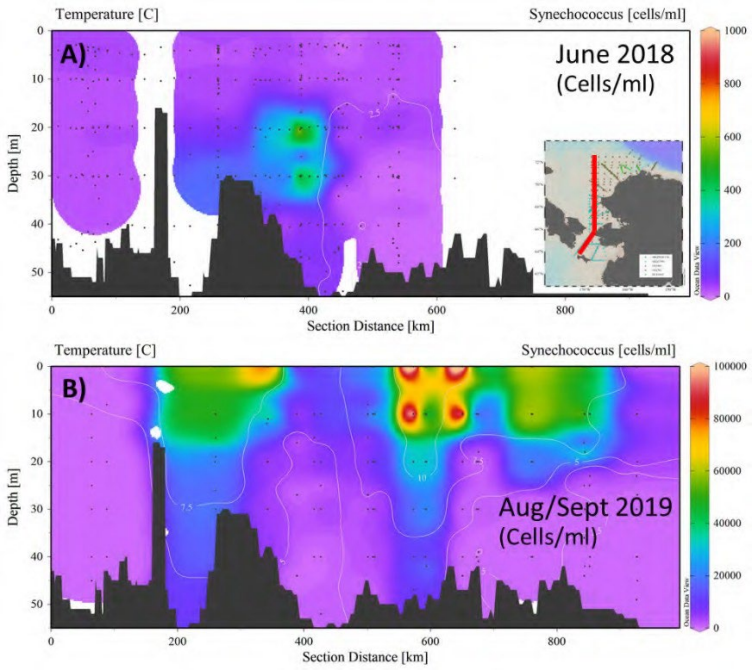

Figure 3. Latitudinal section plot of *Synechococcus* abundance through the study region.

Relationships to environmental parameters. *Synechococcus* cell abundances were highest in waters with temperatures >7oC and salinities <30.5 (**Figure 4a**). The T/S region where *Synechococcus* cell abundances were highest is classified as the warm coastal water (Danielson et al. 2020), although elevated abundances can also be found in the warmer/fresher regions of the warm shelf water. These waters are also depleted in inorganic nitrogen concentrations (**Figure 4b**).

Multiple linear regression (Model 2) analysis suggests that the only environmental variable that is significantly related to *Synechococcus* cell abundance is Temperature (Table 2). Interestingly there are two other nanophytoplankton populations, size-defined nanoeukaryotes, and the specific nanoeukaryote group of the cryptophytes, that are significantly related to *Synechococcus*.

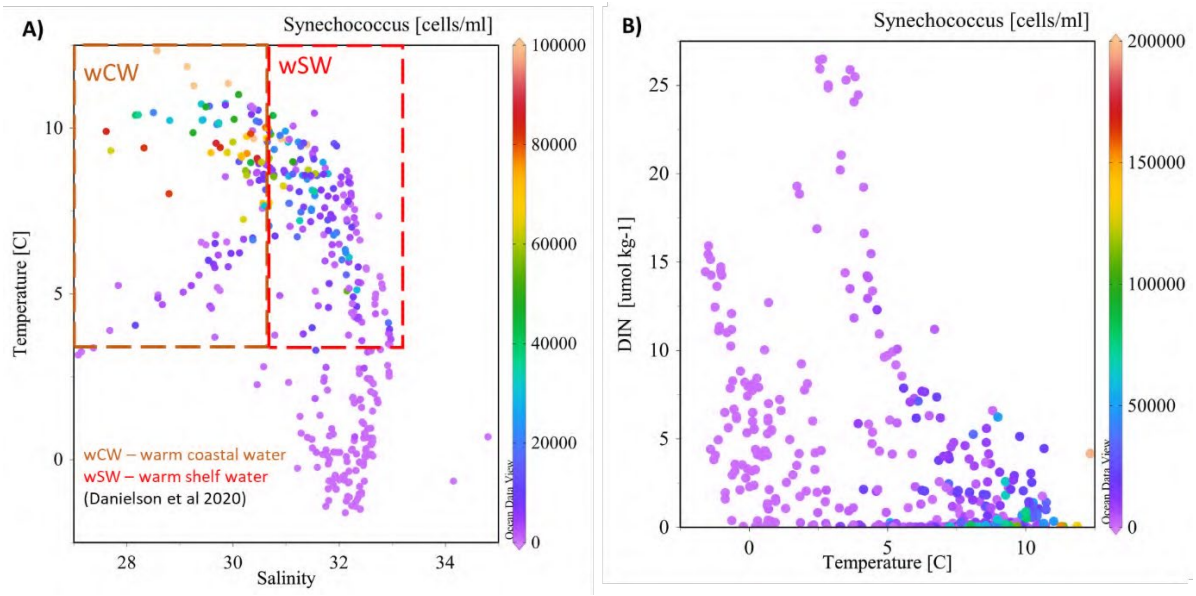

Figure 4. Relationships between *Synechococcus* abundance and environmental variables. A) temperature/salinity plot. Dashed lines bound the warm coastal water (orange) and warm shelf water (red) domain as defined by Danielson et al. 2020. B) temperature/dissolved inorganic nitrogen (DIN) plot. DIN is defined as the sum of NO3, NO2 and NH4.

Table 2. Results of multiple linear regression (Model 2) analysis between *Synechococcus* abundance and environmental and biological variables. Variables significantly related to *Synechococcus* abundance are shown in italic font.

Parameter	**Coefficient**	**Std. Error**	**t-statistic**	**P-value**
Depth (m)	1.019	109.85	0.00928	0.993
Temperature (°C)	*1167.25*	*423.32*	*2.757*	*0.006*
Salinity	-726.06	1010.29	-0.719	0.473
PAR (umol/m^2/s	-3.367	3.377	-0.997	0.320
NH4 (umol/kg)	570.87	1102.50	0.518	0.605
NO2 (umol/kg)	-709.501	28070.55	-0.0253	0.98
NO3 (umol/kg)	-128.84	434.303	-0.297	0.767
PO4 (umol/kg)	5038.518	6061.425	0.831	0.407
SiOH4 (umol/kg)	128.682	259.505	0.496	0.62
PON (umol/L)	-322.204	1555.11	-0.207	0.836
POC (umol/L)	258.215	193.27	1.336	0.183
POP (umol/L)	-10468.379	9413.506	-1.112	0.267
Total Chla (ug/L)	-26.931	493.123	-0.0546	0.956
<5um Chla (ug/L)	-4445.655	2774.185	-1.603	0.11

Picoeukaryotes (cells/ml)	*1.441*	*0.164*	*8.784*	*<0.001*
Nanoeukaryotes (cells/ml)	-0.768	1.383	-0.555	0.579
Cryptophytes	*6.12*	*1.115*	*5.49*	*<0.001*

Contributions to total biomass. Cell abundances were converted to carbon biomass values using the relationship between normalized forward light scatter and cellular carbon (Casey et al., 2013). Total phytoplankton carbon was estimated by multiplying total chlorophyll-a by the slope of the particulate organic carbon to chlorophyll-a ratio. *Synechococcus* carbon, as a percentage of total phytoplankton carbon, increased as total phytoplankton carbon decreased, reaching values as high as 40% of total phytoplankton carbon (**Figure 5**). At chlorophyll-a concentrations ≤2ug/L, a value commonly used to denote a 'bloom', *Synechococcus* could contributed >20% of total phytoplankton carbon and increased to >40% at <1ug/L chlorophyll. Samples from the shallowest depths and warmest temperatures consistently contributed higher fractions of total phytoplankton biomass.

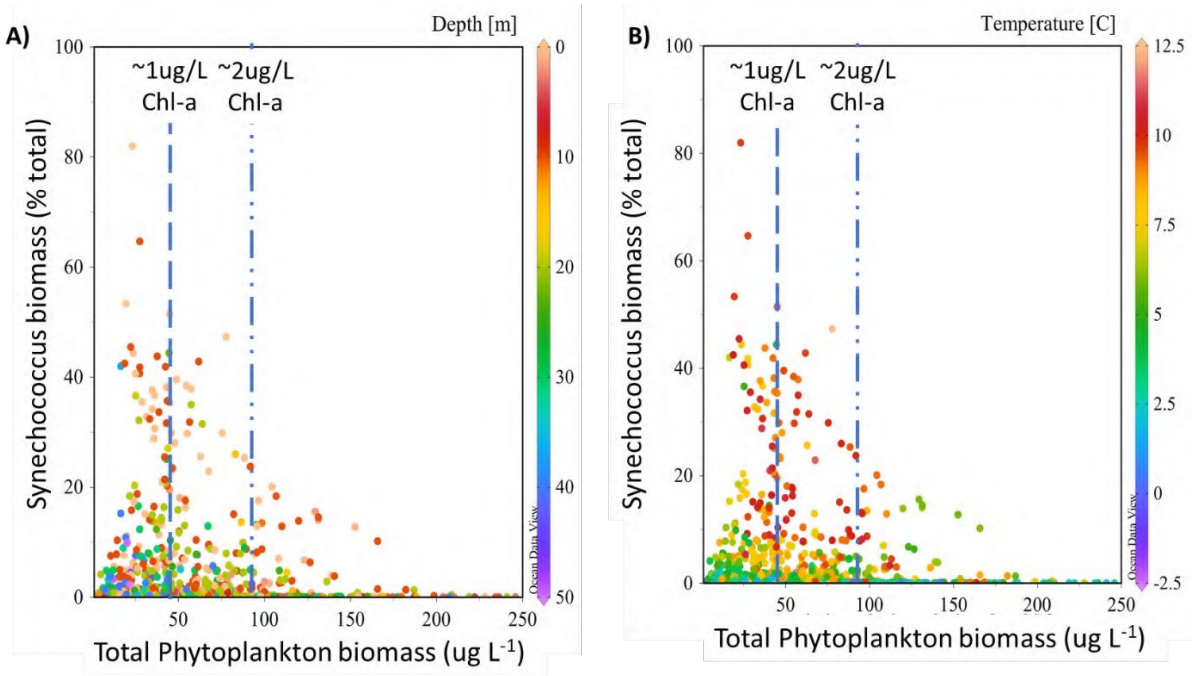

Figure 5. Contributions of *Synechococcus* to total phytoplankton carbon as function of A) depth and B) temperature. Dashed lines denote phytoplankton carbon associated with 1ug/L and 2ug/L chlorophyll.

Discussion

Highly productive systems like the Bering and Chukchi Seas are generally characterized by strong seasonal blooms of large phytoplanktonic diatoms that are rich in fatty acids and serve as an important food source for higher trophic levels. Seasonality of phytoplankton blooms, in particular the 'fall bloom' are gaining increasing recognition as being important in the trophic transfer of carbon and energy (Sigler et al., 2014). In the eastern Bering Sea shelf system, while *Synechococcus* has been observed (e.g., Liu et al., 2002; Moran et al., 2012) their abundances are generally low and represent a minor contribution to total phytoplankton carbon. The data presented in this study suggest that in the Chukchi Sea there is a very different pattern, with a much stronger seasonal amplitude in the abundance of *Synechococcus* and contribution to total phytoplankton carbon. Given the niche that *Synechococcus* fills globally (Flombaum et al., 2013; Visintini et al., 2021), our observations are consistent with *Synechococcus* growing into waters that are warm and nutrient deplete. In other ocean regions, *Synechococcus* abundances are tightly controlled by grazing (e.g., Worden and Binder, 2003), unfortunately there are not *Synechococcus*-specific grazing rates in the Northern Bering and Chukchi Seas. In the Northern Bering and Chukchi Seas, the picoplankton size fraction is tightly controlled by grazers, however, observations were at a time when *Synechococcus* abundances were low (Krause et al., 2021). The extensive net growth of *Synechococcus* during the late summer/fall period suggests a potential disruption to in this grazing control. The ecological impact of the observed increase in *Synechococcus* abundance remains to be fully understood.

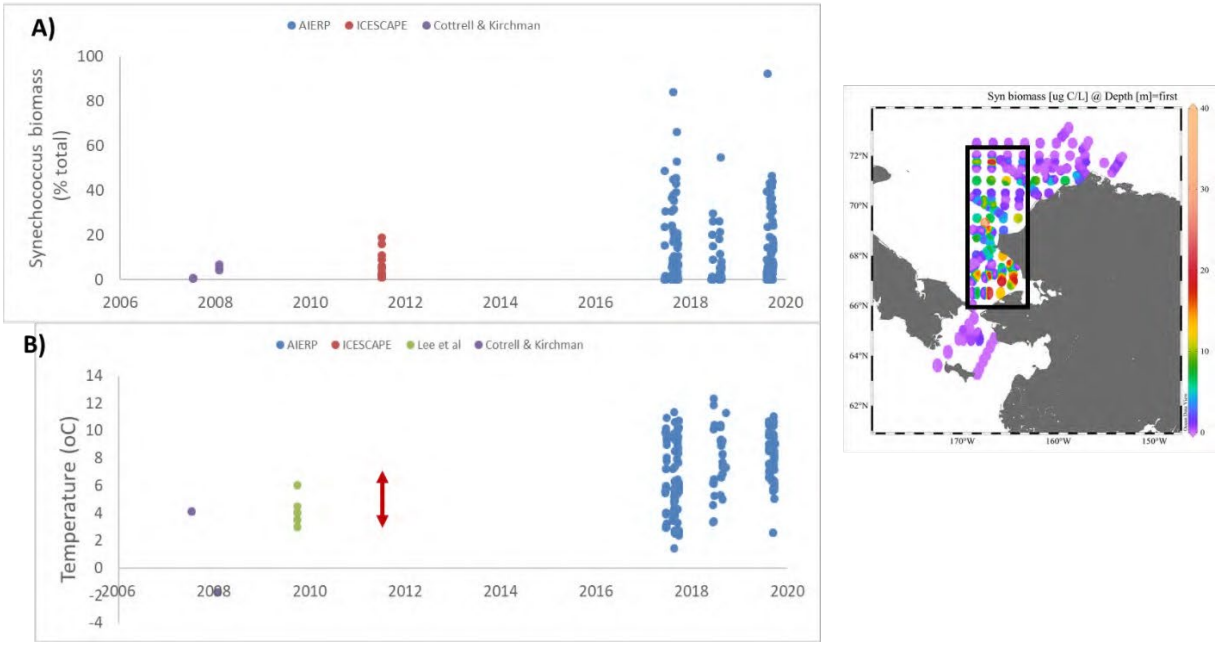

Figure 6. Changes in A) *Synechococcus* biomass and B) sample water temperature from published studies over time. Map inset shows the bounding box (black line) from which our data and those of previously published studies are used for this analysis.

Increasing Synechococcus *in a warming Arctic.* As *Synechococcus* has generally been considered a trivial component of the Arctic phytoplankton community, there are relatively few studies that have

quantified their abundance and from which carbon biomass can be estimated. *Synechococcus* biomass increased over the past decade in the region of Kotzebue Sound and north (Cottrell and Kirchman, 2009; Laney and Sosik, 2014, this study; **Figure 6a**). During this time, water temperatures in this same region increased significantly (Cottrell and Kirchman, 2009; Laney and Sosik, 2014; Lee et al., 2013, this study; **Figure 6b**). This observation is consistent with our environmental analysis from this study where temperature was the only variable that was significantly related to *Synechococcus* abundance. Zhuang et al. (2021) observed that pigments associated with picoplankton, and potentially cyanobacteria, increased from 2008-2016 on a transect in the Chukchi Sea along Icy Cape, consistent with our observations.

References:

Ardyna, M., Gosselin, M., Michel, C., Poulin, M., Tremblay, J.-E., 2011. Environmental forcing of phytoplankton community structure and function in the Canadian High Arctic: contrasting oligotrophic and eutrophic regions. Marine Ecology Progress Series 442, 37-57.

Booth, B., Horner, R.A., 1997. Microalgae on the Arctic Ocean section, 1994: species abundance and biomass. Deep Sea Research II 44, 1607-1622.

Brugel, S., Nozais, C., Poulin, M., Tremblay, J.E., Miller, L.A., Simpson, K.G., Gratton, Y., Demers, S., 2009. Phytoplankton biomass and production in the southeastern Beaufort Sea in autumn 2002 and 2003. Marine Ecology Progress Series 377, 6377.

Carmack, E., Barber, D.G., Christensen, J.P., Macdonald, R.W., Rudels, B., Sakshaug, E., 2006. Climate variability and physical forcing of the food webs and the carbon budget on panarctic shelves. Progress in Oceanography 71, 145-181.

Casey, J., Aucan, J., Goldberg, S., Lomas, M., 2013. Changes in partitioning of carbon amongst photosynthetic pico- and nano-plankton groups in the Sargasso Sea in response to changes in the North Atlantic Oscillation. Deep Sea Research II 93, 58-70.

Cottrell, M.T., Kirchman, D.L., 2009. Photoheterotrophic Microbes in the Arctic Ocean in Summer and Winter. Appl. Environ. Microbiol. 75, 4958-4966.

DuRand, M., Olson, R., 1996. Contributions of phytopankton light scattering and cell concentration changes to diel variations in beam attenuation in the equatorial Pacific from flow-cytometric measurements of pico-, ultra-, and nanoplankton. Deep Sea Research II 43, 891-906.

DuRand, M., Olson, R., Chisholm, S., 2001. Phytoplankton population dynamics at the Bermuda Atlantic Time- series Study station in the Sargasso Sea. Deep-Sea Research Part II 48, 1983-2003.

Flombaum, P., Gallegos, J.L., Gordillo, R.A., Rincon, J., Zabala, L.L., Jiao, N.Z., Karl, D.M., Li, W., Lomas, M., Veneziano, D., Vera, C.S., Vrugt, J.A., Martiny, A.C., 2013. Present and future distributions of the marine cyanobacteria *Prochlorococcus* and *Synechococcus*. Proc. Acad. Nat. Sci. Phila., doi/10.1073/pnas.1307701110.

Gordon, L., Jennings, J., Jr., Ross, A., Krest, J., 1993. A suggested protocol for continuous flow automated analysis of seawater nutrients (phosphate, nitrate, nitrite, and silicic acid) in the WOCE Hydrographic Program and the Joint Global Ocean Fluxes Study. Oregon State University, p. 55.

Hill, V., Cota, G.F., Stockwell, D., 2005. Spring and summer phytoplankton communities in the Chukchi and Eastern Beaufort Seas. Deep Sea Research II 52, 3369-3385.

Krause, J.W., Lomas, M.W., Danielson, S.L., 2021. Diatom growth, biogenic silica production, and grazing losses to microzooplankton during spring in the northern Bering and Chukchi Seas. Deep Sea Research II.

Laney, S.R., Sosik, H.M., 2014. Phytoplankton assemblage structure in and around a massive under-ice bloom in the Chukchi Sea. Deep Sea Research II 105, DOI: 10.1016/j.dsr1012.2014.1003.1012.

Lee, S., Yun, M., Kim, B., Joo, H., Kang, S., Kang, C., Whitledge, T., 2013. Contribution of small phytoplankton to total primary production in the Chukchi Sea. Continental Shelf Research 68, 43-50.

Legendre, L., Gosselin, M., Hirche, H.J., Kattner, G., Rosenberg, G., 1993. Environmental control and potential fate of size-fractionated phytoplankton production in the Greenland Sea (75oN). Marine Ecology Progress Series 98, 297-313.

Li, W., McLaughlin, F., Lovejoy, C., Carmack, E., 2009. Smallest alge thrive as the Arctic Ocean freshens. Science 326, DOI: 10.1126/science.1179798

Liu, H.B., Suzukil, K., Minami, C., Saino, T., Watanabe, M., 2002. Picoplankton community structure in the subarctic Pacific Ocean and the Bering Sea during summer 1999. Mar. Ecol.-Prog. Ser. 237, 1-14.

Lomas, M.W., Steinberg, D.K., Dickey, T., Carlson, C.A., Nelson, N.B., Condon, R.H., Bates, N.R., 2010. Increased ocean carbon export in the Sargasso Sea is countered by its enhanced mesopelagic attenuation. Biogeosciences 7, 57-70.

Lovejoy, C., Vincent, W.F., Bonilla, S., Roy, S., Martineau, M.J., Terrado, R., Potvin, M., Massana, R., Pedros-Alio, C., 2007. Distribution, phylogeny, and growth of cold-adapted picoprasinophytes in Arctic seas. J. Phycol. 43, 78-89.

Moran, S.B., Lomas, M.W., Kelly, R.P., Prokopenko, M., Granger, J., Gradinger, R., Iken, K., Mathis, J.T., 2012. Seasonal succession of net primary productivity, particulate organic carbon export, and autotrophic community composition in the eastern Bering Sea. Deep Sea Research II 65-70, 84-97.

Not, F., Massana, R., Latasa, M., Marie, D., Colson, C., Eikrem, W., Pedros-Alio, C., Vaulot, D., Simon, N., 2005. Late summer community composition and abundance of photosynthetic picoeukaryotes in Norwegian and Barents Seas. Limnol. Oceanogr. 50, 1677-1686.

Odate, T., 1996. Abundance and size composition of the summer phytoplankton communities in the Western North Pacific Ocean, the Bering Sea, and the Gulf of Alaska. Journal of Oceanography 52, 335-351.

Parsons, T.R., Maita, Y., Lalli, C.M., 1984. A manual of chemical and biological methods for seawater analysis. Pergamon Press, New York.

Peterson, B.J., Holmes, R.M., McClelland, J.W., Vorosmarty, C.J., 202. Increasing river discharge to the Arctic Ocean. Science 298, 2171-2173.

Sergeeva, V.M., Sukhanova, I.N., Flint, M.V., Pautova, L., Grebmeier, J.M., Cooper, L.W., 2010. Phytoplankton community in the western Arctic in July-August 2003. Oceanology 50, 1894-1197.

Serreze, M.C., Barrett, A.P., Slater, A.G., Woodgate, R.A., 2006. The large-scale freshwater cycle of the Arctic. . Journal of Geophysical Research 111, C11010.

Sherr, E., Sherr, B., Wheeler, P., Thompson, K., 2003. Temporal and spatial variation in stocks of autotrophic and heterotrophic microbes in the upper water column of the central Arctic Ocean. Deep Sea Research I 50, 557-571.

Sieracki, M.E., Verity, P.G., Stoecker, D.K., 1993. Plankton community response to sequential silicate and nitrate depletion during the 1989 North Atlantic spring bloom. Deep Sea Research II 40, 213-226.

Sigler, M.F., Stabeno, P.J., Eisner, L.B., Napp, J.M., Mueter, F.J., 2014. Spring and fall phytoplankton blooms in a productive subarctic ecosystem, the eastern Bering Sea, during 1995–2011. Deep Sea Research II 109.

Stabeno, P., Sonnerup, R., Mordy, C., Whitledge, T., 2013a. HLY-08-02 CTD and Nutrient Data. Version 4.0. UCAR/NCAR - Earth Observing Laboratory. , https://doi.org/10.5065/D60K26KN.

Stabeno, P., Sonnerup, R., Mordy, C., Whitledge, T., 2013b. HLY-09-02 CTD and Nutrient Data. Version 3.0. UCAR/NCAR - Earth Observing Laboratory, https://doi.org/10.5065/D6SB43R4.

Tremblay, J.E., Gagnon, J., 2009. The effects of irradiance and nutrient supply on the productivity of Arctic waters: A perspective on climate change. , in: Nihoul, J.C.J., Kostianoy, A.G. (Eds.), Influence of Climate Change on the Changing Arctic and Sub-Arctic Conditions. Spring, Dordrecht, Netherlands, pp. 73-93.

Visintini, A., Martiny, A.C., Flombaum, P., 2021. *Prochlorococcus*, *Synechococcus* and picoeukaryotic phytoplankton abundances in the global ocean. Limnology and Oceanography Letters 6, 207-215.

Waleron, M., Waleron, K., Vincent, W.F., Wilmotte, A., 2007. Allochthonous inputs of riverine picocyanobacteria to coastal waters in the Arctic Ocean. FEMS Microbiology Ecology 59, 35365.

Worden, A.Z., Binder, B.J., 2003. Application of dilution experiments for measuring growth and mortality rates among *Prochlorococcus* and *Synechococcus* populations in oligotrophic environments. Aquat. Microb. Ecol. 30, 159-174.

Zhuang, Y., Jin, H., Zhang, Y., Li, H., Zhang, T., Li, Y., Bai, Y., Ren, J., Chen, J., 2021. Incursion of Alaska Coastal Water as a mechanism promoting small phytoplankton in the western Arctic Ocean. Progress in Oceanography, https://doi.org/10.1016/j.pocean.2021.102639.

Phytoplankton and seston fatty acids dynamics in the northern Bering-Chukchi Sea region

Jens M. Nielsen[1,2,*], Louise A. Copeman[3,4,5], Lisa B. Eisner[1], Kelia E. Axler[1], Calvin W. Mordy[2,6] Michael W. Lomas[7]

[1]NOAA Alaska Fisheries Science Center, 7600 Sand Point Way NE, Seattle, WA, 98115, USA

[2]Cooperative Institute for Climate, Ocean, and Ecosystem Studies, University of Washington, Seattle, WA, United States

[3]NOAA Alaska Fisheries Science Center, 2030 SE Marine Science Dr., Hatfield Marine Science Center, Newport, OR, 97365, USA

[4]College of Earth, Ocean, and Atmospheric Sciences, Oregon State University, 104 CEOAS Administration Building, Corvallis, OR, 97331, USA

[5]Cooperative Institute for Marine Ecosystem and Resources Studies, Oregon State University, 2030 SE Marine Science Drive, Newport, OR, 97365, USA

[6]NOAA Pacific Marine Environmental Laboratory, Seattle, WA, USA

[7]Bigelow Laboratory for Ocean Sciences, 60 Bigelow Dr., East Boothbay, ME, 04544, USA

*Corresponding author: jens.nielsen@noaa.gov

KEYWORDS: Fatty acid analysis, Arctic, Chukchi Sea, northern Bering Sea, phytoplankton

ABSTRACT

Arctic and subarctic ecosystems are transitioning due to ocean warming, resulting in conditions that will lead to shifts in phytoplankton communities, their nutritional compositions, and production of fatty acids (FA). FA biomarkers are useful indicators of changing phytoplankton community composition and provide insight into basal resource quality for higher trophic level consumers such as zooplankton, fish, birds and marine mammals, yet phytoplankton FA information is largely lacking from the Bering and Chukchi Sea region. Therefore, we analyzed suspended particulate matter (seston) fatty acids (FA), chlorophyll-a (Chl-a) and environmental data collected from four surveys in the North Bering and Chukchi Seas, two during June of 2017 and 2018 and two during August and September of 2017 and 2019. Our objectives were to determine 1) whether, seston FA composition was correlated with phytoplankton taxonomic composition analyzed using imaging microscope (FlowCAM) techniques, 2) seasonal differences in seston FA concentrations, and 3) how FA concentrations vary with environmental parameters. We found significant seasonal differences in seston FA compositions, with diatom biomarkers more prevalent in spring, followed by a community shift to dinoflagellate and small flagellate FA biomarkers in late fall. These results were overall confirmed by FlowCAM analyses. FA seston concentrations were correlated with total and large size-fractioned Chl-a concentrations, nitrogen concentration and temperature. Lastly, we used a model framework to predict availability of the diatom-associated essential FA, eicosapentaenoic acid (EPA, 20:5n-3). Combined our analysis provide new information on FA phytoplankton dynamics and the important nutritional role of phytoplankton for higher trophic level consumers in the Northern Bering and Chukchi Sea regions.

1. INTRODUCTION

The Bering and Chukchi Seas are some of the most productive areas of the Arctic (Hill et al., 2018). A pronounced diatom spring bloom commonly associated with the timing of ice breakup (Fujiwara et al., 2016; Laney and Sosik, 2014) fuels pelagic and benthic secondary production (Grebmeier et al., 2006; Sigler et al., 2014). Later in the season, once the ocean stratifies, a majority of the large size-fractioned phytoplankton biomass is often present in subsurface water layers (Martini et al., 2016) while smaller sized plankton occur in the surface waters (Giesbrecht et al., 2019). Arctic and subarctic ecosystems, including the Bering and Chukchi Seas are transitioning (Huntington et al., 2020) due to rapid ocean warming. This scenario is projected to continue in the coming decades (Hermann et al., 2019) with changes already affecting sea ice phenology, spring bloom timing and phytoplankton production (Clement Kinney et al., 2020; Song et al., 2021). These changes also influence the production of fatty acids (FA) synthesized by phytoplankton which play a key nutritional role for the growth and functioning of marine consumers. More baseline data on phytoplankton nutrition, including their FA compositions is needed for tracking potential short and long-term changes in the quality and quantity of basal resources in the Bering and Chukchi Sea food webs.

Phytoplankton play a crucial nutritional role in marine ecosystems due to their ability to synthesize dietary FA required by higher trophic level organisms (Budge et al., 2014; Dalsgaard et al., 2003). Marine consumers generally lack the ability to synthesize several essential FA at a sufficient rate to meet their metabolic demand (Helenius et al., 2020), and therefore require FA preformed in their diets (Bell and Tocher, 2009). Several essential polyunsaturated FA (PUFA), including eicosapentaenoic acid (EPA, 20:5n3) and docosahexaenoic acid, (DHA, 22:6n3), are central compounds that regulate cell membrane fluidity, neurological functioning, localized

47 hormones and growth (Bell and Tocher, 2009; Helenius et al., 2019; Tocher et al., 2019). Dietary
48 limitation of essential PUFA directly influence zooplankton fecundity and growth rates (Leiknes
49 et al., 2016; Pond et al., 1996), survival of larval (Copeman and Laurel, 2010) and juvenile fishes
50 (Bell et al., 1995), and lower overall ecosystem productivity (Litzow et al., 2006).
51 The relative amounts of specific FA vary among phytoplankton taxa (Cañavate, 2019;
52 Parrish, 2013), thus changes in phytoplankton community compositions induce shifts in the
53 dietary FA pool available for consuming organisms (Galloway and Winder, 2015). The
54 association between specific FA and certain taxonomic groups also make FA useful biomarkers
55 (Dalsgaard et al., 2003). Yet, the utility of FA biomarkers to partition phytoplankton taxa is
56 known primarily from monoculture experiments (Cañavate, 2019; Dunstan et al., 1993;
57 Jónasdóttir, 2019). Using FA biomarkers to distinguish phytoplankton taxa in field samples is
58 more challenging (Reuss and Poulsen, 2002), variable and less studied (Galloway and Budge,
59 2020; Marmillot et al., 2020). Nonetheless, field studies in other high latitude systems, such as
60 the Beaufort Sea (Connelly et al., 2016; Marmillot et al., 2020), West Greenland Sea (Reuss and
61 Poulsen, 2002), and Barents Sea (Falk-Petersen et al., 1998) have highlighted that changes in
62 phytoplankton compositions, including seasonal shifts from diatoms to flagellates, can be visible
63 in the seston FA pools. Beyond the primary association with a specified phytoplankton
64 taxonomic group, individual FA biomarkers vary with environmental conditions (Sushchik et al.,
65 2004). Although FA provide valuable information about food quality, they are often not
66 diagnostic or species-specific but should rather be viewed as indicative of dominance from broad
67 taxonomic groups (i.e., predominance of diatoms versus flagellates; (Jónasdóttir, 2019),
68 particularly when analysis field data. Therefore, additional species information from microscopy

imaging techniques are also beneficial to validate observed FA biomarker patterns (Marmillot et al., 2020).

Here we use FA biomarkers as indicators of changing phytoplankton community compositions, and of basal resource quality for higher trophic level consumers. We analyzed suspended particulate matter (seston) FA, chlorophyll-a (Chl-a), phytoplankton taxonomic data, and environmental data from four surveys spanning the northern Bering-Chukchi Sea region, two during spring (June) in 2017 and 2018 and two during late summer (August/September) in 2017 and 2019. More specifically, we examine:

1) Seasonal and annual patterns in both absolute FA concentrations and percent FA composition;

2) the relationship between phytoplankton taxonomic data (dinoflagellates and diatoms) determined from imaging microscope analyses (FlowCAM) compared to specific FA biomarkers;

3) the relationship between individual FA biomarkers and physical, chemical, and biological variables; and

4) show how a simple model framework to predict concentrations of the diatom-sourced essential fatty acid, EPA, can provide a measure of consumer nutritional quality at an increased spatial resolution.

2. METHODS

2.1. Data collection

Four surveys were conducted in northern Bering-Chukchi Sea region as part of the Arctic Integrated Ecosystem Research Program (AIERP), during June of 2017 and 2018 (Arctic Shelf

Growth, Advection, Respiration, and Deposition Rate Experiments [ASGARD]) and during August and September (hereafter Aug/Sep) of 2017 and 2019 (Arctic Integrated Ecosystem Survey; Fig. 1). All data are publicly available in the DataONE repository (https://doi.org/10.24431/rw1k5a0). Water samples were collected from 5-12 L Niskin bottles attached to the CTD rosette. At every sampling station, total and size-fractioned (<5, 5-20, >20 μm) Chl-a (mg m^{-3}) samples were collected. Total Chl-a samples were collected at 10 m intervals (~5-6 depths) and filtered through 25 mm Whatman GF/F filters (nominal pore size 0.7 μm). Size-fractionated samples were collected at 2-3 depths using a stacked filtration unit, using 47 mm Whatman GF/F filters for <5 μm, and 47 mm polycarbonate filters with a pore size of 5 and 20 μm, to sample the 5-20 and >20 μm large size fractions. Filters were stored frozen (−80 °C) and analyzed within 6 months with a bench top fluorometer following standard methods (Parsons, 1984). Samples for dissolved inorganic nutrients (nitrate, nitrite, ammonium, phosphate, and silicic acid; μmol kg^{-1}) were collected from each Niskin bottle, filtered through 0.45 cellulose acetate filters, and frozen. Samples were analyzed on a Seal AA3 or Seal AA500 continuous segmented flow analyzer following methods in (Gordon et al., 1993). Ammonium was analyzed using the OPA method (Holmes et al., 1999). At every other station, seston was sampled at 1-2 depths for FA analysis (n =167). Vertical profiles of temperature and salinity were collected from surface to near-bottom at each station using a Sea-Bird Electronics (SBE) 9+ CTD, data processed and averaged into 1-m bins.

Phytoplankton community samples were analyzed for cell abundance using Fluid Imaging Technologies VS Series benchtop FlowCAM (hereafter referred to as FlowCAM) using a 10× objective and 200 μm flow cell in autoimage mode (Álvarez et al., 2014). Samples were counted from surveys in June 2017 and Aug/Sep 2017. Images were grouped into diatoms or

115 dinoflagellates. Diatoms were imaged in both June and Aug/Sep 2017, while dinoflagellates
116 were imaged only in Aug/Sep 2017. Biovolumes of cells were estimated from images using the
117 biovolume estimation function (cylindrical shape) in the VisualSpreadsheet (Scarborough, ME)
118 software provided with the instrument. These estimates compared well with manual estimates of
119 biovolume using standardized shapes and appropriate geometric equations (Menden-Deuer and
120 Lessard, 2000). FlowCAM biovolumes of diatoms and dinoflagellates were compared to
121 concentrations of the FA biomarkers of diatoms and dinoflagellates, and the ratio of DHA: EPA.
122
123 2.2. Fatty acid analyses
124 We collected FA seston samples, which comprise all living and non-living material
125 between 0.7-200 μm, such as phytoplankton, heterotrophic protists, bacteria, mesozooplankton
126 eggs and nauplii, and detritus. During sampling in June and Aug/Sep, phytoplankton commonly
127 constitute the majority of the seston material (Connelly et al., 2016; Hama, 1999) and thus the
128 majority of the seston FA can be attributed to phytoplankton FA. Water samples ranging in
129 volume from 2 L to 6 L were collected for seston fatty acid analysis on each of the four Arctic
130 surveys. Samples were collected from the surface, Chl-a maximum, or at near-bottom depths.
131 Seawater was prescreened through a 200 μm Nitex mesh into 2L sample bottles (1-3 bottles per
132 sample). Each bottle was filtered onto a pre-combusted Whatman 47 mm GF/F filter (0.7 μm
133 nominal pore size), and sample filters were stored aboard the ship at -80°C. Samples were
134 shipped frozen on dry ice to the Hatfield Marine Science Center (HMSC) in Newport, Oregon,
135 and analyzed at the Marine Lipid Ecology Laboratory. To obtain sufficient material, some filters
136 were combined for each sampling depth (1-3 filters), placed into lipid-clean glass tubes and
137 stored in chloroform under nitrogen for less than 3 months prior to extraction. Lipids were

138 extracted using a modified Folch procedure (Folch et al., 1957) using 2:1 chloroform: methanol
139 as described by Parrish et al. (1999). A total of 167 seston samples were processed for FA
140 analyses. An internal standard (23:0 methyl ester) was added to all samples at approximately
141 10% of the total FA concentration, and total lipid extracts were derivatized into their fatty acid
142 methyl esters (FAMEs) using sulphuric acid-catalyzed transesterification (Budge et al., 2006).
143 Resulting FAMEs were analyzed on an HP 7890 GC FID equipped with an autosampler
144 and a DB wax+ GC column (Agilent Technologies, Inc., U.S.A.). The column was 30 m in
145 length, with an internal diameter of 0.25 mm and film thickness of 0.25 μm. The column
146 temperature began at 65 °C and held this temperature for 0.5 min. Temperature was increased to
147 195 °C (@ 40 °C min^{-1}), held for 15 min then increased again (@ 2 °C min^{-1}) to a final
148 temperature of 220 °C, where it was held for 1 min. The carrier gas was hydrogen, flowing at a
149 rate of 2 ml min^{-1}. Injector temperature was set at 250 °C and the detector temperature was
150 constant at 250 °C. Peaks were identified using retention times based upon standards purchased
151 from Supelco (37 component FAME, BAME, PUFA 1, PUFA 3) and in consultation with
152 retention index maps performed under similar chromatographic conditions as our GC-FID
153 (Wasta and Mjøs, 2013). Column function was checked by comparing chromatographic peak
154 areas to empirical response areas using a quantitative FA mixed standard, GLC 487 (NuCheck
155 Prep). Chromatograms were integrated using Chem Station (version A.01.02, Agilent). Select
156 samples were run in triplicate and the coefficient of variation for peaks >1% of the sample, were
157 less than one.
158
159 2.3. Statistical and data analyses

Absolute FA concentrations, the amount of seston FA per volume seawater (reported as mg m^{-3}), were used to infer overall availability of FA as basal resources for consumers. FA data were calculated as percent of total fatty acids, which is a useful metric for quantifying phytoplankton compositional changes in the seston. FA were classified as C:Bn-P, where C is the number of carbon atoms, B the number of double bonds and P the position of the first double bond from the methyl group end (Budge et al., 2006). We considered two aspects of phytoplankton FA composition. Firstly, we focused on phytoplankton biomarkers, such as those indicative of diatoms: 16:1n-7, 16:4n-1, EPA (20:5n-3) and a composite diatom biomarker based on the ratio of 16:1n-7/16:0 (Budge and Parrish, 1998; Dalsgaard et al., 2003). Flagellates are a diverse group, including small autotrophic flagellates, heterotrophic flagellates and dinoflagellates. Therefore, we refer to the biomarkers 18:4n-3, 18:5n-3 and DHA (22:6n-3) as a combination of flagellate and dinoflagellate (dino+flag) FA biomarkers, due to the difficulty in partitioning among these groups using FA biomarkers alone. Secondly, we focused on long-chain PUFA (C_{20+22}) such as EPA and DHA, that are essential in the diet of secondary consumers. In addition, we assessed the ratio of DHA to EPA to denote relative dino+flag: diatom biomarkers in the samples, and a bacterial biomarker, here the sum of all odd carbon FA and branched FAs (Kaneda, 1991).

Type II regressions using $\log_{10}$-transformation were used to assess pairwise relationships between FA seston concentrations, and biological and physical variables including temperature, salinity, nutrients, and total and size-fractioned Chl-a concentrations. One-way Analysis of Variance (ANOVA) with associated post-hoc Tukey Honestly Significant Difference (HSD) was used for group comparisons, such as between seasons, years, depth category (above, below or in the mixed layer) and water mass designations (warm shelf water, cool shelf water, Anadyr water,

183 modified winter water and warm coastal water, Danielson et al., 2020). ANOVA models were
184 assessed for normality and homogeneity of variances of the residuals and variables were log_{10}-
185 transformed when necessary. Non-metric multidimensional scaling (nMDS) using Bray-Curtis
186 distances was used to assess multivariate patterns of the FA percent data, using all FA that
187 constituted more than 1% of the total FA, and the groups saturated FA (SFA), monounsaturated
188 FA (MUFA), PUFA and Bacterial FA.

189 Linear mixed effects models (Zuur et al., 2009) were used to assess how multiple
190 physical and biological parameters influence the FA composition of seston samples, and then to
191 develop a simple model framework that allows prediction of water column (0-50 m) integrated
192 EPA (mg m^{-2}) concentrations over broader spatial or temporal scales. For each FA biomarker a
193 full linear mixed effects model included the following predictor variables: total Chl-a,
194 temperature, nitrogen (sum of nitrate and ammonium), salinity and depth (a categorical variable
195 as described earlier) parameters that are all known to influence FA compositions (Budge et al.,
196 2014; Galloway and Winder, 2015). The different surveys were included as a random effect
197 because we expected that relationships between FA and environmental variables were likely to
198 be independent among years and season. For all models, inspections of residual plots did not
199 reveal obvious deviances from normality or homoscedasticity after log-transformation of
200 variables. In cases of multicollinearity (variance inflation factor (VIF) > 5), we retained only one
201 of those values in the final analysis.

202 Mixed effects models were performed for the following biomarkers: the ratio of DHA:
203 EPA, the ratio of PUFA: SFA, and FA percentage data for diatom biomarkers 16:4n-1 and EPA,
204 and dino+flag biomarkers 18:5n-3 and DHA. We followed the recommendations in (Zuur et al.,
205 2009) for fitting FA mixed effects models. First, the optimal random effect structure (which

206 could be no random effect) was fitted for the full model using restricted maximum likelihood
207 estimation. Second, we used maximum likelihood estimation to determine the most parsimonious
208 fixed effect model structure, with the optimal random structure as determined in step one.
209 Finally, the most parsimonious model for each FA, which included the optimal random and fixed
210 effect structures, was re-fitted with restricted maximum likelihood estimation. Determination of
211 the most parsimonious model in each step was decided using Akaike Information Criterion
212 corrected for small sample sizes (AICc, Burnham and Anderson, 2002). In the instances where
213 more than one model had similar AICc scores (<1 AICc), we chose the model with the lower
214 number of explanatory variables. For simplicity, we report only the final parsimonious model for
215 each FA biomarker in the results.
216 To predict integrated EPA (mg m^{-2}) concentrations, we used a mixed effects model to the
217 EPA concentration data. Because the biological, chemical and physical survey data was sampled
218 at a higher vertical and spatial sampling resolution compared to the FA sampling, these models
219 allowed for predicting integrated water column EPA concentrations for all survey stations.
220 Predictive models were computed using natural log-transformed data, thus a correction was
221 applied to re-convert predicted FA concentrations (Duan, 1983). All analyses were done using R
222 version 3.6 (R Core Team, 2018). Mixed effects models were fitted using the "*nlme*" package
223 (Pinheiro et al., 2017), AICc using the "*AICcmodavg*" package (Mazerolle and Mazerolle, 2019),
224 and type II regressions were computed using the "*smatr*" package (Warton et al., 2012).
225
226 **3. RESULTS**
227 3.1. Spatial patterns of Chl-a and FA concentrations.

228 Generally, areas of higher than average Chl-a were spatially associated with higher total
229 FA concentrations. Average water column (0-50 m) Chl-a measurements were higher in June
230 2017 and 2018 compared to Aug/Sep 2017 and 2019, though high variability existed among
231 stations and across all surveys (Fig. 1). Elevated water column average Chl-a concentrations (>6
232 mg m^{-3}) were present north of St. Lawrence Island within and north of the Bering Strait in both
233 June 2017 and 2018, areas that similarly showed elevated (> 15 mg m^{-3}) concentrations of total
234 FA. Total Chl-a concentrations had significant positive correlations with both the ratio of large
235 (> 5 μm) to small (< 5 μm) particle Chl-a, and the > 20 μm size-fractioned concentrations (Table
236 S1), indicating that communities were comprised of large phytoplankton in areas with high
237 concentrations of total Chl-a.
238
239 3.2. Seasonal dynamics of FA biomarkers
240 Total FA concentrations (mean±SD) in June 2017 were significantly higher than all other
241 surveys (average across stations: 28.2±21.1 mg m^{-3}, $p<0.05$, Tukey HSD, Figs. 1, 2A), followed
242 by FA concentrations in June 2018 (22.2±16.9 mg m^{-3}), Aug/Sep 2019 (18.8±16.5 mg m^{-3}), and
243 Aug/Sep 2017 (12.1±5.4 mg m^{-3}). Overall SFA, and MUFA concentrations were higher in June
244 compared to Aug/Sep (Fig. 2A), however percent PUFA levels were highest in Aug/Sep 2019
245 (Fig. 2D). The diatom biomarkers 16:1n-7, 16:4n-1, and EPA all varied significantly among
246 season and year (Tukey HSD, $F(3,163) = 10.6$, 4.2, and 4.3, respectively, $p< 0.05$, Fig. 2B).
247 Concentrations of 16:1n-7 and 16:4n-1 and EPA were significantly higher in June than in
248 Aug/Sep except for EPA, were values in Aug/Sep 2019 were similar to values in June. The
249 diatom biomarkers (percentage of 16:1n-7, 16:4n-1 and EPA, Fig. 2E) showed similar patterns to
250 the concentration data.

The concentration of dino+flag-associated biomarkers 18:5n-3(0.8± 1.0 mg m^{-3}) and DHA (1.5± 1.6 mg m^{-3}) were significantly higher in Aug/Sep 2019 compared to all other surveys (Tukey HSD, $p<0.05$, Fig. 2C). The dino+flag biomarker 18:4n-3 was significantly higher in Aug/Sep 2019 than in Aug/Sep 2017 (Tukey HSD, $p<0.05$), but otherwise showed no difference among seasons and years. The dino+flag percent FA data and the sum of n-3 PUFA showed overall similar patterns to the concentration data, with Aug/Sep 2019 values being the highest (Fig. 2F). Resultant DHA: EPA ratios were significantly higher in Aug/Sep compared to June (Tukey HSD, $p<0.05$, Fig. 2C). The diatom biomarkers of EPA, 16:1n-7, and 16:4n-1 were all correlated positively for both the concentration (Table S1) and percentage data (Table S2). Similarly, DHA correlated well with the dino+flag biomarkers 18:4n-3 and 18:5n-3 for both the concentration and percentage data (Table S1-S2).

Multivariate nMDS analysis of the FA percentage composition data similarly showed clear differences among seasons and years (Fig. 3). FA biomarkers most responsible for the separation of seasons were diatom biomarkers (i.e., 16:1n-7, 16:2n-4, 16:4n-1 and EPA), which appeared to be more highly associated with the June 2017 and 2018 samples. In contrast, dino+flag markers (i.e., 18:3n-3, 18:4n-3, 18:5n-3, and 22:6n-3) were more closely associated with the Aug/Sep 2017 and 2019 samples. However, substantial variability of the FA compositions within each survey also indicate clear spatial differences in phytoplankton communities across years and seasons.

3.3. Taxonomic comparison of FA biomarkers and FlowCAM images

FlowCAM-measured diatom and dinoflagellate biovolumes correlated positively with their taxa-associated FA biomarkers. Significant positive correlations were observed between

$\log_{10}$-transformed diatom biovolumes and FA concentrations of EPA (Fig. 4A, $r^2 = 0.41$, $p < 0.01$, df = 38), 16:1n-7 (Fig. 4C, $r^2 = 0.45$, $p < 0.01$, df = 38), and 16:4n-1 (Fig. 4E, $r^2 = 0.46$, $p < 0.01$, df = 38) in June 2017 and Aug/Sep 2017. However, when analyzing only the Aug/Sep 2017 diatom data, correlations were not significant ($p > 0.05$, df = 20). Dinoflagellate biovolumes correlated positively with FA concentrations of DHA (Fig. 4B, $r^2 = 0.51$, $p < 0.01$, df = 20) and 18:5n-3 (Fig. 4D, $r^2 = 0.55$, $p < 0.01$, df = 20) in June 2017. Additionally, the ratio of DHA to EPA correlated positively with the FlowCAM-measured ratio of dinoflagellate to diatom biovolumes (Fig. 4F, $r^2 = 0.45$, $p < 0.01$, df = 20) in June 2017.

3.4. Associations between FA biomarkers and environmental variables

Next, we analyzed associations between the individual environmental variables and the FA concentration and percentage biomarkers using $\log_{10}$-transformed data from discrete samples. Some of the main primary pairwise correlations shown in Figure 5 and highlighted below, while all regressions are presented in Table S1 and Table S2.

Overall, the majority of the concentrations of individual FA correlated positively and significantly with total and size-fractionated (<5 µm, 5-20 µm, >20 µm) Chl-a data (Fig. 5A-F, Table S1). The strongest relationship for total FA was with total Chl-a and >20 µm fraction ($r^2 = 0.52$, $p<0.01$), which in turn were highly correlated ($r^2= 0.90$, $p<0.01$) (Fig. 5A, Table S1). Significant correlations were also found for PUFA concentrations, common diatom biomarkers 16:1n-7, and EPA with total and >20 µm Chl-a concentrations (Fig. 5B-D, $r^2 = 0.37$ to 0.52, $p<0.01$, Table S1). In contrast, dino+flag biomarkers 18:5n-3, 18:4n-3 and DHA had the highest correlations with small size fractions of Chl-a (< 5 um) ($r^2 = 0.36$ to 0.67, $p<0.01$, Table S1); positive but weaker correlations were also found with total Chl-a (Fig 5.E, $r^2 = 0.05$ to 0.23,

297 $p<0.05$). Nutrients correlated negatively with temperature and positively with salinity (Fig. 5G,
298 Table S1). We found few significant relationships between FA concentrations and temperature,
299 salinity, and nutrient concentrations and those were weak (Table S1). DHA: EPA ratios were
300 lowest in cold, high salinity waters (Fig. 5H) and correlated negatively with nitrate
301 concentrations (Fig. 5I, $r^2 = 0.31$, $p<0.01$, Table S1).

302 Overall, the percentage FA results suggested that diatoms are higher in relative biomass
303 in colder, high salinity waters and in areas of higher nitrate (Table S2). dino+flag FA biomarker
304 percentages were higher in warmer waters, shallower depths, and in areas with low nutrient
305 concentrations (Table S2). Total and large (>20 μm) size-fractioned Chl-a correlated positively
306 with the percentage diatom biomarkers (16:1n-7, 16:4n-1, 16:2n-4, and EPA) but negatively with
307 the percent contribution of dino+flag-associated FA biomarkers (18:4n-3, 18:5n-3, and DHA)
308 and the ratio of DHA to EPA (Fig. 5F, Table S2). Percentage diatom FA biomarkers associated
309 negatively with the dino+flag and SFA. The percentage contribution from bacterial FA
310 biomarkers correlated positively with the diatom biomarkers, >20 μm, and 5-20 μm and total
311 Chl-a, but negatively with several dino+flag biomarkers. For both the percentage and
312 concentration data, the patterns observed for all 4 surveys combined were generally also visible
313 within each survey (data not shown).

314 Mixed effects models using the FA percentage data showed that several environmental
315 variables influence FA phytoplankton dynamics. The most parsimonious mixed effects models
316 consistently included survey as a random effect. All statistical values are reported in Table S3;
317 below we report the main findings. Percent EPA contribution correlated positively with total
318 Chl-a concentrations and with vertical depth position (Table S3). EPA values were higher below

319 the mixed layer and though the effect of vertical position was included in the final model, its
320 influence was minor (i.e., delta AICc with the vertical position included or not, was small).
321 The diatom biomarker 16:4n-1 showed a significant positive relationship with total Chl-a
322 and nitrogen concentration but a negative relationship with temperature. Percent DHA was
323 positively related to total Chl-a, but negatively related to nitrogen concentrations (Table S3). The
324 dino+flag marker 18:5n-3 was negatively related to both total Chl-a and nitrogen concentrations.
325 DHA: EPA ratios also were negatively related to Chl-a and nitrogen concentrations, while
326 relating positively with salinity and temperature. The ratio of PUFA: SFA increased with Chl-a
327 concentrations, but decreased with nitrogen concentrations and temperature (Table S3).
328 Lastly, we used a mixed effects model to enable predictions of absolute EPA
329 concentrations (Fig. 6). The most parsimonious model, assessed using AICc, included log-
330 transformed total Chl-a and log-transformed nitrogen (sum of nitrate and ammonium) as the
331 fixed effect and a random structure consisting of an interaction of Chl-a and survey (Table S4).
332 Model prediction of EPA correlated overall strongly with measured EPA concentrations (r^2 =
333 0.63, $p < 0.01$, df = 151, Fig. S1A). Variability and thus uncertainty of EPA model predictions
334 were highest in samples with total Chl-a concentrations >5 mg m^{-3} (Fig. S1B). Water column
335 integrated EPA concentrations differed significantly among all four surveys (Fig. 6, Tukey HSD,
336 $p<0.05$), with average values highest in June 2018 (93 ± 60 mg m^{-2}), followed by June 2017 (66
337 ± 46 mg m^{-2}), Aug/Sep 2019 (54 ± 30 mg m^{-2}), and Aug/Sep 2017 (30 ± 8 mg m^{-2}). Throughout,
338 there was high spatial variation in the predictions with the highest concentrations reaching levels
339 of 264 mg m^{-2} and 241 mg m^{-2} in June 2017 and 2018, while highest values in Aug/Sep 2017
340 were 54 mg m^{-2} and 198 mg m^{-2} in Aug/Sep 2019.
341

4. DISCUSSION

Seston FA biomarkers reflected phytoplankton community shifts from diatoms dominating in spring followed by late summer increases of dinoflagellates and small flagellates. High total FA and PUFA concentrations in late spring (June) primarily synthesized by diatoms suggest that phytoplankton FA from this time period provide important dietary subsidies for consumers (Grebmeier et al., 2006). Diatom and dinoflagellate biovolume measurements from FlowCAM images correlated positively with their respective FA biomarkers, confirming that in general FA compositional data can provide reliable information on phytoplankton community dynamics. Measured phytoplankton FA composition (concentrations and percentages) varied with changes in temperature and nutrients, likely due to a combination of species-specific changes in physiology as well as changes in the phytoplankton community composition (Grosse et al., 2019; Jiang and Gao, 2004). Lastly, derived EPA concentrations based a model using commonly sampled survey data (e.g., temperature, nitrogen, and Chl-a) may provide broad-scale water column integrated estimates of dietary EPA availability for consumers in the northern Bering and Chukchi Sea ecosystems.

4.1 FA biomarker and FlowCAM estimates of diatoms and dinoflagellates

Taxonomic information from microscopy imaging techniques generally confirmed that observed FA biomarker patterns can be associated with major phytoplankton taxa groups. Although FlowCAM-measured diatom and dinoflagellate biovolumes correlated positively with diatom and dinoflagellate FA biomarker concentrations, these data also revealed substantial unexplained variance. The combined June and Aug/Sep 2017 data yielded significant trends for diatom biovolumes and their FA biomarkers (16:1n-7, 16:4n-1 and EPA) however, similar

365 diatom trends were insignificant when using only samples from Aug/Sep 2017. Whether the lack
366 of clear correlation was due to variable FA concentrations among diatoms species, less
367 dominance of this taxa compared to spring samples, variable environmental conditions (Sushchik
368 et al., 2004), or FA contributions from other phytoplankton groups is unclear. For example,
369 *Synechococcus,* which can contain 16:1n-7 (Jónasdóttir, 2019), were observed in up to 20% of
370 the phytoplankton carbon biomass during Aug/Sep 2017 (data not shown). Similarly,
371 chlorophytes containing 16:4n-1, or chlorophytes and cryptophytes containing EPA (Jónasdóttir,
372 2019), could have contributed to the FA pools of the diatom associated biomarkers.
373 Differentiating between dinoflagellates, heterotrophic flagellates and flagellates using FA
374 biomarkers alone is challenging. The observable trends between 18:5n-3 and DHA with
375 dinoflagellate identified from the FlowCAM suggest that noticeable FA contributions at least
376 partially originated from dinoflagellates, however, small flagellates, not measured with the
377 FlowCAM analysis, may also be important. Dinoflagellate and small flagellates often co-occur.
378 Higher percentages of 18:1n-9 and 18:0 in some Aug/Sep 2017 samples could indicate increased
379 contributions from smaller flagellates (Reuss and Poulsen, 2002), but these quite ubiquitous FAs
380 that are also present in several other taxa (Cañavate, 2019). The significant association between
381 dinoflagellate biovolumes and their specific FA biomarkers (DHA, 18:5n-3) differ from a recent
382 study by Marmillot et al. (2020) which found no significant relationships for dinoflagellates. We
383 speculate that these differences may be explained by the fact that flagellates are a diverse group
384 of organisms including auto, mixo and heterotrophic species, which can vary substantially in
385 their FA signatures depending on their diet intake and responses to environmental conditions.
386 Overall, and despite considerable variation, our results are in general agreement with previous
387 field studies (Marmillot et al., 2020; Reuss and Poulsen, 2002; Sushchik et al., 2004) and

388 highlights the utility of FA biomarkers for depicting relative contributions of major
389 phytoplankton taxonomic groups.
390
391 4.2. Factors influencing seston FA dynamics
392 Shifting environmental conditions influence seston FA dynamics through both individual
393 phytoplankton species and community composition responses (Cañavate et al., 2019; Miller et
394 al., 2017). Seasonal environmental shifts were clearly visible in the FA biomarkers, with highest
395 abundances of diatom FA in spring followed by increasing dino+flag FA in late summer. These
396 seasonal shifts agree well with phytoplankton taxonomic analysis from the northern Bering and
397 Chukchi Seas (Laney and Sosik, 2014; Lee et al., 2019; Sukhanova et al., 2009) and with FA
398 biomarker studies in other Arctic regions (Connelly et al., 2016; Falk-Petersen et al., 1998). Chl-
399 a concentration was the primary predictor variable for the concentrations of almost all FA
400 biomarkers. These linkages were particularly strong between absolute concentrations of the
401 diatom biomarkers, 16:4n-1, 16:1n-7 and EPA, and the total and the large (>20 μm) size fraction
402 Chl-a. The high positive correlation of >20 μm with total Chl-a suggests that large phytoplankton
403 primarily of diatom origin were driving changes in total Chl-a concentrations.
404 Temperature and nitrogen concentrations also influenced the percentage FA patterns.
405 Temperature correlated negatively with the ratio of PUFA to SFA, a pattern that is likely driven
406 by decreasing PUFA concentrations with warming (Hixson and Arts, 2016; Jiang and Gao,
407 2004), due to both individual species and community compositional responses to variable
408 environmental conditions (Hixson and Arts, 2016). Relative concentration of dino+flag
409 biomarkers increased with decreasing nitrogen concentrations, warmer temperatures and lower
410 salinity, supporting that dinoflagellates and small flagellates are commonly more prevalent in

411 low nutrient environments as observed during summer in the eastern Bering Sea (Moran et al.,
412 2012; Sukhanova et al., 2009). Differences in residual nutrient concentrations among water
413 masses are associated with different phytoplankton communities (Danielson et al., 2017), which
414 likely explain the higher percentages of FA diatom biomarkers in colder, more saline, nutrient-
415 rich waters. Differences in FA compositions with depth also indicate that diatoms are more
416 prevalent in deeper, higher nutrient waters near the subsurface Chl-a maximum which are
417 common phenomena in summer in these ecosystems (Lowry et al., 2015; Martini et al., 2016). In
418 contrast, higher abundance of FA dino+flag biomarkers occurred closer to the surface in waters
419 with lower nutrient concentrations, where they may have an advantage compared to, for example
420 diatoms. Higher surface area to volume ratios of small flagellates allow enhanced access to
421 nutrients at low concentrations (Edwards et al., 2012), while many dinoflagellates maintain
422 higher growth by migrating daily from deeper, nutrient rich water to the surface (Jephson and
423 Carlsson, 2009) and also engage in heterotropy.
424
425 4.3. Importance of dietary FA for consumers
426 Variation in plankton communities and their nutritional quality (i.e. lipid and essential
427 FA) influence spatiotemporal trends in food quality available to consumers (Twining et al.,
428 2016). The availability of essential EPA strongly influences copepod nauplii growth rates
429 (Leiknes et al., 2016), fish (Copeman and Laurel, 2010), juvenile crab (Copeman et al. 2021),
430 benthic organisms (Schollmeier et al., 2018) and overall ecosystem production (Litzow et al.,
431 2006). Using ancillary data from all four surveys, we calculated water column integrated spatial
432 predictions of EPA concentrations. Overall, the modeled EPA predictions compared well to
433 measured EPA concentrations. Modeled EPA data may provide a first step towards a broader

434 characterization of dietary availability of essential FA in these ecosystems. Overall, predicted
435 EPA concentrations were highest in spring with lower concentrations in late summer,
436 particularly Aug/Sep 2017. Our mixed effects model analyses also show that FA spatial
437 predictions vary between seasons and years, as "survey" was a significant explanatory variable in
438 the model. Survey should be considered a proxy for seasonal and inter-annual changes in the FA
439 pools associated with the phytoplankton community composition. Thus, predictive power
440 increases when accounting for inter- and intra-annual differences in FA composition patterns,
441 and best results are retrieved if model predictions are coupled with a smaller subset of FA
442 phytoplankton information from the specific year in question. Additional improvements of the
443 current model framework would be inclusion of data from colder years that may have noticeably
444 different phytoplankton communities (Hill et al., 2005) compared to the years 2017-2019, and
445 laboratory studies of regional zooplankton or benthic invertebrate (e.g., crabs, Copeman et al.
446 2021) growth and reproduction rate responses to dietary availability of essential EPA.
447 An expected future consequence of warming and increased stratification is a shift in
448 phytoplankton community structure towards smaller sized cells (Morán et al., 2010) and a
449 prospective decrease in PUFA concentrations (Hixson and Arts, 2016). Such shifts in FA
450 compositions are due to a combination of direct physiological effects on phytoplankton FA
451 synthesis as well as due to phytoplankton community shifts. How changing sea ice phenology
452 and the resulting effects on ice-associated phytoplankton (Clement Kinney et al., 2020), and
453 spring and summer open water blooms influences the availability of carbon and thus important
454 dietary FA in the northern Bering and Chukchi Sea ecosystems, remains an open question. Our
455 analyses and model framework provide new regional baseline information on phytoplankton FA

seasonal and inter-annual variations. Such information will increase the ability to evaluate the impacts of changing dietary lipid on higher trophic level consumers at broader spatial scales.

DECLERATION OF COMPETING INTEREST

The authors declare no known competing financial interests or personal relationships that could have appeared to influence the work reported in this manuscript.

ACKNOWLEDGEMENTS

We are grateful to Brendan Smith, Miranda Irby, Ed Farley, Anna Mounsey, Haley Cynar, Jeff Krause, Harmony Wayner, and Steven Baer for help during field sampling, for analysis of the nutrient data, and the crews of the *R/V's Ocean Star* and *Sikuliaq*. We are thankful to Lauren Rogers for help with mixed effects models and comments from Jeanette Gann and Fletcher Sewall that substantially helped improve the manuscript. We thank Carlissa Salant Michelle Stowell and Jami Ivory for general analytical assistance in the Marine Lipid Ecology Lab in Newport, OR, and the funding sources; NPRB Arctic IERP (Arctic IES LTL (A92), ASGARD, Phytoplankton Gap proposal (A96), National Science Foundation Office of Polar Programs award numbers OCE-1603460 (ML)). The findings and conclusions in this paper are those of the authors and do not necessarily represent the views of the National Marine Fisheries Service, NOAA. Reference to trade names does not imply endorsement by the National Marine Fisheries Service, NOAA. This is EcoFOCI contribution number EcoFOCI-1005 and PMEL contribution number 5325. This publication was partially funded by the Cooperative Institute for Climate, Ocean, & Ecosystem Studies (CIOCES) under NOAA Cooperative Agreement NA20OAR4320271, Contribution No 2021-1168.

REFERENCES

Álvarez, E., Moyano, M., López-Urrutia, Á., Nogueira, E., Scharek, R., 2014. Routine determination of plankton community composition and size structure: a comparison between FlowCAM and light microscopy. Journal of plankton research 36, 170-184.

Bell, M.V., Batty, R.S., Dick, J.R., Fretwell, K., Navarro, J.C., Sargent, J.R., 1995. Dietary deficiency of docosahexaenoic acid impairs vision at low light intensities in juvenile herring (Clupea harengus L.). Lipids 30, 443.

Bell, M.V., Tocher, D.R., 2009. Biosynthesis of polyunsaturated fatty acids in aquatic ecosystems: general pathways and new directions, Lipids in aquatic ecosystems. Springer, pp. 211-236.

Budge, S.M., Devred, E., Forget, M.-H., Stuart, V., Trzcinski, M.K., Sathyendranath, S., Platt, T., 2014. Estimating concentrations of essential omega-3 fatty acids in the ocean: supply and demand. ICES Journal of Marine Science 71, 1885-1893.

Budge, S.M., Iverson, S.J., Koopman, H.N., 2006. Studying trophic ecology in marine ecosystems using fatty acids: a primer on analysis and interpretation. Marine Mammal Science 22, 759-801.

Budge, S.M., Parrish, C.C., 1998. Lipid biogeochemistry of plankton, settling matter and sediments in Trinity Bay, Newfoundland. II. Fatty acids. Organic Geochemistry 29, 1547-1559.

Burnham, K., Anderson, D., 2002. Model selection and multimodel inference: a practical information-theoretic approach. The University of Chicago Press New York.

Cañavate, J.-P., van Bergeijk, S., Giráldez, I., González-Ortegón, E., Vílas, C., 2019. Fatty Acids to Quantify Phytoplankton Functional Groups and Their Spatiotemporal Dynamics in a Highly Turbid Estuary. Estuaries and Coasts 42, 1971-1990.

Cañavate, J.P., 2019. Advancing assessment of marine phytoplankton community structure and nutritional value from fatty acid profiles of cultured microalgae. Reviews in Aquaculture 11, 527-549.

Clement Kinney, J., Maslowski, W., Osinski, R., Jin, M., Frants, M., Jeffery, N., Lee, Y.J., 2020. Hidden production: on the importance of pelagic phytoplankton blooms beneath Arctic Sea ice. Journal of Geophysical Research: Oceans 125, e2020JC016211.

Connelly, T.L., Businski, T.N., Deibel, D., Parrish, C.C., Trela, P., 2016. Annual cycle and spatial trends in fatty acid composition of suspended particulate organic matter across the Beaufort Sea shelf. Estuarine, Coastal and Shelf Science 181, 170-181.

Copeman, L., Laurel, B., 2010. Experimental evidence of fatty acid limited growth and survival in Pacific cod larvae. Marine Ecology Progress Series 412, 259-272.

Dalsgaard, J., John, M.S., Kattner, G., Müller-Navarra, D., Hagen, W., 2003. Fatty acid trophic markers in the pelagic marine environment.

Danielson, S.L., Eisner, L., Ladd, C., Mordy, C., Sousa, L., Weingartner, T.J., 2017. A comparison between late summer 2012 and 2013 water masses, macronutrients, and phytoplankton standing crops in the northern Bering and Chukchi Seas. Deep Sea Research Part II: Topical Studies in Oceanography 135, 7-26.

Duan, N., 1983. Smearing estimate: a nonparametric retransformation method. Journal of the American Statistical Association 78, 605-610.

522 Dunstan, G.A., Volkman, J.K., Barrett, S.M., Leroi, J.-M., Jeffrey, S., 1993. Essential
523 polyunsaturated fatty acids from 14 species of diatom (Bacillariophyceae). Phytochemistry 35,
524 155-161.
525 Edwards, K.F., Thomas, M.K., Klausmeier, C.A., Litchman, E., 2012. Allometric scaling and
526 taxonomic variation in nutrient utilization traits and maximum growth rate of phytoplankton.
527 Limnology and Oceanography 57, 554-566.
528 Falk-Petersen, S., Sargent, J., Henderson, J., Hegseth, E., Hop, H., Okolodkov, Y., 1998.
529 Lipids and fatty acids in ice algae and phytoplankton from the Marginal Ice Zone in the Barents
530 Sea. Polar Biology 20, 41-47.
531 Folch, J., Lees, M., Stanley, G.S., 1957. A simple method for the isolation and purification of
532 total lipides from animal tissues. Journal of biological chemistry 226, 497-509.
533 Fujiwara, A., Hirawake, T., Suzuki, K., Eisner, L., Imai, I., Nishino, S., Kikuchi, T., Saitoh,
534 S.-I., 2016. Influence of timing of sea ice retreat on phytoplankton size during marginal ice zone
535 bloom period on the Chukchi and Bering shelves. Biogeosciences Discussions 13.
536 Galloway, A.W., Winder, M., 2015. Partitioning the relative importance of phylogeny and
537 environmental conditions on phytoplankton fatty acids. PLoS One 10, e0130053.
538 Galloway, A.W.E., Budge, S.M., 2020. The critical importance of experimentation in
539 biomarker-based trophic ecology. Philosophical Transactions of the Royal Society B: Biological
540 Sciences 375, 20190638.
541 Giesbrecht, K., Varela, D., Wiktor, J., Grebmeier, J., Kelly, B., Long, J., 2019. A decade of
542 summertime measurements of phytoplankton biomass, productivity and assemblage composition
543 in the Pacific Arctic Region from 2006 to 2016. Deep Sea Research Part II: Topical Studies in
544 Oceanography 162, 93-113.
545 Gordon, L.I., Jennings Jr, J.C., Ross, A.A., Krest, J.M., 1993. A suggested protocol for
546 continuous flow automated analysis of seawater nutrients (phosphate, nitrate, nitrite and silicic
547 acid) in the WOCE Hydrographic Program and the Joint Global Ocean Fluxes Study. WOCE
548 hydrographic program office, methods manual WHPO, 1-52.
549 Grebmeier, J.M., Cooper, L.W., Feder, H.M., Sirenko, B.I., 2006. Ecosystem dynamics of the
550 Pacific-influenced Northern Bering and Chukchi Seas in the Amerasian Arctic. Progress in
551 Oceanography 71, 331-361.
552 Grosse, J., Brussaard, C., Boschker, H., 2019. Nutrient limitation driven dynamics of amino
553 acids and fatty acids in coastal phytoplankton. Limnology and Oceanography 64, 302-316.
554 Hama, T., 1999. Fatty acid composition of particulate matter and photosynthetic products in
555 subarctic and subtropical Pacific. Journal of plankton research 21.
556 Helenius, L., Budge, S., Duerksen, S., Devred, E., Johnson, C.L., 2019. Lipids at the plant–
557 animal interface: a stable isotope labelling method to evaluate the assimilation of essential fatty
558 acids in the marine copepod Calanus finmarchicus. Journal of Plankton Research 41, 909-924.
559 Helenius, L., Budge, S.M., Nadeau, H., Johnson, C.L., 2020. Ambient temperature and algal
560 prey type affect essential fatty acid incorporation and trophic upgrading in a herbivorous marine
561 copepod. Philosophical Transactions of the Royal Society B: Biological Sciences 375, 20200039.
562 Hermann, A.J., Gibson, G.A., Cheng, W., Ortiz, I., Aydin, K., Wang, M., Hollowed, A.B.,
563 Holsman, K.K., 2019. Projected biophysical conditions of the Bering Sea to 2100 under multiple
564 emission scenarios. ICES Journal of Marine Science 76, 1280-1304.

565 Hill, V., Ardyna, M., Lee, S.H., Varela, D.E., 2018. Decadal trends in phytoplankton
566 production in the Pacific Arctic Region from 1950 to 2012. Deep Sea Research Part II: Topical
567 Studies in Oceanography 152, 82-94.

568 Hill, V., Cota, G., Stockwell, D., 2005. Spring and summer phytoplankton communities in the
569 Chukchi and Eastern Beaufort Seas. Deep Sea Research Part II: Topical Studies in
570 Oceanography 52, 3369-3385.
571 Hixson, S.M., Arts, M.T., 2016. Climate warming is predicted to reduce omega-3, long-chain,
572 polyunsaturated fatty acid production in phytoplankton. Global Change Biology 22, 2744-2755.
573 Holmes, R.M., Aminot, A., Kérouel, R., Hooker, B.A., Peterson, B.J., 1999. A simple and
574 precise method for measuring ammonium in marine and freshwater ecosystems. Canadian
575 Journal of Fisheries and Aquatic Sciences 56, 1801-1808.
576 Huntington, H.P., Danielson, S.L., Wiese, F.K., Baker, M., Boveng, P., Citta, J.J., De
577 Robertis, A., Dickson, D.M., Farley, E., George, J.C., 2020. Evidence suggests potential
578 transformation of the Pacific Arctic ecosystem is underway. Nature Climate Change, 1-7.
579 Jephson, T., Carlsson, P., 2009. Species-and stratification-dependent diel vertical migration
580 behaviour of three dinoflagellate species in a laboratory study. Journal of plankton research 31,
581 1353-1362.
582 Jiang, H., Gao, K., 2004. Effects of lowering temperature during culture on the production of
583 polyunsaturated fatty acids in the marine diatom Phaeodactylum tricornutum (bacillariophyceae)
584 1. Journal of Phycology 40, 651-654.
585 Jónasdóttir, S.H., 2019. Fatty acid profiles and production in marine phytoplankton. Marine
586 drugs 17, 151.
587 Kaneda, T., 1991. Iso-and anteiso-fatty acids in bacteria: biosynthesis, function, and
588 taxonomic significance. Microbiological reviews 55, 288-302.
589 Laney, S.R., Sosik, H.M., 2014. Phytoplankton assemblage structure in and around a massive
590 under-ice bloom in the Chukchi Sea. Deep Sea Research Part II: Topical Studies in
591 Oceanography 105, 30-41.
592 Lee, Y., Min, J.-O., Yang, E.J., Cho, K.-H., Jung, J., Park, J., Moon, J.K., Kang, S.-H., 2019.
593 Influence of sea ice concentration on phytoplankton community structure in the Chukchi and
594 East Siberian Seas, Pacific Arctic Ocean. Deep Sea Research Part I: Oceanographic Research
595 Papers 147, 54-64.
596 Leiknes, Ø., Etter, S.A., Tokle, N.E., Bergvik, M., Vadstein, O., Olsen, Y., 2016. The Effect
597 of Essential Fatty Acids for the Somatic Growth in Nauplii of Calanus finmarchicus. Frontiers in
598 Marine Science 3, 33.
599 Litzow, M., A. , Bailey, K., M. , Prahl, F., G. , Ron., H., 2006. Climate regime shifts and
600 reorganization of fish communities: the essential fatty acid limitation hypothesis. Marine
601 Ecology Progress Series 315, 1-11.
602 Lowry, K.E., Pickart, R.S., Mills, M.M., Brown, Z.W., van Dijken, G.L., Bates, N.R., Arrigo,
603 K.R., 2015. The influence of winter water on phytoplankton blooms in the Chukchi Sea. Deep
604 Sea Research Part II: Topical Studies in Oceanography 118, 53-72.
605 Marmillot, V., Parrish, C.C., Tremblay, J.-É., Gosselin, M., MacKinnon, J.F., 2020.
606 Environmental and Biological Determinants of Algal Lipids in Western Arctic and Subarctic
607 Seas. Frontiers in Environmental Science.
608 Martini, K.I., Stabeno, P.J., Ladd, C., Winsor, P., Weingartner, T.J., Mordy, C.W., Eisner,
609 L.B., 2016. Dependence of subsurface chlorophyll on seasonal water masses in the Chukchi Sea.
610 Journal of Geophysical Research: Oceans 121, 1755-1770.

611 Mazerolle, M.J., Mazerolle, M.M.J., 2019. Package 'AICcmodavg'.
612 Menden-Deuer, S., Lessard, E.J., 2000. Carbon to volume relationships for dinoflagellates,
613 diatoms, and other protist plankton. Limnology and oceanography 45, 569-579.

Miller, J.A., Peterson, W.T., Copeman, L.A., Du, X., Morgan, C.A., Litz, M.N.C., 2017. Temporal variation in the biochemical ecology of lower trophic levels in the Northern California Current. Progress in Oceanography 155, 1-12.

Moran, S., Lomas, M., Kelly, R., Gradinger, R., Iken, K., Mathis, J., 2012. Seasonal succession of net primary productivity, particulate organic carbon export, and autotrophic community composition in the eastern Bering Sea. Deep Sea Research Part II: Topical Studies in Oceanography 65, 84-97.

Morán, X.A.G., LÓPEZ-URRUTIA, Á., CALVO-DÍAZ, A., Li, W.K., 2010. Increasing importance of small phytoplankton in a warmer ocean. Global Change Biology 16, 1137-1144.

Parrish, C., Arts, M., Wainman, B., 1999. Lipids in freshwater ecosystems. New York, SpringeraVerlag. pp. 5a 20.

Parrish, C.C., 2013. Lipids in marine ecosystems. ISRN Oceanography 2013.

Parsons, T.R., 1984. A manual of chemical & biological methods for seawater analysis. Elsevier.

Pinheiro, J., Bates, D., DebRoy, S., Sarkar, D., Heisterkamp, S., Van Willigen, B., Maintainer, R., 2017. Package 'nlme'. Linear and nonlinear mixed effects models, version 3.

Pond, D., Harris, R., Head, R., Harbour, D., 1996. Environmental and nutritional factors determining seasonal variability in the fecundity and egg viability of Calanus helgolandicus in coastal waters off Plymouth, UK. Marine Ecology Progress Series 143, 45-63.

R Core Team, 2018. R: A Language and Environment for Statistical Computing, R Foundation for Statistical Computing, Austria, 2015. ISBN 3-900051-07-0: URL http://www.R-project. org.

Reuss, N., Poulsen, L., 2002. Evaluation of fatty acids as biomarkers for a natural plankton community. A field study of a spring bloom and a post-bloom period off West Greenland. Marine Biology 141, 423-434.

Schollmeier, T., Oliveira, A., Wooller, M., Iken, K., 2018. Tracing sea ice algae into various benthic feeding types on the Chukchi Sea shelf. Polar Biology 41, 207-224.

Sigler, M.F., Stabeno, P.J., Eisner, L.B., Napp, J.M., Mueter, F.J., 2014. Spring and fall phytoplankton blooms in a productive subarctic ecosystem, the eastern Bering Sea, during 1995–2011. Deep Sea Research Part II: Topical Studies in Oceanography 109, 71-83.

Song, H., Ji, R., Jin, M., Li, Y., Feng, Z., Varpe, Ø., Davis, C.S., 2021. Strong and regionally distinct links between ice-retreat timing and phytoplankton production in the Arctic Ocean. Limnology and Oceanography.

Sukhanova, I.N., Flint, M.V., Pautova, L.A., Stockwell, D.A., Grebmeier, J.M., Sergeeva, V.M., 2009. Phytoplankton of the western Arctic in the spring and summer of 2002: Structure and seasonal changes. Deep Sea Research Part II: Topical Studies in Oceanography 56, 1223-1236.

Sushchik, N.N., Gladyshev, M.I., Makhutova, O.N., Kalachova, G.S., Kravchuk, E.S., Ivanova, E.A., 2004. Associating particulate essential fatty acids of the ω3 family with phytoplankton species composition in a Siberian reservoir. Freshwater Biology 49, 1206-1219.

Tocher, D.R., Betancor, M.B., Sprague, M., Olsen, R.E., Napier, J.A., 2019. Omega-3 long-chain polyunsaturated fatty acids, EPA and DHA: bridging the gap between supply and demand. Nutrients 11, 89.

Twining, C.W., Brenna, J.T., Hairston Jr, N.G., Flecker, A.S., 2016. Highly unsaturated fatty acids in nature: what we know and what we need to learn. Oikos 125, 749-760.

659 Warton, D.I., Duursma, R.A., Falster, D.S., Taskinen, S., 2012. smatr 3–an R package for
660 estimation and inference about allometric lines. Methods in Ecology and Evolution 3, 257-259.
661 Wasta, Z., Mjøs, S.A., 2013. A database of chromatographic properties and mass spectra of
662 fatty acid methyl esters from omega-3 products. Journal of Chromatography A 1299, 94-102.
663 Zuur, A., Ieno, E.N., Walker, N., Saveliev, A.A., Smith, G.M., 2009. Mixed effects models
664 and extensions in ecology with R. Springer Science & Business Media.
665

FIGURES

Figure 1

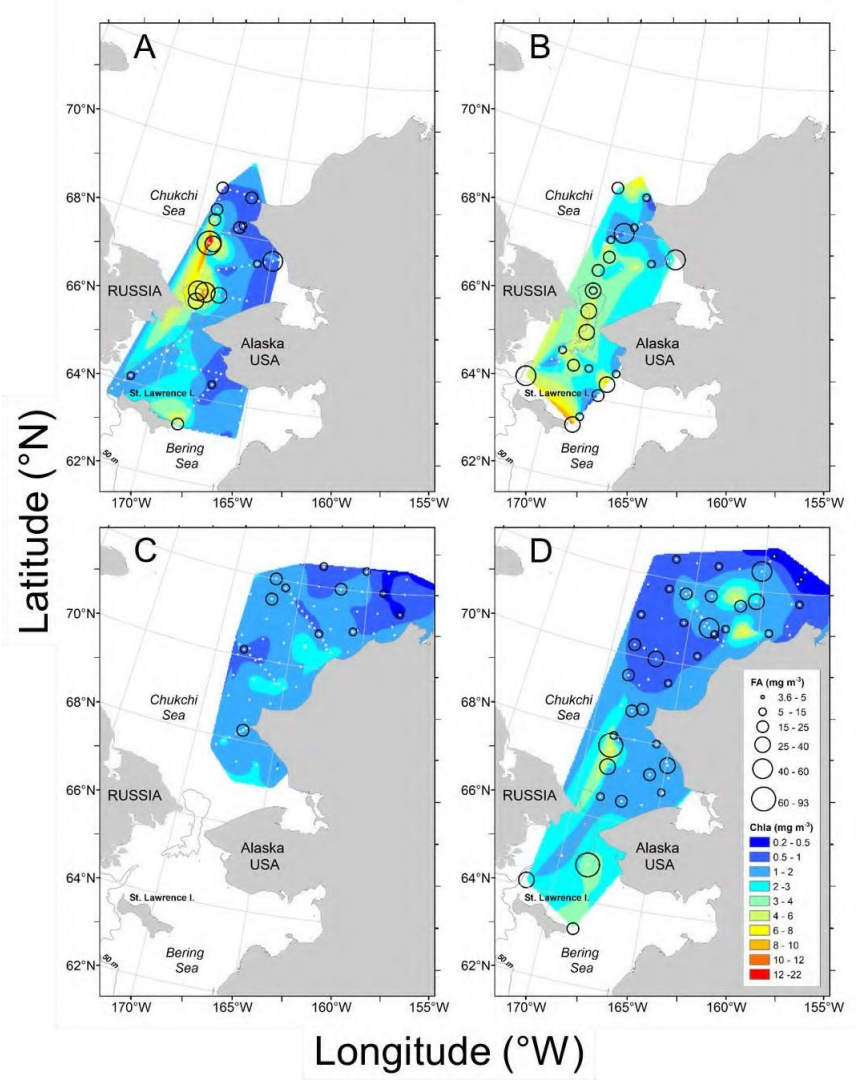

Fig. 1: Mean *in situ* Chl-a [mg m^{-3}] averaged from surface to 50 m and mean total FA concentrations [mg m^{-3}] measured at each station in: **A**) June 2017, **B**) June 2018, **C**) Aug/Sep 2017 and **D**) Aug/Sep 2019 in the northern Bering and Chukchi Seas. White diamonds indicate station locations.

Figure 2

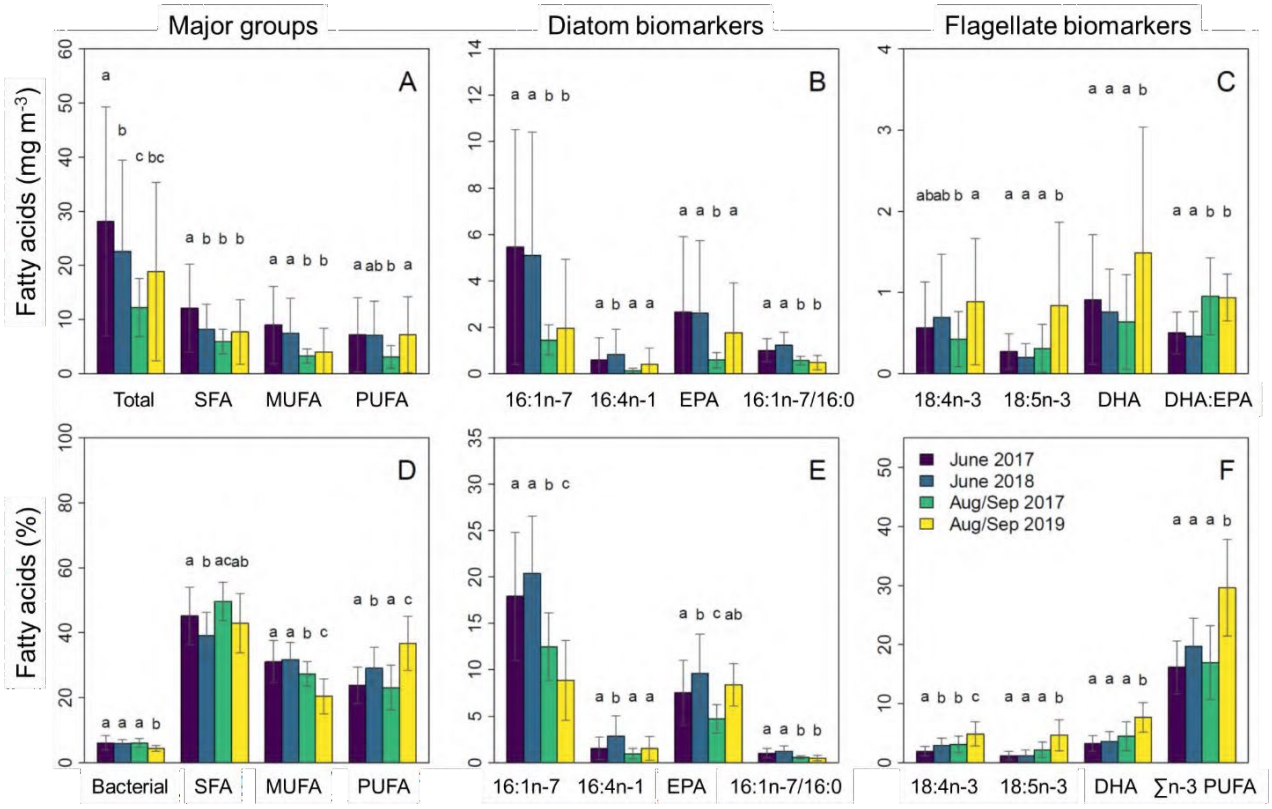

Fig. 2: Differences in June 2017 (n = 45, purple), June 2018 (n = 36, blue), Aug/Sep 2017 (n = 25, green) and Aug/Sep 2019 (n = 61, yellow) FA concentrations (top panel) and percent composition (bottom panel) for total FA, SFA, MUFA, PUFA and Bacterial (sum of all odd carbon FA and branched FAs) (**A, D**), diatom biomarkers 16:1n-7, 16:4n-1 EPA (20:5n-3) and a ratio diatom biomarker (ratio of 16:1n-7/16:0) **(B, E)**, and common dino+flag biomarkers 18:4n-3, 18:5n-3 and DHA (22:6n-3), DHA:EPA ratios, and the sum of n3-PUFA (**C, F**). Letters denote significant group differences based on ANOVA with Tukey HSD ($p<0.05$), with bars showing mean values and error bars denoting standard deviation

Figure 3

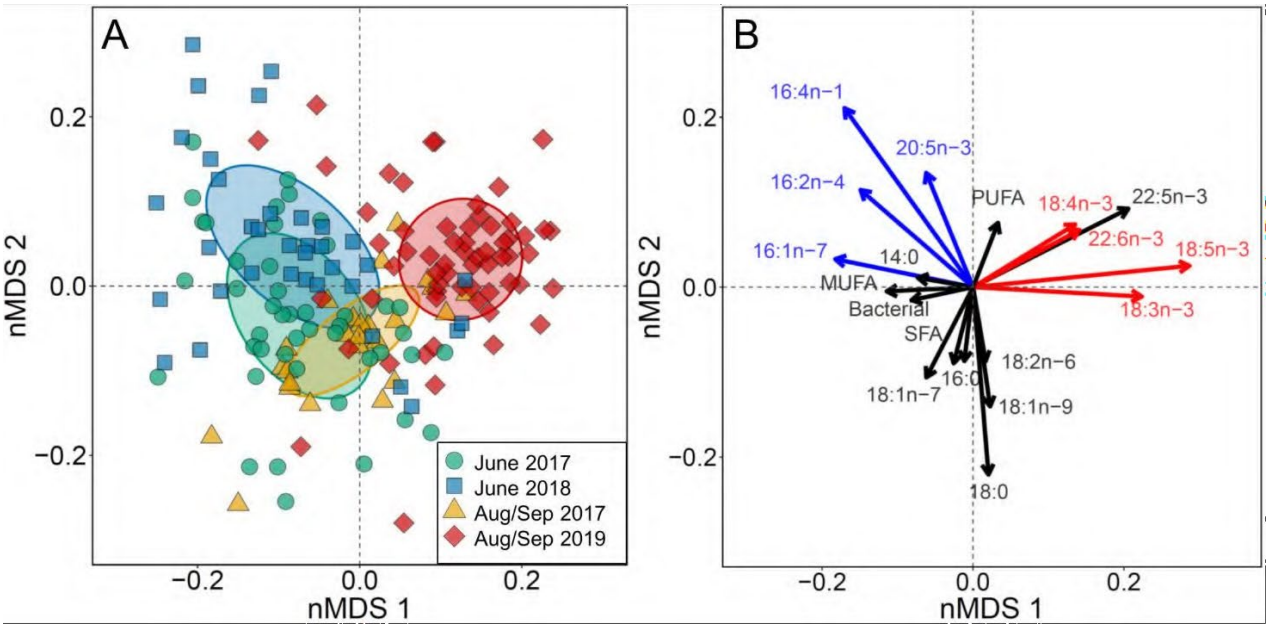

Fig. 3: Non-metric multidimensional scaling (nMDS) of FA percent composition data from each survey, **A**) samples from June 2017 (n = 45, green), June 2018 (n = 36, blue), Aug/Sep 2017 (n = 25, orange) and Aug/Sep 2019 (n = 61, red). Circles denote 50% ellipsoids for each survey. **B**) Vector plot for the nMDS showing individual FA associated with diatoms (blue), dino+flag (red) and shown in black are all non-taxa specific individual FA and major FA biomarker groups (SFA, MUFA, PUFA and bacterial).

Figure 4

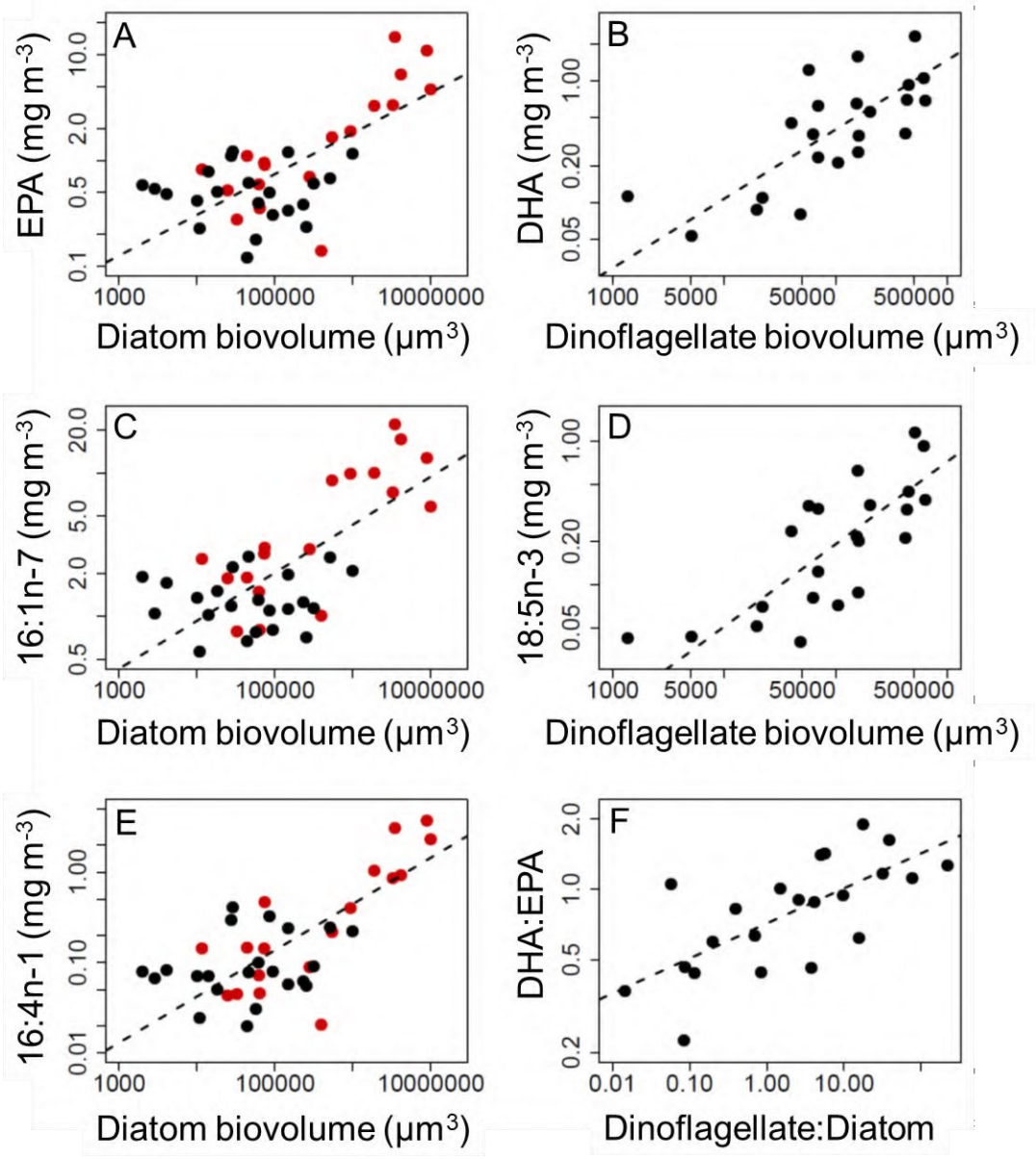

Fig. 4: Comparison of $\log_{10}$ transformed FlowCAM-measured biovolumes and FA biomarker concentration for diatoms in June 2017 (red, n = 18) and diatoms and dinoflagellates in Aug/Sep 2017 (black, n = 22). Comparisons of diatom biovolumes and **A**) EPA, **C**) 16:1n-7, **E**) 16:4n-1; comparison of dinoflagellate biovolumes and **B**) DHA, **E**) 18:5n-3; and **F**) ratios of dinoflagellate to diatom biovolumes compared to the DHA: EPA biomarkers.

Figure 5

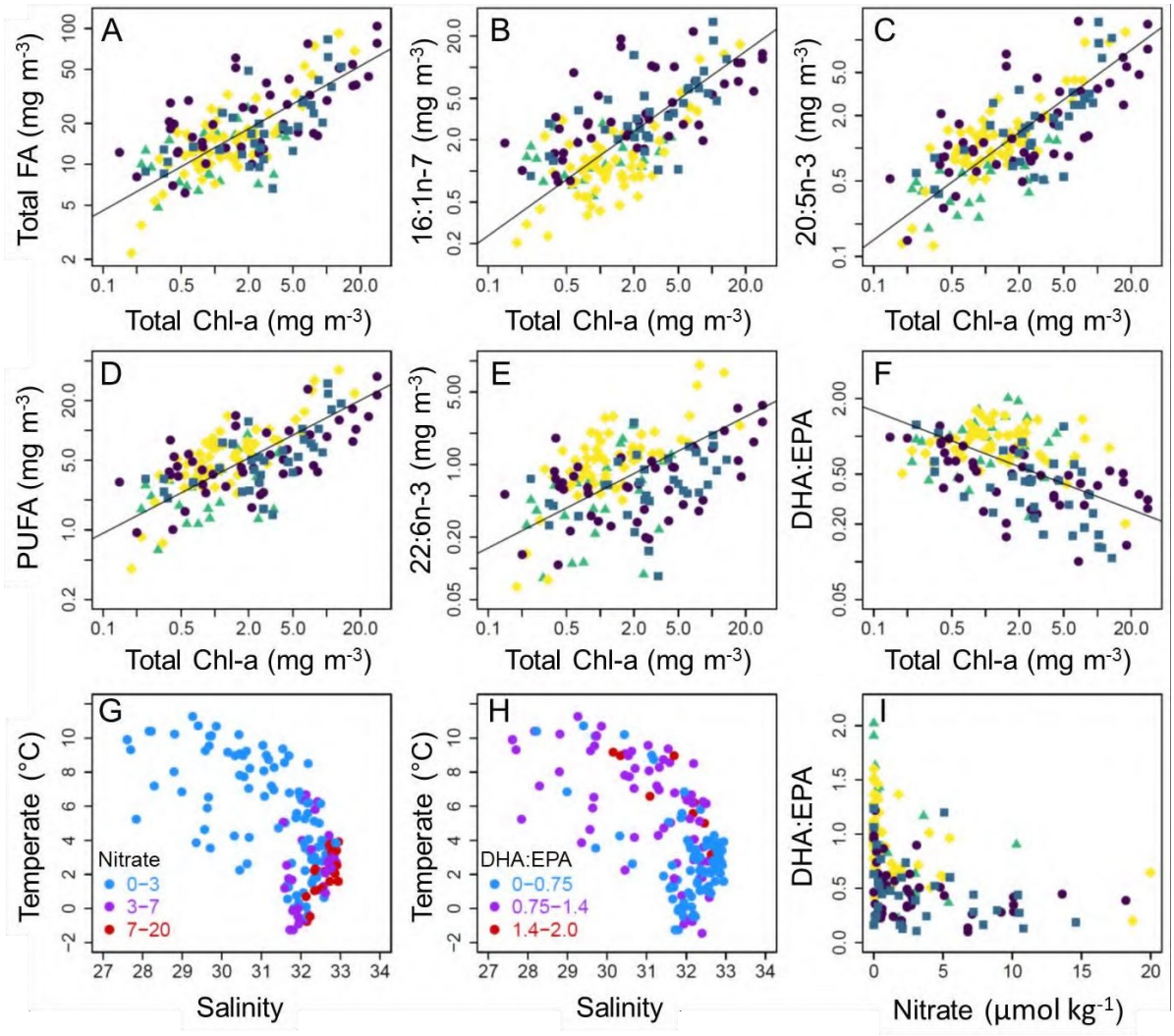

Fig. 5: Selected pairwise Type II regressions using log_{10}-transformed data between *in situ* discrete Chl-a [mg m^{-3}] and FA [mg m^{-3}] samples for **A**) total FA, **B**) 16:1n-7, **C**) EPA, **D**) total PUFA, **E**) DHA and **F**) DHA:EPA ratio. Temperature-salinity plots showing **G**) nitrate concentration (µmol kg^{-1}) and **H**) DHA: EPA ratios, color coded by their values (blue=low, red=high), and I) nitrate to DHA: EPA ratios. Colors in plots **A-F** and **I** denote each survey, with June 2017 (purple circles), June 2018 (blue squares), Aug/Sep 2017 (green triangles) and Aug/Sep 2019 (yellow diamonds).

Figure 6

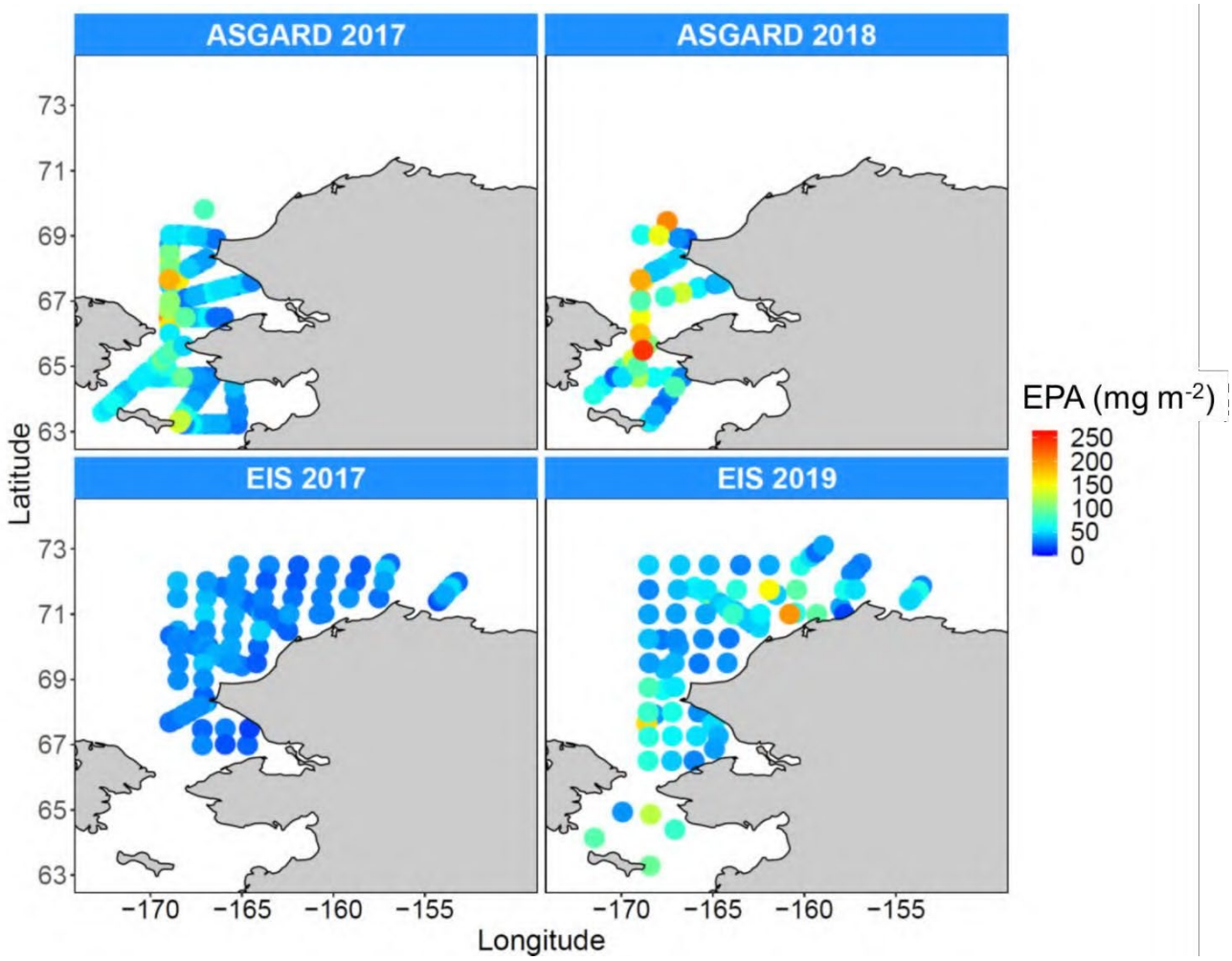

Fig. 6: Mixed effects model results predicting water column integrated EPA concentrations (mg m^{-2}) for each survey using all discrete sample total Chl-a and nitrogen samples as predictor variables (n = 1635, Table S1).

Zooplankton communities of the Arctic's Bering Strait region during the spring bloom, 2017-2018

Russell R. Hopcroft & Caitlin A. Smoot

Institute of Marine Sciences, University of Alaska Fairbanks

Introduction

The Bering Strait region is an important transition zone between the Pacific and Arctic Oceans, being a significant conduit of heat, fresh water, nutrients and entrained plankton (Grebmeier and Maslowski 2014). Four decades ago, it was estimated that 1.8 million metric tons of Bering Sea mesozooplankton were carried into the Chukchi Sea annually (Springer et al. 1989), that were responsible for the higher productivity of the Chukchi Sea than any adjacent regions of the Arctic Ocean. The pronounced changes in sea ice cover that have been occurring for the past two decades (Danielson et al. 2020) are anticipated to have significant consequences on the productivity, function and biodiversity of Arctic regions (Post et al 2013), with consequences for higher trophic levels of subsistence importance (Huntington et al 2020).

Planktonic communities have been shown to serve as useful "beacons of climate change" (Richardson, 2008) due to relatively rapid response changing temperatures and their strong coupling to water mass characteristics. There is now a large body of literature for the Chukchi and Bering Seas that demonstrates the close relationship of zooplankton community structure to water mass distribution (e.g. Hopcroft et al. 2010, Questel et al. 2013, Ershova et al. 2015a, Eisner et al. 2017, Abe et al. 2020), the general occurrence of multiple waters masses within the region, and the Pacific faunal character of much of the Chukchi during late summer. It is however notable that most of these studies have occurred during late summer, when the region is largely ice-free and planktonic productivity is in decline. Thus, we have limited information on what this ecosystem looks like during the spring bloom period that occurs several months in advance of our current window of knowledge. The dynamics of bloom period, both in terms of water temperature and primary productivity, fundamentally shape the magnitude and phenology of the zooplankton community. This in turn alters the fate of phytoplankton export to the seafloor verses retention of carbon within the water column for the remainder of the seasonal cycle.

To address this deficiency, the Arctic Shelf Growth, Advection, Respiration and Deposition Rate Experiments (ASGARD) conducted a pair of cruises in June of 2017 and 2018 to examine the structure and function of communities during the bloom. The broad-scale survey of the zooplankton communities at those times provides context for the vital rates determined within those communities as summarized elsewhere within this report.

Methods

Surveys for zooplankton community assessment during June 2017 and 2018 used a similar set of stations, albeit with fewer of them occupied during the second year (Fig. 1). Smaller-bodied zooplankton were collected with a vertically-hauled 60-cm diameter twin-ring net fitted with 150-µm nets pulled at ~0.5 m s^{-1}. Larger-bodied and more mobile zooplankton were targeted with an obliquely-towed 60-cm diameter Bongo net fitted with 505-µm nets pulled at ~0.5 m s^{-1}. Both nets samples from within 3-5 m of

the seafloor to the surface. Nets were outfitted with annually calibrated flowmeters to estimate volume of water filtered, with ratcheted meters in vertical that only record flow during ascent. Samples were preserved in 10% buffered formalin and returned to the laboratory for processing.

During laboratory processing, samples were subsampled using a Folsom splitter until a given aliquot contained approximately 100 individuals of the most abundant taxa. Increasingly larger fractions were examined for less abundant taxa. Organisms were identified, enumerated, lengths measured, and when appropriate, staged to determine species composition, abundance, and biomass. Typically, 400–600 animals were examined within each sample and organisms were identified to lowest taxonomic level possible. Community similarity was assessed using the Bray-Curtis similarity, and community structure was explored with hierarchical cluster analysis and non-parametric Multi-Dimensional Scaling (nMDS) routines using PRIMER (Clarke et al. 2014).

Results

The zooplankton community was dominated by the copepods *Calanus marshallae/glacialis*, *Pseudocalanus* spp., *Oithona similis*, and *Metridia pacifica* that are best assessed with the 150-µm nets. These copepods were present at nearly all stations during both 2017 and 2018 (Figs. 2-5). The copepod *Acartia* was also present across the sampling domain in both 2017 and 2018 but had a more coastal signal (Fig. 6). We observed higher abundances of Pacific-affinity copepods (*Neocalanus* spp. and *Eucalanus bungii*) in 2017 compared to 2018 (Fig. 7). Multivariate analyses of the combined 2017 and 2018 150-µm datasets revealed five major community groupings (Fig. 8). Group 1 consisted of stations in the northern portion of the sampling domain in 2017. Group 2 consisted of stations to the northwest of St. Lawrence Island in 2017. These stations were characterized by higher abundances of Pacific-affinity copepods, such as *Neocalanus flemingeri*, compared to other groups (Fig. 9). Group 3 consisted primarily of coastal stations in the northern part of the sampling domain in 2017. Group 4 was the largest group, containing stations from both 2017 and 2018. Most stations sampled in 2018 belonged to Group 4. Group 5 also consisted of stations from both 2017 and 2018, and was composed of primarily coastal stations and stations in the southeastern portion of the sampling domain near Norton Sound. The cladocerans *Podon leuckartii* and *Evadne nordmanni* were found nearly exclusively at stations in Group 5 (Fig. 10), characteristic of freshened surface waters. The *Pseudocalanus* spp. population was composed of copepodites in all life stages in both years, but with slightly higher proportion of younger copepodites (Stages 1 & 2) in 2018 (Fig. 11). The *Calanus marshallae/glacialis* population also had a higher proportion of younger copepodites in 2018 (Fig. 12). *Metridia pacifica*, in contrast, did not show a clear dominance of younger copepodite stages (Fig. 13).

Euphausiids, composed of several *Thysanoessa* species, were present across the sampling domain in both years, with slightly higher abundances observed in 2017 (Fig. 14). The euphausiids were also primarily composed of larval calyptopsis and furcilia stages in both years (Fig. 15). Amphipods, decapods, and the predatory chaetognath *Parasagitta elegans* were present in both years across the sampling domain but did not show a particular spatial pattern (Figs. 16-18). *Aglantha digitale*, a common hydrozoan, did not display a strong spatial pattern (Fig. 19). There was often a significant biomass in other jellyfish and ctenophores present in the plankton nets. Multivariate analysis of abundance data from the 505-µm net revealed similar patterns to that of the 150-µm net, although with a few more groupings (Fig. 20). The clustering of stations northeast of St. Lawrence Island observed in the 150-µm net was also

observed in the 505-µm net. Similarly, the cluster of stations in the southeastern portion of the sampling domain in 2017 was observed in the 505-µm net as well.

Abridged Discussion

Not surprisingly, zooplankton community composition observed during the ASGARD cruises was similar to that observed several months later in the season cycle by other studies (e.g. Springer et al. 1989; Questel et al. 2013, Ershova et al. 2015, Eisner et al. 2017, Abe et al. 2020). The abundance and biomass of the crustacean components of the zooplankton fell with the bounds of prior observation, as did many, but not all, gelatinous taxa. The water-mass driven structure in the zooplankton community assemblage was consistent with previously observed patterns for 2017, but not resolved for 2018. The most notable difference between our study years and observations to north was the high abundances of *Neocalanus* copepods during 2017. High abundance of *Neocalanus* was at least partially a reflection of their seasonal occurrence in surface waters of the Gulf of Alaska (Mackas & Tsuda 1999, Coyle and Pinchuk 2003) and their proximity to that source. The individuals collected at that time were lipid-rich Copepodite Stage5 – the final stage before ontological descent – thus it is unclear if they were still actively feeding at the time of our survey. Nonetheless, the large differences in abundance between years suggest greater across-shelf transport was occurring in 2017 compared to 2018.

There were also notable differences in the distribution of developmental stages within key copepod species such as *Calanus* compared to later-season studies (e.g., Ershova et al 2015), with earlier stages being more common in this study. It is notable that the stages were more advanced during 2017 when warmer water temperatures occurred compared to 2018. Further seasonal shifts toward later stage distribution are expected for *Calanus* in this region (Kimura et al. 2020). Exceptions to such stage generalizations have however been observed in the Northeastern Chukchi with early stages sometimes dominating during August when the water over the region is replaced with that originating from the Arctic's basins (Elliot et al. 2017). Developmental stage distributipm was harder to generalize for Metridia, but early stages dominate at many stations In contrast, due to low modulation in the reproductive output of *Pseudocalanus*, seasonal difference in stage distribution were not as pronounced in this genus (Kimura et al 2020), but as observed for Calanus, younger stages were more prominent during the 2018 cruise than in 2017. Euphausiids represented another such example where abundances were high during June and dominated by larval stages. Such elevated transport following the spawning period typical for sub-arctic euphausiids (Pinchuk et al. 2003) is consistent with the belief that euphausiids populations are primarily advected into the Chukchi rather than being a fully resident species (Berline et al. 2008).

References

Abe, Y., Matsuno, K., Fujiwara, A., Yamaguchi, A., 2020. Review of spatial and inter-annual changes in the zooplankton community structure in the western Arctic Ocean during summers of 2008–2017. Progress in Oceanography 186, 102391.

Berline, L., Spitz, Y.H., Ashjian, C.J., Campbell, R.G., Maslowski, W., Moore, S.E., 2008. Euphausiid transport in the Western Arctic Ocean. Mar. Ecol. Prog. Ser. 360, 163-178.

Clarke, K.R., Gorley, R.N., Somerfield, P.J., Warwick, R.M., 2014. Change in marine communities: an approach to statistical analysis and interpretation, 3rd edition. PRIMER-E, Plymouth.

Coyle, K.O., Pinchuk, A.I., 2003. Annual cycle of zooplankton abundance, biomass and production on the northern Gulf of Alaska shelf, October 1997 through October 2000. Fish. Oceanogr. 12, 227-251.

Danielson, S.L., Ahkinga, O., Ashjian, C., Basyuk, E., Cooper, L.W., Eisner, L., Farley, E., Iken, K.B., Grebmeier, J.M., Juranek, L., Khen, G., Jayne, S.R., Kikuchi, T., Ladd, C., Lu, K., McCabe, R.M., Moore, G.W.K., Nishino, S., Ozenna, F., Pickart, R.S., Polyakov, I., Stabeno, P.J., Thoman, R., Williams, W.J., Wood, K., Weingartner, T.J., 2020. Manifestation and consequences of warming and altered heat fluxes over the Bering and Chukchi Sea continental shelves. Deep Sea Research Part II: Topical Studies in Oceanography 177, 104781.

Eisner, L., Hillgruber, N., Martinson, E., Maselko, J., 2013. Pelagic fish and zooplankton species assemblages in relation to water mass characteristics in the northern Bering and southeast Chukchi seas. Polar Biol. 36, 87-113.

Elliott, S.M., Ashjian, C.J., Feng, Z., Jones, B., Chen, C., Zhang, Y., 2017. Physical control of the distributions of a key Arctic copepod in the Northeast Chukchi Sea. Deep Sea Res. II. 144, 37-51.

Ershova, E.A., Hopcroft, R.R., Kosobokova, K.N., 2015. Inter-annual variability of summer mesozooplankton communities of the western Chukchi Sea: 2004–2012. Polar Biol. 38, 1461-1481.

Grebmeier, J.M., Maslowski, W., 2014. The Pacific Arctic Sector: status and trends. . Springer, New York.

Hopcroft, R.R., Kosobokova, K.N., Pinchuk, A.I., 2010. Zooplankton community patterns in the Chukchi Sea during summer 2004. Deep-Sea Res. II. 57, 27-39.

Huntington, H.P., Danielson, S.L., Wiese, F.K., Baker, M., Boveng, P., Citta, J.J., De Robertis, A., Dickson, D.M.S., Farley, E., George, J.C., Iken, K., Kimmel, D.G., Kuletz, K., Ladd, C., Levine, R., Quakenbush, L., Stabeno, P., Stafford, K.M., Stockwell, D., Wilson, C., 2020. Evidence suggests potential transformation of the Pacific Arctic ecosystem is underway. Nature Climate Change 10, 342-348.

Kimura, F., Abe, Y., Matsuno, K., Hopcroft, R.R., Yamaguchi, A., 2020. Temporal changes of zooplankton community and population structure in the northern Bering Sea from June to September in 2017. Deep Sea Res. II. 181-182, 104901.

Mackas, D.L., Tsuda, A., 1999. Mesozooplankton in the eastern and western subarctic Pacific: community structure, seasonal life histories, and interannual variability. Prog. Oceanogr. 43, 335-363.

Pinchuk, A.I., Coyle, K.O., 2008. Distribution, egg production and growth of euphausiids in the vicinity of the Pribilof Islands, southeastern Bering Sea, August 2004. Deep-Sea Res. II. 55, 1792-1800.

Post, E., Bhatt, U.S., Bitz, C.M., Brodie, J.F., Fulton, T.L., Hebblewhite, M., Kerby, J., Kutz, S.J., Stirling, I., Walker, D.A., 2013. Ecological Consequences of Sea-Ice Decline. Science 341, 519-524.

Questel, J.M., Clarke, C., Hopcroft, R.R., 2013. Seasonal and interannual variation in the planktonic communities of the northeastern Chukchi Sea during the summer and early fall. Cont. Shelf Res. 67, 23-41.

Springer, A.M., McRoy, C.P., Turco, K.R., 1989. The paradox of pelagic food webs in the northern Bering Sea - II. Zooplankton communities. Cont. Shelf Res. 9, 359-386.

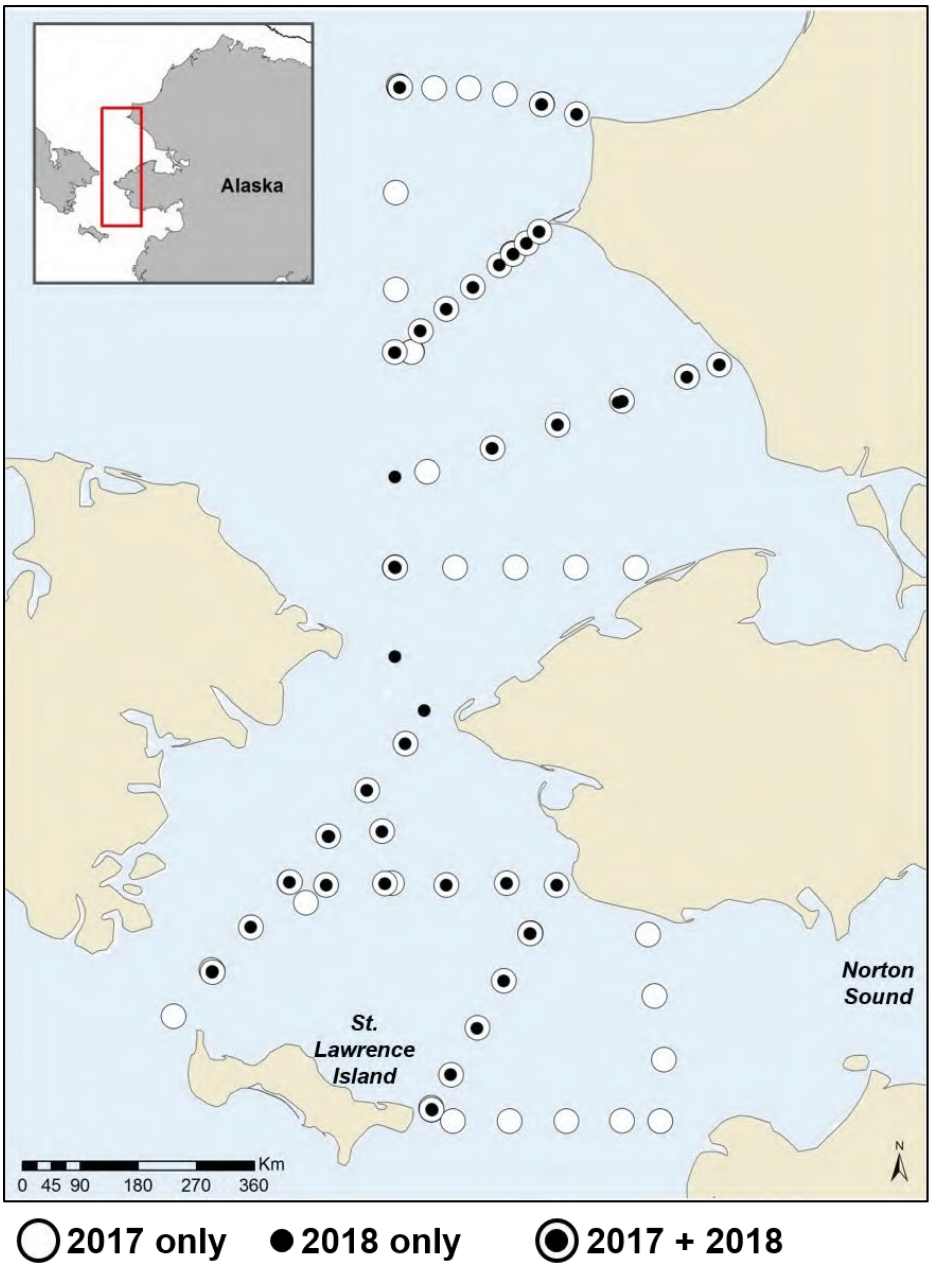

Figure 1. Zooplankton sampling locations during ASGARD 2017 and 2018.

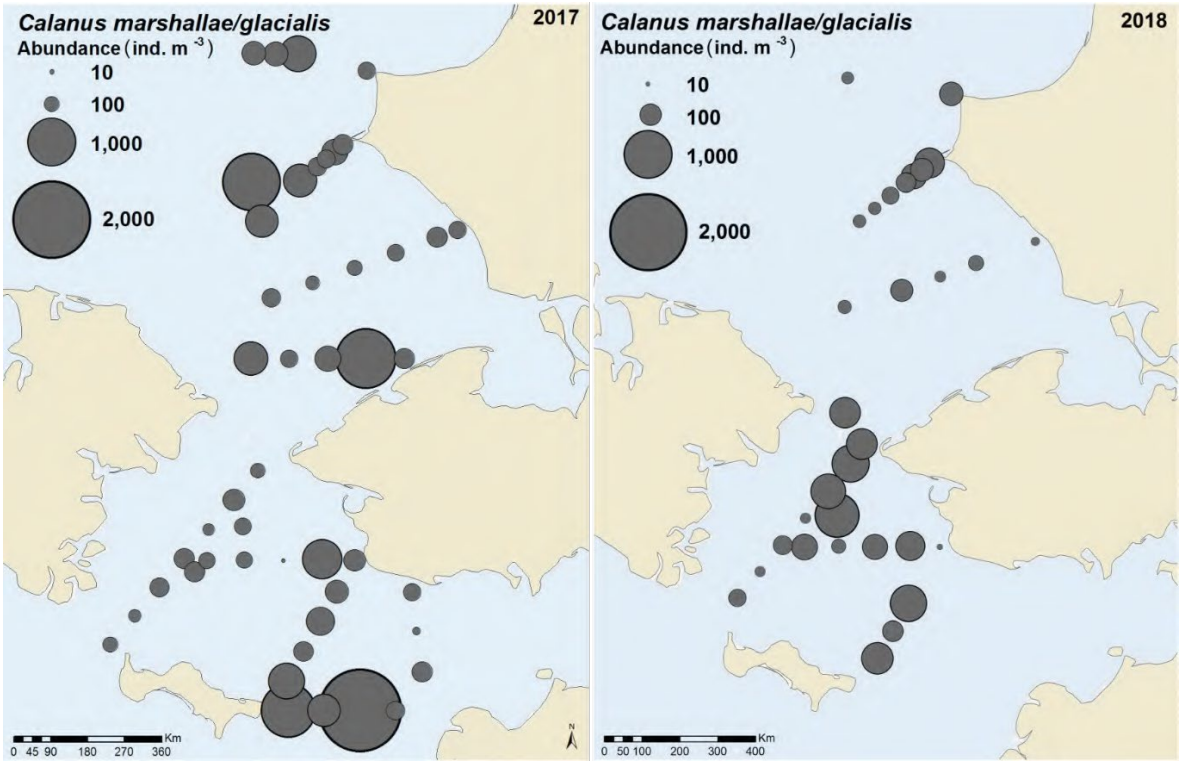

Figure 2. Abundance (ind. m^{-3}) of *Calanus marshallae/glacialis* based on the 150-µm net.

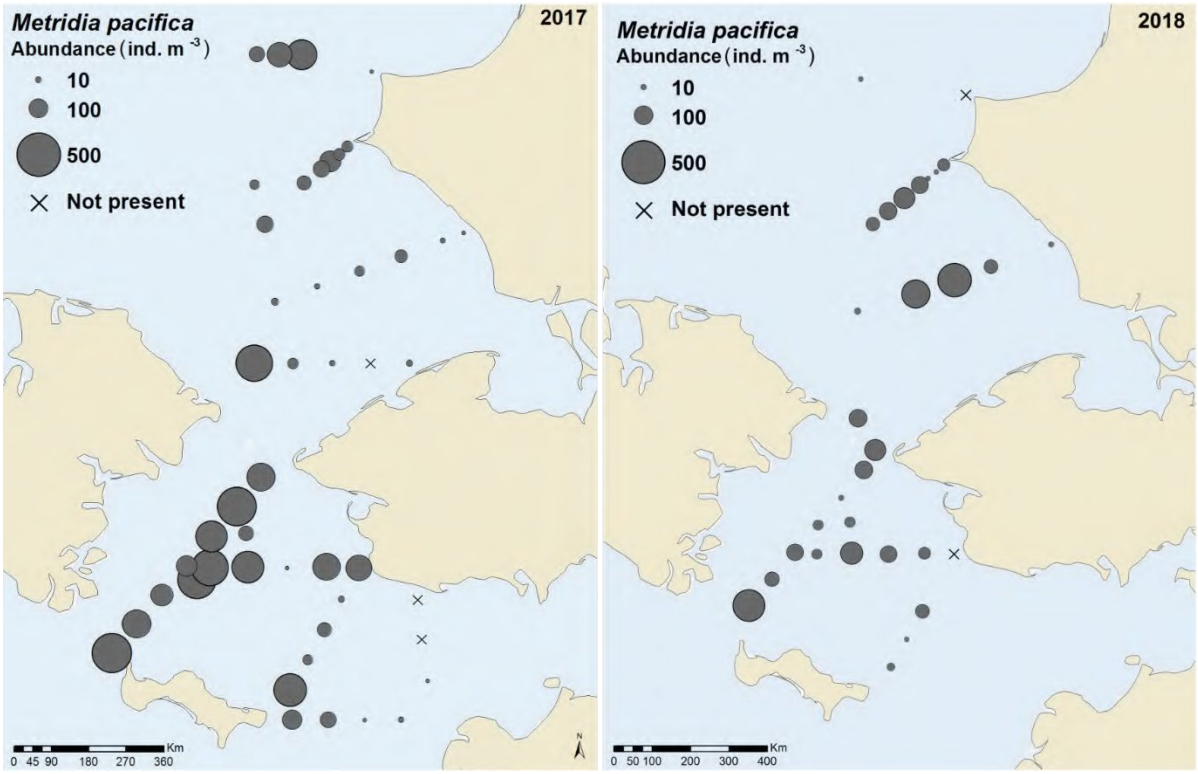

Figure 3. Abundance (ind. m^{-3}) of *Metridia pacifica* based on the 150-µm net.

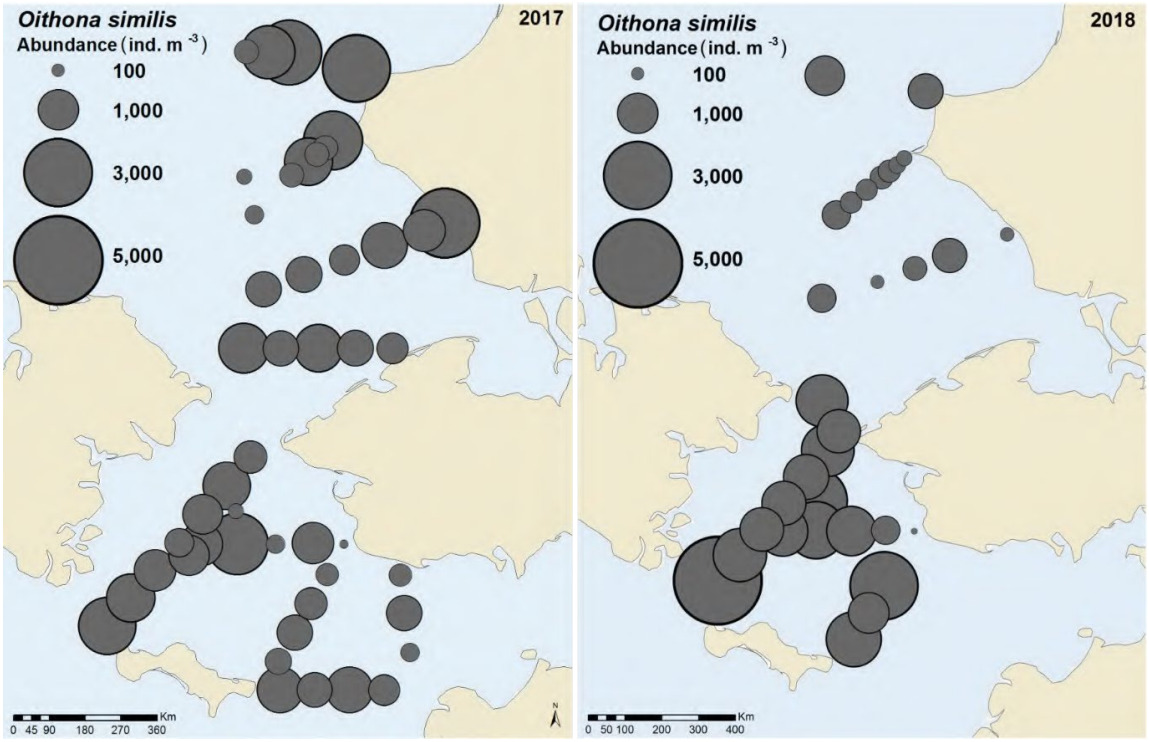

Figure 4. Abundance (ind. m^{-3}) of *Oithona similis* based on the 150-µm net.

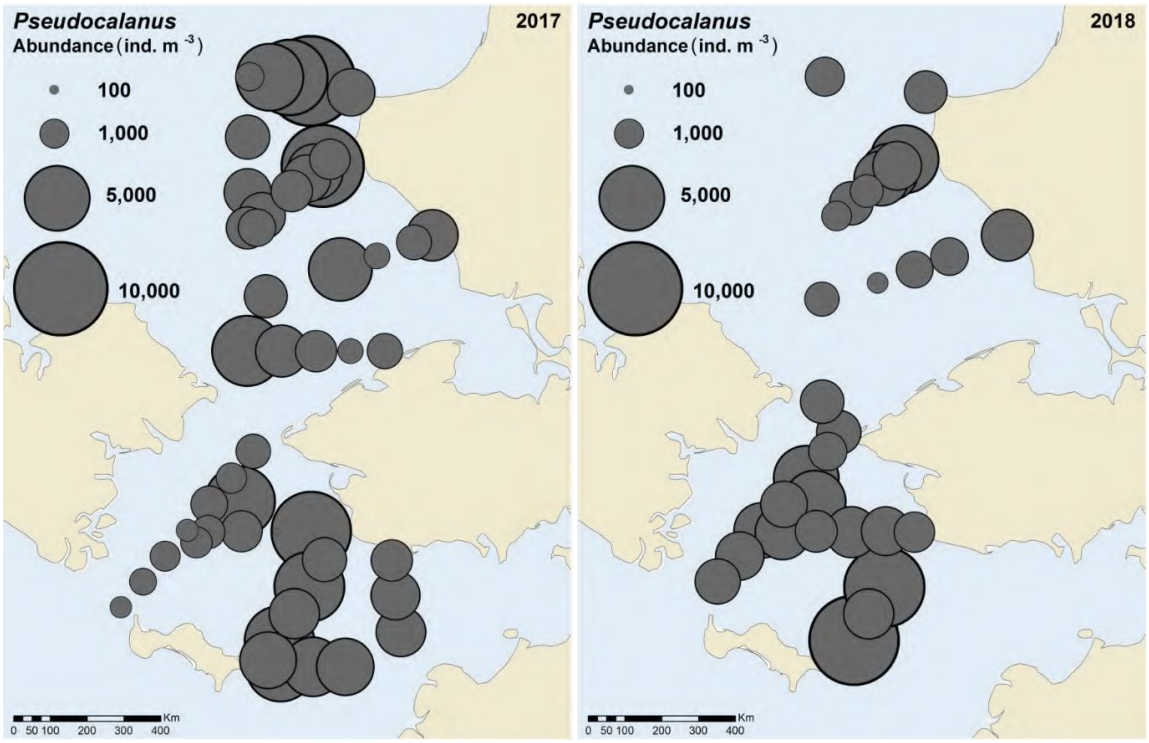

Figure 5. Abundance (ind. m^{-3}) of *Pseudocalanus* spp. based on the 150-µm net.

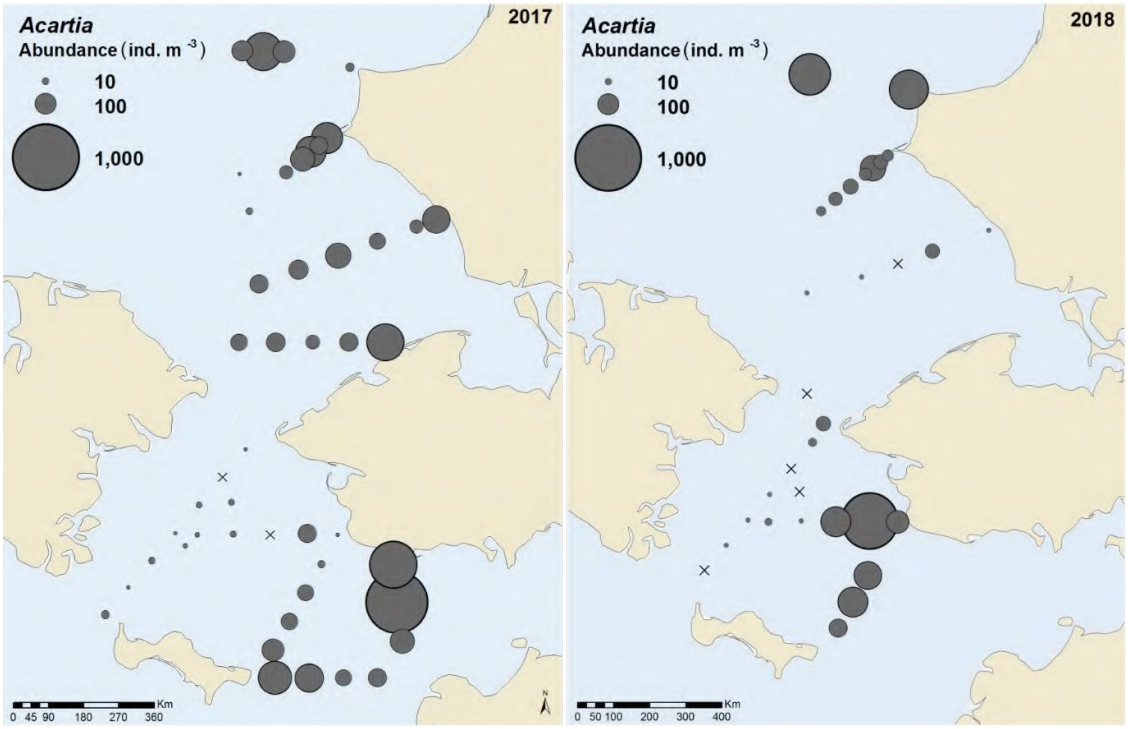

Figure 6. Abundance (ind. m^{-3}) of *Acartia* spp. based on the 150-µm net.

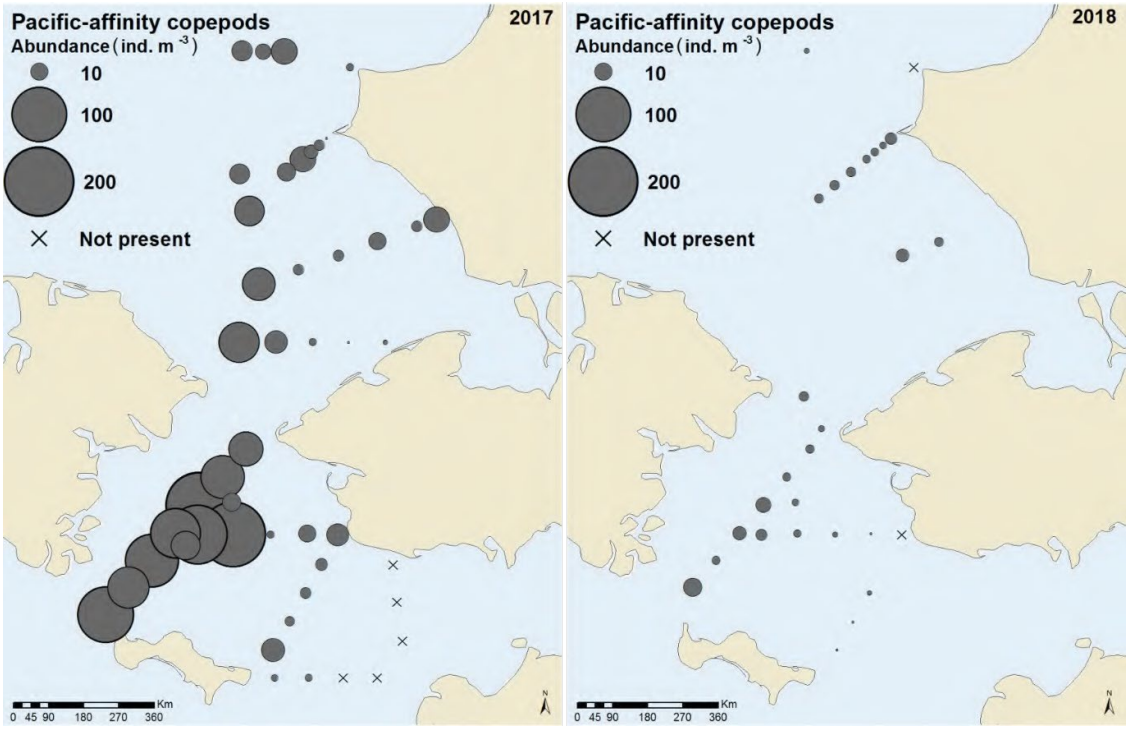

Figure 7. Abundance (ind. m^{-3}) of Pacific-affinity copepods based on the 150-µm net.

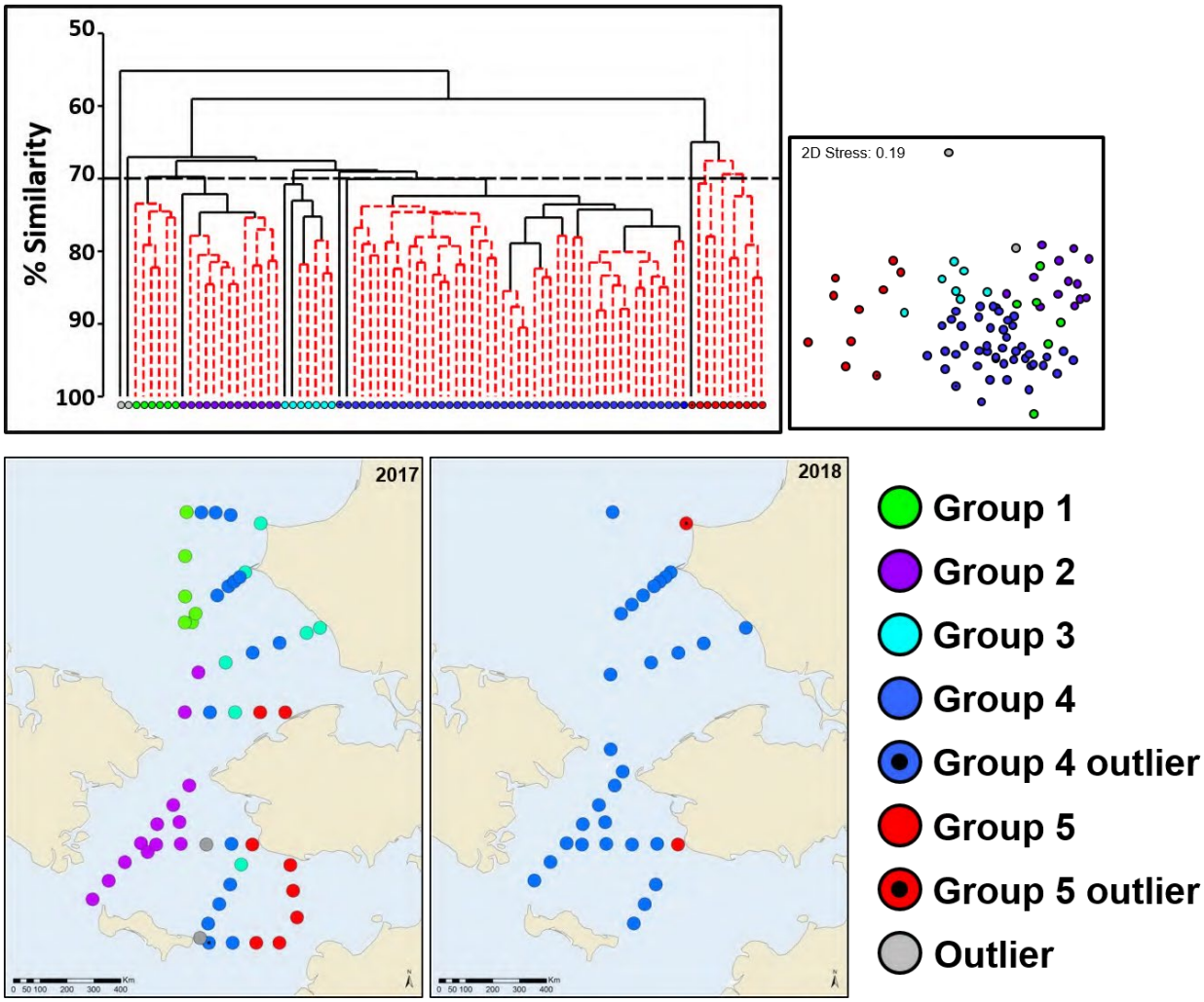

Figure 8. Top left: Bray-Curtis sample similarity as determined by hierarchical clustering of species abundance based on the 150-µm net. Dotted red lines connect samples that are not statistically unique (SIMPROF, $p < 0.05$). Top right: Non-parametric Multidimensional Scaling (nMDS) of zooplankton community overlain with groupings. Bottom: Spatial distribution of community groups.

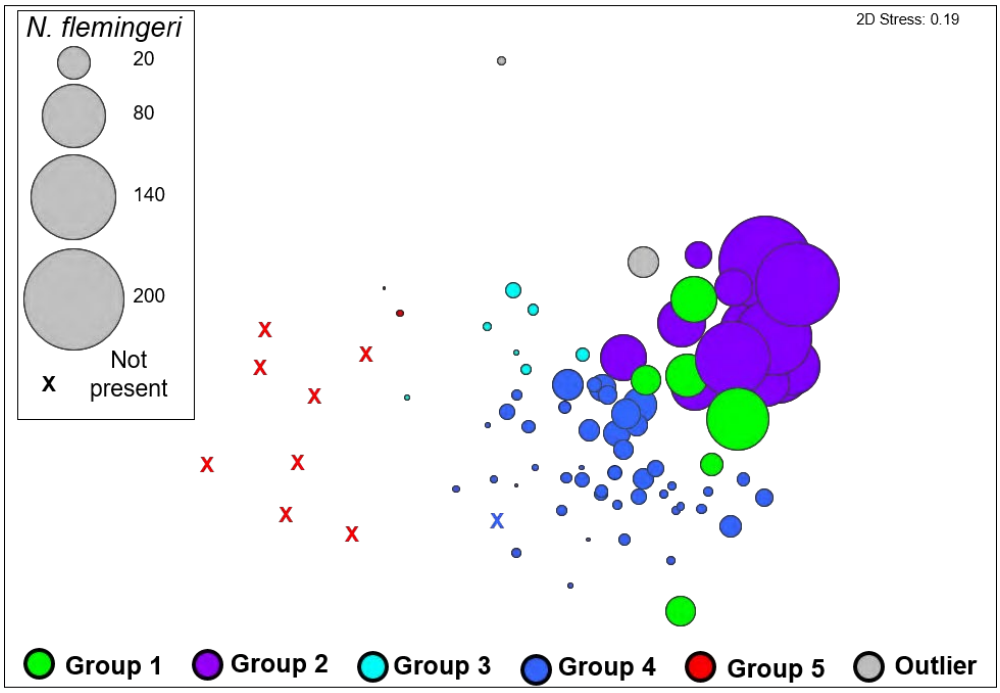

Figure 9. Abundance (ind. m^{-3}) of *Neocalanus flemingeri* superimposed over non-parametric Multidimensional Scaling (nMDS) plot. Based on the 150-µm net.

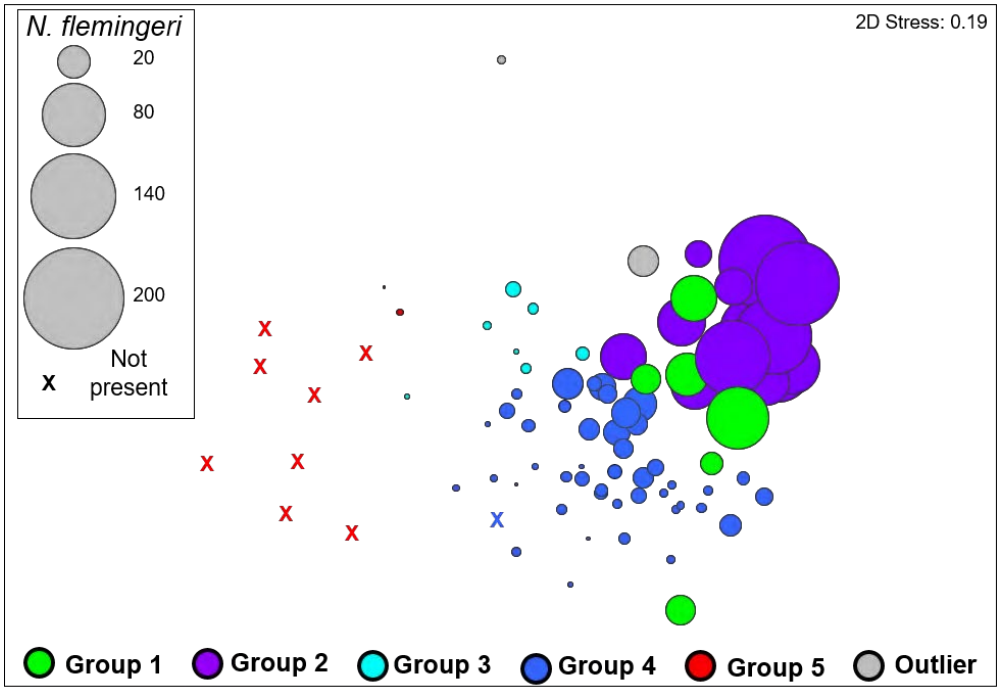

Figure 10. Abundance (ind. m^{-3}) of cladocerans superimposed over non-parametric Multidimensional Scaling (nMDS) plot. Based on the 150-µm net.

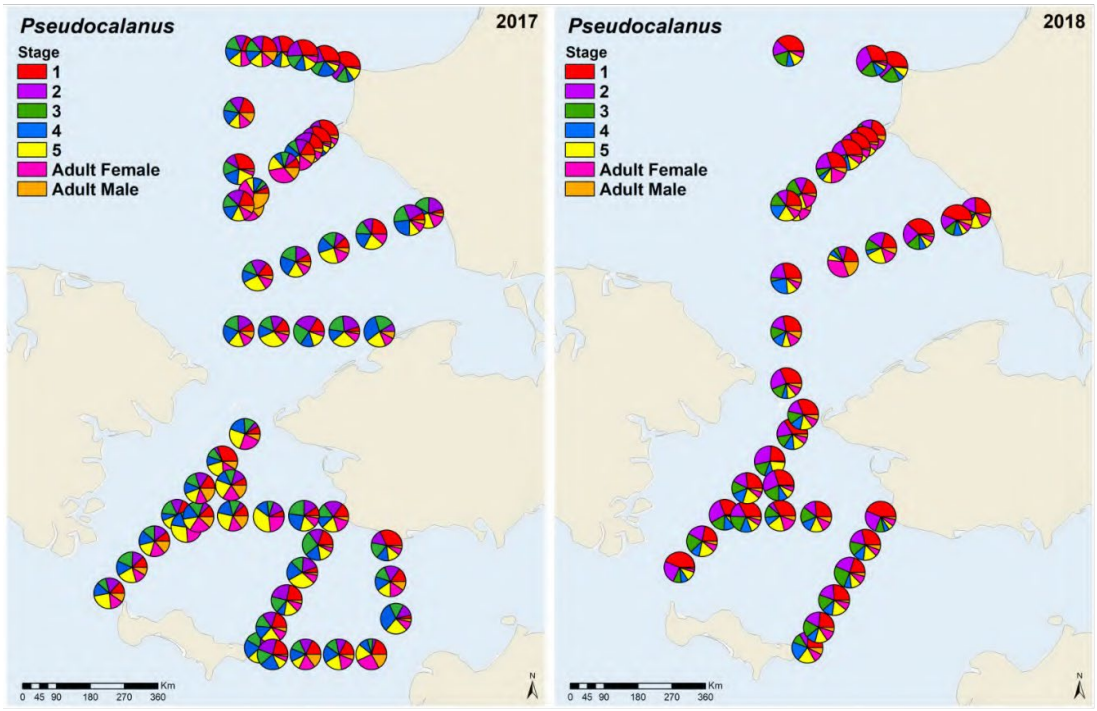

Figure 11. Stage composition of *Pseudocalanus* spp. based on the 150-µm net.

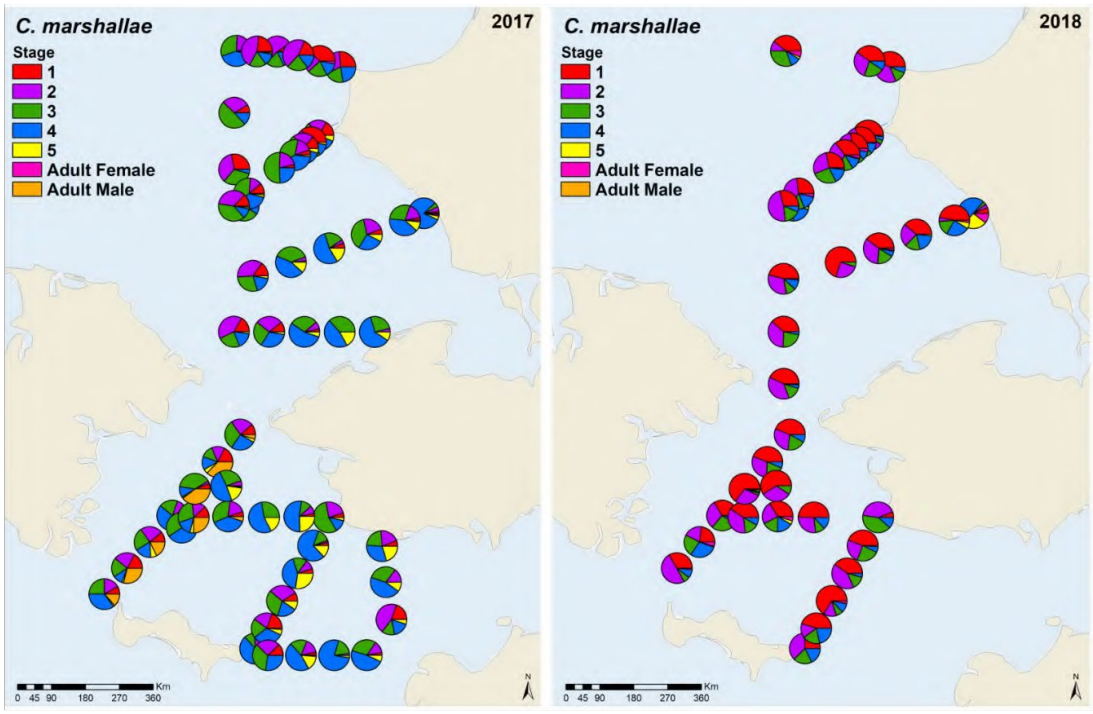

Figure 12. Stage composition of *Calanus marshallae/glacialis* based on the 150-µm net.

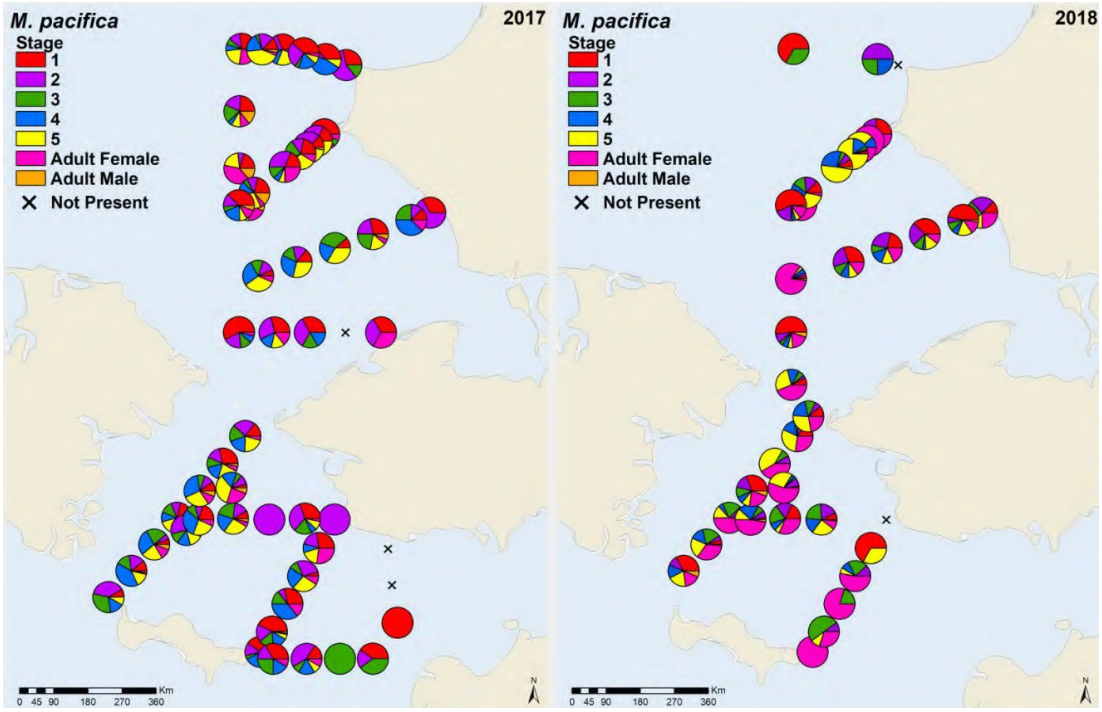

Figure 13. Stage composition of *Metridia pacifica* based on the 150-µm net.

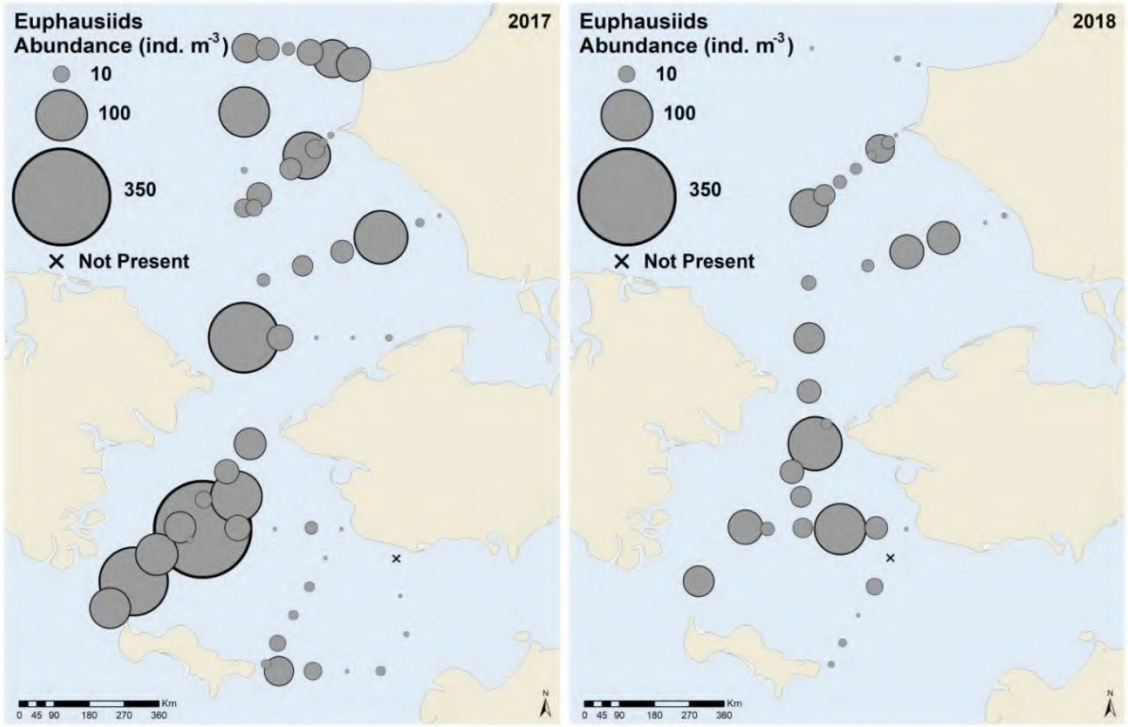

Figure 14. Abundance (ind. m^{-3}) of euphausiids based on the 505-µm net.

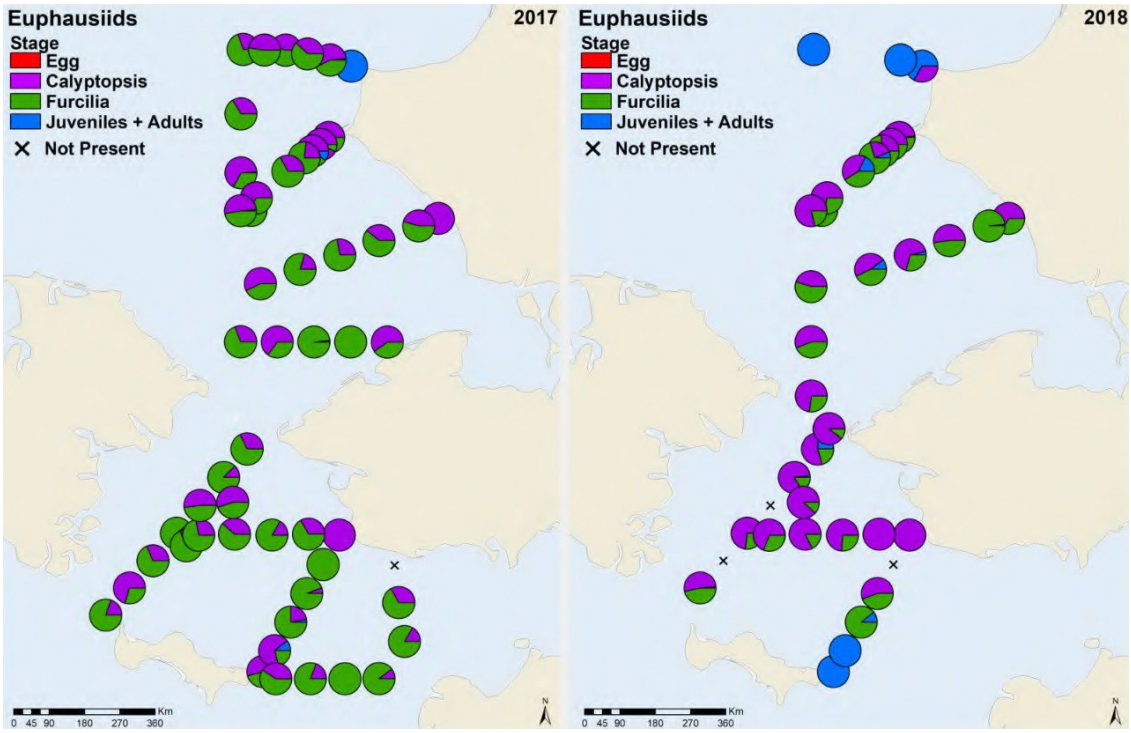

Figure 15. Stage composition of euphausiids based on the 505-µm net.

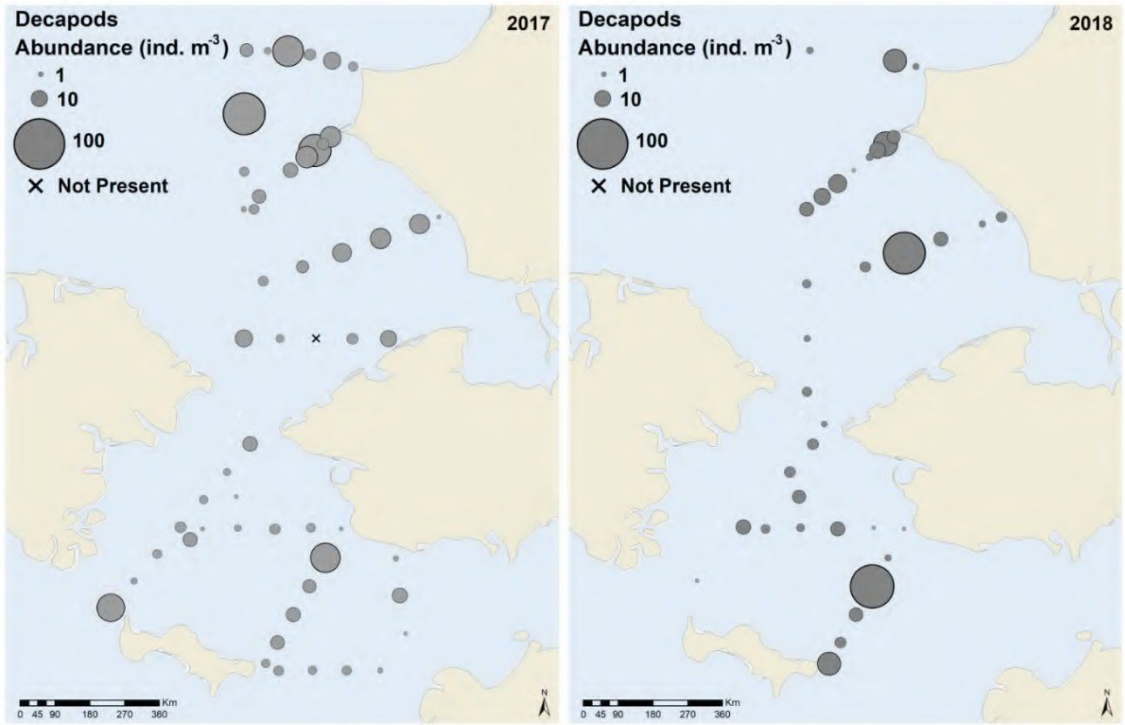

Figure 16. Abundance (ind. m^{-3}) of decapods based on the 505-µm net.

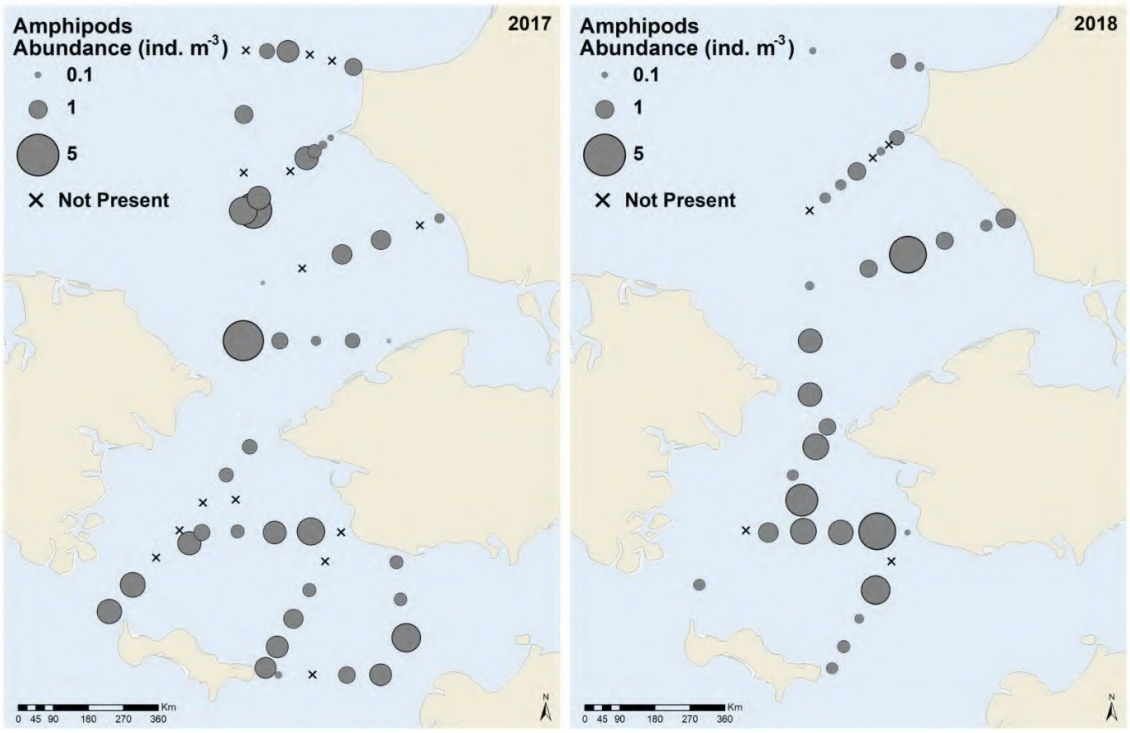

Figure 17. Abundance (ind. m^{-3}) of amphipods based on the 505-µm net.

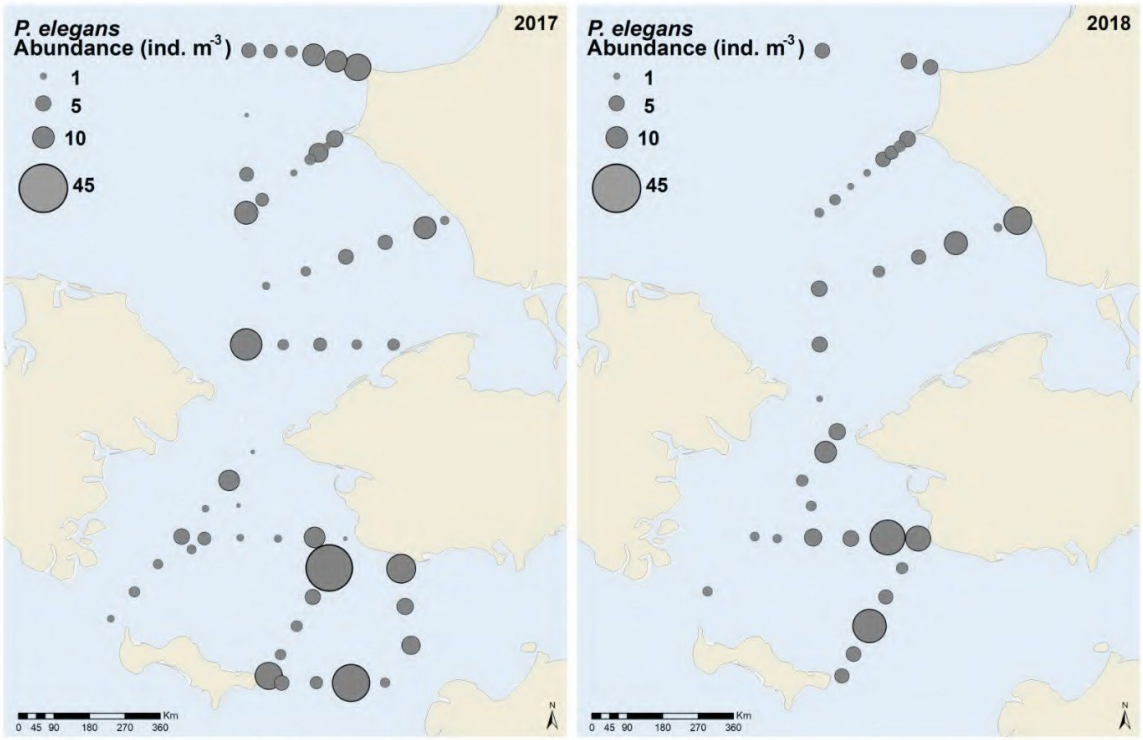

Figure 18. Abundance (ind. m^{-3}) of *Parasagitta elegans* based on the 505-µm net.

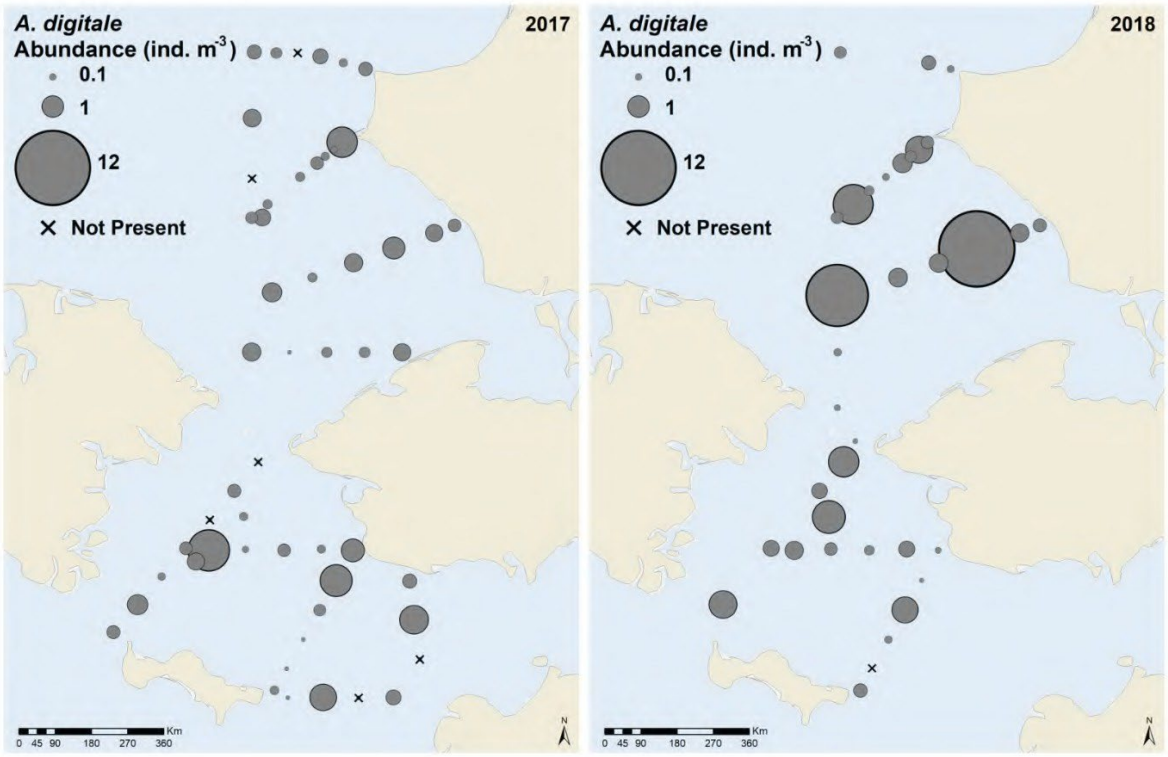

Figure 19. Abundance (ind. m^{-3}) of *Aglantha digitale* based on the 505-µm net.

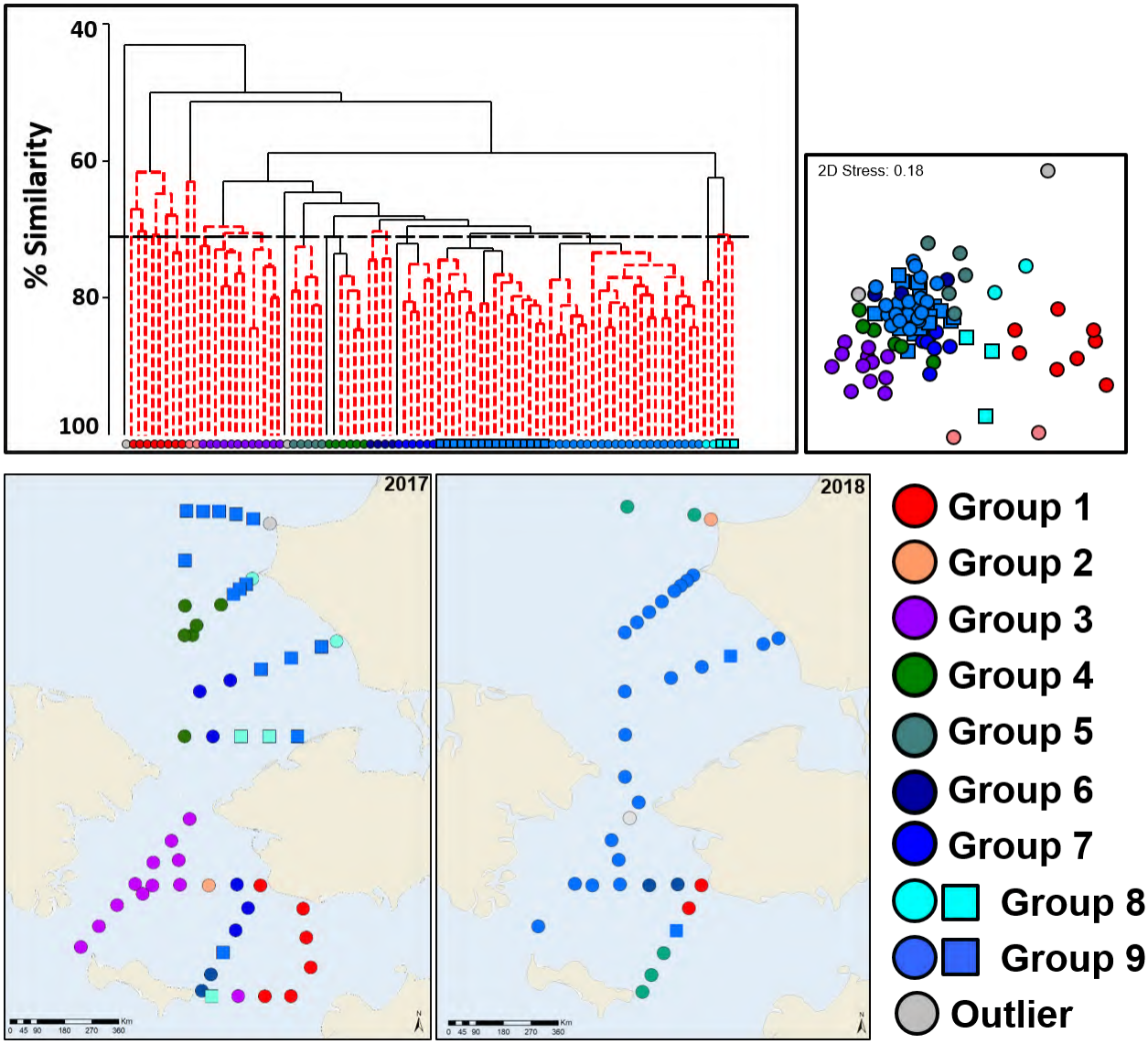

Figure 20. Top left: Bray-Curtis sample similarity as determined by hierarchical clustering of species abundance based on the 505-µm net. Dotted red lines connect samples that are not statistically unique (SIMPROF, $p < 0.05$). Top right: Non-parametric Multidimensional Scaling (nMDS) of zooplankton community overlain with groupings. Bottom: Spatial distribution of community groups.

GROWTH AND REPRODUCTIVE RATES OF CALANOID COPEPODS IN THE NORTHERN BERING AND SOUTHERN CHUKCHI SEAS

By

Alexandra Poje

A Thesis Submitted in Partial Fulfillment of the Requirements

for the Degree of Master of Science

in

Oceanography

University of Alaska Fairbanks

July 2020

APPROVED:

Russ Hopcroft, Committee Chair

Kenneth Coyle, Committee Member

Seth Danielson, Committee Member

Russ Hopcroft, Chair

Department of Oceanography

Brad Moran, Dean

College of Fisheries and Ocean Sciences

Michael Castellini, *Dean of Graduate School*

ABSTRACT

Egg production and copepodite growth rates were measured for the calanoid copepods *Pseudocalanus* spp., *Calanus marshallae/glacialis*, and *Metridia pacifica* in the northern Bering and southern Chukchi Seas during June of 2017 and 2018. For all taxa, instantaneous growth rates generally decreased with increasing copepodite stage, though the differences between most stages was not significant. The growth rates for *Pseudocalanus* spp. averaged 0.03 ± 0.002 day^{-1}, *Calanus* spp. 0.09 ± 0.004 day^{-1}, and *M. pacifica* 0.05 ± 0.03 day^{-1}. Egg production rates increased with prosome length for all species, but when standardized to body weight this trend reversed. All *Pseudocalanus* species had similar weight-specific egg production (SEP): 0.18 ± 0.01 for *P. acuspes*, 0.15 ± 0.00 for *P. newmani*, and 0.11 ± 0.02 for *P. minutus*. The SEP for *Calanus* was considerably lower, 0.09 ± 0.01, while for *M. pacifica* it was 0.11 ± 0.01. These rates suggest considerable discrepancies between growth rates and egg production weights that we propose are due to differences in life history strategies. *Pseudocalanus* reproduce nearly year round, they appear to invest less in somatic growth, preferring to quickly reach their adult stage where they invest heavily into reproduction. *Calanus* spp. have 1 or possibly 2 generations per year in this region, they invest more into somatic growth in order to ensure their population is ready for a reproductive season timed to the spring phytoplankton bloom. The more omnivorous *M. pacifica* is also likely limited to 1 or 2 generations, although their ability to thrive on a wider range of food sources than *Calanus* seems to allow for relatively higher investment in reproduction and perhaps lower investment in somatic growth. Consistent with other studies, global growth models do not match our observations particularly well, likely because they are dominated by egg production estimates at lower latitudes.

TABLE OF CONTENTS

LIST OF FIGURES

Page

LIST OF TABLES

Page

ACKNOWLEDGMENTS

I would like to thank my advisor, Russ Hopcroft, for the support throughout this project. My committee member Seth Danielson and Kenneth Coyle have provided useful feedback during all components of the project. Caitlin Smoot provided invaluable support throughout, particularly in the field and laboratory portions. Cheryl Hopcroft aided in labwork. I would like to thank the many people on the ASGARD project that aided in the setup and breakdown of my experiments, particularly Heidi Mendoza-Islas and Atsushi Yamaguchi. I would also like to acknowledge the UAF CFOS graduate student community for their support throughout this project.

GROWTH AND REPRODUCTIVE RATES OF CALANOID COPEPODS IN THE NORTHERN BERING AND SOUTHERN CHUKCHI SEAS

Formatted for: Journal of Plankton Research

ABSTRACT

Egg production and copepodite growth rates were measured for the calanoid copepods *Pseudocalanus* spp., *Calanus marshallae/glacialis*, and *Metridia pacifica* in the northern Bering and southern Chukchi Seas during June of 2017 and 2018. For all taxa, instantaneous growth rates generally decreased with increasing copepodite stage, though the differences between most stages was not significant. The growth rates for *Pseudocalanus* spp. averaged 0.03 ± 0.002 day^{-1}, *Calanus* spp. 0.09 ± 0.004 day^{-1}, and *M. pacifica* 0.05 ± 0.03 day^{-1}. Egg production rates increased with prosome length for all species, but when standardized to body weight this trend reversed. All *Pseudocalanus* species had similar weight-specific egg production (SEP): 0.18 ± 0.01 for *P. acuspes*, 0.15 ± 0.00 for *P. newmani*, and 0.11 ± 0.02 for *P. minutus*. The SEP for *Calanus* was considerably lower, 0.09 ± 0.01, while for *M. pacifica* it was 0.11 ± 0.01. These rates suggest considerable discrepancies between growth rates and egg production weights that we propose are due to differences in life history strategies. *Pseudocalanus* reproduce nearly year round, they appear to invest less in somatic growth, preferring to quickly reach their adult stage where they invest heavily into reproduction. *Calanus* spp. have 1 or possibly 2 generations per year in this region, they invest more into somatic growth in order to ensure their population is ready for a reproductive season timed to the spring phytoplankton bloom. The more omnivorous *M. pacifica* is also likely limited to 1 or 2 generations, although their ability to thrive on a wider range of food sources than *Calanus* seems to allow for relatively higher investment in reproduction and perhaps lower investment in somatic growth. Consistent with other studies, global growth models do not match our observations particularly well, likely because they are dominated by egg production estimates at lower latitudes.

INTRODUCTION

On the Bering and Chukchi Sea shelves, copepods are the primary component of mesozooplankton and provide an important link in the transfer of energy from primary production to higher trophic levels (Questel *et al.*, 2013; Ershova *et al.*, 2015). Despite this, few direct measurements of copepod production rates have been completed in this region (Vidal and Smith, 1986). Direct rate measurements of the predominant zooplankton are necessary to understand both their grazing potential on primary production and how much energy, in the form of zooplankton, may be available for higher trophic levels.

The Bering and Chukchi Sea shelves are shallow, seasonally ice covered and have extraordinarily productive spring algal blooms, fueled by the input of nutrient-rich waters of the Anadyr Current that originate on the outer Bering Sea, with general northern water transport through the region (Weingartner *et al.*, 2005; Walsh *et al.*, 1989). This region is currently experiencing rapid change, with decreasing winter ice cover, earlier break-up and generally warmer waters, particularly in the northernmost areas (Wood *et al.*, 2015). Impacts of this warming on the ecosystems are yet to be fully understood, and it is possible that the future ecosystem will become increasingly similar to the subarctic North Pacific with Arctic taxa displaced northward (Overland and Stabeno, 2004; Huntington *et al.*, 2020; Sasaki *et al.*, 2016). Due to challenges of accessibility to this region during ice breakup, most studies have occurred during summer and autumn. Thus, there is a general lack of prior observations during the bloom period, and in particular how copepod populations respond during these times.

The predominant mesozooplankton in this high-latitude region are the calanoid copepods *Calanus* spp., *Pseudocalanus* spp., and *Metridia pacifica*. The large bodied, lipid-storing *Calanus* often encompass the highest proportion of the zooplankton biomass depending on the time of the year, whereas *Pseudocalanus* are generally the most abundant zooplankter (Questel *et al.*, 2013; Hopcroft *et al.*, 2010; Eisner *et al.*, 2013). All of these copepods, particularly *Calanus*, are capable of considerable lipid storage, and therefore are important nutritional prey sources for higher trophic levels, as well as for the transfer and repackaging of carbon from primary production (Springer and Roseneau, 1985; Lane *et al.*, 2008). Therefore, *Calanus* and *Pseudocalanus* have been the genera targeted for many zooplankton studies in high latitude regions (e.g. Ershova *et al.*, 2017; Plourde *et al.*, 2005; Smith and Vidal, 1986). The diel migrator *Metridia pacifica*, although less abundant in this system, is also capable of relatively

high lipid storage and may play a role in the daily transfer of carbon within the water column (Takahashi *et al.*, 2009).

In this region there are two co-occurring and morphologically indistinguishable *Calanus* species: *C. marshallae* and *C. glacialis*. Their distributions are largely driven by water transport, with *C. glacialis* generally found in colder Arctic waters and *C. marshallae* in warmer Pacific waters (Nelson *et al.*, 2009). Both species have a life-cycle timed to take advantage of the large phytoplankton bloom that occurs during spring, when they ascend from depth and begin to produce eggs (Conover, 1988). As bottom depths on the Bering and Chukchi shelves are primarily less than 50 m, it is likely that these species overwinter elsewhere and get transported into this region as they arise from depth. *Pseudocalanus* is also a species complex, comprised of *P. minutus*, *P. acuspes*, *P. newmani* and the scarcer *P. mimus* (Questel *et al.*, 2016). These species cannot be morphologically distinguished at the copepodite stages, other than crudely by size. These species also associate well with oceanographic regions, where *P. acuspes* and *P. minutus* are circumpolar species associated with Arctic water and *P. newmani* and *P. mimus* are temperate species common in the North Pacific waters (Ershova *et al.*, 2017). This genus reproduces year round, although production peaks at times with high algal production (Napp *et al.*, 2005). The omnivorous species *Metridia pacifica* often accomplishes 2-3 generations per year in the subarctic Pacific, although due to the cold Bering Sea temperatures and short season in this region they are likely limited to one or two (Padmavati and Ikeda, 2002; Batchelder, 1985), with egg production peaking during spring and summer (Hopcroft *et al.*, 2005).

Copepods have a complex determinate biphasic life-cycle comprised of 6 naupliar stages and 6 copepodite stages, including the final adult stage. The time spent at each life stage varies by species, and can be influenced by water column temperature and food concentration (Bunker and Hirst, 2004; Hirst and Bunker, 2003; Campbell *et al.*, 2001). The vast majority of direct rate measurements for all copepod taxa are egg production measurements (Hirst and Lampitt, 1998). While egg production rates are easy to measure, they are not necessarily representative of growth rates for juvenile stages (Hopcroft and Roff, 1998). Therefore, region-specific measurements of rates specific over the entire copepod lifecycle are needed to understand secondary production within the context of a rapidly changing Pacific Arctic.

To address these gaps, we experimentally determined egg production and somatic growth rates for *Pseudocalanus* spp., *Calanus* spp., and *Metridia pacifica* in the northern Bering and

southern Chukchi Seas during June of 2017 and 2018. These rates add to our understanding of the life-history of these taxa, as well as providing valuable information as to the ecological importance of these taxa in this region during the under-studied spring bloom.

METHODS

Experiments were conducted during cruises on the R/V *Sikuliaq* during June of 2017 and June of 2018 in the northern Bering and southern Chukchi seas as part of the Arctic Shelf Growth, Advection, Respiration and Deposition (ASGARD) project (Fig. 1). Zooplankton were collected using a vertically-hauled 60-cm flow-metered twin-ring net fitted with 150-µm mesh. Nets were hauled through the entire water column (depth ranged 30-56 m) at ~0.5 m s^{-1}. Upon retrieval, only the lowest portion of the nets were lightly rinsed with seawater before removing the cod-end. Zooplankton were quickly diluted with seawater and placed in incubators set at ambient sub-surface seawater temperature until further experimental processing could occur. For community analysis, zooplankton were collected with an additional 150-µm tow, rinsed thoroughly then preserved immediately in formalin. A Seabird 911+ CTD on a 24-place rosette of 12 L Niskin bottles was deployed at each station to collect physical, and chlorophyll profiles as well as the water for incubations. For chlorophyll, 1 L water samples were drawn from CTD casts at 10m intervals. Both total and size-fractionated chlorophyll samples were filtered onto 25mm GF/F filters. Filters were immediately frozen at -80°C aboard ship and transferred frozen back to the laboratory for analysis. Filters were extracted for 24hr in 90% acetone in darkness at -20°C, with chlorophyll *a* and phaeopigment concentrations determined fluorometrically by acidification (Welschmeyer, 1994) with a Turner Designs AU-10 calibrated with purified chlorophyll *a* (Turner Designs).

Community Composition

Samples to document initial communities were processed post-cruise to determine copepod species abundance, composition and biomass. Species-specific (or morphologically similar) length-dry-weight regressions were used to estimate biomass (Questel *et al.*, 2013 - see below). Samples were divided using a Folsom splitter until the smallest fraction contained about 100 organisms. We identified each organism to the lowest taxonomic level possible then counted, staged, and measured them (Roff and Hopcroft, 1985). Increasingly larger fractions

were processed for less abundant taxa, with between 400-600 individual organisms identified from each sample. Only data for the copepods are presented here.

Artificial Cohort

Experiments were conducted to measure copepodite growth rates using the artificial cohort method (Liu and Hopcroft, 2006a; Kimmerer and McKinnon, 1987). Experiments were conducted at all 10 stations during 2018, but only 9 stations (excluding DBO 2.4) during 2017.

Zooplankton from each net tow were size fractioned to create cohorts, using gentle wet sieving, into fractions of 1000-1300, 800-1000, 600-800, 500-600, 400-500, 300-400, 200-300, and 150-200 µm (Liu and Hopcroft, 2008, 2007). A 250 µm sieve was added during 2018, creating 200-250 and 250-300 µm size classes. After creation, each size fraction was then split in two, with half being immediately preserved in formalin.

The other half was incubated for 8-10 days, dependent on available ship time. The incubations occurred within 20 L soft-sided transparent plastic cubic carboys with plankton size-classes diluted using 150-µm pre-screened seawater collected from 10 m depth, where we assumed there was sufficient chlorophyll and nutrients to sustain the incubation. Each size fraction was dispersed across multiple carboys, with the visually-estimated planktonic biomass within the fraction determining how much dilution was necessary. The three dozen carboys employed in each experiment were placed in 1 m^3 insulated commercial fish totes with a constant flow of ambient surface seawater to maintain oceanic temperatures. Water temperatures within the totes were continuously recorded during the incubations using Hobo Tidbits (Onset Inst.). At the end of the incubation the plankton were screened onto 64 µm Nitex and preserved in formalin. The target copepod species were identified and staged, and their prosome lengths (PL) were measured (Roff and Hopcroft, 1985). In addition to the cohort experiments, at 4 stations during 2017 and 7 stations during 2018 individual *Calanus* spp. were live sorted from an additional 150-µm vertical net tow, then dependent upon stage, 35-250 individuals were incubated per carboy and processed as described above.

Weights were predicted using relationships between prosome length and dry weight (DW) established for the region, with the same relationship being applied to all copepodite stages. In both years three copepod genera were numerous enough to calculate growth rates; *Calanus, Metridia* and *Pseudocalanus*. *Calanus* DW was calculated using: $\log_{10}$ DW = 4.024*log PL – 11.561 (Liu and Hopcroft, 2007), *Pseudocalanus* DW was calculated using:

$\log_{10}DW = -7.62 + 2.85*\log_{10}PL$ (Liu and Hopcroft, 2008), and *Metridia* DW calculated using $\log_{10}DW = -8.75 + 3.29*\log_{10}PL$ (Liu and Hopcroft, 2006a). The DW of the average-lengthed individual for each species from the start and end of each incubation were used to calculate the daily growth rate, using the following equation: $g = (\ln W_1 - \ln W_0)\, t^{-1}$, where W_0 is the starting weight, W_1 is the weight at the end of the incubation, and t is the number of days of the incubation. The largest size fractions often did not have an adequate number of animals and were not employed. Growth rates are only presented for experiments where there were a minimum of 30 total copepodites in both the start and end samples, and where apparent mortality was less than 50% (average mortality < 20%).

Egg Production

Egg production experiments were conducted for *Pseudocalanus minutus*, *P. acuspes*, and *P. newmani* during 2017 (n=9) and 2018 (n=10), and for both *Calanus* spp. (n=5) and *Metridia pacifica* (n=6) during 2018 only. Adult female copepods were sorted from the150-µm vertical nets. Water for the incubation was collected from 10 m depth when possible, but occasionally water from 4 m was used. All water was screened through a 150 µm mesh prior to incubation.

For *Pseudocalanus* spp., ~120 sac-less females randomly sorted from each station were placed individually into 70 ml flasks (Napp *et al.*, 2005) incubated under subdued light inside a 4° C walk-in incubator. Copepods were checked every 24 hours for 3 days. Females that had produced egg sacs by the checkpoints were removed and individually preserved with formalin. After three days, all females that had not produced were preserved as a group. All females were later identified to species, their prosome lengths were measured, and the number of eggs produced was counted.

For *Calanus* spp. (n ~ 20 per experiment) and *M. pacifica* (n = 25-48 per experiment), single adult females were placed into 70 ml egg towers within 6-place multiwell trays (Hopcroft *et al.*, 2005). The towers were fitted with a 200 µm mesh allowing eggs to fall through the mesh and be separated from the females during the incubation to prevent damage or cannibalism. Incubations were run for 24 hours, at the end of which the females were preserved in formalin. *Calanus* spp. eggs were preserved with their parent, while *M. pacifica* eggs were counted and their developmental condition noted at the termination of each incubation (Hopcroft *et al.*, 2005). Female prosome lengths were measured from all preserved animals.

Egg production rate (EPR) was calculated using: EPR = (average clutch size*percentage females producing clutch)/experiment duration (days). For *Pseudocalanus* spp., egg production was calculated for experiments with at least 10 individuals within a species. Using egg sizes/weights from previous studies in the Chukchi (Ershova *et al.*, 2017), weight specific egg production rate (SEP) was calculated by taking the ratio of the clutch weight and average weight of the females for each species.

All statistical analyses were performed with R (Version 4.0.2).

RESULTS

Community & stage distribution

During 2017 *Neocalanus flemingeri* had the highest biomass relative to the other calanoid copepods, followed closely by *Pseudocalanus*, then *Calanus, N. cristatus,* and *Metridia*, but the abundance was dominated by *Pseudocalanus* spp. (Table I). The *N. flemingeri* population was primarily composed of copepodite stage-5 (CV), a pre-diapause phase that precluded their use for growth rate or egg production studies (Mackas and Tsuda, 1999). During 2018, *Pseudocalanus* spp. had both the highest biomass and abundance of the copepods, followed by biomass for *Calanus*, *Metridia* and *Neocalanus*. The only other copepod taxa of notable abundance or biomass were *Acartia longiremis* and *Oithona similis*.

In both years the communities were primarily dominated by CI-CV of *Pseudocalanus* spp., *Metridia pacifica* and *Calanus* spp., rather than adults (Figure 2). No clear spatial patterns were observed during either year for any taxa. During 2017 there were higher proportions of CI-III, particularly for *Metridia* and *Calanus*, whereas during 2018 more CIV through adults were present. *Pseudocalanus* generally had the most variability in stage distribution, whereas *Metridia* and *Calanus* tended to have more consistent stage distribution within each cruise.

Somatic Growth Rates

For all taxa, growth rate tended to decrease as stages increased (Figure 3). For *Calanus*, mean stage duration and growth rates with their respective standard errors from the artificial cohort experiments were 8.10 ± 0.36 days and 0.09± 0.004 day^{-1}, respectively. For the stage-selected *Calanus,* mean stage duration and growth rates were 5.85 ± 0.45 days and 0.09 ± 0.006 day^{-1}, respectively, with some variability across stages (Table III). There were no significant differences between the growth rates from the artificial cohort and stage selected *Calanus*

experiments. There were relatively few experiments where *Metridia* were present in high enough abundances to obtain growth rates, however the observed mean stage duration and growth rates were 4.55 ± 0.52 days and 0.05 ± 0.003 day^{-1}, respectively, again with minor variability across stages (Table IV). The high abundance of filamentous algae at most sampling stations interfered with *Pseudocalanus* being well-sorted into cohorts having a distinct single-stage dominance. Most of their cohorts had 2-3 stages with similar abundances, therefore the rates presented reflect a greater mixture of stages for *Pseudocalanus* than for the other taxa. The mean stage duration and growth rates for *Pseudocalanus* were 8.28 ± 0.41 days and 0.03 ± 0.002 day^{-1}, respectively. For *Calanus* and *Pseudocalanus*, an ANOVA revealed significant differences between CIV and younger stage copepodites, but no differences between the CI-CIII stages, while *Metridia* had no significant difference between stages. An ANOVA showed significant differences ($p < 0.05$) between growth rates of *Calanus* and *Pseudocalanus* at all stages, and significant differences between *Metridia* and *Calanus* at all stages. There were no significant differences between *Pseudocalanus* and *Metridia* growth rates.

Growth Rate Drivers

The average temperature during the incubations ranged from 4-5.6°C. Chlorophyll concentrations from the experimental stations ranged from 0.5-6 µg/L. There was no significant relationship between growth rates and temperature or chlorophyll for either *Calanus* or *Pseudocalanus* (Fig. 4). Due to the low number of rates measured for *Metridia,* a comparison of environmental factors to the rates was not undertaken.

For *Calanus*, CI growth rates from the aritifical cohort experiments had a positive linear relationship with average prosome length from the initial experiment, and CIV growth rates from the picked stage experiments had a negative relationship (Figure 5). While such relationships for the other stages was not significant, CI and CII's tended to have a positive relationship between prosome length and growth rate, whereas CIII and CIV's had slight negative relationships.

Egg Production

Clutch size increased as prosome length increased, both within a species and across genera (Fig 6). For *Pseudocalanus* species, egg production rates generally increased with prosome length within the genus, hence *P. newmani* produced the fewest eggs per female and *P. minutus* produced the most (Figure 6). When standardized to weight (i.e. SEP), there was no statistical difference between the *Pseudocalanus* species, with a mean SEP of 0.15 ($p > 0.05$).

For *P. newmani*, mean EPR was 2.32 ± 0.40 day^{-1}, and mean SEP was 0.15 ± 0.00 day^{-1}. For *P. minutus*, mean EPR was 6.67 ± 0.77, and mean SEP was 0.10 ± 0.01. For *P. acuspes,* mean EPR was 4.64 ± 0.26, and mean SEP was 0.18 ± 0.01. *Pseudocalanus* egg production did not have any clear spatial variance, although for all taxa SEP was slightly higher in 2017 than 2018 (Figure 7). The mean EPR and SEP for *Calanus* were 39.7 ± 3.54 and 0.09 ± 0.01, respectively, and for *Metridia* 27.4 ± 1.92 and 0.11 ± 0.01. Between species the only significant difference in SEP was between *Calanus* and *Pseudocalanus*. There was no significant relationship to water column temperature or sampling site chlorophyll concentration for any of these rates.

DISCUSSION

During the 2017 and 2018 spring blooms, the northern Bering and southern Chukchi seas had low diversity copepod communities similar to those reported during summer and fall, with the highest biomass contributed by *Neocalanus flemingeri*, *Calanus* spp., *Pseudocalanus* spp. and *Metridia pacifica* (Questel *et al.*, 2013; Ershova *et al.*, 2015; Eisner *et al.*, 2013; Matsuno *et al.*, 2011). In both years the higher biomass and abundance of copepodite stages rather than adults emphasizes the importance of directly measuring copepodite rates rather than assuming that adult production predominates and provides an adequate proxy for copepodites. *Calanus* spp. and *Metridia pacifica* had similar total biomass, although *M. pacifica* had similar adult and copepodite biomass whereas *Calanus* spp. biomass was primarily as copepodites, likely reflecting differences in how each exploits the spring bloom. Although *Oithona similis* was present in high abundance during both years, their small size limits their contribution to the biomass, and also prevented us from measuring their rates with our experimental design.

For *Calanus* spp., *Pseudocalanus* spp. and *M. pacifica*, within the copepodite stages we found a general decrease in growth rates as the copepodite stages increased, as has been shown previously with these taxa (Liu and Hopcroft, 2007, 2006a, 2008). The prodigious amounts of filamentous algae that prevented clean sorting of *Pseudocalanus* by stage for these experiments likely weakened the observed strength of relationship between growth rate and stage (Table III). Additionally, although the data is more limited for *M. pacifica*, the pattern of lower growth rates at older copepodite stages also emerges for this species, consistent with previously published rates (Table IV).

The apparent correlation between copepod body size and their growth rates, with the large-bodied *Calanus* presenting the highest average growth and *Pseudocalanus* the lowest (Fig.

3), is best explained by differences in life-history strategies. For *Calanus*, despite considerable scatter in growth rates for the younger copepodite stages (CI) growth correlated positively with prosome length (Fig. 5). This within-stage pattern has been observed previously for copepodite growth rate of *Neocalanus* spp., (Liu and Hopcroft, 2006b), another large-bodied sub-arctic copepod. It is probable that size and growth are more dependent on environmental variables during the earlier stages, such that smaller copepodites within a stage are a reflection of poorer conditions for growth, while larger size reflects better growth. Thus, copepods that already had low body condition, then were placed into incubation, likely struggled to grow faster by their next molt. The growth rates determined from the artificial cohort experiments matched relatively well with the rates determined from the stage selected experiments, further indicating that the more time-efficient artificial cohort method is a useful way of determining these rates (Liu *et al.*, 2013).

Within each species, body size appeared to be a main driver for clutch size. Across all taxa there was a trend to have increased eggs per female per day (EPR) with larger body size, yet when egg production was standardized to female weights (SEP), the rates among all the taxa became relatively similar. Although there was no correlation to temperature or chlorophyll for these rates, the former is not surprising given the limited thermal range, whereas preponderance of large filamentous algae during our experiments may have made chlorophyll a poor proxy for the availability of suitable-sized food. It is likely that most copepods were food satiated during these experiments, due to the pronounced spring phytoplankton bloom that occurred concurrent with our sampling.

In general, the growth rates we measured in the Pacific Arctic were lower than those determined for the same taxa in the North Pacific (Gulf of Alaska). It is possible that this is due to colder average temperatures in our study region, although many of the North Pacific rates were Q_{10}-corrected to a similar temperature as occurred in or study, such correction can introduce errors (Liu and Hopcroft, 2007, 2006a, 2008). The *Pseudocalanus* species complex has been the most studied in regards to egg production in this region, likely due to the relative ease of performing the experiments, but such measurements come primarily from summer and fall. Some of the *Pseudocalanus* SEP measured at similar temperatures to ours in this region during early fall (Hopcroft *et al.*, 2010) are only slightly lower than the rates we measured in spring, but others run at colder temperature are substantially lower (Ershova *et al.*, 2017; Lee *et al.*, 2003).

Notably, our EPR is in the lower range measured for these taxa in the North Pacific and southeastern Bering Sea (Napp *et al.*, 2005; Vidal and Smith, 1986). It is therefore likely that a combination of longer-term seasonal variation in food and temperature are driving these rates. While *Calanus* egg production measurements at cold temperatures in our region are limited in number, it has been shown that spring egg production is higher than in summer in the Chukchi and Beaufort Seas (Plourde *et al.*, 2005), likely reflecting the dependence of the *Calanus* lifecycle on the extensive spring bloom in this region. Our rates for *Calanus* egg production were slightly lower than those from the Gulf of Alaska, in part due to colder temperatures, but higher than those measured for the Pacific Arctic (Plourde *et al.*, 2005), likely due to warmer temperatures and presumed food satiation. The growth rates for *Calanus* are surprisingly similar to those measured in the Gulf of Alaska when standardized to similar temperatures (Liu and Hopcroft, 2007). It is however noted that although the Gulf of Alaska rates include measurements throughout spring and summer, they are primarily from the spring bloom period, similar to the rates presented here. For *Metridia pacifica*, our egg production rates are similar to the few rates that have been measured, without apparent differences due to seasonality.

When comparing growth rates to past studies of these taxa, methodology differences become important. The benefits and shortcomings of a variety of methods for estimating growth has been discussed previously (Kimmerer *et al.*, 2007), and it is difficult to determine whether differences in measured rates are due to methodology, location, or environmental conditions. Artificial cohort measurements are rare, and for high latitudes are limited to the Gulf of Alaska, and now the Bering and Chukchi Seas. This complicates any discussion comparing the *in-situ* artificial cohort experiments to laboratory measurements of somatic growth. Overall there are relatively few measurements for the species presented here, but measurements of the same genera are largely available for *Calanus* and *Pseudocalanus* (e.g. Campbell *et al.*, 2001; Vidal, 1980a, 1980b; Smith and Vidal, 1986). When grown at different temperatures, *P. newmani* and *M. pacifica* development time increased with decreasing temperature, indicating potentially different generation times in temperate regions (Lee *et al.*, 2003; Padmavati and Ikeda, 2002). For *C. marshallae*, laboratory growth measurements at 10° C averaged 6.9% body weight per day, which is slighter lower than the estimates presented here (Peterson, 1986). It is likely the lower investment in growth in that study is due to the warmer temperatures, as well that ecosystem's longer productive period.

There were discrepancies between somatic growth rates and the adult egg production rates for all these taxa, and it is clear that the different species are utilizing different life history strategies in terms of where they invest their energy. The large-bodied *Calanus* presented the highest somatic growth rates out of all of the taxa (~15% d^{-1} maximum), but had relatively lower SEP (avg. 9% d^{-1}), although the average growth rate and SEP were not significantly different, likely due to the low growth rates for late-stage copepodites. The small bodied *Pseudocalanus* had considerably lower somatic growth rates (~4 % d^{-1} at the highest), but significantly higher SEP (11-18% d^{-1}). The rates for the omnivorous *M. pacifica* fell between *Calanus* and *Pseudocalanus* for both growth and egg production.

This suggests that *Calanus*, a genus that times its reproductive cycle to take advantage of the seasonal bloom production (e.g. Baier and Napp, 2003), is investing more into somatic growth daily than egg production. Since high-latitude *Calanus* diapause, they must prioritize growth to reach a body size that can contain enough lipids to survive overwintering without feeding. It has been suggested that both *C. glacialis* and *C. marshallae* have a one year lifecycle on the Bering Sea shelf (Baier and Napp, 2003), although in the northern Bering Sea and Arctic they appear to have a two year lifecycle (Smith and Vidal, 1986; Ashjian *et al.*, 2003). In general, high latitude *Calanus* appears to reproduce in late winter and spring, possibly feeding on the ice algae bloom (Durbin and Casas, 2014) while early copepodite development occurs during summer (Ashjian *et al.*, 2003; Peterson and Du, 2015). Thus, *Calanus* diapausing CV's awake, molt to adults and produce eggs during this early productive period, so that younger copepodites can take advantage of the bloom and continue their development throughout summer. Although the bulk of their reproduction appears to be timed to utilize the spring bloom, it has been suggested that late summer or autumn blooms may trigger a second pulse of reproduction (Vidal and Smith, 1986). In the scenario of an autumn bloom it is particularly important for the copepodites to invest heavily into growth in order to reach a lipid storing stage, then load up with lipids to survive the limited food resources during winter.

On the other hand, *Pseudocalanus* invests much less into somatic growth, instead aiming to reach their small adult body size using limited energy, then invest heavily into reproduction whenever there is adequate food. SEP measured in fall in previous studies for *Pseudocalanus* (Ershova *et al.*, 2017; Hopcroft *et al.*, 2010) is only slightly lower than what we measured during spring, indicating sustained investment in reproduction throughout summer and into autumn,

though a slight peak in spring has been indicated for these taxa (Renz *et al.*, 2007). It has been suggested that *Pseudocalanus* have favored slow growth rates to allow for sustainable growth at low chlorophyll levels while maintaining similar development times to other species (Liu and Hopcroft, 2008). This strategy allows them to reliably complete their life cycles under limited food conditions. Therefore, *Pseudocalanus* is prepared to take advantage of any favorable conditions through reproduction, where their apparent energy investment is greatest. Furthermore, their small adult body-size and egg-carrying strategy leads to low predation rates both on the female and their eggs (Hirst and Kiørboe, 2002). It is notable that the different *Pseudocalanus* species directed similar proportionate energy towards egg production, yet they may still occupy slightly different niches and thereby experience different reproductive success under varying oceanographic conditions (Ershova *et al.*, 2017; McLaren *et al.*, 1989).

Metridia pacifica seems to fall somewhere between *Calanus* and *Pseudocalanus*, with average growth rates falling between the two other taxa, and SEP similar to the lower range of *Pseudocalanus*. While *M. pacifica* are larger than the *Pseudocalanus*, and therefore must invest more energy into growth to reach their adult stage, they are a omnivorous species (Campbell *et al.*, 2016; Batchelder, 1985), which may allow them a more extended period where egg production is possible than *Calanus*. It is possible that at these high latitudes *Metridia pacifica* focuses their egg laying to short periods of time optimized to ideal food conditions (Batchelder, 1985), although the Arctic species *Metridia longa* is thought to have the ability to continually reproduce throughout the year (Ashjian *et al.*, 2003). In the North Pacific, *M. pacifica* have been found to have two or three generations per year (Padmavati and Ikeda, 2002; Batchelder, 1985), though at these high latitudes with extreme seasonality they are likely limited to one to two generations. With this limited growing season, they must invest considerable energy into growth to reach their adult stage in time for spawning in fall, or to be at a later, lipid-storing stage in time to overwinter with limited food. It has been noted that the survival of *M. pacifica* eggs during spring is generally low (Halsband-Lenk, 2005; Hopcroft *et al.*, 2005), potentially due to alleochemicals in diatom prey (e.g. Halsband-Lenk, 2005). If we assume this is also the case in the Pacific Arctic, then it is possible that *Metridia* must continue their investment into reproduction throughout a portion of summer to offset low recruitment during the spring bloom. It is uncertain whether the population of *M. pacifica* seen on the Bering and Chukchi shelves are

actually transported to deep waters where they can overwinter, or whether they are advected northward and do not survive, as they are not seen in the higher Arctic .

Despite the notable differences in copepodite growth rates and egg production, and their lack of predictable differences between them, the latter often forms the basis for commonly used global models of copepod production (Hirst and Lampitt, 1998; Hirst and Bunker, 2003). It has already been shown that these models may not match well with direct measurements of somatic growth for the copepodite stages for the species discussed (Liu and Hopcroft, 2007, 2006a, 2008). Rates calculated from these global models, or rates determined at different oceanographic regions, are often used for secondary production estimates but may not result in sufficiently accurate production predictions. Global models are primarily based on egg production (Hirst and Lampitt, 1998), and we show here that egg production and somatic growth rates have substantial differences dependent on the species. For the larger, broadcast spawning species *Calanus* and *Metridia*, egg production rates underestimate production, since juvenile growth rates are higher. For the small sac-spawner *Pseudocalanus,* egg production rates overestimate production, because these species invest more energy into egg production rather than growth.

Additionally, region specific rate measurements are preferable to model estimates, given the impact that environmental variables have on rates (Hirst and Lampitt, 1998). While rates determined at warmer locations can be corrected to cold temperatures using a Q_{10} correction, this introduces an unknown amount of error, given our lack of certainty in the value of Q_{10} that should be applied (Hirst and Bunker, 2003). For comparison to global models (Hirst and Bunker, 2003), using their Q_{10} of 2.7 to standardized to 4°C and our initial weight in each experiment, we predicted model growth rates. For *Calanus*, model estimates for our sampling period for juvenile broadcaster growth rates are 0.09 ± 0.003 day^{-1}, and for adults 0.02 ± 0.002 day^{-1}, that matches with our average juvenile estimates surprisingly well but severely underestimates adult production. This model underestimates *Metridia* juvenile and adult growth, estimating broadcaster rates of 0.08 ± 0.04 day^{-1} for juveniles and 0.04 ± 0.01 day^{-1} for adults. For the sac-spawner *Pseudocalanus*, as expected this model overestimates juvenile production as 0.06 ± 0.01 day^{-1}, but underestimates adult production as 0.08 ± 0.003, which is off by nearly a factor of two.

CONCLUSIONS

We observed that *Calanus* spp., *Pseudocalanus* spp., and *Metridia pacifica* biomass was primarily comprised of copepodites rather than adults during June of 2017 and 2018 within the

northern Bering and southern Chukchi Seas. This is particularly relevant when estimating production because, since we demonstrate that copepodite growth rates can differ substantially from egg production rates for these taxa. The relative differences between adult and juvenile production are not universal and appears to reflect differences in life history strategies employed by different taxa. The large bodied *Calanus* invest considerable energy into growth in order to reach lipid storing CV copepodite stages that are able to diapause by late summer, then emerge to time their reproductive period to the spring bloom. Alternatively, the small-bodied *Pseudocalanus* invest much less into growth, focusing on reaching adulthood where they are primed to invest heavily into reproduction whenever condition allow, regardless of time of year. The life history strategies of *M. pacifica* are less certain, but they too invest a substantial amount into growth, allowing them to reach latter stages that could overwinter. Simultaneously, *M. pacifica* also have higher egg production rates similar to those of *Pseudocalanus* and reproduce when conditions allow, rather than being focused on only the spring bloom. For *Calanus*, global models of rates matched relatively well with our measured juvenile rates, though they underestimated *Metridia* and overestimated *Pseudocalanus* juvenile rates. Global models underestimated adult production for all taxa, highlighting the importance of having directly-measured regional rate measurements.

ACKNOWLEDGMENTS

I gratefully acknowledge the North Pacific Research Board for providing funding for this project. I thank Russ Hopcroft, Seth Danielson and Kenneth Coyle for their feedback on this manuscript. I would also like to thank fellow students plus the captain and crew of the R/V *Sikuliaq* for their assistance with the field portion of this project.

REFERENCES

Ashjian, C. J., Campbell, R. G., Welch, H. E., *et al.* (2003) Annual cycle in abundance , distribution , and size in relation to hydrography of important copepod species in the western Arctic Ocean. *Deep. Res. I*, **50**, 1235–1261.

Baier, C. T. and Napp, J. M. (2003) Climate-induced variability in *Calanus marshallae* populations. *J. Plankton Res.*, **25**, 771–782.

Batchelder, H. P. (1985) Seasonal abundance, vertical distribution, and life history of *Metridia pacifica* (Copepoda: Calanoida) in the oceanic subarctic Pacific. *Deep Sea Res. Part A, Oceanogr. Res. Pap.*, **32**, 949–964.

Bunker, A. J. and Hirst, A. G. (2004) Fecundity of marine planktonic copepods : global rates and patterns in relation to chlorophyll a , temperature and body weight. *Mar. Ecol. Prog. Ser.*, **279**, 161–181.

Campbell, R. G., Ashjian, C. J., Sherr, E. B., *et al.* (2016) Mesozooplankton grazing during spring sea-ice conditions in the eastern Bering Sea. *Deep. Res. Part II*, **134**, 157–172.

Campbell, R. G., Wagner, M. M., Teegarden, G. J., *et al.* (2001) Growth and development rates of the copepod *Calanus finmarchicus* reared in the laboratory. *Mar. Ecol. Prog. Ser.*, **221**, 161–183.

Conover, R. J. (1988) Comparative life histories in the genera *Calanus* and *Neocalanus* in high latitudes of the northern hemisphere. *Hydrobiologia*, **167**–**168**, 127–142.

Durbin, E. G. and Casas, M. C. (2014) Early reproduction by *Calanus glacialis* in the Northern Bering Sea: the role of ice algae as revealed by molecular analysis. *J. Plankton Res.*, **36**, 523–541.

Eisner, L., Hillgruber, N., Martinson, E., *et al.* (2013) Pelagic fish and zooplankton species assemblages in relation to water mass characteristics in the northern Bering and southeast Chukchi seas. *Polar Biol.*, **36**, 87–113.

Ershova, E. A., Hopcroft, R. R., Kosobokova, K. N., *et al.* (2015) Long-term changes in Summer zooplankton communities of the Western Chukchi Sea, 1945–2012. *Oceanography*, **28**, 100–115.

Ershova, E. A., Questel, J. M., Kosobokova, K., *et al.* (2017) Population structure and production of four sibling species of *Pseudocalanus* spp. in the Chukchi Sea. *J. Plankton Res.*, **39**, 48–64.

Halsband-Lenk, C. (2005) *Metridia pacifica* in Dabob Bay, Washington: The diatom effect and the discrepancy between high abundance and low egg production rates. *Prog. Oceanogr.*, **67**, 422–441.

Hirst, A. G. and Bunker, A. J. (2003) Growth of marine planktonic copepods: Global rates and patterns in relation to chlorophyll a, temperature, and body weight. *Limnol. Oceanogr.*, **48**, 1988–2010.

Hirst, A. G. and Kiørboe, T. (2002) Mortality of marine planktonic copepods: Global rates and

patterns. *Mar. Ecol. Prog. Ser.*, **230**, 195–209.

Hirst, A. G. and Lampitt, R. S. (1998) Towards a global model of in situ weight-specific growth in marine planktonic copepods. *Mar. Biol.*, **132**, 247–257.

Hopcroft, R. R., Clarke, C., Byrd, A. G., *et al.* (2005) The paradox of *Metridia* spp . egg production rates : a new technique and measurements from the coastal Gulf of Alaska. *Mar. Ecol. Prog. Ser.*, **286**, 193–201.

Hopcroft, R. R., Kosobokova, K. N., and Pinchuk, A. I. (2010) Zooplankton community patterns in the Chukchi Sea during summer 2004. *Deep. Res. Part II Top. Stud. Oceanogr.*, **57**, 27–39.

Hopcroft, R. R. and Roff, J. C. (1998) Zooplankton growth rates: the influence of female size and resources on egg production of tropical marine copepods. *Mar. Biol.*, **132**, 79–86.

Huntington, H. P., Danielson, S. L., Wiese, F. K., *et al.* (2020) Evidence suggests potential transformation of the Pacific Arctic ecosystem is underway. *Nat. Clim. Chang.*, 342–348.

Kimmerer, W. J., Hirst, A. G., Hopcroft, R. R., *et al.* (2007) Estimating juvenile copepod growth rates: Corrections, inter-comparisons and recommendations. *Mar. Ecol. Prog. Ser.*, **336**, 187–202.

Kimmerer, W. J. and Mckinnon, A. D. (1987) Growth, mortality, and secondary production of the copepod *Acartia tranteri* in Westernport Bay, Australia. *Limnol. Oceanogr.*, **32**, 14–28.

Lane, P. V. Z., Llinás, L., Smith, S. L., *et al.* (2008) Zooplankton distribution in the western Arctic during summer 2002: Hydrographic habitats and implications for food chain dynamics. *J. Mar. Syst.*, **70**, 97–133.

Lee, H. W. U., Ban, S., Ikeda, T., *et al.* (2003) Effect of temperature on development , growth and reproduction in the marine copepod *Pseudocalanus newmani* at satiating food condition. *J. Plankton Res.*, **25**, 261–271.

Liu, H. and Hopcroft, R. R. (2007) A comparison of seasonal growth and development of the copepods *Calanus marshallae* and *C. pacificus* in the northern Gulf of Alaska. *J. Plankton Res.*, **29**, 569–581.

Liu, H. and Hopcroft, R. R. (2006a) Growth and development of *Metridia pacifica* (Copepoda: Calanoida) in the northern Gulf of Alaska. *J. Plankton Res.*, **28**, 769–781.

Liu, H. and Hopcroft, R. R. (2006b) Growth and development of *Neocalanus flemingeri/plumchrus* in the northern Gulf of Alaska: Validation of the artificial-cohort method in cold waters. *J. Plankton Res.*, **28**, 87–101.

Liu, H. and Hopcroft, R. R. (2008) Growth and development of *Pseudocalanus* spp. in the northern Gulf of Alaska. *J. Plankton Res.*, **30**, 923–935.

Liu, H., Hopcroft, R. R., and Bi, H. (2013) Statistical modeling of copepod growth rates: Comparisons for data collections using the artificial cohort (AC) method. *J. Exp. Mar. Bio. Ecol.*, **448**, 271–280.

Mackas, D. L. and Tsuda, A. (1999) Mesozooplankton in the eastern and western subarctic

Pacific: Community structure, seasonal life histories, and interannual variability. *Prog. Oceanogr.*, **43**, 335–363.

Matsuno, K., Yamaguchi, A., Hirawake, T., *et al.* (2011) Year-to-year changes of the mesozooplankton community in the Chukchi Sea during summers of 1991, 1992 and 2007, 2008. *Polar Biol.*, **34**, 1349–1360.

McLaren, I. A., Sevigny, J. M., and Corkett, C. J. (1989) Temperature-dependent development in *Pseudocalanus* species. *Can. J. Zool.*, **67**, 559–564.

Napp, J. M., Hopcroft, R. R., Baier, C. T., *et al.* (2005) Distribution and species-specific egg production of *Pseudocalanus* in the Gulf of Alaska. *J. Plankton Res.*, **27**, 415–426.

Nelson, R. J., Carmack, E. C., McLaughlin, F. A., *et al.* (2009) Penetration of pacific zooplankton into the western arctic ocean tracked with molecular population genetics. *Mar. Ecol. Prog. Ser.*, **381**, 129–138.

Overland, J. E. and Stabeno, P. J. (2004) Is the climate of the bering sea warming and affecting the ecosystem? *Eos (Washington. DC).*, **85**, 1997–2003.

Padmavati, G. and Ikeda, T. (2002) Development of *Metridia pacifica* (Crustacea : Copepoda) reared at different temperatures in the laboratory. *Plankt. Biol. Ecol.*, **49**, 93–96.

Peterson, W. (1986) Development, growth, and survivorship of the copepod *Calanus marshallae* in the laboratory. *Mar. Ecol. Prog. Ser.*, **29**, 61–72.

Peterson, W. and Du, X. (2015) Egg production rates of the copepod *Calanus marhallae* in relation to seasonal and interannual variations in microplankton biomass and species composition in the coastal upwelling zone off Oregon, USA. *Prog. Oceanogr.*, **138**, 32–44.

Plourde, S., Campbell, R. G., Ashjian, C. J., *et al.* (2005) Seasonal and regional patterns in egg production of *Calanus glacialis / marshallae* in the Chukchi and Beaufort Seas during spring and summer , 2002. *Deep Sea Res. II*, **52**, 3411–3426.

Questel, J. M., Blanco-Bercial, L., Hopcroft, R. R., *et al.* (2016) Phylogeography and connectivity of the *Pseudocalanus* (Copepoda: Calanoida) species complex in the eastern North Pacific and the Pacific Arctic Region. *J. Plankton Res.*, **38**, 610–623.

Questel, J. M., Clarke, C., and Hopcroft, R. R. (2013) Seasonal and interannual variation in the planktonic communities of the northeastern Chukchi Sea during the summer and early fall. *Cont. Shelf Res.*, **67**, 23–41.

Renz, J., Peters, J., and Hirche, H. J. (2007) Life cycle of *Pseudocalanus acuspes* Giesbrecht (Copepoda, Calanoida) in the Central Baltic Sea: II. Reproduction, growth and secondary production. *Mar. Biol.*, **151**, 515–527.

Roff, J. C. and Hopcroft, R. R. (1985) High precision microcomputer based measuring system for ecological research. *Can. J. Fish. Aquat. Sci.*, **43**, 2044–2048.

Sasaki, H., Matsuno, K., Fujiwara, A., *et al.* (2016) Distribution of Arctic and Pacific copepods and their habitat in the northern Bering and Chukchi seas. *Biogeosciences*, **13**, 4555–4567.

Smith, S. and Vidal, J. (1986) Variations in the distribution, abundance, and development of

copepods in the southeastern Bering Sea in 1980 and 1981. *Cont. Shelf Res.*, **5**, 215–239.

Springer, A. M. and Roseneau, D. G. (1985) Copepod-based food webs : auklets and oceanography in the Bering Sea. *Mar. Ecol. Prog. Ser.*, **21**, 229–237.

Takahashi, K., Kuwata, A., Sugisaki, H., *et al.* (2009) Downward carbon transport by diel vertical migration of the copepods *Metridia pacifica* and *Metridia okhotensis* in the Oyashio region of the western subarctic Pacific Ocean. *Deep. Res. I*, **56**, 1777–1791.

Vidal, J. (1980a) Physioecology of zooplankton. I. Effects of phytoplankton concentration, temperature, and body size on the growth rate of *Calanus pacificus* and *Pseudocalanus* sp. *Mar. Biol.*, **56**, 111–134.

Vidal, J. (1980b) Physioecology of zooplankton. II. Effects of phytoplankton concentration, temperature, and body size on the development and molting rates of *Calanus pacificus* and *Pseudocalanus* sp. *Mar. Biol.*, **56**, 135–146.

Vidal, J. and Smith, S. (1986) Biomass, growth, and development of populations of herbivorous zooplankton in the southeaster Bering Sea during spring. *Deep. Res.*, **33**, 523–556.

Walsh, J. J., McRoy, C. P., Coachman, L. K., *et al.* (1989) Carbon and nitrogen cycling within the Bering/Chukchi Seas: Source regions for organic matter effecting AOU demands of the Arctic Ocean. *Prog. Oceanogr.*, **22**, 277–359.

Weingartner, T., Aagaard, K., Woodgate, R., *et al.* (2005) Circulation on the north central Chukchi Sea shelf. *Deep. Res. Part II Top. Stud. Oceanogr.*, **52**, 3150–3174.

Welschmeyer, N. A. (1994) Fluorometric analysis of chlorophyll *a* in the presence of chlorophyll *b* and pheopigments. *Limnol. Oceanogr.*, **39**, 1985–1992.

Wood, K. R., Bond, N. A., Danielson, S. L., *et al.* (2015) A decade of environmental change in the Pacific Arctic region. *Prog. Oceanogr.*, **136**, 12–31.

FIGURES

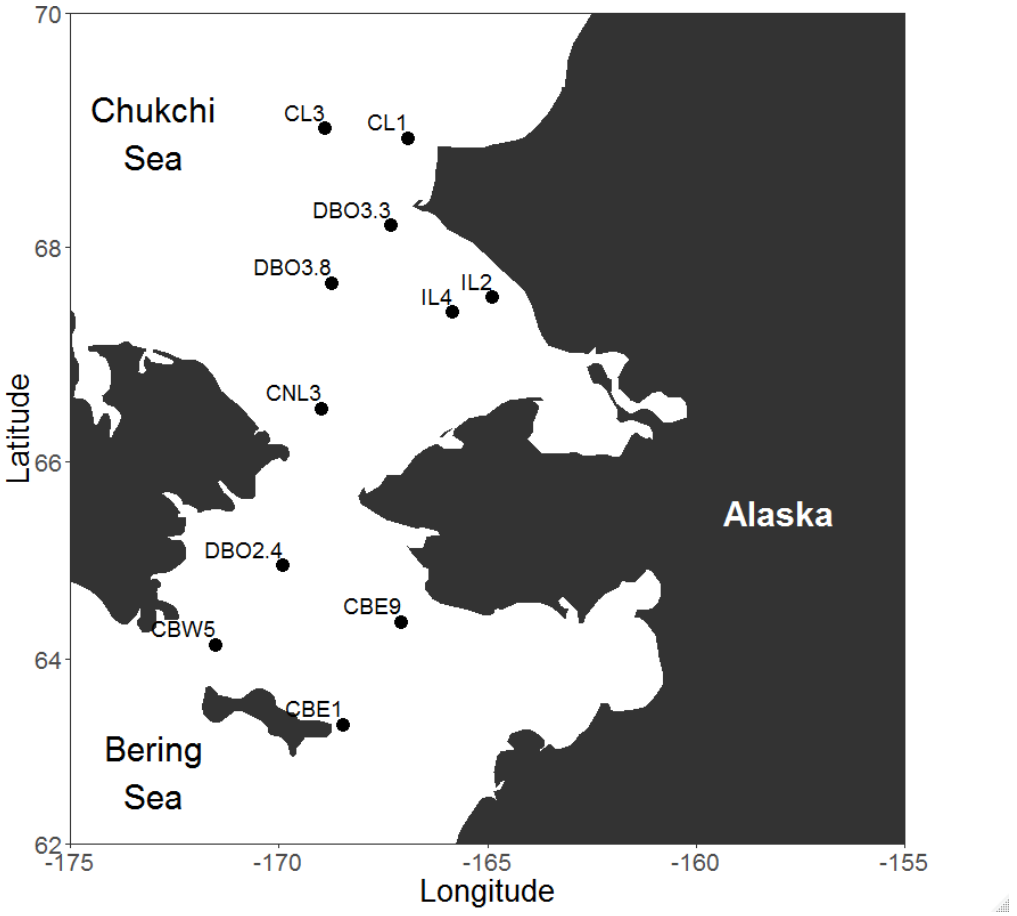

Figure 1: Zooplankton experimental stations for the Arctic Shelf Growth, Advection, Respiration and Deposition project (ASGARD) during 2017 and 2018.

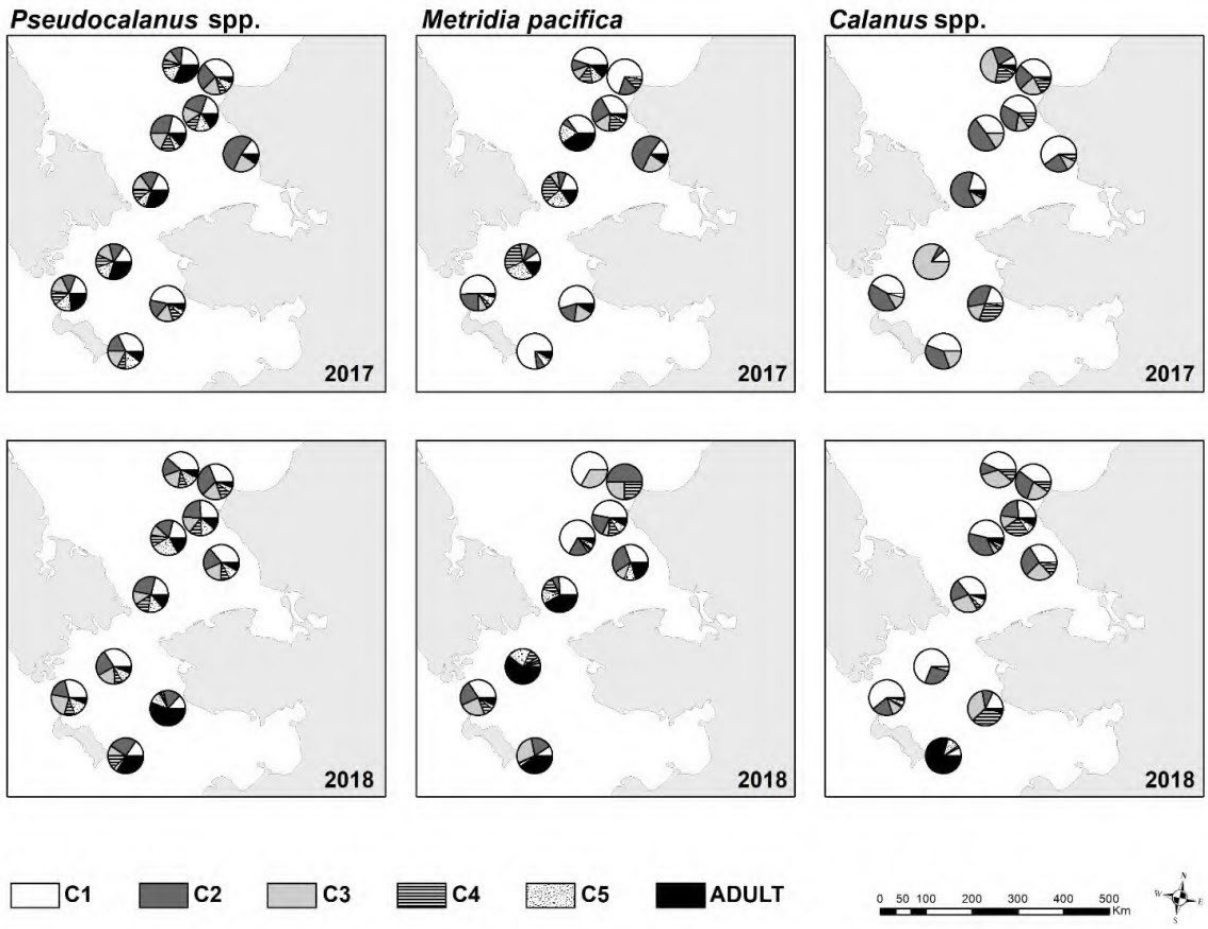

Figure 2: Copepodite abundance for *Pseudocalanus* spp., *Metridia pacifica* and *Calanus* spp. during June 2017 and 2018 in the northern Bering and southern Chukchi Seas

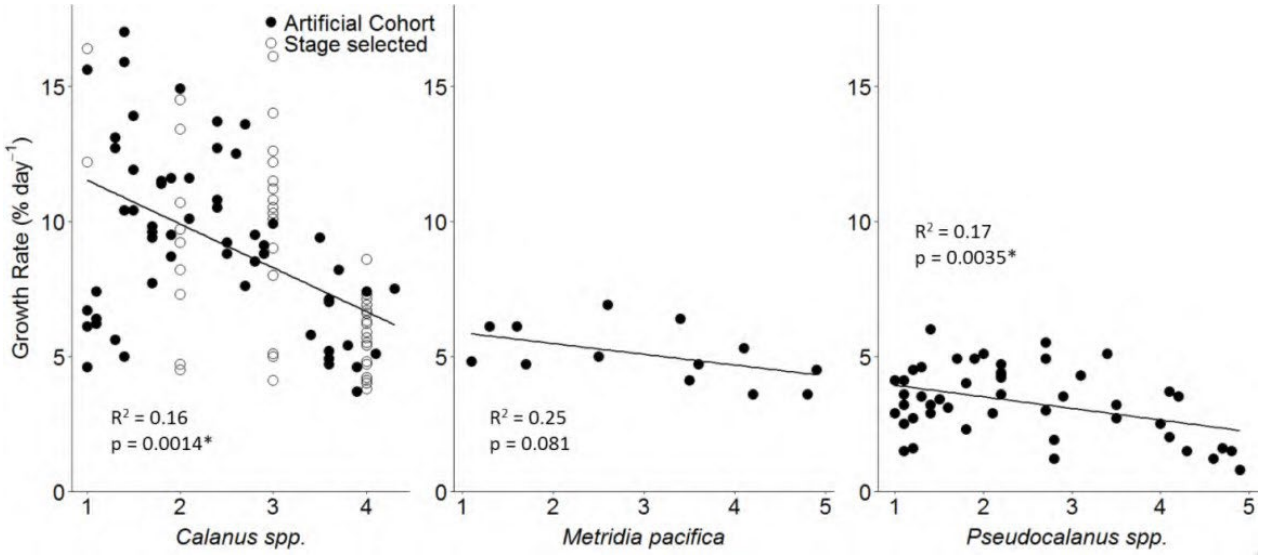

Figure 3: *Calanus* spp., *Pseudocalanus* spp. and *Metridia pacifica* growth rates relative to initial copepodite stage from the artificial cohort experiments (average temperature 4° C) during June 2017 and 2018 in the northern Bering and southern Chukchi seas.

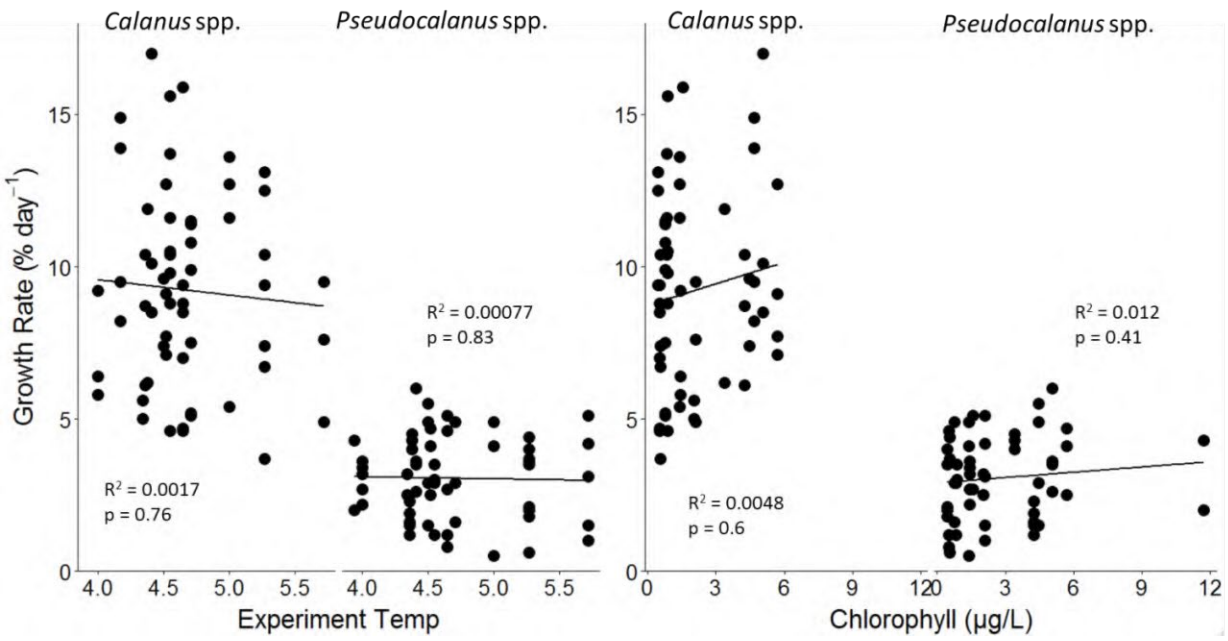

Figure 4: *Calanus* spp. and *Pseudocalanus* spp. growth rates compared to mean experimental temperature and water column chlorophyll from the sampling stations in the northern Bering and southern Chukchi seas during June 2017 and 2018.

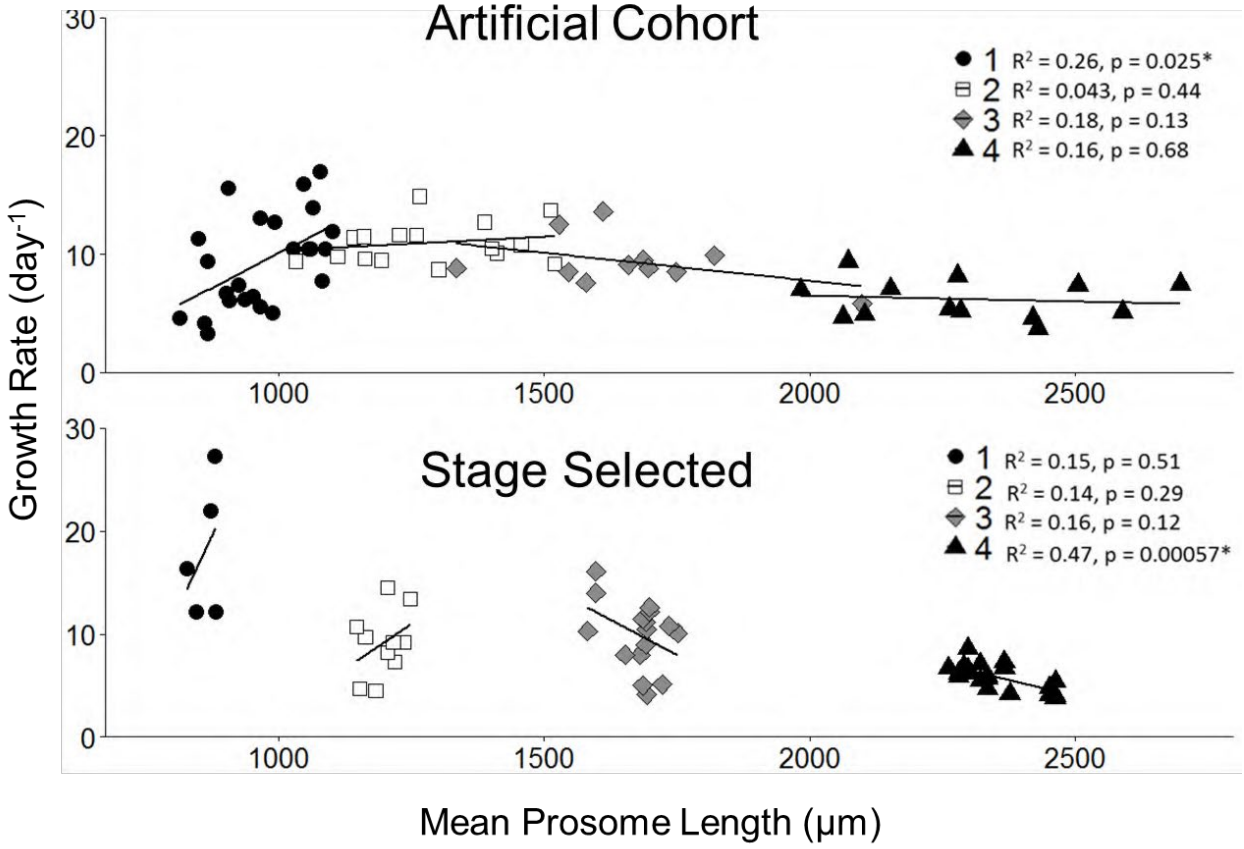

Figure 5: *Calanus* spp. prosome length and growth rate relationship by copepodite stage in the northern Bering and southern Chukchi seas during June 2017 and 2018.

.

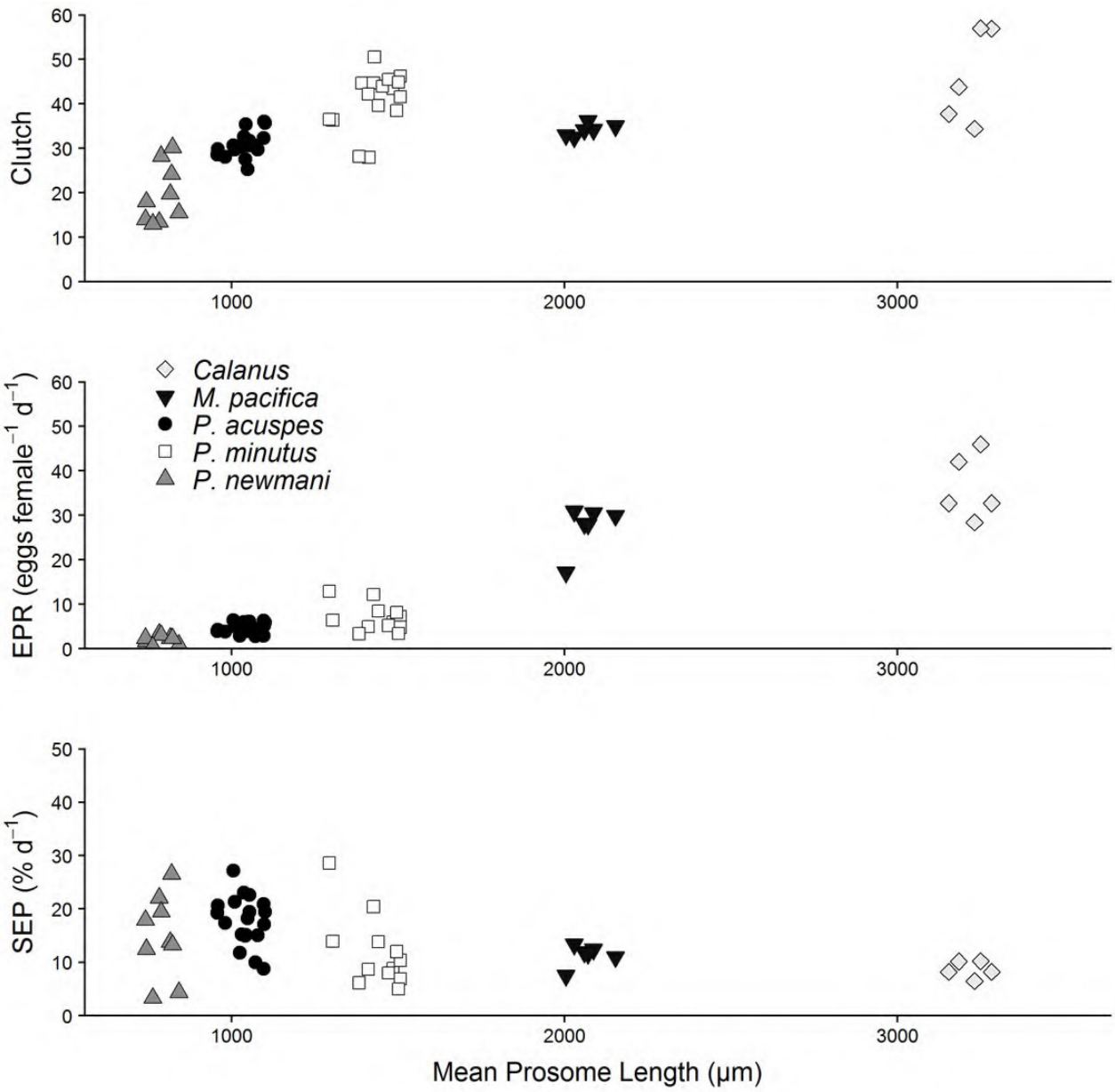

Figure 6: Egg production rates (eggs female^{-1} day^{-1}) and weight specific egg production rates (SEP) compared to prosome length for the three co-occurring *Pseudocalanus* species, *Calanus marshallae/glacialis*, and *Metridia pacifica* in the northern Bering and southern Chukchi seas during June 2017 and 2018.

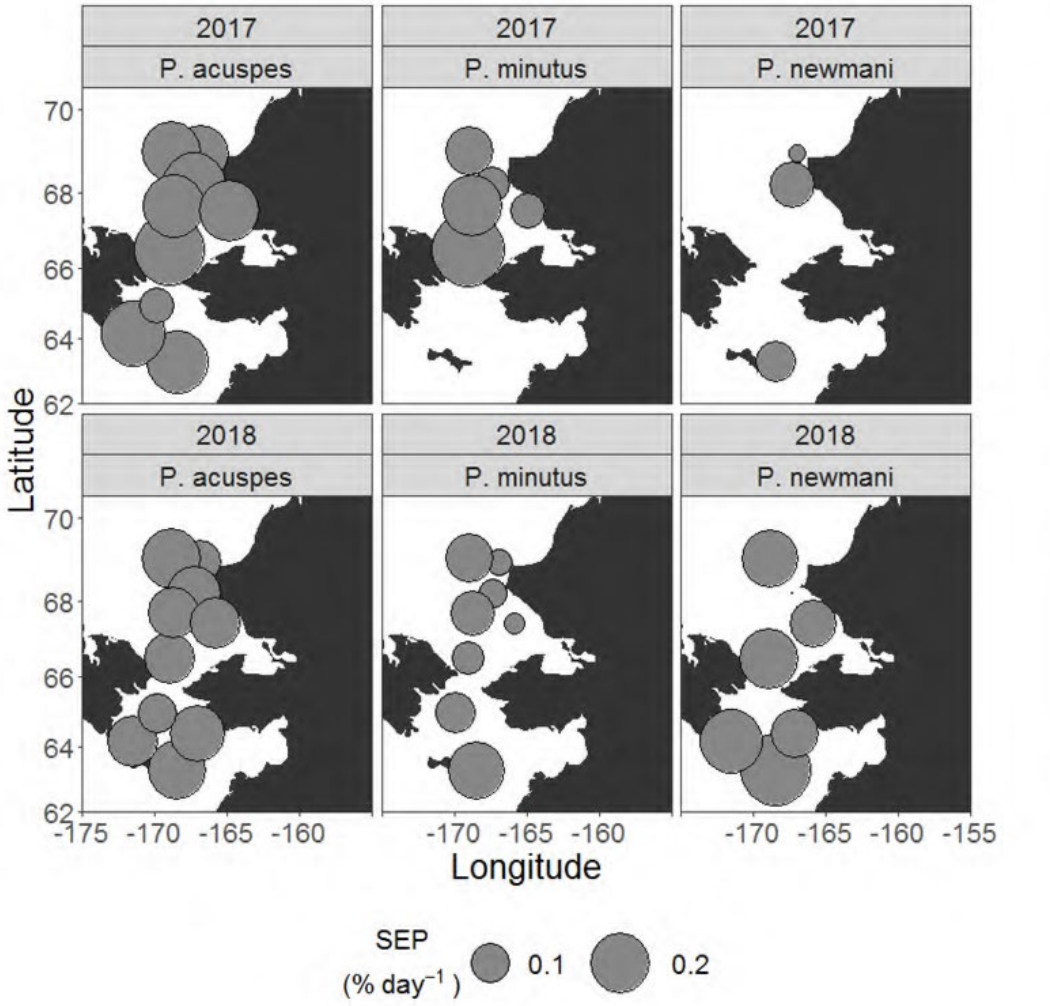

Figure 7: Weight specific egg production rate (SEP) for June of 2017 and 2018 for the three co-occurring *Pseudocalanus* species in the northern Bering and southern Chukchi seas.

TABLES

Table I: Biomass and abundance during June 2017 and 2018 in the Northern Bering and Southern Chukchi Seas of copepodite and adult stages of the most common copepod species. * = species not staged, copepodites and adults grouped

	2017				2018			
	Biomass (mg m^{-3})		Abundance (m^{-3})		Biomass (mg m^{-3})		Abundance (m^{-3})	
Species	copepodite	adult	copepodite	adult	copepodite	adult	copepodite	adult
Calanus spp.	8.14	1.89	338.0	4.69	2.37	1.44	64.8	3.0
Metridia pacifica	1.36	1.39	128.0	11.1	1.08	2.06	100.0	15.6
Neocalanus flemingeri	23.5	0	46.3	0	2.11	0	3.3	0
Neocalanus cristatus	3.63	0	0.9	0	1.52	0	0.4	0
Pseudocalanus spp.	13.90	6.46	7163.0	1002.0	4.70	2.88	1624.0	215.0
Centropages abdominalis	0.04	0.02	3.3	0.54	0.01	>0.01	0.8	>0.01
Eucalanus bungii	0.07	0.06	0.4	0.14	0.04	0.03	0.3	0.1
Acartia longiremis	0.22	0.09	63.3	4.10	0.18	0.09	83.2	14.6
*Oithona similis**	1.72		1265.0		1.38		1186.0	
*Oncaea borealis**	0.42		174.0		0.49		135.0	

Table II: *Pseudocalanus* spp. growth and egg production rates from experiments where experimental temperature was <6ºC or Q_{10} corrected to <6ºC. * = Q_{10} corrected. (^) = development time from hatching to stage. EP = egg production. AC = artificial cohort. T = average experimental temperature. An ANOVA indicated significant differences between mean growth rate and copepodite stage ($p < 0.05$) and a Tukey test indicated the differences were only significant between CIV and the early stages.

Species	T (ºC)	Exp. Type and length	Growth rate (day^{-1}) and development time (in parentheses)					SEP (% day^{-1})	Location and time of year	Source
			CI	CII	CIII	CIV	CV			
P. spp	4	AC 10 d	0.04±0.003 (6.7±0.57)	0.04±0.002 (10.8±0.48)	0.04±0.005 (10.2±0.93)	0.02±0.002 (8.28±0.41)	N/A		Bering & Chukchi Seas (June)	This study
P. acuspes *P. newmani* *P. minutus*	4	EP 2 d						0.18±0.01 0.15±0.00 0.11±0.01		
P. spp	5*	AC 5 d	0.051 (13.9)	0.061 (10.2)	0.046 (10.9)	0.038 (16.1)	0.020 (40.5)		Gulf of Alaska (Mar-Oct avg.)	Liu & Hopcroft (2008)
P. acuspes	4	Moult Rate, EP	.03-0.05 (CI-CIV)				0.04-0.13		Baltic Sea April	Renz et al (2007)
P. acuspes *P. newmani* *P. minutus*	5*	EP 2 d						0.16 ±0.02 0.14±0.02 0.12±0.03	Chukchi Sea (Aug)	Hopcroft & Kosobokova (2010)
P. acupses *P. newmani*	0 3 0 3	EP EP						0.09±0.04 0.09±0.04 0.03±0.02 0.07±0.03	Chukchi Sea (Sep)	Ershova et al. (2017)
P. newmani	3	Ind. inc. EP	37.2±1.1^	43.8±1.8^	51.3±1.1^	58.9±1.5^	66.9±1.6^	0.09	Funka Bay, Japan	Lee et al (2003)
P. newmani *P. mimus* *P. minutus*	5–15	EP						EPR 1.4-9.3	Gulf of Alaska (Apr-Aug)	Napp et al (2005)
P. spp	4			13				EPR 7.5±1.4 SEP 4.8-5.4	SE Bering Sea	Vidal & Smith (1986)

Table III: *Calanus* spp. growth and egg production rates from experiments where experimental temperature was <6ºC or Q_{10} corrected to <6ºC. * = Q_{10} corrected. EP = egg production. AC = artificial cohort. T = average experimental temperature. An ANOVA indicated significant differences between mean growth rate and copepodite stage ($p < 0.05$) for both AC and stage selected experiments, and a Tukey test indicated the differences were only significant between CIV and the early stages.

Species	T (ºC)	Exp. Type and Length	Growth rate (day^{-1}) and development time (days) CI	CII	CIII	CIV	SEP (% d^{-1})	Location	Source
Calanus spp.	4	AC (10d) & EP (1d)	0.09±0.01 (8.31±0.69)	0.11±0.004 (9.65±0.53)	0.09±0.01 (8.06±0.57)	0.06±0.005 (5.73±0.42)	0.09±0.01	Bering & Chukchi Seas (June)	This study
Calanus spp.		Stg. Selected 10d	0.14±0.01 (9.41±0.38)	0.09±0.01 (6.35±0.86)	0.10±0.01 (6.03±0.65)	0.06±0.006 (5.85±0.45)			
Calanus marshallae	5	AC 5d	0.156±0.019 (9.4+01.5)	0.145+0.011 (8.7+0.8)	0.109+0.009 (11+0.8)	0.058+0.009 (18.7+2.5)	10	Gulf of Alaska (Mar-Oct)	Liu & Hopcroft (2008)
Calanus glacialis/ marshallae	-1.7 – -1.25	EP					1-6	Chukchi & Beaufort Seas (May-Aug)	Plourde et al (2005)
Calanus marshallae	0.5 – 6		15 (% day^{-1})		14 (% day^{-1})		EPR 75±15 SEP 6	SE Bering Sea	Vidal & Smith (1986)

Table IV: *Metridia* growth and egg production rates from experiments where experimental temperature was <6ºC or Q_{10} corrected to <6ºC. * = Q_{10} corrected. EP = egg production. AC = artificial cohort. * = development time measured from nauplii to stage. T = average experimental temperature.

Species	T (ºC)	Exp. Type and length	Growth rate (day^{-1}) and development time					SEP (% d^{-1})	Location	Source
			CI	CII	CIII	CIV	CV			
M. pacifica	4	AC 10d	0.06±0.007 (5.23±0.54)	0.06±0.006 (4.57±0.35)	0.05±0.005 (5.57±0.68)	0.04±0.003 (3.21±1.27)			Bering & Chukchi Seas (June)	This study
M. pacifica	4	EP 1d						0.11±0.01		
M. pacifica	5*	AC 5d	0.091±0.010 (16.3±2.3)	0.090±0.008 (13.1±1.4)	0.090±0.007 (11.9±1.5)	0.054±0.009 (19.6±2.6)	0.023±0.009 (46.7±11.1)		Gulf of Alaska (Mar-Oct avg.)	Liu and Hopcroft (2008)
M. pacifica	3	Ind. inc*	(14.5±2.6)	(14.5±3.5)	(20.4±5.8)	(31.7±2.3)	(51.5±4.5)			Padmavati & Ikeda (2002)
M. pacifica	5	EP						avg 10	Gulf of Alaska (Mar-Oct)	Hopcroft et al (2005)
M. pacifica	4	Growth exp.			13-15 (% day^{-1})				SE Bering Sea	Vidal & Smith (1986)

Respiration rates of calanoid copepods during the spring bloom for the Arctic's Bering Strait region

Russell R. Hopcroft & Caitlin A. Smoot

Institute of Marine Sciences, University of Alaska Fairbanks

Introduction

The regions surrounding the Bering Strait are an important transition zone between the Pacific and Arctic Oceans (Grebmeier and Maslowski 2014). Nearly four decades ago, it was estimated that 1.8 million metric tons of Bering Sea mesozooplankton were carried into the Arctic through this region annually (Springer et al., 1989), and that they act as significant consumers of phytoplankton as well as prey for higher trophic levels. The Chukchi has been undergoing pronounced changes in sea ice cover and water temperature for most of this century (Danielson et al. 2020). In its now becoming clear that these changing environmental conditions are propagating to the biological communities with significant implications for the higher trophic levels that of commercial or subsistence importance (Huntington et al 2020). Despite these observations our knowledge of the fundamental rate processes at the organismal level that determine how species will respond to these changes is particularly limited globally and especially so in Arctic waters. The ASGARD program was designed with the goal of significantly increasing of understanding rate process for all trophic components in the Bering Strait region.

Rate processes in zooplankton begin with grazing activity, with calanoid copepods being the dominant components of this grazing community within the Pacific Arctic (Questel et al. 2013, Ershova et al,. 2015). Once food is ingested, a portion of it is assimilated, and the remainder is egested as fecal pellets that sink rapidly to the benthos (O'Daly et al. 2020, LaLande et al. 2020, 2021). Of the matter assimilated, a portion of it is respired, while the remainder goes toward growth, either in the form of body tissue or reproductive products, some may be stored as lipids, and nitrogenous wastes are excreted. Although labor intensive, approaches to estimating growth and egg production in zooplankton are relatively well established, and are reported for this region elsewhere (see Poje chapter). In contrast due to the small size of zooplankton, and in particular of copepods, measurement of respiration has proven particularly difficult to determine routinely. For this reason, in most cases modelers rely on equations determined by global syntheses of respiration rates (Ikeda et al. 2001, Ikeda et al. 2007), that although based on relatively limited data have suggested highly predictive relationships. Nonetheless, if these models prove to be less than universal for all species in all habitats, then significant errors could be introduced in partitioning how much of the food ingested goes into secondary production versus being lost to respiration.

Recent advancement in technologies (e.g., Koster et al. 2008) now allow us to measure respiration for individual copepods in small volumes that was impossible when prior syntheses were undertaken. Most recently this technology has advance to the form of plate readers that allow significant replication. Given these advances we ask the simple question: what are the respiration rates of the dominant zooplankters in the Bering Strait region and how do they compare to the predictions of prior syntheses?

Methods

Experiments were conducted during cruises on the R/V *Sikuliaq* during June of 2017 and June of 2018 in the northern Bering and southern Chukchi seas as part of the Arctic Shelf Growth, Advection, Respiration and Deposition (ASGARD) project (Fig. 1). Zooplankton were collected using a vertically-hauled 60-cm flow-metered twin-ring net fitted with 150-µm mesh. Nets were hauled through the entire water column (depth ranged 30-56 m) at ~0.5 m s^{-1}. Upon retrieval, only the lowest portion of the nets were lightly splashed with seawater before removing the cod-end. Zooplankton were quickly diluted with ambient seawater then placed in incubators set at the typical ambient sub-surface seawater temperature (4°C) until further experimental processing could occur.

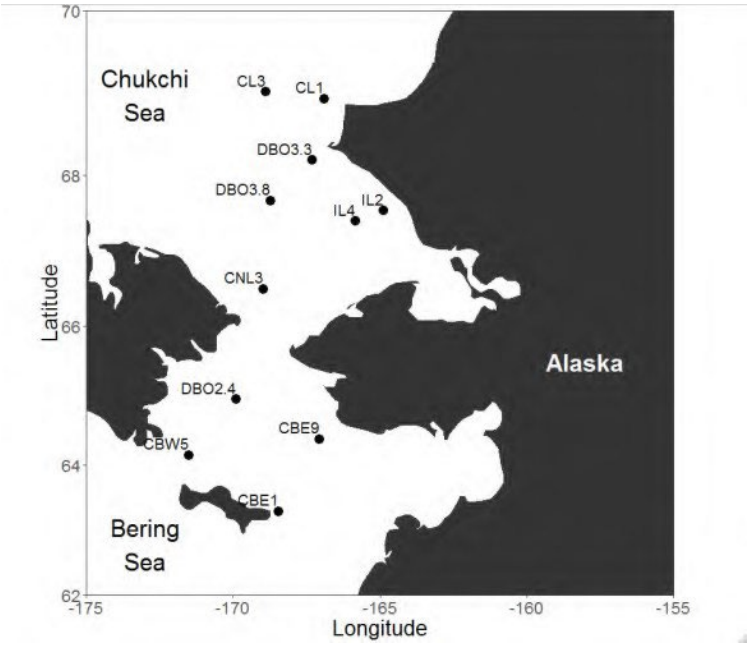

Figure 1: Zooplankton experimental stations for the Arctic Shelf Growth, Advection, Respiration and Deposition project (ASGARD) during 2017 and 2018.

Samples were moved into water-jacketed jars and subsampled for sorting under the microscope to species and stage. Sorted animals were pipetted into water-jacketed trays maintained at 4°C. Most experiments targeted the adult females, although Copepodite-V was targeted for *Neocalanus flemingeri*, and subadults of *Calanus marshallae* were employed on one occasion in 2018. For final sorting, pairs of animals were transferred into each well of a 6-place multiwell plate filled with pre-filtered water. Wells were given several hours to equilibrate oxygen at incubation temperature prior to use. Pre-filtering during 2017 only removed metazoans (~ 20µm) whereas in 2018 we employed 0.2 µm cellulose-acetate filters, and sequentially transferred animals across 3 sets of clean pre-filtered wells immediately prior to being placed in the incubation vial.

Incubations were performed using PreSens oxygen optodes systems (Koster et al. 2008) with SensorVial size scaled to animal size. In 2017 we employed 5-ml vials for *Calanus*, *Neocalanus* and *Metridia*, and 2-ml vials for *Pseudocalanus* and *Metridia* (one occasion only). In 2018 we employed 5-ml vials for *Calanus*, 2-ml for *Metridia*, and custom-made 1-ml vials prototypes for the two dominant species of *Pseudocalanus*. Although animals were sorted in pairs into the 6-well trays, we performed incubations on individual animals. These animals were carefully pipetted with their acclimation water into pre-chilled SensorVial being careful not to introduce or create bubbles any on vial surfaces. From each tray a control vial was filled from an occupied well but leaving both animals behind. Caps were applied then the vial inverted and inspected under the microscope to ensure no bubbles were created during the capping process (a frequent source), or existed on the vial or sensor-dot. Vials were returned to the water baths as quickly as possible. Each experiment consisted of a set of 20 animals and 4 controls filling a 24-place multiwell. Vials were pre-labeled to ensure constant use in the same multiwell position and application of the correct pre-calibrated volume. The multi-well was sealed in a Loligo water bath

that was designed for placement over the SensorDisk plate reader. An alignment guide was 3-D printed to ensure proper placement of the vials and a compressible spacer was employed as needed between the vials and water bath lid. Up to four water baths were connected in series to a Fisher Isotemp circulating chiller that was pre-stabilized thermally and maintained temperature within 0.1°C of the setpoint. At the start of the experiment air was evacuated from each water bath. The entire system was deployed inside a walk-in incubator set at ~4°C and maintained under dim lighting. We learned it was absolutely critical to maintain temperature of all water and vials at the intended setpoint to avoid formation of air bubbles when saturated water warms and because the optodes are highly temperature sensitive.

Figure 2: Water baths each housing 24 sensor vials with a multi-well tray. The water bath has a recessed bottom that aligns directly over an optical plate reader. Hoses connect each to a water bath to maintain thermal stability.

Data was monitored and logged through Presens SDR software (V4) set to read every 15 seconds (2017) or 30 seconds (2018). Experiments were run from 10-24 hours dependent in part on the rate of oxygen change. Despite our best attempts to maintain constant temperature, there was typically a 20-30 minute period at the start of experiment for the vials to stabilize. Presens provides a general calibration for each production-lot of sensors, but our attempts a develop a consistent vial-specific calibration failed, so after removing the pre-stabilization periods, all vials were normalized to the same average oxygen concentration as measured between the first 30-45 minutes of recording. We standardized on using a normalization value of 10.5 mg O_2 L^{-1} which is the saturation value for seawater at 4°C and salinity of 33. Slopes were fit to the 9-point running average the oxygen data for each vial using linear regression. The sensor vials relied on the movement of the animals to maintain a homogenized oxygen concentration, so lines were not always fully linear if a copepod monopolized an end of the vial and/or ceased to generate feeding currents, but in successful experiments linear fits to oxygen concentration were strong (r^2>0.9).

Post-experiment, the identity of experimental animals were confirmed, and their prosome lengths (PL) were measured (Roff and Hopcroft, 1985). Weights were predicted using relationships between prosome length and dry weight (DW) established for the nearby Gulf of Alaska, with the same relationship being applied to all copepodite stages:
Neocalanus DW was calculated using: $\log_{10}$ DW = 3.564*log10[PL] – 10.009 (Liu and Hopcroft, 2006a), *Calanus* DW was calculated using: $\log_{10}$ DW = 4.024*log PL – 11.561 (Liu and Hopcroft, 2007), *Pseudocalanus* DW was calculated using: $\log_{10}$DW = 2.85*$\log_{10}$PL – 7.62 (Liu and Hopcroft, 2008), and *Metridia* DW calculated using $\log_{10}$DW = 3.29*$\log_{10}$PL – 8.75 (Liu and Hopcroft, 2006b).

Where needed, we converted oxygen from mg to ml through multiplication by 0.700 (Molar volume at STP / molar weight of oxygen), and noted that 1 ml O_2 = 44.661 µmol O_2. To further convert to carbon consumption, we assumed the respiration of one carbon atom consumes 1 molecule of oxygen (true at least for glucose), and that carbon was 40% of a copepod's dry-weight (DW).

Results

Failure to adequately prepare controls and remove microbial respiration from sensor vials during 2017 resulted in questionable or low data for most experiments, thus data is not presented. Nonetheless, the 2017 data lead to methodological improvements and highlight the need for both more plate-readers (to consistently encompass the predominant species) and smaller vials to resolve respiration for *Pseudocalanus* species. Even during 2018, experiments at the first 2 process stations failed to produce trustworthy data. By the third process station, CBW5, we were successful in setup up of all 4 predominant calanoid copepod species in our samples: *Calanus marshallae (~3 mm, 500 µg DW)*, *Metridia pacifica (2.1 mm, 150 µg DW)*, *Pseudocalanus minutus* (1.4 mm, 25 µg DW) and *P. acuspes* (1.0 mm, 10 µg DW)(Fig. 3). *Metridia* was not present in adequate number for experimentation at two subsequent stations (CL1 and CL3), while data logging issues at one station compromised both of its *Pseudocalanus* experiments. Due to their short aspect ratio and small sensor-dots, the 1-ml SenorVials proved somewhat more problematic than the larger vials, with jumps in the data possible if the vial shifted position within its plate-holder, or variable data if misaligned to the reader.

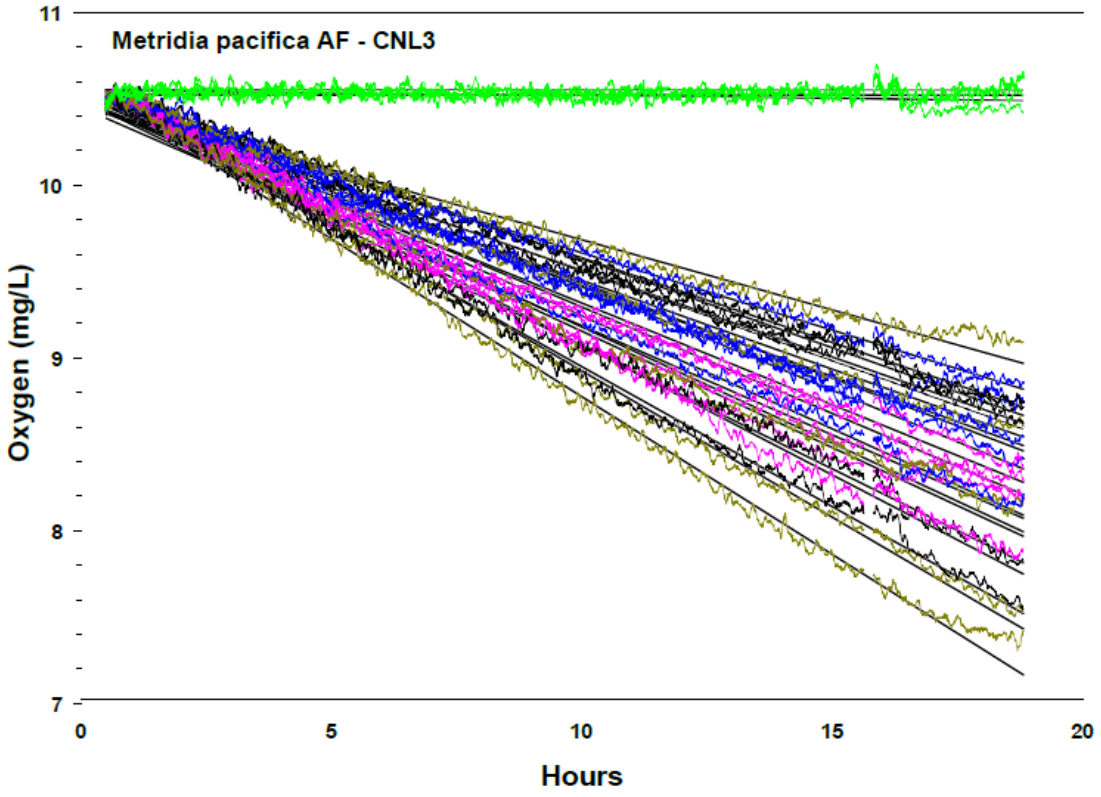

Figure 3. Time-series of oxygen concentration during a respiration experiment for adult female *Metridia pacifica*. The four green lines are controls, with the 20 experimental animals in other colors. Straight lines are linear regressions through data from each vial.

During 2018, the mean respiration for each species was relatively consist across stations (Table 1), with no significant differences between station except for *P. minutus* at station CL1. Gross respiration was greatest the largest species, *Calanus* (~0.9 µg O_2 hr^{-1}), and declined with the body size of species revealing a 20-fold difference to the smallest species, *P. acuspes* (~0.55 µg O_2 hr^{-1}). Variability in respiration rates (as reflected in the standard error) was greatest for the smallest species, *P. acuspes*. This relationship to body size, and particularly body mass is obvious both within and across species when all individual observations are considered (Fig. 4). Standardizing for body mass, specific respiration rate declines with body mass (Fig. 5) from about 5-20% per day in *Pseudocalanus* to 2.5-10% in both *Calanus* and *Metridia*. The data was suggestive of an independent negative relationship to body size within each species.

Table 1. Gross individual respiration rates (µg O_2 hr^{-1}) for calanoid copepods in the Northern Bering and Southern Chukchi Seas during June 2018 at 4°C.

	P. acuspes		*P. minutus*		*Metridia pacifica*		*Calanus marshallae*	
	Mean	STD	Mean	STD	Mean	STD	Mean	STD
CBW5	0.049	0.026	0.091	0.028	0.298	0.051	1.085	0.217
CL1	0.049	0.012	0.069	0.018	-	-	0.844	0.147
CL3	0.054	0.029	0.107	0.022	-	-	0.871	0.133
CNL3	-	-	-	-	0.335	0.076	0.935	0.211
DBO2.4	0.047	0.017	0.081	0.023	0.304	0.066	1.084	0.068
DBO3.3	0.055	0.017	0.100	0.022	0.288	0.068	0.843	0.191
DBO3.8	0.064	0.032	0.112	0.026	0.332	0.059	0.955	0.232
IL4	0.068	0.032	0.094	0.018	0.339	0.077	0.897	0.150

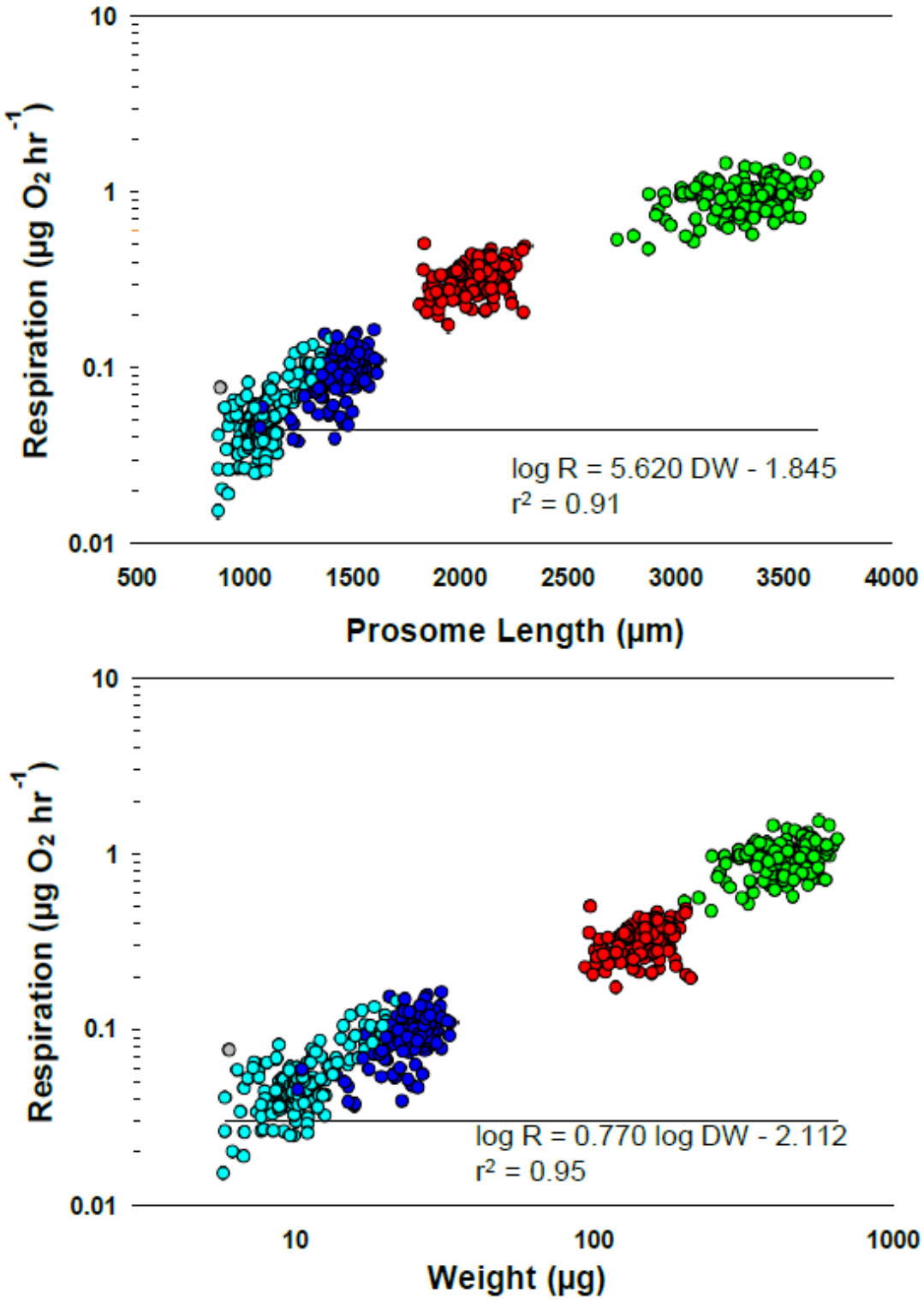

Figure 4. Respiration of calanoid copepods in the Bering Strait region at 4°C as a function of body length and dry-weight body mass.

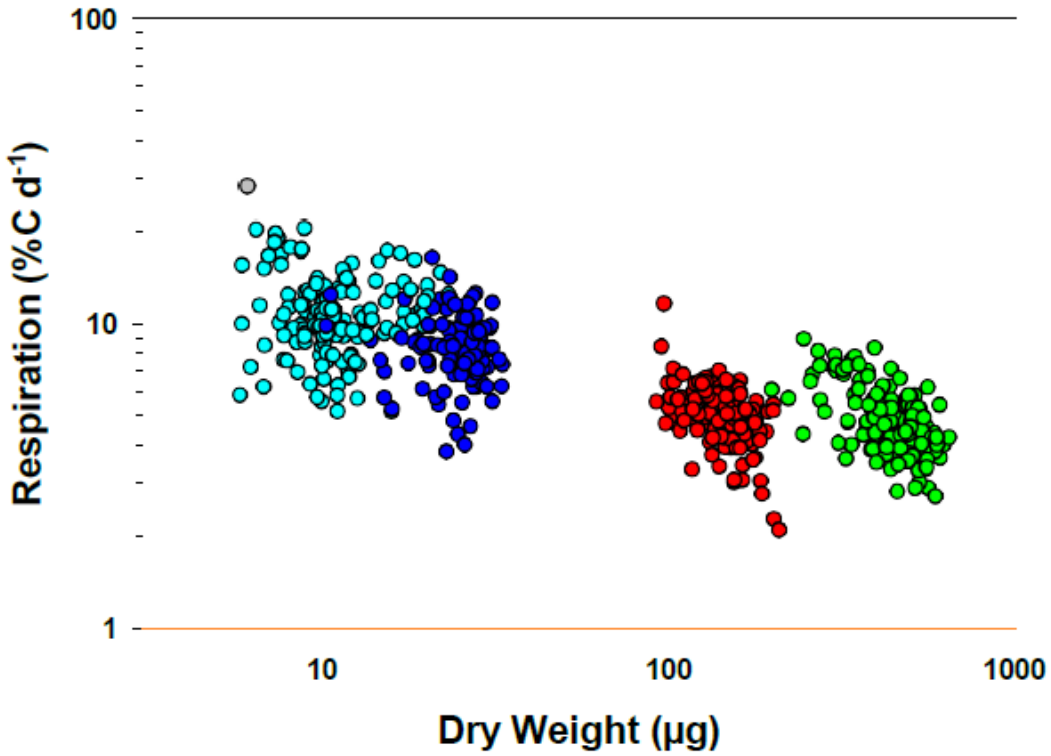

Figure 5. Respiration of calanoid copepods (as carbon equivalents) in the Bering Strait region as a function of body carbon mass at 4°C.

Abridged Discussion

Zooplankton respiration rates determined during the ASGARD program are the first direct determination for this region. They confirm the overall expectation of increasing growth respiration with body size (Ikeda et al. 2001, Ikeda et al. 2007), as well as the recognized decline in weight-specific respiration within increasing body mass (Ikeda et al., 2000). Although optode technology has resulted in some increased reporting of respiration rates, thus far it has still focused on mostly larger species (e.g., Maas et al. 2021). Making such measurements is even more challenging when operating at colder temperatures where respiratory rates are typically low in comparison to warmer waters.

Direct comparison to the relationships established by Ikeda shows the measured rates to be consistently higher than his relationships (Fig. 6). The regression for the data from this study, log R_{10} = 0.779∗log(DM)+0.24 predicts a value almost 3-fold higher than that predicted by the Ikeda relationship (*i.e.,* 0.73 versus 0.26 for a 100 µg copepod). Furthermore, we were able to directly estimate the weight-specific carbon respired and found it to be 5-20%, scaling inversely with body mass. Both of these observations are of significant in understanding the amount of photosynthesized carbon that will be lost to zooplankton respiration, and they set boundaries on the lowest amount of grazing required by zooplankton to meet their basic metabolic needs (i.e., biomass held in steady-state). Our data suggests that despite the cold water temperatures characteristic of the Arctic's marginal seas, respiratory losses by zooplankton are significant and higher than expected and of similar magnitude to that of growth and egg

production for these species (Poje 2020). Failure to appropriately parameterize models with appropriate field observations can be an important source of error in ecosystem models (e.g., Coyle et al. 2019). By combining these respiratory needs with that of zooplankton growth as reported in elsewhere in this report, we can now place boundaries on the grazing rates of the zooplankton community and its potential to impact the biomass of the phytoplankton communities at the time of these experiments.

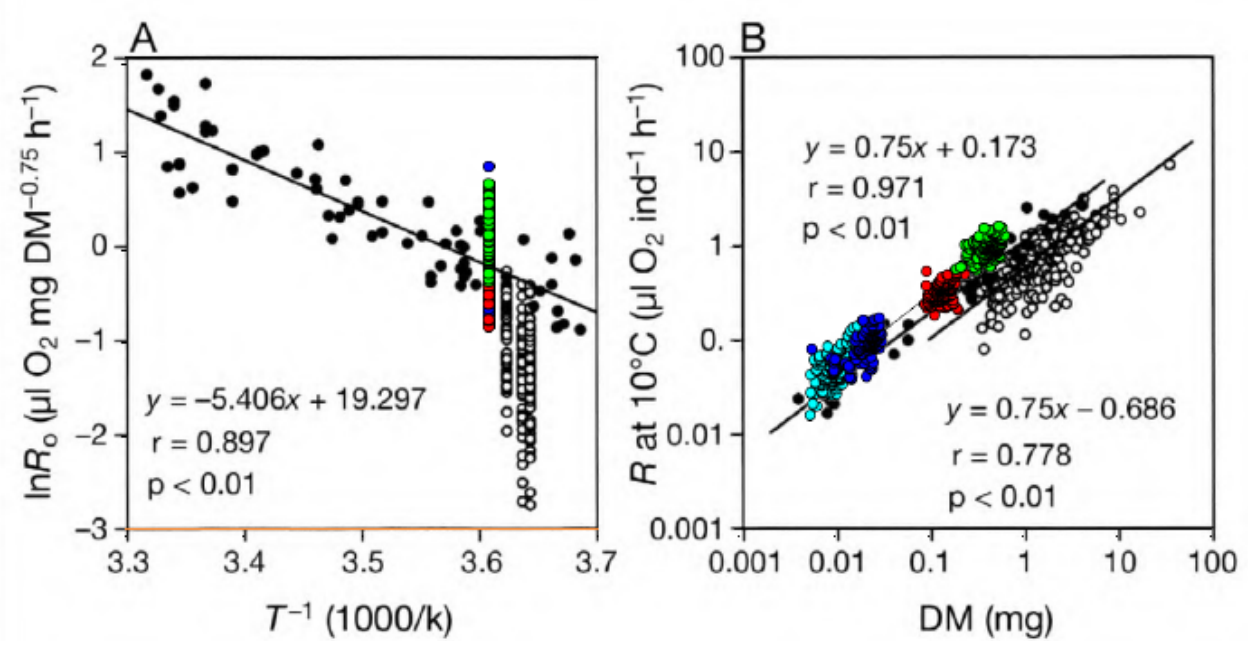

Figure 6. Respiration rates of calanoid copepods in the Bering Strait region compared to the global relationships proposed by Ikeda et al. 2007. The panel at left standardized data to animals of a constant dry mass (1 mg), while the left standardizes data to 10°C. Closed black symbols are epipelagic species, open circles are mesopelagic species. Colors represent species from Bering Strait as in prior figures.

References

Ikeda, T., Sano, F., Yamaguchi, A., 2007. Respiration in marine pelagic copepods: a global-bathymetric model. Marine Ecology Progress Series 339, 215-219.

Ikeda, T., Torres, J.J., Hernandez-Leon, S., Geiger, S.P., 2000. Metabolism, in: Harris, R.P., Wiebe, P.H., Lenz, J., Skjoldal, H.R., Huntley, M. (Eds.), Zooplankton methodology manual. Academic Press, London, pp. 455-532.

Köster, M., Krause, C., Paffenhöfer, G.-A., 2008. Time-series measurements of oxygen consumption of copepod nauplii. Mar. Ecol. Prog. Ser. 353.

Lalande, C., Grebmeier, J.M., Hopcroft, R.R., Danielson, S.L., 2020. Annual cycle of export fluxes of biogenic matter near Hanna Shoal in the northeast Chukchi Sea. Deep Sea Res. II. 177, 104730.

Lalande, C., Grebmeier, J.M., McDonnell, A.M.P., Hopcroft, R.R., O'Daly, S., Danielson, S.L., 2021. Impact of a warm anomaly in the Pacific Arctic region derived from time-series export fluxes. PLoS ONE 16, e0255837.

Liu, H., Hopcroft, R.R., 2006. Growth and development of *Metridia pacifica* (Copepoda: Calanoida) in the northern Gulf of Alaska. J. Plankton Res. 28, 769-781.

Liu, H., Hopcroft, R.R., 2006. Growth and development of *Neocalanus flemingeri/plumchrus* in the northern Gulf of Alaska: validation of the artificial cohort method in cold waters. J. Plankton Res. 28, 87-101.

Liu, H., Hopcroft, R.R., 2007. A comparison of seasonal growth and development of the copepods *Calanus marshallae* and *C. pacificus* in the northern Gulf of Alaska. J. Plankton Res. 29, 569-581.

Liu, H., Hopcroft, R.R., 2008. Growth and development of *Pseudocalanus* spp. in the northern Gulf of Alaska. J. Plankton Res. 30, 923-935.

Maas, A.E., Miccoli, A., Stamieszkin, K., Carlson, C.A., Steinberg, D.K., 2021. Allometry and the calculation of zooplankton metabolism in the subarctic Northeast Pacific Ocean. Journal of Plankton Research 43, 413-427.

O'Daly, S.H., Danielson, S.L., Hardy, S.M., Hopcroft, R.R., Lalande, C., Stockwell, D.A., McDonnell, A.M.P., 2020. Extraordinary Carbon Fluxes on the Shallow Pacific Arctic Shelf During a Remarkably Warm and Low Sea Ice Period. Frontiers in Marine Science 7.

Poje, A., 2020. Growth and reproductive rates of calanoid copepods in the Northern Bering and Southern Chukchi Seas, Oceanography. University of Alaska, Fairbanks, p. 30.

Questel, J.M., Clarke, C., Hopcroft, R.R., 2013. Seasonal and interannual variation in the planktonic communities of the northeastern Chukchi Sea during the summer and early fall. Cont. Shelf Res. 67, 23-41.

Roff, J.C., Hopcroft, R.R., 1986. High precision microcomputer based measuring system for ecological research. Can. J. Fish. Aquat. Sci. 43, 2044-2048.

Polar Biology
https://doi.org/10.1007/s00300-021-02940-2

ORIGINAL PAPER

Seasonal abundance, distribution, and growth of the early life stages of polar cod (*Boreogadus saida*) and saffron cod (*Eleginus gracilis*)

1.1 in the US Arctic

A. L. Deary[1] · C. D. Vestfals[2] · F. J. Mueter[3] · E. A. Logerwell[1] · E. D. Goldstein[1] · P. J. Stabeno[4] · S. L. Danielson[5] · R. R. Hopcroft[5] · J. T. Duffy-Anderson[1]

Received: 26 August 2020 / Revised: 3 September 2021 / Accepted: 6 September 2021

Abstract

Polar cod and saffron cod are dominant components of the fish community in the Chukchi Sea and are ecologically important forage fishes linking plankton to upper-level consumers. In 2017, we conducted a study as part of the Arctic Integrated Ecosystem Research Program to characterize the distribution, abundance, and growth of polar cod and saffron cod early life history stages (ELHS) in late spring and late summer in the Chukchi Sea. Ship-based plankton tows showed that polar cod and saffron cod larvae were centered in Kotzebue Sound in the late spring. By late summer, polar cod juveniles were most abundant in the offshore areas of the northern Chukchi Sea, whereas saffron cod were distributed nearshore in the southern Chukchi Sea around Cape Lisburne. Empirical fish collections were paired with an individual-based biophysical transport model to examine connectivity and relate changes in seasonal distribution to potential environmental variables. Modeled drift trajectories and growth in spring for polar cod and saffron cod matched well with empirical observations, especially along the northern coastline of Kotzebue Sound, offshore of Point Hope/Cape Lisburne. Given the coherence between modeled and observed distributions, Kotzebue Sound is likely a source of gadid ELHS in the nearshore areas of the Chukchi Sea and offshore of Cape Lisburne/Point Hope, although it is not the likely source of polar cod over Hanna Shoal in the late summer. This is the first study to examine seasonal distribution, abundance, and growth of polar cod and saffron cod in the US Arctic and provides data necessary to evaluate the impacts of climate change on forage fishes in the Arctic.

Keywords Gadidae · Ichthyoplankton · Forage fishes · Chukchi Sea · Arctic cod

Introduction

The Arctic has experienced accelerated warming at twice the rate of the global average, making Arctic ecosystems particularly sensitive to climate change (Graham et al. 2017; Tokinaga et al. 2017; Overland et al. 2018). The accumulation of heat in the Arctic has increased significantly since the late 1990s, which correlates to a reduction in sea ice thickness (Maslowski 2014), a 60% loss of multiyear ice, a 75% reduction in sea ice volume (Overland et al. 2018), and lower winter ice extent maxima (Graham et al. 2017). Loss of sea ice is expected to influence Arctic ecosystem dynam- ics through bottom-up changes to lower trophic production (Kahru et al. 2011), community structure (Spear et al. 2019), trophic linkages (Hunt et al. 2013), shifts in benthic-pelagic coupling (Grebmeier et al. 2015 and citations therein), and food web interactions (Li et al. 2009). Ecosystem changes also have potential economic ramifications such as range

* A. L. Deary
alison.deary@noaa.gov

1 Alaska Fisheries Science Center, NOAA, 7600 Sand Point Way NE, Seattle, WA 98115, USA

2 Hatfield Marine Science Center, College of Fisheries and Ocean Sciences, University of Alaska Fairbanks, Newport, OR 97365-5229, USA

3 College of Fisheries and Ocean Sciences, University of Alaska, 17103 Point Lena Loop Rd., Juneau, AK 99801-8344, USA

4 Pacific Marine Environmental Laboratory, NOAA, 7600 Sand Point Way NE, Seattle, WA 98115, USA

5 College of Fisheries and Ocean Sciences, University of Alaska Fairbanks, Fairbanks, AK 99775-7220, USA

Published online: 16 September 2021

extensions of commercially important subarctic gadid species, such as walleye pollock (*Gadus chalcogrammus*), Pacific cod (*Gadus macrocephalus*), and salmonid fishes, into regions north of the Bering Strait (Falardeau et al. 2017; Stevenson and Lauth 2019) in the Pacific Arctic.

Although not fished commercially in the US Arctic (NPFMC 2009), polar cod (*Boreogadus saida*), a circumpolar species, and saffron cod (*Eleginus gracilis*) are crucial forage fishes in Arctic marine ecosystems. Both species support bioenergetic pathways that transfer energy from planktonic food webs to upper-level consumers and apex predators (including humans) and are a dominant component of the fish community in the Chukchi Sea, although polar cod is more abundant than saffron cod (Whitehouse et al. 2014; Logerwell et al. 2015). It is estimated that seabirds and marine mammals consume approximately 75% of the polar cod production (Whitehouse et al. 2014). Changes to the Chukchi shelf ecosystem due to climatic warming, loss of sea ice, and perturbations to sea ice phenology (Graham et al. 2017; Overland et al. 2018) may have serious implications for these ecologically important species.

Despite their ecological importance and abundance in Arctic ecosystems, the life history of polar cod and saffron cod are still relatively unknown (Logerwell et al. 2015; Vestfals et al. 2019). Spawning locations of polar cod in the US Arctic are largely unknown, although it is hypothesized that polar cod spawn under sea ice (Rass 1968) and that peak hatching likely occurs in May and June as the ice edge recedes (Bouchard and Fortier 2008; Vestfals et al. 2019). In the Pacific Arctic, development of larvae and early juve- niles occurs along the shelf (Logerwell et al. 2015; Vestfals et al. 2019). Saffron cod are near-shore, demersal, under-ice spawners that deposit demersal eggs in nearshore areas on sandy-pebbly substrates (Vestfals et al. 2019 and citations therein) but exact locations are unknown in the US Arctic. Peak hatching for saffron cod occurs in April and May, earlier than for polar cod, and offspring are often found concentrated closer to shore and at more southerly locations within the Chukchi Sea (Vestfals et al. 2019). The life histories of polar cod and saffron cod are similar in that both are planktonic in shelf waters after hatching through the first summer, after which polar cod move deeper in the water column while saffron cod become demersal as juveniles (Logerwell et al. 2015; Vestfals et al. 2019).

Growth of polar cod and saffron cod is mediated by temperature (Laurel et al. 2016) and an additional consequence of a warming Arctic is that large calanoid copepod species, an important prey resource for Arctic gadids, will be replaced by smaller, less lipid-rich copepods (Aarflot et al. 2018; Møller and Nielsen 2020; Bouchard and Fortier 2020). Larvae and juveniles will be disproportionally affected by these changes relative to adults due to their higher weight-specific growth rates, and polar cod may be more sensitive than saffron cod because they are a stenothermic species (Laurel et al. 2016). Polar cod are adapted to support high growth and lipid allocation at a narrow range of low temperatures (optimal growth rate at 5 °C), while saffron cod experience high growth and lipid allocation over a wider temperature range, particularly, at high temperatures (optimal growth rate > 16 °C) (Copeman et al. 2016; Laurel et al. 2016). As such, saffron cod may be better able to mitigate the effects of ocean warming in the Arctic than polar cod.

In 2017, the Arctic Integrated Ecosystem Research Program (Arctic IERP), funded by the North Pacific Research Board, conducted its first field season in the US Pacific Arctic. Concurrent with the Arctic IERP surveys, the Distributed Biological Observatory (DBO) project and the Arctic Marine Biodiversity Observation Network (AMBON) survey were also sampling the region, providing more coverage to this region that is often under-researched. In this inaugural year of sampling for the Arctic IERP, it was remarkable that the northern Bering Sea and Chukchi Sea were sampled for ichthyoplankton in both late spring and late summer, a first in the region. These sampling efforts provided an opportunity to assess the seasonal abundance, distribution, and growth of fishes during their early life history stages (ELHS). However, the summer of 2017 in the Chukchi Sea was also remarkable in environmental conditions, with an elevated sea surface temperature (+ 4 °C relative to the historic average) and the lowest recorded March sea ice minimum in the 39-year history of the time series (Perovich et al. 2017; Timmermans et al. 2017), providing us with baseline vital rate data for polar cod and saffron cod, albeit during a warm year. Such baseline data, when coupled with further monitoring and modeling, can be used to determine the impact of climate warming on these two ecologically important species. In addition to empirical sampling, we used an individual-based model (IBM) as a tool to simulate larval transport and examine potential linkages and connectivity in polar cod and saffron cod abundance and distribution between the late spring and late summer sampling events. Our goals for this study were to (1) examine spatial patterns of distribution and abundance of polar cod and saffron cod during their larval (June; late spring) and early juvenile (August–September; late summer) stages in 2017; (2) assess the change in mean length to approximate daily growth rates in the summer for polar cod and saffron cod; and (3) evaluate potential sources of larval polar cod and saffron cod using an IBM to compare observed distributions and sizes with model output. This study coupled empirical observations with IBM output to synthesize, for the first time, the seasonal distribution, abundance, and growth of two co-occurring Arctic forage fishes, providing a means to assess the biological impacts of warming on polar cod and saffron cod ELHS.

Methods

Specimen collection

Polar cod and saffron cod ELHS were collected in 2017, using three different sampling gears, as part of several cooperating research projects (Table 1): the Arctic Integrated Ecosystem Survey (AIES; part of Arctic IERP), AMBON survey, the Arctic Shelf Growth, Advection, Respiration, Deposition (ASGARD; part of Arctic IERP) project, and the DBO project. Larval and early juvenile Arctic gadids were targeted with a 60-cm bongo (bongo hereafter) equipped with a flow meter and a 505-µm mesh net fished obliquely from 10 m off the bottom or a maximum depth of 200 m to the surface in the late spring and late summer during the AIES and DBO surveys and to 5 m off the bottom or a maximum depth of 200 m for ASGARD. Demersal juvenile Arctic gadids (age-0, age-1 +) were targeted with a benthic-sampling 3-m plumb-staff beam trawl (Abookire and Rose 2005) equipped with 7-mm mesh and a 4-mm cod end liner during the late summer AMBON and AIES surveys (Table 1). The beam trawl was deployed from the stern of the vessel and towed at 1.5–2.0 knots for four minutes (Logerwell et al. 2015). Juvenile gadids (age- 0, age-1 +) were also collected from the midwater during AMBON using a 1.5 m wide by 1.8 m high Isaacs-Kidd Midwater Trawl Net (IKMT) equipped with 3-mm mesh and a flowmeter (Table 1). The IKMT was towed double obliquely at 3.5–4.0 knots and these data were used to look at length and growth of Arctic gadids in August, prior to the late summer AIES surveys.

All bongo samples were fixed at sea in 5% formalin buffered with seawater and processed at the Plankton Sorting and Identification Center in Szczecin, Poland. ELHS of all fishes were identified to species, enumerated, and up to 50 specimens per taxon at each station were measured to the nearest 0.1 mm. Since specimens were measured after formalin fixation, we applied a + 1.9% correction factor to the measured lengths to account for shrinkage (D. Blood, B. Laurel, NOAA, unpublished data; Vestfals et al. 2019). The identifications of ELHS gadids were verified by scientists at the National Oceanic and Atmospheric Administration's Alaska Fisheries Science Center using Matarese et al. (1989), Dunn and Vinter (1984), and Ichthyoplank- ton Information System IIS (2019). Due to concerns of Walleye Pollock (*Gadus chalcogrammus*) being misidentified as Polar Cod, the Arctic gadids captured during AIES using the beam trawl were verified using genetic methods following Wildes et al. (2016). No specimens of juvenile Arctic cod (*Arctogadus glacialis*) were detected (S. Wildes, Alaska Fisheries Science Center (AFSC), personal communication), suggesting that *A. glacialis* was not present in our study region since the abundance of later stages is reflective of the abundance of the earlier stages (Bouchard et al. 2016).

Catch per unit effort of polar cod and saffron cod was reported as the number of individuals caught under a sea surface area of 10 m^2 (count per 10 m^2). Trawl samples (IKMT and beam trawl) were processed at sea with all individual fishes being identified, enumerated, and measured to the nearest length in millimeters. Standard length (SL) was measured for individuals at flexion size or larger and notochord length (NL) for individuals smaller than flexion. The reported size of flexion is 11.0 mm for polar cod and saffron cod (IIS 2019). Catch for the AIES and AMBON beam trawl was expressed as number of individuals caught per unit area swept (count per 1000 m^2).

Data analysis

All catch and length data were analyzed using R (ver. 3.5.2; R Core Team 2019). For the length data, to account for only a subset of larvae being measured (n = 50 maximum), the estimated proportion of individuals at each length was multiplied by the standardized catch at that station (catch-weighted length). Individuals of polar cod and saffron cod larger than 70 mm SL were presumed to be one year or older based on a cutoff identified in the length–frequency distribution and were excluded from the subsequent length analyses.

Table 1 Arctic Integrated Ecosystem Research Program 2017 sampling events in the northern Bering and Chukchi Seas

Survey identifier	Sampling program	Dates	Season	# of samples	Gear used
SQ17-01	ASGARD*	10–29 June	Late spring	61	60BON
NM17-01	AMBON	4–23 August	Late summer	75	PSBT
				13	IKMT
OS17-01	AIES*	8 August–25 September	Late summer	72	60BON
				62	PSBT
HE17-02	DBO*	29 August–10 September	Late summer	64	60BON

AIES Arctic Integrated Ecosystem Survey, *AMBON* Arctic Marine Biodiversity Observation Network, *ASGARD* Arctic Shelf Growth, Advection, Respiration, Deposition, *DBO* Distributed Biological Observatory, *60BON* 60-cm bongo, *IKMT* Isaacs-Kidd Midwater Trawl, *PSBT* 3-m plumb-staff beam trawl

Asterisks (*) denotes programs affiliated with Arctic Integrated Ecosystem Research Program

Our use of 70 mm SL to delineate between age-0 and age-1 polar cod is smaller than the size of this transition identi- fied in prior work determining length at age using otoliths [84.0 mm fork length (FL) and 81.6 mm total length (TL), respectively] (Craig et al. 1982; Lønne and Gulliksen 1989) because standard length excludes measuring the caudal fin rays that are often damaged during collection. The transition of saffron cod from age-0 to age-1 is not as definitive as that for polar cod due to an overlap in size at these ages occurring between 55 and 110 mm FL in the Chukchi Sea (Wolotira 1985; Copeman et al. 2016; Helser et al. 2017). However, in Arctic samples collected in 2012 all individuals greater than 75 mm FL were age-1 based on otolith analyses, suggesting our size cutoff is reasonable for the region sampled (Copeman et al. 2016). Specimens were then aggregated into 2-mm length bins. For the AMBON samples collected with the IKMT and the beam trawl, subsamples of fish were measured to the nearest millimeter. Many of the smallest individuals (less than 50 mm) were not measured and were instead sorted into approximate 10-mm size bins, enumerated in the field, and then discarded. The binned individuals were combined with the measured individuals by simulating individual lengths of the binned individuals from a uniform random distribution within their assigned size bin. Other distributions (normal, beta) were considered for simulating lengths of the binned individuals but had minimal impact on the resulting length-frequencies.

Daily growth rates were estimated for each species as the change in mean length from June 19th, 2017, the median date of the late spring (June) ASGARD survey, and each late summer survey (AMBON and AIES) under the assumption that these individuals were from the same cohort. The median date of the AMBON survey was August 13th, 2017 and the median date of the AIES survey was September 1st, 2017. Mean length for late spring was based on all individuals collected during the survey using the bongo. Mean length for the late summer individuals was gear-specific and calculated based on all putative age-0 specimens collected during: (1) AMBON survey using a beam trawl, (2) AMBON survey using an IKMT, (3) AIES and DBO surveys using a bongo, and (4) AIES survey using a beam trawl. Data for these growth analyses did not include estimates from midwater-collected gadids sampled during the late sum- mer AIES and DBO surveys, but they were available from the IKMT fished during the 2017 late summer AMBON survey, providing some estimates of growth of midwater-associated fishes. Daily growth rates are presented as a range; the estimate provided from the late summer bongo collections represents a low estimate as larger gadids tend to escape from the bongo net (Shima and Bailey 1994) and likely represents individuals that are smaller-than-average. Late summer beam trawl collections (AIES) represent a high growth estimate as the coarser mesh size of the trawl may select for larger individuals that are larger-than-average and generally resulted in the greatest mean size. For polar cod, length-dependent mortality results in slightly greater length at age estimates (Thanassekos et al. 2012), suggesting our study will be overestimating growth since we are relying on changes in length of survivors (those individuals captured and measured by the various gear types) to estimate growth. A daily growth rate was also calculated using the IKMT data to explore differences in the apparent growth rates between age-0 fishes that are still pelagic and those that have become demersal by the time of sampling. We expected the apparent growth rate to increase as individuals become more demersal. Size distribution from the IKMT and beam trawl are likely to be directly comparable as the IKMT mesh size (4 mm) was identical to that of the beam trawl liner.

Densities (catch per unit area) of polar cod and saffron cod were mapped to explore the seasonal distribution of ELHS of Arctic gadids in the northern Bering and Chukchi seas relative to sea ice concentration on June 19th and September 1st, 2017. Sea ice concentrations were obtained from the National Snow and Ice Data Center at 25 km by 25 km spatial resolution (Cavalieri et al. 1996; NSIDC 2019).

Individual-based biophysical model for polar cod and saffron cod

Late spring and late summer distributions were compared to simulated distributions from biophysical transport mod- els parameterized for polar cod and saffron cod larval and early juvenile stages (Vestfals et al. 2021). Details on the model parameterization and the results of validation testing are described in Vestfals et al. (2021). These models were developed to simulate the growth and dispersal of early life stages in the northern Bering, Chukchi, and Beaufort seas to identify possible spawning locations, which are largely unknown, as well as to examine gadid connectivity between these seas. An implementation of the Regional Ocean Modeling System (ROMS) (Shchepetkin and McWilliams 2005) set up in a Pan-Arctic (PAROMS) configuration (Danielson et al. 2016) was used to realistically simulate the three-dimensional (3-D) circulation field. PAROMS has a horizontal resolution of ~ 5 km south of the Aleutian Islands to 9 km in the North Atlantic and is approximately 5.5–6.0 km in the Chukchi Sea, and is forced by the Japanese 55-year atmospheric reanalysis JRA55-do (version 1.4) (Tsujino et al. 2018), which also provides estimates of freshwater runoff. Boundary conditions come from the Simple Ocean Data Assimilation (SODA) reanalysis (version 3.3.1) (Carton et al. 2018) prior to 2015 and the Hybrid Coordinate Ocean Model (HYCOM) (Chassignet et al. 2009) for more recent years. The Oregon State TOPEX/Poseidon Global Inverse Solution (Egbert and Erofeeva 2002) provides tidal forcing and the sea ice field is based on the single-category

Budgell ice model (Budgell 2005). To simulate advection and growth of larvae, IBMs for polar cod and saffron cod were developed using the particle tracking tool TRACMASS that calculates Lagrangian trajectories from Eulerian velocity fields (Döös 1995).

Stage-specific and size-specific temperature-dependent growth rates were used to model the growth of polar cod and saffron cod (Porter and Bailey 2007; Laurel et al. 2016; Koenker et al. 2018) to 45 mm in length, the size at which these species are thought to transition from pelagic juveniles to more demersal juveniles, with enhanced swimming abilities. In addition, these stages correspond most closely to the stages captured by the water column sampling gear (bongo and IKMT) during the field campaign allowing for comparison between simulated and observed distributions of the two species. Similar to the growth rates calculated for the 2017 empirical data, mean daily growth rates were estimated for the simulated larvae for each species as the change in mean length from late spring (June 19th) to late summer (September 1st) divided by the number of days elapsed.

Hatching locations were identified through a thorough literature review, anecdotal evidence, and known areas of retention in the Pacific Arctic (Vestfals et al 2021 and references therein). However, due to the preponderance of early-stage individuals encountered in the Kotzebue Sound region during spring 2017, we focused this study on this region as a potential source of polar cod and saffron cod in the US Chukchi Sea. For our study, Kotzebue Sound will include the area that extends from the northwestern tip of Seward Peninsula to Point Hope. Simulations were initialized from all PAROMS grid points falling within the eastern-most part of Kotzebue Sound as hatching location (Fig. 1), with 10 particles released per 5 m depth increment to the bottom at each PAROMS grid point. The Chukchi Sea is often shallower than 40 m, which represents the maximum release depth of particles in the model (Vestfals et al. 2021). Based on results from initial particle simulations, dispersal simulations were conducted with larvae hatching on the 1st and 15th day of each month from March 1st to May 15th, for a total of six hatching events. Temperature-mediated growth and dispersal of larvae were simulated until September 1st, the midpoint of the late summer Arctic field surveys in 2017, so that the simulated distribution and size composition during summer could be compared to the observed distributions and size compositions of individuals captured during the surveys.

IBM parameterization-polar cod

Several vertical behaviors were developed for polar cod based on available literature (Borkin et al. 1986; Bouchard et al. 2016) and from laboratory observations (B. Laurel, AFSC, *unpublished data*). Of the five different vertical behavior routines tested, simulations with surface-oriented individuals, where all stages were found at 5 m matched best with prior field observations from acoustic-trawl surveys conducted in 2012 and 2013 (DeRobertis et al. 2017; Vestfals et al. 2021). Polar cod growth was based on growth equations described in Koenker et al. (2018) and Laurel et al. (2016). Simulated larval sizes and distributions on June 19th (midpoint of the ASGARD survey) and September 1st (midpoint of AIES) from simulations originating in Kotzebue Sound were compared to field observations.

IBM parameterization-saffron cod

Similar vertical behaviors were used for the saffron cod simulations as for polar cod since no information on the vertical distribution of saffron cod larvae is available at present. Preflexion larval growth from hatch to 10 mm in length was based on temperature-dependent growth experiments (B. Laurel, unpublished data; Vestfals et al. 2021). At present, temperature-dependent growth models for saffron cod ELHS > 10 mm in length are not available. As growth of saffron cod at these small sizes is linear and resembles that of walleye pollock (B. Laurel, AFSC, unpublished data), the growth model described in Porter and Bailey (2007) was used to model saffron cod growth from 10 to 45 mm.

Results

Field data

Sea ice

As of June 1st, just prior to the survey, sea ice was present in the Kotzebue Sound region (S. Danielson, University of Alaska Fairbanks (UAF), unpublished data). By June 19th, the mid-point of the late spring survey, sea ice was receding and the entire survey area was ice-free.

Abundance, distribution, and size of polar cod

In June, the highest densities of polar cod (> 640 individuals per 10 m^2) were found at nearshore stations of Kotzebue Sound and Point Hope transects and along the entire Cape Lisburne transect (Fig. 2a). Polar cod density was lower south of the Bering Strait with most individuals being encountered along the northernmost transects sampled in the Chukchi Sea. By late summer (August and September), sea ice remained absent in the survey region south of 75°N, except in the nearshore area of Kotzebue Sound. The overall density of polar cod decreased from an average catch of 1183 individuals per 10 m^2 in the late spring to 7 individuals per 10 m^2 in the late summer in the

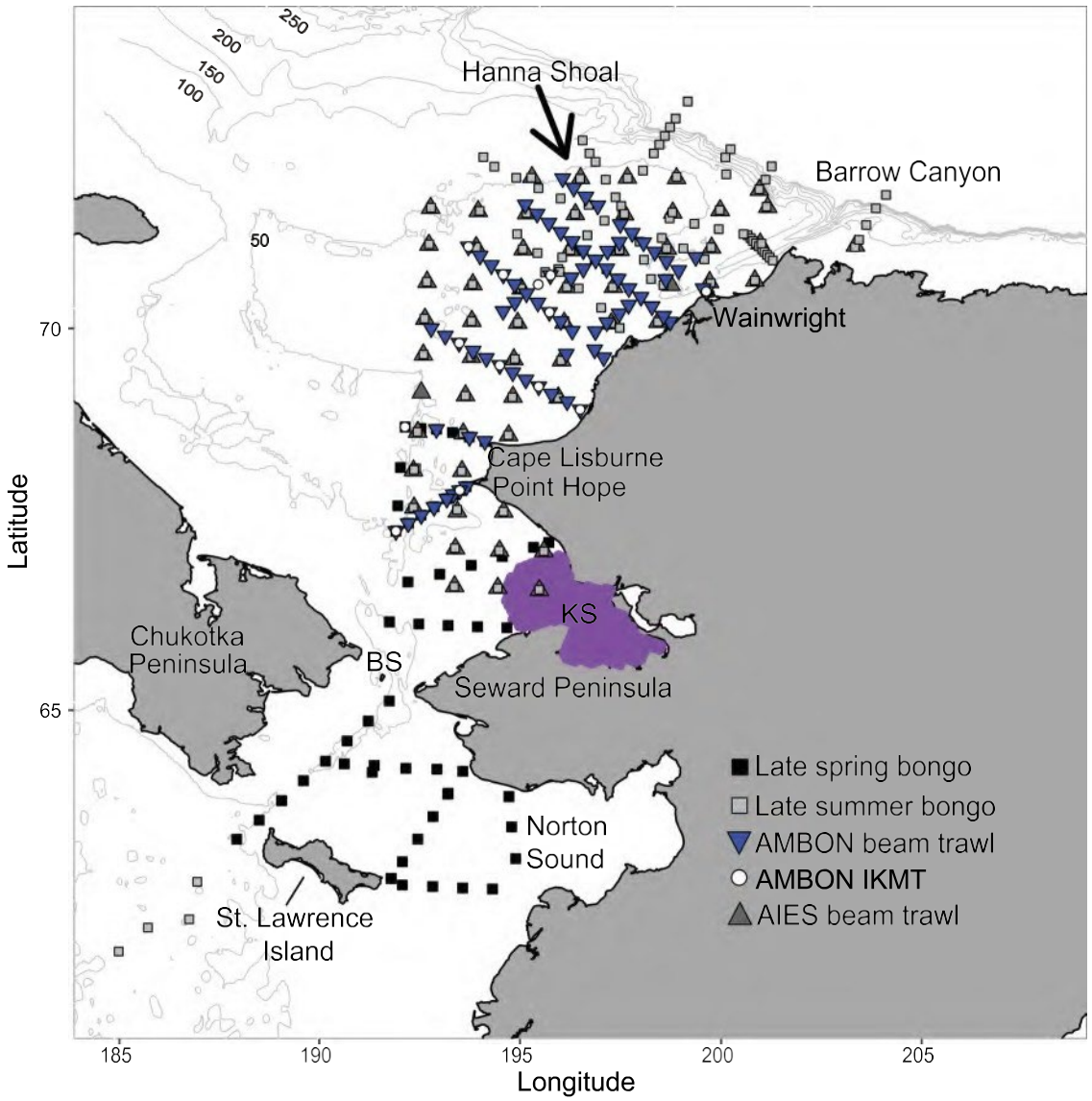

Fig. 1 Survey stations sampled in 2017 in the Chukchi Sea, Bering Strait (BS), and northern Bering Sea. Bongo –Late spring black squares and late summer (August/September) gray squares; beam trawl–AMBON survey (August) blue inverted triangles and AIES (August/September) dark gray triangle; and Isaacs-Kidd Midwater Trawl (IKMT) –AMBON survey (August) white circles. Simulated release locations from the individual-based model in the eastern-most area of Kotzebue Sound (KS), which is shaded in purple. Kotzebue Sound also refers to the broader region from the northwestern tip of Seward Peninsula and Point Hope to the north. Depth contours extend from 50 to 250 m in 50 m increments

water column. The highest densities of polar cod in the water column (> 10 individuals per 10 m^2) were observed in the northern portion of the survey area in the late sum- mer, particularly around Barrow Canyon and Hanna Shoal (Fig. 2b). The distribution of polar cod in the water col- umn was similar to the distribution of demersal individu- als. Demersal catches of juvenile polar cod (< 70 mm SL) were highest offshore in the northern Chukchi Sea in the late summer in areas where bottom water temperatures were below approximately 5 °C (Fig. 3a and b).

In June, the mean length of polar cod larvae in the water column was 9.8 mm NL (n = 850), with most larvae being less than 12.0 mm in length (Fig. 4a; Table 2). By the end of the summer, the length distribution of polar cod had expanded and the mean length increased to 30.1 mm SL ± 0.9 (n = 140) and 30.7 mm SL ± 0.4 (n = 433) for specimens collected in the water column with the bongo and IKMT gears, respectively (Fig. 4c, e; Table 2). In late summer (August–September) the mean length of demersal polar cod was 39.7 mm SL ± 0.4 (n = 718) in the AMBON

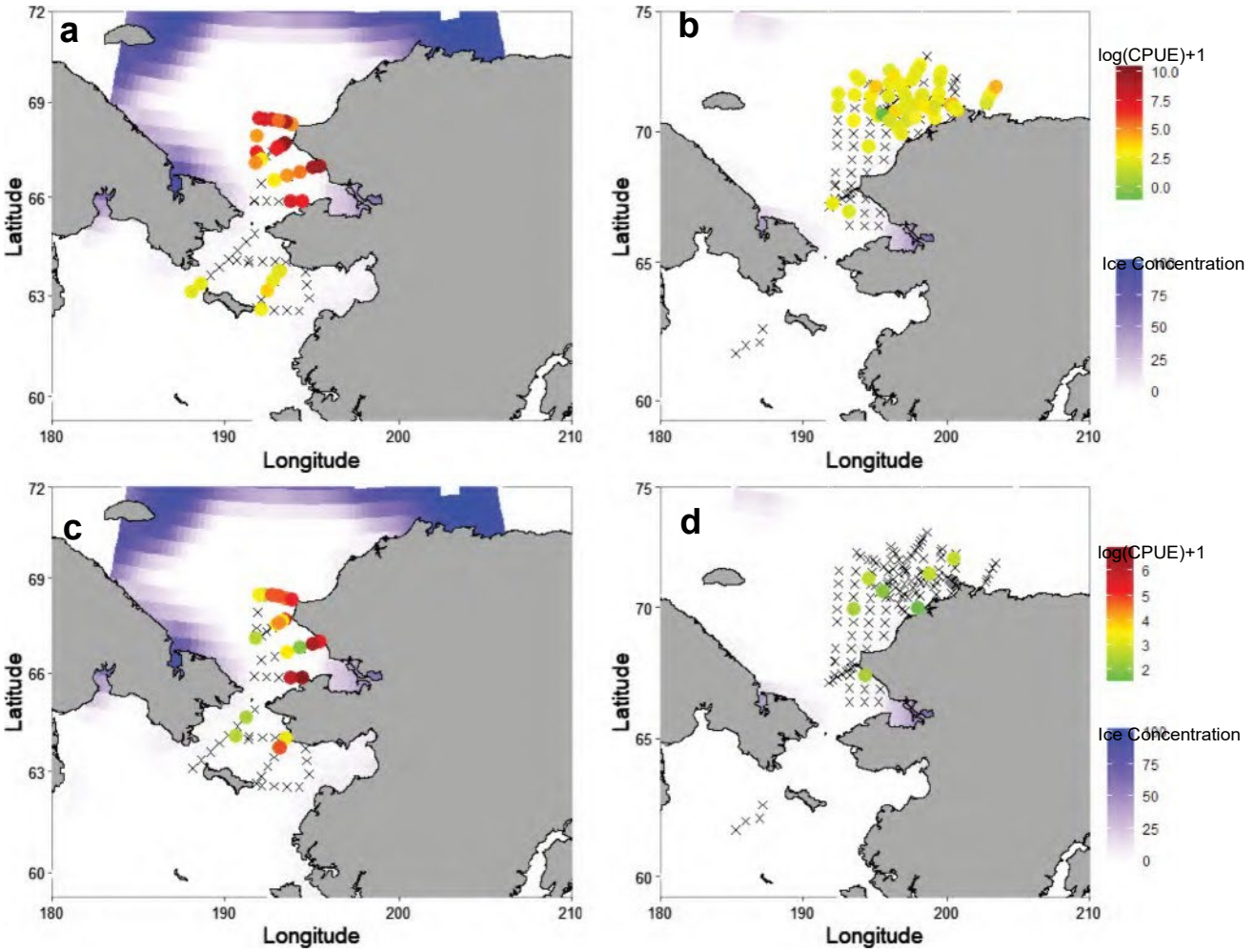

Fig. 2 Distribution of polar cod (*Boreogadus saida*) (**a**, **b**) and saffron cod (*Eleginus gracilis*) (**c**, **d**) in late spring (left column) and late summer (right column) 2017 collected in the water column with the 60-cm bongo net. Catch data are reported as catch-per-unit-effort (CPUE) and log(CPUE)+1 to highlight variability at lower abundances. Ice concentration (% cover) is plotted in the background. Black X's denote sampled stations where polar cod and saffron cod were not caught. Note the different scales for CPUE between the species

beam trawl samples and 47.8 mm SL ± 1.6 (n = 690) in the AIES beam trawl samples (Fig. 4g, i; Table 2). Based on changes in length and an assumption that larvae collected in the late summer surveys were from the same cohort as fish collected in the late spring, the estimated daily growth rate for polar cod during 2017 ranged from 0.27 mm day^{-1} based on individuals in the water column to 0.53 mm day^{-1} based on individuals that had become demersal (Table 3), with an overall mean of 0.39 ± 0.06 mm day^{-1} (n = 4) based on all measured individuals.

Abundance, distribution, and size of saffron cod

The density of pelagic larval saffron cod in June was high- est at the nearshore stations in Kotzebue Sound and Cape Lisburne, which were both ice covered on June 1st, prior to the mid-point of the survey, with densities ranging from 68 to 444 individuals per 10 m^2. The highest observed density of saffron cod was at the innermost station along the southern margin of Kotzebue Sound (Fig. 2c). Catches south of Kotzebue Sound were low (less than 30 individu- als per 10 m^2). Densities of saffron cod were much lower later in the summer (August and September), with most of the stations yielding no saffron cod (Fig. 2d). Unlike saffron cod in the water column, demersal larval and early juvenile saffron cod in later summer were rarely encountered offshore, with most individuals concentrated near Cape Lisburne (Fig. 3c and d). Demersal saffron cod were observed in areas with higher bottom temperatures than demersal polar cod. In early August, saffron cod were con- centrated in areas with bottom water temperatures greater

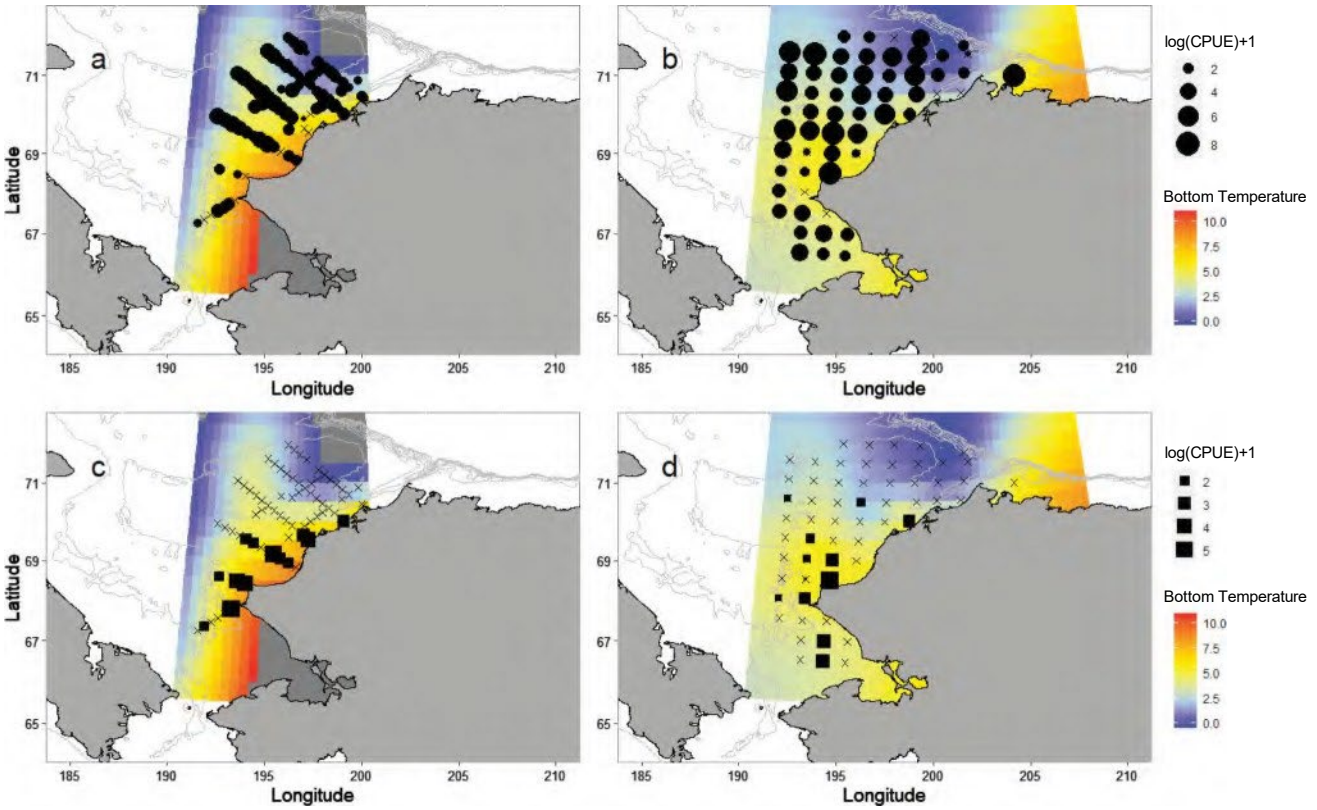

Fig. 3 Late summer distributions of demersal juvenile polar cod (*Boreogadus saida*) from AMBON (**a**) and AIES (**b**) beam trawl collections and of demersal juvenile saffron cod (*Eleginus gracilis*) from the AMBON (**c**) and AIES (**d**) beam trawl collections. The background color denotes bottom temperature in °C. Catch data are reported as catch-per-unit-effort (CPUE) and log(CPUE) + 1 to highlight variability at lower abundances. Note the different scales for CPUE between the species

than 7.5 °C and by September occupied areas with bottom water temperatures greater than 5.4 °C.

Saffron cod had a mean length of 9.3 mm NL ± 0.4 (n = 299) in June, with most individuals measuring less than 14.0 mm in length (Fig. 4b; Table 2). By late summer, the mean length of saffron cod ranged from 18.5 mm SL ± 1.4 (n = 7) in the bongo to 40.3 mm SL ± 1.7 (n = 41) in the IKMT (Fig. 4d, f). The mean length of demer- sal saffron cod was 51.6 mm SL ± 0.4 (n = 318) in the AMBON beam trawl and 55.1 mm SL ± 1.7 (n = 54) in the AIES beam trawl by late summer (Fig. 4h, j; Table 2). The daily growth rate for saffron cod was estimated as 0.12 mm day^{-1} to 0.76 mm day^{-1} (Table 3), with a mean of 0.37 ± 0.16 mm day^{-1} (n = 4).

Comparison of distribution and size of polar cod and saffron cod

Catches of saffron cod were lower relative to polar cod regardless of season. In June, the core distribution of saffron and polar cod overlapped in Kotzebue Sound, with polar cod found farther offshore than saffron cod (Fig. 2). Later in the summer, saffron cod were encountered in bongo samples of the water column at only 7 of the 136 stations sampled. Demersal juveniles of polar cod were observed farther offshore and to the north relative to saffron cod in the late summer. They were also most abundant offshore of the region between Cape Lisburne and Wainwright at stations with bottom water temperatures cooler than 5.0 °C. In contrast, demersal juveniles of saffron cod were most abundant nearshore off Cape Lisburne and in northern Kotzebue Sound where bottom water temperatures were warmer than 7.5 °C (Fig. 3b, d).

Polar cod and saffron cod were similar in mean size in June when their distributions also overlapped. Later in the season, far fewer saffron cod (n = 420) were captured and measured compared to polar cod (n = 1981). Demer- sal saffron cod were larger than those found in the water column in the late summer. The range of daily growth rates was wider for saffron cod than polar cod, but the mean daily growth rate was similar between saffron cod and polar cod at 0.37 ± 0.16 and 0.39 ± 0.06 mm day^{-1}, respectively (n = 4).

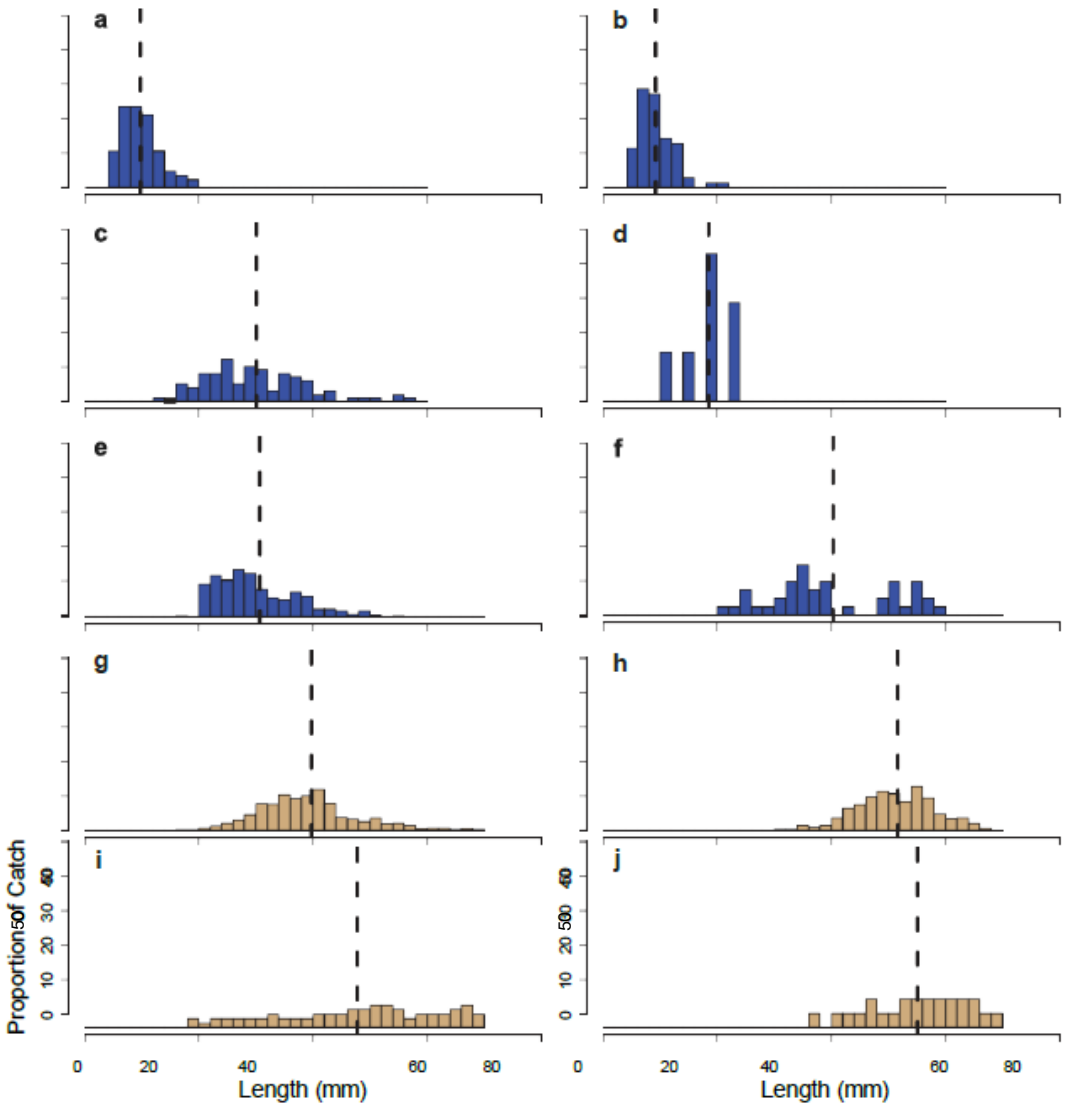

Fig. 4 Length distributions of polar cod (*Boreogadus saida*) (left) and saffron cod (*Eleginus gracilis*) (right) during the late spring (**a**, **b**) and late summer collections with 60-cm bongo (**c**, **d**), Isaacs-Kidd Midwater Trawl (IKMT) (**e**, **f**), AMBON beam trawl (**g**, **h**), and AIES beam trawl (**i**, **j**). Dotted black lines denote the mean length for each histogram. Blue bars represent individuals collected from the water column and brown bars represent those collected along the seafloor. Specimens are binned into 2-mm length intervals and standardized by CPUE when all captured individuals were not measured (i.e., bongo)

IBM simulated data

Simulated distribution and size of polar cod

On June 19th, simulated polar cod hatching in Kotzebue Sound between March 15th and May 15th had similar dispersal trajectories and were mostly found to be retained in and around Kotzebue Sound and in the nearshore region northward to Cape Lisburne (Fig. 5). At Cape Lisburne, some larvae were transported offshore to the north and to the west, and were concentrated in two different trajectories, except for simulated individuals hatched on May 15th. Other individuals were transported northward along the coastline. Based on the 2017 simulations, no individuals were transported to the south in the late spring, though polar cod were observed in the late spring survey around St. Lawrence Island (Fig. 2a; Fig. 5). By September 1st, simulated polar cod were found in the nearshore region from Kotzebue Sound north to Wainwright (Fig. 6). Simulated polar cod were advected offshore, almost due west, at Cape Lisburne/

Table 2 Late spring and late summer 2017 observed length data for polar cod (*Boreogadus saida*) and saffron cod (*Eleginus gracilis*)

Species	Late Spring	Late Summer			
	60BON	60BON	IKMT	AMBON Trawl	AIES Trawl
Polar cod	5.1 NL–19.7 (9.8 ± 0.4 NL, *n* = 850)	13.2–56.1 (30.1 ± 0.9, *n* = 140)	18.0–56.0 (30.7 ± 0.4, *n* = 433)	*18.0–69.0 (39.7 ± 0.4, n = 718)*	*18.5–69.8 (47.8 ± 1.6, n = 690)*
Saffron cod	4.7 NL–21.2 (9.3 ± 0.4 NL, *n* = 299)	11.4–22.4 (18.5 ± 1.4, *n* = 7)	22.0–59.0 (40.3 ± 1.7, *n* = 41)	*31.0–68.0 (51.6 ± 0.4, n = 318)*	*37.9–69.0 (55.1 ± 1.7, n = 54)*

Mean size, standard error, and sample size (*n*) are displayed within the parentheses. Demersal gears are emphasized in italics and all lengths are reported in mm and in standard length, unless noted otherwise

AIES Arctic Integrated Ecosystem Survey, *AMBON* Arctic Marine Biodiversity Observation Network, *60BON* 60-cm bongo, *IKMT* Isaacs-Kidd Midwater Trawl, *NL* notochord length

Table 3 Daily growth rate estimates (mm day^{-1}) for polar cod (*Boreogadus saida*) and saffron cod (*Eleginus gracilis*) in the Chukchi Sea between late spring and late summer

Species	60BON	IKMT	*AMBON Trawl*	*AIES Trawl*	Mean daily
Polar cod	0.27	0.37	*0.53*	*0.51*	0.39 ± 0.06 (*n* = 4)
Saffron cod	0.12	0.56	*0.76*	*0.61*	0.37 ± 0.16 (*n* = 4)

Demersal sampling gears are emphasized in italics

AIES Arctic Integrated Ecosystem Survey, *AMBON* Arctic Marine Biodiversity Observation Network, *60BON* 60-cm bongo, *IKMT* Isaacs-Kidd Midwater Trawl, *n* sample size

Point Hope. Hatch date did not greatly impact the end points of the simulated polar cod on September 1st (Fig. 6). In the late summer, simulated polar cod were abundant offshore of Cape Lisburne/Point Lay and Wainwright but uncommon nearshore along the coastline from Kotzebue Sound to Wainwright (Fig. 6), which was consistent with the empirical data (Fig. 2b; Fig. 3).

The mean size of simulated polar cod individuals hatched between March 1st and April 1st was larger than individuals captured in the field (Fig. 4, Fig. 7). Simulated individuals hatched on May 1st and May 15th were on average smaller than the field samples. For larvae that hatched on April 15th, the average size of simulated polar cod matched the average size of the captured individuals, although the range was broader for the individuals caught in the field compared to the simulated individuals (Table 2, Table 4). In the late summer, the average size of the simulated polar cod was smaller than the wild-caught specimens regardless of hatch date (Fig. 7). The simulated sizes were most similar to polar cod captured using the bongo in the late summer (Table 2, Table 4).

Simulated distribution and size of saffron cod

The simulated distribution of saffron cod in the late spring and late summer was similar to that of polar cod (Fig. 8). Similar to polar cod in the late spring, no simulated saffron cod larvae were found along the southern coastline of Kotzebue Sound, whereas saffron cod larvae were captured along the southern coastline of Kotzebue Sound and northern coastline of Norton Sound (Figs. 2–3). In the late summer, simulated saffron cod were densely concentrated along the coastline extending from Kotzebue Sound to just north of Wainwright with two offshore advection areas at Point Lay/Cape Lisburne and south of Wainwright (Fig. 9). Catches of saffron cod were low in the late summer but the areas with the highest catches corresponded to high den- sity areas identified by the model, particularly offshore of Wainwright and Point Lay/Cape Lisburne (Figs. 2–3; 9).

Regardless of season or hatch date, simulated saffron cod were smaller on average than field captured individu- als (Table 2, Table 4). In addition, the length range of simulated individuals was narrower than the captured individuals in the late spring and late summer (Fig. 10). Unlike simulated polar cod, there was little overlap in the late spring and late summer sizes of simulated saffron cod (Fig. 10). In the late spring, simulated saffron cod did not grow larger than 8.5 mm NL and had a mean size of 5.7 mm NL ± 0.0025–0.0037 for all simulated hatch dates (Fig. 10, Table 4). In the late summer, the average size of simulated saffron cod ranged from 14.6 mm SL ± 0.024 to 14.9 mm SL ± 0.023 (Fig. 10, Table 4).

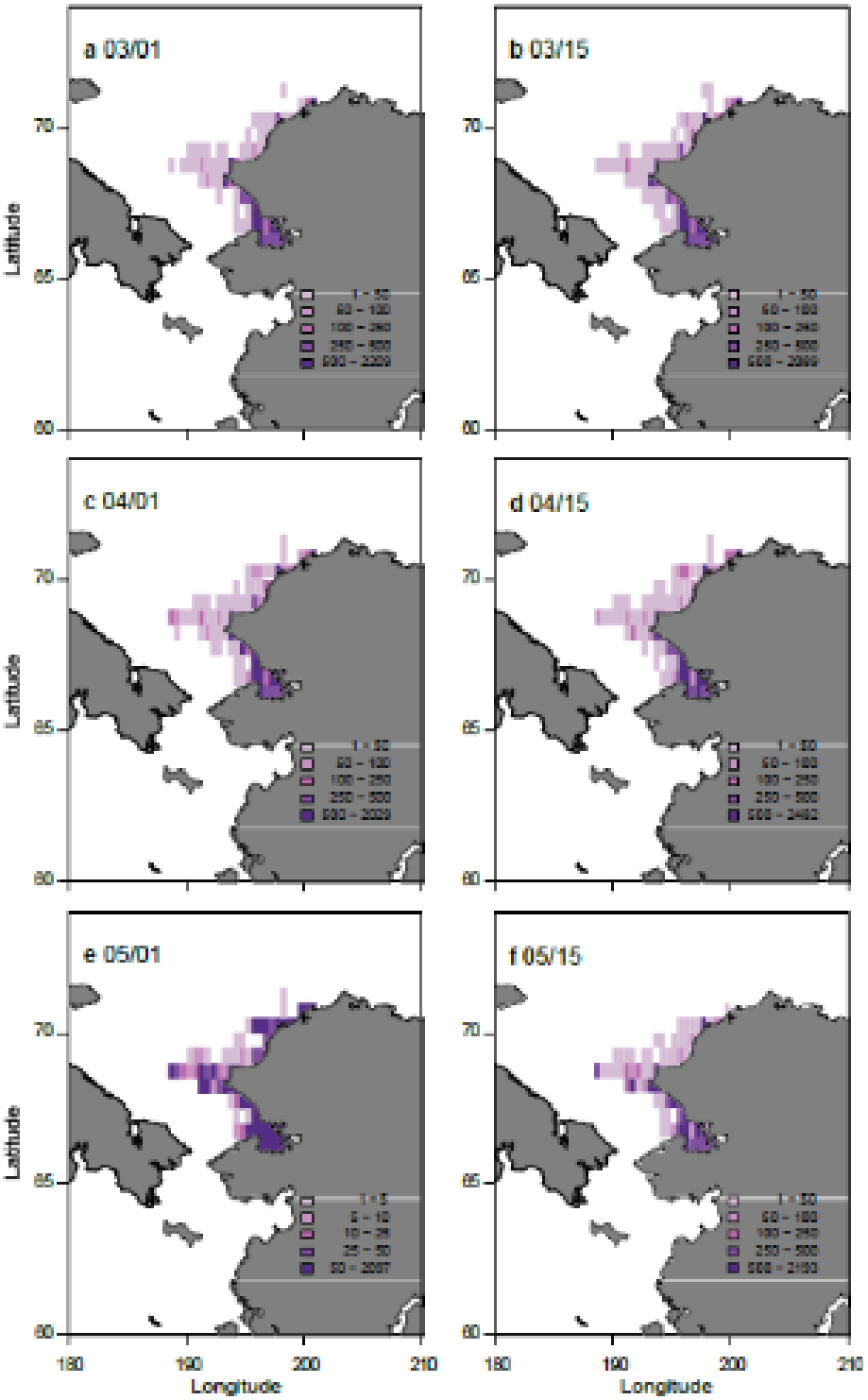

Fig. 5 Density of simulated endpoints from individual-based models in the late spring (June 19th, 2017) for polar cod (*Boreogadus saida*) larvae hatching in Kotzebue Sound. Hatch dates are: **a** March 1st, **b** March 15th, **c** April 1st, **d** April 15th, **e** May 1st, and **f** May 15th. Density is calculated in a 0.5 × 0.5 degree grid

Discussion

Spawning areas and drift

Sea ice was present in Kotzebue Sound at the approximate time of hatch for both polar cod and saffron cod until early June (S. Danielson, UAF, unpublished data; Cavalieri et al. 1996), suggesting that sea ice may be important for the newly hatched larvae of both species. Kotzebue Sound may indeed be a hatching area for polar cod and a source of juveniles to the north later in the summer. One of the main northward currents in the eastern Chukchi Sea is the Alaska

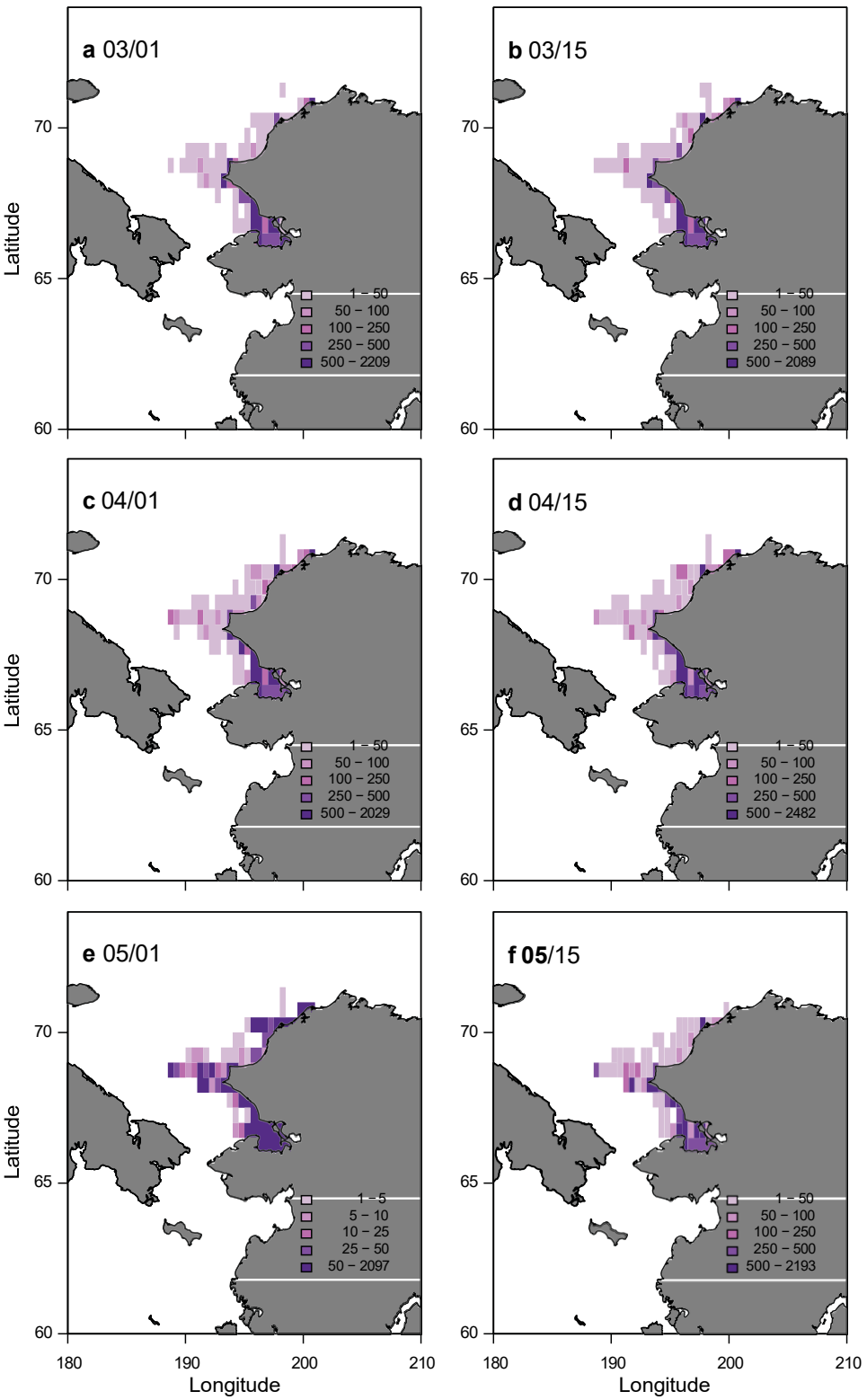

Fig. 6 Density of simulated endpoints from individual-based models in the late summer (September 1st, 2017) for polar cod (*Boreogadus saida*) hatching in Kotzebue Sound. Hatch dates are: **a** March 1st, **b** March 15th, **c** April 1st, **d** April 15th, **e** May 1st, and **f** May 15th. Density is calculated in a 0.5 × 0.5 degree grid

Coastal Current (ACC), which flows through Bering Strait and past the mouth of Kotzebue Sound and it is likely to entrain larvae originating in the Sound. Transport through Bering Strait has been increasing in recent years, which, in turn, has increased heat transport into the Chukchi Sea and the rate of sea ice retreat in the spring (Woodgate et al. 2012; Woodgate 2018), as well as current velocity that may increase the dispersal potential for ELHS entrained in the

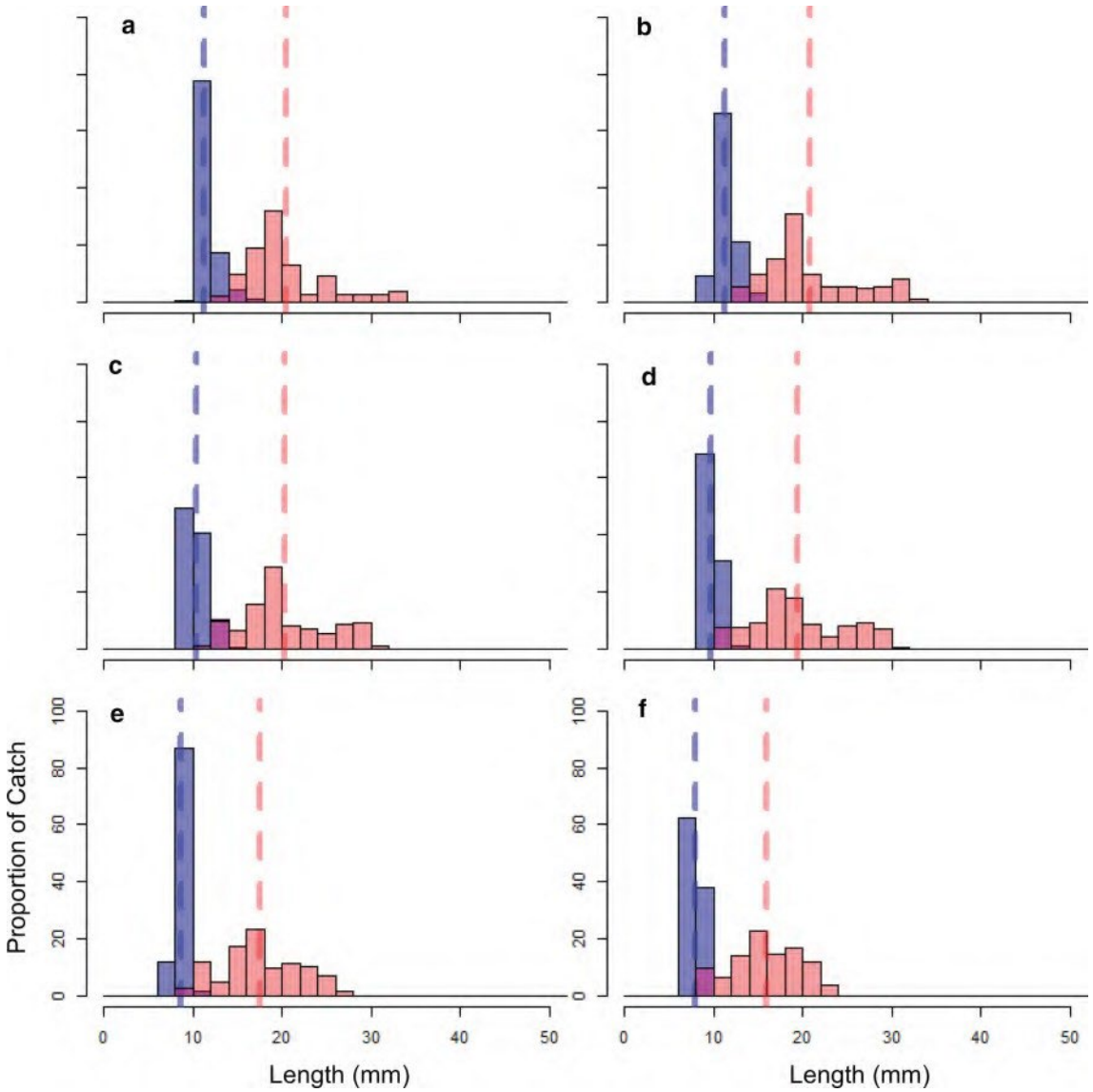

Fig. 7 Length histograms of simulated polar cod (*Boreogadus saida*) larvae by hatch date from the individual-based model in 2017. Hatch dates are: **a** March 1st, **b** March 15th, **c** April 1st, **d** April 15th, **e** May 1st, and **f** May 15th. Blue bars represent late spring (June 19th) lengths and red bars represent late summer (September 1st) lengths. The dashed blue line denotes the mean size of the simulated polar cod in the late spring, whereas the red dashed line denotes the mean size of the simulated polar cod in the late summer. Specimens are binned into 2-mm length intervals

ACC. However, high polar cod abundance in the summer of 2014 corresponded to reduced transport through the Bering Strait (Randall et al. 2019), leading to decreased advection and higher local retention of ELHS. Simulations suggest that polar cod collected along the seafloor and in the water column along the coast and in some offshores areas were likely hatched in Kotzebue Sound and were transported north by the ACC to the northern Chukchi Sea. We believe the likelihood of contamination of polar cod by Arctic cod (*A. glacialis*) is low and not of concern for our analyses. The identity of polar cod collected in the late summer AIES beam trawl was confirmed genetically (S. Wildes, Alaska Fisheries Science Center (AFSC), personal communication). Since the primary currents entering the US Chukchi Sea shelf flow from the south to the north (Danielson et al. 2017), it is unlikely that there is a source of Arctic cod, a high Arctic species, in the southern Chukchi Sea or Bering Strait that would substantially contribute to the larval gadid community of the region (Aschan et al. 2009), especially considering the low sea ice and high water temperatures observed in 2017 (Timmermans et al. 2017; Perovich et al. 2017).

Saffron cod are caught in lower densities than polar cod in the late summer, likely due to their ELHS preferring nearshore habitats not sampled by our surveys (Logerwell

Table 4 Late spring and late summer 2017 simulated length data for polar cod (*Boreogadus saida*) and saffron cod (*Eleginus gracilis*)

Late spring						
	3/1	3/15	4/1	4/15	5/1	5/15
Polar cod	9.8–17.6 (11.3 ± 0.010) *n* = 19,970	9.3–16.7 (11.2 ± 0.0091) *n* = 19,970	8.5–15.1 (10.5 ± 0.0077) *n* = 19,970	7.9–14.1 (9.7 ± 0.0066) *n* = 19,970	7.2–11.7 (8.7 ± 0.0043) *n* = 19,970	6.6–9.7 (7.9 ± 0.0032) *n* = 19,970
Saffron cod	5.1–8.4 (5.7 ± 0.0037) *n* = 19,970	5.1–8.5 (5.7 ± 0.0037) *n* = 19,970	5.1–8.5 (5.7 ± 0.0035) *n* = 19,970	5.1–8.5 (5.7 ± 0.0033) *n* = 19,970	5.1–8.4 (5.7 ± 0.0028) *n* = 19,970	5.1–8.4 (5.6 ± 0.0025) *n* = 19,970
Late summer						
	3/1	3/15	4/1	4/15	5/1	5/15
Polar cod	12.6–33.7 (20.4 ± 0.032) *n* = 19,908	11.4–33.9 (20.8 ± 0.036) *n* = 19,872	10.5–32.0 (20.2 ± 0.034) *n* = 19,895	9.8–30.7 (19.4 ± 0.036) *n* = 19,945	9.1–27.8 (17.6 ± 0.031) *n* = 19,966	8.3–23.5 (15.9 ± 0.026) *n* = 19,947
Saffron cod	9.7–25.3 (14.9 ± 0.023) *n* = 19,919	9.6–25.0 (14.8 ± 0.024) *n* = 19,873	9.6–25.4 (14.7 ± 0.024) *n* = 19,914	9.6–52.7 (14.6 ± 0.024) *n* = 19,940	9.6–35.7 (14.8 ± 0.021) *n* = 19,965	10.7–30.4 (14.9 ± 0.020) *n* = 19,940

Mean size in mm and standard error are reported within the parentheses for each hatching date and sample size (*n*) is reported

et al. 2015; Vestfals et al. 2019). Similar to polar cod, Kotzebue Sound may be a hatching or early nursery area for saffron cod in the late spring. Demersal saffron cod were concentrated in the nearshore, warm waters in northern Kotzebue Sound and around Cape Lisburne, which was similar to the model-predicted distribution, suggesting that saffron cod hatched in Kotzebue Sound were the major source of demersal individuals in the late summer of 2017. Albeit speculative, the few larval saffron cod caught in the water column offshore of Wainwright and Barrow Canyon may be a result of a bet-hedging spawning strategy for saffron cod spawned in Kotzebue Sound and Bering Strait, such as has been documented in other sub-arctic gadids (Laurel et al. 2008; Hutchings and Rangeley 2011). Prolonged hatching periods will result in later hatched saffron cod larvae developing in warmer water where growth rates may be enhanced if mortality related to prey and predators is reduced (Laurel et al. 2008).

Growth and development

The daily growth rates calculated for polar cod and saffron cod were based on individuals collected in the water column and along the bottom using gears that collectively target larvae and juveniles and are used as a coarse estimate of growth in the US Chukchi Sea in the absence of otolith-derived growth rates. Assuming no size-selectivity over the range of sizes that were present, we were able to estimate a range of daily growth rates based on changes in mean length between specimens collected in the late spring and late summer of 2017. Our estimates assume that measured individuals were randomly selected from the same cohort sampled in the late spring and again in the late summer. However, it is probable that individuals from other hatching locations and cohorts were present in the northern Chukchi Sea in the late summer, violating this assumption (e.g., larvae originating from the other side of the U.S. –Russian Federation maritime boundary). In our region in 2017, hatching was observed from January through May, with a peak in April (Z. Chapman, UAF, personal communication), based on the individuals captured during the late spring bongo samples. However, we are likely missing newly hatched larvae in the late spring bongo samples due to the extrusion of these individuals through the 505 μm bongo net mesh (Thanassekos et al. 2012), biasing our samples to individuals that hatched earlier or possessing higher growth rates. The daily growth rate results should be interpreted with caution without a more robust measure of growth using otolith-derived estimates, which is impos- sible for our study due to our specimens being preserved in formalin at sea. Otolith-derived ages would provide refinement of the length-based daily growth rates estimated in this study by determining individual growth rates and allowing for subsequent exploration of differences in growth trajectories by gear type, sampling season, and region. However, we did account for differences in growth rate by gear type and sampling time by estimating daily growth rates as a range, providing a conservative and a maximal estimate each late summer survey and gear type. Our length-based daily growth estimates also assume a constant growth rate over the sampling season, which is likely violated as individuals attain later stages and larger sizes (Thanassekos and Fortier 2012). Daily growth estimated in this study for polar cod ranged from 0.27 mm day^{-1} to 0.53 mm day^{-1} with a mean of 0.39 ± 0.06 mm day^{-1} (n = 4). Our most conservative

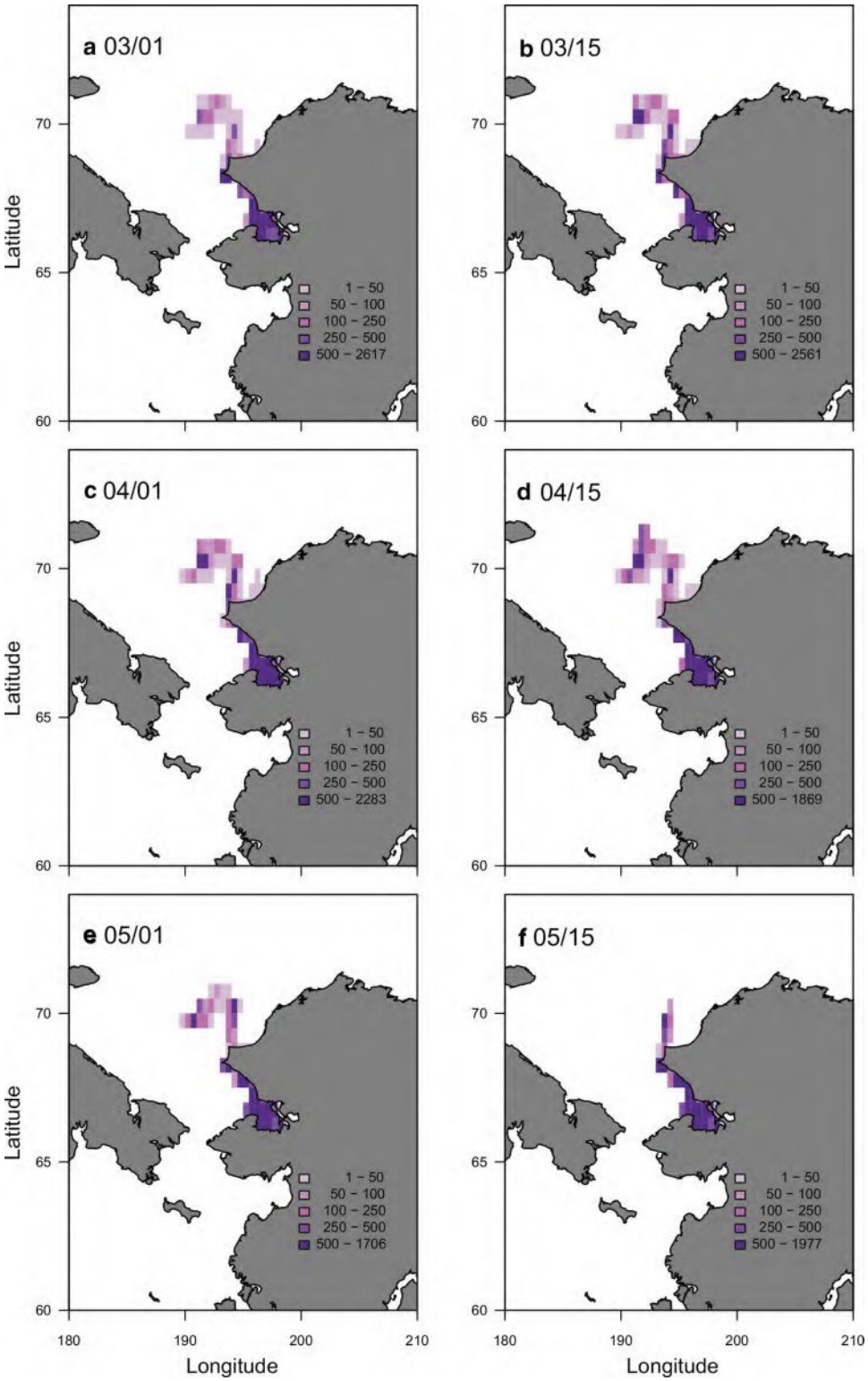

Fig. 8 Density of simulated endpoints from individual-based models in the late spring (June 19th, 2017) for saffron cod (*Eleginus gracilis*) hatching in Kotzebue Sound. Hatch dates are: **a** March 1st, **b** March 15th, **c** April 1st, **d** April 15th, **e** May 1st, and **f** May 15th. Density is calculated in a 0.5 × 0.5 degree grid

growth estimate for polar cod (0.27 mm day^{-1}) agrees well with previous field studies (Bouchard and Fortier 2011; Thanassekos et al. 2012; Vestfals et al. 2019). Daily growth for polar cod in this study may also be higher than is typical due to the elevated water temperatures experienced in 2017. Even though polar cod are adapted to maximize growth at colder temperatures than saffron cod, warmer spring sea surface temperature and earlier ice retreat may be advantageous to larval polar cod due to the availability of zooplankton production supported by earlier

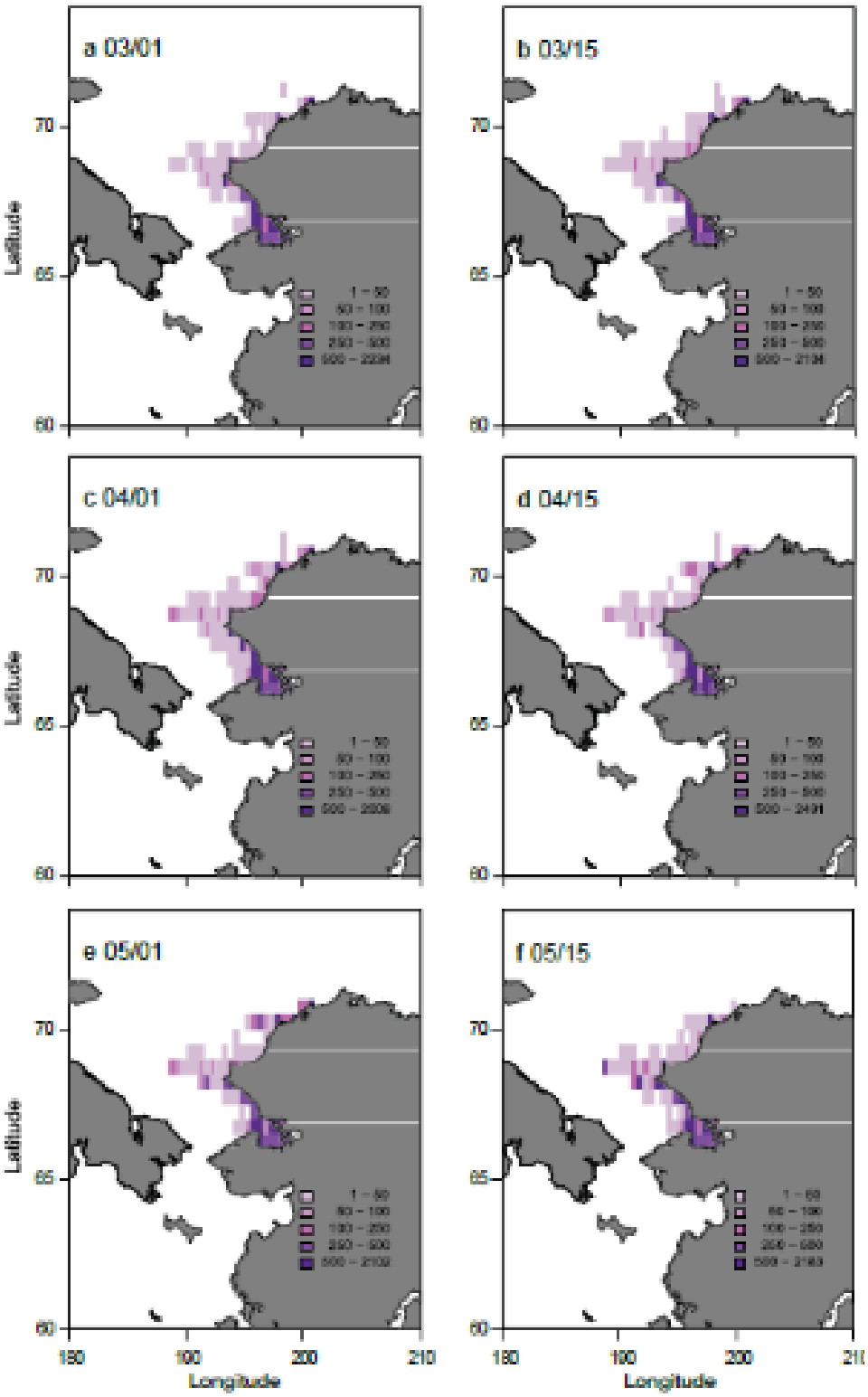

Fig. 9 Density of simulated endpoints from individual-based models in the late summer (September 1st, 2017) for saffron cod (*Eleginus gracilis*) hatched in Kotzebue Sound. Hatch dates are: **a** March 1st, **b** March 15th, **c** April 1st, **d** April 15th, **e** May 1st, and **f** May 15th. Density is calculated in a 0.5 × 0.5 degree grid

ice algae and phytoplankton blooms. This would improve the temporal match of early hatching polar cod with their zooplankton prey (Bouchard et al. 2017). Under scenarios of continued warming in the Arctic, polar cod may lose this growth advantage leading to reduced survival when thermal tolerances of their ELHS are exceeded.

This study is one of the first to estimate daily mean growth for ELHS of saffron cod (0.12–0.76 mm day^{-1};

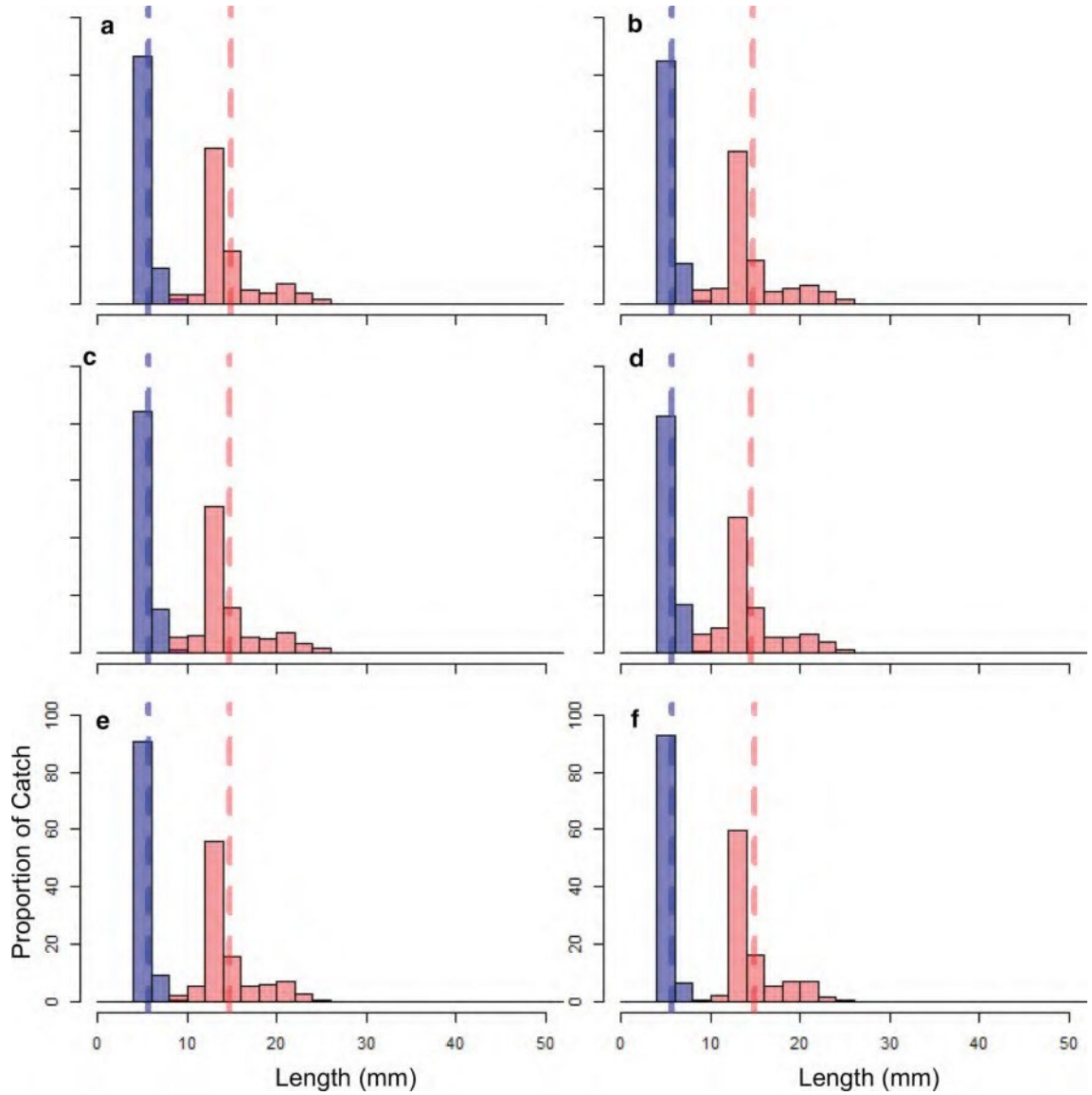

Fig. 10 Length histograms of simulated saffron cod (*Eleginus gracilis*) larvae by hatch date from the individual-based model in 2017. Hatch dates are: **a** March 1st, **b** March 15th, **c** April 1st, **d** April 15th, **e** May 1st, and **f** May 15th. Blue bars represent late spring (June 19th) lengths and red bars represent late summer (September 1st) lengths. The dashed blue line denotes the mean size of the simulated saffron cod in the late spring, whereas the red dashed line denotes the mean size of the simulated saffron cod in the late summer. Specimens are binned into 2-mm length intervals

0.37 ± 0.16 mm day^{-1}; n = 4) collected within the Chukchi Sea. The conservative estimate for daily growth for saffron cod was based on bongo collections in the late summer. The lack of larger saffron cod in the bongo gear compared to the mid-water trawl suggests that larger saffron cod were present in the water column, but avoided the bongo net, which targets smaller individuals (De Robertis et al. 2017; Vestfals et al. 2019). A more realistic lower estimate for daily growth was derived from the mid-water IKMT at 0.56 mm day^{-1}. Saffron cod experience faster growth and better condition at higher temperatures than polar cod (Laurel et al. 2016; Vestfals et al. 2019), consistent with larger sizes and higher apparent growth rates in this study, therefore, a warming Arctic may favor saffron cod over polar cod. The growth advantage for saffron cod at higher temperatures may come at the expense of increased metabolic demands and a shift in the zooplankton community to smaller, less lipid-rich copepod species (Copeman et al. 2017; Aarflot et al. 2018; Møller and Nielsen 2020; Bouchard and Fortier 2020).

Model-data comparison

Kotzebue Sound was selected as the source of simulated polar cod and saffron cod ELHS in this study due to the preponderance of small larvae observed in this area in the late spring, highlighting the region's potential role as a key hatching and/or nursery habitat for the ELHS of these species. The observed distribution of Arctic gadids along the northern coastline of Kotzebue Sound in the late spring matched well with simulated larval distributions from the model. At Point Hope and Cape Lisburne, a portion of the ACC is often deflected offshore (Danielson et al. 2017), which is reflected in both the late spring model simulations and survey catch data. The IBM predicts that larval polar cod and saffron cod will be advected offshore and northward at Cape Lisburne. Consistent with the model simulations, we observed high catches of polar cod and saffron cod offshore of Cape Lisburne during the spring survey. High abundances of polar cod and saffron cod may also be present north of Cape Lisburne in the spring as predicted by the IBM, but we lack the empirical data to test this as sampling did not extend north of Cape Lisburne. Additionally, the simulated distributions for saffron cod and polar cod from the IBM were similar to each other. This is due to the use of a single release location (Kotzebue Sound) for both species and identical behavior routines so that differences in distribution in our study were associated with the species-specific temperature-dependent growth rates used to parametrize the IBMs (Vestfals et al. 2021).

There was no evidence from the model that larvae are advected south from Kotzebue Sound. Any spawning in Kotzebue Sound is likely not the origin of individuals that were caught around St. Lawrence Island or nearshore along the northern Seward Peninsula during spring. Recent modeling work suggests that polar cod hatching south of Bering Strait could be the source of larvae and early juveniles encountered in surveys in the northeastern Chukchi Sea in 2012 while Bering Strait and Kotzebue Sound were likely source regions for saffron cod in 2012 and 2013 (Vestfals et al. 2021).

In the late summer, the IBMs for polar cod and saffron cod indicated high concentrations of larvae and early juveniles nearshore from northern Kotzebue Sound to Wainwright, offshore of Point Hope/Cape Lisburne, and offshore of Wainwright. The modeled distributions agree with the observed late summer distribution of saffron cod where higher abundances were generally nearshore, especially around Point Hope and Cape Lisburne, with abundance decreasing offshore. This suggests that Kotzebue Sound is a center of abundance and potentially serves as an important spawning and hatching area for saffron cod in the Chukchi Sea, a possibility that has been suggested anecdotally (A. Whiting, Village of Kotzebue, personal communication; Vestfals et al. 2021). Larval polar cod were ubiquitous offshore in the Hanna Shoal region during the late summer surveys in 2017, which is consistent with polar cod distributions in other years (Logerwell et al. 2020), but was not captured well by the model, indicating that other hatching locations are major contributors to the observed age-0 aggregations in this area (Vestfals et al. 2021). The simulated distribution overlapped with the distribution of late summer polar cod ELHS individuals offshore of Point Hope and Cape Lisburne, as well as nearshore extending from Cape Lisburne to Wainwright, suggesting Kotzebue Sound may be a potential source of polar cod to these areas in the late summer.

Simulated lengths for both polar cod and saffron cod were smaller than observed specimens collected in the late spring and late summer from the water column or the bottom, with a much larger discrepancy for saffron cod than polar cod. This suggests that the model is underestimating growth, small larvae in the field experience higher mortalities than large larvae, temperatures in the model are underestimates, hatching occurs earlier than assumed, or a combination of these and potentially other factors. The growth equations for polar cod and saffron cod within the IBM are temperature-mediated (Vestfals et al. 2021), making simulated lengths and estimates of daily growth sensitive to thermal conditions in the model, which may differ from those experienced in the field. No growth model exists for ELHS of saffron cod larger than 10 mm in length and the growth model was parameterized using data for walleye pollock due to their similar, linear growth trajectories prior to 10 mm (B. Laurel, AFSC, personal communication; Porter and Bailey 2007; Petrik et al. 2015). However, saffron cod may deviate from linear growth trajectories at later stages or temperatures (Vestfals et al. 2021). Additionally, field estimates of apparent growth tend to be higher than those observed in the lab because of ecological interactions, such as size-selective predation (Houde 2009). The field-based growth calculations were relatively coarse, encompassing all the collected individu- als aggregated from a large spatial area, over a two-month sampling period, and likely originating from multiple spawn locations, whereas the model is based on a single release location.

In the late spring, simulated polar cod hatched before April 15th were larger on average than the individuals captured from the water column, suggesting the model is realistically reflecting the enhanced growth rates of polar cod in the late spring due to earlier ice retreat and warmer water temperatures in 2017 relative to average conditions. The narrow size range of individuals in the model compared to the field collections can indicate several potential scenarios. Firstly, Kotzebue Sound was selected as the source of polar cod and saffron cod larvae, but it is not the only source of larvae in the Chukchi Sea. For example, recent modeling work suggests that Bering Strait and Chukotka

Peninsula were important hatching areas for polar cod in the Chukchi Sea in 2012 and 2013 (Vestfals et al. 2021). Secondly, the presence of smaller polar cod in the catch in the late spring may also suggest a simulated hatch date of April 15th or later, although the model does not capture the full range of observed sizes, particularly at the upper end. We selected to model hatch dates between March 1st and May 15th, which corresponded to the duration of peak hatching for polar cod in 2017, although hatching has been reported as early as January 1st for polar cod in the Arctic (Bouchard and Fortier 2011; Z. Chapman, UAF, personal communication). In polar cod, hatch date explains more variability in length than temperature conditions (Bouchard et al. 2017), therefore, some of the inconsistencies between the sizes, and subsequent calculated growth rates, of field collected and simulated individuals may be due to the hatch date variability. Thirdly, field estimates also differ from those observed under controlled laboratory conditions due to ecological factors that are difficult to account for (Bailey and Houde 1989; Houde 2009; Vestfals et al. 2019) such as patchy prey distribution and small-scale environmental variability (temperature, salinity, etc.). Polar cod are likely able to take advantage of a "big risk, big reward" strategy to forage for limited periods of time in warm, productive waters along thermal-salinity fronts to maximize growth relative to conspecifics (Laurel et al. 2016; Bouchard et al. 2017), which may contribute to the wider size range observed for the field-collected individuals compared to simulated individuals in the late spring.

Differences between simulated and empirical data may also be related to the onset of demersal behavior in polar cod and saffron cod, which is an adaptation to avoid predation, enhance foraging, and find areas of physiological preferred temperature ranges. Given the dominance of gadids by number and biomass in demersal catches in the Arctic (Logerwell et al. 2015), fish predators of ELHS of polar cod and saffron cod are likely conspecifics. Cannibalism has been documented in other subarctic gadids and is mitigated by vertical partitioning between juveniles and adults (Bailey 1975, 1989). Adult walleye pollock in the Bering Sea are semipelagic and cannibalism was highest when juveniles moved deeper in the water column, overlapping with the adults (Bailey 1989). Cannibalism is considered rare for polar cod due to their planktivorous foraging strategy, although fishes do become an important prey category as polar cod grow, and instances of cannibalism have been documented (Bain and Sekerak 1978; Benoit et al. 2010; Christiansen et al. 2012; Whitehouse et al 2017). Polar cod forage primarily on copepod nauplii (e.g., *Pseudocalanus* spp.) when smaller than 25 mm SL and shift to foraging on the copepodite stages of copepods, specifically *Calanus* spp. and *Metridia* spp., and fishes when larger than 25 mm SL (Benoit et al. 2010; Christiansen et al. 2012; Bouchard et al. 2016; Bouchard and Fortier 2020). Saffron cod likely become more piscivorous with increasing size (Laurel et al. 2009), suggesting cannibalism may be more likely in this species than polar cod. Diet data are limited for saffron cod in the Chukchi Sea (Copeman et al. 2016). Increased water temperatures and constriction of available habitat for Arctic taxa may lead to increased cannibalism for polar cod and saffron cod as well as increased competition and predation if subarctic species move into the Chukchi Sea (Bouchard et al. 2017). A number of adult fish species from the Ber- ing Sea, such as walleye pollock and Pacific cod, expanded northward in response to a reduced Cold Pool (bottom water temperatures < 2 °C) over the Bering Sea shelf (Stevenson and Lauth 2019) and are possible competitors as well as predators of Arctic gadids in the Chukchi Sea if climatic warming persists (Marsh and Mueter 2019). Near bottom waters may also act as a thermal refuge for smaller Arctic gadids, particularly small polar cod that are not as tolerant to higher water temperatures as saffron cod (Laurel et al. 2016).

Summary

The late spring distributions of polar cod and saffron cod centered in Kotzebue Sound suggest that sea ice may be an important environmental factor influencing hatching, and it may provide a nursery habitat for newly hatched individuals of both species. Kotzebue Sound was likely a source of ELHS of polar cod and saffron cod offshore of Point Hope/Cape Lisburne and nearshore from Kotzebue Sound to Wainwright during 2017. Without otolith-derived individual growth estimates, it is difficult to know if polar cod and saffron cod experienced greater growth during 2017 compared to other years or regions due to elevated temperatures, although our daily growth estimates were higher than reported in past research (Bouchard and Fortier 2011). Saffron cod should benefit in a warmer Arctic if their ELHS are resilient to the loss of sea ice, and if energetic trade-offs can offset prey-mediated factors that may depress growth (i.e., reduced nutritional value, zooplankton community shift) (Llopiz et al. 2014; Spear et al. 2019) and an increase in competition and predation from sub-Arctic demersal fishes shifting to the north (Stevenson and Lauth 2019). With the forecasted warming in the Arctic and projected changes in sea ice dynamics, studies such as this one synthesizing the seasonal distribution, abundance, and growth of Arctic forage fishes are critical to assess changes in phenology, distributions, and abundance for these species and the impacts of warming on habitat availability for Arctic fishes.

Acknowledgements The authors thank all of the boat and field crews of the USCGC *Healy*, M/V *Ocean Starr*, and R/V *Sikuliaq* who collected these data and without their tireless efforts, this project would not have been possible. We thank the Plankton Sorting and Identification Center in Szczecin, Poland and the ichthyoplankton team at

the Alaska Fisheries Science Center for their taxonomic expertise that makes studies of the ecology of Arctic fishes possible. We also thank Jens Nielsen and Adam Spear for their assistance gathering and plotting the sea ice data as well as intellectual discussions on the interpretation of the data. Finally, we thank Katherine Hedstrom at the University of Alaska Fairbanks for providing the PAROMS model output and Caitlin Smoot and Cheryl Hopcroft, also at the University of Alaska Fairbanks, for facilitating data collection and curation of ASGARD samples. Funding for this project was provided by the North Pacific Research Board through the Arctic Integrated Ecosystem Research Program. AMBON collections were made possible through a National Ocean Partnership Program (NOPP Grant NA14NOS0120158) by the National Oceanic and Atmospheric Administration, the Bureau of Ocean Management and Shell Exploration & Production. The findings and conclusions in the paper are those of the author(s) and do not necessarily represent the views of the National Marine Fisheries Service. Mention of trade names does not imply endorsement by NOAA or any of its subagencies. This is contribution number EcoFOCI-1015 of Ecosystems and Fisheries-Oceanography Coordinated Investigations.

Author contributions ALD, EAL, EDG, and JTD conceived and framed the key questions of the study. CDV conducted all IBM analyses, contributed code to generate figures related to the IBM, and provided text in the *Methods* sections. FJM, SLD, EAL, and RRH provided data that made the analyses possible. ALD wrote the manuscript and generated the figures. All authors read and approved the manuscript.

Declarations

Conflict of interest The authors have no conflict of interest to report.

Ethical approval All field sampling was done in accordance with NOAA NMFS policies, as outlined under the Animal Welfare Act and US Government Principles for the Utilization and Care of Vertebrate Animals Used in Testing, Research, and Training. Collections were made under the following permits approved by the Alaska Regional Office, National Marine Fisheries Service (CF-17-023), a US Fish and Wildlife Service Seabird Salvage Permit (MB035470), and a State of Alaska Resource Permit (CF-16-010).

References

Abookire AA, Rose CS (2005) Modifications to a plumb staff beam trawl for sampling uneven, complex habitats. Fish Res 71:247–254. https://doi.org/10.1016/j.fishres.2004.06.006

Cavalieri DJ, Parkinson CL, Gloersen P, Zwally HJ (1996) Sea Ice Concentrations from Nimbus-7 SMMR and DMSP SSM/I-SSMIS Passive Microwave Data, Version 1. Boulder, Colorado USA. NASA National Snow and Ice Data Center Distributed Active Archive Center. https://doi.org/10.5067/8GQ8LZQVL0VL. [10 April 2019].

Aarflot JM, Skjoldal HR, Dalpadado P, Skern-Mauritzen M (2018) Contribution of *Calanus* species to the mesozooplankton biomass in the Barents Sea. ICES J Mar Sci 75(7):2342–2354

Aschan M, Karamushko OV, Byrkjedal I, Wienerroither R, Borkin IV, Christiansen JS (2009) Records of the gadoid fish *Arctogadus glacialis* (Peters, 1874) in the European Arctic. Polar Biol 32(7):963–970

Bailey RS (1975) Observations on diel behaviour patterns of North Sea gadoids in the pelagic phase. J Mar Biol Assoc UK 55(1):133–142

Bailey KM (1989) Interaction between the vertical distribution of juvenile walleye pollock *Theragra chalcogramma* in the eastern Bering Sea, and cannibalism. Mar Ecol Prog Ser 53:205–213

Bailey KM, Houde ED (1989) Predation on egg and larvae of marine fishes and the recruitment problem. Adv Mar Biol 25:1–83

Bain H, Sekerak AD (1978) Aspects of the biology of Arctic cod (*Boreogadus saida*) in the central Canadian Arctic. LGL Limited, Toronto

Benoit D, Simard Y, Gagne J, Geoffroy M, Fortier L (2010) From polar night to midnight sun: photoperiod, seal predation, and the diel vertical migrations of polar cod (*Boreogadus saida*) under landfast ice in the Arctic Ocean. Polar Biol 33:1505–1520. https://doi.org/10.1007/s00300-010-0840-x

Borkin LV, Ozhigin VK, Shleinik VN (1986) Effect of oceanographical factors on the abundance of the Barents Sea polar cod year classes. In: The effect of oceanographic conditions on distribution and population dynamics of commercial fish stocks in the Barents Sea, vol 169

Bouchard C, Fortier L (2008) Effects of polynyas on the hatching season, early growth and survival of polar cod *Boreogadus saida* in the Laptev Sea. Mar Ecol Prog Ser 355:247–256. https://doi.org/10.3354/meps07335

Bouchard C, Fortier L (2011) Circum-arctic comparison of the hatching season of polar cod *Boreogadus saida*: a test of the freshwater winter refuge hypothesis. Prog Oceanogr 90:105–116. https://doi.org/10.1016/j.pocean.2011.02.008

Bouchard C, Fortier L (2020) The importance of *Calanus glacialis* for the feeding success of young polar cod: a circumpolar synthesis. Polar Biol. https://doi.org/10.1007/s00300-020-02643-0

Bouchard C, Mollard S, Suzuki K, Robert D, Fortier L (2016) Contrasting the early life histories of sympatric Arctic gadids *Boreogadus saida* and *Arctogadus glacialis* in the Canadian Beaufort Sea. Polar Biol 39:1005–1022. https://doi.org/10.1007/s00300-014-1617-4

Bouchard C, Geoffroy M, Leblanc M, Majewski A, Gautheir S, Walkusz W, Reist JD, Fortier L (2017) Climate warming enhances polar cod recruitment, at least transiently. Prog Oceanogr 156:121–129. https://doi.org/10.1016/j.pocean.2017.06.008

Budgell WP (2005) Numerical simulation of ice-ocean variability in the Barents Sea region. Ocean Dyn 55:370–387. https://doi.org/10.1007/s10236-005-0008-3

Carton JA, Chepurin GA, Chen L (2018) SODA3: a new ocean climate reanalysis. J Clim 31(17):6967–6983

Chassignet EP, Hurlburt HE, Metzger EJ, Smedstad OM, Cummings JA, Halliwell GR, Bleck R, Baraille R, Wallcraft AJ, Lozano C, Tolman HL, Srinivasan A, Hankin S, Cornillon P, Weisberg R, Barth A, He R, Werner F, Wilkin J (2009) US GODAE global ocean prediction with the hybrid coordinate ocean model (HYCOM). Oceanography 22:49–59

Christiansen JS, Hop H, Nilssen EM, Joensen J (2012) Trophic ecology of sympatric Arctic gadoids, *Arctogadus glacialis* (Peters, 1872) and *Boreogadus saida* (Lepechin, 1774), in NE Greenland. Polar Biol 35:1247–1257. https://doi.org/10.1007/s00300-012-1170-y

Copeman LA, Laurel BJ, Boswell KM, Sremba AL, Klinck K, Heintz RA, Vollenweider JJ, Helser TE, Spencer ML (2016) Ontogenetic and spatial variability in trophic biomarkers of juvenile saffron cod (*Eleginus gracilis*) from the Beaufort, Chukchi and Bering Seas. Polar Biol 39:1109–1126. https://doi.org/10.1007/s00300-015-1792-y

Copeman LA, Laurel BJ, Spencer M, Sremba A (2017) Temperature impacts on lipid allocation among juvenile gadid species at the Pacific Arctic-Boreal interface: an experimental laboratory approach. Mar Ecol Prog Ser 566:183–198. https://doi.org/10.3354/meps12040

Craig PC, Griffiths WB, Haldorson L, McElderry H (1982) Ecological studies of Arctic cod (*Boreogadus saida*) in Beaufort Sea Coastal

Waters, Alaska. Can J Fish Aquat Sci 39:395–406. https://doi.org/10.1139/f82-057
Danielson SL, Eisner L, Ladd C, Mordy C, Sousa L, Weingartner TJ (2017) A comparison between late summer 2012 and 2013 water masses, macronutrients, and phytoplankton standing crops in the northern Bering and Chukchi Seas. Deep Sea Res Part II 135:7–26. https://doi.org/10.1016/j.dsr2.2016.05.024
Danielson SL, Hedstrom KS, Weingartner TJ (2016) Bering-Chukchi circulation pathways, North Pacific Research Board 2016 Final Report, NPRB project #1308, University of Alaska Fairbanks, Fairbanks, AK
De Robertis A, Taylor K, Williams K, Wilson CD (2017) Species and size selectivity of two midwater trawls used in an acoustic survey of the Alaska Arctic. Deep Sea Res Part II 135:40–50
Döös K (1995) Interocean exchange of water masses. J Geophys Res 100:13499. https://doi.org/10.1029/95jc00337
Dunn JR, Vinter BM (1984) Development of larvae of the saffron cod, *Eleginus gracilis*, with comments on the identification of gadid larvae in Pacific and Arctic waters contiguous to Canada and Alaska. Can J Fish Aquat Sci 41:304–318
Egbert GD, Erofeeva SY (2002) Efficient inverse modeling of barotropic ocean tides. J Atmos Ocean Technol 19:183–204. https://doi.org/10.1175/1520-0426(2002)019%3c0183:EIMOBO%3e2.0.CO;2
Falardeau M, Bouchard C, Robert D, Fortier L (2017) First records of Pacific sand lance (*Ammodytes hexapterus*) in the Canadian Arctic Archipelago. Polar Biol 40:2291–2296. https://doi.org/10.1007/s00300-017-2141-0
Graham RM, Cohen L, Petty AA, Boisvert LN, Rinke A, Hudson SR, Nicolaus M, Granskog MA (2017) Increasing frequency and duration of Arctic winter warming events. Geophys Res Lett 44:6974–6983. https://doi.org/10.1002/2017GL073395
Grebmeier JM, Bluhm B, Cooper LW (2015) Time-Series benthic community composition and biomass and associated environmental characteristics in the Chukchi Sea during the RUSALCA 2004–2012 program. Oceanography 28(3):116–133. https://doi.org/10.5670/oceanog.2015.61
Helser TE, Colman JR, Anderl DM, Kastelle CR (2017) Growth dynamics of saffron cod (*Eleginus gracilis*) and Arctic cod (*Boreogadus saida*) in the Northern Bering and Chukchi Seas. Deep Sea Res Part II 135:66–77. https://doi.org/10.1016/j.dsr2.2015.12.009
Houde ED (2009) Recruitment variability. In: Jakobsen T, Fogarty M, Megrey B, Moksness E (eds) Reproductive biology of fishes: implications for assessment and management. Wiley-Blackwell, Oxford, pp 91–171
Hunt GL, Blanchard AL, Boveng P, Dalpadado P, Drinkwater KF, Eisner L, Hopcroft RR, Kovacs KM, Norcross BL, Renaud P, Reigstad M, Renner M, Skjoldal HR, Whitehouse A, Woodgate RA (2013) The Barents and Chukchi Seas: comparison of two Arctic shelf ecosystems. J Mar Syst 109–110:43–68. https://doi.org/10.1016/j.jmarsys.2012.08.003
Hutchings JA, Rangeley RW (2011) Correlates of recovery for Canadian Atlantic cod (*Gadus morhua*). Can J Zool 89:386–400. https://doi.org/10.1139/Z11-022
Kahru M, Brotas V, Manzano-Sarabia M, Mitchell BG (2011) Are phytoplankton blooms occurring earlier in the Arctic? Glob Chang Biol 17:1733–1739. https://doi.org/10.1111/j.1365-2486.2010.02312.x
Koenker BL, Copeman LA, Laurel BJ (2018) Impacts of temperature and food availability on the condition of larval Arctic cod (*Boreogadus saida*) and walleye pollock (*Gadus chalcogrammus*). ICES J Mar Sci 75(7):2370–2385. https://doi.org/10.1093/icesjms/fsy052
Laurel BJ, Hurst TP, Copeman LA, Davis MW (2008) The role of temperature on the growth and survival of early and late hatching Pacific cod larvae (*Gadus macrocephalus*). J Plankton Res 30:1051–1060. https://doi.org/10.1093/plankt/fbn057
Laurel BJ, Ryer CH, Knoth B, Stoner AW (2009) Temporal and ontogenetic shifts in habitat use of juvenile Pacific cod (*Gadus macrocephalus*). J Exp Mar Bio Ecol 377:28–35. https://doi.org/10.1016/j.jembe.2009.06.010
Laurel BJ, Spencer M, Iseri P, Copeman LA (2016) Temperature-dependent growth and behavior of juvenile Arctic cod (*Boreogadus saida*) and co-occurring North Pacific gadids. Polar Biol 39:1127–1135. https://doi.org/10.1007/s00300-015-1761-5
Li WKW, McLaughlin FA, Lovejoy C, Carmack EC (2009) Smallest algae thrive as the Arctic ocean freshens. Science 326:539. https://doi.org/10.1126/science.1179798
Llopiz JK, Cowen RK, Hauff MJ, Ji R, Munday PL, Muhling BA, Peck MA, Richardson DE, Sogard S, Sponaugle S (2014) Early life history and fisheries oceanography: new questions in a changing world. Oceanography 27(4):26–41
Logerwell E, Busby M, Carothers C, Cotton S, Duffy-Anderson J, Farley E, Goddard P, Heintz R, Holladay B, Horne J, Johnson S, Lauth B, Moulton L, Neff D, Norcross B, Parker-Stetter S, Seigle J, Sformo T (2015) Fish communities across a spectrum of habi- tats in the western Beaufort Sea and Chukchi Sea. Prog Oceanogr 136:115–132. https://doi.org/10.1016/j.pocean.2015.05.013
Logerwell E, Busby M, Mier K, Tabisola H, Duffy-Anderson J (2020) The effects of oceanographic variability on the distribution of larval fishes of the northern Bering and Chukchi Seas. Deep Sea Res Part II. https://doi.org/10.1016/j.dsr2.2020.104784
Lønne OJ, Gulliksen B (1989) Size, age and diet of polar cod, *Boreogadus saida* (Lepechin 1773), in ice covered waters. Polar Biol 9(3):187–91
Marsh JM, Mueter FJ (2019) Influences of temperature, predators, and competitors on polar cod (*Boreogadus saida*) at the southern margin of their distribution. Polar Biol 35:1–20. https://doi.org/10.1007/s00300-019-02575-4
Maslowski W (2014) The pacific arctic region: ecosystem status and trends in a rapidly changing environment. In: Grebmeier JM, Maslowski W (eds) The Pacific Arctic region. Springer, Heidelberg, pp 101–132
Matarese A, Kendall A, Blood D, Vinter B (1989) Laboratory guide to early life history stages of northeast Pacific fishes. NOAA Tech Rep 80:652
Møller EF, Nielsen TG (2020) Borealization of Arctic zooplankton—smaller and less fat zooplankton species in Disko Bay. Western Greenland Limnol Oceanogr 65(6):1175–1188
National Snow and Ice Data Center (NSIDC) (2019) All About Sea Ice. Accessed 15 June 2019. /cryosphere/seaice/index.html
North Pacific Fishery Management Council (NPFMC) (2009) Fishery Management Plan for Fish Resources of the Arctic Management Area. North Pacific Fishery Management Council, Anchorage, AK
Ichthyoplankton Information System (IIS) (2019) National Oceanic and Atmospheric Administration. (7 May 2020) https://apps-afsc.fisheries.noaa.gov/ichthyo/index.php
Overland JE, Wang M, Ballinger TJ (2018) Recent increased warming of the Alaskan marine Arctic due to midlatitude linkages. Adv Atmos Sci 35:75–84. https://doi.org/10.1007/s00376-017-7026-1
Perovich D, Meier W, Tschudi M, Farrell S, Hendricks S, Gerland S, Haas C, Krumpen T, Polashenski C, Ricker R, Webster M (2017). Sea Ice [in Arctic Report Card 2017]. http://www.arctic.noaa.gov/Report-Card
Petrik CM, Duffy-Anderson JT, Mueter F, Hedstrom K, Curchitser EN (2015) Biophysical transport model suggests climate variability determines distribution of Walleye Pollock early life stages in the eastern Bering Sea through effects on spawning. Progr Oceanogr 138:459–474

Porter SM, Bailey KM (2007) The effect of early and late hatching on the escape response of walleye pollock (*Theragra chalcogramma*) larvae. J Plankton Res 29:291–300. https://doi.org/10.1093/plankt/fbm015

R Core Team (2019) R: a language and environment for statistical computing. R Foundation for Statistical Computing, Vienna, Austria. ISBN 3-900051-07-0, http://www.Rproject.org

Randall JR, Busby MS, Spear AH, Mier KL (2019) Spatial and temporal variation of summer ichthyoplankton assemblage structure in the eastern Chukchi Sea 2010–2015. Polar Biol 42:1811–1824

Rass TS (1968) Spawning and development of polar cod. Rapp PV Reun Cons Perm Int Explor Mer 158:135–137

Shchepetkin AF, McWilliams JC (2005) The regional oceanic modeling system (ROMS): a split-explicit, free-surface, topography-following-coordinate oceanic model. Ocean Model 9:347–404. https://doi.org/10.1016/j.ocemod.2004.08.002

Shima M, Bailey KM (1994) Comparative analysis of ichthyoplankton sampling gear for early life stages of walleye pollock (*Theragra chalcogramma*). Fish Oceanogr 3:50–59. https://doi.org/10.1111/j.1365-2419.1994.tb00047.x

Spear A, Duffy-Anderson J, Kimmel D, Napp J, Randall J, Stabeno P (2019) Physical and biological drivers of zooplankton communities in the Chukchi Sea. Polar Biol 42:1107–1124. https://doi.org/10.1007/s00300-019-02498-0

Stevenson DE, Lauth RR (2019) Bottom trawl surveys in the northern Bering Sea indicate recent shifts in the distribution of marine species. Polar Biol 42:407–421. https://doi.org/10.1007/s00300-018-2431-1

Thanassekos S, Fortier L (2012) An individual based model of Arctic cod (*Boreogadus saida*) early life in Arctic polynyas: I. Simulated growth in relation to hatch date in the Northeast Water (Greenland Sea) and the North Water (Baffin Bay). J Mar Syst 93:25–38

Thanassekos S, Robert D, Fortier L (2012) An individual based model of Arctic cod (*Boreogadus saida*) early life in Arctic polynyas: II. Length-dependent and growth-dependent mortality. J Mar Syst 93:39–46

Timmermans ML, Ladd C, Wood K (2017) Sea surface temperature [in Arctic Report Card 2017]. http://www.arctic.noaa.gov/Report-Card

Tokinaga H, Xie S-P, Mukougawa H (2017) Early 20th-century Arctic warming intensified by Pacific and Atlantic multidecadal variability. Proc Natl Acad Sci USA 114:6227–6232. https://doi.org/10.1073/pnas.1615880114

Tsujino H, Urakawa S, Nakano H, Small RJ, Kim WM, Yeager SG, Danabasoglu G, Suzuki T, Bamber JL, Bentsen M, Böning CW (2018) JRA-55 based surface dataset for driving ocean–sea-ice models (JRA55-do). Ocean Model 130:79–139

Vestfals CD, Mueter FJ, Duffy JT, Busby MS, De Robertis A (2019) Spatio-temporal distribution of polar cod (*Boreogadus saida*) and saffron cod (*Eleginus gracilis*) early life stages in the Pacific Arctic. Polar Biol 42(5):969–990. https://doi.org/10.1007/s00300-019-02494-4

Vestfals CD, Mueter FJ, Hedstrom KS, Laurel BJ, Petrik CM, Duffy-Anderson JT, Danielson SL (2021) Modeling the dispersal of polar cod (*Boreogadus saida*) and saffron cod (*Eleginus gracilis*) early life stages in the Pacific Arctic using a biophysical transport model. Prog Oceanogr. https://doi.org/10.1016/j.pocean.2021.102571

Whitehouse GA, Aydin K, Essington TE (2014) A trophic mass balance model of the eastern Chukchi Sea with comparisons to other high-latitude systems. Ocean Model 88:911–939. https://doi.org/10.1007/s00300-014-1490-1

Whitehouse GA, Buckley TW, Danielson SL (2017) Diet compositions and trophic guild structure of the eastern Chukchi Sea demersal fish community. Deep Sea Res Part II 135:95–110

Wildes SL, Whittle J, Nguyen H, Guyon J (2016) *Boreogadus saida* genetics in the Alaskan Arctic. US Dept. of the Interior, Bureau of Ocean Energy Management, Alaska OCS Region. OCS Study BOEM 2011-AK-11-08 a/b. 67 pp—DRAFT REPORT

Wolotira RJ Jr (1985) Saffron cod (*Eleginus gracilis*) in Western Alaska: the resource and its potential. U.S. Dep. Commer., NOAA Tech. Memo. F/NWC-79. 119 p

Woodgate RA (2018) Increases in the Pacific inflow to the Arctic from 1990 to 2015, and insights into seasonal trends and driving mechanisms from year-round Bering Strait mooring data. Prog Oceanogr 160:124–154

Woodgate RA, Weingartner TJ, Lindsay R (2012) Observed increases in Bering Strait oceanic fluxes from the Pacific to the Arctic from 2001 to 2011 and their impacts on the Arctic Ocean water column. Geophys Res Lett. https://doi.org/10.1029/2012GL054092

Polar Biology
https://doi.org/10.1007/s00300-020-02631-4

ORIGINAL PAPER

Spatial patterns, environmental correlates, and potential seasonal migration triangle of polar cod (Boreogadus saida) distribution in the Chukchi and Beaufort seas

Caitlin E. Forster[1] · Brenda L. Norcross[1] · Franz J. Mueter[1] · Elizabeth A. Logerwell[2] · Andrew C. Seitz[1]

Received: 2 April 2019 / Revised: 15 January 2020 / Accepted: 10 February 2020

Abstract

Polar cod (*Boreogadus saida*) is a key forage fish in the Arctic marine ecosystem and provides an energetic link between lower and upper trophic levels. Despite its ecological importance, spatially explicit studies synthesizing polar cod distributions across research efforts have not previously been conducted in its Pacific range. We used spatial generalized additive models to map the distribution of polar cod by size class and relative to environmental variables. We compiled demersal trawl data from 21 cruises conducted during 2004–2017 in the Chukchi and Beaufort seas, and investigated size-specific patterns in distribution to infer movement ecology of polar cod as it develops from juvenile to adult life stages. High abundances of juvenile polar cod (≤ 70 mm) in the northeastern Chukchi Sea and western Beaufort Sea were separated from another region of high abundance in the eastern Beaufort Sea, near the US and Canadian border, suggesting possible population structure in the Pacific Arctic. Relating environmental correlates to polar cod abundance demonstrated that temperature and salinity were related to juvenile distribution patterns, while depth was the primary correlate of adult distribution. A comparison of seasonal 2017 abundances of polar cod in the southern Chukchi Sea found low demersal abundance in the spring when compared to the summer. Seasonal differences in polar cod abundance suggest that polar cod migration may follow a classical 'migration triangle' route between nursery grounds as juveniles, feeding grounds as subadults, and spawning grounds as adults, in relation to ice cover and seasonal production in the Chukchi Sea.

Keywords Polar cod · Pacific arctic · Chukchi sea · Beaufort sea · Harden jones migration triangle

Introduction

Currently, understanding of the basic life history of many marine organisms in the Arctic, including polar cod (*Boreogadus saida*), is based on intermittent "snapshots" of species' presence, abundance, and distribution. While the distribution and movement of polar cod has been investigated in Atlantic Arctic regions such as the East Greenland shelf (Astthorsson 2015), and the Barents, Laptev, and East Siberian seas (Ponomarenko 1968; Lønne and Gulliksen 1989), a comprehensive study synthesizing multiple research efforts to describe the distribution of polar cod is yet to be completed for its range in the Chukchi and Beaufort seas (Mueter et al. 2016).

Polar cod is an abundant, circumpolar forage fish species and is a critical trophic link in the Arctic marine ecosystem (Lowry and Frost 1981; Mecklenburg et al. 2011; Hop and Gjosaeter 2013). This small-bodied species spawns under sea ice in the late fall and early winter and has buoyant eggs

This article belongs to the special issue on the "Arctic Gadids in a Changing Climate," coordinated by Franz Mueter, Haakon Hop, Benjamin Laurel, Caroline Bouchard, and Brenda Norcross.

Electronic supplementary material The online version of this article (https://doi.org/10.1007/s00300-020-02631-4) contains supplementary material, which is available to authorized users.

✉ Caitlin E. Forster
ceforster@alaska.edu

[1] College of Fisheries and Ocean Sciences, University of Alaska Fairbanks, Fairbanks, AK 99775, USA

[2] Alaska Fisheries Science Center, National Marine Fisheries Service, National Oceanic and Atmospheric Administration, 7600 Sand Point Way NE, Seattle, WA 98115, USA

Published online: 21 April 2020

that float to the ice–water interface (Graham and Hop 1995; Bouchard and Fortier 2011). Its diet is composed primarily of zooplankton such as copepods, hyperiid amphipods, and euphausiids in the summer, open water season (Rand et al. 2013; Gray et al. 2016), and ice amphipods and Calanus copepods in the winter, ice-covered season (Kohlbach et al. 2017). In the Pacific Arctic, polar cod is found in high salinity and intermediate water temperatures of the Chukchi Sea shelf (Norcross et al. 2010; Logerwell et al. 2017; De Robertis et al. 2017b). In the Beaufort Sea, polar cod is ubiquitous, present at all depths both on the shelf and the extending seaward down the slope (Benoit et al. 2008; Geoffroy et al. 2011; Norcross et al. 2017).

Body size and ontogeny influence the ability of fishes to exploit available resources and may affect their distribution with respect to these resources. As fish size increases, individuals become stronger swimmers and can exploit larger and more energetically valuable prey (Werner and Hall 1974; Christensen 1996; Clark et al. 2005), while increasing gape size widens the size range of exploitable resources (Scharf et al. 2000; Gray et al. 2017). In the Chukchi and Beaufort seas, body size influences the composition of prey in polar cod diets (Walkusz et al. 2013; Gray et al. 2016). Smaller polar cod are restricted to consuming small-bodied prey (i.e., calanoid and cyclopoid copepods), while larger individuals can also consume large-bodied zooplankton (i.e., hyperiid amphipods and euphausiids) (Gray et al. 2016; Norcross et al. 2017). Therefore, as ontogenetic increases in body size also improve prey resource accessibility, polar cod distribution is likely impacted by size-specific resource distribution.

Differential distribution in fish size with respect to resources can influence species-level life history strategies, including both ontogenetic and seasonal migration patterns. In classic 'migration triangle' theory, species migrate from nursery grounds to feeding grounds and finally to spawning grounds throughout the course of a life cycle (Harden Jones 1968; Secor 2002). Many species in the North Pacific exhibit this life history strategy, including close relatives of polar cod, Pacific cod (*Gadus macrocephalus*), and walleye pollock (*Gadus chalcogrammus*) (Shimada and Kimura 1994; Kotwicki et al. 2005). Seasonal migrations are also common for fish species in the highly seasonal North Pacific ecosystem. Pacific herring (*Clupea pallasii*) and yellowfin sole (*Limanda aspera*), for example, exploit abundant food resources as they migrate between summer feeding grounds and offshore overwintering grounds (Nichol 1998; Tojo et al. 2007). Both the ontogenetic and seasonal migration patterns of polar cod in the Pacific Arctic are not well established and could be improved with additional sampling beyond the August and September open water sampling season.

Global attention has recently shifted to the Arctic, creating a unique opportunity for national and international fisheries management organizations to incorporate precautionary management strategies from the outset. In 2009 the North Pacific Fisheries Management Council (NPFMC) closed US Arctic waters to commercial fishing until sufficient information becomes available to sustainably manage a fishery (NPFMC 2009). Polar cod is listed as one of only two finfish species with commercial potential within the NPFMC Arctic Fisheries Management Plan, and any fishery development would require a review of the life history of the potential target species, as well as an evaluation of the impacts to essential fish habitat. While a number of recent pelagic and demersal trawl surveys conducted by both the National Marine Fisheries Service and academic researchers (Rand and Logerwell 2011; Norcross et al. 2013; De Robertis et al. 2017b) have described broad patterns in polar cod distribution and overall abundance (Logerwell et al. 2015), a study specifically investigating polar cod distribution patterns across multiple years and many cruises is yet to be completed. Accordingly, we generated a comprehensive understanding of polar cod distribution in the Chukchi and Beaufort seas, investigating patterns with respect to size class, environmental covariates, and seasonal data in the southern Chukchi Sea to inform a hypothesis about a polar cod migration triangle.

Methods

Study region

Within US waters, polar cod is abundant in the Chukchi and Beaufort seas, two waterbodies with differing physical and biological conditions. The Chukchi Sea has a wide and shallow shelf with average depths ranging from 40 to 60 m. This sea benefits from an inflow from three primary water masses, nutrient poor Alaska Coastal Water (ACW), nutrient-rich Bering Shelf Water (BSW), and nutrient-rich Anadyr Water (AW) (Fig. 1; Weingartner 1997; Weingartner et al. 2013; Danielson et al. 2017b). There is considerable mixing between the BSW and AW, creating a water mass that has been termed Bering Chukchi Summer Water (BCSW) (Danielson et al. 2017b). The ACW, BSW, and AW originate in the Bering Sea and travel northward through Bering Strait, transporting nutrients and creating areas of high primary production and rich benthic habitats in portions of the Chukchi Sea (Dunton et al. 2005; Grebmeier et al. 2006). The high levels of Chukchi Sea shelf productivity are influenced to a greater extent by nutrient input from BCSW, than by ACW (Grebmeier et al. 1988). In contrast to the Chukchi Sea, the Beaufort Sea has a much narrower shelf with a slope that drops off steeply to the Arctic Basin. In addition to nutrient-rich waters flowing eastward from the Chukchi Sea, oceanographic processes in the Beaufort

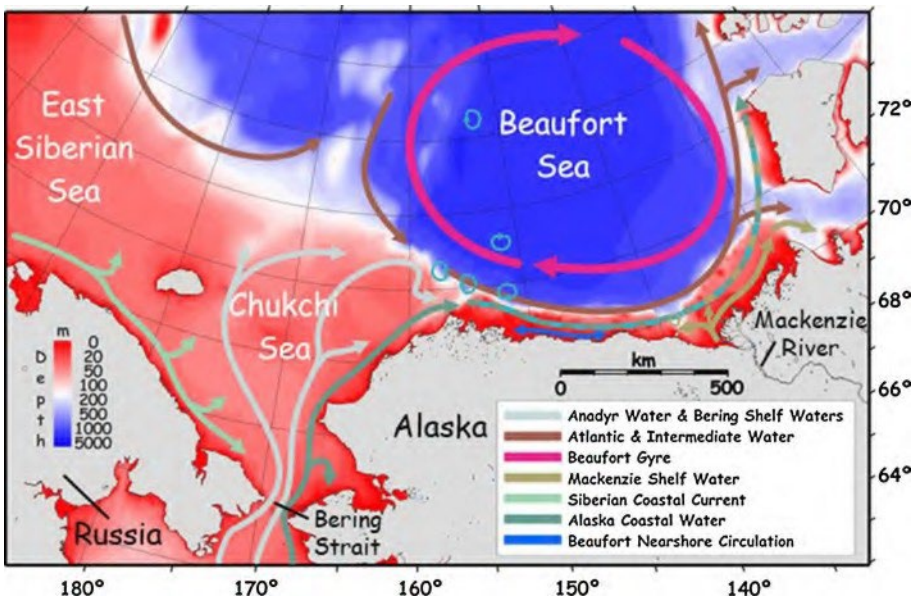

Fig. 1 Schematic of oceanic current flow in the Chukchi and Beaufort seas. After S. Danielson, personal communication

Sea are influenced by water from the Atlantic Ocean, the Beaufort Gyre, and freshwater input from the Mackenzie River (Carmack and Macdonald 2002). Water masses in the Beaufort Sea include a continuation of the eastward flowing ACW from the Chukchi Sea, Summer Shelf Water (SSW) influenced by both sub-Arctic and Arctic currents, and deep Atlantic Water (AtlW) transported west from the Atlantic Ocean (Carmack et al. 1989; Lansard et al. 2012; Norcross et al. 2018). Without nutrient subsidies from richer sub-Arctic waters, production in the Beaufort Sea is much lower than in the Chukchi Sea (Dunton et al. 2005). Regional differences in production create an unequal availability of resources between the Chukchi and Beaufort seas, which may drive both broad-scale patterns of polar cod distribution between the two seas, as well as more fine-scale patterns of polar cod distribution by size class in each respective sea.

Data collection

Data were compiled from 21 research surveys that were conducted during the open water season in the Chukchi and Beaufort seas beginning in 2004 and extending through 2017. Data were available from 16 cruises in the Chukchi Sea and five cruises in the Beaufort Sea (Table 1). In the Chukchi Sea, station locations ranged from approximately 170° W to Point Barrow, 156° W, and from the Bering Strait, 66.4° N, to approximately 73° N. Because the Chukchi Sea is relatively shallow, sampled depths were commonly between 40 and 60 m, with a maximum depth of 90 m. Station locations in the Beaufort Sea extended along the Alaskan coast from Point Barrow and into Canadian waters past the Mackenzie River to 137° W, and offshore to approximately 72° N (Fig. 2). Sampled depths reached nearly 1000 m in the Beaufort Sea. Cruises were divided into two seasons, spring and summer, based on temporal proximity of sampling to sea ice retreat and spring bloom conditions, which has a median date of approximately 20–21 June, based on data collected from 1997–2009 (Kahru et al. 2011). A cruise conducted from 9 to 29 June 2017 in the Chukchi Sea (ASGARD, Table 1), produced some of the earliest seasonal sampling events to ever take place in this region and was categorized as a spring season cruise because sampling occurred at the same time as the spring bloom (Danielson et al. 2017a). The remaining 20 cruises, conducted from 7 July to 10 October, occurred after the initial pulse of spring production from the spring bloom, and were thus categorized as summer season cruises. Because sampling in the spring occurred much earlier than during other cruises, data from this season were excluded from a spatial analysis of the summer distribution of polar cod. Further description of sensitivity analyses regarding seasonal divisions are discussed below.

All polar cod were captured in one of two configurations of a 3-m plumb staff beam trawl (PSBT), either standard (Gunderson and Ellis 1986) or modified with rollers (Abookire and Rose 2005), which were deployed for 1–10 min and towed at a speed over ground of 1.5–2.0 knots. A rigid 3.05 m beam held the net open for an effective swath of 2.26 m; net mesh size was 7 mm in the body with a 4 mm codend liner. In a gear comparison study, neither catch per unit effort (CPUE) of all fishes nor size classes of polar cod were significantly different between these two gear types (Norcross et al. 2018), therefore, abundance data from both gear types were pooled for analysis. Fishing effort for each haul was defined as the total seafloor area swept by the net. Catches were standardized to an area of 1000 m^2 (catch per unit effort or CPUE in no. of fish per 1000 m^2).

Table 1 Cruise information for all surveys used in this study listed by cruise designator, vessel used, year, beginning date of sampling, ending date of sampling, and number of hauls collected

Region	Cruise designator	Vessel	Year	Begin date	End date	No. of hauls
Chukchi	RUSALCA_2004	R/V Professor Khromov	2004	10-Aug	22-Aug	5
Chukchi	OD0710	R/V Oscar Dyson	2007	4-Sep	15-Sep	21
Chukchi	OS180	T/S Oshoro-Maru IV	2007	6-Aug	10-Aug	9
Chukchi	OS190	T/S Oshoro-Maru IV	2008	7-Jul	13-Jul	15
Chukchi	COMIDA_2009	R/V Alpha Helix	2009	27-Jul	11-Aug	30
Chukchi	RUSALCA_2009	R/V Professor Khromov	2009	4-Sep	29-Sep	7
Chukchi	WWW0902	R/V Westward Wind	2009	14-Aug	29-Aug	25
Chukchi	WWW0904	R/V Westward Wind	2009	29-Sep	10-Oct	26
Chukchi	AKCH10	R/V Norseman II	2010	21-Aug	4-Sep	30
Chukchi	WWW1003	R/V Westward Wind	2010	1-Sep	18-Sep	40
Chukchi	AKCH11	R/V Norseman II	2011	4-Sep	17-Sep	28
Chukchi	Arctic EIS_2012	F/V Alaska Knight	2012	14-Aug	18-Sep	40
Chukchi	RUSALCA_2012	R/V Professor Khromov	2012	27-Aug	16-Sep	5
Chukchi	AMBON_2015	R/V Norseman II	2015	11-Aug	3-Sep	68
Chukchi	Arctic IES_2017	R/V Ocean Starr	2017	1-Aug	28-Sep	59
Chukchi	ASGARD_2017	R/V Sikuliaq	2017	9-Jun	29-Jun	8
Beaufort	BOEM_2011	R/V Norseman II	2011	15-Aug	4-Sep	81
Beaufort	TB_2013	R/V Norseman II	2013	12-Aug	2-Sep	90
Beaufort	ANIMIDA_2014	R/V Norseman II	2014	29-Jul	10-Aug	29
Beaufort	TB_2014	R/V Norseman II	2014	14-Aug	2-Sep	68
Beaufort	ANIMIDA_2015	R/V Norseman II	2015	31-Jul	8-Aug	18
					Total no. of hauls	697

Due to difference in sampling seasons, ASGARD_2017 cruise excluded from spatial analysis

In addition, at each haul location a Seabird conductivity-temperature-depth (CTD) recorder was deployed from the vessel separately and used to measure depth (m), bottom water temperature (°C), and bottom water salinity (PSU), hereafter referred to as depth, temperature, and salinity. Fish specimens were measured for total length.

Data analysis

Patterns in polar cod abundance and total length were plotted and inspected prior to statistical analysis. Length frequencies of 6519 and 2752 fish in the Chukchi and Beaufort seas, respectively, were plotted by 10 mm increments (1–10 mm, 11–20 mm, etc.) and examined to inform selection of size classes for analysis (Fig. 3). Visual inspection suggested the presence of three modes, therefore size classes were identified using an expectation–maximization (EM) algorithm to fit a mixture of three Gaussian distributions to the length-frequency data (Benaglia et al. 2009). Based on the results, abundances of polar cod were separated by total length into small (≤ 70 mm), medium (71–130 mm), and large (> 130 mm) size classes. Size classes approximately correspond with age 0, 1, and 2 + polar cod, respectively, based on previously published work (Helser et al. 2017). However, given considerable overlap in length-at-age distributions, the medium size class likely contains a mixture of age-1 and age-2 individuals.

Generalized additive modeling (GAM) was used to relate CPUE of polar cod to spatial and environmental predictor variables. A GAM is a regression technique that uses non-parametric smoothers to allow non-linear relationships between dependent and independent variables (Hastie and Tibshirani 1986; Wood 2006). The GAM approach was chosen to accommodate non-linear relationships between abundance and both spatial (latitude, longitude) and environmental (depth, temperature, salinity) predictors. All models were fit using the 'mgcv' package version 1.8–17 (Wood 2006) in R version 3.4.1 (R Core Team 2017). Analysis may be found in Online Resource 1.

To determine the most appropriate model framework for both the spatial and environmental GAM analyses, preliminary analyses and model diagnostics were conducted prior to selection of final models. Abundance of polar cod was non-normal, including a high proportion of zero-catch hauls, as well as a few hauls with very high abundance values. Exploratory analyses compared models using a Gaussian distribution with log-transformed polar cod CPUE and the identity link function, with negative binomial and tweedie

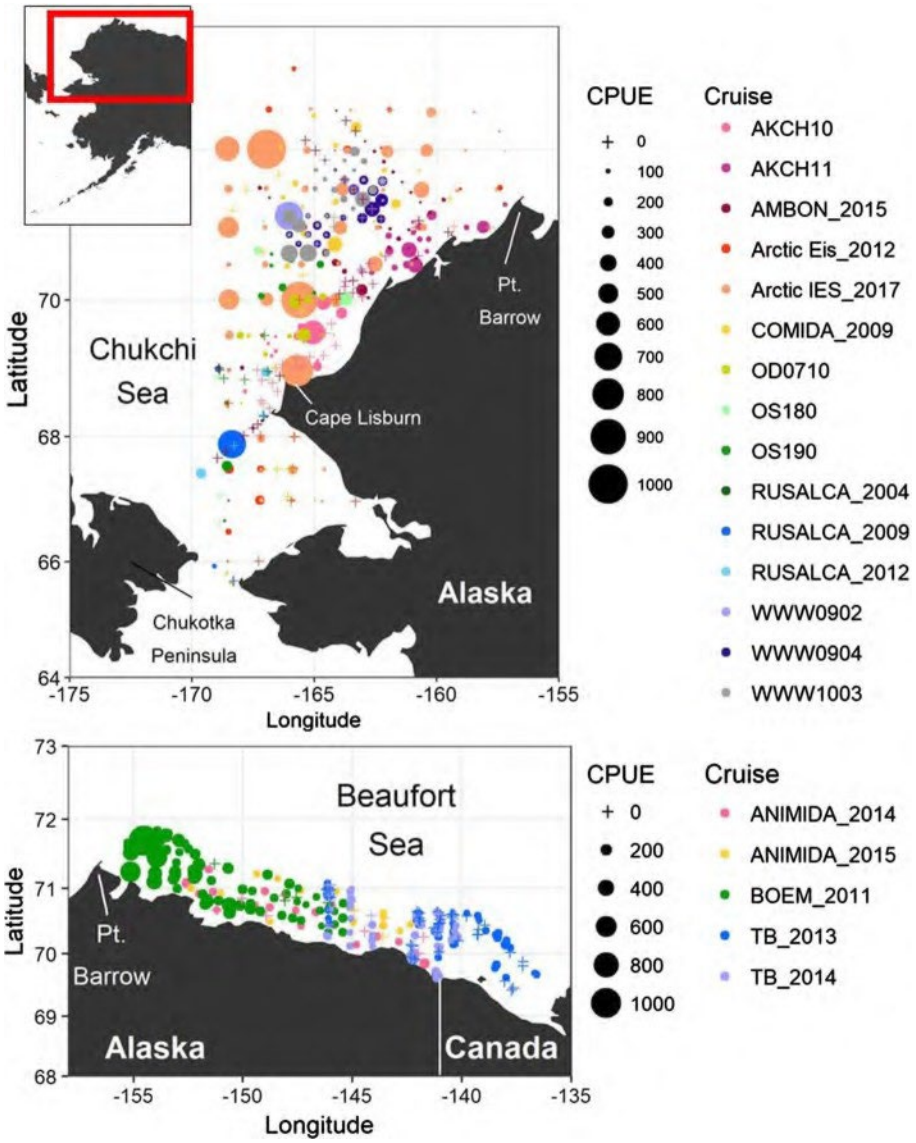

Fig. 2 Catch per unit effort (CPUE, no. of fish per 1000 m²) of polar cod by haul in the Chukchi Sea (top panel) and Beaufort Sea (bottom panel). The + symbol denotes hauls where zero polar cod were caught. Colors correspond to separate cruises. Symbol size is proportional to CPUE. For details about each cruise, see Table 1

distributions using counts of polar cod and the log link function. The negative binomial distribution with a log link was selected as the top performing model based on residual diagnostics, deviance explained, and generalized cross validation scores. This model framework was thereafter used for all GAM analyses. The negative binomial distribution utilizes count data, and is commonly used for analyzing ecological data, as it can accommodate overdispersed observations, or observations with a high proportion of zeros (Zuur et al. 2007). Therefore, we used the count data with a log link and accounted for fishing effort by including the logarithm of area swept (m²) as an offset in the model.

GAM analyses were conducted on cruises conducted in the summer season, defined as open water and more than 30 days after the start of the spring bloom. Two cruises, T/S Oshoro-Maru IV 2008 (Table 1) and WWW0904 2009 were conducted early and late in the summer season (July and October). To verify that it was appropriate to include these cruises in an analysis of polar cod summer distribution patterns, a sensitivity analysis both including and excluding these cruises was conducted. The results of all analyses were virtually identical; therefore, T/S Oshoro-Maru IV 2008 and WWW0904 2009 were included in summer season analyses. Due to considerable differences in oceanographic and bathymetric conditions and due to their spatial separation, analyses were conducted separately for the Chukchi and Beaufort seas.

To describe polar cod distribution patterns and the impact of environmental drivers on those patterns, two separate analyses were undertaken using GAM. The first analysis described the spatial distribution of polar cod abundance using latitude and longitude as covariates. Environmental conditions were strongly confounded with spatial location; for example, in the Beaufort Sea, depth increased with

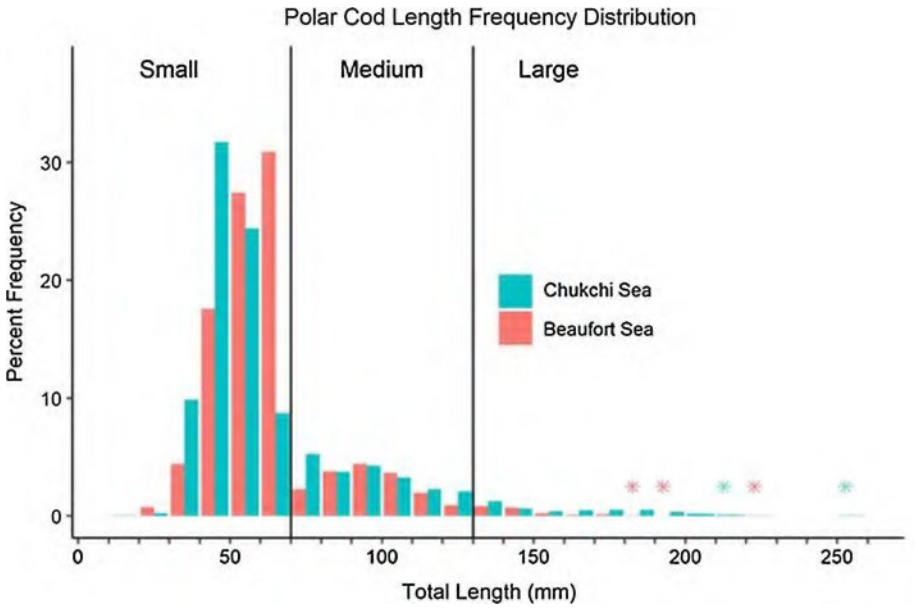

Fig. 3 Length-frequency distribution of polar cod captured in Chukchi Sea (blue) and Beaufort Sea (pink), weighted by station-specific catch per unit effort (CPUE, no. of fish per 1000 m²). Percent frequency is percent of total CPUE for that sea, and bars represent size class in between tick marks. Asterisks above a length bin indicate percentage < 0.1%, color corresponds to sea

latitude as sampling moved both northerly and offshore. Thus, we modeled spatial patterns separately from assessing the effects of environmental covariates. We compared the predicted values of the spatial and environmental models at each station to examine to what extent environmental covariates were able to account for estimated spatial patterns in polar cod distribution. Results of this analysis may be found in Online Resource 2. Spatial and environmental analyses were conducted for each of the three length classes of polar cod in the Chukchi and Beaufort seas. The spatial model was fit as follows:

$$\log(\text{count of polar cod}) \sim s(\text{latitude}, \text{longitude}) + \log(\text{area swept}), \quad (1)$$

where log denotes the natural logarithm and s denotes a smooth function of latitude and longitude estimated using a thin-plate regression spline. The second analysis investigated the impact of environmental correlates by modeling polar cod abundance as a function of selected environmental covariates:

$$\log(\text{count of polar cod}) \sim s(\text{depth}) + s(\text{temperature}) + s(\text{salinity}) + \log(\text{area swept}), \quad (2)$$

where the s_i are smooth functions of the respective covariates estimated using thin-plate regression splines. For the environmental analysis, a model selection approach was used to select a best-fitting model. To evaluate the effect of each environmental covariate on polar cod abundance, a suite of seven models was developed for each size class and in each sea, where every combination of environmental variables was considered. Within a size class and a sea, models were compared and the model with the lowest Akaike Information Criterion (AIC) was selected as the best performing model. Results from the best-fitting model for each size class were visually examined to describe the estimated relationships between polar cod abundance and the environmental predictors. When the best performing environmental model included both temperature and salinity, the temperature and salinity values were used to identify water masses and relate them to polar cod abundance. Literature values characterizing typical water mass temperature and salinity ranges in the Chukchi Sea (Danielson et al. 2017b) or Beaufort Sea (Norcross et al. 2018) were overlaid on relationships of polar cod abundance relative to those variables to determine patterns of polar cod abundance with respect to water mass.

Environmental model residuals suggested some degree of spatial autocorrelation among sites, where sites closer to each other were more similar than sites that were located farther apart. Both spatial and environmental models were tested for residual spatial autocorrelation by plotting the semivariance of model residuals as a function of distance between sampling points by year. Data for all length classes were combined to determine the spatial relationship between stations in each sea within a year. Comparison of AIC between the full model with spatial autocorrelation and the full model without spatial autocorrelation indicated slightly lower values in each sea (Chukchi Sea: ΔAIC = 2; Beaufort Sea: ΔAIC = 10) and thus a modest preference for the models that include a spatially autocorrelated error structure. Each environmental model, therefore, included an exponential decline in residual correlation with distance, as well as a nugget effect, conditioned on sampling year. Spatial correlation scale parameters (range and nugget) were estimated independently for each sea using the full model and were

included in all subsequent models. Due to statistical programming constraints caused by the inclusion of a spatially autocorrelated error structure, the dispersion parameter of the negative binomial distribution was estimated independently using the full model and fixed for each sea. After the incorporation of a spatially correlated error structure in the environmental model, both the spatial models and environmental models met assumptions of independence.

The completion of the spring cruise in the Chukchi Sea in June 2017 provided a seasonal comparison of offshore polar cod abundances. As these data were collected in spring rather than summer, they were not included in the previously described spatial analysis. However, the spring abundance data were directly compared to abundance from a cruise conducted during August and September 2017 in the southern Chukchi Sea. The two research efforts used the same gear and sampled from the Bering Strait (66.4° N) to Cape Lisburne (69.1° N). Due to the small number of sample stations within the area of overlap (spring $n = 9$, summer $n = 14$), we were not able to develop a geostatistical model and instead compared abundance of polar cod between spring and summer using a non-parametric (rank-based) Wilcoxon two-sample test. The test assumes that sampling in each season resulted in independent random samples that were representative of the area of overlap. Several August hauls caught large numbers of fish ≤ 70 mm, a size that was not observed in June. These small fish presumably consist of young-of-the-year fish that were too small to be retained by the beam trawl in June. Therefore, instead of statistically comparing overall seasonal abundances for all sizes of polar cod, we only applied to Wilcoxon two-sample test to compare seasonal abundances for fish > 70 mm, i.e., those fish that were available to be caught by the gear in both spring and summer. Mean values of depth, temperature, and salinity for each season are reported; however, environmental data were not available for two stations sampled in August 2017.

Results

A total of 697 hauls from 21 cruises over 13 years were available for analysis (Table 1). The number of hauls conducted annually ranged from 5 to 88 in the Chukchi Sea and 18 to 97 in the Beaufort Sea. Sampling was conducted from 9 June to 10 October in the Chukchi Sea and from 29 July to 4 September in the Beaufort Sea. Bottom water in the Chukchi Sea ranged from − 1.8 to 10.9 °C, with salinities from 27.2 to 34.5 PSU. In comparison, conditions in the Beaufort Sea lacked the warmest and very coldest temperatures, with a range from − 1.6 to 4.8 °C, and had salinities from 29.2 to 34.9 PSU.

When pooling data across all years, polar cod showed latitudinal patterns in abundance in the Chukchi Sea and a strong longitudinal gradient in the Beaufort Sea. Generally, abundance of polar cod in the Chukchi Sea showed a south to north gradient, with the highest abundance values north of Cape Lisburne (Fig. 2). In the Beaufort Sea, polar cod abundance showed a predominantly west to east gradient, with the highest abundance west of 150° W (Fig. 2). Length frequencies of the catches were similar across both study regions; polar cod ranged from 11 to 260 mm in the Chukchi Sea and from 21 to 230 mm in the Beaufort Sea (Fig. 3).

Spatial analysis

In the Chukchi Sea, GAM analysis of trawl catches revealed distinct patterns of polar cod distribution by size class. The small size class of polar cod was most abundant in the northern Chukchi Sea, north of approximately 68° N (Fig. 4), where the Bering Chukchi Summer Water mass is commonly present, while fewer small polar cod were found south of 68° N. The distribution of the medium size class was different when compared to the distribution of the small size class and did not show the same region of abundance in the NE Chukchi Sea. Medium-sized polar cod were present across the entire Chukchi Sea shelf and showed pockets of high abundance in both nearshore and offshore regions. However, the regions of high abundance for the medium size class were not the same as the regions of high abundance for the small size class offshore at 169° W and north of 70° N (Fig. 4). Finally, the large size class of polar cod was less abundant in the nearshore region and more abundant beginning ~ 80 km offshore and extending seaward, with an area of higher abundance south of Cape Lisburne (Fig. 4). Deviance explained for the small, medium, and large size class models was 24.4%, 20.2%, and 57.5%, respectively (Table 2).

Similar to the Chukchi Sea, the GAM spatial analysis in the Beaufort Sea also found distinct, size-based patterns of polar cod distribution. The small size class was distrib- uted primarily along a west to east gradient, with an area of high abundance west of 150° W, and another smaller area of abundance nearshore and east of 144° W (Fig. 5). There was also a nearshore to offshore gradient, where small polar cod were distributed close to shore; however, the western aggregation was dispersed across the width of the entire Beaufort Sea shelf (to ~ 80 km), more than the eastern aggregation that was generally distributed closer to shore (within ~ 50 km). Abundance of the medium size class showed a less extreme longitudinal gradient than the small size class, and while abundance was highest west of 150° W, medium polar cod were diffuse across the entire Alaskan Beaufort Sea shelf. Unlike the small size class, medium-sized polar cod did not show a separate area of high abundance east of 144° W. The large size class of

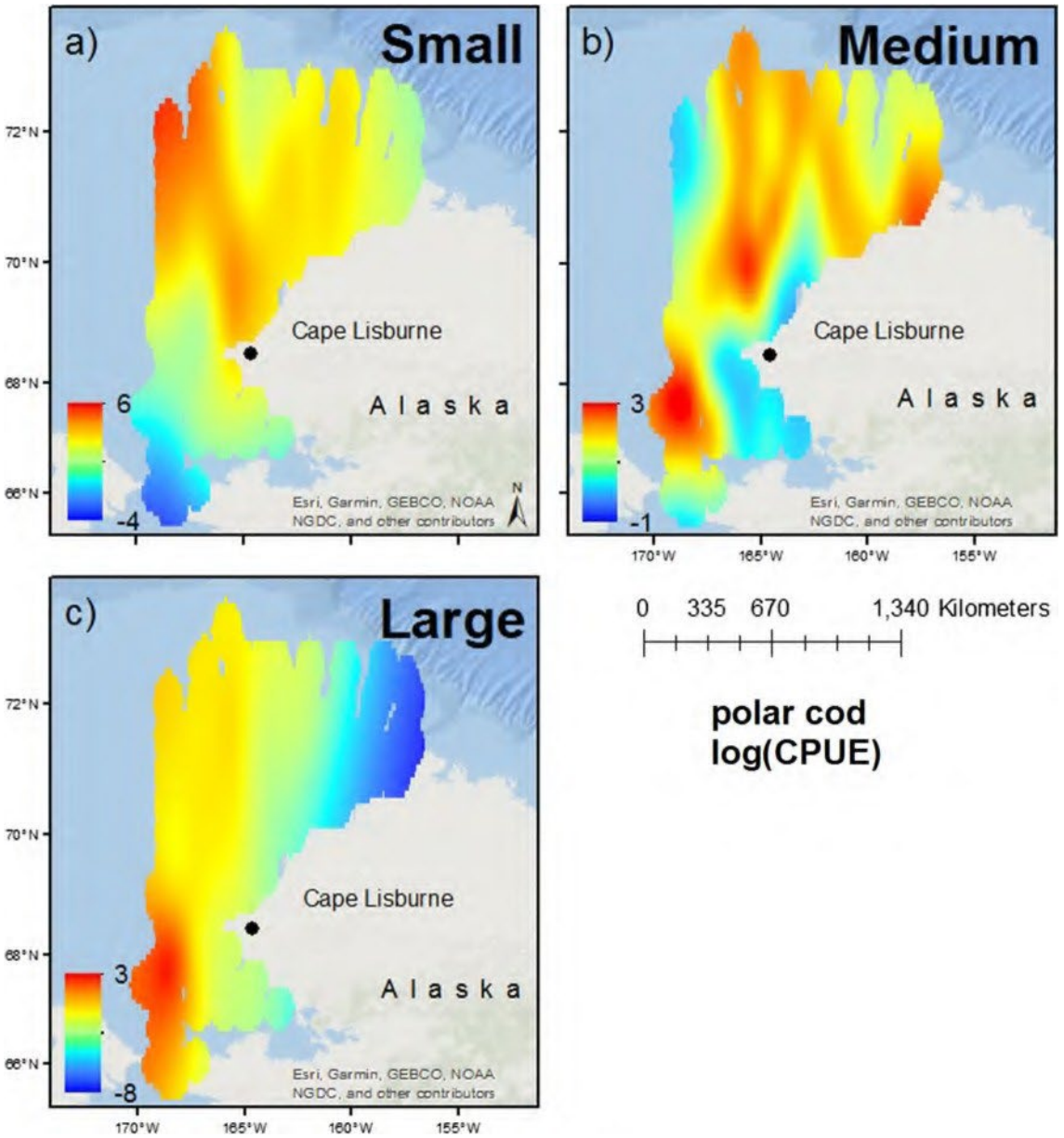

Fig. 4 Spatial distribution of polar cod catch per unit effort (CPUE, no. of fish per 1000 m²) in the Chukchi Sea for **a** small (≤ 70 mm), **b** medium (71–130 mm), and **c** large (> 130 mm) size classes. Abundances as predicted by generalized additive model (GAM) using a smooth function of latitude and longitude, shown on the log scale

polar cod was distributed offshore, beyond ~ 60 km. The deviance explained for the small, medium, and large size class analysis was 62.7%, 22.9%, and 21.7%, respectively (Table 2).

Environmental analysis

In the Chukchi Sea, the influence of the environmental variables on polar cod abundance depended on size class. For the small size class of polar cod, the top performing model included both temperature and salinity (Table 3). A dome-shaped curve described the relationship between polar cod abundance and temperature with a peak at 4–5 °C, while abundances increased linearly with salinity to a maximum of 34.5 PSU (Fig. 6). For polar cod in the medium size class, the top performing model only included depth and abundance increased linearly with depth (Table 3, Fig. 6). The best-fitting model for the large size class of polar cod in the Chukchi Sea also only included depth as a covariate; there was a positive relationship between depth and abundance of large polar cod in the Chukchi Sea (Table 3, Fig. 6).

Table 2 Results of generalized additive models (GAMs) for spatial distribution of polar cod, with latitude and longitude as explanatory variables (see Eq. 1)

Region	Size class	Θ	edf	χ^2	p value	AIC	Deviance explained (%)
Chukchi	Small	0.19	19.5	99.3	< 0.0001	1928.0	24.4
Chukchi	Medium	0.40	26.6	67.0	< 0.0001	1642.0	20.2
Chukchi	Large	0.18	13.7	58.1	< 0.0001	426.9	57.5
Beaufort	Small	0.38	13.4	300.2	< 0.0001	1073.2	62.7
Beaufort	Medium	0.53	7.6	61.4	< 0.0001	1051.0	22.9
Beaufort	Large	0.19	3.0	23.1	< 0.0001	353.9	21.7

Separate models developed in each sea and for each size class. θ parameter used for negative binomial parameterization, estimated degrees of freedom (edf), chi-square statistic, p-value denoting significance of latitude and longitude covariates, Akaike Information Criterion (AIC), and deviance explained

As in the Chukchi Sea, the relationships between environmental variables and abundance of polar cod in the Beaufort Sea were specific to size classes. The best-fitting model for the small size class in the Beaufort Sea included both temperature and salinity (Table 4). Abundance of small polar cod in the Beaufort Sea increased linearly to a maximum temperature of 4.8 °C, which was similar to the Chukchi Sea, and was highest at intermediate salinities; small polar cod were less abundant at the lowest (< 31 PSU) and highest (> 34 PSU) salinity values (Fig. 7). The top performing model for the medium size class in the Beaufort Sea included both depth and temperature (Table 4), unlike the analogous model in the Chukchi Sea, which only included depth. In the Beaufort Sea, abundance of medium polar cod increased with depth to approximately 300 m and then began to decline; medium polar cod abundance increased linearly with temperature (Fig. 7). As in the Chukchi Sea, the top performing model for the large size class included only depth as a covariate (Table 4). Notably, large polar cod abundance increased with depth in the Beaufort Sea to about 400 m, but as depth surpassed 400 m, abundance of polar cod decreased (Fig. 7). The shape of the relationship between depth and abundance was similar for both medium and large polar cod, but the medium size class was more abundant at shallow depths than the large size class of polar cod.

Seasonal analysis

Comparison of polar cod catches between spring and summer in the southern Chukchi Sea revealed striking differences in fish abundance. Overall mean abundance of polar cod was much lower in June 2017 compared to August 2017 (Table 5). During the spring, polar cod was scarce in our nets; only four individuals were captured at three sampling locations (Fig. 8). In contrast, polar cod abundance was higher at locations sampled in August 2017 (Table 5). There were summer hauls that captured high abundances of small-sized polar cod, including one station with an abundance of 832 fish per 1000 m², with individuals ranging from 31 to 70 mm in length. Catch length-frequency composition in the summer contrasts with the polar cod caught in the spring, where only one fish < 70 mm was captured (Fig. 8). Polar cod 31 to 70 mm captured in August were likely young-of-the-year; these small fish were not available to the beam trawl in June due to both their pelagic distribution and small size before the summer growing season. Therefore, to verify that the observed seasonal differences in abundance were truly changes in abundance, and not the result of small fish growing in size and descending to the seafloor to become increasingly represented in the catch as the summer progressed, only spring and summer abundance of individuals > 70 mm were statistically compared. Seasonal differences in abundance were significant, using a Wilcoxon two-sample test, after the exclusion of small, highly abundant polar cod in August (Table 5, $p = 0.02$).

Discussion

By visualizing the distribution patterns of small, medium, and large polar cod, understanding of ontogenetic shifts in distribution as well as possible migration patterns of this species in the Pacific Arctic has been improved. Furthermore, by relating patterns in distribution to environmental variables, we provide insight into potential mechanisms driving polar cod distribution. The importance of environmental covariates varies among the three size classes and suggests that the relative influence of external drivers on polar cod distribution influences life stages differently. A comparison of abundance between spring and summer in the southern Chukchi Sea revealed seasonal differences in polar

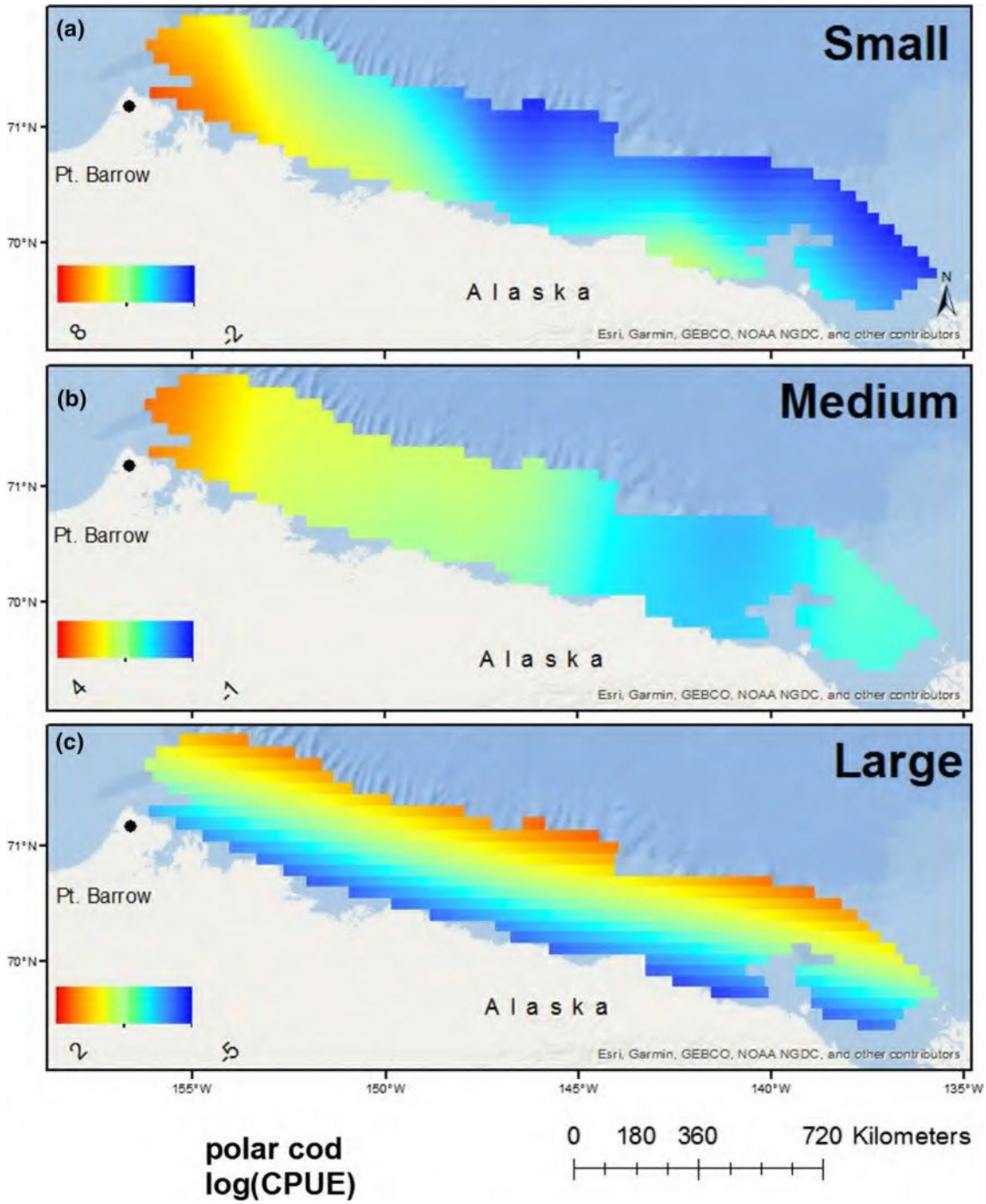

Fig. 5 Spatial distribution of polar cod catch per unit effort (CPUE, no. of fish per 1000 m²) in the Beaufort Sea for **a** small (≤ 70 mm), **b** medium (71–130 mm), and **c** large (> 130 mm) size classes. Abundances as predicted by generalized additive model (GAM) using a smooth function of latitude and longitude, shown on log scale

cod abundance. Finally, we hypothesize that both ontogenetic and seasonal movements of polar cod described in this study are evidence of a migration scenario that may be used to explain polar cod movement patterns in the Pacific Arctic.

There are several assumptions implicit in this analysis that could impact the interpretation of polar cod distribution patterns and potential environmental drivers of those patterns. First, we assume that our sampling gear is reasonably

Table 3 Results of generalized additive models (GAMs) in the Chukchi Sea for environmental covariates, depth, temperature, and salinity (see Eq. 2)

Size class	*s* (depth) (13–90 m)	*s* (bottom temperature) (−1.8 to 10.9 °C)	s (bottom salinity) (27.2–34.5 PSU)	− (logLikelihood)	AIC	ΔAIC	Model rank
Small		+	+	− 1011.1	2034.1	0.0	1
	+	+	+	− 1014.2	2044.3	10.2	2
		+		− 1032.7	2073.5	39.3	3
	+	+		− 1054.5	2121.1	86.9	4
			+	− 1075.7	2159.5	125.4	5
	+		+	− 1081.5	2174.9	140.8	6
	+			− 1115.9	2239.8	205.7	7
Medium	+			− 908.0	1824.0	0.0	1
			+	− 919.7	1847.3	23.4	2
	+		+	− 919.7	1851.3	27.3	3
		+	+	− 920.6	1853.1	29.1	4
	+	+	+	− 920.2	1856.5	32.5	5
	+	+		− 927.8	1867.6	43.6	6
		+		− 933.0	1874.0	50.0	7
Large	+			− 1224.2	2456.4	0.0	1
	+	+		− 1223.7	2459.5	3.1	2
	+		+	− 1247.0	2506.0	49.6	3
	+	+	+	− 1312.7	2641.4	185.0	4
			+	− 1477.5	2962.9	506.5	5
		+	+	− 1574.3	3160.6	704.2	6
		+		− 1595.1	3198.2	741.8	7

Suite of models developed for each polar cod size class, + denotes variables included in each model. The following statistics are reported: − log(likelihood), AIC, ΔAIC. Model performance ranked from best (1) to worst (7) using ΔAIC. ΔAIC calculated as the difference from the lowest AIC value for a size class and sea. θ parameter estimated independently and fixed, $\theta = 0.345$. Inclusion of a spatially autocorrelated error structure precludes the calculation of % deviance explained

effective at capturing all size classes of available polar cod. The 4 mm mesh codend liner ensures that this is an accurate assumption for individuals < 150 mm; however, a gear selectivity study indicates that the PSBT may not be the most effective sampling gear for polar cod > 150 mm (Kotwicki et al. 2017). Despite this selectivity, the results presented here nevertheless capture the bulk of the polar cod length distribution, as similar studies deploying a net with higher selectivity for large fish found that the majority of polar cod catch was < 150 mm in both the Chukchi Sea (Goddard et al. 2016) and the Beaufort Sea (Rand and Logerwell 2011). Second, we assume that the negative binomial distribution is effective at accommodating both the non-normal distribution of abundance and the high proportion of zero catches in the data. Sensitivity analysis comparing the performance of other distribution families (i.e., normal distribution with log-transformed response and tweedie distribution) showed that the top performing model used a negative binomial distribution. Nevertheless, interpretation of analyses for the large size class should be undertaken cautiously, as there is a high proportion of zero-catch hauls for large fish. Patterns in abundance by size class (Online Resource 3) may be compared to GAM analysis output. Finally, by pooling data across years, we assume that the spatial patterns in average fish abundance are not biased by interannual variability in catches. In addition, the environmental analysis is limited in scope to local variables that were measured contemporaneously with at-sea sampling. Additional variables that may be correlated to polar cod distribution, such as mean sea ice coverage or mean distance to sea ice edge in the winter, were ultimately excluded, as we considered it inappropriate to relate the summer distribution of polar cod from multiple cruises conducted at different points in space and time to long-term means of winter sea ice conditions. However, it is important to consider that variable ice conditions dur- ing winter and spring likely also play a role in explaining

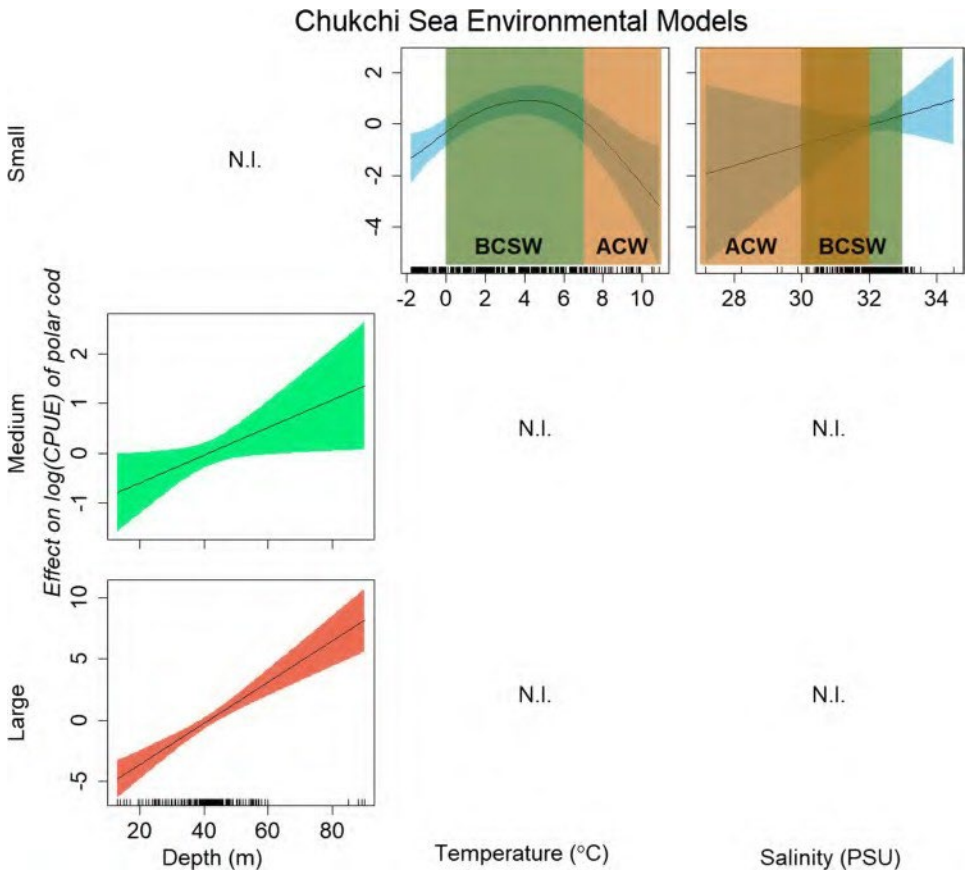

Fig. 6 Estimated effects of three environmental variables on log(CPUE) of three size classes of polar cod in the Chukchi Sea based on generalized additive model (GAM) analysis; *y*-axis is magnitude of effect, rug along *x*-axis marks data values, colored envelopes are 95% confidence intervals. Results from the best model (Table 3) are displayed, and variables excluded from the best model are marked with N.I. (not included). Temperature and salinity measured at the seafloor. Characteristic water mass temperature and salinity values overlaid (*BCSW* Bering Chukchi Summer Water, *ACW* Alaska Coastal Water)

the distribution patterns of polar cod during the following summer.

Spatial analysis

In the Chukchi Sea, visualizing the distribution of the small size class of polar cod suggests oceanic transport of the juvenile life stage of this species. Due to small body size and weak swimming ability, the distribution of small individuals, such as the ≤ 70 mm polar cod considered here, is largely influenced by the direction and speed of the prevailing oceanic currents and sea ice drift (Graham and Hop 1995; David et al. 2016). Because age-0 polar cod descend in the water column throughout their first summer (Geoffroy et al. 2016), the small polar cod captured in the demersal trawl had likely descended to the seafloor recently, after being subjected to movement by pelagic ocean currents. Pelagic acoustic surveys in the Chukchi Sea have also detected large numbers of small, 30–40 mm, age-0 polar cod in the water column in the northern Chukchi Sea (De Robertis et al. 2017a, b), which supports the idea that young-of-the-year polar cod hatch in the spring and are advected from hatch locations via ocean currents.

The primarily northward flow of water through the Bering Strait and across the Chukchi Sea (Weingartner et al. 2013) suggests that the abundance of age-0 polar cod found in the northeast Chukchi Sea in the late summer could have been transported from spawning locations in the southern Chukchi and northern Bering seas in Bering Shelf Water (BSW) and Anadyr Water (AW). Generally, polar cod hatch from buoyant eggs, occupy the water column as larvae, and descend to a demersal environment as they grow (Graham and Hop 1995; Ponomarenko 2000). Though still an area of active research, potential spawning grounds for polar cod in the Pacific Arctic have been proposed near St. Lawrence Island and east of the Chukotka peninsula, Russia (Ponomarenko 1968; Christiansen and Fevolden 2000; Vestfals et al. 2018), and could be the source of age-0 polar cod transported northward and captured in the northeast Chukchi Sea in late summer. However, the detection of larvae throughout the Canadian Arctic (Bouchard and Fortier 2011) indicates that spawning grounds in the Bering and Chukchi seas may be only a few of several spawning regions throughout the Pacific range of polar cod.

As a result of the orientation of the Alaskan coastline, the distribution patterns in the Beaufort Sea of small polar cod display a primarily west to east gradient, coupled secondarily with an inshore to offshore gradient. As in the Chukchi Sea, however, the distribution of small individuals in the Beaufort Sea is likely largely influenced by oceanic currents.

Table 4 Results of generalized additive models (GAMs) in the Beaufort Sea for environmental covariates, depth, temperature, and salinity (see Eq. 2)

Size class	*s* (depth) (9–987 m)	*s* (bottom temperature) (− 1.6 to 4.8 °C)	*s* (bottom salinity) (29.2–34.9 PSU)	− (logLikelihood)	AIC	ΔAIC	Model rank
Small		+	+	− 620.5	1252.9	0.0	1
	+	+	+	− 594.8	1257.2	4.3	2
	+	+		− 700.6	1413.1	160.2	3
	+		+	− 754.5	1521.0	268.1	4
			+	− 756.7	1521.3	268.4	5
		+		− 767.4	1542.8	289.8	6
	+			− 780.7	1569.5	316.6	7
Medium	+	+		− 501.4	1014.7	0.0	1
	+	+	+	− 503.0	1022.0	7.3	2
		+		− 543.7	1095.5	80.7	3
		+	+	− 552.3	1116.6	101.8	4
	+			− 620.7	1249.3	234.6	5
			+	− 629.8	1267.6	252.9	6
	+		+	− 633.1	1278.2	263.5	7
Large	+			− 721.4	1450.9	0.0	1
	+	+		− 724.0	1460.0	9.1	2
		+		− 740.2	1488.4	37.5	3
	+		+	− 764.1	1540.3	89.4	4
			+	− 767.8	1543.6	92.7	5
	+	+	+	− 766.8	1549.5	98.6	6
		+	+	− 775.7	1563.4	112.5	7

Suite of models developed for each polar cod size class, + denotes variables included in each model. The following statistics are reported: − log(likelihood), AIC, ΔAIC. Model performance ranked from best (1) to worst (7) using ΔAIC. ΔAIC calculated as the difference from the lowest AIC value for a size class and sea. θ parameter estimated independently and fixed, $\theta = 0.878$. Inclusion of a spatially autocorrelated error structure precludes the calculation of % deviance explained

A component of the Alaska Coastal Current (ACC), which may play a role in transporting polar cod northward in the Chukchi Sea, continues to flow along the Alaskan Coast, around Point Barrow, and into the Beaufort Sea (Okkonen et al. 2009). Barrow Canyon in the northern Chukchi Sea facilitates the movement of the ACC towards the Beaufort Sea (Pickart et al. 2005) and could effectively transport larval polar cod into the western Beaufort Sea as it does for zooplankton and other small particles (Ashjian et al. 2005; Berline et al. 2008). Further, small polar cod were also detected in the ACC in a plume extending 300 km eastward of Barrow Canyon (Crawford et al. 2012), demonstrating that small fish may be transported into the Beaufort Sea via eastward flowing currents.

Eastern and western aggregations of small polar cod in the Beaufort Sea, separated by a gap from 150° W to 144° W, suggests two separate groupings and perhaps distinct populations. Despite the prevailing eastward flow of water, the spatial separation indicates that polar cod in the eastern Beaufort Sea did not originate in the Chukchi Sea. Larval, juvenile, and adult polar cod are commonly captured in the Canadian Beaufort Sea (Bouchard and Fortier 2011; Geoffroy et al. 2011; Walkusz et al. 2013) and could be a source of small polar cod in the eastern US Beaufort Sea. In 2011, pelagic, larval polar cod were most abundant in the eastern US Beaufort Sea when compared to the western US Beaufort Sea (Gallaway et al. 2017), suggesting that some polar cod in the US Beaufort Sea originate from Canadian sources. The distribution patterns are corroborated by a population genetic study which found that while polar cod comprises a single population, a significant difference in microsatellite alleles between polar cod from the southern Chukchi Sea and the central Beaufort Sea implies some degree of spatial genetic differentiation consistent with an isolation-by-distance pattern (Wilson et al. 2017, 2019). The low abundance of small polar cod between 150° W and 144° W is not an artifact of sparse sampling effort in the middle section, as the station sampling density is similar across the entire Beaufort Sea shelf; nor is it the result of a single year of low polar cod abundance, as this region was sampled over multiple years. Together, spatial and genetic information indicate that small polar cod across the Beaufort Sea shelf belong

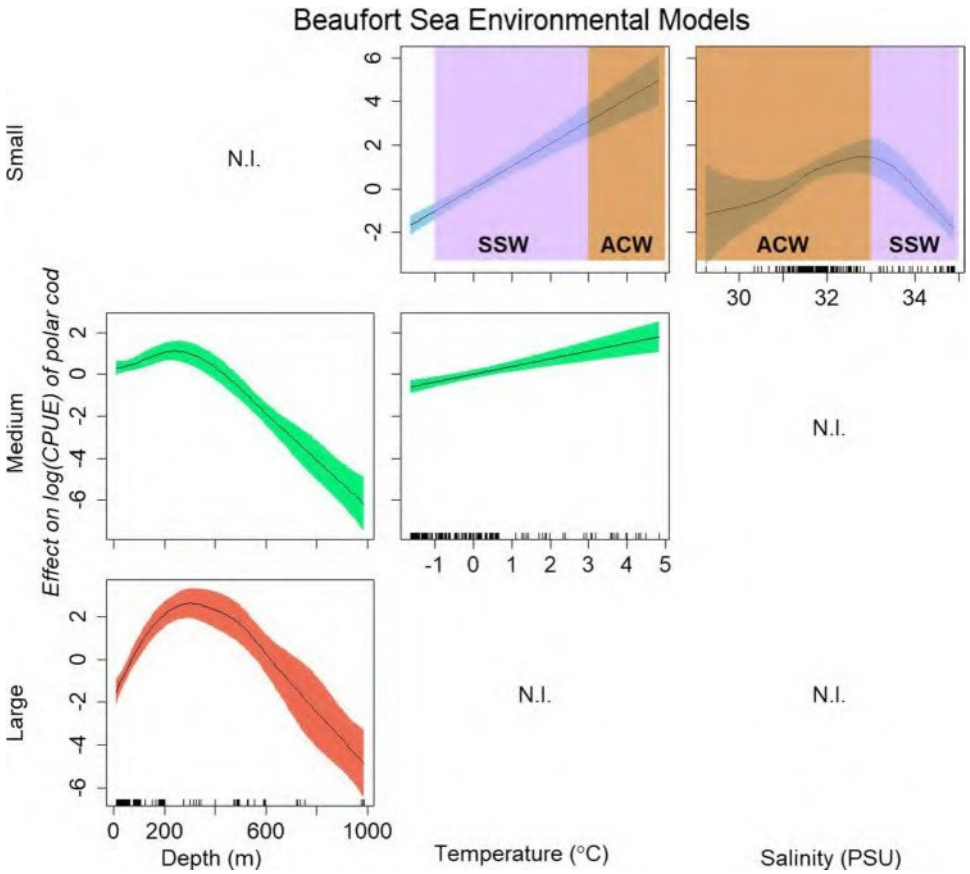

Fig. 7 Estimated effects of three environmental variables on log(CPUE) of three size classes of polar cod in the Beaufort Sea based on generalized additive model (GAM) analysis; *y*-axis is magnitude of effect, rug along *x*-axis mark location of data values, and colored envelopes are 95% confidence intervals. Results from the best model (Table 4) are displayed, and variables excluded from the best model are marked with N.I. (not included). Temperature and salinity measured at the seafloor. Characteristic water mass temperature and salinity values overlaid (*SSW* Summer Shelf Water, *ACW* Alaska Coastal Water)

Table 5. Polar c od mean CPUE in spring and summer 2017 in the southern Chukchi Sea.

Season	Station (*n*)	Depth	Temperature	Salinity	Size class	CPUE
Spring	9	43.1 (9.69)	1.69 (1.22)	32.42 (0.39)	All	0.71 (1.11)
					> 70mm	0.50 (1.04)
Summer	14	39.1 (13)	4.18 (0.95)	32.26 (0.56)	All	70.31 (219.92)

Mean and (standard deviation) environmental conditions reported for depth (m), temperature (°C), salinity (PSU). Mean and (standard deviation) CPUE reported for all polar cod as well as only polar cod > 70 mm. CPUE significantly different ($p < 0.05$) between spring and summer for polar cod > 70 mm

to two spatially segregated groups from different spawning locations.

In both the Chukchi and Beaufort seas, distribution patterns of medium and large polar cod suggest that larger fish actively disperse from areas occupied by the smallest fish. The small size class had a region of high abundance in the northeast Chukchi Sea that was not seen in the medium or large size classes. As fish develop, swimming ability improves (Webb 1994) and juveniles may disperse from nursery grounds to adult habitats (Gillanders et al. 2003). Improved dispersal capabilities gained with increasing body size could explain the spread of the medium size class beyond the confines of the areas occupied by small polar cod in the Chukchi and Beaufort seas. The large size class showed further evidence of offshore ontogenetic movement in both the Chukchi and Beaufort seas, where large polar cod were most abundant beginning around 80 km in the Chukchi Sea and 60 km in the Beaufort Sea and extending seaward. Animals are often distributed with respect to resource availability to maximize fitness and reduce competition (Fretwell and Lucas 1969). The northeast Chukchi Sea and western Beaufort Sea, where there were regions of high abundance of the medium size class, are areas of high summer produc- tion (Walsh et al. 2005; Sigler et al. 2011). Therefore, mid- sized individuals may be maximizing growth by dispersing to productive feeding grounds. Offshore movement of large polar cod may be a component of adult spawning migrations. In the Chukchi Sea, several spawning grounds have been

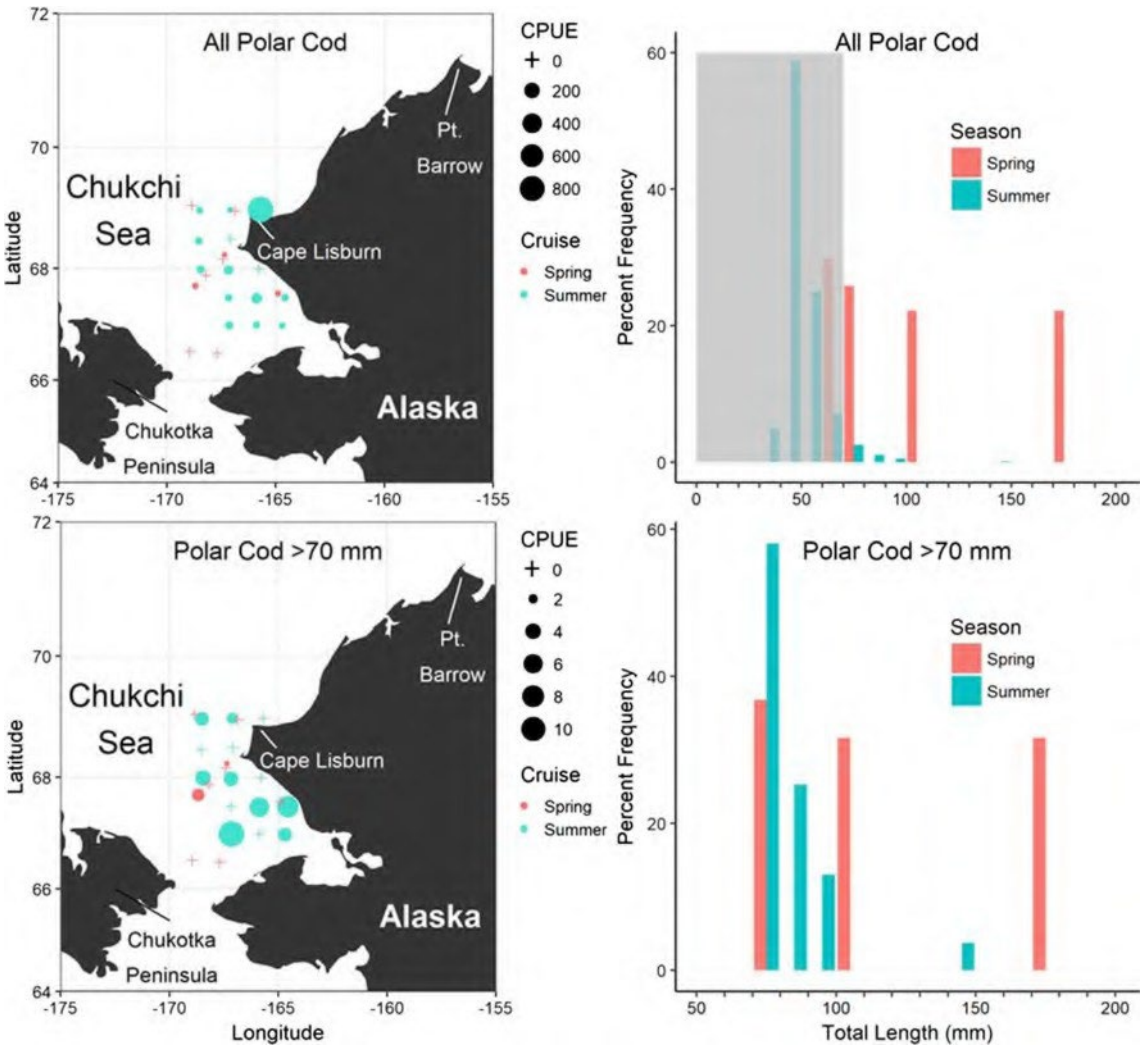

Fig. 8 Distribution and length-frequency of polar cod in the Chukchi Sea in spring and summer 2017. Length-frequency scaled by CPUE. Top two panels are all captured sizes of polar cod, total CPUE (fish per 1000 m^2) spring = 6.43, summer = 984.40. Bottom two panels are only polar cod > 70 mm, total CPUE spring = 4.51, summer = 42.29; gray box in top right shows small fish excluded from lower two plots. Note difference in scale between top left and bottom left plot

proposed in the northern Bering Sea and near the Chukotka peninsula (Ponomarenko 1968; Christiansen and Fevolden 2000; Vestfals et al. 2018). The abundance of the large size class of polar cod, both offshore and south of Cape Lisburne in the late summer, could reflect a movement towards these southern winter spawning locations.

Environmental analysis

Generally, both availability of food resources and temperature influence habitat selection of ectothermic species (Crowder and Magnuson 1983). Food resources are distributed unevenly among water masses (Eisner et al. 2013; Pinchuk and Eisner 2017; Smoot and Hopcroft 2017; Danielson et al. 2017b), which are identified by characteristic temperature and salinity ranges in the Chukchi and Beaufort seas. Temperature also has a direct physiological effect on growth rates of juvenile polar cod (Laurel et al. 2017) and likely influences their distribution. Depth commonly influences distribution patterns and is associated with offshore migrations of other species such as Pacific cod and Pacific halibut (*Hippoglossus stenolepis*), in the neighboring Bering Sea (Shimada and Kimura 1994; Webster et al. 2013). In Alaskan waters, the addition of environmental information to species distribution maps has been identified as a recent research objective in the Alaska Essential Fish Habitat Research Plan, which is mandated by the Magnuson-Stevens Fishery Conservation and Management Act (Sigler et al. 2017). Characterizing the role of environmental conditions for polar cod at different life stages moves towards this

goal and identifies underlying processes influencing spatial patterns in distribution.

In the Chukchi Sea, small polar cod were associated with the intermediate temperature and salinity of the highly productive Bering Chukchi Summer Water (BCSW) mass. BCSW is a commonly detected water mass throughout the northeast Chukchi Sea during the open water season, with temperatures ranging from 0 to 7 °C and salinity from 30 to 33.5 PSU (Danielson et al. 2017b), which were the temperature and salinity ranges most commonly occupied by small polar cod (Fig. 6). Other water masses in the Chukchi Sea include the cooler Bering Chukchi Winter Water (BCWW) with temperatures from − 2 to 0 °C and salinity from 30 to 33 PSU, and the warmer Alaska Coastal Water (ACW) with temperatures from 7 to 12 °C and salinity from 27 to 32 PSU (Danielson et al. 2017b); however, small polar cod were less abundant in these water masses. BCSW is a nutrient-rich water mass with a characteristic zooplankton community of calanoid copepods and euphausiids (Eisner et al. 2013), which are prey for polar cod (Rand et al. 2013; Gray et al. 2016). In contrast, the BCWW and ACW are less nutrient rich, and have smaller-bodied zooplankton communities, including species such as *Oithona similis*, *Calanus abdominalis*, and *Pseudocalanus* spp. (Eisner et al. 2013), which are marginal resources when compared to lipid-rich Calanus copepods (Falk-Petersen et al. 2009). Maximizing energy intake as a result of consuming high-quality prey resources is beneficial to polar cod and results in increased growth rates and improved body condition (Hop et al. 1997). Therefore, distribution patterns of small polar cod in the Chukchi Sea are likely influenced by the abundance and composition of prey resources in different water masses.

In the Beaufort Sea, small polar cod were primarily associated with relatively warm and moderately fresh water found near the Alaskan coast. Environmental conditions in the Beaufort Sea are markedly different from those found in the Chukchi Sea; the warmest sampled Beaufort Sea temperature of 5 °C is comparable to the intermediate temperatures found in the Chukchi Sea. Yet in both the Chukchi and Beaufort seas (Figs. 6, 7), small polar cod were most abundant in water temperatures 4–5 °C. However, the relationship between small polar cod abundance and salinity differed between the Chukchi and Beaufort seas. Unlike in the Chukchi Sea where abundance increased linearly with salinity to a maximum of 34.5 PSU, small polar cod in the Beaufort Sea were less abundant at salinities > 34 PSU. Cold and saline water is associated with Summer Shelf Water (SSW), and our results suggest that the differing effect of salinity between seas is likely due to this association of small polar cod with distinct water masses, characterized by a signature combination of temperature and salinity (Danielson et al. 2017b).

The warm and fresh water occupied by small polar cod in the Beaufort Sea is associated with nearshore coastal habitats and the eastward flowing ACW (Okkonen et al. 2009; Carmack et al. 2015), and could impact growth of individuals in the small size class. This warm coastal water is not nutrient rich (Dunton et al. 2005), but does provide a thermal habitat that is advantageous for polar cod. Though polar cod is a cold-adapted species and capable of surviving in sub-zero temperatures (Osuga and Feeney 1978), it is more commonly found at temperatures above 0 °C (Crawford et al. 2012). Small polar cod in the Beaufort Sea appear to be occupying the warmest available water to maximize growth. Higher growth rates are advantageous for the small, age-0, individuals (Helser et al. 2017). In harsh Arctic winters, survivorship increases dramatically when pre-winter size and body condition are good (Fortier et al. 2006; Heintz and Vollenweider 2010), while large gape size and increased swimming speeds enable better resource exploitation (Scharf et al. 2000). In the Beaufort Sea, the thermal advantages of warm, coastal water appear to be correlated with patterns of distribution of small polar cod. Though warm coastal water may be advantageous for growth in certain scenarios, the cost of occupying low nutrient and low production waters could result in a tradeoff with negative energetic consequences, including a scenario where accelerated growth outstrips resource availability, impacting polar cod growth and survival in the Beaufort Sea.

The positive relationship between depth and abundance (Figs. 6, 7) indicates that depth is a key environmental component correlated with the offshore shift in distribution of the medium and large size classes of polar cod in the Chukchi and Beaufort seas. In the Chukchi Sea, where sampled depths were 13–90 m, the increasing linear relationship with depth suggests that polar cod moves to offshore, somewhat deeper locations as they grow larger. In the Beaufort Sea, where sampled depths reached nearly 1000 m, medium and large polar cod were most abundant at 300 and 400 m, respectively, demonstrating that as individuals increase in size, they move offshore to a specific bottom depth range. A nearly identical pattern was identified in the Canadian Beaufort, where medium and large fish (~ 90+ mm) were encountered at deep, offshore stations and the highest abundances of those fish were found at depths between 350 and 500 m (Geoffroy et al. 2011; Benoit et al. 2014; Majewski et al. 2016). The distribution pattern of polar cod was attributed to distinctly layered water masses in the Canadian Beaufort Sea (Pickart 2004), with polar cod occupying a layer of Atlantic Water, which was warmer than 0 °C and detected from 350 to 500 m depth. In the present study area, Atlantic Water was observed in the US Beaufort Sea at depths > 250 m (Norcross et al. 2017; Smoot and Hopcroft 2017), and this was where large polar cod were most abundant (Fig. 7).

Therefore, polar cod occupies the Atlantic Water mass in both the US and Canadian Beaufort Sea.

Seasonal analysis

Springtime demersal abundance of polar cod in the southern Chukchi Sea was strikingly low compared to late summer abundance. Low springtime abundance of demersal polar cod during 2017, when only four fish were captured, was corroborated the following year when a June 2018 research cruise captured only two polar cod at the same sampling locations (Danielson et al. 2018). While adult polar cod were not present in the demersal environment in the southern Chukchi Sea in the spring, small polar cod (< 20 mm) were captured in Bongo nets (R. Hopcroft, personal communication) concurrently sampled with the bottom trawl in June 2017 and 2018. The bottom trawl gear used in June 2017 and 2018 was identical to the gear used in the late summer collections that successfully captured demersal polar cod in the same region. Though there were approximately half the number of stations sampled in June when compared to August, the stations were distributed across the study area to maximize spatial sampling extent (Fig. 8). It is likely that growth of age-0 polar cod between June and August/September resulted in a higher catch of age-0 polar cod in the late summer. However, the complete lack of larger (> 70 mm), older (age 1 +) individuals, which would be equally susceptible to the net in June and August/September suggests that the collections in June likely truly represent a lower abundance of subadult and adult polar cod near the sea floor in the southern Chukchi Sea in the spring.

Strong linkages between sea ice and polar cod life history suggest that the distribution of polar cod in the southern Chukchi Sea could be influenced by the distribution of sea ice. While polar cod occupies environments that are seasonally ice free, it is often characterized as a sympagic species for a portion of its life cycle (Craig et al. 1982; Lønne and Gulliksen 1989). Polar cod is thought to spawn under sea ice, and buoyant eggs float to the ice–water interface before hatching in early spring (Graham and Hop 1995; Bouchard and Fortier 2011). Sea ice also provides a platform for the growth of sea ice algae, which is not only an important source of primary productivity in the Arctic, but also has a distinct isotopic signature that can be traced throughout Arctic food webs (Iken et al. 2005; Gradinger 2009). Isotopic and fatty acid analyses have linked polar cod to sea-ice-derived carbon, demonstrating the significant influence that sea ice can have on the diet of polar cod (Kohlbach et al. 2017; Dissen et al. 2018). Finally, the seasonal melting of sea ice is a driver of springtime patterns of productivity in the Arctic, with ice-edge blooms typically following the retreat of sea ice, resulting in peak productivity ~ 20 days after ice retreat (Perrette et al. 2011). The spring bloom stimulates and supports secondary productivity, ultimately resulting in planktonic food resources for polar cod (Sigler et al. 2011; Wassmann and Reigstad 2011).

Given the link between sea ice and polar cod life history, sea ice extent and retreat may influence the spring distribution of polar cod in the southern Chukchi Sea. It is possible that polar cod tracks the springtime ice retreat and the wave of productivity that follows. However, in the springs of both 2017 and 2018, when sampling occurred, the sea ice edge had already retreated far north of the sampling region (NASA 2018). If polar cod followed the ice edge in these years, then its distribution would be beyond the northernmost station sampled during the June cruises, explaining the extremely low abundances of subadult and adult polar cod observed in the southern Chukchi Sea. It is unlikely that the low abundances of subadult and adult polar cod in the southern Chukchi Sea can be explained by polar cod moving south into the northern Bering Sea. Though polar cod is found episodically in the northern Bering Sea in association with cold conditions and large ice extent (Wyllie-Echeverria and Wooster 1998; Cui et al. 2009), these conditions did not occur in 2017 or 2018. Furthermore, sampling in the northern Bering Sea from St. Lawrence Island to the Bering Strait caught few polar cod in 2017 and 2018 (Danielson et al. 2018), suggesting that polar cod did not move into the northern Bering Sea.

Movement inferred from size-based and seasonal patterns in distribution describes a plausible migration scenario. In classical fisheries science, the life history of a species that undertakes a migration triangle travels from nursery grounds as juveniles, to feeding grounds as subadults, to spawning grounds upon maturation. The trian- gle is complete when eggs and larvae are passively transported from the spawning grounds to the nursery grounds via oceanic currents and the cycle begins again (Harden Jones 1968; Secor 2002). Small, young polar cod are most abundant in the northeast Chukchi Sea, perhaps indicat- ing that region functions as nursery grounds for juveniles. The northeast Chukchi Sea was also proposed as a nursery area by researchers analyzing the pelagic distribution of age-0 polar cod, though the suggestion remains untested (De Robertis et al. 2017b). The next step in a migration triangle is the movement of subadults to feeding grounds; in the current study, the distribution pattern of the medium size class was different from the small size class, indicating that medium polar cod move away from areas occupied by small fish and disperse across the productive northeast Chukchi Sea shelf (Grebmeier 2012) to take advantage of feeding opportunities. The final component of a classic migration triangle is movement to spawning grounds; the current study cannot address this directly as polar cod spawns in the late fall and early winter under sea ice (Ponomarenko 2000). Several locations in the northern Bering

Sea and near the Chukotka peninsula have been recognized for their potential as polar cod spawning grounds (Ponomarenko 1968; Christiansen and Fevolden 2000; Vestfals et al. 2018); and are geographically close to the late summer distribution of the large size class in this study, which contains the majority of the mature spawners (Nahrgang et al. 2016). Potential spawners in the southern Chukchi Sea in late summer would not have far to travel to proposed spawning grounds during the fall and winter seasons.

Completion of the proposed migration scenario could be achieved via advection of eggs and larvae by the northbound currents traveling through Bering Strait and across the Chukchi Sea (Weingartner et al. 2005). Pelagic (De Robertis et al. 2017b) and demersal distributions are consistent with northward advection of eggs and larvae from southern spawning grounds. The spring absence of polar cod from the southern Chukchi Sea may be explained within the framework of the proposed migration triangle. In the spring, adult polar cod following the seasonal northward retreat of sea ice may be spawners seeking resources to replenish their depleted energy reserves. Spawning is energetically costly and these individuals would likely need to take advantage of the earliest available food resources (Hop et al. 1995). This possible movement scenario synthesizes both size-based and seasonal distribution patterns of polar cod and represents a new effort to characterize polar cod migration patterns in the Chukchi Sea. The migration of a small-bodied, high-latitude fish species is not unprecedented, but there remains much uncertainty surrounding the migration patterns of polar cod in the Chukchi Sea. Other marine fish species, such as Pacific herring and walleye pollock in the Bering Sea, exhibit seasonal migrations between feeding grounds and spawning grounds (Kotwicki et al. 2005; Tojo et al. 2007). Additionally, telemetry studies in the Atlantic Arctic found that polar cod is physically capable of traveling over 100 km in response to rapidly evolving ice conditions (Kessel et al. 2015). The migration triangle proposed here is currently constrained by data collected during open water sampling efforts. Moored acoustics offer an opportunity to confirm and refine understanding of polar cod movement during the Arctic winter and are currently being deployed in the Chukchi and Beaufort seas (Kitamura et al. 2017; Hauri et al. 2018). Patterns in backscatter collected at moorings during the ice-covered season provide information on fish presence and abundance when net sampling is not possible (Kaartvedt et al. 2009). In addition to increased field sampling efforts, modeling studies using tools like ROMS will corroborate the direction and timing of transport of polar cod eggs and larvae in ocean currents, improving understanding of polar cod movement throughout their life cycle in the Chukchi Sea. The scale of detail of the migration triangle proposed here is coarse and based on a small sample size, but nevertheless provides an initial framework against which new information may be tested to advance understanding of polar cod movement patterns in the Chukchi Sea.

Conclusions

Advancing fisheries science in the remote and difficult to access Arctic ecosystem is a significant research challenge. The work presented here compiles a large number of disparate individual sampling efforts to develop a holistic picture describing polar cod summer distribution in the Chukchi and Beaufort seas. The size-based analysis demonstrates ontogenetic shifts in distribution, while consideration of environmental covariates provides insight into potential mechanisms driving these patterns. Though much work remains to be done in understanding polar cod distribution and migration, the comparison between spring and summer abundances shows that polar cod distribution in the Pacific Arctic varies by season and suggests that this species may undertake some form of seasonal migration. The mapping of polar cod distribution in the Chukchi and Beaufort seas improves understanding of one of the most abundant and critical trophic links in the Arctic ecosystem. As the Arctic experiences increased anthropogenic and climatological pressures, thorough knowledge of key components of this system, including species like polar cod, will inform responsible decision making in this dynamic and rapidly changing ecosystem.

Acknowledgements We thank reviewers Kevin Hedges, Wojciech Walkusz, and Hauke Flores for their insightful and constructive review of this manuscript. We thank the scientists, research vessels' captains and crew who collected the data compiled in this study. We also thank past and present members of the UAF Fisheries Oceanography lab for their laboratory work processing specimens. Funds were provided by the North Slope Borough and the Arctic Integrated Research Program sponsored by the North Pacific Research Board (NPRB). In addition, this study was funded in part by material sampled under Award Numbers M10AC0004, M12AC00011, and M13PC00019 of the U.S. Department of the Interior, Bureau of Ocean Energy Management (BOEM), Alaska Outer Continental Shelf Region. In-kind support was contributed by the National Oceanic and Atmospheric Administration (Alaska Fisheries Science Center) and the University of Alaska Fairbanks. This paper represents NPRB publication ArcticIERP-15.

Conflict of interest The authors declare that they have no conflicts of interest.

Ethical approval All applicable national and international guidelines for the care and use of animals were followed. Sample collections in US waters were approved by the Institutional Animal Care and Use Committee (IACUC) of the University of Alaska Fairbanks.

References

Abookire AA, Rose CS (2005) Modifications to a plumb staff beam trawl for sampling uneven, complex habitats. Fish Res 71:247–254. https://doi.org/10.1016/j.fishres.2004.06.006

Ashjian CJ, Gallager SM, Plourde S (2005) Transport of plankton and particles between the Chukchi and Beaufort Seas during summer 2002, described using a Video Plankton Recorder. Deep Sea Res Part II 52:3259–3280. https://doi.org/10.1016/j.dsr2.2005.10.012

Astthorsson OS (2015) Distribution, abundance and biology of polar cod, *Boreogadus saida*, in Iceland-East Greenland waters. Polar Biol 39:995–1003. https://doi.org/10.1007/s00300-015-1753-5

Benaglia T, Chauveau D, Hunter DR (2009) An EM-like algorithm for semi-and nonparametric estimation in multivariate mixtures. J Comput Graph Stat 18:505–526

Benoit D, Simard Y, Fortier L (2008) Hydroacoustic detection of large winter aggregations of Arctic cod (*Boreogadus saida*) at depth in ice-covered Franklin Bay (Beaufort Sea). J Geophys Res 113:1–9. https://doi.org/10.1029/2007jc004276

Benoit D, Simard Y, Fortier L (2014) Pre-winter distribution and habitat characteristics of polar cod (*Boreogadus saida*) in southeastern Beaufort Sea. Polar Biol 37:149–163. https://doi.org/10.1007/s00300-013-1419-0

Berline L, Spitz YH, Ashjian CJ, Campbell RG, Maslowski W, Moore SE (2008) Euphausiid transport in the Western Arctic Ocean. Mar Ecol Prog Ser 360:163–178. https://doi.org/10.3354/meps07387

Bouchard C, Fortier L (2011) Circum-arctic comparison of the hatching season of polar cod *Boreogadus saida*: A test of the freshwater winter refuge hypothesis. Prog Oceanogr 90:105–116. https://doi.org/10.1016/j.pocean.2011.02.008

Carmack EC, Macdonald RW (2002) Oceanography of the Canadian shelf of the Beaufort Sea: a setting for marine life. Arctic 55:S29–S45

Carmack EC, Macdonald RW, Papadakis JE (1989) Water mass structure and boundaries in the Mackenzie shelf estuary. J Geophys Res 94:18043–18055. https://doi.org/10.1029/JC094iC12p18043

Carmack E, Winsor P, Williams W (2015) The contiguous panarctic Riverine Coastal Domain: a unifying concept. Prog Oceanogr 139:13–23. https://doi.org/10.1016/j.pocean.2015.07.014

Christensen B (1996) Predator foraging capabilities and prey antipredator behaviours: pre-versus postcapture constraints on size-dependent predator–prey interactions. Oikos 96:368–380

Christiansen JS, Fevolden S-E (2000) The polar cod of Porsangerfjorden, Norway; revisited. Sarsia 85:89–193. https://doi.org/10.1080/00364827.2000.10414571

Clark DL, Leis JM, Hay AC, Trnski T (2005) Swimming ontogeny of larvae of four temperate marine fishes. Mar Ecol Prog Ser 292:287–300

Craig P, Griffiths W, Haldorson L, McElderry H (1982) Ecological Studies of Arctic Cod (*Boreogadus saida*) in Beaufort Sea Coastal Waters, Alaska. Can J Fish Aquat Sci 39:395–406

Crawford RE, Vagle S, Carmack EC (2012) Water mass and bathymetric characteristics of polar cod habitat along the continental shelf and slope of the Beaufort and Chukchi seas. Polar Biol 35:179–190. https://doi.org/10.1007/s00300-011-1051-9

Crowder LB, Magnuson JJ (1983) Cost-benefit analysis of temperature and food resource use: a synthesis with examples from the fishes. In: Aspey WP, Lustick SI (eds) Behavioral energetics. Ohio State University Press, Columbus, pp 189–221

Cui X, Grebmeier JM, Cooper LW, Lovvorn JR, North CA, Seaver WL, Kolts JM (2009) Spatial distributions of groundfish in the northern Bering Sea in relation to environmental variation. Mar Ecol Prog Ser 393:147–160. https://doi.org/10.3354/meps08275

Danielson S, Ahkinga O, Edenfield L, Eisner L, Forster C, Hardy S, Hartz S, Holladay B, Hopcroft R, Jones B, Krause J, Kuletz K, Lekanoff R, Lomas M, Lu K, Norcross B, O'Daly S, Pretty J, Pham C, Poje A, Roth E, Seabrook S, Shipton P, Smith B, Smoot C, Stafford K, Stockwell D, Yamaguchi A, Zinkann A (2017a) Arctic Shelf Growth, Advection, Respiration and Deposition (ASGARD) rate measurements project. Anchorage AK: North Pacific Research Board. SKQ201709S Cruise Report to the Arctic Integrated Research Program

Danielson SL, Eisner L, Ladd C, Mordy C, Sousa L, Weingartner TJ (2017b) A comparison between late summer 2012 and 2013 water masses, macronutrients, and phytoplankton standing crops in the northern Bering and Chukchi Seas. Deep Sea Res Part II 135:7–26. https://doi.org/10.1016/j.dsr2.2016.05.024

Danielson S, Ahkinga O, Baer S, Chapman Z, Collins E, Edenfeld L, Escajeda E, Forster C, Gonzalez S, Hardy S, Hopcroft R, Iken K, Jones B, Juranek L, Kuletz K, Lomas M, Naber D, Norcross B, McDonnell A, Mendoza H, O'Daly S, Poje A, Roth E, Shipton P, Smith B, Smoot C, Stafford K, Stockwell D, Thurber A (2018) Arctic Shelf Growth, Advection, Respiration and Deposition (ASGARD) Rate Measurements Project. Anchorage AK: North Pacific Research Board. SKQ201813 Cruise Report to the Arctic Integrated Research Program

David C, Lange B, Krumpen T, Schaafsma F, van Franeker JA, Flores H (2016) Under-ice distribution of polar cod *Boreogadus saida* in the central Arctic Ocean and their association with sea-ice habitat properties. Polar Biol 39:981–994. https://doi.org/10.1007/s00300-015-1774-0

De Robertis A, Taylor K, Williams K, Wilson CD (2017a) Species and size selectivity of two midwater trawls used in an acoustic survey of the Alaska Arctic. Deep Sea Res Part II 135:40–50. https://doi.org/10.1016/j.dsr2.2015.11.014

De Robertis A, Taylor K, Wilson CD, Farley EV (2017b) Abundance and distribution of Arctic cod (*Boreogadus saida*) and other pelagic fishes over the U.S. Continental Shelf of the Northern Bering and Chukchi Seas. Deep Sea Res Part II 135:51–65. https://doi.org/10.1016/j.dsr2.2016.03.002

Dissen JN, Oliveira AC, Horstmann L, Hardy SM (2018) Regional and temporal variation in fatty acid profiles of polar cod (*Boreogadus saida*) in Alaska. Polar Biol 41:2495–2510

Dunton KH, Goodall JL, Schonberg SV, Grebmeier JM, Maidment DR (2005) Multi-decadal synthesis of benthic–pelagic coupling in the western arctic: Role of cross-shelf advective processes. Deep Sea Res Part II 52:3462–3477. https://doi.org/10.1016/j.dsr2.2005.09.007

Eisner L, Hillgrubber N, Martinson E, Maselko J (2013) Pelagic fish and zooplankton species assemblages in relation to water mass characteristics in the northern Bering and southeast Chukchi seas. Polar Biol 36:87–113

Falk-Petersen S, Mayzaud P, Kattner G, Sargent JR (2009) Lipids and life strategy of Arctic Calanus. Mar Biol Res 5:18–39

Fortier L, Sirois P, Michaud J, Barber D (2006) Survival of Arctic Cod larvae (*Boreogadus saida*) in relation to sea ice and temperature in the Northeast Water Polynya (Greenland Sea). Can J Fish Aquat Sci 63:1608–1616

Fretwell SD, Lucas HL (1969) On territorial behavior and other fac- tors influencing habitat distribution in birds. Acta Biotheor 19:16–36

Gallaway BJ, Konkel WJ, Norcross BL (2017) Some thoughts on estimating change to arctic cod populations from hypothetical oil spills in the Eastern Alaska Beaufort Sea. Arct Sci 3:716– 729. https://doi.org/10.1139/as-2016-0056

Geoffroy M, Robert D, Darnis G, Fortier L (2011) The aggregation of polar cod (*Boreogadus saida*) in the deep Atlantic layer of ice-covered Amundsen Gulf (Beaufort Sea) in winter. Polar Biol 34:1959–1971. https://doi.org/10.1007/s00300-011-1019-9

Geoffroy M, Majewski A, LeBlanc M, Gauthier S, Walkusz W, Reist JD, Fortier L (2016) Vertical segregation of age-0 and age-1+ polar cod (*Boreogadus saida*) over the annual cycle in the Canadian Beaufort Sea. Polar Biol 39:1023–1037. https://doi.org/10.1007/s00300-015-1811-z

Gillanders BM, Able KW, Brown JA, Eggleston DB, Sheridan PF (2003) Evidence of connectivity between juvenile and adult habitats for mobile marine fauna: an important component of nurseries. Mar Ecol Prog Ser 247:281–295

Goddard P, Lauth R, Armistead C (2016) Results of the 2012 Chukchi Sea bottom trawl survey of bottomfishes, crabs, and other demersal macrofauna. Juneau AK: US Dept. of the Interior, Bureau of Ocean Management, Alaska OCS Region. Report for BOEM agreement Numbers M12AC00009 (UAF), M12PG00018 (AFSC) and M10PG00050 (USF&WS)

Gradinger R (2009) Sea-ice algae: major contributors to primary production and algal biomass in the Chukchi and Beaufort Seas during May/June 2002. Deep Sea Res Part II 56:1201–1212. https://doi.org/10.1016/j.dsr2.2008.10.016

Graham M, Hop H (1995) Aspects of reproduction and larval biology of Arctic Cod (*Boredogadus saida*). Arctic 48:130–135

Gray BP, Norcross BL, Blanchard AL, Beaudreau AH, Seitz AC (2016) Variability in the summer diets of juvenile polar cod (*Boreogadus saida*) in the northeastern Chukchi and western Beaufort Seas. Polar Biol 39:1069–1080. https://doi.org/10.1007/s00300-015-1796-7

Gray BP, Norcross BL, Beaudreau AH, Blanchard AL, Seitz AC (2017) Food habits of Arctic staghorn sculpin (*Gymnocanthus tricuspis*) and shorthorn sculpin (*Myoxocephalus scorpius*) in the northeastern Chukchi and western Beaufort Seas. Deep Sea Res Part II 135:111–123. https://doi.org/10.1016/j.dsr2.2016.05.013

Grebmeier JM (2012) Shifting patterns of life in the Pacific Arctic and sub-Arctic seas. Ann Rev Marine Sci 4:63–78. https://doi.org/10.1146/annurev-marine-120710-100926

Grebmeier JM, McRoy CP, Feder HM (1988) Pelagic-benthic coupling on the shelf of the northern Bering and Chukchi seas. 1. Food supply source and benthic biomass. Mar Ecol Prog Ser 48:57–67

Grebmeier JM, Cooper LW, Feder HM, Sirenko BI (2006) Ecosystem dynamics of the Pacific-influenced Northern Bering and Chukchi Seas in the Amerasian Arctic. Prog Oceanogr 71:331–361. https://doi.org/10.1016/j.pocean.2006.10.001

Gunderson DR, Ellis IE (1986) Development of a plumb staff beam trawl for sampling demersal fauna. Fish Res 4:35–41

Harden Jones FR (1968) Fish migration. Edward Arnold, London

Hastie TJ, Tibshirani RJ (1986) Generalized additive models. Statistical Science 1:297–318

Hauri C, Danielson S, McDonnell AMP, Hopcroft RR, Winsor P, Shipton P, Lalande C, Stafford KM, Horne JK, Cooper LW, Grebmeier JM, Mahoney A, Maisch K, McCammon M, Statscewich H, Sybrandy A, Weingartner T (2018) From sea ice to seals: a moored marine ecosystem observatory in the Arctic. Ocean Sci 14:1423–1433

Heintz RA, Vollenweider JJ (2010) Influence of size on the sources of energy consumed by overwintering walleye pollock (*Theragra chalcogramma*). J Exp Mar Biol Ecol 393:43–50. https://doi.org/10.1016/j.jembe.2010.06.030

Helser TE, Colman JR, Anderl DM, Kastelle CR (2017) Growth dynamics of saffron cod (*Eleginus gracilis*) and Arctic cod (*Boreogadus saida*) in the Northern Bering and Chukchi Seas. Deep Sea Res Part II 135:66–77. https://doi.org/10.1016/j.dsr2.2015.12.009

Hop H, Gjosaeter H (2013) Polar cod (*Boreogadus saida*) and capelin (*Mallotus villosus*) as key species in marine food webs of the Arctic and the Barents Sea. Marine Biol Res 9:878–894. https://doi.org/10.1080/17451000.2013.775458

Hop H, Trudeau VL, Graham M (1995) Spawning energetics of Arctic cod (*Boreogadus saida*) in relation to seasonal development of the ovary and plasma sex steroid levels. Can J Fish Aquat Sci 52:541–550. https://doi.org/10.1139/f95-055

Hop H, Tonn WM, Welch HE (1997) Bioenergetics of Arctic cod (*Boreogadus saida*) at low temperatures. Can J Fish Aquat Sci 54:1772–1784

Iken K, Bluhm BA, Gradinger R (2005) Food web structure in the high Arctic Canada Basin: evidence from 13C and 15N analysis. Polar Biol 28:238–249. https://doi.org/10.1007/s00300-004-0669-2

Kaartvedt S, Røstad A, Klevjer TA, Staby A (2009) Use of bottom-mounted echo sounders in exploring behavior of mesopelagic fishes. Mar Ecol Prog Ser 395:109–118. https://doi.org/10.3354/meps08174

Kahru M, Brotas V, Manzano-Sarabia M, Mitchell BG (2011) Are phytoplankton blooms occurring earlier in the Arctic? Glob Change Biol 17:1733–1739. https://doi.org/10.111 1/j.1365-2486.2010.02312.x

Kessel ST, Hussey NE, Crawford RE, Yurkowski DJ, O'Neill CV, Fisk AT (2015) Distinct patterns of Arctic cod (*Boreogadus saida*) presence and absence in a shallow high Arctic embayment, revealed across open-water and ice-covered periods through acoustic telemetry. Polar Biol 39:1057–1068. https://doi.org/10.1007/s00300-015-1723-y

Kitamura M, Amakasub K, Kikuchia T, Nishinoa S (2017) Seasonal dynamics of zooplankton in the southern Chukchi Sea revealed from acoustic backscattering strength. Cont Shelf Res 133:47–58

Kohlbach D, Schaafsma FL, Graeve M, Lebreton B, Lange BA, David C, Vortkamp M, Flores H (2017) Strong linkage of polar cod (*Boreogadus saida*) to sea ice algae-produced carbon: evidence from stomach content, fatty acid and stable isotope analyses. Prog Oceanogr. https://doi.org/10.1016/j.pocean.2017.02.003

Kotwicki S, Buckley TW, Honkalehto T, Walters G (2005) Variation in the distribution of walleye pollock (*Theragra chalcogramma*) with temperature and implications for seasonal migration. Fish Bull 103:574–587

Kotwicki S, Lauth RR, Williams K, Goodman SE (2017) Selectivity ratio: a useful tool for comparing size selectivity of multiple survey gears. Fish Res 191:76–86. https://doi.org/10.1016/j.fishres.2017.02.012

Lansard B, Mucci A, Miller LA, Macdonald RW, Gratton Y (2012) Seasonal variability of water mass distribution in the southeastern Beaufort Sea determined by total alkalinity and δ18O. J Geophys Res 117:1–19. https://doi.org/10.1029/2011jc007299

Laurel BJ, Copeman LA, Spencer M, Iseri P (2017) Temperature-dependent growth as a function of size and age in juvenile Arctic cod (*Boreogadus saida*). ICES J Mar Sci 74:1614–1621. https://doi.org/10.1093/icesjms/fsx028

Logerwell E, Busby M, Carothers C, Cotton S, Duffy-Anderson J, Farley E, Goddard P, Heintz R, Holladay B, Horne J, Johnson S, Lauth B, Moulton L, Neff D, Norcross B, Parker-Stetter S, Seigle J, Sformo T (2015) Fish communities across a spectrum of habitats in the western Beaufort Sea and Chukchi Sea. Prog Oceanogr 136:115–132. https://doi.org/10.1016/j.pocean.2015.05.013

Logerwell E, Rand K, Danielson S, Sousa L (2017) Environmental drivers of benthic fish distribution in and around Barrow Canyon in the northeastern Chukchi Sea and western Beaufort Sea. Deep Sea Res Part II 152:170–181. https://doi.org/10.1016/j.dsr2.2017.04.012

Lønne OJ, Gulliksen B (1989) Size, age and diet of polar cod, *Boreogadus saida* (Lepechin 1773), in ice covered waters. Polar Biol 9:187–191. https://doi.org/10.1007/bf00297174

Lowry LF, Frost KJ (1981) Distribution, Growth, and Foods of Arctic Cod (*Boreogadus saida*) in the Bering, Chukchi, and Beaufort Seas. Can Field Nat 95:186–191

Majewski AR, Walkusz W, Lynn BR, Atchison S, Eert J, Reist JD (2016) Distribution and diet of demersal Arctic Cod, *Boreogadus saida*, in relation to habitat characteristics in the Canadian Beaufort Sea. Polar Biol 39:1087–1098. https://doi.org/10.1007/s00300-015-1857-y

Mecklenburg CW, Møller PR, Steinke D (2011) Biodiversity of arctic marine fishes: taxonomy and zoogeography. Marine Biodivers 41:109–140

Mueter FJ, Nahrgang J, John Nelson R, Berge J (2016) The ecology of gadid fishes in the circumpolar Arctic with a special emphasis on the polar cod (*Boreogadus saida*). Polar Biol 39:961–967. https://doi.org/10.1007/s00300-016-1965-3

Nahrgang J, Storhaug E, Murzina SA, Delmas O, Nemova NN, Berge J (2016) Aspects of reproductive biology of wild-caught polar cod (*Boreogadus saida*) from Svalbard waters. Polar Biol 39:1155–1164. https://doi.org/10.1007/s00300-015-1837-2

NASA (2018) Sea ice index: data and image archive. https://nsidc.org/data/seaice_index/archives.

Nichol DG (1998) Annual and between-sex variability of yellowfin sole, *Pleuronectes asper*, spring-summer distributions in the eastern Bering Sea. Fish Bull 96:547–561

Norcross BL, Holladay BA, Busby MS, Mier KL (2010) Demersal and larval fish assemblages in the Chukchi Sea. Deep Sea Res Part II 57:57–70. https://doi.org/10.1016/j.dsr2.2009.08.006

Norcross BL, Raborn SW, Holladay BA, Gallaway BJ, Crawford ST, Priest JT, Edenfield LE, Meyer R (2013) Northeastern Chukchi Sea demersal fishes and associated environmental characteristics, 2009–2010. Cont Shelf Res 67:77–95. https://doi.org/10.1016/j.csr.2013.05.010

Norcross BL, Apsens SJ, Bell LE, Bluhm BA, Dissen JN, Edenfield LE, Frothingham A, Gray BP, Hardy SM, Holladay BA, Hopcroft RR, Iken KB, Smoot CA, Walker KL, Wood ED (2017) US-Canada transboundary fish and lower trophic communities: abundance, distribution, habitat and community analysis. Fairbanks AK: US Dept. of the Interior, Bureau of Ocean Energy Management, Alaska OCS Region. Final Report for BOEM Agreement Number M12AC00011

Norcross BL, Holladay BA, Apsens SJ, Edenfield LE, Gray BP, Walker KL (2018) Central Beaufort Sea marine fish monitoring. Fairbanks AK: US Department of the Interior, Bureau of Ocean Energy Management, Final Report for OCS Study BOEM 2017-33

NPFMC (2009) Fishery management plan for fish resources of the arctic management area. North Pacific Fisheries Management Council, Anchorage

Okkonen SR, Ashjian CJ, Campbell RG, Maslowski W, Clement-Kinney JL, Potter R (2009) Intrusion of warm Bering/Chukchi waters onto the shelf in the western Beaufort Sea. J Geophys Res 114:1–23. https://doi.org/10.1029/2008jc004870

Osuga DT, Feeney RE (1978) Antifreeze glycoprotiens from arctic fish. J Biol Chem 253:5338–5343

Perrette M, Yool A, Quartly GD, Popova EE (2011) Near-ubiquity of ice-edge blooms in the Arctic. Biogeosciences 8:515–524. https://doi.org/10.5194/bg-8-515-2011

Pickart RS (2004) Shelfbreak circulation in the Alaskan Beaufort Sea: mean structure and variability. J Geophys Res 109:1–14. https://doi.org/10.1029/2003jc001912

Pickart RS, Weingartner TJ, Pratt LJ, Zimmermann S, Torres DJ (2005) Flow of winter-transformed Pacific water into the Western Arctic. Deep Sea Res Part II 52:3175–3198. https://doi.org/10.1016/j.dsr2.2005.10.009

Pinchuk AI, Eisner LB (2017) Spatial heterogeneity in zooplankton summer distribution in the eastern Chukchi Sea in 2012–2013 as a result of large-scale interactions of water masses. Deep Sea Res Part II 135:27–39. https://doi.org/10.1016/j.dsr2.2016.11.003

Ponomarenko V (1968) Some data on the distribution and migrations of polar cod in the seas of the Soviet Arctic. Rapports et Proces-verbaux des Réunions Conseil International pour l'Éxploration de la Mer 158:131–135

Ponomarenko V (2000) Eggs, larvae, and juveniles of polar cod *Boreogadus saida* in the Barents, Kara, and White Seas. J Ichthyol 40:165–173

R Core Team (2017) R: a language and environment for statistical computing. R Foundation for Statistical Computing, Vienna

Rand KM, Logerwell EA (2011) The first demersal trawl survey of benthic fish and invertebrates in the Beaufort Sea since the late 1970s. Polar Biol 34:475–488. https://doi.org/10.1007/s00300-010-0900-2

Rand KM, Whitehouse A, Logerwell EA, Ahgeak E, Hibpshman R, Parker-Stetter S (2013) The diets of polar cod (*Boreogadus saida*) from August 2008 in the US Beaufort Sea. Polar Biol 36:907–912. https://doi.org/10.1007/s00300-013-1303-y

Scharf FS, Juanes F, Rountree RA (2000) Predator size-prey size relationships of marine fish predators: interspecific variation and effects of ontogeny and body size on trophic-niche breadth. Mar Ecol Prog Ser 208:229–248

Secor DH (2002) Historical roots of the migration triangle. ICES Marine Sci Symp 2002:323–329

Shimada A, Kimura DK (1994) Seasonal movements of Pacific Cod, *Gadus macrocephalus*, in the eastern Bering Sea and adjacent waters based on tag-recapture data. Fish Bull 92:800–816

Sigler M, Renner M, Danielson S, Eisner L, Lauth R, Kuletz K, Logerwell E, Hunt G (2011) Fluxes, fins, and feathers: relationships among the Bering, Chukchi, and Beaufort seas in a time of climate change. Oceanography 24:250–265. https://doi.org/10.5670/oceanog.2011.77

Sigler M, Eagleton M, Helser T, Olson J, Pirtle J, Rooper C, Simpson S, Stone R (2017) Alaska essential fish habitat research plan: a research plan for the National Marine Fisheries Service's Alaska Fisheries Science Center and Alaska Regional Office. Juneau AK: NOAA, National Marine Fisheries Service, Alaska Fisheries Science Center. AFSC Processed Report 2015-05

Smoot CA, Hopcroft RR (2017) Depth-stratified community structure of Beaufort Sea slope zooplankton and its relations to water masses. J Plankton Res 39:79–91. https://doi.org/10.1093/plankt/fbw087

Tojo N, Kruse GH, Funk FC (2007) Migration dynamics of Pacific herring (*Clupea pallasii*) and response to spring environmental variability in the southeastern Bering Sea. Deep Sea Res Part II 54:2832–2848. https://doi.org/10.1016/j.dsr2.2007.07.032

Vestfals CD, Mueter FJ, Hedstrom KS, Laurel BJ, Petrik CM, Duffy-Anderson JT, Danielson SL, De Robertis A, Curchitser EN (2018) Arctic gadids in a changing climate. Anchorage AK: North Pacific Research Board. Final report for NPRB Project Number 1508

Walkusz W, Majewski A, Reist JD (2013) Distribution and diet of the bottom dwelling Arctic cod in the Canadian Beaufort Sea. J Mar Syst 127:65–75. https://doi.org/10.1016/j.jmarsys.2012.04.004

Walsh JJ, Dieterle DA, Maslowski W, Grebmeier JM, Whitledge TE, Flint M, Sukhanova IN, Bates N, Cota GF, Stockwell D, Moran SB, Hansell DA, McRoy CP (2005) A numerical model of seasonal primary production within the Chukchi/Beaufort Seas. Deep Sea Res Part II 52:3541–3576. https://doi.org/10.1016/j.dsr2.2005.09.009

Wassmann P, Reigstad M (2011) Future Arctic Ocean seasonal ice zones and implications for pelagic-benthic coupling. Oceanography 24:220–231. https://doi.org/10.5670/oceanog.2011.74

Webb PW (1994) The biology of fish swimming. In: Maddock L, Bone Q, Rayner JM (eds) Mechanics and physiology of animal swimming. Cambridge University Press, Oxford, pp 45–62

Webster RA, Clark WG, Leaman BM, Forsberg JE, Hilborn R (2013) Pacific halibut on the move: a renewed understanding of adult migration from a coastwide tagging study. Can J Fish Aquat Sci 70:642–653. https://doi.org/10.1139/cjfas-2012-0371

Weingartner T (1997) A review of the physical oceanography of the northeastern Chukchi Sea. In: Fish ecology in Arctic North America. American Fisheries Society Symposium, pp 40–59

Weingartner T, Aagaard K, Woodgate R, Danielson S, Sasaki Y, Cavalieri D (2005) Circulation on the north central Chukchi Sea shelf. Deep Sea Res Part II 52:3150–3174. https://doi.org/10.1016/j.dsr2.2005.10.015

Weingartner T, Dobbins E, Danielson S, Winsor P, Potter R, Statscewich H (2013) Hydrographic variability over the northeastern Chukchi Sea shelf in summer-fall 2008–2010. Cont Shelf Res 67:5–22. https://doi.org/10.1016/j.csr.2013.03.012

Werner EE, Hall DJ (1974) Optimal foraging and the size selection of prey by the Bluegill sunfish (*Lepomis macrochirus*). Ecology 55:1042–1052

Wilson RE, K SG, Sonsthagen SA, Gravley MC, Menning DM, Talbot SL (2017) Genomics of arctic cod. Anchorage, AK: US Dept. of the Interior, Bureau of Ocean Energy Management, Alaska OCS Region. Report for BOEM OSC Study 2017-066

Wilson RE, Sage GK, Wedemeyer K, Sonsthagen SA, Menning DM, Gravely MC, Sexson MG, Nelson RJ, Talbot SL (2019) Micro-geographic population genetic structure within Arctic cod (*Boreogadus saida*) in Beaufort Sea of Alaska. ICES J Mar Sci. https://doi.org/10.1093/icesjms/fsz041

Wood S (2006) Generalized additive models: an introduction with R Taylor and Francis Group, Boca Raton, FL

Wyllie-Echeverria T, Wooster WS (1998) Year-to-year variation in Bering Sea ice cover and some consequences for fish distributions. Fish Oceanogr 7:159–170

Zuur A, Ieno E, Smith G (2007) Analysing ecological data. Springer, New York

ORIGINAL RESEARCH
published: 19 November 2020
doi: 10.3389/fmars.2020.548931

Extraordinary Carbon Fluxes on the Shallow Pacific Arctic Shelf During a Remarkably Warm and Low Sea Ice Period

Stephanie H. O'Daly[1], Seth L. Danielson[1], Sarah M. Hardy[1], Russell R. Hopcroft[1], Catherine Lalande[2], Dean A. Stockwell[3] and Andrew M. P. McDonnell[1]*

[1] College of Fisheries and Ocean Sciences, University of Alaska Fairbanks, Fairbanks, AK, United States, [2] Amundsen Science, Université Laval, Québec, QC, Canada, [3] Institute of Marine Sciences, University of Alaska Fairbanks, Fairbanks, AK, United States

The shallow Pacific Arctic shelf has historically acted as an effective carbon sink, characterized by tight benthic pelagic coupling. However, the strength of the biological carbon pump in the Arctic has been predicted to weaken with climate change due to increased duration of the open-water period for primary production, enhanced nutrient limitation, and increased pelagic heterotrophy. In order to gain insights into how the biological carbon pump is functioning under the recent conditions of extreme warming and sea ice loss on the Pacific Arctic shelf, we measured sinking particulate organic carbon (POC) fluxes with drifting and moored sediment traps, as well as rates of primary production and particle-associated microbial respiration during June 2018. In Bering Shelf/Anadyr Water masses, sinking POC fluxes ranged from 0.8 to 2.3 g C m^{-2} day^{-1}, making them among the highest fluxes ever documented in the global oceans. Furthermore, high export ratios averaging 82% and low rates of particle-associated microbial respiration also indicated negligible recycling of sinking POC in the water column. These results highlight the extraordinary strength of the biological carbon pump on the Pacific Arctic shelf during an unusually warm and low-sea ice year. While additional measurements and time are needed to confirm the ultimate trajectory of these fluxes in response to ongoing climate change, these results do not support the prevailing hypothesis that the strength of the biological carbon pump in the Pacific Arctic will weaken under these conditions.

Keywords: carbon cycling, particulate organic carbon, Bering and Chukchi Sea Shelves, marine particles, marine snow, Arctic, climate change, biological carbon pump

Edited by:
Robyn E. Tuerena, Scottish Association For Marine Science, United Kingdom

Reviewed by:
Henry Ruhl, Monterey Bay Aquarium Research Institute (MBARI), United States
Mark Andrew Stevenson, Newcastle University, United Kingdom

**Correspondence:*
Stephanie H. O'Daly
shodaly2@alaska.edu;
stephanie.odaly@outlook.com

Specialty section:
This article was submitted to Global Change and the Future Ocean, a section of the journal Frontiers in Marine Science

Received: 04 April 2020
Accepted: 27 October 2020
Published: 19 November 2020

Citation:
O'Daly SH, Danielson SL, Hardy SM, Hopcroft RR, Lalande C, Stockwell DA and McDonnell AMP (2020) Extraordinary Carbon Fluxes on the Shallow Pacific Arctic Shelf During a Remarkably Warm and Low Sea Ice Period. Front. Mar. Sci. 7:548931. doi: 10.3389/fmars.2020.548931

INTRODUCTION

Arctic marine systems are currently undergoing rapid and profound changes due to the effects of climate change, including reduced sea ice extent, earlier sea ice retreat, protracted ice-free seasons, warming air and ocean temperatures, and shifts in currents and water column stratification (Vaughan et al., 2013; Richter-Menge et al., 2019). These environmental changes have recently

Abbreviations: ACW, Alaska Coastal Waters; ASGARD, Arctic Shelf Growth, Advection, Respiration, and Deposition rate experiments project; BSAW, Bering Shelf/Anadyr Waters; PN, particulate nitrogen; POC, particulate organic carbon.

accelerated on the Pacific Arctic's Bering and Chukchi Sea shelves (Stabeno and Bell, 2019; Huntington et al., 2020; Thoman et al., 2020). During 2017 and 2018, bottom water temperatures in the Bering Sea were 3°C higher than the 2005–2016 baseline (Stabeno and Bell, 2019), and the four lowest maximum sea ice extents since 1979 in the Bering and Chukchi Seas have occurred after 2015 (Fetterer et al., 2017). Cascading impacts on the regional ecosystems, biogeochemical cycles, climate, and human communities on and around the Pacific Arctic shelf are expected, although the nature and magnitude of these impacts remain largely speculative (Carroll and Carroll, 2003; Grebmeier, 2012; Moore and Stabeno, 2015; Stabeno and Bell, 2019).

The shallow Pacific Arctic shelf, averaging 50 m depth, has historically acted as a strong sink of carbon (Bates, 2006; Chen and Borges, 2009). Water movement on these shelves is generally northward carrying different water masses of Pacific origin into the Arctic (Pickart et al., 2016; Danielson et al., 2017), with a significant seasonal modulation (Woodgate et al., 2015) (see **Supplementary Figure 1** for visualization of currents). This region is also characterized by a strong biological carbon pump having pelagic primary productivity (Walsh et al., 1989; Springer and McRoy, 1993), sedimentation (Naidu et al., 2004), and benthic productivity (Grebmeier and McRoy, 1988; Grebmeier and McRoy, 1989) rates that are all amongst the highest measured in any marine system. When light is sufficient, pelagic primary productivity may reach up to 16 g C m^{-2} day^{-1} and 470–840 g C m^{-2} $year^{-1}$ (Walsh et al., 1989; Springer and McRoy, 1993) due to elevated nutrient concentrations (5–20 μM) (Danielson et al., 2017) advected into the region with the Anadyr current from deep Pacific upwelling (Walsh et al., 1989; Springer and McRoy, 1993). The spring phytoplankton bloom is typically dominated by large, rapidly sinking sympagic or pelagic diatoms (Springer and McRoy, 1993; Gradinger, 1999, 2009) that contributed to an annual particulate organic carbon (POC) flux of up to 145 g C m^{-2} $year^{-1}$ near Hanna Shoal (Lalande et al., 2020) and likely facilitate substantial carbon burial in sediments. Similar to other Arctic shelves (Grebmeier and Barry, 1991), total organic carbon on the Pacific Arctic shelf averages 1% and reaches up to 2% in surface layers (Grebmeier and McRoy, 1989; Grebmeier and Barry, 1991; Bluhm and Gradinger, 2008). This active biological carbon pump supports large populations of benthic-feeding pelagic seabirds and marine mammals (Bluhm and Gradinger, 2008; Moore and Kuletz, 2019), many of which are important to Indigenous communities that rely on subsistence hunting (Hovelsrud et al., 2008).

The strength of the biological carbon pump in the Arctic is predicted to weaken with climate change due to increased duration of the open-water period for primary production and enhanced nutrient limitation (Piepenburg, 2005; Wassmann and Reigstad, 2011; Grebmeier, 2012). Warmer waters could increase metabolic rates of pelagic grazers and heterotrophic bacteria and potentially favor smaller phytoplankton and faster-growing grazers that more rapidly recycle organic matter within the water column (Wassmann and Reigstad, 2011; Neeley et al., 2018). Additionally, increased frequency of storms could increase mixing and efflux of carbon dioxide (Hauri et al., 2013; Slats et al., 2019). If these predictions prove accurate, such mechanisms could accelerate feedback processes on the services supported by the biological carbon pump. While the effects of changing ice conditions and warming water on production on the Pacific Arctic shelf have been investigated for many years (Lee et al., 2012; Arrigo et al., 2014; Hill et al., 2018), few studies have directly measured pathways within the biological carbon pump (Fukuchi et al.,1993; Lalande et al., 2020). As part of the Arctic Shelf Growth, Advection, Respiration, and Deposition rate experiments (ASGARD) project, we measured the strength and efficiency of the biological carbon pump by directly quantifying and comparing rates of primary productivity, sinking POC flux, and microbial respiration associated with trap-collected sinking particulate matter during June of 2018 on the Pacific Arctic Shelf. This study occurred after the winter with the lowest maximum sea ice extent on record and in a prolonged time of abnormally warm water (Stabeno and Bell, 2019; Danielson et al., 2020; Huntington et al., 2020). These unique environmental conditions, described in detail in Huntington et al. (2020), provided an opportunity to test the prevailing hypothesis that the biological carbon pump will decrease in strength with climate change (Piepenburg, 2005; Wassmann and Reigstad, 2011; Grebmeier, 2012).

MATERIALS AND METHODS

Hydrography Sampling

All cruise operations were performed on the R/V *Sikuliaq*. The CTD unit consisted of a Seabird SBE16plus unit coupled with WetLabs fluorometer and transmissometer. A Satlantic SUNA V2 instrument was also mounted to the rosette to measure nitrate. To characterize the water mass at each station, surface salinity and temperature data were retrieved from the CTD profiles at each station, then plotted on a temperature–salinity (T/S) diagram.

Drifting Sediment Trap Sampling

A standard Lagrangian-type surface-tethered drifting sediment trap (KC Denmark model number 28.200) was used to collect sinking particles (Moran et al., 2012) at seven locations (**Figure 1**). Two of the four tubes contained a removable clear-bottomed cup filled with 250 mL of viscous polyacrylamide gel. The cups were fitted with a thin sloping ramp to funnel all sinking particles into the gel within the cup and prevent particles from settling between the inside of the tube and the outside of the cup. All four tubes were filled with chilled (0°C) filtered seawater (0.3 μm) collected in Niskin bottles from the same depth and station at which the drifting sediment trap was deployed. The remaining two tubes collected sinking particles in bulk, maintaining *in situ* chemistry as much as possible. The trap array was deployed at 30 m below the surface at each station, estimated to correspond to the bottom of the euphotic zone, for 3–12 h depending on the timing of other cruise operations (**Table 1**). We used the same depth for consistency and to reduce issues of resuspension by sampling too close to the seafloor. The drifting sediment trap was fitted with an ARGOS beacon and a go-Tele GPS tracker unit to track its real-time location.

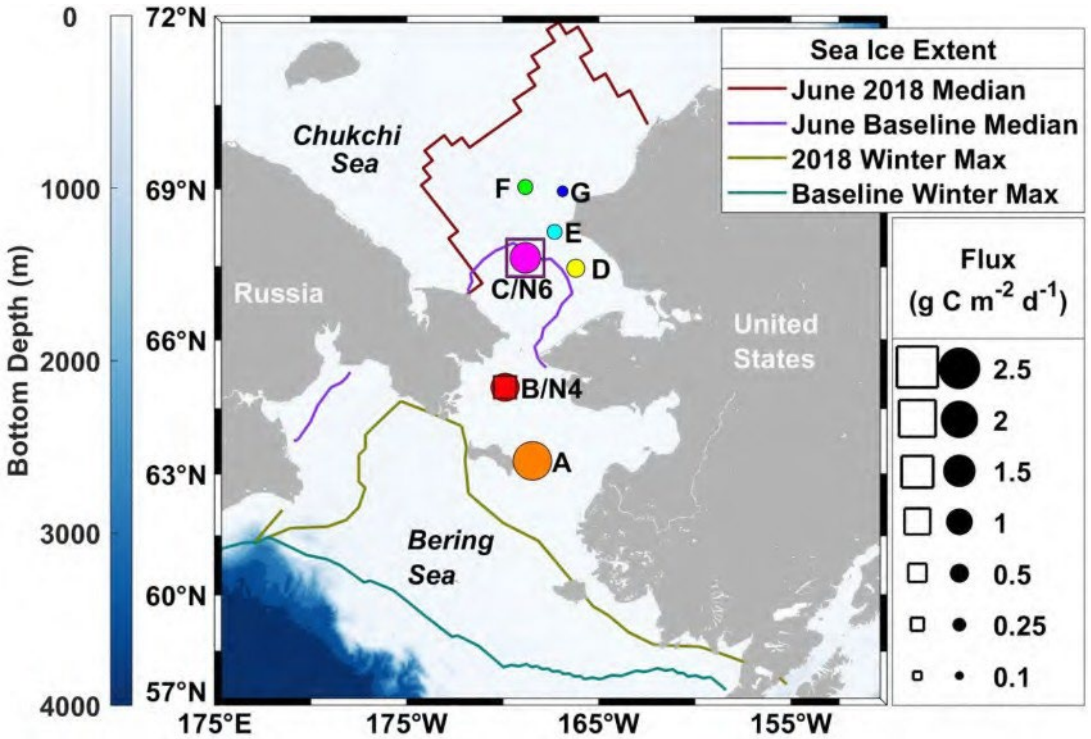

FIGURE 1 Spatial patterns of sinking particulate organic carbon fluxes on the Pacific Arctic shelf in June 2018. Drifting sediment trap measurements are depicted relative to the diameters of the circles, while moored sediment traps fluxes are shown as the length of the squares. Colored lines represent sea ice extent (Fetterer et al., 2017), where the 2018 June median ice extent (maroon) is compared with the 1981–2010 median June baseline (purple) and the record breaking 2018 maximum ice extent (olive) is compared with the 1981–2010 median winter maximum (teal).

TABLE 1 Location and duration of drifting sediment trap deployments 30 m below the sea surface in 2018.

Station name	ASGARD station name	Bottom depth (m)	Latitude deploy (degrees decimal minute)	Longitude deploy (degrees decimal minute)	Date and time of deployment (M/DD HH:MM UTC)	Date and time of recovery (M/DD HH:MM UTC)	Total time of deployment
A	CBE1	41	63° 18.1′	−168° 27.0′	6/07 15:05	6/08 2:40	11h 35m
B	DBO2.4	50	64° 58.6′	−169° 52.8′	6/11 10:59	6/11 17:29	6h 40m
C	DBO3.8	50	67° 40.4′	−168° 50.1′	6/14 23:10	6/15 4:52	5h 42m
D	IL4	42	67° 28.3′	−166° 12.5′	6/13 11:57	6/13 20:44	8h 47m
E	DBO3.3	49	68° 11.1′	−167° 18.6′	6/15 19:30	6/15 22:55	3h 25m
F	CL3	51	69° 2.1′	−168° 49.4′	6/16 19:41	6/17 0:10	4h 29m
G	CL1	46	68° 57.3′	−166° 53.8′	6/17 21:18	6/18 2:20	5h 2m

Flux Rate Measurements

Sinking particles collected in the drifting sediment trap were used to determine POC fluxes. Once the trap was recovered, the following steps were performed as quickly as possible in an environmental chamber that fluctuated in temperature from 3 to 5°C in order to maintain as close to *in situ* conditions for particle-associated microbes as possible. Overlying water was siphoned using a vacuum pump down to a boundary layer above the settled particles at the bottom of all four tubes. In the two bulk particle collection tubes, the material that remained in the tubes after siphoning was quantitatively split into four subsamples using a Folsom plankton splitter. Three subsamples were used for triplicate analytical flux measurements. These subsamples were filtered onto pre-combusted 25-mm Whatman GF/F filters and placed in a dehydrator at 60°C for 12 h. Once dried, the filters were sealed in Petri dishes until further analysis (See section "Elemental POC/PN/$\delta^{13}C$/$\delta^{15}N$ Analysis" for details). Particulate organic carbon values were converted to daily fluxes depending on the deployment period and the collecting area (g C m^{-2} day^{-1}).

Respiration Rate Measurements

One subsample from each of the two drifting sediment trap tubes was used to estimate particle-associated microbial respiration rates. This material was homogenized by swirling the container and pipetted with a wide-bore pipette into eight replicate

2-mL glass vials (Batch PSTS-1721-01) fitted with Pre-Sens Oxygen Optode Sensor Spots (Regensburg, Germany) per drifting sediment trap tube, totaling 16 experimental samples. Filtered seawater controls were obtained from a Niskin bottle closed at 30 m depth during a CTD cast upon recovery of the drifting sediment trap. Water for the control samples was filtered (0.3 μm) to remove particles and particle-associated microbes. The filtrate was pipetted into eight replicate vials that were identical to the experimental vials. All 24 vials were checked for air bubbles, and vials were then placed inside a sealable, clear, plastic water-bath and placed on top of a PreSens SDR SensorDish Reader The water-bath was located inside a dimly lit cold room that varied from 3–5°C and connected to a Fisherbrand Isotemp 500LCSU Circulator, now referred to as a chiller, which maintained temperature at precisely 4.0°C during the incubation. The concentration of oxygen in each vial and temperature in the incubation chamber were recorded every 30 s for the duration of the incubation using PreSens – Sensor Dish Reader Version 4 Software. Incubations lasted for between 3 and 12 h. After the incubations, the remaining material from each vial was filtered onto individual GF/F filters and treated the same as the flux measurement samples.

A few modifications were made to the methods used for measuring particle-associated microbial respiration rates during the course of the study in order to try to improve the accuracy of our measurements. During the first incubation at station A, a low-oxygen micro-environment formed around the sensor spot, located at the bottom of the vial. For all subsequent incubations, the entire incubation chamber was repeatedly inverted for 5 s every 3 min to mix the sample. Additionally, we noticed the concentration of oxygen increased over time in a few of the experimental samples (i.e., at stations A, C, and E), suggesting photosynthetic activity. During the last two incubations at stations F and G, a black cloth was used to cover the incubation chamber in order to prevent any light from reaching the samples, theoretically preventing light reactions associated with photosynthesis. However, it should be noted that dark reactions associated with photosynthesis can continue for several hours after the removal of light in cold water.

The data recorded by the PreSens software were downloaded and analyzed using the following steps in Matlab 2017a computing software. Data collected before the incubation temperature stabilized were trimmed so that only the time during which the incubation temperature remained stable was analyzed. The first 188 min of data after temperature stabilization was used to determine respiration rates. Linear regression analysis was performed on the oxygen concentration data from each vial. The average and standard deviation of the eight replicate control slopes ($r_{control}$) was taken, and for each of the two experimental samples. Then the average slopes for each of the experimental incubations were averaged together and the error was propagated (r_{exp}). We calculated the carbon-specific particle-associated microbial respiration rate (R_PAM) using a 117:170 organic carbon to oxygen molar respiratory quotient ($V_{OC:O2}$), assuming a one to one relationship with organic carbon degradation and carbon dioxide production (Anderson and Sarmiento, 1994), an incubation volume (vol) of 2 mL, and the final concentration of POC at the end of the incubation ([POC]) (Eq. 1).

$$R\_PAM = \frac{(r_{exp} - r_{control}) \times vol \times V_{OC:O2}}{[POC]} \quad (1)$$

The average R_PAM ± 1 standard deviation was compared with those from other studies (Ploug and Jorgensen, 1999; Ploug and Grossart, 2000; Iversen and Ploug, 2010; Collins et al., 2015; McDonnell et al., 2015; Belcher et al., 2016a,b) at different locations.

Sinking Particle Visualization

Collecting particles in polyacrylamide gel kept sinking particles intact and allowed for particle imaging and identification (Ebersbach and Trull, 2008; McDonnell and Buesseler, 2010; Durkin et al., 2015). The contents of the cups were photographed within 6 h of sediment trap recovery using a 42.4 MP digital camera equipped with a 90 mm macro-lens and a flash unit. A length to pixel relationship was determined for each image in Adobe Photoshop CS6. These samples were used to qualitatively determine sinking particle type.

Primary Productivity Rate Measurements

^{13}C-^{15}N dual-isotope tracer technique was used to measure integrated rates of primary productivity at the seven stations following a standard protocol (Dugdale and Goering, 1967; Hama et al., 1983). For primary productivity rate measurements, water was collected at six depths corresponding to the 100, 50, 30, 12, 5, and 1% light levels. The 1% light level is estimated to be the minimum amount of light necessary for photosynthesis to occur, i.e., the bottom of the euphotic zone. The incubations lasted between 4 and 7 h, and measurements were extrapolated to daily production by adjusting to total daylight for each incubation site. At the end of the experiment, contents in each incubation bottle were filtered onto pre-combusted GF/F filters and frozen at −80°C until further analysis. These depth-specific rates were then integrated over the entire depth of the euphotic zone to determine total water column primary productivity rates in units of g C m^{-2} day^{-1}.

Elemental POC/PN/$\delta^{13}C$/$\delta^{15}N$ Analysis

All dried or frozen GF/F filters were processed in the Alaska Stable Isotope Facility at the University of Alaska Fairbanks's Water and Environmental Research Center. Filters were acidified with 10% hydrochloric acid for 24 h to remove particulate inorganic carbon (PIC). The filters were pelletized in tin cups. Stable isotope data were obtained using continuous-flow isotope ratio mass spectrometry. Stable isotope ratios were reported in δ notation as parts per thousand (0) deviation from the international standards VPDB (carbon) and air (nitrogen). Typically, instrument precision was <0.20.

Moored Sediment Trap Sampling

Two 24-cup Hydro-Bios sediment traps were moored at stations B south of Bering Strait (trap depth 37 m, bottom depth 49 m) and C north of Bering Strait (trap depth 35 m, bottom depth

50 m) from June 2017 to June 2018 (see **Table 2** and **Figure 1** for location of traps). Sample cups were filled with a hypersaline (salinity 38) 5% formalin solution in filtered seawater to preserve samples during and after deployment (Lalande et al., 2020). The carousel rotated at pre-programmed intervals ranging from seven to 40 days.

As the trap at station B was recovered before the end of its rotation, the material in the last open cup was excluded from analysis. Subsamples from each cup were filtered onto pre-combusted (500°C overnight) GF/F filters (0.7 μm), exposed to 1 N hydrochloric acid overnight for removal of inorganic carbon, and dried at 60°C overnight before encapsulation for POC measurements (Lalande et al., 2020). Particulate organic carbon measurements were conducted on a Perkin Elmer CHNS 2400 Series II elemental analyzer. Particulate organic carbon measurements were converted to daily flux rates depending on the open cup duration of each sample.

Instruments measuring physical and biological parameters in tandem with sinking POC flux were deployed on the moorings at stations B and C. A 300 kHz RDI workhorse ADCP measured bottom current velocity ~5 m off the seafloor at each site. Lowpass-filtered bottom current velocity were plotted overlaid with a 12-h smoothing. A Seabird SBE16plus unit coupled with a Wetlabs fluorometer measured temperature, salinity and fluorescence at 27 m at station B and 25 m at station C.

Remote Sensing

Daily sea ice concentrations were retrieved from the National Snow and Ice Data Center satellite records for the deployment period at both mooring sites (Fetterer et al., 2017). Wind velocity was obtained from modeled wind reanalysis for the deployment period at both mooring sites (European Centre for Medium-Range Weather Forecasts, 2019). Twenty-four hour smoothing was performed on wind data.

RESULTS

Environmental Conditions

Sea surface temperatures ranged from 1 to 10°C during the ASGARD expedition in June 2018, with the warmest water temperature above 8°C observed south of Nome and west of Norton Sound. These warm waters were characteristically fresher, with salinities ranging from 30 to 30.5, consistent with Alaska Coastal Water (ACW) characteristics and a shift to wind direction from the south (see **Supplementary Figure 1** for a map depicting regional currents in the study area). Wind speed ranged from 0 to 36 kt during the course of the cruise as measured by a vessel-mounted anemometer corrected for ship motion. Throughout the water column, temperatures ranged from −0.5 to 10°C and salinities ranged from 30 to 33.5. Chlorophyll fluorescence ranged from 0 to 15 μg L^{-1} while nitrate concentration ranged from 0 to 20 μmol L^{-1} and was highest along the northernmost Cape Lisburne line. SUNA-derived nitrate concentration measurements were confirmed with bottle-derived nitrate concentration measurements. Sea ice was absent during the cruise. A salinity of 31 delimited stations A, B, and C into the Bering Shelf/Anadyr Waters (BSAW) (salinity > 31) and stations D, E, F, and G into ACW waters (salinity < 31) (**Figure 2**).

Drifting Sediment Trap Flux Rate Measurements

The depth of the water column varied little at our seven stations, ranging from 41 to 51 m and averaging 47 m, 17 m deeper than the drifting sediment traps sampling depths at 30 m (1% Photosynthetically Active Radiation (PAR)). The actual 1% PAR varied from between 16 and 30 m, except for station F having a 1% PAR reaching 38 m (**Table 3**). The overall average depth of the euphotic zone was 26 m, comparable to POC export measurements at 30 m. Sinking POC fluxes were high (up to 2.2 g C m^{-2} day^{-1}) but spatially variable. Bering Shelf/Anadyr Waters were associated with higher fluxes (1.2–2.2 g C m^{-2} day^{-1}) at stations A, B, and C, while lower fluxes (0.2–0.5 g C m^{-2} day^{-1}) were characteristic of ACW at stations D, E, F, and G (**Figure 2**). For stations in the BSAW, sinking particles consisted mostly of aggregated diatoms and viable diatom cells while the ACW stations contained more diverse particles including fecal pellets, zooplankton, and diatom cells (**Figure 3**).

The particulate nitrogen (PN) flux ranged from 0.03 to 0.47 g N m^{-2} day^{-1}. Both the highest and lowest PN flux were measured in the ACW (**Table 3**). PN flux was slightly, though not significantly, higher in the BSAW (0.27 g N m^{-2} day^{-1}) than in the ACW (0.15 g N m^{-2} day^{-1}). Delta ^{13}C ranged from −24.03 to −19.940 with no clear distinction in $\delta^{13}C$ values between the ACW and BSAW. Both the least negative and most negative $\delta^{13}C$ values were located at stations in the ACW. A similar pattern was true for $\delta^{15}N$ values with values ranging from 5.63 to 8.50. There was no spatial pattern in $\delta^{15}N$ values and both the highest and lowest $\delta^{15}N$ values were found in stations in the ACW.

Respiration Rate Measurements

Overall carbon specific particle-associated microbial respiration ranged from −13.7 to 12.8% day^{-1} (**Table 4**). Negative

TABLE 2 Location and duration of moored sediment traps.

Station name	Trap name	Sampling period	Trap depth (m)	Bottom depth (m)	Latitude (degrees decimal minute)	Longitude (degrees decimal minute)
B	N4	June 26, 2017 to June 08, 2018	37	49	64° 55. 7′	−169° 55.1′
C	N6	June 17, 2017 to June 08, 2018	35	50	67° 40.2′	−168° 44.7′

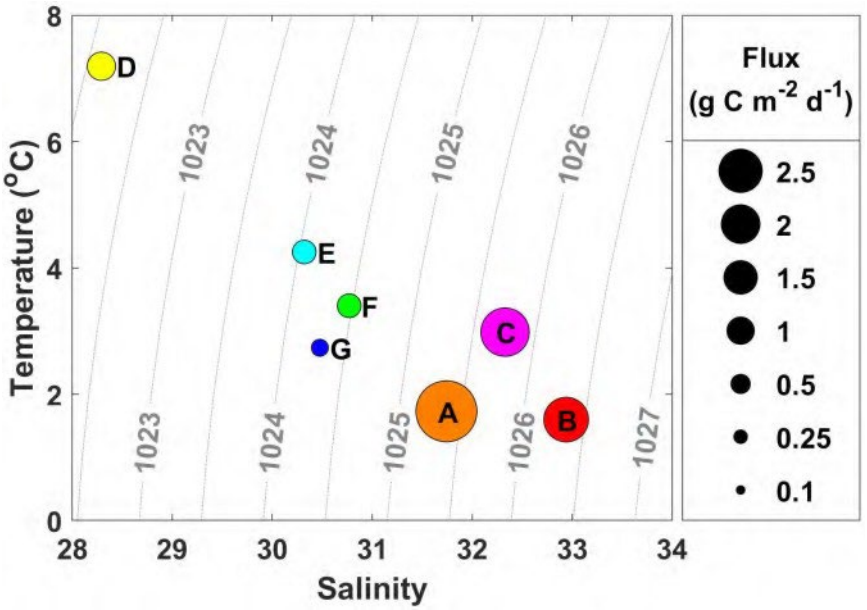

FIGURE 2. Water mass characteristics from each station where drifting sediment traps were deployed. The size of the circle is indicative of the amount of particulate organic carbon (POC) flux, labeled with station name. Warmer, fresher water characteristic of Alaska Coastal Water (ACW) has lower flux values compared with cooler, more saline water characteristic of Bering Shelf/Anadyr Water (BSAW), which has higher flux values.

TABLE 3 Particulate organic carbon (POC) flux, primary productivity, and export ratios at seven stations in the Bering and Chukchi seas at drifting sediment trap sites.

Station Name	Water Mass	Bottom Depth (m)	Euphotic Zone Depth (m)	POC flux (g C m^{-2} day^{-1})	Primary Productivity (g C m^{-2} day^{-1})	Export Ratio	PN (g N m^{-2} day^{-1})	δ13-C of sinking material (‰)	δ15-N of sinking material (‰)
A	BSAW	41	16	2.20 ± 0.19	4.24	0.52 ± 0.05	0.40 ± 0.04	−21.08 ± 0.10	7.51 ± 0.49
B	BSAW	50	24	1.18 ± 0.10	0.87	1.36 ± 0.12	0.21 ± 0.02	−20.27 ± 0.06	6.23 ± 0.50
C	BSAW	50	24	1.39 ± 0.07	2.15	0.65 ± 0.05	0.21 ± 0.01	−19.94 ± 0.92	6.71 ± 0.29
D	ACW	42	26	0.48 ± 0.03**	0.48	1.00 ± 0.07	0.47 ± 0.03**	−19.55 ± 0.04**	7.20 ± 1.43**
E	ACW	49	30	0.34 ± 0.03	0.74	0.45 ± 0.04	0.06 ± 0.01	−21.64 ± 0.43	7.37 ± 0.17
F	ACW	51	38*	0.34 ± 0.05	0.33	1.02 ± 0.14	0.05 ± 0.01	−22.30 ± 0.15	5.63 ± 0.28
G	ACW	46	24	0.17 ± 0.00	0.23	0.75 ± 0.06	0.03 ± 0.00	−24.03 ± 0.53	8.50 ± 1.12

Drifting sediment trap sampled at 30 m depth. BSAW, Bering Shelf/Anadyr Waters; ACW, Alaska Coastal Waters.
**Euphotic zone depth deeper than 30 m, the depth of the drifting sediment trap deployment.*
***Outlier of 3 standard deviations higher than other 3 replicates removed from analysis*
Pacific Arctic's extraordinary carbon fluxes.

carbon specific particle-associated microbial respiration indicates net respiration of carbon while positive values indicate net production of carbon. Five of the seven stations had carbon specific particle-associated microbial respiration that were indistinguishable from zero where carbon specific particle-associated microbial respiration could not be distinguished from free living microbial respiration. The two respiration measurements that were distinguishable from zero were from stations B (−13.7 ± 10.5% day^{-1}) and C (12.8 ± 6.7% day^{-1}), both of which are in BSAW. Therefore, all carbon specific particle-associated microbial respiration from stations in ACW were indistinguishable from zero. Average carbon specific particle-associated microbial respiration from BSAW stations (3.1 ± 14.6% day^{-1}, average ± 1 standard deviation), ACW stations (1.7 ± 2.9% day^{-1}), as well as all stations combined (2.3 ± 8.7% day^{-1}) were indistinguishable from zero. Additionally, there was no statistical difference in carbon specific particle-associated microbial respiration between the ACW and BSAW.

Primary Productivity Rate Measurements

Primary productivity rates were spatially variable with an overall range of 0.23–4.24 g C m^{-2} day^{-1}. Station A had the highest rate of primary productivity and had the highest fluorescence signal of the seven stations (full depth CTD profiles are shown in **Supplementary Figure 2**). Here, a slight chlorophyll-*a* maximum of 10 mg m^{-3} fluorescence was present at 5 m depth and the water column was well-mixed. More pronounced, though lower chlorophyll-*a* maximums occurred at stations C

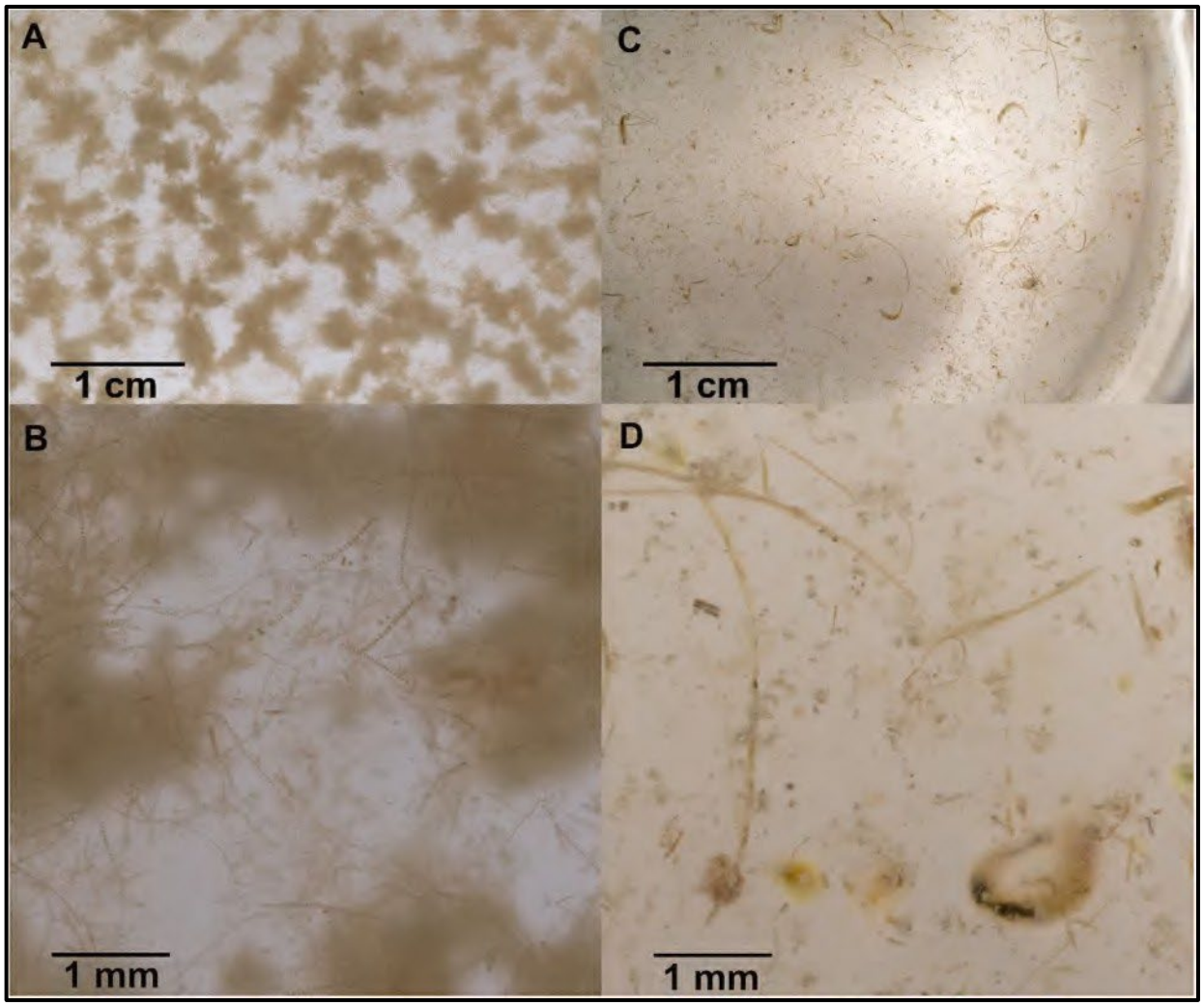

FIGURE 3 Sinking particles collected in polyacrylamide gel traps at station A (A,B) and station D (C,D). Sinking particles at station A are characteristic of Bering Shelf/Anadyr Water stations and consist exclusively of fluffy aggregates made of diatoms and viable diatom chains. Sinking particles at station D are characteristic of Alaska Coastal Water stations and consist of a more diverse set of particles, including fecal pellets, zooplankton swimmers, as well as still viable and senescent diatoms.

TABLE 4. Particle-associated microbial respiration rates and carbon specific rates for sinking material.

Station Name	Water Mass	r_exp (µmol O_2 m^{-1} L^{-1})	r_control (µmol O_2 m^{-1} L^{-1})	r_PAM (µmol O_2 m^{-1} L^{-1})	R_PAM (% day^{-1})
A	BSAW	−0.215 ± 0.120	−0.076 ± 0.086	−0.139 ± 0.147	10.3 ± 24.0
B	BSAW	***−0.073 ± 0.070***	0.017 ± 0.018	***−0.090 ± 0.072***	***−13.7 ± 10.5***
C	BSAW	***0.087 ± 0.044***	−0.001 ± 0.009	***0.088 ± 0.045***	***12.8 ± 6.7***
D	ACW	0.048 ± 0.024	***0.030 ± 0.012***	0.018 ± 0.027	−0.9 ± 5.7
E	ACW	0.019 ± 0.032	−0.001 ± 0.010	0.020 ± 0.033	4.3 ± 8.0
F	ACW	0.007 ± 0.041	***−0.009 ± 0.008***	0.016 ± 0.042	4.2 ± 9.5
G	ACW	−0.008 ± 0.032	−0.003 ± 0.008	−0.005 ± 0.033	−0.8 ± 7.5

Significant rates in bold and italicized. A total of 188 min were analyzed treating all 16 experimental sample as replicates and the final carbon value used to calculate the per carbon rate. r_exp, experimental respiration rate ± 1 SD; r_control, control respiration rate ± 1 SD; r_PAM, particle-associated microbial respiration rate ± 1 SD, R_PAM; carbon specific particle-associated microbial respiration rate ± 1 SD, BSAW; Bering Shelf/Anadyr Waters; ACW, Alaska Coastal Waters.

(30 m) and F (38 m). Station F had the deepest 1% PAR depth of 38 m, co-occurring with the chlorophyll-a maximum, but had the second lowest rate of primary productivity of 0.34 g C m^{-2} day^{-1}. Overall, primary productivity was higher in the BSAW (0.87–4.24 g C m^{-2} day^{-1}) than in the ACW (0.23–0.74 g C m^{-2} day^{-1}). All three stations in the BSAW had

less stratified water columns, while all four stations in the ACW had more stratified water columns.

Export Ratios

Export ratios are a metric that characterizes the efficiency of the biological carbon pump, calculated using Eq. 2.

$$\text{export ratio} = \frac{\text{flux}}{\text{primary productivity}} \quad (2)$$

Higher export ratios indicate a more efficient biological carbon pump and lower ones less efficient. Export ratios ranged from 0.45 to 1.36 with the lowest export ratio observed at station E and the highest at station B (**Table 3**). There was no significant difference in export ratios between water masses (BSAW: 0.84 ± 0.45 and ACW: 0.81 ± 0.27 mean ± 1 SD). Three stations (B, D, and F) had export ratios at or above 1 and the overall study average export ratio was 0.82 ± 0.32 (mean ± 1 SD).

Moored Sediment Trap Time Series Flux Rate Measurements

Moored sediment trap-derived POC fluxes provide independent measures to compare with the fluxes observed with drifting sediment trap sampling. Drifting sediment trap sampling at stations B and C took place three and six days following the end of the moored sediment trap sampling, respectively. Particulate organic carbon fluxes of 0.8 and 1.2 g C m^{-2} day^{-1} at station B and 2.3 and 1.4 g C m^{-2} day^{-1} at station C were obtained with the moored and drifting sediment traps, respectively (**Table 3** and **Figure 4**).

At station B, POC fluxes were generally low (<0.25 g C m^{-2} day^{-1}) from June through October 2017 with brief periods of elevated POC fluxes (0.6–1.3 g C m^{-2} day^{-1}) occurring around the same time as peaks in fluorescence (**Figure 5**). Particulate organic carbon fluxes increased along with wind speed during November and December 2017 (0.9–1.4 g C m^{-2} day^{-1}), decreased during January 2018, and remained relatively low (<0.65 g C m^{-2} day^{-1}) when sea ice was present from January through late April 2018. Fluorescence remained low from mid-October 2017 through April 2018. Sea ice melted at the end of April 2018 and the highest POC fluxes were observed about one month later during late May 2018 (1.5 g C m^{-2} day^{-1}).

At station C, high POC fluxes were recorded from June to mid-July 2017 (1.2–1.7 g C m^{-2} day^{-1}), followed by a period of low POC fluxes from mid-July through mid-October 2017 (<0.5 g C m^{-2} day^{-1}) (**Figure 5**). Spikes in fluorescence occurred sporadically from June until early October 2017. Particulate organic carbon fluxes increased starting in mid-October 2017 and were elevated throughout November and December 2017 (0.9–1.2 g C m^{-2} day^{-1}). Particulate organic carbon flux dramatically decreased when sea ice formed during January 2018. A period of low POC fluxes was observed between January and May 2018 (<0.5 g C m^{-2} day^{-1}), while sea ice was consistently present. The highest POC fluxes were measured at the beginning of June 2018 (2.3 g C m^{-2} day^{-1}), at the same time as the highest peaks of fluorescence soon after sea ice retreated from this station.

The moored sediment trap time series indicates that POC flux had recently peaked at station B before drifting sediment trap sampling took place during early June 2018, but was likely at or near the period of peak annual flux at station C (**Figure 5**). The composition of the material collected in the moored sediment trap samples during June 2018 indicated the occurrence of a pelagic phytoplankton bloom at station B, reflected by the export of the exclusively pelagic centric diatoms *Chaetoceros* spp. and *Thalassiosira* spp. that usually dominate spring blooms on Arctic shelves (Degerlund and Eilertsen, 2010; Lalande et al., 2019). Diatom fluxes, composed of several pennate and centric diatom groups, were nearly three times higher at station C than at station B, reflecting a large diatom bloom.

DISCUSSION

The overall objectives of this study were to characterize the strength and efficiency of the biological carbon pump on the Pacific Arctic shelf during a warm, low-ice year in order to shed light on potential current and future changes in carbon cycling in this region. We addressed this by considering three major aspects of relevance: primary productivity, sinking POC flux, and particle-associated microbial respiration during June of 2018.

Regional Spatial Trends

The largest distinction of regional spatial trends occurred between the two water masses present in this region (ACW and BSAW). Consistent with previous studies, the ACW was warmer and fresher with lower nutrients than the BSAW during June 2018 (Walsh et al., 1989; Springer and McRoy, 1993). Both regions were warmer than normal for this time of year and had experienced much less sea ice than normal (Danielson et al., 2020; Huntington et al., 2020).

We measured consistently lower POC flux rates in ACW than BSAW. These results support the previously untested hypothesis that POC fluxes would be higher in the BSAW compared to ACW (Grebmeier and McRoy, 1989). This distinction in primary productivity and POC flux between the ACW and BSAW could partially be attributed to differences in stratification between these regions; we found a less stratified water column in the BSAW, which could contribute to nutrient input to the surface and allow for higher primary productivity rates. Well-mixed water could also help facilitate POC mixing out of the euphotic zone, however it is more likely that this material could be brought back up to the surface through the same mechanism. The differences in primary productivity and POC flux cannot be fully explained by differences in water column stratification. The two regions were characterized by different types of sinking particles: more uniform aggregated diatoms and viable diatoms were found in the BSAW, while more processed material like fecal pellets and zooplankton were found in the ACW in addition to living diatoms. This distinction suggests more processing of POC by zooplankton or heterotrophic bacteria in the ACW. However, there was no difference in export ratio or particle-associated microbial respiration between

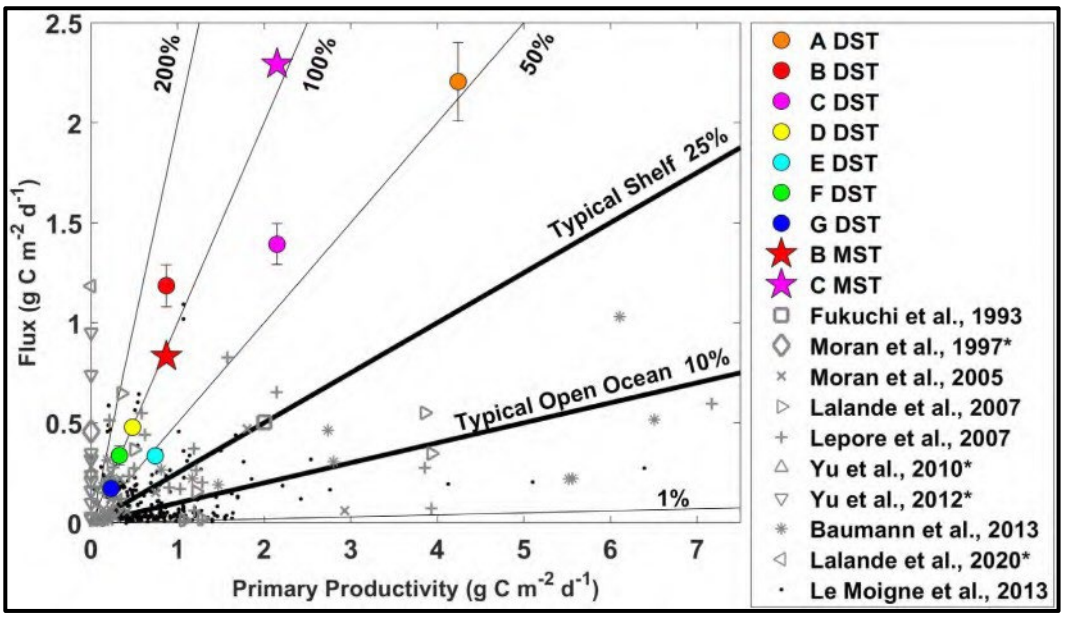

FIGURE 4 Sinking particulate organic carbon fluxes and primary productivity rates with contours of the export ratio between these two parameters measured during June 2018 on the Pacific Arctic shelf. The circles represent flux measurements from the drifting sediment trap. The stars represent the final flux measurement from the moored sediment traps (values plotted against the same primary productivity rates). Gray markers provide regional (Fukuchi et al., 1993; Moran et al., 1997, 2005; Lalande et al., 2007, 2020; Lepore et al., 2007; Yu et al., 2010, 2012; Baumann et al., 2013) and black markers global context (Le Moigne et al., 2013). *No corresponding productivity data with Moran et al., 1997 (Moran et al., 1997), Yu et al. (2010, 2012), and Lalande et al., 2020 (Lalande et al., 2020).

the two water masses, indicating that POC fluxes are mostly regulated by primary production rates rather than heterotrophic processing. The spatially uniform particle associated microbial respiration rates we measured do not support the postulation that the ACW would have higher particle-associated microbial respiration rates (Andersen, 1988; Grebmeier and Barry, 1991). Nonetheless, the higher primary productivity and POC fluxes in the BSAW demonstrate a stronger biological carbon pump in the BSAW region.

PN, $\delta^{13}C$, and $\delta^{15}N$ values were not significantly different between the BSAW and the ACW. Higher PN in sinking material are associated with more nutritious food for the benthos (Grebmeier et al., 1988). Less negative $\delta^{13}C$ values tend to indicate a larger influence of ice algae or a marine signature while more negative $\delta^{13}C$ values tend to indicate a more coastal or terrigenous signature (Wooller et al., 2007). Larger $\delta^{15}N$ values were associated with material that is higher on the food chain (i.e., secondary and tertiary producers), while lower $\delta^{15}N$ values are associated with material lower on the food chain (i.e., primary producers) (Post, 2002).

The ACW had lower primary productivity than the BSAW. This regional pattern has been well described previously (Walsh et al., 1989; Springer and McRoy, 1993) and is attributed to the lower nutrient concentrations in ACW compared with BSAW (Danielson et al., 2017). Primary productivity values in both water masses fell within a typical range for these regions (Lee et al., 2007; Arrigo et al., 2014; Hill et al., 2018). However, a primary productivity rate of 16 g C m^{-2} day^{-1} has been previously observed in the Pacific Arctic Shelf (Walsh et al., 1989; Springer and McRoy, 1993), much higher than what we measured and what is typically measured. If these higher production rates were associated with export ratios similar to what we observed here, then the associated fluxes would be even more remarkable than the values we observed with the DSTs and MSTs during this study.

Stations with higher rates of primary productivity tended to have higher rates of POC flux. However, there was not a perfect relationship between primary productivity and POC flux, which caused some variations in the export ratios. The stations with export ratios over 1 and the high average export ratio indicate an extremely efficient biological carbon pump or temporal or spatial decoupling between primary production and flux.

While the dominant regional patterns were associated with water masses, we also expected some patterns falling along a latitudinal gradient. It is difficult to separate the signal of water mass from latitude because most of the stations that were classified as BSAW were located south of the stations classified as ACW. We found higher daily primary productivity rates and POC fluxes at the southern stations in the BSAW than at the northern stations in the ACW. The annual POC flux was higher at station C (215 g C m^{-2} $year^{-1}$) than at station B (204 g C m^{-2} $year^{-1}$), indicating an increase in POC flux with latitude. However, an annual POC flux lower than these (145 g C m^{-2} $year^{-1}$) was measured at about 200 miles north of our study area (Lalande et al., 2020). Drifting sediment trap sampling at more stations in the southern portion of the ACW and moored sediment trap sampling in the ACW are needed to better

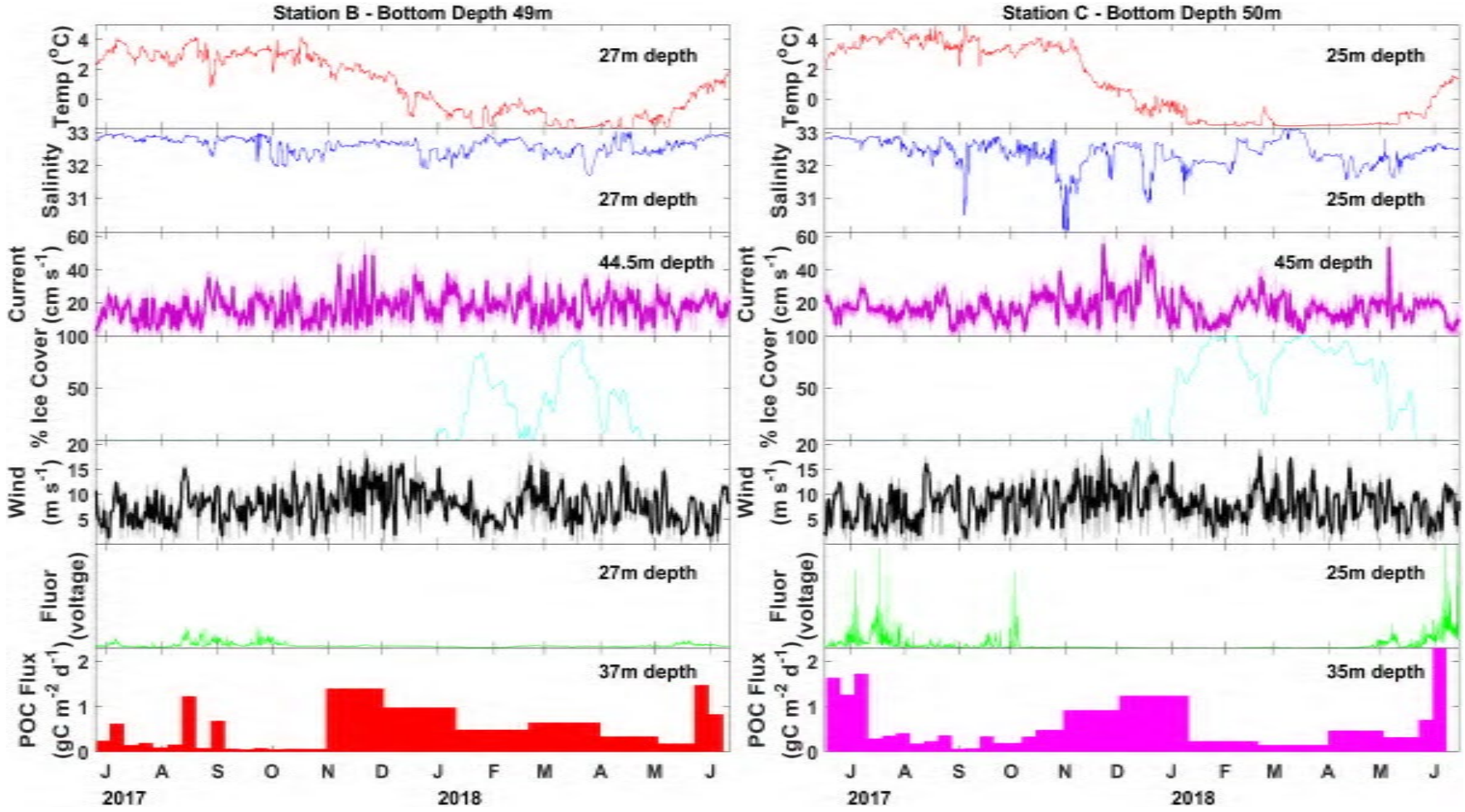

FIGURE 5 Particulate organic carbon flux (colored bars) measured with moored sediment traps at stations N4 and N6 between June 2017 and June 2018. Sea ice percent cover (cyan line) taken from NSIDC satellite records (Fetterer et al., 2017). Wind velocity (black line) taken from modeled wind reanalysis (European Centre for Medium-Range Weather Forecasts, 2019). Twenty-four hour smoothing is shown with the thick black line. Lowpass-filtered current velocity (magenta line) taken from AD, with 12 h smoothing shown with the thick magenta line, temperature (red line), salinity (blue line), fluorescence (green line) taken from seabird SBE16plus unit coupled with a WetLabs fluorometer on each of the moorings.

tease apart the differences associated with latitude and water mass in this region.

The annual pattern of POC flux shows some latitudinal distinction between the more northern station C and the more southern station B. The peak annual flux occurred during early June 2018 at station C, while the peak annual flux occurred a couple of weeks earlier at station B (late May 2018). The spring peak flux was higher at station C (2.3 g C m^{-2} day^{-1}) compared to station B (1.5 g C m^{-2} day^{-1}). Increased POC flux measurements occurred in the absence of peaks in fluorescence at both stations from November 2017 to January 2018 strongly suggesting episodic resuspension events during fall. Particulate organic carbon fluxes decreased in the presence of sea ice, reducing wind mixing and resuspension. This is particularly evident at station C under higher sea ice concentrations. It is likely that these fall high flux events do not represent increased net flux, as they are likely partly the result of material that previously fell to the seafloor being resuspended and collected in the moored sediment trap again.

Role of Heterotrophy in the Water Column

Bacterial production largely controls how much exported POC reaches the seafloor and might increase in Arctic waters under more acidic, warmer, and lower-ice conditions (Garneau et al., 2009; Vaqué et al., 2019), which could result in higher pelagic community carbon demand (Sala et al., 2010). One factor that has received a lot of thought for the Pacific Arctic shelf region is how a reduction in ice algae relative to to pelagic phytoplankton as primary producers might impact the benthic-pelagic coupling, with the prediction that smaller pelagic phytoplankton will have slower sinking rates and will therefore be more likely to be consumed by zooplankton or bacteria in the water column, resulting in less material reaching the seafloor (Carroll and Carroll, 2003; Grebmeier, 2012; Moore and Stabeno, 2015). A slower particle sinking rate will give more time for bacteria to both colonize and degrade sinking particles. In our study, we mostly collected pelagic diatoms in the drifting sediment traps rather than species associated with ice. However, our direct measurements of microbial respiration rates associated with sinking particles were mostly indistinguishable from zero. This is not unprecedented in high latitude regions (McDonnell et al., 2015).

Conducting a comparison of measured particle-associated microbial respiration rates from around the globe, we found that particle-associated microbial respiration generally decreases with increasing latitude (**Figure 6**). In our study, the rate of particle-associated microbial respiration was 2% day^{-1} on average, with a 95% confidence interval ranging from −24.2 to 34.3% day^{-1}. Given the shallow nature of the Pacific Arctic shelf (20 m average distance from base of euphotic zone to seafloor) and rapid sinking velocity of material caught in the traps (greater than 100 m day^{-1}), even under the fastest respiration rate (−24.2% day^{-1}) we calculated that less than 5% of the exported organic carbon would be remineralized within the water column before being deposited on the seafloor. Considering our conservative estimates, the true consumption is likely much smaller than this value. We conclude that particle-associated microbial respiration does not play a large role in recycling POC below the euphotic zone in this region, implying that most of the material that is exported from the euphotic zone will likely reach the shallow seafloor.

One mitigating factor in how much organic matter is deposited on the seafloor is the role zooplankton and free-living heterotrophic microbes play in consuming organic matter in the water column. Historically, zooplankton have not consumed large proportions of organic matter in the water column (Ashjian et al., 2003; Campbell et al., 2009; Hopcroft et al., 2010; Kitamura et al., 2017; Lalande et al., 2020), but it is possible they may play a larger role in the future. One study from just north of our study area found that primary production rates were similar to free-living community microbial respiration rates during the summer, indicating a large proportion of primary production could be consumed by free-living microbes (Cota et al., 1996). High export ratios in the present study point to zooplankton and free-living heterotrophic microbes playing a small role in consuming organic matter within the euphotic zone. It is possible that zooplankton and bacteria may play a larger role in consuming POC later in the summer. We suggest measuring export ratios and particle associated microbial respiration rates in August on the Pacific Arctic shelf to answer this remaining question.

Comparison of Drifting and Moored Sediment Trap POC Fluxes

The POC flux measurements measured with the drifting and moored traps at stations B and C, while of similar magnitude, were not the same. Many factors potentially caused variations between POC flux values obtained with drifting and moored traps. One reason is the different sampling times as POC fluxes may have changed on time scales much shorter than three or six days. In addition, the moored sediment trap measured flux over eight days, while the drifting sediment traps measured flux for six and a half hours and station B and five and a half hours at station C. If there is a diurnal cycle in flux regulated by zooplankton or phytoplankton it can be captured in the drifting sediment trap sampling and masked in the moored sediment trap sampling. Our study took place on a shallow Arctic shelf over the summer solstice. It is unlikely there was a diurnal cycle of primary production due the nearly 24 h of sunlight that were present. Additionally, due to the shallowness of the shelf, zooplankton in this region are not know to exhibit diel vertical migration (Ashjian et al., 2003; Campbell et al., 2009). It is unlikely that any differences in POC flux are a result of any changes in flux as a diurnal cycle, and, if present, are likely due to changes in the rate of primary production controlled by variable cloud cover and nutrient availability. Finally, the locations of the moored sediment trap and drifting sediment trap sampling did not perfectly overlap, although the drifting sediment traps were deployed within half a mile of the moored sediment traps.

Even if the sampling of these two traps perfectly overlapped in time and space, it is unlikely that they would produce the same

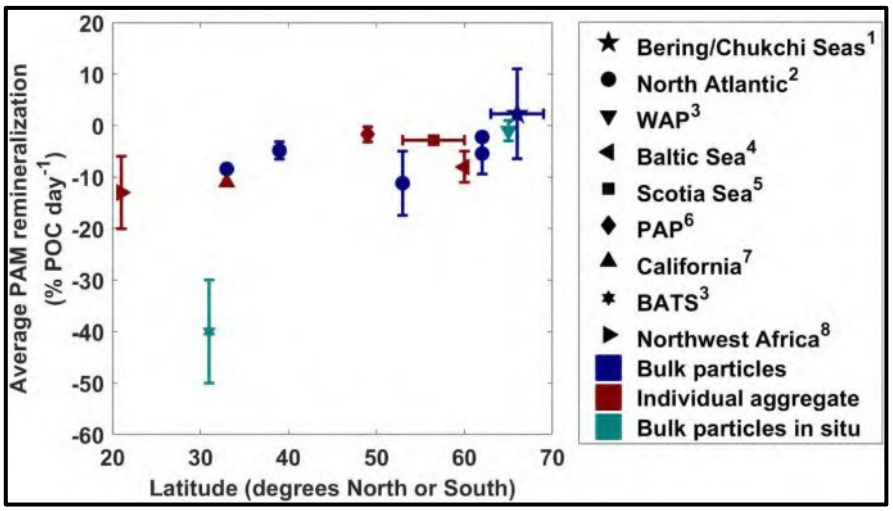

FIGURE 6 Average particle-associated microbial respiration rates (with one standard deviation plotted as vertical error bars) from this study along with previous measurements at other latitudes. Symbols colored with navy indicate bulk particle respiration measurements, teal indicate measurements taken with RESPIRE *in situ* incubator, and maroon indicate rates measured from individual aggregates. WAP, Western Antarctic Peninsula; PAP, Porcupine Abyssal Plain; BATS, Bermuda Atlantic Time Series. Measurements were taken from this study[1], Collins et al. (2015)[2], McDonnell et al. (2015)[3], Ploug and Grossart (2000)[4], Belcher et al. (2016a)[5], Belcher et al. (2016b)[6], Ploug and Jorgensen (1999)[7], and Iversen and Ploug (2010)[8].

POC flux values. One reason is because the moored sediment traps sample with a Eulerian framework, being moored in one location sampling various water masses as they flow, while drifting sediment traps sample with a Lagrangian approach, staying with one parcel of water and sampling it continuously as it moves with the currents. Another reason is that each of these trap designs have their own individual biases. In high current environments moored sediment traps can tilt to the side, affecting the collection of sinking particles. However, no tilt occurred at stations B and C based on CTD data. In contrast, drifting sediment traps may reduce the vertical shear in high current environments by floating freely within the water column. Additionally, we minimized other hydrodynamic concerns by using a bungee to dampen surface motion, tubes with a high aspect ratio, and bottom weighted tubes to keep them upright (Butman et al., 1986; Nodder et al., 2001, Buesseler et al., 2007). However, sinking POC flux may be incorrectly measured with drifting sediment traps because the tubes are open during deployment and recovery, contrary to the moored sediment traps (Buesseler et al., 2007). This source of error is minimized by deploying the drifting sediment traps at a shallow depth (i.e., 30 m).

With these sources of error, it is helpful to have two independent measurements of POC flux using different methods. The overall range of POC flux values in June 2018 was 1.48 to 2.29 g C m^{-2} day^{-1} with the moored sediment traps and 0.17 to 2.20 g C m^{-2} day^{-1} with the drifting sediment traps. Comparable maximum flux magnitudes from these two different methods minimize the concerns of collection biases common with sediment traps and provide some supporting evidence of the validity of POC fluxes of this magnitude.

Comparing POC Flux, Primary Productivity, and Export Ratios

Primary productivity rates, sinking flux, and export ratios were compared with previous measurements from the same study area (Fukuchi et al., 1993; Moran et al., 1997; Yu et al., 2010, 2012; Lalande et al., 2020), the broader Bering and Chukchi shelf system (Moran et al., 2005; Lalande et al., 2007; Lepore et al., 2007; Baumann et al., 2013), the greater Arctic area (**Supplementary Table 1**), and from a global compilation (Le Moigne et al., 2013; **Figure 4**, and **Supplementary Figure 2**). The upper range of our POC flux measurements (2.2 g C m^{-2} day^{-1} from drifting sediment trap and 2.3 g C m^{-2} day^{-1} from moored sediment trap) was unprecedentedly high compared to other measurements in this region and among the highest recorded in the surrounding areas, the broader Arctic, and globally.

Five previous studies report particulate flux estimates for the Bering and Chukchi shelves (Fukuchi et al., 1993; Moran et al., 1997; Yu et al., 2010, 2012; Lalande et al., 2020), two based on sediment trap measurements. A moored sediment trap deployed (36 m water depth, 49 m bottom depth) from late June to late September 1988, about 500 miles south of Bering Strait, measured flux ranging from 253 to 654 mg C m^{-2} day^{-1} (Fukuchi et al., 1993). More recently, a moored sediment trap deployed (37 m water depth, 45 m bottom depth) from August 2015 to July 2016, about 200 miles north of our most northern stations on the Chukchi shelf, measured POC fluxes ranging from 72 to 1184 mg C m^{-2} day^{-1} (Lalande et al., 2020). An estimate of 456 mg C m^{-2} day^{-1} (36 m water depth, 49 m bottom depth) was calculated using the $^{234}Th/^{238}U$ disequilibrium method on the Chukchi Sea shelf in August 1994 (Moran et al., 1997). Yu et al. (2010) measured a POC flux value of 243.8 mg C m^{-2} day^{-1}

(40 m water depth, 50 m bottom depth) using the $^{234}Th/^{238}U$ disequilibrium method sometime between July and September on the Chukchi shelf within the bounds of our study area. Finally, during a study on the Chukchi shelf from July to September, a POC flux measurement of 951.1 mg C m^{-2} day^{-1} (30 m water depth, 40 m bottom depth) was made using the $^{234}Th/^{238}U$ disequilibrium method within the bounds of and to the north of our study area (Yu et al., 2012). We selected the peak annual POC flux value from Lalande et al. (2020) and the flux measurement from Moran et al. (1997) and Yu et al. (2010, 2012) and plotted them directly on the y-axis indicating no known corresponding primary productivity value (**Figure 4**). The spatial extent of these studies are shown along with that of this study in **Supplementary Figure 3**. It should be noted that the $^{234}Th/^{238}U$ disequilibrium method for calculating sinking POC flux has its own biases, especially in areas with non-steady state flux events and advection and dispersion processes (Buesseler et al., 2007), such as on a shallow Arctic shelf. The measurements of POC flux we made in this study were the same or higher than previous measurements made in this region.

We expanded our region of comparison to include the Bering and Chukchi shelf breaks. Particulate organic carbon flux has been estimated more frequently on the Bering and Chukchi shelf breaks, with a maximum flux value at the base of the euphotic zone of 1.381 g C m^{-2} day^{-1} reported slightly south of our study area on the Bering Sea shelf break (40 m water depth, >125 m bottom depth) in July 2010 (**Figure 6**; Baumann et al., 2013). Additionally, our average regional flux for the BSAW, 1.59 ± 0.54 g C m^{-2} day^{-1} (mean ± 1 SD) is much higher than previous average regional flux estimates from the shelf breaks just north and south of this region, which range from 34 mg C m^{-2} day^{-1} (50 m water depth, bottom depth average 1275 m, May and June sampling period) to 376 mg C m^{-2} day^{-1} (50 m water depth, bottom depth average 838 m, May and June sampling period) (Moran et al., 2005, 2012; Lalande et al., 2007; Lepore et al., 2007; Baumann et al., 2013). Although individual measurements of export ratios approaching 1 are somewhat common (Lepore et al., 2007; Baumann et al., 2013), our average export ratio of 0.82 ± 0.32 (mean ± 1 SD) is very high. These observations illustrate the exceptional efficiency and strength of the biological carbon pump in the shallow Pacific Arctic shelf and shelf breaks.

Sinking POC flux and primary productivity values were also compared with a global review of POC flux measurements obtained using the $^{234}Th/^{238}U$ disequilibrium method (Le Moigne et al., 2013). We plotted all values with both POC flux and primary productivity rate measurements from Le Moigne et al. (2013), along with previous measurements from the broader Pacific shelf system, and our specific study area with the values we measured in this study from the drifting sediment traps and the last values of POC flux from the moored sediment traps (**Figure 4**). When available, sinking POC flux measurements at the base of the euphotic zone were selected, a metric shown to be comparable at sites with different bottom and euphotic zone depths (Buesseler et al., 2020). From this analysis, it is evident that the primary productivity rates from this study mostly fall within the upper range of what has been measured in this region before. Flux measurements at the BSAW stations (0.8–2.3 g C m^{-2} day^{-1}) are very high compared to what has been measured previously (0–1.4 g C m^{-2} day^{-1}).

In addition to the global review by Le Moigne et al. (2013), we compiled POC fluxes, primary productivity rates, and export ratios from other high latitude studies. The results of this review can be found in **Supplementary Table 1**. We categorized the studies by region, including the Baffin Bay, Baltic Sea, Barents Sea, Beaufort Sea, Bering Sea, Canadian Archipelago, Chukchi Sea, Fram Strait, Greenland Sea, Hudson Bay, Kara Sea, Labrador Sea, Laptev Sea, North Atlantic, North Sea, White Sea, as well as the high Arctic. We considered studies that measured sinking POC flux rates using drifting, moored, or neutrally buoyant sediment traps, marine snow catchers, or $^{234}Th/^{238}U$ disequilibrium. When possible, we selected samples from as close to the euphotic zone as possible. Primary productivity rates ranged from 0 to 2.6 g C m^{-2} day^{-1} and export ratios ranged from 0.03 to 1.67. These ranges are consistent with the primary productivity and export ratios measured in this study. Out of 79 studies, only nine measured rates of POC flux greater than 1 g C m^{-2} day^{-1} that were measured in the Baffin Bay (Michel et al., 2002), the Barents Sea (Andreassen and Wassmann, 1998; Olli et al., 2002; Lalande et al., 2008; Gustafsson et al., 2013), the Bering Sea (Baumann et al., 2013), the Beaufort Sea (Amiel and Cochran, 2008), the Chukchi Sea (Lalande et al., 2020), and the North Atlantic (Buesseler et al., 1992). The highest POC flux measurement of 2.5 g C m^{-2} day^{-1} was measured in the Beaufort Sea near the Makenzie River drainage in June at 50 m depth and 230 m water depth (Amiel and Cochran, 2008). The second highest POC flux measurement of 1.5 g C m^{-2} day^{-1} was measured in the Barents Sea in May at 30 m depth and 239 m bottom depth (Olli et al., 2002). We also selected some studies of POC flux from known high productivity and/or high flux regions from around the world (**Supplementary Table 2**). These POC flux values ranged from 1 to 620 mg C m^{-2} day^{-1}. Two POC flux values recorded in the present study were among the highest ever recorded at the base of the euphotic zone (2.20 g C m^{-2} day^{-1} at station A with a drifting sediment trap and 2.29 g C m^{-2} day^{-1} at station C with a moored sediment trap). With individual flux values from different methods at different stations ranking among the highest ever recorded, it is clear that the Pacific Arctic shelf exported a massive amount of organic carbon out of the euphotic zone, even in an anomalously warm year with low sea ice.

Limitations and Implications

Even with strong efforts in place to study the processes on the Pacific Arctic Shelf with the ASGARD program, there is still a lack of available data. While POC flux and water column oceanographic measurements are being obtained more frequently with moored sediment traps, temporally overlapping primary productivity rate measurements are not often available, notably later in the summer or earlier in the spring, when production is highest. Previous primary productivity measurements obtained later in the summer (Springer and McRoy, 1993; Lee et al., 2007; Hill et al., 2018) may no longer be representative of current conditions. Additionally, particle-associated microbial respiration rates are likely variable

throughout the spring, summer and fall and therefore cannot be extrapolated beyond spring. Therefore, there are still many unknowns regarding how the Pacific Arctic is responding and will respond to climate change. It is possible that only after many years of consistently warm and low-ice conditions changes in the strength and efficiency of the biological carbon pump on the Pacific Arctic shelf will become apparent.

It has been hypothesized that the strength of the biological carbon pump in the Arctic may weaken with climate change due to increased duration of the open-water period for primary production and enhanced nutrient limitation (Piepenburg, 2005; Wassmann and Reigstad, 2011; Grebmeier, 2012). Warmer waters have been predicted to increase metabolic rates of pelagic grazers and heterotrophic bacteria and potentially favor smaller phytoplankton and faster-growing grazers that more rapidly recycle organic matter within the water column (Wassmann and Reigstad, 2011; Neeley et al., 2018). We postulate that high nutrient concentrations, the shallow nature of the Pacific Arctic shelf, and the large-celled, fast-sinking phytoplankton that dominate pelagic productivity create conditions unique to this Arctic shelf (Springer and McRoy, 1993; Gradinger, 2009). Nutrients are unlikely to become more limited, especially in the BSAW, because of the consistent influx of the Anadyr Current, which is nutrient replete from Pacific upwelling. High nutrient concentrations favor large-cell phytoplankton (Li et al., 2009). Therefore, it is possible the Pacific Arctic shelf will not experience as dramatic of a shift from large cells to small cells with warming conditions when compared to other Arctic shelves. Finally, the Pacific Arctic shelf is shallower than most other Arctic shelves (averaging only 50 m deep). It will never take very long for sinking material leaving the euphotic zone to reach the seafloor, as it only has to sink about 20 m. Even if there is some increased heterotrophy in zooplankton or bacteria or decrease in cell size, the shallow nature of the shelf will allow for a higher proportion of organic matter to reach the seafloor than over deeper shelves, such as the Canadian Arctic Archipelago and European Arctic shelf. Increased frequency of storms are predicted with a changing Arctic (Slats et al., 2019). This could have major implications for the long-term carbon storage that historically has occurred on the Pacific Arctic shelf. Hauri et al. (2013) found that significant portions of carbon once thought to be stored in sediments on the Chukchi shelf are mixed up during fall storms. Given these features, we speculate that this system may retain strong coupling between the pelagic and benthic realms, continue to support highly productive pelagic and benthic ecosystems, and act as a strong sink for atmospheric carbon dioxide, possibly mediated by increased frequency of fall and winter storms. If these results prove to be a sustained feature of the rapidly changing Pacific Arctic, the biological carbon pump could represent an important element of resilience for regional ecosystems and biogeochemical cycles.

CONCLUSION

Measurements from both drifting and moored sediment traps indicate that fluxes of sinking POC on the Pacific Arctic shelf in June 2018 ranged from 0.8 to 2.3 g C m^{-2} day^{-1} in BSAW, making them amongst the highest fluxes ever documented in the global oceans. This region was also characterized by high export ratios and low rates of particle associated microbial respiration. These observations indicate that the biological carbon pump on the Pacific Arctic shelf is exceptionally strong and efficient despite a recent multi-year shift to warmer and relatively ice-free conditions (Fetterer et al., 2017; Stabeno and Bell, 2019; Danielson et al., 2020; Huntington et al., 2020). While the majority of the fluxes we observed during June 2018 were unprecedented relative to the limited number of historical flux measurements from this region, the data are still insufficient to determine whether functioning of the biological carbon pump has changed significantly relative to earlier, colder, and ice-replete years. Nonetheless, our observations do not provide supporting evidence for the common prediction that a weaker biological carbon pump and increased pelagic heterotrophy will prevail on the Pacific Arctic's continental shelves under future change.

DATA AVAILABILITY STATEMENT

The datasets generated for this study section can be found in the DataONE system (doi: 10.24431/rw1k46v).

AUTHOR CONTRIBUTIONS

SO, SD, SH, RH, DS, and AM: conceptualization. SD, SH, RH, DS, and AM: funding acquisition and project administration. SO, RH, CL, DS, and AM: methodology. SO, SD, CL, DS, and AM: investigation and formal analysis. SD, SH, and AM: supervision. SO and RH: software. SO: data visualization, writing-original draft. SO, SD, SH, RH, CL, DS, and AM: writing-reviewing and editing.

FUNDING

Research funded by the NPRB (Grant A91-00a, A91-88 and A91-99a to SD, SH, RH, AM, and DS).

ACKNOWLEDGMENTS

We thank Captain and crew of the R/V Sikuliaq as well as all collaborators in the ASGARD project, for making this project possible. Additionally, we thank S. B. Moran for the use of the drifting sediment traps, the Alaska Stable Isotope Facility for technical support and analytical assistance (University of Alaska, Fairbanks), and the two reviewers for their constructive comments. NPRB Publication Number "ArcticIERP-40".

SUPPLEMENTARY MATERIAL

The Supplementary Material for this article can be found online at: https://www.frontiersin.org/articles/10.3389/fmars.2020.548931/full#supplementary-material

REFERENCES

Amiel, D., and Cochran, J. K. (2008). Terrestrial and marine POC fluxes derived from 234Th distributions and δ13C measurements on the Mackenzie Shelf. *J. Geophys. Res.* 113:C03S06. doi: 10.1029/2007JC004260

Andersen, P. (1988). The quantitative importance of the "Microbial loop" in the marine pelagic: a case study for the North Bering/Chukchi Sea. *Arch. Hydrobiol. Bieh.* 31, 243–251.

Anderson, L. A., and Sarmiento, J. L. (1994). Redfield ratios of remineralization determined by nutrient data-analysis. *Global Biogeochem. Cycles* 8, 65–80. doi: 10.1029/93GB03318

Andreassen, I. J., and Wassmann, P. (1998). Vertical flux of phytoplankton and particulate biogenic matter in the marginal ice zone of the Barents Sea in May 1993. *Mar. Ecol. Prog. Ser.* 170, 1–14. doi: 10.3354/meps170001

Arrigo, K. R., Perovich, D. K., Pickart, R. S., Brown, Z. W., van Dijken, G. L., Lowry, K. E., et al. (2014). Phytoplankton blooms beneath the sea ice in the Chukchi sea. *Deep Sea Res. II* 105, 1–16. doi: 10.1016/j.dsr2.2014.03.018

Ashjian, C. J., Campbell, R. C., Welch, H. E., Butler, M., and Van Keuren, D. (2003). Annual cycle in abundance, distribution, and size in relation to hydrography of important copepod species in the western Arctic Ocean. *Deep Sea Res. I* 50, 1235–1261. doi: 10.1016/S0967-0637(03)00129-8

Bates, N. R. (2006). Air-sea CO_2 fluxes and the continental shelf pump of carbon in the Chukchi Sea adjacent to the Arctic Ocean. *J. Geophys. Res. Ocean* 111, 1–21. doi: 10.1029/2005JC003083

Baumann, M. S., Moran, S. B., Lomas, M. W., Kelly, R. P., and Bell, D. W. (2013). Seasonal decoupling of particulate organic carbon export and net primary production in relation to sea-ice at the shelf break of the eastern Bering Sea: Implications for off-shelf carbon export. *J. Geophys. Res. Ocean* 118, 5504–5522. doi: 10.1002/jgrc.20366

Belcher, A., Iversen, M., Giering, S., Riou, V., Henson, S. A., Berline, L., et al. (2016a). Depth-resolved particle-associated microbial respiration in the northeast Atlantic. *Biogeosciences* 13, 4927–4943. doi: 10.5194/bg-13-4927-2016

Belcher, A., Iversen, M., Manno, C., Henson, S. A., Tarling, G. A., and Sanders, R. (2016b). The role of particle associated microbes in remineralization of fecal pellets in the upper mesopelagic of the Scotia Sea, Antarctica. *Limnol. Oceanogr.* 61, 1049–1064. doi: 10.1002/lno.10269

Bluhm, B. A., and Gradinger, R. R. (2008). Regional variability in food availability. *Ecol. Appl.* 18, S77–S96. doi: 10.1890/06-0562.1

Buesseler, K. O., Bacon, M. P., Livingston, H. D., and Cochrant, K. (1992). Carbon and nitrogen export during the JGOFS North Atlantic Bloom experiment estimated from ^{234}Th: ^{238}U disequilibria. *Deep. Sea Res.* 39, 1115–1137. doi: 10.1016/0198-0149(92)90060-7

Buesseler, K. O., Boyd, P. W., Black, E. E., and Siegel, D. A. (2020). Metrics that matter for assessing the ocean biological carbon pump. *Proc. Natl. Acad. Sci. U.S.A.* 117, 9679–9687. doi: 10.1071/pnas.1918114117

Buesseler, K. O., Chen, M., Harada, K., Gustafsson, O., Trull, T., Rutgers van der Loeff, M., et al. (2007). An assessment of the use of sediment traps for estimating upper ocean particle fluxes. *J. Mar. Res.* 65, 345–416. doi: 10.1357/002224007781567621

Butman, C. A., Grand, W. D., and Stolzenback, K. D. (1986). Predictions of sediment trap biases in turbulent flows, a theoretical analysis based on observations from the literature. *J. Mar. Res.* 44, 601–644. doi: 10.1357/002224086788403024

Campbell, R. G., Sherr, E. B., Ashjian, C. J., Plourde, S., Sherr, B. F., Hill, V., et al. (2009). Mesozooplanktotn prey preference and grazing impact in the western Arctic Ocean. *Deep Sea Res. II* 56, 1274–1289. doi: 10.1016/j.dsr2.2008.10.027

Carroll, M. L., and Carroll, J. (2003). "The arctic seas," in *Biogeochemistry of Marine Systems*, eds K. D. Black and G. B. Shimmield (Boca Raton, FL: CRC Press), 127–156.

Chen, C. A., and Borges, A. V. (2009). Reconciling opposing views on carbon cycling in the coastal ocean: continental shelves as sinks and near-shore ecosystems as sources of atmospheric CO_2. *Deep Sea Res. II* 56, 578–590. doi: 10.1016/j.dsr2.2008.12.009

Collins, J. R., Edwards, B. R., Thamatrakoln, K., Ossolinski, J. E., Ditullio, G. R., Bidle, K. D., et al. (2015). The multiple fates of sinking particles in the North Atlantic Ocean. *Glob. Biogeochem. Cycles* 29, 1471–1494. doi: 10.1002/2014GB005037

Cota, G. F., Pomeroy, L. R., Harrison, W. G., Jones, E. P., Peters, F., Sheldon, W. M., et al. (1996). Nutrients, primary production and microbial heterotrophy in the southeastern Chukchi Sea: arctic summer nutrient depletion and heterotrophy. *Mar. Ecol. Prog. Ser.* 135, 247–258. doi: 10.3354/meps135247

Danielson, S. L., Ahkinga, O., Ashjian, C., Basyuk, E., Cooper, L. W., Eisner, L., et al. (2020). Manifestation and consequences of warming and latered heat fluxes over the Bering and Chukchi Sea continental shelves. *Deep Sea Res. II* 177:104781. doi: 10.1016/j.dsr2.2020/104781

Danielson, S. L., Eisner, L., Ladd, C., Mordy, C., Sousa, L., and Weingartner, T. J. (2017). A comparison between late summer 2012 and 2013 water masses, macronutrients, and phytoplankton standing crops in the northern Bering and Chukchi Seas. *Deep Sea Res. II* 135, 7–26. doi: 10.1016/j.dsr2.2016.05.024

Degerlund, M., and Eilertsen, H. C. (2010). Main species characteristics of phytoplankton spring blooms in NE Atlantic and Arctic waters (68-80° N). *Estuar. Coasts* 33, 242–269. doi: 10.1007/s12237-009-9167-7

Dugdale, R. C., and Goering, J. J. (1967). Uptake of new and regenerated forms of nitrogen in primary productivity. *Limnol. Oceanogr.* 12, 196–206. doi: 10.4319/lo.1967.12.2.0196

Durkin, C. A., Estapa, M. L., and Buesseler, K. O. (2015). Observations of carbon export by small sinking particles in the upper mesopelagic. *Mar. Chem.* 175, 72–81. doi: 10.1016/j.marchem.2015.02.011

Ebersbach, F., and Trull, T. W. (2008). Sinking particle properties from polyacrylamide gels during the KErguelen Ocean and Plateau compared Study (KEOPS): zooplankton control of carbon export in an area of persistent natural iron inputs in the Southern Ocean. *Limnol. Oceanogr.* 53, 212–224. doi: 10.4319/lo.2008.53.1.0212

European Centre for Medium-Range Weather Forecasts (2019). Updated Monthly. ERA5 Reanalysis (0.25 Degree Latitude-Longitude Grid). Research Data Archive at the National Center for Atmospheric Research, Computational and Information Systems Laboratory. Reading: European Centre for Medium-Range Weather Forecasts.

Fetterer, F., Knowles, K., Meier, W. N., Savoie, M., and Windnagel, A. K. (2017). *Updated Daily. Sea Ice Index, Version 3*. Boulder, CO: National Snow and Ice Data Center.

Fukuchi, M., Sasaki, H., Hattori, H., Matsuda, O., Tanimura, A., Handa, N., et al. (1993). Temporal variability of particulate flux in the northern Bering Sea. *Cont. Shelf Res.* 13, 693–704. doi: 10.1016/0278-4343(93)90100-C

Garneau, M. È, Vincent, W. F., Terrado, R., and Lovejoy, C. (2009). Importance of particle-associated bacterial heterotrophy in a coastal Arctic ecosystem. *J. Mar. Syst.* 75, 185–197. doi: 10.1016/j.jmarsys.2008.09.002

Gradinger, R. (1999). Vertical fine structure of the biomass and composition of algal communities in Arctic pack ice. *Mar. Biol.* 133, 745–754. doi: 10.1007/s002270050516

Gradinger, R. (2009). Sea-ice algae: major contributors to primary production and algal biomass in the Chukchi and Beaufort Seas during May/June 2002. *Deep Sea Res. II* 56, 1201–1212. doi: 10.1016/j.dsr2.2008.10.016

Grebmeier, J. M. (2012). Shifting patterns of life in the Pacific Arctic and Sub-Arctic seas. *Ann. Rev. Mar. Sci.* 4, 63–78. doi: 10.1146/annurev-marine-120710-100926

Grebmeier, J. M., and Barry, J. P. (1991). The influence of oceanographic processes on pelagic-benthic coupling in polar regions?: a benthic perspective. *J. Mar. Syst.* 2, 495–518. doi: 10.1016/0924-7963(91)90049-z

Grebmeier, J. M., and McRoy, C. P. (1988). Pelagic-benthic coupling on the shelf of the northern Bering and Chukchi Seas. I. Food supply and source and benthic biomass. *Mar. Ecol. Prog. Ser.* 48, 57–67. doi: 10.3354/meps053079

Grebmeier, J. M., and McRoy, C. P. (1989). Pelagic-benthic coupling on the shelf of the northern Bering and Chukchi Seas. III. Benthic food supply and carbon cycling. *Mar. Ecol. Prog. Ser.* 53, 93–100.

Grebmeier, J. M., McRoy, C. P., and Feder, H. M. (1988). Pelagic-benthic coupling on the shelf of the northern Bering and Chukchi Seas. I. Food supply and source and benthic biomass. *Mar. Ecol. Prog. Ser.* 48, 57–67. doi: 10.3354/meps053079

Gustafsson, Ö, Larsson, U., Andersson, P., Gelting, J., and Roos, P. (2013). An assessment of upper ocean carbon and nitrogen export fluxes on the boreal continental shelf: a 3-year study in the open Baltic Sea comparing sediment

traps, 234Th proxy, nutrient, and oxygen budgets. *Limnol. Oceanogr. Methods* 11, 495–510. doi: 10.4319/lom.2013.11.495

Hama, T., Miyazaki, T., Ogawa, Y., Iwakuma, T., Takahashi, M., Otsuki, A., et al. (1983). Measurement of photosynthetic production of a marine phytoplankton population using a stable 13C isotope. *Mar. Biol.* 73, 31–36. doi: 10.1007/BF00396282

Hauri, C., Winsor, P., Juranek, L. W., McDonnell, A. M. P., Takahashi, T., and Mathis, J. T. (2013). Wind-driven mixing causes a reduction in the strength of the continental shelf carbon pump in the Chukchi Sea. *Geophys. Res. Lett.* 40, 5932–5936. doi: 10.1002/2013GL058267

Hill, V., Ardyna, M., Lee, S. H., and Varela, D. E. (2018). Decadal trends in phytoplankton production in the Pacific Arctic region from 1950 to 2012. *Deep Sea Res. II* 152, 82–94. doi: 10.1016/j.dsr2.2016.12.015

Hopcroft, R. R., Kosobokova, K. N., and Pinchuk, A. I. (2010). Zooplankton community patterns in the Chukchi Sea during summer 2004. *Deep Sea Res. II* 57, 27–39. doi: 10.1016/j.dsri.2009.08.003

Hovelsrud, G. K., Mckenna, M., and Huntington, H. P. (2008). Marine mammal harvests and other interactions with humans. *Ecol. Appl.* 18, 135–147. doi: 10.1890/06-0843.1

Huntington, H. P., Danielson, S. L., Wiese, F. K., Baker, M., Boveng, P., Citta, J. J., et al. (2020). Evidence suggests potential transformation of the Pacific Arctic ecosystem is underway. *Nat. Clim. Chang.* 10, 342–348. doi: 10.1038/s41558-020-0695-2

Iversen, M. H., and Ploug, H. (2010). Ballast minerals and the sinking carbon flux in the ocean: carbon-specific respiration rates and sinking velocity of marine snow aggregates. *Biogeosciences* 7, 2613–2624. doi: 10.5194/bg-7-2613-2010

Kitamura, M., Amakasu, K., Kikuchi, T., and Nishino, S. (2017). Seasonal dynamics of zooplankton in the southern Chukchi Sea revealed from acoustic backscattering strength. *Cont. Shelf Res.* 133, 47–58. doi: 10.1016/j.csr.2016.12.009

Lalande, C., Grebmeier, J. M., Hopcroft, R. R., and Danielson, S. L. (2020). Annual cycle of export fluxes of biogenic matter near Hanna Shoal in the northeast Chukchi Sea. *Deep Sea Res. II* 177:104730. doi: 10.1016/j.dsr2.2020.104730

Lalande, C., Lepore, K., Cooper, L. W., Grebmeier, J. M., and Moran, S. B. (2007). Export fluxes of particulate organic carbon in the Chukchi Sea: a comparative study using 234Th/238U disequilibria and drifting sediment traps. *Mar. Chem.* 103, 185–196. doi: 10.1016/j.marchem.2006.07.004

Lalande, C., Moran, S. B., Wassmann, P., Grebmeier, J. M., and Cooper, L. W. (2008). 234Th-derived particulate organic carbon fluxes in the northern Barents Sea with comparison to drifting sediment trap fluxes. *J. Mar. Syst.* 73, 103–113. doi: 10.1016/j.marsys.2007.09.004

Lalande, C., Nöthig, E. M., and Fortier, L. (2019). Algal export in the arctic ocean in times of global warming. *Geophys. Res. Lett.* 46, 5959–5967. doi: 10.1029/2019GL083167

Le Moigne, F. A. C., Henson, S. A., Sanders, R. J., and Madsen, E. (2013). Global database of surface ocean particulate organic carbon export fluxes diagnosed from the 234Th technique. *Earth Syst. Sci. Data* 5, 295–304. doi: 10.5194/essd-5-295-2013

Lee, S. H., Joo, H. M., Liu, Z. L., Chen, J. F., and He, J. F. (2012). Phytoplankton productivity in the newly opened waters of the Western Arctic Ocean. *Deep Sea Res II* 81-84, 18–27. doi: 10.1016/j.dsr2.2011.06.005

Lee, S. H., Whitledge, T. E., and Kang, S. H. (2007). Recent carbon and nitrogen uptake rates of phytoplankton in Bering Strait and the Chukchi Sea. *Cont. Shelf Res.* 27, 2231–2249. doi: 10.1016/j.csr.2007.05.009

Lepore, K., Moran, S. B., Grebmeier, J. M., Cooper, L. W., Lalande, C., Maslowski, W., et al. (2007). Seasonal and interannual changes in particulate organic carbon export and deposition in the Chukchi Sea. *J. Geophys. Res. Ocean* 112, 1–14. doi: 10.1029/2006JC003555

Li, W. K., McLaughlin, F. A., Lovejoy, C., and Carmack, E. C. (2009). Smallest algae thrive as the arctic ocean freshens. *Science* 326:539. doi: 10.1126/science.1179798

McDonnell, A. M. P., and Buesseler, K. O. (2010). Variability in the average sinking velocity of marine particles. *Limnol. Oceanogr.* 55, 2085–2096. doi: 10.4319/lo.2010.55.5.2085

McDonnell, A. M. P., Boyd, P. W., and Buesseler, K. O. (2015). Effects of sinking velocities and microbial respiration rates on the attenuation of particulate carbon fluxes through the mesopelagic zone. *Glob. Biogeochem. Cycles* 29, 175–193. doi: 10.1002/2014GB004935

Michel, C., Nielsen, T. G., Nozais, C., and Gosselin, M. (2002). Significance of sedimentation and grazing by ice micro- and meiofauna for carbon cycling in annual sea ice (northern Baffin Bay). *Aquat. Microb. Ecol.* 30, 56–68. doi: 10.3354/ame030057

Moore, S. E., and Kuletz, K. J. (2019). Marine birds and mammals as ecosystem sentinels in and near distributed biological observatory regions: an abbreviated review of published accounts and recommendations for integration to ocean observatories. *Deep Sea Res. II* 162, 211–217. doi: 10.1016/j.dsr2.2018.09.004

Moore, S. E., and Stabeno, P. J. (2015). Synthesis of arctic research (SOAR) in marine ecosystems of the Pacific Arctic. *Prog. Oceanogr.* 136, 1–11. doi: 10.1016/j.pocean.2015.05.017

Moran, S. B., Ellis, K. M., and Smith, J. N. (1997). 234Th/238U disequilibrium in the central Arctic ocean: implications for particulate organic carbon export. *Deep Sea Res. II* 44, 1593–1606. doi: 10.1016/S0967-0645(97)00049-0

Moran, S. B., Kelly, R. P., Hagstrom, K., Smith, J. N., Grebmeier, J. M., Cooper, L. W., et al. (2005). Seasonal changes in POC export flux in the Chukchi Sea and implications for water column-benthic coupling in Arctic shelves. *Deep Sea Res. II* 52, 3427–3451. doi: 10.1016/j.dsr2.2005.09.011

Moran, S. B., Kelly, R. P., Iken, K., Mathis, J. T., Lomas, M. W., and Gradinger, R. (2012). Seasonal succession of net primary productivity, particulate organic carbon export, and autotrophic community composition in the eastern Bering Sea. *Deep Sea Res. II* 65-70, 84–97. doi: 10.1016/j.dsr2.2012.02.011

Naidu, A. S., Cooper, L. W., Grebmeier, J. M., Whitledge, T. E., and Hameedi, M. J. (2004). "The continental margin of the north Bering-Chukchi Sea: concentrations, sources, fluxes, accumulation and burial rates of organic carbon," in *The Organic Carbon Cycle in the Arctic Ocean*, eds R. Stein and R. W. Macdonald (Heidelberg: Springer-Verlag), 193–203. doi: 10.1007/978-3-642-18912-8

Neeley, A. R., Harris, L. A., and Frey, K. E. (2018). Unraveling phytoplankton community dynamics in the Northern Chukchi Sea under sea-ice-covered and sea-ice-free conditions. *Geophys. Res. Lett.* 45, 7663–7671. doi: 10.1029/2018GL077684

Nodder, S. D., Charette, M. A., Waite, A. M., Trull, T. W., Boyd, P. W., Zeldis, J., et al. (2001). Particulate transformations and export flux during an *in situ* iron-stimulated bloom in the Southern Ocean. *Geophys. Res. Lett.* 28, 2409–2412. doi: 10.1029/2001GL013008

Olli, K., Riser, C. W., Wassmann, P., Ratkova, T., Arashkevich, E., and Pasternak, A. (2002). Seasonal variation in vertical flux of biogenic matter in the marginal ice zone and the central Barents Sea. *J. Mar. Syst.* 38, 189–204. doi: 10.1016/S0924-7963(02)00177-X

Pickart, R. S., Moore, G. W. K., Chongyuan, M., Bahr, F., Nobre, C., and Weingartner, T. J. (2016). Circulation of winter water on the Chukchi shelf in early summer. *Deep Sea Res. II* 130, 56–75. doi: 10.1016/j.dsr2.2016.05.001

Piepenburg, D. (2005). Recent research on Arctic benthos: common notions need to be revised. *Polar Biol.* 28, 733–755. doi: 10.1007/s00300-005- 0013-5

Ploug, H., and Grossart, H. P. (2000). Bacterial growth and grazing on diatom aggregates: respiratory carbon turnover as a function of aggregate size and sinking velocity. *Limnol. Oceanogr.* 45, 1467–1475. doi: 10.4319/lo.2000.45.7.1467

Ploug, H., and Jorgensen, B. (1999). A net-jet flow system for mass transfer and microsensor studies of sinking aggregates. *Mar. Ecol. Prog. Ser.* 176, 279–290. doi: 10.3354/meps176279

Post, D. M. (2002). Using stable isotopes to estimate trophic position: models, methods and assumptions. *Ecology* 83, 703–718. doi: 10.1890/0012-9658(2002)083[0703:usitet]2.0.co;2

Richter-Menge, J., Druckenmiller, M. L., and Jeffries, M., (eds). (2019). *Arctic Report Card 2019.* https://www.arctic.noaa.gov/Report-Card

Sala, M. M., Arrieta, J. M., Boras, J. A., Duarte, C. M., and Vaqué, D. (2010). The impact of ice melting on bacterioplankton in the Arctic Ocean. *Polar Biol.* 33, 1683–1694. doi: 10.1007/s00300-010-0808-x

Slats, R., Oliver, C., Bahnke, R., Bell, H., Miller, A., Pungowiyi, D., et al. (2019). *Voices from the Front Lines of a Changing Bering Sea. Arctic Report Card 2019.*

Available online at: http://www.arctic.noaa.gov/Report-Card (accessed January 2, 2020).

Springer, A. M., and McRoy, C. P. (1993). The paradox of pelagic food webs in the northern Bering Sea-III. Patterns of primary production. *Cont. Shelf Res.* 13, 575–599. doi: 10.1016/0278-4343(93)90095-F

Stabeno, P. J., and Bell, S. W. (2019). Extreme conditions in the bering Sea (2017-2018): record-breaking low sea-ice extent. *Geophys. Res. Lett.* 46, 8952–8959. doi: 10.1029/2019gl083816

Thoman, R. L., Bhatt, U. S., Bieniek, P. A., Brettschneider, B. R., Brubaker, M., Danielson, S. L., et al. (2020). The record low Bering Sea ice extent in 2018: context, impacts, and an assessment of the role of anthropogenic climate change. *Bull. Am. Meteorol. Soc.* 101, S53–S58. doi: 10.1175/BAMS-D-19-0175.1

Vaqué, D., Lara, E., Arrieta, J. M., Holding, J., Sà, E. L., Hendriks, I. E., et al. (2019). Warming and CO_2 enhance arctic heterotrophic microbial activity. *Front. Microbiol.* 10:494. doi: 10.3389/fmicb.2019.00494

Vaughan, D. G., Comiso, J. C., Allison, I., Carrasco, J., Kaser, G., Kwok, R., et al. (2013). "Observations: Cryosphere," in *Climate Change 2013: The Physical Science Basis. Contribution of Working Group I to the Fifth Assessment of the Intergovernmental Panel on Climate Change*, eds T. F. Stocker, D. Qin, G.-K. Plattner, M. Tignor, S. K. Allen, J. Boschung, et al. (Cambridge: Cambridge University Press), 317–382. doi: 10.1017/CBO9781107415324.012

Walsh, J. J., McRoy, C. P., Coachman, L. K., Goering, J. J., Nihoul, J. J., Whitledge, T. E., et al. (1989). Carbon and nitrogen cycling within the Bering/Chukchi Seas: source regions for organic matter effecting AOU demands of the Arctic Ocean. *Prog. Oceanogr.* 22, 277–359. doi: 10.1016/0079-6611(89)90006-2

Wassmann, P., and Reigstad, M. (2011). Future Arctic Ocean seasonal ice zones and implications for pelagic-benthic coupling. *Oceanography* 24, 220–231. doi: 10.5670/oceanog.2011.74

Woodgate, R. A., Stafford, K. M., and Prahl, F. G. (2015). A synthesis of year-round interdisciplinary mooring measurements in the Bering Strait (1990-2014) and the RUSALCA years (2004-2011). *Oceanography* 28, 46–67. doi: 10.5670/oceanog.2015.57

Wooller, M. J., Zazula, G. D., Edwards, M., Froese, D. G., Boone, R. D., Parker, C., et al. (2007). Stable carbon isotope compositions of eastern beringian grasses and sedges: investigating their potential as paleoenvironmental indicators. *Arctic Antarct. Alpine Res.* 39, 318–331. doi: 10.1657/1523-0430(2007)39[318:scicoe]2.0.co;2

Yu, W., Chen, L., Cheng, J., He, J., Yin, M., and Zeng, Z. (2010). 234Th-derived particulate organic carbon export flux in the western Arctic Ocean. *Chin J. Oceanog. Limnol.* 28, 1146–1151. doi: 10.1007/s00343-010-9933-1

Yu, W., He, J., Li, Y., Lin, W., and Chen, L. (2012). Particulate organic carbon export fluxes and validation of steady state model of 234Th export in the Chukchi Sea. *Deep Sea Res. II* 81–84, 63–71. doi: 10.1016/j.dsr2.2012.03.003

Conflict of Interest: The authors declare that the research was conducted in the absence of any commercial or financial relationships that could be construed as a potential conflict of interest.

PLOS ONE

RESEARCH ARTICLE

Impact of a warm anomaly in the Pacific Arctic region derived from time-series export fluxes

Catherine Lalande[1]*, Jacqueline M. Grebmeier[2], Andrew M. P. McDonnell[3], Russell R. Hopcroft[3], Stephanie O'Daly[3], Seth L. Danielson[3]

1 Amundsen Science, Que´bec City, Canada, **2** UMCES, Cambridge, Maryland, United States of America, **3** College of Fisheries and Ocean Sciences, University of Alaska Fairbanks, Fairbanks, Alaska, United States of America

* catherine.lalande@as.ulaval.ca

Citation: Lalande C, Grebmeier JM, McDonnell AMP, Hopcroft RR, O'Daly S, Danielson SL (2021) Impact of a warm anomaly in the Pacific Arctic region derived from time-series export fluxes. PLoS ONE 16(8): e0255837. https://doi.org/10.1371/journal.pone.0255837

Editor: Alessandro Incarbona, University of Palermo: Universita degli Studi di Palermo, ITALY

Received: March 19, 2021

Accepted: July 23, 2021

Published: August 16, 2021

Data Availability Statement: Datasets generated for this study are available in the DataONE system (DBO2 dataset: https://doi.org/10.24431/rw1k5ag; DBO3 dataset: https://doi.org/10.24431/rw1k5af; DBO4 dataset: https://doi.org/10.24431/rw1k5ah).

Funding: This project was funded in part by the North Pacific Research Board (NPRB) and developed as part of the Arctic Integrated Ecosystem Research Program (IERP; https://www.nprb.org/arctic-program/). ASGARD was funded as part of the Arctic IERP (grant numbers A91-99a

Abstract

Unusually warm conditions recently observed in the Pacific Arctic region included a dramatic loss of sea ice cover and an enhanced inflow of warmer Pacific-derived waters. Moored sediment traps deployed at three biological hotspots of the Distributed Biological Observatory (DBO) during this anomalously warm period collected sinking particles nearly continuously from June 2017 to July 2019 in the northern Bering Sea (DBO2) and in the southern Chukchi Sea (DBO3), and from August 2018 to July 2019 in the northern Chukchi Sea (DBO4). Fluxes of living algal cells, chlorophyll *a* (chl *a*), total particulate matter (TPM), particulate organic carbon (POC), and zooplankton fecal pellets, along with zooplankton and meroplankton collected in the traps, were used to evaluate spatial and temporal variations in the development and composition of the phytoplankton and zooplankton communities in relation to sea ice cover and water temperature. The unprecedented sea ice loss of 2018 in the northern Bering Sea led to the export of a large bloom dominated by the exclusively pelagic diatoms *Chaetoceros* spp. at DBO2. Despite this intense bloom, early sea ice breakup resulted in shorter periods of enhanced chl *a* and diatom fluxes at all DBO sites, suggesting a weaker biological pump under reduced ice cover in the Pacific Arctic region, while the coincident increase or decrease in TPM and POC fluxes likely reflected variations in resuspension events. Meanwhile, the highest transport of warm Pacific waters during 2017–2018 led to a dominance of the small copepods *Pseudocalanus* at all sites. Whereas the export of ice-associated diatoms during 2019 suggested a return to more typical conditions in the northern Bering Sea, the impact on copepods persisted under the continuously enhanced transport of warm Pacific waters. Regardless, the biological pump remained strong on the shallow Pacific Arctic shelves.

Introduction

The Pacific Arctic marine ecosystem is extremely productive due to the persistent flow of nutrient-rich waters fueling high primary production on the shallow northern Bering Sea and Chukchi Sea shelves [1]. Recently, the region showed signs of a warming trend, including

and A91-00a) awarded to AMD and SLD. The CEO project was funded under NPRB Long Term Monitoring program (NPRB grant numbers 1426 and L36) awarded to SLD. JMG received support from the NSF Arctic Sciences Division (OPP grant number 1917469). The funders had no role in study design, data collection and analysis, decision to publish, or preparation of the manuscript.

Competing interests: The authors have declared that no competing interests exist.

drastic reductions in sea ice extent and an increase in the transport of warm Pacific waters delivering more heat and freshwater, and potentially more nutrients and biota, into the Arctic Ocean through the Bering Strait [1–8]. Amid this long-term warming trend, anomalously warm conditions were observed in the Pacific Arctic from 2017 into 2019, including an unprecedented loss of sea ice, even in the context of other recent warm years [1, 9, 10]. Sea ice cover barely extended south of Bering Strait in early January 2017 and remained well below the long-term average during the entire winter [1, 11]. The reduced sea ice cover enhanced oceanic heat uptake during spring months [6] and led to exceptionally high near-bottom ocean temperatures (~4˚C) in the Bering Strait in June 2017 [1]. The anomalously elevated water column heat content combined with winds from the south delayed sea ice formation to late December 2017 and contributed to the highest northward transport of Pacific waters during winter 2017–2018 [1, 6, 12]. Warm winds from the south also contributed to the record-breaking low sea ice extent and concentrations observed in the Pacific Arctic region in February 2018 and to the northern Bering Sea region being mostly ice-free by late March 2018 [1, 13–15]. The early sea ice retreat and reduced input of freshwater from melting sea ice in 2018 delayed the onset of stratification and the spring bloom [14, 16–18], and induced a shift in the composition of the phytoplankton community toward a high abundance of small diatoms [14]. Meanwhile, low abundance of large, lipid-rich copepods and high abundance of small copepods with low lipid content were reported in the northern Bering Sea during 2018 [1, 14–16], affecting the distribution of fish as well as the reproduction and survival of marine birds and mammals [14]. Nevertheless, flux measurements obtained using sediment traps deployed in the Bering Strait region during June 2018 highlighted remarkably high POC fluxes during the warm period [19]. Similar to 2017, accumulated residual heat reflected by record high sea surface temperatures during autumn 2018 [20] delayed freeze-up until December, while unusual southerly winds again forced a large ice retreat in February 2019 that led to the second lowest winter sea ice extent on record during 2018–2019 [1, 13].

While results from several snapshot studies clearly indicated that a sudden shift of the Pacific Arctic ecosystem occurred during the anomalously warm 2017–2019 period, most biological measurements were limited to summer months [1]. To complement these snapshot observations, sinking particles and plankton collected with moored sediment traps deployed at three sites of the Distributed Biological Observatory (Grebmeier et al., this issue) were used to monitor spatial and temporal variations in export fluxes and community composition in the Pacific Arctic region. Continuous flux measurements were obtained at the DBO2 and DBO3 sites from June 2017 to July 2019 and at the DBO4 site from August 2018 to July 2019 (Fig 1). This monitoring effort using sequential sediment traps follows the first time-series flux measurements obtained on the shallow Pacific Arctic shelves at the Chukchi Ecosystem Observatory (DBO4) from August 2015 to July 2016 [21]. Fluxes of living algal cells (with chloroplasts), chlorophyll *a* (chl *a*), total particulate matter (TPM), particulate organic carbon (POC), and zooplankton fecal pellets were measured to monitor carbon export and the seasonal development of the algal bloom in relation to the drastic changes observed during the warm anomaly period. Zooplankton and meroplankton collected in the sediment traps were also identified to track spatial and temporal variations in the composition and development of these communities. The deployment of moored sediment traps represents an invaluable contribution to the DBO as they provided time-series integrative measurements of biological and biochemical parameters at a high temporal resolution during a period of rapid changes in the Pacific Arctic. As warm events are likely to increase in frequency under the current global warming scenario, time-series export fluxes measurements obtained during the 2017–2019 warm period contribute to a better understanding of conditions to expect for the highly productive marine ecosystems of the northern Bering Sea and Chukchi Sea.

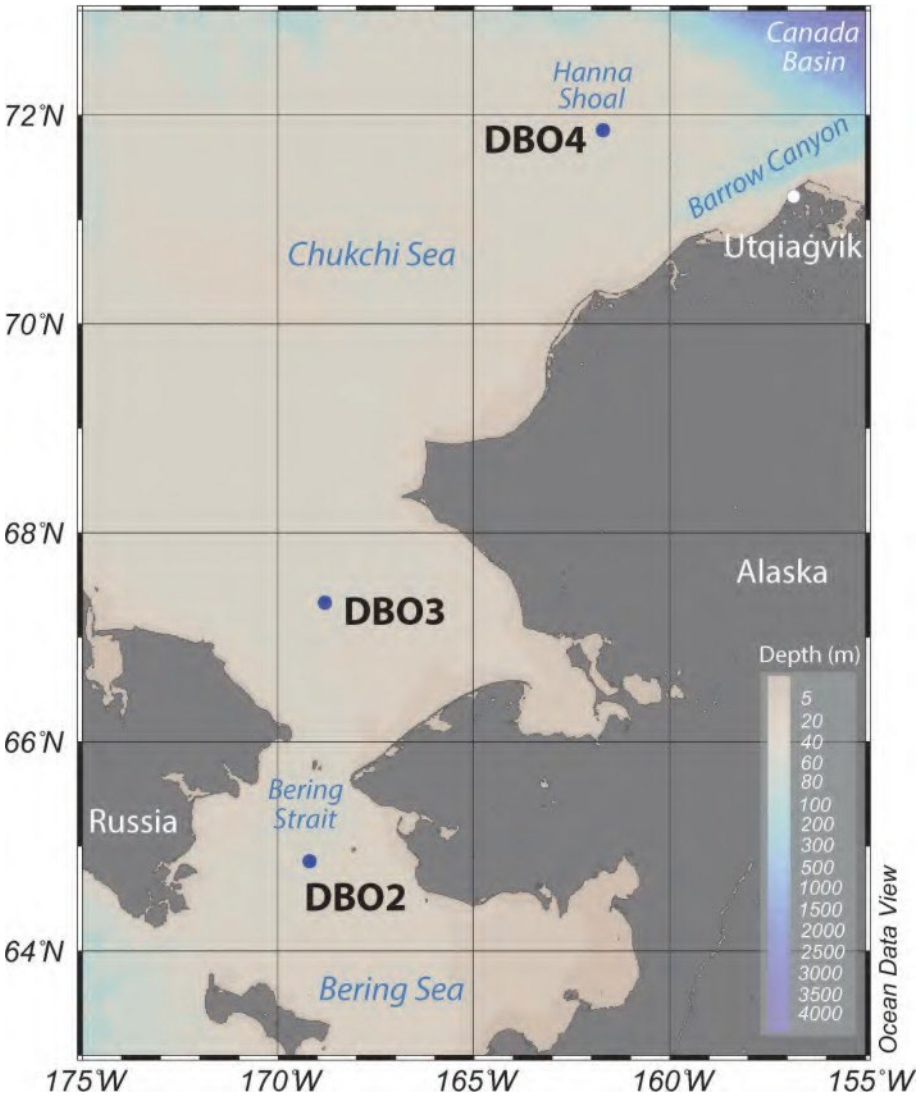

Fig 1. Positions of the three mooring sites at the DBO hotspots in the Pacific Arctic region. Reprinted from Ocean Data View under a CC BY license, with permission from Reiner Schlitzer, original copyright 2021.

https://doi.org/10.1371/journal.pone.0255837.g001

Material and methods

Remote sensing

Daily averaged sea-ice concentrations above each mooring site were retrieved at a 12.5-km resolution from the Centre ERS d'Archivage et de Traitement (CERSAT) service of the French Research Institute for Exploitation of the Sea (http://cersat.ifremer.fr/). Daily sea-ice concentrations were averaged for a 44 x 44 km region above each mooring site (Fig 1; DBO2: 64.7–65.1˚N; 169.3–169.8˚W; DBO3: 67.1–67.5˚N; 168.5–169.0˚W; DBO4: 71.4–71.8˚N; 161.4–161.9˚W).

Mooring

Sequential sediment traps (24 cups, Hydro-Bios, Germany) were deployed at the DBO2 (N4) and DBO3 (N6) sites from June 2017 to July 2019 and at the DBO4 (Chukchi Ecosystem Observatory; CEO) site from August 2018 to July 2019 (Fig 1 and Table 1). No national or

international permitting was required as part of the sample collection efforts, and the field studies did not involve endangered or protected species. At CEO, year-round measurements capture physical and biogeochemical parameters in addition to measures of fish, zooplankton, marine mammals, and other ecosystem components [e.g. 22–24]. Moorings were deployed and recovered from the R/V *Sikuliaq* in June 2017 and June 2018 and recovered from the R/V *Ocean Starr* in July 2019. Sediment trap sample cups were filled with filtered seawater adjusted to a salinity of 38 with NaCl and fixed with formalin (4% final solution) to preserve samples during deployment and after recovery. The carousel holding the sample cups rotated at pre-programmed intervals ranging from one week to one month. As the mooring was recovered before the last rotation of the carousel at DBO2 in June 2018, the sample cup that was open upon recovery was excluded from analysis. Seabird SBE 16plus units were deployed to measure water temperature at three depths at DBO2 and DBO3 and at one depth at DBO4. The unit deployed at the upper depth on each mooring was coupled with a WETStar fluorometer or WET Labs ECO triplet fluorometer to measure fluorescence (Table 1).

Laboratory

In the laboratory, zooplankton and meroplankton were removed from subsamples with forceps and identified to the lowest taxonomic level possible using a dissecting microscope. Sample cups were gently mixed before subsamples (0.1–3 ml) were taken with a modified micropipette to enable the collection of large particles for measurements of chl *a*, algal cells, fecal pellets, TPM, and POC. Subsamples for chl *a* measurements were filtered onto GF/F filters (0.7 μm), extracted in acetone for 24 h at -20˚C and measured on a Turner Design fluorometer following the methods outlined in Welschmeyer [25]. Samples were kept cool and in the dark prior to chl *a* measurements, but may have experienced some degradation. For the enumeration of algal cells, subsample volumes were adjusted to 3 ml with filtered seawater before being placed in an Utermo¨hl chamber. A minimum of 300 algal cells were counted and identified by inverted microscopy at 100X, 200X or 400X depending on cell size according to the Utermöhl method [26]. Using a dissecting scope, the length and width of fecal pellets (broken or intact) were measured with an ocular micrometer and fecal pellet volumes were calculated according to their shape. Cylindrical pellets were attributed to calanoid copepods while ellipsoidal pellets were attributed to appendicularians [27]. Fecal pellet volumes were converted to fecal pellet carbon (FPC) using a volumetric carbon conversion factor of 0.057 mg C mm^{-3} for copepod pellets and 0.042 mg C mm^{-3} for appendicularian pellets [27]. Subsamples for TPM measurements were filtered in triplicate onto pre-combusted (500˚C overnight) and pre-weighed GF/F filters (0.7 μm), rinsed with distilled water to remove salt, dried at 60˚C overnight, and weighed on a microbalance. The filters were then exposed to 1N HCl overnight for removal of inorganic carbon and dried once again at 60˚C overnight before encapsulation for POC measurements. POC was measured using a PerkinElmer CHNS 2400 Series II

Table 1. Mooring and sediment trap deployment information.

Site	Mooring name	Latitude (N)	Longitude (W)	Sampling start date	Sampling end date	Water depth (m)	Sediment trap depth (m)	Fluorometer depth (m)	CTD depth (m)
DBO4	CEO	71˚35	161˚31	August 7 2018	July 30 2019	46	39	33	33
DBO3	N6	67˚40	168˚44	June 17 2017	June 8 2018	50	35	26	26, 35, 45
				June 16 2018	July 13 2019	50	35	25	26, 46
DBO2	N4	64˚55	169˚55	June 26 2017	June 8 2018	49	37	27	27, 35, 44
				June 24 2018	July 13 2019	49	37	25	25, 35, 44

https://doi.org/10.1371/journal.pone.0255837.t001

elemental analyzer. All measurements were converted to daily fluxes depending on sampling duration and integrated to annual fluxes.

Results

Sea ice concentrations

While sea ice was first detected in December 2017 at DBO2 and DBO3, a lasting sea ice cover only formed in January 2018 and sea ice concentrations temporarily decreased in February 2018 at both sites (Fig 2). At DBO2, sea ice concentrations decreased again in early April before complete sea ice melt was observed at the end of April 2018. Sea ice melt was observed one month later at the end of May 2018 at DBO3. Sea ice formed again in early December 2018 at DBO2 and DBO3, two to three weeks earlier than when sea ice formed during 2017. Sea ice concentrations frequently decreased throughout winter 2018–2019, especially at DBO2. At DBO4, sea ice formed in November 2018, two to three weeks earlier than at the other sites, and sea ice concentrations remained >65% throughout winter. Sea ice breakup was observed in early May 2019 at DBO2, a few days later at DBO3, and mid-May at DBO4. While sea ice melted approximately three weeks later in 2019 than in 2018 at DBO2, it disappeared approximately two weeks earlier in 2019 than in 2018 at DBO3.

Water temperatures

Mooring-derived water temperatures were above 2˚C from June to November at all depths sampled at DBO2 and DBO3 (Fig 3). Water temperatures frequently peaked between 6˚C and

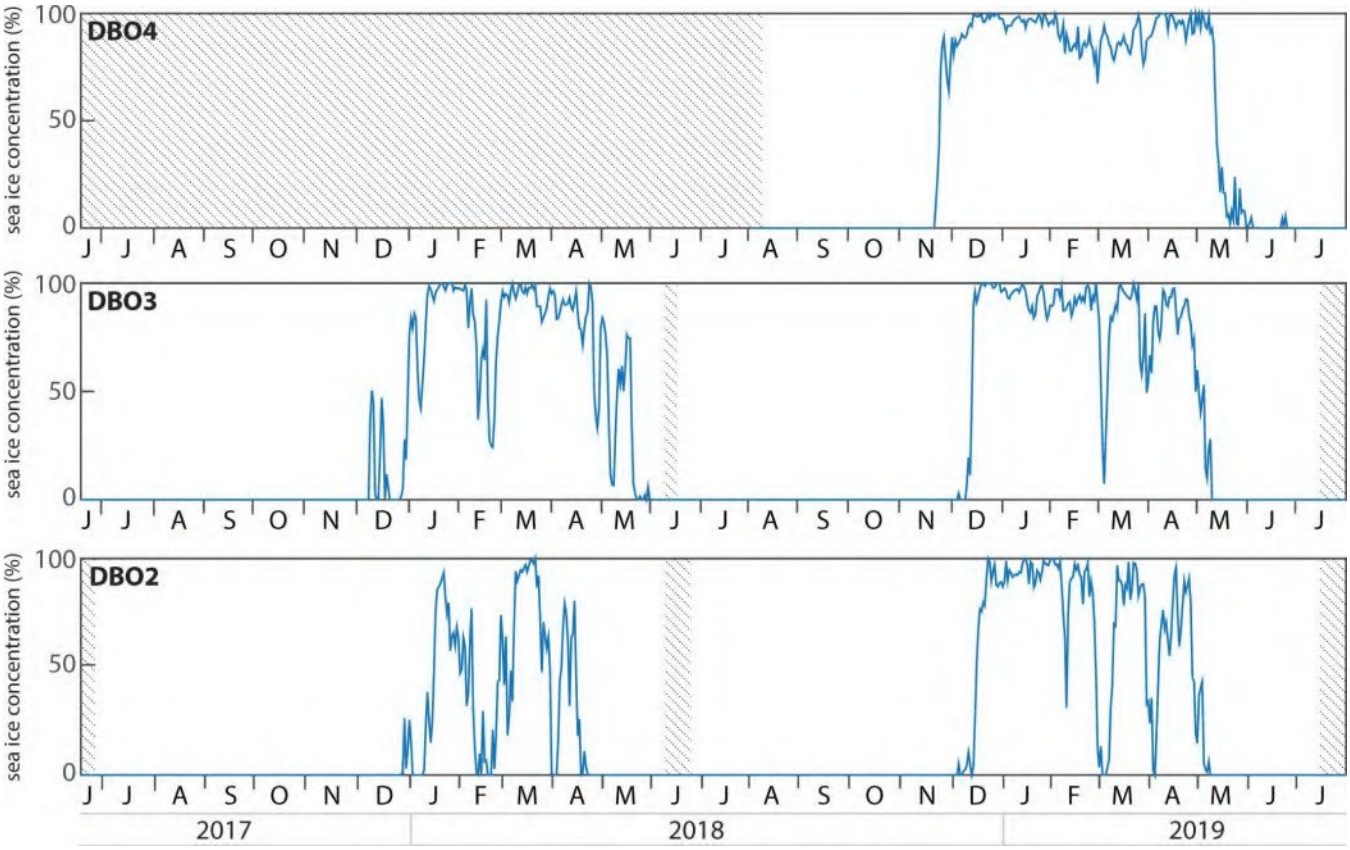

Fig 2. Daily sea ice concentration retrieved for a delimited region above each mooring site. Shaded areas represent periods without data.

https://doi.org/10.1371/journal.pone.0255837.g002

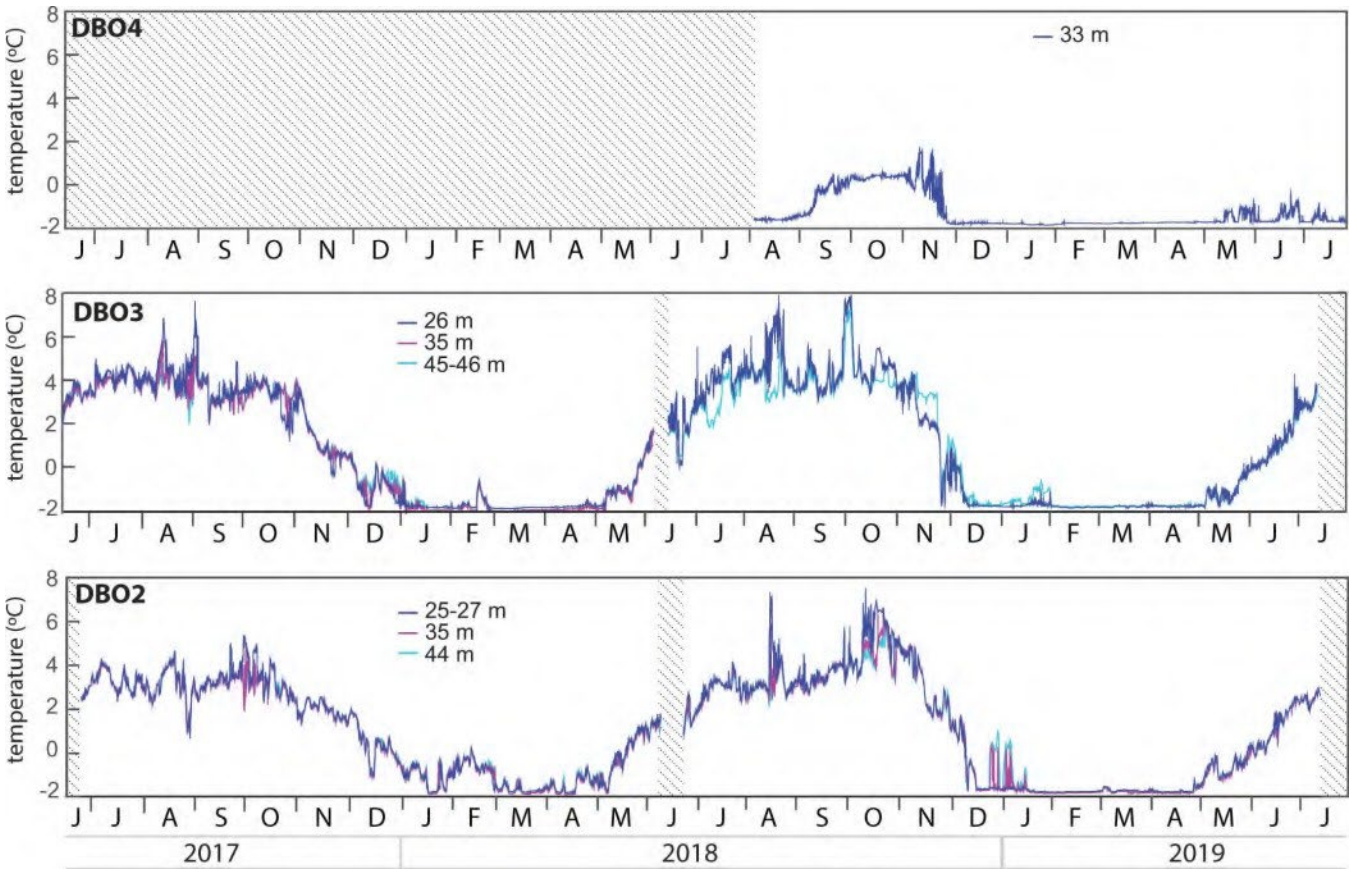

Fig 3. Water temperatures at each mooring site. There are no available data at 35 m for the 2018–2019 cycle at DBO3. Shaded areas represent periods without data.

https://doi.org/10.1371/journal.pone.0255837.g003

8˚C at both sites during late summer and autumn, except at DBO2 in 2017 where they remained below 6˚C. At DBO2, water temperatures slowly decreased to near-freezing point (-1.8˚C) only during very short periods of January, March and April 2018, while in 2019, they decreased more rapidly and remained near the freezing point from January until the end of April. At DBO3, water temperatures were almost continuously near the freezing point from January to early May 2018 and from December 2018 to early May 2019. At DBO4, water temperatures exceeded 0˚C but remained below 2˚C from September to November 2018 and were near the freezing point from the end of November 2018 to May 2019.

Chlorophyll a concentrations and fluxes

While enhanced chl *a* fluxes often coincided with increased suspended chl *a* concentrations recorded by the fluorometer 6 to 10 m above the traps, there were also notable differences between the two measurements (Fig 4). Peak chl *a* fluxes were observed at the end of May and/or early June for every deployment cycle, reaching values >10 mg m^{-2} d^{-1} at DBO2 and DBO3. During 2017, short periods of enhanced chl *a* fluxes were observed in August at DBO2 and during June and July at DBO3. Although there was a period without sampling due to the timing of the mooring turnaround in 2018, elevated chl *a* fluxes (>5 mg m^{-2} d^{-1}) were sustained during approximately five weeks in 2018 and 2019 at DBO2, and during two weeks in 2018 and nine weeks in 2019 at DBO3. At DBO4, relatively low chl *a* fluxes peaked in early June

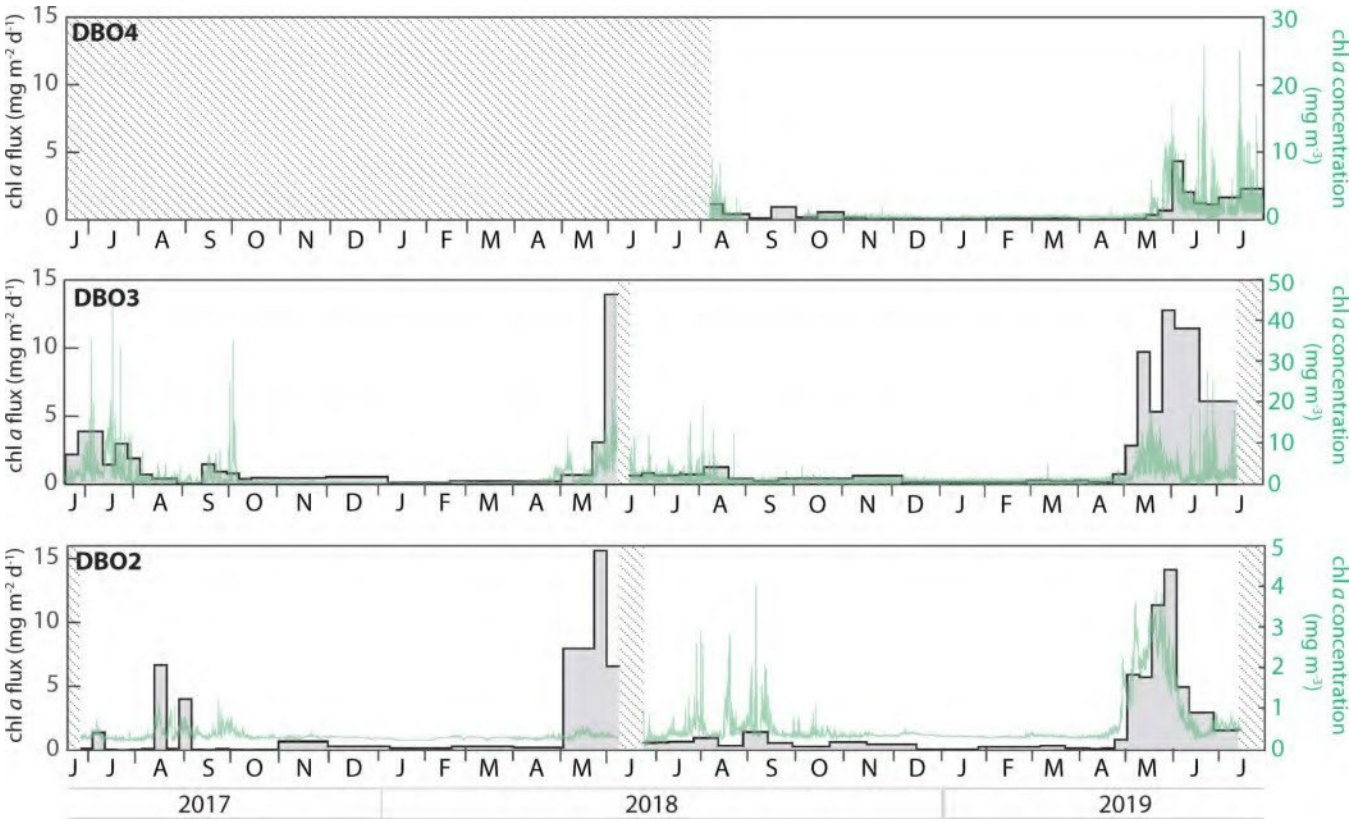

Fig 4. Chlorophyll *a* fluxes (grey bars) and suspended chlorophyll *a* concentration (green line) at each mooring site. Shaded areas represent periods without data.

https://doi.org/10.1371/journal.pone.0255837.g004

2019 (4.3 mg m^{-2} d^{-1}) and remained above >1 mg m^{-2} d^{-1} until the end of the deployment in late July 2019.

Diatom fluxes

Temporal variations in fluxes of diatom cells with chloroplasts were remarkably similar to chl *a* fluxes, with peak diatom fluxes observed at the end of May and/or early June for every deployment cycle (Fig 5). Whereas diatom fluxes were higher at DBO3 than DBO2 during summer 2017, the composition of the fluxes was similar at both sites, with the centric diatoms *Chaetoceros* spp. and *Thalassiosira* spp. and the pennate diatoms *Pseudo-nitzschia*/*Nitzschia* spp. contributing a large proportion of the fluxes. Low fluxes of the pennate diatom *Thalassionema nitzschioides* and the centric diatoms *Leptocylindrus* spp. and *Proboscia* spp. were also frequently observed during summer and autumn 2017. At DBO2, enhanced diatom fluxes with large proportions of the pennate diatoms *Fragilariopsis* spp. and *Neodenticula seminae* in early May 2018 were followed by extremely large fluxes nearly exclusively composed of *Chaetoceros* spp. and *Thalassiosira* spp. during late May and early June 2018. At DBO3, enhanced fluxes during May 2018 were first composed of the pennate diatoms *Pauliella taeniata* and *Fossula arctica* before *Fragilariopsis* spp. and *Thalassiosira* spp. dominated the peak in diatom export in early June 2018. Diatom fluxes at both DBO2 and DBO3 were much lower after mooring turnaround during June 2018, gradually shifting to diatom fluxes dominated by *Thalassiosira* spp. during summer 2018. At DBO4, low diatom fluxes during summer 2018 were mostly composed of *Fragilariopsis* spp., *Pseudo-nitzschia*/*Nitzschia* spp., *Cylindrotheca*

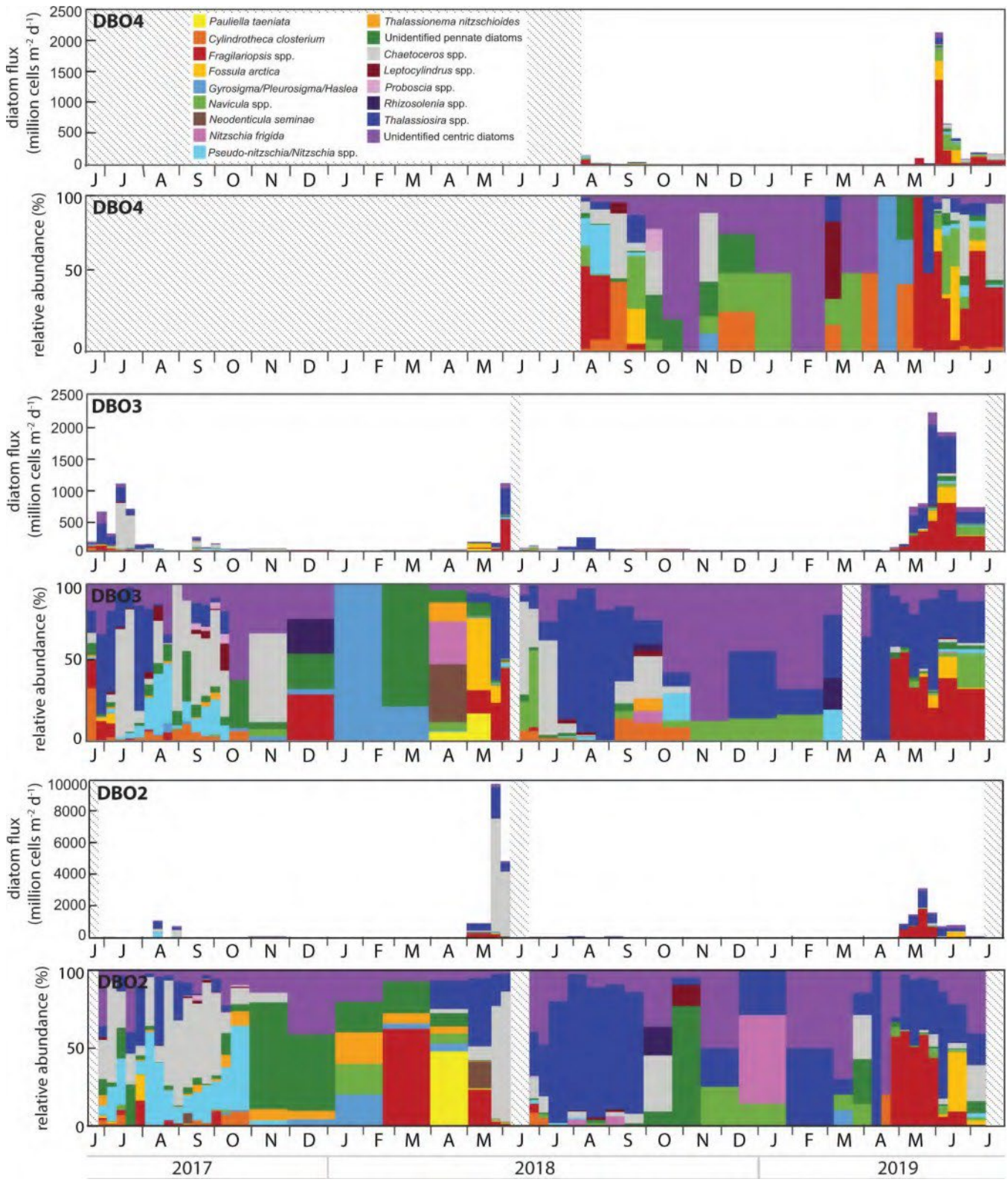

Fig 5. Diatom fluxes and relative abundance of the dominant diatom groups at each mooring site. Note the different scales. Shaded areas represent periods without data.

https://doi.org/10.1371/journal.pone.0255837.g005

closterium, and *Chaetoceros* spp. Diatom fluxes increased again during May 2019 at DBO2 and DBO3 and in early June 2019 at DBO4. The magnitude and composition of the fluxes during spring 2019 was very similar at the three DBO sites, with *Fragilariopsis* spp., *Thalassiosira* spp., *Fossula arctica*, *Navicula* spp., *Pseudo-nitzschia*/*Nitzschia* spp., and *Chaetoceros* spp. contributing to the elevated fluxes.

Zooplankton and meroplankton

Copepods, copepod nauplii, and meroplankton were the most numerous animals collected in the sediment traps, with the highest abundances observed during June or July at DBO2 and DBO3 and during late September at DBO4 (Figs 6–8). As morphological separation of all life stages of several dominant copepod species in the Pacific Arctic is difficult, most species were aggregated and reported at the generic level (e.g. *Calanus glacialis*, *C. marshallae*; *Neocalanus plumchrus*, *N. flemingeri*; *Pseudocalanus minutus*, *P. acuspes*, *P. mimus*, and *P. newmani*), with the exception of *N. cristatus* that is recognizable due to its large size compared to its congeners [28]. A distinct dominance of the Pacific copepods *Neocalanus* was observed at DBO2 and DBO3 from June to August 2017 (Fig 6). The composition of the copepod community shifted to a dominance of *Pseudocalanus* at all sites during spring and/or summer 2018, with varying abundances of *Metridia*, *Calanus*, and *Oncaea* among sites.

Whereas few nauplii of the genera *Calanus*, *Metridia*, and *Pseudocalanus* were collected during summer 2017, large numbers of them were collected during summer 2018 and 2019, especially at DBO3 (Fig 7). At DBO2 and DBO3, nauplii of all stages were often collected simultaneously from May to October, with a larger proportion of nauplii stages N1 and N2

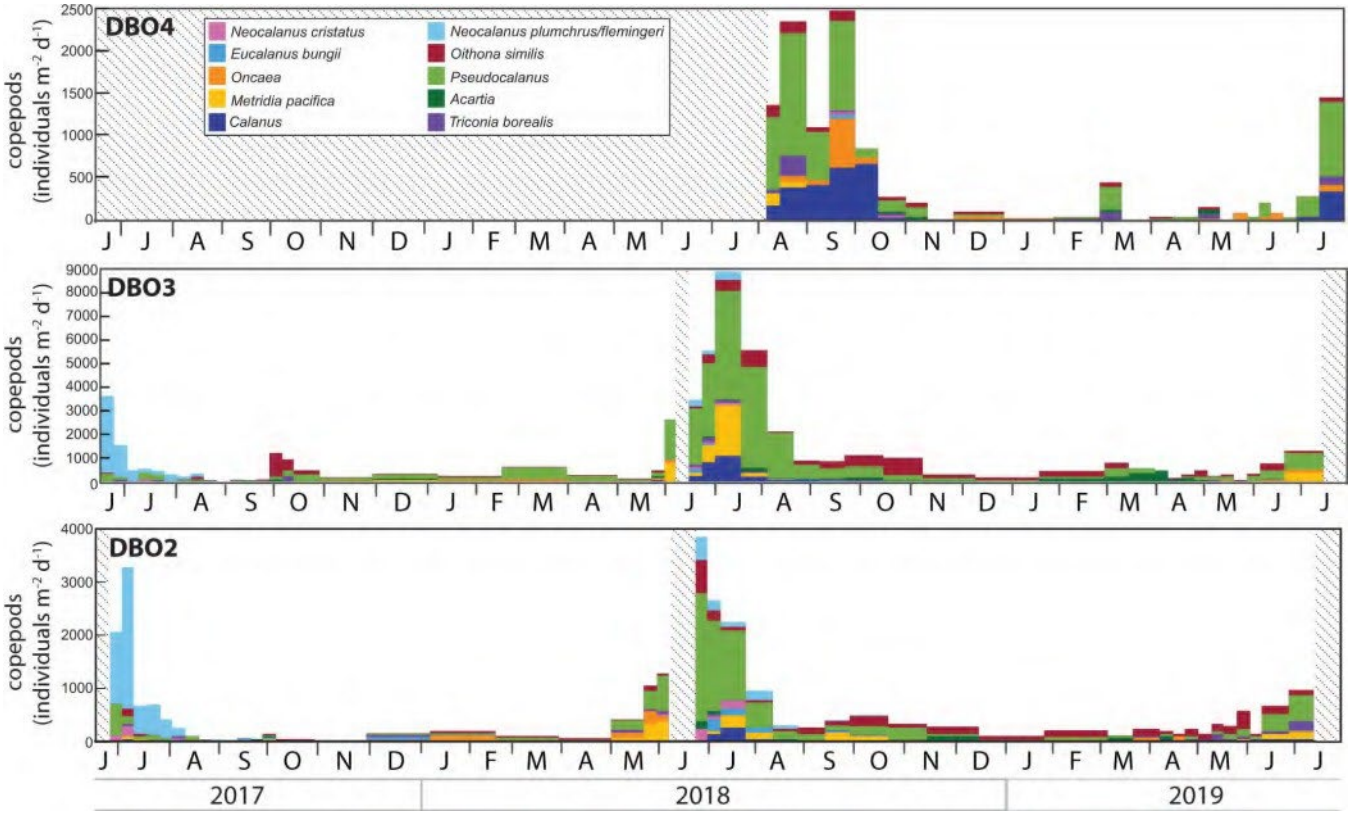

Fig 6. Dominant copepod groups collected in the sediment trap at each mooring site. Note the different scales. Shaded areas represent periods without data.

https://doi.org/10.1371/journal.pone.0255837.g006

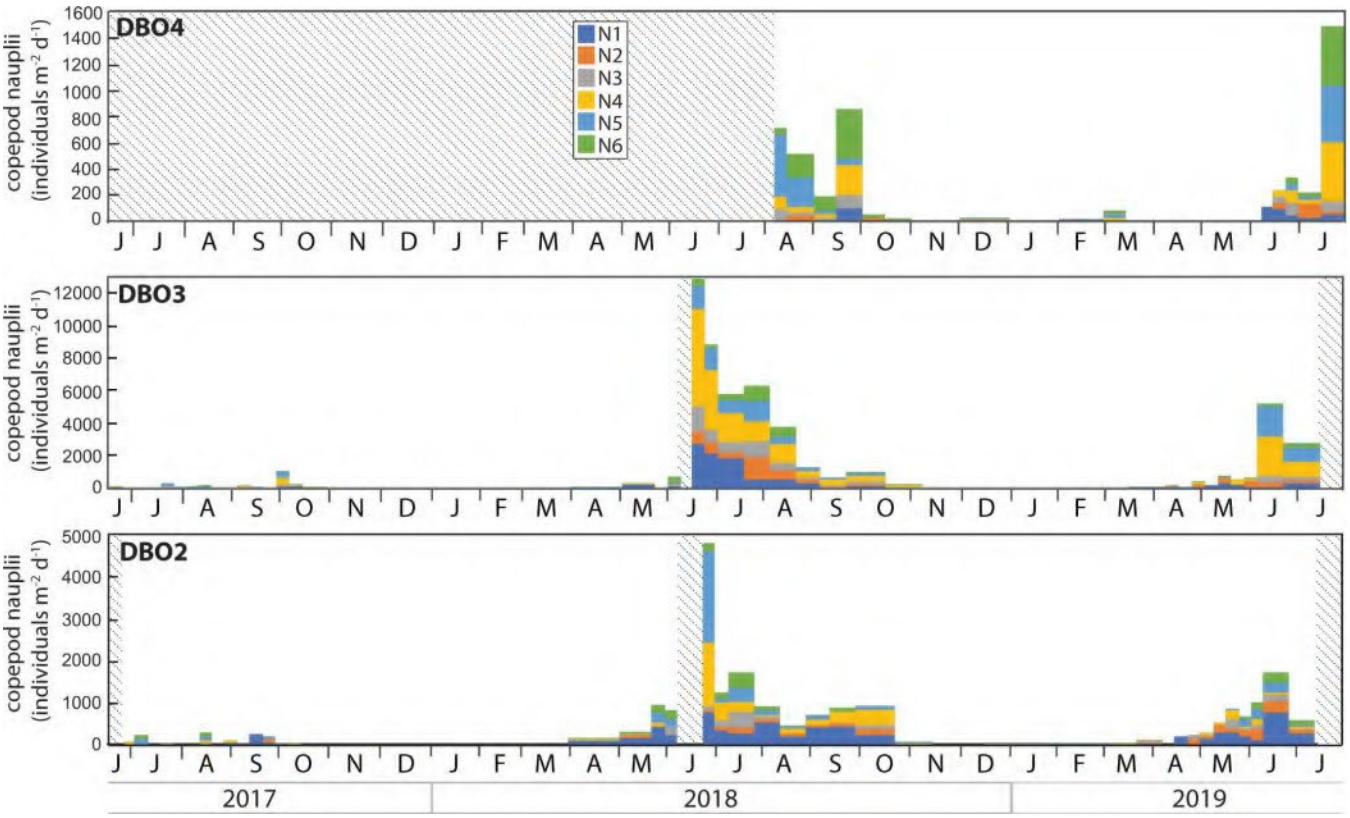

Fig 7. Nauplii of the copepod genus *Calanus*, *Metridia* and *Pseudocalanus* collected in the sediment trap at each mooring site. Note the different scales. Shaded areas represent periods without data.

https://doi.org/10.1371/journal.pone.0255837.g007

collected during April and May and peaks in nauplii abundance recorded in June. At DBO4, a large proportion of stages N5 and N6 was recorded during August and September 2018. Nauplii of all stages were again collected during June 2019 and peaked in abundance at the end of July 2019.

Meroplanktonic stages were dominated by polychaete larvae during summer 2017 at DBO2 and DBO3, while high abundances of bivalve veliger, polychaete larvae, and barnacle larvae blended from spring to autumn 2018 and during spring and early summer 2019 (Fig 8). At DBO4, barnacle larvae contributed to the vast majority of meroplankton collected from August to November 2018, but were absent during June and July 2019 when few bivalve veliger and polychaete larvae were collected.

Particulate organic carbon and total particulate matter fluxes

POC and TPM fluxes displayed similar temporal variations at DBO2 and DBO3 (Fig 9). At DBO2, POC and TPM fluxes increased simultaneously except during spring when TPM fluxes remained relatively low. At DBO3, the highest POC fluxes of the Pacific Arctic region (>2 g m^{-2} d^{-1}) were observed in early June 2018 and from May to July 2019, except for a week at the end of May 2019. At DBO4, peak POC (~1 g m^{-2} d^{-1}) and TPM fluxes (>50 g m^{-2} d^{-1}) were recorded during the second half of May 2019. High POC and TPM fluxes were also observed during autumn and winter at all sites, often in November and/or December. FPC fluxes contributed most to POC fluxes between June and November at all sites, and sporadically contributed to the complete POC flux between August and October 2017 at DBO3 (Fig 9).

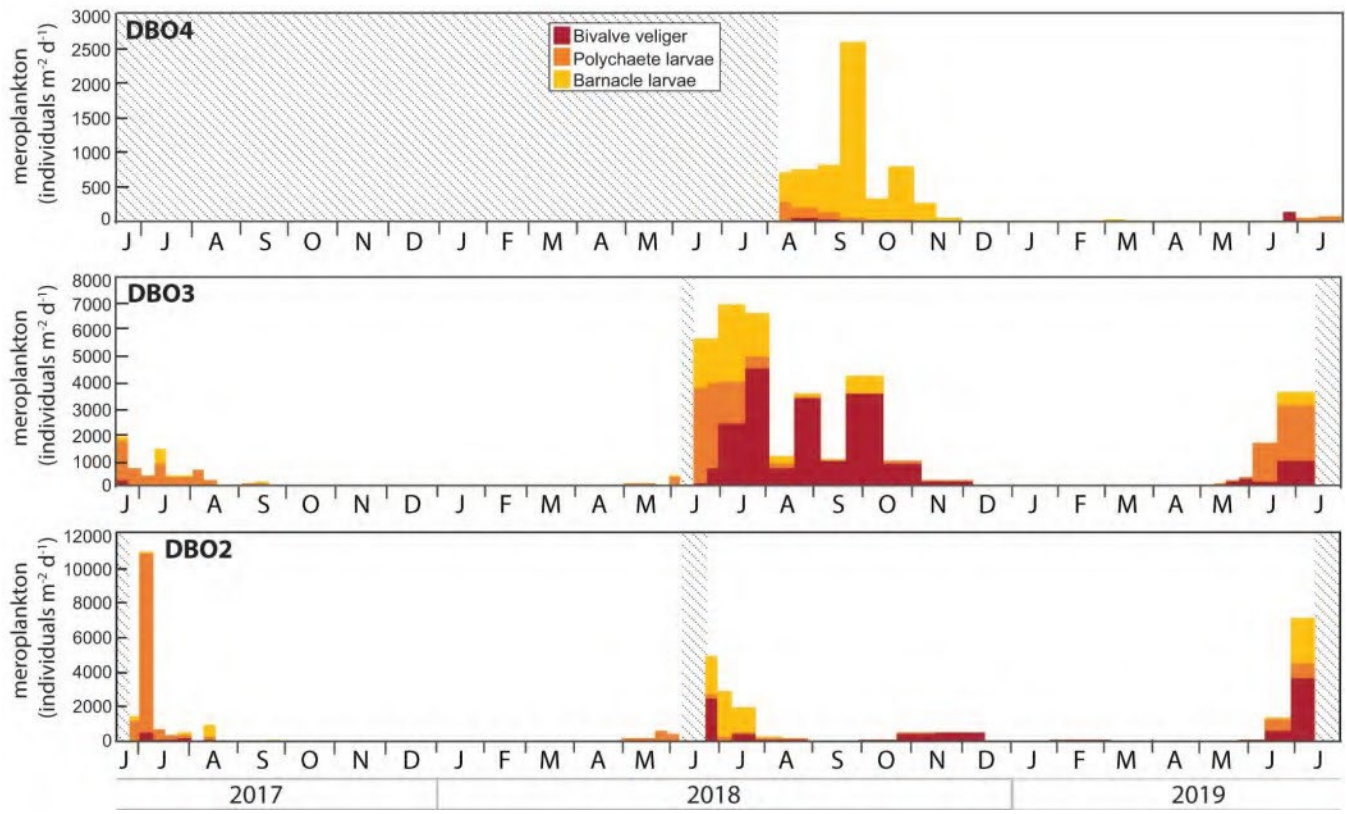

Fig 8. Meroplankton larvae collected in the sediment trap at each mooring site. Note the different scales. Shaded areas represent periods without data.

https://doi.org/10.1371/journal.pone.0255837.g008

Annual fluxes

Annual fluxes of TPM, POC, FPC, chl *a*, and diatoms all increased during the 2018–2019 cycle at DBO2 (Fig 10). Annual fluxes were also higher during the 2018–2019 cycle than during the 2017–2018 cycle at DBO3, except for a lower annual FPC flux. At DBO4, annual TPM, POC, and FPC fluxes obtained from August 2018 to July 2019 were higher than previously measured under extended sea ice cover at the same site from August 2015 to July 2016 [21], while annual chl *a* and diatom fluxes were lower during 2018–2019 than during 2015–2016 [21].

Discussion

A combination of downward export, lateral advection, and resuspension of particles contributed to the fluxes recorded at the three mooring sites of the shallow Pacific Arctic region. As typically observed on Arctic shelves [29, 30], TPM and POC fluxes were strongly correlated ($R^2 = 0.82$, $p<0.01$) at the DBO sites, with POC fluxes consistently contributing to <7% of the TPM fluxes. Whereas enhanced fluxes in April or May most likely resulted from the release of particulate matter from the melting ice [21], algal export contributed to the elevated POC fluxes during May and June. Diatoms usually dominate phytoplankton abundance and biomass in the northern Bering Sea and Chukchi Sea [31–34] and typically represent the most important component of algal fluxes across the Arctic Ocean due to their rapid sinking velocities [21, 30, 35, 36]. Diatoms also dominated algal export during spring at the three DBO sites, contributing to daily POC fluxes that were among the highest ever documented in the global oceans [19].

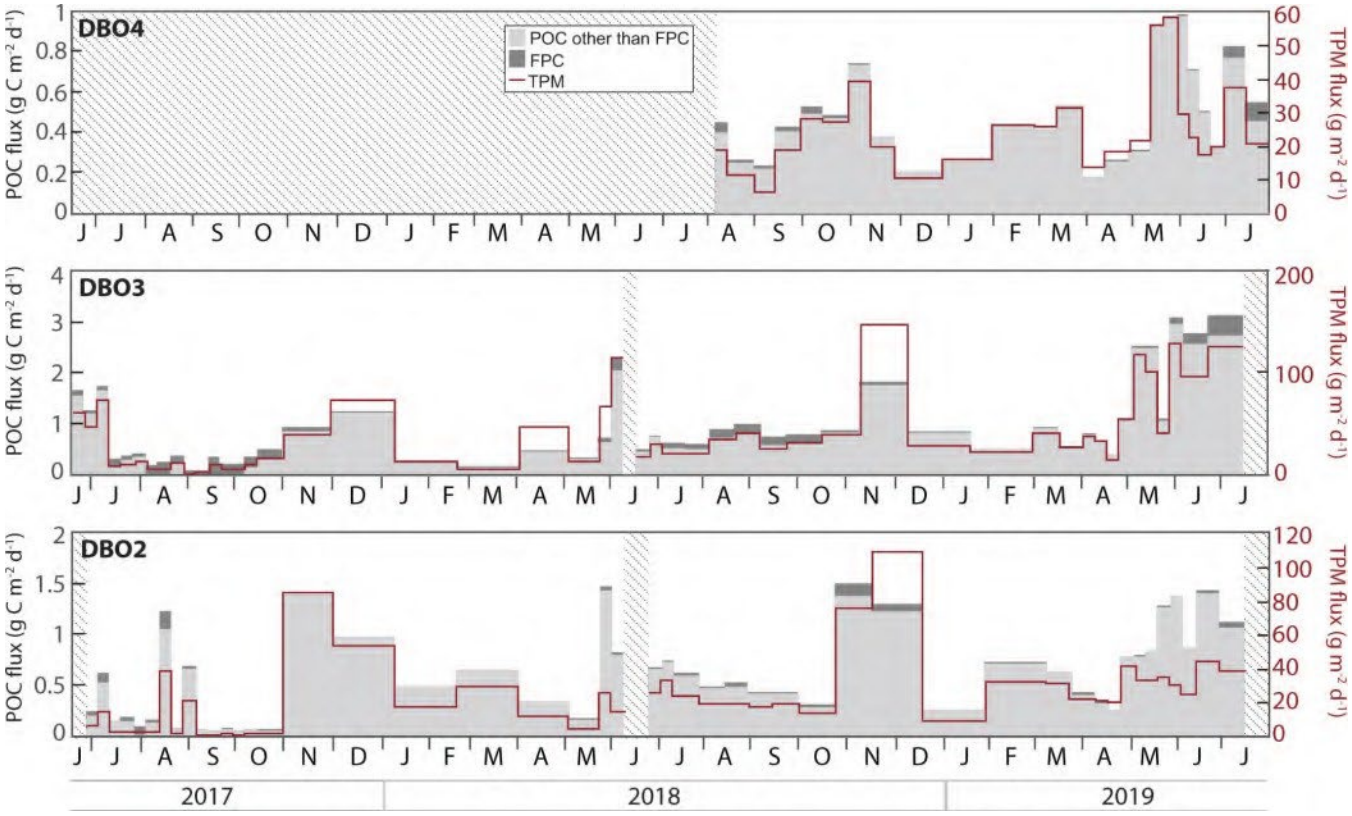

Fig 9. Particulate organic carbon (POC), fecal pellet carbon (FPC), and total particulate matter (TPM) fluxes at each mooring site. Note the different scales. Shaded areas represent periods without data.

https://doi.org/10.1371/journal.pone.0255837.g009

Zooplankton continuously collected at fixed depths indicated a strikingly similar composition of the dominant copepods at the three DBO sites, consistent with the large influence of advection on seasonal zooplankton dynamics in the Pacific Arctic [37, 38]. Copepod grazing certainly reduced diatom fluxes during summer, as supported by enhanced FPC fluxes. Similar to copepod and copepod nauplii abundances, benthic larvae abundance generally increased after the onset of the algal bloom, with large numbers of bivalve veliger, polychaete larvae, and barnacle larvae contributing to the grazing pressure on diatoms during summer and autumn. The lasting presence of planktonic larvae of benthic animals indicated productive conditions conducive to reproduction during several weeks at all sites. While copepod fecal pellets enhanced POC fluxes during summer and autumn, elevated TPM and POC fluxes during autumn and winter likely resulted from wind-induced resuspension and dispersion of sediments, as current speeds reached velocities >40 cm s^{-1} during autumn 2017 at DBO2 and DBO3 [19]. Short-lived increases in chl *a* concentrations, chl *a* fluxes, and diatom fluxes sporadically observed during late summer and autumn further support wind-induced resuspension and dispersion of sediments containing diatoms and chl *a* at the DBO sites. These observations are in agreement with enhanced near-bottom chl *a* concentrations observed during wind-induced high turbidity events during autumn near Bering Strait [39, 40], and with low fluxes of the sympagic diatom biomarker IP_{25} and of diatoms containing chloroplasts throughout the polar night on the northeast Chukchi shelf [21, 41]. In addition to reflecting the seasonal processes influencing the export of particulate matter in the region, the nearly continuous measurements obtained at a high temporal resolution from June 2017 to July 2019

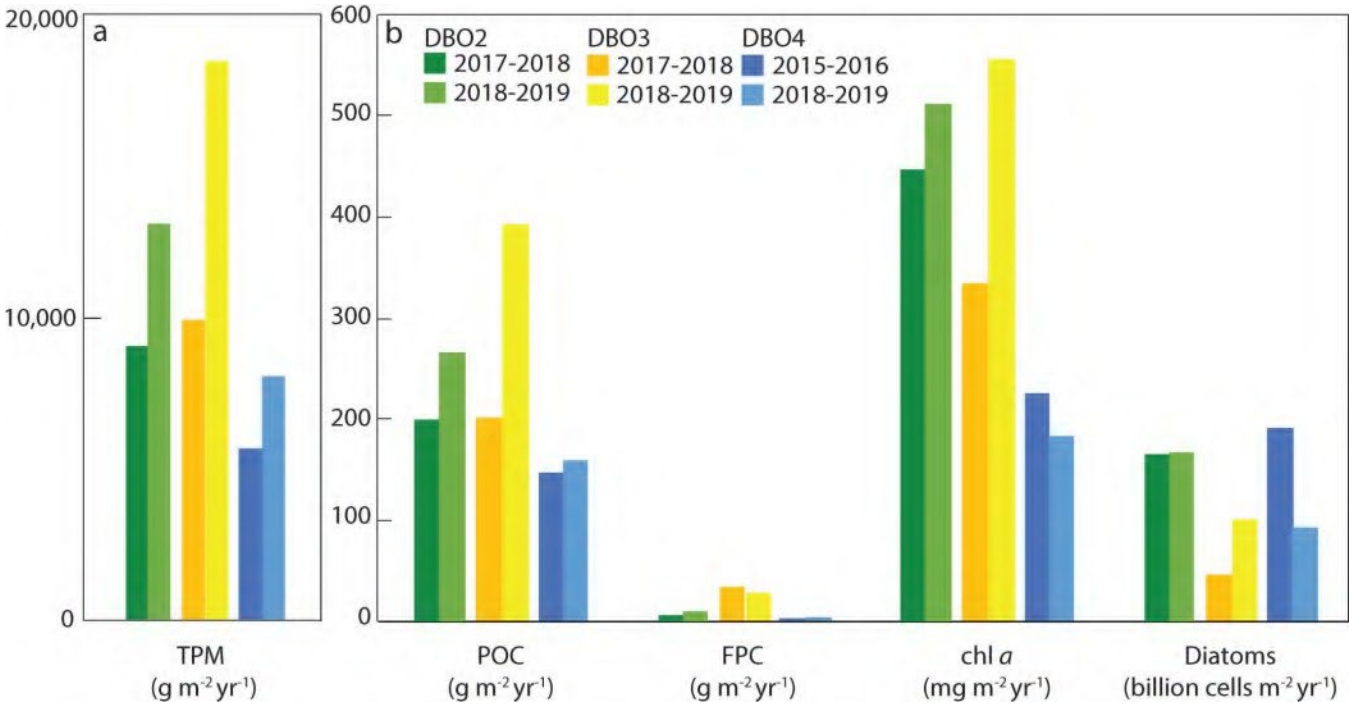

Fig 10. a) Annual total particulate matter (TPM) fluxes, and b) annual particulate organic carbon (POC), fecal pellet carbon (FPC), chlorophyll *a* (chl *a*), and living diatom fluxes at the three mooring sites in the Pacific Arctic region.

https://doi.org/10.1371/journal.pone.0255837.g010

were used to assess the impact of the enhanced transport of warmer Pacific waters and shorter ice-covered duration on the Pacific Arctic marine ecosystem.

June 2017—June 2018

An earlier onset of warming and later onset of cooling in recent years lengthened the warm (±0˚C) water duration to more than 6 months in the Pacific Arctic region [7]. In 2017, the warm period lasted over 7 months and mean June temperatures were 2˚C warmer than climatology when the sediment traps were deployed [7]. A spring bloom probably occurred prior to the onset of sampling at both sites, as indicated by elevated near-bottom chl *a* concentrations revealing the occurrence of a spring bloom during May 2017 at a nearby mooring site in the southern Chukchi Sea [17, 39]. However, relatively high diatom fluxes mostly composed of the exclusively pelagic diatoms *Chaetoceros* spp. and *Thalassiosira* spp. indicated that a pelagic bloom occurred in the DBO3 region during late June and July 2017. The subsequent frequent collection of the boreal diatoms *Proboscia* spp., cosmopolitan diatom *T*. *nitzschioides*, and endemic North Pacific diatom *Neodenticula seminae* [31, 33, 42, 43] during summer and autumn reflected the enhanced inflow of warm Pacific waters across Bering Strait during 2017.

Although zooplankton community composition and distribution have been shown to vary with water properties and the volume of Pacific water transported to the northern Bering Sea and Chukchi Sea [38, 44–47], the most abundant groups are generally found throughout the region and differences between communities often depend on the presence or absence of indicator species [4]. Accordingly, peaks in copepod abundance dominated by the Pacific copepods *Neocalanus* during late June and early July 2017 highlighted an enhanced transport of warm Pacific waters, in agreement with concurrent observations of high abundance of Pacific copepods associated to the inflow of Anadyr Water during June and July 2017 in the northern

Bering Sea [44]. The very low numbers of nauplii collected during 2017 reflected the low abundance of the three copepod groups for which nauplii were identified in the trap samples. In particular, the absence of *Calanus* copepodites and nauplii indicated their decline under warm conditions, as supported by the report of a remarkably low abundance of *Calanus* in the Pacific Arctic during 2017 [1]. The nearly exclusive presence of polychaete larvae during 2017 also suggested their transport with the enhanced inflow of Pacific waters.

Residual heat from the elevated summer water temperatures delayed sea ice formation to December 2017 at both sites [6]. At DBO2, this delay reduced the rejection of salty, cold, and dense brine that typically sinks to the bottom to form a cold water layer, thereby limiting the cooling of the water column during winter and contributing to significant heat input into the Arctic Ocean [13]. At DBO3, oceanic heat loss was sufficient to reduce water column temperature at the freezing point during winter. As oceanic heat flux through Bering Strait triggers the onset of ice melt in the shallow Pacific Arctic region [7], the enhanced heat input during winter presumably contributed to the early ice breakup observed at DBO2 during spring 2018. High chl *a* and diatom fluxes dominated by the exclusively pelagic diatoms *Chaetoceros* spp. and *Thalassiosira* spp. in late May clearly indicated the occurrence of a large open water bloom following the early sea ice breakup in the northern Bering Sea. While biofouling may explain the concurrent low chl *a* concentrations recorded at DBO2 at the end of May, high chl *a* and diatom fluxes at that time were in agreement with the peak near-bottom chl *a* concentrations recorded at a nearby mooring on May 20 2018 [17]. The early collection of low numbers of the ice-associated pennate diatoms *Fragilariopsis* spp., *F. arctica*, and *Navicula* spp. during the sea ice breakup period (sea ice concentration <50%) hinted at a limited ice algae production while ice still drifted in the region in April, inhibiting the seeding of the spring bloom [48] and likely contributing to the shift in the composition of the diatom fluxes. Peak diatom fluxes at the end of May 2018 occurred approximately seven weeks after sea ice breakup at DBO2, likely due to weaker stratification following the extremely low winter sea ice extent and concentration, as observed during July 2018 in the northern Bering Sea [18]. Hence, the early sea ice breakup inhibited the ice-edge bloom and resulted in a large open water bloom in the northern Bering Sea, similar to previous observations following early sea ice breakup in the southeastern Bering Sea [17, 49, 50]. At DBO3, the coincident sea ice breakup and export of ice-associated pennate diatoms in early May was followed approximately three weeks later by a peak in chl *a* and diatom fluxes composed of ice-associated and pelagic diatoms during early June, indicating that colder water temperatures, later sea ice melt, and stronger stratification led to an ice-edge bloom in the southern Chukchi Sea in contrast to the northern Bering Sea. The highest near-bottom chl *a* concentrations recorded in late May and early June 2018 at a nearby mooring in the DBO3 region [17] confirmed that most of the bloom occurred before mooring turnaround in 2018. In response to the enhanced diatom fluxes, the abundances of copepods, copepod nauplii, and polychaete larvae increased at both sites during May 2018.

June 2018—June 2019

Low chl *a* and diatom fluxes mostly composed of *Chaetoceros* spp. and *Thalassiosira* spp. when sampling was resumed during June 2018 at DBO2 and DBO3 indicated a declining pelagic bloom at both sites. From July to September, the centric diatoms *Thalassiosira* spp. dominated the low diatom fluxes, a sharp contrast with fluxes composed of pennate diatoms *Pseudo-nitzschia*/*Nitzschia* spp., *C. closterium*, *Fragilariopsis* spp., *F. arctica*, and centric diatoms *Chaetoceros* spp. collected during the previous summer. This shift in flux composition concurs with a lower abundance of *Chaetoceros* spp. observed during July 2018 than during July 2017 in the Bering Strait region [49]. The large proportion of *Thalassiosira* spp. in the low diatom fluxes

during July 2018 possibly reflected a rapid depletion of nutrients during the large open water bloom taking place in the northern Bering Sea weeks earlier.

Peaks in copepod abundance during late June at DBO2 and early July at DBO3 probably contributed to the low diatom fluxes observed in early summer through grazing pressure. Most of the copepods collected during June and July 2018 consisted of *Pseudocalanus* while the abundance of *Neocalanus* and *Calanus* remained relatively low at both sites. As *Pseudocalanus* copepods are approximately three times smaller than *Neocalanus* and *Calanus*, their dominance supports observations of a zooplankton community dominated by small copepods during 2018 [15]. While small copepods *Pseudocalanus*, *Acartia*, and *Oithona similis* often dominate copepod abundance, large *Calanus* copepods often dominate biomass in late summer in the southern Chukchi Sea [38]. As *C. glacialis* females exploit ice algae to fuel their maturation and egg production [51, 52], the abundance and biomass of *C. glacialis* usually increase under colder conditions in the Bering and Chukchi Seas [53, 54]. The dominance of small copepods in 2018 therefore resulted from a low abundance of *C. glacialis* under warmer conditions. The presence of the Pacific copepods *Neocalanus*, *Eucalanus bungii* and *Metridia pacifica* [32, 44–46] from June to October 2018 further illustrated the influence of warm Pacific waters.

At DBO4, low diatom fluxes composed of *Fragilariopsis* spp., *C. closterium*, *Pseudo-nitzschia/Nitzschia* spp., *Navicula* spp., *Thalassiosira* spp., and *Chaetoceros* spp. at the onset of sampling in August 2018 corresponded to the ice-associated and pelagic diatom groups reported to dominate phytoplankton biomass during summer in the northern Chukchi Sea [33, 55–59], albeit with variations in the relative contribution of each group. Despite the absence of measurements prior to August 2018, the distinct composition of diatoms commonly observed during summer near Hanna Shoal suggests that local algal production was not affected by the anomalous 2018 conditions observed south of Bering Strait. Previous diatom flux measurements at the DBO4 site showed very large fluxes of *C. closterium* from August to October 2015 during a period of strong winds with frequent direction reversals [21]. Similarly, a strong wind event in September 2013 at a nearby site in the Chukchi Sea induced sufficient vertical mixing to enhance phytoplankton productivity and led to high abundances of *C. closterium* and *Leptocylindrus danicus* [60, 61]. However, although high water temperatures recorded at depth during November 2018 indicated storm conditions mixing the water column at DBO4, *C. closterium* fluxes remained low during autumn 2018 when sunlight was sufficient to induce primary production in the region. Peaks in copepod abundance recorded during late August and late September 2018 at DBO4 were dominated by small *Pseudocalanus*, similar to DBO2 and DBO3. The dominance of small copepods in the northern Chukchi Sea also resulted from a low abundance of *C. glacialis* under warmer conditions, as confirmed by *Calanus* that were ~5 times more abundant at DBO4 during August 2015 than during August 2018 while the abundance of *Pseudocalanus* was similar during both years [21]. The collection of Pacific copepods *E. bungii* and *M. pacifica* during August and September further illustrated the transport of warm Pacific waters into the Chukchi Sea. Most meroplankton collected during summer and autumn 2018 consisted of barnacle larvae, in agreement with observations of barnacle larvae contributing to the largest meroplankton biomass from 2008 to 2010 in the northeastern Chukchi Sea [62].

Despite higher water temperatures during summer and autumn 2018, coinciding with record high surface seawater temperatures in the Pacific Arctic [20], water temperatures rapidly decreased and sea ice quickly formed in November at DBO4 and in early December at DBO2 and DBO3, leading to the prolonged presence of cold water at all sites during winter 2018–2019 and to a later sea ice breakup at DBO2 in 2019. Cells of the ice-associated diatoms *Fragilariopsis* spp. were first collected simultaneously to sea ice breakup at the end of April at DBO2 and DBO3 and during mid-May at DBO4, indicative of the latitudinal delay in sea ice

breakup. Peak diatom fluxes were consistently observed approximately three weeks after sea ice breakup, resulting in a 2-week delay between the diatom bloom in the northern Bering Sea (DBO2) and in the northern Chukchi Sea (DBO4). Regardless of the delay in the onset of the bloom, the composition of the diatom fluxes was strikingly similar at the three sites during 2019, with *Fragilariopsis* spp., *F. arctica*, *Navicula* spp., *Pseudo-nitzschia/Nitzschia* spp., *Thalassiosira* spp., and *Chaetoceros* spp. composing most of the fluxes. These observations indicate that algal production was likely back to normal in the northern Bering Sea.

Whereas Pacific copepods were not collected in 2019 despite the enhanced transport of Pacific waters observed until September 2019 across Bering Strait [7], the sustained inflow of warmer waters resulted in the near absence of *Calanus* at DBO2 and DBO3 during June and July 2019. While the majority of *Calanus* copepods present in the Chukchi Sea are believed to originate from the Bering Sea [38], their increasing abundance at DBO4 in July 2019 suggested an alternate source of *Calanus* on the northern Chukchi shelf during summer 2019 [63]. No clear peaks in copepod abundance were observed during June or July 2019, consistent with high seasonal and interannual variability in the Pacific Arctic region [62]. By contrast, peaks in nauplii abundance recorded during June 2018 and 2019 at DBO2 and DBO3 revealed a steady timing in copepod reproduction despite variations in the timing of sea ice breakup. Finally, the concurring absence of diatoms and copepods of Pacific origin at the DBO sites during 2019 suggested that less productive conditions further south may have limited their advection into the region that year.

Less ice led to generally lower annual export fluxes

A comparison of annual fluxes obtained for each deployment cycle highlights the large-scale impact of an early sea ice breakup on export in the Pacific Arctic region. In the northern Bering Sea, lower annual TPM, POC, chl *a*, and diatom fluxes during the June 2017-June 2018 cycle than during the June 2018-July 2019 cycle, despite the export of a large pelagic bloom at the end of May and early June 2018, indicated that elevated fluxes were sustained over a longer period when ice breakup occurred a few weeks later during 2019. It is reasonable to assume that annual fluxes would have been higher for the 2017–2018 cycle without the interruption in sampling during June 2018. However, it is unlikely that these annual fluxes would have been higher than during 2018–2019 as decreasing near-bottom chl *a* concentrations recorded at a close-by mooring indicated a declining bloom during June 2018 [17]. Lower annual chl *a* fluxes during 2017–2018 may have also partly arisen from the dominance of the generally small-sized *Chaetoceros* cells with lower chl *a* content during the 2018 spring bloom. The large abundance of copepodites and nauplii during summer 2018, together with the larger annual FPC flux during 2018–2019, suggest that the massive pelagic bloom enhanced secondary production and grazing pressure in the northern Bering Sea, supporting the hypothesis of a transition to a pelagic-dominated ecosystem under warmer conditions [64]. The dominance of small-sized diatoms and copepods under higher water temperatures and reduced ice cover in the northern Bering Sea concurs with observations in the Atlantic Arctic sector where a shift in the composition of the phytoplankton and zooplankton communities was observed during a period of anomalously warm Atlantic Water inflow and absence of sea ice cover in the eastern Fram Strait [65]. These observations therefore suggest a similar impact of warmer conditions on the Arctic marine ecosystems influenced by the inflow of Pacific and Atlantic waters. Lastly, lower annual TPM and POC fluxes during 2017–2018 along with similar autumn and winter peaks in daily TPM and POC fluxes during both cycles suggest that the intensity and frequency of resuspension events did not significantly increase during the period of unprecedented sea ice loss during 2017–2018 in the northern Bering Sea.

In the southern Chukchi Sea, annual fluxes were also lower during the 2017–2018 cycle than during the 2018–2019 cycle, except for a slightly higher annual FPC flux. The lower chl *a* and diatom fluxes collected at DBO3 during 2017–2018, despite sea ice breakup actually occurring later during 2018 than during 2019, highlighted the influence of advected waters from the northern Bering Sea. Indeed, a shorter period of lower diatom fluxes at DBO3 during May 2018 possibly resulted from a reduced inflow of nutrients into the southern Chukchi Sea following the massive pelagic bloom that occurred during the prior weeks in the northern Bering Sea. Whereas higher annual FPC flux during 2017–2018 may be the result of larger fecal pellets produced by larger copepods during summer 2017, the highest copepod abundance during summer 2018 also contributed to relatively high FPC fluxes at DBO3 during the 2018–2019 cycle, further supporting a transition to a pelagic-dominated ecosystem under warmer conditions [64]. Although annual TPM and POC fluxes were approximately half as high during the 2017–2018 cycle as during 2018–2019, mostly due to the enhanced daily TPM and POC fluxes sustained during the bloom period from May to July 2019, the high springtime POC fluxes recorded during both years when compared with POC fluxes from around the world [19] indicate a persistently strong biological pump in the region due to the highly productive and shallow nature of the shelves.

By contrast to the DBO2 site where sea ice conditions were heavier during 2018–2019 than during 2017–2018, sea ice breakup at the DBO4 site took place more than two months earlier during 2019 than when the same site was previously sampled during 2016 [21]. Considering that the day of sea ice breakup on the Chukchi shelf ranged from mid-May to mid-August between 2010 and 2017 [66], sea ice breakup occurred relatively early during mid-May 2019 at DBO4. This early sea ice breakup led to lower annual chl *a* and intact diatom fluxes during 2018–2019 than under longer lasting sea ice cover during 2015–2016 [21]. While Waga and Hirawake [67] reported an increasing occurrence of fall blooms using satellite remote-sensing data from 2003 to 2017 for the Chukchi Sea, the absence of large diatom fluxes during autumn 2018 in contrast to autumn 2015 partly explains the lower annual chl *a* and diatom fluxes recorded during 2018–2019. However, the lower annual chl *a* and diatom fluxes observed near Hanna Shoal also resulted from the short-lived and smaller peak in diatom fluxes recorded after sea ice melt during spring 2019, while elevated diatom fluxes were sustained during several weeks in the presence of ice cover during spring and summer 2016 [21]. Therefore, a loss of sea ice resulted in a shorter period of enhanced springtime diatom fluxes during 2019 at DBO4, similar to observations during spring 2018 at DBO2 and DBO3. By contrast, annual TPM and POC fluxes were higher during 2018–2019 than during 2015–2016 at DBO4 [21], principally due to high daily TPM and POC fluxes following sea ice melt during spring and summer 2019. Elevated TPM and POC fluxes at a time of lower chl *a* and diatom fluxes during summer 2019 suggest that enhanced resuspension under reduced ice cover likely contributed to these fluxes.

Conclusions

Overall, earlier sea ice breakup resulted in shorter periods of elevated chl *a* and diatom fluxes following sea ice melt at the three DBO sites on the shallow Pacific Arctic shelves. While POC fluxes represent diverse sources of particles, such as material released from the ice, resuspension events, and lateral advection, chl *a* and intact diatom fluxes more reliably reflect the impact of reduced sea ice conditions on the biological pump. Chl *a* and diatom fluxes obtained during the two-year sediment trap time-series therefore suggest that the recent loss of sea ice and ensuing weaker stratification reduced the strength of the biological pump in the Pacific Arctic region. In addition, the sustained transport of warm Pacific waters [7] led to the low

abundance or absence of *Calanus* copepods at the three DBO sites during the study period. The abundance of smaller *Pseudocalanus* copepods instead either increased or decreased FPC fluxes and the efficiency of the biological pump at the DBO sites, highlighting the need for additional export flux measurements to determine long-term trends. As warming of the Arctic and sub-Arctic continues, major ecosystem changes are expected to occur more frequently in the Pacific Arctic region [14]. In this context, sediment trap time-series provided valuable, nearly uninterrupted measurements of biological parameters at a high temporal resolution to complement the other repeated observations made as part of the DBO. Routine sediment trap deployments would help determine if the changes observed under enhanced transport of warmer Pacific waters and shorter ice-covered duration represent an anomalous period or a new normal for the Pacific Arctic marine ecosystem.

Acknowledgments

We would like to thank the Captain and crews of the R/V *Sikuliaq* and R/V *Ocean Starr*. We also thank Thibaud Dezutter, Gabrielle Nadaï, Marie Parenteau, Jade Paradis-Hautcoeur and Julien Claveau for their respective contribution to analyses. This is a contribution to the Arctic Shelf Growth, Advection, Respiration, and Deposition rates measurement (ASGARD) and the Chukchi Ecosystem Observatory (CEO) projects. This manuscript is NPRB Publication ArcticIERP-42.

Author Contributions

Conceptualization: Jacqueline M. Grebmeier, Seth L. Danielson.

Data curation: Catherine Lalande.

Formal analysis: Catherine Lalande, Seth L. Danielson.

Funding acquisition: Andrew M. P. McDonnell, Seth L. Danielson.

Investigation: Catherine Lalande, Stephanie O'Daly.

Methodology: Catherine Lalande.

Project administration: Catherine Lalande, Seth L. Danielson.

Resources: Catherine Lalande.

Visualization: Catherine Lalande.

Writing – original draft: Catherine Lalande.

Writing – review & editing: Catherine Lalande, Jacqueline M. Grebmeier, Andrew M. P. McDonnell, Russell R. Hopcroft, Stephanie O'Daly, Seth L. Danielson.

References

1. Huntington HP, Danielson SL, Wiese FK, Baker M, Boveng P, Citta JJ, et al. Evidence suggests potential transformation of the Pacific Arctic ecosystem is underway. Nature Climate Change. 2020; 10 (4):342–348.
2. Hunt GL, Drinkwater KF, Arrigo K, Berge J, Daly KL, Danielson S, et al. Advection in polar and subpolar environments: Impacts on high latitude marine ecosystems. Prog Oceanogr. 2016; 149:40–81.
3. Danielson SL, Eisner L, Ladd C, Mordy C, Sousa L, Weingartner TJ. A comparison between late summer 2012 and 2013 water masses, macronutrients, and phytoplankton standing crops in the northern Bering and Chukchi Seas. Deep-Sea Res Pt II. 2017; 135:7–26.
4. Ershova EA, Hopcroft RR, Kosobokova KN, Matsuno K, Nelson RJ, Yamaguchi A, et al. Long-term changes in summer zooplankton communities of the western Chukchi Sea, 1945–2012. Oceanography. 2015; 28(3):100–115.

5. Grebmeier JM, Overland JE, Moore SE, Farley EV, Carmack EC, Cooper LW, et al. A major ecosystem shift in the northern Bering Sea. Science. 2006; 311(5766):1461–1464. https://doi.org/10.1126/science.1121365 PMID: 16527980

6. Danielson SL, Ahkinga O, Ashjian C, Basyuk E, Cooper LW, Eisner L, et al. Manifestation and consequences of warming and altered heat fluxes over the Bering and Chukchi Sea continental shelves. Deep-Sea Res Pt II. 2020; 177:104781.

7. Woodgate RA, Peralta-Ferriz C. Warming and Freshening of the Pacific Inflow to the Arctic From 1990–2019 Implying Dramatic Shoaling in Pacific Winter Water Ventilation of the Arctic Water Column. Geophys Res Lett. 2021; 48(9):e2021GL092528.

8. Woodgate RA. Increases in the Pacific inflow to the Arctic from 1990 to 2015, and insights into seasonal trends and driving mechanisms from year-round Bering Strait mooring data. Prog Oceanogr. 2018; 160:124–154.

9. Baker MR, Farley EV, Ladd C, Danielson SL, Stafford KM, Huntington HP, et al. Integrated ecosystem research in the Pacific Arctic–understanding ecosystem processes, timing and change. Deep-Sea Res Pt II. 2020; 177:104850.

10. Baker MR, Kivva KK, Pisareva M, Watson J, Selivanova J. Shifts in the physical environment in the Pacific Arctic and implications for ecological timing and conditions. Deep-Sea Res Pt II. 2020;Special Issue I–Understanding ecosystem processes, timing, and changes in the Pacific Arctic.

11. Thoman RL, Bhatt US, Bieniek PA, Brettschneider BR, Brubaker M, Danielson SL, et al. The Record Low Bering Sea Ice Extent in 2018: Context, Impacts, and an Assessment of the Role of Anthropogenic Climate Change. Bulletin of the American Meteorological Society. 2020; 101(1): S53–S58.

12. Mordy CW, Bell S, Cokelet ED, Ladd C, Lebon G, Proctor P, et al. Seasonal and interannual variability of nitrate in the eastern Chukchi Sea: Transport and winter replenishment. Deep-Sea Res Pt II. 2020; 177:104807.

13. Stabeno PJ, Bell SW. Extreme Conditions in the Bering Sea (2017–2018): Record-Breaking Low Sea-Ice Extent. Geophys Res Lett. 2019; 46(15):8952–8959.

14. Hirawake T, Hunt GL. Impacts of unusually light sea-ice cover in winter 2017–2018 on the northern Bering Sea marine ecosystem–An introduction. Deep-Sea Res Pt II. 2020; 181–182:104908.

15. Siddon EC, Zador SG, Hunt GL. Ecological responses to climate perturbations and minimal sea ice in the northern Bering Sea. Deep-Sea Res Pt II. 2020; 181–182:104914.

16. Duffy-Anderson JT, Stabeno P, Andrews AG III, Cieciel K, Deary A, Farley E, et al. Responses of the Northern Bering Sea and Southeastern Bering Sea Pelagic Ecosystems Following Record-Breaking Low Winter Sea Ice. Geophys Res Lett. 2019; 46(16):9833–9842.

17. Kikuchi G, Abe H, Hirawake T, Sampei M. Distinctive spring phytoplankton bloom in the Bering Strait in 2018: A year of historically minimum sea ice extent. Deep-Sea Res Pt II. 2020; 181–182:104905.

18. Ueno H, Komatsu M, Ji Z, Dobashi R, Muramatsu M, Abe H, et al. Stratification in the northern Bering Sea in early summer of 2017 and 2018. Deep-Sea Res Pt II. 2020; 181–182:104820.

19. O'Daly SH, Danielson SL, Hardy SM, Hopcroft RR, Lalande C, Stockwell DA, et al. Extraordinary Carbon Fluxes on the Shallow Pacific Arctic Shelf During a Remarkably Warm and Low Sea Ice Period. Frontiers in Marine Science. 2020; 7(986).

20. Kodaira T, Waseda T, Nose T, Inoue J. Record high Pacific Arctic seawater temperatures and delayed sea ice advance in response to episodic atmospheric blocking. Scientific Reports. 2020; 10(1):20830. https://doi.org/10.1038/s41598-020-77488-y PMID: 33247199

21. Lalande C, Grebmeier JM, Hopcroft RR, Danielson SL. Annual cycle of export fluxes of biogenic matter near Hanna Shoal in the northeast Chukchi Sea. Deep-Sea Res Pt II. 2020:104730.

22. Danielson SL, Iken K, Hauri C, Hopcroft RR, McDonnell AMP, Winsor P, et al., editors. Collaborative approaches to multi-disciplinary monitoring of the Chukchi shelf marine ecosystem: Networks of networks for maintaining long-term Arctic observations. OCEANS 2017—Anchorage; 2017 18–21 Sept. 2017.

23. Hauri C, Danielson S, McDonnell AMP, Hopcroft RR, Winsor P, Shipton P, et al. From sea ice to seals: a moored marine ecosystem observatory in the Arctic. Ocean Sci. 2018; 14(6):1423–1433.

24. Gonzalez S, Horne J, Danielson SL. Multi-scale temporal variability in biological-physical associations in a high latitude marine ecosystem. Polar Biol. in press.

25. Welschmeyer NA. Fluorometric analysis of chlorophyll a in the presence of chlorophyll b and pheopigments. Limnol Oceanogr. 1994; 39(8):1985–1992.

26. Utermo¨hl vH. Neue Wege in der quantitativen Erfassung des Planktons (Mit besondere Beriicksichtigung des Ultraplanktons). Verh Int Verein Theor Angew Limnol 5, 567–595. 1931.

27. Gonza´lez HE, Gonzalez SR, Brummer G-JA. Short-term sedimentation pattern of zooplankton, faeces and microplankton at a permanent station in the Bjornafjorden (Norway) during April-May 1992. Mar Ecol Prog Ser. 1994; 105:31–45.

28. Hopcroft RR, Kosobokova KN, Pinchuk AI. Zooplankton community patterns in the Chukchi Sea during summer 2004. Deep-Sea Res Pt II. 2010; 57(1–2):27–39.

29. Lalande C, Forest A, Barber DG, Gratton Y, Fortier L. Variability in the annual cycle of vertical particulate organic carbon export on Arctic shelves: Contrasting the Laptev Sea, Northern Baffin Bay and the Beaufort Sea. Cont Shelf Res. 2009; 29(17):2157–2165.

30. Dezutter T, Lalande C, Darnis G, Fortier L. Seasonal and interannual variability of the Queen Maud Gulf ecosystem derived from sediment trap measurements. Limnol Oceanogr. 2021; 66(S1):S411–S426.

31. Zhuang Y, Jin H, Li H, Chen J, Lin L, Bai Y, et al. Pacific inflow control on phytoplankton community in the Eastern Chukchi Shelf during summer. Cont Shelf Res. 2016; 129:23–32.

32. Matsuno K, Ichinomiya M, Yamaguchi A, Imai I, Kikuchi T. Horizontal distribution of microprotist community structure in the western Arctic Ocean during late summer and early fall of 2010. Polar Biol. 2014; 37(8):1185–1195.

33. Wang Y, Kang J, Xiang P, Wang W, Lin M. Short timeframe changes of environmental impacts on summer phytoplankton in the Chukchi Sea and surrounding areas in a regional scaling. Ecological Indicators. 2020; 117:106693.

34. Sukhanova IN, Flint MV, Pautova LA, Stockwell DA, Grebmeier JM, Sergeeva VM. Phytoplankton of the western Arctic in the spring and summer of 2002: Structure and seasonal changes. Deep-Sea Res Pt II. 2009; 56(17):1223–1236.

35. Nadaï G, No¨thig E-M, Fortier L, Lalande C. Early snowmelt and sea ice breakup enhance algal export in the Beaufort Sea. Prog Oceanogr. 2021; 190:102479.

36. Lalande C, No¨thig E-M, Fortier L. Algal Export in the Arctic Ocean in Times of Global Warming. Geophys Res Lett. 2019; 46(11):5959–5967.

37. Kitamura M, Amakasu K, Kikuchi T, Nishino S. Seasonal dynamics of zooplankton in the southern Chukchi Sea revealed from acoustic backscattering strength. Cont Shelf Res. 2017; 133:47–58.

38. Ershova EA, Hopcroft RR, Kosobokova KN. Inter-annual variability of summer mesozooplankton communities of the western Chukchi Sea: 2004–2012. Polar Biol. 2015; 38(9):1461–1481.

39. Abe H, Sampei M, Hirawake T, Waga H, Nishino S, Ooki A. Sediment-Associated Phytoplankton Release From the Seafloor in Response to Wind-Induced Barotropic Currents in the Bering Strait. Frontiers in Marine Science. 2019; 6(97).

40. Nishino S, Kikuchi T, Fujiwara A, Hirawake T, Aoyama M. Water mass characteristics and their temporal changes in a biological hotspot in the southern Chukchi Sea. Biogeosciences. 2016; 13(8):2563–2578.

41. Koch CW, Cooper LW, Lalande C, Brown TA, Frey KE, Grebmeier JM. Seasonal and latitudinal variations in sea ice algae deposition in the Northern Bering and Chukchi Seas determined by algal biomarkers. PLOS ONE. 2020; 15(4):e0231178. https://doi.org/10.1371/journal.pone.0231178 PMID: 32320403

42. Ren J, Chen J, Bai Y, Sicre M-A, Yao Z, Lin L, et al. Diatom composition and fluxes over the Northwind Ridge, western Arctic Ocean: Impacts of marine surface circulation and sea ice distribution. Prog Oceanogr. 2020; 186:102377.

43. Sukhanova IN, Flint MV, Whitledge TE, Stockwell DA, Rho TK. Mass development of the planktonic diatom Proboscia alata over the bering sea shelf in the summer season. Oceanology. 2006; 46(2):200–216.

44. Kimura F, Abe Y, Matsuno K, Hopcroft RR, Yamaguchi A. Seasonal changes in the zooplankton community and population structure in the northern Bering Sea from June to September, 2017. Deep-Sea Res Pt II. 2020; 181–182:104901.

45. Pinchuk AI, Eisner LB. Spatial heterogeneity in zooplankton summer distribution in the eastern Chukchi Sea in 2012–2013 as a result of large-scale interactions of water masses. Deep-Sea Res Pt II. 2017; 135:27–39.

46. Kim J-H, Cho K-H, La HS, Choy EJ, Matsuno K, Kang S-H, et al. Mass Occurrence of Pacific Copepods in the Southern Chukchi Sea During Summer: Implications of the High-Temperature Bering Summer Water. Frontiers in Marine Science. 2020; 7(612).

47. Abe Y, Matsuno K, Fujiwara A, Yamaguchi A. Review of spatial and inter-annual changes in the zooplankton community structure in the western Arctic Ocean during summers of 2008–2017. Prog Oceanogr. 2020; 186:102391.

48. Szymanski A, Gradinger R. The diversity, abundance and fate of ice algae and phytoplankton in the Bering Sea. Polar Biol. 2016; 39(2):309–325.

49. Fukai Y, Abe Y, Matsuno K, Yamaguchi A. Spatial changes in the summer diatom community of the northern Bering Sea in 2017 and 2018. Deep-Sea Res Pt II. 2020; 181–182:104903.

50. Hunt GLJ, Stabeno P, Walters G, Sinclair E, Brodeur RD, Napp JM, et al. Climate change and control of the southeastern Bering Sea pelagic ecosystem. Deep-Sea Res Pt II. 2002; 49(26):5821–5853.

51. Daase M, Falk-Petersen S, Varpe Ø, Darnis G, Søreide JE, Wold A, et al. Timing of reproductive events in the marine copepod Calanus glacialis: a pan-Arctic perspective. Can J Fish Aquat Sci. 2013; 70 (6):871–884.

52. Søreide JE, Leu EVA, Berge J, Graeve M, Falk-Petersen S. Timing of blooms, algal food quality and *Calanus glacialis* reproduction and growth in a changing Arctic. Glob Change Biol. 2010; 16(11):3154–3163.

53. Spear A, Napp J, Ferm N, Kimmel D. Advection and in situ processes as drivers of change for the abundance of large zooplankton taxa in the Chukchi Sea. Deep-Sea Res Pt II. 2020:104814.

54. Eisner LB, Napp JM, Mier KL, Pinchuk AI, Andrews AG. Climate-mediated changes in zooplankton community structure for the eastern Bering Sea. Deep-Sea Res Pt II. 2014; 109:157–171.

55. Booth BC, Horner RA. Microalgae on the arctic ocean section, 1994: species abundance and biomass. Deep-Sea Res Pt II. 1997; 44(8):1607–1622.

56. Coupel P, Jin HY, Joo M, Horner R, Bouvet HA, Sicre MA, et al. Phytoplankton distribution in unusually low sea ice cover over the Pacific Arctic. Biogeosciences. 2012; 9(11):4835–4850.

57. Wang Y, Xiang P, Kang J-h, Ye Y-y, Lin G-m, Yang Q-l, et al. Microphytoplankton community structure in the western Arctic Ocean: surface layer variability of geographic and temporal considerations in summer. Hydrobiologia. 2018; 811(1):295–312.

58. Arrigo KR, Perovich DK, Pickart RS, Brown ZW, van Dijken GL, Lowry KE, et al. Massive Phytoplankton Blooms Under Arctic Sea Ice. Science. 2012; 336(6087):1408–1408. https://doi.org/10.1126/science.1215065 PMID: 22678359

59. Lee Y, Min J-O, Yang EJ, Cho K-H, Jung J, Park J, et al. Influence of sea ice concentration on phytoplankton community structure in the Chukchi and East Siberian Seas, Pacific Arctic Ocean. Deep-Sea Res Pt I. 2019; 147:54–64.

60. Yokoi N, Matsuno K, Ichinomiya M, Yamaguchi A, Nishino S, Onodera J, et al. Short-term changes in a microplankton community in the Chukchi Sea during autumn: consequences of a strong wind event. Biogeosciences. 2016; 13(4):913–923.

61. Nishino S, Kawaguchi Y, Inoue J, Hirawake T, Fujiwara A, Futsuki R, et al. Nutrient supply and biological response to wind-induced mixing, inertial motion, internal waves, and currents in the northern Chukchi Sea. J Geophys Res-Oceans. 2015; 120(3):1975–1992.

62. Questel JM, Clarke C, Hopcroft RR. Seasonal and interannual variation in the planktonic communities of the northeastern Chukchi Sea during the summer and early fall. Cont Shelf Res. 2013; 67:23–41.

63. Elliott SM, Ashjian CJ, Feng Z, Jones B, Chen C, Zhang Y. Physical control of the distributions of a key Arctic copepod in the Northeast Chukchi Sea. Deep-Sea Res Pt II. 2017; 144:37–51.

64. Grebmeier JM. Shifting Patterns of Life in the Pacific Arctic and Sub-Arctic Seas. Annual Review of Marine Science. 2012; 4(1):63–78. https://doi.org/10.1146/annurev-marine-120710-100926 PMID: 22457969

65. Lalande C, Bauerfeind E, No¨thig E-M, Beszczynska-Mo¨ller A. Impact of a warm anomaly on export fluxes of biogenic matter in the eastern Fram Strait. Prog Oceanogr. 2013; 109:70–77.

66. Stabeno PJ, Mordy CW, Sigler MF. Seasonal patterns of near-bottom chlorophyll fluorescence in the eastern Chukchi Sea: 2010–2019. Deep-Sea Res Pt II. 2020; 177:104842.

67. Waga H, Hirawake T. Changing Occurrences of Fall Blooms Associated With Variations in Phytoplankton Size Structure in the Pacific Arctic. Frontiers in Marine Science. 2020; 7(209).

Linking polychaete functional traits and benthic ecosystem function to habitat characteristics on a shallow Arctic shelf[1]

Brittany R. Charrier[a*] and Sarah L. Mincks[a]

[a]College of Fisheries and Ocean Sciences, University of Alaska Fairbanks, AK 99775, USA
[*]Corresponding author: brjones8@alaska.edu

Abstract

In a rapidly changing Arctic, benthic functional traits remain understudied, and baseline metrics of benthic ecosystem function are lacking. Polychaetes are often numerically dominant within the macrofauna and serve essential roles in benthic ecosystem function, such as impacts of sediment oxygenation, organic matter burial, and remineralization within sediments. Macrofauna were collected from 12 stations in June 2017 and 11 stations in June 2018 from the northern Bering and southern Chukchi Sea continental shelves as part of the Arctic Shelf Growth, Advection, Respiration, and Deposition (ASGARD) project. Polychaetes were identified to family level and assigned a functional guild based on feeding mode, motility, and feeding structures. Four clusters of polychaete functional guilds were identified, and a conceptual model was developed to link habitat characteristics to ecosystem function. Sandy stations had a relatively high abundance of selective-feeding, tube-dwelling suspension and surface deposit feeders, reflecting the advective system with rapid current speeds and low deposition. The abundance of tube-dwellers likely results in increased oxygenation of the sediment. The second group of stations displayed characteristics that suggest impacts of fluctuations between high deposition of organic matter and disturbance from scouring. A third group of muddy, offshore Chukchi Sea stations contained large bivalves and large carnivorous polychaetes, promoting high bioturbation rates. The macrofauna at the coastal Chukchi Sea stations in the fourth group were concentrated in the surface layer, and with little bioturbation, anaerobic microbial remineralization of organic matter likely dominates. Overall, polychaete functional composition and vertical distribution reflected the quality and quantity of organic matter input and the depositional environment inferred from grain size, with subsequent impacts on biogeochemical and carbon cycling within the sediment.

Keywords: macrofauna, polychaetes, functional traits, ecosystem function, Pacific Arctic

[1] Charrier, B.R., and S.L. Mincks. Linking polychaete functional traits and benthic ecosystem function to habitat characteristics on a shallow Arctic shelf. *In preparation*.

Introduction

The benthos accounts for a substantial portion of total production in the Pacific Arctic (Walsh et al., 1989). Ecologically important hotspots of high benthic biomass (Grebmeier et al., 2015) serve as critical feeding grounds for marine mammals (Fay, 1982) and birds (Lovvorn et al., 2003). However, the Pacific Arctic is undergoing rapid environmental change (Huntington et al., 2020), with unprecedented environmental conditions in 2017 and 2018 (Baker et al., 2020; Grebmeier et al., 2018). Record low sea ice persistence coincided with low concentrations of ice algae biomarkers in the sediment and high concentrations of pelagic biomarkers (Koch et al., 2020). Emerging evidence also indicates that environmental change has influenced the distribution of macrofaunal biomass (Goethel et al., 2019; Moore et al., 2018) and caused shifts in community structure and composition (Grebmeier, 2012; Waga et al., 2020), likely impacting benthic organic matter consumption and carbon demand (Jones et al., 2021).

Given the rapid environmental change occurring in the Pacific Arctic, it is critical to characterize current benthic ecosystem function to monitor and assess future change. Ecosystem models can be used to predict the impacts of environmental change on ecosystem structure and function (e.g., Lovvorn et al., 2016; Whitehouse et al., 2014) and to inform adaptive ecosystem management and policy decisions. Well-constrained ecosystem models for this region should include quantitative descriptions of spatial patterns in macrofaunal abundance and biomass (Grebmeier et al., 2015) but also functional characteristics of the benthic community (Liu et al., 2019; Sutton et al., 2020). The vertical distribution of macrofauna within the sediment is also critical in understanding biogeochemical, nutrient, and carbon cycling within the benthos (Deng et al., 2020). However, the benthos is often oversimplified in ecosystem models due to a lack of available information, aggregated as the whole benthos or higher taxonomic levels that do not account for differences in functional roles among taxa within these major groups (Whitehouse et al., 2014). For instance, in a Bering Sea modeling study, polychaetes were categorized as deposit-feeders or carnivores (Lovvorn et al., 2016). Yet, the burrowing activities of surface and subsurface deposit feeders have different impacts on important ecosystem functions such as sediment stabilization, oxygenation, organic matter burial, and remineralization in sediments (Aller, 1982; Jumars and Nowell, 1984; Lopez and Levinton, 1987; Rhoads, 1974). Additionally, various types of deposit feeders consume different quality and freshness of organic material (Josefson et al., 2002). For example, tentacle feeders generally select high-quality particles, while non-selective deposit feeders feed on lower quality, diffuse food sources. Consequently, carbon cycling in an area dominated by selective surface feeders will be different from an area dominated by non-selective subsurface deposit feeders.

While taxonomic composition of benthic communities is of interest in understanding biogeographic patterns and drivers of community structure, functional trait analysis elucidates the roles of communities in ecosystem processes. Biological traits can describe ecosystem functions (Degen et al., 2018), such as the ability to avoid disturbance (Hinchey et al., 2006), bioturbation (Mermillod-Blondin et al., 2004), and organic matter and nutrient cycling (Norling et al., 2007). Additionally, taxonomic diversity does not necessarily equate to functional diversity (Snelgrove, 1998). While communities may differ in taxonomic composition, they can share common functional traits, which has been shown in other Arctic benthic communities (Rand et al., 2018; Sutton et al., 2020). Different species often perform similar functions, and the loss of one species can be compensated for by an increase in the abundance of other species that perform similar ecological roles (Bremner et al., 2006; Snelgrove, 1998).

Sediment substrate type, sediment transport, and water depth are critical structuring forces of macrobenthic functional traits in Arctic systems (Liu et al., 2019; Włodarska-Kowalczuk et al., 2012). While taxonomic and functional diversity may follow similar large-scale spatial patterns, functional analyses in the Arctic have revealed additional patterns in the partitioning of ecological niche space and improved understanding of how disturbance may cause ecosystem shifts (Kokarev et al., 2017; Liu et al., 2019; Sutton et al., 2020). Variation in community structure of macrofauna has also been directly linked to differences in ecosystem function in Arctic sediments (e.g., Link et al., 2013; McTigue et al., 2016). Studies have also shown low functional redundancy in some Arctic shelf systems, implying vulnerability to a changing climate (Kokarev et al., 2017; Liu et al., 2019).

Polychaetes are often numerically dominant in the macrofauna (Gontikaki et al., 2011; Gunton et al., 2015) and serve essential roles in the benthic ecosystem (reviewed by Hutchings, 1998). The feeding and bioturbation activities of polychaetes have critical effects on carbon and biogeochemical cycling, such as oxygenation of sediment, reworking of organic material, and alteration of habitat for other infaunal or microbial communities (Aller, 1994; Hutchings, 1998; Pinto and Austen, 2006). Functional trait databases of polychaete families have been established based on morphology and taxonomy (Jumars et al., 2015), making polychaetes an ideal taxonomic group for functional trait analyses. The overall objective of this study was to characterize spatial patterns in macrofaunal communities across the northern Bering and southern Chukchi Sea shelves, with an emphasis on polychaete functional traits. Based on the distribution of polychaete functional guilds, we identified four distinct assemblages in different locations. We present an overview of the major patterns in macrofaunal community structure among these areas and describe differences in functional composition of polychaete assemblages that may influence ecosystem processes. We also examine relationships between polychaete functional traits and environmental characteristics, which may be used to extrapolate functional information to broader areas with similar environmental conditions.

Methods

Study area and sampling

Macrofaunal samples were collected from the northern Bering and southern Chukchi Seas in June 2017 and 2018 from the *R/V Sikuliaq* as part of the Arctic Shelf Growth, Advection, Respiration, and Deposition (ASGARD) project (Table 1; Figure 1). Some sampling locations correspond to long-term monitoring stations in the Distributed Biological Observatory (DBO) regions 2 and 3, also known as the Chirikov and SECS hotspots, respectively (Grebmeier et al., 2015, 2010). The northern Bering and southern Chukchi Sea continental shelves are shallow, seasonally ice-covered, and highly productive. The shelves are characterized by the net northward movement of cold, nutrient-rich Anadyr-Bering Sea Water in the west and warm, more nutrient-poor Alaska Coastal Water in the east (Danielson et al., 2017). Currents accelerate as flow is constricted through Bering Strait (Danielson et al., 2014), promoting water column mixing that locally enhances pelagic primary productivity (Walsh et al., 1989). Downstream of this constriction, the water column fans out over the wide and shallow Chukchi shelf, resulting in the decline of the current speed and allowing suspended particulate material to settle to the seafloor (Grebmeier et al., 2015).

Intact sediment cores were retrieved from 12 stations in 2017 and 11 stations in 2018 using an MC-800 multi-corer with 10-cm diameter tubes (Ocean Instruments, San Diego). Nine stations were sampled in both years (Table 1). Sampling stations ranged from 32 to 59 m in water depth.

The average near-bottom water temperature was 2.02 ± 1.35 °C (ranging from -1.2 to 3.96 °C) in 2017 and 1.15 ± 0.88 °C (ranging from -0.6 to 2.4 °C) in 2018, measured from CTD deployments (Table 1). Given the interdisciplinary nature of the field sampling program, weather constraints, and limits on wire time, statistical replicates for macrofaunal community structure analysis were not collected at all stations. For most stations, at least two intact cores from different multi-core deployments (i.e., sampling replicates) were sectioned into 0-1 cm, 1-5 cm, and 5-10 cm depth intervals and sampled for macrofauna. At some stations, multiple cores were processed from the same deployment (i.e., sampling pseudo-replicates). These pseudo-replicates were averaged into a single mean value for that deployment before combining with other true sampling replicates to calculate a station average. Pseudo-replicates were included to better constrain sampling error, given that the area sampled by a single multi-core tube is relatively small (78.5 cm^2). In 2017, a single core was retrieved at stations CPL8 and DBO2.3. Additional sampling coverage was achieved by including cores used for other purposes, including grain-size analysis and shipboard oxygen-flux incubations. Due to the differences in depth strata sampled in these additional cores, broad-scale spatial patterns in community structure were analyzed using data summed across the upper 10 cm of sediment. We also present more detailed results on the depth distribution of infauna for cores with 0-1, 1-5, and 5-10 cm sections. All cores used for macrofaunal analyses were gently washed over 500-µm mesh using filtered seawater and preserved in 10% buffered formalin.

Macrofauna and polychaetes

Preserved macrofaunal samples were stained with Rose Bengal and transferred to 70% isopropanol for sorting. Macrofauna were generally identified to phylum, class, or order level, counted, and wet mass was determined to 0.1 mg. Polychaetes were identified to family. Higher-level taxonomy was sufficient to meet ASGARD objectives of quantifying total abundance and biomass and examining functional roles of dominant species, which can be assessed based on family-level taxonomy in polychaetes (Jumars et al., 2015).

Polychaete taxa were classified into functional guilds based on feeding mode (microphage, macrophage/carnivore, or omnivore), motility (motile or discretely motile), and feeding structures (tentacles or palps, non-muscular eversible pharynx, or muscular eversible pharynx), according to Jumars et al. (2015; Table 2). Microphage feeders were further classified as suspension-, surface deposit-, or subsurface deposit-feeders. Motility was further distinguished by tube-dwelling, burrowing, crawling, or swimming behaviors. Polychaetes are considered motile if they exhibit burrowing, crawling, or swimming behavior. Discretely motile polychaetes are individuals that actively construct burrows or are tube-dwelling and can rebuild, extend, or move their tubes. Polychaete families can display multiple traits within individual taxa, so only the most common trait or traits were selected (Table 2).

Environmental parameters

Individual multi-core tubes were taken from the same deployments as the macrofaunal cores and allocated for analyses of sediment environmental parameters. One core from each station was allocated for grain-size analysis. Sediment was collected by inserting a 60-cc plastic syringe (6-cm diameter) with the tip cut off into the core surface to a depth of 5 cm. Samples were frozen in Whirl-Pak bags at -20°C until analyzed. Grain size was determined through a combination of wet and dry sieving. Sediment was thawed and homogenized by kneading the bag. To break up sediment aggregates, 20 mL of 2 g L^{-1} sodium hexametaphosphate and 30 mL of reverse osmosis water were added to 30 to 40 g of sediment and stirred for three minutes. The sample was wet

sieved through stainless steel 2-mm and 63-µm sieves. The material retained on each sieve and the <63-µm fraction (silt/clay) was collected into separate glass beakers and dried at 90°C until a constant mass was achieved. The material retained on the 63-µm sieve was then dry sieved through a set of brass stacked sieves on a shaker for 10 min (#18, 35, 60, 120, and 230 mesh sizes). Material retained on each sieve was weighed. The silt/clay fraction was weighed, rehydrated with reverse osmosis water, and 30% hydrogen peroxide (H_2O_2) was added to the sample until effervescence ceased to remove the organics. The beaker was held at 70°C on a block heater for one hour to decompose the H_2O_2 and then stirred for three minutes. The material was dried at 90°C until a constant mass was achieved. Mean phi and sorting coefficient were calculated using the Grain Size Distribution and Statistics (GRADISTAT v.8.0) package (Blott, 2010; Blott and Pye, 2001).

Replicate cores from different multi-core deployments at each station were allocated for analyses of sediment organic matter. Intact sediment cores were sectioned in 0-1, 1-2, 2-3, 3-4, 4-5, 5-7, and 7-10 cm layers, and each layer was then subsampled for different analyses. For chloropigment analyses, samples were sealed in Whirl-Pak bags, wrapped in foil, and frozen at -80°C until analyzed. Samples were thawed, homogenized by kneading the bag, and 1 cc of sediment was subsampled using a syringe and placed in a glass extraction tube. Samples were then suspended in 5 mL of 100% acetone, vortexed, sonicated in an ice bath for 10 minutes, and left to extract in the dark overnight at -20°C. Samples were then centrifuged for five minutes at 3,000 rpm, and the supernatant was removed and transferred to a clean glass tube. Fluorescence of the supernatant was measured using a TD-700 fluorometer (Turner Designs, San Jose, CA, USA). The fluorescence of a blank of 100% acetone was measured and subtracted from the sample fluorescence. Samples were then acidified with 0.15 mL of 0.1 N HCl, briefly vortexed, and allowed to rest for at least 90 seconds. The fluorescence was then measured again to determine phaeopigment concentrations. Each sample was extracted a second time by adding another 5 mL of acetone to the same sediment and following the procedure described above. Afterward, the sediment was dried at 60° until a constant mass was achieved. A standard curve was produced using a chlorophyll-a standard (spinach extract C5753, Sigma-Aldrich) to convert fluorescence into concentrations (adapted from Arar and Collins, 1997). Chlorophyll-a (chl-a) and phaeopigment (phaeo) concentration (µg g^{-1} dry sediment) from both extractions were then summed for each sample, and sediment inventories of chl-a and phaeo (µg cm^{-2}) were calculated for the upper 10 cm of sediment using the volume-to-dry weight conversion derived from the 1-cc sample of sediment extracted. Chloroplastic pigment equivalents (CPE) were calculated as the sum of chl-a and phaeo inventories.

Additional subsamples from these same cores were analyzed for stable carbon isotope signature of surface sediments ($\delta^{13}C$), total organic carbon (TOC) and nitrogen (TN) for the upper 1 cm of sediment (mg cm^{-2}), and carbon to nitrogen ratios (C:N). A subsample of the top 0-1 cm of intact sediment cores were collected, sealed in Whirl-Pak bags, and frozen at -80°C until they were freeze-dried. Between 5 and 10 g of freeze-dried sediment was weighed into 50-mL centrifuge tubes. To remove carbonates, the samples were rinsed with 1 N HCl until effervescence ceased. Samples were rinsed with reverse osmosis water and then freeze-dried again. Between 15 and 50 mg were weighed into 7 mm aluminum boats and submitted to the Alaska Stable Isotope Facility at the University of Alaska Fairbanks Water & Environmental Research Center. Elemental and stable isotope analyses were conducted via continuous-flow isotope ratio mass spectrometry using a Thermo Scientific Flash 2000 elemental analyzer and Thermo Scientific Conflo IV interfaced with a Thermo Scientific DeltaV Plus Mass Spectrometer. Stable isotope ratios were

reported in δ notation as parts per thousand (‰) deviation from the international standard Vienna Pee Dee Belemnite (VPDB; carbon). Typically, instrument precision is <0.2 ‰.

Data analysis

Abundance and biomass were calculated as the number of individuals and total wet weight m^{-2} for spatial comparisons and m^{-3} for comparison among sediment depth layers. The average size of individuals was calculated by dividing total biomass by total abundance (g $indiv.^{-1}$).

Multivariate analyses of community structure were conducted in PRIMER v7 (Clarke and Gorley, 2015) with PERMANOVA+ add-on (Anderson and Gorley, 2008) for macrofauna higher taxonomic levels, polychaete families, and polychaete functional guilds. Echiurans and two unidentifiable polychaetes were excluded from the polychaete analysis so that the polychaete family dataset could be directly compared to the functional guild dataset. Bray-Curtis similarity matrices were calculated on 4^{th}-root transformed data and displayed on non-metric multi-dimensional scaling (nMDS) plots to visualize similarities and differences among samples. Samples with similar taxonomic or functional composition were identified using hierarchical agglomerative clustering with group-average linking. A similarity profile (SIMPROF) procedure was used to delineate statistically significant groupings.

Relationships between polychaete functional guild composition and environmental variables were examined using a distance-based linear model (DistLM) with a stepwise selection criterion based on adjusted R^2, followed by distance-based redundancy analysis (dbRDA). After examining histograms, sediment chl-a inventory, phaeo inventory, chl-a:phaeo, and CPE were log-transformed. All data were normalized. Variables were removed prior to the analysis due to multicollinearity determined by Draftsman plots and Pearson's correlation coefficients (>0.8), including mean phi, percent sand, chl-a inventory, phaeo inventory, and surface TOC.

Univariate descriptors of polychaete functional guild diversity included Margalef's richness (d) and Pielou's evenness (J′), which were calculated using PRIMER. A functional redundancy index was calculated by dividing the number of functional guilds by the number of polychaete families. Differences in diversity indices, abundance, biomass, and size among station groups were examined using analyses of variance (ANOVA) and Tukey's post hoc test, performed in R Studio. ANOVA assumptions were checked using the Shapiro-Wilk test for normality of residuals and Cochran's C test for homogeneity of variances. When assumptions were not met, data were log-transformed.

Results

Overall, there was roughly the same proportion of major macrofaunal taxa at all sampling stations, but total abundance and biomass differed (Table 1; Supplemental Tables 1 and 2). There was no significant spatial pattern in community structure when all macrofauna were examined at higher taxonomic levels. Polychaetes composed an average of 40.2% ± 11.2% (ranging from 22 to 66%) of total macrofaunal abundance. Polychaete abundance relative to total macrofauna increased with sediment depth (67% at the 5-10 cm layer), while the relative abundance of amphipods and bivalves decreased with sediment depth.

Spatial patterns emerged when considering only polychaetes at the family level, with three significant clusters of samples identified. Further spatial structure was revealed when examining patterns based on polychaete functional guilds, yielding four significant clusters (A, B, C, and D; Figures 1 and 2). The fourth cluster (Group C) was composed of stations that had clustered with either Group B or Group D in the family-level analysis. Stations attributed to each of these four

clusters are indicated on the map in Figure 1, and these groupings are used to further explore patterns in community structure, including associations with environmental variables.

Macrofauna

There were no significant differences in total macrofaunal abundance among the four groups ($F_{3,19}$ = 2.70, = 0.07); however, C had the lowest average abundance (Table 3). Total macrofaunal biomass at sites in Group D was significantly lower than Groups B and C ($F_{3,19}$ = 4.36, p = 0.02), and the average size followed a similar pattern ($F_{3,19}$ = 3.54, p = 0.03; Table 3).

Polychaetes were the most abundant macrofaunal taxon in all groups except Group A, where amphipods were the most abundant (Table 4). Groups B and C had similar relative abundances of the major taxa but differed in total macrofaunal abundance (Tables 3 and 4). Group D exhibited different composition than the other groups, with relatively high abundance of ostracods (14%), ophiuroids (5%), echiurans (4%), and echinoids (3%). Bivalves accounted for more than 50% of the biomass in Groups B, C, and D and were particularly high (88%) at sites in groups B and C. In contrast, amphipods had the highest biomass in Group A. Polychaetes had the second-highest biomass in all groups. In all groups, total macrofauna abundance was highest in the 1-cm surface layer (Figure 3). Biomass showed a similar pattern except in Group C, where biomass was highest at the 5-10 cm layer primarily due to bivalves (Figure 3).

Polychaete community structure

Polychaete abundance was significantly different among groups, with the post hoc test revealing that abundance was significantly lower at Group C compared to Group B ($F_{3,19}$ = 5.72, p = 0.006; Table 3). There were no significant differences in polychaete biomass ($F_{3,19}$ = 0.72, p = 0.55) or average body size ($F_{3,19}$ = 0.52, p = 0.67) among the groups; however, average polychaete biomass was highest at Group A (Table 3). Additionally, Group C had a high variance in average polychaete body size.

The most abundant family was different in each group, although some families had high abundance across multiple groups, such as Capitellidae, Spionidae, and Cossuridae (Table 4). One or two families dominated most groups; however, Group C had a relatively even distribution, with many families of similar abundances. The most abundant polychaete families (>10% of relative abundance) at Group A were Paraonidae, Capitellidae, Spionidae, and Terebellidae (Table 4). Group A also had the highest proportion of Maldanidae, which otherwise only occurred among the top 10 families at sites in Group B. Polychaete abundance was highest at Group B stations, where only three families (Capitellidae, Phyllodocidae, and Spionidae) accounted for ~75% of total polychaete abundance (Table 4). Group B also had a high proportion of Polynoidae and Pectinariidae compared to the other groups. The most numerous families in the Group C polychaete assemblage included Nephtyidae, Sigalionidae, Cossuridae, and Flabelligeridae (Table 4). Group C also had low abundance of Sabellidae and Capitellidae compared to other groups, and Syllidae and Paraonidae were notably absent. Family richness was highest at Group D sites, where Cirratulidae, Cossuridae, and Capitellidae were most abundant (Table 4). Group D was the only group containing Apistrobranchidae, Magelonidae, Ophellidae, Owenidae, and Serpulidae.

Overall, 21 polychaete functional guilds were identified, with most guilds represented by only one or two families, suggesting little functional redundancy over the study region when feeding type, motility, and feeding structure were all considered (Tables 2 and 4). Groups B and C were dominated by carnivores (~40 – 45%), although different families comprised the most abundant carnivores in each group, including Phyllodocidae in Group B and Nephtyidae and

Sigalionidae in Group C (Table 4). Subsurface deposit feeders made up the next largest proportion of the polychaetes at these sites (~26 – 36%), with Capitellidae the dominant family overall in Group B and Cossuridae the third most abundant in Group C. Deposit feeders, both surface and subsurface, accounted for ~70% of the polychaetes in Groups A (e.g., Paraonidae and Capitellidae) and D (e.g., Cirratulidae, Cossuridae, and Capitellidae; Table 4). Motile burrowers were the most abundant motility type in all groups (Table 4). Group A had a large portion of tube-dwellers compared to the other stations (37%). The most common feeding structure at Group A was non-muscular eversible pharynx, followed by tentacles/palps. The most common structure at Groups B and C was muscular eversible pharynx (Table 4), followed by non-muscular eversible pharynx in Group B and tentacles/palps in Group C. In Group D, the most common feeding structure was tentacles/palps, followed by muscular eversible pharynx.

Surface and subsurface deposit-feeding motile burrowers with non-muscular eversible pharynges, including guilds I(S/B)M(B)N (Paraonidae) and I(B)M(B)N (Capitellidae and Orbiniidae), accounted for almost half of the polychaetes in Group A, and thus accounted for a large portion of the dissimilarity between groups in pairwise comparisons to other sites (Supplemental Table 3). The subsurface deposit-feeders with non-muscular eversible pharynges (I(B)M(B)N) were also abundant in Groups B and D where they accounted for roughly ~20 – 30% of polychaetes. Mobile and discreetly mobile carnivores, including a combination of burrowing, crawling, and swimming behaviors, were abundant in Group B and C. SIMPER analysis indicated that within-group similarity in Groups A and D were attributed to the five most abundant guilds at those sites, as well as carnivores of lower abundance (Table 5; Figure 4). Groups B and C were distinguished based on abundance of 4 out of 5 of the most abundant guilds. A(C)M/D(C)P (Polynoidae) in Group B and I(B)M(B)P (Cossuridae) in Group C were abundant guilds that did not contribute substantially to within-group similarity at these sites. Guilds that contributed to within-group similarity that were not in the top five of respective groups were A(C)D(B)P (Glyceridae) in all groups, I(S/B)M(B)T (Cirratulidae) in Group B, I(F/S)D(T)T (Spionidae) and A(C)M/D(C)P (Polynoidae) in Group C, and A(C)M/D(C)P (Polynoidae) and A(C)M(B/C/S)P (Nephtyidae) in Group D (Table 5).

There were no significant differences in Margalef's richness (d) of functional guilds among the groups ($F_{3,19} = 2.63$, $p = 0.08$), although Group D had the highest average richness (Table 3). Group B had a low Pielou's evenness (J′) compared to Groups C and D ($F_{3,19} = 4.62$, $p = 0.01$; Table 3). In particular, Group C had low richness but high evenness, while Group D had high richness and high evenness. Group B had low richness and evenness. Additionally, Group D had high functional redundancy (e.g., guilds I(S/B)M)B)T, I(B)M(B)P, I(B)M(B)N, and I(F/S)D(T)T each contained two families) compared to Group B ($F_{3,19} = 4.62$, $p = 0.02$; Table 3). Group A also had high functional redundancy (e.g., guilds I(B)M(B)N and I(S)D(T)T each contained two families).

Polychaete abundance gradually declined with sediment depth at Groups A and D, where abundance was about twice as high in the surface layer compared to the 1-5 cm layer (Figure 3). In contrast, polychaete abundance declined rapidly at Group B, and surface abundance was almost four times higher than the 1-5 cm layer. Group C showed relatively similar abundances in the 0-1 and 1-5 cm layers, with dominance of carnivores at all depths. Groups A and C show an opposite pattern in biomass compared to abundance trends, with biomass maxima in the 5-10 cm layer (Figure 3), primarily attributed to the large carnivore Nephtyidae and high relative abundance of mid-sized subsurface deposit feeders. The large suspension feeder Sabellidae also contributed to the biomass maxima at Group A, and the large surface deposit feeder Pectinariidae contributed to

Group C. In contrast, Group D had the greatest polychaete biomass in the surface layer (Figure 3) due to a high abundance of carnivores (Polynoidae) and a few large surface deposit feeders (Trochochaetidae). Biomass peaked in the 1-5 cm layer at Group B (Figure 3) with particularly high abundance of large carnivores (Nephtyidae) and a high abundance of small subsurface deposit feeders (e.g., Maldanidae, Capitellidae).

The surface layer at Group A had a high relative abundance of suspension and suspension/surface feeders compared to the other groups, although it was still a small portion at only 8%. There was a notably high relative abundance of carnivores at the 1-5 cm layer at Group B and the 1-10 cm layers for Group C. Groups A and D had a high relative abundance of surface/subsurface deposit feeders at depths. However, subsurface deposit-feeders made up 22% of total abundance in the surface layer in Group D and 83% in the 5-10 cm layer where capitellids were abundant. Group D also had a high relative abundance of suspension feeders at the surface layers compared to Groups B and C, but still small at only 4%.

Environmental setting

The selected DistLM model accounted for 53.6% of total variation in polychaete functional guild composition and included TN, chl-a:phaeo, percent silt/clay, depth, CPE, and salinity (Figure 6). Some of the selected environmental predictors were highly correlated with other parameters not included in the model selection. TN was highly correlated with TOC. Percent silt/clay was highly correlated with mean phi, percent sand, and TOC. CPE was highly correlated with chl-a and phaeo inventories.

The first dbRDA axis was most correlated with TN and percent silt/clay, and the second dbRDA axis was highly correlated with chl-a:phaeo, with a lower, negative correlation with depth (Figure 5). These parameters suggest that organic matter and depositional environmental (i.e., muddy vs. sandy substrate) are important correlates of polychaete functional structure. Groups A and B were distinctly separated from Group C along the first dbRDA axis, reflecting differences in sediment type between sandier substrate in the northern Bering Sea and muddier sediments in the central Chukchi Sea. In contrast, distribution of sites in Group D along axis 1 overlaps with the other groups, reflecting more variability in sediment grain size among sites (Figure 6). Stations within Groups C and D further separated from each other along the second dbRDA axis, reflecting differences in surface chl-a:phaeo, which may be driven by a recent deposition of phytodetritus observed during sampling at some Group D sites.

Group A consisted of two sites in the Chirikov basin (DBO2.2 and DBO2.3), which were characterized by sandy sediments and low chl-a:phaeo, as well as higher $\delta^{13}C$ values than the other groups (Figure 6). These latter two metrics taken together suggest freshly deposited phytoplankton detritus at the seafloor, although TOC and TN content were low. Group B included stations directly north (downstream) of the Bering Strait constriction and station CBE3 east of Saint Lawrence Island, near the Yukon River delta. Grain sizes ranged from fine sand to very coarse silt with organic matter content similar to that of Group A. CBE3 had very low salinity (Table 1), reflecting freshwater input from the Yukon River.

Groups C and D were composed of stations in the more northerly portion of the study area, characterized by muddy sediment and high TOC and TN (Figure 6). IL4 was included in Group D in 2017 and Group C in 2018. Group C stations were located in the central Chukchi Sea and included the southeast Chukchi Sea hotspot (DBO3.8, CNL5). Group D was mostly comprised of the coastal stations with lower salinity indicative of the Alaska Coastal Current. CPE inventories were variable but included higher values in Group C, whereas chl-a:phaeo ratios were higher in

Group D (Figure 6), suggesting deposition of phytodetritus in both areas, but perhaps more degradation had taken place at Group C sites by the time of our sampling. Group D stations also had higher C:N and lower $\delta^{13}C$ values, suggesting more refractory organic matter, including terrestrial inputs or material advected from further south. Group D also contained station DBO2.4 in the Chirikov Basin, which had distinct community structure compared to the nearby DBO2.2 and DBO2.3 sites that made up Group A. The temperature at DBO2.4 was comparable to the warm temperature of Groups A and B. DBO2.4 had lower chl-a:phaeo, TOC, TN, and C:N, and higher $\delta^{13}C$ than other Group D stations (Table 1).

Discussion

We identified four distinct polychaete assemblages based on functional guild composition that were associated with specific environmental conditions. Overall, the distribution of these assemblages aligned reasonably well with key benthic environmental variables, including grain size and organic matter content, and with a south-to-north gradient across the Bering Strait, typical of this advective system. Although broad-scale features of the environment, such as substrate type and water mass distribution, are known to influence benthic biomass (Bluhm et al., 2009; Grebmeier et al., 2015), an exploration of the functional characteristics of infaunal communities provides a refined view of benthic ecosystem function in these four distinct regions. For example, sediment grain-size characteristics are well-known to constrain benthic assemblage structure (Rhoads, 1974), as we observed here in the separation between the sandy, southern groups (Groups A and B) and the northern, muddy groups (Groups C and D). However, functional characteristics of infaunal assemblages indicate further differentiation among sites within sandy and muddy areas. We combined community structure and environmental information from these subregions to construct a conceptual model of ecosystem structure and function across the study area (Figure 7).

Benthic "eco-regions" in the Alaskan Arctic

Group A consisted of the two eastern DBO2 stations in the northern Bering Sea, located within the Chirikov Basin and characterized by sandy sediment. Our measurements indicated low amounts of high-quality organic matter (OM) in the sediments at these sites; however, suspended OM likely supports benthic biomass in this area. The sandy sediment suggests high current velocity and lateral advection of particles, thus low phytodetritus deposition to the benthos. Low sediment TOC concentration and low sedimentation rates support this scenario (Grebmeier, 1993). Furthermore, the relatively high proportion of suspension-feeding polychaetes in the surface layer suggests that currents are critical in structuring the macrofaunal community (Gontikaki et al., 2011; Lovvorn et al., 2020).

Characteristics of many of the benthic taxa in Group A also suggest the dependence of a large portion of the assemblage on fresh, high-quality suspended or recently deposited OM. For instance, the Chirikov Basin is a known amphipod hotspot and critical feeding ground for gray whales. Amphipods in this region have been estimated to consume nearly all available carbon (Coyle et al., 2007). Indeed, amphipods were the most abundant taxon and had high biomass at the Group A sites, especially at DBO2.2. The amphipod community in the Chirikov Basin is composed primarily of the tube-dwelling suspension-feeding Ampeliscidae family (Grebmeier et al., 1989), although we found a diverse community of amphipod taxa in our samples, including Ampeliscidae, Lysianassidae, Phoxocephalidae, Photidae, and Tryphosidae. While some ampeliscids are obligate suspension feeders, others can supplement with surface deposit-feeding or preying on small crustaceans (reviewed by Conlan et al., 2019). Group A also had a high portion of tube-dwelling

polychaetes, many of which were tentaculate or palp feeders, such as Spionidae, Terebellidae, Sabellidae, and Ampharetidae. While surface and subsurface deposit feeders were the most abundant feeding type at these sites, there was a relatively high portion of suspension (Sabellidae) and facultative suspension feeders (Spioindae) in the surface layer, both of which exhibit particle selectivity (Cavallo et al., 2007; Guieb et al., 2004; Mincks et al., 2008). Additionally, Spionids display an ontogenetic shift from feeding on labile particles like diatoms as juveniles to detrital feeders as adults (Hentschel, 1998). Suspension feeders need a specific range of current speeds to suspension feed (Bock and Miller, 1997). Many facultative species switch between suspension and deposit-feeding behaviors depending on both fluid velocities and organic composition of suspended particles, entering suspension-feeding mode when the horizontal flux of high-quality particles is sufficient (Bock and Miller, 1997). Spionids have been shown to grow faster when consuming high-quality suspended particles than when deposit feeding (Hentschel, 2004).

Group A also had a high relative abundance of surface/subsurface feeders at depth, such as Paraonidae, which primarily feed in deeper sediment layers and move to the surface to feed after a fresh food pulse (Jumars et al., 2015). Indeed, paraonids were most abundant at the 1-5 cm layer at the Group A stations and had a high relative abundance at the 5-10 cm layer, suggesting they were primarily subsurface feeding. Paraonids and others with non-muscular eversible pharynges are generally non-selective, while those with tentacles display more particle selection behavior (Magalhães and Bailey-Brock, 2017). These non-selective polychaetes likely are consuming more refractory and reworked detritus within the sediment. Similarly, capitellids and orbiniids were also common in Group A, both of which are burrowing subsurface deposit feeders with non-muscular eversible pharynges. Although capitellids are generally subsurface deposit feeders, they can respond to fresh deposits of organic-rich particles on the sediment surface (Tsutsumi et al., 2005). However, in the absence of a fresh depositional event, they are likely consuming primarily refractory material that has been reworked and degraded by bacteria (Gontikaki et al., 2011). Both capitellids and orbiniids are in the same functional group, representing an example of functional redundancy. Overall, in Group A, suspension and surface feeders may take advantage of higher quality suspended material associated with the high fluid velocity, while subsurface feeders may dominate because they can survive on the more refractory buried detritus, suggesting physical resource partitioning of OM between these groups based on vertical stratification within the sediment (Jumars, 1978; North et al., 2014; Whitlatch, 1980).

Even within the Chirikov Basin, heterogeneity existed among polychaete assemblages, illustrating the importance of considering subregional spatial scales. For instance, although also located in the Chirikov Basin, station DBO2.4 clustered with Group D. DBO2.4 had a smaller abundance of certain tube-dwellers [e.g., I(B)D(T)N, I(S)D(T)T, I(F/S)D(T)T] and a higher abundance of certain carnivores [e.g., A(C)M(B/C/S)P and A(C)M/D(B)P] and burrowing deposit feeders [e.g., I(B)M(B)P and I(S/B)M(B)T] compared to Group A stations. During sampling, DBO2.4 was solely in Anadyr Water, while the Group A stations were also influenced by Bering Shelf water (Danielson unpublished data). DBO2.4 also had a low relative abundance of amphipods and a high relative abundance of ostracods and brittle stars compared to Group A, representing Group D composition. Brittle stars have also been found in Anadyr Strait communities to the southwest of our sampling (Grebmeier, 1993).

The fourth station sampled in the Chirikov Basin (CBE3) clustered with Group B, which also included two stations with sandy substrate directly north (downstream) of Bering Strait (CNL3 and CPL8). CBE3 had similar environmental conditions to these more northerly sites, except that salinity was lower due to proximity in the Yukon River plume. The CBE region (measured at

nearby CBE1) had high export flux during the time of sampling in 2018 (O'Daly et al., 2020). The Bering Strait stations in Group B had a larger percent of gravel (1-2%) compared to other stations, suggesting high current velocity. Currents accelerate as water moves through the narrow Bering Strait constriction (Danielson et al., 2014). Currents are strong in the fall and winter, resulting in disturbance and resuspension (Abe et al., 2019). However, currents in the Bering Strait throughflow are weaker in the spring, allowing the spring bloom to settle and leading to high sediment chl-a values (Abe et al., 2019). High dominance of relatively few families, especially the classic opportunists Capitellidae and Spionidae (Rhoads et al., 1978), could suggest a disturbed environment, for example, due to scouring from the strong currents. However, the high abundance of large carnivorous polychaetes observed in Groups B would be less likely in recently disturbed areas and is likely supported by the deposition of the spring bloom during weaker phases of the currents (Abe et al., 2019).

Further north, water fans out over the wide and shallow Chukchi shelf, and velocity decreases, allowing local and advected sources of OM to settle to the seafloor (Feng et al., 2020; Grebmeier et al., 2015). These stations are influenced by the nutrient-rich, highly productive Bering Shelf and Anadyr waters with high export flux of diatom detritus and viable diatom cells (O'Daly et al., 2020). Group C was composed of muddy stations in the central Chukchi, including the benthic "hotspot" area near DBO3.8 and CNL5 (Grebmeier et al., 2015), where large amounts of labile OM are deposited. Interestingly, although Group C had large amounts of OM, it had a low abundance of total macrofauna and low abundance and biomass of polychaetes. However, it had a large biomass and average size of macrofauna. These trends may be due to the competitive advantage of a few large-bodied bivalves. Additionally, Group C was the only group with relatively high abundance of Flabelligeridae, which can feed on fresh phytodetritus, but may also target bacteria particularly in the Chukchi Sea (*Brada* spp.; Iken et al., 2010; Jumars et al., 2015).

The large amounts of sediment OM at Groups B and C supported a high relative abundance of carnivores in both groups. The dominant carnivores at Group B sites were Phyllodocidae, which burrow or crawl and feed with a muscular eversible pharynx (Jumars et al., 2015; Kedra et al., 2012; Sokołowski et al., 2014), and are known to eat other polychaetes (Michaelis and Vennemann, 2005). At Group C sites, Nephtyidae and Sigalionidae were common carnivores, both of which are motile predators with muscular eversible pharynx. Sigalionids may be active hunters or sit-and-wait predators (Jumars et al., 2015). Nephtyids consume a variety of prey, including amphipods, foraminifera, and polychaetes (Gaston, 1987; Redmond and Scott, 1989). Nephtyids were abundant throughout the upper 5 cm of sediment and often burrow right below the sediment-water interface (Jumars et al., 2015).

In contrast to Group C, the coastal Chukchi Sea stations of Group D are generally influenced by the nutrient-poor, low-productivity Alaska Coastal Water (Danielson et al., 2017; O'Daly et al., 2020). These stations likely have a high input of refractory terrestrial material or marine detritus that has been reworked during lateral transport, as suggested by depleted $\delta^{13}C$ values and high C:N (Feder et al., 2007; Iken et al., 2010). We found high chl-a:phaeo at some sites and high TOC and TN in part attributed to a visible layer of newly deposited phytodetritus. Sampling timing compared to depositional events associated with ice-cover and bloom phenology are known to influence measurements of sediment OM (Lovvorn et al., 2020), and we sampled these stations shortly after sea-ice retreat. In addition to the amount of food, the quality of food can influence benthic biomass and abundance, impacting trophic structure and ecosystem function (Campanyà-Llovet et al., 2017).

Sites in Group D had low macrofauna and polychaete biomass and small average body sizes, with the majority of individuals concentrated in the surface layer. However, this area also had the highest number of polychaete families and high functional-guild richness and evenness. This diversity may be sustained by a diversity of food sources due to inputs of both terrestrial and marine sources. Station IL4, which switched from Group D to Group C between years, may be experiencing dynamic frontal or ice-edge conditions that affect advection and deposition of organic material. In contrast to other Group D stations, DBO3.3 had a high abundance and biomass of total macrofauna, which has been found before under the ACW near Point Hope and some stations within the Chukchi Bight, likely supported by advected and resuspended organic material (Feder et al., 2007). Similar to Group A, deposit feeders were the most abundant feeding types in Group D. These tentacle feeders were concentrated in the surface layer, suggesting the predominance of particle-selective surface deposit-feeding. Many subsurface deposit-feeders were also found in the upper 1 cm.

Implications for ecosystem processes

We created a conceptual model demonstrating how substrate type and OM input related to benthic community structure and hypothesized environmental inferences from each of the eco-regions, such as bioturbation potential and remineralization pathways (Figure 7). While some generalizations can be made between the sandy and muddy stations, many essential differences are missed with this generalization. For instance, the vertical distribution of macrofauna within the sediment and their associated functional traits impact biogeochemical cycling through oxygenation and bioturbation of sediment. There was evidence of intense sediment mixing in Groups A, B, and C, which all had subsurface maxima of polychaete biomass. Large, tube-dwelling, head-down deposit-feeders such as Maldanidae (Group A) and Pectinariidae (Group B) were relatively abundant at these sites and are known to influence biogeochemical cycling through oxygenation of the sediment by flushing their tubes (McTigue et al., 2016). Group C contained stations DBO3.6 and DBO3.8, the only stations with a subsurface abundance peak of total macrofaunal abundance. Additionally, these stations had high biomass at the 5-10 cm layer dominated by bivalves. High deposition of labile OM at these stations may stimulate bioturbation by macrofauna, leading to high rates of aerobic remineralization (Aller, 1994). Vertical distribution of sediment microbial communities also suggests intense sediment mixing in these groups, with a homogenous community of aerobic microbes inhabited the upper 7 cm of sediment and evidence of a deep oxic/anoxic boundary at about 7-10 cm (Walker et al. submitted). In contrast, the Group D stations had most of the macrofauna abundance concentrated at the surface and are predicted to have low amounts of bioturbation, with primarily anaerobic remineralization of OM. Furthermore, the microbial community at Group D stations showed a shallow transition from an aerobic to an anaerobic community at 1 cm (Walker et al. submitted). The concentration of macrofauna and polychaetes in the surface layer may be due to shallow anoxic conditions at this site, where anaerobic mineralization of organic matter may be the dominant pathway.

When more than one taxa perform similar ecological roles, functional redundancy can contribute to ecological resiliency to disturbance (Bremner et al., 2006; Snelgrove, 1998), and this relationship has been demonstrated for polychaetes in a variety of settings (e.g., Magalhães and Barros, 2011). Groups A and D had the highest functional redundancy and may be more resilient to disturbance than Groups B and C. However, functional redundancy was low throughout all groups, with most functional guilds represented by only one or two polychaete families. Low functional redundancy was also determined for the whole macrobenthos in the Bering Sea (Liu et

al., 2019). Accordingly, benthic ecosystem function in the Pacific Arctic may be susceptible to species loss or shifts in community structure caused by environmental change.

Alterations in benthic biomass and community composition have already been observed in response to environmental change in the Pacific-Arctic region (Goethel et al., 2019; Grebmeier, 2012; Stabeno et al., 2020; Waga et al., 2020), with likely impacts on carbon cycling (Jones et al., 2021). A decline in phytodetrital input to the seafloor has been predicted (Lee et al., 2013; Moore and Stabeno, 2015), and model results for the Chirikov basin suggest this decline will result in a steady loss of deposit feeders followed by a decline in carnivorous polychaetes (Lovvorn et al., 2016). However, deposit-feeding polychaetes remained relatively constant under simulated declines of different magnitudes south of St. Lawrence Island, and carnivorous polychaetes declined slightly (Lovvorn et al., 2016). These regional differences demonstrate the need for local, high-resolution data to inform the modeling of ecosystem function and potential environmental change impacts. For instance, the four polychaete functional assemblages identified in our study will likely respond differently to projected changes in food input and other environmental changes.

Taxa that rely more on fresh microalgae, such as protists, meiofauna, and tunicates, are likely to be more vulnerable, especially in the short term, to declines in phytodetrital inputs (Lovvorn et al., 2016). This vulnerability might also extend to polychaetes relying on higher-quality food particles, such as suspension and surface deposit feeders (Lessin et al., 2019). Consequently, sites in the Chirikov basin and just north of Bering Strait (Groups A and B) with higher proportions these types of feeders (e.g., Spionidae, Terebellidae) may be particularly at risk. These taxa are also discretely motile tube-dwellers, which, like amphipods, rely on water currents to supply suspended OM, contributing to their likely sensitivity to declines in primary production (Coyle et al., 2007). Additionally, some juveniles rely on discrete, labile food particles. For example, juvenile spionids feed on labile particles like fresh diatoms before experiencing an ontogenetic shift to detrital feeders as adults (Hentschel, 1998). Even if the adult food source is still abundant, a reduction in labile particles could cause a bottleneck in development and a population decline. In contrast, deposit feeders may be somewhat buffered against declines in phytodetrital input by a sediment food bank of labile organic matter (Mincks et al., 2005; Pirtle-Levy et al. 2009). These differing responses to environmental change based on functional traits may indicate that specific traits will be more susceptible, with deposit feeders potentially outcompeting suspension feeders. Consequently, it is possible that large suspension feeders will decline, and these broader areas would transition to assemblages resembling Group D, with small deposit-feeders adapted to less labile food.

Changes in phytodetrital input impact trophic groups differently (Lovvorn et al., 2016). However, the benthos is often oversimplified in ecosystem modeling due to a lack of available information (Whitehouse et al., 2014). This aggregation of the benthos at higher taxonomic levels or generic functional groups likely does not reflect local ecosystem function. For instance, feeding type alone did not distinguish differences in proportional contribution of bacterial, phytoplankton, and terrestrial organic matter sources in the Chukchi Sea food web, suggesting the need to consider other traits, including motility and particle selectivity (Zinkann et al., 2021). Consequently, the differences among the four polychaete functional guild assemblage "eco-regions" identified here, which considered feeding type, feeding structure, and motility, can be used to inform ecosystem models through the Pacific Arctic.

In conclusion, we found that the depositional environment, characterized by grain size and amount and quality of OM deposition, structures the taxonomic, functional, and vertical structure of the Pacific Arctic benthos. These community composition patterns likely impact benthic trophic

food web dynamics and biogeochemical and carbon cycling within the sediment, especially rapid, short-term processing of OM. Consequently, alterations in polychaete functional traits due to changing environmental conditions will likely impact the biogeochemical and carbon cycle of the benthos. Thus, ecosystem modeling and conservation and management would benefit from including representatives of different ecosystem functional systems, such as the different polychaete functional assemblage "eco-regions" and the trophic and biogeochemical carbon cycling they represent.

Acknowledgments

This research was part of the Arctic Integrated Ecosystem Research Program (IERP; http://www.nprb.org/arctic-program/). Funding for the program was provided by the North Pacific Research Board, U.S. Bureau of Ocean and Energy Management, Collaborative Alaskan Arctic Studies Program, and U.S. Office of Naval Research. Generous in-kind support for the program was contributed by the U.S. National Oceanic Atmospheric Administration Alaska Fisheries Science Center and Pacific Marine Environmental Laboratory, University of Alaska Fairbanks, U.S. Fish and Wildlife Service, and U.S. National Science Foundation. Support for this research was also provided by the University of Alaska Dissertation Completion Fellowship. We would like to thank the Captain and crew of the *R/V Sikuliaq* for making sampling possible and Opik Ahkinga, Silvana Gonzalez, Jessica Pretty, Sarah Seabrook, and Andrew Thurber for help with sample collection. We also thank Tibor Dorsaz, Brenda Holladay, and Nana Matsui for their assistance with sample sorting; Hilary Nichols and Max Hoberg for macrofaunal identification; Timothy Howe and others at the Alaska Stable Isotope Facility; and Seth Danielson, Jeroen Ingels, Amanda Kelly, and Andrew Thurber for their guidance and valuable input.

References

Abe, H., Sampei, M., Hirawake, T., Waga, H., Nishino, S., Ooki, A., 2019. Sediment-associated phytoplankton release From the seafloor in response to wind-induced barotropic currents in the Bering Strait. Front. Mar. Sci. 0, 97. doi:10.3389/FMARS.2019.00097

Aller, R.C., 1994. Bioturbation and remineralization of sedimentary organic matter: effects of redox oscillation. Chem. Geol. 114, 331–345.

Aller, R.C., 1982. The effects of macrobenthos on chemical properties of marine sediment and overlying water, in: McCall, Tevesz (Eds.), Animal-Sediment Relations. pp. 53–102.

Anderson, M.J., Gorley, R.N., 2008. PERMANOVA+ for PRIMER: Guide to software and statistical methods.

Arar, E.J., Collins, G.B., 1997. In vitro determination of chlorophyll a and pheophytin a in marine and freshwater algae by fluorescence, National Exposure Research Laboratory Office of Research and Development U.S. Environmental Protection Agency. Cincinnati.

Baker, M.R., Kivva, K.K., Pisareva, M.N., Watson, J.T., Selivanova, J., 2020. Shifts in the physical environment in the Pacific Arctic and implications for ecological timing and conditions. Deep. Res. Part II Top. Stud. Oceanogr. 177. doi:10.1016/j.dsr2.2020.104802

Blott, S.J., 2010. GRADISTAT Version 8.0: A grain size distribution and statistics package for the analysis of unconsolidated sediments by sieving or laser granulometer.

Blott, S.J., Pye, K., 2001. Gradistat: A grain size distribution and statistics package for the analysis of unconsolidated sediments. Earth Surf. Process. Landforms 26, 1237–1248. doi:10.1002/esp.261

Bluhm, B., Iken, K., Mincks Hardy, S., Sirenko, B., Holladay, B., 2009. Community structure of epibenthic megafauna in the Chukchi Sea. Aquat. Biol. 7, 269–293. doi:10.3354/ab00198

Bock, M.J., Miller, D.C., 1997. Particle-bound organic matter as a cue for suspension feeding in tentaculate polychaetes. J. Exp. Mar. Bio. Ecol. 215, 65–80. doi:10.1016/S0022-0981(97)00014-2

Bremner, J., Rogers, S.I., Frid, C.L.J., 2006. Matching biological traits to environmental conditions in marine benthic ecosystems. J. Mar. Syst. 60, 302–316. doi:10.1016/j.jmarsys.2006.02.004

Campanyà-Llovet, N., Snelgrove, P.V.R., Parrish, C.C., 2017. Rethinking the importance of food quality in marine benthic food webs. Prog. Oceanogr. 156, 240–251. doi:10.1016/j.pocean.2017.07.006

Cavallo, D., Pusceddu, A., Danovaro, R., Giangrande, A., 2007. Particulate organic matter uptake. Mar. Pollut. Bull. 5, 622–625. doi:10.1016/J.MARPOLBUL.2006.11.024

Clarke, K.R., Gorley, R.N., 2015. PRIMER v7: User Manual/Tutorial.

Conlan, K.E., Hendrycks, E.A., Aitken, A.E., 2019. Dense ampeliscid bed on the Canadian Beaufort Shelf: an explanation for species patterns. Polar Biol. 42, 195–215. doi:10.1007/s00300-018-2417-z

Coyle, K.O., Bluhm, B., Konar, B., Blanchard, A., Highsmith, R.C., 2007. Amphipod prey of gray whales in the northern Bering Sea: Comparison of biomass and distribution between the 1980s and 2002-2003. Deep. Res. Part II Top. Stud. Oceanogr. 54, 2906–2918. doi:10.1016/j.dsr2.2007.08.026

Danielson, S.L., Eisner, L., Ladd, C., Mordy, C., Sousa, L., Weingartner, T.J., 2017. A comparison between late summer 2012 and 2013 water masses, macronutrients, and phytoplankton standing crops in the northern Bering and Chukchi Seas. Deep Sea Res. Part II 135, 7–26. doi:10.1016/j.dsr2.2016.05.024

Danielson, S.L., Weingartner, T.J., Hedstrom, K.S., Aagaard, K., Woodgate, R., Curchitser, E.,

Stabeno, P.J., 2014. Coupled wind-forced controls of the Bering-Chukchi shelf circulation and the Bering Strait throughflow: Ekman transport, continental shelf waves, and variations of the Pacific-Arctic sea surface height gradient. Prog. Oceanogr. 125, 40–61. doi:10.1016/j.pocean.2014.04.006

Degen, R., Aune, M., Bluhm, B.A., Cassidy, C., Kędra, M., Kraan, C., Vandepitte, L., Włodarska-Kowalczuk, M., Zhulay, I., Albano, P.G., Bremner, J., Grebmeier, J.M., Link, H., Morata, N., Nordström, M.C., Shojaei, M.G., Sutton, L., Zuschin, M., 2018. Trait-based approaches in rapidly changing ecosystems: A roadmap to the future polar oceans. Ecol. Indic. doi:10.1016/j.ecolind.2018.04.050

Deng, L., Bölsterli, D., Kristensen, E., Meile, C., Su, C.C., Bernasconi, S.M., Seidenkrantz, M.S., Glombitza, C., Lagostina, L., Han, X., Jørgensen, B.B., Røy, H., Lever, M.A., 2020. Macrofaunal control of microbial community structure in continental margin sediments. Proc. Natl. Acad. Sci. U. S. A. 117, 15911–15922. doi:10.1073/pnas.1917494117

Fay, F.H., 1982. Ecology and biology of the pacific walrus, *Odobenus rosmarus divergens* Illiger. North Am. Fauna 74, 1–279. doi:10.3996/nafa.74.0001

Feder, H.M., Jewett, S.C., Blanchard, A.L., 2007. Southeastern Chukchi Sea (Alaska) macrobenthos. Polar Biol. 30, 261–275. doi:10.1007/s00300-006-0180-z

Feng, Z., Ji, R., Ashjian, C., Zhang, J., Campbell, R., Grebmeier, J.M., 2020. Benthic hotspots on the Northern Bering and Chukchi continental shelf: Spatial variability in production regimes and environmental drivers. Prog. Oceanogr. 191, 102497. doi:10.1016/j.pocean.2020.102497

Gaston, G., 1987. Benthic Polychaeta of the Middle Atlantic Bight: feeding and distribution. Mar. Ecol. Prog. Ser. 36, 251–262. doi:10.3354/meps036251

Goethel, C.L., Grebmeier, J.M., Cooper, L.W., 2019. Changes in abundance and biomass of the bivalve *Macoma calcarea* in the northern Bering Sea and the southeastern Chukchi Sea from 1998 to 2014, tracked through dynamic factor analysis models. Deep Sea Res. Part II 162, 127–136. doi:10.1016/j.dsr2.2018.10.007

Gontikaki, E., Mayor, D.J., Narayanaswamy, B.E., Witte, U., 2011. Feeding strategies of deep-sea sub-Arctic macrofauna of the Faroe-Shetland Channel: Combining natural stable isotopes and enrichment techniques. Deep. Res. Part I Oceanogr. Res. Pap. 58, 160–172. doi:10.1016/j.dsr.2010.11.011

Grebmeier, J., Bluhm, B.A., Cooper, L.W., Danielson, S.L., Arrigo, K.R., Blanchard, A.L., Clarke, J.T., Day, R.H., Frey, K.E., Gradinger, R.R., Kedra, M., Konar, B., Kuletz, K.J., Lee, S.H., Lovvorn, J.R., Norcross, B.L., Okkonen, S.R., 2015. Ecosystem characteristics and processes facilitating persistent macrobenthic biomass hotspots and associated benthivory in the Pacific Arctic. Prog. Oceanogr. 136, 92–114. doi:10.1016/j.pocean.2015.05.006

Grebmeier, J., Feder, H., McRoy, C., 1989. Pelagic-benthic coupling on the shelf of the northern Bering and Chukchi Seas. II. Benthic community structure. Mar. Ecol. Prog. Ser. 53, 79–91. doi:10.3354/meps053079

Grebmeier, J., Frey, K., Cooper, L., Kędra, M., 2018. Trends in benthic macrofaunal populations, seasonal sea ice persistence, and bottom water temperatures in the Bering Strait region. Oceanography 31, 136–151. doi:10.5670/oceanog.2018.224

Grebmeier, J.M., 2012. Shifting patterns of life in the Pacific Arctic and Sub-Arctic Seas. Ann. Rev. Mar. Sci. 4, 63–78. doi:10.1146/annurev-marine-120710-100926

Grebmeier, J.M., 1993. Studies of pelagic-benthic coupling extended onto the Soviet continental shelf in the northern Bering and Chukchi seas. Cont. Shelf Res. 13, 653–668. doi:10.1016/0278-4343(93)90098-I

Grebmeier, J.M., Moore, S.E., Overland, J.E., Frey, K.E., Gradinger, R., 2010. Biological Response to Recent Pacific Arctic Sea Ice Retreats. Eos, Trans. Am. Geophys. Union 91, 161–162. doi:10.1029/2010EO180001

Guieb, R.A., Jumars, P.A., Self, R.F.L., 2004. Adhesive-based selection by a tentacle-feeding polychaete for particle size, shape and bacterial coating in silt and sand. J. Mar. Res. 62, 260–281. doi:10.1357/002224004774201717

Gunton, L.M., Gooday, A.J., Glover, A.G., Bett, B.J., 2015. Macrofaunal abundance and community composition at lower bathyal depths in different branches of the Whittard Canyon and on the adjacent slope (3500m; NE Atlantic). Deep. Res. Part I Oceanogr. Res. Pap. 97, 29–39. doi:10.1016/j.dsr.2014.11.010

Hentschel, B.T., 2004. Sediment resuspension and boundary layer flow dramatically increase the growth rates of interface-feeding spionid polychaetes. J. Mar. Syst. 49, 209–224. doi:10.1016/j.jmarsys.2003.08.007

Hentschel, B.T., 1998. Intraspecific variations in $\delta^{13}C$ indicate ontogenetic diet changes in deposit-feeding polychaetes, Ecology. doi:10.1890/0012-9658

Hinchey, E.K., Schaffner, L.C., Hoar, C.C., Vogt, B.W., Batte, L.P., 2006. Responses of estuarine benthic invertebrates to sediment burial: The importance of mobility and adaptation. Hydrobiol. 2006 5561 556, 85–98. doi:10.1007/S10750-005-1029-0

Huntington, H.P., Danielson, S.L., Wiese, F.K., Baker, M., Boveng, P., Citta, J.J., De Robertis, A., Dickson, D.M.S., Farley, E., George, J.C., Iken, K., Kimmel, D.G., Kuletz, K., Ladd, C., Levine, R., Quakenbush, L., Stabeno, P., Stafford, K.M., Stockwell, D., Wilson, C., 2020. Evidence suggests potential transformation of the Pacific Arctic ecosystem is underway. Nat. Clim. Chang. doi:10.1038/s41558-020-0695-2

Hutchings, P., 1998. Biodiversity and functioning of polychaetes in benthic sediments. Biodivers. Conserv. 7, 1133–1145. doi:10.1023/A:1008871430178

Iken, K., Bluhm, B., Dunton, K., 2010. Benthic food-web structure under differing water mass properties in the southern Chukchi Sea. Deep Sea Res. Part II 57, 71–85. doi:10.1016/j.dsr2.2009.08.007

Jones, B.R., Kelley, A.L., Mincks, S.L., 2021. Changes to benthic community structure may impact organic matter consumption on Pacific Arctic shelves. Conserv. Physiol. 9. doi:10.1093/conphys/coab007

Josefson, A., Forbes, T., Rosenberg, R., 2002. Fate of phytodetritus in marine sediments: Functional importance of macrofaunal community. Mar. Ecol. Prog. Ser. 230, 71–85. doi:10.3354/meps230071

Jumars, P.A., 1978. Spatial autocorrelation with RUM (Remote Underwater Manipulator): Vertical and horizontal structure of a bathyal benthic community. Deep. Res. 25, 589–604. doi:10.1016/0146-6291(78)90615-X

Jumars, P.A., Dorgan, K.M., Lindsay, S.M., 2015. Diet of worms emended: An update of polychaete feeding guilds. Ann. Rev. Mar. Sci. 7, 497–520. doi:10.1146/annurev-marine-010814-020007

Jumars, P.A., Nowell, A.R.M., 1984. Effects of benthos on sediment transport: difficulties with functional grouping. Cont. Shelf Res. 3, 115–130. doi:10.1016/0278-4343(84)90002-5

Kedra, M., Kuliński, K., Walkusz, W., Legezyńska, J., 2012. The shallow benthic food web structure in the high Arctic does not follow seasonal changes in the surrounding environment. Estuar. Coast. Shelf Sci. 114, 183–191. doi:10.1016/j.ecss.2012.08.015

Koch, C.W., Cooper, L.W., Lalande, C., Brown, T.A., Frey, K.E., Grebmeier, J.M., 2020. Seasonal

and latitudinal variations in sea ice algae deposition in the Northern Bering and Chukchi Seas determined by algal biomarkers. PLoS One 15, e0231178. doi:10.1371/journal.pone.0231178
Kokarev, V.N., Vedenin, A.A., Basin, A.B., Azovsky, A.I., 2017. Taxonomic and functional patterns of macrobenthic communities on a high-Arctic shelf: A case study from the Laptev Sea. J. Sea Res. 129, 61–69. doi:10.1016/j.seares.2017.08.011
Lee, S., Sun Yun, M., Kyoung Kim, B., Saitoh, S., Kang, C.-K., Kang, S.-H., Whitledge, T., 2013. Latitudinal carbon productivity in the Bering and Chukchi Seas during the summer in 2007. Cont. Shelf Res. 59, 28–36. doi:10.1016/J.CSR.2013.04.004
Lessin, G., Bruggeman, J., McNeill, C.L., Widdicombe, S., 2019. Time scales of benthic macrofaunal response to pelagic production differ between major feeding groups. Front. Mar. Sci. 6. doi:10.3389/FMARS.2019.00015
Link, H., Piepenburg, D., Archambault, P., 2013. Are Hotspots Always Hotspots? The Relationship between Diversity, Resource and Ecosystem Functions in the Arctic. PLoS One 8, 1–18. doi:10.1371/journal.pone.0074077
Liu, K., Lin, H., He, X., Huang, Y., Li, Z., Lin, J., Mou, J., Zhang, S., Lin, L., Wang, J., Sun, J., 2019. Functional trait composition and diversity patterns of marine macrobenthos across the Arctic Bering Sea. Ecol. Indic. 102, 673–685. doi:10.1016/j.ecolind.2019.03.029
Lopez, G., Levinton, J., 1987. Ecology of deposit-feeding animals in marine sediments. Q. Rev. Biol. 62, 235–260.
Lovvorn, J., North, C., Kolts, J., Grebmeier, J., Cooper, L., Cui, X., 2016. Projecting the effects of climate-driven changes in organic matter supply on benthic food webs in the northern Bering Sea. Mar. Ecol. Prog. Ser. 548, 11–30. doi:10.3354/meps11651
Lovvorn, J., Rocha, A., Danielson, S., Cooper, L., Grebmeier, J., Hedstrom, K., 2020. Predicting sediment organic carbon and related food web types from a physical oceanographic model on a subarctic shelf. Mar. Ecol. Prog. Ser. 633, 37–54. doi:10.3354/meps13163
Lovvorn, J.R., Richman, S.E., Grebmeier, J.M., Cooper, L.W., 2003. Diet and body condition of spectacled eiders wintering in pack ice of the Bering Sea. Polar Biol. 26, 259–267. doi:10.1007/s00300-003-0477-0
Magalhães, W.F., Bailey-Brock, J.H., 2017. Particle selection and feeding behaviour in two cirratulid polychaetes. J. Mar. Biol. Assoc. United Kingdom 97, 1069–1074. doi:10.1017/S0025315417000522
Magalhães, W.F., Barros, F., 2011. Structural and functional approaches to describe polychaete assemblages: ecological implications for estuarine ecosystems. Mar. Freshw. Res. 62, 918–926. doi:10.1071/MF10277
McTigue, N.D., Gardner, W.S., Dunton, K.H., Hardison, A.K., 2016. Biotic and abiotic controls on co-occurring nitrogen cycling processes in shallow Arctic shelf sediments. Nat. Commun. 2016 71 7, 1–11. doi:10.1038/ncomms13145
Mermillod-Blondin, F., Rosenberg, R., François-Carcaillet, F., Norling, K., Mauclaire, L., 2004. Influence of bioturbation by three benthic infaunal species on microbial communities and biogeochemical processes in marine sediment. Aquat. Microb. Ecol. 36, 271–284. doi:10.3354/ame036271
Michaelis, H., Vennemann, L., 2005. The “piece-by-piece predation” of *Eteone longa* on *Scolelepis squamata* (Polychaetes)-traces on the sediment documenting chase, defence and mutilation. Mar. Biol. 147, 719–724. doi:10.1007/s00227-005-1595-8
Mincks, S., Smith, C., DeMaster, D., 2005. Persistence of labile organic matter and microbial biomass in Antarctic shelf sediments: evidence of a sediment “food bank.” Mar. Ecol. Prog.

Ser. 300, 3–19. doi:10.3354/meps300003
Mincks, S.L., Smith, C.R., Jeffreys, R.M., Sumida, P.Y.G., 2008. Trophic structure on the West Antarctic Peninsula shelf: Detritivory and benthic inertia revealed by $\delta^{13}C$ and $\delta^{15}N$ analysis. Deep Sea Res. Part II 55, 2502–2514. doi:10.1016/j.dsr2.2008.06.009
Moore, S.E., Stabeno, P.J., 2015. Synthesis of Arctic Research (SOAR) in marine ecosystems of the Pacific Arctic. Prog. Oceanogr. 136, 1–11. doi:10.1016/j.pocean.2015.05.017
Moore, S.E., Stabeno, P.J., Grebmeier, J.M., Okkonen, S.R., 2018. The Arctic Marine Pulses Model: linking annual oceanographic processes to contiguous ecological domains in the Pacific Arctic. Deep. Res. II 152, 8–21. doi:10.1016/j.dsr2.2016.10.011
Norling, K., Rosenberg, R., Hulth, S., Grémare, A., Bonsdorff, E., 2007. Importance of functional biodiversity and species-specific traits of benthic fauna for ecosystem functions in marine sediment. Mar. Ecol. Prog. Ser. 332, 11–23. doi:10.3354/MEPS332011
North, C.A., Lovvorn, J.R., Kolts, J.M., Brooks, M.L., Cooper, L.W., Grebmeier, J.M., 2014. Deposit-feeder diets in the Bering Sea: Potential effects of climatic loss of sea ice-related microalgal blooms. Ecol. Appl. 24, 1525–1542. doi:10.1890/13-0486.1
O'Daly, S.H., Danielson, S.L., Hardy, S.M., Hopcroft, R.R., Lalande, C., Stockwell, D.A., McDonnell, A.M.P., 2020. Extraordinary carbon fluxes on the shallow Pacific Arctic shelf during a remarkably warm and low sea ice period. Front. Mar. Sci. 7, 986. doi:10.3389/fmars.2020.548931
Pinto, T.K., Austen, M.C. V, 2006. Effects of macroinfauna sediment disturbance on nematode vertical distribution. Artic. J. Mar. Biol. Assoc. UK. doi:10.1017/S0025315406013075
Pirtle-Levy, R., Cooper, L.W., Larsen, I.L., 2009. Chlorophyll a in Arctic sediments implies long persistence of algal pigments. Deep Sea Res. Part II Top. Stud. Oceanogr. 56, 1326–1338.
Rand, K., Logerwell, E., Bluhm, B., Chenelot, H., Danielson, S., Iken, K., Sousa, L., 2018. Using biological traits and environmental variables to characterize two Arctic epibenthic invertebrate communities in and adjacent to Barrow Canyon. Deep. Res. Part II Top. Stud. Oceanogr. 152, 154–169. doi:10.1016/j.dsr2.2017.07.015
Redmond, M.S., Scott, K.J., 1989. Amphipod predation by the infaunal polychaete, Nephtys incisa. Estuaries 12, 205–207. doi:10.2307/1351825
Rhoads, D., McCall, P., Yingst, J., 1978. Disturbance and Production on the Estuarine Seafloor: Dredge-spoil disposal in estuaries such as Long Island Sound can be managed in ways that enhance productivity rather than diminish it on JSTOR. Am. Sci. 66, 577–586.
Rhoads, D.C., 1974. Organism-sediment relations on the muddy sea floor. Ocean. Mar. Bio. Ann. Rev. 12, 263–300.
Snelgrove, P.V.R., 1998. The biodiversity of macrofaunal organisms in marine sediments. Biodivers. Conserv. 7, 1123–1132. doi:10.1023/A:1008867313340
Sokołowski, A., Szczepańska, A., Richard, P., Kędra, M., Wołowicz, M., Węsławski, J.M., 2014. Trophic structure of the macrobenthic community of Hornsund, Spitsbergen, based on the determination of stable carbon and nitrogen isotopic signatures. Polar Biol. 37, 1247–1260. doi:10.1007/s00300-014-1517-7
Stabeno, P.J., Mordy, C.W., Sigler, M.F., 2020. Seasonal patterns of near-bottom chlorophyll fluorescence in the eastern Chukchi Sea: 2010–2019. Deep. Res. Part II Top. Stud. Oceanogr. 177, 104842. doi:10.1016/j.dsr2.2020.104842
Sutton, L., Iken, K., Bluhm, B., Mueter, F., 2020. Comparison of functional diversity of two Alaskan Arctic shelf epibenthic communities. Mar. Ecol. Prog. Ser. 651, 1–21. doi:10.3354/meps13478

Tsutsumi, H., Taniguchi, A., Sakamoto, N., 2005. Feeding and burrowing behaviors of a deposit-feeding capitelid polychaete, *Capitella* sp. I. Benthos Res. 60, 51–58. doi:10.5179/BENTHOS1996.60.2_51

Waga, H., Hirawake, T., Grebmeier, J.M., 2020. Recent change in benthic macrofaunal community composition in relation to physical forcing in the Pacific Arctic. Polar Biol. 43, 285–294. doi:10.1007/s00300-020-02632-3

Walsh, J.J., McRoy, C.P., Coachman, L.K., Goering, J.J., Nihoul, J.J., Whitledge, T.E., Blackburn, T.H., Parker, P.L., Wirick, C.D., Shuert, P.G., Grebmeier, J.M., Springer, A.M., Tripp, R.D., Hansell, D.A., Djenidi, S., Deleersnijder, E., Henriksen, K., Lund, B.A., Andersen, P., Müller-Karger, F.E., Dean, K., 1989. Carbon and nitrogen cycling within the Bering/Chukchi Seas: Source regions for organic matter effecting AOU demands of the Arctic Ocean. Prog. Oceanogr. 22, 277–359. doi:10.1016/0079-6611(89)90006-2

Whitehouse, G.A., Aydin, K., Essington, T.E., Hunt, G.L., 2014. A trophic mass balance model of the eastern Chukchi Sea with comparisons to other high-latitude systems. Polar Biol. 37, 911–939. doi:10.1007/s00300-014-1490-1

Whitlatch, R., 1980. Patterns of resource utilization and coexistence in marine intertidal deposit-feeding communities. J. Mar. Res. 38, 743–765.

Włodarska-Kowalczuk, M., Renaud, P., Węsławski, J., Cochrane, S., Denisenko, S., 2012. Species diversity, functional complexity and rarity in Arctic fjordic versus open shelf benthic systems. Mar. Ecol. Prog. Ser. 463, 73–87. doi:10.3354/meps09858

Zinkann, A.-C., Wooller, M.J., O'Brien, D., Iken, K., 2021. Does feeding type matter? Contribution of organic matter sources to benthic invertebrates on the Arctic Chukchi Sea shelf. Food Webs e00205. doi:10.1016/J.FOOWEB.2021.E00205

Table 1: Macrofaunal, environmental, and sediment characteristics of each station in 2017 and 2018, including clustering group, latitude (N), longitude (W), macrofaunal abundance (individual m^{-2}), macrofaunal biomass (g m^{-2}), depth (m), near-bottom water temperature (°C), near-bottom water salinity, mean phi, percent silt/clay, surface chl-a, surface phaeopigment, surface chl-a: phaeopigment ratio, 0-10 cm chl-a inventory, 0-10 cm phaeopigment inventory, surface TOC, surface TN, surface C:N, and surface $\delta^{13}C$.

Station	Group	Latitude (°N)	Longitude (°W)	Macrofauna abundance	Macrofauna Biomass	Depth (m)	Temp. (°C)	Sal.	Mean Phi	% Silt/Clay	Surface Chla (ug cm^{-2})	Surf. Phaeo (ug cm^{-2})	Surface Chla: Phaeo	0-10 cm chl-a (ug cm^{-2})	0-10 cm phaeo (ug cm^{-2})	Surface TOC (mg cm^{-2})	Surface TN (mg cm^{-2})	Surf. C:N	Surf. $\delta^{13}C$
2017																			
CL1	D	68.95	-166.91	20879 ± 5534	92 ± 94	48	0.3	32.1	6.16	0.76	81.24	37.89	2.16	127.40	86.19	6.78	0.91	7.51	-22.62
CL3	C	69.03	-168.89	12762 ± 611	347 ± 145	53	2.0	32.8	6.67	0.90	32.83	32.73	1.00	87.42	175.00	6.03	0.85	7.10	-22.22
CNL3	B	66.50	-168.96	26292 ± 4592	2407 ± 1498	56	2.2	32.6	2.34	0.14	22.09	71.29	0.32	75.85	282.49	2.45	0.38	6.37	-21.63
CPL8	B	66.50	-168.54	44181	260	52	3.96	32.6	3.592	0.272	27.73	58.22	0.48	48.84	104.14	3.00	0.40	7.55	-22.34
DBO2.2	A	64.68	-169.10	26229 ± 10084	480 ± 31	46	2.8	32.8	2.91	0.11	12.11	44.03	0.28	40.15	136.80	2.86	0.40	7.08	-22.02
DBO2.3	A	64.67	-168.24	23555 ± 1260	243 ± 26	39	2.4	32.4	2.411	0.084	6.57	15.30	0.43	24.06	37.14	1.64	0.24	6.97	-21.39
DBO2.4	D	64.96	-169.89	8400 ± 2374	673 ± 418	48	2.6	32.8	3.06	0.11	8.20	26.03	0.33	35.79	106.27	4.39	0.65	6.74	-21.77
DBO3.3	D	68.19	-167.31	25055 ± 3280	145 ± 141	48	1.5	32.3	3.05	0.38	15.86	18.45	0.84	54.89	79.32	3.82	0.57	6.75	-22.30
DBO3.6	C	67.90	-168.24	26754 ± 1823	1742 ± 3	59	3.9	32.9	4.63	0.45	23.32	71.78	0.32	142.97	524.72	6.16	0.91	6.75	-21.94
DBO3.8	C	67.67	-168.73	17571 ± 4141	1399 ± 833	50	2.0	32.8	6.75	0.92	24.34	66.44	0.44	192.76	491.08	7.17	1.06	6.75	-21.83
IL2	D	67.54	-164.88	22125 ± 3775	309 ± 238	35	-1.2	31.7	6.17	0.76	38.03	18.75	2.30	87.61	51.15	5.46	0.73	7.52	-22.40
IL4	D	67.40	-165.84	29406 ± 11532	19 ± 13	39	2.8	32.3	6.79	0.93	27.46	27.05	0.87	79.95	134.66	6.22	0.87	7.12	-22.65
2018																			
CBE3	B	63.51	-168.18	15406 ± 4867	208 ± 346	32	1.1	31.7	4.51	0.3	1.20	4.00	0.30	6.82	32.36	4.71	0.68	7.19	-22.48
CL1	D	68.95	-166.91	20924 ± 5475	51 ± 8	46	0.0	31.9	6.16	0.76	4.92	4.03	1.21	12.58	29.42	7.96	1.04	7.74	-23.09
CL3	C	69.03	-168.89	13348 ± 2265	652 ± 117	53	-0.6	32.4	6.67	0.90	2.65	4.66	0.57	9.95	38.96	6.72	0.99	6.86	-22.10
CNL3	B	66.50	-168.96	17698 ± 2042	2100 ± 515	56	1.9	32.5	2.34	0.14	5.85	5.66	1.00	15.66	39.75	4.50	0.70	6.44	-21.88
CNL5	C	67.00	-168.96	10647 ± 3287	1833 ± 911	48	1.5	33.0	5.00	0.48	1.41	4.76	0.30	16.11	39.01	5.52	0.76	7.21	-22.40
DBO2.2	A	64.68	-169.10	28234 ± 8807	386 ± 378	46	2.4	32.3	2.92	0.11	2.90	5.02	0.57	10.08	35.10	3.75	0.55	6.75	-21.72
DBO2.4	D	64.96	-169.89	8149 ± 2049	337 ± 361	48	1.6	32.4	3.06	0.11	2.39	3.89	0.61	7.45	26.90	3.37	0.48	7.01	-21.77
DBO3.3	D	68.19	-167.31	19523 ± 2994	226 ± 107	48	0.5	32.5	3.05	0.38	3.90	2.99	1.29	10.29	30.44	5.18	0.71	7.04	-22.41
DBO3.6	C	67.90	-168.24	11602 ± 4179	535 ± 308	58	0.6	32.7	4.63	0.45	1.95	4.70	0.43	10.05	46.95	5.31	0.79	6.74	-22.03
DBO3.8	C	67.67	-168.96	11255 ± 1594	2702 ± 903	51	1.5	32.8	5.56	0.62	0.80	4.12	0.19	6.94	44.37	6.19	0.93	6.64	-21.86
IL4	C	67.40	-165.84	12669 ± 3121	118 ± 119	39	2.1	32.5	6.79	0.93	3.66	3.42	1.08	15.56	33.97	6.13	0.81	7.55	-22.69

Table 2: (a) Legend of polychaete functional guild codes. (b) Polychaete families and assigned functional guilds (based on Jumars et al. 2015). Codes that have multiple traits in parenthesis are families that are facultative feeders, display multiple modes of movement, or have common species within a family that display different traits.

(a)

Feeding		**Motility**		**Structure**
I: Microphage	(B): Subsurface	D: Discretely motile	(T): Tube	T: Tentacle/palps
A: Macrophage	(S): Surface	M: Motile	(B): Burrow	(N): Non-muscular eversible pharynx
O: Omnivore	(F): Suspension		(C): Crawl	P: Muscular eversible pharynx
	(C): Carnivore		(S): Swim	

(b)

	Detailed guild	**Families**
Macrophage carnivores:	A(C)D(B)P	Glyceridae
	A(C)M(B/C)P	Phyllodocidae
	A(C)M(B/C/S)P	Nephtyidae
	A(C)M/D(B)P	Sigalionidae
	A(C)M/D(C)P	Polynoidae
	A(C)MP	Sphaerodoridae
Microphage subsurface deposit feeders:	I(B)D(T)N	Maldanidae
	I(B)D(T)T	Pectinariidae
	I(B)M(B)N	Capitellidae, Orbiniidae
	I(B)M(B)P	Cossuridae, Sternaspidae
	I(B)M(B/S)N	Opheliidae, Scalibregmatidae
	I(B)M/D(B/T)T	Trichobranchidae
Microphage suspension feeders:	I(F)S(T)T	Sabellidae, Serpulidae
Microphage suspension/surface deposit feeders:	I(F/S)D(T)T	Oweniidae, Spionidae
Microphage surface deposit feeders:	I(S)D(B)T	Flabelligeridae
	I(S)D(T)T	Ampharetidae, Terebellidae, Trochochaetidae
Microphage surface/subsurface deposit feeders:	I(S/B)M(B)N	Paraonidae
	I(S/B)M(B)T	Cirratulidae, Magelonidae
Microphage (unspecified) feeder:	IDT	Apistobranchidae
Omnivores:	OM(B/C)P	Syllidae
	OM(C)P	Dorvilleidae

Table 3: Average macrofauna (including polychaetes) and polychaete abundance (individuals m^{-2}), biomass (g m^{-2}), and body size (g $indiv.^{-1}$) for each group (± standard deviation) for the upper 10 cm of sediment; and polychaete functional guild Margalef's richness (D), Pielou's evenness (J′), and functional redundancy index.

	Group A	**Group B**	**Group C**	**Group D**
Macrofauna				
Abundance	25,815 ± 2,650	25,946 ± 12,963	14,497 ± 5,429	18,852 ± 7,190
Biomass	367 ± 123	1,367 ± 1,129	1,147 ± 881	225 ± 216
Average Size	0.02 ± 0.005	0.07 ± 0.06	0.09 ± 0.08	0.02 ± 0.03
Polychaete				
Abundance	8,769 ± 990	11,903 ± 3,193	5,160 ± 2,203	7,792 ± 3,226
Biomass	78 ± 17	46 ± 5	85 ± 141	37 ± 24
Average Size	0.009 ± 0.003	0.004 ± 0.001	0.02 ± 0.02	0.005 ± 0.004
Functional guild				
Richness	1.29 ± 0.29	1.18 ± 0.19	1.23 ± 0.20	1.48 ± 0.20
Evenness	0.75 ± 0.03	0.64 ± 0.09	0.78 ± 0.06	0.77 ± 0.07
Redundancy	1.16 ± 0.03	1.02 ± 0.04	1.09 ± 0.08	1.16 ± 0.08

Table 4: Relative abundance (%) of dominant macrofauna, polychaete families, polychaete functional guilds, feeding types, motility, and feeding structures within each group of stations indicated in Figure 1 with relative abundances (%). Numbers in parentheses indicate total number of classifications found in each group (i.e., total number of families or total number of functional guilds).

Most abundant macrofauna in each group (>1%)			
Group A	**Group B**	**Group C**	**Group D**
Amphipoda – 36.85	Polychaeta – 45.44	Polychaeta – 35.56	Polychaeta – 41.34
Polychaete – 33.97	Amphipoda – 27.00	Amphipoda – 32.00	Bivalvia – 14.66
Bivalvia – 12.99	Bivalvia – 17.93	Bivalvia – 21.92	Ostracoda – 13.85
Malacostraca – 6.84	Malacostraca – 2.80	Ophiuroidae – 2.97	Amphipoda – 9.41
Ostracoda – 6.72	Echiura – 1.96	Ostracoda – 2.86	Malacostraca – 6.51
Echinoidea – 1.46	Ostracoda – 1.53	Echiura – 1.64	Ophiuroidae – 4.66
	Gastropoda – 1.05	Malacostraca – 1.45	Echiura – 3.96
			Echinoidea – 3.06
			Gastropoda – 1.39
Top 10 polychaete families			
Group A (19 families)	**Group B (17 families)**	**Group C (20 families)**	**Group D (28 families)**
Paraonidae – 26.50 I(S/B)M(B)N	Capitellidae – 31.72 I(B)M(B)N	Nephtyidae – 18.45 A(C)M(B/C/S)P	Cirratulidae – 28.32 I(S/B)M(B)T
Capitellidae – 17.91 I(B)M(B)N	Phyllodocidae – 25.82 A(C)M(B/C)P	Sigalionidae – 15.42 A(C)M/D(B)P	Cossuridae – 15.97 I(B)M(B)P
Spionidae – 14.28 I(F/S)D(T)T	Spionidae – 17.20 I(F/S)D(T)T	Cossuridae – 12.46 I(B)M(B)P	Capitellidae – 14.56 I(B)M(B)N
Terebellidae – 13.13 I(S)D(T)T	Polynoidae – 5.69 A(C)M/D(C)P	Flabelligeridae – 12.11 I(S)D(B)T	Spionidae – 8.04 I(F/S)D(T)T
Maldanidae – 5.87 I(B)D(T)N	Sigalionidae – 4.51 A(C)M/D(B)P	Capitellidae – 9.74 I(B)M(B)N	Sigalionidae – 6.06 A(C)M/D(B)P
Glyceridae – 5.20 A(C)D(B)P	Cirratulidae – 4.35 I(S/B)M(B)T	Spionidae – 8.68 I(F/S)D(T)T	Polynoidae – 4.53 A(C)M/D(C)P
Orbiniidae – 3.69 I(B)M(B)N	Nephtyidae – 2.45 A(C)M(B/C/S)P	Cirratulidae – 6.45 I(S/B)M(B)T	Glyceridae – 3.74 A(C)D(B)P
Polynoidae – 3.51 A(C)M/D(C)P	Maldanidae – 2.28 I(B)D(T)N	Phyllodocidae – 4.35 A(C)M(B/C)P	Orbiniidae – 3.23 I(B)M(B)N
Syllidae – 1.69 OM(B/C)P	Glyceridae – 2.04 A(C)D(B)P	Polynoidae – 3.63 A(C)M/D(C)P	Nephtyidae – 3.17 A(C)M(B/C/S)P
Sigalionidae – 1.57 A(C)M/D(B)P	Pectinariidae – 1.31 I(B)D(T)T	Glyceridae – 3.43 A(C)D(B)P	Phyllodocidae – 2.20 A(C)M(B/C)P
Top 5 polychaete functional guilds			
Group A (17 guilds)	**Group B (16 guilds)**	**Group C (16 guilds)**	**Group D (21 guilds)**
I(S/B)M(B)N – 26.50 Surface/subsurface, motile, burrowing, non-muscular	I(B)M(B)N – 31.94 Subsurface, motile, burrowing, non-muscular	A(C)M(B/C/S)P – 18.45 Carnivore, motile, burrowing/ crawling/swimming, muscular	I(S/B)M(B)T – 28.70 Surface/subsurface, motile, burrowing, tentacles/palps
I(B)M(B)N – 21.60 Subsurface, motile, burrowing, non-muscular	A(C)M(B/C)P – 25.89 Carnivore, motile, burrowing/crawling, muscular	A(C)M/D(B)P – 15.42 Carnivore, motile/discretely motile, burrowing, muscular	I(B)M(B)N – 17.81 Subsurface, motile, burrowing, non-muscular
I(S)D(T)T – 14.46 Surface, discretely motile, tube-dwelling, tentacles/palps	I(F/S)D(T)T – 17.25 Suspension/surface, discretely motile, tube-dwelling, tentacles/palps	I(B)M(B)P – 13.29 Subsurface, motile, burrowing, muscular	I(B)M(B)P – 16.77 Subsurface, motile, burrowing, muscular
I(F/S)D(T)T – 14.28 Suspension/surface, discretely motile, tube-dwelling, tentacles/palps	A(C)M/D(C)P – 5.71 Carnivore, motile/discretely motile, crawling, muscular	I(S)D(B)T – 12.11 Surface, discretely motile, burrowing, tentacles/palps	I(F/S)D(T)T – 8.25 Suspension/surface, discretely motile, tube-dwelling, tentacles/palps
I(B)D(T)N – 5.87 Subsurface, discretely motile, tube-dwelling, non-muscular	A(C)M/D(B)P – 4.52 Carnivore, motile/discretely motile, burrowing, muscular	I(B)M(B)N – 11.49 Subsurface, motile, burrowing, non-muscular	A(C)M/D(B)P – 6.06 Carnivore, motile/discretely motile, burrowing, muscular
Polychaete feeding types			
Group A	**Group B**	**Group C**	**Group D**
Subsurface – 28.31	Carnivore – 40.62	Carnivore – 45.44	Subsurface – 35.60
Surface/subsurface – 27.28	Subsurface – 35.57	Subsurface – 26.74	Surface/subsurface – 30.25

Surface – 14.46	Suspension/Surface – 17.25	Surface – 12.50	Carnivore – 20.23
Suspension/Surface – 14.28	Surface/subsurface – 5.30	Suspension/surface – 8.68	Suspension/surface – 8.25
Carnivore – 12.46	Omnivore – 0.84	Surface/subsurface – 6.45	Suspension – 2.28
Omnivore – 1.69	Surface – 0.29	Suspension – 0.15	Surface – 2.11
Suspension – 1.51	Suspension – 0.13	Omnivore – 0.05	Omnivore – 1.15
Unspecified Microphage – 0.00	Unspecified Microphage – 0.00	Unspecified Microphage – 0.00	Unspecified Microphage – 0.14

Top 5 polychaete motility types

Group A	**Group B**	**Group C**	**Group D**
Motile, burrowing – 48.88	Motile, burrowing – 37.24	Motile, burrowing – 31.22	Motile, burrowing – 64.82
Discretely motile, tube-dwelling – 35.09	Motile, burrowing/ crawling/ swimming – 28.34	Motile, burrowing/ crawling/ swimming – 22.80	Discretely motile, tube-dwelling – 9.60
Discretely motile, burrowing – 5.20	Discretely motile, tube-dwelling – 20.91	Discretely motile, burrowing – 15.54	Motile/discretely motile, burrowing – 6.06
Motile/discretely motile, crawling – 3.51	Motile/discretely motile, crawling – 5.71	Motile/discretely motile, burrowing – 15.42	Discretely motile, burrowing – 5.46
Motile, burrowing/ crawling/ swimming – 1.81	Motile/discretely motile, burrowing – 4.52	Discretely motile, tube-dwelling – 11.03	Motile, burrowing/ crawling/ swimming – 5.37

Polychaete feeding structure types

Group A	**Group B**	**Group C**	**Group D**
Non-muscular eversible pharynx – 54.08	Muscular eversible pharynx – 41.45	Muscular eversible pharynx – 58.78	Tentacles/palps – 41.69
Tentacles/palps – 31.76	Non-muscular eversible pharynx – 35.20	Tentacles/palps – 29.56	Muscular eversible pharynx – 38.15
Muscular eversible pharynx – 14.16	Tentacles/palps – 23.35	Non-muscular eversible pharynx – 11.66	Non-muscular eversible pharynx – 20.17

Table 5: Similarity Percentages (SIMPER) polychaete functional guild contributions to similarity between samples within groups (%) with a 70% cut-off for low contributions. Average group similarity in parenthesis next to group name.

Group A (72.86 avg)	**Group B (74.27 avg)**	**Group C (76.83 avg)**	**Group D (76.55 avg)**
I(B)M(B)N – 15.44 Subsurface, motile, burrowing, non-muscular (Capitellidae, Orbiniidae)	I(B)M(B)N – 15.80 Subsurface, motile, burrowing, non-muscular (Capitellidae, Orbiniidae)	A(C)M/D(B)P – 12.77 Carnivore, motile/discretely motile, burrowing, muscular (Sigalionidae)	I(S/B)M(B)T – 13.15 Surface/subsurface, motile, burrowing, tentacles/palps (Cirratulidae, Magelonidae)
I(S/B)M(B)N – 15.35 Surface/subsurface, motile, burrowing, non-muscular (Paraoinidae)	I(F/S)D(T)T – 13.82 Suspension/surface, discretely motile, tube-dwelling, tentacles/palps (Spionidae)	I(B)M(B)N – 12.50 Subsurface, motile, burrowing, non-muscular (Capitellidae, Orbiniidae)	I(B)M(B)P – 11.72 Subsurface, motile, burrowing, muscular (Cossuridae, Sternapsidae)
I(F/S)D(T)T – 11.81 Suspension/surface, discretely motile, tube-dwelling, tentacles/palps (Spionidae)	A(C)M(B/C)P – 13.48 Carnivore, motile, burrowing/crawling, muscular (Phyllodocidae)	A(C)M(B/C/S)P – 12.04 Carnivore, motile, burrowing/crawling/swimming, muscular (Nephtyidae)	I(B)M(B)N – 11.19 Subsurface, motile, burrowing, non-muscular (Capitellidae, Orbiniidae)
I(S)D(T)T – 11.16 Surface, discretely motile, tube-dwelling, tentacles/palps (Terebellidae, Ampharetidae)	A(C)M/D(B)P – 10.44 Carnivore, motile/discretely motile, burrowing, muscular (Sigalionidae)	I(S)D(B)T – 11.10 Surface, discretely motile, burrowing, tentacles/palps (Flabelligeridae)	I(F/S)D(T)T – 9.32 Suspension/surface, discretely motile, tube-dwelling, tentacles/palps (Spionidae, Oweniidae)
I(B)D(T)N – 10.15 Subsurface, discretely motile, tube-dwelling, non-muscular (Maldanidae)	I(S/B)M(B)T – 8.99 Surface/subsurface, motile, burrowing, tentacles/palps (Cirratulidae)	I(F/S)D(T)T – 9.93 Suspension/surface, discretely motile, tube-dwelling, tentacles/palps (Spionidae)	A(C)M/D(B)P – 9.21 Carnivore, motile/discretely motile, burrowing, muscular (Sigalionidae)
A(C)D(B)P – 9.96 Carnivore, discretely motile, burrowing, muscular (Glyceridae)	A(C)D(B)P – 8.48 Carnivore, discretely motile, burrowing, muscular (Glyceridae)	A(C)M/D(C)P – 9.17 Carnivore, motile/discretely motile, crawling, muscular (Polynoidae)	A(C)M/D(C)P – 8.01 Carnivore, motile/discretely motile, crawling, muscular (Polynoidae)
		A(C)D(B)P – 8.54 Carnivore, discretely motile, burrowing, muscular (Glyceridae)	A(C)M(B/C/S)P – 7.23 Carnivore, motile, burrowing/crawling/swimming, muscular (Nephtyidae)
			A(C)D(B)P – 6.31 Carnivore, discretely motile, burrowing, muscular (Glyceridae)

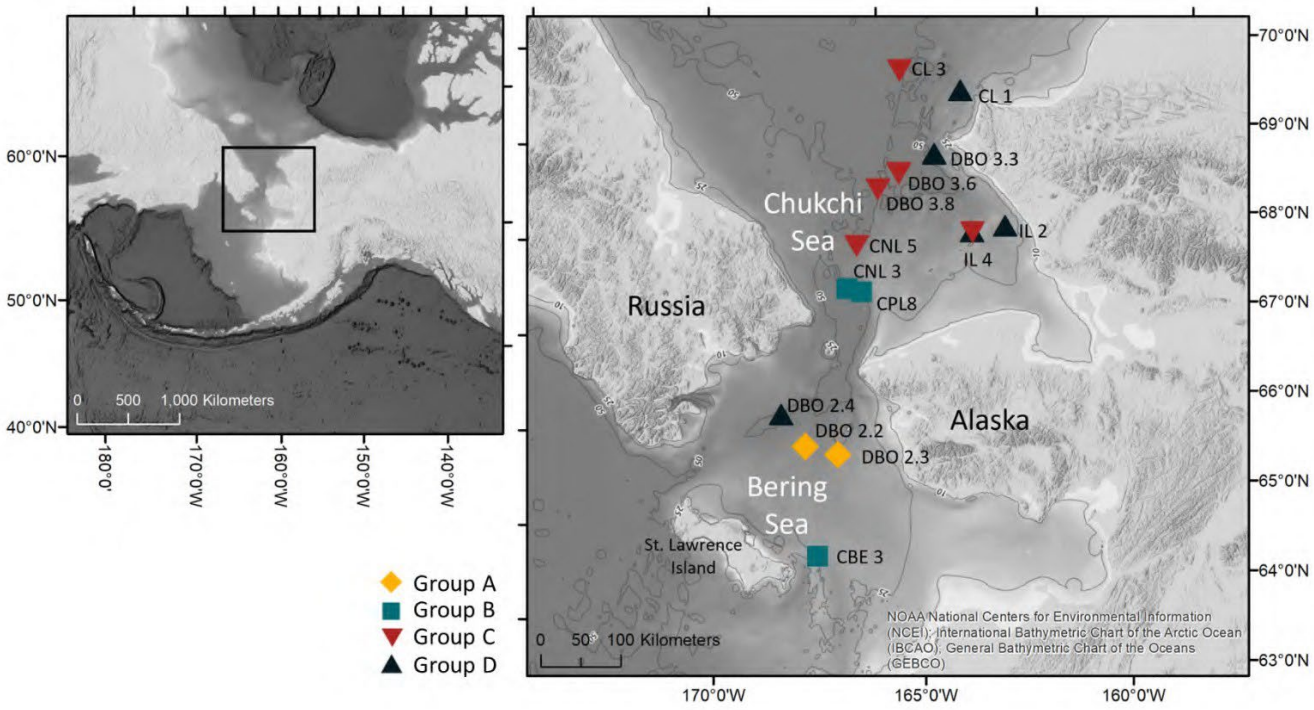

Figure 1: Macrofauna sampling locations in the northern Bering and southern Chukchi Sea in 2017 and 2018. Nine stations were sampled in both years. Symbols based on hierarchical agglomerative clustering of polychaete functional guild abundances from Figure 2. Station IL 4 clustered in Group D in 2017 and Group C in 2018.

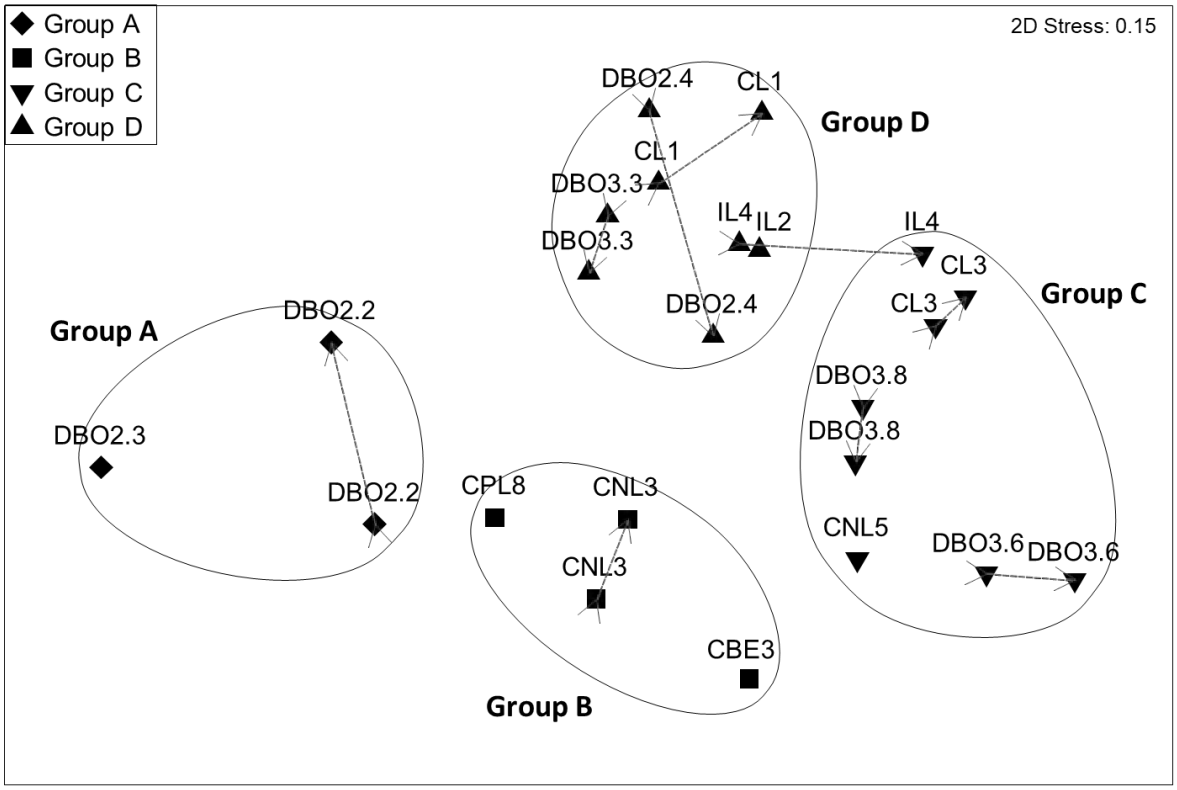

Figure 2: nMDS ordination of polychaete functional guild community structure (indiv. m^{-2}) from 2017 and 2018. Ordination based on hierarchical agglomerative clustering with group-averaged linkage on 4^{th} root transformed data and Bray-Curtis similarity. Four significant station groupings circled in black based on the similarity profile test (SIMPROF). Arrows indicate trajectories from 2017 to 2018 for stations sampled in both years.

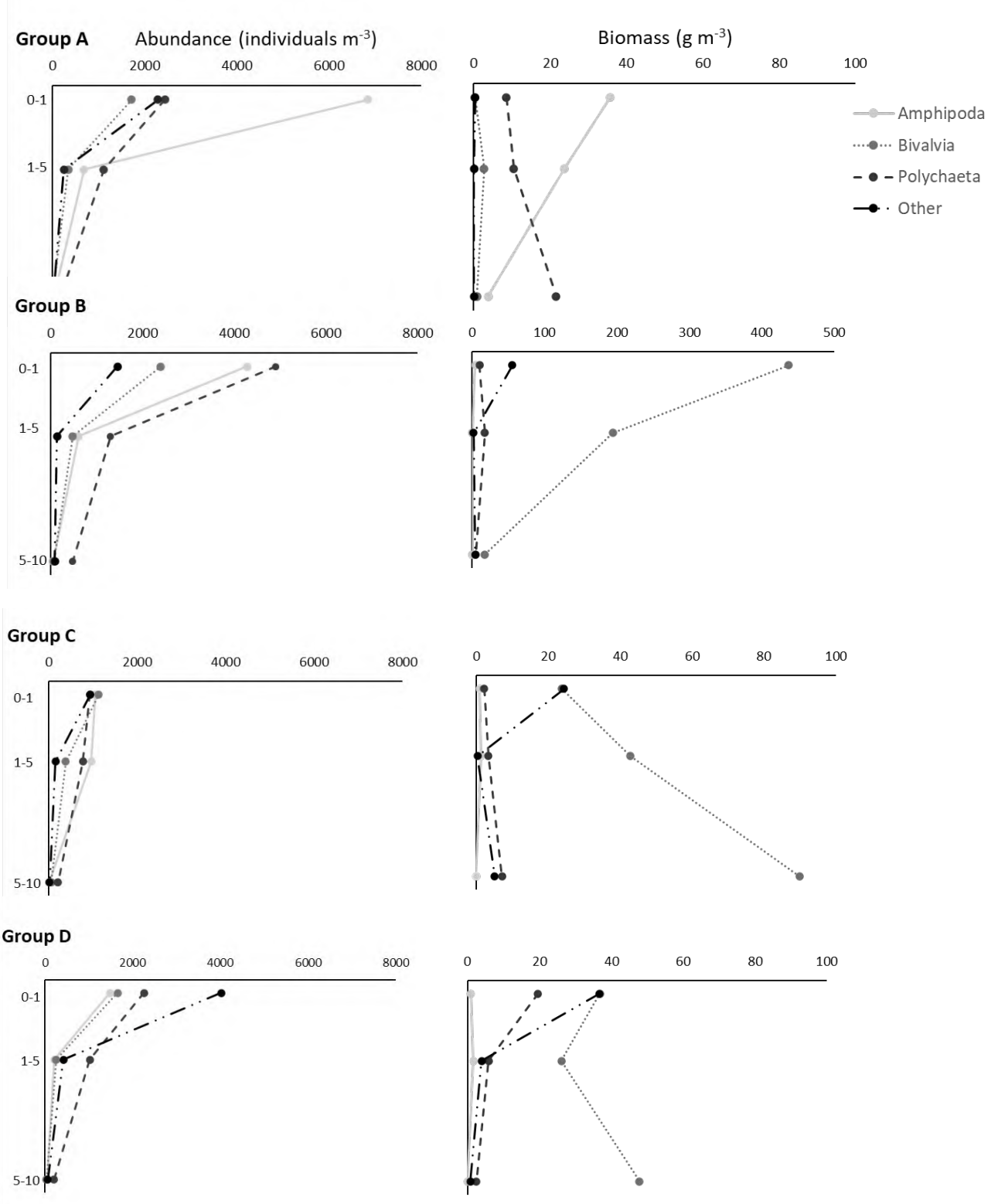

Figure 3: Average abundance (individuals m^{-3}) and biomass (g m^{-3}) within each group of Amphipoda, Bivalvia, Polychaeta, and other macrofaunal taxa for each sediment layer. Scale for Group B biomass is different from other groups. Groups based on hierarchical agglomerative clustering from Figure 2.

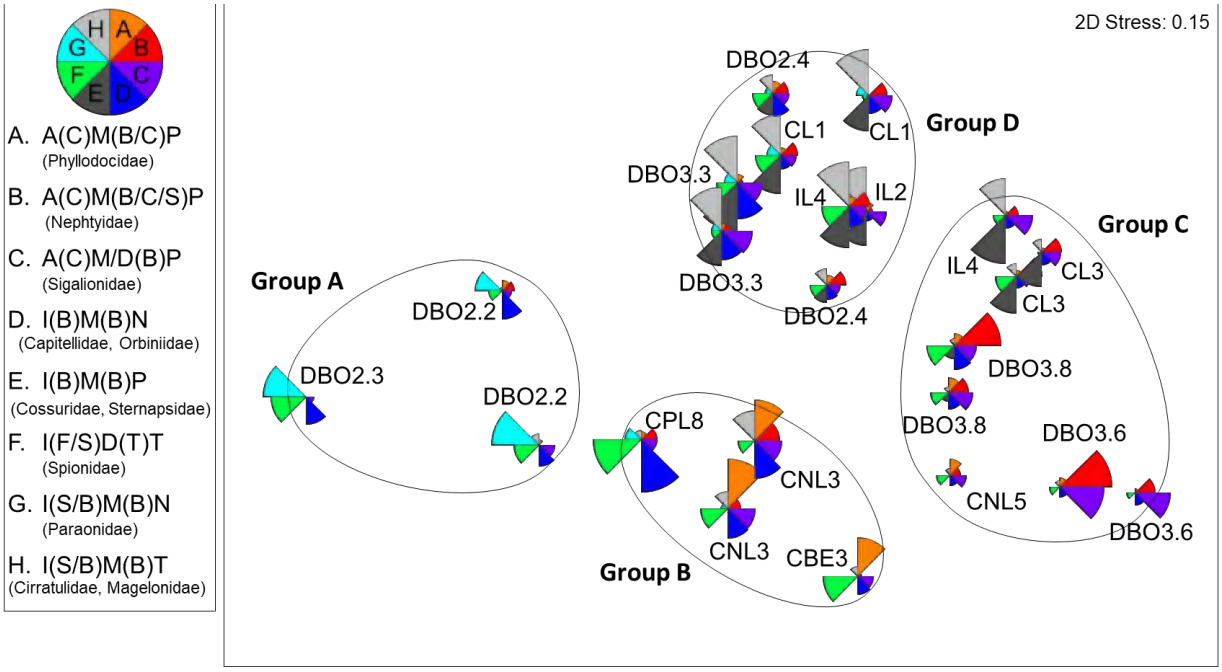

Figure 4: nMDS ordination of polychaete functional guild community structure from 2017 and 2018. Ordination based on hierarchical agglomerative clustering with group-averaged linkage on 4th root transformed data and Bray-Curtis similarity. Significant clusters circled in black based on similarity profile test (SIMPROF). Pie slices represent the abundance of polychaete functional guilds in the top three guilds contributing to within-group similarity in at least one group based on Similarity Percentages (SIMPER) procedure. The first three guilds in the legend are carnivores (A-C), followed by two subsurface deposit feeders (D-E), a suspension/surface deposit feeder (F), and two surface/subsurface deposit feeders (G-H). See Table 2 for detailed guild information.

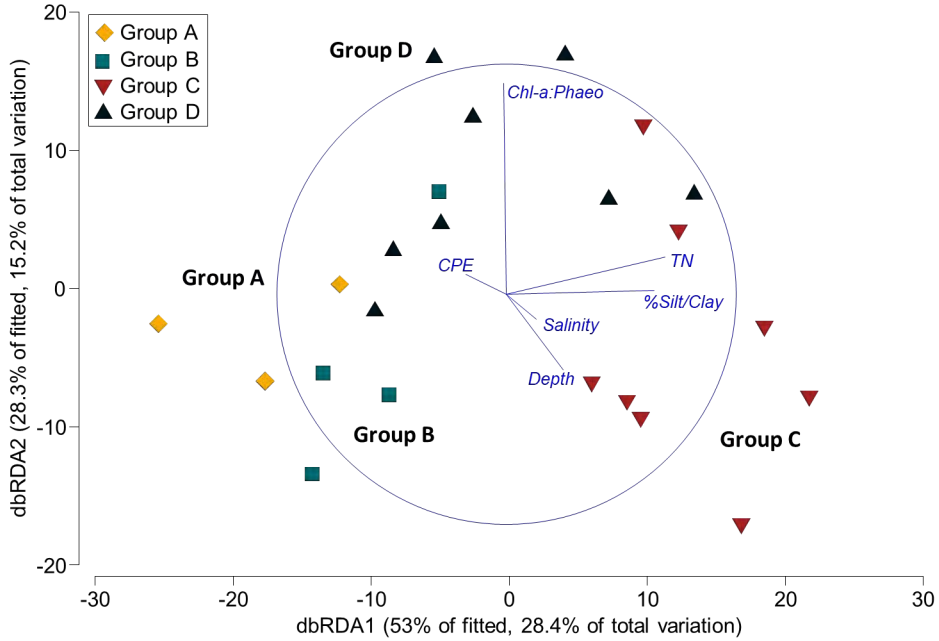

Relationships between dbRDA coordinate axes and orthonormal X variables (multiple partial correlations)

	dbRDA1	dbRDA2	dbRDA3	dbRDA4	dbRDA5	dbRDA6
TN	0.690	0.163	-0.134	0.240	-0.411	0.504
Chl-a:phaeo	-0.014	0.919	-0.243	-0.086	0.290	-0.066
Silt/clay	0.644	0.018	0.518	-0.098	0.270	-0.484
Depth	0.247	-0.329	-0.427	-0.045	0.750	0.288
CPE	-0.175	0.087	0.353	0.855	0.295	0.139
Salinity	0.131	-0.109	-0.590	0.439	-0.156	-0.637

Figure 5: dbRDA displaying the relationship between polychaete functional guild community structure and environmental correlates. The selected model accounted for 53.6% of total variation and included TN, chl-a: phaeopigment, percent silt/clay, depth, CPE, and salinity.

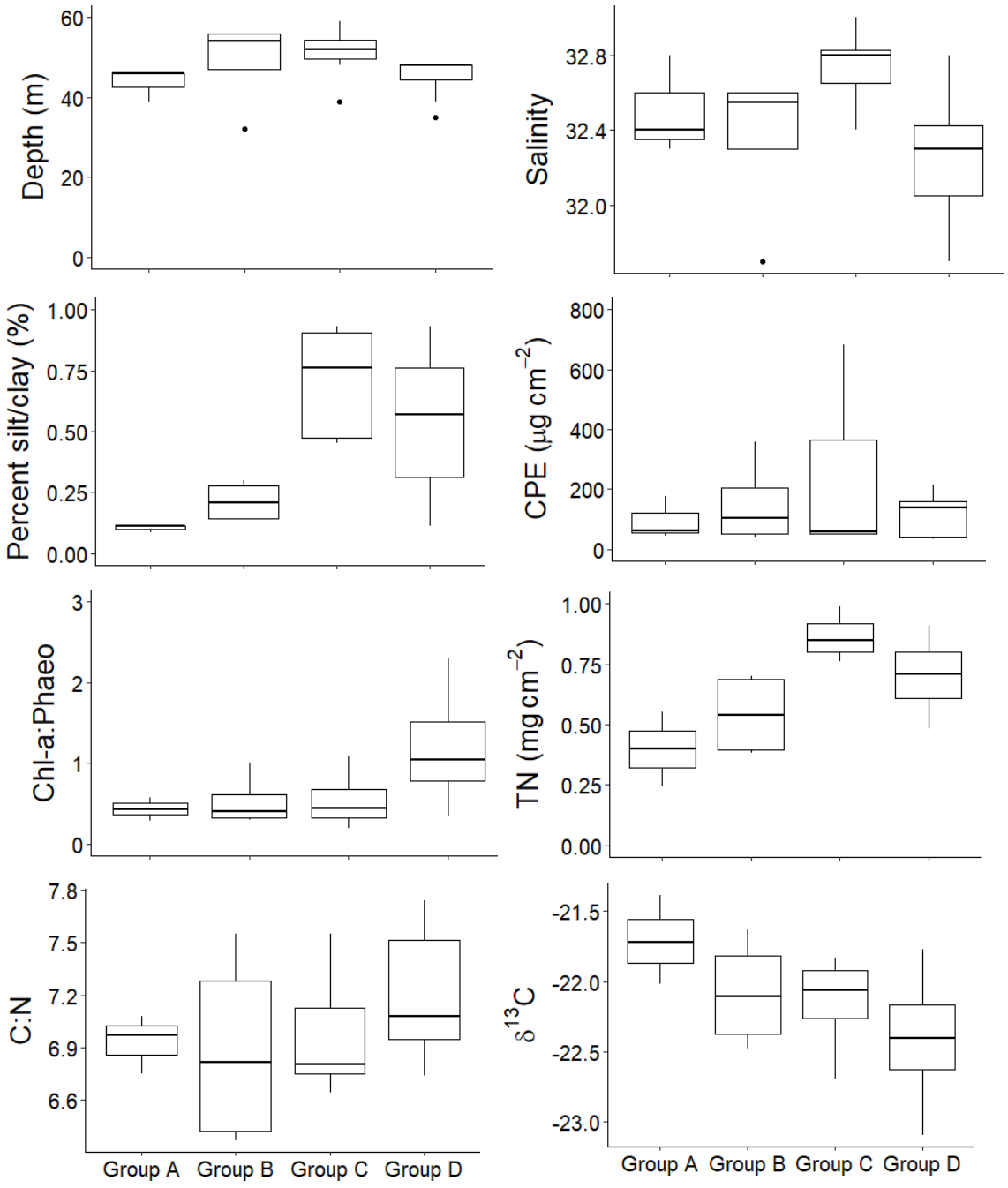

Figure 6: Boxplot of environmental parameters for each group including depth (m), bottom-water salinity, percent silt/clay (%), CPE for the upper 10 cm of sediment (ug cm^{-2}), and chl-a:phaeo, TN (mg cm^{-2}), C:N, and δ^{13}C for the upper 1 cm of sediment. Groups based on hierarchical agglomerative clustering from Figure 2.

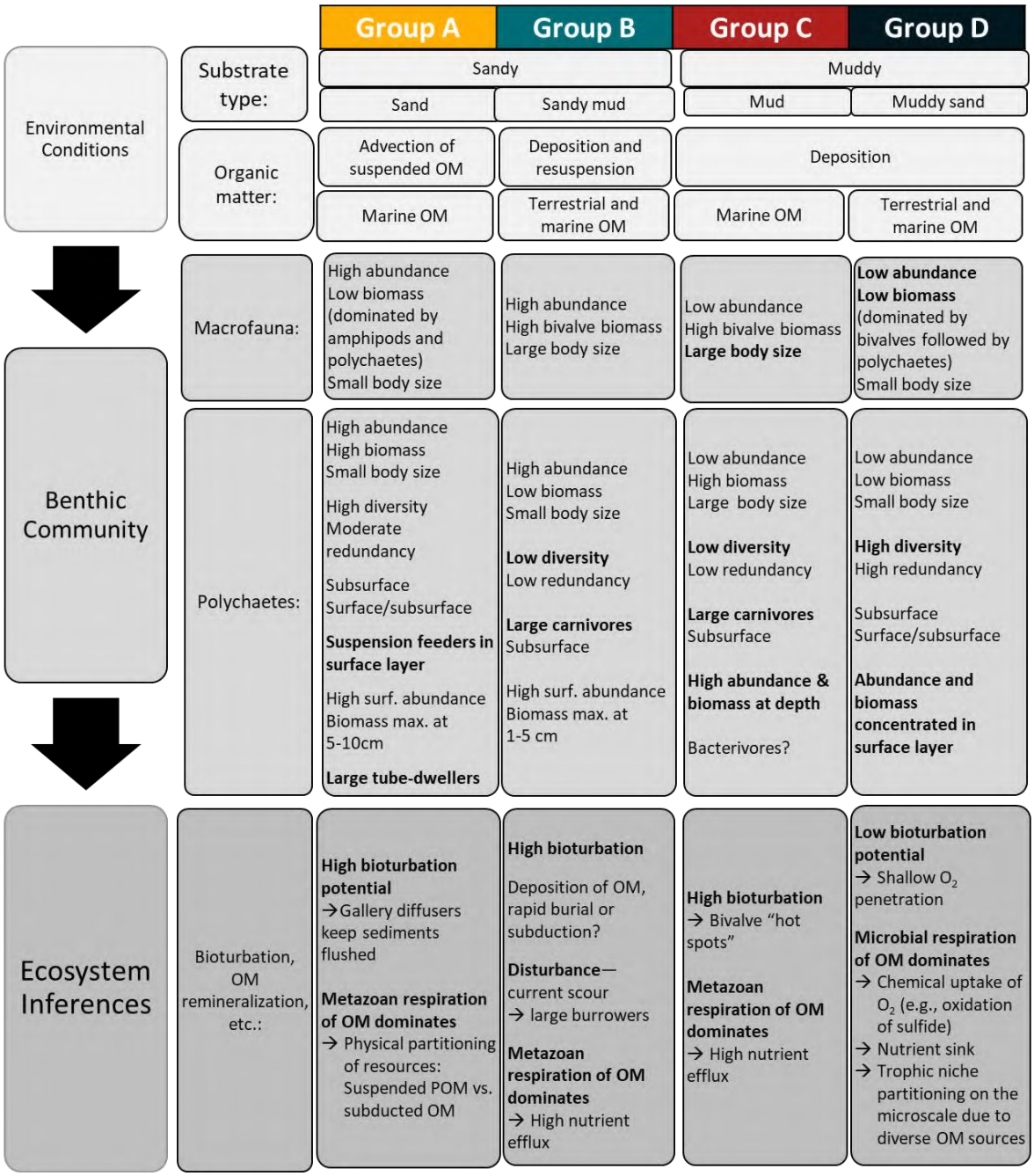

Figure 7: Conceptual model of environmental conditions, benthic community characteristics, and ecosystem function inferences of each benthic "eco-region." Groups ("eco-regions") based on hierarchical agglomerative clustering from Figure 2.

Supplementary Table 1: Average macrofauna abundances (individuals m-2) ± standard deviation for 0-1 cm, 1-5 cm, and 5-10 cm sediment layers.

Station	Year	0-1 cm	1-5 cm	5-10 cm
CBE3	**2017**	-	-	-
	2018	-	-	-
CL1	**2017**	8913 ± 2341	7830 ± 990	891 ± 337
	2018	12223 ± 4190	7555 ± 1974	1528 ± 1088
CL3	**2017**	5220 ± 720	7448 ± 630	467 ± 74
	2018	6069 ± 3658	6451 ± 746	1103 ± 194
CNL3	**2017**	19862 ± 8103	5284 ± 2071	1146 ± 1441
	2018	5814 ± 972	8913 ± 2021	2801 ± 2816
CNL5	**2017**	-	-	-
	2018	3650 ± 1021	5432 ± 588	1146 ± 709
CPL8	**2017**	21645	14642	7894
	2018	-	-	-
DBO2.2	**2017**	13178 ± 4592	12223 ± 4682	828 ± 810
	2018	15279 ± 8643	6684 ± 4412	1337 ± 270
DBO2.3	**2017**	11395 ± 990	9804 ± 2161	1719 ± 90
	2018	-	-	-
DBO2.4	**2017**	3119 ± 630	3247 ± 90	1103 ± 701
	2018	3565 ± 1621	1592 ± 630	191 ± 90
DBO3.3	**2017**	11586 ± 720	10122 ± 6932	1114 ± 225
	2018	7894 ± 459	7682 ± 1155	1867 ± 1476
DBO3.6	**2017**	5475 ± 3061	21900 ± 7203	1082 ± 90
	2018	1995 ± 574	8064 ± 5253	934 ± 389
DBO3.8	**2017**	3183 ± 180	12987 ± 4502	1401 ± 180
	2018	2228 ± 450	7130 ± 0	2165 ± 180
IL2	**2017**	16425 ± 1801	4966 ± 2701	764 ± 662
	2018	-	-	-
IL4	**2017**	17889 ± 990	12732 ± 3241	2706 ± 1756
	2018	3692 ± 709	7215 ± 3130	2928 ± 1254

Supplementary Table 2: Average macrofaunal biomass (g m^{-2}) ± standard deviation for 0-1 cm, 1-5 cm, and 5-10 cm sediment layers.

Station	Year	0-1 cm	1-5 cm	5-10 cm
CBE3	**2017**	-	-	-
	2018	6 ± 5	127 ± 110	338 ± 402
CL1	**2017**	52 ± 71	49 ± 58	2 ± 1
	2018	17 ± 11	22 ± 11	8 ± 6
CL3	**2017**	134 ± 181	125 ± 135	4 ± 15
	2018	327 ± 201	337 ± 25	16 ± 16
CNL3	**2017**	1492 ± 1589	905 ± 97	9 ± 7
	2018	15 ± 12	1479 ± 547	358 ± 347
CNL5	**2017**	-	-	-
	2018	153 ± 243	680 ± 882	589 ± 598
CPL8	**2017**	43	183	34
	2018	-	-	-
DBO2.2	**2017**	63 ± 19	165 ± 125	252 ± 113
	2018	49 ± 2	113 ± 67	93 ± 131
DBO2.3	**2017**	22 ± 1	172 ± 13	49 ± 12
	2018	-	-	-
DBO2.4	**2017**	0.5 ± 0.2	157 ± 120	357 ± 504
	2018	40 ± 54	285 ± 327	43 ± 16
DBO3.3	**2017**	54 ± 71	9 ± 2	52 ± 29
	2018	212 ± 148	46 ± 12	41 ± 31
DBO3.6	**2017**	11 ± 12	333 ± 79	1097 ± 342
	2018	7 ± 6	122 ± 142	246 ± 269
DBO3.8	**2017**	2 ± 1	401 ± 219	996 ± 615
	2018	9 ± 12	96 ± 101	1876 ± 1146
IL2	**2017**	313 ± 329	10 ± 3	9 ± 5
	2018	-	-	-
IL4	**2017**	6 ± 5	4 ± 2	9 ± 9
	2018	1 ± 0.1	3 ± 1	13 ± 9

Supplementary Table 3: Similarity Percentages (SIMPER) polychaete functional guild percentage contributions to dissimilarity between groups (%) with a 70% cut-off for low contributions and average group abundance of transformed data. Average group dissimilarity in parenthesis next to group name. Groups based on hierarchical agglomerative clustering from Figure 2.

Groups A & B (35.90 avg)	**Group Avg abund**	**Group B avg abund**	**Contribution %**
I(S/B)M(B)N	6.81	1.81	12.81
I(S)D(T)T	5.51	0.59	12.44
A(C)M(B/C)P	2.25	6.80	11.82
A(C)M(B/C/S)P	1.21	3.75	7.17
I(S/B)M(B)T	1.90	4.39	6.54
Group A & C 48.16 avg	**Group A**	**Group C**	**Contribution %**
I(S/B)M(B)N	6.81	0.00	14.08
I(S)D(B)T	0.00	4.61	9.49
I(S)D(T)T	5.51	1.25	8.68
I(B)D(T)N	4.61	0.60	8.34
A(C)M(B/C/S)P	1.21	5.04	8.00
Group A & D 38.55 avg	**Group A**	**Group D**	**Contribution %**
I(B)M(B)P	0.00	5.84	13.18
I(S/B)M(B)T	1.90	6.62	10.65
I(S/B)M(B)N	6.81	2.29	10.40
I(S)D(T)T	5.51	1.62	8.82
I(B)D(T)N	4.61	1.65	6.97
Group B & C 33.70	**Group B**	**Group C**	**Contribution %**
A(C)M(B/C)P	6.80	3.54	10.37
I(S)D(B)T	1.34	4.61	9.80
I(B)M(B)P	0.00	3.23	9.64
I(B)D(T)N	3.80	0.60	9.48
I(B)M(B)N	7.46	4.77	8.19
Group B & D 34.41	**Group B**	**Group D**	**Contribution %**
I(B)M(B)P	0.00	5.84	14.98
A(C)M(B/C)P	6.80	3.25	9.42
I(F)S(T)T	0.71	3.37	7.02
I(S/B)M(B)T	4.39	6.62	6.20
I(B)D(T)T	2.69	0.65	6.19
Group C & D 31.95	**Group C**	**Group D**	**Contribution %**
I(S/B)M(B)T	3.21	6.62	10.53
I(B)M(B)P	3.23	5.84	9.45
I(F)S(T)T	0.35	3.37	9.10
I(S)D(B)T	4.61	2.25	8.21
I(S/B)M(B)N	0.00	2.29	6.87

Meiofauna community structure in Pacific Arctic shelf sediments: a comparison of meiofaunal- and macrofaunal-sized nematodes and functional traits[1]

Brittany R. Charrier[1*], Jeroen Ingels[b], and Sarah L. Mincks[a]

[a]College of Fisheries and Ocean Sciences, University of Alaska Fairbanks, AK 99775, USA
[b]Coastal and Marine Laboratory, Florida State University, FL 32358, USA
[*]Corresponding author: brjones8@alaska.edu

Abstract

Meiofauna serve essential roles in benthic ecosystems, such as nutrient cycling and linking microbial and upper-trophic levels of the food web, and they serve as bioindicators of environmental change, particularly nematodes. However, in the rapidly changing Pacific Arctic shelf region, meiofauna remain poorly studied, and baseline data for assessing change is lacking. Sediment samples were collected at ten stations in the northern Bering and southern Chukchi Seas in June 2018 as part of the Arctic Shelf Growth, Advection, Respiration, and Deposition (ASGARD) project. We characterized meiofauna (63-500 µm) community structure and abundance at higher taxonomic levels and evaluated genus-level composition of nematodes in both meiofaunal (63-500 µm) and macrofaunal (>500 µm) size fractions. The nematodes were also classified by trophic feeding groups and life-history strategies. Total meiofauna abundance ranged from 1449 to 12875 ind. 10 cm^{-2} for the upper 5 cm of sediment, and the dry weight (DW) biomass of nematodes in the upper 1 cm of sediment ranged from 33 to 739 µg DW10 cm^{-2}. Four clusters of meiofaunal-sized nematode communities were identified occupying different regions of the Pacific Arctic shelves: the northern Bering shelf, Bering Strait region, central Chukchi Sea, and coastal Chukchi Sea. These nematodes assemblages reflected impacts of food availability and substrate type, and differences suggest these subregions should be considered separately in ecosystem modeling. Additionally, the meiofaunal- and macrofaunal-sized nematodes represented two distinct communities. The taxonomic composition and large standing stock of the macrofaunal-sized nematodes (2 - 215 µg DW 10 cm^{-2}) suggest they are a critical component of the infauna and merit more in-depth research to consider the ecological role they play, including benthic carbon cycling and trophic dynamics. This study provides the first genus-level characterization of nematode communities in the region and among the first measurements of meiofauna standing stock. Thus, the data presented here can serve as a baseline for assessing ecosystem shifts in a rapidly changing Arctic environment.

Keywords: Nematoda, meiofauna, macrofauna, functional traits, trophic diversity, Pacific Arctic

[1] Charrier, B.R., J. Ingels, and S.L. Mincks. Meiofauna community structure in Pacific Arctic shelf sediment: a comparison of meiofaunal- and macrofaunal-sized nematodes and functional traits. *In preparation*.

Introduction

Meiofauna play critical roles in ecosystem functioning (reviewed by Schratzberger and Ingels, 2017), including carbon and nutrient cycling (Bonaglia et al., 2014; Coull, 1999; Rysgaard et al., 2000), linking microbial and upper-trophic levels of the food web (Coull, 1990; Gee, 1989; Kennedy, 1994), and serving as bioindicators of environmental change (Ridall and Ingels, 2021). Tight pelagic-benthic coupling on Arctic shelves supplies substantial inputs of phytodetritus to the benthos (Grebmeier and Barry, 1991; Grebmeier and McRoy, 1989), often supporting abundant meiofauna communities (Górska et al., 2014). Important sources of organic matter (OM) include phytoplankton and ice algal production, and possibly riverine input of microbially processed terrestrial material (McMahon et al., 2006; Zinkann, submitted).

This tight pelagic-benthic coupling sustains high macrofaunal biomass on the Pacific Arctic shelf (Grebmeier et al., 2015). However, the Pacific Arctic meiobenthos remains poorly studied and has been identified as a critical data gap in the region, especially for constraining ecosystem models (Lovvorn et al., 2016; Nelson et al., 2014). Only a handful of meiofaunal studies have been conducted in the Pacific Arctic. One study quantified the abundance and distribution of meiofauna in the Chukchi Sea (Lin et al., 2014) but only identified specimens to higher taxonomic levels (e.g., phylum and class). Community composition and functional diversity of nematodes were not resolved any further, even though nematodes accounted for 96.6% of total meiofauna abundance in the shallow shelf region (Lin et al., 2014). Additionally, meiofaunal abundance and biomass were quantified in the Northeast Chukchi Sea (Hajduk, 2015), and nematode community structure and function were assessed, with *Sabatieria* dominating nematode assemblages (Mincks et al., 2021). However, additional research is needed on meiofauna community structure and functional diversity in the Pacific Arctic, especially in the context of the rapid environmental change and unprecedented environmental conditions observed in recent years, including high temperatures and record low sea ice persistence (Baker et al., 2020; Grebmeier et al., 2018; Huntington et al., 2020).

Nematodes are generally the most abundant metazoan meiofaunal taxa in marine sediment. Additionally, functional traits are reasonably well described for nematode genera, including feeding types and life-history strategies (Bongers et al., 1991; Wieser, 1953). Consequently, nematode communities can be useful in assessing ecosystem function and provide insights into ecological and biogeochemical processes occurring in the benthic ecosystem, such as food availability, hydrodynamic conditions, and sediment biogeochemistry (e.g., Gunton et al., 2017; Ingels et al., 2011b; Román et al., 2018).

While meiofauna, and nematodes in particular, are commonly shown to reflect environmental conditions and ecosystem processes, macrofaunal-sized nematodes are often ignored in infaunal studies. Standardized sieve sizes operationally define meiofauna as individuals that pass through an upper mesh of 300-1,000 µm and are retained on a lower 32-63 µm mesh (Giere, 2009). These size separations align with a trough in the bimodal size distribution of benthic infaunal metazoans, corresponding to a shift in optimizing life-history strategies between small, meiofaunal organisms living interstitially within the sediment and large, macrofaunal organisms actively manipulating the sediment matrix (Warwick, 1984). Thus, macrofaunal-sized nematodes are excluded from meiofaunal studies due to their large size and ignored in macrofaunal studies because they are not considered macrofaunal taxa *sensu stricto*. However, macrofaunal-sized nematodes exhibit distinct assemblage structure and functional diversity relative to meiofaunal nematodes (Baldrighi and Manini, 2015; Sharma et al., 2011) and can contribute substantially to macrofaunal abundance (Baldrighi and Manini, 2015; Gunton et al., 2017).

We characterized the spatial variability of meiofauna communities in the upper 5 cm of sediment on the northern Bering and southern Chukchi Sea shelves. Community composition, abundance, biomass, and function (as reflected by feeding mode and life-history strategy) were also assessed for meiofaunal- and macrofaunal-sized nematode genera in surface sediments, in relation to environmental characteristics. We explored differences in nematode community structure between the two size fractions and evaluated the contribution of macrofaunal-sized nematode abundance and biomass to total macrofaunal standing stock and whether critical information may be lost when they are excluded from benthic research. This study provides the first genus-level characterization and biomass estimates of nematodes in this region.

Methods

Study area and sampling

Meiofauna samples were collected from the northern Bering and southern Chukchi Seas in June 2018 from the *R/V Sikuliaq* as part of the Arctic Shelf Growth, Advection, Respiration, and Deposition (ASGARD) project (Table 1; Figure 1). This shallow shelf area is seasonally ice-covered and influenced by distinct water masses. Cold, nutrient-rich Bering Shelf-Anadyr Water (BSAW) experiences water column mixing that enhances primary productivity as current speeds accelerate through the Bering Strait constriction (Danielson et al., 2017; Walsh et al., 1989). As the BSAW fans out over the Chukchi Sea shelf, the current speed declines resulting in high deposition of suspended particulate material to the seafloor (Grebmeier et al., 2015). In contrast, the warm, nutrient-poor Alaska Coastal Water in the east is characterized by low pelagic production and high terrestrial input (Danielson et al., 2017).

Intact sediment cores with undisturbed surfaces were retrieved from ten stations using an MC-800 multi-corer with 10-cm internal diameter tubes (Ocean Instruments, San Diego, USA). Sampling stations ranged from 39 to 58 m in water depth (Table 1). Average near-bottom water temperature was 1.15°C ± 0.93°C (ranging from -0.6 to 2.4°C), measured from CTD deployments. One core from each station was selected for meiofauna sampling. The cores were sectioned into 1-cm depth intervals down to 5 cm and preserved in 10% buffered formalin.

Meiofauna analysis

Meiofauna were separated from the sediment using a decantation method (Creer et al., 2010), whereby samples were washed over a 63-µm sieve, transferred to 70% isopropanol, and stained with Rose Bengal. Prior to sorting, an upper sieve with a 500-µm mesh size was used to separate macrofaunal- (>500 µm) from meiofaunal-sized (63-500 µm) specimens. All nematodes were counted from the >500 µm samples for each sediment depth. From the surface sediment layers (0-1 cm), the first 120 nematodes were picked out for further taxonomic identification and biomass estimation. All nematodes were identified if there were fewer than 120 individuals.

The 63-500 µm samples were split using a Wet Sample Divider (WSD-10, McLane Research Laboratories, Massachusetts, USA), and 10% of each sediment layer was processed for abundance of metazoan meiofauna, identified to higher taxonomic levels (i.e., phylum, class; Giere, 2009; Higgins and Theil, 1988). For surface sediment layers (0-1 cm), 100-150 nematodes were randomly selected for genus-level identification and biomass estimation using a random number table and a gridded petri dish. This number of individuals generally reflects the composition of the whole nematode community (Soetaert and Heip, 1990), allowing for greater efficiency in taxonomic analysis.

The selected meiofaunal- (N= 1124) and macrofaunal-sized (N = 483) nematodes were transferred to anhydrous glycerin using a glycerol-isopropanol-water solution and evaporated overnight in a drying oven at 50°C (Seinhorst, 1959). Nematodes were then mounted on glass slides and identified to genus under a compound microscope using pictorial keys (Platt and Warwick, 1988) and the Nemys database (Bezerra et al., 2021). Genus-level identification is effective in detecting ecological significance (Somerfield and Clarke, 1995). Specimens that could not be identified to genus level were assigned to family.

Length and width of each mounted nematode were measured using a compound microscope and imaging software. Nematode wet weight (µg) was calculated using the equation $(L * W^2)/(1.5 * 10^6)$, where L is length (µm), and W is the maximum body diameter (µm). This equation is adapted from (Andrassy, 1956), assuming a specific gravity of 1.13 g cm^{-3} for marine nematodes (Ingels et al., 2013; Pape et al., 2013). Wet weight was converted to dry weight using a dry-to-wet weight ratio of 0.25 (Heip et al., 1985) and to carbon weight using a carbon-to-wet weight ratio of 0.124 (Jensen, 1984).

Nematode functional traits were characterized in terms of feeding type and life-history strategy. The feeding type of each nematode was assigned based on their buccal cavity morphology as classified by Wieser (1953): selective deposit feeder (1A), non-selective deposit feeder (1B), epistratum feeder (2A), and predators/scavengers or omnivores (2B). Each nematode was also assigned a life-history strategy based on c-p scores on a scale ranging from 1 (colonizer with short generation times and rapid reproductive rates) to 5 (persister with long generation times and slow reproductive rates), based on Bongers (1990) and Bongers et al. (1991, 1995).

Environmental variables

Sediment cores were collected from multi-core deployments at each station to analyze sediment characteristics (N=1 core) and OM content (N = 3 cores; except DBO2.4 N = 2 cores). Detailed methods for all analyses are presented in Charrier et al. (in preparation). Briefly, grain size analysis was conducted using a subsample of the upper 5 cm of sediment. Samples were suspended in dispersant and then separated into size fractions using a combination of wet and dry sieving. The <63-µm (silt/clay) fraction was treated with 30% hydrogen peroxide (H_2O_2) to remove organic material prior to final weighing. Mean phi was calculated with the Grain Size Distribution and Statistics (GRADISTAT v.8.0) package (Blott, 2010; Blott and Pye, 2001). Percent silt/clay and percent sand were calculated, and porosity was calculated as the ratio of water content to total sediment wet weight.

OM was measured as chloropigment content, total organic carbon (TOC), total nitrogen (TN), and carbon to nitrogen ratio (C:N). Stable carbon isotope signatures were also measured as an indication of carbon source. For these analyses, cores were sectioned in 0-1, 1-2, 2-3, 3-4, 4-5, 5-7, and 7-10 cm layers. Chloropigments were extracted in 100% acetone and analyzed as in Charrier et al. (in preparation) using a TD-700 fluorometer (Turner Designs, San Jose, CA, USA). Fluorescence was converted to concentration units based on a standard curve produced (adapted from Arar and Collins, 1997) using a chlorophyll-a standard (spinach extract C5753, Sigma-Aldrich). Each sediment sample was extracted twice, and the amount of chlorophyll yielded from each extraction was summed. Sediment chlorophyll parameters measured included chlorophyll-a (chl-a), phaeopigment (phaeo), and chloroplastic pigment equivalent (CPE; chl-a + phaeo) inventories (ug cm^{-2}). Chl-a to phaeo (chl-a:phaeo) ratio was also calculated. Stable carbon isotope signatures ($\delta^{13}C$), TOC (mg cm^{-2}), and TN (mg cm^{-2}) were analyzed at the Alaska Stable Isotope Facility at the University of Alaska Fairbanks Water & Environmental Research Center. Stable

isotope data were obtained by continuous-flow isotope ratio mass spectrometry, utilizing a Thermo Scientific Flash 2000 elemental analyzer and Thermo Scientific Conflo IV interfaced with a Thermo Scientific DeltaV Plus Mass Spectrometer. Stable isotope ratios were reported in δ notation as parts per thousand (‰) deviation from the international standard Vienna Pee Dee Belemnite (VPDB; carbon). Typically, instrument precision is <0.2 ‰.

Data analysis

Multivariate analyses of community structure were conducted in PRIMER v7 (Clarke and Gorley, 2015) with the PERMANOVA+ add-on on (Anderson and Gorley, 2008). Bray-Curtis similarity matrices were calculated on $\log_{(x+1)}$ transformed data and displayed on non-metric multi-dimensional scaling (nMDS) plots to visualize similarities and differences among samples. Samples with similar taxonomic composition were identified using hierarchical agglomerative clustering with group-average linking. A similarity profile (SIMPROF) procedure was used to delineate statistically significant groupings. The RELATE routine was used to calculate a Spearman rank correlation coefficient between the meiofaunal- and macrofaunal-sized nematode community Bray-Curtis similarity matrices. Since the abundances of the two size fractions were orders of magnitude different, relative abundances were calculated for further comparisons. A Bray-Curtis similarity matrix was calculated on $\log_{(x+1)}$ transformed relative abundances, and analysis of similarities (ANOSIM) was performed to test for differences between the communities within the two size fractions.

Relationships between meiofaunal-sized nematode community structure, environmental variables, and surface layer sediment variables were examined using a distance-based linear model (DistLM) with a stepwise selection criterion based on adjusted R^2, followed by distance-based redundancy analysis (dbRDA). All environmental data were normalized. Variables were removed prior to the analysis due to multicollinearity determined by Pearson's correlation coefficients (>0.8). Variables allowed in model selection included depth, temperature, salinity, percent silt/clay, and surface sediment layer CPE, chl-a:phaeo, phaeo, TN, and $\delta^{13}C$.

Univariate descriptors of nematode diversity were calculated in PRIMER. Hill's numbers (H_0, H_1, H_2, and H_∞; Heip et al., 1998; Hill, 1973), Pielou's evenness (J′), Shannon-Wiener diversity index (H′), and expected number of genera for 51 individuals (EG(51)) were calculated. The trophic diversity index (TDI) was calculated as the reciprocal of the trophic index (Heip et al., 1998; Ingels and Vanreusel, 2013). The maturity index (MI) was calculated as the sum of the products of the relative proportion of each genus and their c-p score (Bongers, 1990; Bongers et al., 1991; Ingels and Vanreusel, 2013).

Results

Metazoan meiofauna

Total meiofauna abundance (63-500 μm) was 1.7 times higher at the most northern station (CL3) than at any other station, due mainly to a large abundance of small nematodes in the surface layer of sediment (Table 1; Figure 2). The central, offshore Chukchi stations (DBO3.6 and DBO3.8) also had high meiofauna abundance (Table 1; Figure 2). The lowest meiofauna abundances occurred at the stations immediately north of the Bering Strait (CNL3 and CNL5) and the station off the coast of Point Hope (DBO3.3).

Nematodes were the most abundant taxon at all stations and accounted for 88% ± 14% (ranging from 49% at DBO2.4 to 98% at DBO3.8) of total meiofauna abundance (Table 1; Figure 2). Nauplii (6%) were the second most abundant taxa, followed by copepods (4%), bivalves

(0.6%), kinorhynchs (0.4%), polychaetes (0.4%), and ostracods (0.4%). Kinorhynchs were only found at the four coastal Chukchi Sea stations, while ostracods were only found at the two central Chukchi Sea stations (DBO3.6 and DBO3.8). Nauplii abundance at DBO2.4 was 4.8 times higher than at any other station (Figure 2).

Meiofaunal-sized nematodes

There was no significant spatial pattern in community structure when all meiofauna were examined at higher taxonomic levels. However, when surface nematodes (63-500 μm) were considered at the genus level, spatial patterns emerged, and four significant clusters of stations were identified (A, B, C, and D; Figure 3). Group A included stations south of Bering Strait, CNL 3 immediately north of the Strait was distinct (Group B), Group C was composed of three central Chukchi Sea stations, and Group D contained the coastal Chukchi Sea stations (Figure 1). Within-group similarity was driven by a combination of abundant and less abundant genera (Table 2; Figure 4), suggesting that rarer taxa are important in structuring differences among the nematode assemblages in this region. Additionally, some genera were highly abundant across multiple groups. For instance, *Daptonema* was in the top two most abundant genera in Groups A, B, and C (Table 2; results for each station presented in Supplemental Table 1).

Group A had high abundance and biomass of nematodes in the surface 1 cm of sediment, dominated by *Daptonema* and *Oncholaimus* (Table 2; Figure 5). The dominant feeding type in Group A was non-selective deposit feeders (1B; e.g., the Xyalidae family, including *Daptonema* and *Paramonohystera*, and *Monhystrella*), which was also the most abundant feeding type in Groups B and C (Table 3; results for each station presented in Supplemental Table 2). Predators/scavengers (2B; e.g., *Oncholaimus* and *Viscosia*) were relatively more abundant in Group A compared to the other groups, leading to the highest average trophic diversity index (Table 3). However, Group A did not have a higher taxonomic diversity compared to the other groups, demonstrating the importance of assessing both taxonomy and functional diversity. General opportunists (c-p score = 2) were dominant in all groups (Table 3), particularly in Groups B (59%; e.g., *Sabatieria*, *Daptonema*, *Paramonohystera*) and C (81%; e.g., *Daptonema* and *Paramonohystera*). Indeed, Group C consistently had the lowest taxonomic and trophic diversity values among the groups (Table 3). Groups B and C had low nematode abundance and biomass in the upper 1 cm of sediment (Figure 5).

Selective deposit feeders (1A; e.g., *Halalaimus*, *Tricoma*, *Terschellingia*) were dominant in the muddier coastal sites in Group D (Tables 2 and 3). Group D had the highest average maturity index, with a relatively large number of persisters (c-p score = 4; e.g., *Halaimus*, *Tricoma*). Group D was characterized by high abundance and biomass of small-bodied nematodes (Figure 5), although this pattern was heavily influenced by very high abundance at station CL3.

While meiofauna abundance was highest in surface sediments at six sites (Groups A and D), a subsurface abundance peak was detected at the central and southern Chukchi Sea stations (Groups B and C; Figure 6). Overall, the relative abundance of nematodes increased over the first 3 cm of sediment and then remained high at an average of 96 to 97% of total meiofaunal abundance.

Environmental correlates of nematode assemblages

The selected DistLM model for the 63-500 μm surface nematodes community structure accounted for 97.2% of total variation in nematode community structure and included $\delta^{13}C$, chl-a:phaeo, salinity, percent silt/clay, depth, TN, phaeo, and CPE (Figures 7 and 8; environmental

values for each station presented in Supplemental Table 3). Many of these parameters (e.g., $\delta^{13}C$, chl-a:phaeo, TN) suggest the freshness of OM was an important correlate of nematode community structure in this region. The first dbRDA axis was most positively correlated with chl-a:phaeo and negatively correlated with salinity and depth. The second dbRDA axis was highly correlated with $\delta^{13}C$, with a negative correlation with salinity and TN. Some of the selected environmental predictors were highly correlated with other parameters not included in the model selection. The parameter $\delta^{13}C$ was correlated with C:N. Chl-a:phaeo was correlated with chl-a. Percent silt/clay was correlated with mean phi, percent sand, porosity, and TOC. TN was correlated with TOC.

Groups C and D separated from each other along the first dbRDA axis, with higher chl-a:phaeo, lower salinity, and muddier sediments at Group D. Groups A and B fell between Groups C and D along the first axis, with Group B closer to Group C, while Group A was closer to Group D. Group A separated from the other groups along the second dbRDA axis, with higher $\delta^{13}C$ values, sandier sediment, and lower TN.

Macrofaunal-sized nematodes

Macrofaunal-sized nematodes (>500 µm) contributed a small amount to total nematode abundance in the upper 5 cm of sediment (1.1 ± 1%; 16 to 110 ind. 10 cm^{-2}) but a considerable amount to total nematode biomass (16 ± 17%), given their large size (Figure 5), with biomass contribution ranging from 0.2% at CL3 to 58% at DBO3.3. Community structure showed no significant spatial pattern (Supplemental Figure 1) but was distinct from the meiofaunal-sized nematodes (ANOSIM R = 0.356, p = 0.0002; Figure 9). However, spatial patterns of taxonomic composition among stations between meiofaunal- and macrofaunal-sized nematodes were significantly related (RELATE test: rho = 0.37, p = 0.0095), suggesting the two communities followed similar spatial patterns.

The most abundant macrofaunal-sized nematode genus at most stations was either *Paramonohystera* or *Sabatieria*, with exceptions at DBO2.2 (*Cephalanticoma* and *Mesacanthion*) and CL1 (*Setosabatiera)*; Supplemental Table 3). *Paramonohystera* was generally dominant at northern stations, while *Sabatieria* was dominant at the southern Chukchi stations and DBO2.4 (Table 2; Supplemental Table 4).

Of the 67 genera recovered in the meiofaunal size fraction, 45 were not found in the larger fraction, including *Neochromadora* and *Tricoma*, which along with abundant genera contributed to dissimilarity between the two size fractions. Ten genera were only found in the >500 µm size fraction, including *Ledovitia*, *Mesacanthion*, *Symplocostoma*, and *Thalassoalaimus*, and were mainly predators/scavengers (2B) and/or had high c-p scores (3 or 4).

Trophic diversity was lower than that of the meiofaunal nematode assemblage at all stations except CNL5 (Supplemental Table 2). However, as with the smaller size fraction, non-selective deposit feeders (1B) were the dominant feeding type except at DBO2.2, which was dominated by predators/scavengers (2B). Predators/scavengers were also abundant north of Bering Strait (CNL3 and CNL5) and at DBO3.3. At many sites, especially those in Group D, the maturity index was lower in the macrofaunal size fraction compared to the smaller size fraction (Supplemental Table 2), attributed to the high relative abundance of general opportunists (c-p score = 2), such as *Paramonohystera* and *Sabatieria*). Station DBO2.2 also had a high abundance of c-p = 3 and 4.

Discussion

This study is among the first meiobenthic studies in the Pacific Arctic. The most northern portion of our study area overlapped with that of a previous study, which presented abundance

estimates for higher taxonomic levels of meiofauna (>32 µm) down to 10 cm depth (~1200 to 4900 individuals 10 cm^{-2}; Lin et al., 2014) that are somewhat lower than our values of ~1500 to 12000 individuals 10 cm^{-2} for the upper 5 cm. These differences may be due to temporal changes in meiofaunal standing stock during the eight years between sampling events, seasonal differences (June sampling versus July to September sampling), or small-scale spatial variability. Although nematodes accounted for 96.6% of total meiofauna abundance at their shallow stations, the taxonomic and functional diversity of nematodes was not assessed (Lin et al., 2014). Further north in the Northeast Chukchi Sea (NECS), meiofaunal abundance in surface sediments (0-1 cm) was measured as ~90-1300 individuals 10 cm^{-2}, with nematodes accounting for 80.6 to 88% of meiofauna abundance (Hajduk, 2015). We observed higher abundances with 351 to 7322 individuals 10 cm^{-2}. These studies used the same sieve sizes; however, there were many other mythological differences, including sample collection (multi-core versus van Veen grab) and extraction method (decantation versus Ludox extraction).

Four distinct station groups for meiofaunal nematodes

Our study provides the first genus-level characterization and biomass estimates of nematodes in the northern Bering and southern Chukchi Seas. While no significant spatial patterns were detected in the meiofaunal community when examined at the phylum/class level, spatial patterns emerged through higher-resolution analysis of the nematodes identified to genus, demonstrating the value of meiofaunal studies for elucidating ecological patterns. Previous studies have shown that patterns of ecological impact are robust at the species and genus level but are altered at higher levels of taxonomic aggregation (Somerfield and Clarke, 1995). Our study supports this finding.

Four distinct communities of meiofaunal nematodes were identified, occupying different regions of the continental shelves associated with local environmental conditions. **Group A** comprised the Bering shelf stations (DBO2.2 and DBO2.4) within the Chirikov Basin, characterized by sandy sediment and low amounts of labile organic matter in sediments. The Chirikov Basin experiences high-speed flow resulting in low sedimentation rates (Grebmeier, 1993; Lovvorn et al., 2020). The water currents in this region accelerate as they move toward and are constricted by the narrow Bering Strait (Danielson et al., 2014). Notably, the abundance of nauplii at DBO2.4 was nearly five times higher than at any other station, suggesting a recent recruitment event, potentially in response to a pulse of OM following the retreat of the sea-ice edge and subsequent spring bloom. The nematode assemblage in Group A was indicative of a labile food source at the surface. However, while these sites had high abundance and biomass of relatively large-bodied taxa, most of the nematodes were concentrated in the upper 1 cm of sediment and declined rapidly downcore. This pattern has been observed in food-poor environments, where densities are concentrated in the upper sediment layers to access surface food availability (Górska et al., 2014; Lambshead et al., 1995). Group A also had a high relative abundance of predators/scavengers (2B; e.g., *Oncholaimus* and *Viscosia*) in both the meiofauna (18%) and macrofauna (~30-55%) size fractions. In the Northeast Chukchi and Beaufort Seas, these genera and feeding types were also more abundant at sandy nearshore sites compared to other habitats (Mincks et al., 2021). This pattern further suggests a food-limited habitat, where this facultative feeding strategy and greater mobility are advantageous (Baldrighi and Manini, 2015; Sharma and Bluhm, 2010).

Immediately north of the Bering Strait lies station CNL3, the singular station in **Group B**. CNL3 and the station off the coast of Point Hope (DBO3.3; Group D) were the only sites with

gravel (0.9% and 32%, respectively), suggesting these stations may experience hydrodynamic disturbance, such as scouring from strong currents. This disturbance may negatively impact meiofaunal abundance. At DBO3.3, the currents likely speed up as they curve around Point Hope, or the gravel may be caused by ice-rafted debris or ice scouring since this station also has a high portion of silt/clay particles (38%). CNL3 is influenced by constriction of water masses moving through Bering Strait and the deepening topography as the shallow Strait opens onto the Chukchi shelf. The nematode community composition and functional traits at CNL3 also point to a disturbed environment. CNL3 was dominated by non-selective deposit feeders (56%) and general opportunists (c-p = 2), including *Sabatieria*, *Daptonema*, and *Paramonohystera*. *Sabatieria* was the most abundant genus at CNL3 (25%) and is often abundant in disturbed areas, hydrodynamically active sites, or sediments generally under stressed environmental conditions such as low oxygen concentration (Ingels et al., 2011a, 2011b; Mincks et al., 2021). The location downstream of the Bering Strait constriction, sandy and gravelly substrate, and high abundance of *Sabatieria* support the hypothesis of a dynamic and disturbed environment at CNL3. This disturbance is further supported by the high dominance of relatively few families of polychaetes, including the classic opportunist Capitellidae family (Charrier et al. in preparation). *Sabatieria* (37.6%) was the most abundant genera in the upper 1 cm of sediment in the NECS, with the next three most abundant genera being *Daptonema* (10.7%), *Cervonema* (4.5%), and *Dorylaimposis* (3.7%; Mincks et al., 2021). In our study, *Sabatieria* was only the most abundant meiofaunal-sized nematode in Group B, whereas *Daptonema* was highly abundant in groups A, B, and C., and *Cervonema* (CL1, CL3, IL4) and *Dorylaimpsis* (IL4) were only found in Group D which included the northern, coastal stations closest to the NECS, suggesting broader regional patterns that extend beyond our study area and point to the heterogeneous nature of Pacific Arctic benthos.

Group C included three stations in the central Chukchi Sea (CNL5, DBO3.8, and DBO3.6), with muddy sediment and low chloropigment content, but high TOC and TN. Overall, these stations receive large inputs of OM (Feng et al., 2020; O'Daly et al., 2020), which result in high biomass of deposit-feeding macrofauna (Grebmeier et al., 2015) that may subduct this material through feeding activity and bioturbation. The meiofaunal and nematode community in Group C also reflects these large inputs of OM, with high meiofauna abundance in the upper five cm of sediment, especially at DBO3.6 and DBO3.8, and dominance of non-selective deposit feeders (80%) and general opportunists (c-p = 2; 81%) including members of the Xyalidae family and *Sabatieria*. In contrast to the high meiofaunal abundance of small nematodes in Group C, macrofaunal abundance was low at these stations (Charrier et al. in preparation). However, macrofaunal biomass was high and dominated by a few species of large-bodied organisms, particularly bivalves. This abundance and biomass differentiation suggests the meiofauna and macrofauna are responding differently to food input, with meiofauna responding with high abundance and low biomass, while macrofauna respond with low abundance and high biomass.

Group D contained the four coastal Chukchi Sea stations, characterized by muddy sediment with high concentrations of TOC and TN, and evidence of recently deposited phytodetritus at some sites. However, this region is influenced by Alaska Coastal Water, which is generally more nutrient-poor and less productive (Danielson et al., 2017; O'Daly et al., 2020). High C:N ratios and depleted $\delta^{13}C$ values in sediments suggest these relatively large sediment OM pools are partly comprised of refractory terrestrial material or advected particles, which enter the benthic food web in this area (Feder et al., 2007; Iken et al., 2010). This large amount of OM supports high nematode surface abundance and biomass, with meiofaunal abundance 1.7 times

higher at station CL3 than at any other station, although the community also comprised the smallest individuals on average.

The large number of small nematodes (i.e., likely dominated by juveniles) suggests that CL3 recently experienced a recruitment event, potentially in response to the spring bloom. Although other stations had higher sediment chl-a and TOC values, the sediment cores at CL3 had a thin, visible layer of flocculated phytodetritus at the surface (personal observation), suggesting a recent depositional event. Food pulses may be important in regulating nematode size distributions as food inputs can stimulate reproduction (e.g., Ingels et al., 2013). The Pacific Arctic is indeed characterized by large pulses of OM input to the seafloor associated with ice melt and release of ice algae and a strong spring phytoplankton bloom. We sampled these stations shortly after sea-ice retreat and saw evidence of freshly deposited phytodetritus at some of the more northernly stations, likely due to the settlement of the spring bloom. Small organisms, such as meiofauna, respond more rapidly to changes in OM than large organisms and may serve as important indicators of environmental change in these ice-influenced ecosystems.

The nematode and meiofauna communities at Group D stations were representative of assemblages commonly found in muddy locations with high OM. For instance, the most abundant genus was *Halalaimus*, a long, slender nematode that can occupy very fine interstitial space in fine sediments (Sharma et al., 2011). The Desmodoridae family (e.g., *Desmodora* and *Molgolaimus*) was only found at these sites and were also most abundant at muddy stations in the Southern Ocean (Ingels et al., 2006). Kinorhynchs were unique to Group D, and particularly abundant at the muddiest stations CL1, CL3, and IL4, and are generally restricted to muddy sediment with higher OM (Grzelak and Sørensen, 2019; Landers et al., 2019). Overall, these taxa suggest that the muddy substrate and OM quantity at these stations drive community composition.

Group D also had a high trophic diversity index and a high proportion of selective deposit feeders such as *Halalaimus*, *Tricoma*, and *Terschellingia*. Of particular interest is the genus *Terschellingia*, which has been found in abundance in sulphidic, shallow-water habitats and are known to be tolerant of harsh biochemical conditions (Vanreusel et al., 2010). *Terschellingia* is most likely indicative of a shallow redox boundary at Group D sites, corresponding with evidence of a transition from an aerobic microbial community in the upper 1 cm of sediments at these same sites to an anaerobic community below (Walker et al. in preparation).

Meiofauna distributions along the vertical sediment profile across stations groups

The densities of meiofauna generally decline with sediment depth; however, the rate at which this decline occurs can vary. For instance, in the Fram Strait, shallow stations with high food availability on the upper slope exhibited a gradual decrease in meiofauna density with increasing sediment depth, whereas at deeper stations with low food availability, meiofauna densities decreased rapidly to low levels with increasing sediment depth (Górska et al., 2014). Similar trends have been found at continental slope and abyssal sites (Lambshead et al., 1995; Vanaverbeke et al., 1997). These patterns of the vertical distribution of meiofauna in relation to food input align with the patterns we observed in the Pacific Arctic. Meiofauna abundance decreased slowly with sediment depth at the muddy, coastal Chukchi stations (Group D) characterized by high OM inputs and declined more rapidly at the sandy Bering Sea stations with low OM (Group A).

The vertical distribution of meiofauna can also be impacted by other factors such as predation, bioturbation, and downcore movement of OM. Although meiofauna are often concentrated in surface sediment, we found four stations with a subsurface peak of meiofauna

abundance at our southern and central Chukchi Sea stations (Groups B and C). Two of these stations also had a subsurface peak of macrofaunal abundance (Charrier et al. in preparation). Other studies have found subsurface peaks in meiofaunal abundance due to surficial predation pressure (Soltwedel et al., 2003), subsurface peaks of food availability due to bioturbation (Galéron et al., 2001), or physical disturbance (Braeckman et al. 2011). The stations in the Chukchi Sea with the subsurface peaks of meiofaunal abundance generally had a large biomass of bivalves at depth. Thus, the peaks are likely due to bioturbation activity and the subduction of OM to depth.

Role of macrofaunal-sized nematodes in the sediment food web

Macrofaunal-sized nematodes are often ignored in both macro- and meiobenthic studies. However, they have been shown to be distinct from meiofaunal nematodes in terms of taxonomic and functional diversity compared to meiofaunal-sized nematodes (Baldrighi and Manini, 2015; Gunton et al., 2017; Sharma et al., 2011). Similarly, we found that the meiofaunal- and macrofaunal-sized nematodes in the Pacific Arctic represent two distinct communities and should both be considered in future benthic studies and ecosystem modeling.

The macrofaunal-sized nematode communities comprised relatively fewer selective deposit feeders (1B) and epistratum feeders (2A) and higher proportions of non-selective deposit feeders (1B) and predators/scavengers (2B) compared to the meiofaunal-sized nematode communities. Indeed, they were dominated by non-selective deposit feeders, such as *Paramonohystera* and *Sabatieria*. *Sabatieria* was also the dominant genus in Arctic deep-sea macrofaunal-sized nematode assemblages (>250 μm), followed by *Viscosia* (Sharma and Bluhm, 2010). *Viscosia* was present at low abundance in only four of our ten samples, suggesting the taxonomic composition of macrofaunal-sized nematode assemblages is not ubiquitously uniform in the region but varies according to local conditions. Predators/scavengers contributed to a larger relative abundance in the macrofaunal-sized nematode samples compared to the meiofaunal-sized nematode samples. In addition, those genera that were exclusively found in the >500 μm communities were mainly predators/scavengers and/or persisters (c-p = 3 or 4), which tend to be larger and thus better represented in this size fraction (Baldrighi and Manini, 2015; Gunton et al., 2017; Sharma and Bluhm, 2010).

These differences in relative proportions of feeding modes between meiofaunal- and macrofaunal-sized nematodes suggest distinct roles in benthic carbon cycling due to the consumption of different food sources. Many of the meiofaunal-sized nematodes are selective feeders, targeting labile food particles such as fresh phytoplankton cells or bacteria. These nematodes likely depend on a constant supply of freshly deposited OM and would be sensitive to changes in food input (Lovvorn et al., 2016), such as a decline in fresh phytoplankton to the seafloor, which has been predicted for the region (Lee et al., 2013; Moore and Stabeno, 2015). In contrast, non-selective deposit feeders that dominate the macro-sized communities may be utilizing more refractory or reworked material that would go unconsumed and buried in their absence, and additionally are possibly making it more available to other organisms. These taxa may be buffered against declines in the input of fresh phytodetritus to the seafloor through consumption of a sediment food bank of OM (Mincks et al., 2005; Pirtle-Levy et al. 2009). In addition, the predators/scavengers prevalent in macro-sized nematode communities can consume other meiofaunal organisms or the juveniles and scavenged remains of macrofaunal organisms, adding a trophic pathway to sedimentary systems that goes unnoticed when the larger nematodes are ignored. Predators/scavengers were particularly abundant in sandier locations, potentially

because their facultative feeding type and higher mobility are successful strategies for food-limited habitats (Baldrighi and Manini, 2015; Sharma and Bluhm, 2010).

In addition to representing a unique component of the benthos in terms of taxonomic composition and ecosystem function, macrofaunal-sized nematodes contributed substantially to benthic abundance and biomass, and hence benthic carbon cycling. While they only represented 1% of total nematode abundance (16-110 individuals 10 cm^{-2} in the upper 5 cm of sediment; similar to values reported by Gunton et al., (2017)), they accounted for 16% of total nematode biomass, with a high of 58% at DBO3.3. This large biomass and their unique role in the benthic food web imply that macrofaunal-sized nematodes are a critical component of the Pacific Arctic benthic ecosystem and merit more in-depth research. Meiofaunal and macrofaunal studies that do not consider macrofaunal-sized nematodes are ignoring the ecological role they play given their unique set of functional traits, as well as the role of these large infaunal organisms with rapid turnover times in carbon cycling at the seafloor.

Macrofaunal-sized nematodes were also an important component of macrofauna, especially in terms of abundance. They composed an average of 82% ± 17% (ranging from 48% at DBO2.2 to 96% at DBO3.6 and DBO3.8) of total macrofaunal abundance in the upper 5 cm of sediment (macrofaunal data from Charrier et al. in preparation), and 3% ± 8% (ranging from 0.002% at CL3 to 26% at IL4) of macrofaunal biomass in the surface sediment. This contribution of nematodes to total macrofaunal abundance is high compared to other studies. In the Whittard Canyon, nematodes only accounted for up to 15% of total macrofaunal abundance for the upper 5 cm of sediment (Gunton et al., 2017) and between 16-40% at deep-sea sites in the Mediterranean Sea (>300 μm for upper 20 cm; Baldrighi and Manini, 2015). However, these studies counted nematodes in macrofaunal samples that were live sieved prior to preservation, while our estimates were for samples that were sieved after preservation. Sieving live reduces retention of many taxonomic groups of macrofauna, especially soft-bodied, motile polychaetes (Degraer et al., 2007). Indeed, nematode counts from our macrofauna samples that were sieved live yielded estimates of only 28% ± 19% of total macrofauna abundance, which is nevertheless a significant contribution. This discrepancy highlights the well-known potential for methodological bias when comparing results among studies.

Conclusions

The Pacific Arctic is experiencing rapid environmental change (Baker et al., 2020; Huntington et al., 2020), including warming temperatures, declining sea ice, and changes in the timing and magnitude of pelagic production (Arrigo and van Dijken, 2015; Huntington et al., 2020; Ringuette et al., 2002; Selz et al., 2018; Wang and Overland, 2015). These environmental changes impact benthic biomass distribution and community structure (Goethel et al., 2019; Grebmeier, 2012; Moore et al., 2018; Waga et al., 2020), with likely alterations in benthic carbon cycling (Jones et al., 2021). To predict potential impacts of future environmental change on ecosystem structure and function, ecosystem models must be well-constrained and representative of the current ecosystem. However, most benthic research in the Pacific Arctic has focused on the macro- or epibenthos (e.g., Bluhm et al., 2009; Grebmeier et al., 2015), even though meiofauna play critical roles in ecosystem functioning (reviewed in Schratzberger and Ingels, 2017) and achieve high densities in other marginal ice zones (Górska et al., 2014). Due to a lack of available meiofauna data, modeling studies have utilized meiofauna community metrics from other regions (Lovvorn et al., 2016; Nelson et al., 2014). Our study shows four distinct regional benthic communities (using nematodes as a representative component) in the Bering and Chukchi Seas,

providing insight into the heterogeneous nature of the Pacific Arctic sedimentary ecosystem, its distinct communities, and the environmental drivers that shape them. Additionally, the four meiofaunal-sized nematode assemblages identified in our study align well with clusters of stations identified based on polychaete functional guilds (Charrier et al. in preparation), reinforcing the distinctiveness of these "eco-regions."

The data presented here provide critical baseline community metrics for meiofauna in the region, with abundance, biomass, and community structure and function data that can serve as a baseline to assess the impact of environmental change and inform regional ecosystem models. Although more research is needed to better understand the community taxonomic and functional dynamics in the Arctic, particularly across a larger spatial scale and increased temporal resolution, our results suggest the need for small-scale sub-region ecosystem modeling units within the greater Pacific Arctic region. Our research also shows that the size-based separation for infauna (meiofauna versus macrofauna) and the traditional taxonomic focus by scientists within each group leads to exclusion of a benthic component, the macrofauna-sized nematodes, that represent a significant amount of biomass and abundance, and a distinct trophic signature. Future field, experimental, and modeling studies should take into account the potential bias when excluding macrofaunal-sized nematodes and assess their contribution to benthic ecosystem diversity and function.

Acknowledgments

This research was part of the Arctic Integrated Ecosystem Research Program (IERP; http://www.nprb.org/arctic-program/). This manuscript is Publication ArcticIERP-XX. Funding for the program was provided by the North Pacific Research Board, U.S. Bureau of Ocean and Energy Management, Collaborative Alaskan Arctic Studies Program, and U.S. Office of Naval Research. Generous in-kind support for the program was contributed by the U.S. National Oceanic Atmospheric Administration Alaska Fisheries Science Center and Pacific Marine Environmental Laboratory, University of Alaska Fairbanks, U.S. Fish and Wildlife Service, and U.S. National Science Foundation. Funding was also provided by the North Pacific Research Board Graduate Student Research Award and the University of Alaska Dissertation Completion Fellowship. We would like to thank the Captain and crew of the *R/V Sikuliaq* for making sampling possible and Opik Ahkinga, Silvana Gonzalez, and Andrew Thurber for help with sample collection. We would also like to thank Tibor Dorsaz and Alexis Walker for lab assistance, Timothy Howe and others at the Alaska Stable Isotope Facility, and Seth Danielson, Amanda Kelly, and Andrew Thurber for their valuable input and guidance.

References

Anderson, M.J., Gorley, R.N., 2008. PERMANOVA+ for PRIMER: Guide to software and statistical methods.

Andrassy, I., 1956. The determination of volume and weight of nematodes. Acta Zool. 2, 1–15.

Arar, E.J., Collins, G.B., 1997. In vitro determination of chlorophyll a and pheophytin a in marine and freshwater algae by fluorescence, National Exposure Research Laboratory Office of Research and Development U.S. Environmental Protection Agency. Cincinnati.

Arrigo, K.R., van Dijken, G.L., 2015. Continued increases in Arctic Ocean primary production. Prog. Oceanogr. 136, 60–70. doi:10.1016/j.pocean.2015.05.002

Baker, M.R., Kivva, K.K., Pisareva, M.N., Watson, J.T., Selivanova, J., 2020. Shifts in the physical environment in the Pacific Arctic and implications for ecological timing and conditions. Deep. Res. Part II Top. Stud. Oceanogr. 177. doi:10.1016/j.dsr2.2020.104802

Baldrighi, E., Manini, E., 2015. Deep-sea meiofauna and macrofauna diversity and functional diversity: are they related? Mar. Biodivers. 45, 469–488. doi:10.1007/s12526-015-0333-9

Bezerra, T.N.., Eisendle, U.., Hodda, M.., Holovachov, O.., Leduc, D.., Mokievsky, V.., Peña Santiago, R.., Sharma, J.., Smol, N.., Tchesunov, A.., Venekey, V.., Zhao, Z.., Vanreusel, A., 2021. Nemys: World database of nematodes. http://nemys.ugent.be. doi:10.14284/366

Blott, S.J., 2010. GRADISTAT Version 8.0: A grain size distribution and statistics package for the analysis of unconsolidated sediments by sieving or laser granulometer.

Blott, S.J., Pye, K., 2001. Gradistat: A grain size distribution and statistics package for the analysis of unconsolidated sediments. Earth Surf. Process. Landforms 26, 1237–1248. doi:10.1002/esp.261

Bluhm, B., Iken, K., Mincks Hardy, S., Sirenko, B., Holladay, B., 2009. Community structure of epibenthic megafauna in the Chukchi Sea. Aquat. Biol. 7, 269–293. doi:10.3354/ab00198

Bonaglia, S., Nascimento, F.J.A., Bartoli, M., Klawonn, I., Brüchert, & V, 2014. Meiofauna increases bacterial denitrification in marine sediments. Nat. Clim. Chang. 5, 1–9. doi:10.1038/ncomms6133

Bongers, T., 1990. The maturity index: an ecological measure of environmental disturbance based on nematode species composition. Oecologia 83, 14–19. doi:10.1007/BF00324627

Bongers, T., Alkemade, R., Yeates, G., 1991. Interpretation of disturbance-induced maturity decrease in marine nematode assemblages by means of the Maturity Index. Mar. Ecol. Prog. Ser. 76, 135–142.

Bongers, T., de Goede, R.G., Korthals, G.W., Yeates, G.., 1995. Proposed changes of c-p classification for nematodes. Russ. J. Nematol. 3, 61–62.

Braeckman, U., Provoost, P., Moens, T., Soetaert, K., Middelburg, J.J., Vincx, M., Vanaverbeke, J., 2011. Biological vs. physical mixing effects on benthic food web dynamics. PLoS One 6. doi:10.1371/journal.pone.0018078

Clarke, K.R., Gorley, R.N., 2015. PRIMER v7: User Manual/Tutorial.

Coull, B.C., 1999. Role of meiofauna in estuarine soft-bottom habitats. Austral Ecol. 24, 327–343. doi:10.1046/j.1442-9993.1999.00979.x

Coull, B.C., 1990. Are Members of the Meiofauna Food for Higher Trophic Levels? Trans. Am. Microsc. Soc. 109, 233. doi:10.2307/3226794

Danielson, S.L., Eisner, L., Ladd, C., Mordy, C., Sousa, L., Weingartner, T.J., 2017. A comparison between late summer 2012 and 2013 water masses, macronutrients, and phytoplankton standing crops in the northern Bering and Chukchi Seas. Deep Sea Res. Part II 135, 7–26. doi:10.1016/j.dsr2.2016.05.024

Danielson, S.L., Weingartner, T.J., Hedstrom, K.S., Aagaard, K., Woodgate, R., Curchitser, E., Stabeno, P.J., 2014. Coupled wind-forced controls of the Bering-Chukchi shelf circulation and the Bering Strait throughflow: Ekman transport, continental shelf waves, and variations of the Pacific-Arctic sea surface height gradient. Prog. Oceanogr. 125, 40–61. doi:10.1016/j.pocean.2014.04.006

Degraer, S., Moulaert, I., Van Hoey, G., Vincx, M., 2007. Sieving alive or after fixation: effects of sieving procedure on macrobenthic diversity, density and community structure. Helgol. Mar. Res. 2007 612 61, 143–152. doi:10.1007/S10152-007-0062-Y

Feder, H.M., Jewett, S.C., Blanchard, A.L., 2007. Southeastern Chukchi Sea (Alaska) macrobenthos. Polar Biol. 30, 261–275. doi:10.1007/s00300-006-0180-z

Feng, Z., Ji, R., Ashjian, C., Zhang, J., Campbell, R., Grebmeier, J.M., 2020. Benthic hotspots on the Northern Bering and Chukchi continental shelf: Spatial variability in production regimes and environmental drivers. Prog. Oceanogr. 191, 102497. doi:10.1016/j.pocean.2020.102497

Galéron, J., Sibuet, M., Vanreusel, A., Mackenzie, K., Gooday, A.., Dinet, A., Wolff, G.., 2001. Temporal patterns among meiofauna and macrofauna taxa related to changes in sediment geochemistry at an abyssal NE Atlantic site. Prog. Oceanogr. 50, 303–324. doi:10.1016/S0079-6611(01)00059-3

Gee, J.M., 1989. An ecological and economic review of meiofauna as food for fish. Zool. J. Linn. Soc. 96, 243–261. doi:10.1111/j.1096-3642.1989.tb02259.x

Giere, O., 2009. Meiobenthology: The microscopic motile fauna of aquatic sediments, 2nd ed. Springer-Verlag Berlin Heidelberg, Hamburg.

Goethel, C.L., Grebmeier, J.M., Cooper, L.W., 2019. Changes in abundance and biomass of the bivalve *Macoma calcarea* in the northern Bering Sea and the southeastern Chukchi Sea from 1998 to 2014, tracked through dynamic factor analysis models. Deep Sea Res. Part II 162, 127–136. doi:10.1016/j.dsr2.2018.10.007

Górska, B., Grzelak, K., Kotwicki, L., Hasemann, C., Schewe, I., Soltwedel, T., Włodarska-Kowalczuk, M., 2014. Bathymetric variations in vertical distribution patterns of meiofauna in the surface sediments of the deep Arctic ocean (HAUSGARTEN, Fram strait). Deep. Res. Part I 91, 36–49. doi:10.1016/j.dsr.2014.05.010

Grebmeier, J., Bluhm, B.A., Cooper, L.W., Danielson, S.L., Arrigo, K.R., Blanchard, A.L., Clarke, J.T., Day, R.H., Frey, K.E., Gradinger, R.R., Kedra, M., Konar, B., Kuletz, K.J., Lee, S.H., Lovvorn, J.R., Norcross, B.L., Okkonen, S.R., 2015. Ecosystem characteristics and processes facilitating persistent macrobenthic biomass hotspots and associated benthivory in the Pacific Arctic. Prog. Oceanogr. 136, 92–114. doi:10.1016/j.pocean.2015.05.006

Grebmeier, J., Frey, K., Cooper, L., Kędra, M., 2018. Trends in benthic macrofaunal populations, seasonal sea ice persistence, and bottom water temperatures in the Bering Strait region. Oceanography 31, 136–151. doi:10.5670/oceanog.2018.224

Grebmeier, J.M., 2012. Shifting patterns of life in the Pacific Arctic and Sub-Arctic Seas. Ann. Rev. Mar. Sci. 4, 63–78. doi:10.1146/annurev-marine-120710-100926

Grebmeier, J.M., 1993. Studies of pelagic-benthic coupling extended onto the Soviet continental shelf in the northern Bering and Chukchi seas. Cont. Shelf Res. 13, 653–668. doi:10.1016/0278-4343(93)90098-I

Grebmeier, J.M., Barry, J.P., 1991. The influence of oceanographic processes on pelagic-benthic coupling in polar regions: A benthic perspective. J. Mar. Syst. Elsevier Sci. Publ. B.V 2, 495–518.

Grebmeier, J.M., McRoy, C.P., 1989. Pelagic-benthic coupling on the shelf of the northern Bering

and Chukchi Seas. III. Benthic food supply and carbon cycling. Mar. Ecol. Prog. Ser. 53, 79–91.
Grzelak, K., Sørensen, M. V., 2019. Diversity and community structure of kinorhynchs around Svalbard: First insights into spatial patterns and environmental drivers. Zool. Anz. 282, 31–43. doi:10.1016/J.JCZ.2019.05.009
Gunton, L.M., Bett, B.J., Gooday, A.J., Glover, A.G., Vanreusel, A., 2017. Macrofaunal nematodes of the deep Whittard Canyon (NE Atlantic): assemblage characteristics and comparison with polychaetes. Mar. Ecol. 38, e12408. doi:10.1111/maec.12408
Hajduk, M., 2015. Density and distribution of meiofauna in the northeastern Chukchi Sea. University of Alaska Fairbanks.
Heip, C., Herman, P.M.J., Soetaert, K., 1998. Indices of diversity and evenness. Oceanis 24, 61–87.
Heip, C., Vincx, M., Vranken, G., 1985. The ecology of marine nematodes. Oceanogr. Mar. Biol. 23, 399–489.
Higgins, R.P., Theil, H., 1988. Introduction to the study of meiofauna. Smithsonian Institution Press, Washington D.C.
Hill, M.O., 1973. Diversity and Evenness: A Unifying Notation and Its Consequences. Ecology 54, 427–432.
Huntington, H.P., Danielson, S.L., Wiese, F.K., Baker, M., Boveng, P., Citta, J.J., De Robertis, A., Dickson, D.M.S., Farley, E., George, J.C., Iken, K., Kimmel, D.G., Kuletz, K., Ladd, C., Levine, R., Quakenbush, L., Stabeno, P., Stafford, K.M., Stockwell, D., Wilson, C., 2020. Evidence suggests potential transformation of the Pacific Arctic ecosystem is underway. Nat. Clim. Chang. doi:10.1038/s41558-020-0695-2
Iken, K., Bluhm, B., Dunton, K., 2010. Benthic food-web structure under differing water mass properties in the southern Chukchi Sea. Deep Sea Res. Part II 57, 71–85. doi:10.1016/j.dsr2.2009.08.007
Ingels, J., Billett, D.S.M., Kiriakoulakis, K., Wolff, G.A., Vanreusel, A., 2011a. Structural and functional diversity of Nematoda in relation with environmental variables in the Setú bal and Cascais canyons, Western Iberian Margin. Deep. Res. Part II 58, 2354–2368. doi:10.1016/j.dsr2.2011.04.002
Ingels, J., Tchesunov, A. V., Vanreusel, A., 2011b. Meiofauna in the Gollum Channels and the Whittard Canyon, Celtic Margin—How local environmental conditions shape nematode structure and function. PLoS One 6, e20094. doi:10.1371/journal.pone.0020094
Ingels, J., Vanhove, S., De Mesel, I., Vanreusel, A., 2006. The biodiversity and biogeography of the free-living nematode genera *Desmodora* and *Desmodorella* (family Desmodoridae) at both sides of the Scotia Arc. Polar Biol. 29, 936–949. doi:10.1007/s00300-006-0135-4
Ingels, J., Vanreusel, A., 2013. The importance of different spatial scales in determining structural and functional characteristics of deep-sea infauna communities. Biogeosciences 10, 4547–4563. doi:10.5194/BG-10-4547-2013
Ingels, J., Vanreusel, A., Romano, C., Coenjaerts, J., Mar Flexas, M., Zúñiga, D., Martin, D., 2013. Spatial and temporal infaunal dynamics of the Blanes submarine canyon-slope system (NW Mediterranean); changes in nematode standing stocks, feeding types and gender-life stage ratios. Prog. Oceanogr. 118, 159–174. doi:10.1016/J.POCEAN.2013.07.021
Jensen, P., 1984. Measuring carbon content in nematodes. Helgolander Meeresuntersuchungen 38, 83–86.
Jones, B.R., Kelley, A.L., Mincks, S.L., 2021. Changes to benthic community structure may

impact organic matter consumption on Pacific Arctic shelves. Conserv. Physiol. 9. doi:10.1093/conphys/coab007

Kennedy, A., 1994. Carbon partitioning within meiobenthic nematode communities in the Exe Estuary, UK. Mar. Ecol. Prog. Ser. 105, 71–78. doi:10.3354/meps105071

Lambshead, P.J.D., Ferrero, T.J., Wollf, G.A., 1995. Comparison of the vertical distribution of nematodes from two contrasting abyssal sites in the Northeast Atlantic subject to different seasonal inputs of phytodetritus. Int. Rev. der gesamten Hydrobiol. und Hydrogr. 80, 327–331. doi:10.1002/IROH.19950800219

Landers, S.C., Sørensen, M. V., Sánchez, N., Beaton, K.R., Miller, J.M., Ingels, J., 2019. Kinorhynch communities on the Louisiana continental shelf. https://doi.org/10.2988/18-00008 132, 1–14. doi:10.2988/18-00008

Lee, S., Sun Yun, M., Kyoung Kim, B., Saitoh, S., Kang, C.-K., Kang, S.-H., Whitledge, T., 2013. Latitudinal carbon productivity in the Bering and Chukchi Seas during the summer in 2007. Cont. Shelf Res. 59, 28–36. doi:10.1016/J.CSR.2013.04.004

Lin, R., Huang, D., Guo, Y., Chang, Y., Cao, Y., Wang, J., 2014. Abundance and distribution of meiofauna in the Chukchi Sea. Acta Oceanol. Sin. 33, 90–94. doi:10.1007/s13131-014-0493-7

Lovvorn, J., North, C., Kolts, J., Grebmeier, J., Cooper, L., Cui, X., 2016. Projecting the effects of climate-driven changes in organic matter supply on benthic food webs in the northern Bering Sea. Mar. Ecol. Prog. Ser. 548, 11–30. doi:10.3354/meps11651

Lovvorn, J., Rocha, A., Danielson, S., Cooper, L., Grebmeier, J., Hedstrom, K., 2020. Predicting sediment organic carbon and related food web types from a physical oceanographic model on a subarctic shelf. Mar. Ecol. Prog. Ser. 633, 37–54. doi:10.3354/meps13163

Mincks, S., Smith, C., DeMaster, D., 2005. Persistence of labile organic matter and microbial biomass in Antarctic shelf sediments: evidence of a sediment “food bank.” Mar. Ecol. Prog. Ser. 300, 3–19. doi:10.3354/meps300003

Mincks, S.L., Pereira, T.J., Sharma, J., Blanchard, A.L., Bik, H.M., 2021. Composition of marine nematode communities across broad longitudinal and bathymetric gradients in the Northeast Chukchi and Beaufort Seas. Polar Biol. doi:10.1007/s00300-020-02777-1

Moore, S.E., Stabeno, P.J., 2015. Synthesis of Arctic Research (SOAR) in marine ecosystems of the Pacific Arctic. Prog. Oceanogr. 136, 1–11. doi:10.1016/j.pocean.2015.05.017

Moore, S.E., Stabeno, P.J., Grebmeier, J.M., Okkonen, S.R., 2018. The Arctic Marine Pulses Model: linking annual oceanographic processes to contiguous ecological domains in the Pacific Arctic. Deep. Res. II 152, 8–21. doi:10.1016/j.dsr2.2016.10.011

Nelson, R.J., Ashjian, C.J., Bluhm, B.A., Conlan, K.E., Gradinger, R.R., Grebmeier, J.M., Hill, V.J., Hopcroft, R.R., Hunt, B.P. V., Joo, H.M., Kirchman, D.L., Kosobokova, K.N., Lee, S.H., Li, W.K.W., Lovejoy, C., Poulin, M., Sherr, E., Young, K. V., 2014. Biodiversity and biogeography of the lower trophic taxa of the Pacific Arctic region: Sensitivities to climate change, in: The Pacific Arctic Region. Springer Netherlands, Dordrecht, pp. 269–336. doi:10.1007/978-94-017-8863-2_10

O’Daly, S.H., Danielson, S.L., Hardy, S.M., Hopcroft, R.R., Lalande, C., Stockwell, D.A., McDonnell, A.M.P., 2020. Extraordinary carbon fluxes on the shallow Pacific Arctic shelf during a remarkably warm and low sea ice period. Front. Mar. Sci. 7, 986. doi:10.3389/fmars.2020.548931

Pape, E., van Oevelen, D., Moodley, L., Soetaert, K., Vanreusel, A., 2013. Nematode feeding strategies and the fate of dissolved organic matter carbon in different deep-sea sedimentary

environments. Deep Sea Res. Part I Oceanogr. Res. Pap. 80, 94–110. doi:10.1016/J.DSR.2013.05.018
Pirtle-Levy, R., Cooper, L.W., Larsen, I.L., 2009. Chlorophyll a in Arctic sediments implies long persistence of algal pigments. Deep Sea Res. Part II Top. Stud. Oceanogr. 56, 1326–1338.
Platt, H., Warwick, R., 1988. Free-living marine nematodes: Part II. British Chromadorids: pictorial key to world genera and notes for the identification of British species. EJ Brill, Backhuys, Leiden.
Ridall, A., Ingels, J., 2021. Suitability of free-living marine nematodes as bioindicators: Status and future considerations. Front. Mar. Sci. 0, 863. doi:10.3389/FMARS.2021.685327
Ringuette, M., Fortier, L., Fortier, M., Runge, J.A., Bélanger, S., Larouche, P., Weslawski, J.-M., Kwasniewski, S., 2002. Advanced recruitment and accelerated population development in Arctic calanoid copepods of the North Water. Deep Sea Res. Part II 49, 5081–5099. doi:10.1016/S0967-0645(02)00179-0
Román, S., Vanreusel, A., Ingels, J., Martin, D., 2018. Nematode community zonation in response to environmental drivers in Blanes Canyon (NW Mediterranean). J. Exp. Mar. Bio. Ecol. 502, 111–128. doi:10.1016/J.JEMBE.2017.08.010
Rysgaard, S., Christensen, P., Sørensen, M., Funch, P., Berg, P., 2000. Marine meiofauna, carbon and nitrogen mineralization in sandy and soft sediments of Disko Bay, West Greenland. Aquat. Microb. Ecol. 21, 59–71. doi:021059
Schratzberger, M., Ingels, J., 2018. Meiofauna matters: The roles of meiofauna in benthic ecosystems. J. Exp. Mar. Bio. Ecol. 502, 12–25. doi:10.1016/j.jembe.2017.01.007
Seinhorst, J., 1959. A rapid method for the transfer of nematodes from fixation to anhydrous glycerin. Nematolofica 4, 67–69.
Selz, V., Saenz, B.T., van Dijken, G.L., Arrigo, K.R., 2018. Drivers of ice algal bloom variability between 1980 and 2015 in the Chukchi Sea. J. Geophys. Res. Ocean. 123, 7037–7052. doi:10.1029/2018JC014123
Sharma, J., Baguley, J., Bluhm, B.A., Rowe, G., 2011. Do meio-and macrobenthic nematodes differ in community composition and body weight trends with depth? PLoS One 6, 14491. doi:10.1371/journal.pone.0014491
Sharma, J., Bluhm, B.A., 2010. Diversity of larger free-living nematodes from macrobenthos (>250 μm) in the Arctic deep-sea Canada Basin. Mar. Biodivers. 2010 413 41, 455–465. doi:10.1007/S12526-010-0060-1
Soetaert, K., Heip, C., 1990. Sample-size dependence of diversity indices and the determination of sufficient sample size in a high-diversity deep-sea environment. Mar. Ecol. Prog. Ser. 59, 305–307.
Soltwedel, T., Wegener, A., Miljutina, M., Thistle, D., 2003. The meiobenthos of the Molloy Deep (5 600 m), Fram Strait, Arctic Ocean. Vie Milieu 53, 1–13.
Somerfield, P.J., Clarke, K.R., 1995. Taxonomic levels, in marine community studies, revisited. Mar. Ecol. Prog. Ser. 127, 113–119.
Vanaverbeke, J., Soetaert, K., Heip, C., Vanreusel, A., 1997. The metazoan meiobenthos along the continental slope of the Goban Spur (NE Atlantic). J. Sea Res. 38, 93–107. doi:10.1016/S1385-1101(97)00038-5
Vanreusel, A., Fonseca, G., Danovaro, R., Da Silva, M.C., Esteves, A.M., Ferrero, T., Gad, G., Galtsova, V., Gambi, C., Da Fonsêca Genevois, V., Ingels, J., Ingole, B., Lampadariou, N., Merckx, B., Miljutin, D., Miljutina, M., Muthumbi, A., Netto, S., Portnova, D., Radziejewska, T., Raes, M., Tchesunov, A., Vanaverbeke, J., Van Gaever, S., Venekey, V., Bezerra, T.N.,

Flint, H., Copley, J., Pape, E., Zeppilli, D., Martinez, P.A., Galeron, J., 2010. The contribution of deep-sea macrohabitat heterogeneity to global nematode diversity. Mar. Ecol. 31, 6–20. doi:10.1111/j.1439-0485.2009.00352.x

Waga, H., Hirawake, T., Grebmeier, J.M., 2020. Recent change in benthic macrofaunal community composition in relation to physical forcing in the Pacific Arctic. Polar Biol. 43, 285–294. doi:10.1007/s00300-020-02632-3

Walsh, J.J., McRoy, C.P., Coachman, L.K., Goering, J.J., Nihoul, J.J., Whitledge, T.E., Blackburn, T.H., Parker, P.L., Wirick, C.D., Shuert, P.G., Grebmeier, J.M., Springer, A.M., Tripp, R.D., Hansell, D.A., Djenidi, S., Deleersnijder, E., Henriksen, K., Lund, B.A., Andersen, P., Müller-Karger, F.E., Dean, K., 1989. Carbon and nitrogen cycling within the Bering/Chukchi Seas: Source regions for organic matter effecting AOU demands of the Arctic Ocean. Prog. Oceanogr. 22, 277–359. doi:10.1016/0079-6611(89)90006-2

Wang, M., Overland, J.E., 2015. Projected future duration of the sea-ice-free season in the Alaskan Arctic. Prog. Oceanogr. 136, 50–59. doi:10.1016/j.pocean.2015.01.001

Warwick, R., 1984. Species size distributions in marine benthic communities. Oecologia 61, 32–41. doi:10.1007/BF00379085

Wieser, W., 1953. The relationship between the mouth cavity form, feeding habit and occurrence in free-living marine nematodes: An ecological-morphological study. Ark. Zool. 4, 439–484.

Zinkann, A.-C., 2020. Organic matter sources on the Chukchi Sea shelf in a changing Arctic. University of Alaska Fairbanks.

Table 1: Meiofauna metrics of each station sampled in 2018, including cluster group; latitude (°N); longitude (°W); water depth (m); meiofauna, meiofaunal-sized nematode, and macrofaunal-sized nematodes abundances (individuals 10 cm^{-2}) in the upper 5 cm of sediment; and abundance (individuals 10 cm^{-2}), wet weight, dry weight, carbon weight (µg 10 cm^{-2}), and individual size (µg DW $ind.^{-1}$) of meiofaunal- and macrofaunal-sized nematodes in the upper 1 cm of sediment. Groups are based on hierarchical agglomerative clustering and similarity profile test (SIMPROF; Figure 3).

					63-500 µm							>500 µm					
					0-5 cm		0-1 cm--Nematodes					0-5 cm	0-1 cm--Nematodes				
Station	Group	Lat. (°N)	Long. (°W)	Depth (m)	Meio. abund. (ind. 10 cm^{-2})	Nem. abund. (ind. 10 cm^{-2})	Abund. (ind. 10 cm^{-2})	Wet weight (g WW 10 cm^{-2})	Dry weight (g DW 10 cm^{-2})	Carbon weight (g CW 10 cm^{-2})	Avg. individual DW (g DW $ind.^{-1}$)	Nem. abund. (ind. 10 cm^{-2})	Abund. (ind. 10 cm^{-2})	Wet weight (g WW 10 cm^{-2})	Dry weight (g DW 10 cm^{-2})	Carbon weight (g CW 10 cm^{-2})	Avg. individual DW (g DW $ind.^{-1}$)
CL1	D	68.95	-166.91	46	4135	3876	1450	1151	288	143	0.20	19	3	59	15	7	5
CL3	D	69.03	-168.89	53	12875	12457	6920	2958	739	367	0.11	37	1	7	2	1	2
CNL3	B	66.50	-168.96	56	1449	1278	192	251	63	31	0.33	30	4	41	10	5	2
CNL5	C	67.00	-168.96	48	3035	2748	160	131	33	16	0.20	49	1	13	3	2	4
DBO2.2	A	64.68	-169.10	46	3860	3378	1977	1429	357	177	0.18	16	7	234	58	29	8
DBO2.4	A	64.96	-169.89	48	3719	1840	985	1848	462	229	0.47	80	9	247	62	31	7
DBO3.3	D	68.19	-167.31	48	1663	1542	647	626	157	78	0.24	47	22	861	215	107	10
DBO3.6	C	67.90	-168.24	58	7712	7268	598	766	191	95	0.32	102	14	411	103	51	8
DBO3.8	C	67.67	-168.96	51	6906	6775	922	688	172	85	0.19	110	4	33	8	4	2
IL4	D	67.40	-165.84	39	5247	4589	1501	2008	502	249	0.33	46	9	202	50	25	6

Table 2: Relative abundance (%) of the most abundant (>1%) nematode genera per group (0-1 cm sediment layer) for the (a) 63-500 µm and (b) >500 µm size fractions. Groups are based on hierarchical agglomerative clustering and similarity profile test of meiofaunal-sized communities (SIMPROF; Figure 3). Genera highlighted in bold in table (a) contributed >70% to within group similarity based on Similarity Percentages (SIMPER) procedure (Note: Group B only contained one station so a SIMPER could not be performed for this group).

(a)

63- 500 µm:	**Group A**		**Group B**		**Group C**		**Group D**	
	(1b, 2) *Daptonema*	15.28	(1b, 2) *Sabatieria*	24.75	**(1b, 2) *Daptonema***	42.51	**(1a, 4) *Halalaimus***	19.18
	(2b, 4) *Oncholaimus*	11.65	(1b, 2) *Daptonema*	10.89	**(1b, 2) *Paramonohystera***	23.37	**(2a, 2) *Microlaimus***	11.05
	(1b, 1) *Monhystrella*	8.95	(2a, 3) *Marylynnia*	10.89	**(1b, 2) *Sabatieria***	12.67	**(1a, 4) *Tricoma***	8.24
	(1b, 2) *Paramonohystera*	7.67	(1b, 2) *Paramonohystera*	5.94	(2a, 3) *Neochromadora*	11.14	**(1b, 2) *Paramonohystera***	6.26
	(1a, 4) *Halalaimus*	6.55	(1b, 2) Comesomatidae	5.94	**(2a, 3) *Chromadorita***	3.24	(1b, 1) *Thalassomonhystera*	5.59
	(2a, 3) *Neochromadora*	6.46	(1a, 1) *Halomonhystera*	3.96	(1a, 4) *Halalaimus*	2.29	**(1a, 3) *Terschellingia***	4.79
	(2b, 3) *Viscosia*	5.61	(1b, 2) *Metalinhomoeus*	3.96			**(1b, 2) *Sabatieria***	4.49
	(1b, 2) *Sabatieria*	5.18	(1a, 4) *Halalaimus*	2.97			**(1b, 2) *Cervonema***	4.29
	(2a, 2) *Microlaimus*	4.43	(2a, 3) *Neochromadora*	2.97			**(1b, 3) *Campylaimus***	4.12
	(2a, 3) *Actinonema*	3.61	(1b, 1) *Monhystrella*	1.98			**(1a, 4) *Desmoscolex***	3.83
	(1b, 2) *Steineria*	2.70	(2a, 2) *Microlaimus*	1.98			(2a, 3) *Neochromadora*	3.49
	(2a, 3) *Trochamus*	2.70	(1b, 2) Xyalidae	1.98			**(2a, 3) *Aponema***	3.32
	(1a, 1) *Halomonhystera*	2.27	(2a, 3) Cyatholaimidae	1.98			(1b, 2) *Daptonema*	2.54
	(2a, 3) *Chromadorita*	2.15	(1a, 4) *Tricoma*	1.98			(1b, 2) *Eleutherolaimus*	2.00
	(1a, 3) *Diplopeltula*	1.88	(2a, 3) *Pseudomicrolaimus*	1.98			(2a, 2) *Desmodora*	1.79
	(1b, 1) *Thalassomonhystera*	1.33					(1a, 2) *Leptolaimus*	1.73
	(1a, 2) *Leptolaimus*	1.21					(1a, 3) *Diplopeltula*	1.73
							(2a, 3) *Chromadorita*	1.30
							(1a, 3) *Pselionema*	1.28

(b)

>500 µm:	**Group A**		**Group B**		**Group C**		**Group D**	
	Sabatieria	22.97	*Sabatieria*	62.07	*Paramonohystera*	67.70	*Paramonohystera*	32.62
	Cephalanticoma	17.15	*Marylynnia*	13.79	*Sabatieria*	19.85	*Sabatieria*	14.44
	Mesacanthion	12.28	*Metalinhomoeus*	6.90	*Halalaimus*	3.63	*Setosabatieria*	12.53
	Oncholaimus	9.95	*Viscosia*	6.90	*Daptonema*	2.91	*Mesacanthion*	9.92
	Daptonema	6.78	*Crenopharynx*	3.45	*Innocuonema*	1.49	*Oxyonchus*	9.92
	Oxyonchus	5.81	*Oncholaimus*	3.45	*Sphaerolaimus*	1.49	*Rhabdodemania*	5.84
	Metalinhomoeus	4.24	*Symplocostoma*	3.45	*Mesacanthion*	1.43	*Daptonema*	4.67
	Metoncholaimus	4.24					*Dorylaimopsis*	2.21
	Viscosia	4.17					*Thalassoalaimus*	1.24
	Ledovitia	3.30					*Metalinhomoeus*	1.17
	Paramonohystera	2.54						
	Steineria	2.45						
	Subsphaerolaimus	1.69						

Table 3: Hill's numbers (H_0, H_1, H_2, H_∞), Pielou's evenness (J′), Shannon-Wiener diversity index (H′), expected number of genera for 51 individuals (EG(51)), average trophic diversity (Heip et al., 1998), relative abundances of each feeding type, average maturity index (Bongers, 1990; Bongers et al., 1991), and relative abundance of each c-p score for meiofaunal-sized (63-500 µm) nematodes in surface sediments (0-1 cm) for each group. Groups are based on hierarchical agglomerative clustering and similarity profile test (SIMPROF; Figure 3).

	Group A	**Group B**	**Group C**	**Group D**
H_0	26.5	31	12	26
H_1	15.0	16.9	5.0	15.5
H_2	10.3	9.9	3.4	10.1
H_∞	5.1	4.0	2.1	4.5
J′	0.83	0.82	0.62	0.84
H′	2.7	2.8	1.6	2.7
EG(51)	16.7	20.1	8.4	17.0
Trophic Diversity	3.07 ± 0.69	2.42	1.53 ± 0.20	2.67 ± 0.22
Feeding types:				
1A	15.3	12.9	3.3	43.2
1B	43.0	56.4	79.8	32.6
2A	23.3	27.7	15.9	23.7
2B	18.5	3.0	1.1	0.6
Maturity Index	2.61 ± 0.20	2.41	2.25 ± 0.10	2.75 ± 0.24
c-p score:				
2	52.9	66.3	80.7	46.3
3	26.2	26.7	16.0	22.0
4	20.9	6.9	3.3	31.8

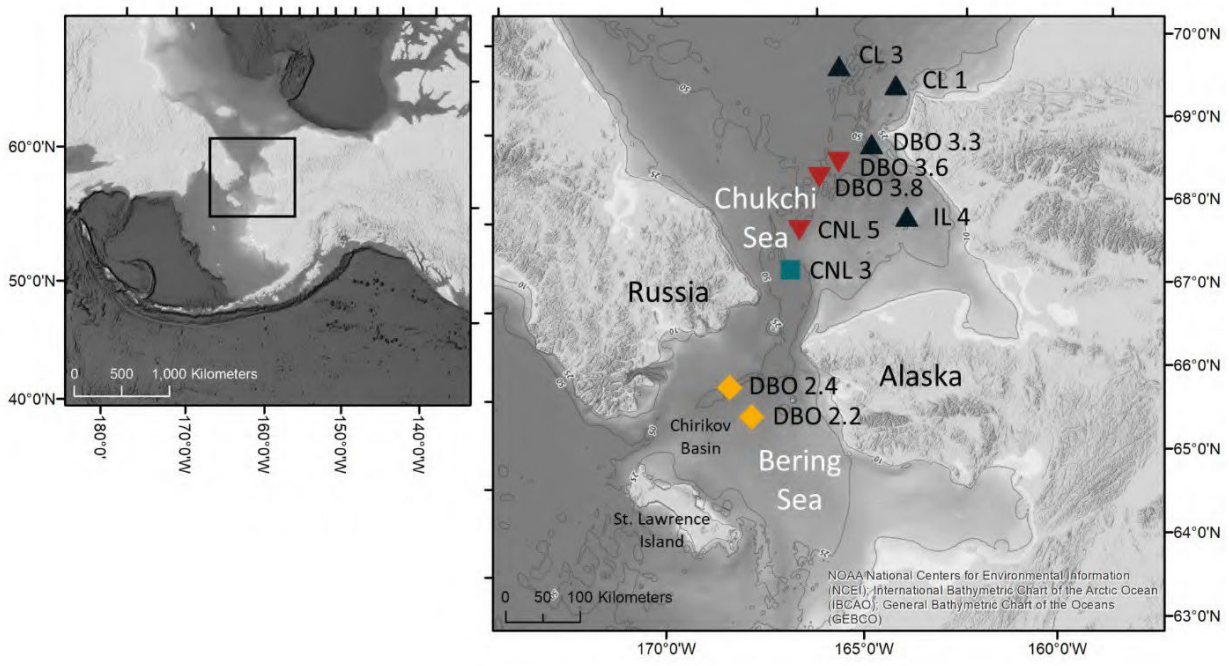

Figure 1: Ten sampling locations in the northern Bering and southern Chukchi Seas in 2018. Symbols based on hierarchical agglomerative clustering of 63-500 µm nematode communities from Figure 3. Group A = yellow diamonds; Group B = blue square; Group C = red inverted triangles; Group D = black upright triangles.

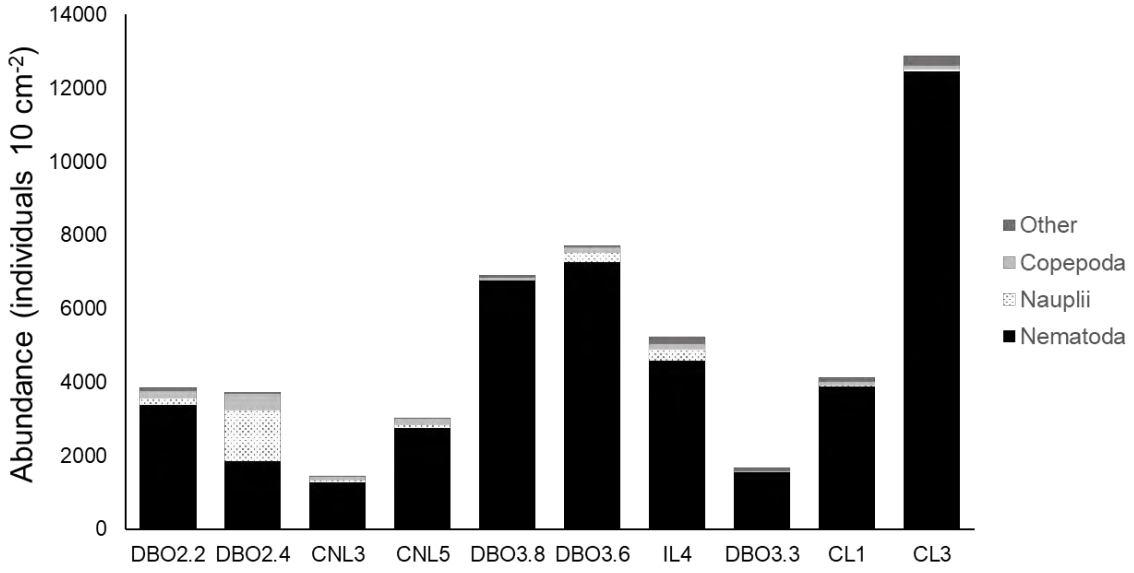

Figure 2: Meiofaunal abundance (ind. 10 cm^{-2}) in the upper 5 cm of sediment at sampling locations on the northern Bering and southern Chukchi Sea continental shelves in 2018.

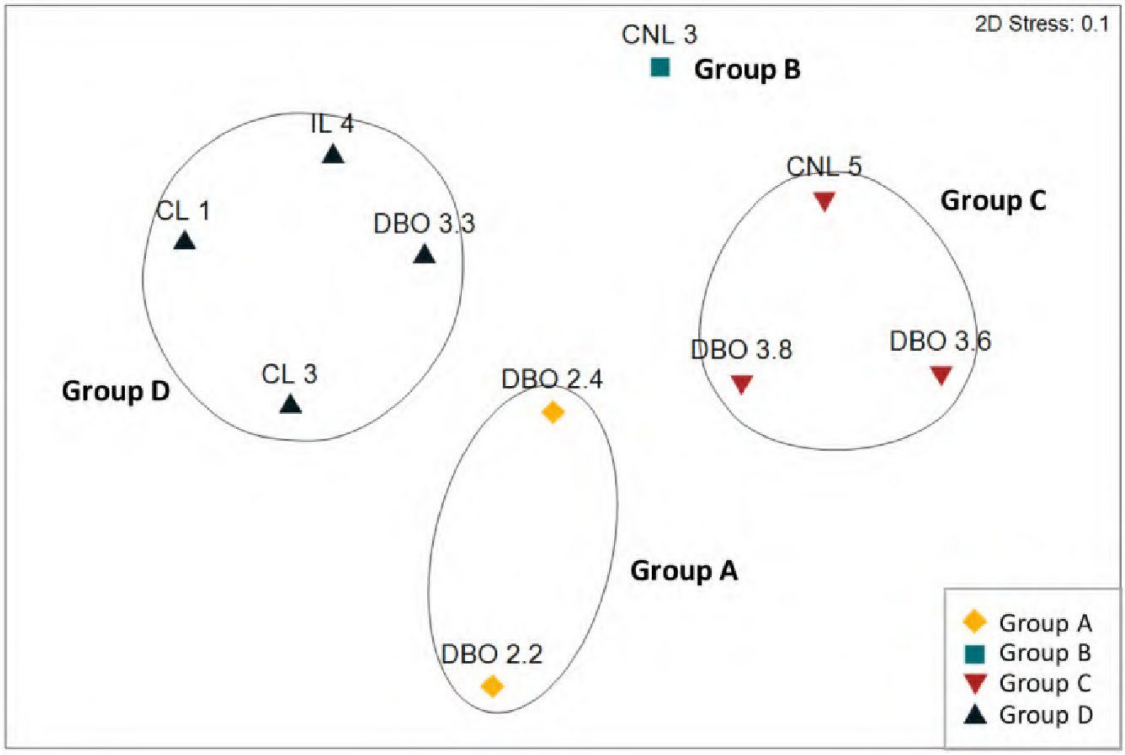

Figure 3: nMDS ordination of meiofaunal-sized (63-500 µm) nematode surface (0-1 cm) community structure (ind. 10 cm^{-2}). Ordination based on hierarchical agglomerative clustering with group-averaged linkage on $\log_{(x + 1)}$ transformed data and Bray-Curtis similarity. Four significant station groupings circled in black or as a singleton station based on the similarity profile test (SIMPROF).

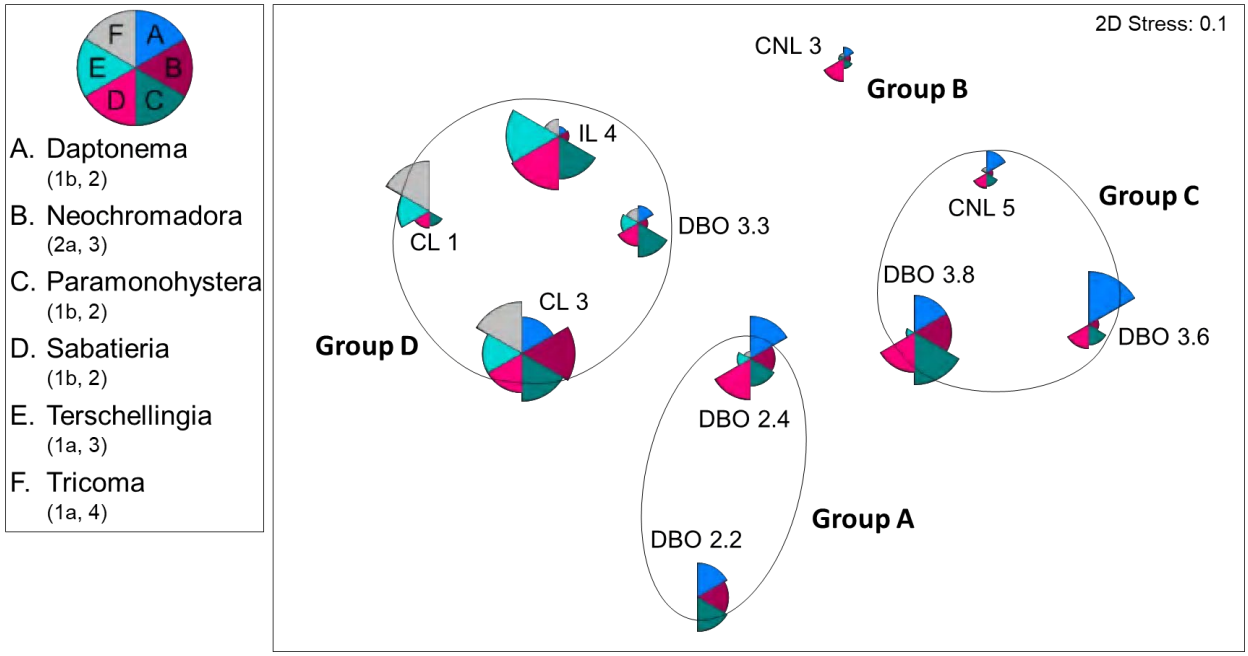

Figure 4: nMDS ordination of meiofaunal-sized (63-500 µm) nematode surface (0-1 cm) community structure (ind. 10 cm^{-2}). Ordination based on hierarchical agglomerative clustering with group-averaged linkage on $\log_{(x + 1)}$ transformed data and Bray-Curtis similarity. Four significant station groupings circled in black or as a singleton station based on the similarity profile test (SIMPROF). Pie slices represent the abundance of nematode genera that are in the top three guilds contributing to within-group similarity in at least one group based on Similarity Percentages (SIMPER) procedure. Feeding type and c-p score of genera in parentheses.

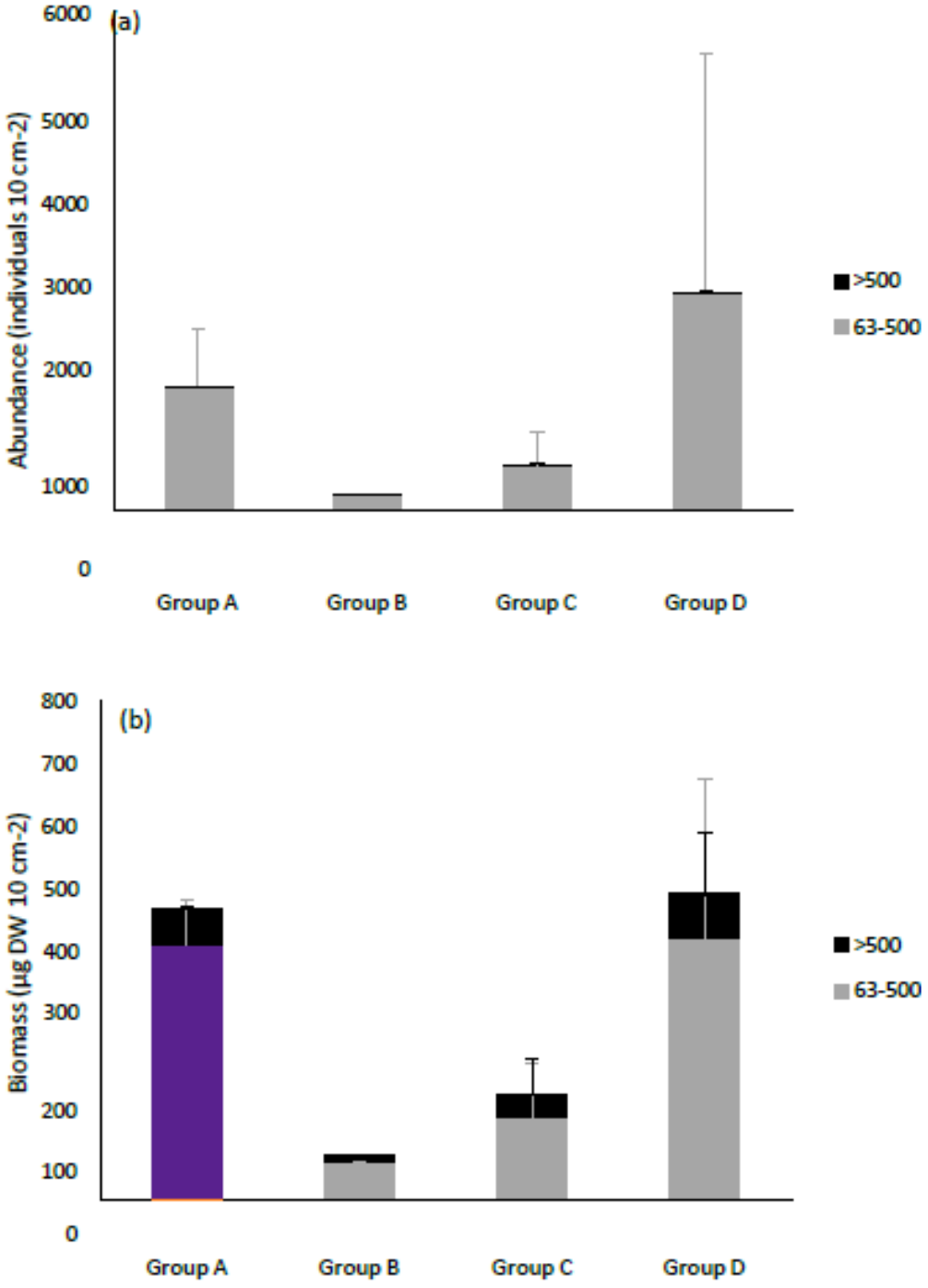

Figure 5: Average meiofaunal-sized and macrofaunal-sized nematode (a) abundance (ind. 10 cm^{-2}) and (b) biomass (µg DW 10 cm^{-2}) in surface sediments (0-1cm) for each group. Groups are based on hierarchical agglomerative clustering and similarity profile test (SIMPROF; Figure 3).

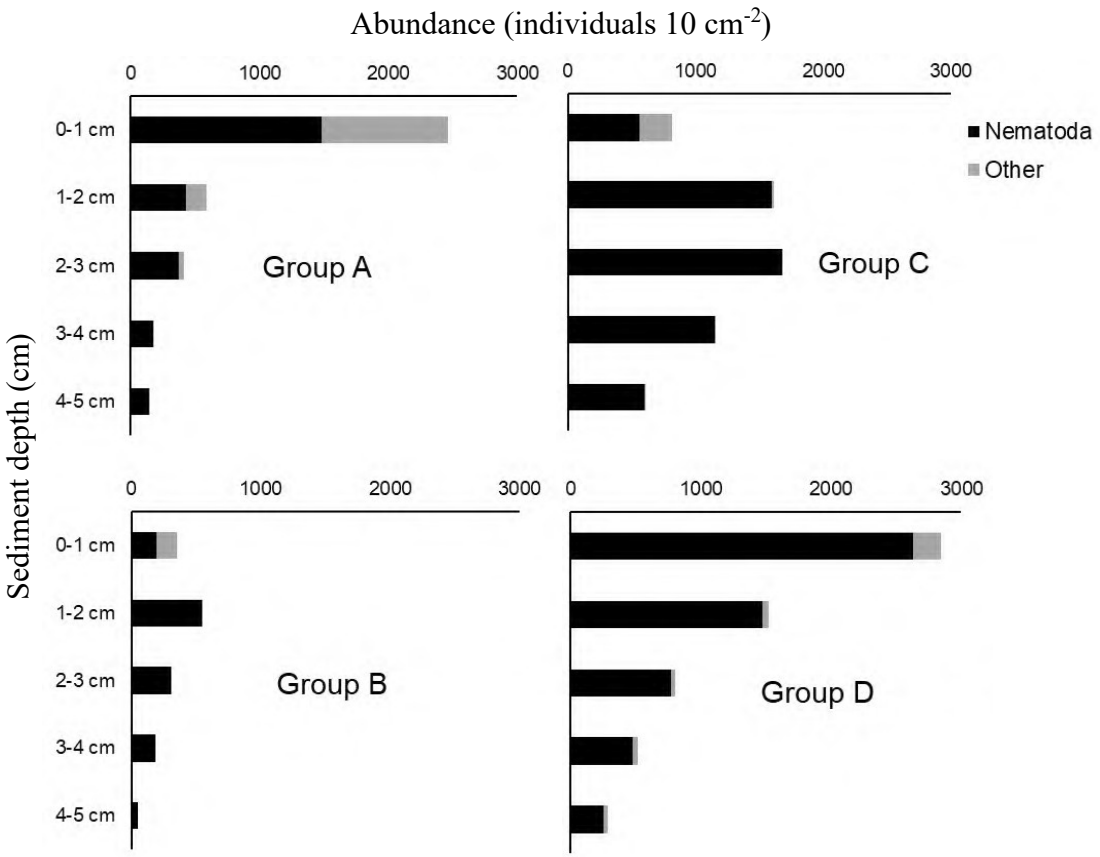

Figure 6: Abundance (individuals $10cm^{-2}$) of nematodes (63-500 µm; black) and other meiofauna (gray) for each sediment depth and group. Groups are based on hierarchical agglomerative clustering and similarity profile test (SIMPROF; Figure 3).

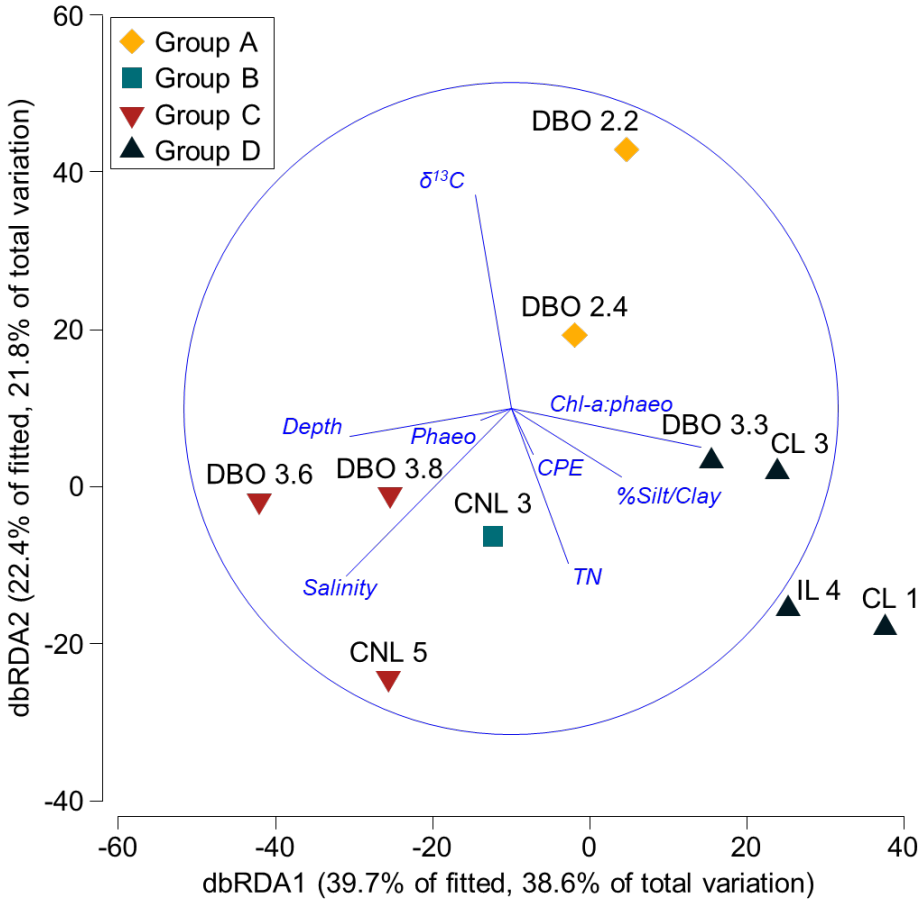

Relationships between dbRDA coordinate axes and orthonormal X variables (multiple partial correlations)

Variable	dbRDA1	dbRDA2	dbRDA3	dbRDA4	dbRDA5	dbRDA6	dbRDA7	dbRDA8
d13C	-0.109	0.653	-0.173	-0.678	0.185	-0.112	0.055	-0.148
Chla:Phaeo	0.579	-0.119	-0.582	0.006	-0.125	-0.029	0.479	-0.257
Salinity	-0.503	-0.512	-0.295	-0.241	-0.135	-0.273	-0.177	-0.464
%Silt/Clay	0.337	-0.211	0.504	-0.531	-0.553	-0.033	0.013	-0.002
Depth (m)	-0.493	-0.087	0.003	-0.089	-0.168	0.094	0.747	0.383
TN inv (mg /cm2)	0.174	-0.474	0.158	-0.340	0.757	0.058	0.127	0.107
Phaeo inv (ug / cm2)	-0.094	-0.036	-0.085	-0.123	-0.061	0.946	-0.087	-0.248
CPE ug/cm2	0.068	-0.140	-0.508	-0.248	-0.144	0.059	-0.394	0.691

Figure 7: dbRDA displaying the relationship between nematode (63-500 µm) community structure for the upper 1 cm of sediment and environmental correlates. The selected model accounted for 97.2% of total variation.

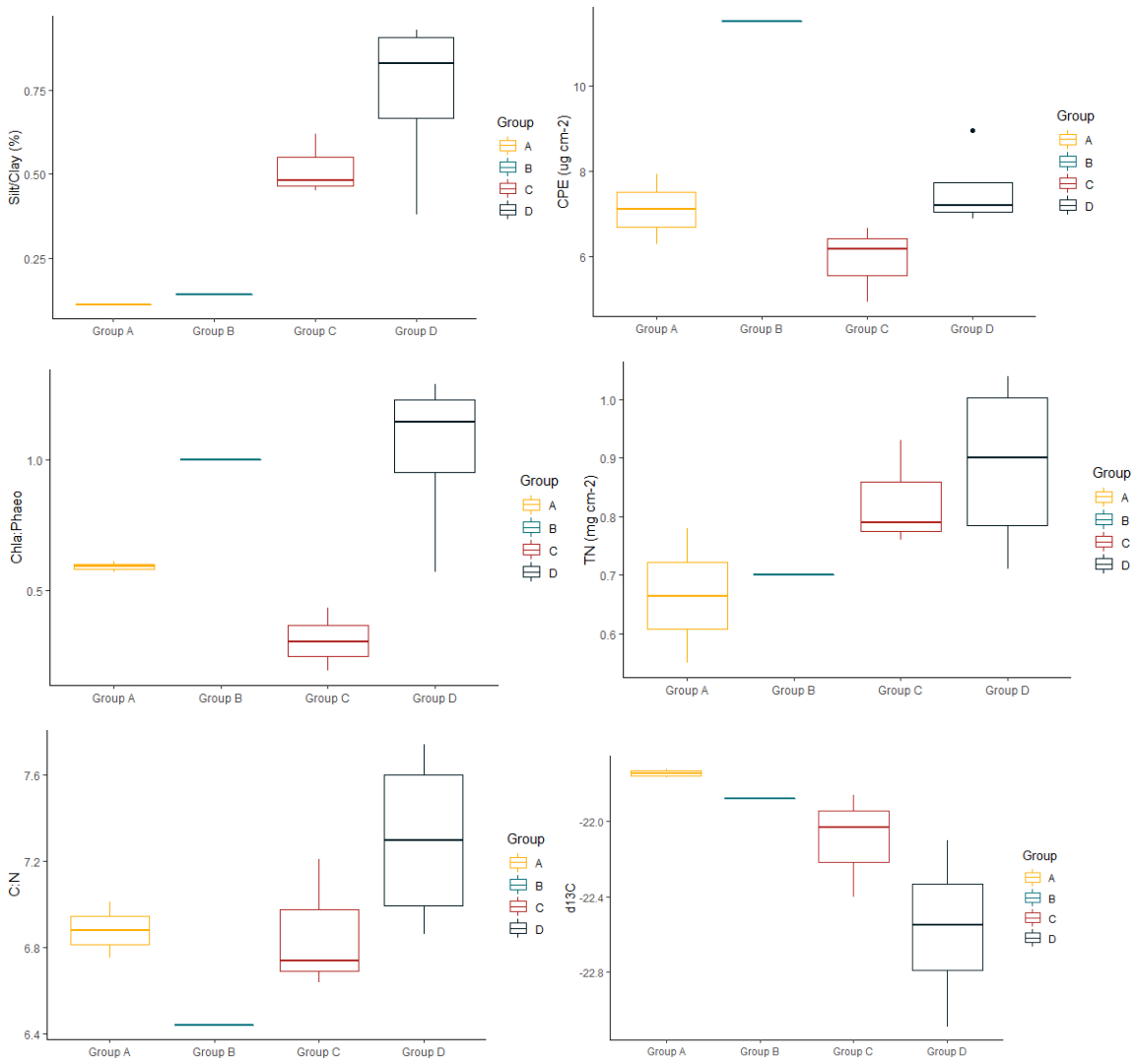

Figure 8: Boxplot of environmental parameters for each group including percent silt/clay (%) and CPE (ug cm^{-2}), chl-a:phaeo, TN (mg cm^{-2}), C:N, and $\delta^{13}C$ for the upper 1 cm of sediment. Groups are based on hierarchical agglomerative clustering and similarity profile test (SIMPROF; Figure 3).

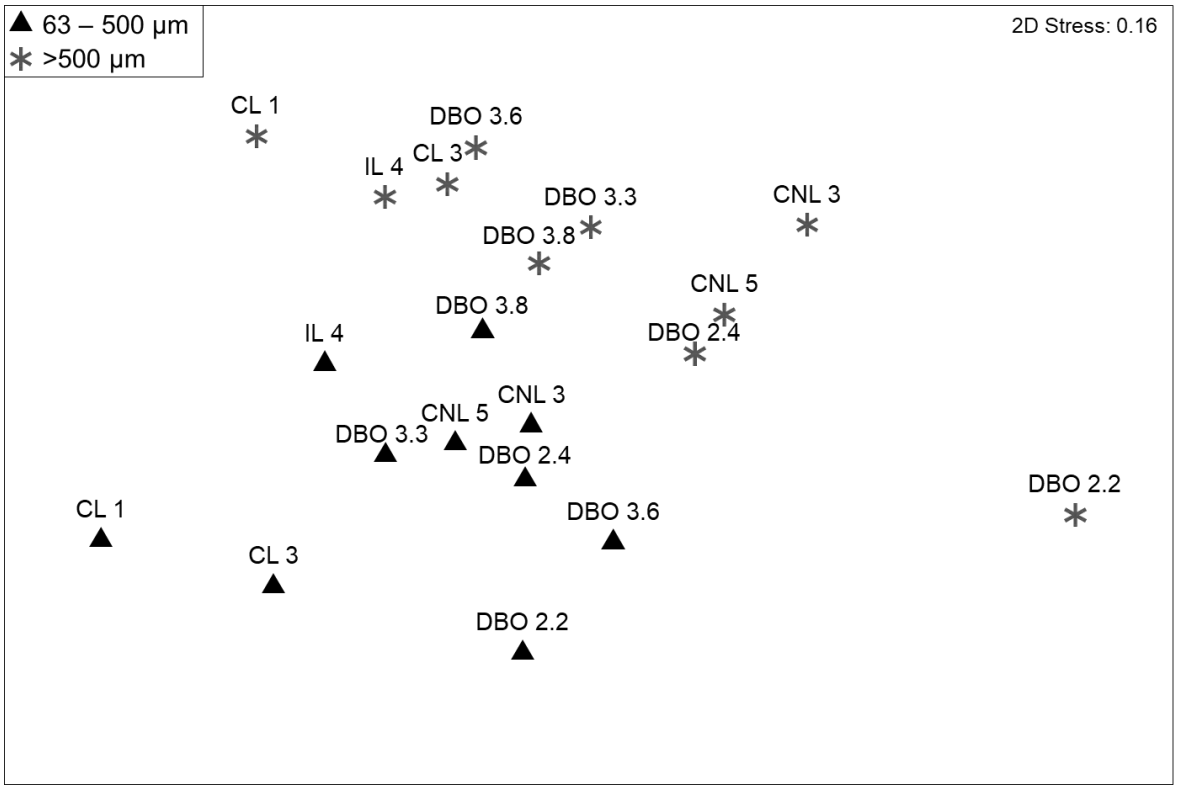

Figure 9: nMDS ordination of meiofaunal- and macrofaunal-sized nematode relative abundance of surface sediment (0-1 cm). Ordination based on hierarchical agglomerative clustering with group-averaged linkage on $\log_{(x + 1)}$ transformed relative abundances and Bray-Curtis similarity. The two size fractions were significantly different (ANOSIM R = 0.356, p = 0.0002). Black triangles are 63-500 µm samples and gray stars are >500 µm sample.

Supplemental Tables and Figures

Supplemental Table 1: Relative abundance (%) of the most abundant (>1%) nematode genera per station (0-1 cm sediment layer, 63-500 µm size fraction).

CL1		CL3		CNL3		CNL5		DBO2.2	
Tricoma	26.36	*Halalaimus*	26.73	*Sabatieria*	24.75	*Daptonema*	45.65	*Oncholaimus*	15.00
Microlaimus	12.73	*Microlaimus*	12.87	*Daptonema*	10.89	*Sabatieria*	13.04	*Monhystrella*	13.00
Desmodora	10.91	*Thalassomonhystera*	7.92	*Marylynnia*	10.89	*Paramonohystera*	11.96	*Daptonema*	9.00
Desmoscolex	10.00	*Tricoma*	5.94	*Paramonohystera*	5.94	*Chromadorita*	5.43	*Halalaimus*	9.00
Aponema	7.27	*Campylaimus*	4.95	Comesomatidae	5.94	*Halalaimus*	4.35	*Viscosia*	8.00
Terschellingia	6.36	*Neochromadora*	4.95	*Halomonhystera*	3.96	*Neochromadora*	3.26	*Paramonohystera*	7.00
Campylaimus	3.64	*Cervonema*	3.96	*Metalinhomoeus*	3.96	*Tricoma*	3.26	*Neochromadora*	6.00
Cervonema	3.64	*Paramonohystera*	3.96	*Halalaimus*	2.97	*Desmoscolex*	3.26	*Microlaimus*	5.00
Pselionema	3.64	*Desmoscolex*	2.97	*Neochromadora*	2.97	*Campylaimus*	2.17	*Actinonema*	5.00
Diplopeltula	2.73	*Aponema*	2.97	*Microlaimus*	1.98	Comesomatidae	1.09	*Halomonhystera*	3.00
Halalaimus	2.73	*Daptonema*	2.97	*Tricoma*	1.98	*Microlaimus*	1.09	*Chromadorita*	2.00
Paramonohystera	1.82	*Eleutherolaimus*	2.97	Cyatholaimidae	1.98	*Aponema*	1.09	*Thalassomonhystera*	2.00
Sabatieria	1.82	*Terschellingia*	1.98	*Monhystrella*	1.98	*Laimella*	1.09	*Diplopeltula*	2.00
		Diplopeltula	1.98	*Pseudomicrolaimus*	1.98	*Linhomoeidae*	1.09	*Trochamus*	2.00
		Sabatieria	1.98	Xyalidae	1.98	*Setosabatieria*	1.09	*Steineria*	2.00
		Leptolaimus	1.98			*Sphaerolaimus*	1.09	*Aponema*	1.00
		Chromadorita	1.98					Xyalidae	1.00
								Leptolaimus	1.00
								Aegialoalaimus	1.00
								Cephalanticoma	1.00
								Dichromadora	1.00
								Haliplectius	1.00
								Metaparoncholaimus	1.00
								Rhynchonema	1.00
								Tripyloides	1.00

DBO2.4		DBO3.3		DBO3.6		DBO3.8		IL4	
Daptonema	27.87	*Paramonohystera*	21.31	*Daptonema*	72.31	*Paramonohystera*	35.04	*Sabatieria*	17.43
Sabatieria	15.57	*Daptonema*	7.38	*Paramonohystera*	8.46	*Daptonema*	22.63	*Terschellingia*	16.51
Paramonohystera	9.02	*Sabatieria*	7.38	*Sabatieria*	8.46	*Neochromadora*	18.25	*Paramonohystera*	14.68
Neochromadora	7.38	*Microlaimus*	4.92	*Chromadorita*	5.38	*Sabatieria*	15.33	*Cervonema*	8.26
Oncholaimus	4.92	*Halalaimus*	4.92	*Neochromadora*	2.31	*Halalaimus*	2.92	*Halalaimus*	6.42
Trochamus	4.10	*Leptolaimus*	4.92			*Chromadorita*	1.46	*Dorylaimopsis*	4.59
Steineria	4.10	*Tricoma*	4.92			*Microlaimus*	1.46	*Molgolaimus*	4.59
Microlaimus	3.28	*Terschellingia*	4.10					*Microlaimus*	3.67
Chromadorita	2.46	*Thalassomonhystera*	4.10					*Tricoma*	2.75
Halalaimus	1.64	Xyalidae	3.28					*Desmoscolex*	2.75
Diplopeltula	1.64	*Chromadora*	2.46					Comesomatidae	1.83
Leptolaimus	1.64	*Oxyonchus*	2.46					Xyalidae	1.83
Desmoscolex	1.64	*Desmodora*	2.46					*Aponema*	1.83
Comesomatidae	1.64	*Neochromadora*	1.64					*Campylaimus*	1.83
Terschellingia	1.64	*Desmoscolex*	1.64					*Laimella*	1.83
Linhomoeus	1.64	*Monhystrella*	1.64						
		Viscosia	1.64						
		Halomonhystera	1.64						
		Linhomoeidae	1.64						
		Aponema	1.64						
		Aegialoalaimus	1.64						
		Campylaimus	1.64						

Supplemental Table 2: Trophic diversity, relative abundances of each feeding type, maturity index, and relative abundance of each c-p score for both the 63-500 µm and >500 µm size fractions for each station.

63-500 µm											
Station	**TDI**	**Feeding type:**	**1A**	**1B**	**2A**	**2B**	**MI**	**c-p score:**	**2**	**3**	**4**
Cl 1	2.38		53.6	11.8	34.5	0.0	3.04		36.4	23.6	40.0
CL 3	2.81		44.6	31.7	23.8	0.0	2.92		43.6	20.8	35.6
CNL 3	2.42		12.9	56.4	27.7	3.0	2.41		66.3	26.7	6.9
CNL 5	1.69		10.9	75.0	13.0	1.1	2.35		76.1	13.0	10.9
DBO 2.2	3.77		18.0	35.0	23.0	24.0	2.81		45.0	29.0	26.0
DBO 2.4	2.38		9.8	59.0	23.8	7.4	2.42		68.9	20.5	10.7
DBO 3.3	2.94		24.6	49.2	17.2	9.0	2.49		66.4	18.0	15.6
DBO 3.6	1.24		0.8	89.2	8.5	1.5	2.12		89.2	10.0	0.8
DBO 3.8	1.67		3.6	74.5	21.2	0.7	2.28		75.9	20.4	3.6
IL 4	2.56		34.9	49.5	15.6	0.0	2.53		59.6	27.5	12.8
IL 4	2.56		34.9	49.5	15.6	0.0	2.53		59.6	27.5	12.8
>500 µm											
CL 1	1.27		5.9	88.2	5.9	0.0	2.18		88.2	5.9	5.9
CL 3	1.47		0.0	80.0	20.0	0.0	2.00		100.0	0.0	0.0
CNL 3	1.94		3.4	69.0	13.8	13.8	2.41		69.0	20.7	10.3
CNL 5	1.81		14.3	71.4	0.0	14.3	2.43		71.4	14.3	14.3
DBO 2.2	2.16		38.9	5.6	0.0	55.6	2.67		51.9	29.6	18.5
DBO 2.4	1.83		1.5	66.7	0.0	31.8	2.45		71.2	12.1	16.7
DBO 3.3	2.06		0.9	53.2	0.9	45.0	2.38		72.5	17.4	10.1
DBO 3.6	1.13		0.0	94.1	2.0	4.0	2.08		94.1	4.0	2.0
DBO 3.8	1.46		14.8	81.5	0.0	3.7	2.33		81.5	3.7	14.8
IL 4	1.35		8.8	85.3	5.9	0.0	2.15		91.2	2.9	5.9

Supplemental Table 3: Environmental and sediment characteristics of each station sampled in 2018, including cluster group; latitude (°N); longitude (°W); station depth (m); near-bottom water temperature (°C); near-bottom water salinity; mean phi; percent silt/clay; percent sand; porosity; chl-a, phaeo, and CPE inventories (μg cm^{-2}) in the surface 1 cm of sediment; surface chl-a:phaeo; TOC and TN inventories (mg cm^{-2}) in the surface 1 cm of sediment; chl-a, phaeo, and CPE inventories (μg cm^{-2}) in the upper 5 cm of sediment; average chl-a:phaeo over the top 5 cm of sediment; TOC and TN inventories (mg cm^{-2}) in the upper 5 cm of sediment; and average C:N and $\delta^{13}C$ over the top 5 cm of sediment. Groups are based on hierarchical agglomerative clustering analysis of meiofaunal-sized (63-500 μm) nematode community structure and similarity profile test (SIMPROF; Figure 3).

											0-1 cm								0-5 cm							
Station	**Group**	**Lat. (°N)**	**Long. (°W)**	**Depth (m)**	**Temp. (°C)**	**Sal.**	**Mean Phi**	**% Silt/ Clay**	**% Sand**	**Porosity**	**Chl-a**	**Phaeo**	**CPE**	**Chl-a: Phaeo**	**TOC**	**TN**	**C:N**	**$\delta^{13}C$**	**Chl-a**	**Phaeo**	**CPE**	**Chl- a:Phaeo**	**TOC**	**TN**	**C:N**	**$\delta^{13}C$**
CL1	D	68.95	-166.91	46	0.0	31.9	6.16	0.76	0.23	0.43	4.92	4.03	8.95	1.21	7.96	1.04	7.74	-23.09	9.05	15.33	24.38	0.52	41.29	4.77	8.85	-23.62
CL3	D	69.03	-168.89	53	-0.6	32.4	6.67	0.90	0.09	0.55	2.65	4.66	7.31	0.57	6.72	0.99	6.86	-22.10	6.67	20.29	26.96	0.32	37.24	5.12	7.29	-22.37
CNL3	B	66.50	-168.96	56	1.9	32.5	2.34	0.14	0.84	0.27	5.85	5.66	11.51	1.00	4.50	0.70	6.44	-21.88	11.50	21.28	32.78	0.49	29.24	4.55	6.45	-21.97
CNL5	C	67.00	-168.96	48	1.5	33.0	5.00	0.48	0.51	0.42	1.41	4.76	6.17	0.30	5.52	0.76	7.21	-22.40	9.13	20.71	29.84	0.48	32.78	4.68	7.00	-22.30
DBO2.2	A	64.68	-169.10	46	2.4	32.3	2.92	0.11	0.89	0.25	2.90	5.02	7.92	0.57	3.75	0.55	6.75	-21.72	7.31	20.10	27.42	0.35	17.03	2.48	6.88	-21.91
DBO2.4	A	64.96	-169.89	48	1.6	32.4	3.06	0.11	0.89	0.26	2.39	3.89	6.28	0.61	3.37	0.48	7.01	-21.77	5.38	16.19	21.57	0.31	18.12	2.57	7.04	-21.96
DBO3.3	D	68.19	-167.31	48	0.5	32.5	3.05	0.38	0.30	0.37	3.90	2.99	6.89	1.29	5.18	0.71	7.04	-22.41	7.50	14.86	22.36	0.50	36.01	4.73	7.53	-22.90
DBO3.6	C	67.90	-168.24	58	0.6	32.7	4.63	0.45	0.54	0.42	1.95	4.70	6.65	0.43	5.31	0.79	6.74	-22.03	6.20	23.38	29.58	0.27	34.22	5.04	6.80	-22.14
DBO3.8	C	67.67	-168.96	51	1.5	32.8	5.56	0.62	0.37	0.52	0.80	4.12	4.92	0.19	6.19	0.93	6.64	-21.86	3.85	21.36	25.21	0.18	37.61	5.67	6.64	-21.84
IL4	D	67.40	-165.84	39	2.1	32.5	6.79	0.93	0.06	0.64	3.66	3.42	7.08	1.08	6.13	0.81	7.55	-22.69	10.06	17.09	27.15	0.59	31.83	4.30	7.42	-22.83

Supplemental Table 4: Relative abundance (%) of all macrofaunal-sized nematode genera per station (0-1 cm, >500 µm).

CL3		CNL3		CNL5		DBO2.2	
64.71	*Paramonohystera*	60.00	*Sabatieria*	62.07	*Sabatieria*	57.14	*Cephalanticoma*	38.89
17.65	*Sabatieria*	20.00	*Marylynnia*	13.79	*Daptonema*	14.29	*Mesacanthion*	25.93
5.88	*Microlaimus*	20.00	*Metalinhomoeus*	6.90	*Halalaimus*	14.29	*Oncholaimus*	12.96
5.88			*Viscosia*	6.90	*Mesacanthion*	14.29	*Oxyonchus*	7.41
5.88			*Crenopharynx*	3.45			*Ledovitia*	5.56
			Oncholaimus	3.45			*Steineria*	5.56
			Symplocostoma	3.45			*Viscosia*	3.70

DBO3.3		DBO3.6		DBO3.8		IL4	
40.91	*Paramonohystera*	31.19	*Paramonohystera*	78.22	*Paramonohystera*	44.44	*Paramonohystera*	38.24
12.12	*Oxyonchus*	15.60	*Sabatieria*	14.85	*Sabatieria*	29.63	*Setosabatieria*	27.94
7.58	*Mesacanthion*	15.60	*Innocuonema*	1.98	*Halalaimus*	14.81	*Sabatieria*	19.12
7.58	*Sabatieria*	11.93	*Sphaerolaimus*	1.98	*Daptonema*	7.41	*Dorylaimopsis*	5.88
7.58	*Rhabdodemania*	9.17	*Daptonema*	0.99	*Mesacanthion*	3.70	*Halalaimus*	2.94
4.55	*Daptonema*	7.34	*Oncholaimus*	0.99			*Thalassoalaimus*	2.94
4.55	*Metalinhomoeus*	1.83	*Symplocostoma*	0.99			*Terschellingia*	2.94
4.55	*Viscosia*	0.92						
3.03	*Subsphaerolaimus*	0.92						
1.52	*Ledovitia*	0.92						
1.52	*Cephalanticoma*	0.92						
1.52	*Dorylaimopsis*	0.92						
1.52	Thoracostomopsidae	0.92						
1.52	*Enoplolaimus*	0.92						
	Xyalidae	0.92						

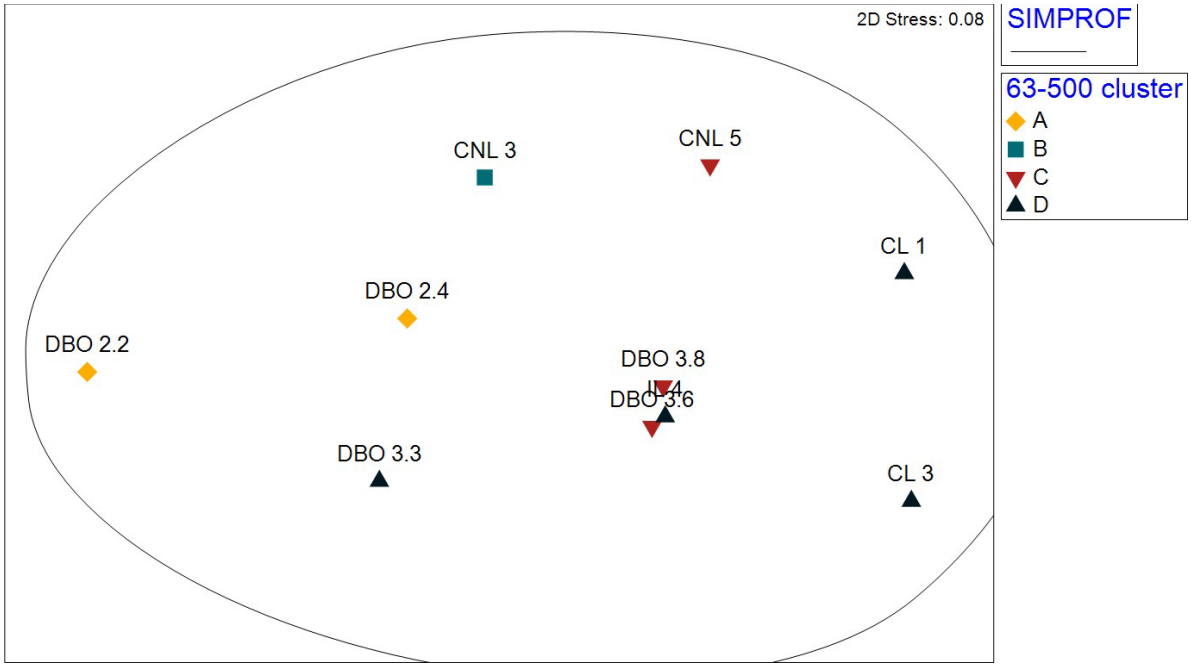

Supplemental Figure1: nMDS ordination of macrofaunal-sized (>500 µm) nematode surface (0-1 cm) community structure (indiv. $10cm^{-2}$). Ordination based on hierarchical agglomerative clustering with group-averaged linkage on $log_{(x+1)}$ transformed data and Bray-Curtis similarity. There was no significant community structure according to the similarity profile test (SIMPROF). Symbols based on clustering analysis of meiofaunal-sized (63-500 µm) nematode community structure.

Conservation Physiology

Volume 9 • 2021 10.1093/conphys/coab007

SEB SOCIETY FOR EXPERIMENTAL BIOLOGY

Research article

Changes to benthic community structure may impact organic matter consumption on Pacific Arctic shelves

Brittany R. Jones*, **Amanda L. Kelley and Sarah L. Mincks**

College of Fisheries and Ocean Sciences, University of Alaska Fairbanks, AK 99775, USA

***Corresponding author**: College of Fisheries and Ocean Sciences, University of Alaska Fairbanks, AK 99775, USA. brjones8@alaska.edu

Changes in species composition and biomass of Arctic benthic communities are predicted to occur in response to environmental changes associated with oceanic warming and sea-ice loss. Such changes will likely impact ecosystem function, including flows of energy and organic material through the Arctic marine food web. Oxygen consumption rates can be used to quantify differences in metabolic demand among species and estimate the effects of shifting community structure on benthic carbon consumption. Closed-system respirometry using non-invasive oxygen optodes was conducted onboard the *R/V Sikuliaq* in June 2017 and 2018 on six dominant species of benthic macrofauna from the northern Bering and southern Chukchi Sea shelves, including five bivalve species (*Macoma* sp., *Serripes groenlandicus*, *Astarte* sp., *Hiatella arctica* and *Nuculana pernula*) and one amphipod species (*Ampelisca macrocephala*). Results revealed species-specific respiration rates with high metabolic demand for *S. groenlandicus* and *A. macrocephala* compared to that of the other species. For a hypothetical 0.1-g ash-free dry mass individual, the standard metabolic rate of *S. groenlandicus* would be 4.3 times higher than that of *Astarte* sp. Overall, carbon demand ranged from 8 to 475 µg C individual^{-1} day^{-1} for the species and sizes of individuals measured. The allometric scaling of respiration rate with biomass also varied among species. The scaling coefficient was similar for *H. arctica*, *A. macrocephala* and *Astarte* sp., while it was high for *S. groenlandicus* and low for *Macoma* sp. These results suggest that observed shifts in spatial distribution of the dominant macrofaunal taxa across this region will impact carbon demand of the benthic community. Hence, ecosystem models seeking to incorporate benthic system functionality may need to differentiate between communities that exhibit different oxygen demands.

Key words: Bivalves, macrofauna, metabolism, oxygen consumption, Pacific Arctic, respiration

Editor: Nann Fangue

Received 9 June 2020; Revised 18 November 2020; Accepted 16 January 2021

Cite as: Jones BR, Kelley AL, Mincks SL (2021) Changes to benthic community structure may impact organic matter consumption on Pacific Arctic shelves. *Conserv Physiol* 9(1): coab007; doi:10.1093/conphys/coab007.

Introduction

Climate change is impacting Arctic marine ecosystems at a rapid pace. Warming temperatures and declining sea ice (IPCC, 2014; Wang and Overland, 2015; Huntington *et al.*, 2020) are resulting in ecosystem-wide changes in the timing and magnitude of primary production (Arrigo and van Dijken, 2015; Selz *et al.*, 2018), secondary production (Ringuette *et al.*, 2002), the strength of pelagic–benthic coupling (Grebmeier *et al.*, 2006; Moore and Stabeno, 2015)

and benthic community structure and function (Grebmeier *et al.*, 2018). These changes are likely to affect metabolic demand of Arctic marine invertebrates and, in turn, the cycling of organic matter in sediments and subsequent exchanges with the water column.

Oxygen consumption rates (MO_2) provide an estimate of metabolic activity in aerobic organisms and serve as a proxy for organic matter consumption and energy flow through the benthic food web. Metabolic rates vary among individuals due to a variety of factors, including developmental stage (Yagi *et al.*, 2010), age (Sukhotin and Pörtner, 2001; Glazier *et al.*, 2015) and body size (Kleiber, 1932). For instance, MO_2 increases with body size in a relatively predictable manner described by the '3/4-power law', wherein the relationship between MO_2 and body size is quantified by a metabolic scaling coefficient of ~0.75 (Kleiber, 1932); however, many exceptions have been reported (reviewed by Glazier, 2005). In addition to physiological differences among individuals and species, MO_2 also varies with environmental factors, such as temperature (Peck *et al.*, 2002; Clarke and Fraser, 2004; Trigos *et al.*, 2015), pH (Liu and He, 2012; Saavedra *et al.*, 2018) and food availability (Brockington and Clarke, 2001; Sejr *et al.*, 2004). Many of these environmental conditions have already changed or are projected to change under future climate scenarios (IPCC, 2014), potentially resulting in alterations to benthic biomass, taxonomic composition and carbon demand.

Estimates of whole sediment-community oxygen consumption rates are available across the Arctic (reviewed in Bourgeois *et al.*, 2017; Grebmeier *et al.*, 2006). However, MO_2 rates of individual species have rarely been reported for the region (Vahl, 1978; Opalinski and Weslawksi, 1989; Sejr *et al.*, 2004; Goethel *et al.*, 2017), hampering efforts to predict how changes in species composition may impact benthic carbon processing rates and ecosystem function (Grebmeier, 2012). In the Pacific Arctic region, the Bering and Chukchi Seas overlie a shallow inflow shelf influenced by distinct water masses: cold, nutrient-rich Anadyr-Bering Sea Water and warm, more nutrient-poor Alaska Coastal Water (Daniel- son *et al.*, 2017). Flows accelerate through the Bering Strait constriction (Danielson *et al.*, 2014), promoting energetic mixing that locally enhances pelagic primary productivity (Walsh *et al.*, 1989). Downstream of this constriction, the current speeds decline, allowing pelagic production and particle flux to settle to the seafloor (Grebmeier *et al.*, 2015b). Such dynamic oceanographic conditions result in a patchy distribution of benthic organisms, with ecologically important hotspots of high benthic biomass up to 32 g C m^{-2} in the Chirikov Basin and southeast Chukchi Sea (Grebmeier *et al.*, 2015b). These hotspots serve as persistent feeding grounds for marine mammals (Fay, 1982) and birds (Lovvorn *et al.*, 2003). Overall, the benthos accounts for a substantial portion of the total food web production in these regions (Walsh *et al.*, 1989), dominated by infaunal bivalves and amphipods (Feder *et al.*, 1994; Grebmeier *et al.*, 2015b).

We quantified metabolic rates of dominant macrofaunal benthos from the northern Bering and southern Chukchi Sea shelves by measuring oxygen consumption rates in laboratory incubations. Experiments were conducted using five bivalve species (*Macoma* sp., *Serripes groenlandicus*, *Astarte* sp., *Hiatella arctica* and *Nuculana pernula*) and one amphipod species (*Ampelisca macrocephala*). These species exhibit diverse life-history strategies and functional traits. For instance, *Astarte* sp., *H. arctica* and *S. groenlandicus* are all suspension feeders, while *N. pernula* is a deposit feeder and *Macoma* sp. is a facultative feeder, capable of switching between deposit and suspension feeding. *Ampelisca macrocephala* is primarily a suspension feeder but can supplement its diet by deposit feeding or consuming small crustaceans. MO_2 was measured for multiple individuals of each species, spanning a range of body sizes in order to establish metabolic scaling relationships for each taxon. Overall, we found species-specific respiration rates and differences in metabolic scaling, which have implications for benthic carbon demand particularly considering altered environmental conditions and shifting species assemblages.

Methods

Sampling

Macrofauna were collected from the northern Bering and southern Chukchi Seas from 13–24 June 2017 and 9–22 June 2018 from the *R/V Sikuliaq* as part of the Arctic Shelf Growth, Advection, Respiration and Deposition (ASGARD) project (Fig. 1, Table 1). Macrofauna were selected from four sampling stations in 2017 and ten stations in 2018 with an average depth of 50 m (ranging from 39 to 59 m). Near-bottom water temperature at sampling location was 2.8 ± 0.7 °C in 2017 and 1.3 ± 0.8 °C in 2018 (Table 1).

Individuals were selected from plumb-staff beam trawl, multi-core (MC-800, Ocean Instruments, San Diego) and 0.1-m^2 Van Veen grab samples. Experiments conducted in 2017 included the bivalves *Macoma* sp. (mostly *M. calcarea*; four small individuals only identified to genus level) and *S. groenlandicus* (Table 1). In 2018, experiments were conducted for additional *Macoma* sp. (one individual only identified to genus) and *S. groenlandicus,* as well as the bivalves *Astarte* sp. (mostly *A. montagui*; one identified only to genus), *N. pernula*, *H. arctica* and the amphipod *A. macrocephala*.

Respirometry

Closed-system respirometry was performed in a temperature-controlled room onboard the *R/V Sikuliaq*. Non-invasive oxygen optodes (PSt3 oxygen sensor spots; PreSens Precision Sensing GmbH, Germany) were used to measure oxygen concentration inside incubation chambers (Gatti *et al.*, 2002). The sensor spots measure oxygen concentration based on the dynamic fluorescence quenching of a luminophore contained in a polymer matrix and have a detection limit of 0.03% oxygen (15 ppb dissolved oxygen). Factory calibration was

Table 1: Station locations, depth (m), near-bottom water temperature from CTD (°C), near-bottom water salinity from CTD and numbers of individuals sampled, by taxon

Year	Station	Latitude (°N)	Longitude (°W)	Depth (m)	Temperature (°C)	Salinity	*Macoma sp.*	*Serripes groenlandicus*	*Astarte* sp.	*Hiatella arctica*	*Nuculana pernula*	*Ampelisca macrocephala*
2017							(*N* = 15)	(*N* = 9)				
	CL3	69.03	−168.89	52	2.4	32.8		5				
	CNL3	66.50	−168.96	56	2.2	32.6	9	1				
	DBO3.6	67.90	−168.24	59	3.9	32.9	4	2				
	DBO3.8	67.67	−168.73	50	2.0	32.8	2	1				
2018							(*N* = 11)	(*N* = 17)	(*N* = 6)	(*N* = 5)	(*N* = 12)	(*N* = 14)
	CBW5	64.15	−171.51	46	0.5	32.3			6	2		
	CL1	68.95	−166.91	46	0.0	31.9					3	
	CL3	69.03	−168.89	54	−0.6	32.4		10			6	
	CNL3	66.50	−168.96	56	1.9	32.5	3	5				
	DBO2.2	64.68	−169.10	46	2.4	32.3						6
	DBO2.4	64.96	−169.89	48	1.6	32.4		2				2
	DBO2.5	64.99	−169.14	48	2.8	32.8						6
	DBO3.3	68.19	−167.31	48	0.5	32.5				3		
	DBO3.8	67.67	−168.96	51	1.5	32.8	8					
	IL4	67.40	−165.84	39	2.1	32.5					3	

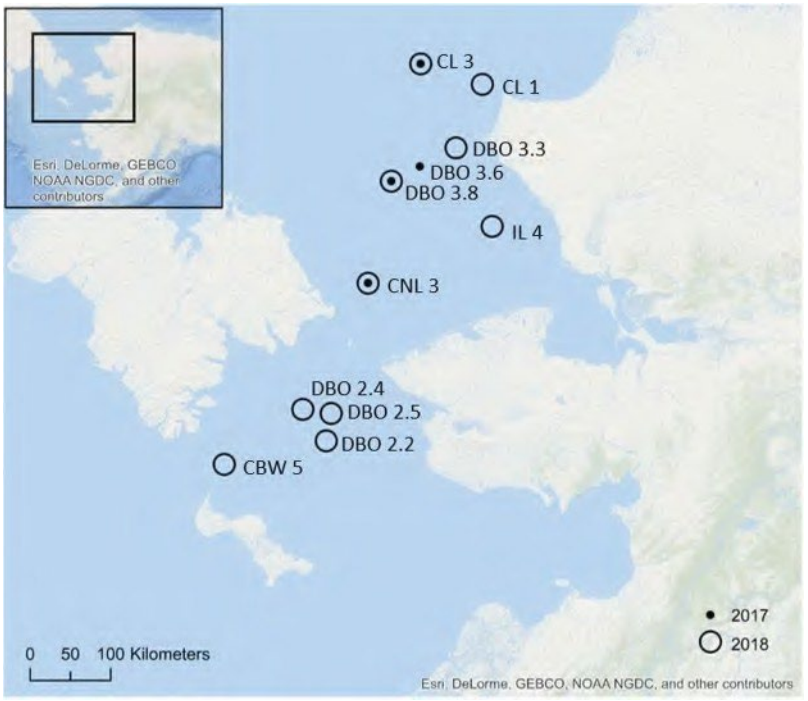

Figure 1: Sampling locations in the northern Bering and southern Chukchi Sea shelves with 2017 in closed circles and 2018 in open circles.

used for new sensor spots purchased in 2017 and 2018. For sensor spots that had been used and stored for a year between field seasons, a two-point calibration was performed per manufacturer's instructions. An aquarium bubbler was used to produce a solution of 100% oxygen air saturation, and a solution of 0% saturation was produced using sodium sulfite and cobalt nitrate (1 g Na_2SO_3 and 50 µL of $Co(NO_3)_2$ dissolved in 100 mL of reverse osmosis water to achieve $\rho(Co) = 1000$ mg L^{-1}; in nitric acid 0.5 mol L^{-1}).

Prior to the start of each experiment, organisms were rinsed with 0.2-µm filtered seawater and bivalve shells were gently scrubbed with a toothbrush to remove microbial films. Each individual was acclimated to experimental conditions by placing it in an incubation chamber submerged in a water bath, which consisted of a plastic tote filled with 0.2-µm filtered seawater aerated with an aquarium bubbler. The temperature-controlled room was set to a target experimental temperature of 0 °C, but recorded temperatures of the seawater baths averaged 0.6 ± 0.3 °C (standard deviation) in 2017 and 0.9 ± 0.2 °C in 2018. Chambers of various sizes (3.7-, 20-, 60-, 120- and 180-ml glass jars) were used to accommodate different sized individuals such that the estimated body volume of each organism did not exceed ~10% of the chamber volume. After organisms were acclimated to experimental conditions for 12 to 24 hours to minimize stress response, each chamber was sealed ensuring no air bubbles were trapped and re-immersed in a water bath to maintain a constant temperature. Organisms were not fed during the acclimation period or incubations to avoid postprandial effects on metabolic rate (Chapelle *et al.*, 1994). Therefore, these measurements of MO_2 estimate the lower bound of carbon consumption for these organisms, given that metabolic rates typically increase following feeding (i.e. a postprandial effect; Brockington and Clarke, 2001; Sejr *et al.*, 2004). In addition, the species inhabit different sediment depths and exhibit different burrowing behaviours *in situ*, which may have influenced species-specific responses to incubation conditions in the absence of sediment for burrowing.

For each incubation, three control chambers (0.2-µm filtered seawater only) of each chamber size were incubated in the water bath alongside the experimental chambers containing organisms. Oxygen concentration of each chamber was measured every 10 to 60 minutes. Average initial oxygen concentration in all incubations was 344.7 µmol O_2 L^{-1} (ranging from 310.9 to 371.8 µmol O_2 L^{-1}). The incubation of each individual chamber was terminated when oxygen concentration declined by ~20% of the initial concentration. For some individuals, the target ratio of body volume:chamber volume was exceeded and oxygen levels declined too rapidly to ensure high-quality data; therefore, data were discarded for incubations lasting less than 1.75 hours. Incubations lasted on average 8.2 hours (ranging from 1.8 to 13.1 hours). In 2017, incubations were repeated three times per individual in order to quantify the variability in respiration rate within an individual. Replicate incubations took place on successive days, and between experiments the organisms were held without

food in open experimental chambers submerged in the aerated water bath. The respiration chambers were sealed with freshly filtered and aerated seawater for each new incubation. In 2018, triplicate incubations were only performed for a subset of individuals from taxa that were not sampled the previous year.

After incubations, bivalve length was measured at the longest part of the shell (Table 2). Length was not measured for amphipods. Organisms were then individually frozen whole at −80 °C. Samples were transported to the laboratory at the University of Alaska Fairbanks and stored at −20 °C for further analysis. Wet mass was measured on thawed, whole organisms. The volume of water in each chamber was determined based on mass measurements. The thawed organism was placed in its original incubation chamber filled with freshwater, and the mass was determined. The mass of water in each chamber was calculated as the mass of the chamber + organism subtracted from the mass of the chamber + organism + water. This water mass was then converted to water volume using a conversion of 1 mL equals 1 g.

Dry mass of each individual was determined by drying at 60 °C until constant mass was achieved. Ash-free dry mass (AFDM) was measured by igniting each individual at 500 °C for 6 hrs. For amphipods, dry mass and AFDM were measured on whole individuals. For bivalves, the soft tissue was removed from the shell and dry mass and AFDM were measured for the soft tissue only.

Data analysis

The linear regression of wet mass versus AFDM was calculated on log-transformed data for all bivalve species taken collectively and for *A. macrocephala* individually, allowing metabolic rates measured here in terms of AFDM to be applied to published estimates of wet biomass from other field studies. Regressions were then expressed as power functions to represent the original data displayed on a log–log scale.

Respiration rates of individuals are typically altered during an initial period of acclimation to the sealed chamber due to handling stress, and the length of this period is variable (Peck and Conway, 2000). The data trend during this acclimation period typically has a different slope than the rest of the incubation. The acclimation period for each individual was thus identified and removed by detecting a breakpoint in the broken-line slope of the linear regression model using a bootstrapped approach, as implemented in the segmented function from the segmented package in R (Muggeo, 2008). Outliers were also identified and removed when standardized residuals were less than −2 or greater than +2. The oxygen consumption rate (MO_2; μmol O_2 L^{-1} min^{-1}) of each individual was then calculated from the linear regression of oxygen concentration versus time. When oxygen concentration significantly changed in the controls, the average rate of the three controls was subtracted from the measured macrofaunal rates of the same incubation to account for background respiration (e.g. by bacteria) or background production. The average rate of change of oxygen concentration in controls was −0.002 μmol O_2 L^{-1} min^{-1} (ranging from −0.015 to +0.013 μmol O_2 L^{-1} min^{-1}).

Rates were converted to μmol O_2 hr^{-1} based on the volume of water contained in each incubation chamber. To model the relationship between MO_2 and AFDM, regressions were calculated on log-transformed data for each taxonomic group:

$$\log MO_2 = b * \log M + \log a,$$

where MO_2 is the respiration rate (standard metabolic rate), b is the slope, M is the AFDM and log a is the y-intercept. The y-intercept (log a) is the metabolic constant and reflects differences in the magnitude of the respiration rate among species. The slope (b) is the metabolic scaling coefficient, relating respiration rate to biomass. Regression equations were then expressed as a power function to represent the original data plotted on a log–log scale:

$$MO_2 = aM^b,$$

where a is the y-intercept at x = 1 on the log–log scale, M is the AFDM and b is the slope. To estimate carbon consumption required to support standard metabolic demand, MO_2 was converted to units of carbon respired (μg C $individual^{-1}$ day^{-1}) based on a respiratory quotient of 0.8 (Witte and Graf, 1996; Ke¸dra *et al.*, 2010).

Mass-specific metabolic rates were calculated by dividing the oxygen uptake rate of each individual by its respective AFDM. Linear regressions on log-transformed data were also calculated for the relationship between mass-specific oxygen uptake rate and AFDM for each taxonomic group and expressed as a power function.

Differences in the intercepts and the slopes of the linear models among species and between years were examined with analysis of covariance (ANCOVA) and Tukey's post hoc test. All analyses were performed in R Studio, and the glht function from the multcomp package was used for Tukey's post hoc (Hothorn *et al.*, 2008). For all comparisons, $\alpha = 0.05$.

Ratios of average measured body length (our study) to maximum length achievable in the field (from the literature) were also calculated to illustrate the potential relationship between metabolic demand and age.

Results

Wet mass and AFDM were strongly related for all bivalve species taken collectively and for *A. macrocephala* individually; therefore, oxygen uptake rates are presented relative to AFDM. The mass conversion relationship was $y = 0.09x^{1.00}$ ($n = 75$, $R^2 = 0.95$, $P < 0.001$) for bivalves (Supplementary Figure 1a) and $y = 0.14x^{0.69}$ ($n = 14$, $R^2 = 0.90$,

Table 2: Power functions of oxygen uptake rate (μmol O_2 h^{-1}) versus ash-free dry mass (g) for taxonomic groups incubated in both years with the R^2, *P*-values and number of individuals (N) associated with each regression; range of maximum length of individuals incubated in each group (mm); average length of incubated individuals (mm ± standard deviation); maximum achievable length (mm) measured in the field taken from the literature; average length to maximum achievable length ratios; average coefficient of variation (CV ± standard deviation) of oxygen uptake rates (MO_2; μmol O_2 h^{-1}) for individuals incubated in triplicate with number of individuals in parentheses; and average mass-specific MO_2 (μmol O_2 hr^{-1} g^{-1} ± standard deviation)

Species	Equation	R^2	*P*-value	N	Length range (mm)	Average length (mm)	Maximum length (mm)*	Avg. length: max. length ratio	Average CV of MO_2	Average mass-specific MO_2 (μmol O_2 hr^{-1} g^{-1})
Macoma sp.	$1.43mass^{0.52}$	0.68	<0.001	26	14.60–57.40	29.3 ± 9.1	57	0.51	0.13 ± 0.11 (*n* = 15)	3.1 ± 1.7
2017 *Macoma* sp.	$1.06mass^{0.44}$	0.78	<0.001	15	-	-	-	-	-	-
2018 *Macoma* sp.	$1.96mass^{0.57}$	0.82	<0.001	11	-	-	-	-	-	-
S. groenlandicus	$7.63mass^{0.94}$	0.88	<0.001	26	7.40–21.80	14.7 ± 4.6	100	0.15	0.14 ± 0.08 (*n* = 9)	9.5 ± 2.7
S. groenlandicus from CNL3	$1.85mass^{0.67}$	0.95	0.001	6	-	-	-	-	-	-
S. groenlandicus excluding CNL3	$7.75mass^{0.89}$	0.97	<0.001	20	-	-	-	-	-	-
Astarte sp.	$1.19mass^{0.77}$	0.99	<0.001	6	11.05–24.05	19.3 ± 4.2	30	0.64	0.14 ± 0.04 (*n* = 5)	2.1 ± 0.5
Hiatella arctica	$2.30mass^{0.74}$	0.96	0.003	5	9.04–31.75	19.6 ± 8.0	45	0.43	0.15 ± 0.04 (*n* = 5)	4.2 ± 1.8
Nuculana pernula	$1.74mass^{0.81}$	0.99	<0.001	12	10.25–31.10	17.6 ± 6.4	30	0.59	0.093 ± 0.04 (*n* = 3)	3.3 ± 0.7
Ampelisca macrocephala	$2.87mass^{0.77}$	0.93	<0.001	14	-	-	-	-	0.22 ± 0.17 (*n* = 4)	6.6 ± 1.5

*(Madsen, 1949; Lubinsky, 1980; Hutchings and Haedrich, 1984; Schaefer et al., 1985; Sejr et al., 2002; Kilada et al., 2007; Sejr and Christensen, 2007)

$P < 0.001$) for *A. macrocephala* (Supplementary Figure 1b), where y is AFDM (g) and x is wet mass (g). Replicate incubations conducted with the same individuals showed little variability in MO_2 based on low coefficients of variation (CV; Table 2), with no consistent increasing or decreasing trend in MO_2 over the three days of incubations.

Macoma sp. and *S. groenlandicus* were incubated in both years, with slight differences in the average incubation temperature (0.6 ± 0.3 °C in 2017 and 0.9 ± 0.2 °C in 2018). The slopes ($F_{1,22} = 0.09$, $P = 0.77$) and intercepts ($F_{1,23} = 1.01$, $P = 0.32$) of the regression relationships relating MO_2 and AFDM were not significantly different between years for *S. groenlandicus* (Fig. 2), indicating no interannual variation, even with the small difference in temperature. Therefore, a single regression is reported for *S. groenlandicus* (Table 2). The slopes ($F_{1,22} = 1.33$, $P = 0.26$) for *Macoma* sp. were not significantly different between years; however, the intercepts ($F_{1,23} = 21.30$, $P < 0.001$) were significantly higher in 2018 compared to 2017 and separate regression relationships are reported for each year (Table 2). For *Macoma* sp., we thus present the regression relationships for each year separately, as well as the pooled 2017 and 2018 data which provides an average value for ease of comparison among species.

There were significant differences in the slopes ($F_{5,81} = 4.47$, $P = 0.001$) and intercepts ($F_{5,86} = 43.40$, $P < 0.001$) for the regressions relating MO_2 and AFDM (Fig. 3a) for all six species (pooled among years). The slope of *S. groenlandicus* was significantly higher than that of *Astarte* sp., *Macoma* sp., *H. arctica* and *N. pernula* (Table 3). Although the slope of *A. macrocephala* (0.77) was lower than that of *N. pernula* (0.81) and the same as that of *Astarte* sp., the standard error of the parameter estimate for *A. macrocephala* was high (0.06), likely reducing the discriminatory power of the post hoc test. The difference was greatest between the slopes of *Macoma* sp. and *S. groenlandicus*, both of which deviated from the ¾- power law for metabolic scaling coefficients (Table 2). The post hoc test showed the intercept of *S. groenlandicus* was significantly higher than that of the other 5 species (Table 4). Over the range of sizes of individuals incubated, MO_2 of *S. groenlandicus* was consistently higher than that of *A. macrocephala*, *H. arctica*, *N. pernula* and *Astarte* sp. (Fig. 3). The intercept for *A. macrocephala* was significantly higher than that of *Macoma* sp., *Astarte* sp. and *N. pernula* (Table 4). Additionally, the intercepts of *H. arctica* and *Macoma* sp. were significantly higher than that of *Astarte* sp. (Table 4).

While MO_2 of *S. groenlandicus* did not differ between sampling years, evidence of spatial variation was observed. Lower MO_2 rates were recorded in individuals collected at station CNL3 compared to individuals from the other stations (Fig. 4). The slopes ($F_{1,22} = 6.28$, $P = 0.020$) and intercepts were significantly different ($F_{1,23} = 79.98$, $P < 0.001$).

Mass-specific respiration rates declined rapidly with increasing body size for all species except *S. groenlandicus* (Fig. 3b). The slope for *S. groenlandicus* was not significantly different from zero ($t = -0.82$, $P = 0.42$), while for all other taxa slopes ranged from −0.19 to −0.48. There were statistical differences in average mass-specific respiration rates among the species ($F_{5,87} = 25.75$, $P < 0.001$; Fig. 5). *Serripes groenlandicus* had a significantly higher rate than the other five species, and the rate for *A. macrocephala* was significantly higher than *Macoma* sp., *Astarte* sp. and *N. pernula* (Fig. 5).

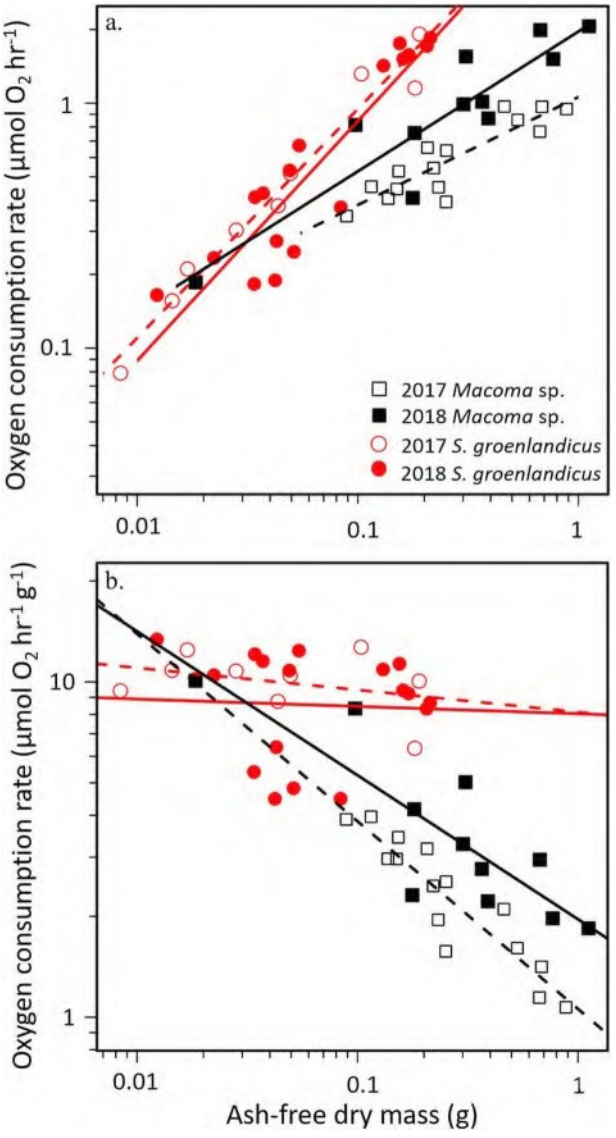

Figure 2: (a) Oxygen uptake rate (µmol O_2 h^{-1}) and (b) mass-specific oxygen uptake rate (µmol O_2 h^{-1} g^{-1}) versus ash-free dry mass (g) for 2017 *Macoma* sp. (black open squares, $n = 15$), 2018 *Macoma* sp. (black closed squares, $n = 11$), 2017 *S. groenlandicus* (red open circles, $n = 9$) and 2018 *S. groenlandicus* (red closed circles, $n = 17$). Dotted lines represent regressions of each species in 2017 and solid lines represent regressions in 2018.

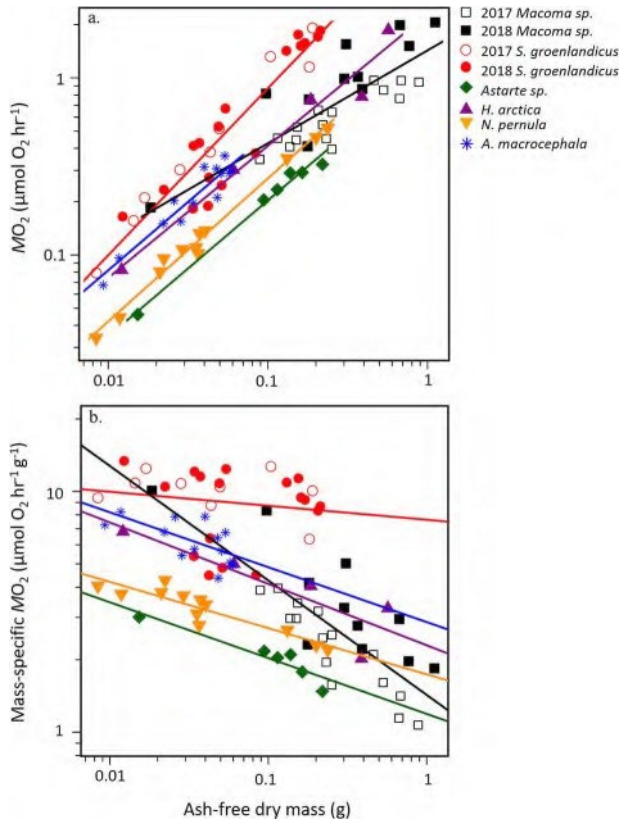

Figure 3: (a) Oxygen uptake rate (µmol O_2 h^{-1}) and (b) mass-specific oxygen uptake rate (µmol O_2 h^{-1} g^{-1}) versus ash-free dry mass (g) for pooled *Macoma* sp. (2017 in open black squares, $n = 15$; 2018 individuals in closed black squares, $n = 11$); pooled *S. groenlandicus* (2017 individuals in open red circles, $n = 9$; 2018 individuals in closed red circles, $n = 17$); and 2018 *Astarte* sp. (green diamonds, $n = 6$), *H. arctica* (purple upright triangles, $n = 5$), *N. pernula* (yellow upside-down triangles, $n = 12$) and *A. macrocephala* (blue asterisks, $n = 14$).

Table 3: Tukey post hoc test statistic (*t*-value) for significant comparisons of slopes of the linear regressions of log-transformed oxygen uptake rate (MO_2; µmol O_2 h^{-1}) versus log-transformed ash-free dry mass (g). See Table 2 for equations and Fig. 3a for plots

Comparison	*t*-value	*P*-value
S. groenlandicus > *Macoma* sp.	10.41	<0.001
S. groenlandicus > *Astarte* sp.	4.69	<0.001
S. groenlandicus > *H. arctica*	3.84	0.003
S. groenlandicus > *N. pernula*	4.23	<0.001

Table 4: Tukey post hoc test statistic (*t*-value) for significant comparisons of y-intercepts of the linear regressions of log-transformed oxygen uptake rate (µmol O_2 h^{-1}) versus log-transformed ash-free dry mass (g). See Table 2 for equations and Fig. 3a for plots

Comparison	*t*-value	*P*-value
S. groenlandicus > *Macoma* sp.	10.35	<0.001
S. groenlandicus > *Astarte* sp.	10.20	<0.001
S. groenlandicus > *N. pernula*	10.56	<0.001
S. groenlandicus > *H. arctica*	4.64	<0.001
S. groenlandicus > *A. macrocephala*	4.86	<0.001
A. macrocephala > *Macoma* sp.	3.34	0.014
A. macrocephala > *Astarte* sp.	5.83	<0.001
A. macrocephala > *N. pernula*	5.18	<0.001
H. arctica > *Astarte* sp.	3.83	0.003
Macoma sp. > *Astarte* sp.	3.53	0.008

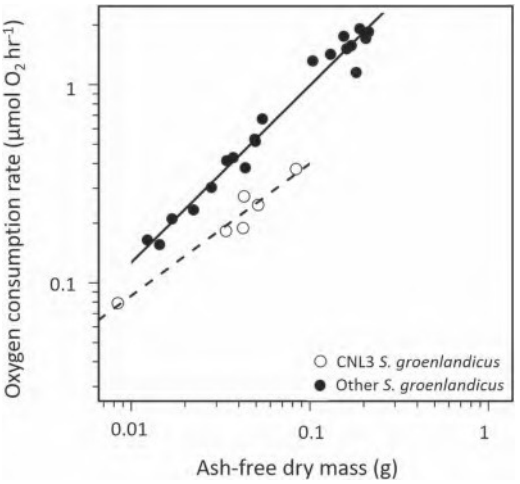

Figure 4: *Serripes groenlandicus* from sampling station CNL3 in open circles and individuals from all other stations in closed circles for both 2017 and 2018.

Discussion

We measured oxygen consumption rates of six dominant macrofauna from the northern Bering and southern Chukchi Sea shelves to determine metabolic demand and organic carbon consumption. Overall, we observed taxonomic variability in metabolic demand with average mass-specific MO_2 rates ranging from 2.1 to 9.5 µmol O_2 hr^{-1} g^{-1}, highlighting the need for species-specific measurements to improve estimates of organic carbon consumption by the benthos. Metabolic scaling coefficients (i.e. slope) also varied among species.

Inter- and intraspecific variation in metabolic rates

We found species-specific standard metabolic rates (MO_2), indicating a wide range in the amount of organic material that benthic species need to consume to maintain baseline metabolic function. For example, the metabolic demand of

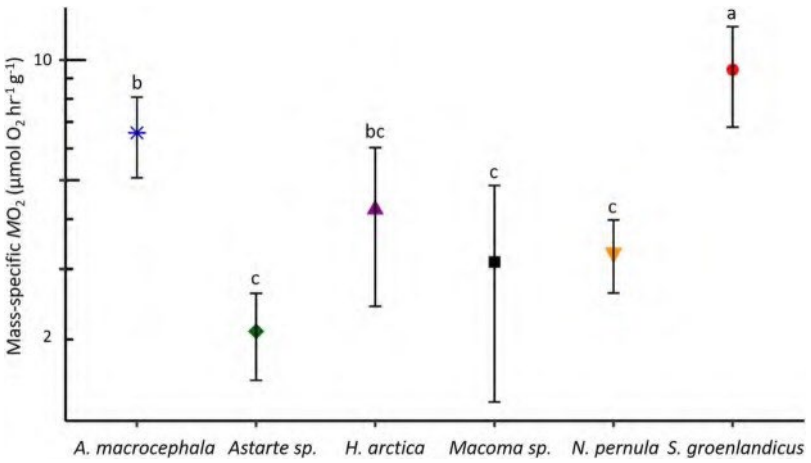

Figure 5: Average mass-specific respiration rates (μmol O_2 hr^{-1} g^{-1}) for each species with standard deviations represented by error bars. *Serripes groenlandicus* had a significantly higher rate than *Macoma* sp. ($t = 9.6$, $P < 0.001$), *Astarte* sp. ($t = 6.8$, $P < 0.001$), *N. pernula* ($t = 7.3$, $P < 0.001$), *H. arctica* ($t = 4.3$, $P < 0.001$) and *A. macrocephala* ($t = 3.1$, $P = 0.028$). The rate for *A. macrocephala* was significantly higher than *Macoma* sp. ($t = 4.7$, $P < 0$ 0.001), *Astarte* sp. ($t = 4.2$, $P < 0.001$) and *N. pernula* ($t = 3.8$, $P = 0.003$).

a hypothetical *S. groenlandicus* with 0.1 g AFDM would be 4.3 times higher than that of a similarly sized individual *Astarte* sp. These rates likely represent conservative estimates of organic carbon consumption. In polar regions, benthic organisms exhibit low metabolic rates when food availability is low, which then increase in response to phytodetrital inputs or elevated food concentrations (Brockington and Clarke, 2001; Sejr *et al.*, 2004).

For the bivalves, these differences in respiration rate among species may be related to the age or life stage of the individuals sampled. The individuals of all species used in our experiments were relatively similar in size (Table 2); however, the maximum achievable length observed in the field varies among species, such that incubated individuals may have been juveniles in some cases. We calculated the ratio of measured body length to maximum achievable length as a proxy to illustrate this relationship (Table 2). In particular, *S. groenlandicus* had the highest average MO_2, but the lowest average measured length to maximum achievable length ratio of only 0.15. Individuals were mostly small, compared to their large maximum achievable size of up to 100 mm in shell length (Lubinsky, 1980; Kilada et al., 2007). In contrast, *Astarte sp*. had the lowest MO_2 and the highest average length to maximum achievable length ratio of 0.64. *Astarte sp*. reach maximum lengths of only 30 mm, but rarely exceed 15 mm (Madsen, 1949; Schaefer et al., 1985), so our individuals were closer to their maximum size compared to *S. groenlandicus*. Overall, individuals selected were likely of different life stages and ages, which can impact respiration rates (Sukhotin and Pörtner, 2001). For instance, all *S. groenlandicus* individuals were smaller than 22 mm in length, which is smaller than the typical size at sexual maturity (Kilada et al., 2007), indicating these individuals were likely all juveniles. A more rapid growth rate that would be expected in these juveniles would thus contribute to the higher MO_2 measured for this species.

In Young Sound, NE Greenland, the respiration rates of 26 individuals of *H. arctica* were measured at −1.3 °C with a constant food supply (Sejr *et al.*, 2004). Adjusting for the differences in temperature using $Q_{10} = 3.64$ (Peck and Conway, 2000) and feeding conditions (using an equation from Sejr *et al.*, 2004), MO_2 for a 0.5 g *H. arctica* was 2 times higher in our study compared to that observed in Sejr *et al.* (2004). Conspecific metabolic rates vary due to numerous factors, such as genotype or environmental conditions during early life stages (Burton *et al.*, 2011). The discrepancies between the rates measured in these studies could also be due to temperature compensation (Rastrick and Whiteley, 2011) or other factors related to differences in experimental design.

The metabolic scaling coefficient, which relates metabolic rate to body mass, is broadly estimated to be 0.75 in a wide variety of taxa (Kleiber, 1932). However, deviations from the '3/4-power law' occur for a variety of reasons in both intra- and interspecific metabolic studies (Glazier, 2005). The metabolic scaling coefficient was close to 0.75 for three of the species measured here, *H. arctica*, *Astarte* sp. and *A. macrocephala* (Table 2), but was much higher for *S. groenlandicus* (b = 0.94) and lower for *Macoma* sp. (b = 0.52). Here again, life stage may be a factor for the high metabolic scaling coefficient of *S. groenlandicus*. Metabolic scaling is often higher in juveniles compared to adults, likely due to greater energetic demands of rapid growth as opposed to somatic tissue maintenance (Glazier, 2005). In 2017, we additionally measured the respiration rates of four large *S. groenlandicus* individuals ranging from 40.6 to 60.0 mm length, which were likely mature adults (Supplementary Figure 2). When MO_2 was calculated for pooled juvenile and adult individuals, the

scaling coefficient declined from b = 0.94 to b = 0.85, suggesting the rate of change of respiration rate with increasing body mass is higher for juveniles than adults (adults-only exponent was b = 0.81; Supplementary Figure 2). Additionally, the slope of the mass-specific oxygen consumption rate for *S. groenlandicus* juveniles was not significantly different from zero, suggesting that the mass-specific respiration rate does not change with increasing biomass. Ontogenetic shifts are known to occur in mass-specific metabolic scaling from near isometry (b = 0) to allometry (b < 0), relating to changes in body shape (Glazier *et al.*, 2015).

Potential environmental effects on metabolic rate

Although we did not sample with the intent to evaluate interannual variability in metabolic rates, we were able to compare data from two years for two species. The small temperature variation in our treatments for each year of about 0.3 ◦C complicates interpretation of this result given the direct effect of temperature on metabolic rate (Peck *et al.*, 2002; Clarke and Fraser, 2004; Trigos *et al.*, 2015). Nonetheless, the respiration rates of *S. groenlandicus* were not significantly different between years, suggesting the temperature difference did not affect our results. Relative thermal independence of metabolic rate has been observed in other benthic species. For instance, the respiration rate of the amphipod *Anonyx nugax* remained constant over the temperature range 1–3 ◦C, suggesting metabolic adaptation to natural variability in environmental conditions (Opalinski and Weslawksi, 1989). In contrast, MO_2 of *Macoma* sp. was significantly higher in 2018. However, if the increased respiration rates were strictly due to temperature, the effect we observed would indicate a Q_{10} of 36 730, which is well beyond typical values (McMahon and Wilson, 1981; Peck and Conway, 2000), suggesting other factors produced this result. Most individuals were collected at different stations in each year, making it difficult to tease apart spatial from temporal differences in the environment as possible influences. Total organic carbon (TOC) concentration was roughly five times higher at station DBO3.8 where most individuals were collected in 2018, compared to station CNL3 where most individuals were collected in 2017, but TOC values were not substantially different between years at either station (Mincks unpublished data). In contrast, chlorophyll-a concentrations in surface sediments were substantially higher in 2017 than in 2018 at both stations due to the timing of ice retreat. Thus, the feeding environment *in situ* may have played a role in producing the interannual differences in MO_2 for *Macoma* sp. Alternatively, this species may simply lack temperature compensation (cf., Rastrick and Whiteley, 2011). Regardless, the experimental temperature difference between the two years is small compared to the seasonal and interannual fluctuations experienced in the region (Danielson *et al.*, 2020).

While the MO_2 of *S. groenlandicus* did not differ between years, evidence of spatial variation was observed, with individuals from one sampling station (CNL3; Fig. 1) exhibiting lower MO_2 compared to individuals from the other stations. This difference may reflect physiological differences related to environmental factors. Intraspecific variation in respiration rate can be related to a variety of factors, such as environmental conditions during early development (Burton et al., 2011). Growth rate of *S. groenlandicus* also varies spatially due to environmental conditions, which likely reflect variations in trophic conditions, and has thus been proposed as an indicator of environmental change (Ambrose et al., 2006; Kilada et al., 2007; Carroll et al., 2009; Gerasimova et al., 2019). While the average depth and other physical variables did not vary substantially at the sampling locations where *S. groenlandicus* was collected (Table 1), sandier sediment and a lower C: N ratio were observed at station CNL3 compared to the other locations (Mincks unpublished data). Both of these variables may reflect feeding conditions, potentially as a function of hydrodynamics at this site where current speeds are high due to the constriction of flow through the Bering Strait (Danielson et al., 2014). The reduced metabolic rate at the sandier CNL3 site seems to contradict evidence of a slower growth rate at stations with high silt fraction reported elsewhere (Gerasimova et al., 2019). However, growth rates and basal metabolic rates do not always align (Sebens, 2002). This spatial difference highlights a need to measure respiration rates from across the region of interest. Individuals with low respiration rates may be buffered against environmental conditions due to their low maintenance costs, which may yield greater fitness in poor trophic conditions (Burton et al., 2011). Not accounting for spatial variability in metabolic rate may bias modelling estimates of regional carbon demand and food web dynamics.

In contrast to *S. groenlandicus*, *Macoma* sp. collected from station CNL3 showed no clear impact of station on respiration rate. However, growth rate of *Macoma* sp. may be less sensitive to environmental conditions than *S. groenlandicus* (Gerasimova *et al.*, 2019) and may be buffered against environmental variability.

Implications for benthic ecosystem functioning

Environmental changes are already resulting in temperature increases, changes in primary production and shifts in benthic species composition, structure and biomass. Species-specific respiration rates suggest these changes will alter organic matter processing and carbon flow pathways in the Pacific Arctic benthos.

Metabolic rate increases with increasing temperature up to an optimal range. Respiration rates were used to estimate the expected increase in metabolic demand of each taxonomic group at a projected future temperature of 5 ◦C (Mora *et al.*, 2013) assuming Q_{10} values between 2.56 and 3.64 (Peck and Conway, 2000) following the equation:

$$R_2 = R_1 Q_{10}^{\frac{T_2 - T_1}{10}}$$

where R_1 is the measured respiration rate at the initial temperature (T_1 = 0.9 °C) and R_2 is the calculated respiration rate at the projected temperature (T_2 = 5 °C). These calculated rates provide an estimate of the increase in carbon demand under projected future warming scenarios. Indeed, bottom-water temperatures of 4 °C are already occurring in the Bering Strait region (Huntington *et al.*, 2020). At a projected future temperature of 5 °C, average mass-specific MO_2 would increase by 48–70% to a value of 14.0–16.1 μmol O_2 hr^{-1} g^{-1} for *S. groenlandicus*, 9.7–11.2 for *A. macrocephala*, 6.2–7.2 for *H. arctica*, 4.8–5.6 for *N. pernula*, 4.6.-5.3 for *Macoma* sp. and 3.1–3.6 for *Astarte* sp., again assuming Q_{10} values between 2.56 to 3.64 (Peck and Conway, 2000) and that an upper critical temperature limit has not been exceeded (Peck *et al.*, 2002). However, Q_{10} likely varies among the species and over different temperature ranges.

With this increase in standard metabolic demand and a potential decline in phytodetrital input to the seafloor (Lee *et al.*, 2013; Moore and Stabeno, 2015; Lovvorn *et al.*, 2016), carbon reserves in the sediment may become depleted, although there are some projections of increased primary production and input to the seafloor in this region (Grebmeier *et al.*, 2015a). Temperature-induced increases in metabolic demand coupled with low food availability can result in reproductive failure, death and a subsequent decline in benthic production and biomass (Hummel *et al.*, 2000). If input of organic carbon to the benthos declines and carbon resources in the sediments are depleted, biomass of bivalves and amphipods in persistent macrobenthic hotspots may then decline, with deleterious impacts on upper trophic levels, such as benthic-feeding marine mammals and birds that depend on these prey items. For instance, in the northern Bering Sea shelf, decline of the spectacled eider population has been associated with a reduction in the biomass of bivalve populations that serve as critical prey for these birds (Lovvorn *et al.*, 2009).

However, species with low metabolic demand may be more adapted to this low-food future scenario. Nuculanidae (which includes *N. pernula*) currently dominate in the northern region of our study area (Grebmeier *et al.*, 2015a). The relatively low respiration rate, and thus low metabolic demand, of *N. pernula* may leave it preadapted to the lower-productivity waters of this area, which is influenced by the Alaska Coastal Current. This low metabolic demand may confer a physiological competitive advantage over other taxonomic groups with higher carbon requirements (Burton *et al.*, 2011; McClain *et al.*, 2020). Therefore, we hypothesize that species with low metabolic rates, such as *Astarte* sp. and *N. pernula*, may dominate under a low-food scenario given their reduced organic carbon requirements necessary to maintain metabolic function. In contrast, species with high metabolic rates, such as *S. groenlandicus* and *A. macrocephala*, may be hindered by higher carbon demands and become food limited. In response to ocean warming, spatial shifts in the frequency and abundance of species associated with differing physiological tolerances has already been identified in many other regions (Sunday *et al.*, 2012).

In the Arctic, emerging evidence indicates environmental change has influenced the distribution of macrofaunal biomass, with declining biomass in some areas and increasing biomass in others (Moore *et al.*, 2018; Goethel *et al.*, 2019). In addition to changes in overall biomass, shifts in community structure and composition are occurring (Grebmeier, 2012; Waga *et al.*, 2020). Shifts in dominant species could impact community metabolic demand even if total biomass remained constant. For instance, if *S. groenlandicus* were outcompeted and replaced by *N. pernula*, carbon demand would decline given the lower MO_2 of *N. pernula*.

In conclusion, the average mass-specific MO_2 of sampled species ranged from 2.1 to 9.5 μmol O_2 hr^{-1} g^{-1}, with species-specific differences up to 4.3 times for a 0.1 g AFDM individual. These differences in MO_2 have implications for the overall carbon demand of the benthic infaunal community as assemblages are likely to continue to change under future climate scenarios.

Supplementary material

Supplementary material is available at *Conservation Physiology* online.

Funding

This research was part of the Arctic Integrated Ecosystem Research Program (IERP; http://www.nprb.org/arctic-program/). This manuscript is Publication ArcticIERP-17. Funding for the program was provided by the North Pacific Research Board, US Bureau of Ocean and Energy Management, Collaborative Alaskan Arctic Studies Program and US Office of Naval Research. Generous in-kind support for the program was contributed by the US National Oceanic Atmospheric Administration Alaska Fisheries Science Center and Pacific Marine Environmental Laboratory, University of Alaska Fairbanks, US Fish and Wildlife Service and US National Science Foundation. Support for this research was also provided by the Robert and Kathleen Byrd Award. This publication was, in part, made possible by the University of Alaska Fairbanks Office of the Vice Chancellor for Research Publication Award.

Acknowledgments

We would like to thank the Captain and crew of the *R/V Sikuliaq* for making sampling possible; and Opik Ahkinga, Lorena Edenfeld, Caitlin Forster, Silvana Gonzalez, Katrin Iken, Jessica Pretty, Sarah Seabrook, Andrew Thurber and Ann Zinkmann for helping collect organisms. We would also like to thank Arny Blanchard for help with experimental design; Max Hoberg for macrofaunal identification; and Seth

Danielson, Jeroen Ingels, Andrew Thurber and Leah Zacher for guidance and comments on this manuscript.

References

Ambrose WG, Caroll ML, Greenacre M, Thorrold SR, McMahon KW (2006) Variation in *Serripes groenlandicus* (Bivalvia) growth in a Norwegian high-Arctic fjord: Evidence for local- and large-scale climatic forcing. *Glob Chang Biol* 12: 1595–1607. https://doi.org/10.1111/j.1365-2486.2006.01181.x.

Arrigo KR, van Dijken GL (2015) Continued increases in Arctic Ocean primary production. *Prog Oceanogr* 136: 60–70. https://doi.org/10.1016/j.pocean.2015.05.002.

Bourgeois S, Archambault P, Witte U (2017) Organic matter remineralization in marine sediments: a Pan-Arctic synthesis. *Global Biogeochem Cycles* 31: 190–213. https://doi.org/10.1002/2016GB005378.

Brockington S, Clarke A (2001) The relative influence of temperature and food on the metabolism of a marine invertebrate. *J Exp Mar Bio Ecol* 258: 87–99. https://doi.org/10.1016/S0022-0981(00)00347-6.

Burton T, Killen S, Armstrong J, Metcalfe N (2011) What causes intraspecific variation in resting metabolic rate and what are its ecological consequences? *Proc R Soc B* 278: 3465–3473. https://doi.org/10.1098/rspb.2011.1778.

Carroll ML, Johnson BJ, Henkes GA, McMahon KW, Voronkov A, Ambrose WG, Denisenko SG (2009) Bivalves as indicators of environmental variation and potential anthropogenic impacts in the southern Barents Sea. *Mar Pollut Bull* 59: 193–206. https://doi.org/10.1016/j.marpolbul.2009.02.022.

Chapelle G, Peck LS, Clarke A (1994) Effects of feeding and starvation on the metabolic rate of the necrophagous Antarctic amphipod *Waldeckia obesa* (Chevreux, 1905). *J Exp Mar Bio Ecol* 183: 63–76. https://doi.org/10.1016/0022-0981(94)90157-0.

Clarke A, Fraser KPP (2004) Why does metabolism scale with temperature? *Funct Ecol* 18: 243–251. https://doi.org/10.1111/j.0269-8463.2004.00841.x.

Danielson SL *et al.* (2020) Manifestation and consequences of warming and altered heat fluxes over the Bering and Chukchi Sea continental shelves. *Deep Res Part II Top Stud Oceanogr* 177: 104781. https://doi.org/10.1016/j.dsr2.2020.104781.

Danielson SL, Eisner L, Ladd C, Mordy C, Sousa L, Weingartner TJ (2017) A comparison between late summer 2012 and 2013 water masses, macronutrients, and phytoplankton standing crops in the northern Bering and Chukchi Seas. *Deep-Sea Res II Top Stud Oceanogr* 135: 7–26. https://doi.org/10.1016/j.dsr2.2016.05.024.

Danielson SL, Weingartner TJ, Hedstrom KS, Aagaard K, Woodgate R, Curchitser E, Stabeno PJ (2014) Coupled wind- forced controls of the Bering-Chukchi shelf circulation and the Bering Strait throughflow: Ekman transport, continental shelf waves, and variations of the Pacific-Arctic sea surface height gradient. *Prog Oceanogr* 125: 40–61 https://doi.org/10.1016/j.pocean.2014.04.006.

Denisenko N, Grebmeier J (2015) Spatial patterns of bryozoan fauna biodiversity and issue of biogeographic regionalization of the Chukchi Sea. *Oceanography* 28: 134–145.

Fay FH (1982) Ecology and biology of the pacific walrus, *Odobenus rosmarus divergens* Illiger. *North Am Fauna* 74: 1–279.

Feder HM, Naidu AS, Jewett SC, Hameedi JM, Johnson WR, Whitledge TE (1994) The northeastern Chukchi Sea: Benthos-environmental interactions. *Mar Ecol Prog Ser* 111: 171–190. https://doi.org/10.3354/ meps111171.

Gatti S, Brey T, Müller WEG, Heilmayer O, Holst G (2002) Oxygen microoptodes: A new tool for oxygen measurements in aquatic animal ecology. *Mar Biol* 140: 1075–1085. https://doi.org/10.1007/s00227-002-0786-9.

Gerasimova AV, Filippova NA, Lisitsyna KN, Filippov AA, Nikishina DV, Maximovich NV (2019) Distribution and growth of bivalve molluscs *Serripes groenlandicus* (Mohr) and *Macoma calcarea* (Gmelin) in the Pechora Sea. *Polar Biol* 42: 1685–1702. https://doi.org/10.1007/s00300-019-02550-z.

Glazier DS (2005) Beyond the "3/4-power law": Variation in the intra- and interspecific scaling of metabolic rate in animals. *Biol Rev* 80: 611–662. https://doi.org/10.1017/S1464793105006834.

Glazier DS, Hirst AG, Atkinson D (2015) Shape shifting predicts ontogenetic changes in metabolic scaling in diverse aquatic invertebrates. *Proc R Soc B Biol Sci* 282:2014302. doi: 10.1098/rspb.2014.2302.

Goethel CL, Grebmeier JM, Cooper LW (2019) Changes in abundance and biomass of the bivalve Macoma calcarea in the northern Bering Sea and the southeastern Chukchi Sea from 1998 to 2014, tracked through dynamic factor analysis models. *Deep-Sea Res II Top Stud Oceanogr* 162: 127–136. https://doi.org/10.1016/j.dsr2.2018.10.007.

Goethel CL, Grebmeier JM, Cooper LW, Miller TJ (2017) Implications of ocean acidification in the Pacific Arctic: Experimental responses of three Arctic bivalves to decreased pH and food availability. *Deep-Sea Res II Top Stud Oceanogr* 144: 112–124. https://doi.org/10.1016/j.dsr2.2017.08.013.

Grebmeier J, Bluhm BA, Cooper LW, Denisenko SG, Iken K (2015a) Time-series benthic community composition and biomass and associated environmental characteristics in the chukchi Sea during the RUSALCA 2004–2012 Program. *Oceanography* 28: 116–133. https://doi.org/10.5670/oceanog.2015.61.

Grebmeier J, Frey K, Cooper L, Ke̦dra M (2018) Trends in benthic macrofaunal populations, seasonal sea ice persistence, and bottom water temperatures in the Bering Strait region. *Oceanography* 31: 136–151. https://doi.org/10.5670/oceanog.2018.224.

Grebmeier JM (2012) Shifting patterns of life in the Pacific Arctic and Sub-Arctic Seas. *Ann Rev Mar Sci* 4: 63–78. https://doi.org/10.1146/annurev-marine-120710-100926.

Grebmeier JM *et al.* (2015b) Ecosystem characteristics and processes facilitating persistent macrobenthic biomass hotspots and associated benthivory in the Pacific Arctic. *Prog Oceanogr* 136: 92–114. https://doi.org/10.1016/j.pocean.2015.05.006.

Grebmeier JM, Cooper LW, Feder HM, Sirenko BI (2006) Ecosystem dynamics of the Pacific-influenced Northern Bering and Chukchi Seas in the Amerasian Arctic. *Prog Oceanogr* 71: 331–361. https://doi.org/10.1016/j.pocean.2006.10.001.

Hothorn T, Bretz F, Westfall P (2008) Simultaneous inference in general parametric models. *Biom J* 50: 346–363. https://doi.org/10.1002/ bimj.200810425.

Hummel H, Bogaards RH, Bachelet G, Caron F, Sola JC, Amiard-Triquet C (2000) The respiratory performance and survival of the bivalve *Macoma balthica* (L.) at the southern limit of its distribution area: A translocation experiment. *J Exp Mar Bio Ecol* 251: 85–102. https://doi.org/10.1016/S0022-0981(00)00208-2.

Huntington HP, Danielson SL, Wiese FK, Baker M, Boveng P, Citta JJ, De Robertis A, Dickson DMS, Farley E, George JC, *et al.* (2020) Evidence suggests potential transformation of the Pacific Arctic ecosystem is underway. *Nat Clim Chang*. doi: https://doi.org/10.1038/s41558-020-0695-2.

Hutchings JA, Haedrich RL (1984) Growth and population structure in two species of bivalves (Nuculanidae) from the deep sea. *Mar Ecol* 17: 135–142.

IPCC (2014) Climate Change 2014: Synthesis Report. Contribution of Working Groups I, II and III to the Fifth Assessment Report of the Intergovernmental Panel on Climate Change. In Core Writing Team, R.K. Pachauri and L.A. Meyer, eds. IPCC. IPCC, Geneva, Switzerland.

Ke˛dra M, Gromisz S, Jaskuła R, Legez˙yn´ska J, Maciejewska B, Malec E, Opanowski A, Ostrowska K, Włodarska-Kowalczuk M, We˛sławski JM (2010) Soft bottom macrofauna of an All Taxa Biodiversity Site: Hornsund (77°N, Svalbard). *Polish Polar Res* 31: 309–326.

Kilada RW, Roddick D, Mombourquette K (2007) Age determination, validation, growth and minimum size of sexual maturity of the Greenland smoothcockle (*Serripes groenlandicus*, Bruguiere, 1789) in Eastern Canada. *J Shellfish Res* 26: 443–450. https://doi.org/10.2983/0730-8000(2007)26[443:ADVGAM]2.0.CO;2.

Kleiber (1932) Body size and metabolism. *Hilgardia* 6: 315–353.

Lee S, Sun Yun M, Kyoung Kim B, Saitoh S, Kang C-K, Kang S-H, Whitledge T (2013) Latitudinal carbon productivity in the Bering and Chukchi Seas during the summer in 2007. *Cont Shelf Res* 59: 28–36. https://doi.org/10.1016/j.csr.2013.04.004.

Liu W, He M (2012) Effects of ocean acidification on the metabolic rates of three species of bivalve from southern coast of China. *Chinese J Oceanol Limnol* 30: 206–211. https://doi.org/10.1007/s00343-012-1067-1.

Lovvorn J, North C, Kolts J, Grebmeier J, Cooper L, Cui X (2016) Projecting the effects of climate-driven changes in organic matter supply on benthic food webs in the northern Bering Sea. *Mar Ecol Prog Ser* 548: 11–30. https://doi.org/10.3354/meps11651.

Lovvorn JR, Grebmeier JM, Cooper LW, Bump JK, Richman SE (2009) Modeling marine protected areas for threatened eiders in a climatically changing Bering Sea. *Ecol Appl* 19: 1596–1613. https://doi.org/10.1890/08-1193.1.

Lovvorn JR, Richman SE, Grebmeier JM, Cooper LW (2003) Diet and body condition of spectacled eiders wintering in pack ice of the Bering Sea. Polar Biol 26: 259–267. https://doi.org/10.1007/s00300-003-0477-0.

Lubinsky I (1980) Marine bivalve mollusca of the Canadian central and eastern Arctic: faunal composition and zoogeography. *Can Bull Fish Aquat Sci* 207: 111.

Madsen F (1949) Marine bivalvia. In *The Zoology of Iceland, Volume IV*. Munksgaard, Reykjavik, pp. 1–116.

McClain CR, Webb TJ, Nunnally CC, Dixon SR, Finnegan S, Nelson JA (2020) Metabolic niches and biodiversity: A test case in the deep sea benthos. *Front Mar Sci* 7: 216. doi: 10.3389/fmars.2020.00216.

McMahon R, Wilson J (1981) Seasonal respiratory responses to temperature and hypoxia in relation to burrowing depth in three intertidal bivalves. *J Therm Biol* 6: 267–277. https://doi.org/10.1016/0306-4565(81)90015-2.

Moore SE, Stabeno PJ (2015) Synthesis of Arctic Research (SOAR) in marine ecosystems of the Pacific Arctic. *Prog Oceanogr* 136: 1–11. https://doi.org/10.1016/j.pocean.2015.05.017.

Moore SE, Stabeno PJ, Grebmeier JM, Okkonen SR (2018) The Arctic Marine Pulses Model: linking annual oceanographic processes to contiguous ecological domains in the Pacific Arctic. *Deep Res II* 152: 8–21. https://doi.org/10.1016/j.dsr2.2016.10.011.

Mora C *et al.* (2013) Biotic and human vulnerability to projected changes in ocean biogeochemistry over the 21st Century. *PLoS Biol* 11(10): e1001682. doi: 10.1371/journal.pbio.1001682.

Muggeo VMR (2008) segmented: an R package to fit regression models with broken-line relationships. *R News* 8: 20–25.

Opalinski KW, Weslawksi JM (1989) Ecology, metabolic rate, and metabolic adaptations in Spitsbergen amphipods. *Pol Arch Hydrobiol* 36: 333–350.

Peck LS, Conway LZ (2000) The myth of metabolic cold adaptation: oxygen consumption in stenothermal Antarctic bivalves. In Harper E, Taylor J, Crame J, eds, *The Evolutionary Biology of the Bivalvia Geological Society of London*, London, pp. 441–450. https://doi.org/10.1144/GSL.SP.2000.177.01.29.

Peck LS, Pörtner HO, Hardewig I (2002) Metabolic demand, oxy- gen supply, and critical temperatures in the Antarctic bivalve *Laternula elliptica*. *Physiol Biochem Zool* 75: 123–133. https://doi.org/10.1086/340990.

Rastrick SPS, Whiteley NM (2011) Congeneric amphipods show differing abilities to maintain metabolic rates with latitude. *Physiol Biochem Zool* 84: 154–165. https://doi.org/10.1086/658857.

Ringuette M, Fortier L, Fortier M, Runge JA, Bélanger S, Larouche P, Weslawski J-M, Kwasniewski S (2002) Advanced recruitment and accelerated population development in Arctic calanoid copepods of the North Water. *Deep-Sea Res II Top Stud Oceanogr* 49: 5081–5099. https://doi.org/10.1016/S0967-0645(02)00179-0.

Saavedra LM, Parra D, Martin VS, Lagos NA, Vargas CA (2018) Local habitat influences on feeding and respiration of the intertidal mussels *Perumytilus purpuratus* exposed to increased pCO2 levels. Estuaries Coasts 41: 1118–1129. https://doi.org/10.1007/s12237-017- 0333-z.

Schaefer R, Trutschler K, Rumohr H (1985) Biometric studies on the bivalves *Astarte elliptica, A. borealis* and *A. montagui* in Kiel Bay (Western Baltic Sea). *Helgoländer Meeresuntersuchungen* 39: 245–253. https://doi.org/10.1007/BF01992772.

Sebens KP (2002) Energetic constraints, size gradients, and size limits in benthic marine invertebrates. *Integr Comp Biol* 42: 853–861. https://doi.org/10.1093/icb/42.4.853.

Sejr MK, Christensen PB (2007) Growth, production and carbon demand of macrofauna in Young Sound, with special emphasis on the bivalves *Hiatella arctica* and *Mya truncata*. In S Ryasgaar, RN Glud, eds, *Carbon Cycling in Arctic Marine Ecosystems.* Bioscience, Meddr, pp. 122–135.

Sejr MK, Petersen JK, Jensen KT, Rysgaard S (2004) Effects of food concentration on clearance rate and energy budget of the Arctic bivalve *Hiatella arctica* (L) at subzero temperature. *J Exp Mar Bio Ecol* 311: 171–183. https://doi.org/10.1016/j.jembe.2004.05.005.

Sejr MK, Sand MK, Jensen KT, Petersen JK, Christensen PB, Rysgaard S (2002) Growth and production of *Hiatella arctica* (Bivalvia) in a high-Arctic fjord (Young Sound, Northeast Greenland). *Mar Ecol Prog Ser* 244: 163–169. https://doi.org/10.3354/meps244163.

Selz V, Saenz BT, van Dijken GL, Arrigo KR (2018) Drivers of ice algal bloom variability between 1980 and 2015 in the Chukchi Sea. *J Geophys Res Ocean* 123: 7037–7052. https://doi.org/10.1029/2018JC014123.

Sukhotin AA, Pörtner HO (2001) Age-dependence of metabolism in mussels *Mytilus edulis* (L.) from the White Sea. *J Exp Mar Bio Ecol* 257: 53–72. https://doi.org/10.1016/S0022-0981(00)00325-7.

Sunday JM, Bates AE, Dulvy NK (2012) Thermal tolerance and the global redistribution of animals. *Nat Clim Chang* 2: 686–690. https://doi.org/10.1038/nclimate1539.

Trigos S, Garcia-March JR, Vicente N, Tena J, Torres J (2015) Respiration rates of the fan mussel *Pinna nobilis* at different temperatures. *J Moll Stud* 81: 217–222. https://doi.org/10.1093/mollus/eyu075.

Vahl O (1978) Seasonal changes in oxygen consumption of the Iceland scallop (*Chlamys islandica* (O.F. Muller)) from 70N. *Ophelia* 17: 143–154. https://doi.org/10.1080/00785326.1978.10425478.

Waga H, Hirawake T, Grebmeier JM (2020) Recent change in benthic macrofaunal community composition in relation to physical forcing in the Pacific Arctic. *Polar Biol* 43: 285–294. https://doi.org/10.1007/ s00300-020-02632-3.

Walsh JJ *et al.* (1989) Carbon and nitrogen cycling within the Bering/Chukchi Seas: Source regions for organic matter effecting AOU demands of the Arctic Ocean. *Prog Oceanogr* 22: 277–359. https://doi.org/10.1016/0079-6611(89)90006-2.

Wang M, Overland JE (2015) Projected future duration of the sea-ice-free season in the Alaskan Arctic. *Prog Oceanogr* 136: 50–59. https://doi.org/10.1016/j.pocean.2015.01.001.

Whitehouse GA, Aydin K, Essington TE, Hunt GL (2014) A trophic mass balance model of the eastern Chukchi Sea with comparisons to other high-latitude systems. *Polar Biol* 37: 911–939. https://doi.org/10.1007/s00300-014-1490-1.

Witte U, Graf G (1996) Metabolism of deep-sea sponges in the Greenland- Norwegian Sea. *J Exp Mar Bio Ecol* 198: 223. https://doi.org/10.1016/0022-0981(96)00006-8.

Yagi M, Kanda T, Takeda T, Ishimatsu A, Oikawa S (2010) Ontogenetic phase shifts in metabolism: links to development and anti-predator adaptation. *Proc R Soc B Biol Sci* 277: 2793–2801. https://doi.org/10.1098/rspb.2010.0583.

Spatial patterns and effects of temperature on rates of organic matter processing in sediments across the northern Bering and southern Chukchi Sea shelf (Manuscript in preparation)

Sarah L. Mincks, Brittany Jones Charrier, Sarah Seabrook, Andrew Thurber

Abstract: Labile organic matter deposited at the seafloor is respired by benthic organisms, and respiration rates are highly temperature dependent in both microbes and metazoan in sediments. In light of changing temperature and productivity regimes across the Pacific-Arctic domain, we measured respiration rates of sediment communities at in situ and elevated temperatures at ten locations across the N Bering and S Chukchi Seas. Intact sediment cores were incubated at 0ºC (ambient) and 5ºC (projected warming). On average, sediment community oxygen demand, a proxy for organic carbon consumption, was ~30% higher in warmer treatments. Substrate type, productivity, and particulate flux rates varied across the study area, resulting in spatial differences in microbial and metazoan biomass. In the southeast Chukchi Sea (DBO 3 region), high biomass of large infaunal species, particularly bivalves, generated somewhat elevated oxygen demand. However, oxygen consumption rates were more consistent across the rest of the study area, with rates increasing more rapidly as a function of microbial biomass than of macrofaunal biomass. Fluxes of dissolved inorganic carbon (DIC) were also measured in incubation experiments as an additional means of quantifying oxygen consumption due specifically to respiration of infauna. DIC fluxes were decoupled from oxygen fluxes at some locations. In some cases, DIC was taken up by sediment communities, suggesting autotrophic production which could have been producing oxygen during experiments, resulting in underestimation of respiration rates by oxygen flux measurement.

Introduction

The processing of organic material by sediment communities has significant consequences for ecosystem functioning and productivity—particularly in the shallow inflow shelf seas of the Pacific-Arctic region, which are characterized by tight benthic-pelagic coupling, high benthic biomass, and high rates of organic matter remineralization in sediments (e.g., Walsh et al. 1989; Whitehouse et al. 2014; Grebmeier et al. 2015; Bourgeois et al. 2017). Organic matter processed by the benthic food web is either respired or assimilated into biomass of benthic organisms; thus, these key processes must be measured in order to characterize the flow of carbon under current conditions, and to project how rates and pathways may change with warming and sea-ice loss (Wassmann and Reigstad 2011).

Organic carbon consumption by Arctic shelf benthos has been estimated as sediment community oxygen consumption (SCOC) (reviewed by Grebmeier et al. 2006; Bourgeois et al. 2017), providing bulk measurement of energy demand for all sediment organisms. Although published data are limited in the Pacific-Arctic region, the majority of the oxygen consumption

(and thus carbon demand) has typically been attributed to macrofaunal organisms (Devol et al. 1997; Clough et al. 2005). For example, in the northern Bering and southern Chukchi seas, amphipods and bivalves were estimated to account for 61% of SCOC (Grebmeier and McRoy 1989). However, bacterial biomass and respiration, which constitute a large portion of SCOC in other regions (Hubas et al. 2007; Franco et al. 2010; Braeckman et al. 2018; Mäkelä et al. 2018), have not been directly measured in sediments on the Pacific-Arctic shelves,.

Bacteria may become increasingly important in organic matter processing on Arctic shelves under future scenarios of increasing temperature and changes in particulate flux to the seafloor. As temperatures increase, heterotrophic bacteria become more efficient, because the activity of extracellular enzymes used by bacteria to hydrolyze high molecular-weight organic matter also increases (Arnosti and Jorgensen 2003; Arnosti 2011). Experimental results are limited for Arctic sediments, but Kritzberg et al. (2010) showed that a 6°C temperature increase resulted in a six-fold increase in pelagic bacterial carbon demand. This and other studies also show strong interactions between the effects of temperature and substrate availability on microbial activity (Pomeroy and Deibel 1986; Wiebe et al. 1992; Canion et al. 2014), which suggests that bacteria may be able to process a larger portion of the sedimentary organic carbon pool at warmer temperatures, potentially affecting food availability for detritivores (cf., Mincks et al. 2005).

We conducted sediment-core incubation experiments in the Northern Bering and Chukchi Seas to measure oxygen consumption of the sediment community at two different temperatures, and estimate rate of organic matter consumption. Microbial and macrofaunal biomass were estimated at the same sites, and patterns in oxygen consumption are considered in light of these biomass patterns as well as other features of the benthic environment.

Methods

To quantify the effect of changing temperatures on the carbon demand of the benthic community, we conducted sediment-core incubation experiments at 13 stations in the Northern Bering and Southern Chukchi Seas in June 2017 and June 2018, during the Arctic Shelf Growth, Advection, Respiration, and Deposition Rates (ASGARD) field program on board *R/V Sikuliaq* (Figure 1). Eight stations were sampled in both years. Station depths ranged from 32 – 58 m (Table 1). Two sampled areas correspond to the Distributed Biological Observatory (DBO) areas 2 and 3, also known as the Chirkov and SECS hotspots, respectively (Grebmeier et al. 2006; Grebmeier 2012). The study area is seasonally ice covered and highly productive, characterized by northward flow of cold, nutrient-rich Anadyr-Bering Sea Water in the west and warmer, more nutrient-poor Alaska Coastal Water in the east (Danielson et al. 2017). Downstream of the Bering Strait constriction, water masses fan out over the shallow Chukchi Sea shelf, resulting in declining current speeds and deposition of suspended particles to the seafloor. Grain-size characteristics generally reflect these patterns, with sandy substrate in the Chirikov Basin south of Bering Strait, and muddier sediments further north in the Chukchi Sea. In turn, composition of macrofauna communities is influenced by grain size and spatial patterns in organic matter

deposition (Grebmeier et al. 2015; Charrier & Mincks, in prep.). The Chirikov Basin is dominated by suspension-feeding amphipods as well as bivalves, whereas large bivalves dominate the infaunal biomass in the central Chukchi with smaller-bodied organisms, mainly polychaetes, dominating in the nearshore areas influenced by Alaska Coastal Water (Charrier & Mincks, in prep.).

Samples were collected using an MC-800 multi-corer with 12 x 10-cm diameter polycarbonate tubes (Ocean Instruments, San Diego, CA). Multi-core samples were retrieved from replicate deployments at each station to obtain true sample replicates. In 2017, the number of cores incubated at each station ranged from one to three per treatment, whereas three cores per treatment were incubated at all stations in 2018 (Table 1). Additional cores were taken from the same multi-core deployments for measurement of environmental variables, including grain size, total organic carbon (TOC), total nitrogen (TN), chloropigment concentration, and stable carbon isotope ($\delta^{13}C$) values. These data and associated methods have been described in detail by Charrier & Mincks (in prep.; see also Study 16, this report).

Sediment community oxygen consumption experiments

High-quality cores with clear top water and undisturbed sediment-water interface were selected for incubation experiments. Most of the top water was siphoned off of each core through a 45-µm screen into a clean bucket, and chilled to experimental temperatures for use during incubations. Each core was then extruded into a shorter 25-cm long x 10-cm diameter acrylic tube to obtain an intact sub-core approximately 15 cm deep. Sediment-community oxygen consumption (SCOC) was measured in each of two different temperature treatments. We targeted 0° and 5°C, simulating ambient and predicted future bottom-water temperatures in the study area (Mora et al. 2013), but actual temperatures fluctuated between 0 – 1°C and 4 – 5°C. Sub-cores were partially submerged in seawater in plastic crates, placed in either a chest freezer (5° C) or in a walk-in environmental chamber (0° C) on board the ship, and allowed to reach the desired temperature. Cores were topped off with the reserved filtered water removed from multi-core tubes upon collection, such that all experimental cores were topped with the same water. In 2018, samples of this water were taken at the start of each experiment for analysis of dissolved inorganic carbon (DIC) concentrations, and in both years were taken for nutrient analysis. Nutrient samples were removed using a syringe filter, and frozen at -20° C, and DIC samples were poisoned with saturated $HgCl_2$. Cores were then capped with rubber stoppers from which a rare-earth magnet was suspended. Small motors were used to rotate a magnetic bar which agitated the magnets inside each core tube, gently stirring overlying water to prevent boundary layer formation. Cores were kept shielded from ambient light during acclimation and incubation periods, except during periodic oxygen measurements.

Oxygen concentration in the incubated cores was measured using non-invasive optodes (PSt3 oxygen sensor spots; PreSens Precision Sensing GmbH, Germany; detection limit = 0.03% oxygen) which were glued to the inside of each core tube. The sensor spots measure changes in oxygen concentration based on the dynamic fluorescence quenching of a luminophore contained

in a polymer matrix. An initial oxygen concentration reading was recorded as soon as tubes were capped, and additional measurements were recorded at consistent intervals throughout each experiment. A temperature probe was placed in the water bath containing submerged core tubes during oxygen readings, and all oxygen concentrations were corrected for temperature by the PreSens meter. Incubations were terminated when oxygen had declined by ~20% of initial concentration (typically 10 - 18 hours after cores were capped). The oxygen consumption rate was then calculated from the linear regression of oxygen concentration versus time. SCOC measurements were converted to estimates of benthic carbon demand using a respiratory quotient of 0.8 (Smith 1978). At the end of the experiment, cores were harvested and either sectioned into discrete depth layers and frozen (2017) or sieved for macrofaunal biomass (2018).

DIC concentrations were analyzed using an Apollo DIC Analyzer AS-C6 following best-practices protocols (Dickson et al. 2007). Nutrient samples were sent to the nutrient analysis lab at Oregon State University for analysis.

Biomass estimation

Bacterial biomass was measured in background cores collected from all stations that were sampled in both years using phospholipid fatty-acid analysis (PLFA). PLFAs were extracted from freeze-dried sediment via a one-step extraction-transesterification method using a transesterification reaction mix of 10:1:1 methanol: chloroform: hydrochloric acid. The resulting fatty-acid methyl esters (FAMEs) were then extracted using 4:1 hexane:chloroform (Lewis et al. 2000). Samples were analyzed using a Thermo-TRACE 1310 gas chromatogram with flame ionization detector (GC-FID). A C19:0 internal standard (Methyl nonadecanoate, CAS 1731-94-8) was added to each sample prior to analysis for FAME quantification, and peaks were identified through comparison to two external standards (Supelco 37 FAME mix CRM47885, and BAME mix 47080-U, Millipore Sigma). Biomass was calculated from the peak areas for known bacteria-specific markers iso15:0, iso16:0, and anteiso15:0 (Boschker and Middelburg 2002; Moodley et al. 2005).

Macrofaunal biomass was measured in background cores (2017) or in the incubated cores (2018). Samples were sieved live on board the vessel over 500 µm mesh using filtered seawater, preserved in 10% buffered formalin, and returned to the lab for sorting and taxonomic identification. Taxa were generally identified to phylum or class, and polychaetes were identified to family. In 2018, a subset of cores (those from the 5°C treatment) received a more detailed analysis with genus- or species-level identification of polychaetes and amphipods.

Results and Discussion:

Stations with replicated sampling in both years were included in a nested ANOVA for temperature treatment, station, and year, which showed no evidence of differences in sediment community oxygen consumption (SCOC) between years ($F = 0.251$, $p = 0.622$). Higher rates were measured in 2018 at station CNL 3, and at DBO 3.8 in the 5°C treatment only; however, only one replicate core was incubated at each temperature at CNL 3 in 20017 so it is difficult to

determine whether the difference is meaningful. Given the lack of detectable difference at most sites between years, samples were pooled among years were for further comparisons, which indicated significant effects of temperature and station on SCOC rate (Table 2). The 5°C temperature difference between treatments resulted in increased SCOC rates at nearly all stations in both years, with increases ranging from 4 to 107% (2017 mean = 38%; 2018 mean = 31%). At DBO 3.8 in 2017, and at DBO 3.3 in 2018, decreases in SCOC of ~10% were observed at the warmer temperature, although these differences may result from high variability among replicates.

Results of Charrier & Mincks (in prep.) indicated four different regions with distinct habitat characteristics and benthic communities, and those station groupings are used here for comparison of SCOC rates (Figure 2). SCOC rates were roughly comparable at most sites (~10 – 20 mmol O_2 m^{-2} d^{-1}), with the exception of sites in the southeast Chukchi Sea benthic 'hot spot' in the DBO 3 area where values ranged from ~20 – 80 mmol O_2 m^{-2} d^{-1} (Table 2, Figure 2). The two stations immediately north of Bering Strait, while situated in close proximity, displayed markedly different results with CNL 3 showing some of the highest rates overall, compared to nearby CPL 8 which was more comparable to other coastal sites. Charrier & Mincks (in prep.) identified similar infaunal communities at these two sites, which suggests macrofauna are not driving this difference. The high SCOC at CNL 3 was mainly observed in 2018, with a rate of 56.5 mmol m^{-2} d^{-1}, compared to 38.7 mmol m^{-2} d^{-1} in 2017. While macrofaunal biomass estimates were similar between years, microbial biomass was 4x higher in 2018. Further, while SCOC rates were roughly similar at coastal and Chirikov Basin sites, macrofaunal biomass varied by as much as two orders of magnitude, again suggesting that macrofauna are not solely responsible for driving spatial variation in SCOC. Organic matter input has been identified as a key driver of SCOC rates in other regions (e.g., Kiesel et al. 2020); we will continue to explore relationships to habitat features and macrofaunal community structure in future analysis.

SCOC rates show strong relationships to both microbial and macrofaunal biomass, although for macrofauna there appear to be two clouds of points representing the southeast Chukchi Sea 'hot spot' sites and the rest of the stations (Figure 3). Our data are more limited for bacterial biomass, but do suggest a steeper relationship between SCOC and biomass which may indicate that smaller changes in microbial biomass may have relatively greater impacts on rate of organic matter consumption.

Change in DIC concentration over the course of the experiment provides an additional estimate of sediment community respiration, and changes in nutrient concentrations provide insights into microbially mediated remineralization pathways occurring in sediments (e.g., Henriksen et al. 1993; Horak et al. 2013). We measured DIC flux across the sediment-water interface in 2018 only, and results show a decoupling between DIC and O_2 fluxes (Figure 4). At the stations with higher macrofaunal biomass, relationships are tighter, whereas coastal sites which may be more heavily influenced by microbial processes show low DIC flux relative to O_2, and even show DIC consumption at station CL 3. This pattern may indicate chemical uptake of O_2 by products of anaerobic microbial respiration (e.g., H_2S). At CL 3, uptake of DIC may

suggest viable photosynthetic cells such as newly settled phytoplankton or benthic microalgae, or other microbial processes. In any case, SCOC measurements alone would likely overestimate true community respiration at these sites. Analysis of microbial community structure in this area does indicate shallow anoxia in sediments, as well as presence of iron reducing and oil degrading species (Walker et al., in prep.).

Table 1. Sampling location information, environmental data, sediment community oxygen consumption (SCOC, averaged across temperature treatments, ± std. dev.), and average biomass for all stations. Stations are grouped into "sampling areas" with similar habitat types, based on differences in benthic community structure and environmental factors as identified by Charrier & Mincks (in prep.; see Study 16, this report). N = number of cores incubated at each experimental temperature at each station. Average macrofaunal biomass (wet weight) ±std. dev is based on analysis of background samples (2017), or experimental cores (2018). Microbial biomass is based on bacterial phospholipid fatty-acid analysis as described in the Methods (n.d. = no data). Inventories of chlorophyll a (Chl-a) in the upper 10 cm of sediment, and total organic carbon and nitrogen (TOC, TN) in the upper 1 cm of sediment provide indicators of organic matter content in sediments.

Station	**Depth (m)**	**Sampling area**	**N**	**SCOC** ($mmol\ O_2\ m^{-2}\ d^{-1}$)	**Macrofauna Biomass** ($g\ WW\ m^{-2}$)	**Microbial Biomass** ($g\ C\ m^{-2}$)	**Chl-a** ($\mu g\ cm^{-2}$)	**TOC** ($mg\ cm^{-2}$)	**TN** ($mg\ cm^{-2}$)
2017									
CL1	48	Coastal	2	17.75 ± 3.97	91.7 ± 94.3	15.9	127.40	6.78	0.91
CL3	53	Central	2	17.49	347.0 ± 145.1	15.2	87.42	6.03	0.85
CNL3	56	B. Strait	1	38.69	2407.4	25.0	75.85	2.45	0.38
CPL8	52	B. Strait	2	22.70	556.2	n.d.	48.84	3.00	0.40
DBO2.2	46	Chirikov	3	16.56 ± 3.85	358.3 ± 212.0	20.9	40.15	2.86	0.40
DBO2.4	48	Chirikov	3	13.99 ± 5.19	672.8 ± 417.6	23.2	35.79	4.39	0.65
DBO3.3	48	Coastal	2	14.21	117.1 ± 69.7	16.7	54.89	3.82	0.57
DBO3.8	50	Central	2	29.06	1398.9	27.6	192.76	7.17	1.06
IL2	35	Coastal	1	12.97	308.8 ± 238.0	n.d.	87.61	5.46	0.73
IL4	39	Coastal	3	22.83 ± 7.64	15.8 ± 11.7	20.1	79.95	6.22	0.87
2018									
CBE3	32	Chirikov	3	11.62 ± 4.86	753.5 ± 485.8	n.d.	6.82	4.71	0.68
CL1	46	Coastal	3	13.95 ± 1.39	49.3 ± 24.2	11.3	12.58	7.96	1.04
CL3	53	Central	3	17.90 ± 3.74	572.5 ± 226.7	17.2	9.95	6.72	0.99
CNL3	56	B. Strait	3	56.45 ± 9.06	2669.1 ± 754.8	96.4	15.66	4.50	0.70
CNL5	48	Central	3	29.90 ± 9.90	1944.5 ± 1057.6	n.d.	16.11	5.52	0.76
DBO2.2	46	Chirikov	3	20.84 ± 3.88	536.2 ± 522.6	18.2	10.08	3.75	0.55
DBO2.4	48	Chirikov	3	10.64 ± 3.40	626.0 ± 608.4	23.2	7.45	3.37	0.48
DBO3.3	48	Coastal	3	17.41 ± 5.42	149.5 ± 130.2	11.8	10.29	5.18	0.71
DBO3.6	58	Central	3	36.31 ± 27.09	967.2 ± 942.2	18.6	10.05	5.31	0.79
DBO3.8	51	Central	3	48.76 ± 19.74	4563.7 ± 1818.5	26.3	6.94	6.19	0.93
IL4	39	Coastal	3	14.01 ± 4.80	148.9 ± 173.9	8.6	15.56	6.13	0.81

Table 2. Results of nested ANOVA for difference in sediment community oxygen consumption (SCOC) rate between temperature treatments. Temperature treatment is nested within station.

	Type III Sum of Squares	df	Mean Square	F	Sig.
Temperature	1485.740	1	1485.740	8.969	0.010
Station	16081.300	12	1340.108	7.442	< 0.001
Temperature(Station)	2160.801	12	180.067	2.883	0.002

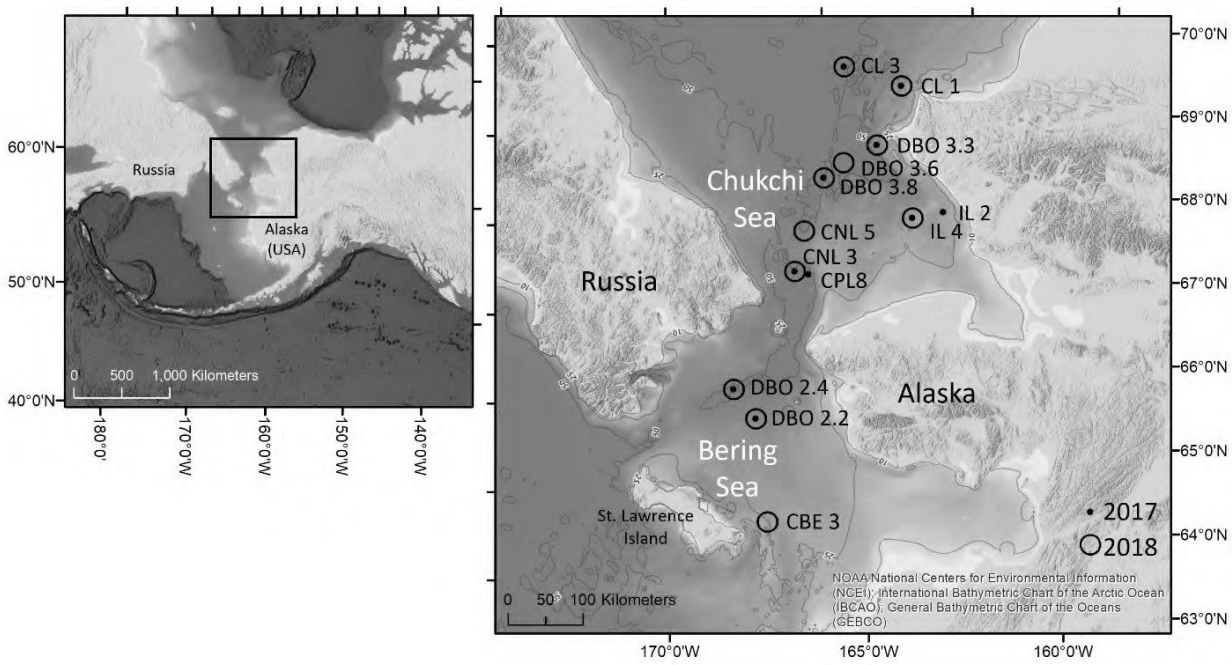

Figure 1. Map of sites where sediment community oxygen consumption experiments were conducted in each year. Stations denoted by a dot within a circle were sampled in both 2017 and 2018.

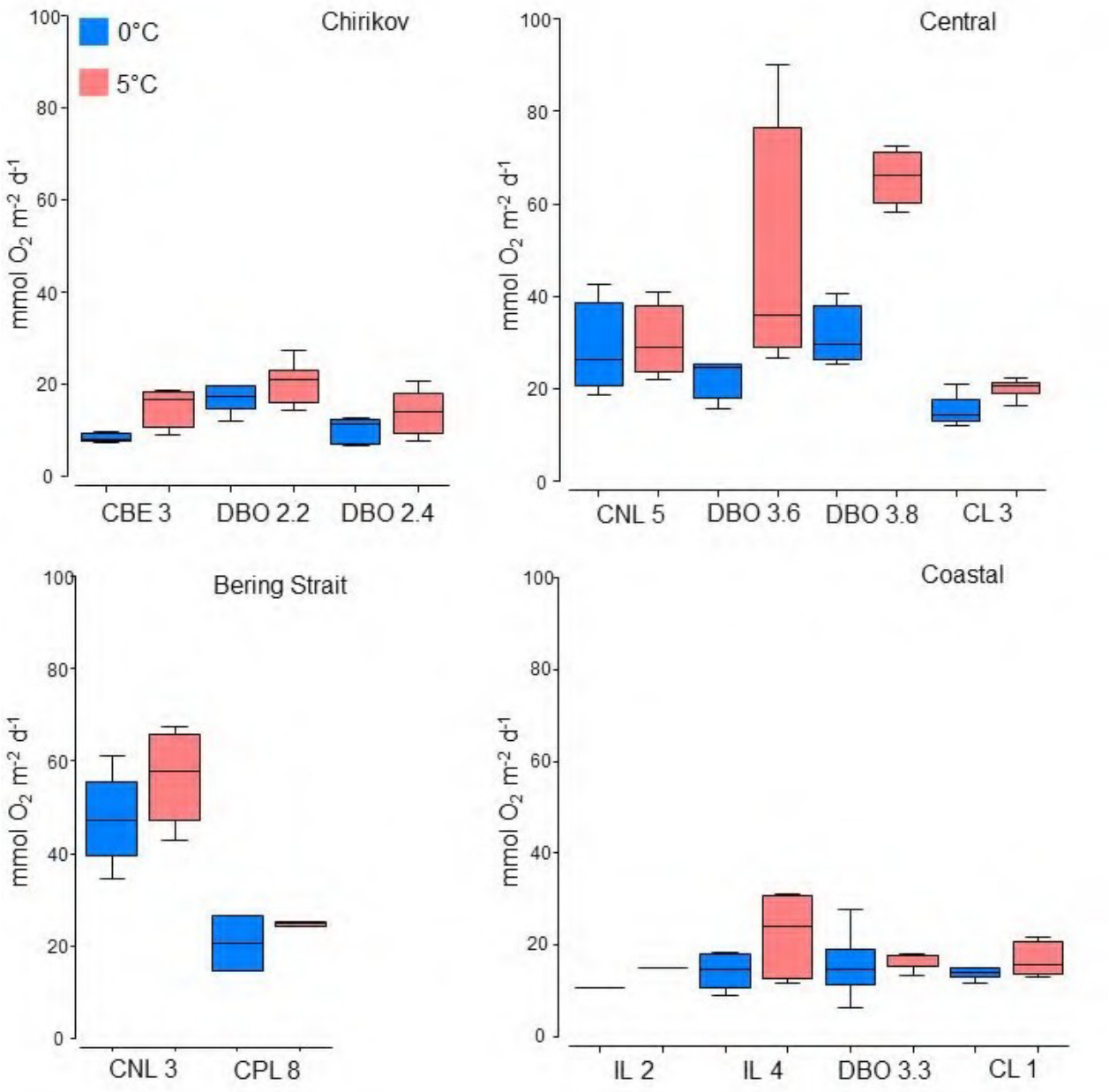

Figure 2. Box plots showing sediment community oxygen consumption at each station, for both 2017 and 2018. Stations are grouped into geographical areas. Boxes extend from first to third quartile, horizontal lines show median values, and whiskers mark minimum and maximum values.

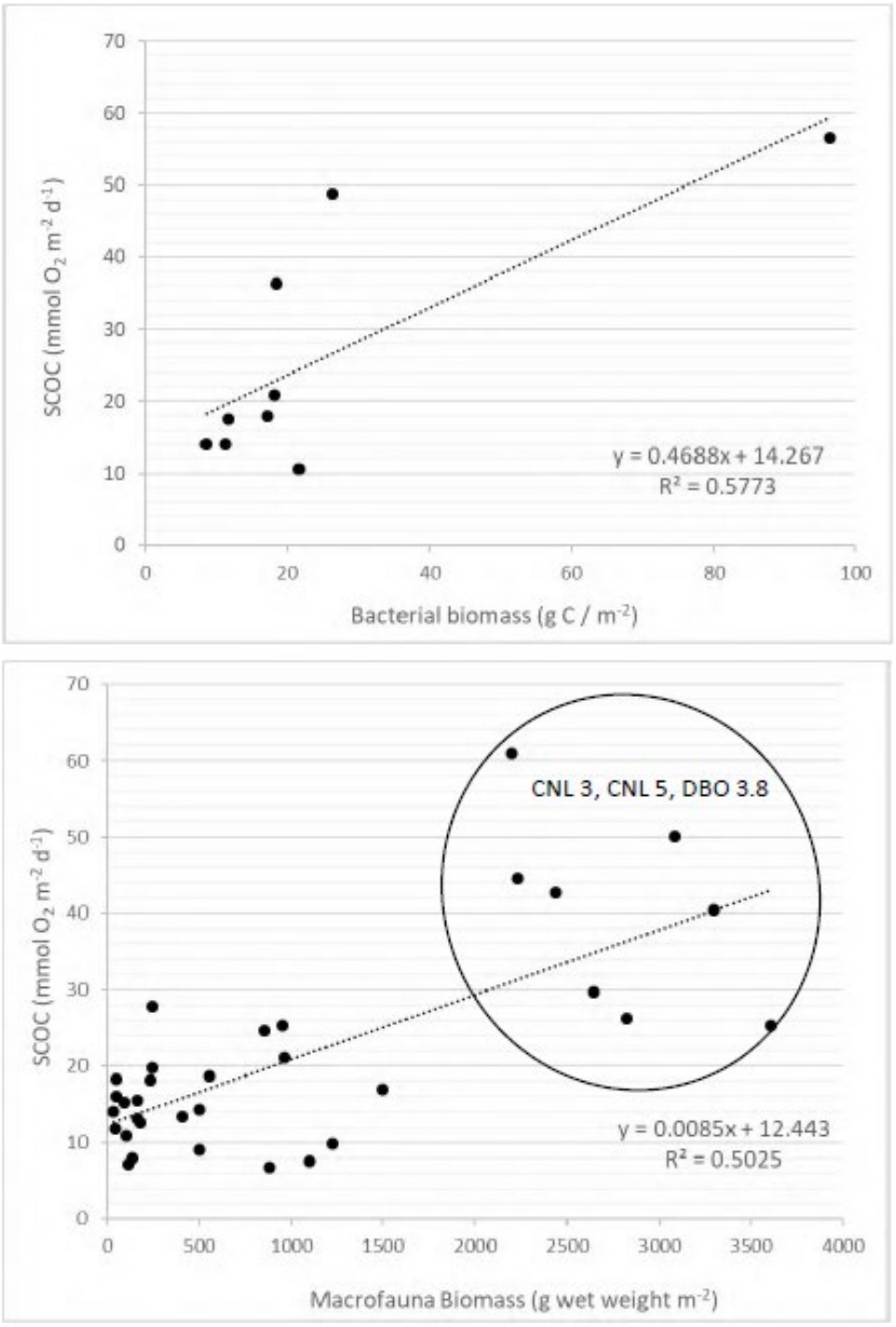

Figure 3. Linear regressions showing relationship between SCOC rates and biomass of bacteria (top) and macrofauna (bottom) in 2018. For bacterial biomass, SCOC rates are means of the two temperature treatments at that station. For macrofauna biomass, paired measurements of SCOC and biomass are plotted for the same core.

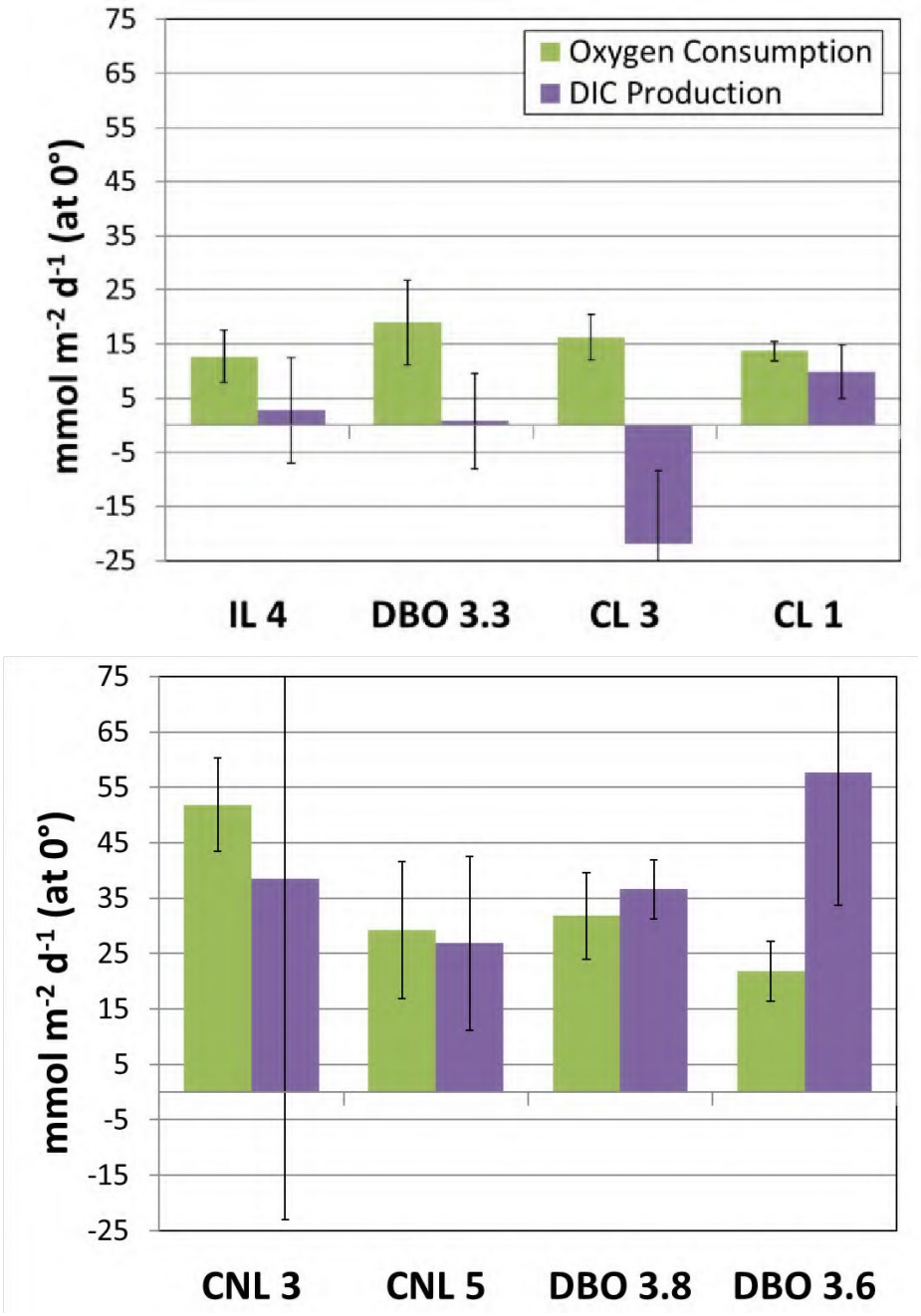

Figure 4. Comparison of sediment community oxygen consumption vs. DIC production rates at 0°C in 2018 for two contrasting settings, with predominantly coastal sites (top) vs. high-biomass sites in the southeast Chukchi Sea 'hot spot' area (bottom). Error bars reflect 1 standard deviation.

References

Arnosti C (2011) Microbial extracellular enzymes and the marine carbon cycle. Annu Rev Mar Sci 3:401-425. https://doi.org/10.1146/annurev-marine-120709-142731

Arnosti C, Jorgensen BB (2003) High activity and low temperature optima of extracellular enzymes in Arctic sediments: Implications for carbon cycling by heterotrophic microbial communities. Mar Ecol Prog Ser 249:15-24

Boschker HTS, Middelburg JJ (2002) Stable isotopes and biomarkers in microbial ecology. FEMS Microbiol Ecol 40:85-95. https://doi.org/10.1111/j.1574-6941.2002.tb00940.x

Bourgeois S, Archambault P, Witte U (2017) Organic matter remineralization in marine sediments: A Pan-Arctic synthesis. Global Biogeochem Cy 31:190-213. https://doi.org/10.1002/2016GB005378

Braeckman U, Janssen F, Lavik G, Elvert M, Marchant H, Buckner C, Bienhold C, Wenzhöfer F (2018) Carbon and nitrogen turnover in the Arctic deep sea: in situ benthic community response to diatom and coccolithophorid phytodetritus. Biogeosciences 15:6537-6557. https://doi.org/10.5194/bg-15-6537-2018

Canion A, Overholt WA, Kostka JE, Huettel M, Lavik G, Kuypers MMM (2014) Temperature response of denitrification and anaerobic ammonium oxidation rates and microbial community structure in Arctic fjord sediments. Environ Microbiol 16:3331-3344. 10.1111/1462-2920.12593

Clough LM, Renaud PE, Ambrose WG, Jr. (2005) Impacts of water depth, sediment pigment concentration, and benthic macrofaunal biomass on sediment oxygen demand in the western Arctic Ocean. Canadian Journal of Fisheries and Aquatic Science 62:1756-1765

Danielson SL, Eisner L, Ladd C, Mordy C, Sousa L, Weingartner TJ (2017) A comparison between late summer 2012 and 2013 water masses, macronutrients, and phytoplankton standing crops in the northern Bering and Chukchi Seas. Deep-Sea Res II 135:7-26. https://doi.org/10.1016/j.dsr2.2016.05.024

Devol AH, Codispoti LA, Christensen JP (1997) Summer and winter denitrification rates in western Arctic shelf sediments. Cont Shelf Res 17:1029-1050. https://doi.org/10.1016/S0278-4343(97)00003-4

Dickson AG, Sabine CL, Christian JR (eds) (2007) Guide to best practices for ocean CO_2 measurements. PICES Special Publication 3. North Pacific Marine Science Organization. 191

Franco MdA, Vanaverbeke J, Van Oevelen D, Soetaert K, Costa MJ, Vincx M, Moens T (2010) Respiration partitioning in contrasting subtidal sediments: seasonality and response to a spring phytoplankton deposition. Mar Ecol 31:276-290. 10.1111/j.1439-0485.2009.00319.x

Grebmeier JM (2012) Shifting patterns of life in the Pacific Arctic and Sub-Arctic seas. Annu Rev Mar Sci 4:63-78. https://doi.org/10.1146/annurev-marine-120710-100926

Grebmeier JM, Bluhm BA, Cooper LW, Danielson SL, Arrigo KR, Blanchard AL, Clarke JT, Day RH, Frey KE, Gradinger RR, Kędra M, Konar B, Kuletz KJ, Lee SH, Lovvorn JR, Norcross BL, Okkonen SR (2015) Ecosystem characteristics and processes facilitating persistent macrobenthic biomass hotspots and associated benthivory in the Pacific Arctic. Prog Oceanogr 136:92-114. http://dx.doi.org/10.1016/j.pocean.2015.05.006

Grebmeier JM, Cooper LW, Feder HM, Sirenko BI (2006) Ecosystem dynamics of the Pacific-influenced Northern Bering and Chukchi Seas in the Amerasian Arctic. Prog Oceanogr 71:331-361

Grebmeier JM, McRoy CP (1989) Pelagic-benthic coupling on the shelf of the northern Bering and Chukchi Seas. III. Benthic food supply and carbon cycling. Mar Ecol Prog Ser 53:79-91

Henriksen K, Blackburn TH, Lomstein BA, McRoy CP (1993) Rates of nitrification, distribution of nitrifying bacteria and inorganic N fluxes in northern Bering-Chukchi shelf sediments. Cont Shelf Res 13:629-651. https://doi.org/10.1016/0278-4343(93)90097-H

Horak REA, Whitney H, Shull DH, Mordy CW, Devol AH (2013) The role of sediments on the Bering Sea shelf N cycle: Insights from measurements of benthic denitrification and benthic DIN fluxes. Deep-Sea Res II 94:95-105. https://doi.org/10.1016/j.dsr2.2013.03.014

Hubas C, Artigas LF, Davoult D (2007) Role of the bacterial community in the annual benthic metabolism of two contrasted temperate intertidal sites (Roscoff Aber Bay, France). Mar Ecol Prog Ser 344:39-48

Kiesel J, Bienhold C, Wenzhöfer F, Link H (2020) Variability in benthic ecosystem functioning in Arctic shelf and deep-sea sediments: Assessments by benthic oxygen uptake rates and environmental drivers. Frontiers in Marine Science 7. 10.3389/fmars.2020.00426

Kritzberg ES, Duarte CM, Wassmann P (2010) Changes in Arctic marine bacterial carbon metabolism in response to increasing temperature. Polar Biol 33:1673-1682. 10.1007/s00300-010-0799-7

Lewis T, Nichols PD, McMeekin TA (2000) Evaluation of extraction methods for recovery of fatty acids from lipid-producing microheterotrophs. J Microbiol Meth 43:107-116. http://dx.doi.org/10.1016/S0167-7012(00)00217-7

Mäkelä A, Witte U, Archambault P (2018) Short-term processing of ice algal-and phytoplankton-derived carbon by Arctic benthic communities revealed through isotope labelling experiments. Mar Ecol Prog Ser 600:21-39

Mincks SL, Smith CR, DeMaster DJ (2005) Persistence of labile organic matter and microbial biomass in Antarctic shelf sediments: Evidence of a sediment "food bank". Mar Ecol Prog Ser 300:3-19

Moodley L, Middelburg JJ, Soetaert K, Boschker HTS, Herman PMJ, Heip CHR (2005) Similar rapid response to phytodetritus deposition in shallow and deep-sea sediments. J Mar Res 63:457-469. 10.1357/0022240053693662

Mora C, Wei C-L, Rollo A, Amaro T, Baco AR, Billett D, Bopp L, Chen Q, Collier M, Danovaro R, Gooday AJ, Grupe BM, Halloran PR, Ingels J, Jones DOB, Levin LA, Nakano H, Norling K, Ramirez-Llodra E, Rex M, Ruhl HA, Smith CR, Sweetman AK, Thurber AR, Tjiputra JF, Usseglio P, Watling L, Wu T, Yasuhara M (2013) Biotic and human vulnerability to projected changes in ocean biogeochemistry over the 21st century. PLOS Biology 11:e1001682. 10.1371/journal.pbio.1001682

Pomeroy LR, Deibel D (1986) Temperature regulation of bacterial activity during the spring bloom in Newfoundland coastal waters. Science 233:359-361

Smith KL (1978) Benthic community respiration in the N.W. Atlantic Ocean: in situ measurements from 40 to 5200 m. Mar Biol 47:337-347. 10.1007/bf00388925

Walsh JJ, McRoy CP, Coachman LK, Goering JJ, Nihoul JJ, Whitledge TE, Blackburn TH, Parker PL, Wirick CD, Shuert PG, Grebmeier JM, Springer AM, Tripp RD, Hansell DA, Djenidi S, Deleersnijder E, Henriksen K, Lund BA, Andersen P, Müller-Karger FE, Dean K (1989) Carbon and nitrogen cycling within the Bering/Chukchi Seas: Source regions for organic matter effecting AOU demands of the Arctic Ocean. Prog Oceanogr 22:277-359. http://dx.doi.org/10.1016/0079-6611(89)90006-2

Wassmann P, Reigstad M (2011) Future Arctic Ocean seasonal ice zones and implications for pelagic-benthic coupling. Oceanography 24:220-231

Whitehouse GA, Aydin K, Essington T, Hunt G, Jr. (2014) A trophic mass balance model of the eastern Chukchi Sea with comparisons to other high-latitude systems. Polar Biol 37:911-939. http://dx.doi.org/10.1007/s00300-014-1490-1

Wiebe WJ, Sheldon WM, Jr., Pomeroy LR (1992) Bacterial growth in the cold: evidence for an enhanced substrate requirement. Appl Environ Microbiol 58:359-364

The Arctic Chukchi Sea food web: simulating ecosystem impacts of future changes in organic matter flow

Ann-Christine Zinkann[1,2], Georgina Gibson[3], Seth Danielson[1], Katrin Iken[1]

[1] College of Fisheries and Ocean Sciences, University of Alaska Fairbanks, 2150 Koyukuk Drive, 245 O'Neill Bldg, Fairbanks 99775, Alaska, USA

[2] Global Ocean Monitoring and Observing Program, National Oceanic and Atmospheric Administration, SSMC3, 1315 East-West Highway, Silver Spring, Maryland 20910

[3] International Arctic Research Center, University of Alaska Fairbanks, 2160 Koyukuk Drive, Fairbanks 99775, Alaska, USA

Correspondence to: Ann-Christine Zinkann (azinkann@alaska.edu, ann-christine.zinkann@noaa.gov, +01-907-347-8291)

Declarations of interest: none

Abstract

The Chukchi Sea continental shelf is a highly productive inflow shelf of the Arctic Ocean that is experiencing climate warming events and declines in seasonal sea ice cover at one of the fastest rates compared to other Arctic shelves. Climate-induced changes in phytoplankton and ice-algal primary production, inflow of terrestrial matter through riverine discharge and coastal erosion, and increases in bacterial production have previously been predicted to cause shifts in the composition and distribution of organic matter supply and energy flow in this system. The goal of this study was to examine potential shifts in the Chukchi Sea ecosystem energy flow under various future climate scenarios. To address these goals, an existing mass balance Chukchi Sea ecosystem model by was updated by incorporating terrestrial matter as an energy source, especially for benthic consumers. Incorporation of the terrestrial matter component allowed us to adjust current model phytoplankton biomass to better match recent empirical measurements and to update the system-wide mass-balance. We also modeled potential impacts of future climate-driven alterations in the composition and flow of organic matter supply on major ecosystem groups for the 2015 – 2050 period. Iterations showed that climate-driven increased retention of phytoplankton biomass in the pelagic realm would depress biomass of most benthic-feeding organisms across several larger ecosystem groups (invertebrates, fishes, mammals). However, simulated increases in both terrestrial matter inflow and bacterial biomass have the potential to compensate for some of the reductions in the energy supply from phytoplankton to the benthic food web, as well as to diversify the supply of organic matter to the seafloor. This diversification could make the Chukchi Sea ecosystem more stable to future climate-driven changes.

Keywords: Ecosystem modelling, Ecopath with Ecosim, benthic food webs, terrestrial matter, bacterial production, future Arctic

Introduction

The Chukchi Sea continental shelf is one of the most productive Arctic shelves (Codispoti et al., 2013); however, patterns in primary productivity and subsequent flow of energy through the Arctic food web are being altered by the rapid atmospheric warming and decline in seasonal sea ice cover (Steele et al., 2008; Serreze et al., 2009; Kumar et al. 2020). Under past conditions of extended seasonal ice cover, up to 70 % of ice-associated and pelagic primary production was exported to the benthos through tight pelagic-benthic coupling, supporting high benthic invertebrate biomass (Grebmeier et al., 1988; Walsh et al., 1989). This high standing stock of benthic invertebrates in the Chukchi Sea supports many benthic-feeding higher trophic levels, e.g., spectacled eiders (*Somateria fischeri*), walruses (*Odobenus rosmarus*), and gray whales (*Eschrichtius robustus*) (Grebmeier et al., 1988; Lovvorn et al., 2003; Dehn et al., 2006; Moore and Huntington, 2008). Changes in atmospheric forcing and sea ice cover can have major impacts at the base of the Arctic food web, including levels of ice algal and phytoplankton production, the strength of pelagic-benthic coupling, and the importance of additional food sources, such as terrestrial matter inflow and bacteria (Bopp et al., 2001; Lavoie et al., 2010; Holmes et al., 2016; Taylor et al., 2018; Zinkann et al. a, in review). Such changes may have repercussions for the energy flow to and between higher trophic levels. Ecosystem models are useful tools to evaluate the potential impacts of changing conditions on the energy flow through a system (e.g., Aydin and Mueter, 2007; Gaichas et al., 2011; Doney et al., 2012; Harvey et al., 2012). Current ecosystem models describe the Chukchi Sea ecosystem as a benthos-dominated system, where much of the primary production is routed through the benthos to higher trophic levels (Christensen and Walters, 2004; Aydin et al., 2007; Whitehouse et al., 2014; Whitehouse and Aydin, 2016); here, we offer perspectives on how changes in primary producer carbon supply and energy flow through the food web may impact the structure and functioning of the Chukchi Sea ecosystem.

In Arctic shelf systems, such as the Chukchi Sea, the benthos represents a cornerstone of the food web (Grebmeier et al., 1988; Aydin et al., 2007; Whitehouse et al., 2014). As organic matter sinks to the seafloor, benthic organisms utilize this material directly as food, while indirectly affecting the detrital distribution and mineralization into nutrients via respiration and bioturbation activities (Heip et al., 1995). The standing stock of the benthic community largely depends on the amount and quality of the detrital material fulfilling the energetic needs of the community (Gooday et al., 1990; Ruhl and Smith, 2004). The reliance of benthic organisms on different organic matter sources (such as from bacteria, phytoplankton, and terrestrial matter) is variable (Zinkann et al. b, in review), and changes in the composition of organic matter to the seafloor can have implications to the benthic community composition.

Ice-algal and phytoplankton production is typically considered the main food source for the Arctic benthos (Grebmeier and Barry, 1991). In regions with abundant seasonal sea ice, the seasonal increase of light and ice melt in late spring results in early-season ice-edge blooms, often dominated by relatively large centric diatoms that sink rapidly and largely ungrazed to the benthos (Grebmeier and McRoy, 1989; Lovvorn et al., 2005). With a reduction of sea ice in warmer years, the ice-algal production in the marginal ice edge may be reduced while phytoplankton blooms are postulated to occur later, once a thermally stratified water column develops (Wassmann and Reigstad, 2011). Increased light availability and a longer growing season in ice-free conditions could allow for an overall increase in Arctic primary production (Brown and Arrigo, 2013). However, a shift towards smaller-celled phytoplankton communities (Li et al., 2009; Morán et al., 2010) and an increase in grazing pressure by zooplankton (Neeley et al., 2018) could result in higher proportions of the primary production being retained in the water column. Such a shift would lead to a weakening of pelagic-benthic coupling in the system with ramifications for the benthos-dependent food web (Lalande et al., 2007; Arrigo et al., 2008; Wassmann and Reigstad, 2011).

Organic matter sources, other than ice algae or phytoplankton, that support the benthic food web on the Chukchi shelf, include terrestrial matter and bacterial production. Arctic river discharge that carries terrestrial matter has increased by 2.6 % per decade since the 1970s (Bopp et al., 2001; McClelland et al., 2006; Lantuit et al., 2012) due to increases in coastal erosion and permafrost thaw (Guo et al., 2004; Semiletov et al., 2011). The presence of terrestrial matter in Chukchi Sea marine sediments and invertebrate diets is high, illustrating the importance of this material to the benthic food web in this region (Yunker et al., 2005; Morris et al., 2015; Rowe et al. 2019; Zinkann et al. b, in review). Although the input of terrestrial matter via rivers and coastal erosion is typically still smaller than the input from marine primary producers, in a warming climate, an increases of terrestrial material to the benthos could affect the direction and efficiency of energy flow through the food web (Dunton et al., 2006). Additionally, sediment bacteria contribute nutritional value to the detrital food supply to and also play an important role in the breakdown and recycling of organic matter (e.g., Newell, 1965; Heip et al., 1995). While Arctic bacterial production and metabolic processes are well adapted to the ambient low temperatures, the predicted increases in bottom water temperature on the Chukchi shelf (Wang et al., 2012) are likely to result in higher bacterial metabolic processes and thus bacterial production (Pomeroy and Deibel, 1986; Kirchman et al., 2009; Zinkann et al. a, in review). This could lead to changes in the carbon cycling of the system, and a potential increase in the importance of bacteria as a benthic food source (Kirchman et al., 2009; McMeans et al., 2013; Bell et al., 2016). Therefore, both terrestrial and bacterial sources should be considered in predictive ecosystem models of the Chukchi Sea.

The goal for this study was to enhance our understanding of trophic pelagic-benthic couplings in the Chukchi Sea ecosystem, and to examine potential ecosystem shifts under future climate scenarios. To address these goals, a recent Chukchi Sea ecosystem mass-balance model (Whitehouse and Aydin, 2016) was updated to include terrestrial matter as a potentially important food source. We determined the necessary terrestrial biomass to balance the ecosystem model with the expected loss in phytoplankton derived organic matter. We accordingly re-defined the routing of phytoplankton, terrestrial, and bacterial matter through the benthic and pelagic food webs. This updated model was then used to determine potential impacts of climate-driven variability in organic matter supply to the food web over time. We hypothesize that weakening of pelagic-benthic coupling would negatively impact benthic biomass and benthos-dependent trophic pathways, but that an increase in terrestrial material and bacterial production would compensate for some of the loss of phytoplankton-derived carbon to the benthos-driven food web.

Materials and Methods

Study area

The Chukchi Sea is a shallow (~ 50 m max), marginal, highly productive shelf of the Arctic Ocean bounded by the Alaskan and Siberian coasts (Fig. 1). Three major water masses (Bering Shelf Water, Anadyr Water, and Alaska Coastal Water) flow through the Bering Strait northward and spread across the shelf (Coachman et al., 1975). Bering Shelf and Anadyr waters mix on the shelf into the salty (30.0 - 33.5), cold (0 – 7 °C), and nutrient-rich Bering Shelf Anadyr Water that flows northwards through the central channel of the Chukchi Sea. Alaska Coastal Water is a nutrient-poor and freshwater-influenced (salinity 20 – 32, 7 - 12°C) water mass that flows along the eastern coast of the Chukchi Sea that carries terrestrial matter from the Yukon River. The Yukon River discharges about 2×10^{11} m^3 freshwater and 2.02×10^{12} g total organic carbon annually into the Bering Sea (Guo and Macdonald, 2006), much of which is advected northward onto the Chukchi shelf (Coachman, 1986; Jorgenson and Brown, 2004; Guo and Macdonald, 2006; Pisareva et al., 2015). In present climate conditions, the Chukchi shelf is sea ice covered for up to 7 months a year (November – May), resulting in short seasonal pulses of ice edge-associated primary production (Walsh et al., 1989). Variations in physical properties and biological dynamics, such as timing and location of phytoplankton blooms, grazing pressure of zooplankton, and organic matter degradation through bacteria, have strong influences on the amount of pelagic-benthic coupling and organic matter pathways in the Chukchi Sea (Walsh et al., 1989; Grebmeier and Barry, 1991).

Modeling Approach

1. *Ecopath modelling framework*

Ecopath (http://ecopath.org/) is a publicly available ecosystem modeling software package that

allows the user to create a mass-balanced snapshot of a system of interest. Configuration of the model requires categorization of the organisms, or groups of organisms, that will be represented and information about how these groups are related though energy flow. The model summarizes and optimizes information on biomass, diet composition, rate of production and consumption, biomass removals from fishery and natural mortality, and information about detrital fate (Christensen and Pauly, 1991; Christensen et al., 2000). Ecopath is based on the assumption of steady state mass-balance over an arbitrary period of time, in this study, a year. The program uses two governing equations to describe both the production and energy balance of each functional group by quantifying the material (biomass) moving in and out of functional groups in a given food web. A functional group can consist of a single species, a set of species, or represent a detrital pool. Following are the master equations in Ecopath that are being applied for each functional group (*i*):

$$P_i = Y_i + B_i * M2_i + E_i + BA_i + P_i\,(1 - EE_i) \quad (1)$$

Production = fisheries catch + predation mortality + biomass accumulation + net migration + other mortality

$$(Q/B)_i * B_i = \left(\frac{P}{B}\right)_i + B_i + R_i + UN_i \quad (2)$$

Consumption = production + respiration + unassimilated food

Definitions of the parameters in the two equations are given in Table 1.

Model parameters can be specified based on observational data, experimental results, or estimated by the model by solving the set of equations. While most parameters are mandatory inputs, optional inputs are the parameters biomass (B), consumption to biomass ratio (Q/B), production to biomass ratio (P/B), and ecotrophic efficiency (EE), as they can be computed by Ecopath given all other parameters. Ecopath links the production of each functional group with the consumption of all other groups and uses the linkages among groups to estimate any missing parameters, using one equation for each functional group. Ecopath works with energy-related currencies and energy output and input must be balanced, so that production of any group is routed to other functional groups within the system, or

out of the system. If not balanced, the EE of a group is >1, indicating that less material is entering the group or box than is consumed. In this study, all production terms represent annual integrations.

2. Update of existing mass-balance model

The most recent version of Ecopath model for the eastern Chukchi Sea shelf was acquired (Whitehouse and Aydin, 2016) (Table 3) and used as baseline model. In the present study, phytoplankton biomass was reduced relative to the baseline to reflect recent estimates of annual production on the Chukchi Sea shelf (Arrigo and van Dijken, 2015). Terrestrial production was added to account for external organic matter input and balance the reduction in phytoplankton biomass. Detrital fates were adjusted to account for the export of material (e.g., waste products) to both terrestrial and phytoplankton detritus pools, and diets of benthic invertebrates were adjusted to reflect our recent findings of organic matter consumption (Zinkann et al. b, in review) (Table 3, Fig. 2).

i. Phytoplankton

In the development of the original Chukchi Sea ecosystem model (Whitehouse et al., 2014), a top-down balance approach was used to estimate phytoplankton production in the system resulting in an annual phytoplankton production of ~170 g C m^{-2} y^{-1}. Subsequent model iterations (Whitehouse and Aydin, 2016) put annual phytoplankton production closer to empirical values, at 141 g C m^{-2} y^{-1}, by reducing the phytoplankton biomass from 27.8 t km^{-2} to 15.0 t km^{-2}, assuming a P/B ratio of 75 and 150 days of growing season for phytoplankton. Whitehouse and Aydin (2016) acknowledged that these annual production and biomass values were still high but were needed to balance an insufficient supply of phytoplankton biomass to the benthic detritus box of the model. Annual primary production estimates for the Chukchi shelf are highly variable, ranging from 20 g C m^{-2} to >400 g C m^{-2} y^{-1} (Sakshaug, 2004), but an average annual primary production of ~141 g C m^{-2} y^{-1} for the entire shelf is likely an overestimate. Annual primary production estimates for the shelf in recent years were closer to ~96 g C m^{-2} y^{-1} (Arrigo and van Dijken, 2011), about 30 % lower than the Whitehouse and Aydin (2016) model requires. To reflect these findings, phytoplankton biomass was reduced by 30 % to 15.0 t km^{-2} in our updated model while keeping P/B values at 75, assuming an average growth rate for Arctic diatoms to be ~0.5 d^{-1} (Connell et al., 2018) and a growing season of ~150 days (Walsh et al., 1989).

ii. Detrital components

Terrestrial organic matter was not included as a food source in any of the previous mass balance Chukchi Sea ecosystem models (Aydin et al., 2007; Whitehouse, 2013; Whitehouse et al., 2014;

Whitehouse and Aydin, 2016). For our updated model, a novel terrestrial production box was added to reflect the terrestrial organic matter that is imported onto the shelf as detritus, where it serves as a food source for the benthic food web. The P/B value for terrestrial production was set to 75, assuming a similar growth rate and 150-day growing period as marine primary producers. The value of 'terrestrial production' biomass was then estimated in an iterative process, starting at 10 t km^{-2}, until the model was balanced (see: Model balancing).

Chukchi Sea benthic invertebrates were permitted to use terrestrial matter and bacteria in our updated model in addition to phytoplankton based on our recent findings (Zinkann et al. b, in review). In the original model (Whitehouse and Aydin, 2016), benthic invertebrates largely fed on benthic detritus, a functional component fueled by inputs from primary pelagic production and secondary production including molts and fecal pellets. For a finer delineation of detrital sources in our updated model, the phytoplankton production component was separated into one that was retained in the pelagic system (phytoplankton retained detritus) and one where phytoplankton was exported to the benthos (phytoplankton export detritus). The phytoplankton export detritus component replaced the 'benthic detritus' box of the original Whitehouse and Aydin (2016) model.

iii. Detrital fate

In our updated model, the phytoplankton export detritus component received ~70 % of total phytoplankton production, while the remaining 30 % were routed into the phytoplankton retained detritus component to reflect the tight pelagic-benthic coupling of the Chukchi Sea shelf (Grebmeier and Barry, 1991). All non-assimilated organic matter by consumers, e.g., due to excretion, was routed in equal amounts to the phytoplankton retained detritus component and the terrestrial detritus component. These proportions are consistent with those used in the Whitehouse and Aydin (2016) model, although in that model all detrital material from non-assimilated food and waste products was routed into the benthic detritus box (Fig. 2). As in the original Whitehouse and Aydin (2016) model, we also assumed that benthic invertebrates directly used benthic bacterial biomass, and parameters for this benthic bacterial box remained unchanged. Finally, detrital flux from fishery discards (in the Chukchi Sea this is related to subsistence or research activity harvests) was routed equally into phytoplankton export and terrestrial detritus components.

iv. Consumer diets

Diets of all functional groups within the original Whitehouse and Aydin (2016) model were set at a fixed diet proportion from prey components or one detrital source. In our updated model, diets of all benthic invertebrates were adjusted based on recent findings that determined the proportions of bacterial, phytoplankton, and terrestrial detrital matter in Chukchi Sea benthic invertebrate diets (Zinkann et al. b, in review). Specifically, the diets of the following benthic invertebrate groups were updated based on the following species: snow crab (*Chionoecetes opilio)*, shrimp (average of *Argis* and *Eualus*), benthic amphipod (*Anonyx*), Bivalvia (average of *Serripes*, *Macoma*, and *Nuculana*), Gastropoda (*Buccinum*), Polychaeta (Maldanidae), and worms etc. (containing bryozoans) (*Alcyonidium*). A mean of all decapod diets (*C. opilio*, *Argis*, *Eualus*) was used for the box "other crabs" (see Table 3). Other benthic invertebrate boxes in the model were updated using a mean of the proportional diet contributions of the three organic matter sources across all benthic taxa from Zinkann et al. b (in review), spanning a multitude of taxonomic groups and feeding characteristics. Diets of pelagic invertebrates, such as Cephalopoda and jellyfish were not updated from the previous model (Whitehouse and Aydin, 2016). In the original Whitehouse and Aydin (2016) model, benthic bacteria were assumed to obtain 100 % of their diet from 'benthic detritus'. Because 'benthic detritus' in our updated model was split into terrestrial detritus and phytoplankton export detritus, benthic bacteria were assumed to consume equal amounts of these two pools. The diets of all higher trophic levels (fish, birds, marine mammals) were kept the same as in Whitehouse and Aydin (2016).

v. Model balancing

Once updated, we re-balanced the model to be based on the reduced phytoplankton production and the added terrestrial production. Because phytoplankton production was set, balancing was achieved by adjusting terrestrial production in a stepwise fashion, increasing production values in 0.1 t km^{-2} increments until the model was in balance (following procedures in Whitehouse and Aydin, 2016).

3. Ecosim framework

Once the updated mass-balanced Ecopath model for the Chukchi Sea was balanced, we used Ecosim simulations (Walters et al., 1997; Christensen et al., 2000; Walters et al., 2000) to run a series of dynamic simulations. Ecosim allows for the manipulation of parameters and analysis of potential impacts of a changing environment on the food web. Ecosim is expressed through a master equation derived from the Ecopath equations (eq. 1 and 2) as follows:

$$dB_i/dt = g_i \sum_j Q_{ji} - \sum_j Q_{ji} + I_i - (MO_i + F_i + e_i) B_i \quad (3)$$

Definitions of the parameters in the equation are given in Table 1.

Ecosim provides the ability to adjust model parameters over time, including the biomass of food web components such as phytoplankton or detrital sources. Ecosim only describes movement of biomass through feeding interactions, so changes in model parameters will affect biomass of the respective functional groups. For the purpose of this study, our updated Ecopath model was assumed to define present steady state conditions. Then, anticipated changes over the 2015-2050 period were cumulatively applied to phytoplankton production, strength of pelagic-benthic coupling, terrestrial matter inflow, and bacterial production (simulations 1-4 below), meaning each subsequent simulation also included the changes of all previous simulations.

4. Model simulations to explore impacts of environmental change

i. Detrital biomass

The biomass of detrital pools reflects the sum of non-assimilated food and organic matter flows from other mortality divided by the P/B ratio of the detritus pool in question:

$$\text{Detritus biomass} = \frac{\left(\frac{B * Q}{B * UN}\right) + \left(\frac{B * P}{B\,[1-EE]}\right)}{P\frac{P}{B_{detritus}}} \quad (4)$$

The P/B ratio in this case is expressed as 1/turnover and reflects the turnover time of detritus. In systems with slow turnover, such as the Arctic, the P/B ratio is usually assumed to be low. Ecosim simulations require detrital biomass to be entered directly. Here, we assumed a P/B ratio of 0.5 as a value that is fast enough to show some detrital dynamics, but slow enough to be stable and reflect detrital burial (Christensen and Pauly, 1993; A. Whitehouse. pers. comm). The sum of flows to each detrital pool was calculated and entered into the basic input in Ecopath.

ii. Simulation 1: Increased phytoplankton biomass

The continued reduction in sea ice cover on Arctic shelves may lead to an increase in phytoplankton production by 10 % between 2015 and 2050 (Arrigo and van Dijken, 2015). To represent a ~10 % increase in phytoplankton production for this simulation, we assumed a linear annual 0.28 % increase in phytoplankton biomass over the targeted time frame (2015-2050), from an initial phytoplankton biomass of 15.0 t km^{-2} in 2015 to 16.5 t km^{-2} by 2050.

iii. Simulation 2: Weakening of pelagic-benthic coupling

Phytoplankton communities are expected to shift to smaller phytoplankton species and an increase in zooplankton grazing on pelagic production is predicted to result in a decrease in the flux of pelagic production to the seafloor (Lalande et al., 2007; Arrigo et al., 2008; Wassmann and Reigstad, 2011). To reflect this change, we assumed in this simulation, in addition to increased phytoplankton biomass (simulation 1), that 30 % rather than 70 % of primary production as in the steady state model is routed to the seafloor; conversely, 70 % of phytoplankton biomass rather than 30 %, as in the steady state model, remains in the pelagic realm.

iv. Simulation 3: Increase in terrestrial matter inflow

Increased river discharge and coastal erosion are expected to increase the influx of terrestrial matter onto the Chukchi Sea shelf (Semiletov et al., 2011). In this simulation, in addition to the increase in phytoplankton production and a weakening in pelagic-benthic coupling (simulations 1 and 2), we assumed that terrestrial matter loading will increase in proportion to the predicted increase of river discharge of 2.6 % per decade (Bopp et al., 2001; McClelland et al., 2006). Accordingly, terrestrial biomass was increased at a linear rate (0.26 % y^{-1}) over 35 years (2015-2050) from an initial biomass value of 15.6 t km^{-2} (see results) to a final value of 29.7 t km^{-2}.

v. Simulation 4: Increase in bacterial production

Bacterial production in Chukchi Sea sediments is known to be temperature dependent, increasing by 182 % within 12 h when the temperature was raised from an ambient 0 °C to 5 °C under replete substrate conditions (Zinkann et al. a, in review). To reflect this response to warming temperatures, in this simulation, we assumed a linear increase of 182 % in benthic bacterial biomass to represent an increase in bacterial production between 2015 and 2050, so that bacterial biomass increased from an initial value of 26.4 t km^{-2} to 74.4 t km^{-2}. Previous model adjustments, i.e., the increase in phytoplankton production, a weakening in pelagic-benthic coupling, and an increase in terrestrial matter inflow (simulations 1-3) were also applied.

Results

Changes in detrital sources at the base of the food web

Following the reduction of phytoplankton biomass, the updated model was initially out of balance due to a higher demand for detritus than the model provided (EE>1 for phytoplankton export detritus).

After the addition of a terrestrial detritus component and updates to diets of benthic invertebrates, the phytoplankton export detritus component was balanced, but the overall model was still out of balance due to insufficient supply of terrestrial detritus (EE>1 for terrestrial detritus). Therefore, terrestrial detritus was increased in 0.1 t km^{-2} increments until the model was in balance at 15.6 t km^{-2} (EE<1 terrestrial detritus).

The throughput representing the size of the entire system in terms of matter flow was calculated by Ecopath directly as 9277.5 t km^{-2} yr^{-1} in our updated model, compared to 8453.1 t km^{-2} yr^{-1} in Whitehouse and Aydin's (2016) model. Most updated model components (mammals, birds, fish, pelagic invertebrates) exhibited similar biomass to that of the Whitehouse and Aydin (2016) model. Adjustments to phytoplankton production values, and the addition of terrestrial detritus, resulted in decreases of overall production of phytoplankton (from 2085 to 1125 t km^{-2} yr^{-1}) and slight increases in bacterial production (from 625 to 730 t km^{-2} yr^{-1}, Fig. 4). While these changes did not lead to strong changes in biomass of the consumer components of the model, energy flow in our updated model was more diversified with the addition of more detrital groups.

Temporal / multi-decadal simulations

Outputs from model simulations are presented as relative biomass. Relative biomass refers to the percentage change in biomass of an ecosystem group relative to its biomass at the beginning of the simulation period. Results show change in relative biomass at the end of the model simulation period (2050) for major ecosystem groups (Fig. 5a-d). An increase in annual phytoplankton production (simulation 1, Fig. 5a) resulted in a slight increase of relative biomass across all ecosystem groups, ranging from 1 to 18 %. The largest increase in relative biomass was observed in pelagic invertebrates (12-18 %; Fig. 6a). Smaller increases in relative biomass occurred in birds and fishes, while benthic invertebrates and marine mammals remained practically unchanged in average relative biomass (Fig. 5). Within these ecosystem groups, larger biomass increases were typically observed in pelagic-feeding functional groups, such as pelagic-feeding birds versus piscivorous birds (see Fig. 6).

When the system was forced into a state of weakened pelagic-benthic coupling in addition to increased phytoplankton biomass (simulation 2, Fig. 5b), average relative biomass increased in pelagic invertebrates and birds, but decreased in benthic invertebrates, fishes, and marine mammals. Relative biomass of pelagic invertebrates increased most (average 26 %) with the enhanced retention of primary production in the pelagic realm. The strongest declines in biomass were observed in benthic invertebrate

groups (9-68 %, average 27 %) with especially large declines for groups that fed on a variety of organic matter sources (Fig. 6b). Fishes showed the largest range in responses with increases in biomass by up to 36 % in some of the pelagic-feeding groups, especially Arctic cod (*Boreogadus saida*), salmon (Salmonidae), and pollock (*Gadus chalcogrammus*), and decreases in relative biomass in mostly benthic-feeding groups, such as small-mouth flatfish (*Etropus microstomus*), sculpins (Cottoidea), and skates (Rajidae) (between 17-47 % decrease) (Fig. 6c). A variable response also was observed in birds, where relative biomass of planktivorous birds (e.g., scolopacids) increased (between 24-32 %), while most piscivorous birds remained stable or decreased in biomass by up to 6 % (e.g., larids, cormorants) (Fig. 6d). Benthic-feeding mammals, including gray whales (*Eschrichtius robustus*), Pacific walrus (*Odobenus rosmarus*), and bearded seals (*Erignathus barbatus*) experienced decreases in biomass ranging from 18 to 26 % (Fig. 6e).

An increase in terrestrial organic matter inflow onto the shelf, in addition to increased phytoplankton production and weakened pelagic-benthic coupling (simulation 3, Fig. 5c), resulted in small increases in relative biomass of most groups, compensating for several of the biomass declines observed in simulation 2. Relative biomass changes of pelagic invertebrates were similar to those in previous simulations, indicating that this ecosystem group was mostly unaffected by the terrestrial matter influx (Fig. 5c, Fig. 6a). Equally, average bird biomass in simulation 3 was similar to levels in simulation 2 but with no functional group experiencing a decrease. Benthic invertebrates, on average, showed a small increase in relative biomass compared to the steady state level and to simulation 2 responses (Fig. 5c), albeit with a large range of biomass changes among functional groups (Fig. 6b). Benthic invertebrate functional groups that showed the largest increases in biomass were snails, benthic urochordates, and sponges (increases by 60 %, 44 %, and 43 %, respectively), while decreases in relative biomass were observed in, e.g., snow crab (*Chionoecetes opilio*) (-17 %) (Fig. 6b). Fishes showed a similar trend to benthic invertebrates with minor increases compared with the steady state level and higher average biomass compared with the previous simulation. The largest biomass increases in fishes (up to 33 %) occurred in mostly pelagic-feeding species, while some benthic-feeding fishes experienced declines in biomass (up to -10 %). Overall, marine mammal biomass remained mostly unchanged compared to steady state conditions with largest increases in biomass observed in pelagic-feeding mammals (+18 %).

Lastly, with the exception of pelagic invertebrates, an increase in annual bacterial production resulted in large average biomass increases in all ecosystem groups, but to varying degrees within each functional group (simulation 4, Fig. 5d). Pelagic invertebrates remained mostly unaffected by the increase

in bacterial production compared with previous simulations. Benthic invertebrates experienced the strongest increases in relative biomass, between 46 – 182 % for different functional groups (Fig. 6b). The second largest increase in biomass occurred in fishes, with strongest responses in benthic-feeding fish groups (up to 170 %, Fig. 6c). The simulated increase in bacterial production also resulted in higher relative biomass of up to 87 % in piscivorous birds, while it only increased in planktivorous birds by up to 32 % (Fig. 6d). With biomass increases of up to 90 % in some benthic-feeding species, marine mammals responded with stronger biomass increases to increased bacterial production than to any prior model adjustment (Fig. 5d).

Discussion

Unprecedented changes occurring on Arctic shelves, such as the Chukchi Sea, have the potential to influence the flow of energy through the ecosystem and alter the supply of organic matter sources in this benthos-dominated system. In an effort to predict potential food web responses of these changes we performed a series of model simulations with an updated Chukchi Sea ecosystem model. We found that the addition of terrestrial matter as a benthic food source diversified the energy flow at lower benthic trophic levels, but overall energy flow through the ecosystem components and biomass of the components remained largely the same as in the previous model version (Whitehouse and Aydin, 2016). Further, cumulative model simulations of climate-driven changes in phytoplankton production, strength of pelagic-benthic coupling, terrestrial matter inflow, and bacterial production were used to assess potential changes in major ecosystem groups of the Chukchi Sea. The biomass of most ecosystem groups increased slightly in response to elevated phytoplankton production, while feeding habits (pelagic-feeding versus benthic-feeding) strongly determined the changes in biomass in subsequent simulations. In several groups, high terrestrial inflow and increases in benthic bacterial production had the potential to compensate for the loss in phytoplankton export to the benthos in a weakened pelagic-benthic coupling scenario.

Annual phytoplankton production in the original Chukchi Sea ecosystem model was estimated at ~141 g C m^{-2}, so that balanced energy flow through the functional groups could be established; however, the authors considered the production value an overestimation (Whitehouse and Aydin, 2016). This suggests that there are food sources in the system that were not included in the original model. One of these food sources could be terrestrial matter. Terrestrial matter has traditionally been assumed a negligible food source in Arctic marine food webs (Schell, 1983), but has recently been identified as a major contributor to at least benthic invertebrate diets in the Arctic (Dunton et al., 2006; Bell et al., 2016;

Harris et al., 2018; Rowe et al., 2019; Zinkann et al. b, in review). For example, ~40 % on average and at some locations up to 80 % of the organic matter in Chukchi Sea sediments can originate from terrestrial matter (Zinkann et al. a, in review). Some consumers like the benthic snail *Buccinum* derived, on average, 81 % of their diet from terrestrial sources on the shelf (Zinkann et al. b, in review). In our model, 15.6 t km^{-2} of terrestrial organic matter were needed to sustain the high benthic biomass and achieve model balance. This may be a high estimate of terrestrial carbon for the Chukchi Sea. One study identified regional benthic carbon concentrations on the Chukchi shelf and reported 5.6 – 7.5 g m^{-2} of organic carbon concentrations (Naidu et al., 1993). Based on our recent work, we estimated 40 % of this to be terrestrial matter (Zinkann et al. a, in review), which would, at maximum, amount to only about a fifth of the terrestrial carbon concentrations that we calculated to balance the model. More in-depth analyses of terrestrial matter concentrations in sediments would improve our ability to model energy flux from the different organic matter sources. However, our updated model provides a new portfolio framework of the Chukchi Sea ecosystem, where a more diversified food base may present a more stable system than previously realized (Huxel et al., 2002).

Arctic benthic invertebrates, especially detritivores, use a variety of organic matter sources deposited to the benthic environment. The use of terrestrial matter by benthic invertebrates has recently been confirmed across various regions of the Alaskan Arctic shelves (Bell et al., 2016; Harris et al., 2018; Rowe et al., 2019; Zinkann et al. b, in review), emphasizing the need to include terrestrial matter into ecosystem models for this region. Information about the proportional contribution of bacteria, phytoplankton, and terrestrial matter to the diets of ten common benthic invertebrate species on the Chukchi shelf, ranging across feeding types and taxonomic groups (Zinkann et al. b, in review), allowed for better resolution of detrital source use in our updated model. What is less well known at this point is the efficiency with which terrestrial matter can be assimilated by these invertebrates. In other Arctic areas, such as the Beaufort Sea, the use of terrestrial matter in benthic food webs increased the trophic steps in the system by reducing the trophic efficiency and the flow of energy to higher trophic levels (Dunton et al., 2006; Bell et al., 2016). Bacterial processes may break down terrestrial matter to facilitate incorporation into marine food webs (Garneau et al., 2009), which increases bacterial production in regions of high terrestrial influx (Figueroa et al., 2016). Energetically, however, the added trophic level of bacterial processing can reduce overall energy transfer efficiency to higher trophic level consumers (Sommer et al., 2002; Berglung et al., 2007). For example, in boreal lake systems, terrestrial organic matter subsidies are abundantly used, but are less effective in supporting consumer population biomass than other food sources (Karlsson et al., 2015). Therefore, trophic transfer efficiency of terrestrial matter in the

Chukchi Sea food web will need to be further investigated to understand the importance of terrestrial matter addition and to appropriately model its incorporation into the energy pathways in the updated model.

Ecosystem model simulations are a valuable tool to discern potential responses of various ecosystem components to anticipated changes in the energy supply and flow of a system. The large changes that Arctic shelf ecosystems are experiencing because of climate change (Steele et al., 2008; Alabia et al. 2020; Huntington et al. 2020) make this a particularly valuable and tractable system for model simulations. Here, we implemented four simulations in a stepwise cumulative fashion, meaning that each subsequent simulation also contained the previous changes. In the natural system, complex ecosystem changes at the base of the marine food web and energy flow are unlikely to happen consecutively, but occur simultaneously and likely not linearly (Doney et al., 2012). However, to discern stepwise responses across the ecosystem, we applied an order where an increase in phytoplankton production (Arrigo and van Dijken, 2015) was followed by weakening of pelagic-benthic coupling (Lalande et al., 2007; Wassmann and Reigstad, 2011), because of greater retention of smaller phytoplankton cells in the water column (Li et al., 2009) and greater grazing pressure in the plankton (Neeley et al., 2018). This enhancement of the pelagic food web may then be countered by an increase in other food subsidies to the benthic system, namely terrestrial matter and subsequent increase of bacterial production (Bopp et al., 2001; Kirchman et al., 2009).

Reductions in sea ice cover allow for a longer growing season and pelagic production has been estimated to increase by 10 % over the next 35 years (Simulation 1, Arrigo and van Dijken, 2015). Enhanced pelagic production resulted in slight increases in relative biomasses of all major ecosystem groups across all trophic levels, reflecting the larger carrying capacity of a more productive system (Christensen and Paul, 1998). Our simulations are only based on feeding interactions and do not take into account other aspects that add complexity to the simulation responses. For example, changes in the physical environment (e.g., warming, Grebmeier et al., 2006; Wang et al., 2012) may cause shifts in community composition that could alter the simulated response to enhanced primary production, which assumes constant community composition. Zooplankton community composition has shifted over the past decades due to larger proportions of Pacific zooplankton species entering the Chukchi shelf in the summer (Matsuno et al., 2011; Ershova et al., 2015; Kim et al., 2020) and trends towards smaller microzooplankton species during warm conditions (Dolan et al., 2014). Similar climate-driven changes have been found in the Atlantic Arctic, with increasing proportions of smaller copepod species due to changes in the

462 phytoplankton community, temperature, and inflow of boreal species (Leu et al., 2011). Such changes in
463 the zooplankton community could influence the efficiency with which the enhanced primary production
464 is channeled through the food web though altered feeding rates, assimilation efficiencies, and lipid
465 storage (Baier and Napp, 2003; Matsuno et al., 2011; Ershova et al., 2015). The increased retention of
466 phytoplankton detritus in the pelagic food web, and subsequent higher zooplankton biomass, may supply
467 larger quantities of prey items to pelagic-feeding mid-trophic level species such as Arctic cod. This, in turn,
468 could lead to increased biomass that supports higher trophic level predators including seals, whales, and
469 birds (Welch et al., 1992; Hop and Gjøsæter, 2013; Marsh et al., 2017). Although increased pelagic food
470 availability could lead to increases in biomass in lower trophic levels, observed trends in zooplankton
471 community composition suggest a shift towards smaller, less lipid-rich copepod species (Matsuno et al.,
472 2011; Ershova et al., 2015), which suggests that subsequent energy transfer through the pelagic food web
473 may eventually be reduced. In addition to possible shifts in energy flow, ice-dependent species, such as
474 Arctic cod may be affected by habitat loss from climate-related changes independent of phytoplankton-
475 driven energy flow. Sea ice is an important habitat for Arctic cod juveniles for feeding as well as protection
476 from predators (Geoffroy et al., 2011). Although Arctic cod biomass responded positively to our simulated
477 ecosystem changes, their likely northward contraction and reduction in juvenile survival rate in response
478 to increased temperature could impact the abundance of this key species in the Arctic food web with
479 implications for higher trophic levels (Darnis et al., 2012). In addition, increased water temperatures are
480 likely going to result in elevated metabolic demands by organisms (Lischka and Rieesell 2017).

481 The Chukchi Sea is known for its tight pelagic-benthic coupling exporting the majority of pelagic
482 production to the benthos and supporting a rich benthic community. These communities serve as an
483 important feeding ground for many higher trophic levels, including fish, birds, and mammals (Moore and
484 Huntington, 2008). It is unsurprising that a weakening in pelagic-benthic coupling (simulation 2) resulted
485 in a strong decline of benthic invertebrate biomass due to the reduced amount of primary production
486 reaching the seafloor in this scenario. In response to this reduction in benthic biomass, benthic-feeding
487 marine mammals and fish showed noticeable declines in biomass (Gray et al., 2017; Jay et al., 2012; Moore
488 and Gulland, 2014). For example, gray whales feed on a broad range of benthic invertebrates, but tend to
489 primarily feed on ampeliscid amphipods (Yablokov and Bogoslovskaya 1984, Nerini 1984). The abundance
490 and biomass of ampeliscids have declined in the Bering Sea, presumably due to changes in the primary
491 production regime, although these changes could have resulted from top-down predation control (Coyle
492 et al., 2007). An ampeliscid decline based on bottom-up factors would be in line with the simulated

493 weakening in pelagic-benthic coupling and a subsequent decline in gray whale biomass and shifts of the
494 foraging area of this top predator (Moore et al., 2003).

495 Increases in terrestrial organic matter source availability (simulation 3) could compensate for
496 some of the biomass loss that several benthic groups experienced under the previous simulation scenario
497 (simulation 2), depending on the composition of organic matter diet composition of benthic functional
498 groups. The addition of this terrestrial material to the model represents a diversification of food sources,
499 which supports notions established for Arctic coastal systems that higher diversity of basal food sources
500 stabilizes the overall food web (McMeans et al., 2013). Benthic functional groups that use high
501 proportions of terrestrial matter (e.g., bivalves and sponges, Harris et al., 2018; Zinkann et al. b, in review)
502 increased the most in relative biomass in the simulation of terrestrial matter addition, while benthic
503 functional groups depending on high proportions of bacteria and phytoplankton in their diet decreased in
504 relative biomass (e.g., snow crab, other crabs and benthic amphipods). Thus, the incorporation of detailed
505 diet compositions in the updated model allowed us to identify some of the more vulnerable functional
506 groups to changes in the organic matter supply to the benthos rather than assuming mostly unified
507 responses across all benthic invertebrates. These results provide new context for potential distribution
508 changes in benthic invertebrate species that are expected to occur in a warmer Arctic, which would
509 consequently influence foraging quality for higher trophic levels (Grebmeier and Dunton, 2000).

510 In addition to the incorporation of terrestrial matter as a food source, the increase in benthic
511 bacterial production further offset some of the expected benthic biomass declines in response to a
512 weakening in pelagic-benthic coupling (simulation 4). A change in organic matter availability may change
513 the habitat suitability for benthic invertebrates. Particularly vulnerable to a decrease in phytoplankton
514 export are benthic-feeding organisms that rely heavily on phytoplankton organic matter sources, e.g.,
515 some crabs; in contrast, taxa relying on bacterial matter would potentially thrive under increased bacterial
516 organic matter availability (e.g., polychaetes, benthic amphipods). Food source availability could,
517 therefore, influence the distribution of ecologically influential species, consequently changing prey quality
518 and foraging areas for important top predators (Alabia et al., 2018). Although biomass of most functional
519 groups increased in this simulation, additional parameters can influence the strength of these effects.
520 These can include temperature effects on growth rates and energy requirements, which will impact
521 energy demands and flow through the system (Ambrose et al., 2006; Bluhm et al., 2009; Węsławski et al.,
522 2011). Higher temperatures could increase metabolic demands of all functional groups, giving rise to a
523 higher demand for food supply, thus reducing the effects seen in our model simulations.

In conclusion, we have provided an updated model of the Chukchi Sea ecosystem and have presented new findings with respect to organic matter supply and use in the Chukchi Sea marine ecosystem. Changes in energy flow and diversification at the base of the Chukchi Sea food web provided a foundation to evaluate the response of major ecosystem components to the changes in energy routing through the pelagic or the benthic food web pathways. The loss in phytoplankton routing to the benthos in a weak pelagic-benthic coupling system may at least partially be offset by an increased inflow of terrestrial matter and in bacterial production. The effects of changes in pelagic or benthic energy flow were detectable throughout all trophic levels and taxonomic groups. However, other ecosystem changes, such as changes in competitive interactions from invading species, energetic composition of key prey items, or changes in trophic transfer efficiency of different organic matter sources, are likely to have effects across trophic levels, but were not reflected in the current model simulations. In future iterations, the model could be used to simulate other climate-driven changes as well as potential external activities, including fishing and oil and gas extraction on the Chukchi shelf. The shelf is home to a variety of fish species and marine mammals that are an important subsistence resource for indigenous residents (Hovelsrud et al., 2008; Zeller et al., 2011). The model presented here is a useful tool to simulate potential changes in the system and manipulate parameters based on those activities (e.g., Harvey et al., 2012). This allows for the assessment of risks to targeted functional groups, guidance to stakeholders, and identification of knowledge gaps (Samhouri et al., 2009).

Acknowledgements

This work was funded in particular through a National Ocean Partnership Program (NOPP grant NA14NOS0120158 to KI) by the National Oceanographic and Atmospheric Administration (NOAA), the Bureau of Ocean Management (BOEM) and Shell Exploration & Production under management of the Integrated Ocean Observing System (IOOS). This publication was also sponsored in part by the Cooperative Institute for Alaska Research with funds from the National Oceanic and Atmospheric Administration under cooperative agreement NA13OAR4320056 with the University of Alaska. SLD acknowledges support from the North Pacific Research Board's Arctic Integrated Ecosystem Program grants A91-99a and A91-00a to the Arctic Shelf Growth, Respiration, Advection and Deposition (ASGARD) rate experiments project. Thanks to Andy Whitehouse (NOAA, NMFS) for his continuous support in the development of this model. Additional thanks to Villy Christensen at the University of British Columbia for providing ACZ with the opportunity to attend the Ecopath class in Vancouver in 2017. We thank Matthew Wooller and Mary Beth Leigh (UAF) for valuable comments on this manuscript.

Literature

Alabia, I.D., García Molinos, J., Saitoh, S.-I., Hirawake, T., Hirata, T., Mueter, F.J., Serra-Diaz, J., 2018. Distribution shifts of marine taxa in the Pacific Arctic under contemporary climate changes. Diversity and Distributions 24, 1583-1597.

Alabia, I.D., Molinos, J.G., Saitoh, S.I., Hirata, T., Hirawake, T. and Mueter, F.J., 2020. Multiple facets of marine biodiversity in the Pacific Arctic under future climate. Science of The Total Environment, 744, p.140913.

Ambrose, W.G., Carroll, M.L., Greenacre, M., Thorrold, S.R., McMahon, K.W., 2006. Variation in *Serripes groenlandicus* (Bivalvia) growth in a Norwegian high-Arctic fjord: evidence for local- and large-scale climatic forcing. Global Change Biology 12, 1595-1607.

Arrigo, K.R., van Dijken, G., Pabi, S., 2008. Impact of a shrinking Arctic ice cover on marine primary production. Geophysical Research Letters 35, 1-6.

Arrigo, K.R., van Dijken, G.L., 2011. Secular trends in Arctic Ocean net primary production. Journal of Geophysical Research 116, 1-15.

Arrigo, K.R., van Dijken, G.L., 2015. Continued increases in Arctic Ocean primary production. Progress in Oceanography 136, 60-70.

Aydin, K., Gaichas, S., Ortiz, I., Kinzey, D., Friday, N., 2007. A comparison of the Bering Sea, Gulf of Alaska, and Aleutian Islands large marine ecosystems through food web modeling. NOAA Technical Memorandum, 1-310.

Aydin, K., Mueter, F., 2007. The Bering Sea—A dynamic food web perspective. Deep Sea Research Part II: Topical Studies in Oceanography 54, 2501-2525.

Baier, C.T., Napp, J., 2003. Climate-induced variability in *Calanus marshallae* populations. Journal of Plankton Research 25, 771-782.

Bell, L.E., Bluhm, B.A., Iken, K., 2016. Influence of terrestrial organic matter in marine food webs of the Beaufort Sea shelf and slope. Marine Ecology Progress Series 550, 1-24.

Berglung, J., Muren, U., Bamstedt, U., Andersson, A., 2007. Efficiency of a phytoplankton-based and a bacteria-based food web in a pelagic marine system. Limnology and Oceanography 52, 121-131.

Bluhm, B.A., Iken, K., Mincks Hardy, S., Sirenko, B.I., Holladay, B.A., 2009. Community structure of epibenthic megafauna in the Chukchi Sea. Aquatic Biology 7, 269-293.

Bopp, L., Monfray, P., Aumont, O., Dufresne, J.-L., Le Treut, H., Madec, G., Terray, L., Orr, J.C., 2001. Potential impact of climate change on marine export production. Global Biogeochemical Cycles 15, 81-99.

Brown, Z.W., Arrigo, K.R., 2013. Sea ice impacts on spring bloom dynamics and net primary production in the Eastern Bering Sea. Journal of Geophysical Research: Oceans 118, 43-62.

Christensen, V., Pauly, D., 1991. Ecopath II -- a software for balancing steady-state ecosystem models and calculating network characteristics. Ecological Modelling 61, 169-185.

Christensen, V., Pauly, D., 1993. Trophic models of aquatic ecosystems. ICLARM, Manila, 1-403.

Christensen, V., Paul, A.J., 1998. Changes in models of aquatic ecosystems approaching carrying capacity. Ecological Applications 8, 104-109.

Christensen, V., Walters, C., Pauly, D., 2000. Ecopath with Ecosim: a User's Guide. Fisheries Centre, University of British Columbia, Vancouver, Canada and ICLARM, Penang, Malaysia, 130 p.

Christensen, V., Walters, C.J., 2004. Ecopath with Ecosim: methods, capabilities and limitations. Ecological Modelling 172, 109-139.

Coachman, L. K., K. Aagaard, and R. B. Tripp, 1975. Bering Strait: the regional physical oceanography. University of Washington Press, Seattle, 172 pp.

Coachman, L.K., 1986. Circulation, water masses, and fluxes on the southeastern Bering Sea shelf. Continental Shelf Research 5, 23-108.

603 Codispoti, L.A., Kelly, V., Thessen, A., Matrai, P., Suttles, S., Hill, V., Steele, M., Light, B., 2013. Synthesis of
604 primary production in the Arctic Ocean: III. Nitrate and phosphate-based estimates of net
605 community production. Progress in Oceanography 110, 126-150.
606 Connell, P.E., Michel, C., Meisterhans, G., Arrigo, K.R., Caron, D.A., 2018. Phytoplankton and bacterial
607 dynamics on the Chukchi Sea shelf during the spring-summer transition. Marine Ecology Progress
608 Series 602, 49-62.
609 Coyle, K.O., Konar, B., Blanchard, A., Highsmith, R.C., Carroll, J., Carroll, M., Denisenko, S.G., Sirenko, B.I.,
610 2007. Potential effects of temperature on the benthic infaunal community on the southeastern
611 Bering Sea shelf: possible impacts of climate change. Deep Sea Research Part II: Topical Studies in
612 Oceanography 54, 2885-2905.
613 Darnis, G., Robert, D., Pomerleau, C., Link, H., Archambault, P., Nelson, R.J., Geoffroy, M., Tremblay, J.-É.,
614 Lovejoy, C., Ferguson, S.H., Hunt, B.P.V., Fortier, L., 2012. Current state and trends in Canadian
615 Arctic marine ecosystems: II. Heterotrophic food web, pelagic-benthic coupling, and biodiversity.
616 Climatic Change 115, 179-205.
617 Dehn, L.-A., Sheffield, G.G., Follmann, E.H., Duffy, L.K., Thomas, D.L., O'Hara, T.M., 2006. Feeding ecology
618 of phocid seals and some walrus in the Alaskan and Canadian Arctic as determined by stomach
619 contents and stable isotope analysis. Polar Biology 30, 167-181.
620 Divine, L.M., Mueter, F.J., Kruse, G.H., Bluhm, B.A., Jewett, S.C., Iken, K., 2019. New estimates of weight-
621 at-size, maturity-at-size, fecundity, and biomass of snow crab, *Chionoecetes opilio*, in the Arctic
622 Ocean off Alaska. Fisheries Research 218, 246-258.
623 Dolan, J.R., Yang, E.J., Kim, T.W., Kang, S.-H., 2014. Microzooplankton in a warming Arctic: a comparison
624 of tintinnids and radiolarians from summer 2011 and 2012 in the Chukchi Sea. Acta
625 Protozoologica, Jagiellonian University 53, 101-113.
626 Doney, S.C., Ruckelshaus, M., Duffy, J.E., Barry, J.P., Chan, F., English, C.A., Galindo, H.M., Grebmeier, J.M.,
627 Hollowed, A.B., Knowlton, N., Polovina, J., Rabalais, N.N., Sydeman, W.J., Talley, L.D., 2012.
628 Climate change impacts on marine ecosystems. Annual Review of Marine Science 4, 11-37.
629 Dunton, K.H., Weingartner, T., Carmack, E.C., 2006. The nearshore western Beaufort Sea ecosystem:
630 circulation and importance of terrestrial carbon in arctic coastal food webs. Progress in
631 Oceanography 71, 362-378.
632 Ershova, E., Hopcroft, R., Kosobokova, K., Matsuno, K., Nelson, R.J., Yamaguchi, A., Eisner, L., 2015. Long-
633 term changes in summer zooplankton communities of the western Chukchi Sea, 1945–2012.
634 Oceanography 28, 100-115.
635 Figueroa, D., Rowe, O.F., Paczkowska, J., Legrand, C., Andersson, A., 2016. Allochthonous carbon-a major
636 driver of bacterioplankton production in the subarctic northern Baltic Sea. Microbial Ecology 71,
637 789-801.
638 Gaichas, S.K., Aydin, K.Y., Francis, R.C., Post, J., 2011. What drives dynamics in the Gulf of Alaska?
639 Integrating hypotheses of species, fishing, and climate relationships using ecosystem modeling.
640 Canadian Journal of Fisheries and Aquatic Sciences 68, 1553-1578.
641 Garneau, M.-È., Vincent, W.F., Terrado, R., Lovejoy, C., 2009. Importance of particle-associated bacterial
642 heterotrophy in a coastal Arctic ecosystem. Journal of Marine Systems 75, 185-197.
643 Geoffroy, M., Robert, D., Darnis, G., Fortier, L., 2011. The aggregation of polar cod (*Boreogadus saida*) in
644 the deep Atlantic layer of ice-covered Amundsen Gulf (Beaufort Sea) in winter. Polar Biology 34,
645 1959-1971.
646 Gooday, A.J., Turley, C.M., Allen, J.A., 1990. Responses by benthic organisms to inputs of organic material
647 to the ocean floor: a review [and Discussion]. Philosophical Transactions of the Royal Society A:
648 Mathematical, Physical and Engineering Sciences 331, 119-138.
649

Gray, B.P., Norcross, B.L., Beaudreau, A.H., Blanchard, A.L., Seitz, A.C., 2017. Food habits of Arctic staghorn sculpin (*Gymnocanthus tricuspis*) and shorthorn sculpin (*Myoxocephalus scorpius*) in the northeastern Chukchi and western Beaufort Seas. Deep Sea Research Part II: Topical Studies in Oceanography 135, 111-123.

Grebmeier, J.M., McRoy, C.P., Feder, H.M., 1988. Pelagic-benthic coupling on the shelf of the northern Bering and Chukchi Seas. I. Food supply source and benthic biomass. Marine Ecology Progress Series 48, 57-67.

Grebmeier, J.M., McRoy, C.P., 1989. Pelagic-benthic coupling on the shelf of the northern Bering and Chukchi Seas. III. Benthic food supply and carbon cycling. Marine Ecology Progress Series 53, 79-91.

Grebmeier, J.M., Barry, J.P., 1991. The influence of oceanographic processes on pelagic-benthic coupling in polar regions: a benthic perspective. Journal of Marine Systems 2, 495-518.

Grebmeier, J.M., Cooper, L.W., Feder, H.M., Sirenko, B.I., 2006. Ecosystem dynamics of the pacific-influenced northern Bering and Chukchi Seas in the Amerasian Arctic. Progress in Oceanography 71, 331-361.

Guo, L., Semiletov, I., Gustafsson, Ö., Ingri, J., Andersson, P., Dudarev, O., White, D., 2004. Characterization of Siberian Arctic coastal sediments: implications for terrestrial organic carbon export. Global Biogeochemical Cycles 18, 1-10.

Guo, L., Macdonald, R.W., 2006. Source and transport of terrigenous organic matter in the upper Yukon River: Evidence from isotope ($\delta^{13}C$, $\Delta^{14}C$, and $\delta^{15}N$) composition of dissolved, colloidal, and particulate phases. Global Biogeochemical Cycles 20, 1-12.

Harris, C.M., McTigue, N.D., McClelland, J.W., Dunton, K.H., 2018. Do high Arctic coastal food webs rely on a terrestrial carbon subsidy? Food Webs 15, 1-14.

Harvey, C.J., Williams, G.D., Levin, P.S., 2012. Food web structure and trophic control in central puget sound. Estuaries and Coasts 35, 821-838.

Heip, C.H., Goosen, N.K., Herman, P.M., Kromkamp, J., Middelburg, J.J., Soetaert, K., 1995. Production and consumption of biological particles in temperate tidal estuaries. Oceanography and Marine Biology - An Annual Review 33, 1-149.

Holmes, R.M., Shiklomanov, A.I., Tank, S.E., McClelland, J.W., Tretiakov, M., 2016. River discharge: in state of the climate in 2015. Bulletin of the American Meteorological Society 97, 147-149.

Hop, H., Gjøsæter, H., 2013. Polar cod (*Boreogadus saida*) and capelin (*Mallotus villosus*) as key species in marine food webs of the Arctic and the Barents Sea. Marine Biology Research 9, 878-894.

Hovelsrud, G.K., McKenna, M., Huntington, H.P., 2008. Marine mammal harvest and other interactions with humans. Ecological Applications 18, 135-147.

Huntington, H.P., Danielson, S.L., Wiese, F.K., Baker, M., Boveng, P., Citta, J.J., De Robertis, A., Dickson, D.M., Farley, E., George, J.C. and Iken, K., Kimmel, D.G., Kuletz, K., Ladd, C., Levine, R., Quakenbush, L., Stabeno, P., Stafford, K.M., Stockwell, D., Wilson, C., 2020. Evidence suggests potential transformation of the Pacific Arctic ecosystem is underway. Nature Climate Change, 10(4), 342-348.

Huxel GR, McCann K, Polis GA. 2002. Effects of partitioning allochthonous and autochthonous resources on food web stability. Ecological Research 17(4): 419-432.

Iken, K., Mueter, F., Grebmeier, J.M., Cooper, L.W., Danielson, S.L., Bluhm, B.A., 2019. Developing an observational design for epibenthos and fish assemblages in the Chukchi Sea. Deep Sea Research Part II: Topical Studies in Oceanography 162, 180-190.

Jay, C.V., Fischbach, A.S., Kochnev, A.A., 2012. Walrus areas of use in the Chukchi Sea during sparse sea ice cover. Marine Ecology Progress Series 468, 1-13.

Jorgenson, M.T., Brown, J., 2004. Classification of the Alaskan Beaufort Sea coast and estimation of carbon and sediment inputs from coastal erosion. Geo-Marine Letters 25, 69-80.

Karlsson, E.S., Brüchert, V., Tesi, T., Charkin, A., Dudarev, O., Semiletov, I., Gustafsson, Ö., 2015. Contrasting regimes for organic matter degradation in the East Siberian Sea and the Laptev Sea assessed through microbial incubations and molecular markers. Marine Chemistry 170, 11-22.

Kędra, M., Moritz, C., Choy, E.S., David, C., Degen, R., Duerksen, S., Ellingsen, I., Górska, B., Grebmeier, J.M., Kirievskaya, D., van Oevelen, D., Piwosz, K., Samuelsen, A., Węsławski, J.M., 2015. Status and trends in the structure of Arctic benthic food webs. Polar Research 34, 1-23.

Kim, J.H., Cho, K.H., La, H.S., Choy, E.J., Matsuno, K., Kang, S.H., Kim, W. and Yang, E.J., 2020. Mass occurrence of Pacific copepods in the southern Chukchi Sea during summer: implications of the high-temperature Bering Summer Water. Frontiers in Marine Science 7:612, 1-11.

Kirchman, D.L., Moran, X.A., Ducklow, H., 2009. Microbial growth in the polar oceans - role of temperature and potential impact of climate change. Nature Reviews Microbiology 7, 451-459.

Kolts, J.M., Lovvorn, J.R., North, C.A., Janout, M.A., 2015. Oceanographic and demographic mechanisms affecting population structure of snow crabs in the northern Bering Sea. Marine Ecology Progress Series 518, 193-208.

Kumar, A., Yadav, J. and Mohan, R., 2020. Global warming leading to alarming recession of the Arctic sea-ice cover: Insights from remote sensing observations and model reanalysis. Heliyon, 6(7), p.e04355.

Lalande, C., Grebmeier, J.M., Wassmann, P., Cooper, L.W., Flint, M.V., Sergeeva, V.M., 2007. Export fluxes of biogenic matter in the presence and absence of seasonal sea ice cover in the Chukchi Sea. Continental Shelf Research 27, 2051-2065.

Lantuit, H., Overduin, P.P., Couture, N., Wetterich, S., Aré, F., Atkinson, D., Brown, J., Cherkashov, G., Drozdov, D., Forbes, D.L., Graves-Gaylord, A., Grigoriev, M., Hubberten, H.-W., Jordan, J., Jorgenson, T., Ødegârd, R.S., Ogorodov, S., Pollard, W.H., Rachold, V., Sedenko, S., Solomon, S., Steenhuisen, F., Streletskaya, I., Vasiliev, A., 2012. The Arctic coastal dynamics database: a new classification scheme and statistics on Arctic permafrost coastlines. Estuaries and Coasts 35, 383-400.

Lavoie, D., Denman, K.L., Macdonald, R.W., 2010. Effects of future climate change on primary productivity and export fluxes in the Beaufort Sea. Journal of Geophysical Research 115.

Leu, E., Søreide, J.E., Hessen, D.O., Falk-Petersen, S., Berge, J., 2011. Consequences of changing sea-ice cover for primary and secondary producers in the European Arctic shelf seas: Timing, quantity, and quality. Progress in Oceanography 90, 18-32.

Li, W.K., McLaughlin, F.A., Lovejoy, C., Carmack, E.C., 2009. Smallest algae thrive as the Arctic Ocean freshens. Science 326, 539.

Lischka, S. and Riebesell, U., 2017. Metabolic response of Arctic pteropods to ocean acidification and warming during the polar night/twilight phase in Kongsfjord (Spitsbergen). Polar Biology, 40(6), pp.1211-1227.

Lovvorn, J.R., Richman, S.E., Grebmeier, J.M., Cooper, L.W., 2003. Diet and body condition of spectacled eiders wintering in pack ice of the Bering Sea. Polar Biology 26, 259-267.

Lovvorn, J.R., Cooper, L.W., Brooks, M.L., De Ruyck, C.C., Bump, J.K., Grebmeier, J.M., 2005. Organic matter pathways to zooplankton and benthos under pack ice in late winter and open water in late summer in the north-central Bering Sea. Marine Ecology Progress Series 291, 135-150.

Marsh, J.M., Mueter, F.J., Iken, K., Danielson, S., 2017. Ontogenetic, spatial and temporal variation in trophic level and diet of Chukchi Sea fishes. Deep Sea Research Part II: Topical Studies in Oceanography 135, 78-94.

Matsuno, K., Yamaguchi, A., Hirawake, T., Imai, I., 2011. Year-to-year changes of the mesozooplankton community in the Chukchi Sea during summers of 1991, 1992 and 2007, 2008. Polar Biology 34, 1349-1360.

McClelland, J.W., Déry, S.J., Peterson, B.J., Holmes, R.M., Wood, E.F., 2006. A pan-arctic evaluation of changes in river discharge during the latter half of the 20th century. Geophysical Research Letters 33, 1-4.

McMeans, B.C., Rooney, N., Arts, M.T., Fisk, A.T., 2013. Food web structure of a coastal Arctic marine ecosystem and implications for stability. Marine Ecology Progress Series 482, 17-28.

Moore, S.E., Grebmeier, J.M., Davies, J.R., 2003. Gray whale distribution relative to forage habitat in the northern Bering Sea: current conditions and retrospective summary. Canadian Journal of Zoology 81, 734-742.

Moore, S.E., Huntington, H.P., 2008. Arctic marine mammals and climate change: Impacts and resilience. Ecological Applications 18, 157-165.

Moore, S.E., Gulland, F.M.D., 2014. Linking marine mammal and ocean health in the 'New Normal' arctic. Ocean & Coastal Management 102, 55-57.

Morán, X.A.G., López-Urrutia, Á., Calvo-Díaz, A., Li, W.K.W., 2010. Increasing importance of small phytoplankton in a warmer ocean. Global Change Biology 16, 1137-1144.

Morris, D.J., O'Connell, M.T., Macko, S.A., 2015. Assessing the importance of terrestrial organic carbon in the Chukchi and Beaufort seas. Estuarine, Coastal and Shelf Science 164, 28-38.

Mueter, F., Litzow, M.A., 2008. Sea ice retreat alters the biogeography of the Bering Sea continental shelf. Ecological Applications 18, 309-320.

Naidu, A.S., Scalan, R.S., Feder, H.M., Goering, J.J., Hameedi, J.M., Parker, P.L., Behrens, E.W., Caughey, M.E., Jewett, S.C., 1993. Stable organic carbon isotopes in sediments of the north Bering- south Chukchi seas, Alaskan-Soviet Arctic shelf. Continental Shelf Research 13, 669-691.

Neeley, A.R., Harris, L.A., Frey, K.E., 2018. Unraveling phytoplankton community dynamics in the northern Chukchi Sea under sea-ice-covered and sea-ice-free conditions. Geophysical Research Letters 45, 7663-7671.

Nerini, M., 1984. A review of ray whale feeding ecology, p. 423-448. In M. L. Jones, S. L. Swartz and S. Leatherwood (editors), The gray whale: *Eschrichtius Robustus*. Academic Press Inc.

Newell, R.C., 1965. The role of detritus in the nutrition of two marine deposit feeders, the prosobranch *Hydrobia ulvae* and the bivalve *Macoma balthica*. Proceedings of the Zoological Society of London 144, 25-45.

Pisareva, M., Pickart, R., Iken, K., Ershova, E., Grebmeier, J., Cooper, L., Bluhm, B., Nobre, C., Hopcroft, R., Hu, H., Wang, J., Ashjian, C., Kosobokova, K., Whitledge, T., 2015. The relationship between patterns of benthic fauna and zooplankton in the Chukchi Sea and physical forcing. Oceanography 28, 68-83.

Pomeroy, L.R., Deibel, D., 1986. Temperature regulation of bacterial activity during the spring bloom in Newfoundland coastal waters. Science 233, 359-361.

Rowe, A.G., Iken, K., Blanchard, A.L., O'Brien, D.M., Doving Osvik, R., Uradnikova, M., Wooller, M.J., 2019. Sources of primary production to Arctic bivalves identified using amino acid stable carbon isotope fingerprinting. Isotopes in Environmental and Health Studies 55, 366-384.

Ruhl, H.A., Smith, K.L., Jr., 2004. Shifts in deep-sea community structure linked to climate and food supply. Science 305, 513-515.

Sakshaug, E., 2004. Primary and secondary production in the Arctic Seas, p. 57-81. In R. Stein and R.M. Macdonald (editors), The Organic Carbon Cycle in the Arctic Ocean. Springer, Berlin; New York.

Samhouri, J.F., Levin, P.S., Harvey, C.J., 2009. Quantitative evaluation of marine ecosystem indicator performance using food web models. Ecosystems 12, 1283-1298.

Schell, D.M., 1983. Carbon-^{13} and Carbon-^{14} abundances in Alaskan aquatic organisms: delayed production from peat in Arctic food webs. American Association for the Advancement of Science 219, 1068-1071.

792 Semiletov, I.P., Pipko, I.I., Shakhova, N.E., Dudarev, O.V., Pugach, S.P., Charkin, A.N., McRoy, C.P.,
793 Kosmach, D., Gustafsson, Ö., 2011. Carbon transport by the Lena River from its headwaters to the
794 Arctic Ocean, with emphasis on fluvial input of terrestrial particulate organic carbon vs. carbon
795 transport by coastal erosion. Biogeosciences 8, 2407-2426.
796 Serreze, M.C., Barrett, A.P., Stroeve, J.C., Kindig, D.N., Holland, M.M., 2009. The emergence of surface-
797 based Arctic amplification. The Cryosphere 3, 11-19.
798 Sommer, U., Stibor, H., Katechakis, A., Sommer, F., Hansen, T., 2002. Pelagic food web configurations at
799 different levels of nutrient richness andtheir implications for the ratio fish production: primary
800 production. Hydrobiologia 484, 11-20.
801 Steele, M., Ermold, W., Zhang, J., 2008. Arctic Ocean surface warming trends over the past 100 years.
802 Geophysical Research Letters 35, 1-6.
803 Taylor, P., Hegyi, B., Boeke, R., Boisvert, L., 2018. On the increasing importance of air-sea exchanges in a
804 thawing Arctic: a review. Atmosphere 9, 1-39.
805 Walsh, J.J., McRoy, C.P., Coachman, L.K., Goering, J.J., Nihoul, J.J., Whiteledge, T.E., Blackburn, T.H.,
806 Parker, P.L., Wirick, C.D., Shuert, P.G., Grebmeier, J.M., Springer, A.M., Tripp, R.D., Hansell, D.A.,
807 Djenidi, S., Deleersnijder, E., Henriksen, K., Lund, B.A., Andersen, P., Mueller, F.E., Dean, K., 1989.
808 Carbon and nitrogen cycling within the Bering/Chukchi Seas: source regions for organic matter
809 effecting AOU demands of the Arctic Ocean. Progress in Oceanography 22, 277-359.
810 Walters, C., Christensen, V., Pauly, D., 1997. Structuring dynamic models of exploited ecosystems from
811 trophic mass-balance assessments. Reviews in Fish Biology and Fisheries 7, 139-172.
812 Walters, C., Pauly, D., Christensen, V., Kitchell, J.F., 2000. Representing density dependent consequences
813 of life history strategies in aquatic ecosystems: EcoSim II. Ecosystems 3, 70-83.
814 Wang, M., Overland, J.E., Stabeno, P., 2012. Future climate of the Bering and Chukchi Seas projected by
815 global climate models. Deep Sea Research Part II: Topical Studies in Oceanography 65-70, 46-57.
816 Wassmann, P., Reigstad, M., 2011. Future Arctic Ocean seasonal ice zones and implications for pelagic-
817 benthic coupling. Oceanography 24, 220-231.
818 Welch, H.E., Bergmann, M.A., Siferd, T.D., Martin, K.A., Curtis, M.F., Crawford, R.E., Conover, R.J., Hop, H.,
819 1992. Energy flow through the marine ecosystem of the Lancaster Sound Region, Arctic Canada.
820 Arctic 45, 343-357.
821 Węsławski, J.M., Kendall, M.A., Włodarska-Kowalczuk, M., Iken, K., Kędra, M., Legezynska, J., Sejr, M.K.,
822 2011. Climate change effects on Arctic fjord and coastal macrobenthic diversity—observations
823 and predictions. Marine Biodiversity 41, 71-85.
824 Whitehouse, A., 2013. Preliminary mass-balance food web model of the eastern Chukchi Sea. NOAA
825 Technical Memorandum, 1-173.
826 Whitehouse, G.A., Aydin, K., Essington, T.E., Hunt, G.L., 2014. A trophic mass balance model of the eastern
827 Chukchi Sea with comparisons to other high-latitude systems. Polar Biology 37, 911-939.
828 Whitehouse, A., Aydin, K., 2016. Trophic structure of the Eastern Chukchi Sea: an updated mass balance
829 food web model. NOAA Technical Memorandum, 1-191.
830 Yablokov, A. V., Bogoslovskaya, L. S., 1984. A review of Russian research on the biology and commercial
831 whaling of the gray whale, p. 465-482. In M. L. Jones, S. L. Swartz and S. Leatherwood (editors),
832 The gray whale: *Eschrichtius Robustus*. Academic Press Inc.
833 Yunker, M.B., Belicka, L.L., Harvey, H.R., Macdonald, R.W., 2005. Tracing the inputs and fate of marine and
834 terrigenous organic matter in Arctic Ocean sediments: a multivariate analysis of lipid biomarkers.
835 Deep Sea Research Part II: Topical Studies in Oceanography 52, 3478-3508.
836 Zeller, D., Booth, S., Pakhomov, E., Swartz, W., Pauly, D., 2011. Arctic fisheries catches in Russia, USA, and
837 Canada: baselines for neglected ecosystems. Polar Biology 34, 955-973.
838 Zinkann, A-C, Wooller, M.J., Leigh, M.B., Danielson, S., Gibson, G., Iken, K., (a) in review. Depth distribution
839 of organic carbon sources in Arctic Chukchi Sea sediments. Deep-Sea Research Part II.

840 Zinkann, A-C, Wooller, M.J., O'Brien, D., Iken, K., (b) in review. Does feeding type matter? Contribution of
841 organic matter sources to benthic invertebrates on the Arctic Chukchi Sea shelf. Food webs.
842
843

Figures and tables

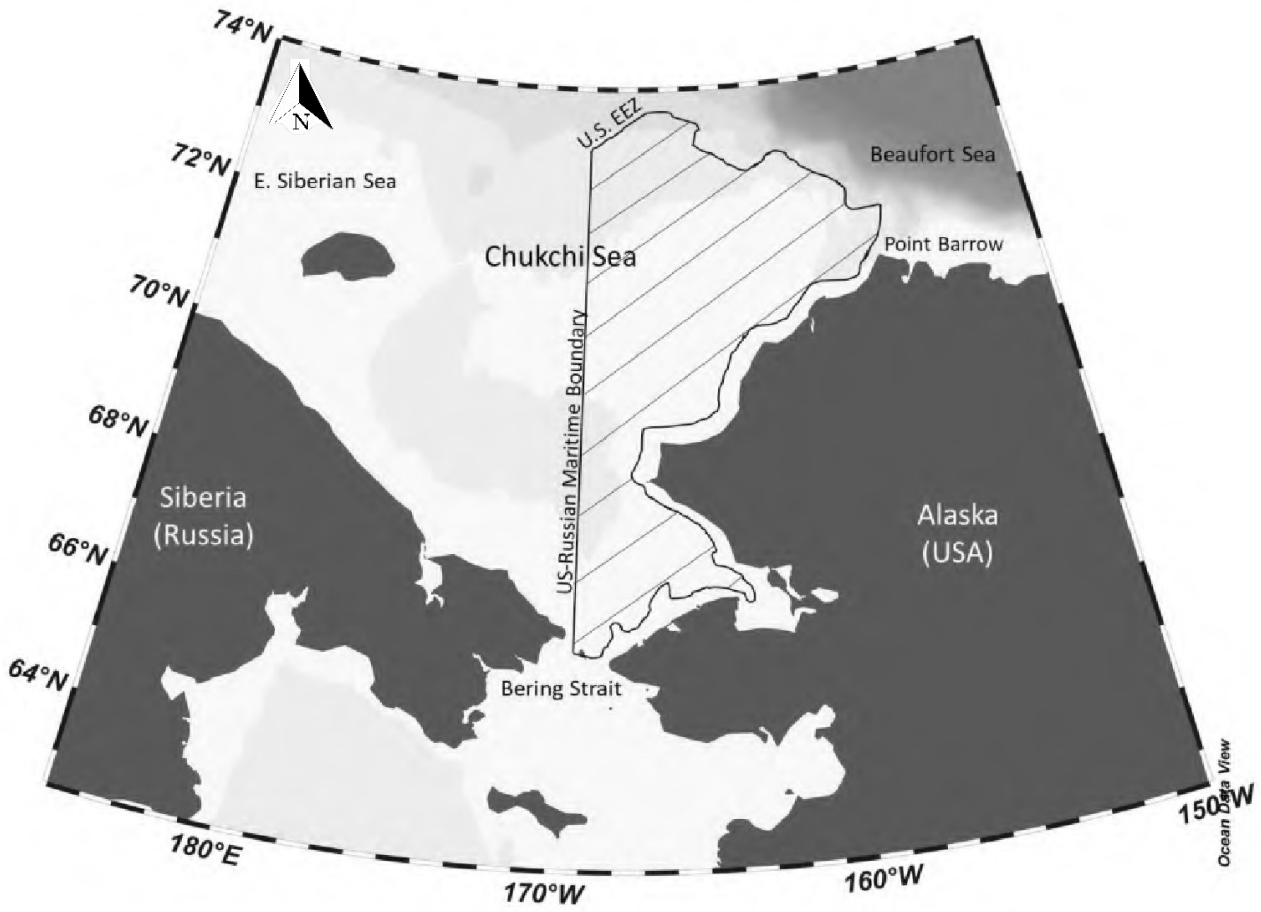

Figure 1. Map of the model area on the eastern Chukchi Sea shelf (hatched area). The model is bounded by the US-Russia maritime border to the west, Bering Strait to the south, Point Barrow to the east, and the US exclusive economic zones along the shelf break to the north.

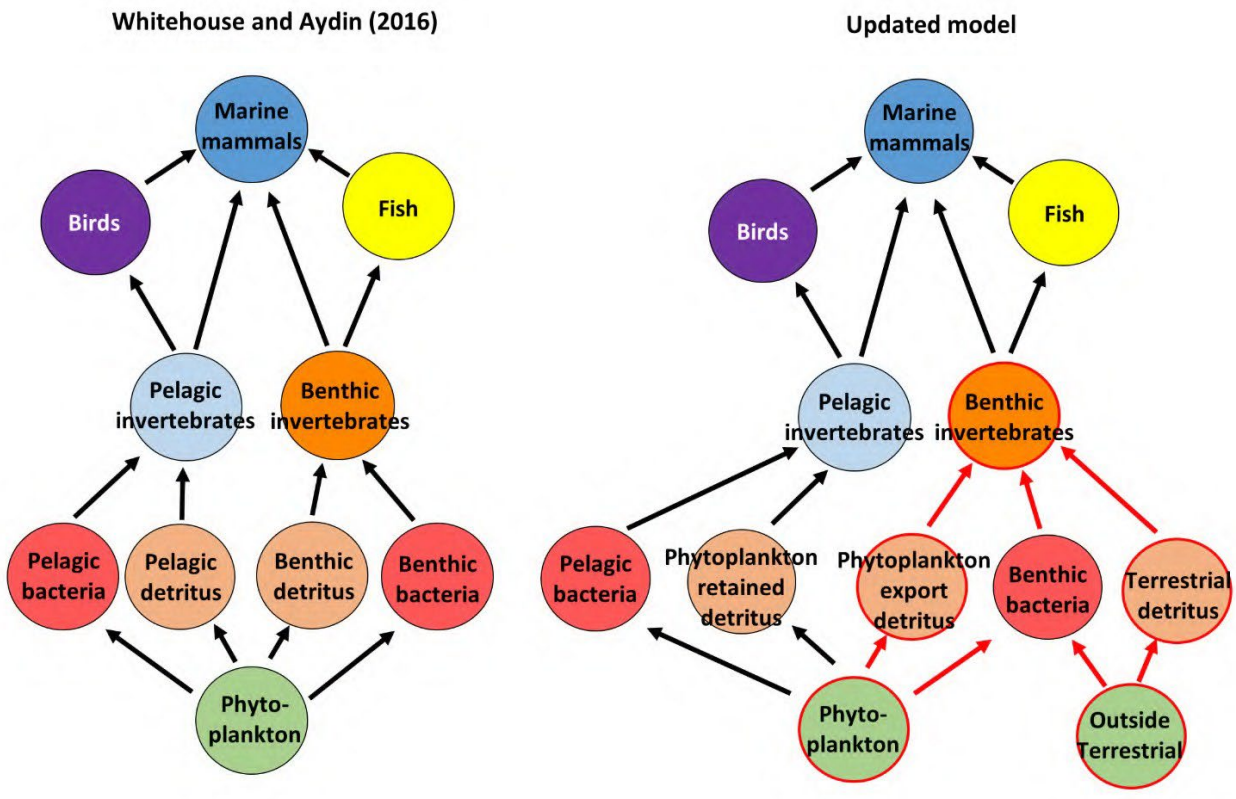

856

857 Figure 2. Comparative schematic of the original Whitehouse and Aydin (2016) and our updated
858 mass-balanced Chukchi Sea ecosystem model. Arrows indicate feeding connections and
859 flow of energy between larger functional groups. Color of circles indicates: brown =
860 detrital pools, green = primary producers, red = bacteria, orange = benthic invertebrates,
861 light blue = pelagic invertebrates, yellow = fish, purple = birds, dark blue = marine
862 mammals. Red outlines and arrows indicate parameters and functional groups that reflect
863 changes in the updated model.

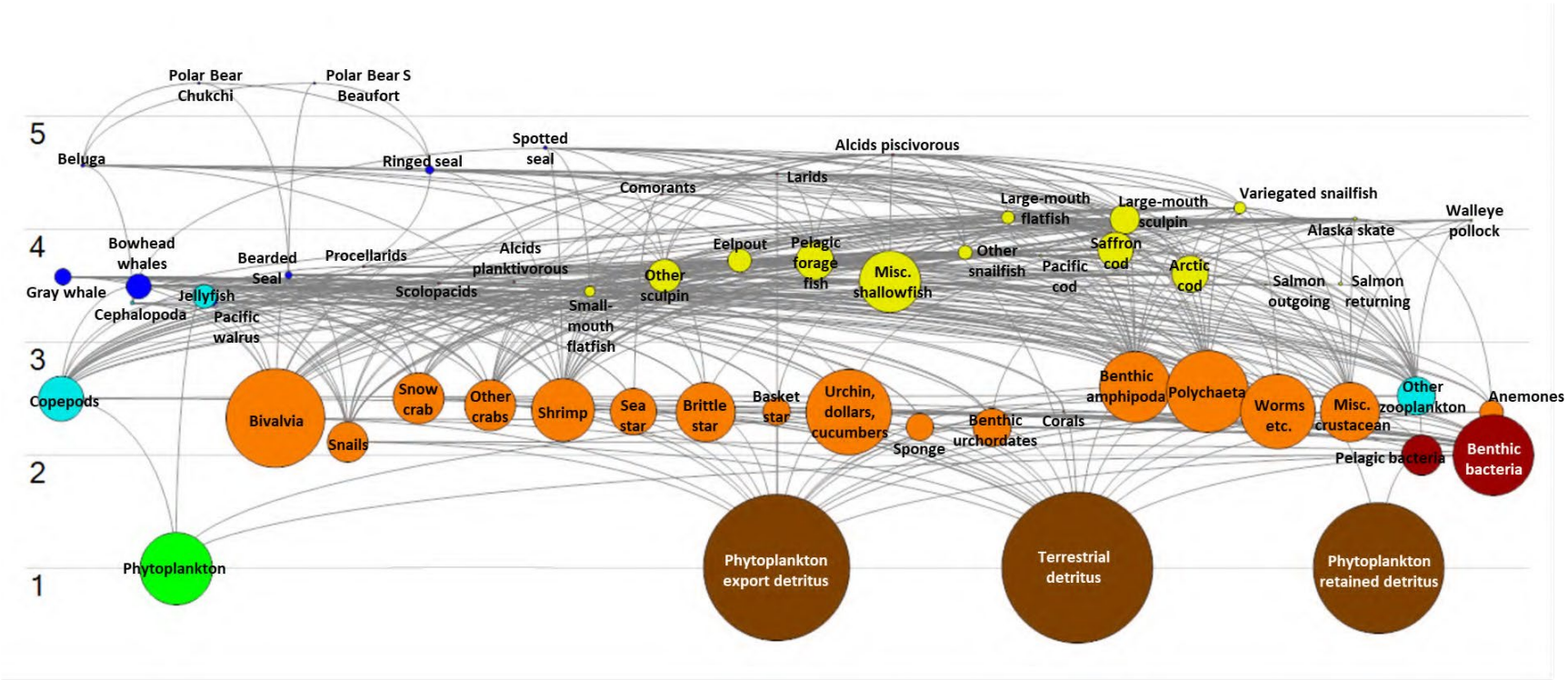

Figure 3. Flow chart for the updated mass-balanced Chukchi Sea ecosystem model. Numbers on the left indicate trophic level, size of nodule indicates biomass of respective functional group, gray lines indicate unidirectional feeding connections and energy flow between functional groups, and colors are indicative of larger functional groupings: brown = detrital pools, green = primary producers, red = bacteria, orange = benthic invertebrates, light blue = pelagic invertebrates, yellow = fish, purple = birds, dark blue = marine mammals.

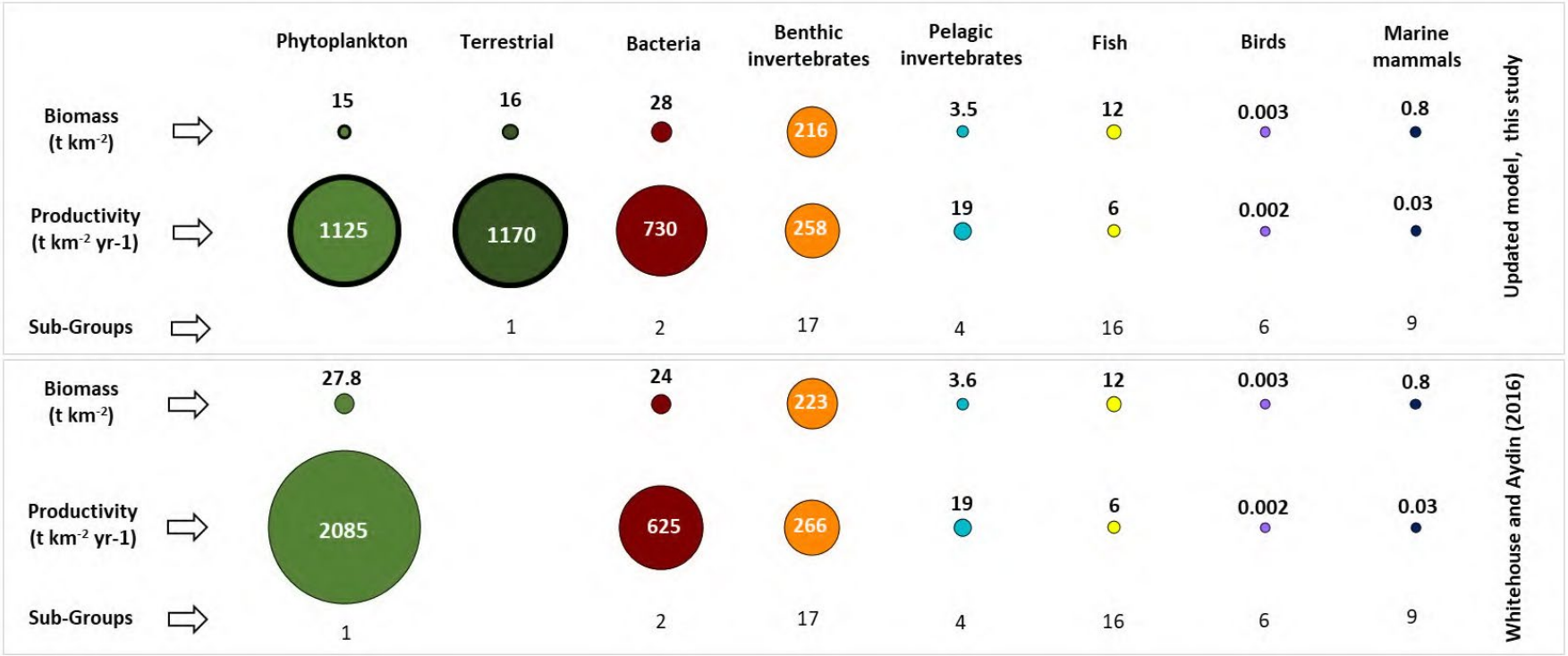

Figure 4. Biomass, productivity of larger functional groups in our updated Chukchi Sea ecosystem model (top panel) and the Whitehouse and Aydin 2016 (bottom panel) model. The figure shows cumulative biomass (t km^{-2}), productivity (t km^{-2} yr^{-1}), and number of subgroups included in each group. Size of circles indicates the representative biomass and production value. Thick black outline indicates the groupings that were updated in the current model: green = primary producers, red = bacteria, orange = benthic invertebrates, light blue = pelagic invertebrates, yellow = fish, purple = birds, and dark blue = marine mammals.

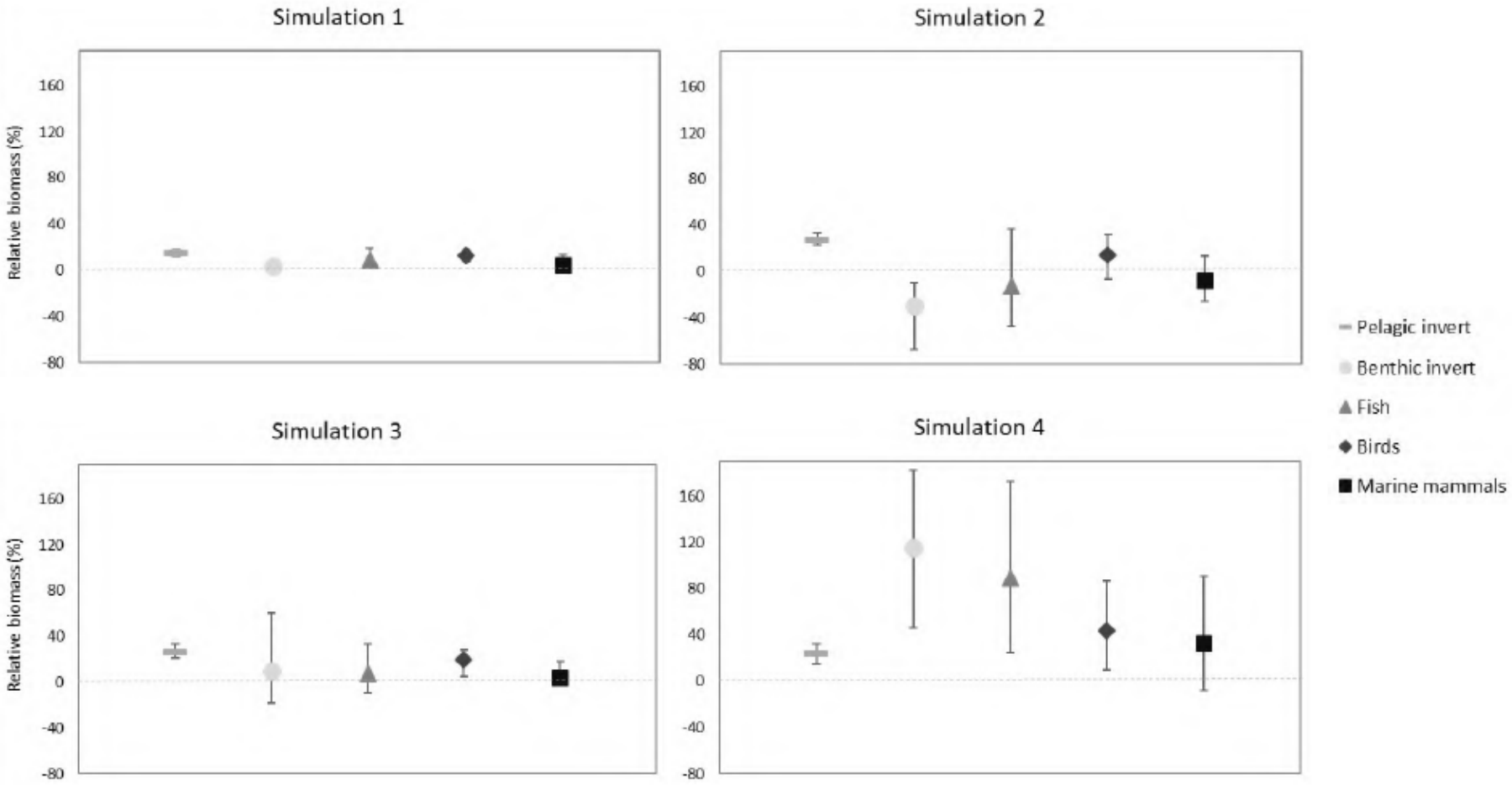

Figure 5. Average relative change in biomass (averaged across functional groups) compared to initial relative biomass (2015) at end of simulation period (2050) based on cumulative Ecosim simulations of the updated mass-balanced ecosystem model of the Chukchi Sea shelf. Error bars for each ecosystem group indicate the minimum and maximum relative biomass values from the functional groups within each ecosystem group (see Fig. 3). Simulation 1 refers to an increase in phytoplankton biomass, simulation 2 refers to an additional weakening in pelagic-benthic coupling, simulation 3 refers to an additional increase in terrestrial matter biomass, and simulation 4 refers to an additional increase in microbial production. The gray line indicates steady state situation with no changes in relative biomass from the initial start year (2015).

Figure 6. Trends in relative biomass (change from initial biomass) for each major ecosystem group (a-e) across the simulation period (2015-2050) based on Ecosim modeling of an updated mass-balanced ecosystem model of the Chukchi Sea shelf. Simulation 1 refers to an increase in phytoplankton biomass, simulation 2 to a weakening in pelagic-benthic coupling, simulation 3 to an increase in terrestrial matter biomass, and simulation 4 to an increase in microbial production. Each simulation also included the changes of all previous simulations. Different shades within some of the larger taxon group indicate functional groupings based on feeding preferences (see legend). Abbreviations in figures refer to specific ecosystem groups: Benthic invertebrates – S (Snails), BU (Benthic urchordates), Sp (Sponges), SC (Snow crab), Birds – S (Scolopacids), L (Larids), C (Cormorants), Fish – AC (Arctic Cod), S (Salmon), P (Pollock), SMF (Small-mouth flatfish), Sc (Sculpin), Sk (Skates), Mammals – G (Gray whales), W (Pacific walrus), S (Bearded seals).

(a) Pelagic invertebrates

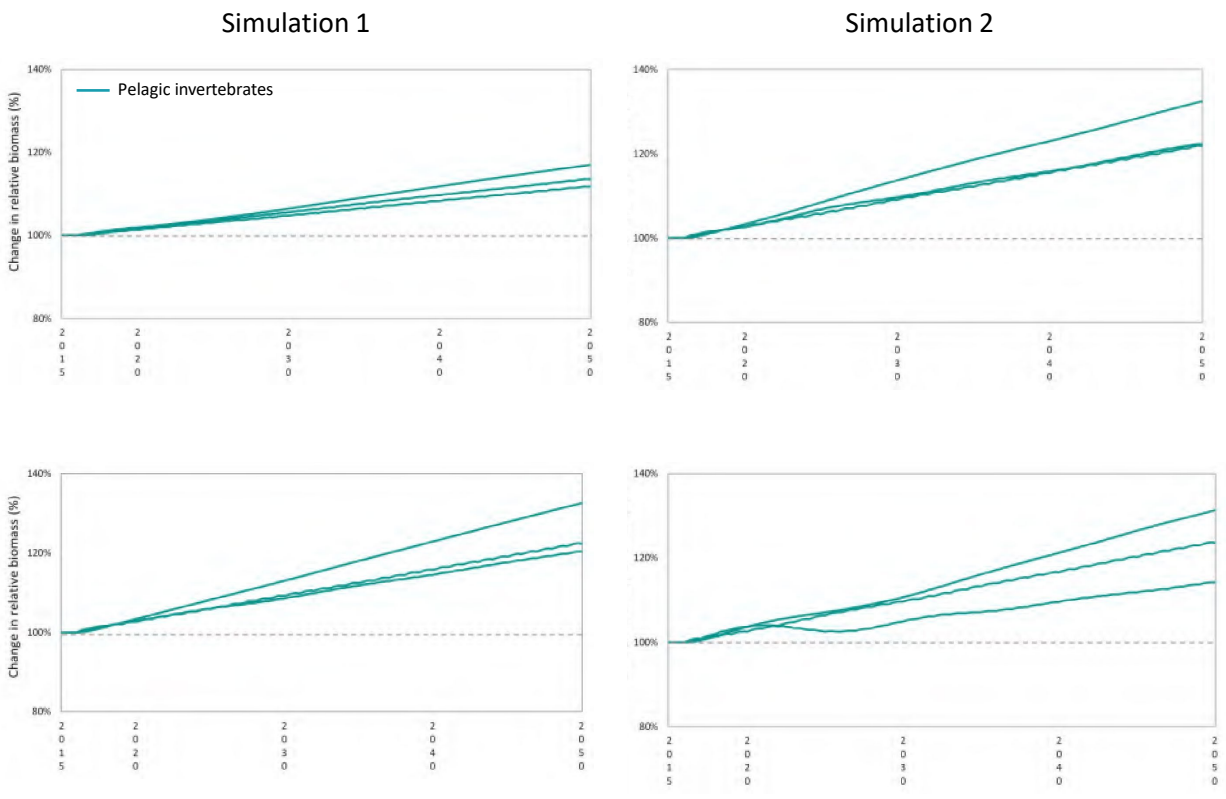

17 *(b) Benthic invertebrates*

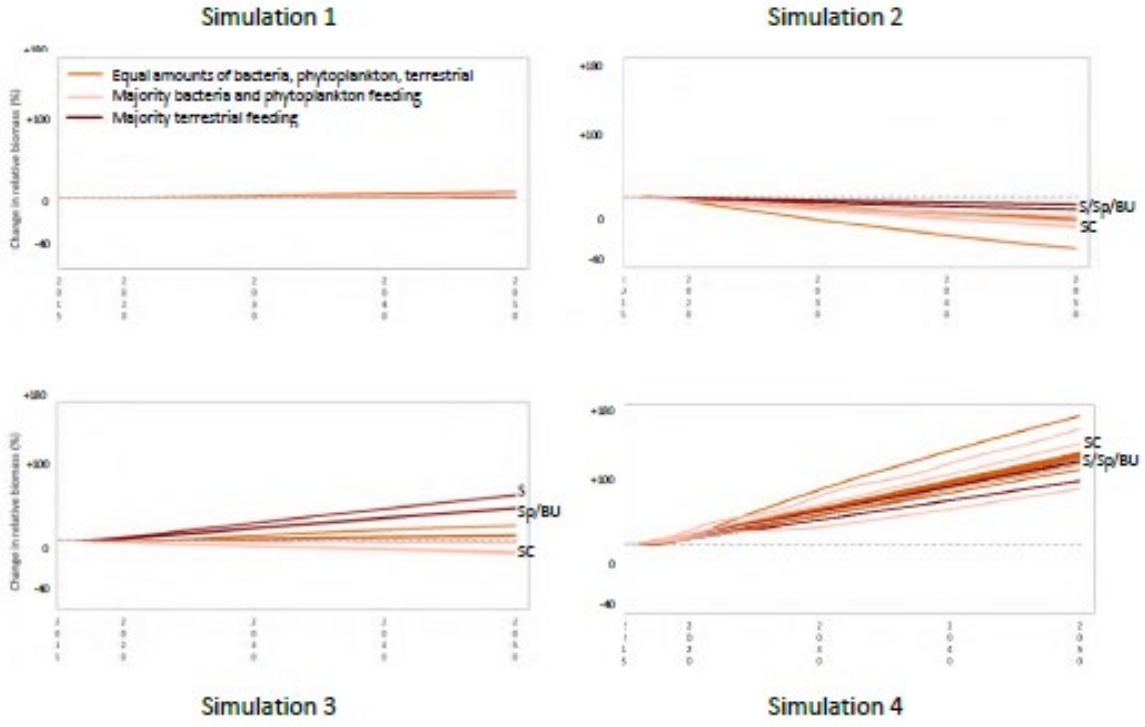

18 *(c) Fish*

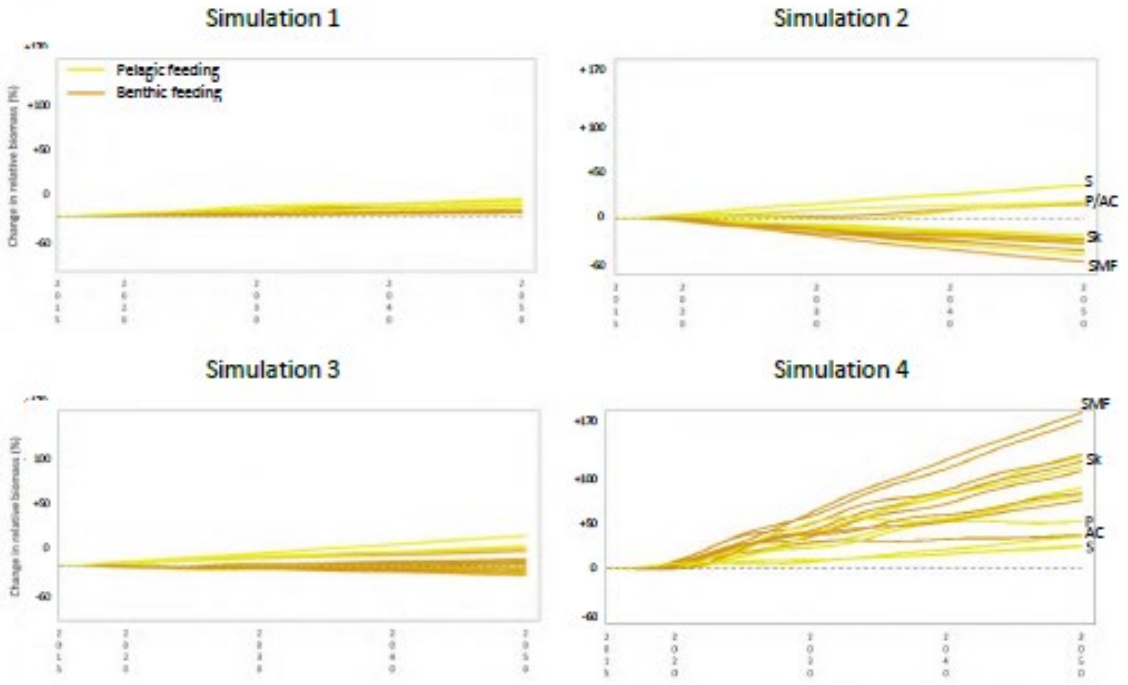

19

(d) Birds

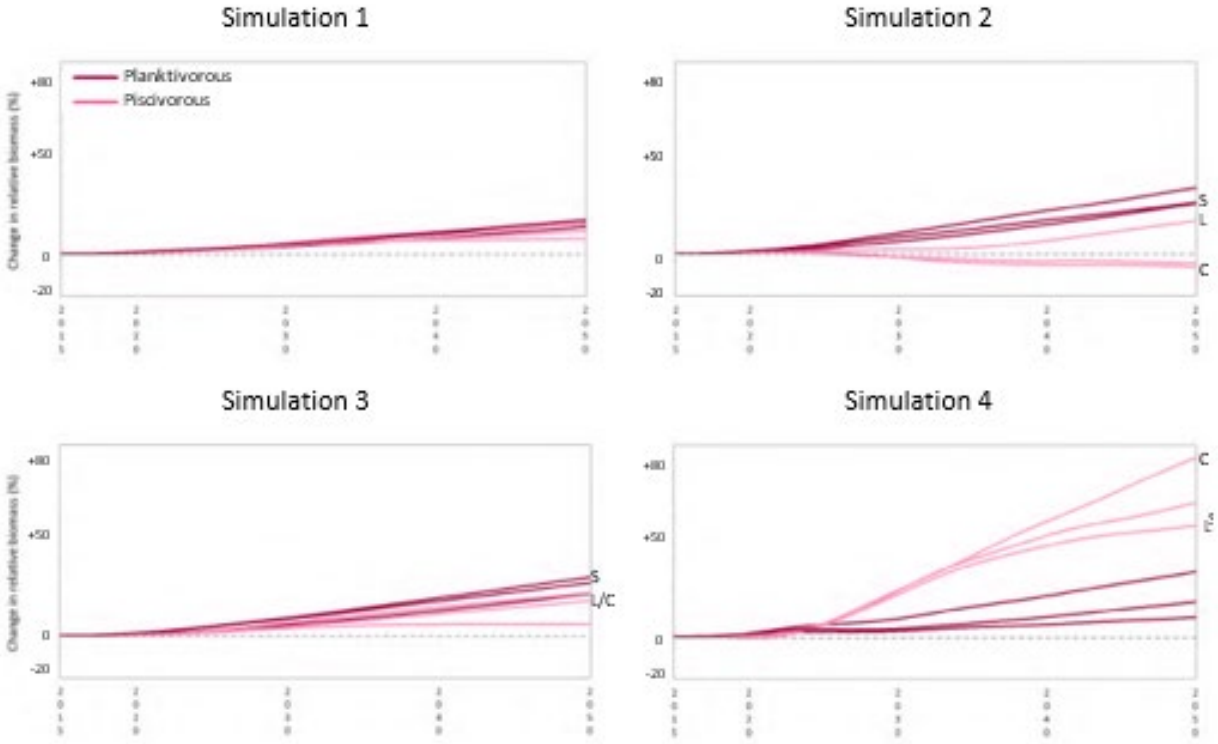

(e) Marine mammals

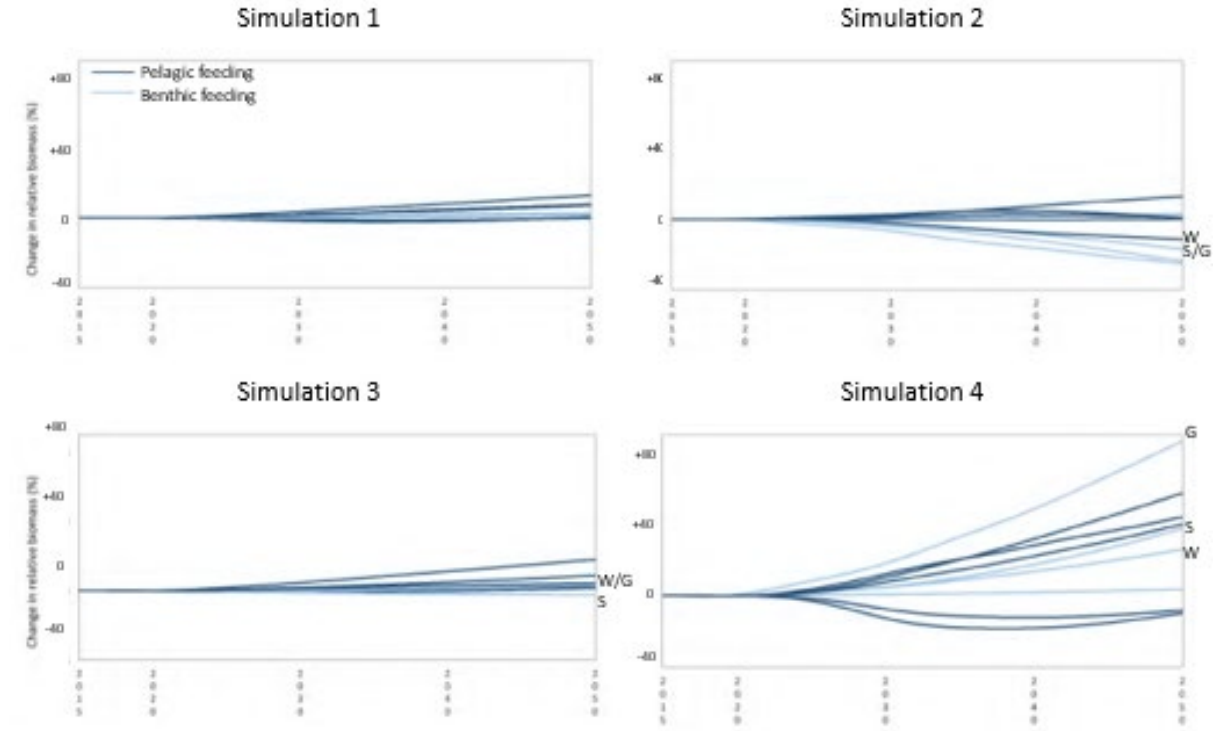

Table 1. Term, descriptions, and units of parameters required for mass-balanced ecosystem model master equations in Ecopath and Ecosim.

Term	Description	Unit
P	Total production rate	t km^{-2} yr^{-1}
Y	Total fishery catch rate (here subsistence harvest)	t km^{-2} yr^{-1}
B	Biomass	t km^{-2}
M2	Instantaneous predation rate	yr^{-1}
E	Net migration rate (emigration-immigration)	t km^{-2} yr^{-1}
BA	Biomass accumulation rate	t km^{-2} yr^{-1}
1-EE	Other mortality	proportion (unitless)
EE	Ecotrophic efficiency	proportion (unitless)
Q/B	Consumption/biomass ratio	yr^{-1}
P/B	Production/biomass ratio	yr^{-1}
R	Respiration of group	t km^{-2} yr^{-1}
UN	Unassimilated food	proportion (unitless)
g	Gross food conversion efficiency (estimated as P/Q ratio)	unitless
Q	Total consumption rate	t km^{-2} yr^{-1}
I	Immigration rate	t km^{-2} yr^{-1}
MO	Instantaneous 'other mortality' rate	yr^{-1}
F	Instantaneous fishing mortality rate	yr^{-1}
e	Emigration rate per unit biomass	t km^{-2} yr^{-1}

Table 2. (Next page). Basic model parameters for the updated Ecopath model for the Chukchi Sea. Parameter inputs into the model were taken from Whitehouse and Aydin (2016). Parameters in bold were computed by the updated model. New functional groups and changed input parameters are highlighted by gray background. TL is trophic level, B is biomass (t km^{-2}), P/B is production to biomass ratio (y^{-1}), Q/B is consumption to biomass ratio (y^{-1}), EE is ecotrophic efficiency, GE is growth efficiency (y^{-1}), UN is unassimilated food, PED is phytoplankton export detritus, TD is terrestrial detritus, and PRD is phytoplankton retained detritus.

Table 2: continued.

	Group name	TL	B	P/B	Q/B	EE	GE	UN	PED	TD	PRD
1	Beluga	4.6	0.012	0.112	14.504	**0.211**	**0.008**	0.2	0.35	0.35	0.3
2	Gray whale	3.6	0.188	0.063	8.873	**0.000**	**0.007**	0.2	0.35	0.35	0.3
3	Bowhead whale	3.5	0.398	0.010	5.260	**0.299**	**0.002**	0.2	0.35	0.35	0.3
4	Polar bear Chukchi	5.3	0.0004	0.060	4.001	**0.663**	**0.015**	0.2	0.35	0.35	0.3
5	Polar bear S Beaufort	5.3	0.0001	0.060	4.001	**0.304**	**0.015**	0.2	0.35	0.35	0.3
6	Pacific walrus	3.4	0.059	0.069	21.662	**0.757**	**0.003**	0.2	0.35	0.35	0.3
7	Bearded seal	3.6	0.039	0.075	12.941	**0.912**	**0.006**	0.2	0.35	0.35	0.3
8	Ringed seal	4.5	0.056	0.088	19.228	**0.895**	**0.005**	0.2	0.35	0.35	0.3
9	Spotted seal	4.7	0.006	0.068	18.705	**0.385**	**0.004**	0.2	0.35	0.35	0.3
10	Procellarids	3.7	0.002	0.067	187.929	**0.000**	**0.0004**	0.2	0.35	0.35	0.3
11	Cormorants	4.3	0.000001	0.163	142.618	**0.000**	**0.001**	0.2	0.35	0.35	0.3
12	Scolopacids	3.5	0.0001	0.163	374.313	**0.000**	**0.0004**	0.2	0.35	0.35	0.3
13	Larids	4.5	0.0001	0.106	205.674	**0.000**	**0.001**	0.2	0.35	0.35	0.3
14	Alcids piscivorous	4.7	0.001	0.104	178.384	**0.741**	**0.001**	0.2	0.35	0.35	0.3
15	Alcids planktivores	3.5	0.0001	0.140	247.507	**0.000**	**0.001**	0.2	0.35	0.35	0.3
16	Large-mouth flatfish	4.1	**0.111**	0.401	1.780	0.800	**0.225**	0.2	0.35	0.35	0.3
17	Small-mouth flatfish	3.5	**0.090**	0.308	1.535	0.800	**0.201**	0.2	0.35	0.35	0.3
18	Large-mouth sculpin	4.1	**0.600**	0.400	2.000	0.800	**0.200**	0.2	0.35	0.35	0.3
19	Other sculpin	3.6	**0.855**	0.459	2.415	0.800	**0.190**	0.2	0.35	0.35	0.3
20	Eelpout	3.7	**0.382**	0.400	2.000	0.800	**0.200**	0.2	0.35	0.35	0.3
21	Pelagic forage fish	3.7	**1.191**	0.543	2.920	0.800	**0.186**	0.2	0.35	0.35	0.3
22	Misc. shallow fish	3.5	**6.498**	0.400	2.000	0.800	**0.200**	0.2	0.35	0.35	0.3
23	Other snailfish	3.8	**0.135**	0.400	2.000	0.800	**0.200**	0.2	0.35	0.35	0.3
24	Variegated snailfish	4.2	**0.099**	0.400	2.000	0.800	**0.200**	0.2	0.35	0.35	0.3
25	Alaska skate	4.1	0.005	0.210	**2.100**	**0.000**	0.100	0.2	0.35	0.35	0.3
26	Walleye pollock	4.1	0.001	0.869	3.008	**0.0001**	**0.289**	0.2	0.35	0.35	0.3
27	Pacific cod	3.8	0.00004	0.548	2.803	**0.744**	**0.195**	0.2	0.35	0.35	0.3
28	Saffron cod	3.8	**0.979**	0.548	2.803	0.800	**0.195**	0.2	0.35	0.35	0.3
29	Arctic cod	3.6	**1.045**	0.869	3.008	0.800	**0.289**	0.2	0.35	0.35	0.3
30	Salmon outgoing	3.5	0.001	1.280	13.560	**0.000**	**0.094**	0.2	0.35	0.35	0.3
31	Salmon returning	3.5	0.005	1.650	11.600	**0.027**	**0.142**	0.2	0.35	0.35	0.3
32	Cephalopoda	3.3	**0.011**	1.770	**8.850**	0.800	**0.200**	0.2	0.45	0.45	0.1
33	Bivalves	2.3	90.288	0.756	**3.778**	**0.029**	0.200	0.4	0.45	0.45	0.1
34	Snails	2.1	1.384	1.770	**8.850**	**0.060**	**0.200**	0.2	0.45	0.45	0.1
35	Snow crab	2.5	3.170	1.000	2.750	**0.082**	**0.364**	0.2	0.45	0.45	0.1
36	Other crabs	2.4	3.067	0.820	**4.100**	**0.187**	0.200	0.3	0.45	0.45	0.1
37	Shrimps	2.4	**7.492**	0.576	2.409	0.800	0.239	0.2	0.45	0.45	0.1
38	Sea stars	2.4	2.180	0.340	**1.700**	**0.014**	0.200	0.2	0.45	0.45	0.1
39	Brittle stars	2.4	5.644	0.485	**2.425**	**0.009**	0.200	0.4	0.45	0.45	0.1
40	Basket stars	2.4	0.510	0.340	**1.700**	**0.002**	0.200	0.2	0.45	0.45	0.1
41	Urchins, dollars, cucumbers	2.4	36.290	0.695	**3.475**	**0.007**	0.200	0.4	0.45	0.45	0.1
42	Sponge	2.2	0.527	1.000	**5.000**	**0.001**	0.200	0.4	0.45	0.45	0.1
43	Anemones	2.4	0.384	1.000	**5.000**	**0.361**	0.200	0.2	0.45	0.45	0.1
44	Benthic urchordate	2.2	1.160	3.580	**17.900**	**0.005**	0.200	0.4	0.45	0.45	0.1
45	Corals	2.4	0.003	0.046	**0.230**	**0.056**	0.200	0.4	0.45	0.45	0.1
46	Jellyfish	3.4	0.372	0.880	3.000	**0.002**	**0.293**	0.2	0.35	0.35	0.3
47	Benthic Amphipoda	2.6	**12.884**	1.000	**5.000**	0.800	0.200	0.4	0.45	0.45	0.1
48	Polychaeta	2.6	27.808	2.916	**14.579**	**0.035**	0.200	0.4	0.45	0.45	0.1
49	Worms etc.	2.4	17.040	2.230	**11.150**	**0.013**	0.200	0.4	0.45	0.45	0.1
50	Misc. crustaceans	2.4	5.581	2.008	**10.040**	**0.103**	0.200	0.4	0.45	0.45	0.1
51	Copepods	2.5	**1.951**	6.000	27.740	0.800	**0.216**	0.2	0.35	0.35	0.3
52	Other zooplankton	2.5	**1.168**	5.475	**15.643**	0.800	0.350	0.2	0.35	0.35	0.3
53	Pelagic bacteria	2.0	**1.421**	26.250	**75.000**	0.800	0.350	0.2	0.35	0.35	0.3
54	Benthic bacteria	2.0	**26.398**	26.250	**75.000**	0.800	0.350	0.2	0.45	0.45	0.1
55	Phytoplankton	1.0	15.000	75.000		**0.100**			0.7	0	0.3
56	Outside Terrestrial production	1.0	15.600	75.000		**0.000**			0	0.7	0.3
57	Phytoplankton export detritus	1.0	3944.760			**0.998**			0	0	0
58	Outside Terrestrial detritus	1.0	2821.520			**0.997**			0	0	0
59	Phytoplankton retained detritus	1.0	2173.080	0.500		**0.040**			0	0	0

Table 3. Proportional contributions of three organic matter sources (bacterial, phytoplankton, terrestrial) to benthic invertebrate functional groups in the Chukchi Sea based on data from Zinkann et al. b, in review. Table shows the functional groups in the model, organisms that were included in each functional group, and diet proportions. See text for details.

Functional group	Organisms included	Bacteria	Phytoplankton	Terrestrial
Snow crab	*Chionoecetes opilio*	0.498	0.360	0.142
Bivalves	Clams, Mytilidae, Cardiidae, Pectinidae, Scaphopoda	0.323	0.302	0.375
Snails	17 species, Buccinidae	0.117	0.072	0.811
Other Crabs	*Hyas* , *Telmessus* , Paguridae, *Paralithodes*	0.437	0.384	0.179
Shrimps	Crangonidae, Hippolytidae, Pandalidae	0.406	0.396	0.197
Sea stars	Solasteridae, Goniopectinidae, Echinasteridae, Asteriidae, Pterasteridae	0.382	0.262	0.357
Brittle stars	*Amphiophiura, Ophiura, Ophiacantha* , and *Ophiopholis*	0.382	0.262	0.357
Basket stars	*Gorgonocephalus*	0.382	0.262	0.357
Urchins, dollars, cucumbers	Clypeasteroida, Holothuroidea, Echinoidea	0.382	0.262	0.357
Sponge	*Halichondria*	0.245	0.112	0.644
Anemones	*Urticina*	0.382	0.262	0.357
Benthic urochordate	*Styela* , *Halocynthia*	0.245	0.112	0.644
Corals	*Gersemia*	0.382	0.262	0.357
Benthic amphipods	Gammaridae, Caprellidae	0.604	0.200	0.196
Polychaetes	All	0.570	0.175	0.255
Worms etc.	Sipuncula, Echiura, Priapula, Nemertea, Brachiopoda, and Bryozoa	0.382	0.262	0.357
Misc. crustaceans	Isopoda, Cumacea, Cirripedia, Pycnogonida, and Ostracoda	0.382	0.262	0.357

Table 4. Time series data used for Ecosim manipulation of biomass for phytoplankton, pelagic-benthic coupling (given as proportions of phytoplankton biomass routed to phytoplankton export detritus and phytoplankton retained detritus), terrestrial matter, and benthic bacterial biomass under predicted changes on the Chukchi Sea shelf from 2015 - 2050. 'Pool code' refers to the number of the functional groups in the Ecopath model, 'Type' to the type of forcing that was set to 'forcing biomass', and numbers 1-4 refer to the simulations.

Simulation	1	2	3	4	
Name	Phytoplankton	Phytoplankton export detritus	Phytoplankton retained detritus	Outside terrestrial	Benthic Bacteria
Pool code	55	57	59	56	54
Type	-1	-1	-1	-1	-1
2015	15.0	2600.8	895.1	15.6	26.4
2016	15.0	2571.0	905.3	16.0	27.8
2017	15.1	2541.3	915.5	16.4	29.1
2018	15.1	2511.6	925.8	16.8	30.5
2019	15.2	2481.9	936.0	17.2	31.9
2020	15.2	2452.1	946.2	17.6	33.3
2021	15.3	2422.4	956.5	18.0	34.6
2022	15.3	2392.7	966.7	18.4	36.0
2023	15.3	2363.0	976.9	18.8	37.4
2024	15.4	2333.3	987.1	19.3	38.7
2025	15.4	2303.5	997.4	19.7	40.1
2026	15.5	2273.8	1007.6	20.1	41.5
2027	15.5	2244.1	1017.8	20.5	42.9
2028	15.6	2214.4	1028.1	20.9	44.2
2029	15.6	2184.6	1038.3	21.3	45.6
2030	15.6	2154.9	1048.5	21.7	47.0
2031	15.7	2125.2	1058.8	22.1	48.3
2032	15.7	2095.5	1069.0	22.5	49.7
2033	15.8	2065.7	1079.2	22.9	51.1
2034	15.8	2036.0	1089.4	23.3	52.5
2035	15.9	2006.3	1099.7	23.7	53.8
2036	15.9	1976.6	1109.9	24.1	55.2
2037	15.9	1946.9	1120.1	24.5	56.6
2038	16.0	1917.1	1130.4	24.9	58.0
2039	16.0	1887.4	1140.6	25.3	59.3
2040	16.1	1857.7	1150.8	25.7	60.7
2041	16.1	1828.0	1161.0	26.1	62.1
2042	16.2	1798.2	1171.3	26.6	63.4
2043	16.2	1768.5	1181.5	27.0	64.8
2044	16.2	1738.8	1191.7	27.4	66.2
2045	16.3	1709.1	1202.0	27.8	67.6
2046	16.3	1679.3	1212.2	28.2	68.9
2047	16.4	1649.6	1222.4	28.6	70.3
2048	16.4	1619.9	1232.7	29.0	71.7
2049	16.5	1590.2	1242.9	29.4	73.0
2050	16.5	1560.5	1253.1	29.8	74.4

Evidence suggests potential transformation of the Pacific Arctic Ecosystem is underway

8 January 2020

Manuscript as accepted by Nature Climate Change; subject to editing, proofreading, etc.

Authors & Affiliations:

Henry P. Huntington, Huntington Consulting, 23834 The Clearing Dr., Eagle River, AK, 99577, USA; henryphuntington@gmail.com
Seth L. Danielson, University of Alaska Fairbanks, Fairbanks, AK, USA
Francis K. Wiese, Stantec, Anchorage, AK, USA
Matthew Baker, North Pacific Research Board, Anchorage, AK, USA
Peter Boveng, NOAA-Alaska Fisheries Science Center, Seattle, WA, USA
John J. Citta, Alaska Department of Fish and Game, AK 99701, USA
Alex De Robertis, NOAA- Alaska Fisheries Science Center, Seattle, WA, USA
Danielle Dickson, North Pacific Research Board, Anchorage, AK, USA
Ed Farley, NOAA-Alaska Fisheries Science Center, Seattle, WA, USA
J. Craighead George, North Slope Borough Department of Wildlife Management, Utqiaġvik, AK, USA
Katrin Iken, University of Alaska Fairbanks, Fairbanks, AK, USA
David G. Kimmel, NOAA-Alaska Fisheries Science Center, Seattle, WA, USA
Kathy Kuletz, U.S. Fish and Wildlife Service, Anchorage, AK, USA
Carol Ladd, NOAA-Pacific Marine Environmental Laboratory, Seattle, WA, USA
Robert Levine, University of Washington, Seattle, WA, USA
Lori Quakenbush, Alaska Department of Fish and Game, Fairbanks, AK 99701, USA
Phyllis Stabeno, NOAA-Pacific Marine Environmental Laboratory, Seattle, WA, USA
Kathleen M. Stafford, University of Washington, Seattle, WA, USA
Dean Stockwell, University of Alaska Fairbanks, Fairbanks, AK, USA
Chris Wilson, NOAA-Alaska Fisheries Science Center (retired), Seattle, WA, USA

Abstract

The highly productive northern Bering and Chukchi marine shelf ecosystem has long been dominated by strong seasonality in sea ice and water temperatures. Extremely warm conditions from 2017into 2019 - including loss of ice cover across portions of the region in all three winters - were a marked change even from other recent warm years. Biological indicators suggest this state change could alter ecosystem structure and function. Here we report observations of key physical drivers, biological responses, and consequences for humans, including subsistence hunting, commercial fishing, and industrial shipping. We consider whether observed state changes are indicative of future norms, whether an ecosystem transformation is already underway, and if so, whether shifts are synchronously functional and system-wide, or reveal a slower cascade of changes from the physical environment through the food web to human society. Understanding of this observed process of ecosystem reorganization may shed light on transformations occurring elsewhere.

The Pacific Arctic, composed of the Chukchi and northern Bering seas (Figure 1), is one of the world's most productive ocean ecosystems (1), characterized by high benthic biomass resulting from persistent, nutrient rich flow through the Bering Strait (2) that fuels high primary production (3). In summer and fall, the region is home to millions of nesting and migratory seabirds, with hotspots of foraging activity shared with marine mammals (4), supporting coastal Indigenous communities. The delivery of nutrients together with the extent and timing of sea ice (5) are dominant environmental factors structuring this ecosystem. Freeze-up in fall and winter eliminates large expanses of open water, causing whales, Pacific walrus (*Odobenus rosmarus divergens*), many seals, and seabirds to migrate southwards into the Bering Sea and beyond (6).

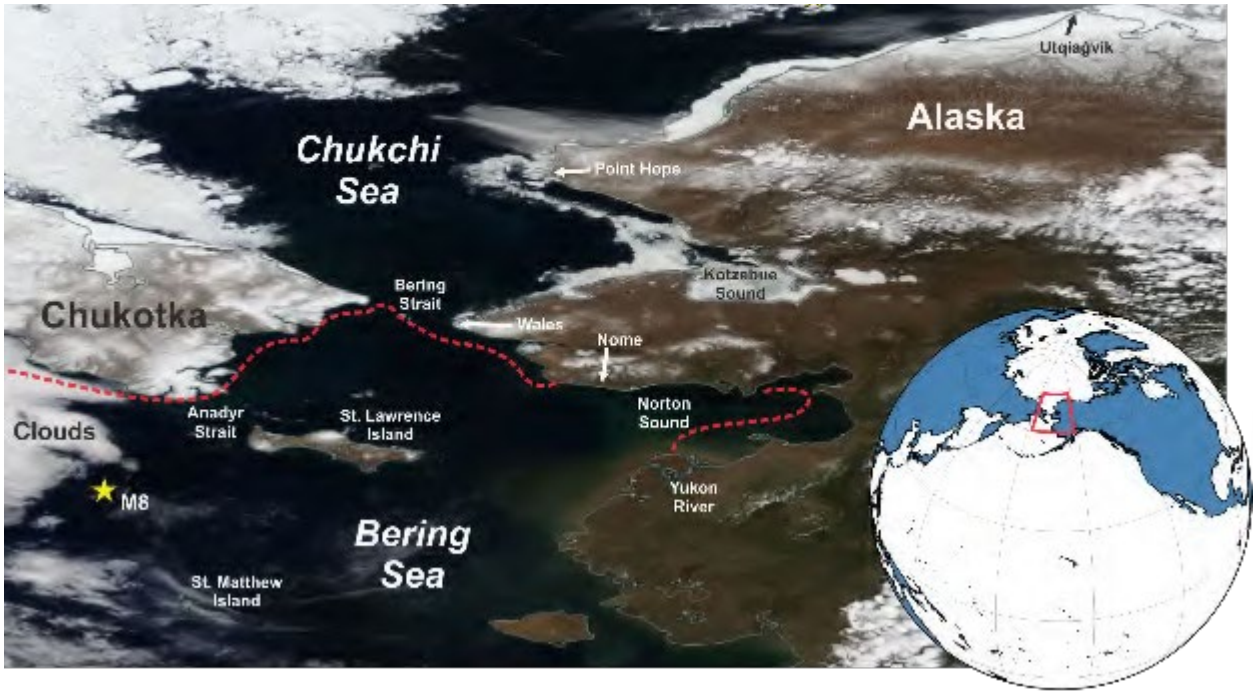

Figure 1. Sea ice changes in recent years. True-color MODIS satellite image showing northern Bering and Chukchi sea ice conditions on 2 June 2017. Red dotted lines denote the 1980-2010 ice edge climatology for June 2nd. Yellow stars denote locations of oceanographic moorings M8 and CEO. Inset locates the study region. Image from NASA Worldview.

In spring, the return of sunlight heralds snow melt, growth of sea ice algae, and a phytoplankton bloom that typically exceeds the consumption capabilities of pelagic consumers, resulting in carbon falling to the seabed, fueling rich benthic communities (7,8). Solar radiation and melting sea ice help stratify the upper water column, impeding the ability of winds to mix surface and subsurface waters. In summer, low-salinity surface waters near the pack ice remain cool relative to the shelf waters warmed by insolation. The Bering Sea cold pool, near-bottom shelf waters cooler than 2°C south of Bering Strait, has long served as a thermal barrier to northward migration of subarctic groundfish (9), which are major stocks for the southeastern Bering Sea's $2 billion fishery and account for about half the seafood landings in the United States (10,11).

Recent Changes in the Pacific Arctic Marine Ecosystem

Declining sea ice in this century has reduced surface albedo in spring and summer, accelerating oceanic heat uptake and causing earlier and more rapid sea ice melt (12). The pack ice and marginal ice zone has retreated north beyond the Chukchi shelf in recent summers, while warmer shelf waters delay sea ice formation in fall. Simultaneously, the northward flow of water through Bering Strait has increased, as has its temperature (2), so that it now delivers more heat, freshwater, nutrients, and biota northwards into the Arctic (13). Near-bottom water temperatures exceed 0°C for a larger portion of the year (Figure 2).

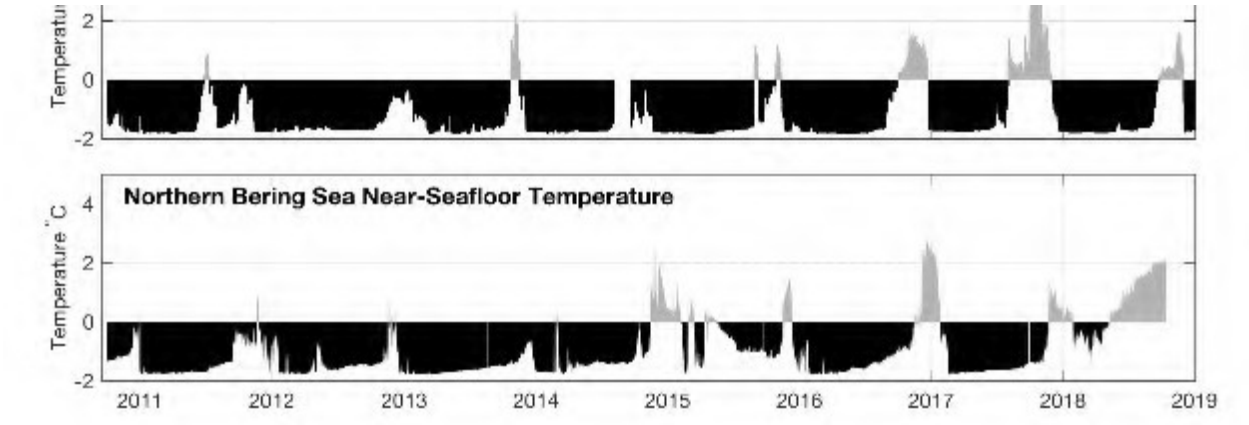

Figure 2. Near-bottom water temperatures. Previously, temperatures in important seafloor habitats remained below 0 ℃ for most of the year. In recent years, an increasing number of months exhibited temperatures well above 0 ℃. Mooring locations are indicated on Figure 1.

Ramifications of these physical changes have included more salmon in the Chukchi and Beaufort seas (14,15), walrus hauling out on shore in northwestern Alaska in late summer instead of on sea ice (16), an increase in the frequency and seasonal duration of killer whale (*Orcinus orca*) presence in the Chukchi Sea (17), an increase in planktivorous seabirds in the Chukchi Sea (18), and a northward shift in the distribution of other seabird species (19,20). For the Indigenous peoples of the region, spring marine mammal hunting opportunities dependent on the presence of sea ice have decreased and shifted in time (21), although the lack of sea ice has allowed additional whaling to occur in fall and early winter in the northern Bering Sea (22).

And Then Came 2017

In 2017, physical conditions in the Pacific Arctic marine shelf ecosystem of the Chukchi and northern Bering seas described above showed signs of a sudden and dramatic shift relative to historical means and even to other recent unusually warm years. In turn, these physical changes seemingly precipitated several significant ecological shifts, with consequences for the region's residents. Based on published and unpublished data from the authors, many changes persisted in 2018 and even into 2019, suggesting that 2017 was not a passing oddity of brief consequence to social-ecological systems, but a sign of what is to come.

In early January 2017, the sea ice edge had barely progressed south of Bering Strait and for the entire winter its extent remained at least $2x10^5$ km^2 below the long-term average. In June, ship-based observations found near-bottom ocean temperatures in Bering Strait of nearly 4 °C, over 3°C and four standard deviations warmer than the 1991-2016 June mean (2). Indeed, by June, the eastern Chukchi shelf was already mostly sea ice-free (Figure 1). In early December 2017, the ice edge was over 1000 km north of its climatological mean position near St. Lawrence Island. There was no sea ice in the Bering Strait in February 2018 and southerly winds forced a large ice retreat again in February 2019 (23). Waters in Norton Sound exceeded 10°C before the end of June 2018 and the cold pool was again minimal by late summer.

Reduced ice cover and warmer seas likely impacted primary production by influencing thermal, light, and stratification conditions. In spring of 2018, in the southern Bering Sea, the bloom was delayed due to a lack of freshwater input from melting sea ice, and chlorophyll concentrations were an order of magnitude lower than usual; however in the northern Bering Sea the ice-associated bloom was early and extensive (24). In addition, the detection of domoic acid in shipboard water samples (Figure 3) and saxitoxin in a few stranded and harvested walruses from Bering Strait villages led to concern about harmful algal blooms and food safety from Indigenous residents, though analytical challenges make the impact difficult to determine (25).

Changes in species distributions had already been observed this century, but not to the extent observed in 2017. The copepods *Calanus glacialis/marshallae* in 2017 were found to be remarkably low in abundance relative to 2012-2015 (Figure 4). Multispecies epibenthic biomass in the southern Chukchi Sea also exhibited a pronounced decline relative to comparable collections in 2004, 2009, 2012, and 2015 (Figure 4). In contrast, acoustic-trawl surveys indicate that age-0 Arctic cod abundance was dramatically higher in the Chukchi Sea in 2017 compared with previous surveys: backscatter in the northern Chukchi Sea (67 N to 71.5 N) was 5.6 times greater than in 2013, and 16.3 times greater than in 2012 (Figure 5), but the fish had low energy content. Juvenile pink salmon (*Oncorhyncus gorbuscha*) catch per unit effort in surface trawl surveys in the northern Bering Sea was two times greater during 2017 than previous years (Figure 4). Juvenile pink salmon return as adults the following year, and the adult pink salmon return to Norton Sound was much stronger than expected during 2018 (27). Adult walleye pollock (*Gadus chalcogramma*), Pacific cod (*Gadus macrocephalus*), and northern rock sole (*Lepidopsetta polyxystra*) biomass in bottom trawl surveys increased in the northeastern Bering Sea during 2017, likely due to northward movement of these fishes in the absence of the Bering Sea cold pool (28).

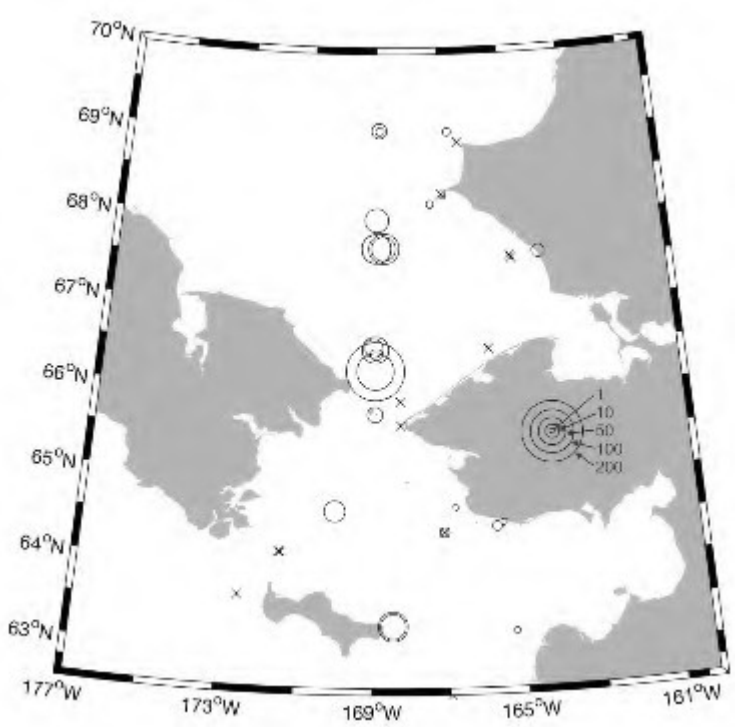

Figure 3. Seawater concentrations of domoic acid, June 2017. NTD = no toxin detected.

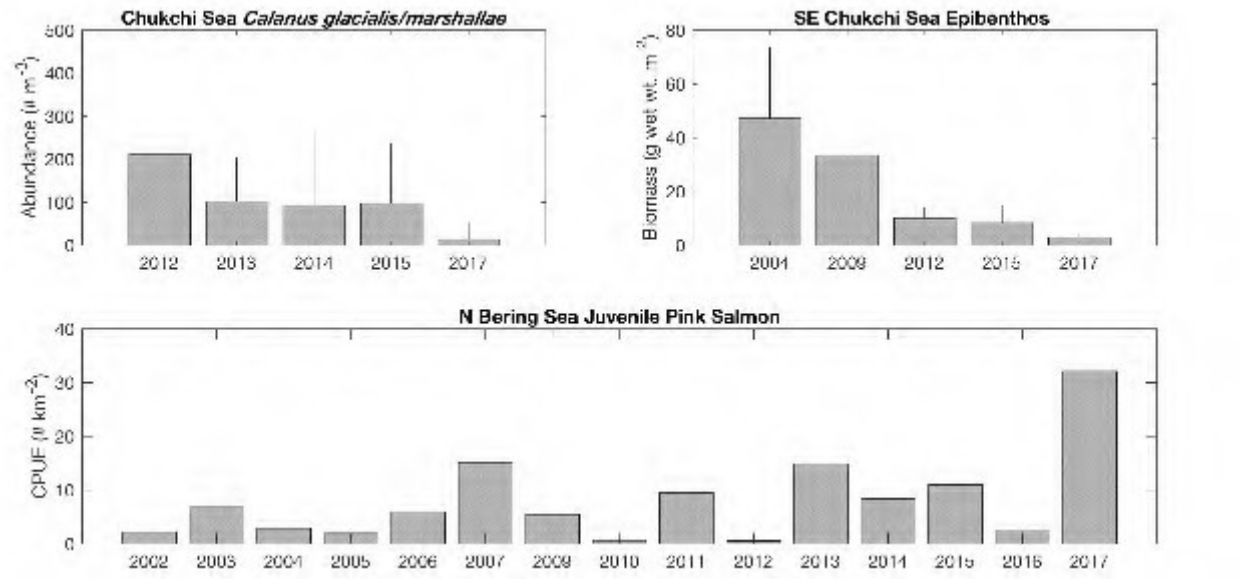

Figure 4. Biological changes in recent years. Observations show declines of Calanus glacialis/marshallae abundance (upper left) and epibenthic biomass (upper right) in 2017

relative to prior years, and an increase in juvenile pink salmon catch per unit effort (CPUE) (bottom). The graphs in upper left and upper right show simple means and standard deviation error bars.

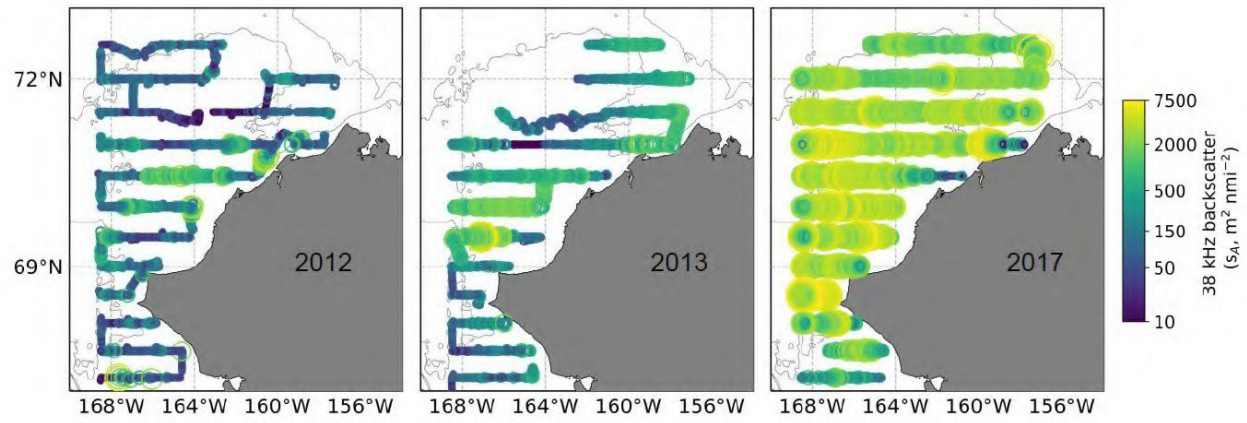

Figure 5. Arctic cod abundance change. Acoustic surveys indicate that the abundance of age-0 Arctic cod increased substantially in 2017 relative to 2012 and 2013. Trawl sampling indicated that Arctic cod dominated acoustic backscatter in this area in 2012 and 2013 (26). This was also the case in 2017: Arctic cod accounted for 95.4% of fish captured in 33 midwater trawl hauls.

In offshore waters, total seabirds declined from 2012-2017 in the southern and northern Bering Sea, but densities were above the long term mean in the Chukchi Sea during most of that period. The increase in the Chukchi Sea in 2015-2017 was primarily due to short-tailed shearwaters (*Ardenna tenuirostris*), which feed primarily on euphausiids, and less pronounced increases in piscivorous black-legged kittiwakes (*Rissa tridactyla*) and murres (*Uria* spp). In contrast, planktivorous auklets (*Aethia* sp.) had low densities in the Chukchi Sea in 2017 and 2018 but increased in the northern Bering Sea those years (24). Reproductive success was low for seabirds in the Bering Sea in 2017-2018, and there were mixed-species die offs there and in the Chukchi Sea (24,29;), with dead birds emaciated. Notably, numbers of murres and kittiwakes attending the large Chukchi Sea colony continued to increase (30) at a rate suggesting immigration of piscivorous nesting birds.

In the spring of 2017, bowhead whales, including females with calves, were seen near Utqiaġvik, Alaska, a month earlier than usual and the Utqiaġvik whale hunt recorded the earliest

known landing, on 13 April. Four bowhead whales equipped with satellite transmitters all wintered (2017/18) in the Chukchi instead of their usual wintering area south of Anadyr Strait in the Bering Sea (31) and a bowhead was recorded singing near Utqiaġvik on 11 January 2018, something never recorded before at that time of year. In 2018/19, the bowheads were again north of Anadyr Strait in winter. Spotted seal (*Phoca largha*) pups in the spring of 2018 were found in poorer condition (less fat and lower mass/length) than in recent years, and almost no ribbon seals (*Histriophoca fasciata*) were seen during those same surveys, raising the specter of a failure in the 2018 year class. In the spring and summer of 2018 and 2019, more than 280 bearded (*Erignathus barbatus*), ringed (*Pusa hispida*), spotted, and unidentified seal carcasses, primarily young and many emaciated, were reported from beaches mostly of the northern Bering and southern Chukchi seas, nearly five times the annual average from 2014-2017, prompting the National Oceanic and Atmospheric Administration to declare an "unusual mortality event" (32).

Anomaly or Transformation?

Changes in sea ice extent, water temperature, currents, zooplankton abundance, animal distribution and health, hunting success, and other aspects of the ecosystem are noteworthy in themselves, but such large-scale changes could conceivably occur without altering basic relationships among ecosystem components. The investigation of specific mechanisms underlying these changes were not part of the cited studies, however it is known from other areas, including the southern Bering Sea, that the spring sea-ice break-up spurs a productive phytoplankton bloom, and its timing together with ocean temperatures determines phytoplankton species composition, carbon export to the benthos, and food quality for zooplankton (24). Changes towards lower-lipid zooplankton reduces over-winter survival of fishes such as salmon and Arctic cod (33), even if they increase numerically in summer due to favorable thermal and oceanographic conditions. Lower zooplankton food quality and increased competition from predatory fish moving north from the Bering Sea might explain seabird and seal mortality.

The ecosystem-wide changes seen in 2017-2019 have the potential to fundamentally reconfigure the Pacific Arctic marine food web. An altered physical environment characterized by warmer waters and a longer open-water season is allowing subarctic species to establish themselves in the Chukchi Sea; seasonally for now, but possibly year-round in the future. Subarctic invaders such as walleye pollock and Pacific cod could fundamentally transform

interactions among pelagic species, benthic invertebrates, groundfish, seabirds, and marine mammals by exerting strong predation pressure on forage fishes and benthic crab, worm, and shrimp communities (10). Predation pressure from these fishes adds top-down stresses to the bottom-up changes associated with altered temperature and primary and secondary productivity. Indigenous hunters may begin to find familiar species of fishes and marine mammals at unusual times of year or unfamiliar species during customary hunting and fishing periods (21).

An interdisciplinary look at the Pacific Arctic marine ecosystem as it changes may provide a rare opportunity to track ecosystem transformation in detail as it unfolds, rather than reconstructing details after the fact. The transformation of an ecosystem may reflect a cascade of sequential changes that take place over multiple years rather than a single shift or tipping point (e.g., 34), though changes to individual ecosystem components may be sudden and dramatic. For example, because of positive feedbacks in the climate system (e.g., 12) it is possible that 2017 marked the crossing of a threshold that precludes return to the system state common just a decade ago. We find that a closely coupled synergy between bottom-up and top-down factors (e.g., 35) appear to best characterize this system's transition, and the interactions among these multiple stressors have important implications for understanding any subsequent reorganization.

The result would be the transformation of an Arctic marine ecosystem into one characterized by subarctic conditions, subarctic species, and subarctic interactions (Figure 6). The Chukchi Sea may soon resemble the east-central Bering Sea shelf in condition, structure, and function, with annual sea ice, warmer bottom water temperatures, and ecosystem productivity derived from forage fishes and pelagic zooplankton rather than the benthos. Changes in the historically strong benthic-pelagic coupling have already been observed in the southeastern Chukchi Sea, where overall epibenthic biomass declined by an order of magnitude from 2004 to 2017; the fact that the most abundant taxa were consistent over time may hint at overall changes in ecosystem productivity or pathways rather than specific habitat changes (36,37). Yet this transformation is more complex than an ecosystem migrating north. For example, the Chukchi Sea would likely retain some characteristics distinguishing it from the Bering Sea shelf, due to higher latitude and downstream location relative to the Bering Strait nutrient supply. How these competing features will combine to create a new state of the Pacific Arctic ecosystem remains to be seen.

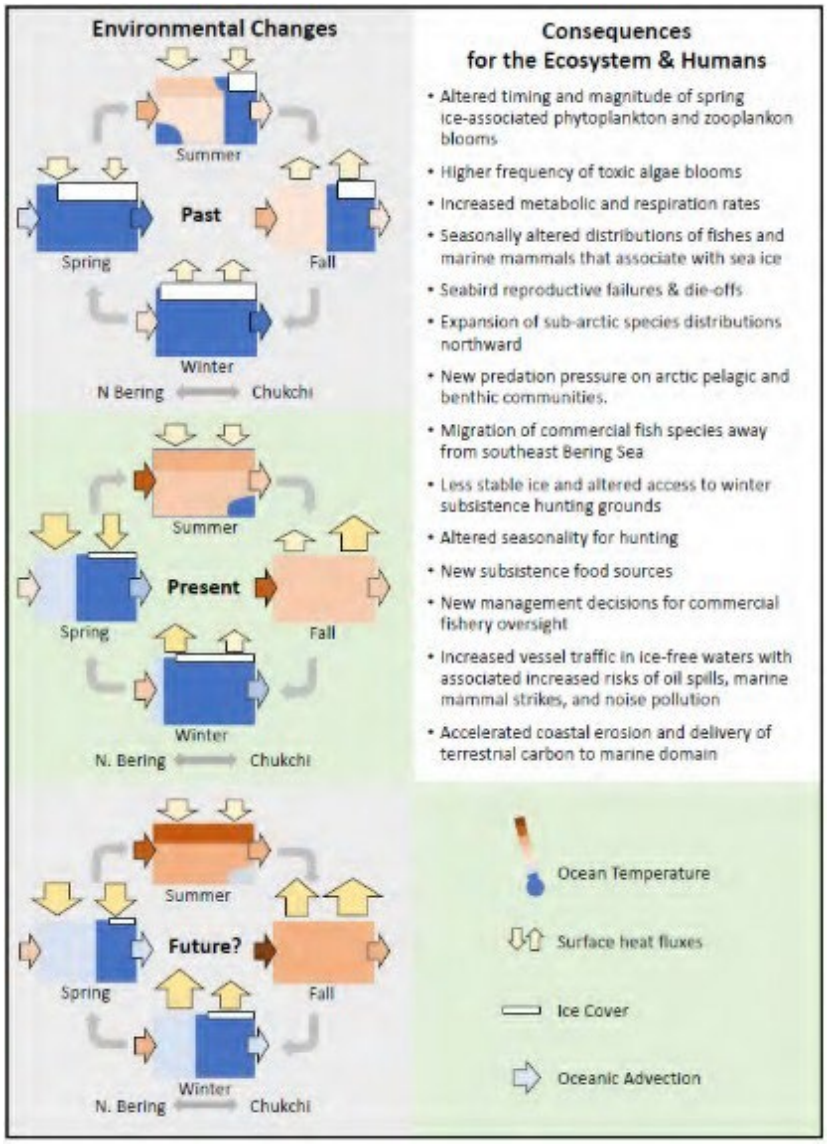

Figure 6. Environmental changes and related consequences. Observed and potential future changes in the physical environment (left panels) in the Northern Bering and Chukchi shelf systems (i.e., bottom-up forcing), along with observed and anticipated consequences for the biological and human components of the ecosystem (right panel).

In addition to its regional significance, the pattern of change underway in the Pacific Arctic may eventually shed light on the progression of ecosystem transformation more generally (38), which manifests as large-scale alterations in the connections and interactions among species and among physical and biological processes. Overpeck et al. (39) suggested the

possibility of such a transformation resulting from the removal of perennial ice in the Arctic, though they focused on "before" and "after" states of the system without describing the transformation in between. The pioneering work of Gunderson and Holling (40) recognized that transformation and reorganization are less predictable and less well understood than a simple shift from stability to instability.

What To Expect Next?

The expectation is for the sea ice season to further shorten and sea ice coverage to diminish (41). Waters will become warmer and stay warm longer into fall and winter. How quickly these changes propagate through and persist in the system, and what additional sudden shifts may occur, are hard to predict. It is likely, however, that there will be differences in the temporal and spatial scales over which physics and biology change (42). Physical conditions that were once anomalous may become normal. The biological response will follow but may not carry over across years until species and behaviors that thrive in the new conditions are able to persist. Hunters and fishers will adjust to some degree but may find it necessary to switch the timing or targets of their efforts (43).

Specific trajectories of these changes and their implications for the Pacific Arctic ecosystem, including Indigenous coastal communities, are still unclear. To stay with or ahead of these system transformations rather than reacting to a new state some years from now, some critical unknowns, especially regarding ecosystem relationships, require further attention and continued monitoring at multiple scales. As sea ice retreats earlier, will some species cling to existing fixed habitats (e.g., depositional zones) and remain largely in place, while others follow shifting habitats (such as the ice edge)? Will subarctic species be able to flourish and persist in the Chukchi Sea year-round, transforming the ecosystem into a locus of groundfish or pelagic predator abundance? Will increased industrial activity such as shipping combine with climate-driven ecosystem changes in ways that amplify the consequences of either alone (44)? How can coastal communities adjust and adapt quickly enough to retain cultural and nutritional security (45)?

Even in this age of information overload, it is how remarkable how scarce (and thus how valuable) the available data are for making statistically robust comparisons of today's conditions versus yesterday's. For example, quantifying changes in primary and secondary productivity

cannot immediately follow the spring retreat of sea ice because previously the ice itself precluded ship-based measurements at locations and times now ice-free. Across the study region, even 15 years of annually collected data is an unusually long time series, and for biological parameters most of these data are confined to summer months. Hence, it is important to learn to distinguish surprises from completely new observations.

A cascade of effects through an ecosystem may include tipping points governed by positive feedbacks for individual components, making recovery to the previous structure and function ever less likely (e.g., 34,46). Top-down changes such as increased predation may result from bottom-up changes such as the removal of thermal barriers to range expansion of predators. The experience to date in the Pacific Arctic by itself will not resolve these questions, but it does suggest that, with regard to cascades versus tipping points or top-down versus bottom-up controls (e.g., 47), ecosystem transformation may be a complex matter of "both and" rather than a simple dichotomy of "either/or."

These questions are more than a curiosity (48). The well-being of coastal communities and the management of human activities in the region, including potential commercial fisheries, depend on reliable information and insight into what is likely to happen next. In Alaska waters, industrial and research activities are planned in ways to reduce interference with Alaska Native subsistence harvests, and conscientious vessel operators communicate with communities and adjust their plans to avoid areas where hunters are active (e.g., 49). Growing uncertainty about the timing of animal migrations and optimal harvest conditions increases the likelihood of conflict and concerns about food security. Coastal communities are likely to face difficult choices between capitalizing on increased economic opportunity and limiting industrial interference with subsistence activities.

The profound shift in ecosystem state and conditions suggest a new framework is needed to replace the paradigm that served well in recent decades. The Pacific Arctic marine ecosystem transformation is not an isolated case. Social-ecological systems worldwide are facing similar pressures from changing physical conditions, with implications that are increasingly uncertain as transformation propagates through the food web and to human outcomes (50). Long-term and multi-scale data are necessary to detect, examine, and respond to such changes. A better understanding of the nature of system transformation will help humans detect transformations

earlier, perhaps in time for more effective response or adaptation, even if prevention may no longer be possible.

Data Availability

All data collected as a part of the North Pacific Research Board's Arctic Integrated Ecosystem Research Program (Arctic IERP) are being curated and preserved. Because the research is actively ongoing, the data are under program embargo through July 2021. At that time, all Arctic IERP data will be publicly released with a CC-0 license from the Research Workspace DataONE Member Node, and this paper will be cited in the DOI for those data, to create a formal link. In the interim, please contact the authors for access to Arctic IERP data.

In Figure 1, we acknowledge the use of imagery from the NASA Worldview application (https://worldview.earthdata.nasa.gov/), part of the NASA Earth Observing System Data and Information System (EOSDIS). Ice-edge marking is from Maslanik, J. and J. Stroeve. 1999. Near-Real-Time DMSP SSMIS Daily Polar Gridded Sea Ice Concentrations, Version 1, F17. Boulder, Colorado USA. NASA National Snow and Ice Data Center Distributed Active Archive Center. doi: https://doi.org/10.5067/U8C09DWVX9LM. Accessed 12-December-2018.

2015 epifauna data are available at https://doi.org/10.25921/b2g4-bs86.

Other data are available on request, pending curation and archiving as part of ongoing studies.

Corresponding Author

Henry P. Huntington is the corresponding author, to whom all requests for materials should be addressed.

Acknowledgments

- Much of the research reported here and preparation of the manuscript was conducted under the Arctic Integrated Ecosystem Research Program (Arctic IERP; http://www.nprb.org/arctic-program/). This manuscript is Publication Arctic IERP-014. Funding for the program was provided by North Pacific Research Board, the U.S. Bureau of

Ocean Energy Management, the Collaborative Alaskan Arctic Studies Program (formerly the North Slope Borough/Shell Baseline Studies Program), and the U.S. Office of Naval Research Marine Mammals and Biology Program. Generous in-kind support was provided by the U.S. National Oceanic and Atmospheric Administration (NOAA; Alaska Fisheries Science Center and Pacific Marine Environmental Laboratory), University of Alaska Fairbanks, U.S. Fish & Wildlife Service, and the U.S. National Science Foundation. The findings and conclusions of this paper are those of the authors and not necessarily those of the agencies and organizations with which the authors are affiliated or which provided support.

- This manuscript is a contribution to the U.S. Marine Biodiversity Observation Network (MBON), the U.S. Integrated Ocean Observing System, and the Group on Earth Observations Biodiversity Observation Network (GEO BON). The work and publication were partially funded under the U.S. National Oceanographic Partnership Program (NOPP) through NOAA award # UAF NA14NOS0120158 Arctic Marine Biodiversity Observing Network (AMBON), with contributions from NOAA, the U.S. Bureau of Ocean Management (BOEM), Shell Exploration & Production under management of the Integrated Ocean Observing System (IOOS), as well as contributions of U.S. National Science Foundation (NSF) grant #1204082.
- We are grateful for the contributions of many colleagues to the research and writing of this paper, including Gay Sheffield.
- This paper is PMEL contribution # 4917.
- Collections of fish specimens were made under the auspices and terms of Scientific Research Permit numbers 2012-11, 2013-8, 2017-2 and 2019-7 issued by the NOAA's Alaska Regional Office and permit numbers CF-12-005, CF-13-016, CF-17-023, and CF-19-018 from Alaska's Department of Fish and Game.

Author Contribution Statement

HPH, SLD, FKW, EF, CL, and KS developed the idea and contributed to writing and editing the paper. MB, PB, JJC, ADR, DD, JCG, KI, DGK, KK, RL, LQ, PS, DS, and CW wrote sections of the paper and contributed to editing of the manuscript. All authors provided data and reviewed the final manuscript and approved it for submission and publication.

Competing Interests

The authors declare no competing interests.

References

1. Grebmeier, J. M., Cooper, L. W., Feder, H. W. & Sirenko, B. I. Ecosystem dynamics of the Pacific-influenced Northern Bering and Chukchi Seas in the Amerasian Arctic, *Prog. Oceanogr*. **71(2–4),** 331 – 361 (2006).
2. Woodgate, R. A. Increases in the Pacific inflow to the Arctic from 1990 to 2015, and insights into seasonal trends and driving mechanisms from year-round Bering Strait mooring data, *Progress in Oceanography* **160,** 124-154 (2018). doi:10.1016/j.pocean.2017.12.007
3. Codispoti, L. A., et al. Synthesis of primary production in the Arctic Ocean: III. Nitrate and phosphate based estimates of net community production. *Progress in Oceanography* **110**, 126-150 (2013).
4. Kuletz, K., et al. Seasonal spatial patterns in seabird and marine mammal distribution in the eastern Chukchi and western Beaufort Seas: Identifying biologically important pelagic areas. *Progress in Oceanography* **136,** 175-200 (2015).
5. Cooper, L. W., et al. The relationship between sea ice break-up, water mass variation, chlorophyll biomass, and sedimentation in the northern Bering Sea. *Deep Sea Research II* **65–70,** 141–162 (2012).
6. Smith, M. A., Goldman, M. S., Knight, E. J. & Warrenchuk, J. *Ecological Atlas of the Bering, Chukchi, and Beaufort Seas* 2nd edition. (Audubon Alaska, 2018.)
7. Grebmeier, J. M., et al. Ecosystem characteristics and processes facilitating persistent macrobenthic biomass hotspots and associated benthivory in the Pacific Arctic. *Progress in Oceanography* **136,** 92–114 (2015). http://dx.doi.org/10.1016/j.pocean.2015.05.006
8. Moore, S. E., Stabeno, P. J., Grebmeier, J. M. & Okkonen, S. R. The Arctic Marine Pulses Model: linking annual oceanographic processes to contiguous ecological domains in the Pacific Arctic. *Deep-Sea Research Part II* **152,** 8-21 (2018).
9. Stabeno, P. J., et al. Comparison of warm and cold years on the southeastern Bering Sea shelf and some implications for the ecosystem. *Deep Sea Research II* **65**, 31-45 (2012).
10. Sigler, M., et al. Fluxes, fins, and feathers: relationships among the Bering, Chukchi, and Beaufort seas in a time of climate change. *Oceanography* **24,** 250–265 (2011).
11. Haynie, A. C. & Pfeiffer, L. Climatic and economic drivers of the Bering Sea walleye pollock (*Theragra chalcogramma*) fishery: implications for the future. *Canadian Journal of Fisheries and Aquatic Sciences* **70,** 841–853 (2013).
12. Stroeve, J. C., et al. The Arctic's rapidly shrinking sea ice cover: a research synthesis. *Climatic Change* **110(3-4)**, 1005-1027 (2012).
13. Hunt Jr, G. L., et al. Advection in polar and sub-polar environments: Impacts on high latitude marine ecosystems. *Progress in Oceanography* **149**, 40-81 (2016).
14. Dunmall, K. M., et al. Pacific salmon in the Arctic: harbingers of change. In: F.J. Mueter, et al., eds. *Responses of Arctic Marine Ecosystems to Climate Change*. (Alaska Sea Grant, University of Alaska Fairbanks, 2013.) Doi:10.4027/ramecc.2013.07.
15. Moore, S. E., et al. Marine fishes, birds and mammals as sentinels of ecosystem variability and reorganization in the Pacific Arctic Region. In: J.M. Grebmeier & W. Maslowski, eds. *The*

413 *Pacific Arctic Region: Ecosystem Status and Trends in a Rapidly Changing Environment*. p.
414 337-392. (Springer, 2014.) DOI 10.1007/978-94-017-8863-2_2.
415 16. Jay, C. V., Taylor, R. L., Fischbach, A. S., Udevitz, M. S. & Beatty, W. S. Walrus haul-out
416 and in water activity levels relative to sea ice availability in the Chukchi Sea. *Journal of*
417 *Mammalogy* **98,** 386-396 (2017). 10.1093/jmammal/gyw195.
418 17. Stafford, K. M. Increasing detections of killer whales (*Orcinus orca*), in the Pacific Arctic.
419 *Marine Mammal Science* **67,** 116 (2018).
420 18. Gall, A. E., Morgan, T. C., Day, R. H. & Kuletz, K. J. Ecological shift from piscivorous to
421 planktivorous seabirds in the Chukchi Sea, 1975-2012. *Polar Biology* **40,** 61-78 (2017). DOI
422 10.1007/s00300-016-1924-z.
423 19. Renner, M., et al. Modeled distribution and abundance of a pelagic seabird reveal trends in
424 relation to fisheries. *Marine Ecology Progress Series* **484,** 259-277 (2013).
425 20. Kuletz, K. J., Renner, M., Labunski, E. A. & Hunt, G. L. Changes in the distribution and
426 abundance of albatrosses in the eastern Bering Sea: 1975-2010. *Deep Sea Research II* **109,**
427 282-292 (2014).
428 21. Huntington, H. P., Quakenbush, L. T. & Nelson. M. Evaluating the effects of climate change
429 on Indigenous marine mammal hunting in northern and western Alaska using traditional
430 knowledge. *Front. Mar. Sci.* **4,** 40 (2017).
431 22. Noongwook, G., the Native Village of Gambell, the Native Village of Savoonga, H.P.
432 Huntington, H. P. & George, J. C. Traditional knowledge of the bowhead whale (*Balaena*
433 *mysticetus*) around St. Lawrence Island, Alaska. *Arctic* **60,** 47–54 (2007).
434 23. Stabeno, P. J. & Bell, S. W. Extreme conditions in the Bering Sea (2017–2018): record-
435 breaking low sea-ice extent. *Geophysical Research Letters* **46** (2019).
436 https://doi.org/10.1029/2019GL083816
437 24. Duffy-Anderson, J. T., et al. Response of the northern Bering Sea and southeastern Bering
438 Sea pelagic ecosystems following record-breaking low winter sea ice. *Geophysical Research*
439 *Letters* **46** (2019). https://doi.org/10.1029/2019GL083396
440 25. Lefebvre, K. A., et al. Prevalence of algal toxins in Alaskan marine mammals foraging in a
441 changing arctic and subarctic environment. *Harmful Algae* **55,** 13–24 (2016).
442 https://doi:dx.doi.org/10.1016/j.hal.2016.01.007
443 26. De Robertis, A., Taylor, K., Wilson, C. & Farley, E. Abundance and distribution of Arctic
444 cod (*Boreogadus saida*) and other pelagic fishes over the U.S. continental shelf of the northern
445 Bering and Chukchi Seas. *Deep-Sea Research II* **135,** 51-65 (2017).
446 27. Brenner, R. E., Munro, A. R. & Larsen, S. J., eds. *Run Forecasts and Harvest Projections for*
447 *2019 Alaska Salmon Fisheries and Review of the 2018 Season*. Special Publication No. 19-07.
448 (Alaska Department of Fish and Game, 2019.)
449 28. Stevenson, D. E. & Lauth, R. R. Bottom trawl surveys in the northern Bering Sea indicate
450 recent shifts in the distribution of marine species. *Polar Biology* **42**, 407-421 (2019).
451 https://doi.org/10.1007/s003000-018-2431-1.
452 29. Siddon, E. & Zador, S. *Ecosystem Considerations 2017: Status of the Eastern Bering Sea*
453 *Marine Ecosystem*. (Alaska Fisheries Science Center, National Marine Fisheries Service,
454 NOAA, 2017.) Available at: www.afsc.noaa.gov/REFM/Docs/2017/ecosysEBS.pdf
455 30. Dragoo, D. E., H. M. Renner, and R. S. A. Kaler. Breeding status and population trends of
456 seabirds in Alaska, 2018. U.S. Fish and Wildlife Service Report AMNWR 2019/03 (2019).
457 31. Quakenbush, L. T., & Citta, J. J. Satellite tracking of bowhead whales: habitat use, passive
458 acoustic, and environmental monitoring. U.S. Dept. of the Interior, Bureau of Ocean Energy

Management, Alaska Outer Continental Shelf Region, Anchorage, AK. *OCS Study BOEM* 2019-076 (2019).
32. NOAA. 2019. 2018-2019 ice seal unusual mortality event in Alaska. National Oceanic and Atmospheric Administration. https://www.fisheries.noaa.gov/alaska/marine-life-distress/2018-2019-ice-seal-unusual-mortality-event-alaska
33. Heintz, R. A., Siddon, E. C., Farley, E. V., & Napp, J. M. Correlation between recruitment and fall condition of age-0 pollock (*Theragra chalcogramma*) from the eastern Bering Sea under varying climate conditions. *Deep Sea Research II* **94**, 150–156 (2013). https://doi.org/10.1016/j.dsr2.2013.04.006
34. Wassman, P. & Lenton, T. M. Arctic tipping points in an earth system perspective. *Ambio* **41(1),** 1-9 (2012). https://dx.doi.org/10.1007%2Fs13280-011-0230-9
35. Lynam, C. P., et al. Trophic and environmental control in the North Sea. *Proceedings of the National Academy of Sciences* 201621037 (2017). DOI: 10.1073/pnas.1621037114
36. Grebmeier, J. M., et al. Time-series benthic community composition and biomass and associated environmental characteristics in the Chukchi Sea during the RUSALCA 2004–2012 Program. *Oceanography* **28,** 116-133 (2015). http://dx.doi.org/10.5670/oceanog.2015.61
37. Iken, K., et al. Developing an observational design for epibenthos and fish assemblages in the Chukchi Sea. *Deep-Sea Research II* **162**, 180-190 (2019). https://doi.org/10.1016/j.dsr2.2018.11.005
38. Scheffer, M., et al. Anticipating critical transitions. *Science* **338,** 344-348 (2012). DOI: 10.1126/science.1225244
39. Overpeck, J. T., et al. Arctic system on trajectory to new state. *EOS* **86(34),** 309, 312-313 (2005).
40. Gunderson, L. & Holling, C. S., eds. 2001. *Panarchy: Understanding Transformations in Human and Natural Systems*. (Island Press, 2001.)
41. IPCC. *Climate Change 2014: Synthesis Report. Contribution of Working Groups I, II and III to the Fifth Assessment Report of the Intergovernmental Panel on Climate Change*. (IPCC, 2014.)
42. Huntington, H.P., et al. A new perspective on changing Arctic marine ecosystems: panarchy adaptive cycles in pan-Arctic spatial and temporal scales. In: S. Arico, ed. *Ocean Sustainability in the 21st Century*. p. 109-126. (Cambridge University Press, 2015.)
43. Huntington, H.P., et al. How small communities respond to environmental change: patterns from tropical to polar ecosystems. *Ecology and Society* 22(3), 9 (2017).
44. Huntington, H.P., et al. Vessels, risks, and rules: planning for safe shipping in Bering Strait. *Marine Policy* **51,** 119-127 (2015).
45. ICC-Alaska. Alaskan Inuit Food Security Conceptual Framework: How to Assess the Arctic from an Inuit Perspective. Technical Report. (Inuit Circumpolar Council-Alaska, 2015.)
46. Huggett, A. J. The concept and utility of ecological thresholds in biodiversity conservation. *Biological Conservation* **124,** 301-310 (2005).
47. Hunt, G. L., et al. Climate change and control of the southeastern Bering Sea pelagic ecosystem. *Deep Sea Research II* **49**, 5821–5853 (2002).
48. Rocha, J., Yletyinen, J., Biggs, R., Blenckner, T. & Peterson. Marine regime shifts: drivers and impacts on ecosystems services. *Philosophical Transactions of the Royal Society B* **370,** 20130273 (2015). https://doi.org/10.1098/rstb.2013.0273

503 49. Konar, B., Frisch, L. & Moran, S. B. Development of best practices for scientific research
504 vessel operations in a changing Arctic: a case study for R/V Sikuliaq. *Marine Policy* **86,** 182-
505 189 (2017).
506 50. Rocha, J. C., Peterson, G. D. & Biggs, R. Regime shifts in the Anthropocene: drivers, risks,
507 and resilience. *PLoS ONE* **10(8),** e0134639 (2015).
508 https://doi.org/10.1371/journal.pone.0134639
509

Synopsis

Synopsis: ASGARD project

Seth Danielson, Russ Hopcroft, Andrew McDonnell, Sarah Mincks, Brenda Norcross, Dean Stockwell

Why we did it
Sea ice is one of the defining characteristics of the Arctic Ocean, and while its timing and extent has already undergone significant human-induced changes, it is projected to further decline in the coming years. The ASGARD project was designed to better refine our knowledge of carbon and nutrient dynamics on the northern Bering and Chukchi sea continental shelves in the face of changing sea ice.

The fundamental science question we addressed is: ***What regulates variations in carbon transfer pathways and how will the changing ice environment alter these pathways and ecosystem structure in the Pacific Arctic and beyond?***

What we did
The ASGARD study consisted of ship-based and mooring-based studies that collected observations of: heat, salt, nutrients and plankton carried by ocean currents; phytoplankton primary productivity; zooplankton growth/reproduction, respiration and fecal pellet production rates; particle deposition rates from the water column to the seafloor; quality of organic matter deposited to the seafloor; benthic respiration and organic matter decomposition rates; abundance and biomass of benthic microbial and metazoan fauna; distribution of fishes at different life history stages; and underwater sound and seasonal distributions of marine mammals.

We sailed to the northern Bering and southern Chukchi shelf in 2017 and 2018 on *R/V Sikuliaq,* occupying "process" stations at which experimental work was carried out, and "survey" stations at which we collected a reduced set of observations. Moorings were deployed in the water from June 2017 to August 2019.

What we learned:
Ample supplies of nutrients delivered to the Southern Chukchi Sea through Bering Strait fuel a high level of Chukchi shelf primary productivity during months in which water column light levels are sufficient to maintain phytoplankton blooms. Portions of the region likely exist in a near-perpetual state of patchy phytoplankton blooms from the spring ice retreat all the into the fall. Export fluxes to the benthos are large because large-celled diatoms sink rapidly to the shallow seafloor and because mesozooplankton often are unable to constrain the phytoplankton bloom by grazing. The benthic community carbon consumption and oxygen turnover rates are sensitive to the bottom water temperature, and are species-specific. Together, these findings suggest that the future Pacific Arctic ecosystem will adjust in species composition and species abundance in a bottom-up response to environmental change. Species that can maintain low basal metabolic rates in the face of larger annual swings in bottom temperature may find a competitive advantage. At the same time, range expansions of sub-Arctic predators into the Chukchi Sea will exert new top-down pressure on both the benthic and pelagic communities. Previously unobserved competition between Arctic and sub-Arctic species will also likely play a role in determining the eventual character of the Chukchi Sea ecosystem.

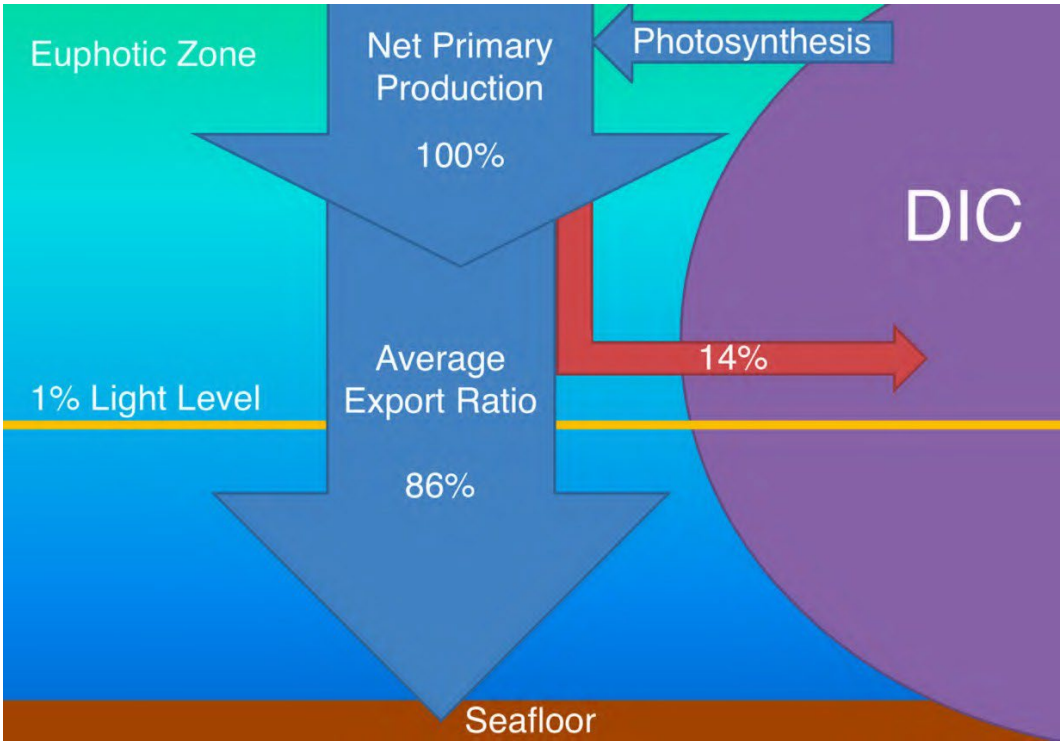

The Chukchi Sea exhibits a highly efficient delivery of carbon from the surface to the seafloor biological community.

*R/V Sikuliaq s*tern deployment of the multi-core instrument, which takes up to eight seafloor samples at one time. Blue totes on deck are incubation chambers for zooplankton growth experiments. Drone photo Brendan Smith.

Synopsis: Bering-Chukchi Heat Budgets

Seth Danielson

Why we did it
To understand how the Pacific Arctic may change in the future, we first must understand the present and the past. Sea ice extent is highly sensitive to oceanic heat content and ocean-atmosphere exchanges of heat. We were interested in how the ocean currents and surface heat fluxes of today's Pacific Arctic shelves differ from the past.

What we did
We assembled an archive of all known conductivity-temperature-depth (CTD) data from the Bering and Chukchi sea continental shelves. Data were found in the Chukchi Sea beginning in 1922 and in the Bering Sea in 1966. We averaged the data on a monthly basis into a spatial "grid", and then analyzed these compiled data for changes through time. Using an atmospheric reanalysis model, we formed heat content budgets and heat flux estimates for the two shelves, constraining the results with the oceanic water column profile observations.

What we learned
Summer and fall ocean temperatures in the Chukchi Sea increased by 1.4 °C over 1922-2018; the rate of warming sharply increased to 0.43 °C per decade after 1990. The average ocean water column temperature of July-October in some recent years was nearly 3 °C higher than in the same months in the 1970s. The Chukchi Sea is an important contributor to the Arctic amplification of atmospheric temperature increases. In recent autumns, the Chukchi shelf has transmitted enough heat to the atmosphere to raise the temperature of the entire Arctic lower atmosphere by 1 °C. We also found that oceanic heat delivered to sea ice melt or the deep basin of the Arctic Ocean has increased significantly relative to years past.

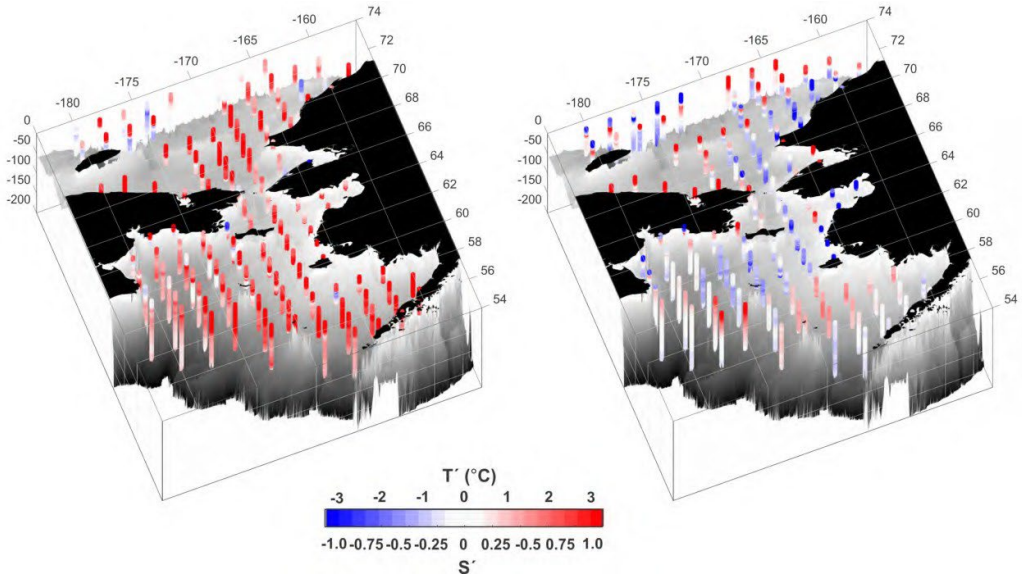

Figure: Perspective view showing water column profiles of summer season temperature anomalies (T'; left) and salinity anomalies (S', right) for 2014-2018 relative to all hydrographic data collected prior to 2014. Seafloor topography (gray shading) is shown only for depths shallower than 200 m.

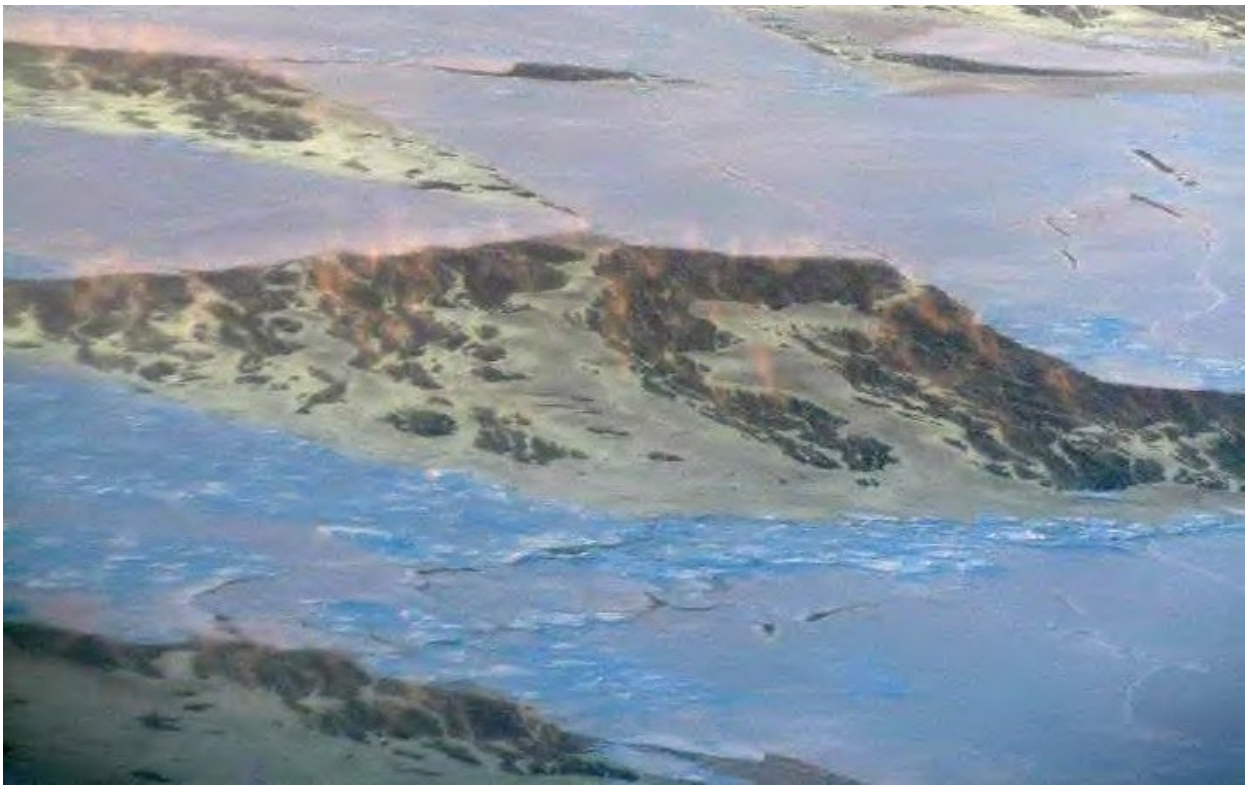

Illuminated by the rising sun, “sea smoke” ice fog rises out of sea ice leads as the Chukchi Sea loses heat to the atmosphere (November 2014). Photo S. Danielson.

Pancakes of new sea ice in the Chukchi Sea (November 2021). Photo S. Danielson.

Synopsis: Biological carbon pump

Andrew McDonnell and Stephanie O'Daly

Why we did it

How will the biological carbon pump change in reaction to the extreme warming and decrease in sea ice in the Pacific Arctic shelf? Warming ocean temperature and decreasing sea ice prevalence on the Pacific Arctic Shelf has been hypothesized to result in changes in the biological carbon pump in a couple of ways such as shifts in predominantly ice algae to ocean phytoplankton production and increased consumption of production in the water by zooplankton grazing and bacterial consumption. If these changes occur, less organic carbon will be deposited on the sea floor of the Pacific Arctic Shelf, which would impact food security in the region and decrease the carbon sink that has historically occurred in this region. We sought to measure the strength and efficiency of the biological carbon pump of the Pacific Arctic Shelf during an unprecedentedly warm and low ice period of time.

What we did

We used sediment traps to measure the amount of carbon that was sinking through the ocean, now called carbon flux. We had two sediment traps tethered to the sea floor that collected sinking particles throughout the year resulting in a time series of organic carbon flux from these two locations. During June of 2018 we also deployed short term drifting sediment traps to collect sinking particles at 7 locations throughout the study area. We also measured rates of organic carbon production using primary productivity experiments in June of 2017 and 2018.

During June of 2018 we also incubated the sinking particles we collected using drifting sediment traps to measure the rate of bacterial respiration associated with the sinking material. We measured the change in oxygen over time and converted that to units of carbon. This is used to estimate how much of the sinking organic carbon will be consumed by bacteria in the ocean before the material lands on the sea floor.

What we learned

We measured a strong and efficient biological carbon pump during June of 2018 in the Pacific Arctic Shelf, despite strong environmental shifts. We measured the highest rates of carbon flux occurring around May or June from the moored sediment traps. We measured relatively normal rates of primary productivity for the region, predominately consisting of pelagic diatoms. We measured an average of 82% of organic carbon production sinking through the ocean, meaning the biological carbon pump is very efficient. Our most notable findings were measuring amongst the highest carbon flux rates ever measured during June of 2018. We measured near zero rates of bacterial degradation of the sinking material. These findings indicate a very strong biological carbon pump.

We are entering the synthesis phase of this project. We will be collaborating more with other groups, specifically the zooplankton and benthic groups, to try to see if we can measure a balanced carbon budget for the region in June. We are also collaborating on an inverse modeling study, which can inform us of holes in our understanding or potentially important features of the system. Additionally we will investigate more about the types of particles collected with the moored sediment trap and how they change over time over the course of the two year study.

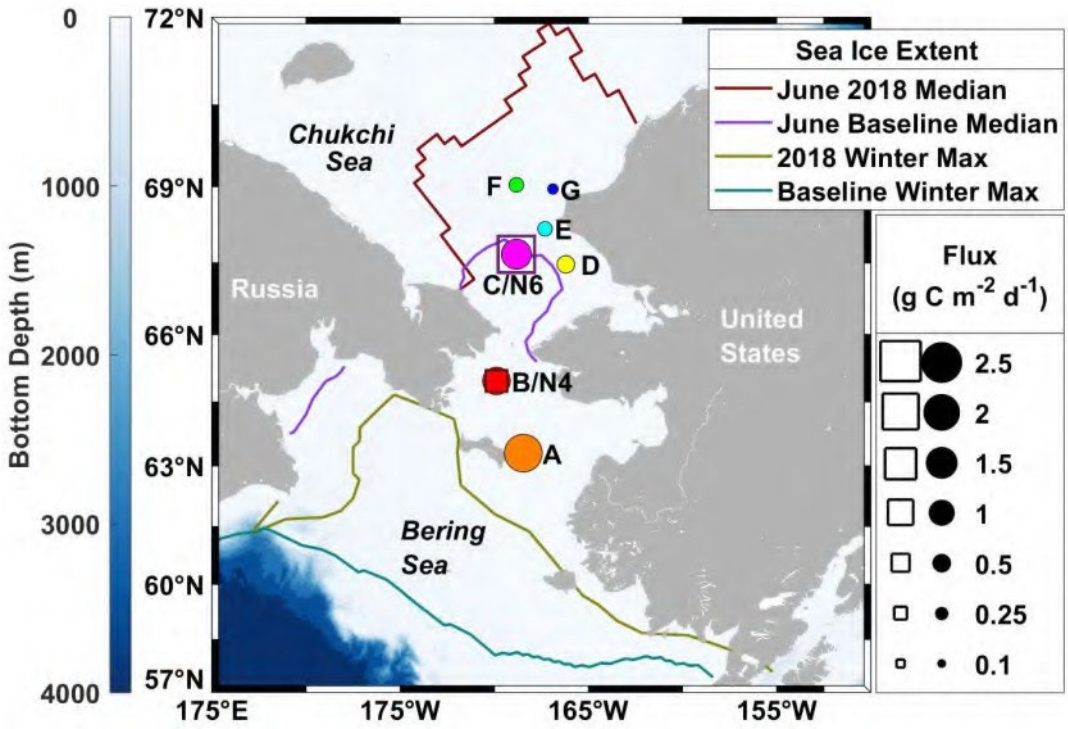

Spatial patterns of sinking particulate organic carbon fluxes on the Pacific Arctic shelf in June 2018. Drifting sediment trap measurements are depicted relative to the diameters of the circles, while moored sediment traps fluxes are shown as the length of the squares. Colored lines represent sea ice extent (Fetterer et al., 2017).

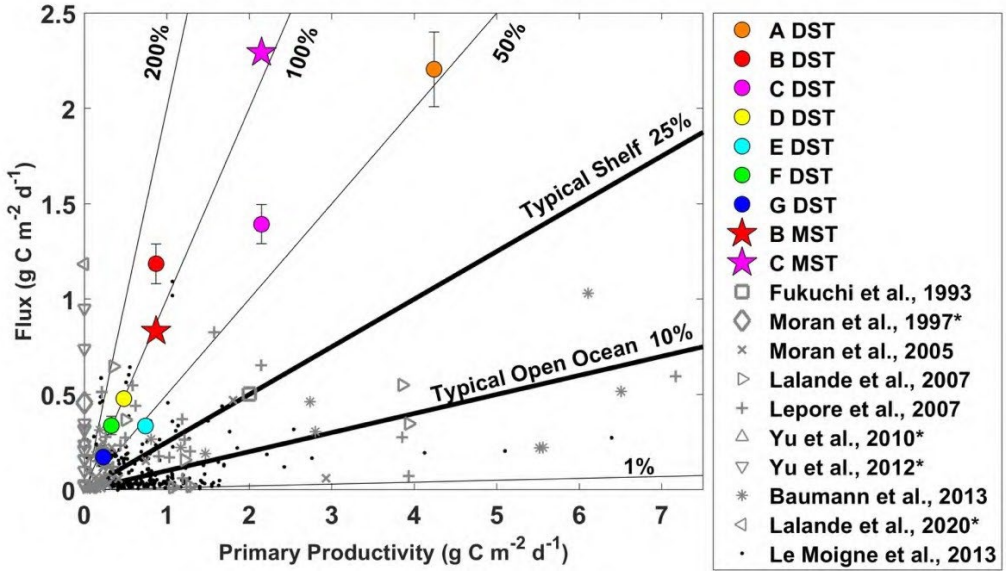

Sinking particulate organic carbon fluxes and primary productivity rates with contours of the export ratio between these two parameters measured during June 2018 on the Pacific Arctic shelf. The circles represent flux measurements from the drifting sediment trap. The stars represent the final flux measurement from the moored sediment traps (values plotted against the same primary productivity rates). Gray markers provide regional and black markers global context.

Synopsis: Benthic carbon cycling

Sarah Mincks and Brittany Charrier

Why we did it

Out on the continental shelf, much of the seafloor is covered with soft sediment which is home to microbial communities as well as many burrowing invertebrates. The energy demands of the sediment community are fueled by phytoplankton and zooplankton that grow in the water column and sink to the seafloor as detritus (waste products, dead and decaying cells or tissue). In the Arctic, much of this detritus falls to the seafloor during the spring and summer productive period. Seafloor organisms, including microbes, play an important role as the decomposers of the marine environment, breaking down this material and releasing nutrients back to the water column. In addition, they serve as food for larger organisms, forming an important component of the food web.

All organisms that eat food must consume oxygen in order to respire, or burn that food to produce the energy that fuels the body's activities. Oxygen's critical role in respiration makes it very useful for measuring metabolism—the rate at which food is burned. Some of that food is also assimilated by the body to make new biomass, so organisms can grow or reproduce. Metabolic rates vary among different types of organisms and among species, due in part to their biology and how they make their living. However, temperature also directly affects metabolic rate. As temperatures increase, the slow metabolic rates of cold-water organisms will increase, and they may need to consume more fuel to compensate. Our goal was to measure the metabolic rate of the sediment community—microbes and small invertebrates—at different temperatures to determine how warming may affect the rate of organic matter consumption.

What we did

We collected sediment cores from multiple sites throughout our study area using a multi-core, and conducted shipboard experiments on board *Sikuliaq* to measure respiration rates of the whole sediment community at two different temperatures (~0° and 5°C). Cores were kept intact to preserve the natural structure of the sediment community, including microbes and microscopic as well as macroscopic invertebrates such as small worms, clams, and crustaceans. We used fiber-optic oxygen sensors to record oxygen consumption during the experiments, as a measure of community metabolism. We also measured the production of nutrients produced via respiration of organic matter. In addition, we collected individuals of larger organisms (clams, amphipods) from bottom trawls to measure the respiration rates of some of the larger sediment-dwelling species that are important prey species and likely responsible for a relatively large fraction of detritus consumption. Multiple individuals of each species were sealed in separate glass chambers, and incubated in a similar manner as whole sediment cores to measure oxygen consumption of each individual organism. These experiments allowed us to compare metabolic rates among different species to determine if shifts in community composition may impact the breakdown of organic matter at the seafloor.

What we learned/Why it matters

A temperature increase of 5°C resulted in an average increase in oxygen consumption rate of about 30%, suggesting this degree of warming will lead to increased consumption of food by seafloor microbes and small invertebrates. Most of the food that supports these organisms all year is produced during the short spring bloom season, so considering that there is only so much food in the fridge which needs to last all winter, increased consumption may lead to a decrease in the amount of organic material stored in sediments to sustain the productive benthic component of the food web.

Results of our experiments with individual benthic organisms showed that the metabolic rate is quite different even among species of clams which one might expect to have similar life habits and

biology. These differences in metabolism result in carbon demand (i.e., amount of food required) that

varies over two orders of magnitude among taxa. With changes in the dominant species of clams already occurring in some areas, these differences in metabolic rate point to consequences of these shifts for the food web. Declines in the amount of organic material available in sediments may favor smaller-bodied species with lower metabolic rates; however, these smaller species may constitute lower quality prey for larger predatory species that feed at the seafloor.

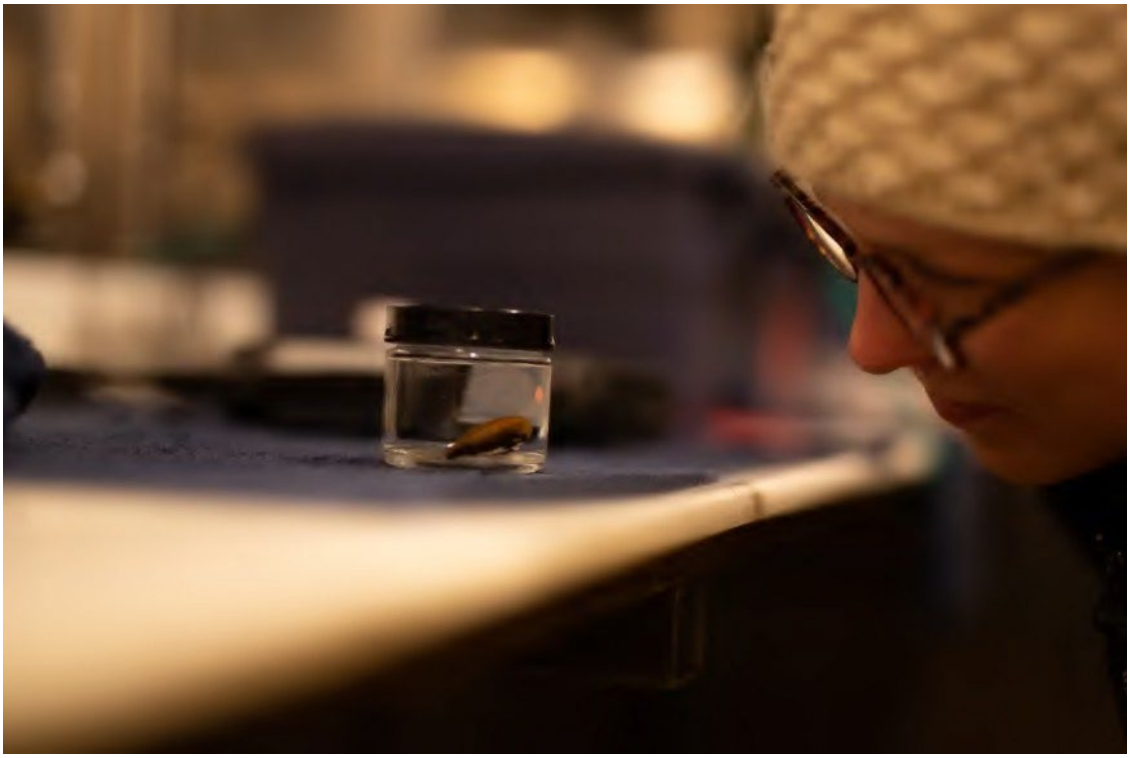

Photo credits: Brendan Smith

Synopsis: Oceanic Nutrient Fluxes

Tyler Hennon, Seth Danielson, Brita Irving, Dean Stockwell, Rebecca Woodgate, and Calvin Mordy

What did we do?
We estimated the transport of nutrients (nitrate, phosphate, and silicate) going through Bering Strait into the Arctic every month from 1998-2018. We used data from two moorings to form our estimates. Mooring N2 was deployed for just one year (2017-2018) and was located in the middle of the Anadyr Current that flows into Chirikov Basin as it passes between St Lawrence Island and the Russian mainland. The Anadyr Current is the major oceanic artery that supplies nutrients to the Arctic from the Pacific Ocean. Mooring A3 is located in the middle of Bering Strait, and now has over 20 years of temperature, salinity, and current data.

By combining the N2 nitrate and salinity data then the A3 salinity data, we developed a method that allows us to estimate the Arctic-bound concentrations nitrate, phosphate, and silicate. Using the estimated nutrient concentration along with the current measurements, we were able to calculate the nutrient transport through Bering Strait for every month between 1998 and 2018.

Why did we do it?
The Arctic environment is undergoing rapid transformation due to climate change. Sea ice is breaking up sooner, and the timing and magnitude of phytoplankton and ice algae blooms depend on light and nutrient availability. To understand phytoplankton growth, phytoplankton species prevalence, and their future trajectories, we must first have a good handle on how much nutrients are available for their growth. Establishing the abundance of phytoplankton and algae is important to understanding the food available to higher trophic levels and the general ecological health of the Arctic.

What did we learn?
We found that nutrient flux through Bering Strait may be up to ~50% higher than previously estimated. We also found a lot of year-to-year (interannual) variability in transport, where some years have high nutrient transport and others are low. There are also large seasonal differences, where April usually has the highest nutrient transport and December has the lowest. Perhaps most importantly, we found that phosphate and silicate nutrient transports increased over the last 20 years, while nitrate had no trend. These results have implications for the distribution, quantity and character of future phytoplankton and ice algae growth.

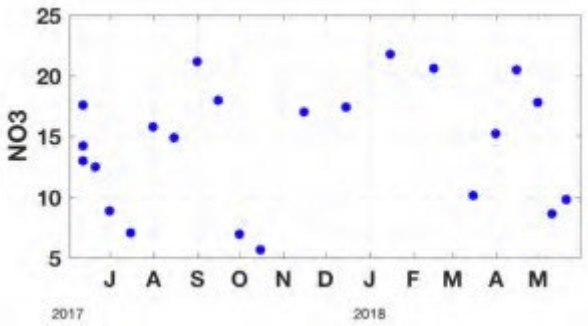

Figure showing nitrate concentration through the deployment year as measured by the discrete water sampler.

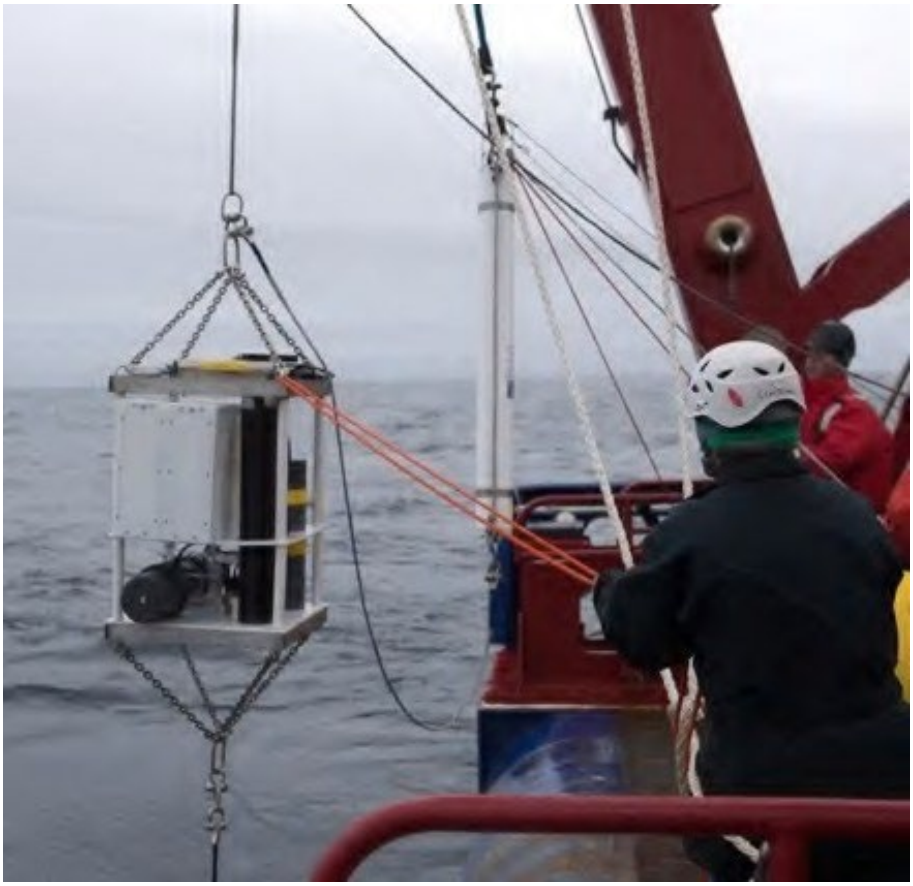

Deployment of moored water sampler, nitrate sensor, and temperature-salinity datalogger. Photo S. Danielson

A rack of IV bags with water samples collected in Anadyr Strait over the course of the 2017-2018 deployment year. Photo S. Danielson.

Setting up a moored Green Eyes water sampler. Roger Topp photograph.

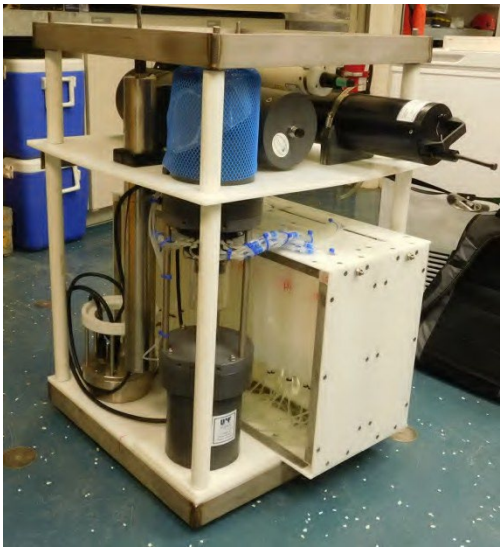

A water sampler mooring recovery.
Roger Topp Photograph.

Synopsis: Phytoplankton Productivity

Dean Stockwell

Why we did it

Phytoplankton form the biological foundation of the food web, converting light and nutrients into biomass. Phytoplankton productivity provides food to the prey consumed by arctic cod, bowhead whales, seals and walrus. This study was designed to improve our understanding of how and where phytoplankton most efficiently grow in the northern Bering Sea and southern Chukchi Sea.

What we did

We conducted phytoplankton growth incubations. Plankton were collected from six light levels from the surface (100% illumination) down to near darkness (1% light level). Productivity was assessed using a ^{13}C-^{15}N dual-isotope tracer technique, measuring carbon and nitrogen uptake rates. The plankton samples were placed into screened polycarbonate incubation bottles and incubated in on-deck incubators that were cooled with running surface seawater. Following an incubation period, samples were filtered and frozen for mass spectrometric analysis at the Alaska Stable Isotope Facility housed at UAF.

What we learned

Phytoplankton productivity is extremely patchy, exhibiting rates as low as 0.1 gC m^2 day^{-1} and as high as 14 gC m^2 day^{-1}. The average productivity measured across all stations and both years was about 2 gC m^2 day^{-1}. These results are consistent with prior studies placing the Bering Strait region as one of the most biologically productive marine systems in the world. Despite a wide range of productivity, a few regions stand out as exhibiting particularly persistent elevated productivity rates. These include locations immediately downstream (north) of Anadyr Strait, the eastern edge of St. Lawrence Island, and Bering Strait. These same regions were also associated with relatively high levels of nitrate (high f-ratio) as the nutrient fueling production, demonstrating the importance of new nitrate brought to the region by the Anadyr Current.

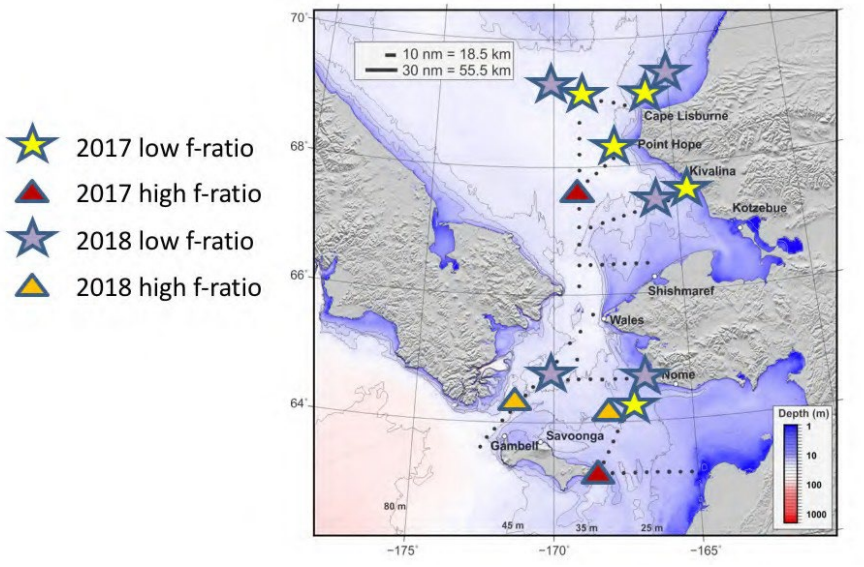

Figure showing locations at which primary productivity exhibit relatively low (stars) and high (triangles) f-ratios. This demonstrates variable sources of nutrients fueling primary production across the study region.

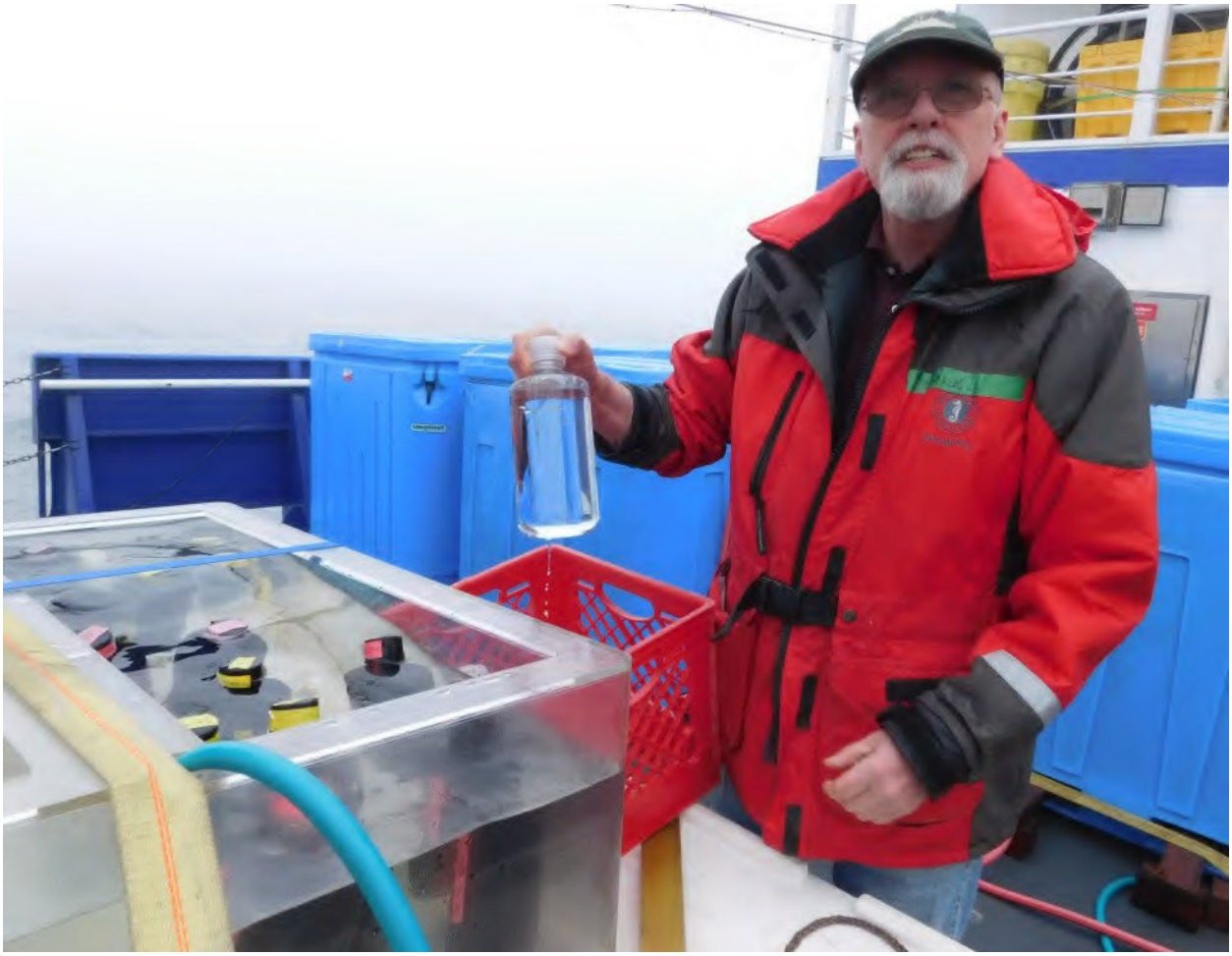

Productivity experiment bottles being loaded into the on-deck incubator. Photo S. Danielson

Synopsis: ASGARD Zooplankton Studies

Russ Hopcroft and Alex Poje

Why we did it. There are few observations of what zooplankton communities look like in the Bering Strait during spring as sea ice retreats and phytoplankton populations explode. A fundamental question is how much of that production may be channeled through the zooplankton at that time and ultimately into water column communities versus falls to the seafloor to feed those benthic communities.

What we did. To address our question, we need knowledge of the rates at which zooplankton grow, and how much of the food they consume is burned off through respiration as they go about their daily activities. We measured the growth rates of the domain zooplankton – copepods – by sorting zooplankton into narrow size ranges and seeing how much they grew over 10 days. We also examined how much energy the adults use to produce eggs each day. We studied respiration by putting individual copepods into tiny vials and constantly monitoring the decline of oxygen over a day. When combined with survey data of how much zooplankton is present we can compute how much phytoplankton they would have need to consume.

Growing copepods during ASGARD. Photo R. Hopcroft

What we learned. Depending on the species, copepods add 3-9% of their weight each day when younger, and adults can convert 9-15% of their weight into eggs daily. Contrary to expectation the largest copepod species grow fastest, while the smaller species are relatively better at producing eggs. Despite the cold temperatures during out study (4°C) adult copepods respire the equivalent of 5-20% of their body mass per day, with highest rates in smaller species. Thus, it appears all species have similar net growth efficiencies (~50%). At the time of our surveys, the given these rates and the biomass of zooplankton, they had limited potential for impacting the phytoplankton production.

Synopsis: ASGARD Fish

Brenda Norcross and Caitlin Forster

Why we did it:
Springtime patterns of biological productivity are driven by seasonal retreat of sea ice in the Chukchi Sea. Despite the biological importance of the ice melt in the Arctic ecosystem, logistical challenges have limited sampling efforts during the spring season. Additionally, there have been significant changes in the timing of the spring-melt season; over the past several decades, the duration of the melt process has decreased by nearly 30 days. The ASGARD cruise, as a part of the Arctic Integrated Ecosystem Program (IERP), investigated the dynamics of the spring season in the northern Bering and southern Chukchi Sea. Of particular interest, Arctic cod (*Boreogadus saida*) is a key forage fish in the Arctic marine ecosystem and provides an energetic link between lower and upper trophic levels. Despite its ecological importance, spatially explicit studies synthesizing polar cod distributions across research efforts have not previously been conducted in its Pacific range.

What we did:
We conducted trawl surveys in June 2017 and June 2018; fishes were targeted with a 3 m plumb-staff beam trawl at 21 stations. We then compiled demersal trawl data from 21 summer-season cruises conducted during 2004–2017 in the Chukchi and Beaufort seas, and investigated size-specific patterns in distribution to infer movement ecology of Arctic cod as it develops from juvenile to adult life stages. Finally, we compared spring and summer patterns in abundance to assess ontogenetic shifts in Arctic cod distribution in the Alaskan Arctic.

What we learned:
Springtime demersal abundance of Arctic cod in the southern Chukchi Sea was strikingly low compared to late summer abundance. Strong linkages between sea ice and Arctic cod life history suggest that the distribution of Arctic cod in the southern Chukchi Sea could be influenced by the distribution of sea ice. It is possible that Arctic cod tracks the springtime ice retreat and the wave of productivity that follows. If Arctic cod followed the ice edge in these years, then its distribution would be beyond the northernmost station sampled during the June (ASGARD) cruises, explaining the extremely low abundances of subadult and adult polar cod observed in the southern Chukchi Sea. Movement inferred from size-based and seasonal patterns in distribution describes a plausible migration scenario where Arctic cod move from nursery grounds as juveniles, feeding grounds as subadults, and spawning grounds as adults.

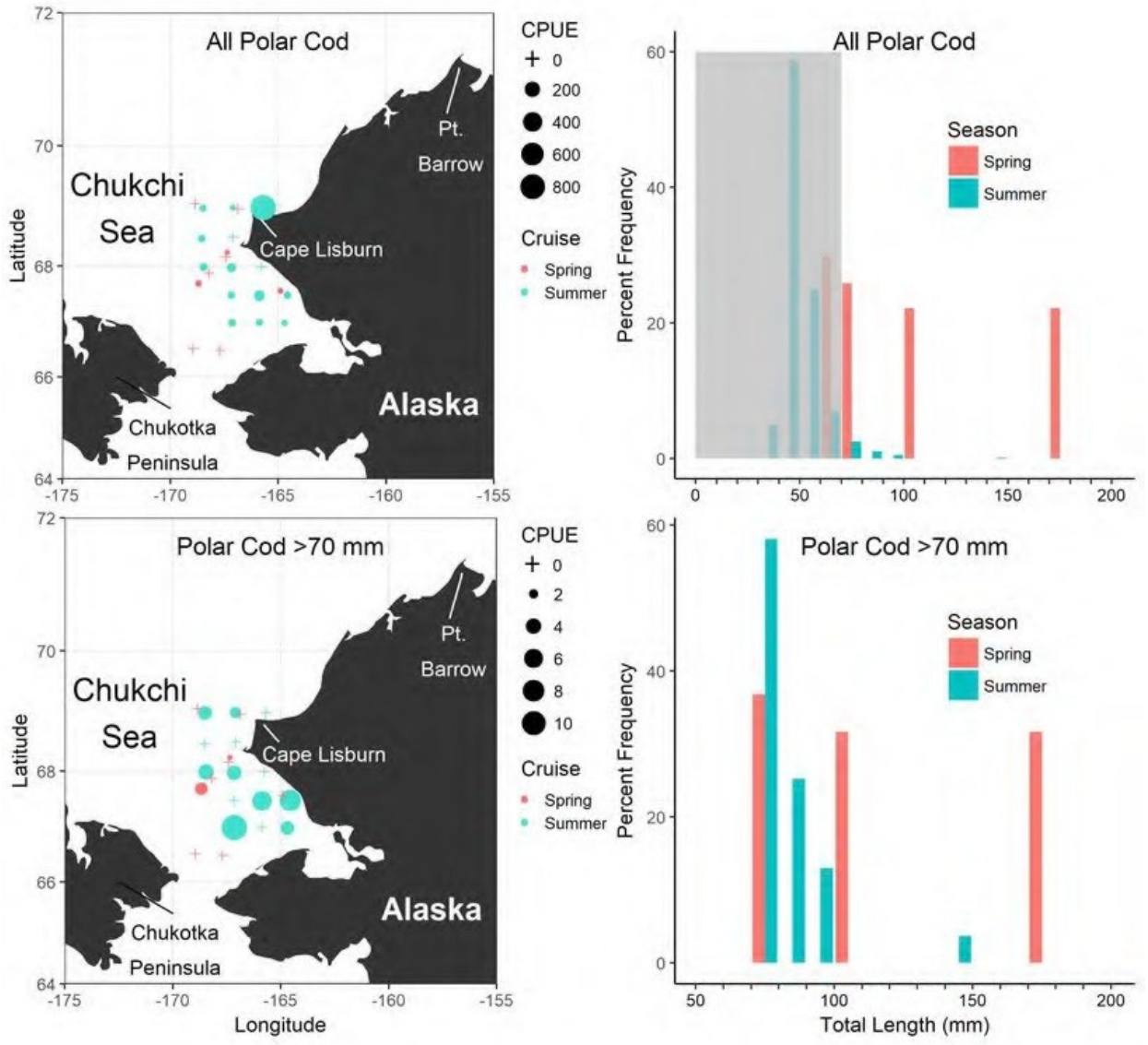

Figure: This is Figure 8, the seasonal Arctic cod distribution figure from Forster et al. 2020 (https://link.springer.com/article/10.1007/s00300-020-02631-4). Caption from publication is below in quotes. Note: figure and caption refer to polar cod, not Arctic cod, which is a naming convention difference in European vs. American journals. They are referring to the same fish species (*Boreogadus saida*)

"Figure 8. Distribution and length-frequency of polar cod in the Chukchi Sea in spring and summer 2017. Length-frequency scaled by CPUE. Top two panels are all captured sizes of polar cod, total CPUE (fish per 1000 m^2) spring = 6.43, summer = 984.40. Bottom two panels are only polar cod > 70 mm, total CPUE spring = 4.51, summer = 42.29; gray box in top right shows small fish excluded from lower two plots. Note difference in scale between top left and bottom left plot."

Photographs:

Photos by Brendan Smith.

Photo by Seth Danielson

Appendix A: ASGARD Project Data

Appendix A contains summaries of data types collected by the ASGARD project, methodologies, and archive locations. Data are archived at DataOne, the UNOLS Rolling Deck to Repository (R2R) and the Arctic IERP Research Workspace that is maintained by Axiom Data Science. Data files are also available directly via the NPRB Arctic IERP Data Portal: https://arctic-ierp.dataportal.nprb.org/.

Data stored at R2R includes seafloor ADCP data, multibeam and single beam sonar data, splitbeam fisheries acoustics sonar, meteorological data, CTD data, navigation data, gravimeter data, and underway thermosalinograph data. Arctic IERP R2R archives can be accessed at the following links: https://www.rvdata.us/search/cruise/SKQ201709S and https://www.rvdata.us/search/cruise/SKQ201813S.

Table A1. ASGARD Process Station laboratory rate measurements.

Measurement Parameters / Sample Type	Experiment Location / Instrument Type
d^{13}C Primary Production	On-deck incubator
Zooplankton growth (Artificial Cohort)	On-deck incubator
Zooplankton egg production (individual females)	Climate-controlled environmental chamber
Zooplankton respiration (individuals)	Climate-controlled environmental chamber
Fecal pellet production (community subsamples)	Climate-controlled environmental chamber
Bioturbation rates (234-Th)	Climate-controlled environmental chamber
Sediment community oxygen consumption and individual macrofaunal respiration rates	Climate-controlled environmental chamber
High resolution particle flux estimates from particle size distribution	LISST & UVP5
Demersal fish age, size, weight, δ^{13}C, δ^{15}N, stomach content	Plumbstaff beam trawl
Pelagic fish age, size, weight, δ^{13}C, δ^{15}N, stomach content	Aluette midwater trawl

- ASGARD process station measurement data files can be accessed at: https://researchworkspace.com/project/1843056/folder/8148675/final-data-archive

Table A2. ASGARD Survey measurements. Measurements listed here were also made at all Process Stations.

Measurement Parameters	Instrument	Locations sampled
Temperature, Conductivity, Salinity, Pressure, Chlorophyll a Fluorescence, PAR, Dissolved Oxygen, Beam Transmittance	SeaBird SBE-911 CTD	Survey stations
NO_3, NO_2, NH_4, PO_4, SiO_4, Total and size-fractionated Chl*a*	CTD Rosette	Survey stations
Quantity & quality of sediment organic matter, and modeled degradation rates within sediments (labile protein, chloropigments, TOC, $d^{13}C$)	Multicore	Process stations
Sediment grain size	Multicore	Process stations
Bacterial biomass in sediments (ATP)	Multicore	Process stations
Abundance, biomass and functional group analysis of benthic meio- and macro-infauna with $d^{13}C$ and $d^{14}N$ of select species	Multicore	Process stations
Metazooplankton composition, abundance, biomass	Plankton nets (150 & 505 µm)	Survey stations
Microzooplankton composition, abundance, biomass	CTD Rosette	Survey stations
Particle size distribution (65 µm - 2.5 cm)	Underwater Vision Profiler 5	Survey stations
Particle Size Distribution (2.5 - 500 µm)	LISST	Survey stations
Mesozooplankton abundance	Underwater Vision Profiler 5	Survey stations

- ASGARD survey station measurements can be accessed at: https://researchworkspace.com/project/1843056/folder/8148675/final-data-archive

Table A3. ASGARD mooring-based measurements.

Measurement Parameters	Instrument	Number of Locations
Water Speed and Direction, Temperature, Signal Strength	Teledyne-RDI 307 KHz ADCP	7 mooring sites*
Temperature, Conductivity, Salinity, Pressure, Chlorophyll *a* Fluorescence, PAR	SeaBird SBE-16+	3 mooring sites
Chlorophyll *a* Fluorescence, OBS, CDOM	Wetlabs Eco-Triplett	3 mooring sites*
Temperature, Conductivity, Salinity, Pressure	SeaBird SBE-37	7 mooring sites*
Sinking fluxes of particulate Mass, Carbon, Nitrogen, and Silica fluxes; Food quality of sinking particles	Hydrobios Sediment Trap	3 mooring sites*
NO_3, NO_2, NH_4, SiO_3, PO_4	GreenEyes Water Sampler	2 mooring sites*
NO_3	Satlantic SUNA V2	3 mooring sites*
Acoustic Backscatter at 38, 125, 200, and 455 KHz	ASL Acoustic Zooplankton Fish Profiler	1 mooring site*
Underwater Sound	AURAL	4 mooring sites*

* = one of the denoted sites includes the CEO mooring site near Hanna Shoal. CEO data are separately archived from the ASGARD data on the Axiom Research Workspace.

- ASGARD Mooring data can be accessed at: https://researchworkspace.com/project/1843033/folder/8148631/final-data-archive
- Data from the CEO mooring are stored at: https://researchworkspace.com/project/302408/folder/302412/data_mooring.

Table A4. ASGARD shipboard underway measurements.

Measurement Parameters	Instrument
Water Speed & Direction, Signal Strength	Teledyne-RDI 307 KHz ADCP
Wind Speed/Direction, Relative Humidity, Air Temperature, PAR, Longwave Downwelling Irradiance, Shortwave Downwelling Irradiance	SKQ Meteorological Instruments
Temperature, Salinity, NO_3, Turbidity, Phycoerytherin, Chlorophyll *a* Fluorescence, Crude Oil	SKQ Seachest Instruments
Ship speed, heading, Speed over Ground, Course over Ground, Speed Through Water, Bottom depth	SKQ Navigation Instruments
Temperature, Conductivity, Salinity, Pressure, Chlorophyll *a* Fluorescence, OBS, CDOM	Acrobat undulating CTD with Eco-Triplett optical sensor (Select transects, only operated in 2018)

- ASGARD shipboard underway measurements can be accessed at: https://researchworkspace.com/project/1843056/folder/8148675/final-data-archive

Arctic Integrated Ecosystem Research Program Final Report for

Arctic Integrated Ecosystem Survey (IES) Phase II: Oceanography and Lower Trophic Level Productivity (A92)

and

Microzooplankton biomass and grazing rates on the Arctic Program Cruises (A70)

C.W. Mordy, K. Axler, L. Copeman, A. Deary, J.T. Duffy-Anderson, L. Eisner, E. Goldstein, H. Tabisola, J.W. Krause, D. Kimmel, C. Ladd, M.W. Lomas, R.M. McCabe, J.M. Nielsen, A. Schnetzer, A. Spear, P. Stabeno

Preamble

The Arctic Integrated Ecosystem Research Program

The Arctic Integrated Ecosystem Research Program (Arctic IERP, 2016-2021) was motivated by the rapid changes occurring in the waters of the northern Bering and Chukchi Seas. While much research has been done in the region, many important questions remain. As a cohesive research endeavor, the Arctic IERP was designed to address a single, overarching question:

How will reductions in Arctic sea ice and the associated changes in the physical environmental influence the flow of energy through the ecosystem in the Chukchi Sea?

The report you are reading now is one of five final reports from the fieldwork phase of the Arctic IERP (a synthesis phase was initiated in 2022 after the completion of the Arctic IERP field-based projects). This preamble provides a brief overview of the Arctic IERP, both to place each final report in the broader context of the whole program, and to encourage readers to examine the other final reports to learn more about the research that was done. More detailed information about the Arctic IERP can be found at https://www.nprb.org/arctic-program.

The spatial domain of interest for the Arctic IERP extended across the Chukchi Sea Large Marine Ecosystem (LME) as redefined by the Arctic Council's Protection of the Arctic Marine Environment (PAME) working group, and the northern Bering Sea (north of 61.5° N) as it strongly influences dynamics in the Chukchi Sea from the upstream direction. The main focus has been on the greater Bering Strait region and the Chukchi Sea. The program included the Arctic Basin and Beaufort Sea insofar as processes in the Chukchi Sea are influenced by these adjacent areas.

Development of the Arctic IERP

Before any Arctic IERP research proposals were written, the NPRB administered an assessment program, the Pacific Marine Arctic Regional Synthesis (PACMARS; https://www.nprb.org/assets/uploads/files/Arctic/PacMARS_Final_Report_forweb.pdf), that applied $1.5M provided by Shell and ConocoPhillips to compile and synthesize existing information about the ecosystem and inform research priorities. This assessment included community meetings in 2013 in Savoonga, Gambell, Kotzebue, Nome, and Barrow (now Utqiaġvik), in which representatives from 17 communities between St. Lawrence Island in the Bering Sea and Barter Island in the Beaufort Sea participated. One major area of emphasis that emerged from these community meetings was concern about food security for the region's residents in light of the rapid environmental changes taking place. Results from the scientific assessment and input provided via the community meetings informed the creation of the Arctic IERP. The PACMARS report informed both the IERP Request for Proposals (https://www.nprb.org/arctic-program/request-for-proposals/) and the submitted proposals.

Following a proposal review process, the Arctic IERP formally began in 2016 with funding from the North Pacific Research Board (NPRB), the Collaborative Alaskan Arctic Studies Program (formerly the North Slope Borough/Shell Baseline Studies Program), the Bureau of Ocean Energy Management (BOEM), and the Office of Naval Research (ONR) Marine Mammals and Biology Program. Generous in-kind support was contributed by the National Oceanic and Atmospheric Administration (NOAA), the

University of Alaska Fairbanks (UAF), the U.S. Fish & Wildlife Service (USFWS), and the National Science Foundation (NSF). This coordinated program was developed in cooperation with the Interagency Arctic Research Policy Committee (IARPC) and the U.S. Arctic Research Commission.

The Research

The Arctic Integrated Ecosystem Research Program (IERP) invested approximately $18.6 million in studying marine processes in the northern Bering and Chukchi Seas in 2017-2021, beginning in the summer of 2017. The research was divided into three main, complementary projects. The Arctic Shelf Growth, Advection, Respiration, and Deposition Rate Experiments (ASGARD) project carried out research in late spring and early summer of 2017 and 2018 aboard R/V Sikuliaq. The Arctic Integrated Ecosystem Survey (Arctic IES) conducted fieldwork aboard R/V Ocean Starr in late summer and early fall 2017 and 2019. In addition to the vessel-based surveys, sub-surface moored sensors were deployed to gather biophysical information continuously from September 2016 to September 2019 and autonomous platforms were brought to bear (e.g., gliders, saildrones, air-deployed profilers).

In addition to the vessel-based work, a team of Arctic residents and social scientists, including members from eight communities in the North Slope and Northwest Arctic Boroughs and the Bering Strait region, met several times during the project to assess and analyze Indigenous observations and experiences with various types of change occurring in the region from Savoonga to Utqiaġvik. This group also compiled an annotated bibliography of Traditional Knowledge or Indigenous Knowledge (available through the data portal described below), to help researchers from other components of the Arctic IERP find information relevant to their studies.

Prior to the commencement of fieldwork, meetings were held in the three hub communities of Nome, Kotzebue, and Utqiaġvik. Scientists from the Arctic IERP and NPRB staff met with community members from each region to discuss the research purpose and plans. Research plans were also shared and discussed at meetings of the Alaska Eskimo Whaling Commission (AEWC), the Indigenous Peoples Council for Marine Mammals (IPCoMM), and with the Tribal Councils of Gambell and Savoonga on St. Lawrence Island. One result of these meetings was a shift in timing of the ASGARD cruises from May until June as well as a shift in timing and survey regions for the Arctic IES cruises, to avoid conflicts with subsistence hunting activities during what is traditionally the time for walrus hunting. Another result was the creation of communication protocols to avoid conflicts by alerting coastal communities to the presence of research vessels and adjusting the ships' routes to avoid areas where hunting was taking place. These communication protocols included regular radio broadcasts and daily emails to community members throughout the research area.

Results from the research are published in a growing list of peer-reviewed journal articles, as well as cruise reports that provide contemporary accounts of the cruises, and many social media postings that are available through the NPRB website. Data are publicly available as described below.

Collaborations

The NPRB collaborated and coordinated with several other U.S. agencies and organizations that fund Arctic marine research. NPRB staff worked closely with the U.S. Interagency Arctic Research Policy Committee (IARPC) and the U.S. Arctic Research Commission. As the Arctic IERP was developed, the

NPRB secured commitments for collaboration from 22 existing research projects that were detailed in Appendix A of the request for proposals, and made connections with new projects as they were funded.

International researchers also collaborated with the Arctic IERP via the Pacific Arctic Group (PAG), the North Pacific Marine Science Organization (PICES), and the Intergovernmental Consultative Committee (US/Russia - bilateral) as well as collaborations developed by individual investigators. PAG participants, including researchers from Canada, China, Japan, Korea, Russia, and the United States, have coordinated their cruise plans to sample standard stations in the Chukchi and Beaufort Seas termed the Distributed Biological Observatory (DBO). The Arctic IERP contributed to this effort. US-Russian data sharing initiatives were hosted in San Diego in 2016 and Vladivostok in 2017 to promote collaboration and exchange and to facilitate collaboration and synthesis of data and trends of patterns observed in the US and Russian waters in the northern Bering and Chukchi seas (PICES Press, Volume 26, Issue 1). ICC collaborations and other connections also brought scientists from the Russian Federal Research Institute of Fisheries and Oceanography (VNIRO), the Russian Pacific Scientific Fisheries Research Center (TINRO), and Hokkaido University to the US to participate in the Arctic IES cruises and co-author results. This collaboration is expected to connect research interests within respective EEZs (Russia/US) of the Chukchi Sea.

COVID-19

While the fieldwork of the Arctic IERP was completed before the outbreak of COVID-19, the final meeting of researchers in November 2020 was changed from an in-person event to an online format. Other plans for in-person events, such as meetings in hub communities within the US Arctic region (Nome, Kotzebue, and Utqiaġvik), were cancelled. Laboratory work and some collaborations were postponed or cancelled due to COVID-related restrictions and concerns. The NPRB made supplemental funds available to assist researchers with unanticipated expenses due to the pandemic. The overall productivity of the Arctic IERP was likely not greatly reduced, due both to good fortune in the fieldwork being completed and to the collaborative relationships that had been built or strengthened during the program.

Data Portal

Axiom Data Science, Inc. provided data management support to the Arctic IERP throughout the field program. Axiom staff assisted the scientists in authoring metadata and publishing the datasets to public archives. The data collected by the Arctic IERP are publicly accessible at https://arctic-ierp.dataportal.nprb.org/.

Executive Summary

The Chukchi Sea is undergoing dramatic sea-ice reductions and temperature increases, but resultant biological and trophic responses are poorly understood. The goal of Arctic IES Phase II (Upper and Lower Trophic Level Teams, UTL and LTL, respectively) was to improve understanding of processes that structure the Arctic ecosystem and influence the distribution, abundance and life history of lower (phytoplankton, zooplankton, ichthyoplankton) and upper (invertebrates, fishes, seabirds, mammals) trophic level species, and evaluate their vulnerability to the rapidly changing environment. The LTL (A92) component sought to better understand the climatological, physical, chemical, and biological processes that influence energy flow from primary producers to zooplankton and ichthyoplankton, and the UTL (A93) component worked to describe and understand how lower trophic processes reverberate through the food web to influence macroinvertebrate, fish, and seabird communities. Together, these programs addressed the following overarching hypothesis:

OVERARCHING HYPOTHESIS OF PROJECT: *Reductions in Arctic sea ice and the associated physical changes to the environment influence the flow of energy through the pelagic ecosystem in the Chukchi Sea. Specifically, we expect lasting changes in the seasonal composition, distribution and production of phytoplankton; in the distribution and standing stocks of large crustacean zooplankton that serve as the prey base for upper trophic level fishes and seabirds; in the assemblages, distributions, and abundances of larval and early juvenile fishes that influence the recruitment success of later life stages, and in the distribution and abundance of adult fishes.*

This report details the LTL program along with a program that was funded to fill a gap in the observational program; the Microzooplankton (A70) gap. We conducted comprehensive ecosystem surveys of Chukchi Sea physics, chemistry, biogeochemistry and biology using an integrated network of moored arrays, autonomous vehicles, and shipboard surveys.

Emerging results from the LTL component were combined with historical data and resulted in a number of insights and new findings.

Northward flow of water from the Bering Sea brings heat, salt and nutrients to the entire Chukchi continental shelf. The higher sea level in the Bering Sea compared to the Arctic Ocean results in a net northward transport. Approximately 40% of the flow through Bering Strait exits the shelf via Barrow Canyon. This flow on the Chukchi Sea is enhanced by northward winds and weakened by southward winds. During the last decade there has been an increase in the magnitude of northward flow on the shelf.

Phytoplankton serve as the energy source for the Arctic marine environment by converting nutrients and sunlight into a food base that ultimately sustains all marine life. In the Chukchi Sea, nitrate is a limiting nutrient for phytoplankton. Year-to-year differences in the amount of nitrate available to sustain spring production varies by about 50%. These differences result from the magnitude of transport through Bering Strait in the fall and winter, and the variability of nitrate concentration in the Bering Sea.

Changing conditions in the Arctic (e.g., warming and reduction in the duration and extent of ice) has altered the distribution, composition and food quality of phytoplankton. Shipboard observations show patchy distributions of phytoplankton and rapidly varying levels of primary productivity. Synechococcus (cyanobacteria) accounted for 20-40% of the total autotrophic biomass by the end of summer in 2019.

This finding suggests that multi-year periods of warmer than average conditions altered the seasonal phytoplankton succession pattern. Phytoplankton fatty acids serve as a measure of the food quality of algae and were used to strengthen predictions of food web functioning and energy transfer to the upper trophic levels in the northern Bering and Chukchi Seas.

Particulate organic matter that falls to the sea floor, including ice algae, dead phytoplankton, and zooplankton fecal pellets, provides nutrition that sustains organisms living in that realm. For example, as ice begins to melt in spring, algae living on the underside of the ice detach and fall to the sea floor. The Chukchi Sea shelf is shallow enough that sunlight can penetrate to depth and detached ice algae can continue to photosynthesize near the seafloor.

There appears to be two distinct communities of zooplankton in the Chukchi Sea: a local, Arctic community related to water masses within the Chukchi Sea, and a community advected from the Bering Sea. Thus, the relative magnitude of annual transport from the Bering Sea influences zooplankton community structure in the Chukchi Sea. Decreased transport and later ice retreat in colder years resulted in zooplankton communities that exhibited more diversity and had higher abundances of fat-rich copepods. In contrast, in years with increased transport from the south, expatriate zooplankton communities from the Bering Sea were prevalent in the Chukchi Sea. If the northward inflow of water into the Chukchi Sea were to increase with concomitant warming, changes in food-web structure and function are likely to result.

Similar to zooplankton, summer ichthyoplankton shifted northward. Shifts in community composition resulted from species-specific responses to temperature changes, ice cover, Bering Strait advection, and changes in the zooplankton prey base. By 2100, some bottom dwelling animals will find themselves in a habitat that is warmer than their preferred temperature range and perhaps even warmer than they can survive. These animals include prey for bottom feeding whales, pinnipeds, seals and walruses, seabirds, and benthic fishes. Snow crabs will likely benefit from warmer bottom ocean temperatures.

Unprecedented warming observed during the course of the Arctic IERP program during the survey years may offer a window into the future Arctic. The biological indicators reported here suggest that increased warming could alter ecosystem structure and function with as yet unknown consequences for the people that depend on marine resources in the region.

Table of Contents

General Introduction

Background

The overall goal of this Lower Trophic Level (LTL) project was to better understand physical, chemical, and biological processes that influence the flow of energy from primary producers to zooplankton and ichthyoplankton in the Chukchi Sea and to determine how a warming climate will influence these processes. This project was directly linked with an Upper Trophic Level (UTL) proposal that examined the distribution, abundance and condition of demersal and pelagic fishes, shellfish and seabirds. Together, these programs addressed factors that influence predator-prey relationships, and provide integrated ecosystem data to examine how relationships and mechanisms may be altered by climate change.

The Overarching Hypothesis embodied both the LTL and UTL components: *Reductions in Arctic sea ice and the associated physical changes to the environment influence the flow of energy through the pelagic ecosystem in the Chukchi Sea. Specifically, we expect lasting changes in the seasonal composition, distribution and production of phytoplankton; in the distribution and standing stocks of large crustacean zooplankton that serve as the prey base for upper trophic level fishes and seabirds; in the assemblages, distributions, and abundances of larval and early juvenile fishes that influence the recruitment success of later life stages, and in the distribution and abundance of adult fishes.*

Changes underway in the Chukchi Sea are unprecedented; the physical environment is experiencing increases in temperature, progressive declines in sea-ice concentration, earlier spring ice retreat, and delayed fall ice formation (Wood et al., 2015, and references therein). In the Arctic, the Chukchi Sea is showing the largest changes in sea-ice duration. In comparison to 1979/80, the region is experiencing later sea-ice advance (1-1.4 months) and earlier sea-ice retreat (1.6-1.9 months), resulting in a shorter ice-season duration of ~3 months (Stammerjohn et al., 2012). Such shifts in timing and physical structure are intimately tied to water column stratification and the magnitude of heat, salt, and nutrients on the shelf. The shift from ice-covered conditions to open-water conditions enhances solar warming of the ocean due to its lower albedo, resulting in increased ocean heat storage (e.g., Jackson et al., 2010). Changes in advective heat flux from the northern Bering Sea through Bering Strait (Woodgate et al., 2012) also play a role in heat content changes in the Chukchi Sea.

The Chukchi Sea consists of a broad shallow shelf incised by two major canyons at the slope – Barrow Canyon in the east and Herald Canyon in the west. Three water types enter the shelf through Bering Strait: Alaska Coastal water (ACW), Bering Water (BW) and Anadyr Water (AW). Water flowing through Bering Strait generally follows three pathways northward through the Chukchi Seat. Nutrient-rich AW flows through the western side of Bering Strait, providing a continuous flux of nutrients into the southwestern Chukchi. Most of the AW flows north towards Herald Canyon with a portion continuing through the canyon and into the basin, and a portion flowing eastward along the shelf break towards Barrow Canyon. In contrast, the ACW is warmer, fresher and nutrient-poor. It typically flows through the eastern side of Bering Strait and is generally confined to the Alaskan coast as it transits northward. BW is a combination of northward flow along the 100-m isobath, outer shelf and slope water (Stabeno et al., 2016). It is slightly fresher and less rich in nutrients than the AW. It flows through the middle of Bering Strait, although mixing of AW and BW does occur. It continues northwestward, with most entering Central Channel, flowing south of Hannah Shoal toward the head of Barrow Canyon. While some (<20%)

of the ACC turns eastward onto the Beaufort shelf, the majority joins the Chukchi Slope Current (Stabeno and McCabe 2020).

Moorings and hydrography along the Icy Cape transect capture flow and characteristics of both ACW and BW. Autumn/winter transport is highly variable while April-July transport is northeastward with lower variability (Stabeno et al., 2018). Monthly mean transport at Icy Cape is 25-50% of the transport through Bering Strait as measured. Transport through Bering Strait has been measured via moorings for over two decades. These moorings remain a high priority in Arctic research and measurements by R. Woodgate continue. In addition, the three moorings across Icy Cape are continuing and are recognized as part of NOAA's Arctic observing system. Mooring time series also show the seasonal variability of the system. In recent years, sea ice arrived at the Icy Cape line in early to mid-November, increasing rapidly to near 100% areal coverage with occasional periods of reduced coverage. The highest turbidity occurred in fall when winds increased while sea-ice coverage remained <80%. Through winter, ice continues to thicken, and nitrate is replenished by a combined influence of Arctic continental slope water and BW flowing up Central Channel.

Historically, the food web of the Chukchi ecosystem has been based on primary production driven by under-ice algal communities. The spring plankton bloom (initially ice algae) likely initiates under and within the ice. Seasonal ice retreat favors the export of aggregates of under-ice algae directly to the benthos, supporting the Arctic's rich, benthic-dominated ecosystem. Increase in percent oxygen saturation is often associated with this export event, suggesting that net primary production continues at depth (Berchok et al., 2015; Stabeno et al., 2020), albeit at a slow rate due to light limitation despite sufficient nutrients. Concentrations of these aggregates occur over large spatial scales and are sufficient to shade the bottom for several weeks.

Rising Arctic temperatures have contributed to reduction in the percentage of thick, multi-year ice and a shift to thinner, first-year ice (Comiso et al., 2008). This shift has contributed to earlier seasonal sea-ice retreat which favors open water phytoplankton primary production and benefits a pelagic ecosystem (Grebmeier et al., 2006; 2015; Moore and Stabeno, 2015). The increase in water column primary production occurs in shallow (<40m) water where light levels are adequate, as long as sufficient nutrients are available. During late summer, due to nutrient exhaustion in the upper mixed layer, phytoplankton in the northeastern Chukchi are typically found below pycnocline (subsurface). Thus changes in stratification will impact primary production through the inverse relationship of light availability from the surface and nutrient availability from depth.

Restructuring in the Chukchi ecosystem is not limited to a change from a benthic to a pelagic dominated system. Physical changes (e.g., increased stratification) are expected to influence nutritional quality of the prey base via a shift in the phytoplankton community to a greater fraction of small cells (Ardyna et al., 2011; Arrigo et al., 2014; Li et al., 2009). This nutritional shift is expected to re-shape zooplankton assemblage composition (Ershova et al., 2015a, 2015b) and energy content, increase food chain length, and decrease the trophic transfer efficiency among food web constituents. When sea ice structures the system, waters are nutrient-rich, prolific blooms of under-ice algae are supported, and the zooplankton community is dominated by large copepods and other large crustaceans that provide a lipid-rich source of energy to upper trophic levels. This food web is short and efficient, supporting large numbers of fish, birds, and mammals. In contrast, under warm, stratified conditions, near-surface waters contain fewer nutrients, the phytoplankton community is dominated by picoplankton and the zooplankton community is dominated by small, lipid-poor copepods. This food web is longer, less efficient, and of poor nutritional

quality (Richardson, 2008). We can examine these two temperature-dependent states using an ecosystem carbon model developed for the Bering Sea shelf. These food web changes will manifest as shifts in upper trophic level species distributions, changes in species assemblages at all trophic levels, seasonal changes in timing of life-cycle events (Beaugrand et al., 2002, 2003), less efficient feeding interactions (Berchok et al., 2015; Norcross et al., 2013; Logerwell et al., 2015), and overall reductions in biomass.

Data collected during Arctic Integrated Ecosystem LTL represents the second phase of arctic ecosystem surveys. Phase 1 was the Arctic Eis surveys in 2012 and 2013 (Mueter et al., 2017). These studies provide examples of interannual differences in the thermohaline properties, nutrients, and phytoplankton communities. Strength of stratification and locations of fronts differed between years primarily because of the regional winds (more persistent southwestward winds in 2013) which weakens the north-eastward flow of the Alaska Coastal Current (ACC), and led to retention of water and biota on the Chukchi shelf in 2013. The increased biomass of Arctic zooplankton in 2013 may also have been due to southeastward flow up Barrow Canyon and onto the shelf from the basin. In contrast, a more northward distribution of Pacific taxa in the Chukchi was observed in 2012. Recent studies show spatial variations in zooplankton community composition associated with variations in water masses, with temperature and salinity as key factors affecting composition (Hopcroft et al., 2010; Eisner et al., 2013). Transport variability through Bering Strait (Woodgate et al., 200) and at Icy Cape (Stabeno et al., 2018) has implications for nutrient availability, and phytoplankton and zooplankton production. Transfer of trophic energy to the pelagic may be intensified if advected North Pacific species are exposed to continued water column production and high phytoplankton or microzooplankton biomass. Increases in water column production are expected to benefit midwater planktivorous and piscivorous fishes, seabirds, and whales. Clearly, regional variations in atmospheric forcing and longer term climate changes have large impacts on the Chukchi shelf ecosystem as a whole.

Variability in physics and lower trophic production subsequently affects recruitment of Arctic fishes. Recruitment success of Arctic Cod (*Boreogadus saida*) and Saffron Cod (*Eleginus gracilis*), key components of the Pacific Arctic Region food web, are important to trophic transfer efficiency and upper trophic functioning. Because survival of the early life history stages is critical to year class strength, study of factors regulating the vital rates of young is central to understanding adult recruitment (Duffy-Anderson et al., 2016). Work from other Alaskan Large Marine Ecosystems has shown that variations in ice dynamics, ocean currents, and primary and secondary production impact survival of gadids through influences on spawning distributions of adults (Petrik et al., 2015), transport pathways of eggs and larvae (Vestfals et al., 2014), spatial overlap of young with zooplankton prey (Siddon et al., 2013), connectivity of spawning areas and juvenile nursery grounds (Cooper et al.,2014), and distributions of eggs and larvae (Boeing and Duffy-Anderson 2008; Atwood et al., 2010, Siddon et al., 2011; Busby et al., 2014). Studies that examine how bottom-up processes influence arctic gadids and other fish species during the early life period offer an opportunity to not only understand critical recruitment bottlenecks for arctic fishes, but also to understand whether those bottlenecks influence species replacements (e.g., Arctic and Saffron Cod) in a warming climate and the resultant implications for seabirds, mammals and humans.

To understand the mechanisms by which the complex interactions of biotic and abiotic forcing influence Arctic ecosystem productivity and functioning, and to refine predictions of future response, we conducted a comprehensive, integrated, multi-disciplinary field-based approach to examine the interacting factors that determine productivity and trophic dynamics in a changing Arctic. Our linked teams (Arctic IES

Phase II; LTL and UTL) expanded on our previous integrated ecosystem assessments, Arctic Eis Phase I and Bering Arctic-Subarctic Integrated Survey (BASIS), by undertaking an intensive, collaborative study of the Chukchi and western Beaufort ecosystems from physics to fish (Beaufort funded with other support).

Hypotheses

Specific hypotheses outlined by the LTL project included:

H1. The source of heat to the Chukchi Sea comprises relatively even contributions from advected heat from the northern Bering Sea and local atmospheric heat fluxes. The contribution of local atmospheric fluxes is expected to increase with future reduction in sea ice.

H2. Earlier ice retreat/melt will result in stronger stratification. The contribution of temperature to stratification is expected to increase, while the contribution of salinity to stratification is expected to decrease or remain unchanged.

H3. In the southern Chukchi Sea, the primary source of nutrients is from Bering Strait; while in the northern Chukchi, nutrient supply is a combination of Bering Strait and upwelled Arctic basin water. Remineralization of organic matter provides a local source of ammonium, and will decrease with earlier ice retreat/melt.

H4. Earlier ice retreat/melt will further shift the balance of spring primary production from ice-associated algae to pelagic phytoplankton, thereby reducing organic matter export to the benthos and increasing organic matter flow to pelagic zooplankton grazers early in the season.

H5. Warming ocean temperatures will increase upper-ocean stratification and reduce vertical nutrient inputs to the mixed layer resulting in the formation of more spatially and temporally extensive subsurface phytoplankton blooms and productivity maxima.

H6. Increased stratification will shift the phytoplankton community to a greater fraction of small cells, thus diverting more energy flow through the microzooplankton community.

H7. Nutritional quality of phytoplankton and their zooplankton grazers will decrease with increased warming (due to increases in stratification and reductions in nutrients).

H8. Summer zooplankton community will shift due to a) increases in the presence of Bering-Pacific fauna and a poleward retraction of arctic species, and b) changes in size structure of the copepod community to smaller-bodied microzooplankton and mesozooplankton as a consequence of the shift in size structure of phytoplankton.

H9. Ichthyoplankton community composition will shift due to a) species-specific responses to temperature changes, and b) changes in species composition and size structure of zooplankton prey base.

Objectives

O1. ***Stratification*** (H1, H2) Quantify the strength of stratification, its temporal evolution, and the relative contribution of temperature and salinity throughout the spring ice melt/retreat.

O2. ***Circulation*** (H3) Quantify transport in Herald Canyon (RUSALCA) and the eastern Chukchi shelf. Identify pathways of flow and their respective heat, salt, and nutrient concentrations.

O3. ***Heat Flux*** (H1, H2, H3) Estimate surface heat fluxes (summer) and compare to estimates of advective heat fluxes.

O4. ***Ice and Phytoplankton*** (H4) Examine the relationship among ice thickness, ice retreat, and the timing and magnitude of near-bottom chlorophyll that fuels benthic-pelagic coupling.

O5. ***Phytoplankton Abundance*** (H4, H5) Quantify the relative abundance of pelagic phytoplankton species compared to sinking ice-associated algae.
O6. ***Primary Production*** (H5, H6) Quantify spatial patterns in rates of total and new production, and phytoplankton community size structure as a function of water column physics and chemistry (nitrate and ammonium).
O7. ***Primary Production Model*** (H4, H5) Use new primary production data to validate and constrain a model of ocean primary productivity and fate in regions where subsurface productivity maxima are important.
O8. ***Secondary Production*** (H8, H9) Quantify the distribution, size, abundance, and species composition of zooplankton and ichthyoplankton throughout the US shelf waters of the Chukchi Sea. Compare data to relative oceanographic conditions and to historical estimates as derived from AFSC sampling 2003- present.
O9. ***Trophic Interactions – Hot Spots*** (H4, H5) Use primary production data to understand spatial variability in net community production and identify 'hot spots' of trophic connections between LTL and UTL, and how these might change in relation to other on-going projects in the region focused on detecting change (e.g., Distributed Biological Observatory [DBO]).
O10. ***Trophic Interactions – Nutrition*** (H6, H7, H8, H9) Determine spatial and temporal relationship between phytoplankton, zooplankton and ichthyoplankton. Link observations to UTL-derived data to provide mechanistic understanding of trophic relationships. Compare fatty acid profiles of seston (primarily phytoplankton) and zooplankton to relate carbon sources to nutritional condition of key forage fish (e.g., Arctic Cod).
O11. ***Ecosystem Connectivity*** (H8, H9) Examine connectivity and exchange of lower trophic biota (zooplankton, ichthyoplankton, juvenile fish) between ecosystems (northern Bering Sea, Chukchi, Beaufort) to determine if each region acts as a source or a sink of ichthyo- and zooplankton stocks.
O12. ***Arctic Cod and Saffron Cod*** (H9) Further resolve spawning and connectivity of Arctic Cod and saffron cod adults, larvae and juveniles by providing new field data on late-stage larvae in summer that will be used to ground truth results from biophysical transport model efforts.
O13. ***US/Russian Chukchi*** (H8, H9) Connect US Chukchi Sea IERP surveys to those planned in the Russian exclusive economic zone (EEZ; 2017, 2019; Melnikov, TINRO; Afanasyev, VNIRO).

Experimental Design and Methods

Physics, nutrients, primary and secondary producers in the eastern Chukchi Sea were concurrently examined using biophysical moorings, shipboard surveys, and uncrewed systems (autonomous vehicles) allowing us to capture the spatiotemporal variability of the ecosystem. Sampling occurred throughout the year. Shipboard measurements in late summer and early fall 2017 and 2019 by the combined LTL and UTL programs provided a comprehensive integrated ecosystem data set (physics to fish to seabirds) of the eastern Chukchi Sea. Year-round measurements were collected over two years from moorings deployed in 2017 (recovered in 2018) and 2018 (recovered in 2019). Moored data were especially valuable in providing critical information during ice-covered months by collecting information on timing of the chlorophyll "dump," drawdown of nutrients, light penetration, and respiration versus primary production (e.g., oxygen saturation). In addition, they provided temporal context for the shipboard measurements that were conducted in late summer and fall of 2017 and 2019, and for autonomous measurements that

sampled the region from ice retreat to freeze-up (e.g., saildrone and ALAMO floats). Close collaboration with our counterparts in the linked UTL component allowed us to understand the effects of these variables on upper trophic biological production. The program also leveraged observations from a number of other teams and programs including EcoFOCI's Bering and Arctic observing programs, NOAA's Marine Mammal program at AFSC, and the Innovative Technology for Arctic Exploration (ITAE) at NOAA's Pacific Marine Environmental Laboratory (PMEL).

Shipboard Work

Integrated ecosystem surveys of the eastern Chukchi Sea occurred from August to early October in each of two field years (2017, 2019) (Figure 1a, 1c). The surveys were conducted in three legs on the R/V *Ocean Starr* (Figure 3) with the first leg dedicated to servicing moorings and conducting hydrographic transects, and Legs 2 and 3 dedicated to gridded fish surveys which were accompanied by additional hydrographic sampling. The hydrographic transects included the Distributed Biological Observatory Line 6 (DBO6) in the Beaufort Sea (2017), and three transects in the Chukchi Sea that have been frequently occupied since 2010; the Icy Cape line, which includes three of PMEL's long-term moorings (C1, C2, C3); the Cape Lisburne line; and DBO3 which includes PMEL's long-term mooring C12. As shown in Figure 2, shipboard activities included CTD casts (1-m resolution of temperature (T), salinity (S), oxygen, chlorophyll-a (Chla) fluorescence, turbidity, and PAR); water samples from Niskin bottles (discrete samples for measurements of nutrients, oxygen, Chla, primary production, and phytoplankton and microzooplankton speciation); and bongo tows for zoo- and ichthyo-plankton.

Biophysical Moorings

This project included two years of time series measurements at three sites; C1, C3, and C4 (Figure 1). EcoFOCI's mooring C2 on the Icy Cape line was leveraged as part of this program. In addition, EcoFOCI has maintained a suite of moorings in the Chukchi Sea since 2010, and in the northern Bering Sea since 2005 (M8 in Figure 1). For this program, moorings were deployed in 2017, recovered and redeployed during a DBO-NCIS cruise on the USCGC Healy in 2018 (Figure 1b), and recovered in 2019. These moorings (C1, C2, C3 and C4) measure current speed and direction (ADCP; RCM-9), near-bottom T and S, oxygen, nitrate (C1, C2, and C3), Chla fluorescence, PAR, bottom pressure and ice thickness (Figure 2). In partnership with AFSC's Marine Mammal program, passive acoustic moorings were also deployed at these sites. Note that measurements were contingent upon successful instrument recovery and operation.

Autonomous Platforms / Uncrewed Systems

This program leveraged ITAE and PMEL deployments of saildrones in 2017 and 2018 and ALAMO floats in 2017-2019. The saildrone is an autonomous vehicle that utilizes wind for propulsion and solar panels to power on-board systems. The saildrone derives its speed from a 4-m wing. Data (returned in real time) include position, atmospheric parameters (sunlight, barometric pressure, wind, air temperature and relative humidity) and oceanic parameters (T, S, Chla, and oxygen). The drones were launched from Dutch Harbor, sailed north through Bering Strait, and traversed the Chukchi Sea. The mission in 2017 was a proof of concept while the mission in 2018 was used primarily to complement UTL surveys in 2017 and 2019. Most of the atmospheric data from these missions were delivered to the Global Telecommunication System (GTS) while salinity, Chla and oxygen data are experimental.

The ALAMO float (Air- Launched Autonomous Micro-Observer [ALAMO]) is an ARGO-like float that is ice reinforced. It was developed by MRV Systems LLC in partnership with ITAE. These floats provide ~100 profiles of T, S and pressure the water column shortly after ice retreat. In partnership with the Woods Hole Oceanographic Institution and PMEL's Arctic Heat program, 29 ALAMO floats were deployed between 2017 and 2019, and that information is available at PMEL's Arctic Heat website (https://www.pmel.noaa.gov/arctic-heat/data).

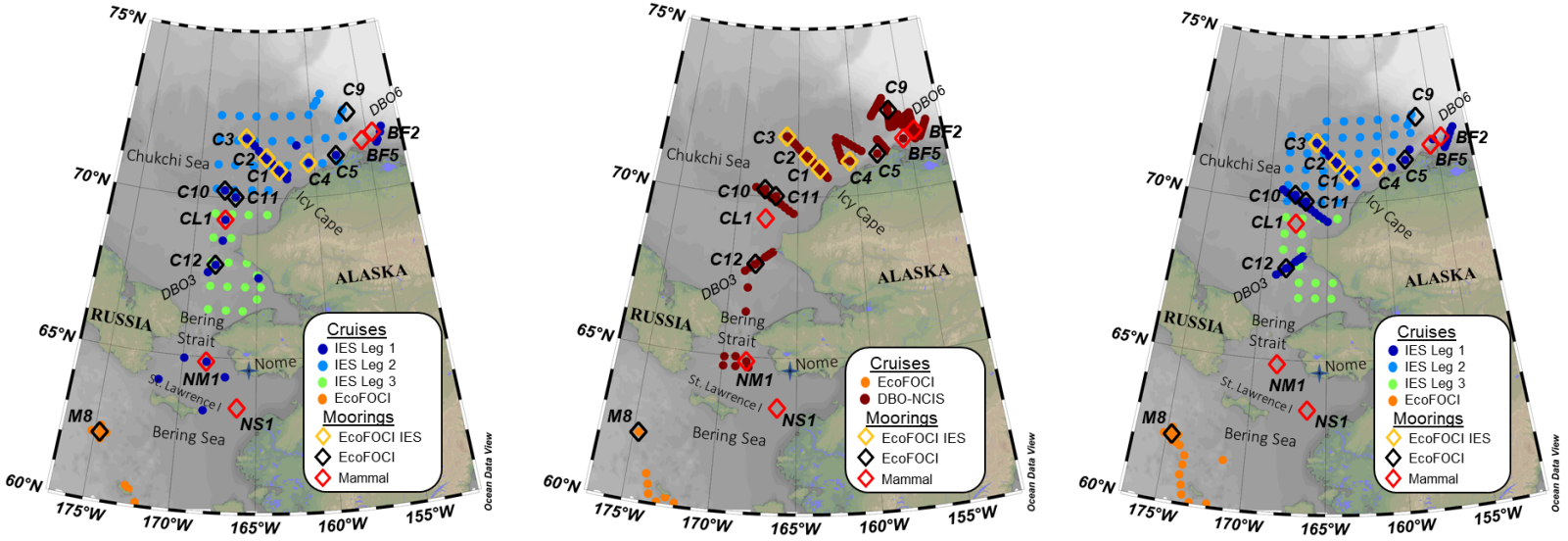

(a) 2017 (b) 2018 (c) 2019

Figure 1: Maps of IES survey stations (dots) and moorings (diamonds) in (a) 2017, (b) 2018, and (c) 2019. Also shown are the following collaborative activities: EcoFOCI hydrographic surveys and the M8 mooring in the Bering Sea, AFSC marine mammal passive acoustic moorings, and the 2018 DBO-NCIS hydrographic and mooring cruise. Not shown are mooring deployment and recovery cruises in 2016 and 2020, saildrone track lines in 2017, 2018 and 2019, and trajectories of satellite-tracked drifters and ALAMO floats. Fall IES cruises OS2017 and OS2019 both had three legs, all involved with data collection.

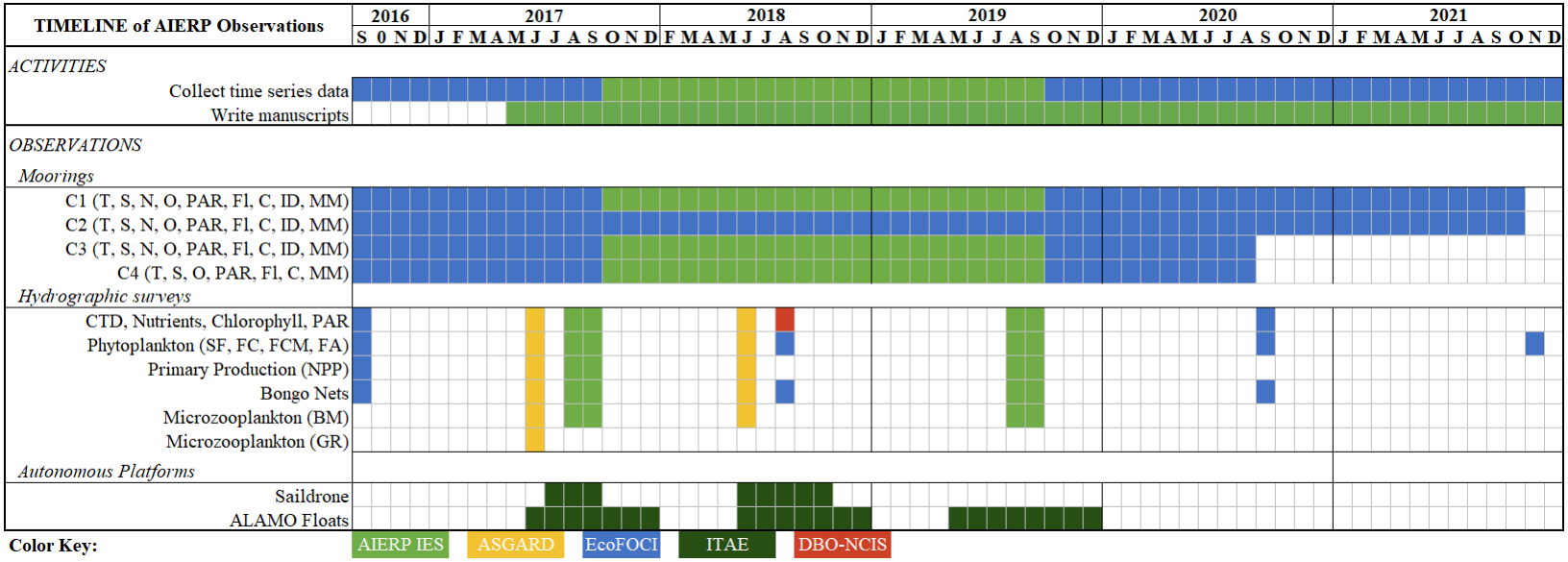

Figure 2. Timeline of activities and observations undertaken by this project. Mooring: Temperature (T), Salinity (S), Nitrate (N), Oxygen (O), Photosynthetically Available Radiation (PAR), Chlorophyll Fluorescence (FL), Currents (C), Ice Draft (ID), Marine Mammals (MM) Note that time series data are contingent upon successful instrument recovery and operation. Phytoplankton: Size Fractionation (SF), FlowCam (FC), Flow Cytometry (FCM), Fatty Acid Content (FA), Net Primary Production (NPP). Microzooplankton: Biomass (BM), Grazing Rates (GR).

Figure 3: R/V Ocean Starr dockside (Stabbert Maritime Inc.). Photo: D. Strausz, NOAA PMEL / CICOES

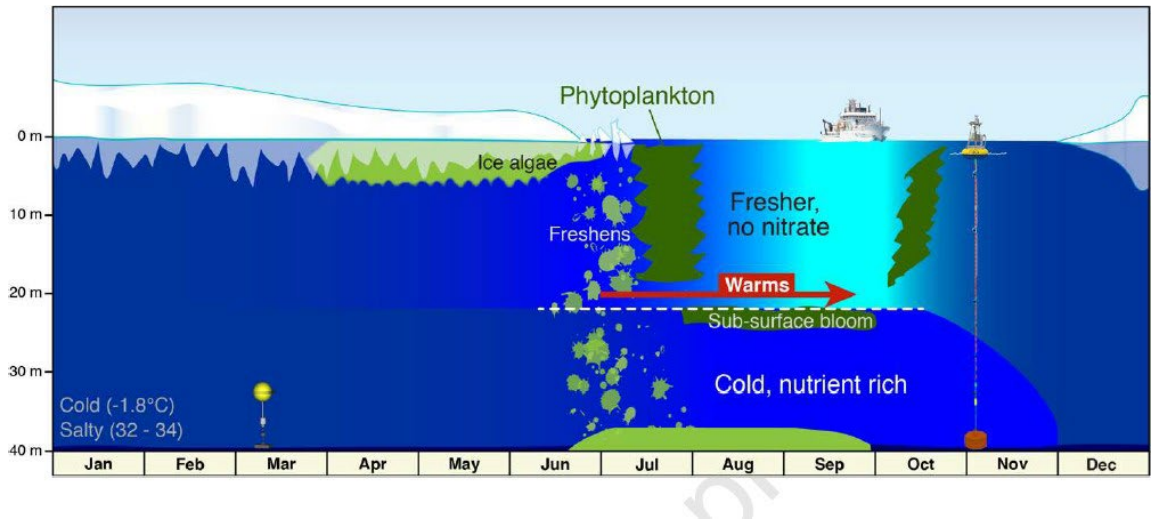

Figure 4. Seasonality of the lower trophic level of the ecosystem on the northeastern Chukchi Sea Shelf. Ice algae bloom occurs beneath the ice in spring, and with ice melt it is exported to the bottom, where there is sufficient light and nutrients to support further production. With ice retreat/melt the water stabilizes with a relatively warm, low salinity surface layer overlaying a cold more saline bottom layer. With this stabilization, a surface phytoplankton bloom can occur consuming the remainder of surface nutrients and support a subsurface bloom. With surface mixing in late summer, a fall phytoplankton bloom may occur (from Chapter 9).

Data and Metadata
Observational data from the A92 EIS program and the microzooplankton A70 programs.

Arctic IES: A92

DATASET	COLLECTION DATE(S)	STORAGE FORMAT	STATUS
Oculus Glider: temperature, salinity, conductivity, and density (EcoFOCI)	Mission delayed until 2022	n/a	n/a
CTD Niskin-bottle: nutrients, oxygen (EcoFOCI)	Fall cruise 2017 (OS1701)	netCDF	Delivered, SEP 2018
Acrobat towed vehicle: T, S, Chla fluorescence, oxygen, nitrate and PAR	Fall cruise 2017 (OS1701)	netCDF or text file	Failed: loss of instrument., SEP 2018
Mooring, two 1-year time series, 3 sites: current speed and direction (ADCP; RCM-9), near-bottom T and S, oxygen, nitrate, Chl-a fluorescence, PAR, bottom pressure and turbidity (EcoFOCI)	Sept 2017- Sept 2019	netCDF	Delivered, 2019-2021
Ice Profiler Mooring, C2: ice draft data (EcoFOCI)	Fall cruise 2017-19 (OS1701, HE1801)	text files	Delivered, SEP 2019-2021
C2 summer mooring: radiation (shortwave, longwave, direct/diffuse), meteorology (wind speed/direction, atmospheric pressure, air temperature, relative humidity, sky camera) and oceanography (T, S, Chla fluorescence, oxygen, nitrate, PAR) at multiple depths in the water column (PMEL, ITAE)	May 2017, summer (HE1701)	netCDF	Delivered, MAY 2018
Pop-up float: near station C2: pressure, tilt, T, PAR, and Chla fluorescence (EcoFOCI)	2017 - 2018	netCDF	Delivered, SEP 2020
ALAMO floats with CTD (plane and ship releases): water-column profiles shortly after ice retreat and during the fall transition. Six ALAMOs were deployed.	Multiple Deployments 2017 - 2019	netCDF or text file	Delivered as a pointer. Metadata completed. Realtime ALAMO data can be found at https://www.pmel.noaa.gov/arctic-heat/data, SEP 2019
Saildrone, oceanographic and acoustic data: position, atmospheric (sunlight, barometric pressure, wind, air temperature and relative humidity) and oceanic parameters (T, S, Chl-a fluorescence, oxygen).	2017 & 2018 Saildrone data	netCDF or text file	Delivered, SEP 2020

DATASET	COLLECTION DATE(S)	STORAGE FORMAT	STATUS
CTD profile data: 1-m resolution of temperature (T), salinity (S), oxygen, chlorophyll-a (Chla) fluorescence, turbidity, and PAR, collected along four transects. (EcoFOCI)	Fall cruise 2017 (OS1701)	netCDF or text file	Delivered, SEP 2018
CTD profile data: 1-m resolution of temperature (T), salinity (S), oxygen, chlorophyll-a (Chla) fluorescence, turbidity, and PAR, collected along four transects. (EcoFOCI)	Fall cruise 2019 (OS1901)	netCDF or text file	Delivered, SEP 2020
Ichthyoplankton abundance and community composition data from a variety of towed nets at fixed stations	Fall cruise 2017 (OS1701)	Oracle (EcoDAAT), to be converted to CSV	Delivered, OCT 2019
Ichthyoplankton abundance and community composition data from a variety of towed nets at fixed stations	Fall cruise 2019 (OS1901)	Oracle (EcoDAAT), to be converted to CSV	Delivered, OCT 2021
Zooplankton abundance and community composition data from a variety of towed nets at fixed stations	Fall cruise 2017 (OS1701)	Oracle (EcoDAAT), to be converted to CSV	Delivered, OCT 2019
Zooplankton abundance and community composition data from a variety of towed nets at fixed stations	Fall cruise 2019 (OS1901)	Oracle (EcoDAAT), to be converted to CSV	Delivered, OCT 2021
CTD Niskin-bottle: microzooplankton speciation	Fall cruise 2017 (OS1701)	netCDF	Delivered, SEP 2020
CTD Niskin-bottle: microzooplankton speciation	Fall cruise 2019 (OS1901)	netCDF	Delivered, SEP 2020
CTD Niskin-bottle: Chl-a (EcoFOCI)	Fall cruise 2017 (OS1701)	netCDF	Delivered, SEP 2018
CTD Niskin-bottle: Chla, nutrients, oxygen	Fall cruise 2019 (OS1901)	netCDF	Delivered, MAR 2021
Primary productivity, particulate phosphate data from bottle samples	Fall cruise 2017 (OS1701)	Excel/Access for conversion to CSV	Delivered, DEC 2018

DATASET	COLLECTION DATE(S)	STORAGE FORMAT	STATUS
Primary productivity, particulate phosphate data from bottle samples	Fall cruise 2019 (OS1901)	Excel/Access for conversion to CSV	Delivered, MAR 2021
Parameter measurements from FlowCam images of phytoplankton	Fall cruise 2017 (OS1701)	CSV file	Delivered, MAR 2021
Parameter measurements from FlowCam images of phytoplankton	Fall cruise 2019 (OS1901)	CSV file	Delayed due to Covid Final data not expected until 2022, DEC 2020
Parameter measurements from flow cytometer - phytoplankton	Fall cruise 2017 (OS1701)	CSV file	Delivered, OCT 2018
Parameter measurements from flow cytometer - phytoplankton	Fall cruise 2019 (OS1901)	CSV file	Delivered, MAR 2021
FlowCam data subset, public library	Fall cruise 2017 (OS1701)	CSV files	Delivered, OCT 2018
FlowCam data subset, public library	Fall cruise 2019 (OS1901)	CSV files	Delayed due to Covid. Final data not expected until 2022, MAR 2021
Satellite imagery: chl-a time-series analysis	n/a	CSV file	Complete*

*For the time-series satellite chlorophyll output, rather than provide a series of static images, the link to the NOAA website allows generation of chlorophyll maps for any region and any time frame. https://coastwatch.pfeg.noaa.gov/erddap/griddap/erdVHNchla8day.graph.

Microzooplankton: A70

DATASET	COLLECTION DATE(S)	STORAGE FORMAT	STATUS
Fatty acid analysis from filtered water	Fall cruise 2017 (OS1701)	Excel/Access for conversion to CSV	Delivered, DEC 2018
Fatty acid analysis of zooplankton	Fall cruise 2017 (OS1701)	Excel/Access for conversion to CSV	Delivered, DEC 2018
Fatty acid analysis of zooplankton	Fall cruise 2019 (OS1901)	Excel/Access for conversion to CSV	Delivered, DEC 2020
Fatty acid analysis from filtered water	Fall cruise 2019 (OS1901)	Excel/Access for conversion to CSV	Delivered, DEC 2020

General Discussion

The overall goal of the Lower Trophic Level (LTL) project was to better understand the mechanisms and processes that structure the ecosystem and influence the distribution, abundance, and life history of lower (phytoplankton, zooplankton, ichthyoplankton) organisms, and their vulnerability to the rapidly changing environment of marine ecosystems in the Arctic. The results of the LTL research was directly linked with results from the Upper Trophic Level (UTL) research component that examined the processes that influence the flow of energy from primary producers, zooplankton and ichthyoplankton to upper trophic species (fishes, seabirds, mammals), and how warming climate will influence these processes.

There were 13 specific objectives for this project. Discussed below are the highlights of our project organized by these objectives. More extensive discussion can be found in the individual Chapters.

Objectives

O1. **Stratification** (H1, H2) Quantify the strength of stratification, its temporal evolution, and the relative contribution of temperature and salinity throughout the spring ice melt/retreat.

Stratification includes thermal and salinity components. Hydrographic transects, surveys and moorings were used to ascertain the relative contribution of these components. During winter the water column is well mixed. In the northern Bering Sea, the water column becomes well mixed in November and begins to stratify in April/May, when ice melts reducing surface salinity and the ocean begins to warm from solar heating. Maximum stratification is in late August/early September. Vertical stratification is due in equal parts to salinity and temperature. Stratification in the Chukchi is also due to both salinity (ice melt) and temperature. Advection, however, modifies this and the influence of advection on stratification is still being resolved (McCabe and Stabeno, Chapter 17; McCabe et al., Chapter 18; Stabeno and McCabe, Chapter 22).

O2. **Circulation** (H3) Quantify transport in Herald Canyon (RUSALCA) and the eastern Chukchi shelf. Identify pathways of flow and their respective heat, salt, and nutrient concentrations.

The RUSALCA program was discontinued shortly after this proposal was funded, so the transport in Herald Canyon could not be resolved directly. Transport on the eastern Chukchi shelf was directly calculated via moorings and drifters and compared to flow through Bering Strait (Stabeno et al., 2018; Stabeno and McCabe, Chapter 22). The annual volume transport near Icy Cape ranged from ~0.3 x 10^6 m^3 s^{-1} (10^6 m^3 s^{-1} = 1 Sv) during September 2011 – August 2012 to ~0.7 Sv during September 2017 – August 2018, with a 10-year average of ~0.4 Sv. This transport accounts for approximately 40% of the flow through Bering Strait and varies seasonally, ranging from >50% of summer transport to only 20% of winter transport in Bering Strait. On an annual basis, there is enough heat exiting the Chukchi shelf through Barrow Canyon to warm the upper 100 m of the Beaufort Sea by approximately 0.5 °C (McCabe and Stabeno, Chapter 17).

In the Chukchi Sea, nitrate is a limiting nutrient for phytoplankton. Year-to-year differences in the amount of nitrate available to sustain spring production varies by about 50%. These differences result from the extent to which the Chukchi Sea is flushed with water from the Bering Sea during

winter, and the variability of nitrate in water being transported from the Bering Sea (Mordy et al., 2021; Hennon et al., Chapter 13; Mordy et al., Chapter 5).

There appears to be two distinct communities of zooplankton in the Chukchi Sea: a local, Arctic community related to water masses within the Chukchi Sea, and a community advected from the Bering Sea. Thus, the relative magnitude of annual transport from the Bering Sea influences zooplankton community structure in the Chukchi Sea. Decreased transport and later ice retreat in colder years resulted in zooplankton communities that exhibited more diversity and had higher abundances of fat-rich copepods. In contrast, in years with increased transport from the south, expatriate zooplankton communities from the Bering Sea were prevalent in the Chukchi Sea. If the northward inflow of water into the Chukchi Sea were to increase with concomitant warming, changes in food-web structure and function are likely to result (Spear et al., Chapter 7; Kimmel and Spear, Chapter 14).

O3. **Heat Flux** (H1, H2, H3) Estimate surface heat fluxes (summer) and compare to estimates of advective heat fluxes.

Danielson et al., (Chapter 2) discusses surface heat flux estimates from an atmospheric reanalysis model (ECMWF ERA5) over the Bering and Chukchi Seas within the context of a compilation of historical and more recent hydrographic profiles that capture significant ocean warming trends in the region. That study documented no trend in the shelf-wide Bering Sea surface heat fluxes (1979-2018). Over the Chukchi shelf, however, there was a trend toward greater surface heat losses during cooling months (October–March) and a trend toward greater heat gains during warming months (April–September). McCabe et al., (Chapter 18) detail in situ estimates of surface heat fluxes over the course of a ~2-month mooring deployment on the central Chukchi shelf in summer 2015 and compare those estimates to those obtained from the ERA5 reanalysis model. It presently appears that both the surface and advective fluxes contribute roughly equally to the total heat flux. McCabe and Stabeno (Chapter 17), quantify a decade-long estimate of the alongshelf transport of heat that transits the eastern Chukchi Sea and enters the Arctic Basin, discussing both the intra- and inter-annual variability. On an annual basis, there is currently enough heat exiting the Chukchi shelf through Barrow Canyon to warm the upper 100 m of the Beaufort Sea by approximately 0.5 °C.

O4. **Ice and Phytoplankton** (H4) Examine the relationship among ice thickness, ice retreat, and the timing and magnitude of near-bottom chlorophyll that fuels benthic-pelagic coupling.

The Chukchi Sea is highly productive even though the growing season is short. Particulate organic matter, including ice algae, dead phytoplankton, and zooplankton fecal pellets, falls to the sea floor providing nutrition that sustains organisms living in that realm. For example, as ice begins to melt in spring, algae living on the underside of the ice detach and fall to the sea floor. The Chukchi Sea shelf is shallow enough that sunlight can penetrate to depth and detached ice algae can continue to photosynthesize.

In Chapter 9 (Stabeno et al.) we identify the occurrence of primary production at multiple layers in the water column and hypothesize that near-bottom production is a result of disassociated ice algae near the seafloor. On the basis of this evidence, we propose the Multiple Production Layer (maple) hypothesis, where high production is promoted by a shallow seafloor, which allows multiple production layers (surface, sub-surface, sympagic ice algae, and disassociated ice algae

near the seafloor)(Figure 4). High production occurs because the amount of light near the seafloor in mid-spring to early fall is similar to that measured beneath a 1.5-m thick ice floe. With sufficient light near the seafloor (~40 m), ice algae continue to photosynthesize, utilizing nitrate and producing oxygen through summer; a unique feature that pertains to this shallow shelf. Bloom onset occurred in summer following ice retreat, whereas the end of the bloom occurred in September following loss of light. While this is a complex system, with multiple feedbacks and thus difficult to predict, our results do suggest certain possibilities. Even in a changing system with ice retreating later and arriving earlier, the primary change will be the timing of the export of ice algae to the bottom. Thus, the duration of near-bottom primary productivity will lengthen, because bloom onset occurs earlier.

O5. **Phytoplankton Abundance** (H4, H5) Quantify the relative abundance of pelagic phytoplankton species compared to sinking ice-associated algae.

The relative distributions of pelagic and ice-associated algae continues to be explored. Eisner et al. (Chapter 24) examined the abundance and production of phytoplankton. The contribution of ice-associated algae were derived from under-ice measurements that provided the timing of ice-algal growth and eventual disappearance as the ice substrate began to erode (Stabeno et al., Chapter 9). Koch et al. (2020) used lipid biomarkers in sinking organic matter to quantify export of ice-associated algae to the benthos. These results were presented by M. Sigler at the 2021 Alaska Marine Science Symposium in 2021 (Seasonal Patterns of Near-Bottom Chlorophyll Fluorescence in the Eastern Chukchi Sea: 2010–2019)

O6. **Primary Production and Phytoplankton Size Structure** (H5, H6) Quantify spatial patterns in rates of total and new production, and phytoplankton community size structure as a function of water column physics and chemistry (nitrate and ammonium).

Samples for total and new production from the ASGARD 2017 and 2018 cruises, and from gridded stations on the IES 2017 and 2019 cruises have been analyzed and rates calculated. Spatial analysis of patterns has not been completed at the time of writing this report, but will be conducted in the near future (Eisner et al., Chapter 24) .

Initial data confirm the stations/depths with highest chlorophyll-a biomass were associated with dominance by the larger size fraction (> 5 um). As expected, in spring diatoms were in higher abundance, primary production rates were higher although more patchy, and subsurface blooms were less prevalent than in fall. In summer, phytoplankton growth in surface waters were nutrient-limited at the majority of stations. Chlorophyll biomass and production of the small (< 5 μm) size fraction was higher in summer 2019 (the warmest year) than 2017. These changes in phytoplankton community, biomass, and primary productivity are likely to result in reduced food quality with potential negative ramifications for higher trophic levels (Lomas et al., Chapter 16; Nielsen et al., Chapter 20; Eisner et al., Chapter 24).

Highly productive ecosystems, such as the Bering and Chukchi Seas, are generally characterized by predominantly large phytoplankton (i.e., pelagic and ice algae diatoms), with picocyanobacteria making trivial contributions to phytoplankton biomass. Our findings challenge this premise by observing high abundances of the picocyanobacteria *Synechococcus*. Indeed, cell counts at some stations/depths exceeded those seen in oligotrophic ocean gyres. These stations with high Synechococcus abundances appear constrained to the warm, nutrient-depleted coastal

and shelf waters. Comparison of the carbon biomass contribution of *Synechococcus* to the total phytoplankton carbon shows that biomass contributions decline as total phytoplankton biomass increases (as expected), but that below a total phytoplankton carbon biomass of ~100 mg C/m^3 (~2 mg Chla/m^3), *Synechococcus* often accounts for 20% to >40% of the biomass. In a compilation of data from prior studies that enumerated *Synechococcus* in the Chukchi Sea, it appears the warming of this region has supported a greater net seasonal growth of *Synechococcus* over the past decade. This finding suggests that multi-year periods of warmer than average conditions are altering the seasonal phytoplankton succession pattern (Lomas et al., Chapter 16).

O7. **Microbial food web model** (H4, H5) Use new primary production data to validate and constrain a model of ocean primary productivity and fate in regions where subsurface productivity maxima are important.

Nielsen et al. (Chapter 21) use new empirical biomass and rate measurements data to validate and constrain a linear inverse microbial food web model. This modeling approach allows reconstruction of trophic flows and quantification of biological rates that are commonly challenging to measure. Preliminary simulations indicate seasonal differences in major carbon pathways. Higher carbon fluxes appeared to be available for benthic consumers in spring (in areas of high primary production) compared to late summer. Our initial analyses also revealed the importance of carbon uptake and transfer in microzooplankton and bacterial compartments, organisms and processes that are often underestimated on many ecosystem models.

O8. **Secondary Production** (H8, H9) Quantify the distribution, size, abundance, and species composition of zooplankton and ichthyoplankton throughout the US shelf waters of the Chukchi Sea. Compare data to relative oceanographic conditions and to historical estimates as derived from AFSC sampling 2003- present.

Zooplankton are the link between phytoplankton and higher trophic levels. Spear et al. (Chapter 7) and Kimmel and Spear (Chapter 14) found that in the warm years of the IERP surveys, fewer *Calanus glacialis* were found during late summer compared to earlier in the decade. *C. glacialis* is the main prey item of juvenile Arctic cod and is also an important prey for bowhead whales and seabirds. As the strength of warming and northward transport increased in 2019, most of the Chukchi Sea was covered in southern associated zooplankton species. These smaller zooplankton are less nutritious prey, having less overall caloric and fat content. Further warming will likely result in increased importance of these smaller zooplankton as the Arctic experiences longer ice-free periods. This will correspond with greater carbon flow through the pelagic as opposed to delivery to the benthos.

O9. **Trophic Interactions – Hot Spots** (H4, H5) Use primary production data to understand spatial variability in net community production and identify 'hot spots' of trophic connections between LTL and UTL, and how these might change in relation to other on-going projects in the region focused on detecting change (e.g., Distributed Biological Observatory [DBO]).

All primary production rates have been calculated and elevated primary production can be seen in regions of high nutrient availability (Eisner et al., Chapter 24). Spatial patterns in primary production rates have not yet been aligned with estimates of net community production, and UTL data to identify 'hot spots' of trophic connectivity, but this will be undertaken in the near future.

O10. **Trophic Interactions – Nutrition** (H6, H7, H8, H9) Determine spatial and temporal relationship between phytoplankton, zooplankton and ichthyoplankton. Link observations to UTL-derived data to provide mechanistic understanding of trophic relationships. Compare fatty acid profiles of seston (primarily phytoplankton) and zooplankton to relate carbon sources to nutritional condition of key forage fish (e.g., Arctic cod).

The determination of temporal and annual links between phytoplankton dynamics and zooplankton lipid storage is work that is currently in progress. Large Arctic zooplankton were found to have elevated lipid storage that is largely dependent on diatom production, which in the Chukchi Sea was found to be elevated in spring and in cold nutrient rich waters (Nielsen et al., Chapter 20). Lipid biomarkers in zooplankton and fish can help us understand the trophic component of their spatial and annual energetic variability. Recent shifts in zooplankton dynamics during warming, such as an increased abundance of small zooplankton (e.g., *Pseudocalanus* spp.), compared to large Arctic zooplankton (e.g., *Neocalanus* sp., *Calanus glacialis*) (Spear et al., Chapter 7; Kimmel and Spear, Chapter 14), have likely resulted in decreased zooplankton lipids available regionally in juvenile fishes diets. We measured a large drop in lipid-based condition metrics of juvenile Chukchi Sea Arctic cod and saffron cod from a current warm year (2017) compared to previous cold years (2012-2013) (Copeman et al., UTL Final Report, Chapter 11). This decline in gadid condition was linked to low *Calanus*- and diatom-sourced fatty acid biomarker in fish tissues. This work remains in progress. Future synthesis efforts will focus on: (1) spatial and annual links between phytoplankton quantity/quality and zooplankton lipids to understand mechanisms driving changes in zooplankton quality; and (2) combining newly generated species-specific Arctic zooplankton lipid values with climate-driven changes in zooplankton species composition to better forecast zooplankton quality that will be available to juvenile fish in a warming Arctic.

O11. **Ecosystem Connectivity** (H8, H9) Examine connectivity and exchange of lower trophic biota (zooplankton, ichthyoplankton, juvenile fish) between ecosystems (northern Bering Sea, Chukchi, Beaufort) to determine if each region acts as a source or a sink of ichthyo- and zooplankton stocks.

In warm years characterized by low sea-ice coverage and strong advection of water masses from the Bering Sea to the Chukchi Sea, we observed a northward shift and range contraction of the late summer Arctic larval fish assemblage (e.g., Arctic Cod, Bering Flounder, Arctic Sand Lance, and Arctic Shanny). Over the same time period, we observed a range expansion of warmer water assemblages (comprised of lower latitude, boreal species such as Yellowfin Sole, Pollock, and Capelin) and increasing species-level abundances in response to Arctic warming. The resulting structural changes to the larval fish community will likely continue with projected ocean warming and sea-ice loss, with consequences for biodiversity, food-web configuration, and trophic pathways in the Arctic (see Axler et al., Chapter 10).

With respect to zooplankton, yearly advection from the Bering Sea influences zooplankton community structure. Increased advection and earlier ice retreat results in zooplankton communities that exhibit less diversity and lower abundances of the lipid-rich copepod Calanus glacialis. These warm-year zooplankton communities are more closely related to water masses that are advected from the south (Spear et al., Chapter 7; Kimmel and Spear, Chapter 14).

O12. **Arctic Cod and Saffron Cod** (H9) Further resolve spawning and connectivity of Arctic Cod and Saffron Cod adults, larvae and juveniles by providing new field data on late-stage larvae in summer that will be used to ground truth results from biophysical transport model efforts.

Arctic Cod (*Boreogadus saida*) and Saffron Cod (*Eleginus gracilis*) are ecologically important forage-fish species in the Arctic. Their life histories have evolved in a system dominated by seasonal sea-ice dynamics, which is currently changing rapidly making these species vulnerable to the effects of climate change. For the first time, we were able to synthesize the seasonal distribution, abundance, and growth of two co-occurring Arctic forage fishes. Kotzebue Sound was likely a source of early-stage Arctic Cod and Saffron Cod found offshore of Point Hope / Cape Lisburne and in nearshore coastal areas to the north. However, Arctic Cod found in the Hanna Shoal region are not likely hatched from Kotzebue Sound, but from other areas such as Bering Strait and Chukotka Peninsula. Growth rates estimated in 2017, an extremely warm year in the Arctic, were higher than in previous studies, although this should be confirmed using otolith-derived growth rates (Deary et al., 2021; Deary et al., Chapter 3).

O13. **US/Russian Chukchi** (H8, H9) Connect US Chukchi Sea IERP surveys to those planned in the Russian exclusive economic zone (EEZ; 2017, 2019; Melnikov, TINRO; Afanasyev, VNIRO).

The IES cruises included participants from TINRO and VNIRO. Eisner, Ladd, and Duffy-Anderson collaborated with Russian oceanographers, Yury Zuenko and Eugene Basyuk at the Pacific Branch of Russian Research Institute of Fisheries and Oceanography (TINRO) to compile surface and bottom water temperature data and pollock abundance data (juveniles and adults) from the eastern and western Bering Sea. This effort resulted in a joint publication (Eisner et al., Chapter 4) with communication ongoing including plans for workshops and a special issue.

Application to Resource Management and Alaskan Communities

Recognizing the potential for commercial fishing activities to expand into the northern Bering Sea and the Arctic, and the lack of baseline information from these areas, the North Pacific Fishery Management Council (NPFMC) has taken several proactive measures to prevent the northward expansion of commercial fishing without prior assessment of fisheries resources. These measures include a ban on non-pelagic trawling in the Northern Bering Sea Research Area until a research plan can be developed and a ban on all commercial fishing in the US Exclusive Economic Zone of the Arctic under the Arctic Fishery Management Plan (FMP, https://www.npfmc.org/arctic-fishery-management/). Implementation of the FMP requires baseline surveys to assess the status of fisheries resources in the Arctic. Information on fish populations collected by this and other projects are critical to informing the NPFMC about the status of fish stocks in the Chukchi Sea and environmental mechanisms underpinning variation in their populations. The Arctic FMP identifies Arctic cod (*Boreogadus saida*), saffron cod (*Eleginus gracilis*) and snow crab (*Chionoecetes opilio*) as potential target species in the Chukchi Sea. An important and required element of any FMP is a description of Essential Fish Habitat (EFH) for each target species in the FMP. Data collected during our surveys already contribute to updating EFH descriptions for the three species named in the Arctic FMP using the best available scientific information.

Together, the LTL and UTL components provide a comprehensive view of the ecosystem and provide clarity on the changing ecosystem for resource managers and Alaskan communities. The LTL program found that there is an increased transport and heat flux into the Arctic basin, substantial interannual variability in the amount of nutrients available to sustain spring production, and that warming will increase the spatial extent of picocyanobacteria Synechococcus, a smaller less energy-rich phytoplankton that will negatively impact the flow of energy to higher trophic levels. There appear to be concomitant reductions in larger sized zooplankton, reducing the amount of prey available for larger, pelagic predators such as bowhead whales and seabirds. There will be winners and losers in the Arctic fishes as climate-driven distribution shifts are restructuring larval fish community composition and bioenergetic pathways that will influence the flow of energy to higher trophic levels. This will have cascading consequences for upper trophic level production that provides the basis for commercial fishing communities, and for local communities in the Arctic that rely on fishes, seabirds and marine mammals for food.

The UTL Arctic Integrated Ecosystem Surveys provide further information on the impact of climate variability on ecosystem function and fitness of fishes and invertebrates. During the research period (2016 to 2021), adult subarctic gadids moved into the northern Bering Sea in large numbers. Commercial fishing for Pacific cod (using longline) commenced within the northern Bering Sea and in Russia's exclusive economic zone in the Chukchi Sea. However, we did not find large numbers of adults of either subarctic or arctic gadids (Arctic cod and saffron cod) within the Chukchi Sea survey region. We did find large numbers of age-0 Arctic cod and saffron cod as well as age-0 subarctic gadids (walleye pollock) within the southern Chukchi Sea region. Pollock were largely absent in previous surveys of the same area in 2005, 2012 and 2013, but were the most abundant pelagic fishes in many areas in 2017 and 2019. In 2019, age-0 Arctic cod were found further north in the survey region than was reported during earlier surveys (Arctic EIS 2012 and 2013). In addition, we found that warming ocean temperatures and increased transport during summer months through the Bering Strait improves habitat quality for juvenile salmon within the southern Chukchi Sea. These changes are related to faster early marine growth and survival of young salmon, potentially leading to higher numbers of adult salmon returns to the Arctic.

Prey quality is likely an important consideration: for example, age-0 Arctic cod are more lipid-rich and energy-dense than walleye pollock. Additionally, environmental factors are likely to play an important role in food quality: although juvenile Arctic cod were very abundant at the end of the warm (2017) summer season, they had only half the fat storage and lower overall energy content than those collected during colder years (2012/2013). Similarly, saffron cod, capelin and sand lance had slightly lower energy content in warmer years. These changes in the distribution of abundant age-0 pelagic fishes are consistent with expectations under continued warming, and will likely continue as the Alaska Arctic continues to warm. These changes in the abundance, distribution and lipid content of small fishes are likely to impact food availability and quality for higher trophic level predators (piscivorous fishes, marine mammals, and birds) and for communities who depend on these food sources. For example, piscivorous seabirds require forage fish of high energy density to raise chicks to fledging during the short Arctic summer. Low quality prey can significantly increase the number of fish needed to raise chicks, increasing foraging effort and extending the chick-rearing period. Late fledging dates and low fledgling weight can reduce overwinter survival. Low recruitment in harvestable seabirds can impact the ability of local communities to gather eggs and adult birds.

In response to changes in prey, some seabirds, such as short-tailed shearwaters and thick-billed murres, have shifted their distribution farther north, and are remaining in the Arctic later into summer or fall, but they must still return south through the Bering Strait. Other marine birds, such as eiders, maintain the timing of their post-breeding southward migration through the Bering Strait region. Due to lack of sea ice, these southward migration patterns now overlap with increased vessel traffic during months of nighttime darkness, potentially resulting in higher risk of vessel-bird collisions. The new overlap of human activities during fall migration of marine birds could pose challenges to bird conservation and to management of vessel traffic lanes throughout the region.

Our results from the Arctic Integrated Ecosystem Survey indicate that our overarching hypothesis:

Reductions in Arctic sea ice and the associated physical changes to the environment influence the flow of energy through the pelagic ecosystem in the Chukchi Sea. Specifically, we expect lasting changes in the seasonal composition, distribution and production of phytoplankton; in the distribution and standing stocks of large crustacean zooplankton that serve as the prey base for upper trophic level fishes and seabirds; in the assemblages, distributions, abundances, and body condition of larval and early juvenile fishes that influence the recruitment success of later life stages, and in the distribution and abundance of adult fishes

is being realized.

Collaborations

C1. **Alaska Ocean Observing System, AOOS.** PI - Stabeno (2020-2022) provides support to improve observations on the northern Bering Sea (NBS) mooring observatory.

C2. **Bureau of Ocean Energy and Management, BOEM:** and Coastal Impact Assistance Program (CIAP) - Arctic Integrated Ecosystem Survey (Eis) Phase 1. PIs - Farley, Mueter, Eisner et al., (NOAA-BOEM IAA-AK-11-08b, 1/1/12-5/31/16). Summer surveys were conducted in the NBS and CS in 2012 and 2013. Observations included pelagic fish and groundfish, zooplankton, oceanography, and total and size fraction Chl-a. We will relate satellite derived estimates of phytoplankton community composition (outcome of our proposal) to in-situ total and size-fraction Chl-a. The validated satellite data can be compared to distributions of zooplankton and fish in this region.

C3. **NOAA Northwest Fisheries Science Center & Woods Hole Oceanographic Institution:** Harmful Algal Blooms. PIs - Duffy-Anderson, Stabeno, Eisner, and Kimmel collaborated with WHOI researcher Don Anderson and NWFSC researcher Kathi Lefebre to collect samples for work on the detection of high levels of paralytic shellfish toxins in Northern Alaskan food webs.

C4. **International Partners.** Russia PIs - Eisner, Ladd, Duffy-Anderson collaborated with Russian oceanographers, Yury Zuenko and Eugene Basyuk at the Pacific Branch of Russian Research Institute of Fisheries and Oceanography (TINRO) to compile surface and bottom water temperature data and pollock abundance data (juveniles and adults) from the eastern and western Bering Sea. This effort resulted in a joint publication (see Chapter 4) with communication ongoing. Canada PIs - Stabeno and Mordy collaborated with Catherine Lalande (Amundsen Science) in an NPRB project to enhance the M8 observatory with sediment traps that will enable the determination of export flux to the benthos.

C5. **NOAA Arctic Research Program - ARP.** PIs - Stabeno, Duffy-Anderson and Mordy supports moorings and annual scientific cruises to the Pacific Arctic region during which U.S. scientists take a wide range of physical, chemical, and biological samplings including Distributed Biological Observatory (DBO). The DBO has designated eight “hot spots" across the Bering, Chukchi, and Beaufort seas where multidisciplinary sampling is focused. We have partnered with the DBO Program to collect a suite of physical and biological measurements in the Chukchi Sea over multiple years and to make these observations available to the AIERP Program. The DBO is a collaboration between multiple U.S. federal agencies and academic institutions as well as from other Arctic nations.

C6. **NOAA Ecosystems and Fisheries-Oceanography Coordinated Investigations (EcoFOCI) Program and Recruitment Process Alliance (RPA) at NOAA PMEL/AFSC**. PIs - Stabeno, Duffy-Anderson, Farley, Axler, Copeman, Deary, Eisner, Gann, Goldstein, Kimmel, McCabe, Mordy, Nielsen, Spear, et al., This is an integrated long-term base-funded NOAA program that conducts research in the US Arctic. It maintains long- term ecosystem moorings in the Bering Sea (since 1995) and Chukchi Sea (CS; since 2010) and spends >100 days at sea each year. Field observations include: temperature, salinity, oxygen, currents, nutrients, phytoplankton (size-fractionated Chl-a, taxa, productivity), zooplankton/ ichthyoplankton, pelagic fish and groundfish. EcoFOCI’s goal is to improve understanding of ecosystem dynamics and apply that understanding to fisheries management. Field, laboratory and modeling studies are integrated to reach this goal.

C7. **NOAA PMEL Innovative Technology for Arctic Exploration program.** PI - Mordy (co-PI C. Meinig, PMEL). To better study arctic marine ecosystems and the rapid changes that are occurring, we are collaborating with the Innovative Technology for Arctic Exploration (ITAE) program as it works to develop innovative technologies, including sensors and platforms, to meet the scientific demand in these regions. The mission of the ITAE program is to conceptualize and build effective research equipment for the assessment of the Arctic environment and ecosystem with the operation of high-resolution sensors on autonomous platforms near sea ice. The dynamic and fine-scale nature of these regions requires responsive, high-resolution data collection over large areas in real time — a logistical challenge ideally suited to fast, mobile autonomous platforms rather than traditional ship-based operations. Existing autonomous platforms are both small and slow, limiting the observational capacity, responsiveness, and deployment capabilities. ITAE is a collaborative research effort by University of Washington (JISAO now CICOES) and NOAA engineers and scientists at the Pacific Marine Environmental Lab (PMEL). This program leveraged saildrone missions and ALAMO float deployments (in collaboration with PMEL's Arctic Heat program).

C8. **NOAA AFSC Marine Mammal Laboratory**. PI - Stabeno collaborates with Catherine Berchok (NOAA AFSC) to assess spatiotemporal variability of marine mammals in the CS and NBS. They coordinate in deploying passive acoustic moorings and in data analysis that helps to elucidate climatic, physical, and biological forcing of marine mammal distributions.

C9. **NOAA National Oceanographic Partnership Program (NOPP)** Expanding exploration and using innovative technologies to assess the rapidly changing Bering and Chukchi Seas. PIs - Stabeno, Mordy, Lomas (Bigelow), Duffy-Anderson, Farley, Logerwell, Berchok, Eisner, Kimmel, Gann, Nielsen, Du (OSU). The US Arctic ecosystems are undergoing dramatic, unprecedented changes in response to ocean warming and declines in sea ice. In addition to the physical changes, biological shifts across all trophic levels have been observed (e.g., phytoplankton community composition and bloom timing; zooplankton dynamics; spatial shifts in fish distributions). This project expands ecosystem observations in NBS and southern CS using traditional and new technologies. Emergent technologies include profiling platforms, speciation techniques ('omics), in-situ visualization, and unmanned vehicles. This project will create new Ecosystem Observatories in the US Arctic.

C10. **NOAA/NASA Joint Polar Satellite System (JPSS)** Satellite analysis of shifts in phytoplankton community composition and energy flow in the new Arctic. PI - Eisner, Lange (Blue Marble Space Institute of Science), Lomas, Mordy, Nielsen, Stabeno; Collaborators Gann (AFSC), Lefebvre (NWFSC, HABs), Robinson (UC Santa Cruz, CoastWatch/PolarWatch), Wilson (SWFSC, CoastWatch/PolarWatch), 6/1/21-5/31/2. The overall goals of this project are to: 1) analyze the variability of phytoplankton community size structure based on spectral slopes of absorption, backscattering, remote-sensing reflectance ($R_{rs}(\lambda)$), and empirical chlorophyll-a (Chl-a) -based algorithms from JPSS satellite data across time and space; 2) modify existing ocean color algorithms to exploit the unique $R_{rs}(\lambda)$ properties of Synechococcus in order to determine changes in this picoplankton group; 3) estimate diatom abundances from Chl-a-specific absorption; and 4) explore correlative methods to assess the probability of occurrence of harmful algae such as Pseudo-nitzschia spp. and Alexandrium spp. using Sentinel 3-A-OLCI satellite products to improve HAB predictions in the North Bering Sea (NBS) and Chukchi Sea (CS). Data from Arctic IERP will be used for ground-truthing satellite data.

C11. **National Science Foundation** What controls the transfer of diatom organic matter to age-0 pollock prey in the Bering Sea ecosystem? PI - Lomas et al., (#OPP-1603460, 11/2016-10/2019). This project explored both physiological responses of polar diatoms in culture, and the ecology (primary production and phytoplankton community) of phytoplankton in the BS and CS. The results from this and other collaborative projects listed below suggest that not only will the nutritional value of diatoms decrease as the BS and CS warm, but also the phytoplankton community, especially in the summer/fall period, will shift to small picoplankton (e.g., Synechococcus).

C12. **North Pacific Research Board (NPRB) and Bureau of Ocean Energy Management (BOEM)** Evaluating historical and future climate-driven changes to Pacific cod spawning habitat in the Bering Sea. PIs - Rogers, Mordy, Stabeno, et al., (NPRB #2003, 7/2020 - 6/2023). This project focuses on exploring the seasonal evolution of ocean temperature across the BS and its impact on spawning of Pacific cod. Specifics goals are to expand observations of seasonal oceanographic conditions in the eastern BS through deployment of an array of low-cost sensors to monitor bottom temperatures; use these data to validate and assess Regional Ocean Model System (ROMS) error and bias with respect to temperature dynamics; formally assimilate new data into ROMS; use ROMS and existing, experimentally-derived relationships between temperature and Pacific cod spawning success to characterize the extent, timing, and distribution of suitable spawning habitat; project the spatial distribution and timing of suitable spawning habitat under future climate scenarios; and introduce this information into the management process for Pacific cod. Changes in phytoplankton species and community structure, which will be directly assessed in the proposed research, impact ecosystem productivity with cascading effects on fish larval abundance and survival and spawning success.

C13. **NPRB** Monitoring export fluxes to detect seasonal and interannual changes in the pelagic ecosystem of the St. Lawrence Island Polynya Region. PIs - Stabeno, Mordy et al., (NPRB #1914, 2020 - 2024, 342,087). Climate change is rapidly affecting the NBS including the St. Lawrence Island Polynya (SLIP) where a large decline in sea-ice cover was observed in 2018, with potentially important consequences for the bird and marine mammal populations of the region. This project will deploy a sequential sediment trap to measure the magnitude and composition of the organic matter supplied to the benthic communities in the region. Sediment trap samples will provide continuous biological samples that will allow the monitoring of several aspects of the marine ecosystem from phytoplankton and zooplankton species to carbon supply to the benthos. This project will provide critical in-situ data for the proposed research, and addresses a pressing need for the long-term monitoring of the BS marine ecosystem to improve our ability to forecast and respond to the effects of climate change and provide deliverables to policy-makers.

C14. **PICES** WG44: NBS and Chukchi IEA. Chair - Logerwell. We are collaborating with PICES WG44 on the northern Bering-Chukchi Sea region to provide detailed assessment of the Pacific Arctic gateway, as well as detailed information that will inform understanding of connectivity of climate and ocean processes, species movements, shelf food web dynamics, fishing, trade, subsistence and food security, and human activities. The northern Bering Sea-Chukchi Sea (NBS-CS) region is experiencing unprecedented ocean warming and loss of sea ice as a result of climate change. Seasonal sea ice declines and warming temperatures have been more prominent in the northern Bering and Chukchi seas as almost all other portions of the Arctic.

C15. **Plankton Sorting and Identification Center,** Gdynia, Poland. Leads - Deary, Kimmel. AFSC collaborates with the Plankton Sorting Center to identify, size, and image zooplankton and ichthyoplankton collected from the northern Bering Sea and Chukchi Sea to document climate-mediated chiefs in plankton and larval fish abundance, size, distribution, and community structure.

Directions for Future Research

Through the combined LTL-UTL AIERP programs, key elements were identified for future research including maintaining long-term observations, incorporating new measurements into the observational programs, enhanced modeling of the region, and operationalizing new technologies. To further advance our understanding of ecosystem variability and climate-induced trends, we recommend the following elements for future research.

Monitoring

To establish baselines that will enable the assessment of trends and variability, we recommend the following activities be continued:

- Maintain moored observatories at key physical (e.g., Icy Cape, M8, C12,) and biological (e.g., C12) hot spots;
- Maintain hydrographic and zooplankton sampling transects (e.g., DBO, Icy Cape) and surveys (e.g., Northern Bering Sea Assessment);
- Continue planktonic monitoring to track ecosystem changes of phytoplankton, zooplankton and ichthyoplankton;
- Continue acoustics surveys and time series of fish as subarctic gadids begin moving into the Chukchi Sea;
- Maintain seabird observations on platforms of opportunity;
- Continue benthic sampling for fishes and invertebrates.

Expanding Observations

To address gaps exposed through this research and other program, we recommend the following:

- Expand the M8, M14, and C12 observatories with traditional (e.g., sediment traps, nitrate sensors, water samplers, eDNA samplers) and new (e.g., RISe profilers, imaging systems) technologies;
- Expand CTD, zooplankton, and fish (ichthyoplankton, juvenile, and adult stages) surveys to the Chukchi and Beaufort shelf break and western Beaufort Shelf;
- Measure taxon-specific grazing (e.g., grazing on Synechococcus) to determine if seasonal variability in growth is due to bottom-up (e.g., warming) or top-down control;

- Measure contributions of the pico fraction, nano-fraction and microplankton fraction to phytoplankton biomass (Chla) and productivity;
- Expand otolith-derived aging and microchemistry of early-stage fish species to enhance our understanding of habitat use, model parameterization, and energy allocation.

Modeling

To provide insights into biophysical processes and ecosystem trends and variability on spatiotemporal scales that cannot be realized through observational programs, we recommend the following:

- Enhance the ROMS based biophysical modeling suite while transitioning to regional MOM6;
- Validate and improve existing models using observational data from the Arctic IES;
- Assimilate observational data through targeted modeling sensitivity experiments;
- Use the modeling suite to understand mechanistic linkages within the biophysical system and align with the Synthesis, Analysis and Products listed below (e.g., quantify the transport of heat/salt, quantify drivers of nutrient flux, quantify extreme events);
- Integrate ROMS/MOM6 LTL modeling (up through zooplankton) with the AFSC Alaska Climate Integrated Modeling Project (ACLIM) that addresses marine ecosystem and fishery dynamics, and incorporates fishery economics.

Synthesis, Analysis and Products

- Quantify the transport of heat and salts;
- Quantify the physical and biological drivers of nutrient flux into the Chukchi Sea;
- Synthesize phytoplankton and zooplankton data to connect to other trophic level work including lipids in phyto- and zooplankton, fish distributions in comparison to plankton, kton, and zooplankton relation to seabird distributions;
- Conduct analysis of adult spawning stock biomass and fish egg data to determine if shifts in the distribution of species are due to increased larval transport and/or changes in spawning locations with warming;
- Conduct analyses of benthic-pelagic coupling to understand if a reorganization of the ecosystem in the northern Bering-Chukchi Seas ecosystem has occurred and what the impact will be on managed and subsistence resources;
- Develop metrics for Arctic ecosystem assessment.

Collaborations

To provide insights on the status of the Arctic ecosystem to stakeholders and the public; partnerships and collaborations must be enhanced. We recommend fostering existing collaborations identified earlier in

this report, and enhance collaborations with local communities and international partners (e.g., Canada, Russia).

New technology

To address observational gaps (e.g., seasonal transitions, phytoplankton and zooplankton speciation, under-ice production), we recommend expanded use of new and emerging technologies:

Imaging and Artificial Intelligence (AI)

- Employ phytoplankton imaging/AI on surface vehicles and moorings to derive speciation and identify and quantify species associated with Harmful Algal Blooms;
- Continue picophytoplankton counts to fill the phytoplankton size spectra and align with imaging methods;
- Monitor zooplankton communities using in-situ imaging/AI;
- Utilize towed and moored cameras with AI to assess decadal changes in the benthic community (e.g., epifauna, fish).

Platforms

- RISe (Refloating Ice Sensing) is a profiling mooring that submerges when ice arrives and refloats in the spring after ice retreat. The system includes a Prawler that moves up and down the mooring line measuring temperature, salinity, chlorophyll, and dissolved oxygen. RISe provides real-time information of the full water column during the entire open water season;
- Pop-up floats are deployed in the late summer/fall and rise to the surface under the ice the following spring. It can measure temperature, salinity, oxygen, fluorescence, PAR, and provide images on the seafloor and under ice;
- The MRV Systems ALAMO (Air Launched Autonomous Micro-Observer) is an autonomous vertically profiling float that is ice-reinforced for sampling through the winter;
- Benthic platforms (e.g., benthic rover, respirometers, microbial incubator, automated samplers) that can be used to assess shifts in the benthic community, nutrient cycling, and production;
- Optimize the use of saildrones and other uncrewed systems equipped with active acoustics to understand age -0 pelagic fish distributions and biomass (Chiodi et al., Chapter 1).

Synopsis

Why We Did it

To understand how reductions in Arctic sea ice and the associated changes in the physical environment influence the flow of energy through the lower trophic levels of the marine ecosystem in the Chukchi Sea.

What We Did

Researchers conducted Integrated Ecosystem Surveys (Arctic IES) aboard the R/V Ocean Starr (Figures 1a, 1c, 3) in late summer and early fall of 2017 and 2019. These surveys examined water properties (physics and chemistry) as well as phytoplankton and zooplankton assemblages. In addition to ship-board measurements, sub-surface moored sensors were deployed to gather biophysical information continuously from September 2016 to September 2019 including winter months when the system is ice covered. Autonomous platforms, such as gliders and saildrones, were used to complement the shipboard observations. .

What We Learned

Northward flow of water from the Bering Sea brings heat, salt and nutrients to the entire Chukchi continental shelf. The higher sea level in the Bering Sea compared to the Arctic Ocean results in a net northward transport. Approximately 40% of the flow through Bering Strait exits the shelf via Barrow Canyon. This flow on the Chukchi Sea is enhanced by northward winds and weakened by southward winds. During the last decade there has been an increase in the magnitude of northward flow on the shelf.

Phytoplankton serve as the energy source for the Arctic marine environment by converting nutrients and sunlight into a food base that ultimately sustains all marine life. In the Chukchi Sea, nitrate is a limiting nutrient for phytoplankton. Year-to-year differences in the amount of nitrate available to sustain spring production varies by about 50%. These differences result from the magnitude of transport through Bering Strait in the fall and winter, and the variability of nitrate concentration in the Bering Sea.

Changing conditions in the Arctic (e.g., warming and reduction in the duration and extent of ice) has altered the distribution, composition and food quality of phytoplankton. Shipboard observations show patchy distributions of phytoplankton and rapidly varying levels of primary productivity. Synechococcus (cyanobacteria) accounted for 20-40% of the total autotrophic biomass by the end of summer in 2019. This finding suggests that multi-year periods of warmer than average conditions altered the seasonal phytoplankton succession pattern. Phytoplankton fatty acids serve as a measure of the food quality of algae and were used to strengthen predictions of food web functioning and energy transfer to the upper trophic levels in the northern Bering and Chukchi Seas.

Particulate organic matter that falls to the sea floor, including ice algae, dead phytoplankton, and zooplankton fecal pellets, provides nutrition that sustains organisms living in that realm. For example, as ice begins to melt in spring, algae living on the underside of the ice detach and fall to the sea floor. The Chukchi Sea shelf is shallow enough that sunlight can penetrate to depth and detached ice algae can continue to photosynthesize near the seafloor.

There appears to be two distinct communities of zooplankton in the Chukchi Sea: a local, Arctic community related to water masses within the Chukchi Sea, and a community advected from the Bering

Sea. Thus, the relative magnitude of annual transport from the Bering Sea influences zooplankton community structure in the Chukchi Sea. Decreased transport and later ice retreat in colder years resulted in zooplankton communities that exhibited more diversity and had higher abundances of fat-rich copepods. In contrast, in years with increased transport from the south, expatriate zooplankton communities from the Bering Sea were prevalent in the Chukchi Sea. If the northward inflow of water into the Chukchi Sea were to increase with concomitant warming, changes in food-web structure and function are likely to result.

Similar to zooplankton, summer ichthyoplankton shifted northward. Shifts in community composition resulted from species-specific responses to temperature changes, ice cover, Bering Strait advection, and changes in the zooplankton prey base. By 2100, some bottom dwelling animals will find themselves in a habitat that is warmer than their preferred temperature range and perhaps even warmer than they can survive. These animals include prey for bottom feeding whales, pinnipeds, seals and walruses, seabirds, and benthic fishes. Snow crabs will likely benefit from warmer bottom ocean temperatures.

Why It Matters

Unprecedented warming observed during the course of the Arctic IERP program during the survey years may offer a window into the future Arctic. The biological indicators reported here suggest that increased warming could alter ecosystem structure and function with as yet unknown consequences for the people that depend on marine resources in the region.

Acknowledgements

We thank the captains, crew, and scientific staff who participated on the research expeditions conducted on the Ocean Starr and Sikuliaq. This study was funded by the North Pacific Research Board and numerous partners as outlined in the preamble. Additional funding was from NOAA PMEL and the Cooperative Institute for Climate, Ocean, & Ecosystem Studies (CIOCES) under NOAA Cooperative Agreements NA20OAR4320271 and NA15OAR4320063. This is contribution 2022-1215 to CICOES and 5330 to PMEL.

General References

Ardyna, M., Gosselin, M., Michel, C., Poulin, M., and Tremblay, J.E., 2011. Environmental forcing of phytoplankton community structure and function in the Canadian High Arctic: contrasting oligotrophic and eutrophic regions, Mar. Ecol. Prog. Ser., 442, 37–57, doi:10.3354/meps09378.

Arrigo, K. R., D. K. Perovich, R. S. Pickart, Z. W. Brown, G. L. van Dijken, K. E. Lowry, M. M. Mills, M. A. Palmer, W. M. Balch, N. R. Bates, C. R. Benitez-Nelson, E. Brownlee, K. E. Frey, S. R. Laney, J. Mathis, A. Matsuoka, B. Greg Mitchell, G. W. K. Moore, R. A. Reynolds, H. M. Sosik, and J. H. Swift., 2014. Phytoplankton blooms beneath the sea ice in the Chukchi Sea. Deep Sea Res. Part II, 105:1-16. DOI: 10.1016/j.dsr2.2014.03.018.

Arrigo, K.R., van Dijken, G.L., 2015. Continued increases in Arctic Ocean primary production. Prog. Oceanogr. 136, 60-70. http://dx.doi.org/10.1016/j.pocean.2015.05.002.

Atwood, E., Duffy-Anderson, J.T., Horne, J.K., Ladd, C., 2010. Influence of mesoscale eddies on ichthyoplankton assemblages in the Gulf of Alaska. Fish. Oceanogr. 19, 493-507. DOI: 10.1111/j.1365-2419.2010.00559.

Beaugrand, G., Brander K. M., Lindley J. A., Souissi S., Reid P. C. 2003. Plankton effect on cod recruitment in the North Sea. Nature. 426:661-664.

Beaugrand. G., Reid P. C., Ibañez F., Lindley J. A., Edwards M. 2002. Reorganisation of North Atlantic marine copepod biodiversity and climate. Science. 296:1692-1694.

Berchok, C.L., J.L. Crance, J.A. Mocklin, P.J. Stabeno, J.M. Napp, M. Wang, and C.W. Clark. 2015. Chukchi Offshore Monitoring In Drilling Area (COMIDA): Factors Affecting the Distribution and Relative Abundance of Endangered Whales. Draft Final Report, OCS Study BOEM 2015. National Marine Mammal Laboratory, Alaska Fisheries Science Center, NMFS, NOAA, 7600 Sand Point Way NE, Seattle, WA 98115-6349.

Busby, M., Duffy-Anderson, J.T., Mier, K.L., and De Forest, L. 2014. Spatial and temporal patterns in summer ichthyoplankton assemblages on the eastern Bering Sea shelf 1996− 2007. Fisheries Oceanography. 23(3): 270-287.

Carmack, E.C., Winsor, P., Williams, W. In press. The contiguous riverine coastal domain. Progress in Oceanography.

Cooper, D., Duffy-Anderson, J.T., Norcross, B., Holladay, B., and Stabeno, P. 2014. Northern rock sole (Lepidopsetta polyxystra) nursery areas in the eastern Bering Sea. ICES J Marine Science. doi:10.1093/icesjms/fst210.

Comiso, J.C., Parkinson, C.L., Gersten, R., Stock. L. 2008. Accelerated decline in arctic sea ice cover. Geophysical Research Letters, 35, L01703, doi:10.1029/2007GL031972.

Duffy-Anderson, J.T., Barbeaux, S., Farley, E., Heintz, R., Horne, J., Parker-Stetter, S., Petrik, C. and Smart, T. 2016. The critical first year of life of walleye pollock in the eastern Bering Sea: implications for recruitment and future research. Deep Sea Res. II. doi: 10.1016/j.dsr2.2015.02.001.

Duffy-Anderson, J.T., Busby, M.S., Mier, K.L., Deliyanides, C.M. and Stabeno, P.J. 2006. Spatial and temporal patterns in summer ichthyoplankton assemblages on the eastern Bering Sea shelf 1996-2000. Fish. Oceanogr. 15, 80-94.

Eisner, L., Hillgruber N., Martinson E., Maselko J. 2013. Pelagic fish and zooplankton species assemblages in relation to water mass characteristics in the northern Bering and southeast Chukchi Seas. Polar Biology, DOI 10.1007/s00300-012-1241-0.

Eisner, L., Napp, J., Mier, K., Pinchuk, A., Andrews A. 2014. Climate-mediated changes in zooplankton community structure for the eastern Bering Sea. Deep Sea Res II, doi: 10.1016/j.dsr2.2014.03.004.

Ershova, E., Hopcroft, R., and Kosobokova, K. 2015a. Inter-annual variability of summer mesozooplankton communities of the western Chukchi Sea: 2004-2012. Polar Biology. doi: 10.1007/s00300-015-1709-9.

Ershova, E., Hopcroft, R., Kosobokova, K., Matsuno, K., Nelson, R., Yamaguchi, A., Eisner, L. 2015b. Long- Term Changes in Summer Zooplankton Communities of the Western Chukchi Sea, 1945–2012. Oceanography 28(3):100-115, http://dx.doi.org/10.5670/oceanog.2015.60.

Grebmeier, J.M., J.E. Overland, S.E. Moore, E.V. Farley, E.C. Carmack, L.W. Cooper, K.E. Frey, J.H. Helle, F.A. McLaughlin, and S.L. Mc Nutt. 2006. A major ecosystem shift in the northern Bering Sea. Science 311: 1461-1464.

Grebmeier, J.A., B.A. Bluhm, L.W. Cooper, S.L. Danielson, K.R. Arrigo, A.L. Blanchard, J.T. Clarke, R.H. Day, K.E. Frey, R.R. Gradinger, M. Kedra, B. Konar, K.J. Kuletz, S.H. Lee, J.R. Lovvorn, B.L. Norcross, and S.R. Okkonen 2015. Ecosystem characteristics and processes facilitating persistent macrobenthic biomass hotspots and associated benthivory in the Pacific Arctic. Progr. Oceanogr. Synthesis of Arctic Research (SOAR) special issue 136: 92-114.

Hopcroft, R.R., Kosobokova K.N., Pinchuk A.I., 2010. Zooplankton community patterns in the Chukchi Sea during summer 2004. Deep-Sea Res II 57:27–29.

Jackson, J.M., Carmack, E.C., McLaughlin, F.A., Allen, S.E., Ingram, R.G., 2010. Identification, characterization, and change of the near-surface temperature maximum in the Canada Basin, 1993–2008. Journal of Geophysical Research: Oceans 115. 10.1029/2009JC005265.

Koch, C.W., Cooper L.W., Grebmeier J.M., Frey K., Brown T.A. 2020. Ice algae resource utilization by benthic macro- and megafaunal communities on the Pacific Arctic shelf determined through lipid biomarker analysis. Mar Ecol Prog Ser 651:23-43. https://doi.org/10.3354/meps13476

Li, W.K.W., McLaughlin F.A., Lovejoy C., Carmack, E.C., 2009. Smallest algae thrive as the Arctic Ocean freshens. Science, 326, 5952–539.

Logerwell, E., Busby, M., Carothers, C., Cotton, S., Duffy-Anderson, J.T., Farley, E., Heintz, R., Holladay, B., Horne, J., Johnson, S., Lauth, R., Moulton, L., Neff, D., Norcross, B., Parker-Stetter, S., Seigle, J., and Sformo, T. 2015. Fish communities across a spectrum of habitats in the western Beaufort Sea and Chukchi Sea. Progress in Oceanography. 136:115-132.

Moore, S.E., and P.J. Stabeno 2015. Synthesis of Arctic Research (SOAR) in marine ecosystems of the Pacific Arctic. Progr. Oceanogr. Synthesis of Arctic Research (SOAR) special issue 136: 11.

Mordy, C.W., L. Eisner, K. Kearney, D. Kimmel, M.W. Lomas, K. Mier, P. Proctor, P.H. Ressler, P. Stabeno, and E. Wisegarver (2021): Spatiotemporal variability of the nitrogen deficit in bottom waters on the eastern Bering Sea shelf. Cont. Shelf Res., 224, 104423, doi: 10.1016/j.csr.2021.104423

Mueter, F. J., Weems, J., Farley, E. V., & Sigler, M. F. (2017). Arctic ecosystem integrated survey (Arctic Eis): marine ecosystem dynamics in the rapidly changing Pacific Arctic Gateway. Deep Sea Research Part II: Topical Studies in Oceanography, 135, 1-6.

Norcross, B., Raborn, S., Holladay, B., Gallaway, B.J., Crawford, S.T., Priest, J., Edenfield, L.E., and Meyer, R. 2013. Northeastern Chukchi Sea demersal fishes and associated environmental characteristics 2009-2010. Continental Shelf Research. 67: 77-95.

Richardson, A.J. 2008. In hot water: zooplankton and climate change. ICES J. Mar. Sci. 65(3): 279-295.

Siddon, E. C., Duffy-Anderson, J.T., and Mueter, F. 2011. Community-level response of ichthyoplankton to environmental variability in the eastern Bering Sea. Mar. Ecol. Prog. Ser. 426: 225-239.

Siddon, E.C., Kristiansen, T., Mueter, F., Holsman, K., Heintz, R., Farley, E. 2013. Spatial match-mismatch between juvenile fish and prey provides a mechanism for recruitment variability across contrasting climate conditions in the eastern Bering sea. PlosOne. DOI: 10.1371/journal.pone.0084526.

Stabeno, P., N. Kachel, C. Ladd, and R. Woodgate (2018): Flow patterns in the eastern Chukchi Sea: 2010–2015. J. Geophys. Res., 123(2), 1177–1195, doi: 10.1002/2017JC013135.

Stabeno, P.J., S. Danielson, D. Kachel, N.B. Kachel, and C.W. Mordy (2016): Currents and transport on the eastern Bering Sea shelf: An integration of over 20 years of data. *Deep-Sea Res. II*, *134*, 13–29, doi: 10.1016/j.dsr2.2016.05.010, Understanding Ecosystem Processes in the Eastern Bering Sea IV

Stabeno, P.J., and R.M. McCabe (2020): Vertical structure and temporal variability of currents over the Chukchi Sea continental slope. Deep-Sea Res. II, 177, 104805, doi: 10.1016/j.dsr2.2020.104805

Stammerjohn, S., Massom, R., Rind, D., Martinson, D., 2012. Regions of rapid sea ice change: An inter-hemispheric seasonal comparison. Geophys. Res. Lett. 39. 10.1029/2012GL050874.

Wood, K.R., N.A. Bond, J.E. Overland, S.A. Salo, P. Stabeno, and J. Whitefield, 2015. A decade of environmental change in the Pacific Arctic region. Prog. Oceanogr., 136, 12–31, doi: 10.1016/j.pocean.2015.05.005.

Woodgate, R.A., Weingartner, T.J., Lindsay, R., 2012. Observed increases in Bering Strait oceanic fluxes from the Pacific to the Arctic from 2001 to 2011 and their impacts on the Arctic Ocean water column. Geophys. Res. Lett. 39. L24603, doi: 10.1029/2012GL054092.

Presentations

Axler K., Goldstein E., Nielsen J., Deary A., Duffy-Anderson J. 2021. Arctic larval fish community changes in relation to recent trends in warming and advection. NOAA in Alaska and the Arctic Seminar Series. November 2021.

Axler, K., Copeman, L., Nielsen, J. Eisner, L. 2020. Seasonal and annual patterns in fatty acid dynamics of Arctic seston from the North Bering-Chukchi Sea regions. AMSS January 2020.

Banas N, Hunter A, Ashjian CA, Keister JE, Campbell RE, Kimmel DG, Eisner LB, Ferreira SA, Zhang J. 2020. Modelling Calanus population dynamics under climate change along the North American Pacific margin from the California Current to the Arctic. Ocean Sciences Meeting. San Diego CA, USA.

Bayley, Y. Influence of the Alaska Coastal Current on Seasonal Patterns of Near-Bottom Chlorophyll Fluorescence in the Eastern Chukchi Sea. AMSS January 2021 virtual meeting.

Bell, S. W., P. J. Stabeno, C. A. Ladd, C. W. Mordy, R. M. McCabe, and K. R. Wood. 2018. Temporal evolution of the vertical structure of the Chukchi Sea water column: investigation from innovative research platforms, Ocean Sci. Meet., Abstract HE44A-2974, Portland, OR, February, 12–16, 2018.

Busby M.S., Duffy-Anderson J.T., Ferm N.C., Goldstein E.D., Kimmel D.G., Logerwell E. Ichthyo- and zooplankton collected in the eastern Chukchi Sea during summer 2017 with emphasis on the Distributed Biological Observatory (DBO) regions. Ocean Sciences Meeting, Portland, OR, USA.

Cynar, H. High-Resolution Biological Net Community Production in the Pacific-Influenced Arctic: A Multi-Method Comparison. AMSS January 2021 virtual meeting.

Deary, A.L. Ecosystem research in Alaska. Friday Harbor Laboratories, University of Washington. Friday Harbor, Washington, November 2019.

Deary, A.L. Fisheries update in the northern Bering Sea and Arctic. Interagency Arctic Research Policy Committee. Washington D.C. July 2019.

Deary, A.L., J.T. Duffy-Anderson, F. Mueter, C.D. Vestfals, E.D. Goldstein, E.A. Logerwell, P. Stabeno, S. Danielson. A synthesis of the early life history of two forage fishes in the US Arctic during a record sea ice minimum in 2017 (Oral). Early Life History Section, American Fisheries Society. Mallorca, Spain, May 2019.

Deary, A.L., J.T. Duffy-Anderson, F. Mueter, C.D. Vestfals, E.D. Goldstein, E.A. Logerwell, P. Stabeno, S. Danielson, R.R. Hopcroft. Seasonal abundance and distribution of larval polar cod (Boreogadus saida) and saffron cod (Eleginus gracilis) in the US Arctic (Oral). Arctic Science Summit Week. International Arctic Science Committee. Lisbon, Portugal (virtual), March 2021.

Deary, A.L. and D.G. Kimmel. 2019. Fisheries research in the United States Arctic (Oral). 45th Anniversary of the American Polish Cooperation Symposium. Gdynia, Poland, May 2019.

Duffy-Anderson, J.T. Cold water science. Gulf of Maine Research institute. Invited. July 2021.

Duffy-Anderson, J.T. A changing arctic: Can we forecast winners and losers? Invited. Savannah State University. October 2020.

Duffy-Anderson, J.T., Stram, D. and Evans, D. Ecosystem Approaches to Management. DFO. Invited. February, 2021.

Duffy-Anderson, J.T., Stram, D. and Evans, D. Ecosystem Approaches to the Arctic. World Fisheries Congress. September, 2021.

Duffy-Anderson, J.T. Long term monitoring in the Pacific Arctic advances ecosystem understanding and resource fisheries management. NOAA Arctic Science Seminar Series. September, 2021.

Duffy-Anderson, J.T. Ecosystem effects of ocean heating in high latitude regions. Invited. Savannah State University. October, 2021.

Eisner, L. 2016. Spatial and temporal variations in late summer chlorophyll a and zooplankton distributions in the northeastern Bering Sea. PICES North Bering Sea workshop 1: The role of the northern Bering Sea in modulating Arctic environments: towards international interdisciplinary efforts. Eisner, lead-PI on workshop with Kivva and Baker. San Diego, CA, October 2016.

Eisner, L. Phytoplankton species identification using the Flow Cam. Public outreach presentation, August 2017, Nome, AK.

Eisner, L. Overview of ASGARD 2017 and Arctic IES 2017 surveys. PICES North Bering Sea workshop 2: The role of the northern Bering Sea in modulating Arctic environments: towards international interdisciplinary efforts, Vladivostok, Russia, September 2017, talk presented by Baker (also in PICES Press winter 2018). Eisner, co-PI on workshop with Kivva and Baker.

Eisner, Lomas, Baer, Ladd. 2018. Variations in Summer Phytoplankton Communities across Water Mass Gradients in the Chukchi and Beaufort Seas. Ocean Sciences February 2018.

Eisner, L., Lomas, M., Nielsen, J. 2019. Variations in spring and summer phytoplankton size structure and composition across water mass gradients in the northern Bering and Chukchi seas. PICES Annual Meeting, 21-25 October 2019, Victoria, B.C., Canada

Eisner, L., S. Danielson, E. Farley, C. Ladd. 2019. Arctic Integrated Ecosystem Research in the Chukchi and North Bering Seas (2019). Second International Science and Policy Conference on Implementation of the Ecosystem Approach to Management in the Arctic, 25-27 June 2019, Bergen, Norway

Eisner, L.B. Environmental impacts on walleye pollock (Gadus chalcogrammus) distribution across the Bering Sea shelf. Invited. AMSS, January 2020. Pollock Conservation Cooperative (PCC) At-sea Processors Association Skippers Meeting. January 2021, NOAA AFSC Fisheries seminar series. March 2021.

Goldstein, E.D. , J.T. Duffy-Anderson, M. Rogers, R. Heintz (2019) High latitude food webs and sensitivities to ecosystem shifts for Arctic gadids during the early life stages. IMBeR Open Science Conference. Brest, France, November 2019

Goldstein, E.D, Cieciel, K., Cooper, D., Duffy-Anderson, J.T., Eisner, L., Farley, E., Kimmel, D., Kuletz, K., Ladd, C., Logerwell, E., Mordy, C., Spear, A., Stabeno, P. Impacts of unprecedented loss of sea ice on multiple trophic levels and ecosystem structure in the Chukchi and Beaufort Seas, Ocean Sciences Meeting, San Diego, CA, USA, February 2020.

Irby M., Kimmel D., Lomas M., Eisner L and Schnetzer A. Microzooplankton Community Structure and Abundance Patterns in the Northern Bering and Chukchi Seas, 2017 and 2019. Aquatic Sciences Meeting, February 2021, virtual meeting.

Kuletz K, Cushing D, Mueter F, Osnas E, Kimmel D, Labunski E, Gall A, Renner H, Dragoo D. 2020. Seabirds signal changes in the Pacific arctic. Alaska Marine Science Symposium, Anchorage, AK, USA.

Lefebvre K, Quakenbush L, Stimmelmayr R, Sheffield G, Hendrix A, Bryan A, Mounsey A, Willis M, Iversen E, Kimmel D, Duffy-Anderson J, Murphy J, Cieciel K, Siddon E, Eisner L, Fergusson E, Showalter S, Yasumiishi E, Gann J, Grebmeier J, Kibler S, Anderson D, Fachon E, Snyder J, Sylvander B. 2020. Algal toxins in Alaskan arctic food webs: krill, clams, benthic worms, fish, ice seals, walruses and whales! Alaska Marine Science Symposium, January 2020, Anchorage, AK, USA.

Levine, R. Where Do They Come from, and Where Do They Go? Abundance, distribution, and transport of age-0 gadids on the Chukchi Shelf. AMSS. January 2021 virtual meeting.

Lomas, Baer, Eisner. 2018. Seasonal distribution of picophytoplankton in the Bering and Chukchi seas. AMSS. January 2018.

Lomas, Eisner, Gann, Ladd, Mordy, Stabeno. 2019. Time series of primary production observations in the eastern Bering Sea: comparison of warm and cold stanzas. AMSS January 2019.

Lomas, M.W., Phytoplankton and Primary Production in a Changing (sub) Arctic. Invited, multiple institutions. Maine Maritime Academy Departmental Seminar. September 2019; University of Maine, Orono Departmental Seminar. October 2019; Duke University Marine Lab Graduate Student Seminar November 2019; Woods Hole Oceanographic Institution. Marine Chemistry and Geochemistry Departmental Seminar. January 2020; Woods Hole Oceanographic Institution. University of Alaska Fairbanks Departmental Seminar. January 2021.

McCabe, R. M., P. J. Stabeno, E. D. Cokelet, and D. Zhang. 2020. An observational description of currents over the Chukchi Sea continental slope, Ocean Sci. Meet., Abstract HE34C-2012, San Diego, CA, February, 16–21, 2020.

McCabe, R. M., P. J. Stabeno, E. D. Cokelet, and D. Zhang. 2020. An observational description of currents over the Chukchi Sea continental slope, Alaska Marine Science Symposium, Anchorage, AK, January, 27–31, 2020.

Mordy C, Duffy-Anderson J, Siddon E, Stabeno P, Andrews A, Deary A, Fugate C, Harpold C, Kimmel D, Lamb J, Porter S. 2018. Response of the Bering Sea Ecosystem to an Ice-Free Winter. AGU Fall Meeting, San Francisco, CA, USA.

Mordy, C.W. Seasonal and Interannual Variability of Nitrate in the Eastern Chukchi Sea: Transport and Winter Replenishment. AMSS January 2021 virtual meeting.

Mordy, C.W. and Chang B. A dive into Chukchi Sea nutrient cycling: New insights and new technology. NOAA EcoFOCI seminar series. March 2021.

Nielsen et al. Seasonal phytoplankton fatty acid dynamics in the North Bering-Chukchi Sea regions. AMSS 2021

Pickart, R. Mean and Seasonal Circulation of the Eastern Chukchi Sea from moored time series in 2013-14. AMSS January 2021 virtual meeting.

Sigler, M. Seasonal Patterns of Near-Bottom Chlorophyll Fluorescence in the Eastern Chukchi Sea: 2010–2019. AMSS January 2021 virtual meeting.

Sigler, M. Climate Change and Alaska Marine Ecosystems: Integrated ecosystem research is a powerful tool for understanding the effect of climate change Invited. NOAA EcoFOCI seminar series. March 2021.

Stabeno, P.J., Fresh Bering Sea Data, Strait Science Talk, October 2020.

Stabeno, P. Flow Patterns over the Chukchi Continental Shelf: 2010-2020. AMSS January 2021 virtual meeting.

Stabeno P, Kimmel D, Ladd C, Mordy C. 2020. Reduction of sea ice in the Bering Sea in 2018 and 2019 and some implications for the ecosystem. Alaska Marine Science Symposium, Anchorage, AK, USA.

Tabisola, H. New Technologies to Quantify a Changing Arctic. Strait Science Series, 17 August 2017, UAF Northwest Campus, Nome, AK

Tabisola, Heather. A Saildrone for Science: Probing the Arctic. Tabor Academy Science at Work Lecture Series, 13 February 2018, Tabor Academy, Marion, MA. Scientist in Residence.

Tabisola, Heather. Innovative Technology to Advance Ocean Observation. Alaska Marine Science Symposium, January 2018, Hotel Captain Cook, Anchorage, AK. Poster Session.

Tabisola, H.M.,Stabeno, P.J., Mordy, C.W. 2020. Innovative Technologies for Arctic Exploration: Successful partnerships to advance ocean research. Ocean Sciences Meeting, Abstract ED14D-3583, San Diego, CA. February 16-21, 2020.

Published Chapters

Chapter 1: Exploring the Pacific Arctic Seasonal Ice Zone with Saildrone USVs

Chiodi, A.M., C. Zhang, E.D. Cokelet, Q. Yang, C.W. Mordy, C.L. Gentemann, J.N. Cross, N. Lawrence-Slavas, C. Meinig, M. Steele, D.E. Harrison, P.J. Stabeno, H.M. Tabisola, D. Zhang, E.F. Burger, K.M. O'Brien, and M. Wang.

Citation:

Chiodi, A.M., Zhang, C., Cokelet, E.D., Yang, Q., Mordy, C.W., Gentemann, C.L., Cross, J.N., Lawrence-Slavas, N., Meinig, C., Steele, M. Harrison, D.E., Stabeno, P.J., Tabisola, H.M., Zhang, D., Burger, E.F., O'Brien, K.M., and Wang, M., 2021. Exploring the Pacific Arctic Seasonal Ice Zone With Saildrone USVs. Frontiers in Marine Science, 8, p.481. doi: 10.3389/fmars.2021.640697.

frontiers in Marine Science

ORIGINAL RESEARCH
published: 03 May 2021
doi: 10.3389/fmars.2021.640697

Exploring the Pacific Arctic Seasonal Ice Zone With Saildrone USVs

Andrew M. Chiodi[1,2], Chidong Zhang[2], Edward D. Cokelet[2], Qiong Yang[1,2†], Calvin W. Mordy[1,2], Chelle L. Gentemann[3,4], Jessica N. Cross[2], Noah Lawrence-Slavas[2], Christian Meinig[2], Michael Steele[5], Don E. Harrison[2], Phyllis J. Stabeno[2], Heather M. Tabisola[1,2], Dongxiao Zhang[1,2], Eugene F. Burger[2], Kevin M. O'Brien[1,2] and Muyin Wang[1,2]*

[1] *Cooperative Institute for Climate, Ocean and Ecosystem Studies, University of Washington, Seattle, WA, United States,* [2] *Pacific Marine Environmental Laboratory, National Oceanic and Atmospheric Administration, Seattle, WA, United States,* [3] *Farallon Institute, Petaluma, CA, United States,* [4] *Earth and Space Research, Seattle, WA, United States,* [5] *Polar Science Center, Applied Physics Laboratory, University of Washington, Seattle, WA, United States*

OPEN ACCESS

Edited by:
Gilles Reverdin, Centre National de la Recherche Scientifique (CNRS), France

Reviewed by:
Christoph Waldmann, University of Bremen, Germany
Alexandre Supply, Laboratoire de physique des océans et de télédétection par satellite (LOPS), France

**Correspondence:*
Andrew M. Chiodi
andy.chiodi@noaa.gov

† Present address:
Qiong Yang, The Climate Corporation, Seattle, WA, United States

Specialty section:
This article was submitted to Ocean Observation, a section of the journal Frontiers in Marine Science

Received: 11 December 2020
Accepted: 12 April 2021
Published: 03 May 2021

Citation:
Chiodi AM, Zhang C, Cokelet ED, Yang Q, Mordy CW, Gentemann CL, Cross JN, Lawrence-Slavas N, Meinig C, Steele M, Harrison DE, Stabeno PJ, Tabisola HM, Zhang D, Burger EF, O'Brien KM and Wang M (2021) Exploring the Pacific Arctic Seasonal Ice Zone With Saildrone USVs. Front. Mar. Sci. 8:640690. doi: 10.3389/fmars.2021.640697

More high-quality, *in situ* observations of essential marine variables are needed over the seasonal ice zone to better understand Arctic (or Antarctic) weather, climate, and ecosystems. To better assess the potential for arrays of uncrewed surface vehicles (USVs) to provide such observations, five wind-driven and solar-powered saildrones were sailed into the Chukchi and Beaufort Seas following the 2019 seasonal retreat of sea ice. They were equipped to observe the surface oceanic and atmospheric variables required to estimate air-sea fluxes of heat, momentum and carbon dioxide. Some of these variables were made available to weather forecast centers in real time. Our objective here is to analyze the effectiveness of existing remote ice navigation products and highlight the challenges and opportunities for improving remote ice navigation strategies with USVs. We examine the sources of navigational sea-ice distribution information based on post-mission tabulation of the sea-ice conditions encountered by the vehicles. The satellite-based ice-concentration analyses consulted during the mission exhibited large disagreements when the sea ice was retreating fastest (e.g., the 10% concentration contours differed between analyses by up to ~175 km). Attempts to use saildrone observations to detect the ice edge revealed that *in situ* temperature and salinity measurements varied sufficiently in ice bands and open water that it is difficult to use these variables alone as a reliable ice-edge indicator. Devising robust strategies for remote ice zone navigation may depend on developing the capability to recognize sea ice and initiate navigational maneuvers with cameras and processing capability onboard the vehicles.

Keywords: Arctic sea ice, saildrone, USVs, satellite sea-ice concentration, remote navigation, air-sea fluxes, surface marine observations, ice navigation

INTRODUCTION

The spring/summertime retreat of Arctic sea ice exposes approximately 10^7 km^2 of the ocean surface to direct exchanges of heat, momentum and carbon dioxide (CO_2) with the atmosphere in an area referred to as the seasonal ice zone (SIZ; Steele and Ermold, 2015). Knowledge of these fluxes is necessary to understand Arctic weather, climate, and ecosystems (Danielson et al., 2020; Lu et al., 2020; Ouyang et al., 2020; Qi et al., 2020; Terhaar et al., 2020). Accurate knowledge of the fluxes and

the surface variables from which they are estimated, such as sea surface temperature (SST), surface pressure, humidity, air temperature, and wind speed and the partial pressure of carbon dioxide (pCO_2) is useful for a variety of applications, including accurate initialization and validation of numerical weather forecast models (Liu et al., 2015; Zhang et al., submitted).

Since satellite-based estimates of sea-ice extent became routinely available in the late 1970s, summertime minimum (September) Arctic ice extent has noticeably declined (Wang and Overland, 2009, 2012; Stabeno and Bell, 2019), the ice season has shortened (Wang et al., 2018; Stabeno, 2019) and Arctic surface temperatures have risen faster than global mean surface temperatures (Serreze and Francis, 2006; Danielson et al., 2020). Results from climate forecast model experiments have projected that Arctic surface temperatures will continue to rise significantly faster than the global mean (Alexander et al., 2018), partly as a result of the coupling between diminishing Arctic sea ice and its effects on the surface to atmosphere heat flux (Walsh, 2014; Kashiwase et al., 2017). Accurate knowledge of surface heat and momentum fluxes and how they change with varying sea-ice concentration is necessary for further development and verification of Earth system models.

Few high-quality, direct measurements of surface oceanic and atmospheric variables are available in the Arctic SIZ. The benefits of using automated, uncrewed sampling platforms to increase our ability to observe the SIZ has been demonstrated by several research programs (see Lee et al., 2017, and references therein). Recent SIZ sampling strategies include deploying instrumentation on or in the ice (e.g., Polashenski et al., 2011; Timmermans et al., 2014; Gallaher et al., 2017), or on autonomous underwater vehicles and open water platforms, such as moored-buoys and wave gliders (Wood et al., 2013). Surface drifters (e.g., Thomson, 2012; Banzon et al., 2020) capable of measuring environmental parameters such as air and water temperature and wind speed, have also been deployed in open water and partial ice cover. Uncrewed surface vehicles (USVs) that can navigate from open water through ice zones, while collecting the observations needed to estimate (Bourassa et al., 2013) surface fluxes, would add a key component to our existing high-latitude observing capability. In summer 2019, a collaboration between NOAA, University of Washington and NASA investigators led to the deployment of five USVs, saildrones, with the objective of collecting such observations and providing a subset of them to forecast centers in real time. Saildrones are wind-driven, solar-powered and outfitted for this mission to measure near-surface wind speed and direction, humidity, air temperature and barometric pressure, upper ocean currents, SST, sea surface salinity (SSS), downward longwave and shortwave radiation, and pCO_2, among other variables (Cokelet et al., 2015; Meinig et al., 2015; Mordy et al., 2017; Zhang et al., 2019). A main mission objective was to measure these quantities in the SIZ up to the ice edge. Other objectives of the mission included collecting *in situ* observations for improving calibration of satellite-based measurements of SST in polar waters, occupying four Distributed Biological Observatory lines (Grebmeier et al., 2019), performing pCO_2 sensor cross-calibration tests with instrumentation aboard the USCGC Healy, ocean current surveys of Hanna Shoal, the Chukchi Shelf Current and the Alaskan Coastal Current (c.f. Li et al., 2019) and collecting data for surface flux estimates over Chukchi Sea regions being sampled simultaneously by Air Launched Autonomous Micro-Observer (ALAMO) profiling floats (Jayne and Bogue, 2017) and Beaufort Sea regions being sampled simultaneously by Seagliders (Eriksen et al., 2001) deployed during the Stratified Ocean Dynamics in the Arctic (SODA) experiment (Lee et al., 2016).

The saildrones were launched from Unalaska, AK, United States, in early May 2019, and sailed northward through Bering Strait in early June 2019. In order to successfully complete the mission, they would need to navigate through the SIZ and return to Unalaska before the combination of the energy stored in the vehicle's batteries and availability of solar power diminished below levels necessary to sustain vital communication, navigation and sensor functionality. Navigational information such as vehicle speed over ground and heading was relayed to the navigational team, with typically a few to several minutes delay. Four cameras mounted on the wing also provided images, which took ~30 min to be transmitted. These photos provided three perspectives: (i) upward-looking views of the sky; (ii) downward views of the vehicle hull and surrounding environs (e.g., **Figure 1A**); and (iii) horizontal views fore and aft of the wing (e.g., **Figure 1B**). The downward-looking photos in particular provided clear confirmation of times when the vehicles were in contact with or immediately next to sea ice.

Modern ice-navigation strategies for ships (e.g., Stoddard et al., 2016; Transport Canada, 2018) pair information about ship structure and capability (e.g., IACS, 2016) with estimates of ice concentration and type to assess risks along a route. Navigation-relevant ice information is available from a variety of sources offering different spatial resolutions and collection intervals (e.g., Hui et al., 2017; Rainville et al., 2020). Satellite information available presently includes passive microwave estimates of ice concentration, optical imagery and synthetic aperture radar (SAR) imagery. SAR offers the advantages of all-weather capability and relatively high spatial resolution compared to passive microwave data (e.g., Zakhvatkina et al., 2017 evaluate ice-water classification from Radarsat-2 ScanSAR images with 50 m × 50 m pixel spacing; see also Bertoia et al., 2004; Hui et al., 2017). The general use of individual wide-swath and relatively high-resolution SAR images, however, is limited by the large proportion of them that are not publicly available (Zakhvatkina et al., 2019). Several national ice centers synthesize ice distribution information from multiple sources and expert analysis to produce weekly to bi-weekly ice charts for strategic planning. The "tactical," or most direct navigational utility of ice-distribution information is usually limited to <24 h from the time it was collected (Scheuchl et al., 2004; Rainville et al., 2020).

The suite of remotely produced ice information potentially available for a USV mission such as ours is basically the same as

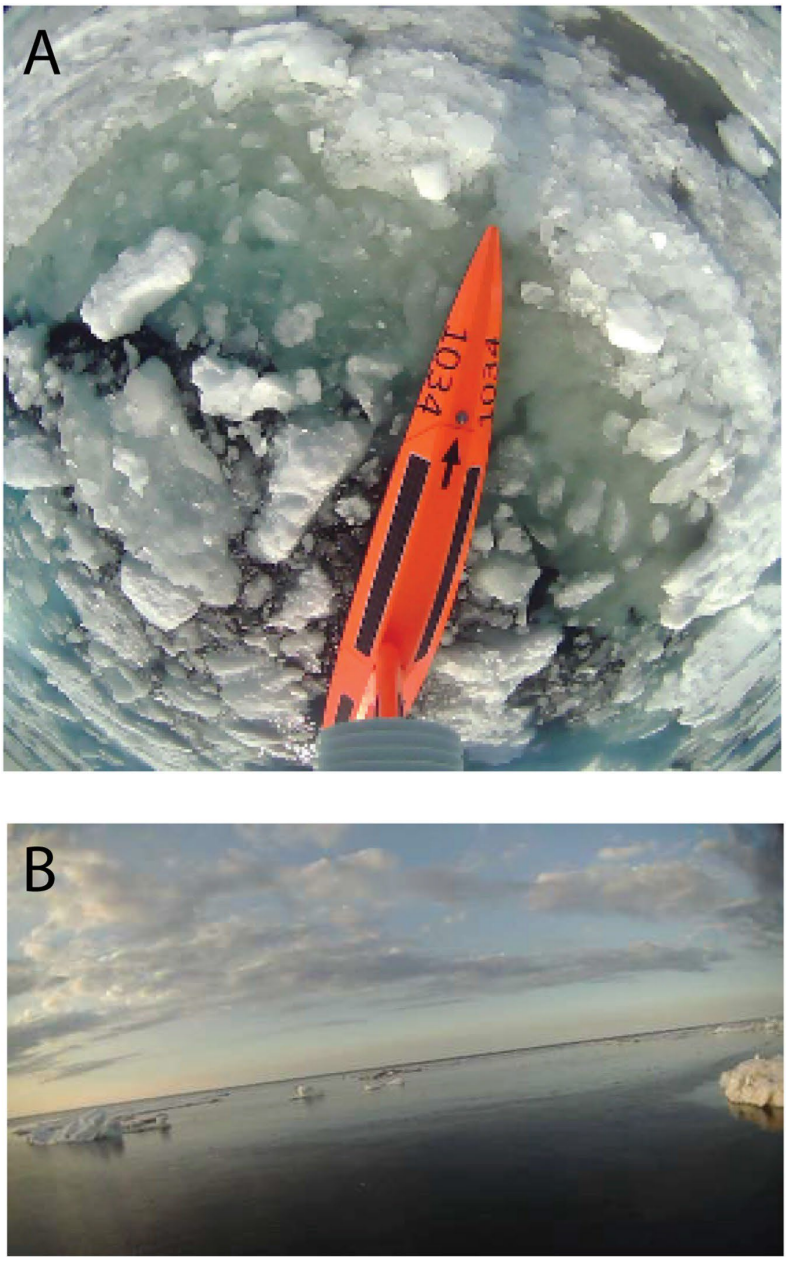

FIGURE 1 | Examples of (A) downward-looking image taken atop the saildrone wing while in sea ice, and (B) horizontal image from the saildrone wing with sea ice floes visible.

for ships. The questions asked of the ice information, however, may be somewhat different in each case. For example, Canadian Arctic experience has shown that sufficiently powered, ice-strengthened ships can make progress through first-year ice in concentrations up to 7/10ths without assistance from an icebreaker (Ice Navigation in Canadian Waters, 2012). Thus, navigating a Polar Class 6 or 7 ship (IACS, 2016) requires, particularly, information about where the ice distribution exceeds these criteria (c.f. Smith and Stephensen, 2013). Saildrones are not specifically designed to withstand collision with or push through sea ice, substantially limiting the range of ice conditions safely navigable compared to ice-strengthened ships. Most ships should also be able to "steer at slow speed around the floes in open pack ice [<6/10ths ice] without coming into contact with very many of them" (Ice Navigation in Canadian Waters, 2012). The capability to steer through floes is perhaps what most clearly distinguishes ship navigation from the situation faced by the USVs on our mission.

Saildrones navigate primarily by controlling the angle of the rudder and the vertically oriented, rigid wing, which

functions in roughly the manner of a mainsail on a traditional sailboat. They automatically navigate from waypoint to waypoint, accounting for wind and currents, while remaining within a specified corridor. The waypoints were decided by scientists and uploaded to the vehicles by Saildrone, Inc. pilots. The saildrones were not equipped during this mission with an automated capability to avoid collision; if their uploaded route intersected a floe, the vehicles would contact the floe unless re-routed by the pilot. In order for the objectives of this mission to be accomplished, the vehicles needed to repeatedly navigate in close proximity to sea ice. Several different types of information were considered or referred to during the mission to help with this navigational challenge. These sources included daily gridded satellite estimates of sea-ice concentration over the study region, natural color (optical) images of the surface provided by satellite radiometric measurements, SAR imagery and the daily 10% sea-ice concentration contour produced via multisensor analysis at the US National Ice Center (NIC). Information collected aboard the vehicles such as near-surface ocean temperature and salinity and the images from the vehicles' wings were also used.

The vehicle images and navigational metrics such as speed-over-ground provide a *de facto* record of when the vehicles were embedded in or in close proximity to ice floes. Here, we examine the relationships between this *de facto* record and the other (potential) sources of sea-ice distribution information that were considered or used while remotely navigating these five saildrones through the SIZ of the Chukchi and Beaufort Seas during May–October 2019. Our focus here is on products available publicly at daily, or higher, frequency and the observations and images collected by the USVs. Our objective in this article is to highlight both the challenges and strategies for improving remote ice navigation with USVs. Results may thereby provide a step forward for our wider objectives of understanding what sort of USV array is needed to monitor the Arctic (or Antarctic) SIZ in support of initializing and assessing the skill of operational numerical weather prediction systems and climate models, and validating numerical and satellite estimates of Arctic surface fluxes.

MATERIALS AND METHODS

In situ Observations

The saildrones deployed on this mission were part of a collaboration between Saildrone, Inc.[1] and the National Oceanographic and Atmospheric Administration (NOAA) Pacific Marine Environmental Laboratory (PMEL; Meinig et al., 2019) through a Cooperative Research and Development Agreement. Saildrones have ~ 7 m long hulls, rigid-wing heights 5 m above the water line, and keel depths of 2.5 m. The saildrone routes were coordinated with members of Alaska's North Slope and Northwest Arctic Boroughs and communicated through the United States Coast Guard Notice to Mariners to avoid potential interference with other uses of the Alaskan waterways. The vehicles' progress was monitored remotely by scientific and engineering team members. Batteries and solar panels power the onboard navigational electronics, which included automated identification system transceivers and Global Positioning System (GPS) navigational systems, as well as scientific instrumentation and satellite telemetry of data and navigational instructions. We designated the five saildrones deployed on this mission *sd-1033, sd-1034, sd-1035, sd-1036, and sd-1037*. Each was equipped with the following sensors: a Rototronic HC2-S3 sensor at 2.3 m height measured air temperature and relative humidity; a Sea-Bird SBE37 Microcat at 0.5 m depth measured seawater conductivity and temperature, which together provide seawater salinity; a Vaisala PTB210 Barometer on the hull (0.2 m height) measured sea level pressure; and a Gill model 1590-PK-020 anemometer atop the wing (5.2 m height) provided three dimensional wind velocity at 10 Hz. These wind measurements, along with synchronous measurements from the onboard inertial measurement unit (VectorNav model VN-300) and GPS, allowed for geo-referenced wind velocity to be calculated onboard and telemetered to the Global Telecommunications System and onshore data repositories as 1-min averages (as described in more detail in Zhang et al., 2019). The higher frequency data were stored onboard for access upon vehicle recovery. Zhang et al. (2019) reported that the auto-corrected saildrone wind speeds measured as a part of the Tropical Pacific Observing System – 2020 pilot study had RMS differences of 0.6 m s^{-1} with respect to the benchmark observations collected on the Salinity Processes in the Upper ocean Regional Study 2 (SPURS-2) buoy. This was based on hourly averages collected while the saildrones were within 12 km of the buoy, during which time the buoy measured a mean speed of 4.2 m s^{-1}, standard deviation of 1.9 m s^{-1} and maximum (minimum) wind speed of ~9.2 (0.2) m s^{-1}. A saildrone's speed over ground is dependent upon wind velocity, ocean current velocity, and navigation. Over the course of this Arctic mission, the vehicles measured an average wind speed of 5.4 m s^{-1}, and their average speed, with respect to the Earth's surface, excluding the times in which they were embedded in or left to drift with sea ice, was 0.96 m s^{-1}, or ~18% of wind speed. The maximum hourly averaged vehicle speed recorded during this mission was 2.9 m s^{-1} at an hourly mean wind speed of 12 m s^{-1} (sd-1035 on 19 July 2019). Sd-1033 and sd-1034 were equipped with Autonomous Surface Vehicle CO2 (ASVCO2; Sutton et al., 2014; Sabine et al., 2020) sensors capable of measuring pCO_2 in both the air and water. Along with wind speed, this pCO_2 information provided the basis for estimating the air-sea flux of carbon dioxide. ASVCO2 systems have been described and evaluated previously by Sabine et al. (2020) and found to provide pCO_2 observations within ±2 μatm of shipboard systems and moored autonomous pCO_2 systems. Sd-1033 and sd-1034 also had instruments capable of measuring solar irradiance, longwave radiation, ocean skin temperature (experimental), ocean color (Chl-a, CDOM), dissolved oxygen, pH and ocean current speed and direction (acoustic Doppler current profilers).

All of these saildrones, except sd-1037, were deployed with cameras mounted on their wings that provided three perspectives: (i) upward-looking views of the sky; (ii) downward views of the vehicle hull and surrounding environs (e.g.,

[1]saildrone.com

Figure 1A); and (iii) horizontal views fore and aft of the wing (e.g., **Figure 1B**). The saildrones sent back images every 5 to 60 min over most of the mission, but cameras were turned off during later stages of the mission to conserve power. The cameras on sd-1035 and sd-1036 collected images at a resolution of 1920 × 1080 pixels. The camera on sd-1034 was lower resolution (500 × 279).

The Saildrone-derived data used in this paper are hosted at PMEL by its Science Data Integration Group. These data are received from Saildrone during the mission and also as a bulk data acceptance post-mission. Data were delivered from Saildrone as discrete sampling geometry NetCDF files that included comprehensive documentation of the observations, including the standard and long names of the observed variables, their units, latitude, longitude and time of collection, as well as the name, vendor, serial number, installation height on the vehicle, installation date, date of last calibration, and sampling schedule of the sensor, among other information. During the mission, data files containing 1 min observations were delivered twice per hour, while high resolution (10 Hz and 1 Hz) data were delivered post-mission.

A subset of the 1-min observations received in near-real time were disseminated on the World Meteorological Organization (WMO) Global Telecommunication Service (GTS). The GTS is an operational network maintained by the WMO for the near-real time dissemination of environmental observations to be used in operational forecasting by global weather services. From this mission, an observation every 10 min was uploaded onto the GTS using the Global Ocean Observing System Observations Coordination Group developed Open Access to GTS framework, in partnership with PMEL and the NOAA National Data Buoy Center. This framework was developed to ease the process of globally distributing data in near-real time on the GTS for data producers such as Saildrone, Inc.

A saildrone (sd-1023) on a previous hydroacoustic survey in the Chukchi Sea (Levine et al., 2020) had a brief encounter with sea ice on 7 August 2018 at 71.5°N, 162°W. We analyzed its position, measurements and photographs with regard to various sea-ice products to obtain a preliminary evaluation of what information might be useful for guiding saildrones in sea ice.

To facilitate comparison between the *in situ* saildrone conditions and other potential sources of sea ice information, we define two *in situ* sea ice-related quantities. The first is called the "*In Situ* Sea Ice (ISSI)" record and is defined as 1 over the periods during which ice was visible in the downward or horizontal saildrone images and 0 when ice was not visible in the saildrone images. We use the term "ice free" in reference to the saildrone images. The resulting time series facilitates examination of the distributions of SST, salinity, and other observations collected while ice was or was not visible in the saildrone images. The second quantity is called "Ice-Blocked Vehicle (IBV)" and keys on the points at which the saildrones were blocked by ice on transects beginning in ice free water. Blockage points were determined based on un-commanded drops in vehicle speed-over-ground and inspection of saildrone images (discussed in more detail in the "Results" section). Knowing these ice-blockage points allows us to tabulate information about the changes in SST and salinity observed while approaching ice floes from open water. We use 3 h as the approach period based on preliminary examination showing that 3 h is long enough to capture some ice-free observations and the maximum negative SST and temperature gradients observed *en route* to the ice, yet short enough that ice-free measurements do not overly dominate the analysis and the vehicle route segments prior to IBVs did not, typically, include substantial changes in direction (e.g., change in USV heading of ~180°).

Satellite Information

The European organization for the exploitation of satellite measurements (EUMETSAT) offers daily gridded sea-ice concentration estimates based on radiances measured by the satellite-born Advanced Scanning Microwave Radiometer (AMSR-2). Hereafter, we refer to EUMETSAT's daily AMSR-2 ice concentration product as EA2. EA2 daily estimates are available starting in September 2016 on a 10 km horizontal resolution polar stereographic grid. Daily EA2 updates were typically available to us in the early local morning hours (Pacific Daylight Time = Universal Coordinated Time – 7 h) and were considered for use in route planning during the mission. The relationship between the EA2 values interpolated to the vehicles' positions and the *in situ* conditions encountered by the vehicles is further examined herein. To facilitate this examination, interpolated EA2 estimates have been binned at 1% concentration intervals with the first bin (labeled 0%) containing all 0% concentration estimates, the second, 1%, containing concentrations >0% and ≤1%, the third, 2%, containing concentrations >1% and ≤2%, and so forth. Herein, we calculate the ice extent of our study region as the area of EA2 grid cells within the region bounded by 145°W–180°W and 66°N–80°N with >10% ice concentration, in keeping with the definition used by the NIC. Lavelle et al. (2016) evaluated EA2 concentrations in reference to weekly ice charts produced by the NIC. This comparison was done on a grid point-by-grid point basis and found that the spatially aggregated percentage of Northern Hemisphere grid points with concentrations within 10% of one another was between 90 and 95% during their 1 January – 31 December 2015 analysis period, with the exception of mid-June through August when this percentage fell below 90% and reached a minimum of ~83% in mid-July. Lavelle et al. (2016) suggest summertime melt caused this drop in weekly ice-chart versus EA2 concentration agreement (c.f. Markus and Dokken, 2002).

A daily analysis of sea-ice information, based on multiple sources of near real-time satellite data, derived satellite products, buoy data, and other weather data was provided to us upon request by the NIC. A main component of this analysis was its ice edge, which is nominally defined as the 10% sea-ice concentration contour. The NIC 10% concentration contour is produced by NIC analysts with the aid of several types of satellite imagery, including Advanced Very High Resolution Radiometer, Special Sensor Microwave Imager, Moderate Resolution Imaging Spectroradiometer (MODIS), Visible Infrared Imaging Radiometer Suite (VIIRS) and SAR (e.g., Lavelle et al., 2016). The latitude and longitude points comprising the daily NIC ice-edge contour are freely available to the public

(U.S. National Ice Center, 2020). The NIC ice edge was consulted during mission days with an ice-navigation component, which included the majority of days when at least one vehicle was north of Bering Strait (5 June 2019 – 28 September 2019).

We occasionally requested extended analysis from NIC when the Radarsat-2 SAR images available to them (c.f. Bertoia et al., 2004) covered the saildrone positions. Radarsat-2 return periods from <1 to 3 days are typical for Chukchi and Beaufort Sea locations [interested readers can freely view reduced-resolution Radarsat-2 images on the European Space Agency Earth Observation Portal[2] as well as the SODA situational awareness data archive[3] (Rainville et al., 2020)]. High-resolution Radarsat-2 imagery, however, is not freely available to the public. The enhanced assistance received from NIC confirmed that the ability to geo-locate USVs on full-resolution SAR imagery within the tactical window (Scheuchl et al., 2004 suggests this to be <6 h) is a critical tool for remote ice navigation.

Satellite imagery from the European Space Agency Sentinel-1 SAR and Sentinel-2 MultiSpectral Instrument (MSI) missions is made freely available from the Sentinel Hub EO Browser[4] and was used during the mission. Sentinel-2 consists of a pair of satellites with MSIs measuring 13 spectral bands in the 443–2203 nm range with 10–60 m horizontal resolution (König et al., 2019). The return period for Sentinel-2 MSI images in the Chukchi and Beaufort Seas was up to 1 per day. Use of MSI imagery for ice detection, however, requires clear sky conditions. Sentinel-1 SAR provides all-weather capability (e.g., Nagler et al., 2015; Karvonen, 2017). Based on the EO Browser repository, however, the Sentinel-1 return period for a specific location in our study area was up to 12 days.

The natural color images made available at the NASA Worldview website[5], offered useful information about ice distribution, provided the local cloud cover was sufficiently sparse. Images are available on a daily basis from this site based on measurements collected by pairs of VIIRS and MODIS instruments aboard four different satellites, with a different image layer for each combination and a nominal horizontal resolution of 250 m. Because the cloud patterns tended to shift more than the ice between the different satellite overpasses during a given day, having multiple sensor-layers (e.g., the MODIS image from the Aqua v. Terra satellite) was sometimes useful for distinguishing sea ice from cloud.

RESULTS

Daily Gridded Sea-Ice Concentration From AMSR Measurements

Illustrations of the EA2 gridded sea-ice concentration estimates are shown in **Figures 2**, **3** on the days of the first and final ice encounter (ISSI and IBV) of the mission, i.e., 14 June 2019 and 23 August 2019, respectively. In these two cases, saildrones encountered sea ice near the NIC 10% concentration lines; however, other ice encounters occurred in a wide range of sea-ice concentrations.

Based on EA2, ice extent over the study region bounded by 180°–145°W and 66°N–80°N was ~10×10^5 km^2 at the start of the mission on 15 May 2019 (**Figure 4**). The vehicles encountered ice during different phases of the ice retreat over this region. A moderately paced decline of -0.92×10^5 km^2/month was observed in June 2019 based on a linear fit to the EA2 concentration estimates. A more rapid decline was seen in July and early August (-3.8×10^5 km^2/month). The pace of the decline in regional ice extent then slowed in mid to late August, during which time ice extent hovered near 2×10^5 km^2. The study area minimum ice extent of 1.28×10^5 km^2 occurred on 15 September 2019. Comparison reveals that the study region experienced an earlier decline in ice cover in 2019 relative to the previous two summers over which EA2 data are available (**Figure 4**). On 28 July 2019, study-region ice extent reached 5×10^5 km^2, a level not reached until 2 August in 2017 and 16 August in 2018. The return of ice to the study region in 2019 was also slower than in the previous 2 years: In 2017 and 2018 ice extent had risen to 5.6 and 6.2×10^5 km^2, respectively, by the end of October but was still at 2.4×10^5 km^2 at the end of October 2019, based on EA2.

The distribution of EA2 sea-ice concentration at the locations of sd-1034, sd-1035 and sd-1036 is shown in **Figure 5**. Based on EA2, these three vehicles collected observations in sea-ice concentrations from 0 to slightly over 20%. The most common EA2 estimate was for 0% concentration at the vehicles' locations (59%). Three percent of the observations have an EA2 estimate of 10% concentration or greater. A secondary maximum occurs at ~16% sea-ice concentration.

For the subset of observations taken while sea ice was visible in the saildrone images, the most common EA2 estimate at the vehicle locations was still 0% sea-ice concentration. A secondary maximum spans 3% and 4% ice concentration, each with ~36 h of saildrone observations (inset of **Figure 5**). There were 8.3 h of observations collected with sea ice visible in the saildrone images and an EA2 estimate of 15% sea-ice concentration. The saildrones encountered ice 1.5% of the time their EA2 concentrations were 0%, 5.8% of the time their EA2 concentrations were 1–10% and 4.1% of the total time they spent in EA2 concentrations >10%, although no sea ice was evident in the vehicle images when the EA2 estimates were >15%.

Ice Edge Information From the U.S. National Ice Center

The EA2 and NIC 10% contours did not always agree, as for example shown in **Figures 2**, **3**. We quantified the uncertainty between these two estimates of the 10% sea-ice concentration edge by calculating the minimum distance between each point on the NIC contour and any point on the EA2 contour, as well as calculating the minimum distance between each point on the EA2 contour and any point on the NIC contour. This calculation was performed in both directions because the ice edge geometry was often sufficiently complex that doing it in

[2] https://directory.eoportal.org/web/eoportal/satellite-missions/r/radarsat-2

[3] http://hdl.handle.net/1773/45592

[4] https://www.sentinel-hub.com/explore/eobrowser/

[5] https://worldview.earthdata.nasa.gov/

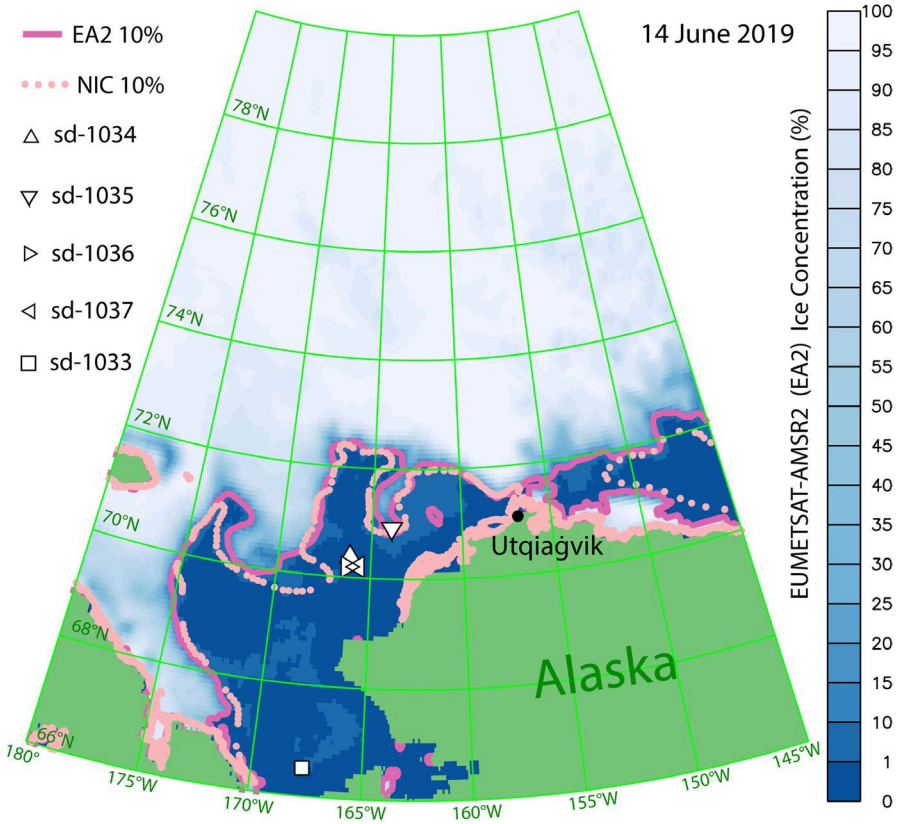

FIGURE 2 | The Eumetsat-AMSR2 (EA2) estimate of sea-ice concentration (blue-white hues) and 10% ice contour (solid purple curve) along with the NIC 'ice edge' 10% contour (pink dotted curve) and locations of saildrones sd-1033 (square), sd-1034, sd-1035, sd-1036, and sd-1037 (triangles) on 14 June 2019, the date of the mission's first ice encounter (sd-1035).

only one direction led to an incomplete estimate of distance. We did this for all points on the 10% contours within our study region (**Figures 2**, **3**) and over water; but not along the coast. The results of averaging these contour-separation distances over each day of the mission (**Figure 6**) reveal that mean minimum-separation distances varied by almost a factor of 20 during the mission, with lows of ~ 10 km in early June, late September and early October and highs near 175 km in August. The mean minimum distance between the EA2 and NIC 10% ice contours was greatest when the sea-ice coverage was declining rapidly (early to mid-August) and hovering (late-August) approximately 50% above the eventual minimum (c.f. **Figures 4**, **6**). Because the NIC 10% contour may be overestimating the extent of ice (see U.S. National Ice Center, 2020, p. 9 and **Figure 7**) we looked for better EA2 versus NIC agreement using 8% and 5% contours from EA2. The **Figure 6** results, however, remained qualitatively and quantitatively similar using these lower concentration EA2 contours. For example, the minimum, maximum and mean of Line C in **Figure 6** changed by ≤7% (see **Supplementary Figure 1**).

Figure 7 shows the number of hours that the saildrones with cameras (sd-1034, sd-1035, and sd-1036) were within a given distance of the NIC 10% ice edge between 5 June when they entered Bering Strait and the end of September when they turned south. Overall, ~40% of this time was spent within 40 km of the NIC ice edge; further, 18% of the period was spent in waters with >10% ice concentration according to NIC. Did the saildrone cameras agree with these NIC ice estimates? The answer is mostly yes; nearly all camera images that showed ice were for vehicles in >10% ice concentration according to NIC and ice free conditions were encountered 99.7% of the time the saildrones were in <10% concentration according to NIC. However, 80% of the images taken while the vehicles were in ≥10% ice concentration according to NIC showed no ice. The results confirm that the NIC ice edge corresponds to the boundary beyond which ice may affect vehicle navigation, although the NIC ice edge might be overestimating the extent of ice.

Satellite Imagery

The Terra/MODIS image shown in **Figure 8A** depicts a zonal ice band that was targeted for exploration on 13 July 2019, with the fleet 130 km to its south. Unfortunately, another clear image did not become available before the fleet contacted sea ice near this location in the first hour (UTC) of 18 July 2019, 5 days later (**Figures 8B–F**). Thus, waypoints estimated at the ice edge based on the 13 July 2019 image, but used for ice navigation on 18 July 2019, did not account for the distances that the targeted ice band might have moved, dispersed or otherwise changed shape over

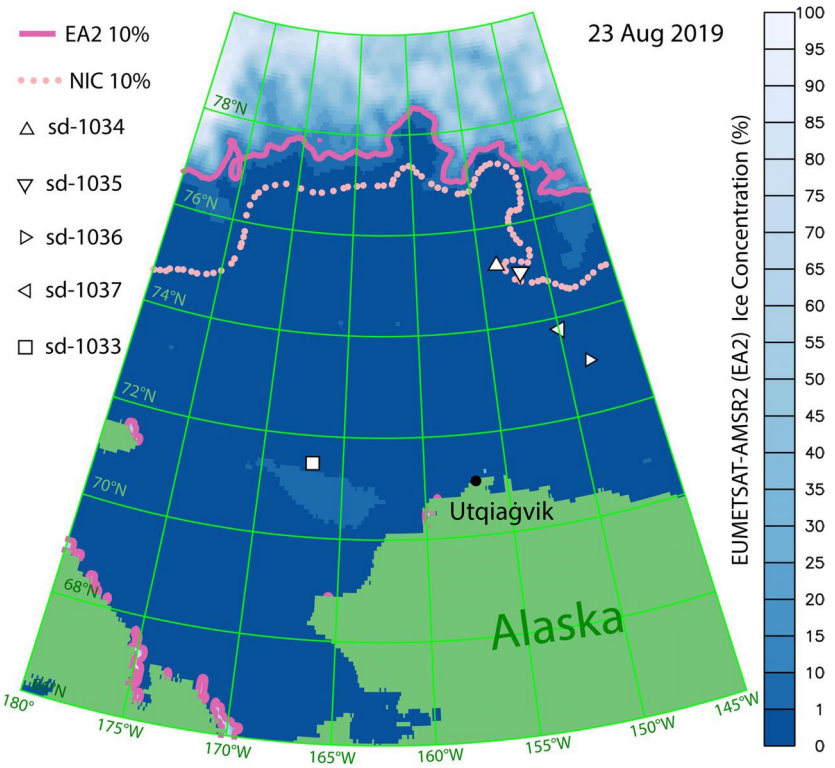

FIGURE 3 | The Eumetsat-AMSR2 (EA2) estimate of ice concentration (blue-white hues) and 10% ice contour (solid purple curve) along with the NIC 'ice edge' 10% contour (pink dotted curve) and locations of saildrones sd-1033 (square), sd-1034, sd-1035, sd-1036, and sd-1037 (triangles) on 23 August 2019, the date of the mission's last ice encounter (sd-1035).

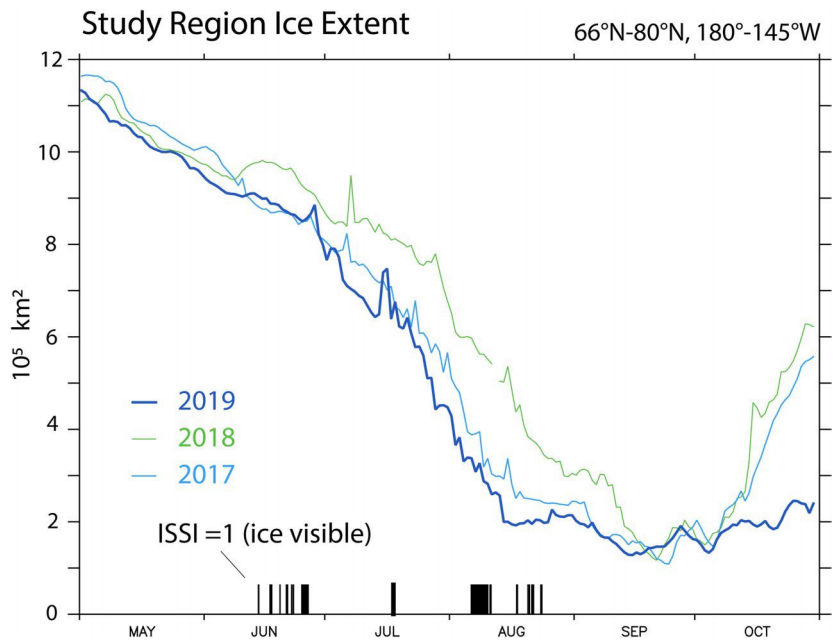

FIGURE 4 | Sea ice extent over the Chukchi and Beaufort Sea study region (180◦–145◦W, 66◦–80◦N) from the AMSR2 based ice concentration estimate provided by the EUMETSAT ocean and sea ice satellite application facility. Vertical lines on the time axis mark times when ISSI = 1, that is, sea ice was visible in either the horizontal or downward saildrone images. ISSI = 0 (images were ice-free) during all other times, which are not marked by vertical lines.

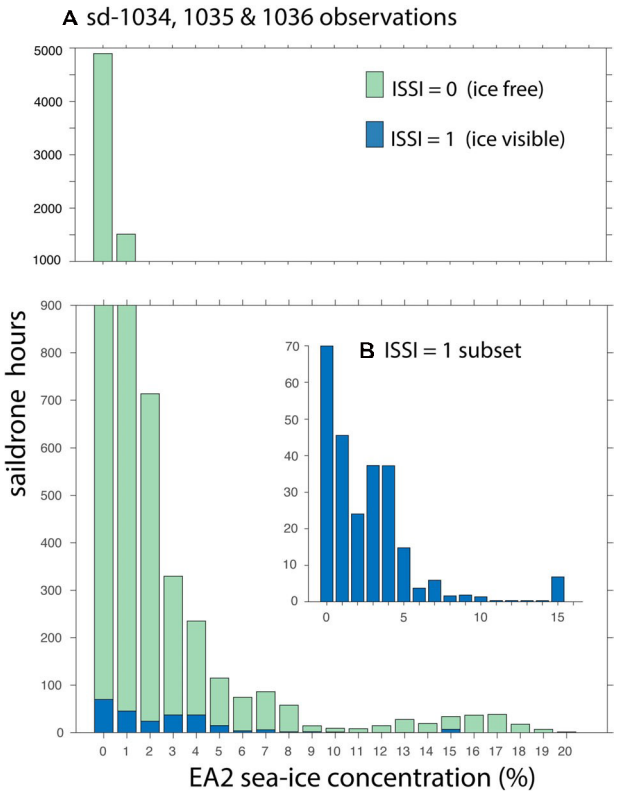

FIGURE 5 | (A) Histogram showing the number of hours saildrones spent in different EA2 sea-ice concentration levels. Data are from sd-1034, sd-1035, and sd-1036 and binned in 1% intervals over the period 5 June 2019 – 30 September 2019. (B) The inset histogram highlights the subset of observations collected when ISSI = 1, meaning sea ice was visible in the images taken from the saildrones.

these 5 days. As it turned out, sd-1034, sd-1036, and sd-1037 encountered sea ice on 18 July 2019 1 to 4 km north of where the southern ice edge was on 13 July 2019.

Visual inspection of the sequence of daily Terra/MODIS images revealed that mostly clear sky conditions, such as seen in **Figure 8A**, occurred over this location on about 70% of the days in June 2019, but only about 20% of the days in July 2019 and even fewer days in August. Such unobstructed images of the surface were useful for ice zone navigation when available. However, they could not be consistently relied upon throughout the mission because of cloud cover.

When cloud cover was sufficiently sparse, Sentinel-2 offered relatively high-resolution images (10–60 m), often ~24 h apart. Example clear-sky images encompassing sd-1034's route on 18 and 19 June 2019 are offered in **Supplementary Figure 2**. At the sensing time of the first image (18 June 2019 22:46), sd-1034 was 9 km south of a sparse band of ice extending east from the southern tip of denser pack ice (upper-left corner of **Supplementary Figure 2A**). By the sensing time of the second image (19 June 2019 23:06), sd-1034 had traveled ~18 km to the northeast and was ~1.5 km east of the dense pack ice. In between these two images, sd-1034 became embedded in ice (vehicle images collected at 19:00 UTC confirm ice in the downward view) and then freed itself around 22:15 UTC by sailing east into open water. This episode served as a reminder that the effective navigational resolution of satellite ice imagery is a function of the spatial resolution of the image, the speed of the vehicle, and the distance that the ice moves after the image is available. The ice moved ~10 km in this case.

A few days prior, at ~09:00 on 17 June 2019, sd-1036 and sd-1037's routes intersected an ice floe visible in the Sentinel-2 image collected at 22:56 on 16 June 2019 (see **Supplementary Figure 3A**). Sd-1036 was able to resume open water sailing within a few hours, but sd-1037 remained blocked by ice until 21 June 2019. Another clear-sky Sentinel-2 image was available on 19 June 2019 (**Supplementary Figure 3B**; collection time 23:05) that indicated sd-1037 was still encumbered in the same flow. While encumbered during these 4 days (17–21 June 2019), sd-1037's average speed-over-ground was 0.15 m s^{-1} and it moved 35 km to the east-northeast (67°).

The Sentinel-1 SAR offered a view of the saildrone study area on 22 June 2019 (**Supplementary Figure 4**). Such images, which offered a chance to detect ice even in cloudy conditions, were useful when available. However, the next Sentinel-1 swath covering the saildrone positions shown in **Supplementary Figure 4** was not available until 12 days later, on 4 July 2019.

Saildrone Photos

The vehicle images taken during the approach to the ice band described above, which was oriented roughly zonally along 73°N in mid-July, exemplifies their potential for navigational use. **Figure 9** shows the images collected at a 5 min interval by sd-1036, while en route to the ice. There are light hues on the horizon (**Figure 9A**) in the transmitted image taken at 00:23 UTC on 18 July 2019 that can be confirmed as sea ice from the following images. At 00:23 UTC, sd-1036 was heading north at 0.41 m s^{-1} and was ~1 km away from its northernmost point on this transect. Five minutes later, a similar image was telemetered with the vehicle ~700 m away from its northernmost point (**Figure 9B**). At 350 m out, the image taken at 00:33 UTC (**Figure 9C**) offers a more distinct view of ice along the horizon. Without this, the previous images could have easily been mistaken for reflections associated with cloud breaks. Sea ice is clearly recognizable below the horizon at 00:38 UTC with the vehicle 50 m out, still heading north at 0.57 m s^{-1} (**Figure 9D**). Five minutes later, sd-1036's northward progress was blocked by sea ice (**Figure 9E**). The time between an image being taken and its availability for viewing on shore was 30–40 min. If remote transmission and processing times were short enough (say, 1 min), vehicle instructions could be tailored based on images like those in **Figures 9C,D** to avoid sailing directly into sea ice. Alternatively, automated decision-making aboard a vehicle (e.g., Jin et al., 2020) might be able to avoid a sea-ice collision. In practice, the delay associated with being able to view the transmitted photos was long enough that the vehicles usually were impeded by the sea ice before a transmitted image revealed it. Vehicle speed and direction information was sent separately and faster than the images so that it was available within a few minutes. Early indications that the saildrones had encountered

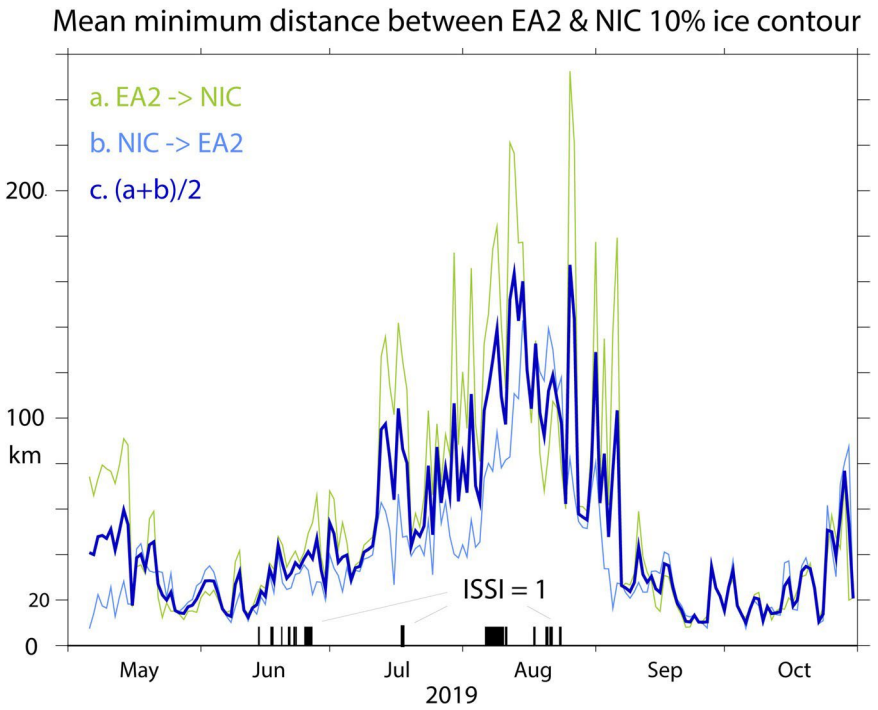

FIGURE 6 | Mean minimum-distances between the 10% ice concentration contour based on the NIC analysis and EA2 data. Vertical lines on the time axis mark times when ISSI = 1. ISSI = 0 during times unmarked by such vertical lines.

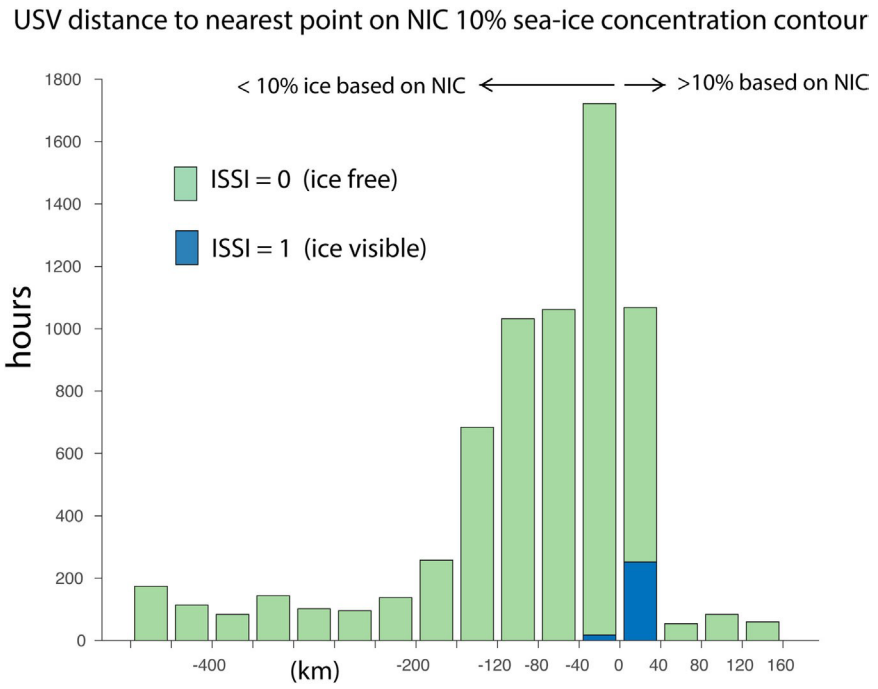

FIGURE 7 | Histogram showing the number of hours that saildrones with cameras (sd-1034, sd-1035, and sd-1036) spent at various distances to the NIC 10% sea-ice concentration contour. Results shown were calculated based on 6-h intervals over the period bounded by their northward transit of Bering Strait on 5 June 2019 through the end of September. The portion of the distribution with sea ice visible from the onboard horizontal or downward photos (ISSI = 1) is shown in blue.

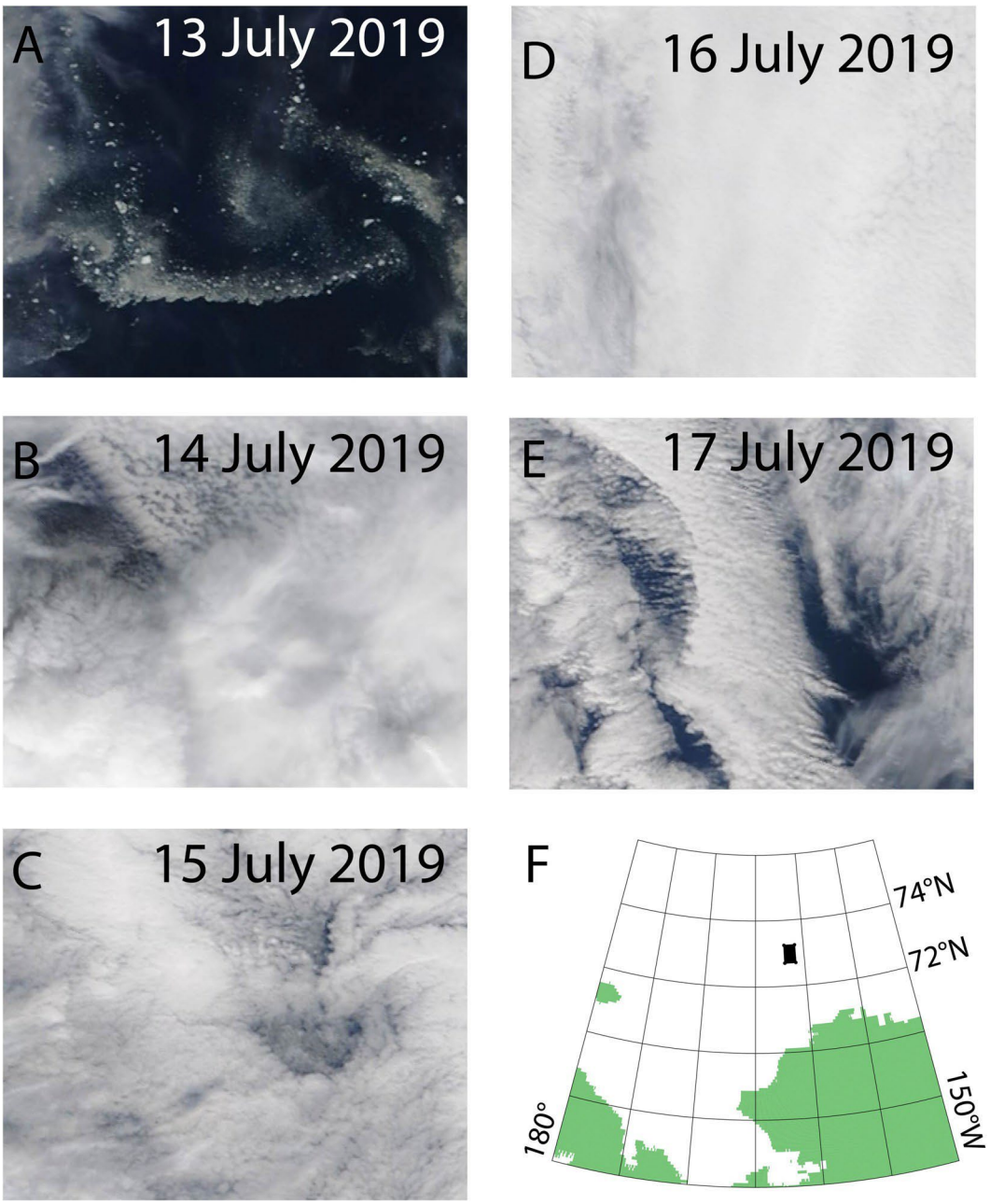

FIGURE 8 | Daily "natural color" images from the MODIS instrument aboard the Terra satellite. These images are centered at 161.46W, 72.97N and span approximately 60 km meridionally (vertical) and 18 km zonally (horizontal). The ice edge visible in panel (A) was targeted for exploration on 13 July 2019, but skies remained cloudy from 14 July through contact with the remnants of the band in the first hour (UTC) of 18 July panels (B–E). The black rectangle in panel (F) shows the location of the images.

sea ice usually included an unanticipated sudden drop in speed and a possible change in direction.

Surface Marine Observations From the Saildrones

Sea ice is known to affect the properties of the seawater around it (e.g., Gallaher et al., 2016; Dewey et al., 2017; Brenner et al., 2020). If the surface marine variables observed in close range of sea ice (say, while ice was visible in the horizontal photos from the vehicles) proved sufficiently distinct from those measured in ice-free water, then they might offer a navigationally useful indicator for the proximity of sea ice. For example, if seawater temperature and salinity falling below a certain level proved to be a sufficiently distinct characteristic of the presence of sea ice, measurements approaching those levels might

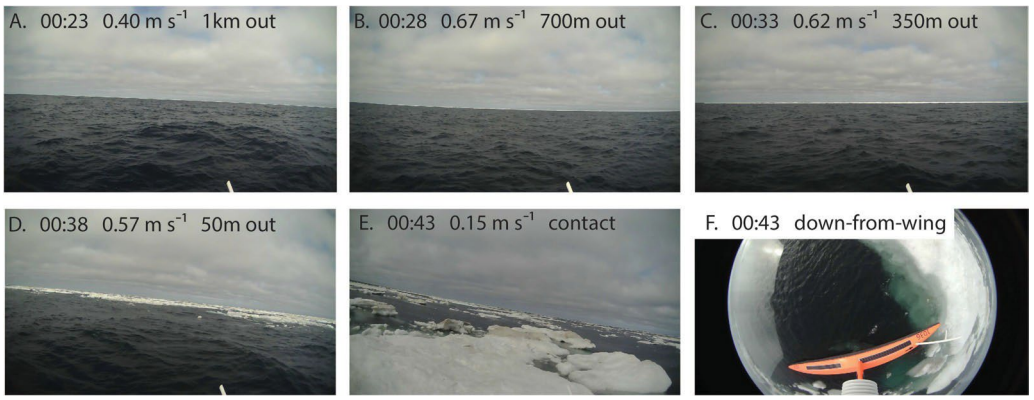

FIGURE 9 | Photos from the camera aboard sd-1036 as it approached the ice band targeted on 18 July 2019. Times in UTC. Distances listed are relative to the vehicle's northernmost point of travel, at which point it was blocked by ice. Panels (A–E) are looking north, along the vehicle's northward route. Photo (F) was taken looking down from the top of the vehicle's wing.

serve as a warning that vehicle contact with ice was imminent. Examination of the 1-min averaged surface marine observations and navigational metrics collected *en route* to ice, however, highlights difficulties associated with using surface marine measurements of temperature and salinity for this purpose.

The sd-1036 ice band approach pictured in **Figure 9** provides a useful example. The vehicle's navigational metrics help pinpoint intervals during which the vehicle's progress was impeded by sea ice. In particular, a drop in vehicle speed from ~ 0.8 to 0.3 m s^{-1} was evident between the 39th and 40th minute of 18 July 2019 (**Figure 10A**; denoted by vertical line). Wind speed remained above ~ 2.5 m s^{-1} and the vehicle's instructions were to maintain course during this time. We thereby infer that ice impeded sd-1036's northward progress between 00:39 and 00:40 UTC of 18 July 2019. As discussed above, an image confirming that sd-1036 was in contact with sea ice was taken at 00:43. The vehicle remained in the ice from ~00:40 to 01:08 UTC, after which it made its way back south.

Density, salinity, and temperature values during the ice-band approach are plotted in **Figures 10B–D** and on a Temperature–Salinity (T–S) plot in **Figure 11**. At the time of the initial ice contact, at 00:40 UTC, the 1-min averaged measurements for temperature and salinity were −0.18°C and 26.12, which equate to a seawater density near 1021 kg m^{-3} (**Figure 10**). A salinity drop of ~2.2 and temperature drop of ~0.2°C were observed in the few minutes following 00:40, which lowered the seawater density to ~1019.5 kg m^{-3}. But this fresher (salinity ~ 24) and cooler (temperature near −0.5°C) water was observed only after sd-1036 became embedded in the ice band. Even once embedded, temperatures remained above the freezing point (**Figure 11**). Prior to contact, there was a discernible increase in salinity observed as the vehicle moved closer to the floe (e.g., ~+0.4 from 00:20 to 00:40). Evidently, at this scale (~1 km), melting ice is not always located at the low end of an open-water, surface salinity gradient.

Seawater conditions observed just before the ice encounter (i.e., temperatures near 0°C and salinities near 26) were also often observed in ice free water. **Figure 12** shows the distribution of 1-min averaged temperatures and salinities collected by sd-1036 during June, July and August, with different symbols differentiating measurements taken while ice was (dots) and was not (open green circles) visible from the vehicle. The low-density (near 1019.5 kg m^{-3}) measurements observed after sd-1036 was embedded in ice on 18 July 2019 are the only ones separated in T–S space from other measurements. The correlation coefficient between sd-1036 temperature (salinity) and the sd-1036 *in situ* sea-ice time series (equal to 1 when ice was visible, and 0 when ice was not visible in the saildrone images) is −0.37 (−0.26). Based on Bootstrap/Monte Carlo sub-sampling, with replacement, of the respective sd-1036 time series (Efron and Tibshirani, 1991), the temperature correlation with *in situ* ice is statistically significant at the 99.9% confidence interval and the salinity correlation is significant at the 90% confidence interval. We thus conclude that temperature was more closely related to ice proximity than salinity (c.f. Johnson, 2011) but attempts to use threshold values of seawater temperature and salinity as a proxy for >0% sea-ice concentration in conditions such as were observed by sd-1036 will have a low probability of success.

The 18 July 2019 ice encounter described above stood out as a prime candidate for close examination in this context because it was associated with some of the coldest and least saline water observed during the mission. The other ice encounters were also examined for surface marine variable precursors to contact with the ice. Although each encounter differed in detail, when viewed from the perspective of trying to anticipate the transition from open water sailing to probable ice contact, they exhibited broadly similar characteristics. The encounter that led to sd-1035 being embedded in ice for approximately 6 h on 14 June 2019, which was the first such occurrence of the mission, exemplifies these characteristics (**Figure 13**). In particular, although the salinity and temperature measured while the vehicle was embedded in the ice were substantially lower than those measured when last sailing through open water – in this case temperature dropped by 1.6°C and salinity by 0.7 between 09:10 and 10:10 UTC – most of these changes occurred after the vehicle hit ice at 09:25 UTC. The important point for ice-avoidance navigation is this: The changes

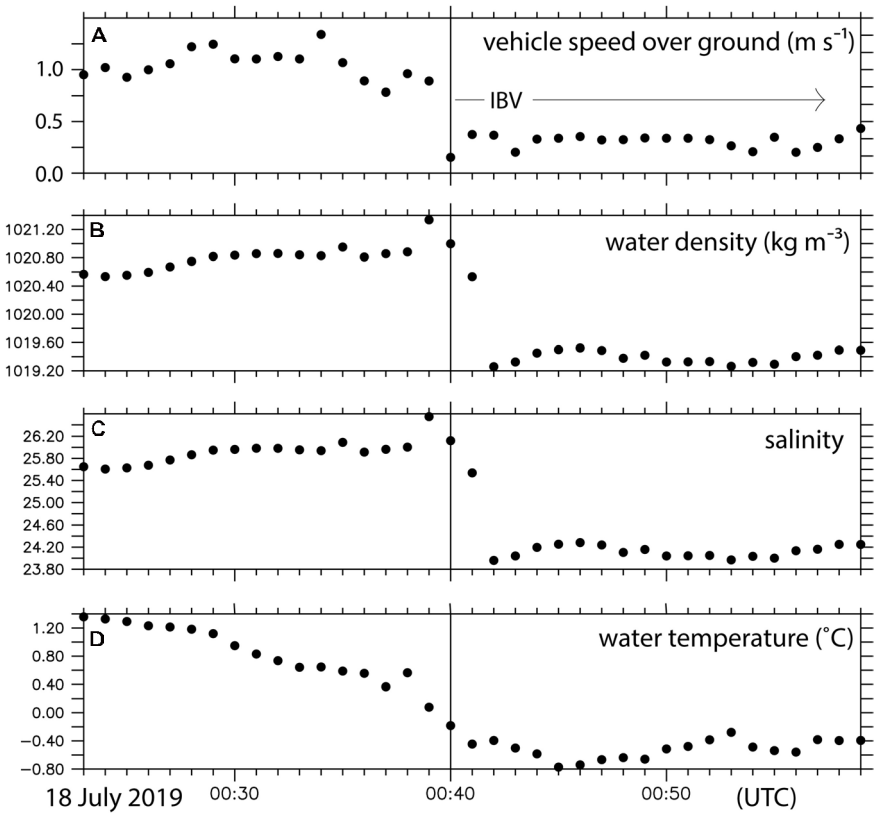

FIGURE 10 | One-minute averaged data just before and after sd-1036 was blocked by sea ice (IBV) on 18 July 2019. (A) The geo-referenced vehicle speed, (B) water density, (C) salinity, and (D) ocean temperature. We infer IBV from the drop in vehicle speed at 00:40 UTC (upper panel; marked with a black vertical line at 00:40 UTC) that sea ice impeded the vehicle's northward progress sometime between 00:39 and 00:40 UTC. An image confirming that ice was surrounding the vehicle was taken at 00:43 (Figure 9E).

observed prior to the point at which the vehicle was impeded by ice – in this case a temperature drop of 0.032°C min^{-1}, or 0.11°C per 100 m based on the 5-min averages centered at 09:10 and 09:23 – were not especially distinct from similar time and space scale changes observed in ice-free water.

We further examined the temperature and salinity gradients observed during the seven times sd-1036 sailed from open water into the marginal ice zone and was impeded by ice. These spatial gradients appear as temporal tendencies in the saildrone time series. The largest negative tendencies (hereafter, LNTs) observed <3 h before ice contact are listed in **Table 1**, based on 5 min averages separated by 20 min. The corresponding 1-min averaged temperature and salinity records from these seven ice encounters are also illustrated in **Supplementary Figures 5–11**. The LNTs preceding four of these seven ice encounters are not very distinct from tendencies seen during periods of ice-free sailing (**Figure 14**). Specifically, for the 23 June, (2) 6 August and 8 August ice encounters, there were 175–371 other, 3 h-long, ice-free periods that had temporal temperature and salinity LNTs lower than those observed *en route* to the ice (**Table 1**). Triggering ice-navigation maneuvers based on temperature and salinity changes in this range ($11S/11t$ = −0.0034 to −0.0082 min^{-1}, $11T/11t$ = −0.0029 to −0.0163°C min^{-1}) would likely introduce unnecessary inefficiency to SIZ sampling strategies because of the apparent abundance of false-positives. Three of these seven ice encounters, however, occurred after traversing stronger gradients than the other 4; the 17 June ice encounter was preceded by a −0.1133°C min^{-1} temperature (−0.158°C per 100 m) gradient located 4840 m from the ice-blockage point, the 22 June ice encounter by a −0.0371 min^{-1} (−0.055 per 100 m) salinity gradient observed just before contact with ice, and the 18 July ice encounter by a temperature gradient of −0.0885°C min^{-1} (−0.119°C per 100 m) and salinity gradient of −0.0686 min^{-1} (−0.092 per 100 m), each at distance of 1480 m from ice contact (**Table 1**). Turning the vehicles around based on gradients far from the ice would leave the remaining section of the vehicle route unobserved; thus, the longer of these distances-to-contact (~1.5 and 5 km) are likely too far for the associated gradients to be used for navigation on their own and still meet our objective of being able to collect observations in close proximity to the ice. The case of navigating based on gradients immediately adjacent to ice presents the opposite issue of needing enough time and space to detect the gradients and turn before contacting the ice; successfully implementing such a system may therefore require

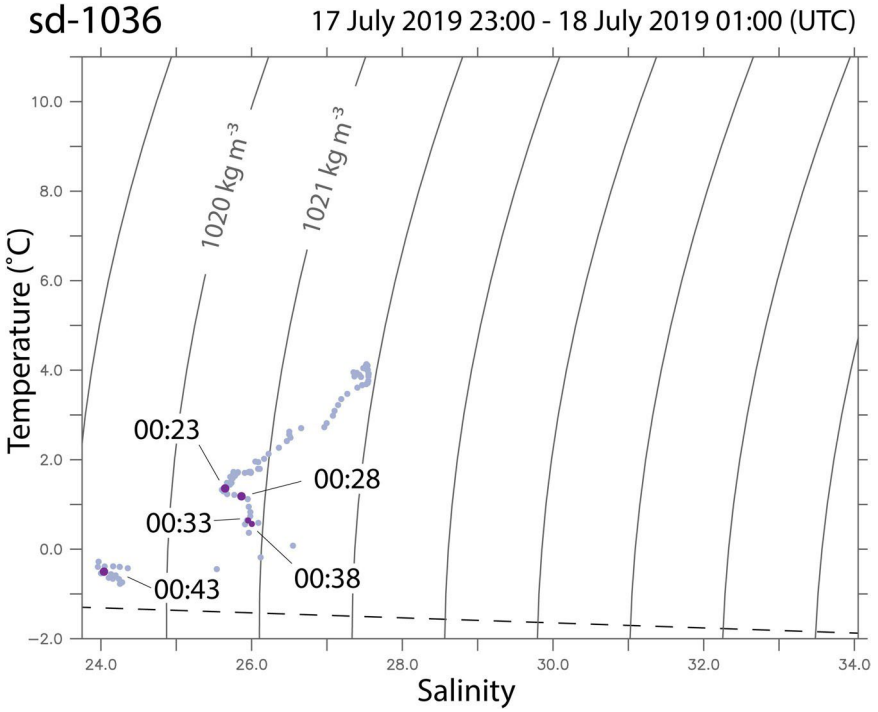

FIGURE 11 | One-minute average temperature and salinity measurements during sd-1036's initial northward transect into an ice band on 18 July 2019. Density contours every 1 kg m^{-3} (solid lines). Seawater freezing temperature calculated based on the equation suggested by Millero and Leung (1976) and used by Fofonoff and Millard (1983) is shown with a dashed line.

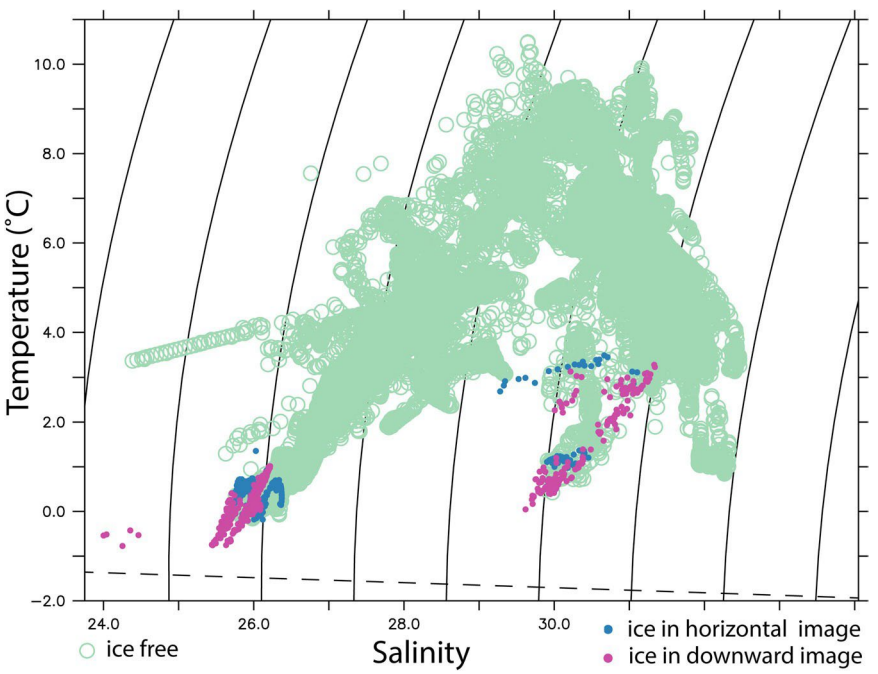

FIGURE 12 | Same as Figure 11 except for seawater temperature and salinity measurements collected by sd-036 during June, July and August of 2019. Light green circles denote times when no ice was visible in the saildrone images; light blue filled dots denote times when ice was visible in the horizontal but not in the downward saildrone photos; magenta dots denote times when ice was visible in the downward-looking saildrone images. Seawater freezing point is shown with a dashed line.

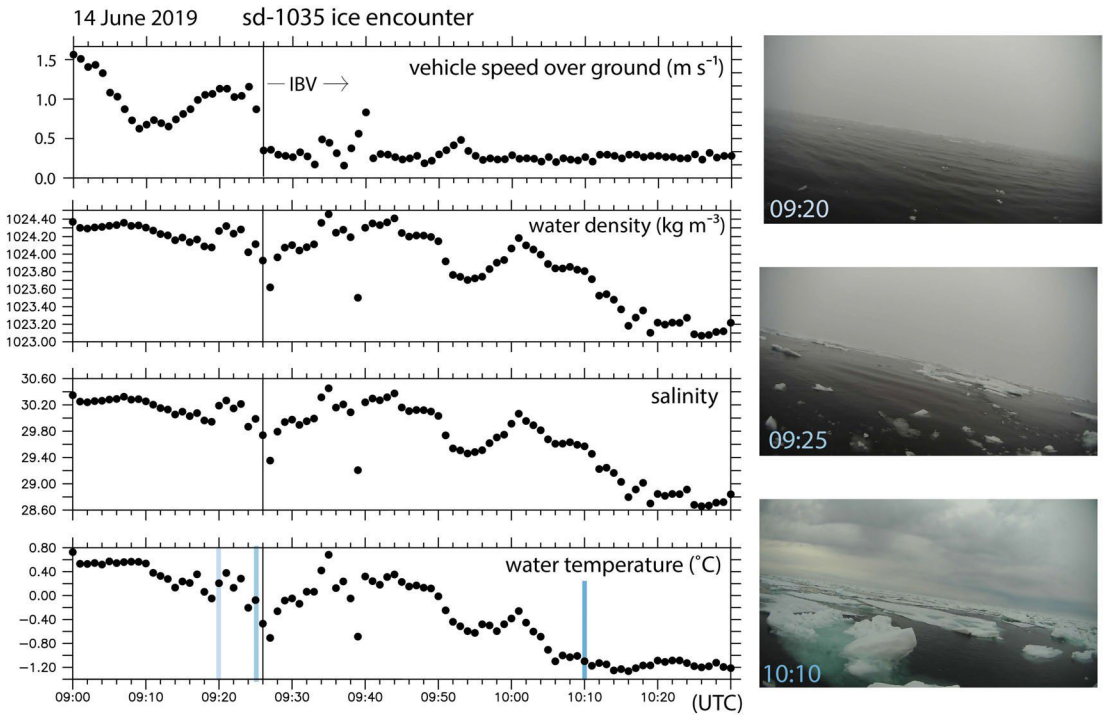

FIGURE 13 | As in Figure 9, except for sd-1035's 14 June 2019 ice encounter. In this case a horizontal photo revealing sparse ice was taken at 09:20 and a downward looking photo confirming ice surrounding the vehicle taken at 09:25 UTC. The drop in vehicle speed over ground between 09:25 and 09:26 (upper-left panel; marked by the IBV-vertical black line in each panel) confirms that the vehicle was impeded then. The blue vertical lines in the near surface water temperature plot (lower left) mark the times of the images shown on the right.

TABLE 1 | Minimum temperature and salinity tendencies observed during seven 3-h-long sd-1036 transects beginning in open water and ending with an IBV (vehicle blocked by sea ice).

Date, Time (UTC)	Largest negative $\Delta S/\Delta t$ (min^{-1})	$\Delta S/\Delta t$ time/distance before ice contact (minutes/meters)	Largest negative $\Delta T/\Delta t$ (C° min^{-1})	$\Delta T/\Delta t$ time/distance before ice contact (minutes/meters)	Open-water exceedances: $\Delta S/\Delta t$, $\Delta T/\Delta t$, combined
17 Jun 2019, 08:26	−0.0240	92/6020	−0.1133	76/4840	39, 7, 5
22 Jun 2019, 16:10	−0.0371	0/0	−0.0286	0/0	19, 111, 13
23 Jun 2019, 00:38	−0.0054	107/5240	−0.0158	50/2470	263, 221, 143
18 Jul 2019, 00:40	−0.0686	42/1480	−0.0885	42/1480	1, 14, 0
6 Aug 2019, 09:08	−0.0057	0/0	−0.0048	0/0	250, 282, 162
6 Aug 2019, 20:42	−0.0082	116/4380	−0.0163	108/3970	175, 213, 102
8 Aug 2019, 17:26	−0.0034	0/0	−0.0029	0/0	371, 345, 236

Date-times listed are for the ice-blockages. Tendencies are calculated based on the change between two 5-min averages separated by 20 min. The distances/times-to-contact listed are between the end of the second 5-min averaging period and the point at which vehicle progress was blocked by ice. The number of 3 h-long, open water sampling windows (non-overlapping) that contain 20-min temperature or salinity tendencies lower (more negative) than the respective ice approach minimums are listed in the open-water exceedances column.

refinement. Nonetheless, the stronger gradients associated with these three ice encounters had far fewer (1–19) open-water analogs relative to the other four sd-1036 ice encounters. This suggests that monitoring for negative temperature and salinity tendencies might be useful if a large enough threshold is selected and if supplemented with other ice-detection strategies (see section "Summary and Discussion").

We also considered other surface marine variables, such as near-surface air temperature and humidity, for use in this context, but failed to find a distinct subset of near-ice values in them (**Supplementary Figure 12**). The distribution of seawater temperature and salinity values observed while sd-1034 and sd-1035 were embedded in ice and sailing in open water were also examined and found to have character qualitatively similar to the distribution shown **Supplementary Figure 12**, in that, the subset of in-ice values was indistinct from other values measured in ice-free conditions (the near-1019.5 kg m^{-3} sd-1036 density values already discussed were the only ones with this distinction). The sd-1034 and sd-1035 temperature and salinity diagrams are therefore not shown for the sake of brevity.

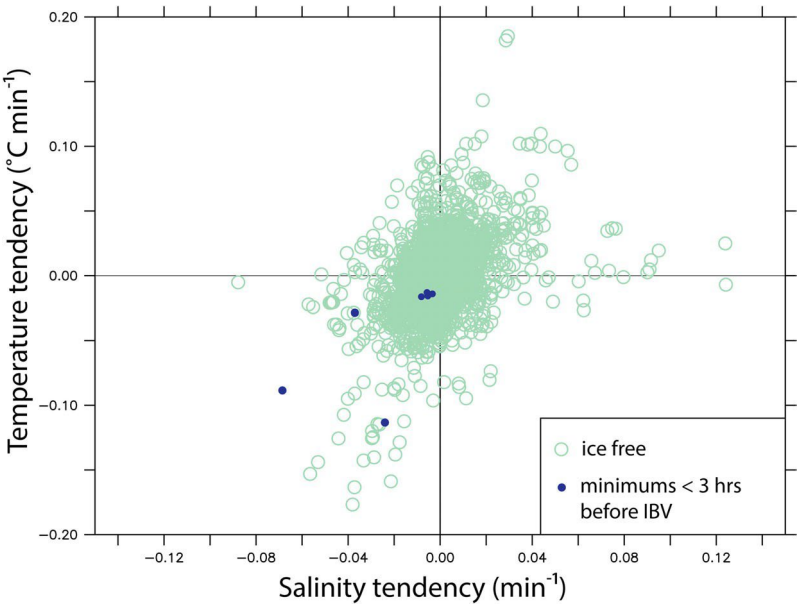

FIGURE 14 | The temperature and salinity tendencies observed while sd-1036 sampled ISSI = 0 conditions (no ice in saildrone images) are plotted with open circles, based on differences between 5 min averages separated by 20 min. The largest negative tendencies observed *en route* to ice (see Table 1) are plotted with dots.

SUMMARY AND DISCUSSION

On 15 May 2019 five saildrones were launched from Unalaska (formerly Dutch Harbor), AK, United States with the objective of observing the air-sea interface within the SIZ of the Chukchi and Beaufort Seas. This mission constituted a test of our ability to use saildrones to observe the SIZ with novel instrumentation packages capable of measuring air-sea fluxes of heat, momentum and CO_2. These saildrones, however, had not been specifically designed to navigate in close proximity to, or collide with, sea ice. Remotely controlled navigation near sea ice was a crux of this mission and will remain critical to future attempts to use similar means to provide high quality, *in situ* observations of surface marine variables in and near the marginal ice zone. Here, we have re-examined the sources of navigational information, based on post-mission tabulation of the sea-ice conditions encountered by the vehicles. Our objectives are to better understand the utility and limitations of this information and to identify opportunities for improving our ability to remotely navigate through the SIZ and near sea ice.

At points in the mission where the vehicles sailed in open water and decisions were being made about where and how to approach marginal ice zones, the EA2 gridded ice-concentration product, pseudo-true color satellite images of the surface and NIC 10% ice concentration contour were initially considered prime candidates for providing regional ice distribution information. However, on most days that the vehicles encountered ice, EA2 estimated zero ice at their location. The chances of seeing ice was not closely linked to EA2 concentration. For example, ice was encountered ~6% of the time EA2 estimated concentrations of 1–10%, but only ~4% of the time EA2 estimated >10% concentration. It was also the case that no ice was encountered or photographed by the vehicles on the handful of days in which EA2 predicted the highest ice concentrations (around 20%) at the vehicle locations. These mismatches between the EA2 estimates and *in situ* conditions encountered by the saildrones made it difficult to reliably use EA2 ice concentration data for SIZ navigation.

We also examined vehicle distances to the daily NIC 10% ice concentration contour on days in which ice was and was not encountered. Our experience with this analysis product largely supports its use as an identifier of ice-free (or nearly so) pathways of navigation over the study region. To put it another way, being on the open water side of the NIC 10% contour proved to be a useful predictor for clear sailing: in only three instances during the mission, specifically on 21 June and 17 August 2019 (sd-1034) and 18 July 2019 (sd-1036) was ice encountered when a vehicle was in waters with discernibly <10% ice concentration according that day's NIC analysis. And in these three cases the vehicles were close to (within a few to several km from) the NIC 10% contour line. Clear sailing was also encountered, however, most (~80%) of the time the vehicles were in >10% ice concentration according to NIC. Thus, other information was needed to plan vehicle routes when the navigational objective was not avoiding but sampling close to ice floes.

Satellite-based surface imagery from radiometric measurements in the near-visible range was at times quite useful in this context. On clear-sky days, Sentinel-2 provided relatively high-resolution (10–60 m) images in which ice floes could be distinguished from water with relative ease using imagery that is generally available to the public. MODIS and VIIRS imagery also provided this capability with moderately coarser, but still useful (up to 250 m) horizontal resolution. But this utility was conditional on skies being free enough from

clouds to offer clear views of the planetary surface, and this was not the norm during the mission. When cloud cover obscured the optical view of the planetary surface and high-resolution SAR imagery was available to us, it proved very useful, confirming the benefits from investments made in this technology by the European (e.g., Sentinel-1) and Canadian (e.g., Radarsat-2) Space Agencies. The combination of Sentinel-1 and Radarsat-2 coverage, however, suffered from significant time and space gaps in our study region.

The use of USV observations such as near-surface ocean temperature and salinity to help determine proximity to sea ice was examined. Unfortunately, the distributions of these variables exhibited a wide enough range of variability in open water that they often overlapped with characteristics observed just prior to coming into contact with ice floes. This was true for the absolute values of the variables as well as their rates of change in time and space. These overlaps likely preclude this approach from providing, on its own, a reliable indicator that a given vehicle is nearing sea ice. Ice detection, however, was not the main motivation for collecting the surface marine observations. We expect them to be valuable in many other respects. These include providing a basis by which high priority targets for improvements of weather forecast model initializations and predictions can be identified (Zhang et al., submitted) and heat transfer between sea ice and sea water can be estimated.

There might be several reasons for the difficulty of using observed temperature and salinity to detect when USVs are approaching sea ice. If ice floes are drifting toward ice-free water, the strongest temperature and salinity gradients would be very close to their edges facing the ice-free water. Likewise, if surface currents are toward ice bands, they would push relatively warm, saline water against the ice bands and cause the strongest temperature and salinity gradients to lie very close to the ice bands. In addition, sea ice can move quickly (~2% of the wind speed; Sullivan et al., 2014) leaving behind swaths of melt water that have complex geometrical relationships to the ice before they are mixed to ocean-gyre scales (e.g., Dewey et al., 2017). Other factors, such as the strength of surface wind that dominantly controls surface heat flux, would further complicate distributions of surface temperature relative to sea ice. Distributions of surface temperature and salinity in the SIZ need to be further characterized using the observations from the saildrones deployed in this Arctic mission to better understand both their relationship to sea ice distribution and the time-space sampling density needed to constrain flux estimates over the SIZ.

Based on a review of images taken from the vehicles as they approached waters containing varying concentrations of sea ice, it is not difficult to imagine that – in true real time – they could usefully aid remote navigation near ice bands. For example, they could be used to trigger navigational instructions to the vehicle to preempt unwanted collisions with the ice, or tailor the sampling to mitigate risk to the vehicles if near-ice sampling remained the objective; perhaps by reducing vehicle speed or steering along rather than into a denser ice band. In practice, we found that the delay associated with being able to view the telemetered images (~ 30–40 min, or 1.8–2.4 km traveling at 1 m s^{-1}) was too long for practical use in this respect. If this transmission time could be greatly reduced, we expect that the images could then play a key role in developing more robust ice zone navigation strategies. However, in the case that this monitoring and navigational decision-making depended upon continued human interaction, the burden this would place on the navigational team during a mission of this length should not be overlooked.

Ideally, artificial intelligence (AI) can be applied to the saildrone images to detect, in real time, sea ice in the distance and either automatically navigate the vehicles to avoid collisions or alert the navigational team. Promising onboard AI navigation strategies have been reported for other USVs previously (e.g., Huntsberger et al., 2011; Carlson et al., 2019; Jin et al., 2020). The power-constraints associated with operating on solar power for months in high-latitudes – and still having power for meteorological and oceanographic sensors – likely preclude many of the specific techniques employed on much shorter missions (e.g., stereo-video cameras, LiDAR) from being very useful for a next generation of Arctic saildrones. However, general advances made recently in image recognition capability (e.g., LeCun et al., 2015) provide a basis for developing this capability. The next generation of saildrones have already been equipped with onboard Artificial Intelligence (AI) navigation for ships (R. Jenkins, pers. comm.). It is unknown if the amount of ice image information collected from this mission is sufficient for a complementary AI application for sea ice. The possibility of applying AI to information from onboard images and *in situ* observations to develop an automated navigation algorithm for endurance-sailing on solar power in the SIZ should be explored; in this context the *in situ* saildrone observations (and perhaps satellite information) can be used to add confidence to the ice image detection algorithms. For example, the confidence associated with a possible ice detection in the image algorithm can be downgraded if temperatures are several degrees above the freezing point (SSTs reached 10°C but ice was not seen above 4°C during this mission) or upgraded if temperatures are low and strong negative salinity or temperature gradients are observed.

Although the limitations associated with the ice navigation information available for this mission made it difficult to consistently answer, in a navigationally useful manner, the question of where the ice was in relation to the vehicles without actually running the vehicles into the ice, the mission was completed in October 2019 with some notable successes; saildrones reached latitudes up to 75.49° N and as far east as ~151°W while traveling over 56,000 km. And although saildrones were not specifically designed to come into contact with ice, they did so on approximately two dozen occasions bracketed by ice-free sailing. Even so, all of the vehicles and the instruments deployed were successfully recovered, although some with damage.

In conclusion, this mission provided understanding toward the potential for USVs to substantially contribute to the development of high-latitude observing systems (e.g., Lee et al., 2017) by providing the capability to accurately monitor surface fluxes of heat, momentum and carbon dioxide throughout the

Earth's SIZ. Improved strategies for remote navigation of the ice zone are needed to accomplish this. Our analysis highlights what appears to be a useful and feasible next step in this process; automated detection of ice from cameras and processors installed on the vehicles that may then trigger navigational maneuvers. The repository of saildrone ice and non-ice images collected on this mission will be key to developing the necessary ice recognition capability. Work is planned to bring this to fruition.

DATA AVAILABILITY STATEMENT

The datasets presented in this study can be found in online repositories. The names of the repository/repositories and accession number(s) can be found below:

https://ferret.pmel.noaa.gov/pmel/erddap/index.html
https://thredds.met.no/thredds/osisaf/osisaf_seaiceconc.html
https://www.natice.noaa.gov/products/daily_products.html
https://worldview.earthdata.nasa.gov/
https://www.sentinel-hub.com/explore/eobrowser/.

AUTHOR CONTRIBUTIONS

AC co-managed the mission, analysis, design, and writing of this manuscript. CZ was a mission Principal Investigator (PI) and helped design, and write this manuscript. QY co-managed the mission. EC and QY studied a previous year's ice encounter. EC provided the seminal post-mission tabulation of sea-ice conditions. CMo and PS provided analysis results and aided the writing. CG was a mission PI. JC was a mission PI and helped write this manuscript. NL-S and CMe were instrumental in equipping the saildrones with the observational packages used during this mission. MS, MW, and DH helped organize and write this manuscript. HT led communications with Alaskan communities, helped coordinate the mission's preparation and progress, and helped write this manuscript. EB and KO'B managed the saildrone data curation, enabled the real-time data feed to the GTS, and helped write this manuscript. All authors contributed to the article and approved the submitted version.

FUNDING

AC was supported by funding from the NOAA Global Ocean Monitoring and Observation program (FundRef # 100007298). This publication is partially funded by the University of Washington's Joint Institute for the Study of the Atmosphere and Ocean under NOAA Cooperative Agreement NA15OAR4320063, Contribution No. 2020-1115. MS and CG were funded by the MISST3 Project, NASA grant 80NSSC18K0837. MW gratefully acknowledges support from National Science Foundation Grant 1751363 and the NOAA Arctic Research Program. This is PMEL contribution 5158 and EcoFOCI contribution 0959-RPPO.

ACKNOWLEDGMENTS

We thank the Saildrone Inc. team that worked on this mission, including pilots K. Neal, D. Nonweiler, and R. Jenkins who, among other tasks, led the effort to rescue sd-1035, which lost its ability to navigate following the mission's final ice encounter on 23 Aug 2019. We also thank the members of the Alaskan communities we corresponded with, including those who provided the small boat for sd-1035's rescue. We thank also Alaska SeaGrant Map Agent Gay Sheffield, NOAA's Candace Nachman and Amy Holman for continued support in communicating the testing of innovative technologies in the US Arctic. CDR Paul Kunicki helped facilitate communication with the US Coast Guard and researched options for sd-1035's rescue. We greatly appreciate the assistance from NIC analysists who shared their ice information expertise with us, including Alexandra Darden, William Walter, Chris Readinger, Katie Quinn, Evan Neuworth, Christopher Szorc and Sofia Montalvo. This mission benefited from collaboration and assistance from Kevin Wood, who led aerial reconnaissance of the saildrone positions on 17 July 2019, capturing thermal imaging video of the drones and deploying nearby airborne expendable bathythermographs. This mission benefited from helpful conversation with Luc Rainville and Craig Lee. Ansley Manke contributed FERRET software that calculated distance between saildrones, facilitating close-sail, inter-vehicle sensor comparisons at the beginning and end of the mission. We are also grateful to Stacey Maenner-Jones for remotely controlling the ASVCO2 systems. The saildrone mission was funded by NOAA PMEL Innovative Technology for Arctic Exploration program.

SUPPLEMENTARY MATERIAL

The Supplementary Material for this article can be found online at: https://www.frontiersin.org/articles/10.3389/fmars.2021.640697/full#supplementary-material

REFERENCES

Alexander, M. A., Scott, J. D., Friedland, K. D., Mills, K. E., Nye, J. A., Pershing, A. J., et al. (2018). Projected sea surface temperatures over the 21st century: changes in the mean, variability and extremes for large marine ecosystem regions of Northern Oceans. *Elem Sci. Anth.* 6:9. doi: 10.1525/elementa.191

Banzon, V., Smith, T. M., Steele, M., Huang, B., and Zhang, H. (2020). Improved estimation of proxy sea surface temperature in the Arctic. *J. Atmos. Ocean. Technol.* 37, 341–349. doi: 10.1175/jtech-d-19-0177.1

Bertoia, C., Manore, M., Andersen, H. S., O'Connors, C., Hansen, K. Q., and Evanego, C. (2004). "'Chapter 20: synthetic aperture radar for operational ice observation and analysis at the U.S., Canadian and Danish National Ice Centers'," in *Synthetic Aperture Radar: Marine User's Manual*, eds J. R. Apel and C. R. Jackson (Washington, DC: U.S. Dept. of Commerce, National Oceanographic and Atmospheric Administration), 417–442.

Bourassa, M. A., Gille, S. T., Bitz, C., Carlson, D., Cerovecki, I., Clayson, C. A., et al. (2013). High-latitude ocean and sea ice surface fluxes: challenges for

climate research. *Bull. Am. Meteorol. Soc.* 94, 403–423. doi: 10.1175/bams-d-11-00244.1

Brenner, S., Rainville, L., Thomson, J., and Lee, C. (2020). The evolution of a shallow front in the Arctic marginal ice zone. *Elem. Sci. Anth.* 8:17. doi: 10.1525/elementa.413

Carlson, D. F., Fursterling, A., Versterled, L., Skovby, M., Pedersen, S. S., Melved, C., et al. (2019). An affordable and portable autonomous surface vehicle with obstacle avoidance for coastal ocean monitoring. *HardwareX* 6:e00059. doi: 10.106/j.ohx.2019.e0059

Cokelet, E. D., Meinig, C., Lawrence-Slavas, N., Stabeno, P. J., Mordy, C. W., Tabisola, H. M., et al. (2015). *The Use of Saildrones to Examine Spring Conditions in the Bering Sea*. Washington: IEEE.

Danielson, S. L., Ahkinga, O., Ashjian, C., Basyuk, E., Cooper, L. E., Eisner, L., et al. (2020). Manifestation and consequences of warming and altered heat fluxes over the Bering and Chukchi Sea continental shelves. *Deep Sea Res. II* 177:104781. doi: 10.1016/j.dsr2.2020.104781

Dewey, S. R., Morison, J .H., and Zhang, J. (2017). An Edge-referenced surface fresh layer in the beaufort sea seasonal ice zone. *J. Phys. Oceanogr.* 47, 1125–1144. doi: 10.1175/JPO-D-16-0158.1

Efron, B., and Tibshirani, R. (1991). Statistical data analysis in the computer age. *Science* 253, 390–395.

Eriksen, C. C., Osse, T. J., Light, R. D., Wen, T., Lehman, T. W., Sabin, P. L., et al. (2001). Seaglider: a long-range autonomous underwater vehicle for oceanographic research. *IEEE J. Ocean. Eng.* 26, 424–436. doi: 10.1109/48.972073

Fofonoff, N. P., and Millard, R. C. Jr. (1983). Algorithms for the computation of fundamental properties of seawater. *Paper Presented at the UNESCO Technical Papers in Marine Sciences 44*. Paris: UNESCO.

Gallaher, S., Stanton, T., Shaw, W., Cole, S. T., Toole, J. M., Wilkinson, J., et al. (2016). Evolution of a Canada Basin ice-ocean boundary layer and mixed layer across a developing thermodynamically forced marginal ice zone. *J. Geophys. Res. Oceans* 121, 6223–6250. doi: 10.1002/2016JC011778

Gallaher, S. G., Stanton, T. P., Shaw, W. J., Kang, S.-H., Kim, J.-H., and Cho, K.-H. (2017). Field observations and results of a 1-D boundary layer model for developing near-surface temperature maxima in the Western Arctic. *Elementa: Sci. Anthropocene* 5:11. doi: 10.1525/elementa.195

Grebmeier, J. M., Moore, S. E., Cooper, L. W., and Frey, K. E. (2019). The distributed biological osbervatory: a change detection array in the pacific arctic – an introduction. *Deep Sea Res. II* 162, 1–7. doi: 10.1016/j.dsr2.2019.05.005

Hui, F., Zhao, T., Li, X., Shokr, M., Heil, P., Zhao, J., et al. (2017). Satellite-based sea ice navigation for Prydz Bay, East Antarctica. *Remote Sens.* 9:518. doi: 10.3390/rs9060518

Huntsberger, T., Aghazarian, H., Howard, A., and Trotz, D. C. (2011). Stereo vision-based navigation for autonomous surface vessels. *J. Field Robot.* 28, 3–18. doi: 10.1002/rob.20380

IACS (2016). *International Association of Classification Societies, Unified Requirements for Polar Class Ships (UR-I). Rev. 2*. Available online at: https://www.iacs.org.uk/download/1803 (accessed March 2021).

Ice Navigation in Canadian Waters (2012). *Ottowa: Icebreaking Program, Maritime Services Canadian Coast Guard Fisheries and Oceans Canada*. Ottowa: Ice Navigation in Canadian Waters, 81–115.

Jayne, S., and Bogue, N. (2017). Air-deployable profiling floats. *Oceanography* 30, 29–31. doi: 10.5670/oceanog.2017.214

Jin, J., Zhang, J., Liu, D., Shi, J., Wang, D., and Li, F. (2020). Vision-based target tracking for unmanned surface vehicle considering its motion features. *IEEE Access* 8, 132655–132664. doi: 10.1109/ACCESS.2020.3010327

Johnson, W. (2011). Correlation and explaining variance: to square or not to square? *Intelligence* 39, 249–254. doi: 10.1016/j.intell.2011.07.001

Karvonen, J. (2017). Baltic sea ice concentration estimation using SENTINEL-1 SAR and AMSR2 microwave radiometer data. *IEEE Trans. Geosci. Remote Sens.* 55, 2871–2883. doi: 10.1109/TGRS.2017.2655567

Kashiwase, H., Ohshima, K. I., Nihashi, S., and Eicken, H. (2017). Evidence for ice-ocean albedo feedback in the Arctic Ocean shifting to a seasonal ice zone. *Sci. Rep.* 7:8170. doi: 10.1038/s41598-017-08467-z

König, M., Hieronymi, M., and Oppelt, N. (2019). Application of Sentinel-2 MSI in arctic research: evaluating the performance of atmospheric correction approaches over arctic sea ice. *Front. Earth Sci.* 7:22. doi: 10.3389/feart.2019.00022

Lavelle, J., Tonboe, R., Pfeiffer, R.-H., and Howe, E. (2016). *Validation Report for the OSI SAF AMSR-2 Sea Ice Concentration, Product OSI-408. Version 1.1*. Available online at: http://saf.met.no/docs/osisaf_cdop2_ss2_valrep_amsr2-ice-conc_v1p1.pdf (accessed March, 2021).

LeCun, Y., Bengio, Y., and Hinton, G. (2015). Deep learning. *Nature* 521, 436–444. doi: 10.1038/nature14539

Lee, C. M., Sylvia, C., Martin, D., James, M., Ruth, M., and Tom, P. (2016). *Stratified Ocean Dynamics in the Arctic: Science and Experiment Plan*. Seattle, WC: Applied Physical Laboratory, University of Washington. Technical Report APL-UW TR 1601.

Lee, C. M., Thomson, J., and the Marginal Ice Zone and Arctic Sea State Teams (2017). An autonomous approach to observing the seasonal ice zone in the western Arctic. *Oceanography* 30, 56–68. doi: 10.5670/oceanog.2017.222

Levine, R., De Robertis, A., Grunbaum, D., Woodgate, R., Mordy, C., Mueter, F. J., et al. (2020). Repeat autonomous vehicle surveys indicate that age-0 gadid fishes are largely retained over the Chukchi Sea shelf in summer 2018. *Limnol. Oceanogr.* [Epub ahead of print].

Li, M., Pickart, R. S., Spall, M. A., Weingartner, T. J., Lin, P., Moore, G. W. K., et al. (2019). Circulation of the Chukchi Sea shelfbreak and slope from moored timeseries. *Prog. Oceanogr.* 172, 14–33. doi: 10.1016/j.pocean.2019.01.002

Liu, Z., Schweiger, A., and Lindsay, R. (2015). Observations and modeling of atmospheric profiles in the arctic seasonal ice zone. *Monthly Weather Rev.* 143, 39–53. doi: 10.1175/MWR-D-14-00118.1

Lu, K., Danielson, S., Hedstrom, K., and Weingarner, T. (2020). Assessing the role of oceanic heat fluxes on ice ablation of the central Chukchi Sea Shelf. *Prog. Oceanogr.* 184:102313. doi: 10.1016/j.pocean.2020.102313

Markus, T., and Dokken, S. T. (2002). Evaluation of late summer passive microwave arctic sea ice retrievals. *IEEE Trans. Geosci. Remote Sens.* 40, 348–356. doi: 10.1109/36.992795

Meinig, C., Burger, E. F., Cohen, N., Cokelet, E. D., Cronin, M. F., Cross, J. N., et al. (2019). Public–private partnerships to advance regional ocean-observing capabilities: a saildrone and NOAA-PMEL case study and future considerations to expand to global scale observing. *Front. Mar. Sci.* 6:448. doi: 10.3389/fmars.2019.00448

Meinig, C., Jenkins, R., Lawrence-Slavas, N., and Tabisola, H. (2015). "The use of Saildrones to examine spring conditions in the Bering Sea: vehicle specification and mission performance," in *Proceedings of the Oceans 2015 MTS/IEEE, Marine Technology Society and Institute of Electrical and Electronics Engineers*, Washington, DC.

Millero, F. J., and Leung, W. H. (1976). The thermodynamics of seawater at one atmosphere. *Am. J. Sci.* 276, 1035–1077. doi: 10.2475/ajs.276.9.1035

Mordy, C. W., Cokelet, E. D., DeRobertis, A., Jenkins, R., Kuhn, C. E., Lawrence-Slavas, N., et al. (2017). Advances in ecosystem research: saildrone surveys of oceanography, fish, and marine mammals in the Bering Sea. *Oceanography* 30, 113–115. doi: 10.5670/oceanog.2017.230

Nagler, T., Rott, H., Hetzenecker, M., Wuite, J., and Potin, P. (2015).The sentinel-1 mission: new opportunities for ice sheet observations. *Remote Sens.* 7, 9371–9389. doi: 10.3390/rs70709371

Ouyang, Z., Qi, D., Chen, L., Takahashi, T., Zhong, W., DeGrandpre, M. D., et al. (2020). Sea-ice loss amplifies summertime decadal CO2 increase in the western Arctic Ocean. *Nat. Clim. Chang.* 10, 678–684. doi: 10.1038/s41558-020-0784-2

Polashenski, C., Perovich, D., Richter-Menge, J., and Elder, B. (2011). Seasonal ice mass-balance buoys: adapting tools to the changing Arctic. *Ann. Glaciol.* 52, 18–26. doi: 10.3189/172756411795931516

Qi, D., Chen, B., Chen, L., Lin, H., Gao, Z., Sun, H., et al. (2020). Coastal acidification induced by biogeochemical processes driven by sea-ice melt in the western Arctic ocean. *Polar Sci.* 23:100504. doi: 10.1016/j.polar.2020.100504

Rainville, L., Wilkinson, J., Durley, M. E., Harper, S., DiLeo, J., Doble, M., et al. (2020). Improving situational awareness in the Arctic Ocean. *Front. Mar. Sci.* 7:581139. doi: 10.3389/fmars.2020.581139

Sabine, C., Sutton, A., McCabe, K., Noah, L. S., Simone, A., Richard, F., et al. (2020). Evaluation of a new carbon dioxide system for autonomous surface vehicles. *J. Atmos. Ocean. Tech.* 37, 1305–1317. doi: 10.1175/jtech-d-20-0010.1

Scheuchl, B., Flett, D., Caves, R., and Cumming, I. (2004). Potential of Radarsat-2 data for operational sea ice monitoring. *Can. J. Remote Sens.* 30, 448–461. doi: 10.5589/m04-011

Serreze, M. C., and Francis, J. A. (2006). The arctic amplification debate. *Clim. Change* 76, 241–264. doi: 10.1007/s10584-005-9017-y

Smith, L. C., and Stephensen, S. R. (2013). New Trans-Arctic shipping routes navigable by midcentury. *Proc. Nat. Adac. Sci. U.S.A.* 110, E1191–E1195. doi: 10.1073/pnas.1214212110

Stabeno, P. J. (2019). The Eastern Bering Sea: declining ice, warming seas, and a changing ecosystem, in State of the Climate in 2018. *Bull. Am. Meteorol. Soc.* 100, S148–S149. doi: 10.1175/2019BAMSStateoftheClimate.1

Stabeno, P. J., and Bell, S. W. (2019). Extreme conditions in the Bering Sea (2017-2018): record breaking low sea-ice extent. *Geophys. Res. Lett.* 46, 8952–8959. doi: 10.1029/2019GL083816

Steele, M., and Ermold, W. (2015). Loitering of the retreating sea ice edge in the Arctic Seas. *J. Geophys. Res. Oceans* 120, 7699–7721. doi: 10.1002/2015JC011182

Stoddard, M. A., Etienne, L., Fournier, M., Pelot, R., and Beveridge, L. (2016). Making sense of arctic maritime traffic using the polar operational limits assessment risk indexing system (POLARIS). *IOP Conf. Ser. Earth Environ. Sci.* 34:e012034.

Sullivan, M. E., Kachel, N. B., Mordy, C. W., Salo, S. A., and Stabeno, P. J. (2014). Sea ice and water column structure on the eastern Bering sea shelf. *Deep Sea Res. II* 109, 39–56. doi: 10.1016/j.dsr2.2014.05.009

Sutton, A. J., Sabine, C. L., Maenner-Jones, S., Lawrence-Slavas, N., Meinig, C., Feely, R. A., et al. (2014). A high-frequency atmospheric and seawater pCO_2 data set from 14 open-ocean sites using a moored autonomous system. *Earth Syst. Sci.* 6, 353–366. doi: 10.5194/essd-6-353-2014

Terhaar, J., Kwiatkowski, L., and Bopp, L. (2020). Emergent constraint on Arctic Ocean acidification in the twenty-first century. *Nature* 582, 379–383. doi: 10.1038/s41586-020-2360-3

Thomson, J. (2012). Wave breaking dissipation observed with "SWIFT" drifters. *J. Atmos. Ocean. Technol.* 29, 1866-1882. doi: 10.1175/JTECH-D-12-00018.1

Timmermans, M.-L., Proshutinsky, A., Golubeva, E., Jackson, J. M., Krishfield, R., McCall, M., et al. (2014). Mechanisms of pacific summer water variability in the arctic's Central Canada Basin. *J. Geophys. Res.* 119, 7523-7548. doi: 10.1002/2014JC010273

Transport Canada (2018). *Arctic Ice Regime Shipping System (AIRSS) Standard*. TP 12259. Canada: Transport Canada.

U.S. National Ice Center (2020). *U.S. National Ice Center Daily Marginal Ice Zone Products, Version 1. Overlay Shapefile and User Guide*. Boulder, CA: NSIDC: National Snow and Ice Data Center.

Walsh, J. E. (2014). Intensified warming of the Arctic: causes and impacts on middle latitudes. *Glob. Planet. Change* 117, 52–63. doi: 10.1016/j.gloplacha.2014.03.003

Wang, M., and Overland, J. E. (2009). A sea ice free summer Arctic within 30 years? *Geophys. Res. Lett.* 36:L07502. doi: 10.1029/2009GL037820

Wang, M., and Overland, J. E. (2012). A sea ice free summer Arctic within 30 years – an update from CMIP5 models. *Geophys. Res. Lett.* 39:L18501. doi: 10.1029/2012GL052868

Wang, M., Yang, Q., Overland, J. E., and Stabeno, P. J. (2018). Sea-ice cover timing in the Pacific Arctic: the present and projections to mid-century by selected CMIP5 models. *Deep Sea Res. II* 152, 22–34. doi: 10.1016/j.dsr2.2017.11.017

Wood, K., Overland, J. E., Salo, S. A., Bond, N. A., Williams, W. J., and Dong, X. (2013). Is there a "new normal" climate in the Beafort Sea? *Polar Res.* 32:19552. doi: 10.3402/polar.v32i0.19552

Zakhvatkina, N., Korosov, A., Muckenhuber, S., Sandven, S., and Babiker, M. (2017). Operational algorithm for ice-water classification on dula-polarized RADARSAT-2 images. *Cryosphere* 11, 33–46. doi: 10.5194/tc-11-33-2017

Zakhvatkina, N., Smirnov, V., and Bychkova, I. (2019). Satellite SAR data-based sea ice classification: an overview. *Geosciences* 9:152. doi: 10.3390/geosciences9040152

Zhang, D., Cronin, M. F., Meinig, C., Farrar, J. T., Jenkins, R., Peacock, D., et al. (2019). Comparing air-sea flux measurements from a new unmanned surface vehicle and proven platforms during the SPURS-2 field campaign. *Oceanography* 32, 122–133. doi: 10.5670/oceanog.2019.220

Conflict of Interest: The authors declare that the research was conducted in the absence of any commercial or financial relationships that could be construed as a potential conflict of interest.

The reviewer CW declared a shared committee with one of the authors EB at time of review.

Chapter 2: Manifestation and consequences of warming and altered heat fluxes over the Bering and Chukchi Sea continental shelves

Danielson, S. L., O. Ahkinga, C. Ashjian, E. Basyuk, L. W. Cooper, L. Eisner, E. Farley, K. B. Iken, J. M. Grebmeier, L. Juranek, G. Khen, S. R. Jayne, T. Kikuchi, C. Ladd, K. Lu, R. M. McCabe, G. W. K. Moore, S. Nishino, F. Ozenna, R. S. Pickart, I. Polyakov, P. J. Stabeno, R. Thoman, W. J. Williams, K. Wood, and T. J. Weingartner.

Citation:

Danielson, S.L., Ahkinga, O., Ashjian, C., Basyuk, E., Cooper, L.W., Eisner, L., Farley, E., Iken, K.B., Grebmeier, J.M., Juranek, L. Khen, G., Jayne, S.R., Kikuch, T., Ladd, C., Lu, K., McCabe, R.M., Moore, G.W.K, Nishimo, S.,Ozenna, F., Pickart, R.S., Polyakov I., Stabeno, P.J., Thoman, R., Williams, W.J., Wood, K., and Weingartner T.J., 2020. Manifestation and consequences of warming and altered heat fluxes over the Bering and Chukchi Sea continental shelves. Deep Sea Research Part II: Topical Studies in Oceanography, 177, p.104781. doi: 10.1016/j.dsr2.2020.104781

Chapter 3: Seasonal abundance, distribution, and growth of the early life stages of polar cod (Boreogadus saida) and saffron cod (Eleginus gracilis) in the US Arctic

Deary, A.L., Vestfals, C.D., Mueter, F.J., Logerwell, E.A., Goldstein, E.D., Stabeno, P.J., Danielson, S.L., Hopcroft, R.R., Duffy-Anderson, J.T.

Citation:

Deary, A.L., Vestfals, C.D., Mueter, F.J., Logerwell, E.A., Goldstein, E.D., Stabeno, P.J., Danielson, S.L., Hopcroft, R.R. and Duffy-Anderson, J.T., 2021. Seasonal abundance, distribution, and growth of the early life stages of polar cod (Boreogadus saida) and saffron cod (Eleginus gracilis) in the US Arctic. Polar Biology, 44, pp.2055-2076. doi: 10.1007/s00300-021-02940-2.

Deary, A.L., Vestfals, C.D., Mueter, F.J., Logerwell, E.A., Goldstein, E.D., Stabeno, P.J., Danielson, S.L., Hopcroft, R.R., Duffy-Anderson, J.T. 2021. Seasonal abundance, distribution, and growth of the early life stages of polar cod (*Boreogadus saida*) and saffron cod (*Eleginus gracilis*) in the US Arctic. *Polar Biology*. https://doi.org/10.1007/s00300-021-02940-2

Abstract

Polar cod and saffron cod are dominant components of the fish community in the Chukchi Sea and are ecologically important forage fishes linking plankton to upper-level consumers. In 2017, we conducted a study as part of the Arctic Integrated Ecosystem Research Program to characterize the distribution, abundance, and growth of polar cod and saffron cod early life history stages (ELHS) in late spring and late summer in the Chukchi Sea. Ship-based plankton tows showed that polar cod and saffron cod larvae were centered in Kotzebue Sound in the late spring. By late summer, polar cod juveniles were centered offshore in the northern Chukchi Sea whereas saffron cod were distributed nearshore around Cape Lisburne. Empirical fish collections were paired with an individual-based biophysical transport model to examine connectivity and relate changes in seasonal distribution to potential environmental variables. Modeled drift trajectories and growth in spring for polar cod and saffron cod matched well with empirical observations, especially along the northern coastline of Kotzebue Sound, offshore of Point Hope/Cape Lisburne. Given the coherence between modeled and observed distributions, Kotzebue Sound is likely a source of gadid ELHS in the nearshore areas of the Chukchi Sea and offshore of Cape Lisburne/Point Hope, although it is not the likely source of polar cod over Hanna Shoal in the late summer. This is the first study to examine seasonal distribution, abundance, and growth of polar cod and saffron cod in the US Arctic and provides data necessary to evaluate the impacts of climate change on forage fishes in the Arctic.

Introduction

The Arctic has experienced accelerated warming at twice the rate of the global average, making Arctic ecosystems particularly sensitive to climate change (Graham et al., 2017; Tokinaga et al., 2017; Overland et al., 2018). The accumulation of heat in the Arctic has increased significantly since the late 1990s, which correlates to a reduction in sea ice thickness (Maslowski 2014), a 60% loss of multiyear ice, a 75% reduction in sea ice volume (Overland et al. 2018), and lower winter ice extent maxima (Graham et al. 2017). Loss of sea ice is expected to influence Arctic ecosystem dynamics through bottom-up changes to lower trophic production (Kahru et al. 2011), community structure (Spear et al. 2019), trophic linkages (Hunt et al. 2013), shifts in benthic-pelagic coupling (Grebmeier et al. 2015 and citations therein), and food web interactions (Li et al. 2009). Ecosystem changes also have potential economic ramifications such as range extensions of commercially important subarctic gadid species, such as walleye pollock (*Gadus chalcogrammus*), Pacific cod (*Gadus macrocephalus*), and salmonid fishes, into regions north of the Bering Strait (Falardeau et al. 2017; Stevenson and Lauth 2019) in the Pacific Arctic.

Although not fished commercially in the US Arctic (NPFMC 2009), polar cod (*Boreogadus saida*), a circumpolar species, and saffron cod (*Eleginus gracilis*) are crucial forage fishes in Arctic marine ecosystems. Both species support bioenergetic pathways that transfer energy from planktonic food webs to upper level consumers and apex predators (including humans) and are a dominant component of the fish community in the Chukchi Sea, although polar cod is more abundant than saffron cod (Whitehouse et al. 2014; Logerwell et al. 2015). It is estimated that seabirds and marine mammals consume approximately 75% of the polar cod production (Whitehouse et al. 2014). Changes to the Chukchi shelf ecosystem due to climatic warming, loss of sea ice, and perturbations to sea ice phenology (Graham et al. 2017; Overland et al. 2018) may have serious implications for these ecologically important species.

Despite their ecological importance and abundance in Arctic ecosystems, the life history of polar cod and saffron cod are still relatively unknown (Logerwell et al. 2015; Vestfals et al. 2019). Spawning

locations of polar cod in the US Arctic are largely unknown, although it is hypothesized that polar cod spawn under sea ice (Rass 1968) and that peak hatching likely occurs in May and June as the ice edge recedes (Bouchard and Fortier 2008; Vestfals et al. 2019). In the Pacific Arctic, development of larvae and early juveniles occurs along the shelf (Logerwell et al. 2015; Vestfals et al. 2019). Saffron cod are near-shore, demersal, under-ice spawners that deposit demersal eggs in nearshore areas on sandy-pebbly substrates (Vestfals et al. 2019 and citations therein) but exact locations are unknown in the US Arctic. Peak hatching for saffron cod occurs in April and May, earlier than for polar cod, and offspring are often found concentrated closer to shore and at more southerly locations within the Chukchi Sea (Vestfals et al. 2019). The life histories of polar cod and saffron cod are similar in that both are planktonic in shelf waters after hatching through the first summer, after which polar cod move deeper in the water column while saffron cod become demersal as juveniles (Logerwell et al. 2015; Vestfals et al. 2019).

Growth of polar cod and saffron cod is mediated by temperature (Laurel et al. 2016) and an additional consequence of a warming Arctic is that large calanoid copepod species, an important prey resource for Arctic gadids, will be replaced by smaller, less lipid-rich copepods (Aarflot et al. 2018; Møller and Nielsen 2020; Bouchard and Fortier 2020). Larvae and juveniles will be disproportionately affected by these changes relative to adults due to their higher weight-specific growth rates, and polar cod may be more sensitive than saffron cod because they are a stenothermic species (Laurel et al. 2016). Polar cod are adapted to support high growth and lipid allocation at a narrow range of low temperatures (optimal growth rate at 5°C), while saffron cod experience high growth and lipid allocation over a wider temperature range, particularly, at high temperatures (optimal growth rate >16°C) (Copeman et al. 2016; Laurel et al. 2016). As such, saffron cod may be better able to mitigate the effects of ocean warming in the Arctic than polar cod.

In 2017, the Arctic Integrated Ecosystem Research Program (Arctic IERP), funded by the North Pacific Research Board, conducted its first field season in the US Pacific Arctic. Concurrent with the Arctic IERP surveys, the Distributed Biological Observatory (DBO) project and the Arctic Marine Biodiversity Observation Network (AMBON) survey were also sampling the region, providing more coverage to this region that is often under-researched. In this inaugural year of sampling for the Arctic IERP, it was remarkable that the northern Bering Sea and Chukchi Sea were sampled for ichthyoplankton in both late spring and late summer, a first in the region. These sampling efforts provided an opportunity to assess the seasonal abundance, distribution, and growth of fishes during their early life history stages (ELHS). However, the summer of 2017 in the Chukchi Sea was also remarkable in environmental conditions, with an elevated sea surface temperature (+4°C relative to the historic average) and the lowest recorded March sea ice minimum in the 39-year history of the time series (Timmermans et al. 2017; Perovich et al. 2017), providing us with baseline vital rate data for polar cod and saffron cod, albeit during a warm year. Such baseline data, when coupled with further monitoring and modelling, can be used to determine the impact of climate warming on these two ecologically important species. In addition to empirical sampling, we used an individual-based model (IBM) as a tool to simulate larval transport and examine potential linkages and connectivity in polar cod and saffron cod abundance and distribution between the late spring and late summer sampling events. Our goals for this study were to (1) examine spatial patterns of distribution and abundance of polar cod and saffron cod during their larval (June; late spring) and early juvenile (August-September; late summer) stages in 2017; (2) assess the change in mean length to approximate daily growth rates in the summer for polar cod and saffron cod; and (3) evaluate potential sources of larval polar cod and saffron cod using an IBM to compare observed distributions and sizes with model output. This study coupled empirical observations with IBM output to synthesize, for the first time, the seasonal distribution, abundance, and growth of two co-occurring

Arctic forage fishes, providing a means to assess the biological impacts of warming on polar cod and saffron cod ELHS.

Methods

Specimen Collection

Polar cod and saffron cod ELHS were collected in 2017, using three different sampling gears, as part of several cooperating research projects (Table 1): the Arctic Integrated Ecosystem Survey (AIES; part of Arctic IERP), AMBON survey, the Arctic Shelf Growth, Advection, Respiration, Deposition (ASGARD; part of Arctic IERP) project, and the DBO project. Larval and early juvenile Arctic gadids were targeted with a 60-cm bongo (bongo hereafter) equipped with a flow meter and a 505-µm mesh net fished obliquely from 10 m off the bottom or a maximum depth of 200 m to the surface in the late spring and late summer during the AIES and DBO surveys and to 5 m off the bottom or a maximum depth of 200 m for ASGARD. Demersal juvenile Arctic gadids (age-0, age-1+) were targeted with a benthic-sampling 3-m plumb-staff beam trawl (Abookire and Rose 2005) equipped with 7-mm mesh and a 4-mm cod end liner during the late summer AMBON and AIES surveys (Table 1). The beam trawl was deployed from the stern of the vessel and towed at 1.5-2.0 knots for four minutes (Logerwell et al. 2015). Juvenile gadids (age-0, age-1+) were also collected from the midwater during AMBON using a 1.5 m wide by 1.8 m high Isaacs-Kidd Midwater Trawl Net (IKMT) equipped with 3-mm mesh and a flowmeter (Table 1). The IKMT was towed double obliquely at 3.5-4.0 knots and these data were used to look at length and growth of Arctic gadids in August, prior to the late summer AIES surveys.

All bongo samples were fixed at sea in 5% formalin buffered with seawater and processed at the Plankton Sorting and Identification Center in Szczecin, Poland. ELHS of all fishes were identified to species, enumerated, and up to 50 specimens per taxon at each station were measured to the nearest 0.1 mm. Since specimens were measured after formalin fixation, we applied a +1.9% correction factor to

the measured lengths to account for shrinkage (D. Blood, B. Laurel, NOAA, unpublished data; Vestfals et al. 2019). The identifications of ELHS gadids were verified by scientists at the National Oceanic and Atmospheric Administration's Alaska Fisheries Science Center using Matarese et al., 1989, Dunn and Vinter 1984, (and Ichthyoplankton Information System (IIS 2019). Due to concerns of Walleye Pollock (*Gadus chalcogrammus*) being mis-identified as Polar Cod, the Arctic gadids captured during AIES using the beam trawl were verified using genetic methods following Wildes et al. (2016). No specimens of juvenile Arctic cod (*Arctogadus glacialis*) were detected (S. Wildes, Alaska Fisheries Science Center (AFSC), personal communication), suggesting that *A. glacialis* was not present in our study region since the abundance of later stages is reflective of the abundance of the earlier stages (Bouchard et al. 2016). Catch per unit effort of polar cod and saffron cod was reported as the number of individuals caught under a sea surface area of 10 m^2 (count per 10 m^2). Trawl samples (IKMT and beam trawl) were processed at sea with all individual fishes being identified, enumerated, and measured to the nearest length in millimeters. Standard length (SL) was measured for individuals at flexion size or larger and notochord length (NL) for individuals smaller than flexion. The reported size of flexion is 11.0 mm for polar cod and saffron cod (IIS 2019). Catch for the AIES and AMBON beam trawl was expressed as number of individuals caught per unit area swept (count per 1000 m^2).

Data Analysis

All catch and length data were analyzed using R (ver. 3.5.2; R Core Team 2019). For the length data, to account for only a subset of larvae being measured (n = 50 maximum), the estimated proportion of individuals at each length was multiplied by the standardized catch at that station (catch-weighted length). Individuals of polar cod and saffron cod larger than 70 mm SL were presumed to be one year or older based on a cutoff identified in the length-frequency distribution and were excluded from the subsequent length analyses. Our use of 70 mm SL to delineate between age-0 and age-1 polar cod is smaller than the size of this transition identified in prior work determining length at age using otoliths

[84.0 mm fork length (FL) and 81.6 mm total length (TL), respectively] (Craig et al. 1982; Lønne and Gulliksen 1989) because standard length excludes measuring the caudal fin rays that are often damaged during collection. The transition of saffron cod from age-0 to age-1 is not as definitive as that for polar cod due to an overlap in size at these ages occurring between 55 and 110 mm FL in the Chukchi Sea (Wolotira 1985; Copeman et al. 2016; Helser et al. 2017). However, in Arctic samples collected in 2012 all individuals greater than 75 mm FL were age-1 based on otolith analyses, suggesting our size cutoff is reasonable for the region sampled (Copeman et al. 2016). Specimens were then aggregated into 2-mm length bins. For the AMBON samples collected with the IKMT and the beam trawl, subsamples of fish were measured to the nearest millimeter. Many of the smallest individuals (less than 50 mm) were not measured and were instead sorted into approximate 10-mm size bins, enumerated in the field, and then discarded. The binned individuals were combined with the measured individuals by simulating individual lengths of the binned individuals from a uniform random distribution within their assigned size bin. Other distributions (normal, beta) were considered for simulating lengths of the binned individuals but had minimal impact on the resulting length-frequencies.

Daily growth rates were estimated for each species as the change in mean length from June 19th, 2017, the median date of the late spring (June) ASGARD survey, and each late summer survey (AMBON and AIES) under the assumption that these individuals were from the same cohort. The median date of the AMBON survey was August 13th, 2017 and the median date of the AIES survey was September 1st, 2017. Mean length for late spring was based on all individuals collected during the survey using the bongo. Mean length for the late summer individuals was gear-specific and calculated based on all putative age-0 specimens collected during: (1) AMBON survey using a beam trawl, (2) AMBON survey using an IKMT, (3) AIES and DBO surveys using a bongo, and (4) AIES survey using a beam trawl. Data for these growth analyses did not include estimates from midwater-collected gadids sampled during the late summer AIES and DBO Project, but they were available from the IKMT fished during the 2017 late summer

AMBON survey, providing some estimates of growth of midwater-associated fishes. Daily growth rates are presented as a range; the estimate provided from the late summer bongo collections represent a low estimate as larger gadids tend to escape from the bongo net (Shima and Bailey 1994) and likely represent individuals that are smaller-than-average. Late summer beam trawl collections (AIES) represent a high growth estimate as the coarser mesh size of the trawl may select for larger individuals that are larger-than-average and generally resulted in the greatest mean size. For polar Cod, length-dependent mortality results in slightly greater length at age estimates (Thanassekos et al. 2012), suggesting our study will be overestimating growth since we are relying on changes in length of survivors (those individuals captured and measured by the various gear types) to estimate growth. A daily growth rate was also calculated using the IKMT data to explore differences in the apparent growth rates between age-0 fishes that are still pelagic and those that have become demersal by the time of sampling. We expected the apparent growth rate to increase as individuals become more demersally oriented. Size distribution from the IKMT and beam trawl are likely to be directly comparable as the IKMT mesh size (4 mm) was identical to that of the beam trawl liner.

Densities (catch per unit area) of polar cod and saffron cod were mapped to explore the seasonal distribution of ELHS of Arctic gadids in the northern Bering and Chukchi seas relative to sea ice concentration on June 19th and September 1st, 2017. Sea ice concentrations were obtained from the National Snow and Ice Data Center at 25 km by 25 km spatial resolution (Cavalieri et al. 1996; NSIDC 2019).

Individual-based biophysical model for polar cod and saffron cod

Late spring and late summer distributions were compared to simulated distributions from biophysical transport models parameterized for polar cod and saffron cod larval and early juvenile stages (Vestfals et al. 2021). Details on the model parameterization and the results of validation testing are described in

Vestfals et al. (2021). These models were developed to simulate the growth and dispersal of early life stages in the northern Bering, Chukchi, and Beaufort seas to identify possible spawning locations, which are largely unknown, as well as to examine gadid connectivity between these seas. An implementation of the Regional Ocean Modeling System (ROMS) (Shchepetkin and McWilliams 2005) set up in a Pan-Arctic (PAROMS) configuration (Danielson et al. 2016) was used to realistically simulate the three-dimensional (3-D) circulation field. PAROMS has a horizontal resolution of ~5 km south of the Aleutian Islands to 9 km in the North Atlantic and is approximately 5.5 – 6.0 km in the Chukchi Sea, and is forced by the Japanese 55-year atmospheric reanalysis JRA55-do (version 1.4) (Tsujino et al. 2018), which also provides estimates of freshwater runoff. Boundary conditions come from the Simple Ocean Data Assimilation (SODA) reanalysis (version 3.3.1) (Carton et al. 2018) prior to 2015 and the Hybrid Coordinate Ocean Model (HYCOM) (Chassignet et al. 2009) for more recent years. The Oregon State TOPEX/Poseidon Global Inverse Solution (Egbert and Erofeeva 2002) provides tidal forcing and the sea ice field is based on the single-category Budgell ice model (Budgell 2005). To simulate advection and growth of larvae, IBMs for polar cod and saffron cod were developed using the particle tracking tool TRACMASS that calculates Lagrangian trajectories from Eulerian velocity fields (Döös 1995).

Stage-specific and size-specific temperature-dependent growth rates were used to model the growth of polar cod and saffron cod (Porter and Bailey 2007; Laurel et al. 2016; Koenker et al. 2018) to 45 mm in length, the size at which these species are thought to transition from pelagic juveniles to more demersal juveniles, with enhanced swimming abilities. In addition, these stages correspond most closely to the stages captured by the water column sampling gear (bongo and IKMT) during the field campaign allowing for comparison between simulated and observed distributions of the two species. Similar to the growth rates calculated for the 2017 empirical data, mean daily growth rates were estimated for the simulated larvae for each species as the change in mean length from late spring (June 19th) to late summer (September 1st) divided by the number of days elapsed.

Hatching locations were identified through a thorough literature review, anecdotal evidence, and known areas of retention in the Pacific Arctic (Vestfals et al 2021 and references therein). However, due to the preponderance of early-stage individuals encountered in the Kotzebue Sound region during spring 2017, we focused this study on this region as a potential source of polar cod and saffron cod in the US Chukchi Sea. For our study, Kotzebue Sound will include the area that extends from the northwestern tip of Seward peninsula to Point Hope. Simulations were initialized from all PAROMS grid points falling within the eastern-most part of Kotzebue Sound as hatching location (Figure 1), with 10 particles released per 5 m depth increment to the bottom at each PAROMS grid point. The Chukchi Sea is often shallower than 40 m, which represents the maximum release depth of particles in the model (Vestfals et al. 2021). Based on results from initial particle simulations, dispersal simulations were conducted with larvae hatching on the 1st and 15th day of each month from March 1st through May 15th, for a total of six hatching events. Temperature-mediated growth and dispersal of larvae were simulated until September 1st, the midpoint of the late summer Arctic field surveys in 2017, so that the simulated distribution and size composition during summer could be compared to the observed distributions and size compositions of individuals captured during the surveys.

IBM parameterization- polar cod

Several vertical behaviors were developed for polar cod based on available literature (Borkin et al. 1986; Bouchard et al. 2016) and from laboratory observations (B. Laurel, AFSC, *unpublished data*). Of the five different vertical behavior routines tested, simulations with surface-oriented individuals, where all stages were found at 5 m matched best with prior field observations from acoustic-trawl surveys conducted in 2012 and 2013 (DeRobertis et al. 2017; Vestfals et al. 2021). Polar cod growth was based on growth equations described in Koenker et al. (2018) and Laurel et al. (2016). Simulated larval sizes

and distributions on June 19th (midpoint of the ASGARD survey) and September 1st (midpoint of AIES) from simulations originating in Kotzebue Sound were compared to field observations.

IBM parameterization- saffron cod

Similar vertical behaviors were used for the saffron cod simulations as for polar cod since no information on the vertical distribution of saffron cod larvae is available at present. Preflexion larval growth from hatch to 10 mm in length was based on temperature-dependent growth experiments (B. Laurel, unpublished data; Vestfals et al. 2021). At present, temperature-dependent growth models for saffron cod ELHS > 10 mm in length are not available. As growth of saffron cod at these small sizes is linear and resembles that of walleye pollock (B. Laurel, AFSC, unpublished data), the growth model described in Porter and Bailey (2007) was used to model saffron cod growth from 10 to 45 mm.

Results

2017 Field Data

Sea Ice

As of June 1st, just prior to the survey, sea ice was present in the Kotzebue Sound region (S. Danielson, University of Alaska Fairbanks (UAF), unpublished data). By June 19th, the mid-point of the late spring survey, sea ice was receding and the entire survey area was ice-free.

Abundance, Distribution, and Size of polar cod

In June, the highest densities of polar cod (> 640 individuals per 10 m^2) were found at nearshore stations of Kotzebue Sound and Point Hope transects and along the entire Cape Lisburne transect (Figure 2a). Polar cod density was lower south of the Bering Strait with most individuals being encountered along the northernmost transects sampled in the Chukchi Sea. By late summer (August and September), sea ice remained absent in the survey region south of 75°N, except in the nearshore area of Kotzebue

Sound. The overall density of polar cod decreased from an average catch of 1183 individuals per 10 m^2 in the late spring to 7 individuals per 10 m^2 in the late summer in the water column. The highest densities of polar cod in the water column (>10 individuals per 10 m^2) were observed in the northern portion of the survey area in the late summer, particularly around Barrow Canyon and Hanna Shoal (Figure 2b). The distribution of polar cod in the water column was similar to the distribution of demersal individuals. Demersal catches of juvenile polar cod (<70 mm SL) were highest offshore in the northern Chukchi Sea in the late summer in areas where bottom water temperatures were below approximately 5°C (Figure 3a and b).

In June, the mean length of polar cod larvae in the water column was 9.8 mm NL (*n*= 850), with most larvae being less than 12.0 mm in length (Figure 4a; Table 2). By the end of the summer, the length distribution of polar cod had expanded and the mean length increased to 30.1 mm SL ± 0.9 (*n*= 140) and 30.7 mm SL ± 0.4 (*n*= 433) for specimens collected in the water column with the bongo and IKMT gears, respectively (Figure 4c, e; Table 2). In late summer (August-September) the mean length of demersal polar cod was 39.7 mm SL ± 0.4 (*n*= 718) in the AMBON beam trawl samples and 47.8 mm SL ± 1.6 (*n* = 690) in the AIES beam trawl samples (Figure 4g, i; Table 2). Based on changes in length and an assumption that larvae collected in the late summer surveys were from the same cohort as fish collected in the late spring, the estimated daily growth rate for polar cod during 2017 ranged from 0.27 mm day^{-1} based on individuals in the water column to 0.53 mm day^{-1} based on individuals that had become demersal (Table 3), with an overall mean of 0.39 ± 0.06 mm day^{-1} (*n*= 4) based on all measured individuals.

Abundance, Distribution and size of saffron cod

The density of pelagic larval saffron cod in June was highest at the nearshore stations in Kotzebue Sound and Cape Lisburne, which were both ice covered on June 1st, prior to the mid-point of the survey, with densities ranging from 68 to 444 individuals per 10 m^2. The highest observed density of saffron cod was

at the innermost station along the southern margin of Kotzebue Sound (Figure 2c). Catches south of Kotzebue Sound were low (less than 30 individuals per 10 m^2). Densities of saffron cod were much lower later in the summer (August and September), with most of the stations yielding no saffron cod (Figure 2d). Unlike saffron cod in the water column, demersal larval and early juvenile saffron cod in later summer were rarely encountered offshore, with most individuals concentrated near Cape Lisburne (Figure 3c and d). Demersal saffron cod were observed in areas with higher bottom temperatures than demersal polar cod. In early August, saffron cod were concentrated in areas with bottom water temperatures greater than 7.5°C and by September occupied areas with bottom water temperatures greater than 5.4°C.

Saffron cod had a mean length of 9.3 mm NL ± 0.4 (*n*= 299) in June, with most individuals measuring less than 14.0 mm in length (Figure 4b; Table 2). By late summer, the mean length of saffron cod ranged from 18.5 mm SL ± 1.4 (*n*= 7) in the bongo to 40.3 mm SL ± 1.7 (*n*= 41) in the IKMT (Figure 4d, f). The mean length of demersal saffron cod was 51.6 mm SL ± 0.4 (*n*= 318) in the AMBON beam trawl and 55.1 mm SL ± 1.7 (*n*= 54) in the AIES beam trawl by late summer (Figure 4h, j; Table 2). The daily growth rate for saffron cod was estimated as 0.12 mm day^{-1} to 0.76 mm day^{-1} (Table 3), with a mean of 0.37 ± 0.16 mm day^{-1} (*n*= 4).

Comparison of distribution and size of polar cod and saffron cod

Catches of saffron cod were lower relative to polar cod regardless of season. In June, the core distribution of saffron and polar cod overlapped in Kotzebue Sound, with polar cod found farther offshore than saffron cod (Figure 2). Later in the summer, saffron cod were encountered in bongo samples of the water column at only 7 of the 136 stations sampled. Demersal juveniles of polar cod were observed farther offshore and to the north relative to saffron cod in the late summer. They were also most abundant offshore of the region between Cape Lisburne and Wainwright at stations with bottom water temperatures cooler than 5.0°C. In contrast, demersal juveniles of saffron cod were most

abundant nearshore off Cape Lisburne and in northern Kotzebue Sound where bottom water temperatures were warmer than 7.5°C (Figure 3b, d).

Polar cod and saffron cod were similar in mean size in June when their distributions also overlapped. Later in the season, far fewer saffron cod (*n*= 420) were captured and measured compared to polar cod (*n*= 1981). Demersal saffron cod were larger than those found in the water column in the late summer. The range of daily growth rates was wider for saffron cod than polar cod, but the mean daily growth rate was similar between saffron cod and polar cod at 0.37 ± 0.16 and 0.39 ± 0.06 mm day^{-1}, respectively (*n*= 4).

IBM Simulated Data

Simulated distribution and size of polar cod

On June 19th, simulated polar cod hatching in Kotzebue Sound between March 15th and May 15th had similar dispersal trajectories and were mostly found to be retained in and around Kotzebue Sound and in the nearshore region northward to Cape Lisburne (Figure 5). At Cape Lisburne, some larvae were transported offshore to the north and to the west, and were concentrated in two different trajectories, except for simulated individuals hatched on May 15th. Other individuals were transported northward along the coastline. Based on the 2017 simulations, no individuals were transported to the south in the late spring, though polar cod were observed in the late spring survey around St. Lawrence Island (Figure 2a; Figure 5). By September 1st, simulated polar cod were found in the nearshore region from Kotzebue Sound north to Wainwright (Figure 6). Simulated polar cod were advected offshore, almost due west, at Cape Lisburne/Point Hope. Hatch date did not greatly impact the end points of the simulated polar cod on September 1st (Figure 6). In the late summer, simulated polar cod were abundant offshore of Cape Lisburne/Point Lay and Wainwright but uncommon nearshore along the coastline from Kotzebue Sound to Wainwright (Figure 6), which was consistent with the empirical data (Figure 2b; Figure 3).

The mean size of simulated polar cod individuals hatched between March 1st and April 1st was larger than individuals captured in the field (Figure 4, Figure 7). Simulated individuals hatched on May 1st and May 15th were on average smaller than the field samples. For larvae that hatched on April 15th, the average size of simulated polar cod matched the average size of the captured individuals, although the range was broader for the individuals caught in the field compared to the simulated individuals (Table 2, Table 4). In the late summer, the average size of the simulated polar cod was smaller than the wild-caught specimens regardless of hatch date (Figure 7). The simulated sizes were most similar to polar cod captured using the bongo in the late summer (Table 2, Table 4).

Simulated distribution and size of saffron cod

The simulated distribution of saffron cod in the late spring and late summer was similar to that of polar cod (Figure 8). Similar to polar cod in the late spring, no simulated saffron cod larvae were found along the southern coastline of Kotzebue Sound, whereas saffron cod larvae were captured along the southern coastline of Kotzebue Sound and northern coastline of Norton Sound (Figures 2-3). In the late summer, simulated saffron cod were densely concentrated along the coastline extending from Kotzebue Sound to just north of Wainwright with two offshore advection areas at Point Lay/Cape Lisburne and south of Wainwright (Figure 9). Catches of saffron cod were low in the late summer but the areas with the highest catches corresponded to high density areas identified by the model, particularly offshore of Wainwright and Point Lay/Cape Lisburne (Figures 2-3; 9).

Regardless of season or hatch date, simulated saffron cod were smaller on average than field captured individuals (Table 2, Table 4). In addition, the length range of simulated individuals was narrower than the captured individuals in the late spring and summer (Figure 10). Unlike simulated polar cod, there was little overlap in the late spring and late summer sizes of simulated saffron cod (Figure 10). In the late spring, simulated saffron cod did not grow larger than 8.5 mm NL and had a mean size of 5.7 mm NL

± 0.0025-0.0037 for all simulated hatch dates (Figure 10, Table 4). In the late summer, the average size of simulated saffron cod ranged from 14.6 mm SL ± 0.024 to 14.9 mm SL ± 0.023 (Figure 10, Table 4).

Discussion

Spawning areas and drift

Sea ice was present in Kotzebue Sound at the approximate time of hatch for both polar cod and saffron cod until early June (S. Danielson, UAF, unpublished data; Cavalieri et al. 1996), suggesting that sea ice may be important for the newly hatched larvae of both species. Kotzebue Sound may indeed be a hatching area for polar cod and a source of juveniles to the north later in the summer. One of the main northward currents in the eastern Chukchi Sea is the ACC, which flows through Bering Strait and past the mouth of Kotzebue Sound and it is likely to entrain larvae originating in the Sound. Transport through Bering Strait has been increasing in recent years, which, in turn, has increased heat transport into the Chukchi Sea and the rate of sea ice retreat in the spring (Woodgate et al. 2012; Woodgate 2018), as well as current velocity that may increase the dispersal potential for ELHS entrained in the ACC. However, high polar cod abundance in the summer of 2014 corresponded to reduced transport through the Bering Strait (Randall et al. 2019), leading to decrease advection and higher local retention of ELHS. Simulations suggest that polar cod collected demersally and in the water column along the coast and in some offshores areas were likely hatched in Kotzebue Sound and were transported north by the ACC to the northern Chukchi Sea. We believe the likelihood of contamination of polar cod by Arctic cod (*A. glacialis*) is low and not of concern for our analyses. The identity of polar cod collected in the late summer AIES beam trawl was confirmed genetically (S. Wildes, Alaska Fisheries Science Center (AFSC), personal communication). Since the primary currents entering the US Chukchi Sea shelf flow from the south to the north (Danielson et al. 2017), it is unlikely that there is a source of Arctic cod, a high Arctic species, in the southern Chukchi Sea or Bering Strait that would substantially contribute to the larval gadid

community of the region (Aschan et al. 2009), especially considering the low sea ice and high water temperatures observed in 2017 (Timmermans et al. 2017; Perovich et al. 2017).

Saffron cod are caught in lower densities than polar cod in the late summer, likely due to their ELHS preferring nearshore habitats not sampled by our surveys (Logerwell et al. 2015; Vestfals et al. 2019). Similar to polar cod, Kotzebue Sound may be a hatching or early nursery area for saffron cod in the late spring. Demersal saffron cod were concentrated in the nearshore, warm waters in northern Kotzebue Sound and around Cape Lisburne, which was similar to the model-predicted distribution, suggesting that saffron cod hatched in Kotzebue Sound were the major source of demersal individuals in the late summer of 2017. Albeit speculative, the few larval saffron cod caught in the water column offshore of Wainwright and Barrow Canyon may be a result of a bet-hedging spawning strategy for saffron cod spawned in Kotzebue Sound and Bering Strait, such as has been documented in other sub-arctic gadids (Laurel et al. 2008; Hutchings and Rangeley 2011). Prolonged hatching periods will result in later hatched saffron cod larvae developing in warmer water where growth rates may be enhanced if mortality related to prey and predators is reduced (Laurel et al. 2008).

Growth and development

The daily growth rates calculated for polar cod and saffron cod were based on individuals collected in the water column and along the bottom using gears that collectively target larvae and juveniles and are used as a coarse estimate of growth in the US Chukchi Sea in the absence of otolith-derived growth rates. Assuming no size-selectivity over the range of sizes that were present, we were able to estimate a range of daily growth rates based on changes in mean length between specimens collected in the late spring and late summer of 2017. Our estimates assume that measured individuals were randomly selected from the same cohort sampled in the late spring and again in the late summer. However, it is probable that individuals from other hatching locations and cohorts were present in the northern Chukchi Sea in the late summer, violating this assumption (e.g., larvae originating from the other side of

the U.S. –Russian Federation maritime boundary). In our region in 2017, hatching was observed from January through May, with a peak in April (Z. Chapman, UAF, personal communication), based on the individuals captured during the late spring bongo samples. However, we are likely missing newly hatched larvae in the late spring bongo samples due to the extrusion of these individuals through the 505 µm bongo net mesh (Thanassekos et al. 2012), biasing our samples to individuals that hatched earlier or possessing higher growth rates. The daily growth rate results should be interpreted with caution without a more robust measure of growth using otolith-derived estimates, which is impossible for our study due to our specimens being preserved in formalin at sea. Otolith-derived ages would provide refinement of the length-based daily growth rates estimated in this study by determining individual growth rates and allowing for subsequent exploration of differences in growth trajectories by gear type, sampling season, and region. However, we did account for differences in growth rate by gear type and sampling time by estimating daily growth rates as a range, providing a conservative and a maximal estimate each late summer survey and gear type. Our length-based daily growth estimates also assume a constant growth rate over the sampling season, which is likely violated as individuals attain later stages and larger sizes (Thanassekos and Fortier 2012).

Daily growth estimated in this study for polar cod ranged from 0.27 mm day^{-1} to 0.53 mm day^{-1} with a mean of 0.39 ±0.06 mm day^{-1} (*n*= 4). Our most conservative growth estimate for polar cod (0.27 mm day^{-1}) agrees well with previous field studies (Bouchard and Fortier 2011; Thanassekos et al. 2012; Vestfals et al. 2019). Daily growth for polar cod in this study may also be higher than is typical due to the elevated water temperatures experienced in 2017. Even though polar cod are adapted to maximize growth at colder temperatures than saffron cod, warmer spring sea surface temperature and earlier ice retreat may be advantageous to larval polar cod due to the availability of zooplankton production supported by earlier ice algae and phytoplankton blooms. This would improve the temporal match of early hatching polar cod with their zooplankton prey (Bouchard et al. 2017). Under scenarios of continued warming in

the Arctic, polar cod may lose this growth advantage leading to reduced survival when thermal tolerances of their ELHS are exceeded.

This study is one of the first to estimate daily mean growth for ELHS of saffron cod (0.12-0.76 mm day^{-1}; 0.37 ± 0.16 mm day^{-1}; *n*= 4) collected within the Chukchi Sea. The conservative estimate for daily growth for saffron cod was based on bongo collections in the late summer. The lack of larger saffron cod in the bongo gear compared to the mid-water trawl suggests that larger saffron cod were present in the water column, but avoided the bongo net, which targets smaller individuals (De Robertis et al. 2017; Vestfals et al. 2019). A more realistic lower estimate for daily growth was derived from the mid-water IKMT at 0.56 mm day^{-1}. Saffron cod experience faster growth and better condition at higher temperatures than polar cod (Laurel et al. 2016; Vestfals et al. 2019), consistent with larger sizes and higher apparent growth rates in this study, therefore, a warming Arctic may favor saffron cod over polar cod. The growth advantage for saffron cod at higher temperatures may come at the expense of increased metabolic demands and a shift in the zooplankton community to smaller, less-lipid rich copepod species (Copeman et al. 2017; Aarflot et al. 2018; Møller and Nielsen 2020; Bouchard and Fortier 2020).

Model-data comparison

Kotzebue Sound was selected as the source of simulated polar cod and saffron cod ELHS in this study due to the preponderance of small larvae observed in this area in the late spring, highlighting the region's potential role as a key hatching and/or nursery habitat for the ELHS of these species. The observed distribution of Arctic gadids along the northern coastline of Kotzebue Sound in the late spring matched well with simulated larval distributions from the model. At Point Hope and Cape Lisburne, a portion of the Alaska Coastal Current (ACC) is often deflected offshore (Danielson et al. 2017), which is reflected in both the late spring model simulations and survey catch data. The IBM predicts that larval polar cod and saffron cod will be advected offshore and northward at Cape Lisburne. Consistent with the model simulations, we observed high catches of polar cod and saffron cod offshore of Cape Lisburne

during the spring survey. High abundances of polar cod and saffron cod may also be present north of Cape Lisburne in the spring as predicted by the IBM, but we lack the empirical data to test this as sampling did not extend north of Cape Lisburne. Additionally, the simulated distributions for saffron cod and polar cod from the IBMs were similar to each other. This is due to the use of a single release location (Kotzebue Sound) for both species and identical behavior routines so that differences in distribution in our study were associated with the species-specific temperature-dependent growth rates used to parametrize the IBMs (Vestfals et al. 2021).

There was no evidence from the model that larvae are advected south from Kotzebue Sound. Any spawning in Kotzebue Sound is likely not the origin of individuals that were caught around St. Lawrence Island or nearshore along the northern Seward Peninsula during spring. Recent modeling work suggests that polar cod hatching south of Bering Strait could be the source of larvae and early juveniles encountered in surveys in the northeastern Chukchi Sea in 2012 while Bering Strait and Kotzebue Sound were likely source regions for saffron cod in 2012 and 2013 (Vestfals et al. 2021).

In the late summer, the IBMs for polar cod and saffron cod indicated high concentrations of larvae and early juveniles nearshore from northern Kotzebue Sound to Wainwright, offshore of Point Hope/Cape Lisburne, and offshore of Wainwright. The modelled distributions agree with the observed late summer distribution of saffron cod where higher abundances were generally nearshore, especially around Point Hope and Cape Lisburne, with abundance decreasing offshore. This suggests that Kotzebue Sound is a center of abundance and potentially serves as an important spawning and hatching area for saffron cod in the Chukchi Sea, a possibility that has been suggested anecdotally (A. Whiting, Village of Kotzebue, personal communication; Vestfals et al. 2021). Larval polar cod were ubiquitous offshore in the Hanna Shoal region during the late summer surveys in 2017, which is consistent with polar cod distributions in other years (Logerwell et al. 2020), but was not captured well by the model, indicating that other hatching locations are major contributors to the observed age-0 aggregations in this area (Vestfals et al.

2021). The simulated distribution overlapped with the distribution of late summer polar cod ELHS individuals offshore of Point Hope and Cape Lisburne, as well as nearshore extending from Cape Lisburne to Wainwright, suggesting Kotzebue Sound may be a potential source of polar cod to these areas in the late summer.

Simulated lengths for both polar cod and saffron cod were smaller than observed specimens collected in the late spring and late summer from the water column or the bottom, with a much larger discrepancy for saffron cod than polar cod. This suggests that the model is underestimating growth, small larvae in the field experience higher mortalities than large larvae, temperatures in the model are underestimates, hatching occurs earlier than assumed, or a combination of these and potentially other factors. The growth equations for polar cod and saffron cod within the IBM are temperature-mediated (Vestfals et al. 2021), making simulated lengths and estimates of daily growth sensitive to thermal conditions in the model, which may differ from those experienced in the field. No growth model exists for ELHS of saffron cod larger than 10 mm in length and the growth model was parameterized using data for walleye pollock due to their similar, linear growth trajectories prior to 10 mm (B. Laurel, AFSC, personal communication; Porter and Bailey 2007; Petrik et al. 2015). However, saffron cod may deviate from linear growth trajectories at later stages or temperatures (Vestfals et al. 2021). Additionally, field estimates of apparent growth tend to be higher than those observed in the lab because of ecological interactions, such as size-selective predation (Houde 2009). The field-based growth calculations were relatively coarse, encompassing all the collected individuals aggregated from a large spatial area, over a two-month sampling period, and likely originating from multiple spawn locations, whereas the model is based on a single release location.

In the late spring, simulated polar cod hatched before April 15th were larger on average than the individuals captured from the water column, suggesting the model is realistically reflecting the enhanced growth rates of polar cod in the late spring due to earlier ice retreat and warmer water

temperatures in 2017 relative to average conditions. The narrow size range of individuals in the model compared to the field collections can indicate several potential scenarios. Firstly, Kotzebue Sound was selected as the source of polar cod and saffron cod larvae, but it is not the only source of larvae in the Chukchi Sea. For example, recent modelling work suggests that Bering Strait and Chukotka Peninsula were important hatching areas for polar cod in the Chukchi Sea in 2012 and 2013 (Vestfals et al. 2021). Secondly, the presence of smaller polar cod in the catch in the late spring may also suggest a simulated hatch date of April 15th or later, although the model does not capture the full range of observed sizes, particularly at the upper end. We selected to model hatch dates between March 1st and May 15th, which corresponded to the duration of peak hatching for polar cod in 2017, although hatching has been reported as early as January 1st for polar cod in the Arctic (Bouchard and Fortier 2011; Z. Chapman, UAF, personal communication). In polar cod, hatch date explains more variability in length than temperature conditions (Bouchard et al. 2017), therefore, some of the inconsistencies between the sizes, and subsequent calculated growth rates, of field collected and simulated individuals may be due to the hatch date variability. Thirdly, field estimates also differ from those observed under controlled laboratory conditions due to ecological factors that are difficult to account for (Bailey and Houde 1989; Houde 2009; Vestfals et al. 2019) such as patchy prey distribution and small-scale environmental variability (temperature, salinity, etc.). Polar cod are likely able to take advantage of a “big risk, big reward” strategy to forage for limited periods of time in warm, productive waters along thermal-salinity fronts to maximize growth relative to conspecifics (Laurel et al. 2016; Bouchard et al. 2017), which may contribute to the wider size range observed for the field-collected individuals compared to simulated individuals in the late spring.

Differences between simulated and empirical data may also be related to the onset of demersal behavior in polar cod and saffron cod, which is an adaptation to avoid predation, enhance foraging, and find areas of physiological preferred temperature ranges. Given the dominance of gadids by number and

biomass in demersal catches in the Arctic (Logerwell et al. 2015), fish predators of ELHS of polar cod and saffron cod are likely conspecifics. Cannibalism has been documented in other subarctic gadids and is mitigated by vertical partitioning between juveniles and adults (Bailey 1975; Bailey 1989). Adult walleye pollock in the Bering Sea are semipelagic and cannibalism was highest when juveniles moved deeper in the water column, overlapping with the adults (Bailey 1989). Cannibalism is considered rare for polar cod due to their planktivorous foraging strategy, although fishes do become an important prey category as polar cod grow, and instances of cannibalism have been documented (Bain and Sekerak 1978; Benoit et al. 2010; Christiansen et al. 2012; Whitehouse et al 2017). Polar cod forage primarily on copepod nauplii (e.g., *Pseudocalanus* spp.) when smaller than 25 mm SL and shift to foraging on the copepodite stages of copepods, specifically *Calanus* spp. and *Metridia* spp., and fishes when larger than 25 mm SL (Benoit et al. 2010; Christiansen et al. 2012; Bouchard et al. 2016; Bouchard and Fortier 2020). Saffron cod likely become more piscivorous with increasing size (Laurel et al. 2009), suggesting cannibalism may be more likely in this species than polar cod. Diet data are limited for saffron cod in the Chukchi Sea (Copeman et al. 2016). Increased water temperatures and constriction of available habitat for Arctic taxa may lead to increased cannibalism for polar cod and saffron cod as well as increased competition and predation if subarctic species move into the Chukchi Sea (Bouchard et al. 2017). A number of adult fish species from the Bering Sea, such as walleye pollock and Pacific cod, expanded northward in response to a reduced Cold Pool (bottom water temperatures < 2°C) over the Bering Sea shelf (Stevenson and Lauth 2019) and are possible competitors as well as predators of Arctic gadids in the Chukchi Sea if climatic warming persists (Marsh and Mueter 2019). Near bottom waters may also act as a thermal refuge for smaller Arctic gadids, particularly small polar cod that are not as tolerant to higher water temperatures as saffron cod (Laurel et al. 2016).

Summary

The late spring distributions of polar cod and saffron cod centered in Kotzebue Sound suggest that sea ice may be an important environmental factor influencing hatching, and it may provide a nursery habitat for newly hatched individuals of both species. Kotzebue Sound was likely a source of ELHS of polar cod and saffron cod offshore of Point Hope/Cape Lisburne and nearshore from Kotzebue Sound to Wainwright during 2017. Without otolith-derived individual growth estimates, it is difficult to know if polar cod and saffron cod experienced greater growth during 2017 compared to other years or regions due to elevated temperatures, although our daily growth estimates were higher than reported in past research (Bouchard and Fortier 2011). Saffron cod should benefit in a warmer Arctic if their ELHS are resilient to the loss of sea ice, and if energetic trade-offs can offset prey-mediated factors that may depress growth (i.e., reduced nutritional value, zooplankton community shift) (Llopiz et al. 2014; Spear et al. 2019) and an increase in competition and predation from sub-Arctic demersal fishes shifting to the north (Stevenson and Lauth 2019). With the forecasted warming in the Arctic and projected changes in sea ice dynamics, studies such as this one synthesizing the seasonal distribution, abundance, and growth of Arctic forage fishes are critical to assess changes in phenology, distributions, and abundance for these species and the impacts of warming on habitat availability for Arctic fishes.

Acknowledgments

The authors thank all of the boat and field crews of the USCGC *Healy*, M/V *Ocean Starr*, and R/V *Sikuliaq* who collected these data and without their tireless efforts, this project would not have been possible. We thank the Plankton Sorting and Identification Center in Szczecin, Poland and the ichthyoplankton team at the Alaska Fisheries Science Center for their taxonomic expertise that makes studies of the ecology of Arctic fishes possible. We also thank Jens Nielsen and Adam Spear for their assistance gathering and plotting the sea ice data as well as intellectual discussions on the interpretation of the data. Finally, we thank Katherine Hedstrom at the University of Alaska Fairbanks for providing the PAROMS model output and Caitlin Smoot and Cheryl Hopcroft, also at the University of Alaska

Fairbanks, for facilitating data collection and curation of ASGARD samples. Funding for this project was provided by the North Pacific Research Board through the Arctic Integrated Ecosystem Research Program. AMBON collections were made possible through a National Ocean Partnership Program (NOPP Grant NA14NOS0120158) by the National Oceanic and Atmospheric Administration, the Bureau of Ocean Management and Shell Exploration & Production. The findings and conclusions in the paper are those of the author(s) and do not necessarily represent the views of the National Marine Fisheries Service. Mention of trade names does not imply endorsement by NOAA or any of its subagencies. This is contribution number EcoFOCI-0XXX of Ecosystems and Fisheries-Oceanography Coordinated Investigations.

Author Contribution Statement

ALD, EAL, EDG, and JTD conceived and framed the key questions of the study. CDV conducted all IBM analyses, contributed code to generate figures related to the IBM, and provided text in the *Methods* sections. FJM, SLD, EAL, and RRH provided data that made the analyses possible. ALD wrote the manuscript and generated the figures. All authors read and approved the manuscript.

Declarations

Conflict of interest The authors have no conflict of interest to report.

Ethical approval All field sampling was done in accordance with NOAA NMFS policies, as outlined under the Animal Welfare Act and US Government Principles for the Utilization and Care of Vertebrate Animals Used in Testing, Research, and Training. Collections were made under the following permits approved by the Alaska Regional Office, National Marine Fisheries Service (CF-17-023), a US Fish and Wildlife Service Seabird Salvage Permit (MB035470), and a State of Alaska Resource Permit (CF-16-010).

References

Aarflot JM, Skjoldal HR, Dalpadado P, Skern-Mauritzen M (2018) Contribution of *Calanus* species to the mesozooplankton biomass in the Barents Sea. ICES J Mar Sci 75(7):2342–2354

Aschan M, Karamushko OV, Byrkjedal I, Wienerroither R, Borkin IV, Christiansen JS (2009) Records of the gadoid fish *Arctogadus glacialis* (Peters, 1874) in the European Arctic. Polar Biol 32(7):963-70

Bailey KM (1989) Interaction between the vertical distribution of juvenile walleye pollock *Theragra chalcogramma* in the eastern Bering Sea, and cannibalism. Mar Ecol Prog Ser 53:205–213

Bailey KM, Houde ED (1989) Predation on egg and larvae of marine fishes and the recruitment problem. Adv Mar Biol 25:1-83

Bailey RS (1975) Observations on diel behaviour patterns of North Sea gadoids in the pelagic phase. J Mar Biol Assoc U K 55(1):133-142

Bain H, Sekerak AD (1978) Aspects of the biology of Arctic cod (*Boreogadus saida*) in the central Canadian Arctic. LGL Limited, Toronto, Ontario, 104 pp

Benoit D, Simard Y, Gagne J, Geoffroy M, Fortier L (2010) From polar night to midnight sun: photoperiod, seal predation, and the diel vertical migrations of polar cod (*Boreogadus saida*) under landfast ice in the Arctic Ocean. Polar Biol 33:1505–1520. doi: 10.1007/s00300-010-0840-x

Borkin LV, Ozhigin VK, Shleinik VN (1986) Effect of oceanographical factors on the abundance of the Barents Sea polar cod year classes. In: The effect of oceanographic conditions on distribution and population dynamics of commercial fish stocks in the Barents Sea, vol. 169

Bouchard C, Fortier L (2008) Effects of polynyas on the hatching season, early growth and survival of polar cod *Boreogadus saida* in the Laptev Sea. Mar Ecol Prog Ser 355:247–256. doi: 10.3354/meps07335

Bouchard C, Fortier L (2011) Circum-arctic comparison of the hatching season of polar cod *Boreogadus saida*: A test of the freshwater winter refuge hypothesis. Prog Oceanogr 90:105-116. doi: 10.1016/j.pocean.2011.02.008

Bouchard C, Fortier L (2020) The importance of *Calanus glacialis* for the feeding success of young polar cod: a circumpolar synthesis. polar Biol. doi: 10.1007/s00300-020-02643-0

Bouchard C, Mollard S, Suzuki K, Robert D, Fortier L (2016) Contrasting the early life histories of sympatric Arctic gadids *Boreogadus saida* and *Arctogadus glacialis* in the Canadian Beaufort Sea. Polar Biol 39:1005–1022. doi: 10.1007/s00300-014-1617-4

Bouchard C, Geoffroy M, Leblanc M, Majewski A, Gautheir S, Walkusz W, Reist JD, Fortier L (2017) Climate warming enhances polar cod recruitment, at least transiently. Prog Oceanogr 156:121–129. doi: 10.1016/j.pocean.2017.06.008

Budgell WP (2005) Numerical simulation of ice-ocean variability in the Barents Sea region. Ocean Dyn 55:370–387. doi: 10.1007/s10236-005-0008-3

Carton JA, Chepurin GA, Chen L (2018) SODA3: a new ocean climate reanalysis. J

Clim 31(17):6967-6983

Cavalieri DJ, Parkinson CL, Gloersen P, Zwally HJ (1996) Sea Ice Concentrations from Nimbus-7 SMMR and DMSP SSM/I-SSMIS Passive Microwave Data, Version 1. Boulder, Colorado USA. NASA National Snow and Ice Data Center Distributed Active Archive Center. doi: https://doi.org/10.5067/8GQ8LZQVL0VL. [10 April 2019].

Chassignet EP, Hurlburt HE, Metzger EJ, Smedstad OM, Cummings JA, Halliwell GR, Bleck R, Baraille R, Wallcraft AJ, Lozano C, Tolman HL, Srinivasan A, Hankin S, Cornillon P, Weisberg R, Barth A, He R, Werner F, Wilkin J (2009) US GODAE Global Ocean Prediction with the HYbrid Coordinate Ocean Model (HYCOM). Oceanography 22:49–59

Christiansen JS, Hop H, Nilssen EM, Joensen J (2012) Trophic ecology of sympatric Arctic gadoids, *Arctogadus glacialis* (Peters, 1872) and *Boreogadus saida* (Lepechin, 1774), in NE Greenland. Polar Biol 35:1247–1257. doi: 10.1007/s00300-012-1170-y

Copeman LA, Laurel BJ, Boswell KM, Sremba AL, Klinck K, Heintz RA, Vollenweider JJ, Helser TE, Spencer ML (2016) Ontogenetic and spatial variability in trophic biomarkers of juvenile saffron cod (*Eleginus gracilis*) from the Beaufort, Chukchi and Bering Seas. Polar Biol 39:1109–1126. doi: 10.1007/s00300-015-1792-y

Copeman LA, Laurel BJ, Spencer M, Sremba A (2017) Temperature impacts on lipid allocation among juvenile gadid species at the Pacific Arctic-Boreal interface: an experimental laboratory approach. Mar Ecol Prog Ser 566: 183-198. doi: 10.3354/meps12040

Craig PC, Griffiths WB, Haldorson L, McElderry H (1982) Ecological Studies of Arctic cod (*Boreogadus saida*) in Beaufort Sea Coastal Waters, Alaska. Can J Fish Aquat Sci 39:395–406. doi: 10.1139/f82-057

Danielson SL, Hedstrom KS, Weingartner TJ (2016) Bering-Chukchi circulation pathways,

North Pacific Research Board 2016 Final Report, NPRB project #1308, University of Alaska Fairbanks, Fairbanks, AK

Danielson SL, Eisner L, Ladd C, Mordy C, Sousa L, Weingartner TJ (2017) A comparison between late summer 2012 and 2013 water masses, macronutrients, and phytoplankton standing crops in the northern Bering and Chukchi Seas. Deep Sea Res Part II 135:7–26. doi: 10.1016/j.dsr2.2016.05.024

De Robertis A, Taylor K, Williams K, Wilson CD (2017) Species and size selectivity of two midwater trawls used in an acoustic survey of the Alaska Arctic. Deep Sea Res Part II 135:40-50

Döös K (1995) Interocean exchange of water masses. J Geophys Res 100:13499. doi: 10.1029/95jc00337

Dunn JR, Vinter BM (1984) Development of larvae of the saffron cod, *Eleginus gracilis*, with comments on the identification of gadid larvae in Pacific and Arctic waters contiguous to Canada and Alaska. Can J Fish Aquat Sci 41:304-318.

Egbert GD, Erofeeva SY (2002) Efficient inverse modeling of barotropic ocean tides. J Atmos Ocean Technol 19:183–204. doi: 10.1175/1520-0426(2002)019<0183:EIMOBO>2.0.CO;2

Falardeau M, Bouchard C, Robert D, Fortier L (2017) First records of Pacific sand lance (*Ammodytes hexapterus*) in the Canadian Arctic Archipelago. polar Biol. 40:2291-2296. doi: 10.1007/s00300-017-2141-0

Graham RM, Cohen L, Petty AA, Boisvert LN, Rinke A, Hudson SR, Nicolaus M, Granskog MA (2017) Increasing frequency and duration of Arctic winter warming events. Geophys Res Lett 44:6974–6983. doi: 10.1002/2017GL073395

Grebmeier JM, Bluhm B, Cooper LW (2015) Time-Series benthic community composition and biomass and associated environmental characteristics in the Chukchi Sea during the RUSALCA 2004– 2012 program. Oceanography 28(3):116-133. doi: 10.5670/oceanog.2015.61

Helser TE, Colman JR, Anderl DM, Kastelle CR (2017) Growth dynamics of saffron cod (*Eleginus gracilis*) and Arctic cod (*Boreogadus saida*) in the Northern Bering and Chukchi Seas. Deep Sea Res Part II 135:66–77. doi: 10.1016/j.dsr2.2015.12.009

Houde ED (2009) Chapter 3. Recruitment variability. In: Jakobsen T, Fogarty M, Megrey B, Moksness E (eds.) Reproductive biology of fishes: implications for assessment and management. Wiley-Blackwell, pp 91-171

Hunt GL, Blanchard AL, Boveng P, Dalpadado P, Drinkwater KF, Eisner L, Hopcroft RR, Kovacs KM, Norcross BL, Renaud P, Reigstad M, Renner M, Skjoldal HR, Whitehouse A, Woodgate RA (2013) The Barents and Chukchi Seas: Comparison of two Arctic shelf ecosystems. J Mar Syst 109–110:43–68. doi: 10.1016/j.jmarsys.2012.08.003

Hutchings JA, Rangeley RW (2011) Correlates of recovery for Canadian Atlantic cod (*Gadus morhua*). Can J Zool 89:386–400. doi: 10.1139/Z11-022

Ichthyoplankton Information System (IIS) (2019) National Oceanic and Atmospheric Administration. (7 May 2020) [<**https://apps-afsc.fisheries.noaa.gov/ichthyo/index.php** >].

Kahru M, Brotas V, Manzano-Sarabia M, Mitchell BG (2011) Are phytoplankton blooms occurring earlier in the Arctic? Glob Chang Biol 17:1733–1739. doi: 10.1111/j.1365-2486.2010.02312.x

Koenker BL, Copeman LA, Laurel BJ (2018) Impacts of temperature and food availability on the condition of larval Arctic cod (*Boreogadus saida*) and walleye pollock (*Gadus chalcogrammus*). ICES J Mar Sci 75(7):2370-2385. doi: 10.1093/icesjms/fsy052

Laurel BJ, Ryer CH, Knoth B, Stoner AW (2009) Temporal and ontogenetic shifts in habitat use of juvenile Pacific cod (*Gadus macrocephalus*). J Exp Mar Bio Ecol 377:28–35. doi: 10.1016/j.jembe.2009.06.010

Laurel BJ, Hurst TP, Copeman LA, Davis MW (2008) The role of temperature on the growth and survival of early and late hatching Pacific cod larvae (*Gadus macrocephalus*). J Plankton Res 30:1051–1060. doi: 10.1093/plankt/fbn057

Laurel BJ, Spencer M, Iseri P, Copeman LA (2016) Temperature-dependent growth and behavior of juvenile Arctic cod (*Boreogadus saida*) and co-occurring North Pacific gadids. polar Biol 39:1127–1135. doi: 10.1007/s00300-015-1761-5

Li WKW, McLaughlin FA, Lovejoy C, Carmack EC (2009) Smallest algae thrive as the Arctic ocean freshens. Science 326:539. doi: 10.1126/science.1179798

Llopiz JK, Cowen RK, Hauff MJ, Ji R, Munday PL, Muhling BA, Peck MA, Richardson DE, Sogard S, Sponaugle S (2014) Early life history and fisheries oceanography: new questions in a changing world. Oceanography 27(4):26-41

Logerwell E, Busby M, Carothers C, Cotton S, Duffy-Anderson J, Farley E, Goddard P, Heintz R, Holladay B, Horne J, Johnson S, Lauth B, Moulton L, Neff D, Norcross B, Parker-Stetter S, Seigle J, Sformo T (2015) Fish communities across a spectrum of habitats in the western Beaufort Sea and Chukchi Sea. Prog Oceanogr 136:115–132. doi: 10.1016/j.pocean.2015.05.013

Logerwell E, Busby M, Mier K, Tabisola H, Duffy-Anderson, J (2020) The effects of oceanographic variability on the distribution of larval fishes of the northern Bering and Chukchi Seas. Deep Sea Res Part II. doi: 10.1016/j.dsr2.2020.104784

Lønne OJ, Gulliksen (1989) Size, age, and diet of polar cod, *Boreogadus saida* (Lepechin 1773), in ice covered waters. Polar Biol 9:187-191

Marsh JM, Mueter FJ (2019) Influences of temperature, predators, and competitors on polar cod (*Boreogadus saida*) at the southern margin of their distribution. Polar Biol 35:1-20 doi: 10.1007/s00300-019-02575-4

Maslowski W (2014) The pacific arctic region: Ecosystem status and trends in a rapidly changing environment. In: Grebmeier JM, Maslowski W (eds.) The Pacific Arctic Region. Springer, Heidelberg, pp 101-132

Matarese A, Kendall A, Blood D, Vinter B (1989) Laboratory guide to early life history stages of northeast Pacific fishes. NOAA Tech Rep 80:652

Møller EF, Nielsen TG (2020) Borealization of Arctic zooplankton—smaller and less fat zooplankton species in Disko Bay, Western Greenland. Limnol Oceanogr 65(6):1175-1188

North Pacific Fishery Management Council (NPFMC) (2009) Fishery Management Plan for Fish Resources of the Arctic Management Area. North Pacific Fishery Management Council, Anchorage, AK, pp 158

National Snow and Ice Data Center (NSIDC) (2019) All About Sea Ice. Accessed 15 June 2019. /cryosphere/seaice/index.html.

Overland JE, Wang M, Ballinger TJ (2018) Recent increased warming of the Alaskan marine Arctic due to midlatitude linkages. Adv Atmos Sci 35:75–84. doi: 10.1007/s00376-017-7026-1

Perovich D, Meier W, Tschudi M, Farrell S, Hendricks S, Gerland S, Haas C, Krumpen T, Polashenski C, Ricker R, Webster M (2017). Sea Ice [in Arctic Report Card 2017]. http://www.arctic.noaa.gov/Report-Card

Petrik CM, Duffy-Anderson JT, Mueter F, Hedstrom K, Curchitser EN (2015) Biophysical transport model suggests climate variability determines distribution of Walleye Pollock early life stages in the eastern Bering Sea through effects on spawning. Progr Oceanogr 138: 459-474.

Porter SM, Bailey KM (2007) The effect of early and late hatching on the escape response of walleye pollock (*Theragra chalcogramma*) larvae. J Plankton Res 29:291–300. doi: 10.1093/plankt/fbm015

R Core Team (2019) R: a language and environment for statistical computing. R Foundation for Statistical Computing, Vienna, Austria. ISBN 3–900051–07-0, URL http://www.Rproject.org

Randall JR, Busby MS, Spear AH, Mier KL (2019) Spatial and temporal variation of summer ichthyoplankton assemblage structure in the eastern Chukchi Sea 2010-2015. Polar Biol 42:1811-1824

Rass TS (1968) Spawning and development of polar cod. Rapp PV Reun Cons Perm Int Explor Mer 158:135–137

Shchepetkin AF, McWilliams JC (2005) The regional oceanic modeling system (ROMS): A split-explicit, free-surface, topography-following-coordinate oceanic model. Ocean Model 9:347–404. doi: 10.1016/j.ocemod.2004.08.002

Shima M, Bailey KM (1994) Comparative analysis of ichthyoplankton sampling gear for early life stages of walleye pollock (*Theragra chalcogramma*). Fish Oceanogr 3:50–59. doi: 10.1111/j.1365-2419.1994.tb00047.x

Spear A, Duffy-Anderson J, Kimmel D, Napp J, Randall J, Stabeno P (2019) Physical and biological drivers of zooplankton communities in the Chukchi Sea. Polar Biol 42:1107–1124. doi: 10.1007/s00300-019-02498-0

Stevenson DE, Lauth RR (2019) Bottom trawl surveys in the northern Bering Sea indicate recent shifts in the distribution of marine species. Polar Biol 42:407–421. doi: 10.1007/s00300-018-2431-1

Thanassekos S, Fortier L (2012) An individual based model of Arctic cod (*Boreogadus saida*) early life in Arctic polynyas: I. Simulated growth in relation to hatch date in the Northeast Water (Greenland Sea) and the North Water (Baffin Bay). J Mar Syst 93:25-38

Thanassekos S, Robert D, Fortier L (2012) An individual based model of Arctic cod (*Boreogadus saida*) early life in Arctic polynyas: II. Length-dependent and growth-dependent mortality. J Mar Syst 93:39-46

Timmermans ML, Ladd C, Wood K (2017) Sea surface temperature [in Arctic Report Card 2017]. http://www.arctic.noaa.gov/Report-Card

Tokinaga H, Xie S-P, Mukougawa H (2017) Early 20th-century Arctic warming intensified by Pacific and Atlantic multidecadal variability. Proc Natl Acad Sci 114:6227–6232. doi: 10.1073/pnas.1615880114

Tsujino H, Urakawa S, Nakano H, Small RJ, Kim WM, Yeager SG, Danabasoglu G, Suzuki T, Bamber JL, Bentsen M, Böning CW (2018) JRA-55 based surface dataset for driving ocean–sea-ice models (JRA55-do). Ocean Model 130:79-139

Vestfals CD, Mueter FJ, Duffy JT, Busby MS, De Robertis A (2019) Spatio-temporal distribution of polar cod (*Boreogadus saida*) and saffron cod (*Eleginus gracilis*) early life stages in the Pacific Arctic. Polar Biol 42(5):969-990. doi: 10.1007/s00300-019-02494-4

Vestfals CD, Mueter FJ, Hedstrom KS, Laurel BJ, Petrik CM, Duffy-Anderson JT, Danielson SL (2021) Modeling the dispersal of polar cod (*Boreogadus saida*) and saffron cod (*Eleginus gracilis*) early life stages in the Pacific Arctic using a biophysical transport model. Prog Oceanogr. doi: 10.1016/j.pocean.2021.102571

Wildes SL, Whittle J, Nguyen H, Guyon J (2016) *Boreogadus saida* genetics in the Alaskan Arctic. US Dept. of the Interior, Bureau of Ocean Energy Management, Alaska OCS Region. OCS Study BOEM 2011-AK-11-08 a/b. 67 pp.—DRAFT REPORT

Whitehouse GA, Aydin K, Essington TE (2014) A trophic mass balance model of the eastern Chukchi Sea with comparisons to other high-latitude systems. Ocean Model 88:911–939. doi: 10.1007/s00300-014-1490-1

Whitehouse GA, Buckley TW, Danielson SL (2017) Diet compositions and trophic guild structure of the eastern Chukchi Sea demersal fish community. Deep Sea Res Part II 135:95-110

Wolotira RJ Jr (1985) Saffron cod (*Eleginus gracilis*) in Western Alaska: the resource and its potential. U.S. Dep. Commer., NOAA Tech. Memo. F/NWC-79. 119 p

Woodgate RA, Weingartner TJ, Lindsay R (2012) Observed increases in Bering Strait oceanic fluxes from the Pacific to the Arctic from 2001 to 2011 and their impacts on the Arctic Ocean water column. Geophys Res Lett 39. doi:10.1029/2012GL054092

Woodgate RA (2018) Increases in the Pacific inflow to the Arctic from 1990 to 2015, and insights into seasonal trends and driving mechanisms from year-round Bering Strait mooring data. Prog Oceanogr 160:124-154

Tables

Table 1. Arctic Integrated Ecosystem Research Program 2017 sampling events in the northern Bering and Chukchi Seas. Abbreviations: AIES, Arctic Integrated Ecosystem Survey; AMBON, Arctic Marine Biodiversity Observation Network; ASGARD, Arctic Shelf Growth, Advection, Respiration, Deposition; DBO, Distributed Biological Observatory; 60BON, 60-cm bongo; IKMT, Isaacs-Kidd Midwater Trawl; PSBT, 3-m plumb-staff beam trawl. Asterisks (*) denotes programs affiliated with Arctic Integrated Ecosystem Research Program.

Survey Identifier	Sampling Program	Dates	Season	# of Samples	Gear Used
SQ17-01	ASGARD*	10-29 June	late spring	61	60BON
NM17-01	AMBON	4-23 August	late summer	75	PSBT
				13	IKMT
OS17-01	AIES*	8 August - 25 September	late summer	72	60BON
				62	PSBT
HE17-02	DBO*	29 August – 10 September	late summer	64	60BON

Table 2. Late spring and late summer 2017 observed length data for polar cod (*Boreogadus saida*) and saffron cod (*Eleginus gracilis*). Mean size, standard error, and sample size (*n*) are displayed within the parentheses. Demersal gears are shaded in grey and all lengths are reported in mm and in standard length, unless noted otherwise. Abbreviations: AIES, Arctic Integrated Ecosystem Survey; AMBON, Arctic Marine Biodiversity Observation Network; 60BON, 60-cm bongo; IKMT, Isaacs-Kidd Midwater Trawl; NL, notochord length.

Species	**late Spring 60BON**	**60BON**	**IKMT**	**late Summer AMBON Trawl**	**AIES Trawl**
polar cod	5.1 NL - 19.7 (9.8± 0.4 NL, n=850)	13.2 - 56.1 (30.1± 0.9, n=140)	18.0 – 56.0 (30.7± 0.4, n=433)	18.0 – 69.0 (39.7± 0.4, n=718)	18.5 – 69.8 47.8± 1.6, n=690)
saffron cod	4.7 NL – 21.2 (9.3± 0.4 NL, n=299)	11.4 - 22.4 (18.5± 1.4, n= 7)	22.0 – 59.0 (40.3± 1.7, n=41)	31.0 – 68.0 (51.6± 0.4, n=318)	37.9 – 69.0 (55.1± 1.7, n=54)

Table 3. Daily growth rate estimates (mm day^{-1}) for polar cod (*Boreogadus saida*) and saffron cod (*Eleginus gracilis*) in the Chukchi Sea between late spring and late summer. Demersal sampling gears are shaded in grey. Abbreviations: AIES, Arctic Integrated Ecosystem Survey; AMBON, Arctic Marine Biodiversity Observation Network; 60BON, 60-cm bongo; IKMT, Isaacs-Kidd Midwater Trawl; *n*, sample size.

Species	60BON	IKMT	AMBON Trawl	AIES Trawl	Mean Daily
polar cod	0.27	0.37	0.53	0.51	0.39±0.06 (*n*= 4)
saffron cod	0.12	0.56	0.76	0.61	0.37±0.16 (*n*= 4)

Table 4. Late spring and late summer 2017 simulated length data for polar cod (*Boreogadus saida*) and saffron cod (*Eleginus gracilis*). Mean size in mm and standard error are reported within the parentheses for each hatching date and sample size (*n*) is reported.

	Late spring					
	3/1	3/15	4/1	4/15	5/1	5/15
polar cod	9.8 – 17.6	9.3 – 16.7	8.5 – 15.1	7.9 – 14.1	7.2 – 11.7	6.6 – 9.7
	(11.3± 0.010)	(11.2± 0.0091)	(10.5± 0.0077)	(9.7± 0.0066)	(8.7± 0.0043)	(7.9± 0.0032)
	n= 19970	*n*= 19970	*n*= 19970	*n*= 19970	*n*= 19970	*n*= 19970
saffron cod	5.1 – 8.4	5.1 – 8.5	5.1 – 8.5	5.1 – 8.5	5.1 – 8.4	5.1 – 8.4
	(5.7± 0.0037)	(5.7± 0.0037)	(5.7± 0.0035)	(5.7± 0.0033)	(5.7± 0.0028)	(5.6± 0.0025)
	n= 19970	*n*= 19970	*n*= 19970	*n*= 19970	*n*= 19970	*n*= 19970
	Late summer					
	3/1	3/15	4/1	4/15	5/1	5/15
polar cod	12.6 – 33.7	11.4 – 33.9	10.5 – 32.0	9.8 – 30.7	9.1 – 27.8	8.3 – 23.5
	(20.4± 0.032)	(20.8± 0.036)	(20.2± 0.034)	(19.4± 0.036)	(17.6± 0.031)	(15.9± 0.026)
	n= 19908	*n*= 19872	*n*= 19895	*n*= 19945	*n*= 19966	*n*= 19947
saffron cod	9.7 – 25.3	9.6 – 25.0	9.6 – 25.4	9.6 – 52.7	9.6 – 35.7	10.7 – 30.4
	(14.9± 0.023)	(14.8± 0.024)	(14.7± 0.024)	(14.6± 0.024)	(14.8± 0.021)	(14.9± 0.020)
	n= 19919	*n*= 19873	*n*= 19914	*n*= 19940	*n*= 19965	*n*= 19940

Figure Captions

Figure 1 Survey stations sampled in 2017 in the Chukchi Sea, Bering Strait (BS), and northern Bering Sea. Bongo --Late spring black squares and late summer (August/September) gray squares; beam trawl– AMBON survey (August) blue inverted triangles and AIES (August/September) dark gray triangle; and

Isaacs-Kidd Midwater Trawl (IKMT) –AMBON survey (August) white circles. Simulated release locations from individual-based models in the eastern-most area of Kotzebue Sound (KS), which shaded in purple. Kotzebue Sound also refers to the broader region from the northwestern tip of Seward peninsula and Point Hope to the north. Depth contours extend from 50 to 350 m in 50 m increments.

Figure 2 Distribution of polar cod (*Boreogadus saida*) (a, b) and saffron cod (*Eleginus gracilis*) (c, d) in late spring (left column) and late summer (right column) 2017 collected in the water column with the 60-cm bongo net. Catch data are reported as catch-per-unit-effort (CPUE) and log(CPUE)+1 to highlight variability at lower abundances. Ice concentration (% cover) is plotted in the background. Black X's denote sampled stations where polar cod and saffron cod were not caught. Note the different scales for CPUE between the species.

Figure 3 Distributions of demersal juvenile polar cod (*Boreogadus saida*) from the late summer. AMBON (a) and AIES (b) beam trawl collections and of demersal juvenile saffron cod (*Eleginus gracilis*) from the AMBON (c) and AIES (d) beam trawl collections. The background color denotes bottom temperature in °C. Catch data are reported as catch-per-unit-effort (CPUE) and log(CPUE)+1 to highlight variability at lower abundances. Note the different scales for CPUE between the species.

Figure 4 Length distributions of polar cod (*Boreogadus saida*) (left) and saffron cod (*Eleginus gracilis*) (right) during the late spring (a, b) and late summer collections with 60-cm bongo (c, d), Isaacs-Kidd Midwater Trawl (IKMT) (e, f), AMBON beam trawl (g, h), and AIES beam trawl (i, j). Dotted black lines denote the mean length for each histogram. Blue bars represent individuals collected from the water column and brown bars represent those collected demersally. Specimens are binned into 2-mm length intervals and standardized by CPUE when all captured individuals were not measured (i.e., bongo).

Figure 5 Density of simulated endpoints from individual-based models in the late spring (June 19th, 2017) for polar cod (*Boreogadus saida*) larvae hatching in Kotzebue Sound. Hatch dates are: a) March 1st, b) March 15th, c) April 1st, d) April 15th, e) May 1st, and f) May 15th. Density is calculated in a 0.5 × 0.5 degree grid.

Figure 6 Density of simulated endpoints from individual-based models in the late summer (September 1st, 2017) for polar cod (*Boreogadus saida*) hatching in Kotzebue Sound. Hatch dates are: a) March 1st, b) March 15th, c) April 1st, d) April 15th, e) May 1st, and f) May 15th. Density is calculated in a 0.5 × 0.5 degree grid.

Figure 7 Length histograms of simulated polar cod (*Boreogadus saida*) larvae by hatch date from the individual-based model in 2017. Hatch dates are: a) March 1st, b) March 15th, c) April 1st, d) April 15th, e) May 1st, and f) May 15th. Blue bars represent late spring (June 19th) lengths and red bars represent late summer (September 1st) lengths. The dashed blue line denotes the mean size of the simulated polar cod in the late spring whereas the red dashed line denotes the mean size of the simulated polar cod in the late summer. Specimens are binned into 2-mm length intervals

Figure 8 Density of simulated endpoints from individual-based models in the late spring (June 19th, 2017) for saffron cod (*Eleginus gracilis*) hatching in Kotzebue Sound. Hatch dates are: a) March 1st, b) March 15th, c) April 1st, d) April 15th, e) May 1st, and f) May 15th. Density is calculated in a 0.5 × 0.5 degree grid.

Figure 9 Density of simulated endpoints from individual-based models in the late summer (September 1st, 2017) for saffron cod (*Eleginus gracilis*) hatched in Kotzebue Sound. Hatch dates are: a) March 1st, b) March 15th, c) April 1st, d) April 15th, e) May 1st, and f) May 15th. Density is calculated in a 0.5 × 0.5 degree grid.

Figure 10 Length histograms of simulated saffron cod (*Eleginus gracilis*) larvae by hatch date from the individual-based model in 2017. Hatch dates are: a) March 1st, b) March 15th, c) April 1st, d) April 15th, e) May 1st, and f) May 15th. Blue bars represent late spring (June 19th) lengths and red bars represent late summer (September 1st) lengths. The dashed blue line denotes the mean size of the simulated saffron cod in the late spring whereas the red dashed line denotes the mean size of the simulated saffron cod in the late summer. Specimens are binned into 2-mm length intervals.

Figure 1

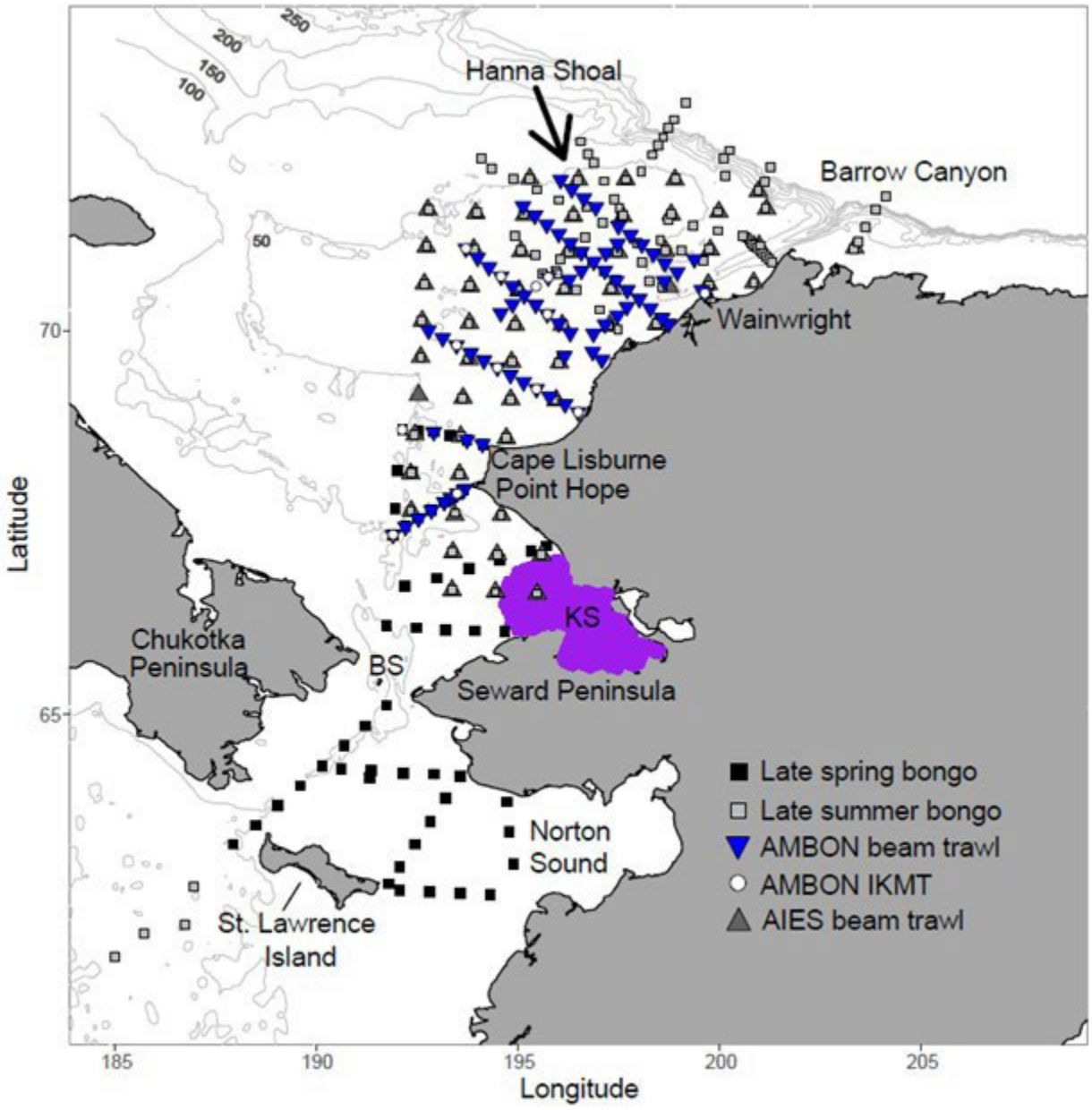
Hanna Shoal
Barrow Canyon
Wainwright
Cape Lisburne
Point Hope
KS
BS
Chukotka
Peninsula
Seward Peninsula
Norton
Sound
St. Lawrence
Island
Late spring bongo
Late summer bongo
AMBON beam trawl
AMBON IKMT
AIES beam trawl
250
200
150
100
50
70
65
Latitude
185
190
195
200
205
Longitude

Figure 2

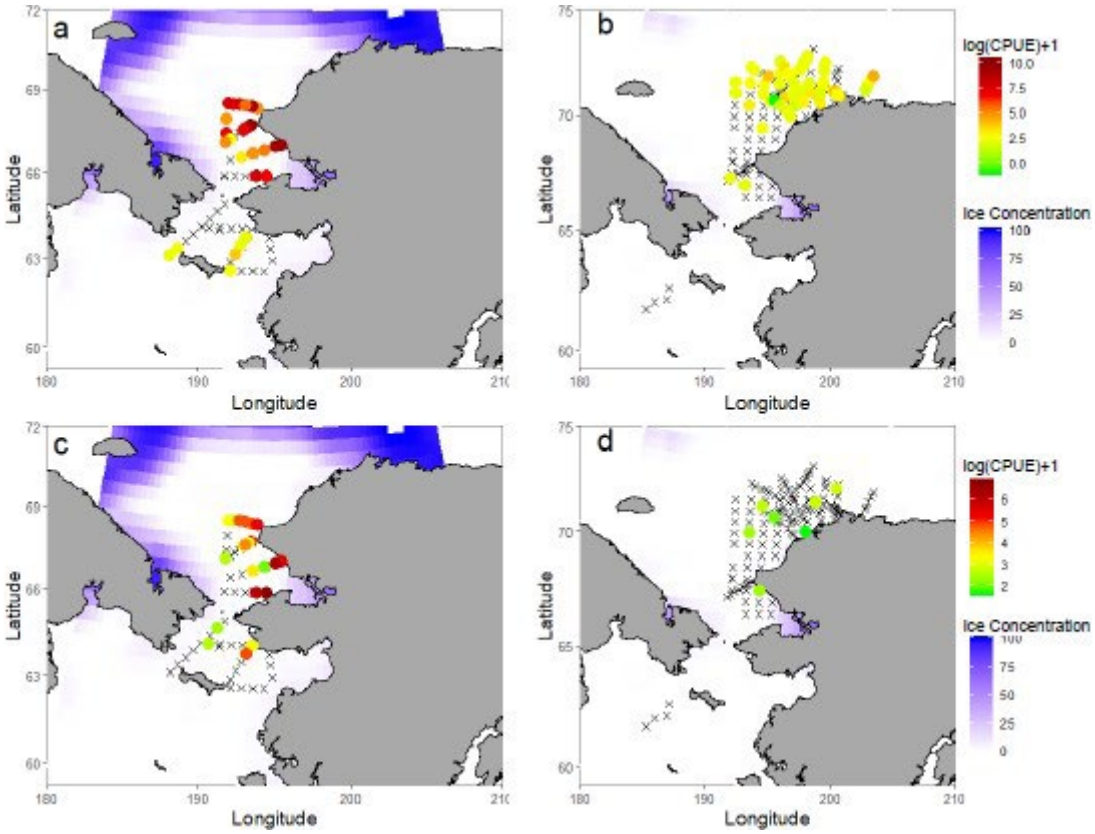

Figure 3

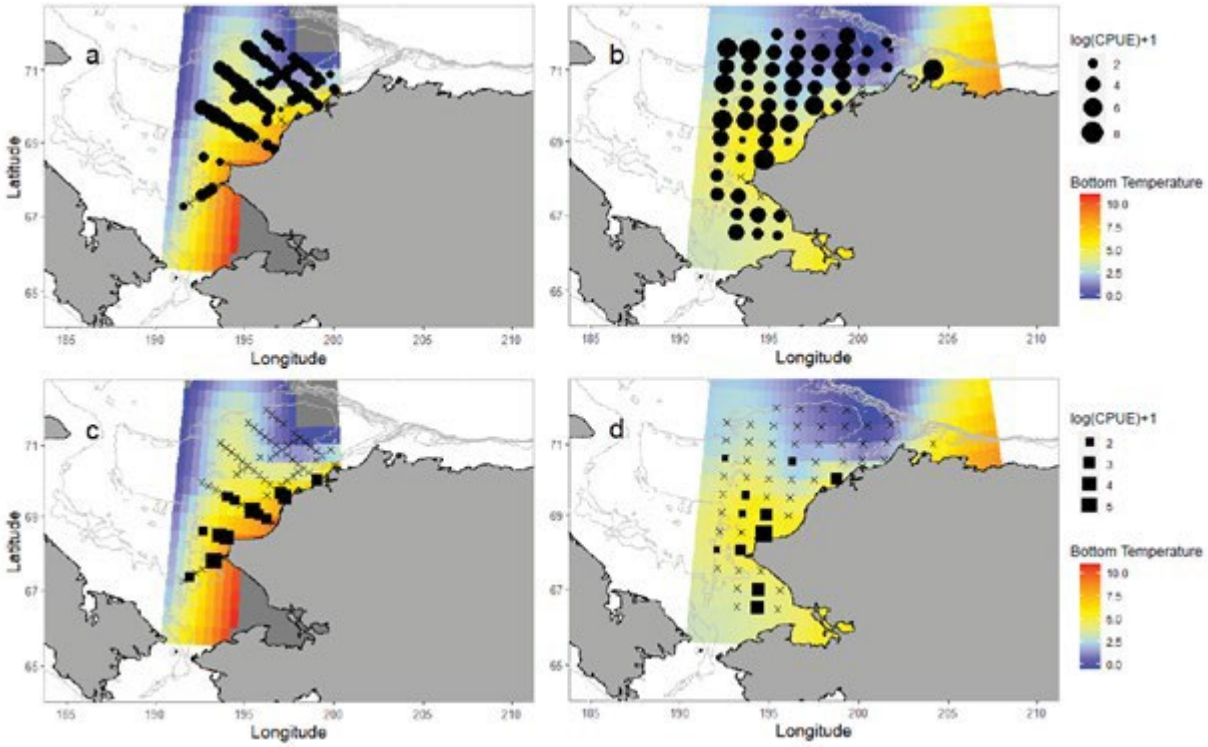

Figure 4

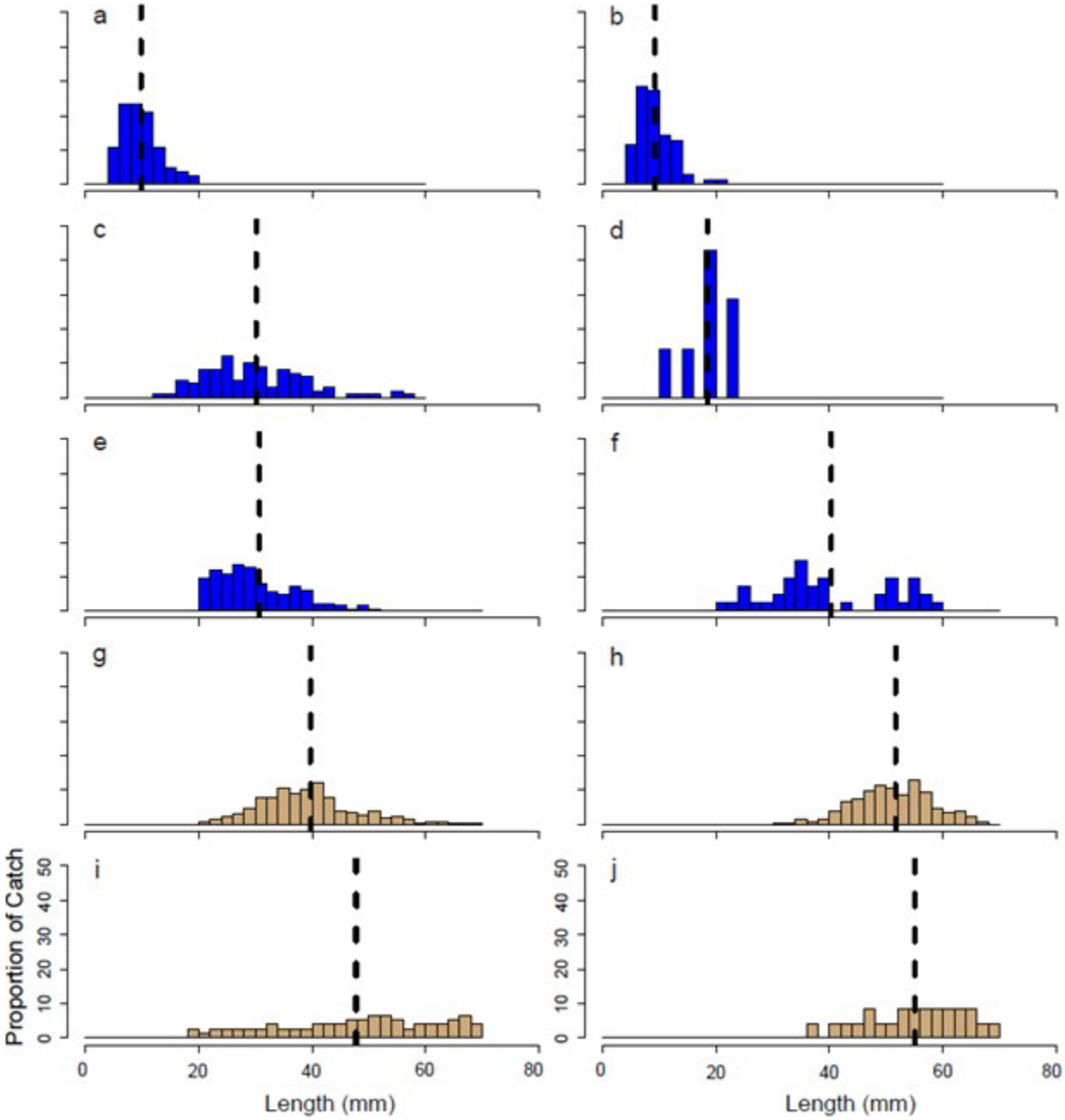
a
b
c
d
e
f
g
h
i
j
Proportion of Catch
0
10
20
30
40
50
0
20
40
60
80
Length (mm)

Figure 5

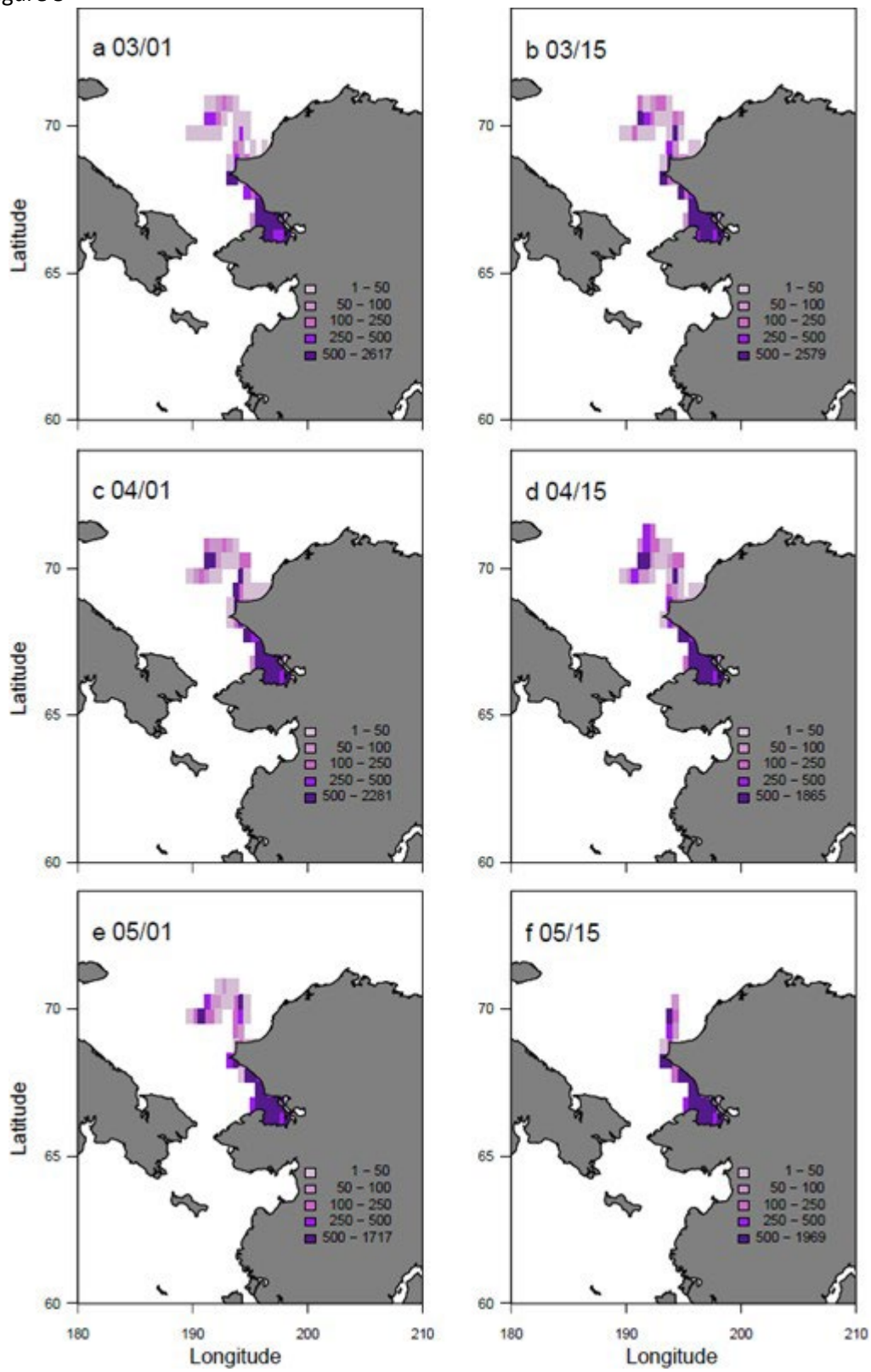
a 03/01
1 – 50
50 – 100
100 – 250
250 – 500
500 – 2617
b 03/15
1 – 50
50 – 100
100 – 250
250 – 500
500 – 2579
c 04/01
1 – 50
50 – 100
100 – 250
250 – 500
500 – 2281
d 04/15
1 – 50
50 – 100
100 – 250
250 – 500
500 – 1865
e 05/01
1 – 50
50 – 100
100 – 250
250 – 500
500 – 1717
f 05/15
1 – 50
50 – 100
100 – 250
250 – 500
500 – 1969
Latitude
Longitude
60
65
70
180
190
200
210

Figure 6

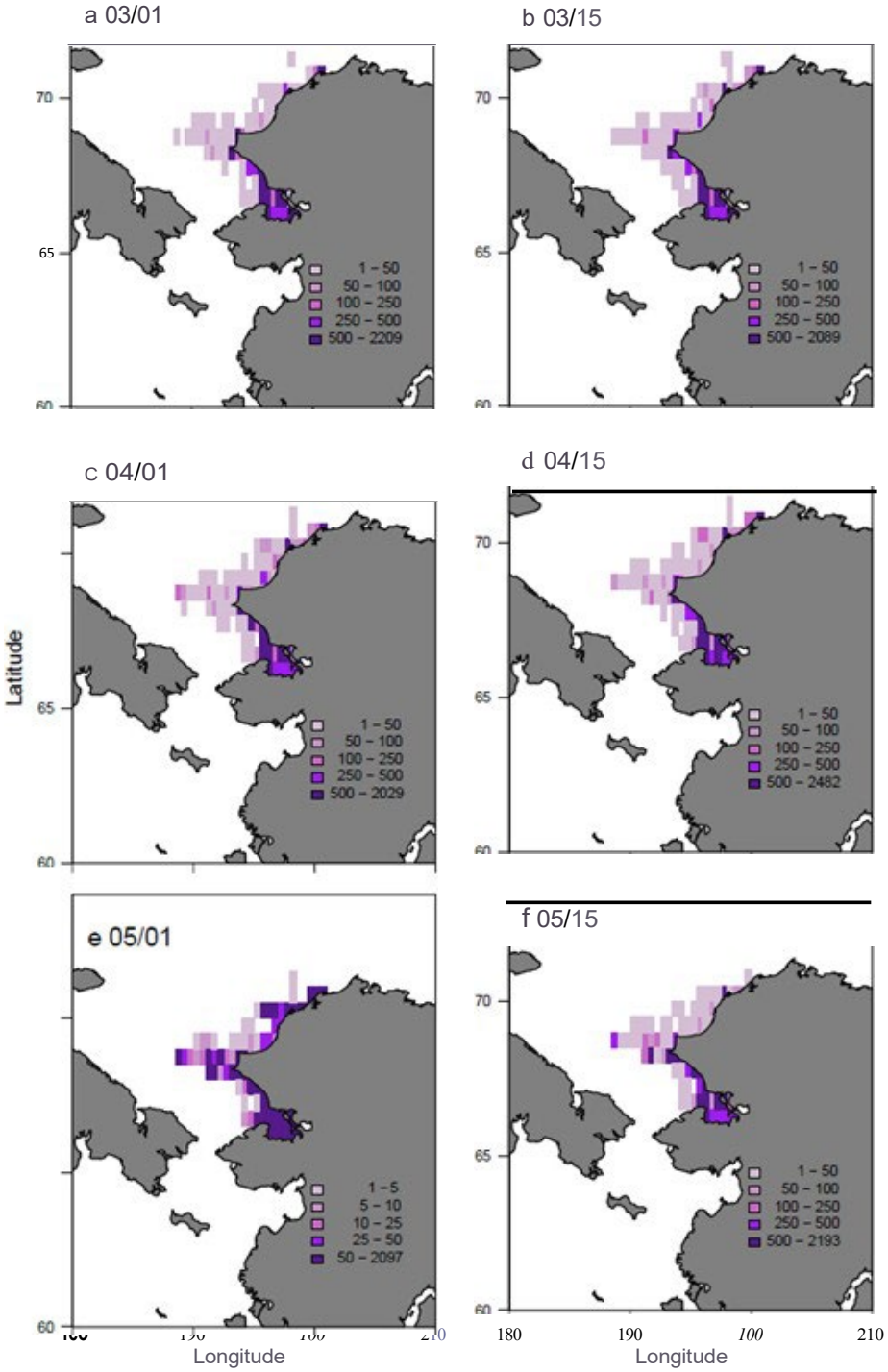
a 03/01
1 – 50
50 – 100
100 – 250
250 – 500
500 – 2209
b 03/15
1 – 50
50 – 100
100 – 250
250 – 500
500 – 2089
c 04/01
1 – 50
50 – 100
100 – 250
250 – 500
500 – 2029
d 04/15
1 – 50
50 – 100
100 – 250
250 – 500
500 – 2482
e 05/01
1 – 5
5 – 10
10 – 25
25 – 50
50 – 2097
f 05/15
1 – 50
50 – 100
100 – 250
250 – 500
500 – 2193
Latitude
70
65
60
180
190
200
210
Longitude

Figure 7

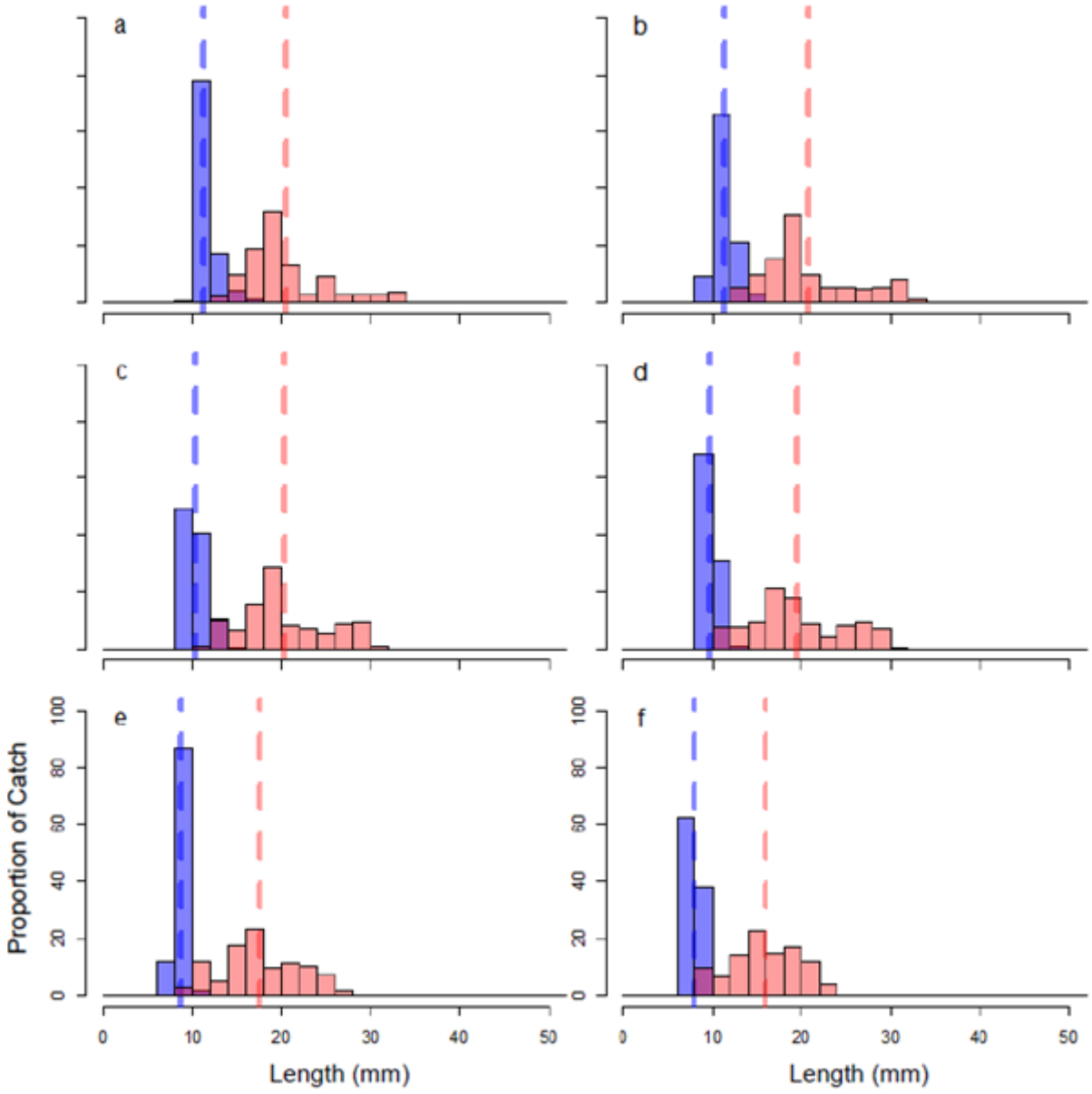
a
b
c
d
e
f
Proportion of Catch
0
20
40
60
80
100
0
10
20
30
40
50
Length (mm)
Length (mm)

Figure 8

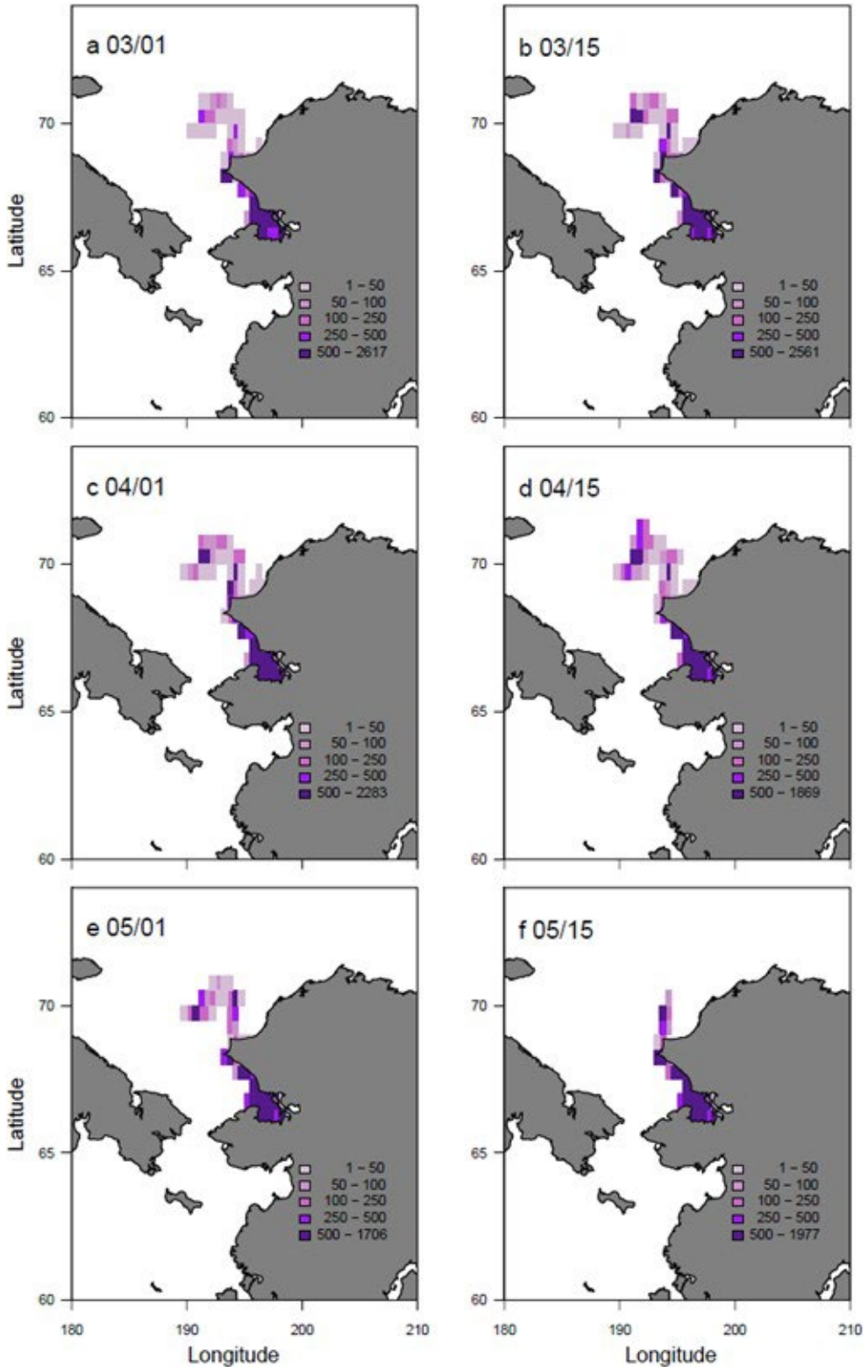
a 03/01
1 – 50
50 – 100
100 – 250
250 – 500
500 – 2617
b 03/15
1 – 50
50 – 100
100 – 250
250 – 500
500 – 2561
c 04/01
1 – 50
50 – 100
100 – 250
250 – 500
500 – 2283
d 04/15
1 – 50
50 – 100
100 – 250
250 – 500
500 – 1869
e 05/01
1 – 50
50 – 100
100 – 250
250 – 500
500 – 1706
f 05/15
1 – 50
50 – 100
100 – 250
250 – 500
500 – 1977
Latitude
70
65
60
180
190
200
210
Longitude

Figure 9

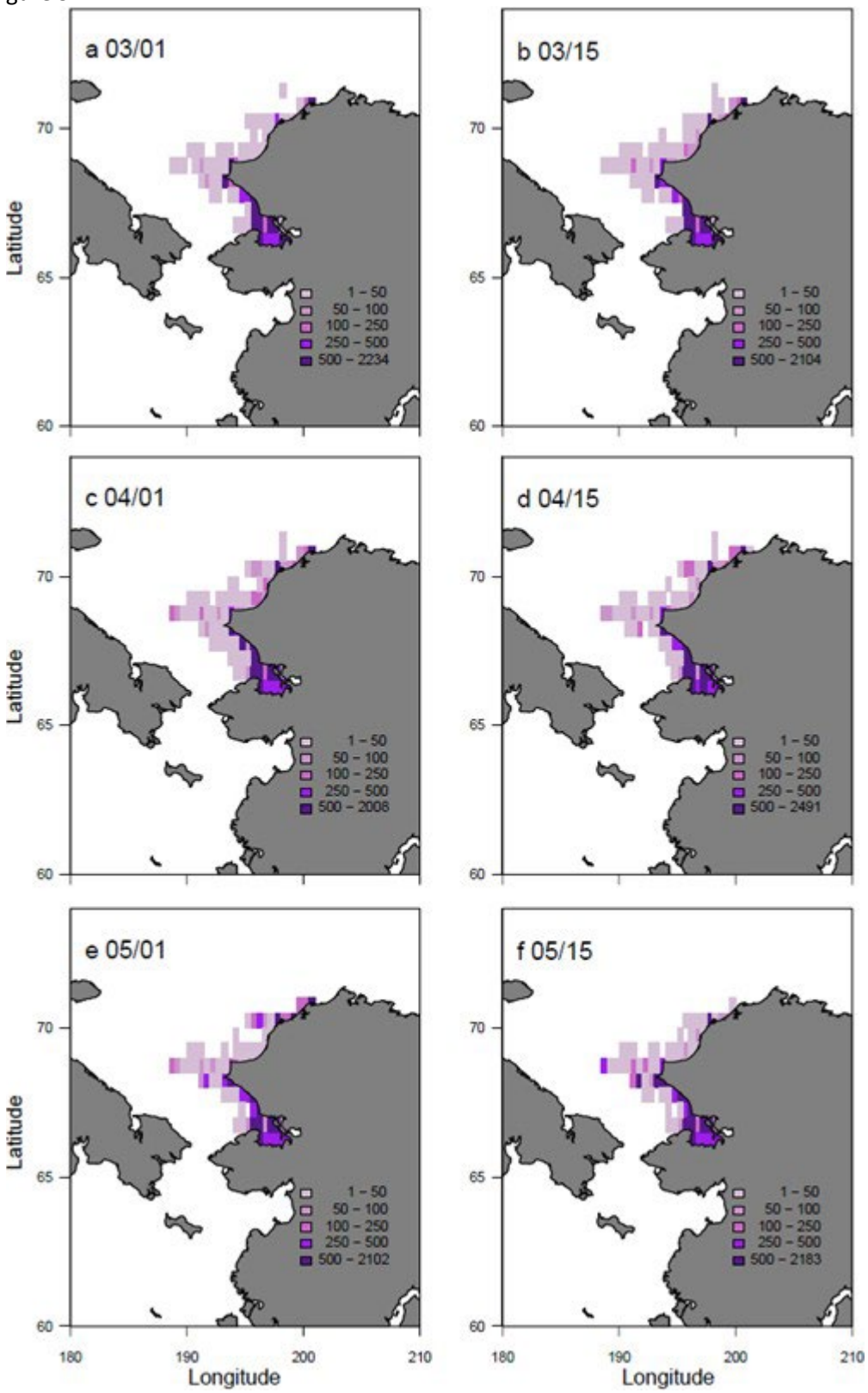
a 03/01
b 03/15
c 04/01
d 04/15
e 05/01
f 05/15
1 – 50
50 – 100
100 – 250
250 – 500
500 – 2234
500 – 2104
500 – 2008
500 – 2491
500 – 2102
500 – 2183
Latitude
Longitude
60
65
70
180
190
200
210

Figure 10

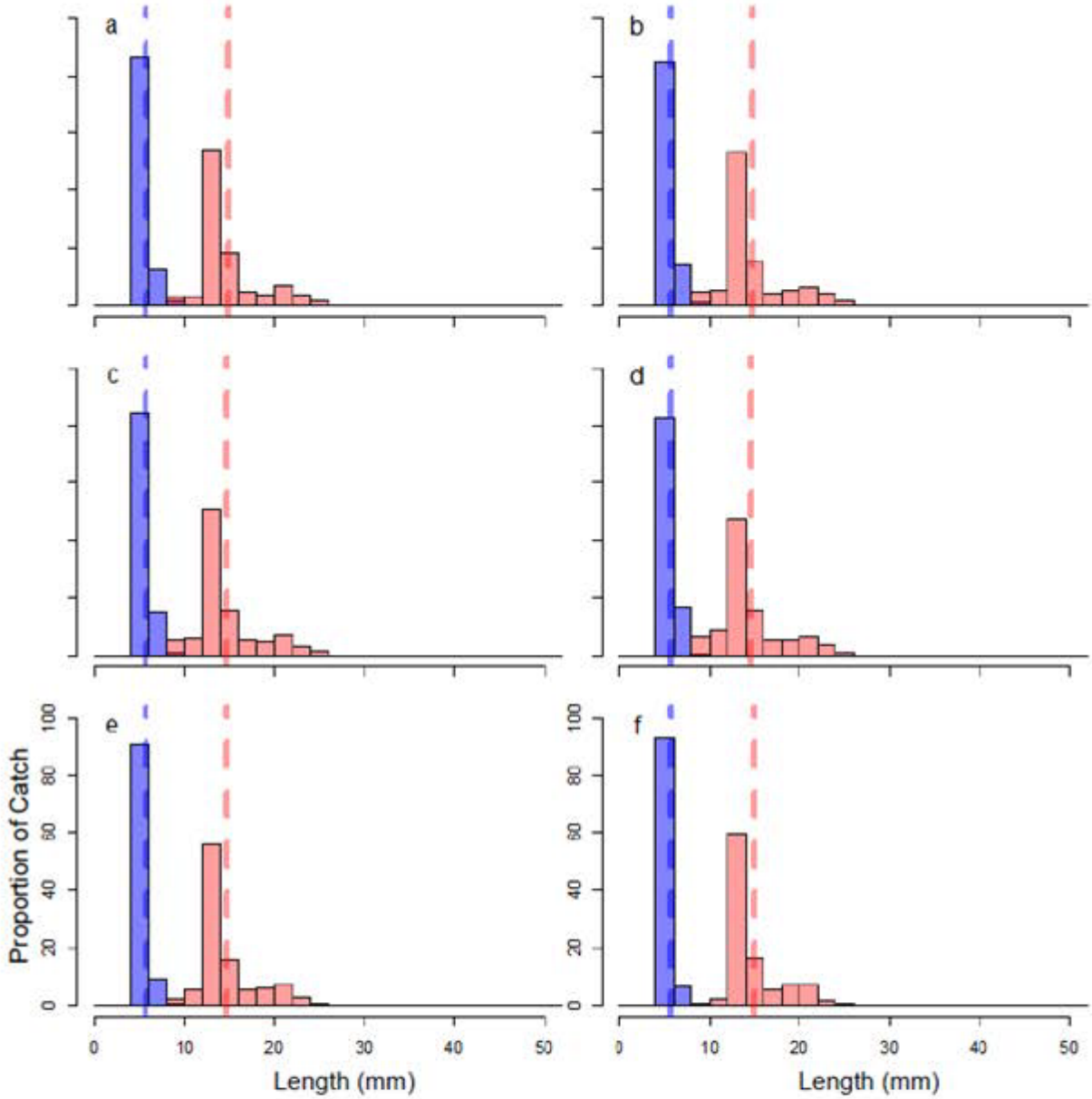
a
b
c
d
e
f
Proportion of Catch
0
20
40
60
80
100
0
10
20
30
40
50
Length (mm)
Length (mm)

Chapter 4: Environmental impacts on walleye pollock (Gadus chalcogrammus) distribution across the Bering Sea shelf

Eisner, L.B., Zuenko, Y.I., Basyuk, E.O., Britt, L.L., Duffy-Anderson, J.T., Kotwicki, S., Ladd, C., Cheng, W.

Citation:

Eisner, L.B., Zuenko, Y.I., Basyuk, E.O., Britt, L.L., Duffy-Anderson, J.T., Kotwicki, S., Ladd, C. and Cheng, W., 2020. Environmental impacts on walleye pollock (Gadus chalcogrammus) distribution across the Bering Sea shelf. Deep Sea Research Part II: Topical Studies in Oceanography, 181-182, p.104881. doi: 10.1016/j.dsr2.2020.104881.

Deep–Sea Research II 181-182 (2020) 104881

Contents lists available at ScienceDirect

Deep-Sea Research Part II

journal homepage: http://www.elsevier.com/locate/dsr2

Environmental impacts on walleye pollock (*Gadus chalcogrammus*) distribution across the Bering Sea shelf

Lisa B. Eisner [a,*], Yury I. Zuenko [b], Eugene O. Basyuk [b], Lyle L. Britt [a], Janet T. Duffy-Anderson [a], Stan Kotwicki [a], Carol Ladd [c], Wei Cheng [c,d]

[a] NOAA Alaska Fisheries Science Center, Seattle, WA, USA
[b] Russian Research Institute of Fisheries and Oceanography, Pacific Branch (TINRO), Vladivostok, Russia
[c] NOAA Pacific Marine Environmental Lab, Seattle, WA, USA
[d] University of Washington, Cooperative Institute for Climate, Ocean and Ecosystem Studies, Seattle, WA, USA

ARTICLE INFO

Keywords:
Walleye pollock
Bering sea
Temperature
Sea ice
Cold pool

ABSTRACT

Adult and juvenile (age-1) walleye pollock (*Gadus chalcogrammus*) were sampled by the US NOAA Alaska Fisheries Science Center summer bottom trawl survey in 2010, 2017, 2018, and 2019 in the northeastern and southeastern Bering Sea, with profiles of temperature collected concurrently. Similarly, the Russian Research Institute of Fisheries and Oceanography, Pacific branch, collected adult and juvenile pollock and temperature profiles on summer bottom trawl surveys in the northwestern Bering Sea. Results from these surveys show that adult pollock abundance in recent years (2017, 2018, 2019) has increased in northern regions of the Bering Sea shelf in both the US and Russian sectors. Lower abundances, compared to historic means, were observed in southern regions of the shelf, suggesting the pollock moved directionally from the south to the north. We relate changes in pollock distribution in recent intermediate (2017) and warm, low-ice years (2018–2019) to a prior cold, high-ice year (2010) and describe how these observations relate to our longer time series. We link temperature data from bottom trawl surveys (US and Russian), sea-ice indices (retreat timing and extent), as well as model-based estimates of ocean circulation to changes in pollock distribution and examine potential environmental factors driving the observed changes. Changes in sea-ice and bottom temperature (e.g., reductions in ice extent and shrinking of the cold pool), and changes in circulation (stronger northward currents over the northeastern shelf in warmer years, particularly in 2018) led to changes in distributions of adult and age-1 pollock. Adult pollock were concentrated north of St. Lawrence Island and had larger longitudinal distributions in warm years, 2017–2019; whereas they had a more southerly and narrow distribution over the outer shelf in the cold year, 2010. Age-1 pollock had higher densities over the inner eastern shelf in 2017–2019 compared to 2010. Northward flow around St. Lawrence Island (particularly in the spring) alternated between stronger flow on the west side of the island in 2010 and 2017 and stronger flow on the east side of the island in 2018 and 2019; variations in flow may have impacted the location of prey and movement of feeding pollock to the Chukchi Sea. Size structure comparisons between NW, NE and SE sections of the Bering Sea shelf suggest that movement of fish between US and Russian waters may have been highest in 2019, one of the two warmest years, and lowest in 2010, the coldest year. Spatial comparisons of distributions and size structure across the Bering Sea help provide a comprehensive view of factors affecting the movement of this highly important commercial fish species.

1. Introduction

Movement of fishes in response to environmental conditions is a well-documented, adaptive response to maximize reproductive success, growth, and survivorship. Typical activating factors include a suite of environmental (temperature and salinity gradients, precipitation and runoff, fluctuating current regimes) and biological variables (e.g., prey resources, habitat optimization, predator and/or competitor avoidance,

* Corresponding author.
E-mail addresses: lisa.eisner@noaa.gov (L.B. Eisner), zuenko_yury@hotmail.com (Y.I. Zuenko), evgeniy.basyuk@tinro-center.ru (E.O. Basyuk), lyle.britt@noaa.gov (L.L. Britt), janet.duffy-anderson@noaa.gov (J.T. Duffy-Anderson), stan.kotwicki@noaa.gov (S. Kotwicki), carol.ladd@noaa.gov (C. Ladd), wei.cheng@noaa.gov (W. Cheng).

https://doi.org/10.1016/j.dsr2.2020.104881
Received 25 March 2020; Received in revised form 22 September 2020; Accepted 30 September 2020
Available online 13 October 2020
0967-0645/Published by Elsevier Ltd.

and mating and reproduction) that serve to initiate behavioral responses, either at the individual, population, or species levels. Climate change, particularly in the sensitive polar regions, exacerbates a number of these known drivers, prompting never-before-seen, population-level, spatial and distributional shifts (McLean et al., 2018; Mueter and Litzow, 2008). In the Pacific Arctic, large scale, northward movements of commercial stocks are underway as previously cold-dominated ecosystems warm and fish move directionally to higher latitude, relatively cooler environments. In the Bering Sea, such migrations have been recently documented among Pacific cod (*Gadus macrocephalus*), Pacific and Greenland halibut (*Hippoglossus stenolepis, Reinhardtius hippoglossoides,* respectively), and walleye pollock (*Gadus chalcogrammus,* hereafter pollock), (Kotwicki and Lauth, 2013; Spies et al., 2019; Stevenson and Lauth, 2019; Vestfals et al., 2016). In particular, shifts in the distribution of pollock are of special concern, as pollock in the eastern Bering Sea and Aleutian Islands (SE and NE shelf, Fig. 1) are the top US commercial fishery by biomass yielding over 1.3 million metric tons annually in recent years (2014–2017) (Fissel et al., 2019). In the western Bering Sea (including the NW shelf, Fig. 1) Russian pollock yearly yields are lower, ~0.4 million metric tons (Khen et al., 2013), but are still a highly important fishery. In addition to their economic importance, pollock are also a key ecological component of the Bering Sea food web across the shelf, serving as a critical link between lower (zooplankton) and upper (fish, seabirds, mammals) trophic levels (Buckley et al., 2016).

Adult and juvenile pollock distributions over the SE shelf have varied between cold, high seasonal sea ice (hereafter, ice) years and warm, low ice years over a 38-year time series (Kotwicki et al., 2005; Kotwicki and Lauth, 2013, Thorson et al., 2017). During cold years, an extensive "cold pool" forms on the eastern Bering Sea shelf below the pycnocline and persists through the summer. Although the cold pool is commonly defined as temperatures below 2 °C (e.g., Stabeno and Bell, 2019; Wyllie-Echeverria and Wooster, 1998), here, we use a cutoff of 0 °C (termed 0 °C cold pool in this manuscript), because adult pollock usually do not form feeding aggregations at temperatures below this threshold in the eastern Bering Sea (Baker, in press). Oceanographically, the eastern shelf has been classified into inner (<50 m), middle (50–100 m) and outer (100–200 m) domains, each separated by an oceanographic front (Coachman, 1986) (Fig. 1); the Aleutian Islands to 60°N, and 60°N to Bering Strait are considered to be the southern and northern Bering Sea respectively. Adults are typically located on the outer shelf outside (west) of the 0 °C cold pool during cold years, with distributions spreading eastward toward the middle shelf in warm years (Baker, in press; Baker and Hollowed, 2014; Kotwicki et al., 2005). Age-1 pollock tend to be distributed more northerly than adult pollock and are likely less able to avoid the 0 °C cold pool (e.g., Kotwicki et al., 2005; Thorson et al., 2017). Pollock over the NW shelf are typically observed off Cape Navarin in southern Anadyr Bay in cold or average years and also are limited by the 0 °C cold pool located northeastward from this area, but spread farther north and northeastward in warm years. Multi-year, warm-cold oscillations of the environment and pollock distribution have been fairly typical over the last 15+ years (Stepanenko and Gritsay, 2016; Zuenko and Basyuk, 2017), though recent years (2018–2019) have been extremely warm (with bottom temperatures anomalies of ~ + 3–4 °C on the northern middle shelf at mooring 8, southwest of St. Lawrence I), and characterized by a lack of sea ice during winter (Stabeno and Bell, 2019), a heretofore unprecedented event. Lack of winter ice has led to a cascade of observed ecosystem changes across multiple trophic levels (Duffy-Anderson et al., 2019; Huntington et al., 2020). During and just prior to this period (2017–2019), summer distributions of adult pollock also changed considerably, with large population biomass observed in the northern reaches of the Bering Sea (north of St. Lawrence Island and in northern Anadyr Bay).

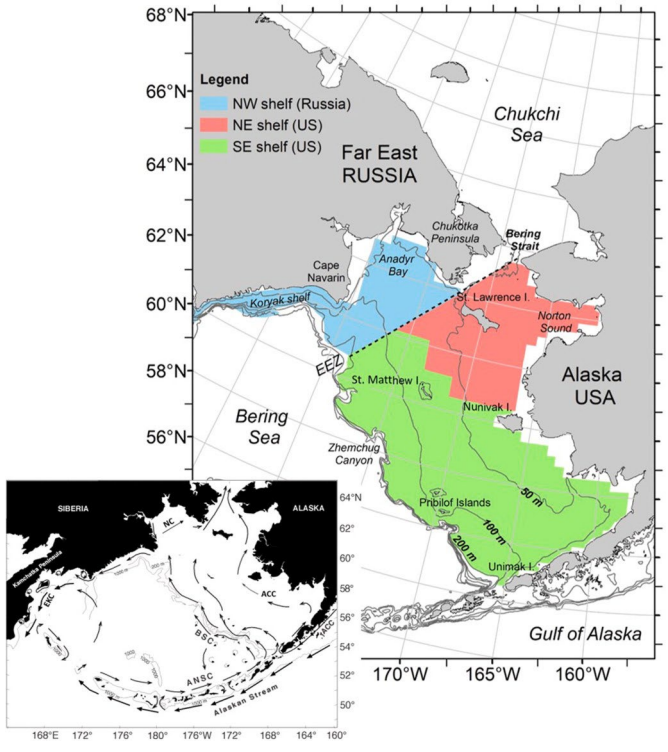

Fig. 1. Study Area. Regions sampled include the northwest (NW) shelf in the Russian EEZ, and the northeast (NE) and southeast (SE) shelf in the US EEZ of the Bering Sea. Contours denote the 50 m, 100 m, and 200 m isobaths. Inset figure shows currents in the Bering Sea. ACC = Alaska Coastal Current, ANSC = Aleutian North Slope Current, BSC = Bering Slope Current, EKC = East Kamchatka Current, and NC = Navarin Current.

Changes in summer pollock distributions are likely related, at least in part, to the extraordinary changes in sea ice and water temperature in the Bering Sea. The summer cold pool extent is determined by late winter ice extent (Wyllie-Echeverria and Wooster, 1998), and recent reductions in ice cover have drastically decreased the extent of the cold pool. In particular, 2018 and 2019 exhibited the smallest cold pool extent observed in at least the last two decades (Basyuk and Zuenko, 2019; Danielson et al., 2020; Overland et al., 2019; Stabeno and Bell, 2019). Retraction of the cold pool may be key to pollock northward distribution. Historically, the 0 °C cold pool was avoided by migrating adults. This effectively served as a barrier to fish passage from the southern to the northern Bering Sea. Profound, climate-mediated shifts in ice dynamics, coupled with associated oceanographic changes, may be altering this division, potentially creating a new paradigm of pollock dynamics across all reaches of the Bering Sea. For example, during fall and winter as ice is forming in the northern Bering Sea, pollock move south to continue feeding in warmer areas. Accordingly, in years with reduced ice extent, there may be less incentive to move to the most southern areas where their traditional spawning grounds are located. Early ice retreat and warmer temperatures during winter can also lead to earlier spawning and an earlier start of feeding migrations (Kotwicki et al., 2005). Changes in hydrography can lead to changes in currents, which then have large impacts on planktonic prey resources for adults (which follow prey) and on juvenile pollock (e.g., age-0 and age-1) and other forage fish species, that are smaller and more susceptible to current flow.

Mean flow on the eastern Bering Sea shelf is weakly (<0.05 m s^{-1}) northwestward (Fig. 1 Inset), along the shelf (e.g., Kinder and Schumacher, 1981; Coachman, 1986). The stronger Bering Slope Current (>0.10 m s^{-1} during winter) flows northwestward along the shelf-break, closer to the shelf-break during winter and farther off-shelf during spring and summer (Ladd, 2014). The Bering Slope Current splits in the northern Bering Sea with most of the flow feeding the southwestward flowing East Kamchatka Current, while a small part of the flow moves

onto the shelf toward Anadyr Bay and ultimately Bering Strait (Stabeno and Reed, 1994; Panteleev et al., 2011). This northward flow from Cape Navarin toward Bering Strait is known in Russia as the Navarin Current (Luchin and Menovshchikov, 1999). The turn to the north is associated with the density gradient between the low-salinity cold pool and the dense, high salinity cold water near the Chukotka coast, formed during winter ice formation. The Navarin Current is the only strong flow that penetrates deeply onto the shelf.

Historically, pollock distribution over the SE shelf is characterized by spatial separation of cohorts, which reduces competition among younger age classes for zooplankton prey, and minimizes cannibalism of younger stages by piscivorous adults (Duffy-Anderson et al., 2003). For example, age-1 pollock (unlike adults) are not able to perform long distance migrations (Kotwicki et al., 2005). Therefore, during their first winter age-1 pollock may not be able to migrate to ice free areas (as adults do), but instead many of them overwinter under the ice and stay in the cold pool throughout the summer. Adults avoid the cold pool, which results in a narrower spatial distribution. A result of this dynamic is a reduction in cannibalism of adults on age-1 pollock during cold years. Separation occurs in both the vertical and horizontal dimensions, and is precipitated by predation dynamics, differences in temperature tolerance, ontogenetic factors, diel shifts, and feeding and diet differences. On the NW shelf, however, spatial separation of pollock cohorts is absent; both adults and juveniles feed in the same area, though often in separate aggregations (Stepanenko and Gritsay, 2016). Climate-mediated shifts in ice and cold pool dynamics could alter the spatial partitioning for both the eastern and the NW Bering Sea, disrupting established feeding, refuging, and migrations across cohorts.

In order to fully assess the potential for broad-scale changes in pollock distribution over the Bering Sea and environmental factors driving these changes, it is critical to evaluate distributions across the entire shelf in both US and Russian sectors. The NOAA Alaska Fisheries Science Center (AFSC) bottom trawl survey now has 4 years of sampling (2010, 2017, 2018, and 2019) in the NE Bering Sea in conjunction with the ongoing annual sampling (1982-present) in the SE Bering Sea. These surveys are used to evaluate adult (age-4+) and juvenile (age-1) pollock distributions. The Pacific branch of Russian Research Institute of Fisheries and Oceanography (TINRO) has conducted similar bottom or midwater trawl surveys on the NW Bering Sea shelf since 1986, including the same 4 years. Our goal is to compare summer distributions and size structure data from SE, NE and NW shelf waters for these years, to decipher the extent of the pollock movement among these regions, and the environmental factors that influence these distributions. We lack information on large scale pollock distributions for seasons other than summer, therefore we are unable to fully evaluate the impact of environmental factors on winter, spring or fall distributions.

1.1. Three main questions will be addressed

1) How do adult and age-1 pollock summer distributions vary across the Bering Sea shelf in high-ice/cold (2010) compared to recent intermediate and low-ice/warm (2017–2019) years?
2) How do environmental factors (ice, water temperature, currents) influence the summer adult and age-1 distributions?
3) Are population size structures similar for US (SE and NE) and Russian (NW) collected pollock (suggesting mixing of the US and Russia origin populations)?

Our evaluations are intended to allow fisheries managers and commercial fishers to gain a better understanding of current changes in stocks and potential factors driving these changes.

2. Methods

2.1. Survey data

Pollock were sampled in 2010 and 2017–2019 on bottom trawl surveys (primarily) during summer months (June–August, Table 1) over the SE, NE and NW Bering Sea shelf (Fig. 1). Timing of the SE and NE surveys was consistent among years. The SE surveys were conducted in June through July with sampling starting with the easternmost stations within Bristol Bay and progressing westward toward the Bering Sea continental slope edge (depths > 200 m) and the US-Russia transboundary line. Sampling for the NE surveys were scheduled to start after the completion of SE survey and a port call to Nome, AK, to re-provision the vessels. NE survey sampling occurred during the first 2–3 weeks of August with a north-to-south progression. The timing of NW surveys varied more, in particular the 2017 survey was conducted in June through July, whereas surveys in the other years occurred from mid/late July to mid-August/early September. Therefore, survey timing overlapped most for the NE and NW surveys in 2010, 2018 and 2019 and for the SE and NW surveys in 2017. Measurements of water temperature were collected at all trawl stations. We lacked the data (e.g., higher temporal resolution data on pollock distribution outside of our survey date) to normalize the trawl data to a specific date (unlike the bottom temperature, described in 2.2.1. below). However, surveys were planned to take into account the timing of pollock movements, and therefore provide a general picture of fish distributions. The differences in survey timing described above can be used to understand finer scale differences among years and regions.

2.1.1. SE and NE bottom trawls

Bottom trawl survey data have been collected by the NOAA AFSC Groundfish Assessment Program on the SE Bering Sea shelf annually during the summer since 1982 (Fig. 1). The survey is based on a systematic design consisting of 376 fixed sampling stations located in the center of 37.04 × 37.04 km (20 × 20 nautical mile) grid squares with the survey ranging from 54.5°N to 62°N latitude and bounded by the 20 m and 200 m isobaths and the US – Russia Convention line to the northwest. Bottom trawl survey data using the same methods were collected

Table 1
Survey timing and mean surface and bottom temperatures (T, °C) for surveys on the SE, NE and NW shelves. See Fig. 7 for differences in areas surveyed among years (e.g., no sampling in Anadyr Bay (NW) in 2019 or Norton Sound (NE) in 2018).

Year	SE	NE	NW
2010	June 3 – August 4	July 23 – August 15	July 10 – September 6
Surface T	5.34	9.35	9.00
Bottom T	1.42	2.01	1.97
2017	June 3 – July 31	August 1 – August 26	June 7 – July 30
Surface T	7.99	9.63	9.08
Bottom T	2.67	4.37	2.46
2018	June 3 – July 30	July 31 – August 14	July 31 – August 18 (midwater trawl)
Surface T	7.59	10.23	9.80
Bottom T	4.14	3.94	2.94
2019	June 3 – July 28	July 29 – August 20	July 26 – August 8
Surface T	9.24	10.85	9.69
Bottom T	4.34	5.75	2.44

in the NE Bering Sea in 2010, 2017, 2018, and 2019. The NE Bering Sea shelf survey was designed as a continuation of the same systematic design established for the SE shelf survey, effectively extending sampling to 65.5°N latitude (Fig. 1). Note that in 2018 the survey extent and station spacing in the NE Bering Sea were non-standard, grid spacing was 55.6 km (30 nm) instead of 37 km (20 nm), and the Norton Sound region was not sampled. Sampling from the bottom trawl surveys in the SE and NE Bering Sea followed standard methods developed by AFSC (Lauth, 2011; Lauth et al., 2019; Stauffer, 2004). Vessels were equipped with 83–112 eastern otter trawls, which have a 25.3 m headrope, 34.1 m footrope, and a 32 mm liner in the codend to aid in retaining smaller animals. The mean effective opening of the trawl is 16.6 m horizontally and 2.7 m vertically.

Catch sampling followed standardized procedures described in detail by Wakabayashi et al. (1985) and Stauffer (2004). Catches with a total weight of 1150 kg or less were sorted and weighed in their entirety, whereas larger catches were randomly subsampled. Fishes were identified and sorted to species to the extent possible, weighed, and counted. For the predominant fish species encountered, including pollock, a random subsample was weighed, sorted by sex, and measured to the nearest centimeter (cm) fork length (FL). Relative abundance was calculated by determining the catch-per-unit-effort (CPUE). CPUE values from each survey are provided for age-1 and adult pollock and were calculated as total weight (kg) per km^2. Based on the results of pollock aging studies, fish were assumed to be age-0 at $<$ ~10 cm FL, age-1 at 10–19 cm, age-2/3 at 20–34 cm, and age-4+ adults at $\geq$ 35 cm (Kimura et al., 2006). Note that the majority of pollock $<$35 cm are less than 4 years old (Fig. A1), and are not consistently caught with the US gear (83–112 eastern otter trawl), with the exception of age-1s (Lauth, 2011).

Temperature and depth profiles were collected using a Sea-Bird Electronics (SBE) 39 datalogger that was attached to the headrope of the trawl. Observations were collected at 3-s intervals during the full duration of each tow. Mean bottom temperature was calculated as the mean temperature sampled between on- and off-bottom events, determined by the bottom contact sensor for each tow.

2.1.2. NW bottom and acoustic/midwater trawls

Bottom trawl data were collected in 2010, 2017, 2019, and a midwater trawl survey coupled with an acoustic survey was conducted in 2018 on the NW Bering Sea shelf and continental slope with bathymetry $<$500 m (Fig. 1). There was no survey in Anadyr Bay in 2019. The bottom trawl gear consisted of a DT-27.1/24.4 net with a horizontal opening of 16.26 m, vertical opening of ~3.6 m and a 10 mm mesh cod end (Savin, 2011). The midwater trawl RT/TM-80/396 had a 40 m opening and a 8 m cod end with 10 mm mesh; the layer from 350 m depth or from the shelf bottom to the sea surface was fished. Acoustics were done with an echo sounder SIMRAD EK-60, using the operating frequencies 38 and 120 kHz; the data were processed with SIMRAD software, with quantitative estimations based on the 38 kHz signals.

For bottom and midwater trawls, every catch was sorted and weighed entirely. Fishes and invertebrates were identified and sorted to species to the extent possible, weighed, and counted. For the predominant fish species encountered, including pollock, a random subsample was weighed, sorted by sex, and measured by centimeter intervals of fork length. Pollock density distribution was estimated following standard methods (Savin, 2011, 2018).

Temperature and salinity data were collected from CTD profiles using a SBE-19plus or SBE-25 deployed to the sea bottom at each station, immediately after trawling. All CTD data were processed with SBE software following standard methods and binned into 1-m bins. Bottom temperature was estimated as the deepest value of the profile.

2.2. Data analysis

2.2.1. Environmental variables

Environmental variables evaluated include sea-ice concentration during the preceding winter, summer bottom temperature, and spring and summer modeled bottom currents for 2010, 2017, 2018, and 2019.

Sea-ice maximum extent and timing of retreat were evaluated using satellite measurements from NOAA/NSIDC Climate Data Record of Passive Microwave Sea Ice Concentration, Version 3 (Meier et al., 2017; Peng et al., 2013) downloaded from the Alaska Ocean Observing System (AOOS) data portal (portal.aoos.org). Ice retreat timing was calculated as the day of year when ice concentration in each pixel reached (and remained) less than 30%. Winters 2009/2010, 2016/2017, 2017/2018 and 2018/2019 were designated as 2010, 2017, 2018 and 2019, respectively.

Bottom temperature data from the SE, NE and NW shelf surveys were combined. The total number of temperature profiles varied from 532 in 2018 to 957 in 2010 (Fig. A2). The following procedure was used to estimate synoptic (normalized to July 15) bottom temperature from the surveys (data collected at different survey dates): 1) climatological bottom temperatures ($T_{clim}(x_i,y_i,t_i)$) were estimated from the World Ocean Atlas 2013 (WOA2013) version 2 monthly climatology (Locarnini et al., 2013) using linear interpolation; 2) for each measurement ($T_i(x_i, y_i,t_i)$), an anomaly from the interpolated climatology was calculated for the observed date and location ($T_{anom}(x_i,y_i,t_i) = T_i(x_i,y_i,t_i)-T_{clim}(x_i,y_i,t_i)$), thus removing any effect of the timing of observation; 3) bottom temperatures were then normalized to July 15 as the sum of the July 15 climatological value and the anomaly ($T_{norm}(x_i,y_i,15\ July) = T_{clim}(x_i,y_i, 15\ July) + T_{anom}(x_i,y_i,t_i)$).

Mean bottom currents for spring (March, April, and May average) and summer (June, July, and August average) over the Bering Sea shelf were examined using output from a regional ocean-sea ice model in the Bering Sea with 10 km horizontal resolution (named Bering10K hereafter). Bering10K is based on ROMS (Regional Ocean Modeling System) (Haidvogel et al., 2008), a terrain following vertical coordinate ocean general circulation model with tides, and is coupled to a dynamic-thermodynamic sea ice model (Budgell, 2005). Over the time period of examination, Bering10K is forced by prescribed surface atmosphere and ocean lateral boundary conditions from NOAA Climate Forecast System Reanalysis (CFSR) and its operational extension (CFSv2-OA). CFSR and CFSv2-OA are reanalyses products where a suite of satellite and in situ observations are assimilated into a coupled climate model (Saha et al., 2010); as such, they represent a best estimate

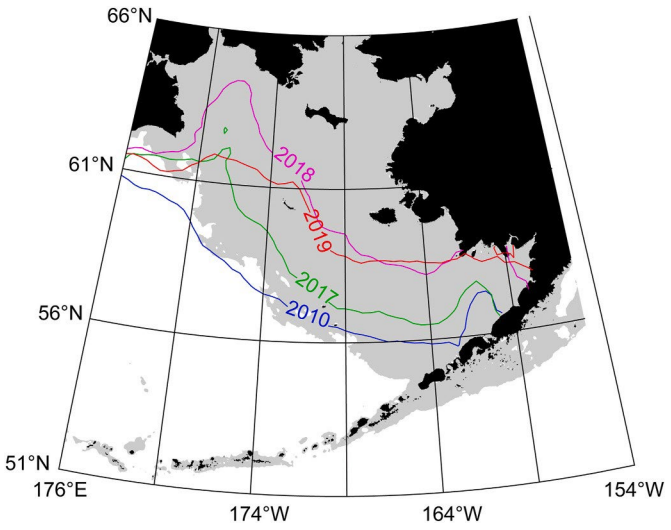

Fig. 2. Maximum sea-ice extent (defined as 30% concentration) in the Bering Sea for 2010, 2017, 2018, 2019.

of past historical climate conditions. The transport through the northern boundary (Bering Strait) is relaxed to the observed value of 0.8×10^6 $m^3 s^{-1}$ (Woodgate and Aagaard, 2005); sensitivity studies tested whether a seasonally varying open boundary condition could better replicate flow patterns in the northern portion of the domain, but the simple relaxation condition was found to perform equally well (Kearney et al., 2020). Bering10K modeling framework and detailed model evaluation are provided in Kearney et al. (2020).

2.2.2. Pollock distribution and size structure

The pollock distribution data were combined from US (SE, NE shelf) and Russian (NW shelf) surveys. Prior to combining data, the US data were corrected for density dependent efficiency of the survey bottom trawl (Kotwicki et al., 2014). The correction was applied using formula $CPUE_o/q$ where $CPUE_o$ is observed CPUE and q averaged 0.75 across years used in analysis and ranged between 0.73 and 0.77. This correction was applied because it has been established that corrected estimates are less biased and more precise with respect to the mean CPUE and variance (Kotwicki and Ono, 2019). The Russian data were not corrected, because for the years used in the analysis we did not have data to compare the efficiency of the US and Russian survey bottom trawls. However, data from years 1982–1990, when both Russian and US surveys were conducted over the SE shelf, suggest that the median sampling efficiency ratio for the Russian survey relative to the US survey for pollock biomass was 0.7 ± 0.16 (O'Leary et al., in review). Because bottom trawl efficiency values in the past were close and we do not have data to estimate these values for the recent surveys we decided that the best approach was to not correct Russian CPUE data. Adult distribution maps were plotted in biomass units (kg km^{-2}), but juveniles (age-1) were plotted in abundance units (number km^{-2}) because of the highly variable weight of juveniles. Maps of pollock distribution overlain with bottom temperature contours (0 °C and 6 °C) were made with ArcMap (version 10.3,2014, ESRI, Inc.) by inverse distance weighting CPUE data (kg/ha) for adult and age-1 pollock in each survey year for the SE and NE shelf.

The preferable bottom temperature and bottom depth range for adult and age-1 pollock was evaluated by comparing mean proportions of pollock abundance relative to bottom temperature and depth for data collected in the SE and NE Bering Sea from 1987 to 2019. We were unable to perform these analyses for pollock collected on the NW shelf.

Pollock size distribution data were plotted as histograms for the three areas of the Bering Sea shelf. Percent frequency of occurrence (proportion of individuals) was plotted for each 1 cm length bin. In 2018, size structure was evaluated only for the NE and SE Bering Sea shelf since the NW pollock data were collected with midwater trawls, which likely collect smaller fish than bottom trawls and could bias the size estimates for comparison. Note that in 2019, the NW fish collection was limited to the Koryak shelf and Cape Navarin (southern part of NW shelf, Fig. 1).

3. Results

3.1. Environmental variables

Of the four years (2010, 2017, 2018, and 2019), maximum sea-ice extent was greatest in the winter of 2010, followed by 2017 (Fig. 2). Maximum extent was comparable in the two years 2018 and 2019 in the eastern Bering Sea. However, on the NW shelf (Anadyr Bay), 2018 exhibited a notable lack of sea-ice compared with the other years. The timing of sea-ice retreat at a given location was much earlier in 2018 and 2019, followed by 2017, then 2010 (Fig. 3). For example, ice retreated southeast of St. Lawrence Island in April 2018 and 2019, May 2017 and June 2010.

Bottom summer temperature data (normalized to July 15) show the

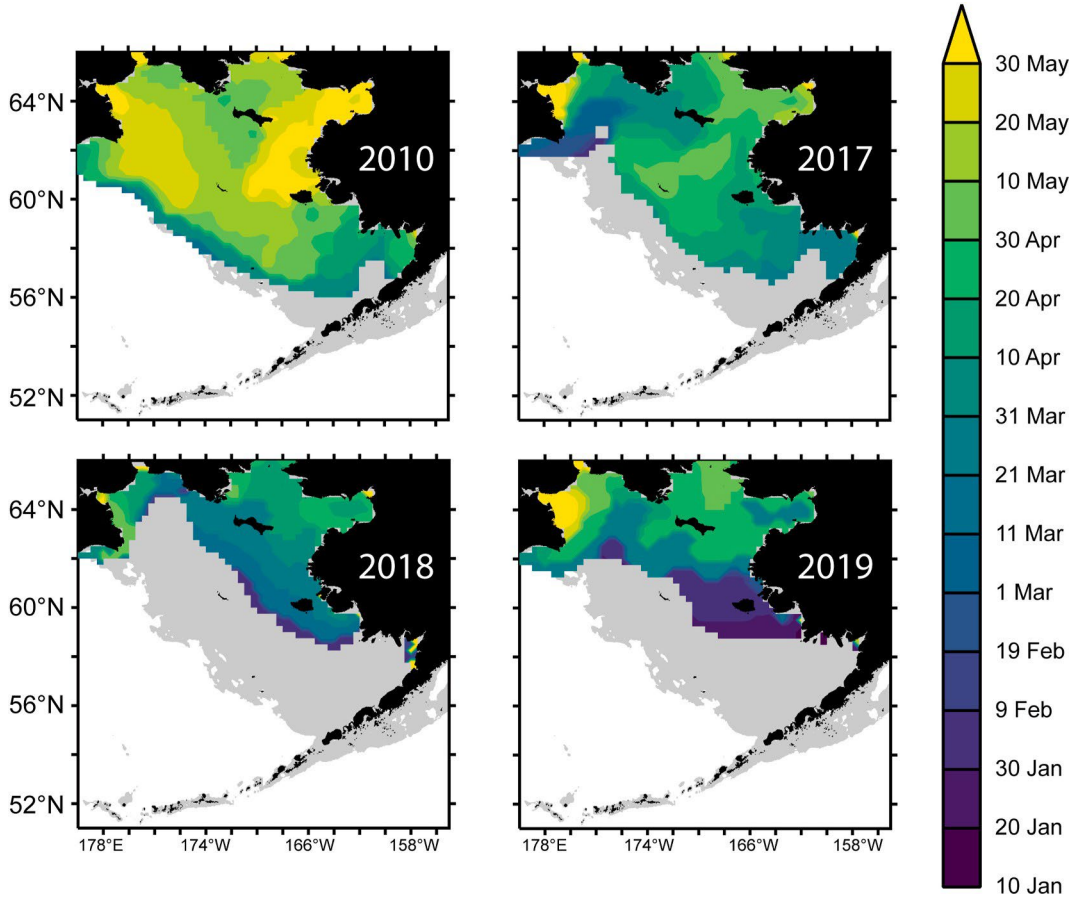

Fig. 3. Ice retreat day of year: the date when sea-ice concentration fell below 30% and remained below 30% for the remainder of the summer.

cold pool extended into the southern shelf in 2010 and 2017, but not in 2018 or 2019 (Fig. 4). Water colder than 0 °C was almost nonexistent in 2018 and was limited to south and west of St. Lawrence Island in 2019. In 2017, on the southern shelf, the water colder than 0 °C was limited to a small area compared to 2010 when the low temperatures extended over almost the entire middle shelf. Bottom temperatures were extremely warm (12–15 °C) along the eastern Inner Domain in 2017, 2018 and 2019, but ≤ 10 °C in the same region in 2010. Otherwise, temperatures in 2010 remained <2 °C, aside from small areas in outer Anadyr Bay (2.5 °C), just north of St. Lawrence Island (3 °C), and outer Norton Sound (2–3 °C). In 2017 and 2018, larger areas with higher temperatures were observed in Anadyr Bay, north of St. Lawrence Island and in Norton Sound. Data were not available for 2019 in Anadyr Bay.

Bottom currents on the northern shelf from Bering10K show that the strongest spring (March, April, May) and summer (June, July, August) currents (>5 cm s^{-1}) in all years were found NW of St. Lawrence Island and in Bering Strait (Figs. 5 and 6). In the spring, northward flow between St. Lawrence Island and the Chukotka Peninsula was strongest in 2010 and 2017 while flow on the east side of St. Lawrence Island was stronger in 2018 and 2019. During summer, flow west of St. Lawrence Island was strongest in 2017 while east of the island, flow was weaker and did not exhibit the same interannual variability as observed in the spring.

In Anadyr Bay during both spring and summer, flow into the bay (toward the northwest) was strongest in 2017, feeding the flow around the Chukotka Peninsula toward Bering Strait. During spring, flow was predominantly out of the bay (toward the southeast) in 2018 and 2019. In 2010, spring flow was weak and spatially variable in the bay but stronger across the bay mouth (toward the northeast). During summer, flow in all years was predominantly directed into the bay but stronger on the southwest side.

3.2. Pollock distribution and size structure

Adult pollock distributions during summer varied among years across the Bering Sea shelf (Fig. 7). In 2010, the pollock were found in high concentrations (>10,000 kg km^{-2}) in the outer shelf from the middle front to the shelf break (100–200 m bathymetry), and in patches north of Unimak Island in the south and outside of Anadyr Bay on the NW shelf (Fig. 7). In 2017 the adult pollock were more widespread across the shelf with high concentrations in western Anadyr Bay and north and west of St. Lawrence Island up to Bering Strait with smaller patches south of the island. In 2018, there was a low abundance of pollock on the SE shelf with small high density patches north of the Aleutians and near the Pribilof Islands; the highest concentrations were found on the northern outer shelf, and north and west of St. Lawrence Island to the Bering Strait, the northern limit of the available bottom trawl survey data. Acoustic data for the NW shelf in 2018 also indicate high densities of pollock south and west of St. Lawrence Island at the mouth of Anadyr Bay (Fig. 8). In 2019, the adults were found over most of the outer and middle shelf with high concentrations also south of Bering Strait. Since there was no 2019 survey in Anadyr Bay, concentrations in that region could not be evaluated.

The adult distributions appear to relate to the seasonal coverage of sea-ice and bottom temperature. In the high and moderate ice years of 2010 and 2017, respectively, the adults were located outside (west) of the 0 °C cold water region (Figs. 4 and 7; Fig. A3). Whereas, in the very low ice years (2018 and 2019) with almost no bottom water colder than 0 °C, the adults were more evenly distributed over the middle and outer shelf. However, these fish were not found in temperatures above 6 °C (Figs. 4 and 7; Fig. A3); thus, distributions in these years may have been constrained by high rather than low temperatures. A comparison of bottom temperature and depth range for adults in the eastern Bering Sea for 1987 to 2019, indicates that most adults are found at temperatures of 0–6 °C. On average only about 2.5% of adults were found below 0 °C and less than 1% above 6 °C (Table 2). Overall, cross-shelf distributions were

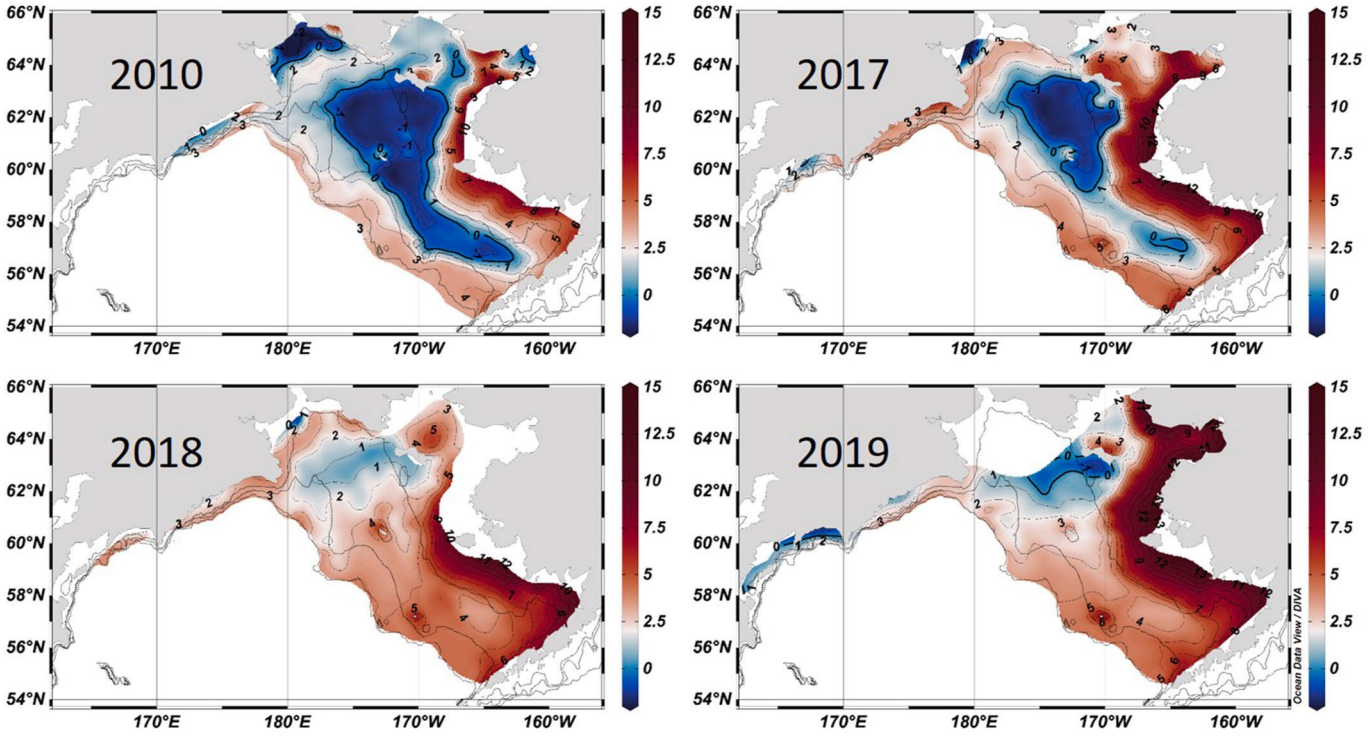

Fig. 4. Bottom temperatures from summer fisheries oceanography surveys for 2010, 2017, 2018, and 2019, normalized to July 15. The cold pool (<2°C) is designated by blue with the 0 °C contour designated by the bold line. (For interpretation of the references to colour in this figure legend, the reader is referred to the Web version of this article.)

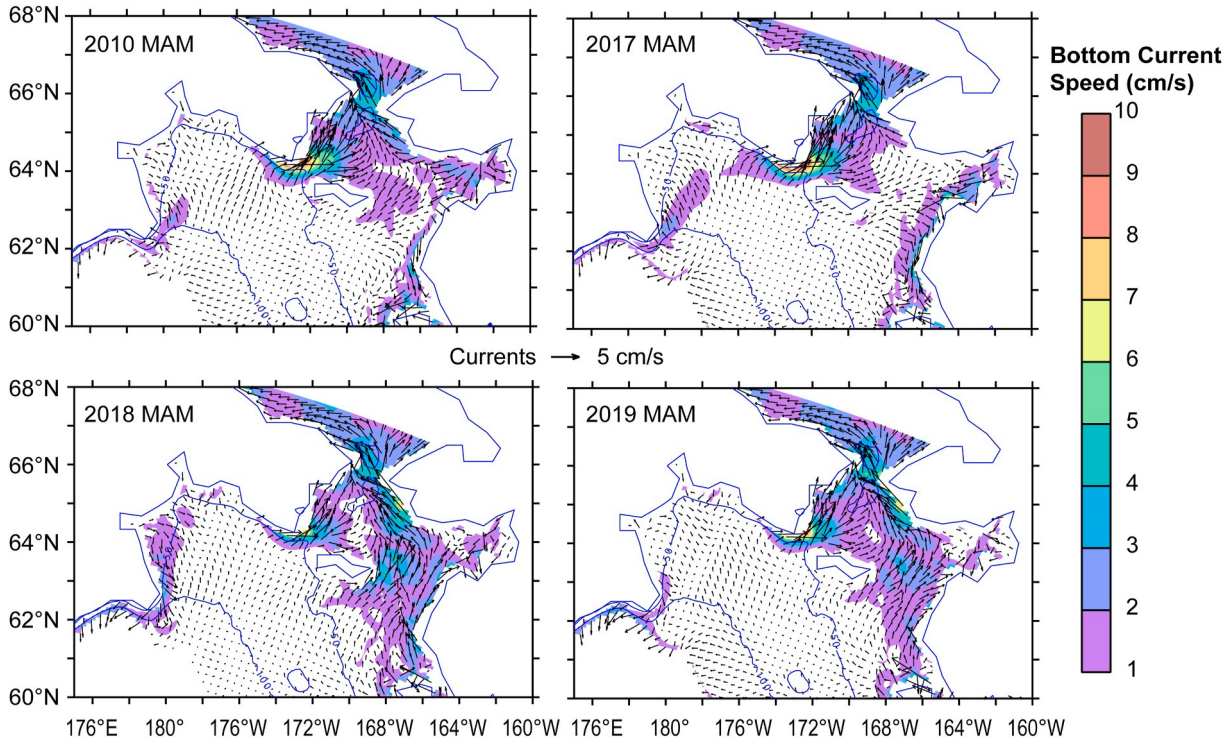

Fig. 5. Bottom currents averaged over March, April and May for 2010, 2017, 2018, and 2019 from the Bering10K model.

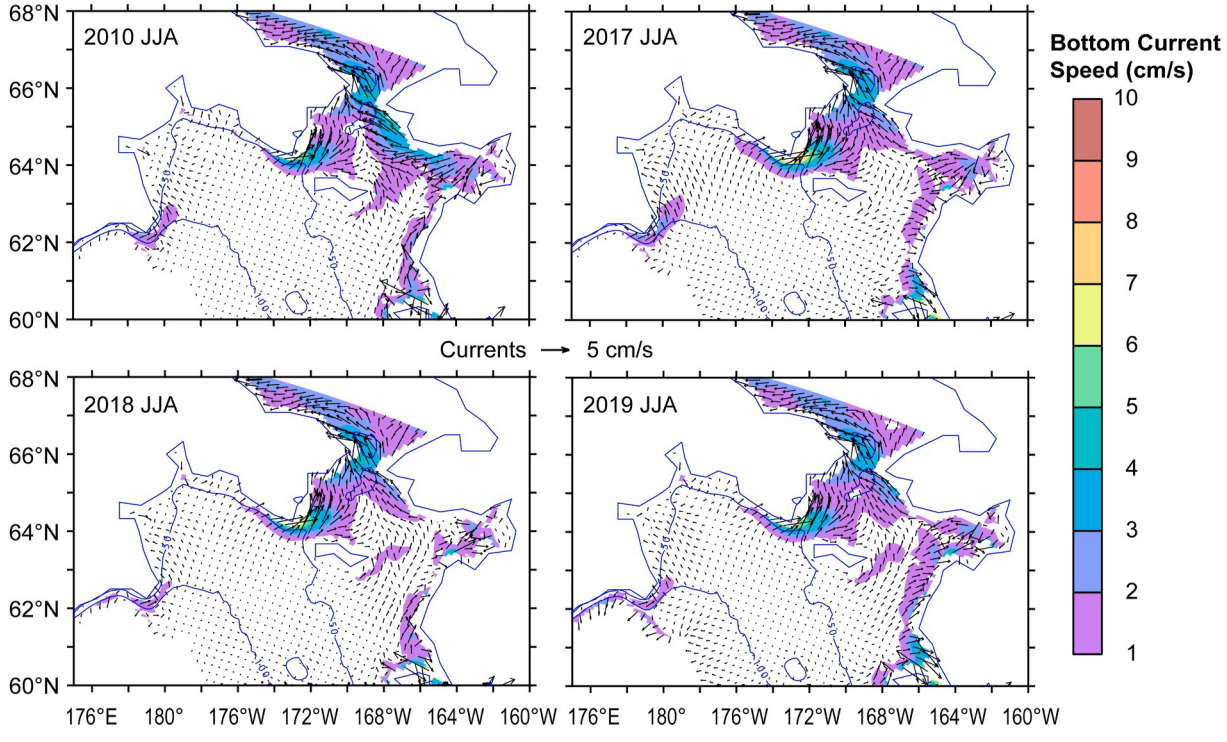

Fig. 6. Bottom currents averaged over June, July and August for 2010, 2017, 2018, and 2019 from the Bering10K model.

larger (extended over a greater depth range) in warm than in cold years. The high adult concentrations located north of St. Lawrence Island and in the NW region in 2017–2019 coincided with areas of higher bottom temperatures. Additionally, high concentrations of pollock were found on the northern middle shelf between St. Matthew and St. Lawrence islands in 2019.

General patterns of the adult distribution in the NW and NE regions may partially relate to the summer currents. In 2010, 2017 and 2018, high concentrations of adults were present in western Anadyr Bay potentially following the Navarin Current. Concentrations of adult pollock were also high to the west and north of St. Lawrence Island toward Bering Strait in 2017–2019, in the region of high currents. In the NE, adult pollock densities were much lower in 2010 compared to the 2017–2019, while in the NW there was not much difference in pollock

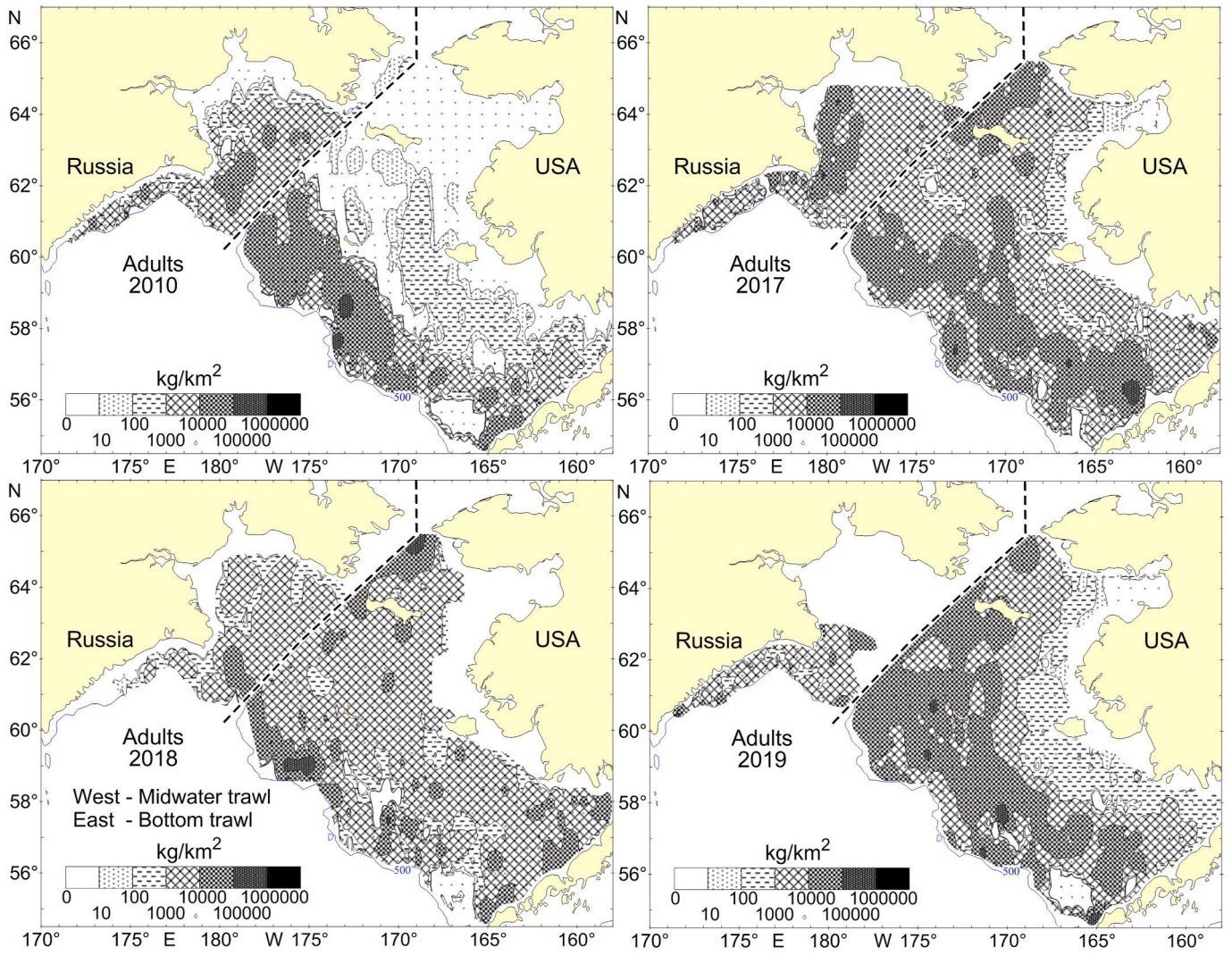

Fig. 7. Adult biomass distribution (kg km^{-2}) for pollock on the Bering Sea shelf from bottom trawls and pelagic (midwater) trawls (2018, NW area) in relatively cold conditions of 2010, intermediate conditions of 2017, and warm conditions of 2018 and 2019 during summer. See Table 1 for surveys dates by region and year. Fisheries sampling stations indicated by dots. US-Russia transboundary shown by dashed line.

densities between these periods.

Age-1 pollock tended to have a more northerly distribution than adults (Figs. 9 and 7). In 2010, age-1 pollock were generally in higher concentration (>1000 km^{-2}) in the outer shelf, but not as far offshore as adults, with smaller patches in the middle shelf, similar to adults, but also had high concentrations in Anadyr Bay (Fig. 9). In 2017, age-1 pollock were found in similar locations on the SE outer shelf and in Anadyr Bay, but were also located on the eastern inner shelf between Nunivak and St. Lawrence islands. In 2018 and 2019, age-1 pollock had a larger cross shelf distribution with the high concentrations located near the eastern inner shelf particularly in 2019 (large area with >10,000 pollock km^{-2}). Fewer age-1 pollock were observed in Anadyr Bay in 2018; there was no survey within Anadyr Bay in 2019, although there is an indication of high concentrations of age-1 pollock south of this area.

Age-1 pollock were found over a greater bottom temperature range than adults (Table 2, Fig. A4). Some age-1 fish were found in temperatures <0 °C, although the highest concentrations were found outside of the 0 °C cold pool. Age-1 pollock on the eastern inner shelf in 2018 and 2019 were found in warm (10 °C) water, much higher than the 6 °C temperature limit for adult distributions. On average age-1 pollock appear to be more widely distributed across bottom temperatures and depths, as indicated by an average 5.7% of age-1 pollock distributed in waters below 0 °C, and 6.7% in waters above 6 °C (Table 2). The high concentrations of age-1 pollock over the eastern inner shelf in 2018 and 2019, in particular, were located in an area with notable northward bottom currents (1–4 cm s^{-1}) south and east of St. Lawrence Island during spring (March–May) (Figs. 9 and 5). Age-1 pollock were not found in this eastern inner shelf area in 2010 when spring (and summer) northward bottom currents were low.

Pollock size structure data indicate differences in several year classes/age groups in the NW compared to SE and NE fish; this is particularly evident in 2010 and 2017 (Fig. 10). For example, in 2017 for NW pollock there were 5 distinct modes in length frequency histograms at ~13, 21, 28, 39, and 48 cm. Only modes similar to the first and last high modes for NW fish were seen in the NE fish at 15 and 49 cm, and in the SE fish at 15 and 45 cm. Age-1 pollock (~10–20 cm, Kotwicki et al., 2005) were found in all regions (NW, NE, and SE) in all years (2010, 2017, 2018, and 2019); the percentage of age-1 pollock were highest in 2010 in the NW and NE, and in 2019 in the NE. In 2010, the cold year, a 40 cm mode was observed both in the SE and NW. Each warm year (2017, 2018, and 2019) appeared to have a different pattern among regions in the size of the largest fish (>35 cm). In 2017, all 3 regions had main modes from 40 to 50 cm, but in the NW there was an additional mode at 39–40 cm. In 2018, the main mode in the NE was larger than in the SE (51 compared to 44 cm), and in 2019 all regions have similar size structure with the

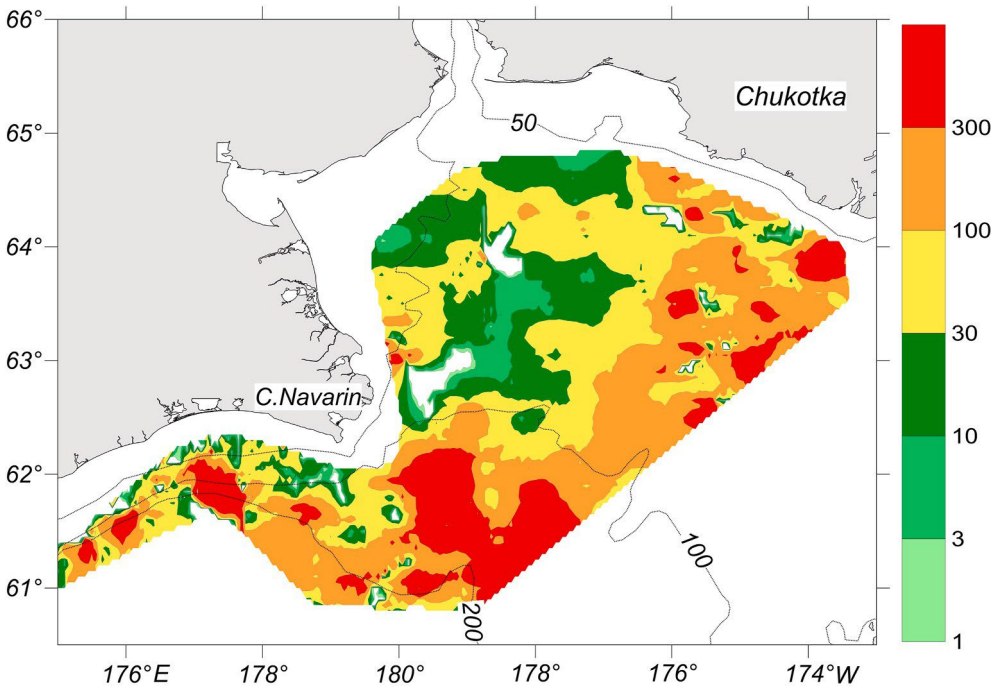

Fig. 8. Pollock distribution in the NW Bering Sea in August 2018 from the acoustic survey. Color bar indicates metric ton/nautical mile^2. The data are kindly presented by Dr. M.Y. Kuznetsov, TINRO. (For interpretation of the references to colour in this figure legend, the reader is referred to the Web version of this article.)

main mode at 46–48 cm and minor modes at 23–25 cm. Spatial differences in size structure were observed even within areas. For example, the two modes for adult pollock in the NW in 2017 reflect the spatial inhomogeneity of size structure within this region. The relatively small fish with the dominant size 39–40 cm were numerous in the southern area (on Koryak shelf), whereas the fish > 50 cm strongly prevailed at the Chukotka coast in the northern Anadyr Bay. Possibly, these two peaks were formed by fish with the same age, but different origin. The same main size group of adults (age-4+ fish, last mode) is observed in all 3 areas in all years, with exception of the NE in 2010 where it was totally absent.

4. Discussion

4.1. Environmental factors related to changes in pollock distribution

Recent changes in adult and age-1 summer pollock distributions in the Bering Sea appear to be related to changes in climate including ice cover, water temperature, and oceanographic currents. Like others have reported earlier, our analyses of US collected data suggest that during cold years when ice is present and extensive, adult pollock are constrained to the outer Bering Sea shelf, limited by the presence of the frigid bottom waters of the 0 °C cold pool (Kotwicki et al., 2005). During warm years when ice is lacking and the cold pool is negligible or absent, pollock are unconstrained by cold bottom temperatures and they shift their distributions northward. However, unique to this study are the inclusion of northwestern Bering Sea (Russian) derived data that demonstrate that not only are pollock distributions north-shifted after ice-reduced winters, but there appears to be more intensive mixing between the Russian stock as it moves north and eastward, and the US stock as it moves north and westward. Specifically we show that pollock expanded their distribution to the area between St. Matthew and St. Lawrence islands in the US, and the area between St. Lawrence Island and Bering Strait in both US and Russian waters. Russia – US stock mixing could portend changes in stock diversity, which has important implications for pollock population resilience, rebuilding, and recovery in the face of climate shifts and anthropogenic pressures.

Several atmospheric and oceanographic factors acted in concert to prompt the spatial shifts described above. Changes in winds during winter impacted the ice and currents in 2017–2019. The seasonally averaged wind anomalies for 2014–2018, compared to 1979–2013, indicate that winds from the south (toward north) were much more prevalent in winter and fall in 2014–2018 (Danielson et al., 2020). These northward winds were correlated to northward water flow in Bering Strait (Danielson et al., 2020), and promoted northward movement of ice (Stabeno and Bell, 2019). In winter 2018, winds from the south occurred in November 2017, and again in February 2018, whereas in winter 2019, more typical winds from the north (and typical ice conditions) occurred in December–January, followed by the return of winds from the south in February 2019 (Stabeno and Bell, 2019). The ice responded to these wind patterns with more ice present in early winter in Anadyr Bay in winter 2019 than in winter 2018, although ice was low elsewhere in the Bering Sea in both winters.

We hypothesize that in 2017, the pollock moved north from their spawning locations over the SE shelf to the NE and NW shelf, stayed farther north than normally over winter due to the low ice conditions, particularly the lack of ice in Anadyr Bay, and remained there in summer 2018 leading to large numbers north of St. Lawrence Island and on the NW shelf, and exceptionally small numbers of pollock in the SE in 2018 (Ianelli et al., 2019). In autumn-winter 2018/2019, adults preferentially moved south as ice concentrations in Anadyr Bay returned to normal in early winter. This may have led to fewer adults north of St. Lawrence Island and more adults in the SE Bering Sea in 2019 compared to 2018 and 2017 (Ianelli et al., 2019). Bottom temperature was shown to be the most significant predictor of pollock distributions for the 1982–2018 time series in the eastern Bering Sea; variables tested included temperature (bottom, surface, minimum, maximum, and range), depth, stratification, substrate, latitude, and longitude. (Baker, in press). Baker (in press) also found that pollock were associated with a bottom temperature range of 0–4 °C.

The high temperature band along the eastern Bering Sea inner shelf in very warm years, 2019 in particular, may limit adults from moving inshore. The increase in metabolic rates at higher temperatures requires pollock to consume more food to avoid starvation and maintain feeding

Table 2

Mean proportions of pollock abundance (% of total weight) for a) adult (>age-2) and b) age-1 pollock, and c) number of successful tows by bottom temperature (°C) and bottom depth (nearest 20 m) from US groundfish bottom trawl surveys (SE and NE), 1987–2019. NA indicates the number of tows = 0. Top 95% of non-zero values are in bold. Darker shading indicates higher values.

a)

Bottom	Mean Bottom Temperature																	
Depth	-2	-1	0	1	2	3	4	5	6	7	8	9	10	11	12	13	14	15
20	NA	0	0	0	0	0	0.001	0.001	0.001	0	0	0	0	0	0	0	0	0
40	0	0.001	0.003	**0.005**	**0.006**	**0.008**	**0.006**	0.003	0.001	0.001	0.001	0	0	0	0	NA	NA	NA
60	0	0.004	**0.009**	**0.015**	**0.022**	**0.038**	**0.028**	**0.019**	**0.005**	0	NA	NA	NA	NA	NA	NA	NA	NA
80	0.002	**0.008**	**0.015**	**0.029**	**0.029**	**0.032**	**0.043**	**0.046**	**0.014**	NA	NA	NA	NA	NA	NA	NA	NA	NA
100	0.002	**0.008**	**0.020**	**0.058**	**0.045**	**0.044**	**0.028**	**0.018**	0.001	0	NA	NA	NA	NA	NA	NA	NA	NA
120	0	0	**0.014**	**0.021**	**0.039**	**0.045**	**0.030**	**0.015**	0	NA	NA	NA	NA	NA	NA	NA	NA	NA
140	NA	NA	0.002	**0.014**	**0.029**	**0.034**	**0.014**	0.001	NA	0	NA	NA	NA	NA	NA	NA	NA	NA
160	NA	NA	0.001	**0.011**	**0.022**	**0.035**	**0.011**	0	0	NA	NA	NA	NA	NA	NA	NA	NA	NA
180	NA	NA	NA	NA	**0.017**	**0.023**	0	NA	NA	NA	NA	NA	NA	NA	NA	NA	NA	NA
200	NA	NA	NA	NA	NA	0.001	0.001	NA	NA	NA	NA	NA	NA	NA	NA	NA	NA	NA
Sum	0.004	0.021	0.064	0.153	0.209	0.260	0.162	0.103	0.022	0.001	0.001	0	0	0	0	0	0	0

b)

Bottom	Mean Bottom Temperature																	
Depth	-2	-1	0	1	2	3	4	5	6	7	8	9	10	11	12	13	14	15
20	NA	0	0	0	0.003	0.004	**0.006**	**0.005**	**0.010**	**0.005**	0.002	0.002	**0.006**	0.002	0.001	0	0	0
40	0	0.004	**0.008**	**0.008**	**0.010**	**0.017**	**0.012**	**0.007**	**0.006**	**0.010**	0.002	0.004	0.002	0.004	0.004	NA	NA	NA
60	0.002	**0.006**	**0.015**	**0.018**	**0.020**	**0.017**	**0.014**	**0.009**	**0.006**	0.001	NA	NA	NA	NA	NA	NA	NA	NA
80	**0.007**	**0.014**	**0.022**	**0.022**	**0.028**	**0.034**	**0.014**	**0.005**	0	NA	NA	NA	NA	NA	NA	NA	NA	NA
100	0.002	**0.021**	**0.041**	**0.050**	**0.092**	**0.054**	**0.014**	0.001	0	0	NA	NA	NA	NA	NA	NA	NA	NA
120	0	0.001	**0.015**	**0.047**	**0.058**	**0.042**	**0.010**	0.001	0	NA	NA	NA	NA	NA	NA	NA	NA	NA
140	NA	NA	**0.005**	**0.026**	**0.053**	**0.032**	0.004	0	NA	0	NA	NA	NA	NA	NA	NA	NA	NA
160	NA	NA	0.001	**0.009**	**0.011**	0.004	0.003	0	0	NA	NA	NA	NA	NA	NA	NA	NA	NA
180	NA	NA	NA	NA	0	0.004	0	NA	NA	NA	NA	NA	NA	NA	NA	NA	NA	NA
200	NA	NA	NA	NA	NA	0	0	NA	NA	NA	NA	NA	NA	NA	NA	NA	NA	NA
Sum	0.011	0.046	0.107	0.18	0.275	0.208	0.077	0.028	0.022	0.016	0.004	0.006	0.008	0.006	0.005	0	0	0

c)

Bottom	Mean Bottom Temperature																	
Depth	-2	-1	0	1	2	3	4	5	6	7	8	9	10	11	12	13	14	15
20	0	0	5	14	16	53	141	103	146	79	56	26	46	29	30	19	8	1
40	2	77	90	133	390	416	489	285	174	65	29	8	5	5	2	0	0	0
60	137	360	374	388	496	396	366	147	62	6	0	0	0	0	0	0	0	0
80	170	346	377	341	473	433	377	109	26	0	0	0	0	0	0	0	0	0
100	21	84	178	249	410	364	294	64	4	0	0	0	0	0	0	0	0	0
120	0	2	32	125	273	319	444	74	1	0	0	0	0	0	0	0	0	0
140	0	0	15	86	319	265	352	32	0	0	0	0	0	0	0	0	0	0
160	0	0	2	12	35	60	118	3	1	0	0	0	0	0	0	0	0	0
180	0	0	0	0	10	16	9	0	0	0	0	0	0	0	0	0	0	0
200	0	0	0	0	0	2	6	0	0	0	0	0	0	0	0	0	0	0

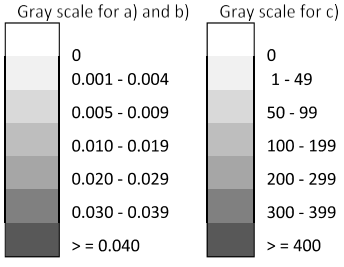

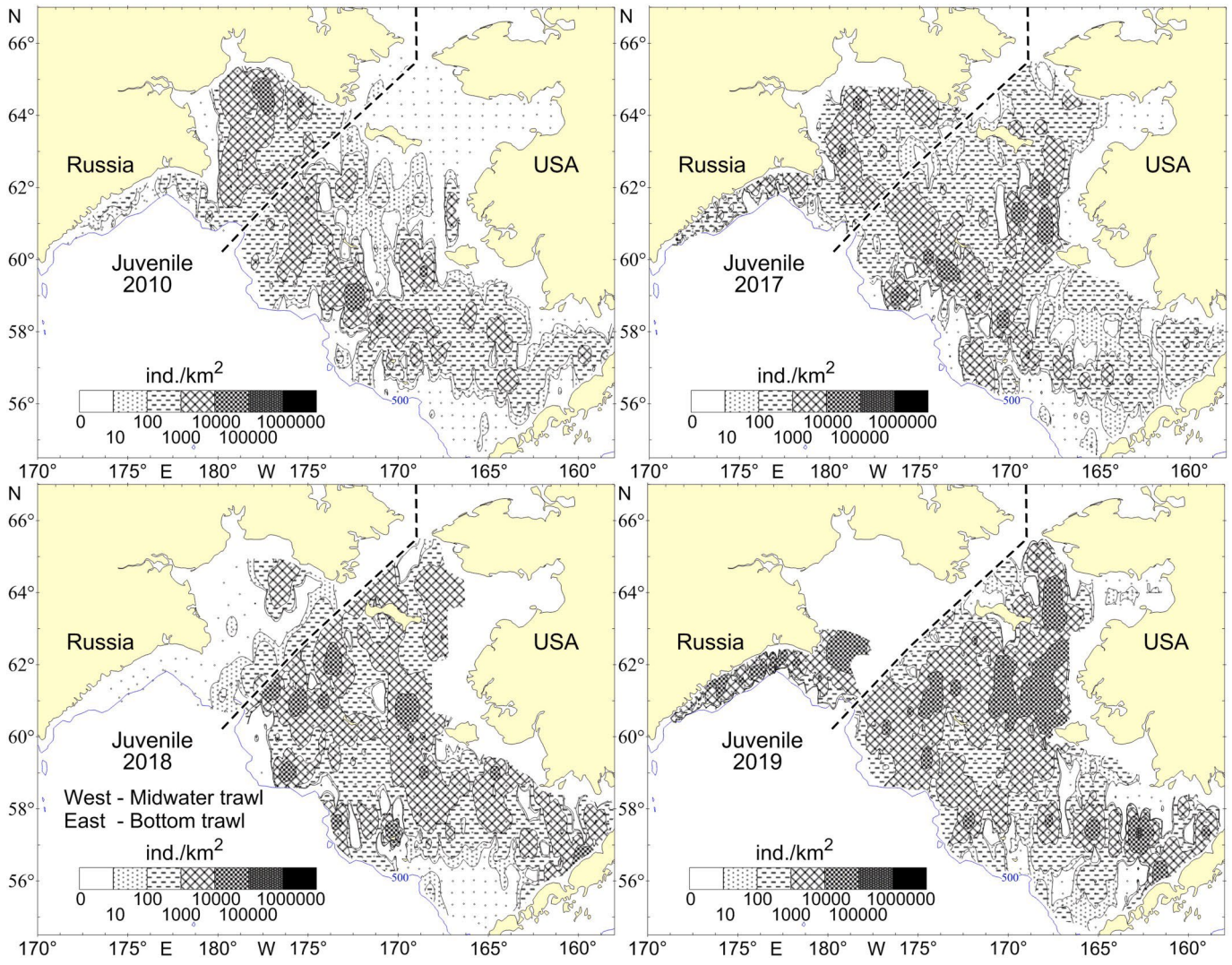

Fig. 9. Age-1 (juvenile) pollock abundance (number km^{-2}) for 2010, 2017, 2018, and 2019 from trawl surveys as described in Fig. 7.

and growth (Smith et al., 1988). The inner shelf varies from the middle and outer shelf ecosystems with differences in taxa and size of zooplankton and forage fish; for example, the inner shelf has smaller-sized and fewer lipid-rich zooplankton taxa (Eisner et al., 2014) and younger/smaller stages of forage fish such as Pacific herring (*Clupea pallasii*) (Andrews et al., 2016). Therefore, adult pollock may avoid or not survive on the inner shelf due to temperature limitation, low prey/food availability or a combination of these or other factors. The presence of age-1 pollock on the inner shelf may reflect the ability of juveniles to tolerate a larger temperature range than adults, as well as differences in preferred prey for adults and juveniles (Buckley et al., 2016). Pollock in the eastern Bering Sea have been shown to move from nearshore to offshore habitats as they progress from juvenile to adult stages (Baker, in press; Barbeaux and Hollowed, 2018; Hollowed et al., 2007).

We also hypothesize that heightened air and sea surface temperature in the northwestern Bering Sea in winter 2018 prevented the water column temperature from becoming cold enough to form a dense lens of water (cold pool) at the shelf bottom. In addition, the stratification was weak in the spring due to the lack of fresh water from ice melt, so the surface warmth could mix deeper, eroding whatever cold pool had formed over the winter(Stabeno and Bell, 2019). As a result, the Navarin Current, usually a strong northeastward flowing current in summer (Favorite et al., 1976; Luchin and Menovshchikov, 1999; Stabeno et al., 2016), was weaker compared to other warm years or sometimes absent. Instead, a northward stream developed that flowed along the eastern shelf and passed east of St. Lawrence Island (Fig. 5). This circulation change likely resulted in a change in pollock summer migration patterns by assisting them to move toward the Chukotka coast using both the Navarin Current and this along-shelf northward stream, as indicated by observations of dense aggregations of pollock in the southern and northern parts of Anadyr Bay (Fig. 8). Accordingly, dense feeding aggregations of pollock were observed at bottom depths throughout Anadyr Bay in 2017–2018 (bottom trawl survey data for 2017 and acoustic survey data for 2018), though their density in the midwater was still lower in the northern part.

4.2. Indications of movement of pollock among regions based on size structure

Size structure data can be used to estimate similarity (and potential mixing) of populations among the SE, NE and NW regions over our 4 study years. In general, the NE and NW have similar modes (first mode indicative of age-1 fish and last mode indicative of age-4+ fish) for all years. General size structure in the Russian sector (NW) is not similar to that in the US sector (SE and NE) in 2010, because of additional minor modes observed in the NW. This suggests that the pollock present in the northeastern part of the Russian EEZ in summer were a mixture of

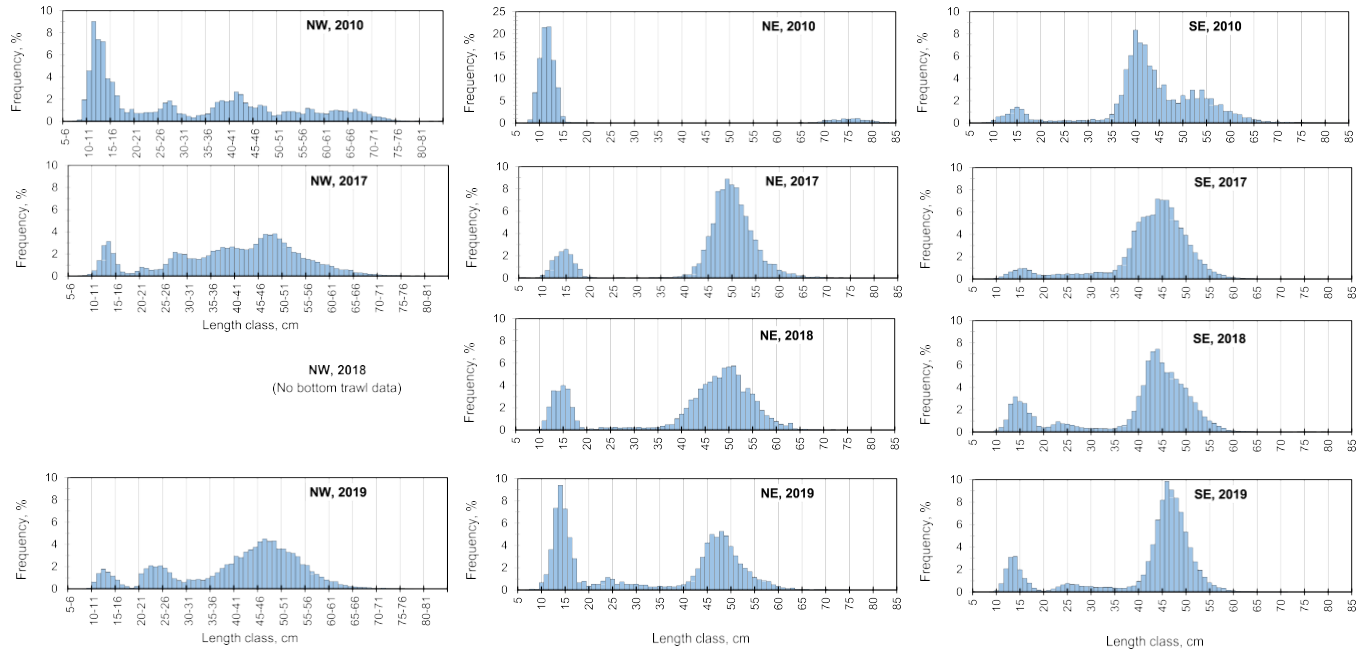

Fig. 10. Size structure of pollock in Russian region (NW) and in US regions (NE, SE). Regions are shown in Fig. 1. Note scale change for NE in 2010. Frequency are % of total individuals. Length data not shown for the NW in 2018 (midwater trawl data).

several stocks that originated from the eastern and western spawning grounds. Kotwicki et al. (2005) hypothesized that timing of feeding migrations is earlier in warm years compared to cold years, which can result in summer distributions that are farther north in warm years compared to cold years. If this is the case, in warm years in the NW and NE we may observe pollock stocks that are more mixed compared to the cold years. Additionally, larger fish can move faster (Kotwicki et al., 2005), leading to slightly larger fish in the north than south. An interesting feature of the pollock length data is a broader size distribution for modal groups for the NW shelf. The US bottom trawl surveys typically only capture age-1 and small numbers of very old and large fish in the 0 °C cold pool. Therefore, the size structure shown in the NE in 2010, where pollock in this region were almost entirely observed within the 0 °C cold pool, is not unusual. Without the cold pool present, pollock distribution demographics may be similar across the international border as suggested by the similar size structure in all regions in 2019. Some of the differences between the NE and NW in the presence or absence of the modes for 2 and 3 year old pollock likely arise from low selectivity of the US bottom trawl survey for these ages (Ianelli et al., 2014). The US bottom trawl survey does not consistently capture age-2 and age-3 pollock because these pollock are often located above the depth of the bottom trawl headrope as demonstrated by higher relative catches of age-2 and age-3 pollock on acoustic surveys (Honkalehto et al., 2013). Differences in the trawl gear (e.g., bottom trawls on Russian surveys have a 3.6 m vertical opening compared to 2.7 m for US surveys) or differences in the depth distribution of the age-2 and age-3 populations can confound interpretation of the size structure data between US and Russian surveys.

4.3. Spawning and feeding migrations

It is unknown whether population-level movement of Bering Sea pollock in response to changing temperatures and ice are temporary shifts that may be reversed if cold stanzas return to the Bering Sea shelf, or whether they are indicative of broader, enduring range alternations that include colonization of higher latitude areas. Pollock are known for their ability to change spawning locations depending on environmental conditions. For example, within the eastern Bering Sea, during warm springs, pollock spawning occurs more to the east (on the middle shelf) while during cold years it is to the west (outer shelf) (Smart et al., 2012). Also, connectivity between spawning and nursery areas is higher during warm years, maximizing dispersal potential (Petrik et al., 2016). Evidence of colonization would include indication of gonad development in adult fishes (spawning condition), and multi-year collections of eggs and early-stage larvae (yolk sac). At present there are comparatively few records of early-stage pollock larvae being collected in the northern Bering and Chukchi seas so it seems unlikely that northern colonization on a large scale has occurred. However, a historic paucity of field sampling during the spawning months (~March–June) in the northerly reaches of the shelf precludes a conclusive assessment. Of those larvae that have been collected, it seems most likely that they were transported from known (Unimak, Bogoslof, or Pribilof islands; Bacheler et al., 2010) or purported (Zhemchug or Navarin canyons) spawning areas rather than being locally produced. Theoretical biophysical transport modeling efforts have demonstrated that pollock larvae spawned from the northern-most known spawning areas in the eastern Bering Sea connect significantly with nursery habitats over the middle and outer shelves in the northern Bering Sea (Petrik et al., 2016), though connectivity from known spawning regions to the Chukchi Sea has not been shown. Connectivity of older early life stages (age-0 juveniles) to northerly regions is also theoretically possible; a combination of favorable currents and directional swimming could enable age-0 pollock to reach northerly regions of the Bering Sea in as little as 4–6 weeks (Duffy-Anderson et al., 2017). Pollock early life stages (<age-2) are unique from adult stages in that, because they have wide thermal tolerance ranges, they are capable of withstanding the frigid (−1.0 – 0 °C; Laurel et al., 2015; Laurel et al., 2018) cold pool temperatures that adults avoid, making young capable of moving northward even during years when a sizable cold pool is present. However, extensive population level migration such as that presented here requires a thermal corridor that permits the large-scale exchange of multiple age classes of pollock, suggesting it can only occur during periods that are warm, ice-free, and cold pool minimal over multiple years.

Movement of fish not only requires appropriate environmental conditions, but also the right biological conditions as well. Of course, spatial scale is a critical issue in these considerations, with biotic

controls exerting sizable influence over smaller scales and abiotic controls exerting influence over larger scales. One significant exception to this general observation is the large-scale seasonal migration (Kotwicki et al., 2005) that pollock undertake post-spawning (spring) to forage areas (summer) and then to overwintering grounds (fall/winter) which is likely motivated by both biotic (reproduction, feeding) and abiotic (temperature) controls. Nevertheless, all life history stages of pollock are able to modify their behavior to exploit food resources that maximize energy intake and growth, and minimize predation risk. While not examined in the present study, the ability of prey (zooplankton) and predators (arrowtooth flounder (*Atheresthes stomias*), seabirds such as murres, and northern fur seals (*Callorhinus ursinus*) to also modify their behavior in response to changing oceanographic conditions is a reasonable assumption. Pollock are zooplanktivores and preferentially prey on euphausiids and large, lipid-rich zooplankton species. Juvenile pollock have been previously demonstrated to shift their vertical distribution (Olla and Davis, 1990; Schabetsberger et al., 2003) in response to shifting prey availabilities, and adults shift horizontal distributions in response to zooplankton occurrence (Barbeaux and Hollowed, 2018). Spatial shifts in pollock as related to predator avoidance have also been documented (Bailey, 1989; Ciannelli et al., 2002), as are shifts in response to presence of competitors (Sturdevant et al., 2001).

4.4. Value of evaluating data across E and W Bering Sea

The inclusion of data from both the eastern and western Bering Sea shelf, across the US–Russia transboundary line is imperative for understanding the movement of pollock and the underlying climatic, environmental and biological drivers for these distribution changes. This is especially relevant in recent warm years (with likely greater movements across international borders, as suggested by the similarity in size structures in 2019). The dramatic northward movement in 2017–2019 and range shifts in pollock also complicate evaluations of stock abundance and provide challenges for management of this large commercial fishery (Baker, in press). It is vitally important for researchers across the Bering Sea shelf to work together to address these recent and future variations in pollock distributions. Moreover, cross border issues are not limited to pollock, but also to other species such as Pacific cod, and flatfish (e.g. Alaska plaice (*Pleuronectes quadrituberculatus*); O'Leary et al., in review). Due to the differences in the survey and density estimation methodology between US and Russian surveys our comparisons of densities on both sides of the border are more qualitative than quantitative. However in the future it is important to improve on these estimates by improving cooperation between Russia and the US to focus not only on data sharing but also on comparisons of catchability and selectivity of survey gears used on both sides of the border. The precision and accuracy of across border fish movement estimates will depend on the ability to estimate accurate selectivity ratios between survey gears (Kotwicki et al., 2017). However, selectivity ratios can only be estimated from experimental paired sampling or by using nearest neighbor techniques (e.g. O'Leary et al., in review). Both of these methods require closer cooperation between US and Russian survey scientists. Good examples of such cooperation existed in the 1980s and 1990s, when it was common for Russian surveys to sample in the eastern Bering Sea; however this sampling has not occurred in the last two decades. Other examples of dedicated international survey efforts include the Russian-American Long-term Census of the Arctic (RUSALCA; Crane and Ostrovskiy, 2015) in the Chukchi Sea and the current Year of the Salmon surveys in the Gulf of Alaska. Continuation of long term monitoring efforts and increased cooperation between monitoring programs for groundfish and habitat variables (e.g., water temperature) by US NOAA and Russian TINRO scientists, will allow researchers to better monitor and understand impacts of climate change on the Bering Sea fisheries and ecosystems.

Coordinated efforts through international organizations (e.g., the North Pacific Marine Science Organization (PICES), the Pacific Arctic Group (PAG), and the North Pacific Anadromous Fisheries Commission (NPAFC)) are also crucial for ongoing communication, data synthesis and the sharing of research ideas and hypotheses. PICES efforts include the North Pacific Ecosystem Status Report, plenary presentations in Vladivostok, Russia in 2017 by Zuenko et al. and Kivva et al. and two workshops on international interdisciplinary efforts to understand the role of the North Bering Sea in modulating arctic environments (Eisner et al., 2017; Baker et al., 2018). Communication has been greatly strengthened by publication of collaborative research, such as Panteleev et al. (2011) on topography, Baker et al. (2020) and Danielson et al. (2020) on oceanography, Beamish et al. (1999) on pelagic fishes, Aydin et al. (2002) on food webs, and O'Leary et al. (in review) on groundfish spatiotemporal variations, in addition to the current manuscript.

4.5. Future considerations

Data presented here on warm-year shifts in pollock distribution between the southern and northern Bering Sea present several important points for consideration. First, are the observed changes presented here harbingers of the future? Ocean heating has already altered the southern Bering Sea shelf such that ice-free winters are now common (2001–2019) and associated warm-year cascading fisheries population and demographic shifts are expected; will the same be true of the northern Bering Sea? Our data show that Russian–US stock mixing over multiple years may be occurring, which can affect the demographic make-up of both populations. Moreover, thermally-mediated differences in age-specific survivorship also could be occurring, given age-selective processes previously described for pollock in the southern Bering Sea during warm stanzas (Heintz et al., 2013).

Stock shifts and stock mixing could pose other problems, as well. Homogenization and loss of diversity (portfolio effects) is known to decrease the ability of a population to adapt to changing conditions, heightening the risk of volatility and exacerbating the potential for failure. Likewise, local population extinctions in areas depleted by northward moving stocks are another topic of concern. Ecologically, local depletions increase the risk of imbalance in food web dynamics, with changes in energy transfer, and potential loss of other co-dependent species. Economically, local depletions of commercial stocks like pollock will require fishers to travel farther to harvest fish, with cascading consequences on cost, time, and resources (Haynie and Huntington, 2016).

Spatial analysis of pollock distributions over the 1982–2018 time series indicated that the highest variance in abundance was outside core habitat areas, suggesting that pollock are able to expand their ranges and utilize areas of more marginal habitat (Baker, in press). In 2018, 2019 adult and juvenile pollock have been observed in high densities in the southern Chukchi Sea on fisheries oceanography surveys, both in the US and Russian sectors (E. Farley, A. Savin, pers. comm.; Orlov et al., 2020). This suggests that pollock have the potential to move northward from the north Bering Sea into the Chukchi Sea as the climate warms and ice diminishes. Whether it will be possible for pollock to colonize these Arctic regions remains an open question that depends, in part, on the magnitude of the climate change in the future, but also on the pollock temperature tolerance, prey resources, reproductive requirements, and predation pressure. Enhanced collaboration among US and Russian researchers is essential for successful evaluation of distribution changes and management of key Bering Sea fisheries in the face of a rapidly changing climate.

CRediT authorship contribution statement

Lisa B. Eisner: Conceptualization, Methodology, Investigation, Writing - original draft, Writing - review & editing, Project administration. **Yury I. Zuenko:** Conceptualization, Methodology, Investigation, Data curation, Visualization, Writing - original draft, Writing - review & editing. **Eugene O. Basyuk:** Conceptualization, Methodology,

Investigation, Data curation, Visualization, Writing - original draft, Writing - review & editing. **Lyle L. Britt:** Conceptualization, Methodology, Investigation, Data curation, Visualization, Writing - original draft, Writing - review & editing. **Janet T. Duffy-Anderson:** Conceptualization, Methodology, Investigation, Writing - original draft, Writing - review & editing. **Stan Kotwicki:** Conceptualization, Methodology, Investigation, Writing - original draft, Writing - review & editing. **Carol Ladd:** Conceptualization, Methodology, Investigation, Visualization, Writing - original draft, Writing - review & editing. **Wei Cheng:** Methodology, Visualization, Writing - review & editing.

Declaration of competing interest

The authors declare that they have no known competing financial interests or personal relationships that could have appeared to influence the work reported in this paper.

Acknowledgements

We thank the captains, crew, and scientific staff who participated on the many Bering Sea fisheries surveys conducted by NOAA AFSC (US) and TINRO (Russia). Funding for surveys and data analysis was provided by NOAA Fisheries, NOAA PMEL, and TINRO. This is PMEL contribution #5082. This is EcoFOCI contribution number EcoFOCI-N957. We greatly appreciate the suggestions from two anonymous reviewers, and we thank Libby Logerwell and Ed Farley for reviews on earlier drafts of the manuscript. We are grateful to PICES for encouraging the international collaborations that led to the production of this manuscript.

Appendix A

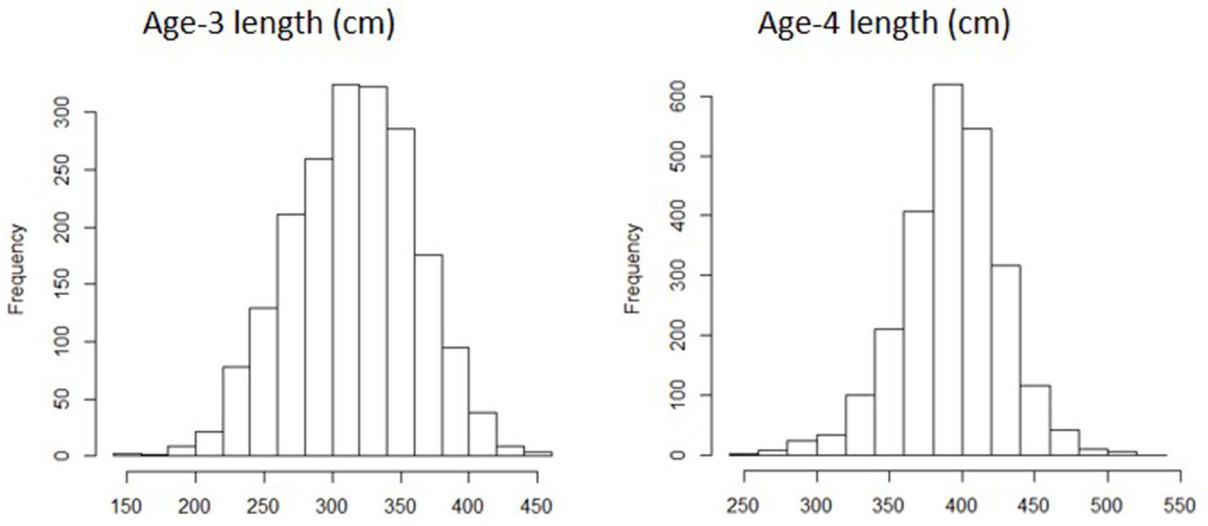

Fig. A.1. Histograms of pollock lengths at age-3 and age-4 from US surveys. Frequency indicates number of individuals.

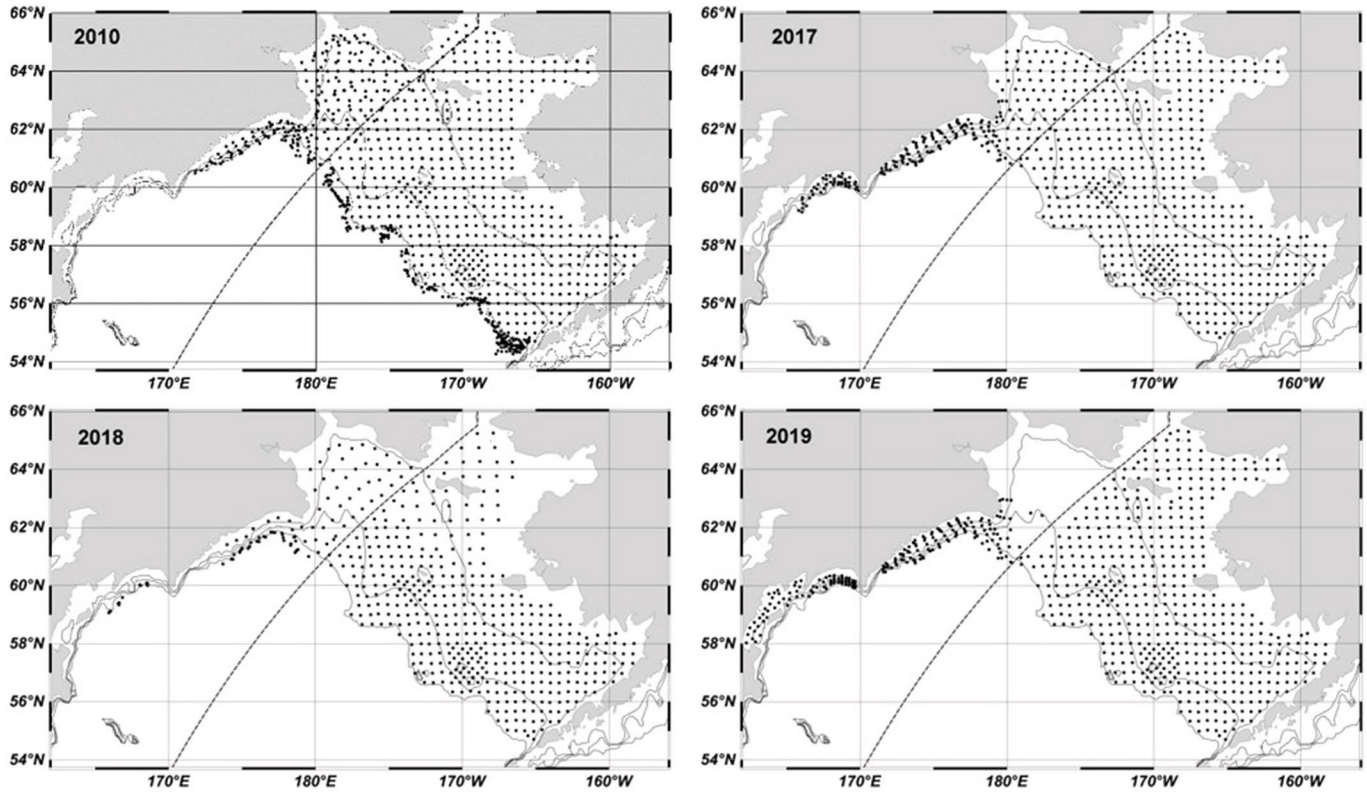

Fig. A.2. Oceanography stations for the US and Russian surveys in 2010, 2017, 2018, and 2019. The isobaths 50, 100, and 250 m are shown by thin lines, and the Russian EEZ border by a dotted line.

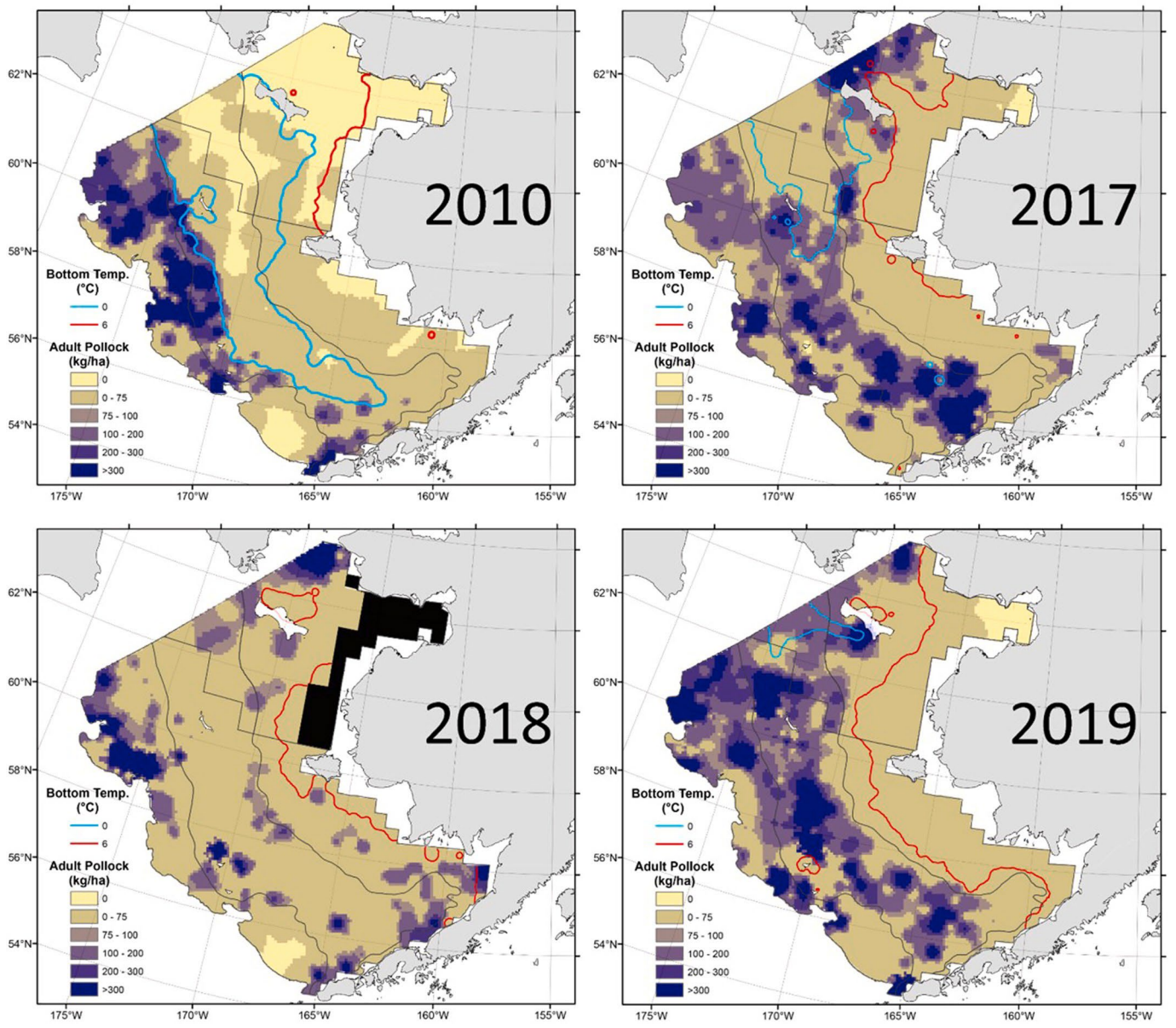

Fig. A.3. Adult pollock biomass (kg/ha) for 2010, 2017, 2018, and 2019 from US NOAA eastern Bering Sea bottom trawl surveys. Bottom temperature <0 °C shown by blue contour and ≥6 °C by red contour.

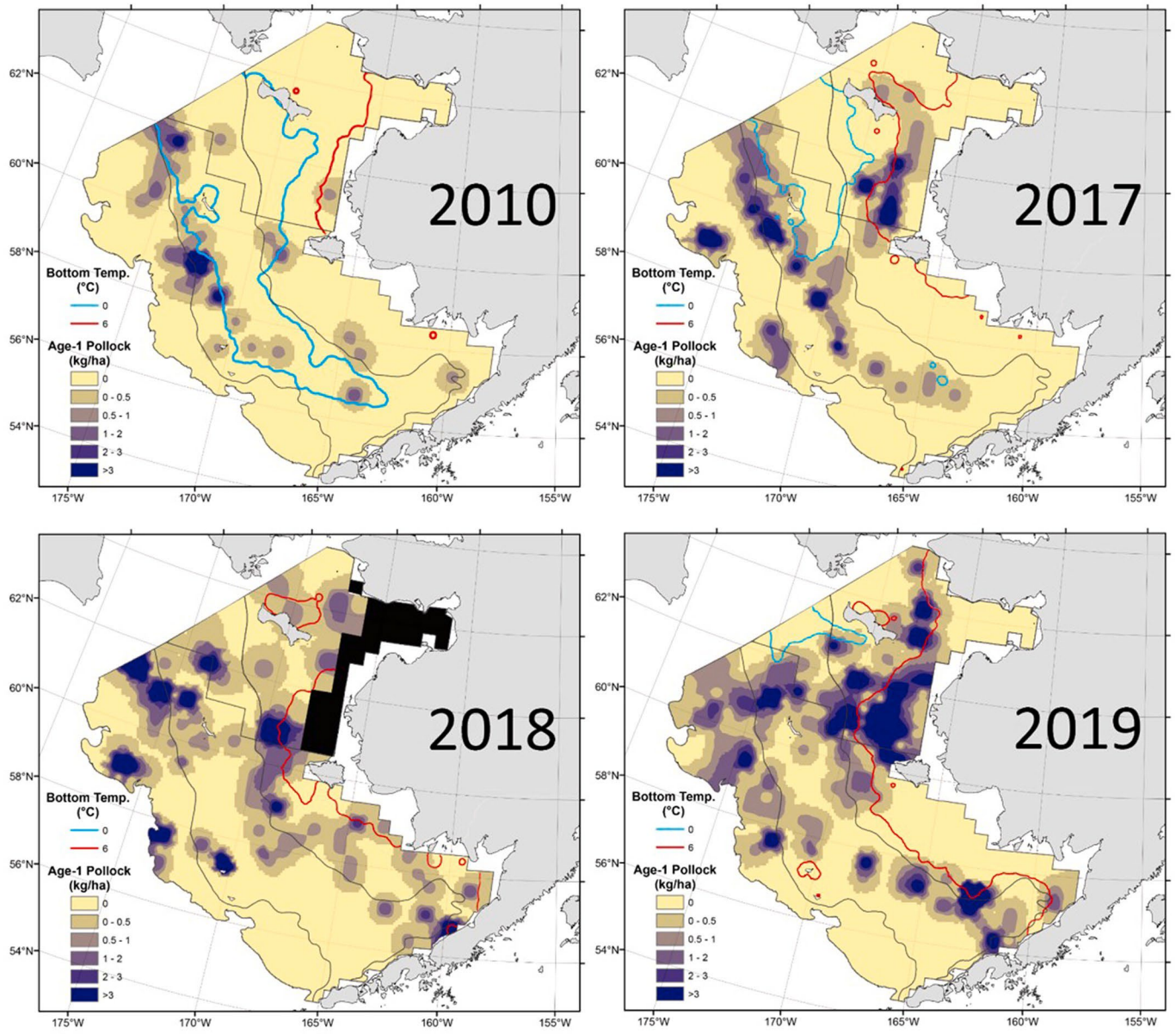

Fig. A.4. Age-1 pollock biomass (kg/ha) for 2010, 2017, 2018, and 2019 from US NOAA eastern Bering Sea bottom trawl surveys. Bottom temperature <0 °C shown by blue contour and ≥6°C by red contour.

References

Andrews, A.G., Strasburger, W.W., Farley, E.V., Murphy, J.M., Coyle, K.O., 2016. Effects of warm and cold climate conditions on capelin (*Mallotus villosus*) and Pacific herring (*Clupea pallasii*) in the eastern Bering Sea. Deep-Sea Res. II. 134, 235–246.

Aydin, K.Y., Lapko, V.V., Radchenko, V.I., Livingston, P.A., 2002. A comparison of the eastern Bering and western Bering Sea shelf and slope ecosystems through the use of mass-balance food web models. NOAA Technical Memorandum NMFS-AFSC 130.

Bacheler, N.M., Ciannelli, L., Bailey, K.M., Duffy-Anderson, J.T., 2010. Spatial and temporal patterns of walleye pollock (*Theragra chalcogramma*) spawning in the eastern Bering Sea inferred from egg and larval distributions. Fish. Oceanogr. 19, 107–120.

Bailey, K.M., 1989. Interaction between the vertical distribution of juvenile walleye pollock *Theragra chalcogramma* in the eastern Bering Sea and cannibalism. Mar. Ecol. Prog. Ser. 53, 205–213.

Baker, M.R. (in press). Contrast of warm and cold phases in the Bering Sea to understand spatial distributions of Arctic and sub-Arctic gadids. Polar Biol.

Baker, M.R., Hollowed, A.B., 2014. Delineating ecological regions in marine systems: integrating physical structure and community composition to inform spatial management in the eastern Bering Sea. Deep-Sea Res. II 109, 215–240. https://doi.org/10.1016/j.dsr2.2014.03.001.

Baker, M., Kivva, K., Eisner, L., 2018. The role of the northern Bering Sea in modulating the Arctic II: international interdisciplinary collaboration. PICES Press 26 (1), 15–19.

Baker, M.R., Kivva, K.K., Pisareva, M.N., Watson, J.T., Selivanova, J., 2020. Shifts in the physical environment in the Pacific Arctic and implications for ecological timing and conditions. Deep -Sea Res II 177. https://doi.org/10.1016/j.dsr2.2020.104802.

Barbeaux, S.J., Hollowed, A.B., 2018. Ontogeny matters: climate variability and effects on fish distribution in the eastern Bering Sea. Fish. Oceanogr. 27, 1–15. https://doi.org/10.1111/fog.12229.

Basyuk, E.O., Zuenko, Y.I., 2019. Bering Sea: 2018 as the extreme low-ice and warm year. Izvestia TINRO (Newsletters of Pacific Fish. Res. Center) 198, 119–142.

Beamish, R.J., Leask, K.D., Ivanov, O.A., Balanov, A.A., Orlov, A.M., Sinclair, B., 1999. The ecology, distribution, and abundance of midwater fishes of the Subarctic Pacific gyres. Prog. Oceanogr. 43 (2–4), 399–442.

Buckley, T.W., Ortiz, I., Kotwicki, S., Aydin, K., 2016. Summer diet composition of walleye pollock and predator–prey relationships with copepods and euphausiids in the eastern Bering Sea, 1987–2011. Deep-Sea Res. II. 134, 302–311.

Budgell, W.P., 2005. Numerical simulation of ice-ocean variability in the Barents Sea region. Ocean Dynam. 55, 370–387.

Ciannelli, L., Brodeur, R.D., Swartzman, G.L., Salo, S., 2002. Physical and biological factors influencing the spatial distribution of age-0 walleye pollock (*Theragra chalcogramma*) around the Pribilof Islands, Bering Sea. Deep-Sea Res. II. 49, 6109–6126.

Coachman, L.K., 1986. Circulation, water masses, and fluxes on the southeastern Bering Sea shelf. Continent. Shelf Res. 5 (1–2), 23–108. https://doi.org/10.1016/0278-4343(86)90011-7.

Crane, K., Ostrovskiy, A., 2015. Russian-American long-term Census of the arctic: RUSALCA. Oceanography 1 (3), 18–23, 28.

Danielson, S.L., Ahkinga, O., Ashjian, C., Basyuk, E., Cooper, L.W., Eisner, L., Farley, E., Iken, K.B., Grebmeier, J.M., Juranek, L., Khen, G., Jayne, S., Kikuchi, T., Ladd, C., Lu, K., McCabe Moore, G.W.K., Nishino, S., Ozenna, F., Pickart, R.S., Polyakov, I., Stabeno, P.J., Thoman, R., Williams, W.J., Wood, K., Weingartner, T.J., 2020. Manifestation and consequences of warming and altered heat fluxes over the Bering and Chukchi Sea continental shelves. Deep-Sea Res. II 177. https://doi.org/10.1016/j.dsr2.2020.104781.

Duffy-Anderson, J.T., Ciannelli, L., Honkalehto, T., Bailey, K.M., Sogard, S.M., Springer, A., Buckley, T., 2003. Distribution of age-1 and age-2 walleye pollock in the Gulf of Alaska and Eastern Bering Sea: sources of variation and implications for higher trophic levels. In: Browman, H., Skiftesvik, A. (Eds.), The Big Fish Bang: Proceedings from the 26th Annual Larval Fish Conference, pp. 381–394.

Duffy-Anderson, J.T., Stabeno, P., Andrews, A., Cieciel, K., Deary, A., Farley, E., Fugate, C., Harpold, C., Heintz, R., Kimmel, D., Kuletz, K., Lamb, J., Paquin, M., Porter, S., Rogers, L., Spear, A., Yasumiishi, E., 2019. Responses of the Northern Bering Sea and Southeastern Bering Sea pelagic ecosystems following record-breaking low winter sea ice. Geophys. Res. Lett. https://doi.org/10.1029/2019GL083396.

Duffy-Anderson, J.T., Stabeno, P.J., Siddon, E.C., Andrews, A.G., Cooper, D.W., Eisner, L. B., Farley, E.V., Harpold, C.E., Heintz, R.A., Kimmel, D.G., Sewall, F.F., Spear, A.H., Yasumiishi, E., 2017. Return of warm conditions in the southeastern Bering Sea: phytoplankton-fish. PloS One 46 (16), 9833–9842. https://doi.org/10.1371/journal.pone.0178955.

Eisner, L., Kivva, K., Baker, M., 2017. The role of the northern Bering Sea in modulating Arctic environments: towards international interdisciplinary efforts. PICES Press 25 (1), 24–29.

Eisner, L., Napp, J., Mier, K., Pinchuk, A., Andrews, A., 2014. Climate-mediated changes in zooplankton community structure for the eastern Bering Sea. Deep Sea Res II 109, 157–171. https://doi.org/10.1016/j.dsr2.2014.03.004.

Favorite, F., Dodimead, A.J., Nasu, K., 1976. Oceanography of the subarctic pacific region, 1960-71. International North Pacific Fisheries Commission Bull 33, 187.

Fissel, B., Dalton, M., Garber-Yonts, B., Haynie, A., Kasperski, S., Lee, J., Lew, D., Lavoie, A., Seung, C., Sparks, K., Szymkowiak, M., Wise, S., 2019. Stock Assessment and Fishery Evaluation Report for the Groundfish Fisheries of the Gulf of Alaska and Bering Sea/Aleutian Island Area: Economic Status of the Groundfish Fisheries off Alaska, 2017. NPFMC. April, 2019. http://www.afsc.noaa.gov/refm/docs/2018/economic.pdf.

Haidvogel, D.B., Arango, H., Budgell, W.P., Cornuelle, B.D., Curchitser, E., Di Lorenzo, E., Fennel, K., Geyer, W.R., Hermann, A.J., Lanerolle, L., Levin, J., McWilliams, J.C., Miller, A.J., Moore, A.M., Powell, T.M., Shchep- etkin, A.F., Sherwood, C.R., Signell, R.P., Warner, J.C., Wilkin, J., 2008. Ocean forecasting in terrain-following coor- dinates: formulation and skill assessment of the Regional Ocean Modeling System. J. Comput. Phys. 227, 3595–3624. https://doi.org/10.1016/j.jcp.2007.06.016.

Haynie, A.C., Huntington, H.P., 2016. Strong connections, loose coupling: the influence of the Bering Sea ecosystem on commercial fisheries and subsistence harvests in Alaska. Ecol. Soc. 21 (4), 6. https://doi.org/10.5751/ES-08729-210406.

Heintz, R.A., Siddon, E.C., Farley Jr., E.V., Napp, J.M., 2013. Climate-related changes in the nutritional condition of young-of-the-year walleye pollock (*Theragra chalcogramma*) from the eastern Bering Sea. Deep-Sea Res. II. 94, 150–156.

Hollowed, A.B., Wilson, C.D., Stabeno, P.J., Salo, S.A., 2007. Effect of ocean conditions on the cross-shelf distribution of walleye pollock (*Theragra chalcogramma*) and capelin (*Mallotus villosus*). Fish. Oceanogr. 16, 142–154. https://doi.org/10.1111/j.1365-2419.

Honkalehto, T., McCarthy, A., Ressler, P., Jones, D., 2013. Results of the acoustic-trawl survey of walleye pollock (*Theragra chalcogramma*) on the U.S. And Russian Bering Sea shelf in june–august 2012 (DY1207). AFSC processed rep. 2013-02. In: Alaska Fish. Sci. Cent., NOAA, Natl. Mar. Fish.Serv., 7600 Sand Point Way NE. Seattle WA 98115, USA.

Huntington, H.P., Danielson, S.L., Wiese, F.K., Baker, M., Boveng, P., Citta, J.J., De Robertis, A., Dickson, D.M.S., Farley, E., George, J.C., Iken, K., Kimmel, D.G., Kuletz, K., Levine, R., Quakenbush, L., Stabeno, P., Stafford, K.M., Stockwell, D., Wilson, C., 2020. Evidence suggests potential transformation of the Pacific Arctic ecosystem is underway. Nature Climate Change. https://doi.org/10.1038/s41558-020-0695-2.

Ianelli, J., Fissel, B., Holsman, K., Honktalehto, T., Kotwicki, S., Monnahan, C., Siddon, E., Stienessen, S., Thorson, J., 2019. Chapter 1: assessment of the walleye pollock stock in the eastern Bering Sea. In: Stock Assessment and Fishery Evaluation Report for the Groundfish Resources of the Bering Sea/Aleutian Islands Regions, Alaska Fisheries Science Center. National Marine Fisheries Service, Anchorage, Alaska, pp. 1–169.

Ianelli, J.N., Honkalehto, T., Barbeaux, S., Kotwicki, S., 2014. Chapter 1: assessment of the walleye pollock stock in the eastern Bering Sea. In: Stock Assessment and Fishery Evaluation Report for the Groundfish Resources of the Bering Sea/Aleutian Islands Regions, Alaska Fisheries Science Center. National Marine Fisheries Service, Anchorage, Alaska, pp. 55–156.

Kearney, K., Hermann, A., Cheng, W., Ortiz, I., Aydin, K., 2020. A coupled pelagic–benthic–sympagic biogeochemical model for the Bering Sea: documentation and validation of the BESTNPZ model (v2019.08.23) within a high-resolution regional ocean model. Geosci. Model Dev. (GMD) 13, 597–650.

Khen, G.V., Basyuk, E.O., Vanin, N.S., Matveev, V.I., 2013. Hydrography and biological resources in the western Bering Sea. Deep-Sea Res. II. 94, 106–120.

Kimura, D.K., Kastelle, C.R., Goetz, B.J., Gburski, C.M., Buslov, A.V., 2006. Corroborating ages of walleye pollock (*Theragra chalcogramma*). Aust. J. Mar. Freshw. Res. 57, 323–332.

Kinder, T.H., Schumacher, J.D., 1981. Circulation over the continental shelf of the southeastern Bering Sea. In: Hood, D.W., Calder, J.A. (Eds.), The Eastern Bering Sea Shelf: Oceanography and Resources. University of Washington Press, Seattle, WA, pp. 53–75.

Kotwicki, S., Lauth, R.R., 2013. Detecting temporal trends and environmentally-driven changes in the spatial distribution of groundfishes and crabs on the eastern Bering Sea shelf. Deep-Sea Res. II. 94, 231–243.

Kotwicki, S., Buckley, T., Honkaletho, T., Walters, G., 2005. Variation in the distribution of walleye pollock with temperature and implications for seasonal migration. Fish. Bull. 103, 574–587.

Kotwicki, S., Ianelli, J.N., Punt, A.E., 2014. Correcting density-dependent effects in abundance estimates from bottom trawl surveys. ICES J. Mar. Sci. 71, 1107–1116.

Kotwicki, S., Lauth, R.R., Williams, K., Goodman, S., 2017. Selectivity ratio a useful tool for comparing size selectivity of multiple survey gears. Fish. Res. 191, 76–86.

Kotwicki, S., Ono, K., 2019. The effect of random and density dependent variation in sampling efficiency on variance of abundance estimates from fishery surveys. Fish Fish. 20 (4), 760–774. https://doi.org/10.1111/faf.12375.

Ladd, C., 2014. Seasonal and interannual variability of the bering slope current. Deep-Sea Res. II. 109, 5–13.

Laurel, B., Copeman, L., Spencer, M., Iseri, P., 2018. Comparative effects of temperature on rates of development and survival of eggs and yolk-sac larvae of Arctic cod (*Boreogadus saida*) and walleye pollock (*Gadus chalcogrammus*). ICES J. Mar. Sci. 75 (7), 2403–2412.

Laurel, B., Spencer, M., Iseri, P., Copeman, L., 2015. Temperature-dependent growth and behavior of juvenile Arctic cod (*Boreogadus saida*) and co-occurring North Pacific gadids. Polar Biol. 39 (6), 1127–1135.

Lauth, R.R., 2011. Results of the 2010 Eastern and Northern Bering Sea Continental Shelf Bottom Trawl Survey of Groundfish and Invertebrate Fauna. United States Department of Commerce, NOAA Technical Memorandum, p. 256. NMFS-AFSC-227.

Lauth, R.R., Dawson, E.J., Conner, J., 2019. Results of the 2017 Eastern and Northern Bering Sea Continental Shelf Bottom Trawl Survey of Groundfish and Invertebrate Fauna. U.S. Dep. Commer. NOAA Tech. Memo, p. 260. NMFS-AFSC-396.

Locarnini, R.A., Mishonov, A.V., Antonov, J.I., Boyer, T.P., Garcia, H.E., Baranova, O.K., Zweng, M.M., Paver, C.R., Reagan, J.R., Johnson, D.R., Hamilton, M., Seidov, D., 2013. World Ocean Atlas 2013, vol. 1: temperature. In: Levitus, S. (Ed.), NOAA Atlas NESDIS, vol. 73, p. 40.

Luchin, V.A., Menovshchikov, V.A., 1999. Chapter 7: non-periodic currents. In: Hydrometeorology and Hydrochemistry of the seas/Volume10: Bering Sea, Part 1. Gidrometeoizdat, Sankt-Peterburg, pp. 193–219.

McLean, M., Mouillot, D., Auber, A., 2018. Ecological and life history traits explain a climate-induced shift in a temperate marine fish community. Mar. Ecol. Prog. Ser. 606, 175–186.

Meier, W.N., Fetterer, F., Savoie, M., Mallory, S., Duerr, R., Stroeve, J., 2017. NOAA/NSIDC climate data record of passive Microwave Sea ice concentration, version 3, boulder, Colorado USA, national snow and ice data center. https://doi.org/10.7265/N59P2ZTG.

Mueter, F.J., Litzow, M.A., 2008. Sea ice alters the biogeography of the Bering Sea continental shelf. Ecol. Appl. 18 (2), 309–320.

Olla, B.L., Davis, M.W., 1990. Behavioral responses of juvenile walleye pollock (*Theragra chalcogramma* Palls) to light, thermoclines, and food: possible role in vertical distribution. J. Exp. Mar. Biol. Ecol. 135, 59–68.

O'Leary, C.A., Kotwicki, S., Hoff, G.R., Thorson, J.T., Kulik, V.V., Ianelli, J.N., Lauth, R. R., Nichol, D.G., Conner, J., Punt, A.E. submitted for publication. Estimating Spatiotemporal Availability of Bering Sea Groundfish Species to Fishery-independent Surveys Using Area-Swept Biomass Indices from Multiple Surveys.

Orlov, A.M., Benzik, A.N., Vedishcheva, E.V., Gafitsk, S.V., Gorbatenko, K.M., Goryanina, S.V., Zubarevich, V.L., Kodryan, K.V., Nosov, M.A., Orlova, S.Yu, Pedchenko, A.P., Rybakov, M.O., Sokolov, A.M., Somov, A.A., Subbotin, S.N., Taptygin, M.Yu, Firsov, YuL., Khleborodov, A.S., Chikilev, V.G., 2020. Fisheries research in the Chukchi sea at the *RV professor levanidov* in August 2019: some preliminary results. Trudy VNIRO 178, 206–220. https://doi.org/10.36038/2307-3497-2019-178-206-220.

Overland, J.E., Stabeno, P., Ladd, C., Wang, M., Bond, N., 2019. Eastern Bering Sea climate - FOCI. In: Siddon, E., Zador, S. (Eds.), Ecosystem Status Report 2019: Eastern Bering Sea. NOAA Fisheries.

Panteleev, G., Yaremchuk, M., Stabeno, P.J., Luchin, V., Nechaev, D.A., Kikuchi, T., 2011. Dynamic topography of the Bering Sea. J. Geophys. Res. - Oceans 116.

Peng, G., Meier, W.N., Scott, D., Savoie, M., 2013. A long-term and reproducible passive microwave sea ice concentration data record for climate studies and monitoring. Earth Syst. Sci. Data 5, 311–318. https://doi.org/10.5194/essd-5-311-2013.

Petrik, C.M., Duffy-Anderson, J.T., Castruccio, F., Curchitser, E.N., Danielson, S.L., Hedstrom, K., Mueter, F., 2016. Modelled connectivity between walleye pollock (*Gadus chalcogrammus*) spawning and age-0 nursery areas in warm and cold years with implications for juvenile survival. ICES J. Mar. Sci. 73 (7), 1890–1900.

Saha, S., Moorthi, S., Pan, H.L., Wu, X., Wang, J., Nadiga, S., Tripp, P., Kistler, R., Woollen, J., Behringer, D., Liu, H., Stokes, D., Grumbine, R., Gayno, G., Wang, J., Hou, Y.T., Chuang, H.Y., Juang, H.M.H., Sela, J., Iredell, M., Treadon, R., Kleist, D., Van Delst, P., Keyser, D., Derber, J., Ek, M., Meng, J., Wei, H., Yang, R., Lord, S., Van Den Dool, H., Kumar, A., Wang, W., Long, C., Chelliah, M., Xue, Y., Huang, B., Schemm, J.K., Ebisuzaki, W., Lin, R., Xie, P., Chen, M., Zhou, S., Higgins, W., Zou, C. Z., Liu, Q., Chen, Y., Han, Y., Cucurull, L., Reynolds, R.W., Rutledge, G.,

Goldberg, M., 2010. The NCEP climate forecast system reanalysis. Bull. Am. Meteorol. Soc. 91, 1015–1057. https://doi.org/10.1175/2010BAMS3001.1.
Savin, A.B., 2011. Methodical recommendations on planning and conducting bottom trawl surveys in the Far Eastern basin. Issled. Vodn. Biol. Resur. Kamchatki i Sev.-Zap. Chasti Tikhogo Okeana (Studies of water biological resources in Kamchatka and North-West Pacific) 22, 68–78.
Savin, A.B., 2018. Fish resources in near-bottom biotopes of the shelf and the upper edge of the continental slope in the northwestern Bering Sea. Russ. J. Mar. Biol. 44 (7), 1–18. ISSN 1063-0740. Original Russian Text © A.B. Savin, 2018, published in Izvestia TINRO.
Schabetsberger, R., Sztatecsny, M., Drozdowski, G., Brodeur, R.D., Swartzman, G.L., Wilson, M.T., Winter, A.G., Napp, J.M., 2003. Size-dependent, spatial, and temporal variability of juvenile walleye pollock (*Theragra chalcogramma*) feeding at a structural front in the southeast Bering Sea. Mar. Ecol. 24, 141–164.
Smart, T., Duffy-Anderson, J.T., Horne, J., 2012. Alternating climate states influence walleye pollock life stages in the southeastern Bering Sea. Mar. Ecol. Prog. Ser. 455, 257–267.
Smith, R.L., Paul, A.J., Paul, J.M., 1988. Aspects of energetics of adult walleye pollock, *Theragra chalcogramma* (Pallas), from Alaska. J. Fish. Biol. 33, 445–454.
Spies, I., Gruenthal, K.M., Drinan, D.P., Hollowed, A., Stevenson, D.E., Tarpey, C.M., Hauser, L., 2019. Genetic evidence of a northward range expansion in the eastern Bering Sea stock of Pacific cod. Evolutionary Applications 13 (2), 362–375. https://doi.org/10.1111/eva.12874.
Stabeno, P.J., Bell, S.W., 2019. Extreme conditions in the Bering Sea (2017–2018): record-breaking low sea-ice extent. Geophys. Res. Lett. 46, 8952–8959. https://doi.org/10.1029/2019GL083816.
Stabeno, P.J., Danielson, S., Kachel, D., Kachel, N.B., Mordy, C.W., 2016. Currents and transport on the eastern Bering Sea shelf: an integration of over 20 years of data. Deep-Sea Res. II. 134, 13–29. https://doi.org/10.1016/j.dsr2.2016.05.010.
Stabeno, P.J., Reed, R.K., 1994. Circulation in the Bering Sea basin observed by satellite-tracked drifters: 1986-1993. J. Phys. Oceanogr. 24, 848–854.
Stauffer, G., 2004. NOAA Protocols for Groundfish Bottom-Trawl Surveys of the Nation's Fishery Resources. United States Department of Commerce. NOAA Technical Memorandum, p. 205. NMFS-F/SPO-65.
Stepanenko, M.A., Gritsay, E.V., 2016. Assessment of stock, spatial distribution, and recruitment of walleye pollock in the northern and eastern Bering Sea. Izvestia TINRO (Newsletters of Pacific Fish. Res. Center) 185, 16–30.
Stevenson, D.E., Lauth, R.R., 2019. Bottom trawl surveys in the northern Bering Sea indicate recent shifts in the distribution of marine species. Polar Biol. 42, 407–421. https://doi.org/10.1007/s00300-018-2431-1.
Sturdevant, M.V., Brase, A.L.J., Hulbert, L.B., 2001. Feeding habits, prey fields, and potential competition of young-of-the-year walleye pollock (*Theragra chalcogramma*) and Pacific herring (*Clupea pallasi*) in Prince William Sounds, Alaska, 1994-1995. Fish. Bull. 99, 482–501.
Thorson, J.T., Ianelli, J.N., Kotwicki, S., 2017. The relative influence of temperature and size-structure on fish distribution shifts: a case-study on walleye pollock in the Bering Sea. Fish Fish. 18 (6), 1073–1084.
Vestfals, C., Ciannelli, L., Hoff, G., 2016. Changes in habitat utilization of slope-spawning flatfish across a bathymetric gradient. ICES J. Mar. Sci. 73 (7), 1875–1889.
Wakabayashi, K., Bakkala, R.G., Alton, M.S., 1985. Methods of the U.S.-Japan demersal trawl surveys, p. 7-29. In: Bakkala, R.G., Wakabayashi, K. (Eds.), Results of Cooperative U.S.-Japan Groundfish Investigations in the Bering Sea during May-August 1979. Int. North Pac. Fish. Comm. Bull. 44.
Woodgate, R.A., Aagaard, K., 2005. Revising the Bering Strait freshwater flux into the arctic ocean. Geophys. Res. Lett. 32 (2) https://doi.org/10.1029/2004GL021747.
Wyllie-Echeverria, T., Wooster, W.S., 1998. Year-to-year variations in Bering Sea ice cover and some consequences for fish distributions. Fish. Oceanogr. 7, 159–170.
Zuenko, Y.I., Basyuk, E.O., 2017. Changing oceanographic conditions influence on species composition and abundance of zooplankton on the fishing grounds at Cape Navarin and their importance for the Russian pollock fishery in the Bering Sea. Izvestia TINRO (Newsletters of Pacific Fish. Res. Center) 189, 103–120.

Chapter 5: Seasonal and interannual variability of nitrate in the eastern Chukchi Sea: Transport and winter replenishment

Mordy, C.W., Bell, S., Cokelet, E.D., Ladd, C., Lebon, G., Proctor, P., Stabeno, P., Strausz, D., Wisegarver, E. and Wood, K.

Citation:

Mordy, C.W., Bell, S., Cokelet, E.D., Ladd, C., Lebon, G., Proctor, P., Stabeno, P.J., Strausz, D., Wisegarver, E. and Wood, K., 2020. Seasonal and interannual variability of nitrate in the eastern Chukchi Sea: Transport and winter replenishment. Deep Sea Research Part II: Topical Studies in Oceanography, 177, p.104807. doi: 10.1016/j.dsr2.2020.104807.

Chapter 6: Multiple life-stage connectivity of Pacific halibut (Hippoglossus stenolepis) across the Bering Sea and Gulf of Alaska

Sadorus, L.L., Goldstein, E.D., Webster, R.A., Stockhausen, WT., Planas, J.V., and Duffy-Anderson, J.T.

Citation:

Sadorus, L.L., Goldstein, E.D., Webster, R.A., Stockhausen, W.T., Planas, J.V. and Duffy-Anderson, J.T., 2021. Multiple life-stage connectivity of Pacific halibut (Hippoglossus stenolepis) across the Bering Sea and Gulf of Alaska. Fisheries Oceanography, 30(2), pp.174-193. doi: 10.1111/fog.12512.

Sadorus, L., Goldstein, E., Webster, R., Stockhausen, W., Planas, J., and Duffy-Anderson, J.T. 2020. Multiple life stage connectivity of Pacific halibut (*Hipppoglossus stenolepis*) across the Bering Sea and Gulf of Alaska. *Fisheries Oceanography*. 2020 (00): 1-20, DOI: 10.1111/fog.12512.

Abstract

Pacific halibut (*Hippoglossus stenolepis*) is managed as a single stock throughout the Gulf of Alaska (GOA) and eastern Bering Sea (BS), but biogeographical barriers and the potential for differential impacts of climate change may alter habitat use and distributions, and restrict connectivity between these ecosystems. To improve our understanding of larval dispersal pathways and migrations of young fish within and between GOA and BS, we (1) examined potential pelagic larval dispersal and connectivity between the two basins using an individual-based biophysical model (IBM) focusing on years with contrasting climatic conditions, and (2) tracked movement of fish up to age-6 years using annual age-based distributions and a spatio-temporal modeling approach. IBM results suggest that the Aleutian Islands constrain connectivity between GOA and BS, but that large island passes serve as pathways between these ecosystems. The degree of connectivity between GOA and BS is influenced by spawning location such that an estimated 47-58% of simulated larvae from the westernmost GOA spawning location arrived in the BS, with progressive reductions in connectivity from spawning grounds further east. From the results of spatial modeling of 2-6 year old fish, we can infer ontogenetic migration from the inshore settlement areas of eastern BS towards Unimak Pass and GOA. The pattern of larval dispersal from GOA to BS, and subsequent post-settlement migrations back from BS toward GOA, provides evidence of circular, multiple life-stage, connectivity between these ecosystems, regardless of climatic variability or year class strength.

Introduction

The Pacific halibut (*Hippoglossus stenolepis*) population in North American waters of the Pacific Ocean and Bering Sea supports vibrant commercial, recreational, subsistence, and tribal fisheries. The management strategy in Alaskan waters encompasses both the Gulf of Alaska (GOA) and the Bering Sea (BS) and uses stock assessment models of spawning biomass combined with agreed management approaches (Stewart & Hicks, 2018) to manage the species as a single, panmictic population, although the International Pacific Halibut Commission (IPHC) also uses current stock distribution to inform harvest distribution. Despite this cross-ecosystem management strategy, the Aleutian Islands are a permeable barrier between the North Pacific and BS ecosystems (Seitz et al., 2011; Spies, 2012; Parada et al., 2016), and there is evidence of differential impacts of climate change across these marine ecosystems such as loss of sea ice in the BS, warm and cold temperature stanzas in the BS (Duffy-Anderson et al., 2017), and warming events in the GOA (Cavole et al., 2016). Such ecosystem discontinuities have the potential to impact species that rely on large geographic domains and multiple habitats throughout their life cycles (Norcross et al., 1999; Mumby et al., 2004; Rochette et al., 2010). For Pacific halibut, fluctuations in year class strength may be determined by conditions during the early life stages that influence growth, survival, and transport to suitable habitats (Bailey et al., 2005). Population age composition of Pacific halibut indicates that a single large year class can dominate the fishery for several years (Stewart & Hicks, 2018), implying that environmental conditions that influence year class strength can have lasting impacts on fishery yield.

Pacific halibut have a complex life-cycle with passive dispersal and active migration stages, and there is evidence to suggest that connectivity between the GOA and BS may occur across multiple life stages. Adults spawn during winter in the deep water of the outer continental shelf and slope throughout the GOA and BS (Thompson & Van Cleve, 1936; Skud, 1977; Sohn et al., 2016). Dispersal occurs during the

pelagic egg and larval stages, and after ~5-7 months, once metamorphosis into the asymmetrical adult form is complete, the juvenile settles to inshore shallow nursery areas (St. Pierre, 1989; Thompson & Van Cleve, 1936). Oceanographically-driven connectivity between the GOA and BS is primarily unidirectional, and fish that are spawned in the GOA may be exported into the BS through Aleutian Island passes (Best, 1977; Skud, 1977; Hinckley et al., 2019). However, mark-recapture studies show that some Pacific halibut during the juvenile and adult life stages migrate from the BS into the GOA (Dunlop et al., 1964; Webster et al., 2013), counteracting the assumed prevailing direction of larval transport. This potential circular transport and migration pathway suggests cross-ecosystem dependence and reliance on habitats in both the GOA and the BS during different life-stages.

Ecosystem changes such as shifts in oceanography (Stabeno et al., 2012), warm and cold climate stanzas, loss of sea ice, and declines in high quality food in the BS (Kimmel, 2018; Duffy-Anderson et al., 2017; Duffy-Anderson et al., 2019) can create survival bottlenecks for species that transition between ecosystems. For example, egg and larval distributions are influenced by the strength and direction of ocean currents that vary among temperature regimes (Stabeno et al., 2012) and seasons (Stabeno et al., 2002; 2016a; 2016b). Shifts in oceanographic currents can profoundly influence the survival of eggs and larvae through favorable transport to hospitable habitats that support growth and survival (Goldstein et al. 2020; Bailey & Picquelle, 2002; Atwood et al., 2010; Napp et al., 2000; Petitgas et al., 2013). Movement by young juveniles, however, is not dictated by oceanographic currents to the same degree as larval dispersal, and there is evidence for counter-current migrations of Pacific halibut (Skud, 1977; St. Pierre, 1989; Clark & Hare, 1998; Webster et al., 2013). Thus, a multiple life-stage approach is required to assess the degree of connectivity between the GOA and the BS and the reliance of Pacific halibut populations on both ocean basins.

Identifying population connectivity across marine ecosystems that incorporates both larval dispersal and active migration could aid in the development of holistic management strategies that reflect habitat requirements across life stages as well as factors that contribute to year class strength. To better understand the geographic continuity of Pacific halibut populations and the vulnerabilities of Pacific halibut to environmental change, we assess life stage-specific distributions and connectivity between the GOA and the BS during years of warm and cold temperature stanzas and opposing year class strength using, (1) empirical larval distributions, (2) an individual-based biophysical larval dispersal model, and (3) spatio-temporal modeling of age-specific data. Incorporating larval dispersal and subsequent ontogenetic migration will provide a holistic understanding of population connectivity, multi-life stage habitat use, and potential vulnerabilities of the Pacific halibut fishery to ecosystem change.

Materials and Methods

Geographic area

The geographic area for this analysis includes the GOA and BS (Figure 1). Within the GOA, the westward flowing Alaskan Stream is the primary water source for flow through multiple Aleutian Island passes connecting the GOA and BS ecosystems (Royer, 1981; Reed & Schumacher, 1986; Stabeno et al., 1995). Originating in the central GOA is the Alaska Coastal Current (ACC) which flows westward along the continental shelf (Stabeno et al., 1999) and is the primary source for flow through Unimak Pass which is the first major pass encountered by the westward flowing current and also the only major connection point between the BS and GOA continental shelves. Based on drifter trajectories, after entering the BS via Unimak Pass, water then flows along the 50-m, 100-m, and 200-m isobaths to the west and north in the BS (Stabeno et al., 2002).–

Catch data

Larval catch and effort data were obtained from the National Oceanic and Atmospheric Administration (NOAA) Alaska Fishery Science Center Ichthyoplankton Information System database (https://access.afsc.noaa.gov/ichthyo/; NOAA 2019). Gear used for data collection most often included a MARMAP (Marine Resources Monitoring, Assessment and Prediction program) type bongo sampler (Posgay & Marak, 1980) with an inside diameter of 60 cm and a 0.333 or 0.505-mm mesh net. Tucker trawl gear was used less often and was composed of cone-shaped fine-mesh nets. Bongo and Tucker gear were determined to fish the same population (Boeing & Duffy-Anderson, 2008) and standardized catches are therefore considered comparable for analysis. Pacific halibut larvae were identified and catches for both gears were standardized to number of individuals caught under 10 m^2 of sea surface area (Smith & Richardson, 1977).

For juvenile and adult fish analyses, catch and effort data from the NOAA Alaska Fisheries Science Center summer bottom trawl survey (NOAA 2020), were coupled with individual fish information, including ages derived from otoliths collected during the surveys (age data available upon request https://www.iphc.int/form/data-request). The NOAA BS bottom trawl survey was conducted annually with stations located on a 20 nautical mile square grid extending from inner Bristol Bay in the eastern Bering Sea within the 200-m depth contour (Figure 1). The standard survey trawl gear and survey design are described in Stauffer (2004) and Clark et al. (1997). The GOA bottom trawl survey was conducted biennially and consisted of a stratified random sampling design based on data from previous surveys (Stauffer, 2004; Clark et al., 1997). Gear for this survey is described in Stauffer (2004). Net mensuration systems recorded net performance, and electronic data loggers recorded temperature and depth during both surveys. Area-swept catch per unit effort was calculated from the distance towed and

net width (Clark et al., 1997). Once settled, Pacific halibut are not routinely monitored until they are captured during the NOAA[A1] Alaska Fisheries Science Center summer bottom trawl surveys at 2 years of age. From various studies it has been observed that age-0 and age-1 Pacific halibut reside in bays and inshore waters from Dixon Entrance to Unimak Pass in the GOA and along the Alaska Peninsula and Bristol Bay in the BS (Best & Hardman, 1982; Norcross et al., 1997; Best, 1977; Stoner & Abookire, 2002). Occasionally, age-1 fish have been caught in the bottom trawl survey, but that number is small, and those in the aging sample and confirmed as age-1 fish, totaled just 57 individuals from 2000-2018 according to the IPHC database. Due to the low numbers of these age-0 and age-1 fish, and lack of standardized monitoring, estimates of relative abundance and modeling of distribution begin at age 2. Thus, catch data from the 2007-2015 bottom trawl surveys were used to examine 2-6 year old fish.

Age data

Age in whole years (2-6 year olds) for demersal juveniles was established using right sagittal otoliths collected during the NOAA Alaska Fisheries Science Center summer bottom trawl surveys. In younger fish (< 5 years), otoliths were surface-aged, i.e. annuli counted on the surface using dissecting microscopes. In older fish or if annuli were indistinct, the break and bake method of aging (described in Forsberg, 2001) was used. While not all trawl stations have Pacific halibut age data collected, the spatial coverage of aged fish was generally comprehensive for the cohorts examined here, particularly in the Bering Sea. Although coverage in the biennial gulf of Alaska survey had some gaps, these were not sufficient to affect our interpretation of the overall distributional patterns.

Cohorts studied

The 2005 and 2009 Pacific halibut year classes were selected as focal cohorts for analysis based on the following rationale: (1) they represent cohorts spawned during distinct BS environmental stanzas (i.e. warm and cold, respectively) (Stabeno et al., 2012), (2) they represent relatively strong and weak year classes, respectively (Stewart & Hicks, 2018), and, 3) the sampling coverage at both the pelagic and settled phases for the two selected cohorts was robust and comparable. The supplemental year classes of 2003, 2004, 2010, and 2011 were added to the larval dispersal modeling and to the subsequent spatio-temporal modeling of older life stages to contrast patterns and strengthen comparisons of advection and migration during warm and cold years. For analytical purposes involving annual cohort analyses, one hatch date (January 1) is assigned per spawning season, regardless of actual spawn date to assign year classes. For example, the 2005 year class includes those larvae spawned from Autumn 2004 through Spring 2005.

Individual-based biophysical model

Larval dispersal, transport, and connectivity were determined using a three dimensional individual based biophysical model (IBM) coupled with daily-averaged output from a hydrodynamic model (ROMS, https://www.myroms.org/). The IBM was developed using the Dispersal Model for Early Life Stages (DisMELS) IBM framework (Stockhausen et al. 2019a) to track transport and dispersal of the pelagic egg and larval stages of marine organisms through earlier life stages from spawning to settlement. Briefly, DisMELS incorporates a Lagrangian particle tracking algorithm and species-specific traits, allowing the model to be parameterized for multiple species (Stockhausen et al., 2019b; Duffy-Anderson et al., 2013; Cooper et al., 2013; Sohn, 2016). The hydrographic ROMS model is a primitive equation, three dimensional ocean circulation model driven by atmospheric forcing (details are available at: myroms.org, Shchepetkin & McWilliams, 2005; Haidvogel et al., 2008). The ocean model used for the present study was the regional Northeast Pacific ROMS model (NEP 6) with ~10 km resolution that spans the GOA and the BS. NEP 6 incorporates sea ice and tidal dynamics that are important for circulation within the study

region (Danielson et al., 2011; Hermann et al., 2013) and has previously been utilized for larval dispersal models in the Bering Sea (Petrik et al., 2016). Output from the ROMS model was saved in daily increments. For the IBM, ROMS daily output was spatially interpolated using bilinear interpolation in order to obtain the physical variables associated with each modeled larvae. Larval locations (latitude, longitude, and depth) were determined using a fourth-order predictor-corrector algorithm that incorporated swimming, buoyancy, and vertical and horizontal random walks for diffusive motion (Stockhausen et al., 2019b). Larval movement was primarily passive (no orientation or directed swimming behavior) except for vertical movement to maintain larvae within preferred depth ranges (Table 1). Larval locations as well as age, size, and development stage were based on 20-minute time steps and saved at daily time steps.

Pacific halibut larval release locations for the IBM were based on known spawning locations (St. Pierre, 1989) that were manually-digitized to create spatial polygons that contained point locations with a 1-km resolution grid for simulated larval release (ESRI ArcMap version 10.6; Figure 2), and were the same for all modelled years. A total of 200 individuals were released from each grid cell. Pacific halibut typically spawn from October-April; however, the exact monthly spawn dates are unknown. Therefore, larvae were released from October-April during each study year from the 25th-28th of each month at midnight to capture the general monthly dispersal patterns. Larval early life history traits generally followed those described in Sohn (2016) and larval mortality was not included in the model. Based on limited nursery habitat information throughout the study domain, all model simulations were terminated once a larvae reached the newly-settled juvenile stage after a pelagic larval duration of 180 days (Table 1). This time- and stage-based model termination limits conclusions that can be made regarding settlement success and post-settlement survival, but provides insight regarding dispersal distance.

Spatio-temporal model

Spatial modeling of trawl survey data allows for a more expansive (but less direct) assessment of cohort movement patterns than is possible using common wire tagging mark-recapture methods. Modeling the 2005 and 2009 year classes provides a look at the similarities and differences between relatively strong and weak cohorts that were spawned during warm and cold environmental stanzas, respectively. Data from other cohorts of intermediate strength (2003-04 and 2010-11 year classes) were also modeled, with results available in supplementary material.

All Pacific halibut caught during the trawl surveys were measured to obtain length data, but spatial coverage for age sampling was often less extensive. To overcome these data limitations, a spatio-temporal modeling approach was utilized (Webster et al., 2020) in order to leverage information about spatial and temporal dependence from observed data to make predictions of abundance within habitat that is unsampled in a given year, as well as improve the quality of estimation elsewhere. For each spatial location (i.e., trawl survey station), the catch-per-unit-effort (CPUE) was computed by dividing catch weight for fish with known age by survey station effort (net width times tow distance), and then adjusting for the sampling fraction in cases where less than 100% of fish were aged. For each aged cohort at each survey station in each year:

$$\text{CPUE} = \frac{W}{E} * \left(\frac{1}{f}\right) \quad (1)$$

where W=catch weight of fish, E=effort (net width x distance) and f=sampling fraction of halibut (proportion aged).

In summary, let $c(s,t)$ be the trawl CPUE value of a given cohort at location s and year t, where s represents the spatial locations of the fished survey stations, taking values $s_1, \ldots, s_n$ and $t = t_1, \ldots, t_T$, corresponding to ages 2 to (T+ 1). In this model, $s_i \hat{I} S^2$, the set of points on the surface of a sphere, and therefore coordinates in longitude and latitude format are converted to Cartesian coordinates on a

sphere for modeling. Data from the trawl surveys contain observations of zero CPUE, due to stations in low-density areas catching no Pacific halibut. The probability that $c(s,t)=0$ is accounted for by using a semi-continuous model, which models the data as a combination of zero and non-zero processes. Two new variables are defined, $x(s,t)$ for presence or absence of Pacific halibut in the catch, and $y(s,t)$ for the CPUE value when Pacific halibut are present:

$$x(s,t)=\begin{cases}0, c(s,t)=0\\ 1, c(s,t)>0\end{cases} \quad (2)$$

$$y(s,t)=\begin{cases}NA, c(s,t)=0\\ c(s,t), c(s,t)>0\end{cases} \quad (3)$$

The *NA* indicates that $y(s,t)$ is a random variable that can only take non-zero values, and is therefore undefined when $c(s,t) = 0$. The variable $x(s,t)$ has a Bernoulli distribution, $x(s,t) \sim \text{Bern}(p(s,t))$, while a gamma distribution is used for the $y(s,t)$, $y(s,t) \sim \text{gamma}(a(s,t), b(s,t))$, which has mean $\mu(s,t) = a(s,t)/b(s,t)$. Only the gamma mean is allowed to vary: the variance, $= a(s,t)/b^2(s,t)$, is assumed invariant over space and time.

Next let the $e(s,t)$ be a Gaussian Field which is shared by both component random variables in the following way:

$$u(s,t) = \text{logit}(p(s,t)) = \beta_x + e(s,t) \quad (4)$$

$$v(s,t) = \log(\mu(s,t)) = \beta_y + \beta_e e(s,t) \quad (5)$$

where β_x and β_y are intercept parameters (which could be generalized to a covariate model) and the parameter β_e is a scaling parameter on the shared random effect. Temporal dependence is introduced through a simple autoregressive model of order 1 (AR(1)), as described in Cameletti et al. (2013), as follows,

$$\varepsilon(s, t) = \rho\varepsilon(s, t - 1) + \eta(s, t) \quad (6)$$

where ρ denotes the temporal correlation parameter and $|\rho| < 1$. For a given year, t, the spatial random field (SRF), $\eta(s, t)$, is assumed to be a Gaussian field with mean zero and covariance matrix Σ. We assume a stationary Matérn model (Cressie, 1993) for the spatial covariance model, which specifies how the dependence between observations at two locations decreases with increasing distance. Models were fitted in R using the R-INLA package (Lindgren & Rue, 2015), which uses a computationally efficient Bayesian approach to fitting spatial and spatio-temporal models. Further details are available in Webster et al. (2020).

Results

Pacific halibut larvae were found during the NOAA ichthyoplankton survey in 2005 east of Kodiak Island, but there was no sampling at those stations in 2009 (Figure 3). Larvae were found in both study years in and around Unimak Pass, and in Bering Canyon. In 2005, larvae were present on the north side of the Alaska Peninsula in the BS and over Bering Canyon, but in 2009, larvae were absent along the north side of the Alaska Peninsula east of the 200 m isobath. Pacific halibut larvae were not found after May in either year. Empirical larval distributions from the supplemental study years were similar to the two focus years (Supplemental Figure 1; Supplemental Table 1).

When comparing larval characteristics of the two primary study years, the month of May was selected because of similar sampling coverage between the two years, and the assumption that spawn timing did not differ substantially between years such that larvae that were present in the water column during a particular month were roughly the same age between years. The catch weighted mean length in 2009 (15.38 mm ± 5.03) was ~87% that of 2005 (17.62 mm ± 6.79) for both the BS and GOA combined, and the average standardized catch of larvae/10 m^2 in 2009 (0.4 larvae/10m^2 ± 2.1) was only 20% that of the 2005 catch (2.0 larvae/10m^2 ± 6.6) (Table 2). When those two annual cohorts were sampled two years later during the NOAA groundfish trawl surveys, the estimated abundance of the 2005 year class was ~53% higher than that of the 2009 year class for the BS and GOA combined, but the average fork length was significantly less for the 2005 cohort than for 2009 both in the GOA and BS (*t*-test *p*-value-0.0027).

Larval dispersal pathways

IBM results from focal study years, 2005 and 2009, and representative spawn locations throughout the GOA and BS showed that, generally, larvae were advected westward away from the spawning subregions in the GOA, and were transported northwest in the BS along the continental slope (ex: 200 m isobath; Figs. 1, 4-6). Larvae spawned in the BS (Spawn Region 1, Figure 2) remained north of the Aleutian Islands throughout their pelagic larval stage (Figure 4) and were transported along the continental slope to arrive at the Pacific coast of Asia within ~3 months. Within 6 months post-release, simulated larvae had the potential for widespread dispersal along the Asiatic coastline and north through the Bering Strait in both the focal and supplemental modeled years (Figure 4; Supplemental Figure 2). In 2005 (Figure 4a), larval dispersal to the western BS was greater than in 2009 (Figure 4b). A portion of the larvae that were spawned in the western GOA (Spawn Region 2; Figure 2) arrived to the

BS from the GOA within 1-3 months and were primarily transported through island passes, including high larval densities near Unimak Pass, in all study years (Figure 5; Supplemental Figure 3). Transport to the northwest in the BS appeared greater in 2005 (a warm year; Figure 5a) compared with 2009 (a cold year; Figure 5b), especially for larvae that were spawned in the earlier months. Larvae that were not transported to the BS were either retained in the western GOA or advected to the eastern Aleutian Islands. A similar pattern of dispersal to the west and through Aleutian Island passes was observed for Spawn Region 3, but there was higher retention of larvae in the GOA and reductions in dispersal to the BS compared with Spawn Region 2 (Figure 2; Supplemental Figure. 4). Dispersal from the GOA to the BS from the easternmost spawn regions was minimal, but dispersal within the GOA was widespread along the GOA coastline (Spawn Regions 4 and 5; Figures 2 and 6; Supplemental Figures 5 and 6). Larvae that originated from Spawn Region 4 arrived to the BS within 4-5 months, but the majority of larvae were retained in the GOA in the vicinity of Unimak Pass and were not transported westward along the Aleutian Islands (Supplemental Figure 5). The easternmost Spawn Region (Spawn Region 5; Figure 2) showed minimal connectivity between GOA and the BS, with indications that only late stage larvae had the potential to traverse the GOA and arrive in the BS after ~6 month pelagic larval duration (Figure 6). A large proportion of the larvae from Spawn Region 5 were retained in the eastern GOA and some were transported southward along the coast as well as offshore (Supplemental Figure 6). Connectivity with the western GOA was greatest in the earlier spawn months and there did not appear to be notable differences between the two primary study years of 2005 and 2009 (Figure 6).

Comparisons among warm (2003-2005) and cold (2009-2011) stanza years showed generally consistent sub-regional patterns in connectivity and transport according to the larval transport model (Table 3). Larvae that originated in the BS (Spawn Region 1), remained within the BS ecosystem throughout their trajectories (Supplemental Figure 2). The highest degree of connectivity as well as the greatest interannual variability in connectivity from GOA spawn locations to the BS occurred from

Spawn Region 2 where 47-58% of the larvae had the potential to be advected into the BS depending on year (Table 3; Supplemental Figure 3). The majority of simulated larvae from Spawn Region 3 remained in the GOA, but ~15-21% had the potential to be advected into the BS (Table 3; Supplemental Figure 4). This contrasted with Spawn Regions 4 and 5 where very few modeled larvae arrived to the BS (<10% and <2%, respectively; Table 3, Supplemental Figures 5 and 6). From Spawn Region 1, there was potential in every modeled year for arrival to north Pacific Asiatic coastal regions and in some years, the Arctic (Supplemental Figure 2). The model also showed that there was potential for the arrival of larvae to the north Pacific Asiatic coast from Spawn Regions 2 and 3 in some years (Supplemental Figures 3 and 4). Larvae from Spawn Regions 4 and 5 were not likely to reach the north Pacific Asiatic coast, but were dispersed throughout the GOA (Supplemental Figures 5 and 6).

Empirical larval observations and IBM trajectories both show concentrations of larvae around island passes and dispersed through the western GOA and eastern Bering Sea along the 200-m isobath (Figures 3-6; Supplemental Figures 1-6). In contrast with empirical larval observations that showed larvae to the east of Unimak Pass in 2005 (Figure 3), almost no IBM trajectories crossed the isobaths along the continental slope to arrive on the continental shelf in the BS (Figures 4- 6; Table 3; Supplemental Figures 2-6). In addition, IBM results did not show larval transport to the western Aleutian Islands where there is a known population of Pacific halibut (Seitz et al. 2008). Large-scale qualitative comparisons are possible as described here, but detailed quantitative comparisons between empirical presence and modelled trajectories are difficult, given that the larval surveys are limited in scope in any given year both spatially and temporally, and Pacific halibut larvae that are caught are not aged so there is no method available to estimate probable origination or settlement locations.

Ontogenetic migration

The spatial model output suggests that as 2 year olds, the 2005 cohort was concentrated in Bristol Bay in the BS and around Kodiak Island in the GOA, and the BS component appears to have stayed aggregated as they began to emerge from Bristol Bay, with distributional centers that moved west and south along the Alaska Peninsula in the immediate subsequent years (Figure 7; Supplemental Figure 7). By age 4, young Pacific halibut were clustered on both sides of Unimak Pass in contrast to younger fish that were concentrated inshore in the southeast BS. Age-5 and age-6 fish appeared less aggregated and were dispersed over a wider range and to deeper depths than younger fish. These patterns in distributional changes over time were generally consistent in other large cohorts from 2003 and 2004 (Supplemental Figures 8 and 9), with apparent dispersal outwards from inside shallow waters of Bristol Bay and south of Nunivak Island (ages 3-4 years), and subsequent aggregation around Unimak Pass (ages 4-6 years).

Model output suggests that the 2009 cohort was more evenly dispersed overall compared to the 2005 cohort at comparable ages (Figure 8; Supplemental Figure 10), lacking the obvious high-density concentrations of the earlier cohort (note the different scales on the two figures). A primary difference from 2005 was that, in addition to a part of the population leaving Bristol Bay and migrating southward along the Alaska Peninsula as seen with the 2005 cohort, a portion of the 2009 year class also continued to occupy the Bristol Bay area as they aged and were not migrating outward to other parts of the BS to the same degree at the 2005 cohort. There was some indication that there were aggregations around Unimak Pass, but there were no obvious aggregations in the GOA. Overall average abundance (Table 2) and sample sizes (Table 4) were relatively low, making it difficult to observe small scale density changes in this cohort. However, according to the model, distributional changes with age were generally similar for other low-density cohorts from 2010 and 2011 (Supplemental Figures 11 and 12; Supplemental Table 2), although with some differences in timing and dispersal (e.g., the 2010 and 2011 cohorts both showed a stronger clustering south of Nunivak Island in 2015).

Discussion

Developing an understanding of cross-ecosystem population connectivity can inform management strategies for Pacific halibut by providing information about dispersal, migration, and habitat use across multiple life stages. Model results suggest consistent and substantial larval connectivity between the western GOA and the BS. Pacific halibut larvae that originated in the western GOA have the potential to be transported to the BS, and those larvae that originated from populations in the BS are likely transported northwest along the isobaths in the BS. In addition to larval dispersal, age-specific distributions of Pacific halibut showed ontogenetic range expansions, suggesting that juveniles radiate from their settlement areas in the BS to regions throughout the continental shelf, and potentially reach the Aleutian Islands and the GOA. Spawning in the GOA may provide access to important settlement habitats in the BS, and the potential reverse migration from the BS to the GOA may be important for access to suitable habitats for older life stages, or for maintaining source populations that facilitate access to juvenile settlement habitats.

Biophysical modeling results suggest that the Aleutian Islands constrain larval connectivity between the GOA and the BS, but that island passes are corridors that connect the two ecosystems. Several studies have highlighted oceanographic connectivity between the GOA and the BS through large island passes (Royer, 1981; Reed & Schumacher, 1986; Stabeno et al., 1995;) with estimates of ~30% of the Alaska Coastal Current (Aagaard et al., 2006) transported from the GOA to the BS through Unimak Pass (Stabeno et al., 2016a). For pelagic larvae, island passes could facilitate connectivity between the GOA and the BS. IBM results suggest a link between the two basins via large island passes in the eastern Aleutian Islands where an estimated average of 35% of larvae that originated in the western GOA (Spawn Regions 2 and 3) were transported into the BS.

The majority of larval dispersal modeling studies in the North Pacific to date have focused on the GOA or the BS in isolation; however, some studies hypothesize that larvae that were spawned in the western GOA and subsequently exited the study area were potentially transported further west to the Aleutian Islands or into the BS (e.g. Gibson et al., 2019). One study to provide evidence of basin connectivity was that of Parada et al. (2016) that modeled walleye pollock (*Gadus chalcogrammus*) larval transport and found evidence for basin connectivity. Coinciding with our results, several studies have highlighted east-west connectivity in the GOA, particularly between spawning grounds in the eastern GOA and nursery areas in the central GOA for sablefish (*Anoplopoma fimbria*) (Gibson et al., 2019), Pacific cod (*Gadus microcephalus*) (Hinckley et al., 2019), arrowtooth flounder (*Atheresthes stomias*) (Stockhausen et al., 2019a), and Pacific ocean perch (*Sebastes alutus*) (Stockhausen et al., 2019b). Dispersal patterns in the BS were typically south to north, coinciding with other modeling studies for walleye pollock (Petrik et al. 2016), northern rock sole (Cooper et al. 2013), and Greenland halibut (Duffy-Anderson et al. 2013). Simulated Pacific halibut larvae in the BS were primarily transported along the continental slope, with some larvae reaching the north Pacific Asiatic coastline or transitioning through the Bering Strait.

The prevailing east to west modelled larval transport in the GOA and the south to north trajectories in the BS along the 50-200 m isobaths agree with the prevailing currents in each respective ecosystem (Stabeno et al., 2002; 2004), and with empirical data showing larval concentrations near island passes. However, smaller-scale comparisons with empirical data suggest that model limitations likely impacted finer scale connectivity patterns and transport trajectories. The absence of simulated larval transport to inshore regions of the BS conflicts with the empirical larval distributions during 2005 where larvae were found north of Unimak Pass along the Alaska Peninsula. In addition, according to catch data from the NOAA Fisheries bottom trawl surveys, young demersal stage Pacific halibut are consistently found in high abundance near shore in the southeastern BS. Together, these empirical data suggest that larval transport to the southeastern BS may be much greater than portrayed in the advection modeling. Thus,

At N2, $NO3_{EST,N2}$ closely tracks both the synoptic and longer period signals captured by the SUNA nitrate sensor ($NO3_{SUNA,N2}$) during the January-April and September-December time frames (Fig. 2d). Although offsets between $NO3_{SUNA,N2}$ and $NO3_{EST,N2}$ are not uniform from September to May (largest in December with instances of 10 μmol differences), the average is 2.5 μmol/kg, which is comparable to the errors and biases discussed in Section 2.1.1.

As with nitrate, correlations with salinity are also significant ($p<0.02$) for Aqua Monitor-measured phosphate and silicate for both January-April and September-December time frames, but neither are significantly correlated during the May-August period. For January-April, May-August, and September-December, the correlation coefficient (r) between SBE salinity and phosphate is 0.89, 0.37, and 0.92, respectively. For salinity and silicate, the correlation coefficients during the same time period are 0.98, 0.12, and 0.91, respectively. Salinity-based estimates of phosphate ($PO4_{EST,N2}$) and silicate ($SiO4_{EST,N2}$) are calculated in identical fashion to $NO3_{EST,N2}$ (Eq. 1).

3.3 Nutrient Fluxes through Anadyr Strait

Using velocity data from the N2 ADCP and the salinity-nutrient regressions described above, we estimate nutrient fluxes through Anadyr Strait by assuming a homogenous flow field through the strait. The homogeneous flow field has been applied to the Bering Strait throughflow with good success by Woodgate and Peralta-Ferriz (2021), despite the presence of the Alaska Coastal Current (ACC) in Bering Strait, which is arguably more problematic than the weaker lateral gradients found in Anadyr Strait. Based on the ADCP current measurements on the N2 mooring, we further assume that the water column is unstratified over November through April such that the salinity and nitrate measurements at 35 m depth are representative of the full water column. For May through October, we assume that the water column is stratified and that the upper 10 m of the water column is nitrate-deplete.

Anadyr Strait is 73 km wide, has a mean depth of ~ 35 m, and is approximately 2.7×10^6 m^2 in cross-sectional area. The major axis of the principal ellipse of the sub-tidal barotropic currents (from the ADCP on N2) is roughly normal to Anadyr Strait (i.e. oriented with the through-flow). If treated as representative for the whole Anadyr Strait, currents along this axis can be used to calculate the volume transport through the strait (T_{AS}). The average speed of the currents along the major axis current is 39 cm s^{-1} for the year-long deployment, which translates to a volume transport of 1.1 Sv to the northeast and is similar to the estimated transport at Bering Strait (1.3±0.3 Sv), based on A3 measurements.

To estimate the nutrient flux through Anadyr Strait, we combine the monthly salinity-based estimates of nutrient concentration at N2 (Section 3.1) with the volume transport through the strait (T_{AS}). Nitrate flux ($F_{NO3,AS}$), for example, is assessed as:

$$F_{NO3,AS} = T_{AS} NO3_{est,N2} \rho_0 \qquad \text{Eq. 2}$$

where ρ_0 is the nominal density of seawater in the region (1025 kg m^{-3}). Fluxes for phosphate and silicate ($F_{PO4,AS}$ and $F_{SiO4,AS}$, respectively) are calculated similarly. From September, 2017 to April 2018 (when salinity nutrient regressions are significant), average nitrate, phosphate, and silicate fluxes are 17±4, 1.8±0.4, and 36±9 kmol s^{-1}. Uncertainty estimates include error from the regressions as well a ±20% assumed error on our transport estimates, as we do not have sufficient in situ data to fully constrain transport

through Anadyr Strait. Changing the assumed transport uncertainty by ±10% modifies flux transport errors by about 2, 0.2, and 3 kmol/s for nitrate, phosphate and silicate, respectively. Using a summertime nutrient depletion depth of 20 m (assumed 10 m here) would reduce these flux estimates by < 10%.

3.4 Nutrient fluxes through Bering Strait

Anadyr and Bering straits are highly covariable. At a 17 day lag, the low-passed (30 day cutoff period) salinity measured at N2 and A3 (both near 35 m) have a correlation coefficient of 0.70 and both time series have similar means and dynamic ranges (Fig. 1d). Given the dominance of the Anadyr Strait-sourced waters in the Bering Strait and the strong co-variability in salinities, we employ the methods of Section 3.3 to estimate the nutrient flux into the Arctic. The foundations of our nutrient flux calculations are estimates of Bering Strait salinity and transport based on observations from the A3 mooring (See Fig. 1a and Section 2.1.2). Although monthly estimates of transport (T_{A3}) and salinity (S_{A3}) begin in 1990, the early data record has gaps so here we focus on the continuous period of the record, starting in fall 1997.

Thus, we apply the monthly salinity measured at A3 (S_{A3}) to Equation 1 to estimate monthly concentrations for nitrate, phosphate, and silicate ($NO3_{EST,BS}$, $PO4_{EST,BS}$, and $SiO4_{EST,BS}$, respectively). Using T_{A3} and these salinity-estimated nutrient concentrations, we employ Eq. 2 to calculate monthly nutrient fluxes through Bering Strait ($F_{NO3,BS}$, $F_{PO4,BS}$, $F_{SiO4,BS}$), Since salinity and nutrients are not significantly correlated at N2 from May-August, we do not use the salinity parameterization (Eq. 1) during these months. Instead, we turn to *in situ* observations from the Russian-American Long-Term Census of the Arctic Program (RUSALCA) program (REF???)to estimate the average nutrient concentrations within the strait. From a set of five separate cruises spanning 2004 to 2010 (all during the month of August), we select stations that are in close proximity to the strait (Fig. 1a). Station locations are transformed to an along-strait coordinate system, and we use objective mapping to estimate the average nutrient section along Bering Strait for each year (See Fig. 1b for nitrate). For all nutrients, objective maps show both subsurface and western enhancement of concentrations, revealing the nutrient depletion near the surface across the whole Strait, nutrient rich subsurface waters from Anadyr Strait in the west, and the nutrient poor waters of the ACC in the east. We compute the mean concentration of each parameter over the entirety of aggregated (all years) objective maps (both in depth and transect distance) and find averages of 12.6, 1.3, and 20.9 μmol/kg for nitrate ($NO3_{RUS,BS}$), phosphate ($PO4_{RUS,BS}$), and silicate ($SiO4_{RUS,BS}$), respectively, which are treated as representative average concentrations for Bering Strait from May to August. While these estimates lack *in situ* data from May to July, SUNA data from N2 suggests that this season is typically the least temporally variable (Fig. 2d), so averages from August should serve as a serviceable but conservative representation for the May-August time frame. Thus, our monthly nutrient fluxes in summer (May-August) combine the variable transport estimate from A3 with a constant nutrient value (rather than the variable nutrients used from January-April and September-December). By combining the RUSALCA-based (May-August) and salinity-based (all other months) we construct a continuous monthly record of nutrient flux through Bering Strait from August 1997-August 2019. The period-of-record mean for nitrate, phosphate, and silicate fluxes are 16±5, 1.5 ± 0.5, and 30 ± 10 kmol s^{-1}, respectively.

Interannual variability is found to be relatively strong with ranges (including error) of approximately 5-25, 0.5-2.5, and 10-50 kmol s^{-1} for nitrate, phosphate, and silicate, respectively (Fig. 3a). There are statistically significant ($p<0.05$) long term temporal trends for annually averaged phosphate ($p<0.01$) and silicate ($p<0.02$), but not for nitrate ($p=0.16$). Sensitivity analysis, where transport (T) and nutrient concentrations

(C) are split into mean and anomaly terms ($T = \overline{T} + T'$, $C = \overline{C} + C'$, and nutrient flux is $T \cdot C$), shows that increasing transport is responsible for the increase in flux for phosphate and silicate ($|T' \cdot \overline{C}| > |\overline{T} \cdot C'|$), while for nitrate decreased nutrient concentrations offset the increased transport ($|T' \cdot \overline{C}| \approx |\overline{T} \cdot C'|$). There is also considerable seasonal variability (Fig. 3b). Monthly average fluxes range between about 5±7 to 27±11, 0.7±0.7 to 2.1±0.7, and 12±13 to 50±18 kmol s^{-1} for nitrate, phosphate, and silicate respectively (± values are standard deviations of monthly fluxes), with maxima in April and minima in December. This timing coincides with the months of maximum and minimum salinity, which is consistent with our salinity-based parameterizations (Eq. 1, and Fig. 2b).

4. Discussion

From 1998 to 2018 we estimate the average poleward flux of nitrate, phosphate, and silicate through Bering Strait is 16±5, 1.6±0.5, and 30±10 kmol s^{-1}, respectively. MacDonald et al. (2010) estimated that 12.4 kmol s^{-1} of nitrogen is needed to support the annual 50 g C m^{-2} y^{-1} of new production in the Chukchi Sea alone, and that the total flux of dissolved inorganic nitrogen was 16.5 kmol s^{-1}, within the uncertainty range the 16±5 kmol s^{-1} of nitrate that we estimate. The wintertime nitrate flux estimates at Bering Strait presented in this work are in relatively good agreement with those found downstream at Icy Cape by Mordy et al. (2020), after accounting for the ~40% of Bering Strait transport that flows by the mooring array used (e.g. 6±2 kmol/s compared to 18±10 kmol/s found here during February). However, our nutrient fluxes are significantly higher than those estimated by Torres-Valdes et al. (2013), ranging between ~25-75% greater. The majority of the discrepancy is rooted in methodological differences, with our single year, but year round time series of nitrate observations providing the basis of our annually-resolved approach. Torres-Valdes et al. (2013) in contrast use temporally static nutrient concentrations along with seasonally changing transport estimates, whereas we use nutrient concentrations that vary over January-April and September-December (only static from May-August). The average nitrate concentration was approximately 10 μmol/kg across Bering Strait during the August, 2005 RUSALCA cruise used in Torres-Valdes et al. (2013), compared to the annually averaged 15.6 μmol/kg estimated here between the years of 1997-2018, which is roughly the same fractional difference between the their nitrate flux estimate and that found here.

Recently, Zhao et al. (2021) used a three-dimensional ocean-sea ice-biogeochemical model to simulate nitrate flux through Bering Strait from 1998-2015 and found values of ~12 kmol s^{-1} during February-May, and ~8 kmol s^{-1} much of the remainder of the year. While that seasonality has loose qualitative agreement with monthly variability found here, their annual average of 9.63 kmol s^{-1} is significantly lower than our 16±5 kmol s^{-1}, and we find higher seasonality (~5-25 kmol s^{-1} versus ~8-12 kmol s^{-1}). A possible explanation for the discrepancy of the annual averages is that Zhao et al. (2020) found simulated nitrate concentrations upstream of Anadyr Strait that were significantly lower than in situ concentrations (~5 umol/kg), which may translate to lower nitrate fluxes through Bering Strait.

Deep water thermohaline and nutrient composition is fairly static (REF), however, the stability of the salinity-nutrient relationships over the multi-decadal period of record (1998-2018) is a central assumption, given these relationships are only estimated from the yearlong N2 mooring deployment (2017-2018). Though lacking in historical data directly at Anadyr Strait, the January-April salinity-nutrient measurements from N2 are near the mixing line between deep nutrient-rich and shallow nutrient-poor waters established

from hydrographic data collected (Fig. 2a) around a decade before the N2 deployment, providing some sign of long-term stability. Brine rejection from sea-ice formation is could also impact our estimates of nutrient flux, as it modifies salinity but not nutrients. However, the wintertime polynyas that are the strongest source of brine are upstream of Anadyr Strait (Danielson et al. 2006), and the pack-ice that is often present between the Anadyr and Bering straits has a weaker influence on salinity. Thus, while some influence of brine rejection is likely implicit in the salinity-nutrient relationships found at N2, these are unlikely to undergo drastic transformations in the wintertime transit time to Bering Strait.

Prominent discontinuities between estimated fluxes on either side of the summer season (May-August, Fig. 3b) mark the changeover between salinity-based nutrient estimates and *in situ* RUSALCA measurements used in calculating nutrient fluxes at Bering Strait. There are different uncertainties associated with each of the different methods, but the discontinuities may also reflect part of the seasonally varying nutrient uptake cycle. Brown et al. (2011) estimate that 54% of the regional annual net primary production occurs from May-July, so phytoplankton blooms during this interval are drawing down nutrient concentrations, thereby reducing the Arctic-bound nutrient flux. The Bering Sea has very high phytoplankton productivity, with 250-300 g C m-2 yr) (Sambrotto et al., 1984, Grebmeier et al. 1988, Springer, 1988, Walsh et al., 1989). Though biotic drawdown during the transit between Anadyr and Bering Strait is unknown, it is possible to construct a crude estimate assuming half the total production (~150 g C m-2) occurs evenly over the ~50 m deep shelf break from May-July. The expected draw down during the two week advective period from Anaydr to Bering Strait is ~ 6 umol N kg^{-1} (assuming a Redfield ratio of 16N:106C), and the remainder of the year is ~ 2 umol N kg^{-1}. Since our flux estimates only use the Anadyr salinity-nutrient relations from September-April, and nutrient concentrations during May-August are based on RUSALCA observations directly at Bering Strait, we expect the error from biotic drawdown in the Anadyr to Bering Strait advection period to be small.

As calculated in Section 3.2, the estimated nitrate, phosphate, and silicate flux in Anadyr Strait for the N2 mooring deployment period when salinity-nitrate relations hold (September, 2017 – April, 2018) was 17±4, 1.8±0.2, and 37±5 kmol s^{-1}, respectively. During the same period at Bering Strait, fluxes are estimated to be 24±8, 2.5±0.8, and 52±16 kmol s^{-1}. Though the uncertainty ranges overlap, it is possible that the larger mean values from Anadyr Strait are partially due to a branch of the Anadyr Current (presumably with the same salinity-nutreint relations) that flows around the southern shore of St. Lawrence Island (Danielson et al., 2006), but we presently lack the data to confirm this.

The estimates of volume transport through Bering Strait (Section 3.3) do not correct for influences from the ACC, which is an additional source of error. However, the fractional correction for the volume transport is ~10% (Woodgate, 2018), and ACC water is well known for being nutrient deplete (Danielson et al., 2017), so it is unlikely that the ACC contributes a significant fraction of the overall nutrient supply to the Arctic.

Woodgate (2018) described a multi-year trend of increasing transport along with a multi-year trend in declining salinity. For our calculation (which assumes a fixed relationship between nutrients and salinity) this introduces competing effects, as increased volume transport favors increased nutrient flux, while decreasing salinity under our parameterizations (Eqs. 1 and 2) translates to lower nutrient concentration and fluxes. Using the salinity-nutrient parameterizations established at N2, we find that silicate and phosphate

fluxes have likely increased significantly from 1998-2018, while nitrate, at best, has a weakly positive trend ($p=0.16$). Though nitrate, phosphate, and silicate are all very well correlated with salinity during non-summer months ($r \geq 0.89$), changes in salinity correspond to a larger fractional change in $NO3_{EST,BS}$ than either $PO4_{EST,BS}$ or $SiO4_{EST,BS}$ (Fig 2 b-d). Thus, the long term decrease in salinity at Bering Strait compensates for the increase in volume flux and $F_{NO3,BS}$ remains relatively steady. Salinity variability causes less fractional change in $PO4_{EST,BS}$ and $SO4_{EST,BS}$, such that the increased transport is the determining factor in long term changes of $F_{PO4,BS}$ and $F_{SiO4,BS}$ (also see Section 3.4).

Bering Strait is an important gateway for supply of Arctic nutrients, and this has major biological implications. Lowry et al. (2015) found that nutrient rich winter water advected north through Bering Strait was strongly associated with phytoplankton blooms in the Chukchi Sea. Torres-Valdes et al. (2013), even with their smaller total flux, found that that Bering Strait is a significant source of annual nutrient supply to the broader Arctic Ocean (21±4%, 35±6%, and 61±11%), for nitrate, phosphate, and silicate, respectively. If, as our analysis suggests, the true nutrient flux is higher than previously estimated, it implies that Bering Strait is an even more significant source of Arctic nutrients than previously appreciated. As temperatures in the Bering Sea rise, the timing of the spring breakup of sea ice shifts to earlier in the year (Danielson et al., 2020). Earlier spring blooms associated with the resulting increased light availability may lead to increased drawdown of the nutrients supplied by the Anadyr Current. By way of biotic consumption, this could reduce the nutrient supply to the Arctic through Bering Strait, although lateral particulate biomass fluxes may increase in turn. Thus, especially since our interannual estimate is calibrated only on one year of year-round data, an urgent requirement is for more year-round measurements of nutrients in the Anadyr Strait and indeed in the Bering Strait to better understand the full scope of Bering Strait region nutrient dynamics.

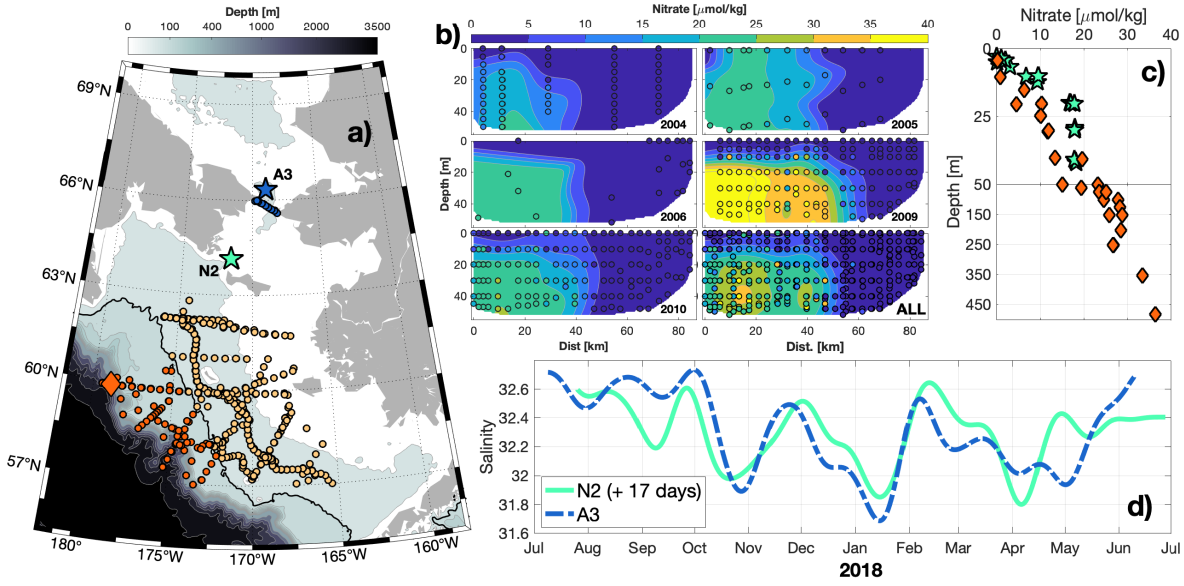

Figure 1: a) A regional map showing hydrography and mooring locations. Orange circles are sites of shipboard hydrography profiles collected mostly during summer from 2008-2018 (see Supplementary Table S2 for sources; dark markers are casts > 100 m), and blue circles mark Bering Strait RUSALCA stations. Stars mark mooring sites (N2,cyan; A3 blue). The dark depth contour is at 100 m. b) RUSALCA nutrient transects collected in August for years 2004, 2005, 2006, 2009 and 2010. Colored circles show measured nitrate values across Bering Strait (blue circles in panel (a)), and the contours are an objective map calculated from observations (smoothing length scales of 10 m and 10 km in the vertical and lateral dimensions, respectively). The lower right subpanel aggregates all years. c) Nitrate profiles collected at N2 (stars) and the Bering continental slope (diamonds). The location of continental slope observations is denoted by the orange diamond in (a). d) Low pass filtered (30 day cutoff period) salinity at N2 (cyan, lagged by 17 days) and A3 (blue).

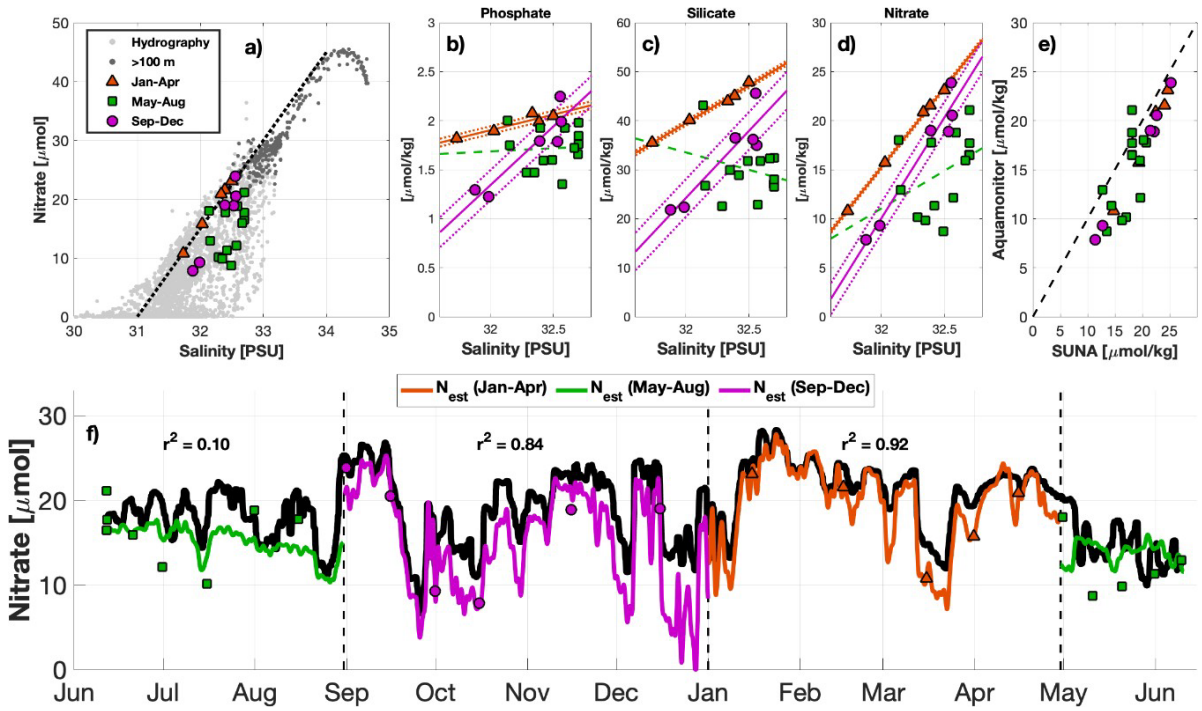

Figure 2 a) Hydrographic samples of nitrate and salinity across the Bering Sea in gray (see Fig. 1a). Darker markers indicate samples taken at > 100 m. Colored markers show 25 nitrate/salinity pairs taken by the Aqua Monitor and SBE at N2, where color corresponds to the seasons denoted in the legend. The dashed box shows the salinity and nitrate ranges plotted in (b). b) Small points show SUNA nitrate versus SBE 35 m salinity at mooring N2 during its 363 day deployment, while larger circles show Aqua Monitor nitrate versus SBE salinity. c) Aqua Monitor nitrate compared to SUNA nitrate (dashed line shows the 1:1 slope). d) SUNA nitrate (thick black) compared to $NO3_{est,N2}$ (colored lines). Colored circles show Aqua Monitor nitrate measurements and vertical dashed lines show delineations for the seasons (Jan-Apr, May-Aug, Sep-Dec). Seasonal color assignments in (b-d) are identical to those in (a).

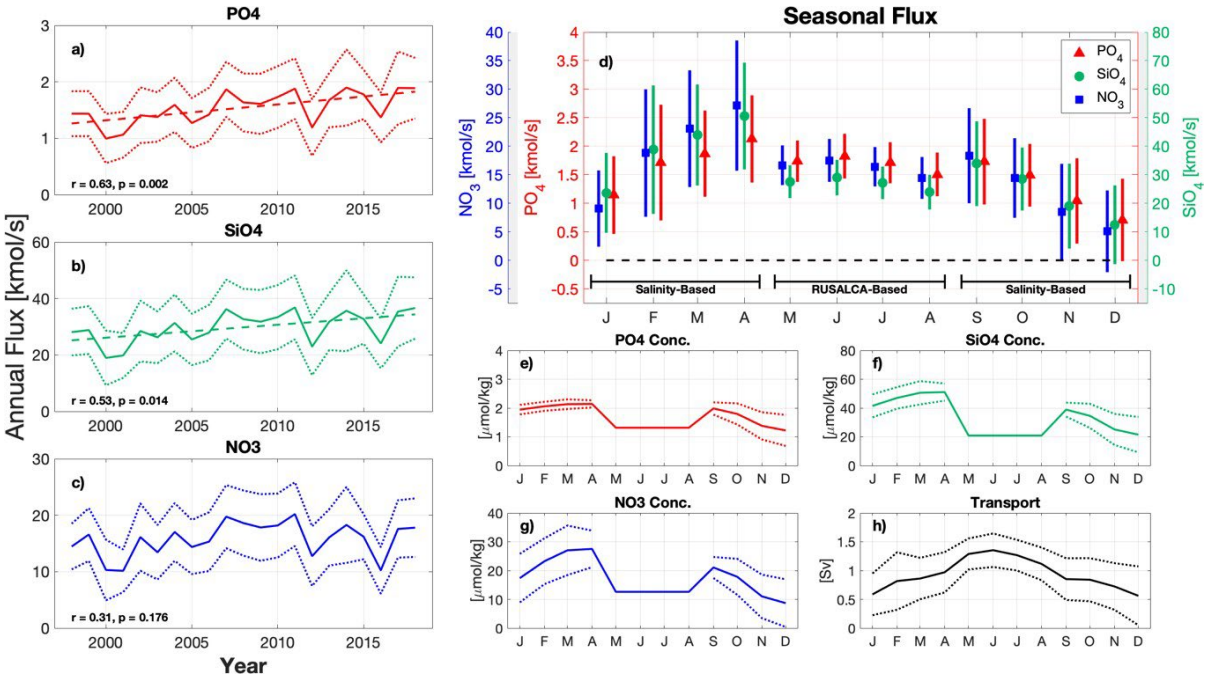

Figure 3: a-c) The annual-average nutrient flux through Bering Strait for each year. Positive values represent a poleward flux, dotted lines show the 95% CI, and dashed lines show the linear regression (if significant). d) The monthly average nutrient flux through Bering Strait spanning 1997-2018. Symbols are the mean and vertical lines show the standard deviation within each month. e-f) The monthly averages (solid line) and standard deviation (dashed lines) of nutrient concentrations and transport estimated at Bering Strait. There are no dashed lines from May-August to reflect the constant concentration assumed during that period.

Supplementary Table A1:

	NO_3 Flux (kmol/s)	PO_4 Flux (kmol/s)	SiO_4 Flux (kmol/s)	Salinity (PSU)	Transport (Sv)
Jan	8.8 (6.5)	1.25 (0.75)	21.8 (12.9)	32.13 (0.52)	0.59 (0.36)
Feb	18.2 (10.8)	1.85 (1.10)	36.0 (20.9)	32.49 (0.49)	0.82 (0.50)
Mar	22.3 (9.9)	2.02 (0.82)	40.9 (16.5)	32.73 (0.53)	0.86 (0.36)
Apr	26.2 (11.0)	2.29 (0.82)	47.1 (17.5)	32.76 (0.39)	0.97 (0.35)
May	17.2 (3.6)	1.78 (0.37)	28.2 (5.9)	32.51 (0.31)	1.29 (0.27)
Jun	18.1 (3.9)	1.87 (0.40)	29.7 (6.4)	32.40 (0.28)	1.36 (0.29)
Jul	17.0 (3.6)	1.75 (0.37)	27.8 (5.8)	32.48 (0.18)	1.27 (0.27)
Aug	14.9 (3.8)	1.54 (0.39)	24.5 (6.2)	32.51 (0.31)	1.12 (0.28)
Sep	16.3 (7.5)	1.87 (0.81)	30.4 (13.5)	32.54 (0.18)	0.85 (0.36)
Oct	12.6 (6.3)	1.63 (0.59)	25.0 (10.3)	32.38 (0.31)	0.84 (0.37)
Nov	7.1 (7.5)	1.16 (0.81)	16.0 (13.6)	32.03 (0.39)	0.72 (0.41)
Dec	4.2 (6.2)	0.80 (0.79)	10.3 (12.1)	31.90 (0.45)	0.56 (0.51)
Year	**15.3 (2.8)**	**1.64 (0.29)**	**28.0 (5.0)**	**32.4 (0.21)**	**0.93 (0.18)**

Caption: The average and standard deviations are presented for nutrient flux, salinity, and transport at Bering Strait. Positive values indicate northward flux and transport through Bering Strait. The standard deviation for annual estimates (bottom row) are computed using the average of each year (rather than all monthly estimates) in order to give a sense of the interannual variability.

Supplementary Table A2:

Program	Cruise	Month/Year	Data
Arctic IERP	SKQ201709S SKQ201813S	6/2017 6/2018	Moorings, CTDs, nutrients
Arctic IES	BE12 BE13	8/2012 8/2012	CTDs, nutrients
Bering Sea IERP	HLY0802 HLY0803 ME0823 KN195 TN249 DY1408	4/2008 7/2008 8/2008 7/2009 5/2010 9/2014	CTDs, nutrients
RUSALCA	Khromov2004 Sever 2005 Sever 2006 Khromov 2009 Khromov 2010	8/2004 8/2005 8/2006 8/2009 8/2010	CTDs, nutrients

Caption: A summary of hydrographic data used in this work, detailing research program, cruise identification, timing, and parameters observed.

Chapter 14: Copepod dynamics in the Chukchi Sea in response to regional climate variation

Kimmel, D., NOAA Fisheries, david.kimmel@noaa.gov

Spear, A.H.

Title: Copepod dynamics in the Chukchi Sea in response to regional climate variation

Authors: David G. Kimmel, Adam H. Spear

NOAA Alaska Fisheries Science Center, 7600 Sand Point Way NE, Seattle, WA 98115, USA

Abstract

High latitude ecosystems are undergoing rapid ecological change. Pacific Arctic waters have experienced sea ice loss and increasing heat flux from the north Pacific Ocean into the Chukchi Sea. The zooplankton community has been shown to correspond to water mass types that are endemic to the Chukchi and Beaufort Seas as well as water masses that are advected from the Bering Sea. Here we examine the zooplankton community composition from a series of surveys in the Chukchi Sea from 2010-2019. The goal was to characterize the spatial variability of the zooplankton community in relation to variability in water masses and examine the temporal change in several key taxa that are critical forage for higher trophic levels. These key taxa include the calanoid copepod *Calanus glacialis*, the dominant large copepod, and *Pseudocalanus* spp., the dominant small copepod. The Chukchi Sea showed evidence of Bering Sea influence in each year as water masses with associated zooplankton communities were advected through Bering Strait. The amount of the Chukchi Sea influenced by these water masses was greatest during 2017 and 2019 when extremely high temperatures were observed. The high temperatures appeared to reduce overall *C. glacialis* abundance throughout the Chukchi Sea. Small copepods, in particular *Pseudocalanus* spp. increased in abundance in locations closer to the Bering Strait in association with warmer temperatures. These community changes agree with prior observations in the Chukchi Sea; however, the more recent surveys had abundances that were approximately an order of magnitude lower than in past years. This suggests that continued warming will result in an altered zooplankton community in the Chukchi that is dominated by smaller-sized copepods. The result would be a shift in trophic connectivity between higher trophic levels in the Chukchi Sea region.

Introduction

Zooplankton form a vital link between primary producers and energy that accumulates in the zooplankton standing stock is transferred to multiple higher trophic levels either directly or indirectly. This is the case along the Chuckchi Sea shelf where zooplankton are consumed by fish such as Arctic (*Boreogadus saida*) and Pacific herring (*Clupea pallasii*) (Eisner et al. 2013), seabirds (Gall et al. 2017), and marine mammals, including a key subsistence species the bowhead whale (*Balaena mysticetus*) (Heide-Jørgensen et al. 2013). Differences among the zooplankton community of the Chukchi Sea are related to differences in hydrography, in particular water masses defined by temperature and salinity characteristics (Eisner et al. 2013, Pinchuk and Eisner 2017). These correlations appear to be robust and have been tracked as water moves from the northern Bering Sea into the Chukchi Sea (Hopcroft et al. 2010, Ershova et al. 2015a, Kim et al. 2020). These zooplankton communities consist of both meroplanktonic larvae and holoplankton, with the latter dominated by copepods (Hopcroft et al. 2010, Questel et al. 2013, Ershova et al. 2015a).

Long-term changes in the zooplankton population in the Chukchi Sea appear to correlate with the amount of ice cover present. Matsuno et al. (2011) compared zooplankton communities in the Chukchi Sea during years with high ice cover (1991-1992) to years with low ice cover (2007-2008) and found a positive impact on zooplankton production in the low ice years due to advection of Pacific species into the Chukchi Sea, but at the expense of the local Arctic species. Other studies also suggest an increase in biomass of zooplankton in the western Chukchi Sea coincident with warming, again pointing to an increased role of Pacific species in general and *Calanus glacialis,* an important lipid-storing copepod, specifically (Ershova et al. 2015a, Ershova et al. 2015b). *Calanus glacialis* populations differ between the NBS and CS (Nelson et al. 2009, Spear et al. 2019, Spear et al. 2020) and may have recently begun to decline in the face of unprecedented warming (Huntington et al. 2020). As the Chukchi Sea experiences less ice with increased warming, the response of the zooplankton community will play an important role should the system become more pelagic.

In this study, we examine the long-term distribution of two dominant zooplankton species in the Chukchi Sea from 2010 to 2019. As the Arctic is already experiencing significant transformation in the face of warming (Huntington et al. 2020), the primary objective was to determine if recent variability in oceanography were correlated to shifts in the abundance of two dominant copepods, *C. glacialis* and *Pseudocalanus* spp. complex (Ershova et al. 2016, Questel et al. 2016). Both species are key members of the food web and affect trophic transfer to higher organisms. We compared the abundances of each species in relation to dominant water masses in the Chukchi Sea over time and determined if specific patterns related to oceanography may be used to make inferences about each species in the face of continued warming. Evidence of shifting populations may also be interpreted as an indicator of future shifts in the food web of the Chukchi Sea from a benthic dominated system to one that is more pelagic (Grebmeier 2012).

Methods

Study area

The Chukchi Sea has a broad, mostly shallow (<50 m) shelf situated between Alaska, USA and Siberia, Russia (Fig. 1). Survey transects varied among years, 2010–2019, depending on the scientific focus for the year, available ship time, and ice distribution. Surveys were primarily conducted in the later summer (August-October) with some variability among years in exact survey timing. Surveys were conducted as part of several different research projects including Arctic Whale Ecology Study (ArcWEST) (Brattström et al. 2019), Chukchi Acoustic Oceanography and Zooplankton Study (CHAOZ) (Berchok et al. 2015), the Distributed Biological Observatory (https://www.pmel.noaa.gov/dbo/), and the Arctic Integrated Ecosystem Research Program (https://www.nprb.org/arctic-program/about-the-program/).

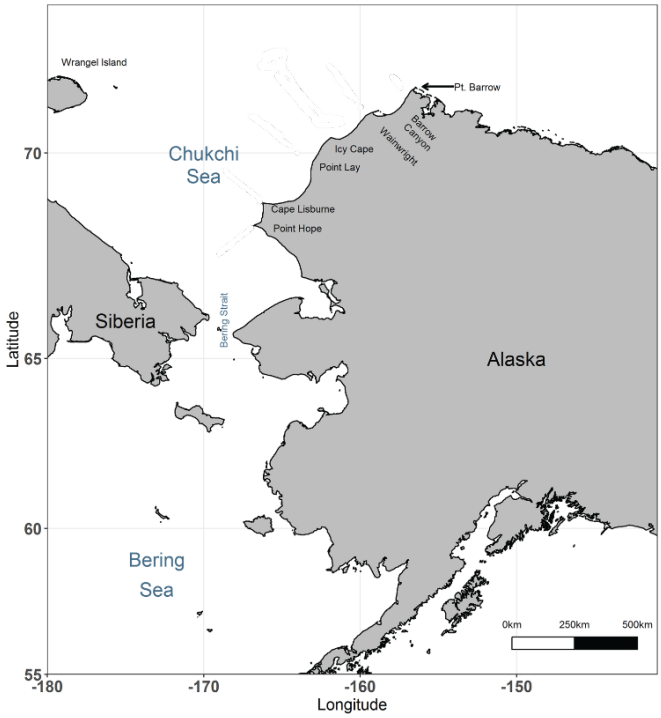

Figure 1.

Physical data

Water temperature (°C) and salinity data were calculated from conductivity temperature depth (CTD) measurements using a FastCat (Sea-bird SBE49) attached to the zooplankton tow cable. During 2019, the conducting winch failed during the second half of the research cruise, thus no FastCAT measurements were made for a portion of the sampling grid. As the zooplankton net samples the entire water column, the mean water column temperature and salinity were calculated over the maximum depth of the zooplankton tow. Based on these mean water temperatures and salinities, each station where a CTD measurement was taken was classified into a particular water mass based on (Danielson et al. 2020) (Table 1).

Table 1. Water mass designations from (Danielson et al. 2020).

Water mass	Abbreviations	Temperature range	Salinity range
Anadyr Water	AnW	$0 < T < 3$	$32.5 < S < 33.8$
Ice Melt Water/cool Coastal Water	IMW/cCW	$-2 < T < 3$	$22.0 < S < 30.8$
Cool Shelf Water	cSW	$0 < T < 3$	$30.8 < S < 32.5$

Warm Coastal Water	wCW	3 < T < 14	18.0 < S < 30.8
Warm Shelf Water	wSW	3 < T < 14	30.8 < S < 33.4
Modified Winter Water	MWW	-1 < T < 0	30.8 < S < 33.8
Winter Water	WW	-2 < T < -1	30.8 < S < 35.0
Atlantic Water	AtlW	-1 < T < 3	34.0 < S < 35.0
Bering Basin Water	BBW	3 < T < 5	33.8 < S < 35.0

Zooplankton data

Zooplankton were collected using multiple gear types over the sampling period. Zooplankton were collected primarily during daylight hours using a multiple-opening and closing 1 m^2 Tucker Sled trawl and sled-like runners at the bottom so that samples could be taken in close proximity to the bottom. A 505 µm (2013–2015) or a 333 µm (2010–2012) mesh net sampled while the sled was towed at a speed of 1.5–2.0 knots along the bottom for 2 min, then mechanically tripped to close and simultaneously open a second net to sample the entire water column from the bottom to the surface (wire retrieval rate 20 m min^{-1}). For smaller taxa, a 25 cm net with 150 µm mesh was suspended in the larger net that profiled the entire water column. Note that this setup is not ideal in cases where clogging in the 20- cm net occurs, thus the possibility of inaccurate volume filtered readings exist in this study. Samples that appeared questionable (e.g. low flowmeter readings, large jellyfish in the net) were excluded from the analysis. Taxa such as *C. glacialis* and *Pseudocalanus* spp. were enumerated in the water column only and not in the epibenthic samples. Both Tucker nets were equipped with a separate calibrated General Oceanics flow meter to estimate volume filtered. In other years, a paired bongo net (20 cm frame, 153 µm mesh for the smaller net and 60 cm frame, 505 µm mesh for the larger net) (Napp et al. 1996, Incze et al. 1997, Kimmel et al. 2018) from 2016-2019.Plankton captured by the nets were washed into the cod-ends, sieved through appropriately-sized wire mesh screens and preserved in glass jars with sodium borate-buffered 5% Formalin. Samples were inventoried at the end of the cruise and then sent to the Plankton Sorting and Identification Center in Szczecin, Poland, for processing. Subsampled taxa were enumerated and identified to lowest possible genera and life stage and returned to the Alaska Fisheries Science Center for verification. Ten percent of the returned samples were checked for quality assurance/quality control of species identification and enumeration.

Results

Water column mean water temperatures were warmer closer to the Alaska coast and in the southern portion of the Chukchi Sea over the study period (Fig. 2). The coldest temperatures were located near Point Barrow (see Fig 1). The warmest temperatures occurred during the latter portion of the study period, from 2017-2019 (Fig. 2). The coldest temperatures were observed in 2013 and 2016, though samples were restricted to northern locations during these years (Fig. 2). Salinity values were variable across the study region, showing no distinct spatial patterns that were repeated across years (Fig. 2). Overall salinity values also showed no temporal pattern (Fig. 2).

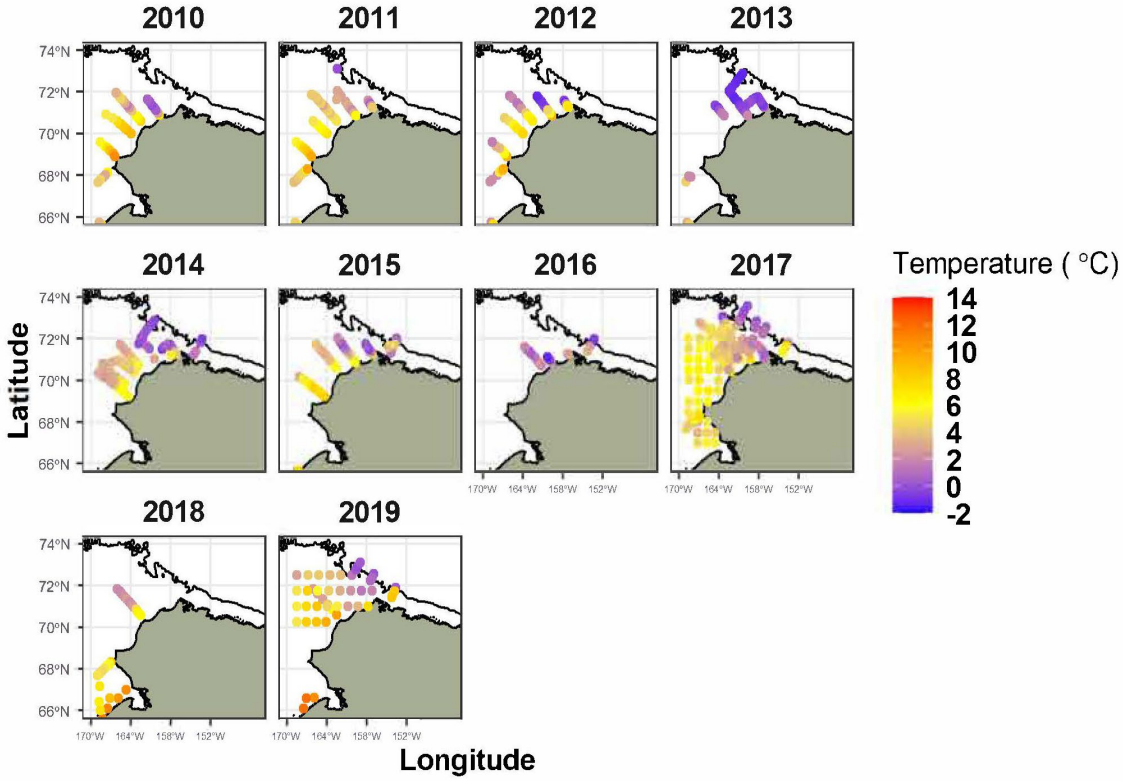
2010
2011
2012
2013
2014
2015
2016
2017
2018
2019
74°N
72°N
70°N
68°N
66°N
170°W
164°W
158°W
152°W
Latitude
Longitude
Temperature (°C)
14
12
10
8
6
4
2
0
-2

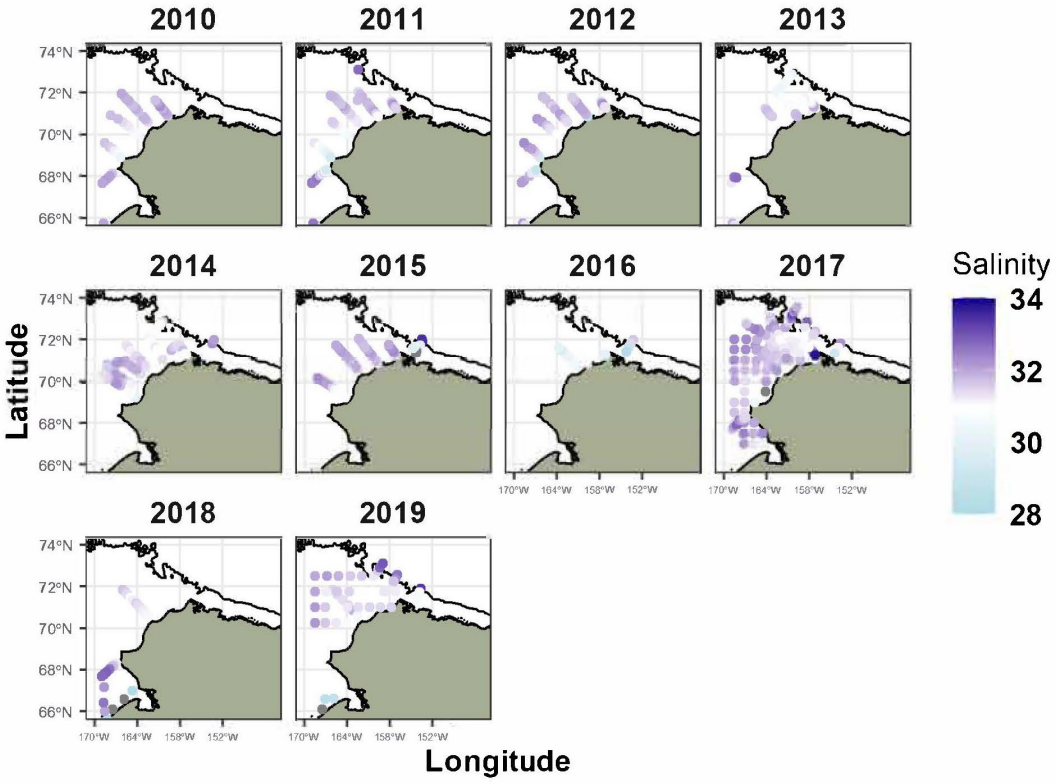
2010
2011
2012
2013
2014
2015
2016
2017
2018
2019
74°N
72°N
70°N
68°N
66°N
170°W
164°W
158°W
152°W
Latitude
Longitude
Salinity
34
32
30
28

Figure 2. Mean water column temperature (°C) and salinity for zooplankton tows.

The predominant water mass (52% of all stations) observed was warm shelf water (wSW, see Table 1). This water mass was widespread during the latter three years of the study period (Fig. 3). The next two most commonly encountered water masses were ice melt water/cool coastal water (IMW, 23% of stations) and cool shelf water (cSW, 22% of stations). These water masses were found in the northern portion of the study region, near Point Barrow and Barrow Canyon (see Fig. 1).

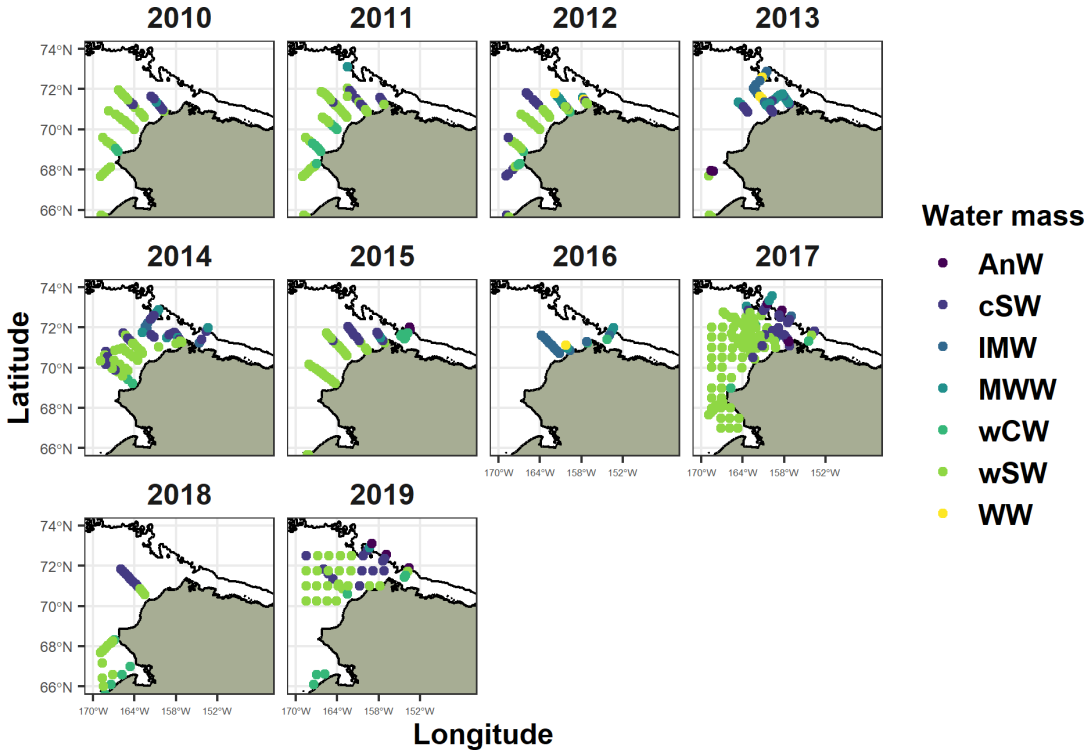

Figure 3. Distribution of water masses based on mean water column water temperature and salinity. Abbreviations for each water mass are defined in Table 1.

The two zooplankton species of interest showed differences in their distribution over the study period. *Calanus glacialis* was most abundant in the northern portion of the study region (Fig. 4). Abundances of *C. glacialis* peaked in 2011 and 2012, with numbers nearly three times as high as any other year (Fig. 4). Numbers for *C. glacialis* were lowest in 2019 (Fig. 4). *Pseudocalanus* spp. were most abundant in the southern portion of the study region, particularly in the latter three years (Fig. 5). *Pseudocalanus* spp. showed variability over time, peaking in 2014 and 2019 (Fig. 5). *C. glacialis* abundances were highest in cool shelf water, with abundances nearly 2.5 times greater than other

water masses (Table 2). In contrast, *Pseudocalanus* spp. was most abundant in warm shelf water and had very low abundances associated with Ice Melt Water (Table 2).

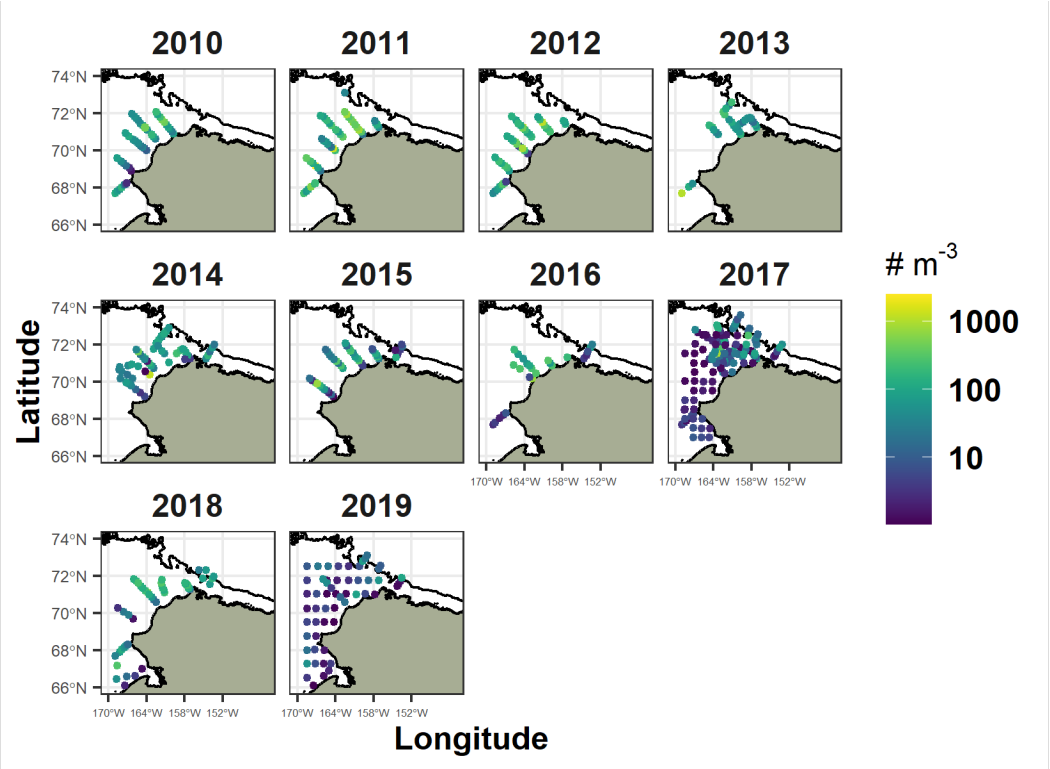

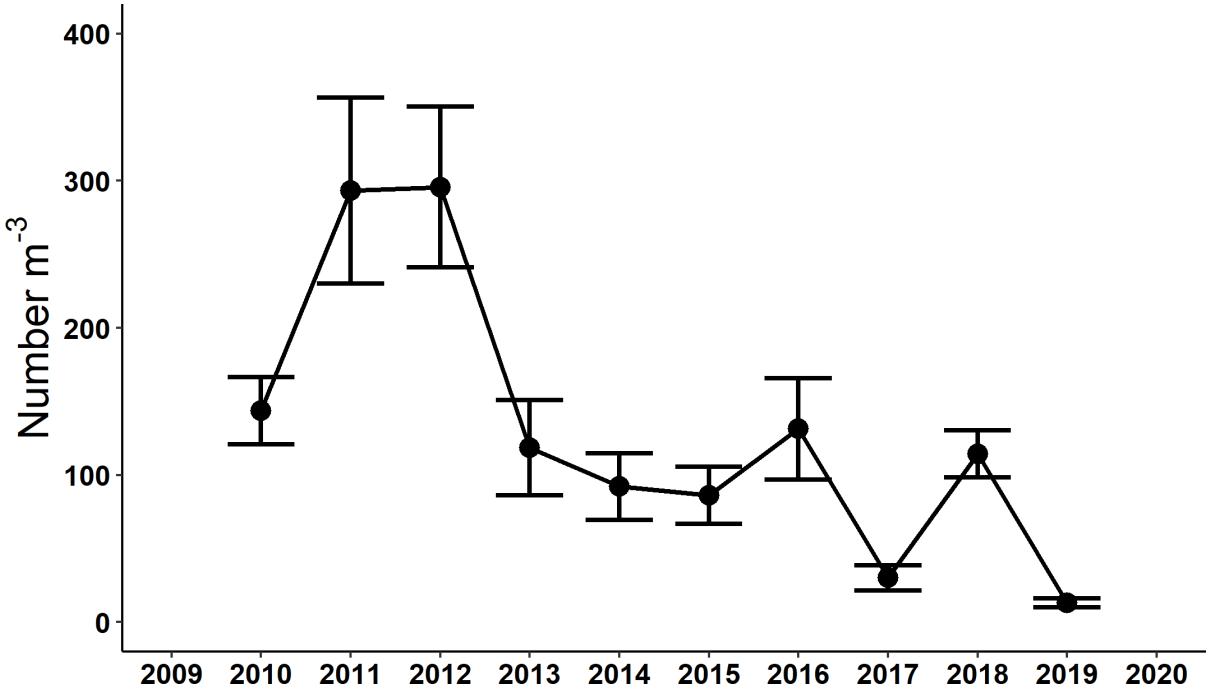

Figure 4. Spatial distribution of *Calanus glacialis* abundance (number m^{-3}) (top panel) and mean (± standard error) annual abundance (number m^{-3}) of *C. glacialis* abundance (bottom panel).

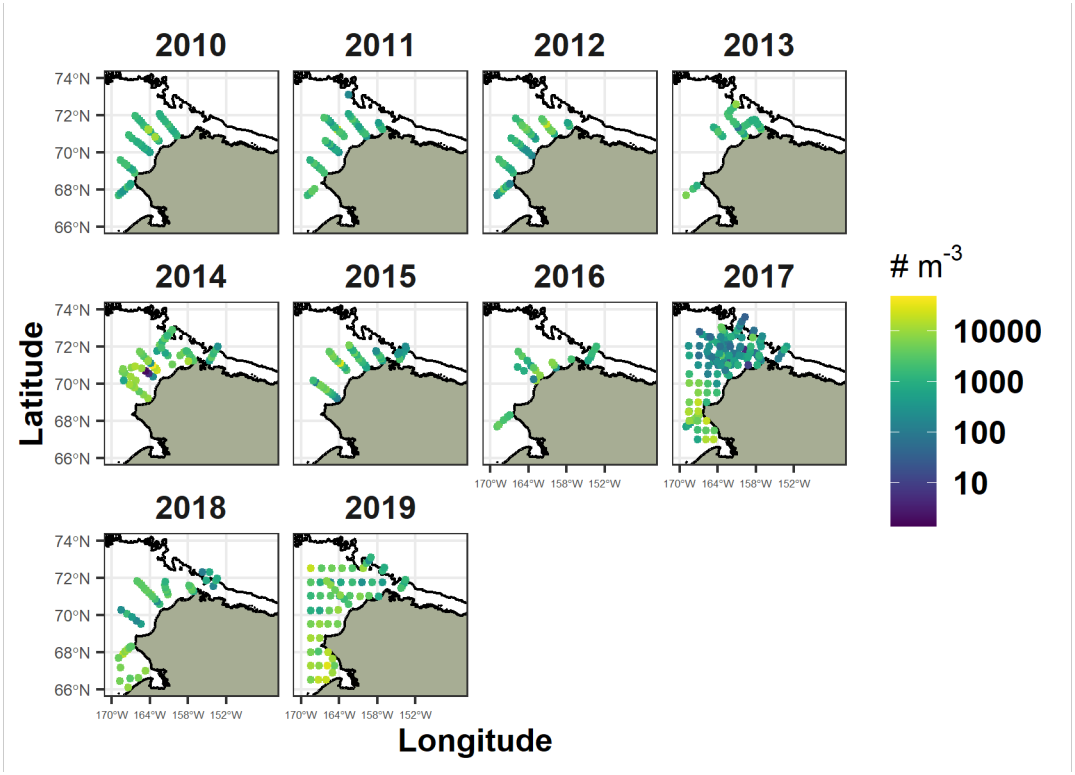

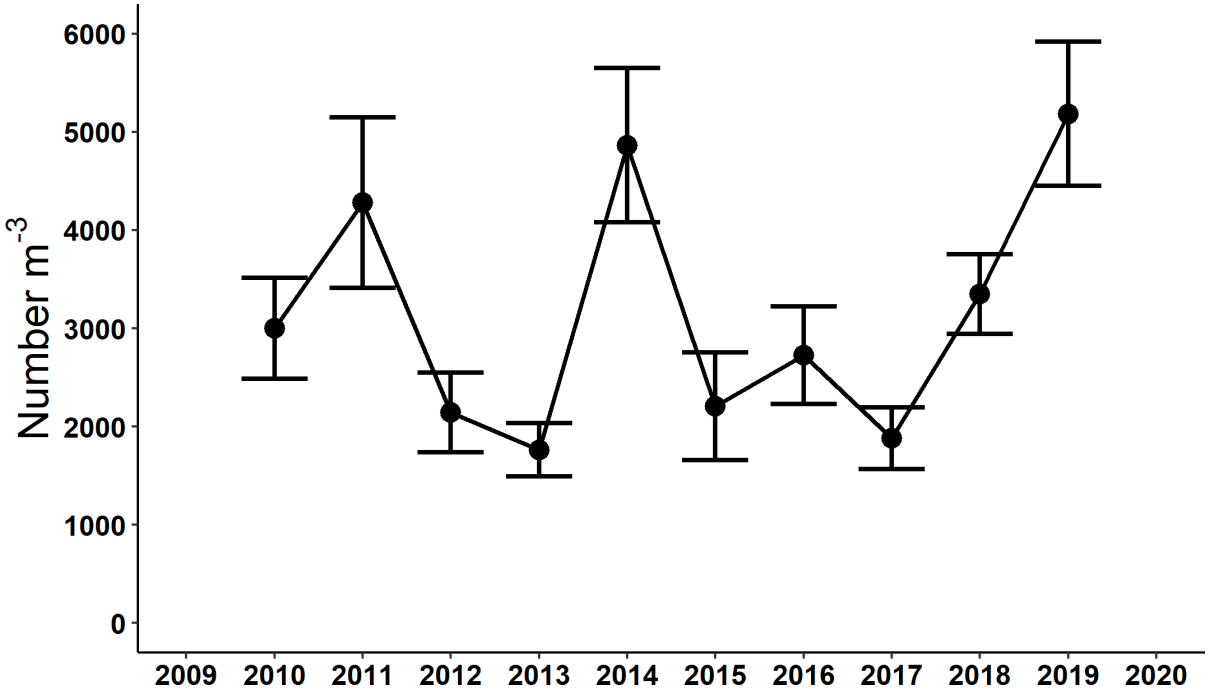

Figure 5. Spatial distribution of *Pseudocalanus* spp. abundance (number m^{-3}) (top panel) and mean (± standard error) annual abundance (number m^{-3}) of *Pseudocalanus* spp. abundance (bottom panel).

Table 2. Mean abundance (± standard deviation) of *C. glacialis* and *Pseudocalanus* spp. for each dominant water mass type

Water mass	Abbreviations	*C. glacialis*	*Pseudocalanus* spp.
Ice Melt Water/cool Coastal Water	IMW/cCW	100.45 (91.33)	1252.32 (1248.65)
Cool Shelf Water	cSW	267.92 (207.34)	5970.26 (4616.67)
Warm Shelf Water	wSW	88.59 (167.35)	6906.64 (7947.72)

Discussion

The two copepod species appeared to respond differently over the 10 year period of observation in the Chukchi Sea. The variability in intrusion of Bering Sea water over time relates strongly to the zooplankton community composition observed (Pinchuk and Eisner 2017, Kim et al. 2020, Spear et al. 2020) and both species were no exception. The copepod *Calanus glacialis* was associated with cold/cooler water and was more abundant during years that featured greater coverage of these water masses. The dominant smaller copepod, *Pseudocalanus* spp., was found in high abundance in both cool shelf water and warm shelf water. The response of both species appears to be related not only to water mass distribution, but also to population structure and species composition. The most striking response over the time-period was the widespread warm conditions in the latter half of the study period, resulting in a steady rise in the abundance of *Pseudocalanus* spp. beginning in 2017 in the southern Chukchi Sea and these species became widespread in 2019. This coincided with a precipitous decline in *C. glacialis* abundance during 2019. This unprecedented event comes after steady warming of the Chukchi Sea (Danielson et al. 2020), recent periods of low ice in the Bering Sea (Stabeno and Bell 2019), and unprecedented influx of heat into the Chukchi Sea (Huntington et al. 2020). Hereafter we attempt to provide context to this observation and present potential implications of a shift in these two species.

The copepod *C. glacialis* is known to be widespread in the shallow shelf of the Chukchi Sea (Hopcroft et al. 2010, Ershova et al. 2015b). Its annual life cycle appears to be related to ice formation and retreat (Søreide et al. 2010) in Arctic waters. However, more complex population dynamics appear to be occurring in the Chukchi Sea as it has been suggested that two distinct populations exist, a northern endemic population and once that is routinely advected from the northern Bering (Pinchuk and Eisner 2017, Spear et al. 2019). This is also supported by genetics (Nelson et al. 2009; Ashjian et al. 2017). Any differences in ecology between these two populations remain unknown; however, differences in temperature sensitivity may be expected as Arctic *Calanus* species have longer life cycles more adapted to longer periods of ice cover (Ji et al. 2012). This difference in temperature sensitivity may impact the number of annual cohorts, diapause timing, and lipid storage dynamics (Banas et al.

2016, Renaud et al. 2018). Therefore, the increasing influx of Bering Sea water (Woodgate 2018) resulting in increased population into the Arctic may result in food web changes related to different life-history behavior of the *C. glacialis* Bering Sea population.

The copepod *Pseudocalanus* spp. is complex of up to four species, two of which are temperate (*P. mimus* and *P. newmani*) and two are Arctic (*P. acuspes* and *P. minutus*) (Ershova et al. 2016, Questel et al. 2016). These species are difficult to distinguish morphologically, but using genetics Ershova et al. (2016) determined that *P. acuspes* is likely the dominant genus in the Chukchi Sea with *P. newmani* occurring as well, though significant variability over time was observed. Only *P. mimus* did not contribute significantly to overall biomass in the Chukchi Sea (Ershova et al. 2016). The presence of multiple species may explain the similar abundance of *Pseudocalanus* spp. in both cool and warm water masses as *P. acuspes/P. minutus* may have been the primary taxa in cooler waters whereas *P. newmani* may have been the representative taxa during the warming event in the latter half of the record. Such differences have important implications for the food web as *P. acuspes* has higher rates of estimated secondary production on average (Ershova et al. 2016), is larger and stores more lipids relative to temperature species (McLaren et al. 1989). Thus, the relative shift to smaller bodied zooplankton predicted for boreal regions may be complicated by differing ecology of these species and *Pseudocalanus* spp. is a prime example.

As the Arctic continues to warm at a rapid pace, changes in the biogeography of the Chukchi Sea should be expected (Sigler et al. 2017). The connectivity between the northern Bering Sea and the Chukchi will increase (Woodgate 2018) with longer periods of reduced ice cover being predicted (Overland and Wang 2007). We reach similar conclusions to others that Pacific species endemic to the Bering Sea will become increasingly prevalent in the Chukchi Sea food web (Matsuno et al. 2011, Sigler et al. 2011, Ershova et al. 2015b, Kim et al. 2020). Such a change will impact the relative timing of zooplankton availability in general and these species specifically. A reduction in overall lipid availability may be one consequence of population shifts, though it has been suggested that species that do not store lipids will fare poorly in Arctic waters (Ershova et al. 2016) or that other mechanisms will compensate for lower lipid occurrence (Renaud et al. 2018). Here we focused only on two key copepod species; however, we aim to examine the community as a whole to elucidate further patterns related to oceanography.

Literature Cited

Ashjian, C.J., Campbell, R.G., Gelfman, C., Alatalo, P., Elliott, S.M., 2017. Mesozooplankton abundance and distribution in association with hydrography on Hanna Shoal, NE Chukchi Sea, during August 2012 and 2013. Deep Sea Research Part II: Topical Studies in Oceanography. **144**:21-36.

Banas, N. S., E. F. Møller, T. G. Nielsen, and L. B. Eisner. 2016. Copepod Life Strategy and Population Viability in Response to Prey Timing and Temperature: Testing a New Model across Latitude, Time, and the Size Spectrum. Frontiers in Marine Science **3**:225.

Berchok, C., J. Crance, E. Garland, J. Mocklin, P. Stabeno, N. JM, B. Rone, S. AH, M. Wang, and C. Clark. 2015. Chukchi Offshore Monitoring in Drilling Area (COMIDA): factors affecting the distribution and relative abundance of endangered whales and other marine mammals in the Chukchi Sea. Final report of the Chukchi Sea Acoustics, Oceanography, and Zooplankton Study. National Marine Mammal Laboratory, Alaska Fisheries Science Center, Nationa Marine Fisheries Service.

Brattström, V., J. A. Mocklin, C. J. L, and N. A. Friday. 2019. Arctic Whale Ecology Study (ARCWEST): Use of the Chukchi Sea by Endangered Baleen and Other Whales (Westward Extension of the BOWFEST). Final Report of the Arctic Whale Ecology Study (ARCWEST). Marine Mammal Laboratory, Alaska Fisheries Science Center, National Marine Fisheries Service, Seattle, WA USA.

Danielson, S. L., O. Ahkinga, C. Ashjian, E. Basyuk, L. W. Cooper, L. Eisner, E. Farley, K. B. Iken, J. M. Grebmeier, L. Juranek, G. Khen, S. R. Jayne, T. Kikuchi, C. Ladd, K. Lu, R. M. McCabe, G. W. K. Moore, S. Nishino, F. Ozenna, R. S. Pickart, I. Polyakov, P. J. Stabeno, R. Thoman, W. J. Williams, K. Wood, and T. J. Weingartner. 2020. Manifestation and consequences of warming and altered heat fluxes over the Bering and Chukchi Sea continental shelves. Deep Sea Research Part II: Topical Studies in Oceanography.

Eisner, L., N. Hillgruber, E. Martinson, and J. Maselko. 2013. Pelagic fish and zooplankton species assemblages in relation to water mass characteristics in the northern Bering and southeast Chukchi seas. Polar Biology **36**:87-113.

Ershova, E. A., R. R. Hopcroft, and K. N. Kosobokova. 2015a. Inter-annual variability of summer mesozooplankton communities of the western Chukchi Sea: 2004-2012. Polar Biology **38**:1461-1481.

Ershova, E. A., R. R. Hopcroft, K. N. Kosobokova, K. Matsuno, R. J. Nelson, A. Yamaguchi, and L. B. Eisner. 2015b. Long-Term Changes in Summer Zooplankton Communities of the Western Chukchi Sea, 1945-2012. Oceanography **28**:100-115.

Ershova, E. A., J. M. Questel, K. Kosobokova, and R. R. Hopcroft. 2016. Population structure and production of four sibling species of Pseudocalanus spp. in the Chukchi Sea. Journal of Plankton Research.

Gall, A. E., T. C. Morgan, R. H. Day, and K. J. Kuletz. 2017. Ecological shift from piscivorous to planktivorous seabirds in the Chukchi Sea, 1975-2012. Polar Biology **40**:61-78.

Grebmeier, J. M. 2012. Shifting Patterns of Life in the Pacific Arctic and Sub-Arctic Seas. Pages 63-78 *in* C. A. Carlson and S. J. Giovannoni, editors. Annual Review of Marine Science, Vol 4.

Heide-Jørgensen, M. P., K. L. Laidre, N. H. Nielsen, R. G. Hanson, and A. Røstand. 2013. Winter and spring diving behavior of bowhead whales relative to prey. Animal Biotelemetry **1**:15.

Hopcroft, R. R., K. N. Kosobokova, and A. I. Pinchuk. 2010. Zooplankton community patterns in the Chukchi Sea during summer 2004. Deep-Sea Research Part Ii-Topical Studies in Oceanography **57**:27-39.

Huntington, H. P., S. L. Danielson, F. K. Wiese, M. Baker, P. Boveng, J. J. Citta, A. De Robertis, D. M. S. Dickson, E. Farley, J. C. George, K. Iken, D. G. Kimmel, K. Kuletz, C. Ladd, R. Levine, L. Quakenbush, P. Stabeno, K. M. Stafford, D. Stockwell, and C. Wilson. 2020. Evidence suggests potential transformation of the Pacific Arctic ecosystem is underway. Nature Climate Change.

Incze, L. S., D. W. Siefert, and J. M. Napp. 1997. Mesozooplankton of Shelikof Strait, Alaska: Abundance and community composition. Continental Shelf Research **17**:287-305.

Ji, R., C. J. Ashjian, R. G. Campbell, C. Chen, G. Gao, C. S. Davis, G. W. Cowles, and R. C. Beardsley. 2012. Life history and biogeography of Calanus copepods in the Arctic Ocean: An individual-based modeling study. Progress in Oceanography **96**:40-56.

Kim, J.-H., K.-H. Cho, H. S. La, E. J. Choy, K. Matsuno, S.-H. Kang, W. Kim, and E. J. Yang. 2020. Mass occurrence of Pacific copepods in the southern Chukchi Sea during summer: Implications of the high-temperature Bering Summer water. Frontiers in Marine Science **7**:612.

Kimmel, D. G., L. B. Eisner, M. T. Wilson, and J. T. Duffy-Anderson. 2018. Copepod dynamics across warm and cold periods in the eastern Bering Sea: Implications for walleye pollock (Gadus chalcogrammus) and the Oscillating Control Hypothesis. Fisheries Oceanography **27**:143-158.

Matsuno, K., A. Yamaguchi, T. Hirawake, and I. Imai. 2011. Year-to-year changes of the mesozooplankton community in the Chukchi Sea during summers of 1991, 1992 and 2007, 2008. Polar Biology **34**:1349-1360.

McLaren, I. A., J. M. Sévigny, and C. J. Corkett. 1989. Temperature dependent development in *Pseudocalanus* species. Canadian Journal of Zoology **67**:559–564.

Napp, J. M., L. S. Incze, P. B. Ortner, D. L. W. Siefert, and L. Britt. 1996. The plankton of Shelikof Strait, Alaska: Standing stock, production, mesoscale variability and their relevance to larval fish survival. Fisheries Oceanography **5**:19-38.

Nelson, R. J., E. C. Carmack, F. A. McLaughlin, and G. A. Cooper. 2009. Penetration of Pacific zooplankton into the western Arctic Ocean tracked with molecular population genetics. Marine Ecology Progress Series **381**:129-138.

Overland, J. E., and M. Wang. 2007. Future regional Arctic sea ice declines. Geophysical Research Letters **34**.

Pinchuk, A. I., and L. B. Eisner. 2017. Spatial heterogeneity in zooplankton summer distribution in the eastern Chukchi Sea in 2012–2013 as a result of large-scale interactions of water masses. Deep Sea Research Part II: Topical Studies in Oceanography **135**:27-39.

Questel, J. M., L. Blanco-Bercial, R. R. Hopcroft, and A. Bucklin. 2016. Phylogeography and connectivity of the *Pseudocalanus* (Copepoda: Calanoida) species complex in the eastern North Pacific and Pacific Arctic Region. Journal of Plankton Research **38**:610-623.

Questel, J. M., C. Clarke, and R. R. Hopcroft. 2013. Seasonal and interannual variation in the planktonic communities of the northeastern Chukchi Sea during the summer and early fall. Continental Shelf Research **67**:23-41.

Renaud, P. E., M. Daase, N. S. Banas, T. M. Gabrielsen, J. E. Søreide, Ø. Varpe, F. Cottier, S. Falk-Petersen, C. Halsband, D. Vogedes, K. Heggland, and J. Berge. 2018. Pelagic food-webs in a changing Arctic: a trait-based perspective suggests a mode of resilience. ICES Journal of Marine Science **75**:1871-1881.

Sigler, M. F., F. J. Mueter, B. A. Bluhm, M. S. Busby, E. D. Cokelet, S. L. Danielson, A. De Robertis, L. B. Eisner, E. V. Farley, K. Iken, K. J. Kuletz, R. R. Lauth, E. A. Logerwell, and A. I. Pinchuk. 2017. Late summer zoogeography of the northern Bering and Chukchi seas. Deep-Sea Research Part Ii-Topical Studies in Oceanography **135**:168-189.

Sigler, M. F., M. Renner, S. L. Danielson, L. B. Eisner, R. R. Lauth, K. J. Kuletz, E. A. Logerwell, and G. L. Hunt, Jr. 2011. Fluxes, Fins, and Feathers Relationships Among the Bering, Chukchi, and Beaufort Seas in a Time of Climate Change. Oceanography **24**:250-265.

Søreide, J. E., E. V. A. Leu, J. Berge, M. Graeve, and S. Falk-Petersen. 2010. Timing of blooms, algal food quality and *Calanus glacialis* reproduction and growth in a changing Arctic. Global Change Biology **16**:3154-3163.

Spear, A., J. Duffy-Anderson, D. Kimmel, J. Napp, J. Randall, and P. Stabeno. 2019. Physical and biological drivers of zooplankton communities in the Chukchi Sea. Polar Biology **42**:1107-1124.

Spear, A., J. Napp, N. Ferm, and D. Kimmel. 2020. Advection and in situ processes as drivers of change for the abundance of large zooplankton taxa in the Chukchi Sea. Deep Sea Research Part II: Topical Studies in Oceanography **177**.

Stabeno, P. J., and S. W. Bell. 2019. Extreme Conditions in the Bering Sea (2017–2018): Record-Breaking Low Sea-Ice Extent. Geophysical Research Letters **46**:8952-8959.

Woodgate, R. 2018. Increases in the Pacific inflow to the Arctic from 1990 to 2015, and insights into seasonal trends and driving mechanisms from year-round Bering Strait mooring data. Progress in Oceanography **160**:124-154.

Chapter 15: Detection of high levels of paralytic shellfish toxins in Northern Alaskan food webs and estimated toxin doses to Pacific walruses and Bowhead whales

Lefebvre, K., et al., NOAA Fisheries, kathi.lefebvre@noaa.gov

Lefebvre, K. et al. (in preparation) ***Paralytic shellfish toxins (PSTs) in Arctic food webs in 2019 during anomalously warm ocean conditions and estimated toxin doses to Pacific walruses and bowhead whales***

Introduction: Climate change-related ocean warming and reduction in Arctic sea-ice extent, duration and thickness increase the risk of cyst germination and toxic blooms of the dinoflagellate, Alexandrium catenella. This algal species produces neurotoxins that impact marine wildlife health and cause the human illness known as Paralytic Shellfish Poisoning (PSP).

Methods: This study reports Paralytic Shellfish Toxin (PST) concentrations quantified in Arctic food web samples which include phytoplankton, zooplankton, benthic clams, benthic worms, and pelagic fish collected in summer 2019 during anomalously warm ocean conditions.

Results and Discussion: PSTs were detected in all trophic levels with the highest concentrations in benthic clams collected offshore on the continental shelf in the Beaufort, Chukchi, and Bering Seas. Most notably, toxic benthic clams (*Macoma calcarea)* were found north of Saint Lawrence Island where Pacific walruses (*Odobenus rosmarus*) are known to forage for a variety of benthic species, including *Macoma*. Fecal samples collected from 13 walruses harvested for subsistence purposes near Saint Lawrence Island during March to May 2019, all contained detectable levels of STX. In contrast, only 64% of fecal samples from zooplankton-feeding bowhead whales (n = 9) harvested between March and September 2019 in coastal waters of the Beaufort Sea near Utqiaġvik (formerly Barrow) and Kaktovik were toxin-positive. This was consistent with the lower concentrations of PSTs found in regional zooplankton prey. These findings raise concerns regarding potential increases in PST/STX exposure risks and health impacts to Arctic marine mammals as ocean warming and sea ice reduction continue.

Intended Journal: Harmful Algae

Author list in order:

1) Kathi A. Lefebvre (Kathi.Lefebvre@noaa.gov) Environmental and Fisheries Science Division, Northwest Fisheries Science Center, National Marine Fisheries Service, NOAA, Seattle, WA 98112, USA

2) Evangeline Fachon efachon@whoi.edu a. Biology Department, Woods Hole Oceanographic Institution, Woods Hole, MA 02543, USA b. Department of Earth, Atmospheric, and Planetary Sciences, Massachusetts Institute of Technology, 77 Massachusetts Ave, Cambridge, MA 02139, USA

3) Emily K. Bowers (Emily.Bowers@noaa.gov) Environmental and Fisheries Science Division, Northwest Fisheries Science Center, National Marine Fisheries Service, NOAA, Seattle, WA 98112, USA

4) David G. Kimmel (david.kimmel@noaa.gov) Alaska Fisheries Science Center, NOAA, National Marine Fisheries Service, Seattle, WA, USA

5) Jonathan A. Snyder (Jonathan_Snyder@fws.gov) US Fish and Wildlife Service

6) Raphaela Stimmelmayr 1 North-Slope Borough Department of Wildlife management, Utqiagvik, Alaska; 2 Institute of Arctic Biology, University of Alaska Fairbanks, Fairbanks, Alaska

7) Jacqueline Grebmeier (jgrebmei@umces.edu) University of Maryland Center for Environmental Science, Chesapeake Biological Laboratory, Solomons, MD 20688, USA

8) Steve Kibler (steve.kibler@noaa.gov) NOAA National Ocean Service, Beaufort Laboratory, Beaufort, NC 28516, Ph: (252) 728-82737, Email: steve.kibler@noaa.gov

9) Donald M. Anderson (danderson@whoi.edu) Biology Department, Woods Hole Oceanographic Institution, Woods Hole, MA 02543, USA

10) David Kulis (dkulis@whoi.edu) Biology Department, Woods Hole Oceanographic Institution, Woods Hole, MA 02543, USA

11) Jim Murphy (jim.murphy@noaa.gov)

12) Jeanette C. Gann (jeanette.gann@noaa.gov) NOAA Alaska Fisheries Science Center, National Marine Fisheries Service, Juneau, AK 99801

13) Dan Cooper (dan.cooper@noaa.gov) Alaska Fisheries Science Center, NOAA, National Marine Fisheries Service, Seattle, WA, USA

14) Lisa B. Eisner (lisa.eisner@noaa.gov) NOAA Alaska Fisheries Science Center, Seattle, WA 98115

15) Janet T. Duffy-Anderson (janet.duffy-anderson@noaa.gov) Alaska Fisheries Science Center, NOAA, National Marine Fisheries Service, Seattle, WA, USA

16) Gay Sheffield (gay.sheffield@alaska.edu); University of Alaska Fairbanks, Alaska Sea Grant / Marine Advisory Program, PO Box 400, Nome, Alaska 99762

17) Robert S. Pickart (rpickart@whoi.edu) Woods Hole Oceanographic Institution, Woods Hole, MA 02543, USA

18) Anna Mounsey (anna.mounseyd@gmail.com) Environmental and Fisheries Science Division, Northwest Fisheries Science Center, National Marine Fisheries Service, NOAA, Seattle, WA 98112, USA

19) Maryjean L. Willis (maryjean.l.willis@noaa.gov) Environmental and Fisheries Science Division, Northwest Fisheries Science Center, National Marine Fisheries Service, NOAA, Seattle, WA 98112, USA

20) Phyllis Stabeno (phyllis.stabeno@noaa.gov)

21) Elizabeth Siddon (elizabeth.siddon@noaa.gov) NOAA Alaska Fisheries Science Center, National Marine Fisheries Service, Juneau, AK 99801

Chapter 16: Growing importance of *Synechococcus* abundance and biomass in the Northern Bering and Chukchi seas

Lomas, M.W., Bigelow Laboratory for Ocean Sciences, mlomas@bigelow.org

Eisner, L.E., Nielsen, J., Danielson, S., Mordy, C.W., Stabeno, P.J., Laney, S.R.

Growing importance of *Synechococcus* abundance and biomass in the Northern Bering and Chukchi seas.

Lomas, M.W.[1], Eisner, L.E.[2,3], Nielsen, J.[4], Danielson, S.[5], Mordy, C.W.[4,6] Stabeno, P.J.[6], Laney, S.R.[7]

[1] Bigelow Laboratory for Ocean Sciences, East Boothbay, ME 04544, USA

[2] NOAA Alaska Fisheries Science Center, Seattle, WA 98115, USA
[3] NOAA Alaska Fisheries Science Center, Auke Bay Laboratories, Juneau, AK 99801, USA
[4] Cooperative Institute for Climate, Ocean, and Ecosystem Studies, University of Washington, Seattle, WA 98115, USA
[5] College of Fisheries and Ocean Science, University of Alaska Fairbanks, Fairbanks, AK 99775, USA
[6] NOAA Pacific Marine Environmental Laboratory, Seattle, WA 98115, USA
[7] Woods Hole Oceanographic Institution, Woods Hole, MA 02543, USA

Key words: Phytoplankton, Bering Sea, Chukchi Sea, Synechococcus

Intended Journal: Oceans

Abstract: Size structure of phytoplankton populations has been shown to be an important determinant of the flow of carbon and energy to higher trophic levels in Arctic ecosystems. Phytoplankton populations dominated by small (<10um) pico- and nanophytoplankton cells are generally dominated by eukaryotic flagellates that are tightly grazed by microzooplankton leading to increases in trophic length. General dogma suggests that the picocyanobacteria *Synechococcus* is detectable but comprises a negligible fraction of phytoplankton carbon in Arctic ecosystems. As part of the Arctic IERP sampling program, we quantified the abundance of the *Synechococcus*, and other picophytoplankton, during the spring to fall period between 2017-2019 in the Northern Bering and Chukchi Seas. *Synechococcus* abundances increased from <500 cells/ml in spring to >50,000 cells/ml in the fall around Kotzebue Sound. Furthermore, the spatial extent of regions with elevated *Synecococcus* abundances in late summer/fall, as well as the absolute abundances, increased from 2017 to 2019, coincident with increasing late summer/fall water temperatures. When integrated over the euphotic zone, *Synechococcus* contributed up to 40% of estimated total phytoplankton carbon during late summer/fall in Kotzebue sound and the region near Icy Cape. These observations support an increased importance of a previously marginal phytoplankton group during a warming period in the Chukchi Sea. The full implications of these changes in the phytoplankton community remain to be resolved.

Introduction: Arctic and subarctic seas are facing many stressors that may lead to significant changes in its function in the future (IPCC 2021). An important change is sea ice loss that when coupled with intensification of the hydrological cycle (Peterson et al., 202; Serreze et al., 2006) will likely lead to increases in stratification in near shore shelf systems, a key controlling factor of the productivity, through negative impacts on nutrient inputs, and structure of marine ecosystems of the Arctic Ocean (Carmack et al., 2006, Carmack 2007). The impact(s) of these

changes on phytoplankton at the base of marine food chains is not completely resolved, particularly changes in phytoplankton community size structure (Tremblay and Gagnon, 2009).

Globally picophytoplankton (<2um) are well known and dominate in the major oligotrophic ocean gyres, but dogma is that they are not quantitatively important in the sub/arctic systems (Buitenhuis et al. 2011, Flombaum et al. 2013). In contrast, numerous measurements of size-fractionated chlorophyll have shown that the picoplankton size fraction can dominate phytoplankton biomass in sub/arctic systems during oligotrophic periods (e.g., summer) and regions (e.g., off-shelf) (e.g., Booth and Horner, 1997; Brugel et al., 2009; Legendre et al., 1993; Li et al., 2009; Odate, 1996). Given that picophytoplankton have a much higher carbon to chlorophyll ratio than microphytoplankton, it is likely that their importance to both carbon cycling and quality as a food source has been further underestimated (Lee et al., 2013). Within the picophytoplankton size class there is a wide diversity of both eukaryotic (e.g., prasinophytes and cryptophytes, Lovejoy et al., 2007; Sergeeva et al., 2010) and prokaryotic (e.g., Cottrell and Kirchman, 2009; Not et al., 2005) organisms. More recent studies have used flow cytometry as a more efficient tool to numerically quantify these <2um cells into operational categories (i.e., pico- and nanophytoplankton; Laney and Sosik, 2014), although some organisms do contain unique pigment signatures that allow them to be distinguished from other similar cells. For example, *Synechoccocus* and cryptophytes both contain the orange pigment phytoerythrin, and thus can be identified as specific groups within the pico- and nanophytoplankton.

In the region between the eastern Beaufort Sea and Baffin Bay picophytoplankton numerically dominate in deeper water stations off shelf, and particularly in the SCM (e.g., Ardyna et al., 2011, Schlooss et al. 2008). In the Chukchi and western Beaufort Seas, it has also been shown that small prasinophytes, other flagellates (e.g., cryptophytes) and non-colonial phaeocystis (<5um) dominated in the deeper basin sites during summer and fall, while diatoms dominated on the shallow shelf (Gosselin et al 1997, Booth and Horner, 1997; Hill et al., 2005; Sergeeva et al., 2010; Sherr et al., 2003). Based upon a few stations in the southern Bering Sea, Liu et al. (2002) observed that picophytoplankton abundance, both *Synechococcus* and eukaryotes decreased from the basin to the shelf. Some eukaryotic picophytoplankton strains have been shown to persist through the winter maintaining growth rates that exceed grazing losses, and have been suggested to represent unique temperature controlled biogeographical clades (Lovejoy et al., 2007). Representatives of this eukaryotic psycrophillic clade are pan-Arctic, with some representatives having maximum growth temperatures of ~12.5◦C, so there may be problems in the future, and could cause disruptions in the food web. In contrast, the picocyanobacteria *Synechococcus,* has been found to be associated with slightly warmer and saltier water than eukaryotic picoplankton (Cottrell and Kirchman, 2009; Not et al., 2005; Tremblay and Gagnon, 2009, Waleron et al., 2007, Gradinger and Lenz 1989). Interestingly, Waleron et al. (2007), using eDNA analysis, identified 6 OTUs similar to *Synechoococcus* from the Mackenzie River system. These OTUs were linked to freshwater *Synechococcus* and it was concluded that they flushed into the system and implied they survived but were not actively growing.

The distributions of picophytoplankton around the sub/Arctic are important to understand, in particularly their contributions to total biomass (not just numbers), as well as the environmental variables that they correlate with to understand the niches that they currently occupy and when

those niche boundaries might be exceeded. In this study we address the following questions. 1) what are the large spatial (i.e., cross shelf) and seasonal patterns of *Synechococcus* abundance and biomass in the Northern Bering and Chukchi Seas; 2) what are the environmental parameters associated with patterns in *Synecococcus* biomass; and 3) is there evidence of long term trends in *Synechococcus* biomass.

Methods: *Sample collection:* Physical, chemical and biological measurements were made as part of the Arctic Integrated Ecosystem Research Program (AIERP, 4 cruises, and one cruise of opportunity) within the Northern Bering and Chukchi Sea region (Table 1, Figure 1). Samples were collected in clean Niskin bottle at roughly 10m spacing throughout the water column. At each station and depth a range of discrete phytoplankton samples were collected including size-fractionated chlorophyll a (Chl-a), picoplankton and nanoplankton counts by quantitative flow cytometry (e.g., Lomas et al., 2010), microplankton counts by inverted microscopy and FlowCAM, and seston particulate organic carbon (POC). Only flow cytometry data data are reported in this study.

Phytoplankton cell counts and carbon biomass estimates: Samples for picoplankton enumeration were generally collected at four to seven depths throughout and just below the euphotic zone, fixed with paraformaldehyde (0.5% final concentration), stored at ~4°C for 1-2 h, before long-term storage at -80°C. Samples were analyzed on a Becton Dickinson (formerly Cytopeia Inc.) Influx or Jazz cytometer using a 488 nm blue excitation laser, appropriate Chl-*a* (692 ± 20 nm) and phycoerythrin (580 ± 15 nm) bandpass filters, and was calibrated daily with 0.53-µm and 3.0-µm fluorescent microbeads (Spherotech Inc. Libertyville, Illinois, USA). Each sample was run for 4-6 min (~0.3-0.5 mL total volume analyzed), with log-amplified Chl-*a* and phycoerythrin fluorescence, and forward and right-angle scatter signals recorded. Data files were analyzed from two-dimensional scatter plots based on Chl.-*a* or phycoerythrin fluorescence and characteristic light scattering properties (e.g., DuRand and Olson, 1996) using FCS Express 3.0 (DeNovo Software Inc. Los Angeles, California, USA) or SortWare (Becton Dickenson, East Rutherford, New Jersey, USA). Picophytoplankton, operationally defined as cells <3.0-um, were identified as *Synechococcus* cells based upon cell size and the presence of phycoerythrin. Based upon these gating criteria, the number of cells in each identified population was enumerated and converted to cell abundances by the volume-analyzed method (Sieracki et al., 1993). Precision of triplicate samples was <10% for cell concentrations >200 cells mL^{-1}. Carbon per cell was estimated for flow cytometrically identified phytoplankton using a calibration curve that related cellular particulate organic carbon (POC) to normalized geometric mean cellular forward scatter (proxy for cell size) (e.g., DuRand et al., 2001, Casey et al. 2013, data specific to the flow cytometer used in this study). Carbon content of each identified population was estimated by multiplying volumetric cell abundance and POC per cell derived from the calibration curve.

Table 1. Summary details associated with cruises included in this analysis.

Cruise ID	Dates	Latitude (°N)	Longitude (°W)
		(min-max)	(min-max)
SKQ-2017-09S	5th June – 26th June 2017	56.4 to 69	-172.6 to -169
OS-1701	6th Aug – 27th Sept 2017	67.0 to 72.5	-169.0 to -152.3
SKQ-2018-13S	7th June – 23rd June 2018	63.3 to 69	-171.5 to -164.4
HLY-1801	8th Aug – 23rd Aug 2018	64.7 to 71.8	-170.0 to -153.8
OS-1901	1st Aug – 2nd Oct. 2019	63.3 to 72.5	-171.5 to -154.2

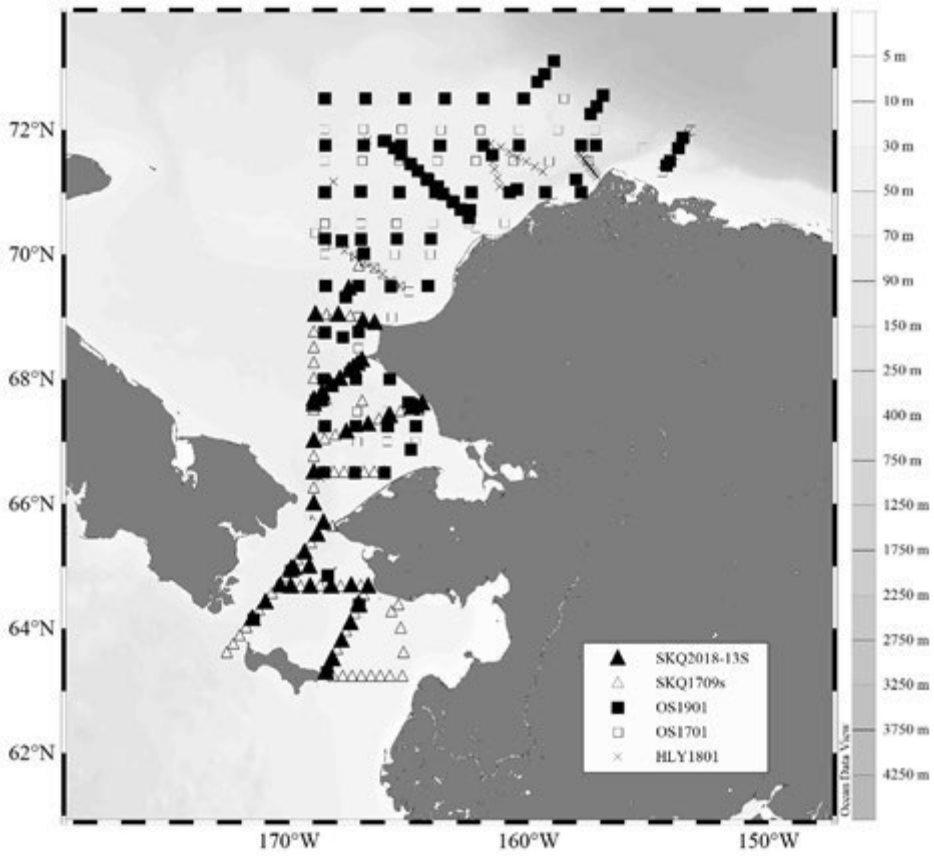

Figure 1. Map of station locations included in this analysis. There are a total of 494 discrete stations, although some are sampled multiple times over multiple cruises within the same program.

Chlorophyll: Sample volumes varied depending upon the cruise, but ranged from 0.1 - 1L, and in all cases were gently vacuum filtered (≤5 mm Hg) for total chlorophyll (Chl-a) analysis onto Whatman GFF (or equivalent) filters (nominal 0.7 µm pore size). At selected stations, size-fractionated chlorophyll concentrations were estimated by filtered paired samples sequentially through a 5 µm Whatman Track Etch polycarbonate filters and then a Whatman GFF filter. After filtration, samples were stored frozen at -80◦C until extraction and analysis. For analysis, samples were extracted in 5 ml of 90% acetone for 24 h at -20◦C. Samples were analyzed on a calibrated fluorometer, either Turner Designs TD-700 or 10-AU, with day-to-day performance of the fluorometer tracked using a commercially available solid standard. Fluorescence readings were taken before and after the addition of 75 µl of 1.2M HCl and concentrations calculated using standard equations (Parsons et al., 1984).

Dissolved nutrients: Samples for nutrient analysis were collected at the same depths as Chl-a and rate process incubation samples. Samples were syringe filtered using 0.45µm cellulose acetate membranes, and collected in 30ml acid washed, high-density polyetehnyel bottles after three rinses. On the BASIS and EcoFOCI cruises, samples were stored frozen at -80◦C and analyzed later at the shore-based facility, while samples from the BEST cruises were stored at 4◦C until analysis at sea, usually within 12 hrs of collection. Phosphate, nitrate, nitrite, and ammonium

concentrations were determined using a combination of analytical components from Alpkem, Perstorp and Technicon. WOCE-JGOFS standardization and analysis procedures (Gordon et al., 1993) were closely followed including reagent preparation, calibration of lab glassware, preparation of primary and secondary standards, and corrections for blanks and refractive index. Nutrient data from the Bering Sea program cruises were accessed from the Bering Sea Project Data Archive (Stabeno et al., 2013a, b), and data from the BASIS and EcoFOCI cruises were provided by co-author CWM.

POC analysis: [to be written]

Data analysis: [to be written]

Results: *Spatial and temporal distribution of* Synechococcus. *Synechococcus* cell abundance showed a clear seasonal variation in each major region (Figure 2). Cell abundance in the spring period were generally low (<1000 cells/ml), with the highest concentrations in the Northern Bering Sea/Bering Strait region. In stark contrast, in late summer/early fall, cell abundances could exceed 100,000 cells/ml. In summer/fall periods highest abundances were in Kotzebue Sound, although between years in the study the spatial extent of high cell abundances increased substantially.

Synechococcus abundances were found to have a seasonal vertical distribution pattern (Figure 3). During spring periods (e.g., June 2018), *Synechococcus* abundances were greater at depth, whereas in late summer/early fall (e.g., Aug/Sept. 2019), greatest *Synechococcus* abundances were restricted to the upper 20m of the water column over the broader spatial range where they were observed.

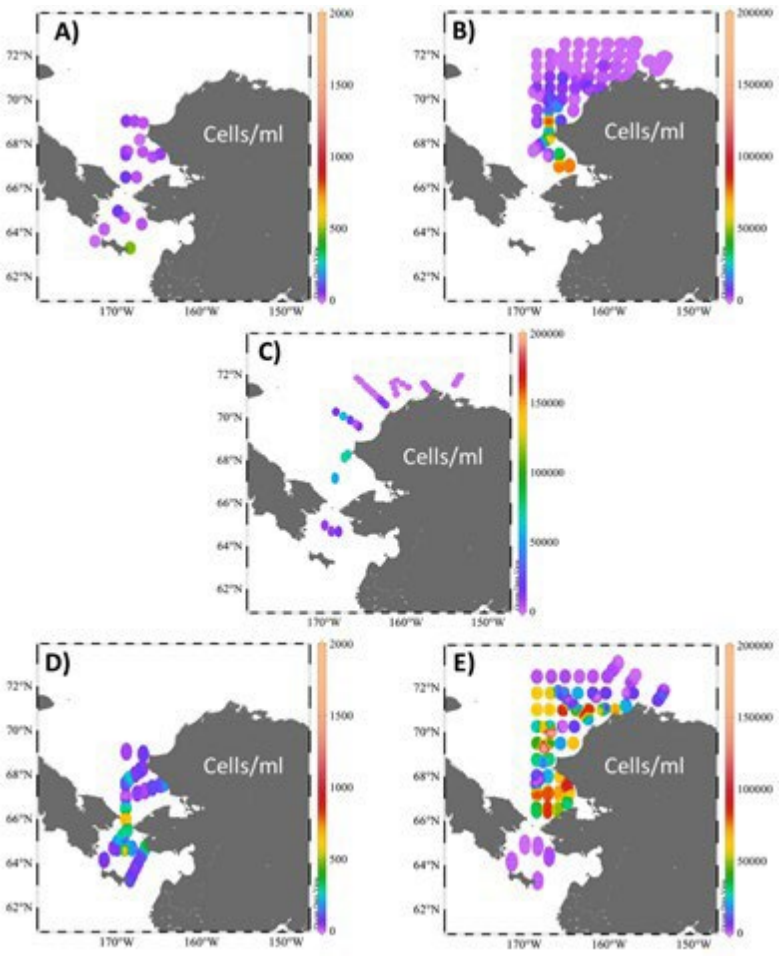

Figure 2. Seasonal patterns of Synechococcus abundance in the Northern Bering and Chukchi Seas. A) spring 2017 (SKQ-2017-09S), B) late summer/early fall 2017 (OS1701), C) summer 2018 (HLY1801), D) spring 2018 (SKQ-2018-13S), and E) late summer/early fall 2019 (OS1901). Note the 100x different in scales between the spring and late summer/early fall cruises.

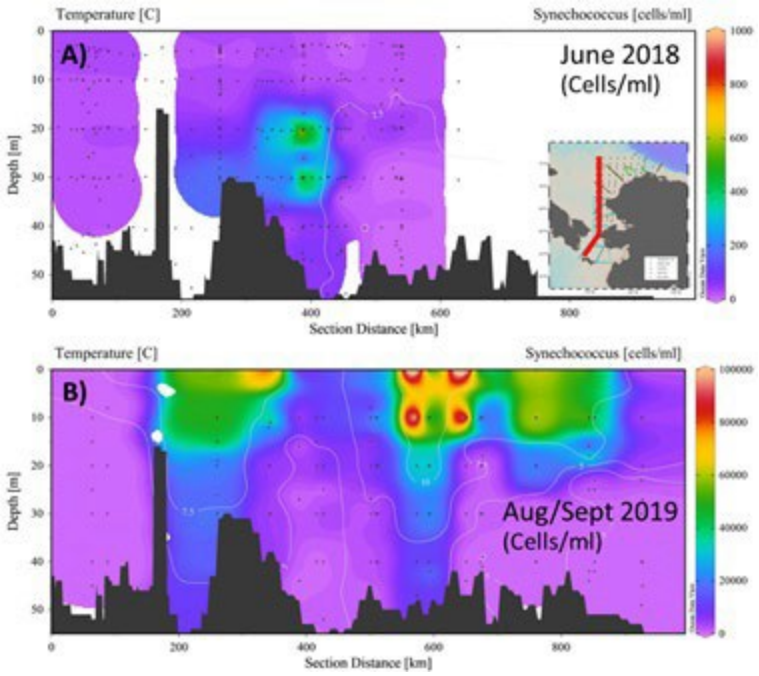

Figure 3. Latitudinal section plot of Synechococcus abundance through the study region.

Relationships to environmental parameters. Synechococcus cell abundances were highest in waters with temperatures >7oC and salinities <30.5 (Figure 4a). The T/S region where *Synechococcus* cell abundances were highest is classified as the warm coastal water (Danielson et al. 2020), although elevated abundances can also be found in the warmer/fresher regions of the warm shelf water. These waters are also depleted in inorganic nitrogen concentrations (Figure 4b).

Multiple linear regression (Model 2) analysis suggests that the only environmental variable that is significantly related to *Synechococcus* cell abundance is Temperature (Table 2). Interestingly there are two other nanophytoplankton populations, size-defined nanoeukaryotes, and the specific nanoeukaryote group of the cryptophytes, that are significantly related to *Synechococcus*.

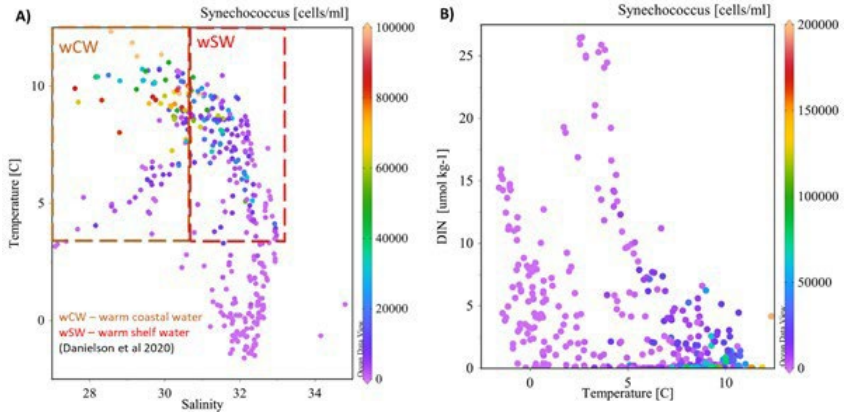

Figure 4. Relationships between Synechococcus abundance and environmental variables. A) temperature/salinity plot. Dashed lines bound the warm coastal water (orange) and warm shelf water (red) domain as defined by Danielson et al. 2020. B) temperature/ dissolved inorganic nitrogen (DIN) plot. DIN is defined as the sum of NO3, NO2 and NH4.

Table 2. Results of multiple linear regression (Model 2) analysis between *Synechococcus* abundance and environmental and biological variables. Variables significantly related to *Synechococcus* abundance are shown in italic font.

Parameter	**Coefficient**	**Std. Error**	**t-statistic**	**P-value**
Depth (m)	1.019	109.85	0.00928	0.993
Temperature (°C)	*1167.25*	*423.32*	*2.757*	*0.006*
Salinity	-726.06	1010.29	-0.719	0.473
PAR (umol/m²/s	-3.367	3.377	-0.997	0.320
NH4 (umol/kg)	570.87	1102.50	0.518	0.605
NO2 (umol/kg)	-709.501	28070.55	-0.0253	0.98
NO3 (umol/kg)	-128.84	434.303	-0.297	0.767
PO4 (umol/kg)	5038.518	6061.425	0.831	0.407

SiOH4 (umol/kg)	128.682	259.505	0.496	0.62
PON (umol/L)	-322.204	1555.11	-0.207	0.836
POC (umol/L)	258.215	193.27	1.336	0.183
POP (umol/L)	-10468.379	9413.506	-1.112	0.267
Total Chla (ug/L)	-26.931	493.123	-0.0546	0.956
<5um Chla (ug/L)	-4445.655	2774.185	-1.603	0.11
Picoeukaryotes (cells/ml)	*1.441*	*0.164*	*8.784*	*<0.001*
Nanoeukaryotes (cells/ml)	-0.768	1.383	-0.555	0.579
Cryptophytes	*6.12*	*1.115*	*5.49*	*<0.001*

Contributions to total biomass. Cell abundances were converted to carbon biomass values using the relationship between normalized forward light scatter and cellular carbon (Casey et al., 2013). Total phytoplankton carbon was estimated by multiplying total chlorophyll-a by the slope of the particulate organic carbon to chlorophyll-a ratio. *Synechococcus* carbon, as a percentage of total phytoplankton carbon, increased as total phytoplankton carbon decreased, reaching values as high as 40% of total phytoplankton carbon (Figure 5). At chlorophyll-a concentrations $\leq$2ug/L, a value commonly used to denote a 'bloom', *Synechococcus* could contributed >20% of total phytoplankton carbon and increased to >40% at <1ug/L chlorophyll. Samples from the shallowest depths and warmest temperatures consistently contributed higher fractions of total phytoplankton biomass.

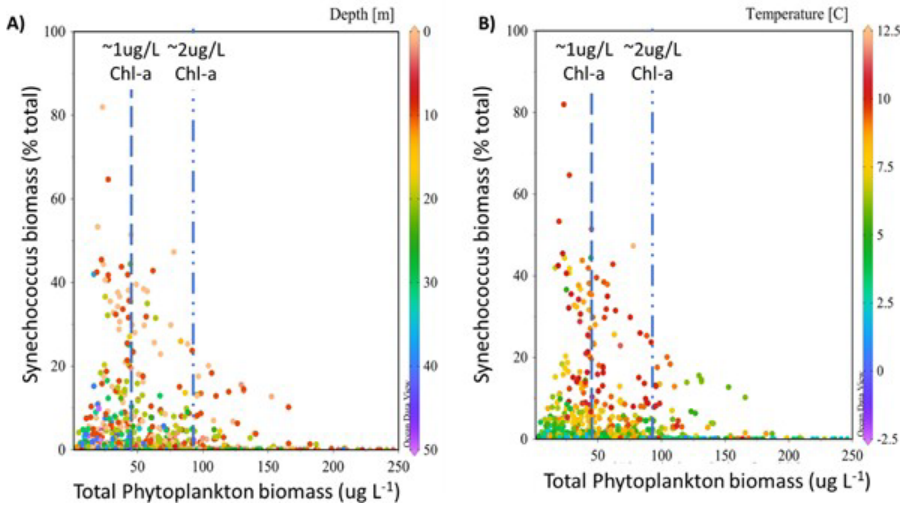

Figure 5. Contributions of Synechococcus to total phytoplankton carbon as function of A) depth and B) temperature. Dashed lines denote phytoplankton carbon associated with 1ug/L and 2ug/L chlorophyll.

Discussion

Highly productive systems like the Bering and Chukchi Seas are generally characterized by strong seasonal blooms of large phytoplanktonic diatoms that are rich in fatty acids and serve as an important food source for higher trophic levels. Seasonality of phytoplankton blooms, in particular the 'fall bloom' are gaining increasing recognition as being important in the trophic transfer of carbon and energy (Sigler et al., 2014). In the eastern Bering Sea shelf system, while *Synechococcus* has been observed (e.g., Liu et al., 2002; Moran et al., 2012) their abundances are generally low and represent a minor contribution to total phytoplankton carbon. The data presented in this study suggest that in the Chukchi Sea there is a very different pattern, with a much stronger seasonal amplitude in the abundance of *Synechococcus* and contribution to total phytoplankton carbon. Given the niche that *Synechococcus* fills globally (Flombaum et al., 2013; Visintini et al., 2021), our observations are consistent with *Synechococcus* growing into waters that are warm and nutrient deplete. In other ocean regions, *Synechococcus* abundances are tightly controlled by grazing (e.g., Worden and Binder, 2003), unfortunately there are not *Synechococcus*-specific grazing rates in the Northern Bering and Chukchi Seas. In the Northern Bering and Chukchi Seas, the picoplankton size fraction is tightly controlled by grazers, however, observations were at a time when *Synechococcus* abundances were low (Krause et al., 2021). The extensive net growth of *Synechococcus* during the late summer/fall period suggests a potential disruption to in this grazing control. The ecological impact of the observed increase in *Synechococcus* abundance remains to be fully understood.

Increasing Synechococcus *in a warming Arctic.* As *Synechococcus* has generally been considered a trivial component of the Arctic phytoplankton community, there are relatively few studies that have quantified their abundance and from which carbon biomass can be estimated. *Synechococcus* biomass increased over the past decade in the region of Kotzebue Sound and north (Cottrell and Kirchman, 2009; Laney and Sosik, 2014, this study; Figure

6a). During this time, water temperatures in this same region increased significantly (Cottrell and Kirchman, 2009; Laney and Sosik, 2014; Lee et al., 2013, this study; Figure 6b). This observation is consistent with our environmental analysis from this study where temperature was the only variable that was significantly related to *Synechococcus* abundance. Zhuang et al. (2021) observed that pigments associated with picoplankton, and potentially cyanobacteria, increased from 2008-2016 on a transect in the Chukchi Sea along Icy Cape, consistent with our observations.

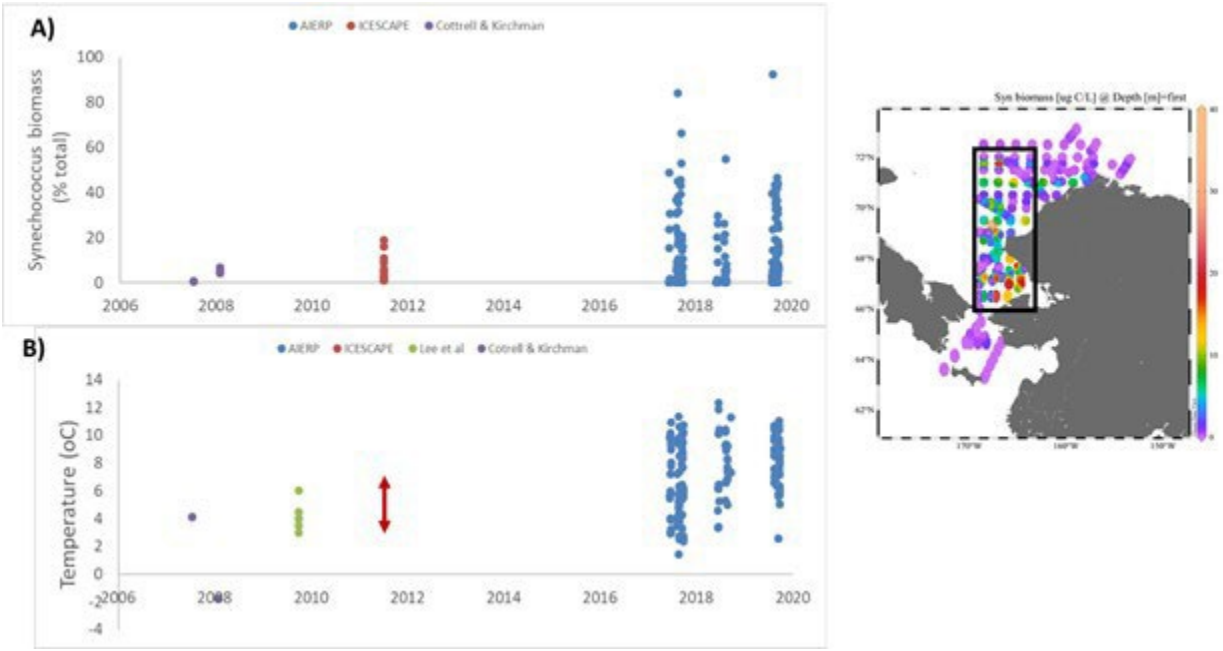

Figure 6. Changes in A) Synechococcus biomass and B) sample water temperature from published studies over time. Map inset shows the bounding box (black line) from which our data and those of previously published studies are used for this analysis.

References:

Ardyna, M., Gosselin, M., Michel, C., Poulin, M., Tremblay, J.-E., 2011. Environmental forcing of phytoplankton community structure and function in the Canadian High Arctic: contrasting oligotrophic and eutrophic regions. Marine Ecology Progress Series 442, 37-57.

Booth, B., Horner, R.A., 1997. Microalgae on the Arctic Ocean section, 1994: species abundance and biomass. Deep Sea Research II 44, 1607-1622.

Brugel, S., Nozais, C., Poulin, M., Tremblay, J.E., Miller, L.A., Simpson, K.G., Gratton, Y., Demers, S., 2009. Phytoplankton biomass and production in the southeastern Beaufort Sea in autumn 2002 and 2003. Marine Ecology Progress Series 377, 6377.

Carmack, E., Barber, D.G., Christensen, J.P., Macdonald, R.W., Rudels, B., Sakshaug, E., 2006. Climate variability and physical forcing of the food webs and the carbon budget on panarctic shelves. Progress in Oceanography 71, 145-181.

Casey, J., Aucan, J., Goldberg, S., Lomas, M., 2013. Changes in partitioning of carbon amongst photosynthetic pico- and nano-plankton groups in the Sargasso Sea in response to changes in the North Atlantic Oscillation. Deep Sea Research II 93, 58-70.

Cottrell, M.T., Kirchman, D.L., 2009. Photoheterotrophic Microbes in the Arctic Ocean in Summer and Winter. Appl. Environ. Microbiol. 75, 4958-4966.

DuRand, M., Olson, R., 1996. Contributions of phytopankton light scattering and cell concentration changes to diel variations in beam attenuation in the equatorial Pacific from flow-cytometric measurements of pico-, ultra-, and nanoplankton. Deep Sea Research II 43, 891-906.

DuRand, M., Olson, R., Chisholm, S., 2001. Phytoplankton population dynamics at the Bermuda Atlantic Time- series Study station in the Sargasso Sea. Deep-Sea Research Part II 48, 1983-2003.

Flombaum, P., Gallegos, J.L., Gordillo, R.A., Rincon, J., Zabala, L.L., Jiao, N.Z., Karl, D.M., Li, W., Lomas, M., Veneziano, D., Vera, C.S., Vrugt, J.A., Martiny, A.C., 2013. Present and future distributions of the marine cyanobacteria *Prochlorococcus* and *Synechococcus*. Proc. Acad. Nat. Sci. Phila., doi/10.1073/pnas.1307701110.

Gordon, L., Jennings, J., Jr., Ross, A., Krest, J., 1993. A suggested protocol for continuous flow automated analysis of seawater nutrients (phosphate, nitrate, nitrite, and silicic acid) in the WOCE Hydrographic Program and the Joint Global Ocean Fluxes Study. Oregon State University, p. 55.

Hill, V., Cota, G.F., Stockwell, D., 2005. Spring and summer phytoplankton communities in the Chukchi and Eastern Beaufort Seas. Deep Sea Research II 52, 3369-3385.

Krause, J.W., Lomas, M.W., Danielson, S.L., 2021. Diatom growth, biogenic silica production, and grazing losses to microzooplankton during spring in the northern Bering and Chukchi Seas. Deep Sea Research II.

Laney, S.R., Sosik, H.M., 2014. Phytoplankton assemblage structure in and around a massive under-ice bloom in the Chukchi Sea. Deep Sea Research II 105, DOI: 10.1016/j.dsr1012.2014.1003.1012.

Lee, S., Yun, M., Kim, B., Joo, H., Kang, S., Kang, C., Whitledge, T., 2013. Contribution of small phytoplankton to total primary production in the Chukchi Sea. Continental Shelf Research 68, 43-50.

Legendre, L., Gosselin, M., Hirche, H.J., Kattner, G., Rosenberg, G., 1993. Environmental control and potential fate of size-fractionated phytoplankton production in the Greenland Sea (75oN). Marine Ecology Progress Series 98, 297-313.

Li, W., McLaughlin, F., Lovejoy, C., Carmack, E., 2009. Smallest alge thrive as the Arctic Ocean freshens. Science 326, DOI: 10.1126/science.1179798

Liu, H.B., Suzukil, K., Minami, C., Saino, T., Watanabe, M., 2002. Picoplankton community structure in the subarctic Pacific Ocean and the Bering Sea during summer 1999. Mar. Ecol.-Prog. Ser. 237, 1-14.

Lomas, M.W., Steinberg, D.K., Dickey, T., Carlson, C.A., Nelson, N.B., Condon, R.H., Bates, N.R., 2010. Increased ocean carbon export in the Sargasso Sea is countered by its enhanced mesopelagic attenuation. Biogeosciences 7, 57-70.

Lovejoy, C., Vincent, W.F., Bonilla, S., Roy, S., Martineau, M.J., Terrado, R., Potvin, M., Massana, R., Pedros-Alio, C., 2007. Distribution, phylogeny, and growth of cold-adapted picoprasinophytes in Arctic seas. J. Phycol. 43, 78-89.

Moran, S.B., Lomas, M.W., Kelly, R.P., Prokopenko, M., Granger, J., Gradinger, R., Iken, K., Mathis, J.T., 2012. Seasonal succession of net primary productivity, particulate organic carbon export, and autotrophic community composition in the eastern Bering Sea. Deep Sea Research II 65-70, 84-97.

Not, F., Massana, R., Latasa, M., Marie, D., Colson, C., Eikrem, W., Pedros-Alio, C., Vaulot, D., Simon, N., 2005. Late summer community composition and abundance of photosynthetic picoeukaryotes in Norwegian and Barents Seas. Limnol. Oceanogr. 50, 1677-1686.

Odate, T., 1996. Abundance and size composition of the summer phytoplankton communities in the Western North Pacific Ocean, the Bering Sea, and the Gulf of Alaska. Journal of Oceanography 52, 335-351.

Parsons, T.R., Maita, Y., Lalli, C.M., 1984. A manual of chemical and biological methods for seawater analysis. Pergamon Press, New York.

Peterson, B.J., Holmes, R.M., McClelland, J.W., Vorosmarty, C.J., 202. Increasing river discharge to the Arctic Ocean. Science 298, 2171-2173.

Sergeeva, V.M., Sukhanova, I.N., Flint, M.V., Pautova, L., Grebmeier, J.M., Cooper, L.W., 2010. Phytoplankton community in the western Arctic in July-August 2003. Oceanology 50, 1894-1197.

Serreze, M.C., Barrett, A.P., Slater, A.G., Woodgate, R.A., 2006. The large-scale freshwater cycle of the Arctic. . Journal of Geophysical Research 111, C11010.

Sherr, E., Sherr, B., Wheeler, P., Thompson, K., 2003. Temporal and spatial variation in stocks of autotrophic and heterotrophic microbes in the upper water column of the central Arctic Ocean. Deep Sea Research I 50, 557-571.

Sieracki, M.E., Verity, P.G., Stoecker, D.K., 1993. Plankton community response to sequential silicate and nitrate depletion during the 1989 North Atlantic spring bloom. Deep Sea Research II 40, 213-226.

Sigler, M.F., Stabeno, P.J., Eisner, L.B., Napp, J.M., Mueter, F.J., 2014. Spring and fall phytoplankton blooms in a productive subarctic ecosystem, the eastern Bering Sea, during 1995–2011. Deep Sea Research II 109.

Stabeno, P., Sonnerup, R., Mordy, C., Whitledge, T., 2013a. HLY-08-02 CTD and Nutrient Data. Version 4.0. UCAR/NCAR - Earth Observing Laboratory. , https://doi.org/10.5065/D60K26KN.

Stabeno, P., Sonnerup, R., Mordy, C., Whitledge, T., 2013b. HLY-09-02 CTD and Nutrient Data. Version 3.0. UCAR/NCAR - Earth Observing Laboratory, https://doi.org/10.5065/D6SB43R4.

Tremblay, J.E., Gagnon, J., 2009. The effects of irradiance and nutrient supply on the productivity of Arctic waters: A perspective on climate change. , in: Nihoul, J.C.J., Kostianoy, A.G. (Eds.), Influence of Climate Change on the Changing Arctic and Sub-Arctic Conditions. Spring, Dordrecht, Netherlands, pp. 73-93.

Visintini, A., Martiny, A.C., Flombaum, P., 2021. *Prochlorococcus*, *Synechococcus* and picoeukaryotic phytoplankton abundances in the global ocean. Limnology and Oceanography Letters 6, 207-215.

Waleron, M., Waleron, K., Vincent, W.F., Wilmotte, A., 2007. Allochthonous inputs of riverine picocyanobacteria to coastal waters in the Arctic Ocean. FEMS Microbiology Ecology 59, 35365.

Worden, A.Z., Binder, B.J., 2003. Application of dilution experiments for measuring growth and mortality rates among *Prochlorococcus* and *Synechococcus* populations in oligotrophic environments. Aquat. Microb. Ecol. 30, 159-174.

Zhuang, Y., Jin, H., Zhang, Y., Li, H., Zhang, T., Li, Y., Bai, Y., Ren, J., Chen, J., 2021. Incursion of Alaska Coastal Water as a mechanism promoting small phytoplankton in the western Arctic Ocean. Progress in Oceanography, https://doi.org/10.1016/j.pocean.2021.102639.

Chapter 17: Estimates of heat transport through the Chukchi Sea to the Beaufort Sea from a decade of in situ observations

McCabe, R.M., NOAA Pacific Marine Environmental Laboratory, ryan.mccabe@noaa.gov
Stabeno, P.J.

McCabe, R. M., P. J. Stabeno, et al. (in preparation) Estimates of heat transport through the Chukchi Sea to the Beaufort Sea from a decade of *in situ* observations

Introduction: An increasing trend in northward volume transport through Bering Strait and into the Chukchi Sea is well established. Analyses of historical water property profiles have similarly quantified a multi-decade warming trend in the Chukchi Sea, with higher rates of increase in recent years. The water column heat content transported across the Chukchi shelf ultimately empties into the Canada Basin where it contributes to an observed accumulation of heat, likely with far reaching consequences. To better understand the amount of, and variations in, heat that gets delivered to the Canada Basin, we use *in situ* observations to construct a decade-long direct estimate of heat transport over the Chukchi Sea continental shelf.

Methods: Water column velocity and near-bottom temperature observations from three mooring sites spanning the eastern Chukchi Sea continental shelf are used to construct a time series of the along-shelf transport of heat from the Chukchi Sea into the Beaufort Sea via Barrow Canyon. In winter months, observations suggest the water column is well mixed such that near-bottom temperature records are sufficient for constructing the heat transport estimates. During ice-free seasons, data from the three primary mooring locations are supplemented with sea surface temperature from satellites, ship-based water property profiles, and from short duration moorings having shallower records.

Results and Discussion: The resulting transport of heat out of Barrow Canyon and into the Beaufort Sea changes seasonally with essentially no northward heat transport in winter months. Variability in monthly heat transport is primarily a result of changes in water column heat content with a smaller contribution from changes in volume transport. Interannual differences in the heat transport are also discussed. On an annual basis, there is enough heat exiting the Chukchi shelf through Barrow Canyon to warm the upper 100 m of the Beaufort Sea by approximately 0.5 °C.

Chapter 18: Surface versus advective heat fluxes on the shallow Chukchi Sea continental shelf

McCabe, R.M., NOAA Pacific Marine Environmental Laboratory, ryan.mccabe@noaa.gov
Stabeno, P.J., Mordy, C.W.

McCabe, R. M., P. J. Stabeno, C.W. Mordy, et al. (in preparation) Surface versus advective heat fluxes on the shallow Chukchi Sea continental shelf

Introduction: The goal of this project was to analyze in situ moored observations of water column temperature and associated atmospheric variables (shortwave and longwave irradiance, wind velocity, air temperature, relative humidity) within the context of a heat budget for the central Chukchi Sea shelf. Ultimately we seek to better understand the relative contributions of heat resulting from two sources: local surface fluxes and oceanic advection of heat from remote locations.

Methods: Bulk algorithms were used to make estimates of the net surface heat flux and its primary components (shortwave, longwave, sensible, and latent) over a roughly two-month period during summer 2015. Satellite sea surface temperature and available shipboard data are used to estimate spatial temperature gradients. When these records are combined with nearby moored velocity records, an advective component of the heat flux can be estimated.

Results and Discussion: Over the first month of the deployment, the cumulative net surface heat flux increased at a nearly constant rate. After mid August, net shortwave irradiance decreased and both the sensible and latent heat fluxes generally increased in magnitude, acting to remove heat from the ocean surface. During this latter half of the record, no additional accumulation of heat was observed. A low-pressure storm system moved into the region in late August, efficiently mixing heat throughout the water column. Analyses of the advective component of the heat flux are ongoing, but, at present, it appears that surface and advective fluxes contribute more or less equivalently to the total heat flux.

Chapter 19: Interannual variability of salts and nutrients at the Distributed Biological Observatory Site DBO 1

Mordy, C.W., CICOES, University of Washington, mordy@uw.edu

Stabeno, P.J., Hristova, H.

Mordy, C.W., P. Stabeno, H. Hristova (in preparation). Interannual variability of salts and nutrients at the Distributed Biological Observatory Site DBO1

Introduction: In winter, nutrient replenishment in the eastern Chukchi Sea is primarily the result of transport of nutrients from the Bering Sea shelf and slope. Along the Ice Cape line in the Chukchi Sea, pre-bloom concentrations of nitrate, a limiting nutrient, were found to vary by ~40%. This variability is driven by interannual differences in both winter transport and the concentration of inorganic nitrogen (nitrate and ammonium) in the Bering Sea source water. Variability in winter transport in the Chukchi Sea is driven by northerly (weakens transport) and southerly (strengthens transport) wind events, with a recent increase in southerly wind events. Unknown are the drivers of nutrient variability in the Bering Sea. The goal of this study is to unravel physical drivers of nutrient variability on the northern Bering Sea shelf.

Method: To study the physical drivers of this variability, we examined surface geostrophic currents from altimetry (anomaly from 1993-2012 mean), velocity data from the M8 and M5 moorings, and the relationship between salinity and DIN (nitrate and ammonium) along the slope to determine variability in the contribution of slope water versus middle shelf water to DBO1.

Results and Discussion: There is considerable spatiotemporal variability in nitrate and ammonium concentrations across the northern Bering Sea. The inner shelf (<50 m) is well-mixed and nutrient poor. The middle shelf (50-100 m) is stratified in summer with nutrient depleted surface water and higher nutrients in the bottom layer. However, in the bottom layer. ~30% of the nitrate typically found in source waters along the slope have been lost to the ecosystem through denitrification. The outer shelf (100-200 m) is more frequently flushed with slope water, and has higher nutrient content and a weaker denitrification signal. Therefore, the relative contributions of slope and shelf water largely determine interannual variability of nutrient content in Bering Sea source water that flows through central Bering Strait. Interannual variability of salinity and DIN were highly correlated, and the salinity at M8 was dependent upon northward transport that includes on-shelf flow of slope water. Since 2005, DIN concentrations around the M8 mooring were lowest in 2016 (11.3 μM) and greatest in 2019 (24 μM). Hence, year-to-year differences in the amount of DIN in source waters that are transported to the eastern Chukchi Sea vary by ~50%, and suggest that net community production over the eastern Chukchi Sea may have varied between ~30 and 70 g C m^{-2} during this time.

Chapter 20: Phytoplankton and seston fatty acids dynamics in the northern Bering-Chukchi Sea region

Nielsen J.M., CICOES, University of Washington, jens.nielsen@noaa.gov

Copeman L.A., Eisner L.B., Axler K.E., Mordy, C.W., Lomas M.W.

Phytoplankton and seston fatty acids dynamics in the northern Bering-Chukchi Sea region

Jens M. Nielsen[1,2,*], Louise A. Copeman[3,4,5], Lisa B. Eisner[1], Kelia E. Axler[1], Calvin W. Mordy[2,6] Michael W. Lomas[7]

[1]NOAA Alaska Fisheries Science Center, 7600 Sand Point Way NE, Seattle, WA, 98115, USA

[2]Cooperative Institute for Climate, Ocean, and Ecosystem Studies, University of Washington, Seattle, WA, United States

[3]NOAA Alaska Fisheries Science Center, 2030 SE Marine Science Dr., Hatfield Marine Science Center, Newport, OR, 97365, USA

[4]College of Earth, Ocean, and Atmospheric Sciences, Oregon State University, 104 CEOAS Administration Building, Corvallis, OR, 97331, USA

[5]Cooperative Institute for Marine Ecosystem and Resources Studies, Oregon State University, 2030 SE Marine Science Drive, Newport, OR, 97365, USA

[6]NOAA Pacific Marine Environmental Laboratory, Seattle, WA, USA

[7]Bigelow Laboratory for Ocean Sciences, 60 Bigelow Dr., East Boothbay, ME, 04544, USA

*Corresponding author: jens.nielsen@noaa.gov

KEYWORDS: Fatty acid analysis, Arctic, Chukchi Sea, northern Bering Sea, phytoplankton

ABSTRACT

Arctic and subarctic ecosystems are transitioning due to ocean warming, resulting in conditions that will lead to shifts in phytoplankton communities, their nutritional compositions, and production of fatty acids (FA). FA biomarkers are useful indicators of changing phytoplankton community composition and provide insight into basal resource quality for higher trophic level consumers such as zooplankton, fish, birds and marine mammals, yet phytoplankton FA information is largely lacking from the Bering and Chukchi Sea region. Therefore, we analyzed suspended particulate matter (seston) fatty acids (FA), chlorophyll-a (Chl-a) and environmental data collected from four surveys in the North Bering and Chukchi Seas, two during June of 2017 and 2018 and two during August and September of 2017 and 2019. Our objectives were to determine 1) whether, seston FA composition was correlated with phytoplankton taxonomic composition analyzed using imaging microscope (FlowCAM) techniques, 2) seasonal differences in seston FA concentrations, and 3) how FA concentrations vary with environmental parameters. We found significant seasonal differences in seston FA compositions, with diatom biomarkers more prevalent in spring, followed by a community shift to dinoflagellate and small flagellate FA biomarkers in late fall. These results were overall confirmed by FlowCAM analyses. FA seston concentrations were correlated with total and large size-fractioned Chl-a concentrations, nitrogen concentration and temperature. Lastly, we used a model framework to predict availability of the diatom-associated essential FA, eicosapentaenoic acid (EPA, 20:5n-3). Combined our analysis provide new information on FA phytoplankton dynamics and the important nutritional role of phytoplankton for higher trophic level consumers in the Northern Bering and Chukchi Sea regions.

1. INTRODUCTION

The Bering and Chukchi Seas are some of the most productive areas of the Arctic (Hill et al., 2018). A pronounced diatom spring bloom commonly associated with the timing of ice breakup (Fujiwara et al., 2016; Laney and Sosik, 2014) fuels pelagic and benthic secondary production (Grebmeier et al., 2006; Sigler et al., 2014). Later in the season, once the ocean stratifies, a majority of the large size-fractioned phytoplankton biomass is often present in subsurface water layers (Martini et al., 2016) while smaller sized plankton occur in the surface waters (Giesbrecht et al., 2019). Arctic and subarctic ecosystems, including the Bering and Chukchi Seas are transitioning (Huntington et al., 2020) due to rapid ocean warming. This scenario is projected to continue in the coming decades (Hermann et al., 2019) with changes already affecting sea ice phenology, spring bloom timing and phytoplankton production (Clement Kinney et al., 2020; Song et al., 2021). These changes also influence the production of fatty acids (FA) synthesized by phytoplankton which play a key nutritional role for the growth and functioning of marine consumers. More baseline data on phytoplankton nutrition, including their FA compositions is needed for tracking potential short and long-term changes in the quality and quantity of basal resources in the Bering and Chukchi Sea food webs.

Phytoplankton play a crucial nutritional role in marine ecosystems due to their ability to synthesize dietary FA required by higher trophic level organisms (Budge et al., 2014; Dalsgaard et al., 2003). Marine consumers generally lack the ability to synthesize several essential FA at a sufficient rate to meet their metabolic demand (Helenius et al., 2020), and therefore require FA preformed in their diets (Bell and Tocher, 2009). Several essential polyunsaturated FA (PUFA), including eicosapentaenoic acid (EPA, 20:5n3) and docosahexaenoic acid, (DHA, 22:6n3), are central compounds that regulate cell membrane fluidity, neurological functioning, localized

47 hormones and growth (Bell and Tocher, 2009; Helenius et al., 2019; Tocher et al., 2019). Dietary
48 limitation of essential PUFA directly influence zooplankton fecundity and growth rates (Leiknes
49 et al., 2016; Pond et al., 1996), survival of larval (Copeman and Laurel, 2010) and juvenile fishes
50 (Bell et al., 1995), and lower overall ecosystem productivity (Litzow et al., 2006).
51 The relative amounts of specific FA vary among phytoplankton taxa (Cañavate, 2019;
52 Parrish, 2013), thus changes in phytoplankton community compositions induce shifts in the
53 dietary FA pool available for consuming organisms (Galloway and Winder, 2015). The
54 association between specific FA and certain taxonomic groups also make FA useful biomarkers
55 (Dalsgaard et al., 2003). Yet, the utility of FA biomarkers to partition phytoplankton taxa is
56 known primarily from monoculture experiments (Cañavate, 2019; Dunstan et al., 1993;
57 Jónasdóttir, 2019). Using FA biomarkers to distinguish phytoplankton taxa in field samples is
58 more challenging (Reuss and Poulsen, 2002), variable and less studied (Galloway and Budge,
59 2020; Marmillot et al., 2020). Nonetheless, field studies in other high latitude systems, such as
60 the Beaufort Sea (Connelly et al., 2016; Marmillot et al., 2020), West Greenland Sea (Reuss and
61 Poulsen, 2002), and Barents Sea (Falk-Petersen et al., 1998) have highlighted that changes in
62 phytoplankton compositions, including seasonal shifts from diatoms to flagellates, can be visible
63 in the seston FA pools. Beyond the primary association with a specified phytoplankton
64 taxonomic group, individual FA biomarkers vary with environmental conditions (Sushchik et al.,
65 2004). Although FA provide valuable information about food quality, they are often not
66 diagnostic or species-specific but should rather be viewed as indicative of dominance from broad
67 taxonomic groups (i.e., predominance of diatoms versus flagellates; (Jónasdóttir, 2019),
68 particularly when analysis field data. Therefore, additional species information from microscopy

imaging techniques are also beneficial to validate observed FA biomarker patterns (Marmillot et al., 2020).

Here we use FA biomarkers as indicators of changing phytoplankton community compositions, and of basal resource quality for higher trophic level consumers. We analyzed suspended particulate matter (seston) FA, chlorophyll-a (Chl-a), phytoplankton taxonomic data, and environmental data from four surveys spanning the northern Bering-Chukchi Sea region, two during spring (June) in 2017 and 2018 and two during late summer (August/September) in 2017 and 2019. More specifically, we examine:

1) Seasonal and annual patterns in both absolute FA concentrations and percent FA composition;

2) the relationship between phytoplankton taxonomic data (dinoflagellates and diatoms) determined from imaging microscope analyses (FlowCAM) compared to specific FA biomarkers;

3) the relationship between individual FA biomarkers and physical, chemical, and biological variables; and

4) show how a simple model framework to predict concentrations of the diatom-sourced essential fatty acid, EPA, can provide a measure of consumer nutritional quality at an increased spatial resolution.

2. METHODS

2.1. Data collection

Four surveys were conducted in northern Bering-Chukchi Sea region as part of the Arctic Integrated Ecosystem Research Program (AIERP), during June of 2017 and 2018 (Arctic Shelf

Growth, Advection, Respiration, and Deposition Rate Experiments [ASGARD]) and during August and September (hereafter Aug/Sep) of 2017 and 2019 (Arctic Integrated Ecosystem Survey; Fig. 1). All data are publicly available in the DataONE repository (https://doi.org/10.24431/rw1k5a0). Water samples were collected from 5-12 L Niskin bottles attached to the CTD rosette. At every sampling station, total and size-fractioned (<5, 5-20, >20 μm) Chl-a (mg m^{-3}) samples were collected. Total Chl-a samples were collected at 10 m intervals (~5-6 depths) and filtered through 25 mm Whatman GF/F filters (nominal pore size 0.7 μm). Size-fractionated samples were collected at 2-3 depths using a stacked filtration unit, using 47 mm Whatman GF/F filters for <5 μm, and 47 mm polycarbonate filters with a pore size of 5 and 20 μm, to sample the 5-20 and >20 μm large size fractions. Filters were stored frozen (−80 °C) and analyzed within 6 months with a bench top fluorometer following standard methods (Parsons, 1984). Samples for dissolved inorganic nutrients (nitrate, nitrite, ammonium, phosphate, and silicic acid; μmol kg^{-1}) were collected from each Niskin bottle, filtered through 0.45 cellulose acetate filters, and frozen. Samples were analyzed on a Seal AA3 or Seal AA500 continuous segmented flow analyzer following methods in (Gordon et al., 1993). Ammonium was analyzed using the OPA method (Holmes et al., 1999). At every other station, seston was sampled at 1-2 depths for FA analysis (n =167). Vertical profiles of temperature and salinity were collected from surface to near-bottom at each station using a Sea-Bird Electronics (SBE) 9+ CTD, data processed and averaged into 1-m bins.

Phytoplankton community samples were analyzed for cell abundance using Fluid Imaging Technologies VS Series benchtop FlowCAM (hereafter referred to as FlowCAM) using a 10× objective and 200 μm flow cell in autoimage mode (Álvarez et al., 2014). Samples were counted from surveys in June 2017 and Aug/Sep 2017. Images were grouped into diatoms or

115 dinoflagellates. Diatoms were imaged in both June and Aug/Sep 2017, while dinoflagellates
116 were imaged only in Aug/Sep 2017. Biovolumes of cells were estimated from images using the
117 biovolume estimation function (cylindrical shape) in the VisualSpreadsheet (Scarborough, ME)
118 software provided with the instrument. These estimates compared well with manual estimates of
119 biovolume using standardized shapes and appropriate geometric equations (Menden-Deuer and
120 Lessard, 2000). FlowCAM biovolumes of diatoms and dinoflagellates were compared to
121 concentrations of the FA biomarkers of diatoms and dinoflagellates, and the ratio of DHA: EPA.
122
123 2.2. Fatty acid analyses
124 We collected FA seston samples, which comprise all living and non-living material
125 between 0.7-200 μm, such as phytoplankton, heterotrophic protists, bacteria, mesozooplankton
126 eggs and nauplii, and detritus. During sampling in June and Aug/Sep, phytoplankton commonly
127 constitute the majority of the seston material (Connelly et al., 2016; Hama, 1999) and thus the
128 majority of the seston FA can be attributed to phytoplankton FA. Water samples ranging in
129 volume from 2 L to 6 L were collected for seston fatty acid analysis on each of the four Arctic
130 surveys. Samples were collected from the surface, Chl-a maximum, or at near-bottom depths.
131 Seawater was prescreened through a 200 μm Nitex mesh into 2L sample bottles (1-3 bottles per
132 sample). Each bottle was filtered onto a pre-combusted Whatman 47 mm GF/F filter (0.7 μm
133 nominal pore size), and sample filters were stored aboard the ship at -80°C. Samples were
134 shipped frozen on dry ice to the Hatfield Marine Science Center (HMSC) in Newport, Oregon,
135 and analyzed at the Marine Lipid Ecology Laboratory. To obtain sufficient material, some filters
136 were combined for each sampling depth (1-3 filters), placed into lipid-clean glass tubes and
137 stored in chloroform under nitrogen for less than 3 months prior to extraction. Lipids were

138 extracted using a modified Folch procedure (Folch et al., 1957) using 2:1 chloroform: methanol
139 as described by Parrish et al. (1999). A total of 167 seston samples were processed for FA
140 analyses. An internal standard (23:0 methyl ester) was added to all samples at approximately
141 10% of the total FA concentration, and total lipid extracts were derivatized into their fatty acid
142 methyl esters (FAMEs) using sulphuric acid-catalyzed transesterification (Budge et al., 2006).
143 Resulting FAMEs were analyzed on an HP 7890 GC FID equipped with an autosampler
144 and a DB wax+ GC column (Agilent Technologies, Inc., U.S.A.). The column was 30 m in
145 length, with an internal diameter of 0.25 mm and film thickness of 0.25 µm. The column
146 temperature began at 65 °C and held this temperature for 0.5 min. Temperature was increased to
147 195 °C (@ 40 °C min^{-1}), held for 15 min then increased again (@ 2 °C min^{-1}) to a final
148 temperature of 220 °C, where it was held for 1 min. The carrier gas was hydrogen, flowing at a
149 rate of 2 ml min^{-1}. Injector temperature was set at 250 °C and the detector temperature was
150 constant at 250 °C. Peaks were identified using retention times based upon standards purchased
151 from Supelco (37 component FAME, BAME, PUFA 1, PUFA 3) and in consultation with
152 retention index maps performed under similar chromatographic conditions as our GC-FID
153 (Wasta and Mjøs, 2013). Column function was checked by comparing chromatographic peak
154 areas to empirical response areas using a quantitative FA mixed standard, GLC 487 (NuCheck
155 Prep). Chromatograms were integrated using Chem Station (version A.01.02, Agilent). Select
156 samples were run in triplicate and the coefficient of variation for peaks >1% of the sample, were
157 less than one.
158
159 2.3. Statistical and data analyses

Absolute FA concentrations, the amount of seston FA per volume seawater (reported as mg m^{-3}), were used to infer overall availability of FA as basal resources for consumers. FA data were calculated as percent of total fatty acids, which is a useful metric for quantifying phytoplankton compositional changes in the seston. FA were classified as C:Bn-P, where C is the number of carbon atoms, B the number of double bonds and P the position of the first double bond from the methyl group end (Budge et al., 2006). We considered two aspects of phytoplankton FA composition. Firstly, we focused on phytoplankton biomarkers, such as those indicative of diatoms: 16:1n-7, 16:4n-1, EPA (20:5n-3) and a composite diatom biomarker based on the ratio of 16:1n-7/16:0 (Budge and Parrish, 1998; Dalsgaard et al., 2003). Flagellates are a diverse group, including small autotrophic flagellates, heterotrophic flagellates and dinoflagellates. Therefore, we refer to the biomarkers 18:4n-3, 18:5n-3 and DHA (22:6n-3) as a combination of flagellate and dinoflagellate (dino+flag) FA biomarkers, due to the difficulty in partitioning among these groups using FA biomarkers alone. Secondly, we focused on long-chain PUFA (C_{20+22}) such as EPA and DHA, that are essential in the diet of secondary consumers. In addition, we assessed the ratio of DHA to EPA to denote relative dino+flag: diatom biomarkers in the samples, and a bacterial biomarker, here the sum of all odd carbon FA and branched FAs (Kaneda, 1991).

Type II regressions using $\log_{10}$-transformation were used to assess pairwise relationships between FA seston concentrations, and biological and physical variables including temperature, salinity, nutrients, and total and size-fractioned Chl-a concentrations. One-way Analysis of Variance (ANOVA) with associated post-hoc Tukey Honestly Significant Difference (HSD) was used for group comparisons, such as between seasons, years, depth category (above, below or in the mixed layer) and water mass designations (warm shelf water, cool shelf water, Anadyr water,

183 modified winter water and warm coastal water, Danielson et al., 2020). ANOVA models were
184 assessed for normality and homogeneity of variances of the residuals and variables were log_{10}-
185 transformed when necessary. Non-metric multidimensional scaling (nMDS) using Bray-Curtis
186 distances was used to assess multivariate patterns of the FA percent data, using all FA that
187 constituted more than 1% of the total FA, and the groups saturated FA (SFA), monounsaturated
188 FA (MUFA), PUFA and Bacterial FA.

189 Linear mixed effects models (Zuur et al., 2009) were used to assess how multiple
190 physical and biological parameters influence the FA composition of seston samples, and then to
191 develop a simple model framework that allows prediction of water column (0-50 m) integrated
192 EPA (mg m^{-2}) concentrations over broader spatial or temporal scales. For each FA biomarker a
193 full linear mixed effects model included the following predictor variables: total Chl-a,
194 temperature, nitrogen (sum of nitrate and ammonium), salinity and depth (a categorical variable
195 as described earlier) parameters that are all known to influence FA compositions (Budge et al.,
196 2014; Galloway and Winder, 2015). The different surveys were included as a random effect
197 because we expected that relationships between FA and environmental variables were likely to
198 be independent among years and season. For all models, inspections of residual plots did not
199 reveal obvious deviances from normality or homoscedasticity after log-transformation of
200 variables. In cases of multicollinearity (variance inflation factor (VIF) > 5), we retained only one
201 of those values in the final analysis.

202 Mixed effects models were performed for the following biomarkers: the ratio of DHA:
203 EPA, the ratio of PUFA: SFA, and FA percentage data for diatom biomarkers 16:4n-1 and EPA,
204 and dino+flag biomarkers 18:5n-3 and DHA. We followed the recommendations in (Zuur et al.,
205 2009) for fitting FA mixed effects models. First, the optimal random effect structure (which

206 could be no random effect) was fitted for the full model using restricted maximum likelihood
207 estimation. Second, we used maximum likelihood estimation to determine the most parsimonious
208 fixed effect model structure, with the optimal random structure as determined in step one.
209 Finally, the most parsimonious model for each FA, which included the optimal random and fixed
210 effect structures, was re-fitted with restricted maximum likelihood estimation. Determination of
211 the most parsimonious model in each step was decided using Akaike Information Criterion
212 corrected for small sample sizes (AICc, Burnham and Anderson, 2002). In the instances where
213 more than one model had similar AICc scores (<1 AICc), we chose the model with the lower
214 number of explanatory variables. For simplicity, we report only the final parsimonious model for
215 each FA biomarker in the results.

216 To predict integrated EPA (mg m^{-2}) concentrations, we used a mixed effects model to the
217 EPA concentration data. Because the biological, chemical and physical survey data was sampled
218 at a higher vertical and spatial sampling resolution compared to the FA sampling, these models
219 allowed for predicting integrated water column EPA concentrations for all survey stations.
220 Predictive models were computed using natural log-transformed data, thus a correction was
221 applied to re-convert predicted FA concentrations (Duan, 1983). All analyses were done using R
222 version 3.6 (R Core Team, 2018). Mixed effects models were fitted using the "*nlme*" package
223 (Pinheiro et al., 2017), AICc using the "*AICcmodavg*" package (Mazerolle and Mazerolle, 2019),
224 and type II regressions were computed using the "*smatr*" package (Warton et al., 2012).
225

226 **3. RESULTS**

227 3.1. Spatial patterns of Chl-a and FA concentrations.

228 Generally, areas of higher than average Chl-a were spatially associated with higher total
229 FA concentrations. Average water column (0-50 m) Chl-a measurements were higher in June
230 2017 and 2018 compared to Aug/Sep 2017 and 2019, though high variability existed among
231 stations and across all surveys (Fig. 1). Elevated water column average Chl-a concentrations (>6
232 mg m^{-3}) were present north of St. Lawrence Island within and north of the Bering Strait in both
233 June 2017 and 2018, areas that similarly showed elevated (> 15 mg m^{-3}) concentrations of total
234 FA. Total Chl-a concentrations had significant positive correlations with both the ratio of large
235 (> 5 μm) to small (< 5 μm) particle Chl-a, and the > 20 μm size-fractioned concentrations (Table
236 S1), indicating that communities were comprised of large phytoplankton in areas with high
237 concentrations of total Chl-a.
238
239 3.2. Seasonal dynamics of FA biomarkers
240 Total FA concentrations (mean±SD) in June 2017 were significantly higher than all other
241 surveys (average across stations: 28.2±21.1 mg m^{-3}, $p<0.05$, Tukey HSD, Figs. 1, 2A), followed
242 by FA concentrations in June 2018 (22.2±16.9 mg m^{-3}), Aug/Sep 2019 (18.8±16.5 mg m^{-3}), and
243 Aug/Sep 2017 (12.1±5.4 mg m^{-3}). Overall SFA, and MUFA concentrations were higher in June
244 compared to Aug/Sep (Fig. 2A), however percent PUFA levels were highest in Aug/Sep 2019
245 (Fig. 2D). The diatom biomarkers 16:1n-7, 16:4n-1, and EPA all varied significantly among
246 season and year (Tukey HSD, $F(3,163) = 10.6$, 4.2, and 4.3, respectively, $p< 0.05$, Fig. 2B).
247 Concentrations of 16:1n-7 and 16:4n-1 and EPA were significantly higher in June than in
248 Aug/Sep except for EPA, were values in Aug/Sep 2019 were similar to values in June. The
249 diatom biomarkers (percentage of 16:1n-7, 16:4n-1 and EPA, Fig. 2E) showed similar patterns to
250 the concentration data.

The concentration of dino+flag-associated biomarkers 18:5n-3(0.8± 1.0 mg m^{-3}) and DHA (1.5± 1.6 mg m^{-3}) were significantly higher in Aug/Sep 2019 compared to all other surveys (Tukey HSD, $p<0.05$, Fig. 2C). The dino+flag biomarker 18:4n-3 was significantly higher in Aug/Sep 2019 than in Aug/Sep 2017 (Tukey HSD, $p<0.05$), but otherwise showed no difference among seasons and years. The dino+flag percent FA data and the sum of n-3 PUFA showed overall similar patterns to the concentration data, with Aug/Sep 2019 values being the highest (Fig. 2F). Resultant DHA: EPA ratios were significantly higher in Aug/Sep compared to June (Tukey HSD, $p<0.05$, Fig. 2C). The diatom biomarkers of EPA, 16:1n-7, and 16:4n-1 were all correlated positively for both the concentration (Table S1) and percentage data (Table S2). Similarly, DHA correlated well with the dino+flag biomarkers 18:4n-3 and 18:5n-3 for both the concentration and percentage data (Table S1-S2).

Multivariate nMDS analysis of the FA percentage composition data similarly showed clear differences among seasons and years (Fig. 3). FA biomarkers most responsible for the separation of seasons were diatom biomarkers (i.e., 16:1n-7, 16:2n-4, 16:4n-1 and EPA), which appeared to be more highly associated with the June 2017 and 2018 samples. In contrast, dino+flag markers (i.e., 18:3n-3, 18:4n-3, 18:5n-3, and 22:6n-3) were more closely associated with the Aug/Sep 2017 and 2019 samples. However, substantial variability of the FA compositions within each survey also indicate clear spatial differences in phytoplankton communities across years and seasons.

3.3. Taxonomic comparison of FA biomarkers and FlowCAM images

FlowCAM-measured diatom and dinoflagellate biovolumes correlated positively with their taxa-associated FA biomarkers. Significant positive correlations were observed between

$\log_{10}$-transformed diatom biovolumes and FA concentrations of EPA (Fig. 4A, $r^2 = 0.41$, $p < 0.01$, df = 38), 16:1n-7 (Fig. 4C, $r^2 = 0.45$, $p < 0.01$, df = 38), and 16:4n-1 (Fig. 4E, $r^2 = 0.46$, $p < 0.01$, df = 38) in June 2017 and Aug/Sep 2017. However, when analyzing only the Aug/Sep 2017 diatom data, correlations were not significant ($p > 0.05$, df = 20). Dinoflagellate biovolumes correlated positively with FA concentrations of DHA (Fig. 4B, $r^2 = 0.51$, $p < 0.01$, df = 20) and 18:5n-3 (Fig. 4D, $r^2 = 0.55$, $p < 0.01$, df = 20) in June 2017. Additionally, the ratio of DHA to EPA correlated positively with the FlowCAM-measured ratio of dinoflagellate to diatom biovolumes (Fig. 4F, $r^2 = 0.45$, $p < 0.01$, df = 20) in June 2017.

3.4. Associations between FA biomarkers and environmental variables

Next, we analyzed associations between the individual environmental variables and the FA concentration and percentage biomarkers using $\log_{10}$-transformed data from discrete samples. Some of the main primary pairwise correlations shown in Figure 5 and highlighted below, while all regressions are presented in Table S1 and Table S2.

Overall, the majority of the concentrations of individual FA correlated positively and significantly with total and size-fractionated (<5 µm, 5-20 µm, >20 µm) Chl-a data (Fig. 5A-F, Table S1). The strongest relationship for total FA was with total Chl-a and >20 µm fraction ($r^2 = 0.52$, $p<0.01$), which in turn were highly correlated ($r^2= 0.90$, $p<0.01$) (Fig. 5A, Table S1). Significant correlations were also found for PUFA concentrations, common diatom biomarkers 16:1n-7, and EPA with total and >20 µm Chl-a concentrations (Fig. 5B-D, $r^2 = 0.37$ to 0.52, $p<0.01$, Table S1). In contrast, dino+flag biomarkers 18:5n-3, 18:4n-3 and DHA had the highest correlations with small size fractions of Chl-a (< 5 um) ($r^2 = 0.36$ to 0.67, $p<0.01$, Table S1); positive but weaker correlations were also found with total Chl-a (Fig 5.E, $r^2 = 0.05$ to 0.23,

297 $p<0.05$). Nutrients correlated negatively with temperature and positively with salinity (Fig. 5G,
298 Table S1). We found few significant relationships between FA concentrations and temperature,
299 salinity, and nutrient concentrations and those were weak (Table S1). DHA: EPA ratios were
300 lowest in cold, high salinity waters (Fig. 5H) and correlated negatively with nitrate
301 concentrations (Fig. 5I, $r^2 = 0.31$, $p<0.01$, Table S1).

302 Overall, the percentage FA results suggested that diatoms are higher in relative biomass
303 in colder, high salinity waters and in areas of higher nitrate (Table S2). dino+flag FA biomarker
304 percentages were higher in warmer waters, shallower depths, and in areas with low nutrient
305 concentrations (Table S2). Total and large (>20 μm) size-fractioned Chl-a correlated positively
306 with the percentage diatom biomarkers (16:1n-7, 16:4n-1, 16:2n-4, and EPA) but negatively with
307 the percent contribution of dino+flag-associated FA biomarkers (18:4n-3, 18:5n-3, and DHA)
308 and the ratio of DHA to EPA (Fig. 5F, Table S2). Percentage diatom FA biomarkers associated
309 negatively with the dino+flag and SFA. The percentage contribution from bacterial FA
310 biomarkers correlated positively with the diatom biomarkers, >20 μm, and 5-20 μm and total
311 Chl-a, but negatively with several dino+flag biomarkers. For both the percentage and
312 concentration data, the patterns observed for all 4 surveys combined were generally also visible
313 within each survey (data not shown).

314 Mixed effects models using the FA percentage data showed that several environmental
315 variables influence FA phytoplankton dynamics. The most parsimonious mixed effects models
316 consistently included survey as a random effect. All statistical values are reported in Table S3;
317 below we report the main findings. Percent EPA contribution correlated positively with total
318 Chl-a concentrations and with vertical depth position (Table S3). EPA values were higher below

319 the mixed layer and though the effect of vertical position was included in the final model, its
320 influence was minor (i.e., delta AICc with the vertical position included or not, was small).
321 The diatom biomarker 16:4n-1 showed a significant positive relationship with total Chl-a
322 and nitrogen concentration but a negative relationship with temperature. Percent DHA was
323 positively related to total Chl-a, but negatively related to nitrogen concentrations (Table S3). The
324 dino+flag marker 18:5n-3 was negatively related to both total Chl-a and nitrogen concentrations.
325 DHA: EPA ratios also were negatively related to Chl-a and nitrogen concentrations, while
326 relating positively with salinity and temperature. The ratio of PUFA: SFA increased with Chl-a
327 concentrations, but decreased with nitrogen concentrations and temperature (Table S3).
328 Lastly, we used a mixed effects model to enable predictions of absolute EPA
329 concentrations (Fig. 6). The most parsimonious model, assessed using AICc, included log-
330 transformed total Chl-a and log-transformed nitrogen (sum of nitrate and ammonium) as the
331 fixed effect and a random structure consisting of an interaction of Chl-a and survey (Table S4).
332 Model prediction of EPA correlated overall strongly with measured EPA concentrations (r^2 =
333 0.63, $p < 0.01$, df = 151, Fig. S1A). Variability and thus uncertainty of EPA model predictions
334 were highest in samples with total Chl-a concentrations >5 mg m^{-3} (Fig. S1B). Water column
335 integrated EPA concentrations differed significantly among all four surveys (Fig. 6, Tukey HSD,
336 $p<0.05$), with average values highest in June 2018 (93 ± 60 mg m^{-2}), followed by June 2017 (66
337 ± 46 mg m^{-2}), Aug/Sep 2019 (54 ± 30 mg m^{-2}), and Aug/Sep 2017 (30 ± 8 mg m^{-2}). Throughout,
338 there was high spatial variation in the predictions with the highest concentrations reaching levels
339 of 264 mg m^{-2} and 241 mg m^{-2} in June 2017 and 2018, while highest values in Aug/Sep 2017
340 were 54 mg m^{-2} and 198 mg m^{-2} in Aug/Sep 2019.
341

4. DISCUSSION

Seston FA biomarkers reflected phytoplankton community shifts from diatoms dominating in spring followed by late summer increases of dinoflagellates and small flagellates. High total FA and PUFA concentrations in late spring (June) primarily synthesized by diatoms suggest that phytoplankton FA from this time period provide important dietary subsidies for consumers (Grebmeier et al., 2006). Diatom and dinoflagellate biovolume measurements from FlowCAM images correlated positively with their respective FA biomarkers, confirming that in general FA compositional data can provide reliable information on phytoplankton community dynamics. Measured phytoplankton FA composition (concentrations and percentages) varied with changes in temperature and nutrients, likely due to a combination of species-specific changes in physiology as well as changes in the phytoplankton community composition (Grosse et al., 2019; Jiang and Gao, 2004). Lastly, derived EPA concentrations based a model using commonly sampled survey data (e.g., temperature, nitrogen, and Chl-a) may provide broad-scale water column integrated estimates of dietary EPA availability for consumers in the northern Bering and Chukchi Sea ecosystems.

4.1 FA biomarker and FlowCAM estimates of diatoms and dinoflagellates

Taxonomic information from microscopy imaging techniques generally confirmed that observed FA biomarker patterns can be associated with major phytoplankton taxa groups. Although FlowCAM-measured diatom and dinoflagellate biovolumes correlated positively with diatom and dinoflagellate FA biomarker concentrations, these data also revealed substantial unexplained variance. The combined June and Aug/Sep 2017 data yielded significant trends for diatom biovolumes and their FA biomarkers (16:1n-7, 16:4n-1 and EPA) however, similar

365 diatom trends were insignificant when using only samples from Aug/Sep 2017. Whether the lack
366 of clear correlation was due to variable FA concentrations among diatoms species, less
367 dominance of this taxa compared to spring samples, variable environmental conditions (Sushchik
368 et al., 2004), or FA contributions from other phytoplankton groups is unclear. For example,
369 *Synechococcus,* which can contain 16:1n-7 (Jónasdóttir, 2019), were observed in up to 20% of
370 the phytoplankton carbon biomass during Aug/Sep 2017 (data not shown). Similarly,
371 chlorophytes containing 16:4n-1, or chlorophytes and cryptophytes containing EPA (Jónasdóttir,
372 2019), could have contributed to the FA pools of the diatom associated biomarkers.
373 Differentiating between dinoflagellates, heterotrophic flagellates and flagellates using FA
374 biomarkers alone is challenging. The observable trends between 18:5n-3 and DHA with
375 dinoflagellate identified from the FlowCAM suggest that noticeable FA contributions at least
376 partially originated from dinoflagellates, however, small flagellates, not measured with the
377 FlowCAM analysis, may also be important. Dinoflagellate and small flagellates often co-occur.
378 Higher percentages of 18:1n-9 and 18:0 in some Aug/Sep 2017 samples could indicate increased
379 contributions from smaller flagellates (Reuss and Poulsen, 2002), but these quite ubiquitous FAs
380 that are also present in several other taxa (Cañavate, 2019). The significant association between
381 dinoflagellate biovolumes and their specific FA biomarkers (DHA, 18:5n-3) differ from a recent
382 study by Marmillot et al. (2020) which found no significant relationships for dinoflagellates. We
383 speculate that these differences may be explained by the fact that flagellates are a diverse group
384 of organisms including auto, mixo and heterotrophic species, which can vary substantially in
385 their FA signatures depending on their diet intake and responses to environmental conditions.
386 Overall, and despite considerable variation, our results are in general agreement with previous
387 field studies (Marmillot et al., 2020; Reuss and Poulsen, 2002; Sushchik et al., 2004) and

388 highlights the utility of FA biomarkers for depicting relative contributions of major
389 phytoplankton taxonomic groups.
390
391 4.2. Factors influencing seston FA dynamics
392 Shifting environmental conditions influence seston FA dynamics through both individual
393 phytoplankton species and community composition responses (Cañavate et al., 2019; Miller et
394 al., 2017). Seasonal environmental shifts were clearly visible in the FA biomarkers, with highest
395 abundances of diatom FA in spring followed by increasing dino+flag FA in late summer. These
396 seasonal shifts agree well with phytoplankton taxonomic analysis from the northern Bering and
397 Chukchi Seas (Laney and Sosik, 2014; Lee et al., 2019; Sukhanova et al., 2009) and with FA
398 biomarker studies in other Arctic regions (Connelly et al., 2016; Falk-Petersen et al., 1998). Chl-
399 a concentration was the primary predictor variable for the concentrations of almost all FA
400 biomarkers. These linkages were particularly strong between absolute concentrations of the
401 diatom biomarkers, 16:4n-1, 16:1n-7 and EPA, and the total and the large (>20 μm) size fraction
402 Chl-a. The high positive correlation of >20 μm with total Chl-a suggests that large phytoplankton
403 primarily of diatom origin were driving changes in total Chl-a concentrations.
404 Temperature and nitrogen concentrations also influenced the percentage FA patterns.
405 Temperature correlated negatively with the ratio of PUFA to SFA, a pattern that is likely driven
406 by decreasing PUFA concentrations with warming (Hixson and Arts, 2016; Jiang and Gao,
407 2004), due to both individual species and community compositional responses to variable
408 environmental conditions (Hixson and Arts, 2016). Relative concentration of dino+flag
409 biomarkers increased with decreasing nitrogen concentrations, warmer temperatures and lower
410 salinity, supporting that dinoflagellates and small flagellates are commonly more prevalent in

411 low nutrient environments as observed during summer in the eastern Bering Sea (Moran et al.,
412 2012; Sukhanova et al., 2009). Differences in residual nutrient concentrations among water
413 masses are associated with different phytoplankton communities (Danielson et al., 2017), which
414 likely explain the higher percentages of FA diatom biomarkers in colder, more saline, nutrient-
415 rich waters. Differences in FA compositions with depth also indicate that diatoms are more
416 prevalent in deeper, higher nutrient waters near the subsurface Chl-a maximum which are
417 common phenomena in summer in these ecosystems (Lowry et al., 2015; Martini et al., 2016). In
418 contrast, higher abundance of FA dino+flag biomarkers occurred closer to the surface in waters
419 with lower nutrient concentrations, where they may have an advantage compared to, for example
420 diatoms. Higher surface area to volume ratios of small flagellates allow enhanced access to
421 nutrients at low concentrations (Edwards et al., 2012), while many dinoflagellates maintain
422 higher growth by migrating daily from deeper, nutrient rich water to the surface (Jephson and
423 Carlsson, 2009) and also engage in heterotropy.
424
425 4.3. Importance of dietary FA for consumers
426 Variation in plankton communities and their nutritional quality (i.e. lipid and essential
427 FA) influence spatiotemporal trends in food quality available to consumers (Twining et al.,
428 2016). The availability of essential EPA strongly influences copepod nauplii growth rates
429 (Leiknes et al., 2016), fish (Copeman and Laurel, 2010), juvenile crab (Copeman et al. 2021),
430 benthic organisms (Schollmeier et al., 2018) and overall ecosystem production (Litzow et al.,
431 2006). Using ancillary data from all four surveys, we calculated water column integrated spatial
432 predictions of EPA concentrations. Overall, the modeled EPA predictions compared well to
433 measured EPA concentrations. Modeled EPA data may provide a first step towards a broader

characterization of dietary availability of essential FA in these ecosystems. Overall, predicted EPA concentrations were highest in spring with lower concentrations in late summer, particularly Aug/Sep 2017. Our mixed effects model analyses also show that FA spatial predictions vary between seasons and years, as "survey" was a significant explanatory variable in the model. Survey should be considered a proxy for seasonal and inter-annual changes in the FA pools associated with the phytoplankton community composition. Thus, predictive power increases when accounting for inter- and intra-annual differences in FA composition patterns, and best results are retrieved if model predictions are coupled with a smaller subset of FA phytoplankton information from the specific year in question. Additional improvements of the current model framework would be inclusion of data from colder years that may have noticeably different phytoplankton communities (Hill et al., 2005) compared to the years 2017-2019, and laboratory studies of regional zooplankton or benthic invertebrate (e.g., crabs, Copeman et al. 2021) growth and reproduction rate responses to dietary availability of essential EPA.

An expected future consequence of warming and increased stratification is a shift in phytoplankton community structure towards smaller sized cells (Morán et al., 2010) and a prospective decrease in PUFA concentrations (Hixson and Arts, 2016). Such shifts in FA compositions are due to a combination of direct physiological effects on phytoplankton FA synthesis as well as due to phytoplankton community shifts. How changing sea ice phenology and the resulting effects on ice-associated phytoplankton (Clement Kinney et al., 2020), and spring and summer open water blooms influences the availability of carbon and thus important dietary FA in the northern Bering and Chukchi Sea ecosystems, remains an open question. Our analyses and model framework provide new regional baseline information on phytoplankton FA

seasonal and inter-annual variations. Such information will increase the ability to evaluate the impacts of changing dietary lipid on higher trophic level consumers at broader spatial scales.

DECLARATION OF COMPETING INTEREST

The authors declare no known competing financial interests or personal relationships that could have appeared to influence the work reported in this manuscript.

ACKNOWLEDGEMENTS

We are grateful to Brendan Smith, Miranda Irby, Ed Farley, Anna Mounsey, Haley Cynar, Jeff Krause, Harmony Wayner, and Steven Baer for help during field sampling, for analysis of the nutrient data, and the crews of the *R/V's Ocean Star* and *Sikuliaq*. We are thankful to Lauren Rogers for help with mixed effects models and comments from Jeanette Gann and Fletcher Sewall that substantially helped improve the manuscript. We thank Carlissa Salant Michelle Stowell and Jami Ivory for general analytical assistance in the Marine Lipid Ecology Lab in Newport, OR, and the funding sources; NPRB Arctic IERP (Arctic IES LTL (A92), ASGARD, Phytoplankton Gap proposal (A96), National Science Foundation Office of Polar Programs award numbers OCE-1603460 (ML)). The findings and conclusions in this paper are those of the authors and do not necessarily represent the views of the National Marine Fisheries Service, NOAA. Reference to trade names does not imply endorsement by the National Marine Fisheries Service, NOAA. This is EcoFOCI contribution number EcoFOCI-1005 and PMEL contribution number 5325. This publication was partially funded by the Cooperative Institute for Climate, Ocean, & Ecosystem Studies (CIOCES) under NOAA Cooperative Agreement NA20OAR4320271, Contribution No 2021-1168.

REFERENCES

Álvarez, E., Moyano, M., López-Urrutia, Á., Nogueira, E., Scharek, R., 2014. Routine determination of plankton community composition and size structure: a comparison between FlowCAM and light microscopy. Journal of plankton research 36, 170-184.

Bell, M.V., Batty, R.S., Dick, J.R., Fretwell, K., Navarro, J.C., Sargent, J.R., 1995. Dietary deficiency of docosahexaenoic acid impairs vision at low light intensities in juvenile herring (Clupea harengus L.). Lipids 30, 443.

Bell, M.V., Tocher, D.R., 2009. Biosynthesis of polyunsaturated fatty acids in aquatic ecosystems: general pathways and new directions, Lipids in aquatic ecosystems. Springer, pp. 211-236.

Budge, S.M., Devred, E., Forget, M.-H., Stuart, V., Trzcinski, M.K., Sathyendranath, S., Platt, T., 2014. Estimating concentrations of essential omega-3 fatty acids in the ocean: supply and demand. ICES Journal of Marine Science 71, 1885-1893.

Budge, S.M., Iverson, S.J., Koopman, H.N., 2006. Studying trophic ecology in marine ecosystems using fatty acids: a primer on analysis and interpretation. Marine Mammal Science 22, 759-801.

Budge, S.M., Parrish, C.C., 1998. Lipid biogeochemistry of plankton, settling matter and sediments in Trinity Bay, Newfoundland. II. Fatty acids. Organic Geochemistry 29, 1547-1559.

Burnham, K., Anderson, D., 2002. Model selection and multimodel inference: a practical information-theoretic approach. The University of Chicago Press New York.

Cañavate, J.-P., van Bergeijk, S., Giráldez, I., González-Ortegón, E., Vílas, C., 2019. Fatty Acids to Quantify Phytoplankton Functional Groups and Their Spatiotemporal Dynamics in a Highly Turbid Estuary. Estuaries and Coasts 42, 1971-1990.

Cañavate, J.P., 2019. Advancing assessment of marine phytoplankton community structure and nutritional value from fatty acid profiles of cultured microalgae. Reviews in Aquaculture 11, 527-549.

Clement Kinney, J., Maslowski, W., Osinski, R., Jin, M., Frants, M., Jeffery, N., Lee, Y.J., 2020. Hidden production: on the importance of pelagic phytoplankton blooms beneath Arctic Sea ice. Journal of Geophysical Research: Oceans 125, e2020JC016211.

Connelly, T.L., Businski, T.N., Deibel, D., Parrish, C.C., Trela, P., 2016. Annual cycle and spatial trends in fatty acid composition of suspended particulate organic matter across the Beaufort Sea shelf. Estuarine, Coastal and Shelf Science 181, 170-181.

Copeman, L., Laurel, B., 2010. Experimental evidence of fatty acid limited growth and survival in Pacific cod larvae. Marine Ecology Progress Series 412, 259-272.

Dalsgaard, J., John, M.S., Kattner, G., Müller-Navarra, D., Hagen, W., 2003. Fatty acid trophic markers in the pelagic marine environment.

Danielson, S.L., Eisner, L., Ladd, C., Mordy, C., Sousa, L., Weingartner, T.J., 2017. A comparison between late summer 2012 and 2013 water masses, macronutrients, and phytoplankton standing crops in the northern Bering and Chukchi Seas. Deep Sea Research Part II: Topical Studies in Oceanography 135, 7-26.

Duan, N., 1983. Smearing estimate: a nonparametric retransformation method. Journal of the American Statistical Association 78, 605-610.

Dunstan, G.A., Volkman, J.K., Barrett, S.M., Leroi, J.-M., Jeffrey, S., 1993. Essential polyunsaturated fatty acids from 14 species of diatom (Bacillariophyceae). Phytochemistry 35, 155-161.

Edwards, K.F., Thomas, M.K., Klausmeier, C.A., Litchman, E., 2012. Allometric scaling and taxonomic variation in nutrient utilization traits and maximum growth rate of phytoplankton. Limnology and Oceanography 57, 554-566.

Falk-Petersen, S., Sargent, J., Henderson, J., Hegseth, E., Hop, H., Okolodkov, Y., 1998. Lipids and fatty acids in ice algae and phytoplankton from the Marginal Ice Zone in the Barents Sea. Polar Biology 20, 41-47.

Folch, J., Lees, M., Stanley, G.S., 1957. A simple method for the isolation and purification of total lipides from animal tissues. Journal of biological chemistry 226, 497-509.

Fujiwara, A., Hirawake, T., Suzuki, K., Eisner, L., Imai, I., Nishino, S., Kikuchi, T., Saitoh, S.-I., 2016. Influence of timing of sea ice retreat on phytoplankton size during marginal ice zone bloom period on the Chukchi and Bering shelves. Biogeosciences Discussions 13.

Galloway, A.W., Winder, M., 2015. Partitioning the relative importance of phylogeny and environmental conditions on phytoplankton fatty acids. PLoS One 10, e0130053.

Galloway, A.W.E., Budge, S.M., 2020. The critical importance of experimentation in biomarker-based trophic ecology. Philosophical Transactions of the Royal Society B: Biological Sciences 375, 20190638.

Giesbrecht, K., Varela, D., Wiktor, J., Grebmeier, J., Kelly, B., Long, J., 2019. A decade of summertime measurements of phytoplankton biomass, productivity and assemblage composition in the Pacific Arctic Region from 2006 to 2016. Deep Sea Research Part II: Topical Studies in Oceanography 162, 93-113.

Gordon, L.I., Jennings Jr, J.C., Ross, A.A., Krest, J.M., 1993. A suggested protocol for continuous flow automated analysis of seawater nutrients (phosphate, nitrate, nitrite and silicic acid) in the WOCE Hydrographic Program and the Joint Global Ocean Fluxes Study. WOCE hydrographic program office, methods manual WHPO, 1-52.

Grebmeier, J.M., Cooper, L.W., Feder, H.M., Sirenko, B.I., 2006. Ecosystem dynamics of the Pacific-influenced Northern Bering and Chukchi Seas in the Amerasian Arctic. Progress in Oceanography 71, 331-361.

Grosse, J., Brussaard, C., Boschker, H., 2019. Nutrient limitation driven dynamics of amino acids and fatty acids in coastal phytoplankton. Limnology and Oceanography 64, 302-316.

Hama, T., 1999. Fatty acid composition of particulate matter and photosynthetic products in subarctic and subtropical Pacific. Journal of plankton research 21.

Helenius, L., Budge, S., Duerksen, S., Devred, E., Johnson, C.L., 2019. Lipids at the plant–animal interface: a stable isotope labelling method to evaluate the assimilation of essential fatty acids in the marine copepod Calanus finmarchicus. Journal of Plankton Research 41, 909-924.

Helenius, L., Budge, S.M., Nadeau, H., Johnson, C.L., 2020. Ambient temperature and algal prey type affect essential fatty acid incorporation and trophic upgrading in a herbivorous marine copepod. Philosophical Transactions of the Royal Society B: Biological Sciences 375, 20200039.

Hermann, A.J., Gibson, G.A., Cheng, W., Ortiz, I., Aydin, K., Wang, M., Hollowed, A.B., Holsman, K.K., 2019. Projected biophysical conditions of the Bering Sea to 2100 under multiple emission scenarios. ICES Journal of Marine Science 76, 1280-1304.

Hill, V., Ardyna, M., Lee, S.H., Varela, D.E., 2018. Decadal trends in phytoplankton production in the Pacific Arctic Region from 1950 to 2012. Deep Sea Research Part II: Topical Studies in Oceanography 152, 82-94.

Hill, V., Cota, G., Stockwell, D., 2005. Spring and summer phytoplankton communities in the Chukchi and Eastern Beaufort Seas. Deep Sea Research Part II: Topical Studies in Oceanography 52, 3369-3385.

Hixson, S.M., Arts, M.T., 2016. Climate warming is predicted to reduce omega-3, long-chain, polyunsaturated fatty acid production in phytoplankton. Global Change Biology 22, 2744-2755.

Holmes, R.M., Aminot, A., Kérouel, R., Hooker, B.A., Peterson, B.J., 1999. A simple and precise method for measuring ammonium in marine and freshwater ecosystems. Canadian Journal of Fisheries and Aquatic Sciences 56, 1801-1808.

Huntington, H.P., Danielson, S.L., Wiese, F.K., Baker, M., Boveng, P., Citta, J.J., De Robertis, A., Dickson, D.M., Farley, E., George, J.C., 2020. Evidence suggests potential transformation of the Pacific Arctic ecosystem is underway. Nature Climate Change, 1-7.

Jephson, T., Carlsson, P., 2009. Species-and stratification-dependent diel vertical migration behaviour of three dinoflagellate species in a laboratory study. Journal of plankton research 31, 1353-1362.

Jiang, H., Gao, K., 2004. Effects of lowering temperature during culture on the production of polyunsaturated fatty acids in the marine diatom Phaeodactylum tricornutum (bacillariophyceae) 1. Journal of Phycology 40, 651-654.

Jónasdóttir, S.H., 2019. Fatty acid profiles and production in marine phytoplankton. Marine drugs 17, 151.

Kaneda, T., 1991. Iso-and anteiso-fatty acids in bacteria: biosynthesis, function, and taxonomic significance. Microbiological reviews 55, 288-302.

Laney, S.R., Sosik, H.M., 2014. Phytoplankton assemblage structure in and around a massive under-ice bloom in the Chukchi Sea. Deep Sea Research Part II: Topical Studies in Oceanography 105, 30-41.

Lee, Y., Min, J.-O., Yang, E.J., Cho, K.-H., Jung, J., Park, J., Moon, J.K., Kang, S.-H., 2019. Influence of sea ice concentration on phytoplankton community structure in the Chukchi and East Siberian Seas, Pacific Arctic Ocean. Deep Sea Research Part I: Oceanographic Research Papers 147, 54-64.

Leiknes, Ø., Etter, S.A., Tokle, N.E., Bergvik, M., Vadstein, O., Olsen, Y., 2016. The Effect of Essential Fatty Acids for the Somatic Growth in Nauplii of Calanus finmarchicus. Frontiers in Marine Science 3, 33.

Litzow, M., A. , Bailey, K., M. , Prahl, F., G. , Ron., H., 2006. Climate regime shifts and reorganization of fish communities: the essential fatty acid limitation hypothesis. Marine Ecology Progress Series 315, 1-11.

Lowry, K.E., Pickart, R.S., Mills, M.M., Brown, Z.W., van Dijken, G.L., Bates, N.R., Arrigo, K.R., 2015. The influence of winter water on phytoplankton blooms in the Chukchi Sea. Deep Sea Research Part II: Topical Studies in Oceanography 118, 53-72.

Marmillot, V., Parrish, C.C., Tremblay, J.-É., Gosselin, M., MacKinnon, J.F., 2020. Environmental and Biological Determinants of Algal Lipids in Western Arctic and Subarctic Seas. Frontiers in Environmental Science.

Martini, K.I., Stabeno, P.J., Ladd, C., Winsor, P., Weingartner, T.J., Mordy, C.W., Eisner, L.B., 2016. Dependence of subsurface chlorophyll on seasonal water masses in the Chukchi Sea. Journal of Geophysical Research: Oceans 121, 1755-1770.

Mazerolle, M.J., Mazerolle, M.M.J., 2019. Package 'AICcmodavg'.

Menden-Deuer, S., Lessard, E.J., 2000. Carbon to volume relationships for dinoflagellates, diatoms, and other protist plankton. Limnology and oceanography 45, 569-579.

Miller, J.A., Peterson, W.T., Copeman, L.A., Du, X., Morgan, C.A., Litz, M.N.C., 2017. Temporal variation in the biochemical ecology of lower trophic levels in the Northern California Current. Progress in Oceanography 155, 1-12.

Moran, S., Lomas, M., Kelly, R., Gradinger, R., Iken, K., Mathis, J., 2012. Seasonal succession of net primary productivity, particulate organic carbon export, and autotrophic community composition in the eastern Bering Sea. Deep Sea Research Part II: Topical Studies in Oceanography 65, 84-97.

Morán, X.A.G., LÓPEZ-URRUTIA, Á., CALVO-DÍAZ, A., Li, W.K., 2010. Increasing importance of small phytoplankton in a warmer ocean. Global Change Biology 16, 1137-1144.

Parrish, C., Arts, M., Wainman, B., 1999. Lipids in freshwater ecosystems. New York, SpringeraVerlag. pp. 5a 20.

Parrish, C.C., 2013. Lipids in marine ecosystems. ISRN Oceanography 2013.

Parsons, T.R., 1984. A manual of chemical & biological methods for seawater analysis. Elsevier.

Pinheiro, J., Bates, D., DebRoy, S., Sarkar, D., Heisterkamp, S., Van Willigen, B., Maintainer, R., 2017. Package 'nlme'. Linear and nonlinear mixed effects models, version 3.

Pond, D., Harris, R., Head, R., Harbour, D., 1996. Environmental and nutritional factors determining seasonal variability in the fecundity and egg viability of Calanus helgolandicus in coastal waters off Plymouth, UK. Marine Ecology Progress Series 143, 45-63.

R Core Team, 2018. R: A Language and Environment for Statistical Computing, R Foundation for Statistical Computing, Austria, 2015. ISBN 3-900051-07-0: URL http://www. R-project. org.

Reuss, N., Poulsen, L., 2002. Evaluation of fatty acids as biomarkers for a natural plankton community. A field study of a spring bloom and a post-bloom period off West Greenland. Marine Biology 141, 423-434.

Schollmeier, T., Oliveira, A., Wooller, M., Iken, K., 2018. Tracing sea ice algae into various benthic feeding types on the Chukchi Sea shelf. Polar Biology 41, 207-224.

Sigler, M.F., Stabeno, P.J., Eisner, L.B., Napp, J.M., Mueter, F.J., 2014. Spring and fall phytoplankton blooms in a productive subarctic ecosystem, the eastern Bering Sea, during 1995–2011. Deep Sea Research Part II: Topical Studies in Oceanography 109, 71-83.

Song, H., Ji, R., Jin, M., Li, Y., Feng, Z., Varpe, Ø., Davis, C.S., 2021. Strong and regionally distinct links between ice-retreat timing and phytoplankton production in the Arctic Ocean. Limnology and Oceanography.

Sukhanova, I.N., Flint, M.V., Pautova, L.A., Stockwell, D.A., Grebmeier, J.M., Sergeeva, V.M., 2009. Phytoplankton of the western Arctic in the spring and summer of 2002: Structure and seasonal changes. Deep Sea Research Part II: Topical Studies in Oceanography 56, 1223-1236.

Sushchik, N.N., Gladyshev, M.I., Makhutova, O.N., Kalachova, G.S., Kravchuk, E.S., Ivanova, E.A., 2004. Associating particulate essential fatty acids of the ω3 family with phytoplankton species composition in a Siberian reservoir. Freshwater Biology 49, 1206-1219.

Tocher, D.R., Betancor, M.B., Sprague, M., Olsen, R.E., Napier, J.A., 2019. Omega-3 long-chain polyunsaturated fatty acids, EPA and DHA: bridging the gap between supply and demand. Nutrients 11, 89.

Twining, C.W., Brenna, J.T., Hairston Jr, N.G., Flecker, A.S., 2016. Highly unsaturated fatty acids in nature: what we know and what we need to learn. Oikos 125, 749-760.

659 Warton, D.I., Duursma, R.A., Falster, D.S., Taskinen, S., 2012. smatr 3–an R package for
660 estimation and inference about allometric lines. Methods in Ecology and Evolution 3, 257-259.
661 Wasta, Z., Mjøs, S.A., 2013. A database of chromatographic properties and mass spectra of
662 fatty acid methyl esters from omega-3 products. Journal of Chromatography A 1299, 94-102.
663 Zuur, A., Ieno, E.N., Walker, N., Saveliev, A.A., Smith, G.M., 2009. Mixed effects models
664 and extensions in ecology with R. Springer Science & Business Media.
665

FIGURES

Figure 1

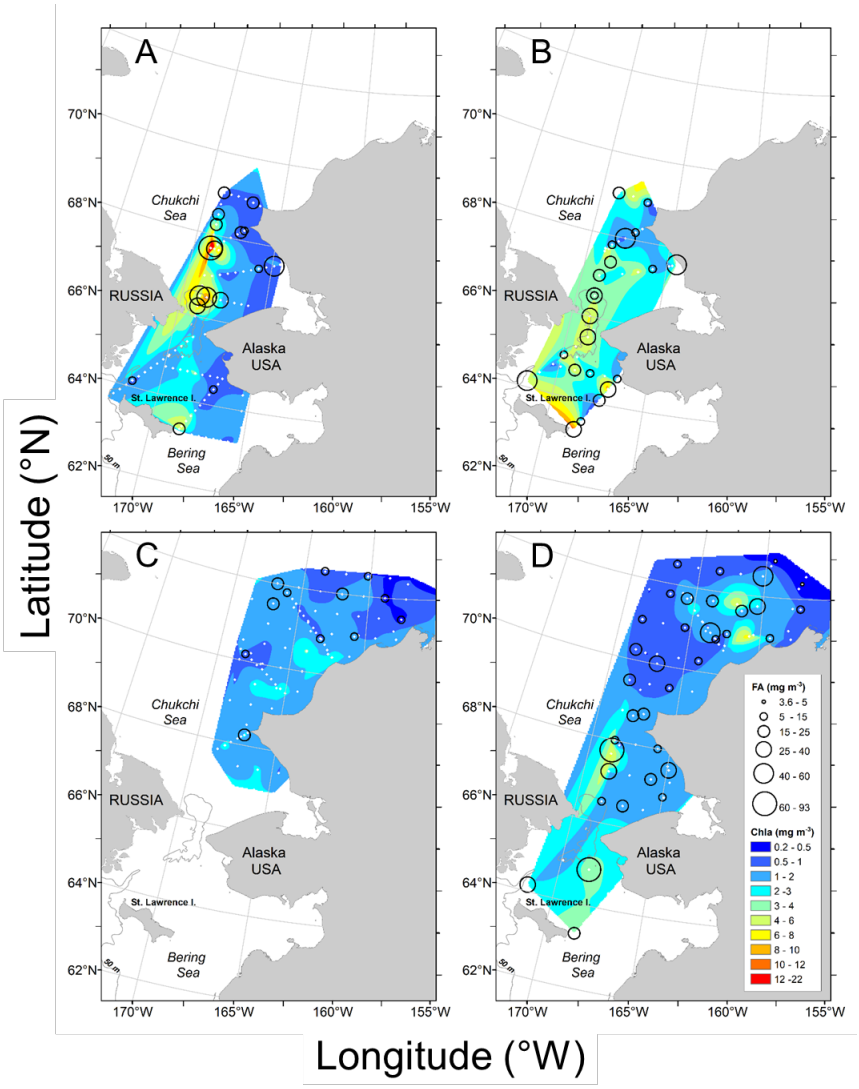

Fig. 1: Mean *in situ* Chl-a [mg m^{-3}] averaged from surface to 50 m and mean total FA concentrations [mg m^{-3}] measured at each station in: **A**) June 2017, **B**) June 2018, **C**) Aug/Sep 2017 and **D**) Aug/Sep 2019 in the northern Bering and Chukchi Seas. White diamonds indicate station locations.

Figure 2

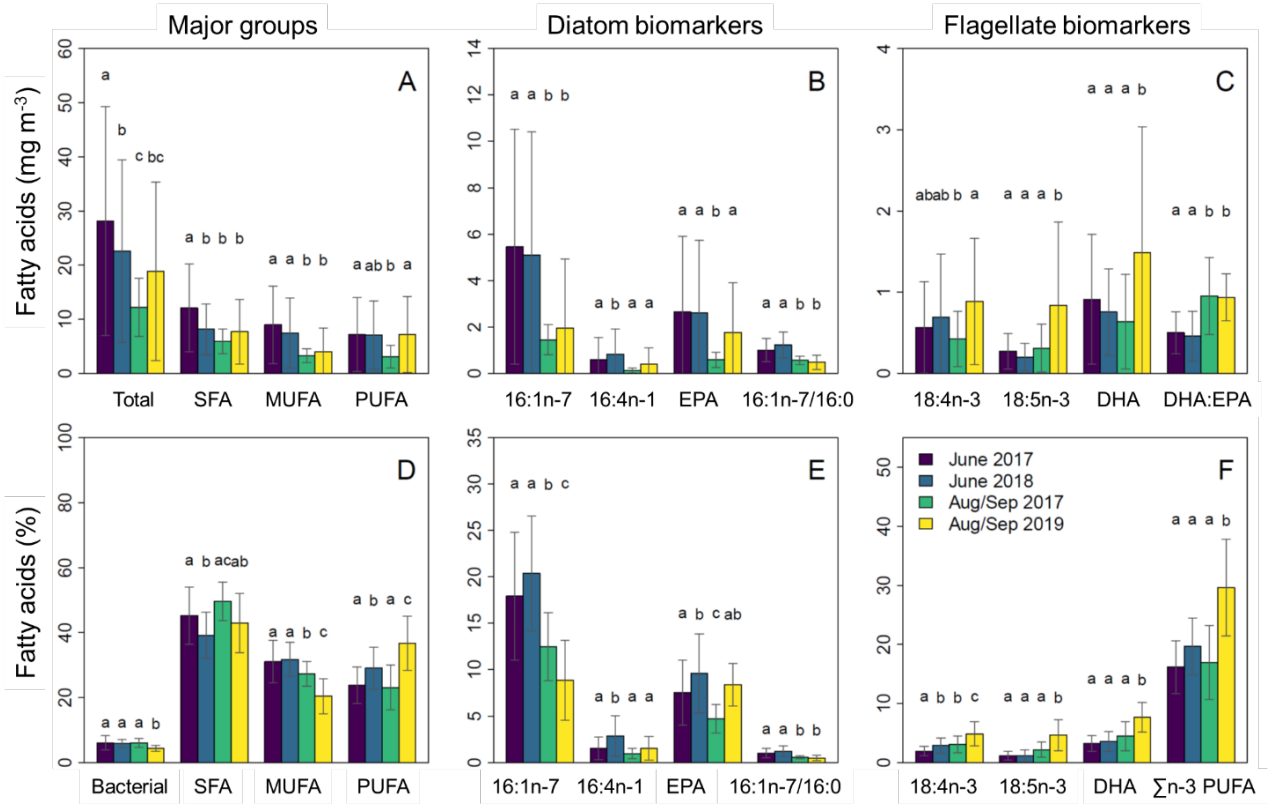

Fig. 2: Differences in June 2017 (n = 45, purple), June 2018 (n = 36, blue), Aug/Sep 2017 (n = 25, green) and Aug/Sep 2019 (n = 61, yellow) FA concentrations (top panel) and percent composition (bottom panel) for total FA, SFA, MUFA, PUFA and Bacterial (sum of all odd carbon FA and branched FAs) (**A, D**), diatom biomarkers 16:1n-7, 16:4n-1 EPA (20:5n-3) and a ratio diatom biomarker (ratio of 16:1n-7/16:0) **(B, E)**, and common dino+flag biomarkers 18:4n-3, 18:5n-3 and DHA (22:6n-3), DHA:EPA ratios, and the sum of n3-PUFA (**C, F**). Letters denote significant group differences based on ANOVA with Tukey HSD ($p<0.05$), with bars showing mean values and error bars denoting standard deviation

Figure 3

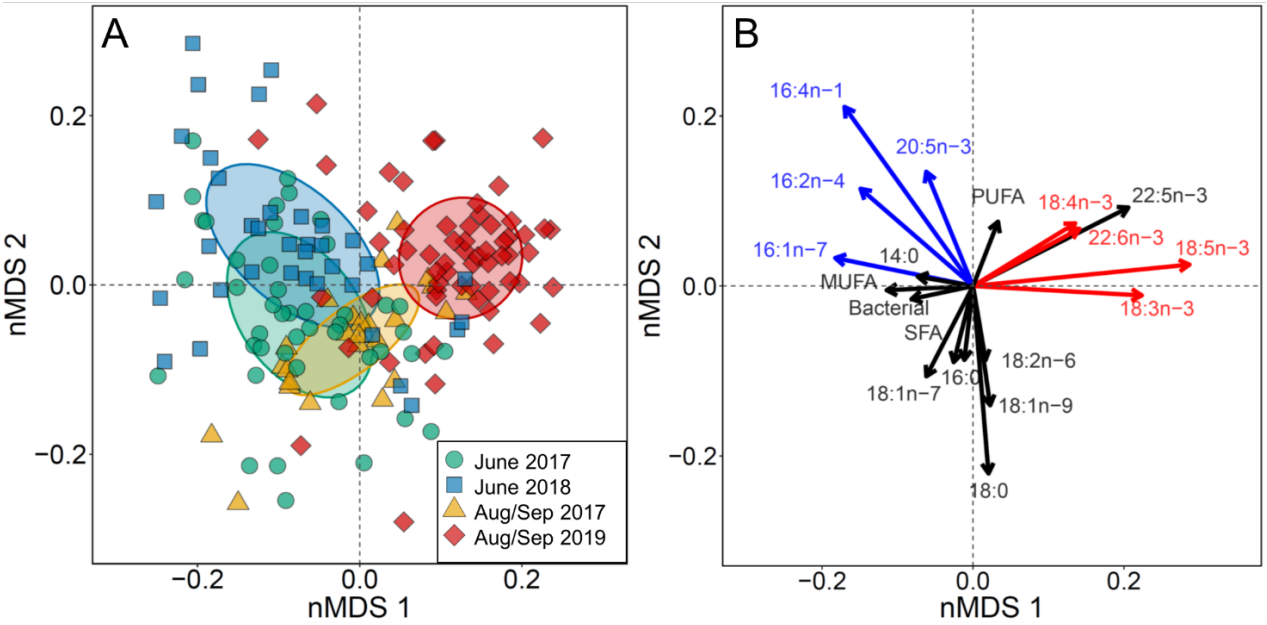

Fig. 3: Non-metric multidimensional scaling (nMDS) of FA percent composition data from each survey, **A**) samples from June 2017 (n = 45, green), June 2018 (n = 36, blue), Aug/Sep 2017 (n = 25, orange) and Aug/Sep 2019 (n = 61, red). Circles denote 50% ellipsoids for each survey. **B**) Vector plot for the nMDS showing individual FA associated with diatoms (blue), dino+flag (red) and shown in black are all non-taxa specific individual FA and major FA biomarker groups (SFA, MUFA, PUFA and bacterial).

Figure 4

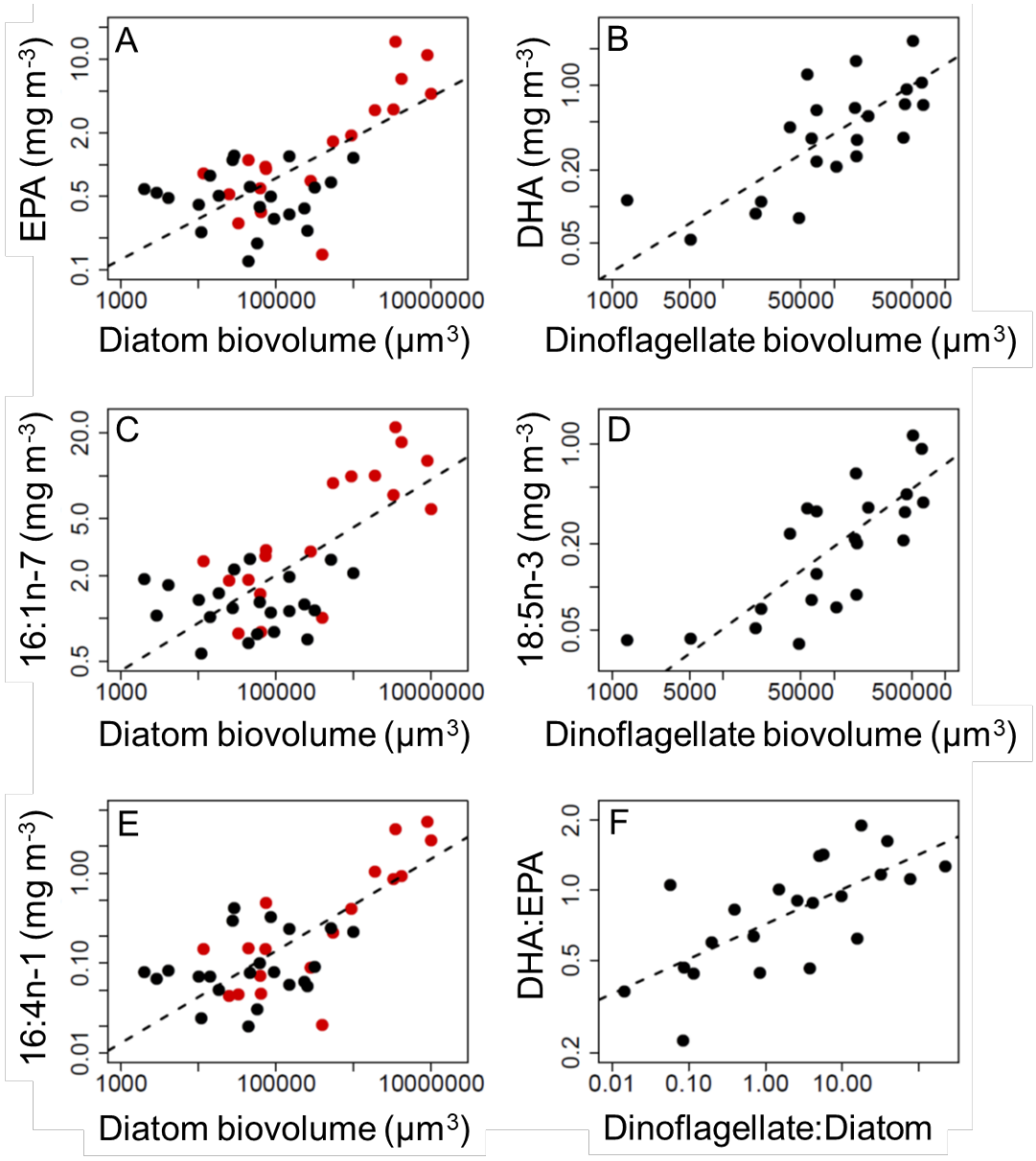

Fig. 4: Comparison of $\log_{10}$ transformed FlowCAM-measured biovolumes and FA biomarker concentration for diatoms in June 2017 (red, n = 18) and diatoms and dinoflagellates in Aug/Sep 2017 (black, n = 22). Comparisons of diatom biovolumes and **A**) EPA, **C**) 16:1n-7, **E**) 16:4n-1; comparison of dinoflagellate biovolumes and **B**) DHA, **E**) 18:5n-3; and **F**) ratios of dinoflagellate to diatom biovolumes compared to the DHA: EPA biomarkers.

Figure 5

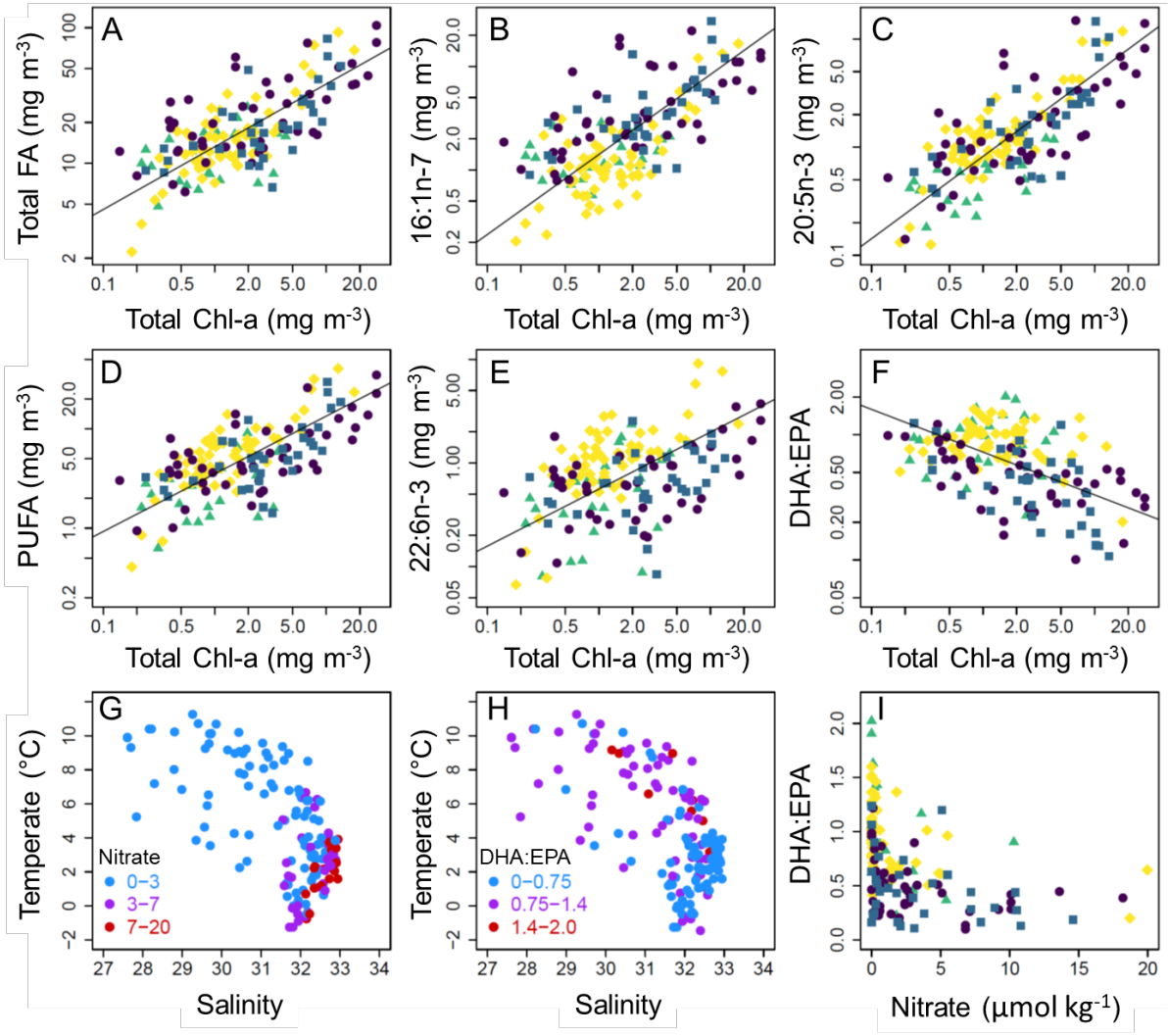

Fig. 5: Selected pairwise Type II regressions using $\log_{10}$-transformed data between *in situ* discrete Chl-a [mg m^{-3}] and FA [mg m^{-3}] samples for **A**) total FA, **B**) 16:1n-7, **C**) EPA, **D**) total PUFA, **E**) DHA and **F**) DHA:EPA ratio. Temperature-salinity plots showing **G**) nitrate concentration (µmol kg^{-1}) and **H**) DHA: EPA ratios, color coded by their values (blue=low, red=high), and I) nitrate to DHA: EPA ratios. Colors in plots **A-F** and **I** denote each survey, with June 2017 (purple circles), June 2018 (blue squares), Aug/Sep 2017 (green triangles) and Aug/Sep 2019 (yellow diamonds).

Figure 6

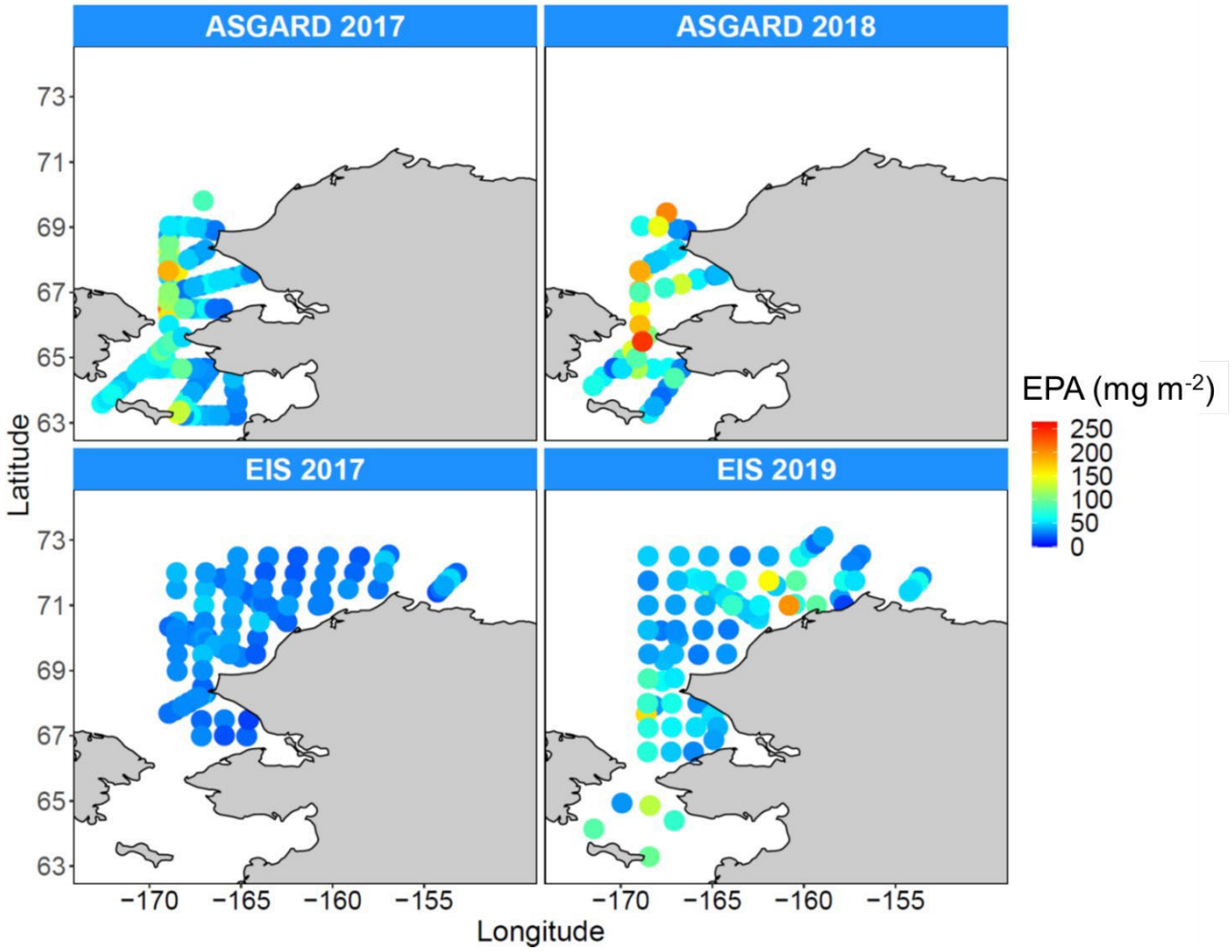

Fig. 6: Mixed effects model results predicting water column integrated EPA concentrations (mg m^{-2}) for each survey using all discrete sample total Chl-a and nitrogen samples as predictor variables (n = 1635, Table S1).

Chapter 21: Dynamics of the microbial food web NSB and Chukchi Seas using a linear inverse modeling approach

Nielsen J.M., CICOES, University of Washington, jens.nielsen@noaa.gov

Lomas M.W., Eisner L.B., Mordy C.W., McDonnell A., Kelly, T.B., O'Daly S., Hopcroft R., Stockwell D., Danielson S., Juranek L., Cynar H., Krause J., Kimmel D., Schnetzer A., Irby M.

Nielsen J.M., Lomas M.W., Eisner L.B., Mordy C.W., McDonnell A., Kelly, T.B., O'Daly S., Hopcroft R., Stockwell D., Danielson S., Juranek L., Cynar H., Krause J., Kimmel D., Schnetzer A., Irby M. Inverse modelling of the microbial food web NSB and Chukchi Seas in spring and late summer

No figure… journal TBD

Introduction: Resolving carbon flows in marine planktonic foodwebs is a fundamental first step for understanding the energy available for higher trophic level consumers and overall food web processes, production and function. Inverse food web modeling is a convenient data driven modeling approach for estimating carbon fluxes in marine food webs.

Methods: Using empirical biomass and rate measurements, inverse food web modeling allows reconstruction of trophic flows and quantification of biological rates that are commonly challenging to measure. Here we use in-situ phytoplankton, microzooplankton, zooplankton, sedimentation and primary production data collected from 4 ecosystem surveys in the Chukchi and Northern Bering seas, June (spring) 2017 and 2018, and August-September (summer) 2017 and 2019.

Results and Discussion: Specifically we assess, 1) partitioning of energy, in terms of carbon, between the pelagic food web and deposition to the benthos, 2) how does transfer and major pathways vary between seasons (June vs August/September), and 3) how does food web carbon pathways vary between nutrient replete and deplete areas. Initial simulations indicate seasonal differences in major carbon pathways. Higher carbon fluxes appeared to be available for benthic consumers in spring (in areas of high primary production) compared to late summer. Our initial analyses also revealed the importance of carbon uptake and transfer in microzooplankton and bacterial compartments, organisms and processes that are often underestimated on many ecosystem models. Overall, our results indicate variable carbon transfer efficiencies among seasons and areas of nutrient replete and deplete conditions, something that should be considered when evaluating larger food web processes.

Chapter 22: Flow patterns over the Chukchi continental shelf: 2010-2020: A decade of observations in the Chukchi Sea

Stabeno, P.J., NOAA Pacific Marine Environmental Laboratory, phyllis.stabeno@noaa.gov

McCabe, R.M.

Stabeno, P. J. and R. M. McCabe (in preparation). Flow patterns over the Chukchi continental shelf: 2010-2020: A decade of observations in the Chukchi Sea. DSRII

Introduction: The Chukchi Sea consists of a broad shallow (<80 m) shelf, extending >800 km northward from its southern boundary at Bering Strait to the shelf break bounding the Arctic basin. The Chukchi continental shelf is generally referred to as an inflow shelf for the Arctic and is the only source of Pacific-origin water to the Arctic Ocean. Most of the flow originates in Bering Strait, and flows northward over the Chukchi shelf. This current system is a major source of heat, nutrients, salt and freshwater to the Arctic.

Methods: From 2010 to 2019, moorings were deployed in the Chukchi Sea at a dozen sites. Deployment duration varied from 10 years at a site off Icy Cape to a single year at a site north of Hanna Shoal. Currents were measured at each site, usually with acoustic Doppler current profilers (ADCPs). In addition, a total of 47 satellite-tracked drifters (drogue depth 25–30 m) were deployed in the region during 2012–2020. A primary goal of these deployments was to better understand the patterns and magnitude of flow on the US Chukchi shelf.

Results and Discussion: Together, these data provided insight into the temporal and spatial variability in the currents over eastern Chukchi continental shelf. There is a 10-year time series of transport at Icy Cape, which accounts for most of the northeastward flow in Barrow Canyon. The annual volume transport near Icy Cape ranged from ~0.3 x 10^6 m^3 s^{-1} (10^6 m^3 s^{-1} = 1 Sv) during September 2011 – August 2012 to ~0.7 Sv during September 2017 – August 2018, with a 10-year average of ~0.4 Sv. This transport accounts for approximately 40% of the flow through Bering Strait and varies seasonally, ranging from >50% of summer transport to only 20% of winter transport in Bering Strait. Anomalous winds toward the north-northeast in the winter of 2017/2018 likely contributed to the higher annual transports in September 2017–August 2018. There are three years (2016–2017, 2017–2018 and 2018–2019) of more intense spatial sampling. For those years, current measurements were made at 8 locations on the eastern Chukchi shelf: southern Chukchi shelf (1 mooring), Central Channel (2 moorings), Icy Cape (3 moorings) and Barrow Canyon (2 moorings). These measurements provide insight into patterns of flow across this shelf. As expected, bathymetry plays an important role in steering the flow patterns on the shelf. Measurements of transport at Icy Cape and in Central Channel indicate that most of the transport at Icy Cape is a continuation of the flow in Central Channel, which flows to the south of Hannah Shoal.

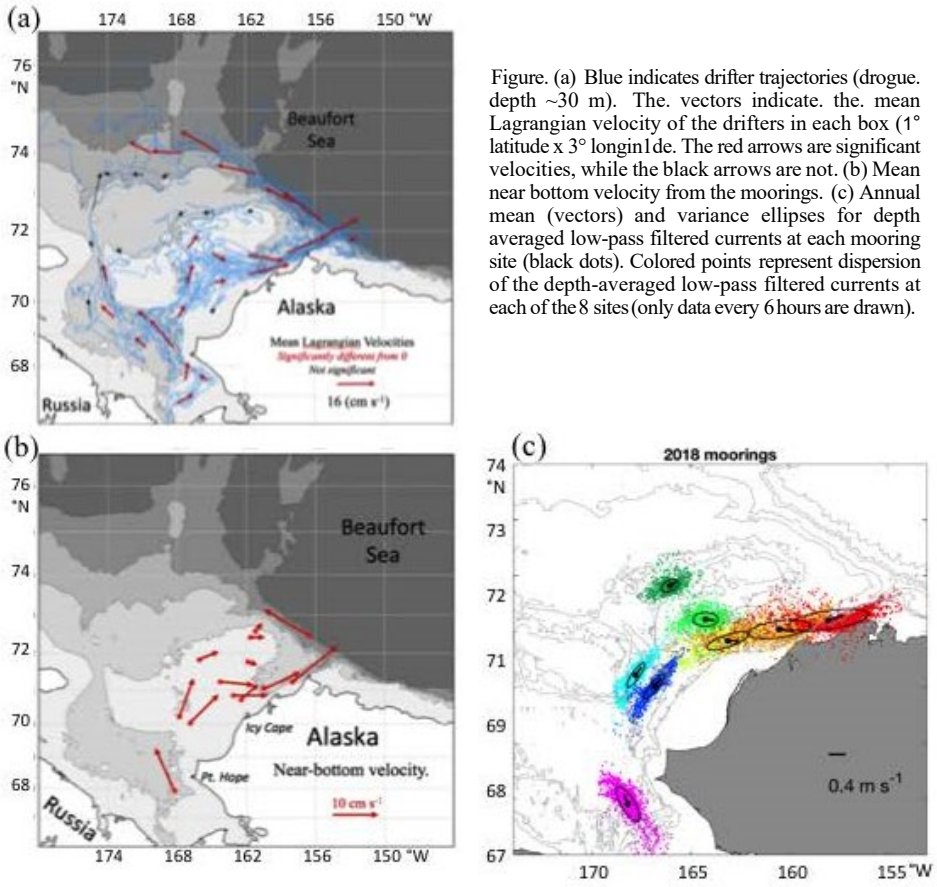

Figure. (a) Blue indicates drifter trajectories (drogue. depth ~30 m). The. vectors indicate. the. mean Lagrangian velocity of the drifters in each box (1° latitude x 3° longin1de. The red arrows are significant velocities, while the black arrows are not. (b) Mean near bottom velocity from the moorings. (c) Annual mean (vectors) and variance ellipses for depth averaged low-pass filtered currents at each mooring site (black dots). Colored points represent dispersion of the depth-averaged low-pass filtered currents at each of the 8 sites (only data every 6 hours are drawn).

Chapter 23: A decade of measurements of ice draft in the Chukchi Sea

Sullivan, M.E., CICOES, University of Washington, peggy.sullivan@noaa.gov

Stabeno, P.J.

A decade of measurements of ice draft in the Chukchi Sea

Sullivan, M.E. and Stabeno, P.J.

Introduction: The Chukchi Sea has seen dramatic warming and sea-ice changes in recent years. Sub-Arctic ice processes, shaped by wind, currents and bathymetry, show a shrinking sea ice season with a longer duration of open water. Changes to this seasonal ice zone imply changes to the ecosystem as a whole, to the success of organisms at all trophic levels, and to the flow of energy within the system.

Methods: Sonar ice draft data were collected, 2010-2019, at multiple mooring locations on the Chukchi Sea shelf to examine the longer-term trend of sea ice changes on the shelf, and related influence on the ecosystem and on marine mammals. Data were collected every second using an ASL Environmental IPS5 ice profiler at 420 kHz and 1.8° beam width. Tilt corrections, removal of atmospheric pressure and removal of outliers occurred during processing. Year-long data are presented in the figure with a focus on three mooring sites (C1, C2 and C3) near 71° N off Icy Cape, Alaska that stretch northwest toward Hanna Shoal, where data collection occurred more frequently. Site C2 data encompass the years 2010 to 2019, fall to fall. Sites C1 and C3 cover most of the same years. Reference is made to three other sites in the region: sites C4 and C5 close to Barrow Canyon, and C6 northeast of C2 near Hanna Shoal, that have fewer data sets. All the sites are in 42-53 meter water depth and were deployed in late summer or fall. We demonstrate localized variations in the larger picture of a changing seasonal ice zone.

Results and Discussion: Fall transition from open water to ice cover can occur November to mid-December, and is a more organized process than the spring melt transition. Cooling of the water column is attributable to cooler air, winds, diminishing solar insolation and advected ice from the north and west. A cycle of ice formation and melt occurs until the water-column temperature cools enough for ice to form and remain. Ice draft data signals clearly show dampening of waves, and a dynamic mix of waves and frazil ice as the winter ice cover forms. This process can extend from a day to a month. Year-to-year trends at sites C1 and C2 show the freeze up trending later in recent years. January-March are mostly ice-covered, with daily mean ice draft values increasing within that time frame: the average of daily median values at C2, 2011-2018, January, February, March, are respectively 0.577, 0.825 and 1.073 m. Deeper ice keels > 20 m occur predominantly April to mid-June and more often occur at C1 and C2, likely due to more open water and polynya exposure, and ice rafting during the spring transition to open water. A very deep keel of 31.3 m occurred at C1 on May 15, 2015. Comparison of VIIRS True Color satellite images with the ice draft signal show cross-shelf ice keel depth variations along the Icy Cape Line, C1, C2, and C3 as the spring breakup chaotically moves ice into and out of the mooring site areas.

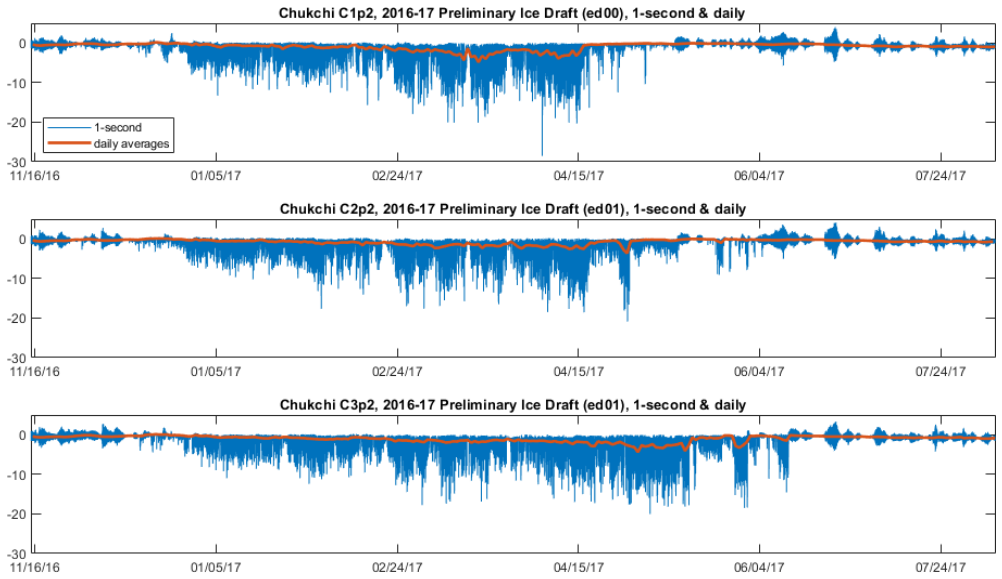

Figure 1. Ice draft data in 2016-2017 from moorings C1 (top), C2 (middle) and C3 (bottom) near 71° N off Icy Cape, Alaska that stretch northwest (C1 to C3) toward Hanna Shoal in the Chukchi Sea.

Chapter 24: Variations in phytoplankton community composition, phytoplankton biomass, and primary production in a warming Arctic

Eisner, L., NOAA Fisheries, lisa.eisner@noaa.gov

Gonzalez, S., Lomas, M., Nielsen, J., Stockwell, D.

Eisner, Gonzalez, Lomas, Nielsen, Stockwell, et al. (in preparation), Variations in phytoplankton biomass, community composition and size structure, and primary production in a warming Arctic.

Introduction: Marine phytoplankton community composition and size structure, biomass and primary production are important to carbon cycling and consequently also the quality and quantity of dietary resources for higher trophic level consumers. Phytoplankton population dynamics can vary considerably between spring and summer, nutrient deplete and replete water masses, and between surface and subsurface depths in Arctic seas.

Methods: Discrete water samples for phytoplankton community composition (e.g., dinoflagellates and diatoms), chlorophyll a (chla) biomass (total and size fractionated for < 5, 5-20, and > 20 µm), and primary productivity (total, < 5, > 5 µm) data were collected during ecosystem process surveys in the Chukchi Sea as part of Arctic ecosystem projects: Arctic Shelf Growth, Advection, Respiration & Deposition (ASGARD) and the Arctic Integrated Ecosystem Survey (Arctic IES) in June (spring 2017 and 2018) and August-September (summer 2017 and 2019), respectively. Phytoplankton taxa were evaluated using Flow Cam analysis (imaging microscope) of live water samples. Chla samples were filtered and stored frozen at -80 °C until later analysis (within 6 months) with a bench top fluorometer following standard acidification methods (Parsons et al. 1984). Water samples for primary productivity stable isotope (^{13}C and ^{15}N) experiments were collected at 4 light levels ranging from 1.5 - 100% surface irradiance, inoculated with isotopes, placed in screen bags (to simulate light levels at the water column depths where samples were collected) and incubated for 6 h encompassing solar noon in an on-deck transparent tank cooled with surface seawater. Samples were then filtered onto GFF (nominal pore size 0.7 µm) and 5 µm filters, and stored frozen at -80 °C until analysis at a shore-based facility; detailed methods described in Lomas et al. (2020). Discrete nutrient samples (nitrate, ammonium, nitrite, phosphate and silicate) were frozen and later analyzed following standard colorimetric methods (Gordon et al. 1993). CTD vertical profiles of temperature, salinity, irradiance (photosynthetically active radiation (PAR)) and chla fluorescence were conducted at each station.

We evaluated spatial variations chlorophyll and primary production for the 4 surveys. We also evaluated seasonal changes in phytoplankton blooms (~ > 1 mg m^{-3} chla) at surface (< 15 m) and subsurface (> 15 m) depths, and the factors limiting phytoplankton growth for data collected in 2017, the year that both seasons were sampled. Nutrients were averaged above and below the mixed layer depth (MLD), defined as the depth where the change in density was greater than 0.1 kg m^{-3} from the 5 m value (Danielson et al. 2011). The measured primary production was compared to modelled phytoplankton growth based on equations incorporating light (PAR), temperature, and nutrient (nitrate) data (Kremer et al. 2017; Palmer et al. 2013).

Results and Discussion:

Chla and Primary Productivity: In June 2017 and 2018, chla integrated over the top 50 m (or to the bottom if shallower than 50 m) was highest in the > 5 µm size fraction (Figure 1). The total chla and the > 5 µm and >20 µm (data not shown) size fractions had very similar concentrations indicating that most cells in June were large particles (e.g., diatom chains). Small phytoplankton were more dominant closer to shore. Large particles and total chla were highest offshore of Point Hope and in the Bering Strait. In August-September, in 2017, low chla was associated with the < 5 µm (small particle) fraction (Figure 2). In 2019, high and low chla were associated with the < 5 µm fraction, depending on station.

In June 2017, total primary productivity (integrated from the surface to the 1% light level) was patchy with the highest production at a station impacted by the nutrient-rich Anadyr Current (Figure 3) offshore of Pt. Hope in an area of high chla. Overall, June 2018 was similar to 2017, with a few stations with slightly higher productivities. In August – September, total primary productivity was generally lower than in June. The fraction of primary production in the < 5µm fraction was quite high in June 2017 (Figure 4). The values in June 2018 and August-September 2017 and 2019 are more in line with expectations at up to 20% in spring, and 20-50% in late summer/fall. Productivities (and chla biomass) were higher in the < 5 µm fraction in late summer 2019 (the warmest year) compared to 2017. The higher abundances of *Synechococcus* sp. (small photosythetic bacteria) in late summer/fall 2019 compared to2017, support these findings (Lomas et al., Chapter 16).

For all 4 surveys, most of the chla was found in larger (> 5 µm) phytoplankton, and the majority of the primary production was from large phytoplankton, particularly in spring. However, small cells are more important to total carbon (C) in both the spring and summer, due to inverse relation of C: Chla ratio and size. Primary production rates and total chla biomass were higher, although more patchy, in spring than in late summer/fall (Figures 1-5).

Subsurface blooms: Subsurface blooms, common features in the Chukchi Sea in summer (Martini et al. 2016), were less prevalent in spring than in late summer/fall in 2017 (Figure 6). In June, 7% of the stations had surface blooms (blue square), 26% had subsurface blooms (blue circle), and 67% had non-blooms (chla < 1 mg m^{-3}, red triangle). In August-September, 8% of the stations had surface blooms, 41% had subsurface blooms, and 51% had non-blooms. Phytoplankton growth depends on nutrient availability and will experience tradeoffs of light and temperature to acquire nutrients. Stratified surface waters (above MLD) often become nutrient-limited, as was observed in summer 2017, leading to subsurface blooms below the nutrient-depleted surface waters (Figures 7-8).

Models of phytoplankton growth: Theoretical models incorporating temperature, irradiance, and nitrate availability were used to predict the realized growth of phytoplankton for a vertical profile in spring and a vertical profile with a subsurface bloom in late summer 2017 (Figure 9). Preliminary results indicate nutrient-limited conditions for the late summer example, but not for the spring example. These models will be further evaluated and generalized using to the entire dataset.

Community composition: As expected, diatoms (primarily large diatom chains) were in higher abundance in spring than fall (data not shown), as also confirmed by fatty acid analysis (Nielsen et al., Chapter 20). Although, diatoms (as well as dinoflagellates) were observed at many stations in summer. Harmful algal bloom (HAB) species *Alexandrium catenella* was observed at several stations in summer with high concentrations off Icy Cape in 2017, an area with known *A. catenella* cyst beds and vegetative cells (Anderson et al. 2021).

Conclusions:

Chla biomass and production of the small (< 5 µm) size fraction was higher in summer 2019 (the warmest year) than 2017. These changes in phytoplankton community dynamics, in addition to reduced biomass and primary productivity, are likely to result in reduced food quality with negative ramifications for higher trophic levels. Small copepods (e.g., *Pseudocalanus* sp.) were also higher in abundance in 2019 (Kimmel et al., Chapter 14), suggesting a small sized planktonic (phytoplankton and zooplankton) community may occur as Arctic waters continue to warm. Future analyses will evaluate the factors

driving seasonal and spatial changes in phytoplankton community composition and size structure, biomass and growth.

References:

Anderson, D.M., Fachon, E., Pickart, R.S., Lin, P., Fischer, A.D. Richlen, M. L., Uva, V. et al. (2021) Evidence for massive and recurrent toxic blooms of *Alexandrium catenella* in the Alaskan Arctic. PNAS 118 (41) e2107387118. https://doi.org/10.1073/pnas.2107387118

Danielson, S., Eisner, L., Weingartner, T., Aagaard, K. (2011). Thermal and haline variability over the central Bering Sea shelf: Seasonal and interannual perspectives. *Continental Shelf Research*, 31(6), 539-554.

Gordon, L., Jennings, J. Jr., Ross, A., Krest, J. (1993) A suggested protocol for continuous flow automated analysis of seawater nutrients (phosphate, nitrate, nitrite, and silicic acid) in the WOCE Hydrographic Program and the Joint Global Ocean Fluxes Study. Oregon State University, Corvallis, OR

Kremer, C. T., Thomas, M. K., Litchman, E. (2017). Temperature- and size-scaling of phytoplankton population growth rates: Reconciling the Eppley curve and the metabolic theory of ecology. *Limnology and Oceanography, 62*(4), 1658-1670. doi:10.1002/lno.10523

Lomas, M.W., Eisner, L.B., Gann, J., Baer, S.B., Mordy, C.W., Stabeno, P.J. (2020). Time-series of direct primary production and phytoplankton biomass in the Southeastern Bering Sea: Responses to cold and warm stanzas. Marine Ecology Progress Series, 642:39-54.

Martini, K., Stabeno, P., Ladd, C., Winsor, P., Weingartner, T., Mordy, C., Eisner, L. (2016). Dependence of subsurface chlorophyll on seasonal water masses in the Chukchi Sea. JGR 121, doi: 10.1002/2015JC011359.

Palmer, M. A., Dijken, G. L., Mitchell, B. G., Seegers, B. J., Lowry, K. E., Mills, M. M., Arrigo, K. R. (2013). Light and nutrient control of photosynthesis in natural phytoplankton populations from the Chukchi and Beaufort seas, Arctic Ocean. *Limnology and Oceanography, 58*(6), 2185-2205. doi:10.4319/lo.2013.58.6.2185

Parsons TR, Maita Y, Lalli CM (1984). A manual of chemical and biological methods for seawater analysis. Pergamon Press, New York, NY

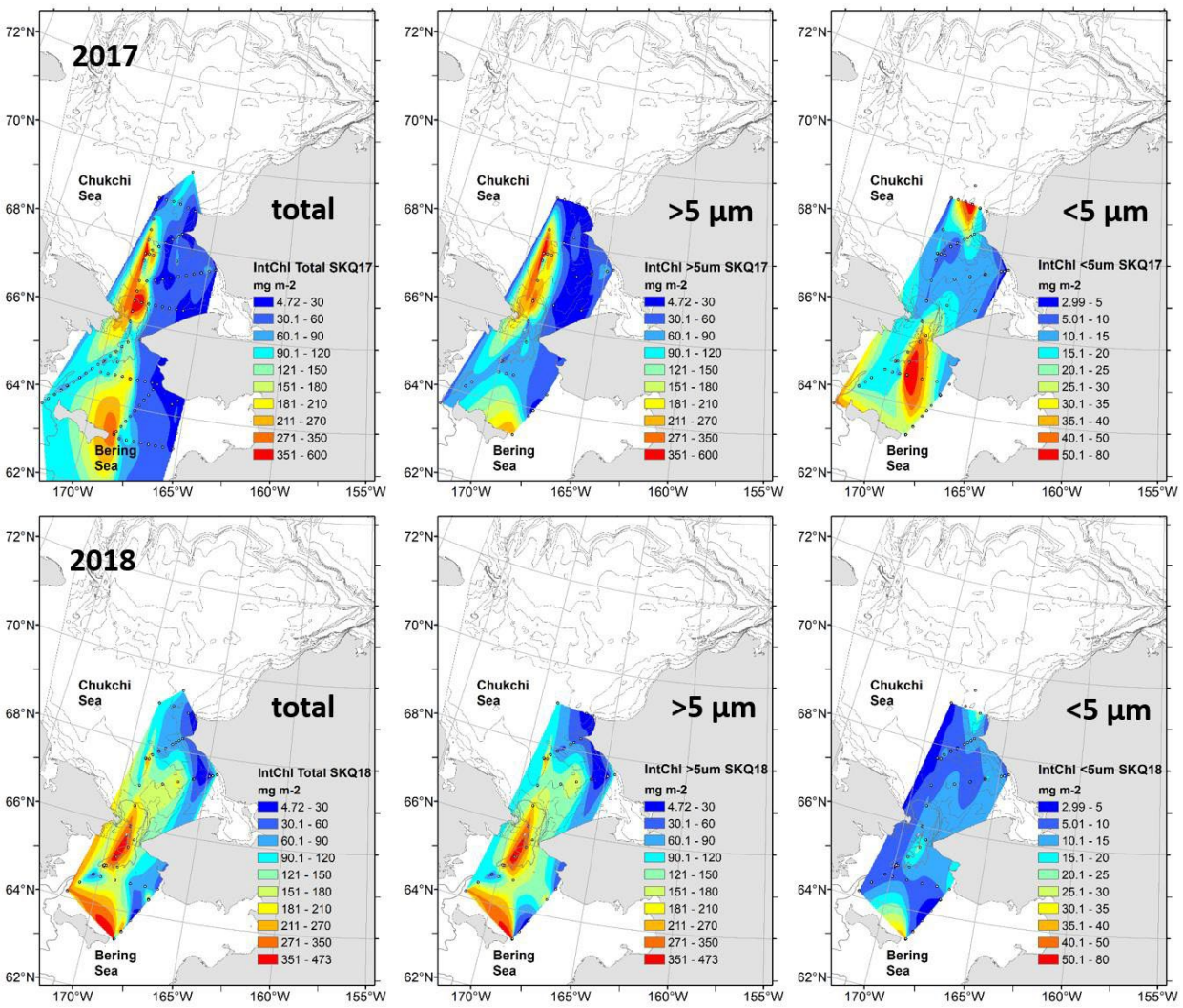

Figure 1. Total >5 µm and <5 µm size fractionated chla integrated over the top 50 m or to bottom if shallower than 50 m for June (spring) ASGARD surveys in 2017 and 2018. Note lower range for < 5 µm fraction.

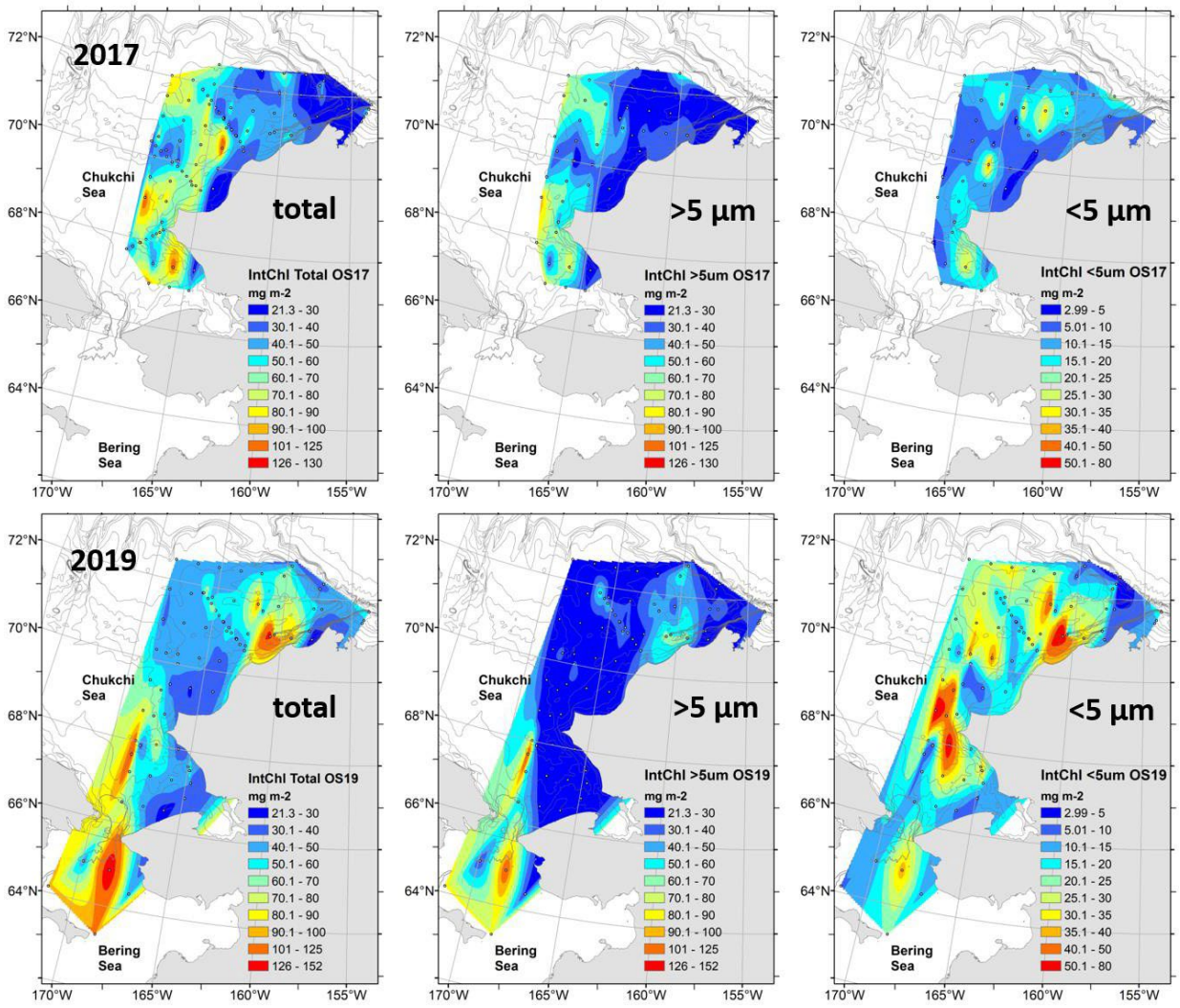

Figure 2. Total >5 µm and <5 µm size fractionated chla integrated over the top 50 m or to bottom if shallower than 50 m for August-September (late summer/fall) Arctic IES surveys in 2017 and 2019. Note lower range for < 5 µm fraction. Total and > 5 um size fraction ranges are lower than in Figure 1 (spring).

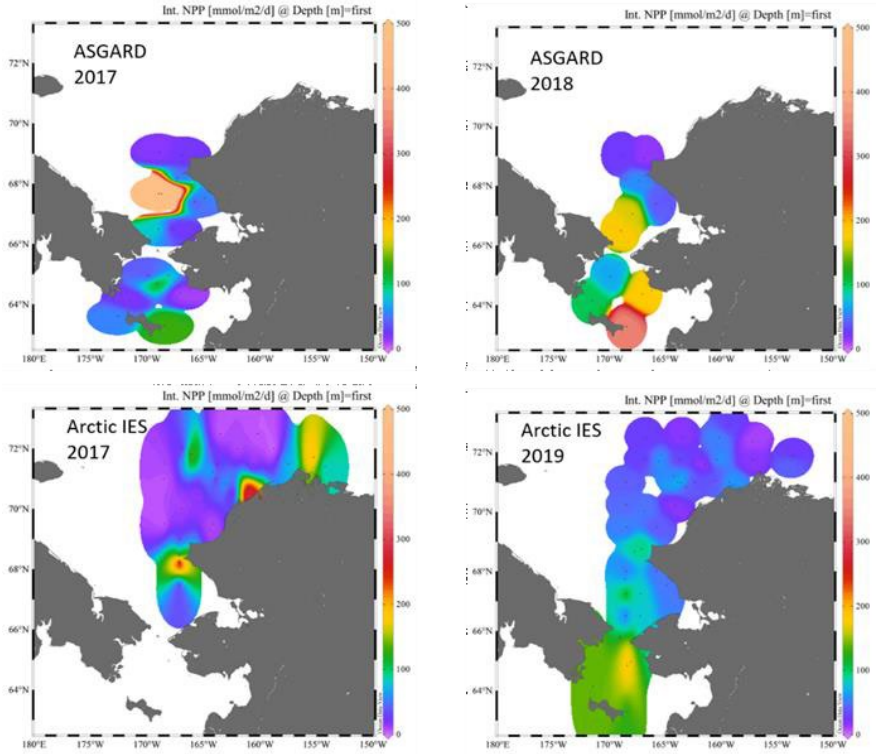

Figure 3. Total primary productivity (mmol m^{-2} d^{-1}) estimates from simulated in situ stable isotope (^{13}C) shipboard experiments.

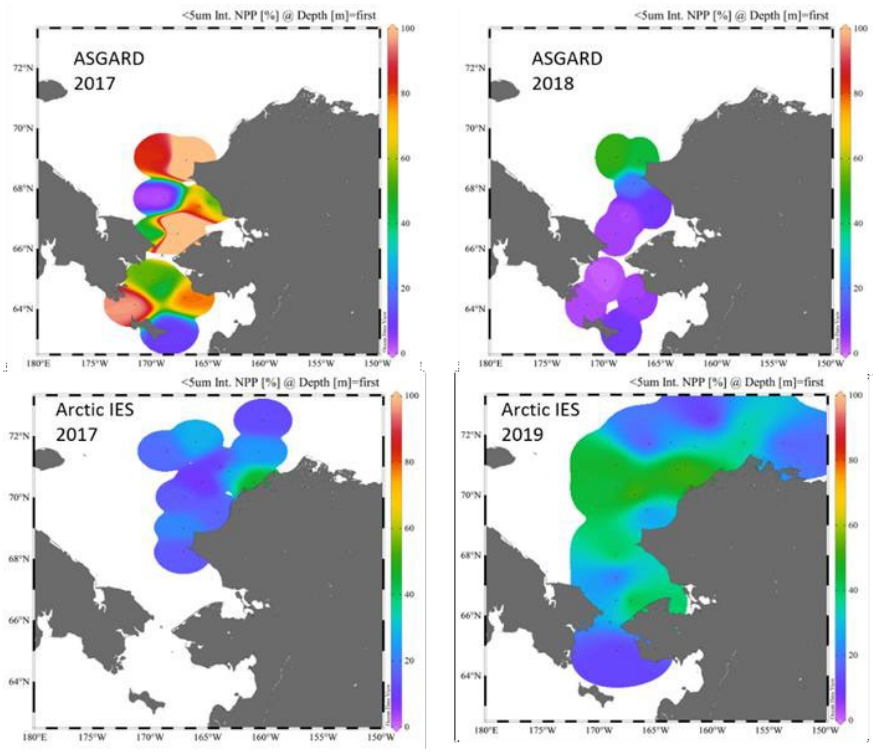

Figure 4. Percent of total primary productivity in the < 5 µm size fraction.

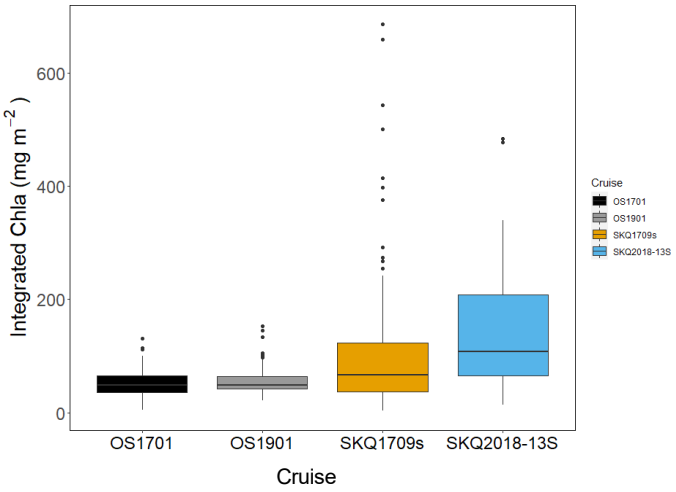

Figure 5. Box plot comparison of chla integrated over the top 50 m or to bottom if shallower than 50 m, for all 4 surveys (OS are August-September surveys and SKQ are June).

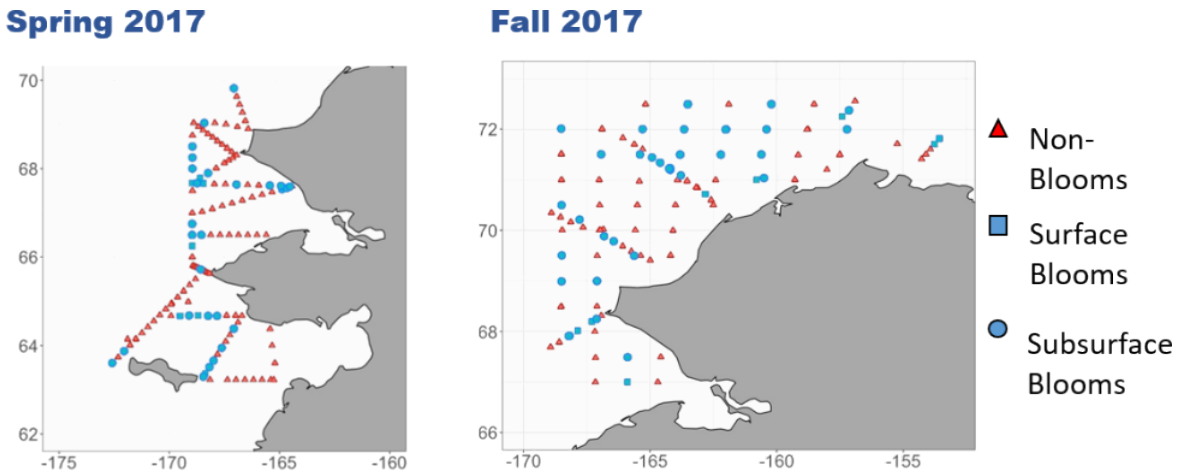

Figure 6. Stations with surface (blue box), subsurface (blue circle) and non-blooms (red triangle) in June (spring) and August –September (late summer/early fall) 2017.

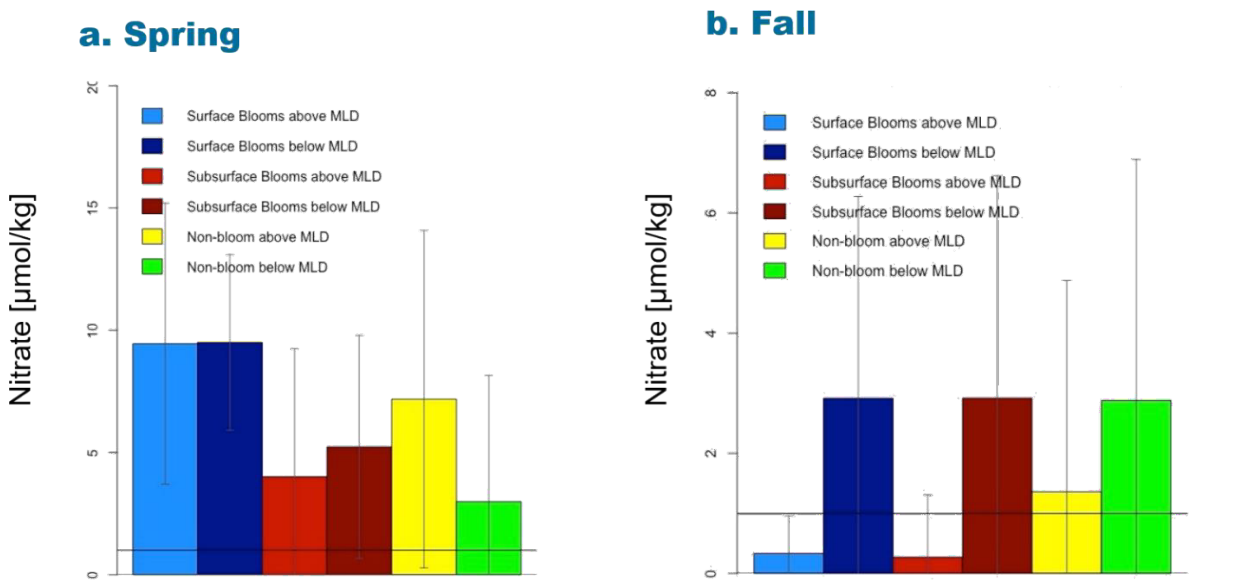

Figure 7. Nitrate Concentrations above and below the MLD for stations with surface blooms (blue), subsurface blooms (red), and non-blooms (yellow/green) for a) June (spring) and b) August –September (late summer/early fall) 2017. The black horizontal line depicts the threshold nitrate concentration of 1 µmol kg^{-1} for nitrate limitation.

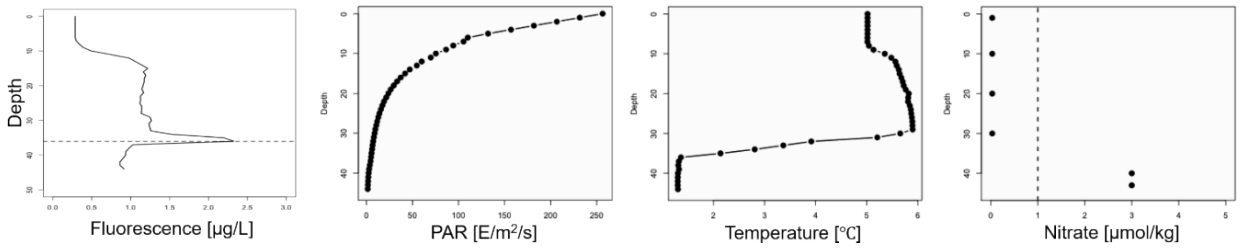

Figure 8. Example subsurface bloom profile from late summer/fall 2017 showing chla from the CTD fluorometer , light (PAR), temperature, and nitrate concentration. Dotted lines depict the threshold concentration for nutrient limitation at 1 µmol kg^{-1}.

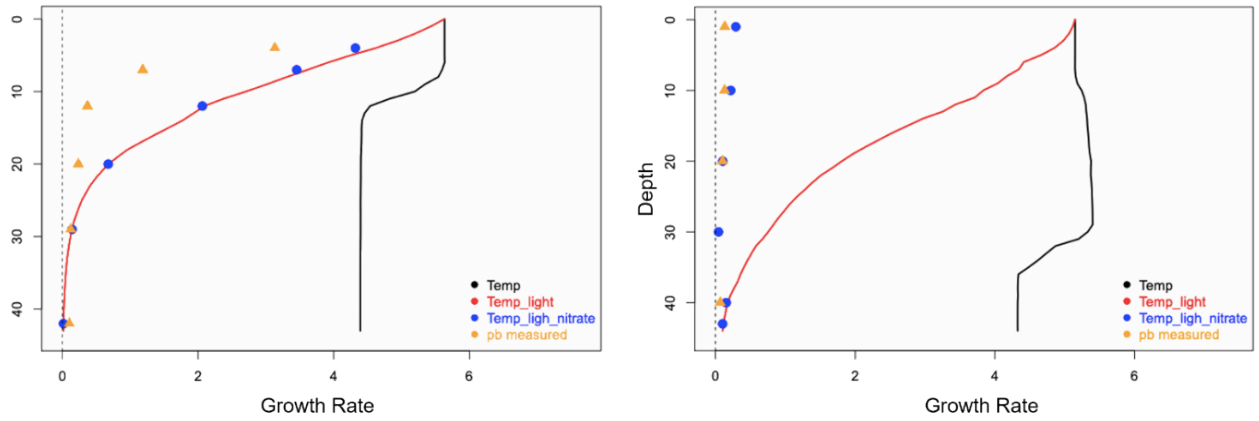

Figure 9. Phytoplankton productivity model examples for left) spring non-nutrient limited, and right) late summer /fall surface nutrient-limited conditions during 2017. The vertical profiles of fluorescence, PAR, temperature and nitrate for the right plot are shown in Figure 8. Models included temperature (black line), temperature + light (red line) and temperature + light + nitrate (blue dots). Pb measured (yellow dots) is phytoplankton specific growth estimated from discrete primary productivity samples. In left plot, nitrate is not limiting (adding nitrate to the model did not improve the model beyond the model with temperature + light and appears to show similarity to the in situ Pb profile data). In contrast, in right plot, adding nitrate to the model appeared to produce results similar to the Pb data.

an understanding of larval access to nurseries is hindered by the probable modeling limitation of under-representing larval transport to inshore habitats in the BS. Another consideration when spatially contemplating nursery occupation, is that demersal-stage juveniles are essentially invisible to survey gear from settlement to 2 years of age and considerable migration may occur during that time. Discrepancies between modeled and empirical abundances of juvenile flatfish in the BS have been observed in the past utilizing an earlier ROMS iteration (Cooper et al., 2013), suggesting that the IBM may be limited in its ability to simulate cross-isobath transport. There are several mechanisms that may impact the ability for the oceanographic model to capture cross-shelf transport. Cross-shelf transport associated with sub-mesoscale eddies or bathymetric steering via seafloor terrain features may play a role in on-shelf movement that can only be captured with higher resolution ocean models (Hermann et al. 2009; Combes et al. 2013; Gibson et al. 2013; Opdal and Vikebø 2016; Vestfals et al. 2014; Mordy et al. 2019). In addition to potential limitations of the physical model, due to lack of empirical data, the IBM did not incorporate orientation to nurseries or directed horizontal swimming behavior that has been observed for some species (Huijbers et al., 2012; Igulu et al., 2013) and has been hypothesized to be relevant for nursery recruitment of sablefish (Gibson et al., 2019). Larval swimming abilities and vertical movement that were not captured by the model may also facilitate transport to settlement habitats (Cowen and Castro 1994). For example, rock sole larvae in the BS are likely transported from the slope to the shelf through vertical movement of larvae that is synchronized with tidal periodicity (Wilderbuer et al., 2016). Modeling constraints due to resolution as well as biological parameterization also have the potential to impact quantitative estimates of transport and connectivity. Unlike cross-shelf transport in the BS, the model did capture larval transport through Unimak Pass; however, model resolution may impact estimates of transport and potentially underestimate the contribution of smaller island passes (Gibson et al. 2013).

Despite these potential limitations, basin-scale larval connectivity of Pacific halibut between the GOA and the BS was consistent across years and larval transport patterns suggest that spawning within the southern BS may subsidize components of the population to the west. Along the north Pacific Asiatic coast there is an established population of Pacific halibut (Schmidt 1934; Best 1979) but details of size composition, growth, and migration rates are largely unknown. Modeling results suggest populations of Pacific halibut along the north Pacific Asiatic coast may be supported by spawning in the southern BS and that juvenile settlement in the BS may be subsidized by larvae that originate in the western GOA.

Our modeling approaches did not provide evidence of possible factors that contribute to the determination of cohort strength, in this case fluctuations in abundance observed with the strong 2005 and the weak 2009 year classes. The Thompson-Burkenroad debate in the early part of the twentieth century discussed fishery and environmental factors as separate and distinct possible causes of fluctuations in Pacific halibut abundance (Skud 1975), but more recent studies have concluded that both factors can affect fish populations. Pacific halibut spawning biomass declined in the period between 2005 and 2009 (Stewart & Hicks, 2018), but it has been shown that cohort strength does not correlate well with spawning biomass (Clark & Hare, 2002). However, given that Pacific halibut is a fully exploited resource, fishing pressure may play a role in cohort strength and distribution, either through direct removals from the population or in combination with climate-related factors that apply stress to the population (Planque et al. 2010). Likewise, other studies have shown that variation in the distribution of fish species can be driven primarily by climatic factors (e.g. Sunday et al., 2015; McLean et al., 2018). Although this modeling effort has illustrated that Pacific halibut early life distributions remained relatively constant over two temperature stanzas, the interaction potential among species occupying a particular habitat can change in response to thermal habitat shifts. (Kleisner et al., 2016). In the case of Pacific halibut, variations in temperature could affect predator and prey species proximity, thus altering Pacific halibut abundance through top down (predation mortality) or bottom-up (food availability)

processes (Ferreira et al. 2020; Durant et al. 2007). Furthermore, Hunt et al. (2011) and Sigler et al. (2014), among others, showed that climate impacts recently experienced in the BS can affect the total caloric energy contained within the biological system so that changes in lower trophic levels influence upper trophic levels. Shifting productivity of spawning grounds (Somarakis et al., 2019) and spatial shifting of spawning grounds (Kanamori et al., 2019), both related to temperature, could also play a role in total productivity.

Movement patterns of juvenile Pacific halibut have not been well understood, particularly within the BS and between the BS and GOA. While there was extensive historical tagging of Pacific halibut in the BS and GOA (Best, 1977), recovery rates were generally low and only broad-scale movement pathways from the BS to GOA (Webster et al. 2013) and from shallow inshore waters to offshore habitats could be inferred from these data (Skud, 1977). In addition to widespread dispersal to deeper habitats, the results of the spatio-temporal modeling of demersal Pacific halibut illustrate the specific dispersal patterns of young fish from settlement grounds to a major inter-basin connection pathway by age-4-6 years. These results suggest that juvenile and adult migration occurs counter to larval dispersal. Compensatory Pacific halibut migration from settlement grounds in the southeastern BS south and east to the GOA is further supported by genetic studies that have found a lack of genetic differences between Pacific halibut in the eastern BS and GOA (Nielsen et al. 2010; Drinan et al. 2016) While there were similarities between year classes in their general direction of movement, there were also notable differences. In this study, the weaker 2009 year class occupied similar post-settlement redistribution pathways to the stronger 2005 year class, but appeared less aggregated overall and continued to occupy settlement grounds in Bristol Bay, whereas the 2005 cohort appeared to be highly aggregated as young fish and migrated away from settlement grounds before becoming more widely dispersed at older ages. The 2009 average size of sampled fish was larger than for 2005. It is unclear if this played a role in the migratory patterns for each cohort, e.g. smaller size could indicate relatively less food and a higher

migration rate to areas with increased food availability. Modeling of the supplemental years reinforced these inter-annual differences, but the general pattern of distribution was consistent across years and temperature stanzas. It is possible that these pattern differences were in part a response to density-dependent processes within the nursery areas (Le Pape & Bonhommeau, 2015) that were not investigated here.

We have used the spatiotemporal modelling to infer patterns of movement for individual Pacific halibut cohorts, but factors other than migration can influence the apparent distribution of fish, including factors affecting gear selectivity. The NMFS trawl survey does not sample the shallowest waters in the BS inside Bristol Bay, and thus young Pacific halibut in such inshore habitats will be missed by the survey. Indeed, this appears to be what happened to the 2011 cohort, which had no age-2 fish captured in 2013, yet the cohort showed up strongly in Bristol Bay the following year (Supplemental Table 2; Supplemental Figure 12). Selectivity to the trawl gear may also be influenced by habitat type, environmental conditions, or sea state, as documented for some other species (e.g., Somerton et al., 2013; Cooper and Nichol, 2016; and Somerton et al, 2018). While acknowledging that such factors may have some effect on the data and thus our model output, the distributional changes we see are both broad-scale and generally consistent among cohorts. This leads us to conclude that movement of Pacific halibut cohorts over time is the most plausible explanation for the patterns described in our work.

This study contributes new knowledge regarding the life cycle of Pacific halibut in the GOA and BS and is a step towards better understanding stock structure. Connectivity driven by dispersal at the larval stage and migration during the early demersal stage impacts species distributions, and leads to large-scale ecosystem connectivity and habitat use. Basin-wide connectivity and habitat use or dependence among life stages suggests that it is imperative for managers to be aware of potential environmental impacts to various geographic components of the stock. The Pacific halibut fishery is currently managed via an

ensemble of stock assessment models that lead to a decision table which outlines risks of various harvest scenarios (Stewart et al. 2020). A better understanding of risk to the spawning biomass and thus the future population as shown here, can lead to improved comprehension of consequences associated with different harvest levels, and provide a connection to how management decisions affecting fish stocks made in one area or region may impact fisheries in other areas, including between ocean basins.

Until recently, details of Pacific halibut early life history dispersal and migration have remained elusive. However, improved data streams and modelling approaches used in this study have supported the notion of broad scale connectivity, as hypothesized in earlier literature. Our building knowledge of Pacific halibut early life history will benefit from future research aimed at improving our understanding of the relative contributions from geographically distinct spawning grounds to nursery habitats, i.e. the sources of replenishment, purported sinks, as well as of the capabilities of young Pacific halibut to actively migrate prior to their detection in standardized surveys as 2-3 year olds.

References

Aagaard, K., Weingartner, T. J., Danielson, S. L., Woodgate, R. A., Johnson, G. C., & Whitledge, T. E. (2006). Some controls on flow and salinity in Bering Strait. Geophys. Res. Ltrs., 33(19). doi:10.1029/2006GL026612

Atwood, E., Duffy-Anderson, J. T., Horne, J. K., & Ladd, C. (2010). Influence of mesoscale eddies on ichthyoplankton assemblages in the Gulf of Alaska. Fish. Oceanogr., 19:493-507. doi:10.1111/j.1365-2419.2010.00559.x

Bailey, K. M., Nakata, H., Van der Veer, H. W. (2005). The planktonic stages of flatfishes: physical and biological interactions in transport processes. Flatfishes: Biology & exploitation: 94-119.
Bailey, K. M., & Picquelle, S. J. (2002). Larval distribution of offshore spawning flatfish in the Gulf of Alaska: potential transport pathways and enhanced onshore transport during ENSO events. Mar. Ecol. Prog. Ser., 236:205-217. doi:10.3354/meps2362015
Best, E. (1977). Distribution and abundance of juvenile halibut in the southeastern Bering Sea. Int. Pac. Hal. Comm. Sci. Rep. 62. 23 p.

Best, E. (1979). Halibut ecology. [In] Fisheries oceanography – eastern Bering Sea shelf. NWAFC Processed Report 79-20, National Marine Fisheries Service. p. 127-165.

Best, E. A. & Hardman, W. H. (1982). Juvenile halibut surveys 1973-1980. Int. Pac. Hal. Comm. Tech. Rep. 20. 38 p.

Boeing, W. J. & Duffy-Anderson, J. T. (2008). Ichthyoplankton dynamics and biodiversity in the Gulf of Alaska: responses to environmental change. Ecol. Indicators, 8:292-302. doi:10.1016/j.ecolind.2007.03.002

Cameletti, M., Lindgren, F., Simpson, D. & Rue, H. (2013). Spatio-temporal modeling of particulate matter concentration through the SPDE approach. Adv. Stat. Anal. 97:109–131. doi:10.1007/s10182-012-0196-3.

Cavole, L. M., Demko, A. M., Diner, R. E., Giddings, A., Koester, I., Pagniello, C. M. L. S., Paulsen, M-L, Ramiriz-Valdez, A., Schwenck, S. M., Yen, N. K., Zill, M. E., & Franks, P. J. S. (2016). Biological impacts of the 2013-2015 warm-water anomaly in the northeast Pacific: Winners, losers, and the future. Oceanography, 29:273-285.

Clark, W. G. & Hare, S. R. (1998). Accounting for bycatch in management of the Pacific halibut fishery. N. American J. Fish. Manag. 18:809-821. doi:10.1577/1548-8675(1998)018<0809:AFBIMO>2.0.CO;2

Clark, W. G. & Hare, S. R. (2002). Effects of climate and stock size on recruitment and growth of Pacific halibut. N. Amer. J. Fish. Manag. 22:852-862. doi:10.1577/1548-8675(2002)022<0852:EOCASS>2.0.CO;2

Clark, W. G., St-Pierre, G., & Brown, E. S. (1997). Estimates of halibut abundance from NMFS trawl surveys. Int. Pac. Halibut Comm. Tech. Rep. 37. 51 p.

Combes, V., Chenillat, F., Di Lorenzo, E., Rivière, P., Ohman, M. D., & Bograd, S. J. (2013). Cross-shore transport variability in the California Current: Ekman upwelling vs. eddy dynamics. Progress in Oceanography 109: 78–89. doi:10.1016/j.pocean.2012.10.001

Cooper, D. W., Duffy-Anderson, J. T., Stockhausen, W. T., & Cheng, W. (2013). Modeled connectivity between northern rock sole (*Leipdopsetta polyxystra*) spawning and nursery areas in the eastern Bering Sea. J. Sea Res., 84, 2-12. doi:10.1016/j.seares.2012.07.001

Cooper, D. W., & Nichol, D. G. (2016). Juvenile northern rock sole (*Lepidopsetta polyxystra*) spatial distribution and abundance patterns in the eastern Bering Sea: spatially dependent production linked to temperature. ICES Journal of Marine Science, 73(4), 1138–1146. doi:10.1093/icesjms/fsw005

Cowen, R. K., & Castro, L. R. (1994). Relation of coral reef fish larval distributions to island scale circulation around Barbados, West Indies. Bulletin of Marine Science 54: 228–244.

Cressie, N. (1993). Statistics for Spatial Data (2nd ed). Wiley, New York, USA. 928 p.

Danielson, S., Curchitser, E., Hedstrom, K., Weingartner, T., & Stabeno, P. (2011). On ocean and sea ice modes of variability in the Bering Sea. J. Geophys. Res., 116(C12). doi:10.1029/2011JC007389

Drinan, D. P., Galindo, H. M., Loher, T., & Hauser, L. (2016). Subtle genetic population structure in Pacific halibut *Hippoglossus stenolepis*, J. Fish. Bio., 89, 2571-2594. doi: 10.1111/jfb.13148

Dunlop, H. A., Bell, F. H., Myhre, R. J., Hardman, W. H., & Southward, G. M. (1964). Investigation, utilization and regulation of the halibut in southeastern Bering Sea. Int. Pac. Hal. Comm. Rep. 35. 72 p.

Duffy-Anderson, J. T., Blood, D. M., Cheng, W., Ciannelli, L., Matarese, A. C., Sohn, D., Vance, T. C., & Vestfals, C. (2013). Combining field observations and modeling approaches to examine Greenland halibut (Reinhardtius hippoglossoides) early life ecology in the southeastern Bering Sea. J. Sea Res., 75, 96-109. doi:10.1016/j.seares.2012.06.014

Duffy-Anderson, J. T., Stabeno, P. J., Siddon, E. C., Andrews, A. G., Cooper, D. W., Eisner, L. B., Farley, E. V., Harpold, C. E., Heintz, R. A., Kimmel, D. G., Sewall, F. F., Spear, A. H., & Yasumishii, E. C. (2017). Return of warm conditions in the southeastern Bering Sea: Phytoplankton – Fish. PLoS ONE, 12, e0178955. doi:10.1371/journal.pone.0178955

Duffy-Anderson, J. T., Stabeno, P., Andrews III, A. G., Cieciel, K., Deary, A., Farley, E., Fugate, C., Harpold, C., Heintz, R., Kimmel, D., Kuletz, K., Lamb, J., Paquin, M., Porter, S., Rogers, L., Spear, A., & Yasumiishi, E. (2019). Responses of the Northern Bering Sea and Southeastern Bering Sea pelagic ecosystems following record-breaking low winter sea ice. Geophys. Res. Lett., 46, 9833-9842. doi:10.1029/2019GL083396

Durant, J. M. Hjermann, D. Ø., Ottersen, G., Stenseth, N. C. 2007. Climate and the match or mismatch between predator requirements and resource availability. Clim. Res., 33: 271-283. doi:10.3354/cr033271

Ferreira, A. S. A., Stige, L. C., Neuheimer, A. B., Bogstad, B., Yaragma, N., Prokopchuk, I., Durant, J. M. (2020). Match-mismatch dynamics in the Norwegian Barents Sea system. Mar. Ecol. Prog. Ser. LFCav5. doi:10.3354/meps13276.

Forsberg, J. E. (2001). Aging manual for Pacific halibut: procedures and methods used at the International Pacific Halibut Commission. Int. Pac. Halibut Comm. Tech. Rep. 46. 56 p.

Gibson, G. A., Coyle, K. O., Hedstrom, K., and Curchitser, E. N. (2013). A modeling study to explore on-shelf transport of oceanic zooplankton in the Eastern Bering Sea. Journal of Marine Systems 121–122: 47–64. doi:10.1016/j.jmarsys.2013.03.010

Gibson, G. A., Stockhausen, W. T., Coyle, K. O., Hinckley, S., Parada, C., Hermann, A. J., Doyle, M., & Ladd, C. (2019). An individual-based model for sablefish: Exploring the connectivity between potential spawning and nursery grounds in the Gulf of Alaska. Deep-Sea Res. Part II, 165, 89-112. doi:10.1016/jdsr2.2018.05.015

Goldstein, E. D., Pirtle, J. L., Duffy-Anderson, J. T., Stockhausen, W. T., Zimmermann, M., Wilson, M. T. and Mordy, C. W. (2020). Eddy retention and seafloor terrain facilitate cross-shelf transport and delivery of fish larvae to suitable nursery habitats. Limnol Oceanogr. doi:10.1002/lno.11553

Haidvogel, D. B., Arango, H., Budgell, W. P., Cornuelle, B. D., Curchitser, E., DiLorenzo, E., Fennel, K., Geyer, W. R., Hermann, A. J., Lanerolle, L., Levin, J., McWilliams, J. C., Miller, A. J., Moore, M., Powell, T. M., Shchepetkin, A. F., Sherwood, C. R., Signell, R. P., Warner, J. C., & Wilkin, J. (2008). Ocean forecasting in terrain-following coordinates: Formulation and skill assessment of the Regional Ocean Modeling System. J. Comp. Phys., 227, 3595-3624. doi:10.1016/j.jcp.2007.06.016

Hermann, A. J., Gibson, G. A., Bond, N. A., Curchitser, E. N., Hedstrom, K., Cheng, W., Wang, M., Stabeno, P. J., Eisner, L., & Cieciel, K. D. (2013). A multivariate analysis of observed and modeled biophysical variability on the Bering Sea shelf: Multidecadal hindcasts (1970-2009) and forecasts (2010-2040). Deep-Sea Res. II: Top. Stud. Oceanogr., 94, 121-139. doi:10.1016/j.dsr2.2013.04.007

Hermann, A. J., Hinckley, S., Dobbins, E. L., Haidvogel, D. B., Bond, N. A., Mordy, C., Kachel, N., & Stabeno, P. J. (2009). Quantifying cross-shelf and vertical nutrient flux in the Coastal Gulf of Alaska with a spatially nested, coupled biophysical model. Deep Sea Research Part II: Topical Studies in Oceanography **56**: 2474–2486. doi:10.1016/j.dsr2.2009.02.008

Hinckley, S., Stockhausen, W. T., Coyle, K. O., Larel, G. J., Gibson, G. A., Parada, C., Hermann, A. J., Doyle, M. J., Hurst, T. P., Punt, A. E., & Ladd, C. (2019). Connectivity between spawning and nursery areas for Pacific cod (*Gadus microcephalus*) in the Gulf of Alaska. Deep-Sea Res. II., 165, 113-126. doi:10.1016/j.dsr2.2019.05.007

Huijbers, C. M., Nagelkerken, I., Lössbroek, P. A. C., Schulten, I. E., Siegenthaler, A., Holderied, M. W., & Simpson, S. D. (2012). A test of the senses: Fish select novel habitats by responding to multiple cues. Ecol., 93, 46-55. doi:10.1890/10-2236.1

Hunt Jr., G. L., Coyle, K. O., Eisner, L. B., Farley, E. V., Heintz, R. A., Mueter, F., Napp, J. M., Overland, J. E., Ressler, P. H., Salo, S., & Stabeno, P. J. (2011). Climate impacts on eastern Bering Sea foodwebs: a synthesis of new data and an assessment of the Oscillating Control Hypothesis. ICES J. Mar. Sci., 68, 1230-1243. doi:10.1093/icesjms/fsr036

Igulu, M. M., Nagelkerken, I., van der Beek, M., Schippers, M., van Eck, R., & Mgaya, Y. D. (2013). Orientation from open water to settlement habitats by coral reef fish: behavioral flexibility in the use of multiple reliable cues. Mar. Ecol. Prog. Ser., 492, 243-257. doi:10.3354/meps10542

Kanamori, Y., Takasuka, A., Nishijima, S., & Okamura, H. (2019). Climate change shifts the spawning ground northward and extends the spawning period of chub mackerel in the western North Pacific. Mar. Ecol. Prog. Ser., 624, 155-166. doi:10.3354/meps13037

Kimmel, D. G., Eisner, L. B., Wilson, M. T., & Duffy-Anderson, J. T. (2018). Copepod dynamics across warm and cold periods in the eastern Bering Sea: Implications for walleye Pollock (*Gadus chalcogrammus*) and the Oscillating Control Hypothesis. Fish. Oceanogr., 27, 143-158. doi:10.1111/fog.12241

Kleisner, K. M., Fogarty, M. J., McGee, S., Barnett, A., Fratantoni, P., Greene, J., Hare, J. A., Lucey, S. M., McGuire, C., Odell, J., Saba, V. S., Smith, L., Weaver, K. J., & Pinsky, M. L. (2016). The effects of sub-regional climate velocity on the distribution and spatial extent of marine species assemblages. PLoS ONE, 11, e0149220. doi:10.1371/journal.pone.0149220

Le Pape, O., & Bonhommeau, S. (2015). The food limitation hypothesis or juvenile marine fish. Fish and Fisheries, 16, 373-398. doi:10.1111/faf.12063

Lindgren, F. & Rue, H. (2015). Bayesian spatial modelling with R-INLA. J. Stat. Soft., 63, 1–27.

McLean, M., Mouillot, D., Lindegren, M., Engelhard, G., Villeger, S., Marchal, P., Brind'Amour, A., & Auber, A. (2018). A climate-driven functional inversion of connected marine ecosystems. Curr. Biol., 28, 3654-3660. doi:10.1016/j.cub.2018.09.050

Mordy, C. W., Stabeno, P. J, Kachel, N. B., Ladd, C., Zimmermann, M., Hermann, A. J., Coyle, K. O., & Doyle, M. J. (2019). Patterns of flow in the canyons of the northern Gulf of Alaska. Deep Sea Research Part II: Topical Studies in Oceanography S0967064519301079. doi:10.1016/j.dsr2.2019.03.009

Mumby, P. J., Edwards, A. J., Arias-González, J. E., Lindeman, K. C., Blackwell, P. G., Gall, A., Gorczynska, M. I., Harborne, A. R., Pescod, C. L., Renken, H., Wabnitz, C. C., & Llewellyn, G. (2004). Mangroves enhance the biomass of coral reef fish communities in the Caribbean. Nature, 427, 533-536. doi:10.1038/nature02286

Napp, J. M., Kendall, A. W., & Schumacher, J. D. (2000). A synthesis of biological and physical processes affecting the feeding environment of larval walleye pollock (*Theragra chalcogramma*) in the eastern Bering Sea. Fish. Oceanogr., 9, 147-162.

National Oceanic and Atmospheric Administration (NOAA). (2019). Ichthyoplankton Information System Database, https://access.afsc.noaa.gov/ichthyo/

National Oceanic and Atmospheric Administration (NOAA). (2020). Alaska Groundfish Bottom Trawl Survey Data, https://www.fisheries.noaa.gov/alaska/commercial-fishing/alaska-groundfish-bottom-trawl-survey-data

Nielsen, J. L., Graziano, S. L., & Seitz, A. C. (2010). Fine-scale population genetic structure in Alaskan Pacific halibut (*Hippoglossus stenolepis*). Conserv. Genet., 11, 999-1012. doi:10.1007/s10592-009-9943-8

Norcross, B. L., Muter, F. J., & Holladay, B. A. (1997). Habitat models for juvenile pleuronectids around Kodiak Is., Alaska. Ocean. Lit. Rev. No. 44, 1548.

Norcross, B. L., Blanchard, A., & Holladay, B. A. (1999). Comparison of models for defining nearshore flatfish nursery areas in Alaskan waters. Fish. Oceanogr., 8, 50-67.

Opdal, A. F. & Vikebø, F. B. (2016). Long term stability in modelled zooplankton influx could uphold major fish spawning grounds on the Norwegian continental shelf. Can. J. Fish. Aquat. Sci. 73: 186-196. doi: 10.1139/cjfas-2014-0524

Parada, C., Hinckley, S., Horne, J., Mazur, M., Hermann, A., & Curchister, E. (2016). Modeling connectivity of walleye Pollock in the Gulf of Alaska: Are there any linkages to the Bering Sea and Aleutian Islands? Deep-Sea Res. II: Top. Stud. Oceanogr., 132, 227-239. doi:10.1016/j.dsr2.2015.12.010

Petitgas, P., Rijnsdorp, A. D., Dickey-Collas, M., Engelhard, G. H., Peck, M. A., Pinnegar, J. K., Drinkwater, K., Huret, M., & Nash, R. D. M. (2013). Impacts of climate change on the complex life cycles of fish. Fish. Oceanogr., 22, 121-139. doi:10.1111/fog.12010

Petrik, C. M., J. T. Duffy-Anderson, F. Castruccio, E. N. Curchitser, S. L. Danielson, K. Hedstrom, and F. Mueter. (2016). Modelled connectivity between Walleye Pollock (Gadus chalcogrammus) spawning and age-0 nursery areas in warm and cold years with implications for juvenile survival. ICES J. Mar. Sci. **73**: 1890–1900. doi:10.1093/icesjms/fsw004

Planque, B., Fromentin, J. M., Cury, P., Drinkwater, K. F., Jennings, S., Perry, R. I., & Kifani, S. (2010). How does fishing alter marine populations and ecosystems sensitivity to climate?. Journal of Marine Systems, 79(3-4), 403-417.

Posgay, J.A. & Marak, R. R. (1980). The MARMAP Bongo Zooplankton Samplers. J. Northw. Atl. Fish. Sci., 1, 91-99.

Reed, R. K. & Schumacher, J. D. (1986). Physical oceanography, [*In*] The Gulf of Alaska. Physical environment and biological resources. Hood, D.W., and Zimmeran, S.T. [*eds*]. U.S. Dept. Comm./NTIS part 2, 57-75.

Rochette, S., Rovot, E., Morin, J., Mackinson, S., Riou, P., & Le Pape, O. (2010). Effect of nursery habitat degradation on flatfish population: Application of Solea solea in the eastern channel (Western Europe). J. Sea Res., 64, 34-44. doi:10.1016/j.seares.2009.08.003

Royer, T. C. (1981). Baroclinic transport in the Gulf of Alaska. Part II. A freshwater driven coastal current. J. Mar. Res., 39, 251-265.

Schmidt, P. J. 1934. On the zoogeographical distribution of the chief marine food fishes in the western part of the Pacific. Pacific Science Congress, 5th, Victoria and Vancouver, B. C. 1933. Proceedings v. 5, p. 3796-3797. Toronto, University Press.

Seitz, A. C., Loher, T., & Nielsen, J. L. (2008). Seasonal movements and environmental conditions experienced by Pacific halibut along the Aleutian Islands, examined by pop-up satellite tags. Int. Pac. Halibut Comm. Sci. Rep. 85. 24 p.

Seitz, A. C., Loher, T., Norcross, B. L., & Nielsen, J. L. (2011). Dispersal and behavior of Pacific halibut *Hippoglossus stenolepis* in the Bering Sea and Aleutian Islands region. Aquat. Biol., 12, 225-239. doi:10.3354/ab00333

Shchepetkin, A. F. & McWilliams, J. C. (2005). The regional oceanic modeling system (ROMS): a split-explicit, free surface, topography-following-coordinate oceanic model. Ocean Model., 9, 347-404. doi:10.1016/j.ocemod.2004.08.002

Sigler, M. F., Stabeno, P. J., Eisner, L. B., Napp, J. M., & Mueter, F. J. (2014). Spring and fall phytoplankton blooms in a productive subarctic ecosystem, the eastern Bering Sea, during 1995-2011. Deep-Sea Res. Part II, 109, 71-83. doi:10.1016/j.dsr2.2013.12.007

Skud, B. E. (1975). Revised estimates of halibut abundance and the Thompson-Burkenroad debate. Int. Pac. Halibut Comm. Sci. Rep. 56. 36 p.

Skud, B. E. (1977). Drift, migration, and intermingling of Pacific halibut stocks. Int. Pac. Halibut Comm. Sci. Rep. 63. 42 p.

Smith, P. E., & Richardson, S. R. (1977). Standard techniques for pelagic fish egg and larva surveys. FAO Fish. Tech. Pap., No. 175. 100 p.

Sohn, D. (2016). Distribution, abundance, and settlement of slope-spawning flatfish during early life stages in the eastern Bering Sea. PhD Dissertation. Oregon State University, Corvallis, OR, U.S.A.

Sohn, D., Ciannelli, L., & Duffy-Anderson, J. T. (2016). Distribution of early life Pacific halibut and comparison with Greenland halibut in the eastern Bering Sea. J. Sea Res., 107, 31-42. doi:10.1016/j.seares.2015.09.001

Somarakis, S., Tsoukali, S., Giannoulaki, M., Schismenou, E., & Nikolioudakis, N. (2019). Spawning stock, egg production and larval survival in relation to small pelagic fish recruitment. Mar. Ecol. Prog. Ser., 617-618, 113-136. doi:10.3354/meps12642

Somerton, D. A., Weinberg, K. L., & Goodman, S. E. (2013). Catchability of snow crab (*Chionoecetes opilio*) by the eastern Bering Sea bottom trawl survey estimated using a catch comparison experiment. Can. J. Fish. Aquat. Sci. 70: 1699–1708 dx.doi.org/10.1139/cjfas-2013-0100

Somerton, D., Weinberg, K., Munro, P., Rugolo, L., & Wilderbuer, T. (2018). The effects of wave-induced vessel motion on the geometry of a bottom survey trawl and the herding of yellowfin sole (*Limanda aspera*). Fish. Bull. 116:21–33. doi: 10.7755/FB.116.1.3

Spies, I. (2012). Landscape genetics reveals population subdivision in Bering Sea and Aleutian Islands Pacific cod. Trans. Am. Fish. Soc., 141(6), 1557-1573. doi:10.1080/00028487.2012.711265

St. Pierre, G. (1989). Recent studies of Pacific halibut postlarvae in the Gulf of Alaska and eastern Bering Sea. Int. Pac. Halibut Comm. Sci. Rep. 73. 31 p.

St. Pierre, G. (1984). Spawning locations and season for Pacific halibut. Int. Pac. Halibut Comm. Sci. Rep. 70. 46 p.

Stabeno, P. J., Reed, R. K., & Schumacher, J. D. (1995). The Alaska Coastal Current: continuity of transport and forcing. J. Geo. Res.: Oceans, 100, 2477-2485. doi:10.1029/94JC02842

Stabeno, P. J., Schumacher, J. D., & Ohtani, K. (1999). Chapter 1: The physical oceanography of the Bering Sea. [*In*] Dynamics of the Bering Sea. Loughlin, T. R. & Ohtani, K. [*eds.*] Alaska Sea Grant, University of Alaska, Fairbanks.

Stabeno, P. J., Reed, R. K., & Napp, J. M. (2002). Transport through Unimak Pass, Alaska. Deep-Sea Res. II, 49, 5919-5930. doi:10.1016/S0967-0645(02)00326-0

Stabeno, P. J., Bond, N. A., Hermann, A. J., Kachel, N. B., Mordy, C. W., & Overland, J. E. (2004). Meteorology and oceanography of the Northern Gulf of Alaska. Cont. Shelf Res., 24, 859-897. doi:10.1016/j.csr.2004.02.007

Stabeno, P. J., Kachel, N. B., Moore, S. E., Napp, J. M., Sigler, M. Yamaguchi, A., & Zerbini, A. N. (2012). Comparison of warm and cold years on the southeastern Bering Sea shelf and some implications for the ecosystem. Deep-Sea Res. II, 65-70, 31-45. doi:10.1016/j.dsr2.2012.02.020

Stabeno, P. J., Bell, S., Cheng, W., Danielson, S., Kachel, N. B., & Mordy, C. W. (2016a). Long-term observations of Alaska Coastal Current in the northern Gulf of Alaska. Deep-Sea Res. II, 132, 24-40. doi:10.1016/j.dsr2.2015.12.016

Stabeno, P. J., Danielson, S. L., Kachel, D. G., Kachel, M. B., & Mordy, C. W. (2016b). Currents and transport on the Eastern Bering Sea shelf: An integration of over 20 years of data. Deep-Sea Res. Part II, 134, 13-29. doi:10.1016/j.dsr2.2016.05.010

Stauffer, G. (2004). NOAA protocols for groundfish bottom trawl surveys of the nation's fishery resources. U. S. Dept. Commerce NOAA Tech. Memo. NMFS-F/SPO-65. 205 p.

Stewart, I. & Hicks, A. (2018). Assessment of the Pacific halibut (*Hippoglossus stenolepis*) stock at the end of 2018. Int. Pac. Halibut Comm. Annual Meeting Report: IPHC-2019-AM095-09.

Stewart, I., Hicks, A., Webster, R., & Wilson, D. (2020) Summary of the data, stock assessment, and harvest decision table for Pacific halibut (*Hippoglossus stenolepis*) at the end of 2019. Int. Pac. Halibut Comm. Annual Meeting Report: IPHC-2020-AM096-09 Rev_2.

Stockhausen, W. T., Coyle, K. O., Hermann, A. J., Blood, D., Doyle, M. J., Gibson, G. A., Hinckley, S., Ladd, C., & Parada, C. (2019a). Running the gauntlet: Connectivity between spawning and nursery areas for arrowtooth flounder (*Atheresthes stomias*) in the Gulf of Alaska, as inferred from a biophysical individual-based model. Deep-Sea Res. II, 165, 127-139. doi:10.1016/j.dsr2.2018.05.017

Stockhausen, W. T., Coyle, K. O., Hermann, A. J., Doyle, M. J., Gibson, G. A., Hinckley, S., Ladd, C., & Parada, C. (2019b). Running the gauntlet: Connectivity between natal and nursery areas for Pacific ocean perch (*Sebastes alutus*) in the Gulf of Alaska, as inferred from a biophysical individual-based model. Deep-Sea Res. II, 165, 74-88. doi:10.1016/j.dsr2.2018.05.016

Stoner, A. W., & Abookire, A. A. (2002). Sediment preferences and size-specific distribution of young-of-the-year Pacific halibut in an Alaska nursery. Fish. Biol., 61, 540-559. doi:10.1111/j.1095-8649.2002.tb00895.x

Sunday, J. M., Pecl, G. T., Frusher, S., Hobday, A. J., Hill, N., Holbrook, N. J., Edgar, G. J., Stuart-Smith, R., Barrett, N., Wernberg, T., Watson, R. A., Smale, D. A., Fulton, E. A., Slawinski, D., Feng, M., Radford, B. T., Thompson, P. A., & Bates, A. E. (2015). Species traits and climate velocity explain geographic range shifts in an ocean-warming hotspot. Ecol. Lett., 18, 944-953. doi:10.1111/ele.12474

Thompson, W. F. & Van Cleve, R. (1936). Life history of the Pacific halibut. Int. Fish Comm. Rep. 9. 205 p.

Vestfals, C. D., Ciannelli, L., Duffy-Anderson, J. T., & Ladd, C. (2014). Effects of seasonal and interannual variability in along-shelf and cross-shelf transport on groundfish recruitment in the eastern Bering Sea. Deep Sea Research Part II: Topical Studies in Oceanography **109**: 190–203. doi:10.1016/j.dsr2.2013.09.026

Webster, R. A., Clark, W. G., Leaman, B. M., & Forsberg, J. E. (2013). Pacific halibut on the move: a renewed understanding of adult migration from a coastwide tagging study. Can. J. Fish. Aquat. Sci., 70, 642-653. doi:10.1139/cjfas-2012-0371

Webster, R. A., Soderlund, E., Dykstra, C. L., & Stewart, I. J. (2020). Monitoring change in a dynamic environment: spatio-temporal modelling of calibrated data from different types of fisheries surveys of Pacific halibut. Can. J. Fish. Aquat. Sci., 77:1421-1432. doi.org/10.1139/cjfas-2019-0240

Wilderbuer, T., Duffy-Anderson, J. T., Stabeno, P., & Hermann, A. (2016). Differential patterns of divergence in ocean drifters: Implications for larval flatfish advection and recruitment. J. Sea Res., 111, 11-24. doi:10.1016/j.seares.2016.03.003

Table 1 Early life history parameters used for the Pacific halibut larval dispersal individual based biophysical model. The model simulation was terminated once a larva reached the newly-settled juvenile stage after 180 days. Information adapted from Table 3.1 in Sohn (2016)

Developmental stage	Duration (days)	Depth range (m)	Vertical swimming speed (m/s)	Vertical diffusion (m/s)
Eggs	20	400-500	0.00006	0.0001
Yolksac/Preflexion larvae	55	100-400	0.002	0.001
Flexion larvae	45	10-100	0.004	0.001
Postflexion larvae	35	10-100	0.006	0.001
Transformation	25	10-100	0.01	0.001
Newly-settled juveniles	N/A	10-100	0.02	0.001

Table 2 Mean catch (number/10m^2) and size (mm) of larval Pacific halibut caught during the NOAA icthyoplankton surveys in May of 2005 and 2009 in the Bering Sea (BS) and Gulf of Alaska (GOA), in addition to estimated abundance (millions of fish) and mean length (cm) of those same year classes when sampled two years later during the NOAA groundfish bottom trawl surveys

Larvae

	Catch-weighted mean length (mm)	Std dev. of Catch- weighted mean length	Min size sample d (mm)	Max size sampled (mm)	# measured	Mean catch/10_m2	Std dev of mean catch	# hauls
2005	17.31	7.23	8.2	21.0	51	2.5	8.0	135
BS GOA	18.04	6.20	10.0	26.0	38	1.6	5.2	163
Combined	17.62	6.79			89	2.0	6.6	298
2009	15.18	5.23	9.7	18.6	12	0.7	2.7	92
BS GOA	19.50	n/a	19.5	19.5	1	<0.1	0.4	66
Combined	15.38	5.03			13	0.4	2.1	158

2 year old fish

	Estimated abundance (Mfish)	Mean length (cm)	Std dev. Of mean length	# measured
2005 year class (BS)	31.42	19.4	3.1	227
2005 year class (GOA)	1.84	24.7	3.4	204
2005 combined	33.26	21.9	4.2	
2009 year class (BS)	13.22	21.4	3.4	30
2009 year class (GOA)	2.34	26.4	3.8	26
2009 combined	15.56	23.7	4.3	

Table 3 Percentage of Pacific halibut larvae arriving in the Bering Sea, based on a division between the GOA and BS along the Aleutian Island chain, from each of five spawn regions (Figure 2) for each study year estimated by the individual-based biophysical model (IBM).

Spawn region	Year					
	Warm			Cold		
	2003	2004	2005	2009	2010	2011
1	100	100	100	100	100	100
2	58.0	51.1	58.1	52.7	51.5	47.0
3	17.6	19.3	15.2	17.2	17.2	20.5
4	8.6	4.5	8.2	4.5	7.0	6.5
5	0.2	0.04	0.6	0.08	1.6	0.04

Table 4 Sample sizes of aged Pacific halibut from NMFS trawl surveys used in the spatio-temporal modelling, by cohort year, body of water, and age (years).

	Cohort			
Age	2005 Bering Sea	GOA	2009 Bering Sea	GOA
2	227	204	30	26
3	510		42	
4	590	633	59	56
5	333		66	
6	411	727	25	48

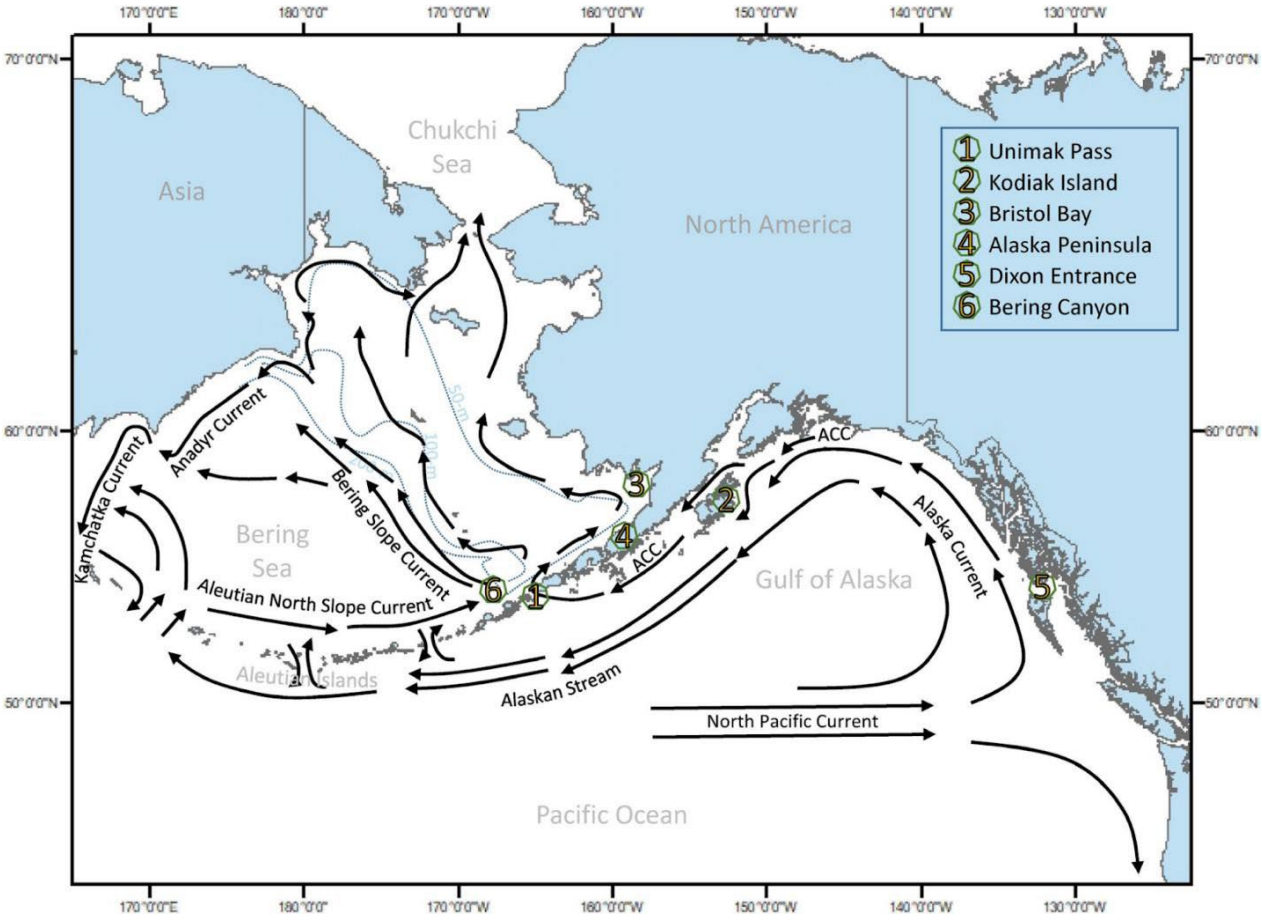

Figure 1 Schematic of major ocean circulation patterns in the Gulf of Alaska and Bering Sea. Compiled from information available in Stabeno et al. (1999), Stabeno et al. (2004), and Stabeno et al. (2016b)

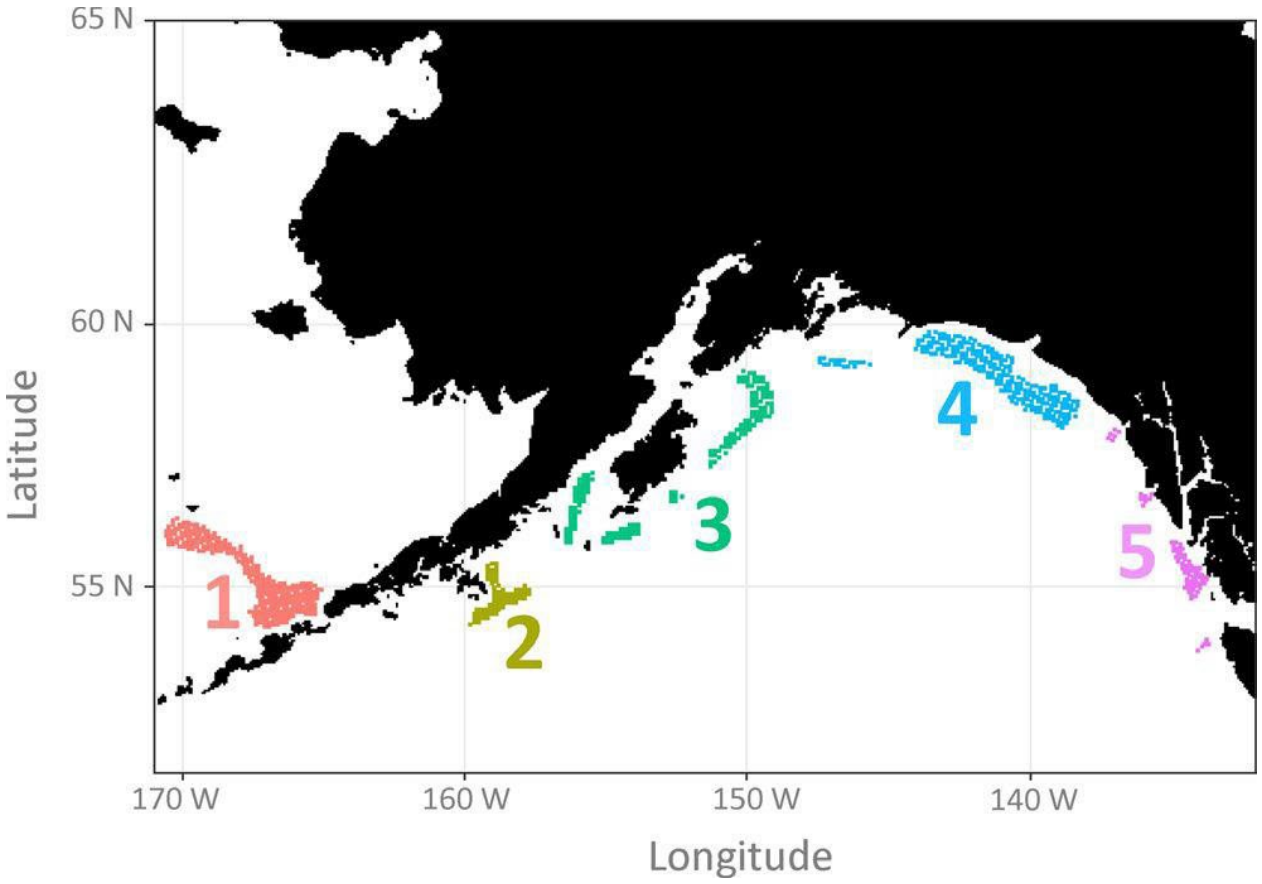

Figure 2 Five regions (color coded) used to define egg/larva origin points for larval advection modeling. Regions are based on major known spawning locations for Pacific halibut identified in St. Pierre (1984).

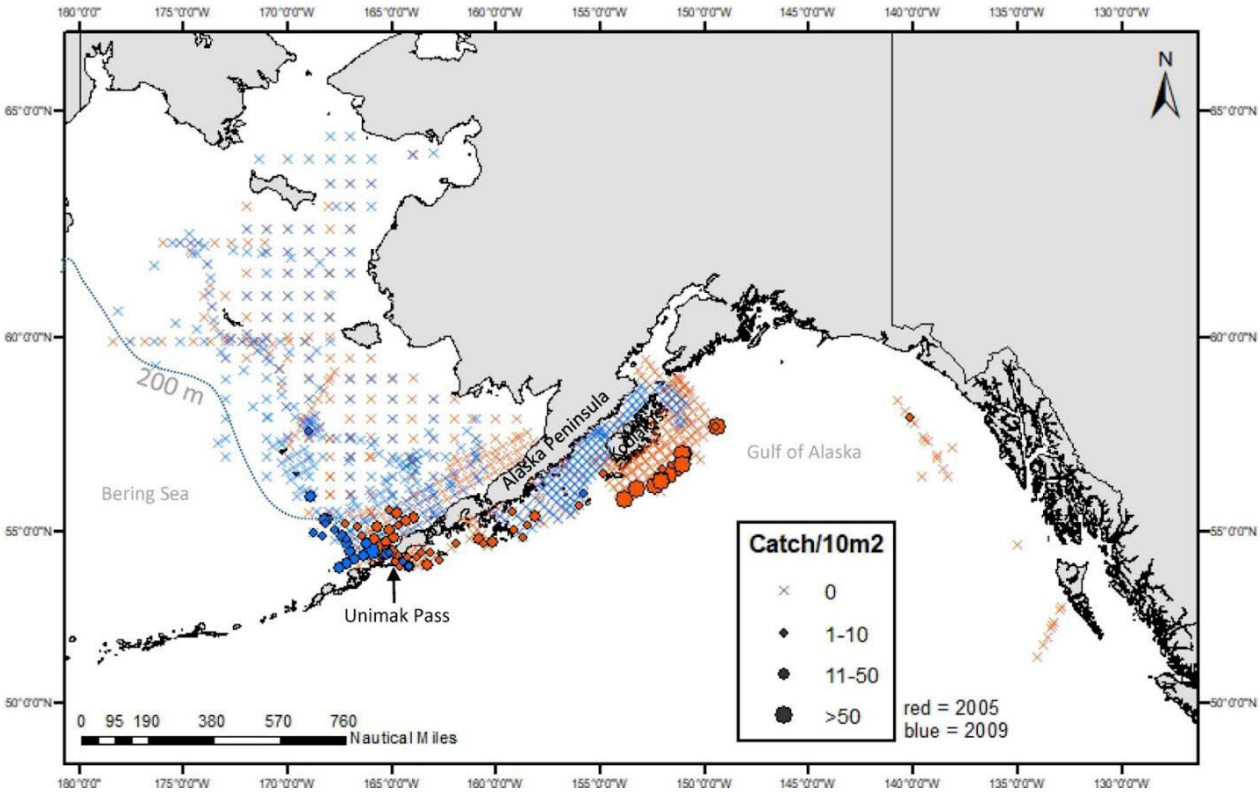

Figure 3 Catch-per-unit-effort (number/10m^2) of Pacific halibut larvae caught during the NOAA Fisheries EcoFOCI Ichthyoplankton surveys in the study years of 2005 (red) and 2009 (blue). Note that sampling occurred in all months February-October in 2005 and those same months excluding August in 2009.

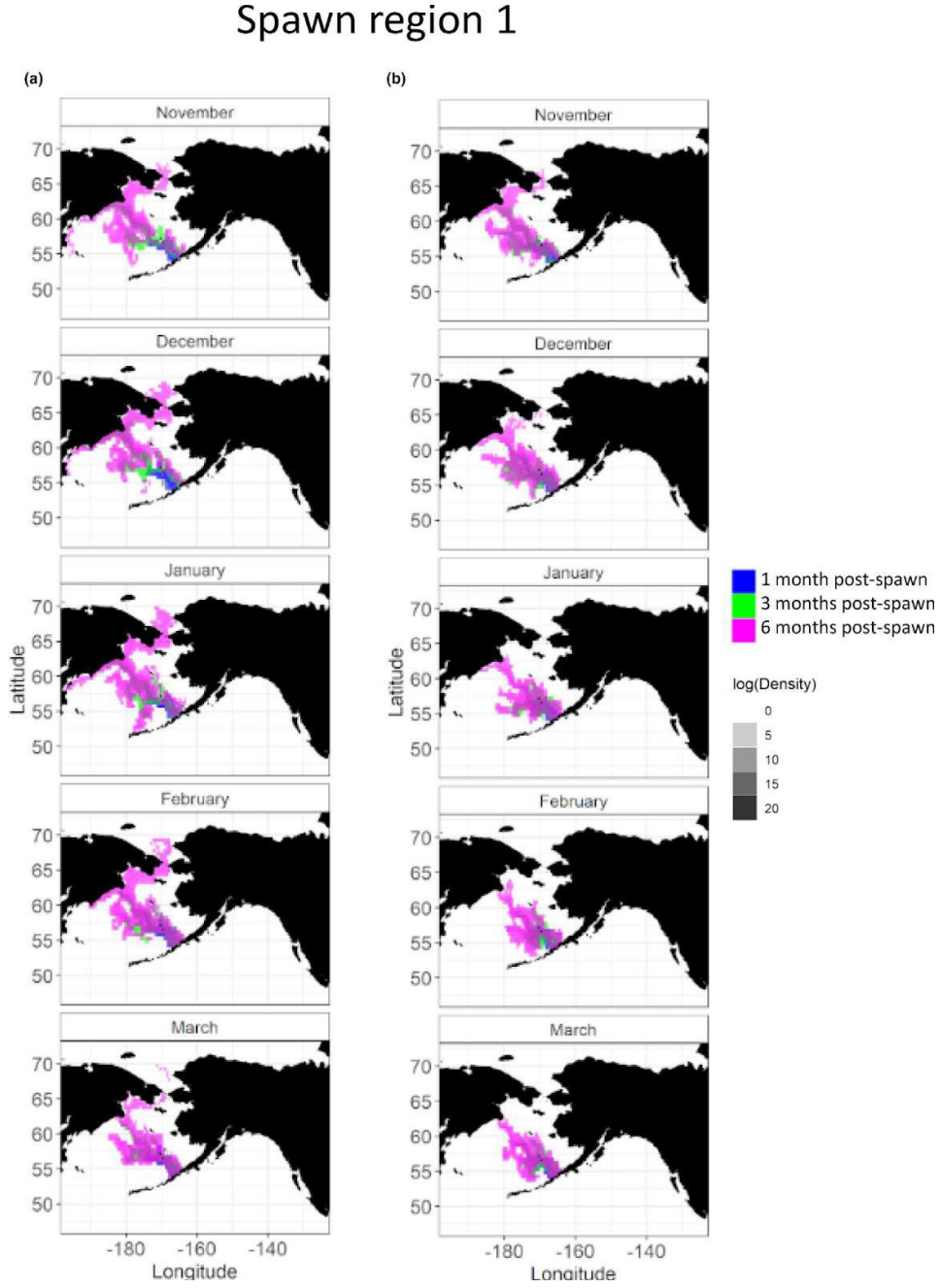

Figure 4 Maps showing simulated larval densities from the Individual-Based Biophysical Model for the (a) 2005 and (b) 2009 year classes with simulated larval release points from Spawn Region 1 (see Figure 2, Panel A). For each spawn month (November-March), counts of individual simulated larvae were summed within 0.5° latitude and longitude grid cells following 1 month (days 0-30), 3 months (days 61-90), and 6 months (days 151-180) post-spawn. The transparency of the color scale reflects larval density in each grid cell and the color shows the time period post-spawning.

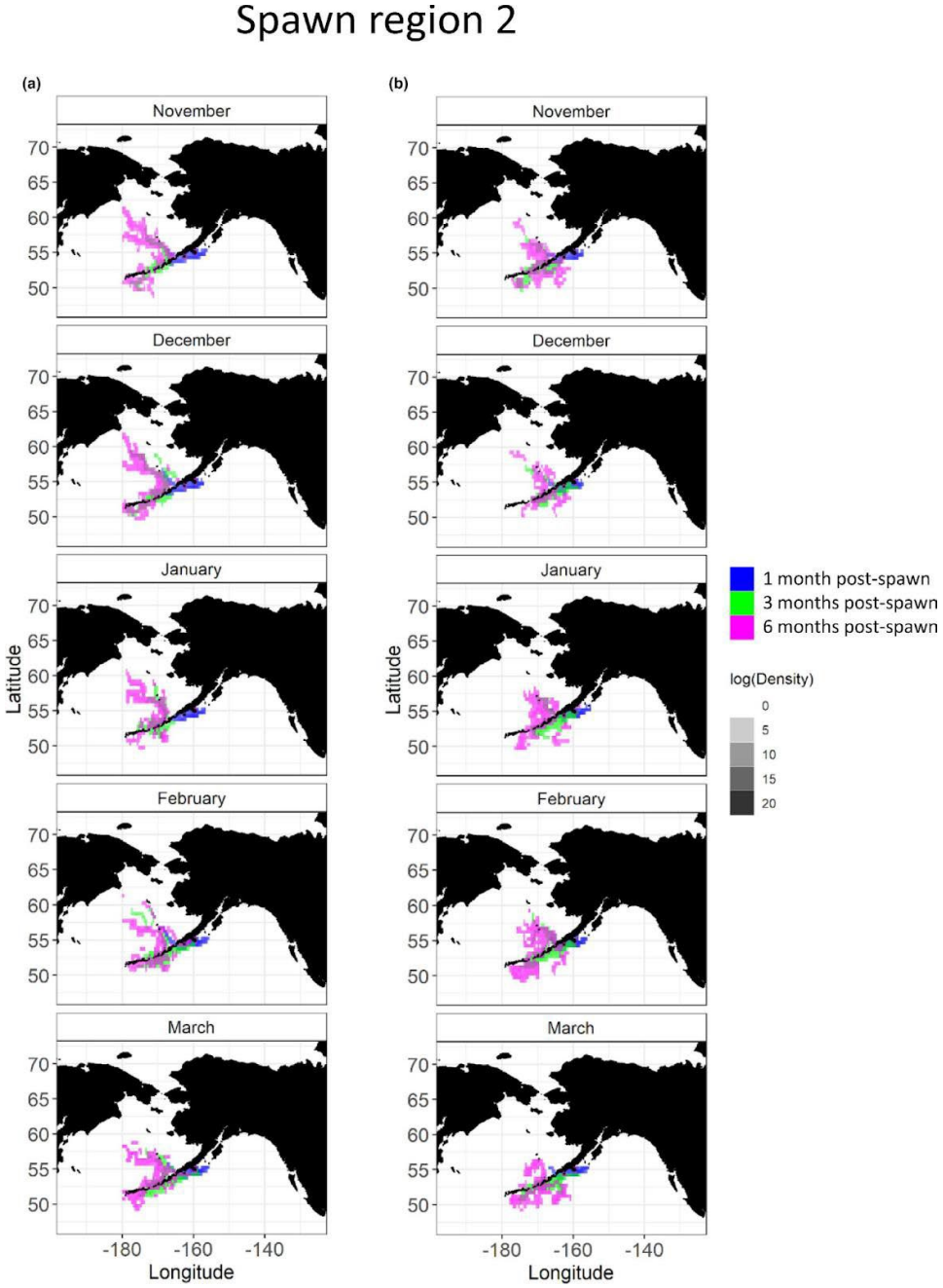

Figure 5 Maps showing simulated larval densities from the Individual-Based Biophysical Model (IBM) for the (a) 2005 and (b) 2009 year classes with simulated larval release points from Spawn Region 2 (see Figure 2, Panel A). For each spawn month (November-March), counts of individual simulated larvae were summed within 0.5° latitude and longitude grid cells following 1 month (days 0-30), 3 months (days 61-90), and 6 months (days 151-180) post-spawn. The transparency of the color scale reflects larval density in each grid cell and the color shows the time period post-spawning.

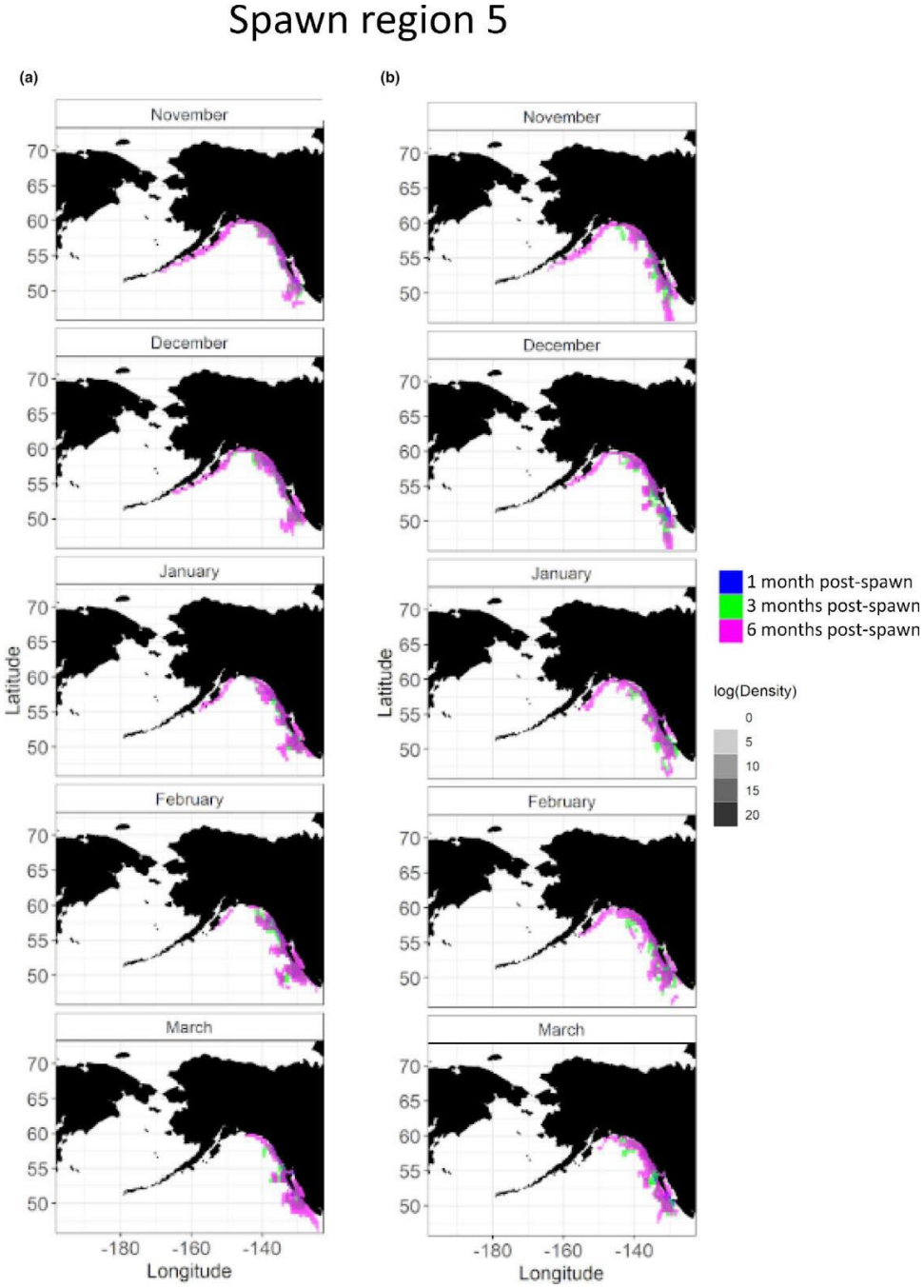

Figure 6 Maps showing simulated larval densities from the Individual-Based Biophysical Model (IBM) for the (a) 2005 and (b) 2009 year classes with simulated larval release points from Spawn Region 5 (see Figure 2, Panel A). For each spawn month (November-March), counts of individual simulated larvae were summed within 0.5° latitude and longitude grid cells following 1 month (days 0-30), 3 months (days 61-90), and 6 months (days 151-180) post-spawn. The transparency of the color scale reflects larval density in each grid cell and the color shows the time period post-spawning.

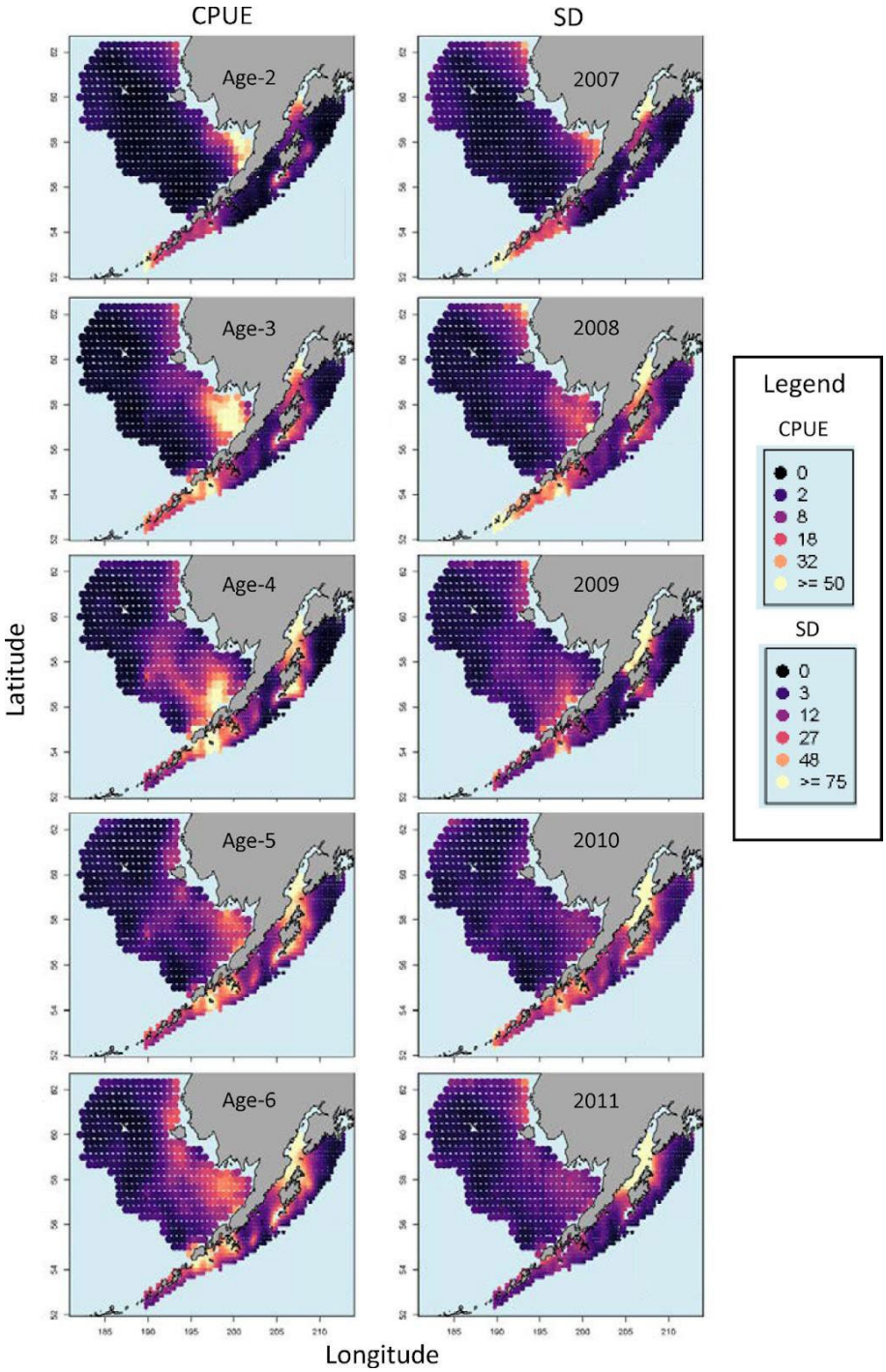

Figure 7 Posterior predictions of catch-per-unit-effort (left) and corresponding posterior standard deviations for 2-6 year old Pacific halibut caught on the NOAA Fisheries groundfish trawl surveys for the 2005 cohort.

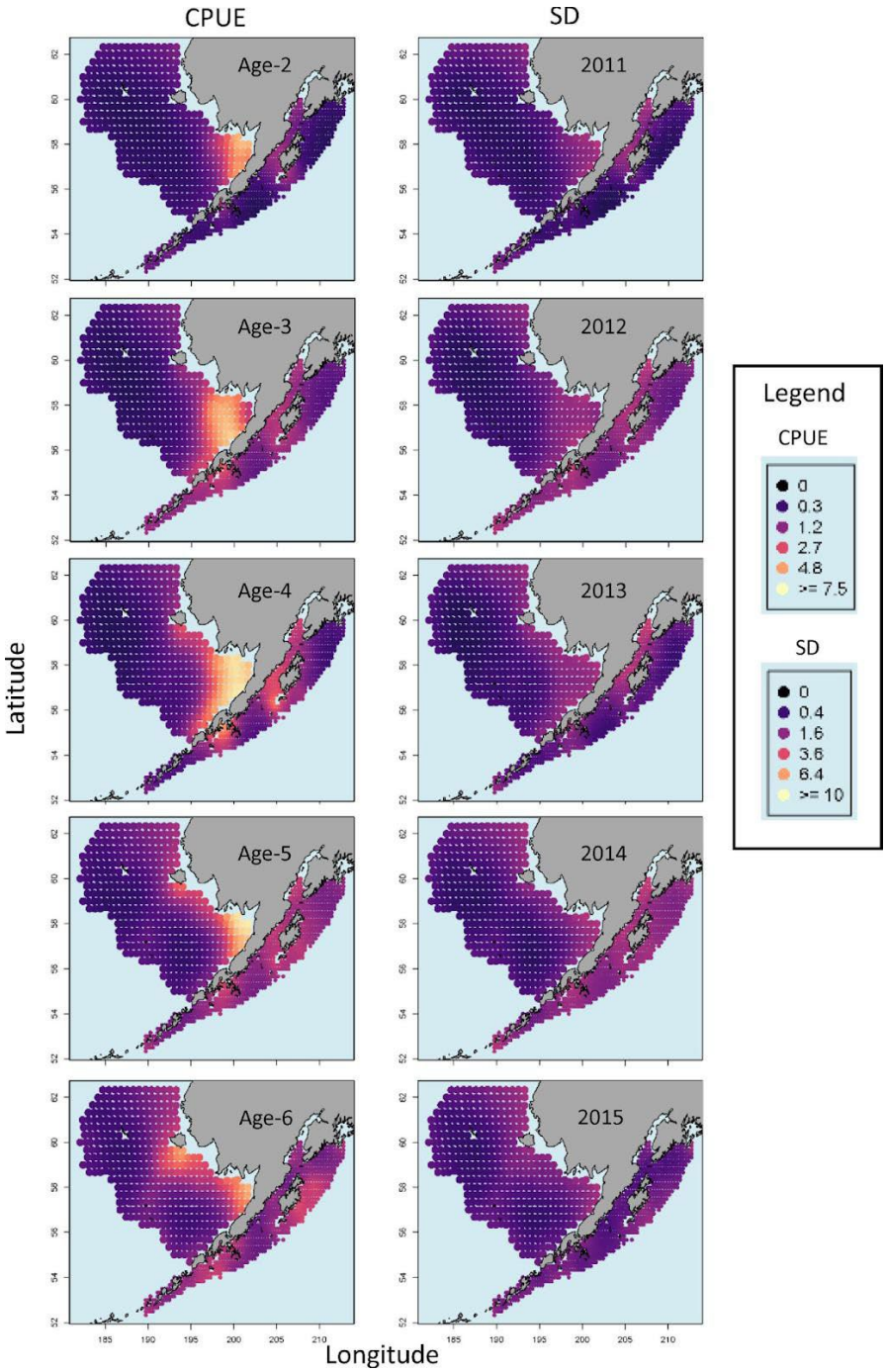

Figure 8 Posterior predictions of catch-per-unit-effort (left) and corresponding posterior standard deviations for 2-6 year old Pacific halibut caught on the NOAA Fisheries groundfish trawl surveys for the 2009 cohort.

Chapter 7: Advection and in situ processes as drivers of change for the abundance of large zooplankton taxa in the Chukchi Sea

Spear, A., Napp, J., Ferm, N., Kimmel, D.

Citation:

Spear, A., Napp, J., Ferm, N. and Kimmel, D., 2020. Advection and in situ processes as drivers of change for the abundance of large zooplankton taxa in the Chukchi Sea. Deep Sea Research Part II: Topical Studies in Oceanography, 177, p.104814, doi: 10.1016/j.dsr2.2020.104814.

Deep–Sea Research II 177 (2020) 104814

Contents lists available at ScienceDirect

Deep-Sea Research Part II

journal homepage: http://www.elsevier.com/locate/dsr2

Advection and in situ processes as drivers of change for the abundance of large zooplankton taxa in the Chukchi Sea

Adam Spear *, Jeff Napp , Nissa Ferm , David Kimmel

Alaska Fisheries Science Center, National Marine Fisheries Service, National Oceanic and Atmospheric Administration, 7600 Sand Point Way NE, Seattle, WA, 98115-6349, USA

ARTICLE INFO

Keywords:
Zooplankton
Euphausiids
Climate
Chukchi sea
Sea ice
Arctic food webs

ABSTRACT

The Chukchi Sea has recently experienced increased water temperatures, increased advection of water from the Bering Sea, declines in sea-ice concentration, and shorter periods of ice coverage. These physical changes are expected to impact trophic food-webs and ecosystem attributes. In this study, a series of research surveys were conducted in the summers of 2011–2015 to characterize the physical environment and its relation to the abundance of large zooplankton. Large zooplankton are key prey for many higher trophic level organisms including seabirds, marine mammals, and fishes. Yearly advection from the Bering Sea influenced the adult large zooplankton abundance, but this influence was less apparent in the earlier development stages. Known development times of stages of zooplankton, along with their location within the study area, suggested that a fraction of the zooplankton standing stock was the result of local production. Decreased advection and later ice retreat resulted in higher abundances of the lipid-rich copepod *Calanus glacialis*. Warmer conditions with increased advection from the Bering Sea resulted in higher abundances of euphausiids. Warming, sea-ice melting, and increases in transport of Bering Sea water and plankton into the Chukchi Sea are ongoing, and changes in food-web structure are likely to result.

1. Introduction

The zooplankton of the Chukchi Sea shelf consist of taxa that are more similar to the Pacific Ocean community than the Arctic Ocean community (Ashjian et al., 2010, 2017; Hopcroft et al., 2010; Eisner et al., 2013; Questel et al., 2013; Pinchuk and Eisner, 2017), a result of the transport of North Pacific water through the Bering Strait into the Arctic. Northward advection through the Bering Strait combines several water masses that results in the transport of relatively warm, nutrient-rich water, as well as primary and secondary producers into the Arctic (Woodgate et al., 2005; Gong and Pickart, 2015; Danielson et al., 2017; Stabeno et al., 2018). Northward advection through the Bering Strait in the summer, along with sea-ice melting and episodic upwelling from the Beaufort Sea on to the shelf and Barrow Canyon, results in a highly productive and complex shelf ecosystem that responds to local, regional and global forcing (e.g. Bond et al., 2018). Adding to the complexity of the Chukchi Sea shelf ecosystem, recent reports have shown dramatic changes in timing and extent of sea-ice coverage, along with considerable increases in sea surface temperatures (National Snow and Ice Data Center, nsidc.org; Timmermans and Ladd, 2019; Perovich et al., 2019).

In summer, the northern Bering and Chukchi seas experience increased day length and melting sea ice, resulting in a phytoplankton bloom. The bulk of the bloom sinks to the bottom due to the shallow depth (<50 m) and relatively low grazing impact on phytoplankton (Campbell et al., 2009), supporting a robust benthic community. Recent studies, however, have shown a temporal decrease in benthic biomass in the northern Bering Sea, suggesting a possible weakening of benthic-pelagic coupling as the ice retreat now occurs earlier in the season (Grebmeier et al., 2006a; Grebmeier et al., 2006b; Grebmeier, 2012). Concurrently, zooplankton biomass in the Chukchi Sea has increased over the past seven decades (Ershova et al., 2015), which can be explained, in part, by increasing temperatures, reduction in sea ice, and an increase in northward water transport through the Bering Strait (Ershova et al., 2015; Woodgate et al., 2015; Woodgate, 2018). These trends suggest a potential ecosystem regime shift is underway in the Pacific Arctic, with consequences for local food webs. These changes emerge from both direct and indirect effects on both the indigenous biota residing in the ecosystem as well as the introduced species. Changes in the timing and type of production within the pelagic and

* Corresponding author.
E-mail address: Adam.Spear@noaa.gov (A. Spear).

https://doi.org/10.1016/j.dsr2.2020.104814
Received 31 July 2019; Received in revised form 3 June 2020; Accepted 3 June 2020
Available online 11 June 2020
0967-0645/Published by Elsevier Ltd.

benthic communities, will result in changes in benthic-pelagic coupling that have the potential to effect higher trophic levels such as birds, marine mammals, fish, and the people who live in the region.

One specific taxon of interest for our studies were bowhead whales (*Balaena mysticetus*) that forage as they migrate southwestward in the fall through the Utqiagvik (formerly known as Barrow) region from the Beaufort Sea (Moore et al., 2010; Quakenbush et al., 2010; Citta et al., 2012). Studies have reported improvements in bowhead body condition in association with earlier ice retreat and increase in the area of open water (George et al., 2015). The observed improvements in bowhead body condition may be the result of increased prey populations, specifically euphausiids and copepods that dominate the prey in stomachs of bowhead whales harvested near Utqiagvik, Alaska (Lowry et al., 2004; Ashjian et al., 2010; Moore et al., 2010; George et al., 2015). Previous studies suggested that euphausiids are advected along the bottom from the northern Bering Sea into the Chukchi Sea, and subsequently concentrated into dense aggregations through upwelling onto the Beaufort Sea shelf towards Barrow Canyon (Berline et al., 2008; Ashjian et al., 2010). Zooplankton sampling in the Chukchi Sea has generally underestimated populations of euphausiids because estimates were based on collections from small (0.25–0.6 cm diameter) aperture size plankton bongo nets (Hopcroft et al., 2010; Eisner et al., 2013; Questel et al., 2013; Ashjian et al., 2017; Pinchuk and Eisner, 2017) and because the predominantly daytime vertical or oblique sampling failed to target krill layers near the bottom (Coyle and Pinchuk, 2002).

The main objectives of this study were 1) to understand the transport pathways of euphausiids from the Bering Strait to Barrow Canyon, 2) evaluate the abundance of other large planktonic prey for whales in the region, and 3) provide data on the status and trends of Chukchi Sea zooplankton communities. This study builds on other research based on conceptualized modeling to explain the dynamics of late-summer euphausiid populations in this region (Berline et al., 2008; Ashjian et al., 2010) by providing empirical data collected from epibenthic and plankton tows that should more accurately reflect the abundance of euphausiid and other epibenthic taxa. We compared epibenthic and pelagic zooplankton abundances to assess whether they were significantly different and to explore whether epibenthic tows were a more accurate reflection of near-bottom taxa. We hypothesized that advection of zooplankton from the Bering Sea to be the main driver of zooplankton abundance in the region. To test this, we compared zooplankton abundance across years and locations, and calculated krill development times to see if euphausiids captured in this study could have reached that stage after having been advected from the Bering Sea.

2. Methods

2.1. Study area

The Chukchi Sea has a broad, mostly shallow (<50 m) shelf situated between Alaska and Siberia (Fig. 1). Survey transects varied among years, 2011–2015, depending on the scientific focus for the year, available ship time, and ice distribution. Surveys were conducted in the late summer, lasting approximately 30 days (~August 5th – September 5th), except for 2014, which was September 22nd – October 12th. For analysis and description purposes, the study area was divided into 'Beaufort', 'Southwest,' 'Central,' and 'Northeast' regions that are established from statistically different oceanographic conditions (Eisner et al., 2013; Randall et al., 2019).

2.2. Physical data

Hydrographic data, including temperature and salinity, were collected using a SBE 911plus and FastCAT SBE 49 systems (SeaBird Electronics). Sea Surface temperatures (SST) were averaged from 5 – 10 m depth. We quantified broad-scale patterns in sea-ice concentration using satellite data. Sea-ice concentration (percentage of ocean covered by sea-ice) and extent data were obtained after the surveys from a Scanning Multichannel Microwave Radiometer (SMMR) on the Nimbus-7 satellite and from the Special Sensor Microwave/Imager (SSM/I) sensors on the Defense Meteorological Satellite Program's (https://nsidc.org; Comiso, 1999). Bering Strait volume transport data were acquired from moored Acoustic Doppler Current Profiler (ADCP)

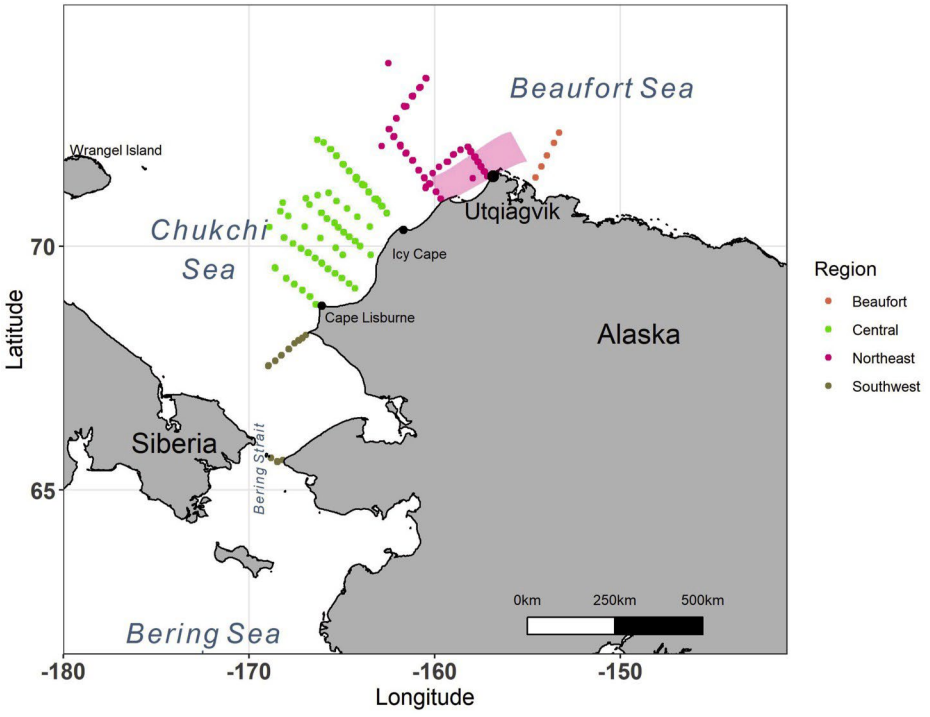

Fig. 1. Study area in the Chukchi Sea. Each region is symbolized by a colored circle. The study area was split up into southwest, central, northeast, and Beaufort regions. The pink shaded region indicates Barrow Canyon.

measurements (Woodgate et al., 2015; Woodgate, 2018). Northeastward water column volume transport, in Sverdrups (Sv), was calculated according to Stabeno et al. (2018) from current data measured at C1, C2, and C3 moorings along the Icy Cape transect. Transport was averaged over 14 and 30 days leading up to the date that the station was sampled.

2.3. Zooplankton net data

Zooplankton were collected primarily during daylight hours using a multiple-opening and closing 1 m^2 Tucker Sled trawl equipped with a FastCAT, and sled-like runners at the bottom so that samples could be taken in close proximity to the bottom. A 505 μm (2013–2015) or a 333 μm (2011–2012) mesh net sampled while the sled was towed at a speed of 1.5–2.0 knots along the bottom for 2 min, then mechanically tripped to close and simultaneously open a second net to sample the entire water column from the bottom to the surface (wire retrieval rate 20 m min^{-1}). For smaller taxa, a 25 cm net with 150 μm mesh was suspended in the larger net that profiled the entire water column. Note that this setup is not ideal in cases where clogging in the 20- cm net occurs, thus the possibility of inaccurate volume filtered readings exist in this study. Samples that appeared questionable (e.g. low flowmeter readings, large jellyfish in the net) were excluded from the analysis. Smaller taxa such as *C. glacialis* and euphausiid furcilia were enumerated in the water column only and not in the epibenthic samples. Both Tucker nets were equipped with a separate calibrated General Oceanics flow meter to estimate volume filtered. Plankton captured by the nets were washed into the cod-ends, sieved through appropriately-sized wire mesh screens and preserved in glass jars with sodium borate-buffered 5% Formalin. Samples were inventoried at the end of the cruise and then sent to the Plankton Sorting and Identification Center in Szczecin, Poland, for processing. Subsampled taxa were enumerated and identified to lowest possible genera and life stage and returned to the Alaska Fisheries Science Center for verification. Ten percent of the returned samples were checked for quality assurance/quality control of species identification and enumeration.

2.4. Zooplankton data analysis

Zooplankton abundance was reported as four general categories in the context of known bowhead whale prey in the region (Lowry et al., 2004; Moore et al., 2010), including: euphausiids (primarily *Thysanoessa raschii*), amphipods (dominant species included *Themisto libellula* and unidentified Gammaridea), mysids (dominant species included *Neomysis rayii* and *Pseudomma truncatum*), and copepods (*Calanus glacialis*). Analysis of variance (ANOVA) was used to examine epibenthic and pelagic variation across years in *T. raschii*, mysid, and amphipod abundance.

Development times of *Thysanoessa* spp. stages were estimated using the formula:

$$R_2 = R_1 * Q_1^{\frac{T_2 - T_1}{10}}$$

where R_1 and R_2 are the development rates (d^{-1}) at temperature T_1 and T_2 (°C), respectively (Teglhus et al., 2015). We used the Q_{10} of 2.04 (Pinchuk and Hopcroft, 2006). The calculated temperature (T_2) and development rate (R_2) were normalized to 5 °C and 0.016 d^{-1} (for furcilia; 0.045 d^{-1} for calyptopis), obtained from Teglhus et al. (2015). We chose the measured rates from Teglhus et al. (2015) because of the similar temperature conditions (5–8 °C) and because a mixed population of krill was used as we also have a mixed community. These were also the slowest known development rates for *Thysanoessa* spp. furcilia compared to previous studies (see Table 3 in Teglhus et al., 2015); this prevented an overestimation of development rates of *Thysanoessa* spp. under conditions that may be significantly influenced by availability of food such as phytoplankton (Pinchuk and Hopcroft, 2007). Development times were then compared to satellite-tracked drifter data (Stabeno et al., 2018) to explore the possibility of recent reproduction in the Chukchi Sea.

We used the mgcv package (Wood, 2011) in R (R Core Team, 2019) to fit generalized additive models (GAM) with Gaussian distribution to relate changes in C2 and C5 stages of *C. glacialis, T. raschii* (adult and juvenile), and euphausiid furcilia mean abundance to environmental variables. These two particular stages in each species were chosen to contrast different ages, with C2 representing younger and C5 representing older *C. glacialis*, and furcilia representing younger and adults/juveniles representing older *T. raschii*. For simplicity, we excluded stages C3 and C4 from the analysis as these stage abundances are correlated to the C5 stage (data not shown). We chose to exclusively use epibenthic abundances of *T. raschii* since most of our sampling occurred primarily during the day and when the vast majority of euphausiids would be at or near the bottom. Restricted Maximum Likelihood (REML) method was used as the smoothing parameter estimation. The model selection was done by assessing deviance explained, R^2, and Akaike information criterion (AIC). Residuals were analyzed to ensure there were no obvious deviations from normal distributions, and we examined the response versus. fitted value for patterns. We assessed ten environmental variables for inclusion in the GAMs including: latitude, longitude, bottom temperature, surface temperature, bottom salinity, surface salinity, 14 and 30-day northeastward transport, year, and day of the year (hereinafter referred to as ordinal day).

3. Results

3.1. Environmental conditions

Sea surface temperatures (SST) were warmest in 2011 (mean SST 6.89 ± 1.35 °C) and coldest in 2013 (mean SST 2.64 ± 2.61 °C). Both 2012 (mean SST 5.46 ± 2.41 °C) and 2015 (mean SST 6.13 ± 2.18 °C) had similar warm SSTs towards the central and southwest portion of the survey, and colder SSTs across the northeast portion; however, 2012 was colder in the northeast region (Fig. 2). Sea surface temperatures in 2014 (mean SST 3.09 ± 1.62 °C) were colder over the entire survey area and had substantially less northeast to southwest variability. Randall et al. (2019) using the mean bottom temperatures in the central region, found 2013 (−1.4 °C) to be the coldest year, with 2011–2012 and 2014–2015 having similar warmer bottom temperatures (~2 °C). Similarly, differences between years were evident from initial dates at which ice concentration was less than 10% (Table 1). Sea-ice remained in the northeast region until mid to late August in years 2012–2014, and melted in mid-to late July in 2011 and 2015.

Monthly mean northward transport (Sv) through the Bering Strait tended to peak in the spring and summer (~May–August), with lower transport in the winter (Fig. 3). Higher spring/summer transport occurred in 2011and 2015, peaking at around 1.92 (±0.09) Sv in May and 1.87 (±0.06) Sv in July of 2015 and 1.91 (±0.10) Sv in June of 2011. Spring and summer transport was moderate in 2014 and lower in 2012 and 2013, with mean values as low as 1.14 (±0.18) and 1.18 (±0.14) in August of 2012 and 2013, respectively.

3.2. Zooplankton abundance

Average pelagic amphipod abundances increased from 2011 to 2015; average benthic abundances were generally higher than pelagic abundances but also increased over the same period (Fig. 4a). Overall, 2013, 2011 had the highest and lowest average amphipod abundance respectively. Mysid epibenthic and pelagic abundances were relatively low across all years (Fig. 4b), but epibenthic abundances were relatively higher in all years and there were no increasing or decreasing trends across the years. The euphausiids community consisted of four species of the genus *Thysanoessa*: *T. inermis, T. longipes, T. spinifera, and T. raschii*; the latter, being the most abundant (approximately 70% of total abundance) of the four, was singled out in this study for purposes of

Fig. 2. Sea surface temperature (°C) averaged from 5-10 m for each year.

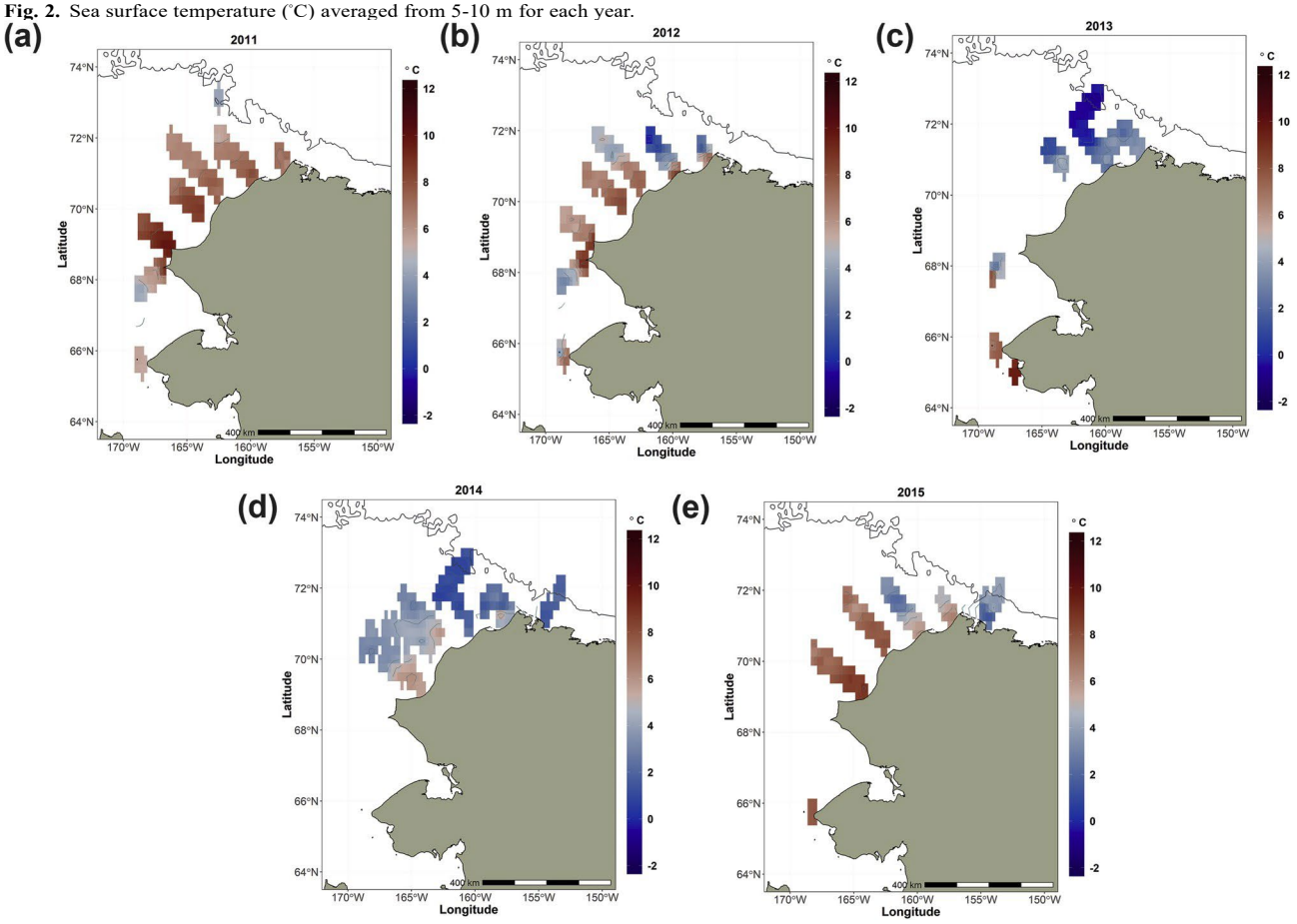

Fig. 2. Sea surface temperature (°C) averaged from 5-10 m for each year.

Table 1
Estimate of the initial date at which ice concentration was less than 10% within the southwest and northeast region of the sampling area.

	Southwest	Northeast
2011	3 June	15 July
2012	22 June	19 August
2013	29 June	31 August
2014	16 June	16 August
2015	14 June	18 July

simplicity. Epibenthic *T. raschii* abundances were lowest in 2013 and highest in 2014 (Fig. 4c). Pelagic *T. raschii* abundance was lowest in 2011 and highest in 2015.

There were no consistent differences in the abundance of *T. raschii*, mysid, and amphipods between the bottom layer and water column when we took into account year and a depth-year interaction in our analyses. ANOVA results did not show significant differences between epibenthic and pelagic *T. raschii* abundances independent of year. However, *T. raschii* abundance did show significant differences between years ($F = 3.20$, $p = 0.01$), independent of depth and depth/year interactions ($F = 5.56$, $p < 0.001$). Similarly, ANOVA results did not show significant differences between epibenthic and pelagic amphipods independent of year ($F = 2.16$, $p = 0.14$). However, amphipod abundances did show significant differences among years independent of depth ($F = 4.467$, $p = 0.001$) and depth/year interactions ($F = 3.294$, $p = 0.01$). ANOVA results showed significant differences between epibenthic and pelagic mysids independent of year ($F = 9.59$, $p = 0.002$), years independent of depth ($F = 4.80$, $p = 0.0008$), and depth/year interactions ($F = 0.84$, $p = 0.50$). Time of day was hypothesized to influence euphausiid

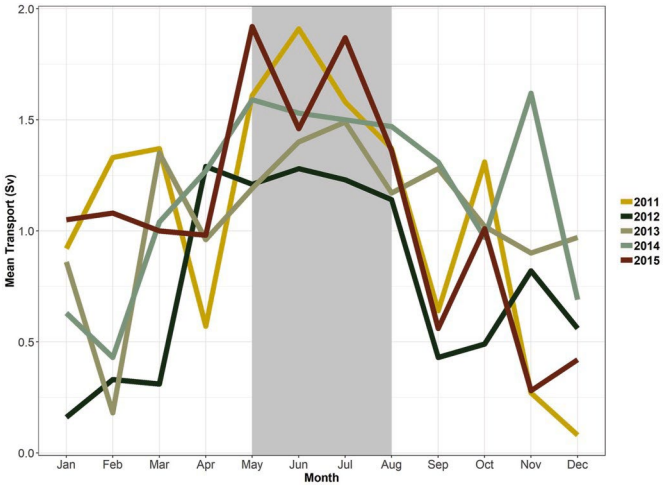

Fig. 3. Mean transport (Sv) of water by month for each year through the Bering Strait. The grey underlay highlights the approximate peak transport months.

abundance, however, ANOVA results did not find differences in day/night sampling abundances of *T. raschii* at the $p < 0.05$ significance level.

A post-hoc Tukey's 'Honest Significant Difference' test of depth-year interactions of *T. raschii*, mysids, and amphipods showed 2014 and 2015 were significantly ($p < 0.05$) different from most previous years (Table 3). Within years 2014 and 2015, *T. raschii* showed significant ($p < 0.05$) differences between epibenthic and pelagic depths. Similarly, both mysids and amphipods showed significant ($p < 0.05$) differences

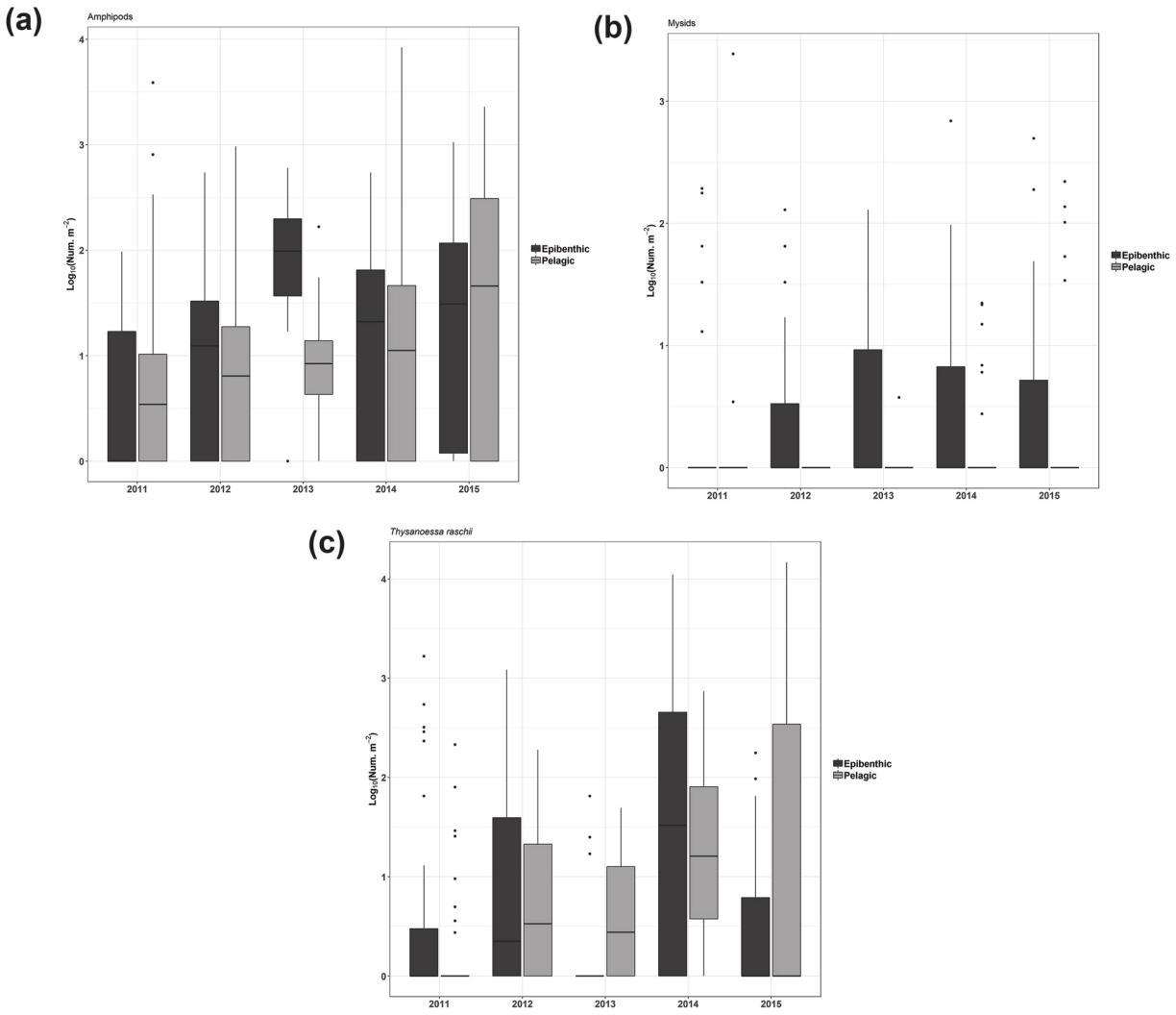

Fig. 4. Yearly epibenthic and pelagic total abundance (Log_{10}(Num m^{-2})) for amphipods (a), mysids (b), and *Thysanoessa raschii* (c).

between epibenthic and pelagic depths within 2014. Overall, we cannot independently assess year without noting whether *T. raschii*, mysids, or amphipods samples were caught in the water column or just above the bottom.

There was a lack of spatial differences among years for amphipods, with positive catches across all regions (Fig. 5a). The highest amphipod frequency of occurrence was in 2013, with complete absence in only one station (epibenthic and pelagic combined). Mysid abundance was low for each year across all regions (Fig. 5b); within years, more mysids were captured in the northeast than other regions. Mysid had the highest frequency of occurrence in 2014 with animals captured at stations in 3 of the 4 regions (epibenthic and pelagic combined). A lack of spatial differences of *T. raschii* among years was evident (Fig. 5c), with positive catches appearing across most regions. The highest *T. raschii* frequency of occurrence was in 2014, with presence detected from at least one station in three of the four areas (epibenthic and pelagic combined). There were no obvious trends in presence/absence or abundance as a function of distance from land.

Abundances of *C. glacialis* were lower in warmer years (2011, 2014, and 2015) and higher in colder years (2012, 2013; Fig. 6). *Calanus glacialis* were ubiquitous across all regions, with presence detected at most stations (Fig. 7).

3.3. Early life stages

Development time calculations suggest that it takes approximately 51 and 78 days at 8 and 2 °C water temperature, respectively, for *Thysanoessa* spp. stages to develop from eggs to furcilia (Table 2). Note that the furcilia counted in this study were not identified to species. Euphausiid furcilia stages were most abundant in the central and southwestern regions of each year (Fig. 8). Euphausiid furcilia were completely absent from the northeastern region in 2012 and 2013. Both 2011, 2014 had similar abundances along the central and southeastern regions, with 2011 having slightly higher abundances in the northeast. In 2015, highest abundances were located in the central region, with lower abundances extending into the northeast. Euphausiid calyptopis, a developmental stage of much shorter duration (~40 days shorter; Teglhus et al., 2015), were only caught in very low abundances (~1.0 log_{10} (Num. m^{-2})) in 2011 at 3 stations (map not shown) from the northeast and southwest regions.

Spear et al. (2019) estimated *C. glacialis* egg to C2 stages have approximate development times of 8 to 12 days at temperatures ranging between 12 and -1.5 °C respectively. *Calanus glacialis* C2 stages were almost exclusively caught in the northeast region, including Icy Cape (Fig. 9). Higher total abundances appeared in both 2012 (4.92 log_{10} (Num. m^{-2})) and 2013 (5.19 log_{10} (Num. m^{-2})), while the lowest total abundances were in 2011 (3.38 log_{10} (Num. m^{-2})).

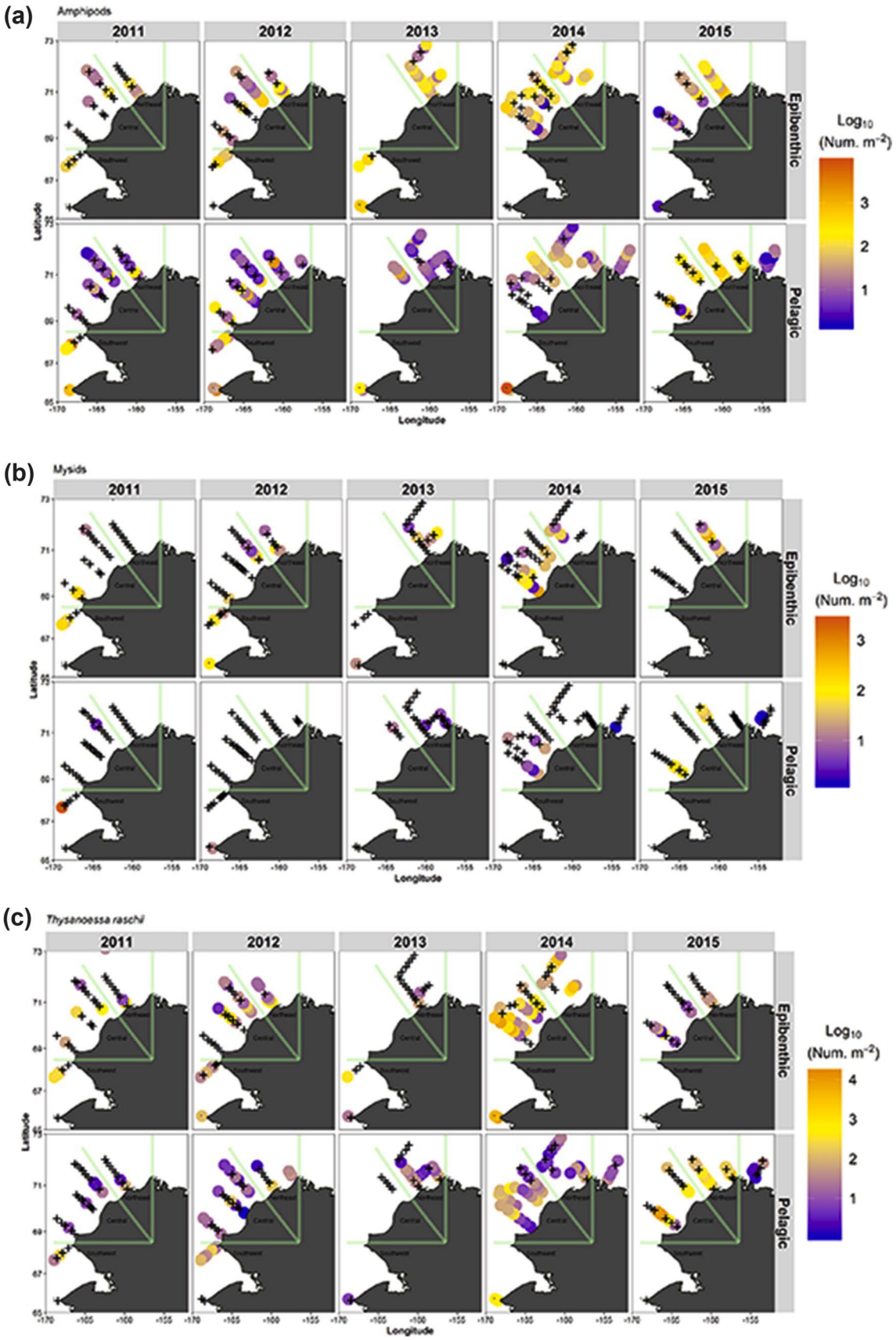

Fig. 5. Yearly maps of epibenthic and pelagic total abundance (Log_{10}(Num m^{-2}))for amphipods (a), mysids (b), and *Thysanoessa raschii* (c). The letter "X" denotes tows where the taxon was absent. Note that the scale differs among taxa.

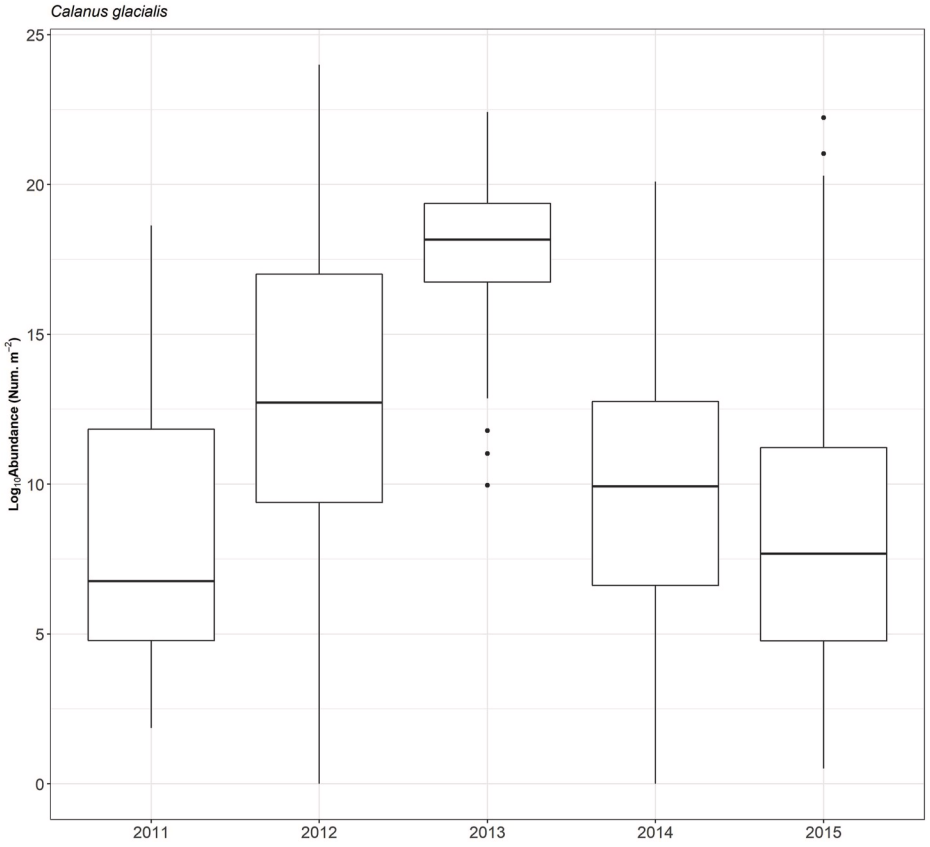

Fig. 6. Yearly pelagic total abundance (Log_{10}(Num m^{-2})) of *Calanus glacialis*.

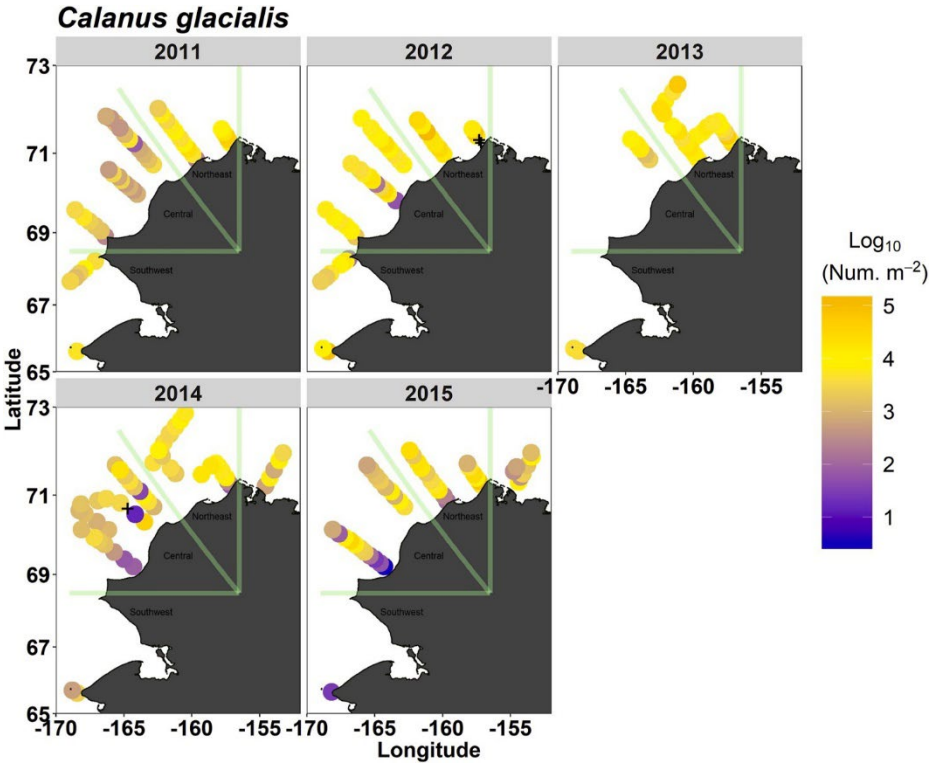

Fig. 7. Yearly maps of pelagic total abundance (Log_{10}(Num m^{-2})) of *Calanus glacialis*. The letter "X" denotes tows where the taxon was absent.

Table 2
Amount of days at different temperatures for *Thysanoessa* spp. stages to develop from eggs.

Stage	12 °C	8 °C	2 °C	−1.5 °C
Calyptopis	13.4	17.8	27.3	35
Furcilia	38.2	50.9	78	100

3.4. Relationships between plankton abundance and physical variables

Bottom temperature, 30-day northeastward transport, longitude, and ordinal day were the most significant variables associated with mean *T. raschii* abundance (Table 4). The model helped explain 42.3% of the deviance with an r^2 of 0.38. Extreme lower and higher bottom temperature conditions were associated with lower *T. raschii* abundance (Fig. 10). There was a positive relationship between 30-day northeastward transport and *T. raschii* abundance. The longitude parameter also showed that *T. raschii* abundance was positively associated with the northeastern and southwestern portions of the study area. The strong positive relationship with ordinal day showed that higher abundances showed up later in the year in 2014. This is because the only year in which we sampled past day of year 260 was 2014. Furcilia abundance had significant relationships with bottom temperature, 14-day northeastward transport, year, ordinal day, and longitude. The model explained 56.8% deviance in abundance for euphausiid furcilia with an r^2 of 0.53 (Table 4). There was not a clear abundance pattern in relation to the bottom temperature (Fig. 11). In contrast to the relationship between transport and *T. raschii* adults, there was a negative relationship with furcilia abundance and 14-day northeastward transport.

The model helped explain 43% of the deviance with an r^2 of 0.39 of the *C. glacialis* C5 stage (Table 4). The most significant parameters included surface salinity, surface temperature, bottom temperature, 14-day transport, ordinal day, and year. Higher surface temperatures had a positive association, while lower surface had a slightly negative association, with C5 abundances (Fig. 12). Conversely, lower bottom temperatures had a positive relationship and higher bottom temperatures had a negative relationship with C5 abundance. Stage C5 abundance was also negatively associated with lower salinity seawater. There was a slight negative association with strong northeastward transport and C5 abundance. Interestingly, there was not a significant association with northeastward transport and *C. glacialis* C2 stages. The C2 stage was similar to C5 stages in the relationship with bottom temperatures, as there was a negative relationship with higher bottom temperatures and a positive relationship lower bottom temperatures (Fig. 13). There was positive association of C2 stages with higher longitudes. Overall, C2 stages had the strongest GAM model, which explained 57% of the deviance and a r^2 of 0.55 (Table 4).

4. Discussion

4.1. Euphausiid transport

T. raschii is an amphiboreal species whose distribution also extends to the Arctic Ocean and associated continental shelves. We observed the presence of *T. raschii* in all years near Utqiagvik, with relatively high abundances in 2014 and 2015. The annual presence of euphausiids there is important as they are a dominant component of the diet for bowhead whales in the region (Lowry et al., 2004; Moore et al., 2010). A positive association with northeastward transport and a positive association with higher longitudes, implies that *T. raschii* were advected from the south. The positive association with lower longitudes may be the result of krill being advected into the Chukchi Shelf from the Beaufort Sea as described by Ashjian et al. (2010); other explanations include lack of sampling in the central region in 2013, sampling later in the 2014, or because of the current patterns that tend to extend farther offshore in the central region (Stabeno et al., 2018), resulting in animal presence just outside of the sampled transect. Overall, these findings support the hypothesis of Berline et al. (2008) and Ashjian et al. (2010) that the

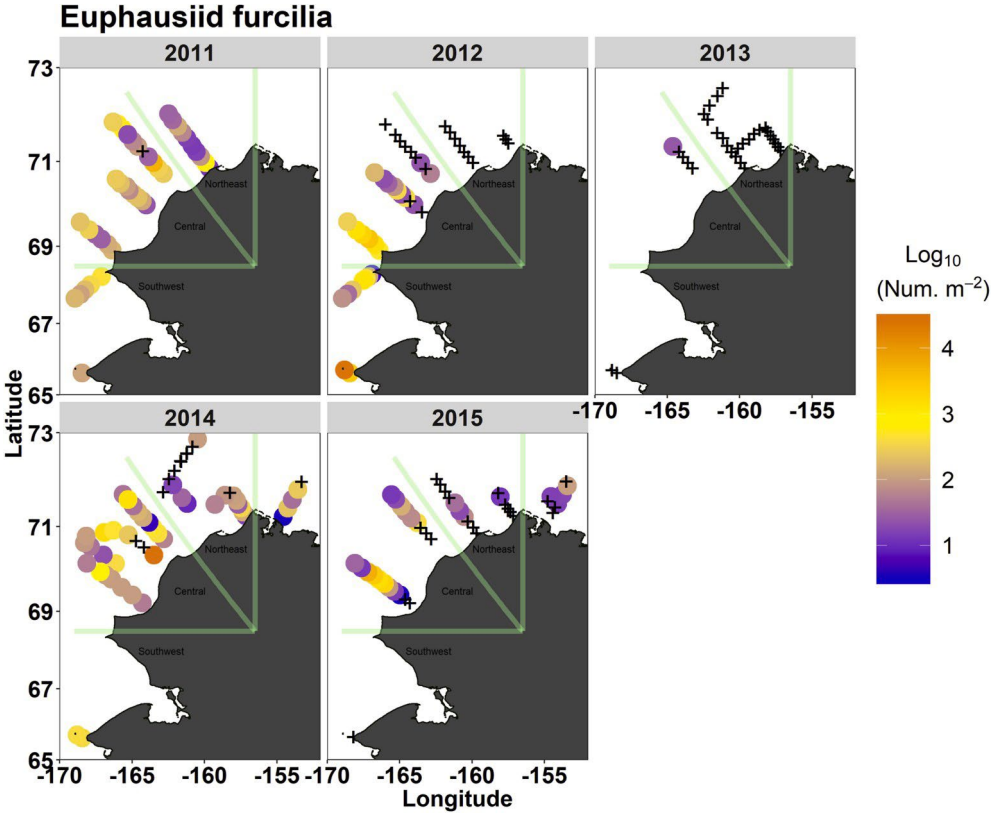

Fig. 8. Yearly maps of pelagic total abundance (Log_{10}(Num m^{-2})) of euphausiid furcilia. The letter "X" denotes tows where the taxon was absent.

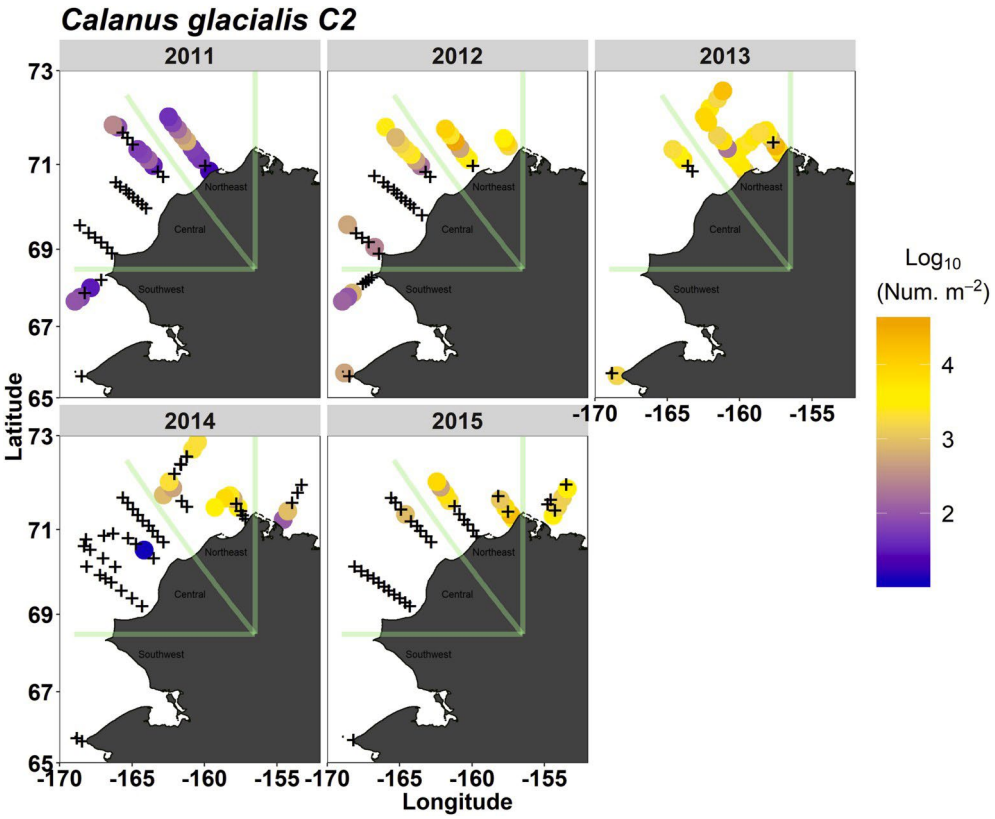

Fig. 9. Yearly maps of pelagic total abundance (Log_{10}(Num m^{-2})) of *Calanus glacialis* C2 stage. The letter "X" denotes tows where the taxon was absent.

Table 3
Post-hoc Tukey's test significant *p* values for the depth-year interactions of each taxon.

	Depth:Year	*p* value
T. raschii	Epibenthic:2014 – Pelagic:2011	0.0200
	Pelagic:2015 – Pelagic:2011	0.0252
	Epibenthic:2014 – Epibenthic:2011	0.0462
	Epibenthic:2014 – Pelagic:2012	0.0179
	Pelagic:2015 – Pelagic:2012	0.0234
	Epibenthic:2014 – Epibenthic:2012	0.0417
	Pelagic:2015 – Epibenthic:2011	0.0494
	Epibenthic:2014 – Pelagic:2014	0.0235
	Pelagic:2015 – Pelagic:2014	0.0307
	Epibenthic:2015 – Epibenthic:2014	0.0342
	Epibenthic:2015 – Pelagic:2015	0.0390
Mysids	Epibenthic:2014 – Pelagic:2011	0.0000
	Epibenthic:2014 – Epibenthic:2011	0.0001
	Epibenthic:2014 – Pelagic:2012	0.0000
	Epibenthic:2014 – Epibenthic:2012	0.0001
	Epibenthic:2014 – Pelagic:2013	0.0008
	Epibenthic:2014 – Epibenthic:2013	0.0009
	Epibenthic:2014 – Pelagic:2014	0.0000
	Epibenthic:2014 – Epibenthic:2015	0.0001
	Epibenthic:2014 – Pelagic:2015	0.0001
Amphipods	Epibenthic:2014 – Pelagic:2011	0.0060
	Epibenthic:2014 – Epibenthic:2011	0.0017
	Epibenthic:2014 – Pelagic:2012	0.0010
	Epibenthic:2014 – Epibenthic:2012	0.0014
	Epibenthic:2014 – Pelagic:2013	0.0101
	Epibenthic:2014 – Epibenthic:2013	0.0087
	Epibenthic:2014 – Pelagic:2014	0.0063
	Epibenthic:2014 – Epibenthic:2015	0.0312
	Epibenthic:2014 – Pelagic:2015	0.0010

Table 4
GAM model significant terms for each taxon with R^2 and the percentage of deviance explained. *$p < 0.05$; **$p < 0.01$; ***$p < 0.001$.

	Significant terms	R^2	Deviance explained
Calanus glacialis C5	Surface Salinity***	0.394	43%
	Surface Temperature*		
	14-day Transport*		
	Bottom Temperature***		
	Ordinal Day***		
	Year***		
Calanus glacialis C2	Mean Bottom Temperature***	0.551	57%
	Mean Surface Temperature**		
	Longitude*		
	Julian Day*		
	Year*		
Thysanoesssa raschii	Mean Bottom Temperature**	0.375	42.3%
	30-day Transport*		
	Longitude***		
	Ordinal Day ***		
Euphausiid furcilia	Mean Bottom Temperature ***	0.53	55.8%
	14-day Transport***		
	Longitude***		
	Ordinal Day***		
	Year***		

euphausiids concentrated by physical processes near Barrow Canyon likely originated from the northern Bering Sea.

Conversely, temperature-dependent euphausiid furcilia development times suggest their extent into the central and northeast regions in warmer conditions was a result of spawning in the Chukchi Sea. Transport of water takes ~90 days to reach Icy Cape from the Bering

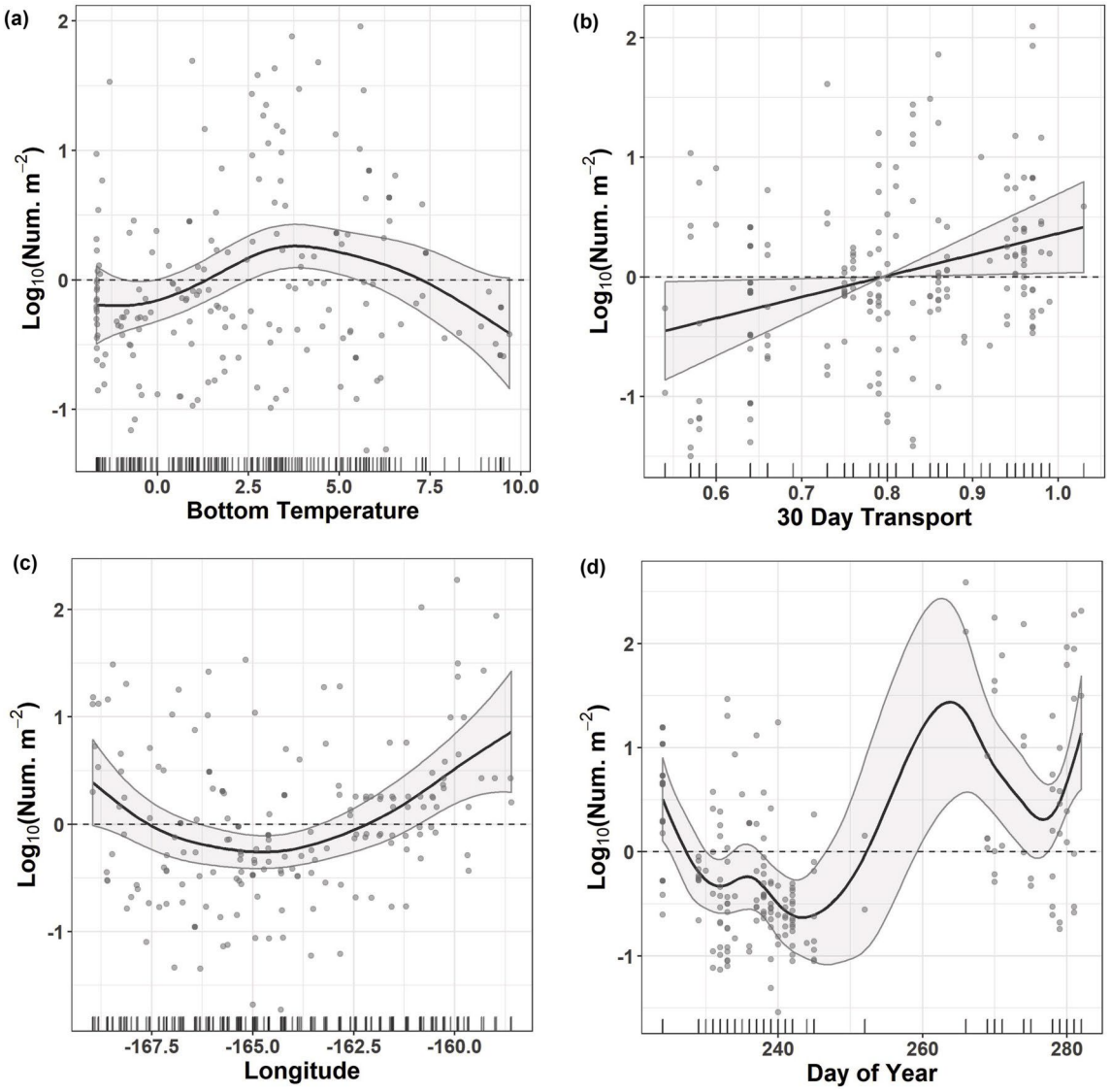

Fig. 10. GAM smooth for the distribution of *Thysanoessa raschii* epibenthic abundance (Log_{10}(Num m^{-2})), 2011–2015. Variables included mean bottom temperature (a), 30-day transport (b), longitude (c), and day of year (ordinal day) (d).

Strait (Stabeno et al., 2018). This is roughly 12 to 40 days longer than the development time from egg to furcilia at comparable temperatures. The hypothesis of local production is also supported by the negative relationship with 14-day transport or lack of clear relationship with bottom temperatures. In particular, the negative relationship with 14-day transport (in addition to a lack of association with 30-day transport) showed that the greater and more recent transport resulted in reduced abundances, suggesting they were likely recently spawned nearby and subsequently transported away.

Adult euphausiids were present in the northeast region in 2012 and 2013, even though overall transport during those years was low. The absence of younger stages could have resulted from a change in the timing of reproduction relative to our sampling, failed spawning, or very high mortality of the larvae because of cold temperatures or high predation. Euphausiid eggs were present in the northeast region in 2014 and 2015, but were absent in 2012 and 2013 (egg data not collected in 2011), suggesting reproduction only occurred when this region was not occupied by colder water masses.

The higher pelagic abundances of euphausiids in 2013 and 2015 were not due to a day/night effect as a comparison of day/night abundances found no significant differences (not shown). The significant increase in abundance of *T. raschii* in 2014, compared to remaining years, suggests that sampling later in the season likely had considerable impact. This is evidenced by the relationship between ordinal day and euphausiid abundance in 2014. Other environmental and physical results did not suggest any other anomalous features that may have caused this significant jump in abundance. Thus, it suggests that because we sampled later in 2014 we observed more euphausiids compared to other years. This is most likely the result of advection timing (as explained in Berline et al., 2008), but may also reflect local recruitment. Alternative explanations for increased abundance include local production or retained for a longer period of time. Most historical surveys have not sampled later than mid-September to avoid disturbing subsistence hunting by Iñupiat whalers as the whales migrate westward from the Beaufort. Thus previous surveys (Grebmeier and Harvey, 2005; Lane et al., 2008) reporting low numbers of euphausiids could be due to the mismatch between euphausiid transport from the south and survey timing.

Our estimates of adult euphausiid abundance may be somewhat improved over prior estimates derived from small mouth plankton nets towed only in the water column (e.g. Eisner et al., 2013). However, euphausiids are difficult to accurately estimate even with larger nets

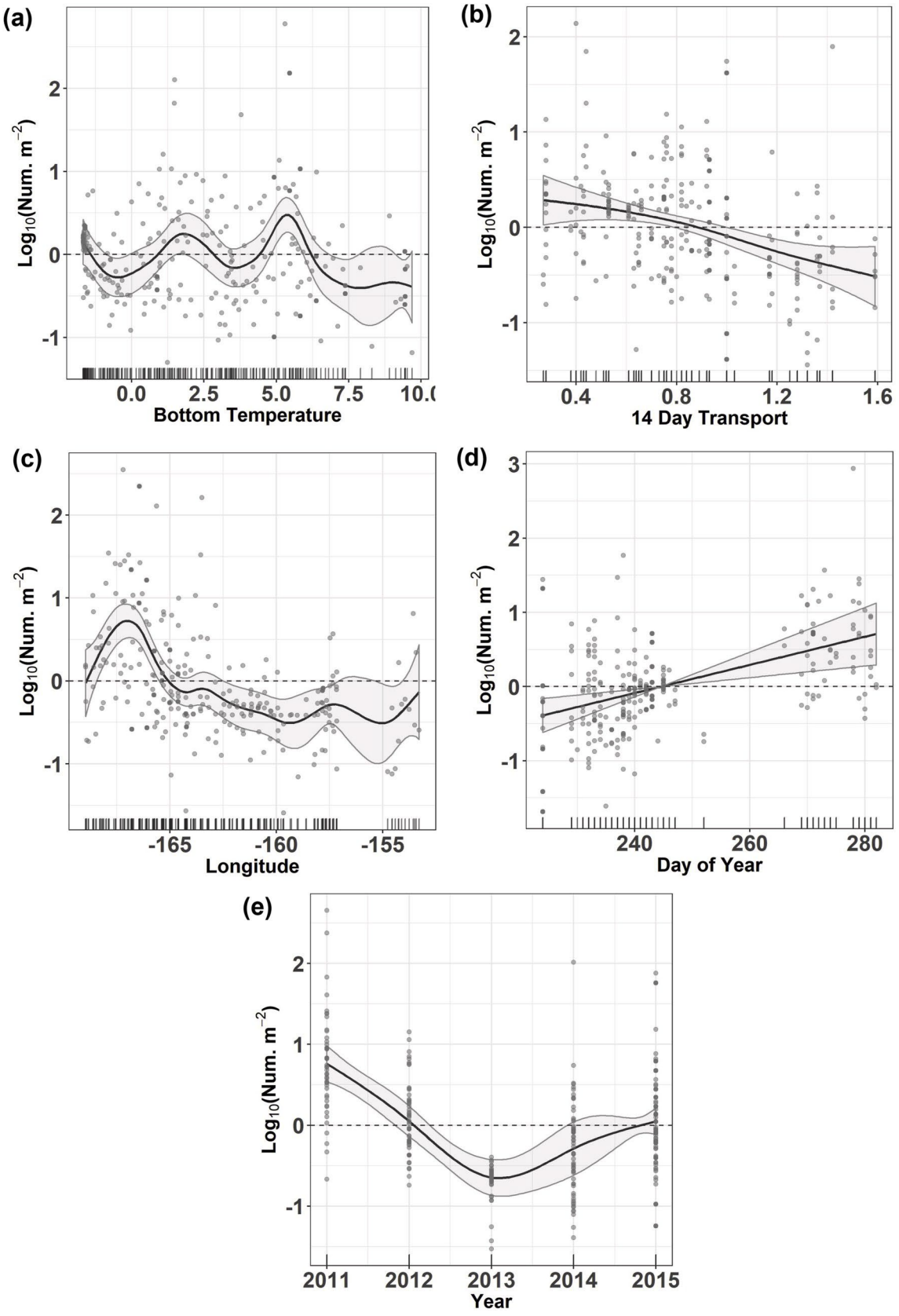

Fig. 11. GAM smooth for the distribution of euphausiid furcilia pelagic abundance (Log_{10}(Num m^{-2})), 2011–2015. Variables included mean bottom temperature (a), 14- day transport (b), longitude (c), day of year (ordinal day) (d), and year (e).

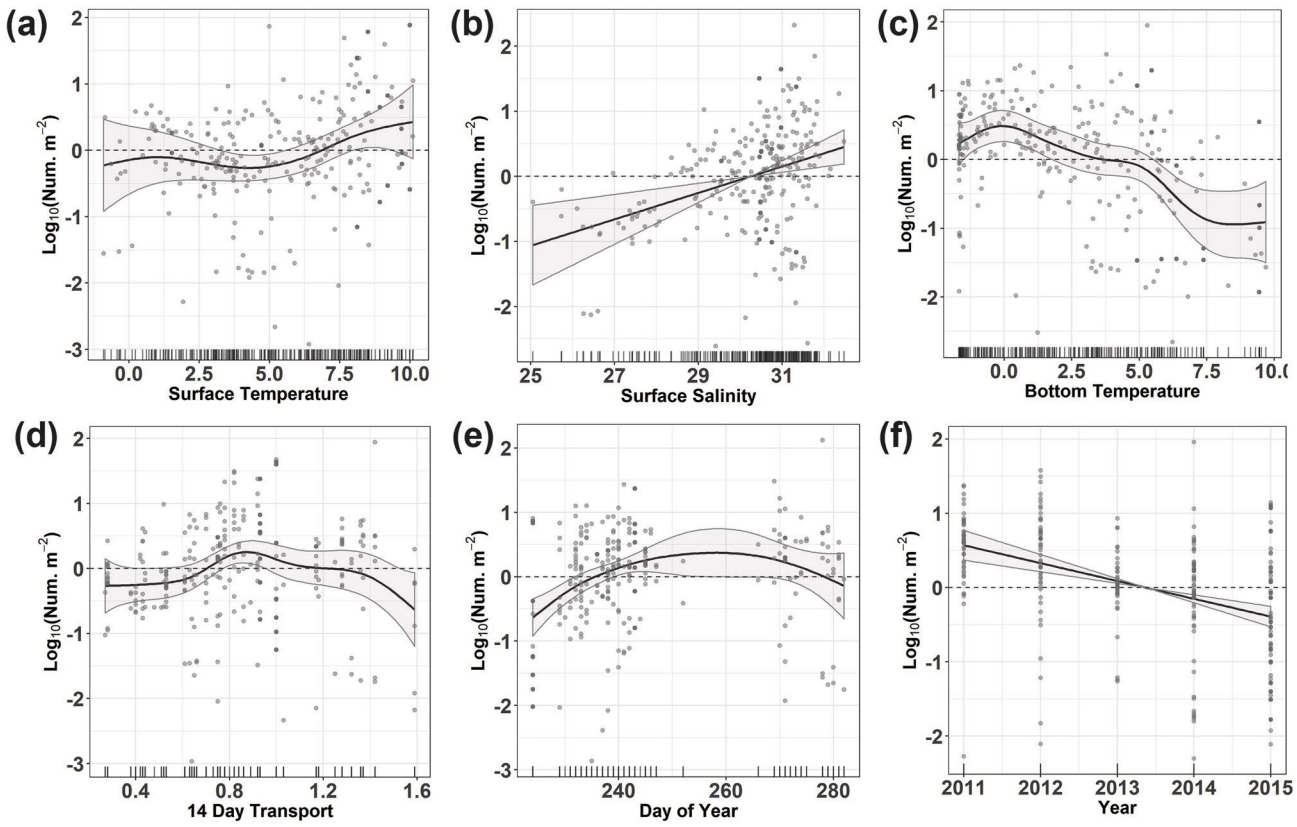

Fig. 12. GAM smooth for the distribution of *Calanus glacialis* C5 stage pelagic abundance (Log_{10}(Num m^{-2})), 2011–2015. Variables included mean surface temperature (a), surface bottom salinity (b), bottom temperature (c), 14-day transport (d), day of year (ordinal day) (e), and year (f).

that sample at faster tow speeds. (e.g. Hunt et al., 2016). Net avoidance by euphausiids has long been recognized as chronic problem in oceanographic studies (e.g. Brinton, 1967; Sameoto et al., 2011; Wiebe et al., 2013). Net avoidance abilities may even extend to the young stages (e.g. Smith, 1991). Future work using acoustical or optical techniques may be able to provide better estimates of euphausiid abundance, although as this study demonstrated there is a need to sample very close to the seafloor.

4.2. Other large zooplankton

We found that *C. glacialis* were most abundant in colder conditions, with the abundance increase being driven by earlier development stages. This finding is supported by research showing that *C. glacialis* were strongly tied to the ice edge algae production, which is increased in colder years (Søreide et al., 2010). Both C2 and C5 stages showed a significant positive association with colder bottom temperatures. The C5 stage, as opposed to the C2 stage, also had a positive association with warmer surface temperatures and significant relationship with northeastward transport, suggesting that C5 stages were more likely to be influenced by advection. The C2 stage had significantly higher abundances in the northeast region, a negative relationship with higher surface temperatures, and lack of a significant relationship with transport, suggesting local production rather than transported from the south. This is supported by previous research showing *C. glacialis* having approximate development times of 8 to 12 days at temperatures between 12 and -1.5 °C, respectively, from egg to C2 stage (Hirst and Lampitt, 1998; Kiørboe and Hirst, 2008; Spear et al., 2019). As described earlier, transport times from the Bering Sea to the northeast region were much longer than development times from egg to C2 Stage. C2 copepodites were also more abundant in 2012 and 2013, when temperatures were coldest in the northeast. This suggests that the overall abundance increases in *C. glacialis* in 2012 and 2013, when temperatures were colder, sea ice melted later in the northeast region, and advection was lower, was primarily due to local reproduction. Abundance increases in the northeast region could also be due to upwelling onto the Chukchi Shelf from the Beaufort Sea (Ashjian et al., 2010). Conversely, the lower abundances of C2 stages in warmer conditions may be a result of faster and earlier development into later stages. Thus the various stages of *C. glacialis* region likely have multiple sources (in situ reproduction and transport from the south and east), and the absolute abundance is a function of local and regional processes. This is a notable result; later stages of *C. glacialis* are known to be the primary prey of bowhead whales around West Greenland (Heide-Jørgensen et al., 2013), and a significant contribution to their diet in the Chukchi and Beaufort seas (Lowry et al., 2004; Moore et al., 2010). In addition, if *C. glacialis* are developing faster, they may enter into diapause earlier creating a mismatch with migrating whales.

The significant differences in pelagic and epibenthic abundance in both mysids and amphipod highlights the importance of sampling near the bottom. Mysids and some amphipod species may spend time in the water column; therefore, sampling the water column and epibenthic layer will yield improved estimates of their abundance. Epibenthic amphipod abundance was significantly higher in 2013 than any other year sampled in this study. This is a notable observation in the context of a changing climate, given that 2013 was also the coldest year and certain species of amphipods, in particular, have known ice-associated and bottom dwelling habits (Vinogradov, 1999; Gradinger and Bluhm, 2004). Both amphipods and mysids are prey for multiple marine mammals, including bearded seals (*Erignathus barbatus*; Cameron et al., 2010), Pacific walrus (*Odobenus rosmarus divergens*; Sheffield and Grebmeier, 2009), beluga whales (*Delphinapterus leucas*; Quakenbush et al., 2015), grey whales (*Eschrichtius robustus*; Nerini, 1984; Darling et al., 1998), and bowhead whales (Lowry et al., 2004). Given the

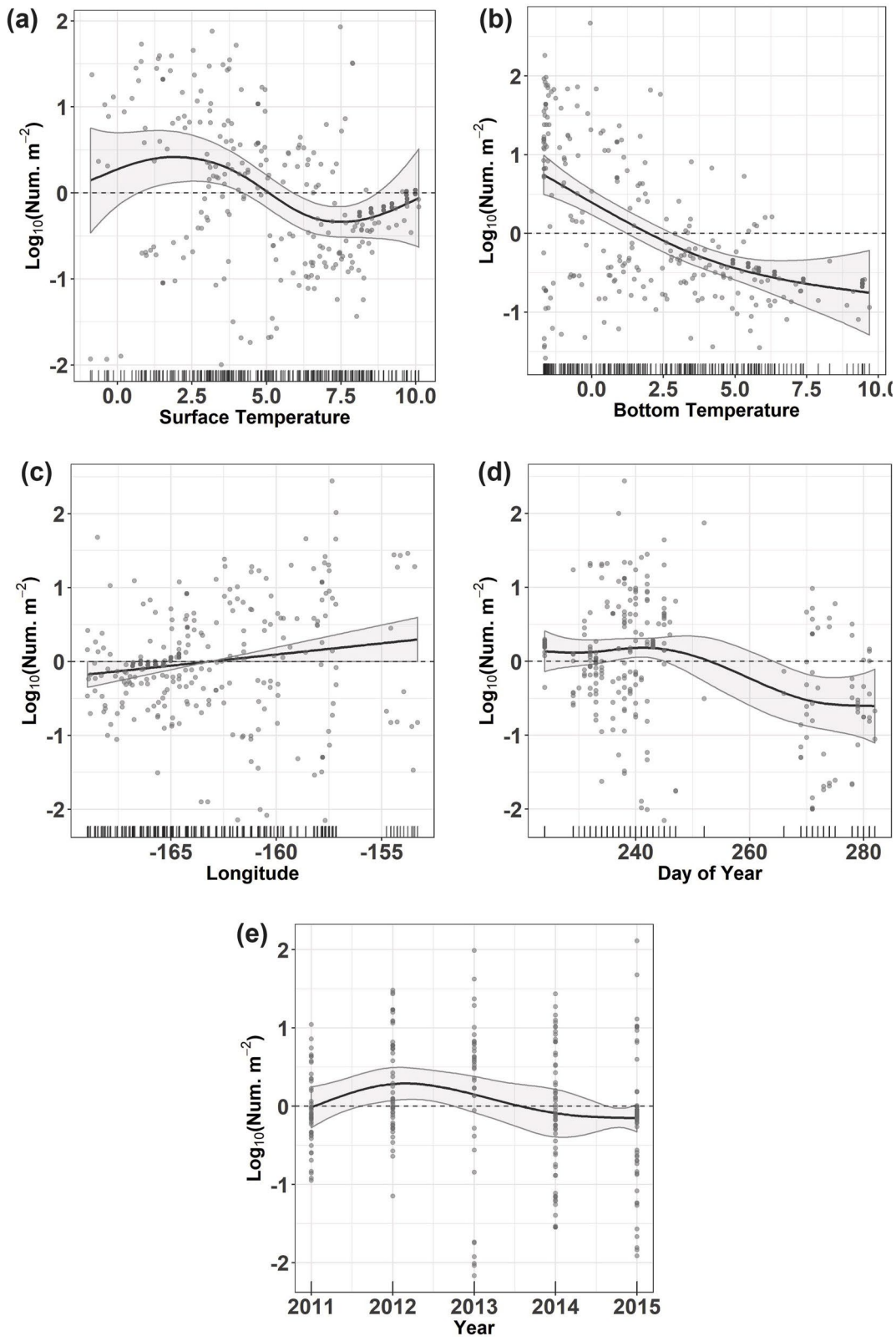

Fig. 13. GAM smooth for the distribution of *Calanus glacialis* C2 stage pelagic abundance (Log_{10}(Num m^{-2})), 2011–2015. Variables included mean surface temperature (a), bottom temperature (b), longitude (c), day of year (ordinal day) (d), and year (e).

importance of mysids and amphipods to Arctic food webs, it is important to monitor their response to changes in ice cover and water temperatures.

4.3. Chukchi Sea large zooplankton status and trends

The findings of this study are relevant to the potential response of lower trophic levels to climate warming, including changes in Arctic

food webs. Recent studies have found a 50% increase in water volume transport through the Bering Strait to the Chukchi Sea from 2001-2014; the immediate impact to the physical environment is an increase in heat flux that is a potential trigger for Arctic sea-ice melt and retreat (Woodgate et al., 2010; 2015; Woodgate, 2018). As the climate warms, increases in primary and secondary production will result in changes in abundance of lipid-rich zooplankton, but it remains to be seen what the overall lipid availability will be (Renaud et al., 2018). Two of the species targeted in this study, *C. glacialis* and *T. raschii*, have an average percent lipid content of approximately 11–15% and 3–5%, respectively, both having a higher average percent lipid content in colder years (Heintz et al., 2013). There is a general consensus that densities of sea ice-associated, lipid-rich *C. glacialis* are expected to decline due to loss of ice in the region. (Tremblay et al., 2012; Grebmeier et al., 2006a; Grebmeier, 2012; Moore and Stabeno, 2015; Renaud et al., 2018). In addition, this study provides evidence that increases in large zooplankton abundance such as euphausiids (which also contain depot lipids) is likely to occur, either via advection from lower latitudes or changes in local production. This is supported by previous studies which found an increase in zooplankton biomass over several decades in the Chukchi Sea (Ershova et al., 2015). An increase in abundance of prey such as euphausiids will likely benefit higher trophic level predators such as planktivorous fish, seabirds and marine mammals. Recently, studies have suggested that the abundance of other planktivores in the northern Bering Sea and Chukchi appear to be changing. For example, in the Bering Sea, there has been a decrease in the lipid-rich nodal species Arctic cod (*Boreogadus saida*) and an increase in the commercial species walleye pollock (*Gadus chalcogrammus*) and Pacific cod (*Gadus macrocephalus*; Stevenson and Lauth, 2019). Walleye pollock have been observed in the Chukchi and Beaufort seas (e.g. Logerwell et al., 2015) and is an important planktivore in the southeastern Bering Sea ecosystem consuming both euphausiids and large copepods (Dwyer et al., 1987; https://access.afsc.noaa.gov/REEM/WebDietData/DietDataIntro.php). Walleye pollock could become an effective competitor for large zooplankton with other fishes, seabirds, and marine mammals if its abundance continues to increase in the northern Bering, Chukchi and Beaufort seas. At present, however, there is evidence of improved body condition of bowhead whales returning from the Beaufort (George et al., 2015). This suggests that the plankton community in their summer feeding grounds has changed in either biomass, species composition or both.

The strong interaction between top-predators (whales, seabirds, and Arctic cod) and copepods/krill in the northern Chukchi appeared to be mediated by both advection and local production related to sea-ice dynamics. What remains to be seen is whether arctic shelf ecosystems will continue to be bottom-up forced by sea-ice dynamics or whether climate-mediated impacts on intermediate trophic levels (e.g. large zooplankton and small fishes) could become the predominant controlling mechanism, e.g. wasp-waist control (Gaichas et al., 2015; Griffiths et al., 2013; Fauchald et al., 2011). If warming continues, the bottom-up dynamics in this location would likely be disrupted by increased advection over longer time-periods as well as a lack of localized, lipid-rich, ice-associated production. Such a shift would greatly impact the trophic dynamics in the region.

5. Conclusions

This study analyzed five successive years of zooplankton abundance over a wide range of physical oceanographic characteristics in the Chukchi Sea to better understand the status and trends in prey availability for baleen whales, seabirds, and planktivorous fish. The coldest year (2013) was highlighted by later summer sea-ice melt, colder sea surface and bottom temperatures, and lower northward transport through the Bering Strait during the spring and summer months. Generally, the warmest years accompanied with earlier summer sea-ice melt, warmer sea surface and bottom temperatures, and higher Bering Strait transport during the spring and summer months. Adult euphausiid abundances differed across warm and cold conditions. These differences appeared most pronounced regionally (NE-SW gradient) and were related to transport, which suggests that most of these euphausiids are transported to the Chukchi Sea from the Bering Sea. The lack of furcilia in 2012 and 2013, (except in the SW), and the presence of furcilia in 2011 and 2014–15, suggests that only in these warmer years with higher advection were earlier stages transported to the northeast region of the Chukchi Sea. We also found that some euphausiids might be locally produced based on the development times. In contrast, the *C. glacialis* C5 stages were found across all years, but C2 stages were found primarily in the northeast and were more abundant under colder conditions which suggests local production of copepods. Thus, the large numbers of euphausiids and copepods that dominate the prey in stomachs of bowhead whales harvested near Utqiagvik, Alaska (Lowry et al., 2004; Ashjian et al., 2010; Moore et al., 2010; George et al., 2015) are likely the result of transport of euphausiids to this location and the contribution of locally produced *C. glacialis,* although *Calanus* found in the region potentially come from several sources or origins.

Declaration of competing interest

The authors declare that they have no known competing financial interests or personal relationships that could have appeared to influence the work reported in this paper.

CRediT authorship contribution statement

Adam Spear: Investigation, Conceptualization, Methodology, Data curation, Formal analysis, Writing - original draft, Visualization. **Jeff Napp:** Investigation, Conceptualization, Methodology, Writing - review & editing, Supervision. **Nissa Ferm:** Data curation, Visualization, Formal analysis. **David Kimmel:** Conceptualization, Methodology, Writing - review & editing.

Acknowledgements

The authors would like to thank Captain Fred Roman, F/V *Mystery Bay*, Captain Kale Garcia, R/V *Aquila*, and Captain/C.O. Robert A. Kamphaus, NOAA ship *Ronald H. Brown*, as well as all crew members. Special thanks also go to Catherine Berchok and Nanci Kachel for their leadership; Bill Floering and David Strausz for assistance at sea, Rebecca Woodgate for suggestions and sharing physical data; the Bering Strait mooring project; Polish Plankton Sorting and Identification Center for processing and enumerating zooplankton samples; and North Pacific Climate Regimes and Ecosystem Productivity (NPCREP) program for support. This research was part of the Chukchi Sea Acoustics, Oceanography and Zooplankton Extension (CHAOZ-X) and Arctic Whale Ecology Study (ArcWEST) which were funded by the Bureau of Ocean Energy Management (BOEM; Contract No. M13PG00026 and M12PG00021). Reference to trade names does not imply endorsement by the National Marine Fisheries Service, NOAA.

References

Ashjian, C.J., Braund, S.R., Campbell, R.G., Gearge, J.C., Kruse, J., Maslowski, W., Moore, S.E., Nicolson, C.R., Okkonen, S.R., Sherr, B.F., 2010. Climate variability, oceanography, bowhead whale distribution, and In˜upiat subsistence whaling near Barrow, Alaska. Arctic 179–194. https://doi.org/10.14430/arctic973.

Ashjian, C.J., Campbell, R.G., Gelfman, C., Alatalo, P., Elliott, S.M., 2017. Mesozooplankton abundance and distribution in association with hydrography on Hanna Shoal. NE Chukchi Sea, during August 2012 and 2013. Deep-Sea Res. II 144, 21–36. https://doi.org/10.1016/j.dsr2.2017.08.012.

Berline, L., Spitz, Y.H., Ashjian, C.J., Campbell, R.G., Maslowski, W., Moore, S.E., 2008. Euphausiid transport in the western Arctic Ocean. Mar. Ecol. Prog. Ser. 360, 163–178. https://doi.org/10.3354/meps07387.

Bond, N., Stabeno, P., Napp, J., 2018. Flow patterns in the Chukchi sea based on an oceano reanalysis. Deep-Sea Res. II 152, 35–47. https://doi.org/10.1016/j.dsr2.2018.02.009. June through October 1979 – 2014.

Brinton, E., 1967. Vertical migration and avoidance capability of euphausiids in the California Current. Limnol. Oceanogr. 12, 451–483. https://doi.org/10.4319/lo.1967.12.3.0451.

Cameron, M.F., Bengtson, J.L., Boveng, P.L., Jansen, J.K., Kelly, B.P., Dahle, S.P., Logerwell, E.A., Overland, J.E., Sabine, C.L., Waring, G.T., Wilder, J.M., 2010. Status review of the bearded seal (*Erignathus barbatus*). U.S. Dep. Commer. NOAA Tech Memo NMFS-AFSC- 211, 246.

Campbell, R.G., Sherr, E.B., Ashjian, C.J., Plourde, S., Sherr, B.F., Hill, V., Stockwell, D. A., 2009. Mesozooplankton prey preference and grazing impact in the western Arctic Ocean. Deep-Sea Res. II 56, 1274–1289. https://doi.org/10.1016/j.dsr2.2008.10.027.

Citta, J.J., Quakenbush, L.T., George, J.C., Small, R.J., Heide-Jorgensen, M.P., Brower, H., Adams, B., Brower, L., 2012. Winter movements of bowhead whales (*Balaena mysticetus*) in the Bering Sea. Arctic 65, 13–34. https://doi.org/10.14430/arctic4162.

Comiso, J., 1999. Bootstrap Sea Ice Concentrations for NIMBUS-7 SMMR and DMSP SSM/I. Digital Media. National Snow and Ice Data Center 10.

Coyle, K., Pinchuk, A., 2002. Climate-related differences in zooplankton density and growth on the inner shelf of the southeastern Bering Sea. Prog. Oceanogr. 55, 177–194. https://doi.org/10.1016/S0079-6611(02)00077-0.

Danielson, S.L., Eisner, L., Ladd, C., Mordy, C., Sousa, L., Weingartner, T.J., 2017. A comparison between late summer 2012 and 2013 water masses, macronutrients, and phytoplankton standing crops in the northern Bering and Chukchi Seas. Deep-Sea Res. II 135, 7–26. https://doi.org/10.1016/j.dsr2.2016.05.024.

Darling, J.D., Keogh, K.E., Steeves, T.E., 1998. Gray whale (*Eschrichtius robustus*) habitat utilization and prey species off Vancouver Island, BC. Mar. Mamm. Sci. 14, 692–720. https://doi.org/10.1111/j.1748-7692.1998.tb00757.x.

Dwyer, D.A., Bailey, K.M., Livingston, P.A., 1987. Feeding habits and daily ration of walleye pollock (*Theragra chalcogramma*) in the eastern Bering Sea with special reference to cannibalism. Can. J. Fish. Aquat. Sci. 44, 1972–1984. https://doi.org/10.1139/f87-242.

Eisner, L., Hillgruber, N., Martinson, E., Maselko, J., 2013. Pelagic fish and zooplankton species assemblages in relation to water mass characteristics in the northern Bering and southeast Chukchi seas. Polar Biol. 36, 87–113. https://doi.org/10.1007/s00300-012-1241-0.

Ershova, E.A., Hopcroft, R.R., Kosobokova, K.N., Matsuno, K., Nelson, R.J., Yamaguchi, A., Eisner, L.B., 2015. Long-term changes in summer zooplankton communities of the western Chukchi Sea, 1945–2012. Oceanography 28, 100–115. https://doi.org/10.5670/oceanog.2015.60.

Fauchald, P., Skov, H., Skern-Mauritzen, M., Johns, D., Tveraa, T., 2011. Wasp-waist interactions in the north Sea ecosystem. PloS One 6, e22729. https://doi.org/10.1371/journal.,pone.0022729.

Gaichas, S., Aydin, K., Francis, R.C., 2015. Wasp waist or beer belly? Modeling food web structure and energetic control in Alaskan marine ecosystems, with implications for fishing and environmental forcing. Prog. Oceanogr. 138, 1–17. https://doi.org/10.1016/j.pocean.2015.09.010.

George, J.C., Druckenmiller, M.L., Laidre, K.L., Suydam, R., Person, B., 2015. Bowhead whale body condition and links to summer sea ice and upwelling in the Beaufort Sea. Prog. Oceanogr. 136, 250–262. https://doi.org/10.1016/j.pocean.2015.05.001.

Gong, D., Pickart, R.S., 2015. Summertime circulation in the eastern Chukchi sea. Deep-Sea Res. II. 118, 18–31. https://doi.org/10.1016/j.dsr2.2015.02.006.

Gradinger, R.R., Bluhm, B.A., 2004. In-situ observations on the distribution and behavior of amphipods and Arctic cod (*Boreogadus saida*) under the sea ice of the High Arctic Canada Basin. Polar Biol. 27, 595–603. https://doi.org/10.1007/s00300-004-0630-4.

Grebmeier, J.M., Harvey, H.R., 2005. The western arctic shelf? Basin interactions (SBI) project: an overview. Deep-Sea Res. II. 52, 3109–3115. https://doi.org/10.1016/j.dsr2.2005.10.004.

Grebmeier, J.M., Cooper, L.W., Feder, H.M., Sirenko, B.I., 2006a. Ecosystem dynamics of the pacific-influenced northern bering and Chukchi seas in the amerasian arctic. Prog. Oceanogr. 71, 331–361. https://doi.org/10.1016/j.pocean.2006.10.001.

Grebmeier, J.M., Overland, J.E., Moore, S.E., Farley, E.V., Carmack, E.C., Cooper, L.W., Frey, K.E., Helle, J.H., McLaughlin, F.A., McNutt, S.L., 2006b. A major ecosystem shift in the northern Bering Sea. Science 311, 1461–1464. https://doi.org/10.1126/science.1121365.

Grebmeier, J.M., 2012. Shifting patterns of life in the pacific arctic and sub-arctic seas. Ann. Rev. Mar. Sci. 4, 63–78. https://doi.org/10.1146/annurev-marine-120710-100926.

Griffiths, S.P., Olson, R.J., Watters, G.M., 2013. Complex wasp-waist regulation of pelagic ecosystems in the Pacific Ocean. Rev. Fish Biol. Fish. 23, 459–475. https://doi.org/10.1007/s11160-012-9301-7.

Heide-Jørgensen, M.P., Laidre, K.L., Nielsen, N.H., Hanson, R.G., Røstand, A., 2013. Winter and spring diving behavior of bowhead whales relative to prey. Anim. Biotel. 1, 15. https://doi.org/10.1186/2050-3385-1-15.

Heintz, R.A., Siddon, E.C., Farley, E.V., Napp, J.M., 2013. Correlation between recruitment and fall condition of age-0 pollock (*Theragra chalcogramma*) from the eastern Bering Sea under varying climate conditions. Deep-sea Res II 94, 150–156. https://doi.org/10.1016/j.dsr2.2013.04.006.

Hirst, A.G., Lampitt, R.S., 1998. Towards a global model of in situ weight-specific growth in marine planktonic copepods. Mar. Biol. 132, 247–257. https://doi.org/10.1007/s002270050390.

Hopcroft, R.R., Kosobokova, K.N., Pinchuk, A.I., 2010. Zooplankton community patterns in the Chukchi Sea during summer 2004. Deep-Sea Res. II 57, 27–39. https://doi.org/10.1016/j.dsr2.2009.08.003.

Hunt, G.L., Ressler, P.H., Gibson, G.A., De Robertis, A., Aydin, K., Sigler, M.F., Ortiz, J., Lessard, E.J., Williams, B.C., Pinchuk, A., Buckley, T., 2016. Euphausiids in the eastern Bering Sea: a synthesis of recent studies of euphausiid production, consumption, and population control. Deep-Sea Res. II 134, 204–222. https://doi.org/10.1016/j.dsr2.2015.10.007.

Kiørboe, T., Hirst, A.G., 2008. Optimal development time in pelagic copepods. Mar. Ecol. Prog. Ser. 367, 15–22. https://doi.org/10.3354/meps07572.

Lane, P.V., Llinás, L., Smith, S.L., Pilz, D., 2008. Zooplankton distribution in the western Arctic during summer 2002: hydrographic habitats and implications for food chain dynamics. J. Mar. Syst. 70, 97–133. https://doi.org/10.1016/j.jmarsys.2007.04.001.

Logerwell, E., Busby, M., Carothers, C., Cotton, S., Duffy-Anderson, J., Farley, E., Goddard, P., Heintz, R., Holladay, B., Horne, J., Johnson, S., Lauth, B., Moulton, L., Neff, D., Norcross, B., Parker-Stetter, S., Siegle, J., Sformo, T., 2015. Fish communities across a spectrum of habitats in the western Beaufort sea and Chukchi sea. Prog. Oceanogr. 136, 115–132. https://doi.org/10.1016/j.pocean.2015.05.013.

Lowry, L.F., Sheffield, G., George, J.C., 2004. Bowhead whale feeding in the Alaskan Beaufort Sea, based on stomach contents analyses. J. Cetacean Res. Manag. 6, 215–223.

Moore, S.E., Stafford, K.M., Munger, L.M., 2010. Acoustic and visual surveys for bowhead whales in the western Beaufort and far northeastern Chukchi seas. Deep-Sea Res. II 57, 153–157. https://doi.org/10.1016/j.dsr2.2009.08.013.

Moore, S.E., Stabeno, P.J., 2015. Synthesis of arctic research (SOAR) in marine ecosystems of the pacific arctic. Prog. Oceanogr. 136, 1–11. https://doi.org/10.1016/j.pocean.2015.05.017.

Nerini, M., 1984. A review of gray whale feeding ecology. The gray whale, Eschrichtius robustus 423–450.

Perovich, D.K., Farrell, S., Gerland, S., Hendricks, S., Kaleschke, L., Meier, W., Ricker, R., Tian-Kunze, X., Tschudi, M., Webster, M., Wood, K., 2019. sea ice [in Arctic Report Card 2019]. http://www.arctic.noaa.gov/reportcard.

Pinchuk, A.I., Eisner, L.B., 2017. Spatial heterogeneity in zooplankton summer distribution in the eastern Chukchi Sea in 2012–2013 as a result of large-scale interactions of water masses. Deep-Sea Res. II 135, 27–39. https://doi.org/10.1016/j.dsr2.2016.11.003.

Pinchuk, A.I., Hopcroft, R.R., 2006. Egg production and early development of *Thysanoessa inermis* and *Euphausia pacifica* (Crustacea: Euphausiacea) in the northern Gulf of Alaska. J. Exp. Mar. Biol. Ecol. 332, 206–215. https://doi.org/10.1016/j.jembe.2005.11.019.

Pinchuk, A.I., Hopcroft, R.R., 2007. Seasonal variations in the growth rates of euphausiids (*Thysanoessa inermis, T. spinifera*, and *Euphausia pacifica*) from the northern Gulf of Alaska. Mar. Biol. 151, 257–269. https://doi.org/10.1007/s00227-006-0483-1.

Questel, J.M., Clarke, C., Hopcroft, R.R., 2013. Seasonal and interannual variation in the planktonic communities of the northeastern Chukchi Sea during the summer and early fall. Continent. Shelf Res. 67, 23–41. https://doi.org/10.1016/j.csr.2012.11.003.

Quakenbush, L.T., Citta, J.J., George, J.C., Small, R.J., Heide-Jørgensen, M.P., 2010. Fall and winter movements of bowhead whales (*Balaena mysticetus*) in the Chukchi Sea and within a potential petroleum development area. Arctic 63, 289–307. https://doi.org/10.14430/arctic1493.

Quakenbush, L., Suydam, R.S., Bryan, A.L., Lowry, L.F., Frost, K.J., Mahoney, B.A., 2015. Diet of beluga whales (*Delphinapterus leucas*) in Alaska from stomach contents, March–November. Mar. Fish. Rev. 77, 70–84.

R Core Team, 2019. R: A Language and Environment for Statistical Computing. R Foundation for Statistical Computing, Vienna, Austria. https://www.R-project.org/.

Randall, R.J., Busby, M.S., Spear, A., Mier, K.L., 2019. Spatial and temporal variation of summer ichthyoplankton assemblage structure in the eastern Chukchi Sea 2010-2015. Polar Biol. 42, 1811–1824. https://doi.org/10.1007/s00300-019-02555-8.

Renaud, P.E., Daase, M., Banas, N.S., Gabrielsen, T.M., Søreide, J.E., Varpe, Ø., Cottier, F., Falk-Petersen, S., Halsband, C., Vogedes, D., Heggland, K., Berge, J., 2018. Pelagic food-webs in a changing Arctic: a trait-based perspective suggests a mode of resilience. ICES J. Mar. Sci. 75, 1871–1881. https://doi.org/10.1093/icesjms/fsy063.

Sameoto, D., Cochrane, N.A., Herman, A., 2011. Convergence of acoustic, optical, and net-catch estimates of euphausiid abundance: use of artificial light to reduce net avoidance. Can. J. Fish. Aquat. Sci. 50, 334–346. https://doi.org/10.1139/f93-039.

Sheffield, G., Grebmeier, J.M., 2009. Pacific walrus (*Odobenus rosmarus divergens*): differential prey digestion and diet. Mar. Mamm. Sci. 25, 761–777. https://doi.org/10.1111/j.1748-7692.2009.00316.x.

Smith, S.L., 1991. Growth, development and distribution of the euphausiids *Thysanoessa raschii* (M.Sars) and *Thysanoessa inermis* (Kroyer) in the southeastern Bering Sea. Polar Res. 10, 461–478. https://doi.org/10.3402/polar.v10i2.6759.

Søreide, J.E., Leu, E., Berge, J., Graeve, M., Falk-Petersen, S., 2010. Timing of blooms, algal food quality and *Calanus glacialis* reproduction and growth in a changing Arctic. Global Change Biol. 16, 3154–3163. https://doi.org/10.1111/j.1365-2486.2010.02175.x.

Spear, A., Duffy-Anderson, J., Kimmel, D., Napp, J., Randall, J., Stabeno, P., 2019. Physical and biological drivers of zooplankton communities in the Chukchi Sea. Polar Biol. 42, 1107–1124. https://doi.org/10.1007/s00300-019-02498-0.

Stabeno, P., Kachel, N., Ladd, C., Woodgate, R., 2018. Flow patterns in the eastern Chukchi sea: 2010–2015. J. Geophys. Res.-Oceans 123, 1177–1195. https://doi.org/10.1002/2017JC013135.

Stevenson, D.E., Lauth, R.R., 2019. Bottom trawl surveys in the northern Bering Sea indicate recent shifts in the distribution of marine species. Polar Biol. 42, 407–421. https://doi.org/10.1007/s00300-018-2431-1.

Teglhus, F.W., Agersted, M.D., Akther, H., Nielsen, T.G., 2015. Distributions and seasonal abundances of krill eggs and larvae in the sub-Arctic Godthåbsfjord, SW Greenland. Mar. Ecol. Prog. Ser. 539, 111–125. https://doi.org/10.3354/meps11486.

Timmermans, M.-L., Ladd, C.. Sea Surface temperature [in Arctic Report Card 2019]. http://www.arctic.noaa.gov/reportcard.

Tremblay, J.-É., Robert, D., Varela, D.E., Lovejoy, C., Darnis, G., Nelson, R.J., Sastri, A.R., 2012. Current state and trends in Canadian Arctic marine ecosystems: I. Primary production. Climatic Change 115, 161–178. https://doi.org/10.1007/s10584-012-0496-3.

Vinogradov, G.M., 1999. Deep-sea near-bottom swarms of pelagic amphipods *Themisto*: observations from submersibles. Sarsia 84, 465–467. https://doi.org/10.1080/00364827.1999.10807352.

Wiebe, P.H., Lawson, G.L., Lavery, A.C., Copley, N.J., Horgan, E., Bradley, A., 2013. Improved agreement of net and acoustical methods for surveying euphausiids by mitigating avoidance using a net-based LED strobe light system. ICES J. Mar. Sci. 70, 650–664. https://doi.org/10.1093/icesjms/fst005.

Wood, S.N., 2011. Fast stable restricted maximum likelihood and marginal likelihood estimation of semiparametric generalized linear models. J. Roy. Stat. Soc. B 73, 3–36.

Woodgate, R.A., Aagaard, K., Weingartner, T.J., 2005. A year in the physical oceanography of the Chukchi Sea: moored measurements from autumn 1990–1991. Deep-Sea Res. II 52, 3116–3149. https://doi.org/10.1016/j.dsr2.2005.10.016.

Woodgate, R.A., Weingartner, T., Lindsay, R., 2010. The 2007 Bering Strait oceanic heat flux and anomalous Arctic sea-ice retreat. Geophys. Res. Lett. 37 (1) https://doi.org/10.1029/2009GL041621.

Woodgate, R.A., Stafford, K.M., Prahl, F.G., 2015. A synthesis of year-round interdisciplinary mooring measurements in the Bering Strait (1990–2014) and the RUSALCA years (2004–2011). Oceanography 28, 46–67. https://doi.org/10.5670/oceanog.2015.57.

Woodgate, R.A., 2018. Increases in the Pacific inflow to the Arctic from 1990 to 2015, and insights into seasonal trends and driving mechanisms from year-round Bering Strait mooring data. Prog. Oceanogr. 160, 124–154. https://doi.org/10.1016/j.pocean.2017.12.007.

Chapter 8: Vertical structure and temporal variability of currents over the Chukchi Sea continental slope

Stabeno, P. J., and McCabe, R.M.

Citation:

Stabeno, P.J. and McCabe, R.M., 2020. Vertical structure and temporal variability of currents over the Chukchi Sea continental slope. Deep Sea Research Part II: Topical Studies in Oceanography, 177, p.104805.doi: 10.1016/j.dsr2.2020.104805.

Deep–Sea Research II 177 (2020) 104805

Contents lists available at ScienceDirect

Deep-Sea Research Part II

journal homepage: http://www.elsevier.com/locate/dsr2

Vertical structure and temporal variability of currents over the Chukchi Sea continental slope

Phyllis J. Stabeno [a,*], Ryan M. McCabe [b]

[a] NOAA Pacific Marine Environmental Laboratory (PMEL), Ocean Environment Research Division, 7600 Sand Point Way NE, Seattle, WA, 98115-6349, USA
[b] Joint Institute for the Study of the Atmosphere and Ocean (JISAO), University of Washington, 3737 Brooklyn Ave NE, Seattle, WA, 98195, USA

A B S T R A C T

Observations from a single mooring site on the northern Chukchi Sea continental slope near the 1000-m isobath are presented. This site was occupied consecutively for three years (spanning September 2014–August 2017). Vertically the flow divides into three depth ranges: the upper ~200 m, ~200—~850 m and near-bottom flow. In the upper ~200 m, the mean flow was northwestward and strongest in the summer months. During winter months, currents decreased in magnitude, and in some years even reversed in direction. Satellite-tracked drifter trajectories (drogue depth ~30 m) show this along-slope flow persists at least from 156 to 165 °W, with an average velocity of ~17 cm s^{-1}. This northwestward flowing current is the Chukchi Slope Current. From ~250 m to ~850 m, the flow reversed; this weak flow is the Arctic-wide cyclonic boundary current advecting Atlantic Water. The mean flow at ~900 m is weak and on an annual time scale not significantly different from 0 cm s^{-1}. It consists of Arctic deep water. In the upper two layers, currents vary on the scale of days to seasons, with short-term reversals common. Currents below 40 m were not significantly correlated with local winds nor wind stress curl. We hypothesize that the northwestward flowing Chukchi Slope Current is a consequence of dynamics associated with the Beaufort Gyre.

1. Introduction

The Chukchi Sea consists of a broad shallow (<80 m) shelf, extending >800 km northward from its southern boundary at Bering Strait to the shelf break bounding the Arctic basin (Fig. 1). Approximately 1 x 10^6 m^3 s^{-1} (1 Sverdrup [Sv]) of Pacific water enters the shelf through Bering Strait (Woodgate et al., 2005a, 2012) and continues generally northward following the bathymetry (Woodgate et al., 2005b). Most of this flow exits the Chukchi Shelf through two canyons—Barrow Canyon in the east (Coachman et al., 1975; Weingartner et al., 2005) and Herald Canyon in the west (Coachman et al., 1975; Pickart et al., 2010). The flow exiting via Barrow Canyon is a combination of the northward flow through Central Channel that joins the coastal flow offshore of Icy Cape. Exiting Herald Canyon, there is a relatively narrow eastward flowing shelfbreak jet (Linders et al., 2017; Corlett and Pickart, 2017; Li et al., 2019).

As Pacific water transits the Chukchi Shelf northward, it is modified through local physical and biological processes. In summer, when sea-ice coverage is marginal or absent, water over the shallow Chukchi Shelf gains heat. A portion of this excess summer heat is advected north from the Bering Sea through Bering Strait (e.g., Woodgate et al., 2012), but the heat gained locally over the Chukchi Shelf through solar radiation can also be substantial (Tsukada et al., 2018). The modified shelf water then flows off the shelf and into the Canada Basin (Shimada et al., 2001; Steele et al., 2004; Watanabe et al., 2017; Fine et al., 2018) where it contributes to the observed accumulation of heat (Timmermans et al., 2014, 2018). Excess subsurface heat, as far west as the Chukchi Abyssal Plain (just to the west of the Chukchi Borderland), was recently identified to have a Pacific origin (Watanabe et al., 2017). Such subsurface heat anomalies can persist for years (Watanabe et al., 2017; Fine et al., 2018) and likely lead to delays in winter freeze-up and an overall decline of sea ice (Steele et al., 2008; Jackson et al., 2012; Timmermans, 2015; Serreze et al., 2016). The pathways of Pacific Water after exiting Barrow Canyon are not well known.

The basin in the vicinity of the Chukchi and Beaufort shelves is influenced by the anti-cyclonic Beaufort Gyre (Aagaard and Carmack, 1989; Regan et al., 2019), which dominates surface flow in the Canada Basin. Along the slope and beneath the Beaufort Gyre is the Arctic Ocean Boundary Current (AOBC; Woodgate et al., 2001), which moves Atlantic water cyclonically around the Arctic basin. The westward flowing Chukchi Slope Current (CSC) resides along the slope from Barrow Canyon to Herald Canyon (Corlett and Pickart, 2017; Stabeno et al., 2018; Li et al., 2019). The recently identified CSC appears to vary seasonally, with the strongest flow in the summer months and weak or even eastward flow dominating in the winter months. From earlier results, it appears to be confined to the upper ~300 m, with an eastward

* Corresponding author.
E-mail address: phyllis.stabeno@noaa.gov (P.J. Stabeno).

https://doi.org/10.1016/j.dsr2.2020.104805
Received 26 August 2019; Received in revised form 8 May 2020; Accepted 23 May 2020
Available online 17 June 2020

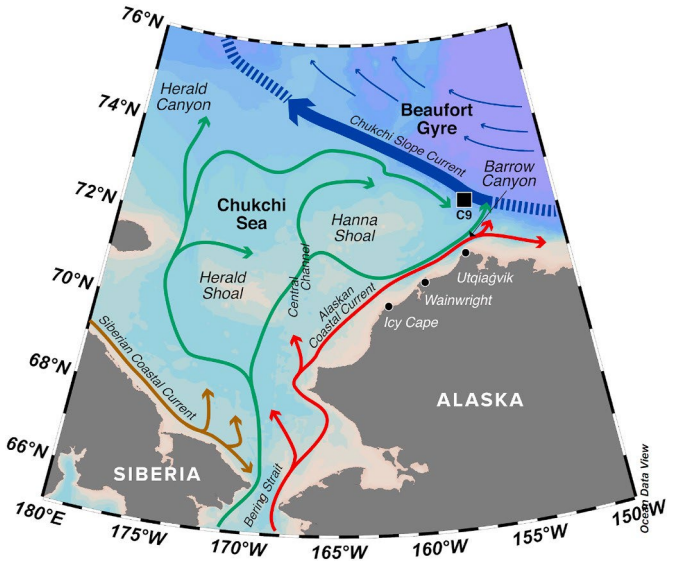

Fig. 1. Schematic map of surface flow patterns over the Chukchi Sea continental shelf and slope (adapted from Stabeno et al., 2018). The location of the C9 mooring, near the 1000-m isobath, is indicated with the black square.

reversal at deeper depths (Stabeno et al., 2018). Analysis by Corlett and Pickart (2017) indicates that it is baroclinically unstable and meanders along the slope. Satellite-tracked drifter trajectories show that the CSC extends from at least Barrow Canyon to near Herald Canyon (Stabeno et al., 2018). Watanabe et al. (2017) used observations and a high-resolution numerical ocean model to demonstrate that Pacific-origin heat gets transported in the CSC as far west as the Chukchi Borderland.

This paper concentrates on a 34-month time series of currents, temperature and salinity collected at a single mooring site on the Chukchi continental slope. A single mooring was deployed in each of three years (2014, 2015 and 2016) in the late summer, near the 1000-m isobath at a site (C9; 72.46°N, 156.55°W) north of Utqiag_ vik (previously Barrow), Alaska. The goal of these deployments was to better understand the flow along the slope and the fate of Chukchi Shelf water exiting Barrow Canyon. Data and handling methods are described in section 2. Results are presented in section 3, including: vertical structure and temporal variability of currents and temperature at C9, relationship of sea ice and winds to flow patterns, variability of Atlantic water and the strength of the AOBC. Section 4 provides a discussion of the results, summary and conclusions.

2. Data sources and methods

2.1. Atmospheric variables

Two different reanalysis products were considered in order to provide a comprehensive record of wind over our region of interest. The first is the European Centre for Medium-Range Weather Forecasts (ECMWF) ERA5 reanalysis (https://climate.copernicus.eu/climate-reanalysis), which is the latest update to the ERA-Interim reanalysis (Dee et al., 2011). Like ERA-Interim, ERA5 solutions are based on a 4D-Var data assimilation routine, but the ERA5 model implements substantial improvements relative to ERA-Interim and includes hourly output at 31 km horizontal resolution (Haiden et al., 2017; Hersbach et al., 2018). At present, no thorough validation exists for ERA5 in the Alaskan Arctic, but we note that an Arctic-focused comparison of seven reanalysis products found that ERA-Interim was among the top-performing models for a number of key parameters (Lindsay et al., 2014). For 10-m winds, which is our focus, ERA-Interim had low biases of $\leq$0.5 m s^{-1} as well as the highest correlations ($\geq$0.85) among the seven different reanalysis models when compared to independent daily-averaged wind records measured from drifting ice stations (Lindsay et al., 2014). Belmonte Rivas and Stoffelen (2019) discuss improvements of ERA5 wind relative to ERA-Interim in comparisons with Advanced Scatterometer satellite wind on a global scale, including a 20% improvement in root mean square wind speed agreement, and reductions in divergence and curl biases; the Arctic, however, was not part of that analysis. Given the model and resolution improvements of ERA5 relative to ERA-Interim, we anticipate model skill that is at least on par with that of ERA-Interim in the Arctic.

The second reanalysis product that we considered is the National Center for Environmental Prediction (NCEP) North American Regional Reanalysis (NARR). It is an extension of the NCEP Global Reanalysis that is run over the North American Region with improvements in both resolution (~32 km) and accuracy (Mesinger et al., 2006). Stegall and Zhang (2012) reported moderate agreement between coastal land- and ocean-based wind observations in northern Alaska and the NARR winds, with correlations of 0.66 for speed and 0.71 for direction. NARR wind variance was close to observed wind variance, but NARR wind speeds were biased low (by as much as 2.5 m s^{-1}). Moore et al. (2008) and Renfrew et al. (2009) reported somewhat better performance in comparisons to buoy and aircraft measurements off southern Greenland (correlations of 0.88 for speed and $\geq$0.92 for direction with a ~1.5 m s^{-1} low bias). NARR data are available eight times daily from 1979 to present. Three-hourly winds at 10 m were obtained from the NOAA Earth System Research Laboratory, Physical Sciences Division in Boulder, Colorado, USA, from their website (https://www.esrl.noaa.gov/psd/).

For both reanalysis products, data spanning 2014–2017 were downloaded and then linearly interpolated onto desired locations or averaged over specific regions as discussed in the text. Because grid-scale noise is present in NARR wind, we first applied a two-dimensional Gaussian filter (standard deviation = 1; 5 grid points wide) to the spatial wind fields before calculating wind stress curl. We then re-gridded the smoothed NARR wind fields onto a regularly spaced 0.2° latitude by 0.6° longitude grid. Wind stress for both NARR and ERA5 was then estimated at each grid point following Large and Pond (1981), and wind stress curl was calculated using a centered-difference approach.

Comparisons with observed wind from the Barrow Atmospheric Baseline Observatory near Utqiag_ vik, Alaska, were also made. Hourly averaged meteorological data recorded at the Barrow Observatory were downloaded from the NOAA ESRL Global Monitoring Division website at https://www.esrl.noaa.gov/gmd/obop/brw/.

2.2. Sea ice

Sea-ice concentration data (2014–2017) used herein were the daily Version 3 Sea-Ice Concentrations from Nimbus-7 SMMR and DMSP SSM/I-SSMIS and were obtained from the National Snow and Ice Data Center (http://nsidc.org/data/nsidc-0079). These data are calculated using NASA's Earth Observing System AMSR-E bootstrap algorithm. Average ice concentrations in a 50 km × 50 km square around the mooring site (72.5°N, 156.5°W) were calculated.

2.3. Moorings

Moorings at C9 were deployed in three consecutive years (spanning September 2014–July 2017) in ~1000 m of water on the Chukchi continental slope northwest of Barrow Canyon (Fig. 1, Table 1). For reference, this site was ~9.8 km offshore of the seaward-most mooring (deployed during the previous year) discussed in Li et al. (2019). Because of the steepness of the slope and the interference of sea ice during deployment, actual C9 bottom depths ranged from 870 m to 970 m. The mooring design included three RCM current meters near ~900 m, ~600 m and ~300 m; an upward looking 75 kHz acoustic Doppler current profiler (ADCP) at a depth of ~300 m; and a Sea-Bird Electronics

Table 1
The duration of deployment, location and bottom depth are indicated in the first column. The instrumentation and depth of instruments are indicated in columns 2–4. MTR refers to miniature temperature recorders.

Deployment/ Recovery Info	Instrument	Measurement	Deployment Depth (m)	Comments
14C9	75 kHz ADCP	Currents	345	16-m bins
10/1/14–9/ 15/15	SBE-37	Temp, Sal	349	
72° 27.5' N	RCM-9	Currents, Temp	350	Inst. at 645 m failed
156° 33.9' W	RCM-11	Currents, Temp	895	
950 m				
15C9	75 kHz ADCP	Currents	372	8-m bins
9/15/15–9/8/ 16	SBE-37	Temp, Sal	382	
72°28.0' N	RCM-9	Currents, Temp	378, 672	
156°33.0' W	RCM-11	Currents, Temp	922	
970 m				
16C9	75 kHz ADCP	Currents	290	16-m bins
9/8/16–8/3/ 2017	MTR	Temp	90, 101, 120, 150, 180, 210, 240, 270	
72°27.8' N	SBE-37	Temp, Sal	45, 460	
156°32.9W	RCM-9	Currents, Temp	311	
870 m	RCM-11	Currents, Temp	467, 822	

(SBE) Microcat near a depth of 400 m (actual instrument depths are listed in Table 1). Additional temperature sensors (miniature temperature recorders or MTRs, and SBE-37 which also measures conductivity) were added in the upper 300 m for the 2016 deployment. Data were collected at hourly intervals except for the ADCP deployed in 2014, which recorded data at 2 h intervals. All instruments were calibrated prior to deployment and data were processed according to manufacturers' specifications. Current meter time series were low-pass filtered with a 35 h, cosine-squared, tapered Lanczos filter to remove tidal and higher-frequency variability, and then resampled at 6 h intervals. Additional analyses were completed using other filters as described in the text (e.g., section 3.4.1). Final processed time series data are accurate to at least $\pm$0.002 °C, $\pm$0.0005 S/m and $\pm$0.5 cm s^{-1} (temperature, conductivity and currents, respectively).

Wavelet analysis was used to examine the dominant frequencies of the low-pass filtered current data. The wavelet function used here was the Morlet wavelet with non-dimensional frequency six, consisting of a sinusoid modulated by a Gaussian. The wavelet power spectra were normalized by the variance of each time series. The 95% significance levels were calculated by comparing each wavelet power spectrum to a red noise background spectrum, modeled as univariate lag-1 autoregressive (AR-1) processes generated with variance equal to that of each time series (Torrence and Compo, 1998).

2.4. Satellite-tracked drifters

From 2012 to 2018, the National Oceanographic and Atmospheric Administration's Ecosystem Fisheries Oceanographic Coordinated Investigations (EcoFOCI) program deployed 45 satellite-tracked drifters in the Chukchi Sea. Drifters were drogued at a depth of 25–35 m using a 10-m long "holey sock" drogue. Each drifter reported position and sea surface temperature via Argos approximately 14 times per day. Data were examined and spurious points were removed by inspection, as were data collected after drogues were lost (as indicated by a sensor), and after drifters grounded or entered into ice (determined from satellite maps of sea-ice extent). The resulting data were linearly interpolated to hourly intervals.

Lagrangian velocities were determined by centered differences using the hourly drifter positions. A low-pass filter (25-h running mean) was applied to the drifter location data. Spatially gridded mean velocities were then calculated following Stabeno and Reed (1994) and Stabeno et al. (2016b). In this analysis, each 2-day period within a grid area was considered an independent estimate. Each rectangular grid cell was 1° latitude by 3° longitude. In addition, three rhomboids of a similar size abutted the slope (Fig. 2).

2.5. Shipboard hydrography

In this paper, temperature and salinity data from a cruise aboard the R/V *Ocean Starr* in late summer 2017 are presented. Conductivity, temperature, depth (CTD) profiles were collected using a Sea-Bird Electronics (SBE) 911*plus* system with dual temperature, conductivity (for salinity) and oxygen (SBE-43) sensors, and single chlorophyll fluorescence (WET Labs WETStar WS3S) and photosynthetically active radiation (PAR; Biospherical Instruments QSP-200 L4S or QSP-2300) sensors. Data were recorded during the downcast, with a descent rate of

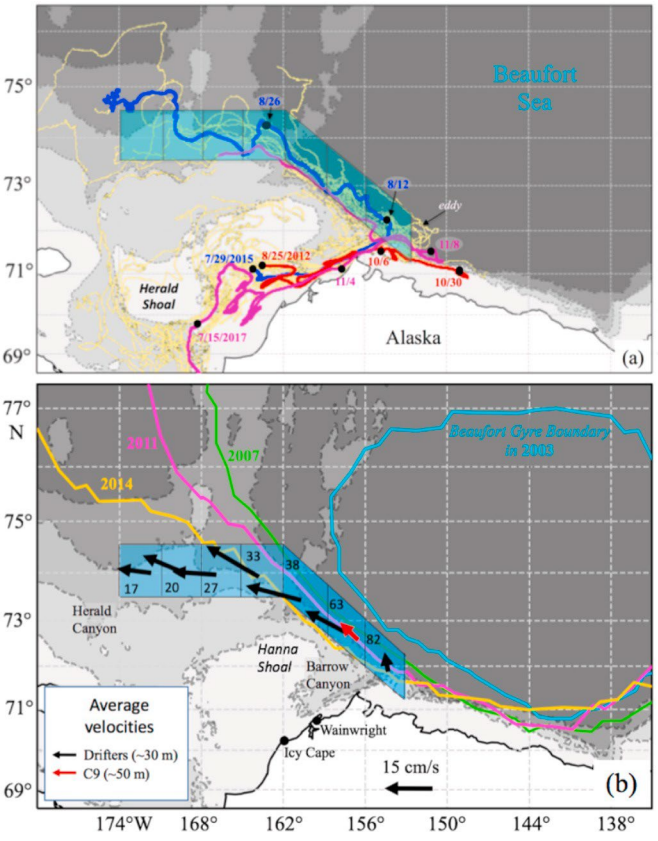

Fig. 2. (a) Drifter trajectories (drogue depth ~30 m). The yellow trajectories indicate drifters deployed in the region. Three pathways are shown in different colors: (1) eastward flow on the Beaufort Shelf (red); (2) first eastward flow and then northwestward flow (magenta); and (3) northwestward flow upon exiting Barrow Canyon (blue). Selected dates are indicated along each trajectory. (b) The position of the edge of the Beaufort Gyre during four different years (adapted from Regan et al., 2019, their Fig. 3). The mean Lagrangian velocity of the drifters in each box (black arrows), with the number of independent estimates that contributed to the mean (black numerals). The red arrow is the mean velocity at ~50 m from the three C9 mooring deployments. (For interpretation of the references to color in this figure legend, the reader is referred to the Web version of this article.)

15 m min^{-1} to a depth of ~30 m, and 30 m min^{-1} at deeper depths. Salinity calibration samples were taken on approximately one-third of the 135 casts and analyzed on a laboratory salinometer. The bottle samples were then used to post-calibrate the CTD data.

In addition to the 2017 R/V *Ocean Starr* data, historical CTD profiles collected aboard a variety of other vessels that were seaward of the shelf-break, within 200 km of the C9 mooring location, and at least 400 m deep are used to describe mean water properties over the Chukchi continental slope. Those historical profiles were taken from the much larger accumulated data set provided by Corlett and Pickart (2017).

3. Results and discussion

3.1. Patterns of variability of flow in the Chukchi Slope Current

3.1.1. Spatial patterns of flow

Trajectories from satellite-tracked drifters (yellow lines Fig. 2a) provide information on general flow patterns during the ice-free season. Drifters deployed in the southern Chukchi Sea (south of 70°N), generally followed one of two trajectories, one northward through Central Channel and the other westward then turning northward through Herald Canyon. Most of the drifters did not enter onto Hanna nor Herald shoals (Fig. 2a). Stabeno et al. (2018) calculated that ~40% of the transport through Bering Strait exits through Barrow Canyon as part of the Alaskan Coastal Current (ACC). The ACC has a buoyant low salinity core, but similar to the Alaska Coastal Current in the Gulf of Alaska (Stabeno et al., 2004, Stabeno et al., 2016), it is wind driven and extends beyond the freshwater core. The strongest transport is in the summer when northward winds dominate the Chukchi Sea. Only about half of the drifters deployed in the Chukchi Sea exited the shelf. The remainder failed to reach the northern boundary before sea ice arrived or before the shifting winds weakened the northward flow. Strong wind-driven reversals are evident in the 2017 (magenta) trajectory (Fig. 2a). It must be noted that except for the low-salinity Alaskan Coastal Water, the water in the ACC is more saline and denser than the melt water that typically resides along the slope. When exiting Barrow Canyon, the ACC water sinks to ~40 m (Stabeno et al., 2018). Thus, once seaward of Barrow Canyon the drifters are not tracking shelf water.

Most of the drifters deployed over the eastern Chukchi continental shelf traveled northward through Central Channel and turned eastward south of Hanna Shoal (Fig. 2; Stabeno et al., 2018). This flow intensifies between Icy Cape and Wainwright into a narrow current (the ACC) that exits the shelf via Barrow Canyon (Stabeno et al., 2018). The trajectories of flow, once the drifters have exited Barrow Canyon, fall into three patterns (Fig. 2a): (1) a sharp westward turn and then continuing along the slope (blue); (2) an eastward turn for a short period (days) followed by a westward trajectory along the slope (magenta); and (3) eastward flow on the Beaufort shelf or along the shelf break (red). Of the 22 drifters that passed through Barrow Canyon, nine followed the first pathway and an equal number followed the second pathway traveling eastward for ~8 days (on average) before turning westward; only four followed the third pathway. The remainder of the 45 drifters that were deployed in the Chukchi Sea did not leave the shelf.

Of the satellite-tracked drifters that joined the westward flowing CSC, most continued northwestward along the slope until sea ice arrived. The remaining drifters ceased transmitting or lost their drogue before the arrival of sea ice. Mean Lagrangian velocities of all of the satellite-tracked drifters that transited along the continental slope were calculated as described in section 2.4, with an integral time scale of 48 h. Velocity was calculated in seven boxes (three rhomboids and four rectangles; Fig. 2). The outflow from Barrow Canyon dominates in the easternmost box. The velocity estimated in this box is biased, because all drifters were deployed on the shelf, so northward flow out of Barrow Canyon dominates the mean flow. The next three boxes (moving westward) all show a well-defined CSC (black arrows, Fig. 2b). Mean velocities from east to west were 14.9 $\pm$ 2.7 (mean $\pm$ standard error), 19.4 $\pm$ 2.5, and 17.3 $\pm$ 2.9 cm s^{-1}, respectively. Fewer drifters survived long enough to travel west of 165°W, and the velocities decreased from 14 $\pm$3.0 to 9.2 $\pm$ 1.6 cm s^{-1} in that region. The mean velocity (at 50 m) from the moorings (red arrow) was weaker than that calculated from the drifters for three reasons. Drogue depths were typically shallower than the uppermost ADCP bin; the Lagrangian velocities were primarily during the summer and early fall months (July–November) when the CSC is at its strongest; and the drifters only entered the CSC when the currents were westward.

The trajectories of drifters in the CSC were often characterized by meanders (wavelength ~100 km). Eddies also were apparent in two trajectories (one is illustrated in Fig. 2a) with radii of 25–50 km. The drifters remained near the slope in a ~70 km wide band, which is similar to the width of the CSC observed by Corlett and Pickart (2017).

It must be noted that the drifter trajectories reveal flow that is limited to the ice-free period. Once entering the ice field the drifters move with the sea ice. A few drifters transmitted locations sporadically during the winter, but most drifters caught in the sea ice were damaged and failed during winter or in spring/summer with the melting of the sea ice.

3.1.2. Temporal variability and vertical structure of flow at C9

Year-long deployments of each C9 mooring were made in late summer of 2014, 2015, and 2016, resulting in 34-month long velocity, temperature and salinity records at a variety of depths (Table 1; Figs. 3–5). During the first two deployments, sea ice arrived in the vicinity of C9 (50 km x 50 km box centered on the mooring site) in October and reached >80% areal ice cover within a month (Figs. 3 and 4, top panels). In the fall of 2016, sea ice arrived a month later in November, with >80% areal cover occurring ~3 weeks later (Fig. 5). Each year, the ice retreat began in June, with areal ice coverage falling below 20% from mid-July to early August.

The current meter records reveal a well-organized flow (Figs. 3–5). In the upper 100 m, the net direction ranged from 300 to 324° (Table 2), which is approximately the along-slope direction at C9. The principal axes were in a similar direction, indicating that most of the variance was also in the along-slope direction. Contours of monthly mean along-slope currents (toward 310°) reveal the mean structure of the surface-intensified CSC (Fig. 6a). During the warm months, the CSC extended to depths of approximately 200–250 m depending on the year, which is consistent with the mean geostrophic description constructed from historical hydrographic profiles by Corlett and Pickart (2017), the modeling results of Watanabe et al. (2017) and the results presented in Li et al. (2019). There was a strong seasonality in the flow, with northwestward flow most common in the warm season, and reversals occurring below 200 m in the cold seasons of 2015 and 2016. September through November of 2016 showed southeastward flow from the surface to at least 500 m (Figs. 5 and 6).

The current measurements deeper in the water column (>250 m) reveal the existence of an along-slope undercurrent that flows southeastward for at least part of the year (Figs. 3–5, Table 2). At C9, daily magnitudes of this southeastward flowing undercurrent were $\leq$10 cm s^{-1}. At ~300 m, there was a strong seasonality in the flow, with northwestward flow during spring shifting to southeastward flow in September 2015, June 2016 and July 2017 (Fig. 6b, solid line).

While the areal sea-ice concentration, and the flow in the upper 200 m and at 300 m all have annual signals, it is not clear that they are related. Depth-averaged flow in the upper 200 m ($V_{0\text{-}200}$) begins to increase before ice retreats in the summer and begins to weaken before the arrival of sea ice in the fall. The relationship between flow in the upper 200 m and at 300 m also appears to be somewhat out of phase, with northwestward flow at 300 m (Fig. 6b, solid line) tending to reverse just as the depth-averaged flow in the upper 200 m reaches its maximum.

On shorter time scales (days to weeks), variability, including flow reversals, was common in both the CSC and the flow below ~200 m (the AOBC; Figs. 3–5). The near-bottom (~900 m) flow was extremely weak during the first two deployments and not statistically different from 0

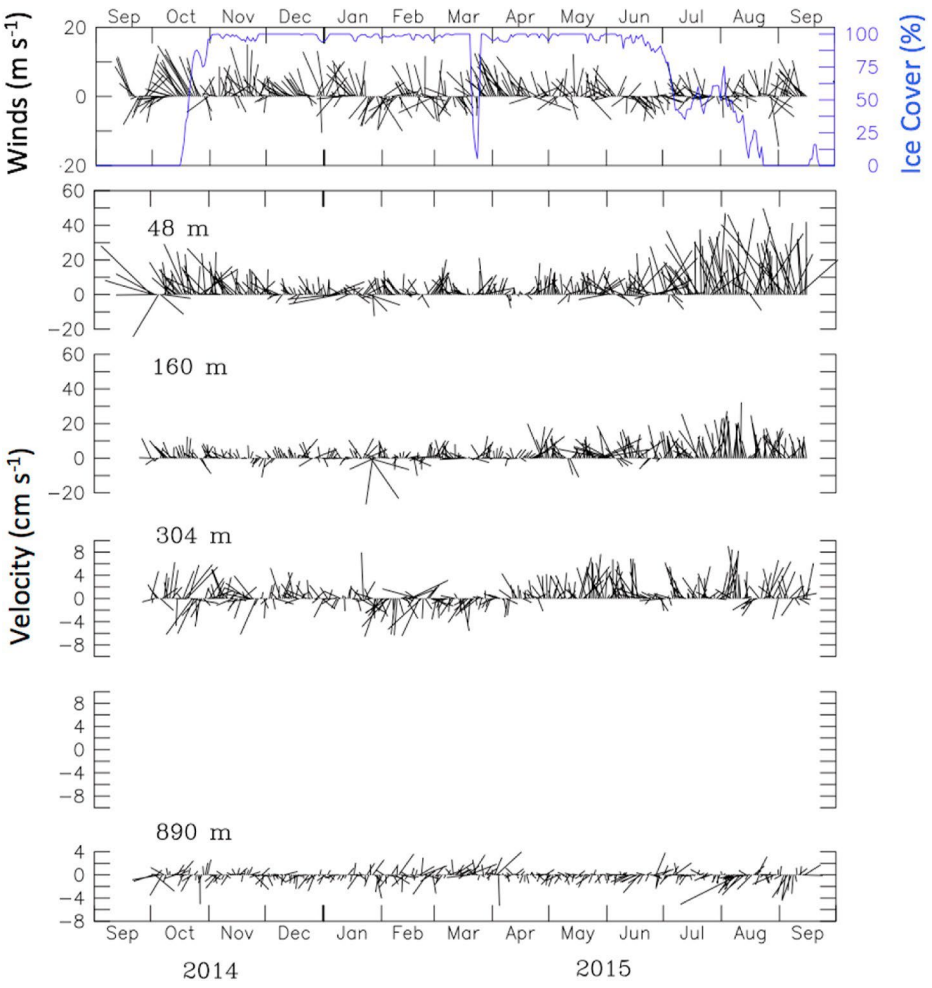

Fig. 3. (top panel) Daily ERA5 wind vectors interpolated onto the C9 mooring location and percent areal ice cover (blue) in a ~50 km x 50 km box centered on C9. (bottom panel) Low-pass filtered current velocities (daily) measured at C9 spanning September 2014–September 2015. The depths of each time series of currents are indicated. Both the wind and velocity were rotated 310° so that upward is approximately northwestward along the continental slope. Note the different velocity scales. (For interpretation of the references to color in this figure legend, the reader is referred to the Web version of this article.)

cm s^{-1}. In the third deployment, the bottom instrument was almost 100 m shallower than during the first two years. During this last year, near-bottom currents were stronger and appeared to be related to the flow above (Fig. 5).

3.1.3. *Vertical variability*

To examine the vertical structure of the currents in more detail, we divide the time series into two parts—the warm (ice free) season (1 July – 31 October) and the cold (ice-covered) season (1 December – 31 May). During the warm season, currents in the upper 200 m were much stronger in 2015 than they were in either of the other years (Fig. 7a). During the cold season, the three years were all comparable (Fig. 7b). A comparison of average flows during the warm and cold seasons shows that currents in the upper 200 m were stronger in the warm season compared to the cold season, as were the reversals below 300 m (Fig. 7c). Reversals were evident below 300 m in the warm season. During the cold season, average currents below 300 m were weak and were not significantly different from zero.

The currents fall into three vertical groups: (1) 0–200 m; (2) 200–850 m; and (3) below 850 m (Fig. 8). Currents in the upper 200 m were well correlated and in phase during each deployment, and the rotation between different depths was near zero. The second vertical group was also in phase and well correlated, with a slightly larger angle of rotation among depths. Currents in groups 1 and 2 were significantly correlated at zero lag, but with a rotation angle of 15–30°. The final group consists of the bottom instrument in the first two deployments. Here the correlations between group 3 and the other two groups were weak, with significant correlation largely limited to group 2. Perhaps more importantly, there was significant rotation of ~140° counter-clockwise and a lag of 2 days between the currents at ~900 m and those at depths >200 m. The third deployment was approximately 70–100 m shallower than the other two deployments and the bottom two depths were significantly, albeit weakly, correlated and in phase with group 2.

This same vertical pattern appears in the empirical orthogonal functions (EOFs) of the along slope component (along 310°) of the time series for each deployment (Fig. 9). There were two significant modes, EOF1 and EOF2. EOF1 accounted for 69%, 51% and 62% of the variability in the 2014, 2015 and 2016 deployments, respectively, and EOF2 accounted for 17%, 33% and 22% of the variability in the 2014, 2015 and 2016 deployments, respectively. EOF1 represents the upper ~250 m of the water column, and EOF2 represents the flow patterns between ~250 and ~850 m. The bottom time series of the 2014 and 2015 deployments were not represented in neither EOF1 nor EOF2 and appeared as a mode by itself that was not statistically significant.

3.2. *Temperature and salinity at the mooring site*

Several water types are recognized on the Chukchi Shelf (Coachman et al., 1975; Gong and Pickart, 2016; Corlett and Pickart, 2017) and are indicated in Fig. 10a. Melt water (MW) results from melting ice earlier in summer. The source of fresh, relatively warm Alaskan Coastal Water (ACW), and the colder more saline Bering Sea Water (BSW) originates in the Bering Sea, entering the Chukchi Sea through Bering Strait. The cold, saline Winter Water (WW) forms locally through cooling and brine rejection during the previous winter. Remnant Winter Water (RWW)

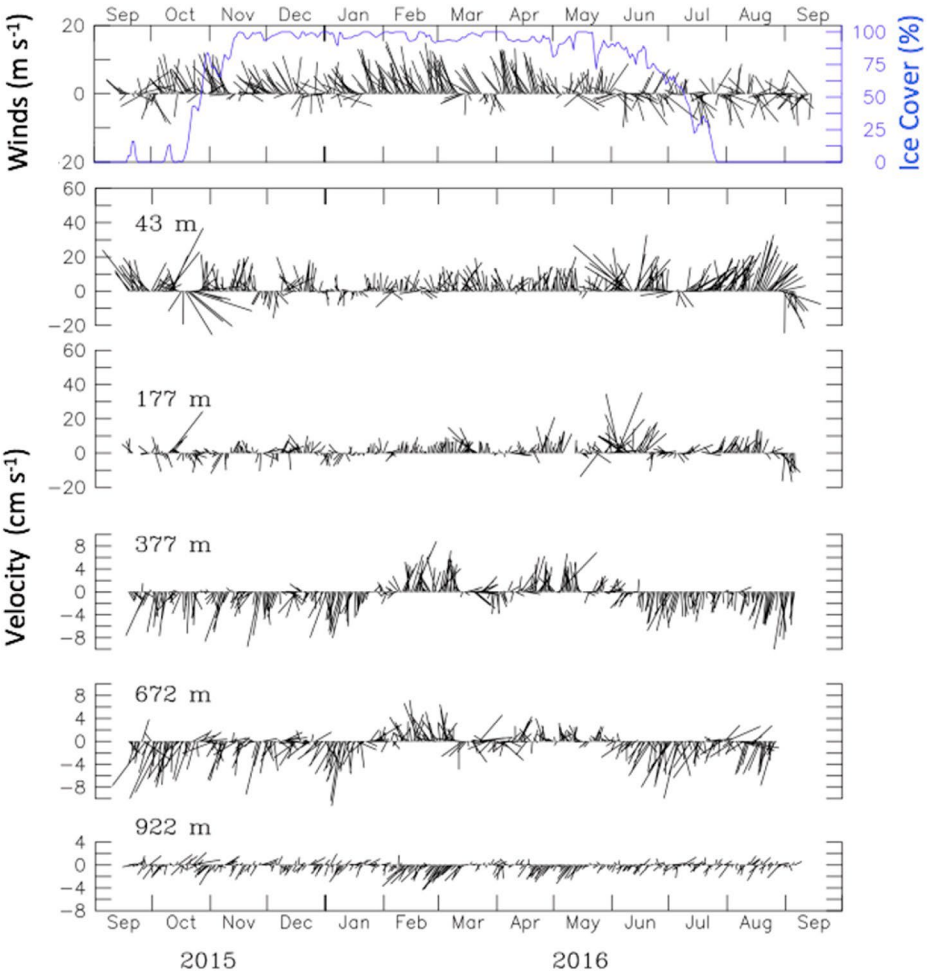

Fig. 4. Same as Fig. 3 except for September 2015–September 2016.

forms as WW warms through heating and mixing processes in the Chukchi Sea. Finally, the relatively warm and saline Atlantic Water (AW) originates in the Atlantic, as its name suggests, flowing cyclonically around the Arctic basin and, occasionally, flows onto the Chukchi Shelf via Barrow Canyon (Bourke and Paquette, 1976; Ladd et al., 2016; Wood et al., 2018; Pisareva et al., 2019).

The C9 data at 45 m in 2016 showed large variability in temperature and salinity, indicating multiple water types (MW, RWW, BSW; cyan dots, Fig. 10a). Salinity varies from <30 to >32, with the least saline water occurring in early December, almost a month after the arrival of sea ice (Fig. 11a), and likely is the result of local ice melt. So, it was not surprising that the water type for this least saline, cold (<-1 ℃) water is categorized as MW (Fig. 10a).

While measurements of salinity were limited to a few depths, in the 2016–2017 deployment 11 temperature sensors were distributed between 45 m and 460 m (Fig. 11b). In the upper 100 m, temperature ranges from −1.8 °C in winter to 3.5 °C in July 2017 after ice retreat (Fig. 10a). Between 100 m and 200 m, there was a band of relatively cold (approximately −1 °C) water. At ~200 m, the temperature begins to increase from approximately −1 °C reaching 0 °C at 258 m ± 10 m (average ± standard deviation) and continuing to warm to a depth of ~400 m. This relatively warm, saline (~0.5 °C, 34.8; Fig. 10b) water below 200 m is Atlantic Water (AW).

Atlantic Water generally inhabits intermediate depths (200–1000 m) over the continental slope in the western Arctic (Corlett and Pickart, 2017). AW contains a large amount of heat (enough to melt all the ice in the Arctic, if it came into direct contact with sea ice; Polyakov et al., 2017). At the C9 location the core of this water mass, with maximum subsurface temperature ~0.65 °C (0.57–0.80 °C) and practical salinities in the range of 34.73–34.86, was consistently found near a depth of 400 m (Fig. 10b) as expected from the historical data (Fig. 10 c–d). The C9 instrument depths varied from 345 m to 460 m dependent upon the year. The 2016 deployment was the deepest (~460 m), and the 2014 deployment was shallowest (~345 m), with the 2015 deployment falling in between (~382 m). All three time series were near the relative maximum in temperature of AW, and varied as expected along the long-term temperature-salinity line. The greatest variability was in the 2014 deployment, which was at the upper edge of the depth of the local temperature maximum. The least variability was at 460 m, while the two shallower instruments showed periods of colder temperatures.

3.3. Temporal variability in the depth of Atlantic Water

To examine the temporal variability in the depth of the warmer Atlantic Water, we chose the 0 °C isotherm (Fig. 11b). There was insufficient vertical instrumentation near 350 m, where the relative maximum of temperature occurs and the water column at the relative minimum (depth <200 m) is influenced by surface processes. The character of the isotherm varies in time. From September through March, there was much higher variability in the depth of the 0° isotherm than later during April–July. This coincides with the variability of the currents (Fig. 5, bottom). At depths shallower than 170 m, prior to mid-March, the currents were highly variable and largely southeastward. This transition was not related to sea-ice cover, since sea-ice cover was extensive (>90%) from mid-January through April (Fig. 5, top).

There are two sharp increases in the depth of the 0 °C isotherm, one

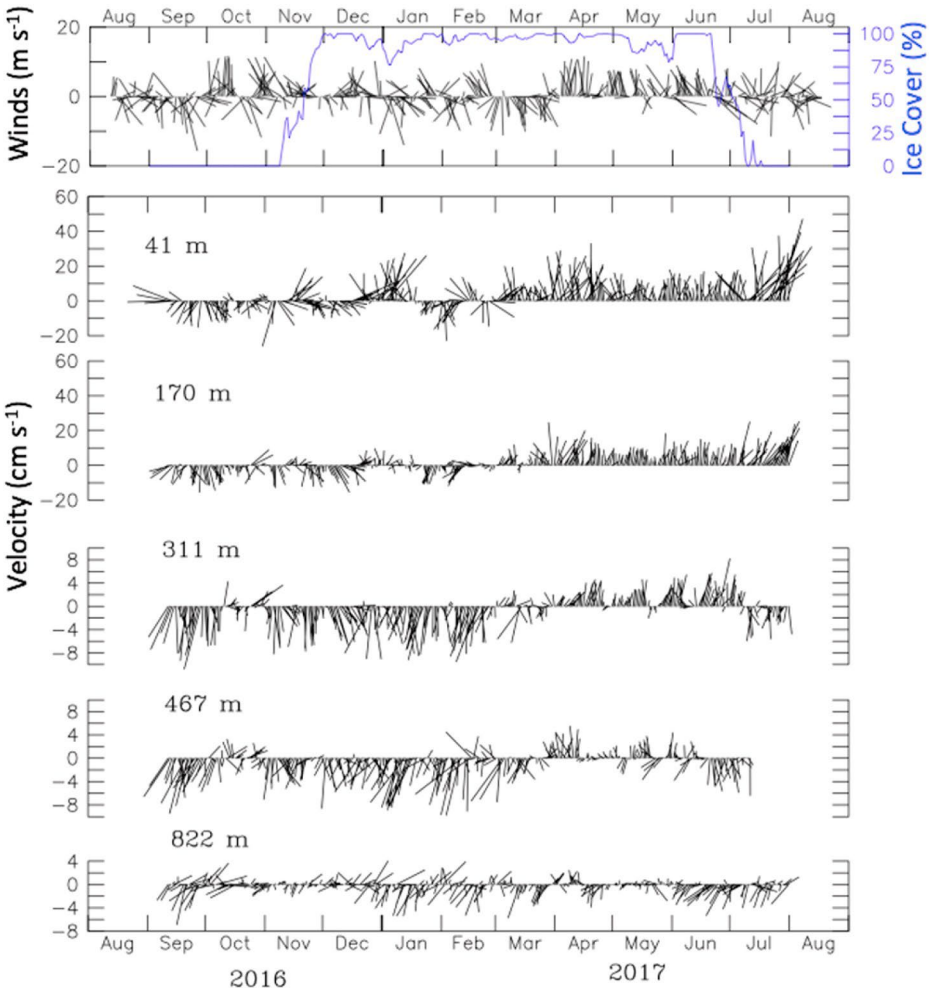

Fig. 5. Same as Fig. 3 except for September 2016–August 2017.

Table 2
Velocity statistics at selected depths distributed through the water column. Maximum speed was calculated from the hourly velocities, while net speed and principal axis were calculated from the low-pass filtered data (35-hr Lanczos).

Mooring	Depth (m)	Maximum Speed (cm s^{-1})	Net speed (Direction) (cm s^{-1} [°])	Prin. Axis (% var) (° [%])
14C9	48	72.1	10.6 (300)	302 (62)
	96	59.1	9.5 (302)	298 (62)
	192	31.1	3.4 (306)	320 (66)
	304	11.5	1.0 (291)	318 (75)
	895	11.4	0.5 (159)	359 (75)
15C9	35	58.6	8.0 (320)	306 (56)
	99	57.8	5.2 (327)	312 (58)
	195	35.9	1.7 (335)	318 (69)
	299	21.6	1.2 (129)	323 (79)
	672	17.0	1.4 (148)	330 (73)
	922	9.1	0.7 (160)	358 (75)
16C9	41	54.5	6.1 (324)	322 (70)
	105	48.7	4.7 (322)	320 (68)
	201	23.1	0.8 (10)	321 (75)
	265	17.4	1.6 (124)	320 (80)
	467	13.2	1.9 (148)	322 (77)
	822	14.4	0.8 (156)	319 (82)

in late October and the second in late December (Fig. 11b). The first event was during a period of no ice and the second during extensive ice cover. Both events had temporal scales consistent with those of longitudinal waves (3–5-day periods; Fig. 12). Interestingly, the greatest depth of the 0° isotherm in October (on the 24th) occurred when the currents were northwestward and the greatest depth of the 0° isotherm in December (on the 27th) occurred when currents were southeastward, but both were during a period of maximum wave amplitude (~20 cm s^{-1}).

Energy in the 3–5 day band is fairly common in the along slope currents at ~240 m (Fig. 13b). It does not appear to be strongly related to the presence of sea ice nor to variations in the winds. At periods >12 days there are only a couple of events in the fall of 2015 and 2016 with significant energy. In contrast, the spectra of the depth-averaged along-slope currents in the upper 200 m appears to be more energetic when sea-ice concentrations are <85% areal coverage (Fig. 13a). There are several periods (e.g. late March 2015) when a sharp decrease in sea ice is associated with an increase in energy at 1–5 days. There also is more energy in the 10- to 20-day band, but once again no significant peaks in energy are present at lower frequencies.

3.4. Forcing mechanisms

3.4.1. Wind

Given the lack of buoy measurements of wind in the Chukchi-Beaufort region, the ECMWF ERA5 reanalysis product was chosen for our analysis. While we also evaluated the NCEP NARR reanalysis,

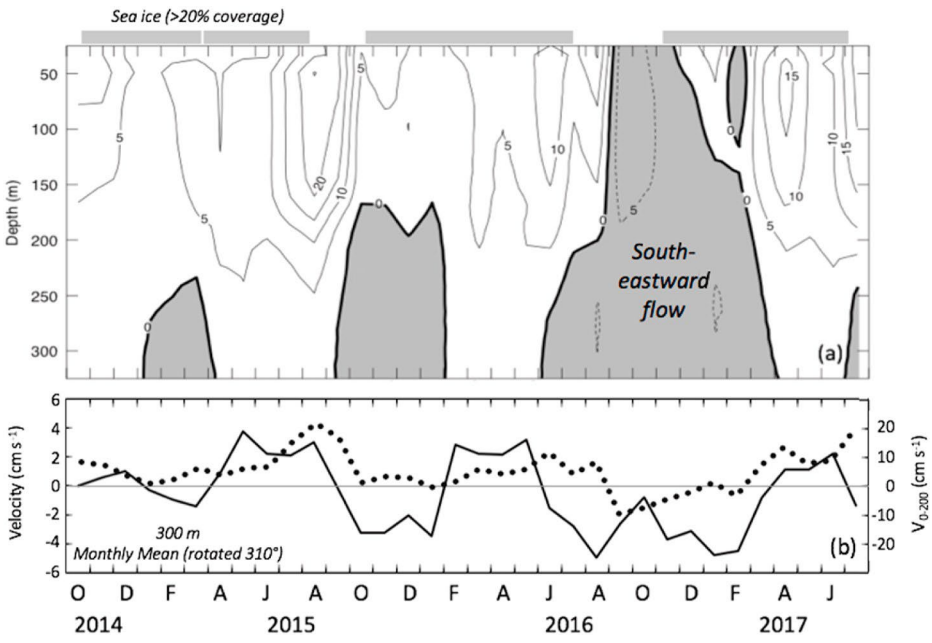

Fig. 6. (a) Contours of monthly mean currents (rotated 310°) measured by the three ADCPs deployed at C9. Positive is approximately northwestward. At the top is the areal sea-ice cover (>20%) in the vicinity of C9. The shaded region represents negative (nominally southeastward) flow. (b) Monthly mean currents at ~300 m (solid line) and depth-averaged velocity, $V_{0\text{-}200}$, in the upper 200 m (dotted line). Positive is northwestward.

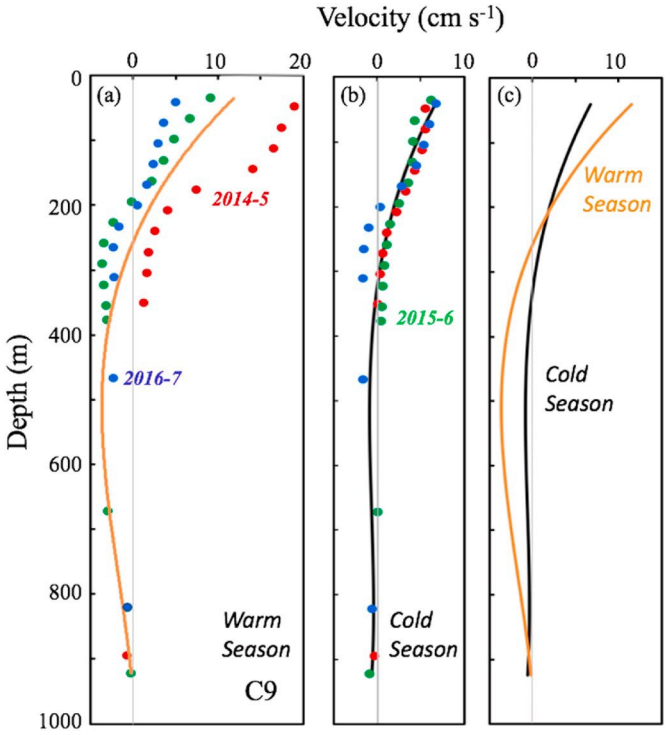

Fig. 7. Mean alongshore flow in (a) the warm season, 1 July – 31 October, and (b) the cold season, 1 December – 31 May. Positive is approximately northwestward (310°). Colored dots represent averages for different deployment years (2014 is red, 2015 is green, 2016 is blue). Solid lines in (a) and (b) represent 3-year seasonal means and are least squares fits of a third-degree polynomial. (c) The 3-year seasonal means are shown separately to facilitate comparison. (For interpretation of the references to color in this figure legend, the reader is referred to the Web version of this article.)

comparisons with observed wind from the Barrow Atmospheric Baseline Observatory near Utqiag_ vik, Alaska, indicated that ERA5 more faithfully reproduced the observations. Zero-lag correlation coefficients for the east-west (north-south) components of 10-m winds spanning the 2014–2017 C9 record were r = 0.96 (0.85) for ERA5 compared to 0.90 (0.70) for NARR. Complex (vector) correlations were r = 0.94 with a 4° clockwise rotation for ERA5 wind compared to observed wind, while NARR wind had r = 0.89 with a 17° clockwise rotation relative to the Barrow observations. As is discussed later, the use of a reanalysis product such as ERA5 further allows for an examination of the spatial structure of the wind field.

We attempted a number of different lagged correlation analyses between both observed and ERA5 winds and the along-slope currents measured at the C9 mooring. For simplicity, we first chose to use currents from the shallowest ADCP bin (52 m, 36 m and 44 m depth for the 2014, 2015 and 2016 deployments, respectively). Correlations between year-long records of low-pass filtered 10-m ERA5 wind interpolated to the C9 location and the low-pass filtered near-surface along-slope current were poor, even when the current was lagged relative to the wind. The highest correlation coefficient (r = 0.36 at zero lag for the cross-slope wind component) was in 2015. This was the year with the shallowest (36 m) current data. Using observed wind or wind stress from the Barrow observatory did not markedly improve the wind-current correlations. Similarly, when we restricted the analysis to the largely ice-free summer season (or conversely to the ice-covered winter season), wind-current correlations remained poor or not significant, despite the ice-free periods generally resulting in stronger relationships. The highest correlation coefficient during an ice-free period was r = 0.46 for the along-slope wind in fall 2014. Correlations between near-surface currents at C9 and remote ERA5 winds at selected sites (e.g. in the East Siberian Sea as suggested by Danielson et al., 2014; Peralta-Ferriz and Woodgate, 2017) were generally lower than with local winds, even with lags.

We next examined wind-current correlations using successively low-frequency filters (5, 10, 15 and 30 day Hanning windows) for both the observed wind and along-slope current records. Again, highest correlations were in 2015, but the values remained low (e.g. r = 0.42 for the cross-slope component of wind with a 15-day Hanning filter applied).

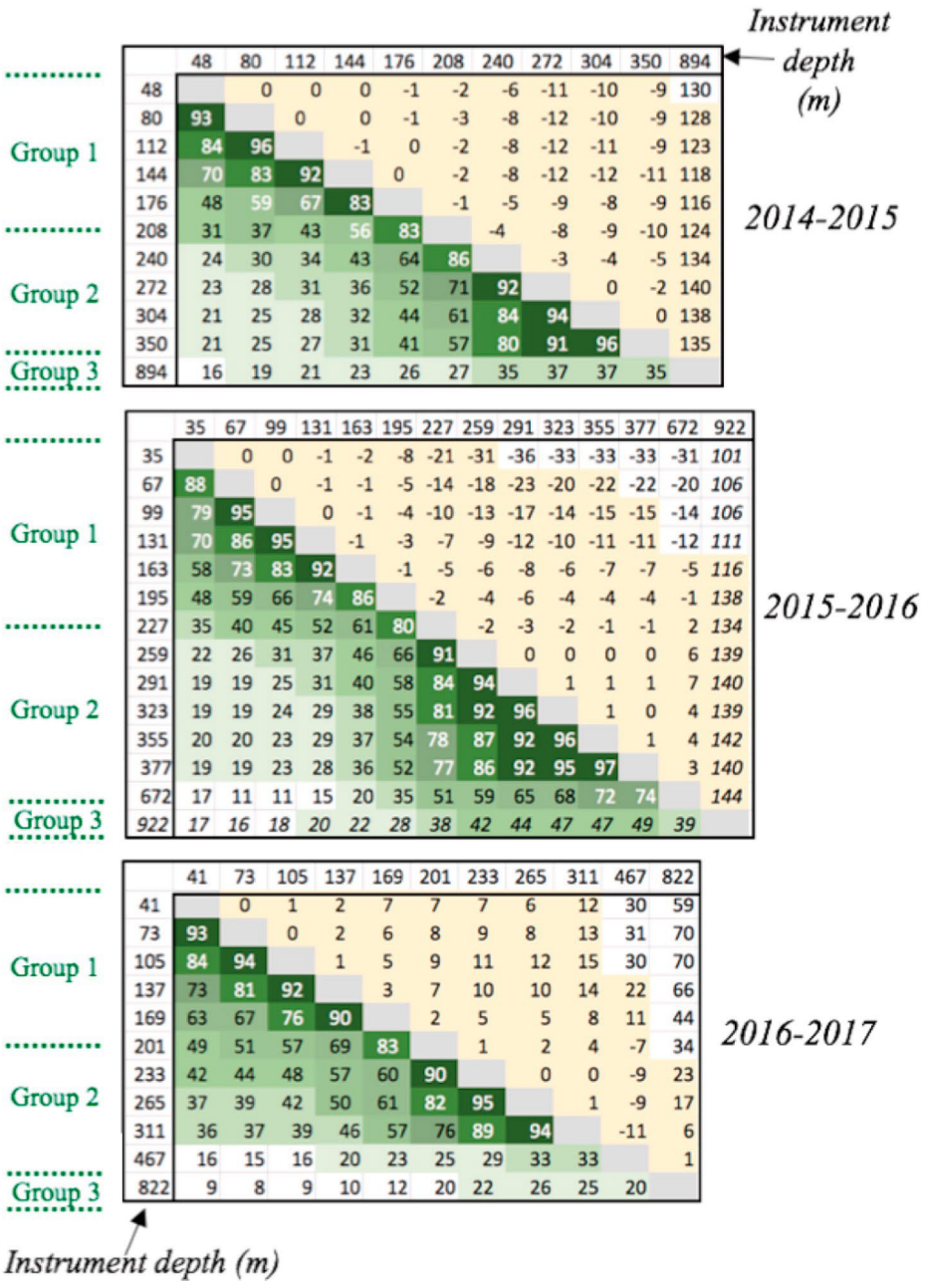

	48	80	112	144	176	208	240	272	304	350	894
48		0	0	0	-1	-2	-6	-11	-10	-9	130
80	93		0	0	-1	-3	-8	-12	-10	-9	128
112	84	96		-1	0	-2	-8	-12	-11	-9	123
144	70	83	92		0	-2	-8	-12	-12	-11	118
176	48	59	67	83		-1	-5	-9	-8	-9	116
208	31	37	43	56	83		-4	-8	-9	-10	124
240	24	30	34	43	64	86		-3	-4	-5	134
272	23	28	31	36	52	71	92		0	-2	140
304	21	25	28	32	44	61	84	94		0	138
350	21	25	27	31	41	57	80	91	96		135
894	16	19	21	23	26	27	35	37	37	35	

	35	67	99	131	163	195	227	259	291	323	355	377	672	922
35		0	0	-1	-2	-8	-21	-31	-36	-33	-33	-33	-31	*101*
67	88		0	-1	-1	-5	-14	-18	-23	-20	-22	-22	-20	*106*
99	79	95		0	-1	-4	-10	-13	-17	-14	-15	-15	-14	*106*
131	70	86	95		-1	-3	-7	-9	-12	-10	-11	-11	-12	*111*
163	58	73	83	92		-1	-5	-6	-8	-6	-7	-7	-5	*116*
195	48	59	66	74	86		-2	-4	-6	-4	-4	-4	-1	*138*
227	35	40	45	52	61	80		-2	-3	-2	-1	-1	2	*134*
259	22	26	31	37	46	66	91		0	0	0	0	6	*139*
291	19	19	25	31	40	58	84	94		1	1	1	7	*140*
323	19	19	24	29	38	55	81	92	96		1	0	4	*139*
355	20	20	23	29	37	54	78	87	92	96		1	4	*142*
377	19	19	23	28	36	52	77	86	92	95	97		3	*140*
672	17	11	11	15	20	35	51	59	65	68	72	74		*144*
922	*17*	*16*	*18*	*20*	*22*	*28*	*38*	*42*	*44*	*47*	*47*	*49*	*39*	

	41	73	105	137	169	201	233	265	311	467	822
41		0	1	2	7	7	7	6	12	30	59
73	93		0	2	6	8	9	8	13	31	70
105	84	94		1	5	9	11	12	15	30	70
137	73	81	92		3	7	10	10	14	22	66
169	63	67	76	90		2	5	5	8	11	44
201	49	51	57	69	83		1	2	4	-7	34
233	42	44	48	57	60	90		0	0	-9	23
265	37	39	42	50	61	82	95		1	-9	17
311	36	37	39	46	57	76	89	94		-11	6
467	16	15	16	20	23	25	29	33	33		1
822	9	8	9	10	12	20	22	26	25	20	

Fig. 8. Complex correlations (below diagonal) and correlation angles (above diagonal) for currents for each of the three mooring deployments: (top) 2014 with 1350 data points; (middle) 2015 with 1372 data points; and (bottom) 2016 with 1200 data points. Instrument depths are in meters. The correlations are color coded from dark (high) to light (low) correlations. Shaded correlations are significant at $p < 0.01$. All lags are zero except for the 922-m record in 2014–15, and the 894-m record in 2015–16. For both of those deployments the deep current record lags the shallower records by 2 days. Divisions into three vertical groups are indicated at the left. (For interpretation of the references to color in this figure legend, the reader is referred to the Web version of this article.)

Unsurprisingly, correlations between ERA5 wind and the 200-m depth-averaged along-slope current, $V_{0\text{-}200}$, over the entire 3-year record (also using 5, 10, 15 and 30-day Hanning window filters) were also poor. Thus, near-surface along-slope flows at C9 do not appear to be significantly correlated with local wind nor with ERA5 wind at select remote sites.

There are specific events, however, in the C9 200-m depth average current record, $V_{0\text{-}200}$, that appear to be in response to local wind forcing (Fig. 14c). For example, the onset of a period of sustained southeastward along-slope flow in September 2016 begins during a reasonably strong southeastward wind event (Fig. 14). Interestingly, such strong along-slope wind events are somewhat rare in the 3-year record, with the September 2016 event being the strongest during an ice-free period. Similarly, the enhancement of northwestward slope flows in April 2017 may be related to the northwestward component of winds at that time. Recall that it is evident from the wavelet analysis (Fig. 13a) that more energy is found in the currents (2–10 day band; 0–200 m average) when areal ice concentrations are <85% and wind can directly force the ocean surface. April through June 2017 was a period of relatively sustained upwelling favorable winds (Fig. 5, top) with corresponding low variability in the depth of 0° isotherm (as mentioned in the previous section; Fig. 11b) and a period of reduced 3–5 day energy in the currents (Fig. 13a). During this time, correlation between the winds and depth of 0° isotherm were significant ($r = 0.48$, $p < 0.01$) with the isotherm depth lagging the winds by 1 day with a decrease in depth of 1.8 m per 1 m s^{-1} increase in wind toward 310° (approximately northwestward). The winds were not well correlated ($r = 0.22$, $p > 0.10$) with the depth of the 0° isotherm for the first part of the record (September 2016–February 2017). We note that Li et al. (2019) also found no correlation between local wind forcing and upwelling events on the Chukchi continental slope at their nearby array site. Watanabe et al. (2017) similarly noted the lack of correspondence between local winds and the current flowing west along the Chukchi Slope in their model.

To briefly summarize, although more synoptic energy (2–10 day

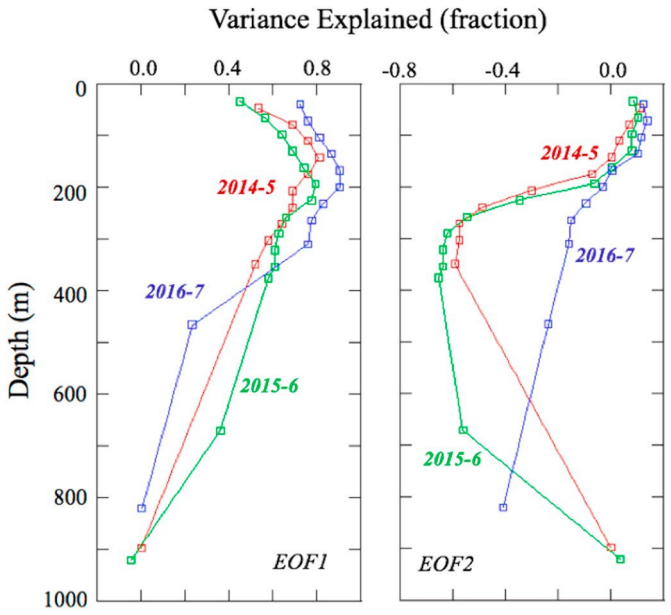

Fig. 9. The first two EOF modes of variability of the along-shelf flow (rotation of 310°) colored by deployment year. The time series were normalized by their respective standard deviations. (a) The fraction of the variance of each time series represented by the first EOF mode (EOF1). (b) The fraction of the variance of each time series represented by the second EOF mode (EOF2). Note that a negative fraction indicates negative correlations between the EOF mode and the time series and positive indicates a positive correlation.

band) is found in the upper water column currents during ice-free periods, on average, local wind does not appear to exert a primary influence on the upper water column along-slope current at the C9 site. Evidence suggests that particularly strong wind events may enhance upper water column currents over the slope, consistent with the findings of Corlett and Pickart (2017). For at least a portion of the C9 data record in 2017, wind influences were instead more readily observed in variation of the depth of the 0° isotherm.

3.4.2. Wind stress curl

Because the C9 mooring was located >100 km from shore, it is unlikely that coastal divergence of surface Ekman transport would be an important mechanism there. Wind stress curl, however, could lead to transport divergence or convergence that, in turn, could drive flow along the continental slope. Using composite averages over multiple northwestward flow events, Li et al. (2019) showed relationships between strong along-slope flows and the wind stress curl averaged over a region of the northeast Chukchi Shelf, suggesting that wind stress curl is a primary forcing agent for strong and weak states of the CSC. Although such extreme states comprised only ~23% of their record, their dominant EOF mode appeared to reflect that variability, suggesting it may be important.

To investigate whether or not wind stress curl impacts currents at C9, we plotted the time variation of mean wind stress curl calculated over a similar portion of the northeast Chukchi Sea shelf (as in Li et al., 2019, Fig. 14a) and compared it with the upper 200-m depth-averaged along-slope current, $V_{0\text{-}200}$, (Fig. 14 d,g). A few characteristics stand out. First, wind stress curl averaged over the northeast Chukchi Shelf is highly variable, often changing sign in as little as three days. On average, the mean wind stress curl is negative, although a few positive events are apparent such as in August 2015, February 2016, and January 2017. Negative wind stress curl over the northeast Chukchi Shelf would lead to flow convergence and geostrophic sea level set-up. Interestingly, high sea level over the shelf (relative to sea level offshore) would tend to force southeastward along-shelf/slope flow, which is opposite to the mean northwestward flow observed at the C9 location (Fig. 14g) and as previously observed for the CSC (Corlett and Pickart, 2017; Stabeno et al., 2018; Li et al., 2019). Thus, on average, it does not appear that the mean wind stress curl over the northeast Chukchi Shelf is itself adequate to explain the observed northwestward flowing CSC at the C9 site. Still, as with some of the wind events described earlier, and in agreement with Li et al. (2019), there is a suggestion of a relationship between portions of the wind stress curl record and the mean along slope currents. For instance, the current decreases and briefly turns southeastward in October and December 2015 when the wind stress curl is strongly negative. Similarly, the current increases to the northwest in early January 2017 when the wind stress curl is significantly positive. Other

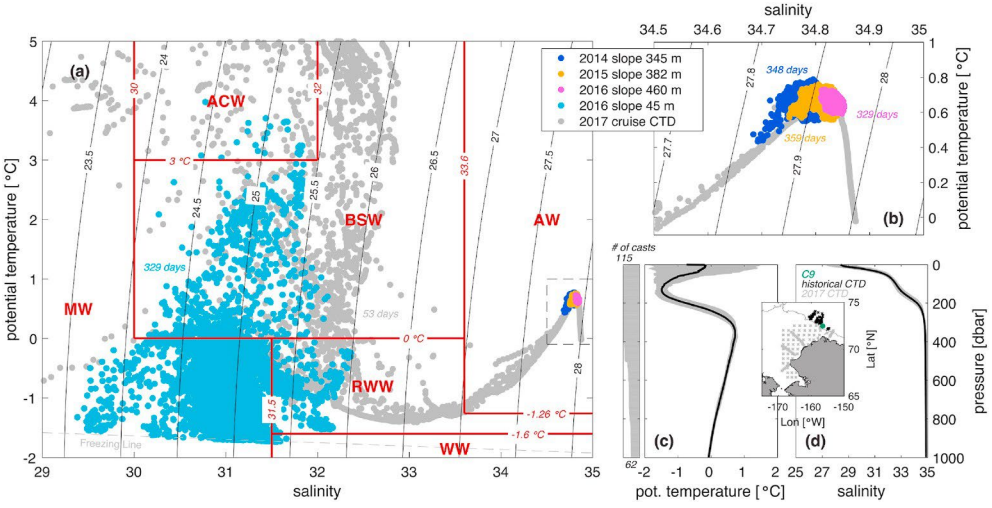

Fig. 10. (a) Potential temperature–salinity diagram, with potential density contours in black, for the Chukchi Shelf and continental slope. Red lines indicate nominal water mass boundaries (after Corlett and Pickart, 2017), and include: melt water (MW), Alaskan Coastal Water (ACW), Bering Sea Water (BSW), Winter Water (WW), Remnant Winter Water (RWW) and Atlantic Water (AW). Hydrographic data from a summer 2017 cruise are shown (gray) for context, with data (45 m) at C9 in 2016–2017 (cyan). Three years of moored data near the core depth of the AW are colored by deployment year, which is expanded in (b). The mean (c) potential temperature and (d) salinity profiles near the C9 location from historical profiles are drawn in black; gray shading represents the standard deviation. The number of profiles used to construct the means is shown to the left of (c). The inset map shows the locations of: C9 (green); the 2017 cruise data (gray) used in (a) and (b); and the historical profiles (black) used to calculate (c) and (d). (For interpretation of the references to color in this figure legend, the reader is referred to the Web version of this article.)

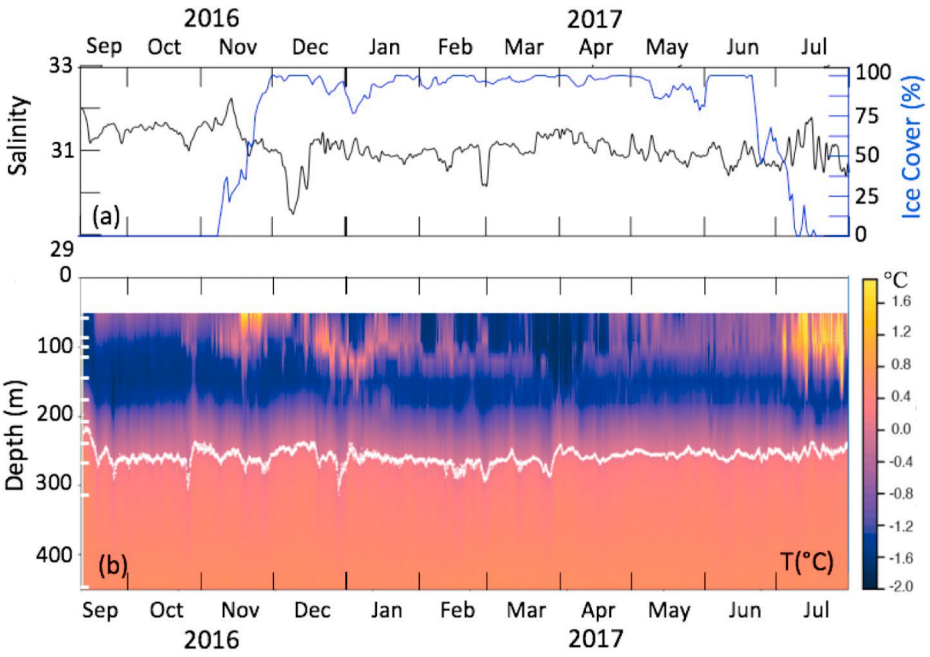

Fig. 11. (a) Time series of salinity at 45 m (black) and the daily percent ice cover (blue) in a 50 km x 50 km box centered at C9. (b) Contours of temperature at the C9 mooring spanning 50–450 m depth from September 2016 to July 2017 (color). Depth of the 0° isotherm is overlaid (white contour). Instrument depths are indicated by the white bars at the left. (For interpretation of the references to color in this figure legend, the reader is referred to the Web version of this article.)

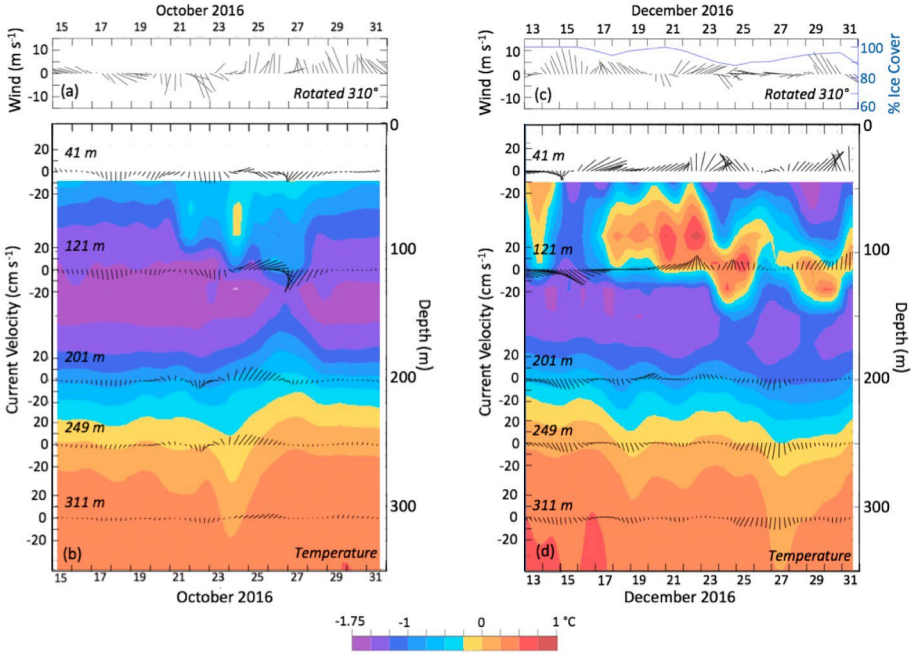

Fig. 12. (a) ERA5 winds at C9, and (b) contours of ocean temperature (color) and current velocity (vectors) at indicated depths during 15–31 October 2016. No ice was near C9 in October. (c) As in (a) during 13–31 December 2016, with percent ice cover indicated in blue. (d) As in (b) except for 13–31 December 2016. The currents are low pass filtered and rotated 310° (upward is approximately northwestward) and ice is percent cover in the 50 km x 50 km box centered on C9. (For interpretation of the references to color in this figure legend, the reader is referred to the Web version of this article.)

events exist, however, that defy such a simple one-to-one explanation. The strengthening of the current in July 2015, a time when the wind stress curl over the northeast Chukchi Shelf was in opposition, is not clearly explained by shelf-average curl. Also, the positive current events spanning June–August 2016 do not appear to be related to wind stress curl over the shelf.

An examination of monthly averaged spatial patterns of wind and wind stress curl throughout the region suggests the possibility of large gradients in wind stress curl near the Chukchi continental slope (not shown); in some cases, positive/negative wind stress curl over the shelf was accompanied by negative/positive wind stress curl offshore. Thus, the induced across-slope geostrophic sea level gradient could potentially be enhanced or diminished as a result of changes in the sign of the wind stress curl across the continental slope. To test this possibility, we averaged wind stress curl over two adjacent boxes: one including a small region of the Chukchi Shelf west of Barrow Canyon parallel to the continental slope, and the other immediately offshelf including the continental slope (Fig. 14a). The difference in mean wind stress curl over these two boxes (shelf value – offshelf value) is illustrated in Fig. 14e. The mean wind stress curl difference is negative, meaning that the wind stress curl induced geostrophic sea level in the offshore box is higher than that over the shelf box (ignoring any otherwise pre-existing shelf-

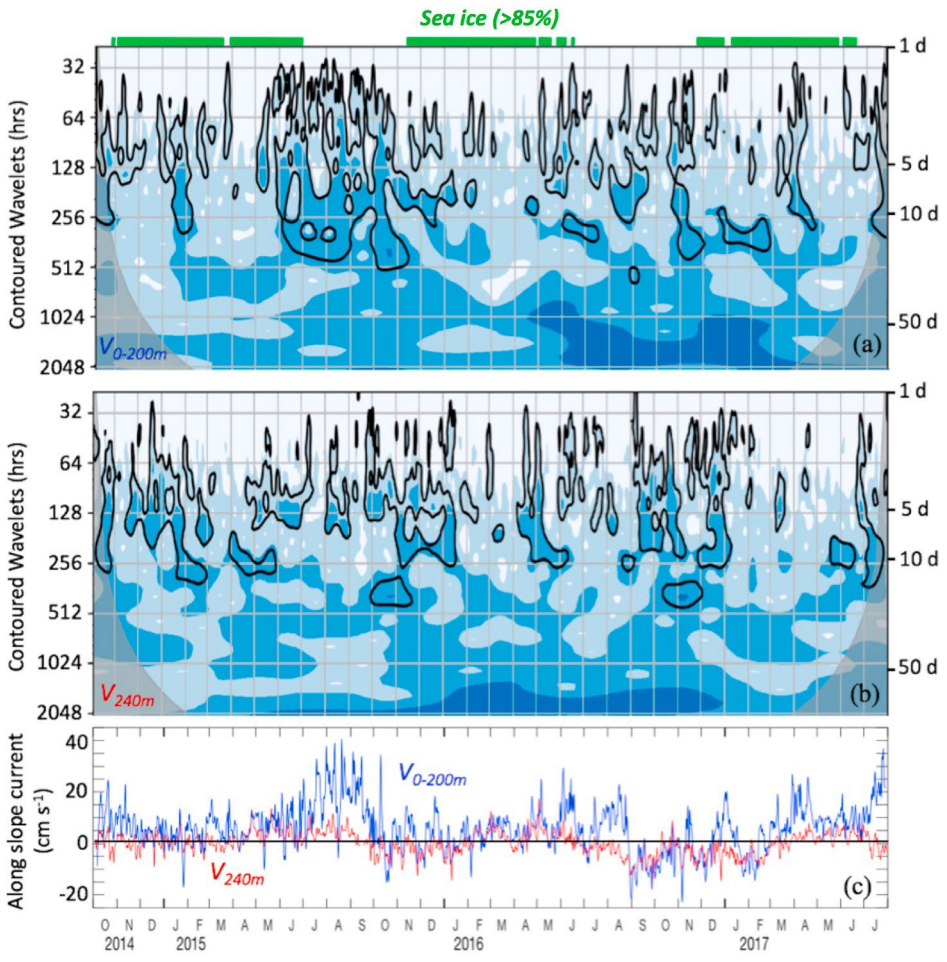

Fig. 13. Wavelet analysis for (a) along slope (rotated 310°), depth average (0–200 m) flow at C9, and (b) along-slope flow at ~240 m for October 2014–July 2017. The blue-shaded contours are quartiles. Closed black contours denote peaks of significant energy. Areal sea-ice concentration (>85%) in a 50 km x 50 km box centered on C9 is indicated in green above (a). (c) Time series used to create (a) and (b) are shown. (For interpretation of the references to color in this figure legend, the reader is referred to the Web version of this article.)

slope sea level gradient), a condition that would favor the northwestward flowing CSC. There is also the suggestion of correspondence between events in the wind stress curl difference and the mean along slope currents. For example, the along-slope current is strong from August through September 2015 when the curl difference is favorable, and then decreases as the curl difference changes sign in late September 2015. A similar series of events occurred during fall 2016. Nevertheless, correlation between the shelf-offshelf curl difference and the 200-m depth-averaged current remains poor over the entire record, even when considering low-pass filtered time series (Fig. 14e, g).

3.4.3. The Beaufort Gyre

The Beaufort Gyre (BG) is a relatively shallow (~250 m), anticyclonic circulation that dominates the Canadian Basin and is driven by the Beaufort Sea High pressure system (e.g. Giles et al., 2012; Moore, 2012). The low salinity (<30) core of the BG sits above more saline Atlantic Water. It is of interest that the depth of the BG along its edge shoals to ~200 m (Doddridge et al., 2019; see their Fig. 1), which is the depth between our observed current groups 1 and 2 discussed in section 3.1.3. The size and strength of the gyre varies on seasonal through interannual time scales. Using sea surface height data from satellite altimetry during the period 2003–2014, the area of gyre and its strength were greatest in the fall and smallest in the summer (Regan et al., 2019). In addition, the size and strength of the BG increased during this time period. Although care must be taken in interpreting dynamic ocean topography near shore and complex bathymetry, it is noteworthy that the edge of the gyre extends in recent years along the continental slope from 130°W westward to the Chukchi Borderland (Fig. 2b).

The location of C9 is at the southern edge of the BG, so it could be argued that the currents measured at C9 are likely related to the BG. The largest slope of dynamic ocean topography is in the region of C9 westward to the Chukchi Borderland (Regan et al., 2019; see their Figs. 4 and 5), where the outer edge of the gyre crosses lines of latitude. This is reminiscent of a western boundary current. Here the bathymetry of the shelf crosses lines of latitude effectively reducing the strength of β, the rate of change of the Coriolis parameter (f) with latitude, to ~20% of its value at a latitude of 45°. Yang et al. (2016) suggest that even though β is small at these latitudes a western boundary current could be supported. Since the BG is driven by the large-scale wind stress curl it is possible that variability in upper 200-m depth-averaged current at C9 would also be related to variability in the basin-scale wind stress curl. A time series of wind stress curl averaged over the Canada Basin is illustrated in Fig. 14f. As with other wind metrics, correlation of this low-pass filtered quantity with low-pass filtered currents was poor ($r = 0.12$ at 37-day lag with a 30-day Hanning filter applied). We also attempted to correlate the currents with running cumulative sums of basin-averaged curl (e.g. summations over 60 days and 90 days), but this too gave similarly poor results.

3.4.4. The Alaskan Coastal Current exiting Barrow Canyon

Using both an idealized model and the year-long moored array observations of Li et al. (2019), Spall et al. (2018) found a relationship between flow in Barrow Canyon and the CSC, with monthly-averaged CSC transport lagging the transport through Barrow Canyon by roughly 2–3 months. Using the Barrow Canyon transport and velocities measured at C9, our results are more ambiguous.

The mean northeastward flow out of Barrow Canyon is ~0.5 Sv (Itoh et al., 2013; Stabeno et al., 2018), with a seasonal signal. The monthly

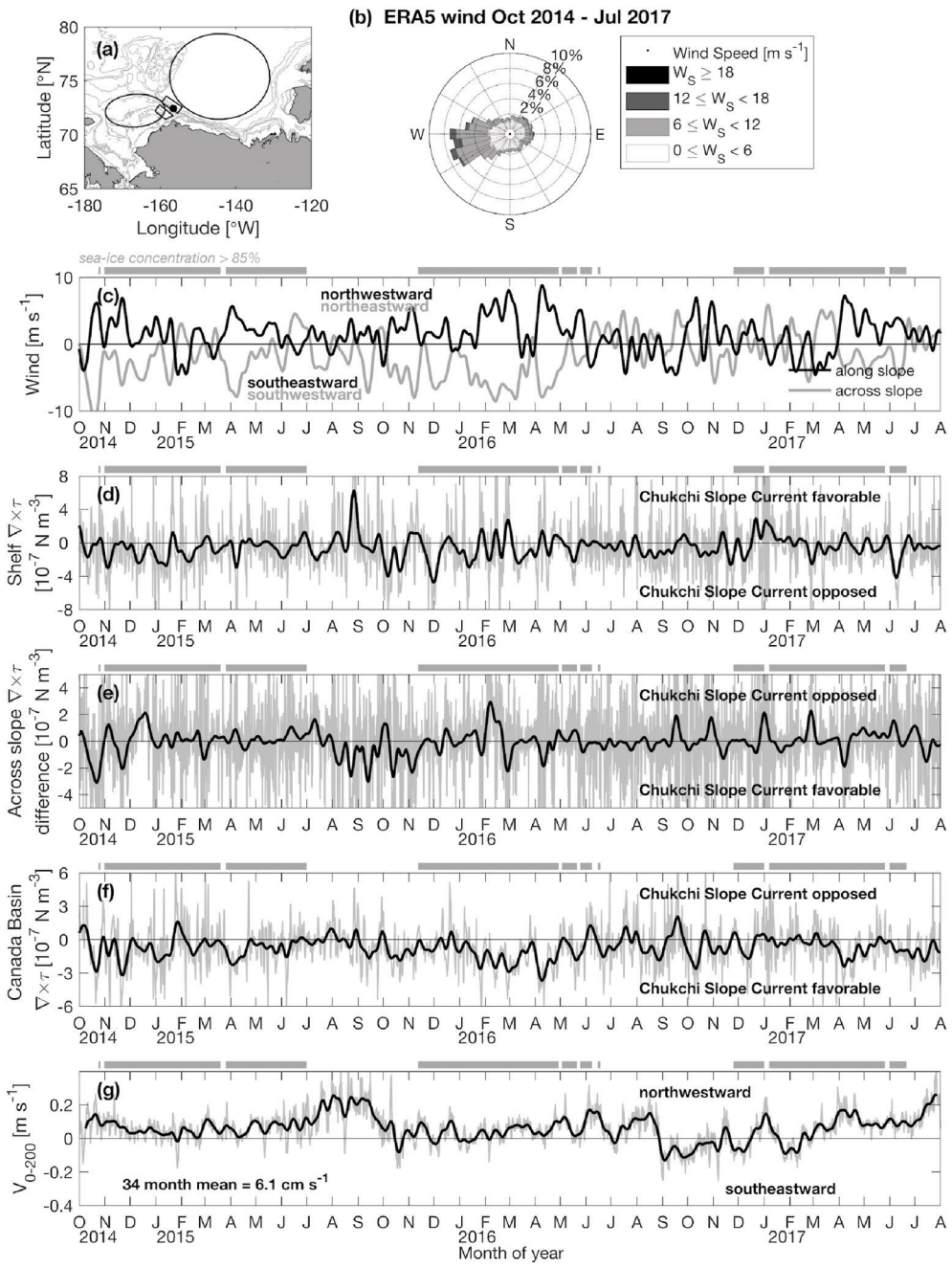

Fig. 14. (a) Map of the Chukchi Sea with the location of the C9 mooring (black dot) and the regions over which wind and wind stress curl were averaged. (b) Histogram of hourly 10-m ERA5 wind averaged over the offshore rectangle encompassing C9 in (a). Wind blows toward the direction indicated. (c) Along- and across-slope components of 10-m ERA5 winds (rotated 310°). Values were averaged over the offshore box encompassing C9 as shown in (a) and low-pass filtered with a 15.5 day Hanning window. (d) Wind stress curl (gray) calculated from the hourly ERA5 winds averaged over the ellipse spanning the northeast Chukchi Sea in (a), and low-pass filtered with a 15.5 day Hanning window (black). (e) Across slope difference of wind stress curl, as a proxy for an across slope sea-surface deformation, calculated from averages over the offshore and shelf boxes in (a). The hourly ERA5 data are gray and the 15.5-day Hanning window filtered time series is black. (f) ERA5 wind stress curl averaged over the Canada Basin as indicated by the large black circle in (a). Hourly values are gray and the 15.5-day Hanning window filtered values are black. (g) The upper 200 m depth average along-slope current measured by the C9 mooring (hourly values - gray, 15.5-day Hanning window filtered values - black).

mean transports in Stabeno et al. (2018) were calculated from hourly currents measured at three mooring sites located off Icy Cape. The number of instruments available varied from three ADCPs deployed in September 2010, 2016, 2017 and 2018 to only one instrument at the central site in 2012. Details of the calculations can be found in Stabeno et al. (2018). The monthly mean northeastward transport along the Chukchi Shelf is strongest in the summer months and weakest in the winter months. As the flow exits Barrow Canyon much of it continues northwestward in the CSC, while a smaller portion turns east forming the Beaufort shelf break current (Nikolopoulos et al., 2009). There is a significant correlation between the monthly mean transport in Barrow Canyon and the upper 200-m depth-averaged velocity, $V_{0\text{-}200}$, observed at C9 ($r = 0.5$, $p < 0.01$; Fig. 15). This significant correlation, however, is a result of six individual months during which the flow in the CSC is above average (Fig. 15a). That is, when monthly mean flow in the CSC is strong, the transport exiting the shelf through Barrow Canyon is also strong. There are even more instances, however, when the Barrow Canyon transport is just as strong yet the monthly averaged flow in the CSC is weak (<10 cm s^{-1}).

As alluded to above, we do not observe a 2–3 month lag between the peaks of monthly-averaged Barrow Canyon transport and currents at C9, although the variability in our record is substantial (Fig. 15). Given an approximate distance of 100 km from Barrow Canyon to the C9 mooring, currents leaving Barrow Canyon should pass the C9 location in 6–17 days, assuming typical speeds of ~6 cm s^{-1} from C9 (Fig. 14g) and ~15 cm s^{-1} from the drifters (drogue depth ~30 m; Fig. 2b).

Thus, using the C9 and Icy Cape current observations the flow out Barrow Canyon does not appear to drive the CSC. Once again there does appear to be an intermittent relationship between possible forcing mechanisms and the magnitude of flow at C9. While the ACC does not drive the CSC, it is a major contributor as discussed in the next section.

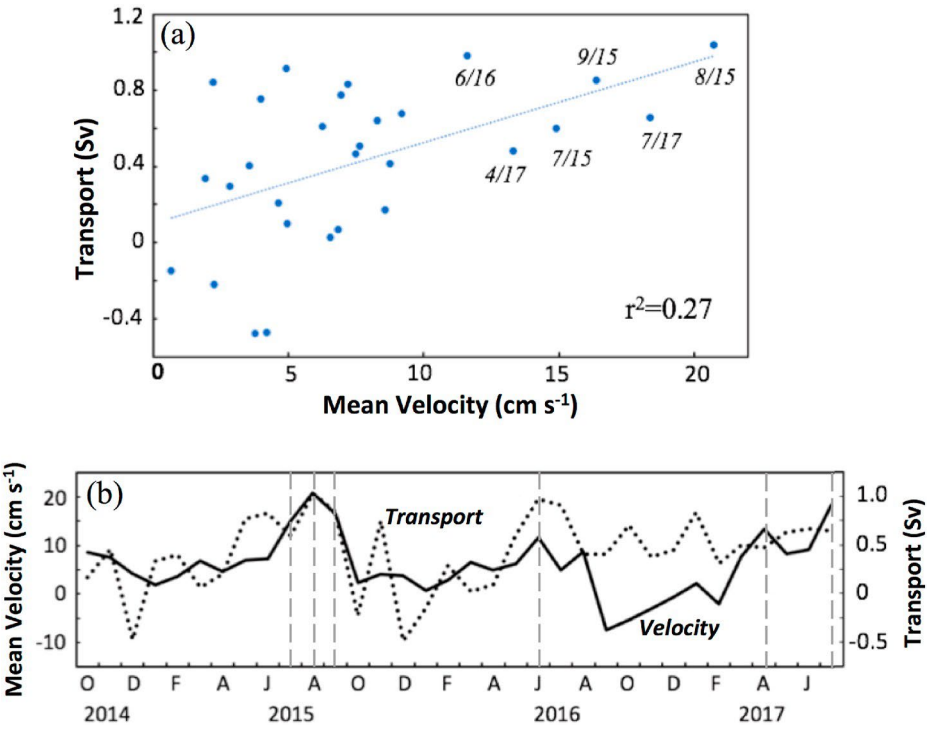

Fig. 15. (a) Monthly depth-averaged (0–200 m) velocity at C9 versus transport at Icy Cape using only data when the mean velocity at C9 was positive (toward the northwest). Best fit line and associated r^2 value are shown. (b) Time series of the depth-averaged (0–200 m) monthly mean velocity at C9 (solid line; left axis) and the monthly mean transport at Icy Cape (dotted line; right axis). The vertical dashed lines represent the timing of the strong velocity events identified in (a).

3.4.5. Volume transport in the CSC

The transport estimate for the CSC can be updated using results from Li et al. (2019) and our C9 results presented herein. Li et al. (2019) estimated transport in the CSC using three year-long moorings deployed in 2013 (spanning 163–356 m bottom depths) and covering an off-slope distance of ~30 km. Their estimate of transport over this area appears to be ~0.35 Sv (their "non-mirrored" value). As noted earlier, our C9 mooring was on the same line of moorings, and ~10 km beyond their outermost site. If we assume that the measurements at C9 are representative of the 20 km beyond the Li et al. (2019) moorings and note that the mean along-slope current in the upper 250 m at C9 was ~5 cm s^{-1}, transport in this region is estimated at 0.25 Sv (width X velocity X depth = 20,000 m X 0.05 m s^{-1} X 250 m). This is likely an under-estimation since the satellite-tracked drifter trajectories provided a width estimate of ~70 km for the CSC. If we do the same calculation assuming that the C9 average velocity is representative of 40 km instead, we obtain an estimate of 0.5 Sv. Although this is likely an over- estimation, it provides a range of transport (including the Li et al., 2019 estimate of 0.35 Sv) in the CSC of 0.60–0.85 Sv.

The mean transport at the Icy Cape moorings for September 2014–August 2017 was 0.42 Sv (following Stabeno et al., 2018). Nikolopoulos et al. (2009) estimated that the eastward transport of Pacific water exiting Barrow Canyon was 0.13 Sv, meaning that 0.29 Sv of the water exiting Barrow Canyon would flow westward. Using these values, the volume of outflow from Barrow Canyon provides between ~34% ([0.42–0.13]/0.85) to ~48% ([0.42–0.13]/0.60) of the CSC volume transport, which as a percentage is less than what was estimated by Li et al. (2019). Alternately, if we use the values explicitly measured from the mooring array, Li et al. (2019) estimated 0.28 Sv of Pacific water in the CSC (their "non-mirrored" value), which is essentially identical to our 0.29 Sv that exits Barrow Canyon and turns westward.

4. Discussion and conclusions

Three years of moored current meter and water property data confirm a well-defined, seasonally varying northwestward surface-intensified flow (the CSC) along the northern Chukchi continental slope. This flow was best defined in the upper 200–250 m of the water column. Below this surface layer was an undercurrent (the AOBC) that flowed predominantly southeastward. Temperature and salinity in this undercurrent (~200 m–~850 m) classified it as Atlantic Water. Vertical correlations among current time series in the AOBC were strong, as were correlations among current time series in the CSC. Only temperature was measured at 900 m in the 2014 and the 2015 deployments, and the average potential temperature at 900 m (below the AOBC) was ~0.0 °C (standard deviation of 0.03 °C), which is typical of Arctic deep water in the Canada Basin.

The C9 mooring site was unknowingly positioned on the southern boundary of the BG (Regan et al., 2019). The BG intensified from 2003 through 2012, reaching a maximum in 2013 and 2014 the end of the analysis period described by Regan et al. (2019). In recent years, the geostrophic transport in the vicinity of C9 has stabilized (Armitage et al., 2017; Zhang et al., 2016), although there remains strong monthly variability in the system, particularly in the fall (Regan et al., 2019). Northwestward velocity appears to be largest in the fall (Regan et al., 2019), but variability also appears to be strongest at that time. In contrast, the flow in the upper 200 m at C9 increased from June through September and then appeared to weaken in the fall. It is unclear whether this apparent disagreement is a result of temporal variability in the system or other mechanisms. For instance, C9 was a single mooring, making it difficult to differentiate between spatial oscillations, such as cross-slope meanders, and temporal variability in the current system. As noted in section 3.1.2, meanders in the system are apparent in the satellite-tracked drifter trajectories. The northwestward trajectory of the drifters followed the trajectory of the southern edge of the BG in 2013 and 2014 (Regan et al., 2019).

The appearance of the CSC has been most evident to the west of Utqiag_ vik, AK (Corlett and Pickart, 2017; Stabeno et al., 2018; Li et al., 2019). According to the analysis by Regan et al. (2019) this is also the region of greatest slope of dynamic ocean topography. Evidence for a

similar current flowing along the Beaufort continental slope is currently lacking. However, we note that the ~1400 m depth mooring of Nikolopoulos et al. (2009) did capture a weak (~2 cm s^{-1}) mean northwestward near-surface flow. Interestingly, the Beaufort mooring array analyzed by Nikolopoulos et al. (2009) was deployed in 2002–2004 before the recent expansion and increase in strength of the BG (Armitage et al., 2017; Regan et al., 2019). It remains unknown whether a more recent mooring array would detect a similar relatively weak northwestward flowing current off the Beaufort continental slope. It should also be noted that the model fields of Watanabe et al. (2017) showed northwestward flow all along the Beaufort continental slope. That the strength of the CSC varied substantially over the three years of our deployment is not surprising, in that the strength and size of the BG also varies interannually (Armitage et al., 2017; Regan et al., 2019).

Recent updates to the freshwater content volume in the BG region indicate that 2015–2017 have the largest total freshwater content volumes on record, with particularly large spatial gradients near the Chukchi continental slope (Proshutinsky et al., 2019; see their Figs. 4 and 5). Thus, our three years of observations at C9 were during a period where the BG was particularly strong.

Li et al. (2019) built upon the results of Corlett and Pickart (2017) by suggesting that wind stress curl over the shelf, rather than westward winds alone, primarily drive variability in the CSC. Our findings indicate that while this may be true in an episodic sense, it is generally not the case over our three-year C9 record. The along-slope currents at C9 were not significantly correlated with local winds, except at depths <40 m. There are several possibilities for this.

One potential explanation for the lack of strong correlations between winds and currents at C9 could be meandering of the current. As mentioned, from a single mooring location, it is difficult to distinguish between temporal variability in currents and inherent spatial changes such as cross-slope meandering of the current.

Secondly, the winds were typically weak, often <10 m s^{-1} (Fig. 14b and c). At present, we remain uncertain about how skillfully the ERA5 reanalysis reproduces the true wind stress curl. Belmonte Rivas and Stoffelen (2019) suggest improvements in ERA5 relative to its predecessor model, but additional ground-truthing is needed, particularly in the Arctic where data for assimilation is sparse.

Remote forcing could provide another possible explanation for the lack of correlation between currents and winds or between the depth of the 0° isotherm and local wind during the first part of the 2016–17 record. Recall that there was significant energy in the currents in the 2–10 day energy band. This energy is likely generated elsewhere, and thus could obscure any correlation between currents and local winds. While we tested for relationships with remote winds at select sites without significant results, a more complete investigation of remote versus local forcing on the Chukchi continental slope is left for future analyses.

Finally, the C9 location is approximately 120 km from the coast north of Utqiag_ vik, AK, where the coastline abruptly changes direction by ~90°. Wind at C9 is usually oriented northeast-southwest, roughly parallel to the Chukchi Sea coast (Fig. 14b; Stabeno et al., 2018), so that it often blows across, rather than along, the continental slope. This general lack of alignment of the wind and continental slope could potentially help explain the lack of correlation between the wind and observed along-slope currents at C9. In contrast, wind blowing along Alaska's Beaufort coastline, where the shelf is much narrower, appears to be effective at forcing along-slope flows (Nikolopoulos et al., 2009). Any oceanic response, however, to changes in wind forcing on the Beaufort continental slope would propagate east in the direction of coastal-trapped waves, rather than toward the C9 site. Finally, the BG is forced by basin-wide winds (the Beaufort High) and modified by the accumulation of freshwater stored in the BG (Armitage et al., 2017; Regan et al., 2019; Petty et al., 2016), so it is not surprising that the CSC at C9 is not locally wind-forced. Although we also found poor correlations between basin-averaged wind stress curl and currents at C9, the fact that the region of highest sea-surface height gradient exists along the Chukchi continental slope from Barrow Canyon to the Chukchi Borderland (Regan et al., 2019) suggests a relationship between the CSC and the BG.

We hypothesize that this northwestward flowing CSC is forced by the edge of the Beaufort Gyre. Corlett and Pickart (2017), while admitting that a dynamical connection could exist, argued that the CSC was not a manifestation of the Beaufort Gyre, citing the relatively strong currents observed on the Chukchi Slope, lack of a similar current off the Beaufort Slope and the presence of Chukchi Shelf water properties in the CSC as evidence. Spall et al. (2018) similarly suggest that the CSC is distinct from the Beaufort Gyre owing to its Bering Strait source and unique water properties. Nevertheless, the fact that the CSC flowed west in the model of Spall et al. (2018) was a result of the basin-scale circulation associated with the BG (their Fig. 16). The body of evidence indicates that the fact that the CSC flows northwestward is a result of the BG dynamics. We suggest that water exiting the Chukchi Shelf via Barrow Canyon is entrained into the western boundary current of the BG flowing northwest along the Chukchi Slope, consistent with the model results of Spall et al. (2018). Dynamically, we expect that the lateral pressure gradient associated with the BG in the region north of, and extending west from, Utqiagvik (Figs. 4 and 5 of Regan et al., 2019) presents an effective "wall" that is more than sufficient to overcome the Coriolis force acting on the flow emanating from Barrow Canyon, resulting in the CSC flowing northwestward along the continental slope.

The shelf-slope system from Barrow Canyon to the Chukchi Borderland is a complex region. The exit of warm, saline water out of Barrow Canyon during summer is a source of subsurface heat to the Arctic Ocean basin (Aagaard and Carmack, 1989; Stabeno et al., 2018; Woodgate et al., 2012). In contrast, the Atlantic Water can enter the Chukchi Shelf via Barrow Canyon (Bourke and Paquette, 1976; Ladd et al., 2016; Wood et al., 2018). An array of moorings across the Chukchi Slope would provide insight into the variability in the boundary of the BG, its strength and the pathways of the outflowing Pacific Water. Clearly, additional observations are required to understand the system.

CRediT authorship contribution statement

Phyllis J. Stabeno: Conceptualization, Methodology, Software, Validation, Formal analysis, Investigation, Resources, Data curation, Writing - original draft, Visualization, Supervision, Project administration, Funding acquisition, Writing - review & editing. **Ryan M. McCabe:** Conceptualization, Methodology, Software, Validation, Formal analysis, Investigation, Resources, Writing - original draft, Visualization, Project administration, Writing - review & editing.

Declaration of competing interest

The authors declare that they have no known competing financial interests or personal relationships that could have appeared to influence the work reported in this paper.

Acknowledgments

Support was provided by the National Oceanic and Atmospheric Administration; the Bureau of Ocean Energy Management CHAOZ, CHAOZ-X and ArcWEST programs; the NPRB Arctic Program (A92-02a, A92-02b); and the Joint Institute for the Study of the Atmosphere and Ocean (JISAO) under NOAA Cooperative Agreement NA15OAR4320063. This is contribution No. 4990 for Pacific Marine Environmental Laboratory and Contribution No. 2019-1048 to University of Washington JISAO. We thank three anonymous reviewers for helping to improve the manuscript.

References

Aagaard, K., Carmack, E., 1989. The role of sea ice and other fresh water in the Arctic circulation. J. Geophys. Res. 94 (14), 485–14,498.

Armitage, T.W.K., Bacon, S., Ridout, A.L., Petty, A.A., Wolbach, S., Tsamados, M., 2017. Arctic Ocean surface geostrophic circulation 2003–2014. Cryosphere 11, 1767–1780. https://doi.org/10.5194/tc-11-1767-2017.

Belmonte Rivas, M., Stoffelen, A., 2019. Characterizing ERA-Interim and ERA5 surface wind biases using ASCAT. Ocean Sci. 15, 831–852. https://doi.org/10.5194/os-15-831-2019.

Bourke, R.H., Paquette, R.G., 1976. Atlantic water on the Chukchi shelf. Geophys. Res. Lett. 3 (10), 629–632. https://doi.org/10.1029/GL003i010p00629.

Coachman, L.K., Aagaard, K., Tripp, R.B., 1975. Bering Strait: the Regional Physical Oceanography. Univ. of Washington Press, Seattle, Wash.

Corlett, W.B., Pickart, R.S., 2017. The Chukchi slope current. Prog. Oceanogr. 153, 50–65. https://doi.org/10.1016/j.pocean.2017.04.005.

Danielson, S.L., Weingartner, T.J., Hedstrom, K.S., Aagaard, K., Woodgate, R., Curchitser, E., Stabeno, P.J., 2014. Coupled wind-forced controls of the Bering-Chukchi Shelf circulation and the Bering Strait throughflow: Ekman transport, continental shelf waves, and variations of the Pacific-Arctic sea surface height gradient. Prog. Oceanogr. 125, 40–61. https://doi.org/10.1016/j.pocean.2014.04.006.

Dee, D.P., Uppala, S.M., Simmons, A.J., Berrisford, P., Poli, P., Kobayashi, S., Andrae, U., Balmaseda, M.A., Balsamo, G., Bauer, P., Bechtold, P., Beljaars, A.C.M., van de Berg, L., Bidlot, J., Bormann, N., Delsol, C., Dragani, R., Fuentes, M., Geer, A.J., Haimberger, L., Healy, S.B., Hersbach, H., Hólm E.V., Isaksen, L., Kållberg, P., Köhler, M., Matricardi, M., Mcnally, A.P., Monge-Sanz, B.M., Morcrette, J.J., Park, B. K., Peubey, C., de Rosnay, P., Tavolato, C., Thépaut, J.N., Vitart, F., 2011. The ERA-Interim reanalysis: configuration and performance of the data assimilation system. Q. J. Roy. Meteorol. Soc. 137, 553–597. https://doi.org/10.1002/qj.828.

Doddridge, E.W., Meneghello, G., Marshall, J., Scott, J., Lique, C., 2019. A Three-way balance in the Beaufort Gyre: the Ice-Ocean Governor, wind stress, and eddy diffusivity. J. Geophys. Res. Oceans 124, 3107–3124. https://doi.org/10.1029/2018JC014897.

Fine, E.C., MacKinnon, J.A., Alford, M.H., Mickett, J.B., 2018. Microstructure observations of turbulent heat fluxes in a warm-core Canada Basin eddy. J. Phys. Oceanogr. 48, 2397–2418. https://doi.org/10.1175/JPO-D-18-0028.1.

Giles, K.A., Laxon, S.W., Ridout, A.L., Wingham, D.J., Bacon, S., 2012. Western Arctic Ocean freshwater storage increased by wind-driven spin-up of the Beaufort Gyre. Nat. Geosci. 5, 194–197. https://doi.org/10.1038/ngeo1379.

Gong, D., Pickart, R.S., 2016. Early summer water mass transformation in the eastern Chukchi Sea. Deep Sea Res. Part II 130, 43–55. https://doi.org/10.1016/j.dsr2.2016.04.015.

Haiden, T., Janousek, M., Bidlot, J., Ferranti, L., Prates, F., Vitart, F., Bauer, P., Richardson, D.S., 2017. Evaluation of ECMWF forecasts, including 2016–2017 upgrades. European Centre for medium-range weather Forecasts. ECMWF Tech. Memo 817, 56. https://doi.org/10.21957/x397za5p5.

Hersbach, H., de Rosnay, P., Bell, B., Schepers, D., Simmons, et al., 2018. Operational global reanalysis: progress, future directions and synergies with NWP. In: European Centre for Medium-Range Weather Forecasts, ERA Report Series, vol. 27, p. 63.

Itoh, M., Nishino, S., Kawaguchi, Y., Kikuchi, T., 2013. Barrow Canyon volume, heat, and freshwater fluxes revealed by long-term mooring observations between 2000 and 2008. J. Geophys. Res. Oceans 118 (9), 4363–4379. https://doi.org/10.1002/jgrc.20290.

Jackson, J.M., Williams, W.J., Carmack, E.C., 2012. Winter sea-ice melt in the Canada basin, Arctic Ocean. Geophys. Res. Lett. 39, L03603. https://doi.org/10.1029/2011GL050219.

Ladd, C., Mordy, C.W., Salo, S.A., Stabeno, P.J., 2016. Winter water properties and the Chukchi Polynya. J. Geophys. Res. Oceans 121, 5516–5534. https://doi.org/10.1002/2016JC011918.

Large, W.G., Pond, S., 1981. Open ocean momentum flux measurements in moderate to strong winds. J. Phys. Oceanogr. 11, 324–336.

Li, M., Pickart, R.S., Spall, M.A., Weingartner, T.J., Lin, P., Moore, G., Qi, Y., 2019. Circulation of the Chukchi Sea shelfbreak and slope from moored timeseries. Prog. Oceanogr. 172, 14–33. https://doi.org/10.1016/j.pocean.2019.01.002.

Linders, J., Pickart, R.S., Bjo€rk, G., Moore, G.W.K., 2017. On the nature and origin of water masses in Herald Canyon, Chukchi Sea: synoptic surveys in summer 2004, 2008, and 2009. Prog. Oceanogr. 159, 99–114. https://doi.org/10.1016/j.pocean.2017.09.005.

Lindsay, R., Wensnahan, M., Schweiger, A., Zhang, J., 2014. Evaluation of seven different atmospheric reanalysis products in the Arctic. J. Clim. 27, 2588–2606. https://doi.org/10.1175/JCLI-D-13-00014.1.

Mesinger, F., DiMego, G., Kalnay, E., Mitchell, K., Shafran, P.C., Ebisuzaki, W., Jovic, D., Woollen, J., Rogers, E., Berbery, E.H., Ek, M.B., Fan, Y., Grumbine, R., Higgins, W., Li, H., Lin, Y., Manikin, G., Parrish, D., Shi, W., 2006. North American regional reanalysis. Bull. Am. Meteorol. Soc. 87, 343–360. https://doi.org/10.1175/BAMS-87-3-343.

Moore, G.W.K., 2012. Decadal variability and a recent amplification of the summer Beaufort Sea High. Geophys. Res. Lett. 39, L10807. https://doi.org/10.1029/2012GL051570.

Moore, G.W.K., Pickart, R.S., Renfrew, I.A., 2008. Buoy observations from the windiest location in the world ocean, Cape Farewell, Greenland. Geophys. Res. Lett. 35, L18802. https://doi.org/10.1029/2008GL034845.

Nikolopoulos, A., Pickart, R.S., Fratantoni, P.S., Shimada, K., Torres, D.J., Jones, E.P., 2009. The western Arctic boundary current at 152 W: Structure, variability, and transport. Deep-Sea Res. Part II 56, 1164–1181. https://doi.org/10.1016/j.dsr2.2008.10.014.

Peralta-Ferriz, C., Woodgate, R.A., 2017. The dominant role of the East Siberian Sea in driving the oceanic flow through the Bering Strait—conclusions from GRACE ocean mass satellite data and in situ mooring observations between 2002 and 2016. Geophys. Res. Lett. 44 (11) https://doi.org/10.1002/2017GL075179, 472–11,481.

Petty, A.A., Hutchings, J.K., Richter-Menge, J.A., Tschudi, M.A., 2016. Sea ice circulation around the Beaufort Gyre: the changing role of wind forcing and the sea ice state. J. Geophys. Res. Oceans 121 (5), 3278–3296. https://doi.org/10.1002/2015JC010903.

Pickart, R.S., Pratt, L.J., Torres, D.J., Whitledge, T.E., Proshutinsky, A.Y., Aagaard, K., Agnew, T.A., Moore, G.W.K., Dail, H.J., 2010. Evolution and dynamics of the flow through Herald canyon in the western Chukchi Sea. Deep-Sea Res. Part II 57 (1–2), 5–26. https://doi.org/10.1016/j.dsr2.2009.08.002.

Pisareva, M.N., Pickart, R.S., Lin, P., Fratantoni, P.S., Weingartner, T.J., 2019. On the nature of wind-forced upwelling in Barrow Canyon. Deep-Sea Res. II 162, 63–78. https://doi.org/10.1016/j.dsr2.2019.02.002.

Polyakov, I.V., Pnyushkov, A.V., Alkire, M.B., Ashik, I.M., Baumann, T.M., 2017. Greater role for Atlantic inflows on sea-ice loss in the Eurasian basin of the Arctic Ocean. Science 356 (6335), 285–291. https://doi.org/10.1126/science.aai8204.

Proshutinsky, A., Krishfield, R., Timmermans, M.-L., 2019. Preface to special issue forum for Arctic Ocean modeling and observational synthesis (FAMOS) 2: Beaufort gyre phenomenon. J. Geophys. Res. Oceans. https://doi.org/10.1029/2019JC015400 (in press).

Regan, H.C., Lique, C., Armitage, T.W.K., 2019. The Beaufort Gyre extent, shape, and location between 2003 and 2014 from satellite observations. J. Geophys. Res. Oceans 124, 844–862. https://doi.org/10.1029/2018JC014379.

Renfrew, I.A., Peterson, G.N., Sproson, D.A.J., Moore, G.W.K., Adiwidjaja, H., Zhang, S., North, R., 2009. A comparison of aircraft-based surface-layer observations over Denmark Strait and the Irminger Sea with meteorological analyses and QuikSCAT winds. Q. J. R. Meteorol. Soc. 135, 2046–2066. https://doi.org/10.1002/qj.444.

Serreze, M.C., Crawford, A.D., Stroeve, J.C., Barrett, A.P., Woodgate, R.A., 2016. Variability, trends, and predictability of seasonal sea ice retreat and advance in the Chukchi Sea. J. Geophys. Res. Oceans 121, 7308–7325. https://doi.org/10.1002/2016JC011977.

Shimada, K., Carmack, E.C., Hatakeyama, K., Takizawa, T., 2001. Varieties of shallow temperature maximum waters in the western Canada Basin of the Arctic Ocean. Geophys. Res. Lett. 28, 3441–3444.

Spall, M., Pickart, R., Li, M., Itoh, M., Lin, P., Kikuchi, T., Qi, Y., 2018. Transport of Pacific water into the Canada basin and the formation of the Chukchi slope current. J. Geophys. Res. Oceans 123, 7453–7471. https://doi.org/10.1029/2018JC013825.

Stabeno, P., Kachel, N., Ladd, C., Woodgate, R., 2018. Flow patterns in the eastern Chukchi Sea: 2010–2015. J. Geophys. Res. Oceans 123, 1177–1195. https://doi.org/10.1002/2017JC013135.

Stabeno, P.J., Danielson, S.L., Kachel, D.G., Kachel, N.B., Mordy, C.W., 2016b. Currents and transport on the Eastern Bering Sea shelf: an integration of over 20 years of data. Deep-Sea Res. II 134, 13–29. https://doi.org/10.1016/j.dsr2.2016.05.010.

Stabeno, P.J., Bell, S., Cheng, W., Danielson, S., Kachel, N.B., Mordy, C.W., 2016. Long-term observations of Alaska Coastal Current in the northern Gulf of Alaska. Deep-Sea Res. II 132, 24–40. https://doi.org/10.1016/j.dsr2.2015.12.016. Understanding Ecosystem Processes in the Gulf of Alaska: Volume 1.

Stabeno, P.J., Bond, N.A., Hermann, A.J., Kachel, N.B., Mordy, C.W., Overland, J.E., 2004. Meteorology and oceanography of the northern Gulf of Alaska. Continent. Shelf Res. 24, 859–897. https://doi.org/10.1016/j.csr.2004.02.007.

Stabeno, P.J., Reed, R.K., 1994. Circulation in the Bering Sea basin observed by satellite-tracked drifters: 1986–1993. J. Phys. Oceanogr. 24 (4), 848–854.

Steele, M., Morison, J., Ermold, W., Rigor, I., Ortmeyer, M., Shimada, K., 2004. Circulation of summer Pacific halocline water in the Arctic Ocean. J. Geophys. Res. 109, C02027. https://doi.org/10.1029/2003JC002009.

Steele, M., Ermold, W., Zhang, J., 2008. Arctic Ocean surface warming trends over the past 100 years. Geophys. Res. Lett. 35, L02614. https://doi.org/10.1029/2007GL031651.

Stegall, S.T., Zhang, J., 2012. Wind field climatology, changes, and extremes in the chukchi-beaufort seas and Alaska north slope during 1979–2009. J. Clim. 25, 8075–8089. https://doi.org/10.1175/JCLI-D-11-00532.1.

Timmermans, M.-L., Proshutinsky, A., Golubeva, E., Jackson, J.M., Krishfield, R., McCall, M., Platov, G., Toole, J., Williams, W., Kikuchi, T., Nishino, S., 2014. Mechanisms of Pacific summer water variability in the Arctic central Canada basin. J. Geophys. Res. Oceans 119, 7523–7548. https://doi.org/10.1002/2014JC010273.

Timmermans, M.-L., 2015. The impact of stored solar heat on Arctic sea ice growth. Geophys. Res. Lett. 42, 6399–6406. https://doi.org/10.1002/2015gl064541.

Timmermans, M.-L., Toole, J., Krishfield, R., 2018. Warming of the interior Arctic Ocean linked to sea ice losses at the basin margins. Sci. Adv. 4 (8), eaat6773 https://doi.org/10.1126/sciadv.aat6773.

Torrence, C., Compo, G.P., 1998. A practical guide to wavelet analysis. Bull. Am. Meteorol. Soc. 79, 61–78. https://doi.org/10.1175/1520-0477(1998)079<0061:APGTWA>2.0.CO;2.

Tsukada, Y., Ueno, H., Ohta, N., Itoh, M., Watanabe, E., Kikuchi, T., Nishino, S., Mizobata, K., 2018. Interannual variation in solar heating in the Chukchi Sea, Arctic Ocean. Polar Sci. 17, 33–39. https://doi.org/10.1016/j.polar.2018.06.003.

Watanabe, E., Onodera, J., Itoh, M., Nishino, S., Kikuchi, T., 2017. Winter transport of subsurface warm water toward the Arctic Chukchi Borderland. Deep-Sea Res. I 128, 115–130. https://doi.org/10.1016/j.dsr.2017.08.009.

Weingartner, T., Aagaard, K., Woodgate, R., Danielson, S., Sasaki, Y., Cavalieri, D., 2005. Circulation on the north central Chukchi Sea shelf. Deep-Sea Res. Part II 52 (24–26), 3150–3174. https://doi.org/10.1016/j.dsr2.2005.10.015.

Wood, K.R., Jayne, S.R., Mordy, C.W., Bond, N., Overland, J.E., Ladd, C., Stabeno, P.J., Ekholm, A.K., Robbins, P.E., Schreck, M., Heim, R., Intrieri, J., 2018. Results of the first Arctic heat open science Experiment. Bull. Am. Meteorol. Soc. 99, 513–520. https://doi.org/10.1175/BAMS-D-16-0323.1.

Woodgate, R.A., Aagaard, K., Weingartner, T.J., 2005a. Monthly temperature, salinity, and transport variability of the Bering Strait through flow. Geophys. Res. Lett. 32, L04601. https://doi.org/10.1029/2004GL021880.

Woodgate, R.A., Aagaard, K., Weingartner, T.J., 2005b. A year in the physical oceanography of the Chukchi Sea: moored measurements from autumn 1990–1991. Deep-Sea Res. Part II 52 (24–26), 3116–3149. https://doi.org/10.1016/j.dsr2.2005.10.016.

Woodgate, R.A., Weingartner, T.J., Lindsay, R., 2012. Observed increases in Bering Strait oceanic fluxes from the Pacific to the Arctic from 2001 to 2011 and their impacts on the Arctic Ocean water column. Geophys. Res. Lett. 39, L24603. https://doi.org/10.1029/2012GL054092.

Woodgate, R.A., Aagaard, K., Muench, R.D., Gunn, J., Bjork, G., Rudels, B., Roach, A.T., Schauer, U., 2001. The Arctic Ocean boundary current along the Eurasian slope and the adjacent Lomonosov Ridge: water mass properties, transports and transformations from moored instruments. Deep-Sea Res. Part I 48 (8), 1757–1792.

Yang, J., Proshutinsky, A., Lin, X., 2016. Dynamics of an idealized Beaufort Gyre: 1. The effect of a small beta and lack of western boundaries. J. Geophys. Res. Oceans 121, 1249–1261. https://doi.org/10.1002/2015JC011296.

Zhang, J., Steele, M., Runciman, K., Dewey, S., Morison, J., Lee, C., Rainville, L., Cole, S., Krishfield, R., Timmermans, M., Toole, J., 2016. The Beaufort Gyre intensification and stabilization: a model-observation synthesis. J. Geophys. Res. Oceans 121, 7933–7952. https://doi.org/10.1002/2016JC012196.

Chapter 9: Seasonal patterns of near-bottom chlorophyll fluorescence in the eastern Chukchi Sea: 2010–2019

Stabeno, P. J., Mordy, C. W., and Sigler, M. F.

Citation:

Stabeno, P.J., Mordy, C.W. and Sigler, M.F., 2020. Seasonal patterns of near-bottom chlorophyll fluorescence in the eastern Chukchi Sea: 2010–2019. Deep Sea Research Part II: Topical Studies in Oceanography, 177, p.104842, doi: 10.1016/j.dsr2.2020.104842.

Deep–Sea Research II 177 (2020) 104842

Contents lists available at ScienceDirect

Deep-Sea Research Part II

journal homepage: http://www.elsevier.com/locate/dsr2

Seasonal patterns of near-bottom chlorophyll fluorescence in the eastern Chukchi Sea: 2010–2019

Phyllis J. Stabeno [a,*], Calvin W. Mordy [a,b], Michael F. Sigler [c]

[a] NOAA Pacific Marine Environmental Laboratory, 7600 Sand Point Way NE, Seattle, WA, 98115-0070, USA
[b] University of Washington, JISAO, 7600 Sand Point Way NE, Seattle, WA, 98115-0070, USA
[c] NOAA Alaska Fisheries Science Center, Retired, 17109 Point Lena Loop Road, Juneau, AK, 99801-8344, USA

ARTICLE INFO

Keywords:
Chukchi Sea
Sea ice
Fluorescence
Ice algae

ABSTRACT

The Chukchi Sea consists of a broad, shallow (<45 m) shelf that is seasonally (November–July) covered by sea ice. This study characterizes the seasonal patterns of near-bottom primary production using moored instruments measuring chlorophyll fluorescence, oxygen, nitrate, and photosynthetically active radiation. From 2010 to 2018, moorings were deployed at multiple sites each year. Instruments were restricted to within 10 m of the seafloor due to ice keels, which can reach 30 m below the surface in this region. Near-bottom blooms were common at all mooring sites. The bloom onset directly followed ice retreat whereas the end of the bloom followed loss of light in September. The intensity of light at the seafloor (~40 m deep) was similar to levels observed under 1–2 m thick ice floes in the spring/early summer, and was sufficient to support photosynthesis near the seafloor, utilizing nitrate and producing oxygen. We hypothesize that the near bottom bloom originated from aggregates of ice algae that sank during ice retreat. As a consequence of climate warming and earlier ice retreat, we predict that the near-bottom bloom onset will occur earlier, but the timing of the end of the near-bottom bloom will remain the same pending a sufficient nutrient supply. The Chukchi Sea is highly productive even though the growing season is short. This production is promoted by a shallow seafloor, which allows multiple production layers (surface open water, bottom of the mixed layer, under-ice algae, and disassociated ice algae which settles near the seafloor). We term this the Multiple Production Layers (MPL) hypothesis.

1. Introduction

The Chukchi Sea consists of a broad shallow shelf, extending >800 km northward from the Bering Strait to the shelf break and the Arctic basin. It is characterized as an inflow shelf for the Arctic (Carmack and Wassmann, 2006) and is the sole source of Pacific water to the Arctic Ocean. The flow through Bering Strait provides heat, freshwater, and salt, including nutrients, to the Chukchi Sea and the Arctic Basin. The northward flow divides into two primary branches — the western branch flows into the Arctic basin through Herald Canyon and the eastern branch flows through Barrow Canyon (Coachman et al., 1975). Sea-ice algae are a major source of carbon to the benthic ecosystem (Grebmeier, 2012; Koch et al., 2020) with an estimated production during spring of 1–2 g C m^{-2} (Gradinger, 2009). Production of ice algae is primarily limited by light (Michel et al., 1988; Welch and Bergmann, 1989) and nutrients (Cota et al., 1987; Castellani et al., 2017).

The spring plankton bloom likely initiates under and within the sea ice (Hill and Cota, 2005; Arrigo et al., 2012; Lowry et al., 2018; Tedesco et al., 2019). Seasonal ice retreat favors the export of aggregates of under-ice algae directly to the benthos (Ambrose et al., 2005; Boetius et al., 2013; Katlein et al., 2015; Koch et al., 2020). This, together with benthic microalgae, support the Chukchi's rich, benthic-dominated ecosystem (Dunton et al., 2014).

There has been a dramatic loss of sea ice in the Chukchi Sea during the last 15 years (Wood et al., 2015, 2018; Serreze et al., 2016; Frey et al., 2015), with earlier ice retreat in the spring/summer and later ice arrival in the fall. This loss of sea ice (including multi-year ice) has increased the atmospheric heat-flux into the Chukchi Sea (Danielson et al., 2020). Earlier ice retreat also impacts the timing of export of ice algae to the seafloor and the timing of open water phytoplankton production (Arrigo et al., 2008; Hill et al., 2017), and favors open water phytoplankton primary production that benefits a pelagic ecosystem (Grebmeier et al., 2006, 2015; Moore and Stabeno, 2015). A longer open-water season is predicted to alter the composition and distribution

* Corresponding author.
E-mail address: phyllis.stabeno@noaa.gov (P.J. Stabeno).

https://doi.org/10.1016/j.dsr2.2020.104842
Received 6 September 2019; Received in revised form 11 July 2020; Accepted 16 July 2020
Available online 25 July 2020
0967-0645/

of phytoplankton communities (Tremblay et al., 2009; Neeley et al., 2018).

The focus in this paper is to examine the relationship among chlorophyll fluorescence, arrival and departure of sea ice, and photosynthetically active radiation (PAR). We utilize a variety of data sources, including hydrographic casts, pop-up buoys (a newly developed technology that measures properties underneath the ice), and a variety of time series collected on moorings. Chlorophyll fluorescence, PAR, oxygen, and nitrate were measured near the seafloor at multiple mooring sites on the U.S. Chukchi Shelf over a 9-year period (Fig. 1). These instruments were all deployed within 8 m of the seafloor to avoid the deep ice keels that can occur on this shelf.

Preliminary analysis indicated that the large export of ice algae to the seafloor coincides with ice retreat (Berchok et al., 2015). In their analysis, an increase in percent oxygen saturation and/or decrease in nitrate concentration were often associated with this export event, suggesting that net primary production due to ice algae continues at depth. We contend that this continued production is not due to subsurface phytoplankton, which lie shallower, but rather near-bottom disassociated ice algae. We present evidence to support this distinction in the results and discussion.

Our objective was to test the multiple production layer or MPL, 'maple', hypothesis that ice algae fall to the seafloor as ice retreats and continue to photosynthesize for weeks or longer (Fig. 2). According to this hypothesis, this near-bottom layer of continued photosynthesis by disassociated ice algae adds to the other layers of primary production (i.e. sympagic algal production, and surface and sub-surface phytoplankton blooms) that together account for the high primary productivity found on the Chukchi Shelf (Hill and Cota, 2005; Arrigo et al., 2012; Codispoti et al., 2013; Hill et al., 2017).

2. Data and methods

2.1. Moorings

Moorings (Fig. 1) were deployed at 8 sites (C1–C8) on the Chukchi Shelf during late summer and recovered the following summer, when new moorings were usually deployed. Listed in Table 1 are the deployment years at each site, mooring locations and instrumentation. All moorings were short, taut wire moorings. During winter and spring, sea-ice keels can be as deep as 30 m below the surface (Stabeno et al., 2018). To avoid these ice keels, each mooring was <10 m tall, keeping the upper float at least 30 m below the surface. This height limitation resulted in two moorings being deployed at each site, because of the limited amount of vertical wire space. Instruments on the moorings collected hourly measurements of the following variables: temperature (SeaBird SBE-37, SBE-39, SeaCat); currents (Acoustic Doppler Current Profiler, RCM-9); salinity (SBE-37, SeaCat); chlorophyll fluorescence (Sea-Bird/WET Labs FLSB ECO Fluorometer); nitrate (Sea-Bird/Satlantic ISUS or SUNA; at selected sites); and PAR (Biospherical Instruments QSP2300). Excluding the ADCP that was deployed at the top of the mooring, the rest of the instruments were deployed 4–8 m above the bottom. All instruments were prepared according to manufacturers' specifications and calibrated prior to deployment (except for calibration of the nitrate sensors which is discussed below). While chlorophyll samples were taken at the mooring sites on deployment and recovery of the moorings, there were insufficient data to improve the conversion of fluorescence to chlorophyll.

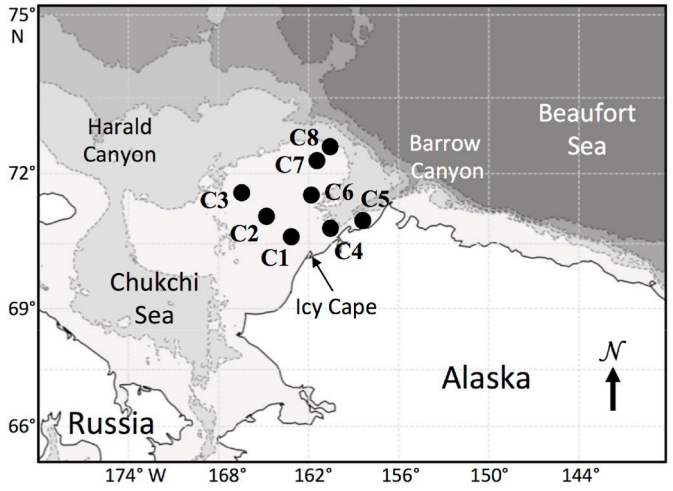

Fig. 1. Map of the Chukchi Sea shelf with bathymetry and place names. The eight shelf mooring sites (C1–C8) are indicated by black dots. The periods of deployments are listed in Table 1.

To reduce biofouling, optical wipers on the Eco Fluorometer and SUNA were engaged prior to each hourly set of measurements, and the ISUS sensors were plumbed into the outflow of a Sea-Bird Scientific SBE-16 with anti-fouling agents mounted on either side of the ISUS flow cell. See Mordy et al. 2020 for further details of data processing of nitrate sensors.

2.2. Hydrography

The conductivity-temperature-depth (CTD) instrument package consisted of a Sea-Bird 911plus with dual sensors measuring temperature, conductivity and oxygen, and single sensors measuring, pressure, and chlorophyll fluorescence. Hydrographic casts were done at each mooring site upon deployment and/or recovery of moorings. While the optical nitrate sensors (ISUS and SUNA) have a reported accuracy of ~2 μM, they must be calibrated with discrete samples. At the depth of the nitrate sensor, discrete samples for nutrients were collected from Niskin bottles and filtered through 0.45 μm cellulose acetate filters. Samples were frozen for analysis at our laboratory in Seattle, WA. See Mordy et al. 2020 for details of the analysis.

On July 18, 2015, aboard the USCGC Healy cruise HE1501, a GoPro camera was attached to the top of the CTD frame and a movie was taken simultaneously with the CTD downcast near the C2 mooring (164.3°W, 71.2°N). Three representative frames were selected from this movie and presented herein, and a short video segment is included in the supplemental material (Supplemental Video).

2.3. Pop-up buoy

During the last four years, pop-up buoys have been developed at the Pacific Marine Environmental Laboratory (Langis et al., 2018). The purpose of this effort was to develop an inexpensive, expendable buoy to make under-ice measurements that could be deployed in summer or fall and rise to the surface in the following winter or spring on a prearranged day. Eventually, when the ice melted, the buoy surfaced and transmitted data back to the laboratory. The instruments collect data during three unique periods: (1) on the seafloor; (2) on the vertical profile as it rises to the surface; and (3) under the ice.

The buoy presented in this manuscript is Generation 3. It consisted of a spherical float (30 cm in diameter). The upper ~5 cm of top had been cut off, and a flat plate (cap) attached at the top. One thermistor (±0.01 °C) was located on the top-cap and a second one at the bottom of the float. A fluorometer (±2%) was located on the bottom of the float facing downwards, while the PAR sensor (±3%) and pressure sensor (±0.21 m) were located on the top-cap. The camera (UCAM III Low-Resolution Digital Camera) was tilted upward at 45° and positioned ~10 cm from the bottom of the ice.

2.4. Sea ice

The Advanced Microwave Scanning Radiometer (AMSR-E) data

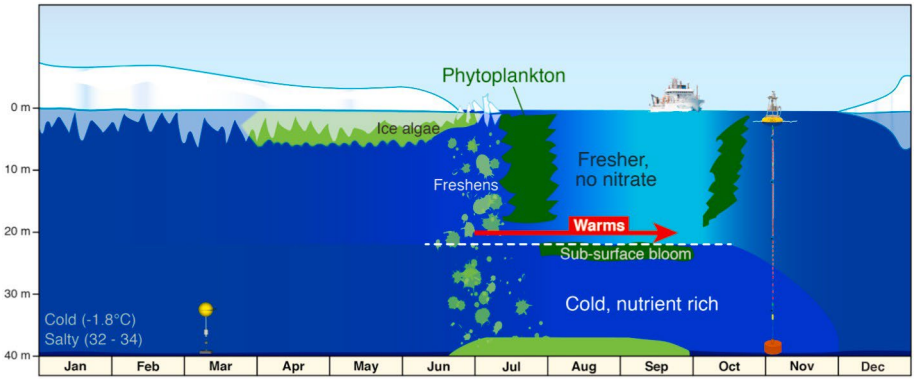

Fig. 2. Seasonality of the lower trophic level of the ecosystem on the northeastern Chukchi Sea Shelf. Ice algae bloom occurs beneath the ice in spring, and with ice melt it is exported to the bottom, where there is sufficient light and nutrients to support further production. With ice retreat/melt the water stabilizes with a relatively warm, low salinity surface layer overlaying a colder, more saline bottom layer. With this stabilization, a surface phytoplankton bloom can occur consuming the remainder of surface nutrients and support a subsurface bloom. With surface mixing in late summer a fall phytoplankton bloom may occur (Adapted from Fig. 136, Berchok et al., 2015).

Table 1
List of moorings (with depth in parentheses) and instruments deployed between 2010 and 2017. F indicates the fluorometer functioned correctly providing data for the entire deployment. Similarly, N is a nitrate sensor, O an oxygen sensor and P a PAR sensor. Bold indicates that the instrument recorded data for only part of the deployment cycle. "Yes" indicates that there was production in the near bottom; "No" indicates that there was no production; and "-" indicates that there were insufficient data to decide. In addition to the variables listed below, currents were measured at most sites. The depths of each instrument were 4–8 m above the bottom.

Site (depth)	Lat. Long.	Aug 2010	Aug 2011	Aug 2012	Aug 2013	Sep 2014	Sep 2015	Aug 2016	Aug 2017
C1	70.835	FNO**P**	F**O**		**FNOP**	NP	FNOP	FNOP	FNP
(45 m)	163.119	yes	–		–	–	yes	yes	yes
C2	71.222	FNOP	FN**OP**	FOP	FOP	FN**OP**	FN**OP**	FNOP	FNOP
(44 m)	164.250	yes	yes	yes	yes	yes	yes	yes	yes
C3	71.825	OP	FN**O**					NP	FNOP
(45 m)	165.975	–	yes					–	yes
C4	71.042			OP	F**OP**	FNP	FOP	FP	FOP
(48 m)	160.493			–	–	yes	yes	–	yes
C5	71.207				FON	**F**NOP		FP	FP
(45 m)	157.999				yes	yes		–	–
C6	71.777				FN	**F**N			
(43 m)	161.875				no	–			
C7	72.424				FN	FN			
(43 m)	161.604				yes	yes			
C8	72.586					FO			
(46 m)	161.215					yes			

(available from the National Snow and ice Data Center, http://nsidc.org/data/amsre/) were used in this manuscript. AMSR is a dataset of sea-ice extent and areal concentration consisting of daily ice concentration data at 12.5 km resolution. Time series of percent areal coverage were calculated in 50 km × 50 km boxes around each mooring site (C1–C8).

2.5. Data analysis

Time series of sea-ice coverage (percent) values were used to determine the timing and duration of the ice-free period in summer. These records were plotted, and the retreat and return dates were assigned (Table S1, Fig. S1). Ice retreat was considered to have occurred when areal sea-ice cover fell below 15% for the first time during each year. Ice return was considered to have occurred when areal ice cover increased above 15% for the last time during each year. The duration of the ice-free period was computed as the difference in days between ice retreat and ice return.

PAR values near the seafloor for each mooring and year were examined to determine the time and duration of the photic period in summer. These records were plotted and the onset, end and maximum value of PAR were assigned (Table S1, Fig. S1). Onset and end of the PAR period were considered to have occurred when the PAR value crossed a threshold of 0.1 μE m^{-2} s^{-1} (Hancke et al., 2018). PAR duration was computed as the difference in days between PAR end and PAR onset.

Chlorophyll values near the seafloor for each mooring and year were examined to determine the time and duration of the bloom in summer (herein we use "bloom" to indicate increased chlorophyll fluorescence). These records were plotted and the onset, end and maximum value of the summer bloom were assigned (Table S1, Fig. S1). Onset and end of the near-seafloor summer bloom ('bloom end') were considered to have occurred when the concentration of chlorophyll crossed 1 μg l^{-1} (Arrigo and van Dijken, 2011). Bloom duration was computed as the difference in days between bloom end and bloom onset.

Annual values of ice retreat, ice return, PAR onset, PAR end, bloom onset, and bloom end were plotted by year and mooring using box plots and the R package 'ggplot2'. The relationships between values (e.g. between bloom onset and ice retreat) were plotted by year and mooring using the R package 'ggplot2' scatter plots. Their relatedness was examined by computing Pearson correlation coefficients *r* (e.g., between bloom onset and ice retreat) and the statistical significance of the *r*-values were estimated using the R package 'Hmisc'.

3. Results

3.1. Sea ice

Typically, ice cover was at or near 100% during winter for most mooring sites (Fig. 3a, Fig. S1). The exceptions were the three most coastal moorings—primarily C4 and C5 and, to a lesser extent, C1. At these sites, winter and spring sea-ice cover was usually reduced when strong winds were out of the east and/or northeast (referred to as a wind-driven polynya) or when warm Atlantic water surfaced (referred to as a sensible heat polynya) (Ladd et al., 2016; Hirano et al., 2016). At these coastal moorings, areal ice concentration during winter was smallest in 2013, 2014, and 2016 (Fig. 3a). The greatest variability in areal ice cover was at C4 and C5, the two moorings nearest the shelf break (Figs. 1 and 3b). At all the mooring sites discussed herein, sea ice eventually retreated in summer, and returned in late summer or fall (Fig. S1).

The timing of sea-ice retreat varied among years with later retreats in 2012–2014 and earlier retreats in 2010–2011 and 2015–2017 (Fig. 4a). The median day of ice retreat was approximately day 170 (mid-June) for 2010–2011, day 205 (late July) for 2012–2014, day 190 (early July) for 2015–2016, and day 135 (mid-May) for 2017. This pattern of two years of early retreat, three of late, two of mid-range, and finally one year of early ice retreat largely occurred regardless of location, with some exceptions. For example, ice retreat at C7 and C8 in 2010 was similar to the later ice retreat observed in 2012–2014. At C4, the early ice retreat in 2012 reflects a brief period of low ice followed by a return of sea ice lasting several weeks (Fig. S1).

The timing of sea-ice return varied less than sea-ice retreat, with most returns occurring between days 300 and 330 (November; Fig. 4d). The range of sea-ice return was much narrower (~50 days, day 294–345) than the range of sea-ice retreat (~100 days, day 133–232) (Table S1). Thus, variability in the duration of the ice-free period was dictated more by ice retreat than ice return and ranged from 67 to 203 days. The median duration of the ice-free period was 127 days.

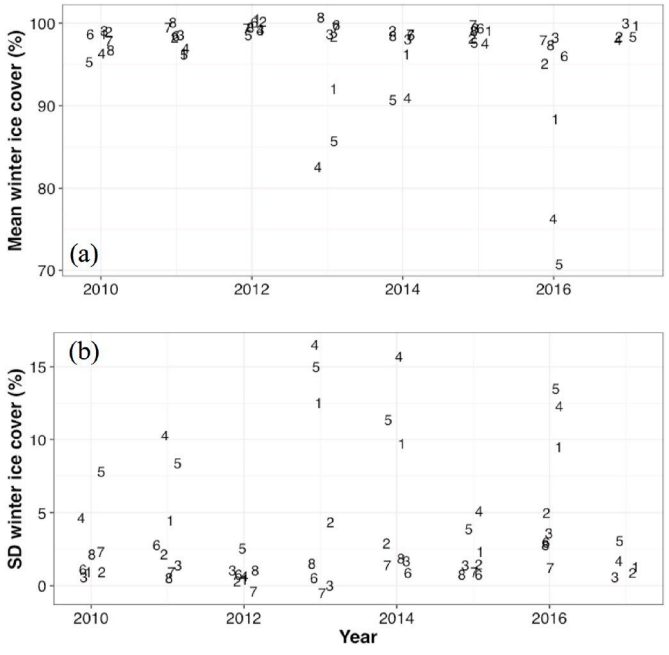

Fig. 3. (a) The mean winter (January–March) ice cover at each mooring site as a function of year. (b) The standard deviation of the mean winter ice cover shown in (a). The individual moorings are indicated by number, so "4" refers to the mooring site C4. The points are randomly offset to reduce overlap. The coastal moorings C1, C4, and C5 had periods of low ice cover and the greatest variability.

3.2. Ice algae

3.2.1. Under-ice data from pop-up buoy

An under-ice (water-ice interface) bloom was observed during spring 2019 from a pop-up buoy that floated to the surface and came to rest at the bottom of an ice floe for approximately two months (May and June). The pop-up buoy was deployed in August 2018 near the C2 mooring (71.2°N, 164.3°W). It remained anchored to the sea floor until April 30, 2019, when the pop-up buoy was released (as designed) and rose to the surface underneath a large (~20 km long) ice floe (Fig. 5a). This distinctive floe was tracked *via* satellite images until 20 June, when the ice floe began to break apart. The floe traveled a distance of ~400 km over a period of 60 days (blue line, Fig. 5b). During this period, the pop-up buoy successfully collected hourly temperature, PAR and fluorescence data just below the bottom of the ice. The top of the buoy rested immediately below the ice at a depth of ~1.5 m (an indication of ice thickness) during the first ~25 days and then began to shoal (an indication of ice thinning) (Fig. 5c).

Chlorophyll fluorescence near the ice-seawater interface began to increase on ~14 May and the bloom continued through early June (Fig. 5d). This bloom occurred under low light conditions (max 2–3 μE m^{-2} s^{-1} prior to 27 May); PAR increased reaching 4–8 μE m^{-2} s^{-1} in early June. In mid-June, the fluorescence disappeared and PAR increased to 20 μE m^{-2} s^{-1}. It was unlikely that the disappearance of the bloom was related to photoinhibition because Cota and Horne (1989) found that, even for ice algae adapted to low light, photo inhibition does not occur until ~40 μE m^{-2} s^{-1}. While nutrient depletion and grazing cannot be discounted, the expectation is that the bloom sank toward the sea floor once the ice substrate began to erode (Fig. 5c), which is consistent with loss of color in the under-ice images (Fig. 5f and g) (Riebesell et al., 1991; Ambrose et al., 2005; Boetius et al., 2013; Ferna´ndez-M´endez et al., 2014; Katlein et al., 2015).

The pop-up buoy remained in the vicinity of moorings C2 and C3 for ~25 days (Fig. 5b). This provided simultaneous time series of fluorescence underneath the ice and near the seafloor (Fig. 6). While in the vicinity of C2 (red line Fig. 6a), the under-ice chlorophyll fluorescence was near-zero as was the near-bottom chlorophyll fluorescence. As the buoy came closer to C3, under-ice fluorescence began to increase (green line). The near bottom fluorescence began to increase at C3 ~20 days after it began to increase at the ice-water interface (green line in Fig. 6b). This lag is consistent with estimates of settling rates of ice algae (0.4–2.7 m d^{-1}, Michel et al., 1993).

3.2.2. Water column data from CTD and video

Vertically, there can be multiple layers of significant chlorophyll fluorescence in the Chukchi Sea (Martini et al., 2016). This multilayer pattern was evident in a hydrographic cast done in 2015 (Fig. 7, left), when a camera was attached to the CTD frame (photos in Fig. 7, right). This CTD cast (164.3◦W, 71.2◦N on July 18, 2015) was taken near C2, approximately 3 days after the ice retreated. Two increases in chlorophyll fluorescence are evident in the cast data, a relatively small one at ~15 m and a larger one below 20 m. The photos show the different quality of the blooms. The photo of the upper water column appears fairly clear (Fig. 7, photo A); the middle photo shows a diffuse chlorophyll peak and likely represents a subsurface phytoplankton bloom associated with the pycnocline (Fig. 7, photo B), while the bottom photo (Fig. 7, photo C) has larger aggregates of cells and extends over ~10 m depth (Fig. 7, left). As the CTD passed the halfway point through the lower layer of fluorescence (~28 m), PAR was fully attenuated. These aggregates are better viewed and clearly visible by video (Supplementary Video), and consistent with reports of sinking aggregates of disassociated ice algae (Riebesell et al., 1991; Ambrose et al., 2005; Boetius et al., 2013; Ferna´ndez-M´endez et al., 2014; Katlein et al., 2015; Koch et al., 2020).

Identifying these aggregates as disassociated ice algae at our moorings is supported by observations at a nearby sediment trap deployed on

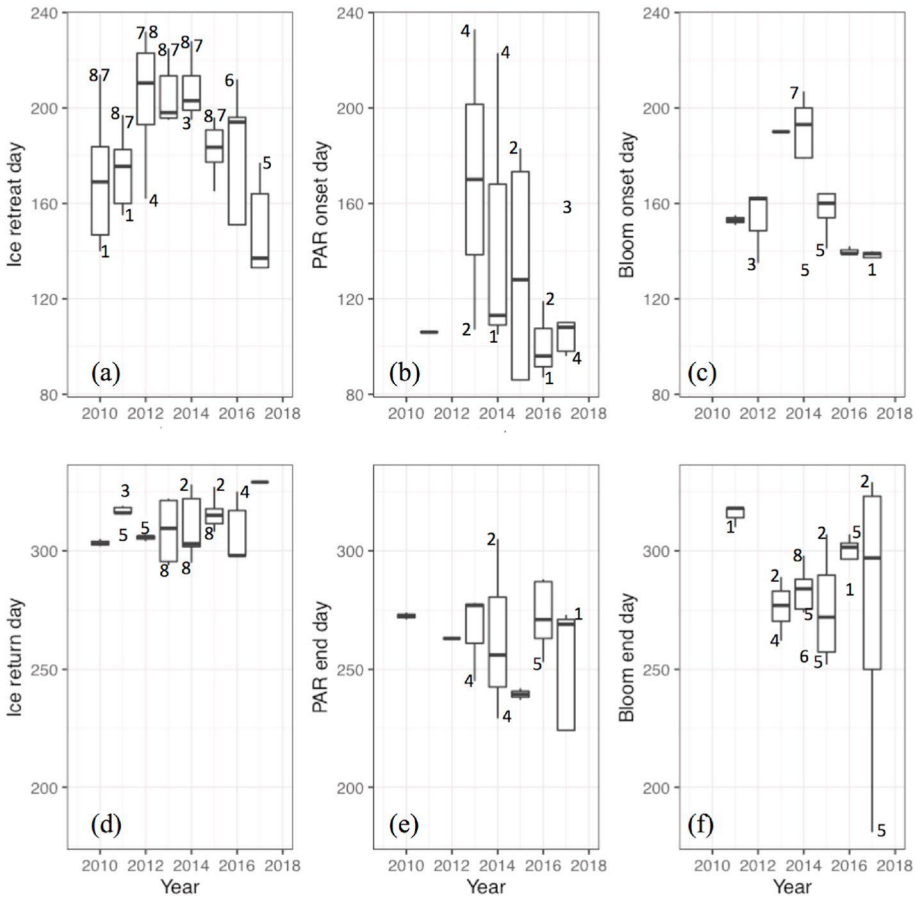

Fig. 4. Box plots indicating (a) day of ice-retreat, (b) day on which the onset of PAR > 0.1 μE m^{-2} s^{-1}, (c) day of bloom onset, (d) day of ice-return, (e) day on which PAR falls below 0.1 μE m^{-2} s^{-1}, and (f) day of bloom end day, all versus year of mooring deployment. The data shown herein are from S1. The numbers in each panel indicate the mooring sites (e.g. "4" refers to C4) that are outside the interquartile range.

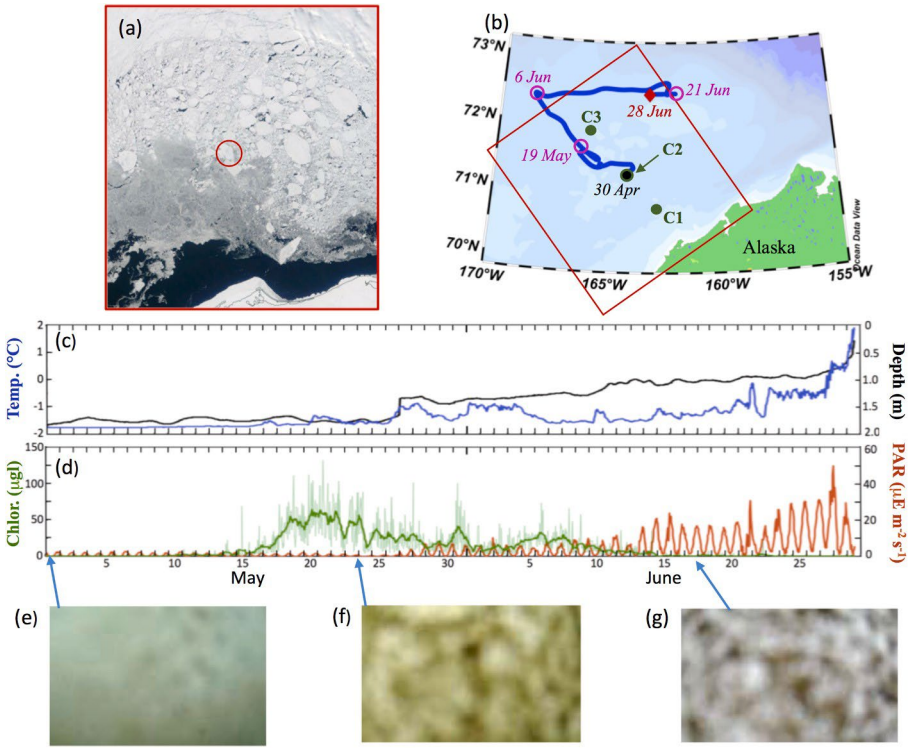

Fig. 5. (a) Satellite image of sea ice on April 30, 2019 when the pop-up buoy surfaced. The red circle indicates the location of where the pop-up buoy was deployed. (b) The trajectory of the ice floe from 30 April to 28 June when it broke apart and the buoy began to transmit location and data (red dot). Selected dates are indicated in purple. Mooring locations are shown and color-coded. The red box is the area shown in (a). (c) Time series of temperature beneath the sea ice and the depth of buoy. The depth of buoy is effectively the thickness of the sea ice at that point because the buoy sits immediately beneath the ice. (d) Time series of chlorophyll fluorescence and PAR measured below the ice by instruments on the pop-up buoy. (e–g) Photos of the water column. (For interpretation of the references to color in this figure legend, the reader is referred to the Web version of this article.)

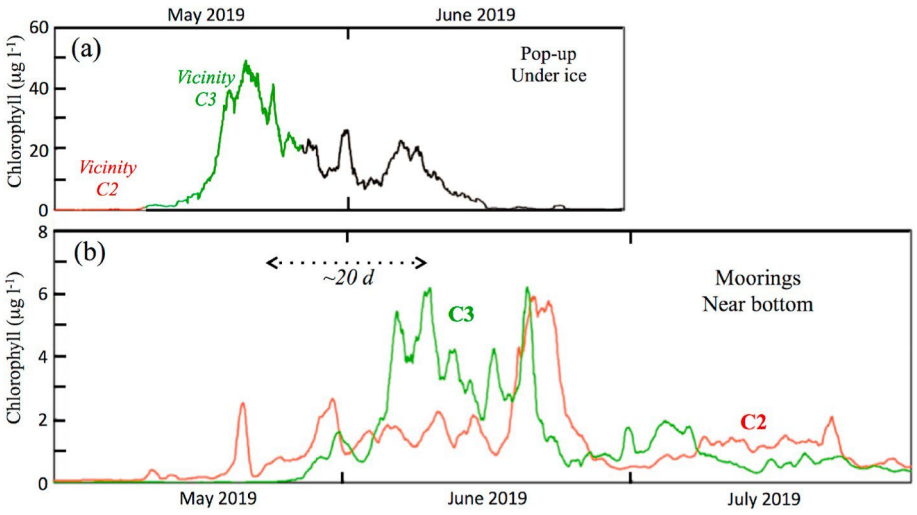

Fig. 6. (a) Low-pass filtered time series of chlorophyll fluorescence measured by pop-up buoy under the ice. It is color coded with red indicating when the buoy was in the vicinity of C2, green in the vicinity of C3, and black in the vicinity of no mooring. (b) Low-pass filtered time series of near-bottom chlorophyll fluorescence measured at C2 (red) and C3 (green). (For interpretation of the references to color in this figure legend, the reader is referred to the Web version of this article.)

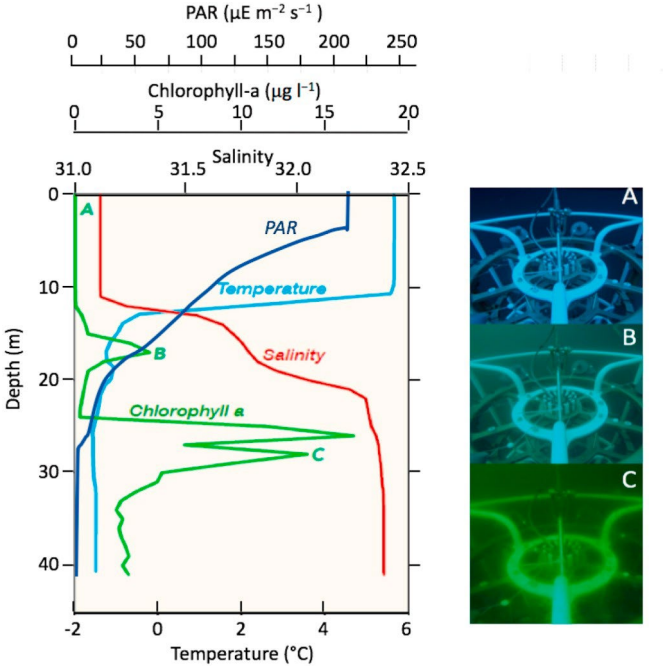

Fig. 7. (left) Hydrographic cast in 2015 near C2 showing multiple subsurface chlorophyll maxima. A smaller subsurface maximum was observed just below the pycnocline, and a larger maximum was observed in the bottom layer. (right) Photos of the water column (taken from a video in the supplemental material): upper layer of relatively clear water; first chlorophyll maximum below the pycnocline; and at the top of the large maximum. The letters A, B, and C correspond to the appropriate depth shown on the left.

the northern Chukchi Shelf in 2016 (Koch et al., 2020). Koch et al. (2020) found that as ice retreated, the flux of sea-ice exclusive diatoms (*Nitzschia frigida* and *Melosira arctica*) increased from ~2 million cells m^{-2} d^{-1} in early June to ~ 30 million cells m^{-2} d^{-1} in early July. This was accompanied by a 10-fold increase in the flux of lipids that are specific to sympagic organisms (from ~100 to 1000 ng m^{-2} d^{-1}). The timing of this flux was concurrent with the increased concentrations of chlorophyll observed at two nearby moorings, C2 (60 km away) and C4 (80 km) (Fig. S1).

3.2.3. Near-bottom data from mooring C2 in 2018

The fate of these sinking aggregates can be seen in the time series (oxygen, nitrate, PAR and fluorescence) collected at the moorings. For example, in 2018 at mooring C2, the ice retreated in mid-May (Fig. 8a), an early date for ice retreat, and there was a sharp increase in chlorophyll fluorescence in the near-bottom water (30–40 m below the surface; Fig. 8b). Accompanying this increase in fluorescence was a sharp increase in the percent saturation of oxygen, from ~90% to >120%, and, at the same time, a decrease in nitrate from ~15 μM to near 0 μM

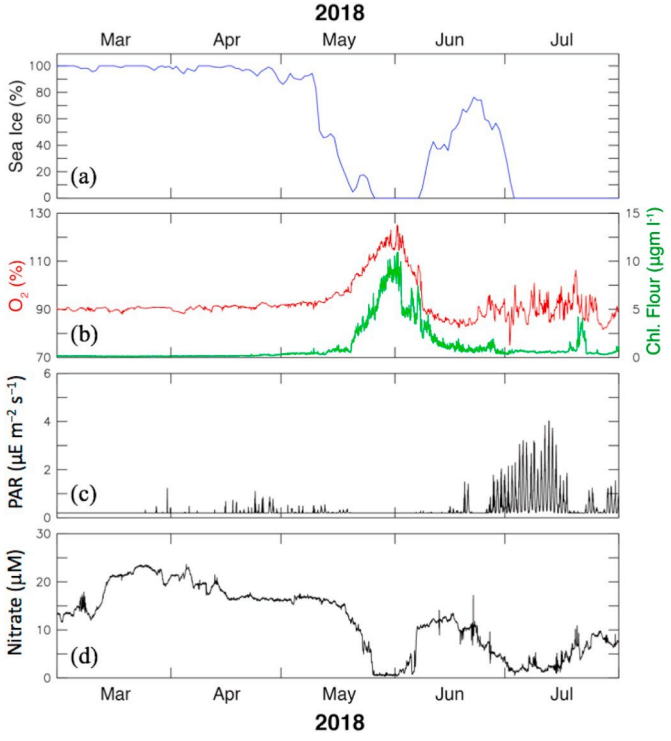

Fig. 8. Time series of: (a) percent ice cover in 50 km × 50 km box centered on C2; (b) percent oxygen saturation (red) and chlorophyll fluorescence (green); (c) PAR; and (d) nitrate. Except for (a), all time series were measured on mooring at C2 within 8 m of the bottom. (For interpretation of the references to color in this figure legend, the reader is referred to the Web version of this article.)

(Fig. 8d) consistent with active photosynthesis in the bottom waters. Light (PAR) was very weak (<2 μE m^{-2} s^{-1}), but measurable through mid-May, decreasing to near zero during the period of high chlorophyll fluorescence; it increased markedly in early July with the disappearance of fluorescence. We suspect that the decrease in PAR to near zero in mid-May was a result of disassociated ice algae descending as a mass through the water column, and the resulting shading prevented most of the light from reaching the seafloor. Such a shading (sharp decrease in PAR) effect was also evident in Fig. 7a, when the CTD entered the region with high chlorophyll. The highest PAR values (Fig. 8c) occurred in July when near-bottom chlorophyll concentrations were low and ice was absent. Vertical mixing in the bottom ~8 m during late May - early June likely exposes the ice algae to sufficient light to continue production; that is, sometimes cells are at the top of the layer and exposed to sufficient light and then mixed downward in this bottom mixed layer.

Near the seafloor, chlorophyll fluorescence began decreasing between 1–6 June, perhaps due to nutrient limitation or grazing (Fig. 8b, d). On 7 June, sea ice returned, and there was a sharp increase in nitrate, and reductions in chlorophyll fluorescence and oxygen saturation (<90%), results consistent with advection of water past the mooring (Mordy et al., 2020) and net respiration. When the ice retreated for the second time in early July, the highest PAR was recorded and yet there was no clear evidence of active photosynthesis as chlorophyll fluorescence remained low and oxygen saturation, while variable, was <100%. Finally, in mid-July there was a small pulse of chlorophyll fluorescence that once again shaded near-bottom waters (low PAR), was coincident with a 5 μM drop in nitrate, and resulted in a short period of >100% oxygen saturation.

3.3. Near-bottom chlorophyll and its relationship to sea ice and light level

Continued fluorescence and photosynthesis near the seafloor following ice retreat was common in our time series. This pattern (described in the previous section for mooring C2 in 2018) of ice retreat, increased fluorescence, increased oxygen (by >20%) and/or decreased nitrate dominates at the mooring sites over the years (2010–2018), occurring 22 out of 23 times (96%) when there are sufficient data to detect this pattern (Table 1). Each of these locations is shallow (<48 m) with measurable light (PAR) reaching the bottom. In MPL, we have hypothesized that the increased fluorescence was likely due to continued photosynthesis by disassociated ice algae near the seafloor, as evidenced by accumulation of sea-ice exclusive diatoms in a sediment trap (Koch et al., 2020) and increasing percent oxygen saturation and/or decreasing nutrients (Fig. 8). In the next few paragraphs, we explore the relationship among the timing and duration of the chlorophyll fluorescence bloom, ice retreat and duration, and the magnitude of PAR.

The timing of PAR onset (>0.1 μE m^{-2} s^{-1}) was earlier for 2011, variable and often later for 2013–2015, and earlier for 2016–2017 (Fig. 4b). The median of PAR onset was approximately days 95–130 for all years except in 2013, when the median was about day 170. Unlike the timing of PAR onset, the timing of PAR end was similar regardless of the year. In general, the range of PAR end (~80 days, day 224–305) was much narrower than the range of PAR onset (~150 days, day 86–233) (Supplemental Table S1). Thus, the duration of the PAR period was dictated more by the timing of PAR onset than the timing of PAR end, ranging from 6 (C4 in 2014) to 200 days. The median duration of the PAR period was 151 days (Table S1).

The timing of the algal bloom onset was earlier for 2011–2012, later for 2013–2014, and earlier for 2015–2017 (Fig. 4c). The median day of bloom onset was approximately day 160 for 2011–2012, 190 for 2013–2014, and 150 for 2015–2017. The timing of bloom end was later for 2011, earlier for 2013–2015, and mid-range for 2016–2017 (Fig. 4f). The median day of the end of the bloom was about day 320 for 2011, 280 for 2013–2015, and 300 for 2016–2017. The median duration of the bloom was 128 days and the range was 41–190 days (Table S1). One unusual observation was mooring C5 in 2014, which had a much earlier bloom onset (approximately day 130) than that year's median (approximately day 190). This bloom began during a period of variable ice cover, but the ice was not so reduced that it reached the 15% threshold that defined ice retreat (Fig. S1).

Comparing the timing of ice, light and the bloom provides evidence that the near-bottom bloom onset occurs at, or prior to, ice retreat, whereas the end of the bloom followed the loss of light in September (Fig. 9). The timing of bloom onset was related to ice retreat ($r = 0.54$, $p = 0.007$) and weakly related to PAR onset ($r = 0.51$, $p = 0.065$) (Fig. 9). The timing of bloom end was weakly related to PAR end ($r = 0.46$, $p = 0.098$) and unrelated to ice return ($r = 0.26$, $p = 0.199$) (Fig. 9). Based on these results, we computed an alternate index of the growing period, the interval between ice retreat and PAR end. We termed this interval the ice retreat-PAR end duration and found that bloom duration is strongly related to ice retreat-PAR end duration ($r = 0.72$, $p = 0.013$) (Fig. 10).

3.4. Annual fluorescence variation during summer

The growing season near the seafloor typically began with the following sequence: ice retreat, a slight increase in PAR, followed by a reduction of PAR concomitant with an increase in near-bottom chlorophyll fluorescence (e.g. Fig. 8). As the ice melted, ice algae were released from the underside of the ice and dropped to the bottom. During the period of the near-bottom bloom (high fluorescence), PAR was particularly low due to self-shading of the bloom. In addition, open-water phytoplankton blooms in the surface layer or below the surface mixed layer (subsurface), common on the northern Chukchi Shelf (Martini et al., 2016), likely contributed to shading of the water column. Another good example of this sequence of events is mooring C2 in 2013 (Fig. S1), where ice cover decreased to 50% in early July and was quickly followed by increased near-bottom chlorophyll concentration. PAR increased concomitant with declining chlorophyll.

As discussed above, sea-ice return did not determine the end of the growing season. Instead the near-bottom bloom was terminated by the seasonal reduction in light during early fall that preceded ice return during our sample years. The usual sequence at the end of the growing season was: PAR becoming undetectable around days 250–270; the near-bottom bloom ending around days 270–300; and ice returning around days 300–320 (Fig. 4).

The near-bottom bloom onset followed directly on ice retreat whereas the end of the bloom followed loss of light in September. As a result, the growing season (bloom duration) near the seafloor was significantly related to the duration of the period between ice retreat and PAR end. In fact, because there was relatively low variability in the ice return day, the PAR end day, and the bloom end day (Fig. 4), the durations of the bloom, PAR, and the ice-free periods were dictated by the timing of their onsets and not their ends.

3.5. Earlier blooms, polynyas and ice-cover variability

Areas of open water during winter and spring occurred in some years. Most often, this happened at mooring sites C1, C4, and C5 (2010, 2011, 2013, 2014, and 2016; Fig. 3). Each of these moorings is near the coast where the Chukchi polynya occurs (Ladd et al., 2016). Intrusion of warmer, saltier Atlantic Water can contribute to or even cause this polynya (Ladd et al., 2016). Earlier blooms were more common in the Chukchi polynya area (C1, C4, and C5) than outside this area. Using the median bloom onset day (day 154) as a threshold to differentiate "early" from "late" bloom onset, 8 of 12 bloom onsets were early in the Chukchi polynya area and only 4 of 12 bloom onsets from this area were late.

Ice retreat is primarily a result of ice melt or of advection forced by local winds and local currents, or a combination of melt and advection (Ladd et al., 2016). The timing of ice retreat (defined here as the first occurrence of areal ice concentration <15%) varied among the five primary moorings (C1–C5 for the period 2001–2016), with earliest

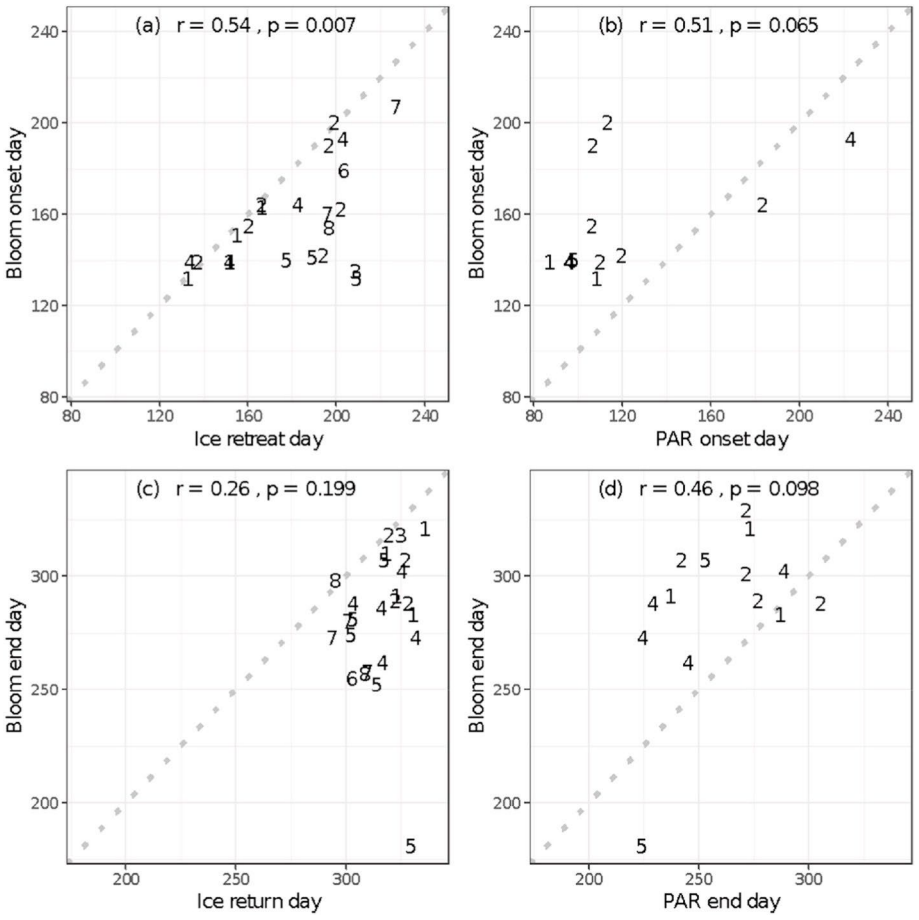

Fig. 9. Scatter plots of the timing of: (a) bloom onset versus ice retreat; (b) bloom onset versus PAR onset; (c) bloom end versus ice return; and (d) bloom end versus PAR end based on near-bottom measurements. The dashed grey line is the 1:1 line.

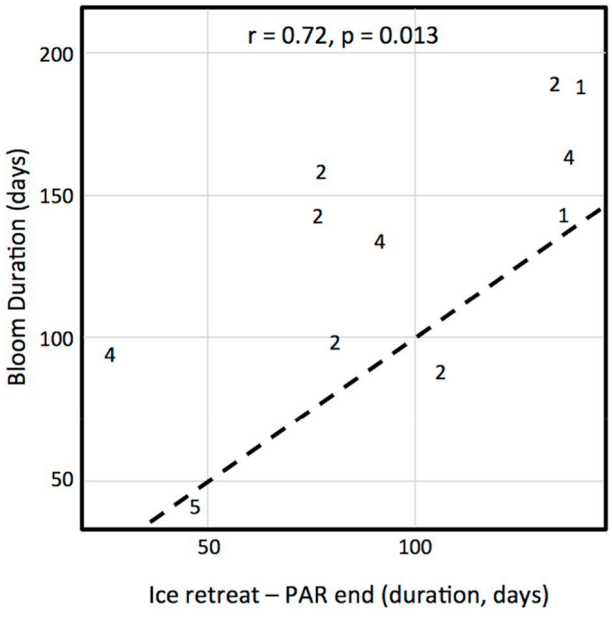

Fig. 10. Scatter plot of the duration of the bloom versus the length of time between ice retreat and PAR end based on near-bottom measurements. The dashed grey line is the 1:1 line.

mean retreat occurring at C1 followed by C4, C2, C3 and, finally, C5. The date of retreat among these five moorings was related with the highest correlation ($r = 0.86$, $p < 0.01$) between the coastal moorings C1 and C4 and the weakest, but still significant, between C1 and C5 ($r = 0.71$, $p < 0.01$). Noting this relationship, the expectation (Fig. 9a) would be that blooms occur earliest at C1 and latest at C3 and C5. Unfortunately, directly examining the timing of the blooms is difficult, because of the limited number of concurrent time series.

Bloom onset was early during years when ice retreated earlier (Fig. 9a) or was episodic in nature. Occasionally ice retreated early, partially returned and then retreated fully for the summer (e.g. mooring C1 in 2012). In this case, a bloom began with the initial ice retreat and continued during the partial return. In other years (e.g. mooring C2 in 2018; Fig. 8) the bloom began with ice retreat and stopped when ice returned. In some years, ice cover was variable during winter and spring (e.g. 2016), PAR increased early (April) and the spring bloom occurred after the early PAR increase (Fig. S1).

Even if ice retreat occurred earlier, an associated chlorophyll maximum was not guaranteed. The earliest observed chlorophyll maxima were during May. For example, a May bloom followed early ice retreat at mooring C5 in 2014 and 2015 (Fig. S1). This can be seen in the 2016 time series; ice cover was irregular in April at moorings C1, C2, and C4, yet substantial fluorescence increases did not occur until May. The lack of a bloom may indicate that either little ice algae were present or the sea ice was advected away (taking its ice algae with it) as opposed to melted.

4. Discussion

4.1. Primary production continues at the seafloor through summer

We found that primary production continued at the seafloor through summer, adding to the primary productivity of the Chukchi Sea, which together with the Chirikov Basin (the region of the northern Bering Sea northeast of St. Lawrence Island) are the most productive regions in the Pacific Arctic (Hill and Cota, 2005; Arrigo et al., 2012; Codispoti et al., 2013; Hill et al., 2017). Virtually all the moorings that successfully measured chlorophyll fluorescence, and either oxygen or nitrate, showed a clear signal of continued production near the seafloor during the summer (Table 1).

We propose that this near-bottom production is due to disassociated ice algae. In most regions with seasonal sea ice, ice algae descend below the photic zone, and thus discontinue to photosynthesize (e.g. Boetius et al., 2013; Rapp et al., 2018). In contrast, much of the Chukchi Sea Shelf is less than 45 m deep and lies within the photic zone. The magnitude of PAR at the Chukchi seafloor was comparable to what was measured beneath the sea ice (Figs. 5d and 8c). Because ice algae can photosynthesize at low levels (Hancke et al., 2018), it is not surprising that photosynthesis by disassociated ice algae may continue near the seafloor. This conclusion is consistent with Koch et al. (2020) who identified disassociated ice algae species together with chlorophyll fluorescence for several months at the seafloor. In addition, the concentration of nitrate in spring and summer is variable, but nitrate usually is sufficient to support some production (see Figs. 2 and 5 in Mordy et al., 2020. With both light and nutrients, the contribution of continued primary production on the seafloor can be substantial and should be considered in estimating primary production in the Chukchi Sea.

4.2. MPL hypothesis

Our results support the hypothesis that continued photosynthesis by disassociated ice algae at the seafloor provides another source of primary production in addition to the spring phytoplankton bloom in the surface mixed layer (Arrigo et al., 2012; Lowry et al., 2014, 2018), the subsurface phytoplankton blooms in the nutrient rich water beneath the surface mixed layer (Lowry et al., 2015; Martini et al., 2016), and the sympagic algal bloom (Gradinger, 2009; Poulin et al., 2011). There is also evidence of a late summer phytoplankton bloom, when summer/fall storms entrain water from the nutrient-rich lower layer (Hill et al., 2017; Ardyna et al., 2014). Together, the various blooms form Multiple Productive Layers that we term the MPL Hypothesis. The MPL hypothesis explains why the Chukchi Sea is highly productive even with a short growing season.

The Chukchi Sea is an inflow shelf (Carmack and Wassmann, 2006). The Arctic Marine Pulses Model describes the Chukchi Sea ecosystem as being dominated by various pulses from the Bering Sea into the Chukchi Sea and from the Arctic basin onto the Chukchi Shelf (Moore et al., 2018). On monthly time scales, inflow through Bering Strait is typically weak in the winter, but in summer this changes with a strong northward flow ($>1 \times 10^6$ m^3 s^{-1}) of relatively warm nutrient-rich, Bering Sea water into the Chukchi Sea (Coachman et al., 1975; Mordy et al., 2020. With the melting of sea ice, a strong pulse of carbon (e.g. ice algae) is exported to the benthic community—an important pelagic-benthic coupling that supports the rich benthic community of the Chukchi Sea (Grebmeier, 2012; Koch et al., 2020). Herein, we add that while there is a sudden pulse of ice algae to the bottom with sea ice melting; in the Chukchi Sea, this near-bottom water remains productive for weeks to months.

4.3. Comparison of Chukchi and Bering Seas

The relationship between the onset of the growing season and ice retreat for the Chukchi Sea also occurs in the northern Bering Sea, but not in the southeastern Bering Sea (Sigler et al., 2014). In the southeastern Bering Sea, the timing of the spring bloom (ice algae and phytoplankton) is dependent on ice and winds (Sigler et al., 2014). If ice retreats early (prior to March 15) or is not present at all, storms continue to mix the upper water column, and the spring bloom commences only after surface waters have warmed enough to stratify the vertical structure. This bloom is only composed of phytoplankton. If ice retreat is late, melt water stabilizes the water column and promotes an early spring, under-ice algal bloom, as well as an open-water phytoplankton bloom near the ice edge. The latter pattern is what occurs in the northern Bering Sea, at least until 2018 (Stabeno and Bell, 2019; Stabeno et al., 2019). In 2018, the lack of sea ice in the northern Bering Sea (mooring M8; 62.2°N, 174.7°W) resulted in a late (June) open water bloom, similar to what occurs in the southeastern Bering Sea during years when there is no ice on the southern shelf after 15 March. While subsurface blooms are uncommon in the southeastern Bering Sea, the northern Bering Sea is similar to the Chukchi Sea, with subsurface blooms being common (Stabeno et al., 2012).

The timing of the spring bloom in the southeastern Bering Sea affects the zooplankton species of the ecosystem, a phenomenon described as the Oscillating Control Hypothesis (OCH) (Hunt et al., 2002, 2011; Stabeno and Hunt, 2002). This control likely is spatially determined and related to the location of the ice edge (Siddon et al., 2013; Sigler et al., 2016). The region where the OCH is effective appears to be moving north as climate warms. For example, the entire eastern Bering Sea Shelf was largely ice free in the winter of 2017–2018, a radical change that was not predicted to occur for at least a few decades (Stabeno et al., 2012; Stabeno and Bell, 2019). The lack of ice had widespread effects on the survival of large crustacean zooplankton and juvenile walleye pollock (Duffy-Anderson et al., 2017). Whether and when the OCH region will move into the Chukchi Sea remains to be examined.

Continued productivity of ice algae that has sunk to the seafloor is probably much greater for the Chukchi Sea Shelf than the eastern Bering Sea Shelf, because the latter's bottom depth is mostly below the photic zone. The eastern Bering Sea Shelf deepens from east to west and the mid-shelf is 50–100 m deep whereas the eastern Chukchi Sea Shelf is predominantly shallower than 45 m. Thus, in the Bering Sea, primary production is limited to under-ice algal blooms, surface mixed layer phytoplankton blooms and subsurface phytoplankton blooms, while in the Chukchi Sea, there is evidence of additional disassociated ice algal production near the seafloor.

4.4. What are the consequences of a shorter ice season?

Sea ice in the Chukchi Sea has been arriving later and retreating earlier for ~30 years (Wood et al., 2015; Serreze et al., 2016; Stroeve et al., 2014) and this pattern is expected to continue (Wang et al., 2018). How changes in ice arrival and retreat will impact primary production in the Chukchi ecosystem is dependent upon how other ecosystem characteristics change. Consider two scenarios (from Berchok et al., 2015). As ice retreats earlier, there will be an earlier export of ice algae to the benthos, but the timing of the spring phytoplankton bloom depends upon wind conditions. If winds are strong, then the water column will be well mixed and the spring phytoplankton bloom will not set up until after winds weaken and water becomes stratified. In contrast, if winds are weak the water column will stratify with a warm, fresher (from ice melt) surface layer. This would support an earlier spring phytoplankton bloom. The first scenario will result in weaker stratification than the second scenario, allowing more short summer blooms supported by input of nutrients during wind events. The complexity of the system makes it difficult to predict how this ecosystem will react to changing ice conditions, but there is consensus on some changes.

With climate warming, there will be a decrease in the duration of sea ice over the Chukchi Sea (Wang et al., 2018). Earlier ice retreat will result in earlier export of ice algae to the seafloor, where there should be sufficient nutrients and light to support a near bottom algal bloom

(Tedesco et al., 2019). The one caveat to this scenario is: can the sea-ice retreat occur "too early". Considering that from our analysis there is insufficient light after the fall equinox to support algal production on the seafloor, it is likely that any ice algae dropping to the seafloor before the spring equinox, also will be non-productive. Ice retreat prior to the spring equinox, however, is not predicted to occur prior to 2050 (Wang et al., 2018). In contrast to earlier ice retreats, delayed ice return will have little impact on near-bottom algal blooms, since they are largely controlled by the availability of light.

Ice algae, however, is only one component in primary production in the Chukchi Sea. Changes in phytoplankton blooms in spring (upper mixed layer), in the summer (sub-pycnocline) and fall (near surface) have been discussed by others. In open water, phytoplankton production may increase, because of a longer growing season (Arrigo and van Dijken, 2015; Arrigo et al., 2008; Brown et al., 2015), although nutrients could be limiting. Once nutrients are consumed in the surface layer, a bloom often forms below the surface mixed layer (e.g. Martini et al., 2016; Lowry et al., 2015). This bloom can be substantial, providing more than a third of primary productivity in the Beaufort Sea (Martin et al., 2013). Churnside et al. (2020) suggest that with reduction in sea ice, the occurrence of these subsurface blooms could increase. These subsurface phytoplankton blooms would likely compete for nutrients with the near-bottom algal blooms and may reduce near-bottom algal production through shading.

5. Summary

The Chukchi Sea is highly productive even though the growing season is short. We provide evidence of production at multiple layers and hypothesize that near-bottom production is a result of disassociated ice algae near the seafloor. On the basis of this evidence, we propose the MPL hypothesis, where high production is promoted by a shallow seafloor, which allows multiple production layers (surface, sub-surface, sympagic ice algae, and disassociated ice algae near the seafloor; Fig. 2). High production occurs because the amount of light near the seafloor in mid-spring to early fall is similar to that measured beneath a 1.5-m thick ice floe. With sufficient light near the seafloor (~40 m deep), ice algae continue to photosynthesize, utilizing nitrate and producing oxygen through summer; a unique feature that pertains to this shallow shelf.

Bloom onset occurred in summer following ice retreat, whereas the end of the bloom occurred in September following loss of light. While this is a complex system, with multiple feedbacks and thus difficult to predict, our results do suggest certain possibilities. Even in a changing system with ice retreating later and arriving earlier, the primary change will be the timing of the export of ice algae to the bottom. Thus, the duration of near-bottom primary productivity will lengthen, because bloom onset occurs earlier.

CRediT authorship contribution statement

Phyllis J. Stabeno: Conceptualization, Methodology, Validation, Resources, Formal analysis, Investigation, Data curation, Writing - original draft, Writing - review & editing, Funding acquisition, Supervision, Visualization. **Calvin W. Mordy:** Conceptualization, Methodology, Validation, Resources, Investigation, Data curation, Funding acquisition, Writing - original draft, Writing - review & editing. **Michael F. Sigler:** Conceptualization, Methodology, Formal analysis, Writing - original draft, Writing - review & editing, Supervision, Visualization.

Declaration of competing interest

The authors declare that they have no known competing financial interests or personal relationships that could have appeared to influence the work reported in this paper.

Acknowledgements

Support was provided by the National Oceanic and Atmospheric Administration; the Bureau of Ocean Energy Management CHAOZ, CHAOZ-X and ArcWEST programs; the NPRB Arctic Program (A92-02a, A92-02b); and the Joint Institute for the Study of the Atmosphere and Ocean (JISAO) under NOAA Cooperative Agreement NA15OAR4320063. We thank S. Bell for data analysis; S. Donohoe for building the pop-up buoys; Leo MacLeod for tracking the ice floe; C. Berchok for being principal investigator on the three BOEM programs, and S. Salo, D. Strausz, G. Lebon, and S. Grassia, for preparing equipment, processing data, and deploying and recovering the moorings. This manuscript is included as part of the North Pacific Research Board (NPRB) Arctic Integrated Ecosystem Research Program, NPRB publication ArcticIERP-09. It is contribution No. 5010 for Pacific Marine Environmental Laboratory, contribution No. 2020–1064 for JISAO, and contribution No. 0933 for NOAA's Ecosystem Fisheries Oceanography Coordinated Investigations.

Appendix A. Supplementary data

Supplementary data to this article can be found online at https://doi.org/10.1016/j.dsr2.2020.104842.

References

Ambrose, W.G., Von Quillfeldt, C., Clough, L.M., Tilney, P.V., Tucker, T., 2005. The sub-ice algal community in the Chukchi sea: large-and small-scale patterns of abundance based on images from a remotely operated vehicle. Polar Biol. 28 (10), 784–795.

Ardyna, M., Babin, M., Gosselin, M., Devred, E., Rainville, L., Tremblay, J.-É., 2014. Recent Arctic Ocean sea ice loss triggers novel fall phytoplankton blooms. Geophys. Res. Lett. 41 (17), 6207–6212. https://doi.org/10.1002/2014GL061047.

Arrigo, K.R., van Dijken, G.L., 2011. Secular trends in Arctic Ocean net primary production. J. Geophys. Res. Oceans 116(C9), C09011. https://doi.org/10.1029/2011JC007151.

Arrigo, K.R., van Dijken, G., 2015. Continued increases in Arctic Ocean primary production. Prog. Oceanogr. 136, 60–70. https://doi.org/10.1016/j.pocean.2015.05.002.

Arrigo, K.R., van Dijken, G., Pabi, S., 2008. Impact of a shrinking Arctic ice cover on marine primary production. Geophys. Res. Lett. 35, L19603. https://doi.org/10.1029/2008GL035028.

Arrigo, K.R., Perovich, D., Pickart, R., Brown, Z., van Dijken, G., Lowry, K., et al., 2012. Massive phytoplankton blooms under Arctic sea ice. Science 336(6087) 1408. https://doi.org/10.1126/science.1215065.

Berchok, C.L., Crance, J.L., Garland, E.C., Mocklin, J.A., Stabeno, P.J., Napp, J.M., Rone, B.K., Spear, A.H., Wang, M., Clark, C.W., 2015. Chukchi Offshore Monitoring In Drilling Area (COMIDA): Factors Affecting the Distribution and Relative Abundance of Endangered Whales and Other Marine Mammals in the Chukchi Sea. Final Report of the Chukchi Sea Acoustics, Oceanography, and Zooplankton Study, OCS Study BOEM 2015-034. National Marine Mammal Laboratory, Alaska Fisheries Science Center, NMFS, NOAA, 7600 Sand Point Way NE, Seattle, WA 98115-6349.

Boetius, A., Albrecht, S., Bakker, K., Bienhold, C., Felden, J., Fern´andez-M´endez, M., Hendricks, S., Katlein, C., Lalande, C., Krumpen, T., Nicolaus, M., 2013. Export of algal biomass from the melting Arctic sea ice. Science 339 (6126), 1430–1432.

Brown, Z.W., Lowry, K.E., Palmer, M.A., van Dijken, G.L., Mills, M.M., Pickart, R.S., Arrigo, K.R., 2015. Characterizing the subsurface chlorophyll *a* maximum in the Chukchi sea and Canada basin. Deep-Sea Res. Part II 118 (A), 88–104. https://doi.org/10.1016/j.dsr2.2015.02.010.

Carmack, E., Wassmann, P., 2006. Food webs and physical-biological coupling on pan-Arctic shelves: unifying concepts and comprehensive perspectives. Prog. Oceanogr. 71, 446–477.

Castellani, G., Losch, m., Lange, B., Flores, H., 2017. Modeling Arctic sea-ice algae: physical drivers of spatial distribution and algae phenology. J. Geophys. Res. Oceans 122, 7466–7487. https://doi.org/10.1002/2017JC012828.

Churnside, J.H., Marchbanks, R.D., Vagle, S., Bell, S.W., Stabeno, P.J., 2020. Stratification, plankton layers, and mixing measured by airborne lidar in the Chukchi and Beaufort seas. Deep-Sea Res. Part II this issue.

Coachman, L.K., Aagaard, K., Tripp, R.B., 1975. Bering Strait: The Regional Physical Oceanography. University of Washington Press, Seattle, WA.

Codispoti, L.A., Kelly, V., Thessen, A., Matrai, P., Suttles, S., Hill, V., Steele, M., Light, B., 2013. Synthesis of primary production in the Arctic Ocean: III. Nitrate and phosphate based estimates of net community production. Prog. Oceanogr. 110, 126–150.

Cota, G.F., Horne, E.P.W., 1989. Physical control of arctic ice algal production. Mar. Ecol. Prog. Ser 52, 111–121.

Cota, G.F., Prinsenberg, S.J., Bennett, E.B., Loder, J.W., Lewis, M.R., Anning, J.L., et al., 1987. Nutrient fluxes during extended blooms of Arctic ice algae. J. Geophys. Res.: Oceans 92 (C2), 1951–1962.

Danielson, S.L., Ahkinga, O., Ashjian, C., Basyuk, E., Cooper, L.W., Eisner, L., et al., 2020. Manifestation and consequences of warming and altered heat fluxes over the Bering and Chukchi Sea continental shelves. Deep-Sea Res. Part II this issue.

Duffy-Anderson, J.T., Stabeno, P.J., Siddon, E.C., Andrews, A.G., Cooper, D.W., Eisner, L. B., Farley, E.V., Harpold, C.E., Heintz, R.A., Kimmel, D.G., Sewall, F.F., Spear, A.H., Yasumishii, E.C., 2017. Return of warm conditions in the southeastern Bering Sea: phytoplankton–fish. PLoS ONE 12(6), e0178955. https://doi.org/10.1371/journal.pone.0178955.

Dunton, K.H., Grebmeier, J.M., Trefry, J.H., 2014. The benthic ecosystem of the northeastern Chukchi Sea: an overview of its unique biogeochemical and biological characteristics. Deep-Sea Res. Part II 102, 1–8. https://doi.org/10.1016/j.dsr2.2014.01.001.

Fernandez-Mendez, M., Wenzho¨fer, F., Peeken, I., Sørensen, H.L., Glud, R.N., Boetius, A., 2014. Composition, buoyancy regulation and fate of ice algal aggregates in the Central Arctic Ocean. PloS One 9 (9), e107452. https://doi.org/10.1371/journal.pone.0107452.

Frey, K.E., Moore, G.W.K., Cooper, L.W., Grebmeier, J.M., 2015. Divergent patterns of recent sea ice cover across the bering, Chukchi, and Beaufort seas of the pacific arctic region. Prog. Oceanography 136, 32–49.

Gradinger, R., 2009. Sea-ice algae: major contributors to primary production and algal biomass in the Chukchi and Beaufort Seas during. Deep-Sea Res. Part II 56 (17), 1201–1212. https://doi.org/10.1016/j.dsr2.2008.10.016. May/June 2002.

Grebmeier, J., 2012. Shifting patterns of life in the Pacific Arctic and sub-arctic seas. Annu. Rev. Mar. Sci. 4, 16, 1–16.6.

Grebmeier, J., Overland, J.E., Moore, S.E., Farley, E.V., Carmack, E.C., Cooper, L.W., Frey, K.E., Helle, J.H., McLaughlin, F.A., McNutt, S.L., 2006. A major ecosystem shift in the northern Bering Sea. Science 311, 1461–1464. https://doi.org/10.1126/science.1121365.

Grebmeier, J., Bluhm, B., Cooper, L., Denisenko, S., Iken, K., Kędra, M., Serratos, C., 2015. Time-series benthic community composition and biomass and associated environmental characteristics in the Chukchi Sea during the RUSALCA 2004–2012 program. Oceanography 28 (3), 116–133.

Hancke, K., Lund-Hansen, L.C., Lamare, M.L., Højlund Pedersen, S., King, M.D., Andersen, P., Sorrell, B.K., 2018. Extreme low light requirement for algae growth underneath sea ice: a case study from Station Nord, NE Greenland. J. Geophys. Res.: Oceans 123, 985–1000. https://doi.org/10.1002/2017JC013263.

Hill, V., Cota, G., 2005. Spatial patterns of primary production on the shelf, slope and basin of the Western Arctic in 2002. Deep Sea Res. Part II 52 (24–26), 3344–3354.

Hill, V., Ardyna, M., Lee, S., Varela, D., 2017. Decadal trends in phytoplankton production in the Pacific Arctic region from 1950 to 2012. Deep-Sea Res. Part II 152, 82–94. https://doi.org/10.1016/j.dsr2.2016.12.015.

Hirano, D., Fukamachi, Y., Watanabe, E., Ohshima, K.I., Iwamoto, K., Mahoney, A.R., Eicken, H., Simizu, D., Tamura, T., 2016. A wind-driven, hybrid latent and sensible heat coastal polynya off Barrow, Alaska. J. Geophys. Res. Oceans 121, 980–997. https://doi.org/10.1002/2015JC011318.

Hunt Jr., G.L., Stabeno, P., Walters, G., Sinclair, E., Brodeur, R.D., Napp, J.M., Bond, N. A., 2002. Climate change and control of the southeastern Bering Sea pelagic ecosystem. Deep-Sea Res. Part II 49 (26), 5821–5853. https://doi.org/10.1016/S0967-0645(02)00321-1.

Hunt Jr., G.L., Coyle, K.O., Eisner, L., Farley, E.V., Heintz, R., Mueter, F., Napp, J.M., Overland, J.E., Ressler, P.H., Salo, S., Stabeno, P.J., 2011. Climate impacts on eastern Bering Sea foodwebs: a synthesis of new data and an assessment of the Oscillating Control Hypothesis. ICES J. Mar. Sci. 68 (6), 1230–1243. https://doi.org/10.1093/icesjms/fsr036.

Katlein, C., Fernandez-Mendez, M., Wenzho¨fer, F., Nicolaus, M., 2015. Distribution of algal aggregates under summer sea ice in the Central Arctic. Polar Biol. 38 (5), 719–731.

Koch, C.W., Cooper, L.W., Lalande, C., Brown, T.A., Frey, K.E., Grebmeier, J.M., 2020. Seasonal and latitudinal variations in sea ice algae deposition in the Northern Bering and Chukchi Seas determined by algal biomarkers. PLoS ONE 15(4), e0231178. https://doi.org/10.1371/journal.pone.0231178.

Ladd, C., Mordy, C.W., Salo, S.A., Stabeno, P.J., 2016. Winter water properties and the Chukchi polynya. J. Geophys. Res. 121 (8), 5516–5534. https://doi.org/10.1002/2016JC011918.

Langis, D., Stabeno, P.J., Meinig, C., Mordy, C.W., Bell, S.W., Tabisola, H.M., October 2018. 2018. Low-cost expendable buoys for under ice data collection. In: Oceans 2018 MTS/IEEE Charleston, Marine Technology Society and IEEE Oceanic Engineering Society. IEEE, Charleston, SC, pp. 22–25. https://doi.org/10.1109/OCEANS.2018.8604752.

Lowry, K.E., van Dijken, G.L., Arrigo, K.R., 2014. Evidence of under-ice phytoplankton blooms in the Chukchi sea from 1998 to 2012. Deep Sea Res. Part II 105, 105–117. https://doi.org/10.1016/j.dsr2.2014.03.013.

Lowry, K.E., Pickart, R.S., Mills, M.M., Brown, Z.W., van Dijken, G.L., Bates, N.R., Arrigo, K.R., 2015. The influence of winter water on phytoplankton blooms in the Chukchi Sea. Deep-Sea Res. Part II 118, 53–72.

Lowry, K.E., Pickart, R.S., Selz, V., Mills, M.M., Pacini, A., Lewis, K.M., et al., 2018. Under-ice phytoplankton blooms inhibited by spring convective mixing in refreezing leads. J. Geophys. Res. Oceans 123 (1), 90–109.

Martin, J., Dumont, D., Tremblay, J.-E´., 2013. Contribution of subsurface chlorophyll maxima to primary production in the coastal Beaufort Sea (Canadian Arctic): a model assessment. J. Geophys. Res. Oceans 118 (11), 5873–5886. https://doi.org/10.1002/2013JC008843.

Martini, K.I., Stabeno, P.J., Ladd, C., Winsor, P., Weingartner, T.J., Mordy, C.W., Eisner, L.B., 2016. Dependence of subsurface chlorophyll on seasonal water masses in the Chukchi Sea. J. Geophys. Res. 121 (3), 1755–1770. https://doi.org/10.1002/2015JC011359.

Michel, C., Legendre, L., Demers, S., Therriault, J.-C., 1988. Photoadaptation of sea-ice microalgae in springtime: photosynthesis and carboxylating enzymes. Mar. Eco. Prog. Ser 50, 177–185.

Michel, C., Legendre, L., Therriault, J._C., Demers, S., Vandevelde, T., 1993. Springtime coupling between ice algal and phytoplankton assemblages in southeastern Hudson Bay, Canadian Arctic. Polar Biol. 13, 441–449. https://doi.org/10.1007/BF00233135.

Moore, S.E., Stabeno, P.J., 2015. Synthesis of arctic Research (SOAR) in marine ecosystems of the pacific arctic. Prog. Oceanography 136, 1–11. https://doi.org/10.1016/j.pocean.2015.05.017.

Moore, S.E., Stabeno, P.J., Grebmeier, J.M., Okkonen, S.R., 2018. The arctic marine pulses model: linking annual oceanographic processes to contiguous ecological domains in the pacific arctic. Deep-sea res. Part II 152. SOAR II 8–21. https://doi.org/10.1016/j.dsr2.2016.10.011.

Mordy, C., Bell, S., Cokelet, E., Ladd, C., Lebon, G., Proctor, P., Stabeno, P., Strausz, D., Wisegarver, E., 2020. This Issue. Seasonal Variability of Nitrate in the Eastern Chukchi Sea. Deep-Sea Res. Part II.

Neeley, A.R., Harris, L.A., Frey, K.E., 2018. Unraveling phytoplankton community dynamics in the northern Chukchi Sea under sea-ice-covered and sea-ice-free conditions. Geophys. Res. Lett. 45 (15), 7663–7671.

Poulin, M., Daugbjerg, N., Gradinger, R., Ilyash, L., Ratkova, T., von Quillfeldt, C., 2011. The pan-Arctic biodiversity of marine pelagic and sea-ice unicellular eukaryotes: a first-attempt assessment. Mar. Biodivers. 41, 13–28. https://doi.org/10.1007/s12526-010-0058-8.

Rapp, J.Z., Fernandez-Mendez, M., Bienhold, C., Boetius, A., 2018. Effects of ice-algal aggregate export on the connectivity of bacterial communities in the central Arctic Ocean. Front. Microbiol. 9, 1035.

Riebesell, U., Schloss, I., Smetacek, V., 1991. Aggregation of algae released from melting sea ice: implications for seeding and sedimentation. Polar Biol. 11 (4), 239–248.

Serreze, M.C., Crawford, A.D., Stroeve, J.C., Barrett, A.P., Woodgate, R.A., 2016. Variability, trends, and predictability of seasonal sea ice retreat and advance in the Chukchi Sea. J. Geophys. Res. Oceans 121 (10), 7308–7325. https://doi.org/10.1002/2016jc011977.

Siddon, E., Heintz, R., Mueter, F., 2013. Conceptual model of energy allocation in walleye pollock (*Theragra chalcogramma*) from age-0 to age-1 in the southeastern Bering Sea. Deep-Sea Res. Part II 94, 140–149. https://doi.org/10.1016/j.dsr2.2012.12.007.

Sigler, M.F., Stabeno, P.J., Eisner, L.B., Napp, J.M., Mueter, F.J., 2014. Spring and fall phytoplankton blooms in a productive subarctic ecosystem, the eastern Bering Sea, during 1995–2011. Deep-Sea Res. Part II 109, 71–83. https://doi.org/10.1016/j.dsr2.2013.12.007.

Sigler, M.F., Napp, J.M., Stabeno, P.J., Heintz, R.A., Lomas, M.W., Hunt Jr., G.L., 2016. Variation in annual production of copepods, euphausiids, and juvenile walleye pollock in the southeastern Bering Sea. Deep-Sea Res. Part II 134, Understanding Ecosystem Processes in the Eastern Bering Sea IV 223–234. https://doi.org/10.1016/j.dsr2.2016.01.003.

Stabeno, P.J., Bell, S.W., 2019. Extreme conditions in the Bering Sea (2017–2018): record-breaking low sea-ice extent. Geophys. Res. Lett. 46 (15), 8952–8959. https://doi.org/10.1029/2019GL083816.

Stabeno, P.J., Hunt Jr., G.L., 2002. Overview of the inner front and southeast Bering Sea carrying capacity programs. Deep-Sea Res. Part II 49 (26), 6157–6168. https://doi.org/10.1016/S0967-0645(02)00339-9.

Stabeno, P.J., Farley, E., Kachel, N., Moore, S., Mordy, C., Napp, J.M., Overland, J.E., Pinchuk, A.I., Sigler, M.F., 2012. A comparison of the physics of the northern and southern shelves of the eastern Bering Sea and some implications for the ecosystem. Deep-Sea Res. Part II 65–70, 14–30. https://doi.org/10.1016/j.dsr2.2012.02.019.

Stabeno, P., Kachel, N., Ladd, C., Woodgate, R., 2018. Flow patterns in the eastern Chukchi sea: 2010–2015. J. Geophys. Res. 123 (2), 1177–1195. https://doi.org/10.1002/2017JC013135.

Stabeno, P.J., Bell, S., Bond, N., Kimmel, D., Mordy, C., Sullivan, M., 2019. Distributed biological observatory region 1: physics, chemistry and plankton in the northern Bering Sea. Deep-Sea Res. Part II 162, 8–21. https://doi.org/10.1016/j.dsr2.2018.11.006.

Stroeve, J.C., Markus, T., Boisvert, L., Miller, J., Barret, A., 2014. Changes in Arctic melt season and implications for sea ice loss. Geophys. Res. Lett. 41, 1216–1225. https://doi.org/10.1002/2013GL058951.

Tedesco, L., Vichi, M., Scoccimarro, E., 2019. Sea-ice algal phenology in a warmer Arctic. Sci. Adv 5 (5), eaav4830. https://doi.org/10.1126/sciadv.aav4830.

Tremblay, G., Belzile, C., Gosselin, M., Poulin, M., Roy, S., Tremblay, J.E´., 2009. Late summer phytoplankton distribution along a 3500 km transect in Canadian Arctic waters: strong numerical dominance by picoeukaryotes. Aquat. Microb. Ecol. 54 (1), 55–70.

Wang, M., Yang, Q., Overland, J.E., Stabeno, P.J., 2018. Sea-ice cover timing in the Pacific Arctic: the present and projections to mid-century by selected CMIP5 models. Deep-Sea Res. Part II 152. SOAR II 22–34. https://doi.org/10.1016/j.dsr2.2017.11.017.

Welch, H.E., Bergmann, M.A., 1989. Seasonal development of ice algae and its prediction from environmental factors near Resolute, NWT, Canada. Can. J. Fish. Aquat. Sci. 46 (10), 1793–1804.

Wood, K.R., Bond, N.A., Overland, J.E., Salo, S.A., Stabeno, P., Whitefield, J., 2015. A decade of environmental change in the Pacific Arctic region. Prog. Oceanography 136, 12–31. https://doi.org/10.1016/j.pocean.2015.05.005.

Wood, K.R., Jayne, S.R., Mordy, C.W., Bond, N., Overland, J.E., Ladd, C., Stabeno, P.J., Ekholm, A.K., Robbins, P.E., Schreck, M.-B., Heim, R., Intrieri, J., 2018. Results of the first. Arctic Heat Open Science Experiment. Bull. Am. Meteorol. Soc. 99 (3), 513–520. https://doi.org/10.1175/BAMS-D-16-0323.1.

Unpublished Chapters

Chapter 10: Arctic larval fish community changes in relation to recent trends in warming and advection

Axler, K.E. NOAA/Fisheries, kelia.axler@noaa.gov

Goldstein, E.D., Deary, A.D., Nielsen, J.M., Duffy-Anderson, J.T.

Kelia E Axler[1]*, Esther D Goldstein[1], Jens M Nielsen[1,2], Alison L Deary[1], Janet T Duffy-Anderson[1]

Arctic larval fish community changes in relation to recent trends in warming and advection (in preparation)

[1]NOAA, Alaska Fisheries Science Center, 7600 Sand Point Way NE, Seattle, WA, 98115, USA

[2]Cooperative Institute for Climate, Ocean, and Ecosystem Studies, University of Washington, Seattle, WA, USA

*Corresponding author: kelia.axler@noaa.gov

Introduction: The Pacific Arctic marine ecosystem is rapidly changing due to ocean warming, sea ice loss, and increased advection via the Bering Strait. These physical changes are expected to impact the distributions of Arctic fish communities, and while climate-mediated range shifts of juvenile and adult fish populations are a major topic under study, less is known about how the early life stages (larvae) are responding.

Methods: In this study, we analyzed time series data of larval fish distributions sampled in the late summer (Aug-Sep) of 2010-2019 relative to ocean conditions in the northern Bering (NBS) and Chukchi Sea region (>60°N).

Results and Discussion: Multivariate analyses revealed the presence of 3 distinct multi-species assemblages in the region across all years: 1) a warmer water (≥7.4°C), lower latitude assemblage dominated by Yellowfin Sole (*Limanda aspera*); 2) a colder water (<4.6°C), higher latitude assemblage dominated by Arctic Cod (*Boreogadus saida*), Bering Flounder (*Hippoglossoides robustus*), and other common Arctic species; and 3) a mixed assemblage (4.6-7.4°C) comprised of the dominant species from the other two assemblages. We used partial least squares models to examine links between oceanographic and climate parameters and the areal coverage and center of distribution of each assemblage. We found that the areal coverage of the warmer water assemblage expanded further into the Chukchi Sea in years with higher NBS sea surface temperature (SST), strong Bering Strait northward advection, and increased southerly winds, while the colder water assemblage retracted its areal coverage in those years. Conversely, the colder water assemblage expanded in years with lower Chukchi Sea SST and greater sea ice area and extent. Additionally, we observed a general northward latitudinal shift of all NBS-Chukchi larval fish assemblages in recent warm years (2018-2019) characterized by strong northward winds and advection. Species-level abundance responses to temperature in the northeast Chukchi Sea varied such that lower latitude larval fish species increased in abundance in response to Arctic warming, whereas higher latitude species decreased in abundance (Fig. 1). Mid-latitude species responses to warming conditions varied, but were far less extreme than high-latitude and low-latitude Arctic species. These findings suggest that Arctic warming is most

significantly driving density changes in the leading and trailing edges of the larval fish community. Further, the patterns observed over the past decade in the region document how quickly larval fish communities track environmental change and suggest that climate warming and associated oceanographic processes could be leading toward a borealization of the Arctic by a warmer-water, lower latitude larval fish assemblage.

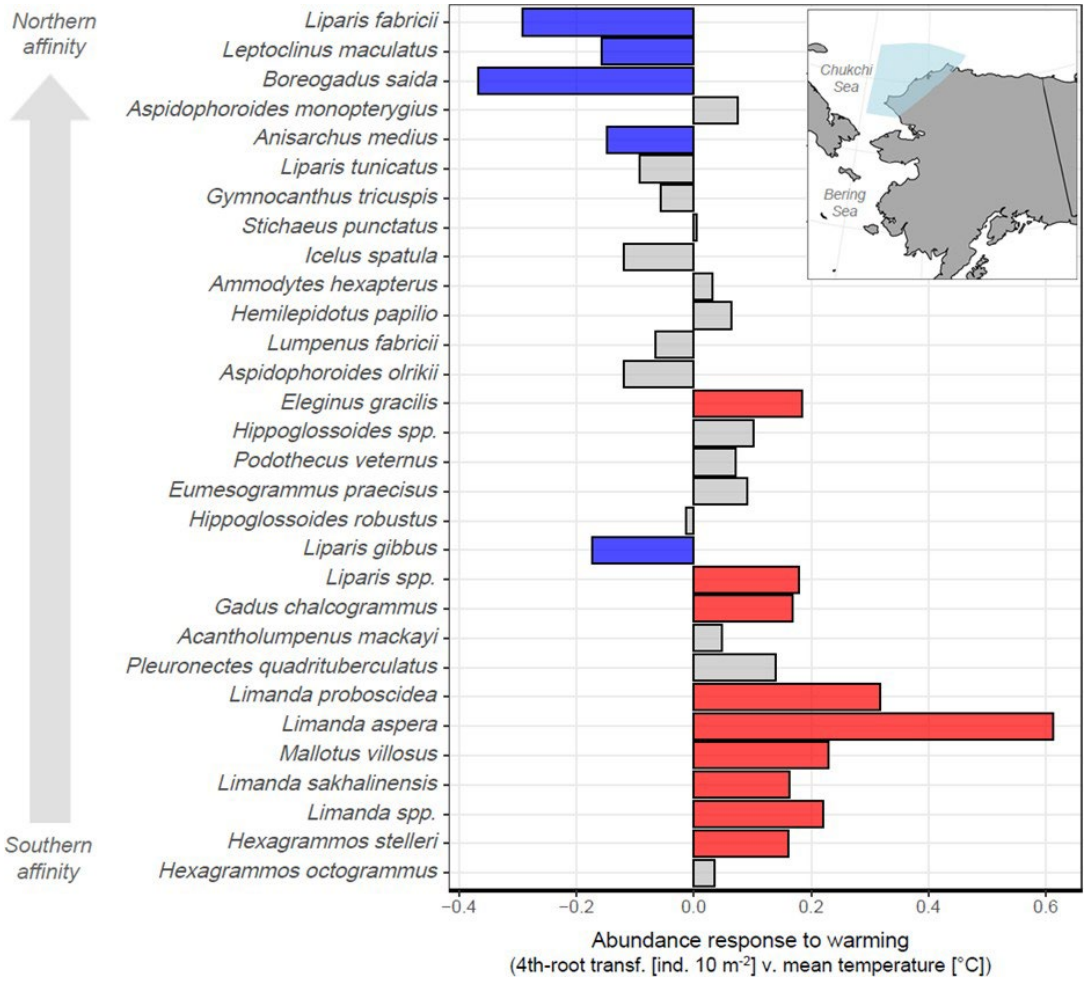

Fig. 1. Mean species-level relationships between the abundance (fourth-root transformed ind. 10 m^{-2}) of all 30 larval fish taxa examined in this study and temperature (°C) for all years pooled (2010-2019) during late summer in the northeast Chukchi Sea (calculated region shown in the blue polygon on the inset map). Spearman correlation coefficient values are given for each species' abundance and temperature pairing; positive correlations are displayed in red (indicating a significant increase in abundance in response to higher water temperatures), negative correlations in blue (indicating a significant decrease in response to warming), and grey indicates no significant response (correlations with $p \geq 0.05$). Taxa are sorted based on their mean latitudinal distribution in cold years (i.e., 2012-2013; proxy for average baseline Arctic conditions).

Chapter 11: High-resolution Biological Net Community Production in the Pacific-influenced Arctic: A Multi-Method Comparison

Cynar, H., CEOAS, Oregon State University, cynarh@oregonstate.edu

Juranek, L.W., Mordy, C.W., Strausz, D, Bell, S.

High-resolution Biological Net Community Production in the Pacific-influenced Arctic: A Multi-Method Comparison

Haley Cynar[1], Lauren W. Juranek[1], Calvin W. Mordy[2,3], David Strausz[2,3], Shaun Bell[3]

[1] College of Earth, Ocean, and Atmospheric Sciences, Oregon State University, Corvallis, USA

[2] Cooperative Institute for Climate, Ocean, and Ecosystem Studies, University of Washington, Seattle, USA

[3] Pacific Marine Environmental Laboratory, National Oceanic and Atmospheric Administration, Seattle, USA

ORCID:

(HC) https://orcid.org/0000-0003-0609-5226

(LWJ) https://orcid.org/0000-0002-4922-8263

(CWM) https://orcid.org/0000-0002-3674-7072

Correspondence: cynarh@oregonstate.edu

Abstract

Spatial and temporal patterns of primary productivity in the Arctic are expected to change with warming-associated changes in ice cover and stratification, yet productivity measurements are historically spatially and temporally limited. An established method to estimate net community production (NCP) rates involves measurement of dissolved oxygen/argon gas ratios (O_2/Ar) from a vessel's underway seawater system. An emerging method that may provide comparable NCP estimates involves measurement of oxygen/nitrogen ratios (O_2/N_2) with a gas tension device (GTD) and optode. The GTD/optode combo has several advantages: it is small, inexpensive, and suitable for autonomous deployments; however, the dissimilarity in solubility between O_2 and N_2 makes this tracer pair less favorable than O_2/Ar. We conducted a side-by-side comparison of a GTD and EIMS during the 2019 Arctic Integrated Ecosystem Survey OS1901-L1 in the Pacific Arctic. NCP from these two approaches were generally consistent throughout this cruise, with median NCP from O_2/Ar and O_2/N_2 of 7.33 ± 2.43 and 9.43 ± 2.73 mmol O_2 m^{-2} day^{-1} in comparable regions, respectively. While O_2/Ar and O_2/N_2 tracked each other in patterns, there were small deviations due to different sensitivities to physical drivers, which included a section in the Bering Strait where wind induced bubbles were the primary driver, followed by a period where both temperature and wind were thought to drive the differences between O_2/Ar and O_2/N_2. These results suggest that the GTD/optode can be used to enhance spatial and temporal coverage of NCP measurements. However, the GTD/optode approach is reliant on well-calibrated oxygen observations, a potential challenge if the GTD/optode is autonomously deployed. Uncertainty in the GTD/optode approach makes it well-suited to regions with strong gradients in NCP, while regions near equilibrium may result in unacceptably high uncertainty.

Chapter 12: Loss of sea ice alters distributions, abundance, and diet carbon sources of young Arctic forage fish in the Chukchi Sea

Goldstein, E.D., NOAA/Fisheries, esther.goldstein@noaa.gov

McCabe, R.M., Rogers, M.C., Deary, A., Duffy-Anderson, J.T.

Loss of sea ice alters distributions, abundance, and diet carbon sources of young Arctic forage fish in the Chukchi Sea

[*1,2]Goldstein E.D., [3]McCabe R.M., [4]Rogers M.C., [2]Deary A., [2,5]Duffy-Anderson J.T.

[1]NOAA Alaska Fisheries Science Center, Resource Ecology and Fisheries Management Division, 7600 Sand Point Way NE, Seattle, WA 98115, USA

[2]NOAA Alaska Fisheries Science Center, Resource Assessment and Conservation Engineering Division, 7600 Sand Point Way NE, Seattle, WA 98115, USA

[3]NOAA Pacific Marine Environmental Laboratory, 7600 Sand Point Way NE, Seattle, WA 98115, USA

[4]NOAA Alaska Fisheries Science Center, Auke Bay Laboratories, 17109 Pt. Lena Loop, Juneau, Alaska, 99801, USA

[5]Gulf of Maine Research Institute, 350 Commercial St., Portland, Maine, 04101, USA

*Corresponding author Esther.Goldstein@noaa.gov

Abstract

Loss of sea ice can alter habitat for forage fish and copepods that function as important energetic links between primary producers and higher trophic levels, potentially impacting spatial distributions and diets with consequences to Arctic marine food webs. To address the impacts of loss of sea ice on pelagic lower trophic level taxa, we focus on the early life stages of two species of forage fish (polar cod: *Boreogadus saida* and saffron cod: *Eleginus gracilis*) and two copepod taxa (*Calanus* spp. and *Pseudocalanus* spp.) in the Chukchi Sea with differing reliance on sea ice environments. We assess distributions throughout years of varying sea ice extent (2010-2013, 2015, 2017-2018) and diets during two unprecedented warm years (2017-2018) using stable isotope analyses [bulk $\delta^{13}C$ and $\delta^{15}N$ and $\delta^{13}C$ compound-specific isotope analysis of amino acids]. *Calanus* spp. and polar cod were found primarily in northern Chukchi Sea in close proximity to recent sea ice, whereas saffron cod were rare and *Pseudocalanus* spp. were more evenly distributed. Spatial patterns in $\delta^{13}C$ stable isotopes were latitudinal but also showed inshore-offshore gradients in regions where ocean current converge suggesting shifts in baseline isotope values as well as the potential for water mass-associated changes in carbon sources. When sea ice was entirely absent from the Chukchi shelf during 2017, all taxa were broadly dispersed but *Calanus* spp. abundance was low, polar cod had a reduced isotopic (diet) breadth, and diet carbon sources for both saffron cod and polar cod differed from those of 2018 when sea ice was also low but not absent. Changes in distributions and diet associated with lack of sea ice in the summer indicate shifts in pelagic habitats that are likely to reverberate up Arctic marine food webs.

Introduction

The Arctic is warming at an accelerated rate compared to lower latitudes, leading to loss of sea ice and feedbacks that amplify the impacts of climate change (Serreze and Barry 2011). Warmer temperatures and an extended ice-free season have multiple impacts on Arctic marine ecosystems such as altering species distributions (Frainer et al. 2017) as well as the phenology

and magnitude of algal blooms (Ji et al. 2013) that impact marine food webs (Griffith et al. 2019). For high latitude taxa that function as important links between primary producers and higher trophic levels, loss of sea ice and changes in primary production may impact pelagic habitats and alter species' distributions and diets with consequences that ripple throughout Arctic food webs.

To better understand the impacts of loss of sea ice and ocean warming on high latitude ecosystems and species that are adapted to sympagic habitats, we focus on important zooplankton taxa and the early life stages of forage fish that are closely tied to changes in primary producers. Specifically, we assess: 1) distributions and abundance of Polar cod (*Boreogadus saida*) and saffron cod: (*Eleginus gracilis*) during years of differing ice extent, 2) spatial variability in $\delta^{13}C$ and $\delta^{15}N$ stable isotopes in anomalously low-ice extent years for Polar and saffron cod as well as co-occurring *Calanus* spp. and *Pseudocalanus* spp. copepods (henceforth *Calanus* and *Pseudocalanus*), and 3) whether loss of sea ice alters carbon sources for forage fish that are important linkages to higher trophic levels.

Methods

We assess spatial distributions from the years 2010-2018 of two forage fish species (Polar cod: *Boreogadus saida* and saffron cod: *Eleginus gracilis*) during the pelagic larval life stage, and two copepod taxa (*Calanus* and *Pseudocalanus*) using a combination of historic and recent survey data collected in the Chukchi Sea available through the National Oceanic and Atmospheric Administration Eco-FOCI Program. Spatial and between-year patterns in diet were determined using stable isotope analyses during two unprecedented warm years (2017 and 2018) using two approaches: bulk stable isotopes and compound-specific isotope analysis of amino acids (CSIAA).

Bulk stable isotope values were measured to address variability in $\delta^{13}C$ and $\delta^{15}N$ due to baseline variation and shifts in diet and trophic position. Copepod and fish isotopic niches, indicative of diet breadth, were assessed for years with low (2018) and no (2017) summer ice by calculating convex hull and standard ellipse areas from bulk $\delta^{13}C$ and $\delta^{15}N$ stable isotope values. Lipids are depleted in ^{13}C compared to other tissues (Post et al. 2007), so bulk $\delta^{13}C$ values were corrected to account for lipids in the tissue samples following (Marsh et al. 2017) using equation (1) for fish that was derived from a combination of aquatic animal whole tissue samples and samples with solely muscle tissue (Post et al. 2007) and equation (2) for copepods (El-Sabaawi et al. 2009):

$$\delta^{13}C_{cor} = \delta^{13}C_{measured} - 3.32 + 0.99 * C{:}N \quad (1)$$

$$\delta^{13}C_{cor} = \delta^{13}C_{measured} - 1.85 + 0.38 * C{:}N \quad (2)$$

Where $\delta^{13}C_{cor}$ (henceforth referred to as $\delta^{13}C$) is the lipid-corrected value, $\delta^{13}C_{measured}$ is the measured value from bulk isotope analyses, and C:N is the carbon to nitrogen ratio for each fish or copepod sample. Several methods were employed to determine interannual variability in isotopic niche. Convex hulls and standard ellipses both incorporate variability in $\delta^{13}C$ and $\delta^{15}N$, but standard ellipse calculations were performed using Maximum Likelihood with a correction for small sample size (SEA_C) as well as a Bayesian framework (SEA_B) to account for bias associated with sample sizes and to allow for comparison among unbalanced datasets (Jackson et al. 2011). Isotopic niche analyses were performed using the R package SIBER (Jackson et al.

2011). Survey and sample coverage differed among study years, therefore the samples included in the analyses were truncated based on the latitudinal extent of the sample collection for each species during the year with the smallest spatial coverage. Specimens collected far from land were also excluded for *Pseudocalanus* in 2018 because no isotope samples were obtained from the region in 2017. Total area of the truncated sample region (excluding land) was calculated for each species and year to compare with isotope niche (SEA_B).

Focusing on forage fish, variation in $\delta^{13}C$ was also assessed using CSIAA to better understand the drivers of variability in baseline carbon sources and potential differences in food web dynamics between years and species. CSIAA has advantages over bulk analyses because essential amino acids (AA) can only be synthesized by bacteria, fungi, and photoautotrophs. Essential AAs therefore show minimal trophic fractionation throughout the food web because they are routed from the diet directly into the tissue of the consumer, thereby minimizing the need for isotopic baseline measurements (McMahon et al. 2010).

Results

High abundances of Polar cod and *Calanus* spp. were generally found farther north in closer proximity to recent sea ice, whereas saffron cod larvae were rare and *Pseudocalanus* spp. were more evenly distributed throughout the Chukchi Sea (Fig.1). For all taxa and years, regardless of sea ice extent, there were consistent regions of aggregation in the northern Chukchi sea near Barrow Canyon (Fig. 1). Based on carbon stable isotope analyses ($\delta^{13}C$: bulk stable isotopes and CSIAA), diet carbon sources were broadly similar for all taxa during the two warm years (Figs. 2 and 3A), but showed some minor difference within species among years (Figs 2B and 3B, C). Spatial patterns in stable isotopes indicated that there were latitudinal and inshore-offshore gradients in bulk $\delta^{13}C$ (Fig. 2A). When late summer sea ice was entirely absent in 2017, basal carbon sources in Polar cod and saffron cod diets were almost indistinguishable (Fig. 3A) and isotope niche breadth was reduced for Polar cod compared to 2018, primarily due to reduced breadth of $\delta^{13}C$ but not $\delta^{15}N$ (Table 1, Fig. 2B).

Discussion

Spatial patterns in distributions and carbon sources suggest interactions between sea ice extent during the summer months and ocean currents that advect warm southerly water northward across the Chukchi shelf, impacting the distributions of copepods and forage fish as well as the composition of primary producers consumed by key taxa in Arctic food webs. Of the four focal taxa, Polar cod and *Calanus* spp. are more ecologically-linked to sea ice habitats than saffron cod and *Pseudocalanus* spp. (Søreide et al. 2010; Leu et al. 2011; Kohlbach et al. 2017; Bouchard and Fortier 2020), implying that these taxa may be more sensitive to shifts in sea ice extent. Indeed, distributions of both taxa were often restricted to the north near recent sea ice and concentrated in regions where ocean currents converge such as Barrow Canyon (Danielson et al. 2017). While *Calanus* spp. and *Pseudocalanus* spp. taxonomic resolution for this study likely includes multiple species, comparisons of distributions among the four taxa suggest that sea ice likely impacts the southerly extent of Arctic species that are closely tied with sympagic habitats, which is not evident for taxa that are less tightly coupled with sea ice ecosystems and sea ice algal blooms.

Polar cod diet breadth and carbon sources shifted between low ice years to a greater degree than other taxa, suggesting that even the impacts of small changes in ice extent on pelagic conditions may affect basal carbon sources and feeding for a key species in Arctic food webs. Polar cod eggs hatch under the ice during the spring (Bouchard and Fortier 2008) and small larvae prey on copepod nauplii that feed on sea ice algae (Kohlbach et al. 2017). As they growth, larval Polar cod transition to broader diets that also include larger prey items such as lipid-rich *Calanus glacialis* copepods (Michaud et al. 1996). During a year with no summer sea ice, Polar cod diet breadth was more restricted and basal carbon sources from CSIAA were almost indistinguishable from saffron cod. In contrast, during 2018 when ice was minimal but present at some sampling stations (*personal observation*), Polar cod diet breadth was greater. Notably, bulk $\delta^{13}C$ values diverged from north to south, suggesting that shifts in diet breadth could be driven by both changes in advection and associated water mass composition as well as loss of sea ice that impacts primary producers. However, carbon source variation based on CSIAA also indicated slight shifts in diet between low ice years, suggesting alterations in baseline carbon sources for Polar cod. Such shifts highlight the sensitivity of Polar cod to changing conditions in the Arctic and suggest that lack of sea ice may force young fish to diverge from ice-associated carbon sources that typically contribute to Arctic food webs. Changes in distributions coupled with altered trophic relationships suggest broad consequences and potentially the borealization of Arctic ecosystems that could impact trophic structure and pelagic food web length and composition.

References

Bouchard C, Fortier L (2008) Effects of polynyas on the hatching season, early growth and survival of polar cod *Boreogadus saida* in the Laptev Sea. Marine Ecology Progress Series 355:247–256. doi: 10.3354/meps07335

Bouchard C, Fortier L (2020) The importance of *Calanus glacialis* for the feeding success of young polar cod: a circumpolar synthesis. Polar Biol. doi: 10.1007/s00300-020-02643-0

Danielson SL, Eisner L, Ladd C, Mordy C, Sousa L, Weingartner TJ (2017) A comparison between late summer 2012 and 2013 water masses, macronutrients, and phytoplankton standing crops in the northern Bering and Chukchi Seas. Deep Sea Research Part II: Topical Studies in Oceanography 135:7–26. doi: 10.1016/j.dsr2.2016.05.024

El-Sabaawi, R., J. F. Dower, M. Kainz, and A. Mazumder. 2009. Characterizing dietary variability and trophic positions of coastal calanoid copepods: insight from stable isotopes and fatty acids. Mar. Biol. **156**: 225–237. doi:10.1007/s00227-008-1073-1

Frainer A, Primicerio R, Kortsch S, Aune M, Dolgov AV, Fossheim M, Aschan MM (2017) Climate-driven changes in functional biogeography of Arctic marine fish communities. Proc Natl Acad Sci USA 114:12202–12207. doi: 10.1073/pnas.1706080114

Griffith GP, Hop H, Vihtakari M, Wold A, Kalhagen K, Gabrielsen GW (2019) Ecological resilience of Arctic marine food webs to climate change. Nat Clim Chang 9:868–872. doi: 10.1038/s41558-019-0601-y

Jackson AL, Inger R, Parnell AC, Bearhop S (2011) Comparing isotopic niche widths among and within communities: SIBER - Stable Isotope Bayesian Ellipses in R: Bayesian isotopic niche metrics. Journal of Animal Ecology 80:595–602. doi: 10.1111/j.1365-2656.2011.01806.x

Ji R, Jin M, Varpe Ø (2013) Sea ice phenology and timing of primary production pulses in the Arctic Ocean. Glob Change Biol 19:734–741. doi: 10.1111/gcb.12074

Kohlbach D, Schaafsma FL, Graeve M, Lebreton B, Lange BA, David C, Vortkamp M, Flores H (2017) Strong linkage of polar cod (Boreogadus saida) to sea ice algae-produced carbon: Evidence from stomach content, fatty acid and stable isotope analyses. Progress in Oceanography 152:62–74. doi: 10.1016/j.pocean.2017.02.003

Leu E, Søreide JE, Hessen DO, Falk-Petersen S, Berge J (2011) Consequences of changing sea-ice cover for primary and secondary producers in the European Arctic shelf seas: Timing, quantity, and quality. Progress in Oceanography 90:18–32. doi: 10.1016/j.pocean.2011.02.004

Marsh, J. M., F. J. Mueter, K. Iken, and S. Danielson. 2017. Ontogenetic, spatial and temporal variation in trophic level and diet of Chukchi Sea fishes. Deep Sea Res. Part II Top. Stud. Oceanogr. **135**: 78–94. doi:10.1016/j.dsr2.2016.07.010

McMahon KW, Fogel ML, Elsdon TS, Thorrold SR (2010) Carbon isotope fractionation of amino acids in fish muscle reflects biosynthesis and isotopic routing from dietary protein: Carbon isotope fractionation of fish muscle amino acids. Journal of Animal Ecology 79:1132–1141. doi: 10.1111/j.1365-2656.2010.01722.x

Michaud JE, Fortier L, Rowe P, Ramseier R (1996) Feeding success and survivorship of Arctic cod larvae, *Boreogadus saida*, in the Northeast Water polynya (Greenland Sea). Fisheries Oceanography 5:120–135. doi: 10.1111/j.1365-2419.1996.tb00111.x

Post, D. M., C. A. Layman, D. A. Arrington, G. Takimoto, J. Quattrochi, and C. G. Montaña. 2007. Getting to the fat of the matter: models, methods and assumptions for dealing with lipids in stable isotope analyses. Oecologia **152**: 179–189. doi:10.1007/s00442-006-0630-x

Serreze MC, Barry RG (2011) Processes and impacts of Arctic amplification: A research synthesis. Global and Planetary Change 77:85–96. doi: 10.1016/j.gloplacha.2011.03.004

Søreide JE, Leu E, Berge J, Graeve M, Falk-Petersen S (2010) Timing of blooms, algal food quality and *Calanus glacialis* reproduction and growth in a changing Arctic: Timing of production in a changing Arctic. Global Change Biology 16:3154–3163. doi: 10.1111/j.1365-2486.2010.02175.x

Table 1. Isotopic niche estimates from bulk $\delta^{13}C$ and $\delta^{15}N$ stable isotope values (Fig. 7b) using specimens from spatial areas outlined in Fig. 7a. Ellipse areas were calculated using maximum likelihood with a correction for small sample size (SEAc) and a Bayesian approach (SEA_B). SEA_B standardized to spatial area was calculated by dividing SEA_B and credible intervals by spatial area for each taxon and year.

Taxa	Year	Spatial area (km^2)	Convex hull area	Ellipse area (SEAc/SEA_B)	SEA_B 95% credible interval (CI) (low, high)	SEA_B standardized to spatial area $‰^2\ km^{-2} * 10^{-5}$ (CI low, CI high)
Polar cod	2017	38495	2.28	0.76/0.76	0.41, 1.13	1.97 (1.07, 2.94)
Polar cod	2018	29717	7.04	3.05/3.09	1.60, 4.82	10.40 (5.38, 16.22)
Saffron cod	2017	na	na	-	-	-
Saffron cod	2018	46422	7.84	4.32/4.52	1.91, 7.66	9.74 (4.11,16.50)
Calanus spp.	2017	78996	3.77	2.07/2.09	1.07, 3.30	2.65 (1.35, 4.18)
Calanus spp.	2018	44133	5.08	2.48/2.62	1.38, 4.00	5.94 (3.13, 9.06)
Pseudocalanus spp.	2017	57974	3.85	2.11/2.24	0.90, 3.87	3.86 (1.55, 6.68)
Pseudocalanus spp.	2018	57126	7.97	2.26/2.31	1.29, 3.45	4.04 (2.26, 6.04)

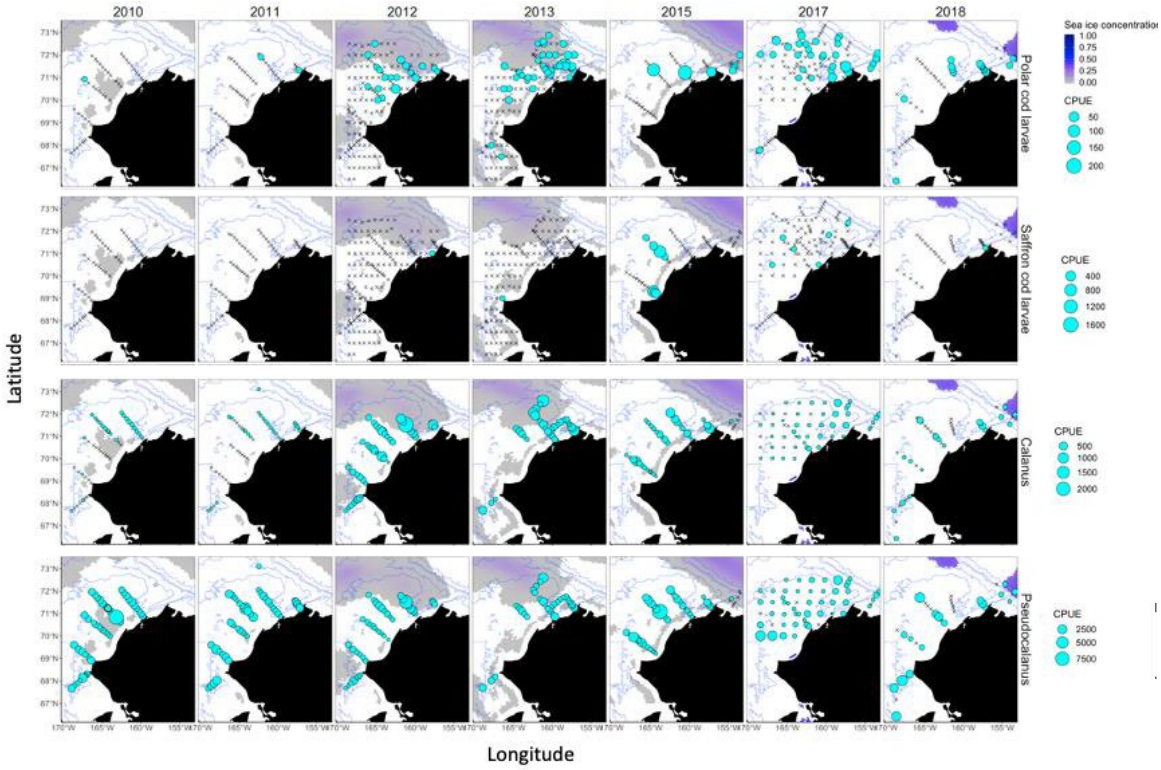

Figure 1. Distributions of larval Polar cod, saffron cod, *Calanus* and *Pseudocalanus* in relation to sea ice from 2010-2018 where CPUE is catch per unit effort (catch per 10 m^{-2} surface area calculated based on the maximum depth of the tow and volume filtered).

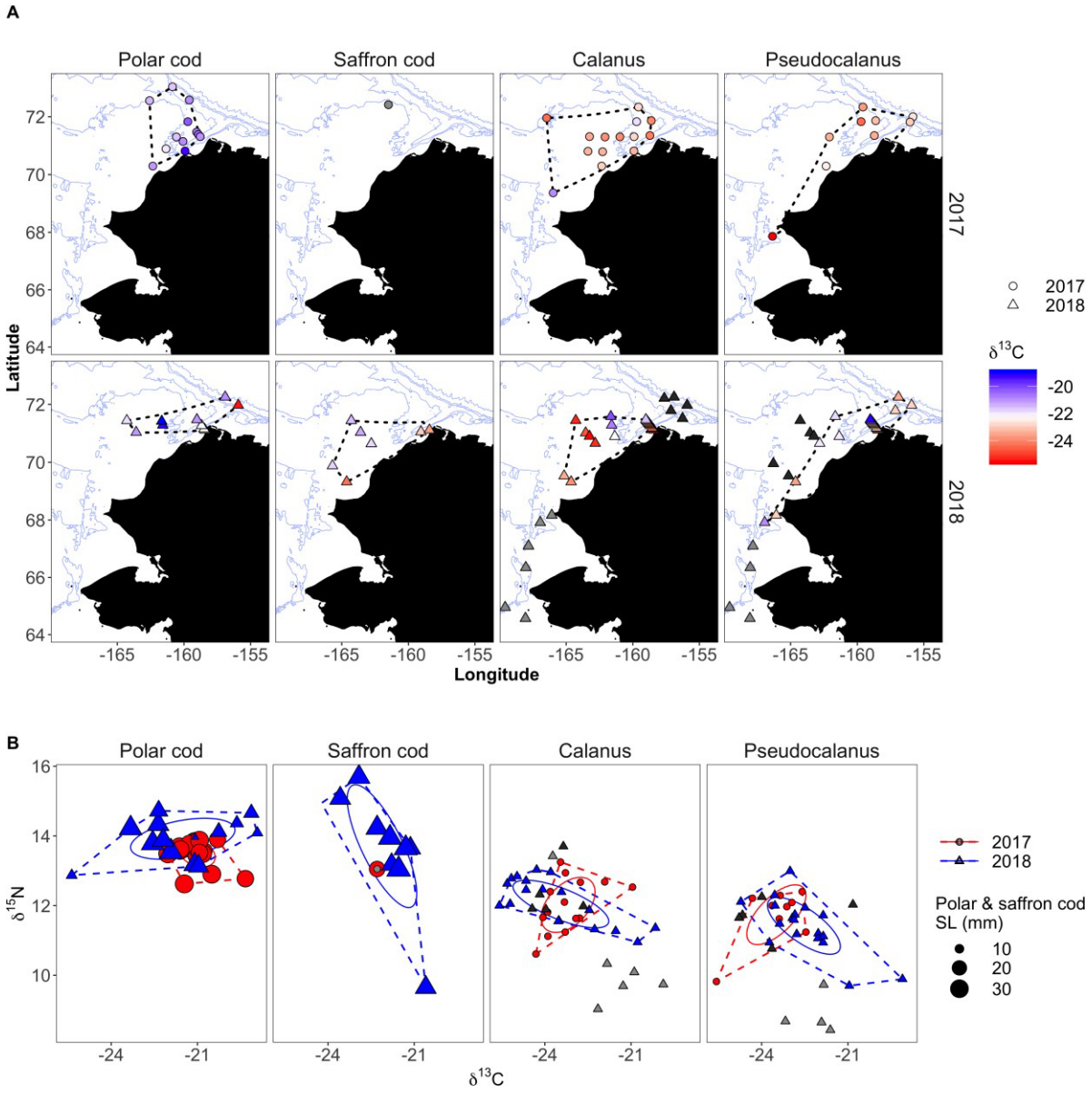

Figure 2. Stable isotope values from the years 2017 and 2018. (A) Maps of specimen collection locations for bulk $\delta^{13}C$ and $\delta^{15}N$ for Arctic cod, saffron cod, *Calanus* spp., and *Pseudocalanus* spp., with the color ramp scale corresponding to $\delta^{13}C$ bulk stable isotope values. (B) Bulk stable isotope values showing isotopic diet breadth as convex hull (dotted lines) and maximum likelihood 95% prediction ellipses (solid lines) based on (Jackson et al. 2011). Grey symbols in A and B were excluded from convex hulls and 95% prediction ellipses because sample collection locations extended beyond the geographic range of collection locations for other taxa or years. Shape denotes sample collection year to facilitate comparisons between (A) and (B). Symbol size in (B) corresponds fish specimen standard length (SL).

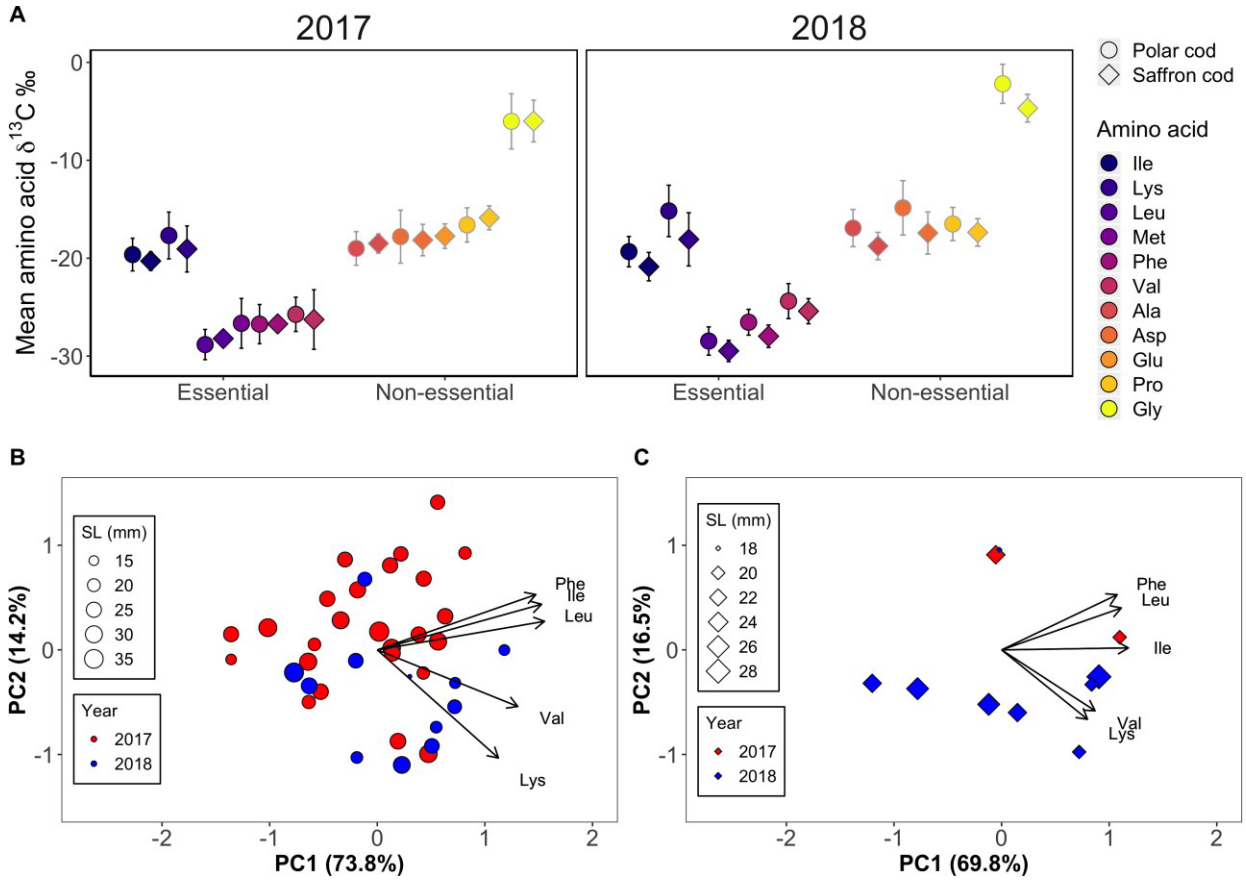

Figure 3. Stable isotope values from the years 2017 and 2018 showing (A) average (±SD) $\delta^{13}C$ from compound specific stable isotopes of amino acids for saffron cod and Arctic cod for essential amino acids that are routed directly from the diet into the tissue of the consumer and non-essential amino acids that are influenced by the complexity of physiological and biochemical processes that impact trophic fractionation. (B and C) Principal component (PC) analyses of a subset of essential amino acid $\delta^{13}C$ values for Polar cod (A) and saffron cod (B) specimens.

Chapter 13: Estimates of monthly flux of oceanic nutrients into the Arctic from 1998 to 2018 based on Anadyr Strait and Bering Strait measurements

Hennon, T.D, University of Alaska, Fairbanks, tdhennon@alaska.edu

Danielson, S.L., Mordy, C.W., Stockwell, D.A., Woodgate, R.A.

Anadyr Current Contributions to the Arctic-bound Oceanic Nutrient Flux

Tyler D. Hennon[1], Seth L. Danielson[1], Brita Irving[1], Dean A. Stockwell[1],
Rebecca A. Woodgate[2], Calvin W. Mordy[3,4]

[1]University of Alaska Fairbanks (UAF), College of Fisheries and Ocean Sciences, Fairbanks, AK, USA
[2]University of Washington (UW), Applied Physics Laboratory (APL), Seattle, WA, USA
[3]Cooperative Institute for Climate, Ocean, & Ecosystem Studies, University of Washington (UW), Seattle, WA, USA
[4]National Oceanographic and Atmospheric Administration (NOAA), Pacific Marine Environmental Laboratory (PMEL), Seattle, WA, USA

23 November 2021

Manuscript in preparation for Geophysical Research Letters

Based on year-round measurements of nutrients from summer 2017-2018 from the Anadyr Strait, we use a combination of year-round mooring-based in situ measurements and salinity-nutrient relationships established at Anadyr Strait are used to estimate Pacific-to-Arctic fluxes of nitrate, phosphate, and silicate for each month spanning 1998-2018. Annually averaged fluxes are 16 ± 5, 1.6 ± 0.5, and 30 ± 10 kmol s^{-1} for nitrate, phosphate, and silicate, respectively, and inter-annual variability can reach ±30% of the means. Maximum fluxes occur in April, exceeding the annual average by ~50%, while minimum fluxes occur in December. Due to biological uptake, the seasonality of nutrient fluxes is more closely tied to nutrient concentration than transport, which peaks in June. Our annually averaged estimates are ~ 50% higher than prior estimates, which may be rooted in methodological differences. We find significant ($p < 0.05$) increasing trends in phosphate and silicate fluxes over 1998-2018 that are associated with increasing transport. In contrast, nitrate exhibits no significant long-term trend, suggesting different nutrient composition ratios between surface and deep waters. Our data, taken from the core of the Anadyr current, will be valuable for assessing biogeochemical model performance at a globally important oceanic chokepoint and can contribute to studies that seek to understand the future trajectory of the Arctic ecosystem.

1 Introduction

The Arctic Ocean is experiencing rapid and accelerating change due to an anthropogenically altered climate (Zhang et al. 2005; Polyakov et al. 2020), including reduction of sea ice extent volume (Comiso et al. 2006, Frey et al. 2015, Wang et al. 2018), and altered growing conditions (e.g., changes in timing, temperature, and light availability) for marine phytoplankton (Arrigo et al. 2008, Codispoti et al. 2009, Neeley et al. 2018, Lewis and Arrigo, 2020). Consequently, the Arctic marine ecosystem may exhibit changes even to the character of the ecosystem services that it provides (Huntington et al., 2020), including critical habitat for marine mammals and seabirds, subsistence harvests vital to indigenous communities, and its globally important role in carbon export and sequestration.

The Arctic has limited connectivity to the rest of the world's oceans. Bering Strait is the only link to the Pacific ocean, and is relatively narrow and shallow, ~ 85 km across, with an average depth ~ 50 m, and an annual average throughflow of about 1.0 Sv (10^6 m^3s^{-1}) (Woodgate, 2018). The Anadyr Current (Fig. 1a) delivers approximately 80% of the Bering Strait transport through Anadyr Strait (Overland and Roach, 1987; Muench et al., 1988; Danielson et al., 2014). The two straits are separated by less than 250 km and the advective time scale is as little as 10 days (Coachman, 1993). Due to characteristically low nutrient concentrations on the eastern Bering shelf (Danielson et al. 2011), the Anadyr Current delivers the vast bulk of nutrients that are advected into the Arctic through Bering Strait. This nutrient-rich flow is thus singularly responsible for maintaining the remarkably high levels of pelagic and benthic biological productivity found downstream in Chirikov Basin and the Chukchi Sea (Grebmeier et al., 2015).

Relatively little work has evaluated Arctic-bound nutrient fluxes directly at Bering Strait. Torres-Valdes et al. (2013) used data from a single cross-strait transect from summer of 2005 in combination with modeled currents to estimate annually averaged fluxes into the Chukchi Sea. They found poleward fluxes of 9.0±0.8, 1.3±0.1, and 20.9±2.4 kmol s^{-1} for nitrate, phosphate, and silicate, respectively. Zhao et al. (2021) used a coupled physical and biogeochemical numerical model to estimate ~10 kmol s^{-1} of nitrate through Bering Strait. Downstream in the Chukchi Sea, Mordy et al. (2020) found considerable variability in winter nitrate flux (ranging between 0-10 kmol s^{-1} during 2010-2018). Here, we seek to build upon these results and provide an updated set of observation-based nutrient flux estimates by using a year of mooring-based measurements from Anadyr Strait (2017-2018) and long term mooring observations in the Bering Strait (1998-2018).

2 Data

2.1 Shipboard Hydrography

Nutrient and CTD hydrographic data from several ship-based observation programs that sampled in the Northern Bering and Southern Chukchi seas are used to characterize the regional nutrient distribution. All cruises took place between April and September (Fig. 1a) and in aggregate the collection includes over 500 vertical profiles (spanning 2004-2018). See supplementary Table A2 for more information on these cruises.

2.2 Moorings

2.2.1 Anadyr Strait Mooring

A subsurface mooring (N2) was deployed in 46 m of water in Anadyr Strait (Fig. 1a) from 12 June 2017 to 9 June 2018. At 64.1545 °N, 174.5260 °W. N2 was equipped with the following: three conductivity-

temperature-depth (CTD) sensors, a fluorometer, an acoustic Doppler current profiler (ADCP), submersible ultraviolet nitrate analyzer (SUNA), and an Aqua Monitor to collect bag samples for nutrient analysis. The SeaBird Electronics CTDs were mounted at 25 m (SBE-16, 120 minute sampling), 35 m and 41 m (SBE-37s with 15 minute sampling) depths. The WetLabs AFL fluorometer was mounted at 25 m depth (120 minute sampling). The upward-looking 300 kHz Teledyne RDI ADCP was mounted at 41 m depth (30 minute ensembles of 1-m bins). The SUNA V2 was mounted at 35 m depth (120 minute sampling). The Green Eyes Aqua Monitor discrete water sampler was mounted at 35 m depth. Between 12 June 2017 and 09 June 2018, twenty five 500 mL water samples were collected, each prepared with 400 μL of saturated mercuric chloride solution to halt microbial growth. Upon recovery, samples were analyzed for nitrate (NO_3), nitrite (NO_2), ammonium (NH_4) phosphate (PO_3) and silicate (SiO_4). All records were subjected to quality assurance protocols that are described in the archived datasets.

Immediately following mooring deployment, the Aqua Monitor collected four samples spanning 45 minutes to estimate repeatability and thereafter once every 9-31 days (averaging once every 17 days, see Supplementary Table S1).

2.2.2 Bering Strait Mooring

At Bering Strait, we employ monthly estimates of salinity and transport (Woodgate et al. 2015, Woodgate 2018) based on measurements from the long-term A3 mooring (Fig. 1a), which has been site of continuous monitoring from 1997 to the present and is representative of the Bering Strait through-flow (Woodgate 2015). Our estimates do not include contributions from the Alaskan Coastal Current (ACC), which contributes ~ 10% of the net transport but is generally nitrate-deplete (Danielson et al., 2017).

3. Results

3.1 Nutrient Biases and Corrections

Niskin bottle nutrient samples from the N2 mooring deployment and recovery cruises provide a means to correct both the SUNA and Aqua Monitor data for offsets and drift (e.g. Daniel et al., 2020). The Niskin samples (not shown) exhibit a well-mixed water column within ± 10 m of the Aqua Monitor at deployment, with average $NO3_{CTD}$=17.7±0.5, $PO4_{CTD}$=1.80±0.02, and $SiO4_{CTD}$=28.1±0.8 μM from 6 samples (± indicates standard deviation). Upon deployment, Aqua Monitor concentrations were as follows: $NO3_{AM}$ = 15±2, $PO4_{AM}$=1.9±0.1, and $SiO4_{AM}$=24±3. These samples suggest initial Aqua Monitor biases of about -3, +0.1, and -4 μM, and measurement uncertainties of ±2, ±0.1, and ±3 μM (nitrate, phosphate, and silicate, respectively). Upon recovery one year later, CTD profiles suggest the water column was well mixed within ±5 m of the Aqua Monitor, with average $NO3_{CTD}$=12.9±0.3, $PO4_{CTD}$=1.75±0.05, and $SiO4_{CTD}$=27±1 μM from 5 samples, where a single Aqua Monitor sample measured $NO3_{AM}$=12.9, $PO4_{AM}$=1.9, $SiO4_{AM}$=23.6. These samples suggest final Aqua Monitor biases of approximately 0, +0.1, and -3 μM (nitrate, phosphate, and silicate, respectively). We assume a linear drift between the deployment and recovery biases over the yearlong deployment, and adjust Aqua Monitor nutrient concentrations accordingly. Similarly, the bias at deployment (recovery) for the SUNA nitrate was 4.1 μM (deployment) and 0.3 μM (recovery), and concentrations were again adjusted assuming linear drift. Post corrections, the two measures of NO_3 at mooring N2 (Aqua Monitor and SUNA) are strongly correlated over the year-long deployment (root-mean-square-difference=2.3 μM, r=0.87 and $p<0.01$, Fig. 2e). The offset between SUNA and Aqua Monitor nitrate does not have a significant temporal trend, and the good agreement between these independent data provide evidence of the proper functioning of both instruments.

3.2 Salinity-nutrient relations

Ship-based hydrography from across the northern Bering Sea shelf and continental slope exhibit a nearly monotonic relationship between salinity (S_{HYD}) and nitrate ($NO3_{HYD}$) for measurements collected >100 m (Fig. 2a, dark grey dots), corresponding to parameter ranges of about S_{HYD}=33-34 and $NO3_{HYD}$=25-45 μM. Extrapolation of this mixing line to full nitrate depletion at salinity ~ 31 PSU closely approximates the maximum observed nitrate concentration for all salinities in the range of 31-34 (Fig. 2a), suggesting that in absence of nitrate draw-down due to biological production, mixing between the nitrate rich slope waters and the nitrate deplete shelf waters (upper 10-20 m throughout the southern Bering Sea) primarily regulates nutrient concentration. While it is not clear exactly what range of depths the Anadyr Current draws its source waters from, near-bottom observations of nitrate up to 30 μM in Anadyr Strait (Walsh et al., 1989) and typical vertical profiles from the slope region (Fig. 1c) suggest that the core of the Anadyr Current must draw slope waters from at least 100 m depth. In the absence of mixing, water from 100 m at the slope would provide a salinity of ~ 33.1 and NO_3 of ~ 28.2 (based on 14 samples taken from 100 m depth over the Bering slope with salinity and nitrate ranges of 33.0-33.3 and 24.5-30.4, respectively). If the Anadyr Current waters mix with lower-salinity shelf waters during their transit to Anadyr Strait, the mean source depth could be even greater.

In the aggregate, nutrient estimates from the Aqua Monitor near 35 m depth at N2 are not tightly coupled with *in situ* salinity (S_{N2}) from the co-located SBE37 instrument but significant relationships emerge when the data are partitioned seasonally (Fig. 2a-d), according to expected nutrient drawdown or regeneration. We divide the mooring data into three intervals, each with different environmental conditions: 1) January to April (cold, ice-covered, dark), 2) May to August (warming, ice-free or declining sea ice conditions, high light availability), and 3) September to December (warm, ice-free, decreasing light availability). The moored S_{N2} data is strongly correlated with $NO3_{AM}$ from January-April (orange) ($r=0.99$, $p<0.01$, $N=6$) and September-December (pink) ($r=0.97$, $p< 0.01$, $N=5$), but the relationship breaks down even at this sub-pycnocline depth for May-August (green) ($r=0.50$, $p=0.10$, $N=13$). The offset between the fall and winter regression lines is attributed to the fall season being at the end of the growing season where nutrients not yet fully replenished from the summer biological drawdown. The winter samples all fall close to the "upper limit" bounding mixing line between high-salinity, high-nitrate slope waters (e.g., salinity=33, nitrate = 30) and low-salinity, low-nitrate shelf waters (e.g., salinity=31, nitrate = 0). These results show that for the weakly stratified fall and winter seasons, salinity is a allows for a potentially useful estimate of nitrate in the Anadyr Current.

While it is possible to modestly improve the salinity-nitrate correlations with different grouping strategies (e.g. finer monthly partitioning), here we seek to avoid over-fitting to the individual year of data collection in favor of a coarser strategy that is generalizable to different years. Using detrended (Section 3.1) Aqua Monitor nitrate and SBE salinity at mooring N2, we perform linear least squares regressions to parameterize nitrate concentration ($NO3_{EST,N2}$) based on a known salinity (S_{N2}), such that

$$NO3_{EST,N2} = C_1 S_{N2} + C_2 \qquad \text{Eq. 1}$$

C_1 and C_2 are coefficients calculated for each of the three seasonal time frames described previously (Fig. 2b).

References

Abookire, A.A., Duffy-Anderson, J., Jump, C. 2007. Habitat associations and diet of young-of-the-year Pacific cod (*Gadus macrocephalus*) near Kodiak, Alaska. Mar. Biol. 150(4):713–726. 10.1007/s00227-006-0391-4.

Abookire, A.A., Piatt, J.F., Norcross, B.L. 2001. Juvenile groundfish habitat in Kachemak Bay, Alaska, during late summer. Alaska Fish. Res. Bull. 8(1):45–56.

Abookire, A.A., Rose, C.S. 2005. Modifications to a plumb staff beam trawl for sampling uneven, complex habitats. Fish. Res. 71(2):247–254. doi.org/10.1016/j.fishres.2004.06.006.

Andriashev, A.P. 1937. A contribution to the knowledge of the fishes from the Bering and Chukchi Seas. Explor. Mers. U.R.S.S. 25:292–355. (English summary).

Antonov, N.P., Emelin, P.O., Maznikova, O.A., Sheibak, A.Yu., Trofimova, A.O., Benzik, A.N., Nosov, M.A., Orlov, A.M. 2021. Walleye pollock *Gadus chalcogrammus* in the western Chukchi Sea: promising target of Arctic fishery? Deep-Sea Res. II: Topical Stud. Oceanogr. (this issue)

Baker, M.R. 2021. Contrast of warm and cold phases in the Bering Sea to understand spatial distributions of Arctic and sub-Arctic gadids. Polar Biol. doi.org/10.1007/s00300-021-02856-x

Barbeaux, S.J., Hollowed, A.B. 2018. Ontogeny matters: Climate variability and effects on fish distribution in the eastern Bering Sea. Fish. Oceanogr. 1:1–15.

Barber, W.E., Smith, R.L., Vallarino, M., Meyer, R.M. 1997. Demersal fish assemblages of the northeastern Chukchi Sea, Alaska. Fish. Bull., U.S. 95:195–209.

Brown, S.C., Bizzarro, J.J., Cailliet, G.M., Ebert, D.A. 2012. Breaking with tradition: redefining measures for diet description with a case study of the Aleutian skate *Bathyraja aleutica* (Gilbert 1896). Environ. Biol. Fishes 95(1):3–20.

Budge, S.M., Iverson, S.J., Koopman, H.N. 2006. Studying trophic ecology in marine ecosystems using fatty acids: A primer on analysis and interpretation. Mar. Mammal Sci. 22:759–801.

Bulatov, O.A. 1986. Distribution of eggs and larvae of codfishes (subfamily Gadinae) in the Pacific waters of Kamchatka and western Bering Sea. In: Codfishes of the Far Eastern seas. Vladivostok, TINRO. pp. 89–102 (In Russian)

Copeman, L.A., Laurel, B.J., Spencer, M., Sremba, A. 2017. Temperature impacts on lipid allocation among juvenile gadid species at the Pacific Arctic-Boreal interface: an experimental laboratory approach. Mar. Ecol. Prog. Ser. 566:183–198. doi.org/10.3354/meps12040.

Danielson, S.L., Ahkinga, O., Ashjian, C., Basyuk, E., Cooper, L.W., Eisner, L., Farley, E. and others. 2020. Manifestation and consequences of warming and altered heat fluxes over the Bering and Chukchi Sea continental shelves. Deep-Sea Res. II: Topical Stud. Oceanogr. 177.

Emelyanova, O.R., Grigorov, I.V., Orlov, A.M., Orlova S.Yu. 2021. Polymorphism of mtDNA gene *Cyt b* of the Chukchi Sea walleye pollock, *Gadus chalcogrammus* (Gadidae, Gadiformes) Deep-Sea Res. II: Topical Stud. Oceanogr. (this issue).

Fadeev, N.S. 2005. Guide to biology and fisheries of fishes of the North Pacific Ocean. Vladivostok, TINRO-Center. 366 p.

Figueira, W.F., Booth, D.J. 2010. Increasing ocean temperatures allow tropical fishes to survive overwinter in temperate waters. Global Change Biol. 16:506–516.

Folch, J., Less, M., Sloane Stanley, G.H. 1956. A simple method for the isolation and purification of total lipids from animal tissues. J. Biological Chem. 22:497–509.

Grebmeier, J.M., Bluhm, B.A., Cooper, L.W., Danielson, S.L., Arrigo, K.R., Blanchard, A.L., Clarke, J.T., Day, R.H., Frey, K.E., Gradinger, R.R., Kedra, M., Konar, B., Kuletz, K.J., Lee, S. H., Lovvorn, J.R., Norcross, B.L., Okkonen, S.R. 2015. Ecosystem characteristics and processes facilitating persistent macrobenthic biomass hotspots and associated benthivory in the Pacific Arctic. Prog. Oceanogr. 136:92–114. doi.org/10.1016/j.pocean.2015.05.006.

Gunderson, D.R., Ellis, I.E. 1986. Development of a plumb staff beam trawl for sampling demersal fauna. Fish. Res. 4(1):35–41. doi.org/10.1016/0165-7836(86)90026-3.

Hill, N.J., Tobin, A.J., Reside, A.E., Pepperell, J.G., Bridge, T.C.L. 2016. Dynamic habitat suitability modeling reveals rapid poleward distribution shift in a mobile apex predator. Global Change Biol. 22:1086–1096.

Hollowed, A.B., Barange, M., Beamish, R., Brander, K., Cochrane, K., Drinkwater, K., Foreman, M., Hare, J., Holt, J., Ito, S-I., Kim, S., King, J., Loeng, H., MacKenzie, B., Mueter, F., Okey, T., Peck, M. A., Radchenko, V., Rice, J., Schirripa, M., Yatsu, A., and Yamanaka, Y. 2013. Projected impacts of climate change on marine fish and fisheries. ICES J. Mar. Sci. 70:1023–1037.

Hurst, T.P. 2007. Causes and consequences of winter mortality in fishes. J. Fish Biol. 71:315–345.

Hurst, T.P., Cooper, D.W., Duffy-Anderson, J.T., Farely, E.V. 2015. Contrasting coastal and shelf nursery habitats of Pacific cod in the southeast Bering Sea. ICES J. Mar. Sci. 72(2):515–527. doi.org/10.1093/icesjms/fsu141.

Hurst, T.P., Laurel, B.J., Ciannelli, L. 2010. Ontogenetic patterns and temperature-dependent growth rates in early life stages of Pacific cod (*Gadus macrocephalus*). Fish. Bull., U.S. 108:382–392.

Hurst, T.P., Miller, J.A., Ferm, N., Heintz, R.A., Farley, E.V. 2018. Spatial variation in potential and realized growth of juvenile Pacific cod in the southeastern Bering Sea. Mar. Ecol. Prog. Ser. 590:171–185. doi.org/10.3354/meps12494.

Hurst, T.P., Moss, J.H., Miller, J.A. 2012a. Distributional patterns of 0-group Pacific cod (*Gadus macrocephalus*) in the eastern Bering Sea under variable recruitment and thermal conditions. ICES J. Mar. Sci. 69:163–174.

Hurst, T.P., Munch, S.B., Lavalle, K.A. 2012b. Thermal reaction norms for growth vary among cohorts of Pacific cod (*Gadus macrocephalus*). Mar. Biol. 159:2173–2183. doi.org/10.1007/s00227-012-2003-9.

Kotwicki, S., Lauth, R.R. 2013. Detecting temporal trends and environmentally-driven changes in the spatial distribution of bottom fishes and crabs on the eastern Bering Sea shelf. Deep-Sea Res. II: Topical Stud. Oceanogr. 94:231–243.

Kotwicki, S. Lauth, R.R., Williams, K., Goodman, S.E. 2017. Selectivity ratio: A useful tool for comparing size selectivity of multiple survey gears. Fish. Res. 191:76 – 86. doi.org/10.1016/j.fishres.2017.02.012.

Laurel, B.J., Copeman, L.A., Hurst, T.P. et al. 2010. The ecological significance of lipid/fatty acid synthesis in developing eggs and newly hatched larvae of Pacific cod (*Gadus macrocephalus*). Mar. Biol. 157:1713–1724 doi.org/10.1007/s00227-010-1445-1

Laurel, B.J., Hunsicker, M.E., Ciannelli, L., Hurst, T.P., Duffy-Anderson, J., O'Malley, R., Behrenfeld, M. 2021. Regional warming exacerbates match/mismatch vulnerability for cod larvae in Alaska. Prog. Oceanogr. 193.

Laurel, B.J., Hurst, T.P., Copeman, L.A., Davis, M.W. 2008. The role of temperature on the growth and survival of early and late hatching Pacific cod larvae (*Gadus macrocephalus*). J. Plankton Res. 30(9):1051–1060.

Laurel, B.J., Knoth, B.A., Ryer, C.H. 2016a. Growth, mortality, and recruitment signals in age-0 gadids settling in coastal Gulf of Alaska. ICES J. Mar. Sci. 73(9): 2227–2237. doi:10.1093/icesjms/fsw039.

Laurel, B.J., and Rogers, L.A. 2020. Loss of spawning habitat and prerecruits of Pacific cod during a Gulf of Alaska heatwave. Canadian J. of Fish. Aquat. Sci. 77(4): 644-650. doi.org/10.1139/cjfas-2019–0238.

Laurel, B.J., Spencer, M., Iseri, P., Copeman, L.A. 2016b. Temperature-dependent growth and behavior of juvenile Arctic cod (*Boreogadus saida*) and co-occurring North Pacific gadids. Polar Biol. 39:1127–1135. doi.org/10.1007/s00300-015-1761-5.

Laurel, J., Stoner, A.W., Ryer, C.H., Hurst, T.P., Abookire, A.A. 2007. Comparative habitat associations in juvenile Pacific cod and other gadids using seines, baited cameras and laboratory techniques. J. Exp. Mar. Biol. Ecol. 351(1–2): 42–55.

Lauth, R.R., Britt, L., Kotwicki, S., Norcross, B. In prep. Differences in catchability between two bottom trawls used in Arctic bottom trawls surveys of bottom fishes, crabs and other demersal macrofauna.

Levine, R.M., De Robertis, A., Grunbaum, D., Wildes, S., Farley, E.V., Stabeno, P.J., Wilson, C.D. This Issue. Climate-driven shift in pelagic fish distributions in a rapidly changing Pacific Arctic.

Logerwell, E., Busby, M., Carothers, C., Cotton, S., Duffy-Anderson, J., Farley, E., Goddard, P., Heintz, R., Holladay, B., Horne, J., Johnson, S., Lauth, B., Moulton, L., Neff, D., Norcross, B., Parker-Stetter, S., Seigle, J., Sformo, T. 2015. Fish communities across a spectrum of habitats in the western Beaufort Sea and Chukchi Sea, Prog. Oceanogr. 136:115–132. doi: http://dx.doi.org/10.1016/j.pocean.2015.05.013.

Matarese, A.C., Blood, D.M., Picquelle, S.J., Benson, J.L. 2003. Atlas of abundance and distribution patterns of ichthyoplankton from the northeast Pacific Ocean and Bering Sea ecosystems based on research conducted by the Alaska Fisheries Science Center (1972–1996). NOAA Prof. Paper NMFS 1, 281 p.

Mecklenburg, C.W., Lynghammar, A., Johannesen, E., Byrkjedal, I., Christiansen, J.S., Dolgov, A.V., Karamushko, T.A., Møller, P.R., Steinke, D., Wienerroither, R.M. 2018. Marine Fishes of the Arctic Region, Volume I. Conservation of Arctic Flora and Fauna Monitoring Series Report 28.

Mecklenburg, C.W., Møller, P.R., Steinke, D. 2011. Biodiversity of arctic marine fishes: taxonomy and zoogeography. Mar. Biodivers. 41:109–140 and online resource 2.

Morley, J.W., Batt, R.D., Pinsky M.L. 2017. Marine assemblages respond rapidly to winter climate variability. Global Change Biol. 23: 2590–2601. doi: 10.1111/gcb.13578

Mueter, F.J., Litzow, M.A. 2008. Sea ice retreat alters the biogeography of the Bering Sea continental shelf. Ecol. Appl. 18:309–320

Neidetcher, S.K., Hurst, T.P., Ciannelli, L., Logerwell, E.A. 2014. Spawning phenology and geography of Aleutian Islands and eastern Bering Sea Pacific cod (*Gadus macrocephalus*). Deep-Sea Res. II: Topical Stud. Oceanogr. 109:204–214. doi.org/10.1016/j.dsr2.2013.12.006.

Nichol, D.G., Honkalehto, T., Thompson, G.G. 2007. Proximity of Pacific cod to the sea floor: Using archival tags to estimate fish availability to research bottom trawls. Fish. Res. 86:129–135.

Nye, J., Link, J., Hare, J., Overholtz, W. 2009. Changing spatial distribution of fish stocks in relation to climate and population size on the Northeast United Sates continental shelf. Mar. Ecol. Prog. Ser. 393:111–129. Doi.org/10.3354/meps08220.

Orlov, A.M., Benzik, A.N., Vedishcheva, E.V., Gafitsky, S.V., Gorbatenko, K.M., Goryanina, S.V., Zubarevich, V.L., Kodryan, K.V., Nosov, M.A., Orlova, S.Yu., Pedchenko, A.P., Rybakov, M.O., Sokolov, A.M., Somov, A.A., Subbotin, S.N., Taptygin, M.Yu., Firsov, Yu.L., Khleborodov, A.S., Chikilev, V.G., 2019. Fisheries research in the Chukchi Sea on the RV ”Professor Levanidov” in August 2019: some preliminary results, Trudy VNIRO 178:206–220. DOI: 10.36038/2307-3497-2019-178-206-220.

Orlov, A.M., Rabazanov, N.I., Nikiforov, A.I. 2020. Transoceanic migrations of fishlike animals and fish: norm or exclusion? J. Ichthyol. 60:242–262. https://doi.org/10.1134/S0032945220020125

Orlov, A.M., Gorbatenko, K.M., Benzik, A.N., Rybakov, M.O., Nosov, M.A., Orlova, S.Y.,. 2021. Biological research in the Siberian Arctic seas in summer–autumn 2019 (cruise of the R/V Professor Levanidov). Oceanology 61:295–296. https://doi.org/10.1134/S0001437021020156,

Overland, J.E., Wang, M., Wood, K.R., Percival, D.B,. Bond, N.A. 2012. Recent Bering Sea warm and cold events in a 95-year context. Deep-Sea Res. II: Topical Stud. Oceanogr. 65–70: 6–13.

Parrish, C.C. 1987. Separation of aquatic lipid classes by chromarod thin-layer chromatography with measurement by Iatroscan flame ionization detection. Canadian J. Fish. Aquat. Sci. 44:722–731.

Pianka, E.R. 1973. The structure of lizard communities. Annu. Rev. Ecol. and Systematics 4: 53–74.

Post, D.M. 2002. Using stable isotopes to estimate trophic position: models, methods, and assumptions. Ecol. 83:703–718.

Post, D.M., Layman, C.A., Arrington, D.A., Takimoto, G., Quattrochi, J., Montana, C.G. 2007. Getting to the fat of the matter: models, methods and assumptions for dealing with lipids in stable isotope analyses. Oecologia 152:179–189.
R Core Team. 2020. R: A language and environment for statistical computing. R Foundation for Statistical Computing, Vienna, Austria. URL https://www.R-project.org/.
Rand, K., Logerwell, E.A. 2010. The first survey of the abundance of benthic fish and invertebrates in the offshore marine waters of the Beaufort Sea since the late 1970s. Polar Biol. 34:475–488.
Rindorf, A., Lewy, P. 2006. Warm, windy winters drive cod north and homing of spawners keeps them there. J. Appl. Ecol. 43: 445–453.
Shuntov, V.P., Volvenko, I.V., Kulik, V.V., Bocharov, L.N. 2014. Benthic macrofauna of the western part of the Bering Sea: occurrence, abundance, and biomass. 1977–2010. Edited by V.P. Shuntov and L.N. Bocharov. Vladivostok : TINRO-Centre, 803 pp.
Siddon, E.C., Zador, S. G., Hunt G. L. 2020. Ecological responses to climate perturbations and minimal sea ice in the northern Bering Sea. Deep-Sea Res. II: Topical Stud. Oceanogr. 181–182. doi.org/10.1016/j.dsr2.2020.104914
Sogard, S.M. 1997. Size-selective mortality in the juvenile stage of teleost fishes: A review. Bull. Mar. Sci. 60:1129–1157.
Stabeno, P.J, Bell, S.W. 2019. Extreme Conditions in the Bering Sea (2017–2018): Record-Breaking Low Sea-Ice Extent. Geophys. Res. Lett. 46(15):8952–8959.
Stabeno, P.J., Bond, N.A., Kachel, N.B., Salo, S.A., Schumacher, J.D. 2001. On the temporal variability of the physical environment over the southeastern Bering Sea. Fish. Oceanogr. 10: 81–98.
Stabeno, P., Moore, S., Napp, J., Sigler, M., Zerbini, A. 2012. Comparison of warm and cold years on the southeastern Bering Sea shelf. Deep-Sea Res. II: Topical Stud. Oceanogr. 65–70: 31–45.
Stark, J.W. 2007. Geographic and seasonal variations in maturation and growth of female Pacific cod (*Gadus macrocephalus*) in the Gulf of Alaska and Bering Sea. Fish. Bull., U.S. 105:396–407.
Stauffer, G. (compiler). 2004. NOAA protocols for groundfish bottom trawl surveys of the nation's fishery resources. NOAA Tech. Memo. NMFS-F/SPO-65, 205 p.
Stevenson, D.E., Lauth, R.R. 2019. Bottom trawl surveys in the northern Bering Sea indicate recent shifts in the distribution of marine species. Polar Biol. 42:407–421. doi.org/10.1007/s00300-018-2431-1.
Thompson, G. 2018. Assessment of the Pacific cod stock in the eastern Bering Sea. Stock assessment and fishery evaluation report for the groundfish resources of the Bering Sea/Aleutian Islands regions. In Stock assessment and fishery evaluation report for the groundfish resources of the Bering Sea/Aleutian Islands regions, North Pacific Fishery Management Council, Anchorage, Alaska.
Thomson, J.A. 1963. On the demersal quality of the fertilized eggs of Pacific cod, *Gadus macrocephalus* Tilesius. J. Fish. Res. Board Canada 20:1087–1088.
Woodgate, R.A. 2018. Increases in the Pacific inflow to the Arctic from 1990 to 2015, and insights into seasonal trends and driving mechanisms from year-round Bering Strait mooring data. Prog. Oceanogr. 160:124–154.
Woodgate R.A., Aagaard, K., Weingartner, T.J. 2005. Monthly temperature, salinity, and transport variability of the Bering Strait through flow, Geophys. Res. Lett., 32, L04601, doi:10.1029/2004GL021880.
Woodgate, R.A., Peralta-Ferriz, C. 2021. Warming and Freshening of the Pacific Inflow to the Arctic from 1990–2019 implying dramatic shoaling in Pacific Winter Water ventilation of the Arctic water column. Geophys. Res. Lett. doi:10.1029/2021GL092528.
Woodgate, R.A., Stafford, K.M., Prahl, F.G. 2015. A synthesis of year-round interdisciplinary mooring measurements in the Bering Strait (1990–2014) and the RUSALCA years (2004–2011). Oceanogr. 28(3):46–67, http://dx.doi.org/10.5670/ oceanog.2015.57.
Woodgate, R.A., Weingartner, T., Lindsay, R. 2010. The 2007 Bering Strait oceanic heat flux and anomalous Arctic sea-ice retreat, Geophys. Res. Lett. 37, L01602, doi:10.1029/2009GL041621.

Wyllie-Echeverria, T., Wooster, W.S. 1998. Year-to-year variations in Bering Sea ice cover and some consequences for fish distributions. Fish. Oceanogr. 7:159–170.
Zakharov E.A., Kruchinin O.N., Mizurkin M.A., Safronov V.A. 2013. Geometric parameters of the bottom trawl 27.1/24.4, and its possible errors in assessment of number of marine organisms. Izv. TINRO. 174:284–292.

Table 1. Summary of trawling effort in the Chukchi Sea included in this study.

Year	Months	Trawl type (model)	Mouth opening	Max. mesh (mm)	Min. mesh (mm)	No. stations	Chukchi Sea Region
2010	Sep.	Large-mesh benthic (DT 27.1/24.4)	16.2 m horiz.	80	10	38	Western
2012	Aug. - Sep.	Large-mesh benthic (83-112)	17.0 m horiz.	100	31	71	Eastern
2012	Aug. - Sep.	Small-mesh benthic	2.1 m horiz.	7	4	40	Eastern
2017	Aug. - Sep.	Surface	18 m horiz. X 24 m vert.	1620	12	17	Eastern
2017	Aug. - Sep.	Midwater	7.5 m horz. X 7.9 m vert.	64	30	33	Eastern
2017	Aug. - Sep.	Small-mesh benthic	2.1 m horiz.	7	4	60	Eastern
2018	Aug. - Sep.	Large-mesh benthic (DT 27.1/24.4)	16.2 m horiz.	80	10	54	Western
2019	Aug. - Sep.	Surface	18 m horiz. X 24 m vert.	1620	12	10	Eastern
2019	Aug. - Sep.	Midwater	7.5 m horz. X 7.9 m vert.	64	30	42	Eastern
2019	Aug. - Sep.	Small-mesh benthic	2.1 m horiz.	7	4	49	Eastern
2019	August	Large-mesh benthic (DT 27.1/24.4)	16.2 m horiz.	80	10	79	Western

Table 2. Prey-specific relative index of importance (PSIRI) for prey taxa by trawl type for Pacific cod small juveniles collected in the eastern Chukchi Sea in 2017. Only prey items with PSIRI greater than 3 are listed.

Trawl Type	Prey Taxa	Prey Group	PSIRI
Small-mesh benthic	Polychaeta	Annelid worm	13.57
Small-mesh benthic	Eurytemora herdmandi	Calanoid copepods, <2.5 mm Total length	13.55
Small-mesh benthic	Nematoda parasite	Unidentified	10.55
Small-mesh benthic	Euphausiidae juv/adult	Euphausiids, j+a	10.00
Small-mesh benthic	Decapoda	Decapoda	8.83
Small-mesh benthic	Cistenides spp.	Annelid worm	5.59
Small-mesh benthic	Margarites spp.	Gastropod	4.41
Small-mesh benthic	Argis spp.	Carideans	3.21
Small-mesh benthic	Paguridae juv/adult	Anomuran crab	3.06
Midwater	Calanoida (<2.5 mm)	Calanoid copepods, <2.5 mm Total length	17.68
Midwater	Actinopterygii	Fish	17.48
Midwater	Caridea	Carideans	17.01
Midwater	Gadiformes	Fish	12.89
Midwater	Cirripedia cypris	Barnacle	8.72
Midwater	Centropages abdominalis	Calanoid copepods, >2.5 mm Total length	8.09
Midwater	Brachyura megalopa	Brachyuran crab	6.80
Midwater	Paguridae zoea	Anomuran crab	6.04
Surface	Centropages abdominalis	Calanoid copepods, >2.5 mm Total length	31.41
Surface	Calanoida (<2.5 mm)	Calanoid copepods, <2.5 mm Total length	31.28
Surface	Decapoda	Decapoda	13.45
Surface	Crustacea	Crustacean	8.33
Surface	Pseudocalanus spp.	Calanoid copepods, <2.5 mm Total length	7.34
Surface	Brachyura megalopa	Brachyuran crab	5.73

Table 3. Comparison of Catch per Unit Effort (CPUE) in this and other studies from Alaskan waters using a similar 3-meter beam trawl based on the design of Gunderson and Ellis (1986). Where noted, the trawls were based on the modified design of Abookire and Rose (2005).

Large Marine Ecosystem	Area	Year	Trawl Design	Mean Pacific cod km^{-2}	Reference
Chukchi Sea	20-29m depth range	2017	Abookire and Rose (2005)	6,200	This study
Chukchi Sea	30-39m depth range	2017	Abookire and Rose (2005)	2,800	This study
Chukchi Sea	20-29m depth range	2019	Abookire and Rose (2005)	0	This study
Chukchi Sea	30-39m depth range	2019	Abookire and Rose (2005)	1,800	This study
Bering Sea	Alaska Peninsula <50m depth	2012	Abookire and Rose (2005)	2,200	Hurst et al., 2015
Gulf of Alaska	Kachemak Bay	1994	Gunderson and Ellis (1986)	100	Abookire et al., 2001
Gulf of Alaska	Kachemak Bay	1995	Gunderson and Ellis (1986)	48,700	Abookire et al., 2001
Gulf of Alaska	Kachemak Bay	1996	Gunderson and Ellis (1986)	0	Abookire et al., 2001
Gulf of Alaska	Kachemak Bay	1997	Gunderson and Ellis (1986)	50,300	Abookire et al., 2001
Gulf of Alaska	Kachemak Bay	1998	Gunderson and Ellis (1986)	200	Abookire et al., 2001
Gulf of Alaska	Kachemak Bay	1999	Gunderson and Ellis (1986)	600	Abookire et al., 2001

Figure 1. Map of the study area in the Chukchi and northern Bering Seas and the surrounding area.

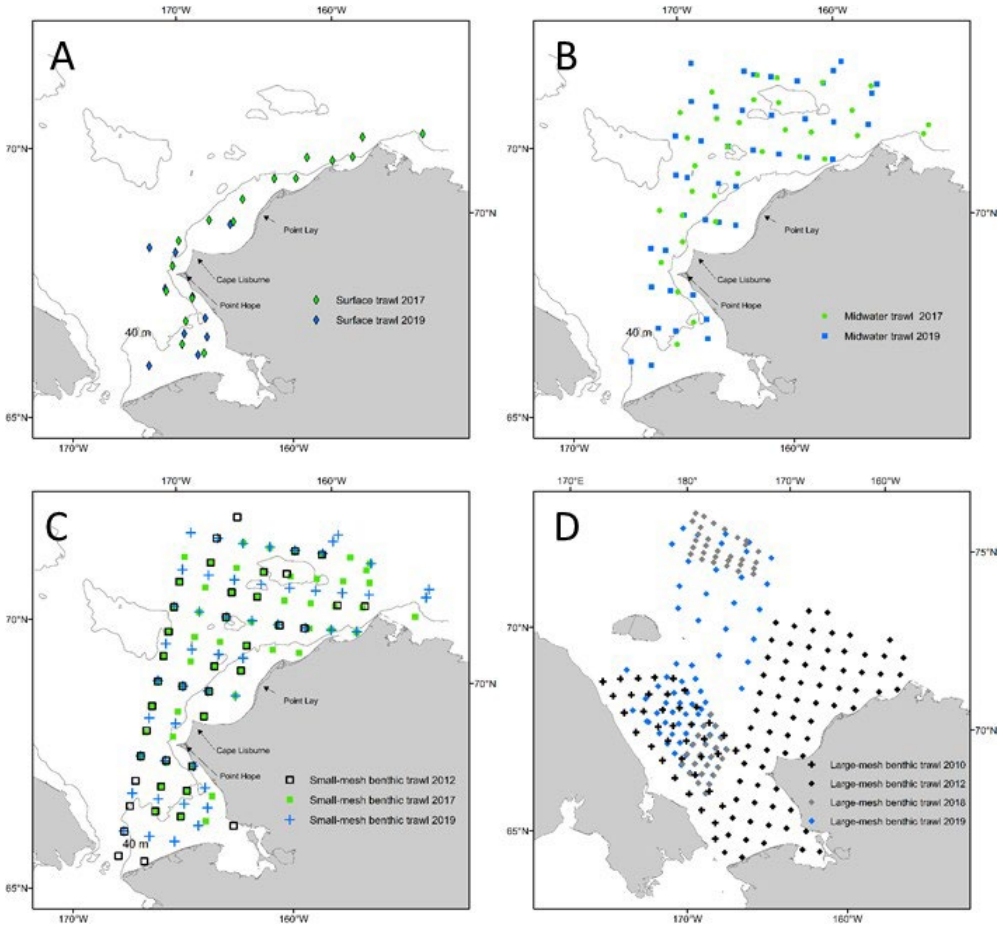

Figure 2. Maps of trawl sampling effort by trawl type and sampling year for A) surface trawl, B) midwater trawl, C) small-mesh benthic trawl, and D) large-mesh benthic trawls.

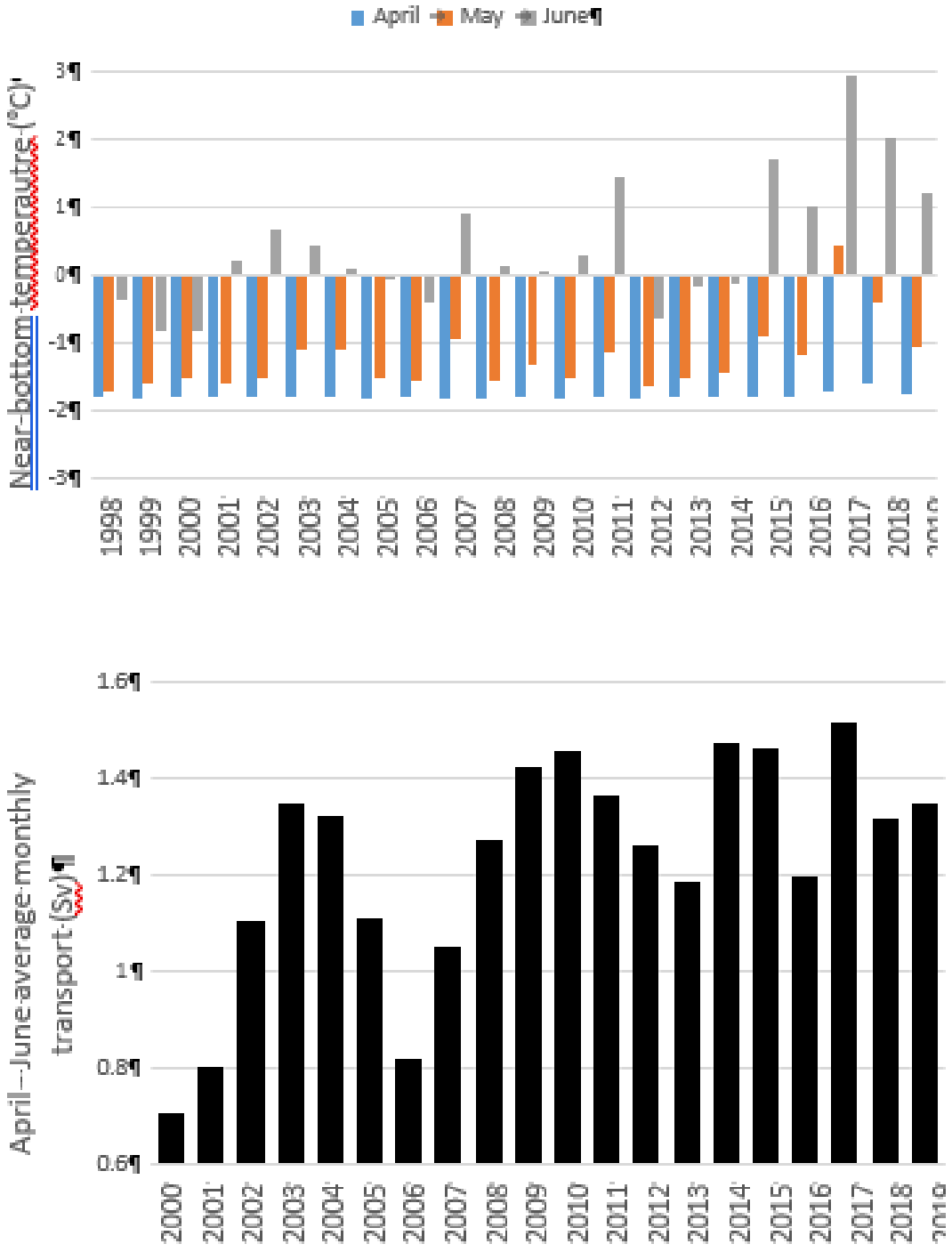

Figure 3. Environmental measurements from the A3 mooring north of the Bering Strait. Monthly-averaged near bottom temperatures in April – June from 1998 through 2019 (Top panel) and mean of average monthly northward transport from April – June in 2000 – 2019 (Bottom panel).

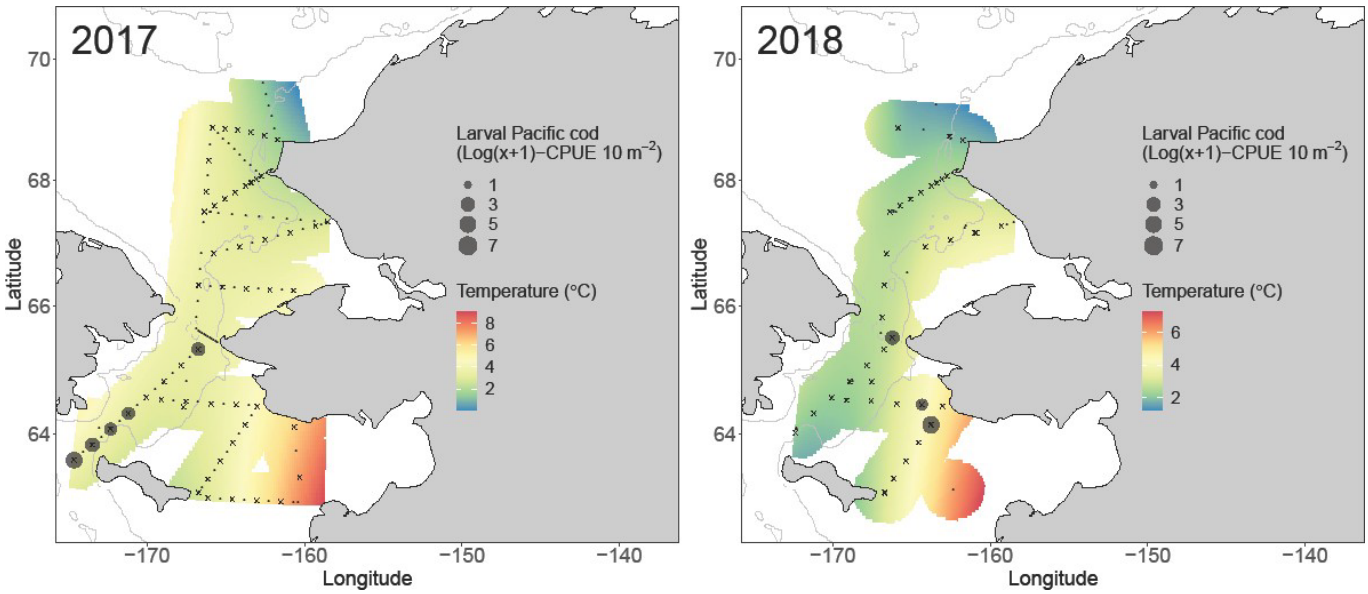

Figure 4. Pacific cod larval distributions and interpolated mean water column temperature in the Northern Bering and Chukchi Seas in June 2017 and 2018. “X” indicates zero catch.

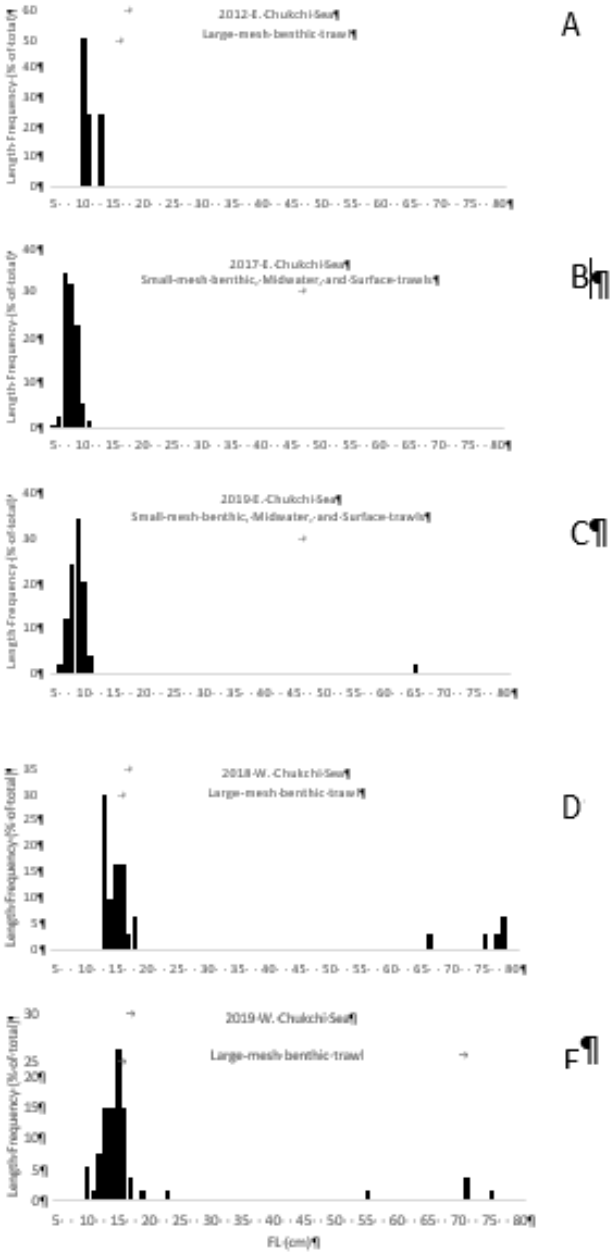

Figure 5. Length frequency distributions for Pacific cod caught in the Chukchi Sea in: A) 2012 in a large-mesh trawl in the eastern Chukchi Sea, B) 2017 in three trawls (small-mesh benthic trawl, midwater trawl, and surface trawl) in the eastern Chukchi Sea, C) 2019 in three trawls (small-mesh benthic, midwater, and surface) in the eastern Chukchi Sea, D) 2018 in a large-mesh benthic trawl in the western Chukchi Sea, and E) 2019 in a large-mesh-benthic trawl in the western Chukchi Sea.

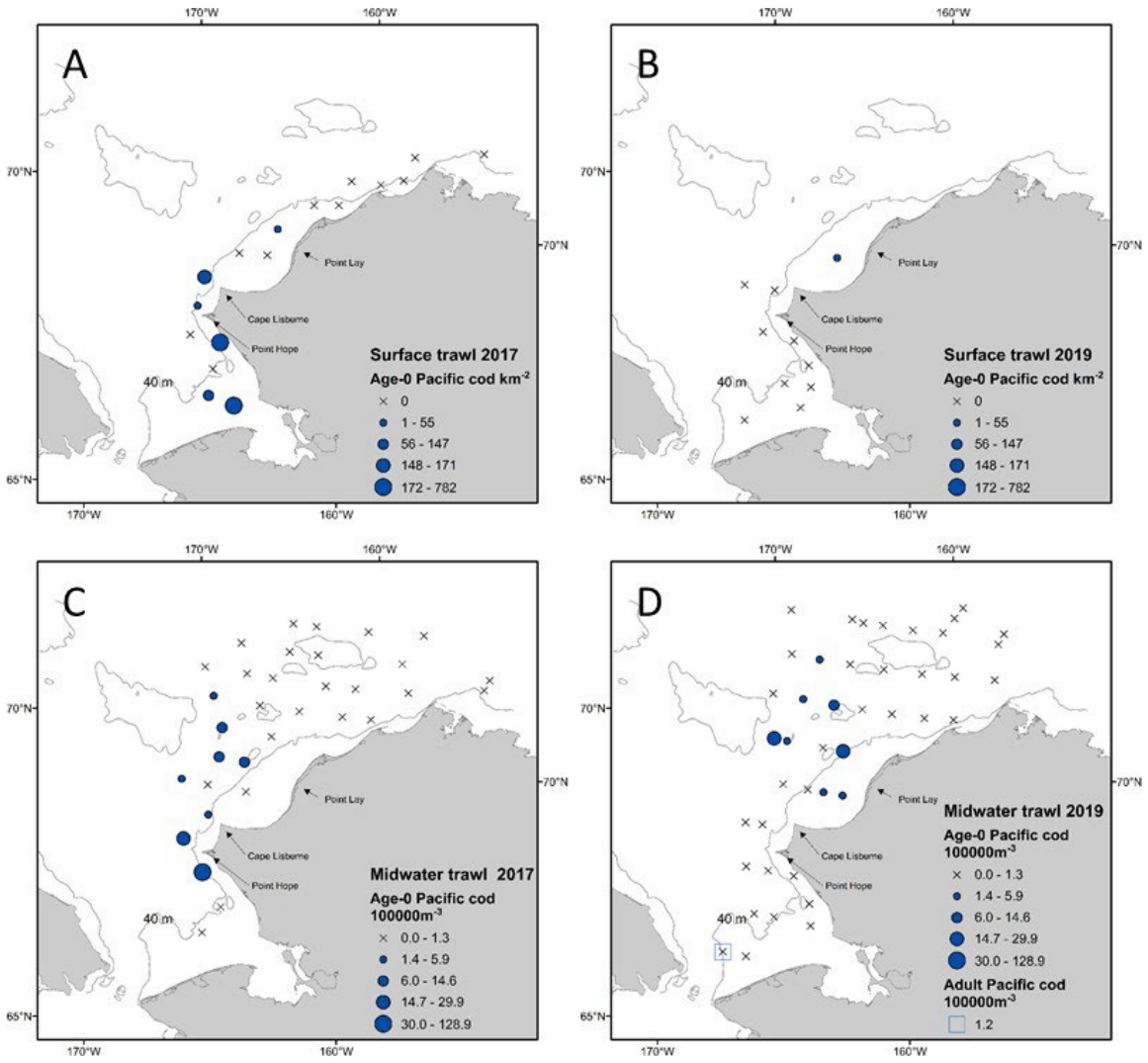

Figure 6. Distribution and catch per unit effort of Pacific cod caught in: A) the surface trawl in 2017; B) the surface trawl in 2019; C) the midwater trawl in 2017; D) the midwater trawl in 2019.

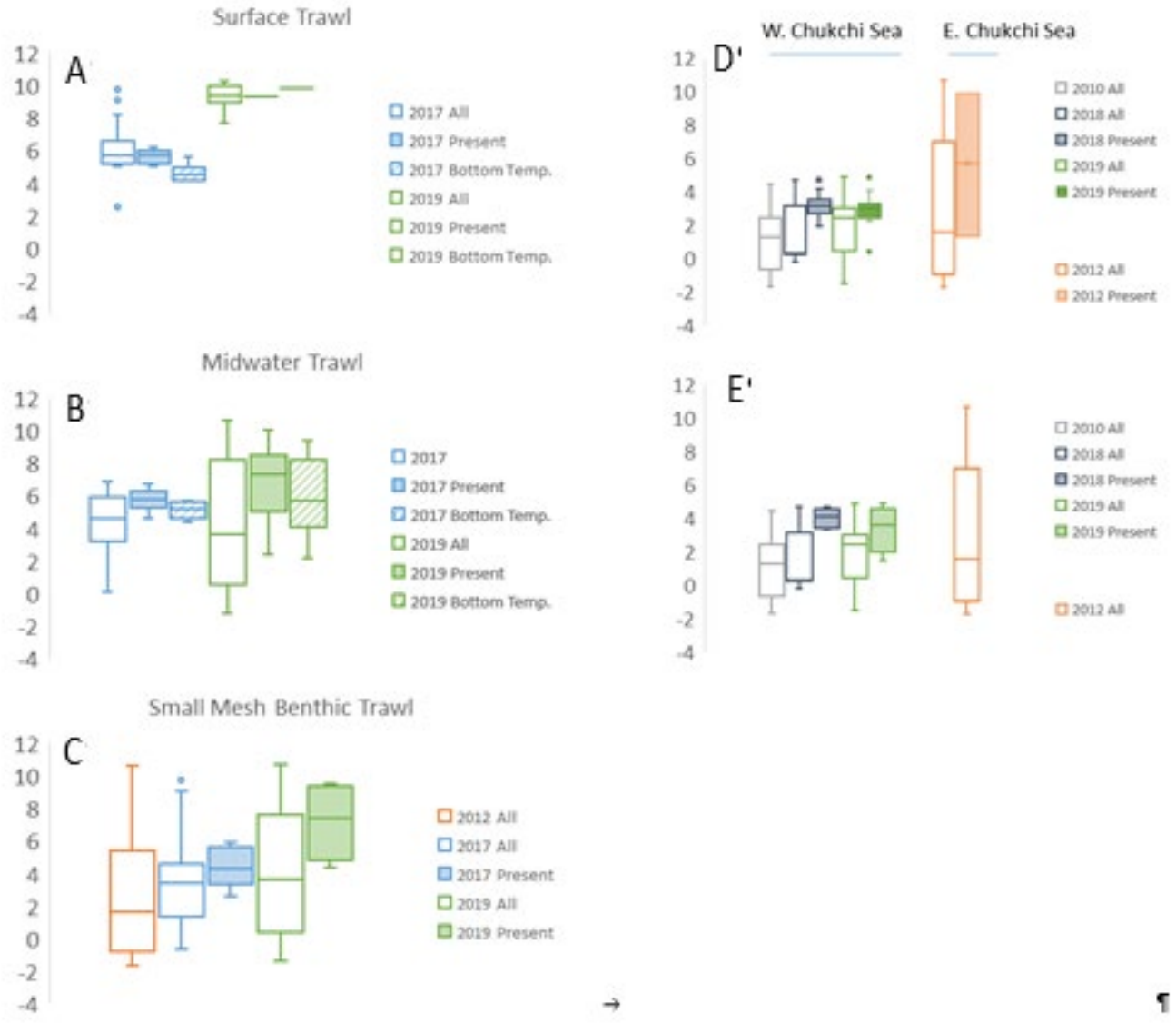

Figure 7. Boxplots of water temperatures at trawl stations in the Chukchi Sea by trawl type and year: A) surface trawl for age-0 Pacific cod sampling, B) midwater trawl for age-0 Pacific cod sampling, C) small-mesh benthic trawl for age-0 Pacific cod sampling, D) Large-mesh benthic trawl for age-1 Pacific cod sampling and E) Large-mesh benthic trawl for adult Pacific cod sampling. Open boxplots represent gear temperatures at all sampled stations. Filled boxplots represent gear temperatures at stations with Pacific cod presence. Striped boxplots represent bottom temperatures at stations where Pacific cod were present in pelagic (surface and midwater) trawls.

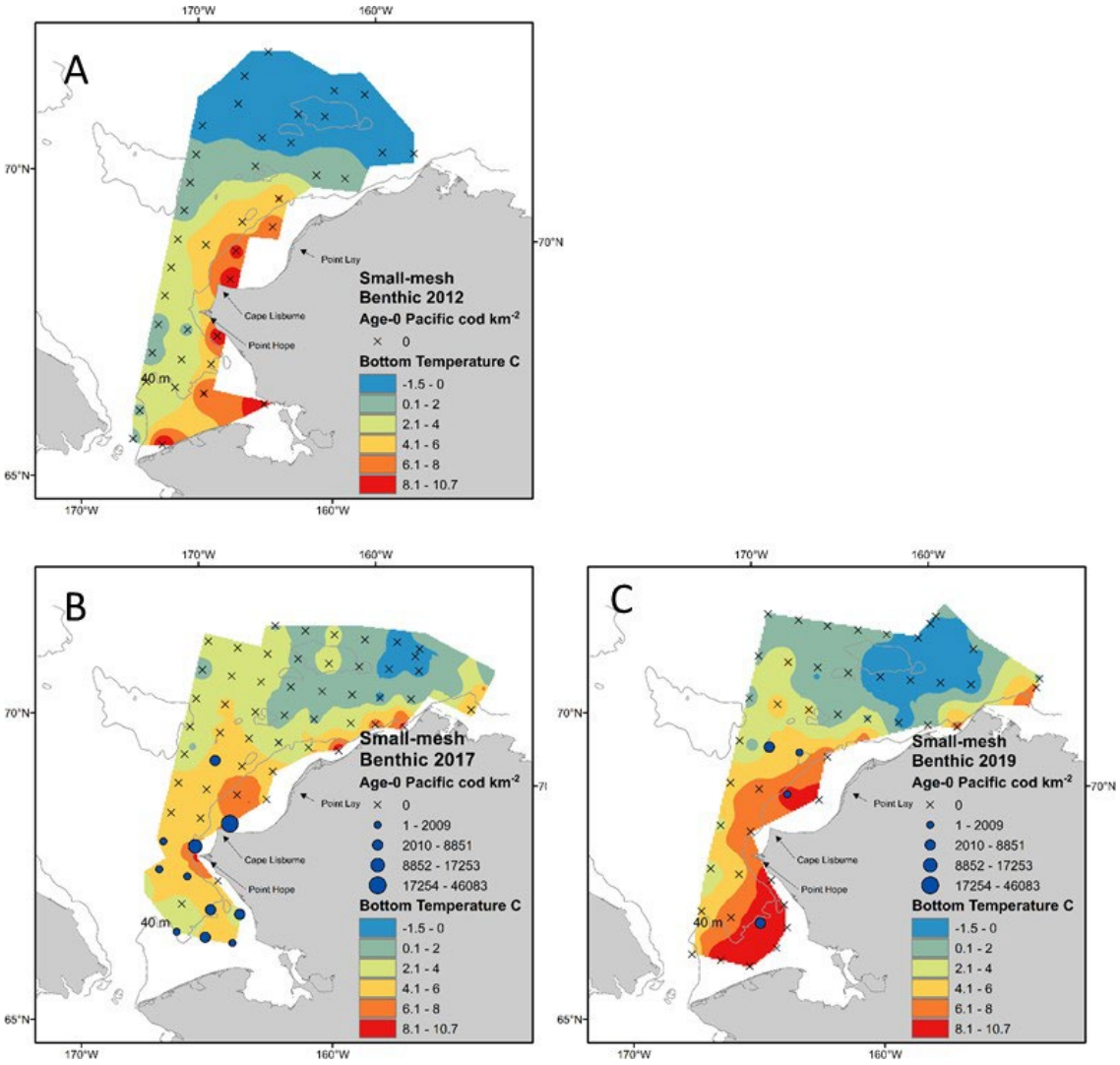

Figure 8. Maps of catch per unit effort of age-0 Pacific cod caught in the small-mesh benthic trawl and interpolated bottom temperatures for three survey years: A) 2012; B) 2017; and C) 2019.

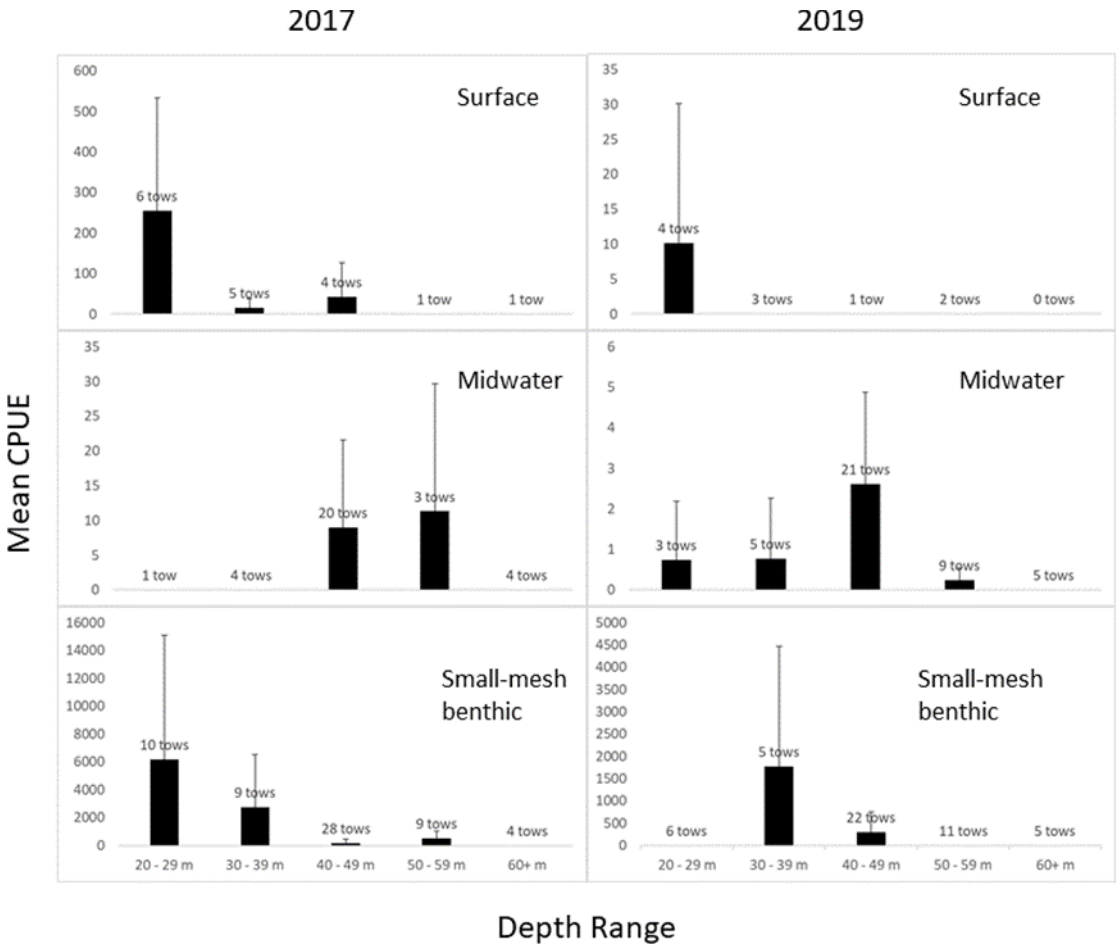

Figure 9. Mean catch per unit effort (CPUE) of age-0 fish by bottom depth range for each gear type in 2017 and 2019. CPUE units are number of fish per km^2 for the surface and small-mesh benthic trawls, and number of fish per 100,000 m^3 for the midwater trawl. Error bars represent 95% confidence interval.

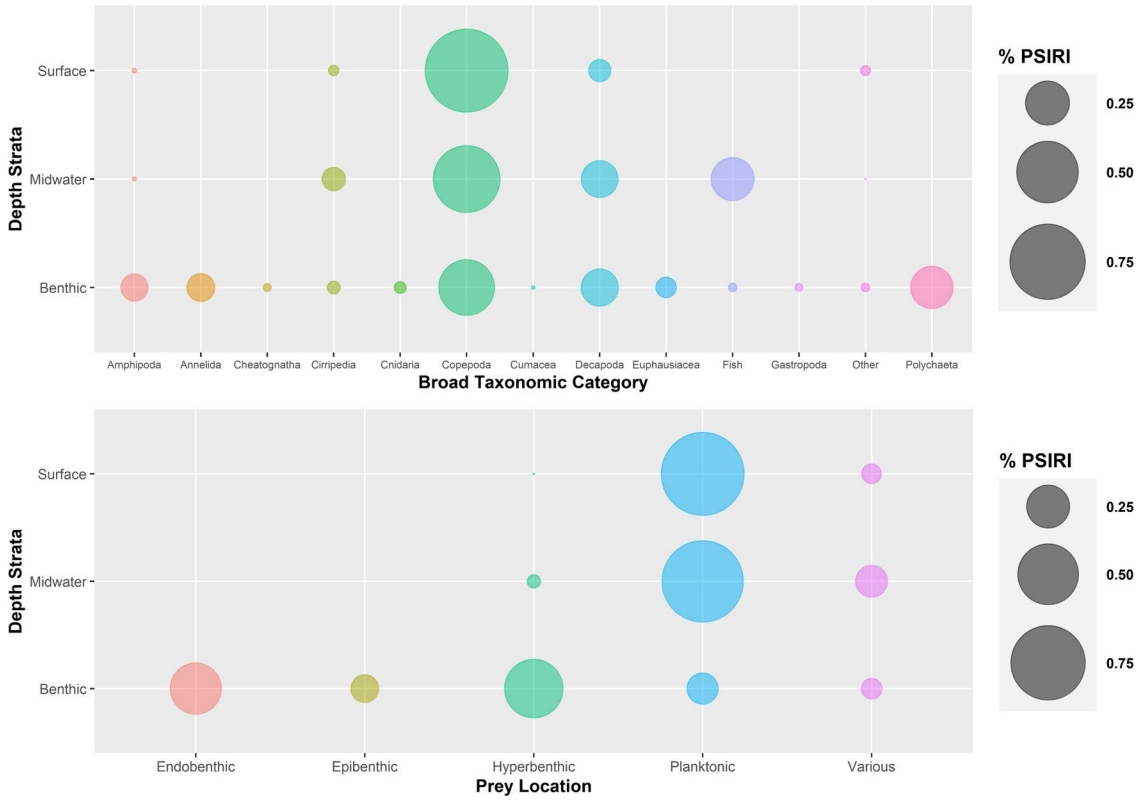

Figure 10. Prey specific relative index of importance (PSIRI) of prey items in the diet of small juvenile Pacific cod caught in 2017. Top panel depicts PSIRI by prey taxonomic groups, and bottom panel depicts PSIRI by prey general habitat classification.

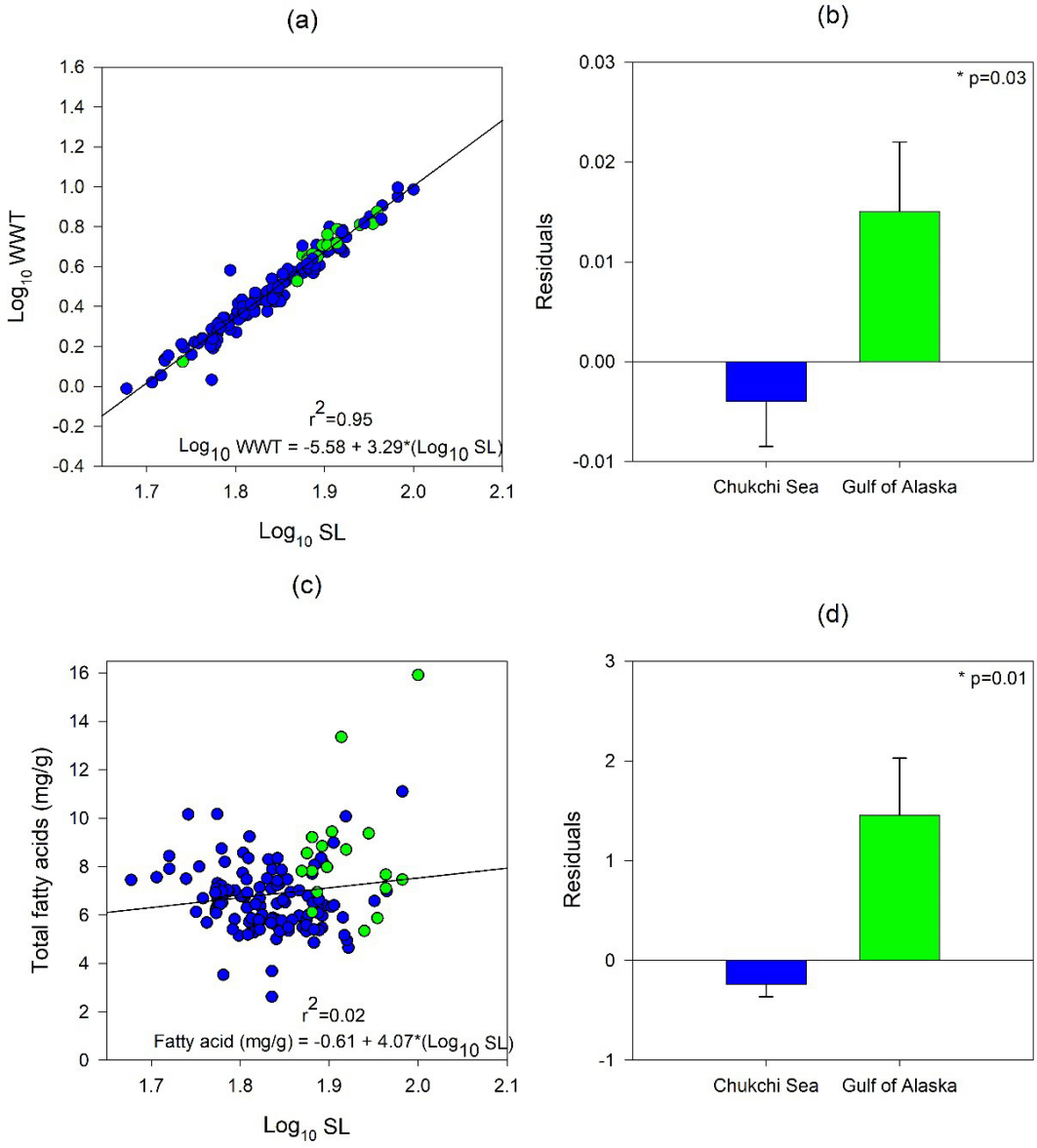

Fig 11. The effect of sampling region on the relationship between age-0 Pacific cod length (Log_{10}, SL, mm) and (a) wet weight (($Log_{10,}$ WWT, g) as well as (c) lipid density. Residuals from these relationships showed a significant effect of region of capture on condition based on length-weight residuals (b) and a significant effect of region on condition based on fatty acids concentrations (d).

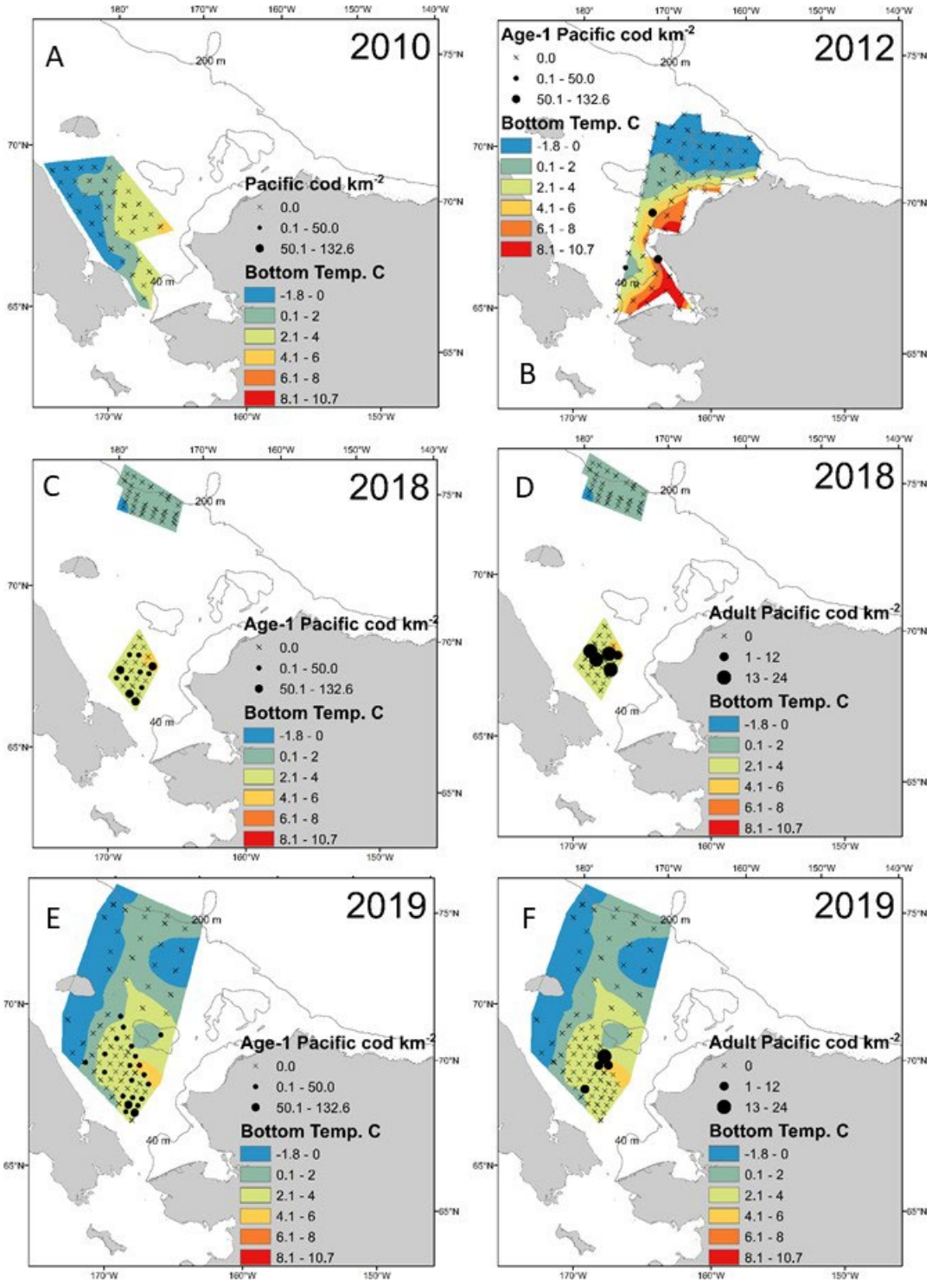

Figure 12. Distribution and catch per unit effort of juvenile (age-1) and adult Pacific cod in large-mesh benthic trawl in the Chukchi Sea: (A) Juveniles and adults in 2010; (B) Juveniles in 2012; (C) Juveniles in 2018; (D) Adults in 2018; (E) Juveniles in 2019; (F) Adults in 2019.

CHAPTER 14 - Response of Pink salmon to climate warming in the northern Bering Sea

Objective 4: Establish the relative abundance, size, and condition of juvenile salmonids that utilize the coastal regions of the PAR.

Farley, E.V., Jr., J.M. Murphy, K. Cieciel, E.M. Yasumiishi, K. Dunmall, T. Sformo, P. Rand. Response of Pink salmon to climate warming in the northern Bering Sea. Deep-Sea Research II https://doi.org/10.1016/j.dsr2.2020.104830.

Abstract

Life-history and life-cycle models of Pink salmon (*Oncorhynchus gorbuscha*) are developed to provide insight into production dynamics of northern Bering Sea Pink salmon. Arctic ecosystems, including freshwater and marine ecosystems in the northern Bering Sea, are warming at a rapid rate. Due to their short, two-year life cycle, Pink salmon are well known to respond rapidly to ecosystem change and can provide unique insight into ecosystem impacts of warming Arctic conditions. Life-cycle models suggest a lack of density-dependence for adult Pink salmon spawners in the Yukon River and potential for some density-dependence for adult Pink salmon spawners in the Norton Sound region. Life-history models identify a positive and significant relationship between the abundance index for juvenile Pink salmon and average Nome air temperature during their freshwater residency (August to June). This relationship supports the notion that warming air temperatures in this region (as a proxy for river and stream temperatures) are contributing to improved freshwater survival or increased capacity of freshwater habitats to support Pink salmon production. Life-history models also identify the number of adult Pink salmon returning to Norton Sound and the Yukon River is significantly related to the juvenile abundance in the northern Bering Sea. This result indicates that much of the variability in survival for northern Bering Sea Pink salmon occurs during early life-history stages and that juvenile abundance is an informative leading indicator of Pink salmon runs to this region.

Introduction

The Pacific Arctic Region (PAR), that is, the northern Bering Sea, and the Chukchi Sea to the East Siberian and Beaufort seas, is experiencing significant warming and extremes in seasonal sea ice extent and thickness (Frey et al., 2014; Baker et al., 2020; Danielson et al., 2020). Over the past two decades, record summer sea-ice minima (2007, 2011, 2012; 2017 and 2018) have occurred, and climate models project that the southern Chukchi Sea will be sea-ice free for 5 months (July to November) within a decade or two (Overland et al., 2014). In the northern Bering Sea, sea ice is projected to be less common during May, but will continue to be extensive through April (Stabeno et al., 2012). However, recent events during 2017 and 2018 in the northern Bering Sea indicate that open water in this region during winter is already occurring (Stabeno and Bell, 2019). The presence of sea ice during winter and into spring is known to influence summer bottom temperatures; however, climate models project that the loss of seasonal sea ice during spring and into fall months is currently resulting in, and expected in the future to lead to, increased sea surface temperatures during summer months in both the northern Bering Sea and Chukchi Sea (Wang et al., 2012). In addition, the reduction in seasonal sea ice is likely contributing to increased primary and secondary production (Arrigo and van Dijken, 2011) that could shift the ecosystem to a more pelagic state (Grebmeier et al., 2006).

These shifts in the PAR ecosystem are likely to have large impacts on the ecology of upper trophic level species such as fishes, birds, and mammals (Sigler et al., 2011). For instance, the community structure of some upper trophic level species already show evidence of changes in the Chukchi Sea, such as the shift from predominantly piscivorous seabirds to planktivorous seabirds in recent decades (Gall et al., 2017).

Large scale distributional shifts of walleye pollock (*Gadus chalcogrammus*) and Pacific cod (*G. microcephalus*) in response to reduced cold pool extent in the northern Bering Sea were also found (Stevenson and Lauth, 2018). Other ecosystem consequences of continued warming have been described elsewhere, such as the Barents Sea, and include changes in zooplankton community structure as well as shifts in species distributions and relative abundances (Hop and Gjøsæter, 2013; Orlova et al., 2013; Fossheim et al., 2015). Because the upper trophic level species are typically top predators, they must adapt via biological responses to physical forcing and thereby are "sentinels" of ecosystem variability and reorganization (Moore et al., 2014). As such, there will likely be fishes that do better under climate warming and those that may not.

The most common salmon species in the PAR include Pink (*Oncorhynchus gorbuscha*) and Chum (*O. keta*) salmon (Nielsen et al., 2013; Carothers et al., 2013; Stephenson, 2006). Of these two salmon species, Pink salmon are the most abundant in the North Pacific Ocean (Ruggerone and Irvine, 2018) and have the broadest distribution in the PAR from the Yukon River to small steams from Point Hope to Point Barrow (Craig and Haldorson, 1986). Vagrants have also been found upstream in the Mackenzie River to Fort Good Hope, Northwest Territories (Dunmall et al., 2018), as far east in the Canadian western Arctic as Paulatuk, Northwest Territories (Dunmall et al., 2013) and Kugluktuk, Nunavut (Dunmall et al., 2018), and along the east coast of Greenland (Dunmall et al., 2013). Spawning Pink salmon have also been documented along the Chukotka Peninsula coastline from the northern Bering Sea, into the Chukchi Sea and as far east as the Kolyma River (Radchenko et al., 2018).

Pink salmon production around the North Pacific Ocean has increased over the last decade (Radchenko et al., 2018). While some authors have expressed concern that Pink salmon may be exerting top-down control on the food web (Batten et al., 2018) and affecting growth and survival of other species reliant on the marine food web (Ruggerone et al., 2016; Oka et al., 2012; Springer et al., 2018), others have illustrated no evidence of Pink salmon abundance on marine production (Radchenko et al., 2018). While Pink salmon abundance in northern regions of their range is still quite low in relation to stocks farther south, there is evidence that the abundance of some northern stocks is increasing during this period of warming.

Pink salmon have a short 2-year life-cycle that include freshwater and marine environments (Radchenko et al., 2018). Adult Pink salmon in the northern regions return to rivers during July to September and their eggs hatch during late winter and into spring. Fry enter the marine environment during late May through June (Howard et al., 2017) and they spend the summer as juveniles in near coastal regions before migrating offshore into the North Pacific Ocean for the winter. After winter, they migrate back to their natal spawning grounds. The 2-year life-cycle creates separate even and odd year brood lines that do not overlap on spawning grounds (Radchenko et al., 2018).

Conditions in both freshwater and marine environments are important to the survival of Pink salmon. In northern regions of Pink salmon distribution, cold river and stream temperatures in the freshwater environment are believed to limit salmon production (Dunmall et al., 2016); however, continued warming air and stream temperatures, and longer periods of ice-free conditions may benefit salmon survival within this environment (Nielson et al., 2013). Two critical periods in the marine environment are believed to be important to marine survival of salmon. The first critical period is during their early marine residence where rapid growth is believed to reduce predation (Parker, 1968). The second critical period is during their first winter at sea where juvenile salmon that attain sufficient size and energy reserves (lipids) during their first summer at sea have higher probability of survival (Beamish and Mahnken, 2001). Both critical periods are linked to ecosystem function (i.e. optimum sea temperatures for growth, quantity and quality of prey resources) during their first summer at sea as juveniles and there is evidence in the PAR that warmer sea temperatures benefit juvenile Pink salmon early marine growth (Moss et al., 2009; Andrews et al., 2009; Wechter et al., 2017). Thus, the expectation is that Pink salmon in the PAR will respond positively to the rapid warming in both freshwater and marine environments.

To better understand Pink salmon dynamics in this region, we examine the total life-cycle productivity for the Yukon River and Norton Sound area (total number of adult returns per spawner; R/S) based on models that relate abundance estimates for adult returns to the number of spawners two years earlier. We include Nome air temperatures as a proxy for river and stream temperatures and estimates of summer sea surface temperature taken from satellite measurements in the northern Bering Sea in the life-cycle productivity models to explore whether temperature in these environments is affecting production. Next, we use surface trawl survey data to examine early marine life-history periods and conditions in these environments that may impact Pink salmon survival. Juvenile Pink salmon caught during the surface trawl survey are most likely from spawning populations (previous year) in this region (Farley et al., 2005); the juveniles return as adults the following summer to western Alaska rivers. For freshwater and early marine effects, we relate juvenile Pink salmon relative abundance to the total number of spawners to the Yukon River and Norton Sound region and to Nome air temperatures as a proxy for river temperature. Strong positive relationships would suggest that the number of spawners along with warmer freshwater temperatures lead to increased relative abundance of juvenile Pink salmon in the northeastern Bering Sea region. Finally, we examine the relationship between the indices of adult Pink salmon returns to the Yukon River and Norton Sound region with the juvenile Pink salmon relative abundance, body size, and summer sea temperatures from satellite estimates. Strong positive relationships would suggest higher numbers of juveniles along with warmer temperatures and increased size lead to greater numbers of adult Pink salmon the following year.

Materials and methods

Life-cycle models

A time series (1995 to 2018) of adult Pink salmon return indices (harvest and spawners) and spawner indices to the Yukon River and Norton Sound were derived from a number of sources. The time series for the number of Yukon River and Norton Sound region Pink salmon returns are from Estensen et al. (2018) and Menard et al. (2020). For the Yukon River, the number of adult Pink salmon spawners is indexed from estimates of passage past the Pilot Station Sonar in the lower river (JTC, 2019), escapement past the East Fork Andreafsky River weir downstream of the sonar (Conitz, 2019), and total harvest of this species in the Yukon River (Estensen et al., 2018). While some lower river escapement of Pink salmon occur in systems downstream of the East Fork Andreafsky River weir and Pilot Station Sonar, a majority of total number of Pink salmon spawners in the Yukon River is accounted for by these assessment projects. For Norton Sound, the adult Pink salmon spawner index includes rivers that contain weirs or counting towers for more accurate values and have long enough time series to compare with our juvenile Pink salmon abundance index. These include the Eldorado, Snake, Kwiniuk, Nome, and North rivers. The annual indices of total Norton Sound adult Pink salmon returns are the sum of total annual harvest from the Norton Sound area, as most salmon harvest occur in marine waters downstream of spawner assessment projects, plus the sum of annual adult Pink salmon spawners to the index rivers.

Annual mean Nome air temperatures (1995 to 2018; August $_{(t)}$ to June $_{(t+1)}$) where *t* represents the year of adult Pink salmon spawning, were obtained from the National Weather Service web site: https://w2.weather.gov/climate/xmacis.php?wfo=pafg. The mean August $_{(t)}$ to June $_{(t+1)}$ air temperature represents the period of incubation (adult Pink salmon that entered freshwater streams and rivers to spawn during late July through August of year *t*) and rearing (over winter to when they leave freshwater as fry to enter the marine environment during late May through June of year *t*+1) of Pink salmon in northern regions of their distribution. We used the annual mean air temperature as a proxy for stream and river temperatures in the northern Bering Sea region for the Pink salmon production models. Air temperatures have been used to estimate seasonal freshwater stream temperatures (McNyset et al., 2015), however we

understand there are caveats given the span of seasons (includes winter) in our use of air temperatures as proxy for stream temperatures in this region.

Annual mean sea surface temperatures (1995 to 2018; SST_{t+1}) within the northeastern Bering Sea, where *t* represents the year of adult Pink salmon spawning, were estimated using data from satellite sources (NOAA Coral Reef Watch, 2018). Daily SST data were averaged within the northeastern Bering Sea (latitudes 60°N to 65°N; longitudes 166°W to 171°W) for each month. We then averaged the monthly mean sea surface temperatures for June to September for each year to represent sea temperature juvenile Pink salmon would experience during their first summer at sea.

The number of adult Pink salmon that return (*R*) to the river each year is a function of the number of adult spawners (*S*) two years prior as well as life-cycle events that occur during freshwater and marine residence. One measure of productivity is to examine the number of adults produced per spawner. Adult Pink salmon return and spawner data for the Yukon River and Norton Sound region are shown in Fig. 1a,b. There is increased variation in return indices at higher spawner index levels for both the Yukon River stocks and Norton Sound region stocks suggesting a multiplicative error structure. To understand between-stock variability in the northern Bering Sea region, we calculated the correlation of ln(*R/S*) between the Norton Sound region stock group and the Yukon River stock group to determine whether their productivity is synchronous. To take into account density dependent effects, we included models that relate the number of spawners to the number of adult returns (see Quinn and Deriso, 1999),

(1) $\ln R_{t+2} = a + \gamma \ln S_t + \epsilon$ Cushing Model (Cushing, 1971)
(2) $\ln (R_{t+2}/S_t) = a - \beta S_t$ Ricker Model (Ricker, 1975)

where *a* is the natural log of the productivity parameter and γ and β are the density-dependence parameters. While the Cushing model includes a density-dependent parameter, this model lacks a peak level of recruitment (Quinn and Deriso, 1999); recruitment continues to increase as spawning level increases. To provide density dependence in the Cushing model, γ must be less than 1. The Cushing model is typically not used for salmon stocks to examine the relationship between the number of returns and spawners due to lack of density dependence at high spawning levels; however, it may be informative for northern river systems experiencing rapid warming with potential for shifts in the underlying capacity of these ecosystems to support higher production. In addition, we included the annual estimates of Nome air temperature, as a proxy for freshwater temperatures, and annual average of sea temperature in the life-cycle models to test whether their inclusion helps explain production dynamics in this region.

A step-wise selection of a linear regression model (S-plus; Insightful Corporation, 2001) was used to determine the most parsimonious life-cycle models that explain production dynamics of Pink salmon in the northern Bering Sea region. In S-plus, the effects of additional terms to the model are determined by comparing the Mallow's C_p statistic estimated by

$$\boldsymbol{C_p = \left(\frac{RSS}{\hat{\sigma}^2}\right) + 2 * p -}$$

where *n* is the sample size, $\boldsymbol{\hat{\sigma}^2}$ is the mean square error of the true regression model, RSS is the residual sum of squares and *p* is the number of parameters in the model, which equals the number of predictors plus 1 if the intercept is included in the model. The stepwise selection process requires an initial model often constructed explicitly as an "intercept-only" model. The step function in S-plus calculates the C_p statistic for the intercept only model as well as those for all reduced and augmented models. If any term has a C_p statistic lower than that of the intercept only model, the term with the lowest C_p statistic is dropped. We also tested the residuals of the most parsimonious models for autocorrelation between consecutive years to see if the other potential factors beyond those in the model could influence adult Pink salmon returns.

Life-history models

The information on juvenile Pink salmon marine ecology in the northern Bering Sea comes from integrated ecosystem surveys conducted during late summer and early fall months of 2003 to 2018 (except 2008) (Fig. 2). For this study, the northern Bering Sea consisted of stations sampled between 60°N to 65°N and juvenile Pink salmon captured in the survey region are assumed to be of wild origin originating from spawning populations within the Norton Sound region and Yukon River. Details on survey design can be found in Murphy et al. (2017). Briefly, juvenile Pink salmon were captured using a model 400/601 rope trawl, made by Cantrawl Pacific Limited of Richmond, British Columbia. The rope trawl was rigged with buoys on the headrope to sample from near surface to approximately 20 to 25 m depth. Sampling stations were generally completed during daylight hours (0730 – 2100, Alaska Daylight Savings Time). All trawl deployments lasted 30 minutes and covered between 2.8 – 4.6 km. A vertical (surface to near bottom depths) conductivity and temperature at depth (CTD) cast was done at each station to measure oceanographic characteristics during the survey. The surveys generally occurred during September; however, there was some variability in start and end dates among years (Table 1). The median year-day for the surface trawl survey during all years (2003 to 2018) was 256 (September 12).

A multi-year distribution map of juvenile Pink salmon in the northern Bering Sea using the standardized catch estimated as:

$$\boldsymbol{C\_std_{i,y}} = \frac{\boldsymbol{C_{i,y}}}{\boldsymbol{E_{i,y}}}\overline{\boldsymbol{E}}$$

where $C_{i,y}$ is the number of juvenile Pink salmon captured at station i during year y, $E_{i,y}$ is the area (km^2) swept by the trawl and E is the average effort (km^2) (Murphy et al., 2017). Zero catch boundary conditions were added to land masses, and the prediction surface was estimated with a neighborhood kriging model (Murphy et al., 2017).

Fish captured in the trawl were sorted to species. Subsamples of up to n=50 juvenile Pink salmon were randomly selected, and these fish were measured to fork length (nearest mm) and weighed (nearest gram). Juvenile pink salmon fork length and weight were adjusted to take into account the annual differences in the surface trawl survey median year-day that could influence our interpretation of juvenile Pink salmon size due to differences in size of juveniles that could occur over the course of the survey period. We estimated adjusted length and weight by:

$$\boldsymbol{L_{J,i,y}} = \left(\boldsymbol{YD_{Capture\,j,i,y}} - \mathbf{256}\right) * \mathbf{1.18}\boldsymbol{mm}$$
$$\boldsymbol{W_{j,i,y}} = \left(\boldsymbol{YD_{Capture\,j,i,y}} - \mathbf{256}\right) * \mathbf{0.2}\boldsymbol{g}$$

where $L_{j,i,y}$ and $W_{j,i,y}$ are the length and weight of a juvenile Pink salmon j caught at station i during year y, $YD_{Capture\ j,\ i,\ y}$ is the year-day of capture of the juvenile Pink salmon j at station i during year y, 256 is the median year-day (September 12) for all years (2003 to 2018) of the surface trawl survey, and 1.18 mm and 0.2 g are the estimated daily growth rate in length (Moss et al., 2009) and weight (Grant et al., 2009) for juvenile Pink salmon.

An abundance index of juvenile Pink salmon for the northern Bering Sea was based on catch per unit effort (CPUE, catch per km^2) where the number of juvenile Pink salmon caught at each station was divided by the area swept by the trawl. We used an index of relative abundance and not actual abundance because juvenile Pink salmon captured at the outer regions of our survey may be from stocks other than Yukon River and North Sound (Farley et al., 2005). Area swept by the trawl at each station was determined by multiplying the distance (km) traveled by the horizontal distance (km) of the trawl opening that was measured by net sonar. The distance traveled was estimated using:

$$\boldsymbol{x} = \mathbf{cos^{-1}}(\mathbf{sin}(\boldsymbol{lat_s}) * \mathbf{sin}(\boldsymbol{lat_e}) + \mathbf{cos}(\boldsymbol{lat_s}) * \mathbf{cos}(\boldsymbol{lat_e}) * \mathbf{cos}(\Delta\mathbf{lon})) * \mathbf{6371},$$

where lat_s is the trawl start latitude position in radians, lat_e is the trawl end latitude position in radians, Δlon is the longitude distance between the start and end trawl positions in radians, and 6371 is the earth radius in km (Murphy et al., 2017).

Mixed-layer depth expansions were applied to the area-swept indices of juvenile Pink salmon to generate an abundance index for juvenile Pink salmon as described in Murphy et al. (2017). Mixed layer depth expansions account for changes in the vertical extent of trawl sampling depths and juvenile habitat over time. Summer sea temperatures below the mixed layer depth in the northern Bering Sea are generally cold (< 2° C), which are not suitable habitat for juvenile salmon (Brett, 1952); therefore, this correction is used to provide a reasonable approximation for the vertical distribution of juvenile salmon in the northern Bering Sea (Murphy et al., 2017). Oceanographic characteristics from the CTD casts were used to determine the mixed layer depth defined as the depth where seawater density (sigma-theta) increased by 0.10 kg m^{-3} relative to the density at five meters (Danielson et al., 2011). Mixed layer depth was set to 5 m off bottom when the entire water column was vertically mixed. The mixed layer depth adjustments applied to annual relative abundance estimates, θ_y, were estimated by

$$\boldsymbol{\theta_y} = \frac{\sum_i \boldsymbol{M_{i,y} C_{i,y}}}{\sum_i \boldsymbol{C_{i,y}}}$$

where $C_{i,y}$ is the number of juvenile Pink salmon captured at station i during year y, and $M_{i,y}$ is equal to the ratio of mixed-layer depth to trawl depth when trawl depth is shallower than mixed layer depth, and 1.0 when trawl depth is below the mixed-layer depth. The juvenile abundance index for Pink salmon was estimated by multiplying the average ln(CPUE) by θ_y

$$\boldsymbol{N_y} = \frac{\sum_i \boldsymbol{ln(CPUE_{i,y})}}{\boldsymbol{n_y}} * \boldsymbol{\theta_y}$$

where n is the number of stations i sampled during year y.

Life-history models were constructed for northern Bering Sea Pink salmon using multiple sources of data. The models included the juvenile Pink salmon abundance index and adjusted average juvenile weight during the northern Bering Sea surface trawl survey. A subset (2003 to 2018) of Nome air temperatures and summer SSTs described above were used in the life-history models to represent freshwater and early marine conditions for relationships with juvenile Pink salmon relative abundance and adult returns. Annual estimates of adult Pink salmon returns and spawners to the Northern Bering Sea region were developed from a subset of the available annual estimates (2003 to 2018) of adult Pink salmon returns and spawners to the Yukon River and Norton Sound region.

Because the juvenile Pink salmon relative abundance is estimated during September, the life-history model for juvenile abundance incorporates potential freshwater and early marine effects

ln (juvenile relative abundance $_t$) = ln (adult spawners$_{(t-1)}$) + Nome air temp + ln (adjusted weight $_t$) + SST_t

and includes the number of adult Pink salmon that spawned during the prior year, stream temperature during their freshwater life history stage, adjusted weight of juvenile salmon during year t, and summer sea surface temperatures during year t.
The life-history model relating early marine effects with adult Pink salmon returns

ln (adult returns $_{(t+1)}$) = ln (juvenile relative abundance $_t$) + SST_t + ln (adjusted weight $_t$)

examined the relationship between the number of adult Pink salmon returning the following year to the region with juvenile abundance, juvenile weight (condition), and sea temperature in the early marine period. We applied the step-wise variable selection procedure described above to select the most

parsimonious life-history models that explain production dynamics of Pink salmon in the northern Bering Sea region.

Results

Life-cycle productivity

The adult Pink salmon return and spawner indices to the Norton Sound region and Yukon River during 1995 to 2018 ranged between a few thousand to several million (Table 2). More adult Pink salmon return during even years than odd years, especially within the Norton Sound region. However, adult returns to the Norton Sound region during the recent odd year of 2017 was much higher (> 2 million) than most of the previous odd years (generally < 1 million except for 2005) within the time series. Overall, productivity (ln *R/S*) appears higher during the late 1990s and from 2013 to 2015 (Fig. 3). The correlation between Yukon River and Norton Sound region productivity was positive and significant ($r = 0.47$, $p = 0.02$).

The average Nome air temperature (proxy for freshwater temperatures) for the period covering adult Pink salmon spawning, fry emergence and smolt migration to the marine environment was below 0°C during each year (Table 2). Coldest temperatures occurred during 1999, 2009 and 2012 with warmer temperatures occurring during 2003 to 2005 and 2014 to 2016. The summer SSTs covering the period of juvenile Pink salmon residence in the northeastern Bering Sea had similar trends with coolest temperatures during the late 1990s and during 2008 to 2012 and warmer temperatures during the early 2000s and from 2015 to 2017 (Table 2). The correlation between Nome air temperatures and summer SSTs was positive and significant ($r = 0.61$, $p = 0.002$).

The life-cycle model fits and results for the Norton Sound region and Yukon River are shown in Fig. 1a,b and Table 3. For the Yukon River, the most parsimonious Cushing model included the natural log of spawners and summer SST which explained 71% of the variation in the natural log of returning adult Pink salmon. However, the parameter estimate for summer SST is not significant ($p = 0.11$) in the model. The most parsimonious Ricker model included SST, explaining 11% of the variation in adult Pink salmon production to the Yukon River; neither parameter estimates for number of spawners and SST were significant ($p = 0.232$ and 0.124, respectively). For Norton Sound stocks, the most parsimonious Cushing model was one that included the natural log of spawners and summer SST, explaining 77% of the variation in the natural log of adult Pink salmon returns to the region. The most parsimonious Ricker model was one that contained spawners and summer SST, explaining 53% of the variation in the natural log of adult Pink salmon production to the region. No significant autocorrelation between consecutive years is evident in the residuals of the most parsimonious models (Fig. 4 a-c). In addition, the gamma parameter for the Cushing model was 0.66 for Norton Sound stocks and 0.82 for the Yukon River stock suggesting that density-dependence on the spawning grounds may be more evident in the Norton Sound stocks than the Yukon River stocks.

Early life-history

Juvenile Pink salmon are distributed throughout the northern Bering Sea during late summer months (Fig. 2). The region of highest catch densities occurred within the shallow (< 50 m) coastal habitats from the northern to southern margins of the northern Bering Sea survey area. Observed average size of juvenile Pink salmon varied from 136 to 193 mm (25.7 to 70.8 g) with an average of 164.6 mm (44.8 g) (Table 1). Adjustments for survey timing increased the overall average size of juvenile Pink salmon to 165.6 mm (44.9 g) with the largest differences occurring during 2005 and 2007. Juvenile Pink salmon were generally smaller during 2006, 2009, 2011 and from 2015 to 2018 (Fig. 5a,b). Moreover, the number of larger fish that occurred as outliers to the sample of juvenile Pink salmon was highest during 2007 and

2016 to 2018 (Fig. 5b), years that coincided with warm sea temperatures. Mixed layer depth corrections ranged from a low of 1.00 (<1%) during 2016 to a high of 1.79 (79%) during 2005 with an overall average of 1.22 (22%) to juvenile Pink salmon relative abundance estimates (Table 4). Juvenile Pink salmon relative abundance was high during 2003 to 2007 and again from 2013 to 2018 with lower abundance during 2009 to 2012.

The step-wise model selection statistics to explore life-history events that may impact Pink salmon production in fresh water and the early marine period are shown in Table 5. For the juvenile abundance model, freshwater effects including the number of spawners and Nome air temperatures were significant and explained 55% of the variation in juvenile Pink salmon relative abundance during September (Fig. 6). The step-wise selection process removed summer SST and the natural log of weight, (both represent early marine effects) as these variables did not contribute to the most parsimious model. For the adult return model, the *Cp* values for the natural log of weight and sea temperature during September were lower than the intercept only model, suggesting these variables could be removed. The most parsimonious model (Fig. 7) that included juvenile Pink salmon relative abundance explained 62% of the variation in adult Pink salmon returns to the northern Bering Sea region.

Discussion

Our analysis provides new insights into production dynamics of Yukon River and Norton Sound Pink salmon stocks. The best fit life-cycle models suggest that density-dependence on the spawning grounds may be low within the Yukon River but may be present within river systems draining into Norton Sound. We interpret this result to indicate that there may be potential for increased freshwater production especially within the Yukon River. The best fit life-history models suggest that the number of juvenile Pink salmon during September is a function of the number of adult Pink salmon spawners and Nome air temperature, reflecting the importance of freshwater production to overall numbers of juvenile Pink salmon. In addition, juvenile Pink salmon relative abundance during September is a good predictor of the number of adult Pink salmon that return the following year indicating that conditions in fresh water and early marine environments are key to our understanding of Pink salmon production dynamics in this region.

Our analysis of the productivity patterns highlights the synchrony (positive, significant correlation) in temporal variation among Pink salmon stocks in the northeastern Bering Sea. These patterns have been found for Pink salmon stocks across western North America (Malick and Cox, 2016) as well as other salmon stocks that show positive correlation at regional scales (Pyper et al., 2001, 2002, 2005; Peterman et al., 1998; Peterman and Dorner, 2012; Dorner et al., 2017). The synchrony in production suggests shared factors that are affecting Pink salmon stocks throughout the study region. The best fit life-cycle models included summer SSTs indicating the potential importance of sea temperature on Pink salmon production in this region. This result is similar to other analyses of salmon productivity in the Northeast Pacific Ocean (Mueter et al., 2002), illustrating the importance of summer sea temperatures to production of Pink salmon in the northeastern Bering Sea.

The best fit life-history models were those that included the number of spawners, Nome air temperatures and the relative abundance of juvenile Pink salmon. For the juvenile abundance model, we found positive, significant relationships between annual juvenile Pink salmon relative abundance and the number of adult Pink salmon spawners the prior year along with annual average Nome air temperatures. This result supports the hypothesis that warming air temperatures in this region (as a proxy for river and stream temperatures) may be improving freshwater production leading to higher numbers of juvenile Pink salmon in the northern Bering Sea region during summer months. For the adult Pink salmon return model, the number of juvenile Pink salmon in the northern Bering Sea region during late summer predict the number of adults returning the following year. While summer SSTs were not included in these

models, we note that there is a significant positive correlation between SSTs and Nome Air temperatures that may indicate that temperature, either fresh water or early marine are important for Pink salmon production in this region.

These relationships suggest a possible connection between changes in fresh water and early marine environments and subsequent adult production. However, the amount of variation in juvenile Pink salmon relative abundance explained by adding adult Pink salmon spawners and Nome air temperatures was less than the amount of variation explained in the adult Pink salmon returns by the juvenile index. This suggests other factors affecting early marine survival of juvenile Pink salmon in the northern Bering Sea during summer months could influence total production or that Nome air temperatures may not fully reflect the freshwater temperature dynamics thereby reducing the influence of juvenile Pink salmon relative abundance.

Although freshwater conditions in the Arctic are known to limit salmon production, it can be difficult to predict how salmon will respond to warming freshwater habitats (Nielson et al., 2013). A case study on projecting effects of climate warming on Atlantic salmon suggested that northern rivers could become more productive with increased colonization success northward and diminished production to river systems in the southern range (Reist et al., 2006). Density-dependent mortality due to too many spawners on the river, temperature, and stream flows are all factors contributing to fluctuations in freshwater survival (Heard, 1991). In addition, stream habitats with a minimum temperature of 4°C during spawning and temperatures above 2°C during egg incubation were found to benefit establishment of Chum and Pink salmon in high latitude and high elevation watersheds (Dunmall et al., 2016). Nome air temperatures from August (spawning year) to June the following year were used as a proxy for freshwater stream temperatures in the region. The average air temperature was below 0°C which is most likely colder than stream temperatures, especially during summer months. Limited information on stream temperatures at various locations along the Pilgrim River (north of Nome, Alaska) during the summer months of 2013 to 2016 show that temperatures varied between 8.4°C to 18.7°C (Carey et al., 2019). These temperatures are well above the minimum temperature of 4°C for successful Pink salmon spawning suggested in Dunmall et al. (2016). In addition, some river systems in the Norton Sound region experienced extremely high temperatures during summer 2019 that were believed to contribute to observed adult Pink salmon die offs on the spawning grounds (pers. Comm. Gay Sheffield). Given the nature of rapid warming in the region with respect to the marine ecosystem (Baker et al., 2020; Danielson et al., 2020; Huntington et al., 2020), it is likely that freshwater temperatures during winter and summer months in the Norton Sound and Yukon River drainage are warming enough to both improve survival and to open new areas along rivers and streams for Pink salmon to establish thereby increasing production potential in this region.

Pink salmon returns to this region are typically higher during even years (odd year juvenile Pink salmon brood), but more recently the returns to the Norton Sound region during odd years have also been high. Studies have indicated that embryonic survival of the even-year broodline for British Columbia Pink salmon is higher than the odd-year broodline in a cold (4°C) incubation environment with higher alevin and fry growth observed (Beacham and Murray, 1988). Increasing dominance of odd-year brood lines has been documented with the inference of favorable survival during period of warming freshwater habitats (Irvin et al., 2014). The difference in temperature tolerance between the even and odd-year brood lines has been linked to dispersal after the Pleistocene Era glaciation some 10,000 years ago (Beacham et al., 2012), where even-year broodlines likely survived the glaciation in the northern refugia (Aspinwall, 1974) and the odd-year brood line may have occupied more southern refugia (McPhail and Linsey, 1970). Therefore, warming freshwater habitats in the northern regions may be improving odd-year broodline survival, leading to more adult Pink salmon returning during odd years.
Earlier studies on juvenile Pink salmon marine ecology in the northern Bering Sea found that warmer sea surface temperatures during spring and summer were positively related to their growth (Andrews et al.,

2009; Farley et al., 2009; Wechter et al., 2017). Presumably, higher growth rates during their early marine period would reduce size-selective mortality and lead to higher survival for juvenile salmon (Parker, 1968). We found that juvenile Pink salmon adjusted weight and length declined over the course of our time series even though sea temperatures were increasing during the survey period. This result was counter-intuitive as growth rates typically increase with temperature. Dispersal, changes in prey quality and quantity, and migratory patterns of juvenile Pink salmon could be contributing to this apparent negative relationship between size and temperature.

Although juvenile Pink salmon were distributed throughout the northern Bering Sea survey region, the vanguard of their distribution can be under sampled, particularly during warm years. Moss et al. (2009) examined juvenile Pink salmon distribution and size within the northern Bering Sea and Chukchi Sea during 2007. They found that the highest catches of juvenile Pink salmon were in the Chukchi Sea and that these juveniles were larger than those in the northern Bering Sea region. The year 2007 was characterized by exceptionally warm sea temperatures in the Chukchi Sea and significantly increased annual mean water transport through the Bering Strait (Woodgate et al., 2010). Moreover, the water flow from the northern Bering Sea through the Bering Strait and into the Chukchi Sea has increased by 50% over the past two decades (Woodgate et al., 2015). Given that the sea temperatures have been much higher during recent years of our survey period, it is possible that juvenile Pink salmon from the northern Bering Sea region were advected north with the largest fish at the vanguard of the migration through the Bering Strait and into the Chukchi Sea and out of the northern Bering Sea survey area.

The large numbers of juvenile Pink salmon found near the Bering Strait could also be related to higher Pink salmon production in the northern regions of the PAR. Adult Pink salmon have become more prevalent in subsistence catches in the high Arctic particularly during even-numbered years (Dumnall et al., 2013; Dunmall et al., 2018). Further, the large catch of juvenile Pink salmon in the Chukchi Sea during 2007 (Moss et al., 2009) coincided with higher adult returns to the Beaufort Sea coast during 2008 (Dunmall et al., 2013; Dunmall et al., 2018). While Pink salmon appear to be poised to take advantage of warm-water thermal refugia within several watersheds of the Arctic (North American North Slope; Dunmall et al., 2016), it is unknown whether spawning has been successful in this region. Adult Pink salmon returns to the northern regions of the Kamchatka peninsula have recently increased (Klovach et al., 2018) and record returns have occurred during most recent years to Norton Sound rivers (Menard et al., 2018). Farley et al. (2005) speculated that juvenile Pink salmon caught offshore in the northern Bering Sea could be of Russian origin. In addition, Kondzela et al. (2009) found that most of the juvenile Chum salmon caught in the Bering Strait area during 2007 were from Anady-Kanchalan rivers in the northern Kamchatka region. In any case, stock-specific juvenile data for Pink salmon are needed to better understand movement and production dynamics during this time of rapid warming.

The significant correlation between juvenile Pink salmon relative abundance and adult returns the following year suggests that the second critical period has not contributed as much to the annual variation in Pink salmon production to the northern Bering Sea region. The addition of sea surface temperature and weight did not improve our model for adult Pink salmon returns to the northern Bering Sea region. Our result is similar to studies that utilized juvenile salmon abundance indices from surface trawl data to predict adult returns. For example, a stock-specific juvenile Yukon River Chinook salmon index collected in the northern Bering Sea is used to provide management advice for expected run sizes (Murphy et al., 2017). Within southeast Alaska, adult Pink salmon returns are predicted using a juvenile Pink salmon index collected during summer months within Icy Strait (Orsi et al., 2016). Both applications are used to inform management decisions and provide more accurate outlooks than previous models.

Lastly, it is important to note results from the life-cycle models that utilize harvest and spawner data for Pink salmon to the Yukon River and Norton Sound regions are limited by incomplete data. Our estimates

of Pink salmon total number of returns and spawners to the Yukon River and Norton Sound region are considered indices of abundance as total accounting of Pink salmon abundance in this region is not currently possible. Total harvest includes stocks not indexed in the spawning escapement and escapement assessment programs are designed to estimate other salmon species and do not fully account for Pink salmon abundance. Productivity values and inferences are presented here to illustrate relative change over time or relationships to environmental parameters, and should not be considered absolute values. Consequently, our interpretation of the results from these models should be considered cautiously. In addition, separate analyses of odd and even year broodlines may be warranted given that they are ecologically and reproductively isolated, suggesting that stock-recruitment relationships may differ between broodlines. The adult return and spawner time series for the region are short, therefore combining the two broodlines allowed a more complete examination of relationships between environmental conditions and indices of productivity in the context of changing climate conditions. Additional analyses into these relationships should be explored in the future, as the extension of time series and collection of new environmental data enable such models.

Continued monitoring of salmon through life-cycle and life-history models will provide insight into how warming Arctic climate conditions are impacting critical periods in salmon production. Our analyses suggest that Pink salmon production in the northeastern Bering Sea is driven by freshwater and early marine habitat dynamics. While we used air temperature as a proxy for stream temperature, broad-scale predictive models of climate change in the Arctic provide little information about feedback processes contributing to local conditions (Nielsen et al., 2013). To explore emerging connections within freshwater habitats, local knowledge regarding stream conditions, salmon abundance and spawning locations will be needed for perspective to current observations. Further monitoring of stream temperatures, flow and ice dynamics will improve our understanding of how climate warming is impacting this important habitat and context to shifts in abundance northward into the high Arctic.

Acknowledgements

The authors sincerely thank two anonymous reviewers for comments that greatly improved the manuscript. We also thank Jordan Watson for providing the summer sea surface temperatures for the northeastern Bering Sea. In addition, the authors thank all captains, crew, and science teams who collected these data. These samples were collected over 18 surveys with support and funding from many different entities including: Bering Sea Fisherman's Association, The Alaska Coastal Impact Assistance Program (Arctic Ecosystem Integrated Survey 2012 and 2013), Bureau of Ocean and Energy Management, The Alaska Sustainable Salmon Fund, NCEAS – State of Alaska's Salmon and People and the Yukon River Drainage Fisherman's Association. This project is a collaborative effort with the Alaska Department of Fish and Game and the North Pacific Anadromous Fish Commission. The northern Bering Sea surface trawl survey is part of the NOAA Alaska Fisheries Science Center's, Bering Arctic Subarctic Integrated Survey (BASIS). This manuscript is a product of the North Pacific Research Board Arctic Integrated Ecosystem Research Program, NPRB publication number ArcticIERP-12.

Table 1. The year, survey timing (start and end day), average date adjustment in days (Adj. days), average observed and adjusted (Adj.) length (L, mm), weight (W, g) and standard error (SE) for the number (N) of juvenile pink salmon sampled in the northeastern Bering Sea during 2003 to 2018. * no survey conducted in the NBS during 2008.

Year	Survey Timing		Adj.	N	L	SE	Adj. L	SE	W	SE	Adj. W	SE
	Start	End	(days)		(mm)		(mm)		(g)		(g)	
2003	21-Aug	8-Oct	8	550	167.0	1.4	176.6	2.4	45.9	1.1	47.5	1.3
2004	10-Sep	30-Sep	8	622	192.6	0.9	202.3	0.9	70.8	1.1	72.5	1.1
2005	17-Sep	3-Oct	16	287	188.6	1.2	207.5	1.3	63.1	1.3	66.4	1.3
2006	31-Aug	19-Sep	-2	353	150.8	0.7	148.5	0.8	29.3	0.4	28.8	0.5
2007	14-Sep	1-Oct	11	1098	186.8	0.5	199.9	0.6	64.4	0.7	66.6	0.7
2009*	30-Aug	13-Sep	-4	365	160.6	0.7	155.7	0.9	38.3	0.6	37.5	0.6
2010	10-Sep	4-Oct	10	189	179.4	1.2	190.9	1.7	54.3	1.3	56.3	1.4
2011	29-Aug	17-Sep	-8	417	145.0	0.9	135.5	1.0	27.9	0.6	26.2	0.6
2012	11-Sep	25-Sep	8	110	157.9	0.9	167.9	1.2	35.4	0.7	37.1	0.7
2013	10-Sep	24-Sep	6	684	174.2	0.5	181.3	0.6	50.6	0.5	51.7	0.5
2014	4-Sep	22-Sep	-1	372	168.7	0.8	167.8	1.0	48.5	0.8	48.3	0.8
2015	2-Sep	16-Sep	-4	983	161.4	0.8	156.2	0.9	42.4	0.7	41.6	0.7
2016	28-Aug	12-Sep	-10	395	153.9	1.2	141.9	1.4	37.3	1.1	35.2	1.2
2017	27-Aug	8-Sep	-9	848	136.4	1.0	125.4	1.0	25.7	0.6	23.9	0.7
2018	3-Sep	15-Sep	-4	1171	152.9	0.5	148.5	0.6	33.4	0.3	32.6	0.3

Table 2. Indices of adult Pink salmon returns and spawners to the Norton Sound region and Yukon River (1995 - 2018), the average Nome Air temperatures (°C, August t to June t+1), and average summer sea surface temperatures during June to September (°C, SST t+1).

Adult	Norton Sound Region		Yukon River		Nome Air	Summer
Year	Returns	Spawners	Returns	Spawners	Temp.	SST
1995	169,496	49,409	55,284	55,137	-4.6	7.2
1996	3,089,682	2,535,593	216,582	214,837	-3.3	6.7
1997	189,439	163,728	4,519	4,301	-3.9	7.5
1998	3,712,761	3,070,848	336,166	330,624	-3.1	6.3
1999	95,302	73,077	4,771	4,716	-5.5	5.7
2000	2,091,074	1,883,867	105,461	104,866	-4.6	6.4
2001	109,878	79,706	3,675	3,666	-2.6	5.7
2002	2,300,537	2,239,565	298,111	289,688	-4.5	7.8
2003	441,387	392,827	17,864	15,673	-1.9	7.8
2004	6,513,682	6,432,486	808,739	799,009	-2.8	9.2
2005	2,652,592	2,594,334	103,255	100,121	-2.6	7.9
2006	5,825,726	5,763,830	384,274	379,366	-5.1	6.5
2007	734,723	708,669	138,492	136,374	-3.3	8.4
2008	4,069,508	3,932,201	793,747	770,035	-4.4	6.6
2009	320,631	275,834	39,225	36,924	-5.4	6.5
2010	1,560,810	1,484,282	1,261,091	1,256,789	-4.7	7.1
2011	231,000	206,127	13,298	10,973	-3.1	6.3
2012	1,265,834	1,013,565	500,227	495,026	-6.2	6.4
2013	102,117	73,928	7,791	6,715	-4.9	7.0
2014	960,447	735,843	799,804	738,121	-1.7	8.2
2015	716,045	626,383	50,632	40,473	-2.0	7.1
2016	4,638,943	4,378,422	1,755,412	1,619,366	-1.1	8.9
2017	2,780,199	2,723,866	199,040	196,573	-2.9	8.9
2018	6,253,239	6,176,411	825,957	785,957	-1.4	9.3

Table 3. Results of the step-wise model selection for Yukon River and Norton Sound region Pink salmon life-cycle models (1995 – 2018). Statistics include C^p, residual standard error (*RSS*), coefficient of variation (R^2), the mean square error of the true regression model $\hat{\sigma}^2$, parameter estimate (Estimate) and standard error (SE), *t* value of the parameter estimate and significance of the estimate (Prob).

Region	Model	*Cp*	*RSS*	$\hat{\sigma}^2$	Estimate	SE	*t* value	Prob	*R2*
Yukon									
	Cushing								
				1.27					0.71
	Intercept Only	1.0	24.2		-0.47	2.07	-0.23	0.821	
	ln(spawners)	42.9	80.1		0.82	0.12	6.80	0.000	
	Summer Sea Surface Temp	1.7	27.6		0.34	0.21	1.69	0.107	
	Ricker								
				1.31					0.11
	Intercept Only	0.5	26.8		-2.44	1.61	-1.52	0.144	
	Summer Sea Surface Temp	1.0	30.1		0.35	0.22	1.60	0.124	
Norton Sound	Cushing								
				0.52					0.77
	Intercept Only	1.4	10.2		1.10	1.59	0.68	0.504	
	ln(spawners)	41.7	32.4		0.66	0.10	6.61	0.000	
	Summer Sea Surface Temp	13.9	17.8		0.54	0.14	3.88	0.001	
	Ricker								
				0.55					0.53
	Intercept Only	1.1	10.5		-3.36	1.04	-3.24	0.004	
	spawners	9.6	16.3		0.00	0.00	-3.32	0.003	
	Summer Sea Surface Temp	14.5	19.0		0.57	0.14	4.02	0.001	

Table 4. Juvenile Pink salmon natural log of the catch per unit effort (CPUE), relative abundance (defined as the natural log of the adjusted CPUE), average sea temperature above the mixed layer depth (°C), and average $August_{t-1}$ to $June_t$ air temperatures (°C) in Nome, Alaska during 2003 to 2018. * no ship board data available for 2008.

Juvenile Year	Mixed Layer Depth Adjustment	ln CPUE	Relative Abundance	Summer SST	Nome Air Temp.
2003	1.78	2.54	4.5	7.8	-1.9
2004	1.46	2.51	3.7	9.2	-2.8
2005	1.79	1.96	3.5	7.9	-2.6
2006	1.20	1.69	2.0	6.5	-5.1
2007	1.18	3.08	3.6	8.4	-3.3
2009*	1.01	1.38	1.4	6.5	-5.4
2010	1.08	1.43	1.5	7.1	-4.7
2011	1.16	1.36	1.6	6.3	-3.1
2012	1.21	0.84	1.0	6.4	-6.2
2013	1.02	3.09	3.1	7.0	-4.9
2014	1.04	2.00	2.1	8.2	-1.7
2015	1.26	4.30	5.4	7.1	-2.0
2016	1.00	2.65	2.7	8.9	-1.1
2017	1.03	3.94	4.1	8.9	-2.9
2018	1.04	4.22	4.4	9.3	-1.4

Table 5. Results of the step-wise model selection for Pink salmon freshwater and early marine life-history events. Statistics include C_p, residual standard error (*RSS*), the mean square error of the true regression model $\hat{\sigma}^2$, coefficient of variation (R^2), parameter estimate (Estimate) and standard error (SE), *t* value of the parameter estimate and significance of the estimate (Prob).

Model	C_p	*RSS*	$\hat{\sigma}^2$	Estimate	SE	*t* value	Prob	R^2
Juvenile Abundance Model								
			0.98					0.55
Intercept Only	17.2	9.8		-9.60	3.50	-2.74	0.018	
ln(spawners)	18.4	14.5		0.35	0.19	1.85	0.090	
Nome Air Temp	25.2	21.3		0.29	0.09	3.26	0.007	
Adult Return Model								
			0.75					0.62
Intercept Only	1.1	8.4		12.3	0.52	23.6	0.000	
Juvenile Index	17.3	22.0		0.74	0.16	4.6	0.000	

a.

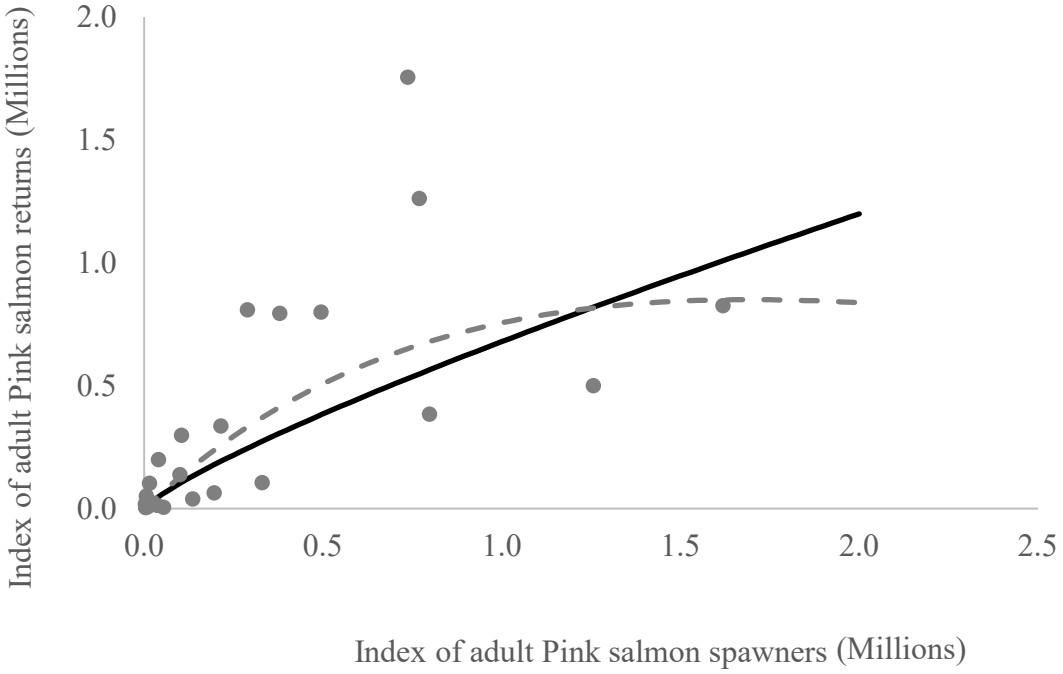

b.

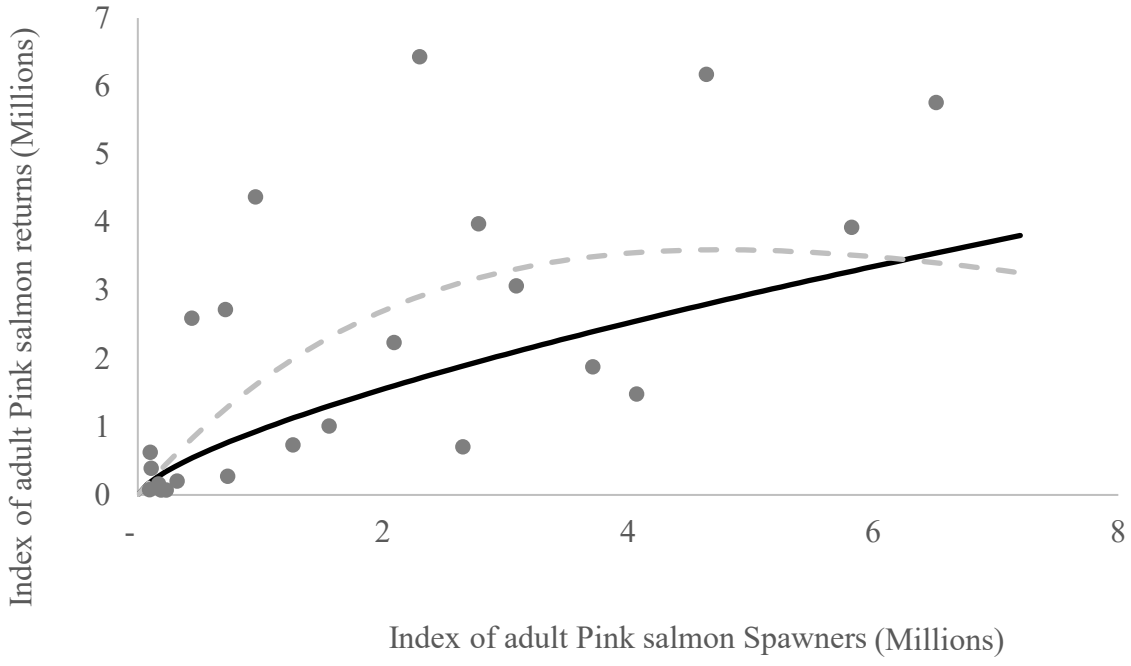

Fig. 1. Indices of adult Pink salmon spawners and returns (spawners plus harvest) to the Yukon River (a) and Norton Sound region (b). The solid line represents the Cushing model fit and the dashed line represents the Ricker model fit to the spawner and return data.

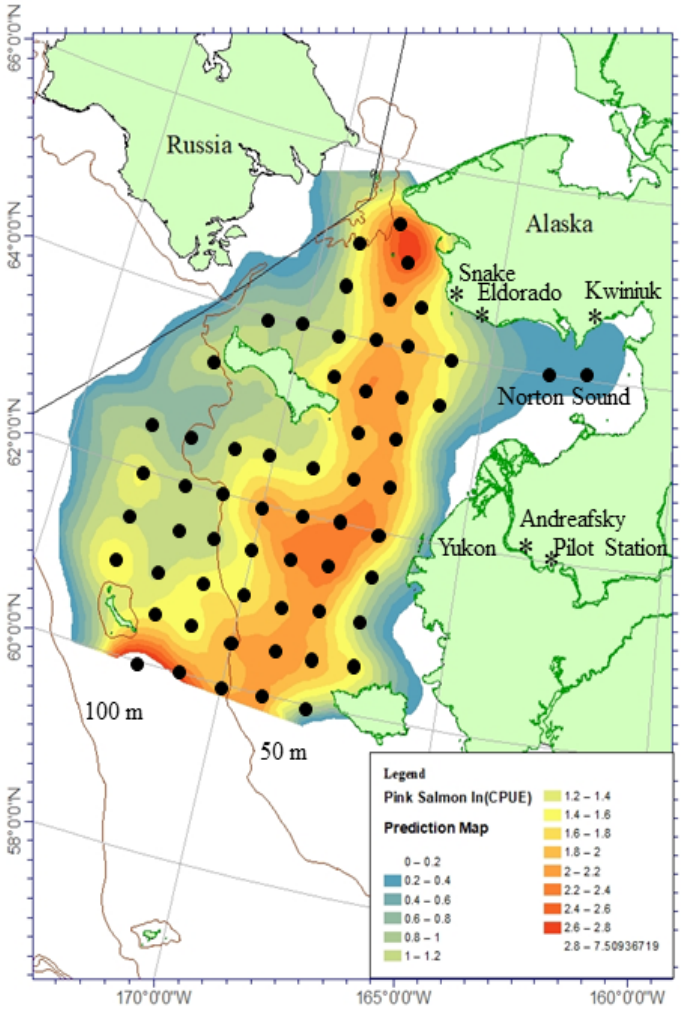

Fig. 2. Typical station grid (black dots) sampled during late August to September (2003 to 2018; excluding 2008) surface trawl surveys of the Northern Bering Sea. Lines indicate the 50 m and 100 m depth contours. Spatial distribution of juvenile Pink salmon based on catch data (ln CPUE, catch per unit effort, scaled to average effort km^2). Color contours are from the neighborhood kriging prediction surface of ln(CPUE). The map includes locations for Norton Sound region and Yukon River adult Pink salmon escapement index rivers (Snake, Eldorado, Kwiniuk, Yukon, Andreafsky) and the Pilot Station index.

Fig. 3. The natural log of adult Pink salmon returns per spawner for the Yukon River (solid line) and Norton Sound region (dashed line) for brood years 1995 to 2017.

a.

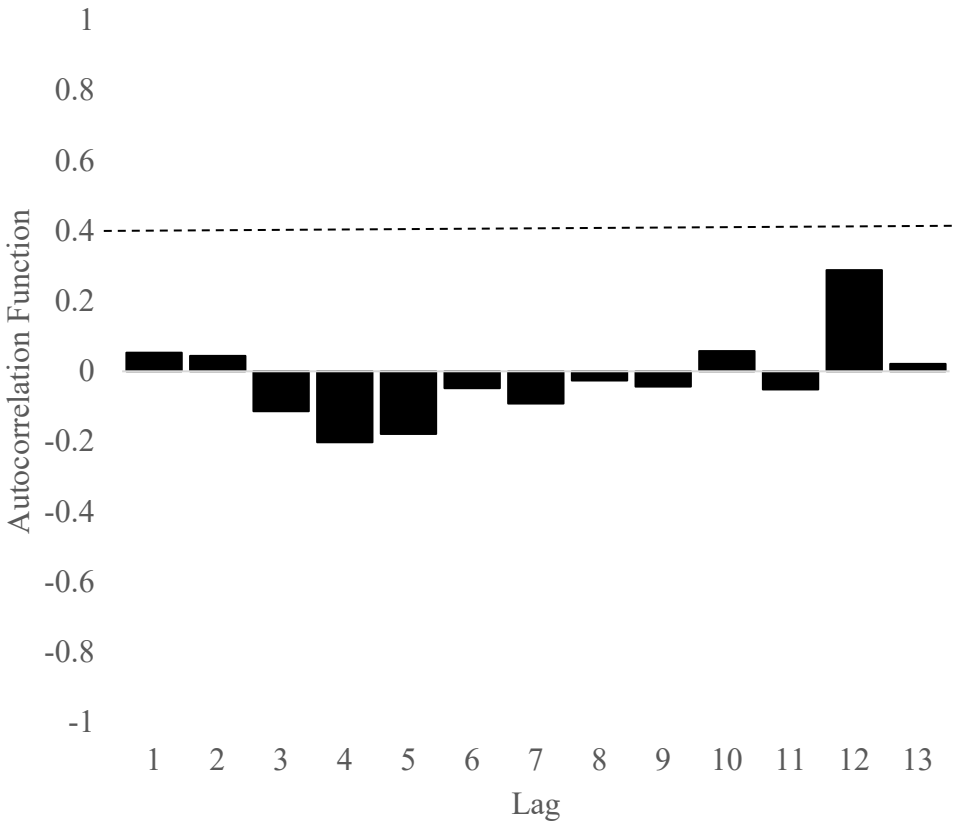
1
0.8
0.6
0.4
0.2
0
-0.2
-0.4
-0.6
-0.8
-1
Autocorrelation Function
1 2 3 4 5 6 7 8 9 10 11 12 13
Lag

b.

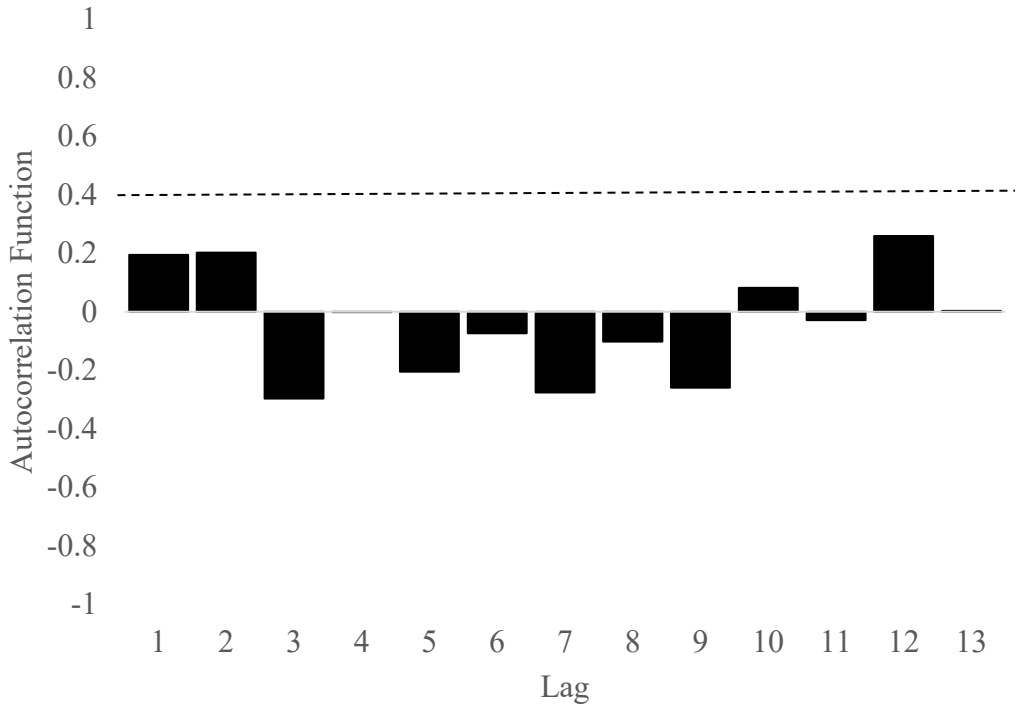
1
0.8
0.6
0.4
0.2
0
-0.2
-0.4
-0.6
-0.8
-1
Autocorrelation Function
1 2 3 4 5 6 7 8 9 10 11 12 13
Lag

c.

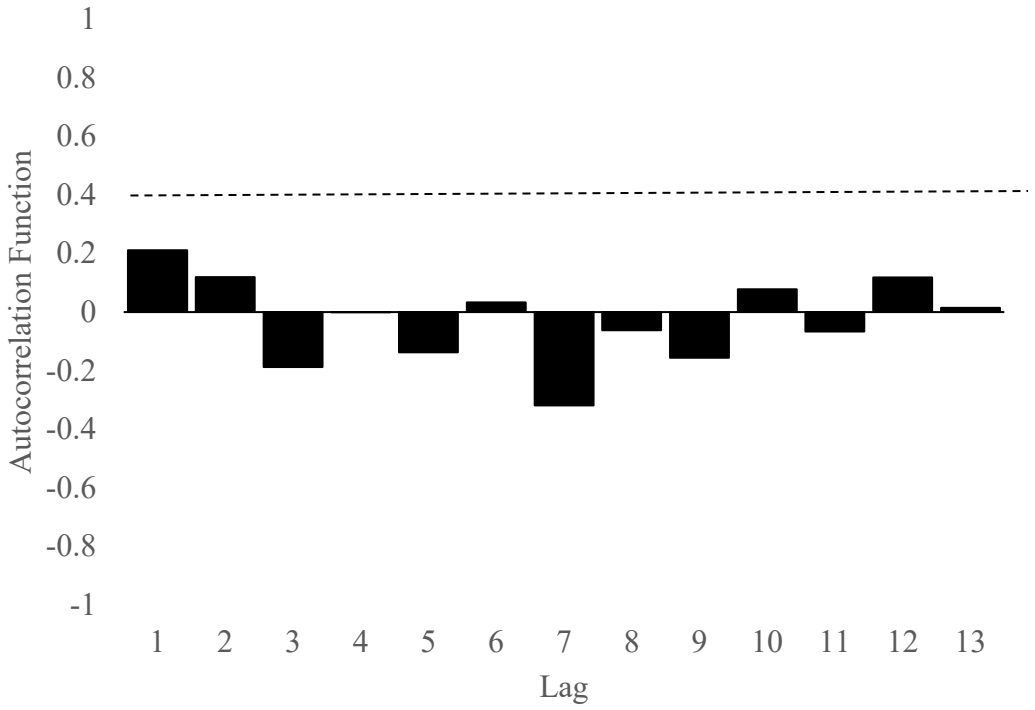

Fig. 4. The autocorrelation functions for residuals of the most parsimonious life-cycle models including the Cushing model for the Yukon River (a), the Cushing model (b) and Ricker model (c) for the Norton Sound region. The dashed lines are the upper and lower bounds for significant autocorrelation.

a.

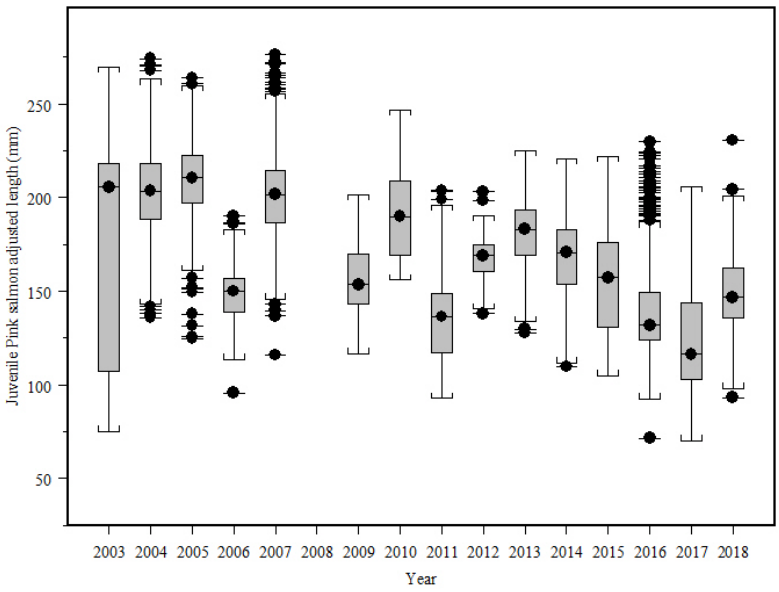

b.

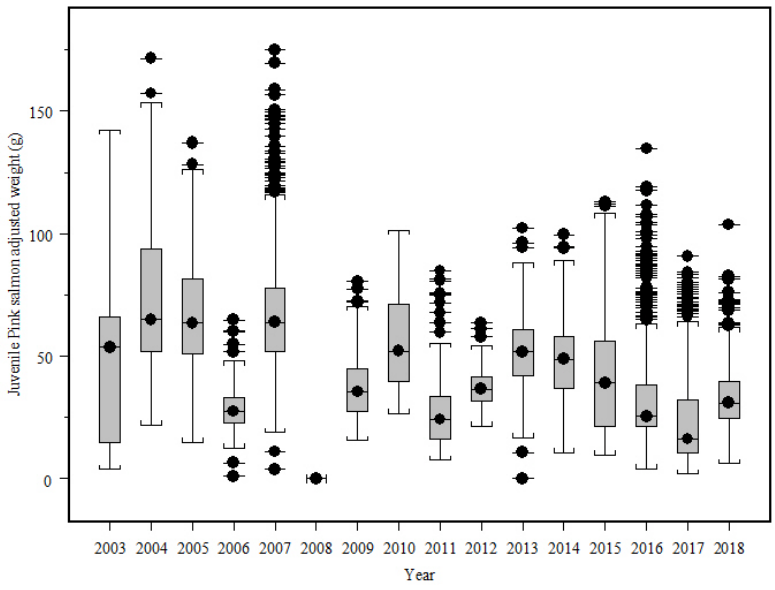

Fig. 5. Box plots of juvenile Pink salmon adjusted a) length (mm) and b) weight (g) during late August to September 2003 to 2018 (no survey was conducted during 2008) in the northeastern Bering Sea. Length and weight were adjusted to September 12 of each year. The solid horizontal line in the box plot is located at the median of the data, and the upper and lower ends of the box are located at the upper quartile and lower quartile of the data, respectively. The lines extending above and below the box indicate the variability outside the upper and lower quartiles.

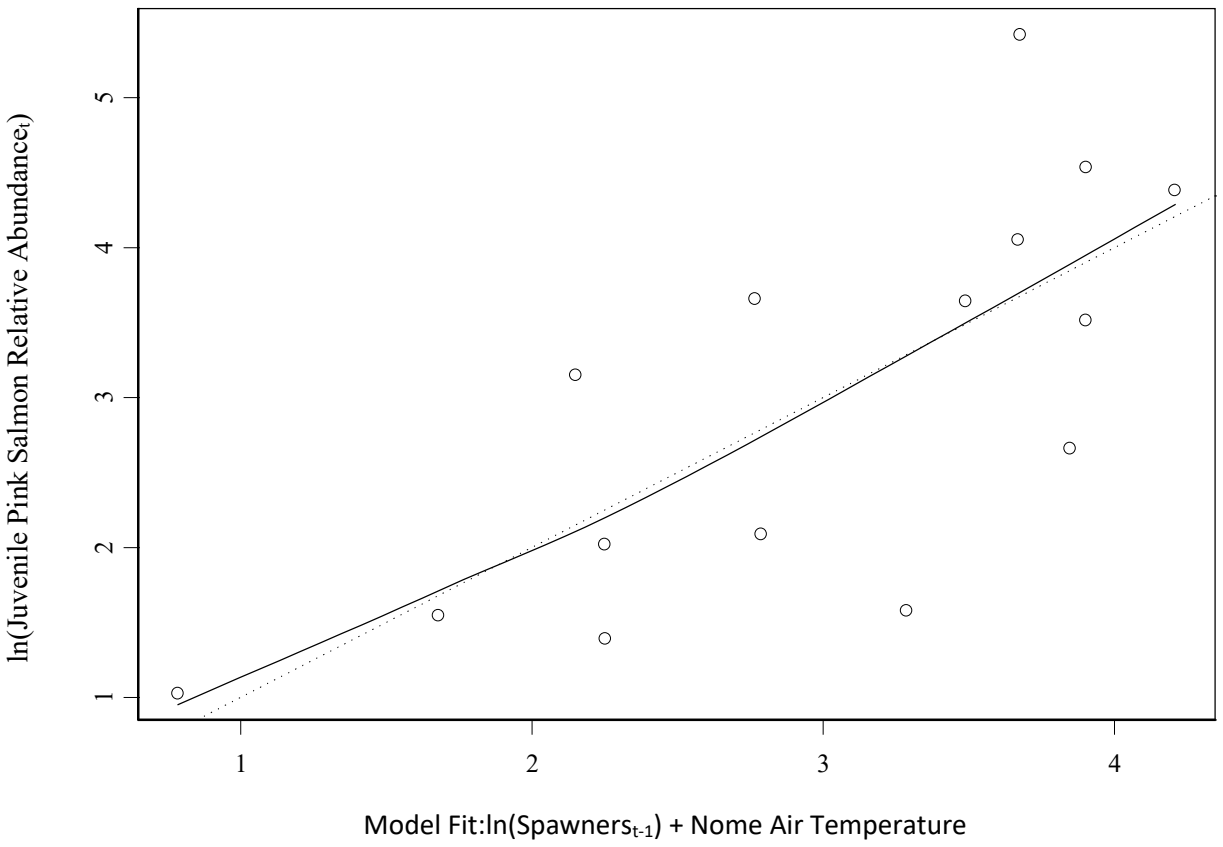

Fig. 6. The relationship (dark line) between the natural log of juvenile Pink salmon relative abundance and the natural log of adult Pink salmon spawner index with Nome Air temperature (open circles; 2003 to 2018).

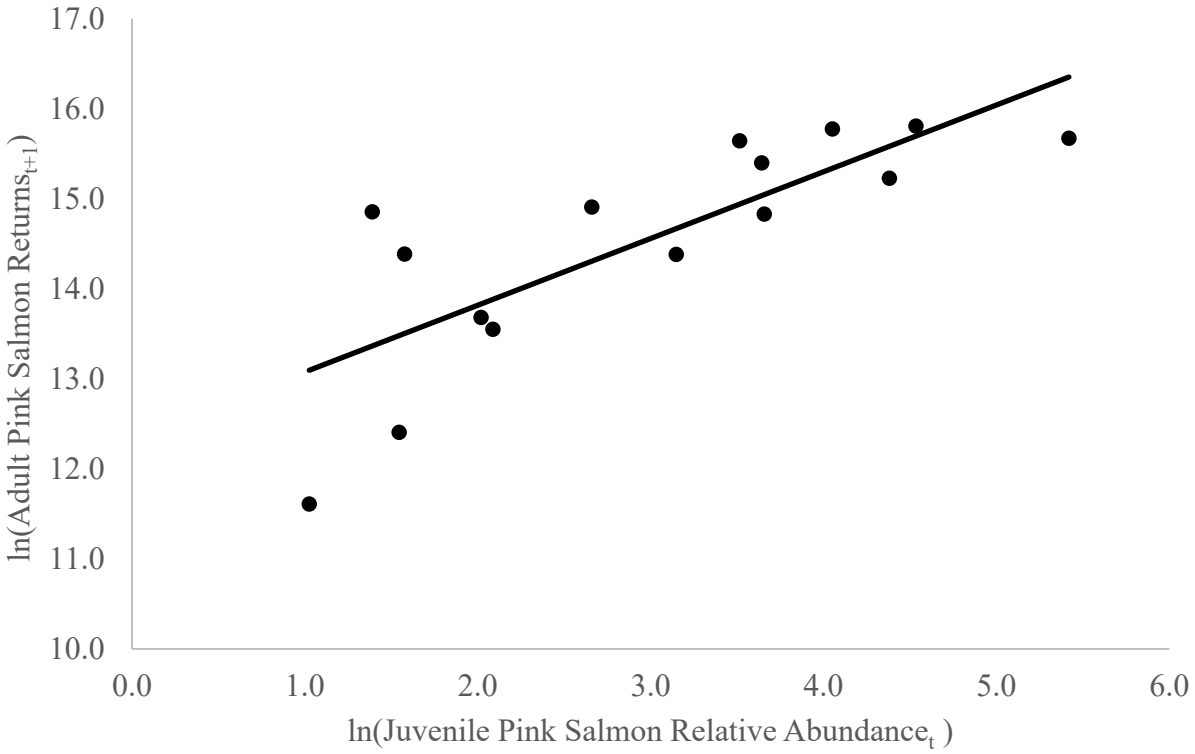

Fig. 7. The relationship (dark line) between the natural log of adult Pink salmon return index to the Yukon River and Norton Sound region and the natural log of the relative abundance of juvenile Pink salmon from the surface trawl surveys (black dots; 2003 to 2018).

References

Andrews, A.G., Farley Jr., E.V., Moss, J.H., Murphy, J.M., Husoe, E.F., 2009. Energy density and length of juvenile Pink salmon (*Oncorhynchus gorbuscha*) in the eastern Bering Sea from 2004 to 2007: a period of relatively warm and cool sea surface temperatures. N. Pac. Anadrom. Fish Comm. 5, 183 – 189.

Arrigo, K.R., van Dijken, G.L., 2011. Secular trends in Arctic Ocean net primary production. J. Geophys. Res. 116, C09011, doi:10.1029/2011JC007151.

Aspinwall, N., 1974. Genetic analysis of North American populations of the Pink salmon, *Onchorhynchus gorbuscha*; possible evidence for the neutral mutation-random droft hypothesis. Evol. 28, 295 – 305.

Baker, M.R., Kivva, K.K., Pisareva, M., Watson, J., Selivanova, J., 2020. Shifts in the physical environment in the Pacific Arctic and implications for ecological timing and conditions. Deep Sea Res. II. (this volume)

Batten, S.D., Ruggerone, G.T., Ortiz, I., 2018. Pink salmon induce a trophic cascade in plankton populations in the southern Bering Sea and around the Aleutian Islands. Fish. Ocean. 27, 548 – 559.

Beacham, T.D., McIntosh, B., MacConnachie, C., Spolsted, B., White, B.A., 2012. Population structure of Pink salmon (*Oncorynchus gorbuscha*) in British Columbia and Washington, determined with microsatellites. Fish. Bull. 110, 242–256.

Beacham, T.D., Murray, C.B. 1988. Variation in developmental biology of Pink salmon (*Oncorhynchus gorbuscha*) in British Columbia. Can. J. of Zool. 66, 2634 – 2648.

Beamish, R.J., Mahnken, C., 2001. A critical size and period hypothesis to explain natural regulation of salmon abundance and the linkage to climate and climate change. Prog. Ocean. 49, 423 – 437.
Brett, J.R., 1952. Temperature tolerance in young Pacific salmon genus Oncorhynchus. J. Fish. Res. Board Can. 9, 265 – 323.
Carey, M.P., Keith, K.D., Schelske, M., Lean, C., McCormick, S.D., Regish, A., Zimmerman, C.E., 2019. Energy depletion and stress levels in Sockeye salmon migrating at the northern edge of their distribution. Trans. Am. Fish. Soc. 148, 785 – 797.
Carothers, C., Cotton, S., Moerlein, K., 2013. Subsistence use and knowledge of salmon in Barrow and Nuiqsut, Alaska. Final Report to OCS study Bureau of Ocean and Energy Management 2013 – 0015.
Chambers, J.M., Hastie, T.J., 1991. Statistical Models in S. Chapman and Hall. London.
Conitz, Jan., 2019. Abundance and Run Timing of Adult Pacific Salmon in the East Fork Andreafsky River, Yukon Delta National Wildlife Refuge, Alaska, 2018. Alaska Fisheries Data Series Number 2019-2.
Craig, P., Haldorson, L., 1986. Pacific salmon in the North American Arctic. Arct. 39:2 – 7.
Cushing, D.H., 1971. Dependence of recruitment on parent stock. J. Fish. Res. Board Can. 30, 1965 – 1976.
Danielson, S., Eisner, L, Weingartner, T., Aagaard, K., 2011. Thermal and haline variability over the central Bering Sea shelf: seasonal and interannual perspectives. Cont. Shelf Res. 31, 539 – 554.
Danielson, S.L., Ahkinga, O., Ashjian, C., Basyuk, E., Cooper, L.W., Eisner, L., Farley, E., Iken, K.B., Grebmeier, J.M., Juranke, L., Khen, G., Jayne, S., Kikuchi, T., Ladd, C., Lu, K., McCabe, R.M., Moore, G.W.K., Nishino, S., Ozenna, F., Pickart, R.S., Polyakov, I., Stabeno, P.J., Thoman, R., Williams, W.J., Wood, K., Weingartner, T.J., 2020. Manifestation and consequences of warming and altered heat fluxes over the Bering and Chukchi Sea continental shelves. Deep Sea Res. II (this volume)
Dorner, B., Catalano, M.J., Peterman, R.M., 2017. Spatial and temporal patterns of covariation in productivity of Chinook salmon populations of the northeastern Pacific Ocean. Can. J. Fish. Aquat. Sci. 75, 1082 – 1095.
Dunmall, K.M., Reist, J.D., Carmack, E.C., Babluk, J.A., Heide-Jorgensen, M.P., Docker, M.F., 2013. Pacific salmon in the Arctic: harbingers of change, in: Mueter, F.J., Dickson, D.M.S., Huntington, H.P., Irvine, J.R., Logerwell, E.A., MacLean, S.A., Quankenbush, L.T., Rosa, C. (Eds.), Responses of Arctic Marine Ecosystems to Climate Change. Alaska Sea Grant, University of Alaska Fairbanks. pp. 141 – 163.
Dunmall, K.M., Mochnacz, N.J., Zimmerman, C.E., Lean, C., Reist, J.D., 2016. Using thermal limits to assess establishment of fish dispersing to high-latitude and high-elevation watersheds. Can. J. Fish. Aquat. Sci. 73, 1750 – 1758.
Dunmall, K.M., McNicholl, D.G., Reist, J.D., 2018. Community-based monitoring demonstrates increasing occurrences and abundances of Pacific salmon in the Canadian Arctic from 2000 to 2017. N. Pac. Anadr. Fish Comm. Tech. Rep. 11
Estensen, J. L., Carroll, H. C., Larson, S. D., Gleason, C. M., Borba, B. M., Jallen, D. M., Padilla, A. J., and Hilton, K. M., 2018. Annual management report Yukon Area, 2017. Alaska Department of Fish and Game, Fishery Management Report No. 18-28, Anchorage.
Farley Jr., E.V., Murphy, J.M., Wing, B.W., Moss, J.H., Middleton, A., 2005. Distribution, migration pathways, and size of western Alaska juvenile salmon along the eastern Bering Sea shelf. Alaska Fish. Res. Bull. 11, 15 – 26.
Farley Jr., E.V., Murphy, J., Moss, J., Feldmann, A., Eisner, L., 2009. Marine ecology of western Alaska juvenile salmon, in Krueger, C.C., Zimmerman, C.E. (Eds.), Pacific Salmon: Ecology and Management of Western Alaska's Populations. American Fisheries Society, Bethesda, Maryland, pp. 307 – 329.

Fossheim, M., Primicerio, P. E., Johannesen, R.B., Ingvaldsen, M.M., Aschan, Dolgov, A.V., 2015. Recent warming leads to a rapid borealization of fish communities in the Arctic. Nature doi:10.1038/NCLIMATE2647.

Frey, K.E., Maslanik, J.A., Kinney, J.C., Maslowski, W., 2014. Recent variability in sea ice cover, age, and thickness in the Pacific Arctic region, in: Grebmeier, J.M., Maslowski, W. (Eds.), The Pacific Arctic Region: Ecosystem Status and Trends in a Rapidly Changing Environment. Springer, the Netherlands, pp. 31-63.

Gall, A.E., Morgan, T.C., Day, R.H., Kuletz, K.T., 2017. Ecological shift from piscivorous to planktivorous seabirds in the Chukchi Sea, 1975 – 2012. Polar Biol. 40, 61 – 78.

Grant, A., Gardner, M., Nendick, L., Sackville, M., Farrell, A.P., and Brauner, C.J., 2009. Growth and ionoregulatory ontogeny of wild and hatchery raised juvenile Pink Salmon (*Oncorhynchus gorbuscha*). Can. J. Zool. 87, 221-228.

Grebmeier, J.M., Overland, J.E., Moore, S.E., Farley, E.V., Carmack, E.C., Cooper, L.W., Frey, K.E., Helle, J.H., McLaughlin, F.A., McNutt, S.L., 2006. A major ecosystem shift in the Norther Bering Sea. Science 311 (5766), 1461 – 1464, doi:10.1126/science.1121365.

Heard, W.R. 1991. Life history of Pink salmon. In Groot, C., and Margolis, L. (eds), Pacific Salmon Life Histories. UBC Press.

Hop, H., Gjosaeter, H., 2013. Polar cod (*Boreogadus saida*) and capelin (*Mallotus villosus*) as key species in marine food webs of the Arctic and Barents Sea. Mar. Biol. Res. 9, 878-894.

Howard, K. G., K. M. Miller, and J. Murphy. 2017. Estuarine fish ecology of the Yukon River Delta, 2014–2015. Alaska Department of Fish and Game, Fishery Data Series No. 17-16, Anchorage.

Huntington, H.P., and others., 2020. Evidence suggests potential transformation of the Pacific Arctic ecosystem is underway. Nat. Clim. Change. https://doi.org/10.1038/s41558-020-0695-2.

IARC (International Arctic Research Center), 2019. https://uaf-iarc.org

Insightful, 2001. S-Plus 6 for Windows Guide to Statistics, Vol. 1. Seattle, WA: Insightful Corporation.

Irvine, J.R., Michielsens, C.J.G., O'Brien, M., White, B.A., Folkes, M., 2014. Increasing dominance of odd-year returning pink salmon. Trans. Am. Fish. Soc. 143, 939 – 956.

JTC (Joint Technical Committee of the Yukon River U.S./Canada Panel), 2019. Yukon River salmon 2018 season summary and 2019 season outlook. Alaska Department of Fish and Game, Division of Commercial Fisheries, Regional Information Report 3A19-01, Anchorage.

Klovach, N.V., Temnykh, O.S., Shevlyakov, V.A., Shevlyakov, E.A., Bugaev, A.F., Ostrovskiy, V.I., Kaev, A.M., Volobuev, V.V., 2018. Current stock assessment of Pacific salmon in the far east of Russia. N. Pac. Anad. Fish Com., Tech. Rep. 11, 12 – 16.

Kondzela, C., Garvin, M., Riley, R., Murphy, J., Moss, J., Fuller, S.A., Gharrett, A., 2009. Preliminary genetic analysis of juvenile Chum salmon from the Chukchi Sea and Bering Strait. N. Pac. Anad. Fish Com. Bull. 5, 25 – 27.

Malick, M.J., Cox, S.P., 2016. Regional-scale declines in productivity of pink and chum salmon stocks in western North America. PLoS One 11(1):e0146009. Doi:10.1371/journal.pone.0146009.

McPhail, J.D., Lindsey, C.C., 1970. Freshwater fishes of northwestern Canada and Alaska. Bull. Fish. Res. Board Can. 173.

Menard, J., Leon, J., Bavilla, J., Neff, L., Joyce, S., 2018. Norton Sound salmon season summary. Alaska Department of Fish and Game, Division of Commercial Fisheries News Release. https://www.adfg.alaska.gov/static/applications/dcfnewsrelease/997457402.pdf

Menard, J., Soong, J., Bell, J., Neff, L., Leon, J.M. 2020. 2018 annual management report Norton Sound, Port Clarence, and Arctic, Kotzebue areas. Fishery Management Report number 20-05. Alaska Department of Fish and Game, Division of Sport Fish and Commmercial Fisheries.

Mueter, F.J, Peterman, R.M., Pyper, B.J., 2002. Opposite effects of ocean temperature on survival rates of 120 stocks of Pacific salmon (*Oncorhynchus* spp.) in the northern and southern areas. Can. J. Fish. Aquat. Sci. 59, 456 – 463.

Murphy, J.M., Howard, K.G., Gann, J.C., Cieciel, K.C., Templin, W.D., Guthrie III, C.M., 2017. Juvenile Chinook salmon abundance in the northern Bering Sea: Implications for future returns and fisheries in the Yukon River. Deep-Sea Res. II. 1235, 156 – 167.

Moss, J.H, Murphy, J.M., Farley, E.V., Eisner, L.B., Andrews, A.G., 2009. Juvenile Pink and Chum salmon distribution, diet, and growth in the northern Bering and Chukchi seas. N. Pac. Anad. Fish Comm. Bull. 5, 191 – 196.

Moore, S.E., Logerwell, E., Eisner, L., Farley Jr., E.V., Harwood, L.A., Kuletz, K., Lovvorn, J., Murphy, J. M., Quakenbush, L.T., 2014. Marine fishes, birds and mammals as sentinels of ecosystem variability and reorganization in the Pacific Arctic Region, in: Grebmeier, J.M., Maslowski, W. (Eds.), The Pacific Arctic Region: Ecosystem Status and Trends in a Rapidly Changing Environment, pp. 337-392

McNyset, K.M., Volk, C.J., and Jordan, C.E., 2015. Developing an effective model for predicting spatially and temporally continuous stream temperatures from remotely sensed land surface temperatures. Water 7, 6827 – 6846.

Nielsen, J.L, Ruggerone, G.T., Zimmerman, C.E., 2013. Adaptive strategies and life history characteristics in a warming climate: Salmon in the Arctic? Environ. Biol. Fish. 96:1187 – 1226. Doi:10.1007/s10641-012-0082-6.

NOAA Coral Reef Watch. 2018, updated daily. NOAA Coral Reef Watch Version 3.1 Daily Global 5-km Satellite Coral Bleaching Degree Heating Week Product, Jun. 3, 2013-Jun. 2, 2014. College Park, Maryland, USA: NOAA Coral Reef Watch. https://coastwatch.pfeg.noaa.gov/erddap/griddap/NOAA_DHW.html. (accessed 07 January 2020).

Oka, G., Holt, C., Irvine, J.R., Trudel, M., 2012. Density-dependent growth of salmon in the North Pacific Ocean: Implications of a limited, climatically varying carrying capacity for fisheries management and international governance. N. Pac. Anad. Fish Comm., Tech. Rep. 8, 112.

Orlova, E.L., Dolgov, A.V., Renaud, P.E., Boitsov,V.D. Prokopchuk, I.P., Zashihina, M.V., 2013. Structure of the macroplankton-pelagic fish-cod trophic complex in a warmer Barents Sea. Mar. Biol. Res. 9, 851-866.

Orsi, J.A., Fergusson, E.A., Wertheimer, A.C., Farley Jr., E.V., Mundy, P.R., 2016. Forecasting Pink salmon production in southeast Alaska using ecosystem indicators in times of climate change. N. Pac. Anad. Fish Comm. Bull. 6, 483 – 499.

Overland, J.E., Wang, J., Pickart, R.S., and Wang, M., 2014. Recent and future changes in the meteorology of the Pacific Arctic, in: Grebmeier J.M., Maslowski, W. (Eds.), The Pacific Arctic Region: Ecosystem Status and Trends in a Rapidly Changing Environment, pp. 17 – 30.

Parker, R.R., 1968. Ocean ecology of the North Pacific salmonids. Univ. of Washington Press, Seattle, WA. p. 179.

Peterman, R.M., Pyper, B.J., Lapointe, M.F, Adkison, M.D., Walters, C.J., 1998. Patterns of covariation in survival rates of British Columbian and Alaska sockeye salmon (*Oncorhynchus nerka*) stocks. Can. J. Fish Aquat. Sci. 55, 2503 – 2517.

Peterman, R.M., Dorner, B.A., 2012. A widespread decrease in productivity of sockeye salmon (*Oncorhynchus nerka*) populations in western North America. Can. J. Fish Aquat. Sci. 69, 1255 – 1260.

Pyper, B.J., Mueter, F.J., Peterman R.M., Blackbourn, D.J., Wood, C.C., 2001. Spatial covariation in survival rates of Northeast Pacific Pink salmon (*Oncorhynchus gorbushcha*). Can. J. Fish Aquat. Sci. 58, 1501 – 1515.

Pyper, B.J., Mueter, F.J., Peterman, R.M., Blackbourn, D.J., Wood, C.C., 2002. Spatial covariation in survival rates of Northeast Pacific Chum salmon (*Oncorhynchus keta*). Trans. Am. Fish Soc. 131, 343 – 363.

Pyper, B.J., Mueter, F.J., Peterman, R.M., 2005. Across-species comparisons of spatial scales of environmental effects on survival rates of Northeast Pacific salmon. Trans. Am. Fish Soc. 134, 86 – 104.

Quinn, T.J., III, and Derison, R.B., 1999. Quantitative fish dynamics. Oxford University Press.
Radchenko, V.I., Beamish, R.J., Heard, W.R., Temnykh, O.S., 2018. Ocean ecology of pink salmon, in: Beamish, R.J. (Ed.), The Ocean Ecology of Pacific Salmon and Trout. American Fisheries Society, Bethesda, pp. 15 – 160.
Reist, J.D., Wrona, F.J., Prowse, T.D., Power, M., Dempson, J.B., Beamish, R.J., King, J.R., Carmichael, T.J., Sawatzky, C.D. 2006. General effects of climate change on Arctic fishes and fish populations. Ambio 35, 370 – 380.
Ricker, W.E., 1975. Computation and interpretation of biological statistics of fish populations. Bull. Fish. Res. Board Can. 191.
Ruggerone, G.T., Agler, B.A., Connors, B.M., Farley Jr., E.V., Irvine, J.R., Wilson, L.E., Yasumiishi, E.M., 2016. Pink and sockeye salmon interactions at sea and their influence on forecast error of Bristol Bay sockeye salmon. N. Pac. Anadr. Fish Comm. Bull. 6, 349 – 361.
Ruggerone, G.T., Irvine, J.R., 2018. Numbers and biomass of natural- and hatchery- origin Pink salmon, Chum salmon, and Sockeye salmon in the North Pacific Ocean, 1925 – 2015. Mar. Coast. Fish. 10, 152 – 168.
Sigler, M.F., Renner, M., Danielson, S.L., Eisner, L.B., Lauth, R.R., Kuletz, K.J., Logerwell, E.A., Hunt Jr., G.L., 2011. Fluxes, fins and feathers: relationships among the Bering, Chukchi, and Beaufort Seas in a time of climate change. Oceanogra. 24, 250 – 265.
Springer, A.M., van Vliet, G.B., Bool, N., Crowley, M., Fullagar, P., Lea, M., Monash, R., Price, C., Vertigan, C., Woehler, E.J., 2018. Transhemispheric ecosystem disservices of pink salmon in a Pacific Ocean macrosystem. PNAS, doi/10.1073/pnas.1720577115.
Stabeno, P.J., Farley Jr., E.V., Kachel, N.B., Moore, S., Mordy, C.W., Napp, J.M., Overland, J.E., Pinchuk, A.I., Sigler, M.F., 2012. A comparison of the physics of the northern and southern shelves of the eastern Bering Sea and some implications for the ecosystem. Deep-Sea Res. II 65 – 70, 14 – 30.
Stabeno, P.J., Bell, S.W., 2019. Extreme conditions in the Bering Sea (2017-2018): Record breaking low sea-ice extent. Geophys. Res. Lett. 46, 8952 – 8959. Doi: 10.1029/2019GL083816.
Stephenson, S.A., 2006. A review of the occurrence of Pacific salmon (*Oncorhynchus* spp) in the Canadian Western Arctic. Arctic, 59, 37 – 46.
Stevenson, D.E., Lauth, R.R., 2018. Bottom trawl surveys in the northern Bering Sea indicate recent shifts in the distribution of marine species. Polar Biol., 42, 407 – 421.
Wang, M., Overland, J.E., Stabeno, P., 2012. Future climate of the Bering and Chukchi Seas projected by global climate models. Deep-Sea Res. II. doi:10.1016/j.drs2.2012.02.022.
Wechter, M.E., Beckman, B.R., Andrews III., A.G., Beaudreau, A.H., McPhee, M.V., 2017. Growth and condition of juvenile Chum and Pink salmon in the northeastern Bering Sea. Deep-Sea Res. II. 135, 145 – 155.
Woodgate, R.A., Weingartner, T., Lindsay, R., 2010. The 2007 Bering Strait oceanic heat flux and anomalous Arctic sea-ice retreat. Geophys. Res. Lett. 37. L01602. doi:10.1029/2009GL041621.
Woodgate, R.A., Stafford, K.M., Prahl, F.G., 2015. A synthesis of year-round interdisciplinary mooring measurements in the Bering Strait (1990 – 2014) and the RUSALCA years (2004 – 2011). Oceanogra. 28, 46 – 67. http://dx.doi.org/10.5670/oceanog.2015.57.

CHAPTER 15 – Northern Bering Sea surface trawl and ecosystem survey cruise report, 2019

Objective 4: Establish the relative abundance, size, and condition of juvenile salmonids that utilize the coastal regions of the PAR.

James Murphy[1], Sabrina Garcia[2], John Dimond[1], Jamal Moss[1], Fletcher Sewall[1], Wesley Strasburger[1], Elizabeth Lee[2], Tyler Dann[2], Elizabeth Labunski[3],Tamara Zeller[3], Andrew Gray[1], Charles Waters[1], Deena Jallen[2], Dave Nicolls[1], Ryan Conlon[4], Kristin Cieciel[1], Kathrine Howard[2], Brad Harris[4], Nathan Wolf[4], and Edward Farley Jr.[1]

[1] Auke Bay Laboratories
Alaska Fisheries Science Center
National Marine Fisheries Service
17109 Point Lena Loop Road, Juneau, AK 99801

[2] Alaska Department of Fish and Game
Division of Commercial Fisheries
333 Raspberry Rd, Anchorage, AK 99518

[3] United States Fish and Wildlife Service
1011 E Tudor Rd # 200, Anchorage, AK 99503

[3] Alaska Pacific University
4101 University Dr., Anchorage, AK 99508

ABSTRACT

The northern Bering Sea (NBS) surface trawl survey is a multi-disciplinary research survey that has supported annual sampling of the inner domain (bottom depths generally less than 55 m) of the NBS (60°N–66.5°N). Average sea surface temperature (SST, 11.5°C, upper 10 m) during the 2019 survey was the warmest on record and contributed to significant changes in the NBS ecosystem. Similar to prior years, the jellyfish species, northern sea nettle (*Chrysaora melanaster*), had the largest surface trawl catch biomass with a total catch of 6,989 kg in 2019. Pacific herring (*Clupea pallasii*) were the most abundant species of fish with a total catch of 142,512 fish. Juvenile pink salmon (*Oncorhynchus gorbuscha*) were the most abundant species of salmon with a total catch of 13,507 fish. Annual catch rates of several pelagic fish species increased with temperature, reflecting the influence of temperature on the distribution (e.g. Bristol Bay juvenile sockeye salmon (*O. nerka*), $\rho = 0.9$) and survival (e.g. juvenile coho salmon (*O. kisutch*), $\rho = 0.7$). The abundance and proportion of juvenile Yukon River Chinook salmon (*O. tshawytscha*) in 2019 were the lowest observed in the northern Bering Sea. The abundance of the Canadian-origin stock group (stock proportion of 30%) was estimated at 575,100 juveniles. The abundance of the Total Yukon River stock group (stock proportion of 65%) was estimated at 1,246,000 juveniles. Projected run-sizes for Yukon River Chinook salmon in 2021 and 2022 are 52,300 and 46,300 for the Canadian-origin stock group and 143,800 and 129,000 for the Yukon River stock group, respectively. The abundance of juvenile pink salmon reached a record high abundance in 2019, resulting in an outlook of 6.5 million pink salmon for Yukon River and Norton Sound in 2020. Average lengths of juvenile salmon were typical of past years except for coho salmon, which had the lowest recorded average length in 2019. The proportion of non-target prey consumed by juvenile coho and chum (*O. keta*) salmon

has increased in recent years suggesting a decrease in preferred prey. A total of 2,870 km of transects were surveyed. We recorded 3,310 birds on transect, comprised of 38 species plus a few unidentified passerines, with the northern fulmar (*Fulmarus glacialis*) the most abundant seabird species encountered.

INTRODUCTION

The northern Bering Sea (NBS) surface trawl survey (NBS survey) is a multi-disciplinary survey that supports research on pelagic fish species and oceanographic conditions in the eastern Bering Sea. Surface trawl surveys in the NBS were initiated by NOAA's Alaska Fisheries Science Center (AFSC) in 2002 as part of the Bering-Aleutian Salmon International Survey (BASIS). BASIS was a basin-wide research program developed by member nations of the North Pacific Anadromous Fish Commission and designed to improve our understanding of the marine ecology of salmon in the Bering Sea. Surface trawl surveys in the NBS were continued through 2007 as part of the BASIS survey for the eastern Bering Sea shelf. The NBS was not sampled in 2008, but it has been sampled on an annual basis since 2009 to support research objectives on the ecology of salmon in the NBS and to improve our understanding of how the NBS ecosystem is changing in response to warming climate and loss of arctic sea ice.

The NBS survey has supported a range of different survey operations and research objectives in the NBS. Survey operations have included the following: surface and midwater trawl sampling for pelagic nekton, midwater acoustics, seabird and marine mammal observations, bongo net sampling for zooplankton and ichthyoplankton, electronic conductivity, temperature, depth (CTD) data, and water collections for chlorophyll-a, phytoplankton, and nutrients. Survey objectives have supported research objectives on salmon and other pelagic fish resources in the NBS, including: juvenile salmon abundance and run-size forecasts (Murphy et al. 2017, Howard et al. 2019, Howard et al. 2020, Farley et al. 2020), size selective mortality (Murphy et al. 2013, Howard et al. 2016), energy allocation (Andrews et al. 2009, Murphy et al. 2013, Moss et al. 2017), diet (Farley et al. 2009, Andrews et al. 2016, Auburn and Sturdevant 2013, Honeyfield et al. 2016, Garcia and Sewall 2021), and species distribution (Murphy et al. 2009, Murphy et al. 2016, Andrews et al. 2016). An emphasis has been given to Chinook salmon over the last 5 to 10 years due to the decline in their survival (ADF&G 2013) and their importance to subsistence fisheries in the Yukon River. The declining sizes of Chinook salmon in the Yukon River has a widespread impact on subsistence fisheries throughout Alaska and the Yukon Territory, and it has had a significant impact on pollock fisheries in the eastern Bering Sea through efforts to reduce Chinook salmon bycatch (Ianelli and Stram 2014, Stram and Ianelli 2014).

The 2019 NBS survey was a cooperative research survey by AFSC, the Alaska Department of Fish and Game (ADF&G), the Alaska Pacific University (APU), and the U.S. Fish and Wildlife Service (USFWS) to improve our understanding of the marine ecosystem in the NBS. Key funding was provided by the Alaska Sustainable Salmon Fund to help maintain research on juvenile salmon in the NBS. The primary objectives of the 2019 NBS surface trawl survey were to 1) conduct surface trawl operations in support of ecosystem science, with a focus on the marine ecology of juvenile fish species; 2) estimate stock-specific abundance of juvenile Chinook salmon and update run-size forecast models for the Yukon River; 3) collect electronic oceanographic data and water samples for temperature, salinity, chlorophyll-a, nutrients, particulate organic carbon, and harmful algal blooms with a SBE-9-11 CTD and Niskin bottles; 4) collect zooplankton and icthyoplankton samples with a 20 cm (150 µm mesh) and 60 cm (505 µm mesh) bongo array; and 5) assess the distribution and abundance of seabirds and marine mammals on the NBS shelf.

METHODS

The 2019 NBS survey began and ended in Dutch Harbor, AK, with a port call in Nome, AK. The survey occurred over 25 days inclusive of mobilization, demobilization, travel, sampling, and weather days aboard the chartered fishing vessel FV *Northwest Explorer*, August 27 to September 20, 2019. The survey crew consisted of scientists from Alaska Fisheries Science Center, Alaska Department of Fish and Game (ADF&G), U.S. Fish and Wildlife Service (USFWS), and Alaska Pacific University (APU) (Table 1).

The survey consisted of 44 stations in the NBS between 60°N–66.5°N and east of 171°W, and three additional stations just north of the Bering Strait (Fig. 1, Table 2). Rough weather conditions at the end of the survey prevented sampling at the distributed biological observatory (DBO) stations in 2019. Each day typically consisted of sampling three stations during daylight hours. The order of operations at each station was 1) a Conductivity Temperature Depth (CTD) instrument system, 2) a Van Veen grab sample to collect benthic organisms and sediment samples for the presence of harmful algal blooms (HABs), 3) an oblique zooplankton net tow with bongo array and a FastCat CTD, and 4) one surface trawl tow. Seabird and marine mammal observations were recorded while travelling between stations.

Oceanographic Conditions

The primary CTD (SeaBird Instruments SBE-9-11+) was outfitted with dual temperature and conductivity (TC) sensors, a Photosynthetically Active Radiation (PAR) spherical sensor (QSP 2300, Biospherical Instruments), chlorophyll-a fluorometer, beam transmissometer (Wet Labs C-star), and two dissolved oxygen sensors (SeaBird Instruments SBE-43). The CTD measured temperature (°C), salinity (psu), and pressure (db) from the surface down to 5 m from the bottom. A SeaBird Instruments SBE-32 carousel water sampler frame with 1.5 liter Niskin bottles was used to collect water samples from the surface down to 5 m from the bottom in 10 m increments. The water samples from the Niskin bottle were filtered following water collection protocols (Appendix A).

The temperature and salinity for each meter of the CTD cast was calculated by averaging the readings from the primary and secondary temperature and salinity sensors. Sea surface temperature (SST) and salinity were estimated by averaging the temperature and salinity measurements from the top 10 m of the water column. Bottom temperature and salinity were equal to the measurements from the deepest cast of the CTD at each station. The average annual SST was estimated for all stations within the NBS (latitudes: 60°N - 65.5°N) and for a restricted spatial range to account for changes in sampling locations over time (longitudes east of 171°W, and latitudes south of 64°N). Norton Sound stations were restricted to three stations along 64°N.

Mixed-layer depth (MLD) was defined as the depth where seawater density (kg/m^3) increased by 0.10 kg/m^3 relative to the density at 5 m (Danielson et al. 2011; Murphy et al. 2017). Seawater density was calculated from temperature and salinity using the oce package (Kelley and Richards 2020) in R (R Core Team 2020). The MLD was set to the maximum depth of the CTD cast when the water column was mixed. The MLD was calculated from the FastCat CTD (SeaBird Instruments SBE-49) when the primary CTD data were not available. Average MLD from adjacent stations was used when both the CTD and FastCat data were not available.

A bongo net array was deployed to sample zooplankton and ichthyoplankton throughout the water column. The bongo array consisted of two 60-cm diameter bongo nets with 505 micron mesh and two 20-cm diameter bongo nets with 153 micron mesh. A FastCat CTD was affixed above the bongo net array to measure depth in real time using a conducting wire. The bongo nets were towed obliquely from the surface down to 5 m off the bottom at a 45° angle. One net from each bongo frame was preserved in 5% buffered formalin, the second bongo net was sorted for on-board Rapid Zooplankton Assessment (RZA) (Appendix A).

RZA was used to provide information on zooplankton abundance and community structure from coarse taxonomic categories of zooplankton during the 2019 NBS survey. Taxonomic categories included small copepods (< 2 mm; example species: *Acartia* spp., *Pseudocalanus* spp., and *Oithona* spp.), large copepods (> 2 mm; example species: *Calanus* spp. and *Neocalanus* spp.), and euphausiids (< 15 mm; example species: *Thysanoessa* spp.). Small copepods were counted from the 153 µm mesh, 20 cm bongo net. Large copepods and euphausiids were counted from the 505 µm mesh, 60 cm bongo net. Bongo net samples were split with Stemple pipettes to reach a total count of at least 100 individuals per sample. This method was first used in the NBS survey in 2018.

Surface Trawl Data

A Cantrawl 400/601 rope trawl from Cantrawl Pacific Ltd. (Murphy et al. 2003) was used to conduct surface trawl operations. All surface trawl tows were 30 min in duration and trawl dimensions were monitored during each tow with a Simrad FS70 net sounder. A SeaBird Instruments SBE-39 temperature and depth sensor mounted to the center of the footrope measured footrope depth and temperature during each tow. The number of fish (or weight of jellyfish) caught in a single tow was divided by the area swept by the trawl (km^2) to estimate catch-per-unit-effort (CPUE) and was used to describe species distribution and abundance. The area swept by the trawl was calculated using the horizontal opening from the net sonar and the distance sampled from GPS positions at the start and end of the trawl set.

Surface trawl catches were sorted by species and life history stage and up to 50 individuals from each species and life history stage combination were measured for length and weight at each station. Individual specimen weights were not recorded for species with weights less than 10 g due to the limited accuracy of ship-board weights. Mixed-species subsamples were used to estimate the catch of a few small and numerous species (typically ninespine stickleback (*Pungitius pungitius*), age-0 Pacific herring (*Clupea pallasii*), and moon jellyfish (*Aurelia* spp.). Total catch weight and average weight of measured individuals were used to estimate the total number of species when a subsample of the catch was measured. Annual sample requests were used to define specimen collection protocols for juvenile salmon (*Oncorhynchus* spp.), immature/mature salmon, and non-salmon species (Appendix A). Subsample sizes for juvenile salmon species were reduced in 2019 to accommodate specimen requests from the unexpectedly large numbers of juvenile pink (*O. gorbuscha*), chum (*O. keta*), and sockeye (*O. keta*) salmon. Subsample sizes for individual jellyfish widths and weights were also reduced to 10 individuals per species per station in 2019. All biological data were recorded in an electronic catch logging system, known as the Catch Logger for Acoustic and Midwater Surveys (CLAMS). Individual specimens collected in surface trawls were assigned a specimen number (barcode number) and electronically scanned into CLAMS to ensure a consistent record of all specimens collected during the survey. Juvenile chum and pink salmon caudal fins were collected for genetic analysis, frozen, and assigned a station number. All Chinook salmon were scanned for missing adipose fins, coded-wire-tags (CWTs), and Passive Integrated Transponder (PIT) tags.

Correlations between CPUE of the most abundant pelagic fish species and SST were plotted using the ggcorrplot package (Kassambara 2019) in R (R Core Team 2020) to provide insight into how the NBS fish community is responding to warming climate conditions in the eastern Bering Sea. Species-specific CPUE indices were based on log-transformed average CPUE adjusted for MLD as

$$\ln(CPUE_y) = ln\left(\frac{\sum_i C_{iy} M_{iy}}{\sum_i a_{iy}}\right),$$

where C_{iy}, and a_{iy} are the catch and effort, at station i, and year y, respectively, and M_{iy} is equal to the ratio of mixed-layer depth to trawl depth when trawl depth is shallower than mixed layer depth at station i, and 1.0 when trawl depth is below the mixed-layer depth. The Optimal Interpolation Sea Surface Temperature (OISSTv2.1) dataset (Huang et al. 2021) provided by NOAA's CoastWatch West Coast Regional Node ERDDAP cite for the eastern Bering Sea shelf (54° to 66°N, and 146° to 176°W) from June through August was used in lieu of *in situ* SST measured by the CTD to enable a broader spatial and temporal scale of temperature. Temperature data at this scale were thought to be more relevant to the overall distribution and abundance of fish species in the NBS; however, *in situ* temperatures were highly correlated with the broader-scale SST data, therefore, the overall conclusions are similar with both temperature datasets.

A multi-year distribution of juvenile Chinook salmon (*O. tshawytscha*) CPUE was created using a simple kriging model with a gaussian semivariogram as part of the geostatistical analyst extension in ArcGIS (ESRI 2019). Juvenile Chinook salmon CPUE was multiplied by average effort (across all years) to scale the distribution to the catch at each station and a first order trend was removed before kriging. The prediction surface was generated with a neighborhood kriging model with a minimum of five and maximum of 20 points within each of four search quadrants. CPUE data from the southern Bering Sea and Chukchi Sea were included to help define the spatial distribution of juvenile Chinook; however, CPUE within Bristol Bay (near the Kuskokwim and Nushagak rivers) were excluded to maintain a focus on the distribution of Chinook salmon within the NBS. The locations of CWT and adipose fin-clipped juveniles from the Whitehorse Rapids Fish Hatchery (WRFH) within the Yukon River were added to the distribution map of juvenile Chinook salmon to highlight the known locations of Yukon River Chinook salmon.

Length-frequency distributions, length-weight relationships, and box plots of lengths were used to describe the size of juvenile salmon and primary non-salmon species captured in the surface trawl. Length-weight relationships were used as a quality control measure to ensure large errors in length or weight were not present. Juvenile salmon lengths (fork length, mm) were standardized to a common capture date using juvenile growth rates calculated from previous NBS surveys (Howard et al. 2019). The common capture date was equal to the average capture date calculated for each species. Growth rates of 1.06 mm/day for Chinook salmon, 1.69 mm/day for chum salmon, and 1.76 mm/day for pink salmon were then used to standardize length (Howard et al. 2019). Growth rates of coho and sockeye salmon in the NBS are not available; therefore, coho salmon were assumed to grow at the same rate as Chinook salmon (1.06 mm/day) and the average growth rate of all juvenile salmon species was used to standardize sockeye salmon lengths (1.50 mm/day). Length frequency distributions of species captured in surface trawls were corrected by the proportion of the catch that was measured at each station to ensure length distributions reflected the total number of fish caught during the survey.

Juvenile Salmon Origin

All juvenile Chinook salmon were scanned for coded-wire-tags (CWTs) and caudal fin clips were collected from all juvenile Chinook and coho salmon and from a subsample of sockeye, pink, and chum salmon captured during the survey. Pectoral fin clips were collected from all immature Chinook and chum salmon. Individual fin clips were placed on Whatman paper cards specific to Chinook, coho, and sockeye salmon and barcode IDs were recorded on the Whatman cards. Caudal fin clips were collected from juvenile chum and pink salmon and were placed on plastic wrap, frozen, and pooled by species for each station. Pelvic fin clips from immature chum salmon were individually labeled and stored in plastic bags. All genetic tissue samples were shipped to the ADF&G Gene Conservation Lab as part of the cooperative NOAA/ADF&G research on salmon stock origin. Genetic mixed stock analysis has not been initiated for sockeye, coho, and pink salmon but samples are being archived to support analyses when funding and specific interest becomes available.

Genetic mixed-stock analysis was completed for juvenile Chinook and chum salmon and immature Chinook salmon, but only stock mixtures of juvenile Chinook salmon are reported here. DNA was extracted from the tissue samples using the NucleoSpin 96 Tissue Kit (Macherey-Nagel, Düren, Germany). Single nucleotide polymorphism (SNP) genotyping of the 80 SNPs common to the AYK baseline of 60 populations (Howard et al. 2019) was performed with standard TaqMan chemistry (Applied Biosystems, Waltham, USA). Quality control analyses included comparison of discrepancy rates between original genotypic data and genotypic data of 8% of individuals that were re-extracted and re-genotyped, removal of individuals missing 20% or more genotypic data, and removal of duplicate individuals. Stock composition was estimated by comparing genotypes of catch samples to reference baseline allele frequencies using the Bayesian statistical approach implemented in the software package BAYES with a flat prior (Pella and Masuda 2001). Contributions of juvenile Chinook salmon from four

reporting groups were estimated: Lower Yukon, Middle Yukon, Upper Yukon, and Other Western Alaska. Estimates from the three intra-Yukon River groups (Lower Yukon, Middle Yukon, and Upper Yukon) were summed to estimate the total Yukon River stock contribution.

Juvenile Chinook Salmon Abundance and Run Forecasts

The methods for estimating juvenile Chinook abundance were initially described in Murphy et al. (2017) and revised in Howard et al. (2019) and Howard et al. (2020). Juvenile Chinook salmon catches are scaled to the MLD by dividing the catch of juvenile Chinook salmon by the proportion of the mixed layer sampled at that station. The NBS was divided into four latitude strata: 1) Lower NBS (60 to 62°N), 2) Upper NBS (62° to 64°N), 3) Norton Sound, and 4) the Bering Strait region. The average CPUE within each stratum *n*, was estimated by dividing the total catch by the total effort as

$$CPUE_n = \frac{\sum_{i=1}^{I} C_{ni}}{\sum_{i=1}^{I} a_{ni}},$$

where C_{ni} and a_{ni} are the MLD adjusted catch and area swept, respectively, for station *i* and stratum *n*, and *I* is the total number of stations in stratum *i* (Quinn and Deriso 1999). The variance of *CPUE* by strata was defined as

$$CPUE_A = \sum_n \frac{A_n}{A} CPUE_n,$$
$$V(CPUE_A) = \sum_n \frac{A_n}{A} V(CPUE_n).$$

The area sampled within each strata (A_n) was calculated from the number of stations in the strata and the average grid area (the average area of the 0.5° latitude by 1° longitude grid, calculated with average latitude). A fixed sample grid area (A_{NS}) was assumed for the Norton Sound stratum as the effective habitat for juvenile Chinook salmon was assumed to be limited by the high turbidity and shallow bottom depths (Murphy et al. 2017). The mean proportion of juvenile Chinook salmon in the Bering Strait (6.7%) and Norton Sound (8.2%) during 2003, 2007, 2009 to 2015, and 2017 were used to adjust abundance estimates in years when these strata were not sampled (2004 to 2006 for Bering Strait and 2016 for Norton Sound). The sum of the individual strata areas was used to estimate the total survey area, *A*. The average *CPUE* for the survey, $CPUE_A$, and variance, V($CPUE_A$), were simply the weighted average based on the strata area as

$$\hat{N} = CPUE_A \cdot A,$$
$$V(\hat{N}) = A^2 \cdot V(CPUE_A).$$

Juvenile abundance ($\hat{N}$) and variance V($\hat{N}$) estimates for the survey were calculated as

$$\hat{N} = CPUE_A \cdot A,$$
$$V(\hat{N}) = A^2 \cdot V(CPUE_A).$$

Juvenile Chinook salmon abundance estimates were apportioned by stock composition to Upper Yukon (hereafter Canadian-origin) and total Yukon River groups (combined Canadian-origin, Middle Yukon, and Lower Yukon stock groups). The variance of stock-specific abundance was derived from a Taylor series approximation to the multiplicative variance of 2 random variables (*X* and *Y*) using the Delta method as

$$V(X,Y) = \mu_Y^2 \sigma_X^2 + \mu_X^2 \sigma_Y^2 + 2\mu_X \mu_Y \sigma_X \sigma_Y \rho,$$

where μ_X and σ_X are the mean and standard deviation of juvenile abundance, μ_Y and σ_Y are the mean and standard deviation of the stock group proportion, and ρ is the correlation between juvenile abundance and stock proportion.

Canadian-origin and Total Yukon Chinook salmon forecasts were generated using juvenile abundance estimates, brood tables, and age at maturity estimates for both Canadian-origin and Total Yukon Chinook

salmon. The number of juvenile Chinook salmon predicted to return to the Yukon River was based on the midpoint and 80% prediction interval of the linear regression model between juvenile abundance and adult returns. The majority of Yukon River Chinook salmon spend a full year growing in fresh water after hatching and therefore juvenile abundance is assumed to be offset from spawner abundance by two years (one year is added to account for overwinter egg incubation). The marine ages of returning adults (typically 2 to 4 years) are used to scale juvenile abundance to run year. Projected run sizes were based on recent 3-year average maturity schedules derived from Canadian-origin brood tables (JTC 2020) and the total Yukon River drainage (Howard et al. 2020).

Juvenile Pink Salmon Abundance

Catch and effort, abundance indices, and forecast models for Yukon River and Norton Sound pink salmon were developed and reported in Farley et al (2020). Mixed layer depth corrections were applied to the annual abundance index as

$$\theta_y = \frac{\sum_i M_{iy} C_{iy}}{\sum_i C_{iy}},$$

where C_{iy} is the catch at station i and year y, and M_{iy} is equal to the ratio of mixed-layer depth to trawl depth when trawl depth is shallower than mixed layer depth, and 1.0

when trawl depth is below the mixed-layer depth. The juvenile abundance index for pink salmon was estimated as

$$N_y = \frac{\sum_i ln\left(CPUE_{iy}\right)}{n_y} \cdot \theta_y,$$

where n_y is the number of trawl stations in year y.

Juvenile Salmon Diet

Stomach contents were examined either at sea or in a laboratory setting between 2004 and 2019. Stomach processing followed standard methods developed by Tikhookeanskiy Nauchno-Issledovatelskiy Institut Rybnogo Khozyaystva I Okeanografiy (Chuchukalo and Volkov 1986, Volkov and Kuznetsova 2007, Moss et al. 2009, Coyle et al. 2011). Typically, the contents of up to 10 stomachs from randomly sampled fish were combined together from each station, and prey composition was recorded as a stomach content index (SCI) and stomach fullness index (SFI). The SCI was calculated as individual prey taxon weight (g) multiplied by 10,000 and divided by predator body weight (g). Multiplying by a factor of 10,000 made these numbers easier to handle, as predator body weight was always much larger than prey taxon weight. The SFI was equal to the sum of all prey SCIs at a given station and gives an indication of fullness as a proportion of prey weight to predator weight. The average SFI was calculated for each year and compared with SST. In some cases, accurate prey weights could not be measured due to movement of the vessel. In these instances, prey taxon weight was estimated based upon percent volume and the assumption of equal body density of all prey items. Laboratory based weights were typically measured at 0.001 g. Prey composition was summarized as %SCI contribution (individual prey category SCI divided by the sum of SCI in a given year). Prey categories occurring in less than 10% of all stomachs within a predator species were combined into broader taxonomic groups. Prey groups were determined by the overall contribution to the diet within a predator species across all years, the proportion of the SFI within years, and in terms

of percent frequency of occurrence over all years. Rare prey items that did not fall into a larger category were placed into an "Other" category. *Thysanoessa* was used as a prey category for sockeye salmon diets because they composed 95% or higher of all the euphausiids while euphausiids was used as a broader prey category for pink and chum diets. All stations where stomachs were analyzed, but no prey was present in stomachs or contents were not identified were removed from this analysis. Years with diet data from less than five stations were not included in the diet summaries/figures.

Juvenile Salmon Energetic Condition

Energetic condition (energy density, ED) of juvenile Chinook salmon from the NBS was obtained using bomb calorimetry on dried samples of homogenized whole fish tissues for 2006-2019 (Fergusson et al. 2010). From 2006 to 2015, samples were heated at 75°C in a drying oven and manually re-weighed until mass was constant. Starting in 2016, the method of sample drying and moisture determination prior to bombing was changed. Since 2016, samples were heated at 135°C to dryness using a LECO Thermogravimetric Analyzer 601. Moisture values obtained by the two methods were known to differ by less than 1% (Vollenweider et al 2011).

Comparing annual average ED among years required use of weighted least squares in Welch's ANOVA (Welch 1951, Day and Quinn 1989) due to unequal variances among years. Testing for differences in ED among years while controlling for fish size was accomplished using one-way ANCOVA and post-hoc Tukey's pairwise comparisons of adjusted means. Due to unequal variances among years, ANCOVA results were compared to results from a rank-based Kruskal-Wallis test performed on the residuals from a simple linear regression of ED against length, followed by Tukey's pairwise comparisons on the ranked residuals.

Spearman's rank correlation test was used to evaluate the effects of SST on ED and nonlinearity in the relationship was described using generalized additive models (GAMs; Wood 2006) limited to 4 knots to avoid overfitting. Multiple linear regression models of fish length and SST on annual average ED were selected based on Akaike Information Criteria (AICc) (Burnham and Anderson 2004).

Seabird and Marine Mammal Observations

The USFWS conducted seabird surveys during the NBS survey. The USFWS was supported by an Interagency Agreement with the Bureau of Ocean Energy Management (project AK-17-03: Marine Bird Distribution and Abundance in Offshore Waters). This study will combine data collected during the NBS survey with data from other USFWS seabird surveys to examine the distribution of marine birds relative to prey and oceanographic properties. It will also be used to describe seasonal and interannual changes in marine birds and their communities in the Beaufort and Chukchi Planning Areas. Marine birds and mammals were surveyed from 28 August to 19 September, 2019. Survey data will be archived in the North Pacific Pelagic Seabird Database (http://alaska.usgs.gov/science/biology/nppsd).

Marine birds and mammals were surveyed from the port side of the bridge using standard USFWS protocols. Observations were conducted during daylight hours while the vessel was underway. The observer scanned the water ahead of the ship using hand-held 10 x 42 binoculars for identification and recorded all birds and mammals. Bird surveys used a modified strip transect methodology with four distance bins from the center line: 0-50 m, 51-100 m, 101-200 m, 201-300 m. Rare birds, large flocks, and mammals beyond 300 m or on the starboard side ('off transect') were also recorded but will not be included in density calculations. We recorded the species, number of animals, and behavior (on water, in air, foraging). Birds on the water or actively foraging were counted continuously, whereas flying birds were recorded during quick 'Scans' of the transect window.

Geometric and laser hand-held rangefinders were used to determine the distance to bird sightings. Observations were directly entered into a GPS-interfaced laptop computer using the DLOG3 program (Ford Ecological Consultants, Inc., Portland, OR). Location data were also automatically written to the

program in 20-second intervals, which allowed us to track survey effort and simultaneously record changing weather conditions, Beaufort Sea State, glare, and ice coverage (no ice was encountered during this cruise). Other environmental variables recorded at the beginning of each transect included wind speed and direction, cloud cover, sea surface temperature, and air temperature.

RESULTS AND DISCUSSION

Oceanographic Conditions

The CTD data were collected at each of the 47 stations sampled in 2019 (Table 2). Surface temperatures (upper 10 m) in the NBS in 2019 ranged from 7.9°C to 13.8°C with an average of 11.5°C, which was 2.9°C above average (restricted SST range, 2003 to 2018) (Fig. 2). Surface and bottom temperatures were highest in the shallow nearshore stations and in Norton Sound. Surface temperatures were coldest at stations northeast of St. Lawrence Island; bottom temperatures were much colder due to the presence of the eastern Bering Sea cold pool and were coldest just south of St Lawrence Island (Fig. 3). Surface salinities ranged from 21.7 PSU to 31.9 PSU. The lowest salinities were in Norton Sound and just outside the Yukon River Delta with salinity increasing with distance from shore (Fig. 4). Mixed layer depths ranged from 7 m to 29 m with an average of 19 m (Table 3, Fig. 5). The MLD estimates from the SBE9-11 CTD for stations 2 and 5 were missing data from the top 11 m of the water column; therefore, the MLD estimates for those stations were derived from the FastCat (SBE49) data collected during the bongo tow.

Small copepods (< 2 mm) were abundant across the sampling area, with abundances approaching 10,000 ind/m^3 (Fig. 6). In contrast, large copepod (> 2mm) abundances were low overall, and copepods were largely absent in many stations between 62°N and 64°N. Large copepods abundances would be expected to be higher in an average year, based on the accumulation of *Calanus* spp. C5 stages later in the year (Stabeno and Bell, 2019). Small copepods have faster turnover times, multiple generations per year, and metabolic rates that scale less dramatically with temperature. Warm temperatures in 2018 and 2019 are likely a contributing factor to the elevated abundance of small versus large zooplankton (Kimell et al. 2018, Kimell et al. 2019). The abundance of small and large copepods declined from 2018 and may indicate an overall decline in productivity during 2019. Euphausiid numbers were also low across the NBS, with no euphausiids recorded north of 62°N. Above average temperatures in 2019 may have caused earlier entry into diapause or increased advection of local populations of *Calanus* spp. into the Chukchi Sea. The low euphausiid abundance was expected; bongo tows typically undersample adult euphausiids due to depth distribution.

Surface Trawl Data

Bottom depths at stations sampled during the survey ranged from 14 m to 63 m (Table 2). Footrope setback chains were shortened to collapse the vertical opening of the trawl when sampling locations with bottom depths less than approximately 22 m. The average horizontal and vertical opening of the trawl was 49.8 m and 17.5 m, respectively. The average footrope depth from the SeaBird SBE39 depth sensor was 18.9 m (Table 4), indicating that the average depth of the center of the headrope (where the net sonar is located) was 1.4 m. The average distance towed during each 30 minute trawl set (based on GPS coordinates of the start and end of each tow) was 3.9 km, which results in a calculated average speed of 4.2 knots. MLD expansions were required at 27 of the 47 stations and ranged from 2% to 33% (Table 4).

Similar to previous years, the species with the largest biomass in the surface trawl catches was the northern sea nettle (*Chrysaora melanaster*) at 6,898 kg, and the species with the largest catch in numbers was Pacific herring at 142,512 individuals (Tables 5-7). Juvenile pink salmon was the most abundant species of salmon at 13,507 fish. Ninespine stickleback were the third most abundant species at 9,464 individuals. The catch of age-0 walleye pollock (*Gadus chalcogrammus*, n = 8,798) was above average, but the catch of other forage fish species, including Arctic or Pacific sand lance (*Ammodytes* spp., n = 2) (Orr et al. 2015) and capelin (*Mallotus villosus*, n = 11) were quite low. Sand lance are able to avoid

capture with trawl gear, therefore, a low catch does not necessarily reflect low abundance. Capelin are known to be less abundant in the NBS during warm years (Andrews et al. 2016).

The spatial distribution of fish and jellyfish captured in surface trawls varied significantly by species (Appendix B). Surface trawl catch rates of the Juvenile chum and pink salmon were the most widely distributed salmon species with relatively high CPUEs across most of the survey area. Unlike previous years, juvenile Chinook salmon were absent in a number of stations between 60°N and 62°N and their highest catch rates were just west of Norton Sound where surface temperatures tended to be a bit colder. Juvenile coho salmon exhibited high CPUEs south of 62°N, in Norton Sound, and just northwest of the Yukon Delta. Juvenile sockeye salmon catches were concentrated at offshore stations south of St. Lawrence Island. sockeye salmon runs in the Yukon River and Norton Sound are relatively small so we suspect the high catches of sockeye salmon encountered during the 2019 survey were of Southern Bering Sea origin. Except for sockeye salmon, all other salmon species were caught at stations north of 66°N. The northern sea nettle, the most abundant of jellyfish, were caught in all but four stations during the 2019 survey. The moon jellyfish were found throughout the survey except just west of Norton Sound. Water jellyfish (*Aequorea* spp.) and the whitecross jellyfish (*Staurophora mertensi*) were encountered infrequently. The highest catch rates of Lion's mane jellyfish (*Cyanea capillata*) were in the shallow nearshore stations. Age-0 walleye pollock had high CPUEs west of 167.5°W and south of 63°N, whereas age-1+ walleye pollock catches were sparsely distributed throughout the survey grid. Both age-0 and age-1+ walleye pollock were caught at stations north of the Bering Strait. Pacific herring were captured throughout the NBS, but catches tended to be higher in Norton Sound and nearshore habitats where age-0 herring occur (Appendix B). Rainbow smelt (*Osmerus mordax*) were caught at nearshore stations and in Norton Sound and were absent west of 168°W. Similar to rainbow smelt, ninespine sticklebacks were constrained to nearshore stations east of 168°W and Norton Sound. Documenting species catch and distribution during NBS surface trawl surveys will help identify northward shifts in species's migration and distribution as the Bering Sea continues to increase in temperature over time.

Approximately half of the primary species captured in the NBS were significantly ($\alpha = 0.5$) correlated with SST (Figs. 7 and 8). Average catch rates of juvenile sockeye salmon had the highest positive correlation with SST ($\rho = 0.9$). Increased catch rates of sockeye salmon with temperature stems from the northward dispersal and increased abundance of juveniles from the southeastern Bering Sea (primarily Bristol Bay) as there are only minor spawning populations of sockeye salmon within the Yukon River and Norton Sound (Estensen et al. 2018, Menard et al. 2020). Spawning locations of walleye pollock also are predominantly in the southeast Bering Sea and therefore the positive correlation between age-0 pollock and SST ($\rho = 0.6$) reflects increased northward dispersal of age-0 pollock with temperature. The relationship between age-0 pollock and temperature in non-linear therefore the correlation coefficient underestimates the significance of temperature to the catch rates of age-0 pollock. There are significant spawning stocks of coho salmon in the Yukon River and Norton Sound (Estensen et al. 2018, Menard et al. 2020); therefore the correlation betwenn CPUE and SST ($\rho = 0.7$) most likely reflects an increase in the abundance of juvenile coho salmon stocks within the NBS. Capelin was the only species with a negative correlation ($\rho = - 0.6$) with SST. Capelin are known to have a preference for cooler water in the eastern Bering Sea (Andrews et al. 2016); therefore, this may also reflect a northward shift in their distribution (into the Chukchi Sea) as temperatures increases in the eastern Bering Sea.

Significant positive correlations were present between catch rates of ninespine stickleback and Pacific herring ($\rho = 0.8$), Arctic lamprey (*Lethenteron camtschaticum*) ($\rho = 0.7$), and Chinook salmon ($\rho = 0.6$) (Fig. 8). Ninespine stickleback are an abundant species within the nearshore habitats of the NBS and nearly all ninespine stickleback are captured in the shallowest stations sampled in the NBS (Appendix B). Although age-0 Pacific herring are likely the dominant species within the nearshore fish community, catches of age-0 Pacific herring are not separated from the older age classes, and could reflect a mixture of herring from the NBS and SEBS (Andrews et al 2016). The highly piscivorous diet of juvenile Chinook salmon (Farley et al. 2009, Auburn and Sturdevant 2013, Honeyfield et al. 2016, Miller et al.

2016, Garcia and Sewall 2021) and Arctic lamprey (Shink et al. 2019) would logically support a dependency of these two species on the nearshore fish community. It is possible that the correlations between CPUE of ninespine stickleback and juvenile Chinook salmon and Arctic lamprey could stem from a dependency of Chinook salmon and Arctic lamprey on the nearshore estuarine fish community in the NBS in general, not necessarily a direct association with ninespine stickleback.

Size Distributions

Length-frequency distributions for the primary species captured in surface trawl catches are summarized in Figs. 9 to 11. Juvenile salmon lengths in 2019 were typical of those encountered in past NBS surveys (Fig. 9). Individual lengths and weights of juvenile salmon (Appendix C) confirm that there is limited error in the size data and that juvenile salmon have a relatively stable relationship between length and weight. Juvenile Chinook salmon lengths ranged from 10 to 24 cm, and averaged 20 cm. Most juvenile Chinook salmon caught in the NBS survey spend one year in fresh water (total age 2); however, smaller juvenile Chinook may be indicative of sub-yearlings (Chinook salmon that migrate to sea without spending a year in fresh water). Due to their multi-year residence in fresh water, coho salmon were the largest juvenile salmon species caught in the survey with lengths between 20 and 30 cm and averaging 25 cm. Chum and pink salmon were the smallest species caught with lengths ranging between 12 and 25 cm. The overlap in juvenile Chum and pink salmon lengths suggests that their growth rates during the early marine stage may be similar. Except for a few larger individuals, juvenile sockeye salmon lengths ranged between 15 and 22 cm.

There was not a consistent trend in the size of juvenile salmon within or between species across the time series (Fig. 12), which emphasizes the importance of species-specific factors in the growth and size of juvenile salmon. The average lengths of juvenile Chinook salmon from recent warm years (2016-2019) are smaller than those from prior warm years (2004, 2014-2015). The average lengths of juvenile coho salmon has declined in the recent warm years. The recent warm temperatures may be limiting the growth of piscivorous species like juvenile Chinook and coho salmon through changes in prey quality and quantity. The average length of juvenile coho salmon in 2019 was the lowest observed since the survey began in 2003. Due to the multiple fresh water ages of coho salmon (predominantly fresh water ages of 1 and 2), the reduced size of coho salmon could also reflect an earlier age of marine entry. Variation in the average length of juvenile chum and pink salmon did not vary consistently with temperature and above and below average lengths were present in warm and cold years. This highlights the importance of dynamic ecosystem impacts on their size and growth, including prey availability. Growth potential models are in development and will clarify the role of warming temperature on pink and chum salmon in the NBS.

The size and growth of juvenile salmon during the early marine life stage have important implications for future marine survival. Larger juvenile salmon are more likely to survive than smaller individuals because they are able to avoid predators and maintain high energy reserves necessary to survive their first winter at sea (Beamish and Mahnken 2001). Prior research on juvenile Chinook salmon correlated growth and size in the early marine stage with increased adult returns (Tomaro et al. 2012). Additionally, scale pattern analyses have shown that small juvenile Chinook, coho, pink, and sockeye salmon are subject to size-selective mortality during their first summer at sea (Beamish et al. and Mahnken 2001, Moss et al. 2005, Howard et al. 2016), providing further evidence that larger juvenile salmon have higher likelihoods of surviving than their smaller conspecifics. Juvenile salmon caught in the NBS are caught in September, after they have spent their first summer in the ocean, and their size at this critical period may inform whether they are likely to survive their first marine winter.

Length measurements were also taken from immature salmon and non-salmon species. Fork lengths were measured for immature chum, sockeye, and Chinook salmon (Fig. 10). Immature sockeye (n = 19) and Chinook salmon (n = 24) are less frequently encountered during the NBS survey compared to immature chum salmon (n = 194). Immature sockeye salmon lengths ranged from 26 cm to 53 cm and averaged 36

cm. Immature Chinook salmon (n = 24) ranged from 31 cm to 79 cm and averaged 43 cm. Immature chum salmon lengths ranged from 29 cm to 79 cm. The bimodal distribution of fork length measurements for immature chum salmon suggest two age classes are encountered during survey operations. Although immature sockeye salmon greater than 45 cm suggest the presence of a separate, older age class, there are not enough samples to categorize age distributions. Bell diameters for moon jellyfish, northern sea nettle, and lion's mane jellyfish were between 10 and 50 cm. Bell diameters were skewed towards smaller sizes between 10 cm and 15 cm for moon jellyfish (mean of 15.3 cm), centered around 23 cm for the Northern Sea Nettle and bimodal at 18 cm and 33 cm for lion's mane jellyfish (Fig. 11, Table 7). Ninespine stickleback were larger than those encountered in the NBS survey in past years, ranging between 4.0 cm and 6.5 cm (Fig. 11, Howard et al. 2020). Pacific herring, rainbow smelt, and walleye pollock length frequencies reflect the multiple age classes of each species encountered during the survey (Fig. 11).

Juvenile Salmon Origin

Juvenile Chinook salmon are distributed within the inner domain (bottom depths less than 55 m) of the NBS and can occur throughout the latitude range of the NBS (Fig. 13). CWT recoveries are particularly useful in characterizing marine distributions of Chinook salmon (Appendix D). All CWTs recovered from juvenile Chinook salmon (including two CWTs in 2019) have been from the Whitehorse Rapids Fish Hatchery (WRFH). All juvenile Chinook salmon released from the WRFH have adipose fin clips and all tagged juveniles exhibit a subyearling migration pattern. Juveniles with an adipose fin clip and not CWT were assumed to be the result of tag shedding and were assumed to be subyearling Chinook salmon from the WRFH. WRFH Chinook salmon had an average length of 151 mm (range: 109 to 207 mm), and an average weight of 43 g. The size of hatchery Chinook salmon were slightly below the average size of pink salmon (164 mm) and chum salmon (177 mm), which migrate to sea during the same year that they hatch. Although hatchery Chinook salmon have been caught throughout the latitude range of the NBS survey, they are most commonly captured in the nearshore stations adjacent to the Yukon River Delta and within Norton Sound (Appendix D).

Although CWTs are useful in identifying the origin of individual Chinook salmon, genetic stock identification is the primary method used to identify the origin of Chinook salmon in the NBS. A total of 125 juvenile Chinook salmon were successfully genotyped for mixed-stock-analysis (MSA) during the 2019 NBS survey. Mean stock composition estimates were: 30% Upper Yukon (hereafter Canadian-origin), 22% Middle Yukon, 14% Lower Yukon, and 35% Other Wester Alaska (non-Yukon River) stocks (Table 8, Fig. 14). The Canadian-origin proportion was lower than the historical average (48%), and the non-Yukon River proportion was higher than the historical average (12%); however, the composition of Lower Yukon and Middle Yukon stocks were similar to historical averages (12% and 27%, respectively). The Canadian-origin stock group had the largest reduction from the historic average (an 18% decrease from average) followed by the Middle Yukon River stock group (6% decrease from average). The proportion of the Lower Yukon River stock group was slightly higher (2%) than the historic average. The increase in non-Yukon stocks (23% increase) may reflect a combination of northward dispersal of Chinook salmon stocks from the southern Bering Sea (e.g., Kuskokwim River Chinook salmon) and possibly an increase in the relative contribution of Norton Sound Chinook salmon.

Juvenile Chinook Salmon Abundance and Run Forecasts

The overall abundance of juvenile Chinook salmon in the NBS during 2019 (2.0 million fish) was significantly below their average abundance during 2003-2018, (3.2 million fish). Abundance estimates of juvenile Chinook salmon were expanded by 10% (MLD adjustment) to account for incomplete sampling of the mixed layer, which was higher than the recent 5-year average of 2%. The abundance of Canadian-origin juvenile Chinook salmon during 2019 was the lowest observed in the NBS at 575,094 fish (sd = 164,126; CV = 29%) (Table 9, Fig. 15), and was less than half of the average abundance (1.57 million) during previous years (2003-2018). Similar to the Canadian-origin stock group, the abundance of Yukon River juvenile salmon was also the lowest observed at 1,246,038 fish (sd = 326,257; CV = 26%), and was

less than half of the 2003-2018 average of 2.75 million fish (Table 10, Fig. 15). The juvenile Chinook salmon caught during the 2019 NBS survey will primarily contribute to adult runs in 2021 (as age-4), 2022 (age-5), and 2023 (age-6).

Juvenile abundance is significantly ($\rho < 0.001$) related to adult Chinook salmon returns up to three years into the future (Fig. 16). Both the Canadian-origin and total Yukon runs are expected to decline over the next two years due to the reduction in juvenile abundance during 2017-2019. The projected run sizes for Canadian-origin Chinook salmon are 52,300 (31,200 to 73,400) fish in 2021, and 46,300 (24,800 to 67,900) fish in 2022. The projected run sizes for the total Yukon River run are 143,800 (95,200 to 192,400) fish in 2021, and 129,000 (79,500 to 178,500) fish in 2022. Although the ranges of possible run sizes are very wide, they indicate an expected decline in abundance of Chinook salmon. New forecast models for the Canadian-origin stock group are being developed by the Joint Technical Committee of the Yukon River Panel which will integrate juvenile and other sibling data into a Bayesian model framework. Similar models are also expected to be developed for the total run of Chinook salmon to the Yukon River. Estimates of future run size to the Yukon River have been of particular interest by managers, biologists, and stakeholders within the Yukon River as it helps support fisheries management decisions needed to protect the spawning stock and subsistence fisheries in the Yukon River (JTC 2020).

The number of Chinook salmon juveniles-per-spawner in 2019 was the lowest observed since 2003 for the Canadian-origin stock group (8.4) and the Yukon River stock group (5.3) (Fig. 17, Tables 9 and 10). The number of juveniles-per-spawner has been quite low for the last three years (2017-2019) and indicates a distinct downward shift in the survival of Yukon River Chinook salmon. Although the cause of the reduced survival is unclear, it may be tied to recent losses of arctic Sea ice and warming of the NBS and Yukon River. The number of juveniles-per-spawner does not vary predictably with spawner abundance for either the Canadian-origin or total Yukon River stocks. Similarly, there is no relationship between the number of spawners and the resulting number of juveniles for either the Canadian-origin or Yukon River stock groups. Juveniles-per-spawner and returns-per-spawner are highly correlated ($\rho = 0.76$) for both the Canadian-origin and Yukon River stock groups (Tables 9 and 10) and therefore the survival of Yukon River Chinook salmon during the initial fresh water and/or marine stages of salmon is the key factor in both the decline and variation in abundance over time.

Measurement error in juvenile abundance is a key limitation in the analysis and interpretation of juvenile survival. There are a number of unique features of the NBS survey that help limit the measurement error of surface trawl estimates of the distribution and abundance of juvenile salmon. We are able to restrict abundance of juvenile Chinook salmon to large stock groups such as the Total Yukon (average proportion of 86%) and the Canadian-origin (average proportion of 47%) stock groups, which minimizes the stock identification error in abundance estimates. The shallow depths and presence of the eastern Bering Sea cold pool play a key role in limiting the vertical distribution of juvenile salmon in the NBS. MLD corrections are used to account for changes in the sampling depth of surface trawls relative to juvenile habitat. The relatively limited dispersal rate of juvenile Chinook salmon in the NBS (compared to coastal habitats in the Gulf of Alaska) allows a single survey to sample through the distribution of juveniles and limits the influence of year to year variation in the migration of juveniles on abundance estimates. There has been limited mixing of juvenile Chinook salmon stocks from regions outside of the Yukon River prior to 2019. This has helped clarify the spatial distribution and dispersal patterns of juvenile Chinook salmon stocks from the NBS and has helped establish survey designs for juvenile Chinook salmon in the NBS. However, caution is still needed when interpreting abundance estimates as measurement has not been stationary over time due to changes in sea states, vessel platforms, juvenile distributions, and survey designs over time.

Juvenile Pink Salmon Abundance

The juvenile pink salmon abundance index ranged from 1.0 to 5.4 with an overall average of 2.9 from 2003 to 2019 (Fig. 19). The index is significantly correlated with pink salmon returns to Yukon and

Norton Sound rivers and provides an informative tool to forecast adult returns to these regions (Fig. 20). The preliminary index for 2019 was 5.3, which forecasted an adult return of 6.5 million pink salmon to the region in 2020.

Juvenile pink salmon abundance has increased along with the recent warming conditions in the eastern Bering Sea. The NBS is experiencing significant warming and extremes in seasonal ice extent and thickness that may benefit the growth and survival of pink salmon stocks in this region. Increased pink salmon abundance in the NBS and overall warming climate conditions are both thought to play an important role in the expansion of pink salmon into the Arctic (Farley et al. 2020). The critical period (Beamish and Mahnken 2001) in the production dynamics of pink salmon in the NBS appears to be more strongly tied to the initial life-history stages (fresh water and initial marine) than later marine life-history stages and may reflect temperature limitations present in high latitude stocks of salmon. Stock-specific information on juvenile pink salmon abundance would significantly improve our understanding of their movement and production dynamics in the NBS. Farley et al. (2005) identified discontinuous distribution in the size of juvenile pink salmon that may stem from the presence of both North American and Russian stocks in the NBS. Support for this interpretation was provided by the observation that 76% of the juvenile chum salmon in the Bering Strait region were from Russia during the 2007 NBS survey (Kondzela et al. 2009).

Juvenile Salmon Diet

Stomach fullness and species composition of juvenile salmon diets are summarized in Figs. 21 to 27 and in Appendix E. Station numbers and the number of stomachs sampled are also summarized in Appendix E.

Chum salmon fed upon gelatinous plankton, fish, hyperiid amphipods, and euphausiids in most years (Fig. 21). The proportion of hyperiid amphipods, which are rich in fatty acids (Persson and Vrede 2006), increased during cool years (2006-2012) (Appendix E). Feeding on prey high in fatty acids and lipids facilitates the accumulation of energy stores which are needed for overwinter survival (Heintz et al. 2013, Rogers et al. 2020).

Pink and sockeye salmon fed on a combination of fish and zooplankton confirming findings from previous investigations (Cook and Sturdevant 2013). Pink and sockeye salmon demonstrated no preference for a single species of zooplankton prey. Fish prey were most common in pink salmon diets during anomalously warm conditions (2003-2006), a transitional period from warm to cool (2007), and during the anomalously warm year of 2015 (Fig. 22). The composition of prey in sockeye salmon diets varied inter-annually and no pattern or prey preference during cool or warm years was apparent (Fig. 23).

Coho salmon preyed primarily upon sand lance, age-0 walleye pollock, capelin, and other fish (Fig. 24). Capelin increased in coho salmon when ocean conditions were cool (2007-2011) and capelin abundance was elevated in the NBS (Andrews et al. 2016). The proportion of decapods and other prey items not commonly consumed by coho salmon increased during warm years (2006-2012, 2014-2019), with the exception of 2007 and 2014, which were years when thermal conditions switched from anomalously warm to cool and cool to warm, respectively. Age-0 walleye pollock accounted for a larger proportion of prey in coho salmon diets during warm years, consistent with increased catches and of age-0 walleye pollock in the NBS and northward with warm temperatures (Fig. 7 and 8).

Chinook salmon fed primarily upon fish in the NBS (Fig. 25) which has also been reported by previous investigations (Cook and Sturdevant 2013, Garcia and Sewall 2021). However, piscivory by juvenile Chinook salmon has decreased as SSTs have increased in the NBS (Fig. 26). There has been a clear decline in piscivory in Chinook salmon relative to other species of juvenile salmon in the NBS. Fish composed 88.9% of the diet of Chinook salmon on average during 2004-2017, but decreased to 72.8% on average during 2018-2019. Age-0 walleye pollock were common in Chinook salmon diets when ocean

conditions were anomalously warm but were rare when conditions were cool. Capelin was a common prey item composing 16.7-68.4% of the diet during 2004-2013, with the exception of one year (2012), when capelin were not detected. The absence of capelin from the 2012 diet is more likely an artifact of the diet processor than an ecological reflection. No fish were identified to species from the 2012 survey, though a large percent of the diet was still fish. The presence of capelin declined to only 4.7-11.0% during 2014-2018 and were absent from the diet in 2019 (Fig. 25). Concurrent with the decrease and disappearance of capelin from the diet was an increase in the consumption of decapod larvae during 2018-2019, which may reflect a decrease in the availability of fish prey or a reduced ability to capture fish resulting from a concurrent decrease in body size. Our findings highlight key features in the feeding ecology of juvenile Chinook salmon in the NBS and identify areas of potential concern.

The level of piscivory in Chinook salmon and the survey design in 2005 were atypical and the therefore the data from 2005 is treated as an outlier in the time series (Fig. 26). The 2005 survey started later than usual in 2005 and stations were sampled from North to South. Stations at the southern end of the NBS were sampled a month later than most years and juveniles had already begun to disperse into the southern Bering at that point. The unusual distribution of juvenile Chinook salmon in 2005 is believed to be contributing to an atypical pattern in their diet.

The average stomach fullness index (SFI) of all juvenile salmon except for coho salmon has declined as SSTs have increased in the NBS (Fig. 27). The overall average SFI was similar for Chinook (157), pink (156), and coho salmon (153), but lower for chum salmon (126). The average SFI in 2019 for Chinook salmon (67) and chum salmon (49) were the lowest on record and less than half of their overall average. Warmer temperatures increase metabolic rates which would require a higher overall amount of prey consumed or an increase in the energetic quality of prey consumed for a fish to realize the same growth rate under cooler conditions. Therefore, the combination of an increase in thermal experience and a decrease in the amount of food consumed will have a larger effect on growth than an increase in thermal experience alone.

Larger body size requires higher energy prey (Schabetsberger et al. 2003). Years in which piscivory decreased for juvenile Coho and Chinook salmon may signal a lack of energy-rich forage. Sand lance and capelin are energetically rich prey (Litzow 2006). In the absence of high quality prey, lower quality prey may be substituted (Weitcamp and Sturdevant 2008), and an increase in prey diversity may indicate more generalized feeding and a greater reliance on non-preferred prey items (Weitcamp and Sturdevant 2008). If ocean conditions continue to warm and alter lower trophic levels in the Bering Sea (Hunt et al. 2011), these changes are likely to cascade up to higher trophic levels and affect salmon growth and survival. This analysis combined all juvenile salmon diets of a given species without regard to habitat (bottom depth) to provide a synoptic view across the entire NBS survey area. Previous studies have noted that certain prey may be more commonly consumed in certain habitats by juvenile salmon (Cook and Sturdevant 2013) and forage fishes (Andrews et al. 2016).

Juvenile Salmon Energetic Condition

The energetic condition of NBS juvenile Chinook salmon varied across the 12 years of available data, partially driven by differences in fish size (Fig. 28). Average ED (kJ/g dry tissue mass) differed significantly among years (Welch's ANOVA, $F = 10.36$, $R^2 = 17.9\%$, $\rho < 0.001$), with 2016 being the highest, 2011 the lowest, and 2019 of intermediate value slightly lower than 2018. Average lengths of analyzed fish also differed among years (Welch's ANOVA, $F = 22.12$, $R^2 = 21.9\%$, $\rho < 0.001$), with 2007 the largest, 2011 the smallest, and 2019 of intermediate size slightly larger than 2018. With all data pooled across years, linear regression analysis indicated that the energetic condition of juvenile Chinook salmon increased with fish length (slope = 0.0230; $R^2 = 39.7\%$; $\rho < 0.001$; Fig. 29). This positive relationship was expected, as energetic condition commonly increases with size in fishes that must store energy prior to winter (Post and Parkinson 2001), and has been previously observed in juvenile Chinook salmon (Murphy et al. 2014). However, this indicated that approximately 60% of the variation in

individual ED was due to factors other than fish size. Including year in addition to length increased the explained variation to 50.9%, with a significant effect of year after controlling for length (ANCOVA, $F_{11,562} = 11.56$, $\rho < 0.001$). Mean size-adjusted energetic condition overlapped significantly among years but was lowest in 2011 and highest in 2018 (Table 11). Similar results regarding yearly comparisons were obtained using a rank-based test and comparisons of ranked residuals from the regression fit of ED versus length (Kruskal-Wallis Test, H = 103.9, $\rho < 0.001$; Table 12). Monitoring yearly differences in autumn energetic condition may help understand and project juvenile survival, as cohorts that are able to store more energy prior to their first winter are more likely to survive (Sogard and Olla 2000).

Differences in ED among years also may be driven by annual differences in SST. Annual mean Chinook ED generally increased with mean autumn SST across years (Spearman's rho = 0.583, $\rho = 0.047$. However, temperature may have a non-linear, dome-shaped relationship to ED, as indicated by a GAM model fit (k = 4, edf = 2.26, adj $R^2 = 36.4\%$, $\rho = 0.108$) in which ED was highest at intermediate SST and appeared to decline at the highest SST observed in 2019 (< 11 °C; Fig. 30). Temperature effects on ED were evaluated in combination with fish size, given that average length alone accounted for 46.5% of the variation in annual average ED (slope = 0.0237; $F_{1,10} = 8.68$, $\rho = 0.015$; Fig. 31) in a simple linear regression model. Temperature combined with length in a multiple regression model explained 64.0% of the variation in average ED ($slope_{SST} = 0.146$, $slope_{LEN} = 0.0211$; $F_{2,9} = 7.99$, $\rho = 0.010$). The effect of SST on ED was marginally not significant ($\rho = 0.066$) in that model and was potentially weakened by collinearity with length due to the non-significant but positive influence of SST on length (slope = 1.72; $F_{1,10} = 0.313$; $R^2 = 3.04\%$, $\rho = 0.588$). The 17.5% improvement in fit versus length alone justified the inclusion of the SST term in the model (ΔAICc = - 0.034).

The positive influence of temperature on juvenile Chinook salmon energetic condition across most of the observed temperature range through 2018 may be expected for fish near the northern limit of their distribution, where temperatures are likely below optimal for growth and condition. Warmer temperatures are expected to have a positive effect up to a species-dependent optimal temperature, given the typical dome-shaped responses of fish growth and condition to temperature (Beauchamp et al 2007; Laurel et al 2016). Warmer temperatures in the past have supported higher survival of northern stocks of pink, chum, and sockeye salmon potentially through indirect effects on prey production (Mueter et al. 2002). However, anomalously warm temperatures seen in 2019 may have exceeded the optimum for juvenile Chinook salmon, and thus led to a decline in ED.

The 2019 decline in ED may have been caused by a combination of increased metabolic rates (Gillooly et al. 2001) and negative impacts on prey quality or quantity associated with unusually warm conditions. Higher ED observed in warmer years through 2018 suggests that juvenile Chinook salmon energetic condition during that period generally was not limited by food energy intake. Juvenile Chinook salmon may have adapted to decreased availability of capelin in warm years (Andrews et al. 2016) by eating more sand lance and early-stage decapods. Diet differences in warmer versus colder years make it difficult to strictly distinguish temperature effects from diet effects on energetic condition. However, despite eating fewer fish and less prey overall in warmer years, NBS juvenile Chinook salmon diets were adequate to support higher energetic condition than in cooler years through 2018. The 2019 decline in ED suggests juvenile Chinook salmon were unable to ingest sufficient energy to support optimal energetic condition, though it is difficult to infer mechanisms or trends based on a single anomalous year. If energetic condition consistently declines in response to anomalously warm conditions, continued ocean warming could lead to decreased survival of juveniles, which in 2019 had among the lowest abundances since monitoring began in 2003. These data indicate juvenile Chinook salmon energetic condition is sensitive to temperature-driven changes in ocean conditions that could impact future returns.

Seabird and Marine Mammal Observations

A total of 2,870 km were surveyed during the cruise with 324 km in the Chukchi Sea, 1,734 km in the NBS, and 809 km in the southern Bering Sea during transit to port in Dutch Harbor, AK. We observed a total of 3,310 birds on transect, comprising 38 species plus several unidentified passerines (Table 13).

The northern fulmar (*Fulmarus glacialis*) was the most abundant seabird species (28%) recorded during the survey. Highest concentrations of fulmars were observed in the southern Bering Sea south of 60°N near the shelf-break and the middle domain (Fig. 32). In the northern Bering and Chukchi seas, fulmar observations were generally lower and fulmars were largely absent on transects offshore of Norton Sound. Short-tailed shearwaters (*Ardenna tenuirostris*) and unidentified shearwaters (*Ardenna* spp.) were a predominant bird species (15%) recorded throughout the study area (Table 13). Shearwaters were widely distributed, with higher numbers in the southern Bering Sea, along with larger concentrations of birds near the Bering Strait (Fig. 33). Another *Procellariidae* species, the fork-tailed storm-petrel, was also common in the Bering Sea, with distribution centered in the southern Bering Sea (Fig. 33).

Aethia auklets (Crested, Least, and Parakeet) combined comprised 6% of the total seabird observations during the survey (Table 13). Crested auklets were primarily observed in two areas, southeast of St. Lawrence Island and near King Island in the NBS (Fig. 34). Least and parakeet auklets were more widely dispersed south of St. Lawrence Island, west of Nunivak Island, and in the southern Bering Sea (Fig. 34). Tufted puffins (3%) and common murres (3%) were other commonly detected *Alcid* species.

Phalaropus spp. consisting of red phalaropes (*P. fulicarius*), red-necked phalaropes (*P. lobatus*), and unidentified phalaropes, comprised 8% of total birds recorded during the survey. Phalaropes were mostly found in the NBS near St. Lawrence Island, the Bering Strait, and extending into the Chukchi Sea (Fig. 35). Black-legged kittiwakes (*Rissa tridactyla*) were the prevalent *Laridae* species recorded and comprised 19% of total seabird observations. Kittiwakes were widely distributed, with the highest numbers detected near the Pribilof Islands, east of St. Matthew Island, and Bering Strait (Fig. 36).

We recorded marine mammals during surveys, but because we used seabird survey protocols our observations cannot be used to calculate marine mammal densities. The USFWS observer recorded 65 marine mammals of seven species, including off-transect individuals (Table 14). northern fur seals (*Callorhinus ursinus*) were the most commonly encountered marine mammal, with individuals observed in the Bering Sea within 200 km of Dutch Harbor. The most common cetacean species observed was the humpback whale (*Megaptera novaeangliae*).

Sandhill cranes (*Grus canadensis*) were observed in five flocks near Bering Strait on 14 and 16 September, totaling 604 birds. We recorded three observations of Aleutian terns (*Onychoprion aleuticus)* totaling four birds in early to mid-September, east of St. Paul Island, north of Nunivak Island, and northeast of St. Lawrence Island. Near Nunivak Island we also observed two female Steller's eiders (*Polysticta stelleri*), and one marbled murrelet *(Brachyramphus marmoratus*) in early September.

Acknowledgements

We wish to thank the captain and crew of the FV *Northwest Explorer* for their exceptional support during the 2019 northern Bering Sea surface trawl survey. We also wish to thank Alex Andrews for his helpful review of this report. The 2019 survey was supported by the Alaska Sustainable Salmon Fund (AKSSF) through the project entitled northern Bering Sea Juvenile Chinook salmon Survey Phase 2 (project #51002), Alaska Fisheries Science Center, Alaska Department of Fish and Game, U.S. Fish and Wildlife Service (with funding from Bureau of Ocean Energy Management, project AK-17-03), and Alaska Pacific University. This report was prepared under award NA19NMF4380229 from the NOAA Cooperative Institute Program and administered by the Alaska Department of Fish and Game. The statements, findings, conclusions, and recommendations are those of the author(s) and do not necessarily reflect the views of NOAA or the Alaska Department of Fish and Game.

CITATIONS

ADF&G Chinook Salmon Research Team. 2013. Chinook salmon stock assessment and research plan, 2013. Alaska Department of Fish and Game, Special Publication No. 13-01, Anchorage, AK.

Andrews, A. G, E. V. Farley Jr., J. H. Moss, J. M. Murphy, and E. F. Husoe. 2009. Energy density and length of juvenile pink salmon, *Oncorhynchus gorbuscha*, in the eastern Bering Sea from 2004 to 2007: a period of relatively warm and cool sea surface temperatures. N. Pac. Anadr. Fish Comm. Bull. 5:182-189.

Andrews, A .G., W. W. Strasburger, E. V. Farley Jr., J. M. Murphy, and K. O. Coyle. 2016. Effects of warm and cold climate conditions on capelin (*Mallotus villosus*) and Pacific herring (*Clupea pallasii*) in the eastern Bering Sea. Deep Sea Res. II. 134:235-246.

Auburn, M., and M. Studevant. 2013. Diet composition and feeding behavior of juvenile salmonids in the northern Bering Sea August - October, 2009 – 2011. [In] Proceedings of the 2013 NPAFC Third International Workshop on Migration and Survival Mechanisms of Juvenile Salmon and Steelhead in Ocean Ecosystems, April 24–25, 2013, Honolulu, HI, U.S.A.

Beauchamp, D. A., A. D. Cross, J. L. Armstrong, K. W. Myers, J. H. Moss, J. L. Boldt, and L. J. Haldorson. 2007. Bioenergetic responses by Pacific salmon to climate and ecosystem variation. N. Pac. Anadr. Fish Comm. Bull. 4: 257–269.

Beamish, R. J., and C. Mahnken. 2001. A critical size and period hypothesis to explain natural regulation of salmon abundance and the linkage to climate and climate change. Prog. Oceanogr. 49:423–437.

Burnham, K. P. and D. R. Anderson. 2004. Multimodel inference understanding AIC and BIC in model selection. Sociol. Method. Res. 33: 261–304.

Chuchukalo, V. I., Volkov, A. F., 1986. Manual for The Study of Fish Diets. TINRO, Vladivostok, p. 32, in Russian.

Coyle, K. O., L. B. Eisner, F. J. Mueter, A. I. Pinchuk, M. A. Janout, K. D. Cieciel, E. V. Farley, and A. G. Andrews. 2011. Climate change in the southeastern Bering Sea: impacts on pollock stocks and implications for the oscillating control hypothesis. Fish. Oceanogr. 20, 139–156.

Danielson, S., E. Curchitser, K. Hedstrom, T. Weingartner, and P. Stabeno. 2011. On ocean and sea ice modes of variability in the Bering Sea. J. Geophys. Res. 116:C12034.

Day, R. W., and G. P. Quinn. 1989. Comparisons of treatments after an analysis of variance in ecology. Ecol. Monogr. 59: 433–463.

ESRI 2019. ArcGIS Desktop: Release 10.7. Redlands, CA: Environmental Systems Research Institute.

Estensen, J. L., H. C. Carroll, S. D. Larson, C. M. Gleason, B. M. Borba, D. M. Jallen, A. J. Padilla, and K. M. Hilton. 2018. Annual management report Yukon Area, 2017. Alaska Department of Fish and Game, Fishery Management Report No. 18-28, Anchorage.

Farley, E. V. Jr., J. M. Murphy, B. W. Wing, J. H. Moss, and A. Middleton. 2005. Distribution, migration pathways, and size of western Alaska juvenile salmon along the eastern Bering Sea shelf. AK. Fish. Res. Bull. 11, 15–26.

Farley, E. V. Jr., J. Murphy, J. Moss, A. Feldmann, and L. Eisner, 2009. Marine ecology of western Alaska juvenile salmon. In: Krueger, C. C., and C. E. Zimmerman (Eds.), Pacific Salmon: Ecology and Management of Western Alaska's Populations. American Fisheries Society, Bethesda, Maryland, pp. 307–329.

Farley, E. J. Murphy, E. Ysumiishi, K. Cieciel, K. Dunmall, T. Sformo, and P. Rand. 2020. Response of pink salmon to climate warming in the northern Bering Sea. Deep Sea Res. II.177:104830. doi.org/10.1016/j.dsr2.2020.104830

Fergusson, E. A., M. V. Sturdevant, and J. A. Orsi. 2010. Effects of starvation on energy density of juvenile chum salmon (*Oncorhynchus keta*) captured in marine waters of Southeastern Alaska. Fish. Bull., AK 108: 218–225.

Garcia, S., and F. Sewall. 2021. Diet and energy density assessment of juvenile Chinook salmon from the northeastern Bering Sea, 2004–2017. Alaska Department of Fish and Game, Fishery Data Series No. 21-05, Anchorage, AK.

Heintz, R. A., E. C. Siddon. E. V. Farley Jr., and J. M. Napp. 2013. Correlation between recruitment and fall condition of age-0 pollock (*Theragra chalcogramma*) from the eastern Bering Sea under varying climate conditions. Deep Sea Res. II 94:150-156.

Honeyfield, D. C., J. M. Murphy, K. G. Howard, W. W. Strasburger, and A. C. Matz. 2016. An exploratory assessment of thiamine status in western Alaska Chinook salmon (*Oncorhynchus tshawytscha*). N. Pac. Anadr. Fish Comm. Bull. 6: 21–31. doi:10.23849/npafcb6/21.31.

Howard, K. G., J. M. Murphy, L. I. Wilson, J. H. Moss, and E. V. Farley Jr. 2016. Size-selective mortality of Chinook salmon in relation to body energy after the first summer in nearshore marine habitats. N. Pac. Anadr. Fish Comm. Bull. 6:1–11. doi:10.23849/npafcb6/1.11.

Howard, K. G., S. Garcia, J. Murphy and T. H. Dann. 2019. Juvenile Chinook salmon abundance index and survey feasibility assessment in the northern Bering Sea, 2014–2016. Alaska Department of Fish and Game, Fishery Data Series No. 19-04, Anchorage.

Howard, K. G., S. Garcia, J. Murphy, and T. H. Dann. 2020. Northeastern Bering Sea juvenile Chinook salmon survey, 2017 and Yukon River adult run forecasts, 2018–2020. Alaska Department of Fish and Game, Fishery Data Series No. 20-08, Anchorage.

Huang, B., C. Liu, V. Banzon, E. Freeman, G. Graham, B. Hankins, T. Smith, and H. M. Zhang. 2021. Improvements of the Daily Optimum Interpolation Sea Surface Temperature (DOISST) Version 2.1. Journal of Climate. 34:2923-2939. DOI 10.1175/JCLI-D-20-0166.1.

Hunt G. L. Jr, K. O. Coyle, L. B. Eisner, E. V. Farley, R. A. Heintz, F. Mueter, J. M. Napp, J. E. Overland, P. H. Ressler, S. Salo, and P. J. Stabeno. 2011. Climate impacts on eastern Bering Sea foodwebs: a synthesis of new data and an assessment of the Oscillating Control Hypothesis. ICES J. Mar. Sci. 68(6): 1230-1243.

Ianelli, J. N. and D. L. Stram. 2014. Estimating impacts of the pollock fishery bycatch on western Alaska Chinook salmon. ICES Journal of Marine Science 72 1159–1172, doi.org/10.1093/icesjms/fsu173

JTC (Joint Technical Committee of the Yukon River U.S./Canada Panel). 2020. Yukon River salmon 2019 season summary and 2020 season outlook. Alaska Department of Fish and Game, Division of Commercial Fisheries, Regional Information Report 3A20-01, Anchorage.

Kassambara, A. 2019. ggcorrplot version 0.1.3: visualization of a correlation matrix using 'ggplot2'. http://www.sthda.com/english/wiki/ggcorrplot.

Kelley, D., and C. Richards. 2020. oce: Analysis of Oceanographic Data. R package version 1.2-0. https://CRAN.R-project.org/package=oce

Kondzela, C., M. Garvin, R. Riley, J. Murphy, J. Moss, S. Fuller, and A. Gharrett, 2009. Preliminary genetic analysis of juvenile chum salmon from the Chukchi Sea and Bering Strait. N. Pac. Anadr. Fish Comm. Bull. 5, 25–27.

Kondzela, C. M., J. A. Whittle, C. T. Marvin, J. M. Murphy, K. G. Howard, B. M. Borba, E. V. Farley, Jr., W. D. Templin, and J. R. Guyon. 2016. Genetic analysis identifies consistent proportions of seasonal life history types in Yukon River juvenile and adult chum salmon. N. Pac. Anadr. Fish Comm. Bull. 6:439-450.

Laurel, B. J., M. Spencer, P. Iseri, and L. A. Copeman. 2016. Temperature-dependent growth and behavior of juvenile Arctic cod (*Boreogadus saida*) and co-occurring North Pacific gadids. Polar Bio. 39(6): 1127–1135.

Litzow, M. A., K. Bailey, F. Prahl, and R. Heintz. 2006. Climate regime shifts and reorganization of fish communities: the essential fatty acid limitation hypothesis. Mar. Ecol. Prog. Ser. 315: 1-11.

Menard, J., J. Soong, J. Bell, L. Neff, and J. M. Leon. 2020. 2018 Annual management report Norton Sound, Port Clarence, and Arctic, Kotzebue Areas. Alaska Department of Fish and Game, Fishery Management Report No. 20-05, Anchorage, AK.

Miller, K., D. Neff, K. Howard, and J. M. Murphy. 2016. Spatial distribution, diet, and nutritional status of juvenile Chinook salmon and other fishes in the Yukon River estuary. U.S. Dep. Commer., NOAA Tech. Memo. NMFS-AFSC-334, 103 p.

Moss, J. H., J. M. Murphy, E. A. Fergusson, and R.A. Heintz. 2017. Energy dynamics and growth of juvenile Chinook (*Oncorhynchus tshawytscha*) and Chum (*Oncorhynchus keta*) salmon in the eastern Gulf of Alaska and northern Bering Sea. N. Pac. Anadr. Fish Comm. Bull. 6:161-168.

Moss, J. H., D. A. Beauchamp, A. D. Cross, K. W. Myers, E. V. Farley, J. M. Murphy, and J. H. Helle. 2005. Evidence for size-selective mortality after the first summer of ocean growth by pink salmon. Trans. Amer. Fish. Soc. 134:1313–1322.

Moss, J. H., J. M. Murphy, E. V. Farley, L. B. Eisner, and A. G. Andrews. 2009. Juvenile pink and chum salmon distribution, diet, and growth in the northern Bering and Chukchi seas. N. Pac. Anadr. Fish Comm. Bull. 5:191–196.

Mueter, F. J., R. M. Peterman, and B. J. Pyper. 2002. Opposite effects of ocean temperature on survival rates of 120 stocks of Pacific salmon (*Oncorhynchus* spp.) in northern and southern areas. Can. J. Fish. Aquat. Sci. 59(3): 456–463.

Murphy, J., O. Temnykh, and T. Azumaya. 2003. Trawl Comparisons and Fishing Power Corrections for the F/V *Northwest Explorer*, R/V *TINRO*, and R/V *Kaiyo Maru* During the 2002 BASIS Survey. (NPAFC Doc. 677 Rev. 1) 25 p. (available at www.npafc.org)

Murphy J. M., W. D. Templin, E. V. Farley, and J. E. Seeb. 2009. Stock-structured distribution of western Alaska and Yukon juvenile Chinook salmon (*Oncorhynchus tshawytscha*) from United States BASIS surveys, 2002–2007. N. Pac. Anadr. Fish Comm. Bull. 5:51–59.

Murphy, J., K. Howard, L. Eisner, A. Andrews, W. Templin, C. Guthrie, K. Cox, and E. Farley. 2013. Linking abundance, distribution, and size of juvenile Yukon River Chinook salmon to survival in the northern Bering Sea. [In]: Proceedings of the 2013 NPAFC Third International Workshop on Migration and survival mechanisms of juvenile salmon and steelhead in ocean ecosystems, April 24–25, 2013, Honolulu, HI, U.S.A.

Murphy, J., K. Howard, A. Andrews, L. Eisner, J. Gann, W. Templin, C. Guthrie, J. Moss, D. Honeyfield, K. Cox, and E. Farley. 2014. Yukon River Juvenile Chinook salmon Survey. AKSSF Project 44606 Final Report. 130 p.

Murphy, J. M., E. V. Farley, Jr., J. N. Ianelli, and D. L. Stram. 2016. Distribution, diet, and bycatch of chum salmon in the eastern Bering Sea. N. Pac. Anadr. Fish Comm. Bull. 6: 219–234. doi:10.23849/npafcb6/219.234.

Murphy, J., K. Howard, J. Gann, K. Cieciel, W. Templin, and C. Guthrie. 2017. Juvenile Chinook salmon abundance in the northern Bering Sea: implications for future returns and fisheries in the Yukon River. Deep Sea Res. II. 135:156–167.

Orr J. W., S. Wildes, Y. Kai, N. Raring, T. Nakabo, O. Katugin, and J. Guyon. 2015. Systematics of North Pacific sand lances of the genus *Ammodytes* based on molecular and morphological evidence, with the description of a new species from Japan. Fish. Bull., 113: 129–156.

Pella, J. J., and M. Masuda. 2001. Bayesian methods for analysis of stock mixtures from genetic characters. Fish. Bull., 99:151–167.

Persson, J., and T. Vrede. 2006. Polyunsaturated fatty acids in zooplankton: variation due to taxonomy and trophic position. Freshwater Biology 51: 887-900.

Post, J. R. and E. A. Parkinson. 2001. Energy allocation strategy in young fish: allometry and survival. Ecology 82(4): 1040–1051.

Quinn, T. J., and R. B. Deriso. 1999. Quantitative fish dynamics. Oxford University Press, Oxford.

R Core Team (2020). R: A language and environment for statistical computing. R Foundation for Statistical Computing, Vienna, Austria. URL www.R-project.org/.

Rogers, L. A., M. T. Wilson, J. T. Duffy-Anderson, D. G. Kimmel, and J. F. Lamb. 2020. Pollock and "the Blob": Impacts of a marine heatwave on walleye pollock early life stages. Fish. Oceanogr., 30(2):142-158.

Schabetsberger, R., C. A. Morgan, R. D. Brodeur, C. L. Potts, W. T. Peterson, and R. L. Emmett. 2003. Prey selectivity and diel feeding chronology of juvenile Chinook (*Oncorhynchus tshawytscha*)

and coho (*O. kisutch*) salmon in the Columbia River plume. Fish. Oceanogr., 12(6): 523-540.
Shink, K. G., T. M. Sutton, J. M. Murphy, and J. A. López. 2019. Utilizing DNA metabarcoding to characterize the diet of marine-phase Arctic lamprey (*Lethenteron camtschaticum*) in the eastern Bering Sea. Can. J. Fish. Aquat. Sci. 76:1993-2002. doi.org/10.1139/cjfas-2018-0299.
Sogard, S. M., and B. L. Olla. 2000. Endurance of simulated winter conditions by age-0 walleye pollock: effects of body size, water temperature and energy stores. J. Fish Bio. 56(1): 1–21.
Stabeno, P. J., and S. W. Bell. 2019. Extreme Conditions in the Bering Sea (2017 - 2018): Record - Breaking Low Sea-Ice Extent. Geophy. Res. Lett. 46:8952–8959.
Stram, D. L., and J. N. Ianelli. 2014. Evaluating the efficacy of salmon bycatch measures using fishery-dependent data. ICES J. Mar. Sci. 72:1173–1180. https://doi.org/10.1093/icesjms/fsu168
Templin, W. D., J. E. Seeb, J. R. Jasper, A. W. Barclay, and L. W. Seeb. 2011. Genetic differentiation of Alaska Chinook salmon: the missing link for migratory studies. Mol. Ecol. Resour. 11(Suppl. 1): 215-235.
Tomaro, L. M., D. J. Teel, W. T. Peterson, and J. A. Miller. 2012. When is bigger better? Early marine residence of middle and upper Columbia River spring Chinook salmon. Mar. Ecol. Prog. Ser. 452:237–252.
Volkov, A. F., and N. A. Kuznetsova. 2007. Results from research on the diets of Pacific salmon in 2002(2003)–2006 under the BASIS program. Izv.TINRO 151, 365–402, in Russian.
Vollenweider, J. J., R.A. Heintz, L. Schaufler, and R. Bradshaw. 2011. Seasonal cycles in whole-body proximate composition and energy content of forage fish vary with water depth. Mar. Bio. 158: 413–427.
Weitkamp, L. A., and M. V. Sturdevant. 2008. Food habits and marine survival of juvenile Chinook and coho salmon from marine waters of southeast Alaska. Fish. Oceanogr. 17: 380-395.
Welch, B.L. 1951. On the comparison of several mean values: an alternative approach. Biometrika 38: 330–336.
Wood, S.N. 2006. Generalized additive models: an introduction with R. Chapman & Hall / CRC, London.

Table 1. -- Name and affiliation of scientific crew members during the northern Bering Sea surface trawl survey, 2019. AFSC—Alaska Fisheries Science Center, Auke Bay Laboratories, Juneau, AK; ADFG—Alaska Department of Fish and Game, Commercial Fisheries Division, Anchorage, AK; USFWS—US Fish and Wildlife Service, Office of Migratory Bird Management, Anchorage, AK; APU—Alaska Pacific University, Anchorage, AK.

Name (Last, First)	Title	Date Embark	Date Disembark	Affiliation
Murphy, Jim	Chief Scientist	8/27/2021	9/20/2021	AFSC
Gray, Andrew	Sup. Fish Biologist	8/27/2021	9/8/2021	AFSC
Sewall, Fletcher	Fish Biologist	8/27/2021	9/8/2021	AFSC
Dimond, Andrew	Fish Biologist	8/27/2021	9/8/2021	AFSC
Jallen, Deena	Fish Biologist	8/27/2021	9/8/2021	ADFG
Labunski, Elizabeth	Seabird Observer	8/27/2021	9/8/2021	USFWS
Waters, Charlie	Fish Biologist	9/8/2021	9/20/2021	AFSC
Garcia, Sabrina	Fish Biologist	8/8/2021	9/20/2021	ADFG
Nicols, Dave	Fish Biologist	9/8/2021	9/20/2021	AFSC
Conlon, Ryan	Student	9/8/2021	9/20/2021	APU
Zeller, Tamara	Seabird Observer	9/8/2021	9/20/2021	USFWS

Table 2. -- Dates, locations, and sampling events completed at each station during the northern Bering Sea surface trawl survey, 2019.

Station	Date	Latitude	Longitude	Bottom Depth (m)	CTD Depth (m)	CAT Depth (m)	Benthic Grab
1	8/30/2019	60.01	-167.98	23	17	16	No
2	8/30/2019	59.99	-168.97	38	31	30	No
3	8/31/2019	59.99	-169.97	51	47	41	No
4	8/31/2019	59.99	-170.98	65	47	56	No
5	8/31/2019	60.51	-170.96	59	52	50	No
6	9/1/2019	60.51	-169.98	45	40	NA	No
7	9/1/2019	60.51	-168.97	35	30	26	No
8	9/1/2019	60.51	-167.96	27	21	18	No
9	9/2/2019	60.51	-167.04	24	19	19	No
10	9/2/2019	60.99	-167.04	19	13	12	No
11	9/2/2019	61	-168.02	27	20	21	Yes
12	9/3/2019	60.99	-169.05	34	29	26	No
13	9/3/2019	60.99	-170.02	44	36	37	No
14	9/3/2019	61.03	-170.98	51	47	45	No
15	9/4/2019	61.49	-170.96	48	41	40	No
16	9/4/2019	61.51	-169.98	42	37	34	No
17	9/4/2019	61.5	-169	32	26	26	No
18	9/5/2019	61.49	-168.01	26	21	21	No
19	9/5/2019	61.54	-167.06	19	16	15	No
20	9/5/2019	61.99	-166.98	26	22	21	Yes
21	9/6/2019	61.98	-167.98	25	21	20	No
22	9/6/2019	62	-169.04	34	29	28	No
23	9/6/2019	62.02	-170.07	41	35	35	Yes
24	9/7/2019	62.01	-170.95	47	41	40	Yes
25	9/7/2019	62.5	-166.96	31	26	24	No
26	9/7/2019	63.01	-165.95	18	15	14	Yes
27	9/8/2019	63.51	-165.96	21	18	17	No
28	9/9/2019	63.49	-166.94	23	19	20	Yes
29	9/9/2019	62.99	-167.03	22	19	18	No
30	9/10/2019	62.49	-167.94	26	20	20	Yes
31	9/10/2019	62.5	-169.04	29	25	26	No
32	9/10/2019	62.48	-170.03	33	29	27	Yes
33	9/11/2019	62.49	-170.98	40	37	36	No
34	9/11/2019	63.49	-167.96	30	26	26	No
35	9/11/2019	64	-167.97	34	28	29	No
36	9/12/2019	64.52	-166.99	24	20	19	No
37	9/12/2019	64.01	-166.96	30	27	25	Yes
38	9/13/2019	64.01	-165.96	19	16	16	No
39	9/13/2019	64.1	-162.54	18	15	13	Yes
40	9/13/2019	64.1	-163.56	21	15	18	Yes
41	9/14/2019	64.1	-164.47	19	15	14	Yes
42	9/14/2019	64.53	-168.01	33	30	27	No
43	9/14/2019	65.02	-167.55	22	19	19	Yes
44	9/15/2019	65.42	-168.04	38	29	33	Yes
45	9/15/2019	66.62	-165.8	16	14	13	Yes

46	9/15/2019	66.61	-166.99	28	25	24	Yes
47	9/16/2019	66.12	-167.45	19	16	15	Yes

Table 3. -- Temperature (°C), salinity (PSU), and mixed layer depth (MLD, m) measurements from CTD (SBE-9-11+) and FastCat (SBE-49) casts during the northern Bering Sea surface trawl survey, 2019. Surface values are average values from the top 10 meters, and bottom values are values at maximum gear depth.

Station	CTD Surface Temp.	CAT Surface Temp.	CTD Surface Salinity	CAT Surface Salinity	CTD Bottom Temp.	CAT Bottom Temp.	CTD Bottom Salinity	CAT Bottom Salinity	Mixed Layer Depth
1	12.42	12.41	31.15	30.77	12.42	12.41	31.12	30.78	17
2	11.84	11.84	NA	31.82	7.66	7.71	31.91	31.91	22
3	11.99	12.08	31.91	31.91	4.17	4.27	32.05	32.05	21
4	11.99	11.54	31.91	32.05	4.17	2.65	32.05	32.23	21
5	11.68	11.67	--	31.95	2.9	2.90	32.18	32.18	26
6	11.76	--	31.89	--	4.88	--	31.97	--	22
7	10.91	10.94	31.56	31.58	10.09	10.42	31.68	31.65	22
8	12.43	12.44	--	30.97	12.43	12.43	30.97	30.96	21
9	12.87	12.88	30.71	30.72	12.85	12.85	30.73	30.73	19
10	13.77	13.77	29.23	29.21	13.74	13.74	29.3	29.3	13
11	12.59	12.59	30.88	30.88	12.57	12.57	30.88	30.88	20
12	11.03	11.03	31.46	31.46	11.02	11.03	31.46	31.46	29
13	11.27	11.27	31.78	31.77	5.68	5.66	31.86	31.86	24
14	11.41	11.41	31.93	31.92	3.13	3.12	32.09	32.09	27
15	11.37	11.36	31.9	31.89	2.73	2.73	32.04	32.04	23
16	10.95	10.93	31.44	31.44	5.74	5.84	31.69	31.69	20
17	11.23	11.23	31.38	31.37	11.23	11.24	31.38	31.36	26
18	11.93	11.9	30.69	30.68	11.93	11.93	30.69	30.65	21
19	12.96	12.96	30.22	30.04	12.96	12.96	30.22	30.2	16
20	12.87	12.89	30.14	29.86	12.88	12.89	30.19	29.82	22
21	11.02	11.04	--	30.63	11.02	11.07	30.81	30.82	21
22	10.89	10.95	--	30.64	8.02	8.08	31.32	31.33	21
23	11.33	11.33	31.5	31.50	3.44	3.43	31.57	31.57	24
24	11.24	11.26	31.64	31.65	1.77	1.77	31.87	31.88	19
25	12.57	12.56	30.1	30.00	12.07	12.1	30.32	30.31	20
26	12.28	12.32	29.78	29.51	12.03	12.04	29.98	29.99	12
27	11.09	11.18	30.74	30.36	10.31	10.4	31.02	31.01	10
28	9.99	10.02	31.24	31.24	9.53	9.71	31.28	31.01	19
29	11.02	11.18	30.89	30.85	10.95	10.96	30.98	30.96	19
30	11.27	11.39	31.05	30.59	10.47	10.48	31.05	31.35	15
31	11.11	11.1	31.28	31.21	2.96	2.95	31.53	31.57	18
32	11.39	11.39	31.37	31.22	2.02	2.03	31.66	31.67	18
33	11.38	11.39	31.37	31.36	1.72	1.72	31.77	31.77	19
34	10.02	9.88	31.67	31.66	6.42	6.42	31.72	31.73	12
35	10.29	10.3	--	31.71	2.80	2.77	32.11	32.16	20
36	10.62	10.63	30.86	30.88	10.45	10.47	30.96	30.66	19
37	8.45	8.46	31.55	31.55	8.00	8.05	31.72	31.73	27
38	10.36	10.37	31.19	31.13	10.37	10.36	31.19	31.18	16
39	12.93	12.9	21.68	21.75	12.97	12.97	22.06	19.9	14
40	12.93	12.43	21.68	21.08	12.97	12.46	22.06	24.01	14
41	12.07	12.14	29.17	29.18	11.91	11.91	29.47	29.57	8
42	7.91	7.86	31.26	31.43	5.66	5.73	31.93	31.93	17
43	11.38	11.67	--	29.42	11.37	11.35	30.23	30.22	19

44	11.45	11.84	29.3	29.63	10.68	10.68	30.76	30.76	6
45	10.79	10.76	29.59	29.58	10.75	10.74	29.6	29.53	14
46	11.89	11.9	28.5	28.35	11.68	11.78	28.88	28.8	14
47	11.97	11.94	27.36	27.5	11.60	11.63	28.37	28.28	10
Average	11.47	11.46	30.37	30.39	8.70	8.77	30.70	30.64	18.66

Table 4. -- Average surface trawl net dimensions (horizontal and vertical spread), average footrope depth (from the SBE39 temperature-depth recorder) and mixed layer depth (MLD) expansions during the northern Bering Sea surface trawl survey, 2019. MLD expansions are used to scale surface trawl catches to the mixed layer.

Station	Horiz. Net Spread (m)	Vert. Net Spread (m)	SBE39 Footrope Depth (m)	Mixed Layer Depth Expansion
1	38.45	17.15	18.72	1.00
2	49.50	19.00	21.59	1.02
3	51.00	16.40	18.11	1.16
4	51.00	18.50	20.27	1.04
5	51.00	19.00	19.95	1.30
6	50.00	19.00	20.45	1.08
7	48.62	20.87	23.17	1.00
8	49.60	19.20	21.23	1.00
9	51.00	12.00	12.80	1.48
10	51.22	15.39	16.53	1.00
11	52.00	15.00	16.44	1.22
12	50.00	22.00	24.58	1.18
13	48.00	21.00	22.94	1.05
14	52.38	17.12	18.87	1.43
15	49.50	20.00	22.30	1.03
16	50.50	16.00	16.74	1.19
17	50.00	19.24	22.02	1.18
18	50.00	20.19	21.33	1.00
19	50.50	16.50	17.46	1.00
20	51.00	18.00	19.03	1.16
21	49.00	17.00	18.41	1.14
22	49.00	17.00	19.56	1.07
23	52.00	17.00	18.43	1.30
24	49.50	19.50	21.22	1.00
25	51.00	17.50	19.19	1.04
26	51.62	15.00	15.02	1.00
27	53.01	15.34	17.23	1.00
28	44.00	17.00	18.66	1.02
29	48.00	18.00	18.96	1.00
30	49.00	17.00	18.75	1.00
31	51.00	16.00	17.09	1.05
32	45.00	17.00	18.29	1.00
33	47.00	17.75	19.07	1.00
34	51.00	21.00	23.22	1.00
35	47.00	19.50	20.11	1.00
36	48.00	16.00	16.17	1.18
37	47.00	18.50	18.83	1.43
38	51.00	16.50	16.97	1.00
39	52.71	14.29	14.39	1.00
40	51.00	15.50	16.08	1.00
41	51.50	15.00	16.27	1.00
42	50.50	19.00	21.48	1.00
43	51.00	17.00	18.98	1.00

44	53.00	20.00	23.10	1.00
45	53.00	13.00	14.10	1.00
46	51.00	18.50	19.65	1.00
47	49.00	14.50	16.61	1.00
Average	49.81	17.47	18.94	1.08

Table 5. -- Average size (length and weight), total catch, and catch-per-unit-effort (CPUE) of salmon species captured during the northern Bering Sea surface trawl survey, 2019.

Common Name	Scientific Name	Life History Stage	Average Length (cm)	Average Weight (g)	Average CPUE (n/km²)	Total Number Caught
pink salmon	*Oncorhynchus gorbuscha*	Juvenile	15.37	34	1,463	13,507
chum salmon	*O. keta*	Juvenile	16.73	49	397	3,660
sockeye salmon	*O. nerka*	Juvenile	18.56	64	277	2,553
coho salmon	*O. kisutch*	Juvenile	24.82	194	20	182
Chinook salmon	*O. tshawytscha*	Juvenile	19.75	97	14	125
chum salmon	*O. keta*	Immature	42.92	1,187	21	194
Chinook salmon	*O. tshawytscha*	Immature	42.17	1,271	3	26
sockeye salmon	*O. nerka*	Immature	36.62	676	2	19
coho salmon	*O. kisutch*	Immature	65.00	3,870	0.1	1

Table 6. -- Average size (bell width and weight), total weight, and catch-per-unit-effort (CPUE) of common jellyfish species captured during the northern Bering Sea surface trawl survey, 2019.

Common Name	Scientific Name	Average Bell Diameter (cm)	Average Weight (g)	Average CPUE (kg/km²)	Total Weight (kg)
northern sea nettle	*Chrysaora melanaster*	22.91	873	6,898	747,341
lion's mane jellyfish	*Cyanea capillata*	22.60	962	610	66,055
moon jellyfish	*Aurelia labiata*	15.32	302	378	40,906
whitecross jellyfish	*Staurophora mertensi*	--	--	69	7,443
water jellyfish	*Aequorea* spp.	15.40	218	23	2,478
fried egg jellyfish	*Phacellophora camtschatica*	--	--	2	182

Table 7. -- Average size (length and weight), total catch, and catch-per-unit-effort (CPUE) of non-salmon species captured during the northern Bering Sea surface trawl survey, 2019.

Life History Stage	Common Name	Scientific Name	Average Length (cm)	Average CPUE (n/km²)	Total Num. Caught	Total Weight Caught (kg)
					142,15	
--	Pacific herring	*Clupea pallasi*	14	15,401	2	1,842
--	salmon shark	*Lamna ditropis*	210	0.2	2	191
--	rainbow smelt	*Osmerus mordax*	13	113	1,040	14
	ninespine stickleback					
--		*Pungitius pungitius*	5	1,025	9,464	10
--	starry flounder	*Platichthys stellatus*	25	3	27	5
--	Arctic lamprey	*Lethenteron camtschaticum*	38	2	20	2
	smooth lumpsucker					
--		*Aptocyclus ventricosus*	NA	0	1	2
--	threespine stickleback	*Gasterosteus aculeatus*	4	159	1,464	1
--	Arctic staghorn sculpin	*Gymnocanthus tricuspis*	29	0.3	3	1
--	crested sculpin	*Blepsias bilobus*	12	1	13	1
--	yellowfin sole	*Limanda aspera*	27	0.3	3	1
		Pleuronectes quadrituberculatus				
--	Alaska plaice		19	0.4	4	0.4
--	greenling	*Hexagrammos spp.*	NA	1	7	0.2
--	capelin	*Mallotus villosus*	11	1	11	0.1
--	northern rock sole	*Lepidopsetta polyxystra*	NA	0.1	1	0.1
--	sturgeon poacher	*Podothecus accipenserinus*	26	0.1	1	0.1
--	armhook squid	*Gonatus spp.*	6	1	9	0.1
--	sand lance	*Ammodytes spp.*	15	0.2	2	0.03
--	longhead dab	*Limanda proboscidea*	3	0.2	2	0.002
Age 1+	walleye pollock	*Gadus chalcogrammus*	42	6	51	27
Age 1+	saffron cod	*Eleginus gracilis*	21	4	35	3
Age 0	walleye pollock	*Gadus chalcogrammus*	7	953	8,798	26
Age 0	rainbow smelt	*Osmerus mordax*	7	255	2,350	4
Age 0	saffron cod	*Eleginus gracilis*	10	2	14	0.1
Age 0	Pacific cod	*Gadus macrocephalus*	8	0.3	3	0.02

Table 8. -- Stock composition percentages (mean, standard deviation) for reporting groups (Upper Yukon, Middle Yukon, Lower Yukon, and Other Western Alaska) of juvenile Chinook salmon captured during the northern Bering Sea surface trawl surveys, 2003-2019. Stock composition estimates are not available for 2008 (no survey), 2012 and 2005 (low sample size), and 2013 (genetic samples contaminated during a flooding event aboard the survey vessel).

	Upper Yukon		**Middle Yukon**		**Lower Yukon**		**Other Western Alaska**	
Year	Mean	SD	Mean	SD	Mean	SD	Mean	SD
2003	48.29	3.5	23.44	3.06	16.55	4.34	11.72	4.13
2004	57.37	4.46	26.26	4.03	5.49	3.72	10.88	4.15
2006	48.98	5.34	26.51	4.8	14.99	5.59	9.52	5.14
2007	50.59	3.49	29.88	3.27	13.84	3.09	5.69	2.5
2009	52.43	4.77	28.06	4.42	6.26	4.25	13.25	4.63
2010	48.78	4.59	27.36	4.13	15.27	4.09	8.59	3.54
2011	46.74	2.88	22.46	2.44	17.53	3.52	13.27	3.38
2014	50.62	3.71	36.6	3.62	8.8	2.64	3.98	2.13
2015	44.17	2.93	30.02	2.79	11.87	3.35	13.94	3.37
2016	54.18	3.47	20.84	2.93	9.54	3.27	15.44	3.49
2017	42.3	3.67	19.94	3.04	9.28	4.32	28.47	4.97
2018	34.43	4.03	30.89	4.02	19.18	5.05	15.51	4.82
2019	29.99	4.5	21.17	4.19	13.88	6.04	34.96	6.63
Average	46.84	3.95	26.42	3.6	12.5	4.1	14.25	4.07

Table 9. -- Juvenile abundance, standard deviation (SD) of abundance, and juveniles-per-spawner for Yukon River Canadian-origin Chinook salmon stock group during the northern Bering Sea surface trawl surveys, 2003-2019 (juvenile years). Canadian-origin Chinook salmon spawner abundance, adult returns, and returns-per-spawner are included.

Brood Year	Juvenile Year	Juvenile Abundance (000s)	Juvenile Abundance (SD) (000s)	Adult Returns (000s)	Spawner Abundance (000s)	Juveniles-Per-Spawner	Returns-Per-Spawner
2001	2003	2,691	506	120	53	51.2	2.3
2002	2004	1,449	298	55	42	34.2	1.3
2003	2005	1,659	485	98	81	20.6	1.2
2004	2006	772	161	56	48	15.9	1.2
2005	2007	1,621	493	78	68	23.8	1.2
2006	2008	--	--	59	63	--	0.9
2007	2009	984	418	45	35	28.2	1.3
2008	2010	974	254	42	34	28.7	1.2
2009	2011	1,843	756	81	65	28.2	1.2
2010	2012	719	292	55	32	22.4	1.7
2011	2013	2,924	881	107	46	63.1	2.3
2012	2014	1,789	412	87	33	54.8	2.7
2013	2015	2,113	677	70	29	73.7	2.4
2014	2016	2,126	746	68	63	33.6	1.1
2015	2017	1,049	219	--	83	12.7	--
2016	2018	888	224	--	69	12.9	--
2017	2019	575	164	--	68	8.4	--
Average		1,511	437	73	54	32	1.6

Table 10. -- Juvenile abundance, standard deviation (SD) of abundance, and juveniles-per-spawner for the Total Yukon River Chinook salmon stock group during the northern Bering Sea surface trawl surveys, 2003-2019 (juvenile years). Total Yukon River Chinook salmon spawner abundance, adult returns, and returns-per-spawner are included.

Brood Year	Juvenile Year	Juvenile Abundance (000s)	Juvenile Abundance (SD) (000s)	Adult Returns (000s)	Spawner Abundance (000s)	Juveniles-Per-Spawner	Returns-Per-Spawner
2001	2003	4,920	878	322	--	--	--
2002	2004	2,249	435	154	113	19.9	1.4
2003	2005	2,952	698	263	264	11.2	1
2004	2006	1426	262	108	150	9.5	0.7
2005	2007	3,020	884	189	207	14.6	0.9
2006	2008	--	--	178	187	--	0.9
2007	2009	1629	676	175	128	12.7	1.4
2008	2010	1824	437	94	147	12.4	0.6
2009	2011	3,422	1391	200	153	22.3	1.3
2010	2012	1279	467	101	114	11.2	0.9
2011	2013	5,204	1285	276	130	40.1	2.1
2012	2014	3,393	724	238	111	30.6	2.2
2013	2015	4,115	1294	220	129	31.8	1.7
2014	2016	3,318	1149	208	173	19.2	1.2
2015	2017	1,773	361	--	151	11.7	--
2016	2018	2181	493	--	163	13.4	--
2017	2019	1246	326	--	236	5.3	--
Average		2,747	735	195	160	17.7	1.3

Table 11. -- Grouping information from post-hoc Tukey pairwise comparisons of energy density (covariate: length) by year, ordered by mean value, for juvenile Chinook salmon caught during the northern Bering Sea surface trawl surveys, 2006–2019. Years that share a common letter do not significantly differ (95% confidence).

Year	N	Mean Energy Density (kJ/g)	Group				
2018	41	22.359	A				
2017	49	22.213	A	B			
2016	36	22.154	A	B	C		
2010	95	22.152	A	B			
2014	87	21.884		B	C	D	
2019	50	21.733			C	D	
2007	49	21.684			C	D	
2006	10	21.594	A	B	C	D	E
2015	69	21.55				D	E
2012	31	21.55				D	E
2009	17	21.548		B	C	D	E
2011	41	21.076					E

Table 12. -- Grouping information from post-hoc Tukey pairwise comparisons of ranked residuals from simple linear regression of energy density versus length, ordered by mean rank, for juvenile Chinook salmon caught during the northern Bering Sea surface trawl surveys, 2006–2017. Years that share a common letter do not significantly differ (95% confidence).

Year	N	Mean Rank	Group				
2018	41	412.6	A				
2017	49	366.7	A	B			
2016	36	356.3	A	B	C		
2010	95	351.8	A	B			
2014	87	285.2		B	C	D	
2019	50	259.3			C	D	E
2007	49	254.9			C	D	E
2012	31	230				D	E
2006	10	213.9		B	C	D	E
2015	69	211.2				D	E
2009	17	206.1				D	E
2011	41	167.3					E

Table 13. -- Number (N) and percent of total (%) of marine birds recorded on transect during the northern Bering Sea surface trawl survey, 2019.

		S. Bering		N. Bering		Chukchi Sea		Total	
Common Name	**Scientific Name**	**N**	**%**	**N**	**%**	**N**	**%**	**N**	**%**
red-throated loon	*Gavia stellata*					2	0.8	2	0.1
Pacific loon	*Gavia pacifica*	2	0.1	10	0.8	5	2	17	0.5
yellow-billed loon	*Gavia adamsii*			1	0.1			1	< 0.1
unid. loon	*Gavia* spp.			4	0.3	2	0.8	6	0.2
red-necked grebe	*Podiceps grisegena*			2	0.2			2	0.1
black-footed albatross	*Phoebastria nigripes*	7	0.4					7	0.2
Laysan albatross	*Phoebastria immutabilis*	3	0.2					3	0.1
northern fulmar	*Fulmarus glacialis*	762	40.7	160	13.5	3	1.2	925	27.9
fork-tailed storm-petrel	*Oceanodroma furcata*	97	5.2	3	0.3	1	0.4	101	3.1
short-tailed shearwater	*Ardenna tenuirostris*	281	15	182	15.3	19	7.5	482	14.6
unid. dark shearwater	*Ardenna* spp.	7	0.4					7	0.2
pelagic cormorant	*Phalacrocorax pelagicus*	3	0.2	4	0.3			7	0.2
harlequin duck	*Histrionicus histrionicus*			3	0.3			3	0.1
long-tailed duck	*Clangula hyemalis*			1	0.1			1	< 0.1
Steller's eider	*Polysticta stelleri*			2	0.2			2	0.1
unid. duck	*Anatinae* spp.			1	0.1			1	< 0.1
unid. eider	*Somateria* spp.			3	0.3			3	0.1
sandhill crane	*Grus canadensis*			9	0.8	14 5	57.5	154	4.7
dunlin	*Calidris alpina*			1	0.1			1	< 0.1
unid. shorebird	*Scolopacidae* spp.			4	0.3			4	0.1
red phalarope	*Phalaropus fulicarius*	14	0.7	170	14.3	20	7.9	204	6.2
red-necked phalarope	*Phalaropus lobatus*	2	0.1	21	1.8			23	0.7
unid. phalarope	*Phalaropus* spp.	2	0.1	21	1.8	15	6	38	1.1
long-tailed jaeger	*Stercorarius longicaudus*	2	0.1					2	0.1
parasitic jaeger	*Stercorarius parasiticus*	5	0.3	2	0.2			7	0.2
pomarine jaeger	*Sterocorarius pomarinus*	4	0.2	5	0.4	3	1.2	12	0.4
unid. jaeger	*Stercocorarius* spp.			1	0.1			1	< 0.1

Common Name	Scientific Name	S. Bering		N. Bering		Chukchi Sea		Total	
		N	%	N	%	N	%	N	%
	Onychoprion aleuticus								
Aleutian tern		1	0.1	1	0.1			2	0.1
Arctic tern	*Sterna paradisaea*	3	0.2	3	0.3			6	0.2
Unid. Tern	*Sterna* spp.	1	0.1					1	< 0.1
black-legged kittiwake	*Rissa tridactyla*	318	17	296	24.9	20	7.9	634	19.2
glaucous gull	*Larus hyperboreus*	2	0.1	16	1.3	10	4	28	0.8
Glacous-winged gull	*Larus glaucescens*	27	1.4	11	0.9			38	1.1
herring gull	*Larus argentatus*	8	0.4	1	0.1			9	0.3
red-legged kittiwake	*Rissa brevirostris*	5	0.3					5	0.2
Sabine's gull	*Xema sabini*	6	0.3	22	1.9			28	0.8
slaty-backed gull	*Larus schistisagus*	2	0.1					2	0.1
unid. gull	*Larid* spp.	6	0.3	7	0.6	3	1.2	16	0.5
common murre	*Uria aalge*	56	3	40	3.4			96	2.9
thick-billed murre	*Uria lomvia*	18	1	13	1.1			31	0.9
unid. murre	*Uria* spp.	14	0.7	17	1.4	1	0.4	32	1.0
ancient murrelet	*Synthliboramphus antiquus*			5	0.4			5	0.2
marbled murrelet	*Brachyramphus marmoratus*			1	0.1			1	< 0.1
crested auklet	*Aethia cristatella*	1	0.1	14	1.2			15	0.5
least auklet	*Aethia pusilla*	30	1.6	52	4.4			82	2.5
parakeet auklet	*Aethia psittacula*	49	2.6	36	3			85	2.6
unid. auklet	*Aethia* spp.	14	0.7	4	0.3			18	0.5
horned puffin	*Fratercula corniculata*	20	1.1	19	1.6	2	0.8	41	1.2
tufted puffin	*Fratercula cirrhata*	97	5.2	15	1.3	1	0.4	113	3.4
unid. alcid	*Alcid* spp.	1	0.1	3	0.3			4	0.1
Passerine spp.	*Passeriformes* spp.			1	0.1			1	< 0.1
unid. bird.	*Aves* spp.	1	0.1					1	< 0.1
Total		1,871		1,187		25		3,310	

Table 14. -- Marine mammals recorded on and off transect during the northern Bering Sea surface trawl survey, 2019.

Common Name	Scientific Name	Southern Bering Sea	Northern Bering Sea	Total
Dall's porpoise	*Phocoenoides dalli*	2	9	11
fin whale	*Balaenoptera physalus*		2	2
harbor seal	*Phoca vitulina*	1		1
humpback whale	*Megaptera novaeangliae*		20	20
killer whale	*Orcinus orca*		3	3
northern fur seal	*Callorhinus ursinus*	2	24	26
unidentified whale	*Cetacea* spp.		2	2
Total		5	60	65

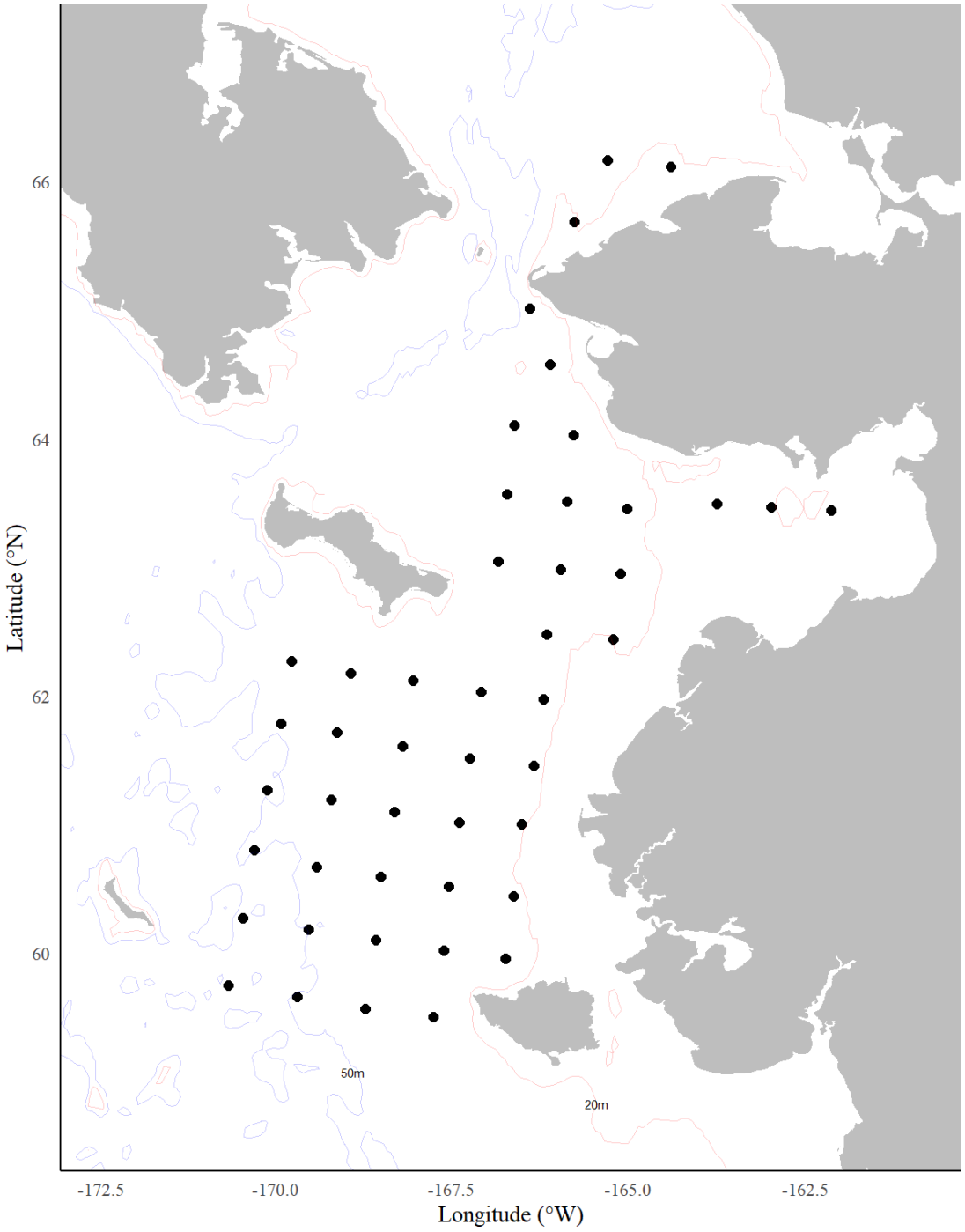

Figure 1. – Map of stations sampled during the northern Bering Sea surface trawl and ecosystem survey, 2019.

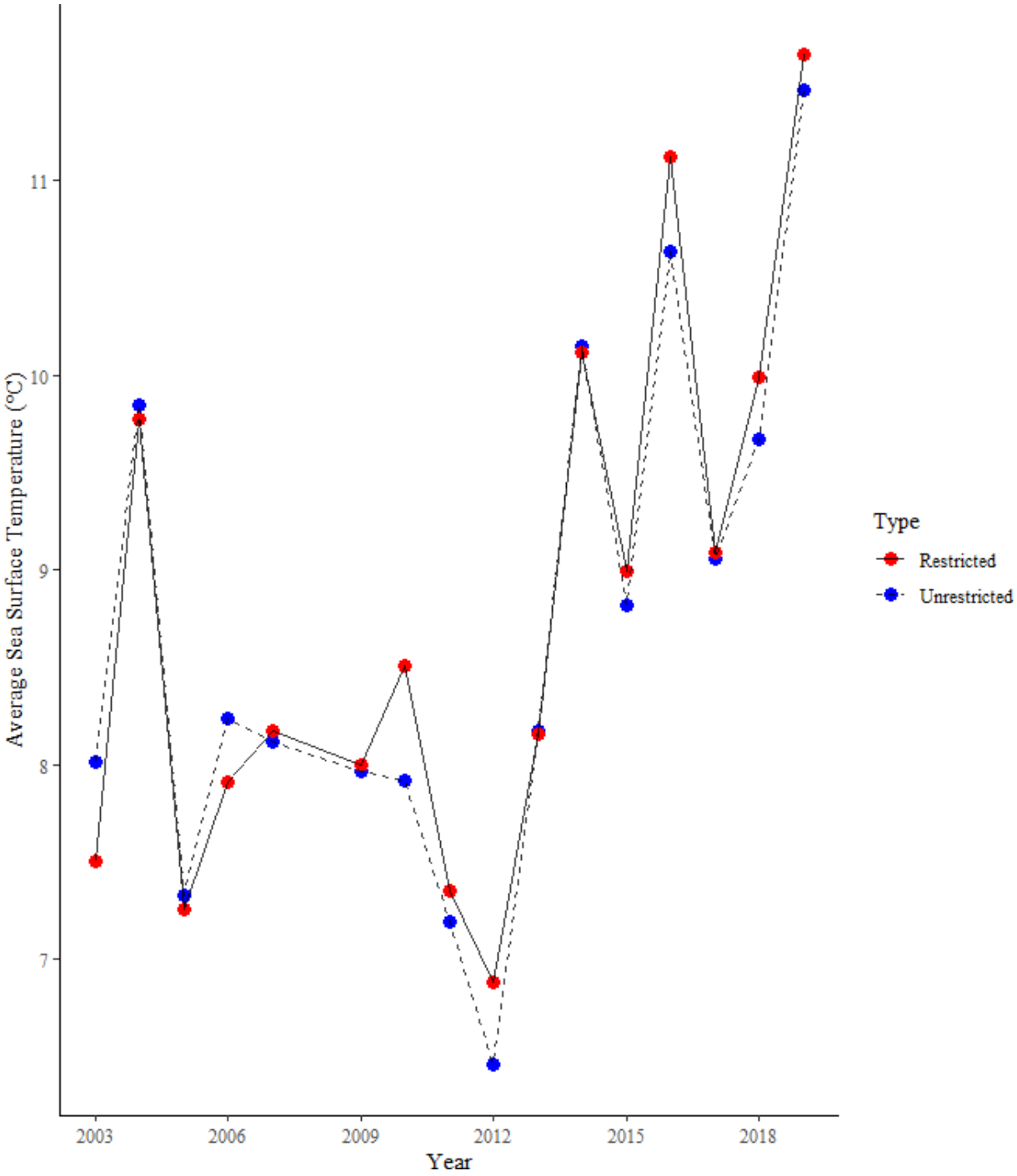

Figure 2. -- Average annual sea surface temperature (top 10 m of the water column) from CTD data collected during the northern Bering Sea surface trawl surveys, 2003-2019.

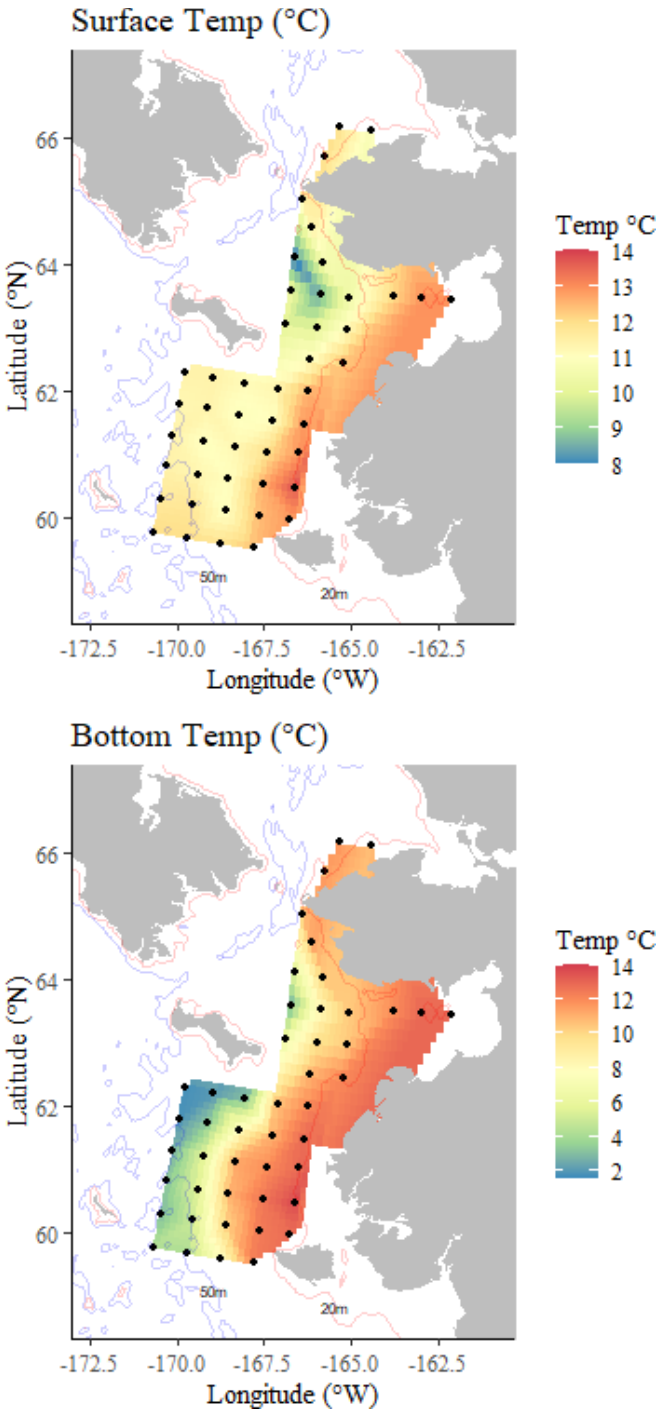

Figure 3. -- Interpolated map of surface (upper 10m) and bottom (deepest depth sampled) temperature (°C) from CTD data collected during the northern Bering Sea surface trawl survey, 2019.

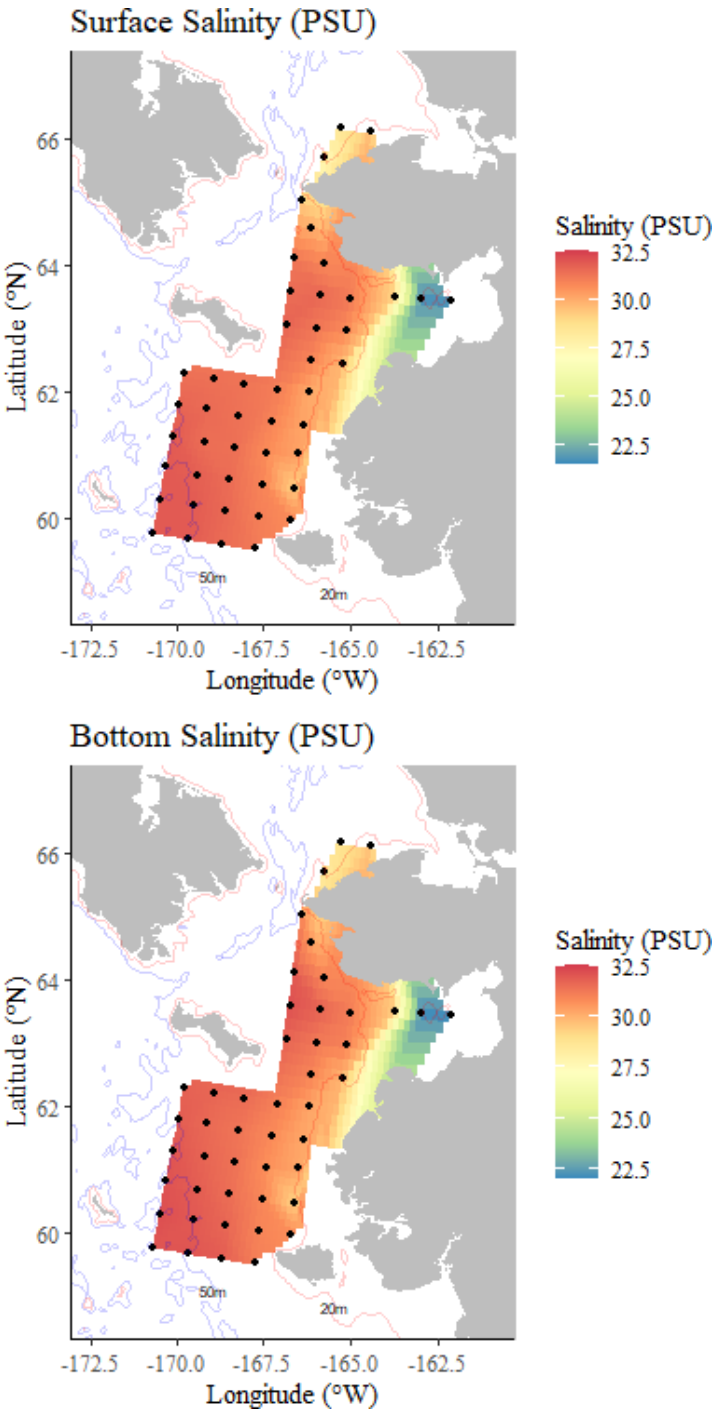

Figure 4. -- Interpolated map of surface (upper 10m) and bottom (deepest depth sampled) salinity (PSU) from CTD data collected during the northern Bering Sea surface trawl survey, 2019.

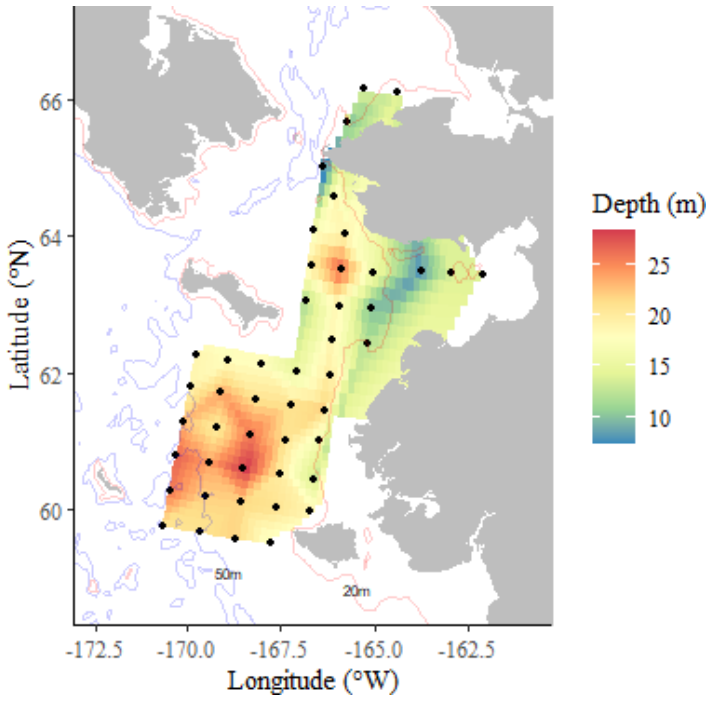

Figure 5. -- Interpolated map of mixed layer depth (m) from CTD data collected during the northern Bering Sea surface trawl survey, 2019.

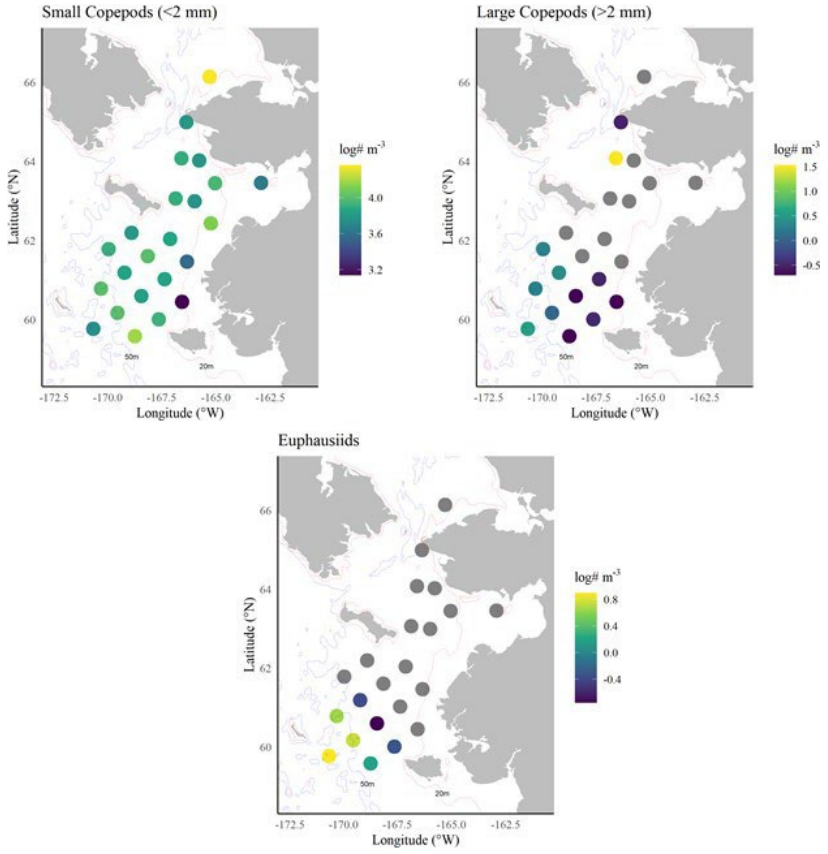

Figure 6. – Distribution of small copepods, large copepods, and euphausiids determined by rapid zooplankton assessment methods during the northern Bering Sea surface trawl survey, 2019.

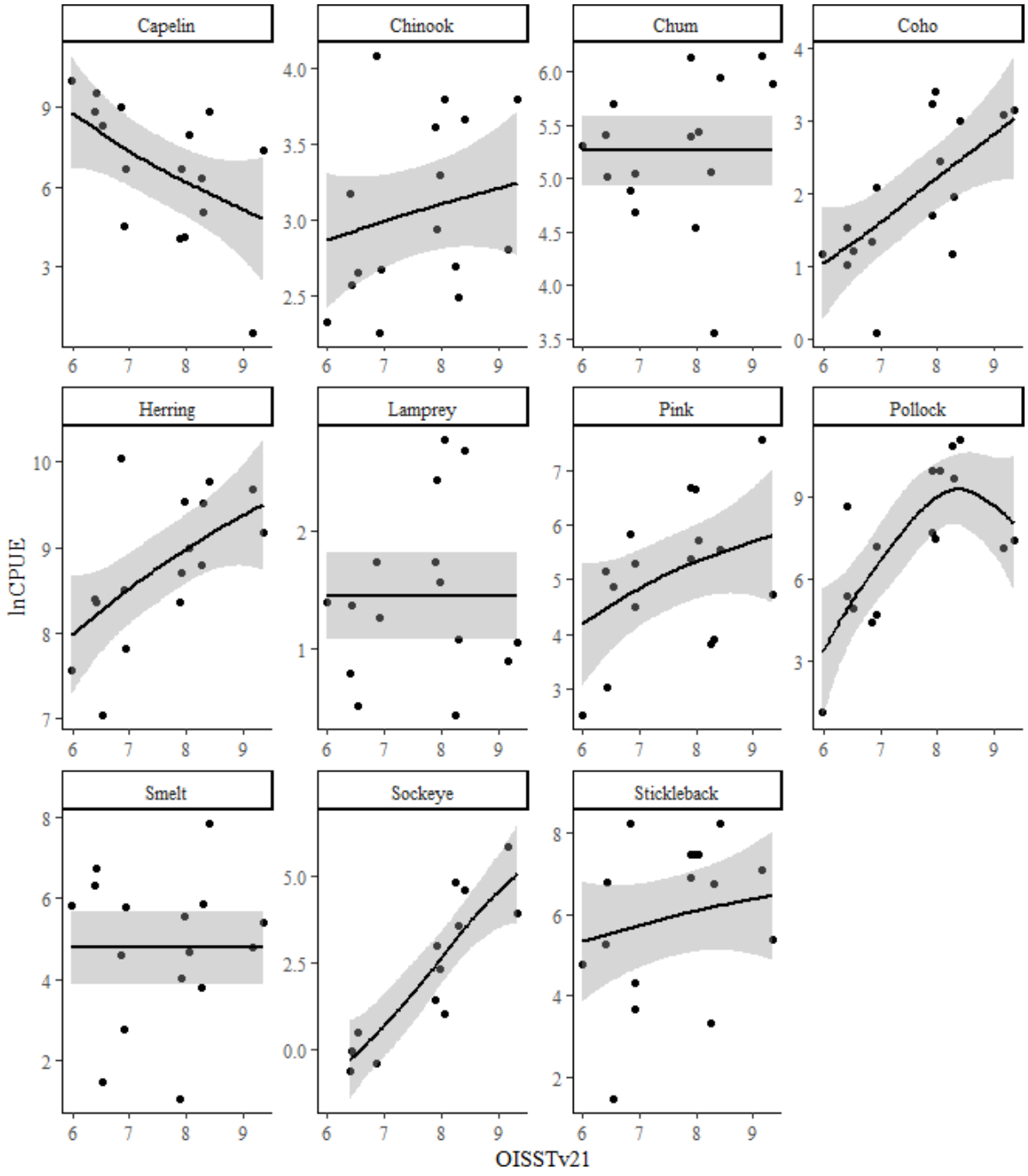

Figure 7. -- General additive model fits (black lines) with 95% confidence intervals (shaded regions) between average summer sea surface temperatures in the northern Bering Sea (OISSTv2.1) and catch rates (lnCPUE) of the primary fish species captured during the northern Bering Sea surface trawl surveys, 2003-2019.

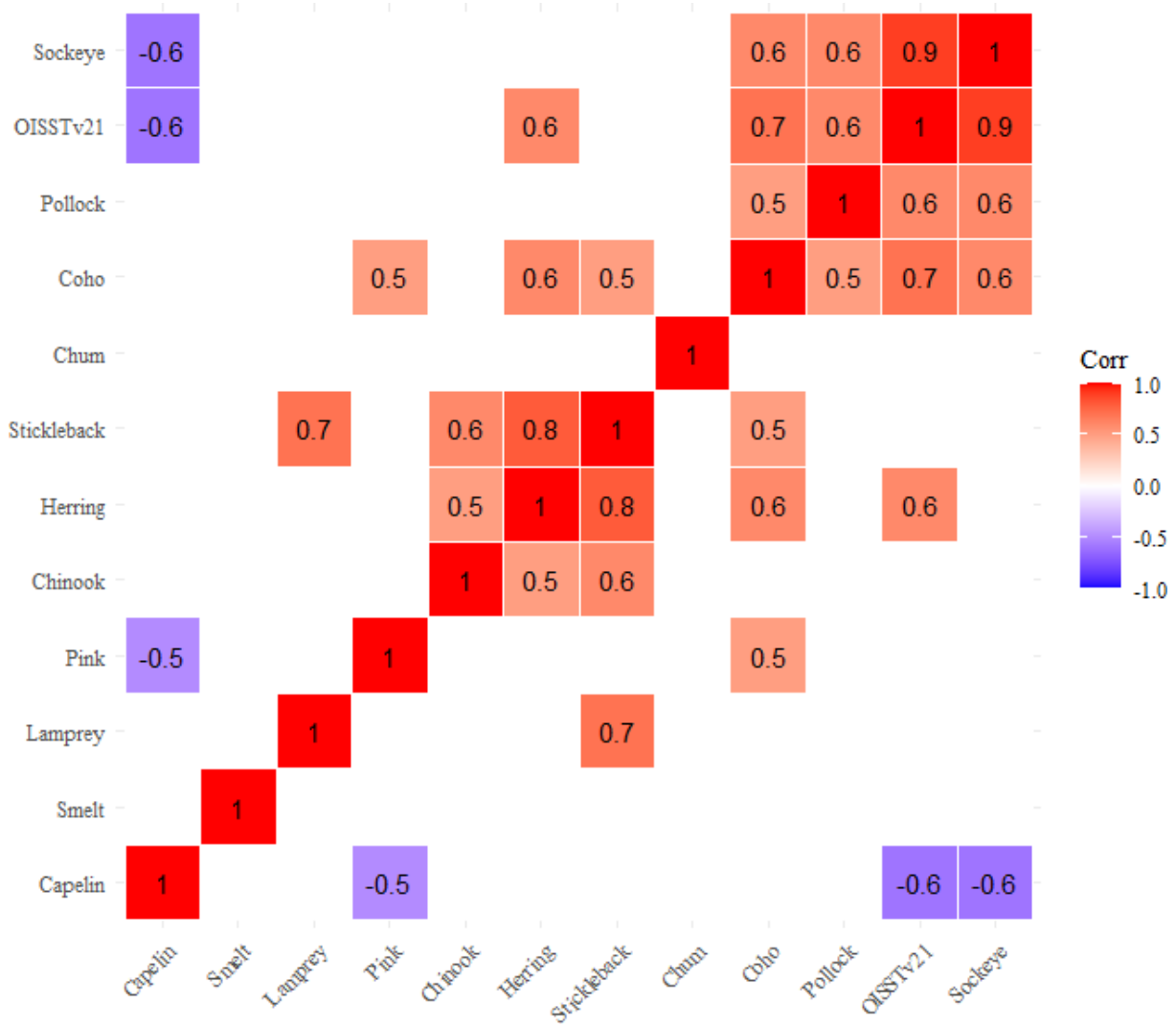

Figure 8. -- Significant correlations (Corr) between average catch rate (ln(CPUE)) of primary species captured during the northern Bering Sea surface trawl surveys and sea surface temperature data (OISSTv2.1), 2003-2019.

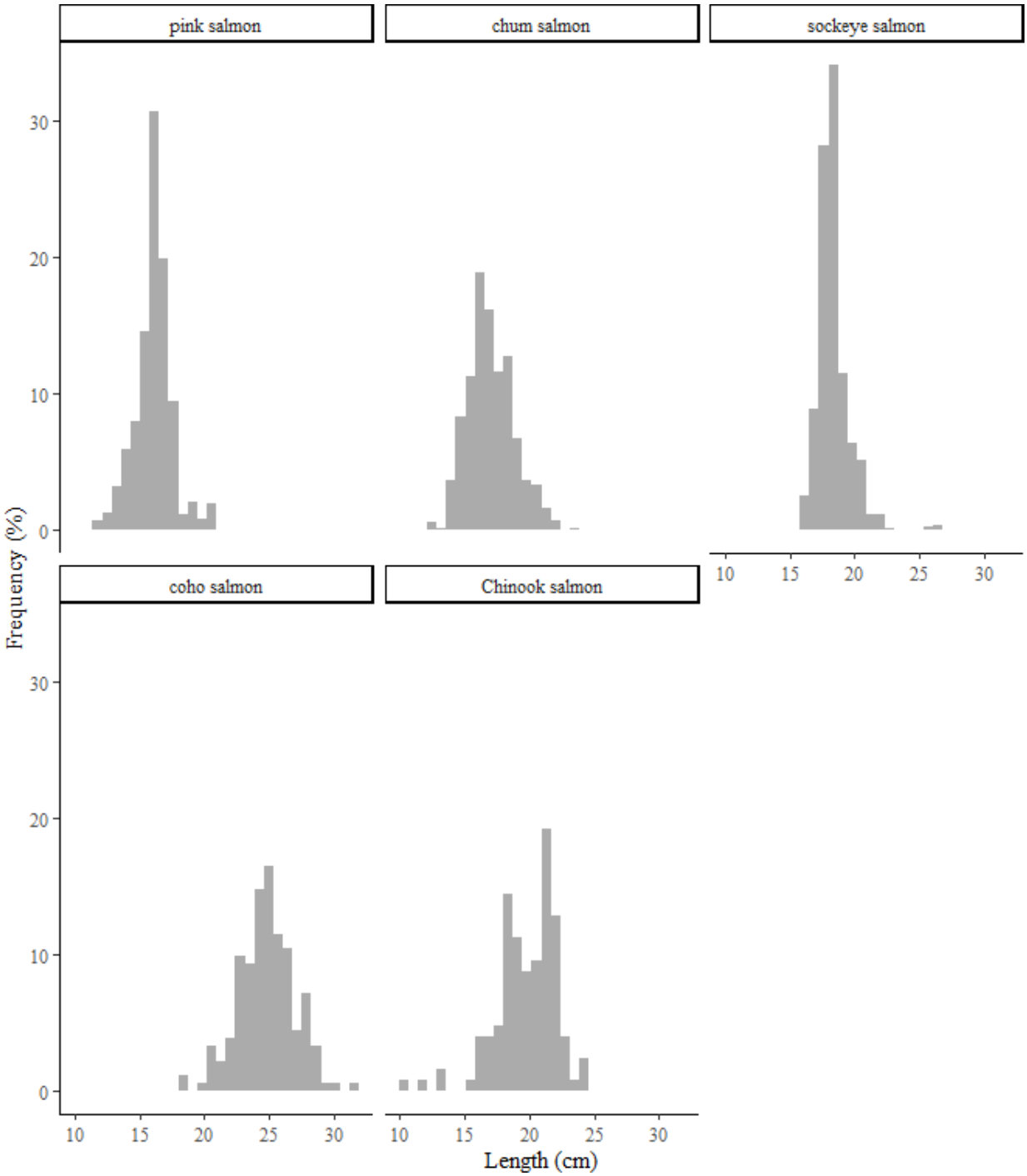

Figure 9. -- Length frequency distributions of juvenile salmon species captured during the northern Bering Sea surface trawl survey, 2019.

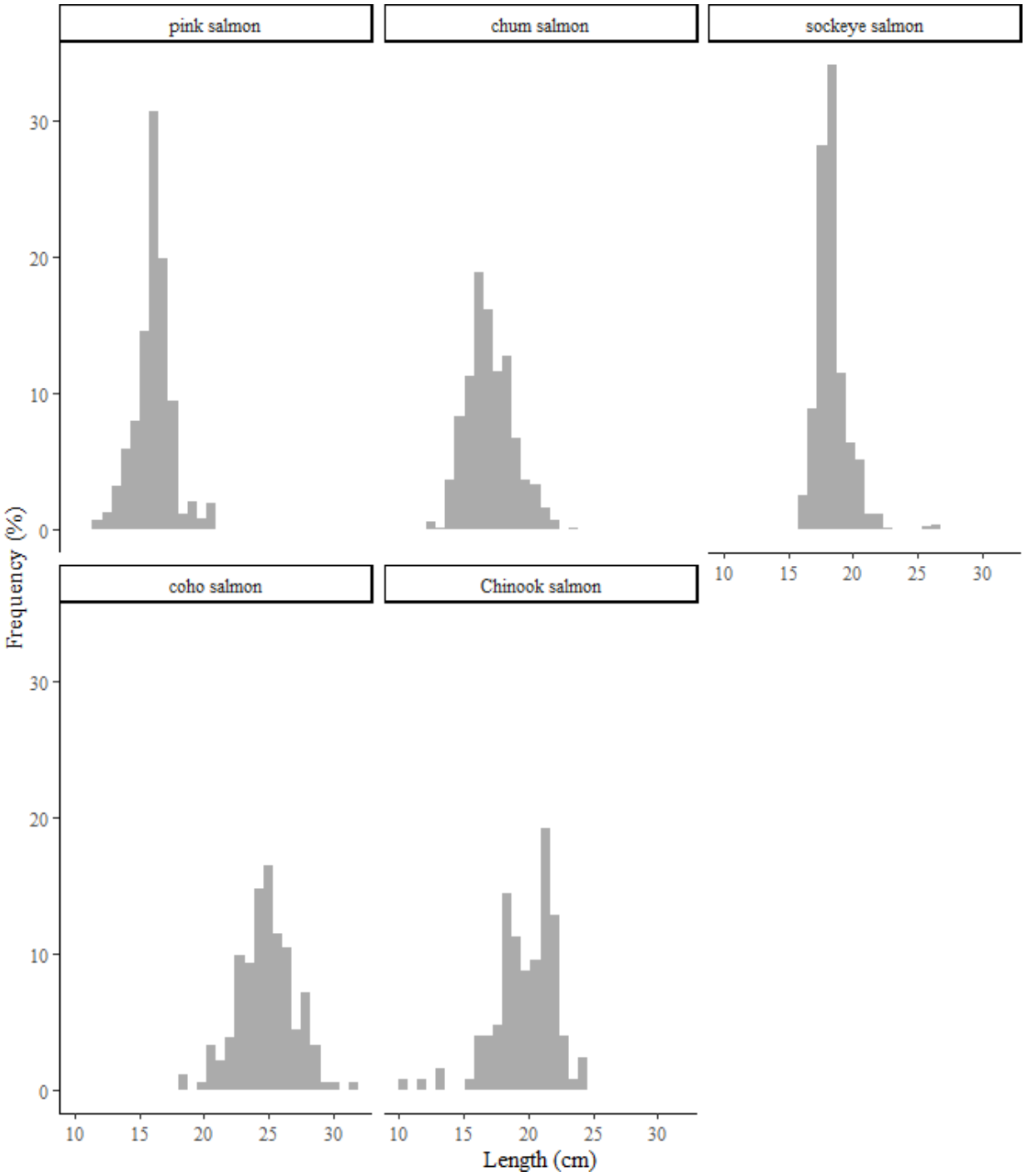

Figure 10. -- Length frequency distributions of immature salmon species captured during the northern Bering Sea surface trawl survey, 2019.

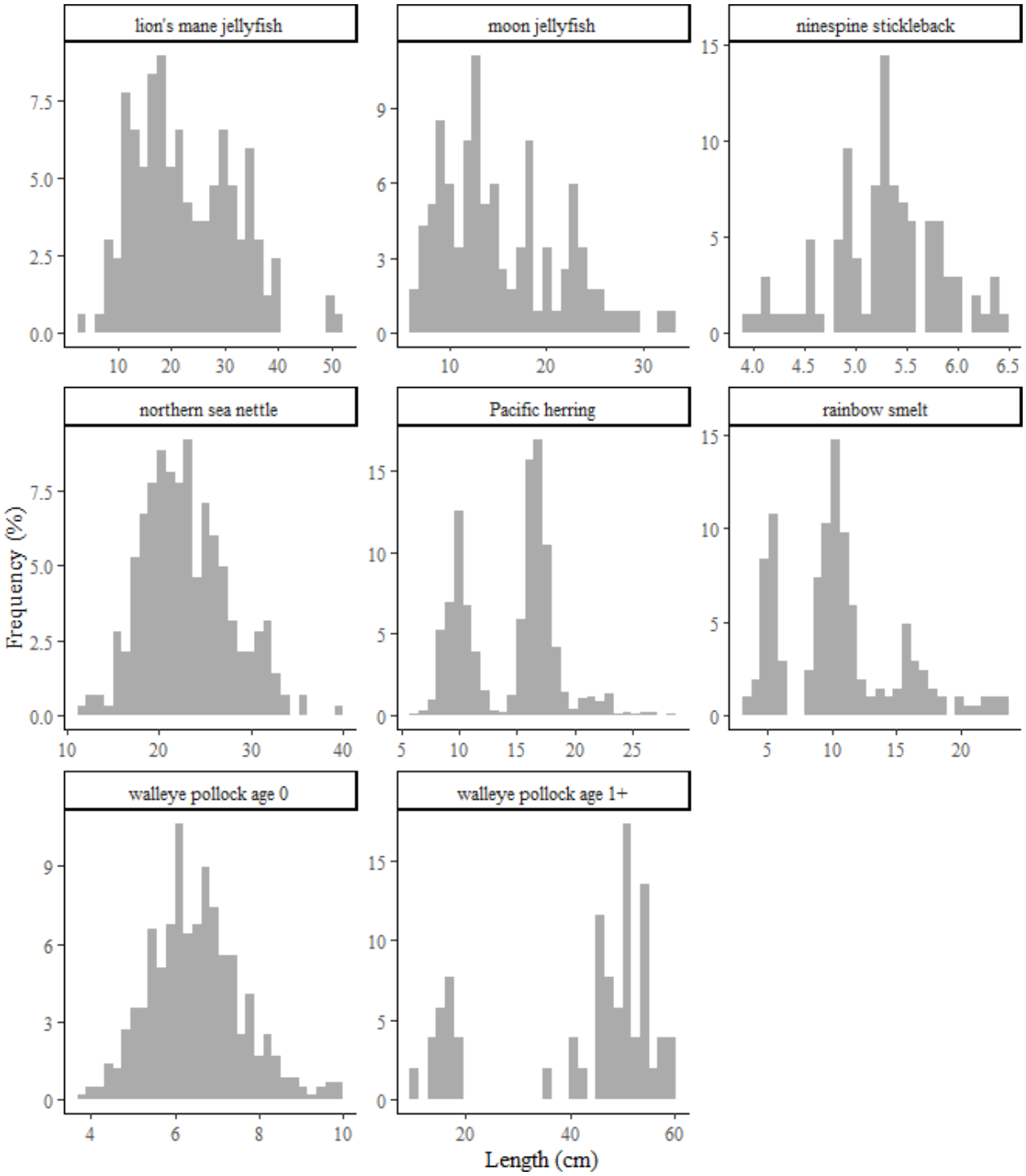

Figure 11. -- Length frequency distributions of the most abundant non-salmon species captured during the northern Bering Sea surface trawl survey, 2019.

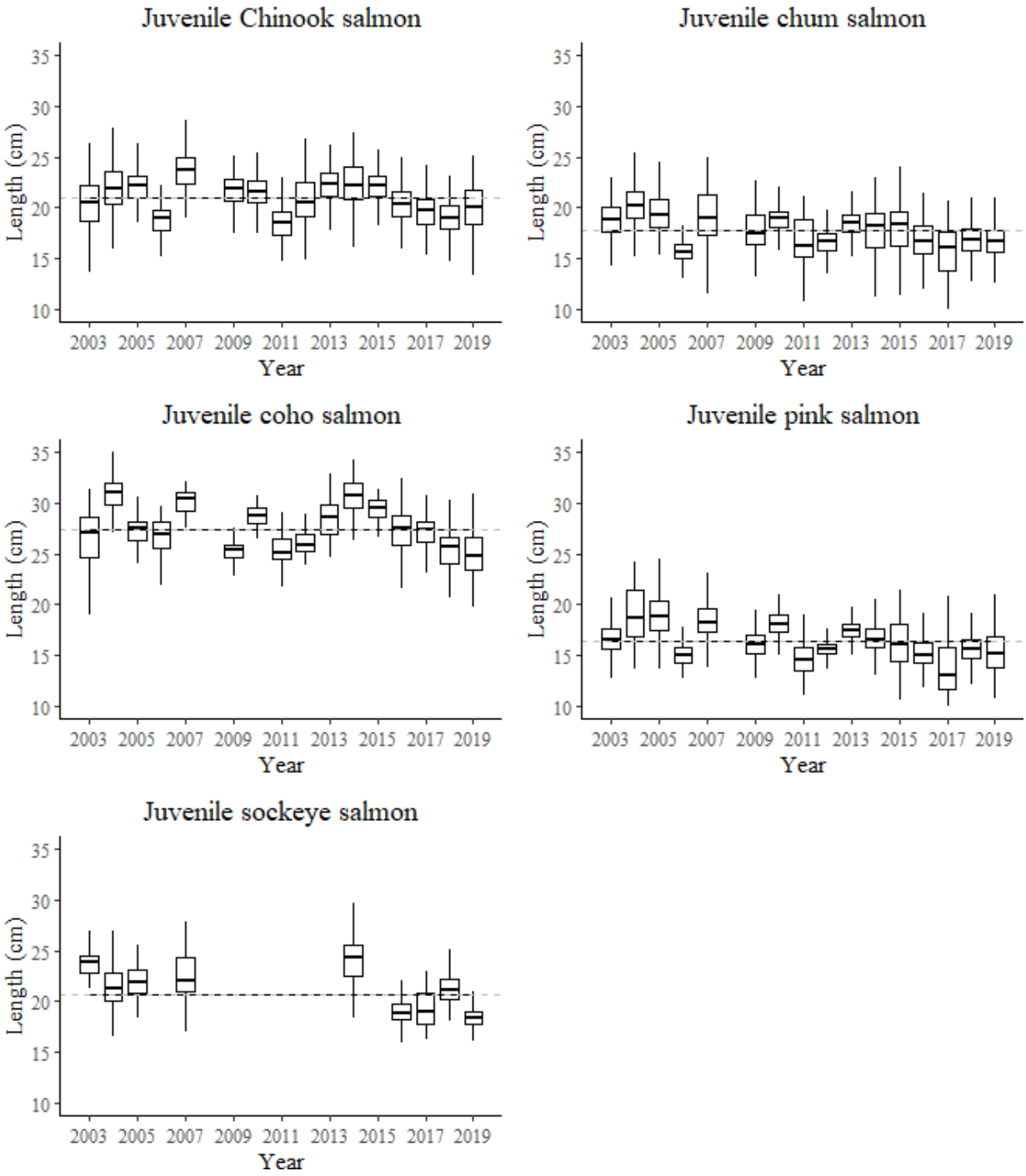

Figure 12. -- Box plots of juvenile salmon fork lengths (cm) sampled during the northern Bering Sea surveys, 2003-2019. The dashed line is the mean length across all years. Sockeye salmon lengths were limited to years where at least 20 lengths were measured.

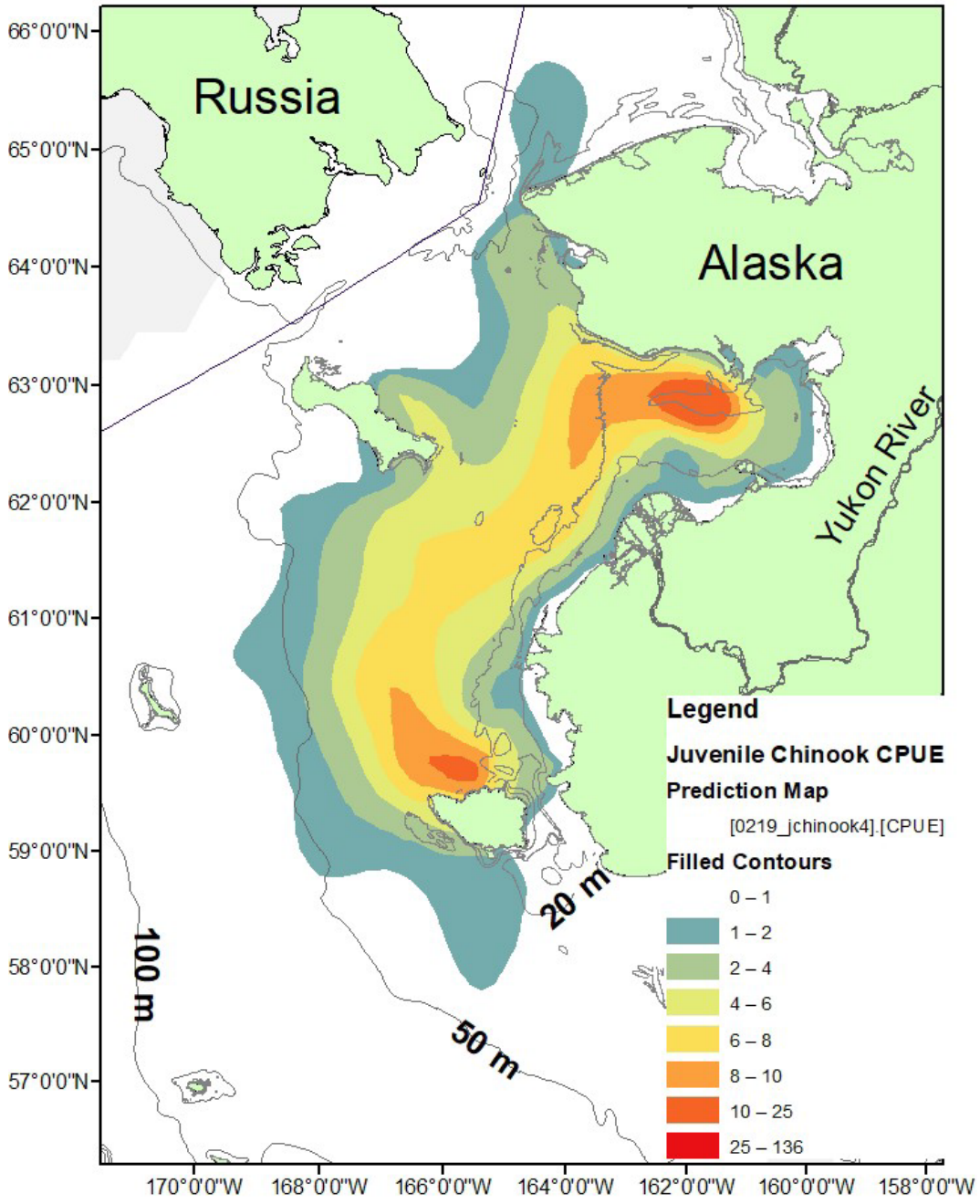

Figure 13. -- A kriging predicted surface of juvenile Chinook salmon catch rates during the northern Bering Sea surface trawl survey, 2003-2019.

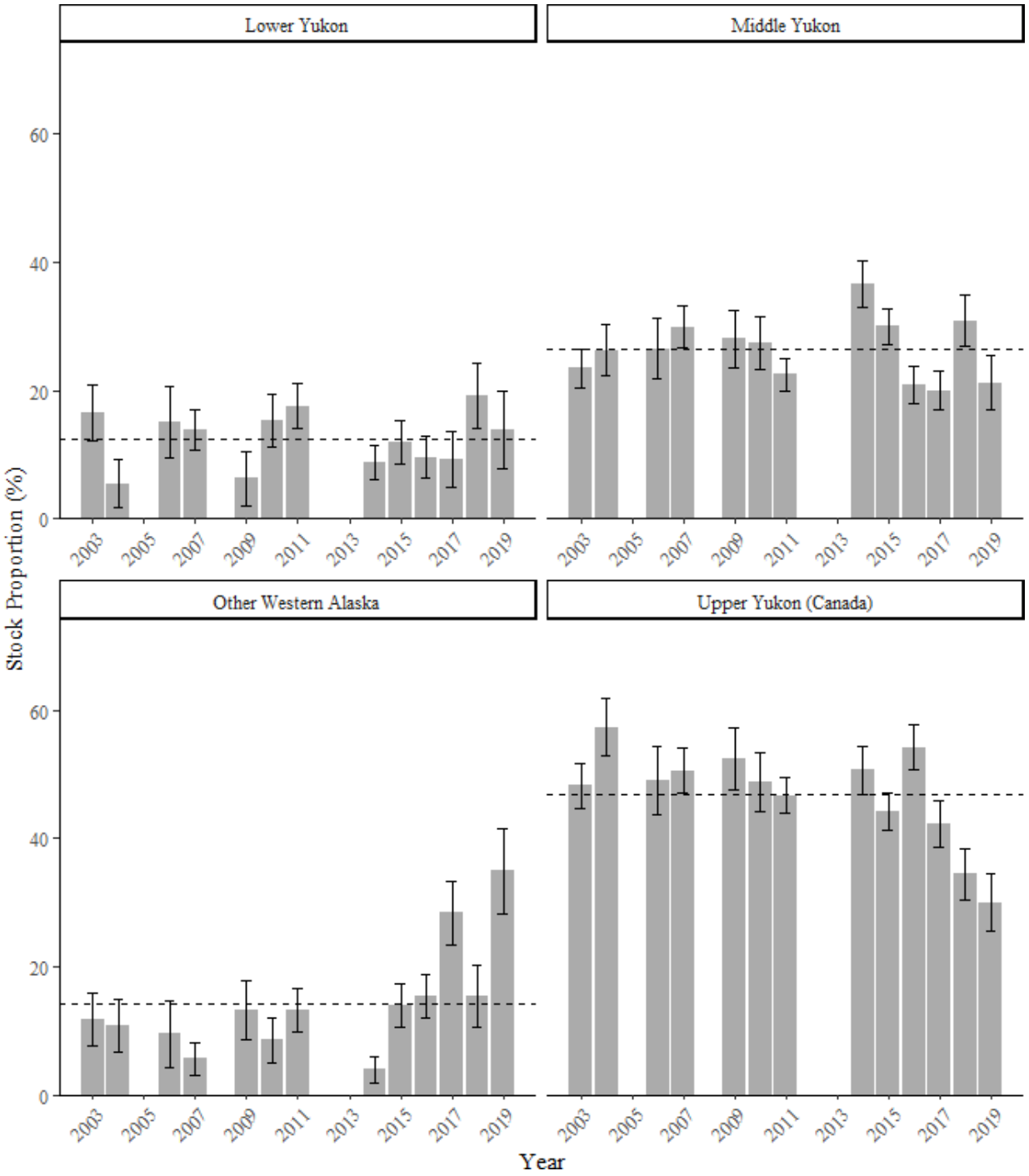

Figure 14. -- Genetic stock proportions of juvenile Chinook salmon captured during the northern Bering Sea surface trawl surveys, 2003-2019. Average stock proportions (dashed line) are included for each stock group.

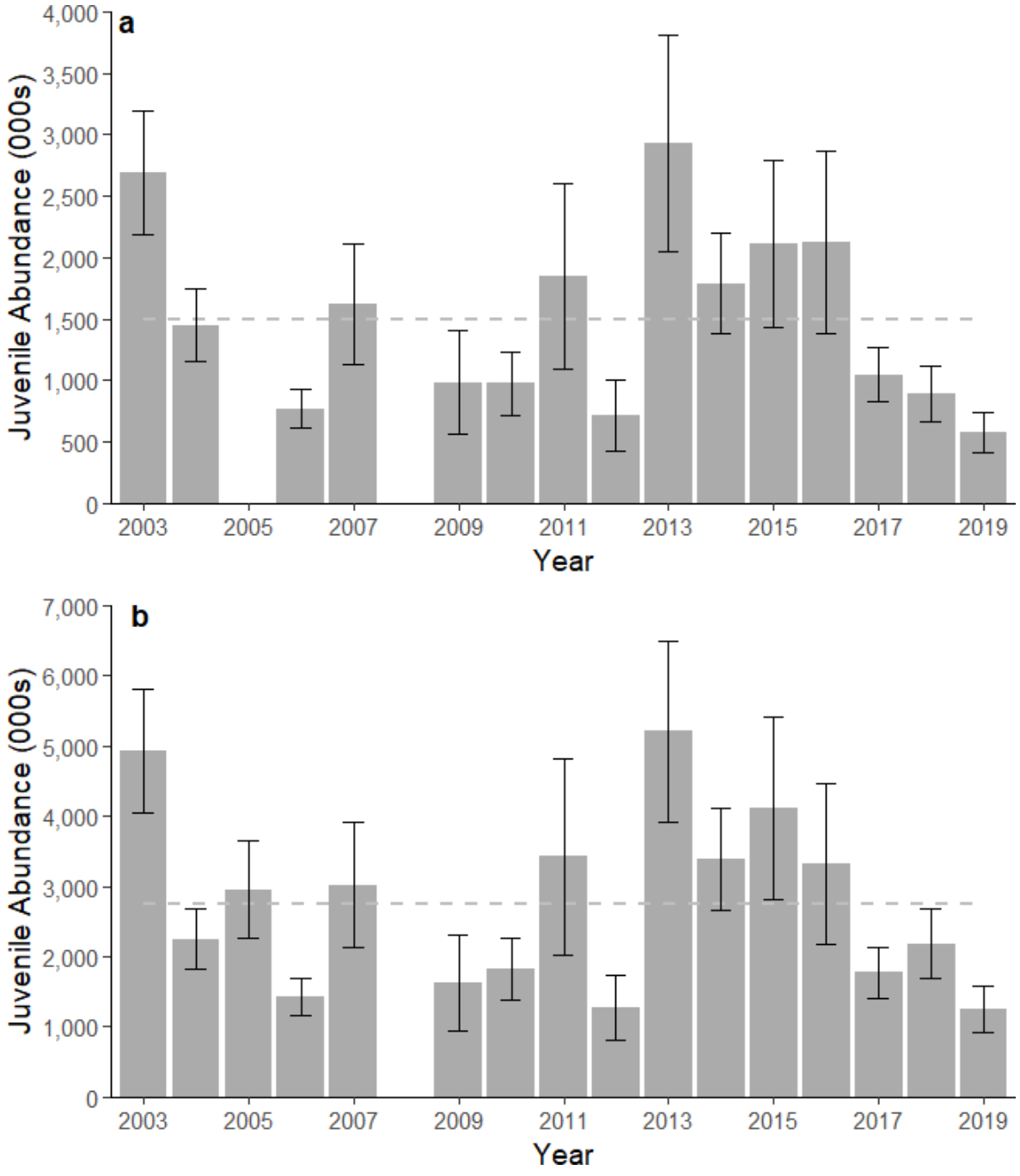

Figure 15. -- Stock-specific abundance estimates of Yukon River Canadian-origin (a) and Total Yukon (b) stock groups of Chinook salmon during the northern Bering Sea surface trawl surveys, 2003-2019. Average abundance for each stock group (solid line) is included.

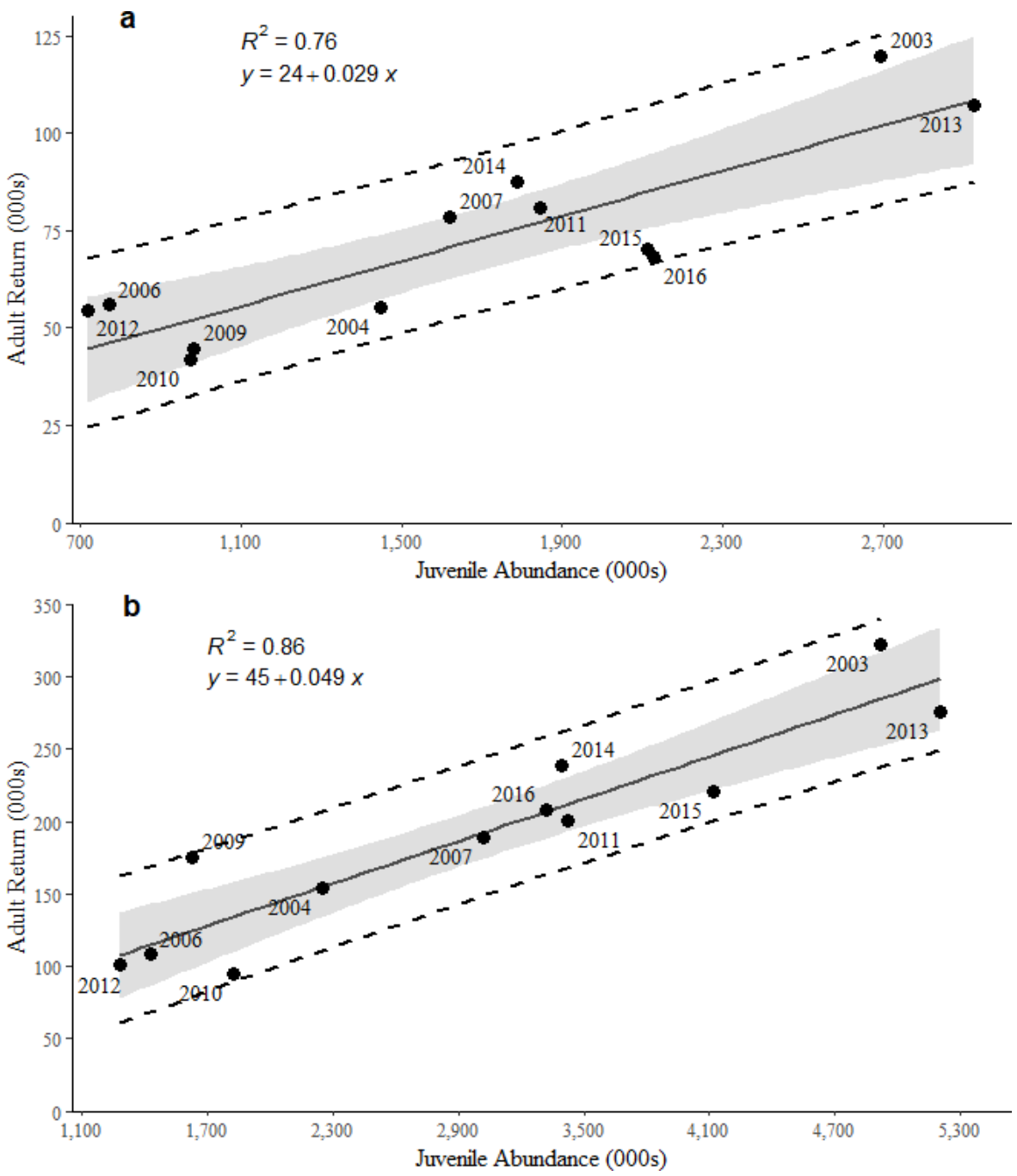

Figure 16. -- Relationships between juvenile abundance and resulting adult returns of Yukon River Canadian-origin (a) and Total Yukon (b) stock groups of Chinook salmon, 2003-2016. The fitted relationship (solid line), 80% prediction interval (dashed lines), 80% confidence interval (shaded region), and survey years (labels) are included.

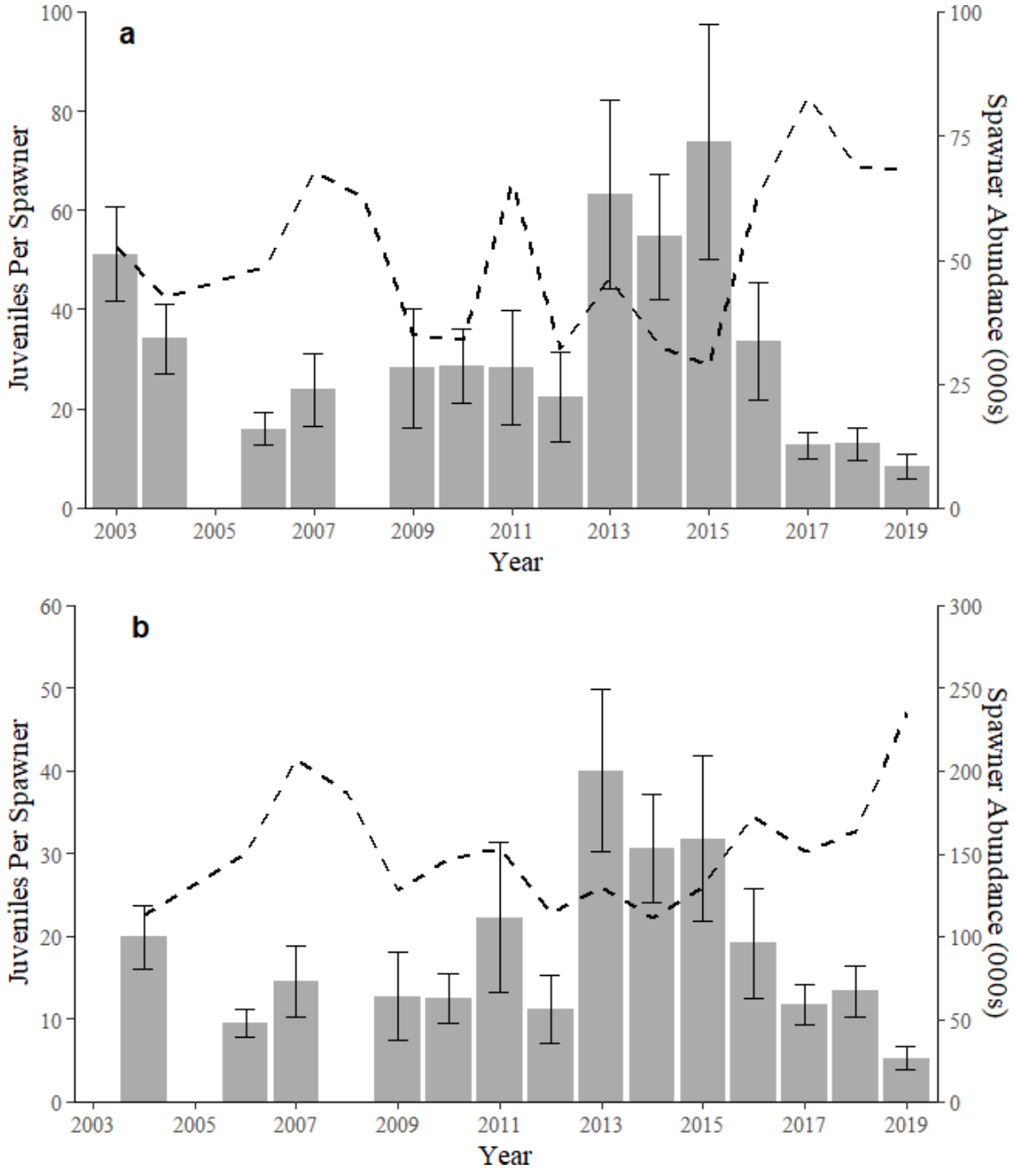

Figure 17. -- The number of juveniles-per-spawner (gray bars) and spawner abundance (dashed line) for the Yukon River Canadian-origin (a) and Total Yukon (b) stock groups of Chinook salmon, 2003-2019.

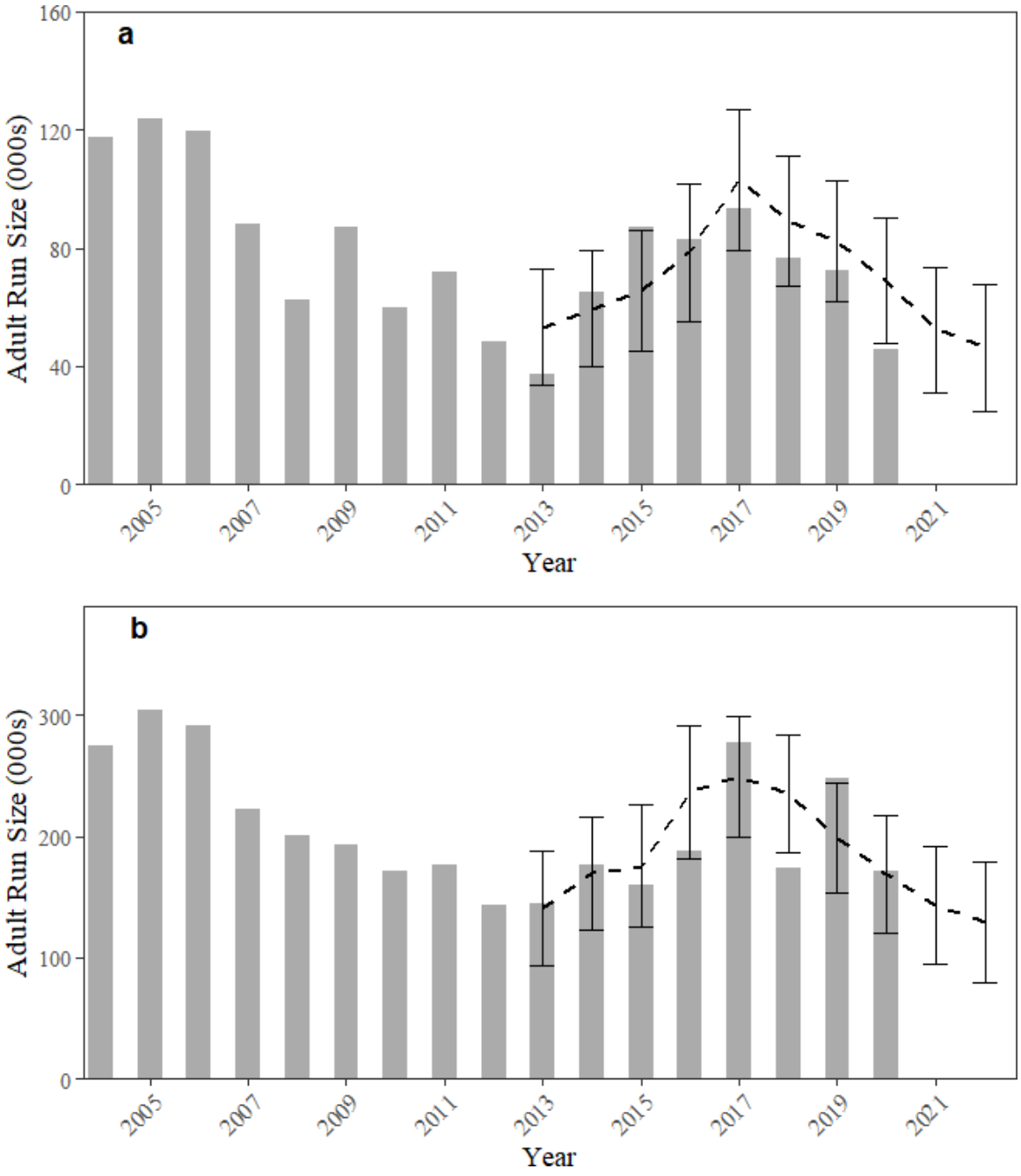

Figure 18. -- Observed (gray bars) and 80% predicted intervals of projected run sizes (black error bars) for the Yukon River Canadian-origin (a) and Total Yukon (b) stock groups of Chinook salmon, 2003-2022.

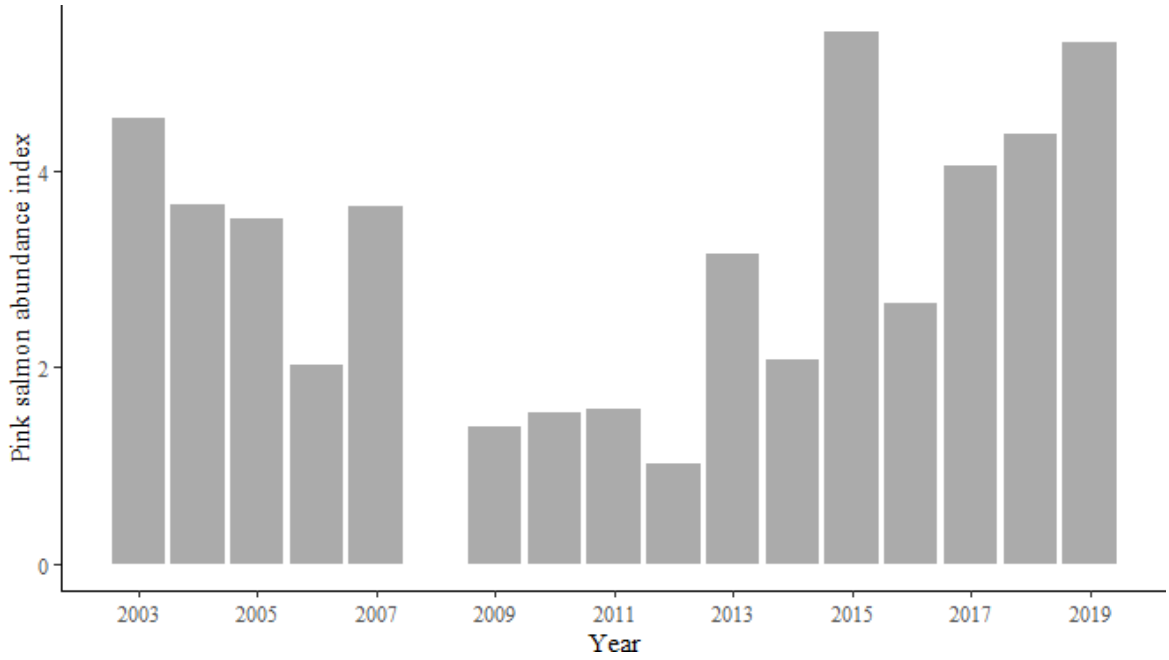

Figure 19. -- The juvenile pink salmon abundance index from the northern Bering Sea surface trawl surveys, 2003-2019.

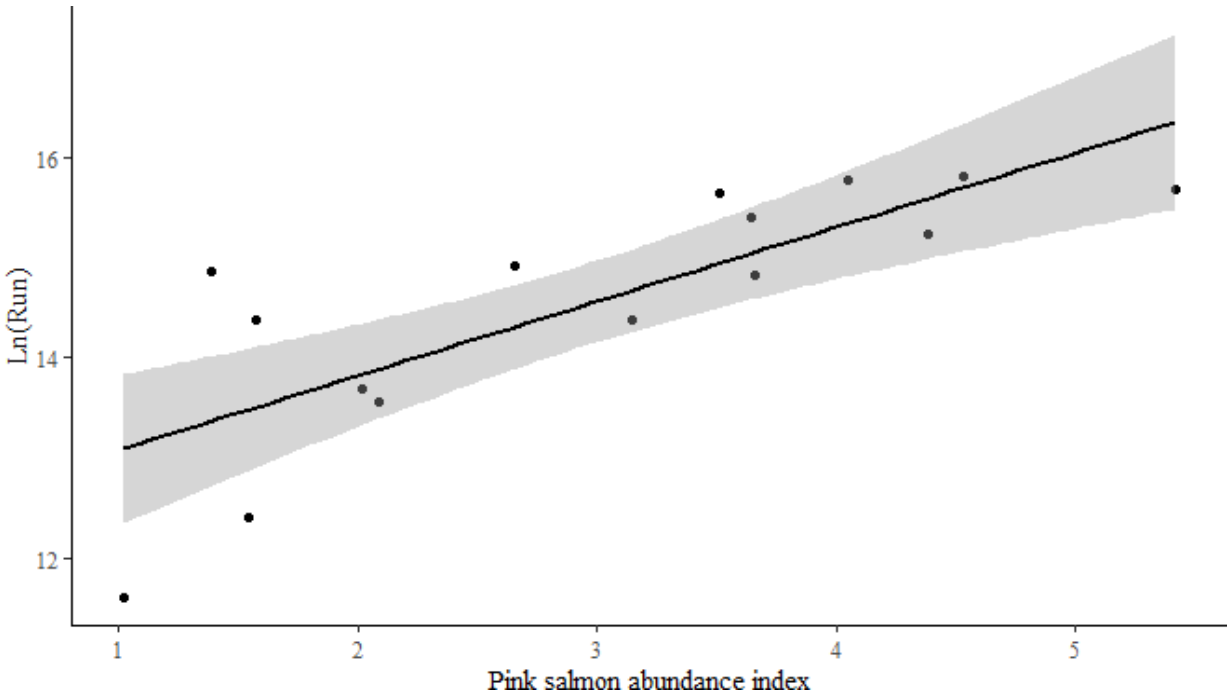

Figure 20. -- A linear regression model fit (black line) with 95% confidence interval (shaded region) between the juvenile pink salmon abundance index from the northern Bering Sea surface trawl surveys (black dots; 2003-2018) and the natural log of the adult pink salmon run index (Yukon River and Norton Sound; 2004-2019).

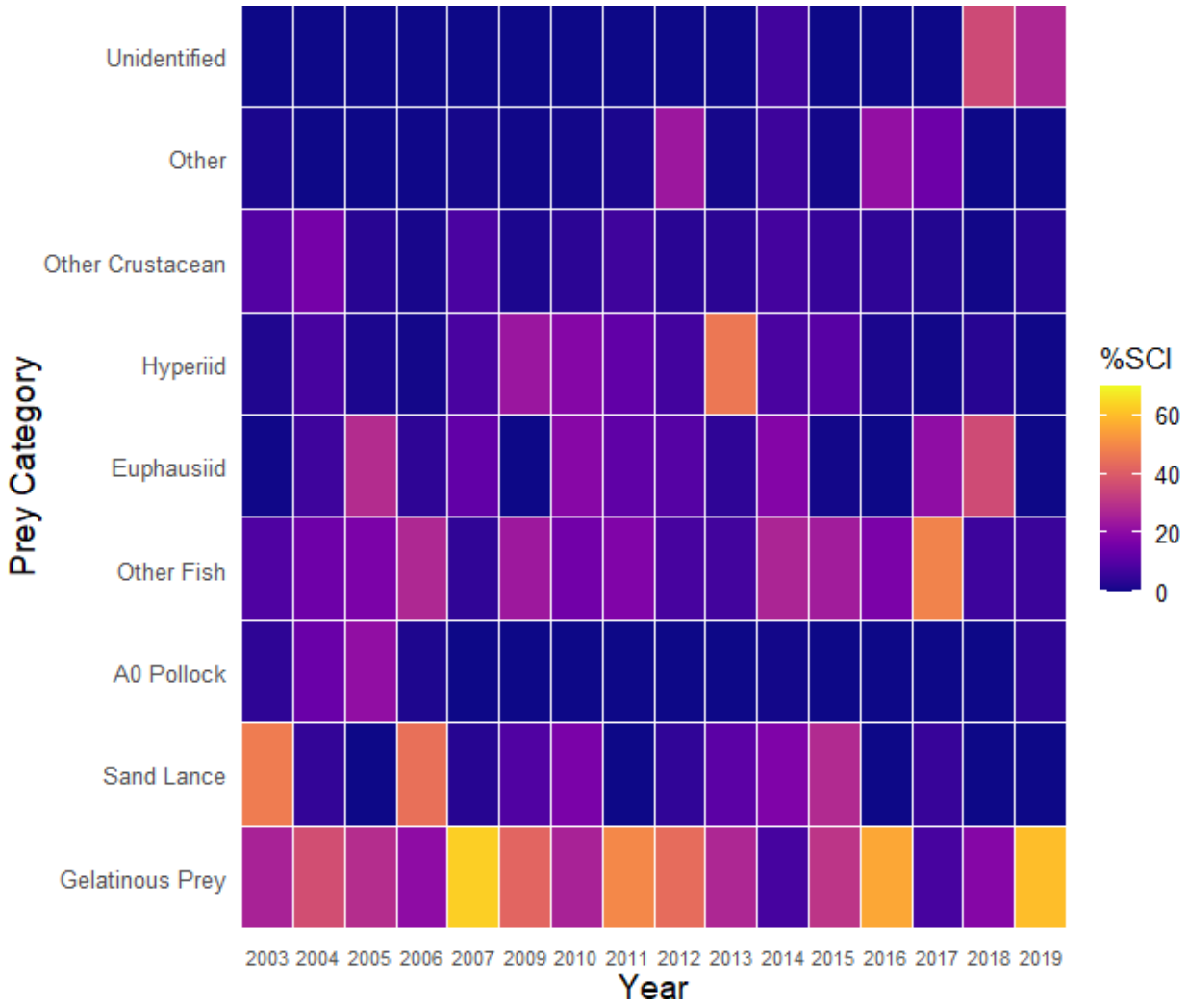

Figure 21. -- The percent of taxonomic prey groups by stomach content index in the stomachs of juvenile chum salmon sampled from the northern Bering Sea surface trawl surveys, 2003-2019.

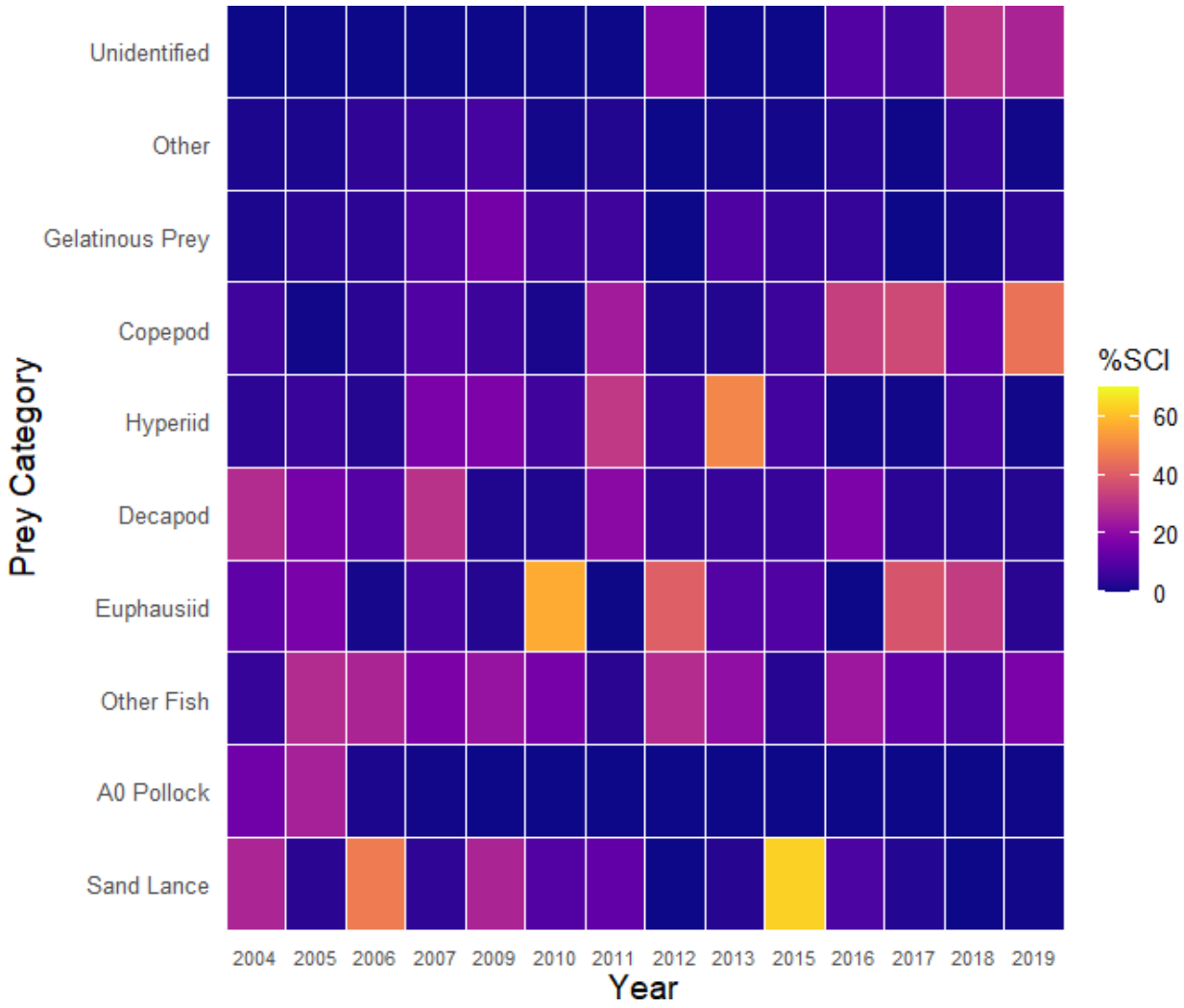

Figure 22. -- The percent of taxonomic prey groups by stomach content index in the stomachs of juvenile pink salmon sampled from the northern Bering Sea surface trawl surveys, 2003-2019.

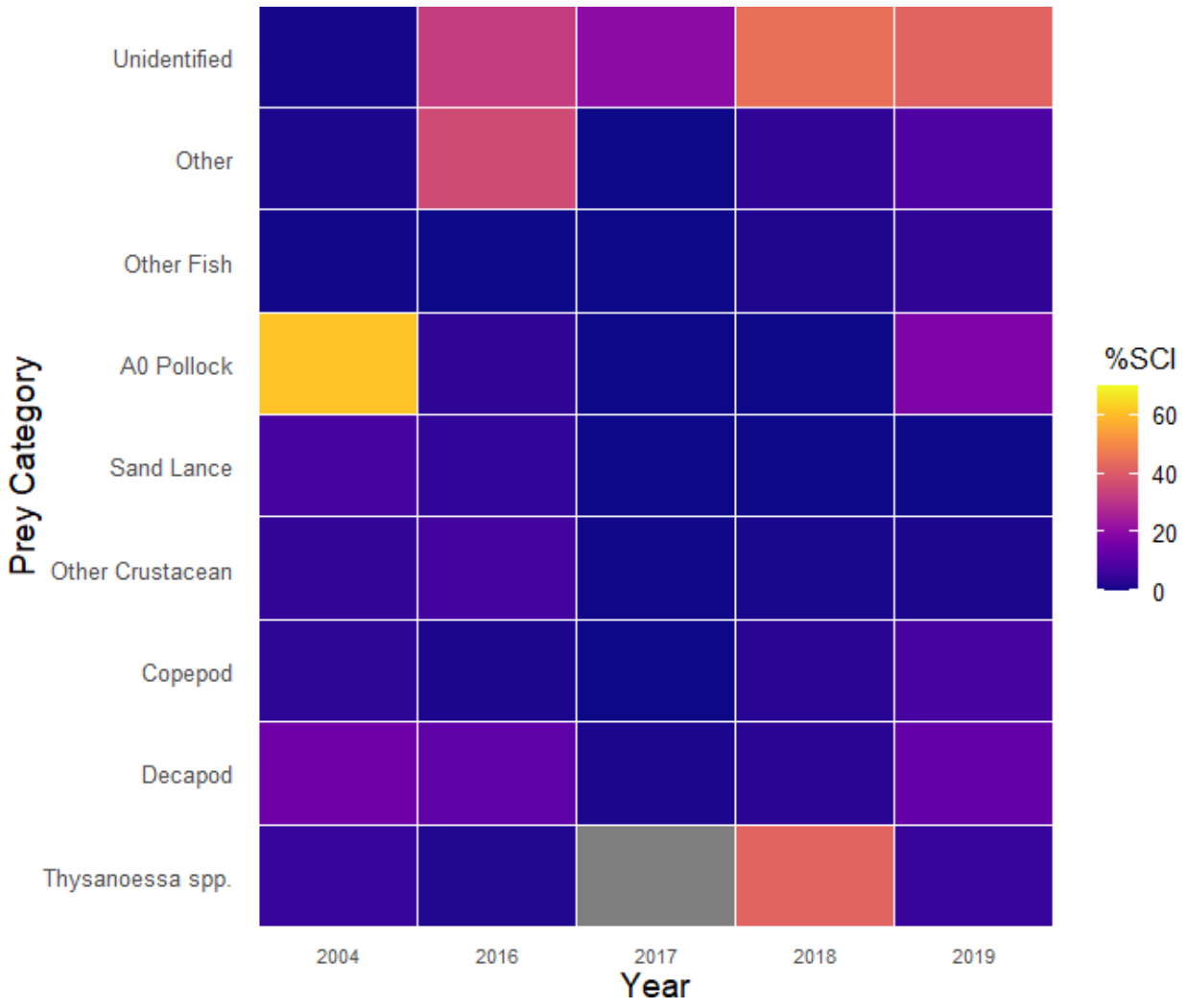

Figure 23. -- The percent of taxonomic prey groups by stomach content index in the stomachs of juvenile sockeye salmon sampled from the northern Bering Sea surface trawl surveys, 2003-2019.

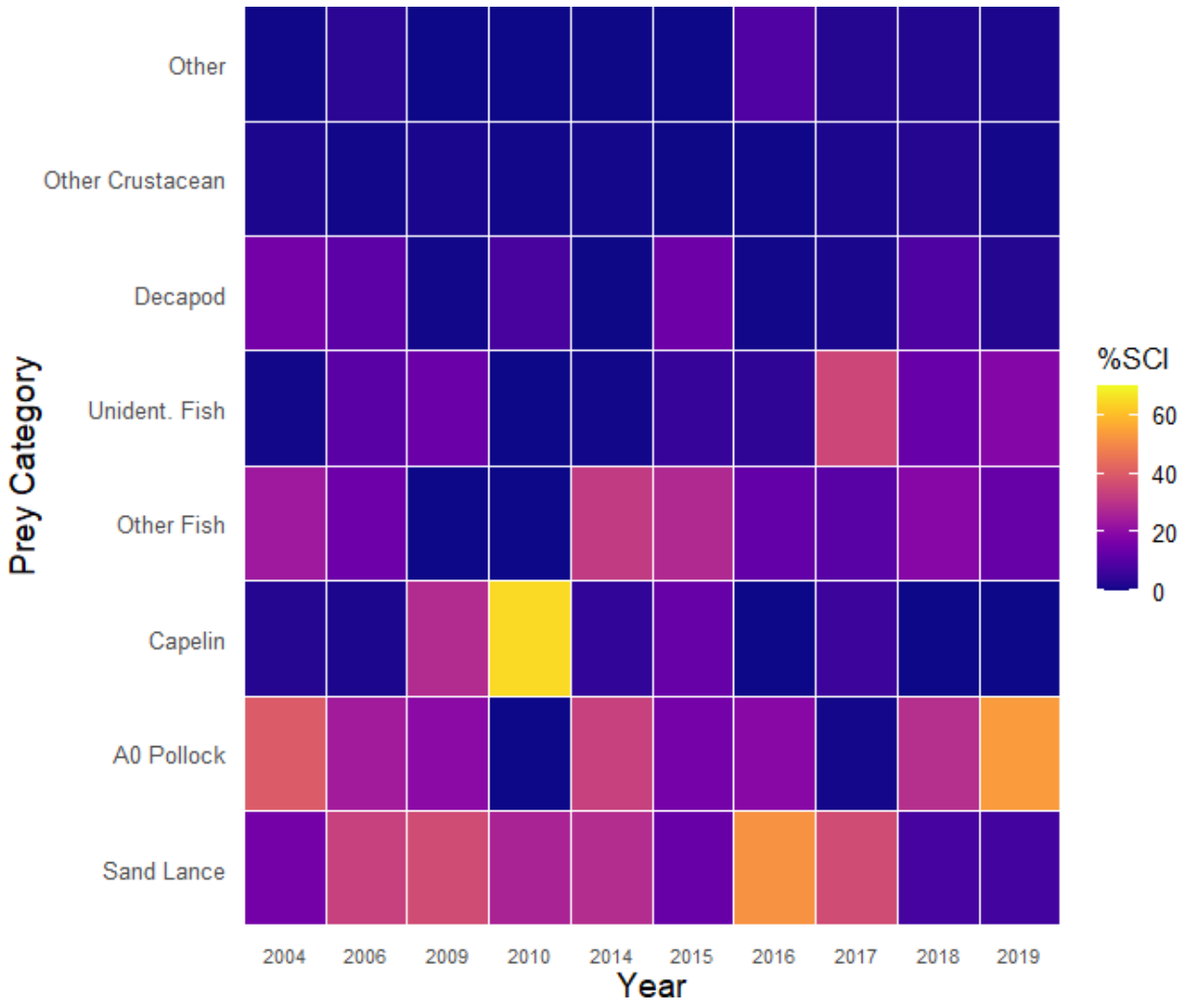

Figure 24. -- The percent of taxonomic prey groups by stomach content index in the stomachs of juvenile coho salmon sampled from the northern Bering Sea surface trawl surveys, 2003-2019.

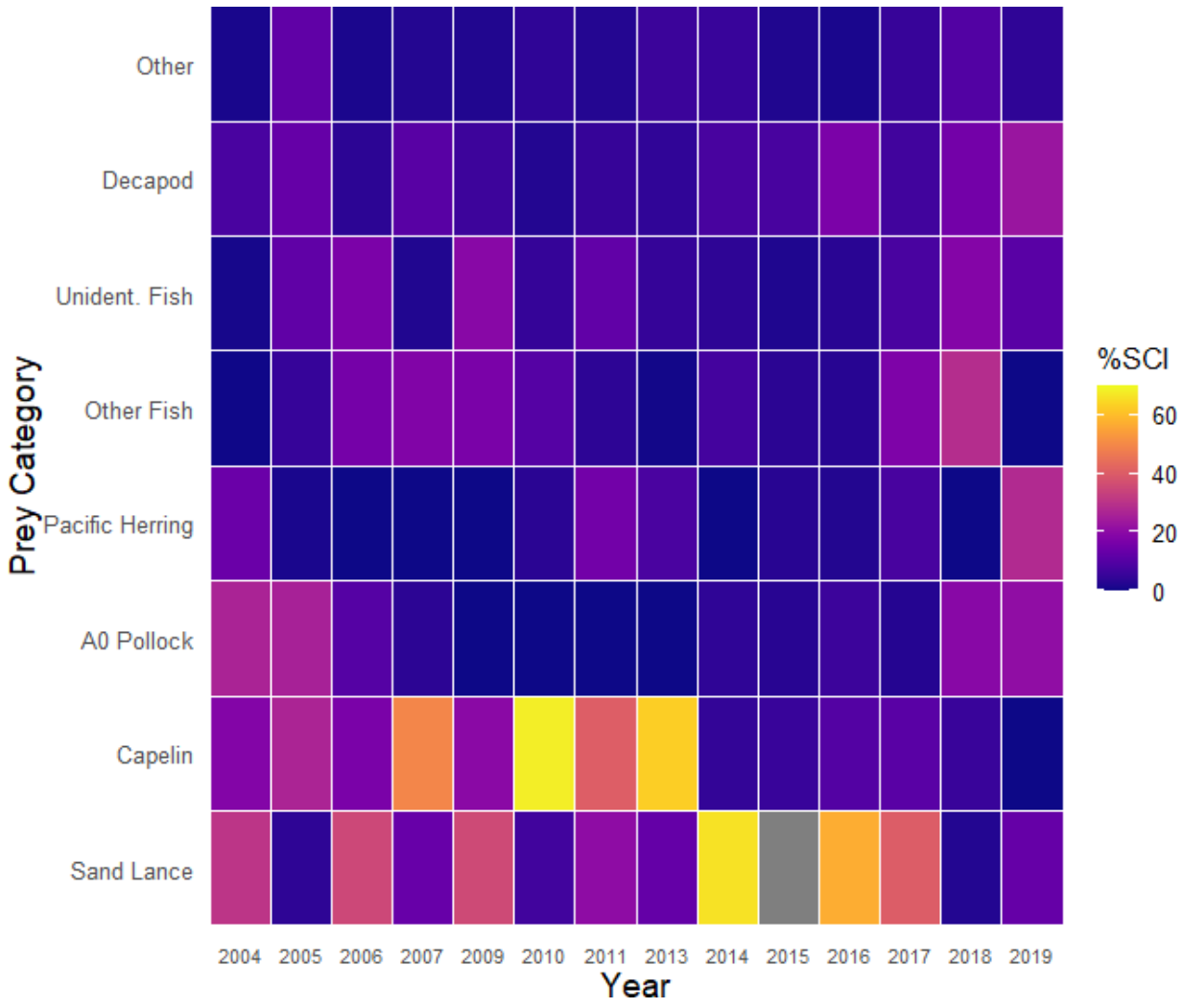

Figure 25. -- The percent of taxonomic prey groups by stomach content index in the stomachs of juvenile Chinook salmon sampled from the northern Bering Sea surface trawl surveys, 2003-2019.

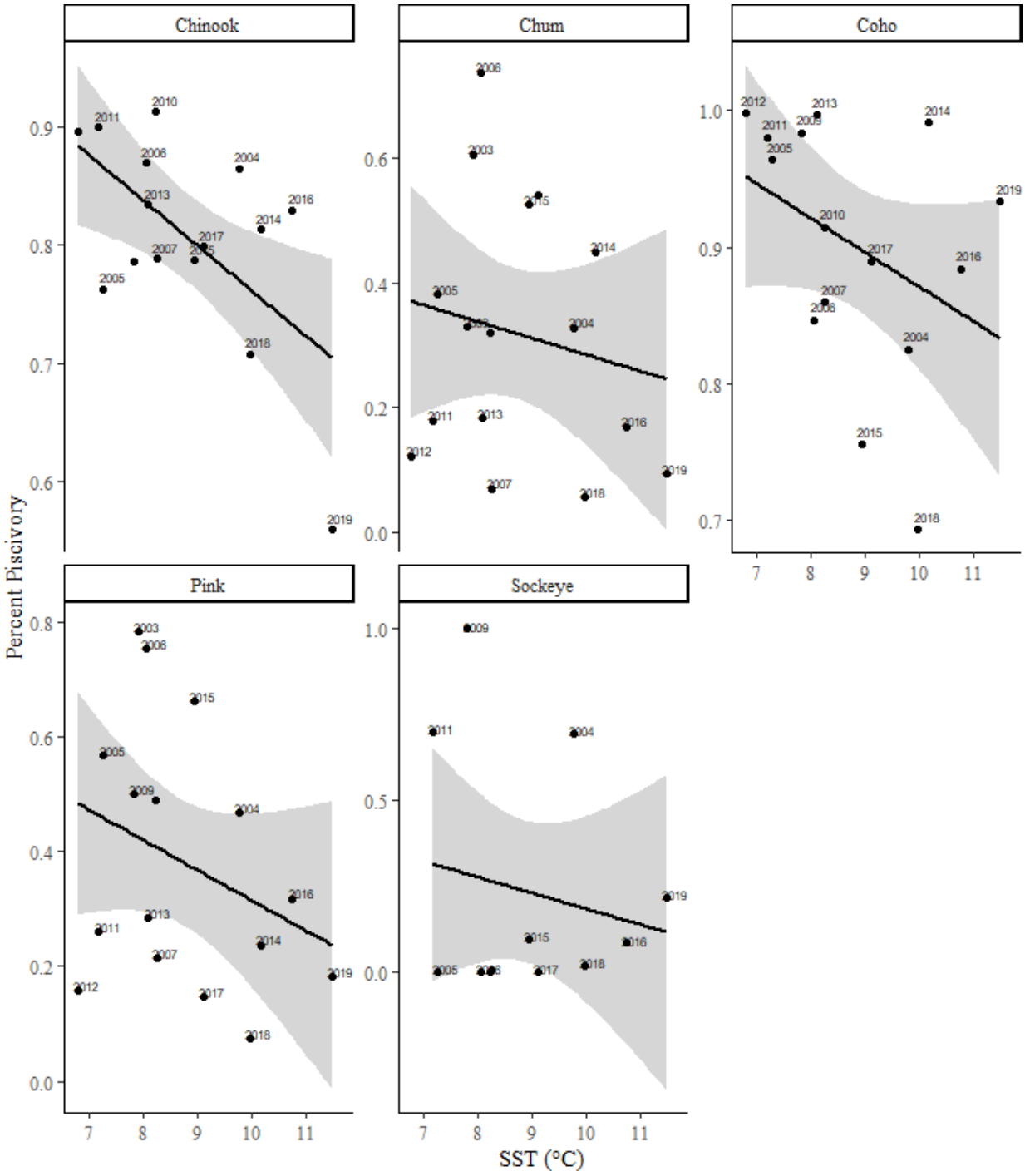

Figure 26. -- Linear regression model fits (black lines) with 95% confidence intervals (shaded regions) between the average percentage of fish in the stomachs of juvenile salmon (piscivory) and sea surface temperature (SST) sampled during the northern Bering Sea surface trawl surveys, 2004-2019. Each point is labeled with the sample year.

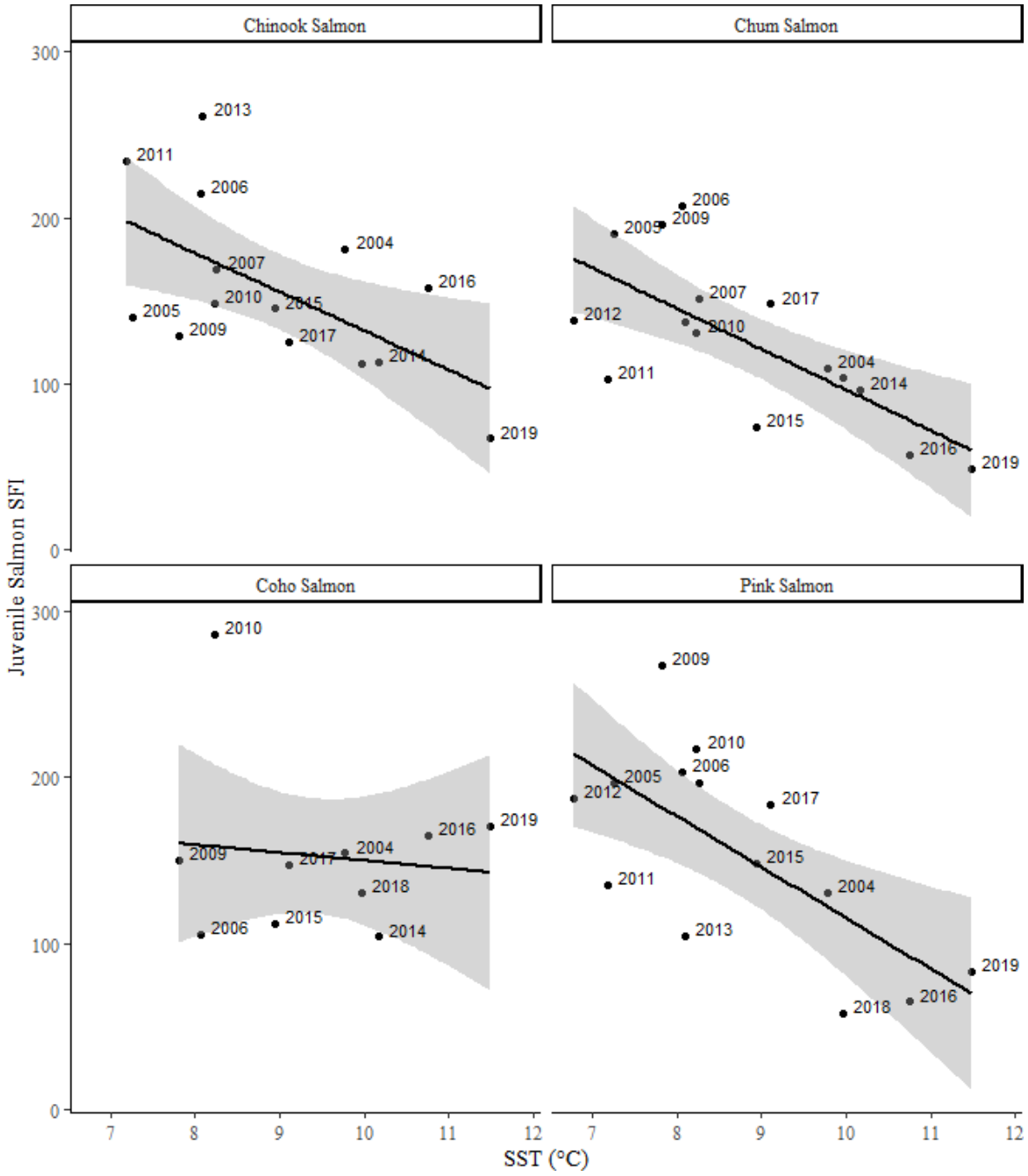

Figure 27. -- Linear regression model fits (black lines) with 95% confidence intervals (shaded regions) between the average stomach fullness index (SFI) of juvenile salmon and sea surface temperature (SST) sampled during the northern Bering Sea surface trawl surveys, 2004-2019. Each point is labeled with the sample year.

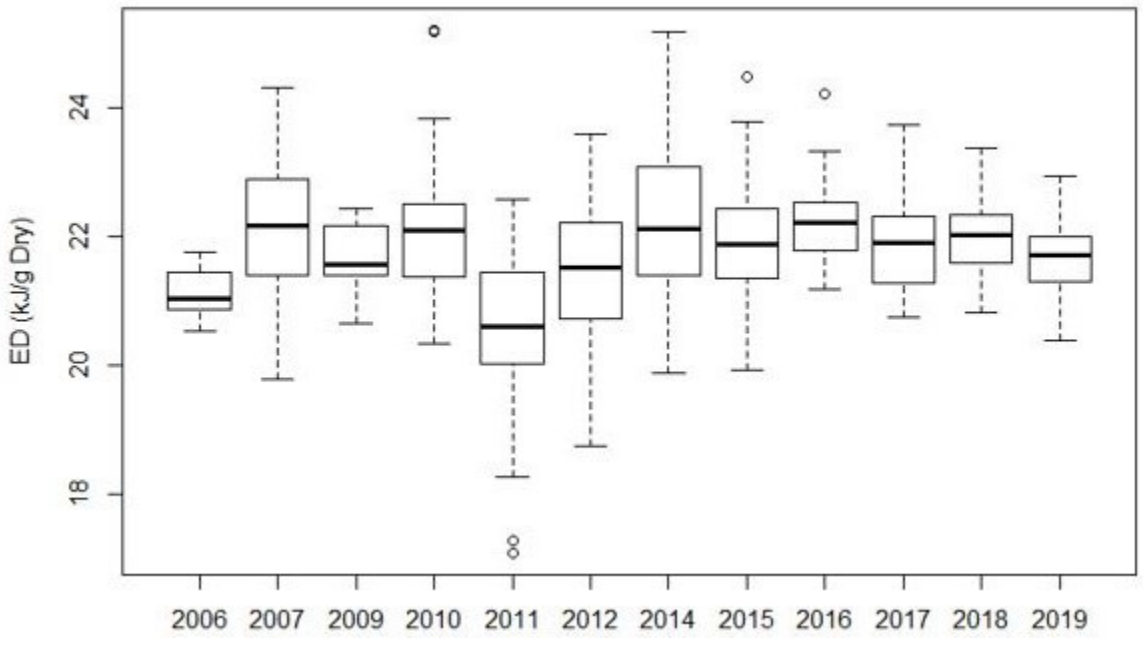

Figure 28. -- Boxplots of juvenile Chinook salmon sampled for energy density (kJ/dry tissue mass, n=575) sampled during northern Bering Sea surface trawl surveys, 2006-2019. Data unavailable for 2008 and 2013. Medians, interquartile ranges (IQR), whiskers (1.5 IQR), and outliers (empty circles, >1.5 IQR) are shown.

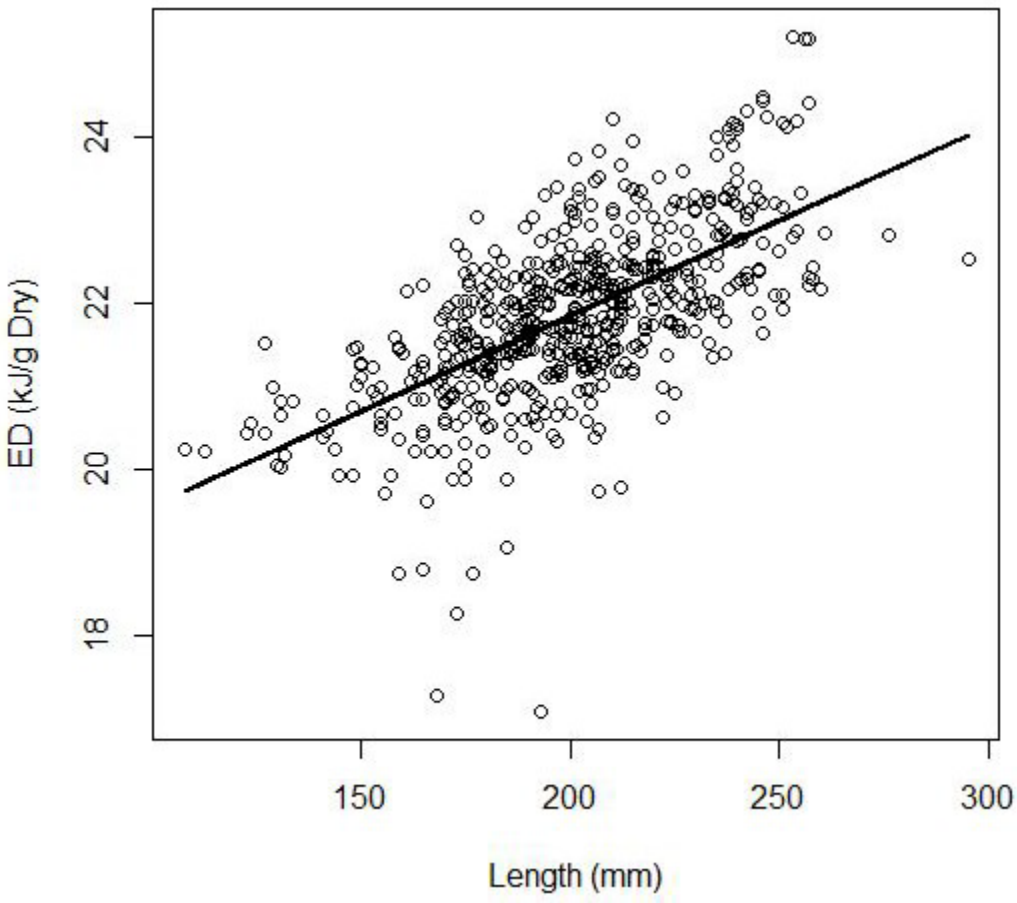

Figure 29. -- Energy density (kJ/g) of dry tissue mass by fork length (mm) of juvenile Chinook salmon caught during the northern Bering Sea surface trawl surveys, 2006-2019. Simple linear regression model fit shown by line (n = 575).

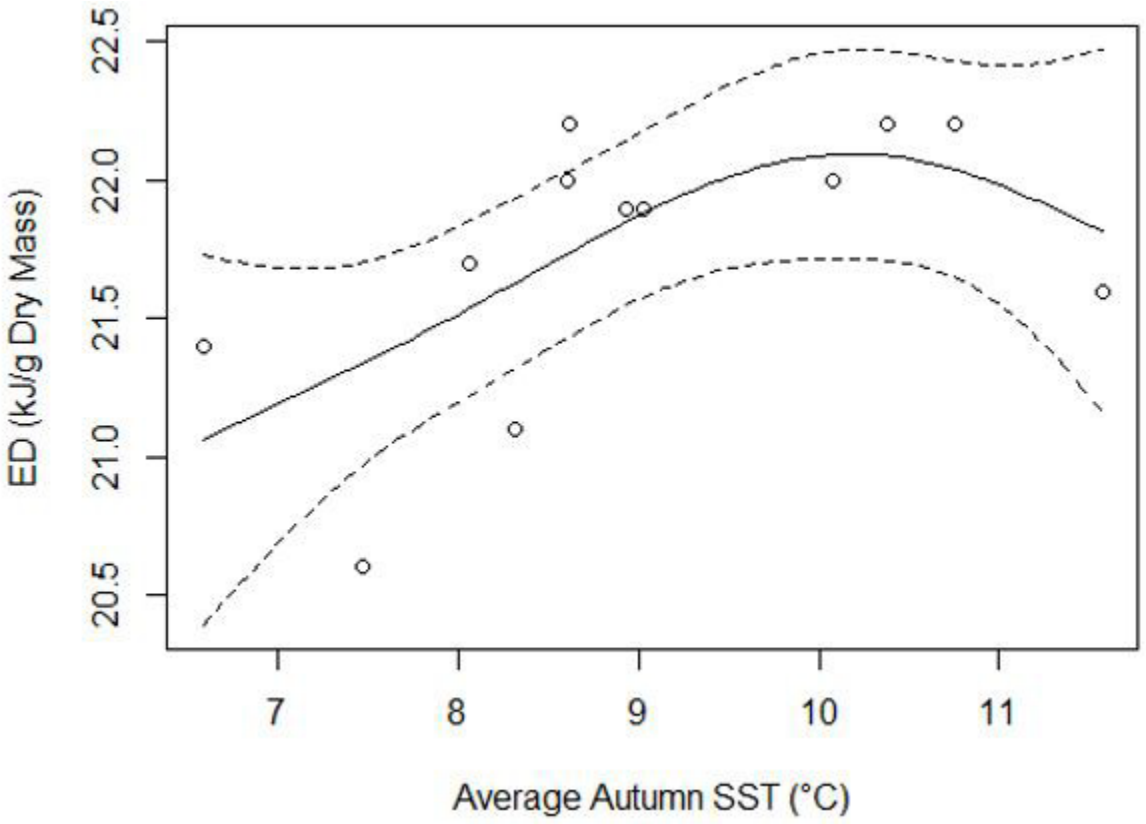

Figure 30. -- Annual mean energy density (kJ/g) of dry tissue mass by average autumn sea surface temperature (°C) for juvenile Chinook salmon caught during the northern Bering Sea surface trawl surveys, 2006-2019. Generalized additive model fit shown by solid line, dashed lines represent ±1 SE. Data unavailable for 2008 and 2013.

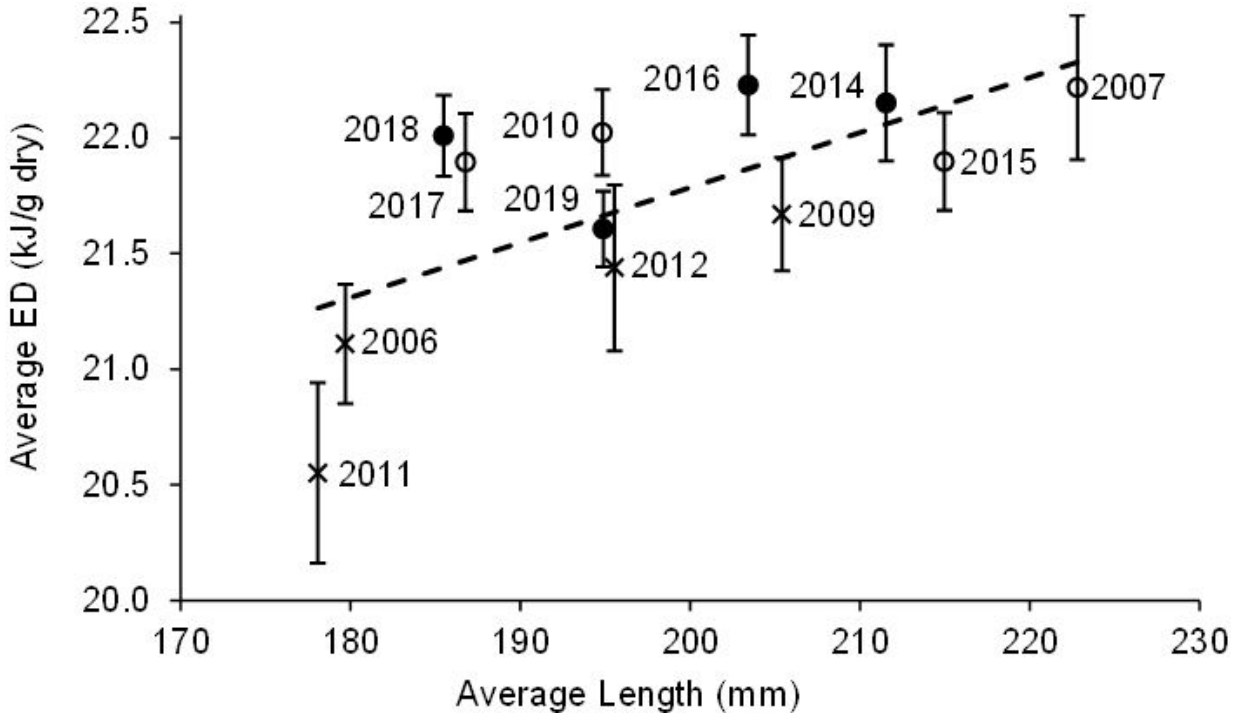

Figure 31. -- Annual mean energy density (kJ/g) of dry tissue mass by fork length (mm) of juvenile Chinook salmon caught during the northern Bering Sea surface trawl surveys, 2006-2019. Simple linear regression model fit shown by dashed line (n = 12 years). Error bars represent 95% confidence intervals. Data unavailable for 2008 and 2013. Symbols indicate four warmest years (filled circles; autumn SST > 9.5 °C), four coldest years (X; autumn SST < 8.5 °C), and four intermediate years (empty circles).

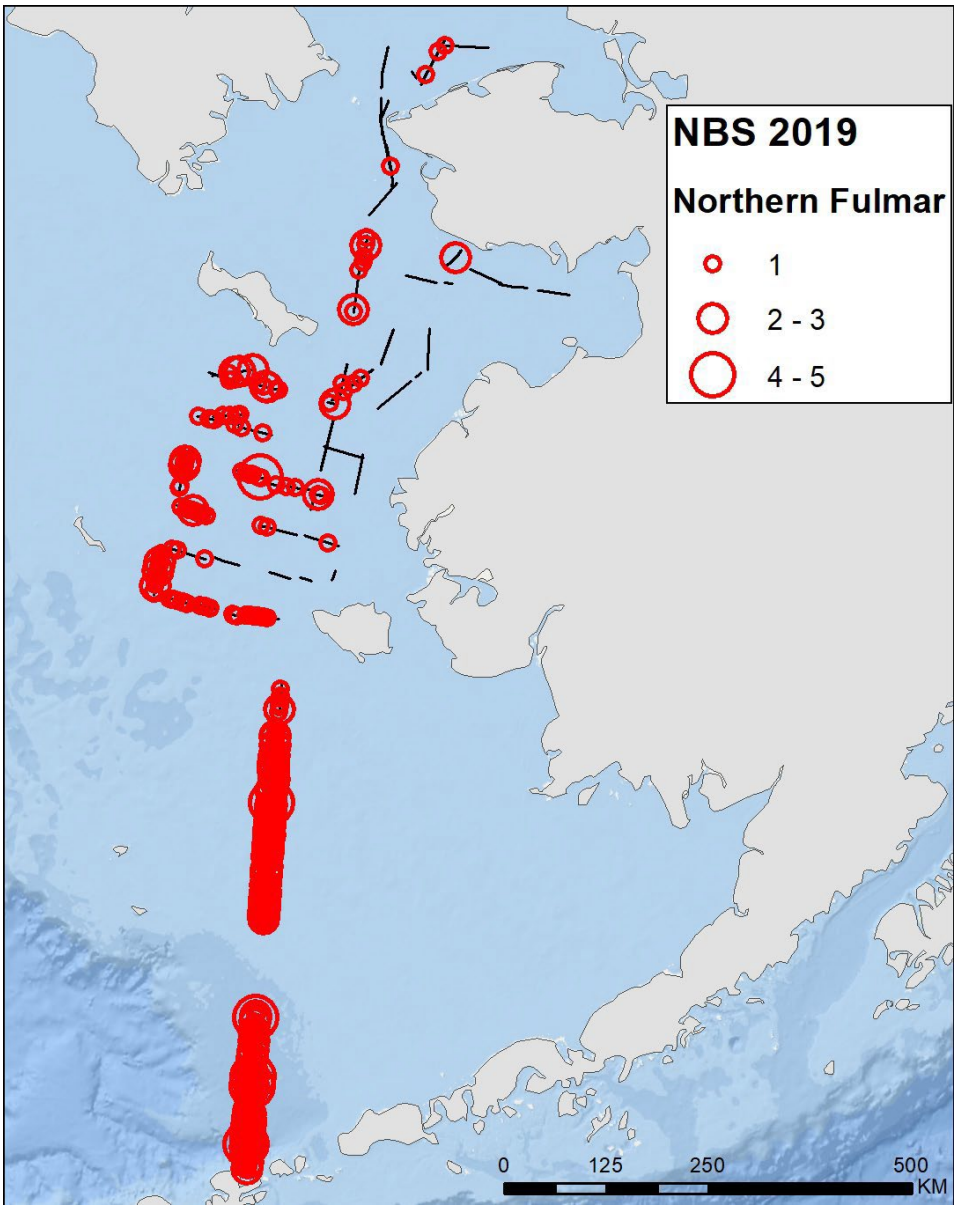

Figure 32. -- Distribution of northern fulmars observed during the northern Bering Sea surface trawl survey, 2019.

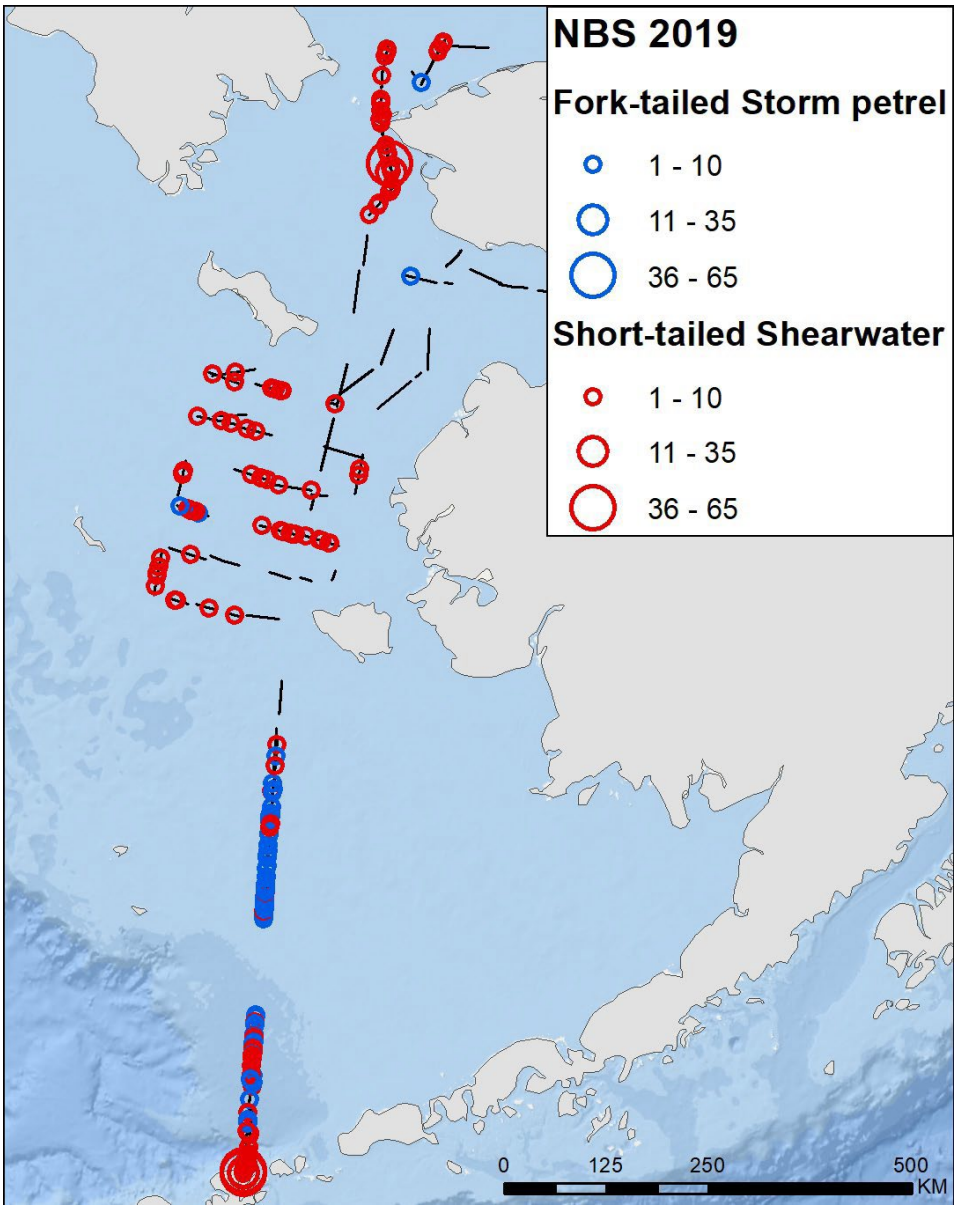

Figure 33. -- Distribution of shearwaters and fork-tailed storm-petrels during the northern Bering Sea surface trawl survey, 2019.

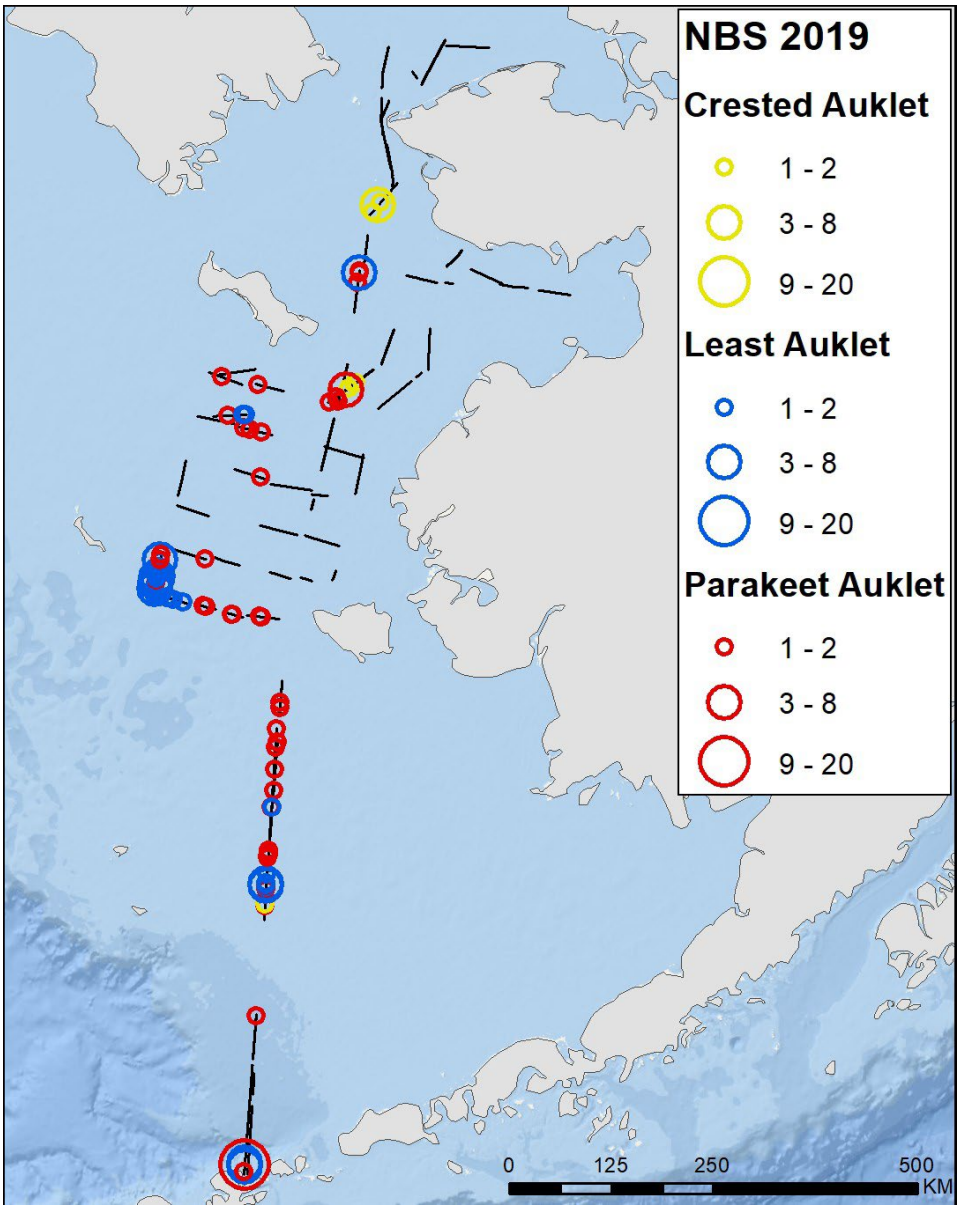

Figure 34. -- Distribution of auklet species during the northern Bering Sea surface trawl survey, 2019.

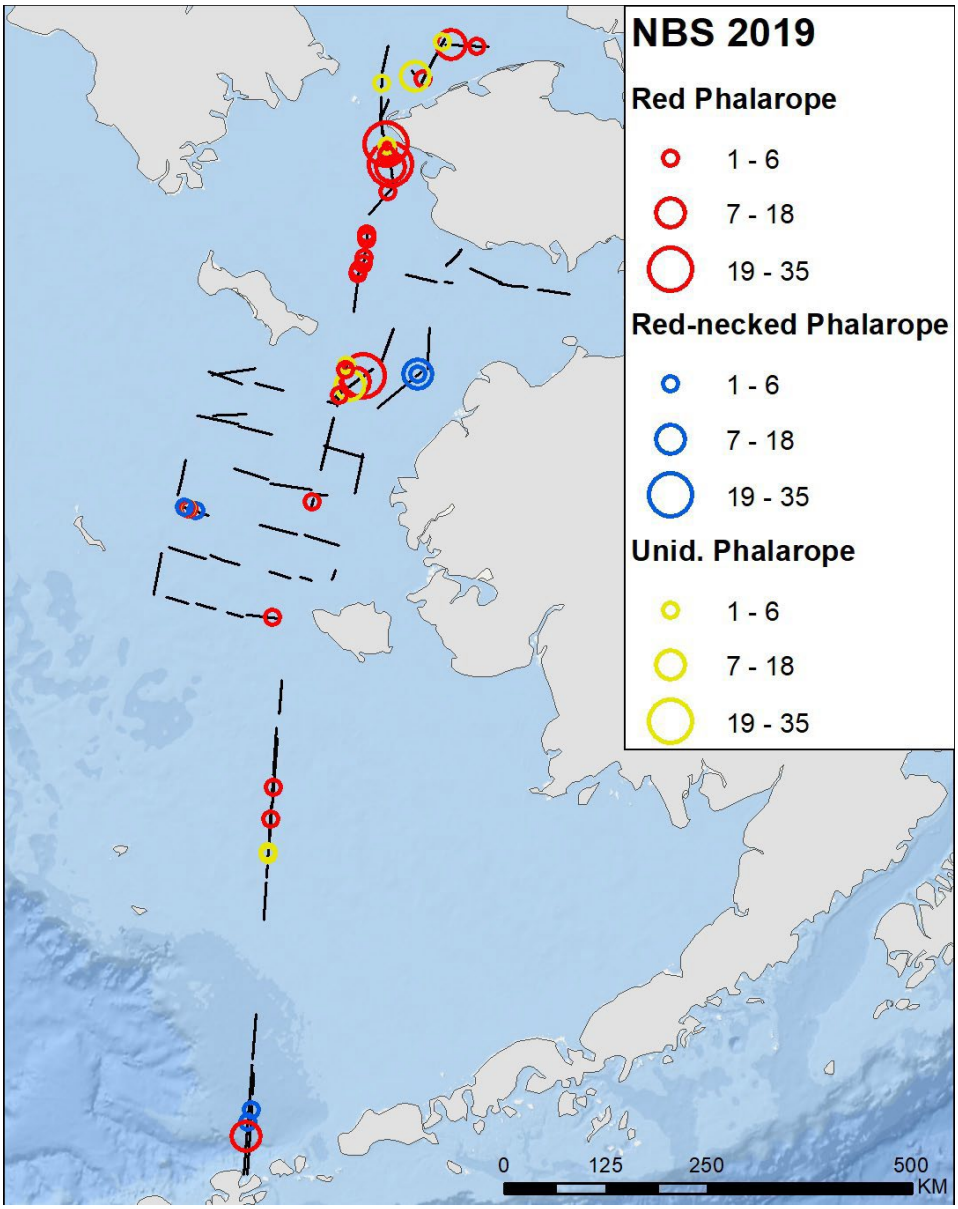

Figure 35. -- Distribution of phalarope species observed during the northern Bering Sea surface trawl survey, 2019.

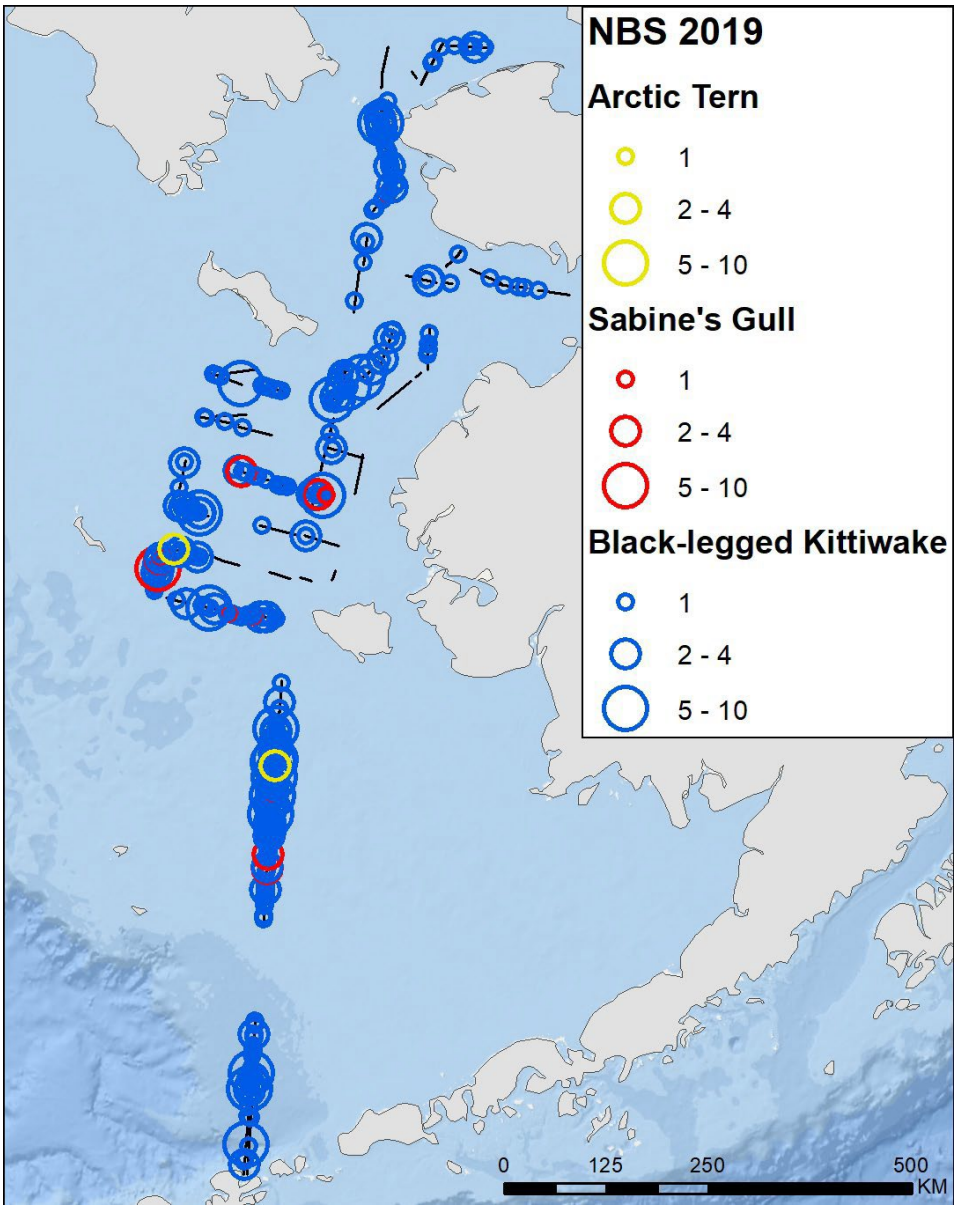

Figure 36. -- Distribution of Arctic tern, Sabine's gull, and black-legged kittiwakes observed during the northern Bering Sea surface trawl survey, 2019.

APPENDIX B. -- Spatial distribution surface trawl catch.

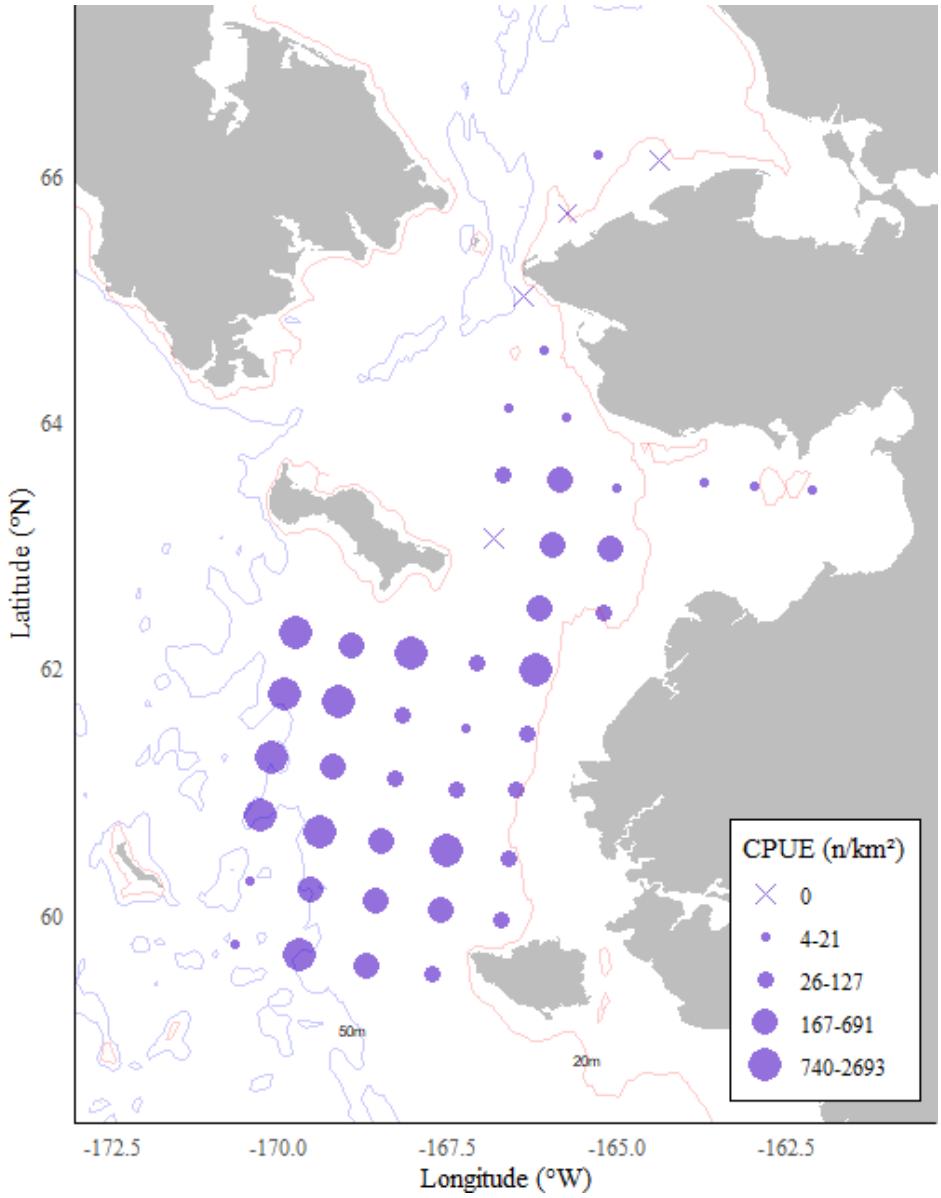

Figure B1. -- Surface trawl catch rates of juvenile chum salmon (CPUE, n/km^2) during the northern Bering Sea surface trawl survey, 2019.

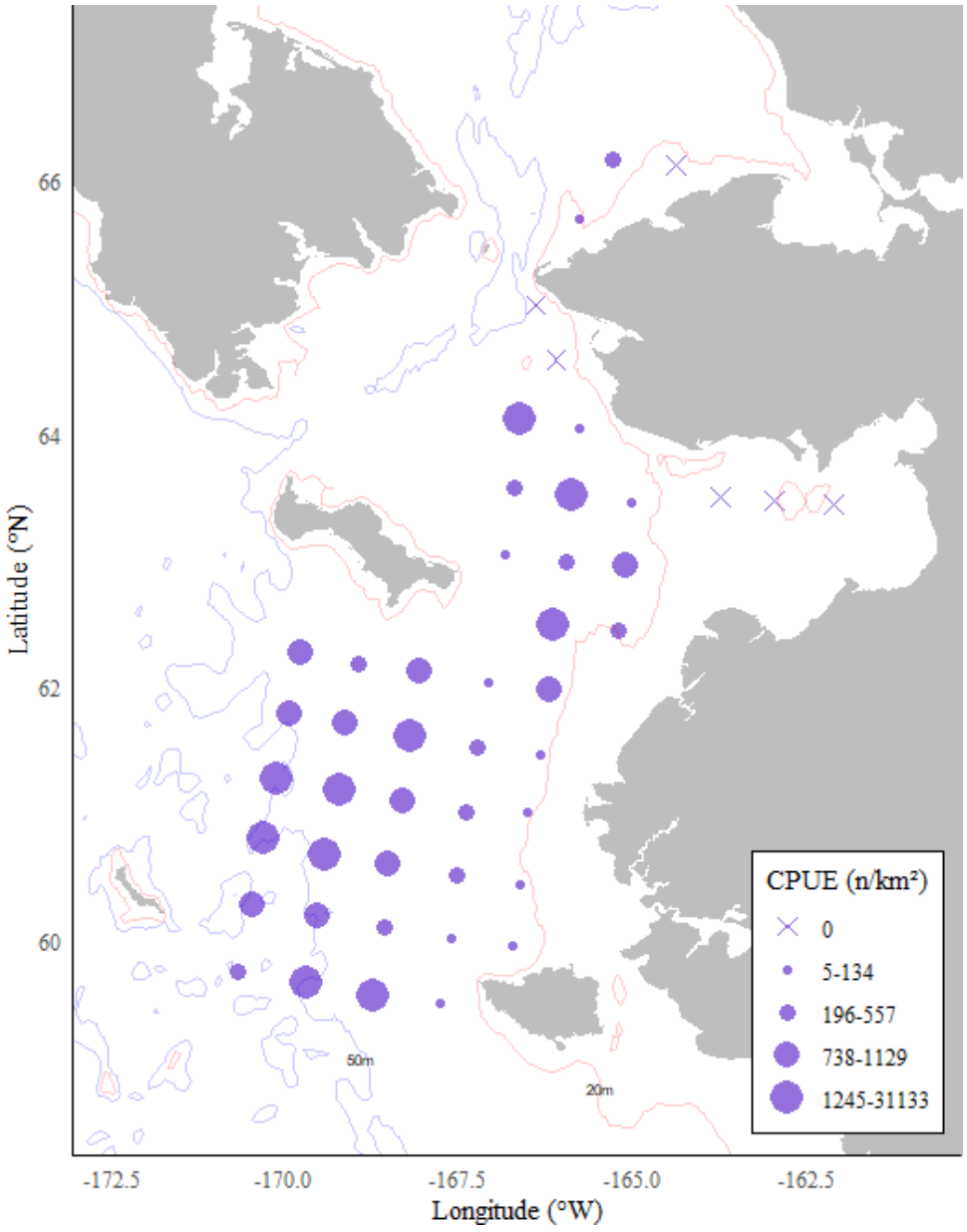

Figure B2. -- Surface trawl catch rates of juvenile pink salmon (CPUE, n/km^2) during the northern Bering Sea surface trawl survey, 2019.

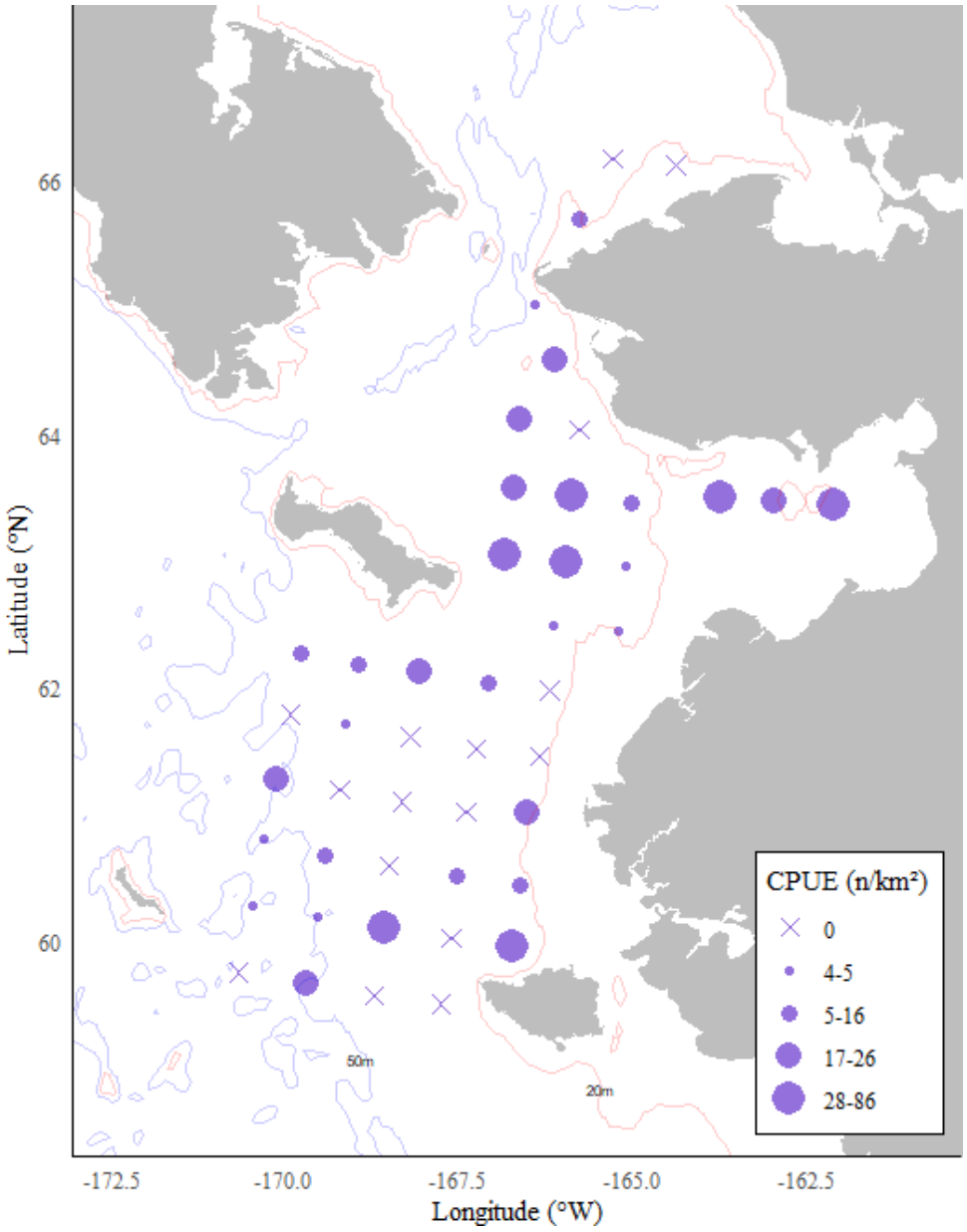

Figure B3. -- Surface trawl catch rates of juvenile Chinook salmon (CPUE, n/km^2) during the northern Bering Sea surface trawl survey, 2019.

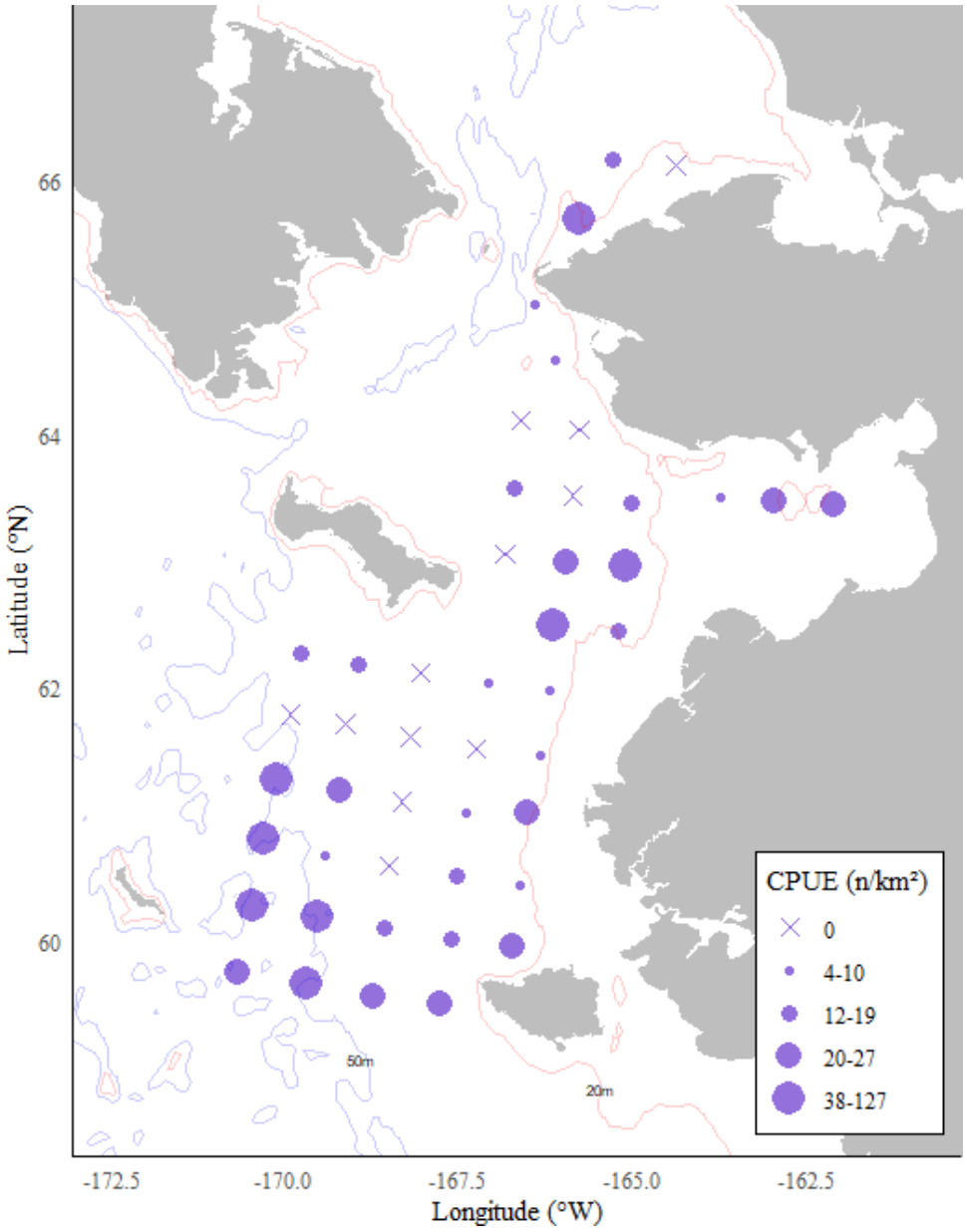

Figure B4. -- Surface trawl catch rates of juvenile coho salmon (CPUE, n/km^2) during the northern Bering Sea surface trawl survey, 2019.

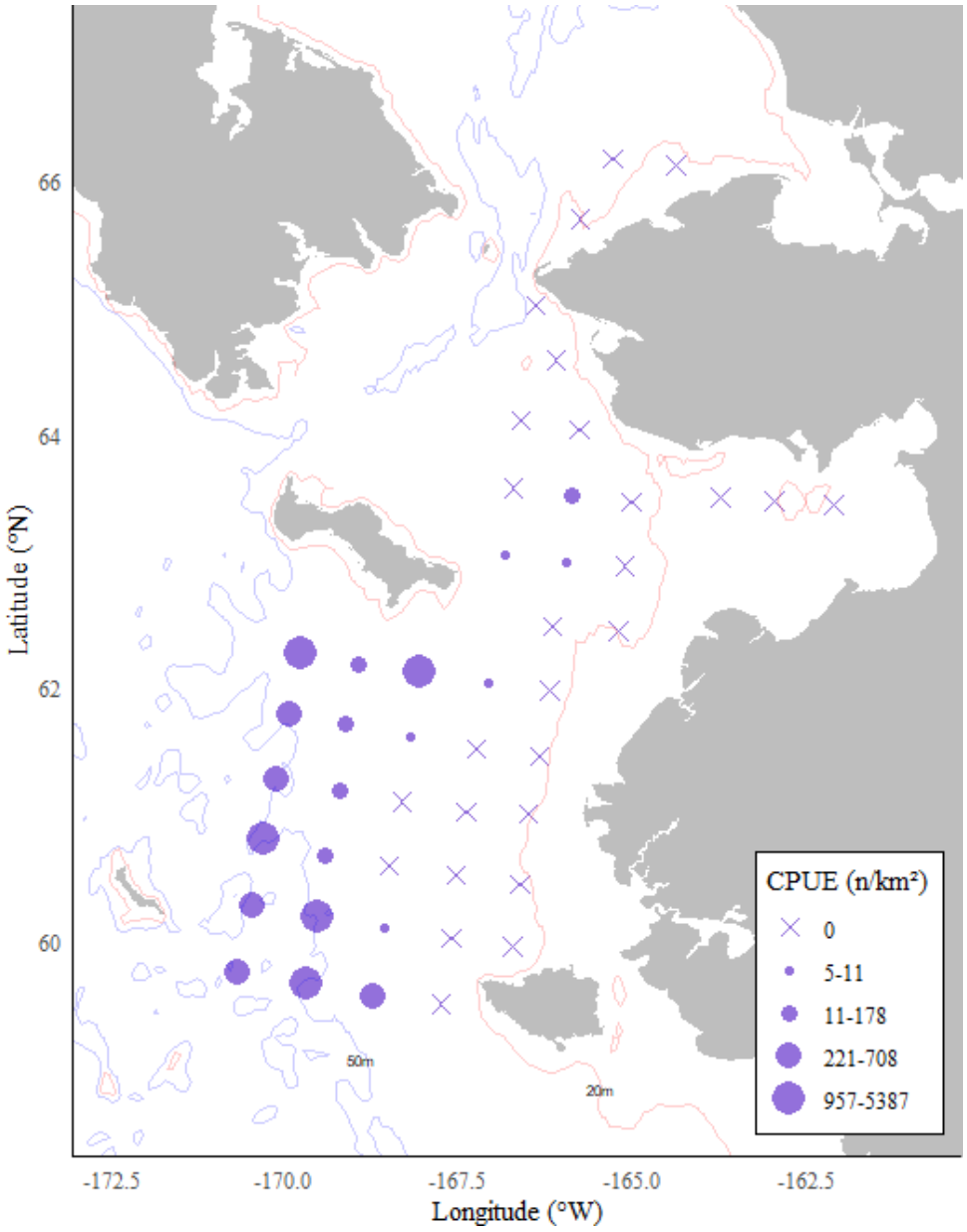

Figure B5. -- Surface trawl catch rates of juvenile sockeye salmon (CPUE, n/km^2) during the northern Bering Sea surface trawl survey, 2019.

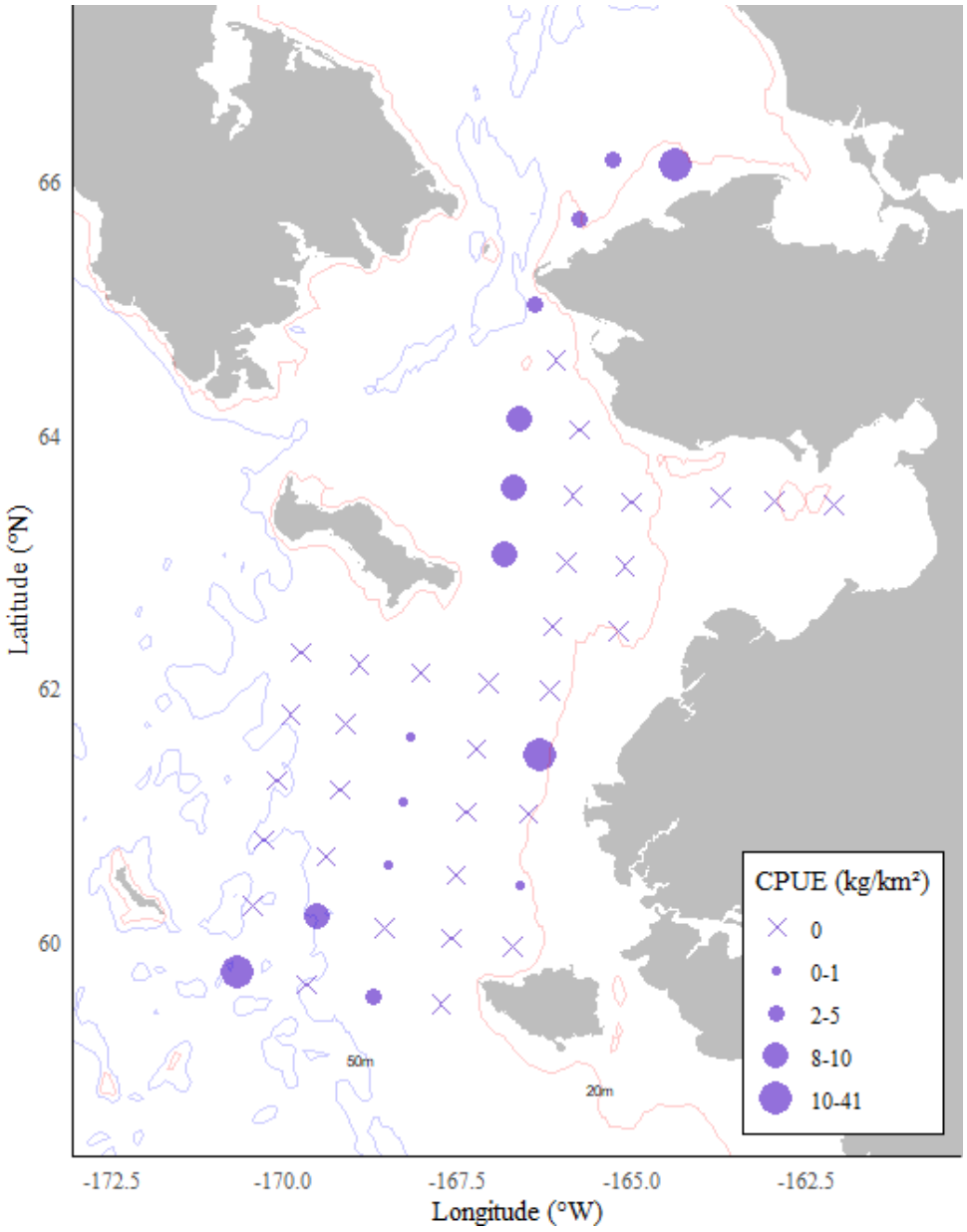

Figure B6. -- Surface trawl catch rates of water jellyfish (*Aequorea* sp.) (CPUE, kg/km^2) during the northern Bering Sea surface trawl survey, 2019.

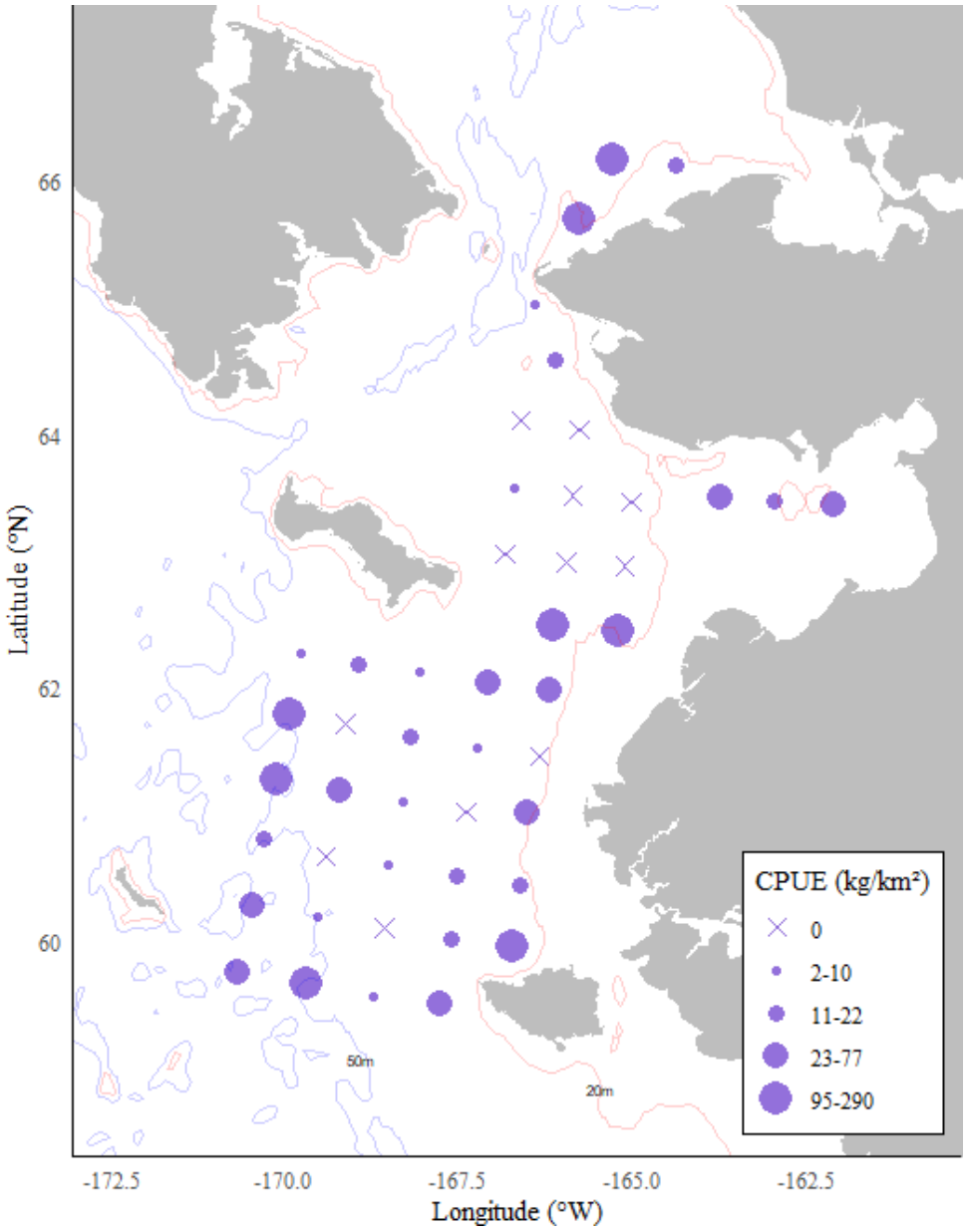

Figure B7. -- Surface trawl catch rates of moon jellyfish (*Aurelia labiata*) (CPUE, kg/km^2) during the northern Bering Sea surface trawl survey, 2019.

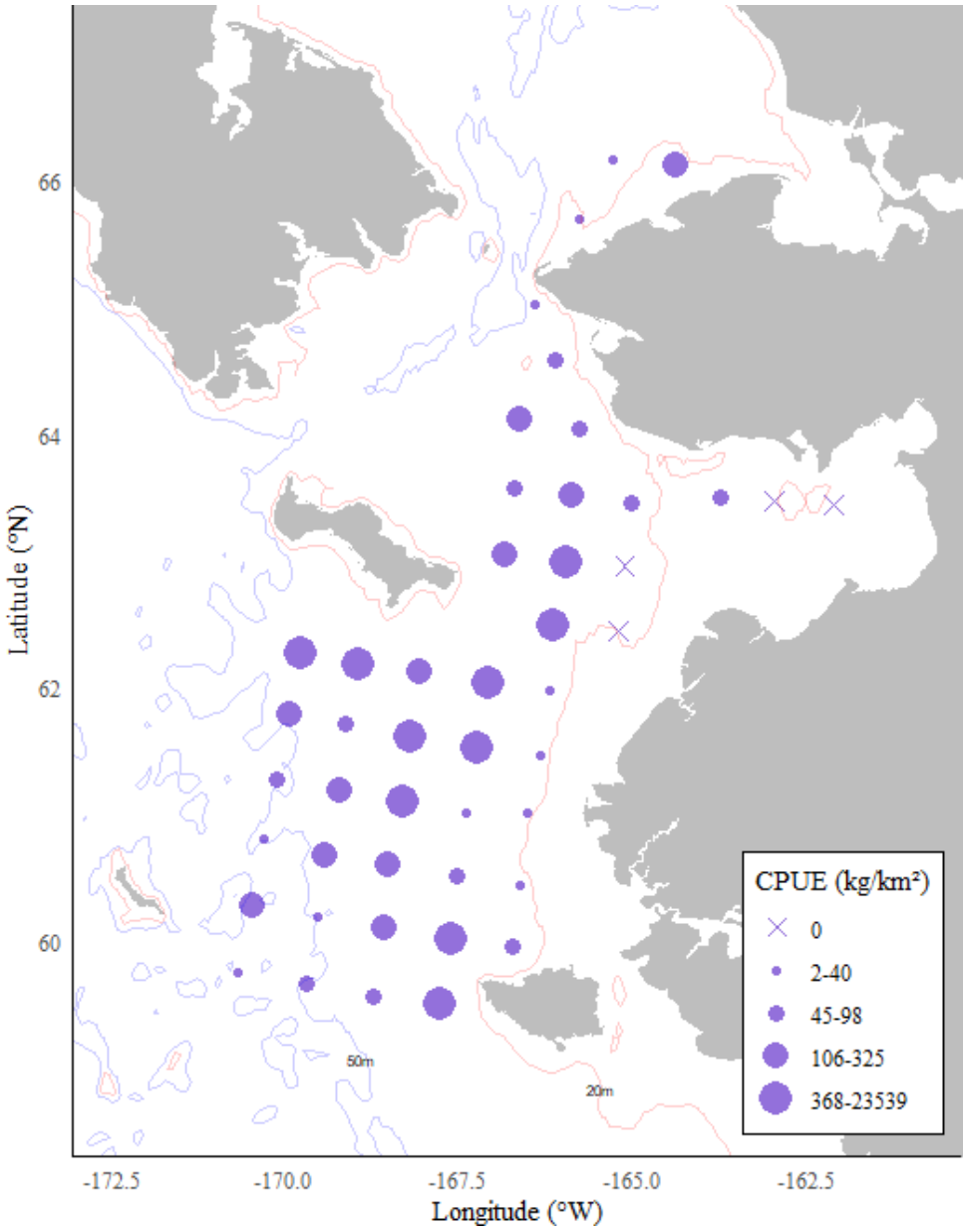

Figure B8. -- Surface trawl catch rates of northern sea nettle (*Chrysaora melanaster*) (CPUE, kg/km^2) during the northern Bering Sea surface trawl survey, 2019.

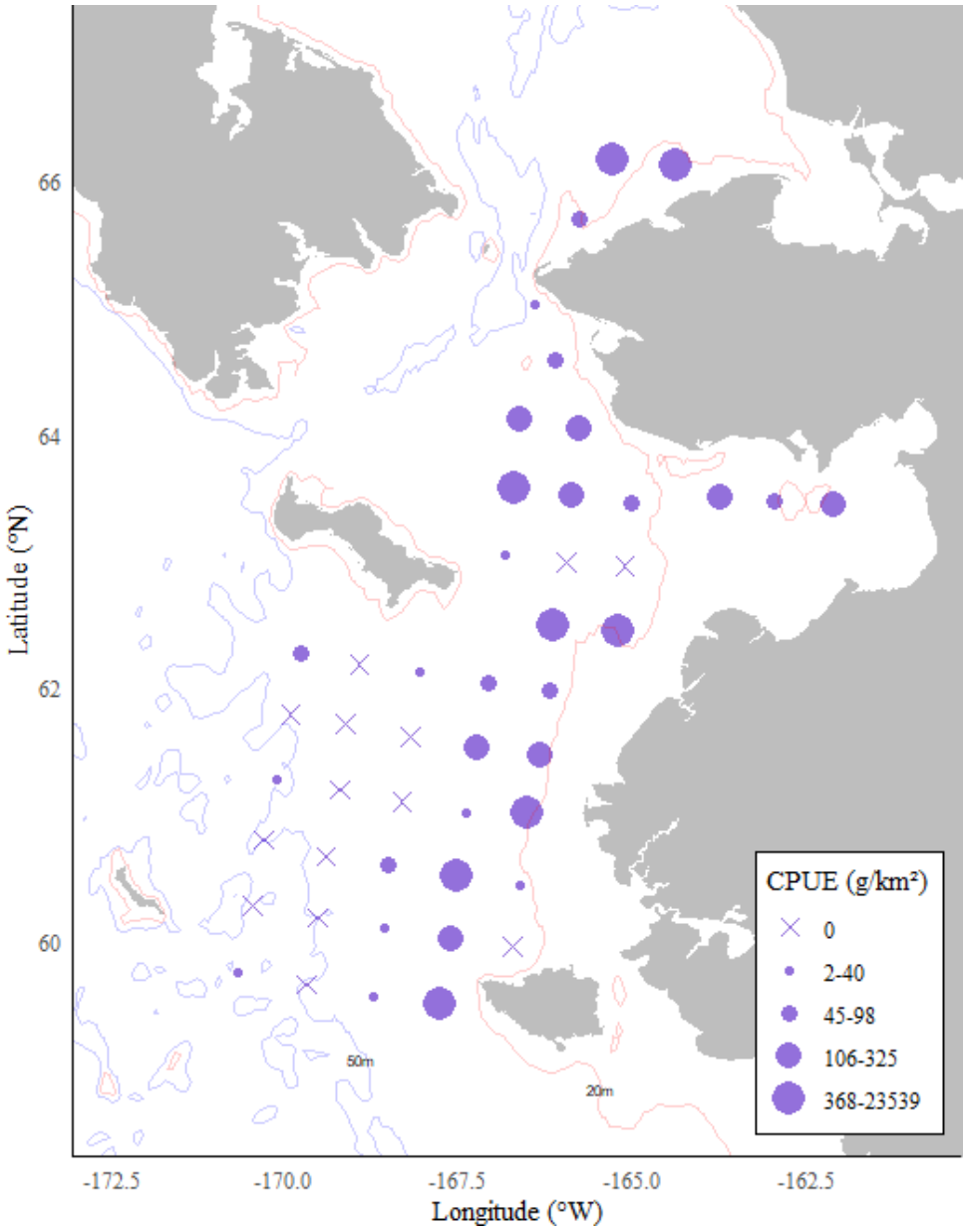

Figure B9. -- Surface trawl catch rates of lion's mane jellyfish (*Cyanea capillata*) (CPUE, g/km^2) during the northern Bering Sea surface trawl survey, 2019.

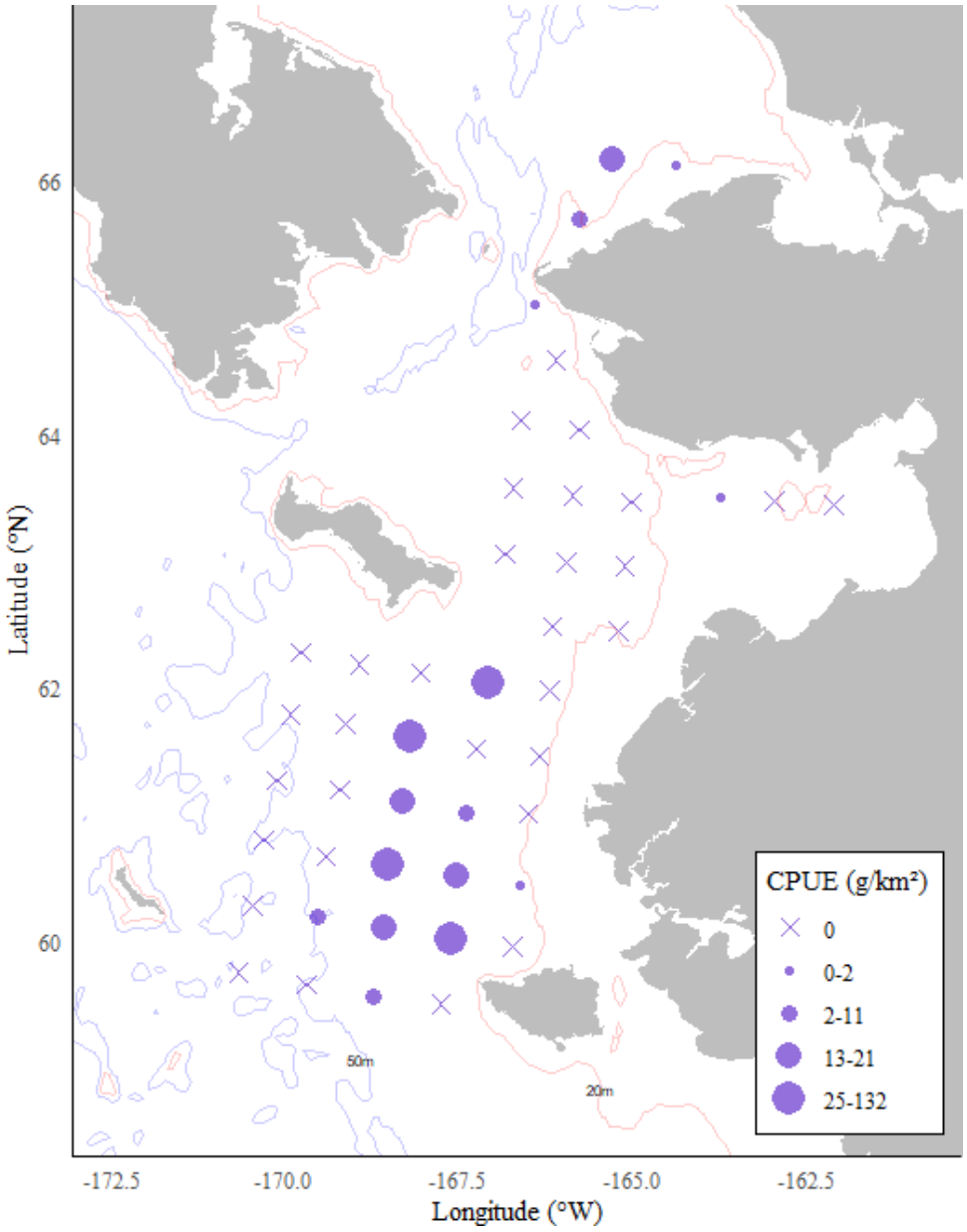

Figure B10. -- Surface trawl catch rates of whitecross jellyfish (*Staurophora mertensi*) (CPUE, g/km^2) during the northern Bering Sea surface trawl survey, 2019.

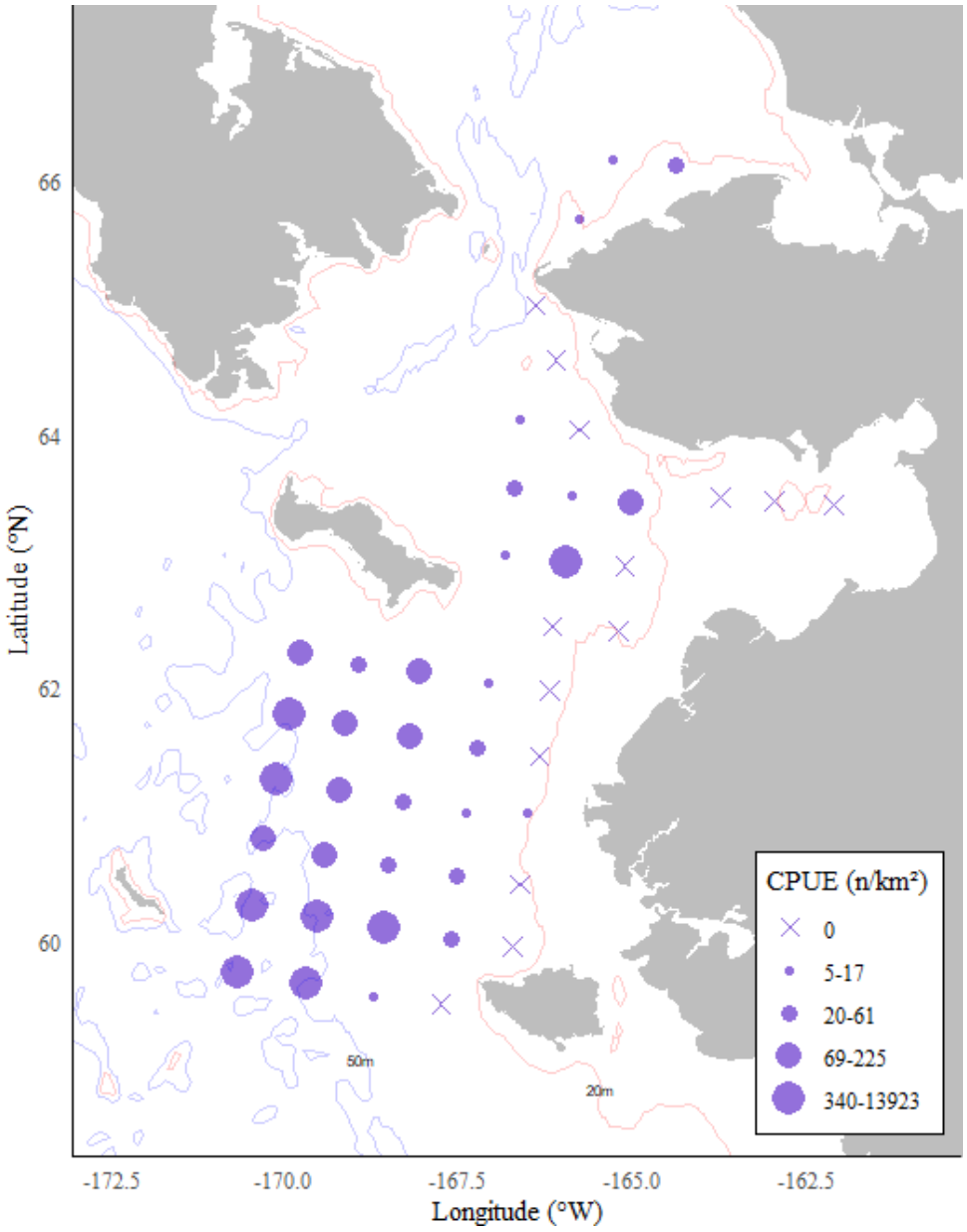

Figure B11. -- Surface trawl catch rates of age-0 walleye pollock (CPUE, n/km^2) during the northern Bering Sea surface trawl survey, 2019.

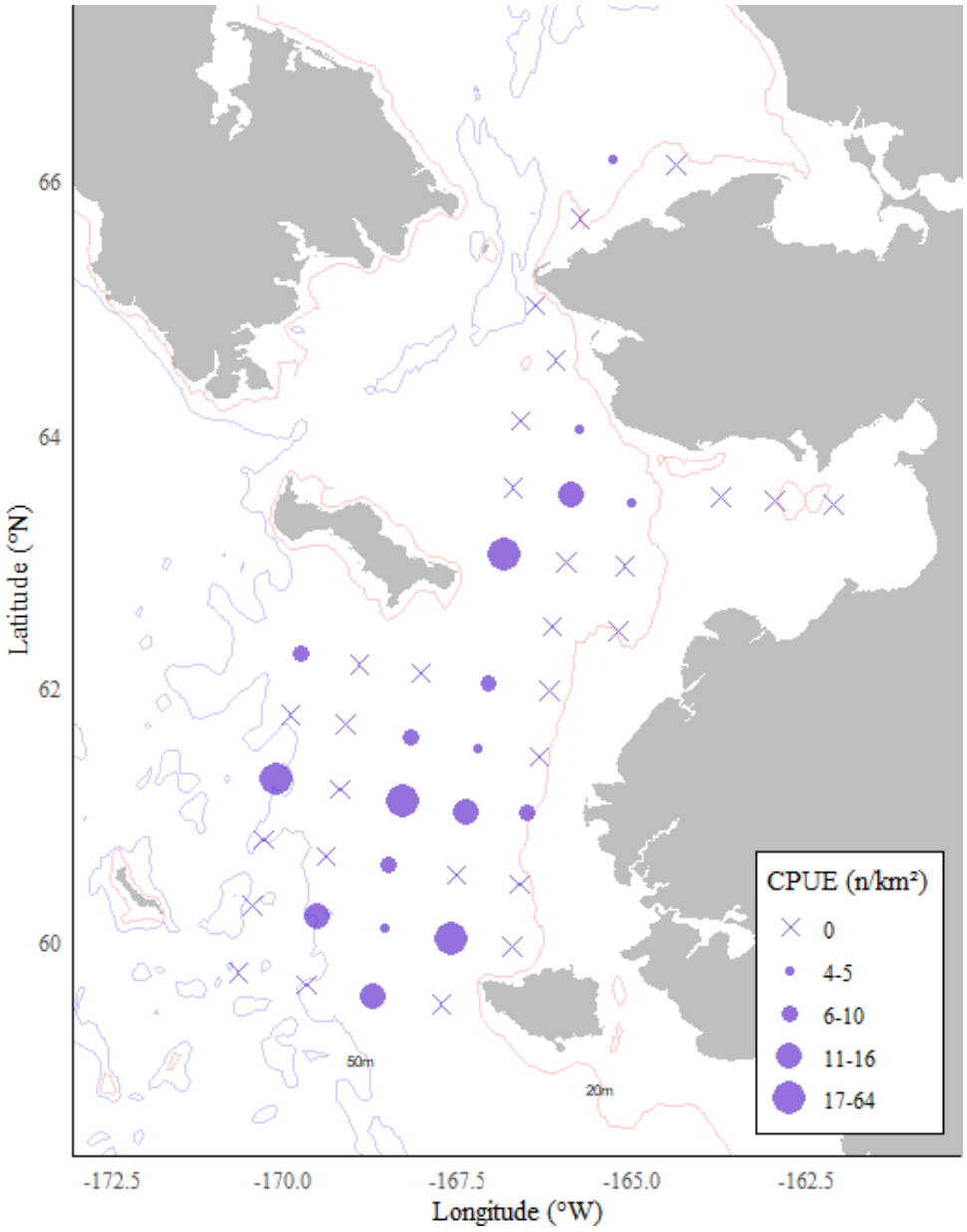

Figure B12. -- Surface trawl catch rates of age-1+ walleye pollock (CPUE, n/km^2) during the northern Bering Sea surface trawl survey, 2019.

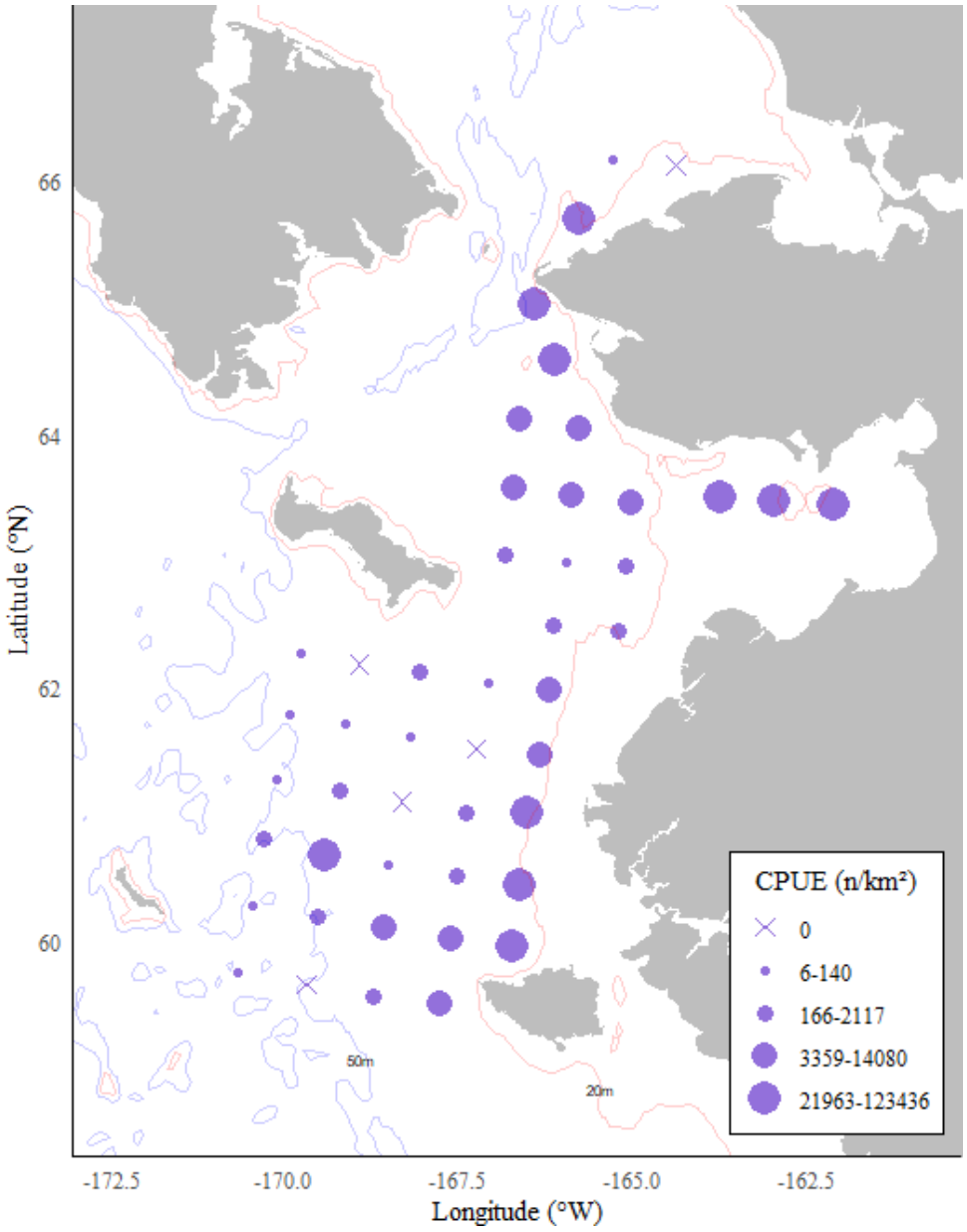

Figure B13. -- Surface trawl catch rates of Pacific herring (CPUE, n/km^2) during the northern Bering Sea surface trawl survey, 2019.

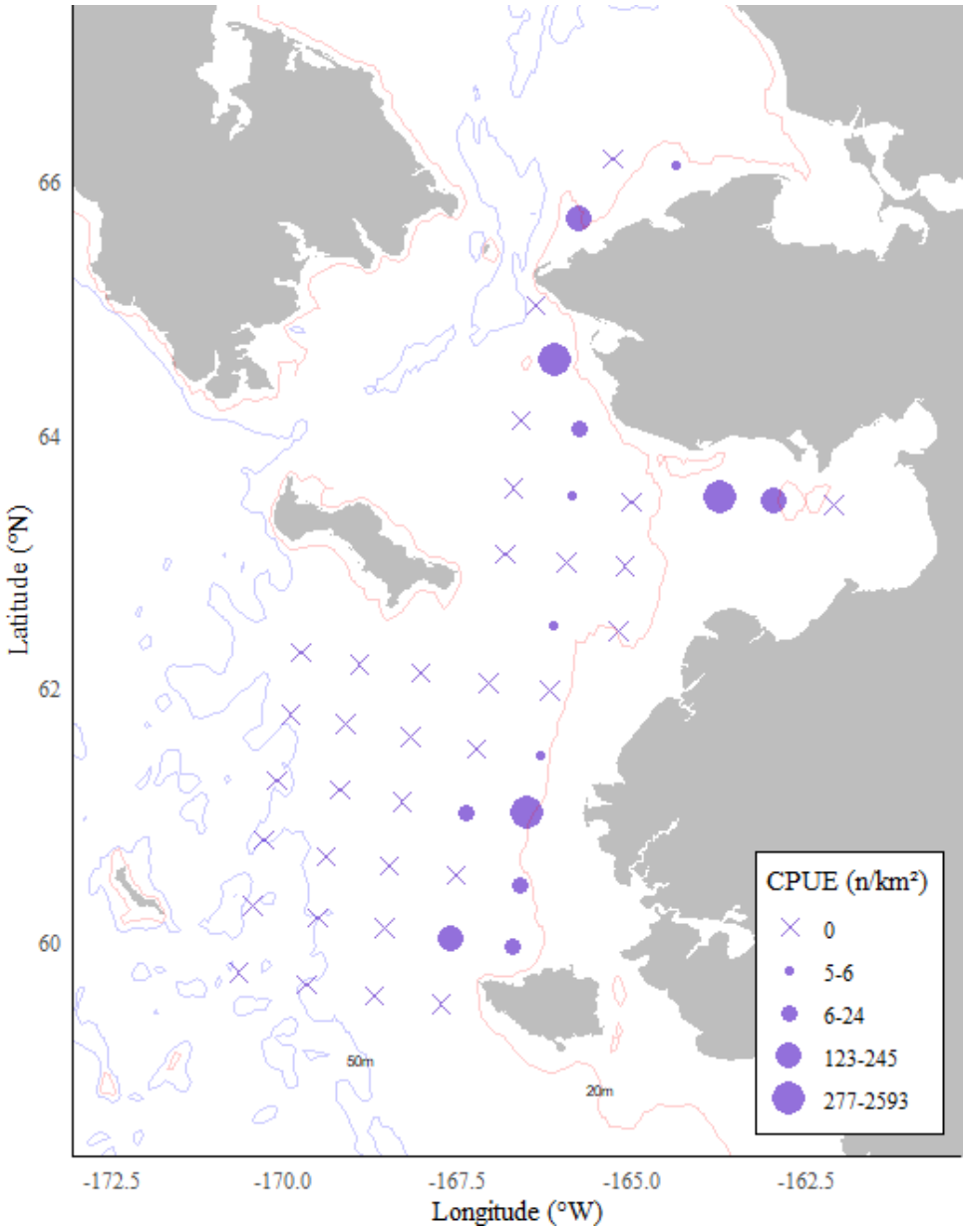

Figure B14. -- Surface trawl catch rates of rainbow smelt (CPUE, n/km^2) during the northern Bering Sea surface trawl survey, 2019.

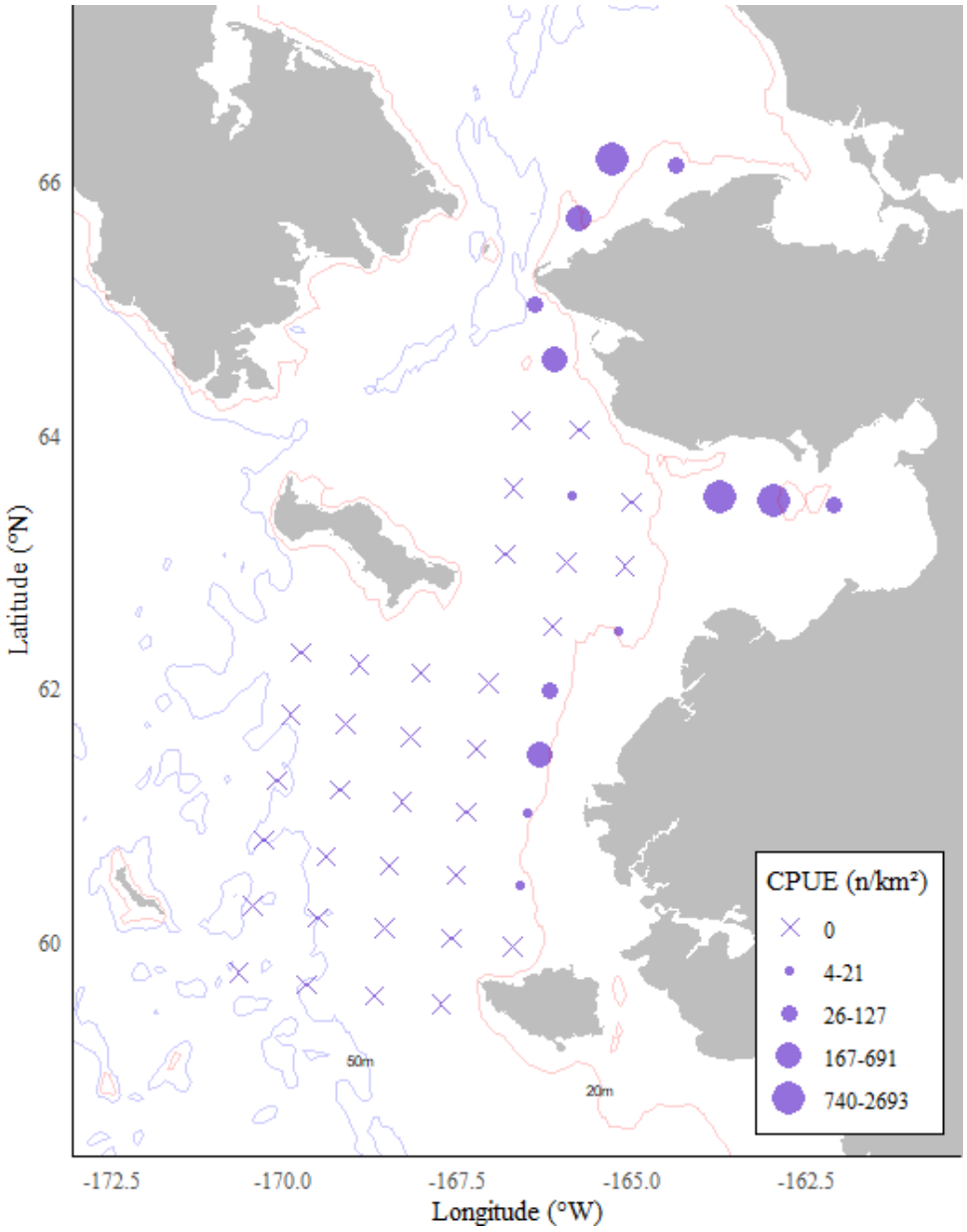

Figure B15. -- Surface trawl catch rates of ninespine stickleback (CPUE, n/km^2) during the northern Bering Sea surface trawl survey, 2019.

APPENDIX C. -- Length-weight relationships.

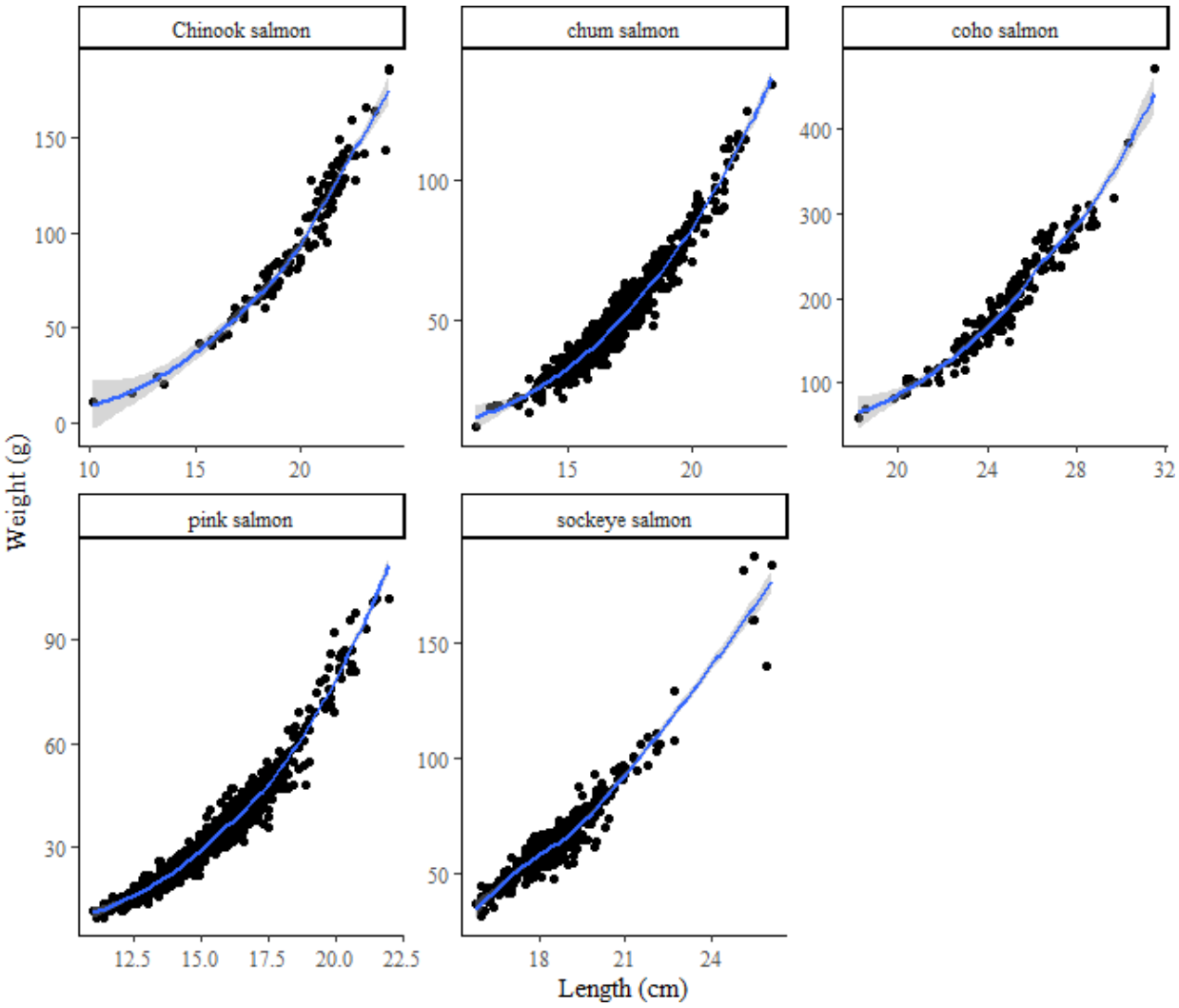

Figure C1. -- Length weight relationships of juvenile salmon species sampled during the northern Bering Sea surface trawl survey, 2019. Lines and shaded regions are from a local regression model (loess) fit and standard error.

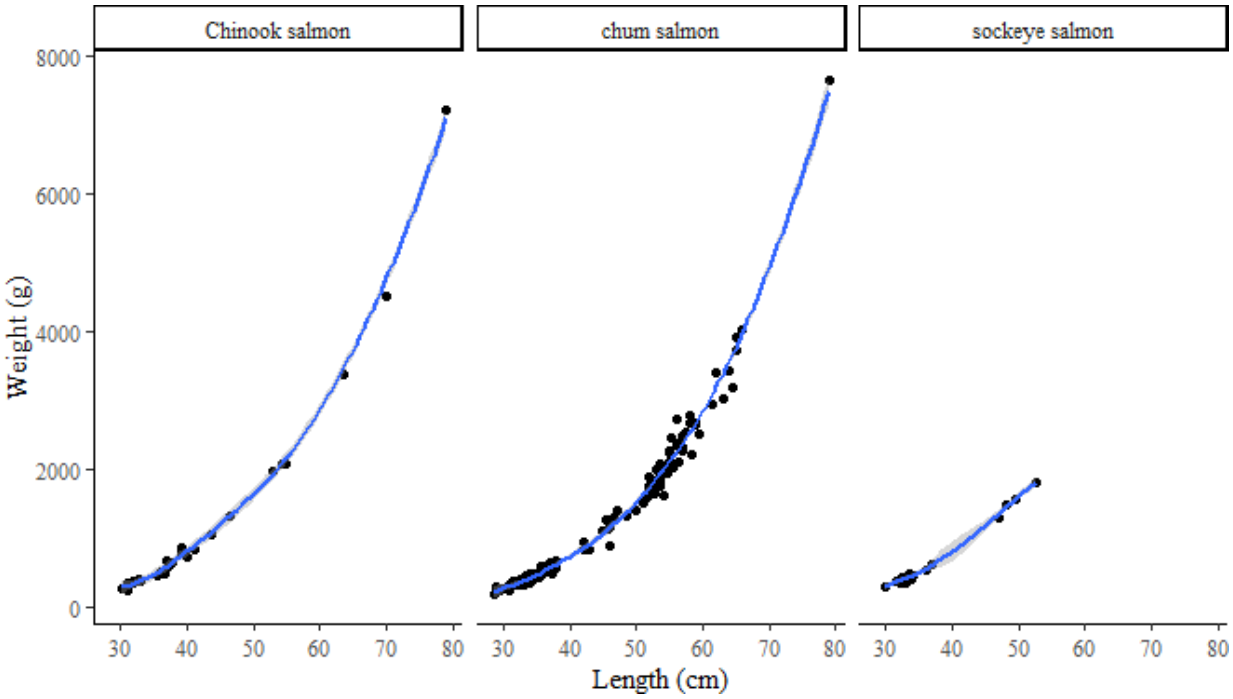

Figure C2. -- Length weight relationships of immature salmon species sampled during the northern Bering Sea surface trawl survey, 2019. Lines and shaded regions are from a local regression model (loess) fit and standard error.

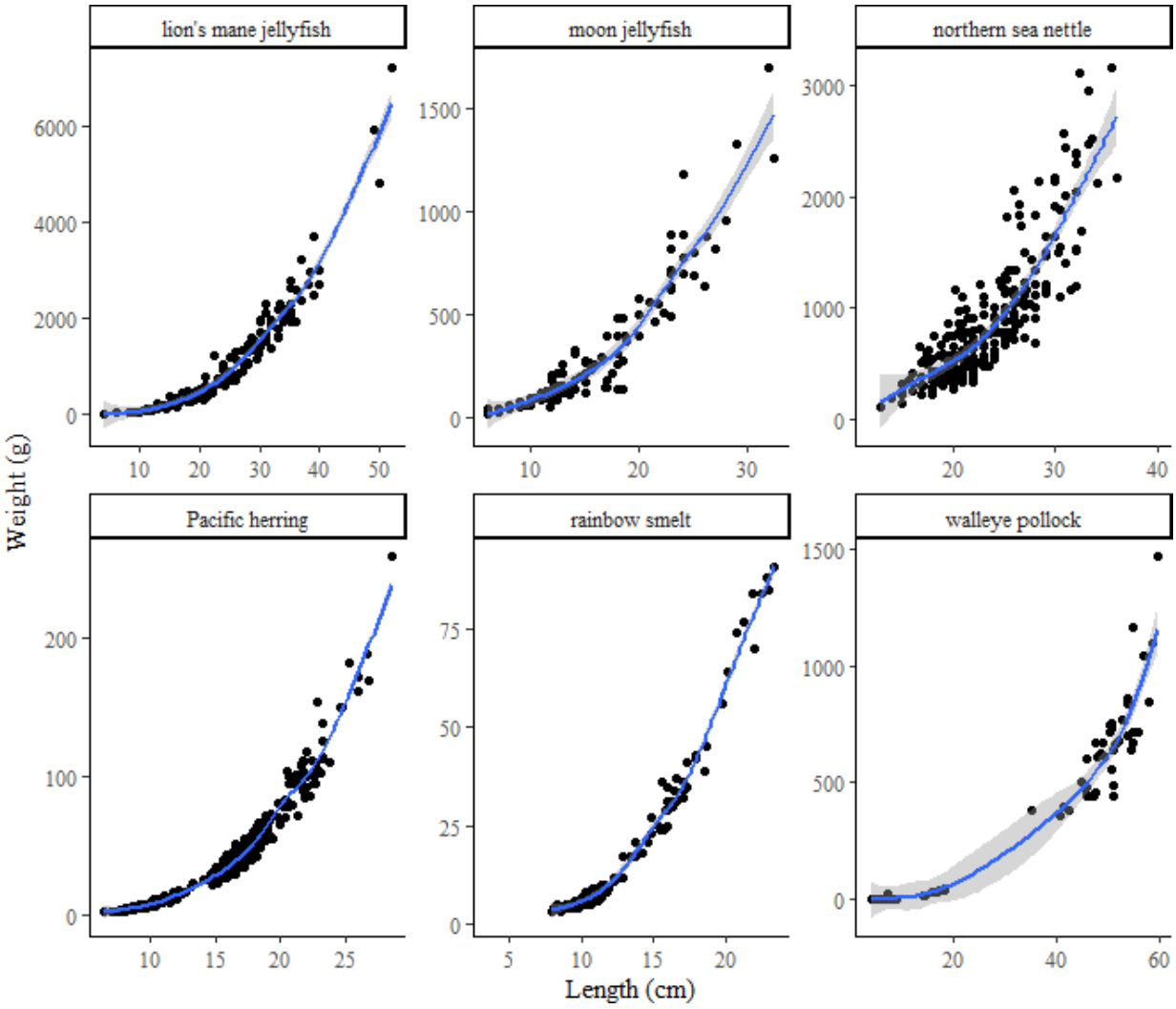

Figure C3. -- Length weight relationships of other key non-salmon species sampled during the northern Bering Sea surface trawl survey, 2019. Lines and shaded regions are from a local regression model (loess) fit and standard error.

APPENDIX D. – Coded-wire-tag recoveries.

Table D1. -- Coded-wire-tag (CWT) recovery information from Whitehorse Rapids Fish Hatchery Chinook salmon captured during the northern Bering Sea surface trawl surveys, 2003-2019.

CWT or Ad-Clip	Brood Year	Release Date	Recovery Date	Latitude (N)	Longitude (W)	Length (mm)	Weight (g)
185106	2001	6/10/2002	10/4/2002	64.1	-164.52	193	79
185102	2001	6/2/2002	10/4/2002	64.1	-164.52	155	46
185061	2001	6/10/2002	10/4/2002	63	-165.97	161	49
18	2006		9/13/2007	65.2	-168.1	125	18
18	2006		9/13/2007	65.2	-168.1	176	58
18	2006		9/13/2007	65.2	-168.1	179	58
18	2009		9/25/2010	64.07	-162.72	164	50
181374	2011	6/6/2012	9/22/2012	61.48	-167	138	28
181779	2011	6/6/2012	9/24/2012	64.1	-163.55	160	45
181779	2011	6/6/2012	9/24/2012	60.98	-168	138	25
182874	2013	6/6/2014	9/5/2014	63.85	-165.97	126	18
183184	2013	6/1/2014	9/6/2014	63.02	-166.05	120	15
183185	2013	6/6/2014	9/14/2014	62.5	-167.08	192	75
183187	2013	6/6/2014	9/14/2014	62.5	-167.08	177	60
183186	2014	6/8/2015	9/8/2015	62.98	-165.97	109	13
183186	2014	6/8/2015	9/14/2015	64	-166.02	120	18
183186	2014	6/8/2015	9/14/2015	64	-166.02	124	21
184064	2014	6/3/2015	9/9/2015	63.02	-167.07	112	13
184065	2014	6/3/2015	9/14/2015	64	-166.02	129	24
184593	2016	6/7/2017	9/3/2017	62	-168	110	12
185573	2018	6/12/2019	9/13/2019	64.12	-162.52	152	42
185587	2018	6/12/2019	9/13/2019	64.12	-162.52	132	24
ad-clip			10/5/2002	63	-167.48	134	23
ad-clip			9/25/2010	63.82	-162.78	190	87
ad-clip			9/12/2012	64.4	-166.07	185	75
ad-clip			9/24/2013	60.52	-167.05	207	108
ad-clip			9/16/2013	63.77	-164.57	183	70
ad-clip			9/19/2013	62.52	-167.03	202	94
ad-clip			9/13/2015	64.02	-167	113	15
ad-clip			9/10/2018	63.5	-166	127	22

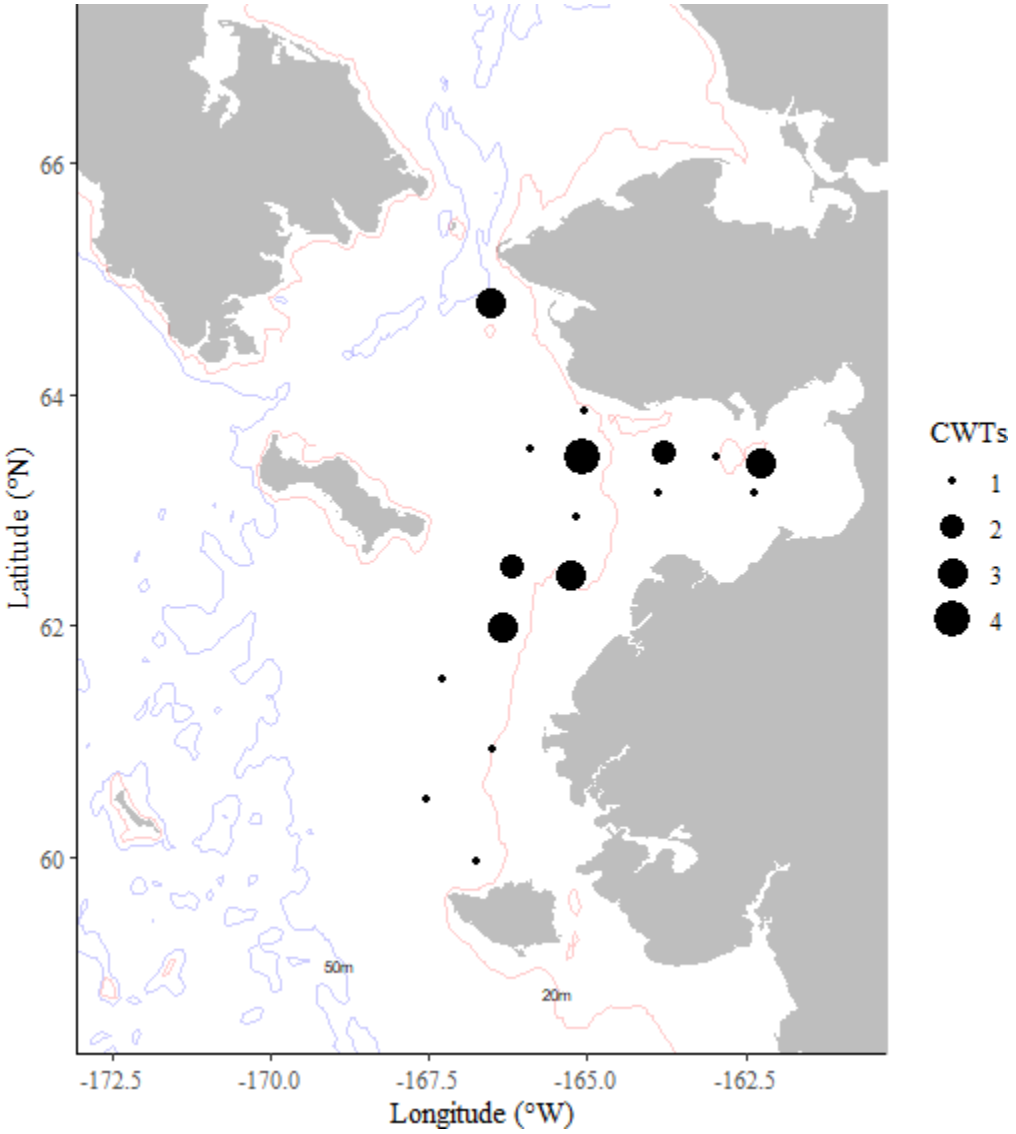

Figure D1. -- Location of CWTs recovered from Whitehorse Rapids Fish Hatchery Chinook salmon during the northern Bering Sea surface trawl surveys, 2003-2019.

APPENDIX E. -- Juvenile salmon diet.

Table E1. -- Juvenile Chinook, coho, chum, pink, and sockeye salmon sample size by number of stations (N), total number of stomachs (n), and the mean fullness index (SFI) sampled during the northern Bering Sea surface trawl surveys, 2004-2019.

Year	Chinook Salmon			Coho Salmon			Chum Salmon		
	Stations (n)	Stomachs (n)	Mean SFI	Stations (n)	Stomachs (n)	Mean SFI	Stations (n)	Stomachs (n)	Mean SFI
2004	37	138	180.85	27	96	154.39	42	261	109.43
2005	16	75	140.42	2	3	280.45	31	142	190.21
2006	28	87	215.00	21	78	105.36	32	213	207.08
2007	18	98	169.02	4	5	183.60	44	294	151.71
2009	11	50	129.02	5	13	150.35	18	138	196.09
2010	16	69	148.55	6	30	286.58	29	229	130.55
2011	15	111	234.26	4	13	151.29	20	177	103.09
2012	6	42	96.55	1	10	170.69	13	126	137.95
2013	20	174	261.07	3	16	292.98	17	148	136.99
2014	29	204	113.43	11	65	104.08	34	332	96.65
2015	27	180	145.26	7	43	111.65	27	215	74.29
2016	22	91	157.60	5	17	164.86	17	165	57.38
2017	28	148	125.21	19	117	147.19	18	167	148.12
2018	24	109	145.36	24	132	117.73	24	227	102.89
2019	10	44	70.47	17	84	173.49	29	252	48.21

Year	Pink Salmon			Sockeye Salmon		
	Stations (n)	Stomachs (n)	Mean SFI	Stations (n)	Stomachs (n)	Mean SFI
2004	48	323	130.29	23	173	95.35
2005	39	171	197.13	1	1	31.30
2006	24	131	203.30	2	2	172.20
2007	47	325	196.95	4	34	157.50
2009	14	121	267.38	1	10	100.90
2010	15	116	217.68	1	6	89.40
2011	14	114	135.51	1	2	105.26
2012	5	43	187.53	0	0	
2013	21	188	104.33	0	0	
2014	0	0		0	0	
2015	24	222	148.23	3	12	54.86
2016	12	97	64.95	11	78	106.75
2017	20	194	183.73	7	42	41.45
2018	31	277	56.43	7	30	37.90
2019	32	320	86.72	13	126	42.84

Table E2. -- Juvenile Chinook salmon diet expressed as percent stomach content index (SCI) during the northern Bering Sea surface trawl survey, 2004-2019.

Year	Sand Lance	Capelin	A0 Pollock	Pacific Herring	Other Fish	Decapod	Other	Unident. Fish
2004	30.75	18.52	26.29	14.01	0.16	8.21	1.11	0.94
2005	3.97	26.63	25.84	1.27	5.14	12.99	12.05	12.11
2006	35.24	16.69	10.22	0	15.95	3.58	1.37	16.95
2007	13.33	49.60	3.62	0	18.03	10.81	2.52	2.11
2009	35.76	19.79	0	0	16.78	6.14	2.03	19.50
2010	6.89	68.39	0	3.24	10.16	2.35	4.02	4.95
2011	20.52	40.65	0	15.38	3.71	5.03	2.50	12.22
2012	0	0	0	0.00	0	4.22	1.00	94.78
2013	12.93	63.05	0	8.33	0.57	4.31	5.86	4.95
2014	66.46	4.68	4.10	0	7.35	7.97	5.52	3.92
2015	73.43	5.44	3.07	3.04	3.37	7.93	1.91	1.82
2016	57.29	9.90	6.06	2.31	2.95	17.01	1.29	3.19
2017	40.37	11.00	2.67	7.95	17.61	6.81	5.30	8.29
2018	2.39	5.59	19.50	0	28.70	15.46	9.79	18.56
2019	12.98	0	21.00	28.08	0	22.78	4.18	10.99

Table E3. -- Juvenile coho salmon diet expressed as percent stomach content index (SCI) during the northern Bering Sea surface trawl surveys, 2004-2019.

Year	A0 Pollock	Capelin	Decapod	Other	Other Crustacean	Other Fish	Sand Lance	Unident. Fish
2004	40.07	2.43	15.71	0.3	1.5	23.75	15.69	0.55
2005	0	0	0.23	3.35	0	95.22	0	1.19
2006	24.35	1.35	11.56	3.44	0.36	14.46	33.36	11.13
2007	0	23.88	14.04	0	0	34.35	22.19	5.53
2009	20.1	28.35	0.42	0	1.21	0	36.18	13.75
2010	0	65.06	8.07	0	0.45	0	26.41	0
2011	0.23	44.41	1.95	0	0	9.35	43.47	0.59
2012	0	0	0	0	0.2	0	0	99.8
2013	0	0	0.17	0.16	0	11.18	88.35	0.14
2014	33.47	4.38	0.09	0.05	0.73	32.09	28.65	0.5
2015	15.92	13.28	14.58	0	0.11	27.66	13.56	5.09
2016	19.48	0	0.36	9.27	0.27	12.75	51.99	4.17
2017	0.59	6.22	1.23	2.46	1.65	10.68	36.36	35.13
2018	29.2	0	8.89	2.21	2.56	19	7.69	13.38
2019	53.93	0	2.51	1.37	0.62	13.28	7.22	18.86

Table E4. -- Juvenile chum salmon diet expressed as percent stomach content index (SCI) during the northern Bering Sea surface trawl surveys, 2004-2019.

Year	Gelatinous Prey	Sand Lance	A0 Pollock	Other Fish	Euphausiid	Hyperiid	Other Crustacean	Other	Unident.
2003	26.07	47.43	3.87	9.25	0.26	1.95	9.83	1.34	0
2004	36.91	4.64	13.72	14.47	6.38	7.84	15.97	0.08	0
2005	28.74	0	21.1	17.04	28.51	1.56	3.05	0	0
2006	20.49	44.64	1.76	27.34	3.88	0.67	1	0.22	0
2007	63.29	2.72	0	4.23	12.31	8.26	8.4	0.79	0
2009	42.23	9.44	0	23.5	0	22.97	1.54	0.33	0
2010	26.07	16.87	0	15.07	19.08	18.86	3.46	0.59	0
2011	49.91	0	0	17.87	11.97	12.37	6.56	1.33	0
2012	43.81	4.32	0	7.8	10.29	7.27	3.2	23.31	0
2013	27.13	11.29	0	6.95	4.03	46.42	3.38	0.8	0
2014	7.73	17.7	0.51	26.7	18.59	8.36	7.42	6.11	6.88
2015	30.65	27.9	0	24.56	0.55	10.61	5.09	0.64	0
2016	56.1	0	0	16.96	0	1.37	4.02	21.55	0
2017	7.86	5.2	0	48.89	20.88	0.41	2.27	14.48	0
2018	18.86	0	0	6.22	35.88	2.92	0.41	0.03	35.67
2019	60.28	0	3.65	5.7	0.06	0.32	2.92	0.01	27.08

Table E5. -- Juvenile pink salmon diet expressed as percent stomach content index (SCI) during the northern Bering Sea surface trawl surveys, 2004-2019.

Year	A0 Pollock	Copepod	Decapod	Other	Gelatinous Prey	Other Fish	Sand Lance	Euphausiid	Hyperiid	Unident.
2003	29.18	0.96	4.75	0	0	40.46	8.66	14.19	1.8	0
2004	14.98	6.55	28.36	1.47	1.4	5.07	26.75	11.83	3.59	0
2005	25.46	0.4	15.86	1.58	3.36	28.19	3.15	16.65	5.35	0
2006	1.48	3.28	10.16	4.21	3.59	26.53	47.26	0.89	2.59	0
2007	0.37	9.5	29.96	5.24	8.97	17.11	3.96	7.86	17.05	0
2008	0	0	30	0	0	0	50	0	20	0
2009	0	6.03	1.92	7.64	15.72	22.27	26.64	2.47	17.32	0
2010	0	1.16	1.96	0.62	6.75	16.3	9.7	56.78	6.72	0
2011	0	24.38	19.73	2.14	6.39	3.14	12.55	0.12	31.55	0
2012	0	1.96	3.95	0	0	28.43	0	40.91	5.72	19.01
2013	0	2.16	5.09	0.56	9.04	21.01	2.69	9.88	49.57	0
2015	0	6.21	5.21	0.73	5.02	2.65	63.49	9.44	7.24	0
2016	0	33.11	17.2	2.62	4.92	23.34	8.47	0	0.61	9.71
2017	0	35.78	3.31	0.25	0	12.24	2.35	38.56	0.59	6.93
2018	0	12.54	2.34	5.08	0.79	8.34	0	32.32	8.24	30.35
2019	0.27	45.45	2.52	0.56	3.73	16.88	0.52	3.15	0.47	26.46

Table E6. -- Juvenile sockeye salmon diet expressed as percent stomach content index (SCI) during the northern Bering Sea surface trawl surveys, 2004-2019.

Year	Copepod	Sand Lance	A0 Pollock	Other Fish	Thysanoessa spp.	Decapod	Other Crustacean	Other	Unident.
2004	3.68	7.87	61.15	0.44	5.17	14.78	4.63	1.55	0.74
2005	0	0	0	0	0	0	0.96	30.03	69.01
2006	0	0	0	0	33.04	47.5	4.73	14.72	0
2007	26.97	0	0	0.49	4.83	0.65	12.08	55.03	0
2009	0	100	0	0	0	0	0	0	0
2010	0	0	0	0	95	0	0	5	0
2011	0	0	0	70	0	30	0	0	0
2015	5.91	0	9.44	0	0.2	73.57	9.45	0.24	1.19
2016	1.42	4.33	4.17	0	2.12	11.85	7.26	36.05	32.8
2017	0	0	0	0	77.67	1.68	0.27	0	20.38
2018	2.98	0	0	1.92	41.9	3.34	1.14	4.05	44.67
2019	7.86	0	17.71	4.19	5.2	12.67	1.49	9.01	41.86

CHAPTER 16 - Multi-Year autonomous observations of Seasonality in movement, behavior, and growth of pelagic fishes in the Chukchi Sea

Objective 5: Further resolve early life history characteristics of Arctic cod and saffron cod and their behavior and connectivity between the Chukchi Sea and western Beaufort Sea.

Robert M. Levine[1*], Alex De Robertis[2], Daniel Grunbaum[1], Christopher D. Wilson[2]

*Corresponding Author, Leviner@uw.edu, 1503 NE Boat St Seattle, WA 98195, USA

[1]School of Oceanography, University of Washington, Seattle, Washington

[2]Alaska Fisheries Science Center, National Marine Fisheries Service, Seattle, Washington

Key words: Arctic cod, polar cod, *Boreogadus saida*, *Gadus chalcogrammus*, acoustics, moorings, transport, Chukchi Sea

Abstract

Recent summer surveys of the Chukchi Sea determined that pelagic fishes were dominated by large numbers of age-0 Arctic cod and walleye pollock, while adult fishes are comparatively scarce. Transport modeling based on regional currents indicates that these age-0 fishes are likely advected to the north in fall. However, the source and fate of these fishes remains unclear, as sampling in this region is impeded by seasonal ice cover. To determine the movement and seasonal variability of this age-0 gadid population, seafloor-moored echosounders were deployed at three locations in the northeastern Chukchi Sea from 2017-2019. Year-round observations indicate that the abundance and composition of the pelagic community on the Chukchi Sea shelf is highly variable over seasonal time scales. Fish abundance was very low in winter, increased in May, and reached peak abundance in late summer in both years. Fish tracking indicated that fish velocities and headings were strongly correlated with local currents. Two modes of direction were apparent; movement was primarily to the northeast with periodic reversals towards the southwest driven by changes in regional wind. The displacement of age-0 gadids to the northeast is consistent with the dominant patterns of advection on the shelf, and the flux of fishes indicates that a large portion of the population present on the Chukchi shelf in summer is likely transported to the northeast, resulting in low abundances of age-1+ fishes present in summer.

Introduction

The Chukchi Sea is a highly seasonally dynamic region, serving as the pathway for Pacific water into the Arctic basin. The shallow continental shelf is covered by sea ice in late winter and spring before warm water from the south initiates the retreat of ice in spring (Woodgate et al., 2010) leading to a largely ice-free summer. Seasonal sea ice extent in the Chukchi has declined over recent decades (Frey et al., 2015) and is predicted to continue to decrease at a rate of 0.94 days year^{-1} (Wang et al., 2018) as temperatures in the region continue to increase (Danielson et al., 2020). These changes are expected to alter the ecology of endemic Arctic fishes and enable further intrusion of boreal species, moving the southern boundary of Arctic species northward and altering composition of the local ecosystem (Mueter et al., 2021).
Age-0 gadids, particularly Arctic cod (*Boreogadus saida*), dominate the pelagic fish community on the Chukchi shelf in summer (De Robertis et al., 2017). Arctic cod is a circumpolar distributed species found throughout the Arctic basin and surrounding shelves (Mecklenburg et al. 2018). Arctic cod are common throughout the region (Lowry and Frost 1981; Rand and Logerwell 2011; De Robertis et al., 2017), where they are a key pelagic component of energy transfer between lower and upper trophic levels (Whitehouse et al., 2014). However, while large numbers of age-0 Arctic cod have been observed in the Chukchi in summer, adult fishes were comparatively scarce (De Robertis et al., 2017; Levine et al., in review). The

observed density of adult Arctic cod does not have the reproductive potential to produce the population of age-0 fishes observed on the shelf in summer and thus these fishes likely originated elsewhere (Marsh et al., 2019). Arctic cod are known to spawn under sea ice (Ponomorenko et al., 2000). Although the source of these age-0 Arctic cod has not been confirmed, modeling studies of regional advection indicate that these age-0 Arctic cod may originate in the southern Chukchi or northern Bering Seas in winter and early spring (Deary et al., 2021; Vestfals et al., 2021).

The composition of the pelagic community is changing under current warming conditions. Boreal species such as walleye pollock (*Gadus chalcogrammus*) make up an increasing portion of the age-0 gadid community (Wildes et al., in review; Levine et al., in review). As a result of recent warming, the distribution of adult pollock in the Bering Sea has shifted, with high densities of mature adults in the northern Bering Sea (Stevensen and Lauth, 2019; Eisner et al., 2020). The age-0 pollock in the Chukchi Sea are hypothesized to originate from this large population of adult fishes south of Bering Strait (Levine et al., in review). Eggs and larvae from this northern Bering population are likely to be transported north along with the movement of water through Bering Strait (Woodgate et al., 2005).

The Chukchi shelf is hypothesized to be an important nursery area for these age-0 fishes in summer (De Robertis et al., 2017; Levine et al., 2021), where relatively warm temperatures support high growth rates for both Arctic cod and pollock (Laurel et al., 2018) that are necessary to maximize growth prior to experiencing winter conditions. However, it remains unclear whether the abundant age-0 fishes observed in summer provide recruits to other areas or act as an ecological sink with fish not surviving through winter (De Robertis et al., 2017). As development of age-0 gadids is largely temperature-dependent (Laurel et al., 2018), the potential fates of populations observed on the Chukchi shelf may depend on their movement into environments conducive to survival during winter. Identifying the mechanisms and pathways by which these fish are distributed across the Chukchi shelf will help to further constrain the fate of this age-0 population and help predict how ongoing environmental changes will further alter their abundance and distribution in the region.

Advection from the south structures the distribution of the planktonic communities in the Chukchi in summer (Eisner et al., 2013; Danielson et al., 2017; Pinchuk and Eisner, 2017; Spear et al., 2020). Northward currents are also hypothesized to exert a strong influence on the gadid populations, as larvae are likely passively transported (Vestfals et al., 2019; Vestfals et al., 2021). Repeat surveys in 2018 indicated that advection played a key role in the distribution of age-0 gadids on the Chukchi shelf in summer (Levine et al., 2021). Periods of on-shelf retention of the population were likely important for growth for these small fishes, prior to their being transported off the shelf towards the Beaufort Sea and Central Basin in fall (Levine et al., 2021). While modeling studies based on summer distributions have hypothesized the passive northward movement of fishes (Deary et al., 2021; Vestfals et al., 2021), there are no direct observations to validate whether the large age-0 population observed in summer is transported to other areas or if this region serves as a sink with fishes failing to survive through winter conditions. If advection is the primary mechanism of distribution, mooring and radar observations and model output of currents provide opportunities to predict changes in distribution of these age-0 fishes on the Chukchi shelf.

Historically, direct observations of fishes in ice covered areas have been rare. Because access to ice-covered areas is limited and traditional trawling gear cannot be used, sampling has been restricted in spatial and temporal extent (Lønne and Gulliksen, 1989; Gradinger and Bluhm, 2004; Melnikov and Chernova, 2013). To monitor fishes during periods of ice cover, acoustic observations of pelagic fishes have been collected from ships (Benoit et al., 2008) and autonomous underwater vehicles operating under sea ice (Fernandes et al., 2003). Net systems designed to sample in ice have made it easier to collect specimens under sea ice over a greater area (Flores et al., 2012; David et al., 2016). However, these methods are logistically difficult and expensive. Winter surveys rely on ships with ice-strengthened hulls to provide access to areas that are seasonally inaccessible, and the deployment of autonomous platforms

or net systems are typically limited to a few discrete locations and collect observations over relatively short periods of time.

In seasonally ice-covered regions, moored instrumentation can be deployed during the ice-free period and left to collect data year-round. In these seasonal ice zones, acoustic doppler current profilers (Wallace et al., 2010) and echosounders (Miksis-Olds et al., 2013; Darnis et al., 2017; Kitamura et al., 2017; Gonzalez et al., 2021) have used acoustic observations to study zooplankton and fish dynamics during extended periods of ice cover. However, moorings have not been previously used to collect long-term observations of fish population movements through ice-covered regions. Moored echosounders can be used to collect continuous data to study fish abundance and fine-scale behavior (Trevorrow, 2005; Kaartvedt et al., 2009; Urmy et al., 2012; Ross et al. 2013; De Robertis et al., 2018). Detection of individual scatterers from split-beam observations can also be used to infer the size composition, transport, and behavior of fishes from moored platforms. While acoustic observations offer limited capacity to identify sound-scattering organisms, in low-diversity regions where backscatter is dominated by a single species or group, moorings can be used to infer information about the population as the primary species are known and interpretation of the acoustic signal is less dependent on the collection of biological samples. For example, if the species of the primary scatterers is known, length can be inferred from acoustic target size using established target strength-length (Traynor, 1996; Geoffroy et al., 2016). Angular information can be used to assess the location of a fish in the water column, and over sequential observations can be used to infer swimming speed and direction (Ehrenberg and Torkelson, 1996).

This study presents two years of near-continuous observations of age-0 gadids collected by seafloor-mounted echosounders at three sites in the northeastern Chukchi Sea. The primary objectives of this study were to characterize the seasonal patterns in pelagic fish abundance in the Chukchi Sea, and to determine the role of advective transport and fish behavior in the movement of age-0 gadids. Year-round observations enabled us to resolve the timing and seasonal dynamics of the pelagic ecosystem, helping to constrain the potential spawning region and determine the fate of the large juvenile population of fishes present during the summer months.

Methods

Mooring deployments

Three moorings were deployed in the northeastern Chukchi Sea in locations where fish densities had previously been observed to be high in summer (De Robertis et al., 2017). The moorings were deployed for two years at 71.03N 160.50W (49 m depth), 70.83N 163.11W (44 m depth), and 70.01N 166.85W (47 m depth) (Figure 4.1). The moorings were initially deployed between 08-15 August 2017, recovered and redeployed between 12-15 August 2018 after data recovery and maintenance, then recovered between 26 August and 05 September 2019 at the completion of the field program.

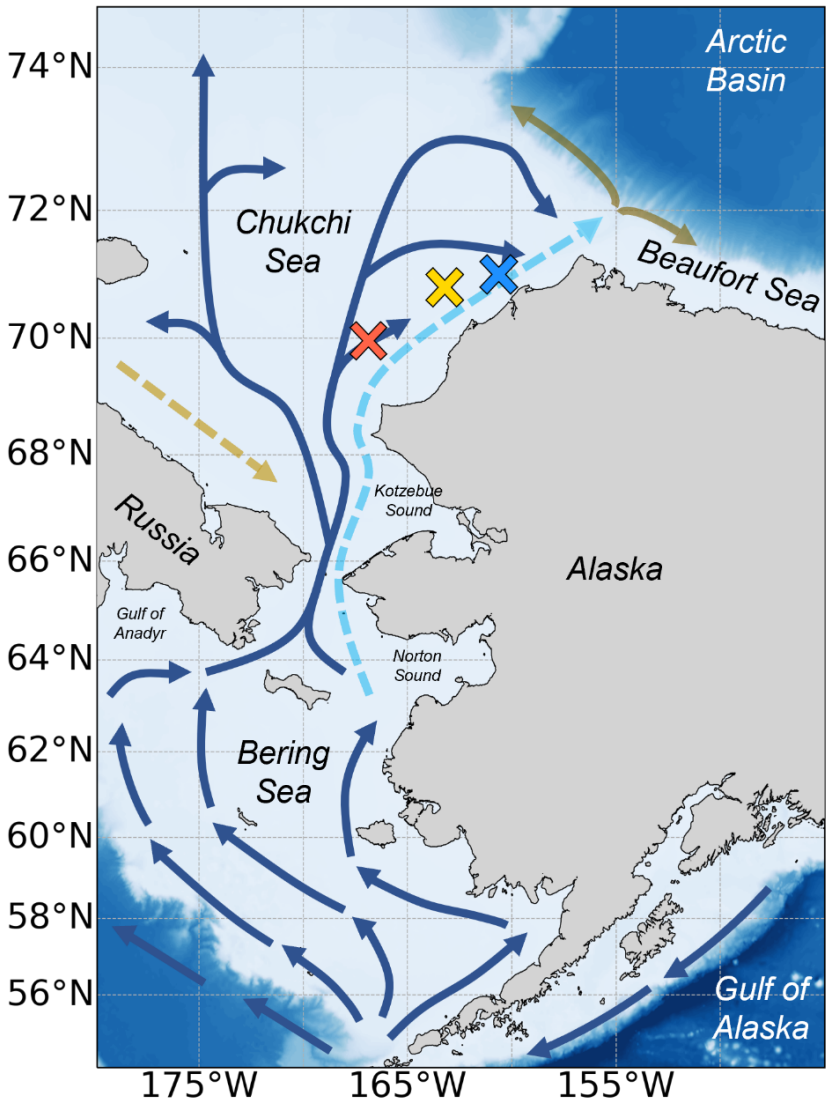

Figure 4.1 Map of the study region, showing the primary transport pathways through the Bering and Chukchi Seas based on Corlett and Pickart (2017) and Levine et al. (2020): Alaskan coastal current (light blue), Bering Sea water (dark blue), Siberian coastal current (gold), slope current (brown, westward) and shelf break jet (brown, eastward). Dashed lines indicate seasonal currents. The locations of the southern (red), central (yellow), and northern (blue) mooring sites are indicated by an x.

Composition of acoustic scatterers

The Chukchi Sea is well-suited for the use of autonomous acoustics. In the low diversity pelagic community of the Chukchi shelf, backscatter is dominated by a single species or group which simplifies the process of inferring species from backscatter. Acoustic-trawl surveys in the northeastern Chukchi Sea in 2012 and 2013 identified age-0 Arctic cod as the primary scatterers (De Robertis et al., 2017). Recent surveys during the mooring deployment period in summer 2017 and 2019 similarly found that age-0 gadids, particularly Arctic cod and walleye pollock, were the dominant pelagic scatters, accounting for 94.3% and 88.3% of the survey backscatter in 2017 and 2019, respectively (Levine et al., in review). Genetic analyses have confirmed that the increase in the proportion of pollock within the gadid community appears to have occurred during the period of these surveys (Wildes et al., in review). Thus,

walleye pollock were likely present throughout the deployment period. Other strong sound scattering pelagic fishes such as capelin (*Mallotus villosus*) and Pacific herring (*Clupea pallasii*) were present only in comparatively low abundances and accounted for < 6% of backscatter during summer surveys in both 2017 and 2019 (Levine et al., in review). Therefore, we assume that the primary contributors to backscatter were age-0 gadids, and that acoustic-based measures of fish density reflect the abundance and distribution of age-0 Arctic cod and walleye pollock.

Mooring Instrumentation

The mooring platforms were designed to be low profile to maximize the range of water column sampled by the echosounder, and to minimize the likelihood of damage due to sea ice. Each mooring was composed of two stacked 1.2 by 1.8 m fiberglass grates, separated with 0.2 m spacers (Supplementary Figure 4.1). The moorings were anchored to the seafloor by 23 kg lead feet positioned on each corner. The feet were replaced with 18 kg steel discs during the second year of deployment to reduce the mooring weight in order to increase the safety margin during recovery. Each mooring contained two acoustic release pop-up recovery packages (EdgeTech PORT-MFE) containing 100 m of recovery line connecting a hoist point on the mooring to a 15.4 cm diameter syntactic foam-filled float. All scientific instrumentation was mounted to the upper grate (Supplementary Figure 4.1).

The moorings were instrumented with battery-powered scientific echosounders (wideband autonomous transceiver, Simrad AS). Each echosounder operated an upwards facing depth-rated 70 kHz 18° split-beam transducer (ES70-18CD), positioned upward in a two-axis gimbal equipped with a 0.7 kg counterweight. Each echosounder also operated a combined 38 kHz 18° split-beam and 200 kHz 18° single-beam transducer (ES38-18/200-18C) mounted to the grating without a gimbal. Both transducer faces were positioned at a height of 0.8 m above the seafloor. During the deployment, the echosounders transmitted an ensemble of 300 pings (200 pings at 70 kHz, 100 pings at 38 and 200 kHz) at a ping rate of 0.4 s every two hours. Data were recorded to a range of 60 m. The echosounders were calibrated at the surface using a 38.1-mm tungsten carbide sphere, following the standard sphere method (Demer et al., 2015; Renfree et al., 2019). Echosounders used in 2017-2018 were calibrated prior to deployment. The echosounders used in 2018-2019 were calibrated following their final recovery, because the transducers recovered in summer 2018 were immediately redeployed. Due to a post-recovery instrument failure, the echosounder and transducer configuration deployed at the southern mooring site could not be calibrated. The average gains of the five other instrument calibrations were used for data processing along with the factory-specified beamwidth. The average gains for each frequency were 19.12 (±0.80 SD) dB at 38 kHz, 19.98 (±0.86 SD) dB at 70 kHz, and 17.98 (±0.55 SD) dB at 200 kHz. These calibrations did not account for potential pressure effects; however preliminary field experiments using the ES70-18CD transducer indicate that targets strength observations vary by <1.2 dB up to 100 m transducer depth (De Robertis, unpublished).

To determine the heading of the transducers when settled on the seafloor, each mooring was deployed with a calibrated compass mounted at a fixed position aligned with the forward direction of the transducers. Deployments used either a custom underwater magnetometer produced by the Engineering Development division of the NOAA Pacific Marine Environmental Lab or an Aaronia GPS Logger (Aaronia AG) sealed in a custom waterproof PVC pressure housing. Measurements were recorded for 0.3 - 385 d of each deployment due to variability in the battery life of each compass. Compasses in four deployments recorded for > 295 d, during which the hourly mean headings varied by < 5° (Supplementary Figure 4.2). These long-duration compass recordings confirmed that mooring orientations were stable throughout the deployment. The mode of all observations collected after deployment, corrected for magnetic declination at each site, was used to represent the mooring orientation (Table S4.1).

Acoustic data processing

Acoustic data were recorded from 8 August 2017 to 26 August 2019 at the southern site, 9 August 2017 to 4 September 2019 at the central site, and 15 August 2018 to 5 September 2019 at the northern site.

Data were not available for the northern mooring site for the 2017-2018 deployment as a result of instrument failure. In addition, the 38 kHz channel at the central mooring site failed during the 2018-2019 deployment. Thus, only the 70 and 200 kHz data were included in analyses. Due to interference (likely from side-lobe reverberation) appearing at 16-20 and 27-30 m depth at 200 kHz at the central mooring site during the 2018-2019 deployment, only data within those ranges where the signal was 10 dB higher than the noise level were included.

Acoustic data were processed using Echoview 12.0 (Echoview Software Pty Ltd). 70 kHz backscatter was used as a proxy for fish abundance. The depth of the sea surface/ice echo was determined by Echoview's threshold offset operator with a minimum detection threshold of -50 dB re 1 m^{-1} below the surface/ice, and manually corrected after visual inspection. The nautical area backscattering coefficient (s_A, m^2 nmi^{-2}; MacLennan et al., 2002) for all frequencies was echo-integrated in 1-m bins from 2 m above the transducer to 2 m below the sea surface/ice echo for every 2-h ensemble. The weighted mean depth ("centre of mass" in Urmy et al., 2012, their Table 1) of s_A was calculated for each ensemble. To investigate seasonality of diel vertical migration, the difference between the weighted mean depth of fishes at maximum and minimum solar altitude was calculated, determined as a function of datetime and location using the Pysolar library for Python (http://pysolar.org/).

The strength of backscatter across frequencies varies as a function of animal scattering properties (reviewed in Benoit-Bird and Lawson, 2016) and can be used to differentiate among key groups of scatterers (Jech and Michaels, 2006; De Robertis et al., 2010). Higher backscatter at 200 kHz than 70 kHz is indicative of scattering from zooplankton, while gadids exhibit higher scattering at 70 kHz than 200 kHz (De Robertis et al., 2010). To investigate potential changes in the composition of acoustic scatterers over the length of the deployment, the difference between the mean 70 kHz and 200 kHz S_v ($\Delta S_{v,70\text{-}200}$, dB) for each ensemble was calculated as used to infer dominant scatterer type.

Fish tracking and flux estimates

Echoes from individual fishes were identified with Echoview's split-beam single target detection (method 2), using a detection threshold of -70 dB re 1 m^{-2}. To minimize the potential bias due to overlapping targets being interpreted as a single fish, single target detection was limited to portions of the water column where density was low. The estimated number of animals per reverberation volume (Nv, Sawada et al., 1993) was calculated in 5-m vertical bins for each ensemble using a target strength of -55.5 dB re 1 m^{-2}, which assumes a mean Arctic cod size of approximately 4.5 cm (Geoffroy et al., 2021; Levine et al., in review). Single targets in grid cells where Nv > 0.04 were excluded as recommended by Sawada et al. (1993). Single targets were joined into individual fish trajectories using Echoview's 4D alpha-beta tracker (Blackman, 1986; see Table S4.2 for parameters). A minimum of 5 single targets was required with a maximum gap of 5 pings (2 s). The mean target strength (TS, dB re 1 m^{-2}) of each tracked fish was calculated as the mean TS of the single targets contained in each track, calculated from the mean of the linear TS values (σ_{bs}, m^2). Fish headings were calculated by fitting a 3-dimensional linear model with respect to time to the single target detections assigned to each fish track. Headings were converted from a coordinate system relative to the transducer into a geographic reference frame based on the compass orientation.

Speed was calculated by dividing the total distance along the model-fit linear track by the duration of the track. In addition to representing the net displacement of tracks through the acoustic beam, the use of the linear model also reduced range-dependent errors associated with the angular resolution of split-beam transducers. As range increases, angular errors as a result of the discrete resolution of 0.1125° in the acoustic data correspond to greater increases in the calculated physical distance between targets, resulting in a range-dependent increase in track speed (Klevjar and Kaartvedt, 2003). This bias was reduced by using a linear model compared with a B-spline or similar curve fitting representations, for tracks in which the distance between control points is likely to be affected by such angular errors (Supplementary Figure 4.3).

Fish density (fish m^{-2}) was calculated at each ensemble using the mean of the observed linear target strengths (σ_{bs}, m^2) and area backscattering coefficient (s_a, m^2 m^{-2}) following MacLennan et al. (2002). The flux of fish (Q, fish m^{-1} s^{-1}) was estimated using the fish density (A) and mean speed and direction of tracks during each ensemble, such that:

$$QQ = AAVV \quad (4.1)$$

Velocity (V) was calculated along the dominant direction of movement, defined as the mode of track headings (in 5° bins) for all tracks observed at each site (hereafter referred to as the reference heading). Thus, flux represents the number of fishes per second crossing underneath a 1 m line of the sea surface perpendicular to the reference heading.

Environmental data

Bottom temperature and salinity were measured using a conductivity, temperature, and depth (CTD, SeaBird 37) sensor mounted on each mooring. Hourly current measurements were derived from acoustic doppler current profilers (ADCP, Teledyne RD Instruments WorkHorse operating at either 300 or 600 kHz varying by site and year) deployed <500 m away from the echosounder moorings (see Stabeno et al., 2018 for details on data processing). To investigate the relationship between currents and fish tracks along a uniform direction, current velocities relative to the reference heading were calculated from the zonal (east-west) and meridional (north-south) components of each depth bin. Fish tracks were matched with the closest ADCP measurement in time and depth.

Sea ice concentrations were obtained from the NOAA/NSIDC Climate Data Record of Passive Microwave Sea Ice Concentration, Version 3 (Peng et al., 2013; Meier et al., 2017). Daily measurements were extracted from the 25 by 25 km grid cell that contained each mooring site. The NCEP/NCAR reanalysis (Kalnay et al., 1996) wind forecasts were used to estimate the wind speed and direction. Near-surface (0.995 sigma level) values of zonal and meridional wind, available in 6-h intervals, were obtained from the 2.5° grid cell nearest to each mooring.

Results

Seasonal characteristics of acoustics scatterers

Backscatter was highest during the late-summer and early fall, decreasing in winter and then increasing the following June/July across all sites during both years of deployment (Figure 4.2). Backscatter was lowest in early spring in all deployments. In early summer of 2018 and 2019, high backscatter first developed in the upper water column, deepening over the course of the summer (Figure 4.2a-c), indicating that the fish increased their depth distribution in summer.

Strong seasonal variability in pelagic community composition is demonstrated by the difference in volume backscatter observed at 70 and 200 kHz ($\Delta S_{v,70\text{-}200}$, Figure 4.3). In winter, $\Delta S_{v,70\text{-}200}$ is consistent with zooplankton-like scatterers at all three sites (blue regions, Figure 3). Fish-like scatterers (red regions, Figure 4.3) appear concurrently with the increase in backscatter in early summer (Figure 4.2). The highest backscatter occurs during periods when $\Delta S_{v,70\text{-}200}$ indicates that the backscatter is dominated by fish-like scatterers ($\Delta S_{v,70\text{-}200}$ > -5 dB, Figure 4.4), consistent with previous summer survey observations of small fishes dominating pelagic backscatter (De Robertis et al., 2017; Levine et al., in review). Thus, further analyses interpreted backscatter as a proxy for fishes (as described in the methods above.)

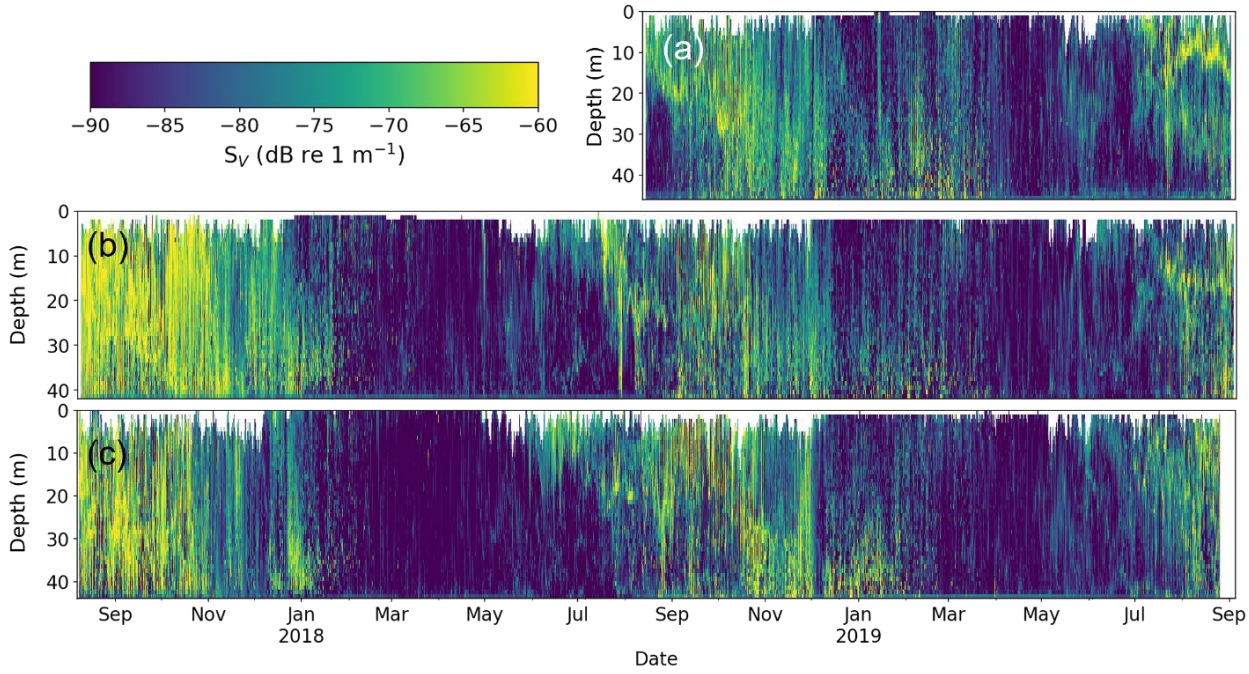

Figure 4.2 Echogram of 70 kHz mean volume backscattering strength (S_v, dB re 1 m^{-1}) recorded during each 2-h ensemble from 7 August 2017 to 06 September 2019 at the (a) northern, (b) central, and (c) southern mooring. Each point represents the mean of all observations in a 1 m depth bin of the water column recorded every 2 hours. White portions of the echogram indicate areas of no data due to the removal of backscatter from the sea surface and ice.

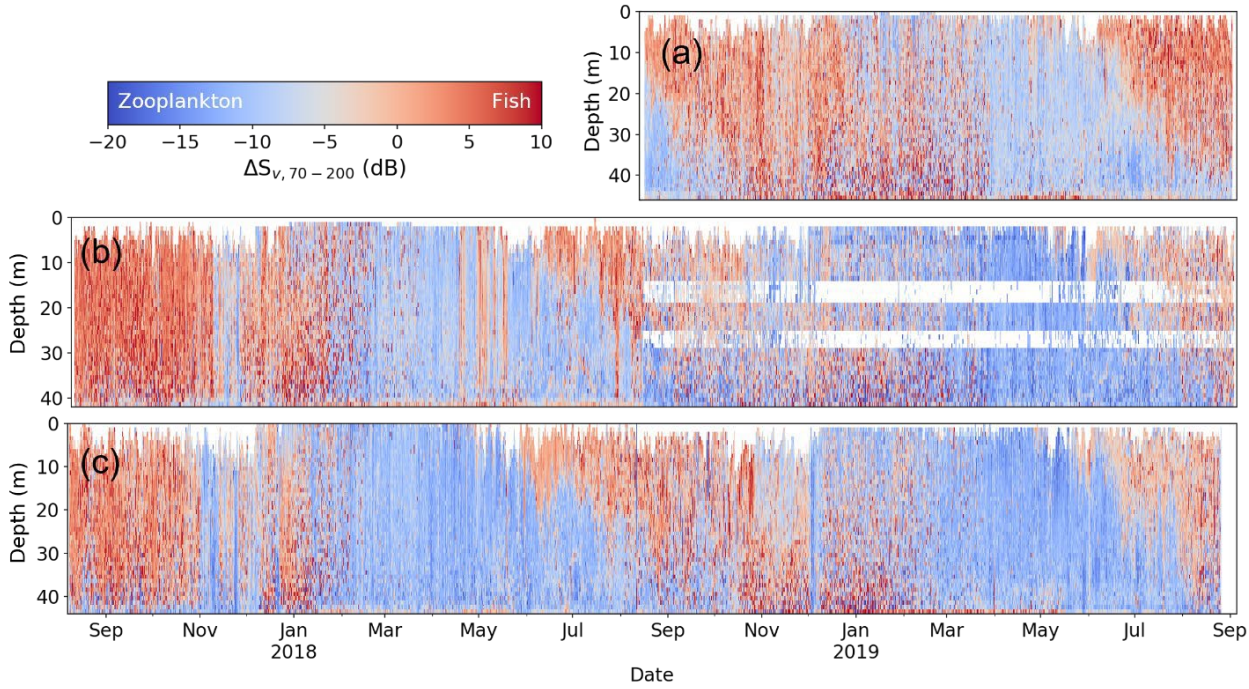

Figure 4.3 Echogram of difference between 70 kHz and 200 kHz volume backscatter ($\Delta S_{v,70\text{-}200}$, dB) for the complete time series at the (a) northern, (b) central, and (c) southern mooring. Red indicates bins where S_v is greater at 70 kHz (fish-like scatterers) and blue indicates bins where s_A is greater at 200 kHz (zooplankton-like scatterers). Each point represents the mean of all observations in a 1 m depth bin of the water column recorded every 2 hours. White portions of the echogram indicate areas of no data due to the removal of backscatter from the sea surface and ice. Due to interference between 16-20 and 27-30 m depth at 200 kHz at the central site during the 2018-2019 deployment, data where the signal was <10 dB higher than the noise level were removed.

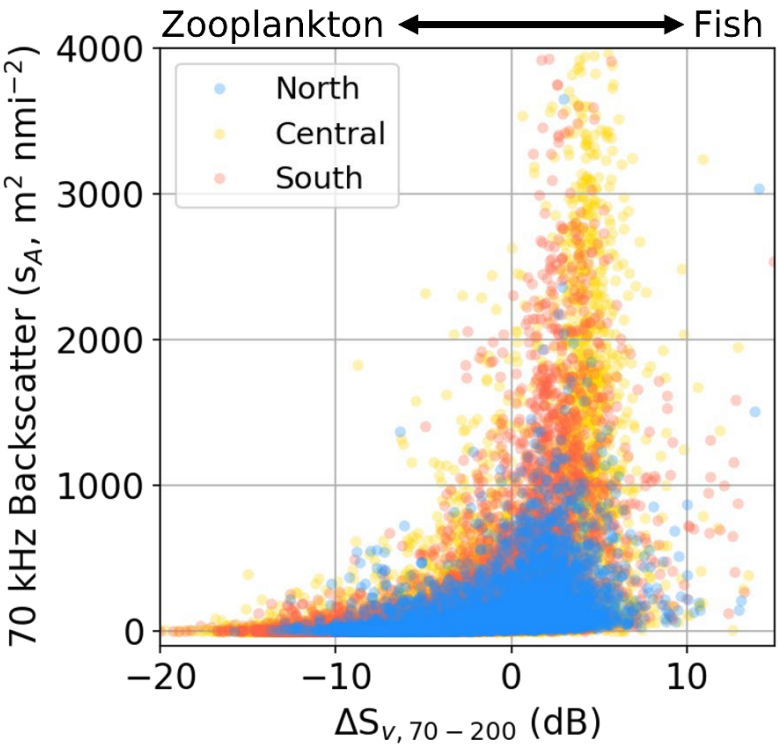

Figure 4.4 Daily mean 70 kHz backscatter (s_A, m^2 nmi^{-2}) as a function of the mean difference between 70 kHz and 200 kHz volume backscatter ($\Delta S_{v,70\text{-}200}$, dB) for each ensemble at the northern (blue), central (yellow), and southern (red) mooring sites. Higher values indicate the prevalence of fish-like scatterers.

Seasonal changes in fish size, abundance, and vertical distribution

Acoustic backscatter indicates that there was strong seasonality in the abundance, size, and vertical distribution of pelagic fishes at all three mooring sites (Figures 4.2, 4.5b, 4.6b, 4.7b). Fish abundance began to increase in July in both 2018 and 2019, peaking in fall. During this period, target strengths were high, consistent with the $\Delta S_{v,70\text{-}200}$ indicating the presence of fishes (Figures 4.5c, 4.6c, 4.7c). Target strengths in summer were consistent with previous observations of scattering from age-0 gadids (TS of ~-55 dB re 1 m^{-2} at 5 cm length, Geoffroy et al., 2016). Given the limited observations of target strengths consistent with large scatterers (e.g., TS ~-35 for a 35 cm adult pollock; Traynor, 1996), there was little evidence of a significant number of larger fishes throughout the deployments (Supplementary Figure 4.4a). Abundance was highest when bottom temperatures were greater than ~1 °C (Figure 4.8a) which was observed at all sites in late summer and fall (Figures 4.5a, 4.6a 4.7a).

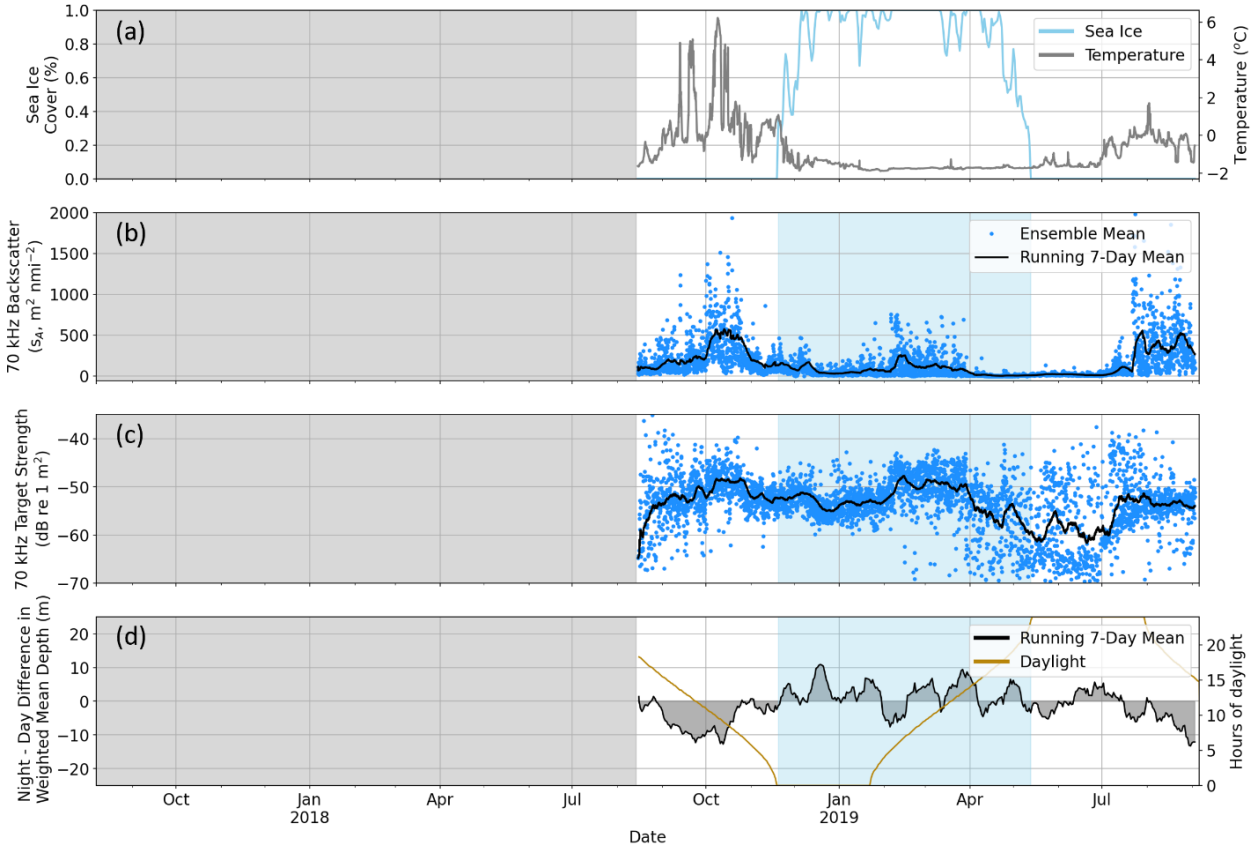

Figure 4.5 Time series of the northern mooring site. (a) Sea ice concentration of the nearest 25 km^2 grid cell of satellite observations (blue line) and bottom temperature recorded by the conductivity, temperature, and depth sensor mounted on the mooring platform (grey line). Mean of each 2-hour ensemble (blue points) and running 7-day mean (black line) of (b) water column 70 kHz backscatter (s_A) and (c) 70 kHz target strength. (d) Running 7-day mean difference in weighted mean depth of 70 kHz backscatter between minimum (night) and maximum (day) solar altitude. The gold line indicates the number of hours of daylight. Blue shading (panels b, c, and d) indicates periods when sea ice concentration was > 20%. Due to instrument failure, data are not available for the northern mooring site from the 2017-2018 deployment (grey region).

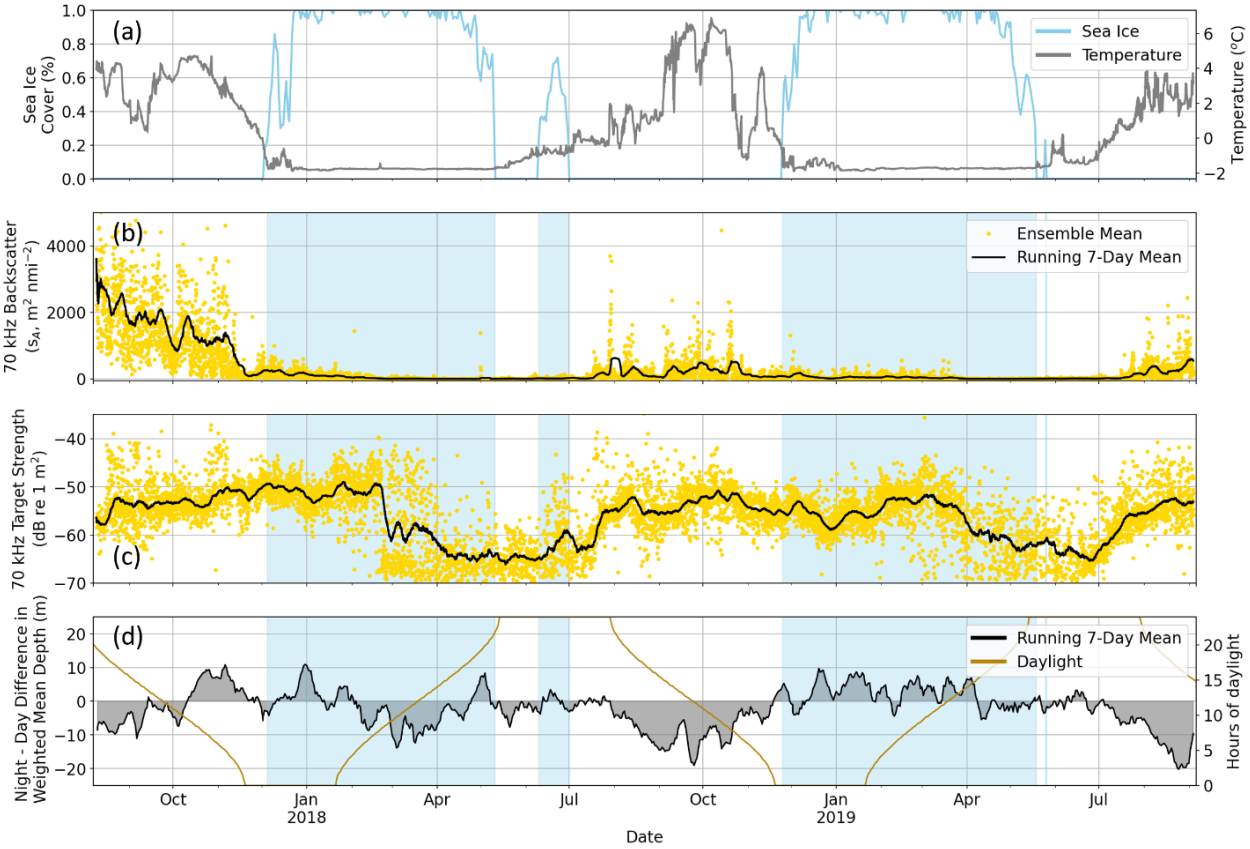

Figure 4.6 Time series of the central mooring site. (a) Sea ice concentration of the nearest 25 km^2 grid cell of satellite observations (blue line) and bottom temperature recorded by the conductivity, temperature, and depth sensor mounted on the mooring platform (grey line). Mean of each 2-hour ensemble (yellow points) and running 7-day mean (black line) of (b) water column 70 kHz backscatter (s_A) and (c) 70 kHz target strength. (d) Running 7-day mean difference in weighted mean depth of 70 kHz backscatter between minimum (night) and maximum (day) solar altitude. The gold line indicates the number of hours of daylight. Positive and negative values are shown in blue and red, respectively. Blue shading (panels b, c, and d) indicates periods when sea ice concentration was > 20%.

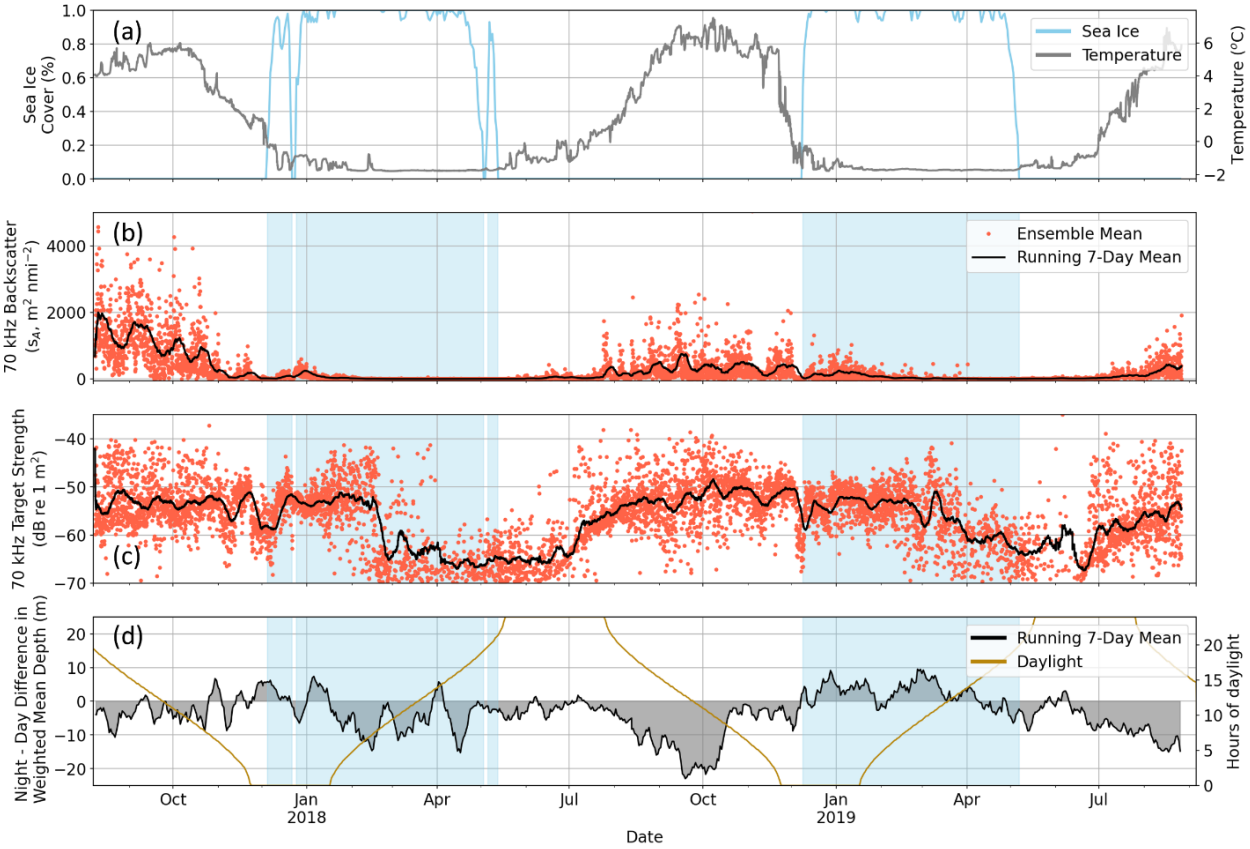

Figure 4.7 Time series of the southern mooring site. (a) Sea ice concentration of the nearest 25 km^2 grid cell of satellite observations (blue line) and bottom temperature recorded by the conductivity, temperature, and depth sensor mounted on the mooring platform (grey line). Mean of each 2-hour ensemble (red points) and running 7-day mean (black line) of (b) water column 70 kHz backscatter (s_A) and (c) 70 kHz target strength. (d) Running 7-day mean difference in weighted mean depth of 70 kHz backscatter between minimum (night) and maximum (day) solar altitude. The gold line indicates the number of hours of daylight. Positive and negative values are shown in blue and red, respectively. Blue shading (panels b, c, and d) indicates periods when sea ice concentration was > 20%.

Between August and October, night-day differences in weighted mean depth of fish increased (Figures 4.5d, 4.6d, 4.7d), with the greatest difference occurring during periods of 14-20 hours of daylight (Figure 4.9). Beginning in October, fish transitioned to be deeper during the day, showing less diel variability as day length shortened (Figures 4.5d, 4.6d, 4.7d, 4.9). As sea ice concentration over the moorings increased in November and December, fish abundance decreased. The onset of sea ice was associated with decreased fish abundance: mean backscatter was 2.8-7.5 times lower at all three mooring sites when sea ice concentration was > 20% (t-test on log-transformed 70 kHz s_A, $p<0.001$ at all sites, Figure 4.8b). However, target strengths remained consistent, indicating that fish of similar size were still present, though in reduced numbers (Figures 4.5, 4.6, 4.7).

In winter, the backscatter observations indicated that fish densities were very low at all three sites, with the lowest abundances occurring in late-winter and early spring. Target strength decreased substantially during this period, reflecting a transition in scatterer type, likely from small swim-bladdered gadids to a zooplankton-dominated pelagic community with lower target strengths (Figures 4.5c, 4.6c, 4.7c). The change in the frequency response also supports this inference. Unlike in summer, where $\Delta S_{v,70\text{-}200}$ was high, higher backscatter was observed at 200 kHz than 70 kHz throughout the water column from

approximately March to May of both years (lower values of $\Delta S_{v,70\text{-}200}$, blue regions Figure 4.3). Among the few periods where fish-like scatterers (> -60 TS) dominated the water column during early winter, vertical distribution remained deep throughout day and night with little evidence of migration (Figure 4.9).

Following the retreat of sea ice in May, bottom temperatures and fish abundance increased. Changes in the $\Delta S_{v,70\text{-}200}$ indicated a transition to fish-like scatterers in June and July beginning near the surface (Figure 4.3). Fishes appeared to grow during this period, as evidenced by increases in target strength (Figures 4.5c, 4.6c, 4.7c). As fish size increased, their night-day depth differences also increased (Figures 4.5d, 4.6d, 4.7d), consistent with the onset of vertical migration behavior. Day-night depth differences peaked in fall when the length of daylight and darkness are approximately equal (Figure 4.9).

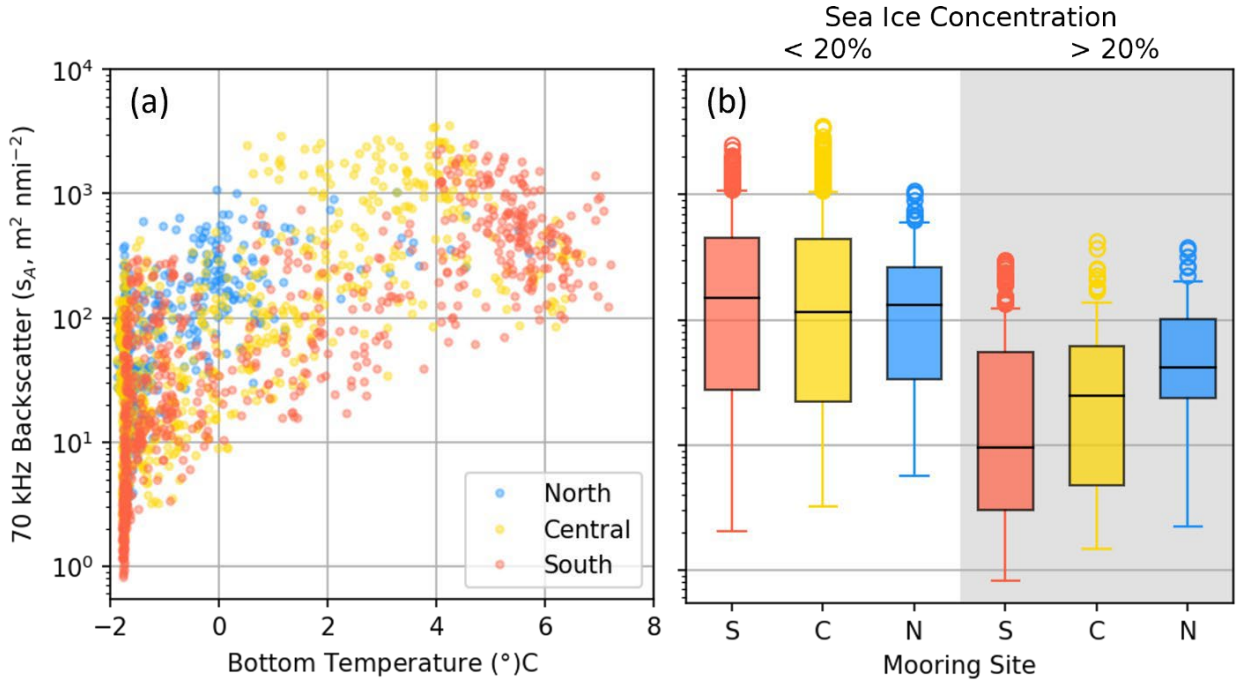

Figure 4.8 (a) Mean daily 70 kHz backscatter (s_A, m^2 nmi^{-2}) as a function of temperature at the northern (blue), central (yellow), and southern (red) mooring sites. (b) Distributions of mean daily 70 kHz backscatter when sea ice concentrations were < 20% (white background) and > 20% (grey background). Boxes indicate the interquartile range, horizontal black lines the median, vertical lines the 5% and 95% intervals. Circles indicate observations beyond the 5% and 95% intervals.

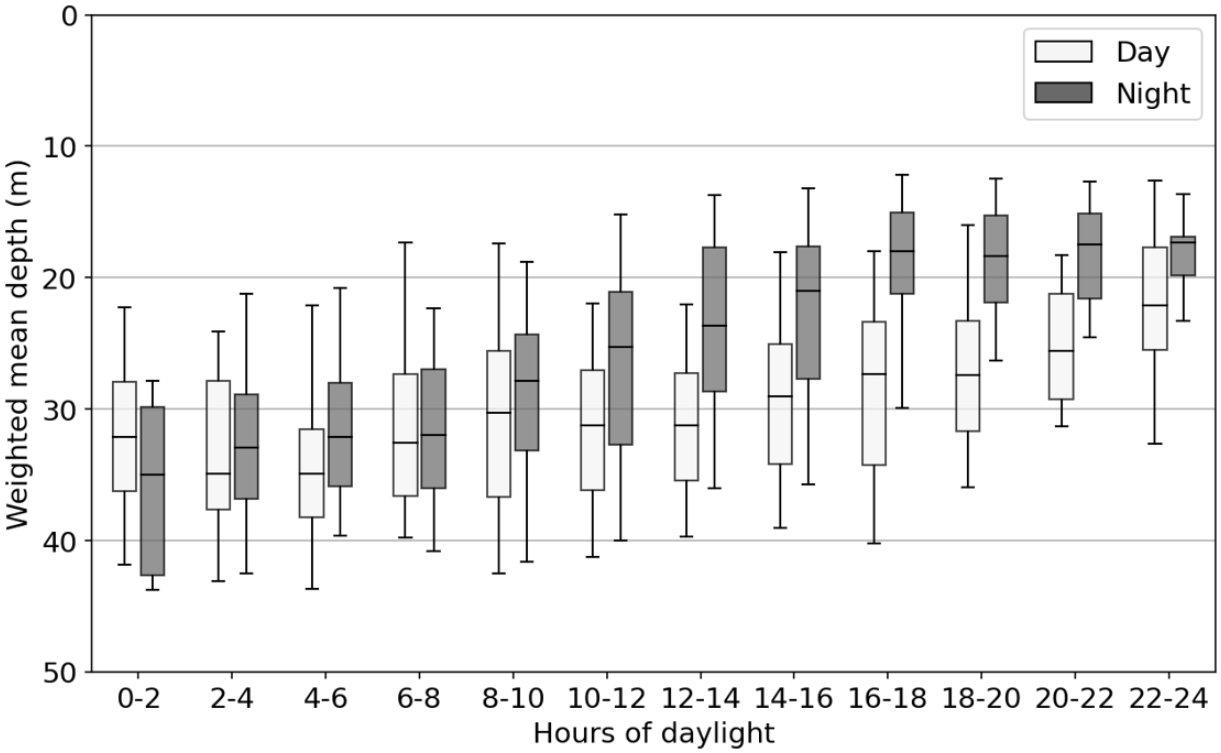

Figure 4.9 Night (minimum solar altitude, grey boxes) and day (maximum solar altitude, white boxes) distributions of weighted mean depth in 2-hour bins of length of daylight. Only ensembles where mean target strength indicate scattering was likely from fishes (TS > -60 dB re 1 m^{-2}) are included.

Drivers of fish movement

Fish tracks and ACDP measurements of currents indicate that fishes were moving largely as passively advected particles. After filtering, a total of 40317, 83024, and 63674 fish tracks were reconstructed from single target measurements at the northern, central, and southern moorings, respectively, during the two years of deployments. The mean track depth was 26.8 (±10.4 SD) m (Supplementary Figure 4.4b). Over the observation period, the majority of track headings were towards the northeast, with the mode of heading distributions (reference headings) for each mooring at 45° (southern), 75° (central), and 65° (northern). The daily mean track heading was correlated to current direction measured independently from the nearby ADCP (R^2=0.58, p<0.001, Figure 4.10a). Two modes were apparent in the current and fish headings corresponding to movement to the northeast and southwest (Figure 4.10a). The mean speed of all individual tracks was 23.4 (±13.5 SD) cm s^{-1}. Daily mean fish track velocities and current velocities calculated along the reference heading for each site were strongly correlated (R^2=0.81, p<0.001, Figure 4.10b), and the mean difference between fish track and current velocities was 0.2 cm s^{-1} (±12.6 cm s^{-1}). Mean track velocities along the reference heading were 8.2 cm s^{-1}, indicating net movement to the northeast.

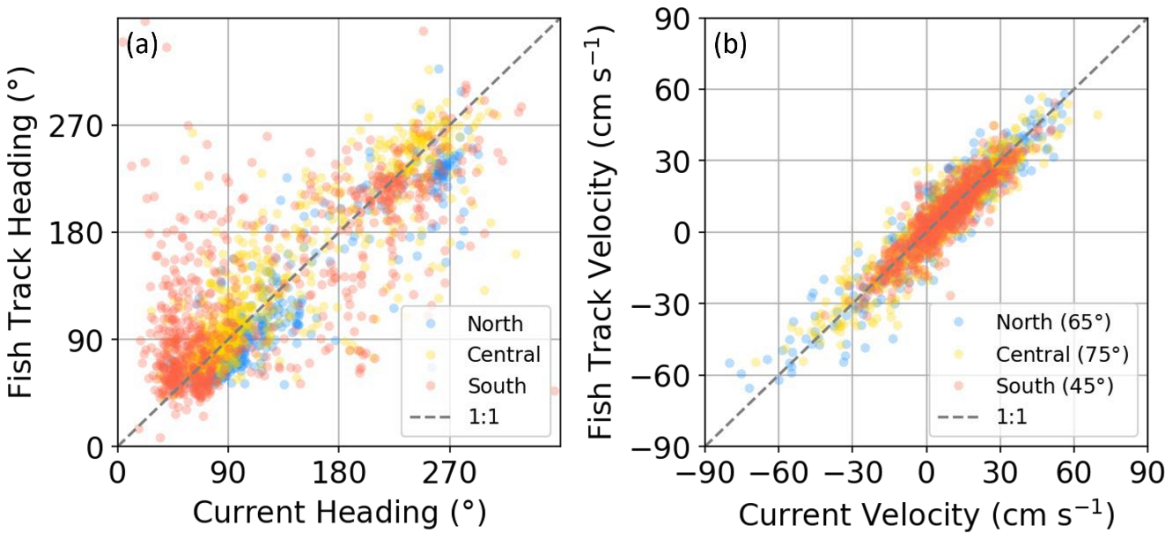

Figure 4.10 (a) Mean daily heading of currents measured from the acoustic doppler current profilers (ADCP) and fish tracks. (b) Mean daily current and fish track velocities along the reference heading (the mode of track headings [in 5° bins] for all tracks observed at each site) indicated in the legend for each site. The 1:1 line on each plot is shown as a reference (grey dashed line).

Table 4.1 Mean flux (Fish m^{-1} s^{-1}) and total cumulative flux over the course of each deployment (Fish m^{-1}) calculated along the reference heading for each mooring.

Deployment	Site	Reference Heading	Mean Flux (Fish m^{-1} s^{-1})	Cumulative Flux (Fish m^{-1})
2017 - 2018	Southern	45°	0.07	1.8×10^6
	Central	80°	0.23	6.8×10^6
2018 - 2019	Southern	45°	0.08	2.8×10^6
	Central	80°	0.09	3.0×10^6
	Northern	75°	0.13	4.4×10^6

The flux of fishes was primarily to the northeast at all three sites (Figure 4.11, Table 4.1). Mean flux was highest at the central site in 2017-2018 and the northern site in 2018-2019, with the lowest estimates of flux at the southern site in both years (Table 4.1). Fluxes were highest during the summer and fall when fish were abundant. The highest mean flux over a 7-day period, 2.6 fish m^{-1} s^{-1}, was observed in September 2017 at the central mooring site (Figure 4.11b). This corresponds with the highest fish abundances observed throughout the deployments (Figure 4.6b). The magnitude of the flux was primarily driven by the abundance (Supplementary Figure 4.5); fluxes were lowest during the ice-covered period when fish were scarce (Figure 4.11). Although current velocities to the northeast were also slower when ice was present at the northern (t-test, $p<0.05$) and central sites ($p<0.1$), velocities did not vary significantly at the southern site ($p=0.8$).

Short episodes of fish movement to the southwest occurred throughout the year (blue bars, Figure 4.11). However, cumulative fluxes indicate net movement of fishes was consistently to the northeast (Table 4.1). These reversals in flux were associated with shifts in wind speed and direction (Figures 4.12, 4.13). Daily mean estimated northward wind speeds during the deployment period ranged from -13.5 to 19.9 m s^{-1} (mean of 0.04 m s^{-1} ±5.5 SD). When wind speeds to the north were high, fish primarily moved to the northeast/east (Figure 4.12). Fish headings became more variable as northward winds weakened, and transitioned to the southwest when winds were strong towards the south (Figure 4.12).

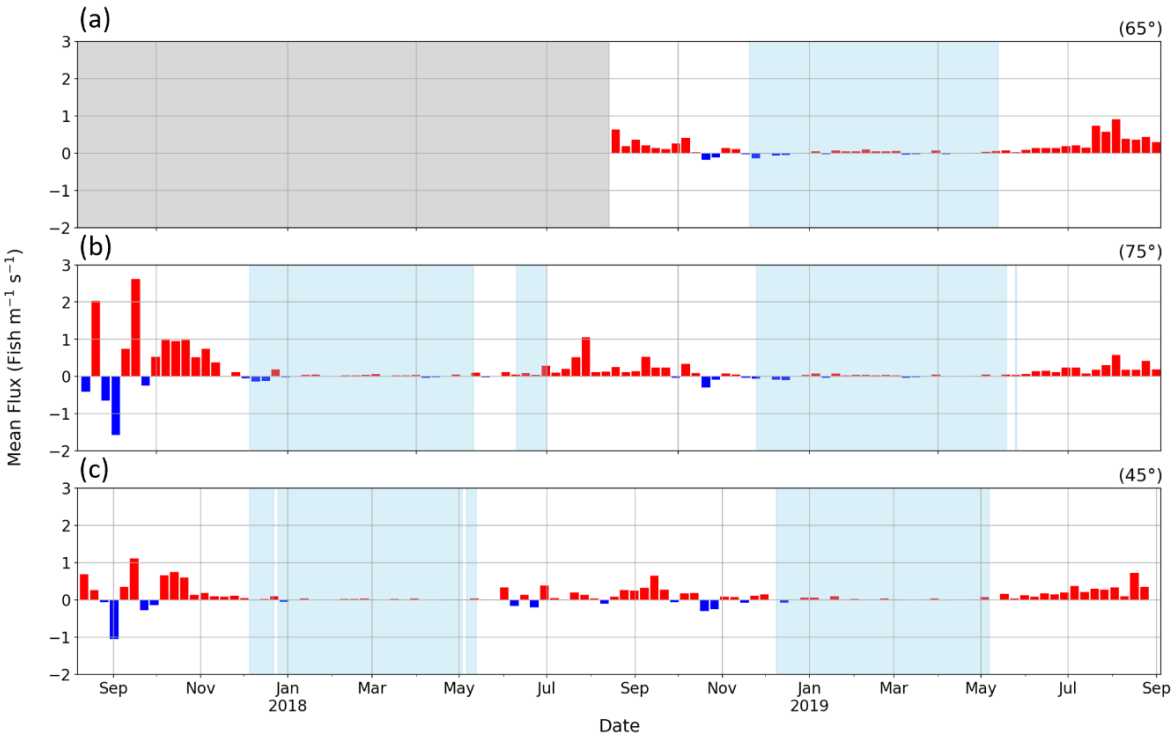

Figure 4.11 Mean flux of fishes (fish m^{-1} s^{-1}) at the (a) northern, (b) central, (d) and southern mooring sites. Each bar represents the mean flux during a single week of deployment. Values represent the number of fish passing through a 1-m line perpendicular to the reference heading (the mode of track headings [in 5° bins] for all tracks observed at each site) indicated in the top right of each panel. Positive (within 90° of the refence heading) and negative (within 90° of 180° from the refence heading) values are shown in red and blue, respectively.

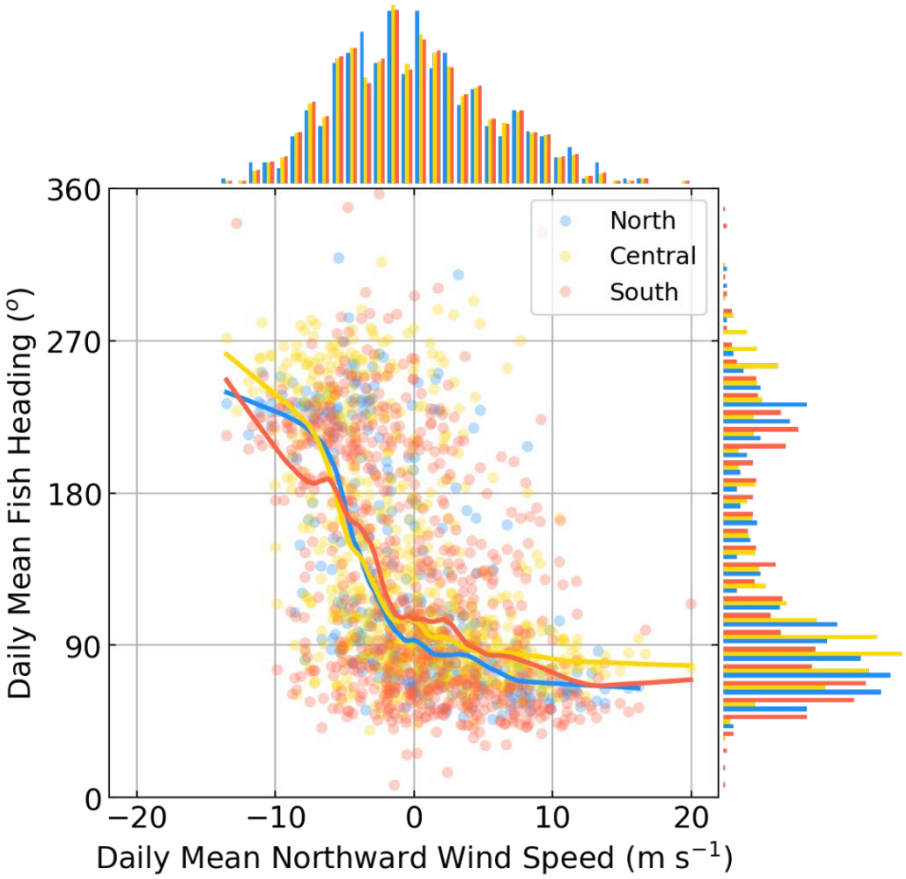

Figure 4.12 Daily mean fish heading as a function of mean northward wind speed at the northern (blue), central (yellow), and southern (red) mooring site. Histograms represent the distribution of wind speeds (top) and fish headings (right) for both years of deployments at each moorings site. The solid lines represent a locally estimated scatterplot smoothing curve (Cleveland, 1979) of the daily means for each mooring to indicate the trend.

Discussion

Seasonality of fishes

The mooring observations provide further evidence of strong seasonality in the composition of the pelagic community on the Chukchi shelf. Large numbers of age-0 gadids have been observed in summer (De Robertis et al., 2017; Levine et al., in review). However, few age-1+ individuals appeared to be present, indicating that either mortality in this region is high or that these fish emigrate to other regions. Using two years of year-round observations from moored echosounders in the northeastern Chukchi Sea, we found that these fishes appear in the region in late summer and disappear in early winter. Using tracking, we found that fish movement correlated with local currents, and estimates of flux indicate that the majority of the age-0 population in summer is likely transported to the north and east off towards the Beaufort Sea and Arctic Basin each fall and winter. These findings support the predictions of passive particle tracking simulations which predict the displacement of the summer age-0 population to the northeast off the Chukchi shelf in fall (Levine et al., 2021).

The presence of fish appears to be strongly associated with seasonal warm waters entering the region. Temperature is a key driver of both Arctic cod and pollock distribution (Sigler et al., 2017; Eisner et al.,

2020; Baker, 2021; Levine et al., in review) and growth (Laurel et al., 2018). The northward transport of warm Bering Sea water in spring and summer into the northeastern Chukchi Sea (Danielson et al., 2017) has been associated with increases in abundance of zooplankton (Eisner et al., 2013; Ashjian et al., 2017; Spear et al., 2020) and fishes (Logerwell et al. 2020; Levine et al., in review). Increases in abundance of fishes in the northeastern Chukchi Sea in summer appear to coincide with the arrival of southern-origin water masses. These flow north into the Chukchi Sea from the Bering Sea shelf (Coachman et al. 1975; Danielson et al. 2017), replacing the colder winter water on the Chukchi shelf (Weingartner et al. 2013). The age-0 gadids observed in the northeastern Chukchi in summer are primarily associated with the warmer (2-8 °C) conditions of these seasonal water masses (De Robertis et al., 2017; Marsh et al., 2019; Levine et al., in review). The observations in this study further indicate that the seasonality of age-0 gadids in the northeastern Chukchi Sea is driven by the advective movement of the fish population within this warm water.

Abundance was much higher in the summer and fall of 2017 than in the following two years at the central and southern sites. This high interannual variability is consistent with survey observations of substantially higher age-0 gadid abundances in 2017 than 2019 (Levine et al., in review). Levine et al., (in review) hypothesized that this increase in gadids was attributed to anomalously warm conditions in spring, resulting in earlier hatch and favorable growth conditions that led to increased length-at-age and thus increased age-0 fish survival. The lower backscatter in both subsequent years is consistent with surveys conducted in 2018 (Levine et al., 2021) and 2019 (Levine et al., in review) which observed similar backscatter during the late summer and fall.

While it was not possible to directly assess the size of fishes, the moorings confirm previous observations that the pelagic community in summer is dominated by small fishes. Mean target strengths during periods dominated by fish-like scattering were consistent with the target strength expected from small (<6 cm) age-0 fishes (Traynor, 1996; Geoffroy et al., 2016; Levine et al., 2021). However, while these reported target strength-length relationships for age-0 gadids are based on ship-based (ventral) observations at 38 kHz (Traynor 1996; Geoffroy et al., 2016), our inferred length from mooring observations are ventral measurements collected at 70 kHz. While target strength of individuals is orientation- and frequency-dependent (Foote 1980; Francis and Foote 2003), the difference in volume backscattering strength at 38 kHz and 70 kHz is small for walleye pollock (De Robertis et al., 2010); we therefore applied the target strength-length relationships estimated at 38 kHz to our observations at 70 kHz with the expectation that the associated error as a result of frequency was minimal. The impact of the use of ventral observations from the moorings is also likely to be low. Most of the variability in target strength of an individual as a result of behavior is due to the change in tilt angle (Horne, 2003) and model predictions estimate that the variability between dorsal and ventral measurements of the same orientation is low (Francis and Foote 2003). Even with these potential sources of variability in the target- strength-length relationship, the scarce observations of high (>-35 dB re 1 m^{-2}) target strengths (Supplementary Figure 4.4a) indicate that larger fishes such as adult pollock were likely not present in significant abundance.

The increase in target strength from July to October, along with the increase in diel vertical migration indicated by increasing difference between day and night weighted mean depth, is evidence of growth in the age-0 population during the late summer (July - October) as observed in summer surveys (Deary et al., 2021; Levine et al., 2021). Arctic cod and pollock are typically surface-associated as eggs and larvae (Spencer et al., 2020). As they increase in size and swimming ability, juveniles begin to move deeper into the water column during the day, a behavioral shift typically occurring at a length of ~ 30 mm in both species (Brodeur et al., 2000; Ponomorenko 2000). The increase in night-day depth difference beginning in July of each year at all three sites is consistent with the onset of diel vertical migration (DVM). The signal of increased diel vertical migration with increasing daylight hours was likely driven primarily by strengthening DVM behaviors, occurring in late summer as the day length is being reduced. We found little evidence of diel vertical migration occurring during polar night and the adjacent periods of minimal daylight, though young Arctic cod have been observed to undergo migration during polar winter in

response to small changes in twilight (Benoit et al., 2010). Thus, the lack of vertical migration observed in winter is consistent with our other observations suggesting that age-0 fishes are virtually absent during March to June.

Fate of age-0 gadids

Advection appears to be the primary mechanism of movement in fishes on the northeastern Chukchi shelf. Fish headings and velocities were consistent with those of the currents, with little evidence of significant horizontal displacement as a result of swimming or other behavior. While age-0 gadids are capable of fast swimming speeds (aerobic threshold of 2-3 body lengths s^{-1}, Hurst, 2007; Kunz et al., 2018), routine speeds are much slower (0.25 – 1 body lengths s^{-1}, Rose et al., 1995; Hurst, 2007). In the fast current velocities observed on the Chukchi shelf, routine swimming behavior is likely to have minimal impact on fish displacement relative to advection. These in situ observations support the assumptions inherent to modelling studies using passive drift to determine horizontal distributions of age-0 gadids in summer (Deary et al., 2021; Vestfals et al., 2021). This work is further evidence that future studies can use direct observations (e.g., ADCPs) or model predictions of regional transport to assess historic and future trends in the source and fate of this age-0 population observed in summer.

We found substantial variability in the flux of age-0 fishes across seasons and between mooring locations. The magnitude of flux was primarily driven by seasonal changes in abundance. However, the variability among sites was likely due to variability in local currents. During 2018-2019, the mean flux was highest at the northern site, although fish abundance was lower than the other sites. Current velocities are typically faster at this mooring site than the central and southern sites (Weingartner et al., 2005; Woodgate et al., 2005; Stabeno et al., 2018), particularly in summer (Stabeno et al., 2018) when we observed the highest fish abundances. Although fish density was comparable between the southern and central sites, (Figures 4.6, 4.7), fluxes were lowest in both years at the southern site. This variability in flux is likely due to the relatively slower velocities typically observed in this portion of the shelf compared to velocities closer in proximity to Barrow Canyon (Stabeno et al., 2018).

The flux of fishes to the northeast provides evidence that the age-0 fishes present in summer are transported out of the ecosystem. This is consistent with particle tracking simulations based on modeled regional advection which predicted that fishes observed in the central portion of the eastern shelf in summer would be transported beyond the shelf break in fall (Levine et al., 2021). If the northern site is representative of the surrounding area of the shelf, we hypothesize that the flux at the northern mooring site may account for a significant portion of the export of age-0 fishes off the shelf. Using the estimate of 4.4×10^6 fish m^{-1} (Table 4.1) observed at the northern mooring site, flux would need to be consistent across <50 km of the eastern Chukchi shelf in order to represent the export of the approximately 1.5×10^{11} fishes reported in the 2019 survey (Levine et al., in review). The ability to extrapolate mooring observations over a wider area is a function of the behavior of the species being observed relative to their environment. When abundances are high, fishes on the Chukchi shelf are relatively evenly distributed over large portions of the shelf (De Robertis et al., 2017; Levine et al., in review), and when moving in a relatively uniform distribution (i.e., large-scale scattering layers rather than discrete schools) moorings are likely to represent abundance over a much broader spatial area than the small area directly observed in the acoustic beam (Brierly et al., 2006; De Robertis et al., 2018). Abundance and distribution of fishes can also be depth-dependent and vary as a function of local topography due to changes in either behavior or advection, therefore extrapolation of mooring observations may only apply within appropriate depth ranges (De Robertis et al., 2018). However, the eastern Chukchi shelf has a relatively consistent depth, thus the moorings may be representative of a larger area.

Age-1+ Arctic cod have been found in low abundance during demersal surveys of the Chukchi shelf in summer (Norcross et al., 2013; Goddard et a., 2014; Logerwell et al., 2017). While the demersal abundances of Arctic cod are significantly lower than pelagic estimates (De Robertis et al., 2017), the presence of these age-1+ fish along the seafloor indicates that Arctic cod likely transition to be more

demersal as they age. Following this transition, these fish would likely not be observable in our mooring data and are inaccessible to pelagic trawls. More work is needed to identify the potential shift of this pelagic age-0 population to demersal habitat on the Chukchi shelf to assess how much of the population remains on the shelf year-round.

Thus, the low densities of age-1+ gadids in the region are likely the result of this continued northward transport of the age-0 population observed in summer. The very low densities of age-1+ gadids in during summer surveys (De Robertis et al., 2017; Levine et al., in review) suggests that the age-0 fishes found in the eastern Chukchi Sea likely originated in other areas. Previous studies using models have hypothesized that the distribution of age-0 fishes observed in summer and fall reflects the northward advection of fishes from southern spawning areas (Deary et al., 2021., Vestfals et al., 2021). Our observations are consistent with these hypotheses: While our study did not observe spawning location, we infer from the strong correlation between fish displacement and currents that age-0 gadids in the Chukchi during summer are likely of southern origin. Larger fish, however, are likely not allowing themselves to be passively transported with their drifting eggs and are more likely to maintain their position in their preferred habitat. Age-1+ fishes have also likely developed the swimming ability required to return to spawning grounds. While we did not identify any high target strength fishes migrating south indicating the return of large fishes to spawning grounds in our observations, some portion of the age-0 population is likely returning as mature adults in order to maintain the spawning population (Forster et al., 2020).

The potential of the age-0 fishes we observed in the Chukchi to survive over winter after being advected into the Arctic remains unclear. Growth and lipid accumulation are temperature-dependent in age-0 gadids (Laurel et al., 2018; Koenker et al., 2018). Based on their body condition, age-0 pollock captured during recent surveys of the Chukchi Sea in summer are unlikely to survive overwinter under Arctic conditions (Copeman, pers. comm.). Thus, while the flux of fishes supports the hypothesis of emigration of the population to other areas as they age, quantifying the mortality of these age-0 pollock in their new environment is still required to address the long-term survival of the population and the ability of boreal species observed seasonally on the shelf to establish permanent populations in the region. However, Arctic cod are widely present throughout the Arctic basin and are capable of surviving Arctic winter conditions. Large aggregations of age-1+ Arctic cod have been observed at depth in Barrow Canyon (De Robertis et al., 2017) and the Beaufort Sea shelf break (Parker-Stetter et al., 2011; Rand and Logerwell, 2011), and genetic studies have not identified any significant population stratification between Arctic cod observed on the Chukchi shelf and those in the western Beaufort Sea (Wilson et al., 2019; Nelson et al., 2020). These populations may recruit from the age-0 Arctic cod being transported off of the Chukchi shelf, though further work is necessary to identify if the western Beaufort is the wintering grounds for the majority of these age-0 fish.

Influence of regional winds

The direction of fish movements appears to be driven primarily by changes in wind speed and direction. On the Chukchi shelf, advective transport that moves water of Bering Sea origin north is driven by the pressure head created by differences in sea surface height between the Pacific and Arctic Oceans (Woodgate et al., 2005; Danielson et al., 2014). This northward flow is restrained by mean winds to the southwest (Pisareva et al., 2019) and variations in the current are primarily wind-driven (Weingartner et al., 2005). Increases in winds to the southwest can slow this northward flow and when strong enough, lead to episodic flow reversals (Woodgate et al., 2005; Stabeno et al., 2018; Pisareva et al., 2019). Conversely, during periods of strong winds to the northeast, the northward flow across the shelf increases. Particle tracking simulations have suggested that this variability in wind and the resulting shift in currents is a major source of interannual variability observed in late-summer distribution of age-0 fishes in the Chukchi Sea (Levine et al., 2021; Vestfals et al. 2021).

We observed two modes in fish displacement, which varied with changes in wind speed on the northeastern shelf. During periods of strong northward wind, current and fish speeds increased, and the

movement of both currents and fish was to the north/east (yellow box, Figure 4.13). When winds were strongly to the south, a reversal was seen in both the currents and fish tracks, with a higher proportion of fish moving to the south/west (purple box, Figure 4.13). During periods of weak and variable winds, fish tracks remained towards the north/east (Figures 4.12, 4.13), consistent with the expected flow on the northeastern shelf (Stabeno et al., 2018). These wind-driven modes of water movement in the northeastern Chukchi have previously been documented and a threshold of 6 m s^{-1} winds towards the southwest (Fang et al., 2017) has been reported as the requirement for transition between states. Our results suggest adjustments to make currents better proxies for fish movements.

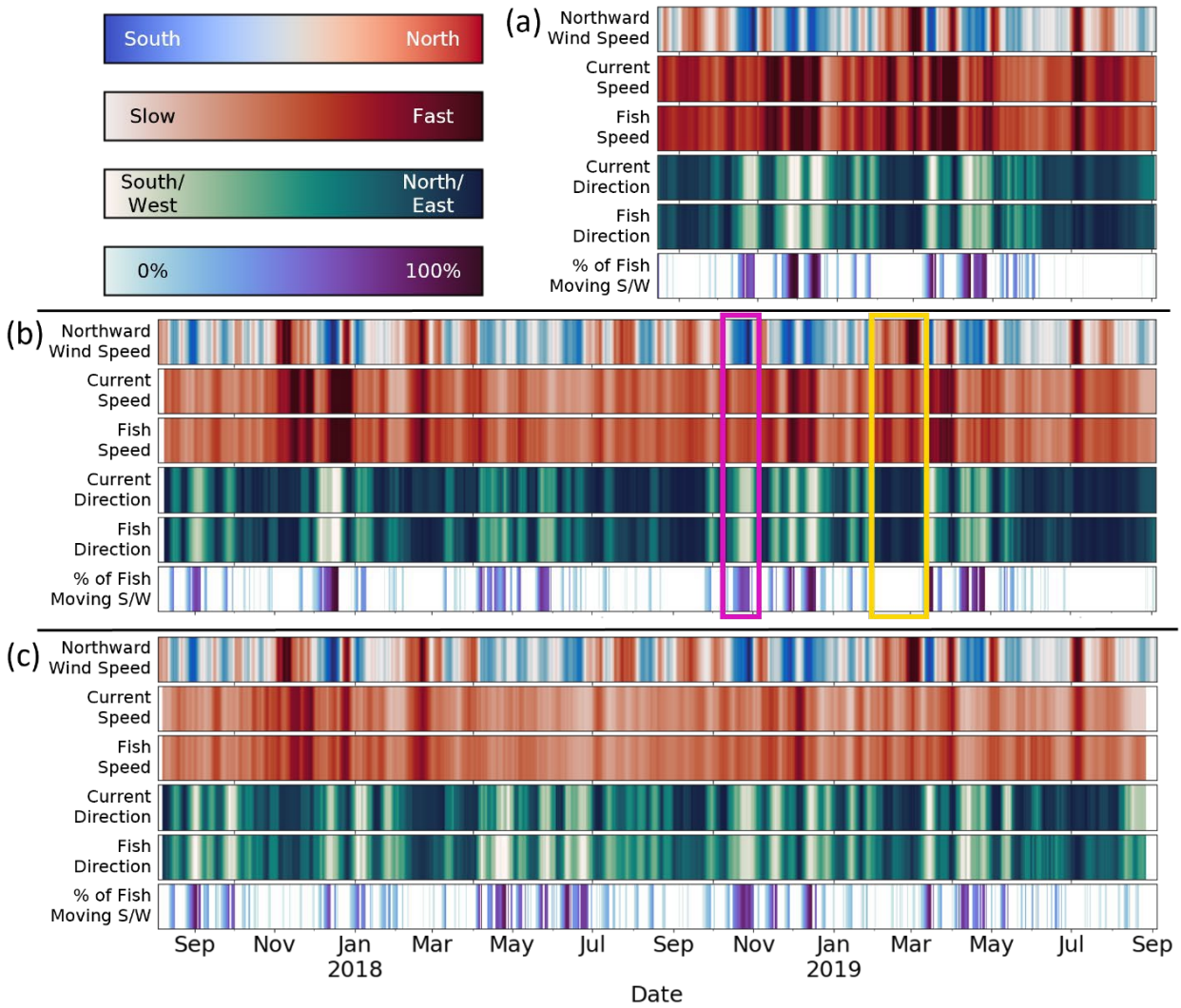

Figure 4.13 Heatmaps of 7-day rolling means of north-south winds, current and fish speeds, and current and fish directions at the (a) northern, (b) central, and (c) southern mooring sites. Within each panel, the top heatmap indicates the northward (meridional component) wind speed, where red indicates strong northward winds and blue indicates strong southward winds. The second and third heatmaps indicate the speed of both the current and fishes, where darker colors indicate faster speeds. The fourth and fifth heatmaps indicate the direction of the current and fishes, where darker colors indicate coherence with the reference heading (towards the northeast, see methods, Figure 4.9). The bottom heatmap shows the % of

fish tracks moving opposed to the reference heading (to the southwest). As examples, the purple box and yellow box highlight a period of strong southward and northward winds, respectively (see results).

Northward winds are expected to increase with future changes in climate. In recent years, the frequency of northward wind events in the region has increased, (Stabeno and Bell 2019). As the region continues to warm, the input of water through the Bering Strait is also predicted to increase (Woodgate, 2018; Danielson et al., 2020), which would increase northward transport across the Chukchi shelf. Transport has already been increasing over recent decades, considerably reducing the amount of time needed to flush and renew the water on the Chukchi shelf (Woodgate et al., 2018). Based on the mean fish track velocity of 8.2 cm s^{-1}, the residence time of fish on the Chukchi shelf is ~85 days (based on ~600 km of transit from Bering Strait to Barrow Canyon). This study occurred during a period of high transport relative to previous decades (Woodgate and Peralta-Ferriz, 2021; Levine et al., in review). This enhanced transport may be more nearly the norm in future decades, and future changes in transport are likely to further decrease the residence time of age-0 gadids on the Chukchi shelf.

Conclusions

The composition of the pelagic community on the Chukchi shelf is highly seasonal. This study provides further evidence that the age-0 gadids observed on the Chukchi shelf in summer are likely temporary residents of the region. Their distribution and movement across the shelf are primarily driven by advection, providing further evidence that these fish are likely originating from the south. However, transport in the region is changing, with potential consequences for the future of this ecosystem and the structure of the summer pelagic community. Enhanced transport from the south is hypothesized to be driving the recent increased presence of boreal species such as pollock in the eastern Chukchi Sea (Levine et al., in review). While these southern-origin species likely cannot survive overwinter in Arctic conditions (Koenker et al., 2018), their increased presence during summer may increase competition with and predation on endemic species, further altering the structure of the summer community. The role of advection in structuring this seasonal population allow us to use observations and predictions of the physical environment to understand how this ecosystem will be structured under future change.

Acknowledgements

This research was conducted under the Arctic Integrated Ecosystem Research Program

(http://www.nprb.org/arctic-program). Funding for the program was provided by North Pacific Research Board, the Bureau of Ocean Energy Management, the Collaborative Alaskan Arctic Studies Program, and the Office of Naval Research. In-kind support was contributed by the National Oceanic and Atmospheric Administration's (NOAA) Alaska Fisheries Science Center and Pacific Marine Environmental Laboratory, the University of Alaska Fairbanks, the U.S. Fish & Wildlife Service, and the National Science Foundation. We would like to thank Ivar Wagnen, Lars Andersen, and Roger Kasinger for their work on the echosounders and assistance with instrument testing and deployment configurations. We would also like to thank Christian Meinig and Steven Anderson for their work in the design and construction of the mooring platform, and Matthew Casari for development of the underwater compasses. The mooring deployments and recoveries would not have been possible without the captains, crews, and science parties of the RV *Ocean Starr* and USCGC *Healy*.

References

Ashjian, C.J., Campbell, R.G., Gelfman, C., Alatalo, P., Elliott, S.M., 2017. Mesozooplankton abundance and distribution in association with hydrography on Hanna Shoal, NE Chukchi Sea, during August

2012 and 2013. Deep. Res. Part II Top. Stud. Oceanogr. 144, 21–36. https://doi.org/10.1016/j.dsr2.2017.08.012
Baker, M.R., 2021. Contrast of warm and cold phases in the Bering Sea to understand spatial distributions of Arctic and sub-Arctic gadids. Polar Biol. 44, 1083–1105. https://doi.org/10.1007/s00300-021-02856-x
Benoit, D., Simard, Y., Fortier, L., 2008. Hydroacoustic detection of large winter aggregations of Arctic cod (*Boreogadus saida*) at depth in ice-covered Franklin Bay (Beaufort Sea). J. Geophys. Res. Ocean. 113, 1–9. https://doi.org/10.1029/2007JC004276
Benoit, D., Simard, Y., Gagné, J., Geoffroy, M., Fortier, L., 2010. From polar night to midnight sun: Photoperiod, seal predation, and the diel vertical migrations of polar cod (*Boreogadus saida*) under landfast ice in the Arctic Ocean. Polar Biol. 33, 1505–1520. https://doi.org/10.1007/s00300-010-0840-x
Benoit-Bird, K.J., Lawson, G.L., 2016. Ecological Insights from Pelagic Habitats Acquired Using Active Acoustic Techniques. Ann. Rev. Mar. Sci. 8, 463–490. https://doi.org/10.1146/annurev-marine-122414-034001
Blackman, S.S., 1986. Multiple-target tracking with radar applications. Artech House, Inc., Dedham, MA.
Brierley, A.S., Saunders, R.A., Bone, D.G., Murphy, E.J., Enderlein, P., Conti, S.G., Demer, D.A., 2006. Use of moored acoustic instruments to measure short-term variability in abundance of Antarctic krill. Limnol. Oceanogr. Methods 4, 18–29. https://doi.org/10.4319/lom.2006.4.18
Brodeur, R.D., Wilson, M.T., Ciannelli, L., 2000. Spatial and temporal variability in feeding and condition of age-0 walleye pollock (*Theragra chalcogramma*) in frontal regions of the Bering Sea. ICES J. Mar. Sci. 57, 256–264. https://doi.org/10.1006/jmsc.1999.0525
Cleveland, W.S., 1979. Robust locally weighted regression and smoothing scatterplots. J. Am. Stat. Assoc. 74, 829–836. https://doi.org/10.1080/01621459.1979.10481038
Coachman, L.K., Aagaard, K., Tripp, R.B., 1975. Bering Strait: The Regional Physical Oceanography, University of Washington Press. University of Washington Press, Seattle. https://doi.org/10.1016/0146-6291(77)90492-1
Copeman, L., Spencer, M., Heintz, R., Vollenweider, J., Sremba, A., Helser, T., Logerwell, L., Sousa, L., Danielson, S., Pinchuk, A.I., Laurel, B., 2020. Ontogenetic patterns in lipid and fatty acid biomarkers of juvenile polar cod (Boreogadus saida) and saffron cod (Eleginus gracilis) from across the Alaska Arctic. Polar Biol. https://doi.org/10.1007/s00300-020-02648-9
Danielson, S.L., Ahkinga, O., Ashjian, C., Basyuk, E., Cooper, L.W., Eisner, L., Farley, E., Iken, K.B., Grebmeier, J.M., Juranek, L., Khen, G., Jayne, S.R., Kikuchi, T., Ladd, C., Lu, K., McCabe, R.M., Moore, G.W.K., Nishino, S., Ozenna, F., Pickart, R.S., Polyakov, I., Stabeno, P.J., Thoman, R., Williams, W.J., Wood, K., Weingartner, T.J., 2020. Manifestation and consequences of warming and altered heat fluxes over the Bering and Chukchi Sea continental shelves. Deep. Res. Part II Top. Stud. Oceanogr. 177. https://doi.org/10.1016/j.dsr2.2020.104781
Danielson, S.L., Eisner, L., Ladd, C., Mordy, C., Sousa, L., Weingartner, T.J., 2017. A comparison between late summer 2012 and 2013 water masses, macronutrients, and phytoplankton standing crops in the northern Bering and Chukchi Seas. Deep. Res. Part II Top. Stud. Oceanogr. 135, 7–26. https://doi.org/10.1016/j.dsr2.2016.05.024
Darnis, G., Hobbs, L., Geoffroy, M., Grenvald, J.C., Renaud, P.E., Berge, J., Cottier, F., Kristiansen, S., Daase, M., E. Søreide, J., Wold, A., Morata, N., Gabrielsen, T., 2017. From polar night to midnight sun: Diel vertical migration, metabolism and biogeochemical role of zooplankton in a high Arctic fjord (Kongsfjorden, Svalbard). Limnol. Oceanogr. 62, 1586–1605. https://doi.org/10.1002/lno.10519
David, C., Lange, B., Krumpen, T., Schaafsma, F., van Franeker, J.A., Flores, H., 2016. Under-ice distribution of polar cod Boreogadus saida in the central Arctic Ocean and their association with sea-ice habitat properties. Polar Biol. 39, 981–994. https://doi.org/10.1007/s00300-015-1774-0

De Robertis, A., Levine, R., Wilson, C.D., 2018. Can a bottom-moored echo sounder array provide a survey-comparable index of abundance? Can. J. Fish. Aquat. Sci. 75, 629–640. https://doi.org/10.1139/cjfas-2017-0013

De Robertis, A., McKelvey, D.R., Ressler, P.H., 2010. Development and application of an empirical multifrequency method for backscatter classification. Can. J. Fish. Aquat. Sci. 67, 1459–1474. https://doi.org/10.1139/F10-075

De Robertis, A., Taylor, K., Wilson, C.D., Farley, E. V., 2017. Abundance and distribution of Arctic cod (Boreogadus saida) and other pelagic fishes over the U.S. Continental Shelf of the Northern Bering and Chukchi Seas. Deep. Res. Part II Top. Stud. Oceanogr. 135, 51–65. https://doi.org/10.1016/j.dsr2.2016.03.002

Deary, A.L., Vestfals, C.D., Mueter, F.J., Logerwell, E.A., Goldstein, E.D., Stabeno, P.J., Danielson, S.L., Hopcroft, R.R., 2021. Seasonal abundance , distribution , and growth of the early life stages of polar cod (*Boreogadus saida*) and saffron cod (*Eleginus gracilis*) in the US Arctic. Polar Biol. https://doi.org/10.1007/s00300-021-02940-2

Ehrenberg, J., Torkelson, T.C., 1996. Application of dual-beam and split-beam target tracking in fisheries acoustics. ICES J. Mar. Sci. 53, 329–334. https://doi.org/10.1006/jmsc.1996.0044

Eisner, L.B., Zuenko, Y.I., Basyuk, E.O., Britt, L.L., Duffy-Anderson, J.T., Kotwicki, S., Ladd, C., Cheng, W., 2020. Environmental impacts on walleye pollock (*Gadus chalcogrammus*) distribution across the Bering Sea shelf. Deep. Res. Part II Top. Stud. Oceanogr. 181–182, 104881. https://doi.org/10.1016/j.dsr2.2020.104881

Eisner, L., Hillgruber, N., Martinson, E., Maselko, J., 2013. Pelagic fish and zooplankton species assemblages in relation to water mass characteristics in the northern Bering and southeast Chukchi seas. Polar Biol. 36, 87–113. https://doi.org/10.1007/s00300-012-1241-0

Fang, Y.C., Potter, R.A., Statscewich, H., Weingartner, T.J., Winsor, P., Irving, B.K., 2017. Surface Current Patterns in the Northeastern Chukchi Sea and Their Response to Wind Forcing. J. Geophys. Res. Ocean. 122, 9530–9547. https://doi.org/10.1002/2017JC013121

Fernandes, P.G., Stevenson, P., Brierley, A.S., Armstrong, F., Simmonds, E.J., 2003. Autonomous underwater vehicles: Future platforms for fisheries acoustics. ICES J. Mar. Sci. 60, 684–691. https://doi.org/10.1016/S1054-3139(03)00038-9

Flores, H., van Franeker, J.A., Siegel, V., Haraldsson, M., Strass, V., Meesters, E.H., Bathmann, U., Wolff, W.J., 2012. The association of Antarctic krill *Euphausia superba* with the under-ice habitat. PLoS One 7. https://doi.org/10.1371/journal.pone.0031775

Foote, K.G., 1980. Effect of fish behaviour on echo energy: the need for measurements of orientation distributions. ICES J. Mar. Sci. 39, 193–201. https://doi.org/10.1093/icesjms/39.2.193

Forster, C.E., Norcross, B.L., Mueter, F.J., Logerwell, E.A., Seitz, A.C., 2020. Spatial patterns, environmental correlates, and potential seasonal migration triangle of polar cod (*Boreogadus saida*) distribution in the Chukchi and Beaufort seas. Polar Biol. 73. https://doi.org/10.1007/s00300-020-02631-4

Francis, D.T.I., Foote, K.G., 2003. Depth-dependent target strengths of gadoids by the boundary-element method. J. Acoust. Soc. Am. 114, 3136–3146. https://doi.org/10.1121/1.1619982

Frey, K.E., Moore, G.W.K., Cooper, L.W., Grebmeier, J.M., 2015. Divergent patterns of recent sea ice cover across the Bering, Chukchi, and Beaufort seas of the Pacific Arctic Region. Prog. Oceanogr. 136, 32–49. https://doi.org/10.1016/j.pocean.2015.05.009

Geoffroy, M., Majewski, A., LeBlanc, M., Gauthier, S., Walkusz, W., Reist, J.D., Fortier, L., 2016. Vertical segregation of age-0 and age-1+ polar cod (*Boreogadus saida*) over the annual cycle in the Canadian Beaufort Sea. Polar Biol. 39, 1023–1037. https://doi.org/10.1007/s00300-015-1811-z

Goddard, P., Lauth, R., Armistead, C., 2014. Results of the 2012 Chukchi Sea Bottom Trawl Survey of Bottomfishes, Crabs, and Other Demersal Macrofauna. U.S Dep. Commer. NOAA Tech. Memorandum, 110.

Gonzalez, S., Horne, J.K., Danielson, S.L., 2021. Multi-scale temporal variability in biological-physical associations in the NE Chukchi Sea. Polar Biol. 44, 837–855. https://doi.org/10.1007/s00300-021-02844-1

Gradinger, R.R., Bluhm, B.A., 2004. In-situ observations on the distribution and behavior of amphipods and Arctic cod (*Boreogadus saida*) under the sea ice of the High Arctic Canada Basin. Polar Biol. 27, 595–603. https://doi.org/10.1007/s00300-004-0630-4

Horne, J.K., 2003. The influence of ontogeny, physiology, and behaviour on the target strength of walleye pollock (*Theragra chalcogramma*). ICES J. Mar. Sci. 60, 1063–1074. https://doi.org/10.1016/S1054-3139(03)00114-0

Hurst, T.P., 2007. Thermal effects on behavior of juvenile walleye pollock (*Theragra chalcogramma*): Implications for energetics and food web models. Can. J. Fish. Aquat. Sci. 64, 449–457. https://doi.org/10.1139/F07-025

Jech, J.M., Michaels, W.L., 2006. A multifrequency method to classify and evaluate fisheries acoustics data. Can. J. Fish. Aquat. Sci. 63, 2225–2235. https://doi.org/10.1139/F06-126

Kaartvedt, S., Røstad, A., Klevjer, T.A., Staby, A., 2009. Use of bottom-mounted echo sounders in exploring behavior of mesopelagic fishes. Mar. Ecol. Prog. Ser. 395, 109–118. https://doi.org/10.3354/meps08174

Kalnay, E., Kanamitsu, M., Kistler, R., Collins, W., Deaven, D., Gandin, L., Iredell, M., Saha, S., White, G., Woollen, J., Zhu, Y., Chelliah, M., Ebisuzaki, W., Higgins, W., Janowiak, J., Mo, K.C., Ropelewski, C., Wang, J., Leetmaa, A., Reynolds, R., Jenne, R., Joseph, D., 1996. The NCEP/NCAR 40-year reanalysis project. Bull. Am. Meteorol. Soc. https://doi.org/10.1175/1520-0477(1996)077<0437:TNYRP>2.0.CO;2

Kitamura, M., Amakasu, K., Kikuchi, T., Nishino, S., 2017. Seasonal dynamics of zooplankton in the southern Chukchi Sea revealed from acoustic backscattering strength. Cont. Shelf Res. 133, 47–58. https://doi.org/10.1016/j.csr.2016.12.009

Koenker, B.L., Copeman, L.A., Laurel, B.J., 2018. Impacts of temperature and food availability on the condition of larval Arctic cod (*Boreogadus saida*) and walleye pollock (Gadus chalcogrammus). ICES J. Mar. Sci. 75, 2370–2385. https://doi.org/10.1093/icesjms/fsy052

Kunz, K.L., Claireaux, G., Pö Rtner, H.-O., Knust, R., Mark, F.C., Pörtner, H.-O., Knust, R., Mark, F.C., 2018. Aerobic capacities and swimming performance of polar cod (*Boreogadus saida*) under ocean acidification and warming conditions. J. Exp. Biol. 221, jeb184473. https://doi.org/10.1242/jeb.184473

Laurel, B.J., Copeman, L.A., Spencer, M., Iseri, P., 2018. Comparative effects of temperature on rates of development and survival of eggs and yolk-sac larvae of Arctic cod (*Boreogadus saida*) and walleye pollock (*Gadus chalcogrammus*). ICES J. Mar. Sci. 75, 2403–2412. https://doi.org/10.1093/icesjms/fsy042

Levine, R.M., De Robertis, A., Grünbaum, D., Woodgate, R., Mordy, C.W., Mueter, F., Cokelet, E., Lawrence-Slavas, N., Tabisola, H., 2021. Autonomous vehicle surveys indicate that flow reversals retain juvenile fishes in a highly advective high-latitude ecosystem. Limnol. Oceanogr. 66, 1139–1154. https://doi.org/10.1002/lno.11671

Logerwell, E.A., Busby, M., Mier, K.L., Tabisola, H., Duffy-Anderson, J., 2020. The effect of oceanographic variability on the distribution of larval fishes of the northern Bering and Chukchi seas. Deep. Res. Part II Top. Stud. Oceanogr. 177, 104784. https://doi.org/10.1016/j.dsr2.2020.104784

Logerwell, E., Rand, K., Danielson, S., Sousa, L., 2017. Environmental drivers of benthic fish distribution in and around Barrow Canyon in the northeastern Chukchi Sea and western Beaufort Sea. Deep Sea Res. Part II Top. Stud. Oceanogr. https://doi.org/10.1016/j.dsr2.2017.04.012

Lønne, O.J., Gulliksen, B., 1989. Size, age and diet of polar cod, *Boreogadus saida* (Lepechin 1773), in ice covered waters. Polar Biol. 9, 187–191. https://doi.org/10.1007/BF00297174

Lowry, L.F., Frost, K.J., 1981. Distribution, growth, and foods of Arctic cod (*Boreogadus saida*) in the Bering, Chukchi and Beaufort Seas. Can. Field-Naturalist 95, 186–191. https://doi.org/10.1017/CBO9781107415324.004

Maclennan, D.N., Fernandes, P.G., Dalen, J., 2002. A consistent approach to definitions and symbols in fisheries acoustics. ICES J. Mar. Sci. 59, 365–369. https://doi.org/10.1006/jmsc.2001.1158

Marsh, J.M., Mueter, F.J., Quinn, T.J., 2019. Environmental and biological influences on the distribution and population dynamics of polar cod (*Boreogadus saida*) in the US Chukchi Sea. Polar Biol. 1971. https://doi.org/10.1007/s00300-019-02561-w

Mecklenburg, C., Lynghammar, A., Johannesen, E., Byrkjedal, I., Christiansen, J.S., Karamushko, O. V, Mecklenburg, T.A., Møller, P.R., Steinke, D., Wienerroither, R.M., 2018. Marine Fishes of the Arctic Region Volume II, in: CAFF Monitoring Series Report 28. Akureyri, Iceland: Conservation of Arctic Flora and Fauna. Akureyri, Iceland.

Meier, W.N., Fetterer, F., Savoie, M., Mallory, S., Duerr, R., Stroeve, J., 2017. NOAA/NSIDC Climate Data Record of Passive Microwave Sea Ice Concentration, Version 3. Boulder, Colorado, USA. NSIDC National Snow Ice Data Center. https://doi.org/https://doi.org/10.7265/N59P2ZTG

Melnikov, I.A., Chernova, N. V., 2013. Characteristics of under-ice swarming of polar cod *Boreogadus saida* (Gadidae) in the Central Arctic Ocean. J. Ichthyol. https://doi.org/10.1134/S0032945213010086

Miksis-Olds, J.L., Stabeno, P.J., Napp, J.M., Pinchuk, A.I., Nystuen, J.A., Warren, J.D., Denes, S.L., 2013. Ecosystem response to a temporary sea ice retreat in the Bering Sea: Winter 2009. Prog. Oceanogr. 111, 38–51. https://doi.org/10.1016/j.pocean.2012.10.010

Mueter, F.J., Planque, B., Hunt Jr, G.L., Alabia, I.D., Hirawake, T., Eisner, L., Dalpadado, P., Drinkwater, K.F., Harada, N., Arneberg, P., Saitoh, S.-I., 2021. Possible future scenarios in the Gateways to the Arctic for Subarctic and Arctic marine systems: Prey resources, food webs, fish, and fisheries. ICES J. Mar. Sci.

Nelson, R.J., Bouchard, C., Fortier, L., Majewski, A.R., Reist, J.D., Præbel, K., Madsen, M.L., Rose, G.A., Kessel, S.T., Divoky, G.J., 2020. Circumpolar genetic population structure of polar cod, *Boreogadus saida*. Polar Biol. 43, 951–961. https://doi.org/10.1007/s00300-020-02660-z

Norcross, B.L., Raborn, S.W., Holladay, B.A., Gallaway, B.J., Crawford, S.T., Priest, J.T., Edenfield, L.E., Meyer, R., 2013. Northeastern Chukchi Sea demersal fishes and associated environmental characteristics, 2009-2010. Cont. Shelf Res. 67, 77–95. https://doi.org/10.1016/j.csr.2013.05.010

Parker-Stetter, S.L., Horne, J.K., Weingartner, T.J., 2011. Distribution of polar cod and age-0 fish in the U.S. Beaufort Sea. Polar Biol. 34, 1543–1557. https://doi.org/10.1007/s00300-011-1014-1

Peng, G., Meier, W.N., Scott, D.J., Savoie, M.H., 2013. A long-term and reproducible passive microwave sea ice concentration data record for climate studies and monitoring. Earth Syst. Sci. Data 5, 311–318. https://doi.org/10.5194/essd-5-311-2013

Pinchuk, A.I., Eisner, L.B., 2017. Spatial heterogeneity in zooplankton summer distribution in the eastern Chukchi Sea in 2012–2013 as a result of large-scale interactions of water masses. Deep Sea Res. Part II Top. Stud. Oceanogr. 135, 27–39. https://doi.org/10.1016/j.dsr2.2016.11.003

Pisareva, M.N., Pickart, R.S., Lin, P., Fratantoni, P.S., Weingartner, T.J., 2019. On the nature of wind-forced upwelling in Barrow Canyon. Deep. Res. Part II Top. Stud. Oceanogr. 162, 63–78. https://doi.org/10.1016/j.dsr2.2019.02.002

Ponomarenko, V.P., 2000. Eggs, larvae, and juveniles of polar cod *Boreogadus saida* in the Barents, Kara, and White Seas. J. Ichthyol. 40, 165–173.

Rand, K.M., Logerwell, E.A., 2011. The first demersal trawl survey of benthic fish and invertebrates in the Beaufort Sea since the late 1970s. Polar Biol. 34, 475–488. https://doi.org/10.1007/s00300-010-0900-2

Rose, G.A., DeYoung, B., Colbourne, E.B., 1995. Cod (Gadus morhua L.) migration speeds and transport relative to currents on the north-east Newfoundland Shelf. ICES J. Mar. Sci. 52, 903–913. https://doi.org/10.1006/jmsc.1995.0087

Ross, T., Keister, J.E., Lara-Lopez, A., 2013. On the use of high-frequency broadband sonar to classify biological scattering layers from a cabled observatory in Saanich Inlet, British Columbia. Methods Oceanogr. 5, 19–38. https://doi.org/10.1016/j.mio.2013.05.001

Sawada, K., Furusawa, M., Williamson, N.J., 1993. Conditions for the precise measurement of fish target strength in situ. J. Mar. Acoust. Soc. Japan 20, 73–79. https://doi.org/10.3135/jmasj.20.73

Sigler, M.F., Mueter, F.J., Bluhm, B.A., Busby, M.S., Cokelet, E.D., Danielson, S.L., Robertis, A. De, Eisner, L.B., Farley, E. V., Iken, K., Kuletz, K.J., Lauth, R.R., Logerwell, E.A., Pinchuk, A.I., 2017. Late summer zoogeography of the northern Bering and Chukchi seas. Deep Sea Res. Part II Top. Stud. Oceanogr. 135, 168–189. https://doi.org/10.1016/j.dsr2.2016.03.005

Spear, A., Napp, J., Ferm, N., Kimmel, D., 2020. Advection and in situ processes as drivers of change for the abundance of large zooplankton taxa in the Chukchi Sea. Deep. Res. Part II Top. Stud. Oceanogr. 177, 104814. https://doi.org/10.1016/j.dsr2.2020.104814

Spencer, M.L., Vestfals, C.D., Mueter, F.J., Laurel, B.J., 2020. Ontogenetic changes in the buoyancy and salinity tolerance of eggs and larvae of polar cod (*Boreogadus saida*) and other gadids. Polar Biol. 43, 1141–1158. https://doi.org/10.1007/s00300-020-02620-7

Stabeno, P.J., Bell, S.W., 2019. Extreme Conditions in the Bering Sea (2017–2018): Record-Breaking Low Sea-Ice Extent. Geophys. Res. Lett. 46, 8952–8959. https://doi.org/10.1029/2019GL083816

Stabeno, P., Kachel, N., Ladd, C., Woodgate, R., 2018. Flow Patterns in the Eastern Chukchi Sea: 2010–2015. J. Geophys. Res. Ocean. 123, 1177–1195. https://doi.org/10.1002/2017JC013135

Stevenson, D.E., Lauth, R.R., 2019. Bottom trawl surveys in the northern Bering Sea indicate recent shifts in the distribution of marine species. Polar Biol. 42, 407–421. https://doi.org/10.1007/s00300-018-2431-1

Traynor, J., 1996. Target-strength measurements of walleye pollock (*Theragra chalcogramma*) and Pacific whiting (*Merluccius productus*). ICES J. Mar. Sci. 53, 253–258. https://doi.org/10.1006/jmsc.1996.0031

Trevorrow, M. V., 2005. The use of moored inverted echo sounders for monitoring meso-zooplankton and fish near the ocean surface. Can. J. Fish. Aquat. Sci. 62, 1004–1018. https://doi.org/10.1139/f05-013

Urmy, S.S., Horne, J.K., Barbee, D.H., 2012. Measuring the vertical distributional variability of pelagic fauna in Monterey Bay. ICES J. Mar. Sci. 69, 184–196. https://doi.org/10.1093/icesjms/fsr205

Vestfals, C.D.C.D., Mueter, F.J.F.J., Hedstrom, K.S.K.S., Laurel, B.J.B.J., Petrik, C.M.C.M., Duffy-Anderson, J.T.J.T., Danielson, S.L.S.L., 2021. Modeling the dispersal of polar cod (*Boreogadus saida*) and saffron cod (*Eleginus gracilis*) early life stages in the Pacific Arctic using a biophysical transport model. Prog. Oceanogr. 196, 102571. https://doi.org/10.1016/j.pocean.2021.102571

Vestfals, C.D., Mueter, F.J., Duffy-Anderson, J.T., Busby, M.S., De Robertis, A., 2019. Spatio-temporal distribution of polar cod (Boreogadus saida) and saffron cod (*Eleginus gracilis*) early life stages in the Pacific Arctic. Polar Biol. 42, 969–990. https://doi.org/10.1007/s00300-019-02494-4

Wang, M., Yang, Q., Overland, J.E., Stabeno, P., 2018. Sea-ice cover timing in the Pacific Arctic: The present and projections to mid-century by selected CMIP5 models. Deep. Res. Part II Top. Stud. Oceanogr. 152, 22–34. https://doi.org/10.1016/j.dsr2.2017.11.017

Weingartner, T., Aagaard, K., Woodgate, R., Danielson, S., Sasaki, Y., Cavalieri, D., 2005. Circulation on the north central Chukchi Sea shelf. Deep Sea Res. Part II Top. Stud. Oceanogr. 52, 3150–3174. https://doi.org/10.1016/j.dsr2.2005.10.015

Weingartner, T., Dobbins, E., Danielson, S., Winsor, P., Potter, R., Statscewich, H., 2013. Hydrographic variability over the northeastern Chukchi Sea shelf in summer-fall 2008-2010. Cont. Shelf Res. 67, 5–22. https://doi.org/10.1016/j.csr.2013.03.012

Wilson, R.E., Sage, G.K., Wedemeyer, K., Sonsthagen, S.A., Menning, D.M., Gravley, M.C., Sexson, M.G., Nelson, R.J., Talbot, S.L., 2019. Micro-geographic population genetic structure within Arctic cod (*Boreogadus saida*) in Beaufort Sea of Alaska. ICES J. Mar. Sci. 76, 1713–1721. https://doi.org/10.1093/icesjms/fsz041

Woodgate, R.A., Peralta-Ferriz, C., 2021. Warming and Freshening of the Pacific Inflow to the Arctic from 1990-2019 implying dramatic shoaling in Pacific Winter Water ventilation of the Arctic water column. Geophys. Res. Lett. https://doi.org/10.1029/2021GL092528

Woodgate, R.A., 2018. Increases in the Pacific inflow to the Arctic from 1990 to 2015, and insights into seasonal trends and driving mechanisms from year-round Bering Strait mooring data. Prog. Oceanogr. 160, 124–154. https://doi.org/10.1016/j.pocean.2017.12.007

Woodgate, R.A., Weingartner, T., Lindsay, R., 2010. The 2007 Bering Strait oceanic heat flux and anomalous Arctic sea-ice retreat. Geophys. Res. Lett. 37, 1–5. https://doi.org/10.1029/2009GL041621

Woodgate, R.A., Aagaard, K., Weingartner, T.J., 2005. A year in the physical oceanography of the Chukchi Sea: Moored measurements from autumn 1990-1991. Deep. Res. Part II Top. Stud. Oceanogr. 52, 3116–3149. https://doi.org/10.1016/j.dsr2.2005.10.016

Supplementary Material

Supplementary Table 4.1 Compass heading and magnetic declination at each mooring deployment site.

Deployment	Site	Compass Heading (°)	Magnetic Declination (°)
2017 - 2018	Southern	335	9.6
	Central	208	11.6
2018 - 2019	Southern	172	10.3
	Central	198	12.2
	Northern	293	13.4

Supplementary Table 4.2 Parameter values used in Echoview's fish four-dimensional alpha-beta fish tracking module.

Parameter	Major axis	Minor Axis	Range	Target Strength	Ping Gap
Alpha	0.6	0.6	0.6		
Beta	0.0	0.0	0.0		
Exclusion Distance (m)	0.7	0.7	0.3		
Missed Ping Expansion (%)	10	10	10		
Parameter Weighting	30	30	30	30	10

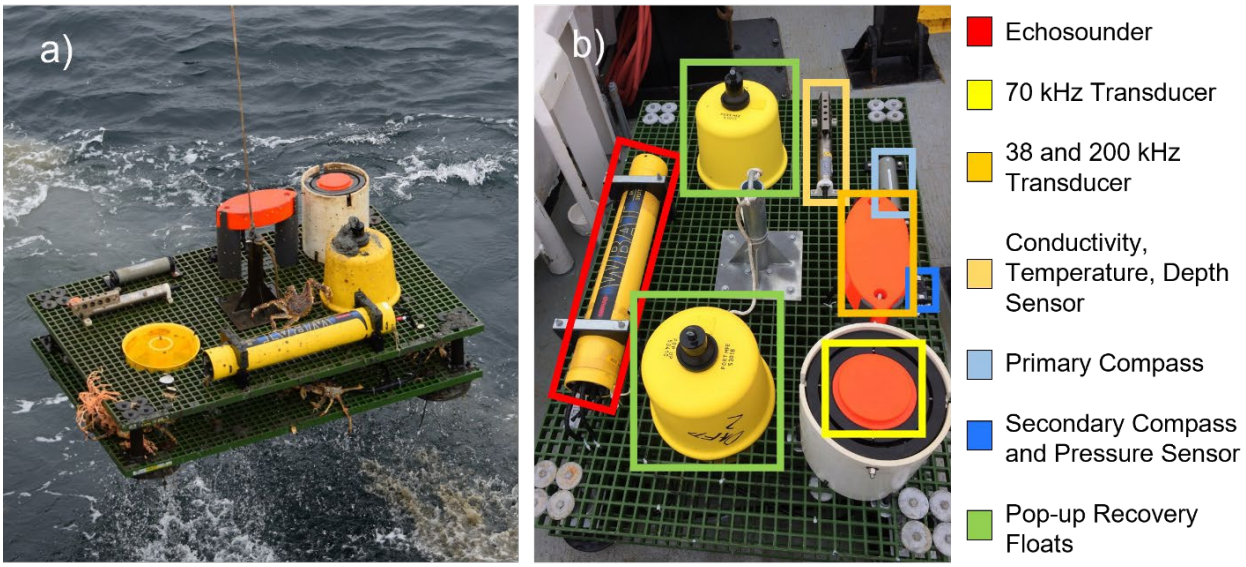

Supplementary Figure 4.1 Photographs of (a) mooring upon recovery and (b) mooring instrumentation.

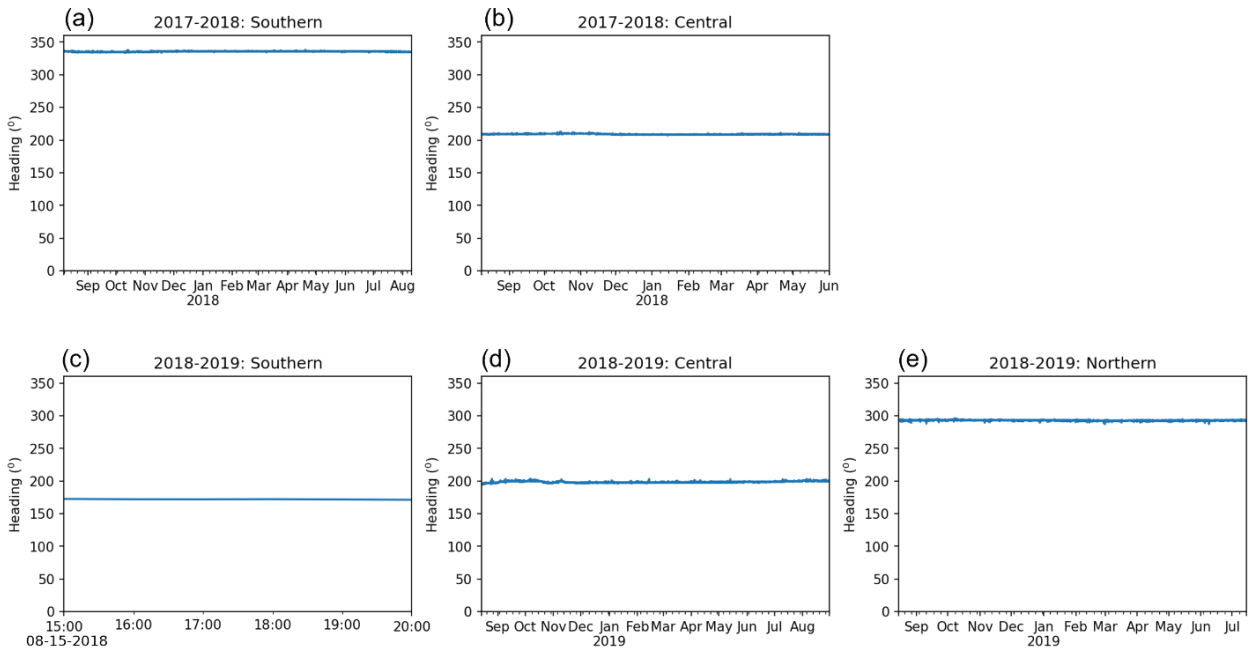

Supplementary Figure 4.2 Heading direction recorded by primary compass during 2017-2018 deployments at the (a) southern and (b) central mooring sites, and during 2018-2019 deployments at the (c) southern, (d) central, and (e) northern mooring sites. Five deployments (a, b, d, and e) were collected by a custom underwater magnetometer produced by the Engineering Development division of the NOAA Pacific Marine Environmental Lab. The short duration of the recording at the southern site in 2018-2019 (c) is due to battery limitations of the Aaronia GPS Logger (Aaronia AG). The secondary compass at this site failed.

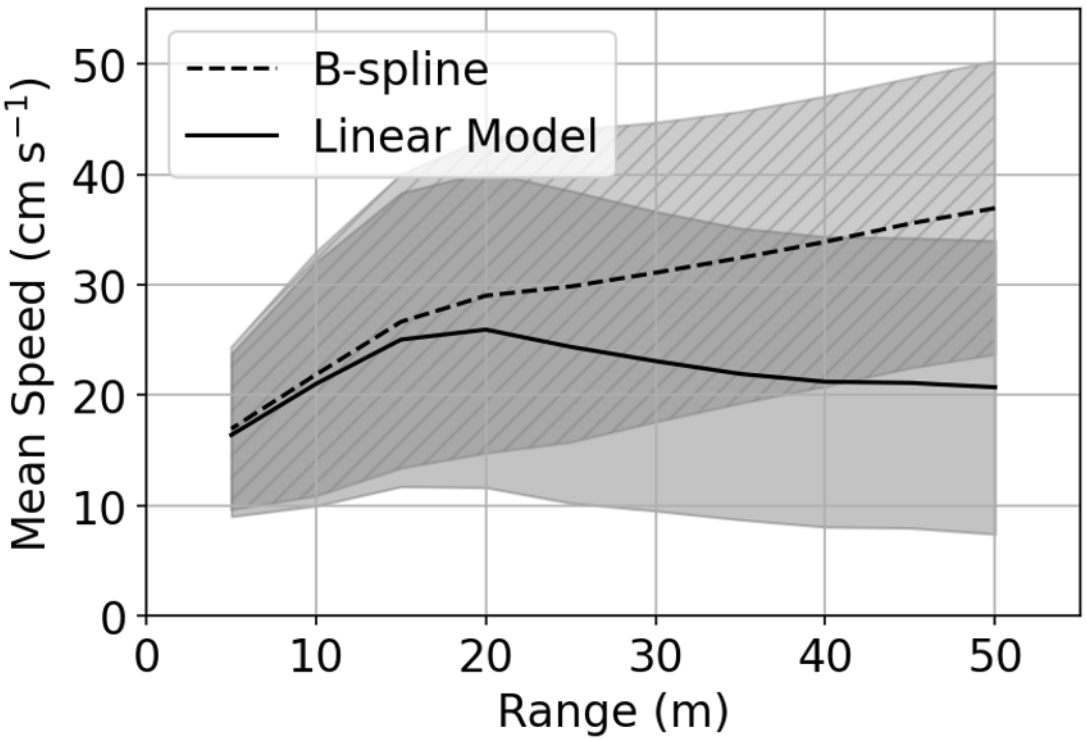

Supplementary Figure 4.3 Mean speed of fish tracks (cm s^{-1}) as a function of range (5-m bins) calculated from the B-spline range (solid line) and linear model (dashed line) representations of all fish tracks. ±1 SD is shown for the linear (solid grey) and B-spline (hatched grey) speeds.

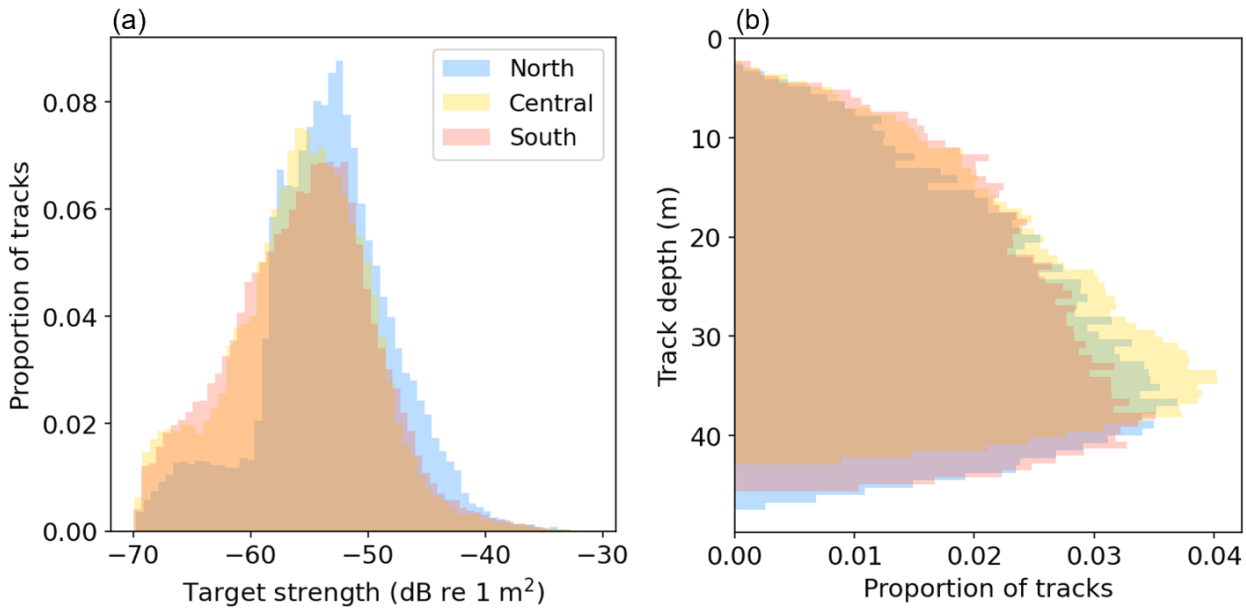

Supplementary Figure 4.4 (a) Distribution of mean target strength (dB re 1 m^{-2}) of all fish tracks at the northern (blue), central (yellow), and southern (red) sites. A threshold of -70 dB re 1 m^{-2} was used for target detection. (b) Depth distribution of fish tracks at all three mooring sites.

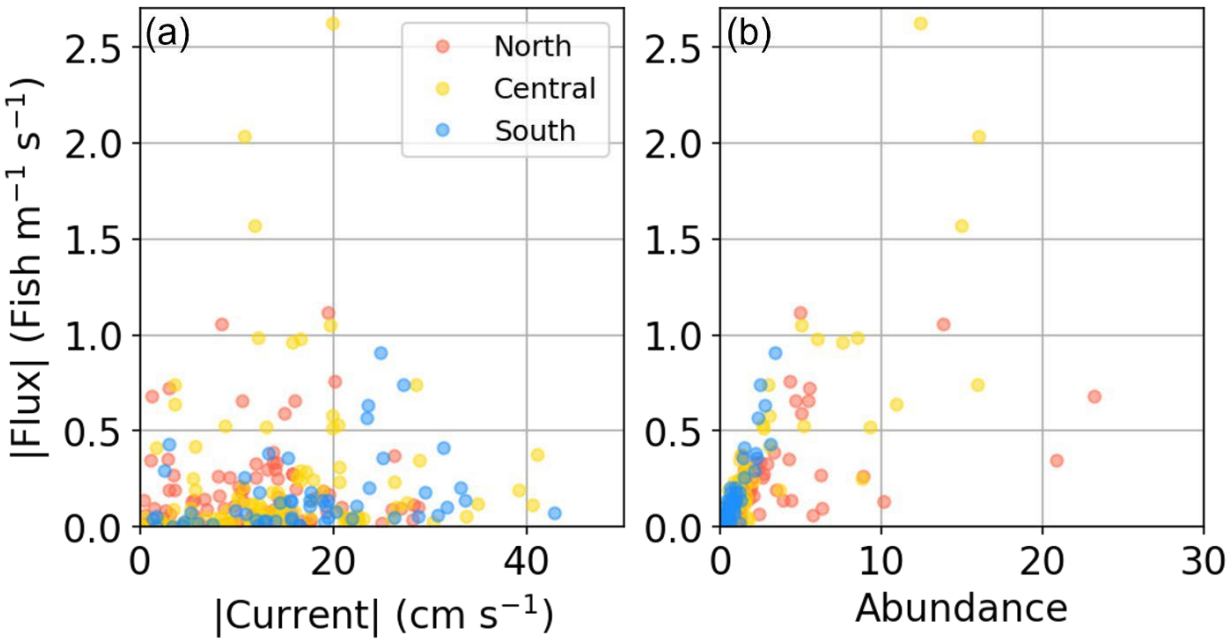

Supplementary Figure 4.5 Absolute value of mean weekly fish fluxes relative to (a) the absolute value of the mean weekly current speed and (b) mean weekly fish abundance at the northern (blue), central (yellow), and southern (red) sites.

CHAPTER 17 - Autonomous vehicle surveys indicate that flow reversals retain juvenile fishes in a highly advective high-latitude ecosystem

Objective 5: Further resolve early life history characteristics of Arctic cod and saffron cod and their behavior and connectivity between the Chukchi Sea and western Beaufort Sea.

Levine, Robert M., Alex De Robertis , Daniel Grünbaum, Rebecca Woodgate, Calvin W. Mordy, Franz Mueter, Edward Cokelet, Noah Lawrence-Slavas, Heather Tabisola. Autonomous vehicle surveys indicate that flow reversals retain juvenile fishes in a highly advective high-latitude ecosystem. Limnol. Oceanogr. 9999, 2020, 1–16. doi: 10.1002/lno.11671

Abstract

Summer surveys of the Chukchi Sea indicate that high densities of age-0 gadid fishes, historically Arctic cod (*Boreogadus saida*) but recently also walleye pollock (*Gadus chalcogrammus*), dominate the pelagic fish community. Adults are comparatively scarce, suggesting that either overwinter survivorship of age-0 gadids is low, or that they emigrate to other areas of the Pacific Arctic. To examine population movement, we conducted repeat acoustic surveys with saildrone autonomous surface vehicles equipped with echosounders throughout summer 2018. The saildrones' range and endurance enabled two large-scale surveys of the U.S. Chukchi shelf. Acoustic backscatter, a proxy for fish density, was highest in regions with sea surface temperatures of 6–8 C, and lowest in areas influenced by recent ice melt. A subarea of the central Chukchi was surveyed a total of four times; backscatter in this subarea increased by > 85% from late-July to mid-September. As summer progressed, fish developed more extensive diel vertical migrations and backscatter from individuals doubled. Both changes suggest increases in backscatter were driven primarily by increasing body size. Particle tracking simulations indicated age-0 gadids were likely retained over the Chukchi shelf by extended periods of wind-driven southward flow during the survey period before strong northward flow in late fall transported them to the north. These findings suggest that in summer 2018, age-0 gadids were advected northward to the Chukchi shelf from the northern Bering Sea, where they were retained during a period of growth until late fall before being advected farther north toward the Chukchi and Beaufort shelf breaks.

Introduction

Arctic gadids, particularly Arctic cod (*Boreogadus saida*), dominate the pelagic fish community in the Pacific Arctic eco- system of the northern Bering, Chukchi, East Siberian, and Beaufort Seas. Arctic cod have a circumarctic distribution and are abundant throughout the shallow shelves of the Arctic marginal seas as well as the Central Arctic Basin (Mecklenburg et al. 2018). Arctic cod are key pelagic secondary consumers that serve as a central trophic link between plankton and higher trophic levels (Bradstreet et al. 1986; Whitehouse and Aydin 2016), supporting large migratory populations of sea- birds (Matley et al. 2012) and marine mammals (Bradstreet et al. 1986). The Pacific Arctic is undergoing rapid changes associated with surface warming and loss of sea ice (Steele et al. 2008; Frey et al. 2015; Woodgate 2018). These changes have the potential to negatively impact Arctic cod growth and survival in this region and alter species distributions.

Recent studies suggest that the warming conditions in the Pacific Arctic are becoming increasingly hospitable for more boreal species such as walleye pollock (*Gadus chalcogrammus*) (Laurel et al. 2016; Huntington et al. 2020). Historically, trawl surveys conducted in the Chukchi Sea have found that pelagic biomass is dominated by age-0 (born within the past year) Arctic cod (Quast 1974; Norcross et al. 2010; Logerwell et al. 2015). Acoustic-trawl surveys conducted in 2017 and 2019 indicate that age-0 walleye pollock have become more abundant on the Chukchi shelf (R. M. Levine unpubl.). As the region changes

due to increasing temperatures, walleye pollock distributions may expand to the north and become a potentially significant component of the gadid community on the Chukchi shelf.

Little is known about the distribution and movements of pelagic fish populations in the region, particularly in the Chukchi Sea. Acoustic-trawl surveys conducted in summer 2012 and 2013 established a baseline of distributions of pelagic fishes in the U.S. northern Bering and Chukchi Seas (De Robertis et al. 2017). These surveys documented large numbers of pelagic age-0 Arctic cod, with the highest abundances in the northern Chukchi Sea where the average length was 3.5 cm and < 0.3% were greater than 6.5 cm (De Robertis et al. 2017). However, this and other surveys in the area indicate that older Arctic cod are comparatively rare on the U.S. Chukchi shelf (Logerwell et al. 2015; De Robertis et al. 2017).

Estimates of the reproductive potential of the Arctic cod population in the survey region indicate that observed densities of adults are likely insufficient to produce the large numbers of age-0 fish observed in the acoustic-trawl surveys (Marsh et al. 2019). It is likely that age-0 Arctic cod observed on the Chukchi shelf in summer are produced by adults that seasonally migrate into the region to spawn, or from eggs and larvae spawned in other areas and subsequently transported into the region. Large-scale horizontal migration of Arctic cod to spawning aggregation sites has been observed in the Barents Sea (Gjøsæter 1995) and Russian Arctic (Ponomarenko 1968). Recent work has hypothesized that a similar pattern of seasonal migration may occur in the Pacific Arctic (Forster et al. 2020). Similarly, walleye pollock have recently become more abundant in the northern Bering Sea (Stevenson and Lauth 2019), and this may have increased the supply of walleye pollock larvae that enter the Chukchi Sea from the south in recent years. The low densities of age-1+ relative to age-0 gadids found on the Chukchi shelf indicate that either overwinter survival of age-0s retained in the area is very low, or that the Chukchi shelf serves only as a summer nursery area, after which age-0s subsequently emigrate or are transported to other areas (De Robertis et al. 2017).

The likelihood of these scenarios is partially constrained by local advective regimes. The Chukchi Sea is a region of seasonally high advection, with strong northward currents that may transport eggs and larvae from the south (Fig. 1). High north- ward transport across the shelf occurs during the summer and fall (Woodgate et al. 2005; Stabeno et al. 2018), yielding residence times of Pacific Waters in the Chukchi of 4–5 months, although this residence time has likely decreased in recent years (Woodgate et al. 2005; Woodgate 2018). This movement of Pacific water toward the Arctic structures the species com- position and distribution of plankton communities in the Chukchi Sea, with many species being transported into the Chukchi Sea from the Bering Sea (Eisner et al. 2013; Ershova et al. 2015; Sigler et al. 2017). Interannual variability in phytoplankton, zooplankton and ichthyoplankton communities is strongly influenced by changes in oceanographic forcing, as indicated by associations between water masses of southern origin and community composition (Norcross et al. 2010; Danielson et al. 2017; Pinchuk and Eisner 2017; Spear et al. 2019).

The reproductive biology of Arctic cod and walleye pollock in the context of the advective regime provides additional clues to the origins of fish observed on the Chukchi shelf. Arctic cod are known to spawn in fall and winter under sea ice on the shallow shelves of the Arctic marginal seas (Ponomarenko 2000). Fertilized eggs are buoyant and develop under ice cover at the ice–water interface (Ponomarenko 2000). Pollock similarly produce pelagic eggs and, as larvae, remain close to the surface (Spencer et al. 2020). Development time in both species is temperature dependent, with time to 50% hatching of Arctic cod in laboratory studies ranging from 31 d at 3.8 C to 67 d at −0.4 C and approximately half of that time across these temperatures for walleye pollock (Laurel et al. 2018). Arctic cod hatching has been observed from December through August, with a peak during May/June (Bouchard and Fortier 2011). Ichthyoplankton surveys and otolith aging of larval and juvenile Arctic cod in other regions of the Arctic indicates that spawning occurs over a period of months, producing an extended distribution of larval fish

throughout the summer rather than a single short pulse or a set of discrete pulses (Bouchard and Fortier 2011; Bouchard et al. 2016). The spawning period of walleye pollock in the Bering Sea extends from early winter into early fall, with spawning in the north- ern Bering shelf highest in early summer (Hinckley 1987).

It is hypothesized that age-0 gadids on the Chukchi shelf are spawned to the south and are advected northward onto the Chukchi shelf in summer. Particle tracking simulations suggest that variations in wind and current patterns drive the interannual variability observed in late-summer distribution in the Chukchi Sea (C. D. Vestfals unpubl.). The age-0 gadids are then advected further to the north in the fall. Observations and modeled transport of larval Arctic cod suggest that spawning occurs at multiple locations in the Pacific Arctic (Vestfals et al. 2019; C. D. Vestfals unpubl.). Three key areas have been proposed as spawning areas for age-0 Arctic cod on the Chukchi shelf: the northern Bering Sea, along the Chukotka Peninsula in western Bering Strait, and the Beaufort Sea (Fig. 1; Kono et al. 2016; Vestfals et al. 2019). Acoustic- trawl abundance estimates in 2012 were lower than those in 2013 which is consistent with the hypothesis that lower annual northward transport in 2012 (e.g., Woodgate 2018) resulted in fewer age-0 Arctic cod originating in the Bering Sea were advected to the northeast Chukchi Sea by the time of the survey (C. D. Vestfals unpubl.). Larval Arctic cod have also been found in the northern Chukchi and western Beaufort Seas, in particular near Barrow Canyon. These fish may have been transported southward via up-canyon advection from aggregations of adult Arctic cod distributed to the north along the Beaufort shelf break (Geoffroy et al. 2011; Parker-Stetter et al. 2011; C. D. Vestfals unpubl.). Although Arctic cod are historically the most abundant species, advective transport is likely the main process driving the presence of all age-0 gadids on the Chukchi shelf. Walleye pollock and saffron cod (*Eleginus gracilis*) are abundant in the northern Bering and southern Chukchi Seas, respectively (De Robertis et al. 2017; Stevenson and Lauth 2019). Eggs and larvae of these species are likely to follow transport pathways similar to Arctic cod on the Chukchi shelf.

In this study, we sought to test the hypothesis that age-0 gadids in the Chukchi Sea are typically advected north during the summer, and that their distribution would shift northward during the open-water season. We used uncrewed surface vehicles (USVs) to conduct repeat acoustic surveys of the northeastern Chukchi Sea to quantify the intraseasonal variability in the spatial distribution of gadids in summer 2018. By conducting repeat surveys, we aimed to: (1) infer the source location of the age-0 gadid population in the northeast- ern Chukchi Sea in summer; (2) evaluate what movements of the fish population may reveal about the role of the northeast- ern Chukchi Sea as a nursery area for age-0 Arctic cod and other gadid fishes; and (3) ascertain whether, when, and how fish were transported out of the study area.

Methods

Survey design and data collection

Two Saildrone generation 5 USVs (SD-1022 and SD-1023, Saildrone, Inc., Fig. 2) were used to conduct an acoustic survey of pelagic sound-scattering organisms on the Chukchi shelf. The vehicles were deployed from Dutch Harbor, Alaska, on 30 June 2018 and recovered in the same location on 06 Octo- ber (98 d). The saildrone is a 7-m long wind-propelled vehicle which uses an actuator-controlled trim tab to manipulate a 5- m wing sail (Mordy et al. 2017; De Robertis et al. 2019). The vehicle autonomously navigates between operator-specified waypoints, with near real-time navigation, data reporting, and instrument control via satellite link. Onboard instrumentation operates on battery power, which is replenished by solar panels on the hull and wing. From 14 July to 24 September 2018 (72 d) the saildrones conducted acoustic surveys of the U.S. continental shelf region of the Chukchi Sea.

To compare the distribution of backscatter during mid and late summer, two large-scale surveys were completed from 20 July to 16 August and 24 August to 11 September. The sur- veys were conducted

between 66.5 N and 72.5 N and 168.6 W and 159.5 W (Fig. 1, area encompassed by the dashed line) along the 0.5 latitude spaced transects as surveyed by research vessels in 2012 and 2013 (De Robertis et al. 2017). Two additional surveys were conducted on a sub- set of four of the transect lines between 69.5 N and 71 N from 20 July to 03 August and from 13 August to 28 August. Along with the two large-scale surveys, this resulted in four replicate small-scale surveys in a region of previously (i.e., 2012 and 2013) observed high acoustic backscatter in the northeastern Chukchi Sea (Fig. 1, area indicated by dotted box). Both large- scale surveys and the additional two small-scale surveys were conducted from north to south along east–west acoustic tran- sects. In total, the two saildrones traveled 7610 nautical miles (14,093 km; hereafter referred to as nmi) in the Chukchi Sea at an average speed of 1.2 m s−1.

To measure backscatter from fishes, each saildrone was out-fitted with a Simrad wideband autonomous transceiver (WBAT-mini) split-beam echosounder with a Simrad ES38-18/200-18C transducer (three-channel split-beam 38 kHz and single-beam 200 kHz, both with a half power beamwidth of 18) gimbal-mounted on the keel at a depth of 1.9 m (see De Robertis et al. 2019 for details on echosounder integration). To manage power consumption, 12-min ping ensembles were transmitted between one and five times per hour (90% of data were collected with the instrument pinging continuously) defined by the operator depending on the battery state. Each ensemble consisted of simultaneous 38 and 200 kHz narrowband pings every 1.5 s using a 0.5-ms pulse duration. Back- scatter was recorded to 75 or 150 m range depending on the bottom depth. Electrical interference from the vehicle's sys- tems precluded the use of the 200 kHz data (this issue has since been resolved by Saildrone). The echosounders were calibrated after deployment using a 60-mm copper sphere for the 38-kHz transducer following the standard sphere method (Demer et al. 2015).

Sensors aboard the saildrone monitored environmental conditions throughout the deployment at 1-min intervals (for a full suite of sensors, see Mordy et al. 2017). Water temperature and salinity at 0.5 m depth were measured using a pair of conductivity, temperature, and depth (CTD) sensors (Saildrone3, RBR Ltd. and Sea-Bird SBE-37) on each USV. In situ comparisons between calibrated sensor pairs agreed to temperatures within ~ 0.01 C and salinities to within ~ 0.02 (PSS-78). Photosynthetically active radiation was measured at 2.5 m above the sea surface (LI-192SA, LI-COR, Inc.), and wind speed was measured using an anemometer mounted on the wing at 5.2 m (1590-PK-020, Gill Instruments Ltd.).

Inferring the identity of acoustic targets

In acoustic-trawl surveys, backscatter is attributed to species based on direct sampling (e.g., trawling) of acoustic scatterers, and by applying knowledge of the abundance and behavior (e.g., schooling characteristics and depth distributions) of the species in the study area (Horne 2000). We were unable to conduct any trawl sampling in 2018, and thus had to rely on observations from other years to interpret the acoustic observations. Surveys in 2012 and 2013 found the age-0 Arctic cod population in the Chukchi Sea to be > 35 times larger than any other observed species (De Robertis et al. 2017). Preliminary results from pelagic trawls conducted in 2017 and 2019 also indicate that most of the acoustic scattering at 38 kHz in this area is attributable to age-0 gadids. However, walleye pol- lock have become more abundant in recent years. Age-0 gadids made up > 95% of the trawl catch per unit effort in 2017 (85% Arctic cod and 10% walleye pollock by number) and > 85% of the catch per unit effort in 2019 (45% Arctic cod and 40% walleye pollock; R. M. Levine and S. Wildes unpubl.). As in previous years (De Robertis et al. 2017), other gadids such as saffron cod and Pacific cod (*Gadus macrocephalus*), and other strong sound scattering pelagic fishes such as capelin (*Mallotus villosus*) and Pacific herring (*Clupea pallasii*), were present in comparatively low abundance in 2017 and 2019 (R. M. Levine unpubl.) and occupied only a small portion of the Chukchi shelf. Although trawl sampling was not conducted during 2018, these surveys from previous and subsequent years strongly suggest that age-0 Arctic cod and walleye pollock likely dominated acoustic backscatter. Therefore, our analysis assumed that the acoustic-based measures

of fish density collected by the saildrones primarily reflect the abundance and distribution of age-0 Arctic cod and walleye pollock.

Acoustic data processing

Acoustic data were processed using Echoview 10.0 (Echoview Software Pty Ltd). Mean volume backscattering strength (Sv, dB re 1 m−1) at 38 kHz was used as a proxy for fish abundance. Sound speed and absorption were determined from 128 CTD casts collected during a 2017 survey of the U.S. continental shelf region of the Chukchi Sea between 67 N and 72.5 N. A mean sound speed of 1466.3 m s−1 was used for acoustic data post-processing, comparable to estimates of mean sound speed of the same region in other years (1470 m s−1 in 2013, 1472 m s−1 in 2019). Estimates fish back- scatter were not sensitive to the sound speed used: if sound speed from any individual cast (range of 1454.6–1484.4 m s−1) was used for the analysis instead of the mean value, backscatter changed by < 1%. In previous acoustic surveys, 38-kHz backscatter was dominated by backscatter with a frequency response consistent with that of fish (~ 96% in 2012 and 2013, De Robertis et al. 2017). During periods of elevated sea state, bubble entrainment caused attenuation of the transmitted signal. These pings were removed following the methods in De Robertis et al. (2019). The nautical area scattering coefficient (SA, m2 nmi−2) was integrated from 4 m below the sea surface to 0.5 m above the sounder-detected seafloor (as determined by Echoview's "best bottom candidate" algorithm and manually corrected after visual inspection where necessary) using a −70 dB re 1 m−1 threshold in 0.1 nmi along-track and 5-m vertical bins. SA is a proxy for fish abundance: it is proportional to fish density if the proportion of incident signal backscattered from the average fish in the population remains constant (MacLennan et al. 2002).

To compare backscatter between repeat surveys, the survey area was gridded into 0.5 latitude by 0.5 longitude cells. For large-scale surveys, only grid cells that contained data from both surveys were included (Fig. 3), resulting in 75 valid grid cells encompassing 993 and 805 nmi of acoustic observations from the first and second surveys, respectively. Mean SA was computed from acoustic measurements within each grid cell. The overall mean SA and the standard errors for all valid grid cells were estimated for each survey by fitting a geostatistical model to the gridded data with a separate mean by survey and constant spatial autocorrelation across surveys. The model was fitted via generalized least squares (GLS) using a Gaussian spatial correlation structure with a nugget effect (Wackernagel 2013). The same gridding and GLS model structure were applied to the four small-scale surveys to calculate mean backscatter and identify variability over time. In each of the four small-scale surveys, a subset of 42 grid cells containing 350 nmi of overlapping trackline was used for analysis (Fig. 5). The mean location of the distribution weighted by mean SA (center of gravity, Eq. 1 in Woillez et al. 2007), and the mean square distance between a measurement and the center of gravity (variance of spatial distribution, Eq. 3 in Woillez et al. 2007), were used to describe changes in the spa- tial distribution of the backscatter.

Measurements of backscattering cross-section (σbs, m2) of individual scatterers during the four small-scale surveys were calculated from single targets identified with Echoview's split- beam single target detection (method 2) algorithm. To minimize potential biases introduced by multiple overlapping targets being interpreted as a single fish, single target detection was limited to areas where density was low. The estimated number of animals per reverberation volume (Nv, Sawada et al. 1993) was determined in 100 ping along-track and 5-m vertical bins based on a target strength (TS, dB re 1 m2; TS = 10 log10(σbs), where σbs is the backscattering cross-section, see MacLennan et al. 2002). Based on previous catch results indicating that Arctic cod were likely the dominant scatterer, Nv was calculated using a TS of −57.3 dB re 1 m2 which assumes a mean Arctic cod size of 3.5 cm (De Robertis et al. 2017) and is similarly appropriate for walleye pollock of the same size class (Table S1). Single targets in grid cells where Nv > 0.04 were excluded from further analyses, as recommended by Sawada et al. (1993).

To investigate changes in acoustic strength of targets during the small-scale surveys, the mean σbs of all targets during each day of each small-scale survey was calculated (79–21,542 targets per day, median of 2893 targets). The daily means were used to model the changes in σbs as a linear function of time (yearday). A TS-length relationship developed primarily from age-0 Arctic cod (Geoffroy et al. 2016) was used to infer fish length at the midpoint of each small-scale survey from σbs, defined as

SL = 10 10 log10 ðσbs Þ +65:13 ,

(Hogan et al. 2014). The particles were seeded in areas where the first large-scale survey suggested (from observed grid cell mean SA and survey-wide mean σbs) that fish were abundant. A single particle was seeded at the center of each model grid cell where observed fish density was ≥ 0.1 fish m−2 (96 of 98 model grid cells) on the start date of the first large-scale survey (20 July).

Particle positions were calculated at 3-h intervals. To evaluate the potential for depth-dependent variability in transport, four separate model runs were conducted seeding particles at fixed depths of either 10, 20, 30, or 40 m. This range of depths encompasses the portion of the water column where most of the fish were located (> 85% of backscatter was observed from 10 to 40 m). To evaluate retention in the northeastern Chukchi Sea, we identified the proportion of particles at each time step that were (1) contained within the small-scale survey where SL is standard length (see Table S1 for additional details). Fish density (fish m−2) at the midpoint of each small-scale survey was calculated using model-predicted σbs following MacLennan et al. (2002).

Vertical distributions of age-0 Arctic cod were quantified by calculating the weighted mean depth of the backscatter from the entire water column in 1-h intervals (Eq. 2 in Woillez et al. 2007). Hourly measurements were classified as day or night based on photosynthetically active radiation measurements from the saildrones' sensors, using a day/night threshold value of photosynthetically active radiation of 10 μmol photons s−1 m−2, with 26% of the survey measurements occurring at night. To investigate linear trends in weighted mean depth over the duration of the surveys, an analysis of covariance was used to model the weighted mean depth of backscatter as a linear function of time (yearday), allowing the intercept and slope to differ between day and night. The model was fit via GLS to account for possible temporal auto- correlation, assuming a continuous first-order autoregressive time series structure (corAR1, Pinheiro et al. 2019).

Particle tracking simulations

The potential for physical retention of fishes in the north- eastern Chukchi Sea was examined using calculations completed using the OceanParcels python library (Lange and van Sebille 2017) which simulates the advection of passive particles from results of a numerical ocean model. Particles were tracked using a 1/12 resolution 3D velocity field obtained from the hybrid coordinate ocean model (HYCOM) global analysis output (https://hycom.org), at 3-h time resolution from 20 July to 18 September 2018. This model has 40 depth levels, with 5-m intervals from 10 to 50 m depth. HYCOM uses the Navy Coupled Ocean Data Assimilation system which assimilates satellite altimeter and sea surface temperature data, and in situ temperature and salinity profiles from ship, drifter, and mooring instrumentation. Surface forcing for the HYCOM run is taken from the Navy Global Environmental Model region or (2) found in the Beaufort Sea or on the Chukchi Sea slope (> 100 m bottom depth).

Results

Repeat large-scale surveys

The saildrones successfully completed two large-scale sur- veys of the U.S. continental shelf of the Chukchi Sea (Fig. 3). Sea-ice north of 71.5 N limited the northern extent of the first survey which was completed from 20 July to 16 August 2018 by a single saildrone. The second survey was completed from 24 August to 11 September 2018 by tasking two saildrones independently with the northern and southern portions of the survey.

Although the mean backscatter in the large-scale survey area increased slightly from a mean SA of 144 (± 37 SE) m2 nmi−2 during the first survey to 188 (± 50 SE) m2 nmi−2 during the second survey, the means were not significantly different (GLS, t-test p = 0.37). Fish distributions were similar in both surveys, suggesting there was no large-scale net advection of the population through the area during the survey period. The center of gravity of the backscatter shifted 18.7 km west (−165.79 W to −166.28 W) and 17.4 km north (from 69.77 N to 69.92 N), while exhibiting a slight decrease in variance of spatial distribution (−0.44 and −0.75 in latitude and longitude, respectively; Fig. 3). During both surveys 50% of the total backscatter occurred between 70 N and 71 N.

Temperature and salinity at 0.5 m depth ranged from−0.7 C to 11.4 C and from 26.5 to 32.8 psu during the large- scale surveys (Fig. 4). The coldest water was encountered north of 71 N, where surface conditions suggested recent mixing with sea ice meltwater (< 7 C and salinity < 30 psu). In areas where meltwater was present at the surface, backscatter was low; 92.9% of backscatter was observed in areas where the sur- face temperature was greater than 6 C and salinity was greater than 29 psu (Figs. 4, S1).

Repeat small-scale surveys

The small-scale surveys (four-transect subarea of the large- scale survey from 69.5 N to 71 N) lasted 12–21 d: 20 July–03 August, 23 July–12 August, 13–28 August (including a 5-d gap in sampling from 17 to 21 August), and 30 August to

11 September (Fig. 5). Mean backscatter within the 42 grid cells of the small-scale survey area varied among surveys, increasing from 197 (± 53 SE) to 369 (± 80 SE) m2 nmi−2 over the course of the summer (GLS, t-test p = 0.03, Table 1). The distribution of the population within the small-scale survey region did not shift appreciably among surveys. The center of gravity shifted slightly to the southwest between the first and last survey (19.4 km to the south and 19.3 km to the west, from −165.56 W 70.37 N to −166.08 W 70.19 N, Fig. 5).

The vertical distribution of fish during the small-scale surveys was consistent with the onset of vertical migration behavior. As the summer progressed, the weighted mean depth of backscatter remained shallow at night, but daytime depth increased after the second survey (Fig. 6a–d). Weighted mean depth during daylight hours increased from 17.7 (± 0.2 SE) to 30.0 (± 0.4 SE) m over the period of 53 d between the 1st and 4th survey (Fig. 6a–d). In contrast, weighted mean depth at night showed less variation, ranging from 16.6 (± 0.5 SE) to 19.6 (± 0.5 SE) m during the four surveys. Daylight hours decreased from 24 h per day at the start of the 1st survey to 14 h per day at the end of the 4th survey. Weighted mean depth differed between day and night (significant interaction in GLS, t-test p = 0.01) and this difference increased as a function of yearday (significant difference in slopes, t-test p = 0.005).

Although the placement of the transducer on the saildrone is shallower than typical on most research vessels, measurements of backscatter and individual acoustic targets were restricted to > 4 m depth. We found no significant difference between day and night backscatter (t-test comparing day and night on all sampling days, p = 0.27), indicating that there were not a significant number of scatterers migrating above the sampling range during the surveys. Although it is possible that some scatterers remained shallower than the transducer at all times, it is unlikely that we missed a large portion of the fish population which would have had to remain above the insonified depth throughout the entire survey period.

Backscattering cross-section (σbs) measurements were obtained from 252,949 acoustic single targets detected during the four small-scale surveys. Daily mean σbs was positively related to yearday (σbs = −7.68 × 10−6 + 4.54 × 10−8 (yearday), $p < 0.001$, $r2 = 0.44$; Fig. 6e), which results in a predicted increase in σbs from 1.7 × 10−6 (± 1.4 × 10−6 SE) to 3.5 × 10−6 (± 1.6 × 10−6 SE) between the midpoints of the first and fourth small-scale survey (Table 1). Estimates of standard length derived from σbs correspond to a change in length of 2.1 cm between the midpoints of the first and last survey 3.4 - 5.5 cm). Using the model-predicted values of σbs from the first day and last day of the small-scale surveys (Fig. 6e), the change in length corresponds to a growth rate of 0.54 mm d−1 over the 53-d period (Table S1). This estimate of growth rate is sensitive to the specific TS–length relationship used to convert scattering strength to fish length, and the use of alternative relationships results in a large range of estimates (0.24–0.89 mm d−1; Table S1).

Particle tracking

The passive particles in the simulation were primarily transported to the northeast (Figs. 7a-e, S2). By the end of the 60-d model run, the majority of particles were dispersed along the slope after being transported through Barrow Canyon (Fig. 7e). Initial movement of particles out of the survey region (Fig. 7a,b) was in two directions; particles in the northwest region of the survey area moved north toward Hanna Shoal, while the remainder of the particles followed the Alaska coast- line to the northeast.

From 20 July to 02 August, particles were advected out of the small-scale survey region at a consistent rate, with the pro- portion remaining in the small-scale survey area decreasing from 49% to 33% (Fig. 7f). The rate of advection out of the small-scale survey region decreased from 02 August to 25 August, when the proportion of particles in the survey region increased to ~ 40% and there were periods where particles returned to the region from the north. Thereafter the rate of export increased, with only 11% of all particles remaining in the survey area by mid-September. Through most of the model run, the proportion of particles along the Beaufort/ Chukchi slope steadily increased. By 18 September, or 60 d after the start of the first small-scale survey, 65% of particles had been advected seaward of the shelf break (> 100 m bottom depth) in the Chukchi and Beaufort Seas (Fig. 7e). The model runs produced similar results with particles tracked across depths of 10–40 m (Fig. 7f), indicating that (1) the system is strongly barotropic, that is, there is little vertical shear to the flow; and (2) inferences drawn from the model are not sensitive to fish depth.

Discussion

Acoustic surveys of age-0 gadids

Although the timing and location of spawning events are not known, large numbers of age-0 Arctic cod have been previously observed in the Chukchi Sea in the late summer and fall (De Robertis et al. 2017). The absence of a large population of age-1+ Arctic cod suggests that age-0 fish found in the eastern Chukchi Sea likely originated elsewhere, and that either over- winter mortality is high or they do not remain in place as they grow to maturity. This mortality and/or emigration is likely also occurring for other gadids including age-0 walleye pol- lock, for which large spawning stocks are observed in the Bering Sea but few age-1+ fish have been reported in the east- ern Chukchi Sea (Goddard et al. 2014). We analyzed repeat acoustic surveys and used particle tracking simulations to gain insights into possible directions of arrival and movement of these age-0 gadids through the eastern Chukchi Sea, and whether the absence of older individuals is most likely due to mortality or emigration of age-0 individuals.

Although we were not able to directly sample acoustic tar- gets, acoustic scatterers throughout the areas surveyed by the saildrones have spatial distributions and scattering properties that are consistent with those expected from age-0 gadids. Backscatter was highest in the northeastern Chukchi Sea, consistent

with observations from previous surveys in which trawl samples in that area were dominated by large numbers of age-0 Arctic cod (Quast 1974; Eisner et al. 2013; De Robertis et al. 2017). The large-scale survey estimates of mean SA (144 and 188 m2 nm−2) are similar in magnitude with estimates observed in previous acoustic surveys in the region (63.6 and 164.9 m2 nm−2 observed in 2012 and 2013), in which age-0 Arctic cod < 6 cm in length were the dominant contributors to 38-kHz backscatter (De Robertis et al. 2017). More recently, preliminary data from midwater trawl surveys in 2017 and 2019 indicate that primary scatterers across the shelf are age-0 gadids < 6 cm in length, and that while Arctic cod are the historically dominant scatterers, age-0 pollock may be becoming more abundant (R. M. Levine unpubl.). The σbs measurements observed in the four small-scale surveys (1.7 × 10−6 to 3.5 × 10−6 m2, Table 1) are consistent with observed in situ observations of both age-0 Arctic cod and walleye pollock < 6 cm (Brodeur and Wilson 1996; Geoffroy et al. 2016) rather than the much higher σbs expected for larger individuals. For example, the σbs for a 15-cm Arctic cod is ~ 8-fold greater than for a 3.5-cm fish (Geoffroy et al. 2016), and ~ 14-fold greater for a 15-cm age-1 pollock than a 3.5-cm age-0 (Brodeur and Wilson 1996; Traynor 1996). Although estimates of length are sensitive to the choice of TS–length relationship (Table S1), the σbs-derived lengths are consistent with the length distributions of age-0 gadids observed in previously collected trawl samples in the region (mean length of 3.5 cm, 99.7% of fish < 6.5 cm in August–September reported in De Robertis et al. 2017). These multiple lines of indirect evidence support our assumption that age-0 gadids dominated contributions to backscatter in the saildrone surveys.

The repeat acoustic surveys indicate that, while the spatial distribution of fishes in the northeastern Chukchi Sea did not change significantly from late July to early September of 2018, acoustic backscatter increased by ~ 87% during this period. The observed increase in acoustic backscatter could have resulted from either an increase in the abundance of scatterers, changes in the composition (i.e., size) of the scatterers, or a combination of both. During the small-scale surveys, σbs between the midpoint of the first and fourth small-scale sur- vey increased 104%. This suggests that the size distribution of fishes in the survey region may have shifted toward larger individuals. Over the same period, estimated fish density derived from the acoustic observations remained consistent (2.0–2.5 fish m−2, with overlapping standard errors, see Table 1). These estimated fish densities are similar to those observed in previous surveys (0.6 age-0 Arctic cod m−2 in 2012 and 2.2 Arctic cod m−2 in 2013, De Robertis et al. 2017).

Despite substantial variability, there is a unimodal distribution of σbs which increases over time, consistent with fish growth (Fig. S3). σbs is largely driven by swimbladder size, and although variability is high, average backscattering strength of individuals increases with length (Traynor 1996; Parker-Stetter et al. 2011). The changes in σbs corresponded to an estimated growth rate of 0.54 mm d−1 during the small-scale survey period. This growth rate is larger than measured rates from previous field and laboratory observations of age-0 Arctic cod (0.26 mm d−1 at 50 mm length, Hop et al. 1997; 0.19–0.24 mm d−1 Bouchard and Fortier 2011). However, growth rate is sensitive to the choice of TS–length relationship (0.24–0.89 mm d−1 depending on the relationship used, Table S1). Furthermore, σbs is orientation dependent (Foote 1980), and these estimates of growth assume consistent average orientation distributions over time. Although the uncertainties are large, the increase in σbs is likely related to growth, and it may ultimately be possible to estimate growth rates of Arctic gadids by measuring target strength in some circumstances. In future work, this uncertainty can be reduced by assessing TS–length relationships directly by coupling these observations with direct sampling of fish lengths.

The observed changes in vertical distribution (change in mean nighttime depth from 17.7 to 30.0 m during small-scale surveys) provide further evidence that growing age-0 gadids may have dominated the acoustic observations. As eggs and larvae, both Arctic cod and walleye pollock are predominantly surface associated (Spencer et al. 2020), drifting until their swimming ability develops and their swimbladder fills. Individuals exhibit an ontogenetic migration, descending deeper in the water column as they age. This transition in Arctic cod and walleye pollock occurs at a length of > 30 mm, when pelagic juveniles

vertically shift to deeper water during day- time, typically observed in late summer (Brodeur et al. 2000; Ponomarenko 2000; Bouchard and Fortier 2011). In the saildrone surveys, diel vertical migration behavior was initiated when mean TS-derived lengths were > 30 mm. This behavior also coincided with the onset of night in late-July during both the first and second small-scale surveys. This change is consistent with expected behavior for gadids as individuals increase in size over time. Together, the observed σbs and increased vertical migration suggest that increasing back- scatter may be due to individual growth.

Suitability of the Chukchi Sea as a nursery

Minimal changes were observed in the spatial distribution of fish during the survey period, which is inconsistent with a single, spatially restricted pulse of fish being advected across the Chukchi shelf. If there was a continuous northward transport, a single short spawning pulse from the south would result in a northward shift in the center of gravity of the population over time, and/or large changes in abundance between surveys. We hypothesized two alternative mechanisms to account for our observations: (1) a greatly extended spawning period that continues late into summer, with fish continuously transported north at a steady rate with balanced immigration and emigration; or, (2) retention of a population established by mid-July for most of the summer. The latter of these scenarios would be consistent with Arctic cod in other regions of the western Arctic where the majority of hatching occurs during a ~ 2-month period in late spring (Bouchard et al. 2016).

Age-0 fish populations may be enhanced by being be retained on the Chukchi shelf in summer to use the region as a nursery. Predation from piscivorous fish is likely low, as large fishes are scarce in the region (Sigler et al. 2011; De Robertis et al. 2017). Piscivorous seabirds are widely distributed and abundant throughout the Bering, Chukchi, and Beaufort Seas (Kuletz et al. 2015), and thus seabird predation pressure during open-water season is relatively consistent throughout the region. In summer, seabird foraging hotspots occur on the boundaries of the Chukchi shelf near Bering Strait and to the north along Barrow Canyon, where there is also a seasonal increase marine mammal presence (Kuletz et al. 2015).

Water temperatures on the Chukchi shelf are also likely to be more conducive for growth than conditions farther north (Laurel et al. 2016). Saildrone measurements of temperature and salinity were limited to the upper 0.5 m, thus it was not possible to directly assess the conditions at the same depths as the fish. However, backscatter was lowest in the northernmost areas of the large-scale survey area (Fig. 3), where low surface water temperatures and salinities suggested recent mixing with the meltwater which typically overlays cold winter water (Weingartner et al. 2013; Danielson et al. 2017). De Robertis et al. (2017) observed that Arctic cod on the Chukchi shelf were largely present at intermediate temperatures (3.4–6.6 C) and high salinities (> 30.4 psu) typical of Bering/Chukchi Summer Water. The Bering/Chukchi Summer Water flows north into the Chukchi Sea from the northern Bering Sea shelf (Coachman et al. 1975; Danielson et al. 2017) and gradually replaces the surface meltwater and deep winter water on the Chukchi shelf (Weingartner et al. 2013). The warmer Bering/ Chukchi Summer Water is within the temperature range (2–8 C) observed for maximum growth in Arctic cod and positive growth potential in both walleye pollock and saffron cod (Laurel et al. 2016).

Advective influences on age-0 fishes

The low backscatter in areas near meltwater indicates that these fish are unlikely to be originating from the north or areas influenced by recent ice melt and are either passively or actively remaining in warmer conditions. The Chukchi shelf is a highly advective environment, where advection is likely to dominate over the directed swimming movements of small fishes. The association of age-0 gadids with warmer water conditions supports the hypothesis that the age-0 gadids observed on the Chukchi shelf are likely advected northward from spawning areas to the south. Advective transport north across the Chukchi shelf

is generally attributed to both local winds and a far field forcing relating to a sea level difference between the Pacific and the Arctic (see Woodgate et al. 2005 for discussion). Since 1990, the annual mean northward velocity of the flow through the Bering Strait has ranged from ~ 18 (± 2) cm s−1 in 2001 to ~ 28 (± 3) cm s−1 in 2014 (lowest and highest annual mean velocities of the 1991–2015 period; Wood- gate 2018). This includes periods of southward flow and thus the northward mode speed is higher (from 20 to 40 cm s−1, Woodgate 2018 their Fig. 4). In the northeastern Chukchi Sea, the mean velocities of the upper 10 m of the water column in summer average 8 cm s−1, ranging from 0.5 to 22.8 cm s−1 from 2010 to 2015 (Stabeno et al. 2018). In respiration experiments, maximum aerobic swim speeds of Arctic cod were 3 to 3.6 body lengths s−1 (12–14 cm s−1 for a 4-cm fish) during burst swimming activity (Kunz et al. 2018). In studies of related gadid species, routine swimming speeds of juvenile fish were 0.5 to 0.6 body lengths s−1 (2–2.4 cm s−1 for a 4-cm fish, Peck et al. 2006). For age-0 gadids of 3.5 cm length, this suggests a routine swimming speed of approximately 1.9 cm s−1, which is an order of magnitude lower than typical advective currents. These estimates support the hypothesis that passive transport likely plays a dominant role determining the distribution of age-0 gadids on the Chukchi shelf, and that swimming behaviors have relatively small impacts on long-term distributions.

In late summer 2018, transport simulations suggest that age-0 gadids were advected northward, likely to the Beaufort and Chukchi slopes and Arctic basin. As expected, the model indicated that net transport was northward, with 90% of modeled particles released in the large-scale survey area dispersed along the shelf or slope to the north of the survey area at the end of the 60-d model run. However, during the month of August, only a few particles left the survey area, and during some periods transport reversed to increase particle abundance within the small-scale survey area (Figs. 7f, S2). The decrease in the rate of particles leaving the survey area and subsequent return of particles suggests that age-0 gadids are retained on the Chukchi shelf by episodic flow reversals. Estimates of retention based on particle transport from the survey area are consistent at 10, 20, 30, and 40 m depth (depths where the bulk of the backscatter occurred throughout the survey period). This suggests that variations in horizontal advection of fishes are likely insensitive to vertical movements or water column position.

Flow reversals similar to those occurring in the 2018 particle tracking model are commonly observed in the northeast- ern Chukchi Sea, and are associated with strong southward winds (Woodgate et al. 2005; Stabeno et al. 2018; Pisareva et al. 2019). De Robertis et al. (2017) speculated that difference in age-0 Arctic cod distribution between 2012 and 2013 may be linked to variability in currents and prey availability, and recent work has proposed variation in wind-driven retention as an explanation (Vestfals et al. 2019). Woodgate et al. (2005) developed a linear model for determining water velocity in the northeastern Chukchi Sea as a function of the pressure head forcing and surface wind speed. Offshore of Cape Lisburne, assuming a baseline pressure head velocity of 9.4 cm s−1 (see Table 3 in Woodgate et al. 2005), surface wind speed would need to exceed 7.2 m s−1 to the south to balance the pressure head forcing, temporarily stopping northward transport. Wind speed measurements from the saildrones indicate that from 01 August to 30 August, the mean velocity of the north–south wind component was 2.3 m s−1 to the south, with 21 days having mean southward winds (Fig. S4). How- ever, during 10.3% of August, wind velocity to the south was 7.2 m s−1, during which predicted net northward transport would be near zero or negative. This simplistic calculation is supported by the particle tracking model which shows this wind reversal was sufficient to account for the particle retention on the shelf. We hypothesize that wind-driven relaxation in northward transport may be responsible for, and predict, retention of age-0 gadids in the northeastern Chukchi Sea.

It also seems reasonable to hypothesize that interannual variations in circulation influence advection and subsequent retention of age-0 gadids in the Chukchi Sea. Transport through the Bering Strait (which is generally indicative of the northward flux through the Chukchi Sea, Woodgate et al. 2005) estimated from near-bottom velocity data indicates that monthly mean transport during summer 2018 (R. A. Woodgate pers. comm.) was similar to the 1990–2004 climatology (Woodgate et al. 2005), even though in the

annual mean, 2018 was higher in flow than the climatology. Thus, as it is summer that most concerns us, it is likely that the observed summer residence time of age-0 gadids in the Chukchi in 2018 is fairly typical, and suggests a hypothesis that cold-adapted species such as Arctic cod may have adapted to spawn at a time and place that more or less reliably places larvae in this apparent nursery area.

The Pacific Arctic is currently undergoing rapid changes, including increased northward transport through Bering Strait in recent decades (Woodgate 2018). These changes in advection, temperature, and ice cover have the potential to alter Arctic gadid populations. Bouchard et al. (2017) proposed that an initial decrease in ice cover, resulting in warmer conditions, would increase survival and growth of larval Arctic cod. However, continued temperature increases beyond their preferred growth range could depress physiological condition and sur- vival of larval Arctic cod, while enhancing conditions for larval walleye pollock (Koenker et al. 2018). Winter spawning provides a lengthy growth period for Arctic cod, during which maximizing prewinter size may be important for survival (Bouchard and Fortier 2011). Increased northward transport in summer may more quickly transport Arctic cod off the shelf and into the Arctic basin, shortening time available for growth in this potentially favorable nursery environment.

Increased input of Pacific water onto the shelf may also increase the presence of subarctic and boreal gadids, increasing competition and predation among pelagic species (Sigler et al. 2011). This transition has already been observed in the Barents Sea, where larger boreal species have expanded their distribution, increasing predation on and competition with smaller Arctic species (Fossheim et al. 2015). Subarctic gadids of high abundance in the Bering Sea such as walleye pollock and Pacific cod may be more likely to be transported north, following the same advective pathways across the Chukchi shelf as Arctic cod. Evidence from recent midwater surveys conducted in the region (R. M. Levine unpubl.) suggest other broadly distributed fishes such as walleye pollock or saffron cod have the potential to move further north, increasing in abundance on the Chukchi shelf as conditions warm (Huntington et al. 2020). The potential for these species to survive overwinter in the Arctic, however, is still unknown.

We found that distributions of age-0 gadids in the Chukchi Sea are strongly driven by two factors: advection and retention within specific water masses. Further studies are needed to better understand specific oceanographic features (e.g., currents, fronts, ice presence, water masses) and to investigate their demographic effects on gadids in the region. For example, in situ observations of fish movement and behavior (e.g., target tracking from moored acoustic instruments; Kaartvedt et al. 2009) paired with direct observations of currents have potential to better constrain potential pathways for transport of fishes, resolve the timing and seasonal dynamics of their development from eggs to juveniles, and predict recruitment into downstream populations along the Beaufort and Chukchi Sea slope.

Insights on Arctic fishes from USV observations

Traditionally, acoustic surveys have relied on trawl sampling of species and size composition to convert acoustic back- scatter into abundance estimates (Simmonds and MacLennan 2005). Recent advances in the integration of echosounders into autonomous platforms have increased our ability to measure acoustic backscatter remotely over long periods (Greene et al. 2014; Mordy et al. 2017; Benoit-Bird et al. 2018; Ohman et al. 2019). We used the endurance of the saildrones to collect a large number of acoustic observations over an extended period of time which would have been pro- hibitively expensive and logistically difficult using ships. These repeat acoustic surveys spanning large spatial and temporal scales enabled us to constrain the movement of age-0 gadid fishes on the Chukchi shelf and made it possible to determine a TS and approximate a growth rate. These insights into the transport, growth, origins, and fate of the age-0 gadid population were made possible by the high spatial and temporal coverage offered by autonomous platforms.

However, with current technology, it remains challenging, in most cases, to validate species composition, size, sex, and other organismal properties by acoustic methods alone (Bassett et al. 2018). Thus, the key challenge going forward is not how to measure acoustic scattering from autonomous vehicles, but how best to use these measurements to under- stand the abundance, distribution, and behavior of marine organisms (De Robertis et al. 2019). While autonomous acoustic surveys cannot definitively identify the species and size composition of acoustic scatterers, they can be effective in regions where other data have shown that a single or distinguishable group of dominant scatterers enables interpretation of acoustic data (Mordy et al. 2017; De Robertis et al. 2019). Low-diversity, high-latitude regions may be favorable for autonomous echosounder measurements because backscatter is often dominated by a single species or group (Geoffroy et al. 2011; De Robertis et al. 2019).

With its low pelagic diversity, the Chukchi Sea provides a good ecosystem for the application of autonomous acoustic survey methods. However, Arctic ecosystems are undergoing changes that may alter species compositions (e.g., Fossheim et al. 2015; Huntington et al. 2020), and the assumptions that make these inferences possible are likely to change with time. The increased presence of species with similar acoustic proper- ties will limit the ability to address species-specific questions without additional sampling in rapidly changing ecosystems such as the Arctic, although inference at the community level (e.g., gadids) may be feasible. Future studies of high-latitude marine environments (e.g., Arctic, Antarctic) may benefit from the use of USVs and other autonomous platforms allowing for acoustic measurement of fish and macrozooplankton populations, with the potential to expand into more complex environments and applications as the methodologies for remote species identification improve.

Conclusions

Repeat saildrone surveys indicated that advection resulted in the retention of age-0 gadids on the Chukchi Sea shelf throughout the summer where they underwent in situ growth. These fish likely originated south of the central Chukchi Sea and were advected onto the northeast shelf. In late summer, transport simulations suggest that advection played a larger role than swimming and that these fishes were passively advected further north to the Beaufort and Chukchi slopes and Arctic basin. Variations in transport rate and trajectory may account for the interannual variability in the density and distribution of pelagic fishes on the Chukchi shelf. In a changing climate, changes in circulation and water column conditions may alter the future structure of pelagic communities in the Pacific Arctic and the suitability of the Chukchi shelf as a favorable nursery area. Although Arctic cod are currently the dominant gadid in the region, increasing temperatures and earlier transport off the Chukchi shelf could limit age-0 growth prior to their first winter, and increased subarctic pelagic fishes such as walleye pollock may lead to increased predation pressure and competition that may further limit the Arctic cod population (Fossheim et al. 2015; Huntington et al. 2020). New technologies such as autonomous vehicles are likely to provide opportunities to better quantify perturbations of this rapidly changing ecosystem.

References

Bassett, C., A. De Robertis, and C. D. Wilson. 2018. Broadband echosounder measurements of the frequency response of fishes and euphausiids in the Gulf of Alaska. ICES J. Mar. Sci. 75: 1131–1142. doi:10.1093/icesjms/fsx204

Benoit-Bird, K. J., T. Patrick Welch, C. M. Waluk, and others. 2018. Equipping an underwater glider with a new echo- sounder to explore ocean ecosystems. Limnol. Oceanogr. Methods 16: 734–749. doi:10.1002/lom3.10278

Bouchard, C., and L. Fortier. 2011. Circum-arctic comparison of the hatching season of polar cod Boreogadus saida: A test of the freshwater winter refuge hypothesis. Prog. Oceanogr. 90: 105–116. doi:10.1016/j.pocean.2011.02.008

Bouchard, C., S. Mollard, K. Suzuki, D. Robert, and L. Fortier.2016. Contrasting the early life histories of sympatric Arctic gadids Boreogadus saida and Arctogadus glacialis in the Canadian Beaufort Sea. Polar Biol. 39: 1005–1022. doi:10.1007/s00300-014-1617-4

Bouchard, C., M. Geoffroy, M. LeBlanc, A. Majewski, S. Gauthier, W. Walkusz, J. D. Reist, and L. Fortier. 2017. Cli- mate warming enhances polar cod recruitment, at least transiently. Prog. Oceanogr. 156: 121–129. doi:10.1016/j. pocean.2017.06.008

Bradstreet, M. S. W., K. J. Finley, A.-D. Sekerak, W. B. Griffiths, C. R. Evans, M. F. Fabijan, and H. E. Stallard. 1986. Aspects of the biology of Arctic Cod (Boreogadus saida) and its importance in Arctic marine food chains. Can. Tech. Rep. Fish. Aquat. Sci. Fish. Aquat. Sci. 1491: 193.

Brodeur, R. D., and M. T. Wilson. 1996. Mesoscale acoustic patterns of juvenile walleye Pollock (Theragra chalcogramma) in the western Gulf of Alaska. Can. J. Fish. Aquat. Sci. 53: 1951–1963. doi:10.1139/cjfas-53-9-1951

Brodeur, R. D., M. T. Wilson, and L. Ciannelli. 2000. Spatial and temporal variability in feeding and condition of age-0 walleye Pollock (Theragra chalcogramma) in frontal regions of the Bering Sea. ICES J. Mar. Sci. 57: 256–264. doi:10.1006/jmsc.1999.0525

Coachman, L. K., K. Aagaard, and R. B. Tripp. 1975. Bering Strait: The regional physical oceanography. Univ. Washington Press, 172 p.

Corlett, W. B., and R. S. Pickart. 2017. The Chukchi slope cur- rent. Prog. Oceanogr. 153: 50–65. doi:10.1016/j.pocean.2017.04.005.

Danielson, S. L., L. Eisner, C. Ladd, C. Mordy, L. Sousa, and T. J. Weingartner. 2017. A comparison between late sum mer 2012 and 2013 water masses, macronutrients, and phytoplankton standing crops in the northern Bering and Chukchi seas. Deep-sea Res. Part II Top. Stud. Oceanogr. 135: 7–26. doi:10.1016/j.dsr2.2016.05.024

De Robertis, A., K. Taylor, C. D. Wilson, and E. V. Farley. 2017. Abundance and distribution of Arctic cod (Boreogadus saida) and other pelagic fishes over the U.S. Continental Shelf of the Northern Bering and Chukchi seas. Deep-Sea Res. Part II Top Stud. Oceanogr. 135: 51–65. doi:10.1016/j.dsr2.2016.03.002

De Robertis, A., N. Lawrence-Slavas, R. Jenkins, and others. 2019. Long-term measurements of fish backscatter from Saildrone unmanned surface vehicles and comparison with observations from a noise-reduced research vessel. ICES J. Mar. Sci 76: 2459–2470. doi:10.1093/icesjms/fsz124

Demer, D.A. and others 2015. Calibration of acoustic instruments. ICES Coop. Res. Rep. No. 326. 133 p.

Eisner, L., N. Hillgruber, E. Martinson, and J. Maselko. 2013. Pelagic fish and zooplankton species assemblages in rela- tion to water mass characteristics in the northern Bering and southeast Chukchi seas. Polar Biol. 36: 87–113. doi:10.1007/s00300-012-1241-0

Ershova, E. A., R. R. Hopcroft, and K. N. Kosobokova. 2015. Inter-annual variability of summer mesozooplankton com- munities of the western Chukchi Sea: 2004–2012. Polar Biol. 38: 1461–1481. doi:10.1007/s00300-015-1709-9

Foote, K. G. 1980. Effect of fish behaviour on echo energy: The need for measurements of orientation distributions. ICES J. Mar. Sci. 39: 193–201. doi:10.1093/icesjms/39.2.193

Forster, C. E., B. L. Norcross, F. J. Mueter, E. A. Logerwell, and A. C. Seitz. 2020. Spatial patterns, environmental correlates, and potential seasonal migration triangle of polar cod (Boreogadus saida) distribution in the Chukchi and Beaufort seas. Polar Biol. 43: 1073–1094. doi:10.1007/s00300-020- 02631-4

Fossheim, M., R. Primicerio, E. Johannesen, R. B. Ingvaldsen, M. M. Aschan, and A. V. Dolgov. 2015. Recent warming leads to a rapid borealization of fish communities in the Arctic. Nat. Clim. Change 5: 673–677. doi:10.1038/nclimate2647

Frey, K. E., G. W. K. Moore, L. W. Cooper, and J. M. Grebmeier. 2015. Divergent patterns of recent sea ice cover across the Bering, Chukchi, and Beaufort seas of the Pacific Arctic region. Prog. Oceanogr. 136: 32–49. doi:10.1016/j. pocean.2015.05.009

Geoffroy, M., D. Robert, G. Darnis, and L. Fortier. 2011. The aggregation of polar cod (Boreogadus saida) in the deep Atlantic layer of ice-covered Amundsen Gulf (Beaufort Sea) in winter. Polar Biol. 34: 1959–1971. doi:10.1007/s00300- 011-1019-9

Geoffroy, M., A. Majewski, M. LeBlanc, S. Gauthier, W. Walkusz, J. D. Reist, and L. Fortier. 2016. Vertical segregation of age-0 and age-1+ polar cod (Boreogadus saida) over the annual cycle in the Canadian Beaufort Sea. Polar Biol. 39: 1023–1037. doi:10.1007/s00300-015-1811-z

Gjøsæter, H. 1995. Pelagic fish and the ecological impact of the modern fishing industry in the Barents Sea. Arctic 48: 267–278. doi:10.14430/arctic1248

Goddard, P., R. Lauth, and C. Armistead. 2014. Results of the 2012 Chukchi Sea bottom trawl survey of Bottomfishes, crabs, and other Demersal macrofauna. U.S. Dep. Commer., NOAA Tech. Memo. NMFS-AFSC-278. 110 p.

Greene, C., and others. 2014. A wave glider approach to fisher- ies acoustics: Transforming how we monitor the Nation's Commercial Fisheries in the 21st century. Oceanography 27: 168–174. doi:10.5670/oceanog.2014.82

Hinckley, S. 1987. The reproductive biology of walleye Pollock, Theragra chalcogramma, in the Bering Sea, with reference to spawning stock structure. Fish. Bull. 85: 481–498.

Hogan, T. F., and others. 2014. The navy global environmental model. Oceanography 27: 116–125. doi:10.5670/ oceanog.2014.73

Hop, H., W. M. Tonn, and H. E. Welch. 1997. Bioenergetics of Arctic cod (Boreogadus saida) at low temperatures. Can. J. Fish. Aquat. Sci. 54: 1772–1784. doi:10.1139/cjfas-54-8-1772

Horne, J. K. 2000. Acoustic approaches to remote species iden- tification: A review. Fish. Oceanogr. 9: 356–371. doi:10. 1046/j.1365-2419.2000.00143.x

Huntington, H. P., and others. 2020. Evidence suggests poten- tial transformation of the Pacific Arctic ecosystem is under- way. Nat. Clim. Change. 10: 342–348. doi:10.1038/s41558-020-0695-2

Kaartvedt, S., A. Røstad, T. A. Klevjer, and A. Staby. 2009. Use of bottom-mounted echo sounders in exploring behavior of mesopelagic fishes. Mar. Ecol. Prog. Ser. 395: 109–118. doi:10.3354/meps08174

Koenker, B. L., L. A. Copeman, and B. J. Laurel. 2018. Impacts of temperature and food availability on the condition of larval Arctic cod (Boreogadus saida) and walleye Pollock (Gadus chalcogrammus). ICES J. Mar. Sci. 75: 2370–2385. doi:10.1093/icesjms/fsy052

Kono, Y., H. Sasaki, Y. Kurihara, A. Fujiwara, J. Yamamoto, and Y. Sakurai. 2016. Distribution pattern of Polar cod (Boreogadus saida) larvae and larval fish assemblages in rela- tion to oceanographic parameters in the Northern Bering Sea and Chukchi Sea. Polar Biol. 39: 1039–1048. doi:10.1007/s00300-016-1961-7

Kuletz, K. J., M. C. Ferguson, B. Hurley, A. E. Gall, E. A. Labunski, and T. C. Morgan. 2015. Seasonal spatial patterns in seabird and marine mammal distribution in the eastern Chukchi and western Beaufort seas: Identifying biologically important pelagic areas. Prog. Oceanogr. 136: 175–200. doi:10.1016/j.pocean.2015.05.012

Kunz, K. L., G. Claireaux, H.-O. Pörtner, R. Knust, and F. C. Mark. 2018. Aerobic capacities and swimming performance of polar cod (Boreogadus saida) under ocean acidification and warming conditions. J. Exp. Biol. 221: jeb184473. doi: 10.1242/jeb.184473

Lange, M., and E. Van Sebille. 2017. Parcels v0.9: Prototyping a Lagrangian Ocean analysis framework for the petascale age. Geosci. Model Dev. 10: 4175–4186. doi:10.5194/gmd-10-4175-2017

Laurel, B. J., M. Spencer, P. Iseri, and L. A. Copeman. 2016. Temperature-dependent growth and behavior of juvenile Arctic cod (Boreogadus saida) and co-occurring North Pacific gadids. Polar Biol. 39: 1127–1135. doi:10.1007/s00300-015-1761-5

Laurel, B. J., L. A. Copeman, M. Spencer, and P. Iseri. 2018. Comparative effects of temperature on rates of develop- ment and survival of eggs and yolk-sac larvae of Arctic cod (Boreogadus saida) and walleye Pollock (Gadus chalcogrammus). ICES J. Mar. Sci. 75: 2403–2412. doi:10.1093/icesjms/fsy042

Logerwell, E., and others. 2015. Fish communities across a spectrum of habitats in the western Beaufort Sea and Chuk- chi Sea. Prog. Oceanogr. 136: 115–132. doi:10.1016/j.pocean.2015.05.013
MacLennan, D. N., P. G. Fernandes, and J. Dalen. 2002. A consistent approach to definitions and symbols in fisheries acoustics. ICES J. Mar. Sci. 59: 365–369. doi:10.1006/jmsc. 2001.1158
Marsh, J. M., F. J. Mueter, and T. J. Quinn. 2019. Environmental and biological influences on the distribution and population dynamics of polar cod (Boreogadus saida) in the US Chukchi Sea. Polar Biol. 43: 1055–1072. doi:10.1007/ s00300-019-02561-w
Matley, J. K., A. T. Fisk, and T. A. Dick. 2012. Seabird predation on Arctic cod during summer in the Canadian Arctic. Mar. Ecol. Prog. Ser. 450: 219–228. doi:10.3354/ meps09561
Mecklenburg, C. W., and others. 2018. Marine fishes of the Arctic Region Volume II. CAFF Monitoring Series Report 28. Akureyri, Iceland: Conservation of Arctic Flora and Fauna.
Mordy, C., and others. 2017. Advances in ecosystem research: Saildrone surveys of oceanography, fish, and marine mammals in the Bering Sea. Oceanography 30: 113–115. doi:10.5670/oceanog.2017.230
Norcross, B. L., B. A. Holladay, M. S. Busby, and K. L. Mier. 2010. Demersal and larval fish assemblages in the Chukchi Sea. Deep-Sea Res. Part II Top. Stud. Oceanogr. 57: 57–70. doi:10.1016/j.dsr2.2009.08.006
Ohman, M. D., R. E. Davis, J. T. Sherman, K. R. Grindley, B. M. Whitmore, C. F. Nickels, and J. S. Ellen. 2019. Zoo- glider: An autonomous vehicle for optical and acoustic sensing of zooplankton. Limnol. Oceanogr. Methods 17: 69–86. doi:10.1002/lom3.10301
Parker-Stetter, S. L., J. K. Horne, and T. J. Weingartner. 2011. Distribution of polar cod and age-0 fish in the U.S. Beaufort Sea. Polar Biol. 34: 1543–1557. doi:10.1007/s00300-011-1014-1
Peck, M. A., L. J. Buckley, and D. A. Bengtson. 2006. Effects of temperature and body size on the swimming speed of larval and juvenile Atlantic cod (Gadus morhua): Implications for individual-based modelling. Environ. Biol. Fishes 75: 419–429. doi:10.1007/s10641-006-0031-3
Pinchuk, A. I., and L. B. Eisner. 2017. Spatial heterogeneity in zooplankton summer distribution in the eastern Chukchi Sea in 2012–2013 as a result of large-scale interactions of water masses. Deep-Sea Res. Part II Top. Stud. Oceanogr. 135: 27–39. doi:10.1016/j.dsr2.2016.11.003
Pinheiro, J., D. Bates, S. DebRoy, D. Sarkar, and R Core Team. 2019. {nlme}: Linear and Nonlinear Mixed Effects Models. Available from https://cran.r-project.org/package=nlme
Pisareva, M. N., R. S. Pickart, P. Lin, P. S. Fratantoni, and T. J. Weingartner. 2019. On the nature of wind-forced upwell- ing in Barrow Canyon. Deep-Sea Res. Part II Top. Stud. Oceanogr. 162: 63–78. doi:10.1016/j.dsr2.2019.02.002
Ponomarenko, V. 1968. Some data on the distribution and migrations of polar cod in the seas of the Soviet Arctic. Rapp. Procès Verbaux Réunions CIEM 158: 131–135.
Ponomarenko, V. 2000. Eggs, larvae, and juveniles of polar cod Boreogadus saida in the Barents, Kara, and White Seas. J. Ichthyol. 40: 165–173.
Quast, J. C. 1974. Density distribution of juvenile Arctic cod, Boreogadus saida, in the eastern Chukchi Sea in the fall of 1970. Fish. Bull., U.S 72: 1094–1105.
Sawada, K., M. Furusawa, and N. J. Williamson. 1993. Conditions for the precise measurement of fish target strength in situ. J. Mar. Acoust. Soc. Jpn. 20: 73–79. doi:10.3135/jmasj. 20.73
Sigler, M., M. Renner, S. Danielson, L. Eisner, R. Lauth, K. Kuletz, E. Logerwell, and G. Hunt. 2011. Fluxes, fins, and feathers: Relationships among the Bering, Chukchi, and Beaufort seas in a time of climate change. Oceanography 24: 250–265. doi:10.5670/oceanog.2011.77
Sigler, M. F., and others. 2017. Late summer zoogeography of the northern Bering and Chukchi seas. Deep-Sea Res. Part II Top Stud. Oceanogr. 135: 168–189.doi:10.1016/j.dsr2.2016.03.005
Simmonds, J., and D. MacLennan. 2005. Fisheries acoustics: Theory and practice, 2nd ed. Blackwell.
Spear, A., J. Duffy-Anderson, D. Kimmel, J. Napp, J. Randall, and P. Stabeno. 2019. Physical and biological drivers of zooplankton communities in the Chukchi Sea. Polar Biol. 42: 1107–1124. doi:10.1007/s00300-019-02498-0

Spencer, M. L., C. D. Vestfals, F. J. Mueter, and B. J. Laurel. 2020. Ontogenetic changes in the buoyancy and salinity tolerance of eggs and larvae of polar cod (Boreogadus saida) and other gadids. Polar Biol. 43: 1141–1158. doi:10.1007/s00300-020-02620-7

Stabeno, P., N. Kachel, C. Ladd, and R. Woodgate. 2018. Flow patterns in the eastern Chukchi Sea: 2010–2015. J. Geophys. Res. Ocean. 123: 1177–1195. doi:10.1002/ 2017JC013135

Steele, M., W. Ermold, and J. Zhang. 2008. Arctic Ocean surface warming trends over the past 100 years. Geophys. Res. Lett. 35: 1–6. doi:10.1029/2007GL031651

Stevenson, D. E., and R. R. Lauth. 2019. Bottom trawl surveys in the northern Bering Sea indicate recent shifts in the dis- tribution of marine species. Polar Biol. 42: 407–421. doi:10. 1007/s00300-018-2431-1

Traynor, J. 1996. Target-strength measurements of walleye Pol- lock (Theragra chalcogramma) and Pacific whiting (Merluccius productus). ICES J. Mar. Sci. 53: 253–258. doi:10.1006/jmsc.1996.0031

Vestfals, C. D., F. J. Mueter, J. T. Duffy-Anderson, M. S. Busby, and A. De Robertis. 2019. Spatio-temporal distribution of polar cod (Boreogadus saida) and saffron cod (Eleginus gracilis) early life stages in the Pacific Arctic. Polar Biol. 42:969–990. doi:10.1007/s00300-019-02494-4

Wackernagel, H. 2013. Multivariate geostatistics: An introduction with applications. Springer Science & Business Media.

Weingartner, T., E. Dobbins, S. Danielson, P. Winsor, R. Potter, and H. Statscewich. 2013. Hydrographic variability over the northeastern Chukchi Sea shelf in summer-fall 2008–2010. Cont. Shelf Res. 67: 5–22. doi:10.1016/j.csr.2013.03.012

Whitehouse, G. A., and K. Y. Aydin. 2016. Trophic structure of the eastern Chukchi Sea: An updated mass balance food web model. U.S. Dep. Commer., NOAA Tech. Memo. NMFS-AFSC-318. 175 p.

Woillez, M., J. C. Poulard, J. Rivoirard, P. Petitgas, and N. Bez. 2007. Indices for capturing spatial patterns and their evolu- tion in time, with application to European hake (Merluccius merluccius) in the Bay of Biscay. ICES J. Mar. Sci. 64: 537–550. doi:10.1093/icesjms/fsm025

Woodgate, R. A. 2018. Increases in the Pacific inflow to the Arctic from 1990 to 2015, and insights into seasonal trends and driving mechanisms from year-round Bering Strait mooring data. Prog. Oceanogr. 160: 124–154. doi:10.1016/ j.pocean.2017.12.007

Woodgate, R. A., K. Aagaard, and T. J. Weingartner. 2005. A year in the physical oceanography of the Chukchi Sea: Moored measurements from autumn 1990-1991. Deep-Sea Res. Part II Top. Stud. Oceanogr. 52: 3116–3149. doi:10.1016/j.dsr2.2005.10.016

Acknowledgments

This work was funded by the North Pacific Research Board Arctic Research Program, NOAA's Pacific Marine Environmental Laboratory's Innovative Technology for Arctic Exploration program, NOAA's Alaska Fisheries Science Center, and the Joint Institute for the Study of the Atmo- sphere and Ocean (JISAO) under NOAA Cooperative Agreement NA15OAR4320063. The saildrone deployments would not have been possible without the contributions of Richard Jenkins and Dave Peacock (Saildrone, Inc.), and Ivar Wagnen (Kongsberg Simrad). We would also like to thank the Alaska Waterways Safety Committee, Alaska Eskimo Whaling Commission, The North Slope Borough, and members of The Vil-lage of Wainwright, AK for their advice and assistance with saildrone oper- ations. We thank the anonymous reviewers for their suggestions which improved this manuscript. This is contribution No. 5091 for Pacific Marine Environmental Laboratory, contribution No. 2020-1063 for JISAO, and contribution No. EcoFOCI-0947 for NOAA's Ecosystem Fisheries Oceanog- raphy Coordinated Investigations. Bering Strait mooring observations are funded by NSF-OPP (1304052 and 1758565) with data available from http://psc.apl.washington.edu/BeringStrait.html. Any use of trade, firm, or product names is for descriptive purposes only and does not imply endorsement U.S. Government. Findings of

this paper do not necessarily represent the views of the National Oceanic and Atmospheric Administration.

Table 1. Summary of small-scale survey observations. The mean SA, model-predicted backscattering cross-section (σ_{bs}) at the midpoint of each small-scale survey, abundance from 38-kHz backscatter, and estimated standard length of gadids are given. Standard errors are given in parentheses. Lengths were calculated from the model-predicted σ_{bs} at each survey midpoint using the TS–length relationship defined for Arctic cod (Geoffroy et al. 2016, Table S1).

	20 Jul-03Aug	**23 Jul-12 Aug**	**13-28 Aug**	**30 Aug-11 Sept**
Mean SA (m^2 nmi^{-2})	197 (53)	177 (76)	281 (79)	369 (80)
σ_{bs} (m^2)	1.7×10^{-6} (1.4×10^{-6})	2.0×10^{-6} (1.4×10^{-6})	2.8×10^{-6} (1.5×10^{-6})	3.5×10^{-6} (1.6×10^{-6})
Abundance index (fish m^{-2})	2.5 (0.6)	2.0 (0.8)	2.2 (0.6)	2.3 (0.5)
Estimated length (cm)	3.4 (1.1, 5.1)	3.7 (1.6, 5.4)	4.7 (2.7, 6.4)	5.5 (3.5, 7.2)

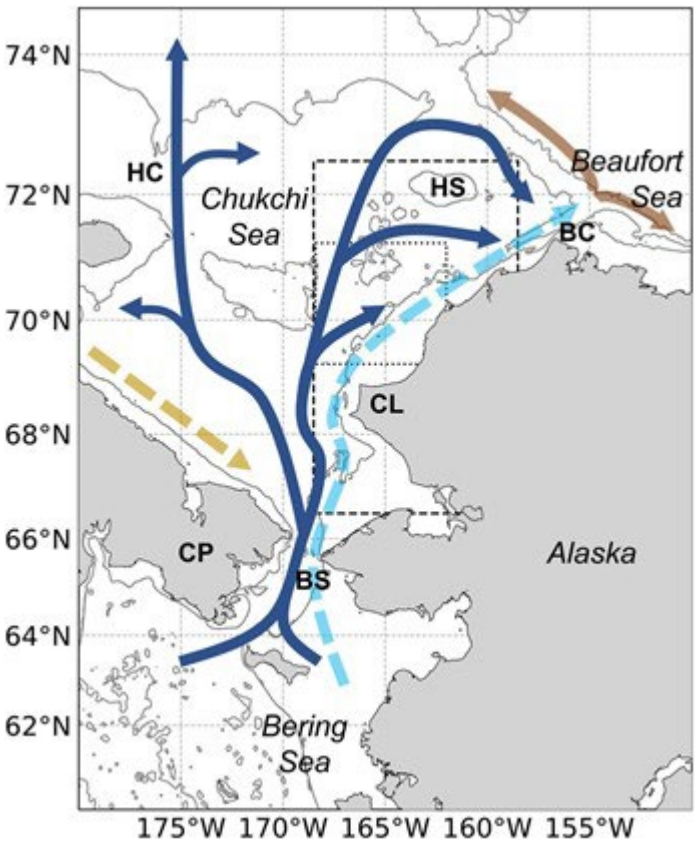

Fig. 1. Map of the study region, showing the primary transport path- ways through the Chukchi Sea based on Corlett and Pickart (2017): Alaskan coastal current (light blue), Bering Sea water (dark blue), Siberian coastal current (gold), slope current (brown, westward) and shelf break jet (brown, eastward). Dashed lines indicate seasonal currents. Survey regions are indicated for the large-scale survey (dashed box) and small- scale survey (dotted box). Geographic features referred to in the text are indicated in bold: Bering Strait (BS), Chukotka Peninsula (CP), Cape Lisburne, (CL), Herald Canyon (HC), Hanna Shoal (HS), and Barrow Can- yon (BC). The 40-, 100-, and 1000-m depth contours are shown.

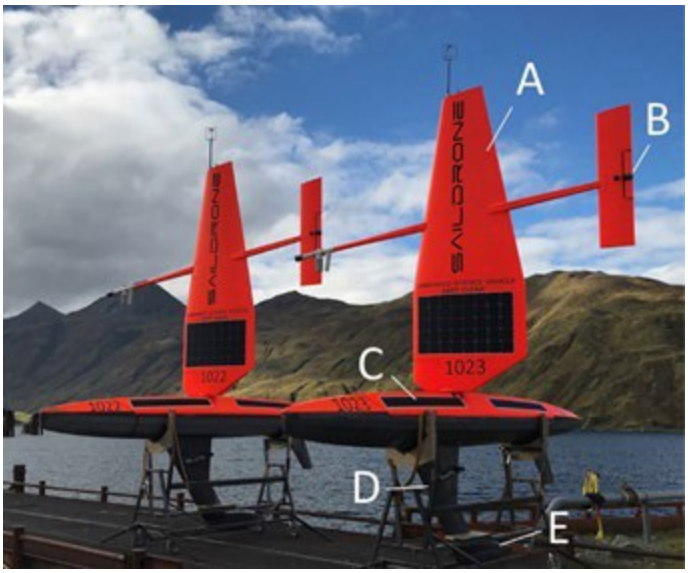

Fig. 2. Saildrone uncrewed surface vehicles upon recovery in Dutch Harbor, Alaska. (a) Wing, (b) trim tab, (c) hull, (d) keel, and (e) transducer mount. Image courtesy of Saildrone, Inc.

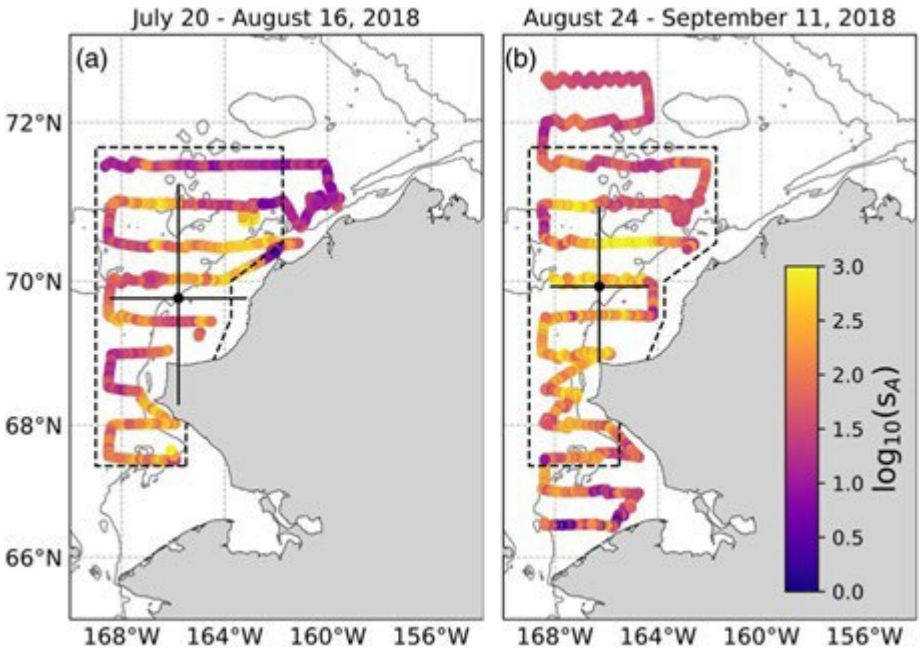

Fig. 3. 38-kHz backscatter (SA, m^2 nmi^{-2}) along the saildrone trackline during the (a) first and (b) second large-scale surveys. Center of gravity and variance of spatial distribution computed from the gridded cells common to both surveys (region encompassed by the dashed line) are indicated by the black circles and lines, respectively. The 40-, 100-, and 1000-m depth contours are shown.

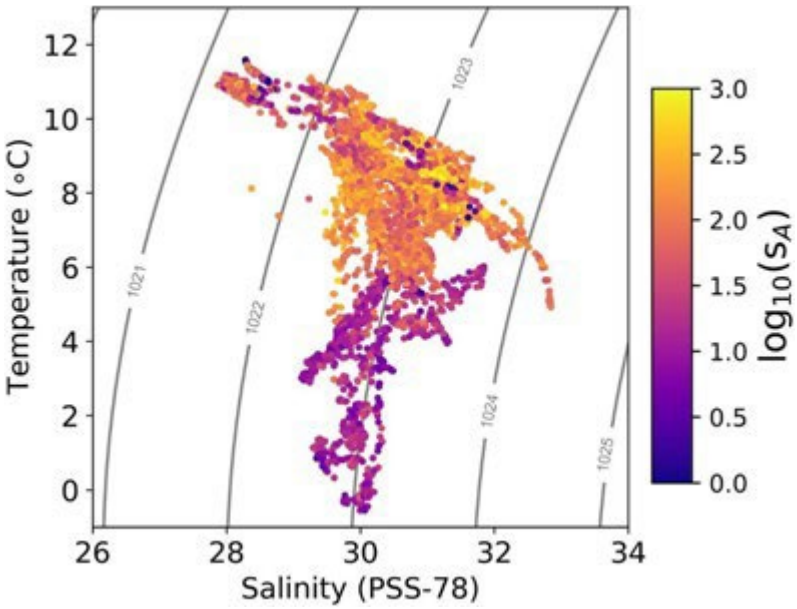

Fig. 4. Ten-minute averaged temperature and salinity at 0.5 m depth measured by sensors on the keel of the saildrone during the large-scale surveys (Fig. 3). Color of points indicates depth-integrated water column 38-kHz backscatter (SA, m^2 nmi^{-2}). Contours indicate potential density.

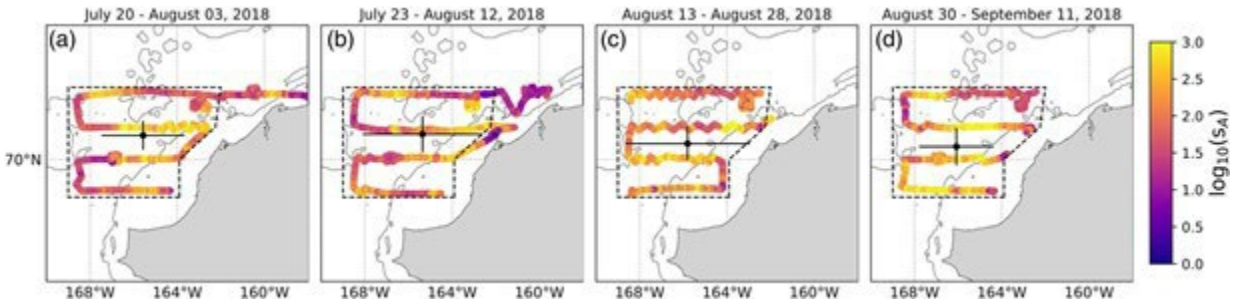

Fig. 5. 38-kHz backscatter (SA, m^2 nmi^{-2}) along the saildrone trackline during the (a) 1st, (b) 2nd, (c) 3rd, and (d) 4th small-scale surveys. The center of gravity and variance of the spatial distribution computed from the gridded cells common to all surveys (region encompassed by the dashed line) is indicated by the black circles and lines, respectively. Note that the first two survey periods overlap in time. The 40- and 100-m depth contours are shown.

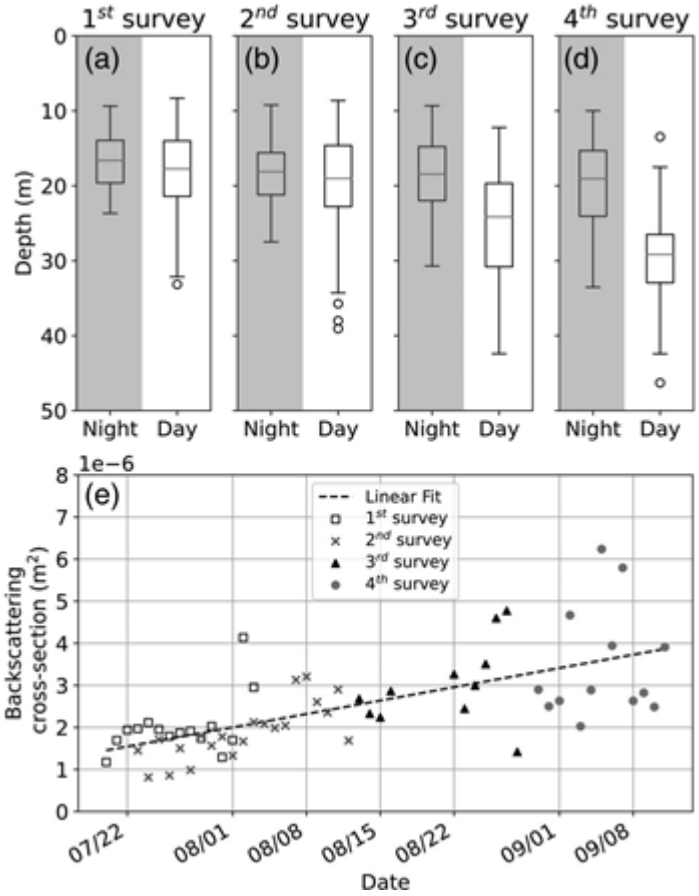

Fig. 6. (a–d) Distributions of nighttime and daytime hourly weighted mean depth of backscatter during the small-scale surveys. Boxes indicate the interquartile range, horizontal gray lines the median, vertical lines the 5% and 95% intervals. Circles indicate observations beyond the whiskers. (e) Daily means of backscattering cross-section (σ_{bs}) of all targets observed in small-scale surveys. Linear fit for the 53-d period is indicated by the black dashed line ($\sigma_{bs} = -7.68 \times 10^{-6} + 4.54 \times 10^{-8}$(yearday), $p < 0.001$, $r^2 = 0.44$.

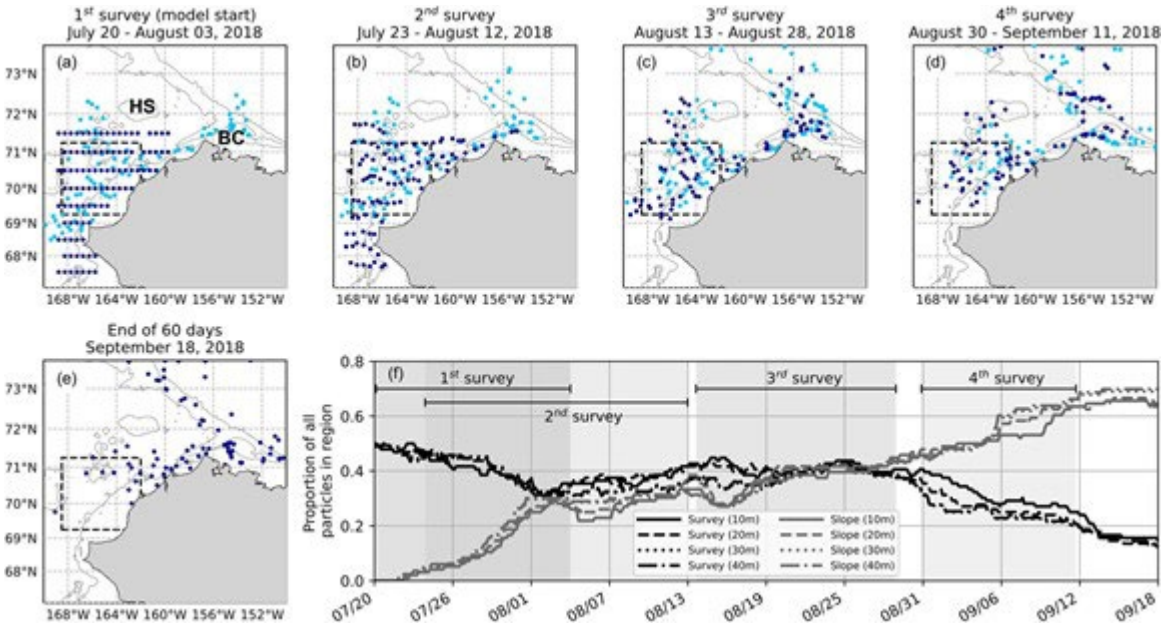

Fig. 7. Results of particle tracking model. (a–d) Locations of particles at 20 m depth at the start (dark blue circles) and end (light blue circles) of the (a) 1st, (b) 2nd, (c) 3rd, and (d) 4th small-scale surveys. Particles were seeded on 20 July at the center of each 0.5 grid cell of the first-large-scale survey (see Fig. S2). The locations of Hanna Shoal (HS) and Barrow Canyon (BC) are indicated in the first panel. (e) Locations of particles seeded at 20 m depth at the end of the 60-d model run. The area indicated by the dashed box represents the small-scale survey region. The 40-, 100-, and 1000-m depth con- tours are shown. (f) Proportion of particles remaining within the small-scale survey region (black lines), and particles transported to the Beaufort Sea and Beaufort/Chukchi slope (> 100 m bottom depth, gray lines) over a period of 2 months from the start of the 1st survey. Model results for particles seeded at fixed depths of 10–40 m are shown. The time periods of the four small-scale surveys are indicated by the gray shaded regions and lines. Note that the 1st and 2nd survey periods overlapped.

CHAPTER 18 - Modeling the dispersal of polar cod (*Boreogadus saida*) and saffron cod (*Eleginus gracilis*) early life stages in the Pacific Arctic using a biophysical transport model

Objective 5: Further resolve early life history characteristics of Arctic cod and saffron cod and their behavior and connectivity between the Chukchi Sea and western Beaufort Sea.

Cathleen D. Vestfals, Franz J. Mueter, Katherine S. Hedstrom, Benjamin J. Laurel, Colleen M. Petrik, Janet T. Duffy-Anderson, and Seth L. Danielson 2021. Modeling the dispersal of polar cod (*Boreogadus saida*) and saffron cod (*Eleginus gracilis*) early life stages in the Pacific Arctic using a biophysical transport model. Progress in Oceanography. 196: 102571. ISSN 0079-6611, https://doi.org/10.1016/j.pocean.2021.102571.

Abstract

Polar cod (*Boreogadus saida*) and saffron cod (*Eleginus gracilis*) are the most abundant and ecologically important forage fishes in the Pacific Arctic marine ecosystem, yet little is known about their spawning locations or the habitats occupied by their early life stages (ELS). We developed a biophysical transport model coupled to a Pan-Arctic hydrodynamic ocean circulation model to identify potential spawning locations and examine connectivity between the northern Bering, Chukchi, and Beaufort seas. We simulated the growth and transport of newly hatched polar cod and saffron cod larvae until the early juvenile stage (to 45 mm in length) using circulation model hindcasts from 2004 – 2015. Analyses identified species-specific differences in dispersal trajectories, despite similar hatch times and locations. Strong interannual variability in growth and dispersal was linked to several global-scale climate indices, suggesting that larval growth and transport may be sensitive to environmental perturbations. Results show that polar cod spawned in the northern Chukchi Sea may be an important source of larvae for the Beaufort Sea and Arctic Basin, while observed larval aggregations in the Chukchi Sea likely originated in the northern Bering and southern Chukchi seas. This study provides new information about potential spawning times and locations for polar cod and saffron cod in the Pacific Arctic and helps to identify important ELS habitat. This knowledge can help improve the management of these species and, by examining how larval connectivity changes in response to changing environmental conditions, improve our ability to anticipate how these species may respond in a rapidly changing Arctic.

Introduction

The Arctic is warming at an unprecedented rate. Surface air temperatures have increased at double the global rate (Screen and Simmonds, 2010) and this warming has also extended to the oceans, resulting in dramatic changes across Arctic ecosystems (Wassman et al., 2011; Huntington et al., 2020). The Pacific Arctic, in particular the Bering Strait region and the Chukchi Sea, is warming rapidly, with water temperatures increasing by 0.43 ºC per decade since 1990 (Danielson et al., 2020a). Sea-ice concentration, extent, and duration have also declined over this period, with an earlier spring ice retreat and delayed fall ice formation increasing the length of the open-water season by ~3 months (Comiso et al., 2008; Stammerjohn et al., 2012). Reduced ice cover, earlier ice melt, and greater freshwater inputs associated with warming in the Arctic are predicted to impact ecosystem dynamics via the poleward movement of boreal species and changes in marine productivity (Meredith et al., 2019). These changes will likely have a profound effect on the distribution and abundance of resident Arctic species. To better understand the consequences of these environmental changes, in this study we examine the early life stages (ELS) of polar cod (Boreogadus saida) and saffron cod (Eleginus gracilis), two of the most abundant and ecologically significant species in the Pacific Arctic marine ecosystem.

Polar cod and saffron cod play an important role in the transfer of energy to higher trophic levels, serving as key prey for piscivorous seabirds and marine mammals, as well as humans, in the northern Bering, Chukchi, and Beaufort seas (Whitehouse, 2011; Moore and Stabeno, 2015). In general, observational data

for Arctic marine fishes are scarce and particularly so for their ELS, such as spawning locations, larval drift pathways, and juvenile nursery areas. Collections are mainly limited to the late spring and summer (but see Lafrance, 2009; Bouchard et al., 2016) due to the challenges and costs of sampling during winter and spring in the remote regions of the Arctic (e.g., difficulties of sampling under the ice, lack of sustained research efforts). As such, identifying major spawning locations of species that spawn under the ice during the winter, such as polar cod and saffron cod, resolving the movement and distribution of their ELS, and understanding their responses to variable climate conditions cannot be achieved through field studies alone.

Advective transport of eggs and larvae is known to play an important role in population regulation of marine fishes and several studies have linked larval transport with variability in year-class strength (Bailey, 1981; Hollowed and Bailey, 1989; Wilderbuer et al., 2002; Govoni 2005; Mueter et al., 2006; Petrik et al., 2015, 2016). Modeling approaches, such as the use of biophysical models that can track and simulate the behavior of eggs and larvae, can provide insights into the movement of ELS and information that would otherwise be unavailable through conventional field sampling. Since eggs and larvae are relatively underdeveloped in the first few months of life, their dispersal is primarily governed by ocean circulation and can be tracked by simulating the transport of passive particles or particles with basic behaviors. Examples include temperature-dependent growth combined with size- or age-dependent vertical migrations, until the larvae grow to a size at which their movements are largely independent of the currents (Leis, 2007). The impacts of circulation on larval dispersal and recruitment has been successfully evaluated using hydrographic modeling approaches in a variety of marine systems (as reviewed in Miller, 2007), including the Gulf of Alaska and the Bering Sea (Hinckley et al., 1996; Parada et al., 2010; Duffy-Anderson et al., 2013; Vestfals et al., 2014; Petrik et al., 2015, 2016; Gibson et al., 2019).

The Chukchi Sea is a broad (> 500 km), shallow (~50 m deep), high-latitude shelf system that extends > 800 km northward from Bering Strait and is highly productive during the spring melt and open-water seasons (Grebmeier et al., 1988). The seasonally fluctuating Pacific-Arctic sea level gradient (Stigebrandt, 1984; Aagaard et al., 2006) drives the northward flow from the Bering Sea through the narrow (~85 km) and shallow (~50 m) Bering Strait. Water entering the Chukchi Sea is often classified into three water masses: cold, relatively saline, and nutrient-rich Anadyr Water (AW) in the west (Coachman et al., 1975; Sambrotto et al., 1984), seasonally present and relatively warm, low-salinity Alaskan Coastal Water (ACW) in the east, and a mixture of the two water masses, Bering Shelf Water (BSW) (Coachman et al., 1975), which originates primarily from 100 m isobath flow (Stabeno et al., 2018). Peak inflow through Bering Strait occurs during summer, bringing relatively fresh water, nutrients, heat, carbon, and organisms into the Chukchi and Beaufort seas (Wyllie-Echeverria et al., 1997; Weingartner et al., 2005; Woodgate et al., 2005a, b; Moore and Stabeno, 2015), while strong southward winds in winter reduce the northward flows (Woodgate et al., 2005a, b; Stabeno et al., 2018).

Inflow through Bering Strait moves across the Chukchi shelf along three main pathways: westward through Hope Valley towards Herald Canyon (Coachman et al., 1975; Weingartner et al., 2005; Woodgate and Aagaard, 2005; Pickart et al., 2010), eastward parallel to the Alaskan coastline into Barrow Canyon (Coachman et al., 1975), and through the Central Channel across the mid-shelf between Herald and Hanna Shoals (Weingartner et al., 2005) (Fig. 1). Flow across the shelf is highly variable and can be modified by local winds and other fluctuations, with particularly strong northerly winds capable of reversing the transport for periods of days to weeks (Coachman and Aagaard, 1981; Weingartner et al., 2005; Woodgate et al., 2005a, b; Danielson et al., 2014, 2017). Flow exits the Chukchi shelf through Barrow Canyon in the east (Coachman et al., 1975; Weingartner et al., 2005) or Herald Canyon in the west (Coachman et al., 1975; Pickart et al., 2010). Water exiting through Barrow Canyon flows either westward along the Chukchi shelf break as the Chukchi Slope Current (Corlett and Pickart, 2017), or eastward into the Beaufort Sea along the shelf break and slope (Pickart, 2004). Low-salinity waters associated with river outflow and solar heating are transported northward during the summer and fall by

the seasonal Alaska Coastal Current (ACC, Coachman et al., 1975). The water column cools to near freezing temperatures in the late fall and early winter and remains near the freezing point until late spring and early summer, when increasing solar radiation and the inflow of warmer water from the Bering Sea leads to rapid warming, melting of sea ice, and increased river discharge (Weingartner et al., 2005; Danielson et al., 2017, 2020a).

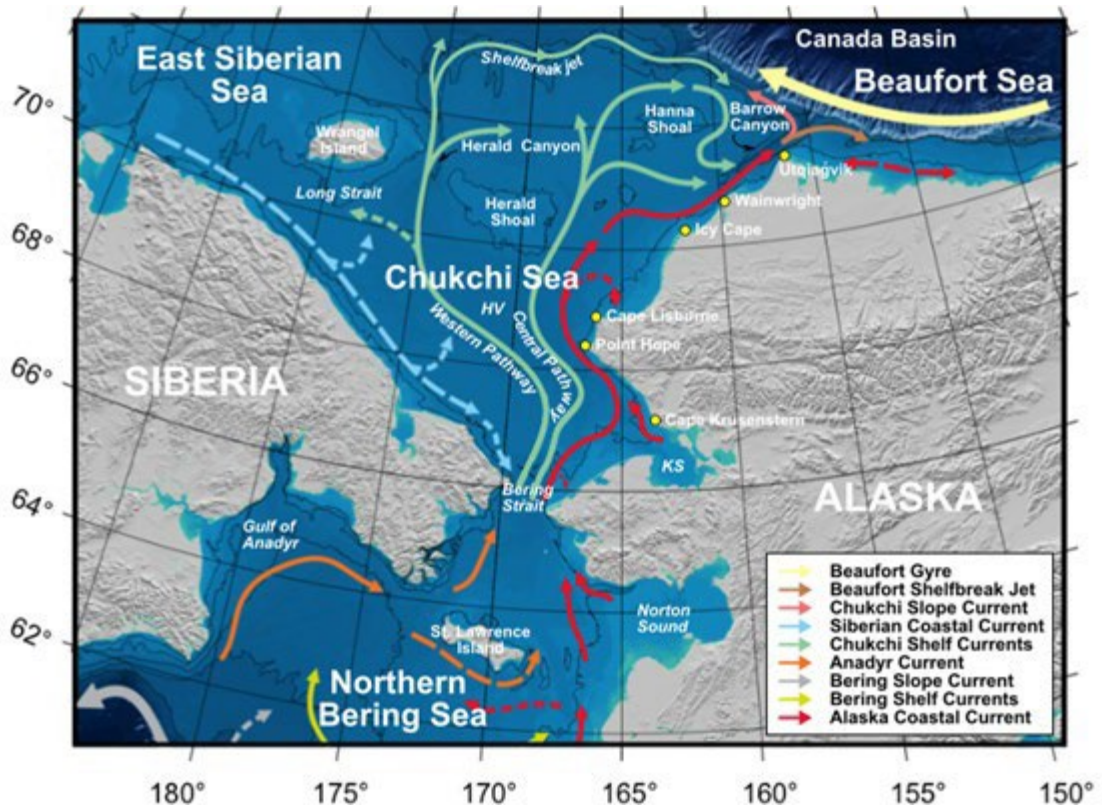

Fig. 1. Map of typical flow pathways of the northern Bering Sea, Chukchi Sea, and western Beaufort Sea based on Danielson et al. (2020a) with water bodies and place names. Persistent currents are shown with solid arrows; intermittent or poorly known flows are shown with dashed arrows. KS denotes Kotzebue Sound and HV denotes Hope Valley. Depth isopleths are contoured with thin black lines at 25, 70, 100, and 200 m.

Building on previous modeling efforts for walleye pollock (Gadus chalcogrammus) in the eastern Bering Sea (Petrik et al., 2015, 2016) and using an ocean circulation model for the Arctic region, we developed biophysical transport models parameterized for larval and early juvenile stages of polar cod and saffron cod. These models were used to simulate the growth and dispersal of their ELS in the northern Bering, Chukchi, and Beaufort seas to identify possible spawning locations, which are currently largely unknown, as well as examine connectivity between these regions. Several behavior scenarios were tested and modeled distributions were compared to known summer distributions of larvae and early juveniles from acoustic-trawl surveys conducted in 2012 and 2013 in the northern Bering and Chukchi seas. Selected behavior scenarios were then used to model their growth and dispersal from 2004 – 2015 to assess interannual variability relative to oceanographic and atmospheric conditions. In addition to providing important information about potential spawning areas and nursery habitats of polar cod and saffron cod, this research helps establish whether observed aggregations of larvae and early juveniles are likely to be retained in the Chukchi Sea, contributing primarily to local populations, or if they are likely to be

transported from the northern Chukchi Sea into the Beaufort Sea, thereby serving as a source population for gadids in the Beaufort Sea. This research also provides valuable information about the growth and dispersal of Arctic gadids under variable climate conditions, which is important for understanding how these species respond to environmental perturbations and how their connectivity between the Chukchi and Beaufort seas may be impacted.

Methods

Circulation model

To realistically simulate the three-dimensional (3-D) circulation field and force the Lagrangian particle-tracking model, we used an implementation of the state-of-the-art, free-surface Regional Ocean Modeling System (ROMS; Shchepetkin and McWilliams, 2005) set up in a Pan-Arctic (PAROMS) configuration (Curchitser et al., 2013, Danielson et al., 2016, 2020b; Lovvorn et al., 2020). The domain of this coupled ocean/sea-ice numerical model spans the Arctic from the Bering Sea in the North Pacific to the North Atlantic. The horizontal resolution varies from ~5 km south of the Aleutian Islands to ~9 km in the North Atlantic and is approximately 5.5 – 6.0 km in the Chukchi Sea. The 50-layer vertical coordinate system is based on terrain-following sigma-layers with finer resolution within the surface and bottom boundary layers. PAROMS is forced by NASA's Modern-Era Retrospective-Analysis for Research and Applications atmospheric reanalysis (Rienecker et al., 2011), with boundary conditions coming from the Simple Ocean Data Assimilation (SODA, Carton and Giese, 2008) for 2008 and prior, and from the Hybrid Coordinate Ocean Model (HYCOM; Chassignet et al., 2009) for more recent years. Tidal forcing is provided by the Oregon State TOPEX/Poseidon Global Inverse Solution (Egbert and Erofeeva, 2002) and the sea ice field is based on the single-category Budgell ice model (Budgell, 2005). For surface fresh water flux, the model uses the method of Dai et al. (2009) south of the Yukon River and that of Whitefield et al. (2015) for the Arctic. A careful model-to-observation comparison of hindcast velocity, temperature, and salinity in the Chukchi and Beaufort seas found that the model exhibited appreciable skill in reproducing the mean velocity directions and magnitudes and the velocity variances at time scales from tidal to annual (Curchitser et al., 2013). The model also captured synoptic and seasonal temperature, salinity, and stratification variations. Offshore ice thicknesses in mid-winter were found by Curchitser et al. (2013) to generally be within 1 m of those estimated from the IceSat satellite missions (Kwok et al., 2009). Without restoring sea ice concentrations to observational data or data assimilation, the model reproduced approximately 50% of both the observed monthly and annual ice concentration anomalies (Curchitser et al., 2013). Additional model-data comparisons that demonstrate model fidelity in reproducing wind-driven SSH anomalies are provided in Danielson et al. (2020b).

Output from the PAROMS 2004 – 2015 hindcast was saved as daily averages to force the offline particle-tracking model, as described below. Specifically, the particle-tracking model used PAROMS-generated velocities, temperature, and salinity.

Particle tracking

To simulate advective transport and growth of larvae, we developed individual-based models (IBMs) for polar cod and saffron cod using the particle tracking tool TRACMASS, which calculates Lagrangian trajectories from Eulerian velocity fields (Döös, 1995). The TRACMASS model is run offline using stored daily output from PAROMS integrations, thus it is less computationally expensive and allows for more calculations of trajectories in comparison to those made online within the circulation model. TRACMASS runs on the 3-D PAROMS grid and solves the trajectory path through each grid cell with an analytical solution of a differential equation, which depends on the horizontal and vertical velocities at the grid cell walls (Döös, 1995). TRACMASS has been used in atmospheric and oceanic studies (Drijfhout et al., 2003; Döös and Engqvist, 2007), as well as for modeling the dispersal of fish and invertebrate larvae (Jacobi and Jonsson, 2011; Berglund et al., 2012; Petrik et al., 2015, 2016).

The particle-tracking time step used in TRACMASS was 1 hour and sub-grid scale turbulence was incorporated by adding a random horizontal turbulent velocity to the horizontal velocity from PAROMS to each trajectory and each horizontal grid wall at every time step (Döös and Engqvist, 2007). A horizontal diffusion value of 4 m2 s-1 was used, based on the relationship between diffusion and model resolution defined in Okubo (1971). Model output of position (latitude and longitude), temperature, salinity, and larval length (see Section 2.3 below) was saved at daily intervals. In addition to particle trajectories, TRACMASS calculated surface light as a function of latitude, longitude, date, and time of day for behavior scenarios that included diel vertical migrations (DVM). While TRACMASS had impermeable boundary conditions at the coast, the incorporation of diffusion into the model allowed for beaching of simulated particles. Trajectories of particles that beached were no longer tracked in the model. Particles rebounded from ice.

We based the number of particles released for each dispersal simulation on the method described in Petrik et al. (2015). In that study, the number of particles released at each time and location (number of simulation repetitions) was determined by calculating the fraction of particles at four random locations downstream of the initial start locations. The minimum number of particles for which those fractions did not change appreciably was determined, with 10 particles per 10 m depth increment per spawning location deemed appropriate for producing stable results (Petrik et al., 2015). For our study, we doubled the number of particles, given that the Chukchi Sea is shallower than the Bering Sea, releasing 10 particles per 5 m depth increment at each PAROMS grid point within each release location (Table 1). Due to the lack of information available about the vertical distributions of post-hatch polar cod and saffron cod larvae in the water column at the time of this study, simulated larvae were released every 5 m from the surface to the bottom. Since saffron cod spawn in close proximity to the bottom (Chen et al., 2008) and their eggs are demersal and adhesive (Berg, 1949; Wolotira, 1985), spawning and hatching locations were assumed to be identical, with dispersal simulations reflecting dispersal from their spawning grounds. For the initial simulations, the minimum and maximum number of particles released were 15,480 and 289,220, respectively, for a total of 623,510 particles released across all locations on each simulation date (Table 1).

Table 1. Hypothesized spawning and/or hatching areas of polar cod (Boreogadus saida) and saffron cod (Eleginus gracilis), region, number of PAROMS grid points, and number of particles released for each dispersal simulation.

Hatch area	Region	# of grid points	# of particles
Gulf of Anadyr	Bering Sea	3,347	289,220
St. Lawrence Island	Bering Sea	235	15,480
Norton Sound	Bering Sea	735	19,370
Bering Strait	Bering Sea	663	48,530
Chukotka Peninsula	Chukchi Sea	888	57,550
Kotzebue Sound	Chukchi Sea	534	20,790
Cape Lisburne	Chukchi Sea	700	45,690
Hanna Shoal	Chukchi Sea	759	68,750
Barrow Canyon	Chukchi Sea	616	58,130
Total:		8,477	623,510

Biological model

Growth

Temperature-dependent growth rates have recently been estimated for larval polar cod and saffron cod in the laboratory (Koenker et al., 2018; Laurel et al., 2018; B. Laurel, National Oceanic and Atmospheric Administration (NOAA), unpublished results). These data provide the information necessary for parameterizing models such as the one presented in this study and provide temperature-dependent growth and developmental rates from the newly hatched larvae to ~25 mm for polar cod and 10 mm for saffron cod. All growth models were based on food 'unlimited' scenarios.

Polar cod

Egg stage: Despite the availability of a temperature-dependent equation for egg development, simulations were initialized at the time of hatching due to uncertainties about where in the water column polar cod eggs occur (e.g., whether they are frozen into the sea ice (Yudanov, 1976) or float at the ice-water interface) and uncertainties about the ability of the PAROMS model to accurately capture small-scale under-ice flow dynamics. Currently, sea ice in PAROMS is modeled as a flat-bottomed surface; however, sea ice is a complex surface that can vary dramatically across even short distances, with ice keels in the Chukchi Sea regularly exceeding 20 m in depth (Hauri et al., 2018). Thus, in an attempt to minimize uncertainties in drift trajectories and ensure more realistic growth and transport of ELS, simulations were restricted to the post-hatch period.

Yolksac larvae: Yolksac larvae were initialized at a random hatch length selected from a normal distribution with a mean standard length (SL) of 5.70 mm and standard deviation (SD) of 0.48 mm. These values were obtained from temperature incubation experiments of polar cod eggs from Beaufort Sea broodstock (Laurel et al., 2018).

Preflexion larvae: Growth from hatch to 10 mm (Fig. 2 a) was modeled as a function of temperature (T) as:

Growth (mm day-1) = 0.0735 + 0.0149*T - 0.0013*T2,

with coefficients determined from a polynomial regression (Koenker et al., 2018).

Post-flexion larvae: Due to the lack of temperature-dependent growth data available for larger sizes, growth from 10 – 25 mm (Fig. 2 a) was modeled using a temperature-dependent growth equation derived for polar cod larvae 10 – 15 mm in length (Koenker et al., 2018):

Growth (mm day-1) = 0.0369 + 0.0583*T - 0.0044*T2

Late-larvae/early juveniles: Growth from 25 – 45 mm (Fig. 2 a) was modeled using a temperature-dependent growth equation for early juveniles between 45 – 70 mm in length (> 10 weeks old, Laurel et al., 2017), as temperature-dependent growth data were not available for these sizes:

Growth (mm day-1) = 0.1377 + 0.0311*T + 0.0041*T2 - 0.0004*T3

Larval length was only updated for nonnegative growth rates, thereby preventing larvae from shrinking at lower temperatures.

Saffron cod

Egg stage: Similar to polar cod, the egg stage of saffron cod was not included in our simulations, despite the availability of information about temperature-dependent egg development. Simulations were initialized at the time of hatching due to uncertainties about the ability of the PAROMS model to accurately capture small-scale under-ice flow dynamics (see Section 2.3.2.1 above). Thus, in an attempt

to minimize uncertainties in drift trajectories and ensure more realistic growth and transport of ELS, simulations were restricted to the post-hatch period.

Yolksac larvae: Yolksac larvae were initialized at a random hatch length selected from a normal distribution with a mean SL of 5.44 mm and SD of 0.30 mm based on values obtained from temperature incubation experiments of saffron cod eggs from Gulf of Alaska broodstock (B. Laurel, NOAA, unpublished results). Size at hatch was not related to incubation temperature.

Preflexion larvae: Growth from hatch to 10 mm (Fig. 2 b) was modeled as:

Growth (mm day-1) = 0.0016 + 0.0088*T

Flexion larvae – early juveniles: At present, temperature-dependent growth models for larval saffron cod > 10 mm in length are not available. Growth of saffron cod at these small sizes is linear and resembles that of walleye pollock (B. Laurel, NOAA, unpublished results). Assuming that growth of larger saffron cod remains similar to that of larger walleye pollock, we used the walleye pollock growth model described in Porter and Bailey (2007) and Petrik et al. (2015) to model saffron cod growth from 10 mm to 45 mm (Fig. 2 b).

Growth (mm day-1) = 0.0902 * log(T) - 0.0147

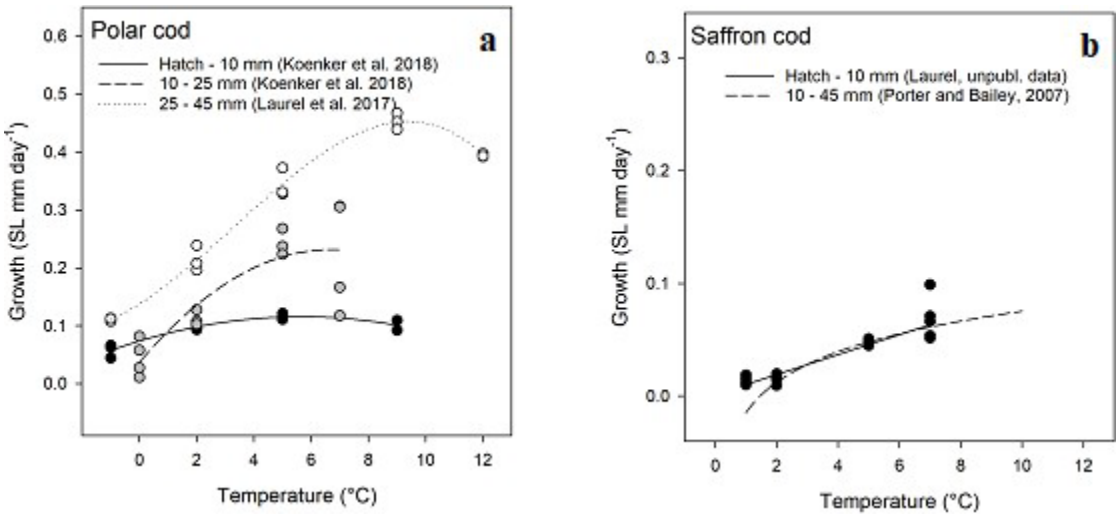

Fig. 2. Temperature-dependent growth rates (in mm day-1) used to model growth of (a) polar cod (*Boreogadus saida*) and (b) saffron cod (*Eleginus gracilis*) early life stages in the individual-based models (IBMs). Growth rates for polar cod yolksac (hatch – 10 mm) and feeding (10 – 25 mm) larvae in the model were based on those derived in Koenker et al. (2018), while early juvenile growth (25 – 45 mm) was based on Laurel et al. (2017). The growth rate for saffron cod yolksac larvae (hatch to 10 mm) was based on unpublished data (B. Laurel, NOAA). For growth of saffron cod preflexion larvae to early juveniles (10 – 45 mm), the walleye pollock (*Gadus chalcogrammus*) growth model described in Porter and Bailey (2007) was used, as a saffron cod- specific growth model for larger sizes is not available and walleye pollock exhibit similar growth (B. Laurel, NOAA, personal communication).

Vertical behavior

Vertical behaviors selected for polar cod were based on values obtained from the literature (Borkin et al., 1986; Bouchard et al., 2016) and from laboratory observations (B. Laurel, NOAA, unpublished results). Similar behaviors were used for the saffron cod simulations, as no information on the vertical distribution of saffron cod larvae is currently available. Five different vertical behavior scenarios were developed and tested: (1) passive (neutrally buoyant) individuals at all stages; (2) surface-oriented individuals such that all stages move to the middle of the 10-m surface layer at 5 m; (3) passive yolksac larvae where older stages move progressively deeper in the water column: preflexion/flexion larvae (5 – 10 m), transformation (10 – 15 m) and early juveniles (20 m); (4) surface-oriented yolksac larvae and older individuals that move progressively deeper in the water column; and (5) surface-oriented yolksac larvae and transformation and early juvenile stages that make diel vertical migrations (DVMs) to the middle of the surface layer (5 m) at night (Table 2). For DVM, day was defined as times when surface light was greater than zero.

Table 2. Model parameters for different behaviors tested for polar cod (*Boreogadus saida*) and saffron cod (*Eleginus gracilis*). Passive = passive (neutrally buoyant) individuals of all stages; Surface = surface-oriented individuals of all stages; Passive & ontogeny = passive yolksac and preflexion larvae with late larvae and early juveniles moving deeper with ontogeny; Surface & ontogeny = surface-oriented yolksac and preflexion larvae with late larvae and juveniles moving deeper with ontogeny; DVM = surface-oriented yolksac and preflexion larvae with late larvae and early juveniles making diel vertical migrations (DVMs) between specified depths during the day, and 5 m during the night. wmax = maximum vertical swimming speed, nb =neutrally buoyant, trans = transformation, early juv. = early juvenile.

Polar cod

Behavior	Length (mm)	Stage	W_{max} (m s^{-1})	Daytime depth (m)	Nighttime depth (m)	Temperature-dependent growth
Passive	Hatch – 10	Yolksac, preflexion	0.002 – 0.003	Nb	Nb	Koenker et al., (2018)
	10 – 25	Post flexion	0.003 – 0.008	Nb	Nb	Koenker et al., (2018)
	25 – 45	Trans – early juv.	0.008 – 0.014	Nb	Nb	Laurel et al., (2017)
Surface	Hatch – 10	Yolksac, preflexion	0.002 – 0.003	5	5	Koenker et al., (2018)
	10 – 25	Post flexion	0.003 – 0.008	5	5	Koenker et al., (2018)
	25 – 45	Trans – early juv.	0.008 – 0.014	5	5	Laurel et al., (2017)
Passive & ontogeny	Hatch – 10	Yolksac, preflexion	0.002 – 0.003	Nb	Nb	Koenker et al., (2018)
	10 – 25	Post flexion	0.003 – 0.008	8	8	Koenker et al., (2018)
	25 – 30	Transformation	0.008 – 0.009	12	12	Laurel et al., (2017)
	30 – 45	Early juvenile	0.009 – 0.014	20	20	Laurel et al., (2017)
DVM	Hatch – 10	Yolksac, preflexion	0.002 – 0.003	5	5	Koenker et al., (2018)
	10 – 25	Post flexion	0.003 – 0.008	8	5	Koenker et al., (2018)
	25 – 30	Transformation	0.008 – 0.009	12	5	Laurel et al., (2017)
	30 – 45	Early juvenile	0.009 – 0.014	20	5	Laurel et al., (2017)

Saffron cod

Behavior	Length (mm)	Stage	W_{max} (m s^{-1})	Daytime depth (m)	Nighttime depth (m)	Temperature-dependent growth
Passive	Hatch – 10	Yolksac, preflexion	0.002 – 0.003	Nb	Nb	Laurel (unpublished data)
	10 – 45	Postflexion – early juv	0.003 – 0.014	Nb	Nb	Porter and Bailey (2007)
Surface	Hatch – 10	Preflexion	0.002 – 0.003	5	5	Laurel (unpublished data)
	10 – 45	Postflexion – early juv	0.003 – 0.014	5	5	Porter and Bailey (2007)
Passive & ontogeny	Hatch – 10	Yolksac, preflexion	0.002 – 0.003	Nb	Nb	Laurel (unpublished data)
	10 – 24	Flexion - postflexion	0.003 – 0.007	8	8	Porter and Bailey (2007)
	24 – 27	Transformation	0.007 – 0.008	12	12	Porter and Bailey (2007)
	27 – 45	Early juvenile	0.008 – 0.014	20	20	Porter and Bailey (2007)
Surface & ontogeny	Hatch – 10	Yolksac, preflexion	0.002 – 0.003	5	5	Laurel (unpublished data)
	10 – 24	Flexion - postflexion	0.003 – 0.007	8	8	Porter and Bailey (2007)
	24 – 27	Transformation	0.007 – 0.008	12	12	Porter and Bailey (2007)
	27 – 45	Early juvenile	0.008 – 0.014	20	20	Porter and Bailey (2007)
DVM	Hatch – 10	Yolksac, preflexion	0.002 – 0.003	5	5	Laurel (unpublished data)
	10 – 24	Flexion - postflexion	0.003 – 0.007	8	5	Porter and Bailey (2007)
	24 – 27	Transformation	0.007 – 0.008	12	5	Porter and Bailey (2007)
	27 – 45	Early juvenile	0.008 – 0.014	20	5	Porter and Bailey (2007)

Vertical swimming speed (w) was parameterized for both polar cod and saffron cod as:

w = wmax * (-tanh(0.2 * (z – zpref)))

where z is depth (m), zpref (m) is the preferred depth (middle of depth range or day-time/night-time preferred depths), and the maximum vertical swimming speed, wmax (m s-1), is

wmax = 0.3 * Llarva *10-3

where Llarva is larval length (mm).

The swimming speed of fish larvae is often overestimated in IBMs (Peck et al., 2006); therefore, we chose a maximum speed of 0.3 body-lengths s−1 as a conservative estimate for sustained swimming. This value aligns well with that used to model polar cod growth in the Greenland Sea and Baffin Bay (Thanassekos and Fortier, 2012) and is comparable to swimming speeds used in studies of Atlantic cod (Gadus morhua) larvae (Sundby and Fossum, 1990; Björnsson, 1993; Vikebø et al., 2007).

Simulations

Release locations and hatch dates

Larvae were released from several hypothesized hatching locations based on information from a review of the literature, anecdotal evidence, and known areas of retention in the region (Craig et al., 1982; Wolotira, 1985; Sunnanå and Christiansen, 1997; A. Whiting, Native Village of Kotzebue, personal communication). In total, nine locations were selected from which to initialize the dispersal simulations: the Gulf of Anadyr, St. Lawrence Island, Norton Sound, Bering Strait, Chukotka Peninsula, Kotzebue Sound, Cape Lisburne, Hanna Shoal, and Barrow Canyon (Table 1). Ellipses were created around the hypothesized hatching locations (Fig. 3) using ArcGIS 10.4 (ESRI, 2017) and simulations were initialized from all PAROMS grid points falling within each ellipse. Points on land were excluded.

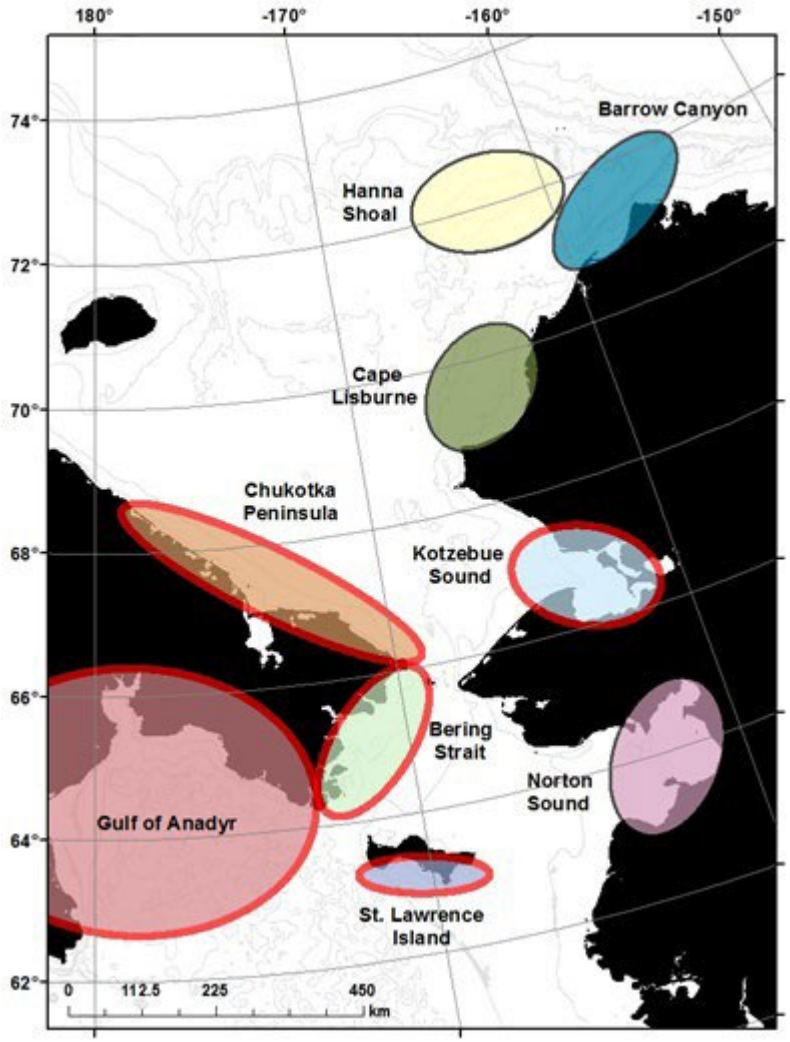

Fig. 3. Map of polar cod (*Boreogadus saida*) and saffron cod (*Eleginus gracilis*) hypothesized spawning and/or hatching locations used to develop the biophysical transport models. All 9 locations were used for the initial dispersal simulations to select plausible release locations. Areas highlighted in red were used to test 5 different behavior scenarios against 2012 and 2013 Arctic Ecosystem Integrated Survey acoustic-trawl survey observations. Simulations for 2004 through 2015 were initiated from the Bering Strait and Chukotka Peninsula locations for polar cod, and the Bering Strait and Kotzebue Sound locations for saffron cod.

In other Arctic seas, peak hatching of polar cod eggs occurs in May and June (Yudanov, 1976; Bouchard and Fortier, 2008), though it can occur as early as December and January in regions warmed by large inputs of fresh water and as late as August in colder regions (Bouchard and Fortier, 2011). In the Chukchi Sea, hatching can occur as late as July (Wyllie-Echeverria et al., 1997). Initial particle releases were based on a hatch date calculated from the midpoint of when polar cod were encountered in the Chukchi Sea portion of the Arctic EIS survey in 2013. The approximate hatch date was estimated by back-calculating

from the average length of age-0 polar cod observed in the survey (~35.2 mm) using the regression of length on hatch date in Bouchard and Fortier (2011). This method resulted in an estimated hatch date of Julian day 72.5 (± 31.5 days SD), with most larvae hatching around early to mid-March (Marsh et al., 2019). Initially, simulated larvae hatched every two weeks from 15 February through 15 May, for a total of 7 hatching events in each year. Simulations were conducted separately for each release location and each hatch date. Results from the initial simulations suggested that larvae did not have sufficient time to achieve the lengths observed in the field, therefore, hatch dates were expanded to include the 1st and 15th day of each month from 1 January through 15 May for a total of 10 polar cod hatching events in each year. This range of hatch dates was also supported by otolith-derived ages of polar cod collected during the Arctic EIS survey (Z. Chapman, University of Alaska Fairbanks, personal communication) and allowed simulated fish lengths to better match field observations. The same range of hatch dates was used for the saffron cod simulations.

Particle tracking

Particle trajectories were tracked forward in time. While tracking particles backward in time can be used to identify potential source locations (e.g., Christensen et al., 2007; Calò et al., 2018), processes such as physical diffusion are not reversible in time (Batchelder, 2006). Backtracking can be complicated by ontogenetic development and the active behavior of larvae due to the stochastic and nonlinear nature of these processes (Christensen et al., 2007). Backtracking may be more suitable for short-duration simulations, but is less effective in shallow, nearshore regions with strong flow–bathymetry interactions (Batchelder, 2006, Bauer et al., 2013). Although inefficient and computationally expensive (Batchelder, 2006; Christensen et al., 2007), tracking particles forward in time can be used to evaluate retention in suitable areas, transport to nursery grounds, or loss to unfavorable habitats (Christensen et al., 2007). Given the shallow Chukchi shelf (~50 m deep), the long drift duration (see Section 2.4.3. below), and the incorporation of diffusion and behavior in our simulations, backtracking was not implemented. The feasibility of tracking fish larvae backwards from observed distributions for several months was unclear, and may have resulted in overly broad distributions. Furthermore, backtracking in TRACMASS at the time did not allow for active behavior of the particles.

Duration of simulated drift

Growth and dispersal of larvae were simulated until 1 September, the midpoint of the Arctic EIS survey, so that the simulated distribution and size composition during summer could be compared to the observed distributions and size compositions in the 2012 and 2013 Arctic EIS acoustic-trawl surveys. Polar cod and saffron cod transition from pelagic juveniles to more demersally-oriented juveniles at approximately 35 – 45 mm (ICES CM, 1988) and between 39 – 60 mm (Wolotira, 1985), respectively, with enhanced swimming abilities that are difficult to capture in an IBM, thus fish larger than 45 mm in length were excluded from further analysis.

Data-model comparison with acoustic-trawl surveys

We used data on the abundance and length composition of larval (preflexion and flexion) and early juvenile polar cod and saffron cod (to 45 mm in length) from acoustic-trawl surveys conducted in the Chukchi Sea as part of the Arctic EIS program (Mueter et al., 2017) to compare with results from the IBMs developed in this study. In late summer 2012 and 2013, the Arctic EIS program conducted comprehensive ecosystem surveys of the U.S. northern Bering Sea and Chukchi Sea shelves (Mueter et al., 2017). Surveys began on 7 August in both years and progressed northward from Bering Strait along designated transects until reaching the Chukchi shelf break by the first week of September, after which sampling recommenced in Bering Strait and progressed southward to 60°N until the last week of September. Acoustic-trawl methods were used to estimate the abundance and distribution of pelagic

organisms in the northern Bering and Chukchi seas (see De Robertis et al., 2017a, b for further details), and provide the best available information about the late summer distributions of age-0 polar cod and saffron cod in the region. The size and species composition of acoustic scatterers were estimated from a combination of surface trawls conducted at pre-determined stations and midwater trawls conducted in areas of high backscatter to convert the measurements of acoustic backscatter into animal abundances. A large Cantrawl rope trawl was used for all surface trawls and for midwater trawls in 2012, while a smaller modified-Marinovich trawl was used for midwater sampling in 2013. In 2013, a series of paired midwater trawls were conducted with the Cantrawl and modified-Marinovich trawls to determine the relative selectivity of the two gear types (De Robertis et al., 2017a). Selectivity-adjusted estimates of abundance (fish m-2) for 10-mm size classes of polar cod and saffron cod ranging from 5 – 305 mm in length were calculated along the acoustic track.

Field distributions of polar cod and saffron cod were compared to simulated distributions by overlaying a 30- x 30-km grid over the 2012 and 2013 Arctic EIS acoustic-trawl survey areas (Fig. S1) in ArcGIS (ESRI, 2017). Survey abundance estimates of fish ≤ 45 mm in length (all size classes ≤ 45 mm in length) were aggregated to each grid cell that overlapped with the survey area in each year. The aggregated abundance estimate for each cell was divided by the total survey abundance to get the proportion of the survey observations of fish ≤ 45 mm in length occurring in each grid cell. A similar process was used to determine the proportion of the simulated larvae falling within each survey grid cell for each release location and each hatch date. The locations of simulated polar cod and saffron cod ≤ 45 mm in length at the end of the simulation (1 September) were plotted and only those that overlapped with the survey grid cells were included in the analysis. The proportion of the simulated distribution that fell within each survey grid cell was calculated by dividing the number of simulated fish ≤ 45 mm in length occurring in each grid cell by the total number of simulated fish falling within the survey area. Note that we chose to analyze release locations and hatch dates separately, as aggregating larval releases over space and time assumes that each release location and time contributes equally, which is almost certainly not the case as the numbers of eggs released and the survival of larvae (which was not modeled) can be expected to vary widely across time and space. While the correlations between observed and simulated particles from a particular release location and time are not expected to be high when multiple hatching events contribute to larvae observed in a given region, significant correlations - even if weak - would strongly suggest that a given release location and time may have contributed to the observed concentrations of larvae.

Initial passive particle trajectory simulations from the northern release locations (Cape Lisburne, Hanna Shoal, and Barrow Canyon) showed poor overlap with the Arctic Ecosystem Integrated Survey (Arctic EIS) acoustic-trawl survey grids (see De Robertis et al., 2017b) used to ground truth the model (see Section 2.5 below), with most particles being advected into the Beaufort Sea and Arctic Basin (Fig. S2). Similarly, particles from the Norton Sound release location had minimal overlap with the acoustic-trawl survey grid and were largely retained in the Bering Sea (Fig. S2). Therefore, subsequent simulations were initialized from the five remaining locations with greater overlap with the acoustic-trawl surveys in 2012 and 2013 (i.e., transport into or retention within the Chukchi Sea), allowing for comparisons between simulated distributions and field observations.

Correlations between simulated distributions and survey observations were calculated for each behavior scenario, spawning location, release date, and release depth using Pearson's Product Moment Correlation, for a total of 525 comparisons per species per year. Correlations were consistent across release depths and are therefore reported for the total, depth-integrated values only.

Interannual variability of simulated distributions

To examine how polar cod and saffron cod dispersal were influenced by variability in climate and oceanographic conditions, the IBMs were run for multiple years (2004 – 2015) over the full range of hatch dates from the release areas that produced the strongest correlations between observed and simulated distributions in 2012 and/or 2013. As simulations with surface-oriented behavior showed the

strongest correlations between observed and simulated distributions for both species, this behavior scenario was used to model polar cod and saffron cod dispersal between 2004 and 2015.

Simulated distributions on 1 September from 2004 – 2015 were compared using a center of gravity (COG) analysis in the R package SDMTools (R Core Team, 2018). Inertia, or the dispersion of simulated particles around the COG (Woillez et al., 2009), was calculated for each year, along with the standard deviations around the major and minor axes. This was done to test for trends in spatial dispersion, which may reflect changes in oceanographic and atmospheric circulation. For example, volume flow through Bering Strait has shown a strong, increasing trend over recent years (Woodgate et al., 2015; Woodgate, 2018). Geographic coordinates (latitude, longitude) were converted to projected coordinates using the North Pole Lambert Azimuthal Equal Area (LAEA) Alaska projection (EPSG: 3572, https://epsg.io/3572, accessed 16 September, 2019) prior to the inertia calculation to minimize the distortion in lengths, areas, and angles at the poles (Skopeliti and Tsoulos, 2013).

Correlations with Climate Indices

To examine how larval growth and connectivity may change under variable climate forcing, we developed COG indices from the simulation output. Anomalies were calculated as deviations from the mean latitude and longitude values for the 2004 – 2015 period normalized by the standard deviation. Larval indices were then compared to several climate indices thought to influence circulation in the Bering and Chukchi seas (Fig. S3). The large-scale climatic indices selected were the winter (December – February) Arctic Oscillation (AO) index, which represents the first empirical orthogonal function (EOF) pattern of sea level pressure (SLP) from 20 – 90°N regressed to the SLP anomaly time series (Thompson and Wallace, 1998); the Arctic Dipole (AD) index, which is the first EOF pattern of 70 – 90°N regressed to the SLP anomaly time series (Wu et al., 2006); and the Siberian-Alaskan (SA) index, which provides a measure of atmospheric circulation based on a correlation between sea ice cover and the 700 hPa geopotential height gradient between Siberia and Alaska, that can be used to estimate thermal conditions in the Bering Sea and ice cover extent (Overland et al., 2002). All indices were obtained from NOAA's Bering Climate website (https://www.beringclimate.noaa.gov/data/index.php, accessed 6 June, 2019).

An index representing ice extent and timing of retreat (IER) was developed for 2005 – 2015 based on the findings of Okkonen et al. (2019), where sea ice areal extent and concentration from April 1 through the third week of August were compared to late August water masses encountered during surveys in Barrow Canyon. Okkonen et al. (2019) found that greater daily sea ice extents and slower/later sea ice retreats occurred in years when the August late season meltwater (LMW) volumes in Barrow Canyon were greater than the 2005–2015 mean (2006, 2008, 2009, and 2012–2014; IER index = 1 in this study), while smaller daily sea ice extents and faster/earlier sea ice retreats occurred in years when August LMW volumes were less than the 2005–2015 mean (2005, 2007, 2010, 2011, and 2015; IER index = 0 in this study).

Correlations between the annual climate indices and the annual COG anomalies between 2004 and 2015 from the selected spawning/hatching areas were calculated for all hatch dates using Pearson's Product Moment Correlation. Correlations with the SA index were calculated for 2004 – 2013, as data beyond 2013 were not available. Similarly, correlations with the IER index were only calculated for 2005 – 2015, as 2004 data were not available. All statistical analyses were carried out in R (R Core Team, 2018).

Results

We found variations in simulated lengths-at-age between hatching areas and hatch dates for both polar cod and saffron cod. Overall, polar cod larvae that hatched from more southerly locations (Gulf of Anadyr, St. Lawrence Island), attained a greater length at the end of the simulation than those originating from the more northerly hatching locations (Fig. 4 a, b). This difference was more apparent in larvae hatched earlier in the year compared to those that hatched at later dates. Differences in length were also

evident between years, with more variability in both simulated and observed polar cod lengths in 2013 compared to 2012 (Fig. 4 a, b). Saffron cod were much smaller in size at the end of the simulation than polar cod (Fig. 4) due to faster growth of polar cod at low temperatures (Fig. 2). While saffron cod lengths differed between southerly and northerly hatching locations, the difference was not as great as that found for polar cod, again, likely due to slower growth of saffron cod at low temperatures. The difference in length remained fairly consistent across hatch dates in 2012, but was less apparent in 2013 (Fig. 4 c, d). Despite some overlap, simulated sizes based on lab-derived growth were smaller than the sizes observed in the Arctic EIS acoustic-trawl survey (Fig. 4). This overlap was much greater for polar cod and nearly absent for saffron cod (Fig. 4).

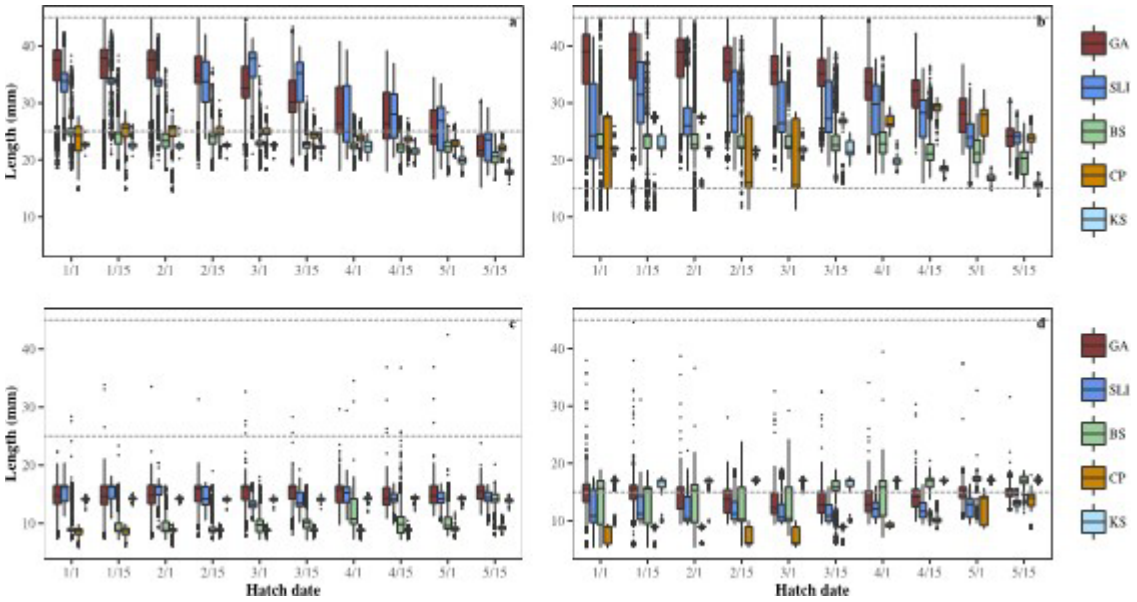

Fig. 4. Simulated lengths of (a, b) polar cod (*Boreogadus saida*) and (c, d) saffron cod (*Eleginus gracilis*) larvae and early juveniles ≤ 45 mm in length located within the Arctic Ecosystem Integrated Survey acoustic-trawl survey area on 1 September (a, c) 2012 and (b, d) 2013. Simulations were initiated from five hypothesized areas on 10 hatch dates. Data presented are from simulations with surface-oriented behavior, which had the strongest correlations with the acoustic-trawl survey data. The dashed grey lines represent the minimum and maximum lengths estimated by the survey (to 45 mm). GA: Gulf of Anadyr; SLI: St. Lawrence Island; BS: Bering Strait; CP: Chukotka Peninsula; KS: Kotzebue Sound. The minimum, first quartile (Q1), median, third quartile (Q3), maximum, and outliers are represented.

Data-model comparison with acoustic-trawl surveys

We found distinct differences in larval distributions between the different behavior scenarios, particularly for those simulations with a passive component (Fig. S4). Behavior scenarios that included a surface component produced relatively similar distributions, especially for the simulations with and without DVM for surface-oriented early larvae that moved deeper with ontogeny, which had almost identical distributions (Fig. S4, Tables 3 and 4). Simulated and observed polar cod larval distributions were not significantly correlated for any of the hatching locations in 2012, except for larvae with surface-oriented behavior that were released around Bering Strait and the Chukotka Peninsula (Table 3). Significant positive correlations were also found for simulations from the Chukotka Peninsula with all other behavioral scenarios except that with DVM (Table 3). Earlier hatching larvae resulted in significant

overlap with observed distributions from the Bering Strait release location, while the correlations for the Chukotka Peninsula simulations were significant across all release dates (Table 3). No significant correlations were found between observed and simulated distributions of polar cod in 2013 (not shown).

Table 3. Correlations between observed distributions of polar cod (Boreogadus saida, larvae and early juveniles ≤ 45 mm in length) in the 2012 Arctic Ecosystem Integrated Survey acoustic-trawl survey and simulated distributions on 1 September from 5 different behavior scenarios. Particles were released at 5 locations (Gulf of Anadyr, St. Lawrence Island, Bering Strait, Chukotka Peninsula, and Kotzebue Sound) on the 1st and 15th of each month from 1 January – 15 May. **p-value < 0.05 (darker shading), *0.05 ≤ p-value < 0.10 (lighter shading). p = p-value, n = number of simulated larvae found within the survey grid.

Gulf of Anadyr	1-Jan		15-Jan		1-Feb		15-Feb		1-Mar		15-Mar		1-Apr		15-Apr		1-May		15-May	
	F	*n*	*F*	*n*	*F*	*n*	*F*	*n*	*F*	*n*	*F*	*n*	*F*	*n*	*F*	*n*	*F*	*n*	*F*	*n*
Passive	0.03	91,390	0.03	91,163	0.02	94,815	0.01	104,614	-0.01	105,849	-0.02	109,275	-0.04	103,251	-0.04	97,109	-0.06	101,004	-0.07	100,556
Surface	-0.02	38,155	-0.02	40,114	-0.02	44,571	-0.02	62,964	-0.02	80,874	-0.02	84,324	-0.02	73,119	-0.02	57,679	-0.02	51,354	0.69	43,574
Passive – ontogeny	-0.02	50,958	-0.03	41,543	-0.02	50,757	-0.02	56,645	-0.02	67,049	-0.02	62,470	-0.02	26,115	-0.02	48,579	-0.02	26,971	-0.02	15,931
Surface – ontogeny	-0.02	52,411	-0.02	53,259	-0.02	52,891	-0.02	62,469	-0.02	73,683	-0.02	79,238	-0.02	76,250	-0.02	55,023	-0.02	39,206	-0.02	45,681
Surface - DVM	-0.02	59,301	-0.02	59,764	-0.02	53,148	-0.02	65,007	-0.02	77,822	-0.02	82,680	-0.02	78,528	-0.02	56,045	-0.02	38,677	-0.02	46,336

St. Lawrence Island	1-Jan		15-Jan		1-Feb		15-Feb		1-Mar		15-Mar		1-Apr		15-Apr		1-May		15-May	
Passive	-0.06	5,791	-0.03	5,495	-0.03	5,348	-0.04	5,149	-0.02	5,172	-0.01	5,720	-0.07	3.976	-0.10	6,569	-0.10	5,379	-0.08	5,677
Surface	-0.02	3,581	-0.02	4,871	-0.02	5,217	-0.03	3,488	-0.05	2,545	-0.05	3,493	-0.03	4,861	-0.04	5,477	-0.04	5,467	-0.04	6,990
Passive – ontogeny	-0.02	3,355	-0.02	3,941	-0.02	2,879	-0.03	1,989	-0.03	145	-0.02	892	-0.03	4,461	-0.04	4,947	-0.05	3,734	-0.05	4,644
Surface – ontogeny	-0.02	4,246	-0.02	4,889	-0.02	4,015	-0.02	3,175	-0.04	1,569	-0.03	2,197	-0.03	6,100	-0.04	5,721	-0.04	4,738	-0.03	6,584
Surface - DVM	-0.02	4,528	-0.02	5,164	-0.02	3,581	-0.03	3,647	-0.05	2,427	-0.04	2,831	-0.03	6,062	-0.04	5,839	-0.04	4,781	-0.03	6,395

Bering Strait	1-Jan		15-Jan		1-Feb		15-Feb		1-Mar		15-Mar		1-Apr		15-Apr		1-May		15-May	
Passive	0.03	11,921	0.04	12,022	0.04	11,877	0.05	12,561	0.06	12,373	0.05	12,948	0.05	16,310	0.10	16,948	0.07	16,368	0.06	20,114
Surface	0.30**	14,816	0.22**	11,223	0.12*	7,934	0.26**	9,829	0.01	9,549	0.01	7,615	0.00	15,331	0.03	16,121	0.01	18,374	-0.03	6,406
Passive – ontogeny	0.05	15,473	-0.01	14,627	0.02	14,611	-0.02	11,453	0.01	8,606	0.05	11,894	0.02	13,646	-0.01	8,174	0.07	11,164	-0.01	7,293
Surface – ontogeny	0.05	17,142	0.06	15,190	0.05	12,913	0.06	15,923	0.04	18,346	0.06	18,840	0.03	19,417	0.06	22,183	0.04	13,247	-0.02	20,114
Surface - DVM	0.05	16,772	0.06	15,186	0.05	12,913	0.06	15,914	0.04	18,337	0.06	18,830	0.03	19,419	0.06	22,214	0.04	13,250	-0.02	6,632

Chukotka Peninsula	1-Jan		15-Jan		1-Feb		15-Feb		1-Mar		15-Mar		1-Apr		15-Apr		1-May		15-May	
Passive	0.02	9,231	0.04	9,526	0.03	8,877	0.06	9,115	0.06	10,106	0.05	10,763	0.03	13,869	0.06	16,530	0.11	20,238	0.18**	20,943
Surface	0.20**	6,801	0.27**	5,390	0.24**	6,904	0.30**	6,749	0.45**	10,653	0.38**	11,016	0.29**	12,042	0.47**	6,867	0.24**	9,976	0.12*	13,498
Passive – ontogeny	0.18**	18,590	0.09	13,126	0.10	11,698	0.06	12,930	0.06	3,933	0.07	4,964	0.10	14,398	0.00	4,611	0.01	877	0.13*	10,356
Surface – ontogeny	0.06	4,189	0.11	6,800	0.06	7,967	0.06	4,789	0.01	7,755	0.05	13,860	0.04	18,649	0.15**	10,708	0.16*	9,084	0.12*	10,836
Surface – DVM	0.05	4,189	0.06	6,804	0.05	7,968	0.06	4,801	0.04	7,747	0.06	13,874	0.03	18,674	0.06	10,689	0.04	9,078	-0.02	10,836

Kotzebue Sound	1-Jan		15-Jan		1-Feb		15-Feb		1-Mar		15-Mar		1-Apr		15-Apr		1-May		15-May	
Passive	0.07	2,983	0.10	2,990	0.11*	2,914	0.09	3,013	0.09	3,762	0.07	3,976	0.06	3,893	0.05	4,366	0.04	4,764	0.13*	4,571
Surface	-0.02	1,056	-0.02	1,200	-0.02	1,379	-0.01	956	-0.02	1,006	-0.02	1,272	-0.02	1,992	-0.02	3,806	-0.02	2,793	-0.02	1,391
Passive – ontogeny	-0.02	1,006	-0.02	3,858	-0.02	3,270	-0.02	1,637	-0.02	2,842	0.01	2,643	0.00	2,643	-0.02	433	-0.02	1,783	-0.02	2,361
Surface – ontogeny	-0.02	1,042	-0.02	1,008	-0.02	1,457	-0.02	1,129	-0.02	1,188	-0.02	1,391	-0.02	2,173	-0.02	4,261	-0.02	3,221	-0.02	1,514
Surface - DVM	-0.02	1,042	-0.02	1,008	-0.02	1,457	-0.02	1,129	-0.02	1,188	-0.02	1,393	-0.02	2,173	-0.02	4,261	-0.02	3,221	-0.02	1,514

For saffron cod, the simulations that produced results most similar to observed field distributions in 2012 were those initiated from Bering Strait and Kotzebue Sound. Simulations initiated from Bering Strait were significantly correlated for all simulation behaviors across most simulation dates, while those initiated from Kotzebue Sound were significant across all behaviors and dates (Table 4). Early passive particle simulations from the Chukotka Peninsula (15 January – 1 March) were also marginally or significantly correlated with observations (Table 4). No significant correlations were found for other release locations. Similar to the 2012 results, most simulations in 2013 from Bering Strait and Kotzebue Sound produced distributions that were significantly correlated to observed distributions of saffron cod in the acoustic-trawl survey (not shown). For both 2012 and 2013 simulations, the majority of correlations were strongest for later release dates (Table 4 for 2012, not shown for 2013). Correlations with release depth did not reveal any patterns for either species, except for saffron cod simulations initiated in Kotzebue Sound, where correlations were significant for all release depths across all behaviors (not shown). Note that most release dates occurred in winter and spring months, when the shallow Chukchi

and Bering shelf water columns exhibit relatively weak stratification. Hence, current-induced turbulent motions can readily redistribute passively floating plankton through the water column at this time of year.

Table 4. Correlations between observed distributions of saffron cod (Eleginus gracilis, larvae and early juveniles ≤ 45 mm in length) in the 2012 Arctic Ecosystem Integrated Survey acoustic-trawl survey and simulated distributions on 1 September from 5 behavior scenarios. Particles were released at 5 locations (Gulf of Anadyr, St. Lawrence Island, Bering Strait, Chukotka Peninsula, and Kotzebue Sound) at bi-weekly intervals from 1 January – 15 May. **p-value < 0.05 (darker shading), *0.05 ≤ p-value < 0.10 (lighter shading). p = p-value, n = number of simulated larvae found within the survey grid.

Gulf of Anadyr	1-Jan		15-Jan		1-Feb		15-Feb		1-Mar		15-Mar		1-Apr		15-Apr		1-May		15-May	
	F	*n*	*F*	*n*	*F*	*n*	*F*	*n*	*F*	*n*	*F*	*n*	*F*	*n*	*F*	*n*	*F*	*n*	*F*	*n*
Passive	0.09	93,331	0.07	93,269	0.05	96,398	0.03	105,121	0.02	106,953	0.02	109,282	0.01	103,251	0.01	97,108	0.01	101,002	-0.01	100,556
Surface	-0.01	43,457	0.01	45,721	-0.02	49,470	-0.02	66,645	-0.02	79,270	-0.01	82,426	-0.01	72,419	-0.02	56,892	-0.02	50,650	-0.02	43,385
Passive – ontogeny	-0.01	54,753	-0.01	41,934	-0.01	60,111	-0.01	79,601	-0.01	88,225	-0.01	80,818	-0.01	77,832	-0.01	82,431	-0.01	30,342	-0.01	27,890
Surface – ontogeny	-0.01	44,123	-0.01	46,344	-0.01	49,833	-0.02	67,621	-0.02	80,369	-0.01	83,384	-0.01	71,798	-0.02	57,966	-0.02	50,017	-0.02	40,788
Surface - DVM	-0.01	43,821	-0.01	46,173	-0.01	52,891	-0.02	67,924	-0.02	80,535	-0.01	83,070	-0.01	71,566	-0.02	57,810	-0.02	50,138	-0.02	40,622

St. Lawrence Island	1-Jan		15-Jan		1-Feb		15-Feb		1-Mar		15-Mar		1-Apr		15-Apr		1-May		15-May	
Passive	-0.03	5,861	-0.01	5,549	0.08	5,349	-0.01	5,149	-0.02	5,172	0.00	5,720	-0.05	5,654	-0.05	6,569	-0.05	5,379	-0.04	5,677
Surface	-0.02	3,565	-0.02	4,957	-0.01	5,315	-0.02	3,364	-0.04	2,478	-0.03	3,393	-0.02	4,836	-0.03	5,502	-0.03	5,440	-0.03	6,971
Passive – ontogeny	-0.01	2,047	-0.01	830	-0.01	1,963	-0.01	194	-0.03	2,394	-0.02	1,007	-0.02	6,967	-0.03	5,076	-0.04	3,643	-0.03	5,685
Surface – ontogeny	-0.02	3,574	-0.01	5,005	-0.01	5,360	-0.02	3,361	-0.03	2,401	-0.03	3,205	-0.02	5,126	-0.02	5,772	-0.03	5,017	-0.02	6,484
Surface - DVM	-0.02	4,246	-0.01	4,889	-0.01	4,015	-0.02	3,175	-0.03	2,398	-0.03	3,205	-0.02	5,132	-0.02	5,772	-0.03	5,017	-0.02	6,484

Bering Strait	1-Jan		15-Jan		1-Feb		15-Feb		1-Mar		15-Mar		1-Apr		15-Apr		1-May		15-May	
Passive	0.48**	11,924	0.46**	12,032	0.46**	11,877	0.44**	12,561	0.55**	12,373	0.53**	12,947	0.99**	16,310	0.47**	16,948	0.51**	16,368	0.81**	20,114
Surface	0.05	15,665	0.21**	12,008	0.18**	7,799	0.12*	9,881	0.07	9,538	0.09	7,558	0.54**	15,149	0.17**	15,947	0.06	18,153	0.54**	6,223
Passive – ontogeny	0.13**	12,915	0.07	12,416	0.27**	11,276	0.42**	9,716	0.35**	13,438	0.30**	20,299	0.56**	15,992	0.19**	16,878	0.22**	11,819	0.72**	7,840
Surface – ontogeny	0.05	15,699	0.24**	12,221	0.20**	8,005	0.14**	10,027	0.08	9,670	0.10	7,684	0.56**	15,620	0.19**	16,207	0.07	18,284	0.99**	6,512
Surface - DVM	0.31**	17,142	0.25**	15,190	0.06	12,913	0.06	15,923	0.02	18,346	0.11	7,725	0.56**	15,666	0.19**	16,170	0.07	18,249	0.99**	6,512

Chukotka Peninsula	1-Jan		15-Jan		1-Feb		15-Feb		1-Mar		15-Mar		1-Apr		15-Apr		1-May		15-May	
Passive	0.10	9,231	0.12*	9,526	0.13**	8,877	0.10	9,115	0.11**	10,106	0.10	10,763	0.10	13,869	0.08	16,529	0.07	20,238	0.05	20,943
Surface	-0.04	7,192	-0.04	4,857	-0.04	7,347	-0.03	6,789	-0.03	10,632	-0.03	10,912	-0.03	11,935	-0.03	6,855	-0.02	9,851	-0.02	13,471
Passive – ontogeny	-0.04	4,321	-0.03	11,390	-0.05	773	-0.03	12,264	-0.02	2,286	-0.03	16,980	-0.04	12,078	-0.03	6,527	-0.02	10,829	-0.04	1,088
Surface – ontogeny	-0.04	7,249	-0.04	4,889	-0.04	7,424	-0.03	6,818	-0.03	10,662	-0.03	10,938	-0.03	12,021	-0.03	6,946	-0.02	9,809	-0.02	13,501
Surface – DVM	-0.02	4,189	-0.03	6,800	-0.03	7,967	-0.03	4,789	-0.03	7,755	-0.03	11,012	-0.03	12,061	-0.03	6,935	-0.02	9,820	-0.02	13,452

Kotzebue Sound	1-Jan		15-Jan		1-Feb		15-Feb		1-Mar		15-Mar		1-Apr		15-Apr		1-May		15-May	
Passive	0.34**	2,983	0.33**	2,990	0.34**	2,914	0.57**	3,013	0.65**	3,762	0.67**	3,975	0.68**	3,893	0.78**	4,366	0.81**	4,764	0.77**	4,571
Surface	0.22**	1,068	0.35**	1,201	0.22**	1,387	0.22**	982	0.22**	1,023	0.28**	1,265	0.71**	1,953	0.75**	3,763	0.76**	2,720	0.41**	1,399
Passive – ontogeny	0.76**	1,097	0.75**	2,636	0.76**	4,678	0.45**	1,648	0.76**	3,664	0.27**	2,970	0.70**	2,979	0.41**	1,106	0.63**	2,453	0.41**	1,953
Surface – ontogeny	0.22**	1,072	0.34**	1,201	0.22**	1,396	0.22**	966	0.22**	1,029	0.29**	1,291	0.72**	2,054	0.75**	4,069	0.76**	3,032	0.45**	1,469
Surface - DVM	0.22*	1,042	0.34**	1,008	0.24**	1,457	0.22**	1,129	0.26**	1,188	0.30**	1,293	0.72**	2,057	0.75**	4,061	0.76**	3,035	0.45**	1,465

Interannual variability in simulated distributions

Large interannual variability in the COGs of simulated particles was found for polar cod, particularly for the Chukotka Peninsula release locations. The COG across simulation years (2004 – 2015) was located in the western portion of the Chukchi Sea, southwest of Herald Shoal (Fig. 5 a), similar to the centers of gravity in 2008, 2013, and 2015. For 2004 – 2006, the COGs shifted to the southwest, while that in 2012 was to the southeast (Fig. 5 a). In 2007, 2011, and 2014, particles were located further north compared to the 2004 – 2015 COG. In 2009, the COG was in the eastern portion of the Chukchi Sea, east of Herald Shoal, while in 2010, it was in the western Chukchi Sea, just south of Wrangel Island (Fig. 5 a). Most of the COGs for the Bering Strait release location were found in close proximity to Cape Lisburne, located north and south of the cape for the majority of the time series. The only exceptions were in 2005, when the COG was located near Herald Shoal, and in 2007, when it was farther north of Cape Lisburne compared to in other years (Fig. 4 a). The COGs of saffron cod released from the Bering Strait region were similar to those of polar cod and were mainly centered around Cape Lisburne (Fig. 5 b). In 2005, the COG was over Herald Shoal, while in 2007 it was located to the north of Cape Lisburne (Fig. 5 b). The COGs for particles released in Kotzebue Sound were found on the north side of the sound, located around Cape Krusenstern (Fig. 5 b), suggesting retention within Kotzebue Sound.

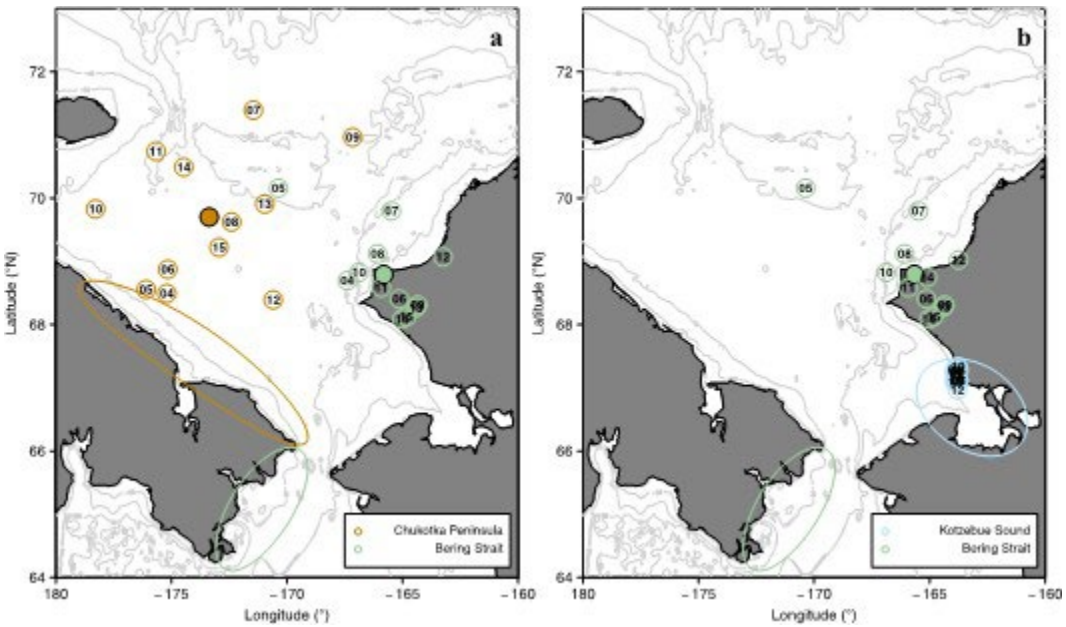

Fig. 5. Mean latitude and longitude of (a) polar cod (Boreogadus saida) and (b) saffron cod (Eleginus gracilis) larvae and early juveniles ≤ 45 mm in length on 1 September from 2004 – 2015. Simulations for polar cod were initiated from Bering Strait (green) and the Chukotka Peninsula (orange). Simulations for saffron cod were initiated from Bering Strait (green) and Kotzebue Sound (blue). Data from simulations with surface-oriented behavior are presented. Solid circles represent overall centers of gravity for 2004 – 2015, color coded to release location. Numbers in circles represent the last two digits of the simulation year. Ellipses represent particle release locations.

Polar cod inertia between 2004 and 2015 was highly variable for both the Bering Strait and Chukotka Peninsula simulations (Fig. 6). Bering Strait had a mean inertia of 97,755 km2 and a SD of the major and minor axes of ± 260,074 km2 and ± 173,542 km2, respectively. The Chukotka Peninsula had a mean inertia of 123,034 km2 and a SD of the major and minor axes of ± 283,059 km2 and ± 207,150 km2, respectively. For Bering Strait releases, inertia declined significantly over time (linear regression, LR: β = -5894, t10 = -3.129, p = 0.011), while it increased over time for simulations originating from the Chukotka Peninsula, although not significantly (LR: β = 4914, t10 = 1.568, p = 0.148). Similar to polar cod, saffron cod inertia for the Bering Strait release location was highly variable (95,729 ± 261,437 and 165,469 km2) and declined significantly over time (LR: β = -5044, t10 = -2.611, p =0.026). Inertia for simulations originating in Kotzebue Sound was very low (15,475 ± 115,195 and 46,956 km2) and remained relatively constant over time (LR: β = -106.2, t10 = -0.384, p = 0.709).

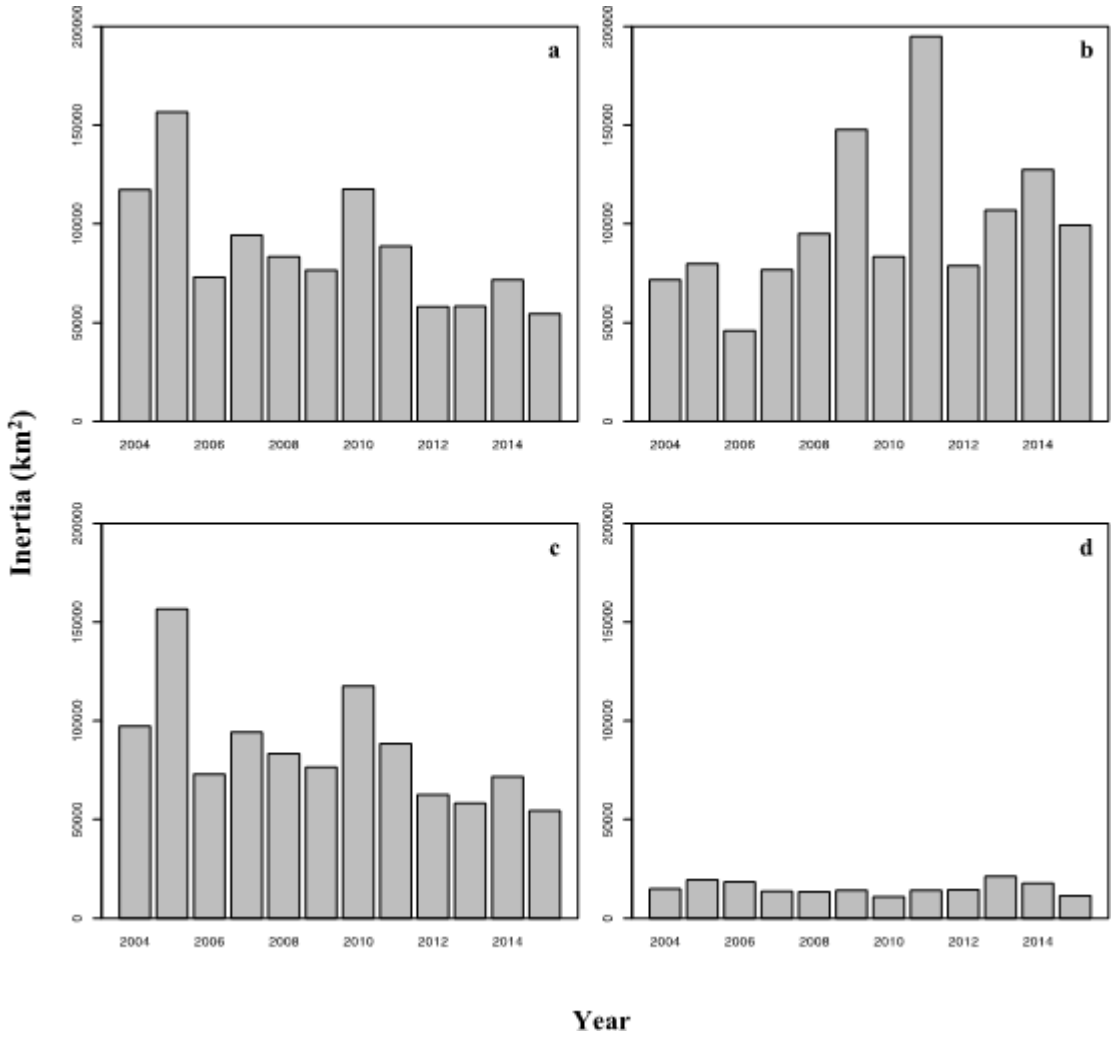

Fig. 6. Inertia (in km2), which measures the dispersion of simulated particles around the center of gravity, for polar cod (Boreogadus saida) simulations from (a) Bering Strait and the (b) Chukotka Peninsula and saffron cod (Eleginus gracilis) simulations from (c) Bering Strait and (d) Kotzebue Sound from 2004 – 2015. Data from simulations with surface-oriented behavior are presented.

Correlations with Climate Indices

Significant correlations were found between latitudinal and longitudinal COG indices for both polar cod and saffron cod at the end of the simulation and several of the climate indices, although correlations were not consistent across release areas or dates (Tables 5, 6). Simulated particles from the Bering Strait region for both species tended to have a more southern and eastern COG during years with a strong summer AD index, a weaker SA index, and more extensive ice (IER index = 1). In most cases, these correlations were stronger for later release dates (March – May). Similarly, the COG of simulated polar cod released at the Chukotka Peninsula were further south and east when the summer AD and AO indices were high and ice was extensive and retreated later (IER index = 1). In contrast to Bering Strait releases, the COG of simulated particles from the Chukotka Peninsula, in particular early releases, occurred further south during years with a stronger SA index, as evidenced by negative correlations with latitude (Table 5). For saffron cod from the Kotzebue Sound release locations, environmental variability appeared to primarily affect the longitudinal COG of early releases but the latitudinal COG from later releases. Simulated

particles from earlier release dates were displaced to the east during years with stronger AO and SA indices and a weaker winter AD index, all indicative of cold winters with heavy ice. Correlations with the latitudinal COG were variable and inconsistent (Table 6).

Table 5. Correlations between latitude and longitude center of gravity (COG) anomalies of simulated polar cod (Boreogadus saida, larvae and early juveniles ≤ 45 mm in length) on 1 September (2004 – 2015) and selected climate indices. AD: Arctic Dipole index, MAM: March, April, May, JJA: June, July, August; AO: Arctic Oscillation index; SA: Siberian/Alaskan index (2004 – 2013); IER: Ice extent/retreat index (2005 – 2015). Simulations were initiated from Bering Strait and Chukotka Peninsula release locations using surface-oriented behavior. **p-value < 0.05 (darker shading), *0.05 ≤ p-value < 0.10 (lighter shading). Red (blue) represents a positive (negative) correlation.

	Bering Strait						Chukotka Peninsula				
Latitude COG Index	**AD (MAM)**	**AD (JJA)**	**AO**	**SA**	**IER**	**Latitude COG Index**	**AD (MAM)**	**AD (JJA)**	**AO**	**SA**	**IER**
Lat, all dates	-0.12	-0.22	0.16	0.39	-0.42	Lat, all dates	0.13	-0.60**	0.07	-0.37	-0.12
Lat, 1-Jan	-0.23	0.19	-0.12	-0.06	-0.43	Lat, 1-Jan	0.16	-0.29	-0.42	-0.47	-0.28
Lat, 15-Jan	-0.08	0.21	-0.08	-0.10	-0.19	Lat, 15-Jan	-0.04	-0.36	-0.20	-0.24	0.07
Lat,1-Feb	-0.22	0.25	-0.11	0.00	0.00	Lat,1-Feb	0.14	-0.53*	-0.01	-0.37	-0.06
Lat, 15-Feb	0.00	0.02	0.07	0.45	-0.28	Lat, 15-Feb	0.27	-0.44	-0.16	-0.54	-0.01
Lat, 1-Mar	0.26	-0.32	0.16	0.16	-0.55*	Lat, 1-Mar	0.16	-0.50*	-0.15	-0.58*	-0.05
Lat, 15-Mar	-0.01	-0.32	0.51*	0.58*	-0.24	Lat, 15-Mar	0.00	-0.64**	-0.12	-0.49	-0.25
Lat, 1-Apr	-0.31	-0.66**	0.44	0.40	0.00	Lat, 1-Apr	-0.08	-0.66**	0.43	-0.18	0.18
Lat, 15-Apr	-0.11	-0.64**	0.02	0.30	-0.53*	Lat, 15-Apr	-0.13	-0.42	0.45	0.18	-0.37
Lat, 1-May	-0.15	-0.38	0.37	0.87**	0.05	Lat, 1-May	0.23	-0.46	0.49	-0.04	-0.15
Lat, 15-May	0.15	-0.33	0.13	0.32	-0.77**	Lat, 15-May	0.17	-0.36	0.54*	0.07	-0.10
Longitude COG Index	**AD (MAM)**	**AD (JJA)**	**AO**	**SA**	**IER**	**Longitude COG Index**	**AD (MAM)**	**AD (JJA)**	**AO**	**SA**	**IER**
Lon, all dates	0.15	0.06	0.17	0.18	0.56*	Lon, all dates	-0.13	-0.10	0.61**	0.09	0.52
Lon, 1-Jan	-0.08	0.34	0.55*	0.13	0.42	Lon, 1-Jan	-0.29	-0.24	0.63**	0.13	0.33
Lon, 15-Jan	0.20	0.12	-0.19	-0.03	0.42	Lon, 15-Jan	-0.13	-0.26	0.54*	-0.10	0.27
Lon,1-Feb	0.36	0.03	0.16	0.13	0.39	Lon,1-Feb	0.04	-0.36	0.48	-0.06	0.36
Lon, 15-Feb	0.41	0.06	-0.02	0.10	0.31	Lon, 15-Feb	0.16	-0.09	0.28	-0.17	0.45
Lon, 1-Mar	0.13	0.26	0.10	0.13	0.72**	Lon, 1-Mar	-0.05	0.08	0.32	-0.06	0.63**
Lon, 15-Mar	-0.25	0.12	0.12	0.42	0.72**	Lon, 15-Mar	-0.20	-0.11	0.49	0.14	0.67**
Lon, 1-Apr	0.03	-0.12	0.14	0.10	0.50	Lon, 1-Apr	-0.09	-0.04	0.46	0.16	0.54*
Lon, 15-Apr	0.02	-0.10	0.50*	0.24	0.50	Lon, 15-Apr	-0.30	0.17	0.56*	0.52	0.35
Lon, 1-May	0.12	-0.12	0.02	0.36	0.37	Lon, 1-May	-0.02	0.03	0.56*	0.14	0.27
Lon, 15-May	0.38	0.01	-0.26	0.02	0.37	Lon, 15-May	0.03	0.09	0.54*	0.11	0.26

Table 6. Correlations between latitude and longitude center of gravity (COG) anomalies of simulated saffron cod (Eleginus gracilis, larvae and early juveniles ≤ 45 mm in length) on 1 September (2004-2015) and selected climate indices. AD: Arctic Dipole index, MAM: March, April May, JJA: June, July, August; AO: Arctic Oscillation index; SA: Siberian/Alaskan index (2004 – 2013); IER: Ice extent/retreat index (2005 – 2015). Simulations were initiated from Bering Strait and Chukotka Peninsula release locations using surface-oriented behavior. **p-value < 0.05 (darker shading), *0.05 ≤ p-value < 0.10 (lighter shading). Red (blue) represents a positive (negative) correlation.

Bering Strait						Chukotka Peninsula					
Latitude COG Index	**AD (MAM)**	**AD (JJA)**	**AO**	**SA**	**IER**	**Latitude COG Index**	**AD (MAM)**	**AD (JJA)**	**AO**	**SA**	**IER**
Lat, all dates	-0.18	-0.27	0.19	0.41	-0.43	Lat, all dates	0.03	0.70*	-0.22	-0.58*	0.07
Lat, 1-Jan	-0.23	0.19	-0.13	-0.07	-0.43	Lat, 1-Jan	-0.14	0.36	-0.06	-0.48	-0.12
Lat, 15-Jan	-0.08	0.21	-0.08	-0.10	-0.19	Lat, 15-Jan	0.13	0.42	-0.22	-0.44	-0.41
Lat,1-Feb	-0.17	0.27	-0.14	-0.11	-0.05	Lat,1-Feb	0.06	-0.07	0.16	-0.06	-0.09
Lat, 15-Feb	-0.30	-0.23	0.19	0.57*	-0.28	Lat, 15-Feb	0.32	0.10	-0.17	-0.56*	0.02
Lat, 1-Mar	0.00	-0.44	0.22	0.26	-0.55*	Lat, 1-Mar	0.06	0.77**	-0.29	-0.51	0.39
Lat, 15-Mar	-0.01	-0.32	0.51*	0.58*	-0.24	Lat, 15-Mar	0.02	0.57*	-0.33	-0.15	-0.10
Lat, 1-Apr	-0.31	-0.66**	0.44	0.40	0.00	Lat, 1-Apr	0.10	0.09	0.13	0.28	-0.24
Lat, 15-Apr	-0.11	-0.64**	0.02	0.30	-0.53*	Lat, 15-Apr	-0.07	-0.23	0.15	0.28	-0.08
Lat, 1-May	-0.15	-0.38	0.37	0.87**	0.05	Lat, 1-May	0.08	-0.63**	0.49	0.00	-0.16
Lat, 15-May	0.15	-0.33	0.13	0.32	-0.77**	Lat, 15-May	0.64*	-0.09	-0.12	-0.35	-0.09
Longitude COG Index	**AD (MAM)**	**AD (JJA)**	**AO**	**SA**	**IER**	**Longitude COG Index**	**AD (MAM)**	**AD (JJA)**	**AO**	**SA**	**IER**
Lon, all dates	0.18	0.07	0.16	0.13	0.55*	Lon, all dates	-0.64**	-0.11	0.71**	0.39	0.47
Lon, 1-Jan	-0.07	0.34	0.55*	0.12	0.41	Lon, 1-Jan	-0.50*	-0.32	0.36	0.60*	0.45
Lon, 15-Jan	0.20	0.12	-0.19	-0.02	0.42	Lon, 15-Jan	-0.27	-0.22	0.61**	0.45	0.01
Lon,1-Feb	0.53*	0.13	-0.04	-0.51	0.13	Lon,1-Feb	-0.58**	-0.04	0.22	-0.15	0.26
Lon, 15-Feb	0.41	0.06	-0.01	0.10	0.31	Lon, 15-Feb	-0.28	0.17	0.34	0.31	-0.03
Lon, 1-Mar	0.18	0.30	0.07	0.10	0.72*	Lon, 1-Mar	-0.21	-0.18	0.39	0.66**	0.23
Lon, 15-Mar	-0.25	0.12	0.12	0.42	0.72*	Lon, 15-Mar	0.22	-0.20	0.41	0.08	0.37
Lon, 1-Apr	0.03	-0.12	0.14	0.10	0.50	Lon, 1-Apr	-0.21	0.02	-0.25	-0.54	0.24
Lon, 15-Apr	0.02	-0.10	0.50*	0.24	0.50	Lon, 15-Apr	0.09	0.23	-0.08	-0.42	-0.10
Lon, 1-May	0.12	-0.12	0.02	0.36	0.37	Lon, 1-May	-0.12	0.65**	-0.44	-0.24	-0.11
Lon, 15-May	0.37	0.01	-0.26	0.02	0.37	Lon, 15-May	-0.13	0.13	0.15	0.02	-0.26

When the five climate indices were compared over the 2004 – 2015 period, no obvious trends were noted (Fig. S3), though the summer AD index was negative from 2004 – 2012 (Fig. S3 b) and the SA index was positive between 2004 – 2008 (Fig. S3 d). Correlations between the climate indices were not significant (Table S1).

Discussion

Results of our biophysical transport modeling study suggest that the source of aggregations of polar cod and saffron cod larvae and early juveniles observed in the Chukchi Sea during the 2012 and 2013 Arctic EIS surveys were most likely from the northern Bering Sea or the southern Chukchi Sea. In particular, Bering Strait and the Chukotka Peninsula were identified as potential spawning and/or hatching locations of polar cod. Our findings support other research that has suggested the existence of a number of nearshore, shallow spawning grounds in the North American and Siberian Arctic (Craig et al., 1982; Thanassekos and Fortier, 2012; Logerwell et al., 2015). In addition, our results align well with those of Ponomarenko (1968) and Sunnanå and Christiansen (1997), which suggested that polar cod spawn in the northern Bering and southern Chukchi seas. For saffron cod, simulations that produced results most similar to observed field distributions were those initiated from Bering Strait and Kotzebue Sound. Saffron cod are believed to spawn demersally under ice in shallow, nearshore areas (Morrow, 1980; Fechhelm et al., 1985; Wolotira, 1985; Johnson, 1995; Mecklenburg et al., 2002) and our results are supported by observations of saffron cod in spawning condition in nearshore areas along the coast, such as Kotzebue Sound (A. Whiting, Native Village of Kotzebue, personal communication). Strong and consistent correlations between field observations and modeled distributions across several behaviors and over a wide range of dates lends further support to the hypothesis that Kotzebue Sound is an important spawning habitat for saffron cod. Furthermore, correlations between simulated and observed saffron cod distributions were strongest from early April to mid-May. These results match well with the timing of

peak hatching for saffron cod, which occurs in April and May, prior to the warming of coastal waters in the Arctic and northern Pacific (Wolotira, 1985).

Simulated distributions and sizes of polar cod overlapped with those estimated by the Arctic EIS program's acoustic-trawl survey in 2012, yet there was poor overlap in 2013, as evidenced by the lack of significant correlations with any of the release locations or dates in that year. A comparison of particle locations on 1 September showed strong variability in dispersal patterns between the two years, with reduced overlap of particles with the Arctic EIS survey grid in 2013 (18.72%) compared to 2012 (22.05%)(Fig. S1). In 2012, simulated particles on the Chukchi Shelf were concentrated along the Central Channel or the Western Pathway towards Herald Canyon. Additional concentrations were found along the Alaskan coastline and formed a thick band between Herald and Hanna shoals, which extended eastward towards the coast between Icy Cape and Wainwright, and towards the head of Barrow Canyon (Fig. S1). High concentrations of simulated larvae in this region are in agreement with other studies that have noted high abundances of polar cod ELS in the northern Chukchi Sea offshore of Wainwright (De Robertis et al., 2017b; Vestfals et al., 2019; Deary et al., in review). In contrast, simulated polar cod in 2013 were mainly distributed outside of the Arctic EIS survey grid (Fig. S1) and found mostly outside of the areas of the shelf that were occupied in 2012. There were some similarities between the two years, mainly along the Alaskan coastline and in the region between Herald and Hanna shoals, towards Icy Cape and Wainwright, although the band in 2013 was narrower (Fig. S5 – S6). Higher concentrations of simulated larvae and early juveniles were found in the western portion of the Chukchi Sea in 2013, along the Chukotka Peninsula and in Long Strait, with additional particles taking a more westward route towards Herald Canyon, over the northern Chukchi shelf, and across the shelf break compared to 2012. While the majority of particles (81.27%) were outside of the Arctic EIS survey area in 2013, limited ichthyoplankton sampling in the western and northern Chukchi Sea in 2004, 2009, and 2012 during the Russian-American Long-Term Census of the Arctic (RUSALCA) program encountered high abundances of polar cod larvae and early juveniles in these areas, and as far west as the East Siberian Sea (Norcross et al., 2006; Vestfals et al., 2019; M. Busby, NOAA, unpublished results).

Simulated distributions of saffron cod from the Bering Strait release location were similar to those of polar cod (Fig. S7). Given that the starting locations and behavior scenarios were identical between species, the distributional differences can be attributed to the different temperature-dependent growth rates used for each species in the IBMs. As fish grow, changes in body length affect their swimming speed. This, in turn, affects their vertical position in the water column, and ultimately, the horizontal transport of their ELS through exposure to different flow schemes (Vikebø et al., 2005; Fiksen et al., 2007; Leis, 2007). Here, the slower growth rates of saffron cod would result in individuals being located in the surface layer for longer in comparison to polar cod. Particles from simulations initiated in Kotzebue Sound were consistently retained within the Sound or were advected northward along the Alaskan coastline (Fig. S8). Age-0 saffron cod are known to occupy shallow, nearshore habitats (Wolotira, 1985; Logerwell et al., 2015; De Robertis et al., 2017b) and have been found in high abundances from Kotzebue Sound to north of Cape Lisburne in late summer (De Robertis et al., 2017b; Vestfals et al., 2019). Recent surveys in the eastern Chukchi Sea in 2017 encountered high abundances of saffron cod larvae around Kotzebue Sound in late spring, though by late summer they were found in nearshore areas from northern Kotzebue Sound to around Cape Lisburne (Deary et al., in review). These findings, combined with our modeling results, suggest that saffron cod spawned in Kotzebue Sound are retained there or are transported northwards by currents to juvenile nursery habitats along the coast. Over time, fish have evolved to spawn in areas where bathymetric features and prevailing currents transport their larvae to or retain them within suitable nursery habitats (Iles and Sinclair, 1982; Bailey and Picquelle, 2002; Bailey et al., 2008; Duffy-Anderson et al., 2013). Satellite tracked drifters with near-surface drogues (Danielson and Whiting, 2016) and numerical modeling (Panteleev et al., 2013) show that a gyre forms in Kotzebue Sound, which was also evident in the PAROMS model output. Hence, the circulation in and around Kotzebue Sound may be especially conducive to larval retention and/or delivery to juvenile nursery

habitats. The retentive nature of Kotzebue Sound is also supported by the results of our analyses, which showed COGs that were consistently located in northern Kotzebue Sound (Fig. 5 b), along with low inertia over the time series (Fig. 6 d).

The strong year-to-year variability in simulated distributions of polar cod and saffron cod suggests that transport of their early life stages is highly sensitive to variations in flow across the Chukchi shelf. Only simulations from Kotzebue Sound showed relatively consistent dispersal patterns between years. Observed differences in simulated particle distributions across the broader Chukchi Shelf in 2012 and 2013 can be linked to differences in oceanographic and atmospheric conditions between the two years. In 2013, persistent northeasterly winds in late summer led to flow reversals over much of the northeast Chukchi Sea, which limited the northward extent of the ACC and advected Arctic waters onto the Chukchi Shelf via Barrow Canyon (Danielson et al., 2017). This is consistent with simulated particles following a more westward pathway along the shelf in 2013, compared to 2012 (Fig. S1). The inflow of Pacific waters through Bering Strait is bathymetrically steered along either Herald Canyon, the Central Channel, or along the Alaskan coast; however, this inflow can be driven towards the western portion of the shelf during periods with easterly winds (Windsor and Chapman, 2004). Similarly, Bond et al. (2018) described a stronger than normal flow pattern through Bering Strait, where a disproportionate portion of the flow travels northwest toward and beyond Wrangel Island rather than joining the ACC, which they linked to anomalous winds from the east-northeast. Indeed, winds were more persistent from the northeast and annual transport through Bering Strait was higher in 2013 (~1.1 Sv) compared to 2012 (~0.7 Sv) (Woodgate et al., 2015).

One curious aspect of the modeled larval aggregations was that they appeared to aggregate in long banded arrangements stretching from the Barrow Canyon region in the NE Chukchi Sea across the shelf toward the west. Examination of the model hydrographic fields in 2012 (Fig. S9) revealed that the larvae were accumulating in the vicinity of the ice-edge frontal zone (Fig. S9 a), which is delineated by a change of density (salinity (Fig. S9 e) and temperature (Fig. S9 c)) from the open water zone south of the marginal ice zone to under the pack ice. Recent investigations into the hydrographic structure associated with ice edge fronts and the melting of ice on the Chukchi shelf has revealed convergent zones associated with the ice and thermohaline fields (Lu et al., 2020a; 2020b). These frontal zones can extend several meters (up to 15 m) below the surface and likely provide enhanced feeding opportunities for surface-oriented larvae and early juveniles by maintaining them in close proximity to the ice edge, where they can take advantage of copepod production fueled by ice-edge phytoplankton blooms (Søreide et al., 2010; Perrette et al., 2011), as well as the higher concentrations of food particles that tend to accumulate in convergent frontal zones (Bakun, 2006). For surface-oriented larvae, these frontal zones may act as a barrier to northward advection, however, this may not be the case for species that live at or migrate to depths below the vertical extent of the frontal zone. Much work remains to be done to determine to what extent polar cod larvae in the field are actually subject to the influences of the convergent ice-edge fronts, but the combination of our work and the ice edge modeling study raises many interesting questions, provides new testable hypotheses, and provides new ways to think about the early life stages of polar cod and other Arctic species.

Correlations between location indices derived from the simulation output and several climate indices provide evidence that dispersal of polar cod and saffron cod ELS are likely sensitive to environmental forcing. During periods that were characterized by colder conditions in the Pacific Arctic (i.e., a positive AO index, with a strong jet stream that retains cold air over the polar region (Thompson and Wallace, 2000); a negative AD index, where more sea-ice remains in the western Arctic (Watanabe et al., 2006; Wu et al., 2006); a positive SA index, with anomalously strong northwesterly winds and heavy ice cover (Fang and Wallace 1994; Overland et al., 2002); and a greater ice extent and later ice retreat (Okkonen et al., 2019)), cod ELS were found farther south and east compared to periods that represented warmer conditions in the region. The findings of our study have important implications for polar cod and saffron cod connectivity between the Chukchi and Beaufort seas. Our results suggest that in warmer years with

greater Pacific inflow and an earlier sea-ice retreat (e.g., 2005, 2010, and 2011 in Figs. S5 – S8), a higher proportion of larvae spawned in the northern Bering or southern Chukchi seas would be transported northwestward towards Herald Canyon and across the northern Chukchi shelf (see Okkonen et al., 2019, their Fig. 6B), which would result in a greater contribution to populations in the northern Chukchi and western Beaufort seas. In contrast, during colder years with reduced Pacific inflow and a later ice retreat (e.g., 2006, 2009, and 2012 in Figs. S5 – S8), larvae would be advected along the ice edge towards the Alaskan coast, with a greater proportion of the population retained in the eastern Chukchi Sea (see Okkonen et al., 2019, their Fig. 6A). The timing and pattern of sea-ice retreat across the Chukchi shelf has been linked to the strength of the Pacific-Arctic pressure head, which is influenced by the strength and location of the Beaufort Sea High pressure cell and its associated winds (Danielson et al., 2014; Okkonen et al., 2019). A stronger Pacific-Arctic pressure head (i.e., 2005, 2007, 2009, 2011, and 2015) was associated with greater northward volume and property fluxes along the Alaskan coast (i.e. a stronger Alaska Coastal Current), which promoted earlier ice retreat across the eastern Chukchi shelf (Okkonen et al., 2019). In contrast, a weaker pressure head (i.e., 2006, 2008, 2010, 2012 – 2014) was associated with lower volume and property fluxes along the Alaskan coast and slower, less directionally-biased ice retreat across the Chukchi shelf (Okkonen et al., 2019). Similarly, Luchin and Panteleev (2014) found that during warm years, the inflow of Pacific water through Bering Strait spread widely along the Siberian coast, with extensive transport through Herald Channel. In cold years, however, the inflow of warm Pacific water was reduced and mostly flowed along the Alaskan coast before exiting the shelf through Barrow Canyon. Thus, as continued Arctic warming further impacts sea-ice extent and timing of sea ice retreat in the Chukchi Sea, we anticipate that polar cod and saffron cod ELS will be affected by concomitant changes in flow across the shelf, which will likely affect population connectivity between the northern Bering, Chukchi and Beaufort seas.

Simulations that produced saffron cod distributions most similar to Arctic EIS field observations were those initiated from Bering Strait and Kotzebue Sound, particularly those with a passive component. This result was not surprising, as saffron cod larvae grow slowly at low temperatures and as such, their dispersal is more likely to be affected by currents than by their behavior. However, larvae are not passive particles that drift along with currents and even first-feeding larvae have the ability to control temperature, salinity, light, turbulence and food concentrations by migrating vertically, which in turn contributes to their horizontal movement (Norcross and Shaw, 1984; Boehlert and Mundy, 1988; Hare and Govoni, 2005; Hurst et al., 2009). Late-stage larvae and pelagic juveniles have also been shown to have considerable control over their speed, direction, and position in the water column (Olla et al., 1996; Leis and Carson-Ewart, 1997, 1999). Even slight differences in behavior can have long-term and large-scale consequences, since vertical positioning influences the drift trajectory of the larva, and thereby the physical environment it experiences along the way (Vikebø et al., 2007). Our simulation results showed that behavior did indeed have a strong effect on larval dispersal (Fig. S4, Tables 3 and 4). While detailed information about the vertical distribution of saffron cod larvae is not currently available, newly hatched larvae spend between 2–3 months as plankton before descending to the bottom in mid-summer, between 39 and 56 mm in length in the Pacific and 55 and 60 mm in the Arctic (Wolotira, 1985); larger age-0 fish can still be found in surface waters in late summer (Eisner et al., 2012). Similarly, polar cod larvae have been shown to be surface-oriented in the first few months of life (Spencer et al., 2020; B. Laurel, unpublished results), moving deeper as they develop (Borkin et al., 1986), with pelagic juveniles descending deeper in the water column in late summer, between 30 and 55 mm in length (Matarese et al., 1989; Ponomarenko, 2000; Bouchard and Fortier, 2011). Recent repeat acoustic surveys in the eastern Chukchi Sea from mid- to late-summer in 2019 indicated that age-0 polar cod moved deeper in the water column and underwent DVM as the season progressed (Levine et al., 2020). While these data were not available at the time of our study, this behavior was considered in our preliminary simulations, as previous research has shown that polar cod undergo DVM in other areas of the Arctic (Borkin et al., 1986; Bouchard et al., 2016). However, the sizes at which fish begin their DVM and the depths to which they migrate had to be estimated for the Chukchi Sea, which is shallower (< 40 m) than the other regions

where DVM behavior has been observed. We ultimately chose the surface-oriented behavior to model growth and dispersal from 2004 – 2005, as this behavior was most strongly correlated with observed distributions in the field, though the overall results and conclusions were similar when based on the more complex surface-oriented behavior for early larval stages that moved deeper with ontogeny (C. Vestfals, unpublished results). The new information provided by the repeat acoustic surveys on the depth distribution of polar cod ELS, the sizes at which they begin to vertically migrate, and the depths to which they migrate (Levine et al., 2020) will be invaluable to future modeling efforts in the Chukchi Sea.

While climate-driven changes in advective transport and mixing will affect the dispersal and ultimately the distribution of larvae, the temperatures they experience during the drift period will, in turn affect their growth rates and their survival (Vikebø et al., 2005, 2007). We found differences in simulated lengths on 1 September between release locations, hatch dates, and species. The greater lengths attained by larvae hatching in southern locations can be attributed to warmer temperatures in the Bering Sea, in general, which results in faster growth of larvae hatching there compared to the Chukchi Sea. In spring, solar heating and the inflow of warmer water from the Bering Sea leads to rapid warming in the Chukchi Sea. Thus, the temperature conditions experienced by larvae hatching at later dates are more similar between regions compared to those hatching during the winter months. While polar cod simulated lengths aligned fairly well with fish ≤ 45 mm in length observed in the Arctic EIS acoustic-trawl survey, those for saffron cod did not, with much smaller simulated sizes than field estimates. The differences in simulated sizes between species result from assuming higher growth rates at lower temperatures for polar cod compared to saffron cod based on laboratory studies (Laurel et al., 2016; B. Laurel, unpublished results). The difference between observed and simulated lengths for saffron cod could have resulted from incorrectly specified growth in the IBM, incorrect temperatures in the model, strong size-selective mortality, incorrect assumptions about hatch dates, or other factors. It should be emphasized that the final estimates of acoustic-trawl survey abundance at length were sensitive to the selectivity parameters used in the calculations, particularly for the smallest size classes, which are poorly retained by the trawls (De Robertis et al., 2017a, b). In particular, 2012 abundance estimates for fish < 25 mm in length were effectively zero for both species across the entire survey region, which was most certainly due to the ineffectiveness of the Cantrawl gear at catching these smaller-sized fish, rather than a lack of presence of these sizes over the eastern Chukchi shelf. While use of the modified Marinovich trawl in 2013 improved the abundance estimates of fish in the 15 – 25 mm range, estimated abundances of fish < 15 mm remained at zero across the entire survey region, which clearly does not reflect their true abundance and distribution. Recent studies of polar cod and saffron cod ELS in the Chukchi Sea have found the presence of larvae < 25 mm in length in the Arctic EIS survey area during late summer (Vestfals et al., 2019; Deary et al., in review). In other regions of the Arctic, polar cod lengths in late summer can vary in size from 10 mm for fish hatched late in July, to 50 mm for young-of-the-year fish hatched early in January (Bouchard and Fortier, 2011). Thus, our simulation results for polar cod from the northern hatching locations (Bering Strait, Chukotka Peninsula, Kotzebue Sound) and saffron cod, in general, may reflect sizes in the field not captured in the acoustic-trawl survey estimates. However, our models clearly underestimated growth in both species. Field-based estimates of polar cod growth range from 0.27 – 0.51 mm day-1 (Bouchard and Fortier, 2011; Vestfals et al., 2019; Deary et al., in review), which are higher than the laboratory estimates used in this study (0.04 – 0.46 mm day−1, Koenker et al., 2018; Laurel et al., 2017), particularly for smaller polar cod larvae and those growing at lower temperatures (Fig. 2). As only the survivors of size-based predation are encountered in field samples, which selects for faster growing individuals (Bailey and Houde, 1989; Litvak and Leggett, 1992), field-based growth estimates are often higher than those derived in the laboratory because fish larvae are known to grow and survive better on natural prey (Sargent et al., 1999; Evjemo et al., 2003).

The laboratory-derived growth rates used in our model likely underestimated saffron cod growth in the field, which contributed to the smaller simulated lengths compared to the lengths estimated by the Arctic EIS acoustic-trawl surveys. Unfortunately, a growth equation for larger stages of saffron cod is not

currently available and we used growth of a related gadid, walleye pollock, to model growth in the IBM. While walleye pollock ELS exhibit linear growth similar to that of saffron cod (Porter and Bailey, 2007; B. Laurel, NOAA, personal communication), some component of saffron growth was not fully captured in our model. Saffron cod may have a specific size or thermal range at which growth increases exponentially, or a particular habitat factor may influence their growth. Growth of saffron cod might be slow and constant during early development, but this could be followed by a period of rapid acceleration in growth. For example, Pacific hake (Merluccius productus), another North Pacific gadiform with a similar trophic role to saffron cod, grow slowly in the first 3 months of life (< 30 mm SL), after which their growth accelerates (Bailey, 1982; Bailey et al., 1982; Woodbury et al., 1995). Saffron cod may also experience faster growth in nearshore regions, with under-ice river plumes in coastal areas providing a thermal refuge for developing eggs and larvae during winter and early spring via relatively warmer freshwater runoff (Bouchard and Fortier, 2011). The solar-heated waters in Kotzebue Sound, Norton Sound, and coastal areas to the south provide a major source of the heat to the Alaska Coastal Current (Coachman et al., 1975; Ahlnäs and Garrison, 1984) and may also provide a thermal habitat conducive for optimal growth in saffron cod. Indeed, temperatures in Kotzebue Sound in July can exceed 12°C (Ahlnäs and Garrison, 1984), which exceeds thermal optima for some gadids, but is near the temperature of maximum growth for age-0 saffron cod (Tmax = 14.8°C) found in the lab (Laurel et al., 2016).

There are some limitations to using observations from the 2012 and 2013 Arctic EIS acoustic-trawl survey to validate our simulation results. The acoustic-trawl surveys were limited in their spatial extent and did not cover the inshore region or more northern areas of the Chukchi and Beaufort seas, or the Arctic Basin. Polar cod and saffron cod larvae may be present in these locations, so without further sampling, it is important not to rule out the northern locations as potential spawning or hatching areas. Results from the initial passive particle simulations showed that polar cod larvae hatching from more northern locations (Cape Lisburne, Hanna Shoal, and Barrow Canyon) were transported into nearshore regions in the northern Chukchi and Beaufort seas, as well as into the Arctic Basin. Due to the lack of overlap between simulated larval distributions and the Arctic EIS survey grids, which prevented model validation with field observations, further simulations from these hatching locations were not explored. However, these northern spawning/hatching locations in the Chukchi Sea may be a source of larvae for the Beaufort Sea and Arctic Basin. Indeed, small polar cod and saffron cod larvae corresponding to the sizes observed in our preliminary simulations from northern hatch locations (see Fig. S2) were collected in August 2008 around Barrow Canyon (Logerwell et al., 2015) and in 2017, small polar cod larvae were collected beyond the Chukchi shelf break in late summer/early fall (M. Busby, NOAA, personal communication.). High abundances of age-0 polar cod may also be present in the western portion of the Chukchi Sea outside the Arctic EIS survey area, as suggested by our simulations. This is consistent with large aggregations of age-0 polar cod along the western edge of the survey area in 2017, and to a lesser extent in 2019 (A. De Robertis, NOAA, R. Levine, UW, personal communication).

The PAROMS model used to drive the polar cod and saffron cod IBMs has been shown to resolve important oceanographic processes [e.g. mean flows and flow variances, wind-driven currents, continental shelf waves, seasonality of ice, and annual volume, heat, freshwater, and ice transport (Curchitser et al., 2013, 2018; Danielson et al., 2016; Danielson et al., 2020) and biological covariates (Rand et al., 2018; Lovvorn et al., 2020). Although PAROMS has relatively fine resolution (e.g. front-resolving and eddy-permitting) for basin-scale models covering a region as broad as the whole Arctic, it undoubtedly fails to accurately reproduce some submesoscale dynamics that could be important in the transport of polar cod and saffron cod larvae to nursery areas. Nonetheless, we believe that our polar cod and saffron cod IBMs can improve our understanding about the growth, transport, and connectivity of these species in the Pacific Arctic and provides an important framework for examining transport in other key arctic species.

Conclusions

We developed the first individual-based, biophysical transport models for polar cod and saffron cod in the Pacific Arctic, which we used to reproduce observed late summer distributions of their ELS in the Chukchi Sea. The results of this study provide important information about these key forage fishes. In particular, we have identified potential spawning locations and nursery habitats for larvae and early juveniles, and have shown how the growth and dispersal of their ELS change in response to variable climate forcing. The source of observed aggregations of polar cod on the Chukchi shelf appear to be from the northern Bering and southern Chukchi seas, while spawning locations in the northern Chukchi Sea may be a source population for the western Beaufort Sea. Kotzebue Sound appears to be both an important spawning and nursery area for saffron cod, as well as a source of larvae and juveniles to nearshore nursery areas. We found strong variability in dispersal patterns among years, which were linked to changes in oceanographic and atmospheric forcing. Observed variability in the dispersal of polar cod and saffron cod ELS is likely related to changes in the strength of the Pacific-Arctic pressure head, which influences the inflow of Pacific waters into the Chukchi Sea and the timing and pattern of sea ice retreat. Understanding how connectivity between the Chukchi and Beaufort seas may change in response to Arctic warming is important if we are to understand the stock structure and population dynamics of polar cod and saffron cod in the region. Such information is essential to spatial management of Alaska's Arctic marine ecosystems.

Declaration of Competing Interest

The authors declare that they have no known competing financial interests or personal relationships that could have appeared to influence the work reported in this paper.

Acknowledgements

This study was supported by a grant from the North Pacific Research Board (NPRB; Project #1508) and was also funded in part by the Bureau of Ocean and Energy Management (BOEM) Award #M12AC00009 and in part with qualified outer continental shelf oil and gas revenues by the Coastal Impact Assistance Program, U.S. Fish and Wildlife Service, U.S. Department of the Interior (Contract #s: 10-CIAP-010; F12AF00188). This paper is EcoFOCI Contribution

No. EcoFOCI-N950. The authors wish to thank the scientists and volunteers that collected data on the Arctic EIS acoustic-trawl surveys, Elizabeth Drenkard, and Joakim Kjellsson for their initial assistance with TRACMASS, Alicia Billings for assistance with data processing, and Alison Deary, Esther Goldstein, and two independent reviewers for their helpful comments on this manuscript. The findings and conclusions in this paper are those of the authors and do not necessarily represent the views of the National Marine Fisheries Service. Reference to trade names does not imply endorsement by the National Marine Fisheries Service, NOAA or any of its subagencies. SLD acknowledges support from NPRB grants A91-99a and A91-00a. This manuscript is a product of the North Pacific Research Board Arctic Integrated Ecosystem Research Program, NPRB publication number ArcticIERP-XX.

Author contributions

Cathleen Vestfals: Methodology, Software, Investigation, Formal Analysis, Data Curation, Writing – Original draft preparation. Franz Mueter: Conceptualization, Methodology, Supervision, Writing – Reviewing and Editing. Katherine Hedstrom: Methodology, Data curation, Software. Benjamin Laurel: Methodology, Investigation, Writing – Reviewing and Editing. Colleen Petrik: Methodology, Software, Writing – Reviewing and Editing. Janet Duffy-Anderson: Conceptualization, Methodology. Seth Danielson: Methodology, Data curation, Writing – Reviewing and Editing.

References

Aagaard, K., Weingartner, T.J., Danielson, S.L., Woodgate, R.A., Johnson, G.C., Whitledge, T.E., 2006. Some controls on flow and salinity in Bering Strait. Geophysical Research Letters 33, L19602.

Ahlnäs, K., Garrison, G.R., 1984. Satellite and oceanographic observations of the warm coastal current in the Chukchi Sea. Arctic 37 (3), 244-254.

Bailey, K.M., 1981. Larval transport and recruitment of Pacific hake Merluccius productus. Marine Ecology Progress Series 6 (1), 1-9.

Bailey, K.M., 1982. The early life history of the Pacific hake Merluccius productus. Fishery Bulletin 80 (3), 589-598.

Bailey, K.M., Abookire, A.A., Duffy-Anderson, J.T., 2008. Ocean transport paths for the early life history stages of offshore spawning flatfishes: a case study in the Gulf of Alaska. Fish and Fisheries 9 (1), 44-66.

Bailey, K.M., Francis, R.C., Stevens, P.R., 1982. The life history and fishery of Pacific whiting, Merluccius productus. NWAFC Processed Report 82-03. Northwest and Alaska Fisheries Center, National Marine Fisheries Service, U.S. Department of Commerce.

Bailey, K.M., Houde, E.D., 1989. Predation on eggs and larvae of marine fishes and the recruitment problem. In: Advances in Marine Biology. Blaxter, J., Douglas, B. (Eds.), Academic Press, Cambridge, MA, Volume 25, pp. 1-83.

Bailey, K.M., Picquelle, S.J., 2002. Larval distribution of offshore spawning flatfish in the Gulf of Alaska: potential transport pathways and enhanced onshore transport during ENSO events. Marine Ecology Progress Series 236, 205-217.

Bakun, A., 2006. Fronts and eddies as key structures in the habitat of marine fish larvae: opportunity, adaptive response and competitive advantage. Scientia Marina 70 (S2), 105-122.

Batchelder, H. P., 2006. Forward-in-time-/backward-in-time-trajectory (FITT/BITT) modeling of particles and organisms in the coastal ocean. Journal of Atmospheric and Oceanic Technology, 23 (5), 727-741.

Bauer, R.K., Stepputtis, D., Gräwe, U., Zimmermann, C., Hammer, C., 2013. Wind-induced variability in coastal larval retention areas: a case study on Western Baltic spring-spawning herring. Fisheries Oceanography, 22 (5), 388-399.

Berg L.S., 1949. Ryby presnykh vod SSSR i sopredel'nykh stran (Freshwater Fishes of the USSR and Adjacent Countries). Zoological Institute of the Academy of Sciences of the USSR, USSR, Leningrad (in Russian).

Berglund, M., Jacobi, M.N., Jonsson, P.R., 2012. Optimal selection of marine protected areas based on connectivity and habitat quality. Ecological Modelling 240, 105-112.

Björnsson, B., 1993. Swimming speed and swimming metabolism of Atlantic cod (Gadus morhua) in relation to available food: a laboratory study. Canadian Journal of Fisheries and Aquatic Sciences 50 (12), 2542-2551.

Boehlert, G.W., Mundy, B.C., 1988. Roles of behavioral and physical factors in larval and juvenile fish recruitment to estuarine nursery areas. In: American Fisheries Society Symposium, Weinstein, M.P. (Ed.), American Fisheries Society, Bethesda, MD, Volume 3 (5), pp. 1-67.

Bond, N., Stabeno, P., Napp, J., 2018. Flow patterns in the Chukchi Sea based on an ocean reanalysis, June through October 1979–2014. Deep Sea Research Part II 152, 35-47.

Borkin, L.V., Ozhigin V.K., Shleinik V.N., 1986. Effect of oceanographical factors on the abundance of the Barents Sea polar cod year classes. In: The effect of oceanographic conditions on distribution and population dynamics of commercial fish stocks in the Barents Sea, vol. 169.

Bouchard, C., Fortier, L., 2008. Effects of polynyas on the hatching season, early growth and survival of polar cod Boreogadus saida in the Laptev Sea. Marine Ecology Progress Series 355, 247-256.

Bouchard, C., Fortier, L., 2011. Circum-arctic comparison of the hatching season of polar cod Boreogadus saida: a test of the freshwater winter refuge hypothesis. Progress in Oceanography 9, 105-116.

Bouchard, C., Mollard, S., Suzuki, K., Robert, D., Fortier, L., 2016. Contrasting the early life histories of sympatric Arctic gadids Boreogadus saida and Arctogadus glacialis in the Canadian Beaufort Sea. Polar Biology 39, 1005-1022.

Budgell, W.P., 2005. Numerical simulation of ice-ocean variability in the Barents Sea region. Ocean Dynamics 55 (3-4), 370-387.

Calò, A., Lett, C., Mourre, B., Pérez-Ruzafa, Á., García-Charton, J.A., 2018. Use of Lagrangian simulations to hindcast the geographical position of propagule release zones in a Mediterranean coastal fish. Marine environmental research, 134, 16-27.

Carton, J.A., Giese, B.S., 2008. A Reanalysis of Ocean Climate Using Simple Ocean Data Assimilation (SODA). Monthly Weather Review 136, 2999-3017. https://doi.org/10.1175/2007MWR1978.1.

Chassignet, E.P., Hurlburt, H.E., Metzger, E.J., Smedstad, O.M., Cummings, J., Halliwell, G.R., Bleck, R., Baraille, R., Wallcraft, A.J., Lozano, C. et al., 2009. U.S. GODAE: Global Ocean Prediction with the HYbrid Coordinate Ocean Model (HYCOM). Oceanography 22 (2), 64-75.

Chen, A., Yoshida, H., Sakurai, Y., 2008. Reproductive behavior of Saffron cod in captivity. Scientific Reports of Hokkaido Fisheries Experimental Station 73, 35-44.

Christensen, A., Daewel, U., Jensen, H., Mosegaard, H., John, M. S., Schrum, C., 2007. Hydrodynamic backtracking of fish larvae by individual-based modelling. Marine Ecology Progress Series, 347, 221-232.

Coachman, L.K., Aagaard, K., Tripp, R.B., 1975. Bering Strait: the regional physical oceanography. University of Washington Press, Seattle.

Coachman, L.K., Aagaard, K., 1981. Re-evaluation of water transports in the vicinity of Bering Strait, The Eastern Bering Sea Shelf: Oceanography and Resources. Hood, D.W., Calder, J.A. (Eds.), National Oceanic and Atmospheric Administration, Washington, D.C., Volume 1, pp. 95–110.

Comiso, J.C., Parkinson, C.L., Gersten, R., Stock, L., 2008. Accelerated decline in the Arctic sea ice cover. Geophysical Research Letters 35, L01703.

Corlett, W.B., Pickart, R.S., 2017. The Chukchi slope current. Progress in Oceanography 153, 50-65.

Craig, P.C., Griffiths, W.B., Haldorson, L., McElderry, H., 1982. Ecological studies of Arctic Cod (Boreogadus saida) in Beaufort Sea coastal waters. Canadian Journal of Fisheries and Aquatic Sciences 39, 395-406

Curchitser, E.N., Hedstrom, K., Danielson, S., Weingartner, T., 2013. Adaptation of an Arctic Circulation Model. U.S. Dept. of the Interior, Bureau of Ocean Energy Management, Headquarters, Herndon, VA. OCS Study BOEM, 2013-202.83 pp. M10PC00116.

Curchitser, E.N., K. Hedstrom, S. Danielson, Kasper, J., 2017. Development of a Very High-Resolution Regional Circulation Model of Beaufort Sea Nearshore Areas. U.S. Dept. of the Interior, Bureau of Ocean Energy Management, Alaska OCS Region, Anchorage, AK. OCS Study BOEM 2018-018. 81 pp.

Dai, A., Qian, T., Trenberth, K.E., Milliman, J.D., 2009. Changes in continental freshwater discharge from 1948 to 2004. Journal of Climate 22 (10), 2773-2792.

Danielson, S.L., Weingartner, T.J., Hedstrom, K.S., Aagaard, K., Woodgate, R., Curchitser, E., Stabeno, P.J., 2014. Coupled wind-forced controls of the Bering-Chukchi shelf circulation and the Bering Strait throughflow: Ekman transport, continental shelf waves, and variations of the Pacific–Arctic sea surface height gradient. Progress in Oceanography 125, 40-61. https://doi.org/10.1016/j.pocean.2014.04.006.

Danielson, S.L., Hedstrom, K.S., Weingartner, T.J., 2016. Bering-Chukchi circulation pathways, North Pacific Research Board 2016 Final Report, NPRB project #1308, University of Alaska Fairbanks, Fairbanks, AK.

Danielson, S.L., Whiting, A. 2016. 2015 Circulation and Hydrographic Structure of Kotzebue Sound. Final Report. Northwest Arctic Borough Science Steering Committee. Native Village of Kotzebue, Kotzebue, AK.

Danielson, S.L., Eisner, L., Ladd, C., Mordy, C., Sousa, L., Weingartner, T.J., 2017. A comparison between late summer 2012 and 2013 water masses, macronutrients, and phytoplankton standing crops in the northern Bering and Chukchi Seas. Deep Sea Research Part II 135, 7-26.

Danielson, S.L., Ahkinga, O., Ashjian, C., Basyuk, E., Cooper, L.W., Eisner, L., Farley, E., Iken, K.B., Grebmeier, J.M., Juranek, L., Khen, G., Jayne, S., Kikuchi, T., Ladd, C, Lu, K., McCabe, R., Moore, GWK, Nishino, S., Okkonen, S.R., Ozenna, F., Pickart, R.S., Polyakov, I., Stabeno, P.J., Wood, K., Williams, W.J., Woodgate, R.A., Weingartner, T.J., 2020a. Manifestation and consequences of warming and altered heat fluxes over the Bering and Chukchi Sea continental shelves. Deep Sea Research Part II 177,104781.

Danielson, S.L., Hennon, T.D., Hedstrom, K.S., Pnyushkov, A.V., Polyakov, I.V., Carmack, E., Filchuk, K., Janout, M., Makhotin, M., Williams, W.J., Padman, L., 2020b. Oceanic routing of wind-sourced energy along the Arctic continental shelves. Frontiers in Marine Science, 7, 509.

Deary, A.L., Vestfals, C.D., Logerwell, E.A., Goldstein, E.D., Stabeno, P.J., Danielson, S.L., Mueter, F.J., Duffy-Anderson, J.T., In Review. Seasonal abundance, distribution, and growth of the early life stages of Polar Cod (Boreogadus saida) and Saffron Cod (Eleginus gracilis) in the US Arctic during a warm year. Polar Biology.

De Robertis, A., Taylor, K., Williams, K., Wilson, C.D. 2017a. Species and size selectivity of two midwater trawls used in an acoustic survey of the Alaska Arctic. Deep Sea Research Part II 135, 40-50.

De Robertis A., Taylor, K., Wilson, C., Farley, E. 2017b. Abundance and distribution of Arctic cod (Boreogadus saida) and other pelagic fishes over the US Continental Shelf of the Northern Bering and Chukchi Seas. Deep Sea Research Part II 135, 51-65.

Döös, K., 1995. Inter-ocean exchange of water masses. Journal of Geophysical Research 100, 13499-13514.

Döös, K., Engqvist, A., 2007. Assessment of water exchange between a discharge region and the open sea – a comparison of different methodological concepts. Estuarine and Coastal Shelf Science 74, 585-597.

Drijfhout, S., de Vries, P., Döös, K., Coward, A., 2003. Impact of eddy-induced transport of the Lagrangian structure of the upper branch of the thermohaline circulation. Journal of Physical Oceanography 33, 2141-2155.

Duffy-Anderson, J.T., Blood, D.M., Cheng, W., Ciannelli, L., Matarese, A.C., Sohn, D., Vance, T.C., Vestfals, C., 2013. Combining field observations and modeling approaches to examine Greenland halibut (Reinhardtius hippoglossoides) early life ecology in the southeastern Bering Sea. Journal of Sea Research 75, 96-109.

Egbert, G.D., Erofeeva, S.Y., 2002. Efficient inverse modeling of barotropic ocean tides. Journal of Atmospheric and Oceanic Technology 19 (2), 183-204.

Eisner, L., Hillgruber, N., Martinson, E., Maselko, J., 2012. Pelagic fish and zooplankton species assemblages in relation to water mass characteristics in the northern Bering and southeast Chukchi seas. Polar Biology 36, 87-113. https://epsg.io/3572, accessed 16 September, 2019.

ESRI, 2017. ArcGIS desktop: release 10.4. Environmental Systems Research Institute, Redlands, CA.

Evjemo, J.O., Reitan, K.I., Olsen, Y., 2003. Copepods as live food organisms in the larval rearing of halibut larvae (Hippoglossus hippoglossus L.) with special emphasis on the nutritional value. Aquaculture 227 (1-4), 191-210.

Fang, Z., Wallace, J.M., 1994. Arctic sea ice variability on a timescale of weeks and its relation to atmospheric forcing. Journal of Climate 7 (12), 1897-1914.

Fechhelm, R.G., Craig, P.C., Baker, J.S., Gallaway, B.J., 1985. Fish distribution and use of nearshore waters in the northeastern Chukchi Sea. In: US Department of Commerce, NOAA, and US Department of the Interior, Minerals Management Service, Outer Continental Shelf Environmental Assessment Program final report. Volume 32, pp. 121-298.

Fiksen, Ø., Jørgensen, C., Kristiansen, T., Vikebø, F., Huse, G. 2007. Linking behavioural ecology and oceanography: larval behaviour determines growth, mortality and dispersal. Marine Ecology Progress Series 347, 195-205.

Gibson, G.A., Stockhausen, W.T., Coyle, K.O., Hinckley, S., Parada, C., Hermann, A.J., Doyle, M., Ladd, C., 2019. An individual-based model for sablefish: Exploring the connectivity between potential spawning and nursery grounds in the Gulf of Alaska. Deep Sea Research Part II 165, 89-112.

Govoni, J.J., 2005. Fisheries oceanography and the ecology of early life histories of fishes: a perspective over fifty years. Scientia marina 69 (S1), 125-137.

Grebmeier, J.M., McRoy, C.P., Feder, H.M., 1988. Pelagic-benthic coupling on the shelf of the northern Bering and Chukchi seas.Food-supply source and benthic biomass. Marine Ecology Progress Series 48, 57-67. https://doi.org/10.3354/ meps048057.

Hauri, C., Danielson, S., McDonnell, A.M., Hopcroft, R.R., Winsor, P., Shipton, P., Lalande, C., Stafford, K.M., Horne, J.K., Cooper, L.W., Grebmeier, J.M., 2018. From sea ice to seals: a moored marine ecosystem observatory in the Arctic. Ocean Science 14 (6), 1423-1433.

Hare, J.A., Govoni, J.J., 2005. Comparison of average larval fish vertical distributions among species exhibiting different transport pathways on the southeast United States continental shelf. Fishery Bulletin 103 (4), 728-736.

Hinckley, S., Hermann, A.J., Megrey, B.A., 1996. Development of a spatially explicit, individual-based model of marine fish early life history. Marine Ecology Progress Series 139, 47- 68.

Hollowed, A.B., Bailey, K.M., 1989. New perspectives on the relationship between recruitment of Pacific hake (Merluccius productus) and the ocean environment. In: Effects of Ocean Variability on Recruitment and an Evaluation of Parameters Used in Stock Assessment Models. Beamish, R.J., McFarlane, G.A. (Eds.), Canadian Special Publication of Fisheries and Aquatic Sciences 108, 207-220.

Hurst, T.P., Cooper, D.W., Scheingross, J.S., Seale, E.M., Laurel, B.J., Spencer, M.L., 2009. Effects of ontogeny, temperature, and light on vertical movements of larval Pacific cod (Gadus macrocephalus). Fisheries Oceanography 18 (5), 301-311.

ICES CM, 1988. Preliminary report of the international 0-group fish survey in the Barents Sea and adjacent waters in August-September 1988. In: ICES Council Meeting

Iles, T.D., Sinclair M., 1982. Atlantic herring: stock discreteness and abundance. Science 215, 627-633.

Jacobi, M.N., Jonsson, P.R., 2011. Optimal networks of nature reserves can be found through eigenvalue perturbation theory of the connectivity matrix. Ecological Applications 21 (5), 1861-1870.

Johnson, J.J., 1995. Description and comparison of two populations of Saffron Cod (Eleginus gracilis) from Western Canadian Arctic Coastal Waters. Master's Thesis, University of Manitoba, Canada, unpublished.

Koenker, B., Laurel, B.J., Copeman, L.A., Ciannelli, L., 2018. Effects of temperature and food availability on the survival and growth of larval Arctic cod (Boreogadus saida) and walleye pollock (Gadus chalcogrammus). ICES Journal of Marine Science 75, 2386-2402.

Kwok, R., Cunningham, G.F., Wensnahan, M., Rigor, I., Zwally, H.J., Yi, D., 2009. Thinning and volume loss of the Arctic Ocean sea ice cover: 2003–2008. Journal of Geophysical Research: Oceans (1978–2012), 114 (C7).

Lafrance, P., 2009. Saison d'éclosion et survie des stades larvaires et juvéniles chez la morue arctique (Boreogadus saida) du sud-est de la mer de Beaufort. Ph.D. thesis. Université Laval, Canada, unpublished (in French, with English Abstract).

Laurel, B.J., Spencer, M., Iseri, P., Copeman, L.A., 2016. Temperature-dependent growth and behavior of juvenile Arctic cod (Boreogadus saida) and co-occurring North Pacific gadids. Polar Biology 39, 1127-1135.

Laurel, B.J., Copeman, L.A., Spencer, M., Iseri, P., 2017. Temperature-dependent growth as a function of size and age in juvenile Arctic cod (Boreogadus saida). ICES Journal of Marine Science 74, 1614-1621.

Laurel, B.J., Copeman, L.A., Spencer, M., Iseri, P., 2018. Comparative effects of temperature on rates of development and survival of eggs and yolk-sac larvae of Arctic cod (Boreogadus saida) and walleye pollock (Gadus chalcogrammus). ICES Journal of Marine Science 75 (7), 2403-2412.
Leis, J.M., 2007. Behaviour as input for modelling dispersal of fish larvae: behaviour, biogeography, hydrodynamics, ontogeny, physiology and phylogeny meet hydrography. Marine Ecology Progress Series 347, 185-193.
Leis, J.M., Carson-Ewart, B.M., 1997. In situ swimming speeds of the late pelagic larvae of some Indo-Pacific coral-reef fishes. Marine Ecology Progress Series 159, 165-174.
Leis, J.M., Carson-Ewart, B.M., 1999. In situ swimming and settlement behaviour of larvae of an Indo-Pacific coral-reef fish, the coral trout Plectropomus leopardus (Pisces: Serranidae). Marine Biology 134 (1), 51-64.
Levine, R. M., De Robertis, A., Grünbaum, D., Woodgate, R., Mordy, C. W., Mueter, F., Cokelet, E., Lawrence-Slavas, N., Tabisola, H. 2020. Autonomous vehicle surveys indicate that flow reversals retain juvenile fishes in a highly advective high-latitude ecosystem. Limnology and Oceanography. doi: 10.1002/lno.11671.
Litvak, M.K., Leggett, W.C., 1992. Age and size-selective predation on larval fishes: the bigger-is-better hypothesis revisited. Marine Ecology Progress Series 81, 13-24.

Logerwell, E., Busby, M., Carothers, C., Cotton, S., Duffy-Anderson, J., Farley, E., Goddard, P., Heintz, R., Holladay, B., Horne, J., Johnson, S., 2015. Fish communities across a spectrum of habitats in the western Beaufort Sea and Chukchi Sea. Progress in Oceanography 136, 115-132.
Lovvorn, J.R., Rocha, A.R., Danielson, S.L., Cooper, L.W., Grebmeier, J.M., Hedstrom, K.S., 2020. Predicting sediment organic carbon and related food web types from a physical oceanographic model on a subarctic shelf. Marine Ecology Progress Series 633, 37-54.
Lu, K., Danielson, S., Hedstrom, K., Weingartner, T., 2020a. Assessing the role of oceanic heat fluxes on ice ablation of the central Chukchi Sea Shelf. Progress in Oceanography.
Lu, K., Danielson, S., Weingartner, T., 2020b. Impacts of short-term wind events on Chukchi hydrography and sea ice retreat, Deep Sea Research II.
Luchin, V., Panteleev, G., 2014. Thermal regimes in the Chukchi Sea from 1941 to 2008. Deep Sea Research Part II: Topical Studies in Oceanography 109, 14-26.
Marsh, J.M., Mueter, F.J., Quinn II, T.J., 2019. Environmental and biological influences on the distribution and population dynamics of polar cod (Boreogadus saida) in the US Chukchi Sea. Polar Biology. doi: 10.1007/s00300-019-02561-w
Matarese, A.C., Kendall, A.W., Blood, D.M., Vinter, B.M., 1989. Laboratory guide to early life history stages of northeast Pacific fishes. U.S. National Archives and Records Administration, College Park.
Mecklenburg, C.W., Mecklenburg, T.A., Thorsteinson, L.K., 2002. Fishes of Alaska, American Fisheries Society, Bethesda, MD.
Meredith, M., Sommerkorn, M., Cassotta, S., Derksen, C., Ekaykin, A., Hollowed, A., Kofinas, G., Mackintosh, A., Melbourne-Thomas, J., Muelbert, M.M.C., Ottersen, G., Pritchard, H., Schuur, E.A.G., 2019. Chapter 3:Polar Regions. In: IPCC Special Report on the Ocean and Cryosphere in a Changing Climate. Pörtner, H-O., Roberts, D.C., Masson-Delmotte, V.,Zhai, P., Tignor, M., Poloczanska, E., Mintenbeck, K., Alegría, A., Nicolai, M., Okem, A., Petzold, J., Rama, B., Weyer, N.M. (Eds.). https://www.ipcc.ch/site/assets/uploads/sites/3/2019/11/07_SROCC_Ch03_FINAL.pdf
Miller, T.J., 2007. Contribution of individual-based coupled physical–biological models to understanding recruitment in marine fish populations. Marine Ecology Progress Series 347, 127-138.
Moore, S.E., Stabeno, P.J., 2015. Synthesis of Arctic Research (SOAR) in marine ecosystems of the Pacific Arctic. Progress in Oceanography 136, 1-11.
Morrow, J.E., 1980. The freshwater fishes of Alaska. Alaska Northwest Publishing Company, Anchorage.

Mueter, F.J., Ladd, C., Palmer, M.C., Norcross, B.L., 2006. Bottom-up and top-down controls of walleye pollock (Theragra chalcogramma) on the Eastern Bering Sea shelf. Progress in Oceanography 68 (2), 152-183.

Mueter, F.J., Weems, J., Farley, E.V., Sigler, M.F., 2017. Arctic ecosystem integrated survey (Arctic Eis): marine ecosystem dynamics in the rapidly changing Pacific Arctic Gateway. Deep Sea Research Part II 135, 1-6.

National Oceanic and Atmospheric Administration, 2019. Bering Climate: A Current View of the Bering Sea Ecosystem and Climate. Accessed 6 June, 2019. http://www.beringclimate.noaa.gov/data/index.php

Norcross, B.L., Shaw, R.F., 1984. Oceanic and estuarine transport of fish eggs and larvae: a review. Transactions of the American Fisheries Society 113 (2), 153-165.

Norcross, B.L., Holladay, B.A., Busby, M.A., Mier, K., 2006. RUSALCA–Fisheries Ecology and Oceanography. Final Report CIFAR# NA17RJ1224.

Okkonen, S., Ashjian, C., Campbell, R.G., Alatalo, P., 2019. The encoding of wind forcing into the Pacific-Arctic pressure head, Chukchi Sea ice retreat and late-summer Barrow Canyon water masses. Deep Sea Research Part II 162, 22-31.

Okubo, A., 1971. Oceanic diffusion diagrams. Deep Sea Research and Oceanographic Abstracts 18, 789-802.

Olla, B.L., Davis, M.W., Ryer, C.H., Sogard, S.M., 1996. Behavioural determinants of distribution and survival in early stages of walleye pollock, Theragra chalcogrammai a synthesis of experimental studies. Fisheries Oceanography 5, 167-178.

Overland, J.E., Bond, N.A., Adams, J.M., 2002. The relation of surface forcing of the Bering Sea to large-scale climate patterns. Deep-Sea Research Part II 49 (26), 5855-5868.

Panteleev, G., Yaremchuk, M., Francis, O., Kikuchi, T., 2013. Configuring high frequency radar observations in the Southern Chukchi Sea. Polar Science 7 (2), 72-81.

Parada, C., Armstrong, D.A., Ernst, B., Hinckley, S. and Orensanz, J.M., 2010. Spatial dynamics of snow crab (Chionoecetes opilio) in the eastern Bering Sea—putting together the pieces of the puzzle. Bulletin of Marine Science 86 (2), 413-437.

Peck, M.A., Buckley, L.J., Bengtson, D.A., 2006. Effects of temperature and body size on the swimming speed of larval and juvenile Atlantic cod (Gadus morhua): implications for individual-based modelling. Environmental Biology of Fishes 75 (4), 419-429.

Perrette, M., Yool, A., Quartly, G.D., Popova, E.E., 2011. Near-ubiquity of ice-edge blooms in the Arctic. Biogeosciences 8 (2), 515-524.

Petrik, C.M., Duffy-Anderson, J.T., Mueter, F., Hedstrom, K., Curchitser, E.N., 2015. Biophysical transport model suggests climate variability determines distribution of Walleye Pollock early life stages in the eastern Bering Sea through effects on spawning. Progress in Oceanography 138, 459-474.

Petrik, C.M., Duffy-Anderson, J.T., Castruccio, F., Curchitser, E.N., Danielson, S.L., Hedstrom, K., Mueter, F., 2016. Modelled connectivity between Walleye Pollock (Gadus chalcogrammus) spawning and age-0 nursery areas in warm and cold years with implications for juvenile survival. ICES Journal of Marine Science 73, 1890-1900.

Pickart, R.S., 2004. Shelfbreak circulation in the Alaskan Beaufort Sea: Mean structure and variability. Journal of Geophysical Research: Oceans, 109 (C4).

Pickart, R.S., Pratt, L.J., Torres, D.J., Whitledge, T.E., Proshutinsky, A.Y., Aagaard, K., Agnew, T.A., Moore, G.W.K., Dail, H.J., 2010. Evolution and dynamics of the flow through Herald Canyon in the western Chukchi Sea. Deep Sea Research Part II 57 (1-2), 5-26.

Ponomarenko, V.P., 1968. Some data on the distribution and migrations of polar cod in the seas of the Soviet Arctic. Rapports et procès-verbaux des reunions/Conseil Permanent International pour l'Exploration de la Mer 158, 131-135.

Ponomarenko, V.P., 2000. Eggs, larvae, and juveniles of polar cod Boreogadus saida in the Barents, Kara, and White Seas. Journal of Ichthyology 40 (2), 165-173.

Porter, S.M., Bailey, K.M., 2007. Optimization of feeding and growth conditions for walleye pollock Theragra chalcogramma (Pallas) larvae reared in the laboratory. AFSC Processed Report 2007-06. Alaska Fisheries Science Center, NOAA, National Marine Fisheries Service, 7600 Sand Point Way NE, Seattle WA 98115. 20 pp.
R Core Team, 2018. R: A language and environment for statistical computing. R Foundation for statistical Computing, Vienna, Austria. http://www.R-project.org/
Rand, K., Logerwell, E., Bluhm, B., Chenelot, H., Danielson, S., Iken, K., Sousa, L., 2018. Using biological traits and environmental variables to characterize two Arctic epibenthic invertebrate communities in and adjacent to Barrow Canyon. Deep Sea Research Part II 152, 154-169.
Rienecker, M.M., Suarez, M.J., Gelaro, R., Todling, R., Bacmeister, J., Liu, E., Bosilovich, M.G., Schubert, S.D., Takacs, L., Kim, G.K., Bloom, S., 2011. MERRA: NASA's modern-era retrospective analysis for research and applications. Journal of Climate 24 (14), 3624-3648.
Sambrotto, R.N., Goering, J.J., McRoy, C.P., 1984. Large yearly production of phytoplankton in the western Bering Strait. Science 225, 1147-1150.
Sargent, J., McEvoy, L., Estevez, A., Bell, G., Bell, M., Henderson, J., Tocher, D., 1999. Lipid nutrition of marine fish during early development: current status and future directions. Aquaculture 179 (1-4), 217-229.
Screen, J.A., Simmonds, I., 2010. The central role of diminishing sea ice in recent Arctic temperature amplification. Nature 464 (7293), 1334-1337.
Shchepetkin, A.F., McWilliams, J.C., 2005. The regional oceanic modeling system (ROMS): a split-explicit, free-surface, topography-following-coordinate oceanic model. Ocean Modelling 9, 347-404.
Skopeliti, A., Tsoulos, L., 2013. Choosing a suitable projection for navigation in the arctic. Marine Geodesy 36 (2), 234-259.
Søreide, J.E., Leu, E., Berge, J., Graeve, M., Falk-Petersen, S., 2010) Timing of blooms, algal food quality and Calanus glacialis reproduction and growth in a changing Arctic. Global change biology 16 (11), 3154-3163.
Spencer, M.H., Vestfals, C.D., Mueter, F.J., Laurel, B.J., 2020. Ontogenetic changes in the buoyancy and salinity tolerance of eggs and larvae of polar cod (Boreogadus saida) and other gadids. Polar Biology. https://doi.org/10.1007/s00300-020-02620-7.
Stabeno, P., Kachel, N., Ladd, C., Woodgate, R., 2018. Flow patterns in the eastern Chukchi Sea: 2010–2015. Journal of Geophysical Research: Oceans 123 (2), 1177-1195.
Stammerjohn, S., Massom, R., Rind, D., Martinson, D., 2012. Regions of rapid sea ice change: an inter-hemispheric seasonal comparison. Geophysical Research Letters 39, L05502.
Stigebrandt, A., 1984. The North Pacific: a global-scale estuary. Journal of Physical Oceanography 14, 464-470.
Sundby, S., Fossum, P. 1990. Feeding conditions of Arcto-Norwegian cod larvae compared with the Rothschild–Osborn theory on small-scale turbulence and plankton contact rates. Journal of Plankton Research 12 (6), 1153-1162.
Sunnanå, K., Christiansen, J.S., 1997. Kommersielt fiske på polar torskerfaringer og potensiale. Fiskeriforsknings Rapportserie 1:20. (In Norwegian).
Thanassekos, S., Fortier, L., 2012. An individual based model of Arctic cod (Boreogadus saida) early life in Arctic polynyas: I. Simulated growth in relation to hatch date in the Northeast Water (Greenland Sea) and the North Water (Baffin Bay). Journal of Marine Systems 93, 25-38.
Thompson, D.W.J., Wallace, J.M., 1998. The Arctic Oscillation signature in wintertime geopotential height and temperature fields. Geophysical Research Letters 25, 1297-1300.
Thompson, D.W.J., Wallace, J.M., 2000. Annular modes in the extratropical circulation. Part I: Month-to-month variability. Journal of Climate 13 (5), 1000-1016.
Vestfals, C.D., Ciannelli, L., Duffy-Anderson, J.T., Ladd, C., 2014. Effects of seasonal and interannual variability in along-shelf and cross-shelf transport on groundfish recruitment in the eastern Bering Sea. Deep Sea Research Part II: Topical Studies in Oceanography 109, 190-203.

Vestfals, C.D., Mueter, F.J., Duffy-Anderson, J.T., Busby, M.S., De Robertis, A., 2019. Spatio-temporal distribution of polar cod (Boreogadus saida) and saffron cod (Eleginus gracilis) early life stages in the Pacific Arctic. Polar Biology 42 (5), 969-990.
Vikebø, F., Jørgensen, C., Kristiansen, T., Fiksen, Ø., 2007. Drift, growth, and survival of larval Northeast Polar cod with simple rules of behaviour. Marine Ecology Progress Series, 347, 207-220.
Vikebø, F., Sundby, S., Ådlandsvik, B., Fiksen, Ø., 2005. The combined effect of transport and temperature on distribution and growth of larvae and pelagic juveniles of Arcto-Norwegian cod. ICES Journal of Marine Science 62 (7), 1375-1386.
Wassmann, P., Duarte, C.M., Agusti, S., Sejr, M.K., 2011. Footprints of climate change in the Arctic marine ecosystem. Global change biology 17 (2), 1235-1249.
Watanabe, E., Wang, J., Sumi, A. and Hasumi, H., 2006. Arctic dipole anomaly and its contribution to sea ice export from the Arctic Ocean in the 20th century. Geophysical Research Letters, 33 (23).
Weingartner, T., Aagaard, K., Woodgate, R., Danielson, S., Sasaki, Y., Cavalieri, D., 2005. Circulation on the north central Chukchi Sea shelf. Deep Sea Research Part II 52, 3150-3174.
Whitefield, J., Winsor, P., McClelland, J., Menemenlis, D., 2015. A new river discharge and river temperature climatology data set for the pan-Arctic region. Ocean Modelling 88: 1-15.
Whitehouse, G.A., 2011. Modeling the eastern Chukchi Sea food web with a mass-balance approach. Ph.D. thesis, University of Washington, unpublished.
Wilderbuer, T.K., Hollowed, A.B., Ingraham, W.J., 2002. Flatfish recruitment response to decadal climatic variability and ocean conditions in the eastern Bering Sea. Progress in Oceanography 55 (1-2), 235-247.
Winsor, P., Chapman, D.C., 2004. Pathways of Pacific water across the Chukchi Sea: A numerical model study. Journal of Geophysical Research: Oceans, 109 (C3).
Woillez, M., Rivoirard, J., Petitgas, P., 2009. Notes on survey-based spatial indicators for monitoring fish populations. Aquatic Living Resources 22 (2), 155-164.
Wolotira, R.J. Jr, 1985. Saffron cod (Eleginus gracilis) in western Alaska: the resource and its potential. Northwest and Alaska Fisheries Center, Kodiak.
Woodbury, D., Hollowed, A.B., Pearce, J.A., 1995. Interannual variation in growth rates and back-calculated spawn dates of juvenile Pacific hake (Merluccius productus). In: Recent Developments in Fish Otolith Research. Secor, D.H., Dean, J.M., Campana, S.E. (Eds.), Belle W. Baruch Institute for Marine Biology and Coastal Research, University of South Carolina Press, Columbia, SC, pp. 481-496.
Woodgate, R.A., 2018. Increases in the Pacific inflow to the Arctic from 1990 to 2015, and insights into seasonal trends and driving mechanisms from year-round Bering Strait mooring data. Progress in Oceanography 160, 124-154.
Woodgate, R.A., Stafford, K.M., Prahl, F.G., 2015. A synthesis of year-round interdisciplinary mooring measurements in the Bering Strait (1990–2014) and the RUSALCA years (2004–2011). Oceanography 28 (3), 46-67.
Woodgate, R.A., Aagaard, K., 2005. Revising the Bering Strait freshwater flux into the Arctic Ocean. Geophysical Research Letters 32 (2). https://doi.org/10.1029/2004GL021747.
Woodgate, R.A., Aagaard, K., Weingartner, T.J., 2005a. Monthly temperature, salinity, and transport variability of the Bering Strait through flow. Geophysical Research Letters 32, L04601. https://doi.org/10.1029/2004GL021880.
Woodgate, R.A., Aagaard, K., Weingartner, T.J., 2005b. A year in the physical oceanography of the Chukchi Sea: moored measurements from autumn 1990–1991. Deep-Sea Research Part II 52 (24-26), 3116-3149.
Wu, B., Wang, J., Walsh, J.E., 2006. Dipole anomaly in the winter Arctic atmosphere and its association with sea ice motion. Journal of Climate 19(2), 210-225.
Wyllie-Echeverria, T., Barber, W.E., Wyllie-Echeverria, S., 1997. Water masses and transport of age-0 Arctic Cod and age-0 Bering flounder into the northeastern Chukchi Sea. In: Fish ecology in

Arctic North America. Reynolds, J.B. (Ed.), American Fisheries Society Symposium 19. American Fisheries Society, Bethesda, MD, pp. 60-67.
Yudanov, I.G., 1976. Zoogeography of polar cod in the Arctic Ocean. Priroda i Khoziaistvo Severa (Nature and Economy of the North), vol 4. KNTs RAN, Apatity, 111-113.

Supplemental Material

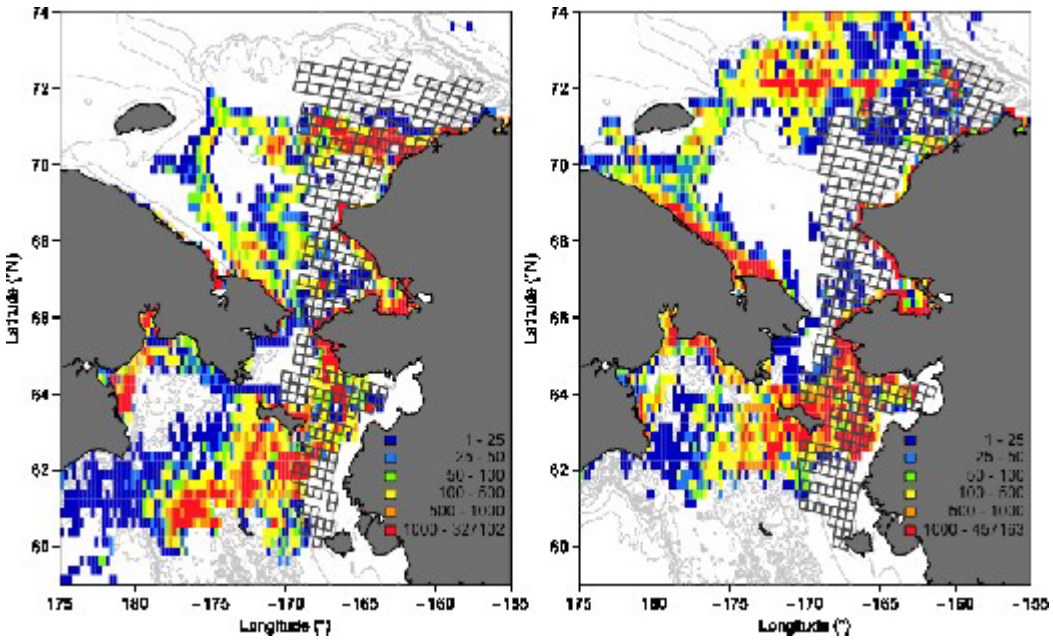

Fig. S1. Simulated particle distributions of polar cod (Boreogadus saida) on 1 September (a) 2012 and (b) 2013 from selected release areas (Gulf of Anadyr, St. Lawrence Island, Bering Strait, Chukotka Peninsula, and Kotzebue Sound) and all release dates (every 2 weeks from 1 January – 15 May) compared to the 30-km x 30-km grid overlaid on the Arctic Ecosystem Integrated Survey (Arctic EIS) acoustic-trawl survey area. These 5 areas were chosen from a total of 9 hypothesized spawning/hatching locations due to the overlap of particles from these locations with the Arctic EIS survey grid. Cell colors represent the total number of particles in each 0.25° x 0.25° grid cell. Dark blue = 1 – 25, light blue = 25 – 50, green = 50 – 100, yellow = 100 – 500, orange = 500 – 1000, red > 1000. Data from simulations with surface-oriented behavior are presented.

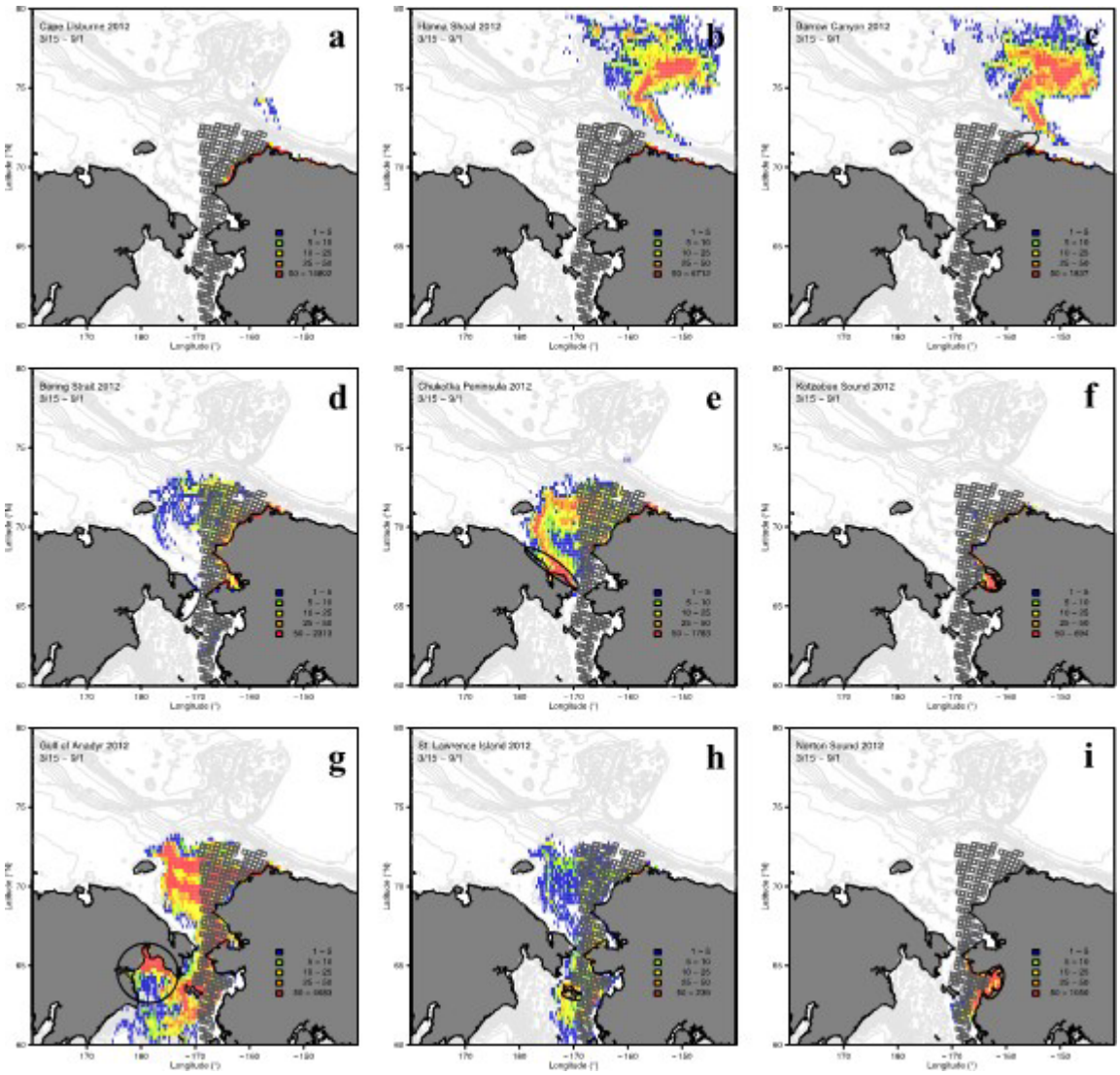

Fig. S2. Distributions of polar cod (Boreogadus saida) on 1 September 2012 from passive particle simulations initiated on 15 March from (a) Cape Lisburne, (b) Hanna Shoal, (c) Barrow Canyon, (d) Bering Strait, (e) Chukotka Peninsula, (f) Kotzebue Sound, (g) Gulf of Anadyr, (h) St. Lawrence Island, and (i) Norton Sound hatching areas. Cell colors represent the total number of particles in each 0.25° x 0.25° grid cell. Blue = 1 – 5, green = 5 – 10, yellow = 10 – 25, orange = 25 – 50, red > 50. Black ellipses represent hatching areas. The 30-km x 30-km grid overlaid on the Arctic Ecosystem Integrated Survey acoustic-trawl survey area for the analysis is shown.

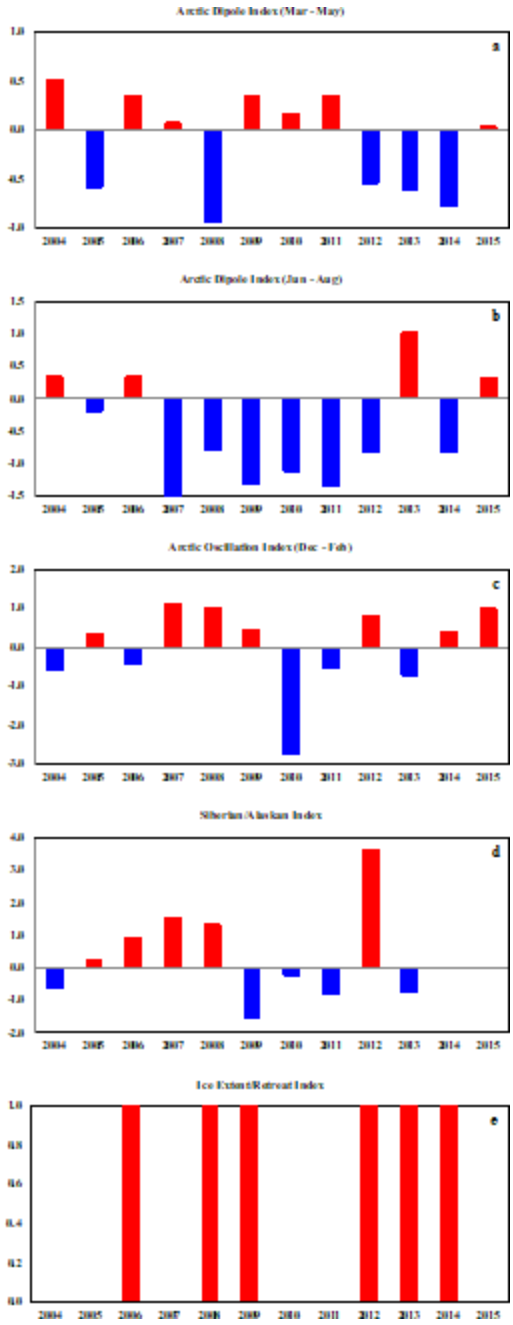

Fig. S3. Index values used in the correlation analyses between latitudinal and longitudinal center of gravities of simulated particles on 1 September and the (a) March – May and (b) June – July Arctic Dipole index, (c) the December – February Arctic Oscillation index, (d) the Siberian/Alaskan index (2004 – 2013), and (d) the Ice extent/retreat (IER) index (2005 – 2015). For the IER, an index value = 0 represents years with smaller daily sea ice extents and faster/earlier sea ice retreats, while an index value = 1 represents years with greater daily sea ice extents and slower/later sea ice retreats. Note that the y-axis scale differs between plots.

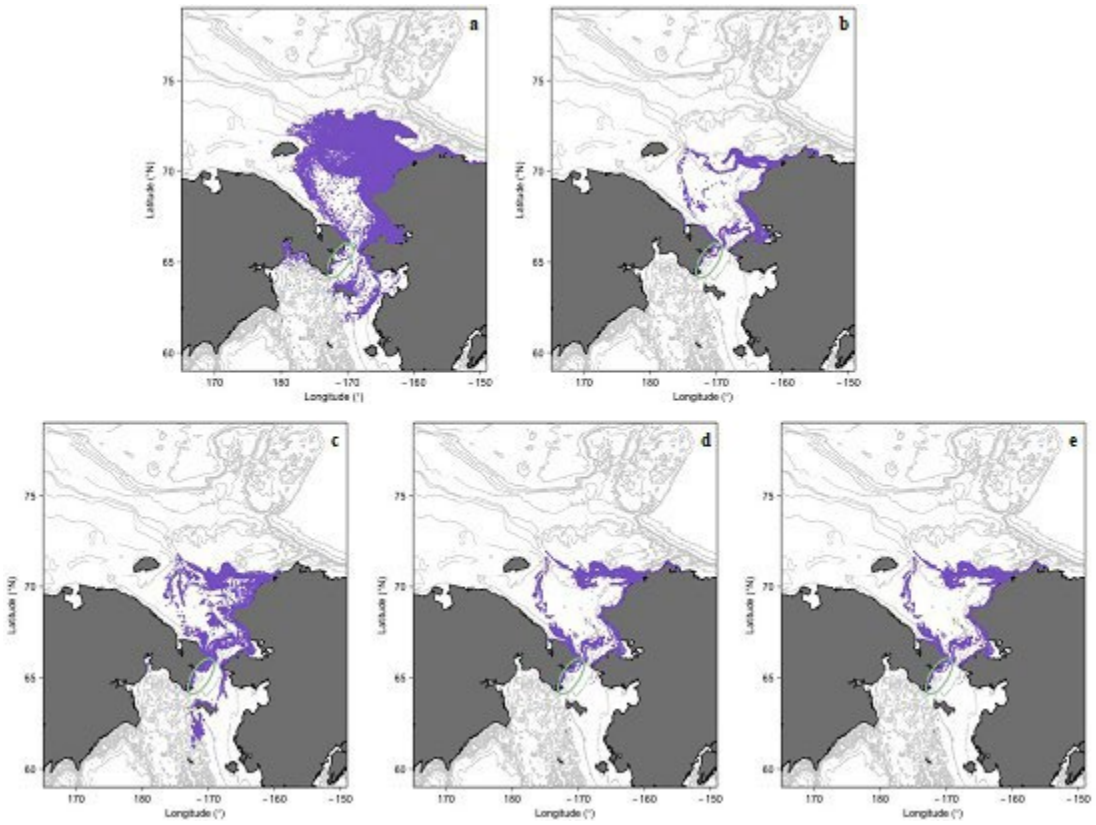

Fig. S4. Distributions of polar cod (Boreogadus saida) on 1 September 2012 from the 5 different behaviors tested; (a) passive (neutrally buoyant) individuals of all stages, (b) surface-oriented individuals of all stages, (c) passive yolksac and preflexion larvae with late larvae and early juveniles moving deeper with ontogeny, (d) surface-oriented yolksac and preflexion larvae with late larvae and juveniles moving deeper with ontogeny, and (d) surface-oriented yolksac and preflexion larvae with late larvae and early juveniles making diel vertical migrations (DVMs) between specified depths during the day, and 5 m during the night.

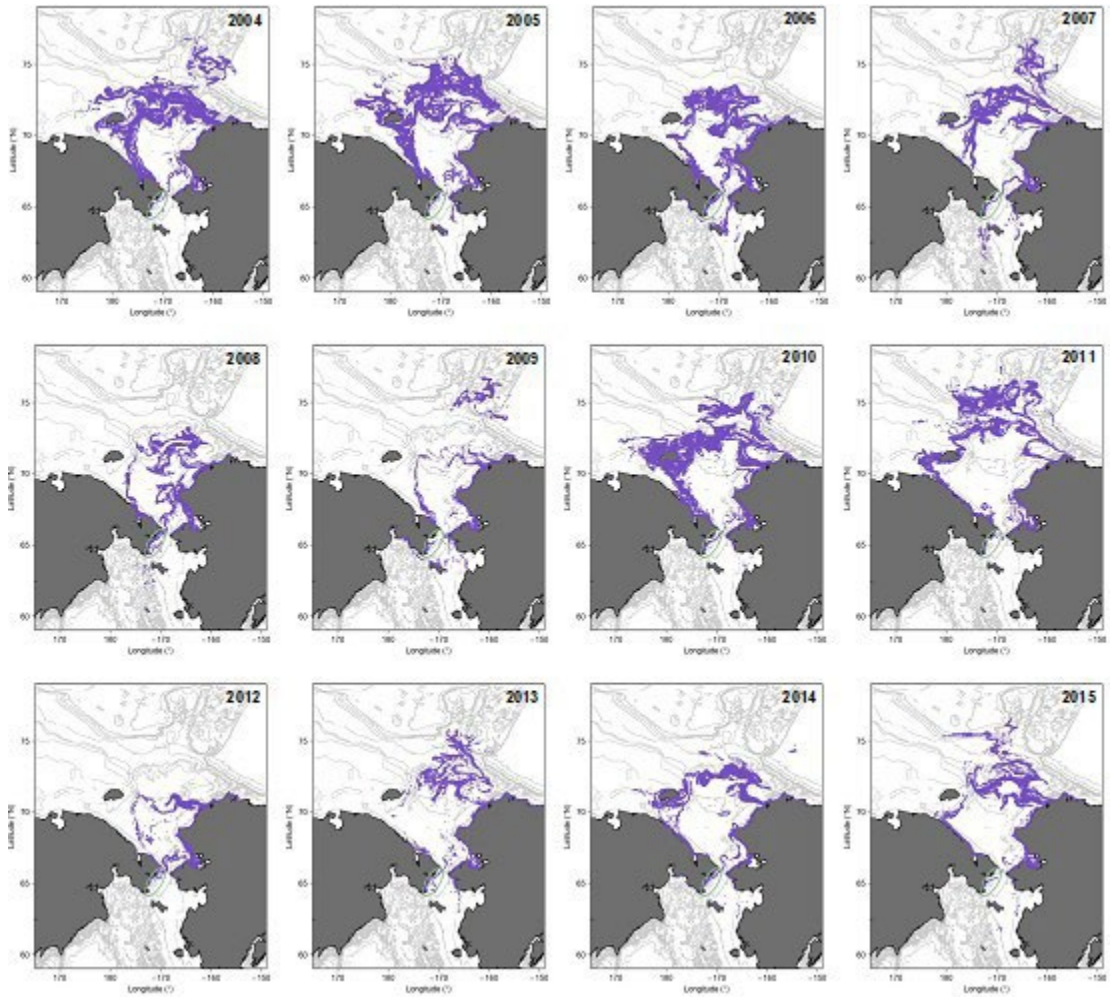

Fig. S5. Simulated particle distributions of polar cod (Boreogadus saida) on 1 September 2004 – 2015 from the Bering Strait release area (green ellipse) for all release dates (every 2 weeks from 1 January – 15 May). Data from simulations with surface-oriented behavior are presented.

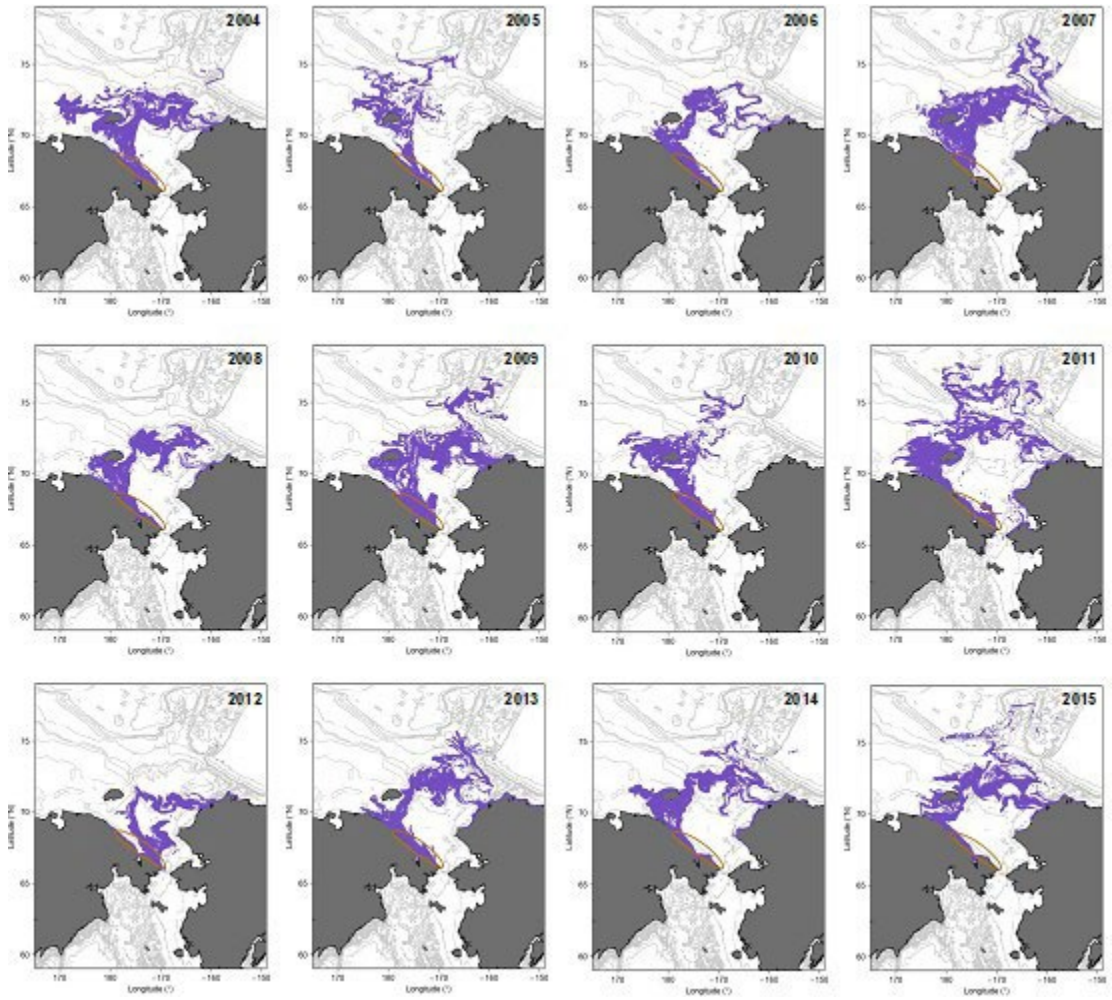

Fig. S6. Simulated particle distributions of polar cod (Boreogadus saida) on 1 September 2004 – 2015 from the Chukotka Peninsula release area (orange ellipse) for all release dates (every 2 weeks from 1 January – 15 May). Data from simulations with surface-oriented behavior are presented.

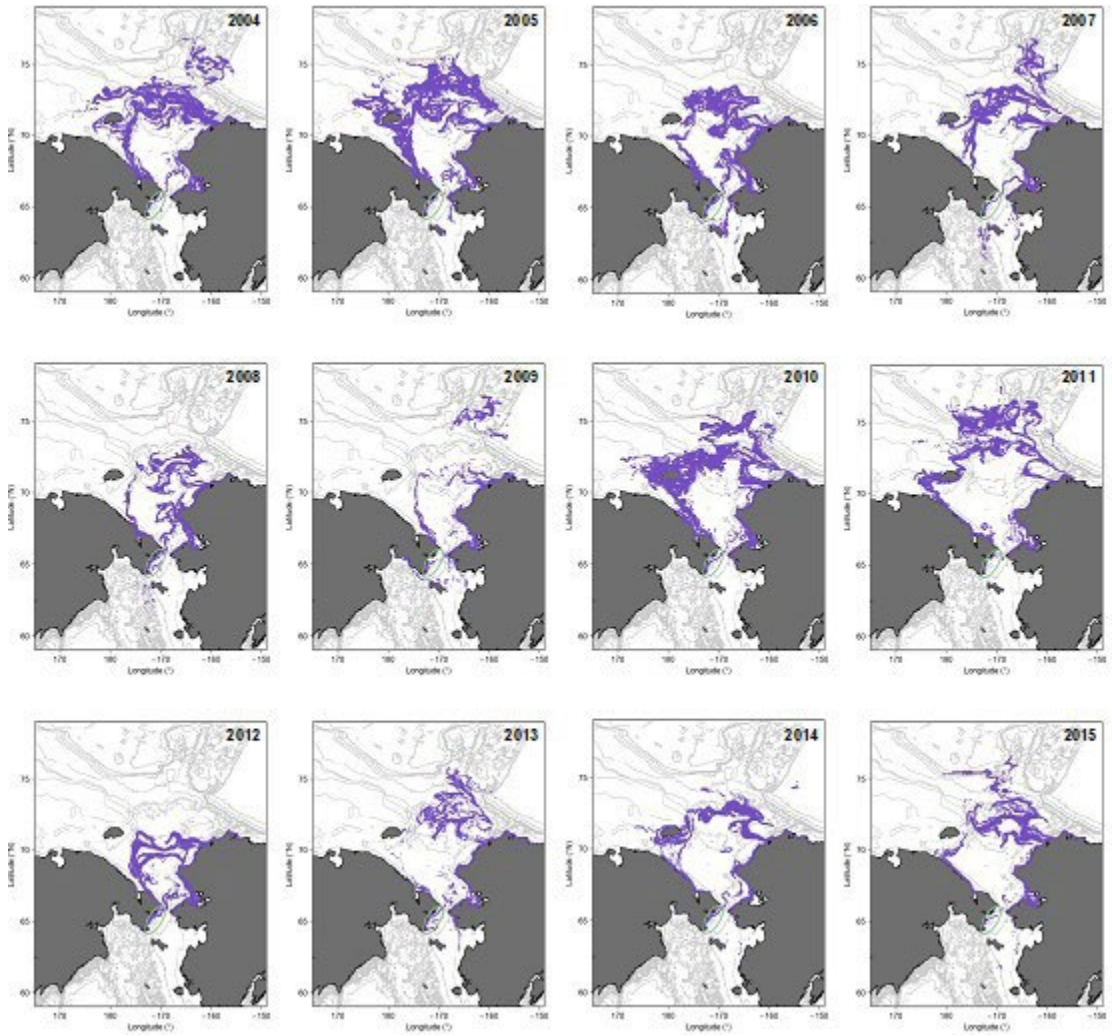

Fig. S7. Simulated particle distributions of saffron cod (Eleginus gracilis) on 1 September 2004 – 2015 from the Bering Strait release area (green ellipse) for all release dates (every 2 weeks from 1 January – 15 May). Data from simulations with surface-oriented behavior are presented.

Fig. S8. Simulated particle distributions of saffron cod (Eleginus gracilis) on 1 September 2004 – 2015 from the Kotzebue Sound release area (blue ellipse) for all release dates (every 2 weeks from 1 January – 15 May). Data from simulations with surface-oriented behavior are presented.

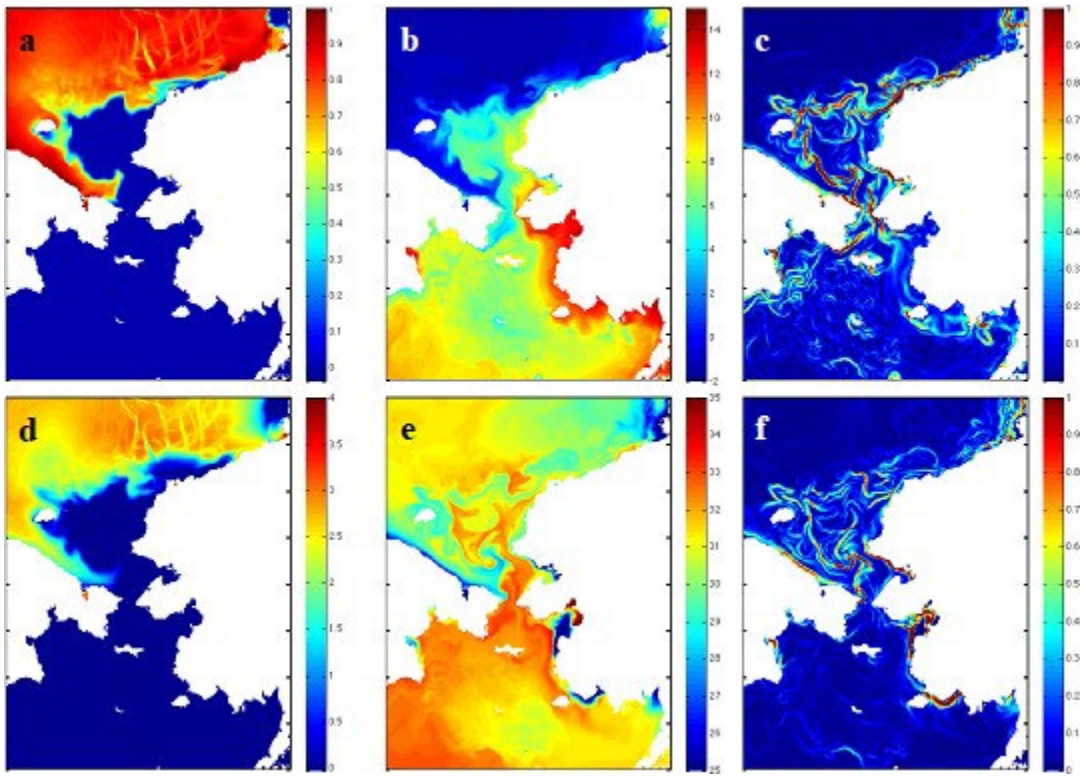

Fig. S9. Pan-Arctic Regional Ocean Modeling System (PAROMS) model (a) ice concentration, (b) sea surface temperature (°C), (c) sea surface temperature gradient (°C 5 km-1), (d) ice thickness (m), (e) sea surface salinity (PSU), and (f) sea surface salinity gradient (PSU 5 km-1) on 30 August, 2012.

Table S1. Correlations between selected climate indices used in the latitude and longitude center of gravity correlation analysis. AD: Arctic Dipole index, MAM: March, April, May, JJA: June, July, August; AO: Arctic Oscillation index; SA: Siberian/Alaskan index (2004 – 2013); IER: Ice extent/retreat index (2005 – 2015), with p-values above the diagonal, and correlations below the diagonal.

	AD (MAM)	AD (JJA)	AO	SA	IER
AD (MAM)	-	0.80	0.24	0.17	0.24
AD (JJA)	-0.37	-	0.73	0.71	0.49
AO	-0.37	-0.17	-	0.17	0.57
SA	-0.42	-0.06	0.45	-	0.64
IER	-0.29	0.44	0.29	0.18	-

CHAPTER 19: Otolith-derived hatch dates and growth rates of Arctic Cod (Boreogadus saida) support existence of several spawning populations in Alaskan waters

Objective 5: Further resolve early life history characteristics of Arctic cod and saffron cod and their behavior and connectivity between the Chukchi Sea and western Beaufort Sea.

Chapman, Z.M.[1], Mueter, F.J.[1], Norcross, B.L.[1], and D.S. Oxman[2]

[1] College of Fisheries and Ocean Sciences, University of Alaska Fairbanks
[2] Mark, Tag and Age Laboratory, Alaska Department of Fish and Game

Prepared for submission to Deep-Sea Research Part II

Abstract

Arctic cod are an important prey species in Arctic marine ecosystems as they provide efficient energy transfer up the food web. They are found throughout the Arctic and have locally high abundances. Little is known about the early life of Arctic Cod in the Pacific Arctic, such as when and where they spawn and hatch, but they have a close relationship with sea ice during incubation and may associate with sea ice through much of their early life history. The goal of this study was to estimate hatch dates and growth rates of first year Arctic Cod, which was accomplished through analysis of otolith growth increments. First-year Arctic Cod were captured in the northern Bering, Chukchi, and Beaufort seas during the spring or summer between 2012 and 2017. Estimated hatch dates ranged widely from November to July with peak hatching occurring from February through May depending on the region of capture. Combined with large individual and regional variability in growth rates, this suggests a bet-hedging strategy to ensure some larvae encounter favorable growth conditions. In addition to regional differences, we identified a clear separation of hatch dates between spring- and summer-caught Arctic Cod, suggesting different origins or strong size-dependent mortality. Finally, differences in hatch dates between pelagic and demersal juveniles support the settlement of older, larger juveniles to the seafloor on deeper portions of the shelf in late summer. Differences in hatch timing and growth in the context of variability in sea ice retreat, river discharge and other environmental conditions can provide new insights into the future of Arctic Cod as the Arctic climate continues to change.

Introduction

Arctic Cod (*Boreogadus saida*) were identified as a keystone species within Alaska's Arctic waters by the Fisheries Management Plan for Marine Resources in the Arctic (NPFMC, 2009). Arctic Cod provide an important pathway for energy transfer from planktonic prey to larger animals. With large abundances, high energy content, and an assimilation efficiency around 80%, Arctic Cod are ideal prey for many Arctic predators (Hop et al., 1997; Bluhm and Gradinger, 2008, Crawford et al., 2016). Many larger predators such as seals, whales, and seabirds depend on Arctic Cod as a source of energy; in turn, polar bears and Alaska Native communities rely on some of these marine mammals for their caloric intake (Welch et al., 1992). Arctic Cod are also targeted by commercial and subsistence fisheries in the Barents Sea (Gjosaeter 1995; Magdanz et al., 2010).

Previous research on Arctic Cod has identified characteristics of their life history as adults; however, less is known about their early life history due to the difficulties associated with sampling early stages. Arctic Cod males reach sexual maturity between 1 and 3 years of age while females reach sexual maturity at 2 or 3 years of age. They have a life span of 7-8 years (Hop and Gjosaeter, 2013), and reportedly spawn mostly between January and March in large groups underneath the ice (Craig et al., 1982; Bouchard and

Fortier, 2011; Gallaway et al., 2017). Based on laboratory studies, Arctic Cod eggs remain suspended at the surface of the water just under the sea ice and can tolerate sub-zero temperatures without affecting survival (Laurel et al., 2015). Artic cod spawning locations and dates, as well as hatch times, are currently unknown, although such information is needed to protect these vulnerable life stages. Early larval stages have been found throughout the spring (Deary et al. in review) and summer sampling seasons (Vestfals et al. 2019), suggesting a broad distribution of spawning and hatching in space and time. However, the bongo nets used in these studies under-sample larger larvae and juveniles in the summer. High abundances of larvae and juveniles have been observed over multiple years on the northeast Chukchi Sea shelf (de Robertis et al 2017; Levine et al. 2021), but their origins remain poorly known. High abundances of larval and juvenile Arctic Cod have also been documented in the western Beaufort Sea (Parker-Stetter et al., 2011; Forster et al., 2020; Vestfals et al., 2019), but it is unclear if this population is connected to Arctic Cod found in the northern Chukchi Sea. In spite of these recent observations of Arctic Cod during their first summer, large gaps remain in the understanding of the reproductive biology and early life history of Arctic Cod in the Pacific Arctic (Mueter et al., 2016; 2020).

The Arctic marine environment is changing rapidly; how this may affect the distribution, abundance, condition, and phenology of Arctic Cod is of great interest to researchers and resource-dependent communities. The Arctic has seen a significant reduction in sea ice, an increase in water temperatures, and a rate of air temperature change that is double the global average (Thoman et al., 2020). These changes are reshaping the ecosystem, allowing southern, warmer-water species such as Capelin (*Mallotus villosus*), Saffron Cod (*Eleginus gracilis*), and other gadids to move north and compete with Arctic Cod for habitat and food resources (Hop and Gjøsæter 2013, Marsh and Mueter, 2020). Arctic Cod have a much lower thermal tolerance than these southern gadid species with high mortalities occurring above 16°C and a peak growth rate at 7.3°C as juveniles (Laurel et al., 2015). The eggs of Arctic Cod have a much narrower temperature tolerance and will not survive in temperatures exceeding 3.8°C (Drost et al., 2016). As the Arctic environment continues to change, the impact of these changes on Arctic Cod will have ripple effects across the Arctic ecosystem.

Arctic Cod growth and hatch timing have been examined in Canadian and European Arctic waters using daily otolith increment deposits. These analyses indicate two hatching patterns: a short hatch event that occurs concurrently with ice break-up and the beginning of increased biological production (May-June) and a protracted hatching pattern that can occur under the sea ice and extend into the summer (January-July) (Bouchard et al., 2017). Hatching patterns, and in particular hatch timing, may be an important determinant of subsequent growth and survival. Early hatching Arctic Cod are able to attain a greater pre-winter size but experience increased mortality during the long larval phase. Later hatching Arctic Cod have reduced pre-winter size, but experience less larval morality. Therefore, there is greater potential for a higher abundance of later hatching fish at the end of the summer season, but these fish are on average smaller than the early hatching Arctic Cod (Fortier et al., 2006; Bouchard and Fortier, 2008) and may experience higher overwinter mortality as a result. If hatch timing is linked to sea-ice retreat, reductions in sea ice and early ice melt may contribute to observed changes in the abundance and distribution of Arctic Cod at the southern end of their range such as the Bering Sea (Marsh and Mueter, 2020). However, the links between changing ice conditions, hatching, and the survival of larval Arctic Cod in the Pacific Arctic are not understood at present.

Understanding the timing and location of spawning and hatching in Alaskan waters, as well as the subsequent growth, movements and survival of eggs and larvae, is critical to identifying habitat requirements for early life history stages of Arctic Cod. This is especially true in areas of potential oil exploration, as Arctic Cod are highly vulnerable to crude oil during their early life history (Gallaway et al., 2017; Laurel et al., 2019). Limited information is available on the distribution of eggs and early larval stages due to the challenges of sampling these life stages. However, field-based information derived from the otoliths of later larval and juvenile stages can be used to inform our understanding of earlier life stages

in several ways. First, information on hatch timing is needed to parameterize biophysical transport models for Arctic Cod (Deary et al., In Review; Vestfals et al., 2021). Such models, in turn, can help identify and protect potential spawning aggregations and can be used to simulate how sea ice reduction and changes in water temperature may affect early life survival. Second, inferred hatch dates can be compared to the known hatch dates for other Arctic Cod stocks to help identify environmental drivers that control hatch timing and to compare the time of hatching across different stocks (Bouchard and Fortier, 2011). Finally, age-length relationships based on otolith-derived ages can be used to estimate growth rates of larval and juvenile Arctic Cod in the field during their first few months and to compare growth rates among regions. A better understanding of the life history and hatching habitats will help inform the conservation and management of Arctic Cod under the NPFMC to ensure that these resources are adequately protected.
To address the gaps in our understanding of Arctic Cod early life history, the goal of this study was to estimate the hatch date distribution of larval and early juvenile Arctic Cod sampled during the spring and summer in the Chukchi and Beaufort seas and to compare inferred hatch dates among regions. Specifically, we estimated age in days of Arctic Cod larvae based on daily otolith growth increments and used age-at-length relationships to infer the distribution of hatch dates from observed length-frequencies. A second objective was to derive field-based estimates of average daily growth rates and to compare realized growth among stocks from different regions and to laboratory-derived and other field-based estimates from the literature. These results will improve the current understanding of early life history dynamics of Arctic Cod and inform ongoing modeling efforts to help better understand ecosystem changes.

Methods

Study Region

Arctic Cod samples were obtained from the Bering, Chukchi and Beaufort seas and were assigned to five distinct regions based on differences in bathymetric and oceanographic characteristics within each of the seas (Fig. 1). From south to north, these regions are northern Bering Sea (NBS), southern Chukchi Sea (SCS), northern Chukchi Sea (NCS), western Beaufort Sea (WBS), and eastern Beaufort Sea (EBS). The NBS is a broad shelf that encompasses Norton Sound and the Chirikov Basin between St. Lawrence Island and Bering Strait, with depths generally less than 50 m. It connects to the Chukchi Sea via the Bering Strait at 56.9°N, which has a depth of less than 50 m. The majority of the Chukchi Sea is a shallow (40-60 m) continental shelf, which was split into a southern and northern region for our analyses due to differences in water masses. Alaska coastal water, Bering shelf water and Anadyr water from the Bering Sea converge in Bering Strait before entering the Chukchi Sea (Danielson et al., 2017; Eisner et al., 2012) and continuing to flow north. These water masses of recent Pacific origin cover a variable portion of the Chukchi Sea shelf, but are typically separated from distinct water masses in the NCS, referred to as Winter Water and recent Melt Water, by a semi-permanent front that extends from the surface to the sea floor (Weingartner 1997). The colder and more saline Winter Water extends as far south as 70°N, therefore 70°N was used as the dividing line between the NCS and SCS for our analyses (Pickart et al., 2010). In contrast to the Chukchi Sea, the Beaufort Sea has a narrow shelf that quickly drops into the Arctic Basin to depths exceeding 2,000m. The Beaufort Sea shelf receives relatively nutrient-poor water via the Alaska Coastal Current entering from the West and is influenced by fresher waters from the Mackenzie Rivers, as well as by deeper Atlantic waters from the East (Carmack and Macdonald 2002, Pickart 2004). For this analysis, the Beaufort Sea was separated into an eastern (samples east of 147°W; EBS) and western region (153 °W to 147 °W; WBS) (Fig. 1), with the EBS experiencing a stronger influence from the Mackenzie River than the WBS (MacDonald et al., 1987). Because of the strong connectivity between the NCS and the westernmost portion of the Beaufort Sea (west of 153° W), we pooled samples from these regions and refer to them collectively as the NCS.
Sample Collection and Processing

Larval and juvenile Arctic Cod used for this analysis were collected during five Arctic surveys that covered the spring (June) and summer (August/September) seasons: the Arctic Shelf Growth, Advection, Respiration and Deposition (ASGARD) rate measurement survey in the NBS and SCS in the spring of 2017 (Danielson et al., 2017), the Arctic Marine Biodiversity Observation Network (AMBON) survey in the Chukchi Sea in the summer of 2017 (Iken et al., 2018), the Arctic Integrated Ecosystem Survey (Arctic IES II) in the Chukchi Sea and WBS in the summer of 2017 (Farley et al., 2017), and the Transboundary Surveys which sampled the summer seasons in the WBS in 2012 (TB12) and in the EBS in 2013 (TB13) and 2014 (TB14) (Norcross et al., 2017; Table 1). Four types of sampling methods were used to collect Arctic Cod: (1) an Isaacs-Kidd Midwater Trawl (IKMT, Methot 1986) with a 3 mm mesh body and 1 mm mesh codend liner was deployed obliquely to collect larval and juvenile pelagic fish from near bottom to the surface during the AMBON, TB12, and TB13 surveys; (2) a modified Marinovich trawl with a 64 mm mesh body which tapered to a 3 mm mesh codend was used to target aggregations identified by acoustic backscatter as part of an acoustic-trawl survey during Arctic IES II (de Robertis et al., 2017); (3) two types of bottom trawls were used to sample demersal fish, including a 3 m modified Plumb Staff Beam Trawl (PSBTA, Abookire and Rose, 2005) with a 7 mm mesh body and a 4 mm liner in US waters during the AMBON, Arctic IES II and transboundary surveys and a Canadian Beam Trawl (CBT, Majewski et al., 2017) with a 10 mm mesh body and a 6 mm liner during the U.S. and Canadian transboundary surveys; and (4) a 60 cm diameter Bongo net with a 505µm mesh was used to sample zooplankton and ichthyoplankton during ASGARD and Arctic IES II surveys.

Two sets of Arctic Cod samples were used for analyses. First, standard lengths of all larval and juvenile Arctic Cod sampled in a given region, season and vertical location (demersal or pelagic) were measured in the field or laboratory to the nearest mm (Table 1). Second, length-stratified sub-samples for otolith aging were obtained from each region and season, except the WBS and 2012 EBS, to estimate region-specific relationships between length and age (Table 2) and to convert observed length-frequencies to estimated hatch date distributions using the approach described below. For summarizing length-frequencies and hatch date distributions and for comparisons, samples from different seasons, regions, and vertical locations were organized in and will be referred to as 'groups'. We defined a total of 10 groups consisting of pelagic spring samples from the NBS (1 group), pelagic spring and pelagic and demersal summer samples from the SCS (3 groups), and pelagic and demersal summer samples from the NCS, WBS, and EBS (2 groups each).

To obtain representative length-frequency distributions for larval and juvenile Arctic Cod for each group, lengths samples from different gear types and cruises were used (Fig. 3, Table 1). Length-frequency distributions during spring were quantified using Bongo samples because larval fish are generally small (< 20 mm) at that time. Although the Bongo may select against some of the larger larvae in the water column because of its small mesh size, Bongo samples were considered to be most representative of the size distribution of larval Arctic Cod in the sampling area during spring. This was supported by opportunistic IKMT samples that indicated larvae were generally less than 20 mm in June. During the summer sampling period, age-0 fish were generally larger than 20 mm and were distributed throughout the water column or had settled to the bottom. We used fish collected by either the Marinovich trawl or the IKMT (when Marinovich was unavailable) to quantify length-frequencies of pelagic juveniles, whereas samples from the bottom trawls (PSBTA or CBT) were used to characterize lengths of demersal fish. The Marinovich has very little size selectivity over the size range of interest (de Robertis et al., 2017; A. de Robertis, NOAA, Seattle, pers. comm.). Similarly, the PSBTA has been estimated to retain all or most age-0 Arctic Cod (Marsh et al., 2020). We focused primarily on the pelagic fish for comparisons among regions because they are assumed to be age-0 fish, whereas the bottom trawl catches may include some small Arctic Cod (< 75 mm) that could be age-1 or older as there is considerable overlap in sizes among ages (Helser et al., 2017). Length data for the Transboundary surveys from both the PSBTA and CBT were combined to characterize the length-frequency distribution of Arctic Cod in the eastern Beaufort Sea because there was no evidence that the size composition of the catches differed significantly

between these gear types (Norcross et al., 2017). The combined gear type will be referred to hereafter as bottom trawl. In summary, pelagic fish in spring were represented by Bongo samples, while in the summer Marinovich and IKMT samples were used to represent pelagic samples, and bottom trawls were used to represent demersal fish.

To assess length frequency distributions of age-0 fish, as well as for aging age-0 fish, we included only fish up to a maximum size of 75 mm in the Bering Sea, Chukchi Sea and WBS and up to 60 mm in the EBS. The upper limits were estimated to be the maximum size of age-0 Arctic Cod in late summer based on the length-frequency distribution of all Arctic Cod sampled in a given region (Fig. A1.1). The estimated cutoff of 75 mm for the southern regions was consistent with that used for age-0 fish sampled in the Chukchi Sea in late summer 2012 and 2013 (Marsh et al., 2020). In the EBS, a cutoff of 60 mm was used as larger fish were clearly separated from a dominant mode of smaller, age-0 fish and were continuous with a mode of larger, presumably age-1 or older fish (Fig. A1.1). This cutoff is consistent with previous studies in the Beaufort Sea (Norcross et al. 2017).

To sample fish for otolith aging, age-0 Arctic Cod were sampled randomly over the full size range of approximately 6 mm to 75 mm. Our sampling goals were to obtain samples for aging that were representative of the full range of sizes of larval Arctic Cod in the spring and of young-of-year Arctic Cod in late summer within each sampling region. We collected size-stratified random subsamples of specimens collected across much of the study region (Fig. 1), subject to other sampling priorities. Lengths were stratified into a small, medium, and large group for each region to ensure that a broad range of lengths was represented for aging. Subsamples of larval and juvenile gadids for otolith analyses were frozen or stored in 95% ethanol and shipped to the University of Alaska Fairbanks in Juneau, Alaska, where they were identified and processed for further analysis. Samples of archived otoliths from the Transboundary surveys in the Beaufort Sea and the corresponding standard lengths were obtained from the Fisheries Oceanography Lab at the University of Alaska Fairbanks (UAF). Of the smaller specimens (< 15 mm) shipped to Juneau, ~ 60% were cross-checked by a larval taxonomist to minimize misidentification. Larger fish are difficult to identify in the field and fish greater than 20 mm captured during the Arctic IES II survey were verified by sequencing the mitochondrial cytochrome oxidase c, subunit 1, and aligning them with known gadid sequences at the National Oceanic and Atmosphere Administration (NOAA) Ted Stevens Marine Research Institute in Juneau, Alaska (Sharon Wildes, NOAA, Seattle, pers. comm.). All samples were processed and analyzed at UAF's Lena Point Fisheries Facility and at the Alaska Department of Fish and Game Mark, Age and Tagging laboratory in Juneau.
Otolith Aging

To estimate ages of juvenile Arctic Cod, sagittal otoliths were examined for daily growth increments. After measuring standard lengths, the sagittal otoliths were removed under a dissecting microscope with fine-tipped forceps. The left otolith was extracted, rinsed with 95% ethanol to remove any organic matter, and mounted to a glass slide using clear, thermal plastic cement. The right otolith was removed, cleaned, and stored dry to be used if the left otolith was damaged or unusable. The mounted otoliths were polished with various grades of lapping film to expose the daily growth increments within the otolith. Due to their uneven shape, some otoliths required polishing on both sides.

To estimate hatch dates, daily growth increments were counted on the otoliths. The deposition of daily growth increments in Arctic Cod was previously confirmed using a tetracycline marking experiment and visual examination under light and scanning electron microscopy (Bouchard and Fortier, 2011). In this study, growth increments were identified under a light microscope at 40x and 100x magnification to confirm adequacy of the otolith preparation for identifying potential daily rings. The otoliths were imaged using Image Pro Plus© (Media Cybernetic), where each visible ring was assumed to represent one day of growth (Fig. 2 A). Using Image Pro Plus© (Media Cybernetic), daily growth increments were counted from the hatch mark to the edge of the otoliths (Fig. 2 B). Hatch marks were identified and validated

using otoliths of lab-reared, known-age Arctic Cod from the Hatfield Marine Science Center in Newport, Oregon (Benjamin Laurel, NOAA Alaska Fisheries Science Center, pers. comm.; Fig. 2 C). The otoliths of lab-reared Arctic Cod were aged to confirm the presence of daily growth increments and test the reader's aging ability. Using the known age of the fish, the location of the hatch mark was then identified and confirmed to further improve age determinations. This method of hatch mark identification is similar to other studies that determined the hatch mark by examining otoliths shortly after the fish hatched (Eckmann and Rey 1987).

To ensure accuracy of otolith aging, all sampled otoliths were aged at least twice and a third time if the first two ages were not within a 5% coefficient of variation (CV). The second and third ages were done at a separate time from the first to avoid any aging bias. If the first two ages fall within a 5% CV of each other the second age was used. In the event the first two ages had a greater than 5% CV then the otoliths was aged a third time and the final age was used if it was within 5% of either the first or second age. Although there are other methods for validating age determinations, the CV is statistically more rigorous and flexible (Chang, 1982; Campana 2001). A subsample of the aged otoliths (n = 15) was examined by a second otolith aging expert to confirm that the images, measurements and ages had no errors.

Growth increments in the center of some otoliths were unreadable because too much material had been removed during polishing. Therefore, the saved otolith was used for aging, but for some of the larger fish (20 - 54mm), the center again became washed out. In these cases, daily ages were counted using the otolith with the most amount of visible increments starting at the first readable growth increment. The number of increments that were unreadable was estimated based on a regression approach using completely aged otoliths from the same region (Appendix 2).

Length-frequency distributions

Length-frequency distributions that best represent the total population of larval or juvenile Arctic Cod were visually examined by season and region, and separately for pelagic and demersal sampling gear. In addition, the mean lengths of demersal and pelagic larvae and juveniles were plotted for each station to visualize spatial patterns in mean size. These representative length-frequency distributions, combined with age-at-length regressions for a given region, provide the basis for determining the hatch date distribution.

Hatch Date Determination

To estimate the distribution of hatch dates for Arctic Cod in each group we first estimated age-at-length relationships and their uncertainty for a subsample of fish using linear regressions. The resulting relationships were then used to convert all observed lengths in a group to estimated ages. Finally, the estimated ages were subtracted from the dates of capture to obtain an estimated hatch-date distribution. We assumed a linear relationship between age and length based on a previous study of Arctic Cod (Bouchard and Fortier, 2011) and visual examinations of age-at-length. Therefore, counts of daily growth increments (hereafter 'age') within each season were modeled as a linear function of length and region with an interaction term to allow for possible differences in age-at-length by region(r):

$$age_{r,i} = a_r + \beta_r \cdot length_{r,i} + \varepsilon_{r,i} \qquad \varepsilon_{r,i} \sim N(0, \sigma_\varepsilon^2)$$

Eq. 1

where and are the estimated age and length of the i^{th} specimen in region r, a_r and b_r are the intercept and slope for region r, and the $\varepsilon_{r,i}$ are residuals that are assumed to be normally distributed with mean 0 and variance . Region-specific coefficients ( ) were only estimated if the interaction term was significant ($p < 0.05$), otherwise a single regression line was estimated across the sampled regions (a, b). Preliminary analyses indicated that the standard deviation in estimated ages increased linearly with the predicted mean

ages, therefore a variance structure accounting for this mean-variance relationship was incorporated into the models. All models were fit using a generalized least squares approach as implemented in the 'nlme' package in R (Pinheiro et al., 2020). Residual diagnostics did not suggest any violations on the linearity or normality assumptions.

To estimate age distributions within each region, we used the best age-at-length model for each region to predict ages from observed lengths. Age data were not available for the WBS and the age-at-length model for the NCS was applied to this region because it is contiguous with and immediately downstream of the NCS. Juveniles from the NCS are likely advected into the western Beaufort Sea (Levine et al. 2021). To appropriately reflect variability in age-at-length arising from individual variations in growth, we randomly simulated up to 10 ages for each observed length based on the estimated mean age and its standard deviation at a given length. Occasionally, the age of a simulated fish exceeded one year due to the large estimated variance in the age of larger fish; those fish were removed from the simulated age distribution. The number of simulated ages per measured individual was arbitrarily chosen to generate at least 10,000 ages for obtaining a smooth age distribution for plotting and this choice did not affect results. The simulated ages were subtracted from the corresponding capture dates to obtain estimated hatch dates for further analyses of hatch date distributions. Regression models to predict ages from lengths for the SCS were fit separately to data from spring and summer surveys due to large differences in the observed length ranges of fish between spring and summer. The SCS was the only region where data from both seasons were available.

Hatch date comparisons

Simulated hatch dates were compared among the groups using graphical and statistical analyses. The full simulated hatch date distributions were visually compared among groups using density plots. To statistically compare these distributions among groups, we calculated the mean hatch dates for each group of Arctic Cod and used a bootstrap approach to construct confidence intervals for the means. Bootstrap samples were generated for each group by randomly re-sampling with replacement both the observed length-frequencies for a given group and the age-length samples used for estimating age-at-length for that group. For each set of bootstrap samples, a hatch date distribution was simulated following the same series of steps used in estimating the hatch date distribution from the original samples and the mean hatch date of the simulated distribution was calculated. This was repeated for each of 10,000 sets of bootstrap samples to construct percentile-based 95% confidence intervals for the mean hatch date of each group, as well as for pairwise differences between groups. If the confidence interval for a pairwise difference did not include zero, mean hatch dates between groups were considered statistically different. In addition, p-values for all pairwise comparisons were computed based on the proportion of simulated differences that were less than or larger than zero, whichever was smaller. The proportion was multiplied by two for a two-sided test because we did not specify *a priori* hypotheses about which groups had earlier or later hatch dates. Mean hatch dates and 95% confidence intervals were visually and statistically compared among groups.

Initial comparisons among regions showed no difference in mean hatch dates between Arctic Cod captured in the most western portion of the Beaufort Sea and the Northern Chukchi Sea from the 2017 Arctic IES survey. This was true for both the pelagic and demersal captured fish with p-values of 0.647 and 0.952 respectively. Due to this lack of significant differences and because of the small sample size (n = 68 pelagic and 77 demersal fish) for length measurements from the Beaufort Sea portion of the Arctic IES survey the two regions were pooled and will be referred to as NCS hereafter. The similarity between the two regions was not surprising given their close proximity and oceanographic connectivity, and the hypothesis that most northern Chukchi and western Beaufort Sea Arctic Cod are advected into those regions from southern hatching locations (Levine et al., 2021).

In the Chukchi Sea during summer, data for both pelagic and demersal Arctic Cod were available from two overlapping surveys and were analyzed separately. Mean hatch dates for pelagic Arctic Cod collected during the transect-based AMBON survey (IKMT) and those collected during the grid-based Arctic IES II survey (Marinovich) (Table 1) were quantified separately as the surveys covered different areas. For comparing hatch dates of fish among regions, we present results for Arctic IES II samples collected in the SCS and NCS using the Marinovich trawl (pelagic fish) or bottom trawl (demersal fish) because the Arctic IES II survey sampled a systematic grid and covered a larger geographical area within each region, providing more representative length-frequency distributions (Fig. 3).

Growth Rates

To obtain field-based estimates of age-0 growth rates for Arctic Cod we fit linear regressions of length on age by region and season. A simple linear regression of length as a function of age was used, where the slope (mm d^{-1}) represents the estimated average growth rate of the sampled population in a given region and season. Growth rates were estimated separately by region to account for differences in temperature, prey availability among regions, and genetic differences among stocks, all of which can affect the rate of growth (Laurel et al., 2015; Helser et al., 2017; Laurel et al., 2018). Growth rates were also estimated by season to account for potential differences between the growth of early larval and juvenile stages and the apparent growth of the surviving age-0 fish sampled later in the summer, whose average growth may differ due to size selective mortality or seasonal changes in temperature.

Results

Otolith-based ages

A total of 181 Arctic Cod otoliths were aged, with ages ranging from 10 to 161 days for Arctic Cod sampled in the spring, and from 55 to 308 days for those collected during summer (Table 2). The age range was greater for samples from the Chukchi Sea (55-308 days) than the Beaufort Sea (76 - 241 days), which may in part be due to smaller sample sizes in the Beaufort Sea (Table 2). The mean CV between first and second age assessments was 0.02 (range: 0.00 to 0.05), indicating acceptable accuracy.

Length-frequency distributions

Length-frequency distributions of age-0 Arctic Cod differed by region, season, and depth of capture. Arctic Cod captured in the spring were much smaller than those captured in the summer (Table 1). In the SCS, where Arctic Cod were sampled in both seasons, pelagic spring caught fish had a mean length of 8 mm (range: 5 - 17 mm) and the pelagic summer captured fish had a mean length of 52 mm (range: 28 - 74 mm). Within seasons, differences in length frequency distribution were observed among regions (Fig. 5). The WBS had the largest mean length of age-0 Arctic Cod followed closely by the SCS (Table 1). Within regions, demersal caught fish were on average larger than fish caught in pelagic nets (Table 1). We also observed differences in mean length among surveys within the same regions sampled during the summer of 2017. Specifically, pelagic captured fish were larger in the Arctic IES II survey (mean length of 52 and 42 mm in SCS and NCS, respectively) than the AMBON survey (mean length of 37 and 29 mm in SCS and NCS respectively). The surveys overlapped spatially, but the Arctic IES II survey took place about one month later (Table 1), which likely accounts for the larger mean sizes. Spatial patterns in mean length across the study region suggest a gradient from larger fish in the south to smaller fish in the north during both spring and summer in the Chukchi Sea (Fig. 3). During summer, the smallest fish were observed in the EBS, while WBS fish were slightly larger on average. These spatial differences are confounded with differences in the timing of sampling as the SCS and WBS were sampled later in the year than the NCS and EBS (Table 1). The number of Arctic Cod captured varied across regions and seasons from 19 cod captured in the NBS during spring to >4,000 captured in the NCS during summer, reflecting differences in average catch-per-unit-effort and differences in the number of stations sampled (Table 1).

Age-at-length regressions

The best age-at-length model included a significant interaction between length and region for spring-caught samples ($F = 12.76$, $p = 0.001$), indicating that slopes differed between the NBS ($\beta_{NBS} = 8.210$, se = 0.561, $R^2 = 0.943$) and SCS ($\beta_{SCS} = 5.485$, se = 0.763, $R^2 = 0.688$; Table 3, Fig. 4A). In contrast, there was no significant interaction between length and region in the summer ($F=0.45$, $p = 0.715$), indicating that age increased at the same rate with length across sampling regions ($\beta = 4.09$, se = 0.24, $R^2 = 0.696$; Table 4, Fig. 4B). However, intercepts differed significantly among regions ($F = 4837$, $p = 0.009$) and fish at a given length were on average 17.5 days older in the NCS compared to the EBS, 22 days older in the SCS compared to the NCS, and 39 days older in the SCS than in the EBS (Table 3). Coefficients from the best model for each season and region were used to predict ages and hatch date distributions from the observed length-frequencies.

Hatch timing

The estimated distribution of hatch dates differed between Arctic Cod sampled in the spring and in the summer, between Arctic Cod from different regions and between pelagic and demersal age-0 Arctic Cod. Within the SCS, spring captured pelagic fish had a mean hatch date that was 131 days later than summer captured pelagic fish (Table 4; Fig. 7). Arctic Cod hatch dates of summer-caught fish differed significantly among regions ($p>0.05$) except for pelagic fish caught in the NCS and WBS ($p=0.957$, ~1-day difference) and demersal fish from the NCS and EBS ($p=0.059$, 12-day difference; Table 5; Fig. 7). Demersal SCS fish sampled during the summer had the earliest mean hatch date (December 27) and pelagic EBS fish had the latest mean hatch date (March 10, Table 4). Summer-caught pelagic fish in the SCS hatched on average 14 days earlier than those in the NCS, 26 days earlier than those in the WBS, and 51 days earlier than EBS pelagic fish (Table 5). Within each region, pelagic Arctic Cod had mean hatch dates significantly later ($p<0.05$) in the year than demersal Arctic Cod, except in the Chukchi Sea where SCS and NCS demersal and pelagic fish did not differ significantly in mean hatch dates. The NCS was the only region where demersal fish hatched later than pelagic fish with a mean hatch date of nine days later (Fig. 7).

Growth rates

Estimated growth rates differed among regions as evident from significant differences in the slopes of the length-age regressions (Table 2). Apparent growth rates of spring-caught Arctic Cod larvae were 37% slower in the NBS (0.115 mm d^{-1}) than in the SCS (0.183 mm d^{-1}) (Table 2; Fig. 8A). Growth rates of Arctic Cod captured in the summer season similarly differed significantly among regions ($F=3.14$, $p=0.047$), ranging from 0.097 mm d^{-1} in the EBS to 0.200 mm d^{-1} in the SCS (Table 2; Fig. 8B).

Discussion

The use of otoliths for age estimation has proven beneficial in furthering the understanding of the early life history of Arctic Cod (Bouchard et al., 2015), and was used in this study to estimate hatch dates within several regions in the Pacific Arctic. We assessed age-at-length relationships for several regions and used those relationships to convert observed length-frequency distributions to hatch date distributions. Arctic Cod from all regions hatched over a protracted period from as early as November through June, with peak hatch dates ranging widely from February through May, depending on the season, region, and vertical location. The observed differences in hatch dates among groups likely reflect gradients in the timing of sea ice retreat, stock-specific differences, and different transport pathways from hatching to sampling due to ocean currents.

Estimated hatch dates ranged from as early as September through August of the following year. This protracted hatching pattern is consistent with previous studies (Bouchard and Fortier, 2011) and maximizes the chances that at least some offspring will hatch during favorable conditions. This bet-hedging strategy helps mitigate against annual variability in environmental conditions (Shama, 2015),

which at high latitudes can impact the timing and magnitude of the spring algal bloom and thereby the timing and abundance of prey for Arctic Cod (LeBlanc et al., 2020). Because of these highly variable conditions, a bet-hedging strategy can impart some resilience to Arctic Cod in a changing environment, as long as some portion of a given year class encounters conditions within an acceptable range. The protracted hatching period can be a result of differences in incubation time or a difference in spawn timing among the regions. The large sizes (>50 mm) of some fish in our samples produced hatch dates that indicate spawning occurred outside of published literature dates (November-March) and prior to ice formation. At least two factors may have contributed to these results. First, early hatch dates could be an artefact of simulating ages based on lengths that exceeded the maximum length in our aging samples. The age-at-length model estimated a strong increase in the variance of age at a given length and could have resulted in unrealistically large simulated ages when extrapolating beyond the maximum length of the estimated age-at-length relationship. The length range we were able to sue to estimate the age-at-length relationship was limited due to the challenges associated with aging larger larvae. Second, some of the Arctic Cod in our length samples may have been age-1 fish. The oldest estimated ages and earliest mean hatch dates were associated with fish sampled in the SCS for both demersal and pelagic samples. Within this region there was a wide range of observed lengths and in particular the demersal samples may have included some age-1 Arctic Cod. Previous studies have reported age-1 Arctic Cod below the cutoff lengths used for this study (Norcross et al., 2017). Both the presence of age-1 fish and unrealistically large variances for the age of larger juveniles are likely causes of the seemingly unrealistic early hatch dates that we estimated.

Seasonal differences in hatch dates

Arctic Cod captured during the spring and summer had different mean hatch dates, with the spring-caught fish hatching later in the year. This result was unexpected and suggests that spring-caught and summer-caught fish in the same region originated from two separate hatch events. Two separate hatch patterns among regions have been previously document, specifically a short hatching event associated with ice break up and a protracted hatching event extending from January to July (Bouchard and Fortier, 2006; Leblanc et al., 2020). The protracted hatch dates were associated with regions that do not experience significant freshwater influence (Bouchard and Fortier, 2006). Larval fish captured in the SCS in June had a mean hatch date in mid-May, suggesting that they originated relatively close to their sampling locations. Within the SCS, Kotzebue Sound has been hypothesized to be a hatching location for Arctic Cod due to the large number of larval fish captured in the outer Sound during the 2017 Arctic IES survey (Deary et al., in Review). In contrast, the summer captured pelagic fish in the SCS had a mean hatch date of mid-February, ranging from January to June. The age of the summer SCS fish indicates that they were likely advected from southern regions as suggested by biophysical transport models (Deary et al., in Review, Vestfals et al., 2021).

Spawning locations of Arctic Cod in the Pacific Arctic are largely unknown, but several areas in the Bering Strait region are believed to serve as spawning grounds, including the waters south of St. Lawrence Island, the Gulf of Anadyr, Kotzebue Sound, and areas along the Russian coast both south and north of the Bering Strait (A. Whiting, Native Village of Kotzebue, personal communication; Craig et al., 1982; Christiansen and Fevolden, 2000; Kono et al., 2016). In 2017, sea ice melt in the NBS occurred in late April and was complete by late May and 99% of estimated hatch dates occurred prior to May 25 with the mean hatch date occurring on April 6th. This indicates that Arctic cod captured in the NBS hatched prior to and during sea ice retreat. Spring-captured fish in the SCS had the latest mean hatch dates of all the regions in this study, possibly reflecting later ice melt in their hatching region. Two spawning sites have been proposed within the SCS, Kotzebue Sound in Alaska and the region along the Chukotka Peninsula in Russia (Deary et al., in Review). Both of these locations had later sea ice recession than the proposed hatching locations in the NBS. The delayed sea ice recession could explain why the spring SCS fish had a later mean hatch date than those caught in the NBS.

The observed length distribution of Arctic Cod sampled in spring 2017 was similar to those of samples collected in 2008 and 2013 from the NBS and SCS regions (Kono et al., 2016). In all three years, lower numbers of larger Arctic Cod were observed in the NBS compared to high abundances of smaller fish in the SCS. For example, the mean catch per unit effort in 2017 was 73 times higher in the SCS than in the NBS (this study). Although Kono et al. (2016) did not determine hatch dates, the observed differences in size and relative abundance of Arctic Cod between the two regions suggest that earlier ice retreat, coupled with warmer waters in the NBS, is associated with earlier hatching (Kono et al., 2016). The earlier hatching larvae experienced a longer period of natural mortality, which can explain their lower abundances in the NBS. Alternatively, larvae may have been advected out of the region prior to sampling.

In contrast to spring-captured fish, the mean simulated hatch date for all summer-captured fish occurred much earlier; with the earliest mean hatch date observed for juveniles caught in the SCS. The summer-caught fish had a mean hatch date 87 days earlier than the spring-caught fish in the SCS which suggests that they originated from a different spawning population than those caught in the spring. Summer-caught fish in the SCS displayed a wide range of hatch dates from January to May (Fig. 6). The protracted range of hatch dates in the SCS may be an indication of multiple spawning events occurring at different times in different areas of the Bering and Chukchi sea. By the time of summer sampling, fish from multiple hatching events may have been advected into the Chukchi Sea, explaining the wide range of hatch dates observed. The earlier hatch dates of summer-captured fish indicate that they likely hatched south of Bering Strait when sea ice was still present in the region, before being advected with the prevailing northward currents through the Bering Strait into the Chukchi Sea (Berline et al., 2008; Vestfals et al., 2021). This is supported by the prevailing currents in the region and by simulations with an individual based particle tracking model, which suggests that age-0 Arctic Cod sampled in the northeast Chukchi Sea during 2012 and 2013 likely originated south of Bering Strait (Vestfals et al., 2021). This model also suggests that age-0 Arctic Cod in the Chukchi Sea must have originated in more southern, warmer waters to grow to the sizes observed during the summer surveys.

Alternatively, spawning could have occurred at similar times in the same region, but differences in development rates driven by environmental influences could have contributed to differences in hatch dates. For example, earlier hatching has been hypothesized to be associated with areas that receive an influx of fresh water such as the Mackenzie River (Bouchard and Fortier, 2008). This could warm the area enough to accelerate egg development and larval growth under the ice, giving juvenile Arctic Cod a physiological advantage over juveniles in colder waters because their increased size likely leads to increased feeding success and predator avoidance (Bouchard and Fortier, 2011; Laurel et al., 2015; Kent et al., 2016).

Another possibility for Chukchi Sea Arctic Cod is that spawning and hatching occurs in association with northern polynyas, such as the recurring polynyas in the eastern Chukchi Sea between Cape Lisburne and Icy Cape. However, this polynya is characterized by high salinity and low but stable temperatures, despite reduced sea ice (Ladd et al., 2016). Thus, temperature conditions do not support the accelerated growth that would be necessary to achieve the observed sizes of summer caught larvae in the NCS. This contrasts with polynyas in the Beaufort Sea, which provide more favorable conditions for EBS Arctic Cod (Bouchard and Fortier, 2011). Moreover, simulations suggest that larvae hatched in the northeast Chukchi Sea would be advected out of the region (Vesfals et al., 2021). Therefore, we conclude that the observed hatch date distributions in the NBS and Chukchi Sea are most consistent with spawning and hatching occurring in the Bering Strait region or south of Bering Strait, with perhaps some contributions from Kotzebue Sound or other coastal areas in the Chukchi Sea. After hatching, larvae are advected northward and may be retained for extended periods over the northeast Chukchi Sea shelf due to wind and flow patterns that favor retention in the summer, before being advected northward off the shelf (Levine et al., 2021).

Seasonal differences in estimated hatch dates could also be impacted by the gear types used for sampling as most sampling gears have some size selectivity. Specifically, the bongo net may not have adequately sampled larger larvae in the spring (Shima and Bailey, 1994) and the Marinovich and IKMT may have excluded small larvae in the summer (de Robertis et al., 2017). This could result in biases towards later hatch dates in the spring because the bongo retains larvae that are smaller and younger on average than those in the water column. In contrast, summer samples could have been biased towards earlier hatch dates because the midwater trawls preferentially select larger and older larvae. Although these differences may partially explain the estimated difference in hatch dates between the spring-and summer-caught Arctic Cod, they are unlikely to account for the large difference in mean hatch dates. While the Bongo may have selected against larger larvae, larvae over 20 mm were not present in IKMT hauls during ASGARD. The similar size composition between the IKMT and bongo tows supports our assumption that the bongo tows provided an adequate representation of the larval Arctic Cod present in the region during the spring.

In addition to gear selectivity, natural mortality can also be size selective as smaller fish are typically more likely to be preyed upon then larger ones (Houde, 1987). Natural mortality of larval Arctic Cod is likely to be very high (Marsh et al., 2020) and may be size dependent. Feeding success and survival typically increase with size, thus faster growing larvae tend to have greater survival rates and may be overrepresented in the summer samples (Pepin et al., 2015). The selection against smaller Arctic Cod due to both natural mortality and gear selectivity may have caused our hatch date estimates to be biased towards earlier hatching, as well as lead to higher growth rate estimates for summer-captured fish.

Seasonal differences in hatch dates may have been further impacted by biased length measurements of preserved larvae. The surveys used two different methods for storing samples: all summer-caught samples were frozen, while most spring-caught samples were preserved in 95% ethanol. Larval fish stored in ethanol have been shown to decrease in length over time. To our knowledge, the effect of ethanol on Arctic Cod has not been studied, but such studies have been conducted on a similar gadid, Walleye Pollock. Larval Walleye Pollock have been observed to shrink between 1.8 and 5.7% in 95% ethanol (Buchheister and Wilson, 2005). To examine the potential bias associated with using preserved fish for aging, we applied the upper shrinkage value estimated for Walleye Pollock (5.7%) to correct the lengths of the spring-caught SCS samples and re-estimated the corresponding age-at-length relationship. Using the corrected relationship to convert field-measured lengths to estimated ages resulted in younger ages at length and in mean hatch dates that were four days later than those based on uncorrected lengths. Because of the uncertain magnitude of the shrinkage and because overall conclusions were not affected, we presented the uncorrected results.

Regional differences in hatch dates

Differences in hatch dates among regions may be partially explained by the timing of sea ice recession, as well as other oceanographic differences among regions. While sea ice formation may affect spawn timing of Arctic Cod (Craig et al., 1982), we focus on the timing of hatch, which is influenced by ice coverage, water temperature (Kent et al., 2016), and potentially genetic differences. Sea ice retreat generally moves in a northerly direction, consistent with fish caught in the southern regions hatching earlier in the season compared to their counterparts in the North. Both pelagic and demersal age-0 Arctic Cod captured during summer had significantly earlier mean hatch dates in the SCS than in the NCS, possibly indicating that they originated from different spawning populations, although there was considerable overlap in hatch date distributions between the two regions. Similarly, pelagic and demersal age-0 fish sampled in the WBS on average hatched earlier compared to those sampled in the EBS. It is important to note that while the differences are significant, each region in the Beaufort Sea was sampled during different years, hence inter-annual variability could contribute to the observed differences.

Similar hatch dates for pelagic captured fish in the NCS and WBS are consistent with oceanographic connections between the two regions. The NCS and WBS are connected via the Alaska Coastal Current, which flows along the coastline of Alaska from the Gulf of Alaska to the Beaufort Sea (Pickart et al., 2005) and has been hypothesized to transport larval and juvenile Arctic Cod from southern hatching locations in the Bering Sea or Chukchi Sea into the WBS (Forster et al., 2020; Levine et al., 2021). Arctic Cod in the NCS and WBS appeared to be distinct from those in the EBS based on a gap in the spatial distribution of age-0 fish (Forster et al., 2020), genetic differences (Wilson et al., 2017a, 2019b; Nelson et al., 2020), and different chemical compositions of age-0 otoliths (Chapter 2). The observed differences in hatch dates provide further evidence that juvenile Arctic Cod in the WBS and EBS originate from two separate spawning populations.

Differences in hatch dates between demersal and pelagic juveniles

Hatch date distributions were different between demersal and pelagic age-0 Arctic Cod in most regions (Fig. 7). Demersal fish were generally older than pelagic fish, supporting previous observations that juveniles descend to the bottom in late summer and throughout the fall as they grow (Geoffroy et al., 2016). Differences in size and inferred hatch date distributions between pelagic and demersal fish are consistent with the general ontogenetic movements of age-0 fish from the surface ocean into deeper waters and settlement to the bottom (Houde et al., 2002; Geoffroy et al., 2016). For example, Arctic Cod in the Chukchi Sea start moving out of the epipelagic layer and descend into the water column when they reach lengths of > 30mm (Levine et al., 2021). In the Beaufort Sea age-0 Arctic Cod have been observed to descend to depths >100 m and are completely out of the epipelagic zone by October (Geoffroy et al., 2011; Bouchard et al., 2015). The observed differences in hatch dates between demersal and pelagic fish were more pronounced in the Beaufort Sea, where the average station depth was 283 m deeper than in the Chukchi Sea with maximum sampling depths of 200 m for the IKMT and 1,000 m for bottom trawls. Deeper stations in the Beaufort Sea allowed for greater stratification of size classes between demersal and mid-water habitats. By contrast, in the NCS region mean hatch dates between pelagic and demersal fish were much smaller and demersal captured fish had a mean hatch date slightly later than the pelagic captured fish. This is likely due to the shallow depth (< 50 m) of the Chukchi Sea shelf, which is less than the depth ranges over which age-0 Arctic Cod are distributed in late summer in the Beaufort Sea (Geoffroy et al., 2016). Thus, daily vertical migrations of juvenile Arctic Cod on the Chukchi shelf are likely to extend to the bottom, limiting the vertical separation by size class.

Interannual variability in hatch dates

Samples in the EBS were collected over two years in 2013 and 2014, providing an opportunity for comparing Arctic Cod hatch dates and growth rates between these two years and between this study and previous estimates. Earlier estimates are available from Bouchard and Fortier (2011), who sampled pelagic age-0 Arctic Cod from 2005 and 2006 approximately 285 km east of our EBS sampling region and from Gallaway et al. (2017) who sampled the WBS and the U.S. side of the EBS in 2011. These comparisons suggest some notable differences that may be due to annual differences in sea ice conditions, sea surface temperatures (SST), or salinity, all of which have been hypothesized to play a large role in Arctic Cod early life history (Doroshev and Arnovich, 1974; Graham and Hop, 1995; Geoffroy et al., 2011). Sea ice thickness and the timing of ice retreat in the EBS varied considerably among years based on satellite-derived estimates for the EBS study region and may explain some of the observed differences.

Pelagic age-0 Arctic Cod from 2013 had the same mean hatch date as samples from 2006 (11 April) but hatched 9 days earlier on average than fish sampled in 2005 (20 April) (Bouchard and Fortier, 2011). Peak hatching in 2011 occurred in late April (Gallaway et al., 2017), similar to 2005. The range of hatch dates was also similar among the four years, beginning in mid to late December and extending through mid-July. There were, however, some differences among years in the peak hatch dates. Specifically, the

hatch date distributions in 2005 and 2006 were bimodal with one peak occurring in early April and the other in mid-May (Fig. 6 in Bouchard and Fortier, 2011). These peaks were more pronounced in 2005, while the 2006 hatch dates were more broadly distributed around these peak dates. In contrast, the hatch date distribution in 2013 showed a single, broad peak in late April (Fig. 6), similar to 2011 (Gallaway et al., 2017). Differences in hatch timing could be due to interannual differences in environmental conditions such as sea ice coverage and freshwater influences. The samples collected in 2006 and 2013 had the same mean hatch date and similar timing of ice retreat compared to an earlier sea ice retreat (Fig. 9) but a later mean hatch date in 2005. Thus, the observed patterns in the EBS are not consistent with a positive association between hatch timing and the timing of sea ice retreat. Alternatively, hatch timing in the EBS may be explained by differences in freshwater discharge. The January-March Mackenzie River discharge, approximately corresponding to the egg incubation period, was 1,266 $m^3 s^{-1}$ higher in 2006 than in 2005 (extracted from https://wateroffice.ec.gc.ca/mainmenu/historical_data_index_e.html on 10/1/2020), and was associated with earlier hatching in 2006. This is consistent with the hypothesis that increased freshwater discharge is associated with earlier hatching due to accelerated egg development in a freshwater lens that has slightly elevated temperatures compared to the surrounding seawater (Bouchard and Fortier, 2011). Thus, differences in freshwater discharge may be more important than the timing of sea ice retreat for determining the timing of hatching of Arctic Cod in the EBS, as previously hypothesized (Bouchard and Fortier, 2011), whereas the timing of sea ice retreat may determine hatch timing in areas without strong freshwater influences such as the Chukchi Sea.

No pelagic samples were collected in the EBS in 2014, but demersal fish captured in 2013 and 2014 had different mean hatch dates with an earlier mean hatch date in 2014 (18 Feb) compared to 2013 (16 March). These differences are consistent with the freshwater discharge hypothesis as the Mackenzie River discharge was considerably higher in 2014 (4655 $m^3 s^{-1}$) compared to 2013 (4022 $m^3 s^{-1}$). The differences were also consistent with the hypothesis that hatch timing is determined by the timing of sea ice retreat. In 2013, sea ice began to decrease in early June and some ice was still present in mid-August in the EBS, whereas ice began to recede in early May and was completely gone by the end of June in 2014 (Fig. 9). Therefore, the observed differences in hatch timing between 2013 and 2014 could be explained by either differences in freshwater discharge, differences in the timing of ice retreat or both.

Arctic Cod growth rates

The growth rates reported here, derived from linear regressions of length on age for each of our study regions, suggest significant regional differences in growth rates that may reflect differences in temperatures, food availability, or genetic differences. Arctic Cod growth rates range from 0.18 - 0.54 mm d^{-1} for field-based estimates (Bouchard and Fortier, 2011; Deary et al., in Review; Levine et al., 2021; Vestfals et al., 2019), whereas laboratory estimates are generally lower, ranging from 0.11 - 0.19 mm d^{-1} (Laurel et al., 201; Koenker et al., 2018). The growth rates from our study fall within the range estimated by Bouchard and Fortier (2011) for the Beaufort Sea, with the exception of the spring NBS and summer EBS samples, which were lower (Table 2). Our low estimate for the EBS could reflect interannual differences but may also be due to the higher uncertainty in our length-age regression for the EBS ($R^2 = 0.397$) relative to other regions (Table 2) and to those reported by Bouchard and Fortier (2011).

Growth rates have been shown to be positively correlated with SST across multiple Arctic seas (Bouchard and Fortier, 2011). That pattern was true for our summer samples as well, with fish in the more southern, warmer regions having higher estimated growth rates. However, spring-caught fish in the NBS had lower growth rates than those in the SCS, despite being caught in warmer waters. The mean temperature across stations sampled for aging in the NBS was 5.57°C whereas the SCS had a mean temperature of 4.35°C across sampling stations. Slower growth in the NBS could be due to the temperature differences at capture not being representative of the average temperatures experienced by larvae since hatching. The

differences in growth could also be an artifact of genetic differences between the stocks as well as differences in food availability (Koenker et al., 2018). Growth rate estimates for Arctic Cod in this and other studies could be affected by methodological differences and the biases associated with them. Among other factors, growth rate estimates are affected by size-selective mortality, gear selectivity and sampling design. Size-selective mortality favors faster growing individuals; thus field-based growth rates based on the survivors, such as in this study, may overestimate the average growth rate for a sampled population (Bailey and Houde, 1989; Litvak and Leggett, 1992). This could have contributed to the lower estimated growth rates for spring-captured larvae in the SCS compared to those captured in the summer, assuming that slower growing Arctic Cod experienced higher predation mortality than larger cod.

Gear selectivity may also bias estimated growth rates. For example, spring-caught Arctic Cod in this study were sampled using a bongo trawl that may have selected against larger, faster-growing larvae, resulting in growth rates that are biased low. In contrast, pelagic Arctic cod in the summer were sampled with a Marinovich trawl that may have selected against smaller larvae due to its large mesh size. These gear-related biases could have contributed to the estimated differences in apparent growth rates between the spring and summer-caught Arctic Cod in this study.

Finally, the sampling design can strongly impact growth rate estimates. Our approach requires age and length samples that are representative of the population of interest. Length samples from two different surveys in the SCS and NCS in 2017 (AMBON and Arctic IES II) were very similar and did not result in a significant different in hatch date distributions (SCS: $p = 0.423$; NCS: $p = 0.107$), despite differences in sampling locations and gear type (Marinovich vs. IKMT). Age samples were collected over a wide range of stations to minimize geographical biases but the extent to which they are representative of the broader populations in the study region is unclear as the population structure and the spatial distribution of different populations is largely unknown. Many studies (e.g. Deary *et al*., in review; Levine *et al*., 2021 for Arctic Cod) have estimated growth rates based on increases in mean length between successive surveys, making the strong assumption that the same population was sampled across surveys. For example, Levine *et al*. (2021) estimated a growth rate for Arctic Cod of 0.54 mm day^{-1} over a relatively short time period and within a region of the NCS where larvae were largely retained over the duration of the study. Their estimate was more than three times the growth rate estimated for the NCS in this study (0.149 mm/day) and higher than most growth rate estimates for Arctic Cod (Bouchard and Fortier, 2011; Koenker *et al*., 2018; Vestfals *et al*., 2021). While their growth rate is sensitive to the assumed relationship between acoustic target strength and length (range: 0.24 – 0.89 mm day^{-1}), higher growth rates could potentially result from favorable growth conditions during the relatively short period of observation during the summer, when temperatures and food availability are high.

Arctic Cod early life history dynamics in a changing climate

Water temperatures in the Arctic are expected to increase by an additional 1.5 ° C by 2100 under current carbon emissions scenarios (Collins et al., 2013). The effects of rising temperatures on Arctic Cod will impact the broader Arctic ecosystem. Warming conditions are expected to initially result in increased growth rates for juvenile Arctic Cod; however, once temperatures exceed 7.3°C, growth rates will begin to decrease (Laurel et al., 2015). Arctic Cod have a growth rate advantage over other gadid species at colder temperatures (< 5°C), but other gadid species grow faster and thus gain a competitive advantage for food resources at higher temperatures. Arctic cod eggs will similarly be disadvantaged in a warming climate as they presumably depend on sea ice cover and experience high mortality and other developmental issues at temperatures above 3.5°C (Kent et al., 2016). If the abundance of Arctic Cod declines in a warming ocean, many predators will have to feed on other species that are not as lipid-rich as Arctic Cod.

In addition to changes in growth rates, continued warming will affect other aspects of Arctic Cod early life history, such as the timing of hatching. Water temperature impacts the egg incubation period of

Arctic Cod, which decreases from an average of 79 days at -1.5°C to as short as 29 days at 3.5°C (Aronovich et al., 1975; Kent et al., 2016; Laurel et al., 2018). Changes in incubation time can result in a potential mismatch with important prey species if larvae emerge early and deplete their yolk sac prior to prey emergence. Decreased incubation time at warmer temperatures also results in decreased length at the time of hatch (Laurel et al., 2018), which limits the size of prey they can ingest and their ability to avoid predation (Cowan et al., 1996). The impact of climate change on Arctic Cod is likely to be more severe at the southern limit of their range in the Bering Sea than in the Chukchi Sea as the former is warmer on average and has experienced more pronounced temperature anomalies in the fall (1.2°C) compared to the Chukchi Sea (0.7°C) (Danielson et al., 2020). Our results, combined with laboratory studies on size at hatch, indicate that, as the Arctic continues to warm, Arctic Cod will hatch earlier in the year and at a smaller size. Our results on Arctic Cod hatch dates provide a benchmark for Arctic Cod emergence and can be compared to future studies to understand how warming ocean conditions impact hatch dates and how changes in hatch dates impact their survival and recruitment to the spawning population.

Management considerations

Arctic Cod are recognized as a critically important forage species in the Arctic and in the US are managed and protected under the Arctic Fishery Management Plan (FMP) (NPFMC, 2009). The FMP requires mapping and periodically updating essential fish habitat, including the distribution of early life history stages and potential spawning areas that were largely unknown at the time the Arctic FMP was written (NPFMC, 2009). After more than a decade of additional research on Arctic Cod in the Pacific Arctic, much has been learned (Mueter et al., 2020), but direct observations of spawning or eggs are still lacking. Our hatch date estimates can provide much needed information for biophysical transport models (Deary et al., in Review; Vestfals et al., 2021) to refine estimates of likely hatching locations. More broadly, this study increases our understanding of the early life history dynamics of Arctic Cod to help predict how their life history and abundance will change under changing Arctic conditions. Important subsistence resources such as ringed seals and beluga whales rely on Arctic Cod as a lipid dense food source and changes in Arctic Cod distribution and abundance will impact the Indigenous people that depend on them (Magdanz et al., 2010; Crawford et al., 2015).

As Arctic waters become more accessible, oil exploration is likely to increase and a better understanding of when and where spawning occurs can inform measures to protect Arctic Cod and mitigate potential impacts from oil development. Larval Arctic Cod exposed to oil for only one hour have a greatly reduced chance of survival to age 1 and mortality would increase if physical or chemical dispersal methods were used to clean up an oil spill (Gallaway et al., 2017; Word et al., 2011). Artic cod eggs may be even more susceptible to oil contamination because their buoyancy increases the chance of interaction with oil spills (Laurel et al., 2019). When exposed to low concentrations of crude oil during the critical period of Arctic Cod it can disrupt the normal development of the jaw and heart, as well as causes changes lipid metabolism and growth (Laurel et al., 2019, Bender et al., 2021). This can lead to degradation of the health of Arctic Cod which would ultimately impact predators that rely on them. If water temperatures are increased by 2.3°C the rate of deformities and mortality during this early stage are significantly increased illustrating the potential an oil spill can have as waters continue to warm (Bender et al., 2021). Bioaccumulation after oil exposure is also a concern as Arctic Cod are a key component of the food web in the Arctic. Indirect exposure to oil thru the consumption of contaminated prey such as *Calanus* spp. can lead to large scale bioaccumulation within Arctic Cod (Agersted et al., 2018). This, in turn, can lead to bioaccumulation in larger animals such as seals, whales, and sea birds that are important subsistence resources. Thus, a spill in an area with high concentrations of Arctic Cod can cause large scale food web impacts for many predatory species in the Arctic, which already face challenges in a changing environment. Modeling efforts to predict the impact of oil spills on the Arctic ecosystem focus on how larval and juvenile Arctic Cod are affected (Word et al., 2014). By estimating how oil spills will impact the recruitment of adult females to the spawning population they can predict the total ecological impact

by extrapolating the loss of critical prey to the Arctic food web. Thus, Arctic Cod can serve as a key indicator for the potential ecological impacts from anthropogenic disturbances.

Transport ships are also known to disrupt and negatively impact survival of Arctic Cod. The sound pollution created by vessel traffic can cause Arctic Cod to move away from vessels and can alter Arctic Cod behavior (Ivanova et al., 2020). The presence of vessels, both moored and when traveling, caused Arctic Cod to spend more time moving away from the source of the noise and less time searching for food. During the summer, when food is most abundant, the trade off in energetics from feeding to fleeing can have a negative impact on Arctic Cod achieving optimal size prior to the winter season (Ivanova et al., 2020). It is important that management strategies account for potential anthropogenic impacts on Arctic Cod, as well as to their essential habitat, to preserve Arctic ecosystem functions.

Conclusions

We used otolith-derived ages to estimate hatch timing and growth rates of Arctic Cod, greatly improving our understanding of the early life history of Arctic Cod in the Pacific Arctic. The wide range of estimated hatch dates provides strong evidence that Arctic Cod use a bet-hedging strategy that distributes offspring over a wide range of environmental conditions by spawning over a protracted time period across multiple locations in the Pacific Arctic. Our results align with previous findings and indicate that regional and interannual variations in hatch dates and growth rates are associated with the timing of sea ice retreat and freshwater discharge, highlighting the sensitivity of Arctic Cod to changing conditions in the Pacific Arctic. Earlier sea ice retreat and increased freshwater discharge under climate warming suggest that Arctic Cod will hatch earlier in the future, with unknown consequences for their early growth and survival. Any impacts of climate change on Arctic Cod have the potential to negatively affect upper trophic level species that rely on Arctic Cod or their consumers as a critical food source, including humans in many local communities that depend on subsistence resources. The regional and seasonal differences in Arctic Cod hatch dates documented here provide evidence for the existence of multiple spawning populations in the Pacific Arctic. However, while our results are suggestive, additional genetic and biological information is required to help differentiate putative populations or sub-populations. Finally, the improved understanding of hatch timing and spawning dynamics can inform the development of measures to protect Arctic Cod during their early life history. Continued monitoring and additional research on Arctic Cod will be required to fully understand how climate change will impact their distribution and abundance and the consequences of these changes for the Arctic ecosystem.

Acknowledgements

The authors thank the boat and field crews of the R/V *Norseman II*, M/V *Ocean Starr*, and R/V *Sikuliaq* for their effort in data collection. We thank Morgan Busby and Alison Deary for their assistance in identifying larval Arctic Cod, and Kristin Cieciel and Sharon Wildes for confirming Arctic Cod identifications through genetic analysis. We also thank Kevin McNeel and Chris Hinds from the Alaska Department of Fish and Game Mark, Age and Tagging laboratory for their resources and knowledge of otolith extraction, preparation and age determination. Thank you to Benjamin Laurel at the Hatfield Marine Science Center for providing lab raised Arctic Cod to test our ageing ability and help determine where the hatch mark is located for Arctic Cod otoliths. Study collaboration and funding were provided by the US Department of the Interior, Bureau of Ocean Energy Management Environmental Studies Program, Washington, DC, under Agreement Numbers M17PG00007, M17AC00016, and M19AC00018. Additional support was provided by the University of Alaska Coastal Marine Institute through a Graduate Student Research Award.

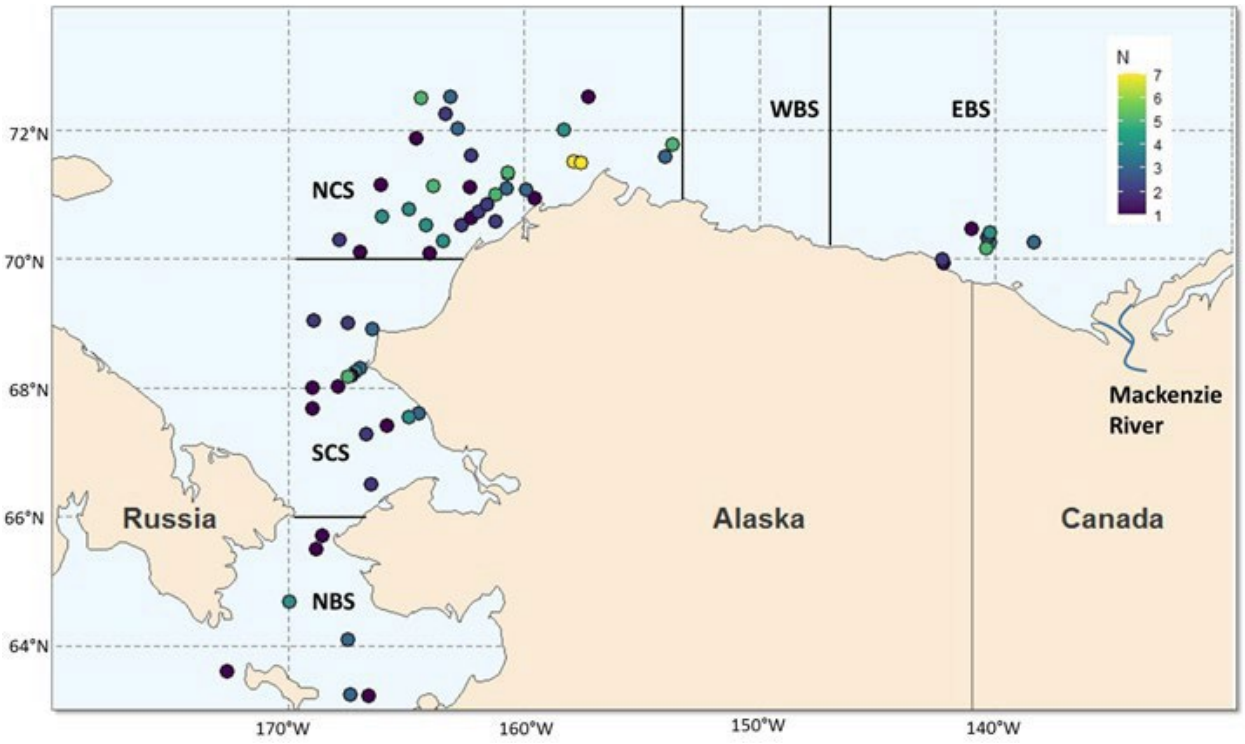

Figure 1: Locations where Arctic Cod for aging were captured. Color change from cool (blue) to warm (yellow) represents the number of specimens captured at a station, where N=7 denotes 7 or more specimens. Study regions are the northern Bering Sea (NBS), southern (SCS) and northern Chukchi Sea (NCS) and western (WBS) and eastern Beaufort Sea (EBS).

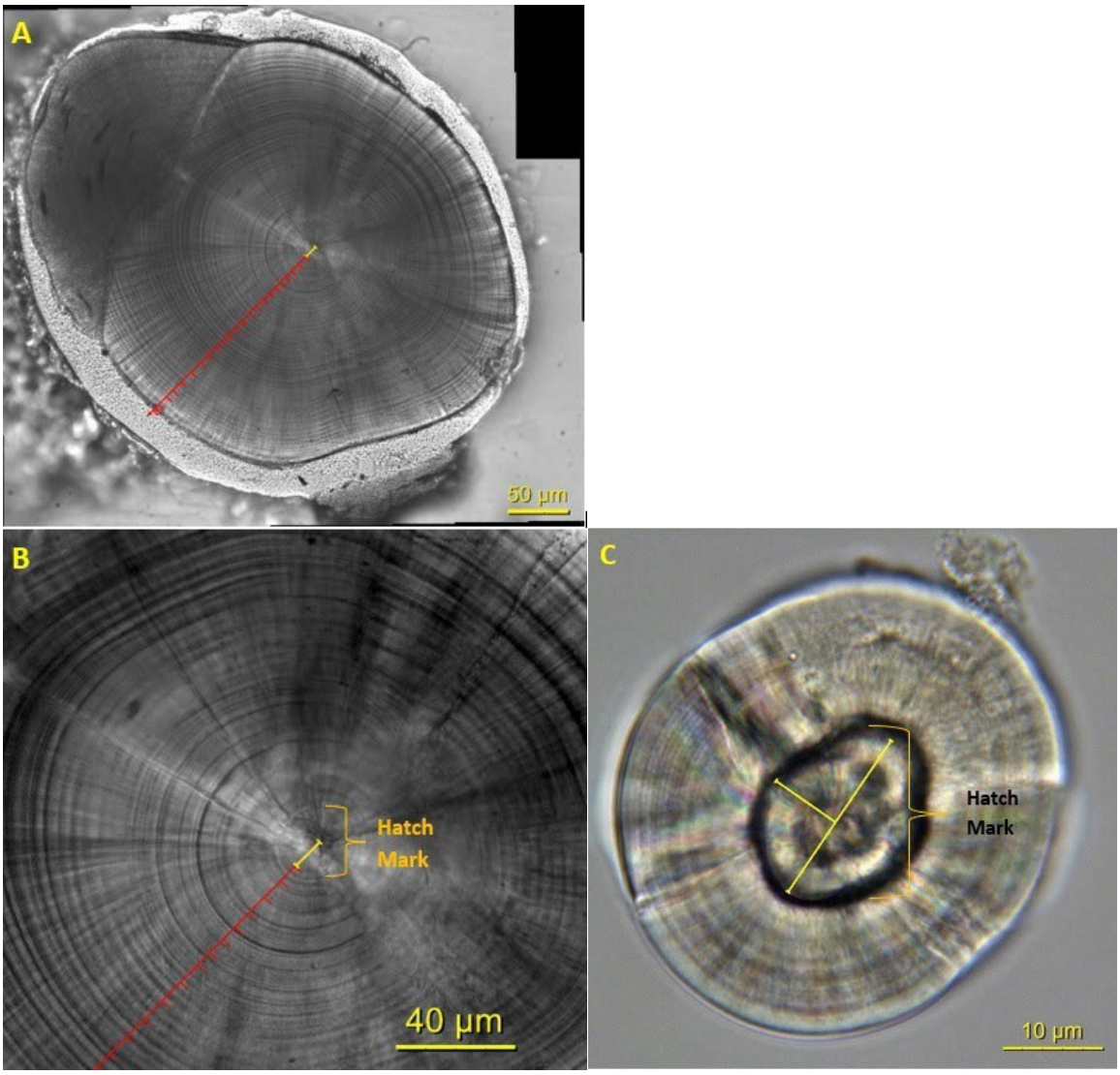

Figure 2: (A) Polished sagittal otolith at 40x magnification with daily growth increments marked at every 5th increment. (B) Cropped image of the same otolith showing the hatch mark. (C) Sagittal otolith at 100X magnification from a lab raised Arctic Cod with the hatch mark outlined.

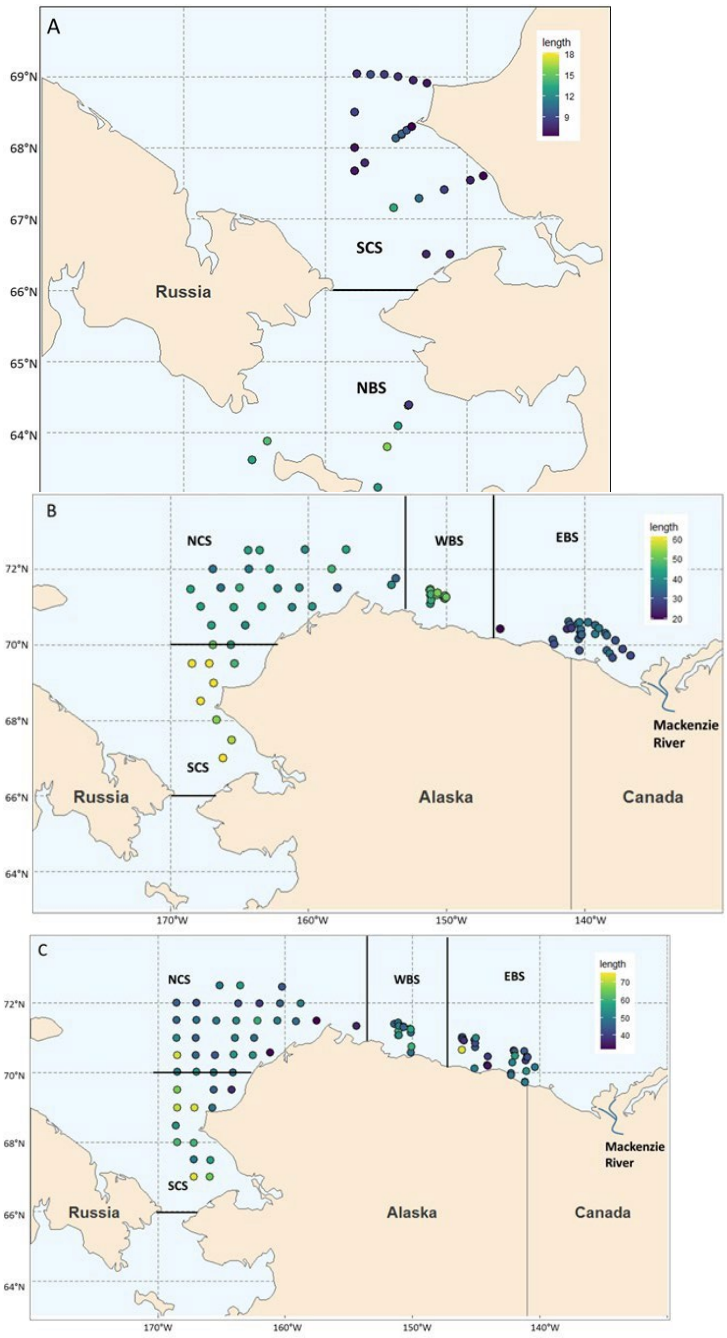

Figure 3: Stations with length data for Arctic Cod. Shading denotes average length by station for Arctic Cod captured during the spring survey in the water column (Bongo nets, A) and during the summer survey in the water column (pelagic trawl, B) and on the bottom (demersal trawl, C).

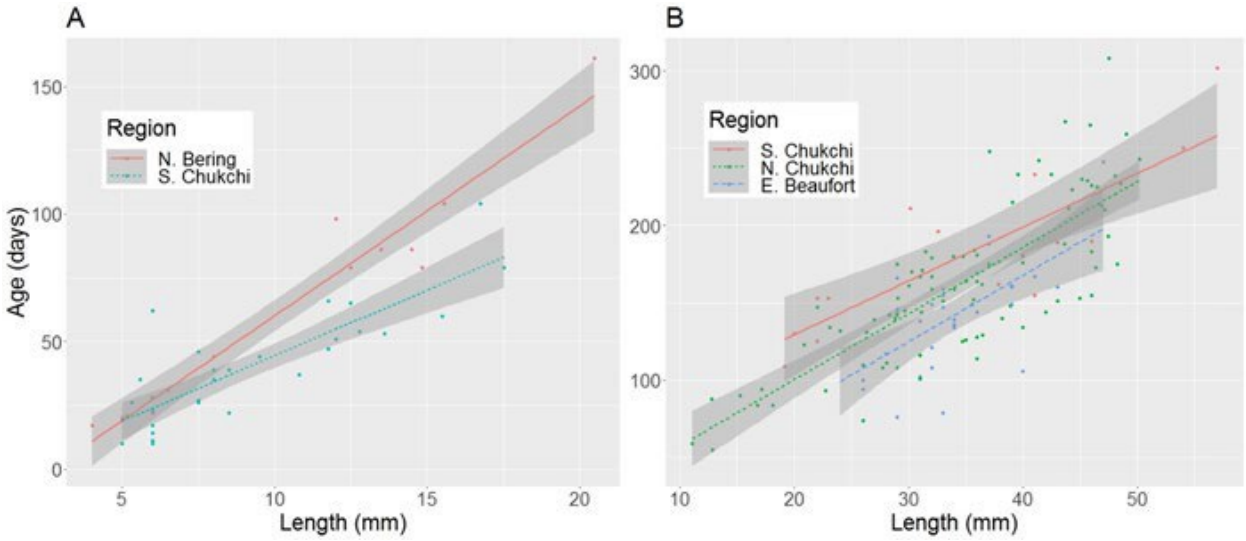

Figure 4: Age-at-length regressions by sampling region for spring (A) and summer (B) captured Arctic Cod with 95% confidence bands. Lengths ranged from 5 to 20 mm in spring (A) and from 10 to 55 mm in summer (B). Ages ranged from 0 to 150 days (A) and 100 to 300 days (B) in the spring and summer, respectively.

Figure 5: Length frequency distributions (x-axis, in mm) of age-0 Arctic Cod sampled in each region by vertical location in the water column. The number of individuals measured in each region is indicated (N).

Figure 6: Estimated hatch date distributions by location in the water column for each region. Northern Bering Sea (NBS); southern Chukchi Sea (SCS); northern Chukchi Sea (NCS); western Beaufort Sea (WBS); eastern Beaufort Sea (EBS).

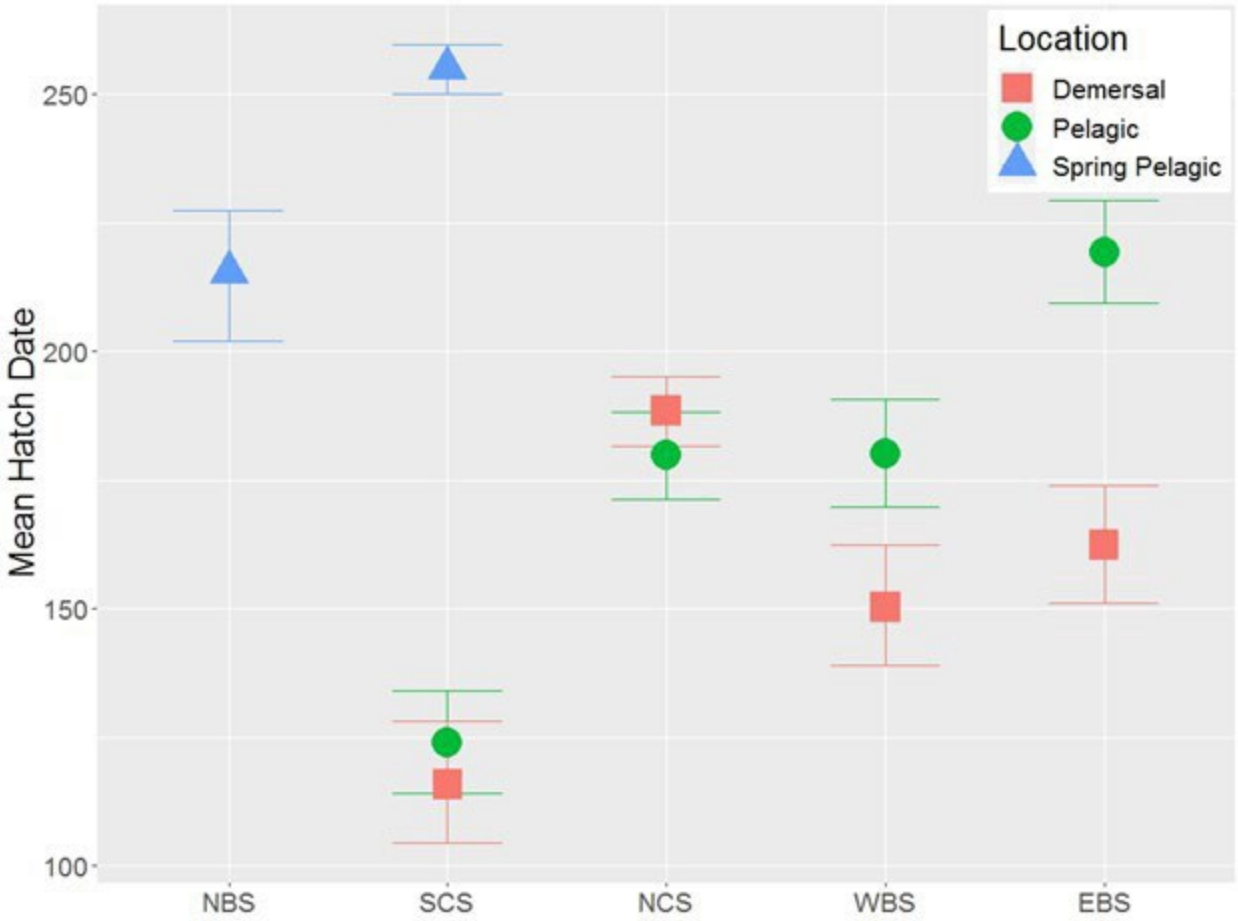

Figure 7: Estimated mean hatch date with 95% confidence limits for each region and vertical location (Pelagic or Demersal). Mean hatch date 100 corresponds to December 12 and hatch date 240 corresponds to May 11.

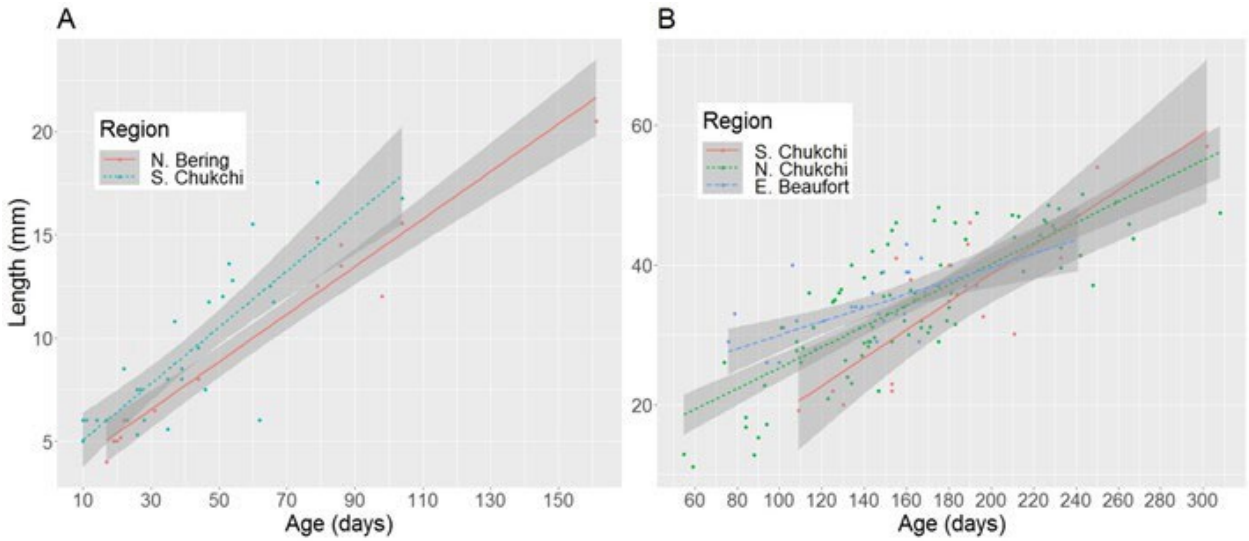

Figure 8: Regressions of length on age to estimate growth rates for spring (A) and summer (B) captured age-0 Arctic Cod by region.

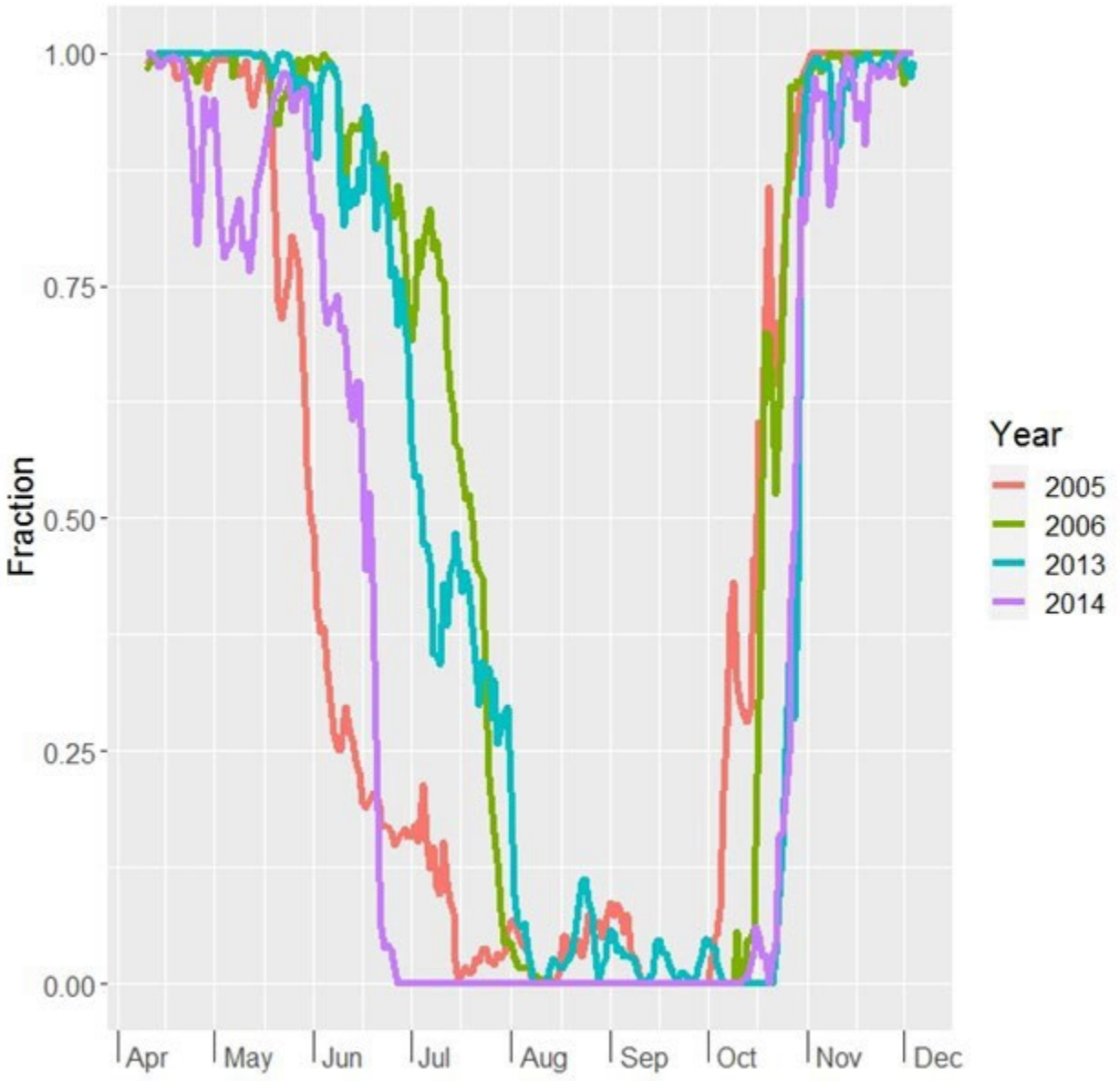

Figure 9: Seasonal trends in sea ice concentration (fraction of area with > 15% sea ice) for the eastern Beaufort Sea sampling region for four selected years with hatch date information.

Table 1: Season, cruise, region, and sampling year with the dates, gear type, number of stations and number of Arctic Cod that were captured with their length range and mean length (mm). Regions are the northern Bering Sea (NBS), southern Chukchi Sea (SCS), northern Chukchi Sea (NCS), western Beaufort Sea (WBS) and eastern Beaufort Sea (EBS). Bongo, IKMT, and Marinovich trawls sampled fish in the pelagic zone and bottom trawls sampled fish in the demersal zone.

Season	Cruise	Region	Year	Sampling Dates	Gear Type	# of Stations	Polar Cod Captured	Length Range	Mean Length
Spring	ASGARD	NBS	2017	Jun-10 – Jun-28	Bongo	7	19	6-19	12
Spring	ASGARD	SCS	2017	Jun-28 – Jun-23	Bongo	23	838	5-17	8
Summer	AMBON	SCS	2017	Aug-6 – Aug-21	IKMT	4	91	18-56	37
Summer	AMBON	SCS	2017	Aug-6 -Aug-21	Bottom Trawl	11	584	28-68	50
Summer	AMBON	NCS	2017	Aug-18 – Aug-22	IKMT	6	1,076	21-51	29
Summer	AMBON	NCS	2017	Aug-9 – Aug-22	Bottom Trawl	50	2,841	11-73	38
Summer	Arctic IES	SCS	2017	Sep13 – Sep-27	Marinovich	9	666	28-74	52
Summer	Arctic IES	SCS	2017	Sep-12 – Sep-27	Bottom Trawl	14	190	34-74	52
Summer	Arctic IES	NCS	2017	Aug-8 – Sep-13	Bongo	25	54	13-40	25
Summer	Arctic IES	NCS	2017	Aug-13 – Sep-13	Marinovich	19	1,256	25-71	42
Summer	Arctic IES	NCS	2017	Aug-10 – Sep-14	Bottom Trawl	30	463	22-73	48
Summer	TB12	WBS	2012	Sep-21 – Sep-29	Bottom Trawl	12	480	15-71	54
Summer	TB12	WBS	2012	Sep-22 – Sep-30	IKMT	13	254	22-71	46
Summer	TB13	EBS	2013	Sep-15 – Sep-30	Bottom Trawl	11	15	30-42	35
Summer	TB13	EBS	2013	Aug-13 – Aug-30	IKMT	27	351	17-47	33
Summer	TB14	EBS	2014	Aug-19 – Aug-31	Bottom Trawl	27	264	27-73	46

Table 2: Number of age-0 Arctic Cod aged by season and region with the range of standard lengths (mm) and estimated ages (days), and parameters of the length-at-age regressions with the slope representing estimated growth rates in mm d^{-1}.

					Length-age regressions		
Season	**Region**	**Total aged**	**Length range (mm)**	**Age range (days)**	**Slope**	**Intercept**	**R^2**
Spring	N. Bering	14	4-21	17-161	0.115	3.075	0.943
Spring	S. Chukchi	29	5-18	10-104	0.183	1.804	0.912
Summer	S. Chukchi	15	19-57	109-302	0.200	-1.290	0.673
Summer	N. Chukchi	77	11-50	55-308	0.149	10.435	0..631
Summer	E. Beaufort	31**	24-47	76-241	0.097	20.250	0.397

** 27 were aged from 2013 survey and four were aged from 2014 survey.

Table 3: Model coefficients, estimates, standard errors and Wald's t-test results for regressions of age in days on standard length (mm) by season. Region-specific intercepts (α) and slopes (β) were estimated in the spring; a common slope was estimated in the summer. Subscript for regions are Northern Bering Sea (NBS), southern (SCS) and northern Chukchi Sea (NCS) and eastern Beaufort Sea (EBS).

Season	Region	Coefficient	Estimate	Std. Error	t-value	P value
Spring	NBS	α_{NBS}	-21.967	6.148	-3.573	0.001
	NBS	β_{NBS}	8.210	0.541	15.185	0.001
	SCS	α_{SCS}	10.484	8.163	1.284	0.207
	SCS	β_{SCS}	5.485	0.763	7.189	0.001
Summer	SCS	α_{SCS}	42.342	9.144	4.631	0.001
	NCS	α_{NCS}	20.538	5.412	3.795	0.002
	EBS	α_{EBS}	3.038	8.973	0.339	0.735
	All	β	4.092	0.238	17.178	0.001

Table 4: Mean and range of hatch dates (HD) by season, region and vertical location in water column. Dates marked with * are from the previous year. Regions are Northern Bering Sea (NBS), southern (SCS) and northern Chukchi Sea (NCS) and western (WBS) and eastern Beaufort Sea (EBS).

Season and Region	Vertical Location	Mean HD	Earliest	Latest
Spring				
NBS	Pelagic	Apr-06	Jan-02	Jun-09
SCS	Pelagic	May-16	Feb-26	Jun-22
Summer				
SCS	Pelagic	Jan-04	Sep-27*	Jul-22
SCS	Demersal	Dec-27*	Sep-27*	Jun-07
NCS	Pelagic	Mar-01	Sep-27*	Aug-06

Table 5: Pairwise comparisons of mean hatch dates among regions by season and vertical location in the water column with bootstrap-based p-values and estimated difference in mean hatch dates. Negative differences in mean HD imply that the first region had an earlier hatch date than the second region.

Regional comparisons	Season	Vertical location	P-value	Difference in Mean HD
Spring				
NBS – SCS	Spring	Pelagic	0.002	-40
Summer				
SCS – NCS	Summer	Pelagic	0.002	-55
SCS – WBS	Summer	Pelagic	0.002	-56
SCS – EBS	Summer	Pelagic	0.002	-95
NCS – WBS	Summer	Pelagic	0.957	0
NCS – EBS	Summer	Pelagic	0.002	-39
WBS – EBS	Summer	Pelagic	0.002	-39
SCS – NCS	Summer	Demersal	0.002	-72
SCS – WBS	Summer	Demersal	0.002	-34
SCS – EBS	Summer	Demersal	0.002	-46
NCS – WBS	Summer	Demersal	0.002	38
NCS – EBS	Summer	Demersal	0.002	-26
WBS – EBS	Summer	Demersal	0.059	-12

References

Abookire, A.A., Rose, C.S., 2005. Modifications to a plumb staff beam trawl for sampling uneven, complex habitats. Fish. Res. 71 (2), 247-254. https://doi.org/10.1016/j.fishres.2004.06.006

Agersted, M., Møller, E., Gustason, K., 2018. Bioaccumulation of oil compounds in the high-Arctic copepod *Calanus hyperboreus*. Aquat. Toxicol. 195, 8-14. https://doi.org/10.1016/j.aquatox.2017.12.001.

Aronovich, T., Doroshev, S., Spectorova, L., Makhotin, V., 1975. Egg incubation and larval rearing of navaga (*Eleginus navaga pall*.), Polar cod (*Boreogadus saida lepechin*) and arctic flounder (*Liopsetta glacialis pall*.) in the laboratory. Aquaculture. 6 (3), 233 - 242. https://doi.org/10.1016/0044-8486(75)90043-5

Bailey, K.M., Houde, E.D., 1989. Predation on eggs and larvae of marine fishes and the recruitment problem. Adv Mar Biol. 25, 1-83. https://doi.org/10.1016/S0065-2881(08)60187-X

Bender, M.L., Giebichenstein, J., Teisrud, R.N., Laurent, J., Frantzen, M., Meador, J.P., Sørensen, L., Hansen, B.H., Reinardy, H.C., Laurel, B., Nahrang, J., 2021. Combined effects of crude oil exposure and warming on eggs and larvae of an arctic forage fish. Sci Rep. 11, 8410. https://doi.org/10.1038/s41598-021-87932-2

Berline, L., Spitz, Y.H., Ashjian, C.J., Campbell, R.G., Maslowski, W., Moore, S.E., 2008. Euphausiid transport in the Western Arctic Ocean. Mar. Ecol. Prog. Ser. 360, 163-178. https://doi.org/10.3354/meps07387

Bluhm, B., Gradinger, R., 2008. Regional variability in food availability for arctic marine mammals. Ecol Appl. 18 (2), 77-96. https://doi.org/10.1890/06-0562.1

Bouchard, C., Fortier, L., 2008. Effects of polynyas on the hatching season, early growth and survival of Arctic cod *Boreogadus saida* in the Laptev Sea. Mar. Ecol.: Prog. Ser. 355, 247-256 https://doi.org/10.3354/meps07335

Bouchard, C., Fortier, L., 2011. Circum-arctic comparison of the hatching season of Arctic cod.

Boreogadus saida: A test of the freshwater winter refuge hypothesis. Prog. Oceanogr. 90, 105-116. https://doi.org/10.1016/j.pocean.2011.02.008
Bouchard, C., Thorrold, S., Fortier, L., 2015. Spatial segregation, dispersion and migration in early stages of Arctic cod *Boreogadus saida* revealed by otolith chemistry. Mar Biol. 162, 855-868. https://doi.org/10.1007/s00227-015-2629-5
Bouchard, C., Fortier, L., 2020. The importance of *Calanus glacialis* for the feeding success of young Arctic cod: a circumpolar synthesis. Polar Biol. 43, 1095-1107. https://doi.org/10.1007/s00300-020-02643-0
Buchheister, A., Wilson, M.T., 2005. Shrinkage correction and length conversion equations for *Theragra chalcogramma*, *Mallotus villosus* and *Thaleichthys pacificus*. J. Fish Biol. 67(2), 541-548. https://doi.org/10.1111/j.0022-1112.2005.00741.x
Campana, S.E., 2001. Accuracy, precision and quality control in age determination, including a review of the use and abuse of age validation methods. J. Fish Biol. 59 (2), 197-242. https://doi.org/10.1111/j.1095-8649.2001.tb00127.x
Campana, S.E., 1999. Chemistry and composition of fish otoliths: pathways, mechanisms and applications. Mar. Ecol.: Prog. Ser. 188, 263-297. https://doi.org/10.3354/meps188263
Carmack, E.C., Macdonald, R.W., 2002. Oceanography of the Canadian Shelf of the Beaufort Sea: A Setting for Marine Life. Arctic. 55 (5), 29-45. https://doi.org/10.14430/arctic733
Chang, W.Y.B., 1982. A statistical method for evaluating the reproducibility of age determination. Can. J. Fish. Aquat. Sci. 39 (8), 1208-1210. https://doi.org/10.1139/f82-158
Christiansen, J.S., Fevolden, S.E., 2000. The Arctic cod of Porsangerfjorden, Norway; revisited, Sarsia. 85 (3), 189-193. https://doi.org/10.1080/00364827.2000.10414571
Collins, M., Knutti, R., Arblaster, J., Dufresne, J.-L., Fichefet, T., Friedlingstein, P., Gao, X., Gutowski, W.J., Johns, T., Krinner, G., Shongwe, M., Tebaldi, C., Weaver, A.J., Wehner, M., 2013. Long-term Climate change: projections, commitments and irreversibility. In: Stocker, T.F., Qin, D., Plattner, G.-K., Tignor, M., Allen, S.K., Boschung, J., Nauels, A., Xia, Y., Bex, V., Midgley, P.M. (Eds.), Climate Change 2013: The Physical Science Basis. Contribution of Working Group I to the Fifth Assessment Report of the Intergovernmental Panel on Climate Change. Cambridge, United Kingdom and New York, NY, USA.
Cowen, J.H., Houde, E.D., Rose, K.A., 1996. Size-dependent vulnerability of marine fish larvae to predation: an individual-based numerical experiment. ICES. J. Mar. Sci. 53, 23-37. https://doi.org/10.1006/jmsc.1996.0003
Craig, P., Griffiths, W., Haldorson, L., McElderry, H., 1982. Ecological studies of Arctic cod (*Boreogadus saida*) in Beaufort Sea coastal waters, Alaska. Can. J. Fish. Aquat. Sci. 39 (3), 395-406. https://doi.org/10.1139/f82-057
Crawford, J.A., Quakenbush, L.T., Citta, J.J., 2015. A comparison of ringed and bearded seal diet, condition and productivity between historical (1975-1984) and recent (2003-2012) periods in the Alaskan Bering and Chukchi seas. Prog. Oceanogr. 136, 133-150. https://doi.org/10.1016/j.pocean.2015.05.011
Danielson, S.L., Eisner, L., Ladd, C., Mordy, C., Sousa, L., Weingartner, T.J., 2017. A comparison between late summer 2012 and 2013 water masses, macronutrients, and phytoplankton standing crops in the northern Bering and Chukchi Seas. Deep Sea Res. Part II 135, 7-26. https://doi.org/10.1016/j.dsr2.2016.05.024
Danielson, S., Ahkinga, O., Edenfield, L., Eisner, L., Forster, C., Hardy, S., Hartz, S., Holladay, B., Hopcroft, R., Jones, B., Krause, J., Kuletz, K., Lekanoff, R., Lomas, M., Lu, K., Norcross, B., O'Daly, S., Pretty, J., Pham, C., Poje, A., Roth, E., Seabrook, S., Shipton, P., Smith, B., Smoot, C., Stafford, K., Stockwell, D., Yamaguchi, A., Zinkann, A., 2017a. Arctic Shelf Growth, Advection, Respiration and Deposition (ASGARD) rate measurements project. Anchorage AK: North Pacific Research Board. SKQ201709S Cruise Report to the Arctic Integrated Research Program.

De Robertis, A., Taylor, K., Wilson, C.D., Farley, E.V., 2017. Abundance and Distribution of Arctic cod (*Boreogadus saida*) and other Pelagic Fishes over the U.S. Continental Shelf of the Northern Bering and Chukchi Seas. Deep Sea Res. Part II. 135, 51-65. https://doi.org/10.1016/j.dsr2.2016.03.002

Doroshev, S., Aronovich, T., 1974. The effects of salinity on embryonic and larval development of *Eleginus navga* (Pallas), *Boreogadus saida* (Lepechin) and *liopsetta glacialis* (Pallas). Aquaculture 4, 353-362. https://doi.org/10.1016/0044-8486(74)90064-7

Drost, H., Lo, M., Carmack, E., Farrell, A., 2016. Acclimation potential of Arctic cod (*Boreogadus saida*) from the rapidly warming Artic Ocean. J. Exp. Biol. 219, 3114-3125. https://doi.org/10.1242/jeb.140194

Eisner, L., Hillgruber, N., Martinson, E., Maselko, J., 2012. Pelagic fish and zooplankton species assemblages in relation to water mass characteristics in the northern Bering and southeast Chukchi seas. Polar Biol. 36, 87-113. https://doi.org/10.1007/s00300-012-1241-0

Eckmann, R., Rey, P., 1987. Daily increments on the otoliths of larval and juvenile *Coregonus* spp., and their modifications by environmental factors. Hydrobiologia 148, 137-143. https://doi.org/10.1007/BF00008399

Eriksen, E., Huserbråten, M., Gjøsæter, H., Vikebø, F., Albretsen, J., 2020. Arctic cod egg and larval drift patterns in the Svalbard archipelago. Polar Biol. 43, 1029-1042. https://doi.org/10.1007/s00300-019-02549-6

Farley, E., Cieciel, K., Vollenweider, J., Ladd, L., Duffy-Anderson, J., Eisner, L., Kimmel, D., Lomas, M., McCabe, R., Mordy, C., Stabeno, P., Copeman, L., De Robertis, A., Levine, R., Guyon, J., Kulets, K., Logerwell, L., Mueter, F., Wilson, C., Vestals, C., Lebon, G., Berchok, C., Ferm, N., Wayner H., Reedy, M., Salo, S., Andrews, A., Grigorov, I., Baer, S., Cooper, D., Johnson G., Somoff, A., Kuznetsova, N., Flores, A., Goldstein, E., Wisegarver, E., Spear, A., Doyle, T., Pohlen, Z., 2017. Arctic integrated ecosystem survey. Anchorage AK: North Pacific Research Board. Cruise Report to the Arctic Integrated Research Program.

Forster, C., Norcross, B., Mueter, F., Logerwell, E., Seitz, A. 2020. Spatial patterns, environmental correlates, and potential seasonal migration triangle of Arctic cod (*Boreogadus saida*) distribution in the Chukchi and Beaufort seas. Polar Biol. 43, 1073-1094. https://doi.org/10.1007/s00300-020-02631-4

Fortier, L., Sirois, P., Michaud, J., Barber, D., 2006. Survival of Arctic cod larvae (*Boreogadus saida*) in relation to sea ice and temperature in the Northeast Water Polyna (Greenland Sea) Can. J. Fish. Aquat. Sci. 63 (7), 1608-1616. https://doi.org/10.1139/f06-064

Gallaway, B.J., Konkel, W.J., Norcross, B.L., 2017. Some thoughts on estimating change to Arctic Cod populations from hypothetical oil spills in the eastern Alaska Beaufort Sea. Arct. Sci. 3 (4), 716-129. https://doi.org/10.1139/as-2016-0056

Gjøsæter, H., 1995. Pelagic fish and the ecological impact of the modern fishing industry in the Barents Sea. Arctic. 48 (3), 267-279. https://www.jstor.org/stable/40511661

Geoffroy, M., Robert, D., Darnis, G., Fortier, L., 2011. The aggregation of Arctic cod (*Boreogadus saida*) in the deep Atlantic layer of ice-covered Amudsen Gulf (Beaufort Sea) in winter. Polar Biol. 34, 1959-1971. https://doi.org/10.1007/s00300-011-1019-9

Geoffroy, M., Majewski, A., LeBlanc, M., Gauthier, S., Walkusz, W., Reist, J., Fortier, L., 2016. Vertical segregation of age-0 and age-1+ polar cod (*Boreogadus saida*) over the annual cycle in the Canadian Beaufort Sea. Polar Biol. 39, 1023-1037. https://doi.org/10.1007/s00300-015-1811-z

Grahm, M., Hop, H., 1995. Aspects of reproduction and larval biology of Arctic cod (*Boreogadus saida*). Arctic. 48 (2), 130-135. https://www.jstor.org/stable/40511636

Gray, B., Norcross, B., Blanchard, A., Beaufreau, A., Seitz, A., 2016. Variability in the summer diets of juvenile polar cod *(Boreogadus saida*) in the northeastern Chukchi and western Beaufort seas. Polar Biol. 39, 1069-1080. https://doi.org/10.1007/s00300-015-1796-7

Gradinger, R., Bluhm, B., 2004. In-situ observations on the distribution and behavior of amphipods and Artic Cod (*Boregadus saida*) under the sea ice of the High Arctic Canada Basin. Polar Biol. 27, 595-603. https://doi.org/10.1007/s00300-004-0630-4

Harding, M.M., Anderberg, P.I., Haymet, A.D.J., 2003. 'Antifreeze' glycoproteins from polar fish. Eur. J. Biochem. 270 (7), 1381-1392. https://doi.org/10.1046/j.1432-1033.2003.03488.x

Helser, T.E., Colman, J.R., Anderl, D.M., Kastelle, C.R., 2017. Growth dynamics of saffron cod (*Eleginus gracilis*) and Arctic cod (*Boreogadus saida*) in the Northern Bering and Chukchi Seas. Deep Sea Res. Part II. 135, 66-77. https://doi.org/10.1016/j.dsr2.2015.12.009

Hop, H., Gjøsæter, H., 2013. Arctic cod (*Boreogadus saida*) and capelin (*Mallotus villosus*) as key species in marine food webs of the Arctic and the Barents Sea. Mar. Biol. Res. 9 (9), 878-894. https://doi.org/10.1080/17451000.2013.775458

Houde, E., 1987. Fish early life dynamics and recruitment variability. Am. Fish. Soc. Symp. 2, 17-29.

Hovde, S., Albert, O., Nilssen, E., 2002. Spatial, seasonal and otogenetic variation in diet of Northeast Arctic Greenland halibut (*Reinhardtius hippoglossoides*). J. Mar. Sci. 59 (2), 421-437. https://doi.org/10.1006/jmsc.2002.1171

Iken, K., Mueter, F., Grebmeier, J.M., Cooper, L.W., Danielson, S.L., Bluhm, B.A., 2018. Developing an observational design for epibenthos and fish assemblages in the Chukchi Sea. Deep Sea Res. Part II. 162, 180-190. https://doi.org/10.1016/j.dsr2.2018.11.005

Ivanova, S., Kessel, S., Espinoza, M., McLean, M., O'Neill, C., Landry, J., Hussey, N., Williams, R., Vagel, S., Fish, A., 2020. Shipping alters the movement and behavior of Arctic cod (*Boreogadus saida*), a keystone fish in Arctic marine ecosystems. Ecol. Appl. 30 (3), e02050. https://doi.org/10.1002/eap.2050

Kent, D., Drost, H., Fisher, J., Oyama, T., Farrell, A., 2016. Laboratory rearing of wild Arctic cod *Boreogadus saida* from egg to adulthood. J. Fish Biol. 88 (3), 1241-1248. https://doi.org/10.1111/jfb.12893

Koenker, B., Laurel, B., Copeman, L., Ciannelli, L., 2018. Effects of temperature and food availability on the survival and growth of larval Arctic cod (*Boreogadus saida*) and walleye pollock (*Gadus chalcogrammus*). ICES J. Mar. Sci. 75 (7), 2386-2402. https://doi.org/10.1093/icesjms/fsy062

Kono, Y., Sasaki, H., Kurihara, Y., Fujiwara, A., Yamamoto, J., Sakurai, Y., 2016. Distribution pattern of Arctic cod (*Boreogadus saida*) larvae and larval fish assemblages in relation to oceanographic parameters in the northern Bering Sea and Chukchi Sea. Polar Biol. 39, 1039-1048. https://doi.org/10.1007/s00300-016-1961-7

Ladd, C., Mordy, C.W., Salo, S.A., Stabeno P.J., 2016. Winter water properties and the Chukchi polynya. J. Geophys. Res.: Oceans. 121, 5516-5534. https://doi.org/10.1002/2016JC011918.

Laurel, B., Spencer, M., Iseri, P., Copeman, L., 2015. Temperature-dependent growth and behavior of juvenile Arctic cod (*Boreogadus saida*) and co-occurring North Pacific gadids. Polar Biol. 39, 1127-1135. https://doi.org/10.1007/s00300-015-1761-5

Laurel, B., Copeman, L., Spencer, M., Iseri, P., 2017. Temperature-dependent growth as a function of size and age in juvenile Arctic cod (*Boreogadus saida*). ICES J. Mar. Sci. 74 (6), 1614-1621. https://doi.org/10.1093/icesjms/fsx028

Laurel, B., Copeman, L., Spencer, M., Iseri, P., 2018. Comparative effects of temperature on rates of development and survival of eggs and yolk-sac larvae of Arctic cod (*Boreogadus saida*) and walleye Pollock (*Gadus chalcogrammus*). ICES J. Mar. Sci. 75, 2403-2412. https://doi.org/10.1093/icesjms/fsy042

Laurel, B., Copeman, L., Iseri, P., Spencer, M., Hutchinson, G., Nordtug, T., Donald, C., Meier, S., Allan, S., Boyd, D., Ylitalo, G., Cameron, J., French, B., Linbo, T., Scholz, N., Incardona, J., 2019. Embryonic crude oil exposure impairs growth and lipid allocation in a keystone arctic forage fish. iScience 19: 1101 - 1113. https://doi.org/10.1016/j.isci.2019.08.051

Leblanc, M., Geoffroy, M., Bouchard, C., Gauthier, S., Majewski, A., Reist, J., Fortier, L., 2020. Pelagic production and recruitment of juvenile Arctic cod (*Boreogadus saida*) in Canadian Arctic seas. Polar Biol. 43, 1043-1054. https://doi.org/10.1007/s00300-019-02565-6

Litvak, M.K., Leggett, W.C., 1992. Age and size-selective predation on larval fishes: the bigger-is-better hypothesis revisited. Mar. Ecol. Prog. Ser. 81, 13-24. www.jstor.org/stable/24827347.
Logerwell, E., Busby, M., Carothers, C., Cotton, S., Duff-Anderson, J., Farley, E., Goddard, P., Heintz, R., Holladay, B., Horne, J., Johnson, S., Lauth, B., Moulton, L., Neff, D., Norcross, B., Parker-Stetter, S., Seigle, J., Sformo, T., 2015. Fish communities across a spectrum of habitats in the western Beaufort Sea and Chukchi Sea. Prog. Oceanogr. 136, 115-132. https://doi.org/10.1016/j.pocean.2015.05.013
MacDonald, R., Wong, C., 1987. The Distribution of Nutrients in the Southeastern Beaufort Sea: Implications for Water Circulation and Primary Production. J. Geophys. Res., 92, 2939-2952. https://doi.org/10.1029/JC092iC03p02939
Magdanz, J.S., Braem, N.S., Robbins, B.C., Koster, D.S., 2010. Subsistence harvests in Northwest Alaska, Kivalina and Noatak, 2007. Alaska Department of Fish and Game Division of Subsistence Technical Paper No. 354, Kotzebue.
Majewski, A.R., Atchison, S., MacPhee, S., Eert, J., Niemi, A., Michel, C., Reist, J.D., 2017. Marine fish community structure and habitat associations on the Canadian Beaufort shelf and slope. Deep Sea Res. Part I. 121, 169-182. https://doi.org/10.1016/j.dsr.2017.01.009
Marsh, J.M., Mueter, F.J., Quinn II, T.J. 2020. Environmental and biological influences on the distribution and population dynamics of Arctic cod (*Boreogadus saida*) in the US Chukchi Sea. Polar Biol. 43 (8), 1055-1072. https://doi.org/10.1007/s00300-019-02561-w
Marsh, J.M. 2019. Diets, distribution and population dynamics of Arctic cod (*Boreogadus saida*) in Arctic shelf ecosystems. Dissertation, College of Fisheries and Ocean Sciences, University of Alaska Fairbanks, Fairbanks, Alaska
Marsh, J.M., Mueter, F.J., 2020. Influences of temperature, predators, and competitors on Arctic cod (*Boreogadus saida*) at the southern margin of their distribution. Polar Biol. 43, 995-1014. https://doi.org/10.1007/s00300-019-02575-4
Marsh, J.M., Mueter, F.J., Thorson, J.T., Britt, L., Zador, S., 2020. Shifting fish distributions in the Bering Sea. In: State of the Climate 2019. Bull. Amer. Meteor. Soc. 101 (8), S254-S256. https://doi.org/10.1175/BAMS-D-20-0086.1
Methot R.D., 1986. Frame trawl for sampling pelagic juvenile fish. CALCOFI Rep. 27, 267-278.
Mueter, F., Bouchard, C., Hop, H., Laurel, B., Norcross, B., 2020. Arctic gadids in a rapidly changing environment. Polar Biol. 43 (8), 945-950. https://doi.org/10.1007/s00300-020-02696-1
Mueter, F.J., Nahrgang, J., John Nelson, R., Berge, J., 2016. The ecology of gadid fishes in the circumpolar Arctic with a special emphasis on the Arctic cod (*Boreogadus saida*). Polar Biol. 39 (6), 961-967. https://doi.org/10.1007/s00300-016-1965-3
Mueter, F., Weems, J., Farley, E., Sigler, M., 2017. Arctic Ecosystem Integrated Survey (Arctic Eis): Marine ecosystem dynamics in the rapidly changing Pacific Arctic Gateway. Deep Sea Res. Part II. 135, 1-6. https://doi.org/10.1016/j.dsr2.2016.11.005
Nelson, R.J., Bouchard, C., Fortier, L., Majewski, A.R., Reist, J.D., Præbel, K., Madsen, M.L., *et al.,* 2020. Circumpolar genetic population structure of Arctic cod, *Boreogadus saida*. Polar Biol. 43, 951-961. https://doi.org/10.1007/s00300-020-02660-z.
Norcross, B.L., Apsens, S.J., Bell, L.E., Bluhm, B.A., Dissen, J.N., Edenfield, L.E., Frothingham, A., *et al.,* 2017. US-Canada Transboundary Fish and Lower Trophic Communities: Abundance, Distribution, Habitat and Community Analysis. BOEM 2017-034. 463 pp + appendices.
NPFMC, 2009. Fishery management plan for fish resources of the Arctic management area. North Pacific Fishery Management Council, 605 W. 4th Ave., Suite 306, Anchorage, AK 99501, Anchorage.
Parker-Setter, S., Horne, J., Weingartner, T., 2011. Distribution of Arctic cod and age-0 fish in the U.S. Beaufort Sea. Polar Biol. 34, 1543-1557. https://doi.org/10.1007/s00300-011-1014-1
Pepin, P., Robert, D., Bouchard, C., Dower, J.F., Falardeau, M., Fortier, L., Jenkins, G.P., et al., 2015. Once upon a larva: revisiting the relationship between feeding success and growth in fish larvae. ICES J. Mar. Sci. 72 (2), 359-373. https://doi.org/10.1093/icesjms/fsu201

Pickart, R., 2004. Shelfbreak circulation in the Alaskan Beaufort Sea: Mean structure and variability. J. Geophys. Res., 109, C04024. https://doi.org/10.1029/2003JC001912
Pickart, R.S., Weingartner, T.J., Pratt, L.J., Zimmermann, S., Torres, D.J., 2005. Flow of winter-transformed Pacific water into the Western Arctic. Deep Sea Res. Part II. 52, 3175-3198. https://doi.org/10.1016/j.dsr2.2005.10.009
Pinheiro, J., Bates, D., DebRoy, S., Sarkar, D., R Core Team (2020). nlme: Linear and Nonlinear Mixed Effects Models. R package version 3.1-147, https://CRAN.R-project.org/package=nlme
R Core Team, 2016. R: A language and environment for statistical computing. R Foundation for Statistical Computing, Vienna, Australia
Richter-Menge, J., Overland, J.E., Mathis, J.T., Eds., 2019: Arctic Report Card 2019, http://www.arctic.noaa.gov/Report-Card.
Shama, L., 2015. Bet hedging in warming ocean: predictability of maternal environment shapes offspring size variation in marine sticklebacks. Glob. Change Biol. 21 (12), 4387-4400. https://doi.org/10.1111/gcb.13041
Shima, M., Bailey, K.M., 1994. Comparative analysis of ichthyoplankton sampling gear for early life stages of walleye pollock (*Theragra chalcogramma*). Fish. Oceanogr. 3, 50-59. https://doi.org/10.1111/j.1365-2419.1994.tb00047.x
Simons, R.A. 2019. ERDDAP. https://coastwatch.pfeg.noaa.gov/erddap . Monterey, CA: NOAA/NMFS/SWFSC/ERD.
Thoman, R., Richter-Menge, J., Druckenmiller, M., Eds, 2020. Arctic Report Card 2020, https://doi.org/10.25923/mn5p-t549
Tourangeau, S., Runge, J., 1991. Reproduction of *Calanus glacialis* under ice in spring in southeastern Hudson Bay, Canada. Mar. Biol. 108, 227-233. https://doi.org/10.1007/BF01344337
Vestfals, C., Mueter, F., Duffy-Anderson, J., Busby, M., De Robertis, A., 2019, Spatio-temporal distribution of Arctic cod (*Boreogadus saida*) and saffron cod (*Eleginus gracilis*) early life stages in the Pacific Arctic. Polar Biol. 42, 969-990. https://doi.org/10.1007/s00300-019-02494-4
Vestfals, C. D., Mueter, F.J., Hedstrom, K. S. , Laurel, B. J., Petrik, C. M., Duffy-Anderson, J. T., Danielson, S. L., 2021. Modeling the dispersal of polar cod (*Boreogadus saida*) and saffron cod (*Eleginus gracilis*) early life stages in the Pacific Arctic using a biophysical transport model. Prog. Oceanogr. 196, 102571. https://doi.org/10.1016/j.pocean.2021.102571
Yank, Y., Bai, X., 2020. Summer Changes in Water Mass Characteristics and Vertical Thermohaline Structure in the Eastern Chukchi Sea, 1974-2017. Water. 12 (5), 1434. https://doi.org/10.3390/w12051434
Yamamoto-Kawai, M., McLaughlin, F.A., Carmack, E.C., Nishino, S., Shimada, K., Kurita, N., 2009. Surface freshening of the Canada Basin, 2003-2007: River runoff versus sea ice meltwater, J. Geophys. Res., 114, C00A05. https://doi.org/10.1029/2008JC005000.
Walkusz, W., Majewski, A., Reist, J., 2013. Distribution and diet of the bottom dwelling Arctic cod in the Canadian Beaufort Sea. J. Mar Syst. 127, 65-75. https://doi.org/10.1016/j.jmarsys.2012.04.004
Welch, H., Crawford, R., Hop, H., 1993. Occurrence of Arctic cod (*Boreogadus saida*) schools and their vulnerability to predation in the Canadian High Arctic. Arctic. 46 (4), 331-339. https://doi.org/10.14430/arctic1361
Weingartner, T.J., 1997. A review of the physical oceanography of the northeastern Chukchi Sea. In: Fish ecology in Arctic North America. Am. Fishe. Soc. Sym. 19, 40-59, Bethesda, Maryland.
Wilson, R.E., Sage, G.K., Sonsthagen, S.A., Gravely, M.C., Menning, D.M., Talbot, S.L., 2017. Genomics of Arctic Cod. Anchorage, AK: US Dept. of the Interior, Bureau of Ocean Energy Management, Alaska OCS Region. Report for BOEM OSC Study 2017-066.92 p.
Wilson R., Sage G., Wedemeyer K., Sonsthagen S., Menning D., Gravley M., Sexson M., Nelson R., Talbot S., 2019. Micro-geographic population genetic structure within Arctic cod (*Boreogadus saida*) in Beaufort Sea of Alaska. ICES J. Mar. Sci. 76, 1713-1721.
Word J., Stoekel D., Greer C., Coelho G., Clark J., Staves J., Essex L., et al., 2014. Environmental impacts of Arctic oil spills and Arctic spill response technologies. Arctic oil spill response

technology joint industry programme. Available at https://neba.arcticresponsetechnology.org/assets/files/Environmental%20Impacts%20of%20Arctic%20Oil%20Spills%20-%20report.pdf [Accessed 23 February, 2021]

Word J., Word L., Gardiner W., Word J., McFarlin K., Perkins R., 2011. Joint industry program to evaluate biodegradation and toxicity of dispersed oil in cold water environments of the Beaufort and Chukchi Seas. Phase 1 and Phase 2 final report. University of Alaska Fairbanks. Available at: https://neba.arcticresponsetechnology.org/media/1109/jip-ph-1-2-final-report-12-04-11.pdf [Accessed 23 February 2021]

CHAPTER 20 - Arctic Cod (*Boreogadus saida*) otolith microchemistry supports regional differences in hatching habitats off Alaska

Objective 5: Further resolve early life history characteristics of Arctic cod and saffron cod and their behavior and connectivity between the Chukchi Sea and western Beaufort Sea.

Chapman, Z.M.[1], Mueter, F.J.[1], Norcross, B.L.[1], and D.S. Oxman[2]

[1] College of Fisheries and Ocean Sciences, University of Alaska Fairbanks
[2] Mark, Tag and Age Laboratory, Alaska Department of Fish and Game

Abstract

The early life history of many fish species is sometimes poorly understood because of the difficulties observing spawning and sampling early life stages. This is especially true for Arctic Cod (Boreogadus saida), which may hatch in remote areas of the Arctic making direct observations difficult. Although larval and early juvenile Arctic Cod have been collected throughout the Alaskan Arctic, their spawning and hatching locations remain unknown. Otolith microchemistry offers one approach to identifying possible habitat conditions associated with hatching. Therefore, we measured the ratio of eight trace elemental concentrations relative to Calcium near the hatch marks of otoliths sampled in the Chukchi and Beaufort seas using laser ablation inductively coupled mass spectrometry. Trace elemental concentrations were used to compare the regions and to infer the water characteristics during the time of hatching. This was done using previously established relationships between elemental ratios and water properties. The results showed no significant difference in hatch mark chemical signatures between the northern Chukchi Sea and the western Beaufort Sea. The results also indicated at least two hatching populations based on significant differences in five of the eight trace elemental ratios from the eastern Beaufort Sea and samples from the western regions. Differences in trace elemental ratios indicated that Arctic Cod from the eastern Beaufort Sea hatched in less saline waters than those from the western regions, possibly a result of hatching within the relatively fresh Mackenzie River plume. Some samples from the northern Chukchi Sea had elevated levels of Zinc near the hatch mark, which could be due to hatching in Kotzebue Sound, where Zinc concentrations may be elevated due to mining. The results of this study expanded our knowledge of Arctic Cod early life history and showed promise for using otolith microchemistry to improve our understanding of Arctic Cod hatch locations.

Introduction

Arctic Cod (*Boreogadus saida*) have a circumpolar distribution in the Arctic and are a primary food source for many predators. They have a narrow thermal range and are sensitive to high temperatures, especially during their larval stage (Laurel et al, 2015; Kent et al, 2016), making them vulnerable to a changing climate. Because of this vulnerability and their importance to the Arctic ecosystem, understanding their early life history is critical to management and conservation (NPFMC, 2009). Several important aspects of the early life history of Arctic Cod in the Pacific Arctic remain poorly understood, especially with regards to vital hatching and spawning locations. Here I present a pilot study that examines the potential of otolith chemical signatures to differentiate stocks and infer habitat characteristics of Arctic Cod during hatching.

Environmental variables such as water temperature and salinity can be reconstructed by analyzing the chemical composition of fish otoliths (Campana, 1999). Otoliths are acellular and metabolically inert and therefore store many elements in proportion to their concentration in the water masses they inhabit (Campana, 2005). Because otoliths are not reabsorbed, they provide a permanent record of environmental

conditions encountered during an individual's lifetime (Campana, 1999). The concentrations of many trace elements differ among water masses and these differences are recorded in the chemical composition of otoliths. Moreover, the rate at which certain elements are incorporated into the otoliths may depend on environmental conditions such as temperature and salinity, as well as somatic growth rate (Bath et al., 2000; Bath and Thorrold, 2005). Incorporation of Barium and Strontium occurs independent of growth rates, whereas Manganese and Magnesium can be dependent (Bath et al., 2000; Bath and Thorrold, 2005).

Elements used commonly for otolith analyses include Barium (Ba), Lithium (Li), Magnesium (Mg), Manganese (Mn), and Strontium (Sr) because change in these elements can be used to infer changes in temperature and salinity (Bouchard et al., 2015). Elemental concentrations of Ba, Li, Mg, and Sr from the otolith edge are positively correlated with salinity, whereas Mn has a negative relationship with salinity in their environment (Bouchard et al., 2015). Water temperature also plays a role in the elemental composition of the otolith as Li and Mn concentrations are both negatively correlated with water temperature near the time of capture (Bouchard et al., 2015). Other elements such as Zinc (Zn) and Copper (Cu) can be used as identifiers of environmental conditions as they may be associated with freshwater runoff from drainages or mines (Saquet et al., 2002, Halden et al., 2000). Zinc is frequently associated with fresh water sources. In Arctic Char (*Salvelinus alpinus*), zinc concentrations are greatest near the otolith core which is likely associated with a near-shore distribution during their first year (Halden et al., 2000). Using the concentrations of these elements within otoliths may therefore help identify the type of water mass fish inhabited during different life stages.

The elemental composition of otoliths provides a timeline of environmental conditions because of the incremental nature of otolith development. The elemental composition of growth rings along the current edge of the otolith reflects the water mass within a few days of capture because of a lag between the ambient water characteristics and the incorporation into the otolith (Miller, 2011). Similarly, the elemental composition near the hatch mark reflects conditions at the time of hatching when the hatch mark formed. To identify possible hatch locations of juveniles requires calibrating the chemical signature by relating elemental concentrations to water mass characteristics such as temperature and salinity. Calibration should ideally be performed using larvae captured shortly after hatching and these calibrations can be used to determine the origin of juveniles or adults caught at later stages, based on the chemical composition of their otolith cores. For example, otoliths from recently hatched Capelin (*Mallotus villosus*) were analyzed for chemical signatures to create a relationship between these signatures and the chemical concentrations in their environment (Davoren et al., 2015). Using the chemical signatures from the hatch mark of adults from the same brood year, their natal origins can be determined. If early larvae from putative spawning locations or from different known populations are not available, calibration may be performed using relationships between the chemical composition at the otolith edges of juvenile or adult samples and the water masses at the capture location. However, applying water mass associations established for juvenile or adult stages to identify hatch locations based on their core chemical composition can be problematic if larvae occur at different depths with varying chemical compositions (Bouchard et al., 2015). Trace elemental composition may also change seasonally and the rate of uptake of trace elements may change with ontogeny (Hüssy et al., 2020). Nevertheless, establishing relationships between environmental conditions and elemental composition can provide valuable information about potential hatching areas and habitat use during early life (Bouchard et al., 2015).

Several studies on Arctic Cod have used otolith microchemistry to identify relationships between chemical composition and environmental conditions. Trace elemental composition along the edge of Arctic Cod otoliths have been used to infer bottom water mass occupancy across the Chukchi Sea with high confidence, indicating the potential for using trace elements to determine habitat associations of early life stages (Gleason et al., 2016). This study showed that benthic temperatures play a larger role than benthic salinity in differentiating among demersal habitats based on otolith chemical compositions of Arctic Cod because temperature is typically more variable among water masses than salinity (Gleason et

al., 2016). Significant differences in environmental conditions must exist among habitats if the composition of otoliths is to be useful for making inferences about habitat use and distribution. Otolith trace elemental composition along the edge and in the core of Arctic Cod differed between each other and among six different regions across the circumpolar Arctic (Bouchard et al., 2015). Trace elemental concentrations at the otolith edge were related to salinity and temperature at the capture locations. Based on the identified relationship between chemical composition and salinity, otolith trace elemental composition near the otolith core was used as a proxy for salinities at the time of hatching to predict the extent to which hatching occurs in locations influenced by freshwater discharge.
In the Pacific Arctic, the stock structure of Arctic Cod and their spawning and hatching locations are not well known. Therefore, the goal of this study was to assess the use of chemical signatures from the hatch mark of otoliths for differentiating possible hatching populations of Arctic Cod in the Pacific Arctic. Specifically, our objectives were to (1) compare the trace elemental composition of otoliths sampled in three different regions of the Alaskan Arctic and (2) infer habitat differences of early larval stages and possible hatching locations based on previously established relationships between the otolith elemental composition of Arctic Cod and surface water salinity and temperature.

Methods

Study area

Arctic Cod were sampled in three distinct regions, the northern Chukchi Sea (NCS), the western Beaufort Sea (WBS), and the eastern Beaufort Sea (EBS) (Fig 1). Samples in the NCS were all collected on the shallow shelf north of 70° latitude and west of 155° longitude. Samples from the WBS region were collected east of 155°W, while the EBS samples were collected near the U.S Canadian Border near 140°W.

Sample Collection

Arctic Cod samples for this study were collected from three different surveys: The 2017 Arctic Integrated Ecosystem Survey (Arctic IES II) and the 2013 (TB13) and 2014 (TB14) US/Canada Transboundary surveys (Table 1). The samples from the Arctic IES II survey were collected using a Marinovich Trawl, the TB13 samples were collected using an Isaacs—Kidd Midwater Trawl (IKMT), and the TB14 samples were collected with a Plumb—Staff Beam Trawl. All larval and juvenile gadids for this analysis were retained and stored in 95% ethanol or frozen. Arctic IES II samples were shipped to the University of Alaska Fairbanks (UAF) lab in Juneau, Alaska. About 60% of these specimens were validated to be Arctic Cod by larval taxonomists from the National Oceanic and Atmosphere Administration (NOAA). The remaining 40% of the samples were identified by the author after training from NOAA larval taxonomists. The TB13 and TB14 samples were identified, measured for length and weight, had sagittal otoliths removed, and archived at the Fisheries Oceanography lab at UAF. Archived otoliths were shipped to the UAF lab in Juneau, Alaska, for this analysis. All otoliths were extracted, cleaned, and polished and were mounted to slides with thermal plastic cement for laser ablation.
Otolith Chemistry

To address my objectives, I measured the concentration of Calcium (Ca^{40}), Lithium (Li^{7}), Magnesium (Mg^{24}), Manganese (Mn^{55}), Copper (Cu^{64}), Zinc (Zn^{65}), Strontium (Sr^{88}), and Barium (Ba^{137}) along a transect from the center to the edge of 133 otolith samples (Fig. 2). I then selected measurements corresponding to the hatch mark, approximately 11.5 μm from the center of the otolith, to infer habitat conditions at the time of hatching and identify possible hatch locations. The identification of the hatch mark was validated through the use of laboratory raised Arctic Cod from the Hatfield Marine Science Center in Newport, Oregon (Fig.3; Benjamin Laurel, NOAA Alaska Fisheries Science Center, pers. comm.). The ablation at 11.5 μm did not include the hatch mark but was within the first week of life and

reflects water conditions just after hatching. A point just outside of the core was selected to avoid any maternal chemical imprinting. Otoliths were analyzed at the University of Alaska Fairbanks Advanced Instrumentation Laboratory using a New Wave UP213 Laser with an Agilent 7500ce Inductively Coupled Plasma Mass Spectrometer (LA—ICP—MS). Nine otoliths were placed on a slide and processed in a single run. Prior to each run Nist610 and Febs pellets were ablated to ensure a consistent standard. The transects were ablated at 5 μm/s, using a beam width of 25 μm with a pulse frequency of 10 Hz at 55% laser power. Data from the LA—ICP—MS were processed using Igor Pro version 6.37® (WaveMetrics) and Iolite software package version 3.0®. To ensure data quality all transect profiles were analyzed to check for and eliminate unrealistic elemental spikes that are caused by elemental fractionation, which is the transport of aerosol particles from the ablation chamber to the ICP and is not representative of the actual elemental abundance (Limbeck et al., 2015). For statistical analysis all measurements were expressed as ratios relative to Ca to standardize the results for the amount of material ablated.

Statistical Analysis

Multivariate and univariate statistical analyses were conducted to compare otolith elemental compositions among collection regions. Prior to analysis, trace elemental ratios were log—transformed to achieve approximate multivariate normality and were standardized to a mean of zero and a standard deviation of one. Pairwise Euclidean distances among samples were calculated to visualize differences in the elemental composition of the hatching location among regions using a multivariate ordination based on a Principle Components Analysis (PCA). Multivariate analysis of variance (MANOVA) was used to test for overall differences in chemical composition among regions. When overall differences were significant ($p < 0.05$), these were followed by individual ANOVAs to determine which of the elemental ratios differed among regions. Significant ANOVA results were followed by Tukey Honest Significant Difference (HSD) post hoc tests to assess pairwise differences between regions for significance. All analyses were performed using the R statistical computing environment version 3.5.3 (R Core Team, 2019). Samples in the EBS were collected during two different years and were assess for interannual variability in their otolith elemental composition. There was no significant difference between 27 samples collected in 2013 and 10 samples from 2014 for most elements; therefore, samples from the EBS region were pooled to increase the sample size for comparisons with other regions.

Results

The results indicated that the otolith chemical composition around the time of hatching differed between the EBS and the two western regions, but not between the WBS and NCS. Within the EBS, no significant differences were found between 2013 and 2014 for most trace elemental ratios, except for Mg/Ca (t-test: $p = 0.001$) and Ba/Ca ($p=0.042$). The PCA ordination showed considerable overlap in trace elemental compositions among regions (Fig. 4). However, there was an overall statistical difference in the mean elemental composition among regions (MANOVA: Pillai's trace = 0.299, $p = 0.004$). Specifically, the elemental ratios for Mn, Zn, Sr88 and Ba differed significantly among regions (ANOVAs: $p = 0.012$, 0.003, 0.002 and 0.035, respectively, Fig. 5). The Mn/Ca ratio was significantly higher in the EBS than the NCS ($p = 0.011$). Zn/Ca was significantly lower in the EBS than in the NCS ($p = 0.008$) and the WBS ($p = 0.013$). At a 90% significance level, the ratios of Sr88/Ca, and Ba/Ca were all significantly lower in the EBS than in the NCS ($p = 0.009$ and $p = 0.074$, respectively) and WBS ($p=0.062$, $p = 0.008$, and $p = 0.070$). In summary, there were no significant differences for any element between the NCS and the WBS; in contrast, seven out of 15 pairwise comparisons between the EBS and the other two regions were significant (Table 2).

Discussion

The chemical analyses suggest considerable overlap in the trace—elemental compositions of the hatch mark in otoliths from the NCS, WBS, and EBS. Nevertheless, small but statistically significant

differences in individual elemental ratios among regions were found, likely reflecting differences in the range of habitats where hatching occurs within each region. Similarly, Bouchard et al. (2015) found significant differences in several of the same trace elements (Mn, Sr, and Ba) across multiple circumpolar regions. Bouchard et al. (2015) found that Mn/Ca was negatively correlated with salinity, while Sr/Ca and Ba/Ca were positively correlated with salinity. In this study, I found a higher ratio for Mn and reduced ratios for Ba, Sr86, and Sr88 in the EBS compare to the other two regions, suggesting that EBS Arctic Cod hatched in waters with lower salinity than those in the WBS and NCS. Arctic Cod captured in the EBS may have hatched in nearshore waters off the Mackenzie River (Bouchard and Fortier, 2008), a region that receives large amounts of freshwater runoff and is characterized by low salinities (Lansard et al., 2012), consistent with the chemical signature of larval Arctic Cod from the EBS. The high—salinity signature in the otoliths of larvae sampled in the other two regions suggests that they originated in areas with higher salinity, consistent with their hypothesized origin near the Bering Strait region (Vestfals et al., 2021). Otolith elemental compositions at both the core and the edge also differed between Arctic Cod from the same transboundary cruises as this study and samples from the Chukchi Sea near the Wrangel Islands in Russian waters (Frothingham et al., 2020). The difference in elemental composition between these two locations was more pronounced than in this study, likely because of their greater geographical separation, whereas the smaller distances among samples from this study may have resulted in some mixing among regions. However, the observed differences in otolith chemistry support the existence of at least two unique spawning populations in the Beaufort and Chukchi seas, consistent with previous studies on Arctic Cod genetics (Wilson et al., 2017, 2019, Nelson et al., 2020), spatial distribution (Forster et al, 2020) and hatch date distributions (Chapman et al. unpublished manuscript).

Differences between the EBS, which was sampled in 2013/14, and the two western regions, which were sampled in 2017, could have resulted from inter—annual variability in environmental conditions. The chemical signatures for both years are consistent with a low salinity origin. The higher Mg and Ba signatures in 2014 compared to 2013 may reflect lower discharge from the Mackenzie River during the April-June hatching period in 2014 (12.57 thousand m^3/s on average) compared to 2013 (14.00 thousand m^3/s) (https://wateroffice.ec.gc.ca/mainmenu/historical_data_index_e.html, accessed on 10/1/2020). However, other environmental variables could have resulted in the observed differences in elemental compositions between these years such as rain, ice melt, and wind mixing.

The lack of significant differences in chemical signatures between Arctic Cod sampled in the NCS and in the WBS during the 2017 survey suggests that they originated from waters with similar chemical compositions. This supports the hypothesis that they are part of the same spawning population, consistent with similarities in hatch dates (Chapman et al. unpublished manuscript), oceanographic connectivity between the two regions (Forster et al., 2020), and model results suggesting transport of larvae from the Chukchi Sea into the western Beaufort Sea (Levine et al. 2021).

Although the mean concentrations of several elements that reflect salinity variations differed among regions, there was considerable overlap in chemical composition among regions as evident in the PCA ordination. In particular, the concentrations of Lithium, a trace element that primarily reflects temperature variations in the environment (Bouchard et al., 2015), did not differ among regions. Temperature affects otolith elemental concentrations by modifying the uptake of trace elements from the water into the otolith (Collingsworth et al., 2010), thus the lack of significant differences in Li suggest similar temperature conditions across regions at the time of hatching. This is not surprising considering that hatching typically occurs under the ice at temperatures near freezing (Bouchard and Fortier, 2011). Like Li, Mn tends to be negatively correlated with temperature, but also has a negative relationship with salinity (Bouchard et al., 2015). Therefore, the lack of difference in Li in the otoliths among regions suggests that the observed elevated Mn concentrations are due to lower environmental Mn concentrations related to lower salinities in the EBS. Alternatively, the observed difference in Mn could be due to slightly elevated temperatures in the EBS region associated with the Mackenzie River freshwater plume. Arctic Cod hatching in freshwater

plumes are hypothesized to experience slightly elevated temperatures and increased growth rates compared to regions without a strong freshwater influence such as the NCS and WBS (Bouchard et al., 2015). However, the lack of a difference in Li concentrations among regions and lower growth rates in the EBS (Chapman et al. unpublished manuscript) are not consistent with the hypothesis that EBS larvae experienced elevated temperatures at the time of hatching compared to larvae in the NCS and WBS. Differences in most elemental ratios provide some insight regarding salinity and temperature conditions at the time of hatching, but trace elements such as Zn may be associated with anthropogenic sources. Zinc is a biologically important nutrient and occurs naturally in freshwater and seawater. Increased levels of Zn in otolith hatch marks of fishes can be caused by Zn runoff from mine tailings near the hatching area (Saquet et al., 2002; Halden and Friedrich, 2008). In the current study, Zinc levels from the NCS and WBS Arctic Cod were significantly higher than those captured in the EBS. One of the hypothesized hatching areas for Arctic Cod is Kotzebue Sound (Deary et al., in Review), which is located about 50 miles downstream from the world's largest Zinc mine, possibly explaining the higher mean levels of Zn in NCS and WBS Arctic Cod. More targeted sampling of environmental Zinc as a tracer and of Arctic Cod at a range of distances from the potential discharge location are required to support this tentative conclusion and would also help determine the relative importance of Kotzebue Sound as a hatch location.

Conclusion

The results of this study, combined with previous studies on Alaskan Arctic Cod, have provided further evidence of at least two separate populations within the Pacific Arctic. While there was considerable overlap between the regions, statistical differences in several otolith elemental concentrations support the existence of two unique hatching populations. The analysis indicated that the EBS Arctic Cod hatched in waters with a lower salinity than those from the western regions. This is consistent with hypothesized hatching in the Mackenzie River plume. The elevated levels of Zinc in the NCS and WBS fish may be attributed to hatching occurring in Kotzebue Sound downstream from the Red Dog mine. While this study has provided greater insight into Arctic Cod populations within Alaska's waters and where they may hatch, more studies will be needed to accurately pinpoint the hatching locations of Arctic Cod. Using the method from this study with a larger sample size collected over an expanded geographic range where sampling occurred can help better identify the multiple spawning populations that inhabit Alaskan waters.

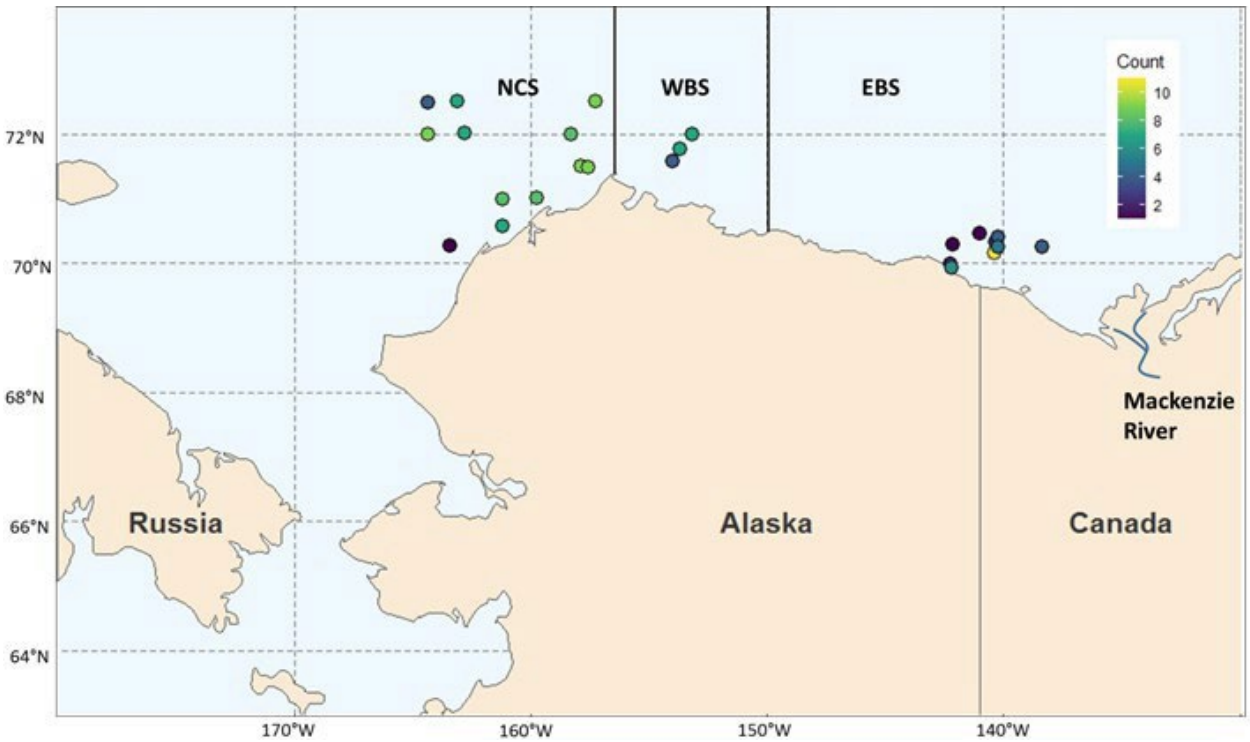

Figure 1: Location of samples from which otoliths were collected for microchemistry analysis from the Arctic IES and Transboundary surveys in the northern Chukchi Sea (NCS), western Beaufort Sea (WBS) and eastern Beaufort Sea (EBS). The number of samples analyzed from each station is indicated by the color change from cool (blue) to warm (yellow).

Figure 2: Polished otolith with ablation scar from laser ablated inductively coupled plasma mass spectrometer for determining trace elemental concentrations. The ablation point used for analysis was at 11.5 µm from the center just past the hatch mark.

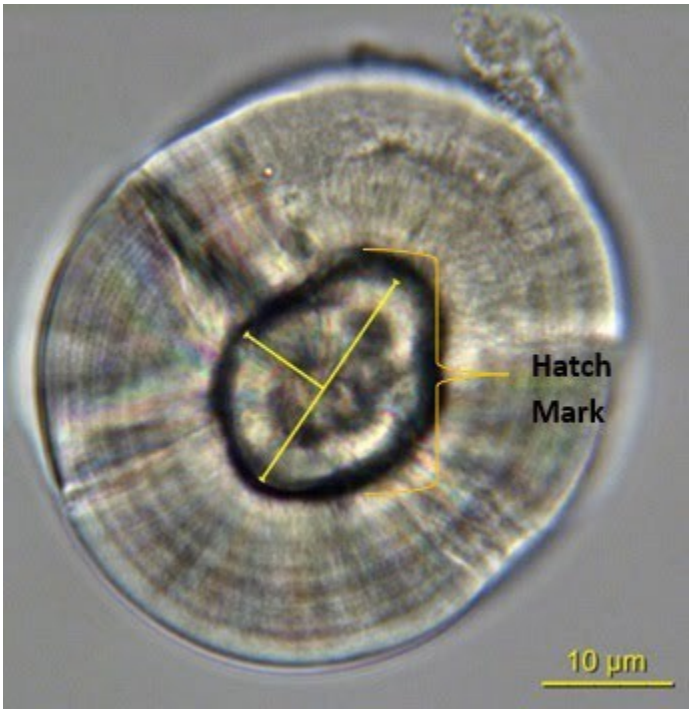

Figure 3: Sagittal otolith at 100X magnification from a lab raised Arctic Cod with the hatch mark outlined.

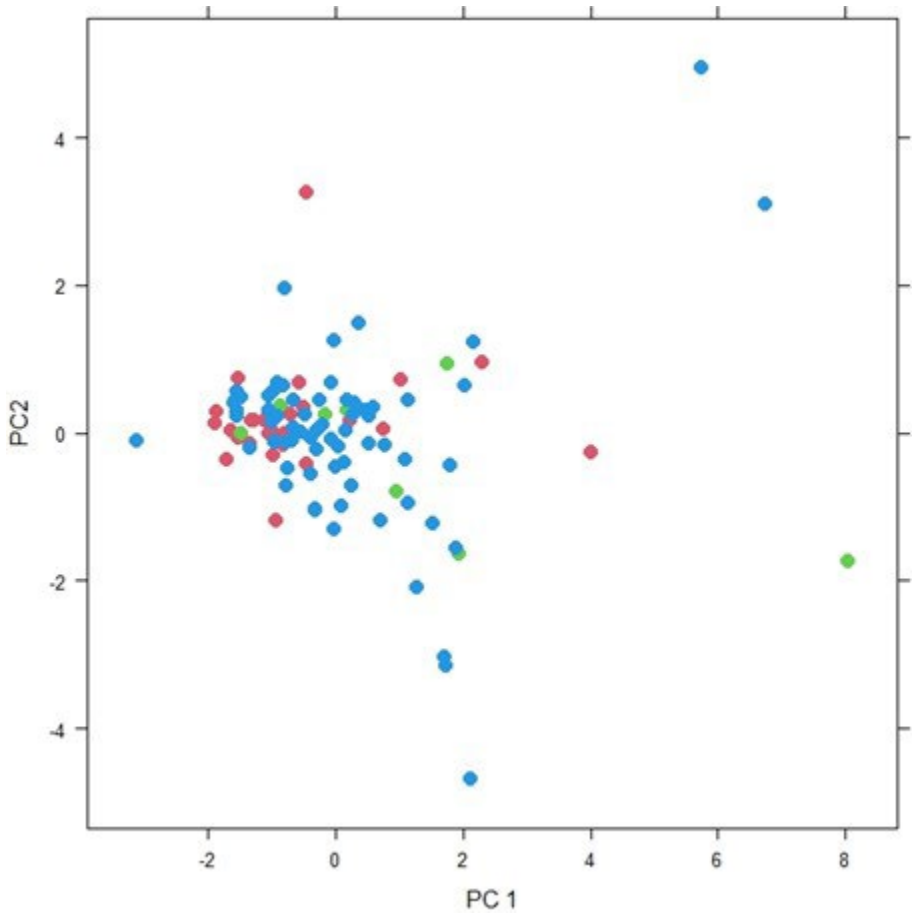

Figure 4: PCA ordination of 104 individual otoliths collected in the northern Chukchi Sea (NCS, blue), western Beaufort Sea (WBS, green), and eastern Beaufort Sea (EBS, red) based on the concentrations of seven trace elements standardized relative to Ca.

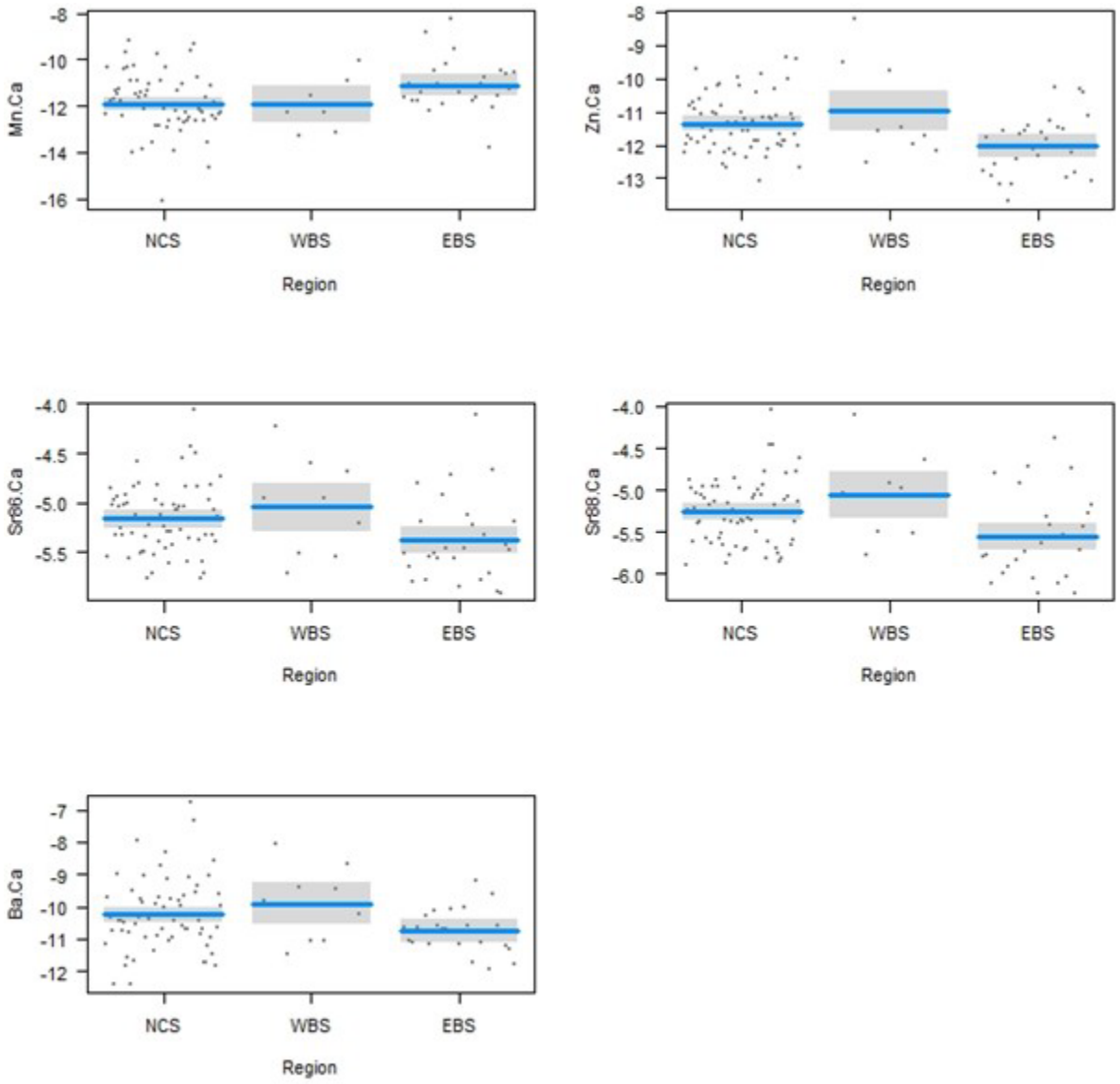

Figure 5: Box plots of mean log—transformed elemental ratios (blue bar) with 95% confidence intervals (grey shading) and partial residuals (black dots) for the five ratios that differed significantly among three regions (Eastern Beaufort Sea (EBS), Western Beaufort Sea (WBS), and Northern Chukchi Sea (NCS).

Table 1: Summary of the sample size, mean, standard deviation, median, and range of the log—transformed elemental ratios for fish captured in the northern Chukchi Sea (NCS), western Beaufort Sea (WBS) and eastern Beaufort Sea (EBS).

Element	Region	Sample Size	Mean	SD	Median	Min	Max
Li/Ca	NCS	68	-12.279	0.898	-12.091	-15.502	-10.544
Mg/Ca	NCS	68	-7.590	0.686	-7.570	-8.926	-5.9132
Mn/Ca	NCS	68	-11.812	1.226	-11.908	-16.114	-9.214
Cu/Ca	NCS	68	-10.905	1.677	-10.987	-13.891	-7.314
Zn/Ca	NCS	68	-11.338	0.934	-11.452	-13.069	-8.196
Sr/Ca	NCS	68	-5.212	0.402	-5.195	-5.899	-4.050
Ba/Ca	NCS	68	-10.129	1.069	-10.292	-12.423	-6.774
Li/Ca	WBS	9	-12.450	1.228	-12.060	-15.502	-11.458
Mg/Ca	WBS	9	-7.538	0.434	-7.517	-8.286	-6.843
Mn/Ca	WBS	9	-11.937	1.009	-12.009	-13.287	-10.065
Cu/Ca	WBS	9	-10.295	1.202	-9.883	-12.290	-8.406
Zn/Ca	WBS	9	-10.985	1.468	-11.568	-12.506	-8.196
Sr/Ca	WBS	9	-5.059	0.504	-5.039	-5.767	-4.093

Ba/Ca	WBS	9	-9.909	1.153	-9.789	-11.489	-8.055
Li/Ca	EBS	27	-12.453	1.053	-12.363	-14.992	-10.007
Mg/Ca	EBS	27	-7.777	0.507	-7.816	-8.923	-6.795
Mn/Ca	EBS	27	-11.093	1.085	-11.174	-13.783	-8.231
Cu/Ca	EBS	27	-11.370	1.372	-11.369	-14.094	-8.720
Zn/Ca	EBS	27	-12.004	0.915	-11.839	-13.689	-10.249
Sr88/Ca	EBS	27	-5.554	0.506	-5.639	-6.229	-4.384
Ba/Ca	EBS	27	-10.754	0.621	10.740	-11.923	-9.209

Table 2: Pairwise Tukey HSD comparison of elemental ratios between regions for four trace elements that showed significant differences among regions (ANOVA). All elemental concentrations are expressed as a ratio relative to calcium. Regions are the northern Chukchi Sea (NCS), western Beaufort Sea (WBS), and eastern Beaufort Sea (EBS). Differences that were significant at the 90% significance level are highlighted.

Element Ratio	Regions	P-Value
Manganese	WBS-NCS	0.995
	EBS-NCS	0.011
	EBS-WBS	0.160
Zinc	WBS-NCS	0.481
	EBS-NCS	0.008
	EBS-WBS	0.013
Strontium	WBS-NCS	0.389
	EBS-NCS	0.008
	EBS-WBS	0.009
Barium	WBS-NCS	0.602
	EBS-NCS	0.070
	EBS-WBS	0.074

References

Bath, G., Thorrold, S., Jones, C., Campana, S., McLaren, J., Lam, J., 2000. Strontium and barium uptake in aragonitic otoliths of marine fish. Geochim. Cosmochim. Acta. 64 (10), 1705-1714. https://doi.org/10.1016/S0016-7037(99)00419-6.

Bath Martin, G., Thorrold, S., 2005. Temperature and salinity effects on magnesium, manganese, and barium incorporation in otoliths of larval and early juvenile spot *Leiostomus xanthurus.* Mar. Ecol. Prog. Ser. 293, 223-232. https://doi.org/10.3354/meps293223.

Bender, M.L., Giebichenstein, J., Teisrud, R.N., Laurent, J., Frantzen, M., Meador, J.P., Sørensen, L., Hansen, B.H., Reinardy, H.C., Laurel, B., Nahrang, J., 2021. Combined effects of crude oil exposure and warming on eggs and larvae of an arctic forage fish. Sci. Rep. 11, 8410. https://doi.org/10.1038/s41598-021-87932-2.

Bouchard, C., Fortier, L., 2011. Circum—arctic comparison of the hatching season of Arctic cod *Boreogadus saida*: A test of the freshwater winter refuge hypothesis. Prog. Oceanogr. 90, 105—116. https://doi.org/10.1016/j.pocean.2011.02.008.

Bouchard, C., Thorrold, S., Fortier, L., 2015. Spatial segregation, dispersion and migration in early stages of Arctic cod *Boreogadus saida* revealed by otolith chemistry. Mar. Biol. 162, 855-868. https://doi.org/10.1007/s00227-015-2629-5.

Campana, S.E., 1999. Chemistry and composition of fish otoliths: pathways, mechanisms and applications. Mar. Ecol. Prog. Ser. 188, 263—297. https://doi.org/10.3354/meps188263.

Campana, S.E., 2005. Chapter 12 - Otolith Elemental Composition as a Natural Marker of Fish Stocks. In: Stock Identification Methods: Applications in Fisheries Science. Edited by Cadrin, S.X., Friedland, K.D., Waldman, J.R. Academic Press, pp. 227-245. https://doi.org/10.1016/B978-012154351-8/50013-7.

Chapman, Z.M., Mueter, F.J., Norcross, B.L., Oxman, D.S. Unpublished manuscript. Otolith-derived hatch dates and growth rates of Arctic Cod (*Boreogadus saida*) support existence of several spawning populations in Alaskan waters. Prepared for submission to Deep Sea Res. Part II.

Collingsworth, P., Van Tassell, J., Olesik, J., Marschall, E., 2010. Effects of temperature and elemental concentration on the chemical composition of juvenile yellow perch (*Perca flavescens*) otoliths. Can. J. Fish. Aquat. Sci. 67 (7), 1187-1196. https://doi.org/10.1139/F10-050.

Craig, P., Griffiths, W., Haldorson, L., McElderry, H., 1982. Ecological studies of Arctic cod (*Boreogadus saida*) in Beaufort Sea coastal waters, Alaska. Can. J. Fish. Aquat. Sci. 39 (3), 395-406. https://doi.org/10.1139/f82-057.

Davoren, G., Woloschiniwsky, C., Halden, N., Wang, F., 2015. Does otolith chemistry indicate the natal habitat of Newfoundland capelin *Mallotus villosus*? J. Exp. Mar. Biol. Ecol. 464, 88-95. https://doi.org/10.1016/j.jembe.2014.10.025.

De Robertis, A., Taylor, K., Wilson, C., Farley, E., 2017. Abundance and Distribution of Arctic cod (*Boreogadus saida*) and other Pelagic Fishes over the U.S. Continental Shelf of the Northern Bering and Chukchi Seas. Deep Sea Res., Part II. 135, 51-65. https://doi.org/10.1016/j.dsr2.2016.03.002.

Forster, C., Norcross, B., Mueter, F., Logerwell, E., Seitz, A. 2020. Spatial patterns, environmental correlates, and potential seasonal migration triangle of Arctic cod (*Boreogadus saida*) distribution in the Chukchi and Beaufort seas. Polar Biol. 43, 1073—1094. https://doi.org/10.1007/s00300—020—02631—4.

Frothingham A., 2020. Age, growth, and movement dynamics of Arctic cod (*Boreogadus saida*) in the Chukchi and Beaufort Seas. Master's thesis, College of Fisheries and Ocean Sciences, University of Alaska Fairbanks, Fairbanks, Alaska.

Gallaway, B.J., Konkel, W.J., Norcross, B.L., 2017. Some thoughts on estimating change to Arctic Cod populations from hypothetical oil spills in the eastern Alaska Beaufort Sea. Arct. Sci. 3 (4), 716—129. https://doi.org/10.1139/as—2016—0056.

Gleason, C., Norcross, B., Spaleta, K., 2016. Otolith chemistry discriminates water mass occupancy of Arctic fish in the Chukchi Sea. Mar. Freshwater Res. 67 (7), 967-979. https://doi.org/10.1071/MF15084.

Halden, N., Mejia, S., Babaluk, J., Reist, J., Kristofferson, A., Campbell, J., Teesdale, W., 2000. Oscillatory zinc distribution in Arctic char (*Salvelinus alpinus*) otoliths: The result of biology or environment? Fish. Res. 46, 289-298 https://doi.org/10.1016/S0165-7836(00)00154-5.

Halden, N., Freidrich, L., 2008. Trace-element distributions in fish otoliths: natural markers of life histories, environmental conditions and exposure to tailings effluence. Mineral. Mag. 72 (2), 593-605. https://doi.org/10.1180/minmag.2008.072.2.593.

Hüssy, K., Limburg, K., de Pontual, H., Thomas, O., Cook, P., Heimbrand, Y., Blass, M., Sturrock, A., 2020. Trace element patterns in otoliths: The role of biomineralization. Rev. Fish. Sci. Aquacult. 1-33. https://doi.org/10.1080/23308249.2020.1760204.

Kent, D., Drost, H., Fisher, J., Oyama, T., Farrell, A., 2016. Laboratory rearing of wild Arctic cod *Boreogadus saida* from egg to adulthood. J. Fish Biol. 88 (3), 1241—1248. https://doi.org/10.1111/jfb.12893.

Laurel, B., Spencer, M., Iseri, P., Copeman, L., 2015. Temperature-dependent growth and behavior of juvenile Arctic cod (*Boreogadus saida*) and co-occurring North Pacific gadids. Polar Biol. 39, 1127-1135. https://doi.org/10.1007/s00300-015-1761-5.

Lansard, B., Mucci, A., Miller, L., Macdonald, R., Gratton, Y., 2012. Seasonal variability of water mass distribution in the southeastern Beaufort Sea determined by total alkalinity and $\delta^{18}O$. J. Geophys. Res., 117, C03003. https://doi.org/10.1029/2011JC007299.

Levine, R.M., De Robertis, A., Grünbaum, D., Woodgate, R., Mordy, C.W., Mueter, F., Cokelet, E., Lawrence-Slavas, N., Tabisola, H., 2021. Autonomous vehicle surveys indicate that flow reversals retain juvenile fishes in a highly advective high-latitude ecosystem. Limnol. Oceanogr. 9999, 1-6. https://doi.org/10.1002/lno.11671.

Limbeck, A., Galler, P., Bonta, M., Bauer, G., Nishkauer, W., Vanhaecke, F., 2015. Recent advances in quantitative LA-ICP-MS analysis: challenges and solutions in the life sciences and environmental chemistry. Anal. Bioanal. Chem. 407 (22), 6593-6617. https://doi.org/10.1007%2Fs00216-015-8858-0.

Miller, J.A., 2011. Effects of water temperature and barium concentration on otolith composition along a salinity gradient: Implications for migratory reconstructions. J. Exp. Mar. Biol. Ecol. 405, 42-52. https://doi.org/10.1016/j.jembe.2011.05.017.

Nelson, R.J., Bouchard, C., Fortier, L., Majewski, A.R., Reist, J.D., Præbel, K., Madsen, M.L., *et al.,* 2020. Circumpolar genetic population structure of Arctic cod, *Boreogadus saida*. Polar Biol. 43, 951—961. https://doi.org/10.1007/s00300—020—02660—z.

NPFMC, (2009) Fishery management plan for fish resources of the Arctic management area. North Pacific Fishery Management Council, 605 W. 4th Ave., Suite 306, Anchorage, AK 99501, Anchorage.

Saquet, M., Halden, N., Babaluk, J., Campbell, J., Nejedly, Z., 2002. Micro-PIXE analysis of trace element variation in otoliths from fish collected near acid mine tailings: Potential for monitoring contaminant dispersal. Nucl. Instrum. Methods Phys. Res., B. 189, 196-201. https://doi.org/10.1016/S0168-583X(01)01041-2.

Thorisson, K., Jósdóttir, I., Marteinsdottir, G., Campana, S., 2011. The use of otolith chemistry to determine the juvenile source of spawning cod in Icelandic waters. ICES J. Mar. Sci. 68 (1), 98-106 https://doi.org/10.1093/icesjms/fsq133.

Wilson, R.E., Sage, G.K., Sonsthagen, S.A., Gravely, M.C., Menning, D.M., Talbot, S.L., 2017. Genomics of Arctic Cod. Anchorage, AK: US Dept. of the Interior, Bureau of Ocean Energy Management, Alaska OCS Region. Report for BOEM Study 2017—066.92 p.

Wilson R, Sage G, Wedemeyer K, Sonsthagen S, Menning D, Gravley M, Sexson M, Nelson R, Talbot S, (2019) Micro—geographic population genetic structure within Arctic cod (*Boreogadus saida*) in Beaufort Sea of Alaska. ICES J. Mar. Sci, 76, 1713—1721.

CHAPTER 21 - Distributional shifts among seabird communities of the Northern Bering and Chukchi seas in response to ocean warming during 2017-2019.

Objective 6: Quantify the distribution, abundance, and prey association of seabirds in the PAR in relation to oceanographic conditions, prey abundance, and feeding guilds.

Kuletz, Kathy, Daniel Cushing, Elizabeth Labunski. 2020. Distributional shifts among seabird communities of the Northern Bering and Chukchi seas in response to ocean warming during 2017-2019. *Deep Sea Research II*, 181-182: 104913. https://doi.org/10.1016/j.dsr2.2020.104913

Abstract

In the northern Bering Sea and eastern Chukchi Sea, 2017-2019 were record-breaking years for warm ocean temperatures and lack of sea ice. The region supports millions of seabirds that could be affected by shifts in prey distribution and availability caused by changing environmental drivers. However, seabirds are highly mobile and often flexible in diet, and might alter their foraging distributions accordingly. To determine if there was evidence of long-term changes in abundance of seabirds, or if seabirds used the offshore habitat differently during recent warm years, we compared species richness, community composition, and distribution and abundance of selected species and Total seabirds (all species combined) between two periods, 2007-2016 and 2017-2019. We also evaluated annual changes in abundance during 2007-2019. We used 79,426 km of transects from vessel-based surveys conducted July through September. Total seabird density for the entire study area increased by ~20% during 2017-2019, but changes were not consistent across the study area, nor among species, and species richness declined except for a slight increase in the northern Chukchi Sea. Total seabird density declined most in the northern Bering Sea (-27%), although it increased in the Chirikov Basin by 73%. During 2017-2019, abundance of piscivorous murres (*Uria* spp.) decreased everywhere, whereas planktivorous *Aethia* auklet density increased by 70% in Chirikov Basin; auklets apparently abandoned their post-breeding migration to the Chukchi Sea. Short-tailed shearwaters (*Ardenna tenuirostris*) expanded farther into the northern Chukchi Sea, with nearly twice the density of the previous decade. We identified five seabird community types, three of which (all dominated by an alcid species) contracted spatially in the later period, and shifted south or near colonies. In contrast, a short-tailed shearwater dominated community expanded northward, and a community defined by low seabird density expanded throughout the eastern portion of both the northern Bering and Chukchi seas, suggesting higher-density communities had shifted westward. The variable responses among species correspond to documented changes in the environment as well as their natural history.

Introduction

The Bering and Chukchi seas have been undergoing warming events and subsequent alteration of biological ecosystem components over the last 20 years (Grebmeier et al., 2006; Stabeno and Bell, 2019). However, events during 2017-2019 appear to have been distinctively disruptive of long term physical and biological patterns. Sea ice plays a critical role in primary productivity of these marine ecosystems. The formation of ice algae feeds phytoplankton blooms as the ice retreats (Brown and Arrigo, 2013), supporting zooplankton production (Campbell et al., 2016; Stabeno et al., 2010), and ultimately upper trophic levels. Early ice retreat, or lack of sea-ice formation, impacts these mechanisms with repercussions throughout the food web (Hunt et al., 2011). In the northern Bering Sea, warm conditions lead to early ice retreat, resulting in early and high primary productivity, particularly near the ice edge (Brown et al., 2011; Brown and Arrigo, 2013).

During 2017, sea ice formed over the eastern Bering Sea shelf, but there was an unusual and early retraction of ice over the northwestern Bering Shelf, attributed to persistent southerly winds. As a result, the northern Bering Sea was characterized by ice conditions similar to those of a 'warm' year, despite ice coverage farther south (Siddon and Zador, 2018). In 2018 and again in 2019, ocean temperatures were above normal in winter, and ice extent in the Bering Sea was the lowest recorded in four decades. In both years, sea ice retreated north of Bering Strait before spring (Siddon and Zador, 2018, 2019; Cornwall, 2019). The extremely low ice cover during 2017-2019 in the northern Bering Sea and Chukchi Sea resulted in altered oceanographic and biological conditions; these were most evident in 2018, and included impacts to lower and upper trophic levels (Duffy-Anderson et al., 2019).

Seabirds are indicators of ocean conditions (Murphy, 1936; Piatt et al., 2007 and references therein; Velarde et al., 2019). By understanding responses of seabirds to broad-scale ecological shifts we may better predict impacts to upper trophic-level taxa in a rapidly changing environment. In the Bering Sea, recent responses of seabirds to ocean warming have included mass mortality (Jones et al., 2019), failed nesting attempts and low reproductive success (Dragoo et al., 2020; Romano et al., this issue). Since 2015, seabird mass mortality events have occurred almost annually in the Bering Strait region (Duffy-Anderson et al., 2019). Species-specific mortality events and seabird reproductive success at monitored colonies can be indicative of food web changes (Abraham and Sydeman, 2004; Jones et al. 2019; Piatt et al., 2020). However, these metrics do not necessarily provide insight into how the broader seabird community has responded to an altered ecosystem.

Seabirds are long-lived, with adaptations to buffer variability in their environment. Forgoing a breeding season or undergoing a few years of low breeding success may not necessarily lead to substantial population-level repercussions (Cairns, 1992; Velarde and Ezcurra, 2018). Seabirds are also highly mobile, and can search for prey over a large area, particularly when not attending a colony. Further, seabirds spend most of their lives at sea, and their temporal and spatial distribution across the seascape often reflects the productivity and foraging conditions of large marine areas (Ballance et al., 1997; Gall et al. 2013; Suryan et al., 2012; Yen et al., 2006). Here, we examine broad-scale responses of seabirds to a warm period (2017-2019) in the Northern Bering and Chukchi Sea Large Marine Ecosystem (LME) relative to the preceding decade (2007-2016). Specifically, we use vessel-based surveys to assess how seabirds differed in species-specific and community-level abundance and distribution between these two time periods.

Methods

Study area

Our study area encompassed offshore waters of two regions, the northern Bering Sea (hereafter, Bering Sea) and eastern Chukchi Sea (hereafter, Chukchi Sea) (Fig. 1), and we considered southern and northern subregions within each region. We refer to the subregions (Fig. 2) as the Northern Bering (59.5°N to St. Lawrence Island; distinct from the general northern Bering Sea), the Chirikov Basin (St. Lawrence Island to Bering Strait at ~65.8°N, including Little Diomede Island), the Southern Chukchi (Bering Strait to 70°N) and Northern Chukchi (70°N to 72.5°N). The western boundary of all regions followed the U.S. Exclusive Economic Zone to 175°W and the eastern boundary followed an offshore buffer bordering coastal Alaska, to include only waters where our surveys occurred in most years (Fig. 2).

The northern Bering Sea is hydrographically and biologically distinct from the southern Bering Sea, separated at approximately 60°N (Stabeno et al., 2010; Sigler et al., 2011, 2017). The shallow continental shelf of the northern Bering Sea includes the Inner Shelf domain (<50 m deep) and Middle Shelf domain (50-100 m deep), with some influence from the more dynamic Outer Shelf and slope domains, which are beyond our study area. The Inner Shelf is bordered by the Alaska Coastal Current on the east side and the

more saline, colder and nutrient rich waters of the Anadyr Current in the west (Fig. 1). Both of these water masses pass through Bering Strait and, as Bering Sea Water, facilitate structure of the Chukchi Sea. The Chukchi Sea is also structured by the Siberian Current, which flows eastward along the northern coast of Russia. The Chukchi Sea, particularly in the north, is also heavily influenced by fresh, cold winter water, derived from sea-ice melt (Coachman et al., 1975; Weingartner et al., 2005, 2013). North of Bering Strait, the Bering Sea waters split and branch westward and eastward, encircling the bathymetrically complex, shallow, and nutrient rich Hanna Shoal in the northern Chukchi Sea (Coachman et al., 1975; Dunton et al., 2017; Fig. 1).

Sea-ice is a primary driver of both Bering and Chukchi ecosystems. The extent of ice coverage and the timing of ice retreat in the spring drives annual primary productivity by affecting sea surface temperatures and light availability for photosynthesis, and by providing a platform for epontic algal growth (Arrigo, 2003). Ultimately, the effects of spring conditions cascade to lower and upper trophic levels (Stabeno et al., 2010; Hunt et al., 2011, 2018). Sea ice generally retreats north of Bering Strait throughout late spring and summer, with the ice minimum occurring between September and October. However, ice extent and duration was minimal overall during 2017-2019 (Siddon and Zador, 2018, 2019).

The study area includes large seabird colonies (Stephensen et al., 2003) with an estimated 12 million birds nesting in the Northern Bering and Southern Chukchi subregions (USFWS, 2014). The largest colonies are on St. Matthew and St. Lawrence islands in the Northern Bering, the two Diomede islands in the Bering Strait, and Cape Thompson and Cape Lisburne in the Southern Chukchi (Fig. 1). In late summer and early fall this LME is also used by equal numbers of migratory birds (Kuletz et al., 2015, 2019), particularly short-tailed shearwaters (*Ardenna tenuirostris*), which nest in the southern hemisphere. Other seasonal visitors that nest south of the study area include members of the Alcidae and Laridae families, as well as waterfowl (Anatidae), phalaropes (Scolopacidae), and loons (Gaviidae), which pass through from Alaska's North Slope after breeding.

Data collection

At-sea distribution and abundance of seabirds were obtained from surveys conducted from research vessels using U.S. Fish and Wildlife Service protocols (Kuletz et al., 2008). A single observer recorded all birds on one side of the vessel, within 300 m and a 90° arc from the centerline of travel. The observer recorded species, number of individuals, and behavior (on water, on ice, foraging, in air) and perpendicular distance from the centerline (using distance bins). Birds were identified to the lowest taxonomic level possible, using 10x binoculars, and sometimes a digital camera, to assist with species identification. Birds on water or actively foraging were recorded continuously, whereas birds in the air (not actively foraging by touching the water surface) were recorded during quick scans within the transect window, at approximately $1 \cdot min^{-1}$ (varying with respect to vessel speed), and avoiding double counting. Surveys were conducted with seas of Beaufort scale ≤ 6 and were discontinued when dense fog or precipitation impeded visibility. Observations were entered into a laptop computer connected to a Global Positioning System (GPS), using software DLog3 (R.G. Ford, Portland, OR). Every record entry was stamped with time, latitude and longitude, and environmental conditions, and automatically updated at 20 sec intervals to record effort. We divided survey transect lines into ~3 km segments, with the segment centroid serving as sample location, and calculated density of birds ($birds \cdot km^{-2}$) for each transect segment. Transect widths were narrowed from 300 m to 200 m or based on observation conditions.

Data treatment and analysis

Survey effort (Table 1, Fig. 2) within the study area during 2007-2019 totaled 79,426 km, using only surveys conducted 1 July to 30 September; these months reflect peak breeding season for seabirds in the study area, and omit June, when we had little survey effort. We compared species richness, community

composition, and abundance of key species within the subregions between two time periods, 2007-2016 and 2017-2019. The latter years were characterized by anomalously low sea-ice coverage in the study region, with the warmest year (2018) exhibiting the highest record of seabird mortalities and reproductive failure (Duffy-Anderson et al., 2019; Romano et al., this issue). We also examined annual differences in abundance of key species and Total seabirds (all species combined, including phalaropes and seaducks but excluding other shorebirds, waterfowl, land birds, and birds of prey; Appendix A).

Species richness

Because sampling effort was not consistent among the four subregions and two time periods, we used rarefaction curves to examine species richness during each time period and within each subregion. We randomly resampled 3-km segments (without replacement) and generated plots of number of species observed vs. number of segments sampled, with 95% confidence intervals calculated using quantiles from 2000 random draws for each sample size. During surveys, it was not always possible to identify sightings to the species level, for example due to a brief or inadequate view. In the rarefaction analysis, a higher-order taxon was counted as a unique species if and only if a corresponding lower-order taxon was not present in the sample. For example, an unidentified murre (*Uria* spp.) would be counted as a species if and only if no common murres (*U. aalge*) or thick-billed murres (*U. lomvia*) occurred in a sample.

For the remaining analyses, we applied a 30-km hexagonal cell grid to the study area, and derived density of each species by cell using the mean of 3-km segments within each cell. Birds that had not been identified to species were apportioned from higher-order taxa to species based on the ratio of identified birds within a cell and year. If there were no identified species within a higher-order taxon in a given cell and year (ranging from 0-7% of cells, with an average of 1%, depending on taxon), unidentified birds were prorated to species based on spatial interpolation of species ratios derived from kriging surrounding cells; kriging applied a cutoff distance of 60 km (~ 2 grid cells).

The number of sampled cells within a subregion varied among years, ranging from 98 to 371 cells for a given year. Because spatial differences in sampling among years could bias comparisons, we imputed species densities for grid cells missing years using methods described in Renner et al. (2013) and Kuletz et al. (2014). Species densities of grid cells not surveyed in a given year were interpolated through time (not space). Within each grid cell, densities in any missing years were imputed using linear interpolation. Any missing values at the beginning or end of the time-series were imputed by replacing missing values with the closest neighbor in time (rather than projecting trends).

Abundance and distribution

During preliminary analyses, we examined the distribution and abundance of four foraging guilds (surface planktivore, diving planktivore, surface piscivore, diving piscivore) along with individual species. Because the foraging guild patterns were largely driven by the most abundant species within each guild, here we present results for Total seabirds and seven focal species: thick-billed murre, common murre, crested auklet (*Aethia cristatella*), least auklet (*A. pusilla*), northern fulmar (*Fulmarus glacialis*), black-legged kittiwake (*Rissa tridactyla*), and short-tailed shearwater. We selected these focal species because they were widespread in the study area (Appendix B) and relatively abundant during all years (Appendix A). Five of them were the predominate species for seabird communities identified in this LME during 2007-2015 (Kuletz et al., 2019).

We used two methods to evaluate distribution and abundance of these species and groups. First, we calculated annual density estimates for species or species groups from the cell means within a subregion and year. The grid cell means for each species were used to plot standardized mean anomalies for each subregion and time period (2007-2016 and 2017-2019). Near the coastline, some cells were truncated,

thus we used weighted averages based on the area of each hexagon cell; this avoided over-representation in the overall average due to the presence of large flocks in small cells. Second, we examined the spatial distribution of increases or decreases in seabird densities (by species) by subtracting mean densities (by cell) for 2007-2016 from mean densities for 2017-2019, and mapping these differences.

Community composition

To identify seabird communities in the study area and compare their distribution between the two time periods, we used K-Means Cluster analysis (Hartigan and Wong, 1979). In the first step, we grouped the 30-km hexagon grid cells based on similarity in densities of birds, using log-transformed densities. Clustering was based on species densities, not geographic coordinates, and performed on all years combined, 2007-2019. Five communities were identified in the study area, based on the inflection point of within-group sum of squares vs. the number of clusters (Hartigan and Wong, 1979). In the second step, the clusters were then redistributed to their respective time-period maps (2007-2016 or 2017-2019).

We used R functions and scripts for analyses (R Core Team, 2015), with kriging for species' ratios applying function *krige* in package gstat (Pebesma, 2004). Cluster analysis used the R function *kmeans* (Hartigan and Wong, 1979).

Results

Species richness

Estimated species richness was higher in the Bering Sea (~40 species) than in the Chukchi Sea (~30 species) during both time periods. Within the two Bering subregions, species richness was slightly lower during 2017-2019, whereas it remained similar overall in the two Chukchi subregions (Fig. 3). However, in both the Bering and Chukchi regions, there was a reversal in richness between subregions; i.e. during the later period the Chirikov Basin had slightly higher species richness than the Northern Bering, and the Northern Chukchi had higher richness than the Southern Chukchi (Fig. 3).

Spatial changes in density

Compared to 2007-2016, Total seabird density was higher in 2017-2019 (Table 2), but the direction of changes in density were not equal across the study area, nor among species. Mean densities indicated both murre species declined in the later period, whereas both auklet species and black-legged kittiwakes increased slightly, and short-tailed shearwaters nearly doubled in density (Table 2). During the later time period, Total seabird density increased along the Anadyr Current, and in the northern Hope Basin, the western portion of the Northern Chukchi, and over Barrow Canyon (Fig. 4a). Decreases occurred in most of the Northern Bering, but also in the eastern Chirikov Basin to southern Hope Basin and the eastern coastal waters of the Northern Chukchi. This pattern largely reflects that of short-tailed shearwaters, a numerically dominate species, although shearwaters also showed large increases in 2017-2019 northwest of Cape Lisburne and over the Hanna Shoal and Barrow Canyon areas (Fig. 4b). Northern fulmars did not have a clear pattern of spatial change, with both increases and decreases scattered throughout the study area and large areas with no change (Fig. 4c). Black-legged kittiwakes also showed little evidence of a clear pattern, although there were more increases in Hope Basin and northwest of Cape Lisburne (Fig. 4d).

Common murres showed few increases in abundance, with those mainly in the Northern Bering, and they otherwise decreased, particularly in the Southern Chukchi (Fig. 4e). Thick-billed murres increased in later years northwest of Cape Lisburne, but primarily decreased throughout the study area, including near the St. Matthew colony (Fig. 4f). Least auklets had large increases in the Chirikov Basin, but mainly

decreased throughout the Chukchi Sea (Fig. 4g). Crested auklets increased near the Anadyr Current in the Chirikov Basin and in the northern edge of the Northern Chukchi, but declined in other areas of the Northern and Southern Chukchi (Fig. 4h).

Annual trends in abundance

For Total seabirds, the annual trends in abundance indicated a general northward shift in distribution. This shift began around 2014 in the Bering Sea, 2015 in the Southern Chukchi, and 2016 in the Northern Chukchi, although relative abundance was below the long-term mean in 2019 for all but the Northern Chukchi (Fig. 5a). In contrast, abundance in the Northern Bering was below the long-term mean for most years after 2013. This general pattern reflected the influence of the most abundant avian species in the study area, the short-tailed shearwater, the least auklet, and the crested auklet (Table 2). Short-tailed shearwaters differed from Total seabirds in having extremely high abundance in the Chirikov Basin and the Southern Chukchi in 2015 (Fig. 5b). Trends of northern fulmars were mixed, with fluctuations between subregions of the Bering and in the Southern Chukchi, but generally lower use of the Northern Chukchi after 2010 (Fig. 5c). Abundance of black-legged kittiwakes shifted from the Northern Bering during 2007-2011 to the Chirikov Basin during 2012-2015, and to the Chukchi subregions from 2014-2019 (Fig. 5d).

In general, the diving alcids declined in recent years in the Chukchi, with the *Aethia* auklets increasing in the Chirikov Basin and Northern Bering, and the murres mostly decreasing throughout the study area after 2013. Starting in 2014 both common murres (Fig. 5e) and thick-billed murres (Fig. 5f) showed steadily declining trends in the Northern Bering and below average abundance (common murre) or very low abundance (thick-billed murre) in the Chirikov Basin. Abundances of both murre species were below the long term mean in the Chukchi subregions for most years after 2013. In contrast, least auklets, which were highly abundant in the Chukchi during 2010 to 2012, increased abruptly in the Chirikov Basin and Northern Bering during 2017-2019 (Fig. 5g). Crested auklets showed a similar pattern, although they were sporadically abundant in the Northern Chukchi and did not substantially increase in the Chirikov Basin until 2018 (Fig. 5h).

Seabird communities

Within our study area we identified five clusters of grid cells that differed from each other in seabird community composition and densities (Appendix C). Four of the clusters had the same primary species as the community types identified by Kuletz et al. (2019); these clusters were dominated by thick-billed murres, least auklets, crested auklets, and short-tailed shearwaters, plus a 'Low Density' cluster type defined by low total densities and no definitive predominant species (no species had a mean density of >0.54 birds·km^{-2}). A sixth community type identified by Kuletz et al. (2019), dominated by northern fulmars, was not distinguished in this new analysis, reflecting the omission of more southerly waters of the outer Bering Sea shelf that were part of the previous study.

The distribution maps for the five community clusters in each time period depicted a spatial contraction of the thick-billed murre, crested auklet, and least auklet-dominated clusters during 2017-2019 (Fig. 6). During the late period the thick-billed murre cluster was less extensive throughout the study area and was located primarily near St Matthew Island in the Northern Bering and the Cape Thompson and Cape Lisburne colonies in the Southern Chukchi. The crested auklet cluster covered a much smaller area and was concentrated in the northeastern portion of its previous range in the Chukchi Sea, although there were also isolated, scattered cells between Chirikov Basin and Hope Basin (Fig. 6). The least auklet cluster also covered less area in 2017-2019, and was found primarily south of Bering Strait, abandoning its earlier occupation of Hope Basin.

In contrast to the three alcid-dominated clusters, the short-tailed shearwater-dominated cluster expanded during 2017-2019, and was located primarily in the Chukchi Sea. Its increase was greatest in Hope Basin and contiguously along the western edge of the study area and in a band from Hanna Shoal to Wainwright and Point Barrow – the Barrow Canyon area (Fig. 6). The Low-Density cluster also expanded in the later period. During 2017-2019, this cluster covered more area (compared to 2007-2016) throughout the Bering Sea shelf, particularly in the Northern Bering subregion. Its distribution in the Southern Chukchi did not change much between time- periods, but in the eastern half of the Northern Chukchi, it greatly expanded during 2017-2019 (Fig. 6).

Discussion

During the exceptionally warm, low-ice years of 2017-2019, we found evidence of broad-scale shifts in distribution of individual species and of identified seabird communities compared to the previous decade. Sea-ice extent in the northern portion of the Bering Sea was the lowest on record during the late period of our study. In 2017, sea ice failed to form over the northwestern Bering Shelf due to atypical southerly wind patterns. Unprecedented open water predominated throughout the Northern Bering and Southern Chukchi subregions in 2018 and 2019 as well (Siddon and Zador, 2018, 2019). Nonetheless, density of Total seabirds increased approximately 20% during this period, with the increase largely due to short-tailed shearwaters in the Chukchi Sea, and least and crested auklets in the Chirikov Basin.

Short-tailed shearwaters breed on islands off Australia's southern coast during the austral summer. After breeding they migrate to Alaska for the boreal summer, and reach the northernmost extent of their migrations in the Chukchi Sea. Untethered from nesting colonies during their non-breeding season, shearwaters can readily respond to shifts in prey distribution. In contrast, the two species of auklet nest during summer in dense colonies on islands in the Chirikov Basin and Northern Bering, although some auklets in the offshore waters could have originated from colonies in the Aleutian Archipelago (Will et al., 2017) or the Siberian coast (USFWS, 2014). What all three species have in common is a diet primarily composed of zooplankton. The short-tailed shearwater is considered an omnivore, with a varied diet that includes euphausiids, copepods, cephalopods, amphipods, and larval and juvenile fish (Hunt et al., 2002; Ogi et al., 1980), but recent studies suggest it primarily feeds on euphausiids while in Alaska (Nishizawa et al., 2017, this issue). Both auklet species are planktivorous, with the smaller-bodied least auklet feeding mainly on *Neocalanus* copepods, and the larger crested auklet feeding on a variety of large copepod taxa, euphausiids, and occasionally, larval fish (Sheffield-Guy et al., 2009; Gall et al., 2006).

The Chukchi Sea has a late seasonal plankton bloom tied to the timing of ice retreat, long daylight hours, and stratification, which makes copepods available into late summer (Weingartner et al., 2013, 2017; Danielson et al., 2017). In comparison to historic patterns (1940s to 1990s), seasonally early ice retreat in the 2000s was associated with higher primary productivity and larger biomasses of lipid-rich copepods (such as *Calanus glacialis*), euphausiids (*Thysanoessa* spp.) and amphipods (*Themisto* spp.) (Ershova et al., 2015; Matsuno et al., 2011). This may be why Gall et al. (2017) found higher predicted abundance of short-tailed shearwaters and crested auklets with earlier ice retreat, based on survey data from the Chukchi Sea during 1975-2012. Our shearwater observations during 2017-2019 are consistent with that model. However, planktivorous seabirds, primarily short-tailed shearwaters and crested auklets, did not predominate in the offshore waters of the Chukchi Sea until sometime between the 1980s and 2007 (Gall et al., 2017). The late summer and fall presence of crested and least auklets far from breeding colonies were presumed to be post-breeding birds replenishing body reserves before migrating back to the Bering Sea for winter (Kuletz et al., 2019; Will et al., 2017).

During the current decade, sea ice has further diminished. Zooplankton communities in the Chukchi Sea have shown highly localized influences of shifting water masses, resulting in high interannual variability (Pinchuk and Eisner, 2017; Spear et al., 2019). The irregular pattern of abundance exhibited by crested

auklets in the Northern Chukchi may reflect these localized fluctuations (Fig. 5h). Preliminary examination of zooplankton samples from the Northern Chukchi found that large copepods were more abundant in 2017 than in 2019, albeit both years had lower copepod abundance than during cooler years of 2012-2015 (D. Kimmel, unpubl. data). Our observations suggest that crested auklets and short-tailed shearwaters took advantage of aggregations of large copepods and euphausiids in the Northern Chukchi, particularly in 2017 (Fig. 5 b, h).

The abundance of crested auklets in the Northern Chukchi suggests that a portion of the Alaska-wide metapopulation rely on the prey in these cooler waters. However, the dynamics of sea ice, water temperature, primary productivity, and zooplankton are complex. Longer periods of open water and thinner sea ice have been linked to increased open water primary productivity in the Arctic (Arrigo et al., 2008; Brown et al., 2011) and an increase in advected Pacific-Bering zooplankton (Ershova et al., 2015). At the same time, warm, low-ice conditions have been associated with a decrease in production by ice algae, which are rich in long-chain omega-3 fatty acids (Søreide et al., 2010), and also with potentially lower local production of Arctic zooplankton fauna, including *C. glacialis* (Spear et al., 2019). In studies during the relatively cool years of 2010-2012, Spear et al. (2019) found highest concentrations of *C. glacialis* along the eastern waters of the Northern Chukchi, from Icy Cape to Barrow Canyon. Indeed, during those years the crested auklet community cluster extended well into these waters (Kuletz et al., 2019), whereas during the warmer period of 2017-2019 (this study), the Low Density seabird community predominated in this area (Fig. 6).

Although least auklets also appear to move into the Chukchi Sea in summer and fall, they primarily occur in the Southern Chukchi (Kuletz et al., 2015, 2019). Small copepods, which least auklets consume, are often abundant in Hope Basin and remained available there in 2017 and 2019 (no data are available for 2018; Kimmel, unpubl. data). Small copepod taxa (*Acartia* spp., *Pseudocalanus* spp., and *Oithona* spp.), were also abundant in the Northern Bering and Chirikov Basin in 2018 (Kimmel et al., 2018), when least auklets shifted to those subregions (Fig. 5g).

Concurrent with decreases in sea ice, northward flow from the Bering Sea has been increasing (Woodgate et al., 2012), which could increase advection of zooplankton and larval fish from the Bering shelf to Hope Basin and Hanna Shoal in the Chukchi Sea (Grebmeier et al., 2006; Dunton et al., 2017). Since the 2000s, zooplankton biomass has also increased along the Chukchi shelf break (Lane et al., 2008). Despite unusually high densities of least and crested auklets in the Chirikov Basin during 2017-2019, the Chukchi Sea will likely remain important post-breeding foraging habitat for these species, as evident in their overall distributions (Appendix B) and observed increases in some locations of the Northern Chukchi (Fig. 4 g, h).

An important feature of the Northern Chukchi is Barrow Canyon, which is a recognized hotspot of seabird activity (Kuletz et al., 2015), and where we found increased densities of several species in 2017-2019. Abundance of short-tailed shearwaters, and to lesser extent black-legged kittiwakes and northern fulmars, increased in the Barrow Canyon area during the late period. These surface feeders may forage over the canyon and adjacent waters because of the associated upwelling and concentration of euphausiids (Okkonen et al., 2011), as well as a variety of forage fishes attracted to large biomasses of copepods there (Logerwell et al., 2018).

The northward distributional shift observed for seabirds during this study was most evident for short-tailed shearwaters; higher densities began in the Chirikov Basin in 2014, the Southern Chukchi in 2015, and the Northern Chukchi in 2016, although shearwater abundance was near the long-term mean in 2018 and 2019 (Fig. 5b). This pattern coincides with seabird mortality events that included shearwaters in the Bering Strait region in summers of 2017-2019. The short-tailed shearwater was the main species impacted by the largest die off in the Bering Sea in recent years, in the southeast Bering Sea in 2019 (Siddon and

Zador, 2019; USFWS, unpubl. data). Necropsies revealed birds were emaciated and starved, thus the large increases in shearwaters observed in the Chukchi Sea suggest foraging conditions were forcing ever-farther migration north to obtain energy stores for the migration back to breeding grounds. The extra distance may have contributed to the late arrival of shearwaters to breeding sites in Australia recorded in October-November of 2019 (Liao 2019).

Piscivorous seabirds could also have been impacted by changes in their prey. A variety of forage fish are available in the study area, with the lipid-rich Arctic cod (*Boreogadus saida*) the most abundant (De Robertis et al., 2017; Logerwell et al., 2018). Age-0 Arctic cod were particularly abundant in the Northern Chukchi during 2012 and 2013, suggesting it is an important nursery ground for the species (De Robertis et al., 2017). In the northern Bering Sea, forage fish biomass in summer 2019 was low compared to previous years, indicating poor conditions for fish growth and survival, or alternatively, that the fish migrated north for better foraging (Yasumiishi et al., 2019). Arctic cod prefer cold, high salinity water masses, where there tends to be high biomass of large copepods (De Robertis et al, 2017; Logerwell et al., 2020). While the effects of warm conditions during 2017-2019 are not yet fully understood, evidence suggests that key seabird prey species, at least in the Bering Sea, were either low in abundance or shifted distribution (Duffy-Anderson et al., 2019; Siddon and Zador, 2018, 2019). These changes in prey availability could have differentially affected breeding seabirds, or birds that have restricted foraging ranges. Murres, which have high wing loading, tend to forage where prey patches are persistent and highly aggregated, or forage closer to their colony (Decker and Hunt, 1996; Sigler et al., 2012).

Both species of murres also experienced mass mortality events in the Bering Sea during 2017-2019, with evidence of starvation (Romano et al., this issue; Siddon and Zador, 2018, 2019) and potentially avian disease (A. Will et al., this issue). The low numbers of murres at colonies in 2018 (Romano et al., this issue; Will et al., this issue), together with broad-scale reductions in offshore densities (this study) concurrent with the mortality events, suggest major reductions in murre populations have probably occurred. Notably, Piatt et al. (2020) speculated that based on satellite-tagged murres, the huge mass mortality of common murres in the Gulf of Alaska during the winter of 2015-2016 could have included birds from the Bering Sea. This would be consistent with the trend of lower abundance in offshore waters of our study area, although we show a decline in abundance of murres starting in 2014 (Fig. 5e, f). In addition, euphausiids make up a high proportion of the diets of adult thick-billed murres, but not common murres. The greater dietary diversity of thick-billed murres may be one reason their densities were more stable than that of common murres, particularly in the Chukchi Sea.

Despite broad-scale declines in abundance at sea, murre (and kittiwake) plot counts at the Cape Lisburne colony in the Southern Chukchi increased at a rate of 6-7% in 2019, with an average increase of ~ 4% per annum over the past decade (Dragoo et al., 2020). The unusually high rate of growth would likely require immigration (D. Dragoo, pers. comm.), perhaps an indication of better foraging conditions near Cape Lisburne. In contrast, the murre colony at Cape Thompson (~100 km over water to the south) has decreased since the 1960s (Dragoo et al. 2000), indicating that murre breeding population trends have not been consistent among Chukchi Sea colonies. Nonetheless, it is noteworthy that at least the northernmost large colony in the Chukchi Sea shows increases in murres and kittiwakes, while the four colonies monitored by the Alaska Maritime National Wildlife Refuge in the southern Bering Sea show evidence of declines in murres, particularly common murre, and three of these colonies show declines in kittiwakes (Dragoo et al. 2000). The decrease in abundance of murres that we detected in offshore waters may reflect population declines in murres throughout the Bering Sea. Black-legged kittiwakes show a similar but less conclusive pattern of convergence between colony and offshore trends.

During 2017-2019, seabird species richness of the Northern Chukchi increased, while richness of other subregions converged at a slightly lower level than during the prior decade. This suggests that less-abundant seabird species were occurring in the Northern Chukchi with increasing frequency during the

later period. The convergence of species richness estimates between the Bering and Chukchi regions was mainly due to a decrease in species richness in the Bering Sea, and was concurrent with the expansion of the Low Density community cluster. Notably, the expansion of the Low Density community during the three warmest years (2017-2019) was nearly entirely along the eastern side of the study area. This expansion occurred in the Northern Bering and Chirikov Basin throughout the Inner Shelf, including areas east and south of St. Lawrence Island, which has large seabird colonies (Fig. 6). The Low Density community primarily displaced the short-tailed shearwater and thick-billed murre community clusters in the Bering Sea, and in the Northern Chukchi it displaced the short-tailed shearwater, thick-billed murre, and crested auklet communities. Thus, multiple foraging guilds appear to have been affected by conditions that concurrently led to the expansion of the Low Density community type.

The Inner Shelf waters of the Bering Sea, influenced by the fresher, warmer waters of the Alaska Coastal Current, have long been recognized as being nutrient-poor. These waters tend to have smaller zooplankton species, lower fish biomass (Eisner et al., 2013) and fewer seabirds compared to Anydyr waters to the west (Piatt and Springer, 2003; Sigler et al., 2017). The expansion of a Low Density seabird community in recent years suggests that large-scale ecosystem changes are altering the Inner Shelf, and to some degree the Middle Shelf and associated currents, thereby expanding the area of low productivity. In contrast, seabird density remained high near the Anadyr Current and western portions of the northern Bering and Chukchi seas. However, we lack sufficient data on seabird distribution west of the International Dateline to determine how far west those conditions exist. A long-term examination of marine fish from the Bering and Chukchi seas found that taxa respond to climate-related changes at different spatial and temporal scales (Alabia et al., 2018); similarly, we show that seabird species demonstrate a diversity of distributional responses, which may provide some level of resilience to their long-term prospects in the Pacific Arctic.

Acknowledgements

The seabird survey data was collected by the authors and a number of dedicated observers throughout the years. The surveys were supported by funding from the North Pacific Research Board (NPRB Projects 637,2007-2008 and B64,2008-2010), and by Intra-Agency Agreements from the Bureau of Ocean Energy Management (2010-2019; BOEM IAs M10PG00050, M17PG00017, and M17PG00039). We thank the many research vessel crews, chief scientists, and collaborating researchers that made our surveys possible, including but not limited to the Arctic Integrated Ecosystem Research Project (E. Farley, F. Mueter), Arctic Marine Biodiversity Observing Network (K. Iken), the Distributed Biological Observatory (J. Grebmeier, J. Nelson), Hokkaido University (T. Hirawake, Y. Watanuki), various National Science Foundation funded studies (C. Ashjian, S. Danielson, R. Pickart, R. Hopcroft), and NOAA Surveys (C. Berchock, J. Murphy). The findings and conclusions in this article are those of the authors and do not necessarily represent the views of the US Fish & Wildlife Service, the NPRB, or BOEM.

References

Abraham, C.L., Sydeman, W.J., 2004. Ocean climate, euphausiids and auklet nesting: inter-annual trends and variation in phenology, diet and growth of a planktivorous seabird, *Ptychoramphus aleuticus.* Mar.Ecol. Progr. Ser. 274, 235-250. doi:10.3354/meps274235

Alabia, I.D., García Molinos, J., Saitoh, S.I., Hirawake, T., Hirata, T., Mueter, F.J., 2018. Distribution shifts of marine taxa in the Pacific Arctic under contemporary climate changes. Divers. Distrib. 24, 1583–1597. https://doi.org/10.1111/ddi.12788

Arrigo, K. R., 2003. Primary production in sea ice. *In* Sea Ice-An Introduction to Its Physics, Chemistry, Biology and Geology, edited by D. N. Thomas and G. S. Dieckmann, pp. 143–183, Blackwell Sci., Oxford, U.K.

Arrigo, K.R., van Dijken, G., Pabi, S., 2008, Impact of a shrinking Arctic ice cover on marine primary production. Geophys. Res. Lett. 35, L19603, doi:10.1029/2008GL035028
Ballance, L., Pitman, R., Reilly, S., 1997. Seabird community structure along a productivity gradient: importance of competition and energetic constraint. Ecology 78, 1502–1518.
Brown, Z.W., Arrigo, K.R., 2013. Sea ice impacts on spring bloom dynamics and net primary production in the Eastern Bering Sea, J. Geophys. Res. Oceans 118, 43–62. https://doi.org/10.1029/2012JC008034.
Brown, Z. W., van Dijken, G. L., Arrigo, K. R., 2011. A reassessment of primary production and environmental change in the Bering Sea J. Geophys. Res. Oceans 116, C08014, doi:10.1029/2010JC006766.
Cairns D.K., 1992. Population regulation of seabird colonies. pp. 37-61, *in* Power D.M., editor. Current Ornithology. vol 9. Springer, Boston, MA.
Campbell, R.C., Ashjian, C.J., Sherr, E.B., Sherr, B.F., Lomas, M.W., Ross, C., Alatalo, P., Gelfman, C., van Keuren, D., 2016. Mesozooplankton grazing during spring sea-ice conditions in the eastern Bering Sea. Deep-Sea Res. Part II 134, 157–172. https://doi.org/10.1016/j.dsr2.2015.11.003.
Coachman, L.K., Aagaard, K., Tripp, R.B., 1975. Bering Strait: The regional and physical oceanography. University of Washington Press, Seattle, Washington.
Cornwall, W., 2019. Vanishing Bering Sea ice poses climate puzzle. Science 364, 616–617.
Danielson, S.L., Eisner, L., Ladd, C., Mordy, C., Sousa, L., Weingartner, T. J., 2017. A comparison between late summer 2012 and 2013 water masses, macronutrients, and phytoplankton standing crops in the northern Bering and Chukchi Seas. Deep-Sea Res. Part II 135, 726. http://doi.org/10.1016/j.dsr2.2016.05.024.
Decker, M.B., Hunt, G.L.,Jr., 1996. Foraging by murres (*Uria* spp.) at tidal fronts surrounding the Pribilof islands, Alaska, USA. Mar. Ecol. Prog. Ser. 139, 1–10.
De Robertis, A., Taylor, K., Wilson, C.D., Farley, E.V., 2017. Abundance and distribution of Arctic cod (*Boreogadus saida*) and other pelagic fishes over the U.S. Continental Shelf of the Northern Bering and Chukchi Seas, Deep-Sea Res. Part II 135, 51-65, ISSN 0967-0645, https://doi.org/10.1016/j.dsr2.2016.03.002.
Dragoo, D.E., Renner, H.M., Kaler, R.S.A., 2020. Breeding status and population trends of seabirds in Alaska, 2019. U.S. Fish and Wildlife Service Report AMNWR 2020/01. Homer, Alaska, unpublished.
Duffy-Anderson, J.T., Stabeno, P., Andrews III, A.G, Cieciel, K., Kimmel, D., Kuletz, K., Lamb, J., Paquin, M., Porter, S., Rogers, L., Spear, A., Yasumiishi. E., 2019. Responses of the northern Bering Sea and southeastern Bering Sea pelagic ecosystems following record-breaking low winter ice. Geophys. Res. Lett. 46, 9833–9842. https://doi.org/10.1029/2019GL083396
Dunton, K. H., Grebmeier, J. M., Trefry, J. H., 2017. Hanna Shoal: An integrative study of a high Arctic marine ecosystem in the Chukchi Sea. Deep-Sea Res. Part II 144, 1–5. https://doi.org/10.1016/j.dsr2.2017.09.001
Eisner, L., Hillgruber, N., Martinson, E., Maskelo, J., 2013. Pelagic fish and zooplankton species assemblages in relation to water mass characteristics in the northern Bering and southeast Chukchi seas. Polar Biol. 36, 87–113.
Ershova, E.A., Hopcroft, R.R., Kosobokova, K.N., Matsuno, K., Nelson, R.J., Yamaguchi, A., Eisner, L.B., 2015. Long-term changes in summer zooplankton communities of the Western Chukchi Sea, 1945–2012. Oceanography 28, 100-115.
Gall, A.E., Day, R.H., Weingartner, T.J., 2013. Structure and variability of the marine-bird community in the northeastern Chukchi Sea. Cont. Shelf Res. 67, 96–115. doi:10.1016/j.csr.2012.11.004
Gall, A.E., Morgan, T.C., Day, R.H., Kuletz, K.J., 2017. Ecological shift from piscivorous to planktivorous seabirds in the Chukchi Sea, 1975-2012. Polar Biol. 40, 61–78. https://doi.org/10.1007/s00300-016-1924-z.
Gall, A.E., Roby, D.D., Irons, D.B., Rose, I.C., 2006. Differential response in chick survival to diet in least and crested auklets. Mar. Ecol. Prog. Ser. 308, 279–291.

Grebmeier, J.M., Cooper, L.W., Feder, H. M., Sirenko, B.I., 2006. Ecosystem dynamics of the Pacific-influenced Northern Bering and Chukchi Seas in the Amerasian Arctic. Prog. Oceanogr. 71, 331–361.
Hartigan, J. A., Wong, M. A., 1979. A K-means clustering algorithm. Appl. Stat. 28, 100–108.
Hunt Jr, G.L., Baduini, C., Jahncke, J., 2002. Diets of short-tailed shearwaters in the southeastern Bering Sea. Deep-Sea Research Part II 49, 6147–6156.
Hunt Jr, G.L., Coyle, K.O., Eisner, L.B., Farley, E.V., Heintz, R.A., Mueter, F., Napp, J.M., Overland, J.E., Ressler, P.H., Salo, S., 2011. Climate impacts on eastern Bering Sea foodwebs: a synthesis of new data and an assessment of the Oscillating Control Hypothesis. ICES J. Mar. Sci. 68, 1230–1243.
Hunt Jr., G.L., Renner, M., Kuletz, K.J., Salo, S., Eisner, L., Ressler, P., Ladd, C., Santora, J.A., 2018. Timing of sea-ice-retreat affects the distribution of seabirds and their prey in the southeastern Bering Sea. Mar. Ecol. Prog. Ser. 593, 209–230.
Jones, T., Divine, L.M., Renner, H., Knowles, S., Lefebvre, K.A., Burgess, H.K., Wright, C., Parrish, J.K., 2019. Unusual mortality of tufted puffins (*Fratercula cirrhata*) in the eastern Bering Sea. PLoS ONE 14, e0216532.
Kimmel, D., Lamb, J., Ferm, N. Fugate, C., Harpold, C., 2018. Rapid zooplankton assessment for 2018 – distribution, abundance, and lipid content – and historical time series. In: Siddon, E., Zador, S., 2018. Ecosystem Status Report 2019: Eastern Bering Sea, Stock Assessment and Fishery Evaluation Report, North Pacific Fishery Management Council, 605 W 4th Ave, Suite 306, Anchorage, AK 99501.
Kuletz, K., Cushing, D.A., Osnas, E.E., Labunski, E.A., Gall, A.E., 2019. Representation of the Pacific Arctic seabird community within the Distributed Biological Observatory array, 2007-2015. Deep-Sea Res. Part II 162, 191 –210. https://doi.org/10.1016/j.dsr2.2019.04.001
Kuletz, K.J., Ferguson, M.C., Hurley, B., Gall, A.E., Labunski, E.A., Morgan, T.C., 2015. Seasonal spatial patterns in seabird and marine mammal distribution in the eastern Chukchi and western Beaufort seas: identifying biologically important pelagic areas. Prog. Oceanogr. 136, 175–200.
Kuletz, K.J., Labunski, E.A., Renner, M., Irons, D., 2008. The North Pacific pelagic seabird observer program. NPRB Project 637 Final Report, North Pacific Research Board (NPRB), Anchorage, Alaska.
Kuletz, K.J., Renner, M., Labunski, E.A., Hunt., G.L., Jr., 2014. Changes in the distribution and abundance of albatrosses in the Eastern Bering Sea: 1975-2010. Deep-Sea Res. Part II 109, 282 – 292.
Lane, P, Llinas, L., Smith, S., Pilz, D., 2008. Zooplankton distribution in the western Arctic during summer 2002: hydrographic habitats and implications for food chain dynamics. J. Mar. Syst. 70, 97–133. https://doi.org/10.1016/j.jmarsys.2007.04.001
Liao, K. 2019. Where have all the short-tailed shearwaters gone? Audubon News. URL: https://www.audubon.org/news/where-have-all-short-tailed-shearwaters-gone.
Logerwell, E.A., Busby, M., Mier, K.L., Tabisola, H., Duffy-Anderson, J., 2020. The effect of oceanographic variability on the distribution of larval fishes of the northern Bering and Chukchi seas, Deep-Sea Res. Part II, 104784, https://doi.org/10.1016/j.dsr2.2020.104784.
Logerwell, E.A., Rand, K., Danielson, S., Sousa, L., 2018. Environmental drivers of benthic fish distribution in and around Barrow Canyon in the northeastern Chukchi Sea and western Beaufort Sea. Deep-Sea Res. Part II 152, 170-181, ISSN 0967-0645, https://doi.org/10.1016/j.dsr2.2017.04.012.
Matsuno, K., Yamaguchi, A., Hirawake, T., et al., 2011. Year-to-year changes of the mesozooplankton community in the Chukchi Sea during summers of 1991, 1992 and 2007, 2008. Polar Biol. 34, 1349–1360. https://doi.org/10.1007/s00300-011-0988-z
Murphy, R. C. 1936. Oceanic birds of South America. Vol. I. New York, American Museum of Natural History

Nishizawa, B., Matsuno, K., Labunski, E.A., Kuletz, K.J., Yamaguchi, A., Watanuki. Y., 2017. Seasonal distribution of short-tailed shearwaters and their prey in the Bering and Chukchi Seas. Biogeosciences 14, 1–12, https:// doi.org/ 10.5194/bg-14-1-2017.

Nishizawa, B., Yamada, N., Hayashi, H., Wright, C., Kuletz, K., Ueno, H., Mukai, T., Yamaguchi, A., Watanuki, Y. This issue. Sea-ice retreat and seabird-prey association in the northern Bering Sea. Deep Sea Res. Part II

Ogi, H. Kubodera, T., Nakamura, K., 1980. The pelagic feeding ecology of the Short-tailed Shearwater *Puffinus tenuirostris* in the Subarctic Pacific Region**.** J. Yamashina Instit. Ornithol.12, 157–182.

Okkonen, S.R., Ashjian, C.J., Campbell, R.G., Clarke, J.T., Moore, S.E., Taylor, K.D., 2011. Satellite observations of circulation features associated with a bowhead whale 'hotspot' near Barrow, Alaska. Remote Sens. Environment. 115, 2168–2174.

Pebesma, E.J., 2004. Multivariable geostatistics in S: the gstat package. Computers. Geosci. 30, 683–691.

Piatt, J.F., Parrish, J.K., Renner, H.M., Schoen, S.K., Jones, T.T., Arimitsu, M.L., Kuletz, K.J., et al., 2020. Extreme mortality and reproductive failure of common murres resulting from the northeast Pacific marine heatwave of 2014-2016. PLoS ONE 15, e0226087. https://doi.org/10.1371/journal.pone.0226087

Piatt, J.F., Springer, A.M., 2003. Advection, pelagic food webs and the biogeography of seabirds in Beringia. Mar. Ornithol. 31, 141–154.

Piatt, J., Sydeman, W., Wiese, F., 2007. Introduction: A modern role for seabirds as indicators. Mar. Ecol. Prog. Ser. 352, 199-204.

Pinchuk, A.I., Eisner, L.B., 2017. Spatial heterogeneity in zooplankton summer distribution in the eastern Chukchi Sea in 2012–2013 as a result of large-scale interactions of water masses. Deep-Sea Res. Part II 135, 27-39, ISSN 0967-0645, https://doi.org/10.1016/j.dsr2.2016.11.003.

R Core Team., 2015. R: A language and environment for statistical computing. R Foundation for Statistical Computing, Vienna, Austria. URL https://www.R-project.org/.

Renner, M., Parrish, J.K., Piatt, J.F., Kuletz, K.J., Edwards, A.E., Hunt, G.L. Jr., 2013. Modeled distribution and abundance of a pelagic seabird reveal trends in relation to fisheries. Mar. Ecol. Prog. Ser. 484, 259–277.

Romano, M.D., Renner, H.M., Kuletz, K.J., Parrish, J.K., Jones, T., Burgess, H.K., Cushing, D.A., Causey, D., This issue. Die-offs and reproductive failure of murres in the Bering and Chukchi Seas in 2018. Deep-Sea Res. Part II.

Siddon, E.C., Zador, S., 2018. Ecosystem status report 2018: Eastern Bering Sea. North Pacific Fishery Management Council, Anchorage, AK. 230 pp. https://access.afsc.noaa.gov/REFM/REEM/ecoweb/pdf/2018ecosysEBS-508.pdf

Siddon, E.C., Zador, S., 2019. Ecosystem status report 2019: Eastern Bering Sea. North Pacific Fishery Management Council, Anchorage, AK. 223 pp. https://access.afsc.noaa.gov/REFM/REEM/ecoweb/pdf/2019EBSecosys.pdf

Sigler. M.F., Kuletz, K.J., Ressler, P.H., Friday, N.A., Wilson, C.D., Zerbini, A.N., 2012. Marine predators and persistent prey in the southeast Bering Sea. Deep-Sea Res. Part II 65, 292-303.

Sigler, M.F., Mueter, J., Bodil, A., Bluhm, B., Busby, M.S., Cokelet, E.D., Danielson, S.L., De Robertis, A., Eisner, L.B., Farley, E.V., Iken, K., Kuletz, K.J., Lauth, R.R., Logerwell, E.A., Pinchuk, A.I., 2017. Late summer zoogeography of the northern Bering and Chukchi seas. Deep-Sea Res. Part II 35, 168–189. https://doi.org/10.1016/j.dsr2.2016.03.005

Sigler, M.F., Renner, M., Danielson, S.L., Eisner, L.B., Lauth, R.R., Kuletz, K.J., Logerwell, E.A., Hunt, Jr., G.L., 2011. Fluxes, fins, and feathers: Relationships among the Bering, Chukchi, and Beaufort Seas in a time of climate change. Oceanography 24, 250–265.

Sheffield-Guy, L.M., Roby, D.D., Gall, A.E., Irons, D.B., Rose, I.C., 2009. The influence of diet and ocean conditions on productivity of auklets on St. Lawrence Island, Alaska. Mar. Ornithol. 37, 227–236.

Søreide, J.E., Leu, E., Berge, J., Graeve., M., Falk-Petersen, S., 2010. Timing of blooms, algal food quality, and *Calanus glacialis* reproduction and growth in a changing Arctic. Glob. Change Biol. 16, 3154–3163.

Spear, A., Duffy-Anderson, J., Kimmel, D, Napp, J., Randall, J., Stabeno, P., 2019. Physical and biological drivers of zooplankton communities in the Chukchi Sea. Polar Biol. 42, 1107–1124. https://doi.org/10.1007/s00300-019-02498-0.

Stabeno, P.J., Bell, S.W., 2019. Extreme conditions in the Bering Sea (2017–2018): Record-breaking low sea-ice extent. Geophys. Res. Lett. 46, 8952–8959.

Stabeno, P., Napp, J., Mordy, C., Whitledge, T., 2010. Factors influencing physical structure and lower trophic levels of the eastern Bering Sea shelf in 2005: Sea ice, tides and winds. Prog. Oceanogr. 85, 180–196.

Stephensen, S.W., Irons, D.B., 2003. A comparison of colonial breeding seabirds in the eastern Bering Sea and Gulf of Alaska. Mar. Ornithol. 31, 167–173.

Suryan, R.M., Santora, J.A., Sydeman, W.J., 2012. New approach for using remotely sensed chlorophyll *a* to identify seabird hotspots. Mar. Ecol. Prog. Ser. 451, 213-225. https://doi.org/10.3354/meps09597

USFWS (U.S. Fish and Wildlife Service), 2014. North Pacific Seabird Colony Database. http://axiom.seabirds.net/maps/north-pacific-seabirds.

Velarde, E., Anderson, D.W., Ezcurra, E., 2019. Seabird clues to ecosystem health. Science 365, 116–117. DOI: 10.1126/science.aaw9999

Velarde, E., Ezcurra, E., 2018. Are seabirds' life history traits maladaptive under present oceanographic variability? The case of Heermann's Gull (*Larus heermanni*). Condor 120, 388–401, https://doi.org/10.1650/CONDOR-17-5.1

Weingartner, T., Aagaard, K., Woodgate, R., Danielson, S., Sasaki, Y., Cavalieri, D., 2005. Circulation on the north central Chukchi Sea shelf. Deep-Sea Research Part II 52, 3150–3174.

Weingartner, T., Dobbins, E., Danielson, S., Winsor, P., Potter, R., Statscewich, H., 2013. Hydrographic variability over the northeastern Chukchi Sea shelf in summer-fall 2008–2010. Cont. Shelf Res. 67, 5–22. https://doi.org/10.1016/j.csr.2013.03.012.

Weingartner, T., Fang, Y.C., Winsor, P., Dobbins, E., Potter, R., Statscewich, H., Mudge, T., Irving, B., Sousa, L., Borg, K., 2017. The summer hydrographic structure of the Hanna Shoal region on the northeastern Chukchi Sea shelf: 2011-2013. Deep-Sea Res. Part II 144, 6–20.

Will, A., Thiebot, J., Takahashi, A., Kitaysky, A. 2017. Following Least Auklets (*Aethia pusilla*) into the winter. Poster presentation at Alaska Marine Science Symposium, January 2017, Anchorage, Alaska.

Will, A., Thiebot, J., Ip, H.S., Shoogukwruk, P., Annogiyuk, M., Takahashi, A., Shearn-Bochsler, V., Killian, M.L., Torchetti, M., Kitaysky, A., this issue. Investigating causes of the 2018 thick-billed murre (*Uria lomvia*) die-off on St. Lawrence Island. Deep-Sea Res. Part II

Woodgate, R. A., Weingartner, T. J., Lindsay, R., 2012. Observed increases in Bering Strait oceanic fluxes from the Pacific to the Arctic from 2001 to 2011 and their impacts on the Arctic Ocean water column. Geophys. Res. Lett. 39, L24603. doi:10.1029/2012GL054092.

Yasumiishi E., Cieciel. K., Murphy, J., Andrews, A., 2019. Trends in the Abundance of Forage Fish in the Northern Bering Sea, 2002–2019. In Siddon, E., and Zador, S., 2019. Ecosystem Status Report 2019: Eastern Bering Sea, Stock Assessment and Fishery Evaluation Report, North Pacific Fishery Management Council, 605 W 4th Ave, Suite 306, Anchorage, AK 99501.

Yen, P.P.W., Sydeman, W.J., Bograd, S.J., Hyrenbach, K.D., 2006. Spring-time distributions of migratory marine birds in the southern California Current: Oceanic eddy associations and coastal habitat hotspots over 17 years. Deep-Sea Res. Part II 53, 399−418.

Table 1. Survey effort during two time periods, 2007-2016 and 2017-2019.

	2007-2016	2017-2019	Total
Subregion	Number of km surveyed		
Northern Chukchi	16969	9096	26065
Southern Chukchi	11393	7335	18728
Chirikov Basin	7212	5110	12322
Northern Bering	16268	6043	22311
	Number of 30-km grid cells		
Northern Chukchi	608	299	907
Southern Chukchi	425	197	622
Chirikov Basin	306	164	470
Northern Bering	820	295	1115

Table 2. Mean density (birds·km^{-2}), by subregion, of 7 focal species and for Total Birds (includes all species in Appendix A), during two time periods, 2007-2016 and 2017-2019.

		2007-2016					2017-2019				
		Mean density					Mean density				
Common Name	**Latin name**	Northern Bering	Chiriko v Basin	Southern Chukchi	Northern Chukchi	all Regions	Northern Bering	Chiriko v Basin	Southern Chukchi	Northern Chukchi	all Regions
Common Murre	*Uria aalge*	0.91	0.78	0.92	0.08	0.62	0.37	0.48	0.37	0.05	0.28
Thick-billed Murre	*Uria lomvia*	0.88	0.87	1.79	0.35	0.91	0.29	0.53	1.29	0.23	0.52
Least Auklet	*Aethia pusilla*	0.07	6.98	2.85	0.43	1.87	0.16	10.48	0.64	0.12	1.95
Crested Auklet	*Aethia cristatella*	0.15	1.97	0.57	2.27	1.21	0.24	4.70	0.34	1.74	1.50
Black-legged Kittiwake	*Rissa tridactyla*	0.61	0.71	0.82	0.38	0.60	0.75	0.68	1.66	0.31	0.78
Northern Fulmar	*Fulmarus glacialis*	0.95	0.59	0.42	0.23	0.54	0.73	0.99	0.22	0.22	0.49
Short-tailed Shearwater	*Ardenna tenuirostris*	1.79	3.71	5.74	4.22	3.76	1.27	3.06	6.46	11.48	6.05
Total Birds*		6.24	18.70	15.76	8.58	11.02	4.53	23.29	14.68	14.83	13.16
* Includes all species observed, see Appendix A											

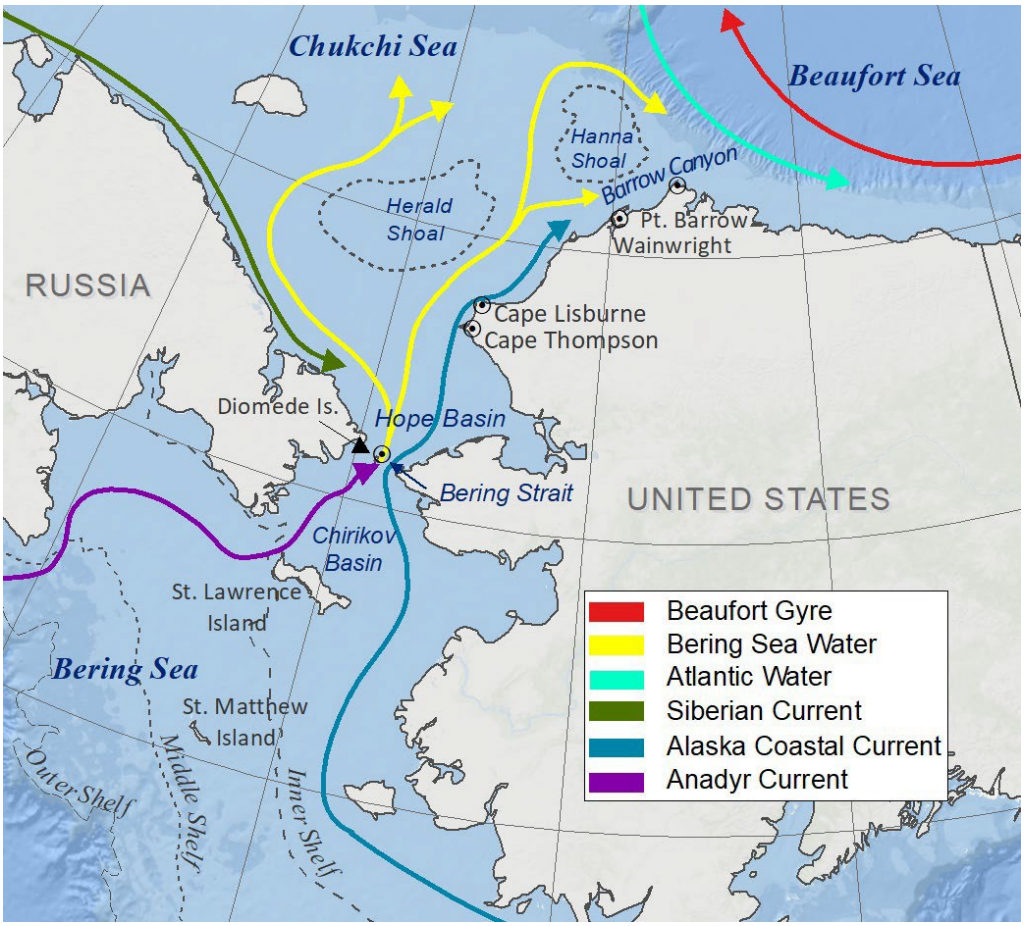

Figure 1. The Bering Sea and Chukchi Sea study area, showing generalized trajectories of major water masses. Map by EAL, based on Dunton et al. (2017).

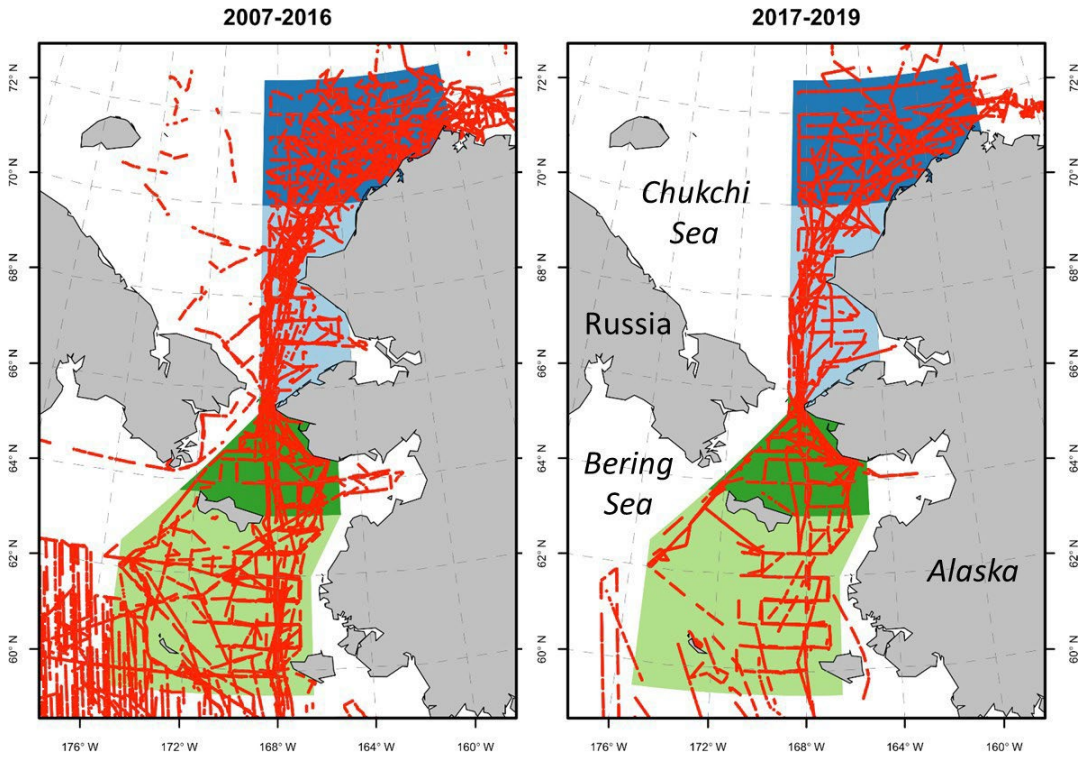

Figure 2. Four subregions of the study area: Northern Bering (light green), Chirkov Basin (dark green), Southern Chukchi (light blue) and Northern Chukchi (dark blue), with seabird survey transects overlaid for each time period.

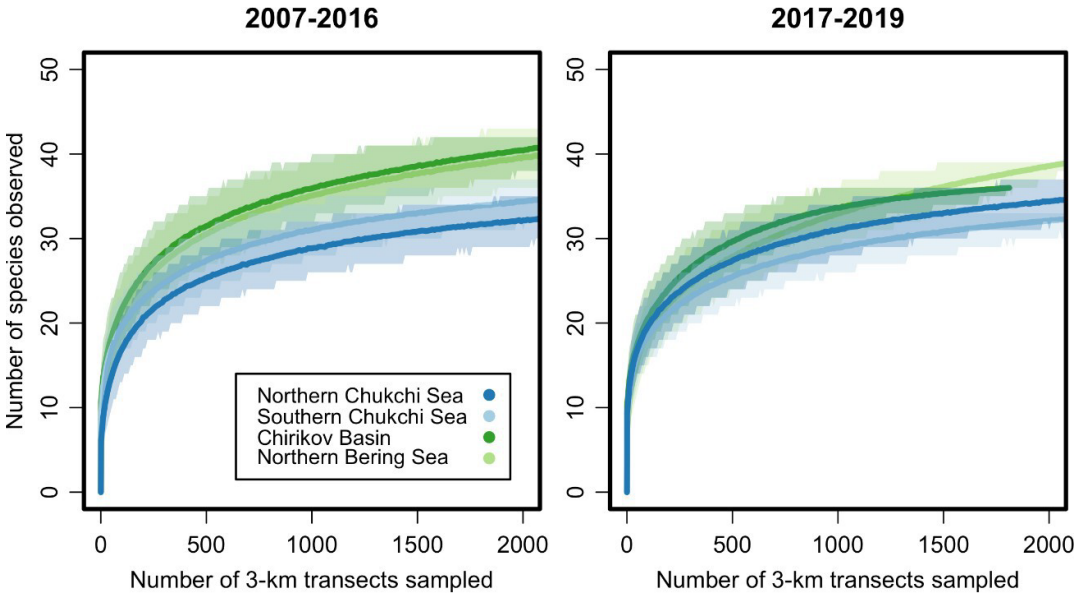

Figure 3. Species richness (rarefaction curves) in four subregions of the study area, for 2007-2016 and 2017-2019. Mean (solid lines) and 95% confidence intervals (shading) were derived from random selection of 3-km transect segments from surveys conducted during each time period and subregion.

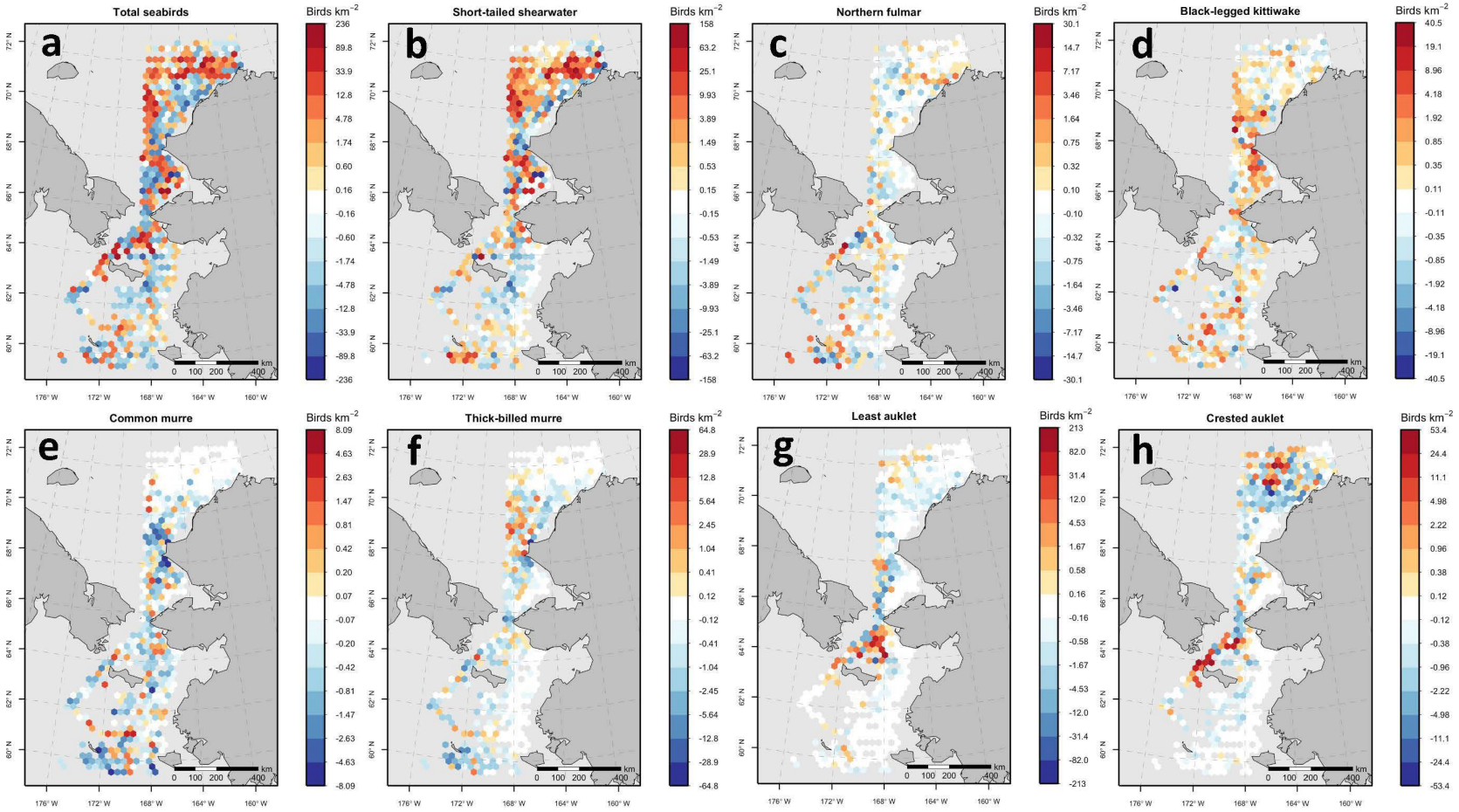

Figure 4. Distribution of increases (oranges) and decreases (blues) in densities of Total Seabirds and seven focal species in 2017-2019, compared to 2007-2016. Mean densities were calculated per 30-km grid cell within each time period for cells surveyed in both time periods.

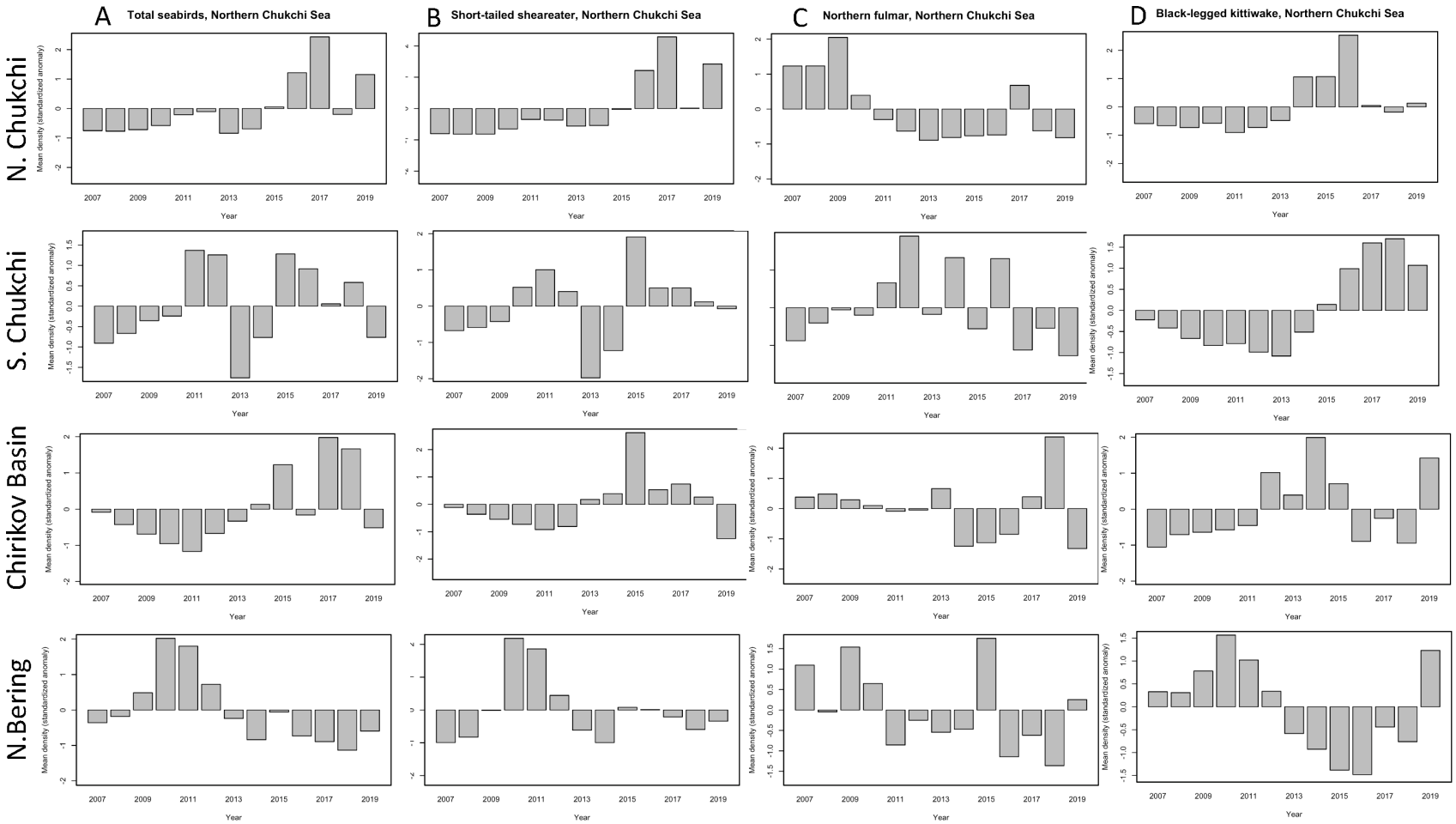

Figure 5. Standardized mean anomalies for Total Seabirds and seven focal species, for each subregion across all years, 2007-2019.

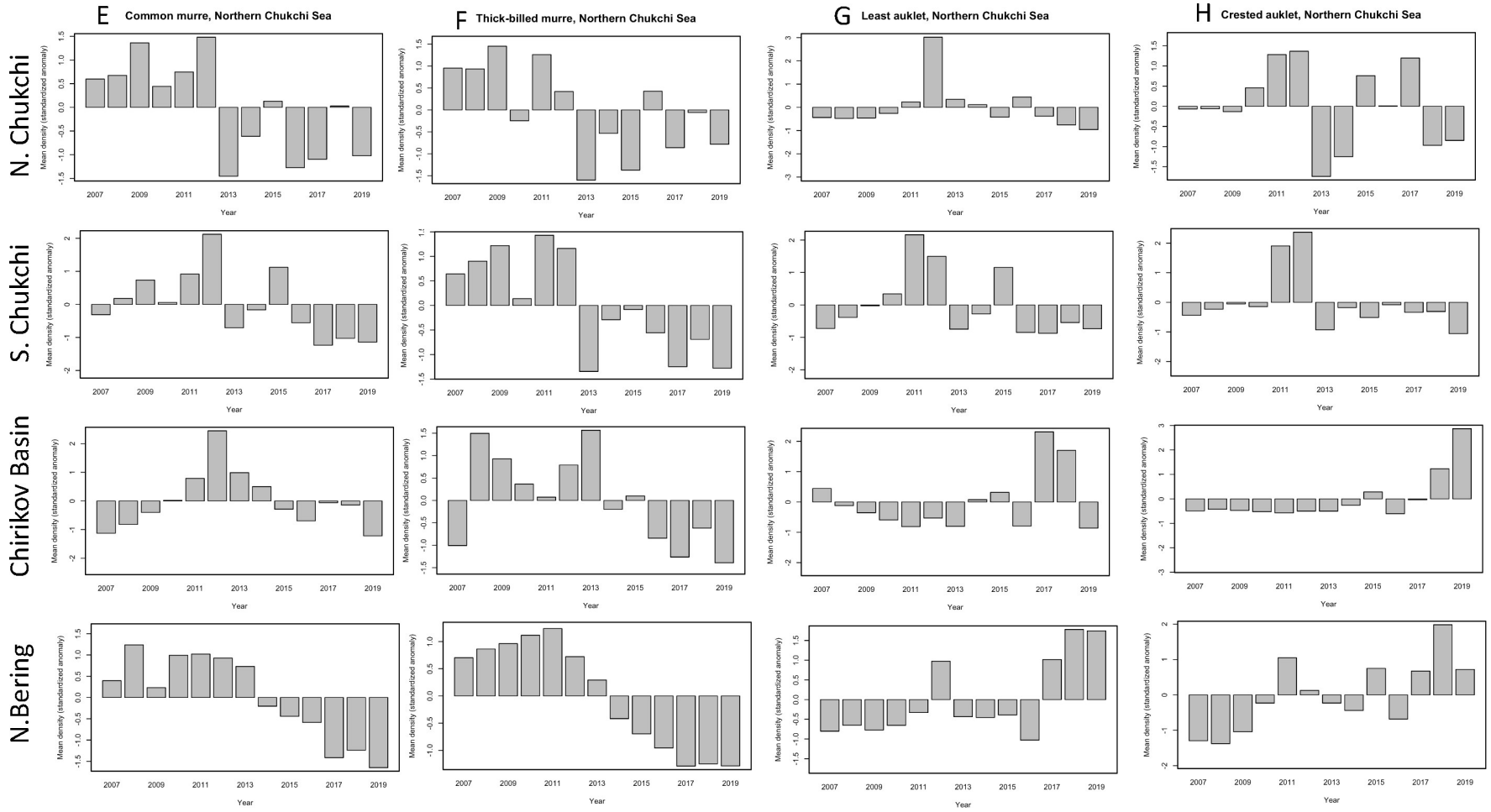

Figure 5. continued

Appendix A. Mean densities (birds/km^2), by species, and subregion, during two time periods, 2007-2016 and 2017-2019. Asterisk indicates densities were < 0.01.

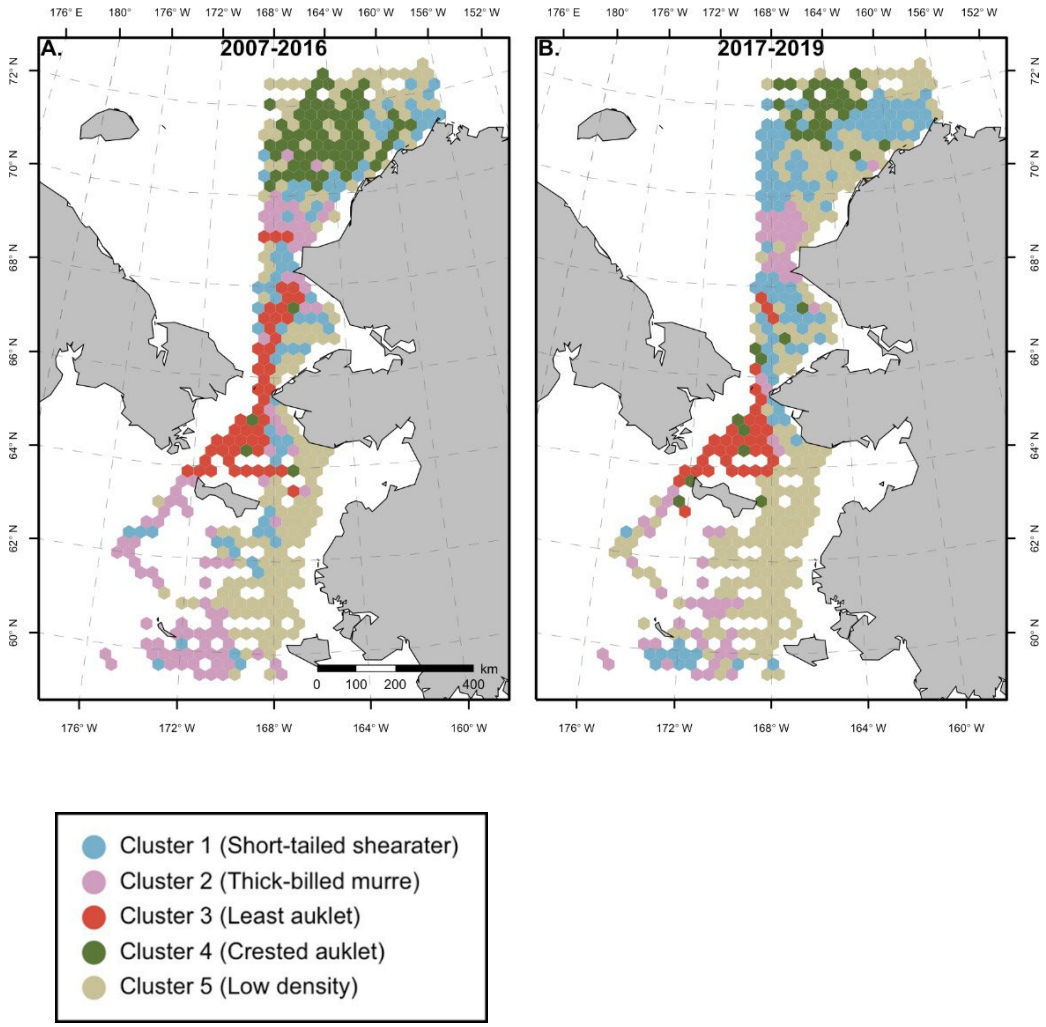

Figure 6. Distribution of five identified seabird community types (clusters) during two time periods, based on K-means Cluster Analysis. Colors represent community types referred to by the most abundant species (Clusters 1 – 4), or by low density and lack of a dominant species (Cluster 5).

Appendix A. Mean densities (birds/km^2), by species, and subregion, during two time periods, 2007-2016 and 2017-2019. Asterisk indicates densities were < 0.01.

		2007-2016					2017-2019				
		Mean density to 0.00 or <.01 (*)					Mean density to 0.00 or <.01 (*)				
Common Name	**Latin name**	Northern Bering	Chirikov Basin	Southern Chukchi	Northern Chukchi	All Regions	Northern Bering	Chirikov Basin	Southern Chukchi	Northern Chukchi	All Regions
Steller's Eider	*Polysticta stelleri*	0	*	0	0	*	*	*	0	0	*
Spectacled Eider	*Somateria fischeri*	0	0	0	*	*	0	*	*	*	*
King Eider	*Somateria spectabilis*	*	0.04	*	*	*	*	0.01	0.03	*	*
Common Eider	*Somateria mollissima*	*	*	0.04	*	0.01	0	0	0.04	*	*
Harlequin Duck	*Histrionicus histrionicus*	*	*	*	0	*	*	0	0	0	*
Surf Scoter	*Melanitta perspicillata*	0	*	*	0	*	0	0	0	0	0
White-winged Scoter	*Melanitta fusca*	0	*	0	0	*	*	*	*	0	*
Black Scoter	*Melanitta americana*	*	0	0	0	*	0	0	0	0	0
Long-tailed Duck	*Clangula hyemalis*	*	*	0.04	0.02	0.02	*	*	0.04	0.07	0.03
Red-necked Grebe	*Podiceps grisegena*	*	0	0	0	*	0	0	*	0	*
Red-necked Phalarope	*Phalaropus lobatus*	0.03	0.25	0.21	0.13	0.14	0.08	0.06	0.01	0.01	0.04
Red Phalarope	*Phalaropus fulicarius*	0.14	1.21	1.49	0.21	0.63	0.1	0.82	2.89	0.27	0.86
Pomarine Jaeger	*Stercorarius pomarinus*	0.04	0.05	0.13	0.03	0.06	0.02	0.05	0.03	0.03	0.03
Parasitic Jaeger	*Stercorarius parasiticus*	*	0.01	0.03	0.01	0.02	*	*	*	0.02	*
Long-tailed Jaeger	*Stercorarius longicaudus*	*	*	*	*	*	0	*	*	*	*
Dovekie	*Alle alle*	*	*	*	*	*	*	*	0	0	*
Common Murre	*Uria aalge*	0.91	0.78	0.92	0.08	0.62	0.37	0.48	0.37	0.05	0.28
Thick-billed Murre	*Uria lomvia*	0.88	0.87	1.79	0.35	0.91	0.29	0.53	1.29	0.23	0.52
Black Guillemot	*Cepphus grylle*	0	*	*	*	*	0	*	0	*	*
Pigeon Guillemot	*Cepphus columba*	*	*	*	*	*	*	*	0	0	*
Marbled Murrelet	*Brachyramphus marmoratus*	*	*	*	0	*	*	*	0	0	*
Kittlitz's Murrelet	*Brachyramphus brevirostris*	0	0	0.04	0.02	0.01	0	0	*	*	*
Ancient Murrelet	*Synthliboramphus antiquus*	0.18	0.11	0.08	0.05	0.1	0.06	0.08	0.07	0.05	0.06
Cassin's Auklet	*Ptychoramphus aleuticus*	*	*	*	0	*	*	*	0	*	*

Appendix A. Mean densities (birds/km^2), by species, and subregion, during two time periods, 2007-2016 and 2017-2019. Asterisk indicates densities were < 0.01.

Parakeet Auklet	*Aethia psittacula*	0.14	0.74	0.24	0.03	0.21	0.16	0.64	0.23	0.07	0.23
Least Auklet	*Aethia pusilla*	0.07	6.98	2.85	0.43	1.87	0.16	10.48	0.64	0.12	1.95
Whiskered Auklet	*Aethia pygmaea*	0	0	0	0	0	0	0	0	0	0
Crested Auklet	*Aethia cristatella*	0.15	1.97	0.57	2.27	1.21	0.24	4.7	0.34	1.74	1.5
Horned Puffin	*Fratercula corniculata*	0.09	0.17	0.13	*	0.08	0.03	0.23	0.12	*	0.07
Tufted Puffin	*Fratercula cirrhata*	0.07	0.34	0.15	*	0.11	0.11	0.34	0.09	*	0.11
Black-legged Kittiwake	*Rissa tridactyla*	0.61	0.71	0.82	0.38	0.6	0.75	0.68	1.66	0.31	0.78
Red-legged Kittiwake	*Rissa brevirostris*	*	*	*	0	*	*	0	0	0	*
Ivory Gull	*Pagophila eburnea*	0	0	0	0	0	0	0	0	0	0
Sabine's Gull	*Xema sabini*	*	0.01	*	0.02	0.01	0.02	*	*	0.04	0.02
Ross's Gull	*Rhodostethia rosea*	0	0	0	*	*	0	0	0	0	0
Mew Gull	*Larus canus*	0	0	0	0	0	0	0	0	*	*
Herring Gull	*Larus argentatus*	0.01	*	*	*	*	*	*	*	0	*
Iceland Gull	*Larus glaucoides*	*	0	*	0	*	0	0	0	0	0
Slaty-backed Gull	*Larus schistisagus*	*	*	0	0	*	*	0	0	0	*
Glaucous-winged Gull	*Larus glaucescens*	0.04	0.02	*	*	0.02	0.06	*	*	0	0.02
Glaucous Gull	*Larus hyperboreus*	0.04	0.09	0.04	0.05	0.05	0.04	0.03	0.08	0.05	0.05
Aleutian Tern	*Onychoprion aleuticus*	0	0	*	0	*	0	*	0	0	*
Arctic Tern	*Sterna paradisaea*	*	*	*	0.02	*	*	*	0.01	0.05	0.02
Red-throated Loon	*Gavia stellata*	*	*	*	*	*	0	*	*	0	*
Pacific Loon	*Gavia pacifica*	0.01	0.02	0.03	0.03	0.02	0.01	0.01	0.06	0.02	0.03
Common Loon	*Gavia immer*	*	0	0	*	*	*	0	*	*	*
Yellow-billed Loon	*Gavia adamsii*	*	*	0	*	*	*	*	*	*	*
Laysan Albatross	*Phoebastria immutabilis*	0.02	0	0	0	*	*	0	0	0	*
Short-tailed	*Phoebastria albatrus*	*	0	0	0	*	*	0	0	0	*

		2007-2016 Mean density to 0.00 or <.01 (*)					2017-2019 Mean density to 0.00 or <.01 (*)				
Common Name	**Latin name**	Northern Bering	Chirikov Basin	Southern Chukchi	Northern Chukchi	all Regions	Northern Bering	Chirikov Basin	Southern Chukchi	Northern Chukchi	all Regions

Albatross												
Northern Fulmar	*Fulmarus glacialis*	0.95	0.59	0.42	0.23	0.54		0.73	0.99	0.22	0.22	0.49
Mottled Petrel	*Pterodroma inexpectata*	*	0	0	0	*		0	0	0	0	0
Short-tailed Shearwater	*Ardenna tenuirostris*	1.79	3.71	5.74	4.22	3.76		1.27	3.06	6.46	11.48	6.05
Sooty Shearwater	*Ardenna grisea*	*	0	0	0	*		0	0	0	0	0
Fork-tailed Storm-Petrel	*Oceanodroma furcata*	0.06	0.02	*	*	0.02		0.03	0.08	*	*	0.02
Red-faced Cormorant	*Phalacrocorax urile*	*	0	*	0	*		*	0	0	0	*
Pelagic Cormorant	*Phalacrocorax pelagicus*	0.01	0.01	0	0	*		*	0.02	*	0	*
Total density		6.24	18.7	15.76	8.58	11.02	0	4.53	23.29	14.68	14.83	13.16

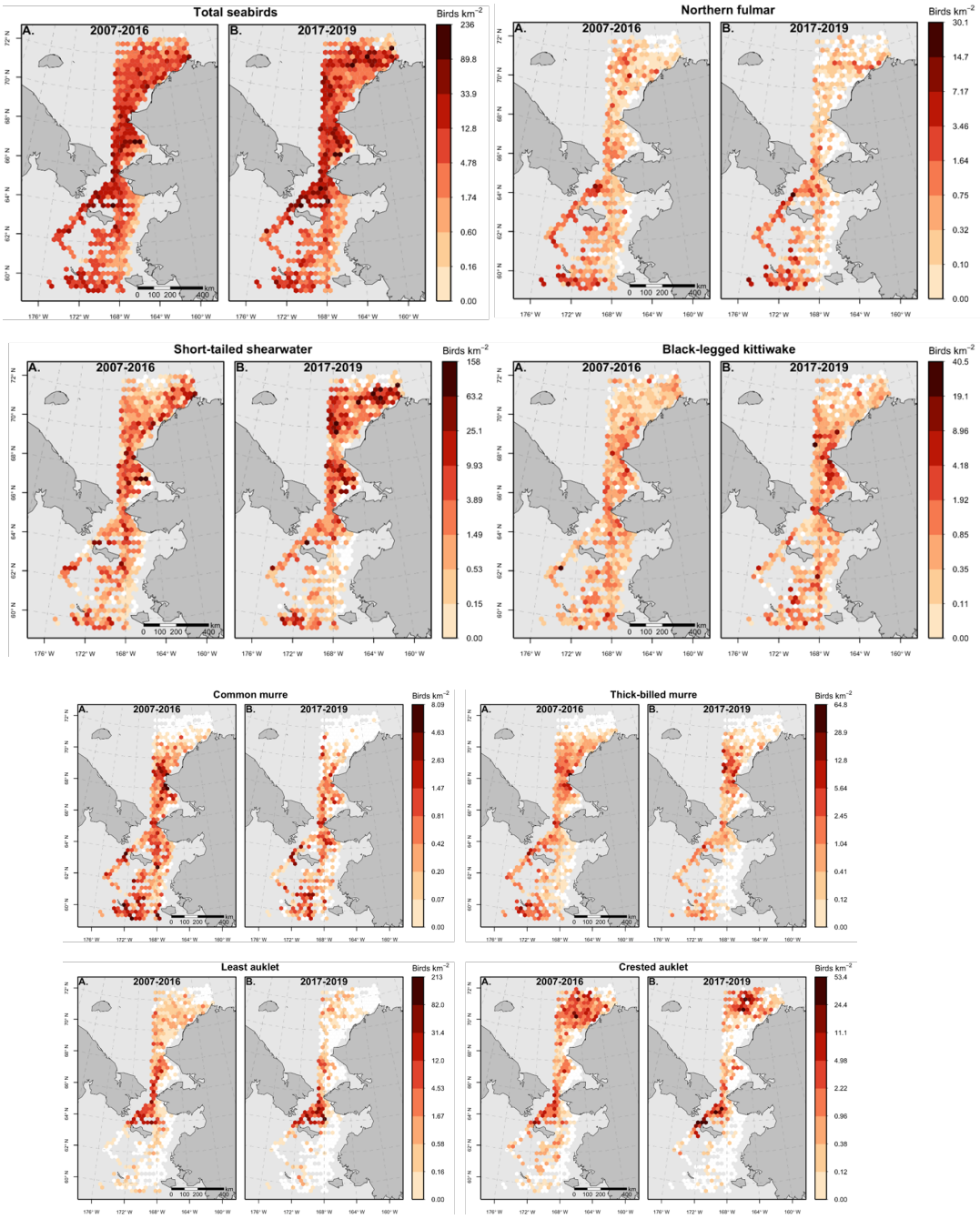

Appendix B. Distribution of total birds and key species for two time periods, 2007-2016 (A) and 2017-2019 (B). All 30-km hexagon cells surveyed during each time period are shown, including those not surveyed in both periods. White cells indicate survey effort, but the species was not observed.

Appendix C. Species composition and mean densities (birds·km^{-2}) for five cluster types identified for the Northern Bering- Chukchi Sea study area, 2007-2019 (July – September) combined. Shaded cells indicate predominate species for that cluster. Asterisks indicate density < 0.01, but above zero. Clusters are named for their most abundant species or Low Density (LowDen); STSH = short-tailed shearwater, TBMU = thick-billed murre, LEAU = least auklet, CRAU = crested auklet.

			Cluster Type				
			1	2	3	4	5
Family	**Common Name**	**Latin name**	**STSH**	**TBMU**	**LEAU**	**CRAU**	**Low Den**
Anatidae	Steller's Eider	*Polysticta stelleri*	*	*	*	0	*
	Spectacled Eider	*Somateria fischeri*	0.01	*	0	0	0.01
	King Eider	*Somateria spectabilis*	0.01	*	0.01	0	0.01
	Common Eider	*Somateria mollissima*	0.01	0.01	*	*	*
	Harlequin Duck	*Histrionicus histrionicus*	*	*	*	0	*
	Surf Scoter	*Melanitta perspicillata*	*	0	*	0	0
	White-winged Scoter	*Melanitta fusca*	*	*	0.01	0	*
	Black Scoter	*Melanitta americana*	0	0	0	0	*
	Long-tailed Duck	*Clangula hyemalis*	0.07	0.01	*	0.02	0.02
Podicipedidae	Red-necked Grebe	*Podiceps grisegena*	0	*	0	0	*
Scolopacidae	Red-necked Phalarope	*Phalaropus lobatus*	0.07	0.07	0.34	0.09	0.07
	Red Phalarope	*Phalaropus fulicarius*	2.00	0.15	2.28	0.34	0.23
Stercorariidae	Pomarine Jaeger	*Stercorarius pomarinus*	0.07	0.04	0.07	0.03	0.03
	Parasitic Jaeger	*Stercorarius parasiticus*	0.02	0.02	0.01	0.01	0.01
	Long-tailed Jaeger	*Stercorarius longicaudus*	*	0.01	0.00	*	*
Alcidae	Dovekie	*Alle alle*	*	*	*	*	*
	Common Murre	*Uria aalge*	0.32	1.28	0.84	0.11	0.21
	Thick-billed Murre	*Uria lomvia*	0.53	2.81	1.49	0.30	0.12
	Black Guillemot	*Cepphus grylle*	*	*	0.01	*	*
	Pigeon Guillemot	*Cepphus columba*	0.01	*	0.01	*	*
	Marbled Murrelet	*Brachyramphus marmora*	*	*	*	0	*
	Kittlitz's Murrelet	*Brachyramphus brevirost*	0.01	0.01	*	0.01	*
	Ancient Murrelet	*Synthliboramphus antiqu*	0.09	0.16	0.09	0.05	0.06
	Cassin's Auklet	*Ptychoramphus aleuticus*	*	*	*	*	*
	Parakeet Auklet	*Aethia psittacula*	0.21	0.20	0.91	0.11	0.10
	Least Auklet	*Aethia pusilla*	0.34	0.22	17.16	0.67	0.07
	Crested Auklet	*Aethia cristatella*	0.50	0.21	5.42	5.15	0.11
	Horned Puffin	*Fratercula corniculata*	0.07	0.16	0.21	0.02	0.04
	Tufted Puffin	*Fratercula cirrhata*	0.07	0.13	0.50	0.04	0.04
Laridae	Black-legged Kittiwake	*Rissa tridactyla*	0.97	1.39	0.61	0.35	0.54
	Red-legged Kittiwake	*Rissa brevirostris*	*	0.01	*	0	*
	Sabine's Gull	*Xema sabini*	0.02	0.02	0.01	0.02	0.01
	Ross's Gull	*Rhodostethia rosea*	0	0	0	*	0
	Mew Gull	*Larus canus*	*	0	0	*	0
	Herring Gull	*Larus argentatus*	*	0.01	*	*	*
	Iceland Gull	*Larus glaucoides*	*	*	0	0	0
	Slaty-backed Gull	*Larus schistisagus*	*	*	*	0	*
	Glaucous-winged Gull	*Larus glaucescens*	0.02	0.05	0.01	0.00	0.02
	Glaucous Gull	*Larus hyperboreus*	0.06	0.05	0.05	0.03	0.05
	Aleutian Tern	*Onychoprion aleuticus*	0	0	*	0	*
	Arctic Tern	*Sterna paradisaea*	0.03	*	*	0.01	0.02
Gaviidae	Red-throated Loon	*Gavia stellata*	*	*	*	*	*
	Pacific Loon	*Gavia pacifica*	0.05	0.02	0.01	0.02	0.02
	Common Loon	*Gavia immer*	*	0	0	*	*
	Yellow-billed Loon	*Gavia adamsii*	*	*	*	*	*
Diomedeidae	Laysan Albatross	*Phoebastria immutabilis*	*	0.02	0	0	*
	Short-tailed Albatross	*Phoebastria albatrus*	0	*	0	0	*
Procellariidae	Northern Fulmar	*Fulmarus glacialis*	0.35	1.43	1.49	0.36	0.27
	Mottled Petrel	*Pterodroma inexpectata*	0	*	0	0	0
	Short-tailed Shearwater	*Ardenna tenuirostris*	18.51	1.66	5.37	1.09	0.61
	Sooty Shearwater	*Ardenna grisea*	*	*	0	0	*
Hydrobatidae	Fork-tailed Storm-Petre	*Oceanodroma furcata*	0.01	0.14	0.06	0.01	*
Phalacrocoracidae	Red-faced Cormorant	*Phalacrocorax urile*	*	0	*	0	*
	Pelagic Cormorant	*Phalacrocorax pelagicus*	0.00	*	0.01	0	0.01
Total Density			24.43	10.28	36.96	8.85	2.65

CHAPTER 22 - Growth rate potential for juvenile Chum salmon in rapidly warming northern Bering and southern Chukchi seas.

Objective 7: Develop spatially explicit bioenergetics models for Arctic cod and saffron cod as well as for juvenile pink and chum salmon and test the impact of warming summer temperatures on their growth and distribution

Edward V. Farley, Jr.[a], Ellen M. Yasumiishi[b], Jamal H. Moss[b], Wesley Strasburger[b], David Kimmel[c], James M. Murphy[b], Fletcher Sewall[b], Alexei Pinchuk[d]

[a] Corresponding author, NOAA/NMFS, Alaska Fisheries Science Center, Ted Stevens Marine Research Institute, Auke Bay Laboratories, 17109 Point Lena Loop Road, Juneau, AK 99801, ed.farley@noaa.gov, (907) 789-6085
[b] NOAA/NMFS, Alaska Fisheries Science Center, Ted Stevens Marine Research Institute, Auke Bay Laboratories, 17109 Point Lena Loop Road, Juneau, AK 99801
[c] NOAA/NMFS, Alaska Fisheries Science Center, Sand Point, Seattle, WA
[d] University of Alaska Fairbanks, School of Fisheries and Ocean Sciences, Juneau, AK 99801

Key Words
Chum Salmon, Western Alaska, Chukchi Sea, Growth Rate Potential, Distribution

Abstract

A spatially explicit bioenergetics model was used to estimate the growth rate potential (GRP; %body weight per day) of juvenile Chum salmon in the northern Bering and Chukchi seas. Annual averages of GRP ranged from a low of 0.9 (2003) to a high of 12.3 (2007) in the northern Bering Sea and from 0.1 (2003) to 39.3 (2007) in the Chukchi Sea. Analyses of juvenile Chum salmon spatial distribution in relation to GRP within each region indicated that they were generally not distributed in regions of higher GRP. There was a significant positive relationship between average seasonal transport through the Bering Strait and juvenile chum salmon GRP, suggesting summer transport of heat (and likely pelagic prey) improves early marine growth potential for juvenile chum salmon in the southern Chukchi Sea region. The year 2007 stands out as an anomaly within the 18 year time series with the highest GRP and catch per unit effort of juvenile chum salmon in both regions. In addition, further examination of juvenile Chum salmon stomach contents and relative abundance are warranted to better understand how anomalous warming during 2017 through 2019 may be linked to the dramatic decline in adult Chum salmon returns to the regions during 2020 and 2021.

Introduction

Marine environments in the Arctic regions (including the northern Bering, Chukchi, and Beaufort seas) are experiencing accelerated warming and extremes in seasonal sea ice extent (Frey et al., 2014; Baker et al., 2020; Danielson et al., 2020). Loss of seasonal sea ice is linked to increased primary and secondary production during spring and summer months (Arrigo and van Dijken, 2011) and advection of sub-Arctic waters and biota into the polar basins, creating conditions favorable for increased heat and expansion of Pacific species into the Arctic interior (Polyakov et al., 2020; Levine et al., 2020). These changes could shift colder Arctic marine ecosystems from benthic to pelagic state (Grebmeier et al., 2006).

Pacific salmon spend much of their marine life history feeding and growing in the pelagic waters of the North Pacific Ocean. The most common salmon species in the Pacific Arctic include Pink and Chum salmon (Nielsen et al., 2013; Carothers et al., 2013; Stephenson, 2006). Of these two salmon species, Chum salmon have the highest biomass in the North Pacific Ocean (Ruggerone and Irvine, 2018) and are broadly distributed in the Arctic from the Yukon River to the Mackenzie River. Adult Chum salmon in the northern regions return to rivers during July to October to spawn and their eggs hatch during late winter and into spring (Urawa et al., 2018). Fry enter the marine environment during late May through July (Vega et al., 2016; Howard et al., 2017), and they spend the summers as juveniles in the near coastal regions and then migrate offshore to spend one or more additional years in the North Pacific Ocean before returning to spawn.

Early marine research on juvenile Chum salmon in the northern Bering Sea and Chukchi Sea suggest that these salmon will likely do better under warming ocean conditions. In the northern Bering Sea, warm spring thermal regimes was linked to increased energy allocation and growth of juvenile Chum salmon (Wechter et al., 2017). During 2007, large numbers of juvenile Chum salmon were captured in the southern Chukchi Sea, and those juvenile salmon were larger and fed upon higher energy prey than those sampled in the northern Bering Sea (Moss et al., 2009). Interannual differences in the size and lipid storage of Pacific salmon during their early marine residence can have a strong influence on survival during subsequent marine life-history periods (Parker, 1968; Willette et al., 1999; Beamish and Mahnken, 2001; Farley et al., 2009). For temperate fishes, energy is generally allocated to growth early on when fish are small, but shifts to lipid accumulation during late summer and fall when fish are larger (Post and Parkinson, 2001). For juvenile salmon, rapid growth during early marine residence may reduce size- selective predation (Parker, 1968), whereas the size and lipid storage attained after their first summer at sea may affect winter survival (Beamish and Mahnken, 2001).

To develop a better understanding of the link between juvenile Chum salmon prey demand and supply, we use a bioenergetics model to estimate growth rate potential (GRP) over a 16-year period within the northern Bering Sea and 10-year period within the Chukchi Sea. Previous bioenergetics models for Chum salmon on the eastern Bering Sea shelf indicate that years with warmer spring and summer sea temperatures had higher annual averages of GRP (Farley and Moss, 2009). That model used a 4-year time series of data collected along the eastern Bering Sea shelf; we plan to extend the time series by 12 years for the northern Bering Sea and include data from the Chukchi Sea thereby capturing a period warm, cool and extremely warm sea temperatures (see Stabeno and Bell, 2019; Thoman et al., 2020) within this region. In addition, we report new estimated temperature and weight dependence parameters for juvenile Chum salmon obtained from laboratory experiments. The model estimates of body size and growth using the newly developed parameters more closely align with observed juvenile Chum salmon body size and growth as compared with model estimates using Pink salmon model parameters. The objective of this study is to compare juvenile Chum salmon GRP among years and between the northern Bering Sea and Chukchi Sea to examine the changes in juvenile salmon habitat quality during this period of rapid warming.

Materials and methods

Study Area and Sampling Protocols

Stations along the northern Bering Sea and southern Chukchi Sea shelf were sampled during August-September, 2003 – 2019 (except 2008) and during 2003, 2007, 2012, 2013, 2017-2019, respectively (Fig. 1). Juvenile Chum salmon were collected using a model 400/601 rope trawl, made by Cantrawl Pacific Limited of Richmond, British Columbia. The rope trawl was 198 m long and constructed with hexagonal mesh in the wings and body, and a 1.2-cm mesh liner in the codend. The trawl was rigged with buoys on

the headrope to sample from near surface to approximately 20–25 m depth. During 2019, juvenile Chum salmon in the Chukchi Sea were sampled using a Nordic 264 rope trawl.

Sampling stations were generally completed during daylight hours (0730–2100 Alaska Daylight Savings Time). All trawl deployments lasted 30 min and covered between 2.8 and 4.6 km. Sampling stations were located along longitudinal meridians spaced every ? (i.e., along longitudinal meridians at stations spaced every ? degrees of latitude). A Seabird SBE-911 conductivity-temperature-depth (CTD) device was deployed at each station to measure the vertical profiles (from near bottom to surface) of ocean temperature. Observed sea surface temperatures at 5 m depth taken from CTD profiles were used for bioenergetics modeling. At each trawl station, juvenile Chum salmon were selected at random (maximum 50) and standard biological attributes, including fork length (nearest 1.0 mm) and body weight (nearest 1.0 g) were measured on board. Subsamples of juvenile Chum salmon from each trawl were frozen whole and taken back to the laboratory for energetic analyses. The catch per unit effort (number/km2) of juvenile Chum salmon at each station was estimated by multiplying the the number of juvenile Chum salmon caught at each station by the distance traveled (km) when the trawl net was fishing and the estimated trawl net opening (km) during fishing operations.

Bioenergetics Model

GRP of juvenile Chum salmon (see Table 1 for details) for the northern Bering Sea and Chukchi Sea shelf was estimated using the bioenergetics model developed by Ware (1978), incorporated modifications to the model developed by Trudel and Welch (2005) and Farley and Trudel (2009), and utilized new parameters for consumption rates of juvenile Chum salmon developed here (see Appendix A). The GRP model:

$$G_{i,s} = \tau \cdot I_{i,s} - (SMR_{i,s} + ACT_{i,s}) \quad (1)$$

accounts for optimal cruising speed, where $G_{i,s}$ is the GRP (cal/s) for juvenile Chum salmon during year i at station s, τ is the proportion of food that can be metabolized (Trudel and Rasmussen 2006), $I_{i,s}$ is the feeding rate (cal/s), $SMR_{i,s}$ and $ACT_{i,s}$ are, respectively, the standard metabolic rate (cal/s) and activity costs (cal/s). For simplicity, we assumed that τ was constant and not affected by water temperature, as the sum of fecal and urinary losses and specific dynamic action is often nearly constant in bioenergetics models (Trudel and Rasmussen 2006).

The relationship between salmon feeding rate and prey density was assumed to be described by a type II functional response (Holling 1965; Ware 1978):

$$I_{i,s} = ED_{i,s} \cdot \frac{\rho_{i,s}\gamma_{i,s}U_{i,s}}{1 + \rho_{i,s}\gamma_{i,s}h_{i,s}U_{i.s}} \quad (2)$$

where ρ is prey density (g/cm^3), γ is the cross-sectional area of the reactive field (cm^2), U is the optimum swimming speed (cm/s), h is handling time of prey (s/g), and ED is sum of prey caloric content (cal/g$_{wet}$) estimated as:

$$I_{i,s} = ED_{i,s} \cdot \frac{\rho_{i,s}\gamma_{i,s}U_{i,s}}{1 + \rho_{i,s}\gamma_{i,s}h_{i,s}U_{i.s}} \quad (3)$$

where p = the number of prey species z. Consumption rates were equal to zero when no prey were available.

The equations for handling time were developed in Farley and Trudel (2009):

$$h = \underline{W_i}^{CB-1}/(CA * f(T)) \quad (4)$$

where $\overline{W}_i$ is the average Chum salmon weight (g) during year *i*, *CA* and *CB* are, respectively, the weight coefficient and exponent for maximum feeding rate for Chum salmon, and *f(T)* is the Thornton and Lessem (1978) temperature dependence function for cold-water fish species (see Table 1 for definition and parameters).

The energetic costs associated with the standard metabolic rates and activity costs of juvenile Chum salmon were estimated using empirical models derived for Sockeye salmon by Trudel and Welch (2005). Specifically, standard metabolic rates were modeled as a function of weight and water temperature (ºC):

$$SMR_{i,s} = \alpha_1 \overline{W}_i^{\beta} e^{\varphi T_{i,s}} \quad (5)$$

where α_1, β, and ϕ are regression coefficients (Table 1). Activity costs were modeled as a function of weight and swimming speed:

$$ACT_{i,s} = \alpha_0 \overline{W}_i^{\delta} U_{i,s}^{\lambda} \quad (6)$$

where α_0, δ, and λ are regression coefficients. We used the optimal cruising speed model derived by Trudel and Welch (2005) to estimate the swimming speed of juvenile Chum salmon (Table 1).

Chum salmon Energy Density

Energy density of juvenile Chum salmon was determined using bomb calorimetry on dried samples of homogenized whole fish tissues following procedures modified from Fergusson et al. (2010). Samples through 2015 were dried to constant mass by heating at 55°C in a drying oven, and samples from 2016-2019 were dried by heating at 135°C in a LECO Thermogravimetric Analyzer 701. The two drying methods were known to yield moisture estimates differing by less than 1% (Vollenweider et al 2011) and thus had negligible effects on dry mass energy estimates. Calorimetry data accuracy was verified using benzoic acid and internal fish tissue standards, and precision verified using sample replicates. The energy density units (Joules/g_{wet}) were converted to (cal/g_{wet}) by dividing the value by 4.184.

For the NBS region, energy density data were available for all years except 2006, 2007, and 2013. To enable estimates of GRP for years that data were not available, we used the average energy density for all available data across years from the NBS region (average = 1,164 cal/gram, n = 673). For the SCS region, energy density data were available for all years except 2017 and 2019. To enable estimates of GRP for years that data were not available, we used the average energy density for all available data across years from the SCS region (average = 1,253 cal/g, n = 55)

Chum Salmon Stomach Contents (Prey)

Stomach contents were examined either at sea or in a laboratory setting. Stomach processing followed standard methods developed by Tikhookeanskiy Nauchno-Issledovatelskiy Institut Rybnogo Khozyaystva I Okeanografiy (Chuchukalo and Volkov, 1986; Volkov and Kuznetsova, 2007; Moss et al., 2009; Coyle et al., 2011). Typically, the contents of up to 10 stomachs from randomly sampled juvenile Chum salmon were combined from each station. Contents were removed from the esophagus to the pylorus. Prey taxa were identified to the lowest possible resolution using a dissecting microscope. Prey composition was recorded as a stomach content index (SCI) and a stomach fullness index (SFI). The SCI represents individual prey item weight (g), scaled by predator body weight (g), and multiplied by 10,000. Prey items were typically weighed to 0.001 g, when possible. The SCI for a given prey taxa *x* at the *i*-th station was calculated as:

$$SCI_{i,x} = [\ Prey_{i,x}/Predator_i * 10{,}000\ ]$$

where $Prey_{i,x}$ was the weight (g) of prey taxa *x* at station i and $Predator_i$ was the weight (g) of the predator at station *i*.

$$SFI_{i,} = \sum SCI_{x\text{-}n,i}$$

The SFI_i is the sum of all SCI values from prey items *i-n* at a given station *x*.

Stomach content data was pooled into broader categories prior to calculating the percent SCI composition for each predator species. Categories were selected either as prey of interest (*Calanus glacialis*), or as similar prey types. Categories that represented less than 10% of the total SCI were grouped together. Any categories that could not be grouped within a taxonomic or functional group were combined into an "Other" category.

Prey Biomass

Zooplankton prey were collected using a 60 cm bongo sampler with 505 μm mesh net. The net was towed obliquely to near bottom (max 200 m depth) and the volume of water flowing through the net was measured using a General Oceanics 2030R flowmeter. Zooplankton samples were preserved in a buffered-formalin (5%) solution and processed at the University of Alaska Fairbanks (see: Coyle and Pinchuk 2002) laboratory and the Plankton Sorting and Identification Center (PSIC) in Szczecin, Poland (see: Napp et al. 1996, Incze et al. 1997, Kimmel et al. 2018). Samples identified at the PSIC were verified at the Alaska Fisheries Science Center, Seattle, Washington, USA. Zooplankton abundances were converted to biomass using individual weights in g (Table 2).

Zooplankton prey density (g/cm^3) at each station was determined as:

$$\rho_{i,s} = \sum_{z=1}^{p} N_{i,s,z} \cdot \bar{W}_{i,s,z} \quad (10)$$

where $N_{i,s,z}$ and $W_{i,s,z}$ are the number and average weight of zooplankton species z (z = 1 to p) at station s during year i. The stomach content analysis did reveal that juvenile Chum salmon feed upon small fishes such as age-0 walleye Pollock and small sandlance (Fig. 2). Sandlance are not captured very frequently in the surface trawl (n < 5 over the time series) and age-0 walleye Pollock were only found in stomach contents of juvenile Chum salmon during 2003 and 2004, even though age-0 walleye Pollock were consistently captured in the NBS throughout the time series (reference).

GRP in cal/s (calories per second) was converted to cal/d (calories per day) by multiplying $I_{i,s}$ by the number of seconds in a 15-hour day (estimated time juvenile Chum salmon spend feeding per day during August and September) and by multiplying $SMR_{i,s}$ and $ACT_{i,s}$ by the number of seconds in a 24-hour day. Estimated daily GRP (cal/d) at each station s was then expressed as a percentage of body weight (% body weight/d) for each station s by dividing estimated daily GRP (cal/d) by the total energy per fish (cal) as in (Perry et al. 1996):

$$\underline{E_{i,s}} = \underline{ED_i} * \underline{W_i} \quad (11)$$

where $\overline{E}_{i,s}$ is the average total energy per fish (cal), $\underline{ED_i}$ is the average caloric content in juvenile Chum salmon (cal/g_{wet}) during year i, and $\overline{W}_i$ is the average weight (g) of juvenile chum salmon. Annual averages of juvenile Chum salmon weight and energy density were used as opposed to average weight and energy density of these fish at each station because there were stations within a year where no juvenile Chum salmon were caught.

Inputs into the GRP model including sea surface temperature at each station, caloric content for zooplankton prey, annual mean estimates of juvenile Chum salmon caloric content, and annual average juvenile Chum salmon weight are provided in appendix 1.

Model Applications

Temporal and spatio-temporal estimates of mean GRP and catch per unit effort (CPUE) were estimated using the VAST package (version 3.7.0, cpp 13_0_0) and FishStatsUtils package (version 2.9.1) with RStudio (version 1.2.1335) (RStudio Team 2020) (Thorson et al. 2015, Thorson et al. 2016, a, b; Thorson 2019a). The GRP and CPUE estimates were initially separated by region: 1) northern Bering Sea (59.5° N to 65.5° N, -173 to -161.5) during 2003 to 2019 (missing 2008) and southern Chukchi Sea (65.54° N to 68° N, -168.5 to -164) during 2003, 2007, 2012, 2013, 2017-2019. Initial efforts found that the VAST model would not converge for GRP or CPUE data within the southern Chukchi Sea region. Therefore, we modeled these data over the entire survey area (NBS and SCS) and then separated the spatial-temporal estimates of GRP and CPUE by region for our analysis.

The VAST model is a delta geostatistical model that includes two linear predictors, one for the probability of encounter and the other for positive catch rate (Thorson et al. 2015, Thorson 2019a, b). Each linear predictor includes spatial and spatio-temporal effects to improve density predictions under a spatially- unbalanced sample design, in areas with few or missing data (Shelton et al. 2014). The first linear predictor, encounter probability for sample *i* is given as:

$$p_1(i) = \sum_{f=1}^{n_{\omega 1}} \omega_1(s_i) + \sum_{f=1}^{n_{\varepsilon 1}} \varepsilon_1(s_i, t_i) + \sum_{p=1}^{n_p} \gamma_1(t_i, p) X(x_i, t_i, p)$$

where $\sum_{f=1}^{n_{\omega 1}} \omega_1(s_i)$ is the spatial effect and $\sum_{f=1}^{n_{\varepsilon 1}} \varepsilon_1(s_i, t_i)$ is the spatio-temporal effect. Symbols include s_i for knot location, t_i is year, and *i* is sample or station. We specified effects of covariates using linear and nonlinear formulas. Parameters include omega (ω), epsilon (ε), and gamma (γ). Positive catch rates $p_2(i)$ the second component given as

$$p_2(i) = \sum_{f=1}^{n_{\omega 2}} \omega_2(s_i) + \sum_{f=1}^{n_{\varepsilon 2}} \varepsilon_2(s_i, t_i) + \sum_{p=1}^{n_p} \gamma_2(t_i, p) X(x_i, t_i, p)$$

These linear predictors are used to predict indices of density and abundance, see Thorson (2019) for additional model details. Including spatio-temporal variation in the estimates of density can improve predictions in areas with little data (Shelton et al., 2014), ideal for our survey with limited coverage in some areas and years (Fig. 1).

Total biomass $\big(I(t)\big)$ of juvenile chum salmon in the surveyed area was predicted from density for the entire survey area by year *t* (Thorson et al. 2015):

$$I(t) = \sum_{s=1}^{n_s} \big(a(s) \times d(s,t)\big)$$

where $a(s)$is the area associated with extrapolation-cell s (Shelton et al., 2014; Thorson et al., 2015). Standard error was calculated with Template Model Builder, an auto differentiation software library and plotted (Kristensen et al., 2016) where the average GRP or catch per unit effort was:

$$\underline{d}(t) = \sum_{s=1}^{n_s} \frac{a(s) \times d(s,t)}{I(t)} d(s,t)$$

For GRP, we model the 2nd linear predictor and not the 1st linear predictor, due to the 100% occurrence of the GRP index, a value at each sample location. A Poisson-link delta-model for positive catch rates with fixed encounter probability=1 for all years because GRP was given for all observations (ObsModel=c(1,4)) and set area swept to a constant 1. For Catch, we used a conventional delta-model for encounter probability and a lognormal model for positive catch rates, but fixing encounter probability=1 for any year where all samples encounter the species. The number of knots was 60 for the predicted surface and knot locations for regions identified using a k-means algorithm based on the location of survey observations across years. An extrapolation area of 75 km from the center of each knot allows for overlap in space among regions around knots. We specified 20000 extrapolation points in VAST per year. Model performance was examined with expected probability and observed frequency of encounter for encounter probability, quantile plots for residuals of the positive catch rates, and spatial trends in the Pearson residuals for encounter probability and positive catch rate components by knot.

To visualize the distribution of juvenile chum salmon with respect to spatial variation in GRP we plotted estimated GRP at each extrapolation point and overlaid with the station level log CPUE of juvenile chum salmon. To show uncertainty in the GRP estimates we plotted the standard errors of predicted densities of GRP at each extrapolation point. This plot was used to illustrate uncertainty in GRP especially offshore where we have little or no data.

Pearson correlation coefficients and p-values were estimated to test the relationships among sea temperature, mean body weight, log CPUE, and log GRP for the northern Bering Sea. For the southern Chukchi Sea, we included estimates of transport (mean May to August) through the Bering Strait (Woodgate et al.), sea temperature, mean body weight, log CPUE, and log GRP for the southern Chukchi Sea correlation analyses were used to examine relationships between annual GRP, CPUE, and physical and biological indices for the north eastern Bering and southern Chukchi seas. The VAST model did not converge for the southern Chukchi Sea, so we estimated densities for GRP and Catch for the two regions combined. Next, we separated the density estimates at each extrapolation by region. Finally, means and SEs of the means of the density estimates were calculated by region. GRP and CPUE were then log transformed. We also calculated means for GRP from the raw data for the correlation analysis and comparison of the SEs.

An analysis of variance (ANOVA, Fixed Effects) was performed to test for significant differences in estimates of GRP among years within each region and among regions and years. We used the area specific VAST density estimates at the extrapolation points (n=2000) that were then separated by region and year. If a significant difference ($P < 0.05$) occurred, a Sidak multiple comparison test was used to calculate the 95% ($\alpha = 0.05, 0.01, 0.001$) confidence intervals for all pairwise differences between the dependent variable means. The level of significance between the pairwise differences was determined by examining those confidence intervals that excluded zero for the three values of α.

Results

Juvenile Chum salmon diet

Within the northern Bering Sea, juvenile Chum salmon fed upon a variety of zooplankton prey as well as small age-0 fishes (Fig. 2). From 2003 to 2007, the percentage of Cnidaria in the juvenile Chum salmon SCI ranged from 16% to 43%. The percentage of Cnidaria in juvenile Chum salmon SCI increased

during 2016 through 2019, ranging from 25% through 93%. The percentage of Oikolpeura spp. in the juvenile Chum salmon SCI was highest during 2007 through 2015, ranging from 14% to 76% and was only a small percentage of their SCI during the other years ranging from 0% to 8%. Similarly, the percentage of Themisto libellula was highest during 2007 through 2015 ranging from 0.5% to 52%, but was absent from the juvenile Chum salmon SCI during the other years. The percentage of fishes in the juvenile Chum salmon SCI varied among the years with sand lance comprising the largest percentage of their SCI ranging from 3% during 2007 to 55% during 2006. Small capelin and age-0 walleye pollock were also found in juvenile Chum salmon stomach contents ranging from 0.5% during 2004 to 14% during 2005 and 1% during 2015 to 16.5% during 2004, respectively.

There were fewer prey items found in juvenile Chum salmon stomachs in the southern Chukchi Sea (Fig. 3). Oikopleura spp. dominated juvenile Chum salmon SCI 2013 and 2018, whereas Epilabidocera amphitrites was 100% of the SCI during 2019. Juvenile Chum salmon fed upon Themisto libellula with an SCI range of 2% during 2007 to 10% during 2013. Several prey species were present in juvenile Chum salmon SCI during only one or two years including Hyperia spp. (2012, 42%), Euphausiid (2012, 25%), and Thysanoessa raschii (2007, 38%; 2012, 32%). Fishes were only found in the Juvenile Chum salmon SCI during 2007 (Lumpenus fabricii, 25%).

Growth rate potential and catch by regions

VAST model estimates of the annual mean and standard error of growth rate potential for juvenile Chum salmon indicate variation in the GRP among years and regions in the Chukchi Sea and northern Bering Sea (Table 3). In general, GRP was lower in the Chukchi Sea than in the northern Bering Sea, except for during 2003, 2007 and 2017. Temporal trends in the GRP were increasing from 2003 to 2007, decreasing from 2007 to 2012, relatively stable through 2015, and from 2015 to 2019 increased in the northern Bering Sea and was variable and low in the Chukchi Sea.

Model estimates of the annual mean and standard error of juvenile Chum salmon biomass also illustrate variation among years within the Bering Sea and Chukchi Sea (Fig. 4). Juvenile Chum salmon biomass was higher in the Chukchi Sea during 2007 and 2018 than in 2003, 2012, and 2013. Within the northern Bering Sea tended to be as high, or higher from 2014 to 2019 than previous years with the exception of 2017. The years with the highest estimated mean biomass of juvenile Chum salmon were 2018 within the Chukchi Sea and 2014 in the northern Bering Sea.

Spatio-temporal variation in growth rate potential and catch

The VAST model indicated significant spatial and spatio-temporal variation in the estimated means and standard errors of GRP of juvenile chum salmon (Figs. 5 and 6). When overlaying the CPUE of juvenile chum salmon at each station (black squares) on the VAST estimates of the GRP we see higher CPUE in regions of lower GRP for the northern Bering Sea. Standard error of the mean estimates show significant error in the model estimate for regions where we lack data. In general, higher GRP occurred farther offshore and in the southern regions of the survey area. Years with the highest GRP included 2007, 2011, and 2006.

Plots of SEs of log GRP show more uncertainty in the offshore regions to the west, and closer to shore in the eastern Bering Sea. Years without data in the SCS and low sampling offshore show higher levels of error.

Correlation analysis of growth rate potential and catch with physical and biological data

Growth rate potential of juvenile chum salmon was more significantly correlated with physical and biological indicators in the Chukchi Sea than in the north eastern Bering Sea (Figs. 7 and 8). In the NBS, VAST estimates of GRP were positively correlated with sea surface temperature, but not CPUE or body weight of the juvenile chum salmon. In the Chukchi Sea, GRP was positively correlated with flux rates from the Bering Strait into the Chukchi Sea, body weight, and sea surface temperatures. CPUE and body weight were positively correlated with sea surface temperatures but not with flux rates.

ANOVA (in process)

The ANOVA model results indicate significant differences in GRP among years within the NBS and SCS regions.

Discussion (in development)

Using a growth rate *potential* model for juvenile Chum salmon within the northeastern Bering Sea and southern Chukchi Sea, we found that GRP varied significantly among years and regions. The strength of northward transport during summer months tended to coincide with years of higher juvenile Chum salmon GRP in the CS, indicating the possibility that northward advection of heat, nutrients, phytoplankton and zooplankton (see Polyakov et al., 2020) improves the potential for early marine growth of these juvenile salmon in this region. Within the NBS, juvenile Chum salmon GRP was highest during years with anomalous warming conditions on the shelf. higher during ?years and within ? LME's, and that transport plays an important role in increased GRP within the ?.

Our longer time series of juvenile Chum salmon GRP within the northern Bering Sea region revealed similar results to Farley and Moss (2009) that also showed a mismatch between areas of higher GRP on the eastern Bering Sea shelf and juvenile Chum salmon distribution.

- our model did not include sandlance, which are found in the area that j. chum salmon are distributed.
- Sandlance are good prey and this likely would increase GRP
- However, there are no good estimates of sandlance in coastal areas of the NBS
- Of note - j. chum salmon were not feeding on sandlance during (years) and instead were feeding primarily on lower quality prey.

Table 1: Equations and parameter description of the Chum salmon bioenergetics model. Note that subscripts i and s represent year (i =2003 to 2019; 2008 not sampled in the NBS) and station, and overbars denote mean quantities within the definitions of i.

Symbol	Equation and parameter description	Value	Source
Growth: $G_{i,s} = \tau \cdot I_{i,s} - (\mathrm{SMR}_{i,s} + \mathrm{ACT}_{i,s})$			
G	Growth rates (cal/s)		
τ	Proportion of food that can be metabolized (dimensionless)	0.7	1
I	Feeding rates (cal/s)		
SMR	Standard metabolic rates (cal/s)		
ACT	Activity costs (cal/s)		
Consumption: $I = \mathrm{ED}_{i,s} \cdot (\rho \cdot \gamma \cdot U/(1 + \rho \cdot \gamma \cdot h \cdot U))$			
ED	Prey energy density (cal/g_{wet})		
ρ	Prey density (g/cm3)		
γ	Cross-sectional area of the reactive field (cm2)		
U	Swimming speed (cm/s)		
h	Handling time (s/g)		
Cross-sectional area of the reactive field: $\gamma = \alpha_2 \cdot \overline{W_i}^{\beta 2}$			
α_2	Intercept (cm^2)	1	1
β_2	Coefficient, γ versus W	0.69	1
$\overline{W}$	Average Chum salmon weight (g)		
Handling time: $h = \overline{W_i}^{CB-1}/(CA \cdot f(T))$			
CA	Intercept for maximum feeding rates (g/s)	0.1298	2
CB	Allometric exponent of maximum feeding rate	-0.2881	2
$f(T)$	Temperature adjustment for maximum food consumption rates		
T	Sea surface temperature (◦ C; 5 m below surface)		
Temperature adjustment function: $f(T) = K_a \cdot K_b$			
K_a	$= (CK1 \cdot L1)/(1 + CK1 \cdot (L1 - 1))$		
$L1$	$= \exp(G1 \cdot (T - \mathrm{CQ}))$		
$G1$	$= (1/(CTO - CQ)) \cdot \ln((0.98 \cdot (1 - CK1))/(CK1 \cdot 0.02))$		
$CK1$	= 0.3761		2
CTO	= 8.5°C		2
CQ	= 3°C		
K_b	$= (CK4 \cdot L2)/(1 + CK4 \cdot (L2 - 1))$		
$L2$	$= \exp(G2 \cdot (CTL - T))$		
$G2$	$= (1/(CTL - CTM)) \cdot \ln((0.98 \cdot (1 - CK4))/(CK4 \cdot 0.02))$		
$CK4$	= 0.8923		2
CTL	= 23°C		2
CTM	= 8.5°C		2
Standard metabolic rates: $\mathrm{SMR}^1 = \alpha_1 \cdot \overline{W_i}^{\beta} \cdot e^{\phi \cdot T}$			
α_1	Intercept (cal/s)[3]	4.76 × 10−5	3
β	Coefficient, SMR versus $\overline{W}$	0.871	3
ϕ	Coefficient, SMR versus T (1/◦ C)	0.064	3
Swimming costs: $\mathrm{ACT}^2 = \alpha_0 \cdot W^{\delta} \cdot U^{\lambda}$			
α_0	Intercept (cal/s)[4]	1.74 × 10−6	3
δ	Coefficient, ACT versus W	0.72	3
λ	Coefficient, ACT versus U	1.6	3
Swimming speed[5]: $U = \omega \cdot W^{\nu} \cdot e^{(\kappa \cdot T)}$			
ω	Intercept (cm/s)	11.1	3
ν	Coefficient, U versus W	0.097	3
κ	Coefficient, U versus T (1/°C)	0.040	3

(1) Ware 1978; (2) this study; (3) Trudel and Welch 2005

[1]SMR model parameters from equation A1 in Table 3 of Trudel and Welch (2005)

[2]ACT model parameters from equation A3 in Table 3 of Trudel and Welch (2005)

[3]The oxygen consumption rates were converted from mg O_2/h to cal/s using an oxycalorific equivalent to 3.24 mg O_2/cal = $\exp(-2.94) * 3.24/3600$

[4]The oxygen consumption rates were converted from mg O_2/h to cal/s using an oxycalorific equivalent to 3.24 mg O_2/cal = $\exp(-6.25) * 3.24/3600$

[5]*U* model parameters from equation 8 in Trudel and Welch (2005)

Table 2 is in development.

Table 3. Growth rate potential of juvenile chum salmon. VAST means were calculated from the estimated densities at the 2000 extrapolation points from the VAST model.

	Northern Bering Sea					Southern Chukchi Sea				
		VAST		Raw			VAST		Raw	
Year	n	Mean	SE	Mean	SE	n	Mean	SE	Mean	SE
2003	46	0.97	0.14	0.31	0.17	12	0.12	0.26	0.13	0.19
2004	55	1.05	0.15	0.96	0.38					
2005	47	4.03	0.36	2.95	0.44					
2006	51	5.29	0.44	4.71	0.51					
2007	54	12.29	1.46	15.01	2.89	12	39.35	6.33	41.60	13.11
2008										
2009	45	5.41	0.47	4.24	0.82					
2010	34	2.61	0.35	1.85	0.44					
2011	59	10.85	0.64	7.55	1.22					
2012	53	3.45	0.25	2.72	0.48	26	1.61	0.20	1.65	0.27
2013	39	3.84	0.30	1.75	0.27	26	1.26	0.10	1.26	0.23
2014	62	2.49	0.31	2.04	0.37					
2015	46	3.01	0.28	2.32	0.41					
2016	44	1.87	0.31	1.47	0.42					
2017	47	1.82	0.40	1.69	0.76	9	1.32	0.27	1.41	0.46
2018	44	3.21	0.36	2.62	1.17	6	2.76	0.95	2.38	2.14
2019	46	4.42	0.60	7.43	3.76	15	3.58	0.72	3.89	1.68

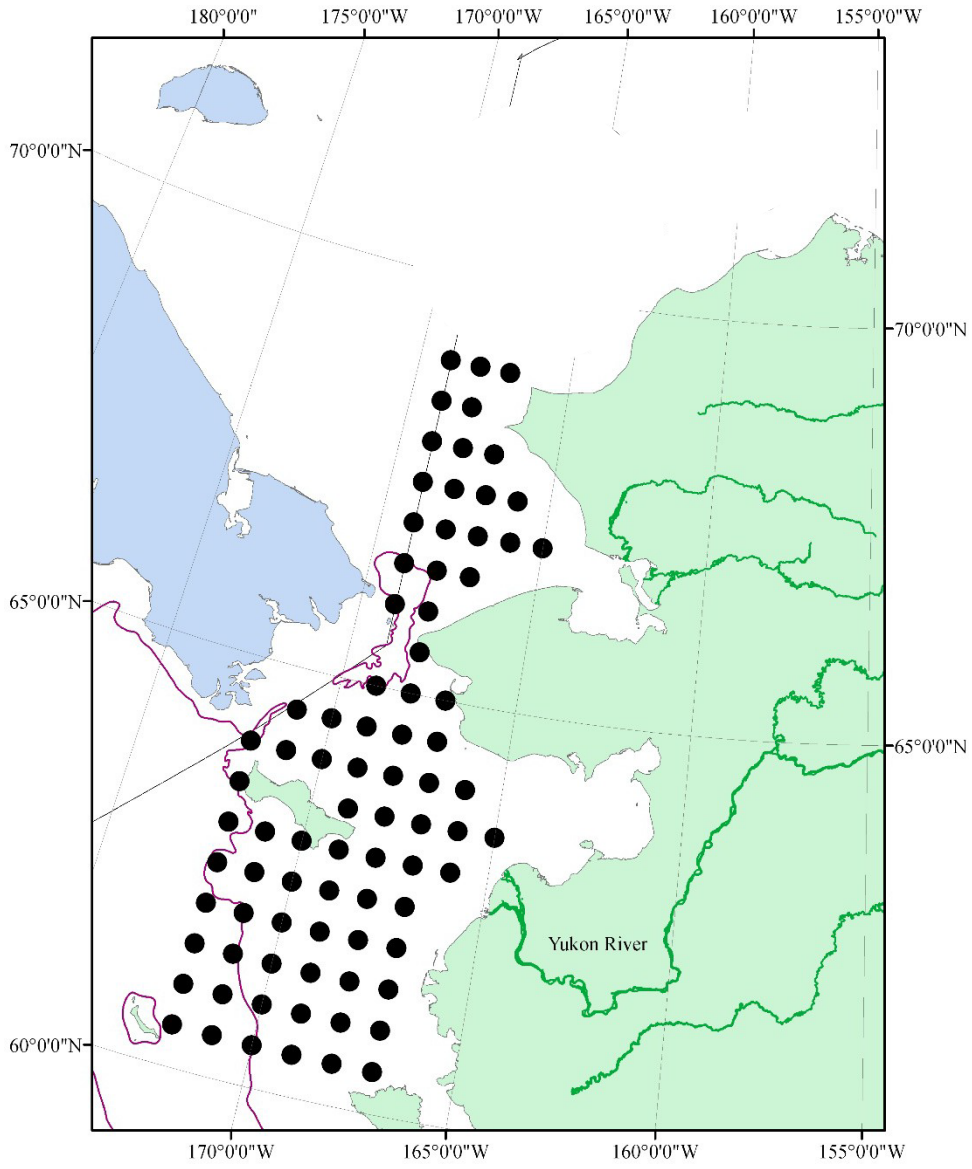

Figure 1. General station locations for surveys conducted in the northern Bering Sea (NBS) and southern Chukchi Sea (SCS) regions.

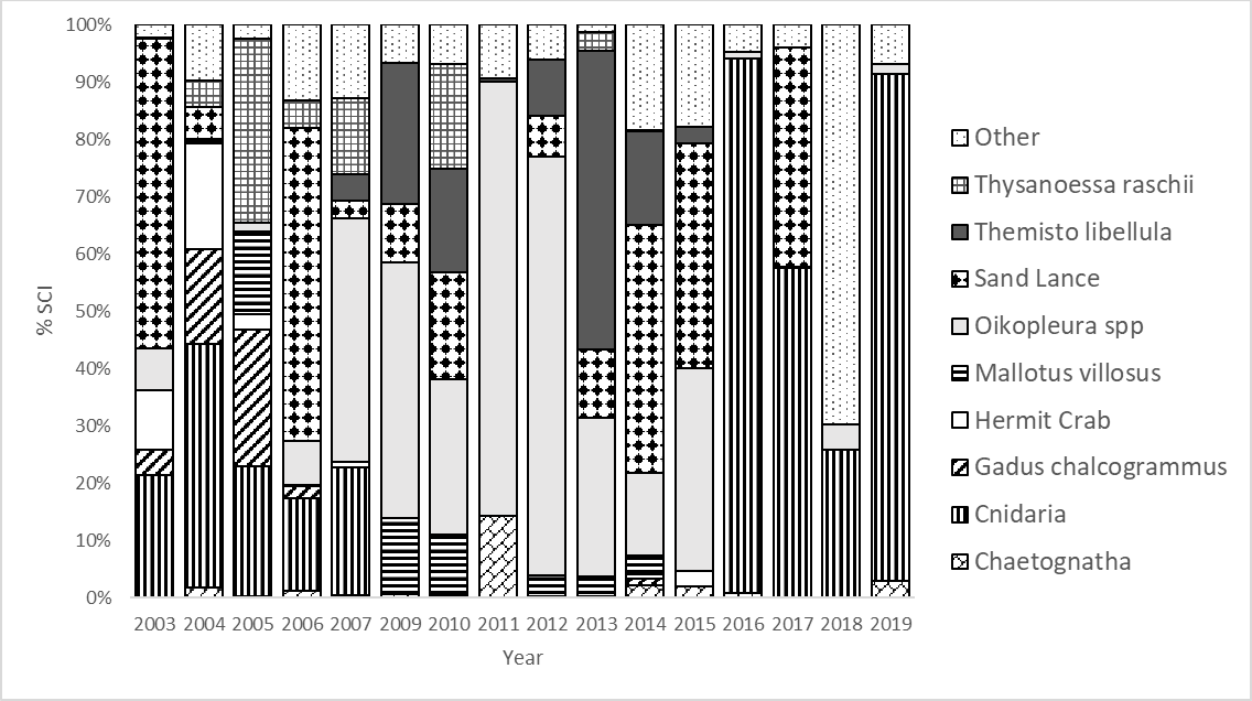

Figure 2. Stomach content index (percent SCI) for juvenile chum salmon captured in the northern Bering Sea during late summer 2003 to 2019.

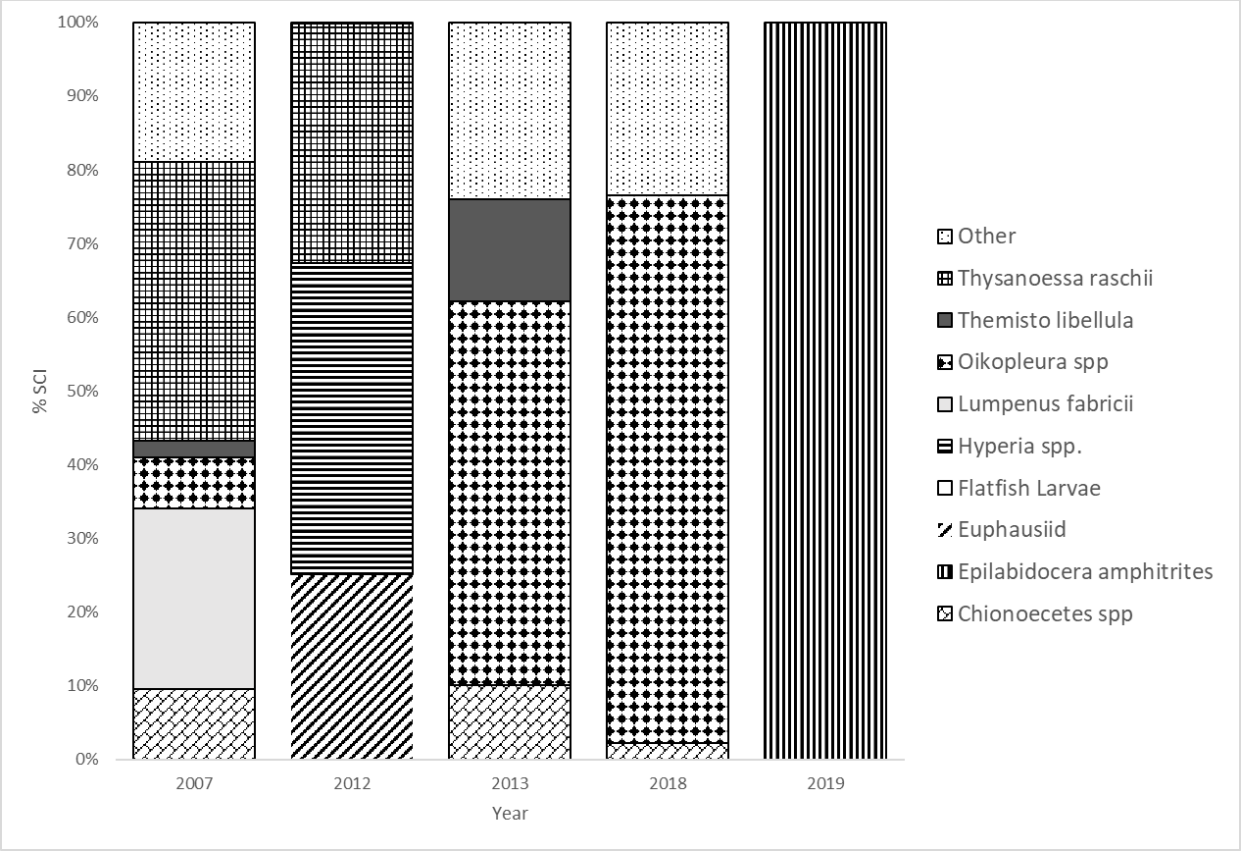

Figure 3. Stomach content index (percent SCI) for juvenile chum salmon caught in the southern Chukchi Sea during late summers 2007 2012, 2013, 2018, and 2019. (no diet data available for 2003 or 2017).

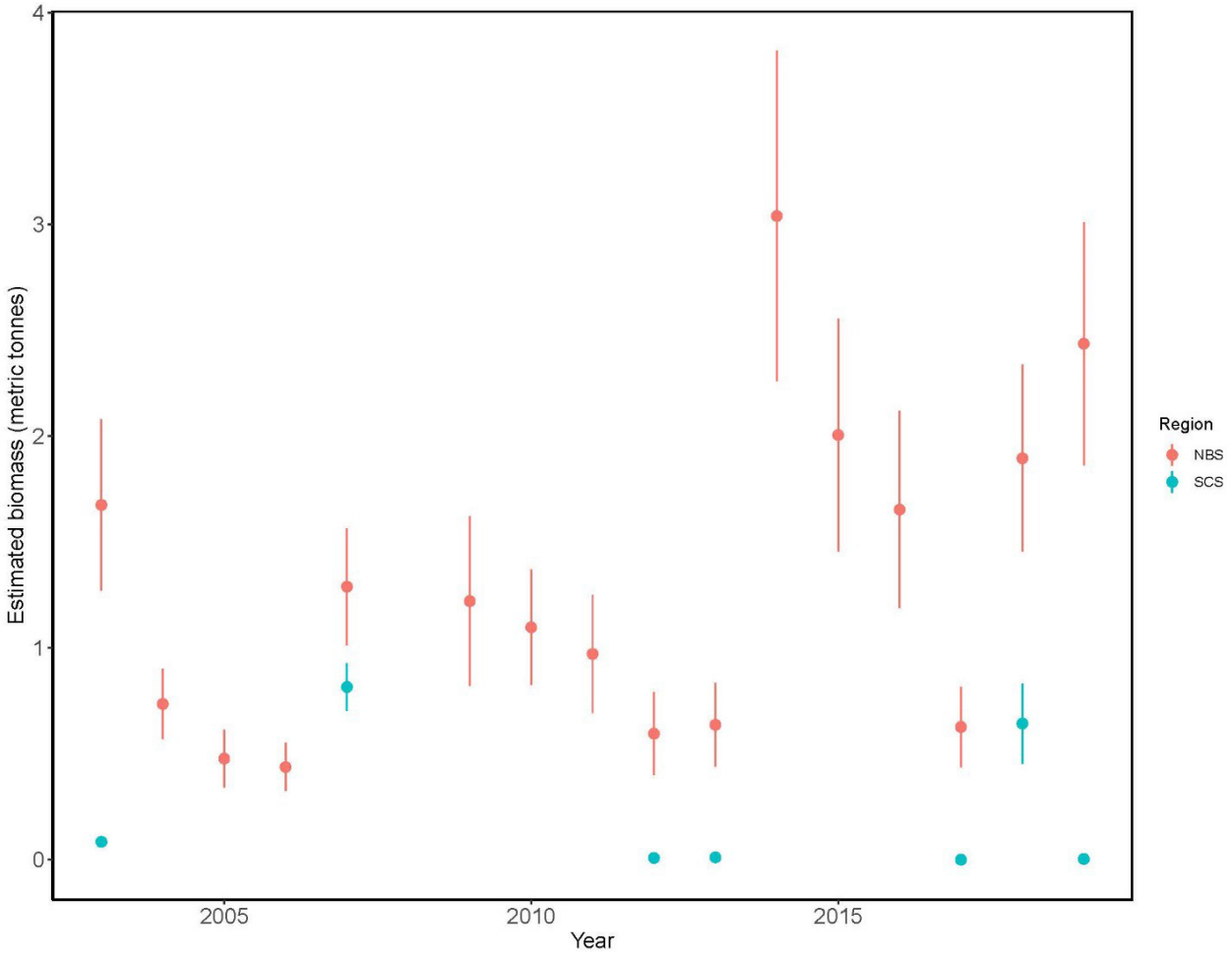

Figure 4. Estimated biomass (VAST estimates in metric tonnes) of juvenile chum salmon in the northern Bering Sea (NBS; red) and southern Chukchi Sea (SCS; blue) regions.

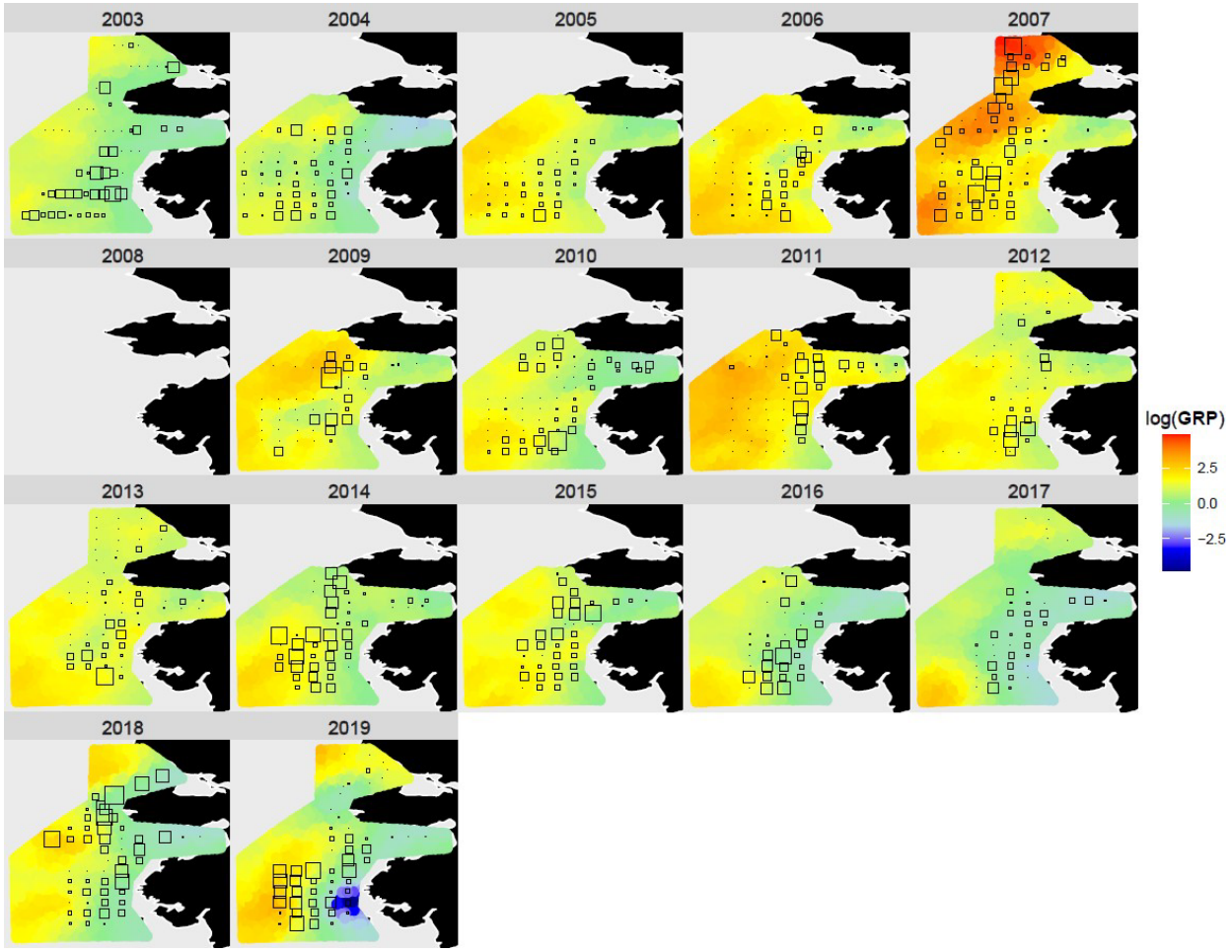

Figure 5. Spatio-temporal variation in catch per unit effort log(kg/km2) (squares) and VAST estimates of growth rate potential per kilometer (heat map) for juvenile chum salmon in the survey area of the Chukchi Sea and northern Bering Sea during late summer, 2003-2019, excluding 2008.

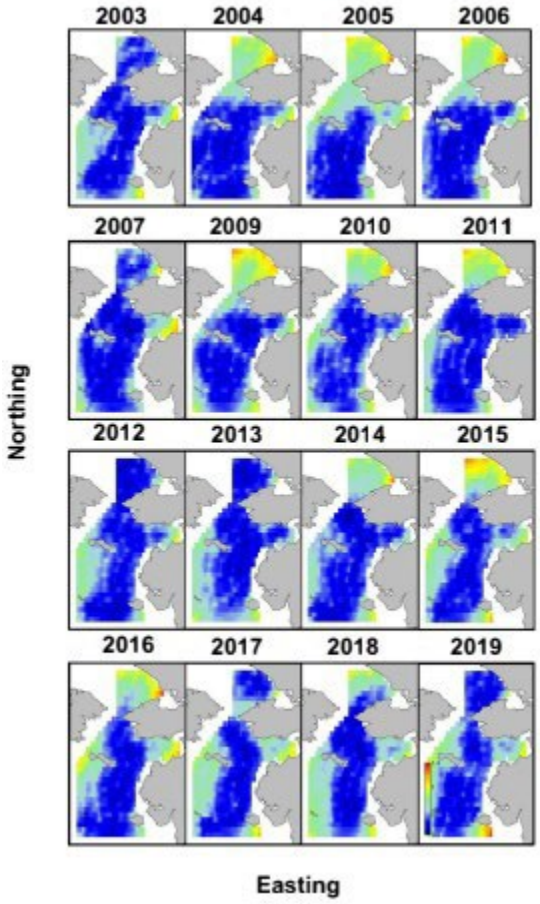

Figure 6. VAST estimates of the standard error of growth rate potential per kilometer for juvenile chum salmon in the survey area of the Chukchi Sea and northern Bering Sea during late summer, 2003-2019, excluding 2008.

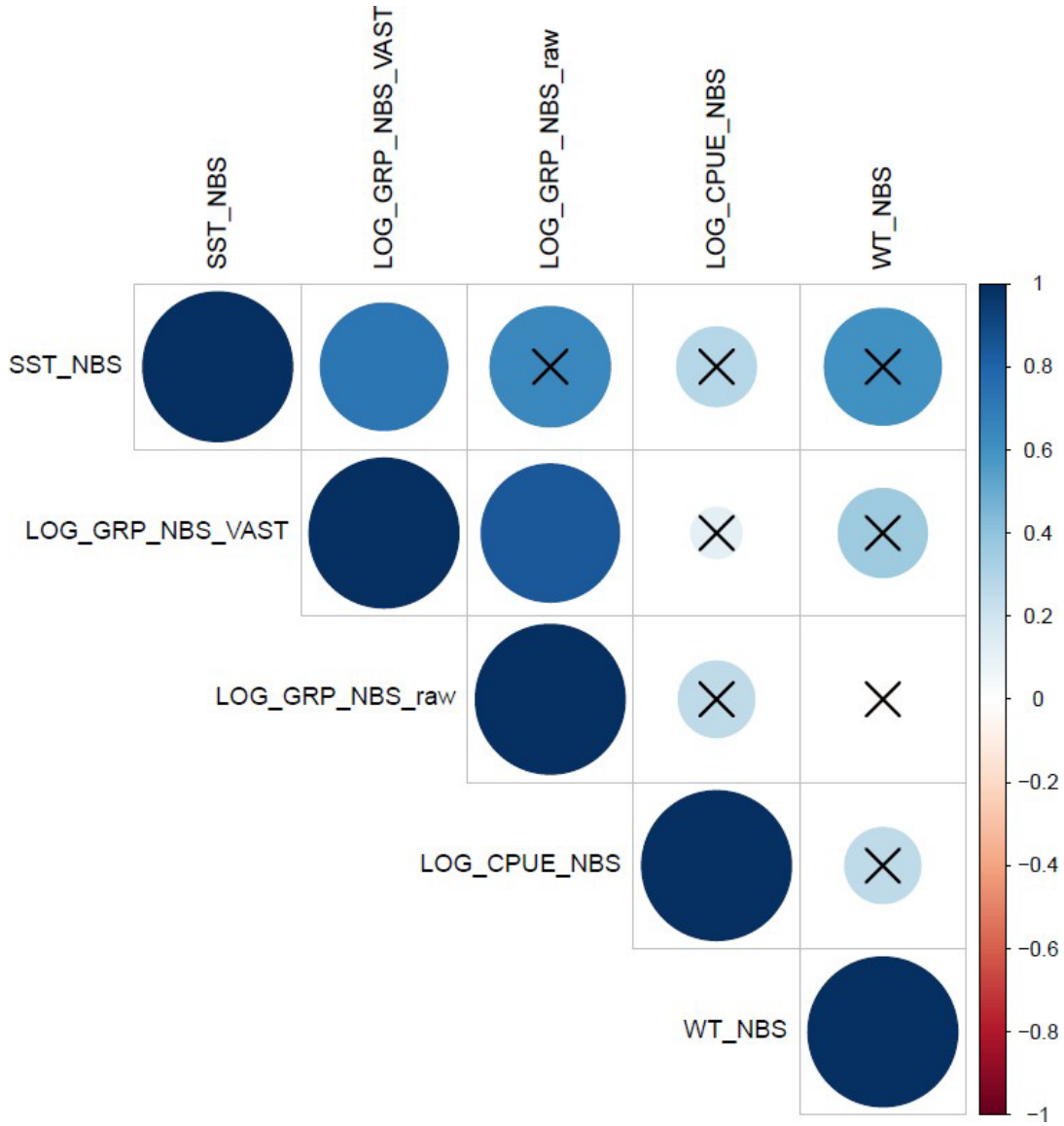

Figure 7. Correlation coefficients relating indices of summer sea temperatures (SST), body weight (Wt), log catch per unit effort (CPUE), and log growth rate potential (GRP) of juvenile chum salmon in the southern Chukchi Sea during summer, 2003, 2007, 2011, 2012, 2017-2019. The x symbol indicates a lack of significance.

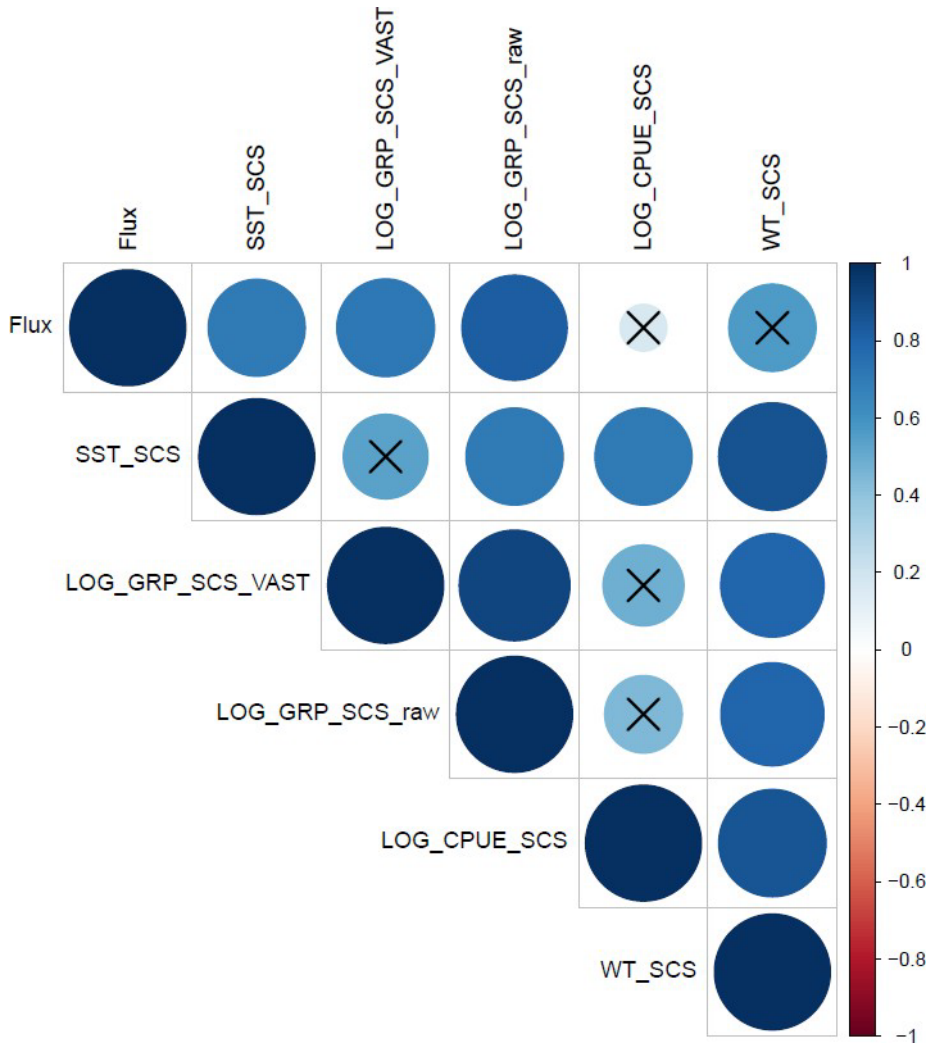

Figure 8. Correlation coefficients relating indices of summer sea temperatures (SST), body weight (Wt), log catch per unit effort (CPUE), and log growth rate potential (GRP) of juvenile chum salmon in the southern Chukchi Sea during summer, 2003, 2007, 2011, 2012, 2017-2019. The x symbol indicates a lack of significance.

References

Arrigo, K.R., van Dijken, G.L., 2011. Secular trends in Arctic Ocean net primary production. J. Geophys. Res. 116, C09011, doi:10.1029/2011JC007151.

Baker, M.R., Kivva, K.K., Pisareva, M., Watson, J., Selivanova, J., 2020. Shifts in the physical environment in the Pacific Arctic and implications for ecological timing and conditions. Deep Sea Res. II.

Beamish, R.J., Mahnken, C., 2001. A critical size and period hypothesis to explain natural regulation of salmon abundance and the linkage to climate and climate change. Prog. Ocean. 49, 423 – 437.

Carothers, C., Cotton, S., Moerlein, K., 2013. Subsistence use and knowledge of salmon in Barrow and Nuiqsut, Alaska. Final Report to OCS study Bureau of Ocean and Energy Management 2013 – 0015.

Coyle,K.O., Pinchuk, A.I. 2002. Climate-relateddifferencesinzooplanktondensity and growth on the inner shelf of the southeastern Bering Sea. Prog. Oceanogr. 55, 177–194.

Coyle,K.O., Eisner, L.B., Mueter, F.J., Pinchuk, A.I., Janout, M.A., Cieciel, K.D., Farley, E. V., Andrews, A.G., 2011.Climate change in the southeastern Bering Sea:impacts on Pollock stocks and implications for the oscillating control hypothesis. Fish. Oceanogr. 20, 139–156.

Danielson, S.L., Ahkinga, O., Ashjian, C., Basyuk, E., Cooper, L.W., Eisner, L., Farley, E., Iken, K.B., Grebmeier, J.M., Juranke, L., Khen, G., Jayne, S., Kikuchi, T., Ladd, C., Lu, K., McCabe, R.M., Moore, G.W.K., Nishino, S., Ozenna, F., Pickart, R.S., Polyakov, I., Stabeno, P.J., Thoman, R., Williams, W.J., Wood, K., Weingartner, T.J., 2020. Manifestation and consequences of warming and altered heat fluxes over the Bering and Chukchi Sea continental shelves. Deep Sea Res. II

Farley Jr., E.V., and J.M. Moss. 2009. Growth rate potential of juvenile chum salmon on the eastern Bering Sea shelf: an assessment of salmon carrying capacity. North Pacific Anadromous Fish Commission Bulletin 5: 265 – 277.

Farley Jr., E.V., Murphy, J., Moss, J., Feldmann, A., Eisner, L., 2009. Marine ecology of western Alaska juvenile salmon, in Krueger, C.C., Zimmerman, C.E. (Eds.), Pacific Salmon: Ecology and Management of Western Alaska's Populations. American Fisheries Society, Bethesda, Maryland, pp. 307 – 329.

Farley, E.V., Jr., and M. Trudel. 2009. Growth rate potential of juvenile sockeye salmon in warmer and cooler years on the eastern Bering Sea shelf. J. Mar. Biol. vol. 2009, Article ID 640215. 10 pp.

Fergusson, E. A., M.V. Sturdevant, and J. A. Orsi. 2010. Effects of starvation on energy density of juvenile chum salmon (Oncorhynchus keta) captured in marine waters of Southeastern Alaska. Fishery Bulletin 108: 218–225.

Frey, K.E., Maslanik, J.A., Kinney, J.C., Maslowski, W., 2014. Recent variability in sea ice cover, age, and thickness in the Pacific Arctic region, in: Grebmeier, J.M., Maslowski, W. (Eds.), The Pacific Arctic Region: Ecosystem Status and Trends in a Rapidly Changing Environment. Springer, the Netherlands, pp. 31-63.

Grebmeier, J.M., Overland, J.E., Moore, S.E., Farley, E.V., Carmack, E.C., Cooper, L.W., Frey, K.E., Helle, J.H., McLaughlin, F.A., McNutt, S.L., 2006. A major ecosystem shift in the Norther Bering Sea. Science 311 (5766), 1461 – 1464, doi:10.1126/science.1121365.

Holling, C.S. 1965. The functional response of predators to prey density and its role in mimicry and population regulation. Mem. Entomol. Soc. Can. 45: 1–60.

Howard, K. G., K. M. Miller, and J. Murphy. 2017. Estuarine fish ecology of the Yukon River Delta, 2014–2015. Alaska Department of Fish and Game, Fishery Data Series No. 17-16, Anchorage.

Kristensen, K., Nielsen, A., Berg, C.W., Skaug, H., Bell, B.M., 2016. TMB: Automatic Differentiation and Laplace Approximation. *J. Stat. Softw.* 70(5), 1–21. doi: 10.18637/jss.v070.i05

Levine, R.M., A. De Robertis, D. Grunbaum, R. Woodgate, C.W. Mordy, F. Mueter, E. Cokelet, N. Lawrence-Slavas, H. Tabisola. 2020. Autonomous vehicle surveys indicate that flow reversals retain juvenile fishes in a highly advective high-latitude ecosystem. Limnology and Oceanography; doi: 10.1002/lno.11671.

Moss, J.H, Murphy, J.M., Farley, E.V., Eisner, L.B., Andrews, A.G., 2009. Juvenile Pink and Chum salmon distribution, diet, and growth in the northern Bering and Chukchi seas. N. Pac. Anad. Fish Comm. Bull. 5, 191 – 196.

Nielsen, J.L, Ruggerone, G.T., Zimmerman, C.E., 2013. Adaptive strategies and life history characteristics in a warming climate: Salmon in the Arctic? Environ. Biol. Fish. 96:1187 – 1226. Doi:10.1007/s10641-012-0082-6.

Parker, R.R., 1968. Ocean ecology of the North Pacific salmonids. Univ. of Washington Press, Seattle, WA. p. 179.

Polyakov, I.V., M.B. Alkire, B.A. Bluhm, K.A. Brown, E.C. Carmack, M. Chierici, S.L. Danielson, I. Ellingsen, E.A. Ershova, K. Gardfeldt, R.B. Ingvaldsen, A.V. Pnyushkov, D. Slagstad, and P. Wassmann. 2020. Borealization of the Arctic Ocean in response to anomalous advection from sub-Arctic seas. Frontiers in Marine Science, doi:10.3389/fmars.2020.00491.

Post, R.R., and E.A. Parkinson. 2001. Energy allocation strategy in young fish: allometry and survival. Ecology 82(4): 1040 – 1051.

RStudio Team (2020). RStudio: Integrated Development for R. RStudio, PBC, Boston, MA URL http://www.rstudio.com/.

Ruggerone, G.T., Irvine, J.R., 2018. Numbers and biomass of natural- and hatchery- origin Pink salmon, Chum salmon, and Sockeye salmon in the North Pacific Ocean, 1925 – 2015. Mar. Coast. Fish. 10, 152 – 168.

Stabeno, P.J., Bell, S.W., 2019. Extreme conditions in the Bering Sea (2017-2018): Record breaking low sea-ice extent. Geophys. Res. Lett. 46, 8952 – 8959. Doi: 10.1029/2019GL083816.

Stephenson, S.A., 2006. A review of the occurrence of Pacific salmon (*Oncorhynchus* spp) in the Canadian Western Arctic. Arctic, 59, 37 – 46.

Thoman, R.L., U.S. Bhatt, P.A. Bieniek, B.R. Brettschneider, M. Brubaker, S.L. Danielson, Z. Labe, R. Lader, W.N. Meier, G. Sheffield, and J.E. Walsh. 2020: The record low Bering Sea ice extent in 2018: context, impacts, and an assessment of the role of anthropogenic climate change [in "Explaining Extremes of 2018 from a Climate Perspective"]. *Bull. Amer. Meteor. Soc*., **101 (1)**, S17–S22, doi:10.1175/BAMS-D-19-0233.1.

Thornton, K.W., and A.S. Lessem. 1978. A temperature algorithm for modifying biological rates. Trans. Am. Fish. Soc. 107: 248–287.

Thorson, J.T., Shelton, A.O., Ward, E.J. & Skaug, H.J. Geostatistical delta-generalized linear mixed models improve precision for estimated abundance indices for West Coast groundfishes. *ICES J. Mar. Sci.* https://doi.org/10.1093/icesjms/fsu243 (2015).

Thorson, J.T., Pinsky, M.L. & Ward, E.J. Model-based inference for estimating shifts in species distribution, area occupied, and center of gravity. *Meth. Ecol. Evol*. **7**(8), 990–1008 https://doi.org/10.1111/2041-210X.12567 (2016a).

Thorson, J.T., Rindorf, A., Gao, J., Hanselman, D.H. & Winker, H. Density-dependent changes in effective area occupied for sea-bottom-associated marine fishes. *Proc*. *R*. *Soc*. B **283**(1840), 20161853. https://doi.org/10.1098/rspb.2016.1853 (2016b).

Thorson, J.T. Guidance for decisions using the Vector Autoregressive Spatio-Temporal (VAST) package in stock, ecosystem, habitat and climate assessments. Fish. Res. 210, 143–161 (2019).

Trudel, M., and D.W. Welch. 2005. Modeling the oxygen consumption rates in Pacific salmon and steelhead: model development. Trans. Am.Fish. Soc. 134: 1542–1561.

Trudel, M., and J.B. Rasmussen. 2006. Bioenergetics and mercury dynamics in fish: a modeling perspective. Can. J. Fish. Aquat. Sci. 63: 1890–1902.

Urawa, S., T.D. Beacham, M. Fukuwaka, and M. Kaeriyama. 2018. Ocean ecology of chum salmon, in: Beamish, R.J. (Ed.), The Ocean Ecology of Pacific Salmon and Trout. American Fisheries Society, Bethesda, pp. 161 – 317.

Vega, S.T., T.M. Sutton, and J.M. Murphy. 2016. Marine-entry timing and growth rates of juvenile Chum salmon in Alaskan waters of the Chukchi and northern Bering seas. Deep-Sea Research II. http://dx.doi.org/10.1016/j.dsr2.2016.02.002.

Vollenweider, J. J., R.A. Heintz, L. Schaufler, and R. Bradshaw. 2011. Seasonal cycles in whole-body proximate composition and energy content of forage fish vary with water depth. Marine Biology 158: 413–427.

Ware, D.M. 1978. Bioenergetics of pelagic fish: theoretical change in swimming speed and ration with body size. J. Fish. Res. Board Can. 35: 220–228.

Wechter, M.E., B.R. Beckman, A.G. Andrews III, A.H. Deaudreau, and M.V. McPhee. 2017. Growth and condition of juvenile chum and pink salmon in the northeastern Bering Sea. Deep-Sea Research II. http://dx.doi.org/10.1016/j.dsr2.2016.06.001.

Shelton, A.O., Thorson, J.T., Ward, E.J. & Feist, B.E. Spatial semiparametric models improve estimates of species abundance and distribution. *Can. J. Fish. Aquat. Sci.* **71**, 1655–1666. https://doi.org/10.1139/cjfas-2013-0508 (2014).

CHAPTER 23 - Environmental drivers of productivity for two endemic Arctic forage fish, juvenile Arctic cod (*Boreogadus saida*) and saffron cod (*Eleginus gracilis*), and an invading subpolar species, juvenile walleye pollock (*Gadus chalcogrammus*) in the Chukchi Sea

Objective 7: Develop spatially explicit bioenergetics models for Arctic cod and saffron cod as well as for juvenile pink and chum salmon and test the impact of warming summer temperatures on their growth and distribution

Vollenweider et al. (in preparation)

Abstract

The rapidly warming Arctic is creating newly accessible, ice-free areas, spurning interest in potential commercial fisheries. Arctic cod (*Boreogadus saida*) and saffron cod (*Eleginus gracilis*) are endemic to the Chukchi Sea and have been identified for harvest, as well walleye pollock (*Gadus chalcogrammus*) that has recently invaded the region in growing numbers. To provide a foundation for fishery management, we quantified how productivity of each of these gadids fluctuates in response to environmental conditions. We modeled the impact of interannual environmental conditions on productivity over the course of four years, 2012, 2013, 2017 and 2019 in the U.S. region of the Chukchi Sea. Specifically, growth rate potential was calculated for each species using the Wisconsin Bioenergetics Model 4.0 with inputs of size-dependent fish energy, temperature, diet, and diet energy. Growth rate potential was scaled up from stations spaced 30 nautical miles apart and summed across the station grid for overall ecosystem productivity. Gadid productivity is likely correlated with temperature and food availability conferred by specific water masses and conducive to the growth of each species. Species-specific ecological and physiological requirements likely results in different water masses conferring maximum productivity to each species. Large interannual wind and pressure-driven fluctuations in the strength and extent of water masses structures interannual differences in gadid productivity. The link between these atmospheric processes and gadid productivity will inform fishery management and provide forecasting potential.

Keywords: spatially-explicit bioenergetics model, growth rate potential, Wisconsin Bioenergetics Model 4.0, water mass

Introduction

Declines in Arctic sea ice extent and duration have spurned interest in developing fisheries in newly ice-free, accessible regions. In federally managed US Arctic waters, comprised of the eastern Chukchi Sea and the western Beaufort Sea, all commercial harvests of fish are prohibited until sufficient information is available to support sustainable conservation and management (North Pacific Fishery Management Council, 2009). A core requirement for commercial harvest is an estimate of maximum sustained yield (MSY), which is calculated based on unfished biomass, age at maturity, natural mortality rate, and stock-recruitment parameters. None of these life history traits are known for even the most basic harvest model for two potential commercial fish species, Arctic cod (*Boreogadus saida*) and saffron cod (*Eleginus gracilis*) (North Pacific Fishery Management Council, 2009). Another Gadidae that may garner future enthusiasm for harvest in the US Arctic is walleye pollock (*Gadus chalcogrammus*) (Hollowed et al., 2013). Walleye pollock is currently fished in adjacent waters of the Bering Sea (Ianelli et al., 2019) and has recently expanded into the Chukchi Sea with increasing abundance (Wildes et al., In Draft; De Robertis et al., In Draft). Complex models for commercial harvest are used for walleye pollock in the Bering Sea (Ianelli et al., 2019), but need to be evaluated for applicability in the Chukchi Sea (North Pacific Fishery Management Council, 2009). Once life history traits are quantified for the multiple

species of gadids in the Chukchi Sea, they need to be revisited periodically to adjust for changing environmental conditions that impact growth and productivity. This will be most pronounced in the Arctic, where oceanographic conditions are changing more rapidly than the rest of the globe (Koenigk et al., 2020; NSIDC, 2020).

Changing environmental conditions may have the highest impact on early life stages of fish. Small fish have high metabolic rates and a low capacity for storing energy, pushing them to their energetic limits (Sogard, 1997). Additional stresses imposed by unfavorable environmental conditions may likely exceed their ability to maintain their basic energetic needs. This is particularly true during their first year of life, a critical period (Howard et al., 2016; Farley et al., 2015; Heintz et al. 2013). Throughout summer, age-0 fish must grow quickly to evade predators and simultaneously store sufficient energy to sustain themselves through winter when food is limited. Consequently, the size and energy content of age-0 fishes in autumn reflects their summer growing conditions and indicates their preparedness to survive winter. This link has been made for walleye pollock in the Bering Sea, where total energy content in autumn correlates highly with their survival to recruitment two years later (Heintz et al., 2013). This concept should hold true for age-0 gadids in the Chukchi Sea, with their autumn body condition predictive of their future production.

Environmental fluctuations will impact the growth and production of age-0 gadids in the Chukchi Sea differentially based on their distinct ecological and physiological niches. Oceanographic conditions such as temperature and salinity that promote optimal growth are generally reflected by fish distribution. Age-0 Arctic cod and recently age-0 walleye pollock are distributed throughout salty (> 30.4 PSU) marine waters from the shoreline to the central Chukchi Sea, though Arctic cod are most prevalent in cooler water (2.6 — 6.7 °C) north of 69.5 °N while walleye pollock are more abundant in relatively warmer water (> 7 °C) south of that latitude (De Robertis et al., In Draft; De Robertis et al., 2017). Lab studies further substantiate Arctic cod and walleye pollock's thermal tolerances, with optimal growth for age 0 occurring at 7.3 °C and 13.0 °C, respectively (Laurel et al., 2015). In contrast, age-0 saffron cod are confined to shallow, coastal regions (> 7 °C, 28 - 31 PSU) in the Chukchi Sea and exhibit optimal growth at 14.8 °C in lab studies (Laurel et al., 2015). Spatial distributions are also driven in part by life history constraints such as ice-associated spawning and early feeding for Arctic cod (Graham and Hop, 1995; Craig et al., 1982) and estuarine spawning in brackish water for saffron cod (Pokrovskaya, 1960). Consequently, temperature and salinity impact growth and production of these gadids.

The Chukchi Sea is characterized by distinct ocean currents with unique temperature and salinity profiles that influence fish productivity. One of the most pervasive surface currents covering much of the Chukchi Sea is the Bering-Chukchi Summer Water, which originates from the Bering Sea and the Gulf of Anadyr (Danielson et al., 2017; Figure 2). This water mass is intermediate in temperature and salinity to other water masses. Along the Alaskan coastline of the Chukchi Sea, the Alaska Coastal Water flows northward from its inception in the Gulf of Alaska en route to the Arctic Basin. The Alaska Coastal Water is fresh and nutrient-rich from terrestrial freshwater runoff. Shallow coastal depths and high turbidity increase solar absorption, making the water mass up to 5 °C warmer than the Bering-Chukchi Summer Water (Danielson et al., 2017). The surface waters in the northern region of the Chukchi Sea, known as Ice Melt Water, which are left over from melted sea ice, are fresh and cold. The different oceanographic conditions of the dominant water masses provide different growing conditions for the three age-0 gadid species.

Another aspect that creates spatial heterogeneity in habitat quality for age-0 gadids in the Chukchi Sea is prey availability. Diets of age-0 Arctic cod and saffron cod in the Chukchi Sea are dominated by calanoid and harpacticoid copepods, as well as *Thysanoessa* sp. euphausids, and to a lesser degree mysids (Gray and Norcross, 2018; Sousa et al., 2018; Gray et al., 2015). Walleye pollock, in comparison, consume primarily euphausiids in the Chukchi and Northern Bering Seas (Cieciel et al., In Draft; Moss et al., 2009). The prominent water masses in the Chukchi Sea have distinct zooplankton assemblages, stemming

from the origination of currents (Pinchuk et al., 2017; Eisner et al., 2013). The Bering-Chukchi Summer Water is dominated by large zooplankton such as copepods (*Eucalanus bungii, Calanus glacialis/marshallae, Metridia pacifica)* and euphausiids (*Thysanoessa raschii*). These species are generally lipid-rich and high-quality prey (Vollenweider et al., Chapter 9). In contrast, the small zooplankton such as bivalve larvae and *Pseudocalanus* copepods characteristic of Alaska Coastal Water (Pinchuk et al., 2017; Eisner et al., 2013) have lower lipid content (Vollenweider et al., Chapter 9). Together, the spatial heterogeneity in oceanographic conditions and prey availability defines the habitat suitability for fish and consequently their growth potential.

Fish growth rate potential is a measure of individual fish growth and productivity and consequently overall ecosystem production. Growth rate potential incorporates fish size and energy content, density of prey by size and their energy content, and the physical environment to simulate fish growth. Both size- and temperature-specific bioenergetics models are needed for each gadid species to calculate growth rate potential. A bioenergetics model has been fully developed for walleye pollock (Buckley and Livingston, 1994), but not for Arctic cod or saffron cod. Growth rate potential is then scaled up by fish density to compute system productivity (Farley and Moss, 2009; Brandt et al., 1992). Growth rate potential should be evaluated on a fine spatial scale to account for heterogeneity in the environment and localized density-dependent processes (Brandt et al., 1992) associated with the different Chukchi water masses (Danielson et al., 2017). The location and extent of these water masses change from year to year primarily as a function of wind fields (Danielson et al., 2017; Pinchuk et al., 2017; Eisner et al., 2013) and are likely a major driver in the interannual productivity of gadids.

We evaluated the influence of spatial and interannual environmental variation on the productivity of three species of gadids in the US region of the Chukchi Sea (60.004° – 43.044° N, 170.000° – 153.179° W) to provide a foundation for emerging harvest strategies and ecosystem sustainability. We examined the age-0 stage of three potential commercial species, including two species endemic to the Arctic, Arctic cod and saffron cod, as well as expanding walleye pollock. Specifically, we used a spatially-explicit bioenergetics model to relate interannual differences in gadid productivity to variable oceanographic conditions observed in the US Chukchi Sea in 2012, 2013, 2017, and 2019 to test the following hypotheses:

- Arctic cod growth and productivity will be elevated in cool water masses, such as Ice Melt Water, and total production will be higher in colder years when these water masses are more pronounced;
- Saffron cod growth and productivity will continue to be restricted to warmer, nearshore Alaskan Coastal Water and will increase during warmer years; and
- Walleye pollock growth will flourish in warm years when Arctic cod production is diminished and constrained to smaller areas.

Methods

We used spatially-explicit bioenergetics models to quantify the influence of oceanographic conditions on the growth and productivity of three species of gadids, Arctic cod, saffron cod, and walleye pollock, with varying niches in the Chukchi Sea. Data for the modeling effort was collected from acoustic-trawl surveys conducted across the US Chukchi Sea in four of eight years, August – September of 2012, 2013, 2017, and 2019 (Figure 1). At each station, temperature and salinity were measured throughout the water column using a Seabird 19+ Conductivity Temperature Depth (CTD) instrument. Mean annual surface water temperature and salinity were calculated by averaging the values in the top 20 m at each station and then averaging over all stations. Zooplankton species assemblages and density were measured using a vertically-towed 60 cm, 505 µm mesh bongo net. Fish were sampled with a 200 m long CanTrawl 400/601 surface trawl with a 122 m headrope, a fished vertical opening of 19 m, and 162 – 1.2 cm mesh (De Robertis et al., 2015). While the vessel traveled between stations, a SIMRAD© hydroacoustic echosounder located fish deeper in the water column than the surface trawl could collect. If additional fish

were found, they were sampled with a modified Marinovich mid-water trawl with 12 m headrope, a fished vertical opening of 6 m, and 6.4 – 0.3 cm mesh (De Robertis et al., 2015).

Approximately 10 age-0 fish were subsampled from each haul and frozen at sea. In the laboratory, each fish was measured for total length (nearest mm) and wet mass (nearest 0.01 g). Stomach contents were extracted, weighed to the nearest 0.01 g, and species were identified to the lowest possible taxon to quantify diet. Diet energy was calculated using published values of lipid content of zooplankton from the Chukchi Sea (Vollenweider et al., In Draft). Individual fish were dried to a constant weight using Thermogravimetric Analysis and homogenized. Energy density (kJ/g dry mass) of each fish was measured using a Parr 6725 semi-micro bomb calorimeter following standard methods (Vollenweider et al., In Draft). Briefly, 30 – 200 mg of dried sample homogenate were pressed into pellets, combusted, and the emitted heat was measured and converted to energy.

We parameterized the Fish Bioenergetics 4.0 model (Deslauriers et al., 2017) for Arctic and saffron cod using published mass and temperature specific values of consumption (C), growth rate (G), respiration (R), specific dynamic action (SDA), and feces (F; Krieger et al., 2020). The core thermodynamic equation used was:

$$C_{ij} = G_{ij} - (R_{ij} + SDA_{ij} + U_{ij} + F_{ij}) \quad \text{(Equation 1)}$$

where consumption (C) is a measure of growth (G) minus losses for respiration (R), specific dynamic action (SDA), urine (U), and feces (F) for a given sized fish *i* at a given temperature *j*. Equation 1 requires size and temperature specific equations to derive each variable (Table 1). Equation parameters were collated from the literature and used to construct models for Arctic cod (Drost et al., 2016; Laurel et al., 2016; Hop et al., 1997; Hop and Graham, 1995; Jensen et al., 1991; Holeton, 1974) and saffron cod ((Laurel et al., 2016; Chen, 1989; Chen and Mishima, 1986).

For each of the four survey years, the Fish Bioenergetics 4.0 model (Deslauriers et al., 2017) was used to calculate the size-dependent growth-rate potential of individual fish for all three gadid species at each station following methods in Farley et al. (2009). Specifically, model inputs for field observations were station-specific values for water temperature, fish diet, and caloric density of individual fish. For each of the three species, annual ecosystem production was calculated across the US region of the Chukchi Sea. Fish production is a measure of the increase in fish biomass within a period of time and was calculated as:

$$\text{system-wide production} = \sum G_{ij} \ast\times N_{ij} \quad \text{(Equation 2)}$$

where G_{ij} is the calculated fish growth potential (g * d^{-1}) from the Wisconsin bioenergetics model at station *i* for a given size *j*, and N_{ij} is the number of fish at station *i* for a given size *j* in 10 mm length bins (Brandt et al. 1992). Sensitivity analyses were conducted to evaluate the robustness of the model and input parameters via Monte Carlo simulation using parameter error rates of 5%, 10%, 15%, and 20% following Bartell et al. (1986).

Results

In progress

Discussion

Interannual variation in the production of the three prominent Arctic gadids in the Chukchi Sea is likely governed by the extent of the prominent water masses. Each of these water masses undergoes significant interannual differences in their strength and spatial extent, with greater deviations anticipated in the future. Ice Melt Water is derived from melting sea ice. Arctic sea ice extent has declined over the 41-year satellite record and is the second lowest on record, and was well below average in the Chukchi Sea in 2019 and 2017 (National Snow and Ice Data Center, accessed 4/22/2020). The Chukchi Sea has had increased persistence of open water in winter and earlier ice retreats in the spring, in large part from

increased ocean heat transport from the Bering Sea (Serreze et al., 2019). Arctic cod productivity is likely linked to characteristics of these water which effect growth, as well as the nutritionally-rich sea-ice diatoms that are passed up the food chain to juvenile fish (Falk-Petersen 1998). Continued reductions in Ice Melt Water likely influences gadid productivity.

Greater heat transport into the Chukchi Sea will diminish sea ice and may decrease productivity of endemic gadids while increasing production of walleye pollock. The dominant water mass in the Chukchi Sea is the Bering-Chukchi Summer Water which is derived from the Bering Sea and the Anadyr Currents. Transport through the Bering Strait is driven by differences in sea level pressure and wind (Serreze et al., 2019; Aagaard et al., 2006). Though sea level differentials and wind fields are hard to predict, general ocean warming in the Bering Sea in coming decades will likely increase ocean heat transport through the Bering Strait (Serreze et al., 2019). With greater influx of water from the Bering Sea, which supports one of the world's largest fisheries on walleye pollock (Ianelli et al., 2019), pollock production is anticipated to increase in the Chukchi Sea. Furthermore,

A second major water mass flowing north through the Bering Strait and into the Chukchi Sea is the Alaskan Coastal Water; for which the strength and spatial extent are driven by wind and freshwater input (Morris, 2019). Enormous quantities of freshwater river discharge along the eastern Bering Sea coast promote this current, including the Yukon, Kuskokwim, Nushagak and Kvichak rivers and to a lesser extent from riverine input from the Gulf of Alaska (Aagaard et al., 2006). River discharge is anticipated to increase as warming continues due to large contributions of freshwater from melting glaciers and permafrost (Chikita et al., 2007). Increasing prominence of the Alaskan Coastal Current in the Chukchi Sea may enhance saffron cod productivity, which are historically distributed along the Alaskan coast. Similar to the Bering-Chukchi Summer Water, the Alaskan Coastal Current transports a large heat flux to the Chukchi Sea, and is instrumental in sea ice melting by as much as 30% of the seasonal sea ice loss area (Woodgate et al., 2010). Consequently, increases in Alaskan Coastal Water prominence in the Chukchi Sea negatively influence the productivity of other gadid species.

Our findings will show that significant changes are occurring in the productivity of gadids in the Chukchi Sea in response to changing environmental conditions. Understanding the disparate trends in production among Arctic cod, saffron cod, and walleye pollock are foundational for developing commercial fisheries in a newly accessible region. Physical processes underlying the distribution and strength of the prominent ocean currents in the Chukchi could be a key indicator used in management strategy to understand and predict fish stocks, determine sustainable harvest levels, and maintain a sustainable ecosystem.

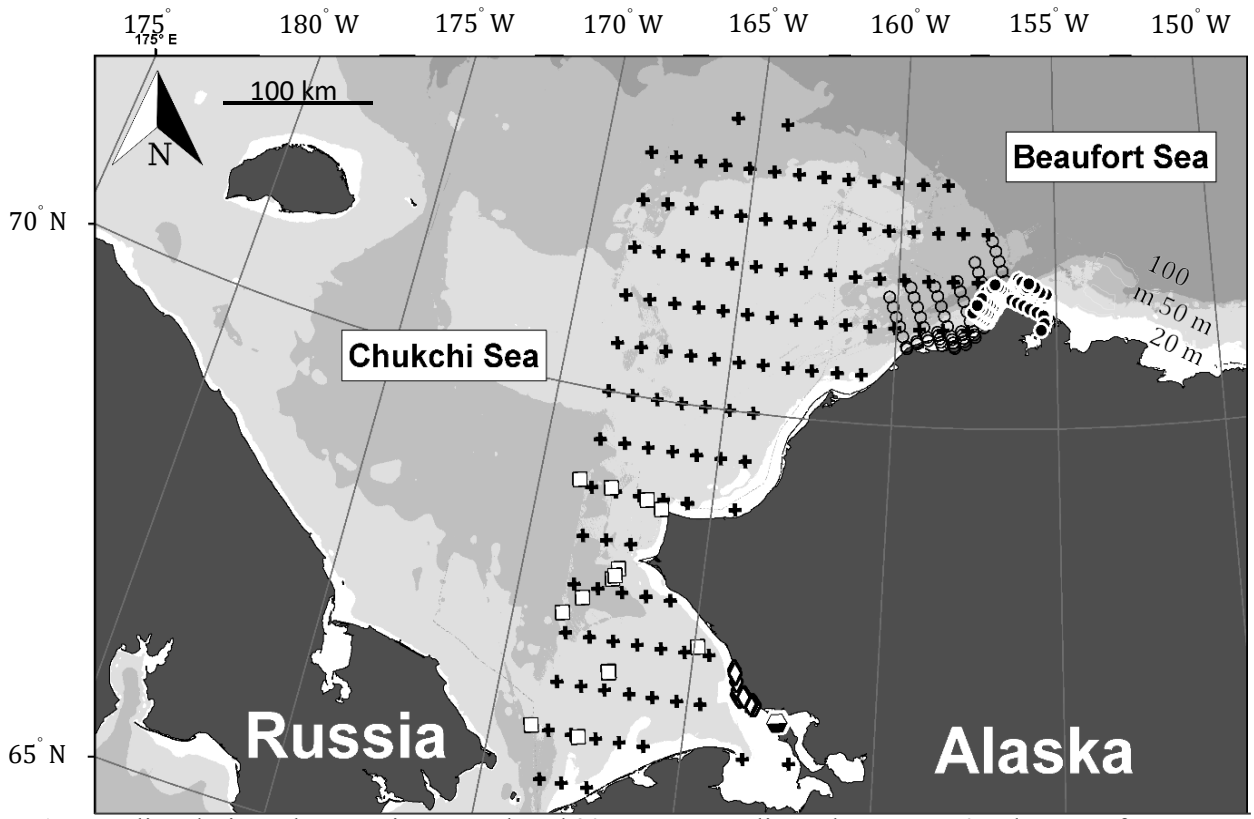

Figure 1. Sampling design where stations are placed 30 nm apart on lines along every 0.5 degrees of latitude in the US region of the Chukchi Sea.

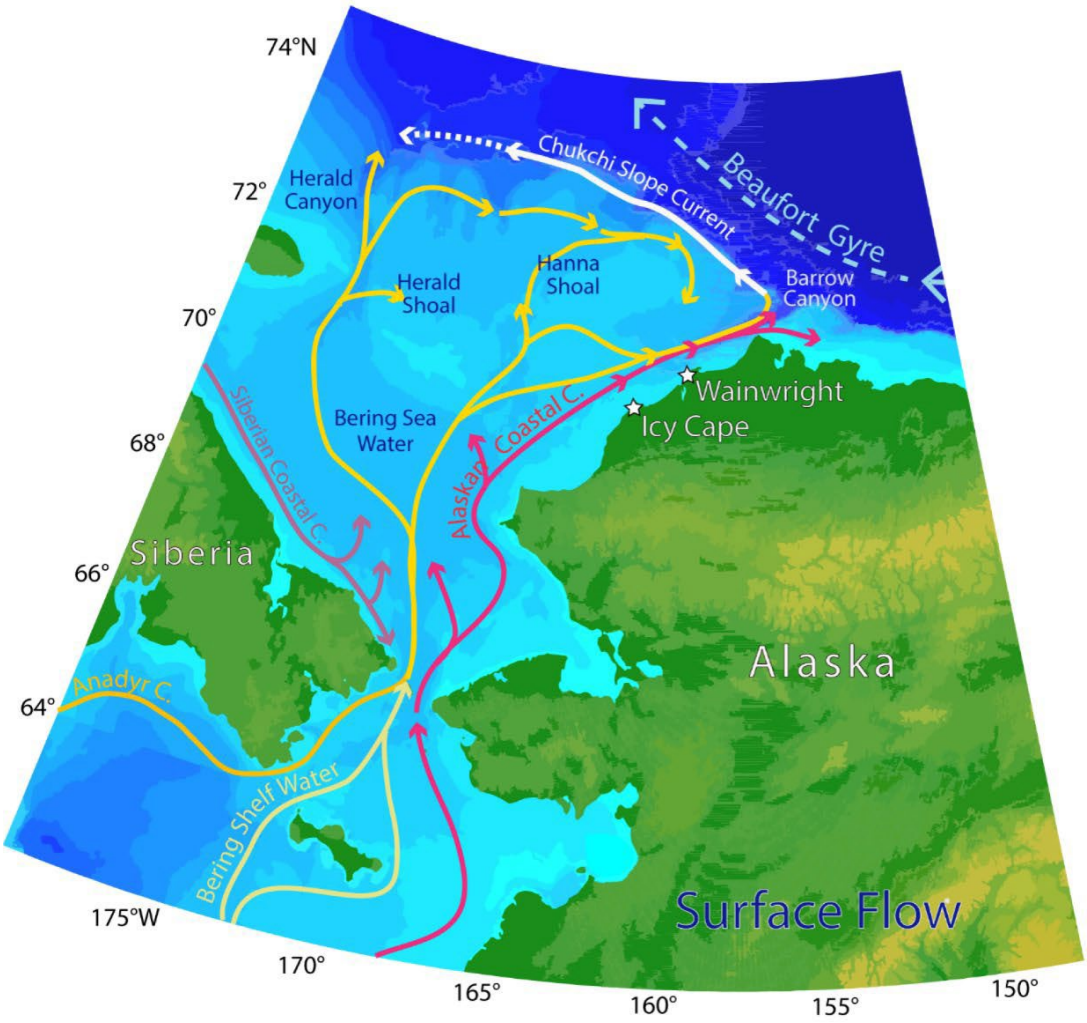

Figure 2. Prominent ocean surface currents in the Chukchi Sea from Stabeno et al., 2018.

Table 1. Size-dependent bioenergetics equations used to parameterize the Fish Bioenergetics 4.0 model for Arctic cod and saffron cod. Equations for each parameter were derived based on methods described in Krieger et al. (2020). Parameter definitions and values are described in Table 2.

Broad Equation	Sub-level equations
$R = RA * W^{RB} * f_R(T) * ACT * w$	$f_R(T) = RV^{RX} * e^{(RX * (1-RV))}$
	$RV = (RTM - T)/(RTM-RTO)$
	$RX = RZ^2 * (1+(1+40/RY)^{0.5})^2)/400$
	$RX = \frac{RZ^2}{400}\left(1 + \sqrt{1 + \frac{40}{RY}}\right)^2$
	$RZ = \ln(RQ) * (RTM - RTO)$
	$RY = \ln(RQ) * (RTM - RTO + 2)$
	$w = 13{,}560\ J * g\ O2^{-1}$
$C = CA * W^{CB} * P * f_C(T)$	$f_C(T) = VX * e^{(X * (1-V))}$
	$V = (CTM - T)/(CTM-CTO)$
	$X=Z^2 * (1+1+40/Y)^{0.5})^2)/400$
	$Z = \ln(CQ) * (CTM - CTO)$
	$Y = \ln(CQ) * (CTM - CTO +2)$
$S = SDA * (C - F)$	
$F = FA * C$	
$U + UA * (C-F)$	

Table 2. Parameter definitions, values, and data sources for Arctic cod and saffron cod bioenergetics models.

Parameter	Description	Arctic Cod		Saffron Cod		Walleye Pollock	
		Value	Source	Value	Source	Value	Source
ACT	activity coefficient						
C	consumption						
CA	intercept of consumption allometric mass function (g g^{-1} d^{-1})						
CB	slope for consumption allometric mass function						
CQ	Q_{10} or temperature effect for consumption						
CTM	maximum temperature for consumption (◦C)						
CTO	optimal temperature for consumption (◦C)						
F	waste loss due to egestion						
FA	constant proportion of consumption						
$f_R(T)$	temperature dependent function for respiration						
$f_C(T)$	temperature dependent function for consumption						
P	proportion of maximum consumption						
R	respiration						
RA	intercept of the respiration allometric function (g O_2 g^{-1} d^{-1})						
RB	slope for the respiration allometric mass function						
RQ	Q_{10} or temperature effect for respiration						
RTM	maximum temperature for respiration (◦C)						
RTO	optimal temperature for respiration (◦C)						
S	specific dynamic action coefficient						
SDA	specific dynamic action						
T	temperature						
U	excretion						
UA	constant proportion of excretion						
V	calculated coefficient						
w	oxy-calorific coefficient						
W	weight of fish						
X	calculated coefficient						
Y	calculated coefficient						
Z	calculated coefficient						

Table 3. Mean annual growth (g * g^{-1} * d^{-1}), energy density (kJ), abundance (n), and productivity (kilograms/day) averaged over all sampling stations in the Chukchi Sea ± standard deviation for each of the three gadids. (Results in progress)

	2012	2013	2017	2019
Arctic cod				
Energy density	X ± X	X ± X	X ± X	X ± X
Growth rate potential	X ± X	X ± X	X ± X	X ± X
Abundance	X ± X	X ± X	X ± X	X ± X
Productivity	X ± X	X ± X	X ± X	X ± X
Saffron cod				
Energy density	X ± X	X ± X	X ± X	X ± X
Growth rate potential	X ± X	X ± X	X ± X	X ± X
Abundance	X ± X	X ± X	X ± X	X ± X
Productivity	X ± X	X ± X	X ± X	X ± X
Walleye pollock				
Energy density	X ± X	X ± X	X ± X	X ± X
Growth rate potential	X ± X	X ± X	X ± X	X ± X
Abundance	X ± X	X ± X	X ± X	X ± X
Productivity	X ± X	X ± X	X ± X	X ± X

References

Chen A (1989) Relation between food-intake and growth of immature saffron cod, Eleginus gracilis (Tilesius) in captivity. Bull Fac Fish Hokkaido Univ 40(4):228-237

Chen A, Mishima S (1986) Oxygen consumption of saffron cod, Eleginus gracilis (Tilesius). Bull Fac Fish Hokkaido Univ 37(4):303-308

Chikita KA, Wada T, Kudo I, Kido D, Narita Y, Kim Y (2007) Modelling discharge, water chemistry and sediment load from a subarctic river basin: the Tanana River, Alaska. Water Quality and Sediment Behaviour of the Future: Predictions for the 21st Century. Proceedings of Symposium, Perugia, July 2007.

Cieciel K et al. (In Draft) Diet of Arctic cod, saffron cod, and walleye pollock in the Chukchi Sea.

Craig PC, Griffiths WB, Haldorson L, McElderry H (1982) Ecological studies of Arctic cod (*Boreogadus saida*) in Beaufort sea coastal waters, Alaska. Can J Fish Aquat Sci, 39(3): 395-406.

Danielson SL, Eisner L, Ladd C, Mordy C, Sousa L, Weingartner TJ (2017) A comparison between late summer 2012 and 2013 water masses, macronutrients, and phytoplankton standing crops in the northern Bering and Chukchi Seas. Deep Sea Res Part II 135:7-26.

De Robertis A, et al. (In Draft) Interannual distribution of gadids in the Chukchi Sea, 2017 & 2019.

De Robertis A, Taylor K, Williams K, Wilson CD (2015) Species and size selectivity of two midwater trawls used in an acoustic survey of the Alaska Arctic. Deep Sea Res II 135:40-50.

De Robertis A, Taylor K, Wilson CD, Farley EV (2017) Abundance and distribution of Arctic cod (*Boregadus saida*) and other pelagic fishes over the U.S. continental shelf of the northern Bering and Chukchi Seas. Deep Sea Res II 135:51-65.

Dorn MW, Deary AL, Fissel BE, Jones DT, Lauffenburger NE, Palsson WA, Rogers LA, Shotwell SK, Spalinger KA, Zador SG (2019) Chapter 1: Assessment of the walleye pollock stock in the Gulf of Alaska. In: North Pacific Fishery Management Council Gulf of Alaska SAFE. p. 1-155.

Drost HE, Lo M, Carmack EC, Farrell AP (2016) Acclimation potential of Arctic cod (*Boreogadus saida*) from the rapidly warming Arctic Ocean. J Exper Biol 219:3114-3125.

Eisner L, Hillgruber N, Martinson E, Maselko J (2013) Pelagic fish and zooplankton species assemblages in relation to water mass characteristics in the northern Bering and southeast Chukchi seas. Polar Biol 36:87-113.

Falk-Petersen S, Sargent JR, Henderson J, Hegseth EN, Hop H, Okolodkov YB (1998) Lipids and fatty acids in ice algae and phytoplankton from the marginal ice zone in the Barents Sea. Polar Biol 20:41-47.

Farley EV, Heintz RA, Andrews AG, Hurst TP (2015) Size, diet, and condition of age-0 Pacific cod (*Gadus microcephalus*) during warm and cool climate states in the eastern Bering Sea. Deep Sea Res II.

Graham M, Hop H (1995) Aspects of reproduction and larval biology of Arctic cod (*Boreogadus saida*). Arctic 48(2):130-135.

Gray BP, Norcross BL (2018) Fish diets in 2013 and 2014. In: Ecology of Forage Fishes in the Arctic Nearshore. Eds. Vollenweider, JJ, Heintz RA, Boswell KM, Norcross BL, Li C, Barton MB, Sousa L, Pinchuk A, Danielson S, George C. Final Report to the North Slope Borough, Shell Baselin Studies Program, July 2018, 480 p.

Gray BP, Norcross BL, Blanchard AL, Beaudrea AH, Seitz AC (2016) Variability in the summer diets of juvenile polar cod (*Boreagadus saida*) in the northeastern Chukchi and western Beaufort Seas. Polar Bio 39:1069-1080.

Heintz RA, Siddon EC, Farley EV, Napp JM (2013) Correlation between recruitment and fall condition of age-0 pollock (*Theragra chalcogramma*) from the Eastern Bering Sea under varying climate conditions. Deep Sea Res II 94:150-156.

Holeton GF (1974) Metabolic cold adaptation of polar fish: fact or artefact? Physiol Zool 43(3):137.

Hollowed AB, Planque B, Loeng H (2013) Potential movement of fish and shellfish stocks from the sub-Arctic to the Arctic Ocean. Fish Oceanogr 22(5): 355-370.

Hop H, Graham M (1995) Respiration of juvenile Arctic cod (Boreogadus saida): effects of acclimation, temperature, and food intake. Polar Biol 15:359-367.
Hop H, Tonn WM, Welch HE (1997) Bioenergetics of Arctic cod (Boreogadus saida) at low temperatures. Can J Fish Aquat Sci 54:1772-1784.
Howard K, Murphy JM, Wilson L, Moss J, Farley EV Jr (2016) Size-selective mortality of chinook salmon in relation to body energy after the first summer in nearshore marine habitats. N Pac Anadr Fish Comm Bull 6:1-11.
Ianelli J, Fissel B, Holsman K, Honkalehto T, Kotwicki S, Monnahan C, Siddon E, Stienessen S, Thorson J (2019) Chapter 1: Assessment of the walleye pollock stock in the eastern Bering Sea. In: North Pacific Fishery Management Council SAFE. p. 1-161.
Jensen T, Ugland KI, Anstensrud M (1991) Aspects of growth in Arctic cod, *Boreogadus saida* (Lepechin 1773). Pp 547-552 in Sakshaug E, Hopkins CCE, Oritsland NA (eds) Proceedings of the Pro Mare Symposium on Polar Marine Ecology, Trondheim, 12-16 May 1990. Polar Res 10(2).
Koenigk T, Key J, Vihma T (2020) Climate change in the Arctic. in: Kokhanovsky A, Tomasi C (Eds.), Physics and Chemistry of the Arctic Atmosphere. Spring Polar Sciences. Springer, Cham, pp. 673-705.
Laurel BJ, Spencer M, Iseri P, Copeman LA (2016) Temperature-dependent growth and behavior of juvenile Arctic cod (*Boregadus saida*) and co-occurring North Pacific gadids. Polar Biol 39(6):1127-1135.
Morris BA (2019) Seasonality and forcing factors of the Alaskan Coastal current in the Bering Strait from July 2011 to July 2012. Ms Thesis, Univ Washington, 86p.
Moss JH, Falrey EV Jr, Feldmann AM, Ianelli JN (2009) Spatial distribution, energetic status and food habits of Eastern Bering Sea age-0 walleye pollock. Trans Amer Fish Soc 138(3):497-505.
National Snow and Ice Data Center. http://nsidc.org/arcticseaicenews/. Accessed Feb 17, 2020.
North Pacific Fishery Management Council (2009) Fishery management plan for fish resources of the Arctic management area. Anchorage, AK. 158 p.
Pinchuk AI, Eisner LB (2017) Spatial heterogeneity in zooplankton summer distribution in the eastern Chukchi Sea in 2012-2013 as a result of large-scale interactions of water masses. Oceanogr 135:27-39.
Pokrovskaya TN (1960) Geographical variability in the biology of the navaga (genus *Eleginus*) Tr Inst Okeanol Akad Nauk SSR 31: 19-110. In Russ.
Serreze MC, Barrett AP, Crawford AD, Woodgate RA (2019) Monthly variability in Bering Strait oceanic volume and heat transports, links to atmospheric circulation and ocean temperature, and implications for sea ice conditions. J Geophys Res Oceans 124:12:9317-9337.
Sogard SM (1997) Size0selective mortality in the juvenile stage of teleost fishes: a review. Bull Mar Sci 60(3): 1129-1157.
Sousa L, Pinchuk AI, Vollenweider JJ (2018) Fish diets in Elson Lagoon and adjacent nearshore marine environment in the Chukchi and Beaufort Seas. In: Ecology of Forage Fishes in the Arctic Nearshore. Eds. Vollenweider, JJ, Heintz RA, Boswell KM, Norcross BL, Li C, Barton MB, Sousa L, Pinchuk A, Danielson S, George C. Final Report to the North Slope Borough, Shell Baselin Studies Program, July 2018, 480 p.
Stabeno P, Kachel N, Ladd C, Woodgate R (2018) Flow patterns in the eastern Chukchi Sea: 2010 – 2015. J Geophys Res, 123(2):1177-1195.
Vollenweider et al. (In Draft) Variation in Nutritional quality of Arctic zooplankton and fish. Chapter 9.

Publications, Presentations, and Collaborations

Publications

The following manuscripts are published in peer-reviewed journals

De Robertis, A., Taylor, K., Wilson, C., and Williams, K. in press. Corrigendum to: "Species and size selectivity of two midwater trawls used in an acoustic survey of the Alaska Arctic" (Deep-Sea Res. II 135 (2017) 40-50). Deep Sea Research II https://doi.org/10.1016/j.dsr2.2021.104997.

Farley, E.V., Jr., J.M. Murphy, K. Cieciel, E.M. Yasumiishi, K. Dunmall, T. Sformo, P. Rand. Response of Pink salmon to climate warming in the northern Bering Sea. Deep-Sea Research II https://doi.org/10.1016/j.dsr2.2020.104830.

Huntington, H. P., Danielson, S. L., Weise, F. K., Boveng, P., Baker, M., Citta, J., De Robertis, A., et al. 2020. Evidence suggests potential transformation of the Pacific Arctic Ecosystem is underway. Nature Climate Change, https://doi.org/10.1038/s41558-020-0695-2.

Kuletz, K., D. Cushing, E. Labunski. 2020. Distributional shifts among seabird communities of the Northern Bering and Chukchi seas in response to ocean warming during 2017-2019. *Deep Sea Research II*, 181-182: 104913. https://doi.org/10.1016/j.dsr2.2020.104913

Levine, R.M., A. De Robertis , D. Grünbaum, R. Woodgate, C.W. Mordy, F. Mueter, E. Cokelet, N. Lawrence-Slavas, H. Tabisola. 2021. Autonomous vehicle surveys indicate that flow reversals retain juvenile fishes in a highly advective high-latitude ecosystem. Limnol. Oceanogr. 66: 1139-1154. https://doi.org/10.1002/lno.11671

Logerwell, E.A., Busby, M., Mier, K.L., Tabisola, H., Duffy-Anderson, J., 2020. The effect of oceanographic variability on the distribution of larval fishes of the northern Bering and Chukchi seas. Deep Sea Res. Part II Top. Stud. Oceanogr. 104784. https://doi.org/10.1016/j.dsr2.2020.104784

Murphy, J., S. Garcia, J. Dimond, J. Moss, F. Sewall, W. Strasburger, E. Lee, T. Dann, E. Labunski, T. Zeller, A. Gray, C. Waters, D. Jallen, D. Nicolls, R. Conlon, K. Cieciel, K. Howard, B. Harris, N. Wolf, and E.V. Farley Jr.[1]. 2021. Northern Bering Sea surface trawl and ecosystem survey cruise report, 2019. NOAA Tech Memo

Piatt, John F., David C. Douglas, Mayumi L. Arimitsu, Michelle L. Kissling, Erica N. Madison, Sarah K. Schoen, Kathy J. Kuletz, Gary S. Drew. 2021. Kittlitz's Murrelet Seasonal Distribution and Post–breeding Migration from the Gulf of Alaska to the Arctic Ocean. *Arctic* 74 (4): 482-495. https://doi.org/10.14430/arctic73992.

Romano, Marc, Heather M. Renner, Kathy J. Kuletz, Julia K. Parrish, Timothy Jones, Hillary K. Burgess, Daniel A. Cushing, Douglas Causey. 2020. Die-offs and reproductive failure of murres in the Bering and Chukchi Seas in 2018. *Deep Sea Research II,* vol 181-182, https://doi.org/10.1016/j.dsr2.2020.104877

Vestfals, C.D., F.J. Mueter, K.S. Hedstrom, B.J. Laurel, C.M. Petrik, J.T. Duffy-Anderson, and S.L. Danielson 2021. Modeling the dispersal of polar cod (*Boreogadus saida*) and saffron cod (*Eleginus gracilis*) early life stages in the Pacific Arctic using a biophysical transport model.

Progress in Oceanography. 196: 102571. ISSN 0079-6611, https://doi.org/10.1016/j.pocean.2021.102571.

The following manuscripts are currently in review.

Cooper, D.W., K. Cieciel, L. Copeman, P.O. Emelin, E. Logerwell, N. Ferm, J. Lamb, R. Levine, K. Axler, R.A. Woodgate, L. Britt, R. Lauth, B. Laurel, and A.M. Orlov (in review). Pacific cod or tikhookeanskaya treska (*Gadus macrocephalus*) in the Chukchi Sea during recent warm years: Distribution by life stage and age-0 diet and condition. DSR II Special Issue

Gall, Adrian E., Alexander K. Prichard, Katherine J. Kuletz[2], Seth L. Danielson. *In review*. Influence of water masses on the summer structure of the seabird community in the northeastern Chukchi Sea. Deep Sea Research Part II Special Issue.

Levine, R.M., A. De Robertis, D. Grunbaum, S. Wildes, E.V. Farley, Jr., P.J. Stabeno, C.D. Wilson (in review) Climate-driven shifts in pelagic fish distributions in a rapidly changing Pacific Arctic. DSR II Special Issue

Logerwell, E., M. Wang, L. Jorgensen, and K. Rand (in review). Winners and Losers in a Warming Arctic: Potential Habitat Gain and Loss for Epibenthic Invertebrates of the Chukchi and Bering Seas. DSR II Special Issue

Marsh J.M., Mueter F.J., Pirtle J.L. 2021. Model-based Fish Distributions and Habitat Descriptions for Arctic Cod (Boreogadus saida), Saffron Cod (Eleginus gracilis) and Snow Crab (Chionoecetes opilio) in the Alaskan Arctic. Anchorage (AK): U.S. Department of the Interior, Bureau of Ocean Energy Management. 58 p. Report No.: OCS Study BOEM 2021-056. Contract No.: M19AC00009.

The following manuscripts are in preparation for submission to peer-reviewed journals.

Chapman, Z.M., F.J. Mueter, B.L. Norcross, and D.S. Oxman (in preparation). Otolith-derived hatch dates and growth rates of Arctic Cod (Boreogadus saida) support the existence of several spawning populations in Alaskan waters. Deep-Sea Research II special issue

Chapman, Z.M., F.J. Mueter, B.L. Norcross, and D.S. Oxman (in preparation). Arctic Cod (*Boreogadus saida*) otolith microchemistry supports regional differences in hatching habitats off Alaska. Deep-Sea Research II special issue

Copeman, L., C. Salant, M. Stowell, M. Ottmar, M. Spencer, P. Iseri, B. Laurel (in preparation). The role of temperature on overwinter survival, condition and lipid storage in juvenile polar cod (*Boreogadus saida*): a laboratory experiment. (to be submitted to DSR II Special Issue).

Copeman, L., C. Salant, M. Stowell, M. Spencer, et al. (in preparation). Annual and spatial variation in the condition and lipid biomarkers of four juvenile gadid species from the Chukchi Sea during a recent period of dramatic warming (2012 to 2019). (to be submitted to DSR II Special Issue).

De Robertis, A., R. Levine, K. Williams, and C.D. Wilson (in NOAA internal review). Modifying a pelagic trawl to better retain small Arctic fishes. (DSR II Special Issue)

Farley, E.V., Jr., E. Yasumiishi, W. Strasburger, D. Kimmell, J. Moss, J. Murphy, F. Sewall (in preparation). Growth rate potential for juvenile Chum salmon in rapidly warming northern Bering and southern Chukchi seas. (in prep for DSR II special Issue).

Levine, R.M., A. De Robertis, D. Grünbaum, C.D. Wilson (in preparation). Multi-Year autonomous observations of Seasonality in movement, behavior, and growth of pelagic fishes in the Chukchi Sea. (in prep for Canadian Journal of Fisheries and Aquatic Sciences)

Mueter, F.J., Iken, K., Cooper, D., Grebmeier, J., Hopcroft, R., Kuletz, K., Danielson, S. (In Prepreview). Trade-offs among sampling designs for monitoring biodiversity and abundance of marine organisms in the Chukchi Sea.

Vollenweider, J.J., R. Heintz, B. Norcross, L. Sousa, A. Pinchuk, M. Robards, R. Bradshaw. (in preparation) Variation in Nutritional Quality of Arctic Zooplankton and Fish (in prep for DSR II special issue)

Vollenweider et al. (in preparation) Environmental drivers of productivity for two endemic Arctic forage fish, juvenile Arctic cod and saffron cod, and an invading subpolar species, juvenile walleye pollock in the Chukchi Sea. (Journal to be determined)

Weems et al. (in preparation). Interannual comparison of late summer distribution and abundance of pelagic larval crab communities, including blue king crab and snow crab, in the Pacific Arctic Gateway. Deep-Sea Research II special issue

Wildes, S., J. Whittle, Hv. Nguyen, M. Marsh, K. Karpan, K. DAmelio, A. Dimond, K. Cieciel, A. De Robertis, R. Levine, W. Larson, and J. Guyon (in review). Walleye Pollock breach the Bering Strait: A change of the cods in the Arctic. DSR II special Issue

The following graduate theses are in preparation or have been submitted.

Chapman, Z. 2021. Otolith derived hatch dates, growth rates, and microchemistry of Arctic cod (*Boreogadus saida*) support the existence of several spawning populations in Alaskan waters (M.S. thesis). University of Alaska Fairbanks, Fairbanks, Alaska. December 2021.

Levine, R. 2021. Climate-driven changes in the composition and distribution of pelagic fishes in the Chukchi Sea (Doctoral dissertation). University of Washington, Seattle, WA.

Presentations

Cieciel, K. 2016. Alaska Fisheries Science Center in the Bering Strait: past, present and future. Strait Science, October 2016, Nome, AK

Cooper, D., Logerwell, E., Emelin, P., Cieciel, K., Levine, R., Axler, K., Britt, L., Woodgate, R., Orlov, A. 2020. Pacific cod or Treska (Gadus macrocephalus) in the Chukchi Sea. Alaska Marine Science Symposium, January 2020, Anchorage, AK.

Copeman LA, Laurel B (2017) The interaction of temperature and diet quality in determining the condition of juvenile saffron cod (*Eleginus gracilis*) and Arctic cod (*Boreogadus saida*): results from combined laboratory and field based approaches. Oral Presentation. Ecosystem Studies of SubArctic Seas Annual Science Meeting, Tromso, Norway, June 11-15, 2017.

Copeman LA, Koenker BL, Laurel BJ (2018) Impacts of temperature and food availability on the condition of larval Arctic cod (*Boreogadus saida*) and walleye pollock (*Gadus chalcogrammus*). Oral Presentation. 42nd Annual Larval Fish Conference, Victoria, Canada, June 24-28, 2018.

Copeman LA, Heintz R (2018) Lipid storage and fatty acid biomarkers in juvenile Arctic cod (*Boreogadus saida*) and saffron cod (*Eleginus gracilis*) from the Beaufort and Chukchi Seas. Oral Presentation. International Symposium on Okhotsk Sea and Sea Ice. Mombetsu, Japan, February 19-21, 2018.

Copeman L, Laurel B, et al. 2019 The effects of temperature and food quality on the lipid condition and trophic biomarkers of juvenile polar cod (*Boreogadus saida*) and co-occurring Alaskan cogeners. Oral Presentation. Arctic Ecosystem Session at the annual Integrated Marine Biosphere Research Conference, Brest France, June 18, 2019.

Copeman L, et al. 2020. Divergent thermal effects on the over-winter survival, condition and lipid storage of juvenile age-0 and age-1 Arctic cod (*Boreogadus saida*). Poster Presentation. Alaska Marine Science Symposium, Anchorage Alaska, January 27-31, 2020.

Copeman L. 2021. The importance of marine lipids in warming Arctic food webs: tales of juvenile fish and crab. RACE_NOAA seminar series. (on-line) April 20th, 2021

De Robertis, A, Levine, R., Williams, K., Wilson, C. 2021 Modifying a pelagic trawl to better retain small Arctic Fishes. ICES Joint Workshop on Fishing Technology, Acoustics and Behavior. April, 2021 [Online]

Dickson, D. 2016 (on behalf of the Arctic IES PI's). Arctic integrated ecosystem research program; proposed late summer research surveys 2017 and 2019. Providers Conference, November 2016, Anchorage, AK

Farley, E.V., Jr. (Arctic IES PI's) 2016. Arctic integrated ecosystem research program; proposed late summer research surveys 2017 and 2019. Hub meeting in Kotzebue, AK, November 2016, Kotzebue, AK.

Farley, E.V., Jr., (Arctic IES PI's) 2016. Arctic integrated ecosystem research program; proposed late summer research surveys 2017 and 2019. Alaska Eskimo Whaling Commission, July 2016 and December 2016, Anchorage, AK

Farley, E.V., Jr., (Arctic IES PI's). 2016. Arctic integrated ecosystem research program; proposed late summer research surveys 2017 and 2019. Arctic Waterways Safety Committee, December 2016, Anchorage, AK.

Farley, E.V. Jr. (Arctic IES PI's) 2017. Arctic (Bering Sea and Chukchi Sea) integrated ecosystem overview. Hub meeting, February 2017, Nome, AK.

Farley, E.V. Jr. (Arctic IES PI's) 2017. Arctic (Bering Sea and Chukchi Sea) integrated ecosystem overview. Strait Science Presentation, February 2017, Nome, AK.

Farley, E.V. Jr. (Arctic IES PI's) 2017. Arctic (Bering Sea and Chukchi Sea) integrated ecosystem overview. Hub meeting, February 2017, Utquiagvik, AK.

Farley, E.V., Jr., (Arctic IES PI's) 2017. Arctic integrated ecosystem survey phase II. Poster at Alaska Marine Science Symposium, January 2017, Anchorage, AK

Farley, E.V., Jr., (Arctic IES PI's) 2017. Arctic integrated ecosystem research program; proposed late summer research surveys 2017 and 2019. Intergovernmental Consultative Committee Annual Meeting, September 2017, La Jolla, CA.

Farley, E.V., Jr., (Arctic IES PI's) 2018. Arctic integrated ecosystem survey phase II., 2017 summary and proposed 2019 survey. North Slope Borough, Fish and Game Management meeting, September 2018, Utqiagvik, AK.

Farley, E.V., Jr., (Arctic IERP PI's) 2020. The Arctic Integrated Ecosystem Research Program: Are we experiencing the future Arctic? AMSS, January 2020, Anchorage, AK.

Farley, E.V., Jr., (Arctic IERP PI's) 2020. Arctic IERP results. North Slope Subsistence Regional Advisory Council, November 2020, virtual.

Farley, E.V., Jr., 2020. Response of pink salmon to climate warming in the northern Bering Sea. Strait Science, November 2020, virtual.

Flores, A. 2017. Sailing to the Arctic. Strait Science, September 2017, Nome, AK.

Forster, C., B. Norcross, and F. Mueter. 2018. Assessing spatial patterns of Arctic Cod (*Boreogadus saida*) abundance and distribution in the Chukchi and Beaufort seas. ESSAS annual science meeting, June, 2018, Fairbanks, AK.

Kuletz, K, K. Cushing, E. Osnas, E. Labunski, A. Gall, and T. Morgan. 2018. Seabirds as indicators for the distributed biological observatory and other long-term marine monitoring programs. AMSS, January 2018, Anchorage, AK.

Kuletz, K., D. Cushing, E. Osnas, E. Labunski, A. Gall. 2019. Pacific Arctic seabird communities: a decade of change viewed through the lens of the Distributed Biological Observatory's at-sea surveys. American Ornithological Society Annual Meeting, June 24-28, 2019, Anchorage, Alaska.

Kuletz, K. 2020. Seabirds signal changes in the Pacific Arctic. AMSS, January 2020, Anchorage, AK.

Kuletz, K. 2021. Seabirds in a changing Arctic. Panel presentation in "Connecting Alaska's Marine and Coastal Biodiversity to the Circumploar Arctic. AMSS, January 2021, virtual.

Kuletz, KJ and L Yeates. 2021 The parallel adventures of short-tailed shearwaters and cross-hemispheric art project: from Australia to Alaska and back in the year of covid-19. Poster at the Alaska Marine Science Symposium, virtual, January 2021. A similar poster was presented at the Pacific Seabird Group annual meeting, February 2021.

Kuletz KJ, Cushing D, Labunski EL. 2021 Short-tailed Shearwater timing and movement though Alaska's seas, based on at-sea surveys 2007-2019. Oral presentation at Pacific Seabird Group annual meeting, virtual, February 2021.

Kuletz, KJ, 2021. Responding to warming waters: Seabirds at sea. Presentation (virtual) as part of the Strait Science Series, sponsored by Alaska Sea Grant and the University of Alaska, Fairbanks, Northwest Campus, Nome AK, February 11, 2021.

Kuletz, K., D. Cushing, F. Mueter, E. Osnas, D. Kimmel, E. Labunski, R. Levine, A. De Robertis. 2021 Peak ocean temperatures cap long term warming in the eastern Pacific Arctic and slams seabirds. World Seabird Conference (virtual), Symposium on "Mechanisms by which extreme heat anomalies impact seabirds", 5 October 2021.

Kuletz, K.J. 2021 Seabirds and shorebirds of the North Pacific: Class No. 2: Seabird responses to changing conditions. *OLÉ!* Course (Opportunity for Lifelong Education, University of Alaska, Anchorage), 2 November 2021 (virtual).

Laurel, B. and L.A., Copeman. 2018. Size- and temperature-dependent overwintering success in age-0 juvenile polar cod (*Boreogadus saida*) and walleye pollock (*Gadus chalcogrammus*). ESSAS annual science meeting, June, 2018, Fairbanks, AK.

Levine, R. 2017. Overview of the acoustic component of the Arctic IES. University of Washington, November 2017, Seattle, WA.

Levine, R. 2018. Preliminary results of the 2017 acoustic-trawl survey, and planned mooring and saildrone operations. AMSS (poster), January, 2018, Anchorage, AK.

Levine, R. 2018. Results of the 2017 Arctic IES survey and future field work. University of Washington Biological Oceanography Seminar Series, January 2018, Seattle, WA.

Levine, R. 2020. Summer 2018 repeat autonomous vehicle surveys indicate age-0 Arctic cod are largely retained over the Chukchi Shelf. Ocean Sciences Meeting (Poster), February 2020, online.

Levine, R. 2020. Summer 2018 repeat autonomous vehicle surveys indicate age-0 Arctic cod are largely retained over the Chukchi Shelf. AMSS (Poster), January 2020, Anchorage, AK

Levine, R., A. De Robertis, C. Wilson, E. Farley, and D. Grünbaum. 2018. Field Studies to Investigate the Fate of Juvenile Arctic cod in the U.S. Continental Shelf Region of the Chukchi Sea. ESSAS annual science meeting, June, 2018, Fairbanks, AK.

Levine, R. 2020. Preliminary results of a 2019 acoustic-trawl survey in the U.S. Continental Region of the Chukchi Sea.. AMSS (Poster), January 2020, Anchorage, AK.

Levine, R. 2021. Go with the flow: Climate-driven transition of the pelagic fish community in the Chukchi Sea. University of Washington Biological Oceanography Spring Seminar Series. May 2021.

Levine, R. 2021 A multiplatform investigation of pelagic fishes in a changing Pacific Arctic. NOAA Northwest Fisheries Science Center Monster Seminar Jam 2021 Spring Seminar Series. May 2021.

Levine, R., De Robertis, A., Grünbaum, D., Wilson, C., Farley, E., Mordy, C., Stabeno, P. 2021 A multiplatform acoustic-based approach to classifying abundance, distribution, and transport of age-0 gadids on the Chukchi shelf. ICES Working Group on Fisheries Acoustics, Science and Technology. April 2021; virtual.

Logerwell, E. 2017. Arctic integrated ecosystem research program. Strait Science, August 2017, Nome, AK.

Logerwell, E. 2018. Distribution of fish and invertebrate species from the 2017 Arctic IES. Alaska Marine Science Symposium (poster), January 2018, Anchorage, AK

Logerwell, E., M. Busby, K. Mier, H. Tabisola, and J. Duffy-Anderson. 2018. The effect of oceanographic variability on the distribution of Arctic cod of the Northern Bering and Chukchi Seas. ESSAS annual science meeting, June, 2018, Fairbanks, AK

Logerwell, E., Wang, M. 2020. Winners and Losers in a Warming Arctic: Potential Habitat Gain and Loss for Epibenthic Invertebrates of the Chukchi and Bering Seas. Alaska Marine Science Symposium, January 2020, Anchorage, AK.

Logerwell, E. 2020. Winners and Losers in a warming Arctic: Potential Habitat Gain and Loss for Epibenthic invertebrates of the Chukchi and Bering seas. Ocean Sciences Meeting, February 2020, Virtual.

Marsh, J. and F. Mueter. 2018. Influences of temperature, predators and competitors on the southern distribution of Arctic cod (*Boreogadus saida*). ESSAS annual science meeting, June, 2018, Fairbanks, AK.

Mueter, F. and Flores, H. 2018. Current and future research on *Boreogadus saida.* ESSAS annual science meeting, June, 2018, Fairbanks, AK.

Vestfals, C., F.J. Mueter, K.S. Hedstrom, B.J. Laurel, C.M. Petrik, J. Duffy-Anderson, S.L. Danielson, A. De Robertis, and E.N. Curchitser. 2018 Gender specific reproductive strategies of an Arctic key species (*Boreogadus saida*) and implications of climate change. ESSAS annual science meeting, June, 2018, Fairbanks, AK.

Wayner, H. 2017. A summer at sea. Strait Science, August 2017, Nome, AK.

Weems, J., G. Eckert, F. Mueter (2016) Early life history ecology of larval and juvenile blue king crab in the U.S. Subarctic. North Pacific Marine Science Organization Annual Meeting (PICES) Northern Bering Sea Workshop. November. San Diego, California. Oral Presentation

Weems, J., F. Mueter, A. I. Pinchuk (2018) Three sides of the same coin: Distribution of three stages of planktonic crab larvae in the northeast Bering Sea and Chukchi Sea in 2012. AMSS. January. Anchorage, Alaska. Poster Presentation

Weems, J., and F. Mueter. 2018. Stage-specific distribution of crab larvae, including snow and blue king crab from the 2012 Arctic Eis survey. AMSS (poster, January, 2018, Anchorage, AK

Weems, J., F. Mueter, E. Farley, G. Eckert, W. C. Long (2019) Arctic IES Program research update and insights on king crab recruitment. Bering Strait Science Series, UAF Northwest Campus. September. Nome, Alaska. Oral Presentation

Weems, J., W. C. Long, F. Mueter, A. I. Pinchuk, G. L. Eckert (2020) Alaska blue king crab: Fishing, habitat, and climate induced vice-grip on recruitment of subarctic Paralithodes platypus. Alaska Marine Science Symposium (AMSS). January. Anchorage, Alaska. Oral Presentation

Collaborations

BOEM Arctic Integrated Ecosystem Survey (Arctic IES), Phase II – PI's Mueter, Kuletz, Farley, Ladd et al. (Alaska Fisheries Science Center (NOAA), M17PG00007; University of Alaska Fairbanks (UAF), M17AC00016; US Fish and Wildlife Service (USFWS), M17PG00017. $2,200,000). Support ship contract costs, data analysis and seabird observations/analyses for the Arctic Integrated Ecosystem Survey.

BOEM and Coastal Impact Assistance Program (CIAP) *Arctic Ecosystem Integrated Survey (EIS) Phase 1.* PIs - Farley, Mueter, Eisner et al., (NOAA-BOEM IAA-AK-11-08b, 1/1/12-5/31/16, $3,000,000). Summer surveys were conducted in the NBS and CS in 2012 and 2013. Observations included pelagic fish and groundfish, zooplankton, oceanography, and total and size fraction Chl-a. We will relate satellite derived estimates of phytoplankton community composition (outcome of our proposal) to *in-situ* total and size-fraction Chl-a. The validated satellite data can be compared to distributions of zooplankton and fish in this region.

DBO. The Distributed Biological Observatory (DBO) is a multidisciplinary Arctic ocean sampling program supported by the NOAA's Arctic Research Program (ARP). ARP supports an annual scientific cruise to the Pacific Arctic region during which U.S. scientists take a wide range of physical, chemical, and biological samplings. The DBO has designated eight "hot spots" areas across the Bering, Chukchi, and Beaufort seas where multidisciplinary sampling is focused. We have partnered with the DBO Program to collect a suite of physical and biological measurements in the Chukchi Sea over multiple years and to make these observations available to the AIERP Program. The DBO is a collaboration between multiple U.S. federal agencies and academic institutions as well as from other Arctic nations.

Harmful Algal Blooms. PIs Duffy-Anderson, Stabeno, Eisner, and Kimmel collaborated with WHOI researcher Don Anderson and NWFSC researcher Kathi Lefebre to collect samples for work on the detection of high levels of paralytic shellfish toxins in Northern Alaskan food webs.

International Partners

RUSSIA. PIs Eisner, Ladd, Duffy-Anderson collaborated with Russian oceanographers, Yury Zuenko and Eugene Basyuk at the Pacific Branch of Russian Research Institute of Fisheries and Oceanography (TINRO) to compile surface and bottom water temperature data and pollock abundance data (juveniles and adults) from the eastern and western Bering Sea. This effort resulted in a joint publication (see above) with communication ongoing.

Intergovernmental Consultation Committee: PI's Farley and Melnikov (TINRO Center Deputy Director) collaborated through the ICC to place Russian scientists on 2017 and 2019 surveys to compile on board fish diets, zooplankton biomass from a Juday net, and on board fish processing.

ITAE: To better study arctic marine ecosystems and the rapid changes that are occurring, we are collaborating with the Innovative Technology for Arctic Exploration (ITAE) program as it works to develop innovative technologies, including sensors and platforms, to meet the scientific demand in these regions. The mission of the ITAE program is to conceptualize and build effective research equipment for the assessment of the Arctic environment and ecosystem with the operation of high-resolution sensors on autonomous platforms near sea ice. The dynamic and fine-scale nature of these regions requires responsive, high-resolution data collection over large areas in real time — a logistical challenge ideally suited to fast, mobile autonomous platforms rather than traditional ship-based operations. Existing autonomous platforms are both small and slow, limiting the observational capacity, responsiveness, and deployment capabilities. ITAE is a collaborative research effort by University of Washington (JISAO) and NOAA engineers and scientists at the Pacific Marine Environmental Lab (PMEL).

National Oceanographic Partnership Program (NOPP). *Expanding exploration and using innovative technologies to assess the rapidly changing Bering and Chukchi Seas.* PIs - Stabeno, Mordy, Lomas, Eisner, Nielsen, et al. The US Arctic ecosystems are undergoing dramatic, unprecedented changes in response to ocean warming and declines in sea ice. In addition to the physical changes, biological shifts across all trophic levels have been observed (e.g., phytoplankton community composition and bloom timing; zooplankton dynamics; spatial shifts in fish distributions). This project expands ecosystem observations in NBS and southern CS using traditional and new technologies. Emergent technologies include profiling platforms, speciation techniques ('omics), *in-situ* visualization, and unmanned vehicles. This project will create new Ecosystem Observatories in the US Arctic.

NOAA Joint Polar Satellite System (JPSS) funded proposal: Satellite analysis of shifts in phytoplankton community composition and energy flow in the new Arctic. PIs: Eisner, Lange (Blue Marble Space Institute of Science), Lomas, Mordy, Nielsen, Stabeno; Collaborators Gann (AFSC), Lefebvre (NWFSC, HABs), Robinson (UC Santa Cruz, CoastWatch/PolarWatch), Wilson (SWFSC, CoastWatch/PolarWatch). 6/1/21-5/31/24, $515,966. The overall goals of this project are to: 1) analyze the variability of phytoplankton community size structure based on spectral slopes of absorption, backscattering, remote-sensing reflectance ($R_{rs}(\lambda)$), and empirical chlorophyll-a (Chl-a) -based algorithms from JPSS satellite data across time and space; 2) modify existing ocean color algorithms to exploit the unique $R_{rs}(\lambda)$ properties of *Synechococcus* in order to determine changes in this picoplankton group; 3) estimate diatom abundances from Chl-a-specific absorption; and 4) explore correlative methods to assess the probability of occurrence of harmful algae such as *Pseudo-nitzschia* spp. and *Alexandrium* spp. using Sentinel 3-A-OLCI satellite products to improve HAB predictions in the North Bering Sea (NBS) and Chukchi Sea (CS). Data from Arctic IERP will be used for ground-truthing satellite data.

NSF COLLABORATIVE RESEARCH: *What controls the transfer of diatom organic matter to age-0 pollock prey in the Bering Sea ecosystem?* PI - Lomas et al., (#OPP-1603460, 11/2016-10/2019; $108,908). This project explored both physiological responses of polar diatoms in culture, and the ecology (primary production and phytoplankton community) of phytoplankton in the BS and CS. The results from this and other collaborative projects listed below suggest that not only will the nutritional value of diatoms decrease as the BS and CS warm, but also the phytoplankton community, especially in the summer/fall period, will shift to small picoplankton (e.g., *Synechococcus*).

Ecosystems and Fisheries-Oceanography Coordinated Investigations (EcoFOCI) Program and Recruitment Process Alliance (RPA) at NOAA PMEL/AFSC. PIs - Stabeno, Duffy-Anderson, Eisner, Nielsen, Mordy, Farley et al. This is an integrated long-term base-funded NOAA program that conducts research in the US Arctic. It maintains long- term ecosystem moorings in the BS (since 1995) and CS (since 2010) and spends >100 days at sea each year. Field observations include: temperature, salinity, oxygen, currents, nutrients, phytoplankton (size-fractionated Chl-a, taxa, productivity), zooplankton/ichthyoplankton, pelagic fish and groundfish. EcoFOCI's goal is to improve understanding of ecosystem dynamics and apply that understanding to fisheries management. Field, laboratory and modeling studies are integrated to reach this goal. On average 19 (11-32) articles are published per year on all aspects of these ecosystems. Collaborators include: Pacific Marine Environmental Lab (PMEL)'s *Innovative Technology for Arctic Exploration* (ITAE, PIs - Mordy et al., $1.3M /year) which supports new technology to improve ocean observations; *AOOS* (PI - Stabeno, 2020-2022, $100K to EcoFOCI) which provides support to improve observations on northern BS (NBS) mooring observatory; and *NOAA's Arctic Research Program* (PIs - Stabeno, Mordy et al., ~$280K /year to EcoFOCI) which supports moorings and an ecosystem cruise (in collaboration with EcoFOCI) each year to the NBS and CS. Data collected under this consortium contributes to the Distributed Biological Observatory - an international effort to conduct opportunistic sampling at biological hotspots in the US Arctic.

North Pacific Research Board (NPRB) and Bureau of Ocean Energy Management (BOEM). Recent awards relevant to this project include the following:

Evaluating historical and future climate-driven changes to Pacific cod spawning habitat in the Bering Sea PIs - Rogers, Mordy, Stabeno, et al. (NPRB #2003, 7/2020 - 6/2023, $599,719). This project focuses on exploring the seasonal evolution of ocean temperature across the BS and its impact on spawning of Pacific cod. Specifics goals are to expand observations of seasonal oceanographic conditions in the eastern BS through deployment of an array of low-cost sensors to monitor bottom temperatures; use these data to validate and assess Regional Ocean Model System (ROMS) error and bias with respect to temperature dynamics; formally assimilate new data into ROMS; use ROMS and existing, experimentally-derived relationships between temperature and Pacific cod spawning success to characterize the extent, timing, and distribution of suitable spawning habitat; project the spatial distribution and timing of suitable spawning habitat under future climate scenarios; and introduce this information into the management process for Pacific cod. Changes in phytoplankton species and community structure, which will be directly assessed in the proposed research, impact ecosystem productivity with cascading effects on fish larval abundance and survival and spawning success.

Monitoring export fluxes to detect seasonal and interannual changes in the pelagic ecosystem of the St. Lawrence Island Polynya Region PIs - Stabeno, Mordy et al., (NPRB #1914, 2020 - 2024, 342,087). Climate change is rapidly affecting the NBS including the St. Lawrence Island Polynya (SLIP) where a large decline in sea-ice cover was observed in 2018, with potentially important consequences for the bird and marine mammal populations of the region. This project will deploy a sequential sediment trap to measure the magnitude and composition of the organic matter supplied to the benthic communities in the region. Sediment trap samples will provide continuous biological samples that will allow the monitoring of several aspects of the marine ecosystem from phytoplankton and zooplankton species to carbon supply to the benthos. This project will provide critical *in-situ* data for the proposed research, and addresses a pressing need for the long-term monitoring of the BS marine ecosystem to improve our ability to forecast and respond to the effects of climate change and provide deliverables to policy-makers.

PICES WG44: NBS and Chukchi IEA (Logerwell chair). We are collaborating with PICES WG44 on the Northern Bering-Chukchi Sea region to provide detailed assessment of the Pacific Arctic gateway, as well as detailed information that will inform understanding of connectivity of climate and ocean processes, species movements, shelf foodweb dynamics, fishing, trade, subsistence and food security, and human activities. The Northern Bering Sea-Chukchi Sea (NBS-CS) region is experiencing unprecedented ocean warming and loss of sea ice as a result of climate change. Seasonal sea ice declines and warming temperatures have been more prominent in the northern Bering and Chukchi seas as almost all other portions of the Arctic.

Synopsis

Why We Did it:

To understand how reductions in Arctic sea ice and the associated changes in the physical environment influence the flow of energy through the ecosystem in the Chukchi Sea.

What We Did

Researchers conducted Integrated Ecosystem Surveys (Arctic IES) aboard the R/V Ocean Starr (Figure 1) in late summer and early fall of 2017 and 2019. Fish observations from collaborative ship-based surveys were incorporated to provide a broader perspective (ASGARD). In addition to the vessel-based surveys, sub-surface moored sensors were deployed to gather biophysical information continuously from September 2016 to September 2019 and autonomous platforms were used to make observations to augment the ship-based surveys (e.g., gliders, saildrones, air-deployed profilers).

What We Learned

Subarctic walleye pollock were found in large numbers within the Chukchi Sea during our survey years, while Arctic cod were distributed further north than in previous survey years (2005, 2012, 2013).

Acoustic estimates of age-0 gadid abundance indicated that Age-0 walleye pollock, which were historically scarce in the region, were the most abundant species in many areas in 2017 and 2019. Small pollock and Arctic cod are difficult to distinguish in the field, and genetic techniques were used to identify age-0 gadids during these and previous surveys. This revealed that the species composition in the eastern Chukchi Sea shelf has shifted dramatically in recent years with the arrival of subarctic species (i.e. walleye pollock) in the region..

Warmer sea temperatures impacted fish fat storage and are predicted to decrease biodiversity

Juvenile Arctic cod at the end of the warm (2017) summer season had only half the fat storage and lower overall energy content than those collected during colder years (2012/2013). Similarly, saffron cod, capelin and Pacific sand lance had slightly lower energy content in warmer years. Reduced body condition of fish in the fall of warm years may reduce overwinter survival of fish. In addition, rising bottom temperatures in the Bering and Chukchi seas is predicted to reduce benthic invertebrate species diversity through loss of suitable temperature habitat. Taxa most impacted include gastropods and mussels, prey for adult gadids and other benthic feeders such as Pacific walrus. The taxa least impacted werebasketstars.

Warmer sea temperatures in the Chukchi Sea may improve overwinter survival of subarctic gadids.

Age-1 Pacific cod were observed in the western Chukchi Sea in 2018 and 2019, indicating possible overwinter survival of age-0 fish, although there was little evidence that they survive and/or remain in the Chukchi Sea to age-2. Adult Pacific cod were also observed in the Chukchi Sea during 2018 and 2019. Although densities in the western Chukchi Sea were very low compared to the Bering Sea, the adults are the first known (to us) in the Chukchi Sea.

Transport through the Bering Strait influences summer fish abundance and juvenile salmon habitat in the Chukchi Sea.

Observations from moorings, autonomous vehicles, and transport models indicate that the abundance of pelagic fish over the Chukchi shelf is tightly coupled to ocean current transport. Pelagic fish abundance is highly variable over the course of a year. Very few fish are present in winter. The abundance of pelagic fishes increases dramatically in summer and fall as they are advected to the area from the south, and are

ultimately transported northwards by fall. Increased transport through the Bering Strait is connected with improved early marine growth rate potential (a measure of habitat quality) for juvenile Chum salmon in the southern Chukchi Sea.

A biophysical transport model suggests that Arctic cod spawned in the northern Chukchi Sea may be an important source of larvae for the Beaufort Sea and Arctic Basin, while observed larval aggregations in the Chukchi Sea likely originated in the northern Bering and southern Chukchi seas.

Estimated hatch dates for Arctic cod in the northern Bering, Chukchi, and Beaufort seas ranged from November to July with peak hatching occurring from February to May. There was clear separation of hatch dates between Arctic cod caught in the spring and summer, suggesting different origins or strong size-dependent mortality.

Why It Matters

Unprecedented warming observed during the course of the Arctic IERP program may offer a window into the future Arctic (Figure 2). The biological indicators reported here suggest that increased warming could alter ecosystem structure and function with as yet unknown consequences for the people that depend on marine resources in the region.

Fig. 1 Chartered survey vessel, R/V Ocean Starr in Nome Alaska. Photo courtesy of Cathleen Vestfals

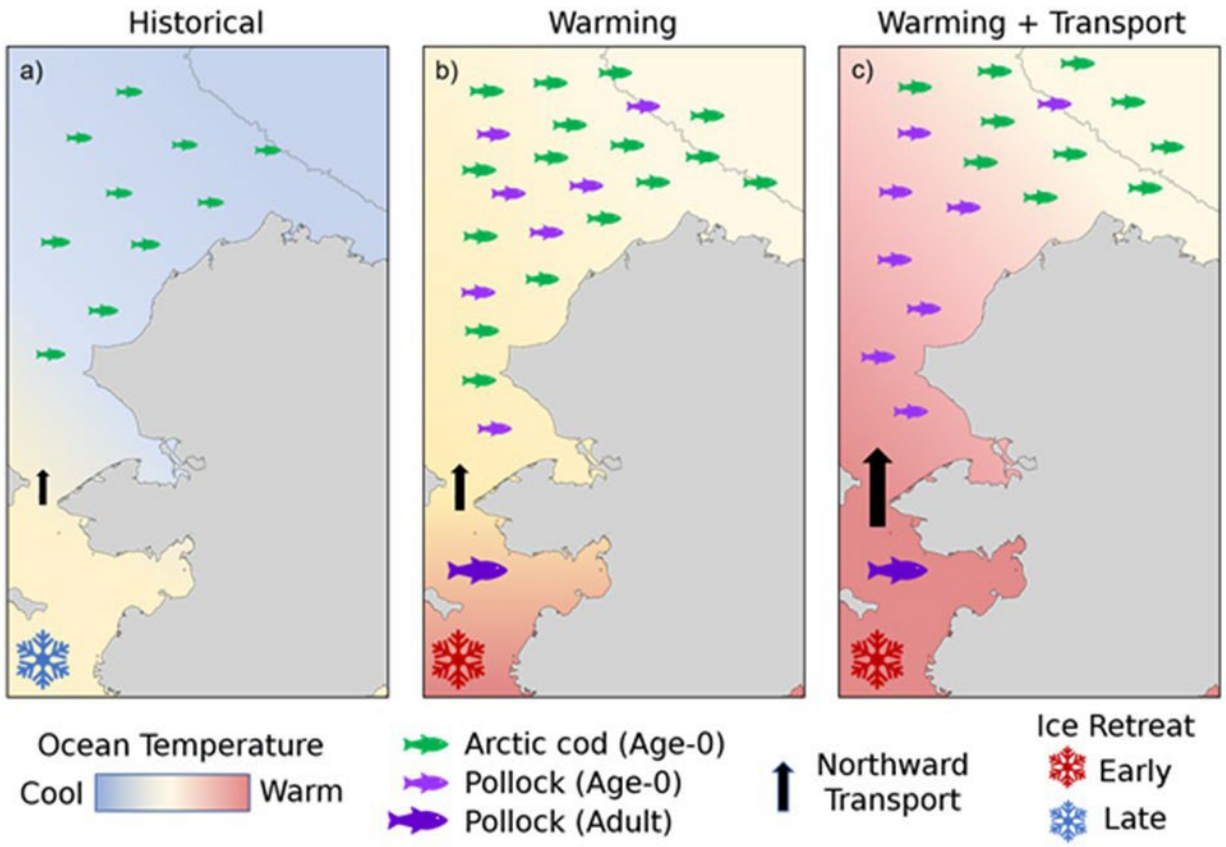

Fig. 2. Hypothesized scenarios based on observations of the Chukchi Sea gadid community. (a) Under historical conditions of later ice retreat, Arctic cod are observed in intermediate and cool waters across the Chukchi Shelf. (b) With increased warming and early ice retreat, age-0 Arctic cod increase in abundance and size across as a result of increasing temperatures. Increased presence of adult walleye pollock in the northern Bering Sea results in the transport of age-0 pollock into the Chukchi, where conditions are favorable for both gadid species. (c) With increased transport of warmer waters from the Bering Sea, Arctic cod are displaced further north along with the intermediate temperature waters. Age-0 pollock from the northern Bering Sea are transported with the warmer waters and become the dominant gadid in the southern portion of the shelf. The 1000-m depth contour is shown to indicate the Chukchi shelf break. (Levine et al. in preparation).

Datasets

Dataset	Collection date(s)	Storage format	To be submitted	Status
Fish lipid composition (Arctic cod and saffron cod)	Fall cruise 2017	Excel, to be converted to CSV	winter 2018	On Schedule
Fish fatty acid composition (Arctic cod and saffron cod)	Fall cruise 2017	Excel, to be converted to CSV	winter 2018	On Schedule
Fish lipid composition (Arctic cod and saffron cod)	Fall cruise 2019	Excel, to be converted to CSV	winter 2020	On Schedule
Fish fatty acid composition (Arctic cod and saffron cod)	Fall cruise 2019	Excel, to be converted to CSV	winter 2020	On Schedule
Fish condition	Fall cruise 2017	Access for Conversion to CSV	winter 2018	On Schedule
Fish condition	Fall cruise 2019	Access for conversion to CSV	winter 2020	On Schedule
Primary productivity, chlorophyll a, particulate phosphate data from bottle samples	Fall cruise 2017	Excel/Access for conversion to CSV	December 2018	On Schedule
At-sea productivity experiments	Fall cruise 2017	Excel/Access for conversion to CSV	December 2018	On Schedule
Fatty acid analysis from filtered water	Fall cruise 2017	Excel/Access for Conversion to CSV	December 2018	On Schedule
Primary productivity, chlorophyll a, particulate phosphate data from bottle samples	Fall cruise 2019	Excel/Access for conversion to CSV	December 2020	On Schedule
At-sea productivity experiments	Fall cruise 2019	Excel/Access for conversion to CSV	December 2020	On Schedule
Fatty acid analysis from filtered water	Fall cruise 2019	Excel/Access for conversion to CSV	December 2020	On Schedule
Fish count, length, weight, and disposition.	Fall cruise 2017	Oracle db for conversion to CSV	March 2018	On Schedule (Delivered)
Fish count, length, weight, and disposition.	Fall cruise 2019	Oracle db for conversion to CSV	March 2020	On Schedule (Delivered)
CLAMS cruise & events log	Fall cruise 2017	Oracle db for conversion to CSV	March 2018	On Schedule (Delivered)
CLAMS cruise & events log	Fall cruise 2019	Oracle db for conversion to CSV	March 2020	On Schedule (Delivered)

Dataset	Collection date(s)	Storage format	To be submitted	Status
Acoustic Backscatter from echosounders (Raw and acoustic quantities)	Fall cruise 2017	Oracle db for conversion to CSV	Raw & acoustic quantities: October 2018; Biological densities: 2021	On Schedule (Acoustics Delivered)
Acoustic Backscatter from echosounders	Fall cruise 2019	Oracle db for conversion to CSV	Raw & acoustic quantities: October 2020; Biological densities: 2021	On Schedule (Acoustics Delivered)
Acoustic Backscatter from moorings	Recovered fall 2018	Oracle db for conversion to CSV	October 2019	On Schedule (Delivered)
Acoustic Backscatter from moorings	Recovered summer 2019	Oracle db for Conversion to CSV	October 2020	On Schedule (Delivered)
Fish genotype for Arctic cod	Fall cruise 2017	CSV files	winter 2018	On Schedule
Fish genotype for salmon	Fall cruise 2017	CSV files	winter 2018	On Schedule
Fish genotype for Arctic cod	Fall cruise 2019	CSV files	winter 2020	On Schedule
Fish genotype for salmon	Fall cruise 2019	CSV files	winter 2020	On Schedule
Allele summary tables/ appendices for genetic population assessment	2020	unknown	winter 2020	On Schedule
Marine bird observations	Spring cruise 2017	CSV file	May 2018	On Schedule
Marine bird density estimation (density value and summary graphic)	Spring cruise 2017	CSV file	October 2018	Delayed but completed May 2019
Marine mammal observations	Spring cruise 2017	JPG/PNG files	October 2018	On Schedule
Marine bird observations	Fall cruise 2017	CSV file	October 2018	On Schedule
Marine bird density estimation (density value and summary graphic)	Fall cruise 2017	CSV file	October 2018	On Schedule
Marine mammal observations	Fall cruise 2017	JPG/PNG files	October 2018	On Schedule
Marine bird observations	Spring cruise 2019	CSV file	May 2020	On Schedule
Marine bird density estimation (density value and summary graphic)	Spring cruise 2019	CSV file	May 2020	On Schedule
Marine mammal observations	Spring cruise 2019	JPG/PNG files	May 2020	On Schedule
Marine bird observations	Fall cruise 2019	CSV file	October 2020	On Schedule

Dataset	Collection date(s)	Storage format	To be submitted	Status
Marine bird density estimation (density value and summary graphic)	Fall cruise 2019	CSV file	October 2020	On Schedule
Marine mammal observations	Fall cruise 2019	JPG/PNG files	October 2020	On Schedule
Benthic fish and invertebrate weight and length data	Fall cruise 2017	Oracle (EcoDAT), to be converted to CSV	October 2018; final processed invert data: October 2019	On Schedule
Trawl specimen catch list	Fall cruise 2017	Oracle (EcoDAT), to be converted to CSV	October 2018	On Schedule
Beam trawl deployment data	Fall cruise 2017	Oracle (EcoDAT), to be converted to CSV	October 2018	On Schedule
Beam trawl catch photos	Fall cruise 2017	JPG/PNG files	October 2018	On Schedule
Benthic fish and invertebrate weight and length data	Fall cruise 2019	Oracle (EcoDAT), to be converted to CSV	October 2020; final processed invert data: 2021	On Schedule
Trawl specimen catch list	Fall cruise 2019	Oracle (EcoDAT), to be converted to CSV	October 2020	On Schedule
Beam trawl deployment data	Fall cruise 2019	Oracle (EcoDAT), to be converted to CSV	October 2020	On Schedule
Beam trawl catch photos	Fall cruise 2019	JPG/PNG files	October 2020	On Schedule
Parameter measurements taken from FlowCam images of phytoplankton	Fall cruise 2017	CSV file	October 2018	On Schedule
Parameter measurements taken from flowcytometer	Fall cruise 2017	CSV file	October 2018	On Schedule
Public library of subsetted FlowCam images	Fall cruise 2017	JPG/PNG files	October 2018	On Schedule
Time-series analysis outputs of satellite chl-a imagery	-	CSV file	May 2020	On Schedule
Microzooplankton abundance, biomass, grazing rates	Fall cruise 2017	CSV file	May 2020	On Schedule
Parameter measurements of bulk Particulate Organic Phosphorus	Fall cruise 2017	CSV file	May 2020	On Schedule
Microzooplankton abundance, biomass, grazing rates	Fall cruise 2019	CSV file	May 2020	On Schedule
Microzooplankton abundance, biomass, grazing rates	Fall cruise 2019	CSV file	May 2020	On Schedule
Parameter measurements taken from FlowCam images of phytoplankton	Fall cruise 2019	CSV file	October 2020	On Schedule

Dataset	Collection date(s)	Storage format	To be submitted	Status
Parameter measurements taken from flowcytometer	Fall cruise 2019	CSV file	October 2020	On Schedule
Public library of subsetted FlowCam images	Fall cruise 2019	JPG/PNG files	October 2020	On Schedule

Final Report

November 30, 2021

Revised June 2022

Project title: A93 - Arctic Integrated Ecosystem Survey, Phase II; Upper Trophic Level (UTL)

Principal Investigator(s): Ed Farley, Kristin Cieciel, Dan Cooper, Louise Copeman, Alex De Robertis, Jeff Guyon, Ron Heintz, Kathy Kuletz, Elizabeth Labunski, Robert Levine, Libby Logerwell, Franz Mueter, Johanna Vollenweider, Jared Weems, Sharon Wildes, and Chris Wilson

Table of Contents

Executive Summary

The Chukchi Sea is undergoing dramatic sea-ice reductions and temperature increases, but resultant biological and trophic responses are poorly understood. The overall goal of this Upper Trophic Level (UTL; A93) project is to better understand the mechanisms and processes that structure the ecosystem and influence the distribution, abundance, and life history of lower (phytoplankton, zooplankton) and upper trophic species (fishes, seabirds, mammals), and their potential vulnerability to the rapidly changing environment of marine ecosystems in the Arctic. The Pacific Arctic Region (PAR) is experiencing significant warming and extremes in seasonal sea ice extent and thickness. To better understand the impact of warming on the PAR ecosystem, we linked this proposal with the Lower Trophic Level proposal (LTL; A92) and completed integrated ecosystem surveys, laboratory processing of samples and experimental projects to assess fish energetics and growth, along with analyses of data to address the following overarching hypothesis:

Reductions in Arctic sea ice and the associated physical changes to the environment influence the flow of energy through the pelagic ecosystem in the Chukchi Sea. Specifically, we expect lasting changes in the seasonal composition, distribution and production of phytoplankton; in the distribution and standing stocks of large crustacean zooplankton that serve as the prey base for upper trophic level fishes and seabirds; in the assemblages, distributions, and abundances of larval and early juvenile fishes that influence the recruitment success of later life stages, and in the distribution and abundance of adult fishes.

This report details the results of the UTL program. We conducted comprehensive ecosystem surveys of Chukchi Sea physics, chemistry, biogeochemistry and biology using an integrated network of moored arrays, autonomous vehicles, shipboard surveys, and laboratory experiments.

Specific hypotheses addressed by the UTL project include:

H1: Cods in the Arctic - *Loss of sea ice and continued warming of sea temperatures during summer in the Chukchi Sea will restructure the food web, decreasing the amount of fat available to higher tropic level predators.*

H2: Cod habitat in the Arctic: *The northern Chukchi serves as a nursery area for young-of-the-year Arctic cod, supplying juveniles to other areas of the Arctic.*

H3: Salmon expansion into a warming Arctic: *Summer surface waters in the northeastern Bering Sea will continue to warm and be a source of heat advected to the Pacific Arctic Region, providing new marine habitat for juvenile salmon.*

H4: Seabird community structure and seabird-prey dynamics: *The current predominance of planktivorous seabirds in the Arctic may shift back towards piscivorous seabirds, if warming sea temperatures restructure the food web*.

Emerging results from the UTL component were combined with historical data to demonstrate that:

1. Genetic techniques used to identify age-0 gadids during the 2017 and 2019 surveys, revealed the species composition in the eastern Chukchi Sea shelf has shifted dramatically in recent years with the arrival of subarctic species (i.e. walleye Pollock) in the region.

2. Acoustic estimates of age-0 gadid abundance indicated that Age-0 walleye pollock, which were historically scarce in the region, were the most abundant species in many areas in 2017 and 2019.

3. Observations from moorings, autonomous vehicles, and transport models indicate that the abundance of pelagic fish over the Chukchi shelf is tightly coupled to transport. Pelagic fish abundance is highly variable over the course of a year. Very few fish are present in winter. The abundance of pelagic fishes increases dramatically in summer and fall as they are advected to the area from the south.

4. Age-1 Pacific cod were observed in the western Chukchi Sea in 2018 and 2019, indicating possible overwinter survival of age-0 fish, although there was little evidence that they survive and/or remain in the Chukchi Sea to age-2. Adult Pacific cod were also observed in the Chukchi Sea during 2018 and 2019. Although densities in the western Chukchi Sea were very low compared to the Bering Sea, the adults are the first known (to us) records from the Chukchi Sea.

5. Analyses on juvenile Pink salmon ecology revealed that much of the variability in survival for northern Bering Sea stocks occurs during early life-history stages and that juvenile abundance is an informative leading indicator of Pink salmon runs to this region.

6. Juvenile Arctic cod at the end of the warm (2017) summer season had only half the fat storage and lower overall energy content than those collected during colder years (2012/2013). Similarly, saffron cod, capelin and sand lance had slightly lower energy content in warmer years.

7. Juvenile Chum salmon took advantage of high growth rate potential (GRP) in the southern Chukchi Sea during 2007; however, GRP was lower overall in the southern Chukchi Sea than within the northern Bering Sea even during the more recent warm years.

8. Rising bottom temperatures in the Bering and Chukchi seas is predicted to reduce benthic invertebrate species diversity through loss of suitable temperature habitat. Taxa most impacted include gastropods and mussels, prey for adult gadids and other benthic feeders such as Pacific walrus. Taxa least impacted include basketstars.

9. Estimated hatch dates for Arctic cod in the northern Bering, Chukchi, and Beaufort seas ranged from November to July with peak hatching occurring from February to May. There was clear separation of hatch dates between spring and summer caught Arctic cod, suggesting different origins or strong size-dependent mortality.

10. A biophysical transport model suggests that polar cod spawned in the northern Chukchi Sea may be an important source of larvae for the Beaufort Sea and Arctic Basin, while observed larval aggregations in the Chukchi Sea likely originated in the northern Bering and southern Chukchi seas.

Preamble

The Arctic Integrated Ecosystem Research Program

The Arctic Integrated Ecosystem Research Program (Arctic IERP, 2016-2021) was motivated by the rapid changes occurring in the waters of the northern Bering and Chukchi Seas. While much research has been done in the region, many important questions remain. As a cohesive research endeavor, the Arctic IERP was designed to address a single, overarching question:

How will reductions in Arctic sea ice and the associated changes in the physical environmental influence the flow of energy through the ecosystem in the Chukchi Sea?

The report you are reading now is one of five final reports from the fieldwork phase of the Arctic IERP (a synthesis phase was initiated in 2022 after the completion of the Arctic IERP field-based projects). This preamble provides a brief overview of the Arctic IERP, both to place each final report in the broader context of the whole program, and to encourage readers to examine the other final reports to learn more about the research that was done. More detailed information about the Arctic IERP can be found at https://www.nprb.org/arctic-program.

The spatial domain of interest for the Arctic IERP extended across the Chukchi Sea Large Marine Ecosystem (LME) as redefined by the Arctic Council's Protection of the Arctic Marine Environment (PAME) working group, and the northern Bering Sea (north of 61.5° N) as it strongly influences dynamics in the Chukchi Sea from the upstream direction. The main focus has been on the greater Bering Strait region and the Chukchi Sea. The program included the Arctic Basin and Beaufort Sea insofar as processes in the Chukchi Sea are influenced by these adjacent areas.

Development of the Arctic IERP

Before any Arctic IERP research proposals were written, the NPRB administered an assessment program, the Pacific Marine Arctic Regional Synthesis (PACMARS; https://www.nprb.org/assets/uploads/files/Arctic/PacMARS_Final_Report_forweb.pdf), that applied $1.5M provided by Shell and ConocoPhillips to compile and synthesize existing information about the ecosystem and inform research priorities. This assessment included community meetings in 2013 in Savoonga, Gambell, Kotzebue, Nome, and Barrow (now Utqiaġvik), in which representatives from 17 communities between St. Lawrence Island in the Bering Sea and Barter Island in the Beaufort Sea participated. One major area of emphasis that emerged from these community meetings was concern about food security for the region's residents in light of the rapid environmental changes taking place. Results from the scientific assessment and input provided via the community meetings informed the creation of the Arctic IERP. The PACMARS report informed both the IERP Request for Proposals (https://www.nprb.org/arctic-program/request-for-proposals/) and the submitted proposals.

Following a proposal review process, the Arctic IERP formally began in 2016 with funding from the North Pacific Research Board (NPRB), the Collaborative Alaskan Arctic Studies Program (formerly the North Slope Borough/Shell Baseline Studies Program), the Bureau of Ocean Energy Management (BOEM), and the Office of Naval Research (ONR) Marine Mammals and Biology Program. Generous in-kind support was contributed by the National Oceanic and Atmospheric Administration (NOAA), the University of Alaska Fairbanks (UAF), the U.S. Fish & Wildlife Service (USFWS), and the National Science Foundation (NSF). This coordinated program was developed in cooperation with the Interagency Arctic Research Policy Committee (IARPC) and the U.S. Arctic Research Commission.

The Research

The Arctic Integrated Ecosystem Research Program (IERP) invested approximately $18.6 million in studying marine processes in the northern Bering and Chukchi Seas in 2017-2021, beginning in the summer of 2017. The research was divided into three main, complementary projects. The Arctic Shelf Growth, Advection, Respiration, and Deposition Rate Experiments (ASGARD) project carried out research in late spring and early summer of 2017 and 2018 aboard R/V Sikuliaq. The Arctic Integrated Ecosystem Survey (Arctic IES) conducted fieldwork aboard R/V Ocean Starr in late summer and early fall 2017 and 2019. In addition to the vessel-based surveys, sub-surface moored sensors were deployed to gather biophysical information continuously from September 2016 to September 2019 and autonomous platforms were brought to bear (e.g., gliders, saildrones, air-deployed profilers).

In addition to the vessel-based work, a team of Arctic residents and social scientists, including members from eight communities in the North Slope and Northwest Arctic Boroughs and the Bering Strait region, met several times during the project to assess and analyze Indigenous observations and experiences with various types of change occurring in the region from Savoonga to Utqiaġvik. This group also compiled an annotated bibliography of Traditional Knowledge or Indigenous Knowledge (available through the data portal described below), to help researchers from other components of the Arctic IERP find information relevant to their studies.

Prior to the commencement of fieldwork, meetings were held in the three hub communities of Nome, Kotzebue, and Utqiaġvik. Scientists from the Arctic IERP and NPRB staff met with community members from each region to discuss the research purpose and plans. Research plans were also shared and discussed at meetings of the Alaska Eskimo Whaling Commission (AEWC), the Indigenous Peoples Council for Marine Mammals (IPCoMM), and with the Tribal Councils of Gambell and Savoonga on St. Lawrence Island. One result of these meetings was a shift in timing of the ASGARD cruises from May until June as well as a shift in timing and survey regions for the Arctic IES cruises, to avoid conflicts with subsistence hunting activities during what is traditionally the time for walrus hunting. Another result was the creation of communication protocols to avoid conflicts by alerting coastal communities to the presence of research vessels and adjusting the ships' routes to avoid areas where hunting was taking place. These communication protocols included regular radio broadcasts and daily emails to community members throughout the research area.

Results from the research are published in a growing list of peer-reviewed journal articles, as well as cruise reports that provide contemporary accounts of the cruises, and many social media postings that are available through the NPRB website. Data are publicly available as described below.

Collaborations

The NPRB collaborated and coordinated with several other U.S. agencies and organizations that fund Arctic marine research. NPRB staff worked closely with the U.S. Interagency Arctic Research Policy Committee (IARPC) and the U.S. Arctic Research Commission. As the Arctic IERP was developed, the NPRB secured commitments for collaboration from 22 existing research projects that were detailed in Appendix A of the request for proposals, and made connections with new projects as they were funded.

International researchers also collaborated with the Arctic IERP via the Pacific Arctic Group (PAG), the North Pacific Marine Science Organization (PICES), and the Intergovernmental Consultative Committee (US/Russia - bilateral) as well as collaborations developed by individual investigators. PAG participants, including researchers from Canada, China, Japan, Korea, Russia, and the United States, have coordinated their cruise plans to sample standard stations in the Chukchi and Beaufort Seas termed the Distributed Biological Observatory (DBO). The Arctic IERP contributed to this effort. US-Russian data sharing initiatives were hosted in San Diego in 2016 and Vladivostok in 2017 to promote collaboration and

exchange and to facilitate collaboration and synthesis of data and trends of patterns observed in the US and Russian waters in the northern Bering and Chukchi seas (PICES Press, Volume 26, Issue 1). ICC collaborations and other connections also brought scientists from the Russian Federal Research Institute of Fisheries and Oceanography (VNIRO), the Russian Pacific Scientific Fisheries Research Center (TINRO), and Hokkaido University to the US to participate in the Arctic IES cruises and co-author results. This collaboration is expected to connect research interests within respective EEZs (Russia/US) of the Chukchi Sea.

COVID-19

While the fieldwork of the Arctic IERP was completed before the outbreak of COVID-19, the final meeting of researchers in November 2020 was changed from an in-person event to an online format. Other plans for in-person events, such as meetings in hub communities within the US Arctic region (Nome, Kotzebue, and Utqiaġvik), were cancelled. Laboratory work and some collaborations were postponed or cancelled due to COVID-related restrictions and concerns. The NPRB made supplemental funds available to assist researchers with unanticipated expenses due to the pandemic. The overall productivity of the Arctic IERP was likely not greatly reduced, due both to good fortune in the fieldwork being completed and to the collaborative relationships that had been built or strengthened during the program.

Data Portal

Axiom Data Science, Inc. provided data management support to the Arctic IERP throughout the field program. Axiom staff assisted the scientists in authoring metadata and publishing the datasets to public archives. The data collected by the Arctic IERP are publicly accessible at https://arctic-ierp.dataportal.nprb.org/.

General Introduction

Boreogadus saida, known as the polar cod or as the Arctic cod, is a fish of the cod family Gadidae. The General Introduction and Discussion refer to *B. saida* as the Arctic cod. Individual chapters within the final report may refer to *B. saida* as polar cod or Arctic cod.

Background

The Pacific Arctic Region (PAR) is experiencing significant warming and extremes in seasonal sea ice extent and thickness (Frey et al. 2014). Over the past decade, record summer sea ice minima (2007, 2011, 2012) have occurred and climate models predict that the southern Chukchi Sea will be sea ice free for 5 months (July to November) within a decade or two (Overland et al. 2014). The impact of loss of summer sea ice on the PAR ecosystem is not fully understood, but a longer period of open water during summer is expected to increase primary production (Arrigo and van Dijken 2011) and, in addition to potential transport of additional heat from southern seas, is expected to increase summer sea temperatures by 4 to 8°C by the end of the century (Mahlstein and Knutti 2011). These shifts to the PAR ecosystem are likely to have large impacts on the ecology of upper trophic level species (UTL, fishes, birds, and mammals; see Sigler et al. 2011). For instance, the community structure of some UTL already show evidence of changes in the Chukchi Sea, such as the shift from predominantly piscivorous seabirds to planktivorous seabirds in recent decades (Gall et al. 2017). Other ecosystem consequences of continued warming have been described for the Barents Sea and include changes in zooplankton community structure as well as shifts in species distributions and relative abundance (Hop and Gjosaeter 2013; Orlova et al. 2013; Fossheim et al. 2015).

Arctic fishes such as Arctic cod (*Boreogadus saida*) and saffron cod (*Eleginus gracilis*) are key components of the PAR food web (Lowry and Frost 1981, Welch et al. 1992) and contribute to supporting large numbers of seabirds (Matley et al. 2012) and marine mammals (Bradstreet et al. 1986; Holst et al. 2001) which migrate to the Arctic to take advantage of high seasonal production. Arctic cod are particularly abundant in the PAR (see Moore et al. (2014) and references therein) and along with snow crab and saffron cod, are recognized as potential target species for new fisheries in this region (Arctic Fishery Management Plan 2009). We expect continued loss of sea ice and continued warming in the PAR to restructure the food web, negatively impacting Arctic cod growth and survival (Laurel et al. 2015), an important prey for seabirds and marine mammals (Welch et al. 1992; Holst et al. 2001; Matley et al. 2012). For instance, age-0 Arctic cod have a low thermal tolerance (< 7°C) for growth and survival; whereas saffron cod have a much wider tolerance and are expected to thrive at higher temperatures (Laurel et al. 2015). Age-0 Arctic cod have 2.7 times more lipid per unit body mass than Age-0 saffron cod (Ron Heintz, personal communication). We therefore hypothesize (H1) that within two to three decades, the Chukchi Sea shelf will experience a reduction in lipid-rich prey (Arctic cod) with negative consequences to other fishes and post-breeding seabirds, similar to that experienced by walleye pollock (Heintz et al. 2013) and Pacific cod (Farley et al. 2014) in the southeastern Bering Sea during a recent warming event (see Coyle et al. 2011).

Arctic Ecosystem Integrated Surveys (Arctic EIS) during late summer and fall 2012 and 2013 found high densities of age-0 Arctic cod in the northern Chukchi Sea (Fig. 1), but relatively few age 1+ fish (De Robertis et al. 2016, Goddard et al. 2014) suggesting this region may be an important nursery ground to examine climate impacts on the ecology of these age-0 fish. The distributions of age-0 Arctic cod were largely confined to the northern region of the Chukchi Sea in both years. Within the northern region of the Chukchi Sea, age-0 Arctic cod were three times more abundant and their distribution extended farther south in 2013 than during 2012 (Fig. 1, De Robertis et al. 2016). This observation was consistent with interannual differences in ocean currents and plankton populations during this period. For example, the Alaska Coastal Current was weaker and there was more "Chukchi winter and ice melt water" on the northern shelf in summer 2013, which was associated with less zooplankton of Pacific origin and lower

Chl *a* concentrations and a shift to larger cell sizes in 2013 (Danielson et al. 2016, Pinchuk and Eisner 2016). Additionally, drifters placed in areas of high age-0 Arctic cod abundance were advected off the shelf in 2012 but not in 2013 (Danielson et al. 2016), indicating potential fish transport to different areas. Together, these observations suggest there is much to be learned regarding mechanisms of dispersal to other areas of the Arctic and associated population dynamics of this species in this region of the Arctic (H2).

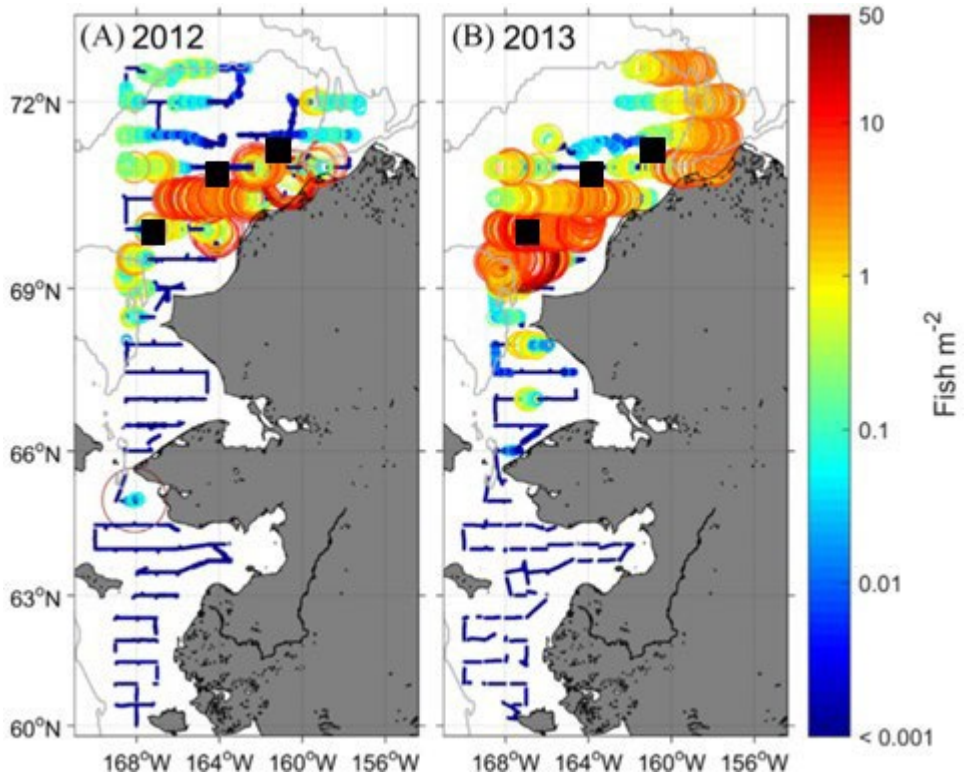

Figure 1. Density of Arctic cod blue to red represents increasing density) estimated by acoustic-trawl methods in A) 2012 and B) 2013. Fish are almost all age-0 except for an aggregation south of Bering Strait in 2012. The locations of the echosounder moorings deployed as part of the AIERP program are represented by the black squares.

In addition, we hypothesize that continued warming of surface temperatures will increase the likelihood of salmon production in the Arctic (H3). During 2007, summer sea temperatures in the Chukchi Sea were anomalously warm (Eisner et al. 2013). BASIS surveys conducted in the Arctic during 2007 documented relatively high abundances of juvenile pink and chum salmon in the Chukchi Sea (Moss et al. 2009). The abundant juvenile salmon returned as adults to the coastal regions of the PAR in relatively high numbers during 2008 (pink salmon) and 2009/10 (chum salmon) as reported by subsistence users in coastal communities (Carothers et al. 2013; Taquilik Hepa, personal communication). These events (anomalously warm summer sea temperatures, historic summer sea ice minima, and highly abundant juvenile pink and chum salmon in the Chukchi Sea) were all "surprises" in that they were large variations from predicted anthropogenic effects on temperatures and sea ice loss from climate models (Overland 2011). We hypothesize that these "surprises" will become the norm in the not too distant future and while the presence of maturing salmon in Arctic waters north of known salmon producing drainages likely reflects

straying and not colonization (Stephenson 2006), continued warming in marine, terrestrial and riverine environments may make it possible for these salmon to become permanently established in the Arctic.

It is also highly likely that climate warming in the Arctic will impact the abundance and distribution of seabird species. Seabird distribution is often influenced by oceanographic characteristics that promote productivity and concentrate prey (Piatt et al. 1991; Gall et al. 2013). In the Chukchi Sea, 'hotspots' of seabird abundance varied among foraging guilds (i.e., surface or diving foragers) and between summer (breeding season) and fall (post-breeding and migration), but were often associated with persistent topographic features such as shelf breaks and underwater canyons (Kuletz et al. 2015). During Arctic EIS, the distribution of planktivorous and piscivorous seabirds reflected the distribution of their prey at broad spatial scales (Arctic EIS reports: see https://web.sfos.uaf.edu/wordpress/arcticeis/). Gall et al. (2017) have also shown a decadal-scale shift from a predominantly piscivorous seabird community to one dominated by planktivores. If warming seas lead to longer ice-free conditions and generally higher productivity, this trend could continue (H4a). However, an alternative hypothesis (H4b) is that these conditions lead to smaller zooplankton and thus less suitable prey to support high densities of planktivorous seabirds, resulting in a shift back towards a predominantly piscivorous seabird community. Furthermore, lack of high-lipid prey (Arctic cod) near breeding colonies could result in low reproductive success and high nutritional stress (see Paredes et al. 2014).

Chapter Content

Each chapter addresses the objectives of the project in relation to the broader hypotheses.

Objective 1: *Quantify the distribution, abundance, and condition of demersal fishes and shellfishes*
Objective 2: *Quantify the distribution, abundance, and condition of pelagic marine fishes, in particular young-of-the-year Arctic gadids and other forage fishes*
Objective 3: *Combine results from previous Arctic surveys (Arctic EIS, Phase 1, BASIS) and planned surveys (Arctic IES Phase 2) to assess variability in pelagic and demersal fish ecology over time relative to ocean conditions.*
Objective 4: *Establish the relative abundance, size, and condition of juvenile salmonids that utilize the coastal regions of the PAR.*
Objective 5: *Further resolve early life history characteristics of Arctic cod and saffron cod and their behavior and connectivity between the Chukchi Sea and western Beaufort Sea.*
Objective 6: *Quantify the distribution, abundance, and prey association of seabirds in the PAR in relation to oceanographic conditions, prey abundance, and feeding guilds.*
Objective 7: *Develop spatially explicit bioenergetics models for Arctic cod and saffron cod as well as for juvenile pink and chum salmon and test the impact of warming summer temperatures on their growth and distribution*

Experimental Design and Methods

We conducted two 65-day integrated ecosystem surveys of the Chukchi and western Beaufort seas during August through early October in 2017 (Fig. 2; see 2017 Cruise Report) and 2019 (Fig. 3; see 2019 Cruise Report). The surveys followed the protocols developed for Arctic EIS (Arctic Ecosystem Integrated Survey 2014) and BASIS (Farley et al. 2005). Sampling was conducted on the R/V OCEAN STARR, capable of deploying bio/physical oceanographic gear (i.e. Arctic IES Phase II LTL), fish trawls (pelagic/surface) and demersal trawls (3-m plumb-staff beam trawl). Acoustic measurements along survey transects (gridded regions from east to west) along with modified Marinovich midwater trawl samples were used to estimate the distribution and abundance of midwater young-of-the-year cods and other forage fishes in the survey area. Surface trawls (Cantrawl 400/600) were used at nearshore stations to assess juvenile salmon. Demersal trawls (3-m plumb-staff beam trawl (PSBT)) were utilized along

gridded stations to assess older age classes of Arctic cod and crab. Oceanography and plankton sampling was coordinated with the Arctic Integrated Ecosystem Survey Phase II LTL team.

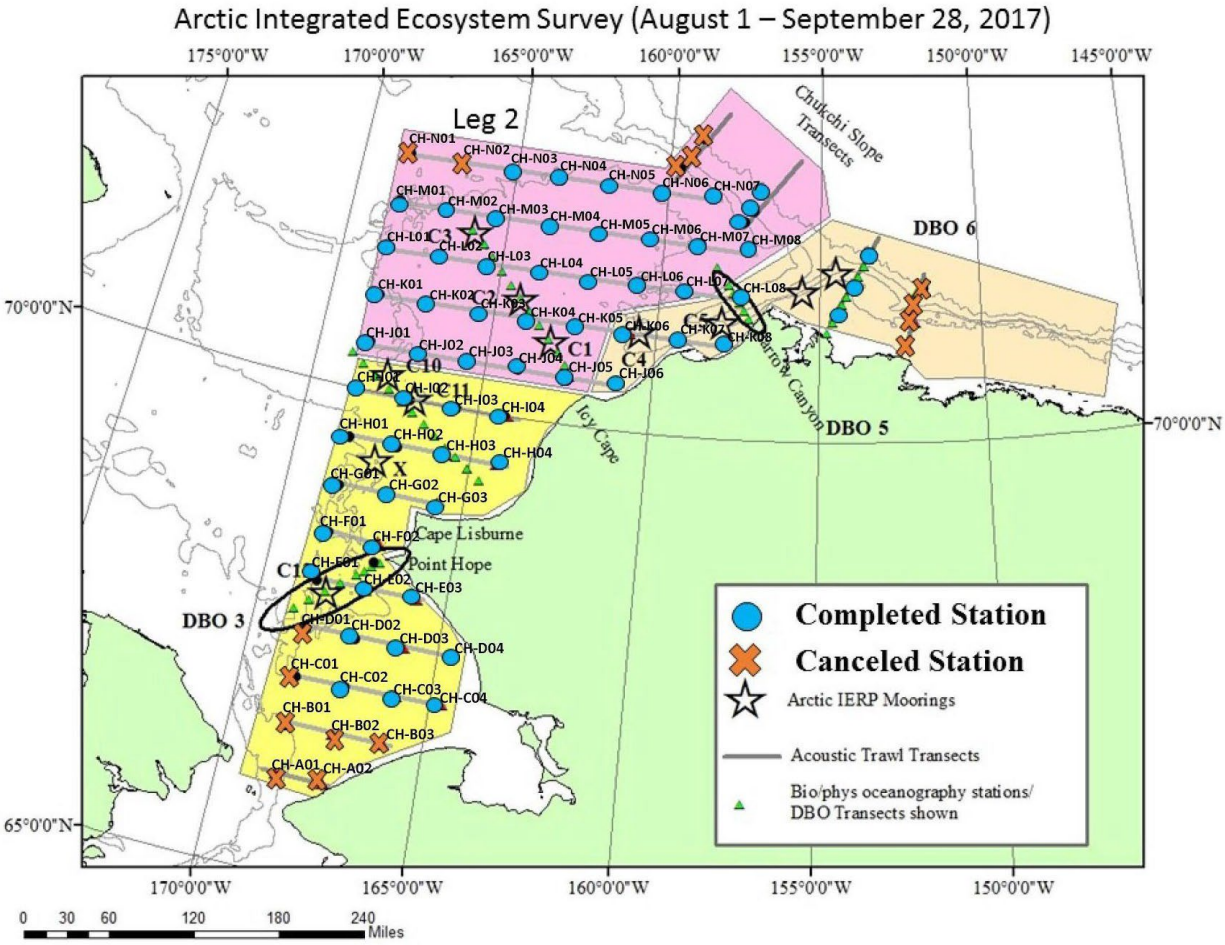

Figure 2. Research survey stations (blue dots -completed; orange crosses -canceled), acoustic transects (grey lines), oceanographic transects (green triangles), and moorings (black stars) for the Arctic Integrated Ecosystem Survey on board the Research Vessel, **OCEAN STARR** during August - October 2017.

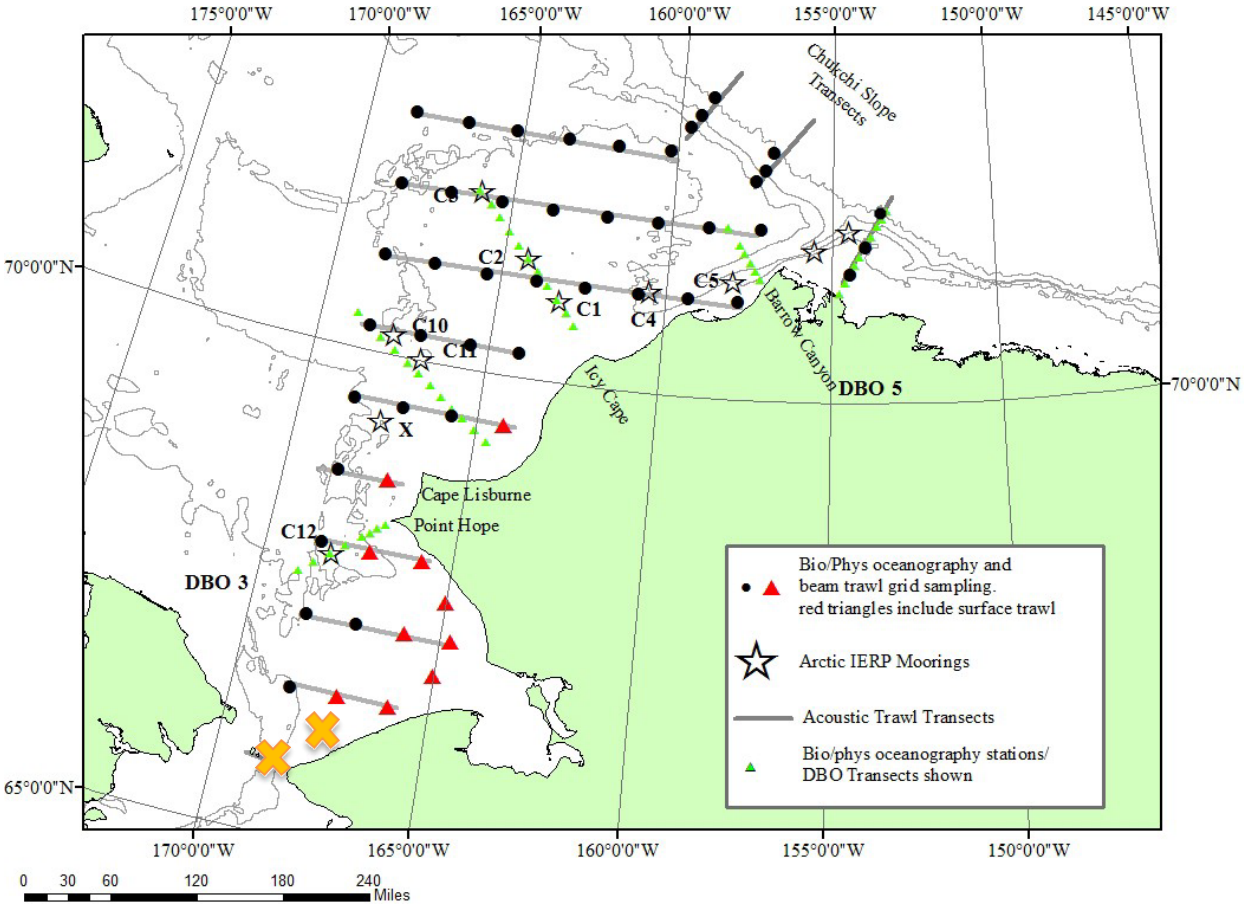

Figure 3. Research survey stations (black dots and red triangles), moorings (stars), oceanographic transects (green diamonds), and acoustic transects (grey lines) for the August 1 to October 4, 2019 Arctic Integrated Ecosystem Survey (Arctic IES) on board the Research Vessel, **OCEAN STARR**. Two stations were canceled (orange cross) due to weather.

General Discussion

The overall goal of this Upper Trophic Level (UTL) project was to better understand the mechanisms and processes that structure the ecosystem and influence the distribution, abundance, and life history of lower (phytoplankton, zooplankton) and upper trophic species (fishes, seabirds, mammals), and their potential vulnerability to rapidly changing marine Arctic environments. This approach was outlined in Moore et al. (2014) whereby fishes, seabirds, and mammals (UTL) respond to biological and physical changes in the ecosystem and thus serve as sentinels producing a continued record of ecosystem response to rapid climate change in the Pacific Arctic Region. The results of the UTL research were directly linked with results from the Lower Trophic Level (LTL) research that examined the climatological, physical, chemical and biological processes influencing the flow of energy from primary producers to zooplankton and ichthyoplankton in the Chukchi Sea and how a warming climate will influence these processes.

During current AIERP surveys, we tested how sampling gear types and survey designs affected the catchability and selectivity of different species and sizes to better understand sampling bias for small fishes and biodiversity measures (Chapters 7, 10 and 12). A correction to estimates of size and species selectivity of two survey trawls was determined necessary. The primary application of the new selectivity relationships was to estimate selectivity-corrected species and size distributions from trawl catches to decrease uncertainty in acoustic-trawl abundance estimates and allow for interannual comparisons. A case study to examine the power to detect changes in diversity of the demersal fish community found no apparent bias in diversity estimates for reduced survey designs, including those with spatially restricted sampling, but substantial increases in uncertainty was found as sample sizes decrease. In contrast, most of the sampling designs (such as Arctic IES) had substantial power for detecting changes in abundance of common species.

To address our overall goal and objectives, scientific analyses were structured around four major hypotheses, which are discussed separately below.

H1: Cods in the Arctic - *Loss of sea ice and continued warming of sea temperatures during summer in the Chukchi Sea will restructure the food web, decreasing the amount of fat and energy available to higher trophic level predators.*

Data from laboratory thermal experiments combined with evidence of declining lipid storage during warming ocean events in the central Chukchi Sea suggest that the southern and central Chukchi Sea regions are warming beyond the thermal limits of Arctic cod (Chapter 8 & 11). Age-0 cod survived the longest at -1 ℃ (~150 days) with reduced survival times measured with increasing temperatures up to the lowest survival duration at 5 ℃ (~90 days).

Increased ocean temperatures are affecting North Pacific fish both via direct thermal effects on their physiology as well as through indirect changes to available food quality and quantity (Chapter 11). During 2017 and 2019, the Chukchi Sea was nearly 4°C warmer than the previous 30-year average. The effect of anomalous warming on the energetic status of Arctic gadids was apparent. Juvenile Arctic cod at the end of the warm (2017) summer season had roughly half the fat storage and lower overall energy content than those collected during colder years (2012/2013). Similarly, saffron cod, capelin and sand lance had slightly lower energy content in warmer years. During 2017 both Arctic cod and saffron cod showed decreased lipid storage compared to fish from 2013 and 2012, respectively. This reduction in total lipid, triacylglycerols and diatom- and *Calanus*-sourced fatty acids was particularly significant in Arctic cod collected over the central Chukchi shelf in 2017.

This project documented a dramatic recent shift in the species composition of age-0 gadids, with age-0 pollock colonizing the Chukchi shelf in the most recent survey years (Chapters 4 and 6). Late summer surveys in the Chukchi Sea during 2012, 2013, 2017 and 2019 indicate that Age-0 Arctic cod were the

most abundant pelagic fish in all four survey years. However, age-0 walleye pollock (*Gadus chalcogrammus*) were present at high abundance throughout the Chukchi shelf in 2017 and 2019 and were the most abundant pelagic fishes in many areas (Chapter 6). In contrast, pollock were scarce and confined to the southern Chukchi Sea in the 2005, 2012 and 2013 surveys. Age-0 Arctic cod were substantially more abundant in 2017 than in any other year. This was possibly due to increased survivorship of larvae under warming conditions. However, given their poor body condition, these fish may have had poor over-winter survival following their first summer. Arctic cod and pollock were spatially separated in 2019, with Arctic cod primarily present in the northeastern portion of the survey area, which was characterized by cooler surface and bottom temperatures. The substantial increase in age-0 pollock in recent years suggests that environmental conditions now allow this species to extend its northern range into the central and southern Chukchi Sea, at least on a seasonal basis. The increased supply of juvenile pollock onto the Chukchi shelf may be linked to the high abundance of adult pollock in the northern Bering Sea in recent years, as well as increased flow through the Bering Strait. We hypothesize that the changes in abundance and species composition based on our 2012-2019 time series are tightly coupled to recent changes in temperature and the transport of Bering Sea waters onto the Chukchi shelf as reductions in sea ice and increases in warming and transport during 2017 and 2019 led to an increase in Pacific-origin waters on the Chukchi shelf in summer.

Survey data also indicated that Age-0 juvenile gadids showed interspecific differences in the spatial distribution of high condition individuals, with Arctic cod showing the highest lipid-based condition in the northern ice-associated region of Hanna Shoal (Chapter 11). In 2019, Arctic cod were only present in the northern Chukchi Sea but maintained a higher region-specific lipid storage than measured in 2017. Age-1 Pacific cod were observed in the western Chukchi Sea in 2018 and 2019, indicating possible overwinter survival of age-0 fish, although there was little evidence that they survive and/or remain in the Chukchi Sea to age-2 (Chapter 13). Low lipid storage of both walleye pollock and Pacific cod juveniles (Chapter 11 & 13) compared to published reports from the Gulf of Alaska and Bering Sea, make it implausible that 'boreal' gadids are successfully surviving winter on the Chukchi Shelf. If lower-fat fish such as walleye pollock or Pacific cod displace Arctic cod, Arctic predators will need to consume more fish to meet their energy requirements.

One of our objectives was to understand how warming sea temperatures and loss of seasonal sea ice may impact the epibenthic invertebrate community (Chapters 1 - 3). Survey data were used to determine "preferred" bottom temperatures for all taxa; modeled projections of bottom temperatures to mid-century and beyond in these regions were used to determine potential habitat gain or loss. The analysis indicated that by mid-century (2050) there will be a 50% decrease in suitable thermal habitat for many invertebrate species as the best thermal habitats contracted northward. By the end of the century (2100), projections indicate very little thermal habitat for almost all invertebrate species, except basketstars, assuming that most invertebrates cannot adapt to the pace of warming. Other data summaries and modeling suggest that larval snow crab are both advected from the northern Bering Sea and are also supplied by mature adults within the Chukchi or Beaufort seas. Warmer sea temperatures are accelerating either pelagic larval development or adult spawning and hatching times. However, sea temperature fluctuations (modeled) had limited influence on adolescent snow crab habitat suitability, whereas mature male snow crab were the most sensitive to changes in temperature.

H2: Cod habitat in the Arctic: *The northern Chukchi serves as a nursery area for young-of-the-year Arctic cod, supplying juveniles to other areas of the Arctic.*

Our project provided critical information on the early life history of Arctic cod through examination of their otoliths, modeling efforts, seasonal and time/space scale observations, and observations through late summer survey efforts. Trace elemental concentrations revealed at least two hatching populations based on significant differences in five of the eight trace elemental ratios from the eastern Beaufort Sea and

samples from the western regions (Chapter 19). Differences in trace elemental ratios indicated that Arctic cod from the eastern Beaufort Sea hatched in less saline waters than those from the western regions, possibly a result of hatching within the relatively fresh Mackenzie River plume (Chapter 20). Some samples from the northern Chukchi Sea had elevated levels of Zinc near the hatch mark, which could be due to hatching in Kotzebue Sound, where Zinc concentrations may be naturally elevated or as a result of mining. Estimated hatch dates ranged widely from November to July with peak hatching occurring from February through May depending on the region of capture (Chapter 19). We also identified a clear separation of hatch dates between spring- and summer-caught Arctic cod, suggesting different origins or strong size-dependent mortality. Finally, differences in hatch dates between pelagic and demersal juveniles support the settlement of older, larger juveniles to deeper shelf seafloor habitats in late summer.

A biophysical transport model coupled to a Pan-Arctic hydrodynamic ocean circulation model revealed potential spawning locations and regional connectivity between the northern Bering, Chukchi, and Beaufort Seas (Chapter 18). Analyses of simulated growth and transport models of newly hatched Arctic cod and saffron cod larvae identified species-specific differences in dispersal trajectories, despite similar hatch times and locations used in the model. Strong interannual variability in growth and dispersal was linked to several global-scale climate indices, suggesting that larval growth and transport may be sensitive to environmental perturbations. The model results show that Arctic cod spawned in the northern Chukchi Sea may be an important source of larvae for the Beaufort Sea and Arctic Basin, while observed larval aggregations in the Chukchi Sea likely originated in the northern Bering and southern Chukchi seas.

To determine seasonal movement and variability of age-0 gadids, bottom-moored multifrequency echosounders were deployed at three locations in the northeastern Chukchi Sea from 2017-2019 (Chapter 16). These observations indicate that the abundance and composition of the pelagic community on the Chukchi Sea shelf is highly variable over seasonal time scales. Fish abundance was very low in winter, increased in May, and reached peak abundance in late summer. Target strength and diel vertical migration of fishes increased in summer, indicating that this is a key period of growth for Arctic gadids. Tracking of acoustic targets indicates that age-0 gadids were displaced to the northeast, consistent with the dominant advection on the shelf. Fish speeds and headings were strongly correlated with local currents, providing evidence that these small age-0 fishes are primarily being passively transported and behavior plays a limited role in population distribution. Occasional reversals of fish transport were observed: when winds blow strongly towards the south, a reversal is seen in both current flow and fish tracks, with a higher proportion of fishes moving to the south and west.

Acoustic surveys with saildrone autonomous surface vehicles equipped with echosounders throughout summer 2018 provide further evidence that juvenile gadids are likely spawned in the south, are retained on the Chukchi shelf in summer, and are ultimately advected nortwards off the Chukchi shelf break in fall (Chapter 17). A subarea of the central Chukchi Sea was surveyed a total of four times in a single season; acoustic backscatter, a proxy for fish density, in this subarea increased by > 85% from late-July to mid-September. As summer progressed, fish developed more extensive diel vertical migrations and backscatter from individuals doubled. Both changes suggest that the observed increase in backscatter was driven primarily by increasing body size (i.e. individual growth) rather than changes in abundance. Across the survey area, backscatter was highest in regions with sea surface temperatures of 6-8 C, and lowest in areas influenced by recent ice melt. Particle tracking simulations indicated age-0 gadids were likely retained over the Chukchi shelf by extended periods of wind-driven southward flow during the survey period before strong northward flow in late fall transported them to the north. These findings suggest that in summer 2018, age-0 gadids were advected northward to the Chukchi shelf from the northern Bering Sea, where they were retained during a period of growth until late fall before being advected farther north toward the Chukchi and Beaufort shelf breaks.

Pelagic habitat requirements of Arctic larval fishes (including Arctic cod) and the effects of interannual variability of ocean conditions on their distribution was also investigated (Chapter 5). There was no significant difference in larval fish distribution among the two years examined (2012 and 2013), despite marked changes in annual water mass characteristics. In both years, larval Arctic cod were found in cold, high salinity water masses that contained higher biomass of large copepods. These large copepods are high in fat content (Chapter 9) providing high quality prey to larval Arctic cod and other larval fishes in the Chukchi Sea. In addition, a model for growth rate potential of Arctic cod indicated that temperature and food availability conferred by specific water masses was conducive to their growth (Chapter 23).

H3: Salmon expansion into a warming Arctic: *Summer surface waters in the northeastern Bering Sea will continue to warm and be a source of heat advected to the Pacific Arctic Region, providing new marine habitat for juvenile salmon.*

A multi-disciplinary research survey within the northern Bering Sea (NBS) has supported annual sampling (2002 to present) of the inner domain (bottom depths generally less than 55 m) during late summer (late August to late September) from 60°N to 66.5°N (Chapter 15). Oceanographic measurements within the NBS reveal that average annual sea surface temperature (SST, 11.5°C, upper 10 m) was warmest from 2014 to the present with 2019 being the warmest on record. In general, the catch per unit effort of juvenile pink, sockeye, and coho salmon were positively related to summer sea surface temperatures. This relationship likely reflects the influence of temperature on the distribution (e.g. Bristol Bay juvenile sockeye salmon (*O. nerka*), $\rho = 0.9$) and survival (e.g. juvenile coho salmon (*O. kisutch*), $\rho = 0.7$) of these juvenile salmon species.

Life-cycle models (adult return and escapement) of pink salmon (*Oncorhynchus gorbuscha*) reveal a lack of density-dependence for adult pink salmon spawners in the Yukon River and potential for some density-dependence for adult pink salmon spawners in the Norton Sound region (Chapter 14). Life-history (freshwater and early marine) models identify a positive and significant relationship between the abundance index for juvenile pink salmon and average Nome air temperature during their freshwater residency (August to June). This relationship supports the notion that warming air temperatures in this region (as a proxy for river and stream temperatures) are contributing to improved freshwater survival or increased capacity of freshwater habitats to support pink salmon production. Life-history models also show that the number of adult pink salmon returning to Norton Sound and the Yukon River is significantly related to the juvenile abundance in the northern Bering Sea. This result indicates that much of the variability in survival for northern Bering Sea pink salmon occurs during early life-history stages and that juvenile abundance is an informative leading indicator of pink salmon runs to this region.

A spatially explicit bioenergetics model was used to estimate the growth rate potential (GRP; %body weight per day) of juvenile chum salmon in the northern Bering and Chukchi seas (Chapter 22). Annual averages of GRP ranged from a low of 0.9 (2003) to a high of 12.3 (2007) in the northern Bering Sea and from 0.1 (2003) to 39.3 (2007) in the Chukchi Sea. Juvenile chum salmon were generally not distributed in regions of higher GRP with the exception being 2007 within the Chukchi Sea. There was a significant positive relationship between average seasonal transport through the Bering Strait and juvenile chum salmon GRP, suggesting summer transport of heat (and likely pelagic prey) improves early marine growth potential for juvenile chum salmon in the southern Chukchi Sea region. The year 2007 stands out as an anomaly within the 18 year time series with the highest GRP and catch per unit effort of juvenile chum salmon in both regions.

H4: Seabird community structure and seabird-prey dynamics: *The current predominance of planktivorous seabirds in the Arctic may shift back towards piscivorous seabirds, if warming sea temperatures restructure the food web*.

Recent loss of sea ice and warmer ocean temperatures could impact seabirds directly (due to lack of prey or lower quality prey) and indirectly (if low-quality zooplankton reduces forage fish availability; Chapter 21). In the northern Bering Sea and eastern Chukchi Sea, 2017-2019 were record-breaking years for warm ocean temperatures and lack of sea ice. The region supports millions of seabirds that could be affected by shifts in prey distribution and availability caused by changing environmental drivers. However, seabirds are highly mobile and often flexible in diet, and might alter their foraging distributions accordingly. To determine if there was evidence of long-term changes in abundance of seabirds, or if seabirds used the offshore habitat differently during recent warm years, we compared species richness, community composition, and distribution and abundance of selected species and all seabirds between two periods, 2007-2016 and 2017-2019. We also evaluated annual changes in abundance during 2007-2019. We used 79,426 km of transects from vessel-based surveys conducted July through September.

Total seabird density for the entire study area increased by ~20% during 2017-2019, but changes were not consistent across the study area, nor among species, and species richness declined except for a slight increase in the northern Chukchi Sea (Chapter 21). Total seabird density declined most in the northern Bering Sea (-27%), although it increased in the Chirikov Basin. During 2017-2019, abundance of piscivorous murres (*Uria* spp.) decreased everywhere, whereas planktivorous *Aethia* auklet density increased by 70% in Chirikov Basin; auklets apparently abandoned their post-breeding migration to the Chukchi Sea. Short-tailed shearwaters (*Ardenna tenuirostris*) expanded farther into the northern Chukchi Sea, with nearly twice the density of the previous decade. We identified five seabird community types, three of which (all dominated by an alcid species) contracted spatially in the later period, and shifted south or near colonies. In contrast, a short-tailed shearwater-dominated community expanded northward, and a community defined by low seabird density expanded throughout the eastern portion of both the northern Bering and Chukchi Seas, suggesting higher-density communities had shifted westward.

The retraction of the auklet community from the Chukchi Sea to the northern Bering Sea during the warm years of 2017-2019 was consistent with the hypothesized shift back to a piscivorous seabird community, although further monitoring would be required to determine if that trend continues. However, the increase in abundance and northward movement of short-tailed shearwaters, which often consume primarily euphausiids, appears to contradict the hypothesis. This shearwater is an omnivore and consumes small fish, fish larvae, and cephalopods, thus its diet is more plastic than that of the least and crested auklets. In addition, the Lisburne seabird colony monitored by the Alaska Maritime National Wildlife Refuge continues to show increases in numbers of nesting murres and kittiwakes, which are piscivores. Thus the shift southwards of auklets (strictly planktivorous), continuous presence of omnivorous shearwaters, and growing colonies of piscivorous seabirds, together provide correlative support for the hypothesis that continued warming could shift the seabird community of the Chukchi Sea back to a predominance of piscivorous, or at least omnivorous species.

Application to Resource Management and Alaska Communities

Recognizing the potential for commercial fishing activities to expand into the northern Bering Sea and the Arctic, and the lack of baseline information from these areas, the North Pacific Fishery Management Council (NPFMC) has taken several proactive measures to prevent the northward expansion of commercial fishing without prior assessment of fisheries resources. These measures include a ban on non-pelagic trawling in the Northern Bering Sea Research Area until a research plan can be developed and a ban on all commercial fishing in the US Exclusive Economic Zone of the Arctic under the Arctic Fishery Management Plan (FMP, https://www.npfmc.org/arctic-fishery-management/). Implementation of the FMP requires baseline surveys to assess the status of fisheries resources in the Arctic. Information on fish populations collected by this and other projects are critical to informing the NPFMC about the status of fish stocks in the Chukchi Sea and environmental mechanisms underpinning variation in their populations. The Arctic FMP identifies Arctic cod (*Boreogadus saida*), saffron cod (*Eleginus gracilis*) and snow crab (*Chionoecetes opilio*) as potential target species in the Chukchi Sea. An important and required element of any FMP is a description of Essential Fish Habitat (EFH) for each target species in the FMP. Data collected during our surveys already contribute to updating EFH descriptions for the three species named in the Arctic FMP using the best available scientific information.

Together, the LTL and UTL components provide a comprehensive view of the ecosystem and provide clarity on the changing ecosystem for resource managers and Alaskan communities. The LTL program found that there is an increased transport and heat flux into the Arctic basin, substantial interannual variability in the amount of nutrients available to sustain spring production, and that warming will increase the spatial extent of picocyanobacteria Synechococcus, a smaller less energy-rich phytoplankton that will negatively impact the flow of energy to higher trophic levels. There appear to be concomitant reductions in larger sized zooplankton, reducing the amount of prey available for larger, pelagic predators such as bowhead whales and seabirds. There will be winners and losers in the Arctic fishes as climate-driven distribution shifts are restructuring larval fish community composition and bioenergetic pathways that will influence the flow of energy to higher trophic levels. This will have cascading consequences for upper trophic level production that provides the basis for commercial fishing communities, and for local communities in the Arctic that rely on fishes, seabirds and marine mammals for food.

The UTL Arctic Integrated Ecosystem Surveys provide further information on the impact of climate variability on ecosystem function and fitness of fishes and invertebrates. During the research period (2016 to 2021), adult subarctic gadids moved into the northern Bering Sea in large numbers. Commercial fishing for Pacific cod (using longline) commenced within the northern Bering Sea and in Russia's exclusive economic zone in the Chukchi Sea. However, we did not find large numbers of adults of either subarctic or Arctic gadids (Arctic cod and saffron cod) within the Chukchi Sea survey region. We did find large numbers of age-0 Arctic cod and saffron cod as well as age-0 subarctic gadids (walleye pollock) within the southern Chukchi Sea region. Pollock were largely absent in previous surveys of the same area in 2005, 2012 and 2013, but were the most abundant pelagic fishes in many areas in 2017 and 2019. In 2019, age-0 Arctic cod were found further north in the survey region than was reported during earlier surveys (Arctic EIS 2012 and 2013). In addition, we found that warming ocean temperatures and increased transport during summer months through the Bering Strait improves habitat quality for juvenile salmon within the southern Chukchi Sea. These changes are related to faster early marine growth and survival of young salmon, potentially leading to higher numbers of adult salmon returns to the Arctic.

Prey quality is likely an important consideration: for example, age-0 Arctic cod are more lipid-rich and energy-dense than walleye pollock. Additionally, environmental factors are likely to play an important role in food quality: although juvenile Arctic cod were very abundant at the end of the warm (2017) summer season, they had only half the fat storage and lower overall energy content than those collected during colder years (2012/2013). Similarly, saffron cod, capelin and sand lance had slightly lower energy content in warmer years. These changes in the distribution of abundant age-0 pelagic fishes are consistent with expectations under continued warming, and will likely continue as the Alaska Arctic continues to

warm. These changes in the abundance, distribution and lipid content of small fishes are likely to impact food availability and quality for higher trophic level predators (piscivorous fishes, marine mammals, and birds) and for communities who depend on these food sources. For example, piscivorous seabirds require forage fish of high energy density to raise chicks to fledging during the short Arctic summer. Low quality prey can significantly increase the number of fish needed to raise chicks, increasing foraging effort and extending the chick-rearing period. Late fledging dates and low fledgling weight can reduce overwinter survival. Low recruitment in harvestable seabirds can impact the ability of local communities to gather eggs and adult birds.

In response to changes in prey, some seabirds, such as short-tailed shearwaters and thick-billed murres, have shifted their distribution farther north, and are remaining in the Arctic later into summer or fall, but they must still return south through the Bering Strait. Other marine birds, such as eiders, maintain the timing of their post-breeding southward migration through the Bering Strait region. Due to lack of sea ice, these southward migration patterns now overlap with increased vessel traffic during months of nighttime darkness, potentially resulting in higher risk of vessel-bird collisions. The new overlap of human activities during fall migration of marine birds could pose challenges to bird conservation and to management of vessel traffic lanes throughout the region.

Our results from the Arctic Integrated Ecosystem Survey indicate that our overarching hypothesis:

Reductions in Arctic sea ice and the associated physical changes to the environment influence the flow of energy through the pelagic ecosystem in the Chukchi Sea. Specifically, we expect lasting changes in the seasonal composition, distribution and production of phytoplankton; in the distribution and standing stocks of large crustacean zooplankton that serve as the prey base for upper trophic level fishes and seabirds; in the assemblages, distributions, abundances, and body condition of larval and early juvenile fishes that influence the recruitment success of later life stages, and in the distribution and abundance of adult fishes

is being realized.

Directions for Future Research

Through the combined LTL-UTL AIERP programs, key elements were identified for future research including maintaining long-term observations, incorporating new measurements into the observational programs, enhanced modeling of the region, and operationalizing new technologies. To further advance our understanding of ecosystem variability and climate-induced trends, we recommend the following elements for future research.

Monitoring - To establish baselines that will enable the assessment of trends and variability, we recommend the following activities be continued:

- Maintain moored observatories at key physical (e.g., Icy Cape, M8, C12,) and biological (e.g., C12) hot spots;
- Maintain hydrographic and zooplankton sampling transects (e.g., DBO, Icy Cape) and surveys (e.g., Northern Bering Sea Assessment);
- Continue planktonic monitoring to track ecosystem changes of phytoplankton, zooplankton and ichthyoplankton;
- Continue acoustics surveys and time series of fish as subarctic gadids begin moving into the Chukchi Sea.
- Maintain seabird observations on platforms of opportunity.
- Continue benthic sampling for fishes and invertebrates.

Expanding Observations - To address gaps exposed through this research and other program, we recommend the following:

- Expand the M8, M14, and C12 observatories with traditional (e.g., sediment traps, nitrate sensors, water samplers, eDNA samplers) and new (e.g., RISe profilers, imaging systems) technologies;
- Expand CTD, zooplankton, and fish (ichthyoplankton, juvenile, and adult stages) surveys to the Chukchi and Beaufort shelf break and western Beaufort Shelf;
- Measure taxon-specific grazing (e.g., grazing on *Synechococcus*) to determine if seasonal variability in growth is due to bottom-up (e.g., warming) or top-down control;
- Measure contributions of the pico fraction, nano-fraction and microplankton fraction to phytoplankton biomass (Chla) and productivity;
- Expand otolith-derived aging and microchemistry of early-stage fish species to enhance our understanding of habitat use, model parameterization, and energy allocation.

Modeling - To provide insights into biophysical processes and ecosystem trends and variability on spatiotemporal scales that cannot be realized through observational programs, we recommend the following:

- Enhance the ROMS based biophysical modeling suite while transitioning to regional MOM6;
- Validate and improve existing models using observational data from the Arctic IES;
- Assimilate observational data through targeted modeling sensitivity experiments;
- Use the modeling suite to understand mechanistic linkages within the biophysical system and align with the Synthesis, Analysis and Products listed below (e.g., quantify the transport of heat/salt, quantify drivers of nutrient flux, quantify extreme events);
- Integrate ROMS/MOM6 LTL modeling (up through zooplankton) with the AFSC Alaska Climate Integrated Modeling Project (ACLIM) that addresses marine ecosystem and fishery dynamics, and incorporates fishery economics.

Synthesis, Analysis and Products

- Quantify the transport of heat and salts;
- Quantify the physical and biological drivers of nutrient flux into the Chukchi Sea;

- Synthesize phytoplankton and zooplankton data to connect to other trophic level work including lipids in phyto- and zooplankton, fish distributions in comparison to plankton, kton, and zooplankton relation to seabird distributions;
- Conduct analysis of adult spawning stock biomass and fish egg data to determine if shifts in the distribution of species are due to increased larval transport and/or changes in spawning locations with warming;
- Conduct analyses of benthic-pelagic coupling to understand if a reorganization of the ecosystem in the Northern Bering-Chukchi Seas ecosystem has occurred and what the impact will be on managed and subsistence resources;
- Develop metrics for Arctic ecosystem assessment.

Collaborations - To provide insights on the status of the Arctic ecosystem to stakeholders and the public partnerships and collaborations must be enhanced. We recommend fostering existing collaborations identified in the collaborations section of this report, and enhance collaborations with local communities and international partners (e.g., Canada, Russia).

New technology - To address observational gaps (e.g., seasonal transitions, phytoplankton and zooplankton speciation, under-ice production), we recommend expanded use of new and emerging technologies:

Imaging and Artificial Intelligence (AI)

- Employ phytoplankton imaging/AI on surface vehicles and moorings to derive speciation and identify and quantify species associated with Harmful Algal Blooms;
- Continue picophytoplankton counts to fill the phytoplankton size spectra and align with imaging methods;
- Monitor zooplankton communities using *in-situ* imaging/AI;
- Utilize towed and moored cameras with AI to assess decadal changes in the benthic community (e.g., epifauna, fish).

Platforms

- *RISe* (**R**efloating **I**ce **Se**nsing) is a profiling mooring that submerges when ice arrives and refloats in the spring after ice retreat. The system includes a *Prawler* that moves up and down the mooring line measuring temperature, salinity, chlorophyll, and dissolved oxygen. RISe provides real-time information of the full water column during the entire open water season;
- *Pop-up* floats are deployed in the late summer/fall and rise to the surface under the ice the following spring. It can measure temperature, salinity, oxygen, fluorescence, PAR, and provide images on the seafloor and under ice;
- The MRV Systems *ALAMO* (Air Launched Autonomous Micro-Observer) is an autonomous vertically profiling float that is ice-reinforced for sampling through the winter;
- Benthic platforms (e.g., benthic rover, respirometers, microbial incubator, automated samplers) that can be used to assess shifts in the benthic community, nutrient cycling, and production;
- Optimize the use of *Saildrones* and other uncrewed systems equipped with active acoustics to understand age -0 pelagic fish distributions and biomass.

General References

Arctic Ecosystem Integrated Survey. 2014. 2013 Surface/Midwater trawl and oceanographic survey of the northeastern Bering Sea and Chukchi Sea. UAF-AFSC Joint Submission to CIAP, BOEM, and AYKSSI. 63pgs.

Arctic Fishery Management Plan 2009. Fishery Management Plan for fish resources of the Arctic Management Area. North Pacific Fishery Management Council, Anchorage, Alaska. 158 Pgs.

Arrigo, K.R., and G.L. van Dijken. 2011. Secular trends in Arctic Ocean net primary productivity. Journal of Geophysical Research 116, C09011, doi:10.1029/2011JC007151Beacham, T.D., J.R. Candy, C. Wallace, S. Urawa, S. Sato, N. V. Varnavskaya, K.D. Le, and M. Wetklo. (2009) Microsatellite stock identification of chum salmon on a Pacific Rim basis. N. Am. J. Fish. Manage. 29: 1757–

Bradstreet, M.S.W., K.J. Finley, A.D. Sekerak, W.B. Griffiths, C.R. Evans, M.F. Fabijan, and H.E. Stallard. 1986. Aspects of the biology of Arctic cod (*Boreogadus saida*) and its importance in Arctic marine food chains. Canadian Technical Report of Fisheries and Aquatic Sciences 1491. 193pgs.

Carothers, C., S. Cotton, and K. Moerlein. 2013. Subsistence use and knowledge of salmon in Barrow and Nuiqsut, Alaska. Final Report to OCS study Bureau of Ocean and Energy Management 2013 – 0015. 58 pgs.

Coyle, K.O., L.B. Eisner, F.J. Mueter, A.I. Pinchuk, M.A. Janout, K.D. Cieciel, E.V. Farley, and A.G. Andrews. 2011. Climate change in the southeastern Bering Sea: impacts on pollock stocks and implications for the oscillating control hypothesis. Fisheries Oceanography 20(2):139-156.

Danielson, S.L., L. Eisner, C. Ladd, C. Mordy, L. Sousa, and T. Weingartner. 2016. A comparison between late summer 2012 and 2013 water masses, macronutrients, and phytoplankton standing crops in the northern Bering and Chukchi Seas. Deep-Sea Research II 135:7–26.

De Robertis, A., K. Taylor, C. Wilson, and E. Farley. 2016. Abundance and distribution of Arctic cod (*Boreogadus saida*) and other pelagic fishes over the U.S. Continental Shelf of the northern Bering and Chukchi seas. Deep Sea Research II. 135:51–65.

Eisner, L., N. Hillgruber, E. Martinson, and J. Maselko. 2013. Pelagic fish and zooplankton species assemblages in relation to water mass characteristics in the northern Bering and southeast Chukchi seas. Polar Biology 36:87-113.

Farley, E.V., Jr., J.M. Murphy, B.W. Wing, J.H. Moss, and A. Middleton. 2005. Distribution, migration pathways, and size of western Alaska juvenile salmon along the eastern Bering Sea shelf. Alaska Fisheries Research Bulletin 11:15-26.

Farley, E.V., Jr., R.A. Heintz, A.G. Andrews, and T.P. Hurst. 2014. Size, diet, and condition of age-0 Pacific cod (*Gadus macrocephalus*) during warm and cool climate states in the eastern Bering Sea. Deep-Sea Research II, http://dx.doi.org/10.1016/j.dsr2.2014.12.011.

Fossheim, M., P. E. Primicerio, R.B. Johannesen, M.M. Ingvaldsen, Aschan, and A.V. Dolgov. 2015. Recent warming leads to a rapid borealization of fish communities in the Arctic. Nature doi:10.1038/NCLIMATE2647.

Frey, K.E., J.A. Maslanik, J.C. Kinney, and W. Maslowski. 2014. Recent variability in sea ice cover, age, and thickness in the Pacific Arctic Region. Pages 31-64, in J.M. Grebmeier and W. Maslowski (eds.), The Pacific Arctic Region: Ecosystem Status and Trends in a Rapidly Changing Environment, DOI 10.1007/978-94-017-8863-2_2.

Gall, A.E., R.H. Day, and T.J. Weingartner. 2013. Structure and variability of the marine-bird community in the northeastern Chukchi Sea. Continental Shelf Research 67:96-115.

Gall, A.E., T.C. Morgan, R.H. Day, and K.J. Kuletz. 2017. Ecological shift from piscivorous to planktivorous seabirds in the Chukchi Sea, 1975–2012. Polar Biology, 40(1):61 – 78.

Heintz, R.A., E.C. Siddon, E.V. Farley, Jr., and J.M. Napp. 2013. Correlation between recruitment and fall condition of age-0 pollock (*Theragra chalcogramma*) from the eastern Bering Sea under varying climate conditions. Deep-Sea Research II 94:150-156.

Holst, M., I. Stirling, and K.A. Hobson. 2001. Diet of ringed seals (*Phoca hispida*) on the east and west sides of the north water polynya, northern Baffin Bay. 2001. Marine Mammal Science 17(4):888-908.

Hop, H., and H. Gjosaeter. 2013. Polar cod (*Boreogadus saida*) and capelin (*Mallotus villosus*) as key species in marine food webs of the Arctic and Barents Sea. Marine Biology Research 9(9):878-894.

Kuletz, K., M. Ferguson, A. Gall, B. Hurley, E. Labunski, and T. Morgan. 2015. Seasonal Spatial Patterns in Seabird and Marine Mammal Distribution in the Eastern Chukchi and Western Beaufort Seas: Identifying Biologically Important Pelagic Areas. Progress in Oceanography 136: 175–200.

Laurel, B.J., M. Spencer, P. Iseri, L.A. Copeman. 2015. Temperature-dependent growth and behavior of juvenile Arctic cod (*Boreogadus saida*) and co-occurring North Pacific gadids. Polar Biology.

Lowry, L.F., and K.J. Frost. 1981. Distribution, growth, and foods of Arctic cod (*Boreogadus saida*) in the Bering, Chukchi, and Beaufort Seas. Canadian Field-Naturalist 95(2):186-191.

Mahlstein, I., and R. Knutti. 2011. Ocean heat transport as a cause for model uncertainty in projected Arctic warming. Journal of Climate 24:1451-1460.

Matley, J. K., A. T. Fisk, and T. A. Dick. 2012. Seabird predation on Arctic cod during summer in the Canadian Arctic. Marine Ecology Progress Series 450:210-228.

Moore, S.E., E. Logerwell, L. Eisner, E.V. Farley, Jr., L.A. Harwood, K. Kuletz, J. Lovvorn, J. M. Murphy, and L.T. Quakenbush. 2014. Marine fishes, birds and mammals as sentinels of ecosystem variability and reorganization in the Pacific Arctic Region. Pgs. 337-392 *In* J.M. Grebmeier and W. Maslowski (eds.), The Pacific Arctic Region: Ecosystem Status and Trends in a Rapidly Changing Environment, DOI 10.1007/978-94-017-8863-2_2.

Moss, J.H., J.M. Murphy, E.V. Farley, Jr., L.B. Eisner, and A.G. Andrews. 2009b. Juvenile pink and chum salmon distribution, diet, and growth in the northern Bering and Chukchi Seas. North Pacific Anadromous Fish Commission Bulletin 5:191-196.

Orlova, E.L., A.V. Dolgov, P.E. Renaud, V.D. Boitsov, I.P. Prokopchuk, and M.V. Zashihina. 2013. Structure of the macroplankton-pelagic fish-cod trophic complex in a warmer Barents Sea. Marine Biology Research 9(9):851-866.

Overland, J.E. 2011. Potential Arctic change through climate amplification processes. Oceanography 24(3):176-185.

Overland, J. E., J. Wang, R.S. Pickart, and M. Wang. 2014. Recent and future changes in the meteorology of the Pacific Arctic. Pages 17-30, *In* J.M. Grebmeier and W. Maslowski (eds.), The Pacific Arctic Region: Ecosystem Status and Trends in a Rapidly Changing Environment, DOI 10.1007/978-94-017-8863-2_2.

Paredes, R., R.A. Orben, R.M. Suryan, D.B. Irons, D.D. Roby, et al. 2014. Foraging Responses of Black-Legged Kittiwakes to Prolonged Food-Shortages around Colonies on the Bering Sea Shelf. PLoS ONE 9(3): e92520. doi:10.1371/journal.pone.0092520.

Piatt, J.F., J.L. Wells, A. MacCharles, and B.S. Fadely. 1991. The distribution of seabirds and fish in relation to ocean currents in the southeastern Chukchi Sea. *In*: W.A. Montevecchi and A.J. Gaston (eds), Population Biology and Conservation of Marine Birds Symposium, St. Joh's, NF. Occasional Papers of the Canadian Wildlife Service, Ottawa, ON.

Pinchuk, A.I., and L.B. Eisner. 2016. Spatial heterogeneity in zooplankton summer distribution in the eastern Chukchi Sea in 2012-2013 as a result of large-scale interactions of water masses. Deep-Sea Research II 135:27–39.

Sigler M.F., M. Renner, S.L. Danielson, L.B. Eisner, R.R. Lauth, K.J. Kuletz, E.A. Logerwell, and G.L. Hunt. 2011. Fluxes, fins, and feathers relationships among the Bering, Chukchi, and Beaufort Seas in a time of climate change. Oceanography 24:250-265.

Stephenson, S.A. 2006. A review of the occurrence of Pacific salmon (*Oncorhynchus* spp.) in the Canadian Western Arctic. Arctic 59(1):37-46.

Welch, H.E., M.A. Bergmann, T.D. Siferd, K.A. Martin, M.F. Curtis, R.E. Crawford, R.J. Conover, and H. Hop. 1992. Energy flow through the marine ecosystem of the Lacaster Sound region, Arctic Canada. Arctic 45(4):343-357.

CHAPTER 1 – Winners and Losers in a Warming Arctic: Potential Habitat Gain and Loss for Epibenthic Invertebrates of the Chukchi and Bering Seas

Objective 1: Quantify the distribution, abundance, and condition of demersal fishes and shellfishes

Elizabeth Logerwell (NOAA), Muyin Wang (PMEL), Lis Jorgensen (IMR), Kimberly Rand (NOAA Affiliate)

Abstract

Our goal was to examine how the epibenthic invertebrate community in the Pacific Arctic Region might be affected by continued increases in ocean temperatures. We used epibenthic invertebrate catch and bottom temperature data collected on groundfish assessment and ecosystem surveys from 2009-2018 in the Bering and Chukchi seas to determine the "preferred" temperature of all taxa. We grouped taxa into five clusters according to their similarity in median temperature and temperature range. We then used an ensemble of eight climate models to project bottom temperature to mid-century and end of the century. Based on these projections, we show how the amount and distribution of cluster-specific thermal habitat might change with ocean warming. We found that by mid-century (2050) there was a 50% decrease in thermal habitat for all clusters except for the most eurythermic cluster, and that thermal habitat contracted to the north. By the end of the century (2100) there was very little thermal habitat for all clusters, except the most eurythermic cluster, and habitat was further contracted to the north. The cold-water and stenothermic cluster, hypothesized to be the most vulnerable to ocean warming, had virtually no projected thermal habitat by the end of the century. These "losers" were primarily gastropods and the mussel *Musculus* sp. These taxa are prey to endangered Pacific walrus (*Odobenus rosmarus*), which is harvested as a food resource in native Alaskan communities; and are prey for commercial groundfishes such as Pacific cod (*Gadus macrocephalus*) and Alaska pollock (*Gadus chalcogrammus*). By 2100 the most eurythermic cluster, hypothesized to be the least vulnerable to warming, had projected suitable thermal habitat throughout most of the Bering and Chukchi Seas, except nearshore coastal regions. The most abundant species of these "winners" was the basketstar *Gorgonocephalus cf. arcticus*. The loss of thermal habitat for all but the "winners" could impact species diversity of the Bering and Chukchi Seas because the "winner" cluster accounted for only 26 taxa or 8% of all taxa observed. Temperature is one determinant of habitat, so a full habitat and ecosystem model is needed to provide more detailed predictions. In addition, more laboratory studies of thermal acclimation potential of Arctic benthic invertebrates are needed. Nonetheless, our results provide the first indications that the epibenthic invertebrate community in the Bering and Chukchi seas, which supports marine mammals, seabirds and human communities, may be seriously impacted by future ocean warming.

Keywords: epibenthic invertebrate community, thermal habitat, climate change, climate projections

Introduction

Loss of sea ice and rise of ocean temperature are impacting Arctic ecosystems around the globe (Huntington et al., 2020; Polyakov et al., 2020; Renaud et al., 2015). Ocean warming has been shown to impact Arctic plankton (Dalpadado et al., 2020; Eisner et al., 2014), fish (Aune et al., 2018; Mueter and Litzow, 2008; Wisz et al., 2015), infaunal invertebrates (Grebmeier, 2012; Solan et al., 2020), seabirds (Gall et al., 2016) and marine mammals (Davis et al., 2020; Laidre et al., 2015). In contrast, the potential impacts of ocean temperature increase on the epibenthic invertebrate community have not been extensively examined. This is a critical knowledge gap because the epibenthic invertebrate community, along with the infauna, supports a number of key upper trophic level predators including commercial groundfish, marine mammals, and seabirds (Bluhm and Gradinger, 2008; Packer et al., 1994; Whitehouse et al., 2017). Arctic native communities depend heavily on many of these predators (cetaceans, pinnipeds,

and sea ducks) for nutrition and for cultural and spiritual fulfillment (Hovelsrud et al., 2008; Huntington et al., 2020).

Despite the critical need to understand the impacts of temperature on epibenthic invertebrates, very few temperature-dependent rate measurements of benthic macrofauna have been made. The physiological capacity of benthic organisms to acclimate or adapt to warming or otherwise changing conditions is also understudied (Pörtner, 2010). A macrophysiological approach can be useful in this situation. Macrophysiology is the study of interpopulation, interspecific and high taxonomic variation in physiological traits over large geographical and temporal timescales. The overall goal of the approach is to understand the reasons for variation in physiological traits and the subsequent ecological implications, particularly in the face of substantial environmental change (Chown et al., 2004).

We took a macrophysiological approach, as described above, to study the potential impacts of ocean warming by using the range of temperatures at which all sampled epibenthic invertebrate taxa over the US Pacific Arctic have been observed over the past decade. We posit that cold-water and stenothermic taxa would be highly susceptible to ocean warming (a.k.a the "losers"), whereas warm-water and eurythermic taxa would be relatively tolerant of warming (a.k.a. the "winners"). Instead of defining taxa *a priori* to be Arctic or boreal, as other investigators have done (Renaud et al., 2015), we used cluster analysis to group taxa by the median and the range of temperatures at which they have been observed. We took advantage of a decade's worth of epibenthic invertebrate catch and temperature data from groundfish assessment surveys (Lauth et al., 2019) and ecosystem surveys of the Bering and Chukchi seas (including the Arctic Ecosystem Integrated Survey and the Arctic Integrated Ecosystem Research Program (Baker et al., 2020; Mueter et al., 2017)). We used an ensemble of eight coupled climate models that participated in the Coupled Model Intercomparison Project Phase 5 (CMIP5) to predict the mean increase in bottom temperature from present to mid-century as well as to the end of the century and calculated the amount and distribution of seafloor thermal habitat (that is, the area within the temperature range of each cluster of taxa). We then discuss the impacts of projected changes in thermal habitat on epibenthic community diversity and Arctic foodwebs.

Methods

The study area for this work encompassed the Bering and Chukchi seas which are seasonally ice-covered shelves (<200 m depth) with currents typically flowing northward due to the difference in sea level between the Pacific and the Arctic (Aagaard et al., 1981). South and north of the shelf breaks are the Aleutian Basin and Central Arctic Ocean, respectively, and the two seas are separated by Bering Strait which is 88 km wide (Fig. 1a). The water masses of the Bering Sea include the nutrient-rich Anadyr Water, Bering Shelf Water, and the comparatively fresh and nutrient-poor Alaska Coastal Water (Coachman, 1986; Danielson et al., 2016). These water masses bring freshwater, nutrients, and organix matter into the Chukchi Sea through Bering Strait (Danielson et al., 2016; Walsh et al., 1989). Near-bottom resident cold and salty water in both the Bering and Chukchi seas is also present, the result of previous winter cooling (Danielson et al., 2016). The Bering Sea is home to some of the most productive and lucrative demersal fisheries in the world. Alaska fisheries as a whole accounted for 57% of the weight and 3% of the ex-vessel value of total U.S. domestic landings in 2020 (Hiatt et al., 2021). In comparison, the Chukchi Sea currently lacks large stocks of commercial groundfish and it is closed to commercial fishing in the US EEZ (North Pacific Fishery Management Council, 2009). There are several human communities that relay on the northern Bering and Chukchi seas for food security through subsistence harvest of marine mammals, fish and seabirds. In addition, the Arctic ecosystem provides these communities with a means for social and cultural expression (Huntington, 2000).

The epibenthic communities of the Bering Sea and Chukchi Sea were sampled during groundfish assessment and ecosystem surveys conducted by National Oceanic and Atmospheric Administration

(NOAA) National Marine Fisheries Service, Alaska Fisheries Science Center (AFSC) (Baker et al., 2020; Lauth, 2011; Lauth et al., 2019; Mueter et al., 2017; Rand et al., 2018). While the Southeast Bering Sea has been surveyed annually for epibenthos since 1975, the other areas were surveyed less often and only since the 2000s. To minimize the effect of long-term trends, catch data were used from surveys from 2009-2018 in the Southeast Bering Sea; 2010 and 2017 in the North Bering Sea; 2012 and 2017 in the Chukchi Sea shelf; and 2013 in the Northeast Chukchi Sea around Barrow Canyon (Fig. 1b). The 83-112 Eastern bottom trawl was used for sampling in all years (Stauffer, 2004), with the exception of the 2017 Chukchi Sea survey which employed a 3-meter plumb staff beam trawl (Abookire and Rose, 2005). For both nets, net mensuration equipment coupled with a GPS feed was used to calculate area swept and catch-per-unit effort (CPUE (kg km^{-2})). Net width was not measured for the beam trawl because the beam keeps the net width constant. Catch was enumerated, weighed, and identified to the lowest taxonomic level feasible on board or from voucher specimens and photographs after the surveys, on land. Catch data of fish were removed before further analysis.

Bottom water temperature data were collected at each trawl station using a Sea-Bird bathythermograph continuous data recorder attached to the headrope of the net. In addition, temperature and salinity with depth were measured with CTDs during the 2012 and 2017 Chukchi Sea surveys. The median temperature at all stations where each invertebrate species (or lowest taxa identified) occurred in the data set was calculated. The temperature range of each taxa was calculated as the 10th and 90th percentiles of temperatures at all stations where it occurred. K-means clustering was used to group taxa by median temperature and range. K-means clustering is a method of vector quantization that partitions n observations into k clusters in which each observation belongs to the cluster with the nearest mean (Bock, 2008). K-means clustering minimizes the within-cluster variances (i. e., the squared Euclidean distances). The number of clusters (k) was chosen as a balance between the number of groups and the variance within groups. Bigger k results in a lower variance to the extreme case of k=n which results in variance of 0. The final k was selected by plotting the variance (sum of squares) within groups by the number of groups and observing the ‘elbow’, or where the slope of the decrease in variance changes from steep to shallow.

The diversity represented by each cluster was assessed by calculating the number of taxa and the percent of all taxa (a.k.a., alpha-diversity). The relative abundance of megabenthic invertebrates in each cluster was calcuated as the mean of the percent CPUE (kg km^{-2}) at all stations, where percent CPUE at each station was calculated as CPUE for each species at that station dividied by total CPUE at that station over all years.

To select climate models for bottom temperature projections, model summer ocean temperature data from Representative Concentration Pathway (RCP) 8.5 scenarios were interpolated on to the survey stations (by latitude, longitude and bottom depth). RCP8.5 combines assumptions about high population and relatively slow income growth with modest rates of technological change, leading in the long term to high energy demand and high greenhouse gas emissions in the absence of climate change policies (IPCC, 2014). This high emissions scenario is frequently referred to as “business as usual”, suggesting that it is a likely outcome if society does not make concerted efforts to cut greenhouse gas emissions. Among the 22 models downloaded, 8 showed relatively good agreement with observations. The data points were combined and separated into a north (>= 66° N), and a south (< 66° N) domain because the whole domain spans a large latitudinal range (54° N - 74°N) which may contain large meridional gradients. Model projections for July and August were averaged because those months were when the surveys occurred. Decadal average bottom temperatures were calculated for 2008-2017 (“present”), 2045-2054 (“mid-century”), and 2091-2100 (“end-of-century”).

Maps of the bottom temperature projections were generated by averaging model output within 100 km^2 grid cells. The 8 projection models had varying spatial resolutions (from 0.18° Longitude to 1.71° Longitude), and the 100 km^2 grid cell sized captured at least one data point for each model.
The amount of thermal habitat available for each cluster of species was calculated as the proportion of the total study area projected to be within the temperature range for that cluster. Thermal habitat was calculated for each cluster for present, mid-century and end-of-century projections of bottom temperature. Maps of the distribution of thermal habitat for all clusters and decadal projections were also produced. ArcGIS Desktop 10.6, version: 10.6.0.8321 (www.esri.com) was used to create maps.

Results

Variance within k-means cluster groups declined rapidly as group number increased from 1 to 5 in all regions (Fig. 2). For group numbers larger than 5 variance decreased less rapidly. So group size (k) was chosen to be 5 for further analysis.

The five k-means clusters were given qualitative descriptors arbitrarily based on average median and range of temperature for taxa in the cluster. Clusters for which median temperatures were 0.6° or less were designated as representing "cold-water" taxa. Clusters for which median temperatures were 2.5° or greater were designated as "warm-water". "Stenothermic" clusters were those with a range of 2.8° or less and "eurythermic" clusters were those with a range of 5.5° to 6°; "highly eurythermic" was a range of 9.0° (Table 1).

Cluster A, the "cold, stenothermic" cluster and Cluster E, the "warm, high eurythermic" cluster contained the lowest proportion of taxa (12% and 8%, respectively). Cluster D, "warm, eurythermic", contained the greatest proportion of taxa (38%). Cluster B, "cold, eurythermic" and Cluster C "warm, stenothermic" contained intermediate proportions of taxa (21% and 19%, respectively). Clusters B and D had the greatest proportional catch density (49% and 38%). The other clusters had catch densities less than 10% of total catch (Table 1).

The most abundant taxa (in terms of biomass density) in Cluster A, "cold, stenothermic", were Gastropoda and *Musculus* sp., at 3.8% and 3% of total catch density, respectively. Other taxa, occurring at less than 1% of catch density but greater than 0.1%, included echinoderms, sipunculids, and arthropods (Table 2). The most abundant taxa in Cluster B, "cold, eurythermic", were *Ophiura sarsii* and *Ophiura* sp. at 39% of total catch density. Other taxa in this cluster included echinoderms, mollusks, chordates, gastropods, cnidarians, arthropods, and annelids. The most abundant taxon in Cluster C, "warm, stenothermic", was *Nuculana radiata*. The other taxa caught at densities greater than 0.1% were a gastropod and a bryozoan. The most abundant taxon in Cluster D "warm, eurythermic", was *Chionoecetes opilio*, at 9% of total catch density. Other taxa in this cluster included echinoderms, cnidarians, bryozoans, sponges (Porifera), arthropods, gastropods, mollusks, cnidarians, chordates, and annelids. The most abundant taxon in Cluster E "warm, highly eurythermic" was *Gorgonocephalus cf. arcticus*. Other taxa in this cluster included arthropods, cnidarians and echinoderms.

Observed temperatures from CTD data collected in 2017 and 2019 fell within the range of model projections for both domains and were very close to the ensemble mean of the model in the north domain (Fig. 3). However, in general, these eight models overestimated the mean bottom temperature in the southern domain. The spread in the projected temperature is larger in the Northern domain compared with Southern domain. This is more obvious in the latter half of the 21st century. Looking forward to the future decadal changes, model projections indicated an increase in average bottom temperature in the north domain from 0.98 °C at present to 2.25 °C by mid-century (an increase of 1.27 °C) and to 5.60 °C by the end of century (an increase of 4.62 °C). Model projections of the South domain indicate an increase from

3.83 °C at present to 5.15 °C by mid-century (an increase of 1.32 °C); and to 8.10 °C by the end of the century (an increase of 4.27 °C) (Table 3).

The spatial distribution of model projections of bottom temperature shows coldest water in the north and warmest to the south and nearshore, as expected (Fig. 4). The range of the coldest water shrinks to the north from present to mid-century to end-of-century; and waters to the south warm. Bottom waters less than 0 °C virtually disappear by the end of the century.

The proportion of the study area within the temperature range of each cluster, based on model projections of bottom temperature at present, indicated that there was proportionally the least thermal habitat for Cluster A "cold, stenothermic" (31%) and the most for Cluster E "warm, highly eurythermic" (96%) (Table 4). The other two eurythermic clusters, Clusters B and D, also had a relatively large proportion of thermal habitat available to them, 88% for both. There was an intermediate proportion of thermal habitat available for Cluster C, "warm, stenothermic" (61%).

The amount of thermal habitat decreased for all clusters from present to mid-century, except for Cluster E for which there as an increase of 2%. The amount of thermal habitat available at mid-century ranged from a low of 13% for Cluster A and a high of 98% for Cluster E. The decrease in thermal habitat from mid-century to end-of-century was even greater than from present to mid-century. Thermal habitat for Cluster A virtually vanished by the end of the century, at 2%. There was 10% or less thermal habitat available for Clusters B and C; and there was 13% available for Cluster D. 72% of thermal habitat was available for Cluster E at the end of the century.

Available thermal habitat, based on present-day model projections, was similar for all clusters, except Cluster A, "cold, stenothermic", for which thermal habitat was confined to the north and west; and Cluster C, "warm, stenothermic", whose thermal habitat did not extend as far north as the others (Fig. 5). Projected available thermal habitat contracts to the north for all clusters from present to mid-century, except for Cluster E, the most eurythermic (Fig. 6). By the end of the century the contraction to the north is so great that there is projected to be suitable thermal habitat for Clusters A-D only north of 65° N, in the northern Chukchi Sea; and thermal habitat for Cluster A is only found at the slope between the Chukchi Sea and Central Arctic Ocean (Fig. 7). The distribution of thermal habitat for Cluster E at mid-century contracts very slightly to the north, and more noticeably to the west.

Discussion

An ensemble of eight coupled climate models projected a mean increase in summer bottom temperature in the Bering to Chukchi Sea region of around 1.3 °C by mid-century and an even greater increase of around 4.5 °C by the end of the century. Warmer waters were projected to expand north, as expected; and the nearshore area, the location of the typically warm and low salinity Alaska Coastal Current (Coachman et al., 1975), was projected to be the warmest by the end of the century, up to 10 °C and greater. These projections are consistent with the reduction of sea ice cover, and earlier sea ice retreat in the region (Wang et al., 2018).

Cold-water and stenothermic taxa, which we suggest would be the most vulnerable to ocean warming, were projected to experience the greatest decline in the proportion of thermal habitat available. Thermal habitat for these taxa, "the losers", decreased by more than 50% by mid-century; and by the end of the century only 2% of the total Bering-Chukchi Sea region was projected to be within their temperature range. The scant thermal habitat that was projected to be available was distributed at the far north on the shelf break and slope between the northern Chukchi Sea and the deep Central Arctic Ocean basin. Temperature projections of the Arctic slope and basin were not examined for this study, but we suggest that even if bottom temperatures were projected to be suitable, the depth of slope and basin would not

match the habitat requirements of these shelf-occupying taxa. In other words, retreat of shelf benthos can only continue until they reach the northern shelf break and slope, with local extinctions a likely consequence. Similar to our predictions, Parada et al. (2010) have documented range contractions to the north of the commercially important snow crab (*Chionoecetes opilio*), driven by ocean warming and the shrinking of the Bering Sea cold pool.

Warm-water and highly eurythermic taxa, hypothesized to be the least vulnerable to ocean warming, were projected to experience the least decline in the proportion of thermal habitat available. Thermal habitat for these taxa, the "winners", increased slightly from present to mid-century and then decreased from 98% to 72% of the study area by the end of the century. There was virtually no latitudinal shift in the available thermal habitat for these taxa, the reduction in available habitat was the result of a slight westward contraction away from the area of the Alaska Coastal Current.

A similar examination of thermal thresholds of Arctic epibenthic invertebrates and predicted changes in bottom temperature was published by (Renaud et al., 2015). They combined geographical observations with model projections of bottom temperature through the end of the century to define temperature thresholds and project future spatial distributions as we did, except that they defined species as "Arctic" or "boreal" *a priori* based on published literature and expert opinion. They also limited their study to 65 benthic taxa. In addition, the geographical scope of their study was different than ours, encompassing all of the Arctic.

Of the species Renaud et al. (2015) analyzed only seven of the Arctic species had clear upper temperature thresholds, and these ranged between 2 °C and 6 °C. These species are analogous to our Clusters A through D which had upper temperature thresholds ranging from 2 °C to 5.1 °C. Similar to our conclusion that these clusters may experience a northward contraction of suitable thermal habitat, Renaud et al. (2015) concluded that the northward progression of low-temperature isotherms suggest shrinking distribution ranges for these taxa in the future. Fourteen of the boreal species that Renaud et al. (2015) studied showed clear lower temperature thresholds, ranging from 4 °C to 10 °C. By this definition, our data did not include any boreal species, the lower temperature thresholds of the taxa we examined ranged from -1.5 °C to 1.8 °C. Renaud et al. (2015) concluded that the boreal species with the lowest thresholds are expected to be the first to expand into the Arctic. In contrast, we did not project northward expansions of thermal habitat, only contractions of habitat to the north. This could be due to the fact that most of our taxa were cold-water "Arctic" taxa, as defined by Renaud et al. (2015). In addition, as we suggest above, even if we had expanded our study area south and included more "boreal" taxa, the Bering Sea slope may represent a habitat boundary between the shallow Bering Sea shelf and the deep Aleutian Basin.

The conclusions of the Renauld et al. (2015) study, although it did include the Bering and Chukchi seas in bottom temperature projections, were driven by taxa occurring outside our study area. 68% of the Arctic taxa and all but two of the boreal species are found only in the Barents, Norwegian, North Atlantic and/or Beaufort seas, (EOL.org). The Barents Sea and surrounding waters are warmer than the Pacific Arctic at a given latitude due to warm Atlantic and coastal waters which flow into the southwestern part and keep the southern Barents Sea relatively warm and ice free, compared to the Chukchi Sea which receives winter-cooled waters from the Bering Sea (Hunt et al., 2013). In addition, the taxonomic composition of the Arctic and boreal species in the Renaud et al. (2015) study was limited compared to our study: 67% of the 28 Arctic species they examined were annelids and 72% of the boreal species were annelids.
In contrast to Renaud et al.'s (2015) study of benthic invertebrates and other studies on the distribution of fishes, our projections of thermal habitat did not predict range expansions to the north, only contractions of habitat to the north and offshore. Mueter and Litzow (2008) and Alabia et al. (2018) have documented changes in the distributions and trophic levels of Bering Sea epibenthic communities from 1982-2016 with ocean warming. They observed a northward expansion of sub-Arctic fish and crustacean species and an increase in community trophic level (more large groundfish) over time. In contrast to our analysis,

which was of the entire epibenthic invertebrate community (at least as reflected in our catch data), their analysis was limited to catch data on 36 fish and 10 crustacean (crab and shrimp) species. There is also evidence for northward range expansions of demersal fish and shrimp species in the Barents Sea and Western Eurasion Basin (Polyakov et al., 2020). These previous studies documenting distributional shifts northward with ocean warming focused on fishes and a few crustaceans, not the epibenthic invertebrate community we examined. A comparative analysis of the temperature tolerances of fishes and invertebrates is beyond the scope of this paper. The reasons that the response of fish distributions to ocean warming may have a different geographic manifestation than that of the invertebrate community require future study.

Our projections of changes in the distribution and extent of thermal habitat do not address the potential for changes in benthic invertebrate biomass over time. Grebmeier (2012) and Grebmeier et al. (2018, 2006) have documented decreases over the past three decades in biomass of benthic infauna (mostly bivalves, amphipods, polychaetes, and sipunculids) in the Northern Bering Sea and increases in the southeast and northeast Chukchi Sea. They attribute decreases in the Bering Sea to the loss of sea ice and a breakdown in the benthic-pelagic coupling that provides pelagic carbon to the benthos. They attribute increases in the Chukchi Sea to higher export of pelagic production to the benthos resulting from a longer open water season. Bluhm et al (2009) have documented increases in epibenthic biomass (mostly ophiuroids, snow crab *Chionoecetes opilio*, holothurians, and urchins) in the southeast Chukchi Sea, Norton Sound and the southeast Bering Sea (Bluhm et al., 2009). In particular, snow crab abundance increased from the late 1970s to the 2000s in the Chukchi Sea. Recent surveys, however, show that snow crab stocks in the Bering Sea are in decline. Biomass of crab was the lowest on record in 2021, continuing a declining trend that began in 2015 (Zacher et al., 2021). To address changes in biomass, an ecosystem model that incorporates projections of primary production, pelagic consumption, supply of pelagic carbon to the benthos, benthic biomass and bottom temperature; and that includes both the infaunal and epifaunal benthic community would be enlightening likely next step.

These predicted changes in amount of thermal habitat available to epibenthic invertebrates could have reverberating impacts on whole Arctic food webs. The most abundant taxa (in terms of biomass) in the cold-water and stenothermic cluster, a.k.a. the “losers”, were gastropods and the mussels *Musculus* sp. These taxa are prey to endangered Pacific walrus (*Odobenus rosmarus*), which is harvested as a food resource in native Alaskan communities (Hovelsrud et al., 2008; Sheffield et al., 2001; Sheffield and Grebmeier, 2009). They are also among the most frequently occurring prey taxa in the stomachs of commercial groundfish such as Pacific cod (*Gadus macrocephalus*) and Alaska pollock (*Gadus chalcogrammus*) in the Northern Bering Sea (A. Whitehouse, pers. com.; Alaska Fish Stomach Database https://www.fisheries.noaa.gov/resource/data/alaska-fish-stomach-database) and flatfish (yellowfin sole) in the Chukchi Sea (Whitehouse et al., 2017). The most abundant species in the warm-water and highly eurythermic cluster, a.k.a. the “winners”, was *Gorgonocephalus cf. arcticus*. They prey on zooplanktonic prey, such as euphausiids using their sticky tube feet and a sophisticated system of spines and hooks (Rosenberg et al., 2005). They have little nutritional value so likely have few predators.

The predicted changes in thermal habitat could also impact species diversity of the region. Thermal habitat for all taxa (except those with the broadest temperature range) contracted to the north, such that by the end of the century the projection was that south of 65 °N (Point Hope) there would only be suitable thermal habitat for the “winners”. This could have an impact on taxonomic diversity of the Bering-Chukchi Sea region because this cluster accounted for only 26 taxa or 8% of all taxa observed. Our diversity calculations are based on data with varying levels of taxonomic resolution, so this estimate may be biased low because of the inclusion of catch data at resolutions higher than species.

We did not examine whether North Pacific epibenthic invertebrate taxa, found south of the Bering Sea might find suitable habitat in a warming Bering Sea. However, the relatively shallow depths of the Bering

Sea shelf, compared to the depth of the slope and basin, might make the "new" habitat unsuitable for southern taxa. Analogous to the situation to the north, we suggest that the possibility of new species invading from the south with warming ocean temperatures might be constrained by the southern shelf break and slope. We also did not examine whether epibenthic invertebrates in the Gulf of Alaska could expand into the Bering Sea with ocean warming; this deserves further study.

A key assumption of our approach was that observed temperature ranges were representative of species physiological tolerances. Laboratory studies of thermal acclimation potential of Arctic epibenthic invertebrate megafauna are scarce. Richard et al. (2012) conducted laboratory experiments to determine the temperature limit of 4 species from Kongsfjorden in Svalbard: a sea urchin (*Strongylocentrotus droebachiensis*), a gastropod mollusk (*Margarites helicinus*), a bivalve mollusk (*Serripes groenlandicus*), and an amphipod of the genus Onisimus. They found that the sea urchin and the gastropod could acclimate to the highest experimental temperature, 10.3 °C. These two species were in the "warm, broad range" cluster in our analysis, although their temperature range (as defined by the 5th and 95th percentiles) was up to only 5.1 °C. Richard et al. (2012) conclude that their results that Arctic species could acclimate to high temperatures "appear anomalous", most likely because the Gulf Stream increases sea temperatures in Svalbard in summer to an average of 4 °C to 6.5 °C, more similar to temperate regions than to other polar regions. Indeed, these temperatures are higher than most of our study area. The climate variability hypothesis predicts that high seasonal variation in ocean temperature, such as observed in temperate regions (and in Svalbard), will result in greater ability to acclimate to increased temperature compared to environments with less seasonal temperature variability such as the tropics and polar regions (Stevens, 1989). Supporting this hypothesis, a number of thermal tolerance experiments have been conducted with Antarctic species and most have demonstrated a narrow thermal tolerance range (Morley et al., 2011; Peck et al., 2010, 2009b, 2009a). Laboratory acclimation experiments of Arctic taxa occurring in less variable and colder temperatures than Richard et al studied are needed. It's also important to note that temperature increases within physiological tolerance extremes, but outside the 'normal operating temperature range' of an organism can result in lower growth and reproduction (Pörtner and Knust, 2007; Wang and Overgaard, 2007).

Another key assumption of our work is that there will be no significant evolutionary adaptation to warming temperatures. Climate change in the Arctic has been rapid. Sea temperatures have risen 1-3 degrees in 40 years (Timmermans and Labe, 2020), and our projections are that sea temperatures are predicted to rise 4 degrees over the next 80 years. This increase is more rapid than has been observed over the past million years or on record over the last glacial cycle (PAGES 2k Consortium et al., 2019) and is faster than normal evolutionary timescales (Peck et al., 2009b). So we suggest that it is unlikely that Arctic benthic macrofauna will be able to evolutionarily adapt to such a rapid increase in ocean temperature.

Model projections of ocean bottom temperature suggest that by the end of the century there will be suitable thermal habitat available for only a small number of Arctic epibenthic invertebrate taxa. Temperature is one determinant of habitat, a full habitat model incorporating other parameters such as sediment type and export production coupled with an ecosystem model that captures trophic and competitive interactions would provide a more detailed picture of the possible future of Arctic benthic communities. In addition, more laboratory studies of thermal acclimation potentials of Arctic benthic invertebrates are clearly needed. Finally, continued monitoring of the distribution, abundance and species composition is needed to track changes and refine predictions about the future of this diverse and productive community that supports a number of upper trophic taxa including Arctic human communities.

Acknowledgements

The authors would like to acknowledge the efforts of all field-going personnel from the Alaska Fisheries Science Center Resource Assessment and Conservation Engineering Program. The ideas for this project were generated at workshops supported by the Nordic Council, AG-FISK (Project number: (159)-2017-Arctic biodiversity). Louise Copemen and Mike Litzow (NOAA AFSC) provided valuable comments that improved to quality of the manuscript. This manuscript is a product of the NPRB Arctic Integrated Ecosystem Research Program [NPRB publication number: ArcticIERP-XX]; and is FOCI Publication #XXXX.

References

Aagaard, K., Coachman, L.K., Carmack, E., 1981. On the halocline of the Arctic Ocean. Deep Sea Res. Part A. Oceanogr. Res. Pap. 28, 529–545.

Abookire, A.A., Rose, C.S., 2005. Modifications to a plumb staff beam trawl for sampling uneven, complex habitats. Fish. Res. 71, 247–254.

Alabia, I.D., García Molinos, J., Saitoh, S.I., Hirawake, T., Hirata, T., Mueter, F.J., 2018. Distribution shifts of marine taxa in the Pacific Arctic under contemporary climate changes. Divers. Distrib. 24, 1583–1597. https://doi.org/10.1111/ddi.12788

Aune, M., Aschan, M.M., Greenacre, M., Dolgov, A. V., Fossheim, M., Primicerio, R., 2018. Functional roles and redundancy of demersal Barents sea fish: Ecological implications of environmental change. PLoS One 13, 1–21. https://doi.org/10.1371/journal.pone.0207451

Baker, M.R., Farley, E. V., Ladd, C., Danielson, S.L., Stafford, K.M., Huntington, H.P., Dickson, D.M.S., 2020. Integrated ecosystem research in the Pacific Arctic – understanding ecosystem processes, timing and change. Deep Sea Res. Part II Top. Stud. Oceanogr. 177, 104850. https://doi.org/10.1016/j.dsr2.2020.104850

Bluhm, B.A., Gradinger, R., 2008. Regional variability in food availability for arctic marine mammals, in: Ecological Applications. pp. S77–S96.

Bluhm, B.A., Iken, K., Hardy, S.M., Sirenko, B.I., Holladay, B.A., 2009. Community structure of epibenthic megafauna in the Chukchi Sea. Aquat. Biol. 7, 269–293.

Bock, H.-H., 2008. Origins and extensions of the k-means algorithm in cluster analysis. J. Électronique d'Histoire des Probab. la Stat. [electronic only] 4.

Chown, S.L., Gaston, K.J., Robinson, D., 2004. Macrophysiology: large-scale patterns in physiological. Funct. Ecol. 18, 159–167.

Coachman, L.K., 1986. Circulation, water masses, and fluxes on the southeastern Bering Sea shelf. Cont. Shelf Res. 8, 758–772.

Coachman, L.K., Aagaard, K., Tripp, R.B., 1975. Bering Strait: The Regional Physical Oceanography. University of Washington Press.

Dalpadado, P., Arrigo, K.R., van Dijken, G.L., Skjoldal, H.R., Bagøien, E., Dolgov, A. V., Prokopchuk, I.P., Sperfeld, E., 2020. Climate effects on temporal and spatial dynamics of phytoplankton and zooplankton in the Barents Sea. Prog. Oceanogr. 185, 102320. https://doi.org/10.1016/j.pocean.2020.102320

Danielson, S.L., Eisner, L., Ladd, C., Mordy, C., Sousa, L., Weingartner, T.J., 2016. A comparison between late summer 2012 and 2013 water masses, macronutrients, and phytoplankton standing crops in the northern Bering and Chukchi Seas. Deep Sea Res. Part II Top. Stud. Oceanogr. 1–20. https://doi.org/10.1016/j.dsr2.2016.05.024

Davis, G.E., Baumgartner, M.F., Corkeron, P.J., Bell, J., Berchok, C., Bonnell, J.M., Bort Thornton, J., Brault, S., Buchanan, G.A., Cholewiak, D.M., Clark, C.W., Delarue, J., Hatch, L.T., Klinck, H., Kraus, S.D., Martin, B., Mellinger, D.K., Moors-Murphy, H., Nieukirk, S., Nowacek, D.P., Parks, S.E., Parry, D., Pegg, N., Read, A.J., Rice, A.N., Risch, D., Scott, A., Soldevilla, M.S., Stafford, K.M., Stanistreet, J.E., Summers, E., Todd, S., Van Parijs, S.M., 2020. Exploring movement patterns and changing distributions of baleen whales in the western North Atlantic using a decade of passive acoustic data. Glob. Chang. Biol. 26, 4812–4840. https://doi.org/10.1111/gcb.15191

Eisner, L.B., Napp, J.M., Mier, K.L., Pinchuk, A.I., Andrews, A.G., 2014. Climate-mediated changes in zooplankton community structure for the eastern Bering Sea. Deep. Res. Part II Top. Stud. Oceanogr. 109, 157–171. https://doi.org/10.1016/j.dsr2.2014.03.004

Fedewa, E.J., Jackson, T.M., Richar, J.I., Gardner, J.L., Litzow, M.A., 2020. Recent shifts in northern Bering Sea snow crab (Chionoecetes opilio) size structure and the potential role of climate-mediated range contraction. Deep. Res. Part II Top. Stud. Oceanogr. 181–182, 104878. https://doi.org/10.1016/j.dsr2.2020.104878

Gall, A.E., Morgan, T.C., Day, R.H., Kuletz, K.J., 2016. Ecological shift from piscivorous to planktivorous seabirds in the Chukchi Sea, 1975–2012. Polar Biol. https://doi.org/10.1007/s00300-016-1924-z

Grebmeier, J.M., 2012. Shifting Patterns of Life in the Pacific Arctic and Sub-Arctic Seas. Annu. Rev. Mar. Sci. Vol 4 4, 63–78. https://doi.org/10.1146/annurev-marine-120710-100926

Grebmeier, J.M., Frey, K.E., Cooper, L.W., Kędra, M., 2018. Trends in benthic macrofaunal populations, seasonal sea ice persistence, and bottom water temperatures in the bering strait region. Oceanography 31, 136–151. https://doi.org/10.5670/oceanog.2018.224

Grebmeier, J.M., Overland, J.E., Moore, S.E., Farley, E. V, Carmack, E.C., Cooper, L.W., Frey, K.E., Helle, J.H., McLaughlin, F.A., McNutt, S.L., 2006. A major ecosystem shift in the northern Bering Sea. Science (80-.). 311, 1461–1646.

Hiatt, T., Dalton, M., Felthoven, R., Fissel, B., Garber-yonts, B., Haynie, A., Himes-Cornell, A., Kasperski, S., Lee, J., Lew, D., Pfeiffer, L., Sepez, J., Seung, C., 2021. Stock Assessment and Fishery Evaluation Report for the Groundfish Fisheries fo the Gulf of Alaska and Bering Sea/Aleutian Islands Area: Economic Status of the Groundfish Fisheries Off Alaska, 2010. 292.

Hovelsrud, G., McKenna, M., Huntington, H.P., 2008. Marine mammal harvests and other interactions with humans. Ecol. Appl. 18, 135–147.

Hunt, G.L., Blanchard, A., Boveng, P.L., Dalpadado, P., Drinkwater, K.F., Eisner, L.B., Hopcroft, R.R., Kovacs, K.M., Norcross, B.L., Renaud, P., Reigstad, M., Renner, M., Skjoldal, H.R., Whitehouse, A., Woodgate, R.A., 2013. The Barents and Chukchi Seas: Comparison of two Arctic shelf ecosystems. J. Mar. Sys. 109-110: 43-68

Huntington, H.P., 2000. Impacts of changes in sea ice and other environmental parameters in the Arctic. Final Report of the Marine Mammal Commission Workshop, Girdwood, Alaska, 15-17 February 2000. 135 p.

Huntington, H.P., Danielson, S.L., Wiese, F.K., Baker, M., Boveng, P., Citta, J.J., De Robertis, A., Dickson, D.M.S., Farley, E., George, J.C., Iken, K., Kimmel, D.G., Kuletz, K., Ladd, C., Levine, R., Quakenbush, L., Stabeno, P., Stafford, K.M., Stockwell, D., Wilson, C., 2020. Evidence suggests potential transformation of the Pacific Arctic ecosystem is underway. Nat. Clim. Chang. 10, 342–348. https://doi.org/10.1038/s41558-020-0695-2

IPCC, 2014. Climate Change 2014: Synthesis Report. Contribution of Working Groups I, II and III to the Fifth Assessment Report of the Intergovernmental Panel on Climate Change. IPCC, Geneva, Switzerland. https://doi.org/10.1016/S0022-0248(00)00575-3

Laidre, K.L., Stern, H., Kovacs, K.M., Lowry, L., Moore, S.E., Regehr, E. V, Ferguson, S.H., Wiig, Ø., Boveng, P., Angliss, R.P., Born, E.W., Litovka, D., Quakenbush, L., Lydersen, C., Vongraven, D., Ugarte, F., 2015. Arctic marine mammal population status , sea ice habitat loss , and conservation recommendations for the 21st century 00, 1–14. https://doi.org/10.1111/cobi.12474

Lauth, R.R., 2011. Results of the 2010 Eastern and Northern Bering Sea Continental Shelf Bottom Trawl Survey of Groundfish and Invertebrate Fauna. NOAA Tech. Memo. NMFS-AFSC-227. 265 p.

Lauth, R.R., Dawson, E.J., Conner, J., 2019. Results of the 2017 Eastern and Northern Bering Sea Continental Shelf Bottom Trawl Survey of Groundfish and Invertebrate Fauna. NOAA Tech. Memo. NMFS-AFSC-396. 270 p.

Morley, S.A., Lemmon, V., Obermüller, B.E., Spicer, J.I., Clark, M.S., Peck, L.S., 2011. Duration tenacity: A method for assessing acclimatory capacity of the Antarctic limpet, Nacella concinna. J. Exp. Mar. Bio. Ecol. 399, 39–42. https://doi.org/10.1016/j.jembe.2011.01.013

Mueter, F.J., Litzow, M.A., 2008. Sea ice retreat alters the biogeography of the Bering Sea continental shelf. Ecol. Appl. 18, 309–20.
Mueter, F.J., Weems, J., Farley, E. V, Sigler, M.F., 2017. Arctic Ecosystem Integrated Survey (Arctic Eis): Marine ecosystem dynamics in the rapidly changing Pacific Arctic Gateway. Deep Sea Res. II 135, 1–6. https://doi.org/10.1016/j.dsr2.2016.11.005
North Pacific Fishery Management Council, 2009. Fishery Management Plan for Fish Resources of the Arctic Management Area. North Pacific Fishery Management Council 605 W. 4th Avenue, Suite 306 Anchorage, Alaska 99501. 146 p.
Packer, D.B., Watling, L., Langton, R.W., 1994. The population structure of the brittle star Ophiura sarsi Lütken in the Gulf of Maine and its trophic relationship to American plaice (*Hippoglossoides platessoides* Fabricius). J. Exp. Biol. Ecol. 179, 207–222.
PAGES 2k Consortium, Neukom, R., Barboza, L.A., Erb, M.P., Shi, F., Emile-Geay, J., Evans, M.N., Franke, J., Kaufman, D.S., Lücke, L., Rehfeld, K., Schurer, A., Zhu, F., Brönnimann, S., Hakim, G.J., Henley, B.J., Ljungqvist, F.C., McKay, N., Valler, V., von Gunten, L., 2019. Consistent multidecadal variability in global temperature reconstructions and simulations over the Common Era. Nat. Geosci. 12, 643–649. https://doi.org/10.1038/s41561-019-0400-0
Parada, C., Armstrong, D.A., Ernst, B., Hinckley, S., Orensanz, J.M., 2010. Spatial dynamics of snow crab (*Chionoecetes opilio*) in the eastern bering sea-putting together the pieces of the puzzle. Bull. Mar. Sci. 86, 413–437.
Peck, L.S., Clark, M.S., Morley, S.A., Massey, A., Rossetti, H., 2009a. Animal temperature limits and ecological relevance: Effects of size, activity and rates of change. Funct. Ecol. 23, 248–256. https://doi.org/10.1111/j.1365-2435.2008.01537.x
Peck, L.S., Massey, A., Thorne, M.A.S., Clark, M.S., 2009b. Lack of acclimation in Ophionotus victoriae: Brittle stars are not fish. Polar Biol. 32, 399–402. https://doi.org/10.1007/s00300-008-0532-y
Peck, L.S., Morley, S.A., Clark, M.S., 2010. Poor acclimation capacities in Antarctic marine ectotherms. Mar. Biol. 157, 2051–2059. https://doi.org/10.1007/s00227-010-1473-x
Polyakov, I. V., Alkire, M.B., Bluhm, B.A., Brown, K.A., Carmack, E.C., Chierici, M., Danielson, S.L., Ellingsen, I., Ershova, E.A., Gårdfeldt, K., Ingvaldsen, R.B., Pnyushkov, A. V., Slagstad, D., Wassmann, P., 2020. Borealization of the Arctic Ocean in Response to Anomalous Advection From Sub-Arctic Seas. Front. Mar. Sci. 7. https://doi.org/10.3389/fmars.2020.00491
Pörtner, H., Knust, R., 2007. Climate change affects marine fishes through the oxygen limiation of thermal tolerance. Science. 315, 95–97. https://doi.org/10.1259/0007-1285-53-633-920-b
Pörtner, H.O., 2010. Oxygen- And capacity-limitation of thermal tolerance: A matrix for integrating climate-related stressor effects in marine ecosystems. J. Exp. Biol. 213, 881–893. https://doi.org/10.1242/jeb.037523
Rand, K., Logerwell, E., Bluhm, B., Chenelot, H., Danielson, S., Iken, K., Sousa, L., 2018. Using biological traits and environmental variables to characterize two Arctic epibenthic invertebrate communities in and adjacent to Barrow Canyon. Deep. Res. Part II Top. Stud. Oceanogr. 152, 154–169. https://doi.org/10.1016/j.dsr2.2017.07.015
Renaud, P.E., Sejr, M.K., Bluhm, B.A., Sirenko, B., Ellingsen, I.H., 2015. The future of Arctic benthos: Expansion, invasion, and biodiversity. Prog. Oceanogr. 139, 244–257. https://doi.org/10.1016/j.pocean.2015.07.007
Richard, J., Morley, S.A., Deloffre, J., Peck, L.S., 2012. Thermal acclimation capacity for four Arctic marine benthic species. J. Exp. Mar. Bio. Ecol. 424–425, 38–43. https://doi.org/10.1016/j.jembe.2012.01.010
Rosenberg, R., Dupont, S., Lundälv, T., Sköld, H.N., Norkko, A., Roth, J., Stach, T., Thorndyke, M., 2005. Biology of the basket star *Gorgonocephalus caputmedusae* (L.). Mar. Biol. 148, 43–50. https://doi.org/10.1007/s00227-005-0032-3
Sheffield, G., Fay, F.H., Feder, H., Kelly, B.P., 2001. Laboratory digestion of prey and interpretation of walrus stomach contents. Mar. Mammal Sci. 17, 310–330. https://doi.org/10.1111/j.1748-7692.2001.tb01273.x

Sheffield, G., Grebmeier, J.M., 2009. Pacific walrus (*Odobenus rosmarus divergens*): Differential prey digestion and diet. Mar. Mammal Sci. 25, 761–777. https://doi.org/10.1111/j.1748-7692.2009.00316.x

Solan, M., Ward, E.R., Wood, C.L., Reed, A.J., Grange, L.J., Godbold, J.A., 2020. Climate-driven benthic invertebrate activity and biogeochemical functioning across the Barents Sea polar front. Philos. Trans. R. Soc. A 378, 20190365.

Stauffer, G.D., 2004. NOAA protocols for groundfish bottom trawl surveys of the nation's fishery resources. U.S. Dep. Commer., NOAA Tech Memo NMFS-SPO-6, 205 p.

Stevens, G.C., 1989. The Latitudinal gradient in geographical range : How so many species coexist in the tropics. Am. Nat. 133, 240–256.

Timmermans, M.-L., Labe, Z., 2020. Sea Surface Temperature. NOAA Arctic Rep. Card 2020, 53–57. https://doi.org/10.25923/v0fs-m920

Walsh, J., McRoy, C., Coachman, L.K., Goering, J.J., Nihoul, J.J., Whitledge, T.E., Blackburn, T.H., Parker, P.L., Wirick, C.D., Shuert, P.G., Grebmeier, J.M., Springer, A.M., Tripp, R.D., Hansell, D.A., Djenidi, S., Deleersnijder, E., Henriksen, K., Lund, B.A., Andersen, P., Muller-Krager, F.E., Dean, K., 1989. Carbon and nitrogen cycling within the Bering/Chukchi Seas: Source regions for organic matter effecting AOU demands of the Arctic Ocean. Prog. Oceanogr. 22, 277–359.

Wang, M., Yang, Q., Overland, J.E., Stabeno, P., 2018. Sea-ice cover timing in the Pacific Arctic: The present and projections to mid-century by selected CMIP5 models. Deep. Res. Part II Top. Stud. Oceanogr. 152, 22–34. https://doi.org/10.1016/j.dsr2.2017.11.017

Wang, T., Overgaard, J., 2007. The heartbreak of adapting to global warming. Science 315, 49–50. https://doi.org/10.1126/science.1137359

Whitehouse, G.A., Buckley, T.W., Danielson, S.L., 2017. Diet compositions and trophic guild structure of the demersal fish community in the eastern Chukchi Sea. Deep. Res. Part II 135, 95-110. https://doi.org/10.1016/j.dsr2.2016.03.010

Wisz, M.S., Broennimann, O., Grønkjær, P., Møller, P.R., Olsen, S.M., Swingedouw, D., 2015. Arctic warming will promote Atlantic – Pacific fish interchange. Nat. Clim. Chang. 1–5. https://doi.org/10.1038/NCLIMATE2500

Zacher, L.S., Richar, J.I., Litzow, M.A., 2021. The 2021 Eastern Bering Sea Continental Shelf Trawl Survey: Results for Commercial Crab Species. Draft NOAA Tech. Memo. NMFS-AFSC, 193 p.

Table 1. Median temperature and range for each cluster and percent of species in each cluster. “Cold” clusters are those which median temperatures 0.6° C or less and “warm” clusters are those with median temperatures 2.5° C or greater (arbitrarily defined). “Stenothermic” clusters are those with a range (5^{th} to 95^{th} percentile) of 3.5° C or less; “eurythermic” clusters are those with a range of 5.5° to 6° C and the “highly eurythermic” cluster has a range of 9.0° C (arbitrarily defined). Number and percent of taxa and percent catch biomass density are also shown

Cluster	Median temperature	Temperature range (°C)	Magnitude of range	Qualitative descriptors	# of taxa	% kg km_2
A	-0.3	-1.5° – 2.0°	3.5°	cold, stenothermic	40 (12%)	9%
B	0.6	-1.4° – 4.6°	6.0°	cold, eurythermic	65 (21%)	49%
C	3.4	1.8° – 4.6°	2.8°	warm, stenothermic	60 (19%)	2%
D	2.5	-0.5° – 5.1°	5.5°	warm, eurythermic	119 (38%)	38%
E	2.8	-0.7° – 8.3°	9.0°	warm, highly eurythermic	26 (8%)	3%

Table 2. Percent catch by species (or lowest taxon) in each cluster. Taxa with percent catch greater than or equal to 0.1% are shown, the rest of the catch is summed and shown as 'Other'.

Cluster A "cold, stenothermic" taxa	
Taxon	% kg km^{-2}
Gastropoda	3.8%
Musculus sp.	3.0%
Urasterias lincki	0.4%
Solaster dawsoni	0.3%
Golfingia (Golfingia) margaritacea	0.3%
Myriotrochus rinkii	0.2%
Naticidae	0.2%
Buccinum glaciale	0.1%
Margarites	0.1%
Pandalidae	0.1%
Other	0.2%
Grand Total	9%

Cluster C "warm, stenothermic" taxa	
Taxon	% kg km^{-2}
Nuculana radiata	1%
Pyrulofusus sp.	0.4%
Alcyonidium gelatinosum	0.1%
Other	0.04%
Grand Total	2%

Cluster D "warm, eurythermic" taxa	
Taxon	% kg km^{-2}
Chionoecetes opilio	9%
Bivalvia	4%
Ctenodiscus crispatus	4%
Asterias amurensis	3%
Actiniaria	2%
Echinarachnius parma	2%

Alcyonidium disciforme	1%
Gorgonocephalus sp.	1%
Strongylocentrotus sp.	1%
Porifera	1%
Pagurus trigonocheirus	1%
Hyas coarctatus	1%
Solaster sp.	1%
Neptunea heros	1%
Ennucula tenuis	0.4%
Evasterias echinosoma	0.4%
Cyanea capillata	0.4%
Neptunea sp.	0.4%
Neocrangon communis	0.4%
Gersemia sp.	0.3%
Eucratea loricata	0.3%
Stomphia sp.	0.3%
Cryptonatica affinis	0.3%
Buccinum scalariforme	0.2%
Strongylocentrotus droebachiensis	0.2%
Bryozoa	0.2%
Gorgonocephalus eucnemis	0.2%
Labidochirus splendescens	0.2%
Chrysaora melanaster	0.2%
Pyrulofusus deformis	0.2%
Boltenia ovifera	0.1%
Styela rustica	0.1%
Neptunea communis	0.1%
Scyphozoa	0.1%
Eualus fabricii	0.1%
Ascidiacea	0.1%
Lethasterias nanimensis	0.1%
Eualus belcheri	0.1%
Pagurus capillatus	0.1%
Cistenides sp.	0.1%

Hyas lyratus	0.1%
Anonyx sp.	0.1%
Beringius sp.	0.1%
Neptunea ventricosa	0.1%
Tachyrhynchus erosus	0.1%
Crangon dalli	0.1%
Other	0.6%
Grand Total	37.5%

Cluster E "warm, highly eurythermic" taxa	
Taxon	% kg km^{-2}
Gorgonocephalus cf. arcticus	2%
Argis lar	0.3%
Balanus sp.	0.3%
Sclerocrangon boreas	0.2%
Urticina crassicornis	0.1%
Argis dentata	0.1%
Stegophiura nodosa	0.1%
Other	0.1%
Grand Total	3%

Table 3. Mean survey bottom temperature, decadal averages from the ensemble mean of the bottom temperature projection models, and temperature increases from present to mid-century and end-of-century (°C)

Domain	Survey	2008-2017	2045-2054	2091-2100	Present to mid-century	Present to end-of-century
North	1.77	0.98	2.25	5.60	1.27	4.62
South	2.86	3.83	5.15	8.10	1.32	4.27

Table 4. Proportion of area within temperature range of each cluster based on model projections of bottom temperature at present (2008-2017), mid-century (2045-2054), and end of century (2091-2100).

			Proportion of area within temperature range			
Cluster	**Temperature range**	**Qualitative descriptors**	**Present**	**Mid-century**	**End- century**	**# of Species**
A	-1.5° – 2.0°	cold, stenothermic	31%	13%	2%	40 (12%)
B	-1.4° – 4.6°	cold, eurythermic	88%	51%	10%	65 (21%)
C	1.8° – 4.6°	warm, stenothermic	61%	38%	8%	60 (19%)
D	-0.5° – 5.1°	warm, eurythermic	88%	64%	13%	119 (38%)
E	-0.7° – 8.3°	warm, highly eurythermic	96%	98%	72%	26 (8%)

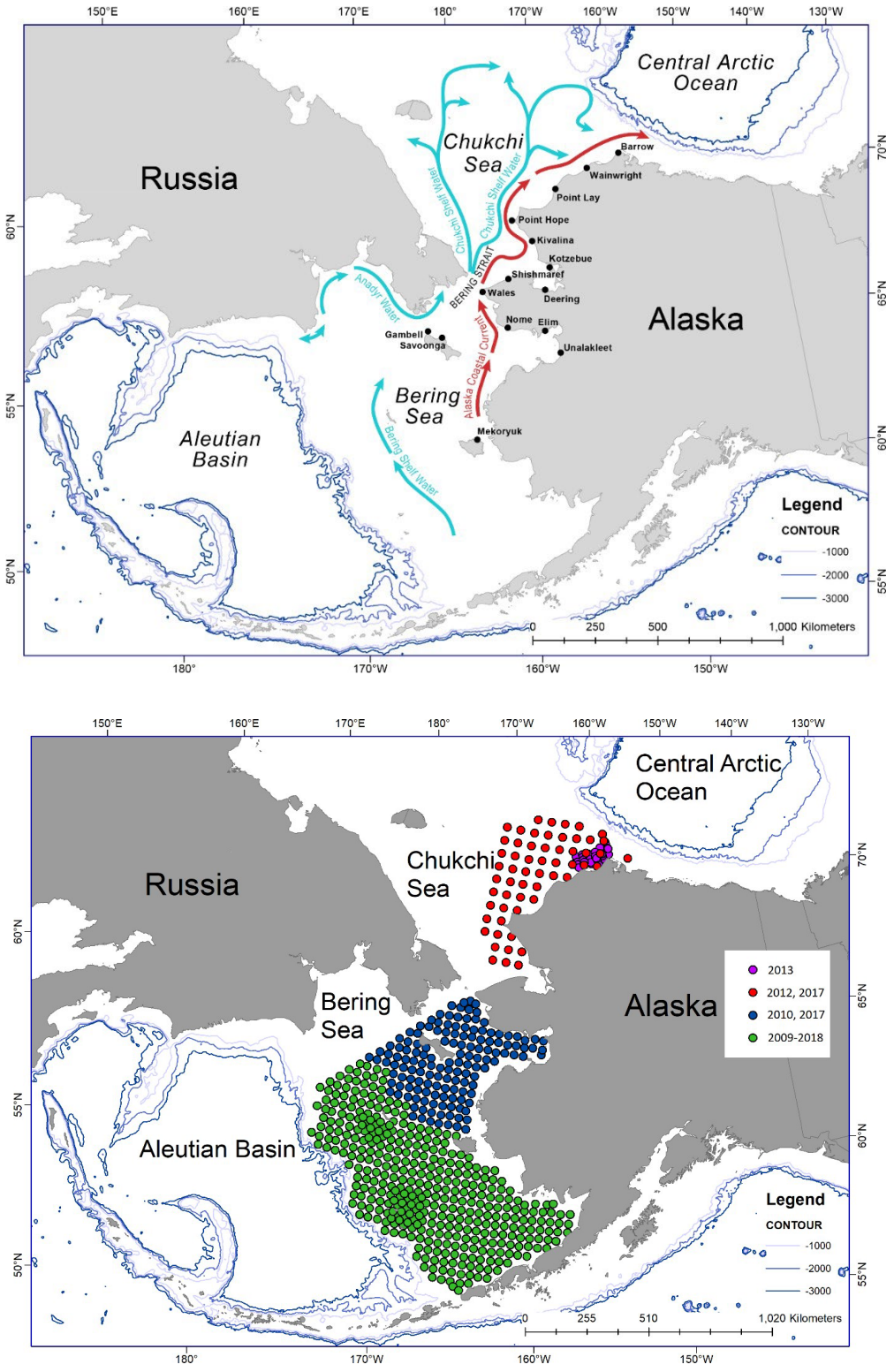

Figure 1. a) The Bering Sea and Chukchi Sea study area showing shelf breaks, Aleutian Basin, Central Arctic Ocean, Bering Strait, currents and/or typical water mass pathways and coastal human communities, b) Stations and years of survey data used in the analysis.

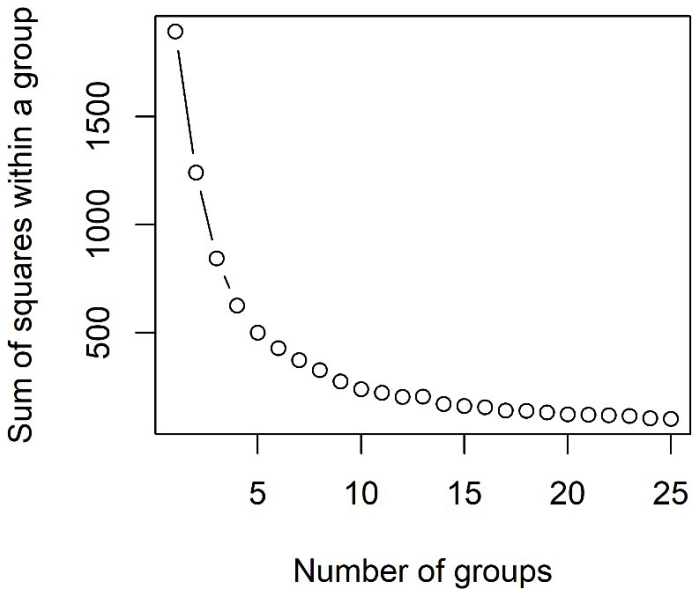

Figure 2. Relationship between number of groups in k-means clustering and within-cluster variance (sum of squares).

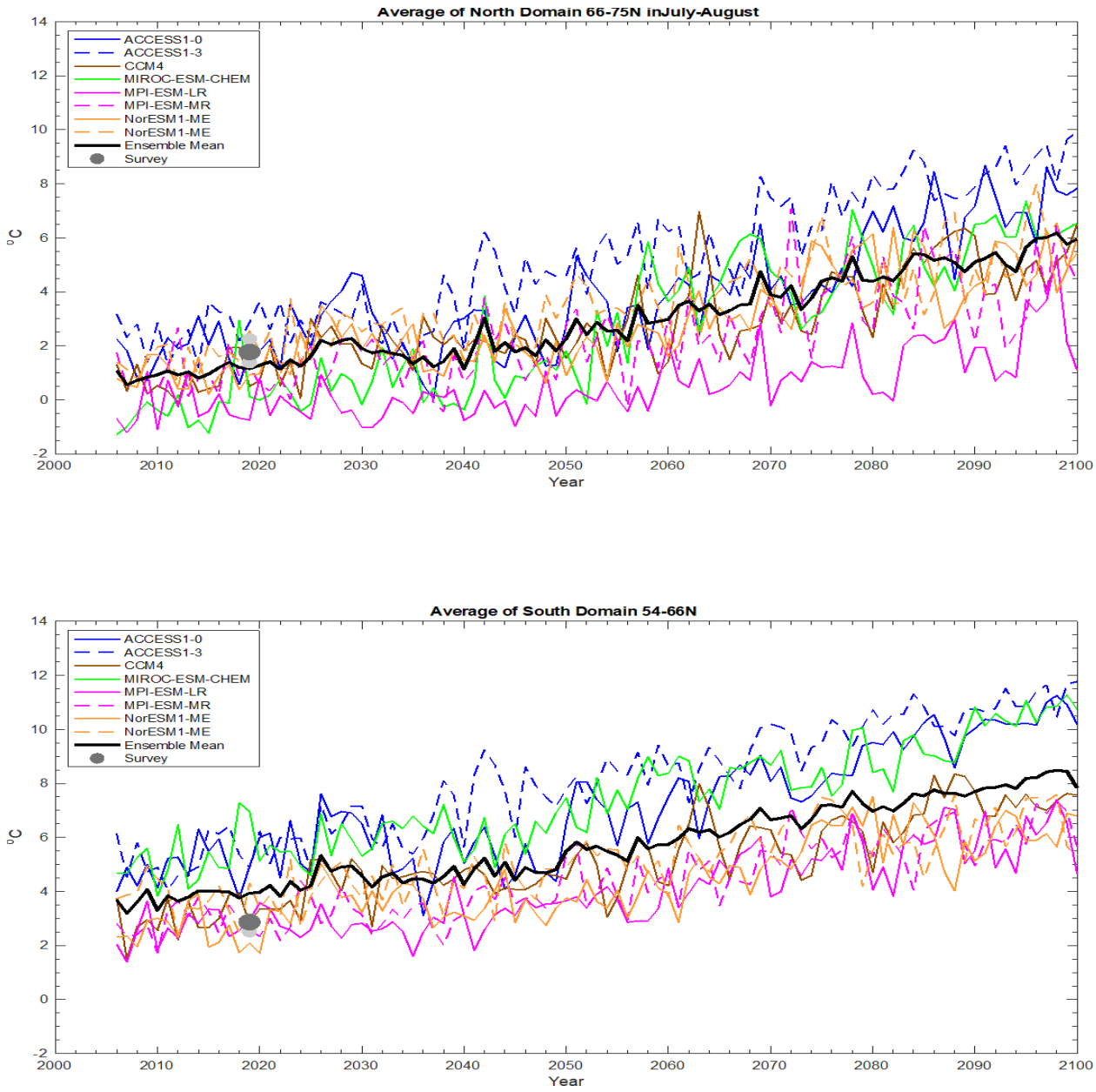

Figure 3. Time series of July and August bottom temperature interpolated to the survey grid and then averaged over the Northern (66-75 °N) and southern (54-66 °N) domain. Thin colored lines are based on each individual model, and thick black line indicates the ensemble mean of the eight models. Grey dots are the based on survey data (light grey dots are survey mean bottom temperature interpolated on the grid of each model; dark grey dot is the mean).

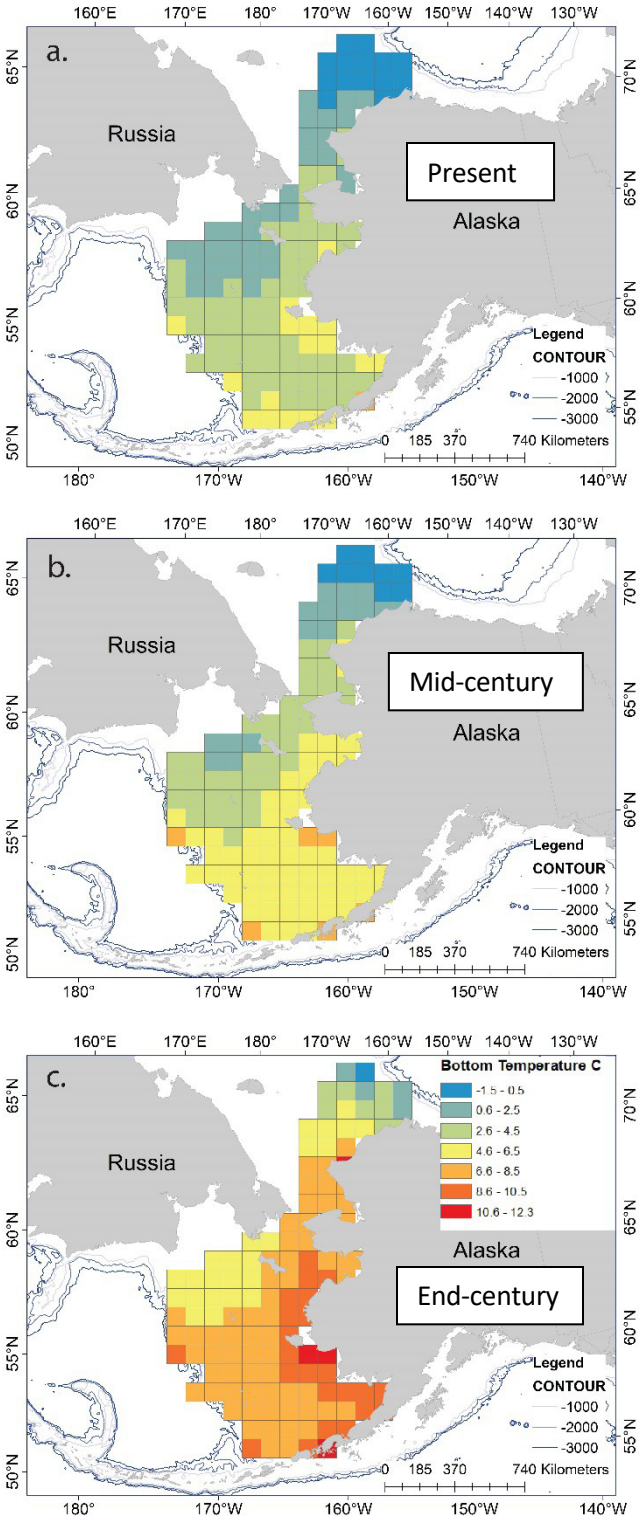

Figure 4. Maps of bottom temperature forecasts (average of 8 models): a) present (2008-2017), b) mid-century (2045-2054), c) end of century (2091-2100).

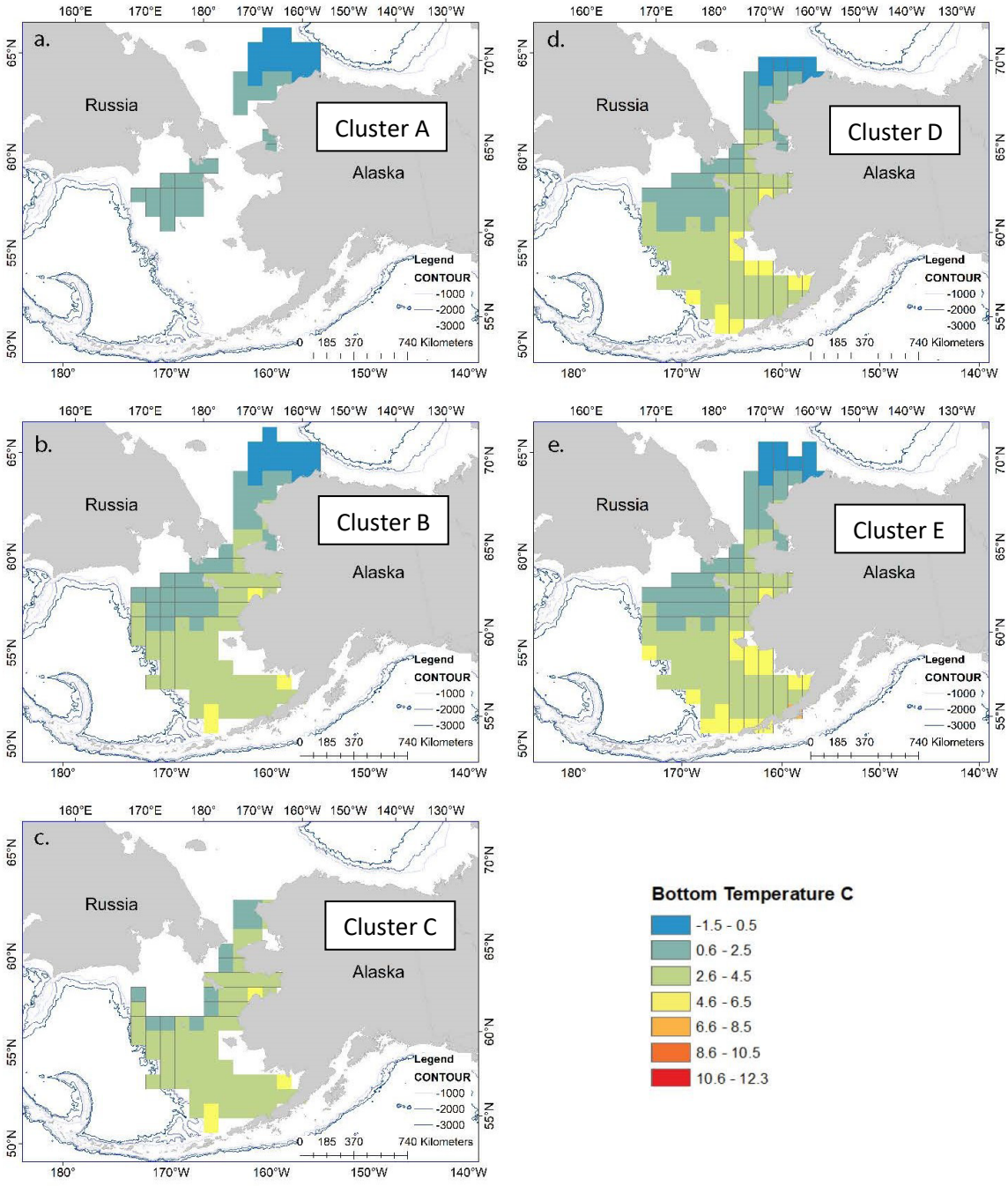

Figure 5. Maps of temperature-defined habitat for each cluster based on present day model forecasts.

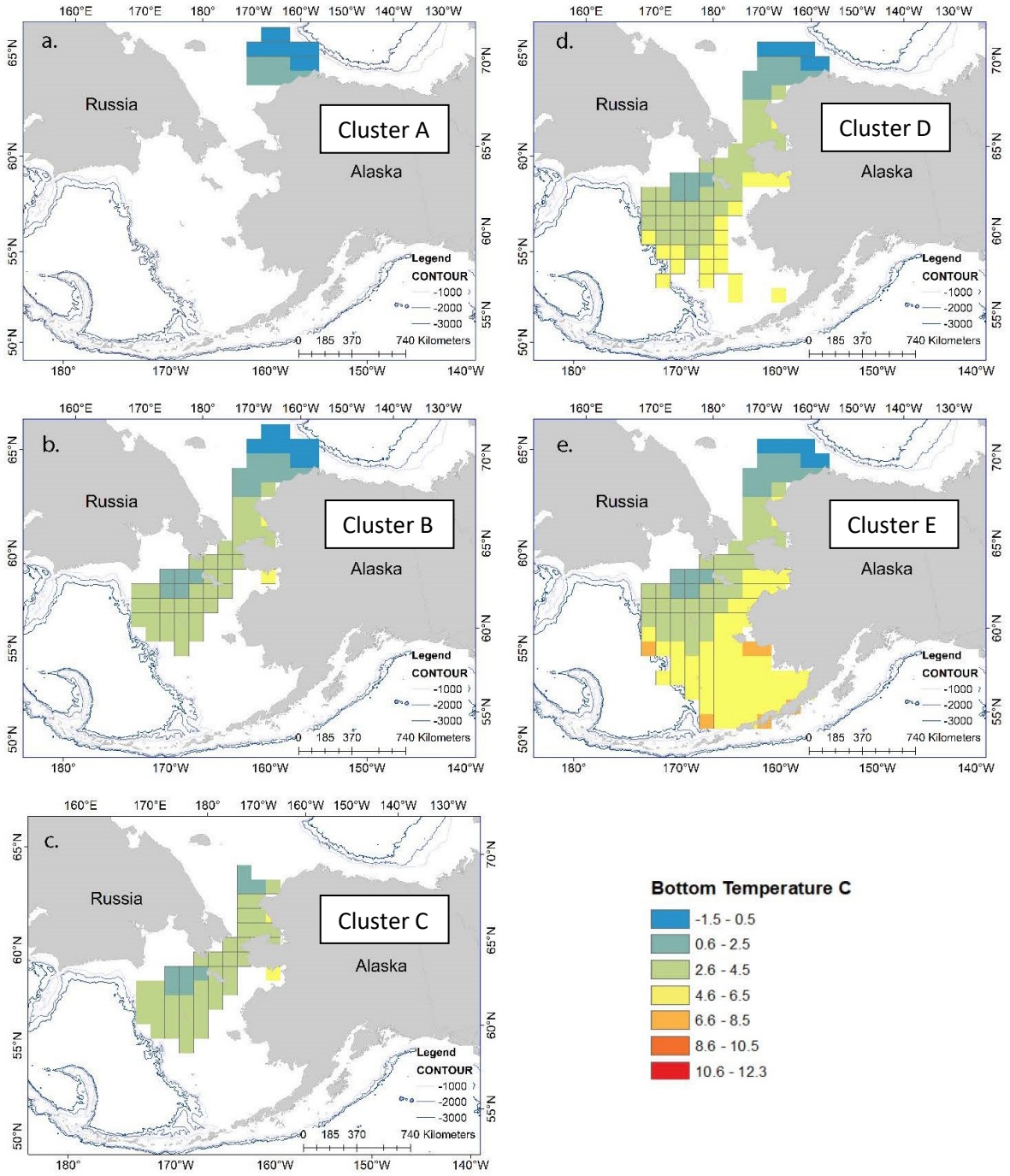

Figure 6. Maps of temperature-defined habitat for each cluster based on mid-century model forecasts.

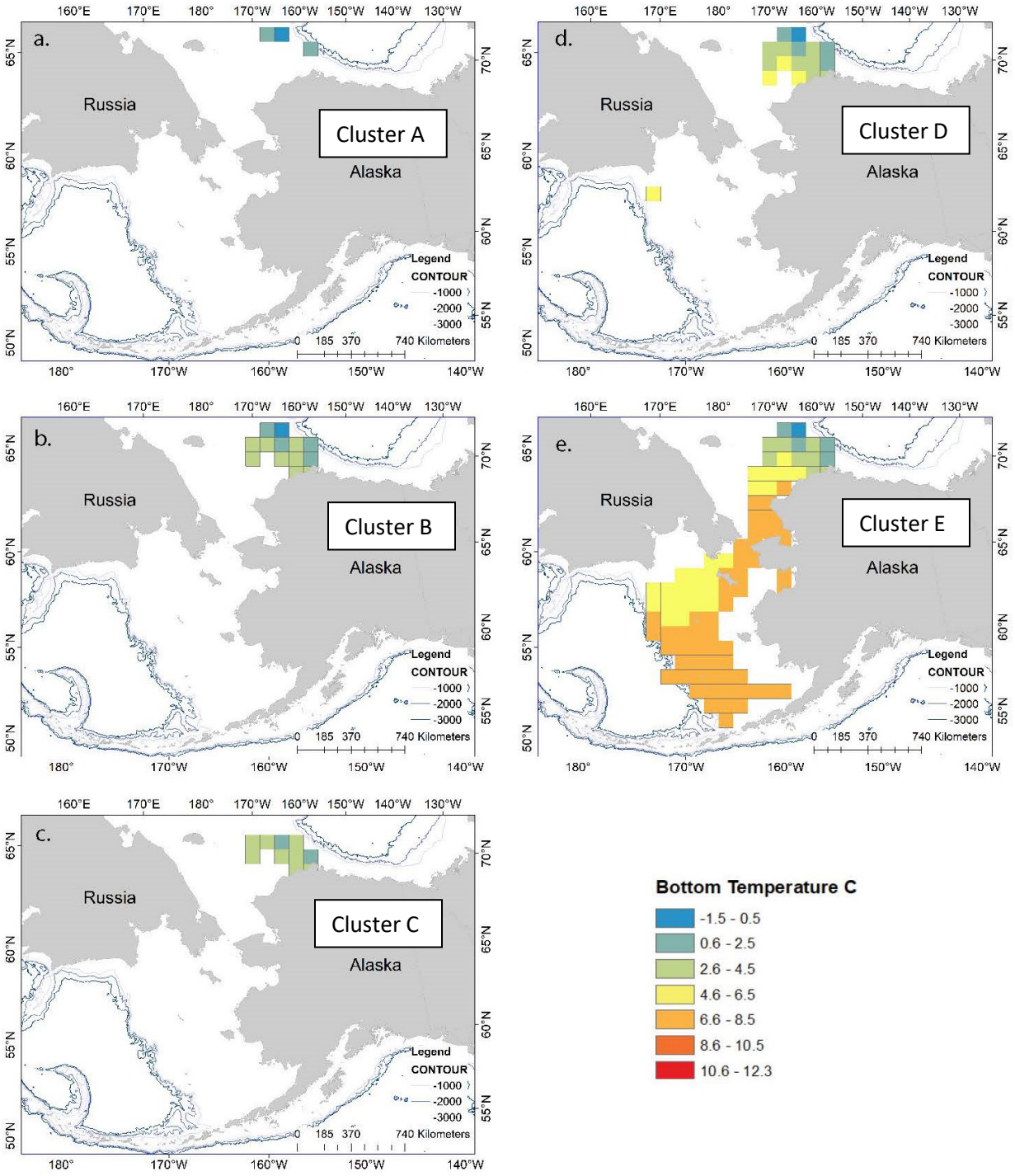

Figure 7. Maps of temperature-defined habitat for each cluster based on end-of-century model forecasts.

CHAPTER 2 - Late summer distribution and abundance of pelagic larval crab communities, including blue king crab and snow crab, in the Pacific Arctic Gateway

Objective 1: Quantify the distribution, abundance, and condition of demersal fishes and shellfishes

Jared Weems[1], Alexei Pinchuk[1], David Kimmel[2], and Franz Mueter[1]
[1]UAF, College of Fisheries and Ocean Sciences, Juneau, AK
[2] NOAA, Alaska Fisheries Science Center, Seattle, WA

Abstract

This multiyear study establishes a critical baseline of late summer larval crab abundance and distribution across the northern Bering and Chukchi seas. We present a snapshot of larval crab community dynamics over space and time for three environmentally contrasting years: 2012 (cold), 2013 (average), and 2017 (warm). Preliminary data summaries suggest spaciotemporal differences in larval crab communities across years are driven by both survey design (sampling date) and variable environmental conditions (temperature, salinity, and water mass distribution). Snow crab larval stages, the most abundant and ubiquitously distributed species in our datasets, provide evidence that mature female crab inhabiting the northern Bering Sea, Chukchi Shelf, and deeper waters in Barrow Canyon and on the Chukchi and Beaufort slopes all potentially supply larvae to the Chukchi Shelf in late summer through hypothesized south-north advection and north-south upwelling processes. Additionally, the Chirikov Basin appears to be an important megalopae settlement area for snow crab larvae advected into the region with southern Bering Sea Shelf Waters (BSSW) or western Anadyr Water. Rare observations of blue king crab larvae were associated with colder BSSW in the southern and central Chukchi Sea in 2012, suggesting that they originated in northern Bering Sea nearshore island habitats known to harbor adult spawners. Larval community distributions remained relatively consistent across years and regions, though abundances were variable. Comparison of stage groups by region suggests possible advanced development in warmer years (2013 & 2017) relative to the colder year (2012). Warming conditions may accelerate either pelagic larval development or benthic adult spawning and hatch release timing. These results provide the most comprehensive assessment of pelagic crab in the northern Bering Sea and Chukchi Sea to date. Future analyses of these data could provide information on early life history survivorship in changing pelagic environments and potentially identify nursery areas for settling post-larval and early instar crabs in the benthos.

Introduction

Planktonic crab larvae are common constituents of zooplankton communities over the Pacific Arctic shelf during summer (Eisner et al., 2013; Landeira et al., 2017). Few studies have examined the distribution and abundance of pelagic larval and settling crabs in Pacific Arctic large marine ecosystems (e.g. Ershova et al., 2019; Landeira et al., 2017). The paucity of crab early life history data severely limits our understanding of crab settlement dynamics and benthic recruitment throughout the region. Current impediments include under-reported or Family aggregated larval abundance estimates, lack of taxonomic and stage-specific resolution in species of non-commercial interest, and poor understanding of larval crab biology in Arctic environments. Recently described larval crab planktonic communities at select areas in the Bering and Chukchi seas show distinct species-specific spatial distributions between two sampling years (Landeira et al., 2017). While Landeira et al. provided the first taxonomically complete description of crab larvae in the Chukchi Sea, comprehensive species and stage-specific distributions and abundances have not been described and associations with adult populations and environmental conditions remain vague.

Pacific subarctic crabs are important subsistence and socioeconomic resources in the region. Adult and juvenile snow crabs are ubiquitous and abundant throughout the Bering Sea and Chukchi Sea (Bluhm et al., 2009; Zheng and Kruse, 2006). Mechanisms for advection of larvae and recruitment of post-larval settlers to the benthos have been hypothesized, such as the Environmental Ratchet Hypothesis for southeastern Bering Sea snow crab (Orensanz et al., 2004; Parada et al., 2010) and variable larval transport of Bristol Bay red king crab with climate change (Daly et al., 2020). To the north in the Chirikov Basin, a hot spot for settling megalopae has been hypothesized based on an over-abundance of early juvenile instars observed in bottom trawls (Kolts et al., 2015). These studies describe oceanographic advection and the location of adult female spawners as primary factors contributing to successful settlement of crab in the Bering Sea. These results rely heavily on model-estimated larval transport; however, model validation is difficult and the parameterization of larval behaviors are largely based on laboratory studies. Without integration of field-observed larval data, we cannot verify model assumptions about early life history dynamics for important crab species. Additional environmental unknowns and complex oceanographic conditions in the marginal ice zone throughout the Bering and Chukchi Seas provide uncertainty. Zooplankton and fish communities are structured by oceanographic domains with contrasting water masses. For example, cold temperatures limit the distribution of temperate species while providing ideal habitat and a thermal refuge for Arctic species (Danielson et al., 2020; Eisner et al., 2013; Hollowed et al., 2013; Pinchuk and Eisner, 2017). It is unknown if the distribution of crab larvae is similarly structured by environmental conditions or if their distribution primarily reflects adult preferences.

To better understand larval crab biology and their seasonal abundance and spatial distribution, we examined the species and stage composition of crab larvae relative to environmental variation using late summer samples from three sampling years. Objectives for this report include quantifying crab species and stage group catch-per-unit-effort (CPUE) to compare distributions across years relative to surface and bottom seawater water mass designations (summarized oceanographic and pelagic production indices) and infer the possible origin for larvae observed. Future analyses based on this report will test community assemblage relationships and commercial crab species abundance and distribution responses to environmental gradients.

Methods

Survey area and regions

Samples were collected in the Chukchi Sea and northern Bering Sea in August through September of 2012 and 2013 as part of the Arctic Ecosystem Integrated Survey (Arctic EIS) Program (Mueter et al., 2017) and August through September of 2017 as part of the Arctic Integrated Ecosystem Survey Phase II (Arctic IES Phase II) Program (Baker et al., 2020). Surveys were conducted using a square grid-based design of equidistant sampling stations approximately 30 nautical miles apart across all years between 60-73.5°N latitude and 155-170°W longitude. Additional oceanographic and plankton sampling every 15 nautical miles occurred in the Chukchi Sea in both 2012 and 2013. Sequential gear deployments at each station collected data on oceanography, zooplankton, and pelagic and benthic macroinvertebrates and fishes; from which all data presented here were acquired.

For seasonal and regional comparisons, we subdivided the study region into three areas: northern Bering Sea (NBS) south of the Bering Strait at 66°N, southern Chukchi Sea (SCS) between 66°N and 69.5°N, and northern Chukchi Sea (NCS) north of 70°N based on sampling design. Surveys conducted in 2012 and 2013 on board the F/V Bristol Explorer were nearly identical in timing and station coverage. Sampling began the first week of August in the southern Chukchi Sea and proceeded northward to approximately 73°N along the Chukchi Sea slope, concluding by early September. Thereafter, surveys of

the northern Bering Sea occurred north to south from Bering Strait to 60°N and concluded by late September. In contrast, the 2017 survey on board the R/V Ocean Starr started in the northern Chukchi Sea and proceeded south with the majority of grid-based sampling events occurring between the last week of August to late September. The 2017 northern Bering Sea survey was conducted on board the F/V Northwest Explorer concurrently from late August through late September using identical methods, however proceeded south to north from 60°N to Bering Strait.

Field sampling and processing

Conductivity-temperature-depth (CTD) profiles of the water column were collected with Sea-Bird Electronics Inc. SBE 911 or SBE 25 units attached to a Niskin bottle rosette steel frame or with a SBE 49 unit in-line with zooplankton net tows. Raw oceanographic data was processed by the Alaska Fisheries Science Center (NOAA) FOCI Program (Danielson et al., 2017). For this study, surface (0-10 m depth) and near-bottom (deepest 10 m) layer mean temperatures (ST / BT, °C), mean salinities (SS / BS, psu), and mean integrated water column chlorophyll a (mChla, mg m^{-3}) were computed. Surface and bottom water mass designations / origin were determined according to Danielson et al. (2020) using the above T/S values.

Zooplankton samples were collected with a 60 cm MARMAP-style bongo frame with 505µm mesh net. Calibrated General Oceanics Inc. mechanical flowmeters were used to estimate seawater filtrate volume. Net rinsed and sieved codend samples were fixed in 1 L glass jars with 5% buffered formalin 150 µm filtered sea water solution. Laboratory zooplankton community processing employed sequential Folsom sampling splitting methods to quantify community composition (Pinchuk and Eisner, 2017). Mean zooplankton abundances (ind. m^{-3}) at each station were aggregated into three groups for analysis: total zooplankton (Z), a 'Pacific' zooplankton indicator group (PZ), and an 'Arctic' zooplankton indicator group (AZ) based on Eisner et al. (2013). PZ and AZ species groupings have previously been used to track water masses of Pacific and Arctic origin, respectively (Eisner et al., 2013; Pinchuk and Eisner, 2017). All oceanographic, chlorophyll a (primary production index) and zooplankton community (secondary production index) estimates were calculated by station to compare to larval crab communities in future analyses.

Crab larvae were processed and removed from complete, non-Folsom split zooplankton samples (Weems and Pinchuk, 2015). Larvae were identified to species and classified into life stage (molt stage) based on best available taxonomic descriptions. Crab life stages were aggregated for each species for cross-species comparisons due to different numbers of larval molts needed to compete the larval cycle across species. Hereafter aggregated life stages are termed 'stage groups'. Biologically, stage groups reflect increasing size, mobility (swimming ability), and pelagic larval duration (PLD, planktonic time) as larvae grow from hatching to benthic settlement and carcinization (development of crab-like form). Stage groups used for analysis include small early stage zoeae (EZ, approximate age 0-4 weeks), larger late stage zoeae (LZ, 4-8 weeks), and relatively large megalopa/glaucothoe decapodite stages (MG, > 8 weeks) which most resemble adult crab morphology. All individuals in each stage group were counted and catch-per-unit-effort (CPUE, individuals per unit volume seawater filtrate) was calculated for each group by station.

Analysis

In this report, we provide maps and qualitative descriptions for larval community and species / stage group abundance and distribution by year and region relative to basic environmental conditions. A future manuscript and dissertation chapter, Weems et al. (in prep), will provide further analysis correlating larval community structure and species-specific distribution to regional environmental covariates and water masses, as well as test blue king crab and snow crab larval response to environmental conditions using a generalized additive modeling framework.

Database preparation and quality control were maintained with Microsoft® Excel®. Maps of CPUE were produced using ArcGIS® (ESRI, 2014) software. Water mass figures and all data summaries and statistical analyses were conducted using R Version 3.5.2 (R Core Team 2021).

Results

Larval crab abundance and distribution

A total of 23,550 crab larvae were observed, categorized by species / stage, and counted across 347 stations spanning all study years. Specimens of uncertain taxonomy and poor condition were excluded from analyses (n = 1,417 individual Pagurid hermit crabs). Standardized abundances (CPUE in ind. $1000m^{-3}$) by species and region are summarized in Table 1. Visual assessments of CPUE by species / stage group (ind. m^{-3}) and proportional contribution of stage groups are mapped by year and station for the total larval community and separately for *P. platypus* and *C. opilio* (Figure 1). Additional maps for all species including *P. ochotensis*, *P. trigonochirus* (cf), *L. splendescens*, *H. grebnitzkii*, *T. cheiragonus*, *O. gracilis*, *H. coarctatus*, *P. camtschaticus*, and *C. bairdi* are included in Supplementary Figures. Very rare commercial species *P. camtschaticus* (n = 1) and *C. bairdi* (n = 7) were mapped in years where present but not further summarized.

Crab larvae were found at nearly all stations sampled. Larval abundance, distribution, and stage composition reveal a few species / stage groups are found regionally in relatively high abundance. Interannual comparison of total community abundance and distribution by region was relatively consistent, except for the southern Chukchi Sea in 2017 due to lower numbers associated with later sampling (Figures 1A-F). Blue king crab, *P. platypus*, occurred as late stage zoea and glaucothoe in low abundances in the Chukchi Sea in 2012 and 2013 but were entirely absent in 2017. Abundances were 3-10 times larger in 2012 compared to 2013 (Figures 1G-L). In contrast, snow crab, *C. opilio,* was the most ubiquitous species across all sampling regions and years. Estimated abundances and proportional contributions by stage group varied by region (Figures 1M-R). Early stage zoeae *C. opilio* occurred nearly exclusively in the North Chukchi Sea region but in relatively low abundances. Late stage zoeae *C. opilio* were the dominate larval group across the entire Chukchi Sea shelf in late summer. Near-settling stage megalopae *C. opilio* were most abundant in the offshore waters of the North Bering Sea in September, though they also occur throughout the Chukchi Sea. Two additional commercial crab larval species were rarely observed. One red king crab, *P. camtschaticus,* was caught in the eastern Chirikov Basin, Bering Sea in 2012. The second ever recorded observation of Southern Tanner crab, *C. bairdi*, larvae in the Chukchi Sea occurred at CH-D03 on Aug 13, 2013 (Landeira et al., 2018), while a few individuals were also seen in the southern region of the North Bering Sea.

Other crab species were important constituents of the larval community, typically observed either in high abundances over constricted ranges or in lower abundances across larger regions (Table 1, Supplementary Figures 3-68). Four Infraorder Anomuran species, taxonomically related to king crab, were significant contributors to the overall community. The Alaskan hermit, *P. ochotensis,* was highly abundant as early stage zoeae in the northern Bering Sea in mainland nearshore areas of Norton Sound across all years. Larger late stage zoeae and glaucothoe stages of the fuzzy hermit (*P. trigonochirus* (cf) and splendid hermit (*L. splendescens*) were moderately abundant and ubiquitous across the Bering and Chukchi Seas offshore regions. The northern hairy king crab, *H. grebnitzkii,* occurred only in the Chukchi Sea in early sampling years with trends similar to blue king crab only in higher abundance. Three Infraorder Brachyuran species, taxonomically related to snow and Southern Tanner crab, were observed in three distinct patterns. The Arctic lyre crab, *H. coarctatus,* mirrored *C. opilio* in observed distribution but had lower abundances. The helmet crab, *T. cheiragonus,* had a consistently high abundance of megalopa stage decapodites in the northern Chukchi Sea region across years. In contrast, the megalopae of the Pacific decorator crab, *O. gracilis,* were primarily found in the southern, nearshore areas of the North Bering Sea region.

Environmental and oceanographic conditions

Sampling was largely restricted to the shallow northern Bering Sea and Chukchi Sea shelves with a mean sea floor depth of 38.6 m (± 13.6) (plus standard deviation, SD) Two stations were sampled off the shelf near Barrow Canyon in 2017 with a sea floor depth greater than 200 m, thus oceanographic data was only analyzed to 150 m depth to match the maximum zooplankton net tow depth.

Water mass characteristics and measures of primary and secondary production are summarized by year and region in Table 2 and water masses were defined and mapped for each year (Figure 2A, B). Anadyr Water (AnW) originates in Russia and is typically colder, more dense water overlain by Alaska origin water masses in more western stations across all regions. The Bering Sea Shelf water includes three distinct water masses that flow onto the Chukchi Shelf, including 1) warm Shelf Water (wSW) warmed by summer seasonal heat, 2) cool Shelf Water (cSW) warmed to a lesser extent due to sub thermo- and halocline entrapment, and 3) Winter Water (WW/MWW) consisting of subzero, cold waters originating under the previous winter's annual sea ice. Alaska Coastal water (wCW, cCW) was relatively warm and less saline due to terrestrial freshwater runoff. Finally, Melt Water (MW) is indistinguishable from cool Alaska Coastal water but originates from recently melted sea ice.

All water masses are distinct and consistently present across all years and provide evidence supporting vertical and horizontal segregation of water masses on regional scales (Figure 2A). In 2012, late summer cold air and ocean conditions prevailed and were driven by southwesterly winds pinning the Alaska Coastal Water along shore flowing northward into the Arctic. Cool summer Bering Sea Shelf Water propagated in the surface waters across the Bering and Chukchi corridors. Cold conditions in 2012 contributed to a relatively strong (extent, thickness) ice cover in spring 2013. However, by late summer 2013 warmer conditions and northeasterly wind fields were consistent, a reversal in contrast to 2012. These southwesterly flowing winds both 'shut-down' the north Chukchi ACC nearshore flow through Barrow Canyon and drove warmer, less saline coastal surface waters offshore across all regions. In 2017, warm conditions were pronounced. More recent years have been characterized by anomalously low winter sea ice concentration coupled with warm to hot air and water temperatures, decreased salinity, and southerly winds driving more heat north into the Arctic.

Discussion

Larval community trends relative to environmental conditions

Larval community catch was variable and generally a low proportion of total zooplankton abundance in zooplankton samples). Species identification and stage descriptions were ascertained and confirmed in this analysis through available literature sources (Table 1). Species *P. trigonochirus* and *H. grebnitzkii* do not have complete larval descriptions, however we are confident in species identifications based on available literature and adult distributions identified in associated benthic bottom trawls.

We hypothesized that seasonality in biological processes and water masses are the primary drivers of larval community structure. Observed species and stage distributions are linked to crab biology by larval hatch area and timing, pelagic larval duration, and preferred settlement habitat. Meroplanktonic crab larvae are seasonally produced from a bottom-dwelling female's egg brood whereby they are hatched and released to disperse into the pelagic water column to growth, feed, swim, disperse from the natal habitat, and reduce predation pressure (Possingham and Roughgarden, 1990; Strathmann, 1985). Over several weeks or months, multiple shell molting cycles take place before larvae settle to a preferred benthic substrate. Survival during early pelagic stages ultimately may determine successful recruitment to adult populations (Strathmann et al., 2002). Consistent adult stock range or spawning habitat (i.e. larval origin) in the Pacific Arctic, as detailed in Loggerwell et al. (this issue, AIERP-UTL Report), Mueter et al. (2017), and historically observed in the NOAA Eastern Bering Sea Bottom Trawl Survey, would be

important information to consider relative to species-specific inferred migration triangle migration pathways (Harden Jones, 1968).

Larval crabs found as one or few stages in a spatially constricted space could reflect a specific adult spawning stock of origin and/or larval advection mechanism. Larvae originating from a specific adult population would likely have similar release time and location and therefore develop under similar pelagic conditions and transport processes. We observed spatially consistent aggregations of several species and stage groups between years with evidence of possible upstream spawning stocks. These included: 1) snow crab early zoea in the northern Chukchi sea, which likely originated from potential spawning stocks in deeper waters of Barrow Canyon and along the Beaufort Sea Slope. 2) Snow crab megalopae in the northern Bering Sea (Chirikov Basin), which likely originate from spawning stocks on the northeastern Bering Sea and Anadyr shelves. 3) Blue king crab late stage larvae and post-larvae in offshore waters of the southern Chukchi Sea with possible spawning stocks to the south in the northern Bering Sea and Bering Strait region associated with nearshore rocky island habitats. 4) Alaskan hermit crab early stage larvae with likely origins in near-coastal areas of the northern Bering Sea and Norton Sound. Across species, we suggest mature female crab chose preferred spawning grounds with consistent, directional oceanographic flow to promote larval advection to optimal nursery habitat for settlement. If predictable transport mechanisms and settlement habitats are maintained, annual environmental conditions would more directly impact yearly benthic recruitment through larval survivorship.

Larval crab that were ubiquitous across all regions could suggest expansive adult stocks employing slow bet-hedging larval release strategies. By spreading larvae over space and time, females selectively limit larval death under poor conditions and reduce competition under optimal conditions. Therefore, the possibility of failure of an entire larval cohort is reduced (Laaksonen, 2004; Pineda et al., 2010). We suggest the following larval species and stage groups reflect non-specific adult spawner habitat selection and prolonged hatching periods. 1) Highly abundant snow crab late stage zoea and megalopae throughout the Chukchi Sea present in all years across the majority of stations, and similarly 2) Arctic lyre crab late stage zoea and megalopae. 3) The fuzzy and splendid hermit crabs of the Chukchi Sea were observed in multiple stages per sampling event, suggesting an even more prolonged spawning period. Overall, we suggest expansive hatching or settlement of larvae is reflective of generalist species occupying a large niche space. Thus, high losses of larvae in one area may be compensated for in another area to maintain high abundances and distributional ranges.

Larval species and stage distributions are linked to local, seasonal, and climatically driven environmental conditions. Stability of water masses in the Pacific Arctic is driven by presence or absence of sea ice, as impacted by atmospheric forcing (Danielson et al., 2017, 2014). We observed all water masses in all years though distribution of those water masses were dramatically different across years. Danielson et al. (2017; 2020). Community level analysis does show some species appear to inhabit only certain water masses, such as shelf waters or coastal waters (Pinchuk and Eisner, 2017; Kimmel et al., AIERP-LTL Report). Typically, cold water species such as snow crab, Arctic lyre crab, blue king crab, and northern hairy king crab were major larval community constituents in colder, offshore shelf waters. Blue and hairy king crab in particular fit this pattern as adults are thought to occur and spawn in rocky and shell island habitats of the north Bering Sea, which were not overlain with Alaska Coastal Water. This suggests they occupy and are advected in the bottom water layer below or near the pycnocline. However, abundant and ubiquitous species like snow crab, Arctic lyre crab, fuzzy hermits, and splendid hermits occur in both offshore and coastal waters, which is consistent with adult distributions across the northern Bering Sea and Chukchi Sea epibenthic communities (Divine et al., 2019; Mueter et al., 2017; Jewett & Feder, 1981). All species exhibited interannual variation as reflected by presence/absence and stage of occurrence and may be influenced by temperature conditions and water mass flow. We suggest with increased warming and regional climate shifts, long term population fluctuation will be a species-specific dynamic response integrating annual larval survivorship and settlement dynamics.

Future Analyses

Trends identified above will be further explored in Weems et al. (in prep) by modeling community and species-specific response to environmental covariates. We will attempt to identify community-level environmental drivers, determine species-specific relationships to important covariates, then test blue king crab and snow crab stages specific response to environmental drivers over space and time.

Multivariate community structure analysis

To characterize the composition of the larval crab community (by species and stage group) during late summer over multiple years relative to environmental conditions, we used 1) non-metric multidimensional scaling (nMDS) ordination to visualize annual community dissimilarities relative to best ranked subset of explanatory environmental covariates. 2) PERMANOVA to statistically test for differences in community composition by region and water masses, and 3) indicator species analysis to identify species with strong affinities for specific water masses or regions.

Blue king crab and snow crab community modeling

To further examine regional patterns in abundance and distribution of our primary target species, snow crab and blue king crab, we will use generalized additive models (GAM) to examine individual counts relative to location and environmental parameters. General hot spot models will assess inter-annual consistency in spatio-temporal peaks of abundance in snow crab larvae distribution in the northern Chukchi Sea by early zoeae stages and in the northern Bering Sea / Chirikov Basin by megalopae stage larvae. Interannual assessment of potential differences in development rate in larvae relative to environmental drivers will focus on late zoea to megalopae transition in snow crab and presence or absence of late stage zoea and glaucothoe in blue king crab within the Chukchi Sea from 2012 and 2013.

Conclusions

Larval crab analysis across a cold, average and warm year in the North Bering Sea and Chukchi Sea sampled during the Arctic EIS and IES II Programs show relatively high consistency in community composition across years by region and water mass. Abundance was variable, but spatiotemporally consistent within regions where sampling occurred at the same time of year. Variation in species distribution was suspected to be driven by water mass position, while variation in stage groups by species could be driven by physiological responses to increasing temperatures or sampling season. In 2012, late summer cold air and ocean conditions prevailed and were driven by southwesterly winds pinning the ACC along shore and northward into the Arctic. Cool summer BSSW propagated in the surface waters across the Bering and Chukchi corridors. This cold year appears to have delayed either crab spawning or physiology (molt frequency, pelagic larval duration) in several species, likely contributing to the presence of blue king crab at the time of sampling. Cold conditions in 2012 contributed to a more extensive and thicker ice cover in spring 2013. However, in late summer 2013 warmer conditions and northeasterly wind fields were consistent and warmed most surface waters relative to 2012. These Arctic winds 'shut-down' the north Chukchi Alaska Coastal Water flow into the Arctic and promoted offshore winds driving warmer, less saline coastal surface waters offshore across all regions leading to strong vertical stratification. Larval communities appeared to be more spread out and overlapping, but strong stratification would likely have limited mixing of communities and excluded cold bottom water larvae from surface waters. In 2017, warming conditions were pronounced in both surface and bottom waters across all regions. More recent years (2014-2020) have been characterized by anomalously low winter sea ice concentration coupled with average to hot air and water temperatures, decreased salinity, and southerly winds driving more heat north. Larval community response is difficult to assess due to survey design discrepancies between programs, however decreased abundances in the Chukchi Sea could be explained by faster development, higher molt frequency, and earlier settlement. However, we cannot rule

out poor larval recruitment or survival. With continued warming and further northward movement of temperate species into the Chukchi Sea, we might expect increased variability in larval community production due to changes in water mass stratification and advection, local food production or prey mismatch, and predation pressure from temperate fishes (e.g., Walleye pollock, Pacific cod).

References

Baker, M.R., Farley, E. V., Ladd, C., Danielson, S.L., Stafford, K.M., Huntington, H.P., Dickson, D.M.S., 2020. Integrated ecosystem research in the Pacific Arctic – understanding ecosystem processes, timing and change. Deep. Res. Part II Top. Stud. Oceanogr. https://doi.org/10.1016/j.dsr2.2020.104850

Bluhm, B., Iken, K., Mincks Hardy, S., Sirenko, B., Holladay, B., 2009. Community structure of epibenthic megafauna in the Chukchi Sea. Aquat. Biol. 7, 269–293. https://doi.org/10.3354/ab00198

Daly, B., Parada, C., Loher, T., Hinckley, S., Hermann, A.J., Armstrong, D., 2020. Red king crab larval advection in Bristol Bay: Implications for recruitment variability. Fish. Oceanogr. 29, 505–525. https://doi.org/10.1111/fog.12492

Danielson, S.L., Ahkinga, O., Ashjian, C., Basyuk, E., Cooper, L.W., Eisner, L., Farley, E., Iken, K.B., Grebmeier, J.M., Juranek, L., Khen, G., Jayne, S.R., Kikuchi, T., Ladd, C., Lu, K., McCabe, R.M., Moore, G.W.K., Nishino, S., Ozenna, F., Pickart, R.S., Polyakov, I., Stabeno, P.J., Thoman, R., Williams, W.J., Wood, K., Weingartner, T.J., 2020. Manifestation and consequences of warming and altered heat fluxes over the Bering and Chukchi Sea continental shelves. Deep Sea Res. Part II Top. Stud. Oceanogr. 177, 104781. https://doi.org/10.1016/j.dsr2.2020.104781

Danielson, S.L., Eisner, L., Ladd, C., Mordy, C., Sousa, L., Weingartner, T.J., 2017. A comparison between late summer 2012 and 2013 water masses, macronutrients, and phytoplankton standing crops in the northern Bering and Chukchi Seas. Deep Sea Res. Part II Top. Stud. Oceanogr. 135, 7–26. https://dx.doi.org/10.1016/j.dsr2.2016.05.024

Danielson, S.L., Weingartner, T.J., Hedstrom, K.S., Aagaard, K., Woodgate, R., Curchitser, E., Stabeno, P.J., 2014. Coupled wind-forced controls of the Bering-Chukchi shelf circulation and the Bering Strait throughflow: Ekman transport, continental shelf waves, and variations of the Pacific-Arctic sea surface height gradient. Prog. Oceanogr. 125, 40–61. https://doi.org/10.1016/j.pocean.2014.04.006

Divine, L.M., Mueter, F.J., Kruse, G.H., Bluhm, B.A., Jewett, S.C., Iken, K., 2019. New estimates of weight-at-size, maturity-at-size, fecundity, and biomass of snow crab, Chionoecetes opilio, in the Arctic Ocean off Alaska. Fish. Res. 218, 246–258. https://doi.org/10.1016/J.FISHRES.2019.05.002

Eisner, L., Hillgruber, N., Martinson, E., Maselko, J., 2013. Pelagic fish and zooplankton species assemblages in relation to water mass characteristics in the northern Bering and southeast Chukchi seas. Polar Biol. 36, 87–113. https://doi.org/10.1007/s00300-012-1241-0

Ershova, E., Descoteaux, R., Wangensteen, O., Iken, K., Hopcroft, R., Smoot, C., Grebmeier, J.M., Bluhm, B.A., 2019. Diversity and distribution of meroplanktonic larvae in the Pacific Arctic and connectivity with adult benthic invertebrate communities. Front. Mar. Sci. 6, 1–21. https://doi.org/10.3389/fmars.2019.00490

Harden Jones, F.R., 1968. Fish Migration, Internationale Revue der gesamten Hydrobiologie und Hydrographie. Edward Arnold Ltd., London. https://doi.org/10.1002/iroh.19700550328

Hollowed, A.B., Planque, B., Loeng, H., 2013. Potential movement of fish and shellfish stocks from the sub-Arctic to the Arctic Ocean. Fish. Oceanogr. 22, 355–370. https://doi.org/10.1111/fog.12027

Jewett, S.C., Feder, H.M., 1981. Epifaunal invertibrates of the continental shelf of the eastern Bering and Chukchi Seas, in: Hood, D.W., Calder, J.A. (Eds.), The Eastern Bering Sea Shelf: Oceanography and Resources. Univeristy of Washington Press, Seattle, Washington, pp. 1131–1153.

Kolts, J.M., Lovvorn, J.R., North, C.A., Janout, M.A., 2015. Oceanographic and demographic mechanisms affecting population structure of snow crabs in the northern Bering Sea. Mar. Ecol. Prog. Ser. 518, 193–208. https://doi.org/10.3354/meps11042

Laaksonen, T., 2004. Hatching asynchrony as a bet-hedging strategy - an offspring diversity hypothesis. Oikos 104, 616–620. https://doi.org/10.1111/j.0030-1299.2004.12858.x

Landeira, J.M., Matsuno, K., Tanaka, Y., Yamaguchi, A., 2018. First record of the larvae of tanner crab Chionoecetes bairdi in the Chukchi Sea: A future northward expansion in the Arctic? Polar Sci. 16, 86–89. https://doi.org/10.1016/j.polar.2018.02.002

Landeira, J.M., Matsuno, K., Yamaguchi, A., Hirawake, T., Kikuchi, T., 2017. Abundance, development stage, and size of decapod larvae through the Bering and Chukchi Seas during summer. Polar Biol. 40, 1805–1819. https://doi.org/10.1007/s00300-017-2103-6

Mueter, F.J., Weems, J., Farley, E.V., Sigler, M.F., 2017. Arctic Ecosystem Integrated Survey (Arctic Eis): Marine ecosystem dynamics in the rapidly changing Pacific Arctic Gateway. Deep. Res. Part II Top. Stud. Oceanogr. 135. https://doi.org/10.1016/j.dsr2.2016.11.005

Orensanz, J., Ernst, B., Armstrong, D.A., Stabeno, P., Livingston, P., 2004. Contraction of the geographic range of distribution of snow crab (Chionoecetes opilio) in the eastern Bering Sea: An environmental ratchet? Calif. Coop. Ocean. Fish. Investig. Reports 45, 65–79.

Parada, C., Armstrong, D.A., Ernst, B., Hinckley, S., Orensanz, J.M., 2010. Spatial dynamics of snow crab (Chionoecetes opilio) in the eastern bering sea - putting together the pieces of the puzzle. Bull. Mar. Sci. 86, 413–437.

Pinchuk, A.I., Eisner, L.B., 2017. Spatial heterogeneity in zooplankton summer distribution in the eastern Chukchi Sea in 2012–2013 as a result of large-scale interactions of water masses. Deep Sea Res. Part II Top. Stud. Oceanogr. 135, 27–39. https://dx.doi.org/10.1016/j.dsr2.2016.11.003

Pineda, J., Porri, F., Starczak, V., Blythe, J., 2010. Causes of decoupling between larval supply and settlement and consequences for understanding recruitment and population connectivity. J. Exp. Mar. Bio. Ecol. https://doi.org/10.1016/j.jembe.2010.04.008

Possingham, H.P., Roughgarden, J., 1990. Spatial population dynamics of a marine organism with a complex life cycle. Ecology 71, 973–985.

Strathmann, R.R., 1985. Feeding and nonfeeding larval development and life-history evolution in marine invertebrates. Annu. Rev. Ecol. Syst. Vol. 16 339–361.

Strathmann, R.R., Hughes, T.P., Kuris, A.M., Lindeman, K.C., Morgan, S.G., Pandolfi, J.M., Warner, R.R., 2002. Evolution of local recruitment and its consequences for marine populations. Bull. Mar. Sci. 70, 377–396.

Weems, J., Pinchuk, A.I., 2015. Is splitting up hard to do? Comparing zooplankton sample processing methods by estimating larval crab abundance. Poster Presentation. Alaska Marine Science Symposium, Anchorage, Alaska.

Zheng, J., Kruse, G.H., 2006. Recruitment variation of eastern Bering Sea crabs: Climate-forcing or top-down effects? Prog. Oceanogr. 68, 184–204.

Table 1: Crab larvae species observed in 2012, 2013 and 2017 in the northern Bering Sea and eastern Chukchi Sea with mean catch-per-unit-effort (CPUE ind. $1000m^{-3}$) during late summer averaged across years and stations. Total pelagic larval duration (PLD) estimates from the literature values are temperature dependent. Taxonomic descriptions allowed for reliable identification.

Family	Species	Larval Stage(s)	Larval Group	Mean Annual Late Summer CPUE (ind. $1000m^{-3}$; SE) N. Bering	S. Chukchi	N. Chukchi	PLD (Days) min; max	Literature Citations for Larval Taxonomy and Total PLD
Infraorder: Anomura								
Paguridae	Ochre / Alaskan hermit	Zoeae 1-2	EZ	414.3 ± 220.5	6.5 ± 4.1	0.7 ± 0.6	49; 90	Lough 1975; Quintana and Iwata 1987;
	Pagurus ochotensis	Zoeae 3-4	LZ	92.5 ± 31.9	2.5 ± 1.4	0.2 ± 0.2		McLaughlin et al. 1992
		Glaucothoe	MG	2.2 ± 1.1	0.4 ± 0.4	0.1 ± 0.1		
Paguridae	Fuzzy hermit	Zoeae 1-2	EZ	3.4 ± 3.4	64.8 ± 27.4	27.7 ± 6.5	na	Quintana and Iwata 1987
	Pagurus trigonochirus (cf)	Zoeae 3-4	LZ	5.3 ± 2.4	96.4 ± 23.7	142.3 ± 25.5		
		Glaucothoe	MG	0.6 ± 0.4	3.4 ± 1.3	32.1 ± 8.0		
Paguridae	Splendid hermit	Zoeae 1-2	EZ	0.9 ± 0.5	15.4 ± 2.5	8.7 ± 4.0	86; 104	Nyblade and McLaughlin 1975
	Labidochirus splendescens	Zoeae 3-4	LZ	18.2 ± 8.3	34.5 ± 12.6	24.3 ± 5.9		
		Glaucothoe	MG	2.6 ± 1.5	3.2 ± 1.4	3.5 ± 1.2		
Hapalogasteridae	Northern hairy stone crab	Zoeae 1-2	EZ	0 ± 0	0.3 ± 0.3	0 ± 0	27; 49	Hynes 1983, (*H. dentata* , Konishi 1986)
	Hapalogaster grebnitzkii	Zoeae 3-4	LZ	0 ± 0	7.4 ± 1.5	0.6 ± 0.3		
		Glaucothoe	MG	0 ± 0	3.2 ± 0.9	0.9 ± 0.5		
Lithodidae	Blue king crab	Zoeae 1-2	EZ	0 ± 0	0.6 ± 0.4	0.2 ± 0.2	54; 79	Kurata 1963; Hoffman 1968;
	Paralithodes platypus	Zoeae 3-4	LZ	0 ± 0	1.9 ± 0.6	0.2 ± 0.2		Jensen et al.1990
		Glaucothoe	MG	0 ± 0	0.8 ± 0.5	0.2 ± 0.1		
Infraorder: Brachyura								
Cheiragonidae	Helmet crab	Zoeae 1-2	EZ	0 ± 0	0.1 ± 0.1	0 ± 0	75+	Kurata 1963; Konishi and Shikatani 2000;
	Telmessus cheiragonus	Zoeae 3-5	LZ	0 ± 0	2.6 ± 1.4	0.3 ± 0.3		Scherbakova and Korn 2012
		Megalopae	MG	0.5 ± 0.4	22.7 ± 5.7	65.0 ± 40.6		
Oregoniidae	Decorator crab	Zoea 1	EZ	0 ± 0	0 ± 0	0 ± 0	35	Hart 1960; Lough 1975; Oh and Ko 2010
	Oregonia gracilis	Zoea 2	LZ	0.1 ± 0.1	0 ± 0	0 ± 0		
		Megalopae	MG	45.3 ± 19.4	0 ± 0	0 ± 0		
Oregoniidae	Arctic lyre crab	Zoea 1	EZ	0 ± 0	2.4 ± 1.5	8.4 ± 3.6	69; 100	Kurata 1963; Christiansen 1973;
	Hyas coarctatus	Zoea 2	LZ	0.2 ± 0.2	180.4 ± 91.1	192.5 ± 3.6		Davidson and Chin 1991; Pohle 1991
		Megalopae	MG	47.4 ± 18.3	16.1 ± 5.7	46.2 ± 19.7		
Oregoniidae	Snow crab	Zoea 1	EZ	0 ± 0	2.0 ± 0.6	26.5 ± 7.8	69.3; 73.3	Haynes 1973, 1981; Motoh 1973;
	Chionoecetes opilio	Zoea 2	LZ	3.3 ± 1.6	199.8 ± 118.5	91.8 ± 26.4		Wencker et al. 1982; Pohle 1991;
		Megalopae	MG	186.0 ± 88.7	14.0 ± 5.6	9.9 ± 5.2		Davidson and Chin 1991

- Total larvae count (N observed) = 23,550. Larvae excluded in analyses = 1,417 including red king crab (*P. camtschaticus* , N = 1), Tanner crab (*C. bairdi* , N = 7), and unknown Pagurid larvae.

Table 2: Arctic Eis and Arctic JES Phase II sampling information, number of zooplankton samples processed for larval counts, and mean environmental parameter values by region. Sampling years 2012 and 2013 have consistent overlap in dates across regions, while only Chirikov Basin and northern N. Chukchi in 2017 overlap consistently enough to include in interannual analyses. Physical and biological oceanographic mean values are restricted to matching larval stations only, where data was available.

						Physical Oceanography				Biological Oceanography			
			Sampling Dates (AKDST)		Larvae Stations	Temperature ('C)		Salinity (psu)		mChla	Total Zoop	Pacific Zoop	Arctic Zoop
Year	Region	Cruise-Leg	Calendar Day	Julian Day	N	Sur (SE)	Bot (SE)	Sur (SE)	Bot (SE)	Ug r^{1} (SE)	ind.rri3 (SE)	ind.rri3 (SE)	ind.rri 3 (SE)	ind.rri3 (SE)
2012	N. Chukchi	BE12-0l-02	Aug. 16- Sep.8	229-252	46	5.3 ± 0.4	2.6 ± 0.5	302 ± 0.2	32.1 ± *02*	1.1 ± 0.2	262.8 ± 30.4	3.6 ± 0.8		*01* ± 0.1
	S. Chukchi	BE12-01	Aug. 7 - 16	220-229	39	7.6 ± 0.3	5.4 ± 0.5	30.3 ± 0.3	31.1 ± 0.3	1.3 ± 0.1	349.9 ± 37.7	12.4 ± 2.3		0 ± 0
	N. Bering	BE12-03	Sept. 10 -24	254 - 268	36	6.6 ± 0.3	5.3 ± 0.5	302 ± 0.4	31.0 ± 0.3	1.9 ± 0.3	148.9 ± 30.5	22.1 ± 12.4		0 ± 0
2013	N. Chukchi	BE13-02	Aug.22 - Sep. 4	234-247	46	3.8 ± 0.3	-0.1 ± 0.3	29.5 ± 0.3	32.4 ± 0.0	0.7 ± 0.1	222.5 ± 44.3	1.5 ± 0.3		1.5 ± 0.5
	S. Chukchi	BE13-01	Aug. 7 - 16	219-228	40	7.8 ± 0.3	4.7 ± 0.4	30.7 ± 0.2	31.6 ± 0.1	±	510.5 ± 111.6	145.0 ± 34.4		0 ± 0
	N. Bering	BE13-03	Sept.JO -24•	253 -267	43	8.0 ± 0.3	4.8 ± 0.6	29.8 ± 0.3	31.0 ± *02*	1.4 ± 0.2	136.7 ± 28.6	30.5 ± 13.1		0 ± 0
2017	N. Chukchi	OSI 7-02-03	Aug. 9 - Sep. 13	221 -256	42	5.4 ± 0.3	2.8 ± 0.4	31.0 ± 0.2	32.2 ± 0.1	1.3 ± 0.1	29.8 ± 12.7	0.01 ± 0.00		0.3 ± 0.1
	S. Chukchi	OSI 7-03	Sept. 19-26	262-269	18	5.6 ± *01*	4.7 ± 0.3	31.3 ± 0.2	32.1 ± 0.1	1.8 ± 0.2	7.0 ± 2.0	0.6 ± 0.5		0 ± 0
	N. Bering	:NW! 7-05	Aug.27 - Sep. 9	239-252	41	8.5 ± 0.3	6.8 ± 0.5	30.5 ± 0.3	31.2 ± *02*	2.1 ± 0.4	16.9 ± 4.9	8.0 ± 3.8		0 ± 0

- Region latitude delineation: N. Bering (60-65.5'N), S. Chukchi (66-09.5°:N), and N. Chukchi (70-73.5°N). Longitude bounds are< 1800\V (Int. Dateline) and> 150°\V (Alaska coast).

•- Northernmost N. Bering Sea Station sampled Aug. 7,2013. Remaining 42 stations sampled within time period stated.

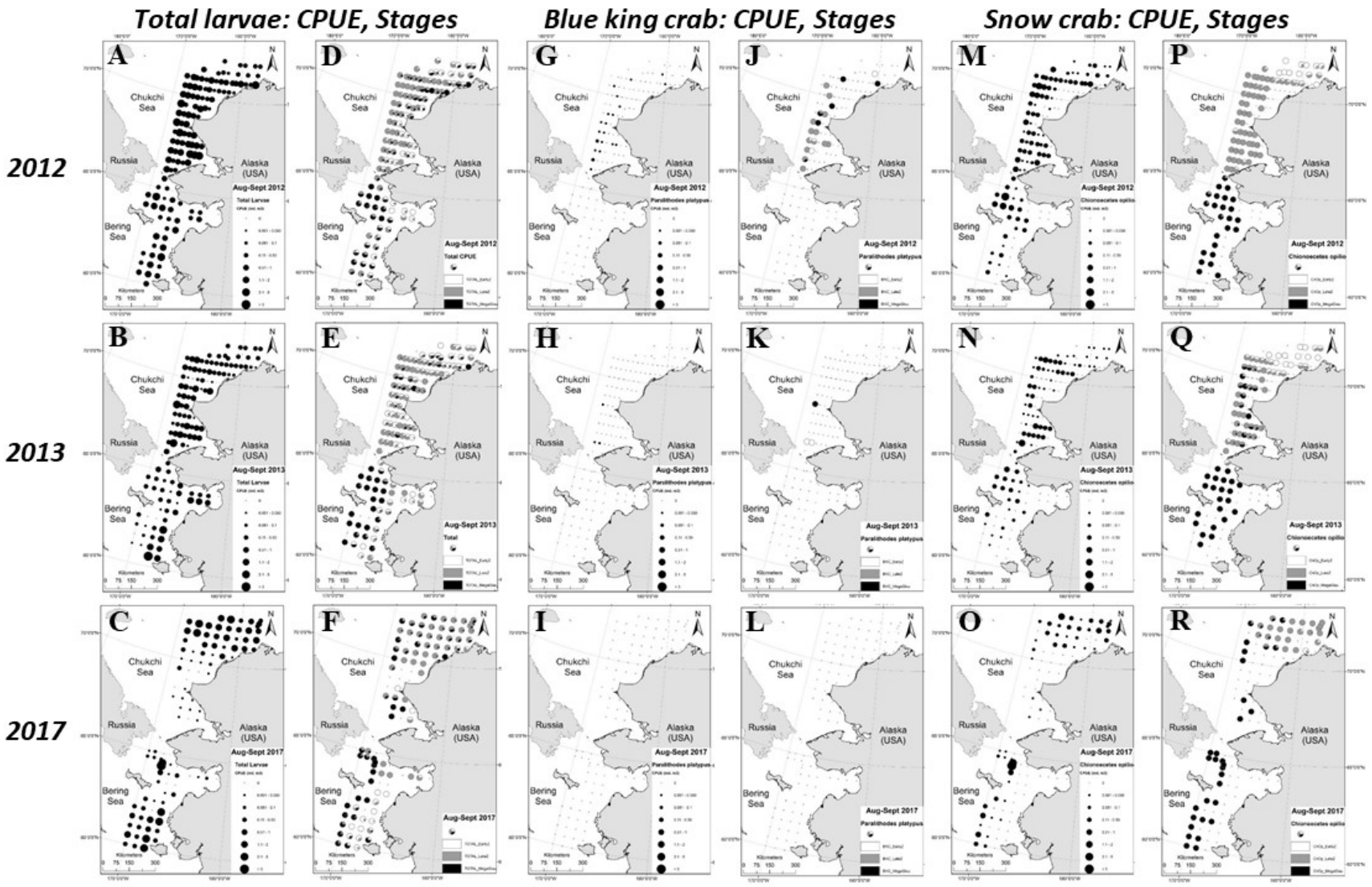

Figure 1. Total crab larval community, blue king crab, and snow crab CPUE (ind. m-3) and stage group proportional contribution of early zoeae, late zoeae, and megalopae/glaucothoe to total catch by station from 2012, 2013, and 2017. (Larger versions repeated below for closer inspection.)

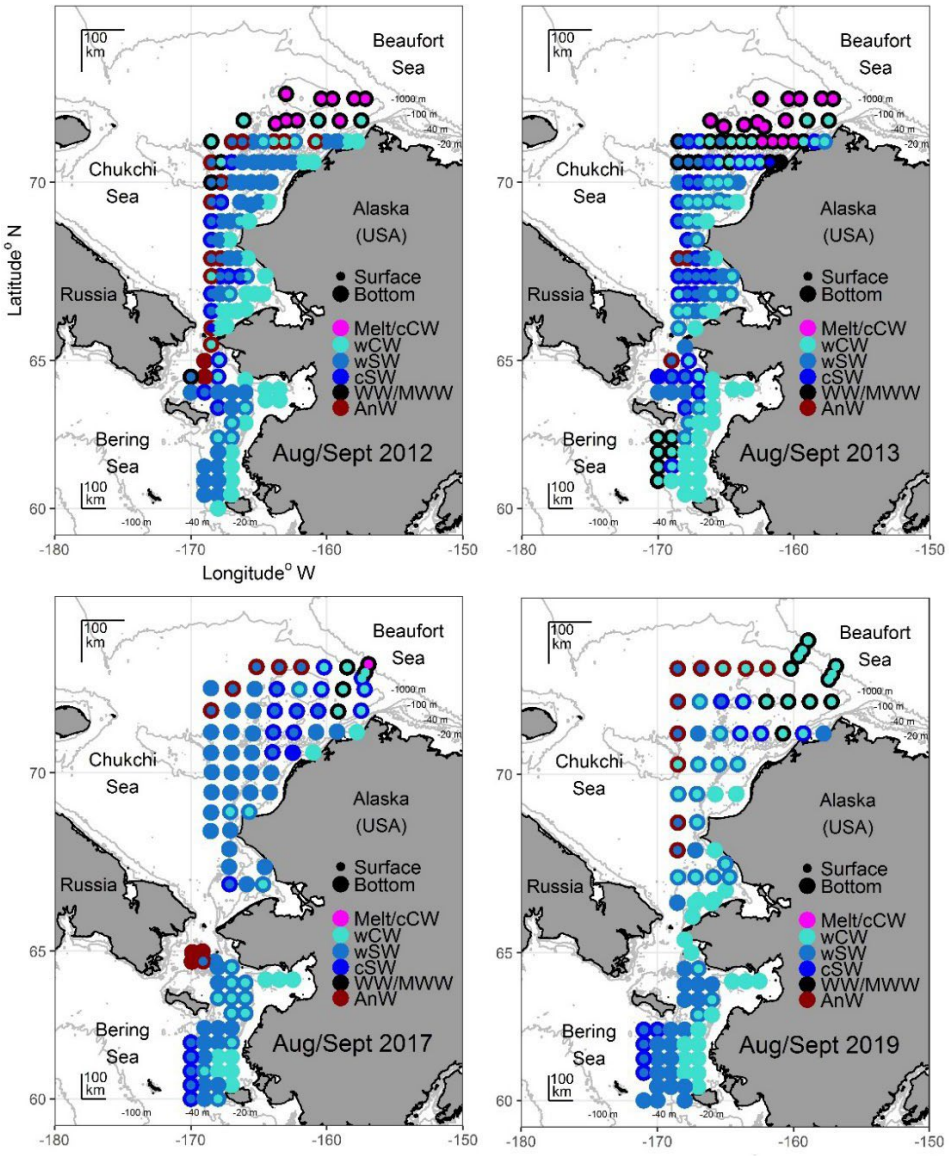

Water Mass	Abbreviations	Temperature Range	Salinity Range
Anadyr Water	AnW	0 < T < 3	32.5 < S < 33.8
Ice Melt Water & Cool Coastal Water	IMW cCW	-2 < T < 3	22 < S < 30.8
Cool Shelf Water	cSW	0 < T < 3	30.8 < S < 32.5
Warm Coastal Water	wCW	3 < T < 14	18 < S < 30.8
Warm Shelf Water	wSW	3 < T < 14	30.8 < S < 33.4
Modified Winter Water	MWW	-1 < T < 0	30.8 < S < 33.8
Winter Water	WW	-2 < T < -1	30.8 < S < 35
Atlantic Water & Bering Basin Water	AtlW & BBW	-1 < T < 3 3 < T < 5	34 < S < 35 33.8 < S < 35

Figure 2. Oceanography, zooplankton, and larval crab survey samples as represented by color coded surface water mass (small foreground circles) and bottom water mass (large background circles) by station from 2012, 2013, 2017. Similarly, 2019 was also characterized though no crab larvae were sampled. Additional table shows water mass specific temperature and salinity characteristics as established by Seth Danielson (UAF).

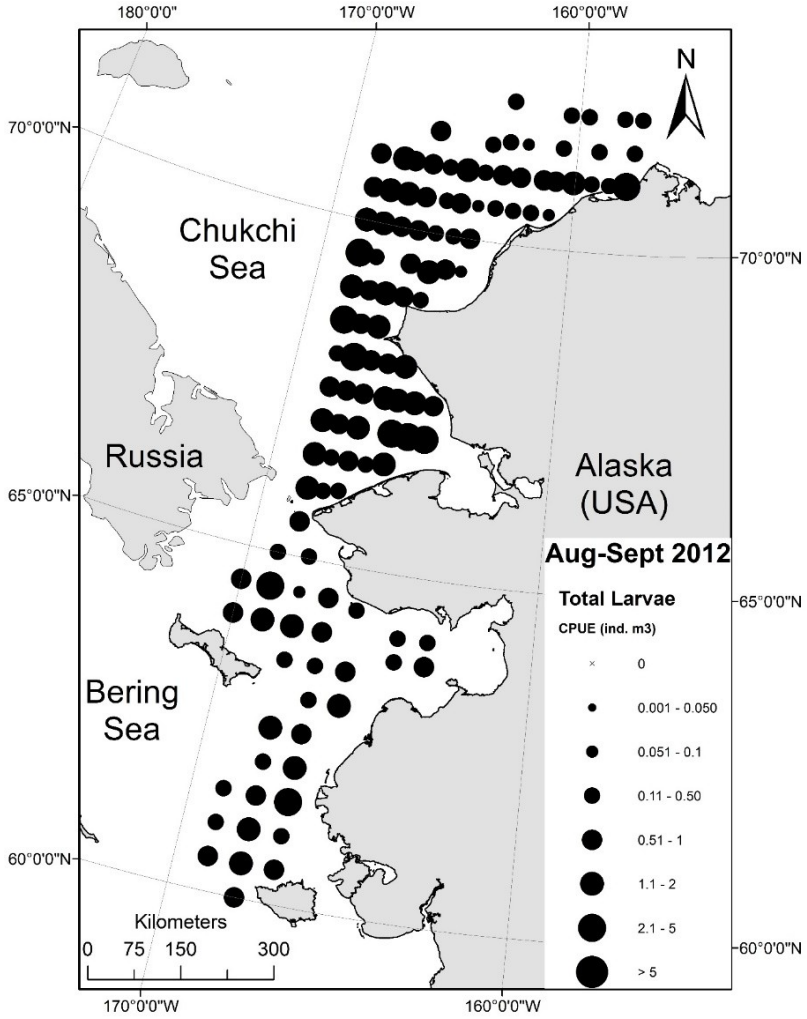

Figure 3. Total crab larval community CPUE (ind. m-3) by station from 2012.

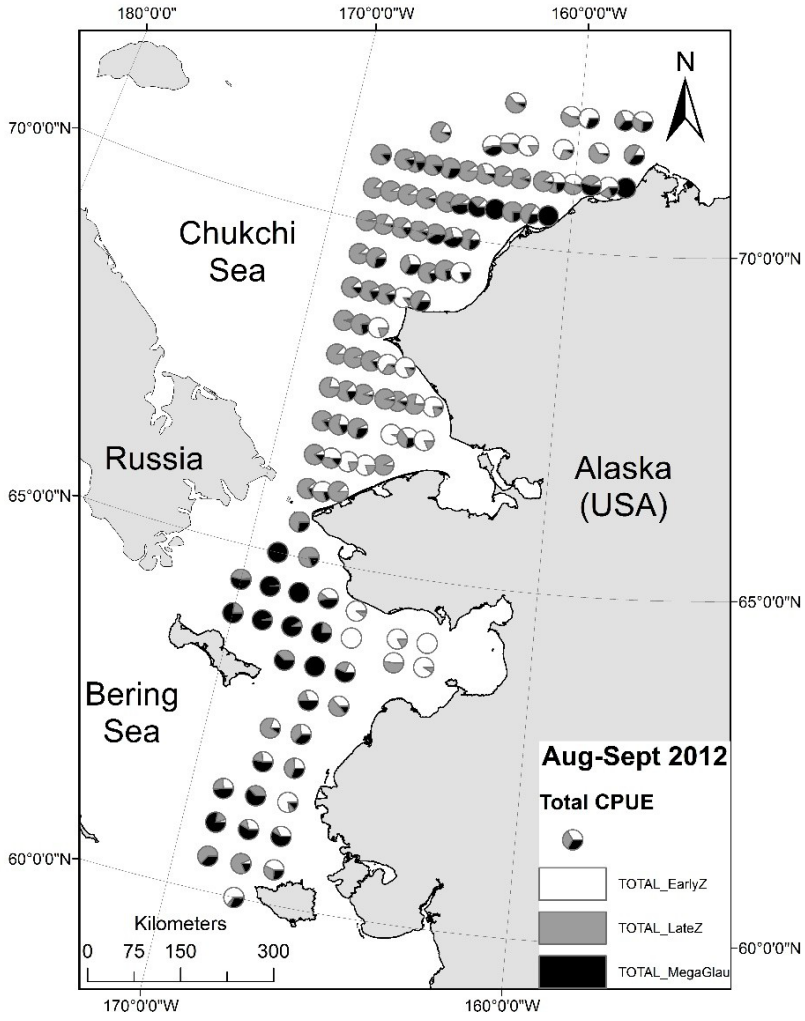

Figure 4. Total crab larvae stage group proportional contribution of early zoeae, late zoeae, and megalopae/glaucothoe to total catch by station from 2012.

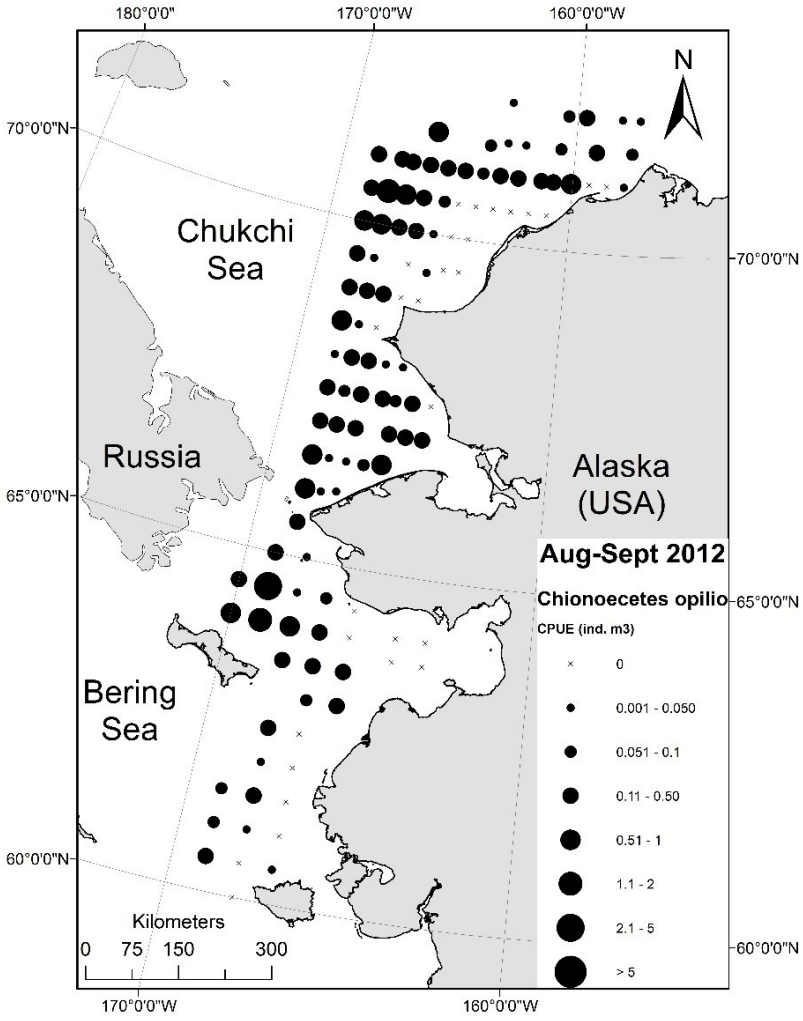

Figure 5. Snow crab (*Chionoecetes opilio*) CPUE (ind. m-3) by station from 2012.

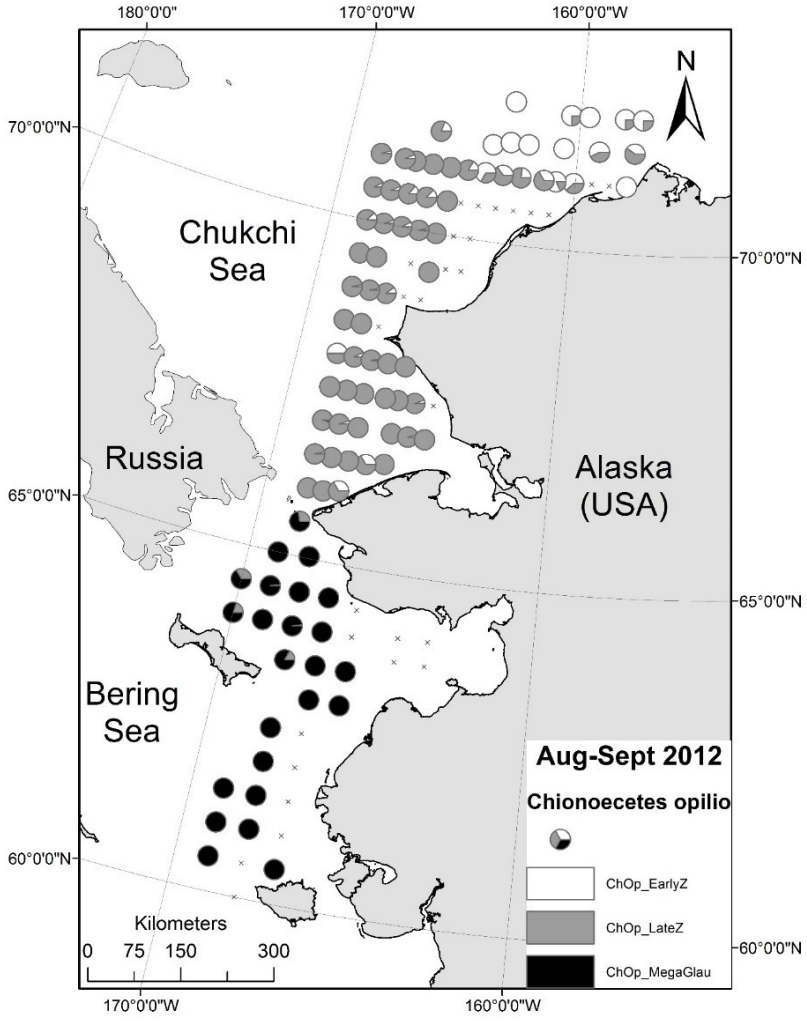

Figure 6. Snow crab (*Chionoecetes opilio*) stage group proportional contribution of early zoeae, late zoeae, and megalopae to species catch by station from 2012.

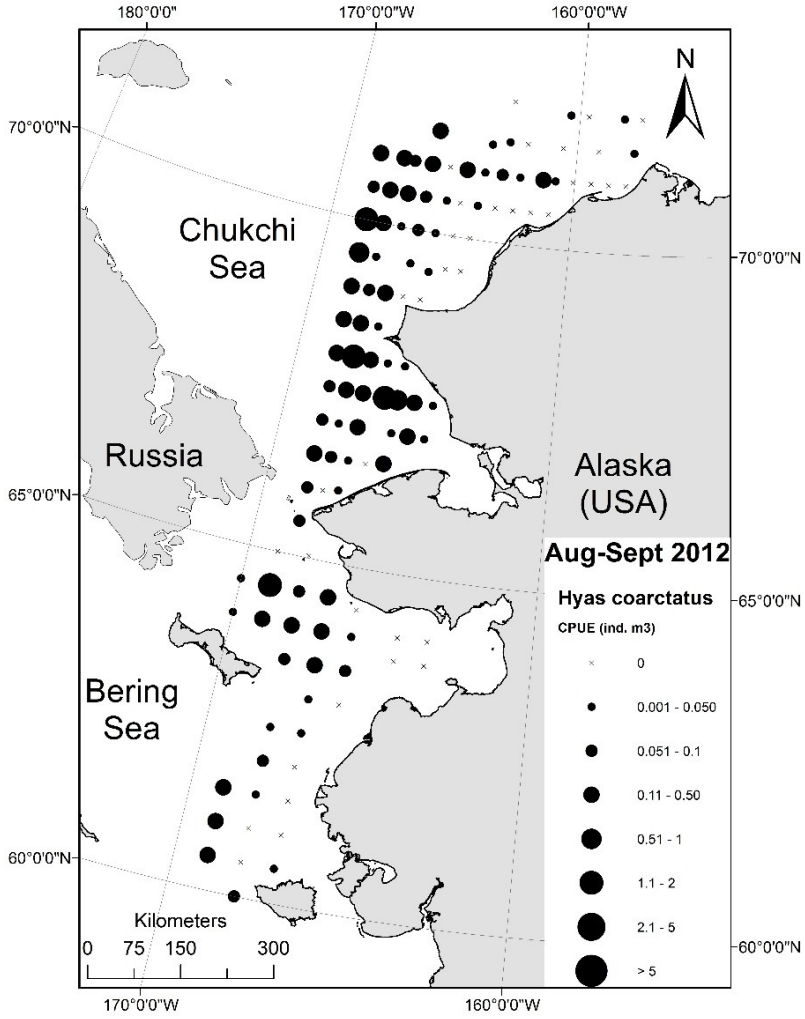

Figure 7. Arctic lyre crab (*Hyas coarctatus*) CPUE (ind. m-3) by station from 2012.

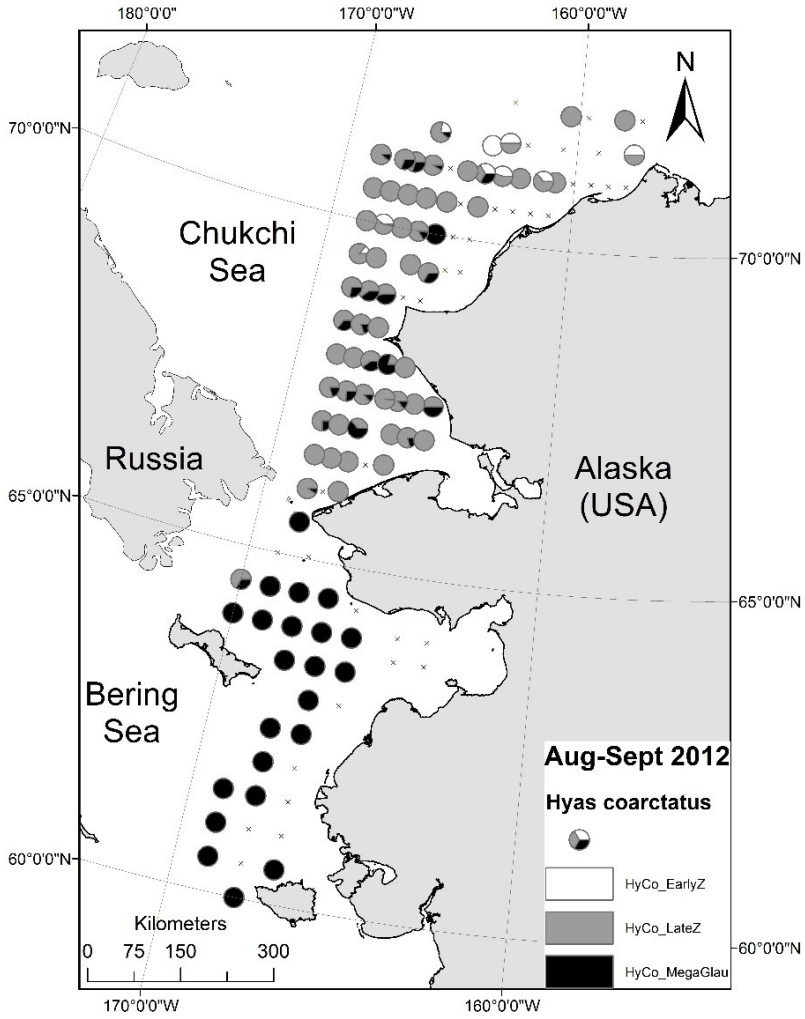

Figure 8. Arctic lyre crab (*Hyas coarctatus*) stage group proportional contribution of early zoeae, late zoeae, and megalopae to species catch by station from 2012.

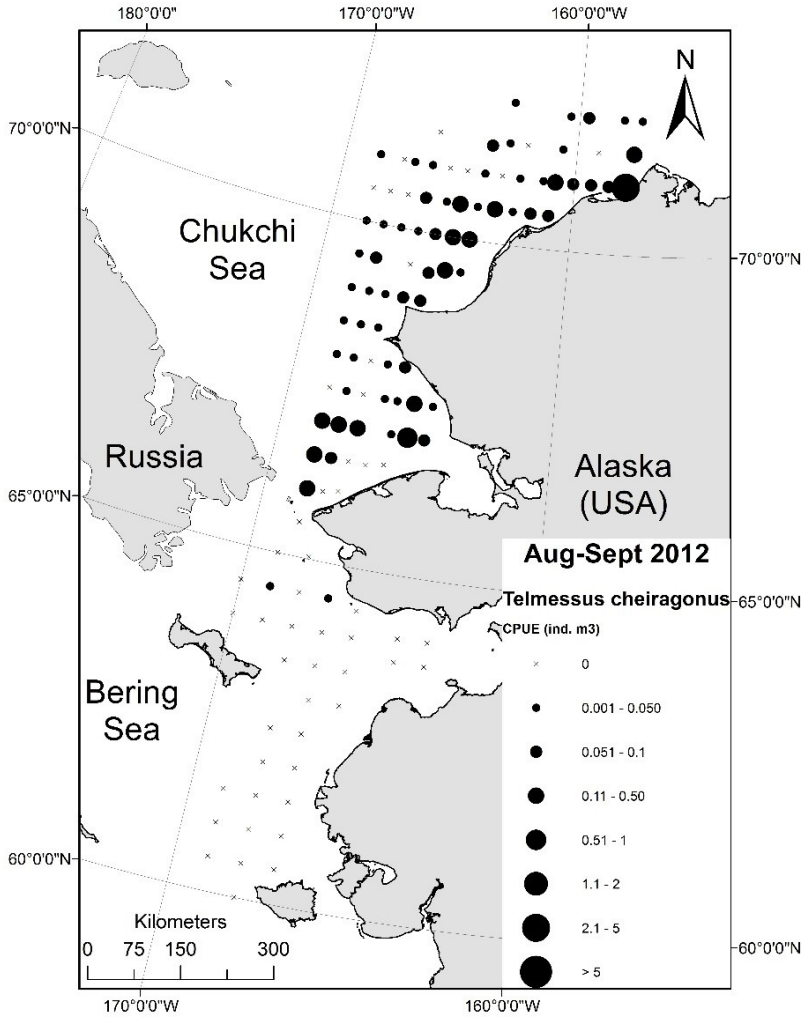

Figure 9. Helmet crab (*Telmessus cheiragonus*) CPUE (ind. m-3) by station from 2012.

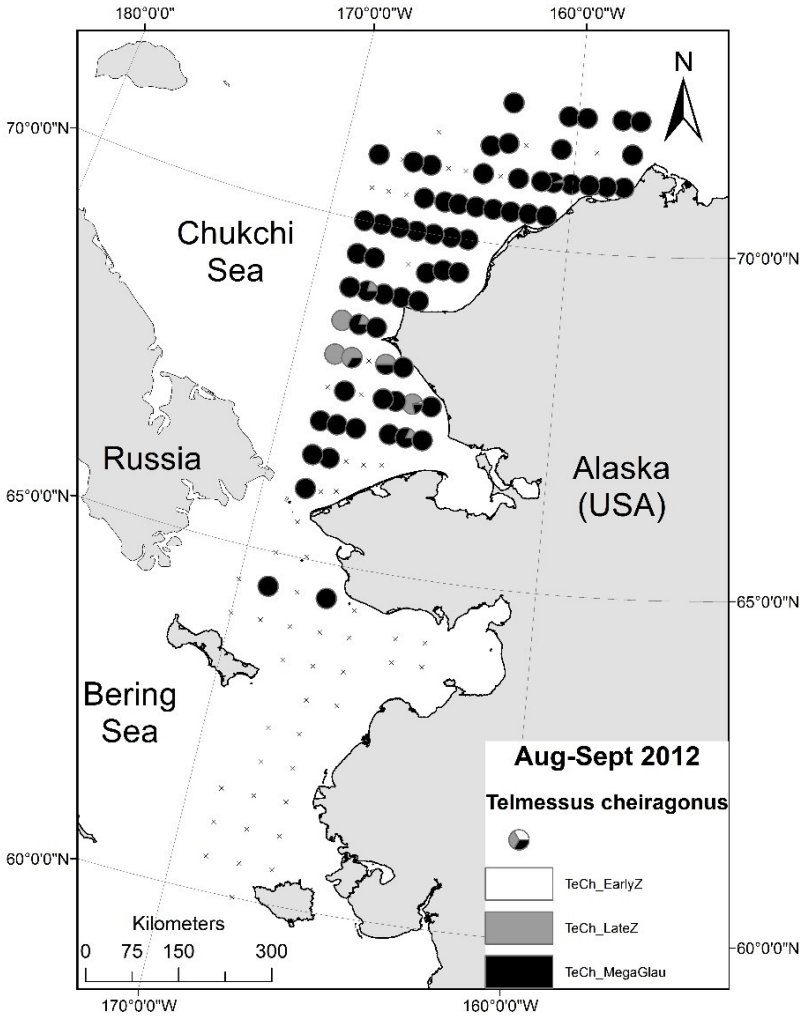

Figure 10. Helmet crab (*Telmessus cheiragonus*) stage group proportional contribution of early zoeae, late zoeae, and megalopae to species catch by station from 2012.

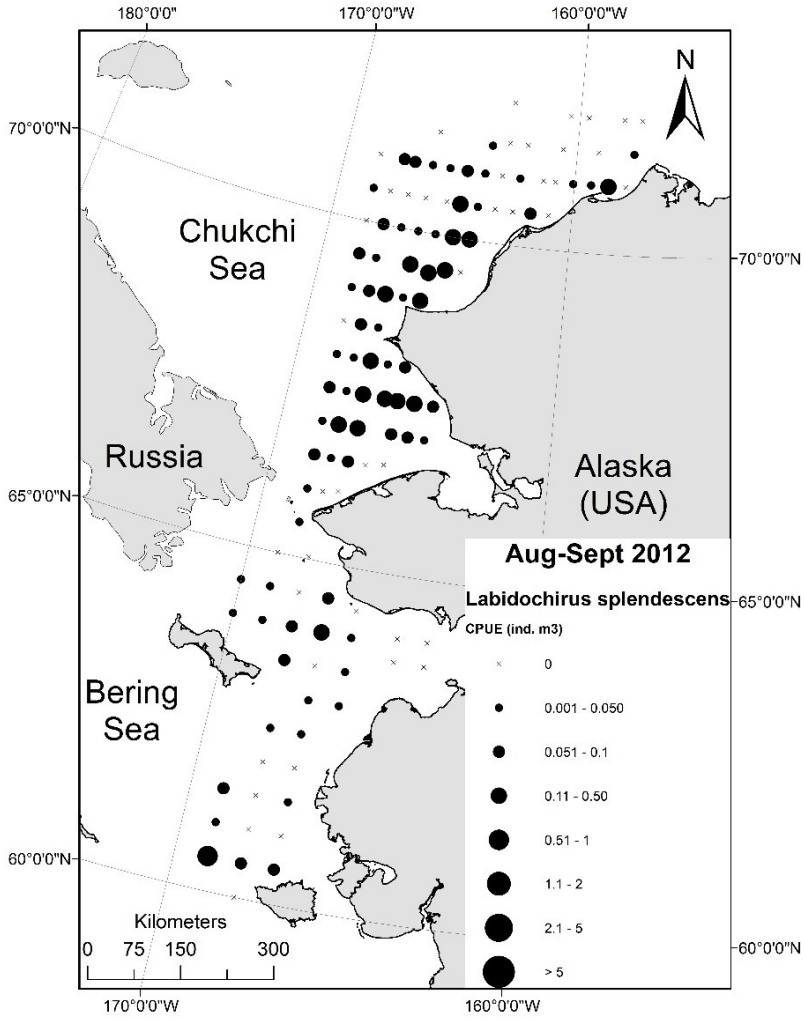

Figure 11. Splendid hermit crab (*Labidochirus splendescens*) CPUE (ind. m-3) by station from 2012.

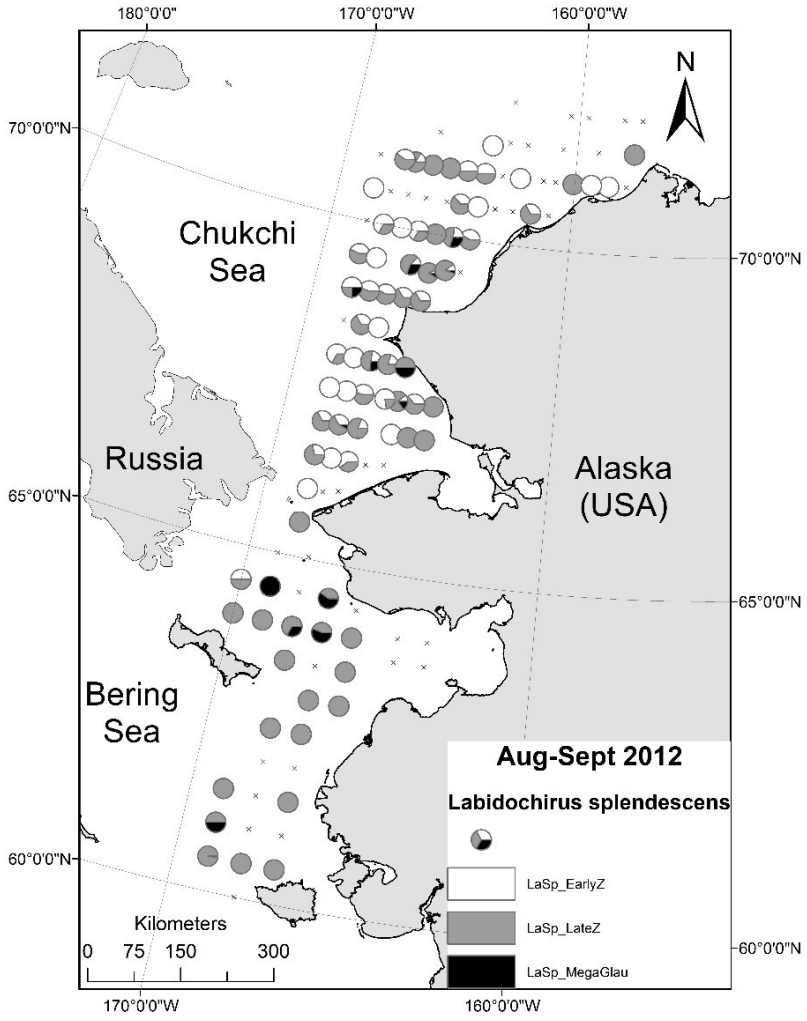

Figure 12. Splendid hermit crab (*Labidochirus splendescens*) stage group proportional contribution of early zoeae, late zoeae, and glaucothoe to species catch by station from 2012.

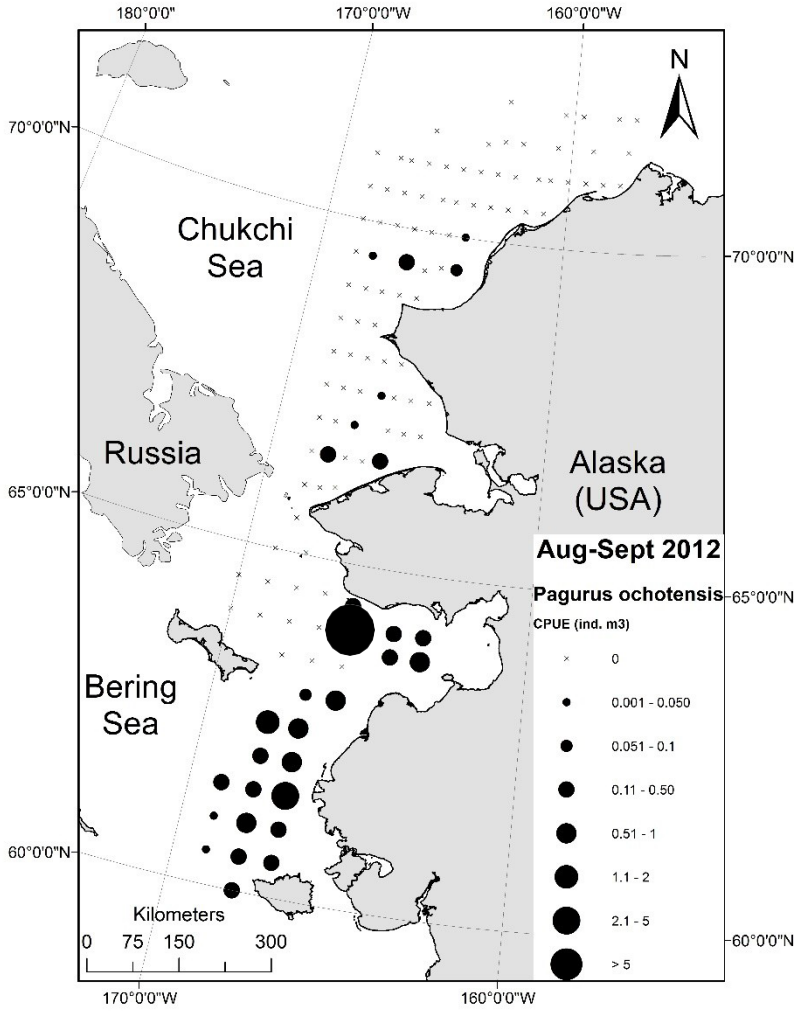

Figure 13. Ochre/Alaskan hermit crab (*Pagurus ochotensis*) CPUE (ind. m-3) by station from 2012.

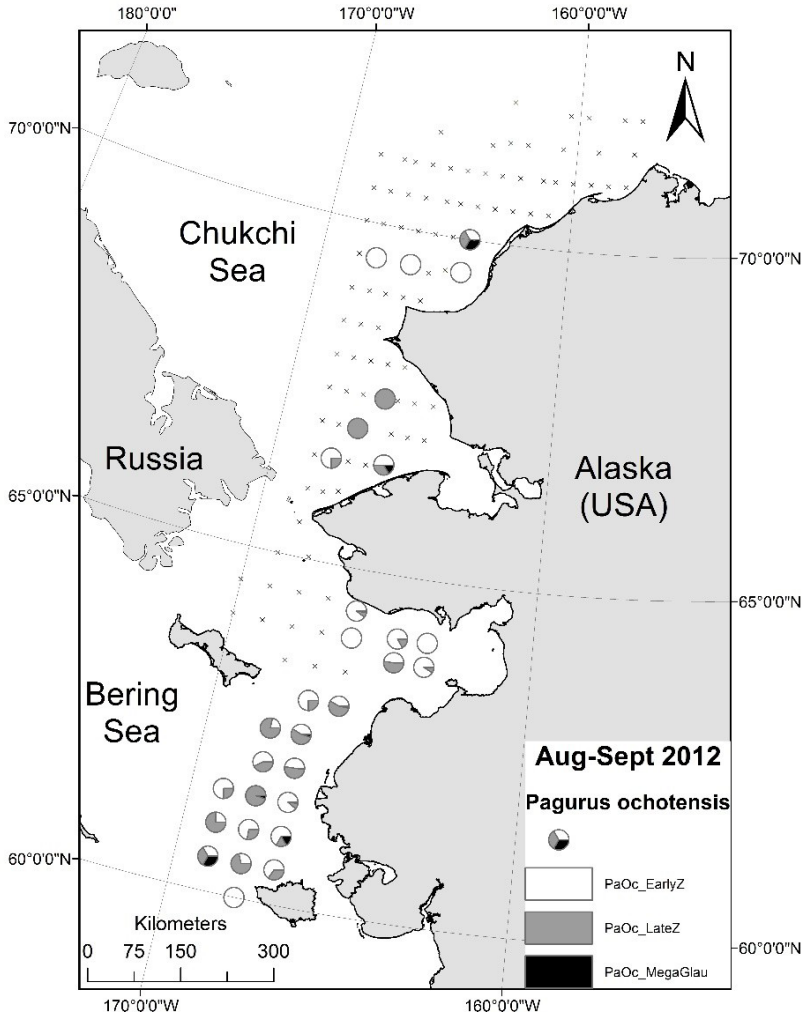

Figure 14. Ochre/Alaskan hermit crab (*Pagurus ochotensis*) stage group proportional contribution of early zoeae, late zoeae, and glaucothoe to species catch by station from 2012.

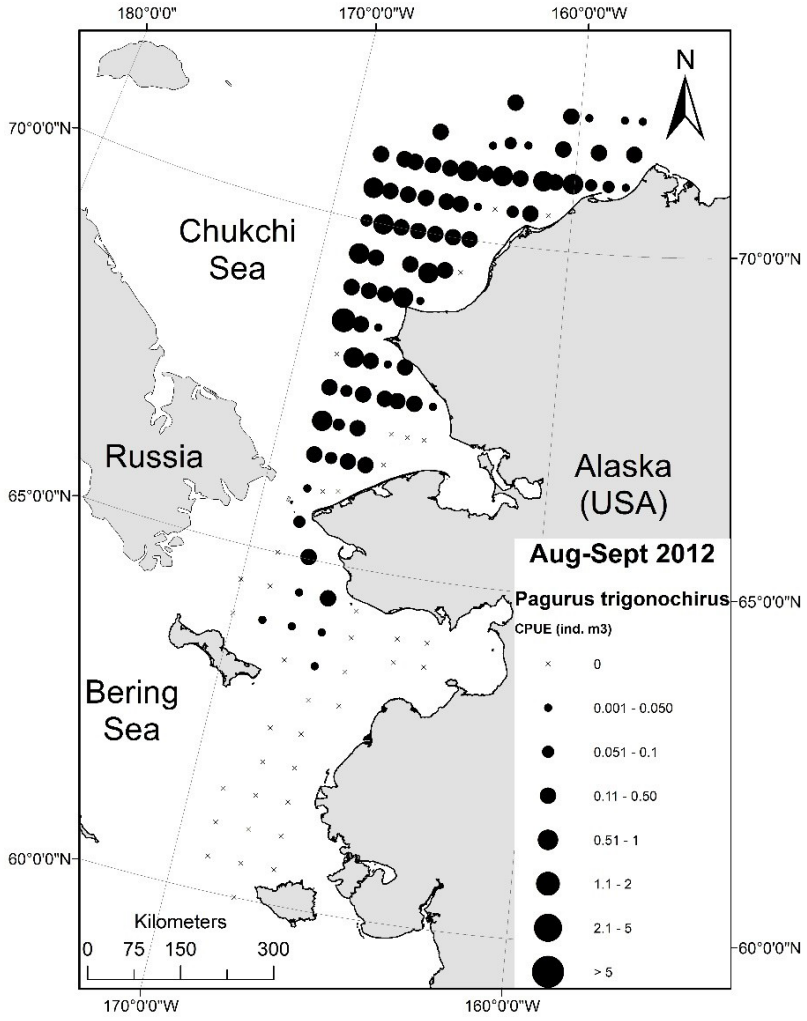

Figure 15 Fuzzy hermit crab (*Pagurus trigonochirus* cf) CPUE (ind. m-3) by station from 2012.

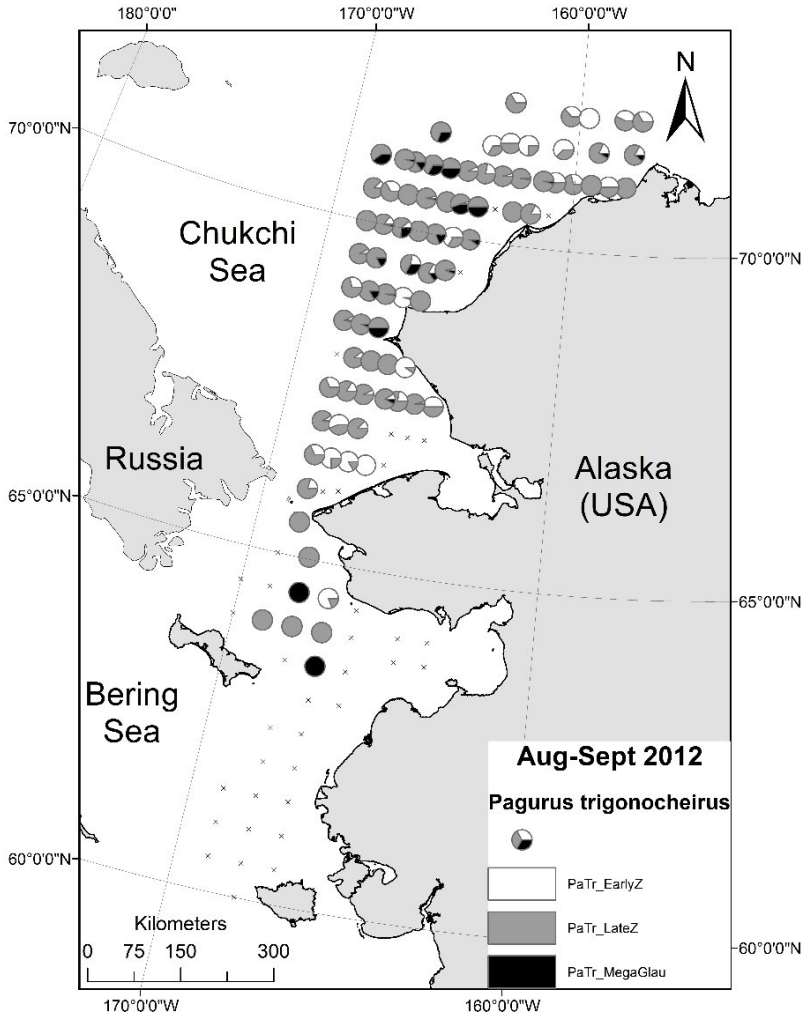

Figure 16. Fuzzy hermit crab (*Pagurus trigonochirus* cf) stage group proportional contribution of early zoeae, late zoeae, and glaucothoe to species catch by station from 2012.

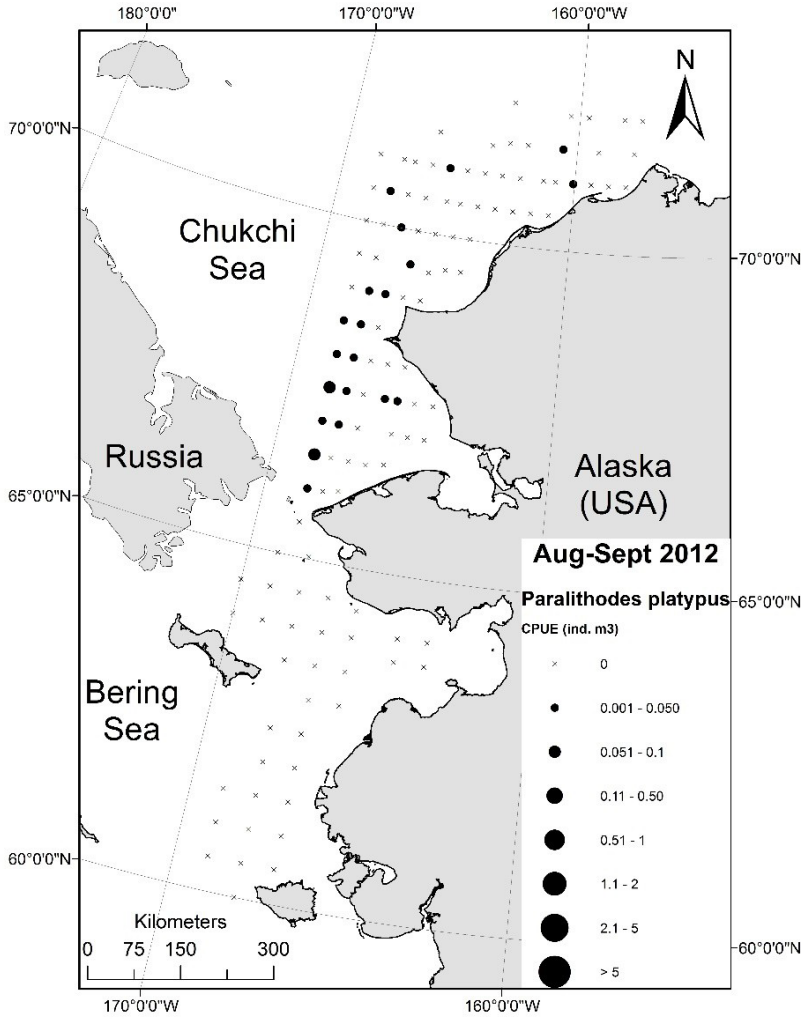

Figure 17. Blue king crab (*Paralithodes platypus*) CPUE (ind. m-3) by station from 2012.

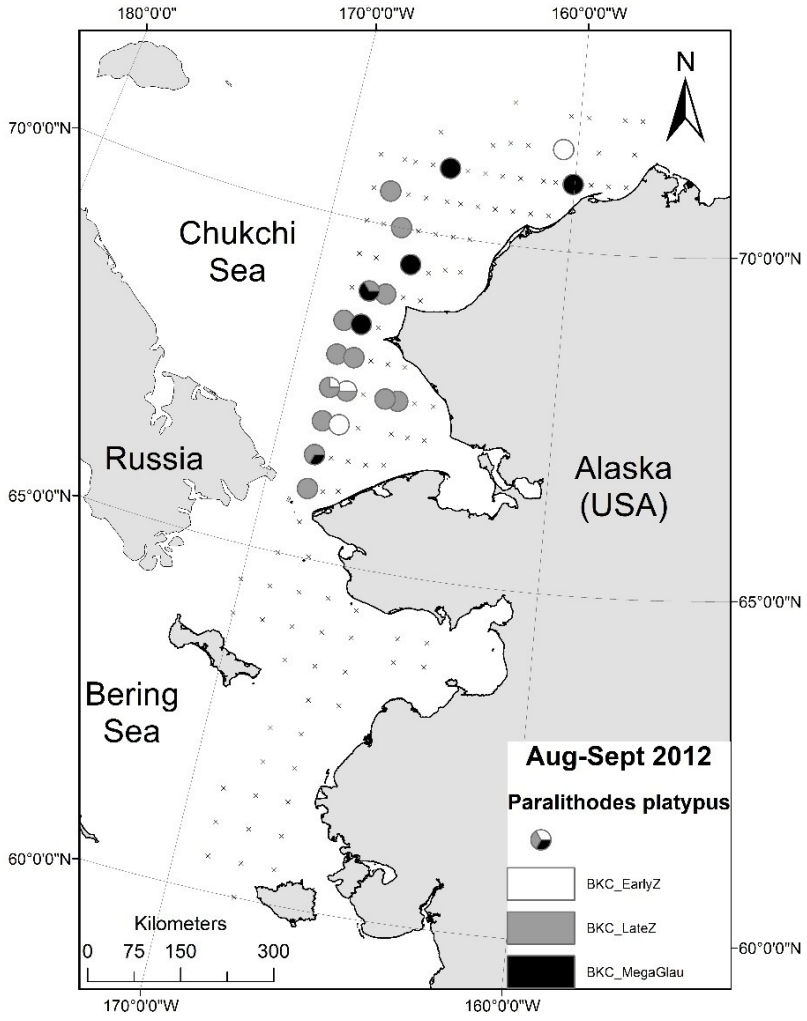

Figure 18. Blue king crab (*Paralithodes platypus*) stage group proportional contribution of early zoeae, late zoeae, and glaucothoe to species catch by station from 2012.

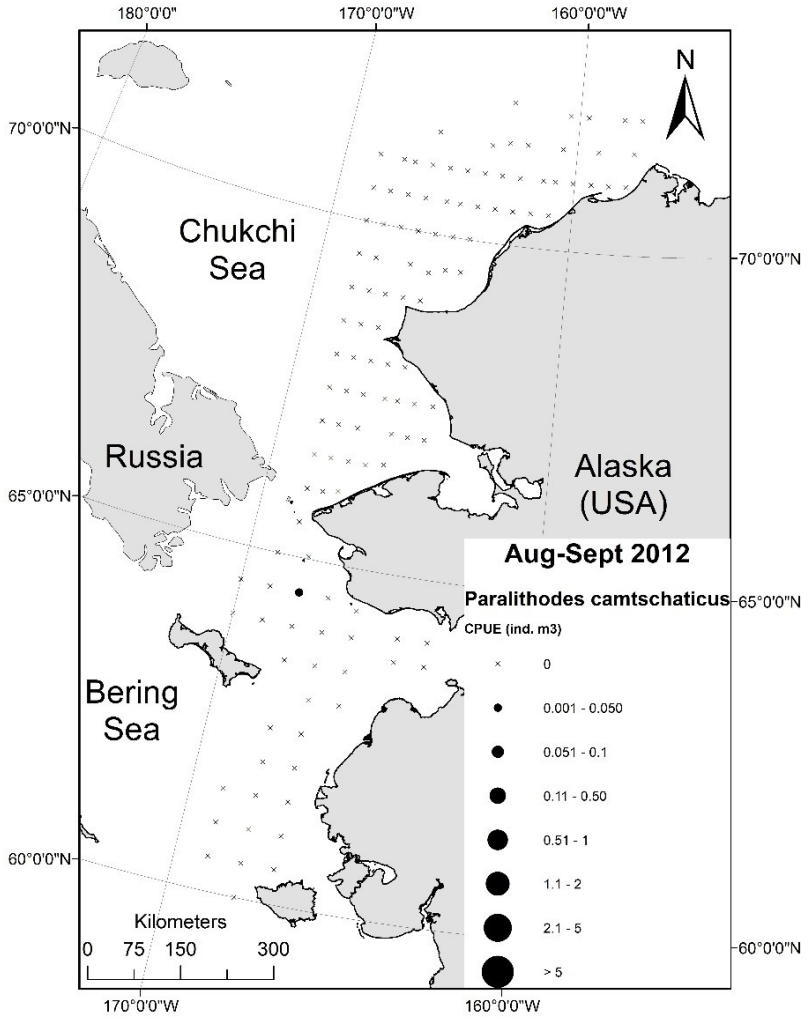

Figure 19. Red king crab (*Paralithodes camtschaticus*) CPUE (ind. m-3) by station from 2012.

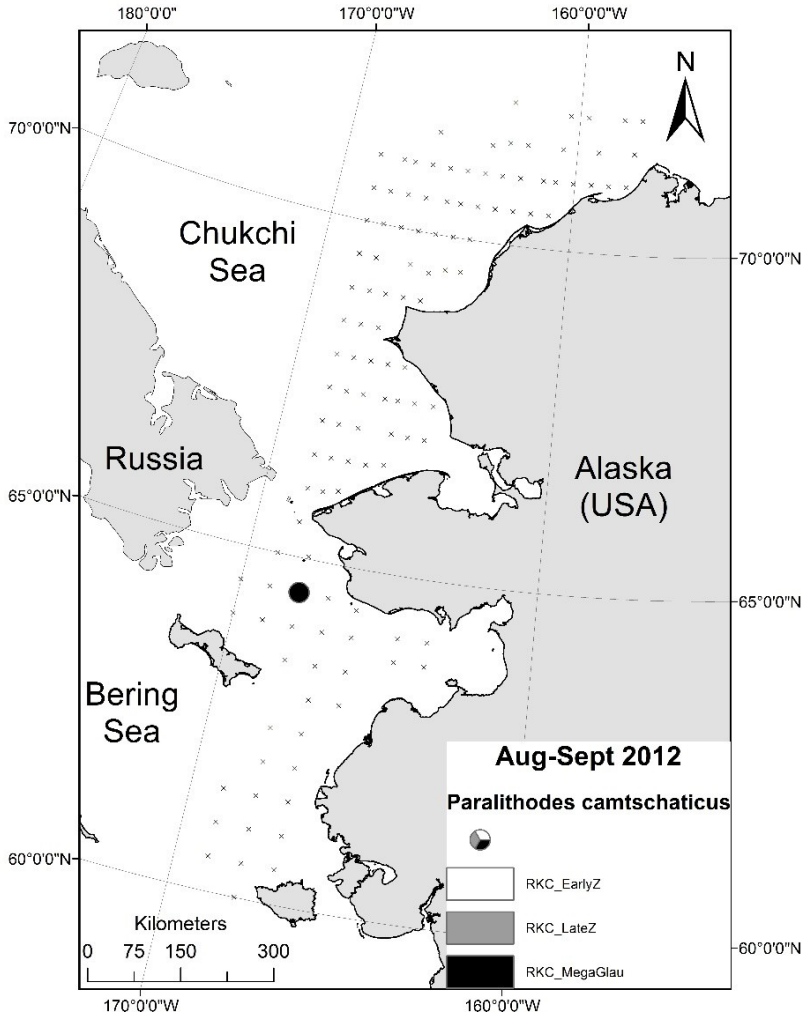

Figure 20. Red king crab (*Paralithodes camtschaticus*) stage group proportional contribution of early zoeae, late zoeae, and glaucothoe to species catch by station from 2012.

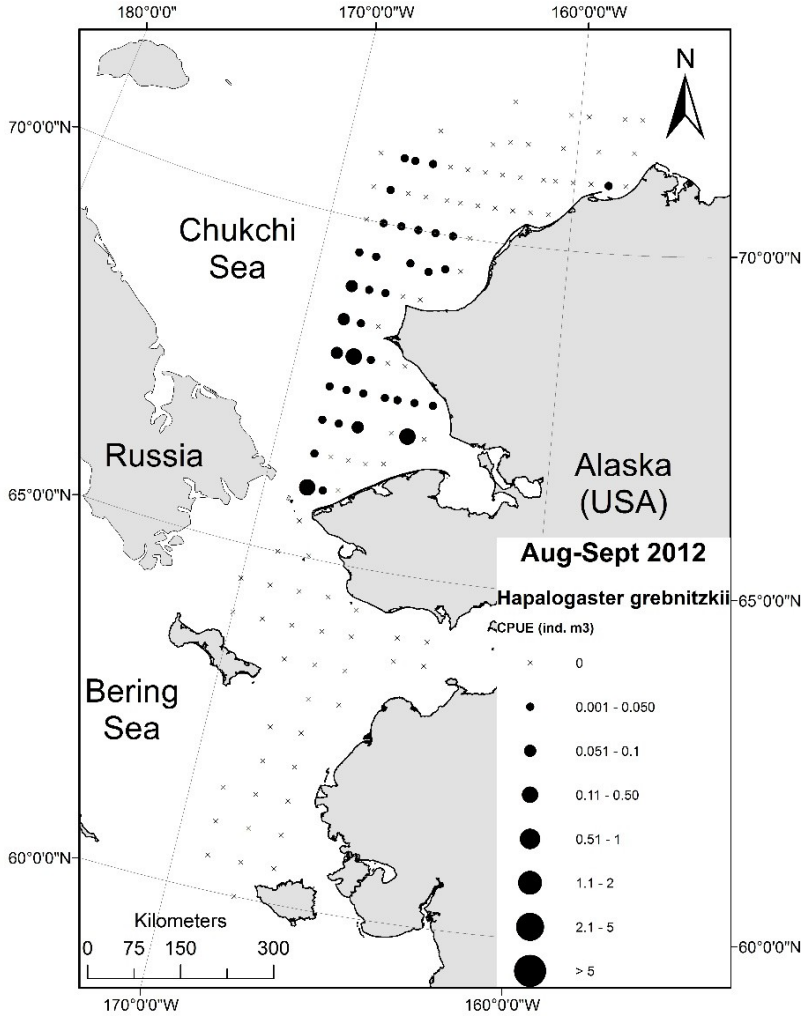

Figure 21. Northern hairy king crab (*Hapalogaster grebnitzkii*) CPUE (ind. m-3) by station from 2012.

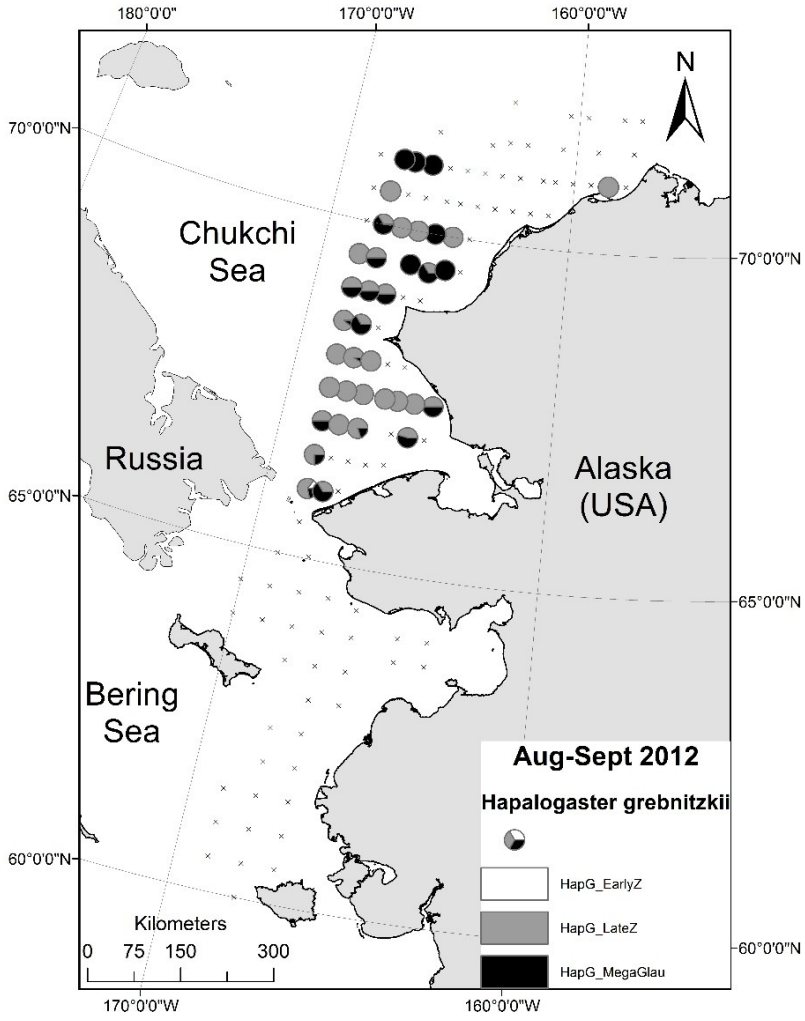

Figure 22. Northern hairy king crab (*Hapalogaster grebnitzkii*) stage group proportional contribution of early zoeae, late zoeae, and glaucothoe to species catch by station from 2012.

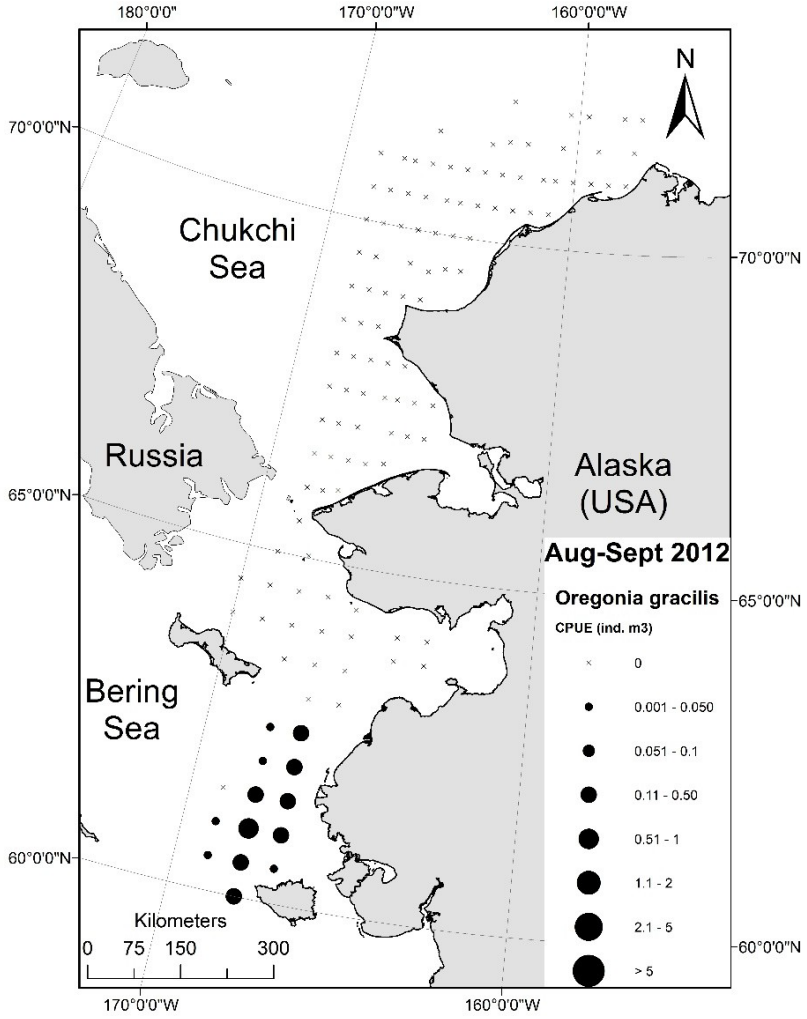

Figure 23. Graceful decorator crab (*Oregonia gracilis*) CPUE (ind. m-3) by station from 2012.

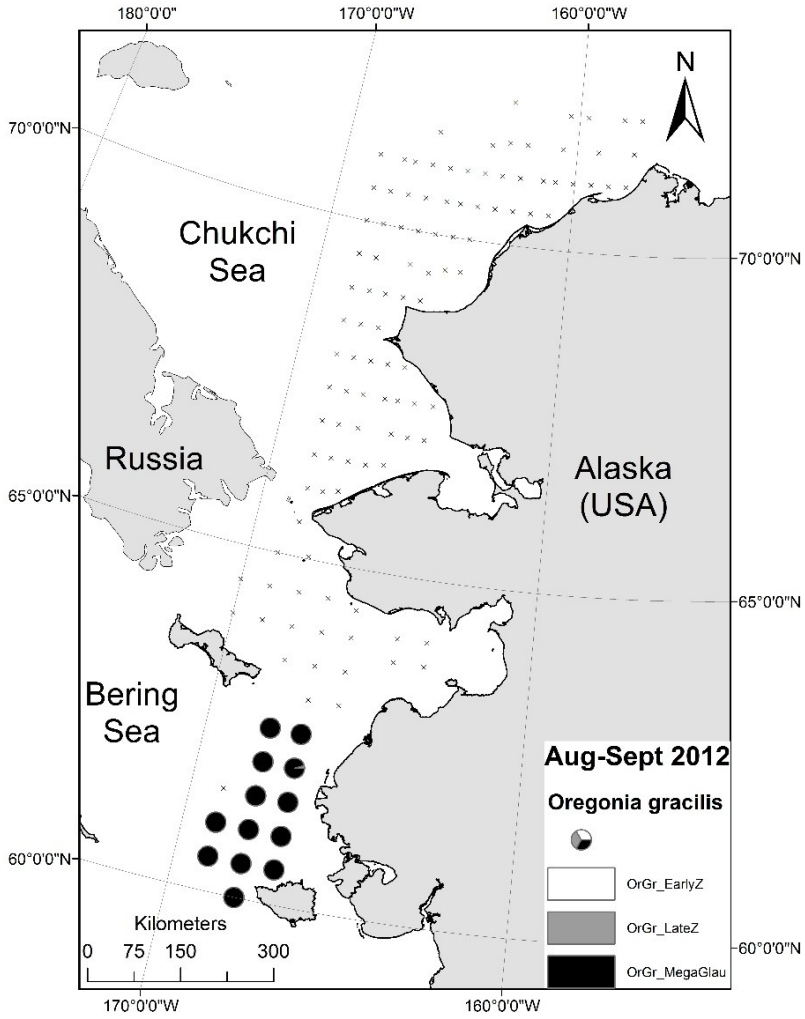

Figure 24. Graceful decorator crab (*Oregonia gracilis*) stage group proportional contribution of early zoeae, late zoeae, and megalopae to species catch by station from 2012.

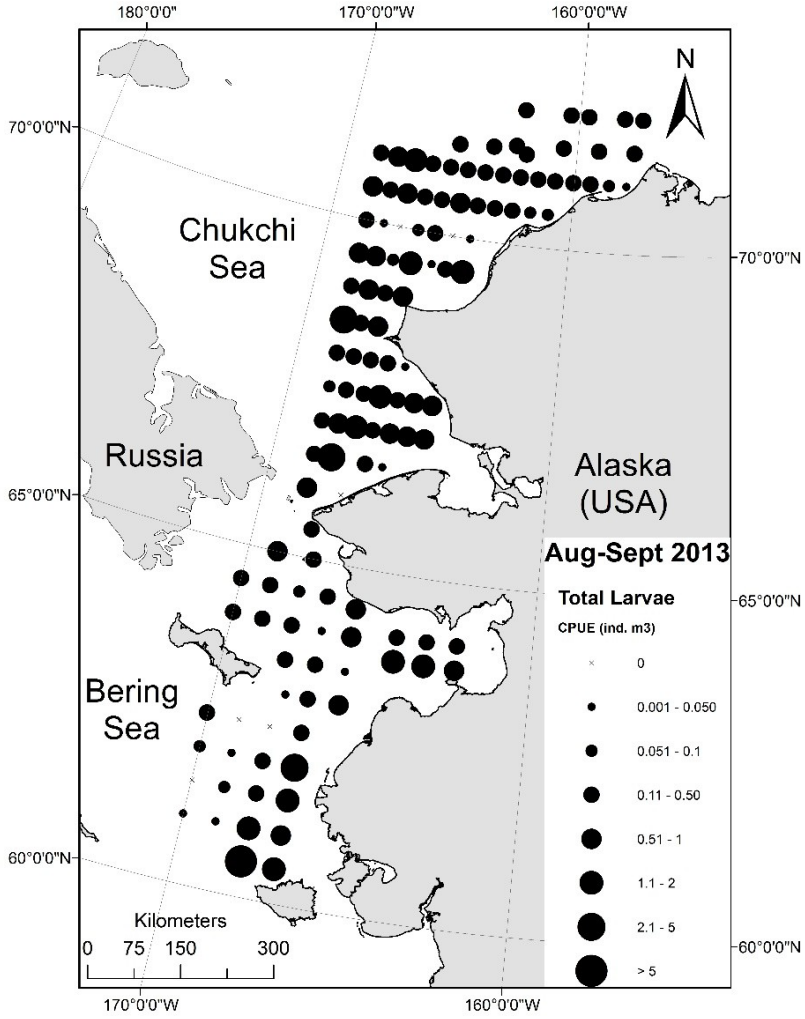

Figure 25. Total crab larval community CPUE (ind. m-3) by station from 2013.

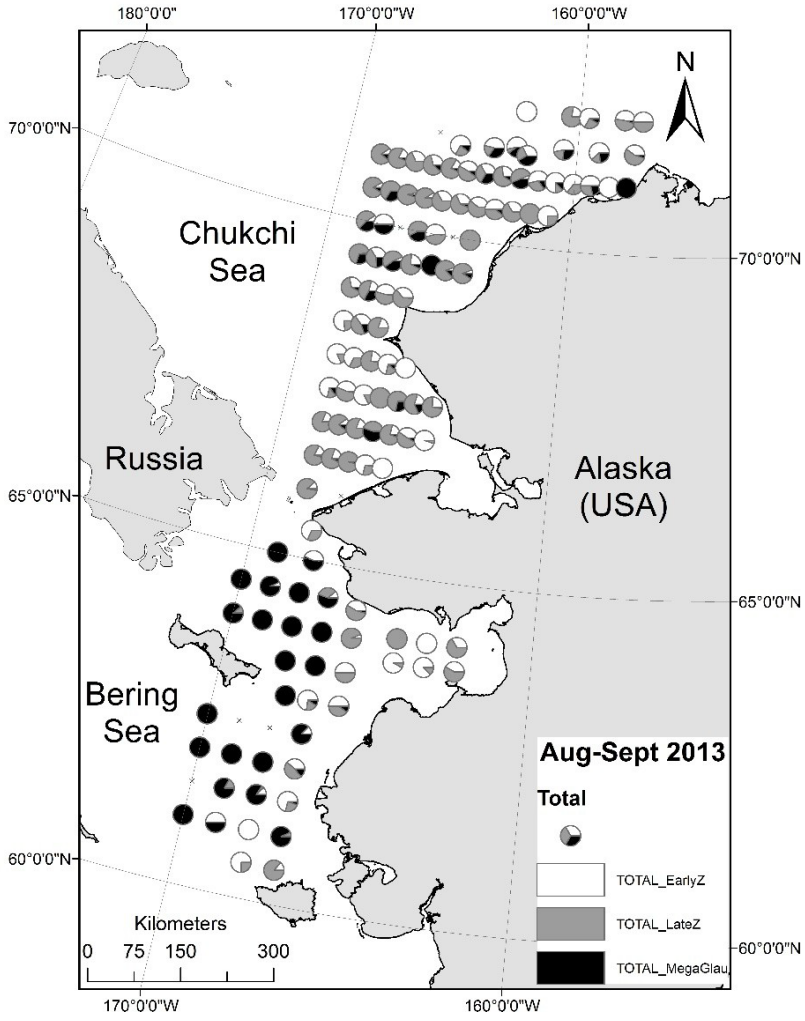

Figure 26. Total crab larvae stage group proportional contribution of early zoeae, late zoeae, and megalopae/glaucothoe to total catch by station from 2013.

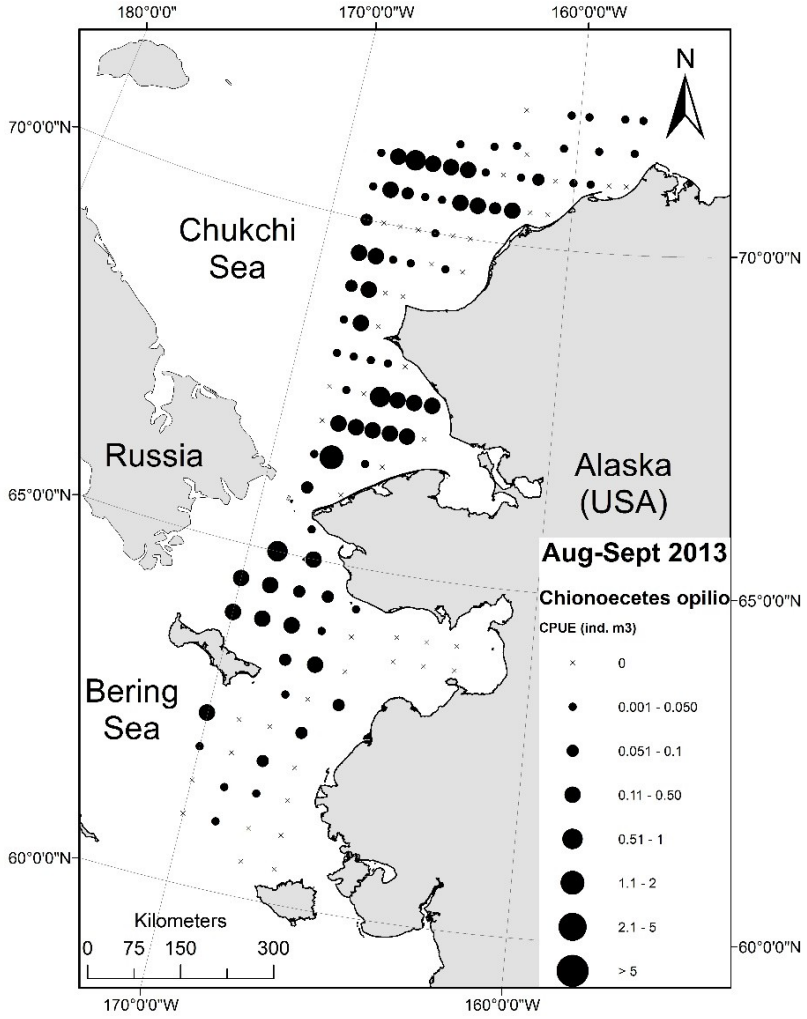

Figure 27. Snow crab (*Chionoecetes opilio*) CPUE (ind. m-3) by station from 2013.

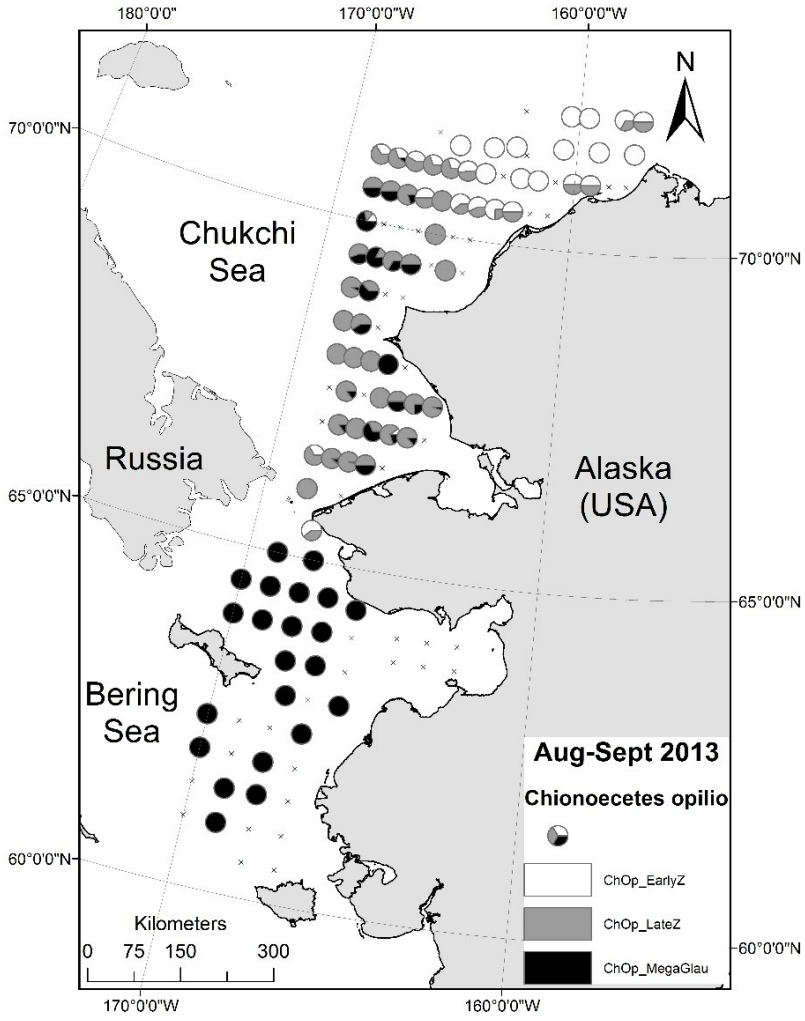

Figure 28. Snow crab (*Chionoecetes opilio*) stage group proportional contribution of early zoeae, late zoeae, and megalopae to species catch by station from 2013.

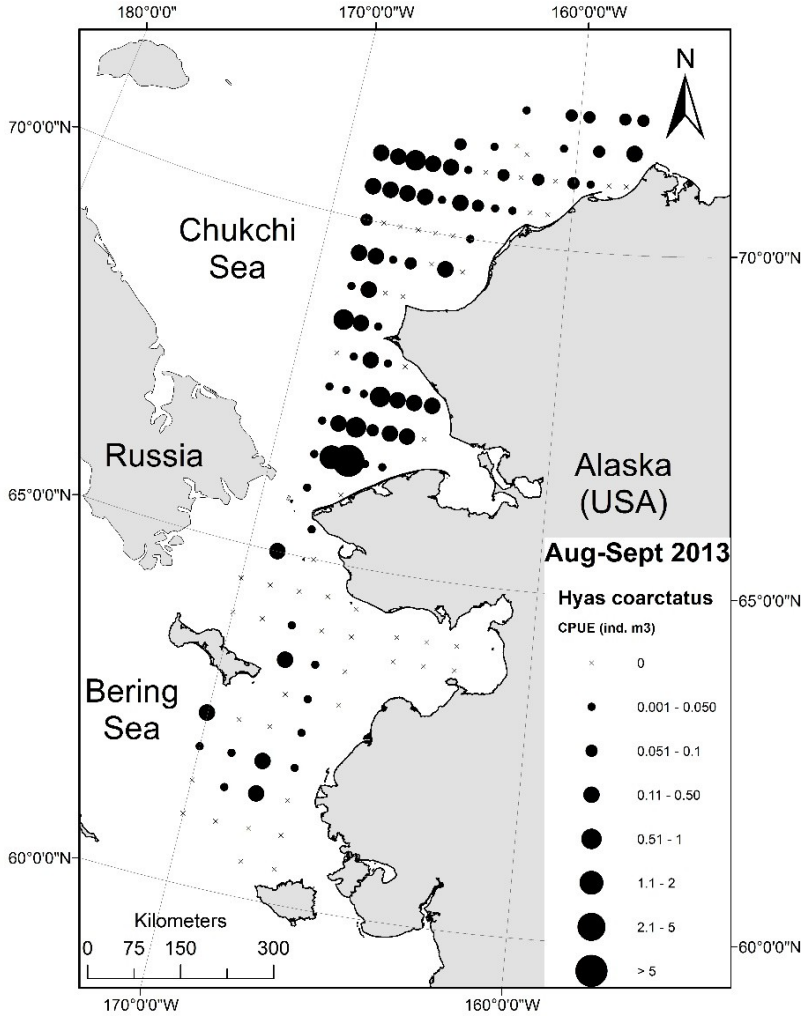

Figure 29. Arctic lyre crab (*Hyas coarctatus*) CPUE (ind. m-3) by station from 2013.

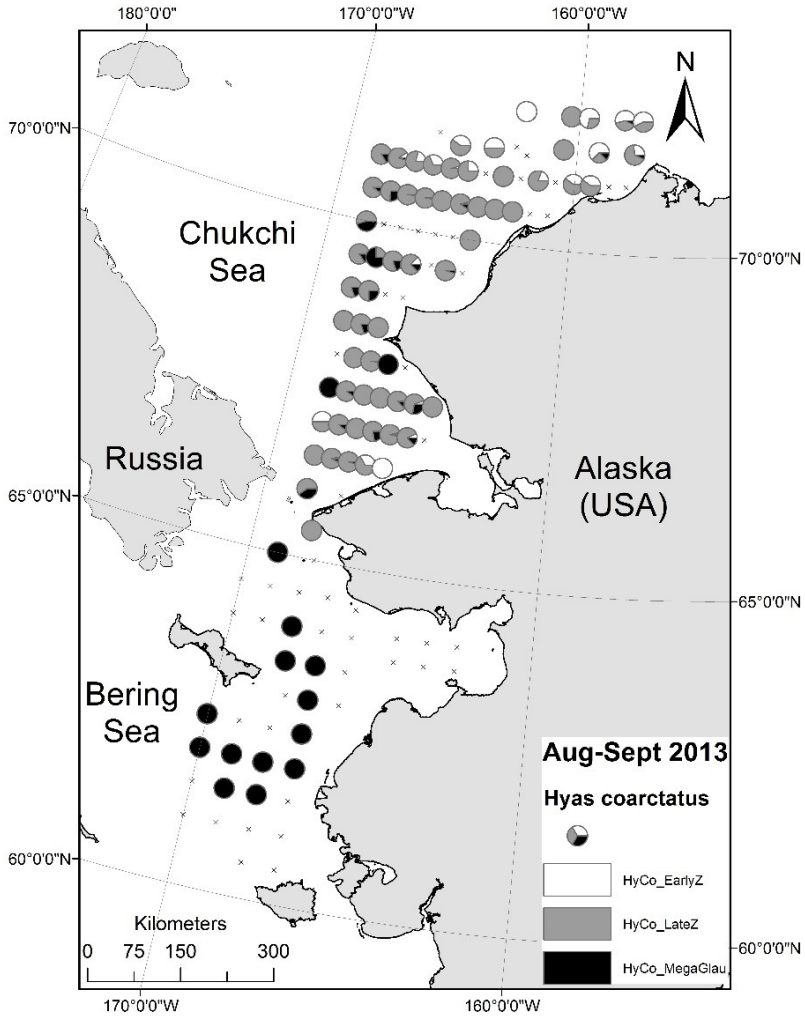

Figure 30. Arctic lyre crab (*Hyas coarctatus*) stage group proportional contribution of early zoeae, late zoeae, and megalopae to species catch by station from 2013.

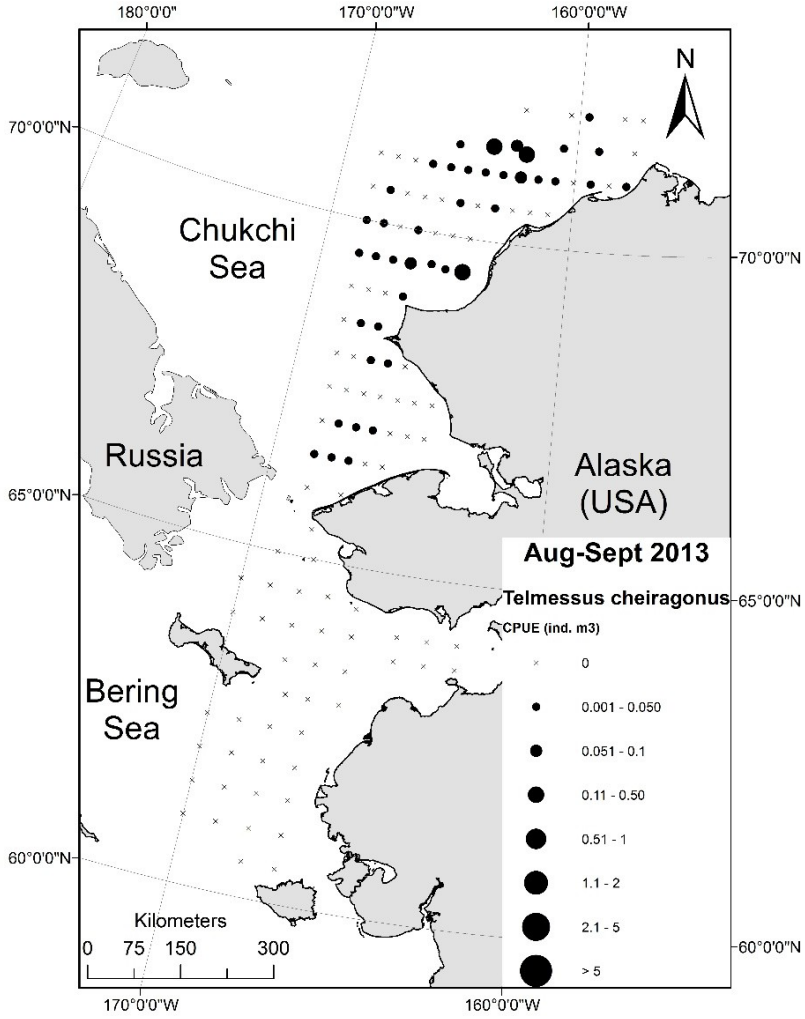

Figure 31. Helmet crab (*Telmessus cheiragonus*) CPUE (ind. m-3) by station from 2013.

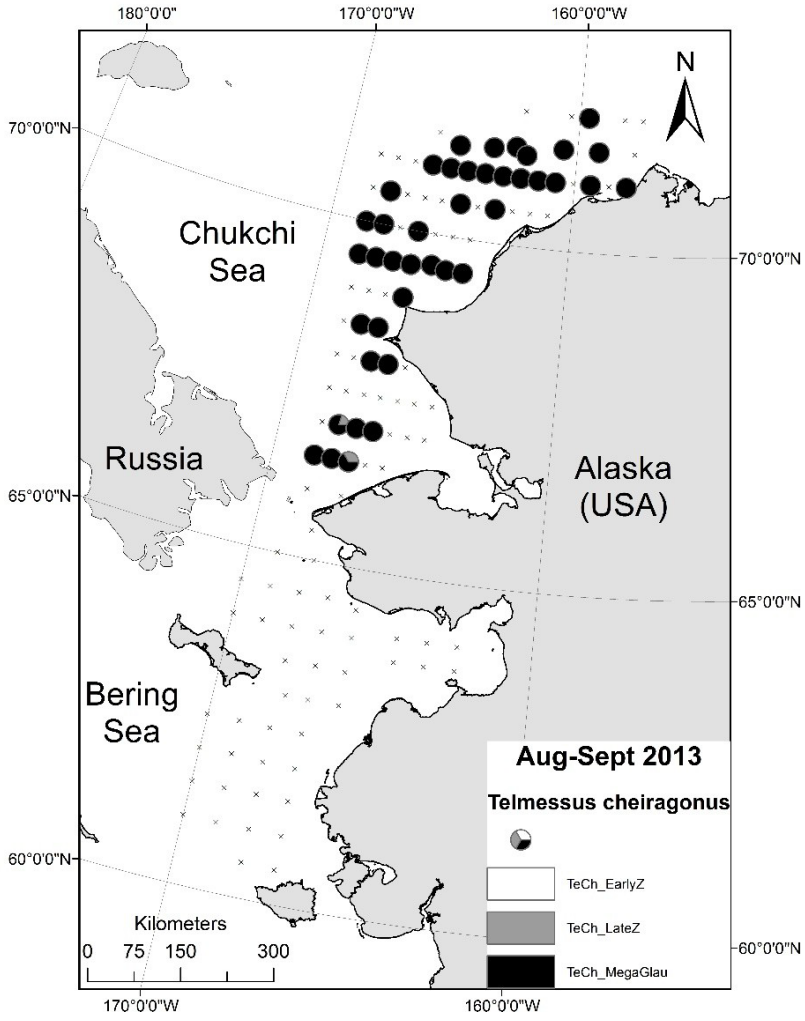

Figure 32. Helmet crab (*Telmessus cheiragonus*) stage group proportional contribution of early zoeae, late zoeae, and megalopae to species catch by station from 2013.

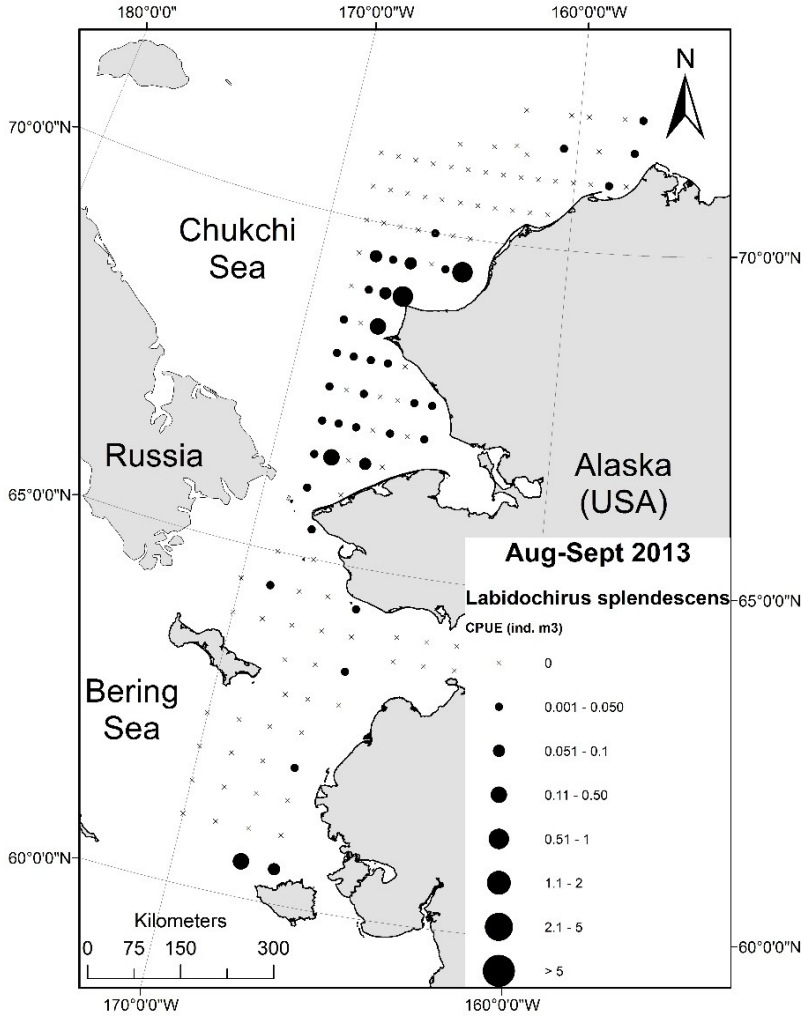

Figure 33. Splendid hermit crab (*Labidochirus splendescens*) CPUE (ind. m-3) by station from 2013.

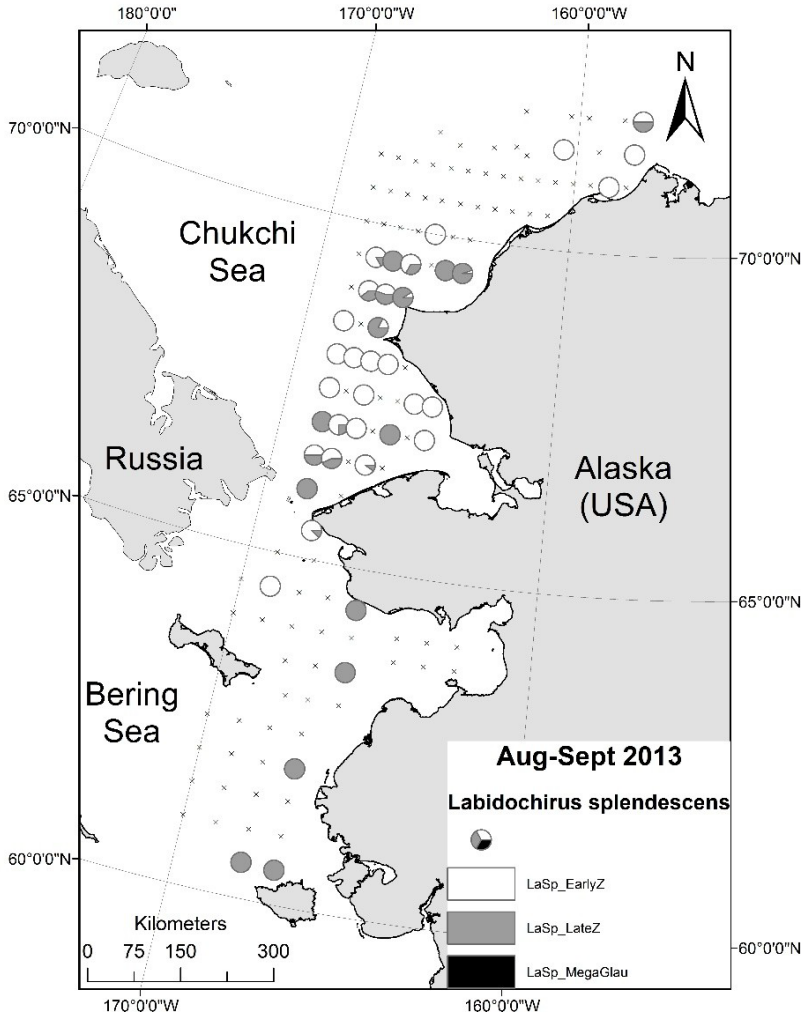

Figure 34. Splendid hermit crab (*Labidochirus splendescens*) stage group proportional contribution of early zoeae, late zoeae, and glaucothoe to species catch by station from 2013.

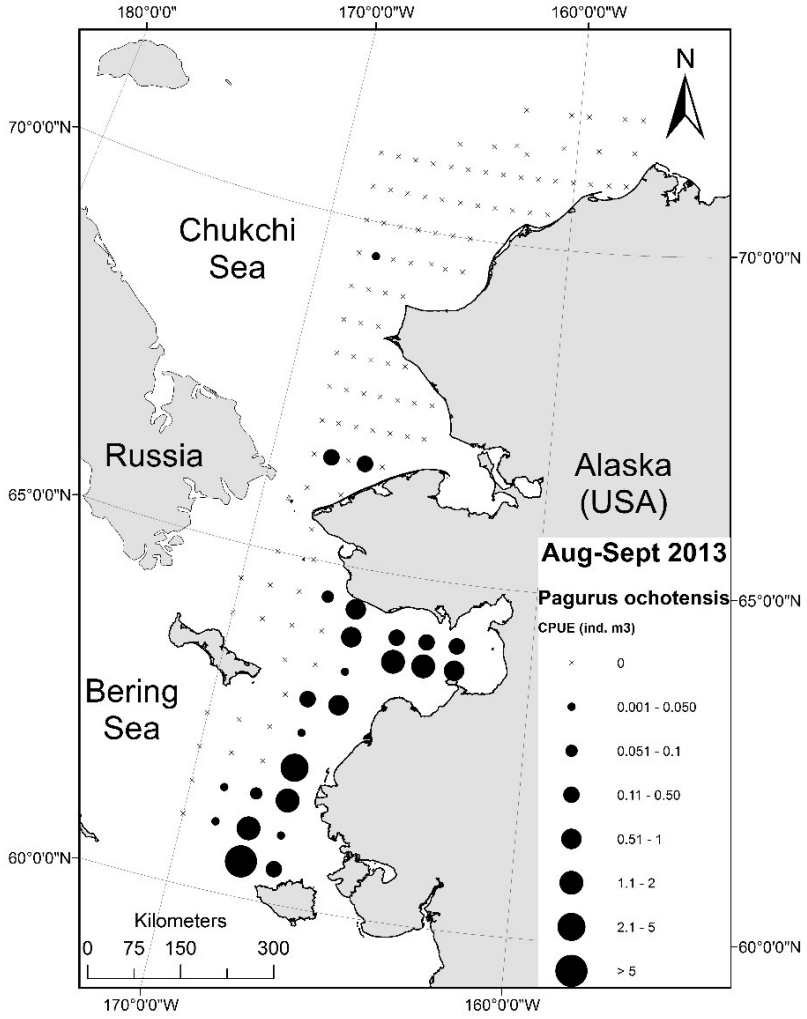

Figure 35. Ochre/Alaskan hermit crab (*Pagurus ochotensis*) CPUE (ind. m-3) by station from 2013.

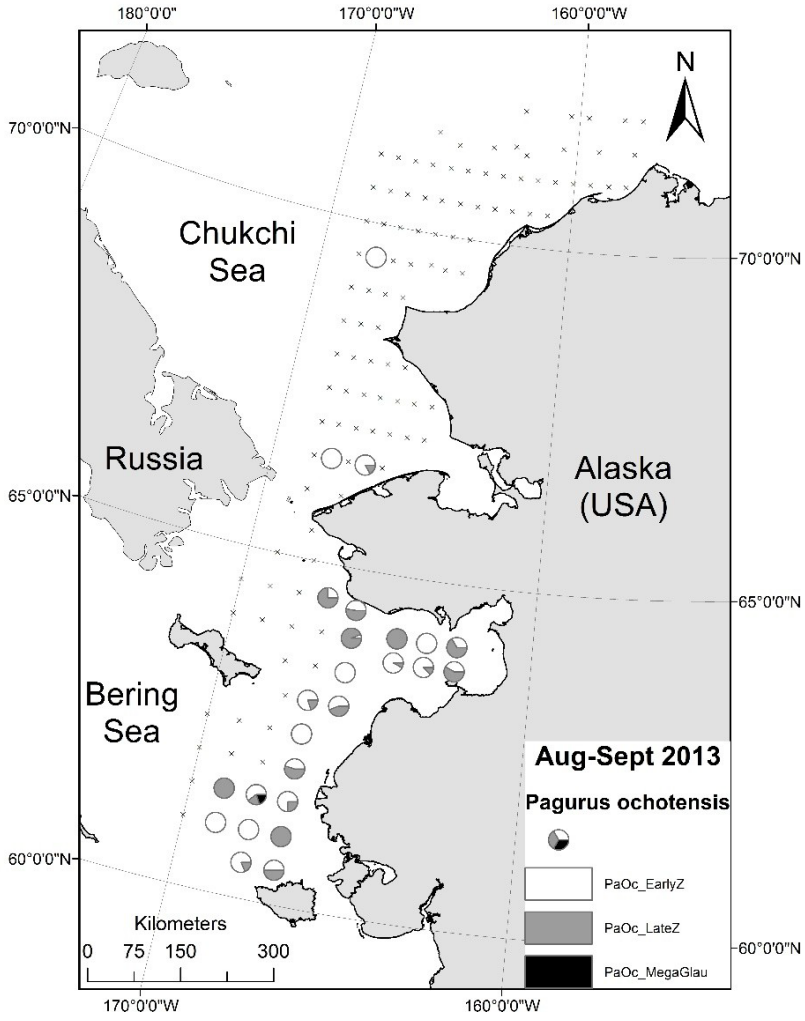

Figure 36. Ochre/Alaskan hermit crab (*Pagurus ochotensis*) stage group proportional contribution of early zoeae, late zoeae, and glaucothoe to species catch by station from 2013.

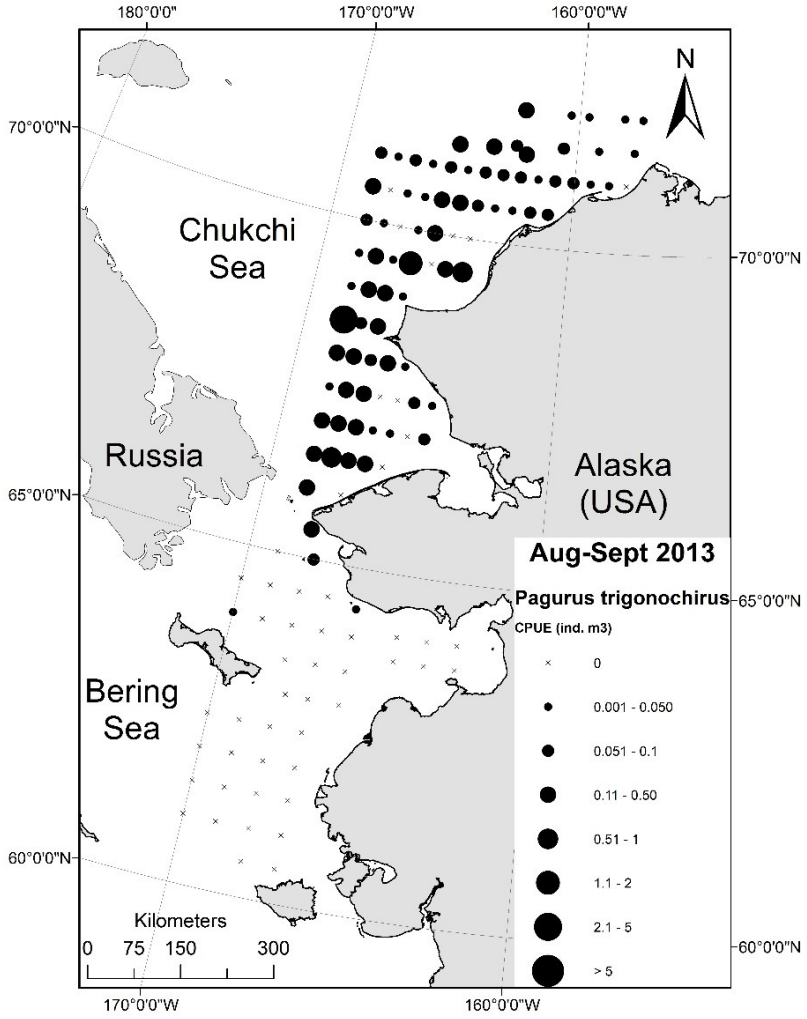

Figure 37. Fuzzy hermit crab (*Pagurus trigonochirus* cf) CPUE (ind. m-3) by station from 2013.

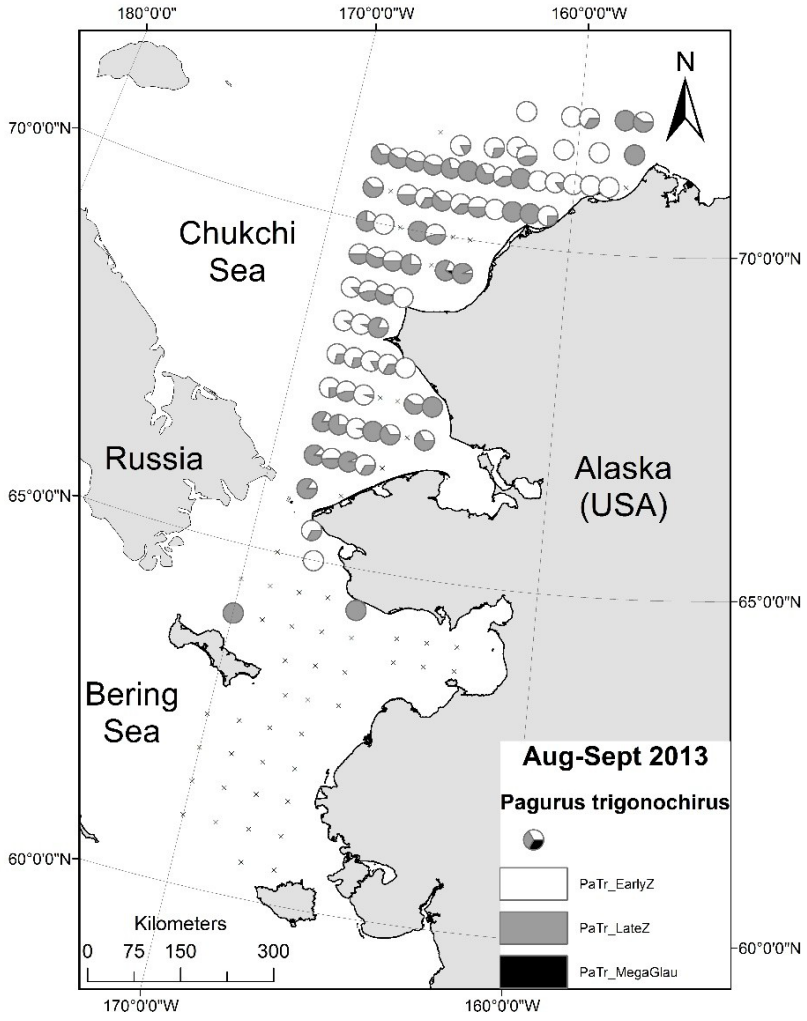

Figure 38. Fuzzy hermit crab (*Pagurus trigonochirus* cf) stage group proportional contribution of early zoeae, late zoeae, and glaucothoe to species catch by station from 2013.

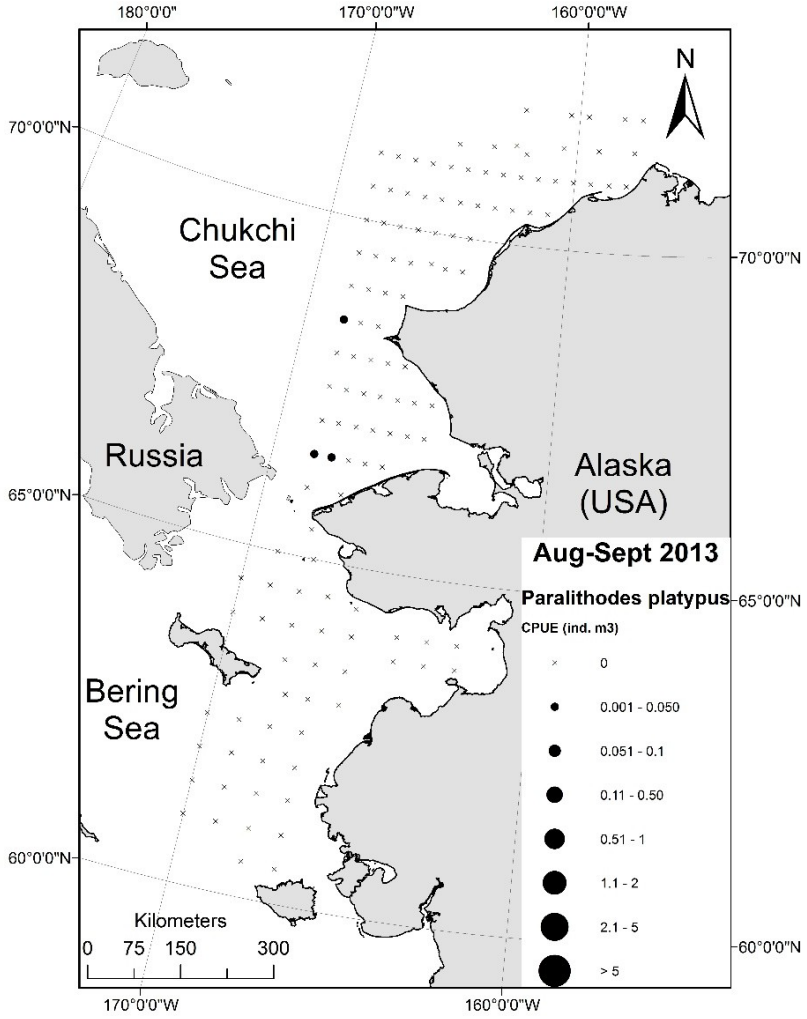

Figure 39. Blue king crab (*Paralithodes platypus*) CPUE (ind. m-3) by station from 2013.

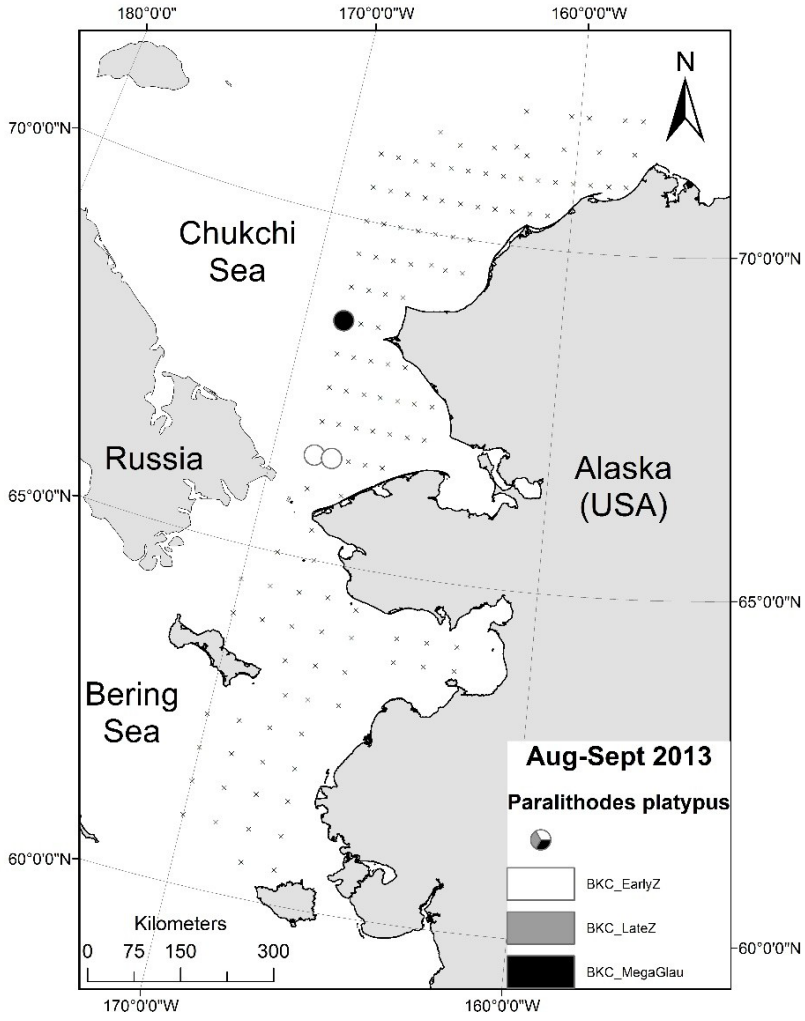

Figure 40. Blue king crab (*Paralithodes platypus*) stage group proportional contribution of early zoeae, late zoeae, and glaucothoe to species catch by station from 2013.

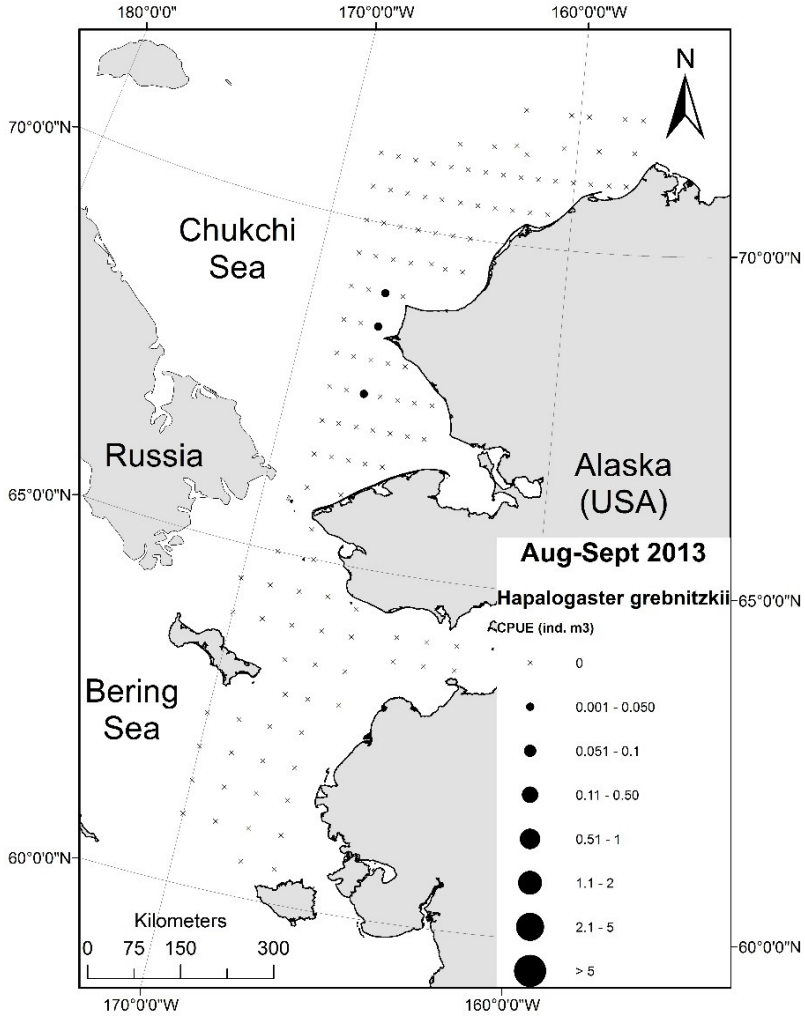

Figure 41. Northern hairy king crab (*Hapalogaster grebnitzkii*) CPUE (ind. m-3) by station from 2013.

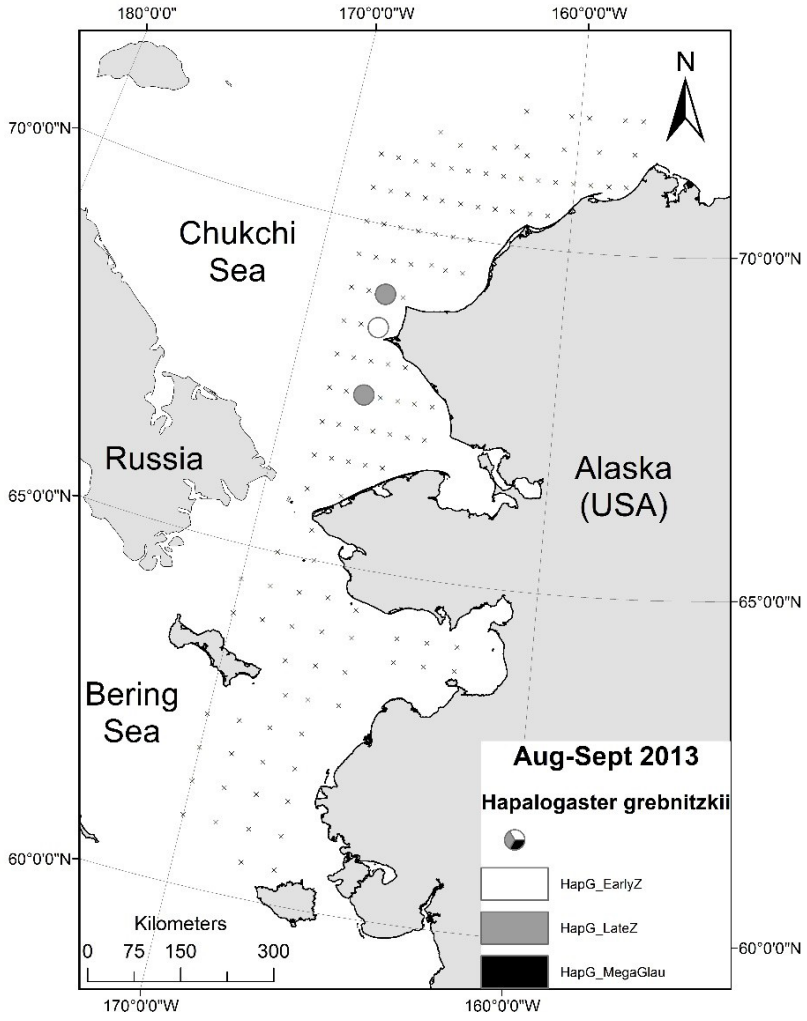

Figure 42. Northern hairy king crab (*Hapalogaster grebnitzkii*) stage group proportional contribution of early zoeae, late zoeae, and glaucothoe to species catch by station from 2013.

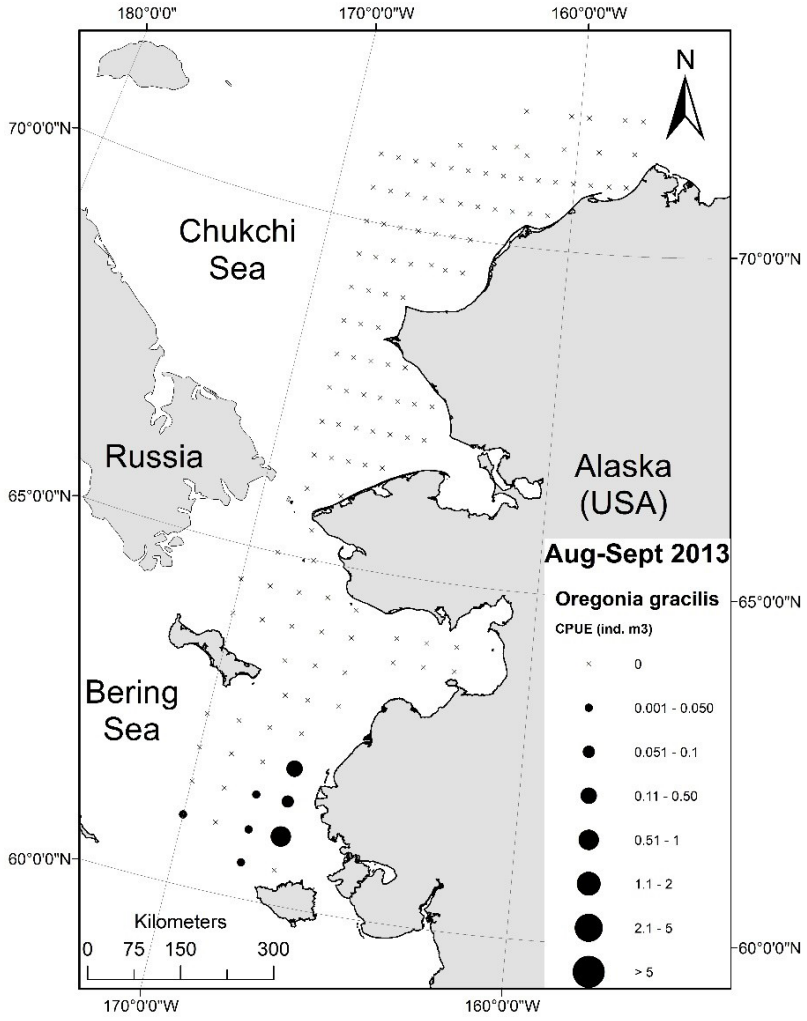

Figure 43. Graceful decorator crab (*Oregonia gracilis*) CPUE (ind. m-3) by station from 2013.

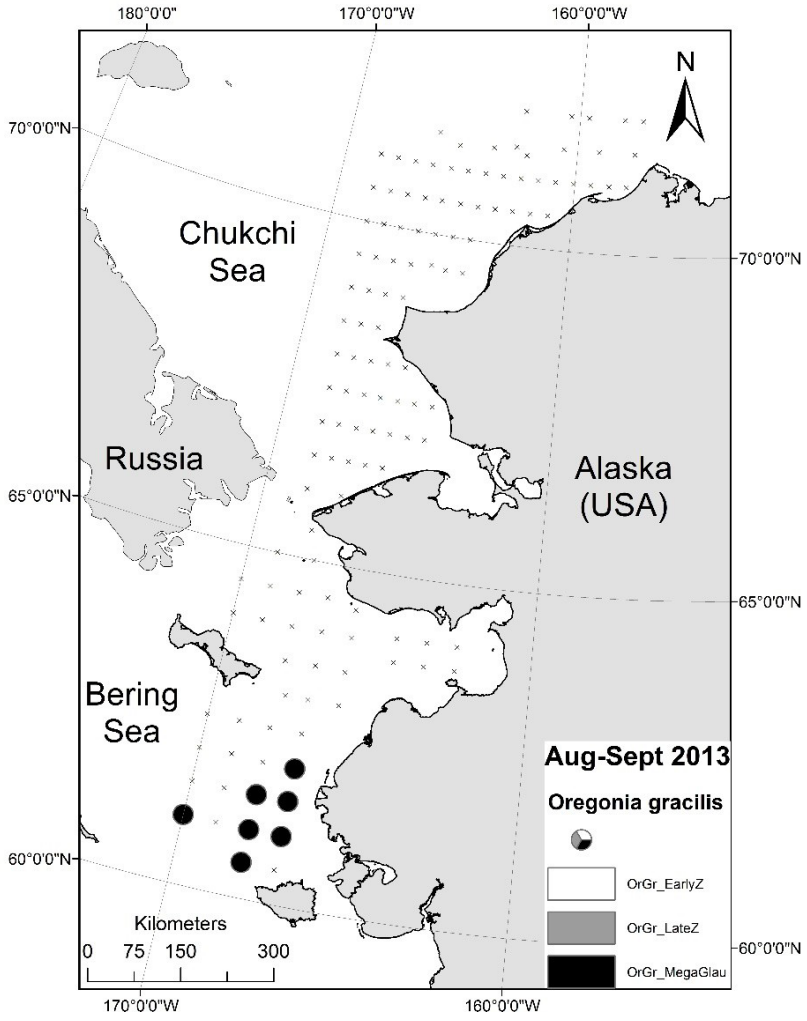

Figure 44. Graceful decorator crab (*Oregonia gracilis*) stage group proportional contribution of early zoeae, late zoeae, and megalopae to species catch by station from 2013.

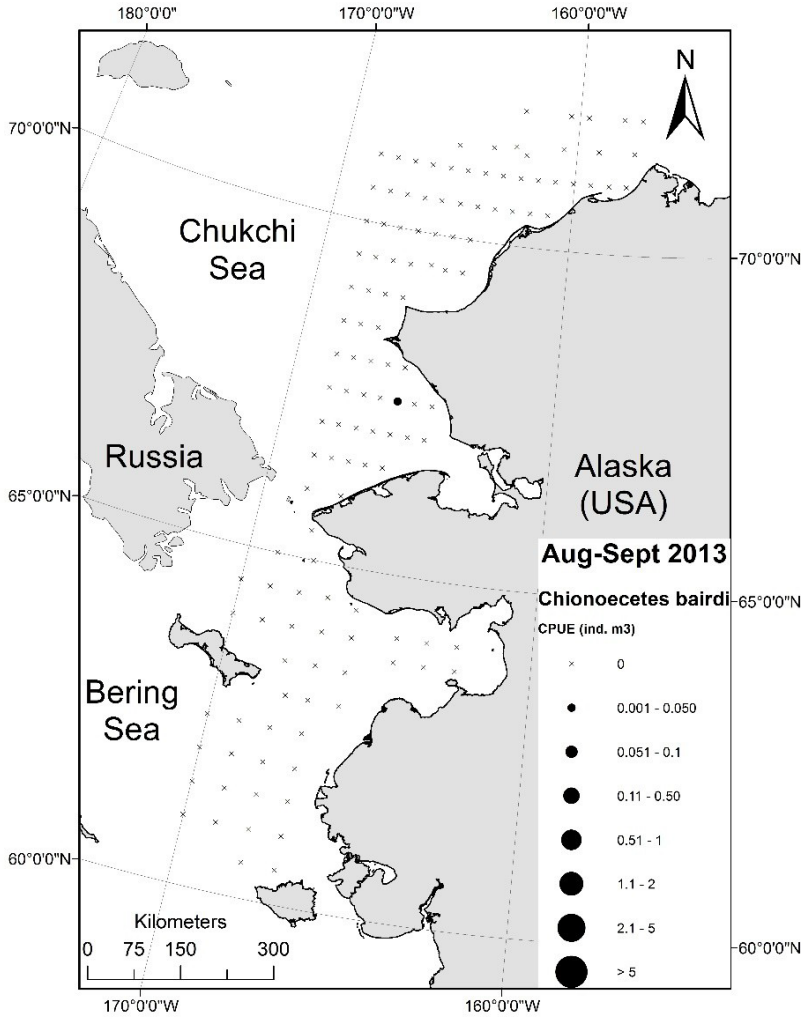

Figure 45. Southern Tanner crab (*Chionoecetes bairdi*) CPUE (ind. m-3) by station from 2013.

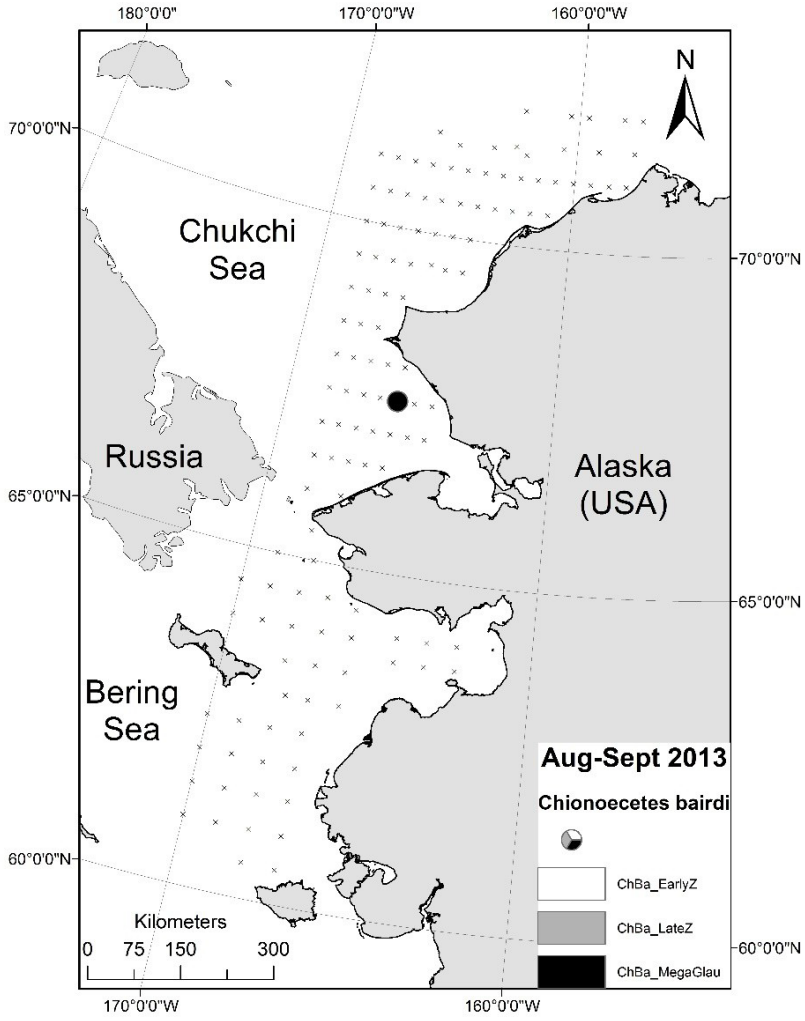

Figure 46. Southern Tanner crab (*Chionoecetes bairdi*) CPUE stage group proportional contribution of early zoeae, late zoeae, and megalopae to species catch by station from 2013.

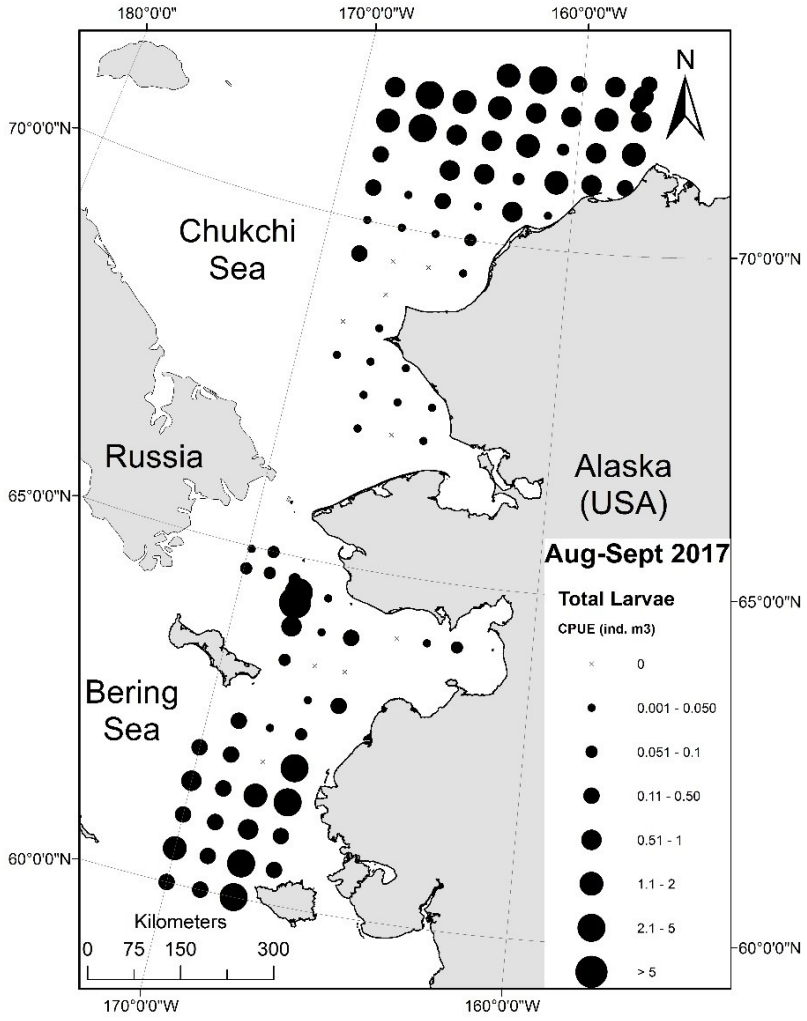

Figure 47. Total crab larval community CPUE (ind. m-3) by station from 2017.

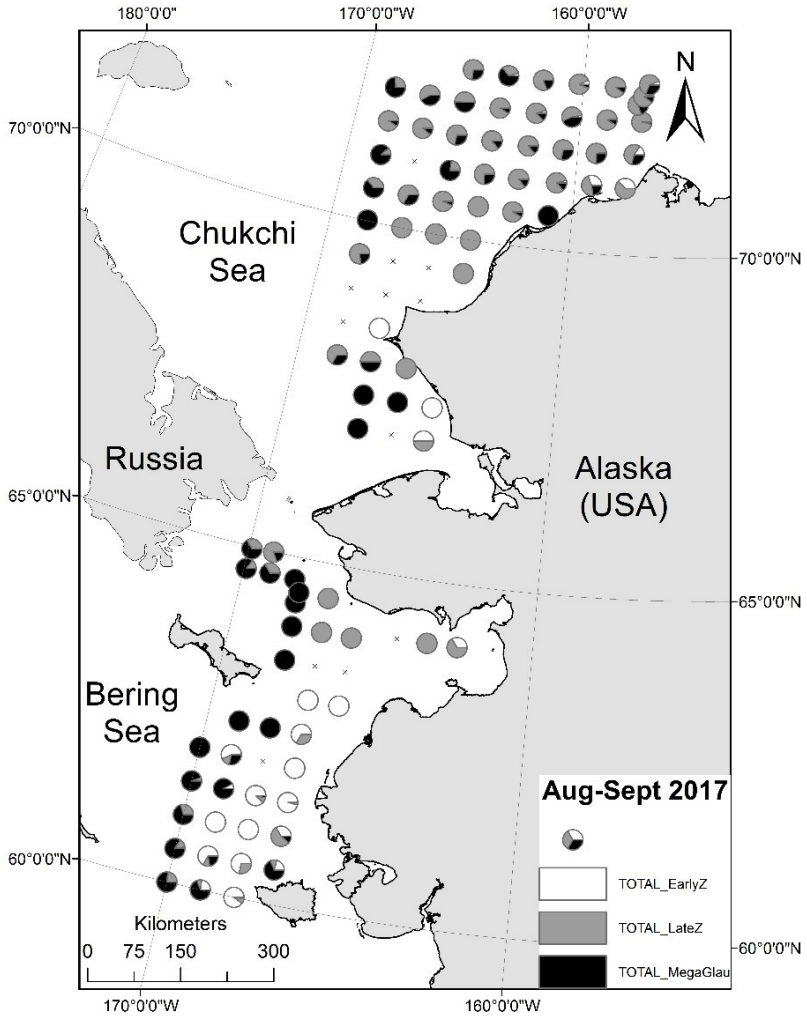

Figure 48. Total crab larvae stage group proportional contribution of early zoeae, late zoeae, and megalopae/glaucothoe to total catch by station from 2017.

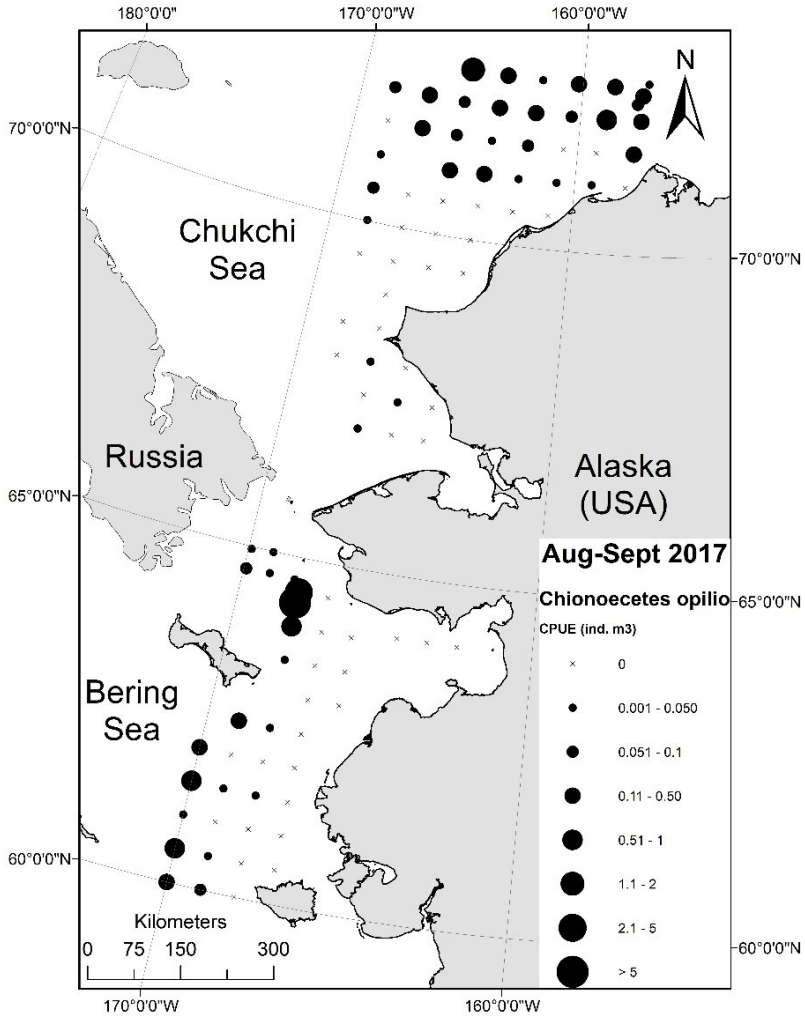

Figure 49. Snow crab (*Chionoecetes opilio*) CPUE (ind. m-3) by station from 2017.

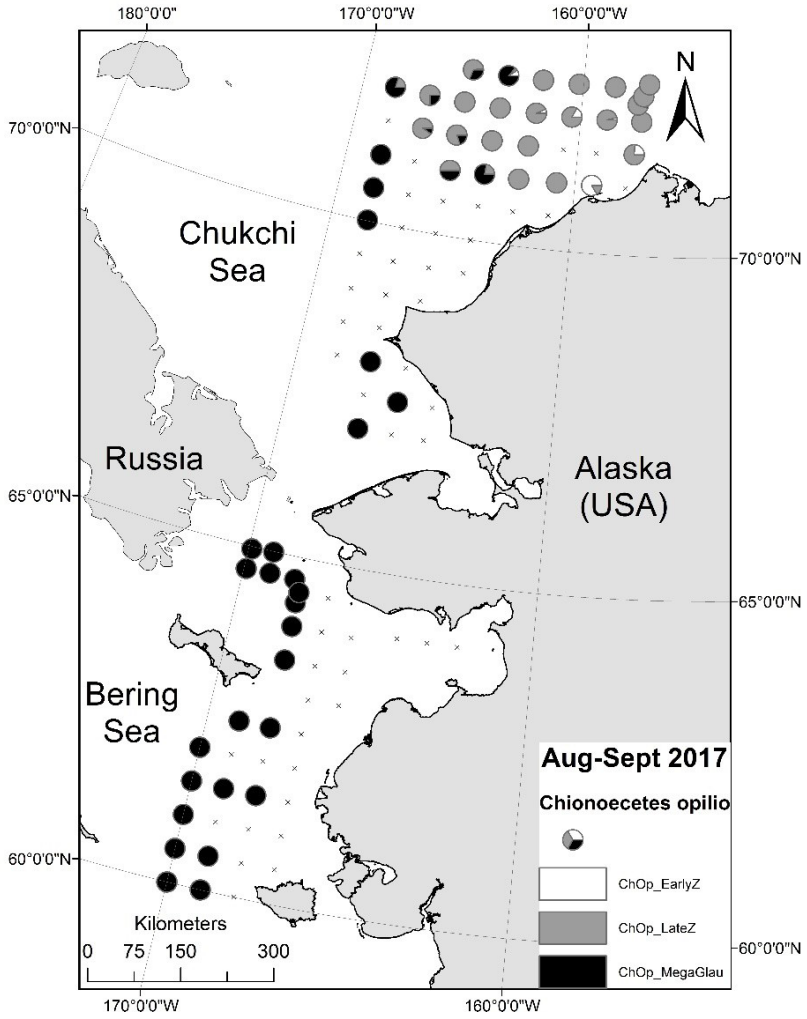

Figure 50. Snow crab (*Chionoecetes opilio*) stage group proportional contribution of early zoeae, late zoeae, and megalopae to species catch by station from 2017.

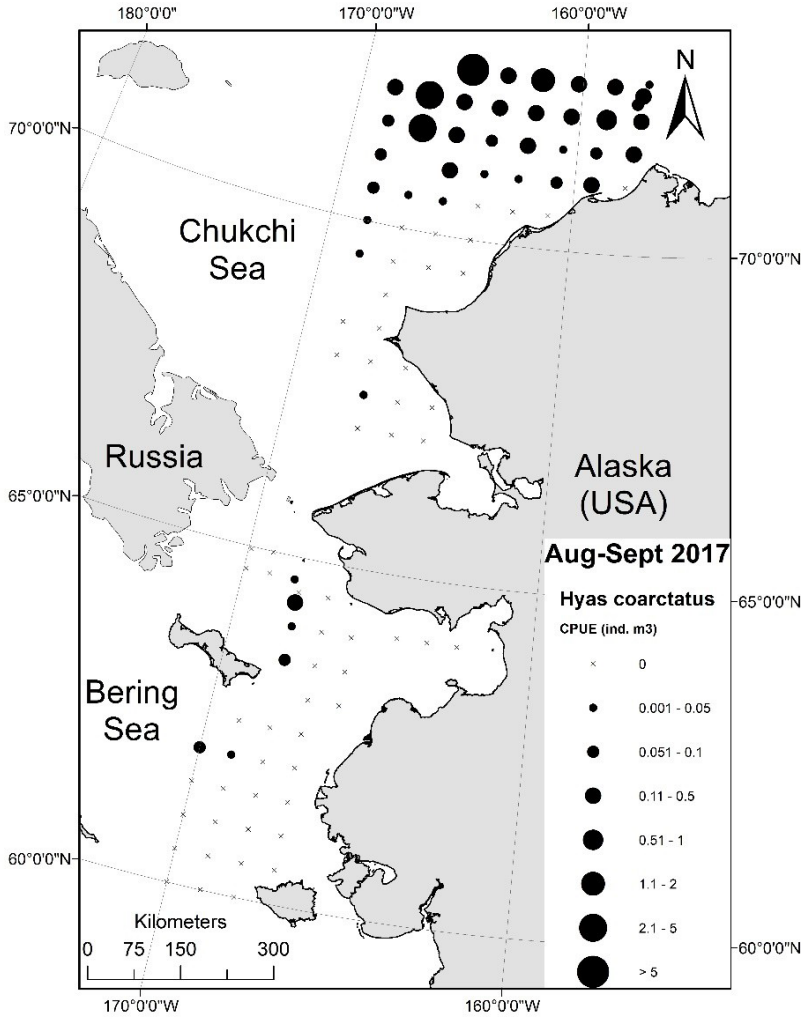

Figure 51. Arctic lyre crab (*Hyas coarctatus*) CPUE (ind. m-3) by station from 2017.

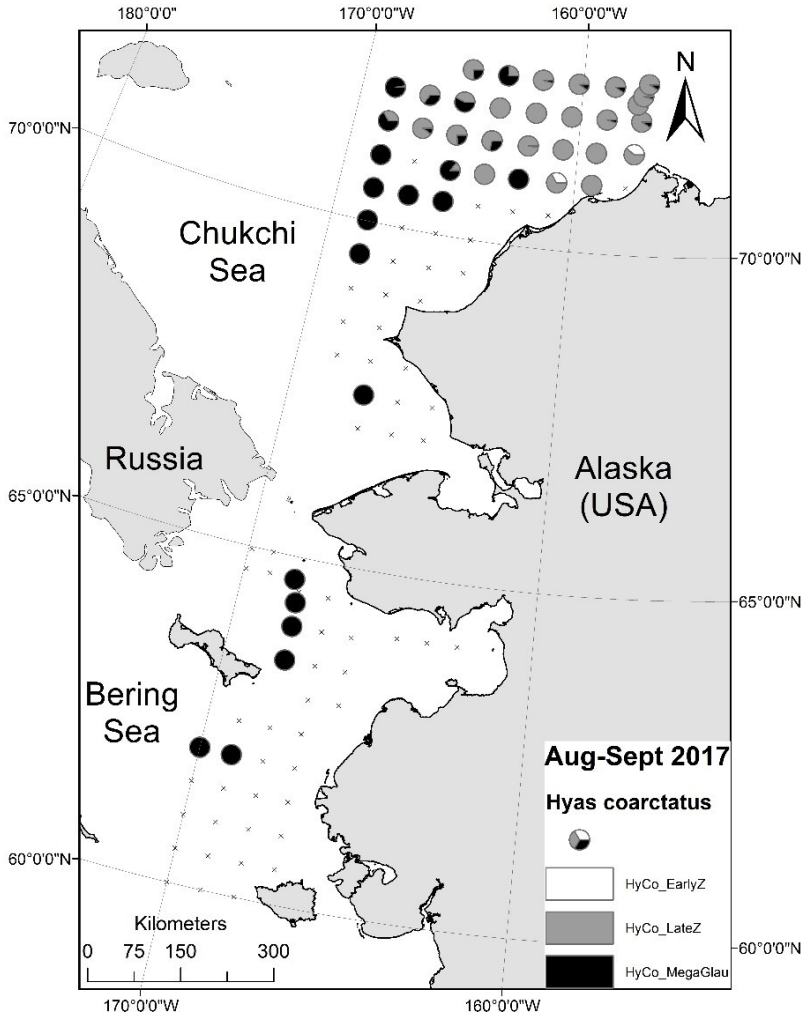

Figure 52. Arctic lyre crab (*Hyas coarctatus*) stage group proportional contribution of early zoeae, late zoeae, and megalopae to species catch by station from 2017.

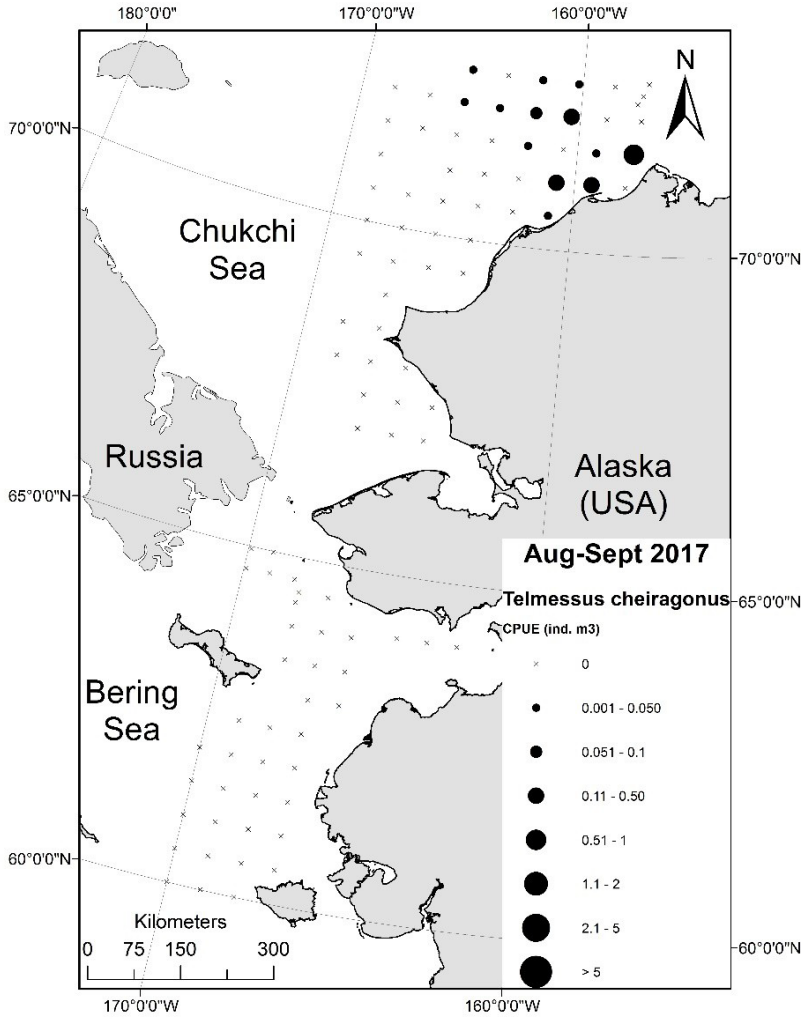

Figure 53. Helmet crab (*Telmessus cheiragonus*) CPUE (ind. m-3) by station from 2017.

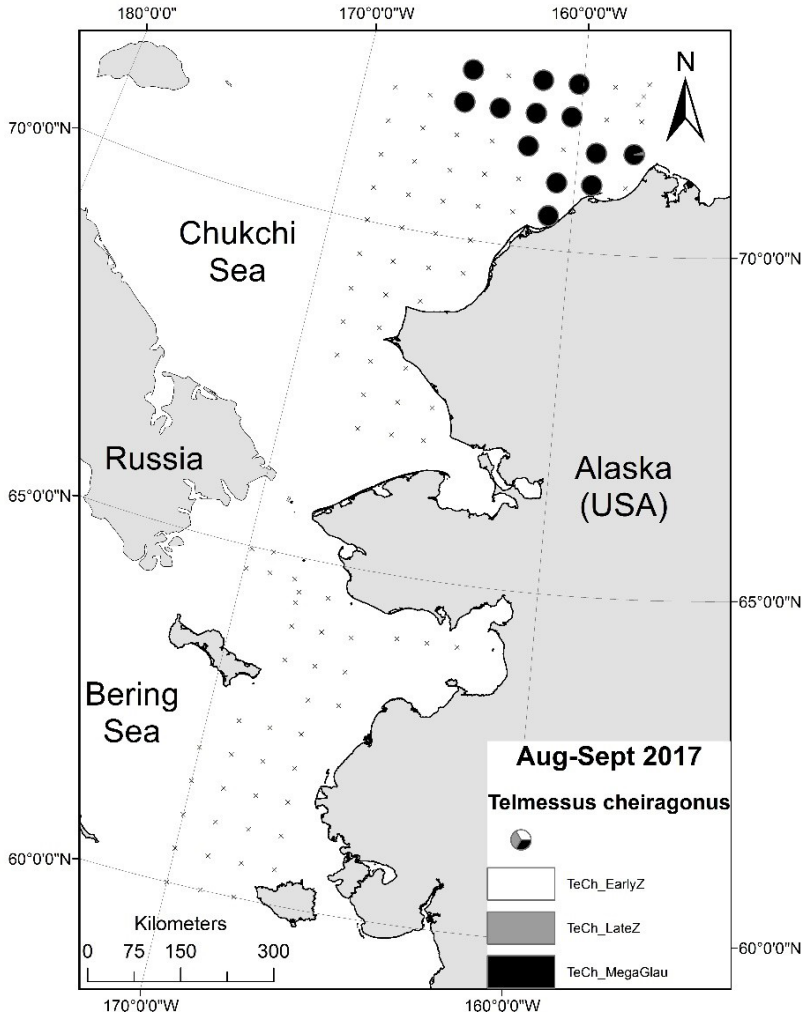

Figure 54. Helmet crab (*Telmessus cheiragonus*) stage group proportional contribution of early zoeae, late zoeae, and megalopae to species catch by station from 2017.

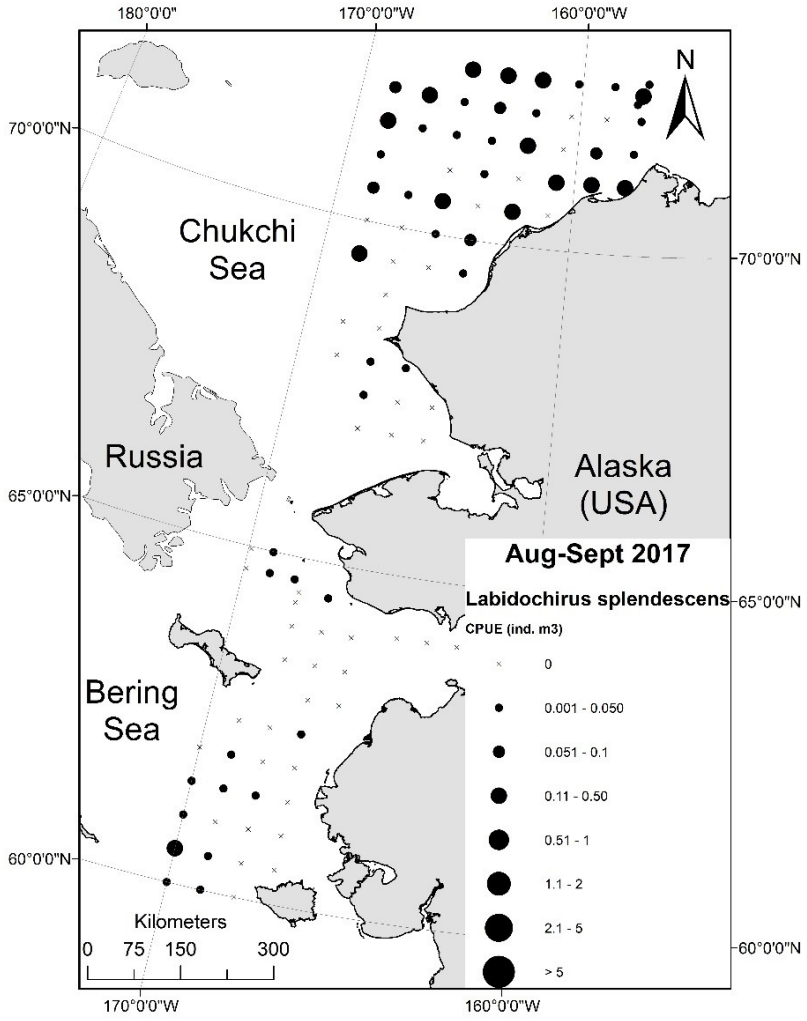

Figure 55. Splendid hermit crab (*Labidochirus splendescens*) CPUE (ind. m-3) by station from 2017.

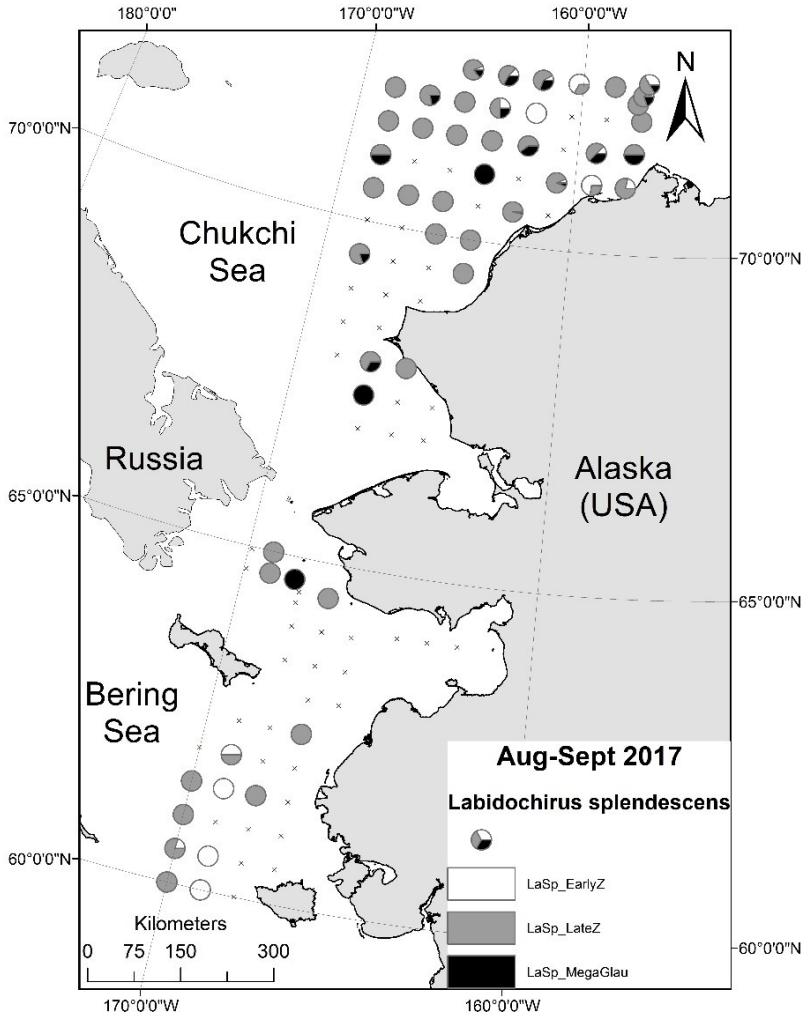

Figure 56. Splendid hermit crab (*Labidochirus splendescens*) stage group proportional contribution of early zoeae, late zoeae, and glaucothoe to species catch by station from 2017.

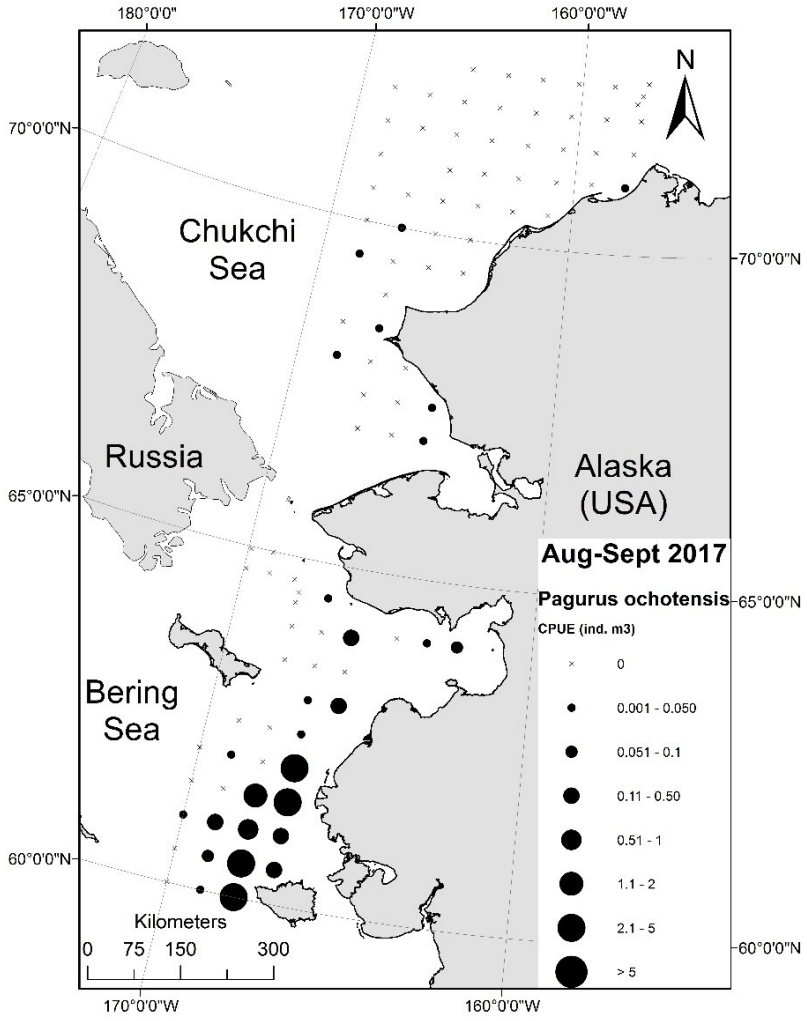

Figure 57. Ochre/Alaskan hermit crab (*Pagurus ochotensis*) CPUE (ind. m-3) by station from 2017.

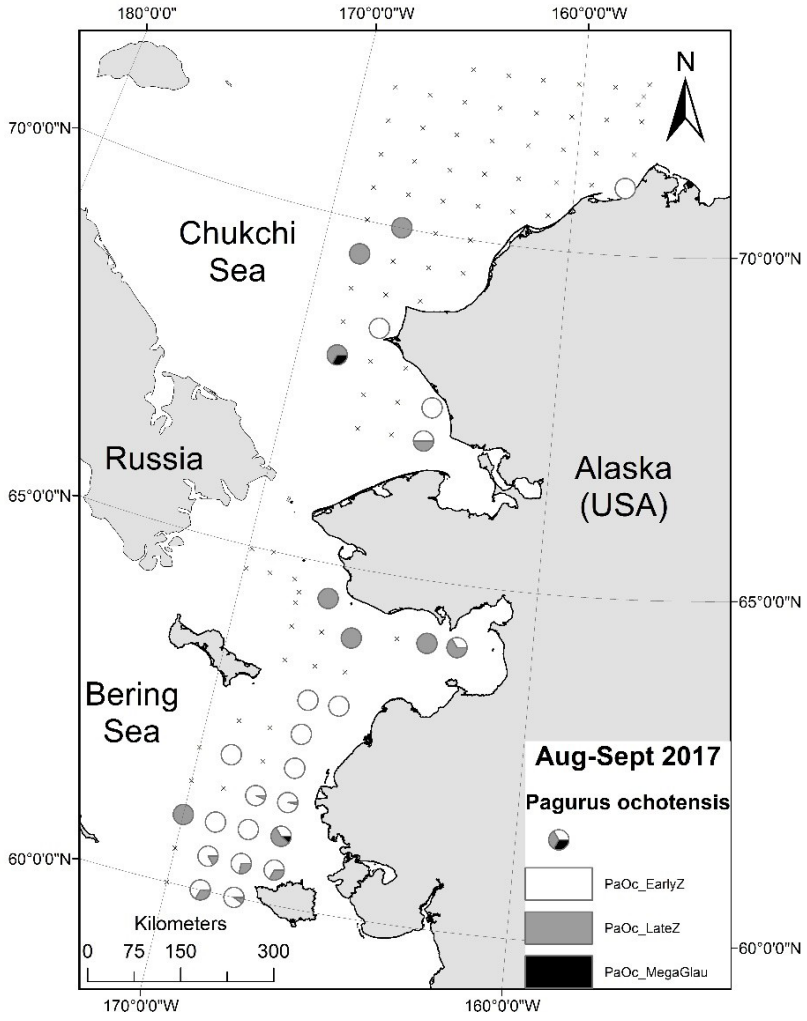

Figure 58. Ochre/Alaskan hermit crab (*Pagurus ochotensis*) stage group proportional contribution of early zoeae, late zoeae, and glaucothoe to species catch by station from 2017.

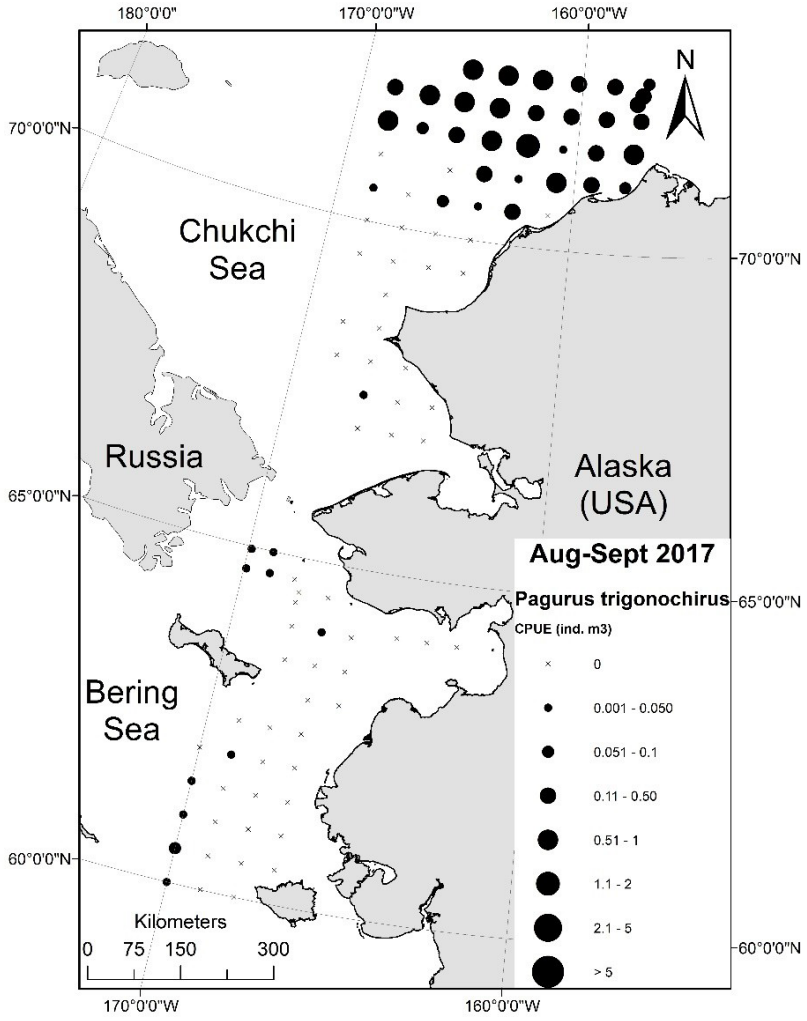

Figure 59. Fuzzy hermit crab (*Pagurus trigonochirus* cf) CPUE (ind. m-3) by station from 2017.

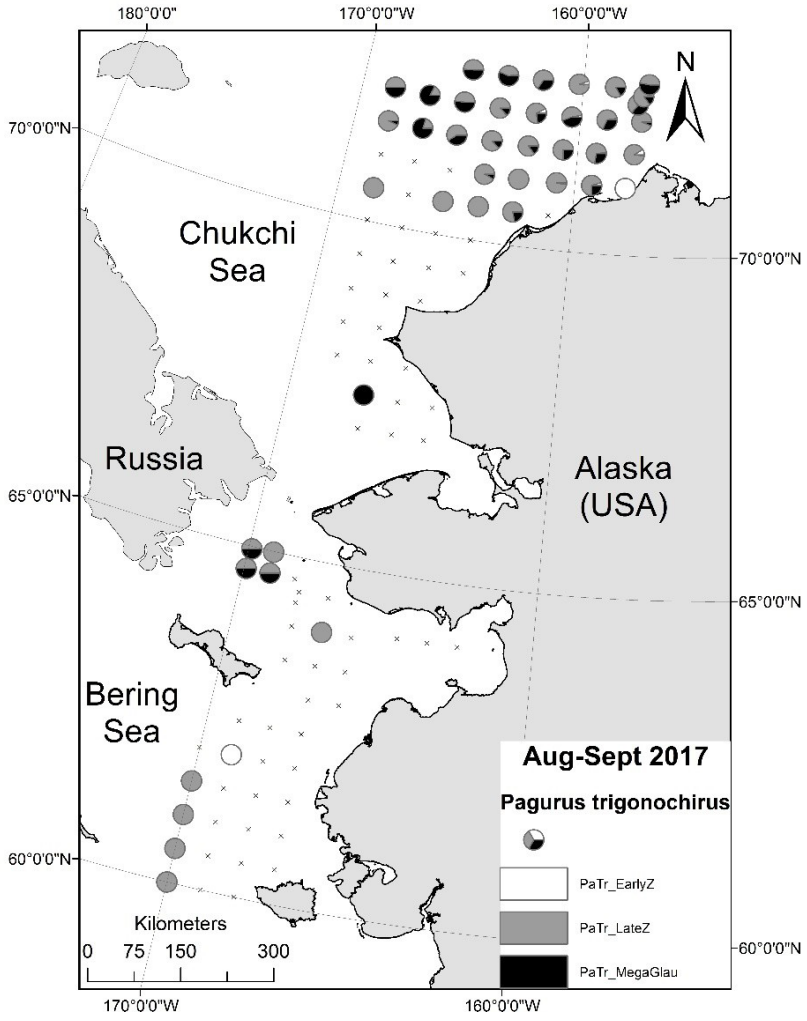

Figure 60. Fuzzy hermit crab (*Pagurus trigonochirus* cf) stage group proportional contribution of early zoeae, late zoeae, and glaucothoe to species catch by station from 2017.

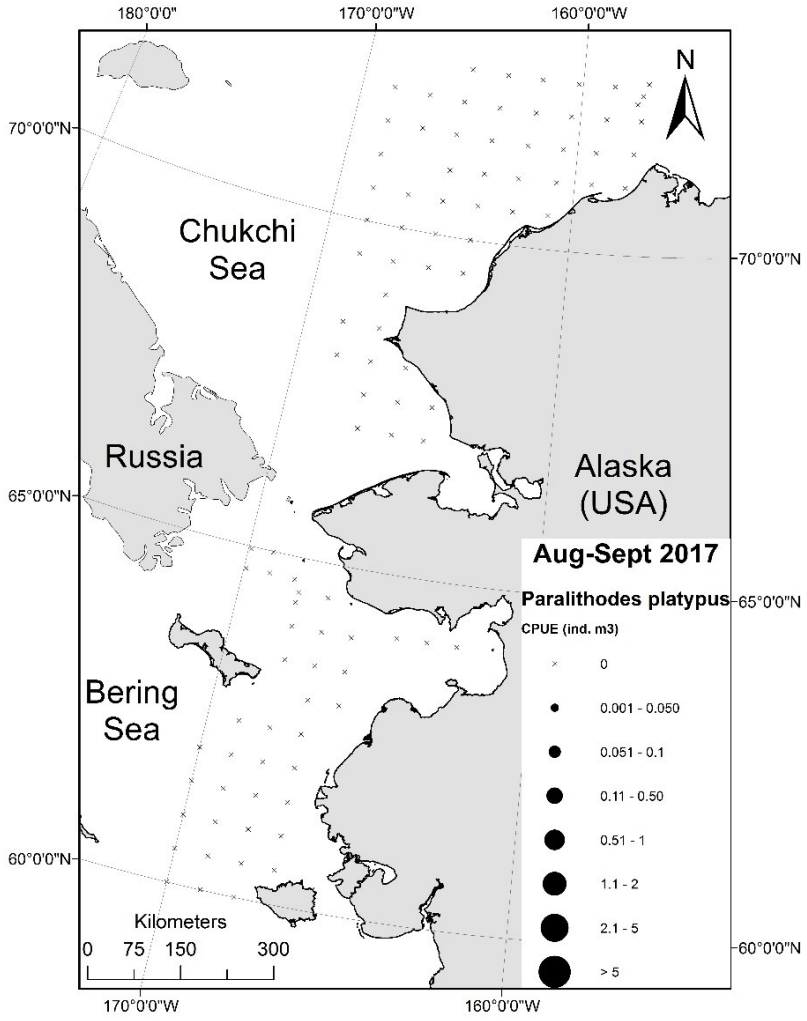

Figure 61. Blue king crab (*Paralithodes platypus*) CPUE (ind. m-3) by station from 2017.

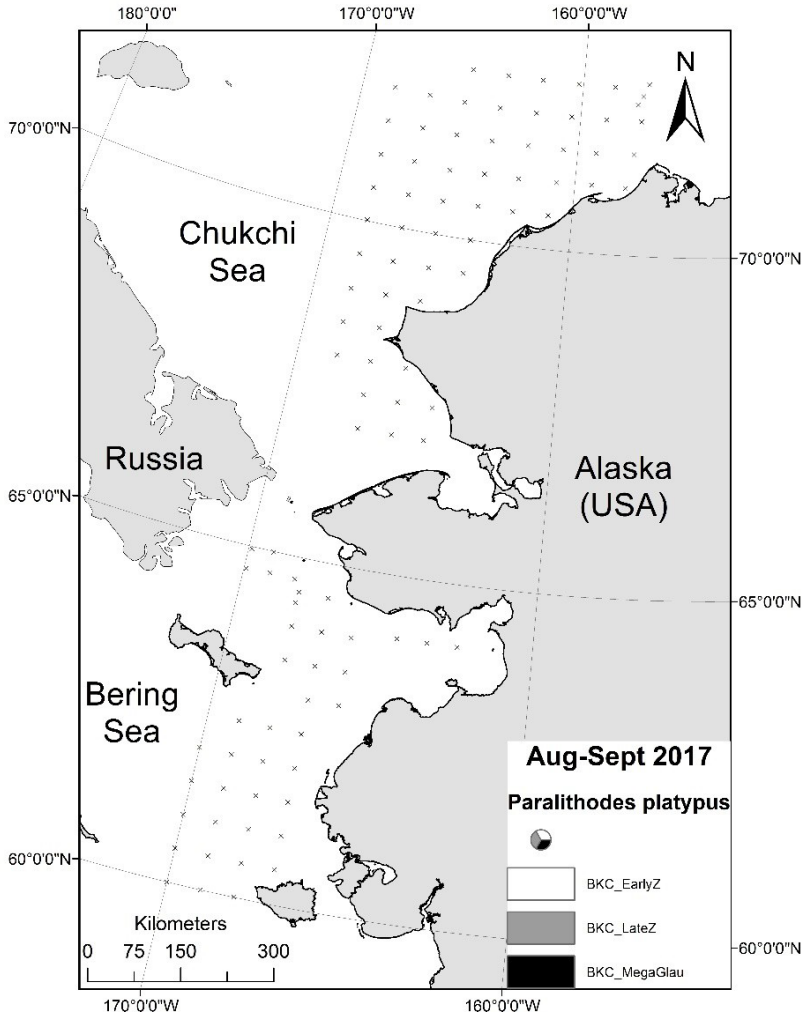

Figure 62. Blue king crab (*Paralithodes platypus*) stage group proportional contribution of early zoeae, late zoeae, and glaucothoe to species catch by station from 2017.

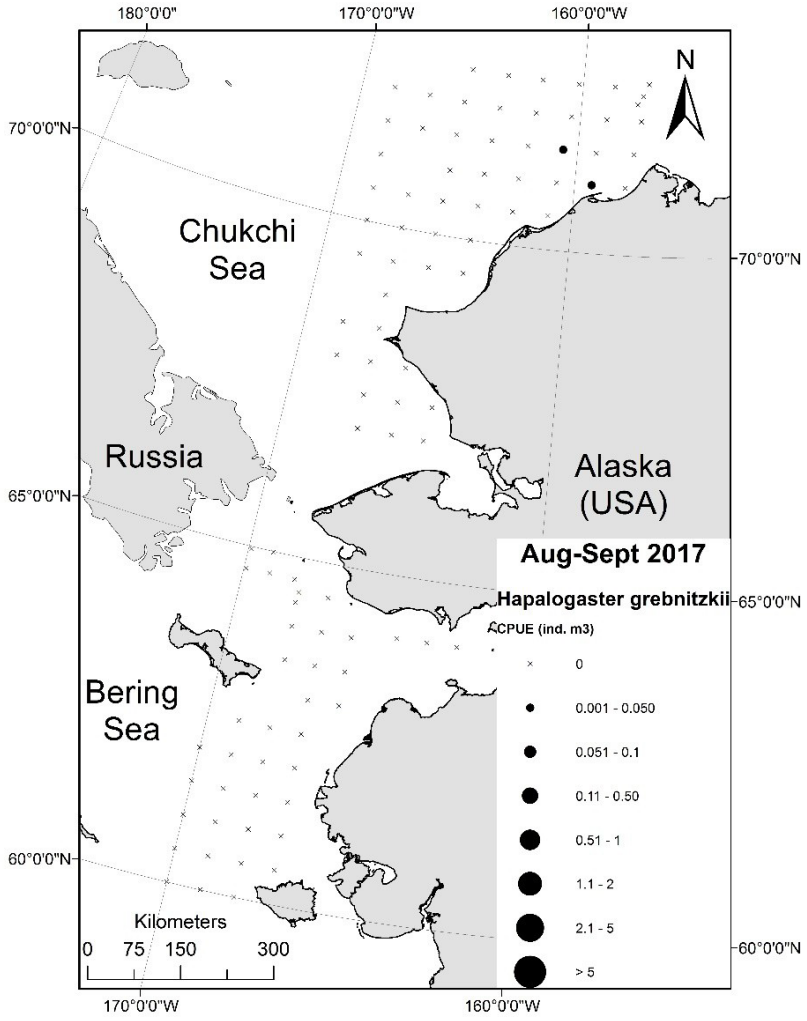

Figure 63. Northern hairy king crab (*Hapalogaster grebnitzkii*) CPUE (ind. m-3) by station from 2017.

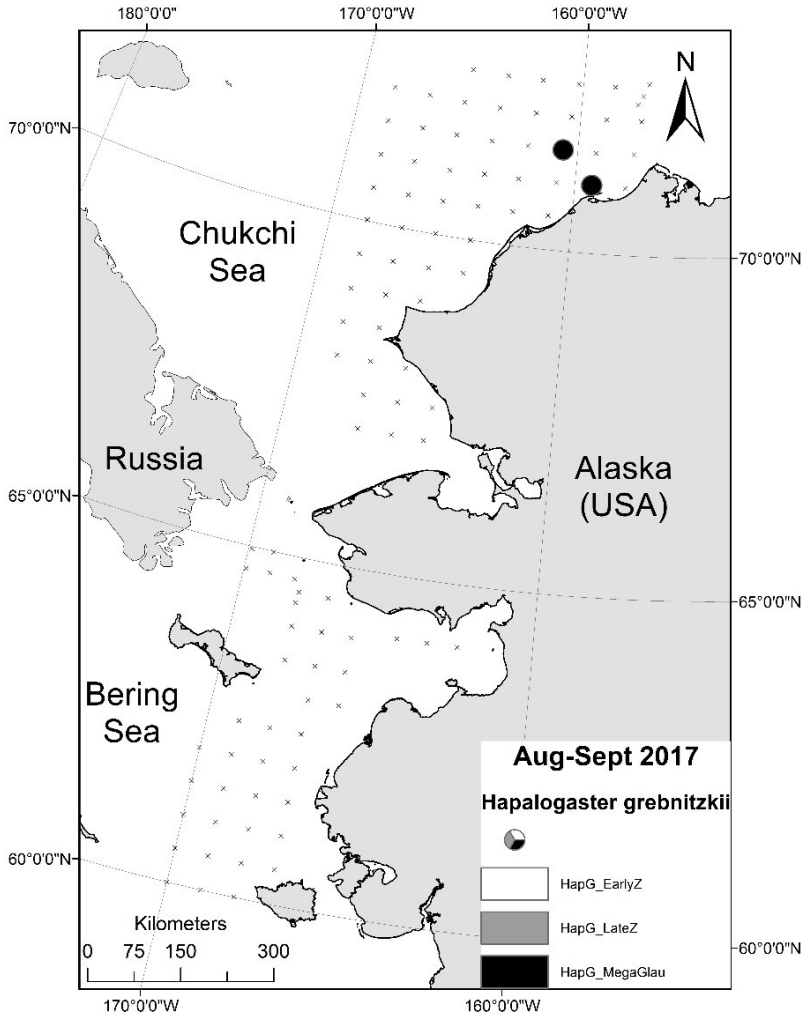

Figure 64. Northern hairy king crab (*Hapalogaster grebnitzkii*) stage group proportional contribution of early zoeae, late zoeae, and glaucothoe to species catch by station from 2017.

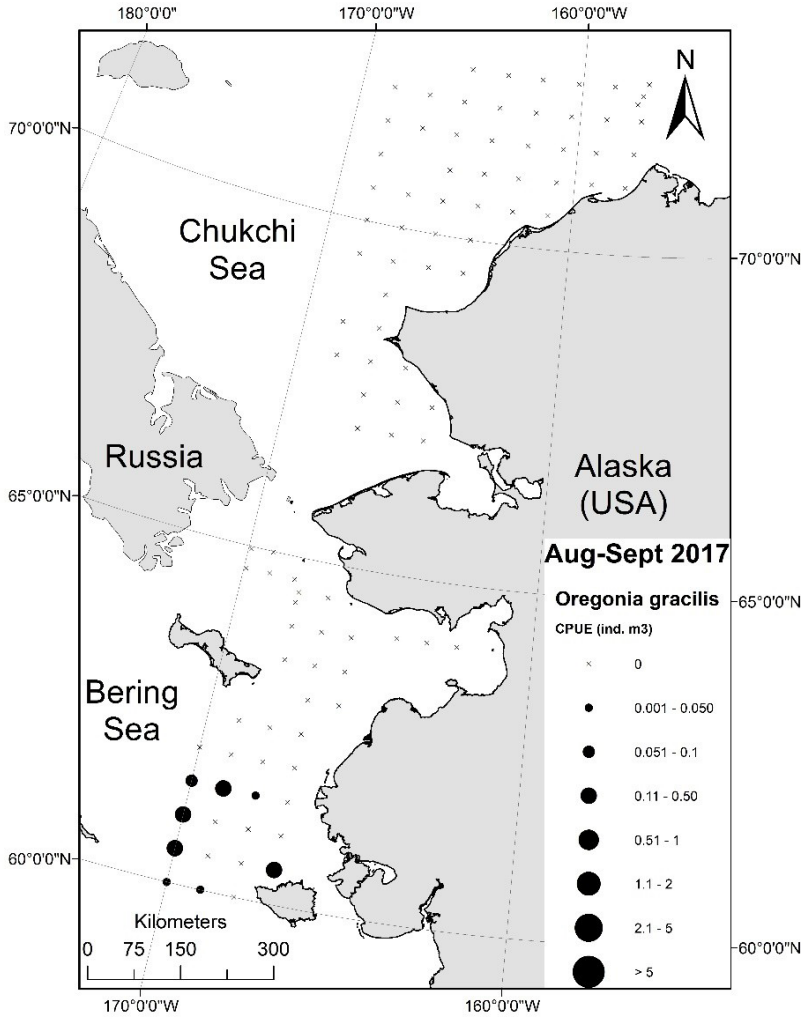

Figure 65. Graceful decorator crab (*Oregonia gracilis*) CPUE (ind. m-3) by station from 2017.

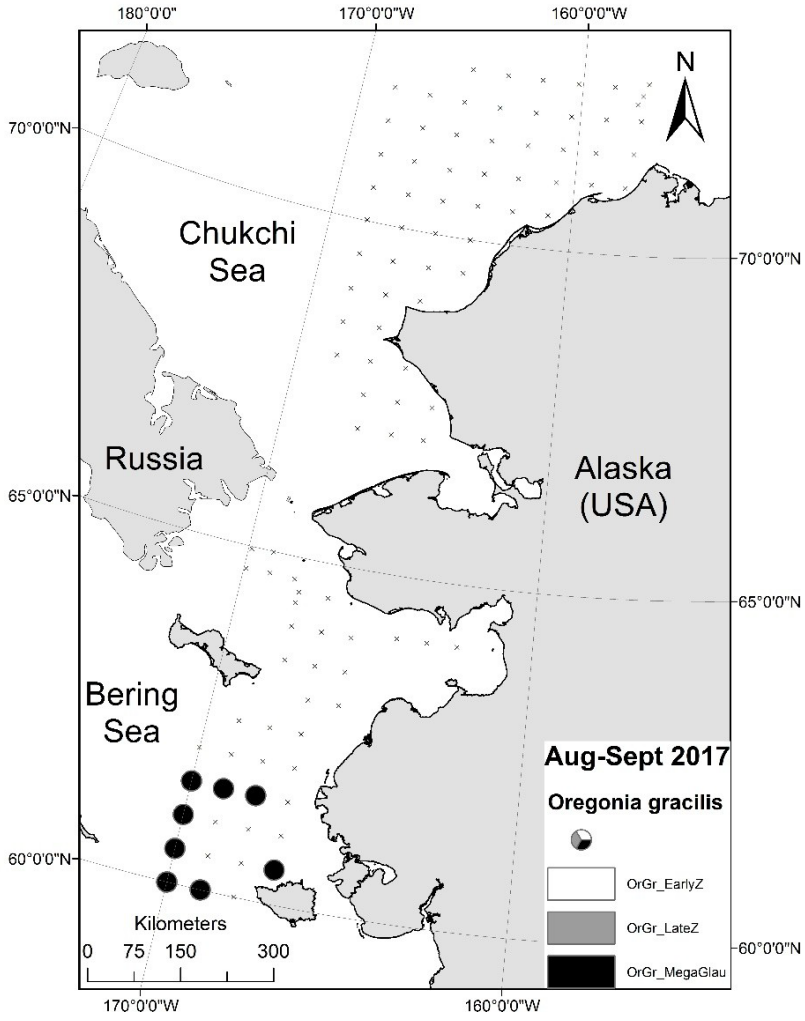

Figure 66. Graceful decorator crab (*Oregonia gracilis*) stage group proportional contribution of early zoeae, late zoeae, and megalopae to species catch by station from 2017.

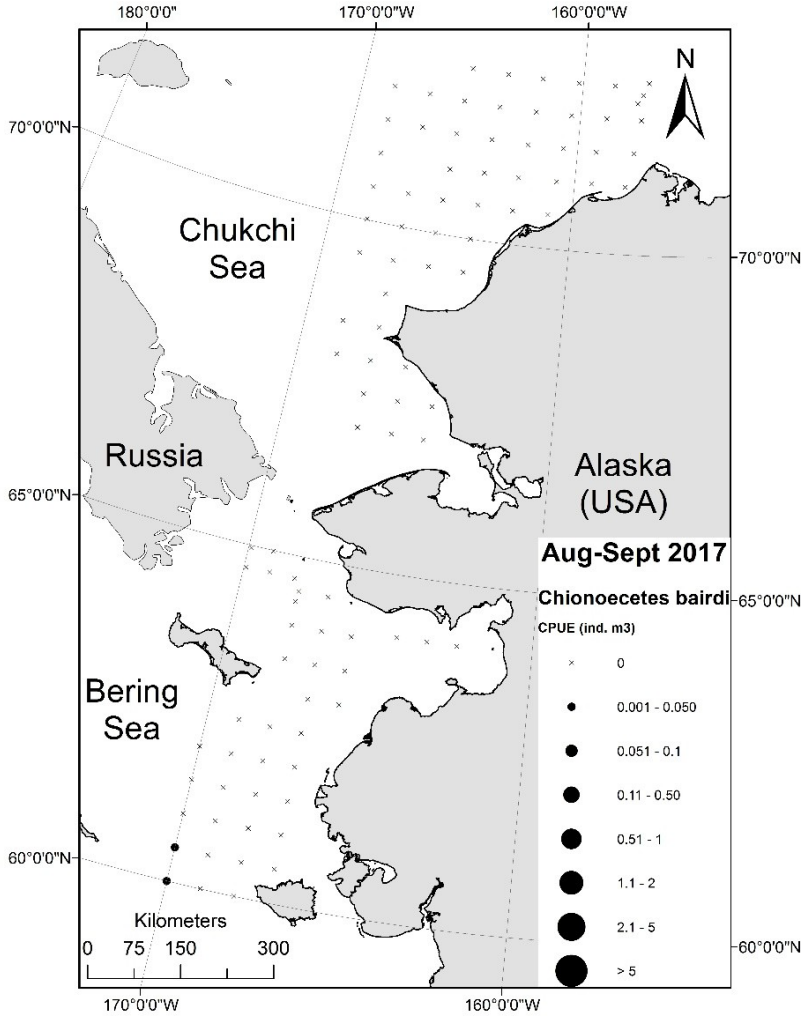

Figure 67. Southern Tanner crab (*Chionoecetes bairdi*) CPUE (ind. m-3) by station from 2017.

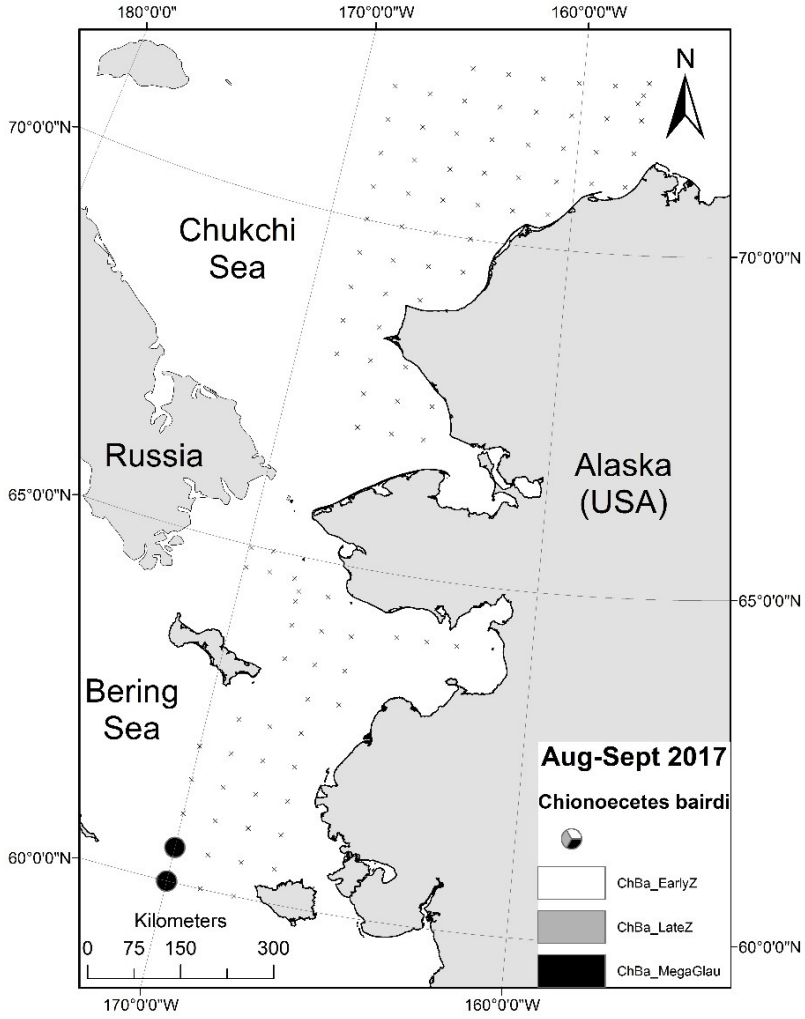

Figure 68. Southern Tanner crab (*Chionoecetes bairdi*) CPUE stage group proportional contribution of early zoeae, late zoeae, and megalopae to species catch by station from 2017.

CHAPTER 3 - Model-based Fish Distributions and Habitat Descriptions for Arctic Cod (*Boreogadus saida*), Saffron Cod (*Eleginus gracilis*) and Snow Crab (*Chionoecetes opilio*) in the Alaskan Arctic

Objective 1: Quantify the distribution, abundance, and condition of demersal fishes and shellfishes

Marsh, J.M., Mueter, F.J., Pirtle, J.
[1] College of Fisheries and Ocean Sciences, University of Alaska Fairbanks
[2] Habitat Conservation Division, Alaska Region, NOAA Fisheries

Abstract

In the 2009 Arctic Fisheries Management Plan (FMP) the North Pacific Fishery Management Council (NPFMC) identified Arctic cod (*Boreogadus saida*), saffron cod (*Eleginus gracilis*) and snow crab (*Chionocetes opilio*) as the three potential target species in the Arctic Management Area (AMA) (NPFMC 2009). For the FMP and for an update to the definition of Essential Fish Habitat (EFH) in 2017, qualitative assessments of these species based on presence-absence survey data were done for late juvenile and mature life stages. To improve on these EFH assessments, we used a quantitative approach based on Maximum Entropy (MaxEnt) species distribution models to link habitat characteristics to species occurrence data from surveys for larval, juvenile and mature life stages. In addition, we used the best-fit models for each species and life stage to predict the distribution of suitable habitat separately for warm and cold years. In this summary, we present the probability of suitable habitat for each life stage of these species in the AMA (US Chukchi and Beaufort Seas). Shifts in the predicted probability of suitable habitat during warm and cold conditions varied by species and life stage. These predicted differences in response to changing temperatures provide insight into future shifts in distribution with climate change.

Introduction

The climate and oceans are rapidly warming in the Alaskan Arctic and will likely have far reaching impacts on marine ecosystems, including the distribution of fishes. Currently, Essential Fish Habitat (EFH) definitions for Arctic species identified as potential target species in the Arctic FMP are qualitative based on presence-absence data. We refined EFH for Arctic cod, saffron cod and snow crab in the Beaufort and Chukchi Seas within the AMA (Fig. 1) using the most recent and best available science. Specifically, we use species distribution models to link habitat characteristics to species occurrence data from numerous surveys. Preliminary maximum entropy (MaxEnt) models were developed by the lead author with support from Alaska Sea Grant and NOAA's Habitat Conservation Division. These models were applied to combined juvenile and adult life stages to produce maps of potentially suitable habitat for each species. Here, we further refined these models by incorporating new survey data from the Beaufort Sea, Barrow Canyon, and nearshore surveys dividing the survey catch data by life stage, as well comparing predicted distributions in warm and cold conditions. The ultimate goal is to refine the EFH text and maps for juvenile, adult and possibly larval life stages of Arctic cod, saffron cod and snow crab for the next 5 year EFH revision.

Objectives

1. Identify core habitat characteristics most important to the distribution and habitat suitability of larval (where data are available), juvenile and adult Arctic cod, saffron cod and snow crab.
2. Refine text descriptions of what constitutes EFH for all life stages (larval, juvenile, and adult) of Arctic cod, saffron cod and snow crab in the Beaufort and Chukchi Seas.

3. Refine maps depicting spatial habitat distributions, by life stage (larval, juvenile, and adult), for Arctic cod, saffron cod, and snow crab in the Beaufort and Chukchi Seas.
4. Develop separate maps of distribution and habitat linkages for life stages of saffron cod, Arctic cod and snow crabs during warm and cold periods.
5. Develop maps indicating distribution shifts between warm and cold periods
6. Develop maps of growth potential for juvenile Arctic cod overall, and separately for warm and cold periods.

Methods

We used environmental and biological survey data from 2000 - 2018 within the AMA to model the probability of suitable habitat for larval, juvenile and mature Arctic cod, saffron cod and snow crab using MaxEnt models. First, we compiled available survey data from 2000 - present and divided occurrences by species and life stage (based on body length and carapace width). We created rasters of potential habitat explanatory variables and selected a suite of independent variables (Table 1). Using explanatory habitat variable rasters and presence data from surveys we modeled the probability of suitable habitat by species and life stage and identified key habitat characteristics in each model. A given species and life stage was considered absent in grid cells that had a probability of suitable habitat less than 5%. Habitat suitability maps were created showing the smallest possible habitat area encompassing a given percentile of the cumulative habitat suitability over all grid cells. Cells where the probability of suitable habitat for a given species and life stage was greater than or equal to 5% were sorted in decreasing order and areas containing the upper 95%, 75%, 50%, and 25% of habitat suitability values were mapped (Figs. 2-4). We consider areas representing the top 25% to be hotspots with the highest probability of suitable habitat and the top 50% to be the "core habitat". The 95% level of areas where the species is present corresponds to the definition of EFH area in Alaska (Sigler et al. 2012). We also used the best-fit models to predict habitat suitability under warm and cold conditions by fitting the models to habitat raster sets from cold and warm years, respectively. Finally, we created potential growth rate maps for age 0 and juvenile Arctic cod and juvenile saffron cod using published, temperature-dependent, laboratory-based grow rate models (Laurel et al. 2016; 2017) and temperature rasters.

Results

For each species and life stage, distribution maps show key habitat areas including the core habitat area defined as the top 50% of suitable area (Figs. 2-4). Temperature was an important habitat covariate for predicting the probability of suitable habitat for many of the life-stage species combinations. Early life stages of Arctic cod were more sensitive to temperature changes and had larger fluctuations in suitable habitat between warm and cold years. The area of suitable habitat decreased for Arctic cod in warm years and increased in cold years indicating climate warming may limit their distribution in the Chukchi Sea. Like early life stages of Arctic cod, larval saffron cod were limited to cooler temperatures. For all older life stages of saffron cod, habitat suitability increased with temperature. Suitable habitat was greatest during warm periods for age-0 saffron cod, but was similar for older life stages. For adolescent snow crab, temperature fluctuations had limited influence on changes in habitat suitability. Mature males snow crabs were the most sensitive to changes in temperatures.

Conclusions

Increases in data availability from numerous surveys conducted since 2009 and advances in species distribution modeling allowed us to update and substantially refine habitat descriptions for three species by life stage in the Alaskan Chukchi Sea and Beaufort Sea. Model performance was acceptable or good in most cases, suggesting that our models provide an adequate basis for updated EFH descriptions for the target species. Moreover, the available data support the development of separate habitat models for warm

and cold conditions as an essential step towards dynamic EFH descriptions. Finally, we showed that estimates of growth potential based on temperature-dependent growth rates from laboratory studies, where available, can be combined with abundance estimates to further improve habitat descriptions by estimating the potential productivity.

References

Laurel BJ, Spencer M, Iseri P, Copeman LA. 2016. Temperature-dependent growth and behavior of juvenile Arctic cod (Boreogadus saida) and co-occurring North Pacific gadids. Polar Biol. 39:1127-1135.

Laurel BJ, Copeman LA, Spencer M, Iseri P. 2017. Temperature-dependent growth as a function of size and age in juvenile Arctic cod (Boreogadus saida). ICES Journal of Marine Science. 74:1614–1621. https://doi.org/10.1093/icesjms/fsx028

Marsh JM , Mueter FJ, Pirtle JL. 2021. Model-based Fish Distributions and Habitat Descriptions for Arctic Cod (*Boreogadus saida*), Saffron Cod (*Eleginus gracilis*) and Snow Crab (*Chionoecetes opilio*) in the Alaskan Arctic. Anchorage (AK): U.S. Department of the Interior, Bureau of Ocean Energy Management. 58 p. Report No.: OCS Study BOEM 2021-056. Contract No.: M19AC00009.

[NPFMC] North Pacific Fisheries Management Council. 2009. Fishery management plan for fish resources of the Arctic management area. http://www.npfmc.org/wpcontent/PDFdocuments/fmp/Arctic/ArcticFMP.pdf

Sigler MF, Cameron MF, Eagleton MP, Faunce CH, Heifetz J, Helser TE, Laurel BJ, Lindeberg MR, McConnaughey RA, Ryer CH, Wilderbuer TK. 2012. Alaska Essential Fish Habitat Research Plan: a research plan for the National Marine Fisheries Service's Alaska Fisheries Science Center and Alaska Regional Office. AFSC Processed Rep. 2012-06

Table 1. Habitat Covariates Used as Explanatory Variables in Species Distribution Models

Variable	Unit	Description of Prediction Raster	Interpolation method
Depth	meters (m)	Bathymetry of the seafloor based on acoustic seafloor mapping data and digitized, position corrected NOS charts (Lewis)	Natural neighbor
Bottom temperature	°C	Seafloor ocean temperature predicted from the Pacific Arctic ROMS (Danielson & Hedstrom) averaged for the bottom 5m across years (2000-2018) during summer months (Jul-Sep)	Inverse distance weighting
Minimum bottom temperature	°C	Seafloor ocean temperature predicted from the Pacific Arctic ROMS (Danielson & Hedstrom) averaged for the bottom 5m across summer months and years (2000-2018)	Inverse distance weighting
Bottom current Eastward velocity	$m \cdot sec^{-1}$	Seafloor ocean current components predicted from the Pacific Arctic ROMS (Danielson & Hedstrom) averaged for the bottom 5m across summer months and years (2000-2018)	Inverse distance weighting
Bottom current Northward velocity	$m \cdot sec^{-1}$	Seafloor ocean current components predicted from the Pacific Arctic ROMS (Danielson & Hedstrom) averaged for the bottom 5m across summer months and years (2000-2018)	Inverse distance weighting
Bottom current Eastward velocity variability	$m \cdot sec^{-1}$	Pooled standard deviation of seafloor ocean current velocities ROMS (Danielson & Hedstrom) from the bottom 5m across summer months and years (2000-2018)	Inverse distance weighting
Bottom current Northward velocity variability	$m \cdot sec^{-1}$	Pooled standard deviation of seafloor ocean current velocities ROMS (Danielson & Hedstrom) from the bottom 5m across summer months and years (2000-2018)	Inverse distance weighting
Sediment grain size	phi	Sediment grain size derived from sampling in the Alaskan Arctic and curated in the DBseabed database (Jenkins)	Ordinary kriging
Organic Carbon	--	Percent organic carbon from sampling sediment in the Alaskan Arctic and curated in the DBseabed database (Jenkins)	Ordinary kriging
Longitude*	m	Grid points spaced every 1 km^2 within the Arctic Management Area in Alaska Albers Equal Area conic projection	--
Sea Surface temperature	°C	Seafloor ocean temperature predicted from the Pacific Arctic ROMS (Danielson & Hedstrom) averaged for the bottom 5m across years (2000-2018) during summer months (Jul-Sep)	Inverse distance weighting
Minimum bottom temperature	°C	Seafloor ocean temperature predicted from the Pacific Arctic ROMS (Danielson & Hedstrom) averaged for the bottom 5m across summer months and years (2000-2018)	Inverse distance weighting
Surface current Eastward velocity	$m \cdot sec^{-1}$	Seafloor ocean current components predicted from the Pacific Arctic ROMS (Danielson & Hedstrom) averaged for the bottom 5m across summer months and years (2000-2018)	Inverse distance weighting
Surface current Northward velocity	$m \cdot sec^{-1}$	Seafloor ocean current components predicted from the Pacific Arctic ROMS (Danielson & Hedstrom) averaged for the bottom 5m across summer months and years (2000-2018	Inverse distance weighting
Surface current Eastward velocity variability	$m \cdot sec^{-1}$	Pooled standard deviation of seafloor ocean current velocities ROMS (Danielson & Hedstrom) from the bottom 5m across summer months and years (2000-2018)	Inverse distance weighting
Surface current Northward velocity variability	$m \cdot sec^{-1}$	Pooled standard deviation of seafloor ocean current velocities ROMS (Danielson & Hedstrom) from the bottom 5m across summer months and years (2000-2018)	Inverse distance weighting

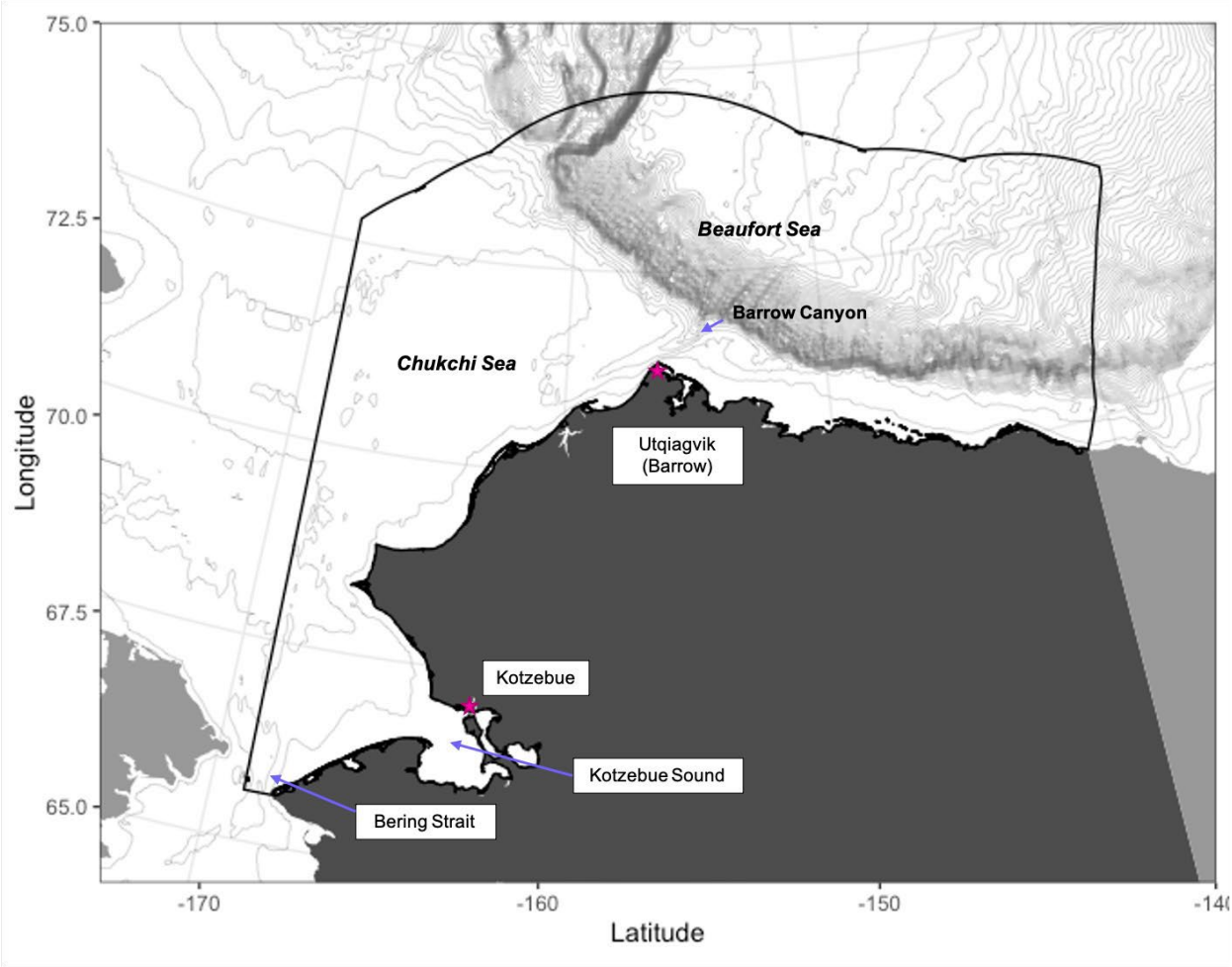

Figure 1: US Arctic Management Area (AMA). The AMA is outlined in black. Isobaths displaying depths of 25 m and from 50 m – 4000 m spaced every 50 m are in grey.

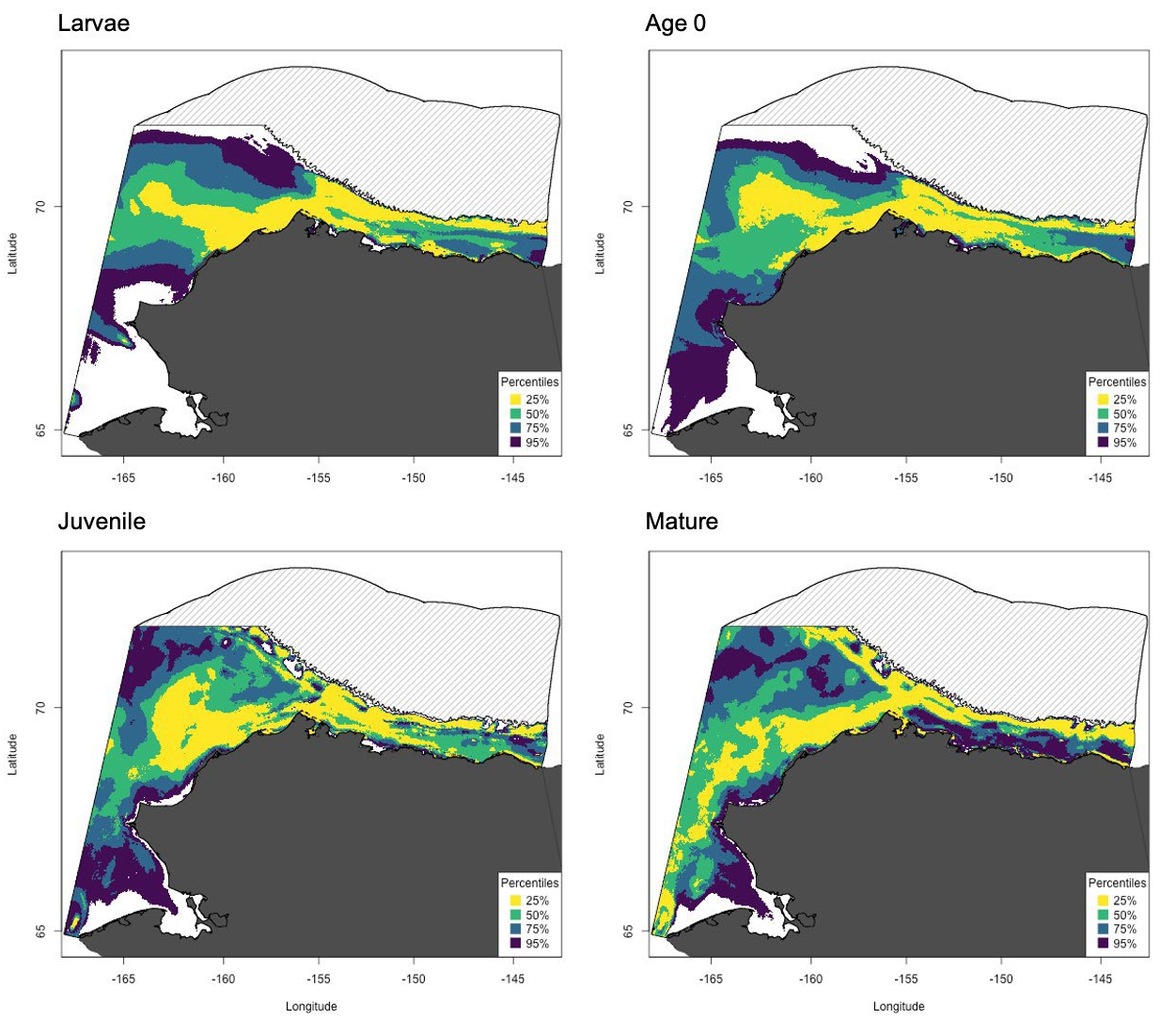

Figure 2: Key Habitat Areas for Larval, Age 0, Juvenile and Mature Arctic Cod, including the upper 95%, 75%, 50%, and 25% of habitat suitability values.

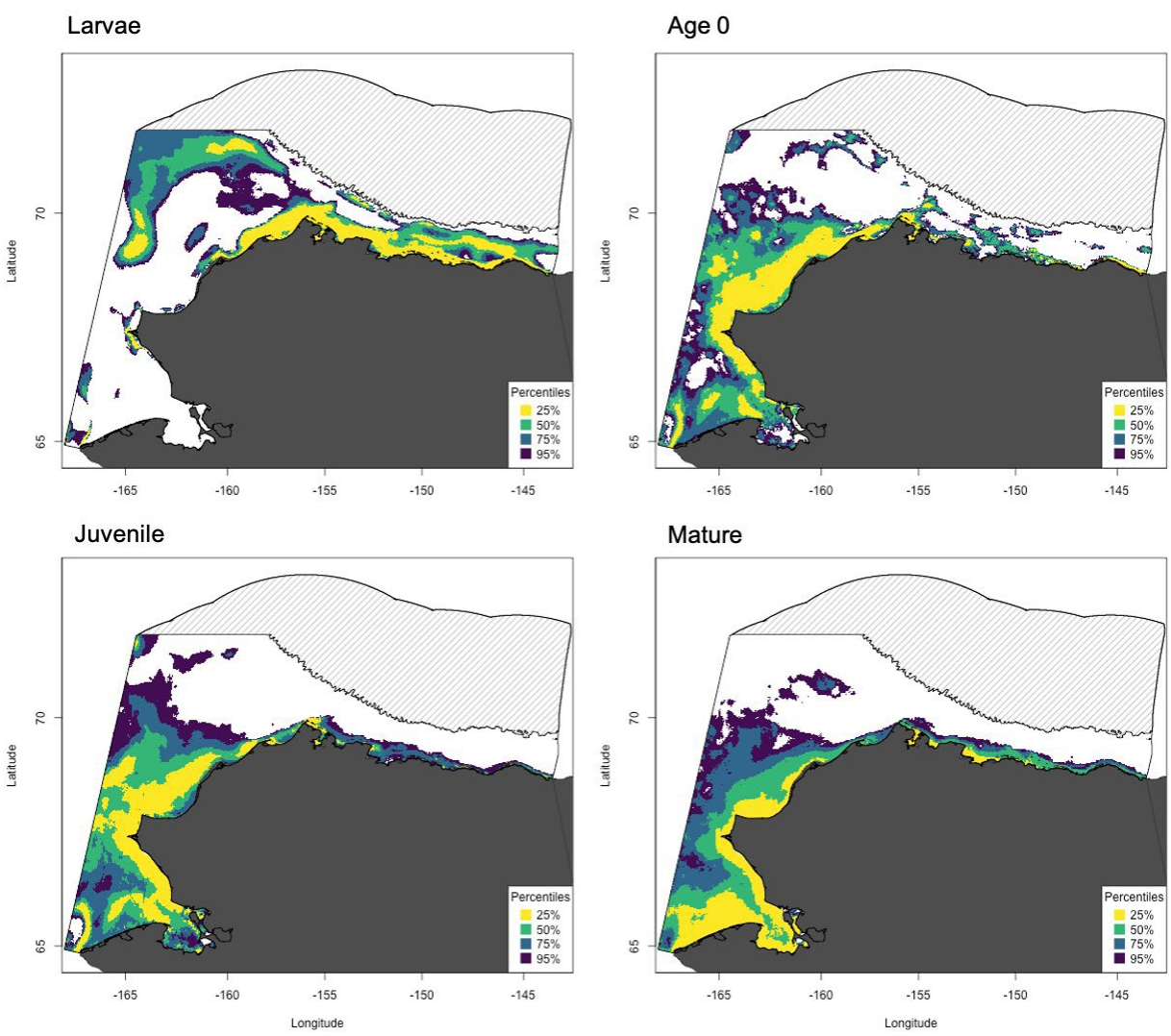

Figure 3: Key Habitat Areas for Larval, Age 0, Juvenile and Mature Saffron Cod, including the upper 95%, 75%, 50%, and 25% of habitat suitability values.

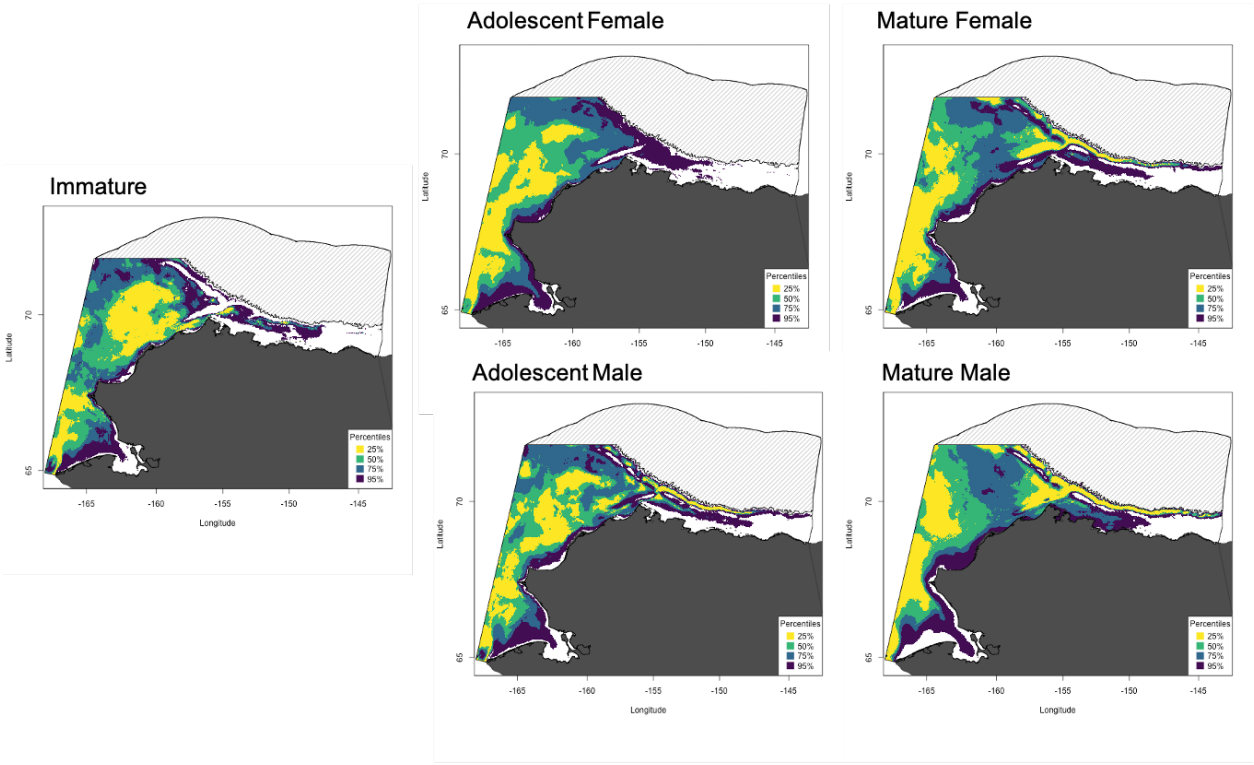

Figure 4: Key Habitat Areas for Immature, Adolescent and Mature Snow Crab, including the upper 95%, 75%, 50%, and 25% of habitat suitability values.

CHAPTER 4 - Walleye Pollock breach the Bering Strait: A change of the cods in the Arctic

Objective 2: Quantify the distribution, abundance, and condition of pelagic marine fishes, in particular young-of-the-year Arctic gadids and other forage fishes

S. Wildes[1], J. Whittle[1], Hv. Nguyen[1], M. Marsh[1], K. Karpan[1], K. DAmelio[1], A. Dimond[1], K. Cieciel[1], A. De Robertis[2], R. Levine[3], W. Larson[1], and J. Guyon[1]

[1]Alaska Fisheries Science Center, National Marine Fisheries Service, Juneau, Alaska
[2]Alaska Fisheries Science Center, National Marine Fisheries Service, Seattle, Washington
[3]School of Oceanography, University of Washington, Seattle, Washington

Abstract

We used genetic techniques to identify gadids (cods) to species in the Pacific Arctic during a time of substantial physical changes in the marine ecosystem, between 2012 and 2019. The dominant fish species in the upper trophic level of the Chukchi Sea is Arctic Cod (*Boreogadus saida*); however other cods such as Saffron Cod (*Eleginus gracilis*), Pacific Cod (*Gadus macrocephalus*) and Walleye Pollock (*Gadus chalcogrammus*) have been observed. Two aims in this study were to evaluate the accuracy of at sea morphological identification with genetic species identification and to document the change in species composition and distribution of gadids in the Pacific Arctic. The morphologically cryptic nature of these gadids, particularly among young-of-the-year fish can lead to misidentification. Microsatellite and mtDNA genetic results revealed that most *B. saida* collected in the Chukchi Sea in 2012 and 2013 were correctly identified at sea. Conversely, results from samples collected in 2017 and 2019 revealed a large number of *G. chalcogrammus* and some *G. macrocephalus* and *E. gracilis* that were initially identified at sea as *B. saida*. The majority of misidentification occurred between *B. saida* and *G. chalcogrammus*. This study indicates a northward shift of *G. chalcogrammus* and *B. saida*. In addition, juvenile Polar Cod (*A. glacialis*), which is not typically found in the Chukchi Sea and was not identified at sea, was genetically detected at 3 hauls on the northern Chukchi shelf, outside of its documented distribution. Accurate species identification, especially during a time of changing marine landscapes, is not only important for survey abundance estimates but for downstream analyses as well. This emphasizes the value of implementing strategies for correct identification of the gadid species in order to better capture and monitor this change. Our results provide strong evidence of distributional shifts and range expansions of gadid species in the Arctic, which may be the result of changing climactic conditions.

Introduction

As changes in the ocean environment unfold in the Arctic, resident species will need to adjust, relocate or perish. Elevated water temperatures, melting sea ice, and other physical changes (Baker et al., 2020; Huntington et al., 2020; Danielson et al., 2020), will usher in an ecologically altered food web (Meuter and Litzow, 2008; Bluhm and Gradinger, 2008) as species seek their optimal habitat. In the past decade, geographic range expansions of species in areas of environmental change around the globe have been reported, such as the movement of *Dosidicus gigas* (Humboldt Squid) toward both poles in the Pacific Ocean (Zeidberg & Robison, 2007), advancement of *Gadus morhua* (Atlantic Cod) and *Mallotus villosus* (Capelin) into the Barents Sea (Howell and Filin, 2014), and shifts in distribution of the cods in the northern Bering Sea (Baker, 2021). Hundreds of species have already exhibited range shifts (Molinos et al., 2017; Pinsky, 2020; Poloczanska et al, 2013, 2016) and future shifts are projected for more species (Cheung et al., 2013; Molinos et al., 2015; Morley et al., 2018; Grebmeier, 2006). An altered ecosystem

in the Arctic will inevitably lead to winners and losers (Sigler, 2011; Fossheim, 2015; Bouchard, 2017; Moore and Stabeno, 2015; Kleisner et al., 2017). Restructuring of the ecosystem will benefit some species but will be detrimental to others. It is yet uncertain which species can take advantage of increased growth potential from warmer temperatures and freshwater input from coastal shelf areas (Copeman, 2016). For some of the northernmost cold-loving species like *Boreogadus saida* (Arctic Cod[1]) and *Arctogadus glacialis* (Polar Cod), there may ultimately be no refuge in a warming Arctic.

Here we focus on species of gadids in two marginal seas of the Pacific Arctic. The Chukchi Sea and the Bering Sea to the south are connected by the narrow Bering Strait. This is one of the world's most productive ocean ecosystems and is characterized by large continental shelves (Grebmeier et al., 2015) with high benthic biomass resulting from persistent nutrient, carbon, and heat flow through the Bering Strait (Woodgate et al., 2005; 2018; Carmack and Wassmann, 2006; Danielson et al., 2020). This flow from the Bering Sea into the Chukchi fuels high primary productivity (Huntington et al., 2020). Recent estimates of net community production (NCP) identify the northern Bering and Chukchi shelves as the single most productive region across the entire Arctic marine system (Codispoti et al., 2013). However, it is a system currently undergoing rapid change (Danielson et al., 2020; Huntington et al., 2020).

In the Bering Sea, the climate over the past 40 years has shifted from high inter-annual variability to multi-year regimes of warmer and colder years (Stabeno, et al., 2012; 2017; Stevenson and Lauth, 2012; Duffy-Anderson, et al., 2017). The Bering Sea cold pool, an area of bottom shelf waters cooler than 2° C resulting from ice melt (Wyllie-Echeverria and Wooster, 1998), has diminished in size in the recent warm years (Conner and Lauth, 2017), particularly in the summers of 2017–2019 (Stevenson and Lauth, 2019). The cold pool has long served as a thermal barrier preventing northward migration of subarctic groundfish (Stevenson and Lauth 2019; Baker, 2020). Ice formation was delayed in the winter of 2017/2018 and even later in 2018/2019, resulting in low abundance of ice algae which lead to low abundances of lipid-rich copepods and a high number of small, lipid-poor copepods, and subsequent cascading impacts on higher trophic levels in the northern Bering Sea marine ecosystem (Siddon et al., 2020). Temperature changes in the Bering Sea have led to an increase in water flow north into the Chukchi Sea (Woodgate et al., 2018), which has experienced similar environmental shifts with increased temperatures, earlier ice melts, and longer ice-free seasons (Frey, 2015; Wood, 2015).

The dominant fish species of the Chukchi Sea has historically been *Boreogadus saida* (Arctic Cod) (De Robertis, et al., 2017; Logerwell et al., 2015), followed by *Eleginus gracilis* (Saffron Cod) (Datsky, 2016; Whitehouse et al., 2014; Goddard et al., 2014; Logerwell et al., 2015). *B. saida* is a circumpolar species, and is usually associated with ice covered waters (Gradinger and Bluhm, 2004). In the Chukchi, *B. saida* is found in a temperature range of 2 to 6.7 °C (Ponomarenko, 1968, Wyllie-Echeverria, 1995, De Robertis et al., 2017), although age-0 fish have been found to grow optimally in the laboratory at 9°C (Laurel et al., 2018). Eggs of *B. saida* are typically associated with ice and develop normally in -1.0°C to 3.5°C, but not >5°C (Drost et al., 2016; Kent et al, 2016). *E. gracilis* has an Arctic-boreal Pacific distribution and occupy nearshore regions from the Korea Peninsula to southeast Alaska and to Dease strait in the Canadian Arctic (Mecklenburg et al., 2002; Vestfals et al., 2019). *E. gracilis* tolerates higher temperatures (>7.5°C), than *B. saida* (Copeman et al., 2016; Laurel et al., 2016), and tolerates areas of lower salinity (Wolotira, 1985) than *B. saida* (De Robertis et al., 2017). In colder years, both *B. saida* and *E. gracilis* are also found in the Bering Sea (Baker et al., 2021; Lauth, 2011).

[1] The common names, Arctic Cod and Polar Cod, are used interchangeably for *Boreogadus saida* and *Arctogadus glacialis* in the literature. In this article we use latin names or follow the most current list of common names published by the American Fisheries Society (Page et al., 2013), and capitalize all common names per ASIH and AFS policy.

Two abundant gadids in the Bering Sea are *Gadus chalcogrammus* (Walleye Pollock) and *Gadus macrocephalus* (Pacific Cod). The geographic distribution of *G. chalcogrammus* is primarily boreal Pacific, with records south to California and Korea and also in the N. Atlantic (Mecklenberg et al., 2011). It is among the top fished species in the world, with the major fishing grounds in the Bering Sea and Sea of Okhotsk (Bulatov, 2014). *G. macrocephalus* occur on continental shelves and slopes from 34-63 N latitude on both sides of the North Pacific from the Yellow Sea to the Okhotsk an Bering Seas, and across the northeastern Pacific to Oregon (Allen & Smith, 1988; Canino et al., 2010). Both *G. chalcogrammus* and *G. macrocephalus* prefer waters above 0°C (Wyllie-Echeverria and Wooster, 1998; Kotwicki and Lauth, 2013) but otherwise tolerate a large temperature range (Baker and Hollowed, 2014).

Gadids in the Pacific Arctic are morphologically similar, and species can be difficult to distinguish. *G. chalcogrammus* and *B. saida* larvae (<60 mm) are particularly cryptic. A few characteristics are reported in Matarese et al., (1989) involving mostly pigmentation differences. Additional distinguishing characteristics emerge with larger fish, but in general, larval gadids, particularly *G. chalcogrammus* and *B. saida*, are difficult to identify in the field.

In this study, we genetically examine these four gadid species in the Pacific Arctic during a time of substantial physical changes in the marine ecosystem, 2012–2019. We have two aims: 1.) To evaluate the accuracy of at sea morphological identifications with genetic species identification and 2.) To document the change in species composition and distribution of gadids sampled in the North Pacific Arctic in 2012, 2013, 2017 and 2019.

Methods

Sample collection

Gadids were collected by vessels operating in the eastern Chukchi Sea in 2012, 2013, 2017, and 2019 (Table 1). Samples were collected through a combination of bottom trawl (a 3-m plumb-staff beam trawl) and a mid-water/surface trawl (a modified Marinovich midwater trawl). An additional collection of *B saida* was opportunistically collected in the Bering Sea in 2010 when present in bottom trawls. In 2012, 2013, 2017, and 2019, *B. saida* was targeted for genetic sampling in the Chukchi Sea to examine its population structure. In 2012, *B. saida* samples were collected by bottom trawl and up to 36 fish were randomly sampled from each haul. Conversely, in 2013 and 2017, *B. saida* were collected by mid-water/surface trawl. In 2013, larger sample sizes (150+) were retained from each haul. The 2017 *B. saida* collections included some individually barcoded samples and some bulk samples (n=50).

Initial genetic screening of the 2017 samples of *B. saida* detected large numbers of *G. chalcogrammus* in the southern Chukchi Sea that had not been identified in the field. This prompted a decision to collect a larger subsample of cods in 2019 for genetic identification, as well as some additional 2017 samples. Sampling in 2019 was also conducted primarily by midwater/surface trawls. Lengths and weights of up to 60 specimens of each cod species were subsampled from each trawl. Fish were frozen whole at sea at -80°C.

Additional fish identified as *B. saida* from the N. Bering Sea collected in 2010 by surface/mid-water trawl, were added for comparison of samples to an earlier, cooler, year, and to illustrate the southern reaches of this species during some years.

Laboratory

DNA was extracted from 7,009 cod tissue samples using Qiagen DNeasy[2] Tissue kit protocols. We took a two-phase approach to distinguishing among candidate gadiid species (*B. saida, E. gracilis, G. chalcogrammus, G. macrocephalus, and Arctogadus glacialis* [Polar Cod]). Because the initial objective was to examine population structure of *B. saida*, all samples were first examined with microsatellite markers. After analysis of the 2017 collections, it was determined that species other than *B. saida* were present in the sample. One microsatellite marker was highly diagnostic, *Sai25*, in distinguishing *B. saida* from the other gadids. Next, for all non-*B. saida*, we sequenced a partial cytochrome oxidase c, subunit I (COI) fragment to distinguish the remaining cods.

Microsatellites

We developed a microsatellite marker, *Sai25*, using methods derived from Glenn and Schable (2005) that was diagnostic for *B. saida*. Adult *B. saida*, *G. chalcogrammus*, *E. gracilis*, and *G. macrocephalus* were morphologically identified by a skilled taxonomist, and tissue samples were used as reference samples in the initial microsatellite investigations of samples collected in 2012. Reactions were prepared according to manufacturers' instructions with primers (*Sai25*F: 3'CAGTTGACCACATCCCACCA and *Sai25*R:3'ATTTCACGTCCCATACCCCG), Qiagen master mix and RNase-free water. Thermal cycling was performed under the following conditions: 95°C for 15 min, 28 cycles of amplification (94°C for 30 sec, 60°C annealing temperature for 90 sec, and 72°C for 60 sec), and a final extension cycle of 72°C for 30 min. Fragments were analyzed on a 16 capillary ABI 3130xl DNA Analyzer (Applied Biosystems [AB]), and genotypes were determined with Genemapper 5.0® (AB) software. Samples which exhibited a size range of 280-283 base pairs (bp) at microsatellite marker *Sai 25* were clearly identified as *B. saida*. All other gadids exhibited fragment sizes larger than 300 bp and overlapping in size: *E. gracilis*, 302-324*, G. chalcogrammus*, 308-400*,* and *G. macrocephalus,* 304-382.
mtDNA.

To identify the species of individuals with *Sai25* alleles outside the allele size range for *B. saida*, a partial region of the mtDNA gene cytochrome oxidase I (COI) was sequenced. This ~170 bp segment of COI was amplified using the coi.175f and coi.345r primers described in Collins et al. (2019). We confirmed that this region contained SNPs that could differentiate each of the 5 possible gadid species (*B. saida*, *G. chalcogrammus*, *E. gracilis*, *G. macrocephalus*, and *A. glacialis*) using sequence data downloaded from the National Center for Biotechnology Information. Specifically, we downloaded COI sequences from the following species: 7 sequences from *A. glacialis*, 31 sequences from *B. saida,* 75 sequences from *E. gracilis,* 64 sequences from *G. macrocephalus*, and 233 sequences from *G. chalcogrammus*. Most of the sequences were vouchered specimens; this was especially true for species with less available sequences. We then used the software Geneious (https://www.geneious.com/) to align and compare reference sequences. Visual comparisons revealed at least one diagnostic SNP between each species, with many more for most comparisons. Additionally, we did not notice any potentially misidentified specimens in the database, as diagnostic SNPs were consistent across specimens.

Amplicon libraries were prepared for COI sequencing using a slightly modified genotyping-in-thousands by sequencing protocol (Campbell, et al., 2014; described in Gehri eta al., 2020). Libraries were sequenced on an Illumina MiSeq using 2x75 bp chemistry. R1 and R2 sequences were processed separately and grouped into unique variants using the R package Dada2 (Callahan et al., 2016). Sequences were then compared to existing COI sequences for gadids (described above) using nBLAST, and species were identified based on the best alignment for each sequence. Samples were only assigned a species ID if the best aligning sequence contained > 100 reads, species identification for the R1 and R2 sequences matched, and at least one of the reads (R1 or R2) produced an unambiguous alignment (i.e., best match to

[2] Mention of trade names or commercial companies is for identification only.

a single species). Some samples were not able to be resolved due to poor sample quality (127 of the 2,139 samples from 2017 and 133 samples of the 3,611 samples from 2019) and were removed from analyses.

Analyses

Field species identification was evaluated for accuracy with a confusion matrix using the caret package in R (Kuhn et al., 2016). The matrix allows for examination of the classification of each of the five gadid species. It provides a visual of how many fish were correctly identified at sea (true positives and true negatives), and how many were incorrectly identified at sea (false positives: *B. saida* at sea but non-*B. saida* in the lab and false negatives: non-*B. saida* at sea, but *B. saida* in the lab). From the confusion matrix we calculated the sensitivity (SE) for a given species *s*,

$$SEs = \frac{TPs}{TPs + |\ FNs}$$

where TP is the number of true positives and FN is the number of false negatives. The specificity (SP) for each species was calculated as

$$SPs = \frac{TNs}{TNs + |\ FPs}$$

where TN is the number of true negatives and FP is the number of false positives. The average of SE and SP provides the balanced accuracy (BA) and gives an estimate of the overall accuracy of at sea species identification. Analyses were conducted separately for small and large size classes of fish from 2017 and 2019. Fish sizes of 60 mm or smaller were classified as age-0 (Helser et al., 2017) and fish larger than 60 mm were classified as age 1+.

Results

Analysis of microsatellite marker *Sai25* was completed for all gadids (N=7,014) collected in the Bering Sea in 2010 (N=89) and the Chukchi Sea in 2012 (N=575), 2013 (N=860), 2017 (N=2,012), and 2019 (N=3,478) (Table 1). A subset of these samples (N=2,949) were also sequenced at a partial COI fragment (2010, N=54; 2012, N=175; 2013, N=122; 2017, N=744; 2019, N=1854 (Appendix 1)). A summary of the results was created by amalgamating the number of each species detected in 2° latitudinal increments for each year (Table 2). Genetic analysis of the 2010, 2012 and 2013 samples exhibited mostly *B. saida*, with a few *G. chalcogrammus* (0/89 individuals in 2010, 3/575 individuals in 2012 and 1/860 individuals in 2013) (Table 2; Fig. 1a). Fish caught in 2017 and 2019 revealed the presence of 4 species of gadids: *B. saida*, *G. chalcogrammus*, *G. macrocephalus*, and *E. gracilis*, and the presence of a fifth species, *Arctogadus glacialis*, in the 2019 collection. The 2017 collection contained 1,492/2,012 *B. saida*, 428/2,012 *G. chalcogrammus*, 66/2,012 *G. macrocephalus*, and 26/2,012 *E. gracilis* (Table 2, Fig. 1b). The 2019 collection was comprised of 1,753/3,478 *B. saida*, 1,474/3,478 *G. chalcogrammus*, 46/3,478 *G. macrocephalus*, 182/3,478 *E. gracilis*, and 13/3,478 *Arctogadus glacialis* (Table 2, Fig. 1c).

Sampling efforts in 2010, 2012, 2013, and 2017 targeted collection of *B. saida*, and the 2010, 2012, 2013 collections exhibited 99.99% correct identification of *B. saida* at sea. Conversely, genetic identification of 2,012 fish caught in 2017 revealed that 21.6% were misidentified at sea. Because of this misidentification, a subsample of all species of cods was retained for genetic identification of the 2019 collection. Genetic identification of the 3,478 fish caught in 2019 revealed that 19.8% were misidentified at sea.

In the 2017 collection, 1,924 fish were identified at sea as *B. saida*; however 433 of those were genetically identified to be 420 *G. chalcogrammus*, 8 *G. macrocephalus*, and 5 *E. gracilis* (Table 3a-b). Additionally, 3 of the 62 *G. macrocephalus* identified at sea were genetically identified as *G.*

chalcogrammus. In both size classes, 0 specimens were identified at sea as *G. chalcogrammus* in 2017 (Fig. 2a & b). *G. chalcogrammus* at sea species IDs that were not identified as *G. chalcogrammus* (specificity, SP), for both small and large size classes, was 0.00. A zero SP means zero *G. chalcogrammus* were correctly identified at sea. The balanced accuracy (BA) = 0.50, is the same as correct identification by random chance (Table 3a-b). The high sensitivity for *B. saida* (SE = 1.0) indicates all genetically identified *B. saida* were correctly identified as *B. saida* at sea, but the low specificity (SP = 0.01) indicates many fish identified at sea as *B. saida*, were genetically identified as something else (Table 3a-b). The balanced accuracy of evaluating *B. saida* is slightly better for larger fish (BA = 0.51 in small fish and 0.75 in larger fish) (Table 3a-b). Smaller *G. macrocephalus* and *E. gracilis* were correctly identified at sea more often than at random (in 2017, BA = 0.62 and 0.69) while, larger *G. macrocephalus* and *E. gracilis* had a high accuracy of at sea identification (BA = 0.96 and 1.0; Table 3a-b).

In the 2019 collection, 2,398 fish were identified at sea as *B. saida*. Of those specimens, 676 were genetically identified as: 654 *G. chalcogrammus*, 13 *A. glacialis*, 7 *E. gracilis*, and 2 *G. macrocephalus* (Table 3c-d). Additionally, 21 of the 853 *G. chalcogrammus* identified at sea, were genetically determined to be *B. saida*. Most samples of *G. macrocephalus* and *E. gracilis* were correctly identified at sea. Of 45 *G. macrocephalus*, 2 were genetically identified as *B. saida* and of 182 *E. gracilis*, 7 were misidentifed as: 5 *B. saida*, one *G. chalcogrammus* and one *G. macrocephalus* (Table 3c-d). The accuracy of species identification at sea for both large and small size classes improved in 2019. The accuracy of both *B. saida* and *G. chalcogrammus* produced a BA of 0.74 for small fish sizes and 0.86 and 0.87 for larger fishes. The accuracy for *G. macrocephalus* and *E. gracilis* identification was high for smaller fishes (BA = 0.83 and 0.91) and very high for larger fish (BA=0.99; Table 3c-d). Juvenile *A. glacialis* was not identified at sea, but genetic identification detected this species at 3 hauls in the northernmost areas of the cruise. In 2019, 13 age-0 *Arctogadus glacialis* (Polar Cod) were detected in the northernmost area of the survey (Fig. 3a & b)

Discussion

Monitoring the compositions of marine species in a changing Arctic is not only important for understanding the overall effects on the ecosystem, but for understanding of local food sources, commercial fishery management, and resource protection. This study provides evidence of a distributional shift to the north of *G. chalcogrammus* and *B. saida*. In the colder years of 2012 and 2013, *B. saida* was the primary cod species in the Chukchi Sea, with little observation of the other cods except for *E. gracilis* which was also present in the Chukchi Sea as noted by De Robertis (et al., 2017). The warmer years of 2017 and 2019 revealed a progressive infusion of *G. chalcogrammus* and to a lesser extent, *G. macrocephalus*. *G. chalcogrammus*, while detected in small numbers (< 1% of the catch) in the Chukchi and Beaufort seas in the cooler years of 2008-2013 (Goddard et al., 2014; Logerwell et al., 2015) accounted for 42% overall of the gadid specimens collected for genetic analysis in 2019, and was present in high densities in the southern Chukchi Sea and Kotzebue Sound (Levine et al, 2021).

B. saida is also moving north, whether due to competition with *G. chalcogrammus* or physical marine changes is unknown. *B. saida*, was detected at lower latitudes in the cooler years, as far south as latitude 60° N in the Northern Bering Sea in 2010 (this study). By 2019, only 14 *B. saida* individuals were genetically detected in gadid samples collected south of latitude 70° N. This is corroborated by observations by the AFSC groundfish survey: Arctic cod had a 99% decline in biomass in the northern Bering Sea between 2017 (4,000 mt) and 2019 (47 mt) (AFSC survey, 2019). Fishes that prefer colder water conditions, such as Arctic Cod (*B. saida*), showed declines in abundance in the northern Bering Sea from previous survey years (Baker, 2021). While age-0 *B. saida* is thought to be able to maximize growth at the elevated temperatures seen during 2017 and 2019 (Laurel et al., 2018), we speculate the reasons for the movement north may be more related to increased water flow from the Bering Sea (Woodgate 2018),

bringing a shift in *B. saida* prey and competition from the incoming *G. chalcogrammus*. Along with warmer boreal waters from the south come more boreal lipid poor copepods which displace the Arctic lipid rich copepods (Siddon et al., 2020). Early ice breakup and warmer growing conditions enhance the survival of *B. saida* because of early hatching, an extended growth season, and optimal growth temperatures, however, competition and predation from invading subarctic species will likely negate these positive effects (Bouchard et al., 2017). Scenarios of lower salinity are also predicted for coastal and shelf areas as warming temperatures increase river runoff (Bluhm and Gradinger, 2008), which would favor *E. gracilis* over *B. saida*.

Another gadid species which was unexpectedly detected in our sample is *Arctogadus glacialis*. *A. glacialis* is common in the Canadian, Russian, and northeast Atlantic Arctic, however documentation for occurrence in the Pacific Arctic is scarce (Mecklenburg et al., 2014). Only 3 records of its presence has been previously noted in the literature in the northern Chukchi Sea area. Andriashev (et al., 1980) reports *A. glacialis* in Siberia on the deeper border waters of the Chukchi Sea to 81°N, 178° W and two records (age 1+, 98 mm and 221mm) in the Chukchi Borderlands: 76° N, 164° W (Mecklenburg, 2014). We identified 13 specimens of age-0 *A. glacialis* (37-50 mm) from three different trawl sites in our 2019 collection. These specimens were all collected in waters at approximately latitude 72° N and longitude 161° W.

Arrival in a new region does not guarantee establishment and subsequent positive population growth (Burgess et al. 2012, Sadowski et al. 2018). A range expansion may occur if the species are able to adapt to a broad range of environmental conditions. A successful invasion or colonization requires a species to disperse to a new location and maintain positive growth through either self-persistence or ongoing immigration (Bridle and Vines 2007). A leading edge of both *G. chalcogrammus* and to a lesser extent, *G. macrocephalus* were noted in the Chukchi Sea in 2017 and 2019, but it is unknown if these fish are able to over winter in the freezing temperatures and ice formation in the Arctic winter (Woodgate et al., 2005). Northward expansion of Atlantic croaker (*Micropogonias undulatus*) along the east coast of the United States in the 1990s has been linked to sequential warm winters that allowed cold-sensitive juveniles to survive through the winter and subsequently establish north of the species' historical range (Hare and Able, 2007). Lionfish juveniles, by contrast, have appeared as far north as New York (implying no lack of dispersal abilities) but have not become established above Cape Hatteras because they fail to survive through the winter (Grieve et al., 2016). In the Barents Sea, recent warming has led to a change in spatial distribution of fish communities (Fossheim et al., 2015). Along the western coast of Svalbard, an influx of warm Atlantic water produced a northward expansion of boreal Atlantic cod (*Gadus morhua*) and haddock (*Melanogrammus aeglefinius*) into areas dominated by the native *Boreogadus saida* (Renaud et al., 2012). Continued warming is likely to enable Atlantic croaker, lionfish, and other species to survive year-round at higher latitudes (Grieve et al. 2016, Hare and Able, 2007).

Pertaining to the Chukchi Sea, perspectives during the cooler sea surface temperatures of 2008-2013 were that bottom water temperatures in the Arctic were too cold to support spawning *G. chalcogrammus*, and that the sub-adult fish caught at high latitudes may have been advected by currents from spawning locations in the Bering Sea (Hollowed, et al., 2013). Few adult pelagic fish were detected in the hydroacoustic survey or captured in the midwater trawl in 2017 and 2019 in the survey area (Levine et al., 2021). We speculate that the warmer waters and ice reduction of the warmer years of 2017-2019 have continued to reduce barriers to subarctic fish (Bering cold pool; Eisner et al., 2020) and have increased water transport from the Bering Sea, carrying sub-adult gadids into the Chukchi (Levine et al., 2021). It is yet unknown whether these age-0 invaders are able to overwinter in these arctic waters and spawn, and whether this constitutes a true range expansion.

Due to the reported distributions of previous surveys, the presence of *G. chalcogrammus* was not anticipated by collectors in 2017. Previous surveys indicated the primary pelagic fish species in the

Chukchi Sea were *B. saida* and *E. gracilis*. After reviewing the 2017 field collection misidentifications, shipboard scientists were able to more accurately identify these age-0 cods at sea with the help of a microscope. Counts of pyloric caeca were conducted on a subsample of specimens from each trawl and for individuals which could not be easily identified as *B. saida* or *G. chalcogrammus*. Specimens with <40 pyloric caeca were classified at sea as *B. saida* (W. Strausburger & N. Kuznetsova, personal communication September 2017). Without additional investment of time, species ID of these small (< 60 mm) fish are difficult. Next generation genetic techniques are able to provide high throughput, reliable species identification at affordable costs in a reasonable period of time. Future surveys may benefit from identifying to genus at sea, and retaining fish (or a small piece of tissue) for post survey genetic species identification.

Correct species identification may also have implications for historic data. *G. chalcogrammus* and *G. macrocephalus* have previously been noted in low abundances in the Chukchi Sea (Goddard et. al., 2014; Logerwell et al., 2015). Surveys in the Chukchi and Beaufort Seas in 2008 detected low abundance for both *G. chalcogrammus* and *G. macrocephalus* (< 1% for both) of the catch (Logerwell et al., 2015). The catch of these species in both seas were of sizes greater than 90 mm (age 1+). Species identification of fish in 2017 and 2019 seemed to improve with size, and supports the idea that the larger size class from the 2008 surveys were correctly identified. Additionally, ichthyoplankton tows in the Beaufort Sea in 2008 revealed a small presence of *G. chalcogrammus* larvae, although adults were not observed in the Chukchi or Beaufort Sea (Logerwell et al., 2015). Surveys of the Chukchi in 2012 also reported low abundance of both *G. chalcogrammus* and *G. macrocephalus* (Goddard et al., 2014). Genetic identification revealed that at sea species identification was mostly accurate in 2012 and 2013 with < 1% misidentification of specifically targeted *B. saida* and very few *G. chalcogrammus* were identified in pelagic trawls in the Chukchi Sea in 2012 (18 age 1+ and 10 age-0 specimens, De Robertis et al., 2017). Even with the unlikely potentiality of misidentification of juvenile cods in the 2008 (Logerwell et al., 2015) and 2012 (Goddard et al., 2014) Chukchi surveys, the increase in juvenile *G. chalcogrammus* in summer waters of the Chukchi Sea in 2017 and 2019 is noteworthy: 21% of the genetic sample in 2017, and 42% in 2019.

Accurate species identification, especially during a time of changing marine landscapes, is not only important for survey abundance estimates (Levine et. al., 2020; 2021), but for downstream analyses as well. Laboratory analyses such as ageing, diet, stable isotopic composition, and energetics, rely on accurate species identification. Age-0 cods, particularly *G. chalcogrammus* and *B. saida* have been recognized as difficult to differentiate in the field. One study suggests that *G. chalcogrammus* may be a genealogically recent hybrid of *B. saida* and *G. morhua* (Arnason and Halldorsdottir, 2019). The two species at early life stages are identical at most exterior characteristics (Matarese et al., 1989; Mecklenberg et al., 2018). The presence of *G. chalcogrammus* and *G. macrocephalus* in the southern Chukchi Sea in 2017 highlights the importance of genetics in identifying morphologically similar species and comparing with at sea identifications.

Our results provide strong evidence of a change of gadids in the Pacific Arctic (at least in summer). The change in species composition of juvenile cods in the Chukchi Sea between the summer of 2012 and 2019 is dramatic. Because of the difficulty in distinguishing between external morphologies of these species, major increases in the abundance of age-0 *G. chalcogrammus* in the Chukchi, and the northern shift of the distribution of *B. saida* would not have been detected without genetic sampling of the survey catch. This emphasizes the importance of implementing strategies for correct identification of the cod species in the Arctic in order to better capture and monitor the ecology of this rapidly changing region.

Acknowledgements

This research was conducted under the Arctic Integrated Ecosystem Research Program

(IERP; http://www.nprb.org/arctic-program/). This manuscript is Publication ArcticIERP-XX. Funding for the program was provided by North Pacific Research Board, the Bureau of Ocean Energy Management, the Collaborative Alaskan Arctic Studies Program, and the Office of Naval Research. In-kind support was contributed by the National Oceanic and Atmospheric Administration (NOAA) Alaska Fisheries Science Center and Pacific Marine Environmental Laboratory, the University of Alaska Fairbanks, the U.S. Fish & Wildlife Service, and the National Science Foundation.

We thank Jay Orr for early manuscript review and Allison Deary, Wes Strausburger and Natalia Kuznetsova for information on morphological identification markers.

References

AFSC Survey 2019: fisheries.noaa.gov/Alaska/science data/Alaska fisheries science center surveys arctic 2019 preliminary findings #adult groundfish, crab and bottom dwelling species survey of northern Bering Sea, summer 2019.

Allen, M.J., Smith, G.B. 1988. Atlas and zoogeography of the common fishes in the Bering Sea and northeastern Pacific. *NOAA Technical Report NMFS*, 66, 151.

Andriashev, A. P., Mukhomedigarov, B. F. & Pavshtiks, E. A., 1980. On the mass accumulations of cryopelagic cods (Boreogadus saida and Arctogadus glacialis) in 1350 A. D. JORDAN ET AL. # 2003 The Fisheries Society of the British Isles, Journal of Fish Biology 2003, 62, 1339–1352 the circumpolar regions of the Arctic. In Biology of the Central Arctic Basin (Vinogradov, M. E. & Melnikov, I. A., eds), pp. 196–211. Moscow: Nauka (in Russian).

Arnason, E., Halldorsdottir, K., 2019. Codweb: Whole-genome sequencing uncovers extensive reticulations fueling adaptation among Atlantic, Arctic, and Pacific gadids. Science Advances 5 (3). doi: 10.1126/sciadv.aat8788.

Baker, M.R., Hollowed, A.B., 2014. Delineating ecological regions in marine systems: Integrating physical structure and community composition to inform spatial management in the eastern Bering Sea. Deep Sea Research II (109) 215-240. doi:10.106/J.DSR2.2014.03.001.

Baker, M.R., Farley, E.V., Danielson, S, Huntington, H.P., Ladd, C., Stafford, K.M, Dickson, D., 2020. Integrated ecosystem research in the Pacific Arctic – understanding ecosystem processes timing and change. Deep Sea Research II. doi: 10.1016/j.dsr2.2020.104850.

Baker, M.R., 2021. Contrast of warm and cold phases in the Bering Sea to understand spatial distributions of Arctic and sub-Arctic gadids. Polar Biology. doi: 10.1007/s00300-021-02856-x

Bluhm, B., Gradinger, R., 2008. Regional variability in food availability for arctic marine mammals. Ecological Applications 18 (2 Suppl) S77:96. doi: 10.1890/06-0562.1

Bouchard, C., Geoffroy, M., LeBlanc, M., Majewski, A., Gauthier, S., Walkusz, W., Reist, J.D., Fortier, L., 2017. Climate warming enhances polar cod recruitment, at least transiently, Progress in Oceanography, V. 156, pp. 121-129, ISSN 0079-6611, doi.org/10.1016/j.pocean.2017.06.008

Bridle J.R., Vines T.H., 2007. Limits to evolution at range margins: When and why does adaptation fail? TrendsEcol. Evol. 22:140–47

Bulatov, O.A. 2014. Walleye Pollock: global overview. Fish. Sci. 80, 109-116. doi.org/10.1007/s12562-014-0715-0

Burgess S.C., Treml E.A., Marshall D.J., 2012. How do dispersal costs and habitat selection influence realized population connectivity? Ecology 93:1378–87

Callahan, B.J., McMurdie, P.J., Rosen, M.J., Han, A.W., Johnson, A.J.A., Holmes, S.P., 2016. DADA2: High resolution sample inference from Illumina amplicon data. Nat. Methods 13(7) pp. 581-583.

Campbell, N.R., Harmon, S.A., Narum, S.R. 2014. Genotyping-in-thousands by sequencing (GT-seq): A cost effective SNP genotyping method based on custom amplicon sequencing. Molecular Ecology Resources 15(4) pp. 855-867. doi.org/10.1111/1755-0998.12357

Canino, M.F., Spies, I.B., Cunningham, K.M., Hauser, L. and Grant, W.S. 2010. Multiple ice-age refugia in Pacific cod, Gadus macrocephalus. Molecular Ecology, 19: 4339-4351. doi.org/10.1111/j.1365-294X.2010.04815.x

Carmack, E., Wassmann, P., 2006. Food webs and physical-biological coupling on pan-Arctic shelves: Unifying concepts and comprehensive perspectives. Progress in Oceanography 71(2):446-477. doi: 10.1016/j.pocean.2006.10.004

Cheung, W.W.L, Watson, R., Pauly, D., 2013. Signature of ocean warming in global fisheries catch. Nature Research Letter. V. 497, pp. 365-369. doi:10.1038/nature12156

Codispoti, L.A., Kelly, V., Thessen, A., Matrai, P., Suttles, S., Hill, V., Steele, M., Light, B., 2013. Synthesis of primary production in the Arctic Ocean: III. Nitrate and phosphate based estimates of net community production. Progress in Oceanography (110) 126-150.

Collins, R.A., Bakker, J., Wangensteen, O.S., Soto, A.Z., Corrigan, L., Sims, D.W., Genner, M.J., Mariani, S., 2019. Non-specific amplification compromises environmental DNA metabarcoding with COI. Methods in Ecology and Evolution. V10 (11) pp. 1985-2001. doi/10.1111/2041-210X.13276.

Conner, J., and R. R. Lauth. 2017. Results of the 2016 eastern Bering Sea continental shelf bottom trawl survey of groundfish and invertebrate resources. U.S. Dep. Commer., NOAA Tech. Memo. NMFS-AFSC352,159 p.

Copeman, L.A., Laurel, B.J., Boswell, K.M., Sremba, A.L., Klinck, K., Heintz, R.A.,Vollenweider, J.J., Helser, T.E, Spencer, M.L. 2016. Ontogenetic and spatial variability in trophic biomarkers of juvenile saffron cod (Eleginus gracilis) from the Beaufort, Chukchi, and Bering Seas. Polar Biology 39:1109-1126. doi 10.1007/s00300-015-1792-y

Danielson, S.L., Ahkinga, O., Ashjian, C., Basyuk E., Cooper, L.W., Eisner, L., Farley, E., Iken K.B., Grebmeier, J.M., Juranek, L., Khen, G., Jayne, S.R., Kikuchi, T., Ladd, C., Lu, K.,McCabe, R.M., Moore, G.W.K., Nishino, S., Ozenna, F., Pickart, R.S., Polyakov, I., Stabeno, P.J., Thoman, R., Williams, W.J., Wood, K., Weingartner, T.J., 2020. Manifestation and consequences of warming and altered heat fluxes over the Bering and Chukchi sea continental shelves. Deep-Sea Research Part II, 177, 104781. doi.org/10.1016/j.dsr2.2020.104781

Datsky, A.V., 2016. Biological features of the common fish species in Olyutorsky-Navarin region and the adjacent waters of the Bering Sea: 1. Gadidae (cods) family. Journal of Ichthyology (56) 868-889.

De Robertis, A., Taylor, K., Wilson, C.D., Farley, E.V., 2017. Abundance and distribution of arctic cod (Boreogadus saida) and other pelagic fishes over the U.S. continental shelf of the northern Bering and Chukchi Seas. Deep Sea Research II (135) 51-65. doi.org/10.1016/j.dsr2.2016.03.002

Drost, H.E., Fisher, J., Randall, F., Kent, D., Carmack, E.C., Farrell, A.P., 2016. Upper thermal limits of the hearts of Arctic cod Boreogadus saida: adults compared with larvae. Journal of Fish Biology (88) 718-726. doi:10.1111/jfb.12807

Duffy-Anderson, J.T., Stabeno, P.J., Siddon, E.C., Andrews, A.G., Cooper, D.W., Eisner, L.B., Farley, E.V., Harpold, C.E., Heintz, R.A., Kimmel, D.G., Sewall, F.F., Spear, A.H., Yasumishii, E.C., 2017. Return of warm conditions in the southeastern Bering Sea: Phytoplanton – fish. PLOS ONE. doi.org/10.1371/journal.pone.0178955

Eisner, L.B., Zuenko, Y.I., Basyuk, E.O., Britt, L.L., Duffy-Anderson, J.T., Kotwicki, S., Ladd, C., Cheng, W. 2020. Environmental Impacts on walleye Pollock (Gadus chalcogrammus) distribution across the Bering Sea shelf. Deep Sea Research II, V. 181-182. doi.org/10.1016/j.dsr2.2020.104881

Fossheim, M., Primicerio, R., Johannesen, E., Ingvaldsen, R.B., Aschan, M.M., Dolgov, A.V., 2015. Recent warming leads to a rapid borealization of fish communities in the arctic. Nature Climate Change. doi: 10.1038/NCLIMATE2647

Frey, K.E., Maslanik, J.A., Clement Kinney, J., Maslowski, W., 2014. Recent variability in sea ice cover, age, and thickness in the Pacific Arctic region. In: Grebmeier, J., Maslowski, W., (eds). The Pacific Arctic Region. Springer, Dordrecht. doi.org/10.1007/978-94-017-8863-2_3

Glenn, T.C. and Schable, N.A., 2005. Isolating microsatellite DNA loci. Methods in Enzymology 395:202-222.

Goddard, P., Lauth, R., Armistead, C., 2014. Results of the 2012 Chukchi Sea bottom trawl survey of bottomfishes, crabs, and other demersal macrofauna. U.S. Dep. Commer., NOAA Tech. Memo. NMFS-AFSC-278, p. 110.

Gradinger and Bluhm. 2004. In situ observations on the distribution and behavior of amphipods and Arctic cod (Boreogadus saida) under the sea ice of the high Arctic Canadian Basin. Polar Biol., 27. P. 595-603.

Grebmeier, J.M., Overland, J.E., Moore, S.E., Farley, E.V., Carmack, E.C., Cooper, L.W., Frey, K.E., Helle, J.H, McLaughlin, F.A., McNutt, S.L. 2006. A major ecosystem shift in the northern Bering Sea. Science. Mar 10:311(5766):1461-4. doi: 10.1126/science.1121365. PMID: 16527980.

Grebmeier, J.M., B.A. Bluhm, L.W. Cooper, S.G. Denisenko, K. Iken, M. Kędra, and C. Serratos. 2015. Time-series benthic community composition and biomass and associated environmental characteristics in the Chukchi Sea during the RUSALCA 2004–2012 Program. Oceanography 28(3):116–133, doi.org/10.5670/ oceanog.2015.61.

Grieve, B.D., Curchitser, E.N., Rykaczewski, R.R., 2016. Range expansion of the invasive lionfish in the Northwest Atlantic with climate change. Marine Ecology Progress Series. 546, pp. 225-237. doi.org/10.3354/meps11638

Hare, J.A. and Able, K.W., 2007. Mechanistic links between climate and fisheries along the east coast of the United States: explaining population outbursts of Atlantic croaker (Micropogonias undulatus). Fish. Oceanogr. 16:1, pp. 31-45.

Helser, T.E., Colman, J.R., Anderl, D.M., Kastelle, C.R., 2016. Growth dynamics of saffron cod (Eleginus gracilis) and Arctic cod (Boreogadus saida) in the Northern Bering and Chukchi Seas. Deep-Sea Res. II, doi.org/10.1016/j.dsr2.2015.12.009

Hollowed, A.B., Barange, M., Beamish, R.J., Brander, K., Cochrane, K., Drinkwater, K., Foreman, M.G.G., Hare, J.A., Holt, J., Ito, S., Kim, S., King, J.R., Loeng, H., MacKenzie, B.R., Mueter, F.J., Okey, T.A., Peck, M.A., Radchenko, V.I., Rice, J.C., Schirripa, M.J., Akihiko Yatsu, A., Yamanaka, Y. 2013. Projected impacts of climate change on marine fish and fisheries. Ices Journal of Marine Science 70 (5), pp. 1023-1037. doi.org/10.1093/icesjms/fst081

Howell, D., Filin, A., 2014. Modelling the likely impacts of climate - driven changes in cod – capelin overlap in the Barents Sea. ICES Journal of Marine Science (2014), 71(1), 72–80. doi:10.1093/icesjms/fst172

Huntington, H.P., Danielson, S.L., Wiese, F.K., Baker, M.R., Boveng, P., Citta, J.J., De Robertis, A., Dickson, D.M.S., Farley, E., Craighead George, J., Iken, K., Kimmel, D.G., Kuletz, K., Ladd, C., Levine, R., Quakenbush, L., Stabeno, P., Stafford, K.M., Stockwell, D., Wilson, C. 2020. Evidence suggests potential transformation of the Pacific Arctic ecosystem is underway. Nature Climate Change. doi: 10.1038/s41558-020-0695-2.

Kent, D., Drost, H. E., Fisher, J., Oyama, T., Farrell, A.P., 2016. Laboratory rearing of wild Arctic cod Boreogadus saida from egg to adulthood. J. Fih Biol. 88, 1241-1248.

Kleisner, K.M., Fogarty, M.J., McGee, S., Hare, J.A., Moret, S., Perretti, C.T., Saba, V.S., 2017. Marine species distribution shifts on the U.S. northeast continental shelf under continued ocean warming. Progress in Oceanography. V. 153, pp. 24-36. doi: 10.1016/j.pocean.2017.04.001

Kotwicki, S., Lauth, R.R. 2013. Detecting temporal trends and environmentally-driven changes in the spatial distribution of bottom fishes and crabs on the eastern Bering Sea shelf. Deep Sea Research II 94:231-243. doi:10.1016/j.dsr2.2013.03.017

Kuhn, M., Wing, J., Weston, S., Williams, A. Keefer C, Engelhardt, A., Cooper, T., Maer, Z., Kenkel, B., R Core Team, Benesty, M., Lescarbeau, R., Ziem, A., Scrucca, L.,Tang, Y., and Candam, C. 2016. Caret:lassification and regression training [Online]. Available: https://cran.r-project.org/package=caret.

Laurel, B.J., Spencer, M., Iseri, P., Copeman, L.A., 2016. Temperature-dependent growth and behavior of juvenile arctic cod (Boreogadus saida) and co-occurring North Pacific gadids. Polar Biology 39:1127-1135. doi: 10.1007/s00300-015-1761-5

Laurel, B.J., Copeman, L.A., Spencer, M., Iseri, P., 2018. Comparative effects of temperature on rates of development and survival of eggs and yolk-sac larvae of Arctic cod (Boreogadus saida) and walleye Pollock (Gadus chalcogrammus). ICES Journal of Marine Science 75:2403-2412. doi:10.1093/icesjms/fsy042

Levine, R.M., De Robertis A., Grunbaum, D., Woodgate, R., Mordy, C.W., Mueter, F., Cokelet, E., Lawrence-Slavas, N., Tabisola, H., 2020. Autonomous vehicle surveys indicate that flow reversals retain juvenile fishes in a highly advective high-latitude ecosystem. Limnol. and Oceanogr. 66, pp. 1139-1154. doi: 10.1002/lno.11671

Levine, R.M., De Robertis, A., Grunbaum, D., Wildes, S.L., Farley, E.V., Stabeno, P.J., Wilson, C. D. 2021. In prep

Logerwell, E., Busby, M., Carothers, C., Cotton, S., Duffy-Anderson, J., Farley, E., Godard, P., Heintz, Holladay, B., Horne, J., Johnson, S., Lauth, B., Moulton, L., Neff, D., Norcross, B., Parker-Stetter, S., Seigle, J., Sformo, T., 2015. Fish communities across a spectrum of habitats in the western Beaufort Sea and the Chukchi Sea. Progress in Oceanography (136) 115-132.

Matarese, A.C., Kendall, A.W., Blood, D.M., Vinter, B.M. 1989. Laboratory guide to early life history stages of Northeast Pacific fishes. NOAA Tech. Rep. NMFS 80.

Mecklenburg, C.W., Byrkjedal, I., Karamushko, O.V., Møller, P.R., 2014. Atlantic fishes in the Chukchi Borderland. Mar Biodivers 44:127–150

Mecklenburg, C.W., Lynghammar, A., Johannesen, E., Byrkjedal, I., Christiansen, J.S., Dolgov, A.V., Karamushko, O.V., Mecklenburg, T.A., Møller, P.R., Steinke, D., and Wienerroither, R.M. 2018. Marine Fishes of the Arctic Region. Conservation of Actic Flora and Fauna, Akureyri, Iceland. ISBN: ISBN 978-9935-431-70-7.

Meuter, F.J., Litzow, M.A., 2008. Sea ice retreat alters the biogeography of the Bering Sea continental shelf. Ecological Applications, 18(2), pp. 309-32. DOI: 10.1890/07-0564.1 Molinos, J.G., Halpern, B.S., Schoeman, D.S., Brown, C.J., Kiessling, W., Moore, P.J., Pandolfi, J.M., Poloczanska, E.S., Richardson, A.J., Burrows, M.T., 2015. Climate velocity and the future global redistribution of marine biodiversity. Nature Climate Change. doi: 10.1038/NCLIMATE2769

Molinos, J.G., Burrow, M.T., Poloczanska, E.S., 2017. Ocean currents modify the coupling between climate change and biogeographical shifts. Nature Scientific Reports. 7: 1332 | doi:10.1038/s41598-017-01309-y

Moore, S.E., Stabeno, P.J., 2015. Synthesis of arctic research (SOAR) in marine ecosystems of the Pacific Arctic. Progress in Oceanography. V. 136, pp. 1-11.

Morley, J.W., Selden, R.L., Latour, R.J., Frolicher, T.L., Seagraves, R.J., Pinsky, M.L., 2018. Projecting shifts in thermal habitat for 686 species on the North American continental shelf. PLOS ONE 13(5): e0196127. doi.org/10.1371/journal.pone.0196127

Mueter, F.J., Litzow, M.A. 2008. Sea ice retreat alters the biogeography of the Bering Sea continental shelf. Ecological Applications (18)2, p. 309-320. doi: 10.1890/07-0564.1

Page, L. M., H. Espinosa-Pérez, L. T. Findley, C. R. Gilbert, R. N. Lea, N. E. Mandrak, R. L. Mayden, and J. S. Nelson (editors). 2013. Common and Scientific Names of Fishes from the United States, Canada, and Mexico. Seventh Edition, American Fisheries Society, Special Publication, 34, 243 pp.

Pinsky, M.L., Selden, R.L., Kitchel, Z.J., 2020. Climate – Driven shifts in marine species ranges:scaling from organisms to communities. Annu. Rev. Mar. Sci. 2020. 12:153–79. doi.org/10.1146/annurev-marine-010419-010916

Poloczanska, E.S., Brown, C.J., Sydeman, W.J., Kiessling, W., Schoeman, D.S., Moore, P.J., Brander, K., Bruno, J.F., Buckley, L.B., Burrow, M.T., Duarte, C.M., Halpern, B.S., Holding, J., Kappel C.V., O'Connor, M.I., Pandolfi, J.M., Parmesan, C., Schwing, F., Thompson, S.A., Richardson, A.J.,

2013. Global imprint of climate change on marine life. Nature climate change 3, pages 919–925. doi.org/10.1038/nclimate1958

Poloczanska, E.S., Burrows, M.T., Brown, C.J., Molinos, J.G., Halpern, B.S., Hoegh-Guldberg, O., Kappel C.V., Moore, P.J., Richardson A.J., Schoeman, D.S., Sydeman, W.J., 2016. Responses of Marine Organisms to climate change across oceans. Front. Mar. Sci. 3:62. doi: 10.3389/fmars.2016.00062

Ponomarenko, V.P., 1968. Some data on the distributions and migrations of polar cod in the seas of the Soviet Arctic. Rapp P-V Reun Cons Perm Int Explore Mer 158:131-133.

Renaud, P.E., Berge, J., Varpe, O., Lonn, O.J., Nahrgang, J, Ottensen, C., Hallanger, I., 2012. Is the poleward expansion by Atlantic cod and haddock threatening native polar cod (Boreogadus saida)? Polar Biol. 35, 401-412. doi.org/10.1007/s00300-011-1085-z

Sadowski J.S., Gonzalez J.A., Lonhart S.I., Jeppesen R., Grimes T.M., Grosholz E.D., 2018. Temperature-induced range expansion of a subtropical crab along the California coast. Mar. Ecol. 39:e12528

Siddon, E.C., Zador, S.G., Hunt, G.L. Jr., 2020. Ecological responses to climate perturbations and minimal sea ice in the northern Bering Sea. Deep Sea Research II 181-182. doi.org/10.1016/j.dsr2.2020.104914.

Sigler, M.F., Renner, M., Danielson, S.L., Eisner, L.B., Lauth, R.R., Kuletz, K.J., Logerwell, E.A., Hunt, G.L., 2011. Fluxes, fins and feathers: Relationships among the Bering, Chukchi, and Beaufort Seas, in a time of climate change. Oceanography 24(3):250–265, doi. org/10.5670/oceanog.2011.77.

Stabeno, P.J., Kachel, N.B., Moore, S.E., Napp, J.M., Sigler, M., Yamaguchi, A., Zerbini, A.N., 2012. Comparison of warm and cold years on the southeastern Bering Sea shelf and some implications for the ecosystem. Deep Sea Research II. (65-70) 31-45

Stabeno, P.J., Duffy-Anderson, J.T., Eisner, L.B., Farley, E.V., Heintz, R.A., Mordy, C.W., 2017. Return of warm conditions in the southeastern Bering Sea: Physics to fluorescence. PLOS ONE 12(9): e0185464. https://doi.org/10.1371/journal.pone.0185464

Stevenson, D.E., Lauth, R.E., 2012. Latitudinal trends and temporal shifts in the catch composition of bottom trawls conducted on the eastern Bering Sea shelf. Deep Sea Research II (65-70) 251-259.

Stevenson, D.E., Lauth, R.R., 2019. Bottom trawl surveys in the northern Bering Sea indicate recent shifts in the distribution of marine species. Polar Biology 42:407-421. doi.org/10.1007/s00300-018-2431-1

Vestfals, C.D, Mueter, F.J., Duffy-Anderson, J.T., Busby, M.S., DeRobertis, A. 2019. Spatio-temporal distribution of polar cod (Boreogadus saida) and saffron cod (Eleginus gracilis) early life stages in the Pacific Arctic. Polar Biol., doi.org/10.1007/s00300-019-02494-4

Whitehouse, G.A., Aydin, K., Essington T.E., Hunt, G.L. Jr., 2014. A trophic mass balance model of the eastern Chukchi Sea with comparisons to other high-latitude systems. Polar Biology (37) 911-939. doi.org/10.1007/s00300-014-1490-1

Wolotira RJ Jr. 1985. Saffron cod (Eleginus gracilis) in western Alaska: the resource and its potential. Northwest and Alaska Fisheries Center, Kodiak.

Wood, K.R, Bond, N.A., Danielson, S.L., Overland, J.E., Salo, S.A., Stabeno, P.J., Whitefield, J., 2015. A decade of environmental change in the Pacific Arctic region. Progress in Oceanography (136) 12-31. doi.org/10.1016/j.pocean.2015.05.005

Woodgate, R.A., Aagaard, K, 2005. Revising the Bering Strait freshwater flux into the Arctic Ocean. Geophysical Research Letters. V. 32. doi.org/10.1029/2004GL021747

Woodgate, R.A., Increases in the Pacific inflow to the Arctic from 1990 to 2015, and insights into seasonal trends and driving mechanisms from year-round Bering Strait mooring data. 2018. Progress in Oceanography. V. 160. Pp. 124-154. doi:10.1016/j.pocean.2017.12.007

Wyllie-Echeverria, T.I., Seasonal sea ice, the cold pool, and gadid distribution on the Bering Sea shelf (Doctoral dissertation U. of Alaska, Fairbanks). 1995. hdl.handle.net/11122/9457.

Wyllie-Echeverria, T.I., Wooster, W.S. 1998. Year-to-year variations in Bering Sea ice cover and some consequences for fish distributions. Fisheries Oceanography 7(2):159. doi.org/10.1046/j.1365-2419.1998.00058.x

Zeidberg, L.D., Robison, B.H., 2007. Invasive range expansion by the Humboldt squid, Dosidicus gigas, in the eastern North Pacific. PNAS. 104 (31) 12948-12950; doi.org/10.1073/pnas.0702043104

Table 1. Sample collection of gadids by year, gear used, general area sampled, range of latitude (N) and range of longitude (W), number of hauls, dates of cruises, and approximate numbers of fish collected for this study.

Year	Gear	Area	Lat (N)	Long (W)	# Hauls	Date Range	# Fish
2010	Bottom Trawl	E. Bering Sea	60 – 65	162 – 172	9	9/11 – 10/04	89
2012	Bottom Trawl	Chukchi Sea	66 – 73	157 – 169	23	8/07 – 9/24	575
2013	Marinovich	Chukchi Sea	70 – 72	155 – 166	6	8/07 – 9/25	860
2017	Marinovich	Chukchi Sea	66 – 73	157 – 169	79	8/10 – 9/27	2012
2019	Marinovich	Chukchi Sea	66 – 73	153 – 169	88	8/15 – 9/09	3478

Table 2. Sample collection of gadids by year, range of latitude (N) and range of longitude (W), size range (mm) of individuals in the sample, and number of genetically verified individuals of each species (*Boreogadus saida*, *Gadus chalcogrammus*, *Gadus macrocephalus*, *Elegius gracilis*, and *Arctogadus glacialis*).

Year	Latitude (N)	Longitude (W)	Size range (mm)	*said.*	*chal.*	*macro.*	*grac.*	*glac.*	Total N
2010	60 – 62	171	108 – 110	23	0	0	0	0	23
2010	62 – 64	164 – 168	110 – 129	31	0	0	0	0	31
2010	64 – 66	162 – 169	112 – 142	35	0	0	0	0	35
2012	66 – 68	164 – 169	87 – 155	144	0	0	0	0	144
2012	68 – 70	165 – 169	146 – 137	108	2	0	0	0	110
2012	70 – 72	166 – 168	78 – 150	80	0	0	0	0	80
2012	70 – 72	157 – 160	71 – 137	109	1	0	0	0	110
2012	72+	166 – 169	85 – 185	97	0	0	0	0	97
2012	72+	157 – 159	81 – 125	34	0	0	0	0	34
2013	70 – 72	161 – 166	47 – 53	312	1	0	0	0	313
2013	70 – 72	155 – 159	36 – 52	547	0	0	0	0	547
2017	66 – 68	164 – 169	44 – 93	21	148	30	7	0	206
2017	68 – 70	165 – 169	35 – 112	350	73	28	15	0	466
2017	70 – 72	162 – 169	28 – 189	483	65	7	2	0	557
2017	70 – 72	153 – 162	22 – 105	259	90	1	2	0	352
2017	72+	162 – 167	28 – 147	161	39	0	0	0	200
2017	72+	153 – 162	26 – 86	218	13	0	0	0	231
2019	66 – 68	164 – 169	37 – 230	5	179	5	49	0	238
2019	68 – 70	164 – 169	30 – 201	9	436	11	66	0	522
2019	70 – 72	162 – 168	21 – 160	425	755	28	34	0	1242
2019	70 – 72	153 – 162	26 – 143	479	48	0	5	0	532
2019	72+	163 – 169	29 – 150	295	4	0	26	0	325

2019	72+	156 – 162	24 – 239	540	52	2	2	13	609

Table 3a-d. Confusion matrices for gadid species identification age-0 and age 1+ collected in the Chukchi Sea in 2017 and 2019. Field IDs are listed as rows (total the row). Genetic IDs are listed in columns. Shaded diagonal indicates correct field ID verifed by genetics. SE=sensitivity or the proportion of true positive ID's for that species. SP=specificity or the proportion of true negatives. BA=balanced accuracy or the average of SE and SP. 3a=2017, ≤ 60 mm fish, 3b=2017, >60 mm fish, 3c=2019 ≤ 60 mm fish, and 3d 2019 > 60mm fish.

a.	N=1712		Genetic	ID's				
	2017 small fish	*saida*	*chalco.*	*macro.*	*gracilis*	SE	SP	BA
	B. saida	1350	349	3	5	1.00	0.01	0.51
	G. chalcogrammus	0	0	0	0	0.00	1.00	0.50
	G. macrocephalus	0	1	1	0	0.25	0.99	0.62
	E. gracilis	0	0	0	3	0.38	100	0.69

b.	N=295		Genetic	ID's				
	2017 large fish	*saida*	*chalco.*	*macro.*	*gracilis*	SE	SP	BA
	B. saida	141	71	5	0	1.00	0.51	0.75
	G. chalcogrammus	0	0	0	0	0.00	1.00	0.50
	G. macrocephalus	0	2	58	0	0.92	0.99	0.96
	E. gracilis	0	0	0	18	1.00	1.00	1.00

c.	N=2660		Genetic	ID's					
	2019 small fish	*saida*	*chalco.*	*macro.*	*gracilis*	*glacialis*	SE	SP	BA
	B. saida	1567	529	2	6	13	0.99	0.49	0.74
	G. chalcogrammus	17	492	0	0	0	0.48	0.99	0.74
	G. macrocephalus	0	0	4	0	0	0.67	1.00	0.83
	E. gracilis	0	1	0	29	0	0.83	0.99	0.91
	A. glacialis	0	0	0	0	0	0.00	1.00	0.50

d.	N=818		Genetic	ID's				
	2019 large fish	*saida*	*chalco.*	*macro.*	*gracilis*	SE	SP	BA
	B. saida	155	125	0	1	0.93	0.81	0.87
	G. chalcogrammus	4	340	0	0	0.73	0.99	0.86
	G. macrocephalus	2	0	39	0	0.98	0.99	0.99
	E. gracilis	5	0	1	146	0.99	0.99	0.99

a.

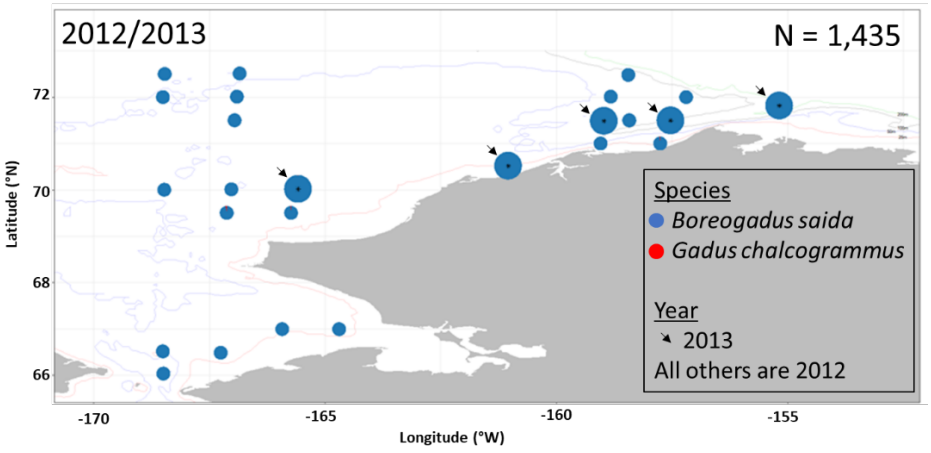

b.

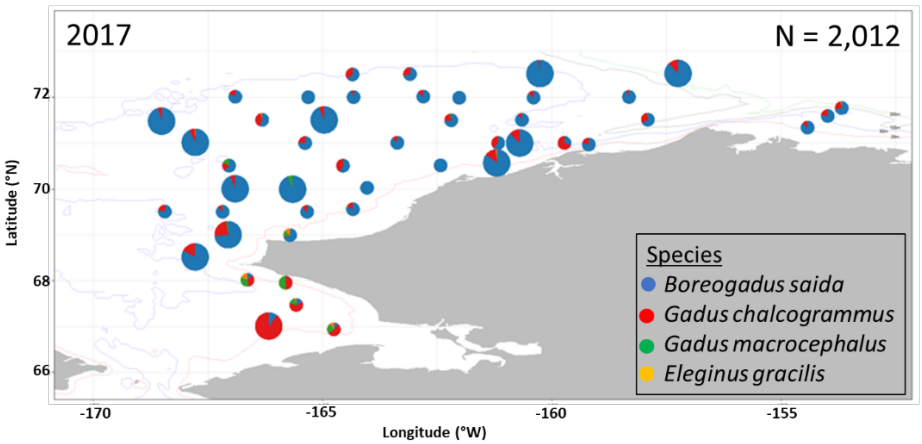

c.

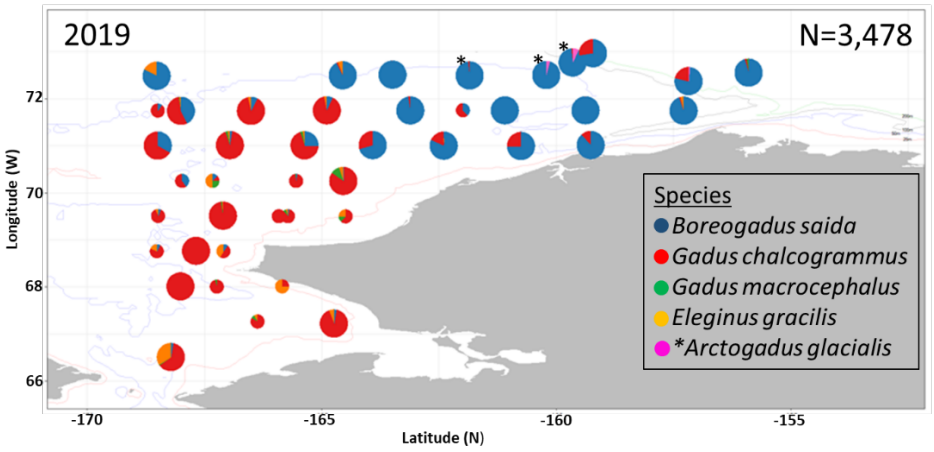

Figure 1 a-c. Genetically identified gadid specimens collected in the Chukchi Sea in a.) 2012 and 2013; b.) 2017; and c.) 2019. The number of individuals represented is reported in the upper right corner of each figure. The size of individuals indicates mostly age 1+ of the 2012 collection and age 0 of the 2013 collections. The 2017 and 2019 are a mix of age 0 and age 1+.

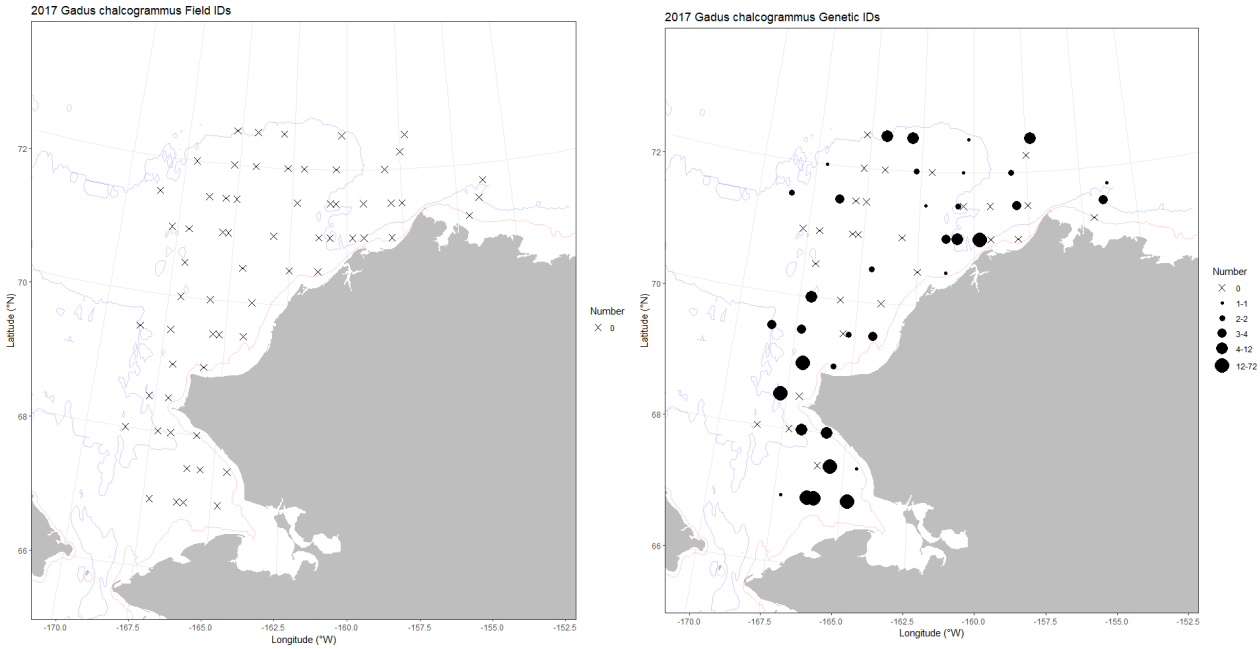

Figure 2a-b. At sea identification (a.) and genetic identification (b.) of *G. chalcogrammus* collected in the Chukchi Sea in 2017.

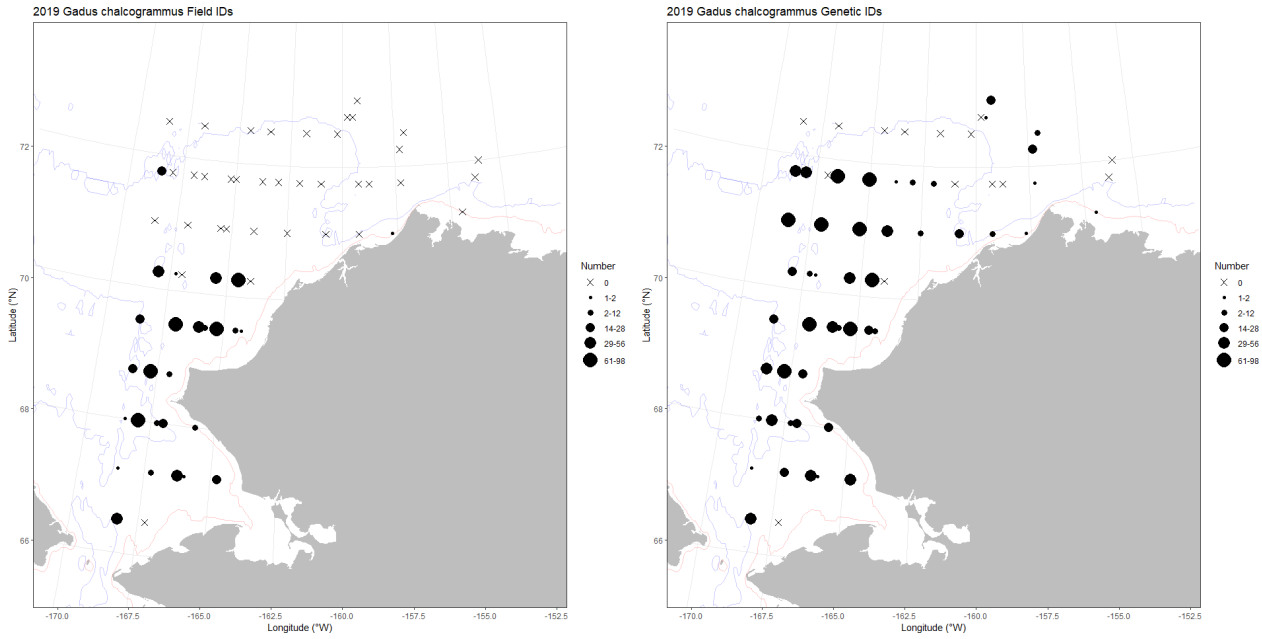

Figure 3a-b. At sea identification (a.) and genetic identification (b.) of *G. chalcogrammus* collected in the Chukchi Sea in 2019.

CHAPTER 5 - The effect of oceanographic variability on the distribution of larval fishes of the northern Bering and Chukchi seas

Objective 2: Quantify the distribution, abundance, and condition of pelagic marine fishes, in particular young-of-the-year Arctic gadids and other forage fishes

Logerwell, E.A., Busby, M., Mier, K.L., Tabisola, H., Duffy-Anderson, J., 2020. The effect of oceanographic variability on the distribution of larval fishes of the northern Bering and Chukchi seas. Deep Sea Res. Part II Top. Stud. Oceanogr. 104784. https://doi.org/10.1016/j.dsr2.2020.104784

Abstract

We investigated the pelagic habitat requirements of Arctic larval fish and the effects of interannual variability of ocean conditions on their distribution. We examined the distribution of larval Arctic cod, Bering flounder, yellowfin sole and capelin in the Chukchi and northern Bering seas during two years with different oceanographic conditions. We found that despite marked changes in water mass distribution, the distributions of larval fishes were not significantly different between the two years. In both years, Arctic cod and Bering flounder were found in cold, high salinity shelf waters advected from the south and influenced by winter cooling (Chukchi Winter Water and Anadyr Water mix). Yellowfin sole and capelin distributions were also similar from year-to-year but they were only found in warm, low salinity Alaska Coastal Water. The cold, high salinity water masses had elevated large copepod biomass, and the Alaska Coastal Water had elevated small copepod biomass. Thus, we propose that these water masses provided different but nonetheless potentially profitable foraging habitat for the four species of larval fishes. We conclude by suggesting that the timing and location of spawning of these species has evolved such that larval offspring are distributed in suitable foraging habitat despite interannual variability in ocean conditions. This study provides a baseline of Arctic larval fish distribution and insight into the degree of climate variability that might be expected to impact early life history stages of larval fish. Our results also increase the knowledge of the mechanistic links between oceanography and the early life history of fish. Because growth and survival of early life stages of fish often drives population change, our results contribute to the understanding of the impacts of climate change on Arctic fish populations.

Keywords: USA, Alaska, Chukchi Sea, Fish larvae, Climate changes, Polar waters, Habitat

Introduction

The Arctic climate is rapidly changing. Ocean temperatures have been warming at over two times the global rate since the mid-20th century (Huang et al., 2017). Sea ice extent, duration and thickness have been declining at an increasing pace (Kwok and Rothrock, 2009; Meier et al., 2012; Wang and Overland, 2015). Embedded within these long-term trends is a high degree of interannual variability in sea ice timing, duration, extent and thickness, as well as ocean temperature and currents (Day et al., 2013; Wang and Overland, 2015; Woodgate et al., 2015). It is not known with certainty how changes in Arctic climate will impact fish, although impacts are expected. Increased water temperatures may affect growth rates negatively or positively depending on the fish's optimum growth temperature and food availability (Björnsson et al., 2001; Laurel et al., 2015). Reductions in sea-ice extent may negatively impact fish that depend on sea ice for spawning, such as Arctic cod (Rass, 1968). On the other hand, an increase in the open water period due to loss of sea ice may result in increased primary production which could benefit fish feeding (Arrigo et al., 2008). The timing of spring season sea ice retreat is also an important factor. Earlier sea-ice retreat with ocean warming may change the timing

and intensity of the spring bloom of phytoplankton resulting in a reduction in productivity and/or a mismatch between the timing of larval first feeding and the availability of prey (Grebmeier, 2012). The survival of early life history stages of fish is generally thought to be an important determinant of variability in the abundance of subsequent older age classes (Hjort, 1914; Lasker, 1981). Furthermore, early life stages of fish are particularly sensitive to changes in their environment such as variability in transport to nursery habitat, exposure to predators and changes in food availability (e.g. Siddon et al., 2011). Thus, an understanding of the impacts of interannual variability and long-term climate trends on Arctic fish populations benefits from information on Arctic fish early life history.

Our work was part of the Arctic Ecosystem Integrated Survey (Arctic EIS), a University of Alaska College of Fisheries and Ocean Sciences program conducted in 2012 and 2013 to document physical and biological oceanography, zooplankton, ichthyoplankton, demersal fish and pelagic fish. The overarching goals of the program were to understand the environmental forcing that impacts northern Bering and Chukchi sea ecosystems and to predict the future effects of reduced sea ice and ocean warming on these ecosystems (Mueter et al., 2017). The goal of the work presented here was to study Arctic fish larval distributions and oceanographic habitat associations. The northern Bering and Chukchi seas are mostly shallow shelves (< 60 m depth) with currents typically flowing northward due to the difference in sea level between the Pacific and the Arctic (Aagaard et al., 2006). Local winds can slow the northward flow or even redirect the flow to the south or west, depending on the direction of the winds (Panteleev et al., 2010). Water masses in the northern Bering and Chukchi seas include warmer, fresher Alaska Coastal Water flowing along the eastern shore and Anadyr/Bering Summer Water flowing across the shelf with moderate temperatures and salinities (Fig. 1). The Anadyr/Bering Summer Water transforms to Chukchi Summer Water as it flows north over the Chukchi Sea shelf. Near-bottom cold and salty Bering and Chukchi Winter Waters are the result of previous winter cooling and are resident to each shelf area. Finally, Melt Water is colder, fresher water at the surface formed by melting of sea ice and in summer is only found in the northern Chukchi Sea (Danielson et al., 2017). These different water masses have different nutrient concentrations and productivity. The colder shelf and winter waters are typically nutrient-rich and productive whereas the Alaska Coastal Water is low in nutrients and productivity (Danielson et al., 2017; Springer and McRoy, 1993).

Atmospheric and oceanographic conditions observed during the Arctic EIS surveys were different between 2012 and 2013, leading to subsequent variations in water mass distribution (Danielson et al., 2017). Sea level pressure and the resulting wind fields strongly contrasted between years. In 2012, low pressure was centered over the northwestern Chukchi Sea resulting in the typical winds from the southwest. In 2013, zonally (longitudinally) elongated low pressure over the Bering Sea resulted in zonal winds from the east. Drifter and high-frequency radar data suggest that the result of these wind differences was that the freshwater core of the Alaska Coastal Current was mostly absent from the Northeast Chukchi Sea during 2013. These differences in winds and currents resulted in pronounced differences in the distribution of water masses. In 2012, Alaska Coastal Water was observed close to shore from the northern Bering Sea all the way to the Northeast Chukchi Sea (Point Barrow). In contrast, in 2013, Alaska Coastal Water was only observed as far north as Ledyard Bay in the Chukchi Sea; and it spread at least 100 km farther offshore in the Northern Bering Sea compared to 2012. Along with more extensive northerly distribution of Alaska Coastal Water in 2012 the Anadyr/Bering Summer Water/Chukchi Summer Water mix extended farther north in 2012 than in 2013. There were also interannual differences in temperature, salinity, nutrients and chlorophyll biomass (Danielson et al., 2017). Surface waters were warmer and near-bottom waters were less saline in 2013 than 2012. Macronutrients, particularly in surface waters, were also different between years: there was less surface nitrate, ammonium and phosphate in 2013 than in 2012, likely leading to nutrient limitation of phytoplankton growth in 2013. In fact, average integrated chlorophyll was lower in 2013 than in 2012

(Danielson et al. 2017). Sea-ice conditions in 2012 and 2013 were similar. Winter sea ice was relatively high but June sea-ice concentrations were below normal in both years.
To investigate the potential impact of interannual variability in water mass distribution, we compared the spatial distribution of fish larvae collected in the northern Bering and Chukchi seas in 2012 and 2013. Our expectation was that larvae would be distributed farther north in 2012, and farther offshore in 2013. We propose that this would be a result of spawning location and subsequent advection within the water masses. To understand larval fish habitat associations, we mapped the distribution of larvae relative to water mass and to explore the potential foraging value of water masses, we examined their biological characteristics in terms of chlorophyll and zooplankton biomass. We also mapped the distribution of eggs and compared larval length frequency distributions for clues about spawn timing and location. The overall goal of our research presented here is to define larval oceanographic habitat and to improve our understanding of the mechanisms and the magnitude of climate variability that impact Arctic fish early life history.

Methods

Ichthyoplankton and oceanographic data were collected at stations spaced 28 or 55 km apart, depending on location, over a survey grid that spanned the U.S. northeastern Bering Sea and Chukchi Sea shelves (157–170°W, 60–72°N, Fig. 2). Sampling occurred from 7 August – 24 September in both years, with a similar order of station occupations. Ichthyoplankton were collected at the primary stations (55-km spacing) and at the higher resolution stations (28-km) with a 60-cm bongo sampler fitted with two 0.505 mm mesh nets with detachable codends at 138 stations in 2012 and 143 stations in 2013. During all cruises, quantitative oblique tows were made to a maximum depth of 200 m (or to within 10 m of the substratum), resulting in vertically integrated estimates of larval fish abundance. The ship speed was monitored and adjusted (1.5 to 2.5 knots) throughout each tow to maintain a wire angle of 45° from the ship to the bongo net. The nets were equipped with a calibrated flow meter; therefore, catch rates were standardized to effort and converted to catch 10 m^{-2} of sea surface area (CPUE; number 10 m^{-2}). Sampling occurred during daylight hours as per ship protocol. Samples were preserved in 5% formaldehyde-sea water solution buffered with sodium borate.

Samples were sorted and fish eggs, larvae and juveniles identified to the lowest taxonomic level possible at the Plankton Sorting and Identification Center in Szczecin, Poland. Taxonomic identifications were verified at the Alaska Fisheries Science Center (AFSC) in Seattle, WA, following Matarese et al. (1989), Busby et al. (2017), and the Ichthyoplankton Information System (https://access.afsc.noaa.gov/ichthyo/). Some fish eggs and larvae were categorized as taxonomic groups (e.g. *Limanda* spp., *Liparis* spp.) due to limitations associated with identifying egg and larval stages to the species level. In the case of *Limanda* spp. eggs, *Limanda aspera* were by far the most common species of *Limanda* larvae, so we treated *Limanda* spp. eggs as *L. aspera* in the analyses. In some cases, identifications of damaged specimens were made at the family level. In these instances, the identifications were not included in counts of species richness or diversity because they were considered to be of taxa that could normally be successfully identified. Taxonomic nomenclature follows (Mecklenburg et al., 2018), except for Bering flounder (*Hippoglossoides robustus*) which, according to Mecklenburg et al. should now be classified as flathead sole (*Hippoglossoides elassadon*) in the Arctic. However, the American Fisheries Society (Page et al., 2013) still lists the occurrence of flathead sole as Pacific only, and Bering flounder as Pacific and Arctic. We defer to the latter source and use Bering flounder in this paper. We use Arctic cod for the common name of *Boreogadus saida* after Mecklenburg and Steinke (2015).

Fish were measured for standard length (SL) to the nearest 1.0 mm. The separation point between the larval and juvenile stages for *B. saida* is 25.0 mm standard length (SL) based on the size at transformation of *Gadus chalcogrammus* determined by Brown et al. (2001). For other taxa, definition

of the juvenile stage follows Kendall et al. (1984) as a fish having complete adult complements of fin elements, scales and "the appearance of a small adult". The only taxa for which we caught juveniles was *B. saida*. Macro- and mesozooplankton were also collected with the 60-cm bongo frame (505 um mesh). Meso- and microzooplankton were sampled with a 20-cm PairVet net with 150 µm mesh attached to the array with the 60-cm frame. PairVet samples were only analyzed for the 2012 cruise, due to loss of data sheets at sea during 2013. All samples were preserved in 5% formalin, buffered with seawater for later processing. In the laboratory, each net sample was subsampled and taxa were identified, staged, counted and weighed. All animals in the samples were identified to the lowest taxonomic category possible. Sibling species *Calanus marshallae* and *C. glacialis* co-occurring in the Bering and Chukchi seas (e.g. Nelson et al., 2009) were not discriminated and are named as *C. glacialis* hereafter. Recent studies confirm that the vast majority of *Calanus* spp. in the northern Bering Sea are *C. glacialis* (Campbell et al., 2014). Copepodites stages were identified and recorded. Biomass values by station were computed for each species in grams m^{-3}. See Pinchuk and Eisner (2016) for details of zooplankton sampling and laboratory analyses. At the primary stations (55-km spaced), ocean temperature and salinity were determined from conductivity-temperature-depth measurements collected with a Sea-Bird (SBE) 911 or SBE 25 CTD equipped with a Wetlabs Wet-Star fluorimeter to estimate in vivo Chl*a*. In addition, a SBE 49 or SBR19+ CTD was towed with the bongo net to obtain hydrographic data at higher spatial resolution (between primary stations). At the primary stations, water samples for total Chl*a* were collected at ~10 m depth intervals.

Danielson et al. (2017) identified four different bottom water masses-based on T/S diagrams derived from the survey oceanographic data: Alaska Coastal Water (ACW), Anadyr Water/Bering Shelf Water/Chukchi Shelf Water (AW Mix), Bering Winter Water (BWW) and Chukchi Winter Water (CWW). ACW was the warmest and freshest (7 – 12 °C; 20 – 32 salinity). CWW and BWW were the coldest and most saline (-2.0 to 0 °C; 30 – 33.5 salinity). The AW Mix was intermediate in temperature and high in salinity (0 – 7 °C; 30-33.5 salinity). Surface water masses were: Melt Water, which was relatively cool and fresh (-2 – 7 °C; 25 – 30 salinity); and AW Mix and ACW (as defined above). Ichthyoplankton distributions were overlaid on water mass distributions using ArcMap 10.5 (ver 10.5.0.6491).

A statistical test based on a generalized two-sample Cramér-von Mises test was employed to test for differences between the spatial distributions of ichthyoplankton between years (Syrjala, 1996). The null hypothesis for this specific test is that across the study area, the distributions of the populations are the same. The alternative hypothesis for this test is that there is some unspecified difference in the underlying distributions. The distributions are normalized so the test is sensitive to differences in the way populations are distributed across space, but insensitive to differences in abundance. The test is nonparametric, so no assumptions are required about the distributions of the populations. The test was implemented in R version 3.3.2 (R Core Team, 2016) using the "syrjala" function. The Kruskal-Wallis rank sum test was employed to test for differences in chlorophyll and zooplankton biomass density among water masses. A non-parametric test was used because the skewed distributions and heterogeneity of variances could not be remedied by data transformation. The test was implemented in R version 3.3.2 (R Core Team 2016).

Results

A total of 1057 individuals and 31 taxa of larvae and juveniles were sampled by the ichthyoplankton nets in 2012 and 2013 (Table 1). The four most abundant taxa collected were Pacific capelin (*Mallotus catervarius*), Arctic cod (*Boreogadus saida*), Bering flounder (*Hippoglossoides robustus*) and yellowfin sole (*Limanda aspera*). These four taxa were the focus of further analysis. Juvenile fish caught in the nets were all Arctic cod. Eggs of only 5 taxa were caught, mostly Bering flounder and yellowfin sole. Walleye pollock (*Gadus chalcogrammus*) eggs were only caught in the northern Bering Sea.

Bering flounder eggs were distributed in the north Chukchi Sea over the shelf during 2012 (Fig. 3 a). Very few eggs were caught in 2013, but they were found in a similar area as in 2012 (Fig. 3 b). In contrast, yellowfin sole eggs were found farther south, in the northern Bering Sea, and in the south/central Chukchi Sea, and relatively close to shore compared to Bering flounder (Fig. 4). No eggs of either Arctic cod or Pacific capelin were caught during the surveys.

Arctic cod larvae and juveniles were distributed in the north and northeast area of the survey in both years (Fig. 5a, b.). Arctic cod were the only taxa for which we caught juvenile fish. The distributions of the two life stages overlapped, such that for further analyses, we combined the data. The Cramer von-Mises test indicated that there was not enough evidence to support a statistically significant difference in the distribution of Arctic cod between years (ψ=3.233, P=0.165). Bering flounder larvae were distributed throughout the Chukchi Sea, and in the northern Bering Sea (Fig. 5b, c). The catch density of Bering flounder in 2013 was much less than 2012. Similar to Arctic cod, the Cramer von-Mises test indicated that there was not enough evidence to support a statistically significant difference in the distributions between 2012 and 2013 (ψ=1.498, P=0.767).

Yellowfin sole and capelin larvae had more southerly distributions than Arctic cod and Bering flounder (Fig. 6). Similar to the other two taxa, there was no statistically significant difference in the distributions between 2012 and 2013 (yellowfin sole: ψ=3.216, P=0.065; capelin: ψ=2.462, P=0.779).

Flatfish larval length-frequency distributions were examined along with their egg distributions (reported above) for information on spawning locations that could explain the distribution of larvae. No eggs of either Arctic cod or capelin were caught. Bering flounder larvae distribution was discontinuous around 70°N in 2012 (Fig. 5c). Very few larvae were caught in 2013. There was little overlap in the length-frequency distributions north and south of 70°N (Fig. 7) – larvae were smaller north of 70°N and larger south. Yellowfin sole larvae distribution was discontinuous at around 65.5°N (Fig. 6a, b). However, in contrast with Bering flounder, the length- frequency distributions of yellowfin sole larvae were similar north and south of 65.5°N in both years (Fig. 8).

Overlaying the distribution of ichthyoplankton on bottom water masses shows that Arctic cod were only present in the CWW and AW Mix in both years (Fig. 5a, b). Similarly, Bering flounder were most abundant in the CWW and AW Mix (Fig. 5c, d). The relatively northerly extension of the AW Mix and ACW in 2012, reported by Danielson et al. (2017), is also evident. The distributions of yellowfin sole and capelin (Fig. 6) are shown overlaid on surface water mass distributions because there was spatial coherence between larvae and both bottom and surface ACW and the oceanographic signal of ACW was more pronounced in surface waters. BWW and CWW were not evident in surface waters (Fig. 6), only in waters at depth (Fig. 5). The ichthyoplankton tows were not depth-discrete, so it is unknown at which depths the larvae occurred. Yellowfin sole and capelin were distributed in the southern two-thirds of the study area and were virtually restricted to ACW in both years (Fig. 6), in contrast to the more northerly Arctic cod and Bering flounder, which occurred in the cold, high salinity water masses as described above.

The difference in integrated chlorophyll biomass among water masses was statistically significant in 2012 (Kruskal-Wallis Chi-squared = 12.085, p-value = 0.002), but not in 2013 (Kruskal-Wallis Chi-squared = 3.4023, p-value = 0.182) (Fig. 9 a, b). Post-hoc tests showed that chlorophyll biomass was significantly greater in ACW compared to CWW and greater in AW Mix compared to CWW in 2012 (Fig 9 a). There was no significant difference in chlorophyll biomass between ACW and AWMix. Post-hoc tests comparing BWW with other water masses were not conducted, because BWW was only observed at one station (n=1).

The difference in *Calanus glacialis* biomass density among all water masses was significant in 2012 (Kruskal-Wallis Chi-squared = 25.724, p-value <0.001), and marginally significant in 2013 (Kruskal-Wallis Chi-squared = 4.5013, p-value = 0.10) (Fig. 9 c, d). Post-hoc tests showed that *Calanus glacialis* biomass density was significantly greater in AW Mix than ACW in both years; and significantly greater in CWW than ACW in 2012. The smaller-sized stages of *Calanus glacialis* copepodites (C2 and C3) were proportionally most abundant in CWW in 2012 (Fig. 10) and even more so in 2013 (Fig. 11). C2 stages were only found in CWW in both years.

In contrast to *Calanus glacialis,* the biomass density of nauplii and smaller taxa of copepods (sampled with the PairVet net) was similar or higher in ACW compared to the other water masses in 2012. The PairVet net samples collected in 2013 were not analyzed due to loss of data sheets at sea. Calanoida nauplii biomass density was significantly different among water masses (Fig. 12 a; Kruskal-Wallis Chi-squared = 8.1041, p- value < 0.05). Post-hoc tests showed that nauplii biomass density was significantly greater in ACW compared to AW Mix. *Pseudocalanus* spp. biomass density was not significantly different among water masses (Fig. 12 b; Kruskal- Wallis Chi-squared = 1.8085, p-value = 0.40). *Acartia* spp. and *Oithona* spp. biomass densities were significantly different among water masses (*Acartia*: Kruskal-Wallis Chi-squared = 34.34, p-value <0.001. *Oithona*: Kruskal-Wallis Chi-squared = 32.5, p-value < 0.001) (Fig 12 c, d). Post-hoc tests showed that *Acartia* and *Oithona* biomass densities were greater in ACW compared to AW Mix and compared to CWW. *Oithona* biomass density was also significantly greater in AW Mix compared to CWW.

In summary, Arctic cod and Bering flounder were most abundant in cold, high salinity water masses (AW Mix and CWW), which had elevated large copepod (*Calanus glacialis*) biomass density compared to Alaska Coastal Water. In contrast, yellowfin sole and capelin were only found in warm, low salinity Alaska Coastal Water that was high in Calanoida nauplii and small copepod biomass density (*Acartia* spp. and *Oithona* spp.) compared to the cold, high salinity water masses (AW Mix and CWW).

Discussion

Arctic cod, Bering flounder, yellowfin sole and capelin were the four most abundant species in the ichthyoplankton catch during the 2012 and 2013 Arctic EIS surveys. Previous ichthyoplankton surveys have caught a similar mix of species (Busby et al., in review; Norcross et al., 2010; Randall et al., 2019; Wyllie-Echeverria et al., 1997), although Randall et al. (2019) also caught relatively high numbers of Arctic sand lance (*Ammodytes hexapterus*) and Arctic shanny (*Stichaeus punctatus*); and Busby et al. (in review) caught relatively high numbers of snailfish (*Liparis gibbus*). Arctic cod and capelin are important energy-rich prey for upper trophic level predators (Hop and Gjøsæter, 2013). Arctic cod are consumed by beluga whales (*Delphinapterus leucas*), ringed seals (*Pusa hispida*), bearded seals (*Erignathus barbatus*), harp seals (*Pagophilus groenlandicus*), black guillemot (*Cepphus grylle*) and thick-billed murres (*Uria lomvia*) (Bradstreet, 1976; Bradstreet et al., 1986; Bradstreet and Cross, 1982; Huntington and The communities of Buckland, Elim, Koyuk, Point Lay, 1999).

Alaska Arctic communities on the Chukchi Sea coast rely on many of these marine mammal species for subsistence use (Hovelsrud et al., 2008; Huntington and The communities of Buckland, Elim, Koyuk, Point Lay, 1999). Capelin are preyed upon by mammal, bird and fish predators such as harp seals (Stenson et al., 1997), thick-billed murres (Provencher et al., 2012) and Atlantic cod (Mehl and Sunnana, 1991; Rose and O'Driscoll, 2002). Flatfishes are also important subsistence and ecological resources in the Arctic (Grebmeier et al., 2006a). Furthermore, yellowfin sole is one of the most abundant flatfish species in the eastern Bering Sea and currently is the target of the largest flatfish fishery in the world (Wilderbuer et al., 2017).

There were no statistically significant differences between 2012 and 2013 in the distributions of Arctic cod, Bering flounder, yellowfin sole and capelin larvae. This was observed despite wind-driven changes in water mass distribution between 2012 and 2013 (Danielson et al., 2017). We expected that larvae would be distributed less far north and further offshore in 2013 due to the reduced northerly extension of the Alaska Coastal Water and Anadyr Water Mix; and the offshore spread of Alaska Coastal Water. We did observe fewer Bering flounder larvae in 2013 compared to 2012. Perhaps the lower nutrient concentration and phytoplankton biomass observed in 2013 (Danielson et al., 2017) reduced the magnitude or delayed the timing of Bering flounder spawning and/or negatively impacted the survival of early larvae. The larval densities of the three other species were similar during the two years.
In both years, Arctic cod and Bering flounder larvae were found in cold water masses that we suggest provided good foraging opportunities. Arctic cod were only found in the northern third of the survey area in the Anadyr Water/Bering Shelf Water/Chukchi Shelf Water Mix (AW Mix) and Chukchi Winter Water (CWW). Bering flounder were similarly virtually restricted to these two cold and high salinity water masses. We suggest that the association of larval fish with particular water masses is the result of spawning location and subsequent entrainment of eggs and larvae in the currents that are associated with the water masses. Arctic cod spawn under the ice in late winter. Eggs are buoyant and develop near the surface, beginning under the ice cover and ending near the surface in ice-free areas after melting of the ice cover (Rass, 1968). Bering flounder spawn from April to June on the Bering and Chukchi sea shelves (Stark, 2004). It is not surprising that Arctic cod larvae are found in the north, given that they spawn under the ice in late winter. In addition, Arctic cod and Bering flounder were not found in Alaska Coastal Water which was expected given that they spawn in shelf waters.

AW Mix is formed from Bering Shelf Water, Chukchi Shelf Water and Anadyr Water. Anadyr Water is cold, saline and nutrient-rich that is delivered across the Gulf of Anadyr to the Bering Strait. This exogenous nutrient supply fuels much of the summer production on the Chukchi Sea shelf (Danielson et al., 2017). The two other components of the AW Mix, Bering Shelf Water and Chukchi Shelf Water, are cold and saline because of cycles of freezing, brine rejection and then summer warming (Danielson et al., 2017). Chukchi Winter Water (CWW) is the cold remnant of the previous winter's heat loss (Danielson et al., 2017). We found that these two cold water masses (AW Mix and CWW) had elevated large copepod (*Calanus glacialis*) biomass, compared to the warmer, fresher Alaska Coastal Water (ACW). The smallest stages of *Calanus* (C2) were proportionally most abundant in CWW.
Published information about the diets of larval Arctic cod supports the idea that the colder water masses were good foraging areas. We caught Arctic cod larvae from 10 mm to 55 mm SL, spanning flexion larvae to post-flexion larvae to juvenile stages (Ponomarenko, 2000). Arctic cod flexion larvae sampled from the Canadian Beaufort Sea consumed copepod nauplii and C1-C2 *Calanus glacialis* copepodites. Post-flexion larvae consumed copepod nauplii, *Pseudocalanus* spp. and C1-C2 *Calanus glacialis* copepodites. Arctic cod juveniles (26-55 mm length) consumed C2-C4 *Calanus glacialis* copepodites (Walkusz et al., 2011). No Arctic cod larval diet data are available for the Chukchi Sea, but if larval diets are comparable across adjacent seas, then the AW Mix and CWW could be hypothesized to be good foraging areas for Arctic cod larvae in the Chukchi Sea.

There is no published information on larval Bering flounder diets. In a review of latitudinal and taxonomic patterns in larval feeding ecology, Llopiz (2013) found that 85% of the diet of flatfish (Order: Pleuronectiformes) was comprised of appendicularians, nauplii, and calanoids. Other studies of specific flatfish taxa showed similar results. American plaice (*Hippoglossoides platessoides*) and Yellowtail flounder (*Limanda ferruginea*) relied on nauplii and copepodites of *Pseudocalanus*, *Oithona similis* and *Temora longicornis* (Pepin and Penney, 1997). Copepods (*Copepoda*) have been found to make up 88% to 99% of the total gut contents of Greenland halibut (*Rheinhardtius hippoglossoides*) (Simonsen et al., 2006). Bering flounder likely consume smaller prey than Arctic cod, however the colder water masses could provide sufficient biomass of some smaller prey taxa such as *Pseudocalanus* spp. and C2 stages of *Calanus glacialis*.

Advection and the timing of seasonal sea-ice retreat contribute to the formation and productivity of the cold, high salinity water masses (AW Mix and CWW), which we suggest are good foraging habitat for Arctic cod and Bering flounder. Advection through the Bering Strait brings nutrients and plankton-rich Pacific Ocean water into the Chukchi Sea, across the shelf and through Barrow Canyon (Pickart et al., 2005; Woodgate et al., 2015). The seasonal sea-ice zone provides ice algae and early stabilization of the water column by melting ice, which initiates a spring bloom of phytoplankton. Both of these features, advection and sea ice retreat, have been shown to be impacted by global climate change. Ocean warming has resulted in reduction in seasonal sea-ice extent and earlier sea-ice retreat (Frey et al., 2014; Grebmeier et al., 2006b). This change in timing of ice break up means that although ice melt still stabilizes the water column, sunlight is not sufficient to initiate an intense spring bloom (Clement, 2004), suggesting a lowering of overall primary production. Alternatively, earlier sea-ice breakup could result in increased primary production due to a longer growing season, as has been observed in the Arctic Ocean (Arrigo et al., 2008). The second process of interest here, advection through the Bering Strait, has increased by almost 50% from 2001 to the present (Woodgate et al., 2015). A larger-scale analysis of flow patterns from 1979 to 2014 shows, in contrast, that there was slightly less poleward advection across the Chukchi Sea shelf since the turn of the century (Bond et al., 2018). Although the present study from two years' surveys suggests some potential mechanisms, further research over multiple years and over a broader study area is needed to confirm how the dynamics of advection and sea-ice retreat impact the habitat of larval fishes.

In contrast to Arctic cod and Bering flounder, yellowfin sole and capelin larvae were found more towards the south and exclusively in nearshore Alaska Coastal Water (ACW) in both years. Yellowfin sole spawn in June and July in nearshore waters (Nichol and Acuna, 2001), and capelin spawn in summer on beaches (Frost and Lowry, 1987). So it is perhaps not surprising that the larvae of both species would be entrained in the ACW. Alaska Coastal Water was the warmest and freshest water observed in the survey, and it is typically low in nutrients, chlorophyll-*a* and phytoplankton productivity after the spring bloom of phytoplankton and associated nutrient depletion (Springer and McRoy, 1993). We observed reduced large copepod (*Calanus glacialis*) biomass in ACW during our surveys. However, copepod nauplii and small copepod biomass (*Acartia* spp. and *Oithona* spp.) were relatively high, compared to the other water masses.

Due to a paucity of relevant published diet information, it is difficult to assess whether ACW could be good foraging habitat for larval yellowfin sole and capelin. There are no published diet data for yellowfin sole larvae. The larval diets of a related species, common dab (*Limanda limanda*) collected in the southern North Sea, were comprised mainly of nauplii and copepodites of the copepod *Temora longicornis* (Last, 1978). Yellowtail flounder (*Limanda ferruginea*) caught off the coast of Newfoundland similarly relied on nauplii and copepodites of *Pseudocalanus*, *Oithona similis* and *Temora longicornis* (Pepin and Penney, 1997). There are no studies of capelin diets in the Pacific arctic or subarctic. Studies of capelin diets in the Barents and Norwegian seas showed that larvae were feeding on *Calanus* eggs and nauplii (Bjorke, 1976; Karamushko and Reshetnikov, 1994). Capelin diets off the coast of Newfoundland were comprised of nauplii and copepodites of *Pseudocalanus*, *Oithona similis* and *Temora longicornis* (Pepin and Penney, 1997). Other forage fish taxa, such as Pacific herring (*Clupea harengus*) and sandlance (*Ammodytes* spp.) similarly consume copepod nauplii and copepodites, including *Acartia* spp. (Fortier et al., 1995; Robert et al., 2013). If copepod nauplii and small copepods such as *Acartia* and *Oithona* are suitable prey for yellowfin sole and capelin larvae in the Chukchi Sea and Northern Bering Sea, then the ACW could provide good foraging habitat. Previous ichthyoplankton surveys of the Chukchi Sea have made similar conclusions about the distribution of Arctic fish larvae in relation to water masses. Surveys in 1990-1991 (Wyllie-Echeverria et al., 1997) and in 2004 (Norcross et al., 2010) found Arctic cod in cold offshore water and yellowfin sole in nearshore ACW. Wyllie-Echeverria et al. (1997) also found capelin in ACW; Norcross et al. (2010) did not catch any capelin in 2004. One conflict among these results is that Norcross et al. (2010)

found Bering flounder larvae in cold offshore waters, similar to what we observed, but Wyllie-Echeverria et al. (1997) showed Bering flounder associated with ACW. Randall et al. (2019) documented species assemblages of ichthyoplankton during marine mammal and plankton surveys in 2010-2015 and found interannual associations between communities and the dominant water masses similar to our results. For instance, in years where ACW occupied more of the study area, the ichthyofauna was characterized by a yellowfin sole-driven community. In years when there was more cold water on the shelf, a community typified by Arctic cod was present at most stations.
The distribution and large size of Arctic cod larvae was expected given what is known about the timing and location of Arctic cod spawning. The transport pathways between Arctic cod hatching locations and larval distributions have been investigated using a biophysical transport model that simulates larval growth and dispersal (Vestfals et al., in prep). The results of this modeling effort indicate that Arctic cod larvae caught during the Arctic EIS surveys were likely spawned in the northern Bering Sea or southern Chukchi Sea in winter and then transported to the north by late summer.

Flatfish larvae in the Chukchi Sea could have resulted from local (Chukchi Sea) or remote (Bering Sea) spawning. Our data on egg distributions and larval length-frequency patterns provided clues about flatfish spawning areas. Bering flounder eggs were caught in the northern Chukchi Sea and there was an aggregation of larvae in the same area. There were also Bering flounder larvae in the southern Chukchi Sea and northern Bering Sea, but no eggs were found in those areas. The length-frequency distributions of the northern versus the southern Bering flounder larvae were different. The larvae to the north were smaller, consistent with later spawning and/or slower larval growth rates. The larvae to the south were larger, consistent with earlier spawning and/or faster growth rates. These patterns in egg distribution and larval length-frequencies could indicate that Bering flounder larvae in the northern Chukchi Sea were spawned locally, in the northern Chukchi Sea, later than flounder to the south and in colder water resulting in slower growth and smaller size. In contrast, larvae in the southern Chukchi Sea could have been spawned to the south in the Bering Sea earlier and in warmer water resulting in faster growth rate, and were then transported north, in the Bering Shelf and/or Anadyr Current. It is unlikely that larvae in the south were advected from the north where we caught eggs because this is in the opposite direction of the prevailing currents. An alternative mechanism is that Bering flounder larvae in the southern Chukchi Sea were spawned locally, but sufficiently earlier that eggs were no longer present when that area was surveyed.

Yellowfin sole eggs were found throughout the survey area and larval length-frequency distributions were similar to the north and south. This is consistent with local spawning of yellowfin sole larvae in the southern Chukchi Sea and northern Bering Sea at the same time of year. An alternative mechanism is that yellowfin sole spawning only occurred in the southern Bering Sea and their eggs and larvae were transported to the northern Bering Sea and Chukchi Sea in the Alaska Coastal Current.
Currents across the Chukchi Sea shelf are slow, on average, around 5 cm s^{-1} (Stabeno et al., 2018; Weingartner et al., 2005; Woodgate et al., 2005), such that it is less likely that larval flatfish found in the Chukchi Sea were transported from the south. At 5 cm s^{-1} (4.32 km day^{-1}), it would take an egg or larvae 179 days to transit the 777 km from the Bering Strait to the northernmost station in the survey. Pelagic durations of flatfish larvae are less than that transit time, on the order of 30-60 days for yellowfin sole in the Gulf of Alaska, and 30-120 days for *Hippoglossoides platessoides* (American plaice) in the North Atlantic (Duffy-Anderson et al., 2015). Randall et al. (2019), analyzing data from a collection of other ichthyoplankton surveys conducted in 2010-2015 as part of marine mammal studies (CHAOZ and ArcWest), similarly concluded that Bering flounder in the Chukchi Sea were likely to have been spawned locally.

Conclusions

The distributions of Arctic fish larvae were not statistically different between 2012 and 2013 despite the differences in water mass distribution between the two years. Larvae of Arctic cod, Bering flounder, yellowfin sole and capelin were found in similar locations in both years and were associated with water masses that had elevated biomass of zooplankton taxa that could potentially have been prey. We suggest that the distribution of larvae is a product of spawning behavior that results in the larvae being located in habitat suitable for successful foraging even as oceanographic processes vary from year-to-year. In other words, Arctic fishes have evolved spawn timing and location such that larval distributions are resilient to the degree of interannual climate variability observed between 2012 and 2013. Biophysical transport models such as Vestfals, et al. (in prep) can demonstrate the advective connections between spawning location and larval distribution and can be used to explore this hypothesis. This study describes the habitat for larval Arctic cod, Bering flounder, capelin and yellowfin sole and provides baseline information on their early life history. Understanding the associations between larval oceanographic habitat and spawning-related resilience helps us to better understand the mechanisms and the degree of oceanographic change due to ocean warming and loss of sea ice which may have the potential to impact the early life histories of Arctic fishes.

Acknowledgments

We thank the captain and crew of the FV *Bristol Explorer*, and all of the Arctic EIS scientists who helped carry this program forward, particularly Franz Mueter and Jared Weems. Thanks also to the Bureau of Ocean and Energy Management program manager Catherine Coon. Thank you to C. Ladd and C. Vestfals for reviews of earlier drafts of this manuscript and to two anonymous reviewers and the editor for journal review. This is Eco-FOCI contribution #0920. Reference to trade names does not imply endorsement by the National Marine Fisheries Service, NOAA.

Funding: This work was supported by the Coastal Impact Assistance Program (AKDNR/USFWS), the University of Alaska Fairbanks [10-CIAP-010 and F12AF00188], Bureau of Ocean Energy Management and the University of Alaska Fairbanks [M12AC00009].

This manuscript builds on research associated with the North Pacific Research Board Arctic (NPRB) Integrated Ecosystem Research Program and is NPRB publication ArcticIERP-11.

References

Aagaard, K., Weingartner, T.J., Danielson, S.L., Woodgate, R.A., Johnson, G.C., Whitledge, T.E., 2006. Some controls on flow and salinity in Bering Strait. Geophys. Res. Lett. 33, 1–5. https://doi.org/10.1029/2006GL026612

Arrigo, K.R., van Dijken, G., Pabi, S., 2008. Impact of a shrinking Arctic ice cover on marine primary production. Geophys. Res. Lett. 35, 1–6. https://doi.org/10.1029/2008GL035028

Bjorke, H., 1976. Some preliminary results on food and feeding of young capelin larvae. ICES Counc. Meet. 1976/H 37.

Björnsson, B., Steinarsson, A., Oddgeirsson, M., 2001. Optimal temperature for growth and feed conversion of immature cod (Gadus morhua L.). ICES J. Mar. Sci. 58, 29–38. https://doi.org/10.1006/jmsc.2000.0986

Bond, N., Stabeno, P., Napp, J., 2018. Flow patterns in the Chukchi Sea based on an ocean reanalysis, June through October 1979–2014. Deep. Res. Part II Top. Stud. Oceanogr. 152, 35–47. https://doi.org/10.1016/j.dsr2.2018.02.009

Bradstreet, M.S.W., 1976. Summer feeding ecology of seabirds in eastern Lancaster Sound, 1976. Report, LGL Ltd. Toronto.

Bradstreet, M.S.W., Cross, W.E., 1982. Trophic relationships at high Arctic ice edges. Arctic 35, 1–12.

Bradstreet, M.S.W., Finley, K.J., Sekerak, A.D., Griffiths, W.B., Evans, C.R., Fabijan, F.F., Stallard, H.E., 1986. Aspects of the biology of Arctic cod (*Boreogadus saida*) in Arctic marine food chains. Can. Tech. Rep. Fish. Aquat. Sci. 1491.

Brown, A.L., Busby, M.S., Mier, K.L., 2001. Walleye pollock *Theragra chalcogramma* during transformation from the larval to juvenile stage: otolith and osteological development. Mar. Biol. 139, 845–851. https://doi.org/10.1007/s002270100641

Busby, M.S., Holladay, B.A., Mier, K.L., and Norcross, B.L., in reviw. Ichthyoplankton of the Chukchi Sea 2004-2012: Russian-American Long-term Census of the Arctic. Polar Biol.

Busby, M. S., Blood, D. M., Matarese, A. C. 2017. Identification of larvae of three Arctic species of Limanda (Family Pleuronectidae). Polar Biol. 40, 2411–2427. doi.org/10.1007/s00300-017-2153-9

Campbell, R.G., Gelfman, C., Dennis, M., McCoy, I., and Ashjian, C.J., 2014. Population genetics of the *Calanus glacialis/marshallae* species complex in the Bering and Western Arctic seas. in: Proceedings of the Ocean Sciences Meeting. Honolulu, Hawaii, USA, 23-28 February.

Clement, J.L., 2004. Late winter water column and sea ice conditions in the northern Bering Sea. J. Geophys. Res. 109, 1–16. https://doi.org/10.1029/2003JC002047

Danielson, S.L., Eisner, L., Ladd, C., Mordy, C., Sousa, L., Weingartner, T.J., 2017. A comparison between late summer 2012 and 2013 water masses, macronutrients, and phytoplankton standing crops in the northern Bering and Chukchi Seas. Deep Sea Res. II 135, 7–26.

Day, R.H., Weingartner, T.J., Hopcroft, R.R., Aerts, L. A. M., Blanchard, A.L., Gall, A.E., Gallaway, B.J., Hannay, D.E., Holladay, B. a., Mathis, J.T., Norcross, B.L., Questel, J.M., Wisdom, S.S., 2013. The offshore northeastern Chukchi Sea, Alaska: A complex high-latitude ecosystem. Cont. Shelf Res. 67, 147–165. https://doi.org/10.1016/j.csr.2013.02.002

Duffy-Anderson, J.T., Bailey, K.M., Cabral, H.N., Nakata, H., Van Der Veer, H.W., 2015. The planktonic stages of flatfishes: Physical and biological interactions in transport processes, in: Gibson, R.N., Nash, R.D.M., Geffen, A.J. and Van der Veer, H.W. (Eds.), Flatfishes: Biology and Exploitation: Second Edition. pp. 132–170. https://doi.org/10.1002/9781118501153.ch6

Fortier, L., Ponton, D., Gilbert, M., 1995. The match/mismatch hypothesis and the feeding success of fish larvae in ice-covered southeastern Hudson Bay. Mar. Ecol. Prog. Ser. 120, 11–27. https://doi.org/10.3354/meps120011

Frey, K.E., Maslanik, J.A., Kinney, J.C., Maslowski, W., 2014. Recent variability in sea ice cover, age, and thickness in the Pacific Arctic region, in: Grebmeier, J.M., Maslowski, W. (Eds.), The Pacific Arctic Region: Ecosystem Status and Trends in a Rapidly Changing Environment. Springer-Verlag, Dordrecht, pp. 31–64.

Frost, K.J., Lowry, L.F., 1987. Marine mammals and forage fishes in the southeastern Bering Sea, in: Conference Proceedings of Forage Fishes of the Southeastern Bering Sea. 4-5 November 1986, Anchorage, AK. Prepared for U.S. Department of the Interior, Mineral Management Service, Alaska OCS Region. pp. 11–18.

Grebmeier, J.M., 2012. Shifting patterns of life in the Pacific Arctic and Sub-Arctic Seas. Annu. Rev. Mar. Sci. Vol 44, 63–78. https://doi.org/10.1146/annurev-marine-120710-100926

Grebmeier, J.M., Cooper, L.W., Feder, H.M., Sirenko, B.I., 2006a. Ecosystem dynamics of the Pacific-influenced Northern Bering and Chukchi Seas in the Amerasian Arctic. Prog. Oceanogr. 71, 331–361. https://doi.org/10.1016/j.pocean.2006.10.001

Grebmeier, J.M., Overland, J.E., Moore, S.E., Farley, E. V, Carmack, E.C., Cooper, L.W., Frey, K.E., Helle, J.H., McLaughlin, F.A., McNutt, S.L., 2006b. A major ecosystem shift in the northern Bering Sea. Science (80-.). 311, 1461–1646.

Hjort, J., 1914. Fluctuation in the great fisheries of northern Europe. Rapp. Proc.-Verb. des Reun. Cons. Int. Explor. Mer. 20, 1–228.

Hop, H., Gjøsæter, H., 2013. Polar cod (*Boreogadus saida*) and capelin (*Mallotus villosus*) as key species in marine food webs of the Arctic and the Barents Sea. Mar. Biol. Res. 9, 878–894. https://doi.org/10.1080/17451000.2013.775458
Hovelsrud, G., McKenna, M., Huntington, H.P., 2008. Marine mammal harvests and other interactions with humans. Ecol. Appl. 18, 135–147.
Huang, J., Zhang, X., Zhang, Q., Lin, Y., Hao, M., Luo, Y., Zhao, Z., Yao, Y., Chen, X., Wang, L., Nie, S., Yin, Y., and Xu, Y., 2017. Recently amplified arctic warming has contributed to a continual global warming trend. Nat. Clim. Chang. 7, 875–880. https://doi.org/10.1038/s41558-017- 0009-5
Huntington, H.P., The communities of Buckland, Elim, Koyuk, Point Lay, and S., 1999. Traditional knowledge of the ecology of beluga whales (*Delphinapterus leucas*) in the Eastern Chukchi and Northern Bering Seas, Alaska. Arctic 52, 49–61.
Karamushko, O., Reshetnikov, Y., 1994. Daily Rations of larval capelin , *Mallotus villosus villosus*, and cod , *Gadus morhua morhua* , in the Barents and Norwegian Seas. J. Ichthyol. 34, 112–127.
Kendall, A.W., Ahlstrom, E.H., Moser, H.G., 1984. Early life history stages and their characters, in: Moser, H.G., Richards, W.J., Cohen, D.M., Fahay, M.P., Kendall, A.W., Richardson, S.L. (Eds.), Ontogeny and Systematics of Fishes - Ahlstrom Symposium, 15-18 August, 1983, La Jolla, CA. Am Soc Ich Herpetol Special Publ 1. Am Soc Ich Herpetol Special Publ 1, pp. 11–22.
Kwok, R., Rothrock, D.A., 2009. Decline in Arctic sea ice thickness from submarine and ICESat records: 1958-2008. Geophys. Res. Lett. 36, 1–5. https://doi.org/10.1029/2009GL039035
Lasker, R., 1981. Factors contributing to variable recruitment of the Northern Anchovy (*Engraulis mordax*) in the California current: contrasting years, 1975 through 1978. Rapp. P.-V. Reun. Cons. int. Mer 178, 375–388.
Last, J.M., 1978. The food of four species of pleuronectiform larvae in the eastern English Channel and southern North Sea. Mar. Biol. 45, 359–368.
Laurel, B.J., Spencer, M., Iseri, P., Copeman, L.A., 2015. Temperature-dependent growth and behavior of juvenile Arctic cod (*Boreogadus saida*) and co-occurring North Pacific gadids. Polar Biol. https://doi.org/10.1007/s00300-015-1761-5
Llopiz, J.K., 2013. Latitudinal and taxonomic patterns in the feeding ecologies of fish larvae : A literature synthesis. J. Mar. Syst. 109–110, 69–77. https://doi.org/10.1016/j.jmarsys.2012.05.002
Matarese, A. C., Kendall Jr., A. W., Blood, D. M., Vinter, B. M., 1989. Laboratory guide to early life history stages of northeast Pacific fishes. In NOAA Technical Report NMFS (Vol. 80).
Mecklenburg, C., Lynghammar, A., Johannesen, E., Byrkjedal, I., Christiansen, J.S., Karamushko, O. V, Mecklenburg, T.A., Møller, P.R., Steinke, D., Wienerroither, R.M., 2018. Marine Fishes of the Arctic Region Vol I and II. CAFF Monitoring Series Report 28. Conservation of Arctic Flora and Fauna, Akureyi, Iceland.
Mecklenburg, C.A., Steinke, D., 2015. Ichthyofaunal baselines in the Pacific Arctic region and RUSALCA study area. Oceanography 28, 158–189.
Mehl, S., Sunnana, K., 1991. Changes in growth of Northeast Arctic cod in relation to food consumption in 1984-1988. ICES Mar. Sci. Symp. 193., 103-112
Meier, W.N., Stroeve, J., Barrett, A., Fetterer, F., 2012. A simple approach to providing a more consistent Arctic sea ice extent time series from the 1950s to present. Cryosphere 6, 1359–1368. https://doi.org/10.5194/tc-6-1359-2012
Mueter, F.J., Weems, J., Farley, E. V, Sigler, M.F., 2017. Arctic Ecosystem Integrated Survey (Arctic Eis): Marine ecosystem dynamics in the rapidly changing Pacific Arctic Gateway. Deep Sea Res. II 135, 1–6. https://doi.org/10.1016/j.dsr2.2016.11.005
Nelson, R.J., Carmack, E.C., McLaughlin, F.A., Cooper, G.A., 2009. Penetration of pacific zooplankton into the western arctic ocean tracked with molecular population genetics. Mar. Ecol. Prog. Ser. 381, 129–138. https://doi.org/10.3354/meps07940
Nichol, D.G., Acuna, E.I., 2001. Annual and batch fecundities of yellowfin sole, Limanda aspera, in the eastern Bering Sea. Fish. Bull. 99, 108–122.

Norcross, B.J., Holladay, B.A., Busby, M.S., Mier, K.L., 2010. Demersal and larval fish assemblages in the Chukchi Sea. Deep Sea Res. II 57, 57–70.
Page, L. M., Espinosa-Perez, H., Findley, L. T., Gilbert C. R., Lea, R. N., Mandrak, N. E., Mayden, R. L., Nelson, J.S., 2013. Common and scientific names of fishes from the United States, Canada, and Mexico. American Fisheries Society Special Publication 34.
Panteleev, G., Nechaev, D.A., Proshutinsky, A., Woodgate, R., Zhang, J., 2010. Reconstruction and analysis of the Chukchi Sea circulation in 1990-1991. J. Geophys. Res. Ocean. 115, 1–22. https://doi.org/10.1029/2009JC005453
Pepin, P., Penney, R.W., 1997. Patterns of prey size and taxonomic composition in larval fish: are there general size-dependent models? J. Fish Biol. 51, 84–100. https://doi.org/10.1111/j.1095-8649.1997.tb06094.x
Pickart, R.S., Weingartner, T., Pratt, L.J., Zimmerman, S.T., Torres, D.J., 2005. Flow of winter-transformed Pacific water into the western Arctic. Deep Sea Res. II 52, 3175–3198.
Pinchuk, A.I., Eisner, L.B., 2016. Spatial heterogeneity in zooplankton summer distribution in the eastern Chukchi Sea in 2012–2013 as a result of large-scale interactions of water masses. Deep Sea Res. Part II Top. Stud. Oceanogr. 0–1. https://doi.org/10.1016/j.dsr2.2016.11.003
Ponomarenko, V.P., 2000. Eggs, larvae, and juveniles of polar cod Boreogadus saida in the Barents, Kara and White Seas. J. Ichthyol. 40, 165–173.
Provencher, J.F., Gaston, A.J., O'Hara, P.D., Gilchrist, H.G., 2012. Seabird diet indicates changing Arctic marine communities in eastern Canada. Mar. Ecol. Prog. Ser. 454, 171–182. https://doi.org/10.3354/meps09299
R Core Team, 2016. R: A language and environment for statistical computing.
Randall, J.R., Busby, M.S., Spear, A.H., Mier, K.L., 2019. Spatial and temporal variation of late summer ichthyoplankton assemblage structure in the eastern Chukchi Sea : 2010 – 2015. Polar Biol. 42, 1811–1824. https://doi.org/10.1007/s00300-019-02555-8
Rass, T.S., 1968. Spawning and development of polar cod. Rapp. Procés-Verbaux des Réunions du Cons. Int. pour l'Exploration la Mer 158, 135–137.
Robert, D., Murphy, H.M., Jenkins, G.P., Fortier, L., 2013. Poor taxonmical knowledge of larval fish prey preference is impeding our ability to assess the existence of a "critical period" driging year-class strength. ICES J. Mar. Sci. https://doi.org/10.1093/icesjms/fst198
Rose, G.A., O'Driscoll, R.L., 2002. Multispecies interactions capelin are good for cod: Can the northern stock rebuild without them? ICES J. Mar. Sci. 59, 1018–1026. https://doi.org/10.1006/jmsc.2002.1252
Siddon, E.C., Duffy-Anderson, J.T., Mueter, F.J., 2011. Community-level response of fish larvae to environmental variability in the southeastern Bering Sea. Mar. Ecol. Prog. Ser. 426, 225–239. https://doi.org/10.3354/meps09009
Simonsen, C., Munk, P., Folkvord, A., Pedersen, S., 2006. Feeding ecology of Greenland halibut and sandeel larvae off West Greenland. Mar. Biol. 149, 937–952. https://doi.org/10.1007/s00227-005-0172-5
Springer, A.M., McRoy, C.P., 1993. The paradox of pelagic food webs in the northern Bering Sea. III. Patterns of primary production. Cont. Shelf Res. 13, 575–579.
Stabeno, P.J., Kachel, N.B., Ladd, C., Woodgate, R.A., 2018. Flow patterns in the Eastern Chukchi Sea: 2010-2015. J. Geophys. Res. Ocean. 123, 1177–1195. https://doi.org/10.1002/2017JC013135
Stark, J.W., 2004. A comparison of the maturation and growth of female flathead sole in the central Gulf of Alaska and south-eastern Bering Sea. J. Fish Biol. 64, 876–889. https://doi.org/10.1111/j.1095-8649.2004.00356.x
Stenson, G.B., Hammill, M.O., Lawson, J.W., 1997. Predation by harp seals in Atlantic Canada: preliminary consumption estimates for Arctic cod, capelin and Atlantic Cod. J. Northwest Atl. Fish. Sci. 22, 137–154. https://doi.org/10.2960/J.v22.a12
Syrjala, S.E., 1996. A Statistical Test for a Difference between the Spatial Distributions of Two Populations. Ecology 77, 75–80.

Vestfals, C.D., Mueter, F.J., Hedstrom, K.S., Laurel, B.J., Petrik, C.M., Duffy-Anderson, J.T., Danielson, S.L., De Robertis, A., and E.N. Curchitser Vestfals, C.D., Mueter, F.J., Hedstrom, K.S., Laurel, B.J., Petrik, C.M., Duffy-Anderson, J.T., Danielson, and E.N.C., in prep. Modeling the dispersal of Arctic cod (Boreogadus saida) and saffron cod (Eleginus gracilis) early life stages in the Pacific Arctic using a biophysical transport model. Polar Biol.

Walkusz, W., Paulic, J.E., Williams, W.J., Kwasniewski, S., Papst, M.H., 2011. Distribution and diet of larval and juvenile Arctic cod (Boreogadus saida) in the shallow Canadian Beaufort Sea. J. Mar. Syst. 84, 78–84. https://doi.org/10.1016/j.jmarsys.2010.09.001

Wang, M., Overland, J.E., 2015. Projected future duration of the sea-ice-free season in the Alaskan Arctic. Prog. Oceanogr. 136, 50–59. https://doi.org/10.1016/j.pocean.2015.01.001

Weingartner, T., Okkonen, S.R., Danielson, S.L., 2005. Circulation and Water Property Variations in the Nearshore Alaskan Beaufort Sea, Final Report, OCS Study MMS.

Wilderbuer, T.K., Nichol, D.G., Ianelli, J.N., 2017. Assessment of the yellowfin sole stock in the Bering Sea and Aleutian Islands. In Bering Sea and Aleutian Islands Stock Assessment and Fishery Evaluation report to the North Pacific Fishery Management Council, 605 W. 4th Avenue, Anchorage AK 99510.

Woodgate, R., Stafford, K., Prahl, F.G., 2015. A synthesis of year-round interdisciplinary mooring measurements in the Bering Strait (1990-2014) and the RUSALCA years (2004-2011). Oceanography 28, 46–67. http://dx.doi.org/10.5670/oceanog.2015.57

Woodgate, R.A., Aagaard, K., Weingartner, T.J., 2005. A year in the physical oceanography of the Chukchi Sea: Moored measurements from autumn 1990-1991. Deep. Res. Part II Top. Stud. Oceanogr. 52, 3116–3149. https://doi.org/10.1016/j.dsr2.2005.10.016

Wyllie-Echeverria, T., Barbera, W.E., and Wylle-Echeverria, S., 1997. Water masses and transport of young-of-the-year fish into the northeastern Chukchi Sea., in: Reynolds, J. (Eds.), Fish Ecology in Arctic North America Symposium. American Fisheries Society, Fairbanks, AK, pp. 60–67.

Table 1. Numbers of fish eggs, larvae, and juveniles collected in bongo tows from the Chukchi and northern Bering seas (NBS) during the 2012 and 2013 Arctic Ecosystem Integrated Survey (Arctic Eis) surveys.

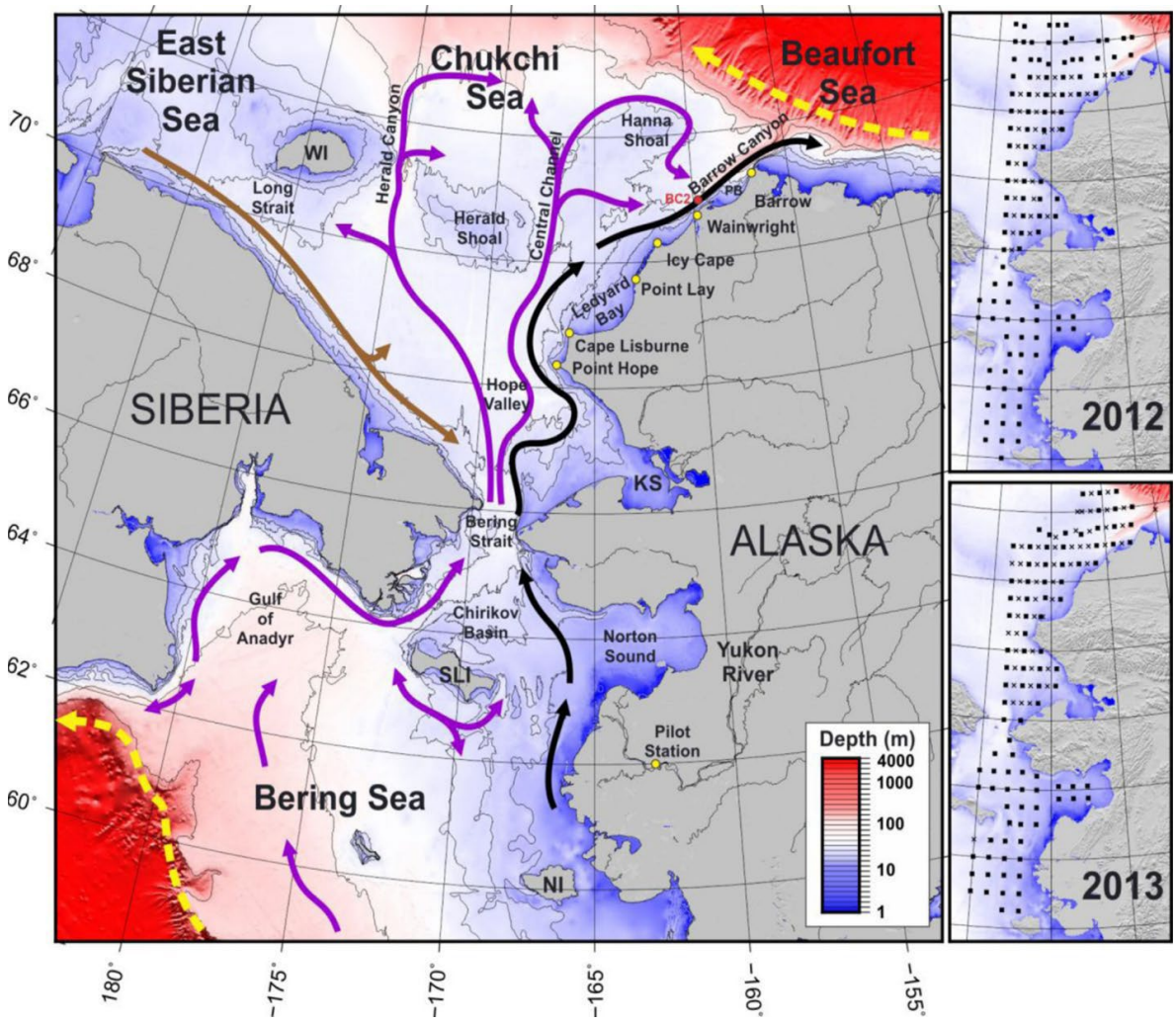
East Siberian Sea
Chukchi Sea
Beaufort Sea
WI
Long Strait
Herald Canyon
Herald Shoal
Central Channel
Hanna Shoal
Barrow Canyon
BC2
PB
Barrow
Wainwright
Icy Cape
Point Lay
Ledyard Bay
Cape Lisburne
Point Hope
Hope Valley
SIBERIA
KS
Bering Strait
ALASKA
Gulf of Anadyr
Chirikov Basin
Norton Sound
Yukon River
SLI
Pilot Station
Bering Sea
NI
Depth (m)
4000
1000
100
10
1
2012
2013
70°
68°
66°
64°
62°
60°
180°
−175°
−170°
−165°
−160°
−155°

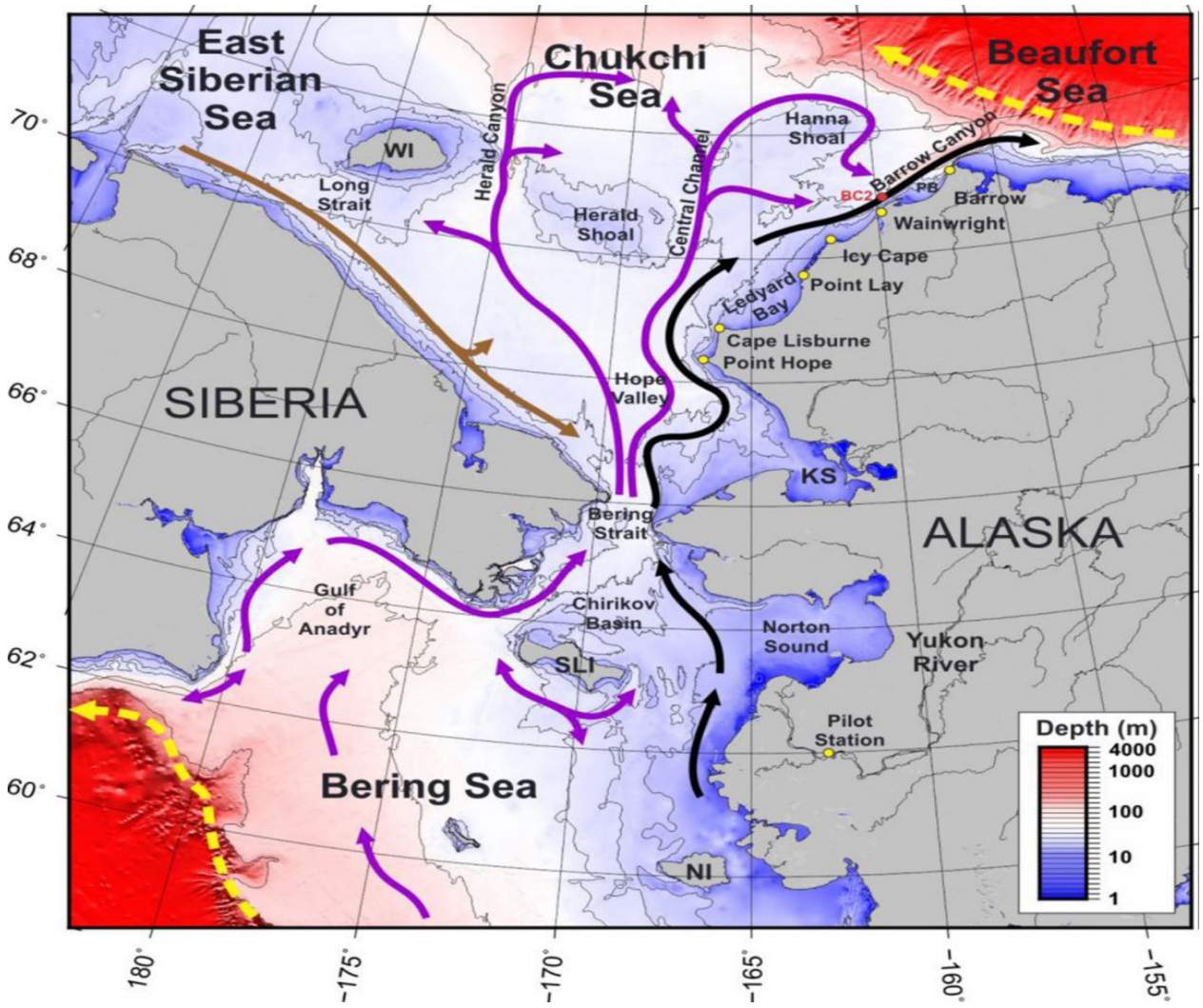

Fig. 1. Study area map with bathymetric depths and overview of general currents in the region. Mean flow pathways are color coded to denote current systems. Yellow=Bering Slope Current and Beaufort Gyre; Black=Alaska Coastal Current; Brown=Siberian Coastal Current; Purple=pathways of Bering shelf, Anadyr, and Chukchi shelf waters (Danielson et al. 2017).

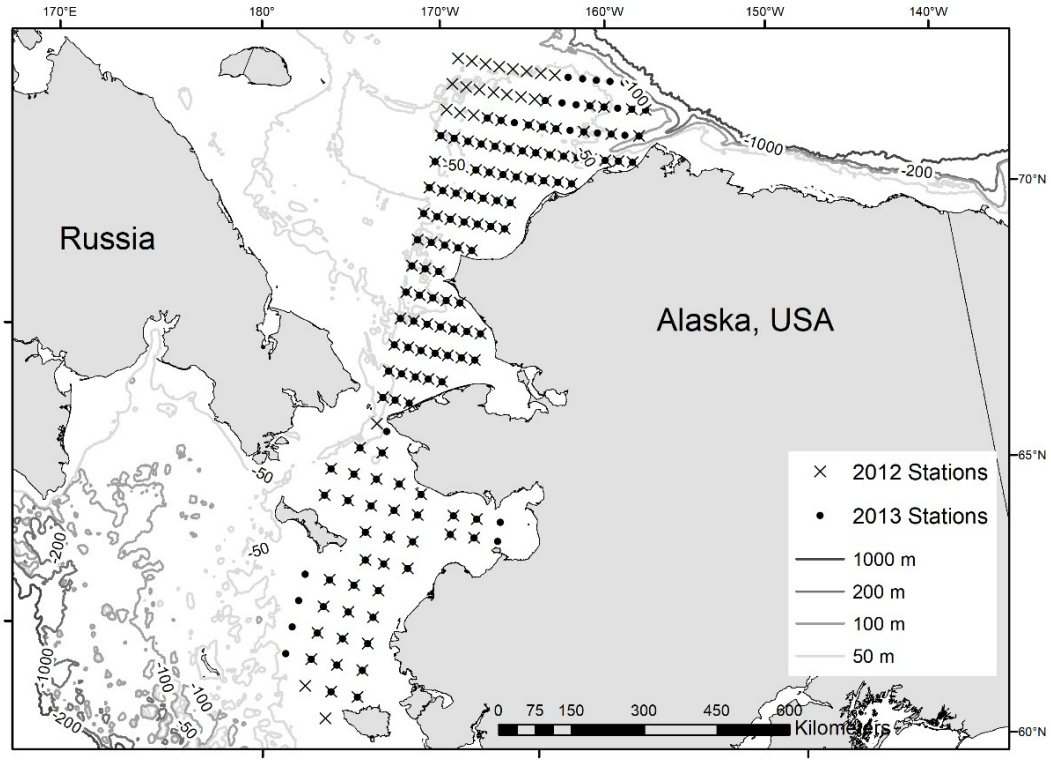

Fig. 2. Survey area and stations sampled in 2012 (x-symbols) and 2013 (solid circles). Depth contours in meters.

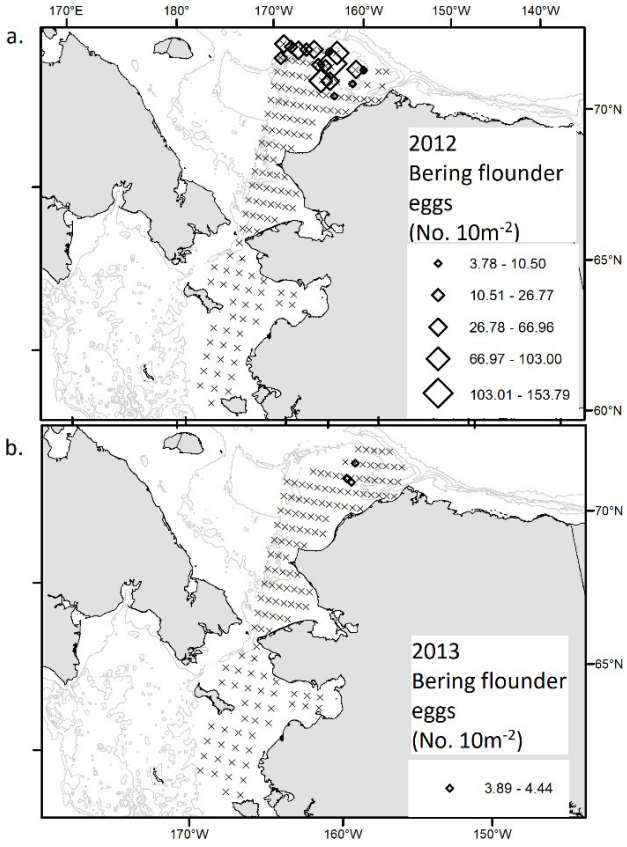

Fig. 3. Distribution of Bering flounder egg catch density (No./10 m^2) in a) 2012 and b) 2013.

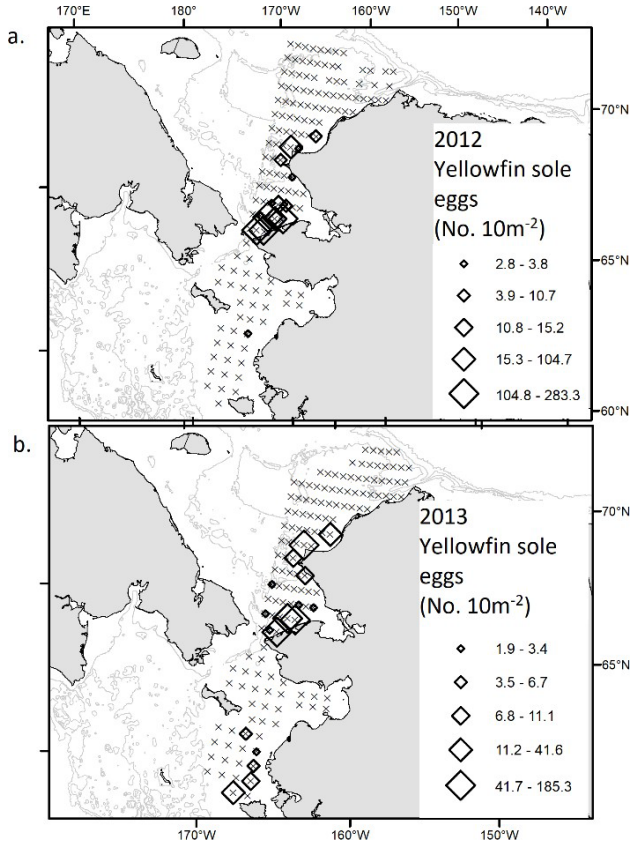

Fig. 4. Distribution of yellowfin sole egg catch density (No./10 m^2) in a) 2012 and b) 2013.

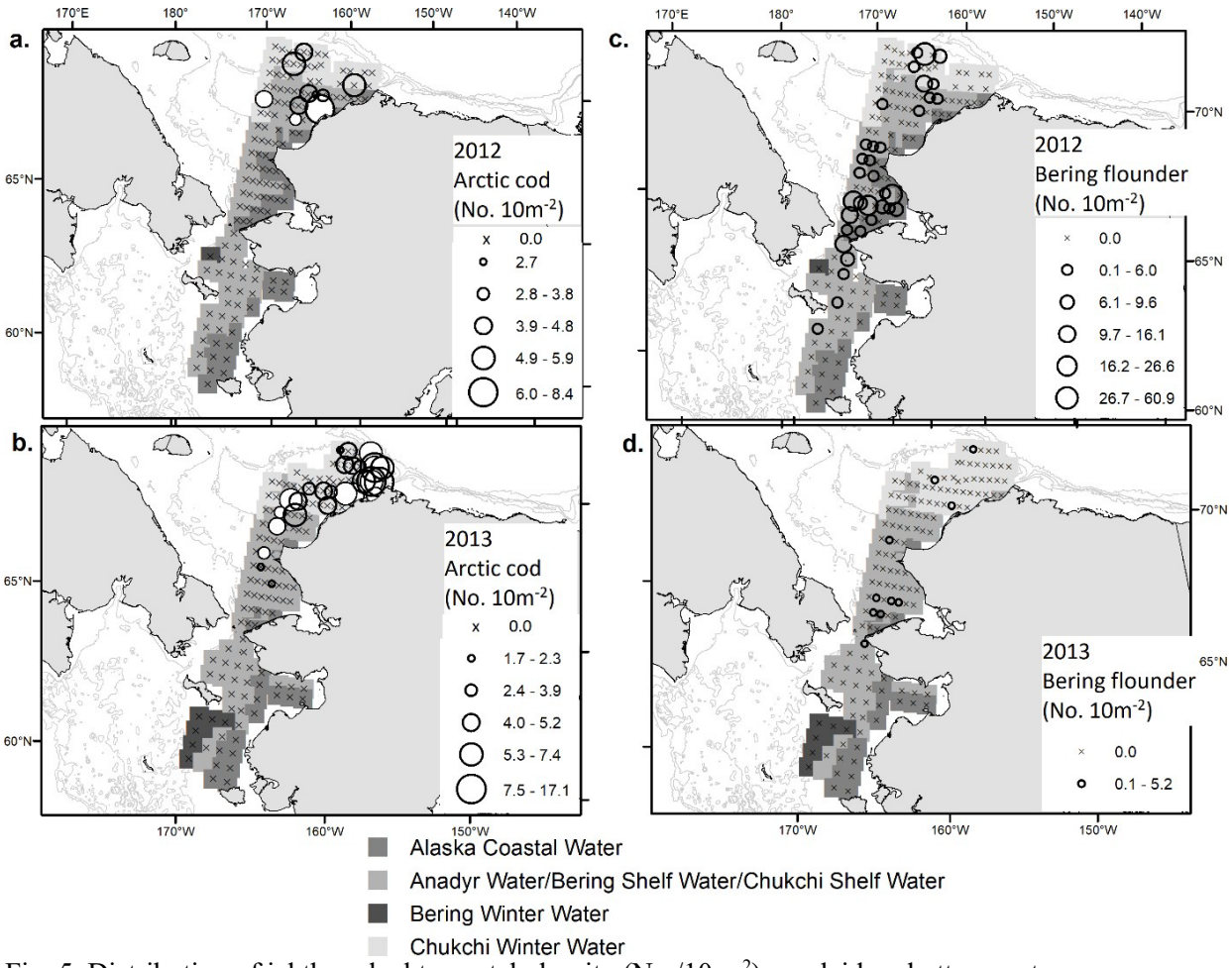

Fig. 5. Distribution of ichthyoplankton catch density (No./10 m^2) overlaid on bottom water mass type. a) 2012 Arctic cod, b) 2013 Arctic cod, c) 2012 Bering flounder, and d) 2013 Bering flounder. Open circles are larval fish, filled circles are juvenile fish. Arctic cod were the only taxa for which juvenile fish were caught. Water mass data courtesy of S. Danielson.

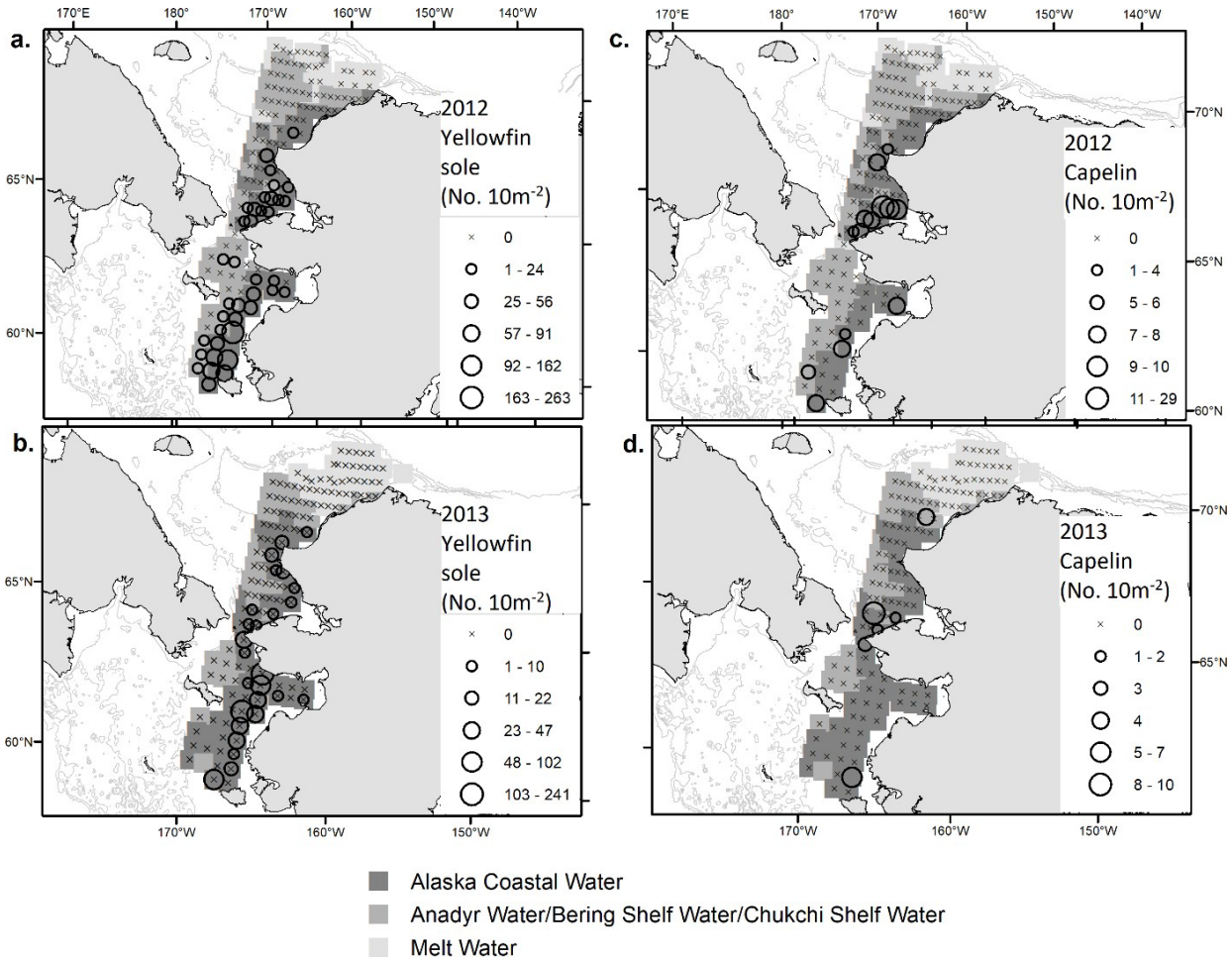

Fig. 6. Distribution of ichthyoplankton catch density (No./10 m^2) overlaid on surface water mass type. a) 2012 yellowfin sole, b) 2013 yellowfin sole, c) 2012 capelin, and d) 2013 capelin ichthyoplankton. Water mass data courtesy of S. Danielson.

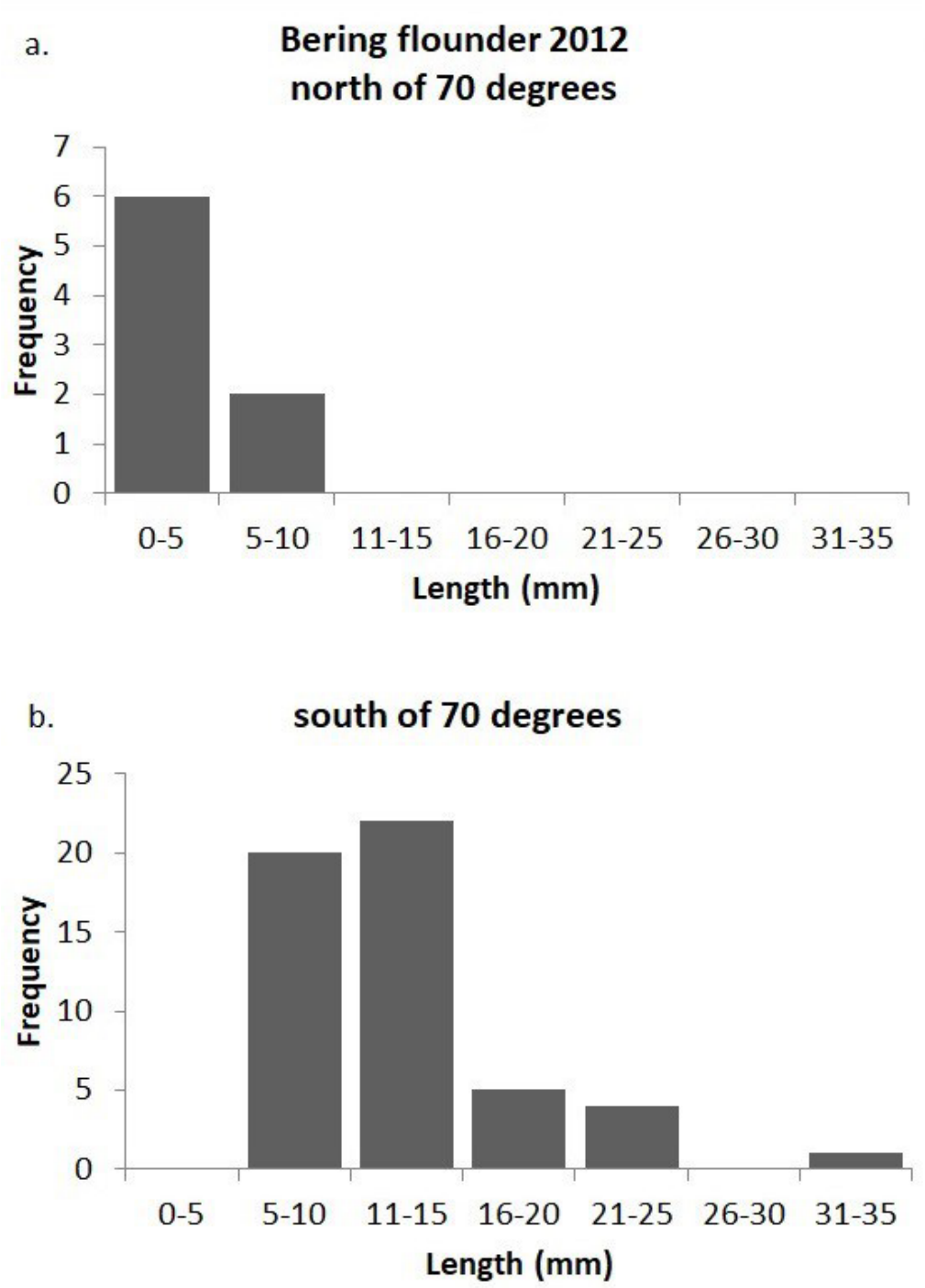

Fig. 7. Length-frequency distributions (number of fish) of Bering flounder larvae from 2012: a) north of 70° latitude (n=8) and b) south of 70° latitude (n=52).

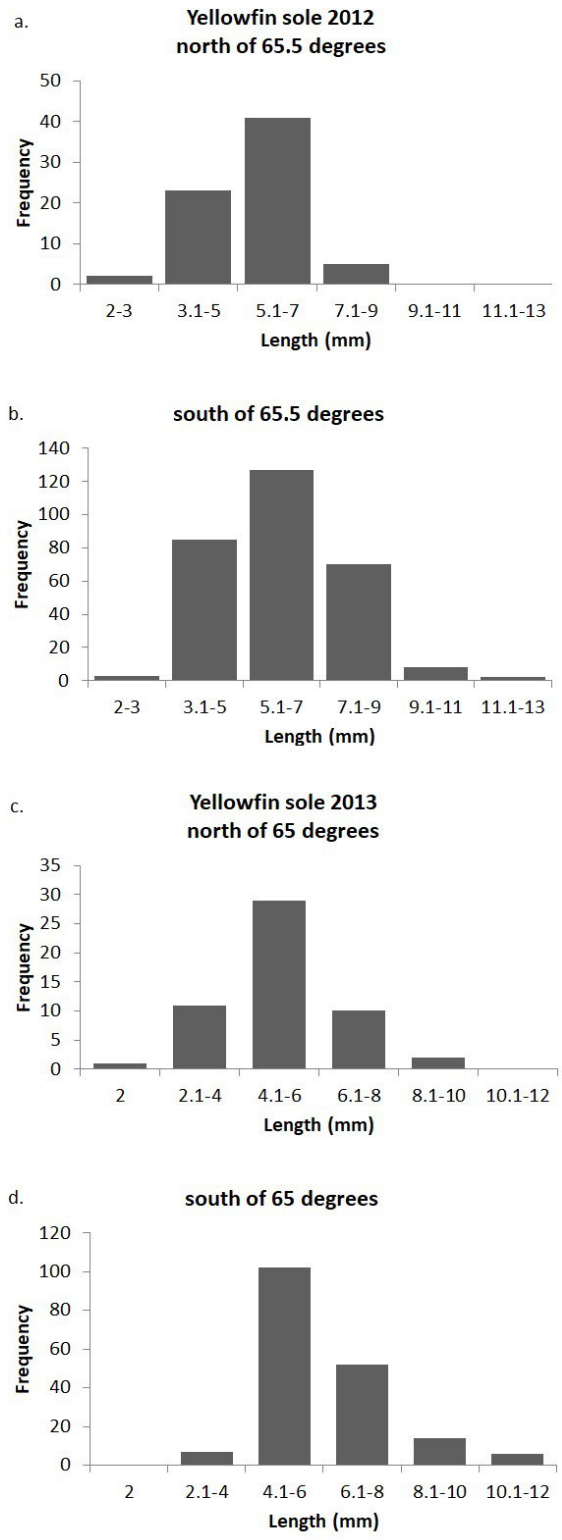

Fig. 8. Length-frequency distributions (number of fish) of yellowfin sole larvae from: a) 2012, north of 65.5° latitude (n=71); b) 2012, south of 65.5° latitude (n=295); c) 2013, north of north of 65.5° latitude (n=53); and d) 2013, south of 65.5° (n=181).

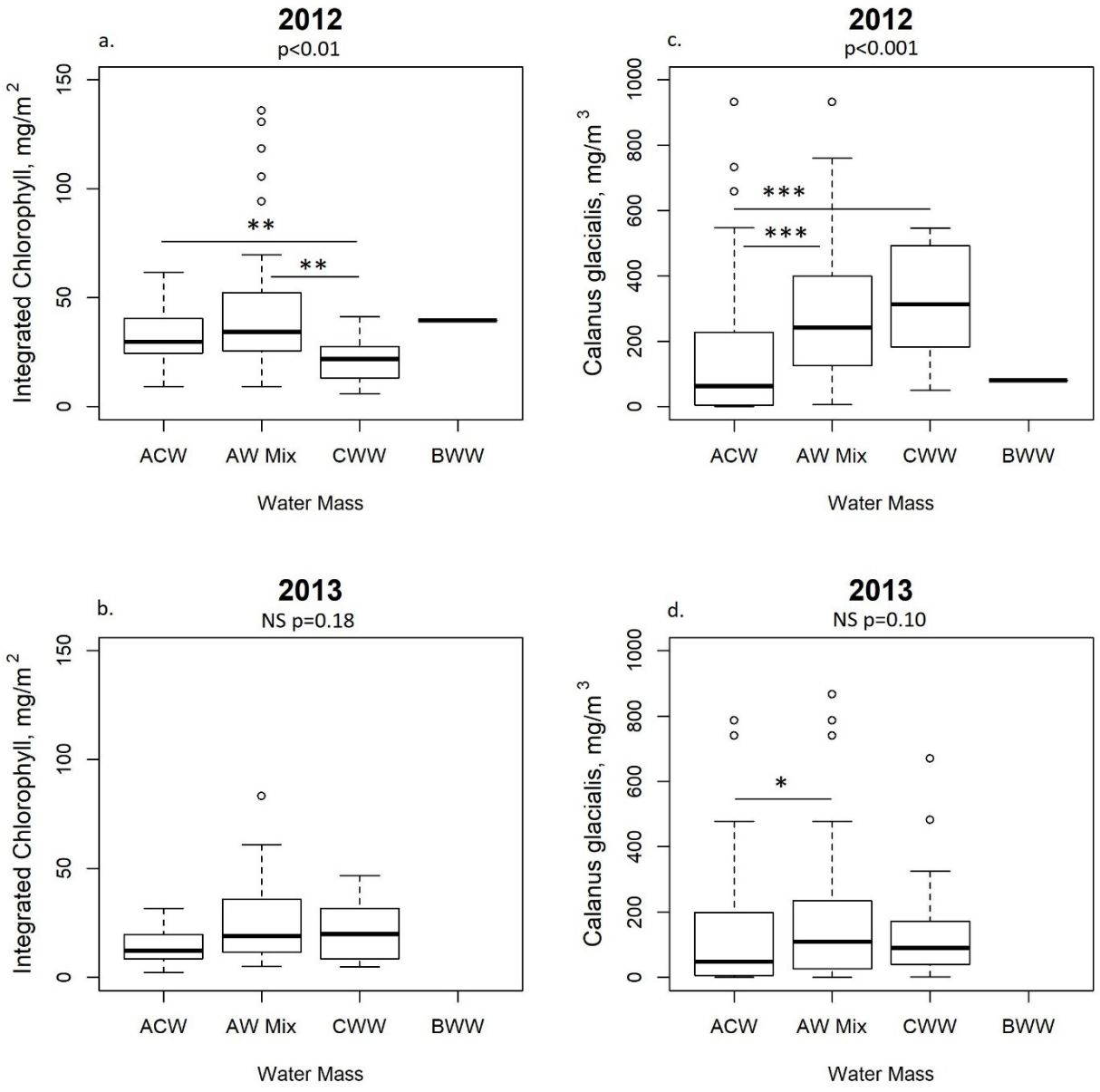

Fig. 9. Water mass characteristics for Alaska Coastal Water (ACW) at the surface; and Anadyr Water/Bering Shelf Water/Chukchi Shelf Water (AW Mix), Chukchi Winter Water (CWW) and Bering Winter Water (BWW) at depth. Box plots show median (horizontal line), first and third quartile (box), minimum and maximum (whiskers) and outliers (points). p-value from Kruskal-Wallis rank sum test for comparisons among all water masses is shown at upper right of each box plot. Significant p-values for post-hoc Kruskal-Wallis rank sum test comparisons between pairs of water masses are indicated by bars and asterix. * $p<0.05$, ** $p<0.01$, *** $p<0.001$; a) 2012 integrated chlorophyll (mg m^{-2}), b) 2013 integrated chlorophyll (mg m^{-2}), c) 2012 *Calanus glacialis* (mg m^{-3}), and d) 2013 *Calanus glacialis* (mg m^{-3}).

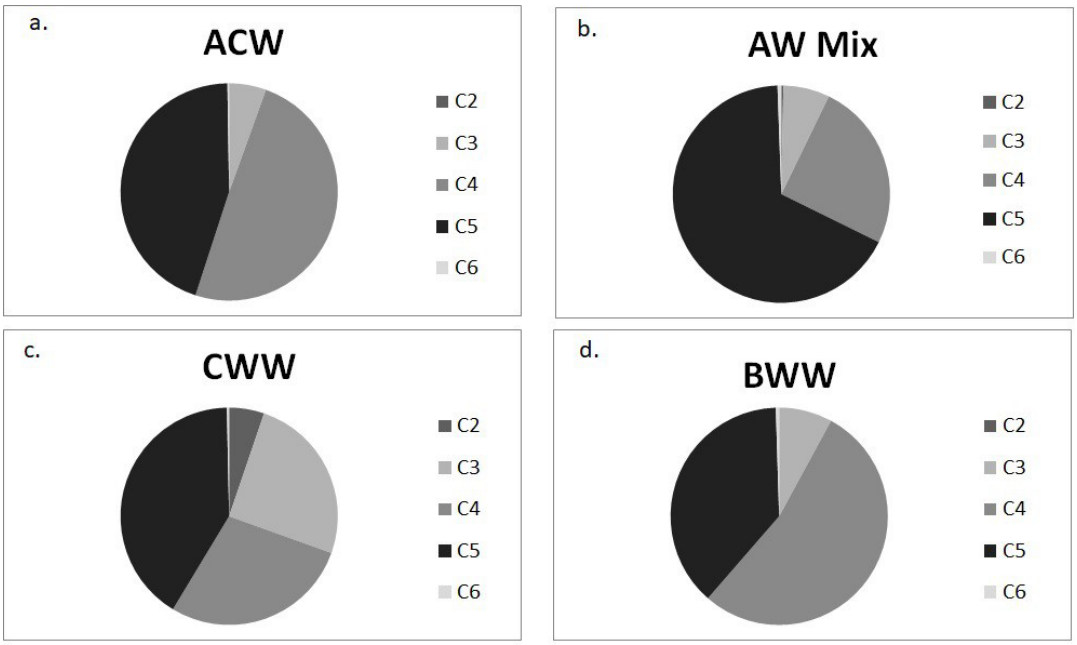

Fig. 10. Proportion of *Calanus glacialis* copepodite stages C2-C6 in each water mass in 2012: a) Alaska Coastal Water (ACW), b) Chukchi Winter Water (CWW), c) Anadyr Water/Bering Shelf Water/Chukchi Shelf Water (AW Mix), d) Bering Winter Water.

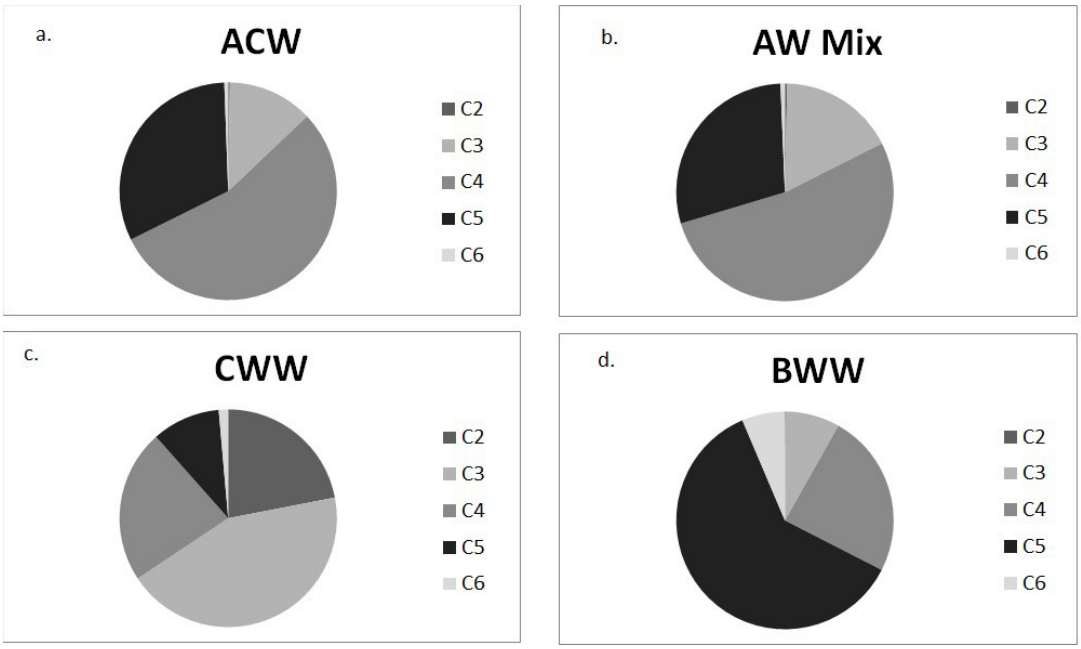

Fig. 11. Proportion of *Calanus glacialis* copepodite stages C2-C6 in each water mass in 2013: a) Alaska Coastal Water (ACW), b) Chukchi Winter Water (CWW), c) Anadyr Water/Bering Shelf Water/Chukchi Shelf Water (AW Mix), d) Bering Winter Water.

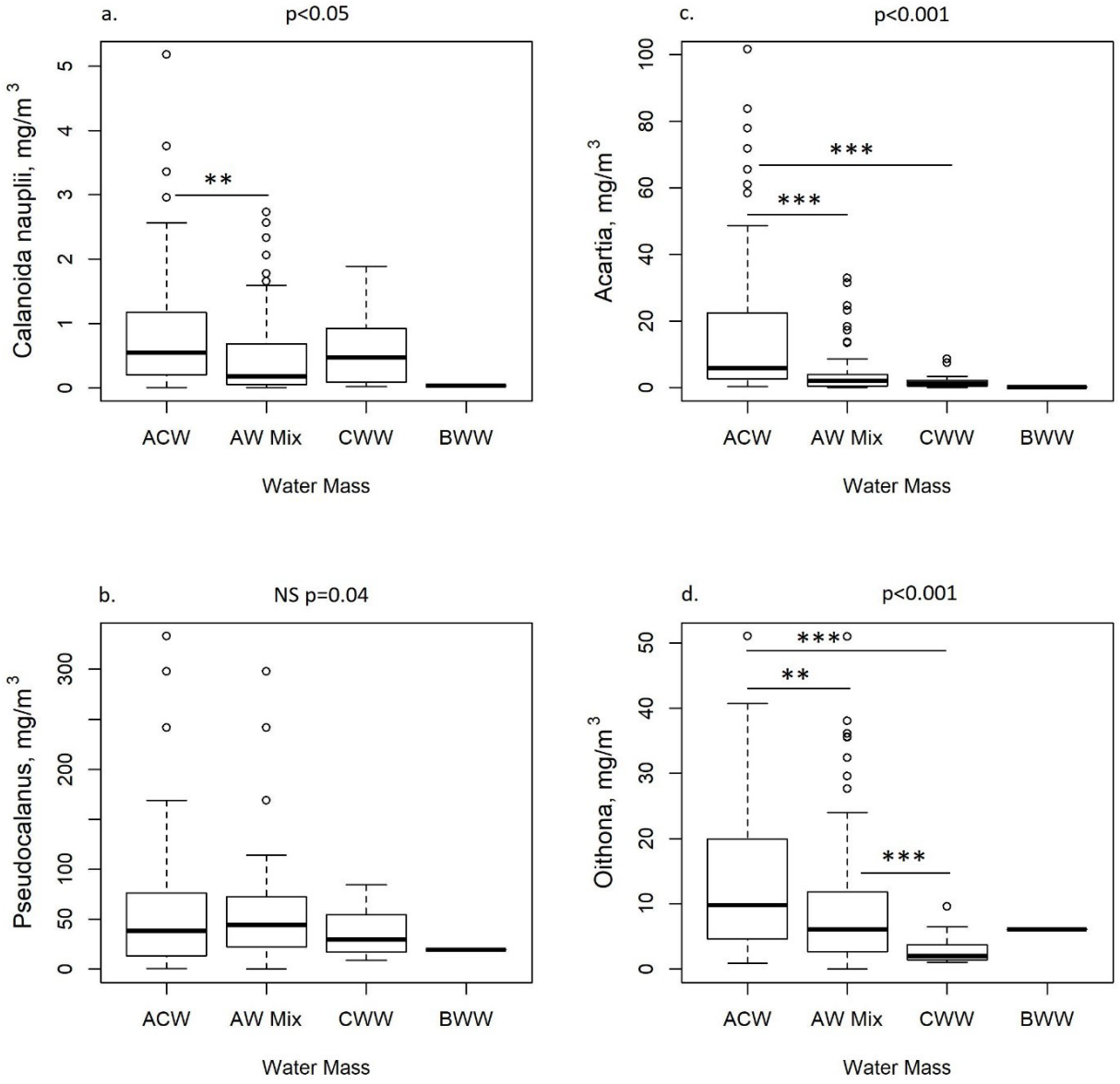

Fig. 12. Biomass density (mg m^{-3}) of small copepods in Alaska Coastal Water (ACW), Anadyr Water/Bering Shelf Water/Chukchi Shelf Water (AW Mix), Chukchi Winter Water (CWW) and Bering Winter Water (BWW) in 2012. No small (20-mm) PairVet net samples were analyzed for 2013 due to loss of data sheets at sea. Box plots show median (horizontal line), first and third quartile (box), minimum and maximum (whiskers) and outliers (points). p-value from Kruskal-Wallis rank sum test for comparisons among all water masses is shown at upper right of each box plot. Significant p-values for post-hoc Kruskal-Wallis rank sum test for comparisons between pairs of water masses are indicated by bars and asterix. * $p<0.05$, ** $p<0.01$, *** $p<0.001$; a) Calanoida nauplii, b) *Pseudocalanus* sp., c) *Acartia* spp., and d) *Oithona* spp.

CHAPTER 6 - Climate-driven shifts in pelagic fish distributions in a rapidly changing Pacific Arctic

Objective 2: Quantify the distribution, abundance, and condition of pelagic marine fishes, in particular young-of-the-year Arctic gadids and other forage fishes

Robert Levine, Alex De Robertis, Daniel Grunbaum, Sharon Wildes, Edward V. Farley, Phillis J. Stabeno, Christopher D. Wilson (in preparation)

Abstract

Age-0 Arctic cod (*Boreogadus saida*) have historically dominated the pelagic fish community in the Chukchi Sea in summer, with few adults present in the region. Recently, reductions in sea ice and increases in warming and transport have led to an increase in Pacific-origin waters on the Chukchi shelf in summer. To examine the potential effects of these environmental changes on the pelagic community in this rapidly changing environment, we extended a time series of acoustic-trawl surveys originally conducted in 2012 and 2013 with additional surveys in 2017 and 2019. Age-0 Arctic cod were the most abundant pelagic fish in all four survey years. However, age-0 walleye pollock (*Gadus chalcogrammus*), which were scarce and confined to the southern Chukchi in the 2012 and 2013, were present at high abundance throughout the Chukchi shelf in 2017 and 2019. Age-0 Arctic cod was substantially more abundant in 2017 than in any other year. This was possibly due to increased survivorship of larvae under warming conditions. Arctic cod and pollock were spatially separated in 2019, with Arctic cod primarily present in the northeastern portion of the survey area, which was characterized by cooler surface and bottom temperatures. The substantial increase in age-0 pollock in recent years suggests that environmental conditions now allow this species to extend its northern range into the central and southern Chukchi Sea, at least on a seasonal basis. We hypothesize that the changes in abundance and species composition based on our 2012-2019 time series are tightly coupled to recent changes in temperature and the transport of Bering Sea waters onto the Chukchi shelf.

Introduction

Arctic gadids, particularly Arctic cod (Boreogadus saida, also referred to as polar cod), have historically dominated the pelagic fish community in the Pacific Arctic ecosystem of the northern Bering, Chukchi, East Siberian, and Beaufort Seas (Quast, 1974; Logerwell et al., 2015; De Robertis et al., 2017). Arctic cod are a circumpolar-distributed species found throughout the Central Arctic Basin and surrounding marginal seas (Mecklenberg et al., 2018). The relatively abundant Arctic cod are lipid-rich (Copeman et al., 2017; Copeman et al., 2020), and serve as an energy-dense trophic link between lower trophic levels and piscivores such as seabirds and marine mammals (Bradstreet et al., 1986; Matley et al., 2012). Trophic mass balance models for the Chukchi Sea indicate that Arctic cod are central to the food web and represent a substantial portion of seabird (>20%) and piscivorous mammal (>40%) diets (Whitehouse et al., 2014). The Chukchi Sea and the entirety of the Pacific Arctic is experiencing substantial and rapid warming (Danielson et al., 2020), and the impacts of these environmental changes on pelagic fishes such as Arctic cod remains unclear.

The Chukchi Sea is warming rapidly: mean summer/fall water column temperatures in the Chukchi Sea have increased by 0.1 °C decade^{-1} over the past century (Danielson et al., 2020). This warming is likely to accelerate as air temperatures in the Arctic are anticipated to increase by >5 °C by 2100 (Overland et al., 2019). Climate predictions (Wang et al., 2018) suggest that the duration of seasonal ice cover will continue to decrease at a rate of -0.94 days year^{-1} as transport of water and heat into the region continue to increase.

Increased input of warm Pacific Water into the Chukchi Sea has created a feedback loop which further increases heating in the region (Danielson et al., 2020; Huntington et al., 2020). The Chukchi is highly advective, with substantial transport of warm water from the Pacific entering through the Bering Strait in spring and summer (Woodgate et al., 2005; Stabeno et al., 2018). This transport through the Bering Strait has been increasing from its previous climatology of ~0.8 Sv at a rate of ~0.01 Sv $year^{-1}$ in recent decades (Woodgate, 2018). The associated northward heat flux helps to initiate the retreat of the Chukchi shelf sea ice (Woodgate et al., 2010). Shorter periods of ice cover further reduce the albedo of the sea surface in spring and summer which increases solar warming, further accelerating ice melt in spring and delaying ice formation in fall (Danielson et al., 2020).

The physiology and recruitment success of Arctic gadids is highly temperature dependent and species specific (Mueter et al., 2011; Laurel et al., 2016; Koenker et al., 2018). Changes in habitat suitability that result from changes in Bering Strait transport are particularly important for early life stages when recruitment is largely dependent on the ability to maximize growth prior to winter (Bouchard et al., 2017). Thus, changes in transport and input of heat into the Chukchi are likely to affect the abundance and role of fishes in energy transfer within Arctic food webs. Increased warming may affect the relative abundance and distributions of different species (Laurel et al., 2016; Baker, 2021). For example, boreal (subarctic) species such as walleye pollock (Gadus chalcogrammus, hereafter pollock) and Pacific cod (Gadus macrocephalus) may benefit from warming (Marsh and Mueter, 2020), while Arctic species may be negatively impacted by reduced habitat (Baker, 2021) and increased competition (Bouchard et al., 2017).

Globally, boreal species have expanded their distributions northwards into the Arctic as high-latitude regions have warmed (Wassman et al., 2011). The Barents Sea, for example, is a shallow marginal sea of the Arctic Ocean which shares many commonalities with the Chukchi Sea (Hunt et al., 2013). Rapid warming in that region has changed the spatial distribution of fish communities as subarctic species expand northward (Fossheim et al., 2015). These spatial shifts in pelagic community structure can alter ecosystem function due to changes in food web structure (Kortsch et al., 2015). Evidence for this is seen in the distribution of adult fishes in the Bering Sea, where boreal species such as pollock and Pacific cod have expanded their range northwards (Stevenson and Lauth, 2019; Eisner et al., 2020; Spies et al., 2020). Similarly, the southern limits of Arctic species such as Arctic cod have shifted further north, with boreal species taking their place (Marsh and Mueter, 2020; Baker, 2021).

Northward advection from the Bering Sea contributes to the structure of the species composition of pelagic communities in the Chukchi Sea. This transport from the south brings planktonic organisms of Pacific-origin onto the Chukchi shelf (Eisner et al. 2013; Sigler et al., 2017). Northward advection across the Chukchi shelf is also hypothesized to structure the spatial distributions of age-0 fish, as the current speeds surpass their swimming abilities (Levine et al., 2020; Vestfals et al., 2021). Age 1+ gadids are scarce in the Chukchi Sea (De Robertis et al., 2017), likely because they are transported northward off the shelf as juveniles by the prevailing currents (Levine et al., 2020; Vestfals et al., 2021). Increased transport may further reduce the residence time for growth in regions of high productivity on the Chukchi shelf (Levine et al., 2020).

Acoustic-trawl (AT) surveys were conducted in 2012 and 2013 by De Robertis et al. (2017) to establish a baseline of the distribution of pelagic fishes in the northern Bering and Chukchi Seas. Similar to previous observations in the region (Norcross et al., 2013; Logerwell et al., 2015), large numbers of Arctic cod were observed, with the greatest abundances in the northern Chukchi Sea. However, these were primarily age-0 fish with an average length of 3.5 cm and <0.3% greater than 6.5 cm (De Robertis et al., 2017). Given the relatively high abundances of age-0 fish at a critical life stage, the Chukchi shelf may serve as an important nursery area (De Robertis et al., 2017; Levine et al., 2020). However, continued warming of the Chukchi has the potential to negatively impact the growth and survival of this population. Further investigations to address how environmental factors influence Arctic cod abundance and distribution are needed to better understand how changing climate will potentially alter this ecosystem.

To examine longer-term trends in pelagic fishes in this rapidly changing environment, we extended the time series of observations collected in 2012 and 2013 with additional AT surveys in 2017 and 2019. The AT methodology provided extensive spatial coverage and comparable measurements to previous surveys. This enabled us to address the impacts of temperature and transport on the distribution of the pelagic fish population in this highly dynamic region. The primary objectives of this study were 1) to characterize the abundance and distribution of the major pelagic fishes in the Chukchi Sea and 2) identify environmental drivers that influence the Chukchi Sea pelagic fish community. Future changes in sea ice, temperature, and transport that result from a changing climate on the Chukchi shelf are likely to be dramatic and the consequences for the age-0 Arctic cod population are unclear. Our goal is to better understand the mechanisms structuring the pelagic fish community in the Chukchi Sea, as this can improve predictions of how future environmental changes will affect these populations.

Methods

Acoustic-trawl surveys were conducted in the U.S. continental shelf region of the Chukchi Sea and coastal regions of the western Beaufort Sea (Fig. 1). The surveys occurred from 1 August to 27 September 2017 and 27 August to 26 September 2019 on the R/V Ocean Starr. Bottom depths were <60 m in 93% of the survey area in 2017 and 91% of the survey area in 2019. Stations were arranged on a 1° longitude and 0.5° latitude grid in 2017. Transect spacing was increased to a 0.75° latitude grid in 2019. Sampling stations were occupied as the vessel reached these locations along the transects. The survey began in the northern Chukchi Sea and progressed south. Acoustic data were collected as the ship transited at ~3.3 m s^{-1} along survey transects oriented in an east/west direction during daylight. Observations collected during daylight while transiting between transects were included in the analysis.

Survey methods were consistent with previous work conducted in 2012 and 2013 (De Robertis et al., 2017). The 2012 and 2013 surveys of the Chukchi Sea both took place from 7 August to 8 September. This was approximately 3 weeks earlier than the surveys in 2017 and 2019. These earlier surveys transited from south to north along the same transects indicated in Figure 1a, with equal sampling station spacing as the 2017 survey.

Acoustic data collection

Acoustic backscatter at 38 and 120 kHz was measured using a split-beam Simrad EK60 echosounder operating ES38B and ES120-7C transducers mounted at 3.7 m depth on the vessel's hull. Data were collected using a pulse length of 0.5 ms at a ping rate of 2 Hz. In deep water (>250 m depth), longer pulse lengths (1 ms at 120 kHz, 4 ms at 38 kHz) were used to increase signal-to-noise ratios, and the ping rate was slowed to ~0.3-0.5 Hz. The echosounders were calibrated at the beginning and end of each survey using the standard sphere technique (Demer et al., 2015). Results from the two calibrations were averaged before being applied in post-processing. Calibration results were consistent among surveys. Gains from the averaged pre- and post-survey calibrations for the 0.5 ms pulse length differed by 0.09 dB (2.2%) at 38 kHz and 0.17 dB (4.0%) at 120 kHz. Gains at the longer pulse lengths used in deeper waters differed between years by 0.04 dB (0.2%) at 38 kHz and 0.4 dB (8.9%) at 120 kHz.

Midwater trawl sampling

The composition of pelagic acoustic scatterers was determined from targeted midwater trawls in areas of high backscatter. Backscatter was generally evenly distributed throughout the survey area. Many trawl hauls were conducted at the survey sampling stations for logistical convenience, but hauls were targeted to the depth of greatest backscatter. Acoustically observed fish aggregations were sampled using a modified Marinovich herring trawl equipped with a fine-mesh 2 by 3 mm codend liner used in previous surveys (De Robertis et al., 2017). Prior to the 2017 survey, this trawl was modified with a redesigned aft section which resulted in lower selectivity and better retention of small fishes (De Robertis et al. in prep). Midwater trawls were conducted at 33 sites in 2017 and 43 sites in 2019 (Fig. 1), with an average ship

speed of 1-1.5 m s^{-1} during trawling. Net openings and depths were monitored with either a Simrad FS70 or Marport Trawl Explorer net sounder attached to the headrope. The trawl opening was approximately 8 m horizontal by 7.5 m vertical, with a mean headrope depth of 27.1 m (range 11.4-46.7 m) in 2017 and 34.9 m (range 13.2-227.9 m) in 2019.

Trawl catches were weighed, sorted, and identified to species. Fish lengths (3392 in 2017, 9124 in 2019) and jellyfish bell diameters (1211 in 2017, 751 in 2019) were measured on a subsample of individuals (up to 60 gadids, 10 of all other species) to the nearest 1.0 mm using an electronic measuring board (Towler and Williams, 2010). Length measurement methodology varied among years for the key gadid species. Age-0 gadids length was measured as fork length in 2012 and 2013, total length in 2017, and standard length in 2019. To account for these differences, we conducted repeat measurements of fork, total and standard length on the same individuals and calculated linear models to convert among length types (Table S1). Tissue samples from a subsample of measured gadid fishes (894 in 2017, 3155 in 2019) were collected and used to confirm field identifications based on genetic markers. Genetic analyses indicated that field identifications of gadids were unreliable, particularly when distinguishing between age-0 Arctic cod and pollock (see Wildes et al., in prep for details). For gadids with a tissue sample (40% and 56% of gadids specimens in 2017 and 2019, respectively), the species identifications were updated based on the genetic identifications. For the remaining gadid specimens with no genetic sampling, species was assigned probabilistically based on the length-dependent species composition of the genetically identified individuals in that haul (see supplementary material S2).

A subsample of gadid specimens collected in 2012 and 2013 (De Robertis et al., 2017) were validated using the same genetic analyses. This indicated that few pollock were present in the survey region during this period (Wildes et al., in prep). This provided confidence for further comparison of the 2017/2019 surveys with the historical 2012/2013 data despite the lack of a genetic-based species assignment in the 2012/2013 surveys.

Data processing and abundance estimation

Fish abundances were estimated by combining backscatter measurements and size and species composition information from genetically corrected trawl samples following methods in De Robertis et al. (2017). 38 kHz acoustic backscatter was integrated in 0.5 nmi along-transect intervals with a minimum Sv threshold of -70 dB re 1 m^{-1}, excluding data shallower than 6.5 m and deeper than 0.5 m above the seafloor. Trawl catches were corrected for size- and species-dependent net selectivity based on fine-mesh recapture nets mounted to the trawl to account for the size and species-specific likelihood of capture (De Robertis et al., in prep). The corrected size and species composition estimates were combined with size- and species-specific scattering properties to allocate observed acoustic backscatter to each species in the catch. Target strength relationships from the literature were used to estimate acoustic scattering for each species in the trawl catch (Table 1 in De Robertis et al., 2017). The proportion of total areal backscatter attributable to each species was then calculated along acoustic transects using species and size compositions from the nearest trawl (De Robertis et al., their equations 1-7). The AT method is best-suited for abundant, strongly-scattering species (Simmonds and MacLennan, 2005). The analysis thus was limited to Arctic cod, pollock, Pacific cod, saffron cod (Eleginus gracilis), Pacific herring (Clupea pallasii), and capelin (Mallotus catervarius), which accounted for 96.2% and 67.7% of fish by number in the trawl catch in 2017 and 2019, respectively. The contribution of other less abundant or weakly scattering species to backscatter was estimated, but abundance estimates were not made. For example, as in previous surveys, we were unable to estimate Arctic sand lance (Ammodytes hexapterus) abundance using AT methods with confidence because they are weak acoustic scatterers due to their lack of a swimbladder, which results in high uncertainty if stronger scatters are misclassified as sand lance (Yasuma et al., 2009; De Robertis et al., 2017). Pelagic fish abundances from surveys conducted in 2012 and 2013 were used in our analyses (De Robertis, 2021).

Environmental data collection and processing

Water column properties were measured using a conductivity, temperature, and depth (CTD, Sea-Bird Electronics 911plus) sensor. At all stations a CTD sensor was deployed from surface to ~5 m above seafloor. Mean water column temperature and salinity in 2017 and 2019 were calculated at each station for the upper 10 m (hereafter referred to as surface temperature/salinity), and the deepest 5 m (hereafter referred to as bottom temperature/salinity) of each cast. Equivalent measures were available for the CTD casts from the 2012 and 2013 surveys (Danielson et al., 2017). Measurements were included from 68 stations in 2012, 55 stations in 2013, 39 stations in 2017, and 46 stations in 2019. To associate fish with environmental conditions, each 0.5 nmi interval of transect was assigned to the nearest CTD station, and the average fish abundances (fish m^{-2}) for each grouping of intervals were calculated. Water mass classifications from Danielson et al. (2017) were used to describe station conditions based on temperature; 2 °C and 7 °C were used to represent the boundaries between Alaskan Coastal Water (>7 °C), Bering/Chukchi Summer Water (2-7 °C), and Bering Chukchi Winter Water (<2 °C).

Results

Trawl catches

Catch rates were >6-fold higher in 2017 (mean catch per unit effort for all fishes of 0.247 fish m^{-3} in 2017 and 0.037 fish m^{-3} in 2019) primarily due to high abundances of Arctic cod (0.209 fish m^{-3} in 2017 and 0.017 fish m^{-3} in 2019). Trawl catches were dominated by small fishes (80% <7.3 cm in 2017 and <8.0 cm in 2019). Gadids (Arctic cod, pollock, saffron cod, Pacific cod), Arctic sand lance, pricklebacks (Stichaedae), Pacific herring, and capelin accounted for 98.6% of catch by number (16.0% by weight) in 2017, and 93.4% of catch by number (6.7% by weight) in 2019 (Fig. 2a, b). With the exception of pollock, the same species accounted for 95.2% and 87.3% of the catch by number in 2012 and 2013, respectively (De Robertis et al., 2017). Jellyfish composed a small portion of the catch by number (0.7% in 2017, 5.5% in 2019), but a large portion of the catch by weight (83.8% of the biomass in 2017, 93.1% in 2019). Chrysaora melanaster was prevalent throughout the survey area in both years and accounted for 60.8% of all jellyfish by weight in 2017 and 58.3% in 2019.

Age-0 Arctic cod dominated the catch throughout the survey region in 2017 except in the southern Chukchi (south of 68.5 °N) where the catch composition was highly variable (Fig. 2a). Age-0 pollock were widely distributed and captured at lower abundance throughout the survey area (Fig. 2a). The catch composition was much more spatially stratified in 2019, with Arctic cod primarily restricted to the northeastern part of the survey area (Fig. 2b). The northwestern portion of the survey area was dominated by pollock and Arctic sand lance. South of 71 °N, pollock were the most abundant fishes in the trawl catches, with capelin and Pacific herring occurring at some nearshore locations (Fig. 2b).

Acoustic backscatter

In the region north of Bering Strait (>66 °N), mean backscatter in 2017 was 3.1-fold higher than in 2019 (Table 1), 4.3-fold higher than 2013, and 15.5-fold higher than 2012. Acoustic backscatter in 2017 was high throughout the survey region north of 68 °N, which coincided with the areas where age-0 Arctic cod were numerically abundant in trawl catches (Fig. 2c). The greatest backscatter levels in 2019 were found between 70 and 72 °N, where both age-0 Arctic cod and pollock were the dominant species in the catch (Fig. 2b, d). Patchy high-backscatter schools in the southern Chukchi Sea in 2019 were attributed to Pacific herring (Figs. 2d, S2). Similar to the trawl catches, Arctic cod, pollock, saffron cod, and Pacific cod were the dominant acoustic scatterers. These species accounted for 93.6% of the backscatter in 2017 and 85.6% in 2019. Capelin and Pacific herring were the next most abundant sound scattering pelagic species in the catch. Together, they accounted for 2.3% of the backscatter in 2017 and 7.1% in 2019. Although jellyfish dominated the biomass, they have a much lower mass-specific target strength than fishes with swimbladdders (De Robertis and Taylor, 2014) and were not major contributors to the observed backscatter (<1.3% in both years). Thus, the primary contributors to 38 kHz backscatter were age-0 gadids.

Fish abundance and distribution

Gadids dominated the acoustic-trawl abundance estimates in 2017 and 2019. They composed 98% of fishes in 2017 and 96% in 2019. Arctic cod was particularly abundant and composed 89.5% of fish abundance in 2017 and 65.1% in 2019. Arctic cod also dominated AT abundance estimates for the 2012 and 2013 surveys. Relatively large pollock abundance estimates were also observed in 2017 and 2019. Pollock made up 7.4% of fishes in 2017 and 29.8% in 2019. This was not the case in earlier survey years; pollock only accounted for 0.1% of fishes in 2012 and <0.001% of fishes in 2013 in the catches north of 66 °N. Abundances of Arctic cod and pollock in 2017 were 7.3- and 1.3-fold greater than in 2019, respectively (Table 1). Arctic cod and pollock densities in 2017 were greater in the central and northern Chukchi compared to other survey years (Fig. 3). Furthermore, the relatively high densities of Arctic cod in 2017 were widespread and extended throughout much of the shelf. Pollock were also distributed throughout the survey region at much greater densities than previously observed (Fig. 3e, f).

The lengths of Arctic cod and pollock were consistent with age-0 fish for these species (Figure 4, Brodeur et al., 2002; Helser et al., 2017). The mean length of Arctic cod was 4.4 cm (±0.5 cm SD) in 2017, and 4.8 (±0.5 cm SD) cm in 2019 (Fig. 4a). The Arctic cod in 2017 and 2019 were on average ~1 cm larger than those observed north of the Bering Strait in 2012 and 2013 (3.5 cm in both years, Fig. 4a). Pollock mean length was 5.1 cm (±0.6 cm SD) in 2017 and 5.0 cm (±0.5 cm SD) in 2019 (Fig. 4b).

Environmental conditions and associations

Arctic cod and pollock densities were highest in regions of intermediate surface waters in all surveys (Fig. 5). Surface temperature and salinity at sampling stations ranged from 2.5 to 7.5 °C and 25.4 to 32.3 in 2017 (Fig. 5g), and 3.2 to 10.6 °C and 27.1 to 32.1 in 2019 (Fig. 5h). Relative to other years, surface temperatures in 2017 were within a relatively narrow band of intermediate temperatures. Bottom temperature and salinity ranged from -0.7 to 6.5 °C and 31.0 to 34.7 in 2017 (Fig. 5g), and -1.4 to 10.6 °C and 29.1 to 34.7 in 2019 (Fig. 5h). The coldest surface and bottom waters were encountered in the northeastern portion of the survey area in both years (Fig. S1).

Arctic cod and pollock distributions overlapped broadly and inhabited similar water masses in 2017 (Figs. 3d, g, 5e, f). In contrast, the two species were spatially separated and largely present in different thermal environments in 2019 (Figs. 3d, h, 5g, h). That is, pollock were the primary gadids in the southern and western portion of the survey area in 2019 (Fig. 3h), which exhibited warm (>7 °C) surface temperatures that typify the Alaskan Coastal Water and warm (>2 °C) bottom waters typical of Bering/Chukchi Summer Water (Figs. 5g, h, S1). Conversely, Arctic cod were largely restricted to the northeastern region of the survey area in 2019 (Fig. 3d), where surface temperatures were <7 °C (Figs. 5g, S1d) and bottom temperatures were <2 °C, typical of Bering/Chukchi Winter Water (Figs. 5h, S1h). Arctic cod were observed in 2012 and 2013 in similar surface water conditions but in the full range of bottom temperatures observed (Fig. 5).

Arctic cod and pollock were higher in the water column in regions with cold bottom water (Fig. 6). Fish were relatively evenly distributed throughout the water column in 2017 (Fig. 6a, b) when water across the shelf was well mixed (Figs. 5e, f, S1c, g), and >65% of the total survey abundance was in areas with bottom water >2 °C. Only 25% of abundance was in areas with bottom water >2 °C in 2019, and fish in these locations were more evenly distributed throughout the water column (Fig. 6c, d), with only 28% of the abundance shallower than 25 m. Arctic cod were largely restricted to areas with bottom waters <2 °C in 2019, which was not the case in previous years (Fig. 5h). In the colder regions of the survey area (bottom temperature <2 °C), >55% of the fish were shallower than 25 m in 2019, driven by the relatively large abundance of Arctic cod high in the water column (Fig. 6c).

Discussion

Abundance and distribution of fishes

Observations from four surveys spanning a seven-year period suggest that the pelagic fish community in the Chukchi Sea is changing. We observed that age-0 gadids continue to dominate the pelagic fishes on the Chukchi shelf (Quast 1974; Logerwell et al., 2015; De Robertis et al., 2017). However, their abundance and species composition was highly variable. Age-0 gadids were substantially more abundant in 2017 relative to the other years, which was apparent in both the AT abundance estimates and the trawl catch rates. This was due to both a large increase in Arctic cod and an influx of pollock which were sparse in previous years. While age-0 Arctic cod continue to be the dominant pelagic fish in much of the Chukchi Sea, age-0 pollock, which were previously near-absent in the region, were present in 2017 and 2019.

Arctic cod, pollock, saffron cod, Pacific cod, and capelin were the most abundant species in 2017 and 2019. Pacific herring were also present in the southern portion of the survey area within Kotzebue Sound in 2019 (Table 1, Fig. S2). With the exception of pollock, these same species groups were dominant in the 2012 and 2013 AT survey observations (De Robertis et al., 2017) and in previous surveys of the Pacific Arctic (Eisner et al., 2013; Goddard et al., 2014; Logerwell et al., 2015). Although we were unable to confidently estimate their abundance using acoustic-trawl methods due to their weak acoustic scattering, Arctic sand lance were abundant in trawl catches in the central and northwestern portion of the survey region in 2019 (Fig. 2b).

Few age-1+ gadids were present in the region, consistent with previous surveys of the eastern Chukchi Sea (Goddard et al., 2014; Logerwell et al., 2015; De Robertis et al., 2017). Gadid lengths from both surveys support the acoustic observations made with a USV in 2018 which concluded that pelagic fishes were primarily age-0 gadids based on the strength of echoes from individuals (target strength) and found little evidence of scattering from adults (Levine et al., 2020). In addition, no large gadids were caught in surface trawls conducted using a large Nordic rope trawl (184 m long, ~315 m^2 net opening) during the 2017 and 2019 surveys (Farley and Levine, 2021a; Farley and Levine, 2021b). The absence of large gadids in 2017 and 2019 is not likely due to gear selectivity, as the Marinovich herring trawl used in this study has retained larger individuals when used in other regions. For example, pollock up to 61 cm were caught in several Marinovich herring trawl hauls in the Bering Sea (Honkalehto and McCarthy, 2015). A bottom trawl (3 m vertical and 12 m horizontal trawl opening) similar in size to the Marinovich has also been effective at capturing adult pollock when fished in midwater (Kotwicki et al., 2017). Thus, we are confident that relatively few pelagic adult gadids were present within the survey area based on our trawl sampling.

Small pollock and Arctic cod are difficult to distinguish based solely on external morphological characteristics in field collections (Mecklenberg et al., 2018). Without genetic analyses, we would have failed to identify the unexpected presence of pollock within the survey area in 2017 due to the unavailability of suitable field identification characteristics to differentiate pollock from Arctic cod (Wildes et al., in prep). Post-survey genetic identification was necessary to accurately estimate abundances and distributions of each species (see supplementary material S2 for details). Although the spatial coverage of specimens from previous surveys is limited, the same genetic analyses conducted on specimens from 2012 and 2013 suggests that pollock were not abundant in the survey region (Wildes et al., in prep). This supports the hypothesis that the dramatic increase in age-0 pollock in the Chukchi Sea is a recent occurrence, rather than the result of historical errors in species identification.

Temperature impacts on Arctic cod populations

The spatial distribution of Arctic cod and pollock closely resembles the distribution of warm and cold waters across the Chukchi shelf. The distributions of Arctic cod and pollock overlapped broadly in 2017 (Fig. 3c, g), with both species co-occurring in the relatively narrow range of surface and bottom temperatures found in the survey area compared to other years (Fig. 5e, f). In contrast, in 2019, Arctic cod and pollock were spatially distinct (Fig. 3d, h) and were associated with different water masses (Fig. 5g, h). Minimum temperatures observed in 2019 were colder than in 2017, and cold water (<2 °C) was more

widespread (Figure S1). In 2019, Arctic cod were primarily found on the northeast Chukchi shelf where bottom temperatures were <2 °C, which is typical of the colder water that forms in winter on the Bering and Chukchi shelves (Coachman et al., 1975; Woodgate et al., 2005). These Arctic cod were shallow (Fig. 6b), likely remaining in the intermediate temperatures between >2 °C in the upper water column. It is unlikely that this shallow distribution is due to limited vertical migration resulting from reduced swimming ability as the size of Arctic cod in 2019 was similar to that in 2017 when fish were relatively evenly distributed throughout the water column (Fig. 6a). This change in vertical distribution is likely behavioral. That is, Arctic cod may be avoiding colder waters at depth or remaining at depths where food availability is high.

Arctic cod in 2017 and 2019 were on average ~1 cm larger than those observed north of the Bering Strait in 2012 and 2013. We attribute this increase in length to a combination of the differences in survey timing and temperatures in the region. The summer is a period of rapid growth for age-0 gadids on the Chukchi shelf (Levine et al., 2020), and the recent surveys in 2017 and 2019 occurred approximately 3 weeks later than those in 2012 and 2013. For a 3.5 cm Arctic cod at a temperature of 9 °C (temperature of maximum growth, Laurel et al., 2017) an additional 21 days to account for the later surveys in 2017 and 2019 could explain an approximate 0.5 cm increase in length (based on Laurel et al., 2017, their Table 2 model B_0). However, even at this maximum growth rate, this would only account for approximately half of the increased size observed in 2017 and 2019.

Warmer water temperatures are also likely to have contributed to recent increases in gadid body size and higher gadid abundance. Mean water temperatures at Bering Strait (A3 mooring site, 66.29 °N, 168.96 °W, Woodgate, 2018; Woodgate and Peralta-Ferriz, 2021) in 2017 and 2019 were 0.5-1.5 °C warmer than in 2012 and 2013 between the approximate timing of Arctic cod spawning and the survey dates (January to August, Fig. 7; Bouchard and Fortier 2011). This was principally driven by warmer conditions in spring and summer (Fig. S3). Exceptionally warm temperatures in spring 2017 were observed at the Bering Strait (Fig. S3a), which were 0.5 °C warmer than 2019 and >1 °C warmer than in 2012 and 2013 (Fig. 7). Increased growth rates resulting from warmer temperatures may have led to larger individuals in 2017 and 2019 due to increased growth rates (Laurel et al., 2017). Based on the growth rates of age-0 Arctic cod laboratory specimens reported in Laurel et al., (2017), the ~1 °C difference in temperature between the spawning period and survey (Fig. 7) could account for a ~0.5 cm increase in length by the time of the survey in September.

Increased survival of early-hatched Arctic cod larvae may have also contributed to increased mean size in 2017 and 2019. Observations of Arctic cod in the Canadian Arctic suggest that higher temperatures reduce time-to-hatch and improve the survival of early hatching larvae (Bouchard and Fortier 2011; Bouchard et al., 2017). Dupont et al. (2020) proposed that increased early-season survival rates would lead to an increase in mean age and length during surveys. As length is strongly associated with hatch date (Bouchard et al., 2017), a greater proportion of older individuals leads to an increase in the mean length in the population. Improved early larval survival may also lead to increased size and lower mortality of age-0 fishes (Dupont et al., 2020), which may have contributed to the high abundances of age-0 Arctic cod observed in 2017.

Drivers of age-0 pollock appearance in the Chukchi Sea

The high abundances of age-0 pollock in the Chukchi Sea in recent years may be indirectly driven by increased temperatures in the northern Bering Sea, which resulted from decreased ice extent. Few pollock of any age class have been observed north of the Bering Strait in previous surveys (Quast 1974; Norcross et al., 2013; Logerwell et al., 2015; De Robertis et al., 2017). Ice cover in the Bering Sea has historically supported the formation of an extensive "cold pool" on the eastern Bering Sea shelf, a region where cold bottom waters (<2 °C) persist through the ice-free period (Wyllie-Echeverria and Wooster, 1998; Stabeno and Bell, 2019). Adult pollock typically avoid the cold pool and reside on the outer shelf region of the Bering Sea when the cold pool is large (Kotwicki et al., 2005; Stevenson and Lauth, 2019). Reduced ice

formation in warm years results in a less extensive cold pool, which reduces the barrier for adult pollock to remain on the inner and northern shelf throughout the year.

The Bering Sea has experienced extreme warming in recent years, which reduced the size of the cold pool in both 2017 and 2019 (Stabeno and Bell, 2019). Pollock distributions shifted northward during this period, which resulted in high densities of adult pollock in the northern Bering Sea (Stevenson and Lauth, 2019; Eisner et al., 2020). High abundances of juvenile and adult pollock were also observed in the Russian sector of the southern Chukchi Sea in 2019 (Orlov et al., 2020). This northern pollock population was likely not present during the 2012 and 2013 surveys due to the presence of an extensive cold pool (O'Leary et al., 2020). Our interpretation is that the recent northward movement of pollock resulted in increased production of pollock larvae in the northern Bering Sea, which were then transported into the Chukchi Sea by the prevailing northward transport (Vestfals et al., 2021).

Cold (<2 °C) Winter Water which forms during ice formation is gradually displaced to the north after seasonal ice melt by water entering the shelf from the Bering Sea (Lowry et al., 2015; Woodgate, 2018; Danielson et al., 2020). The intermediate temperatures of 2 to 7 °C and relatively high salinities (>30.4) observed in surface waters are typical of Bering/Chukchi Summer Water. Bering/Chukchi Summer Water originates in the Chukchi and northern Bering Seas (Danielson et al., 2017) and replaces the Winter Water and meltwater on the Chukchi shelf in summer (Weingartner et al., 2013). The temperature range of the Bering/Chukchi Summer Water is favorable for growth of both Arctic cod and pollock (Laurel et al., 2016).

We hypothesize that the spatial separation between pollock and Arctic cod distributions in the Chukchi observed in 2019 was driven by the association of each species with distinct water masses, which remained separate while undergoing increased transport from the Bering Sea. Bering Strait transport during the period between the approximate time of first spawning of Arctic cod and the survey (January to August) was substantially higher in 2019 relative to previous years (Fig. 7). Surface temperatures at the time of the 2019 survey exceeded 8 °C in the central and southern half of the survey area where pollock were abundant (Figs. 3, 5). These temperatures closely resembled the composition of Alaskan Coastal Water, which primarily originates on the inner Bering Sea shelf, driven by river input in spring and summer (Coachman et al., 1975; Woodgate et al., 2005). In previous surveys, this water was found in the nearshore regions of the eastern Chukchi. However, the Alaskan Coastal Water was found as far north as 72 °N and extended well offshore in 2019 (Fig. S1), which was likely due to southward winds forcing the current away from the coast (Woodgate et al., 2015; Morris, 2019). Age-0 pollock were likely advected within this Bering-origin water mass and may explain their widespread distribution in the Chukchi Sea. Similarly, the increased transport likely displaced age-0 Arctic cod northwards. Arctic cod were largely present in areas where bottom waters still reflected the conditions of Winter Water (Fig. 5f), which was present over the shelf prior to the input of warm water in spring. While age-0 pollock were found in high abundance in summer, it is unclear if these fish are able to establish permanent populations given the near-freezing temperatures they would experience on the shelf in winter (Woodgate et al., 2005; Stabeno et al., 2018).

The future of the Chukchi shelf pelagic community

If lower energy content subarctic species such as pollock continue to displace age-0 Arctic cod, the transition in gadid community structure could reduce energy available to higher trophic levels in the Chukchi Sea (Copeman et al., 2017). Our analysis suggests that the anticipated continued warming of the Chukchi shelf (Danielson et al., 2020) will substantially alter ecosystem function. We propose that the observations of gadids across the years encompassed by our survey data can be described by a conceptual model encompassing three environmental regimes. Under "historical" conditions (Fig. 8a), ice in the northern Bering Sea retreats in May and June (Frey et al., 2015), the Chukchi Sea remains relatively cool and surface waters reflect a mix of melt water, Bering/Chukchi Summer Water, and Alaskan Coastal Water (Danielson et al., 2017). In this regime, age-0 Arctic cod that are likely spawned to the south

(Vestfals et al., 2021) are the dominant gadids on the Chukchi shelf. They are primarily present in the northeastern Chukchi Sea where they experience intermediate temperatures as Winter Water warms in summer. These fish are then advected northwards during the fall towards the Chukchi and Beaufort shelf breaks and the central basin (Levine et al., 2020).

Under warming ocean conditions (Fig. 8b), when ice retreats from the northern Bering Sea earlier in spring (Wang et al., 2018), we propose a "warming" regime where temperatures are warmer across the shelf as a result of decreased sea ice extent. With a reduced cold pool in the Bering Sea, the density of adult pollock near the Bering Strait increases and leads to an increased supply of age-0 pollock on the Chukchi shelf, advected from the northern Bering Sea (Eisner et al., 2020; Baker, 2021). Hatch success for all gadids also increases as a result of warmer conditions on the Chukchi shelf and results in larger age-0 individuals in fall (Bouchard et al., 2017), prior to being advected farther north.

Under a third, "warming and increased transport" regime, northward transport increases along with temperature (Fig. 8c; Woodgate, 2018). Pelagic age-0 pollock and Arctic cod continue to be present on the Chukchi shelf in summer. As a result of increased transport, the residence time of age-0 gadids on the Chukchi shelf decreases. Arctic cod, which are known to spawn under sea ice (Ponomorenko, 2000), originate under this regime further north than pollock. Adult pollock increasingly overwinter and spawn in the ice-free central and northern Bering Sea. The population of age-0 Arctic cod is displaced to the Chukchi shelf break and Beaufort Sea earlier in the summer season, as the water present on the Chukchi shelf is transported north more rapidly. The consequences of this displacement are unknown for Arctic cod. For example, the displacement may result in a potential timing mismatch of their ontogenetic migration to take advantage of warmer Atlantic water along the Chukchi and Beaufort shelf breaks during transport off the Chukchi shelf in fall (Geoffroy et al., 2016). Age-0 pollock that may originate further south in the northern Bering Sea would be transported into the Chukchi along with the warmer water masses to subsequently dominate the gadid distribution on the central and southern shelf in late summer. Although adult pollock do not appear to be present in appreciable densities, under continued warming they may eventually colonize the Chukchi as they have the northern Bering (Eisner et al., 2020). While our time series of survey observations is limited, the 2012 and 2013 surveys are representative of the cooler historical regime (Fig. 8a), 2017 represents the warming regime (Fig. 8b), and 2019 represents the warming and increased transport regime (Figs. 7, 8c).

The spawning population that produces the age-0 Arctic cod observed in the northern Chukchi remains unknown. A migration path between spawning and feeding grounds for Arctic cod has been proposed (Forster et al., 2020) where fish spawn under sea ice in the northern Bering Sea, follow the ice retreat north to seasonal feeding areas, and return to the spawning grounds in late fall. This proposed migration may be altered by continued warming, as the reduction in suitable habitat (bottom temperatures <2 °C) for Arctic cod in the northern Bering Sea has led to decreases in summer populations (Baker, 2021). Modelling efforts based on regional advection have identified likely spawning grounds (Vestfals et al., 2021). However, spawning Arctic cod are difficult to sample due to seasonal ice cover. Without direct observations and tracking of spawning populations, our understanding of the spatio-temporal distributional patterns exhibited by age-0 gadids as they develop and return as adults, and the key environmental drivers that determine juvenile and adult survival and reproductive success is limited. Year-round in situ observations of Arctic cod migration and transport, for example through moorings or autonomous vehicles, are needed to further confirm and quantify the roles of transport in the distribution and movement of these fish (Levine et al., 2020).

If the ongoing changes observed in the physical oceanography of the Chukchi Sea influence growth and transport of age-0 gadids as we hypothesize, indirect environmental measurements could provide a basis for predicting future summer-time distributions of pelagic fishes in this region. Mooring-, satellite-, and shore-based observations as well as model-based predictions of ice, temperature, and transport are well established in the region (Frey et al., 2015; Woodgate, 2018; Janzen et al., 2019; Wang et al., 2018).

These data sources are the basis for the predictions of continued warming and higher transport into the Chukchi Sea. Northward shifts in the distribution of other marine animals have been associated with these changes in the physical environment. For example, changes in water mass transport have strongly influenced shifts in zooplankton distributions (Spear et al., 2020), which in turn, have influenced distribution shifts of their mobile predators (e.g., seabirds, Kuletz et al., 2020). These shifts in populations, which are now also documented in the pelagic fish community, provide insight into potential future states of the Chukchi ecosystem. Developing a mechanistic understanding of how the anticipated rapid increases in warming and transport in the Pacific Arctic will affect fishes is key to understanding future impacts on pelagic fish communities, their role in the ecosystem, and effective management of these species.

Acknowledgements

This research was conducted under the Arctic Integrated Ecosystem Research Program. Funding for the program was provided by North Pacific Research Board, the Bureau of Ocean Energy Management, the Collaborative Alaskan Arctic Studies Program, and the Office of Naval Research. In-kind support was contributed by the National Oceanic and Atmospheric Administration (NOAA) Alaska Fisheries Science Center and Pacific Marine Environmental Laboratory, the University of Alaska Fairbanks, the U.S. Fish & Wildlife Service, and the National Science Foundation. Bering Strait mooring observations are funded by NSF-OPP (1304052 and 1758565) with data available at http://psc.apl.washington.edu/BeringStrait.html. We would like to thank the Captain, crew, and science party of the R/V Ocean Starr for their assistance at sea. Any use of trade, firm, or product names is does not imply endorsement by the U.S. Government. The findings of this paper do not necessarily represent the views of the National Oceanic and Atmospheric Administration.

References

Baker, M.R., 2021. Contrast of warm and cold phases in the Bering Sea to understand spatial distributions of Arctic and sub-Arctic gadids. Polar Biol. https://doi.org/10.1007/s00300-021-02856-x

Bouchard, C., Fortier, L., 2011. Circum-arctic comparison of the hatching season of polar cod Boreogadus saida: A test of the freshwater winter refuge hypothesis. Prog. Oceanogr. 90, 105–116. https://doi.org/10.1016/j.pocean.2011.02.008

Bouchard, C., Geoffroy, M., LeBlanc, M., Majewski, A., Gauthier, S., Walkusz, W., Reist, J.D., Fortier, L., 2017. Climate warming enhances polar cod recruitment, at least transiently. Prog. Oceanogr. 156, 121–129. https://doi.org/10.1016/j.pocean.2017.06.008

Bradstreet, M.S.W., Finley, K.J., Sekerak, A.-D., Griffiths, W.B., Evans, C.R., Fabijan, M.F., Stallard, H.E., 1986. Aspects of the Biology of Arctic Cod (Boreogadus saida) and its Importance in Arctic Marine Food Chains, Canadian Technical Report of Fisheries and Aquatic Sciences. https://doi.org/10.1002/aic.12482

Brodeur, R.D., Wilson, M.T., Ciannelli, L., Doyle, M., Napp, J.M., 2002. Interannual and regional variability in distribution and ecology of juvenile pollock and their prey in frontal structures of the Bering Sea. Deep. Res. Part II Top. Stud. Oceanogr. 49, 6051–6067. https://doi.org/10.1016/S0967-0645(02)00333-8

Coachman, L.K., Aagaard, K., Tripp, R.B., 1975. Bering Strait: The Regional Physical Oceanography, University of Washington Press. University of Washington Press, Seattle. https://doi.org/10.1016/0146-6291(77)90492-1

Copeman, L.A., Laurel, B.J., Spencer, M., Sremba, A., 2017. Temperature impacts on lipid allocation among juvenile gadid species at the Pacific Arctic-Boreal interface: An experimental laboratory approach. Mar. Ecol. Prog. Ser. 566, 183–198. https://doi.org/10.3354/meps12040

Copeman, L., Spencer, M., Heintz, R., Vollenweider, J., Sremba, A., Helser, T., Logerwell, L., Sousa, L., Danielson, S., Pinchuk, A.I., Laurel, B., 2020. Ontogenetic patterns in lipid and fatty acid

biomarkers of juvenile polar cod (Boreogadus saida) and saffron cod (Eleginus gracilis) from across the Alaska Arctic. Polar Biol. https://doi.org/10.1007/s00300-020-02648-9
Danielson, S.L., Eisner, L., Ladd, C., Mordy, C., Sousa, L., Weingartner, T.J., 2017. A comparison between late summer 2012 and 2013 water masses, macronutrients, and phytoplankton standing crops in the northern Bering and Chukchi Seas. Deep. Res. Part II Top. Stud. Oceanogr. 135, 7–26. https://doi.org/10.1016/j.dsr2.2016.05.024
Danielson, S.L., Ahkinga, O., Ashjian, C., Basyuk, E., Cooper, L.W., Eisner, L., Farley, E., Iken, K.B., Grebmeier, J.M., Juranek, L., Khen, G., Jayne, S.R., Kikuchi, T., Ladd, C., Lu, K., McCabe, R.M., Moore, G.W.K., Nishino, S., Ozenna, F., Pickart, R.S., Polyakov, I., Stabeno, P.J., Thoman, R., Williams, W.J., Wood, K., Weingartner, T.J., 2020. Manifestation and consequences of warming and altered heat fluxes over the Bering and Chukchi Sea continental shelves. Deep. Res. Part II Top. Stud. Oceanogr. 177. https://doi.org/10.1016/j.dsr2.2020.104781
[Dataset] De Robertis, A., 2021. De Robertis et al., 2017 – Chukchi shelf acoustic-trawl survey (corrected). Mendeley Data, v1. https://doi.org/10.17632/py3859yhnf.1
De Robertis, A., Taylor, K., 2014. In situ target strength measurements of the scyphomedusa Chrysaora melanaster. Fish. Res. 153, 18–23. https://doi.org/10.1016/j.fishres.2014.01.002
De Robertis, A., Taylor, K., Wilson, C.D., Farley, E. V., 2017. Abundance and distribution of Arctic cod (Boreogadus saida) and other pelagic fishes over the U.S. Continental Shelf of the Northern Bering and Chukchi Seas. Deep. Res. Part II Top. Stud. Oceanogr. 135, 51–65. https://doi.org/10.1016/j.dsr2.2016.03.002
Demer, D.A., Berger, L., Bernasconi, M., Bethke, E., Boswell, K., Chu, D., Domokos, R., Dunford, A., Fassler, S., Gauthier, S., Hufnagle, L.T., Jech, J.M., Bouffant, N., Lebourges-Dhaussy, A., Lurton, X., Macaulay, G.J., Perrot, Y., Ryan, T., Parker-Stetter, S., Stienessen, S., Weber, T., Williamson, N., 2015. Calibration of acoustic instruments. ICES Cooperative Research Reports 326.
Dupont, N., Durant, J.M., Langangen, Ø., Gjøsæter, H., Stige, L.C., 2020. Sea ice, temperature, and prey effects on annual variations in mean lengths of a key Arctic fish, Boreogadus saida, in the Barents Sea. ICES J. Mar. Sci. https://doi.org/10.1093/icesjms/fsaa040
Eisner, L., Hillgruber, N., Martinson, E., Maselko, J., 2013. Pelagic fish and zooplankton species assemblages in relation to water mass characteristics in the northern Bering and southeast Chukchi seas. Polar Biol. 36, 87–113. https://doi.org/10.1007/s00300-012-1241-0
Eisner, L.B., Zuenko, Y.I., Basyuk, E.O., Britt, L.L., Duffy-Anderson, J.T., Kotwicki, S., Ladd, C., Cheng, W., 2020. Environmental impacts on walleye pollock (Gadus chalcogrammus) distribution across the Bering Sea shelf. Deep. Res. Part II Top. Stud. Oceanogr. 181–182, 104881. https://doi.org/10.1016/j.dsr2.2020.104881
[Dataset] Farley, E., Levine, R., 2021a. Surface Trawl Dataset, Arctic Integrated Ecosystem Research Program, August - September 2017. Research Workspace, v10.24431_rw1k58b_20210608T181300Z. https://doi.org/10.24431/rw1k58b
[Dataset] Farley, E., Levine, R., 2021b. Surface Trawl Dataset, Arctic Integrated Ecosystem Research Program, August - September 2019. Research Workspace, v10.24431_rw1k58a_20210608T172806Z. https://doi.org/10.24431/rw1k58ba
Forster, C.E., Norcross, B.L., Mueter, F.J., Logerwell, E.A., Seitz, A.C., 2020. Spatial patterns, environmental correlates, and potential seasonal migration triangle of polar cod (Boreogadus saida) distribution in the Chukchi and Beaufort seas. Polar Biol. 73. https://doi.org/10.1007/s00300-020-02631-4
Fossheim, M., Primicerio, R., Johannesen, E., Ingvaldsen, R.B., Aschan, M.M., Dolgov, A. V., 2015. Recent warming leads to a rapid borealization of fish communities in the Arctic. Nat. Clim. Chang. 5, 673–677. https://doi.org/10.1038/nclimate2647
Frey, K.E., Moore, G.W.K., Cooper, L.W., Grebmeier, J.M., 2015. Divergent patterns of recent sea ice cover across the Bering, Chukchi, and Beaufort seas of the Pacific Arctic Region. Prog. Oceanogr. 136, 32–49. https://doi.org/10.1016/j.pocean.2015.05.009

Geoffroy, M., Majewski, A., LeBlanc, M., Gauthier, S., Walkusz, W., Reist, J.D., Fortier, L., 2016. Vertical segregation of age-0 and age-1+ polar cod (Boreogadus saida) over the annual cycle in the Canadian Beaufort Sea. Polar Biol. 39, 1023–1037. https://doi.org/10.1007/s00300-015-1811-z

Goddard, P., Lauth, R., Armistead, C., 2014. Results of the 2012 Chukchi Sea Bottom Trawl Survey of Bottomfishes, Crabs, and Other Demersal Macrofauna. NOAA Tech. Memo. NMFS-AFSC-, 123.

Helser, T.E., Colman, J.R., Anderl, D.M., Kastelle, C.R., 2017. Growth dynamics of saffron cod (Eleginus gracilis) and Arctic cod (Boreogadus saida) in the Northern Bering and Chukchi Seas. Deep Sea Res. Part II Top. Stud. Oceanogr. 135, 66–77. https://doi.org/10.1016/j.dsr2.2015.12.009

Honakalehto, T., McCarthy, A., 2015. Results of the acoustic-trawl survey of walleye pollock (Gadus chalcogrammus) on the U.S. and Russian Bering Sea Shelf in June - August 2014 (DY1407). AFSC Processed Rep. 2015-07, 63 p. Alaska Fish. Sci. Cent., NOAA, Natl. Mar. Fish. Serv., 7600 Sand Point Way NE, Seattle WA 98115.

Hunt, G.L., Blanchard, A.L., Boveng, P., Dalpadado, P., Drinkwater, K.F., Eisner, L., Hopcroft, R.R., Kovacs, K.M., Norcross, B.L., Renaud, P., Reigstad, M., Renner, M., Skjoldal, H.R., Whitehouse, A., Woodgate, R.A., 2013. The barents and chukchi seas: Comparison of two Arctic shelf ecosystems. J. Mar. Syst. 109–110, 43–68. https://doi.org/10.1016/j.jmarsys.2012.08.003

Huntington, H.P., Danielson, S.L., Wiese, F.K., Baker, M., Boveng, P., Citta, J.J., De Robertis, A., Dickson, D.M.S., Farley, E., George, J.C., Iken, K., Kimmel, D.G., Kuletz, K., Ladd, C., Levine, R., Quakenbush, L., Stabeno, P., Stafford, K.M., Stockwell, D., Wilson, C., 2020. Evidence suggests potential transformation of the Pacific Arctic ecosystem is underway. Nat. Clim. Chang. https://doi.org/10.1038/s41558-020-0695-2

Janzen, C.D., McCammon, M., Danielson, S.S.L., Weingartner, T., Statscewich, H., Page, E., Heim, B., 2019. Innovative real-time observing capabilities for remote coastal regions. Front. Mar. Sci. 6, 1–8. https://doi.org/10.3389/fmars.2019.00176

Koenker, B.L., Copeman, L.A., Laurel, B.J., 2018. Impacts of temperature and food availability on the condition of larval Arctic cod (Boreogadus saida) and walleye pollock (Gadus chalcogrammus). ICES J. Mar. Sci. 75, 2370–2385. https://doi.org/10.1093/icesjms/fsy052

Kortsch, S., Primicerio, R., Fossheim, M., Dolgov, A. V., Aschan, M., 2015. Climate change alters the structure of arctic marine food webs due to poleward shifts of boreal generalists. Proc. R. Soc. B Biol. Sci. 282. https://doi.org/10.1098/rspb.2015.1546

Kotwicki, S., Buckley, T.W., Honkalehto, T., Walters, G., 2005. Variation in the distribution of walleye pollock (Theragra chalcogramma) with temperature and implications for seasonal migration. Fish. Bull. 103, 574–587.

Kotwicki, S., Lauth, R.R., Williams, K., Goodman, S.E., 2017. Selectivity ratio: A useful tool for comparing size selectivity of multiple survey gears. Fish. Res. 191, 76–86. https://doi.org/10.1016/j.fishres.2017.02.012

Kuletz, K., Cushing, D., Labunski, E., 2020. Distributional shifts among seabird communities of the Northern Bering and Chukchi seas in response to ocean warming during 2017–2019. Deep. Res. Part II Top. Stud. Oceanogr. 181–182, 104913. https://doi.org/10.1016/j.dsr2.2020.104913

Laurel, B.J., Copeman, L.A., Spencer, M., Iseri, P., 2017. Temperature-dependent growth as a function of size and age in juvenile Arctic cod (Boreogadus saida). ICES J. Mar. Sci. 74, 1614–1621. https://doi.org/10.1093/icesjms/fsx028

Laurel, B.J., Spencer, M., Iseri, P., Copeman, L.A., 2016. Temperature-dependent growth and behavior of juvenile Arctic cod (Boreogadus saida) and co-occurring North Pacific gadids. Polar Biol. 39, 1127–1135. https://doi.org/10.1007/s00300-015-1761-5

Levine, R.M., De Robertis, A., Grünbaum, D., Woodgate, R., Mordy, C.W., Mueter, F., Cokelet, E., Lawrence-Slavas, N., Tabisola, H., 2020. Autonomous vehicle surveys indicate that flow reversals retain juvenile fishes in a highly advective high-latitude ecosystem. Limnol. Oceanogr. 9999, lno.11671. https://doi.org/10.1002/lno.11671

Logerwell, E., Busby, M., Carothers, C., Cotton, S., Duffy-Anderson, J., Farley, E., Goddard, P., Heintz, R., Holladay, B., Horne, J., Johnson, S., Lauth, B., Moulton, L., Neff, D., Norcross, B., Parker-Stetter, S., Seigle, J., Sformo, T., 2015. Fish communities across a spectrum of habitats in the western Beaufort Sea and Chukchi Sea. Prog. Oceanogr. 136, 115–132. https://doi.org/10.1016/j.pocean.2015.05.013

Lowry, K.E., Pickart, R.S., Mills, M.M., Brown, Z.W., van Dijken, G.L., Bates, N.R., Arrigo, K.R., 2015. The influence of winter water on phytoplankton blooms in the Chukchi Sea. Deep. Res. Part II Top. Stud. Oceanogr. 118, 53–72. https://doi.org/10.1016/j.dsr2.2015.06.006

Marsh, J.M., Mueter, F.J., 2020. Influences of temperature, predators, and competitors on polar cod (Boreogadus saida) at the southern margin of their distribution. Polar Biol. 43, 995–1014. https://doi.org/10.1007/s00300-019-02575-4

Matley, J.K., Fisk, A.T., Dick, T.A., 2012. Seabird predation on Arctic cod during summer in the Canadian Arctic. Mar. Ecol. Prog. Ser. 450, 219–228. https://doi.org/10.3354/meps09561

Mecklenburg, C., Lynghammar, A., Johannesen, E., Byrkjedal, I., Christiansen, J.S., Karamushko, O. V, Mecklenburg, T.A., Møller, P.R., Steinke, D., Wienerroither, R.M., 2018. Marine Fishes of the Arctic Region Volume II. CAFF Monitoring Series Report 20. Akureyri, Iceland: Conservation of Arctic Flora and Fauna.

Morris, B.A., 2019. Seasonality and forcing factors of the Alaskan Coastal Current in the Bering Strait from July 2011 to July 2012. University of Washington.

Mueter, F.J., Bond, N.A., Ianelli, J.N., Hollowed, A.B., 2011. Expected declines in recruitment of walleye pollock (Theragra chalcogramma) in the eastern Bering Sea under future climate change. ICES J. Mar. Sci. 68, 1284–1296. https://doi.org/10.1093/icesjms/fsr022

Norcross, B.L., Raborn, S.W., Holladay, B.A., Gallaway, B.J., Crawford, S.T., Priest, J.T., Edenfield, L.E., Meyer, R., 2013. Northeastern Chukchi Sea demersal fishes and associated environmental characteristics, 2009-2010. Cont. Shelf Res. 67, 77–95. https://doi.org/10.1016/j.csr.2013.05.010

O'Leary, C.A., Thorson, J.T., Ianelli, J.N., Kotwicki, S., 2020. Adapting to climate-driven distribution shifts using model-based indices and age composition from multiple surveys in the walleye pollock (Gadus chalcogrammus) stock assessment. Fish. Oceanogr. 29, 541–557. https://doi.org/10.1111/fog.12494

Orlov, A.M., Benzik, A.N., Vedishcheva, E.V., Gafitsky, S.V., Gorbatenko, K.M., Goryanina, S.V., Zubarevich, V.L., Kodryan, K.V., Nosov, M.A., Orlova, S.Y., Pedchenko, A.P., Rybakov, M.O., Sokolov, A.M., Somov, A.A., Subbotin, S.N., Taptygin, M.Y., Firsov, Y.L., Khleborodov, A.S., Chikilev, V.G., 2019. Fisheries research in the Chukchi Sea at the RV Professor Levanidov in August 2019: some preliminary results. Tr. VNIRO 178, 206–220. https://doi.org/10.36038/2307-3497-2019-178-206-220

Overland, J., Dunlea, E., Box, J.E., Corell, R., Forsius, M., Kattsov, V., Olsen, M.S., Pawlak, J., Reiersen, L.O., Wang, M., 2019. The urgency of Arctic change. Polar Sci. 21, 6–13. https://doi.org/10.1016/j.polar.2018.11.008

Ponomarenko, V.P., 2000. Eggs, larvae, and juveniles of polar cod Boreogadus saida in the Barents, Kara, and White Seas. J. Ichthyol. 40, 165–173.

Quast, J.C., 1974. Density distribution of juvenile Arctic cod, Boreogadus saida, in the eastern Chukchi Sea in the fall of 1970. Fish. Bull. 72, 1094–1105.

Sigler, M.F., Mueter, F.J., Bluhm, B.A., Busby, M.S., Cokelet, E.D., Danielson, S.L., Robertis, A. De, Eisner, L.B., Farley, E. V., Iken, K., Kuletz, K.J., Lauth, R.R., Logerwell, E.A., Pinchuk, A.I., 2017. Late summer zoogeography of the northern Bering and Chukchi seas. Deep Sea Res. Part II Top. Stud. Oceanogr. 135, 168–189. https://doi.org/10.1016/j.dsr2.2016.03.005

Simmonds, J., MacLennan, D., 2005. Fisheries Acoustics: Theory and Practice, 2nd ed. Blackwell.

Spear, A., Napp, J., Ferm, N., Kimmel, D., 2020. Advection and in situ processes as drivers of change for the abundance of large zooplankton taxa in the Chukchi Sea. Deep. Res. Part II Top. Stud. Oceanogr. 177, 104814. https://doi.org/10.1016/j.dsr2.2020.104814

Spies, I., Gruenthal, K.M., Drinan, D.P., Hollowed, A.B., Stevenson, D.E., Tarpey, C.M., Hauser, L., 2020. Genetic evidence of a northward range expansion in the eastern Bering Sea stock of Pacific cod. Evol. Appl. 13, 362–375. https://doi.org/10.1111/eva.12874

Stabeno, P.J., Bell, S.W., 2019. Extreme Conditions in the Bering Sea (2017–2018): Record-Breaking Low Sea-Ice Extent. Geophys. Res. Lett. 46, 8952–8959. https://doi.org/10.1029/2019GL083816

Stabeno, P., Kachel, N., Ladd, C., Woodgate, R., 2018. Flow Patterns in the Eastern Chukchi Sea: 2010–2015. J. Geophys. Res. Ocean. 123, 1177–1195. https://doi.org/10.1002/2017JC013135

Stevenson, D.E., Lauth, R.R., 2019. Bottom trawl surveys in the northern Bering Sea indicate recent shifts in the distribution of marine species. Polar Biol. 42, 407–421. https://doi.org/10.1007/s00300-018-2431-1

Towler, R., Williams Kresimir, K., 2010. An inexpensive millimeter-accuracy electronic length measuring board. Fish. Res. 106, 107–111. https://doi.org/10.1016/j.fishres.2010.06.012

Vestfals, C.D., Mueter, F.J., Hedstrom, K.S., Laurel, B.J., Petrik, C.M., Duffy-Anderson, J.T., Danielson, S.L., 2021. Modeling the dispersal of polar cod (Boreogadus saida) and saffron cod (Eleginus gracilis) early life stages in the Pacific Arctic using a biophysical transport model. Prog. Oceanogr. 102571. https://doi.org/10.1016/j.pocean.2021.102571

Wang, M., Yang, Q., Overland, J.E., Stabeno, P., 2018. Sea-ice cover timing in the Pacific Arctic: The present and projections to mid-century by selected CMIP5 models. Deep. Res. Part II Top. Stud. Oceanogr. 152, 22–34. https://doi.org/10.1016/j.dsr2.2017.11.017

Wassmann, P., Duarte, C.M., Agustí, S., Sejr, M.K., 2011. Footprints of climate change in the Arctic marine ecosystem. Glob. Chang. Biol. 17, 1235–1249. https://doi.org/10.1111/j.1365-2486.2010.02311.x

Weingartner, T., Dobbins, E., Danielson, S., Winsor, P., Potter, R., Statscewich, H., 2013. Hydrographic variability over the northeastern Chukchi Sea shelf in summer-fall 2008-2010. Cont. Shelf Res. 67, 5–22. https://doi.org/10.1016/j.csr.2013.03.012

Whitehouse, G.A., Aydin, K., Essington, T.E., Hunt, G.L., 2014. A trophic mass balance model of the eastern Chukchi Sea with comparisons to other high-latitude systems. Polar Biol. 37, 911–939. https://doi.org/10.1007/s00300-014-1490-1

Woodgate, R.A., Peralta-Ferriz, C., 2021. Warming and Freshening of the Pacific Inflow to the Arctic from 1990-2019 implying dramatic shoaling in Pacific Winter Water ventilation of the Arctic water column. Geophys. Res. Lett. https://doi.org/10.1029/2021GL092528

Woodgate, R.A., Aagaard, K., Weingartner, T.J., 2005. A year in the physical oceanography of the Chukchi Sea: Moored measurements from autumn 1990-1991. Deep. Res. Part II Top. Stud. Oceanogr. 52, 3116–3149. https://doi.org/10.1016/j.dsr2.2005.10.016

Woodgate, R.A., Weingartner, T., Lindsay, R., 2010. The 2007 Bering Strait oceanic heat flux and anomalous Arctic sea-ice retreat. Geophys. Res. Lett. 37, 1–5. https://doi.org/10.1029/2009GL041621

Woodgate, R.A., 2018. Increases in the Pacific inflow to the Arctic from 1990 to 2015, and insights into seasonal trends and driving mechanisms from year-round Bering Strait mooring data. Prog. Oceanogr. 160, 124–154. https://doi.org/10.1016/j.pocean.2017.12.007

Wyllie-Echeverria, T., Wooster, W.S., 1998. Year-to-year variations in Bering Sea ice cover and some consequences for fish distributions. Fish. Oceanogr. 7, 159–170. https://doi.org/10.1046/j.1365-2419.1998.00058.x

Yasuma, H., Nakagawa, R., Yamakawa, T., Miyashita, K., Aoki, I., 2009. Density and sound-speed contrasts, and target strength of Japanese sandeel Ammodytes personatus. Fish. Sci. 75, 545–552. https://doi.org/10.1007/s12562-009-0091-3

Table 1: Mean fish backscatter and total number of fish for each key pelagic sound scattering species estimated with acoustic-trawl methods in 2017 and 2019. The total area of the survey region was 1.48 x 10^5 km^2 in 2017 and 1.53 x 10^5 km^2 in 2019, with >92% of the survey area overlapping between both years.

	2017	2019
Mean fish backscatter (s_A, m^2 nmi^{-2})	1118.5	354.8
Arctic cod	8.7×10^{11}	1.2×10^{11}
Walleye pollock	7.2×10^{10}	5.7×10^{10}
Capelin	1.5×10^{10}	3.7×10^{9}
Saffron cod	4.6×10^{9}	1.8×10^{9}
Pacific cod	9.4×10^{9}	8.9×10^{8}
Pacific herring	Not present	3.1×10^{9}

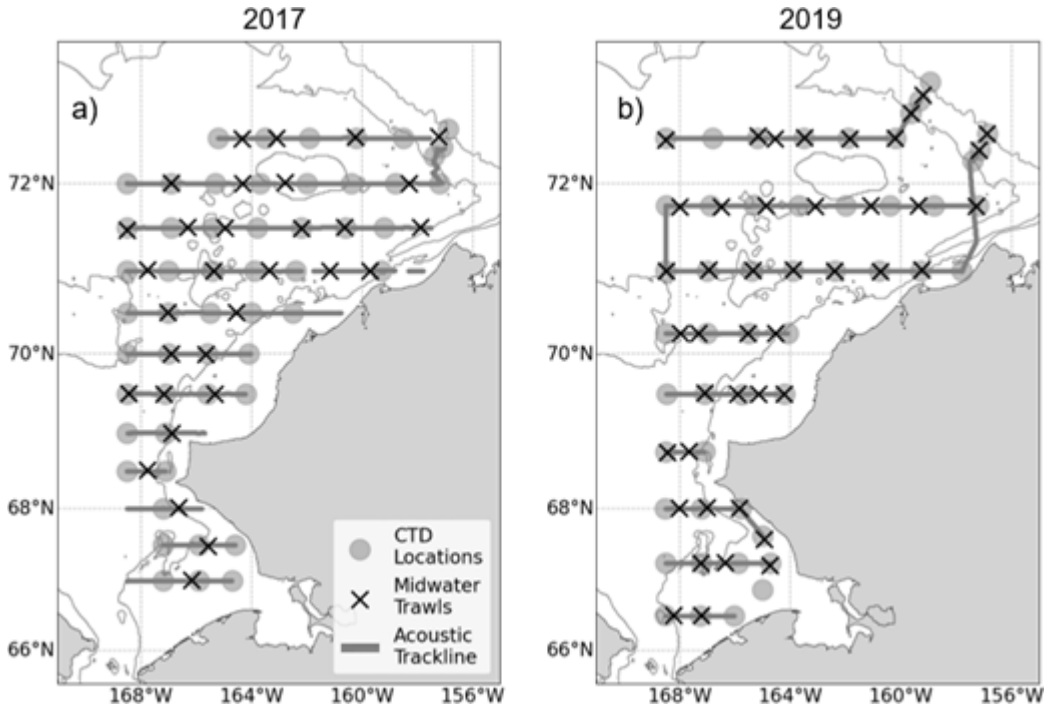

Fig. 1: Study area in (a) 2017 and (b) 2019. The 40-, 100-, and 1000-m depth contours are shown.

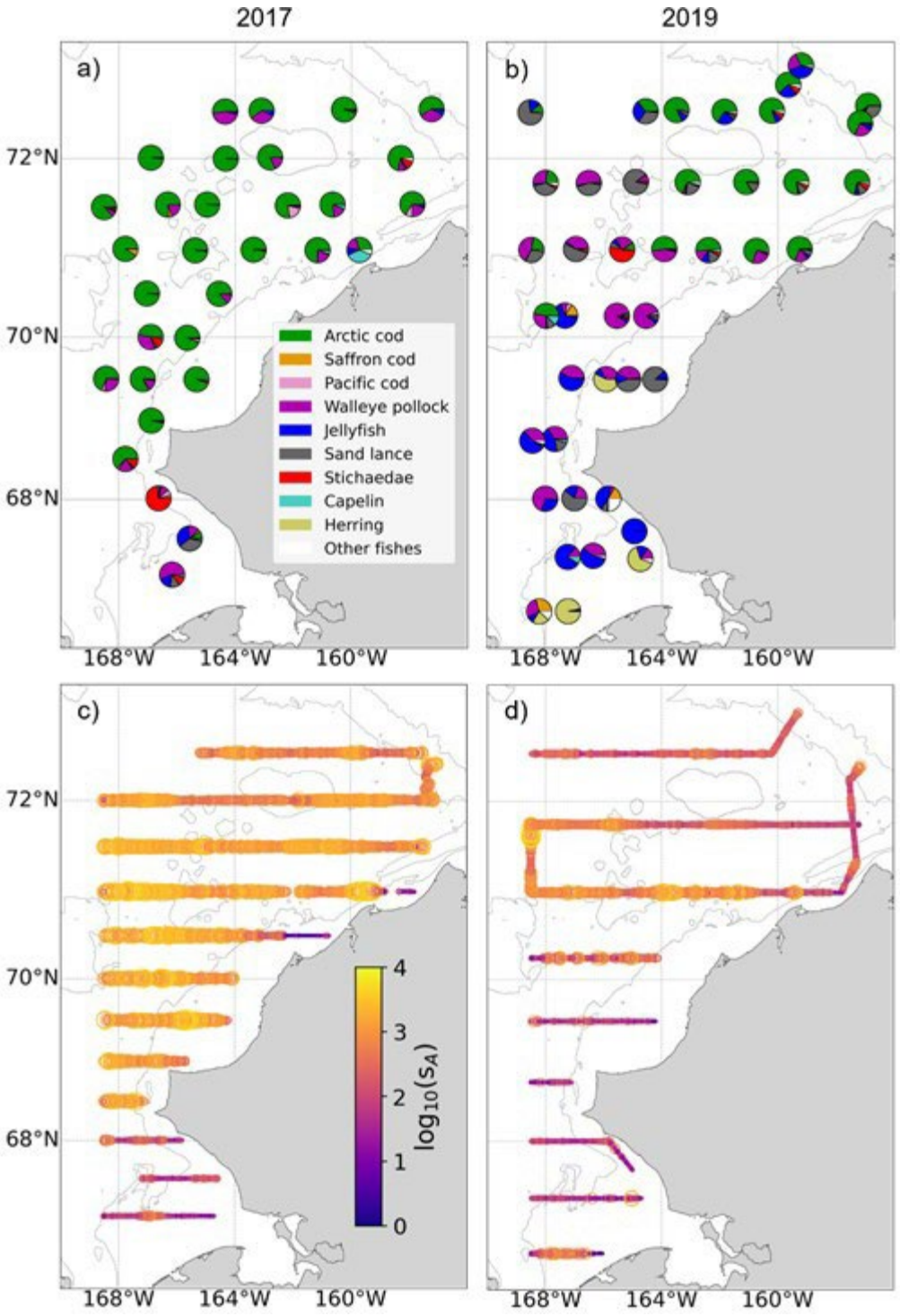

Fig. 2: Catch composition as proportion of individuals captured in each midwater trawl in (a) 2017 and (b) 2019. 38 kHz backscatter from fishes (s_A, m^2 nmi^{-2}) along the survey transects during the c) 2017 and d) 2019 surveys. The 40-, 100-, and 1000-m depth contours are shown.

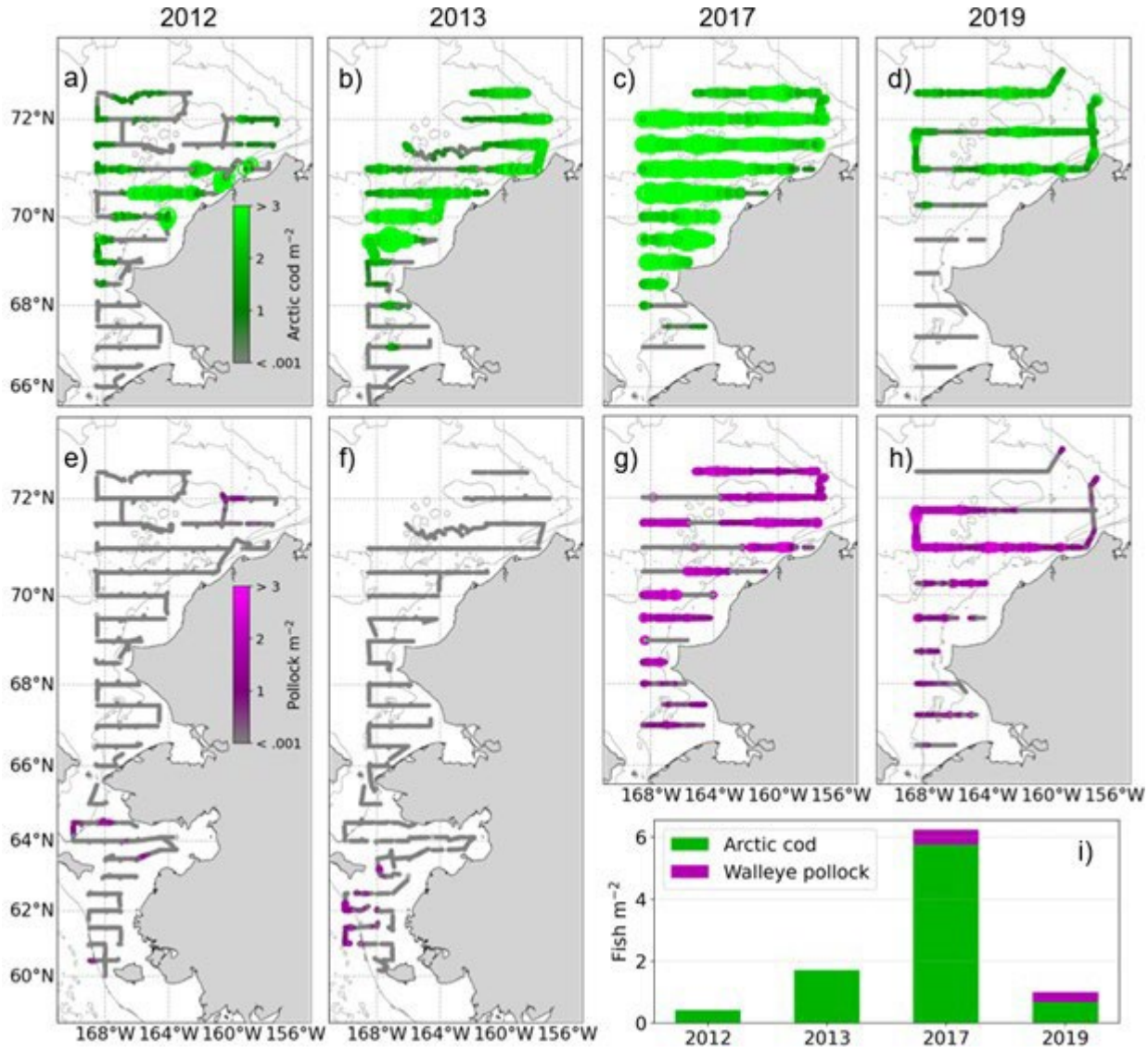

Fig. 3: Density of Arctic cod as estimated by acoustic-trawl methods in 0.5 nmi along-transect intervals in (a) 2012, (b) 2013, (c) 2017, and (d) 2019. Density of walleye pollock in (e) 2012, (f) 2013, (g) 2017, and (h) 2019. The 40-, 100-, and 1000-m depth contours are shown. In 2017 and 2019, the entire survey extent is shown. In 2012 and 2013, plots for Arctic cod (a, b) show only the region north of the Bering Strait (66 °N). This encompasses all Arctic cod except for an aggregation of large (age 1+) individuals captured in one trawl in 2012 at 65 N (not shown; see De Robertis et al., 2017, their Figure 2). (i) Mean areal density (fish m^{-2}) of Arctic cod and pollock north of 66 °N. Pollock were present in 2012 but their density was too low to be visible in the chart.

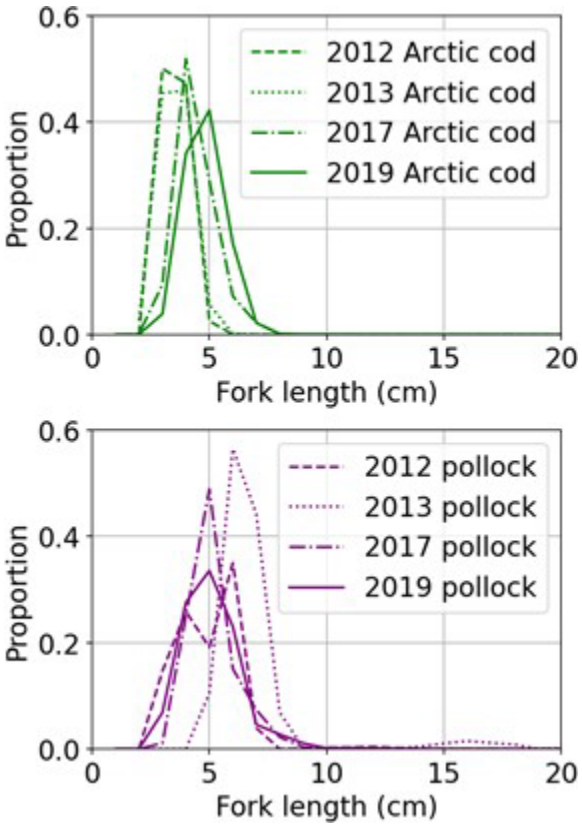

Fig. 4: Size distributions estimated by acoustic-trawl methods of (a) Arctic cod and (b) pollock in each survey year.

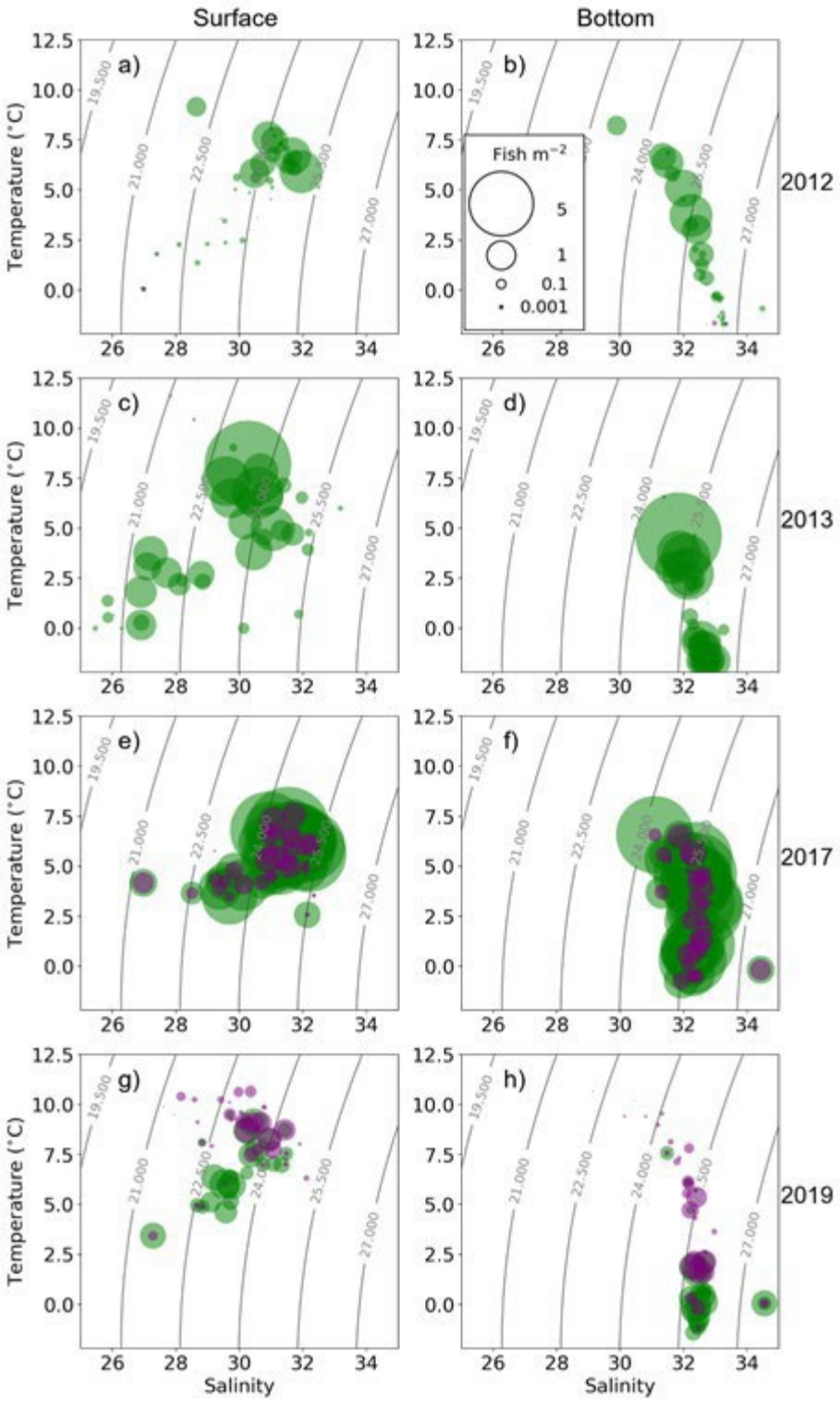

Fig. 5: Surface and bottom temperature and salinity at CTD stations in (a, b) 2012, (c, d) 2013, (e, f) 2017, and (g, h) 2019, where the size of each point indicates the abundance of Arctic cod (green) and walleye pollock (purple) in the transect intervals associated with the station (see methods for details).

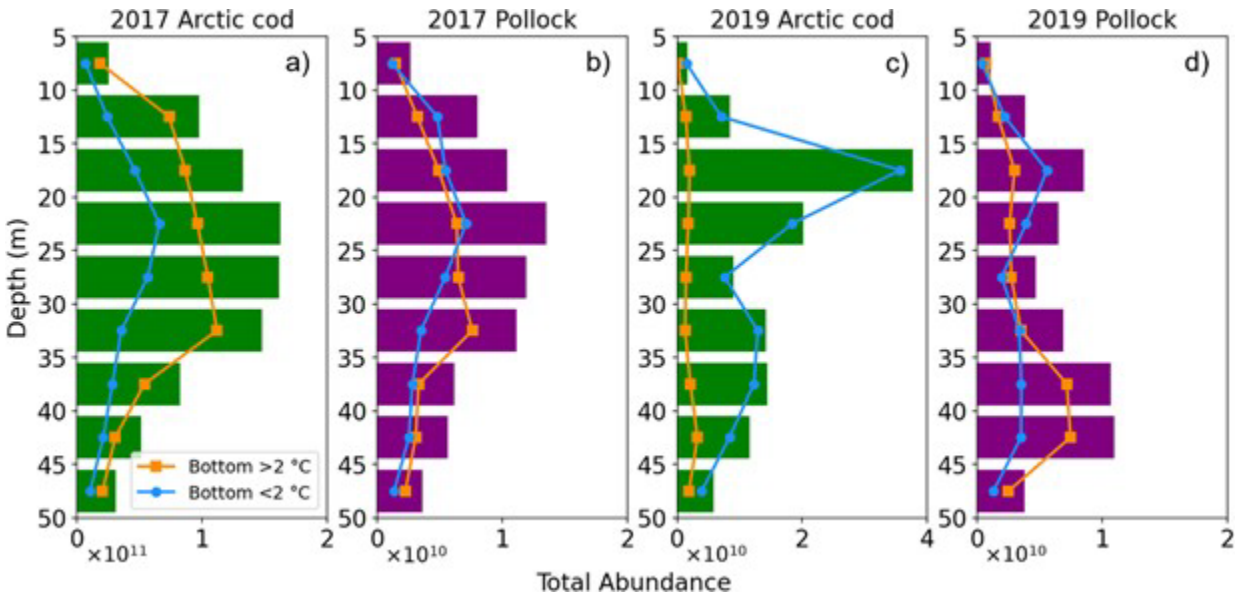

Fig. 6: Total abundance of Arctic cod (green) and pollock (purple) by depth in the water column in (a, b) 2017 and (c, d) 2019. The lines in each panel break down the total abundance into regions where bottom temperatures were >2 °C (orange) <2 °C (blue).

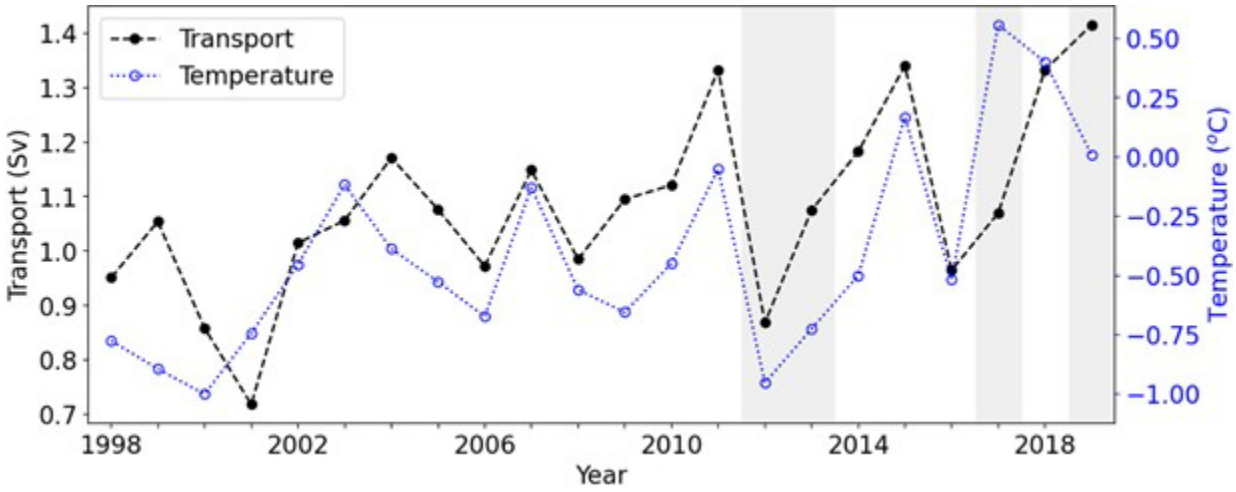

Fig. 7: Mean transport (black dashed line) and bottom temperatures (blue dotted line) measured at Bering Strait (A3 mooring, Woodgate, 2018; Woodgate and Peralta-Ferriz, 2021) from January to August of each year (1998 - 2019). Years of acoustic-trawl surveys (2012, 2013, 2017, 2019) are indicated by the grey-shaded regions.

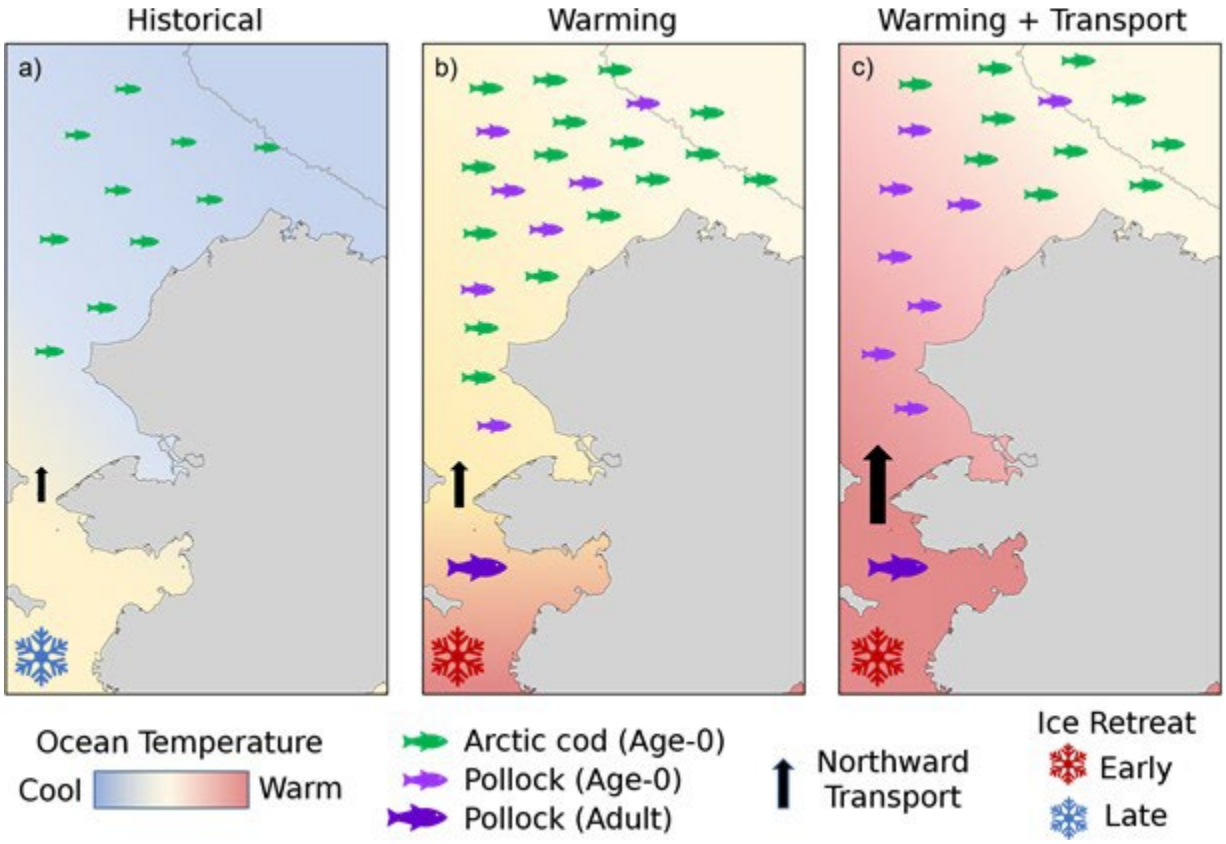

Fig. 8: Hypothesized scenarios based on observations of the Chukchi Sea gadid community. (a) Under historical conditions of later ice retreat, Arctic cod are observed in intermediate and cool waters across the Chukchi Shelf. (b) With increased warming and early ice retreat, age-0 Arctic cod increase in abundance and size across as a result of increasing temperatures. Increased presence of adult walleye pollock in the northern Bering Sea results in the transport of age-0 pollock into the Chukchi, where conditions are favorable for both gadid species. (c) With increased transport of warmer waters from the Bering Sea, Arctic cod are displaced further north along with the intermediate temperature waters. Age-0 pollock from the northern Bering Sea are transported with the warmer waters and become the dominant gadid in the southern portion of the shelf. The 1000-m depth contour is shown to indicate the Chukchi shelf break.

S1 Supplementary Figures and Tables

Table S1: Linear models used to convert TL to SL, TL to FL, and SL to FL based on the different length measurements taken on the same fish specimen. Number of observations (n) and the range of lengths used to fit each model are included. All models were significant ($p<0.001$).

Species	X	Y	n	Length range in model (mm)	Intercept	Slope	R^2
Arctic cod	TL	SL	1,055	18-189	0.364	0.909	0.999
	TL	FL	192	28-189	-0.137	0.967	0.999
	FL	SL	190	27-230	0.496	0.936	0.998
	SL	FL	190	28-230	-0.39	1.066	0.998
Walleye pollock	TL	SL	103	41-108	1.135	0.902	0.996
	TL	FL	38	71-108	-0.636	0.991	0.997
	FL	SL	77	37-106	-1.711	0.948	0.997
	SL	FL	77	42-106	2.031	1.051	0.997
Saffron cod	TL	SL	195	17-268	-0.177	0.92	1
	TL	FL	18	106-222	-0.681	0.991	0.999
	FL	SL	42	54-260	-9.703	0.972	0.996
	SL	FL	42	68-260	10.755	1.025	0.996
Pacific cod	TL	SL	120	47-110	1.284	0.902	0.987
	TL	FL	0	N/A	N/A	N/A	N/A
	FL	SL	11	51-78	-0.663	0.952	0.97
	SL	FL	11	55-78	2.701	1.019	0.97

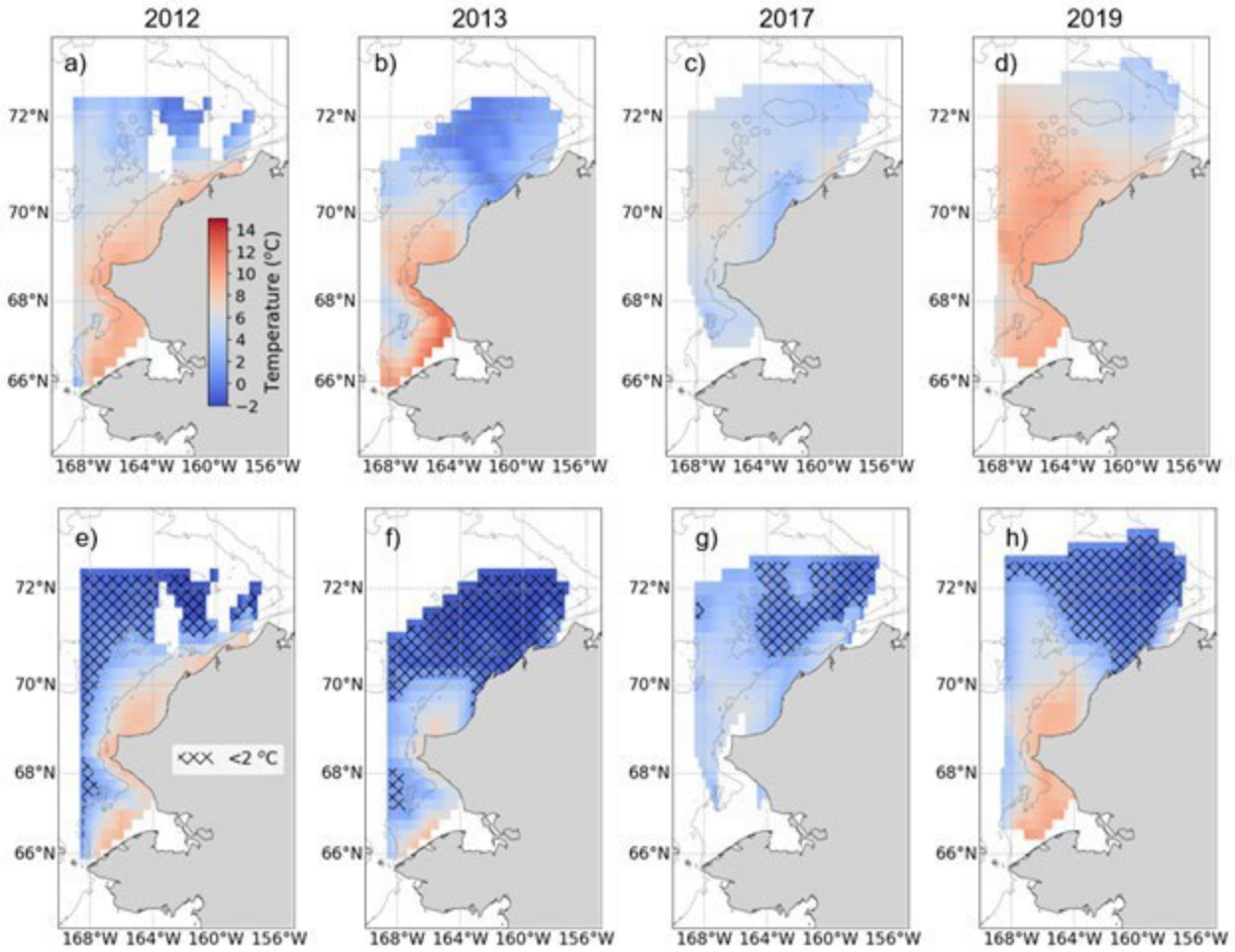

Fig. S1: Linearly interpolated mean surface (top row) and bottom (bottom row, see methods for details) temperatures observed in CTD casts in (a, e) 2012, (b, f) 2013, (c, g) 2017, and (d, h) 2019. Region where bottom temperatures were <2 °C indicated by the hatching (e, f).

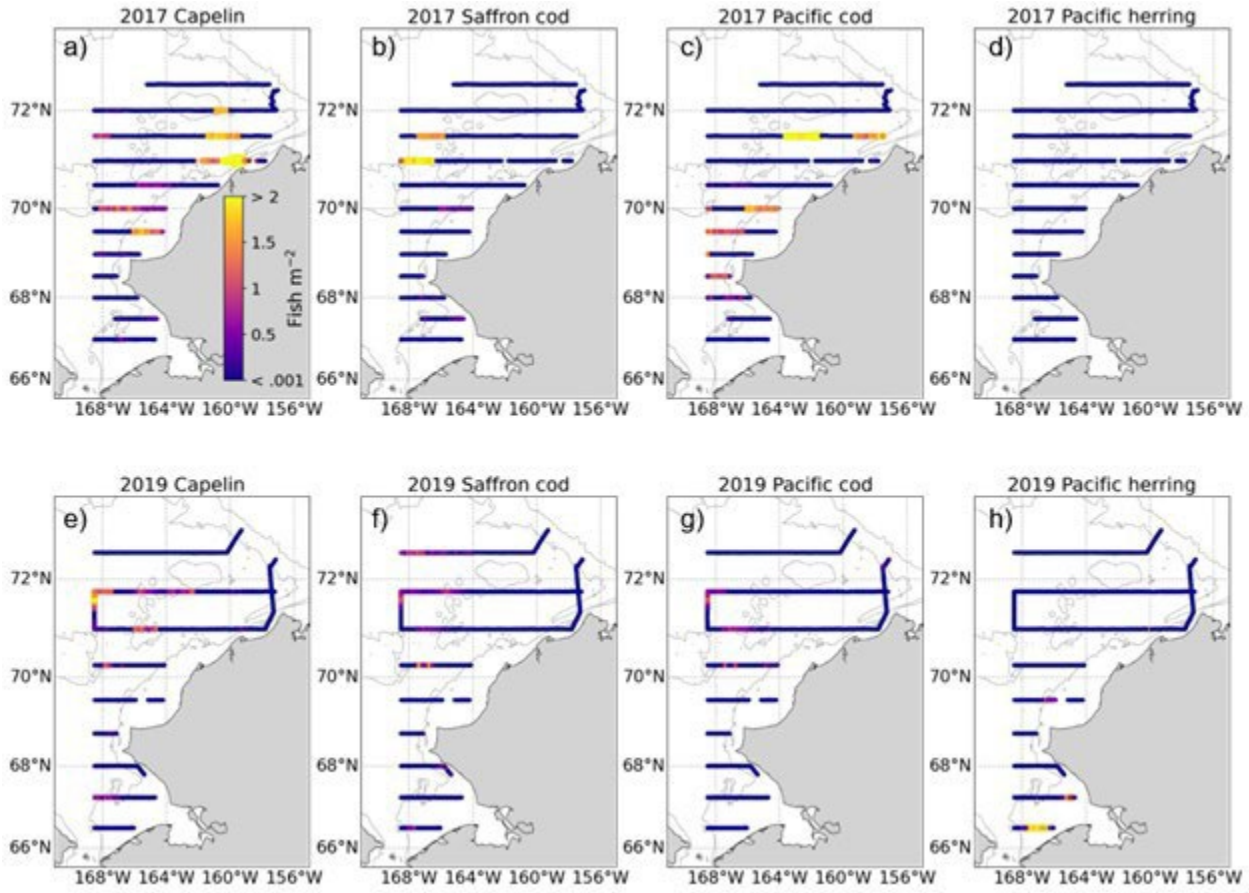

Fig. S2: Density (fish m-2) of (a, e) capelin, (b, f) Saffron cod, (c, g) Pacific cod, and (d, h) Pacific herring estimated by acoustic-trawl methods in 0.5 nmi along-track intervals in 2017 (top row) and 2019 (bottom row). The 40-, 100-, and 1000-m depth contours are shown.

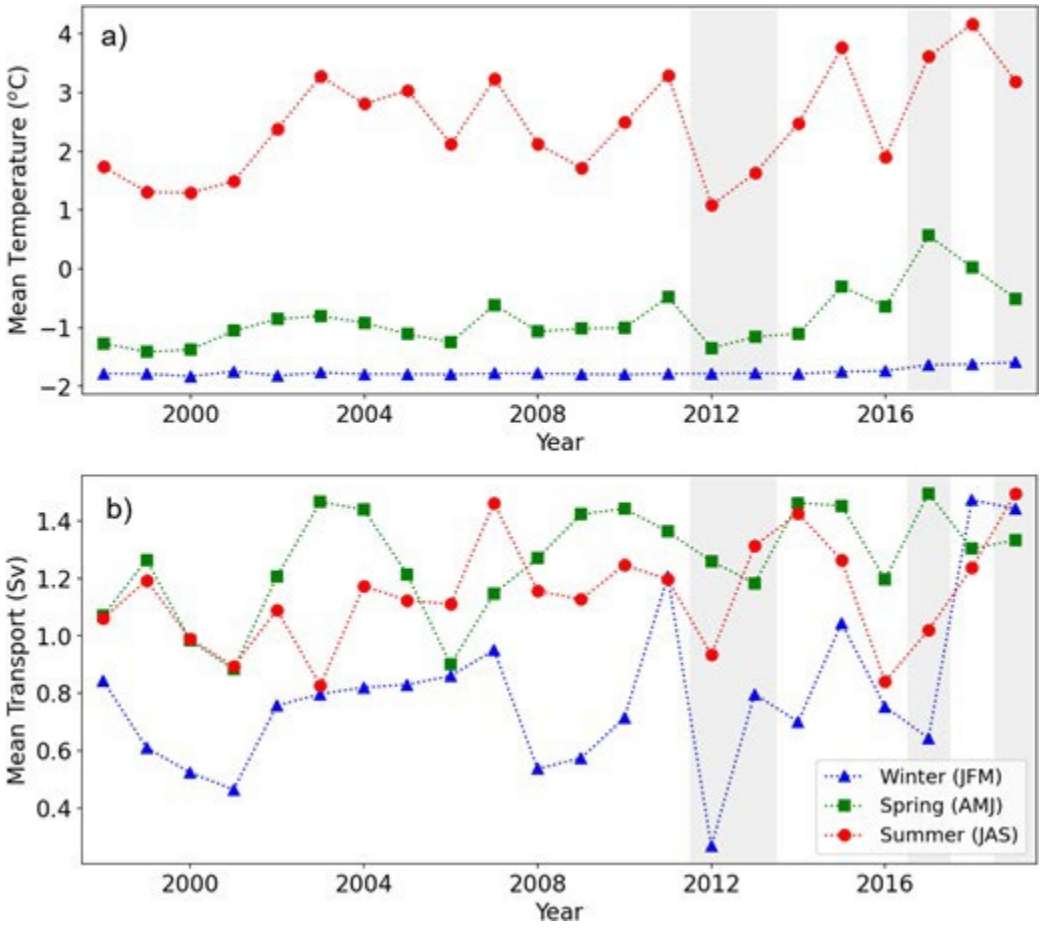

Fig. S3: Mean winter (January, February, March), spring (April, May, June) and summer (July, August, September) a) bottom temperature and b) transport observed at Bering Strait A3 mooring. Years of acoustic-trawl surveys (2012, 2013, 2017, 2019) are indicated by the grey-shaded regions.

References

Woodgate, R.A., 2018. Increases in the Pacific inflow to the Arctic from 1990 to 2015, and insights into seasonal trends and driving mechanisms from year-round Bering Strait mooring data. Progress in Oceanography 160: 124-154, doi:10.1016/j.pocean.2017.12.007.

Woodgate, R.A., and C. Peralta-Ferriz, 2021. Warming and Freshening of the Pacific Inflow to the Arctic from 1990-2019 implying dramatic shoaling in Pacific Winter Water ventilation of the Arctic water column. Geophysical Research Letters, doi:10.1029/2021GL092528.

S2 Genetic correction of gadid species assignment

Species identifications made during field sampling were modified based on the genetic verification of species identity described in Wildes et al. (in prep). In the midwater trawls, 40% of all (n = 2244) gadid specimens in 2017 and 56% of all (n = 5676) fish specimens in 2019 were genetically confirmed. Unverified specimens <24 cm in length were assigned to a species as a function of the gadid species proportion-at-length in each trawl as described below. In practice, only 59 specimens >10 cm in length were modified as a result of the model reassignment, which constitutes 0.3 % of all measured specimens. All fish >= 24 cm retained their species identification as determined in the field.

For a given trawl, the proportions of each of the five gadid species (B. saida, G. chalcogrammus, E. gracilis, G. macrocephalus, and A. glacialis) were determined from the genetically confirmed specimen. Proportions were calculated for specimen grouped into the following length classes: 2 cm <= standard length (SL) < 4 cm, 4 <= SL < 6 cm, and 6 cm <= SL < 30 cm. The proportion (P) of a species s of length class l in trawl t was calculated from the number of genetically confirmed individuals (N) of species s of length class l from trawl t,

$$P_{s,t,l} = \frac{N_{s,t,l}}{\sum_s N_{s,t,l}}$$

For each specimen that was not genetically analyzed, a species was assigned based on the determined genetically identified proportions. For example, trawl t contains the following probabilities P for length class l: P_(s_1,t,l)=0.55, P_(s_2,t,l)=0.25, P_(s_3,t,l)=0.2, P_(s_4,t,l)=0, and P_(s_5,t,l)=0. A value x is randomly generated where 0 <x≤1. The specimen is assigned to species s based on the following conditions:

$$s = \begin{cases} s_1, & x \leq P_{s_1,t,l} \\ s_2, & P_{s_1,t,l} < x \leq P_{s_1,t,l} + P_{s_2,t,l} \\ & \dots \\ s_n, & P_{s_1,t,l} + P_{s_2,t,l} \dots P_{s_{n-1},t,l} < x \leq P_{s_1,t,l} + P_{2,t,l} \dots P_{s_n,t,l} \end{cases}$$

To evaluate the performance of the genetic reassignment model, the identity of all genetically identified specimens were predicted using a leave-one-out method. The identity of each individual was predicted based on the other genetically identified gadid specimens from the same trawl haul. The model-predicted species matched the genetic identification for >80% for individuals in both years. The allocation of acoustic backscatter from trawl data is based on the length distribution and the proportion of each species in the catch, thus the model was also evaluated based on the ability to predict the proportions of each gadid species in each trawl and the impact of reassignment on the length distributions of each species.

The model reassignment introduces a random element due to the probabilistic species assignment of the specimens which were not genetically identified. However, the species compositions of gadids in a given haul after reassignment exhibited very little difference to those derived from the genetically identified specimens (Fig. S4). The mean of the absolute difference between the proportions of Arctic cod and pollock from only genetic specimens and all specimens for each haul was <5% in 2017 and <3% in 2019. The higher variability in 2017 is likely due to both a greater spatial overlap between species, and greater overlap in their size composition (Figure S5) and a higher proportion of unconfirmed identifications than in 2019.

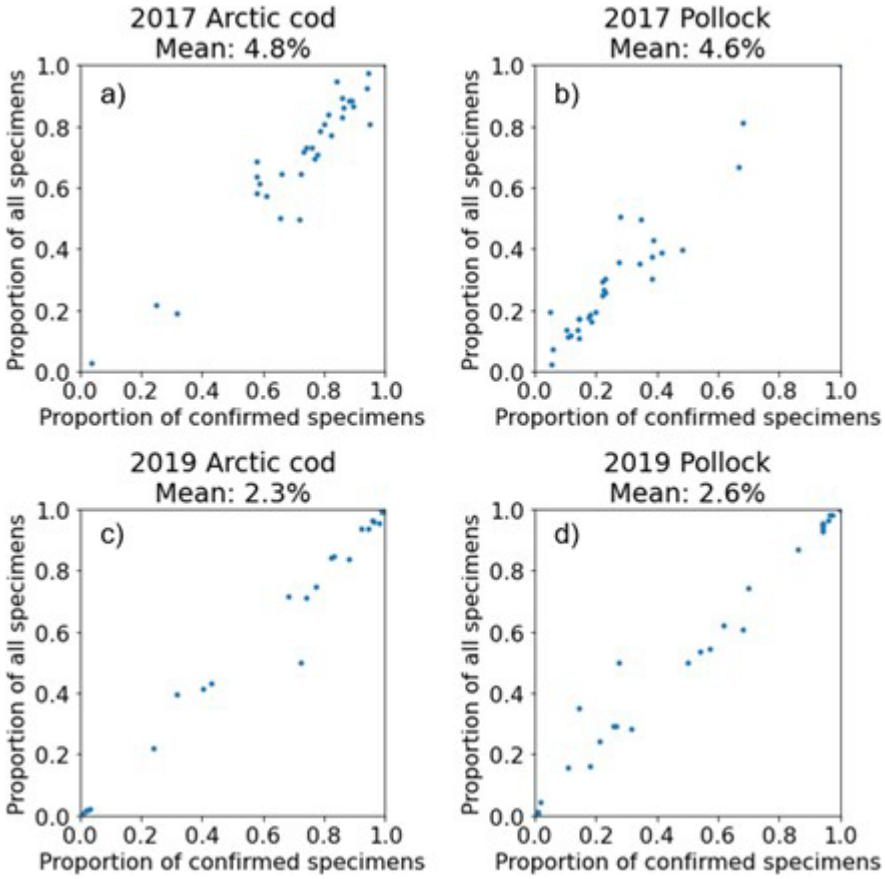

Fig. S4: Comparison of the proportion of (a, c) Arctic cod and (b, d) walleye pollock in each trawl determined from only the genetically confirmed specimens, and from all specimens after model reassignment. Mean absolute difference between the proportions from only genetic specimens and all specimens for each haul is indicated for each set of measurements.

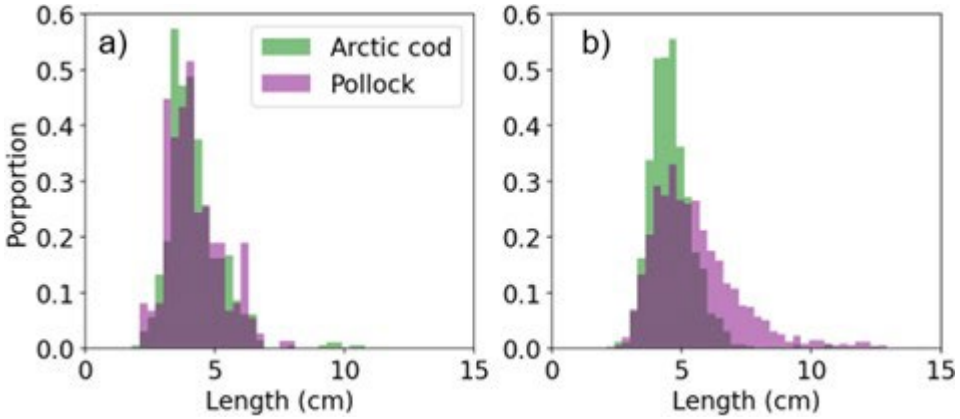

Fig. S5: Proportion at length of genetically identified Arctic cod and pollock in (a) 2017 and (b) 2019.

To quantify agreements in length between genetically identified versus all specimens, we calculated the two-sample Kolmogorov-Smirnov (KS) test between the known and model-assigned lengths for each gadid species in each trawl. The KS statistic was not significant in any trawls, indicating no significant differences between the length-frequency distributions between the genetically confirmed specimens and all specimens after model reassignment. Mean absolute differences between known and reassigned mean species length in each trawl haul was < 0.5 cm for both Arctic cod and pollock in both years (pollock: 0.43 in 2017 and 0.23 in 2019, Arctic cod: 0.07 in 2017 and 0.09 in 2019).

When catches were subsampled, total catch weights and abundances were modified based on the updated identifications of specimens to accurately reflect the final species composition in each trawl catch. This can introduce changes in the weight and number of individuals of a given species in a trawl haul due to the extrapolation from the measured subsamples to the total catch (Figs. S6, S7). To evaluate the potential changes to the total catch resulting from species reassignments, total weight, total number, sampled weight, and sampled number of each gadid species in each trawl in both years were calculated from the original field assignments and the genetically reassigned data. Changes to these measures as a result of reassignment were typically <0.5% (total samples of each gadid species in all trawls = 106 in 2017, and 92 in 2019), with only 5 samples across both years showing changes in any of the metrics by >1% (Figs. S6 and S7). These errors were identified as a result of rounding errors for the mean weight of individuals (i.e., mean individual weights were assigned as .002 kg rather than .001) introduced by the 0.001 kg precision used in the field collection database.

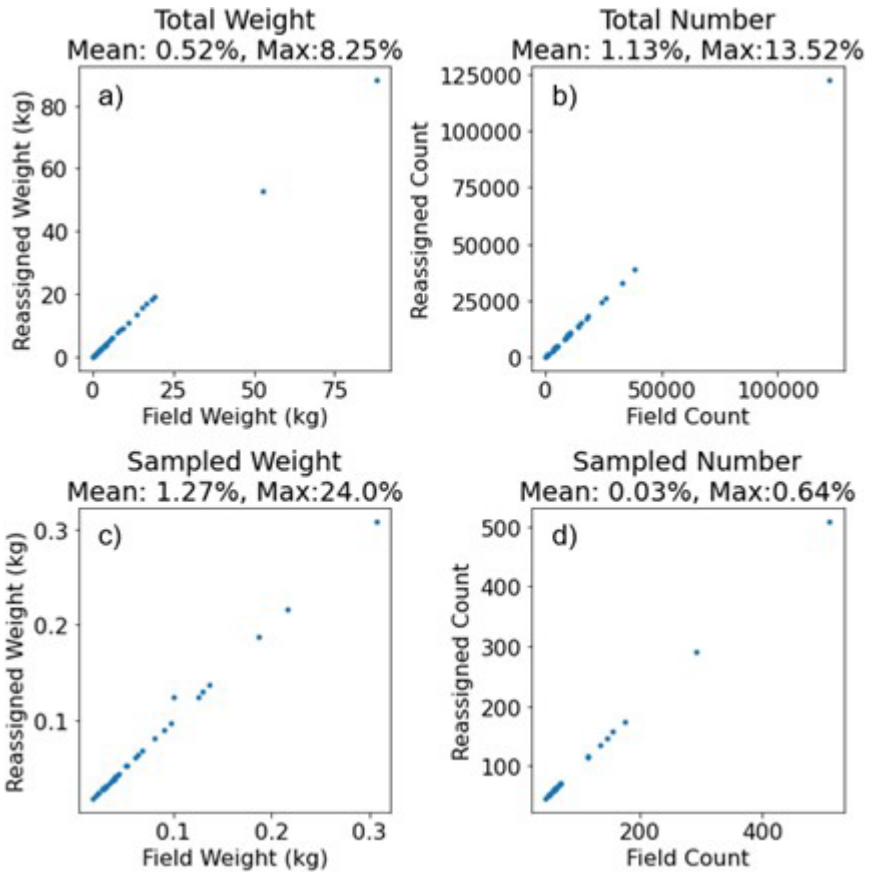

Fig. S6: Comparison of field and reassigned (a) total weight, (b) total number, (c) sampled weight, and (c) sampled number of gadids for all 2017 trawls. Each point represents the total for a single gadid species in a trawl. Mean and maximum values of the absolute difference between the field and reassigned values for each haul are indicated for each set of measurements.

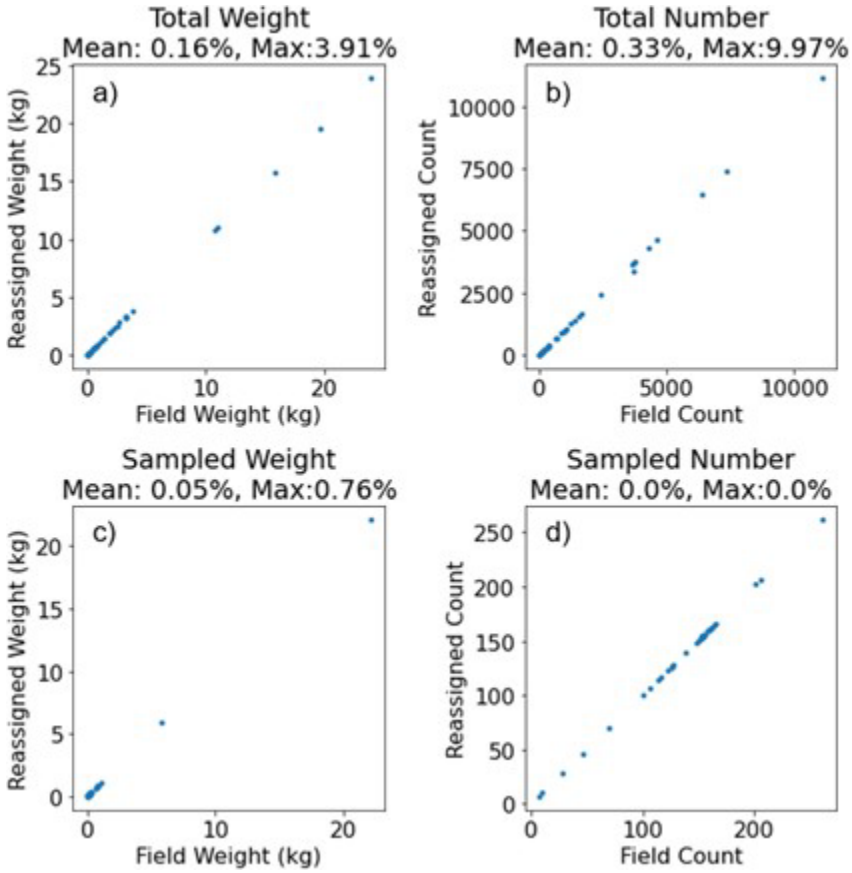

Fig. S7: Comparison of field and reassigned (a) total weight, (b) total number, (c) sampled weight, and (c) sampled number of gadids 2019 for all trawls. Each point represents the total for a single gadid species in a trawl. Mean and maximum values of the absolute difference between the field and reassigned values for each haul are indicated for each set of measurements.

CHAPTER 7 - Modifying a pelagic trawl to better retain small Arctic fishes

Objective 2: Quantify the distribution, abundance, and condition of pelagic marine fishes, in particular young-of-the-year Arctic gadids and other forage fishes

Alex De Robertis, Robert Levine, Kresimir Williams, and Chris Wilson

Abstract

The small, abundant pelagic fishes of the Alaska Arctic are challenging to sample with trawls. They are sufficiently motile to avoid small fine-mesh trawls, but small enough to escape through the meshes of pelagic trawls designed to capture larger fishes. A pelagic herring trawl equipped with a fine-mesh codend liner was used to quantify the size and species composition of pelagic fishes during a baseline acoustic-trawl survey of the Chukchi shelf. Subsequent experiments with recapture nets attached to the outside of the trawl web suggested that escapement of small fishes was substantial, particularly in the aft net section. Thus, the trawl was further modified by reducing the taper in the aft net section, and adding a small-mesh section in front of the codend to potentially reduce escapement. Further use of recapture nets during two subsequent acoustic-trawl surveys confirmed that this trawl modification substantially increased retention of small fishes, and resulted in less size selectivity. These improvements will reduce biases in estimates of abundance, size and species composition of pelagic Arctic fishes. This work highlights the importance of quantifying escapement from survey trawls, and demonstrates that escapement estimates can guide successful trawl modifications.

Introduction

Pelagic trawls are one of the primary methods of sampling midwater fishes, and are widely used in pelagic and acoustic-trawl surveys. These trawls rely on behavior to capture fishes, as the majority of meshes are much larger than the fish being targeted. Pelagic trawls typically gradually decrease in diameter and mesh size from the trawl mouth, leading to a long intermediate section followed by a small-mesh codend. Most meshes in the trawl forward and intermediate sections are large enough to allow fish to escape. However, fish are reluctant to pass through these larger meshes, and instead orient themselves parallel to the netting (Glass et al., 1993). The fish tire, becoming increasingly concentrated as they fall back towards the smaller diameter codend where they are retained in smaller meshes (Kennelly and Broadhurst, 2021). This graduated mesh and gradual narrowing (low taper) of this trawl design reduces drag so larger nets can be deployed to improve catch rates. However, if herding behaviors are species and size-specific (He, 1993), the catch composition will not be representative of the fish the trawl mouth opening. These fish herding behaviors have been extensively exploited to reduce commercial catches of unwanted species and/or size classes (Kennelly and Broadhurst, 2002). Thus, the primary goal of trawl gear designed for commercial fishing is to increase size and species selectivity to maximize the catch rates of target species while reducing the proportion of unwanted species and size classes in the catch.

The requirements for research survey trawls differ from those of commercial fish trawls. Ideally, a survey trawl should be unselective, and capturing all species and size classes with equal efficiency. This is rarely, if ever possible in practice, so a more attainable goal should be to design trawls that capture all species and sizes of interest at high and constant efficiencies. Trawl catches can then be corrected for species/size selectivity if these average size- and species-dependent probabilities of capture (i.e. selectivity) are known (Bethke et al., 1999; Kotwicki et al., 2017). If species and size selectivity were known without error, the corrections would fully account for trawl selectivity. In practice, corrections are imprecise (Williams et al., 2011; De Robertis et al., 2017a). Thus, designing survey trawl gear with high catch rates important, as when the probability of retention is high, the absolute corrections for selectivity will be smaller, and uncertainties in the correction result in smaller impacts abundance estimates.

Selectivity corrections are particularly desirable in the context of acoustic-trawl surveys, as species and size compositions derived from trawl sampling are used in combination with scattering models to convert acoustic backscatter into animal densities (Simmonds and MacLennan, 2005). If the proportion of one species or size class is under-estimated relative to others, its abundance will not only be under-estimated, but the abundance of other species and sizes will also be over-estimated (McClatchie and Coombs, 2005; De Robertis et al., 2017b). Therefore, selectivity corrections are desirable for acoustic-trawl surveys, as errors in species or size composition introduced by trawl selectivity affect the abundance estimates of all the other organisms present.

While substantial effort has gone into making trawls more selective to reduce unwanted bycatch (Kennelly and Broadhurst, 2021), comparatively little work has been conducted to design less selective pelagic trawls for research surveys, or to quantify the selectivity of these survey trawls. Pelagic trawls designed for commercial fishing are regularly used as survey trawls (Bethke et al., 1999; Williams et al., 2011). Fishes that escape from pelagic trawls are generally smaller than those that are retained (Matsushita et al., 1993; Suuronen et al., 1997) and a small-mesh liner is often added to the codend to improve retention of smaller fishes (Simmonds et al., 1992). This is a pragmatic and simple first step as selection in the codend is often high (Matsushita et al., 1993; Wileman et al., 1996; Kennelly and Broadhurst, 2021). However, this does not address escapement from the meshes forward of the codend, which can be substantial, particularly for smaller organisms large enough to be retained in the codend but not the rest of the trawl (Williams et al., 2011; Herrmann et al., 2018).

Although trawl selectivity can be investigated via gear comparisons (Kotwicki et al., 2017), acoustic and optical imaging (Williams et al., 2013, Underwood et al., 2020), or small-mesh recapture nets to capture fishes escaping through the trawl meshes (Matsushita et al., 1993; Skúvadal et al., 2011), the selectivity of most survey trawls is unknown. In many applications, it is implicitly assumed that all species and size classes are equally likely to be retained by the survey trawl (Simmonds et al., 1992). While this assumption is sometimes acceptable, it is tenuous in other situations such as in areas of mixed species and size aggregations. Quantifying trawl selectivity allows selectivity corrections to be implemented, thus reducing a major source of uncertainty in acoustic-trawl abundance (Williams et al., 2013).

The Pacific Arctic, which was sampled as part of the Arctic Integrated Ecosystem Research Program (AIERP), presents a challenging case in terms of the potential for biases to be introduced by trawl selectivity. The dominant pelagic fishes are small (~5 cm), and it is highly probable that they will be poorly retained in large-mesh trawls. However, they are also sufficiently mobile to avoid smaller fine-mesh nets designed for larval fishes and invertebrates (Kwong et al., 2018). Acoustic-trawl surveys of the Chukchi Sea required the ability to sample both large and small fishes, and a large Cantrawl pelagic trawl was used in an initial baseline survey (De Robertis et al., 2017b). A smaller Marinovich herring trawl was introduced in a subsequent survey after it became clear that small fishes likely to escape from the Cantrawl dominated this Arctic pelagic fish community. The Marinovich trawl was equipped with a small mesh codend liner in an effort to better retain small fishes (De Robertis et al., 2017a; De Robertis et al., in press). Although the Marinovich captured pelagic fishes in the Chukchi Sea more efficiently than the larger Cantrawl, experiments with a recapture nets indicated that escapement and size-selectivity remained high, particularly in the aft area of the Marinovich trawl (De Robertis et al., 2017a; see De Robertis et al., in press for a corrigendum). Specifically, the Marinovich trawl was selective in the size range of most pelagic fishes in this Arctic region. For example, only ~23% of 4 cm Arctic cod, the most common species and size class in this environment were retained. Retention of Arctic cod was highly size dependent: ~10% at 3 cm and ~45% at 5 cm. Given the relatively low catch efficiency and substantial size selectivity of the trawl, the aft section of the Marinovich trawl was further modified for continued use during the AIERP program in an effort to improve retention of all small fish species and to reduce the trawl size-selectivity. This study thus has two aims: 1) establish size-dependent selectivity curves for abundant fish species to correct the retained catch for escapement for use in acoustic-trawl abundance estimates of fish abundance (Levine et al., in review), and 2) evaluate whether the Marinovich trawl modifications increased the catch rates of small fishes present in this Arctic region.

Materials and Methods

Trawl modification

The mod-1 Marinovich herring trawl used in previous surveys of the Chukchi shelf in 2013 (De Robertis et al., 2017b) is a symmetrical 4-seam box trawl constructed of diamond (T0) meshes (Fig. 1a). It was modified from the original design by fitting the codend with a 2 by 3 mm oval mesh liner to improve retention of small organisms and enlarging the wings to allow it to be fished with oversized doors as the logistics of this project required fishing both the Marinovich and a larger pelagic trawl without swapping trawl doors (De Robertis et al., 2017b).

The trawl was further modified (Fig. 1b) in an effort to better retain the small fishes observed in the study area (this trawl is hereafter referred to as mod-2 Marinovich). The aim was to increase capture rates of the small fishes to reduce the uncertainties in estimates of animal size and species composition used to convert measurements of acoustic backscatter to estimates of abundance by species and size (De Robertis et al., 2017b). Given that escapement was substantially higher in the aft area of the net, we focused on this part of the trawl.

The mod-1 trawl was modified by replacing the 3.8 cm mesh panel immediately forward of the codend with two new panels after reviewing the recapture net results and consulting with trawl manufacturers and commercial fishers. One panel was redesigned with the same mesh (3.8 cm T0 meshes) but with a lower taper (Fig. 1b). A second panel of 1.9 cm T0 meshes was added immediately aft of the first new section, increasing the overall length of the mod-2 trawl by 249x1.9 cm meshes (Fig. 1b). The codend liner covered the codend and 26.5 of the 1.9 cm meshes of the second new panel (Fig. 1b). These modifications increased the overall length of the net, reduced the taper towards the rear of the net and reduced the mesh size in the area immediately forward of the lined codend where escapement was greatest (De Robertis et al., in press). Hereafter, the two forward panels of the mod-2 Marinovich are referred to jointly as the forward section, the two middle panels are referred to as the middle section, and the new small-mesh panel as the aft section (Fig. 1b).

Recapture nets

The Marinovich trawls were fitted with small-mesh recapture nets designed to quantify the degree to which fish escape through the mesh panels of the trawl (Nakashima, 1990; Williams et al., 2011). The recapture nets were constructed with the same 2 by 3 mm oval mesh material as the codend liner. They were designed with a diamond-shaped mouth equivalent to a 2.4 m stretched diamond mesh, a 2.6 m long tapered body, and codend (see De Robertis et al., in press, their Fig. S1.2 for details). The recapture nets were dyed black to reduce visibility and permanently attached to the trawl netting on the outside of the trawl.

The mod-1 trawl was fitted with 8 recapture nets, one in the forward section and one in the aft section on each of the four sides of the trawl (i.e., top, bottom, port and starboard). The recapture nets were placed at the center of each section (i.e. same number of meshes in front of and behind the recapture net, Fig. 1a). The number of meshes covered by the recapture nets were counted, and the proportion of the area covered by the recapture net was computed (see De Robertis et al., in press, their section S2). The recapture nets covered 6.5% of the area in the front section and 13.2% of the area in the aft section.

The Mod-2 trawl was fitted with 9 recapture nets in the center of the forward, middle, and aft sections of the net (Fig. 1). Recapture nets were mounted on the top, bottom and starboard sides. To reduce the effort required to process the catch, we did not mount nets on the port side and assumed equal escapement from the port and starboard sides of the net. The recapture nets covered 6.5% of mesh area in the front section, 12.7% of mesh area in the middle section, and 30.5% of the unlined mesh area in the aft section.

Field Sampling

The mod-1 Marinovich equipped with recapture nets was used in 30 hauls as part of an acoustic-trawl survey of the continental shelf of the US Chukchi Sea in 2013. These deployments are described

elsewhere (De Robertis et al., 2017a), but results are included here as a reference to judge the effectiveness of the subsequent modifications made to the mod-2 Marinovich.

The mod-2 Marinovich equipped with recapture nets was used in acoustic-trawl surveys in 2017 and 2019, which sampled the same area as the previous survey with the mod-1 trawl (Fig. 2). The mod-2 Marinovich was fished with Nor'Eastern Trawl Systems 3 m^2 Series 2000 doors, synthetic rigging with 55 m long bridles, and 170 kg weights on each wingtip. A Simrad FS70 3rd wire trawl sonar was mounted on the headrope to monitor trawl geometry and fish entering the net. A total of 75 hauls with the Mod-2 trawl (Fig. 2, n=32 in 2017, n=43 in 2019) were conducted during daytime as part of an acoustic-trawl survey (Levine et al., this issue). Most trawls were shallow (average depth of 31.7 ± 32.3 m (mean ± SD), range 11.6 - 228.8 m), with 95% of trawls < 40.2 m. The trawl was fished at 1.2 ± 0.2 m s^{-1}, and exhibited a vertical mouth opening of 7.8 ± 0.9 m and a horizontal opening of 7.5 ± 0.6 m while fishing.

Biological sampling

Catches in the codend and the recapture nets were weighed, subsampled if large, sorted to species and enumerated. The lengths of individuals in the codend (up to 60 for gadids and 20 for other species) and in each recapture net (up to 20) were measured to the nearest mm using an electronic measuring board (Towler and Williams, 2010). For species other than gadids and Arctic sand lance (*Ammodytes hexapterus*), fork length was measured. Gadid lengths were not measured consistently across years: in 2013, fork length was measured, in 2017, total length was measured, and in 2019, standard length was measured. These measurements were converted to standard length using species-specific linear regressions (see Levine et al., in review, their appendix A) for further analysis.

Small gadids (particularly age-0 Arctic cod (*Boreogadus saida*), and pollock (*Gadus chalcogrammus*) could not be reliably identified at sea based on external morphology (Wildes et al, this issue). Thus, species for juvenile gadids in 2017/2019 were assigned probabilistically based on size-dependent genetic sampling of the catch (see Levine et al., in review, their appendix B). Pollock were almost absent in 2013, and saffron cod (*Eleginus gracilis*) which easier to distinguish at this size were spatially distinct from that of Arcitc cod (De Robertis et al., 2017b). The identifications of juvenile gadids in the 2013 survey are thus believed to be generally reliable (Levine et al., in review; Wildes et al., in review).

Estimation of trawl selectivity

The most abundant fishes in the catch (Arctic cod, saffron cod, walleye pollock, capelin (*Mallotus catervarius*), Arctic sand lance) were aggregated by species for analysis. In addition, a grouping for 'other fishes' (i.e. all other fishes pooled) was defined. In the mod-1 deployments, catches of 'other fishes' were dominated by pricklebacks (*Stichaeidae*, 40%), sculpins (*Cottidae*, 33.3%), and snailfishes (*Liparidae*, 13.5%). In the mod-2 deployments, catches of other fishes were dominated by pricklebacks (41.9%), sculpins (16.3%), and Pacific herring (16.2%). A selectivity relationship was fitted to the 'other fishes' complex as an approximate selectivity relationship is required to correct the size and species composition of low-abundance species encountered in the acoustic-trawl survey (Levine et al., this issue). However, given the differences in species and size composition, the selectivity of the 'other fishes' group should not be compared directly between the mod-1 and mod-2 Marinovich trawl designs. For each species grouping listed above, hauls in which >10 individuals were measured were used for further analyses.

Each specimen (i.e. a measured fish) was associated with a scaling factor indicating the total number of individuals that fish represents in the total catch if in the codend, or the total number of fish escaping from the trawl meshes if in the recapture nets. The scaling factor W for each measured individual i in the catch is defined as

$$W_{i,s,j} = \frac{1}{p_{i,j,s}} \cdot \frac{1}{c_j} \quad (1)$$

where $p_{i,j,s}$ is the proportion of individuals of species s in captured in trawl location j (referring to the codend or recapture net location) that were measured , and c_j is the proportion of the area in location j covered by the recapture nets or codend liner. In the case of the mod-1 Marinovich, c_j = 0.065 for the front recapture nets and 0.132 for the aft recapture nets. In the case of the mod-2 Marinovich, in the top and bottom sides of the trawl, c_j was 0.065 for the front recapture nets, 0.127 for the middle recapture nets, and 0.305 for the aft recapture nets. Given that only the starboard side of the net was fitted with recapture nets, escapement was assumed to be the equivalent from both sides. Escapement from both the port and starboard sides was approximated from the catch on the starboard side by fixing c_j to account for the fraction of meshes on both sides of the trawl covered by the starboard recapture nets (front = 0.033, middle= 0.064, aft =0.152). The codend was fully covered by the 2 by 3 mm oval mesh, thus c_j = 1 for both trawls.

Thus, the total number of fish of species s escaping from the trawl (E_s) can be determined by summing the scaling factors for all fish measured from the recapture nets

$$E_s = \sum_i (W_{i,s,j=recapture\ net}). \quad (2)$$

Likewise, the total number of fish retained in the codend (R_s) is estimated as

$$R_s = \sum_i (W_{i,s,j=codend}). \quad (3)$$

Selectivity estimates

Selectivity was treated as a binomial process, where a fish entering the net is either retained in the codend or escapes through the meshes. To model this as a length-dependent process, a logistic curve was used. To estimate the parameters of the logistic curve, a generalized linear model was fitted (Millar and Fryer, 1999) where the dependent binomial data are logit transformed into a linear variable and two linear coefficients are estimated (i.e. the slope a and intercept b).

The selectivity, as a function of length, l, is described as

$$S(l) = \frac{\exp(a+bl)}{1+\exp(a+bl)}, \quad (4)$$

where $S(l)$ represents the length-dependent probability of being caught in the codend.

These coefficients can be re-defined (Williams et al., 2011) in terms of the length at which 50% of the fish are retained (L_{50}= -(a/b)), and the selection range (SR = (2 $\log_e(3)$)/b which represents the length range between 25% and 75% retention). A length-dependent logistic function was parametrized from L_{50} and SR as

$$S(l) = (1 + \exp^{\left(\frac{k(L_{50}-l)}{SR}\right)})^{-1}, \quad (5)$$

where l is length in cm and k = 2 $\log_e(3)$ (Millar, 1993).

Bootstrap estimates of confidence intervals

Uncertainty in the fitted selectivity relationships was estimated using a 2-stage bootstrap approach (Millar, 1993; Kotwicki et al., 2017). In the first stage, between-haul variation was simulated by selecting n hauls with replacement from the n hauls used to fit equation 4 for each species. In the second stage, within-haul variation was simulated by separately resampling the same number of fish measured in the codend and the recapture nets as in the original haul. The approach mimics the sampling of individual fishes in the catch by separately sampling the escapees captured in the resample nets and the retained fish in the codend. The probability of selecting a given measured specimen, i was equivalent to its contribution to the proportion of the fish retained in or escaping from the net (i.e. W_i). Given that the total

number of escaped fish depends on the expansion factors of randomly drawn fish, which differ among the recapture nets, the total number of escapees varies between bootstrap replicates in a given haul.

Selectivity curves for each of 5000 bootstrap replicates was computed following equations 1-4. The approximate 95% confidence intervals were computed for each size class by computing the 2.5% and 97.5% percentiles of the selectivity curves at that length. Confidence intervals for other descriptive parameters of interest (e.g. the proportion of fish or sizes of fish escaping from a given area of the net) were computed in an analogous fashion from the bootstrapped data sets.

Results

Similar species were captured in the mod-1 and mod-2 deployments. However, pollock were much more abundant in the mod-2 catches, and Arctic sand lance and saffron cod represented a larger proportion of the catch in the mod-1 trawl hauls (Fig. 3). Given the time differences (≥ 4 years) between sampling the differences in species composition between trawls primarily reflect temporal changes in species composition in the study area (Levine et al., in review). Small fishes continued to be abundant in the study area, and large numbers were captured in the codend and recapture nets during the mod-2 deployments (Table 1). For example, 355,390 Arctic cod were captured in the codend, 7596 in the recapture nets, and 6386 Arctic cod were measured.

The recapture net catches indicated that that a consistently higher proportion of fishes entering the trawl mouth were retained in the codend of the mod-2 Marinovich than previously observed with the mod-1 trawl (Fig. 4a). Escapees tended to be smaller than retained fish for both trawls (Table1, Fig. 4b), and the ratios of mean size for retained and escaped fish were similar for the mod-1 and mod-2 trawls (Fig. 4b). The mod-2 Marinovich trawl exhibited lower and more uniform escapement from the top, side, and bottom of the trawl, and forward, middle and aft sections of the trawl than the mod-1 trawl (Fig. 5). The mod-2 Marinovich trawl exhibited less escapement from the aft section of the trawl than the mod-1 trawl, (Fig. 5). As the aft section of the mod-1 trawl was converted into the middle and aft sections of the mod-2 trawl (Fig.1) it is informative to note that the combined escapement in the mod-2 middle and aft sections was less than the escapement in the equivalent aft section of the mod-1 trawl (Fig. 5, panels on right side). Escapement was highest in the middle section of the mod-2 trawl, and escapement was low in the new aft section of the mod-2 trawl (Fig. 5), likely due to the low taper and small meshes (Fig. 1). Although the retained fish tended to be larger than the escapees, escapees in the top/side/bottom and the forward/middle/aft areas of the trawl were, in general, of consistent size (Fig. 6). Taken together, this indicates that the modification to the aft section of the mod-2 Marinovich trawl reduced escapement, and that escapement no longer disproportionately occurred in a particular area of the mod-2 trawl.

For all species and length classes, a higher proportion of fish were retained in the mod-2 Marinovich trawl compared to the mod-1 trawl (Fig. 7, compare the histograms). The fitted selectivity curves demonstrate that the estimated probability of retention increased with length for all species, particularly for the smallest size classes (Fig. 7). Retention of Arctic cod, capelin and Arctic sand lance was substantially higher for mod-2 than mod-1 for all size classes (Fig. 7, Table 2). The modifications also reduced size selectivity: this is evidenced when comparing the probability of capturing a large and small individual of each species. For example, the fitted selectivity curves in Fig. 7a indicate that a 5 cm Arctic cod was 5.2 times more likely to be retained in the mod-1 trawl (i.e. a mod-2/mod-1 selectivity ratio of 0.47/0.09), but only 1.3 times more likely to be retained (0.91/0.71) in the mod-2 trawl. This indicates that the mod-2 Marinovich exhibited both higher capture rates and lower size selectivity. Uncertainty in the fitted selectivity relationships was lowest for more abundant species and size classes (Fig 7). For example, the bootstrapped 95% confidence estimates of the selectivity curve for saffron cod for the mod-2 were very wide (Fig. 7b) as only 6 hauls with sufficient catch were available (Table 2). Similarly, few capelin were captured in the mod-2 recapture nets, and some bootstrap realizations led to predictions that larger fish were less likely to be retained than smaller ones (Fig. 7d). Overall, the differences in selectivity across species for mod-2 were similar to those for the mod-1. Arctic sand lance were less likely to be retained

than other species at a given size (likely due to their elongated morphology), as were saffron cod (which may have more developed escape responses).

Discussion

The reduced catches in the recapture nets of the mod-2 Marinovich compared to previous sampling with the mod-1 Marinovich indicate that the modifications to the aft section of the Marinovich trawl substantially decreased escapement of small Arctic fishes. Escapement was lower and no longer occurred disproportionately in a single area of the mod-2 trawl, indicating that further alteration of a limited area of the mod-2 trawl is unlikely to produce a substantial benefit. The mod-2 Marinovich also exhibited less size selectivity over the size range of fishes encountered. The increased capture rates and lower size selectivity of the mod-2 Marinovich trawl will reduce biases in estimates of abundance, size and species composition (Williams et al., 2011). The selectivity relationships derived from these data were applied in an acoustic-trawl survey to correct survey trawl catches for the size- and species-specific probability of escapement from the trawl (Levine et al., in review). Applying these selectivity relationships, avoids the need to assume that all organisms are captured with equal efficiency, which reduces biases in the abundance estimates (Williams et al., 2011; De Robertis et al., 2017b).

The mod-2 Marinovich was modified to decrease the rate of taper in the aft areas of the net and a small-mesh panel was added in front of the codend (Fig. 1). The changes were motivated by previous work with recapture nets which indicated that escapement in the aft part of the mod-1 trawl was high (De Robertis et al., 2017a; De Robertis et al., in press). As we had hoped, the additional modifications successfully decreased escapement in the aft area of the net compared to the mod-1 Marinovich trawl (Fig. 5). Escapement of small fishes often increases in the aft trawl sections (Matsushita et al., 1993; Williams et al., 2011; Kennelly and Broadhurst, 2021), likely due to increased interaction with the netting due to increased concentration of organisms as the net reduces in diameter, and decreased flow rates near the codend.

Pelagic trawls are designed to exploit the herding responses of large fish, and are unlikely to be optimized to capture smaller indivisuals. Small fishes have limited swimming abilities, and are likely to exhibit different behavioral responses during the capture process (He, 1993; Kwong et al., 2018). For example, a 5 cm fish would have to swim at 24 body lengths s^{-1} to keep pace with the forward progress of trawl, which is above their burst swimming capability (He, 1993). In this context, one should recognize that the modifications to the Marinovich trawl share common elements with commercial krill trawls, which are designed to capture small animals with relatively limited swimming capabilities. Krill trawls are long, comprised of small meshes, and have small mouth openings compared to pelagic trawls designed to capture large fishes (Herrmann et al., 2018). The gradual reduction in diameter (i.e. low taper) results in animals encountering meshes with a relatively low angle of attack, reducing escapement (Krag et al., 2014). Although we did not directly observe the interaction of fish with the Marinovich trawl during the hauls, we surmise that the behavioral interactions of the small Arctic fishes with our trawl gear during the capture process may be more similar to those of krill (Herrmann et al., 2018) rather than those of large fishes due to lower swimming speeds and endurance (He, 1993). That is, the combined effects of encountering trawl meshes at lower angles due to the reduced taper, the presence of smaller meshes in the aft portion of the net where fish are more likely to encounter the netting likely contributed to the higher catch rates of the mod-2 Marinovich.

The selectivity of the pelagic trawls used in many survey applications is unknown. One reason for this is that field experiments to estimate selectivity are time consuming and expensive (Kotwicki et al., 2017). A practical advantage of the recapture net approach (Matsushita et al., 1993; Williams et al., 2011) employed here is that the trawling was conducted as part of a survey (De Robertis et al., 2017b; Levine et al., in review) and did not require dedicated vessel time. This approach allowed a relatively large sample size (number of hauls and individuals captured) to be collected at minimal cost. Another benefit of conducting the recapture net study during a survey is that the trawls were conducted under the size and species compositions relevant to that survey. Furthermore, environmental conditions potentially

influencing the capture process (e.g. temperature and light level, He, 1993; Ryer and Olla, 2000) will also be representative of those encountered during a survey.

It is also important to recognize the limitations of the recapture net method. The recapture net method allows one to quantify the probability that a fish entering the trawl will be retained in the codend (i.e. mesh selection). Although selection within the body of the trawl is an important source of trawl selectivity (Nakashima, 1990; Williams et al., 2011), recapture nets do not address the probability that a fish within the trawl path will actually enter the trawl opening. In other words, the approach does not account for reactions to the vessel or the trawl gear affecting the probability that the fish will enter the trawl (Handegard and Tjøstheim, 2005; Kaartvedt et al., 2012). The magnitude of these reactions can be established by comparing trawl catches to other measurements of abundance such as acoustic observations (Handegard and Tjøstheim, 2005; Somerton et al., 2011; Underwood et al., 2020). While these factors are currently not characterized for Arctic fishes, small fishes may be less likely to avoid the net or to be herded into the net due to their limited swimming ability (He, 1993).

When selectivity is quantified using modified gear such as the recapture nets, the resulting selectivity may not be representative of the unmodified gear (Kotwicki et al., 2017). This was less of an issue in our case with the Marinovich modifications as the recapture nets are permanently mounted for the duration of the survey, and are considered integral to the trawl (i.e. the recapture nets will be used on future surveys). However, the recapture nets were mounted in the center of trawl sections, and the observed escapement was assumed to be representative of escapement in the other uncovered meshes. Although we did not evaluate how the recapture nets affected the trawl, previous observations with cameras have indicated that recapture nets of similar design do not appreciably distort the shape of pelagic trawls or alter fish behavior compared to uncovered meshes (Matsushita et al., 1993; Williams et al., 2011). While escape reactions prior to entering the trawl mouth and biases related to sampling with recapture nets remain important areas for further study, our view is that these limitations should not deter future uses of recapture nets until better or more comprehensive methods to characterize trawl selectivity become available as they provide a practical method to quantify mesh selection during the trawl capture process.

One advantage of a using a sizeable pelagic trawl to sample small fishes rather than using a smaller trawl is that the gear is also able to capture large fishes if they are present. For example, during initial testing of the mod-2 Marinovich in the Bering Sea, adult pollock up to 61 cm in length were captured (Honkalehto and McCarthy, 2015). The ability to identify the presence of large fishes, is important in rapidly changing environments such as the Alaska Arctic. For example, there is potential for adult gadids to colonize the Chukchi Sea from the south as the environment warms as has happened in the Northern Bering Sea to the south (Stevenson and Lauth, 2019). The lack of adult gadids in the mod-2 Marinovich catches described here provides evidence that pelagic adult gadids are not abundant during the 2017 and 2019 AIERP program surveys (Levine et al., in review).

Trawls with both known and high capture probabilities are advantageous as these characteristics lead to more accurate estimates of species composition, organism abundance, and size distribution. In the application of Arctic acoustic-trawl surveys examined here, the size and species selectivity has been reduced relative to the mod-1 Marinovich, and the probability of capture as a function of species and size has been established. This reduces uncertainty (because selectivity has been quantified), and biases (because small fishes are more likely to be retained) in future uses of the catch data, including acoustic-trawl surveys (Levine et al., in review). Although the probability of retaining small fishes has been improved, as with all trawls, the trawl remains species and size selective. It is thus best practice to correct the observed trawl catch ($catch_{obs}$) of a given species with the fitted selectivity relationships (i.e. $Catch_{corr,l} = \frac{\mathrm{Catch}_{obs,l}}{S_l}$, where S is the probability of retention in the trawl codend, and l is length) rather than assuming that the trawl catch is unbiased.

The use of trawls with characterized selectivity allows for the requirement for methodological consistency in order to maintain a consistent sampling bias to be relaxed in a survey time series. If selectivity has been

quantified, corrections for selectivity can be implemented and catches from different sampling gears can be combined. This is advantageous as it allows for improved trawl gear to be introduced as surveys are developed. This was the case for development of our acoustic-trawl surveys of the Chukchi sea. That is, a large pelagic trawl was replaced with the mod-1 Marinovich after it became clear that fishes were small (De Robertis et al., 2017b). Then, the mod-2 Marinovich was developed after it became clear that there was substantial escapement in the aft area of the mod-1 net (Levine et al., this issue). Gear with known selectivity would also improve confidence in conclusions drawn from the comparison of sampling with different gears (e.g., Logerwell et al., 2015; Deary et al., 2021). This is particularly relevant to environments such as the Alaska Arctic which lack well-established monitoring programs and data are scarce and sampling methods are not standardized.

Although this study focused on a particular application and ocean region, the principles are transferable to a broad range of applications with pelagic trawls. The primary situations where understanding trawl selectivity are most important are those where estimates of absolute abundance are desired (as escapees will not be enumerated), or cases where size and species composition are required, but there are large differences in the probability of capture. For example, in the case of acoustic-trawl surveys, situations characterized by mixed aggregations of fish species spanning a large size range will be most impacted by trawl selectivity (Williams et al., 2011; Davison et al., 2015). Likewise, acoustic trawl-surveys with mixed species aggregations of strong and weak acoustic scatters (e.g. fishes with and without gas-filled swimbladders) are highly sensitive to selectivity-induced biases in trawl species composition (McClatchie and Coombs, 2005; Davison et al., 2015). For instance, work with recapture nets may prove useful in constraining uncertainties in global abundance estimates of mesopelagic fishes, which remain poorly quantified. Both trawl and acoustic-trawl abundance estimates of mesopelagic fishes are highly dependent on trawl selectivity (Koslow et al., 1997; Davison et al., 2015; Kwong et al., 2018), and characterizing trawl selectivity will reduce the uncertainty in these estimates.

This work highlights the utility of quantifying the size and species selectivity of pelagic survey trawls. The use of recapture nets allowed the primary area of escapement from within a survey trawl to be identified, corrected by modification of the trawl, and finally the improved performance could be quantified. Estimates of trawl selectivity were used to reduce biases in both the abundance and size composition of acoustic-trawl abundance estimates of small Arctic fishes (De Robertis et al., 2017b; Levine et al., in review). The trawl gear was improved to reduce selectivity during these surveys, and catches from the three different trawls used in this survey could be integrated into a consistent abundance survey time series by estimating and then accounting for the impact of selectivity on abundance estimates. The work demonstrates that recapture nets can improve abundance estimates derived from sampling with midwater trawls, and that survey trawls can, and should, be modified to improve performance for specific applications.

Acknowledgements

Poul Pedersen of Dantrawl Inc. proposed the modifications to the Marinovich trawl and the staff at the Alaska Fisheries Science Center's (AFSC) net shed modified the trawl. We thank the cruise participants who processed many recapture net catches. This work was funded by the Arctic Integrated Ecosystem Research Program (IERP; http://www.nprb.org/arctic-program/), and is NPRB Publication ArcticIERP-XX. This paper is dedicated to the memory of the AFSC net shed's leader David King who was a fine co-worker and friend and a patient and encouraging teacher.

References

Bethke, E., Arrhenius, F., Cardinale, M., and Håkansson, N. 1999. Comparison of the selectivity of three pelagic sampling trawls in a hydroacoustic survey. Fisheries Research, 44: 15-23.

Davison, P., Lara-Lopez, A., and Koslow, J. A. 2015. Mesopelagic fish biomass in the southern California current ecosystem. Deep Sea Research Part II: Topical Studies in Oceanography, 112: 129-142.

De Robertis, A., Taylor, K., Williams, K., and Wilson, C. D. 2017a. Species and size selectivity of two midwater trawls used in an acoustic survey of the Alaska Arctic. Deep Sea Research II, 135: 40-50.

De Robertis, A., Taylor, K., Wilson, C., and Farley, E. 2017b. Abundance and Distribution of Arctic cod (*Boreogadus saida*) and other Pelagic Fishes over the U.S. Continental Shelf of the Northern Bering and Chukchi Seas Deep-Sea Research II, 135: 51-65.

De Robertis, A., Taylor, K., Wilson, C., and Williams, K. in press. Corrigendum to: "Species and size selectivity of two midwater trawls used in an acoustic survey of the Alaska Arctic" (Deep-Sea Res. II 135 (2017) 40-50). Deep Sea Research II.

Deary, A. L., Vestfals, C. D., Mueter, F. J., Logerwell, E. A., Goldstein, E. D., Stabeno, P. J., Danielson, S. L., et al. 2021. Seasonal abundance, distribution, and growth of the early life stages of polar cod (Boreogadus saida) and saffron cod (Eleginus gracilis) in the US Arctic. Polar Biology, 10.1007/s00300-021-02940-2.

Glass, C. W., Wardle, C. S., and Gosden, S. J. 1993. Behavioral studies of the principles of mesh penetration by fish. ICES mar Sci. Symp., 196: 92-97.

Handegard, N. O., and Tjøstheim, D. 2005. When fish meet a trawling vessel: examining the behaviour of gadoids using a free-floating buoy and acoustic split-beam tracking. Canadian Journal of Fisheries and Aquatic Sciences, 62: 2409-2422.

He, P. G. 1993. Swimming speeds of marine fish in relation to fishing gears. ICES mar. Sci. Symp., 196: 183-189.

Herrmann, B., Krag, L. A., and Krafft, B. A. 2018. Size selection of Antarctic krill (Euphausia superba) in a commercial codend and trawl body. Fisheries Research, 207: 49-54.

Honkalehto, T., and McCarthy, A. 2015. Results of the acoustic-trawl survey of walleye pollock (*Gadus chalcogrammus*) on the U.S. and Russian Bering Sea Shelf in June - August 2014 (DY1407). AFSC Processed Rep. 2015-07, 62 p. Alaska Fish. Sci. Cent., NOAA, Natl. Mar. Fish. Serv., 7600 Sand Point Way NE, Seattle WA 98115. http://www.afsc.noaa.gov/Publications/ProcRpt/PR2015-07.pdf.

Kaartvedt, S., Staby, A., and Aksnes, D. L. 2012. Efficient trawl avoidance by mesopelagic fishes causes large underestimation of their biomass. Marine Ecology Progress Series, 456: 1-6.

Kennelly, S. J., and Broadhurst, M. K. 2002. By-catch begone: changes in the philosophy of fishing technology. Fish and Fisheries, 3: 340-355.

Kennelly, S. J., and Broadhurst, M. K. 2021. A review of bycatch reduction in demersal fish trawls. Reviews in fish biology and fisheries, 31: 289-318.

Koslow, J. A., Kloser, R. J., and Williams, A. 1997. Pelagic biomass and community structure over the mid-continental slope off southeastern Australia based on acoustic and midwater trawl sampling. Marine Ecology Progress Series, 149: 21-25.

Kotwicki, S., Lauth, R. R., Williams, K., and Goodman, S. E. 2017. Selectivity ratio: A useful tool for comparing size selectivity of multiple survey gears. Fisheries Research, 191: 76-86.

Krag, L. A., Herrmann, B., Iversen, S. A., Engås, A., Nordrum, S., and Krafft, B. A. 2014. Size Selection of Antarctic Krill (*Euphausia superba*) in Trawls. Plos One, 9: e102168.

Kwong, L. E., Pakhomov, E. A., Suntsov, A. V., Seki, M. P., Brodeur, R. D., Pakhomova, L. G., and Domokos, R. 2018. An intercomparison of the taxonomic and size composition of tropical macrozooplankton and micronekton collected using three sampling gears. Deep Sea Research Part I: Oceanographic Research Papers, 135: 34-45.

Levine, R., De Robertis, A., Grunbaum, D., Wildes, S., Farley, E., Stabeno, P. J., and Wilson, C. D. in review. Climate-driven shifts in the pelagic fish community of the Chukchi Sea.

Logerwell, E. A., Busby, M., Carothers, C., Cotton, S., Duffy-Anderson, J., Farley, E., Goddard, P., et al. 2015. Fish communities across a spectrum of habitats in the western Beaufort Sea and Chukchi Sea. Progress in Oceanography, 136: 115-132.

Matsushita, Y., Inoue, Y., Shevchenko, A. I., and Norinov, Y. G. 1993. Selectivity in the codend and in the main body of the trawl. ICES mar. Sci. Symp., 196: 170-177.

McClatchie, S., and Coombs, R. F. 2005. Low target strength fish in mixed species assemblages: the case of orange roughy. Fisheries Research, 72: 185-192.
Millar, R. B. 1993. Analysis of trawl selectivity studies (addendum): implementation in SAS. Fisheries Research, 17: 373-377.
Millar, R. B., and Fryer, R. J. 1999. Estimating the size-selection curves of towed gears, traps, nets and hooks. Reviews in fish biology and fisheries, 9: 89-116.
Nakashima, B. S. 1990. Escapement from a Diamond IX midwater trawl during acoustic surveys for capelin (*Mallotus villosus*) in the Northwest Atlantic. J. Cons. int. Explor. Mer., 47: 76-82.
Ryer, C. H., and Olla, B. L. 2000. Avoidance of an approaching net by juvenile walleye pollock *Theragra chalcogramma* in the laboratory: the influence of light intensity. Fisheries Research, 45: 195-199.
Simmonds, E. J., and MacLennan, D. N. 2005. Fisheries Acoustics 2nd. Ed. Blackwell Science LTD, Oxford, UK 437 p.
Simmonds, E. J., Williamson, N. J., Gerlotto, R., and Aglen, A. 1992. Acoustic survey design and analysis procedure: a comprehensive review of current practice. ICES Cooperative Research Report, 187: 127 pp.
Skúvadal, F. B., Thomen, B., and Jacobsen, J. A. 2011. Escape of blue whiting *(Micromesistius poutassou*) and herring (*Clupea harengus*) from a pelagic survey trawl. Fisheries Research, 111: 65-73.
Somerton, D. A., Williams, K., von Szalay, P. G., and Rose, C. S. 2011. Using acoustics to estimate the fish-length selectivity of trawl mesh. Ices Journal of Marine Science, 68: 1558-1565.
Stevenson, D. E., and Lauth, R. 2019. Bottom trawl surveys in the northern Bering Sea indicate recent shifts in the distribution of marine species. Polar Biology, 42: 407-421.
Suuronen, P., Lehtonen, E., and Wallace, J. 1997. Avoidance and escape behavior by herring encountering midwater trawls. Fisheries Research, 29: 13-24.
Towler, R., and Williams, K. 2010. An inexpensive millimeter-accuracy electronic length measuring board. Fisheries Research, 106: 107-111.
Underwood, M. J., García-Seoane, E., Klevjer, T. A., Macaulay, G. J., and Melle, W. 2020. An acoustic method to observe the distribution and behaviour of mesopelagic organisms in front of a trawl. Deep Sea Research Part II: Topical Studies in Oceanography, 180: 104873.
Wildes, S., Whittle, J., Nguyen, H., Marsh, M., Karpan, K., DeMelio, K., Dimon, A., et al. in review. Walleye Pollock breach the Bering Strait: A change of the cods in the Arctic. Deep Sea Research II.
Wileman, D. A., Ferro, R. S. T., Fonteyen, R., and Millar, R. B., (Eds), 1996. Manual of methods of measuring the selectivity of towed fishing gears. ICES Cooperative Research Report 215, 126 pp.
Williams, K., Punt, A. E., Wilson, C. D., and Horne, J. K. 2011. Length-selective retention of walleye pollock, *Theragra chalcogramma*, by midwater trawls. Ices Journal of Marine Science, 68: 119-129.
Williams, K., Wilson, C., and Horne, J. K. 2013. Walleye pollock (*Theragra chalcogramma*) behavior in midwater trawls. Fisheries Research, 143: 109-118.

Table 1. Summary of the most abundant fishes captured in mod-2 Marinovich hauls equipped with recapture nets. The number of hauls in which >10 fish were measured is given, and the total numbers of individuals captured in the codend and all recapture nets combined are listed. The mean and standard error of the standard length of the specimens and the number of specimens measured also given. See De Robertis et al., 2017, their Table 1 for an equivalent summary of catches for the mod-1 Marinovich hauls.

Species	# hauls	Total # captured	# in codend	# in recapture nets	Length (cm) in codend $\bar{x}$ ± SE, (n)	Length (cm) in recapture nets $\bar{x}$ ± SE, (n)
Arctic cod	51	362986	355390	7596	4.5 ± 0.0 (4094)	4.0 ± 0.0 (2292)
Saffron cod	6	1206	1137	68	7.9 ± 0.2 (291)	4.9 ± 0.3 (38)
Pollock	57	116885	114501	2384	5.7 ± 0.1 (3197)	3.9 ± 0.0 (997)
Capelin	19	6967	6944	23	9.5 ± 0.1 (495)	8.7 ± 0.3 (23)
Arctic sand lance	34	27442	26125	1317	7.8 ± 0.1 (1899)	6.3 ± 0.1 (618)
Other fishes	57	29914	28456	1458	7.1 ± 0.1 (1823)	4.9 ± 0.0 (1047)

Table 2. Parameters of logistic selectivity curves fitted to for catch data from the mod-1 and mod-2 Marinovich pelagic trawl. *L50* represents the length in cm at which 50% of individuals are retained, the selection range (*SR*) is the length in cm between 25 and 75% retention. Bootstrap estimates of the 95% confidence intervals of *L50* and *SR* are given in parentheses. A negative *SR* indicates a prediction that small fish are more likely to be retained than larger fish. Insufficient pollock were captured during mod-1 deployments to compute a selectivity curve. Other fishes refers to the grouping of all fishes other than those specifically listed below.

Species	**Marinovich mod-1**		**Marinovich mod-2**	
	L50	*SR*	*L50*	*SR*
Arctic cod	5.1 (4.6, 5.9)	2.0 (1.3, 3.0)	1.8 (-0.3, 2.6)	3.1 (2.1, 6.2)
Saffron cod	8.8 (6.6, 30.7)	4.6 (2.5, 23.6)	3.5 (-6.1, 45.1)	5.0 (-30.7, 24.9)
Pollock	n/a	n/a	2.1 (-0.2, 2.9)	2.7 (1.7, 5.4)
Capelin	10.2 (-14.5, 34.2)	6.0 (-40.4, 49.4)	-19.0 (-156.7, 125.6)	17.4 (-72.0, 95.4)
Arctic sand lance	11.3 (6.9, 25.5)	6.1 (2.4, 24.2)	5.2 (3.3, 5.8)	3.6 (2.5, 6.5)
Other fishes	3.8 (3.6, 5.2)	0.7 (0.5, 2.0)	5.0 (4.0, 6.0)	2.9 (1.7, 4.3)

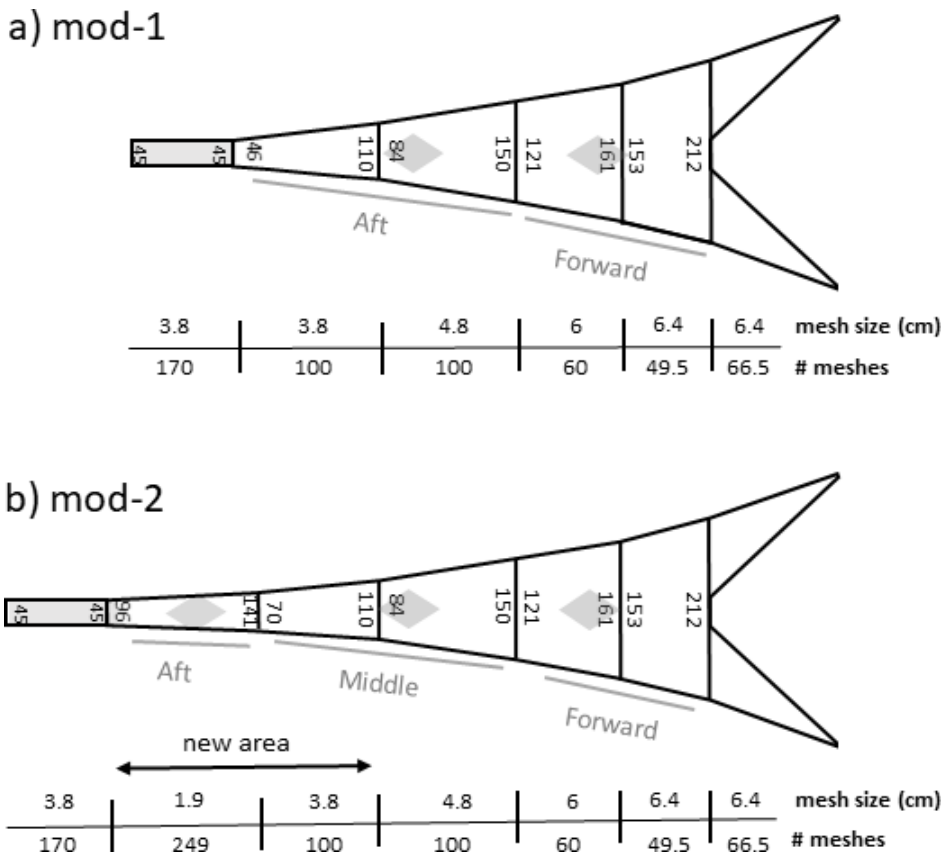

Fig. 1. Schematic of the a) mod-1 and b) mod-2 Marinovich trawls. The Mod-2 trawl was modified from the by replacing the aft-most 3.8 cm mesh panel of the mod-1 trawl forward of the codend with a new 3.8 cm mesh panel with reduced taper, and adding a smaller mesh section forward of the codend (the modified sections are annotated as "new area"). The size and number of meshes of each panel is annotated. This "box" trawl is symmetrical with an equivalent top, side and bottom. Only one view is depicted. For the purposes of analysis, the trawl body was divided into forward, middle and aft sections of similar mesh size. The approximate location of the recapture nets in the center of each section is given by the gray diamonds, and the 2 by 3 mm liner is indicated by gray shading.

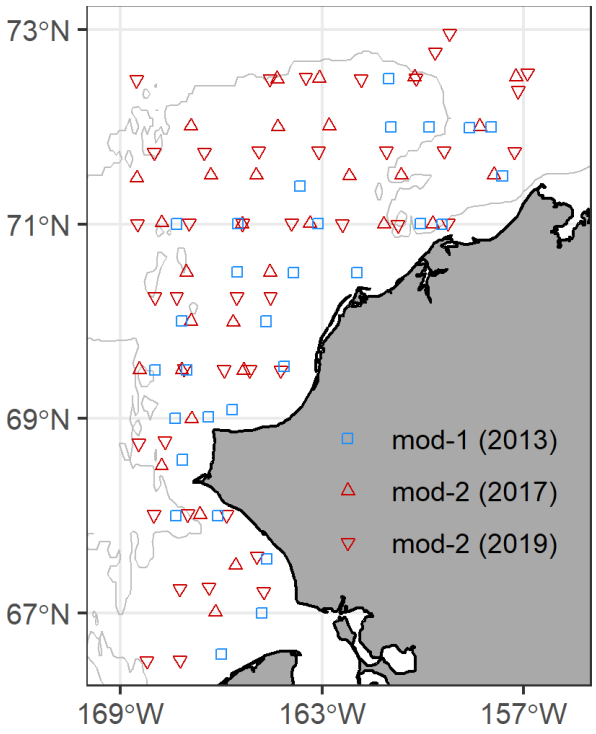

Fig. 2. Map of the study area indicating where locations where the mod-1 and mod-2 Marinovich trawls were fished during acoustic-trawl surveys. The 50 m depth contour is shown as a grey line.

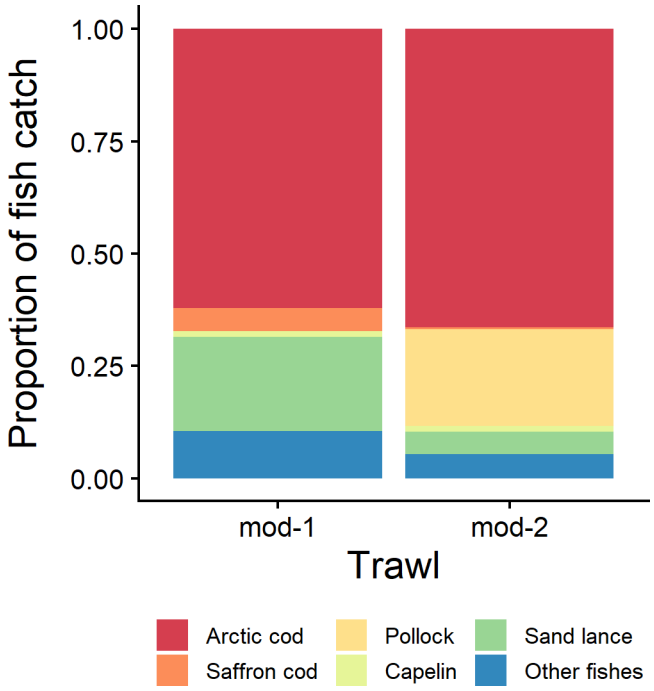

Fig. 3 Fish species composition based on codend catches of trawl hauls conducted with the Marinovich mod-1 and mod-2 trawls.

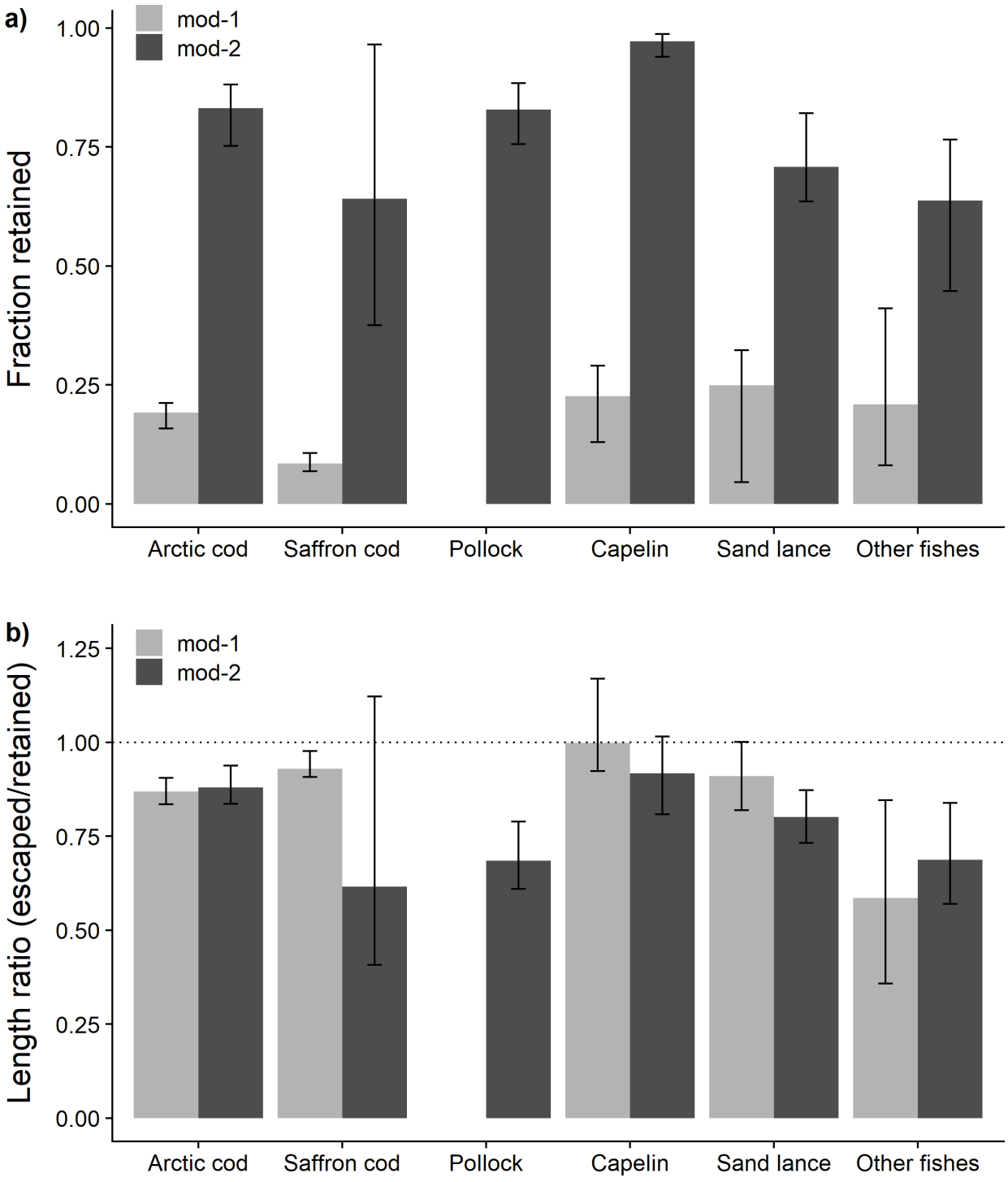

Fig. 4 Summary of a) proportion of fish entering the trawl that were retained in the codend and b) ratio in the mean standard length of the escaped/retained fish for the mod-1 and mod-2 Marinovich trawls. The error bars show the observed values (all hauls pooled) and the error bars are 95% confidence intervals computed via bootstrapping of the hauls catches and measured fish specimen lengths.

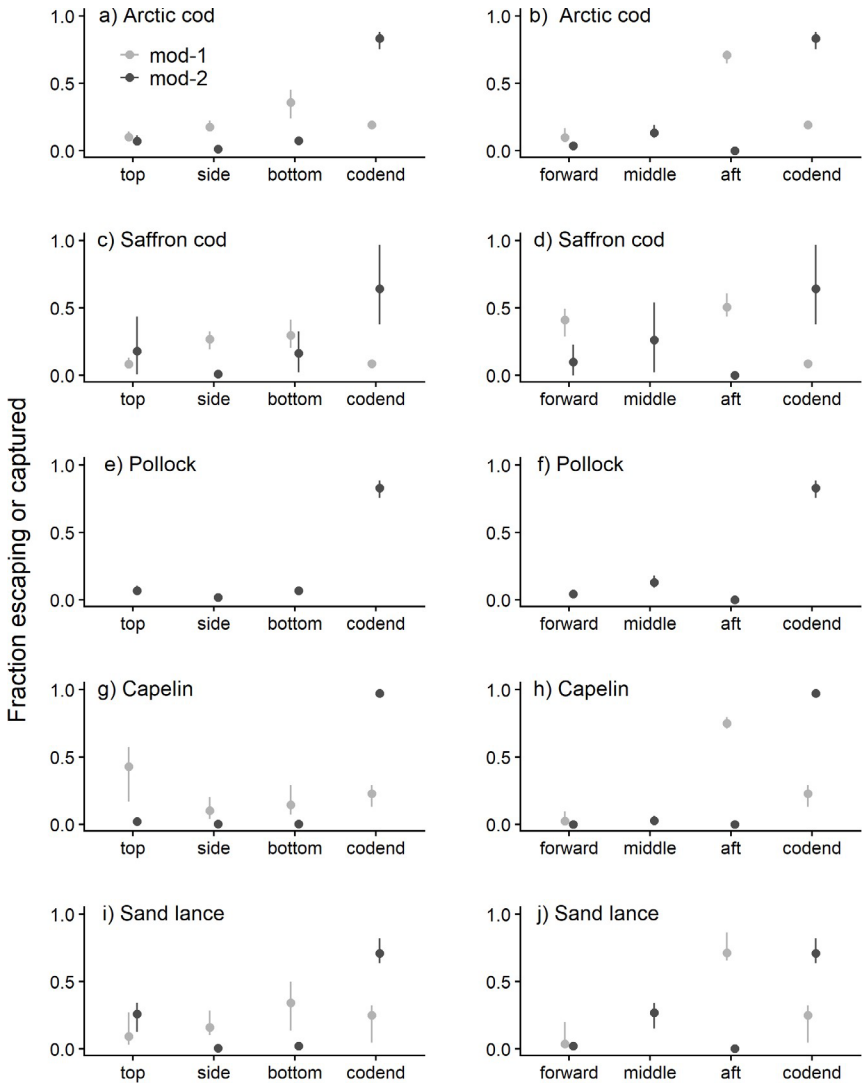

Fig. 5. Escapement pattern in mod-1 and mod-2 Marinovich trawl derived from recapture net and codend catches. a,b) Arctic cod, c,d) saffron cod, e,f) pollock, g,h) capelin, and i,j) Arctic sand lance. Panels to the left depict the estimated proportion of individuals escaping through the meshes in the top, each side, or bottom of the trawl, or retained in the codend. The mod-1 Marinovich lacks a middle section (see Fig. 1). Panels to the right indicate the estimated proportion of fish entering the trawl mouth escaping through the forward middle, or aft net sections or retained in the codend. The points represent the observed means, and error bars represent 95% bootstrap confidence intervals. In some cases, error bars are small and obscured by the symbols.

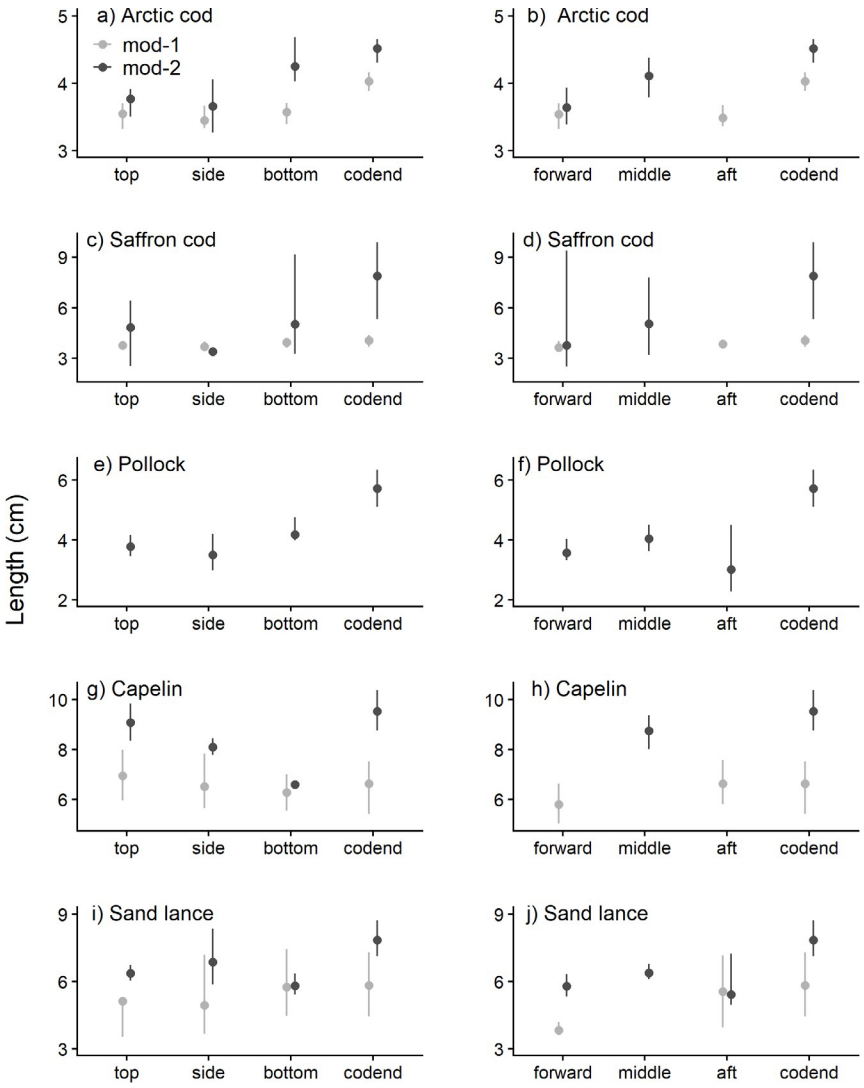

Fig. 6. Standard length of fishes caught in recapture nets and codend of mod-1 and mod-2 Marinovich trawl. a,b) Arctic cod, c,d) saffron cod, e,f) pollock, g,h) capelin, and i,j) Arctic sand lance. Panels to the left depict the lengths of fish caught in recapture nets on the top, side, bottom, or codend of the trawls. Panels to the right indicate the size of fish caught in the forward middle, or aft net sections or the codend. The mod-1 Marinovich lacked a middle section (see Fig. 1). The points represent the observed means, and error bars represent 95% bootstrap confidence intervals. Note that no capelin were captured in the forward and aft recapture nets of the mod-2 Marinovich, and that few were captured in the side (n=3) and bottom (n=2).

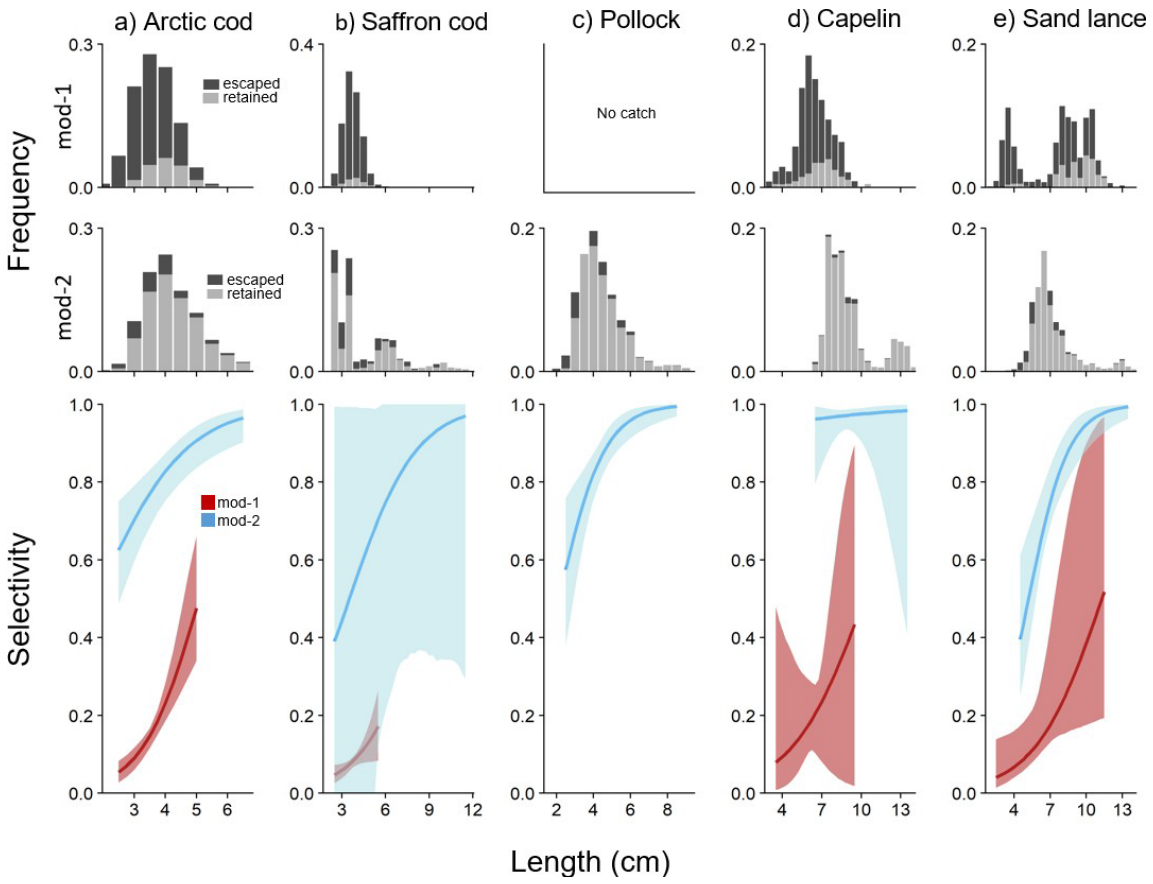

Fig. 7. Summary of escapement and fitted selectivity curves for a) Arctic cod, b) saffron cod c) walleye pollock, d) capelin, and e) Arctic sand lance. The top panel shows a size histogram with color shading representing the proportion of fish escaping through the meshes (dark gray) or captured in the codend (light grey) of the mod-1 Marinovich trawl. The middle panel shows an equivalent histogram for the mod-2 Marinovich trawl. The bottom panels compare the fitted selectivity curve and bootstrapped 95% confidence intervals for the mod-1 and mod-2 Marinovich. Pollock were effectively absent in the mod-1 data set.

CHAPTER 8 - The role of temperature on overwinter survival, condition and lipid storage in juvenile polar cod (*Boreogadus saida*): a laboratory experiment.

Objective 2: Quantify the distribution, abundance, and condition of pelagic marine fishes, in particular young-of-the-year Arctic gadids and other forage fishes

Copeman L, Salant C, Stowell M, Ottmar M, Spencer M, Iseri P, Laurel B

Abstract

In the Arctic, winter warming and loss of sea ice pose largely unknown risks to keystone species and the marine ecosystem they support. Young of the year juvenile polar cod, *Boreogadus saida*, are energy-rich forage fish that accumulate high levels of lipid in the summer but retain a relatively small body size during the winter. To address winter bioenergetics and survival, we held age-0 juveniles under simulated winter conditions (food deprived, 24-hr darkness) throughout a range of four constant temperatures (-1, 1, 3, 5 ℃). Our goals were to: 1) determine how small fish utilize lipid energy in muscle and liver across varying temperatures and durations of food deprivation, and 2) develop temperature-dependent survival trajectories based on energy loss (lipid, condition metrics, body weight) that would be useful for projecting winter outcomes of polar cod sampled pre-winter i.e, when fish are more easily sampled in the field. As expected, juvenile cod were able to better conserve lipids and survive longer at colder temperature in the absence of food. Further, there was no negative impact of freezing temperatures on this trend e.g. 50% mortality at ~170 days at -1℃ versus 94 days at 5℃. During the first 28 days of winter, polar cod preferential catabolized triacylglycerols (TAG) from muscle tissue and then shifted to storage lipids in the liver and muscle until starvation. Mortality occurred when whole body lipid concentrations fell below 12 mg. g^{-1} WWT within each temperature treatment. The temperature-dependent decline in morphometric condition (Hepatosomatic index (HSI) and Fulton's K) and lipid content were parameterized and a series of winter survival trajectory models are presented based on varying condition metrics. Using the lipid model on field collected fish, we demonstrate that winter survival is highly sensitive to small changes in temperature between -1 and 1 °C when fish are in good summer condition (e.g. 2013), alternatively polar cod will be required to continue foraging throughout the winter when in poor late summer condition (e.g. 2017). Collectively, these results suggest lipid-based indices (not size) offer a sensitive means of predicting overwintering success for polar cod experiencing climate-driven changes in summer and winter habitats in the Arctic.

Introduction

Overwintering ecology is a logistically challenging process to examine in cold and ice-covered marine systems (Berge et al. 2020b), but may be the most significant in terms of regulating species distribution and population dynamics in the era of climate change (Hurst 2007, Heintz et al. 2013, Siddon et al. 2013a). In the Arctic, winter conditions are particularly severe (long, cold, dark, and ice-extensive) and likely require specific physiological adaptations for survival e.g., cold-tolerance, energy allocation. Therefore, climate change impacts on species distributions within and adjacent to the Arctic may be limited by their ability to capitalize on warmer summer growth conditions (e.g., grow fast while storing fat) while also having the physiology to survive persistently harsh dark overwintering environments (Copeman et al. 2017, Copeman et al. 2020, Geoffroy & Priou 2020, Geissinger et al. 2021). The vulnerability of Polar cod (*Boreogadus saida*) to seasonal climate forcing are particularly concerning, given their tremendous ecological importance as a mid-trophic forage fish and role in channeling energy from plankton to upper trophic levels such as marine mammals, birds, and other fish (Hop & Gjosaeter 2013, Whitehouse et al. 2014). Estimates from the Canadian Arctic indicate that polar cod can funnel up to 75% of the carbon between zooplankton and top predators, such as seabirds and whales (Welch et al. 1992). Changes in the distribution and abundance of polar cod will therefore likely lead to broad trophic, subsistence hunting and economic impacts (Huserbråten et al. 2019, Huntington et al. 2020, Marsh & Mueter 2020), but studying these and other Arctic fish species is logistically challenging outside the summer, open-ice period (Geoffroy & Priou 2020).

Laboratory studies provide a tractable way of examining overwintering processes in high-latitude marine fish that are otherwise difficult to sample under the ice (Flores et al. 2015, David et al. 2016). Juvenile gadids have been focal species in recent laboratory experiments with results being used to validate several field observations of size-dependent overwintering mortality (Sogard 1997, McCollum et al. 2003, Shoup & Wahl 2011). Experimental studies also provide a means of tracking rates of energetic loss in juveniles during the overwintering period (Gotceitas 1999; Sogard and Olla 2000). Finally, overwintering environments (e.g., food, temperature) can be manipulated in the laboratory to examine impacts on survival and condition which in the future will allow annual forecasting of fish recruitment under different oceanographic conditions (Gotceitas et al. 1999, Sogard & Olla 2000, Kooka 2012, Geissinger et al. 2021).

The physiological response of polar cod to environmental variability provides an indication whether and how these species will persist with continuing climate change. Juvenile gadids must develop, grow and store lipid reserves rapidly during their 1st year to minimize predation and maximize overwintering survival (Copeman et al. 2008, Geissinger et al. 2021). This is especially important in the Arctic where the summers are short and prolonged winter-spring temperatures are <0°C (Bouchard & Fortier 2008). Food availability is highly seasonal in Arctic systems (Wassmann 2006) with consumers utilizing elevated summer lipid storage as a strategy to survive extended winter conditions characterized by lower food availability (Kattner et al. 2007, Falk-Petersen et al. 2009, Leu et al. 2011, Copeman et al. 2016). In general, high latitude fish are presumed to have physiology adapted to grow faster at colder summer temperatures than fish from lower latitudes, but within a narrower range of temperature preference and tolerance (stenothermic, Farrell and Steffensen (2005), (Pörtner & Farrell 2008)). Recent experimental studies have supported these assumptions (Laurel et al. 2016), but it is also clear that the thermal response of polar cod, shifts across ontogenetic stages (Laurel et al. 2017, Koenker et al. 2018b, Laurel et al. 2018). These results strongly emphasize the need to gather species-specific thermal response information spanning development across multiple critical time periods.

There are currently no studies on the overwintering processes of Arctic gadids, and how these and more well-studied boreal species may respond to new winter growth environments resulting from climate change. It is possible that juvenile polar cod utilize alternative developmental and energy storage

strategies to maximize overwintering survival compared to boreal congeners (Copeman et al. 2020). Field studies indicate that saffron cod (*Eleginus gracilis*) overwinter at a smaller size in more northern extremes of their range (Chukchi and Beaufort Seas) than in more southern areas (Gulf of Alaska and South East Bering Sea) (Helser et al. 2017). Further, Copeman et al. (2016) found that age-0 saffron cod from the Chukchi Sea were smaller (<55 mm) and had a much higher lipid concentrations (19 $mg.g^{-1}$ WWT) at the end of their 1st summer than larger (>75 mm) age-0 saffron cod from the Bering sea (12 $mg.g^{-1}$). These findings suggest that gadids living at high latitudes are under selection to store seasonal pulses of food as lipid energy rather than prioritizing accelerated growth. Comparative studies of gadids also indicate that age-0 polar cod store higher concentrations of lipid in their tissues (31 $mg.g^{-1}$, $mg.g^{-1}$ WWT) compared to other gadid species (i.e. saffron cod, ~16 $mg.g^{-1}$, Copeman et al. (2020), Copeman et al. (2017)). High levels of lipid storage in polar cod muscle tissue may offset limited capacity to store energy reserves in the liver at a small size; proportionally large lipid-rich livers are not found in gadids until > 60 mm in standard length which represents the 2nd year of growth for Arctic gadids compared to the 1st in Boreal gadids (Laurel et al. 2007, Helser et al. 2017)).

The goal of this study is to determine the size-, energy- and temperature-dependence of overwintering survival in juvenile polar cod held under simulated winter conditions in the laboratory. Our specific objectives were to parameterize the rates of juvenile mortality and energy loss (growth, condition, lipid) as well as determine the minimum energetic state for survival. We hypothesize that high energy density (pre-winter) and cold thermal conditions (winter) are necessary for elevated overwintering survival in juvenile polar cod.

Methods

Culture of juvenile polar cod

Juveniles used in these experiments were reared from incubated eggs of captive broodstock. Cod adults were originally collected as juveniles (age-0) in the Beaufort Sea (Prudhoe Bay, AK, 70.383°N - 148.552°W) and were held at the Alaska Fisheries Science Center (NOAA) laboratory in Newport, Oregon. Broodstock (age 3+) were maintained in a 6-m tank under seasonally adjusted temperatures ranging from 5 °C in the summer to 0.5 °C in the winter. In 2016, fish showed signs of maturity in early March and were checked daily by gently squeezing the abdomen to determine if eggs were freely flowing, clear and hydrated. Egg batches were made by combining the free-flowing eggs of a single female with the milt of three males in a dry, stainless steel bowl nested in crushed ice (following protocols described by Laurel et al. (2018)). A total of four egg batches were constructed in this manner and then transferred to corresponding meshed 4 L baskets floating in 2 °C water baths for incubation.

After 4 weeks, eggs were then transferred to a series of larger 400 L upwelling tanks to hatch and be cultured on live food. Larvae were reared at 2 to 3 °C on a 12:12 dark-light cycle and fed enriched rotifers at a density of 5 prey mL^{-1} 2x daily for a 4 wk period. After 4 wks, enriched *Artemia* were provided at a density of 1.5 prey mL^{-1} in addition to rotifers. After 10 wks, live prey consisted entirely of *Artemia* supplemented with dry food (Otohime A) 2x daily (Koenker et al. 2018a, Koenker et al. 2018b). At 20 wks, juvenile fish were transferred to 3-m diameter round tanks with flow-through seawater maintained at 5 °C and gradually weaned onto a gel food (diet details as in Copeman et al. (2017) and Copeman et al. (2013)). Juvenile fish (40 to 65 mm SL) were available for the experiment at ~7 months after initial egg fertilization in the laboratory. Juvenile fish were of similar size and lipid density (~55 mm; 30 mg lipids/g WWT) to those measured in late summer/fall collections in the Chukchi Sea during 2013 (Copeman et al. (2020), 2017 and 2019 (Copeman et al. in prep this report).

Temperature-dependent overwintering experiment

On October 13, 2016, age-0 juvenile polar cod were transferred from their large holding tank and separated into a series of smaller experimental tanks (n=12; dimensions 66L × 46H × 38W cm) held in an adjacent laboratory. Following transfer, fish were gradually acclimated (<0.5 ℃ in any day) to their respective overwintering temperatures (-1, 1, 3 or 5 ℃) and held with flow-through, temperature-controlled seawater over the course of the experiment. Three replicate tanks were used per temperature with each tank containing 50 fish. Fish were fed during the 12-day acclimation period but were not fed during the simulated overwintering experimental period. All tanks were covered in black tarp to keep fish in dark conditions throughout the entire experiment. Tanks were checked daily for mortalities using a red-lense flashlight. Daily fish mortalities were retained frozen (-80 ℃) for subsequent condition and lipid analysis (see below).

On October 25, 2016, the experiment was initiated by lethally subsampling 10 fish per tank for length (SL, mm, 0.01mm) and wet weight (WWT, 0.01 g). Variation in fish size (42 - 64 mm SL; 0.55 to 2.34 g) was equal across all temperature treatments (i.e. length, ANOVA $F_{3,8}$=1.31, p=0.34). All sub-sampled fish were frozen (-80 ℃) for later condition analyses based on both WWT (n=10), DWT (n=7) and tissue-specific lipid content (n=3, sampling numbers as in Table 1). After an additional 28 days of winter, 6 fish per replicate tank were measured and frozen for later condition analyses based on WWT (n=6), DWT (n=3) and lipid content (n=3). The final sampling period occurred when a temperature treatment approached 50% survival of the population, after adjusting for fish removals due to sampling events. At this time, all surviving fish in the tank were euthanized and processed for length and weight (n = 9 to 24 per tank) and frozen for later condition analyses based on WWT (n=7 to 20), DWT (7-10) and lipids (n=3, Table 1).

Condition metrics and weight loss

During morphometric and lipid processing, fish were removed from the -80 ℃ freezer in small batches (n<10) and were kept on ice during sampling to prevent lipid break-down. Fish were rinsed with water, patted dry and immediately measured for standard length (tip of the snout to end of the notochord, SL, mm) and wet weight (WWT, g, ± 0.001). Fish intestinal tracts were removed and livers were dissected and weighed on a microbalance (0.001 mg). A subset of eviscerated bodies and livers were dried separately at 65 ℃ to a constant weight (~1 week) and reweighed to calculate Fulton's K and hepatosomatic index (HSI) based on DWT (equations below). Conversion factors between tissue-specific WWT and DWT were also calculated and used to express lipids per DWT of tissue. Liver and body weights were used to calculate the following condition factors on both sampled fish and mortalities:

- Fulton's K_{wet} = (Whole body WWT(g)/(SL(cm)^3) * 100
- Fulton's K_{dry} = (Whole body DWT(g)/(SL(cm)^3) * 100
- HSI_{WET} = (Liver WWT(mg)/Whole Body WWT(mg)) * 100
- HSI_{DRY}= (Liver DWT(mg)/Whole Body DWT(mg)) * 100
- Concentration of total lipids per WWT = (Iatroscan summed lipid classes (µg))/ (weight of tissue (mg))
- Concentration of total lipids per DWT = (Iatroscan summed lipid classes (µg))/(WWT of tissue, (mg) * temperature and time-specific conversion factor (DWT:WWT))

Relative body weight loss (BW_l) was determined by subtracting the measured fish WWT from the WWT estimated from the length-weight relationship at the beginning of the experiment (see Fig.3) assuming negligible change in SL (mm).

BW_l was determined using the following equations:

$$BW_l=100-(e^{g}-1)$$

where g is the instantaneous growth coefficient obtained by the equation:

$$g=(\ln 〚WWT〛_2-\ln 〚WWT〛_1)/(t_2-t_1)$$

where WWi is the measured or estimated wet weight of an individual fish at time ti. Temperature-dependent BW_l was described using a 3-parameter polynomial function (SigmaPlot 14). Tank replicates (mean BW_l) was used as the level of observation for the temperature-dependent weight loss model.

Tissue-specific lipid analyses

Tissue-specific lipid analyses of muscle and liver were conducted for total lipids and lipid classes. Lipid analyses were based on whole livers and ~300 mg samples of dorsal muscle that excluded the skin. All samples for lipid analyses were stored in chloroform under nitrogen in a -20 °C freezer and were extracted and analyzed within 6 months of sampling. Total lipids were determined using thin layer chromatography with flame ionization detection (TLC/FID) with a MARK V Iatroscan (Iatron Laboratories, Tokyo, Japan) as described by Lu et al. (2008) and Copeman et al. (2017). Extracts were spotted on duplicate silica-gel-coated Chromarods, and a three-stage development system was used to separate wax esters, triacylglycerols, free fatty acids, sterols and polar lipids. Polar lipids are mostly phospholipids, with minor amounts of other acetone mobile polar lipids. The first rod development was in a chloroform: methanol: water solution (5:4:1 by volume) until the leading edge of the solvent phase reached 1 cm above the spotting origin. The rods were then developed in hexane: diethyl ether: formic acid solution (99:1:0.05) for 48 min, and finally rods were developed in a hexane: diethyl ether: formic acid solution (80:20:0.1) for 38 min. After each solvent development, rods were dried (5 min) and conditioned (5 min) in a constant humidity chamber (~32%) that was saturated with aqueous $CaCl_2$. Following the last development, rods were scanned using Peak Simple software (ver. 3.67, SRI Inc.) and the signal detected in millivolts was quantified with calibration curves using the following commercial standards from Sigma (St Louis, MO, USA): cholesteryl stearate (wax ester), glyceryl tripalmitate (triacylglycerols), palmitic acid (free fatty acids), cholesterol (sterols), L-alpha-phosphatidylcholine (polar lipids). Calibrated relationships between lipid class areas and standard lipid amounts (µg) had correlations with an r^2 >0.98 for all classes.

Temperature and size effects on survival

The effect of temperature on days to 80% and 50% population mortality for age-0 polar cod was investigated using a one-way ANOVA with Tukey's multiple comparison test on tank values (n=3 per temperature). The effect of size and temperature on days to mortality was investigated using a one-way ANCOVA but inequality of error variance required that we describe the effect of size using separate temperature-dependent linear regression models. Residuals from the regression of length and days to mortality were tested for temperature effects using a one-way ANOVA. A two-way ANOVA was used to investigate the effect of temperature and survival status on the mean SL (mm) of age-0 polar cod when the population reached 50% survival.

Effects of temperature on condition loss

Temperature-specific effects of starvation duration on condition metrics were analyzed by fitting linear and exponential decay functions (SigmaPlot 14). To describe the continuous temperature effect on rate-loss functions, we fit linear regressions between temperature and the slopes of the temperature-specific (-1, 0, 3 and 5 °C) relationships between condition and days of starvation. Hepatosomatic indices were nature log transformed to improve the fit of the models. Condition factors are expressed per WWT and per DWT. All analyses are run on tank means (n=3) with individuals sampled by tank as in Table 1.

The days to starvation over a wide range of winter temperatures were visualized for age-0 polar cod from both this experiment along-side field-collected fish with mean end of summer lipid levels from a divergent cold (2013) and a warm (2017) years (Central Chukchi Sea, see Table 5). Starvation levels (12.5 mg.g-1 WWT, Fig. 7d) as well as a lipid loss model ((mg.g^{-1} WWT).day^{-1} = -0.1879 -0.02122 (T), r^2=0.77 (Fig. 7d)) were determined from experimental treatments. Days to starvation were calculated as the days required to decrease in lipid concentration from end of summer levels (2013, 34.7 mg.g^{-1} and 2017, 16.0 mg.g^{-1}) to starvation status, 12.5 mg.g^{-1}.

Results

Survival

Temperature significantly affected starvation resistance of polar cod, with fish at colder temperatures surviving long than fish at warmer temperatures (Fig. 1). The duration to 80% and 50% population mortality were significantly different across temperature treatments (ANOVA 80%: $F_{3,8}$=22.12, p<0.001, ANOVA 50%: $F_{3,8}$=92.93, p<0.001). Polar cod had a mean survival time to 50% population mortality of 170 ± 11 days at -1°C compared to only 94 ± 1 days at 5 °C (Fig. 1).

Within fish that died, size only weakly explained survival time. The temperature-dependent slopes of this relationship were only significant at 1 and 3 °C (p<0.05) with the strongest correlation between size and survival time noted at 1°C (r^2 = 0.26, Fig. 2a). Size de-trended residuals for the relationship between size and time to mortality showed a significant effect of temperature treatment (ANOVA, $F_{3,190}$=136.37, p<0.001, Fig. 2b.), with fish at 5 °C having the lowest size de-trended survival duration.

At 50% mortality, we compared the effect of temperature and mortality status on the size (SL, mm) of polar cod (Fig. 2c). There was no interaction between temperature and mortality status and no significant difference in size due to temperature (ANOVA, $F_{3,18}$=2.66, p=0.08). However, fish that died were significantly smaller (mean SL of 53.5 ± 0.8) than fish that survived (mean SL of 61.1 ± 0.7 mm, ANOVA, $F_{1,18}$=51.44, p<0.001, Fig 2c), indicating that larger size provided some overwinter survival advantage.

Weight and morphometric condition loss

Length-weight relationships for age-0 polar cod at the beginning of the experiment ('pre-winter') were compared to this relationship at the time of mortality ('winter mortality', Fig 3). The winter mortality length-weight model is the theoretical lower weight threshold juvenile fish must maintain for winter survival. Temperature-dependent weight loss (Fig. 4) was determined using the difference in weight at the time of dead to length-based relationships of the pre-winter model. The rate of temperature-dependent weight loss for age-0 juvenile polar cod was well explained by the following 3 parameter polynomial function:

Growth loss (% WWT (g) day^{-1}) = -0.59 - 0.051(T) - 0.0015(T^2), r^2=0.93.

Temperature-specific Fulton's K based on both WWT (Fig. 5a) and DWT (Fig. 5c) were explained by the duration of winter conditions (r^2 ranged from 0.83 to 0.98). The relationship between the rate of change in Fulton's K_{dry} and K_{wet} and overwintering temperature were defined using the following linear regressions:

$K_{wet}.day^{-1} = -2.130e^{-3} - 1.721e^{-4}$ (T), r^2=0.90 (Fig. 5b)

$K_{dry}.day^{-1} = -2.922e^{-4} - 3.37e^{-5}$ (T), r^2=0.97 (Fig. 5d)

Condition measurements taken on mortalities allowed us to define the mean ± SD starvation condition for K_{wet} and K_{dry} as 0.44 ± 0.063 and 0.066 ± 0.0058, respectively.

Temperature-specific HSI based on both WWT (Fig. 6a) and DWT (Fig. 6c) were explained by an exponential decay in condition over the duration of the winter exposure (r^2 ranged from 0.83 to 0.98). The relationship between the rate of change in natural log transformed HSI_{dry} and HSI_{wet} and overwintering temperature were defined using the following linear regressions:

Ln $(HSI_{wet+1}).day^{-1} = -6.280e^{-3} - 6.96e^{-4}$ (T), r^2=0.87 (Fig. 6b)

Ln $(HSI_{dry}).day^{-1} = -0.0174 - 1.536e^{-3}$ (T), r^2=0.89 (Fig. 6d)

HSI metrics taken on fish that died allowed us to define the mean mortality stage for HSI_{wet} and HSI_{dry} as 0.65 ± 0.35 and 0.87± 0.5, respectively.

Lipid loss models

At time-0, fish ranged in SL from 42 to 66 mm and showed no significant relationship between length and whole body lipid storage per WWT (r^2=0.002, slope p>0.05). Temperature-specific lipid composition was calculated for whole fish over the duration of the experiment (Table 2) from measurements of tissue-specific levels in liver (Table 3) and muscle (Table 4). At time-0, fish had an average of 46.1 ± 15.4 mg of lipid per individual which dropped to 9.1 ± 4.0 mg at the time of 50% population mortality. Most of the lipid loss was due to decreased neutral storage lipids, triacylglycerols (TAG), which decreased from 86% in the liver and 56% of the lipids in the muscle to 8% and 2%, respectively (Tables 3 & 4). Fish that died were characterized by low total lipid concentrations (12 mg. g^{-1} WWT) and high relative proportions of polar lipid (PL, ~70%) and sterols (ST, ~20%), a state indicative of only membrane structures remaining with little lipid-based energy storage.

Across all temperatures, we measured a rapid decline in muscle tissue lipids from 29.1 ± 5.5 mg. g^{-1} WWT at time-0 to 20.8 ± 3.8 after day-28 of simulated winter (Fig. 7b). The opposite trend was measured in liver tissue, that increased in lipid density from 290.3 ± 56.7 at time-0 to 334.9 ± 62.3 mg. g^{-1} at day-28 (Fig 7a). Polar cod have small amounts of liver tissue relative to muscle mass and they store high proportions of lipid (TAG) in their muscle, which explains the general decrease in whole body lipid concentrations from day-0 (41.4 ± 5.3 mg. g^{-1} WWT) until day-28 (33.1 ± 6.0 mg. g^{-1}, Fig. 7c). The same trends were measured for total tissue-specific lipids based on DWT (Fig. 8a & 8b). Both muscle and liver tissue decreased rapidly in lipids from day-28 until 50% population mortality (Fig 7 & 8, Tables 3 & 4).

Temperature-specific lipid concentrations for whole fish based on both WWT (Fig. 7c) and DWT (Fig. 8c) were explained by the duration of winter exposure (r^2 ranged from 0.86 to 0.99). The temperature-dependent rate of whole body lipid loss based on WWT and DWT were explained using the following linear regressions:

Lipid loss (mg. g^{-1} WWT). day^{-1} = -0.1879 -0.02122 (T), r^2=0.77 (Fig. 7d)

Lipid loss (mg. g^{-1} DWT). day^{-1} = -0.9018 -0.08749 (T), r^2=0.64 (Fig. 8d)

Lipid measurements on fish that died allowed us to define the mean lipid composition at death based WWT and DWT as 12.1 ± 2.0 mg. g^{-1} and 65.3 ± 10.9 mg. g^{-1}, respectively.

The importance late summer lipid storage and winter temperatures on survival for age-0 polar cod is shown in Table 5 and Fig. 9. Tissue concentrations of lipids in polar cod from the Central Chukchi Sea in 2013 (from Copeman et al. 2020) and 2017 (Copeman et al. this report) were used with the equation for lipid loss (mg. g^{-1} WWT). day^{-1} = -0.1879 -0.02122 (T), r^2=0.77 (Fig. 7d) to calculate survival times. Specifically, we calculated the time need to achieve a change in lipid concentration equaled the difference between end of summer levels and starvation concentrations (12.5 mg. g^{-1}) (Table5) across a wide range of continuous simulated winter temperatures from -2 to 10 °C (Fig. 9). Starvation resistance at -1 °C was projected to be over 4.5 months compared to less than 1 month in fish from 2013 (cold) versus 2017 (warm), respectively. Further, small changes in temperature at the cold end of the overwintering range made a large difference in survival to high lipid fish (i.e. 1-month difference from -1 to 1 °C in 2013) but little difference to low lipid fish (i.e. 6 days difference from -1 to 1 °C for 2017 fish, Table 5, Fig. 9). Survival of high condition fish is dependent on winter temperatures while poor condition fish had low survival times across a full range of temperatures (24 to 13 days starvation resistance between -1 to 5 °C) (Fig. 9, Table 5).

Discussion

The importance of pre-winter lipid condition and winter temperature were highly apparent in our study. Age-0 polar cod conserved lipids and survived longest in our coldest temperature treatments (-1°C). Although fish that survived to 50% of population levels were categorically larger than those that died, juvenile body size only weakly explained survival times of fish that died (between 42-64 mm SL). In the field, we contend that polar cod overwintering success will be highly dependent on summer lipid storage as well as the availability of cold winter habitats that can minimize energy loss in the Arctic.

Small body size and energy allocation

As predicted, high mortality occurred when energy reserves (e.g., lipids) were exhausted during winter starvation (e.g., Thompson et al. 1991; Ludsin and DeVries 1997). Here, this level was found to be 12.5 mg. g^{-1} lipid per WWT of whole body tissues across all thermal conditions. However, counter to our expectations, there was no overall relationship between fish size and lipid storage at the beginning of the experiments (mg. g^{-1}). Although there was a modest size-effect on survival (~1mm = +1 day of survival), the size covariate in the survival model explained very little variation within any given temperature treatment (r^2 ranged 10 to 26%). We suspect small fish either have slightly higher metabolic requirements or behavioral activity (Kerr 1971), but size by itself appears to be a poor indicator of overwintering success for juvenile polar cod within the size range tested.

In contrast to size, application of laboratory rates to realized variability in the lipid storage of field-collected polar cod (Copeman et al. 2020) indicate that lipid content has an important bearing on winter survival potential. The annual differences in lipid density of field collected fish from the Central Chukchi Sea (2013: 34.7 ± 18.7 versus 2017: 16.0 ± 6.4) were particularly striking despite being similar in size (2013: 43.4 ± 3.9 versus 2017: 47.2 ± 10.3). The starvation models illustrate how winter thermal conditions are either highly important following summers that support fish in good conditions (e.g., 2013) or potentially irrelevant when the preceding summer conditions result in a poor energetic state for age-0 juveniles e.g., 2017, ‘dead fish swimming’. It also appears that small changes in temperature between -1

and 2°C have a dramatic effect on survival of fish entering winter in a high energetic state (Fig. 9). The importance of summer-fall prey availability and pre-winter condition are important processes regulating winter survival and thus recruitment of walleye Pollock (*Gadus chalcogramma*) in the Eastern Bering Sea (Hunt Jr et al. 2011, Mueter et al. 2011, Heintz et al. 2013). Regardless, the high prioritization for energy storage observed in small-bodied juvenile polar cod suggest there is a high winter mortality risk in the Arctic and that this risk is more likely due to starvation than predation (Ivan et al. 2015).

Size-dependent overwintering success may be more important in lower latitude regions where late fall/winter density-dependent predation rates are high (Laurel et al. 2003, Lough & O'Brien 2012) and size demographics are more variable in the summer and fall period (Geissinger et al in review). Overwintering survival has been shown to increase through size-advantages due to earlier spawning (Henderson et al. 1988, Morley et al. 2013) or growth (Mogensen & Post 2012) in more temperate systems. In the Eastern Bering Sea, young-of-the-year Pollock rarely survive their first winter following poor fall growth and lipid storage conditions (Heintz & Vollenweider 2010). Such size advantages are often attributed to reduced winter predations risk (Post & Evans 1989, Pangle et al. 2004, Morley et al. 2013), although size-dependent predation preceding winter may actually be more important (Jonsson et al. 2010). In such instances, it is generally assumed that size-dependent winter survival is linked to higher energy storage in larger fish (e.g., Heermann et al. (2009)) or lower metabolic rates (Werner & Gilliam 1984, Byström et al. 2006).

Condition loss models

We present three types of condition metrics: Fulton's K, a morphometric condition index that indicates the relationship between weight and length (Froese 2006, Nash et al. 2006), 2); HSI, a morphometric index that expresses liver weight relative to body weight and is often referred to as a metric of lipid storage due to high proportions of lipid in the liver ((Guy & Brown 2007, Aune et al. 2021)) and lastly, tissue-specific and whole body explicit measurements of lipid. The use of multiple different condition metrics allows our data to be broadly interpreted in relation to other field collections or laboratory experiments that may have only one metric, such as length-weight. The easy of performing morphometric condition measures can allow for the processing of larger numbers of individuals. However, morphometric condition in larval and juvenile marine organisms has shown a general lack of sensitivity (Suthers 1998, Copeman et al. 2008, Copeman et al. 2018), likely because they are insensitive to changes in high energy lipid storage. Polar cod store high concentrations of lipid in their muscle tissues relative to other boreal congeners (Copeman et al. 2017) making HSI potentially insensitive to changes in the lipid dynamics of polar cod. At time-0 polar cod had 29.9 ± 1.5 mg of lipid in their muscle tissues compared to 16.2 ± 1.6 mg in their liver but by the time of 50% population mortality almost all the remaining lipid was found in muscle storage (8.9 ± 3.9 per fish). The importance of muscle tissue was also demonstrated during the first month of our study when fish preferentially utilized muscle lipid over liver lipid. For future analyses of large field campaigns, age-0 polar cod whole body homogenates should be saved for lipid analyses. Dissections of livers from age-0 polar cod are incredibly time consuming and difficult due to both the small size and delicate nature of the liver tissue.

Future research

Understanding the impact of winter feeding scenarios will be an important component of future laboratory and field research. Small amounts of food during winter can dramatically improve survival of age-0 Atlantic cod with the addition of minimum rations to winter experiments resulting in prolonged survival and growth at low temperatures (-0.8 to 2.7 °C) (Geissinger et al. 2021). Field studies indicate active under-ice zooplankton production in the Arctic winter (Berge et al. 2020a, Geoffroy & Priou 2020), but we know of no such field studies in the Chukchi Sea region. Polar cod have specialized large eyes that enable more successful feeding at lower light intensities than boreal gadids (Wagner et al. 1998) and this

has been proposed as an additional barrier to the establishment of boreal gadid populations in Arctic regions (Kaartvedt 2008). In the waters surrounding Svalbard, Norway, adult polar cod and invading boreal gadids have been shown to forage during the polar night, although at a lower stomach fullness than in summer (Geoffroy & Priou 2020). However, adults were found to switch from zooplankton to larger prey such as fish (Cusa et al. 2019) during the winter. Prey switching was proposed as a solution to reduced light and a polar cod's limited ability to visually capture small zooplankton. Due to gape limitation, it is uncertain if small age-0 polar cod (30-60 mm) can also successfully switch to larger prey items during the winter. Although Polar Regions are becoming 'brighter' with climate change (Kristiansen et al. in review), the projected foraging gains to visual feeders will be mostly limited to the summer months as the polar night will continue to be dark regardless of sea-ice loss (Langbehn & Varpe 2017).

Overwintering processes may become logistically less challenging in the future as the Arctic will have increase periods of open-water and better technology for sampling polar cod and their prey under thin ice (David et al. 2015, Kohlbach et al. 2017). As polar cod tissue samples become available from these efforts, fall/winter lipid storage and trophic dynamics can be used to ground truth some of the survival trajectories from this study, all of which have implications for recruitment dynamics in Alaskan waters (Hurst 2007a, Farley et al. 2011, Heintz et al. 2013, Siddon et al. 2013). Currently, efforts to understand the bioenergetics of polar cod rely on models with many assumptions about physiological rates, consumption rates and trophic relationships (Hansen et al. 1993). The simple models we report do not account for trophic dynamics, however, they are stage-specific and provide an understanding of tissue lipid compartmentalization that are not typically captured in Wisconsin bioenergetics (Munch & Conover 2002).

Conclusions

Age-0 polar cod were able to minimize energy loss at temperatures <0°C with no apparent impact on survival before they reached the point of energetic starvation (Lipids per WWT = 12.5 mg. g-1, HSI_{wet} = 0.67, K_{wet} = 0.62). It is likely that they utilize antifreeze proteins in the liver and/or gills as a metabolically cost-effective way to utilize these extremely cold habitats (Chen et al. 1997, Fletcher et al. 2001). Energy density increases with body size for most fish species during the juvenile phase (pre-reproductive; Martin et al. (2017)), but Chukchi Sea polar cod enter their 1st winter at ~50% the size of similarly aged gadids from the Bering Sea (Siddon et al. 2013a, Siddon et al. 2013b) and the Gulf of Alaska (Laurel et al. 2017). Such contrasting energy storage strategies may set the distributional limits for small polar cod to minimize winter energy loss. Based on summer field collections from the Chukchi Sea (De Robertis et al. 2016), age-0 polar cod are the major gadids in the Chukchi Sea, but changing climatic conditions in the summer and winter could disrupt these distribution boundaries and result in a more boreal summer fish assemblage (Levin et al. this report). It remains uncertain whether boreal gadids can successfully overwinter at temperatures routinely <1°C, such as those common to the Chukchi and Beaufort Sea shelves.

Successful overwintering for polar cod will be highly dependent on seasonal conditions in both the winter and summer. The survival trajectories described in this study demonstrate how summer lipid allocation and cold winters theoretically improve overwintering success while also indicating that winter foraging is necessary when fish are in poor pre-winter condition or Arctic winter thermal habitats are warmer. However, the transition from age-0 to age-1 will remain a poorly understood component of population dynamics without increased seasonal observational data during this period (Heintz & Vollenweider 2010, Geoffroy et al. 2016, Boudreau et al. 2017, Geoffroy & Priou 2020). Winter studies on diet will be especially critical, as will information on regional predation pressure that may impact strategies for energy allocation (e.g., growth) or thermal habitat preferences. The survival trajectory models described

here will therefore remain a theoretical framework for field validation studies and models examining population impacts under varying climate projection scenarios.

.

Table 1: Allocation of samples from age-0 polar cod overwintering experiment. Sampled fish and mortalities were processed for condition metrics based on WWT (526), DWT (374) and detailed tissue-specific lipid classes (n=140).

Temperature	-1°C	1°C	3°C	5°C
Replicate tanks	3	3	3	3
Fish per tank	50	50	50	50
Day-0: October 24, 2016	**Number of fish sacrificed per tank**			
Total fish sampled per tank	10	10	10	10
Condition: hepatosomatic index WWT	10	10	10	10
Condition: hepatosomatic index DWT	7	7	7	7
Tissue specific lipid class analyses	3	3	3	3
Day-28: November 22nd, 2016	**Number of fish sacrificed per tank**			
Total fish sampled per tank	6	6	6	6
Condition: hepatosomatic index WWT	6	6	6	6
Condition: hepatosomatic index DWT	3	3	3	3
Tissue specific lipid class analyses	3	3	3	3
50 % mortality	**Number of fish sacrificed per tank**			
Total fish sampled per tank	8-9	9	5-10	5-8
Condition: hepatosomatic index WWT	8-9	9	5-10	5-8
Condition: hepatosomatic index DWT	13-15	9-19	2-7	2-5
Tissue specific lipid class analyses	3	3	3	3
Mortalities	**Number of mortalities**			
Total fish sampled per tank	13-15	15	10-16	10-14
Condition: hepatosomatic index WWT	13-15	15	13-20	8-16
Condition: hepatosomatic index DWT	7-9	9	4-10	4-8
Tissue specific lipid class analyses	3	3	3	3

Table 2: Mean and standard deviations of the estimated whole bodied total lipids, total lipid concentrations per WWT and total lipid concentrations per DWT ($\mu g.mg^{-1}$) from polar cod sampled at time-0, day-28, in surviving cod at the time of 50% population mortality and in fish that died (n=9 fish per temperature-time).

Sampling time	Temp		Total lipid per fish (mg)	Total lipid concentration per WWT ($\mu g.mg^{-1}$)	Total lipid concentration per DWT ($\mu g.mg^{-1}$)
Day-0	- 1	Mean	37.48	41.97	210.79
		St. Dev	12.58	5.61	26.48
	1	Mean	43.14	40.03	194.25
		St. Dev	10.26	4.21	20.07
	3	Mean	53.48	44.60	217.63
		St. Dev	16.98	2.95	20.15
	5	Mean	49.29	38.41	189.44
		St. Dev	15.37	5.57	28.97
Day-28	- 1	Mean	36.32	36.16	186.40
		St. Dev	12.49	6.33	26.46
	1	Mean	27.27	32.06	165.76
		St. Dev	7.93	7.74	35.95
	3	Mean	39.70	33.52	178.88
		St. Dev	14.37	3.13	14.54
	5	Mean	32.57	30.72	175.56
		St. Dev	10.64	4.79	26.79
Survivors at 50% population mortality	- 1	Mean	8.23	10.87	60.82
		St. Dev	1.89	1.32	7.61
	1	Mean	7.81	10.36	59.64
		St. Dev	1.24	1.57	8.82
	3	Mean	9.53	9.58	55.82
		St. Dev	3.00	1.29	8.05
	5	Mean	10.95	12.00	74.07
		St. Dev	6.49	4.60	28.08
Mortalities	- 1	Mean	5.68	11.80	61.07
		St. Dev	.84	1.06	5.24
	1	Mean	5.21	14.14	74.97
		St. Dev	1.84	6.40	34.30
	3	Mean	5.57	12.59	71.03
		St. Dev	1.12	2.36	20.06
	5	Mean	6.24	11.57	66.24
		St. Dev	1.52	2.23	12.71

Table 3: Mean and standard deviations of the lipid composition in liver of polar cod that were sampled at time-0, day-28, in survivors at the time of 50% population mortality and in fish that died (n=9 fish per temperature-time). Data are shown for total lipids per whole liver (mg), total lipid concentrations per WWT (µg.mg^{-1}), total lipid concentrations per DWT (µg.mg^{-1}), proportions of total lipid as triacylglycerols (TAG), free fatty acids (FFA), sterols (ST) and polar lipids (PL).

Sample Type	Time	Temp		Total lipid in tissue (mg)	Total tissue lipid concentration per WWT (µg.mg^{-1})	Total tissue lipid concentration per DWT (µg.mg^{-1})	% TAG	% FFA	% ST	% PL
Liver	Day-0	-1	Mean	12.11	298.48	485.82	87.25	8.11	1.25	3.39
			St. Dev	7.67	52.27	85.07	3.03	2.37	.55	.63
		1	Mean	18.11	303.47	493.96	85.73	7.77	2.03	4.47
			St. Dev	8.07	78.76	128.20	5.50	2.87	.80	2.42
		3	Mean	18.83	288.76	469.92	88.86	5.61	1.67	3.86
			St. Dev	12.02	41.20	67.05	3.88	1.58	.97	1.64
		5	Mean	16.27	274.95	458.48	85.06	8.78	2.11	4.06
			St. Dev	8.93	63.81	106.40	3.40	2.86	.75	1.22
	Day-28	-1	Mean	14.87	334.61	554.16	89.84	5.51	1.07	3.58
			St. Dev	6.90	46.61	77.20	4.90	4.31	.46	1.41
		1	Mean	9.62	320.67	541.94	91.41	4.68	.84	3.07
			St. Dev	4.39	47.28	79.90	2.23	1.86	.16	1.58
		3	Mean	16.54	338.74	556.17	89.62	5.62	1.05	3.71
			St. Dev	7.61	40.53	66.54	4.05	2.16	.26	1.95
		5	Mean	14.15	345.58	669.51	90.97	4.71	1.06	3.26
			St. Dev	6.31	102.76	199.08	2.90	1.63	.28	1.46
	Survivors at 50%	-1	Mean	.13	13.26	58.38	.71	25.20	14.34	59.74

population mortality		St. Dev	.09	1.96	8.61	1.73	8.15	3.00	7.57
	1	Mean	.16	14.32	61.83	5.72	19.80	14.54	59.94
		St. Dev	.18	8.62	37.20	13.36	3.98	4.03	12.42
	3	Mean	.32	16.76	73.08	6.46	20.38	11.76	61.40
		St. Dev	.35	7.71	33.62	12.42	8.92	2.85	14.68
	5	Mean	.32	24.23	103.79	17.42	24.68	9.69	48.22
		St. Dev	.27	12.61	54.01	16.97	7.00	4.63	17.56
Mortalities	-1	Mean	.06	11.31	55.96	.00	13.22	14.69	72.10
		St. Dev	.04	2.44	12.16	.00	7.83	1.26	8.50
	1	Mean	.04	9.04	45.16	.00	17.20	15.46	67.34
		St. Dev	.01	2.07	10.32	.00	12.29	2.93	11.97
	3	Mean	.05	10.21	52.96	.00	16.09	16.81	67.10
		St. Dev	.04	3.64	19.52	.00	9.04	4.40	7.78
	5	Mean	.10	13.18	72.96	3.90	17.96	14.99	63.15
		St. Dev	.13	7.24	40.07	8.49	15.75	5.58	13.43

Table 4: Mean and standard deviations of the lipid composition in muscle from polar cod that were sampled at time-0, day-28, in survivors at the time of 50% mortality and in fish that died (n=9 fish per temperature-time). Data are shown for total muscle lipids per fish (mg), total lipid concentrations per WWT($\mu g.mg^{-1}$), total lipid concentrations per DWT ($\mu g.mg^{-1}$), and proportions of total lipid as triacylglycerols (TAG), free fatty acids (FFA), sterols (ST) and polar lipids (PL).

Sample Type	Time	Temp		Total lipid in tissue (mg)	Total tissue lipid concentration per WWT ($\mu g.mg^{-1}$)	Total tissue lipid concentration per DWT ($\mu g.mg^{-1}$)	% TAG	% FFA	% ST	% PL
Muscle	Day-0	- 1	Mean	25.37	30.67	173.97	56.37	8.22	5.54	29.87
			St. Dev	6.67	5.43	30.40	4.82	1.43	1.13	3.32
		1	Mean	25.04	25.01	140.44	52.37	9.63	6.33	31.67
			St. Dev	3.46	2.64	14.80	3.89	1.41	.70	2.90
		3	Mean	34.65	31.68	178.25	58.10	7.30	5.67	28.94
			St. Dev	9.04	5.59	31.45	4.36	.73	.82	3.11
		5	Mean	33.02	27.56	153.61	54.40	8.56	6.18	30.87
			St. Dev	9.06	5.42	30.18	6.49	1.27	.71	5.76
	Day-28	- 1	Mean	21.45	22.77	132.97	50.46	5.81	5.85	37.88
			St. Dev	6.48	2.65	15.48	6.25	1.19	.73	5.37
		1	Mean	17.65	21.52	123.24	39.89	6.72	8.75	44.63
			St. Dev	5.71	5.71	32.72	15.58	2.04	4.40	9.63
		3	Mean	23.16	20.64	124.10	49.04	6.10	6.83	38.03
			St. Dev	7.99	2.33	14.02	3.31	1.09	.66	3.62
		5	Mean	18.43	18.44	115.87	42.60	6.59	7.52	43.28
			St. Dev	4.92	2.80	17.62	7.49	2.40	1.07	5.43
			Mean	8.05	10.86	60.54	.00	7.36	18.97	73.67

Survivors at 50% population mortality	-1	St. Dev	1.83	1.35	7.53	.00	3.61	1.45	4.02
	1	Mean	7.65	10.28	58.89	.65	7.57	19.54	72.24
		St. Dev	1.22	1.53	8.76	1.95	1.04	1.43	2.29
	3	Mean	9.21	9.45	54.48	.06	6.49	18.74	74.70
		St. Dev	2.83	1.39	8.01	.19	4.56	1.40	4.99
	5	Mean	10.63	11.83	73.07	6.94	10.85	16.99	65.23
		St. Dev	6.49	4.72	29.19	18.07	4.45	4.29	12.66
Mortalities	- 1	Mean	5.62	11.79	60.32	.00	6.03	20.02	73.96
		St. Dev	.87	1.12	5.46	.00	3.27	1.87	4.55
	1	Mean	4.80	13.04	68.52	.00	3.66	20.16	76.18
		St. Dev	1.51	2.10	10.84	.00	2.07	1.21	2.33
	3	Mean	4.82	13.08	69.72	.00	5.33	18.97	75.70
		St. Dev	2.08	2.65	15.51	.00	2.29	2.24	3.92
	5	Mean	6.14	11.53	65.30	.00	4.27	19.86	75.87
		St. Dev	1.49	2.35	13.31	.00	2.68	1.27	3.57

Table 5: The importance of energetic condition and winter temperatures on days of starvation resistance in age-0 polar cod. Lipid concentrations in polar cod from the central Chukchi Sea in 2013 (Copeman et al. 2020) and 2017 (Copeman et al. this report) are used to demonstrate variability in time to starvation for field collected fish of different nutritional status. The equation for lipid loss ($mg.g^{-1}$ WWT).day^{-1} = -0.1879 -0.02122 (T), r^2=0.77 (Fig. 7d) was used to calculate the days to starvation lipid storage levels under the 4 different experimental temperatures. Data are mean ± standard errors of field-collected age-0 polar cod in the Central Chukchi Sea (68.25 - 70.74°N) region as defined in Buckley and Whitehouse (2017). Extrapolated over a continuous temperature range from -2 to 10 °C in Fig. 9.

Year	Lipids concentration in polar cod from the Central Chukchi Sea	Change in lipid concentration (µg.mg^{-1}, WWT) between end of summer and mortality levels	Duration of starvation resistance at -1 °C (days)	Duration of starvation resistance at 1 °C (days)	Duration of starvation resistance at 3 °C (days)	Duration of starvation resistance at 5 °C (days)
2013 (n=30)	34.73 ± 3.42	22.63	136	108	90	77
2017 (n=35)	16.03 ± 1.08	3.93	24	18	16	13
Mortality levels	12.5					

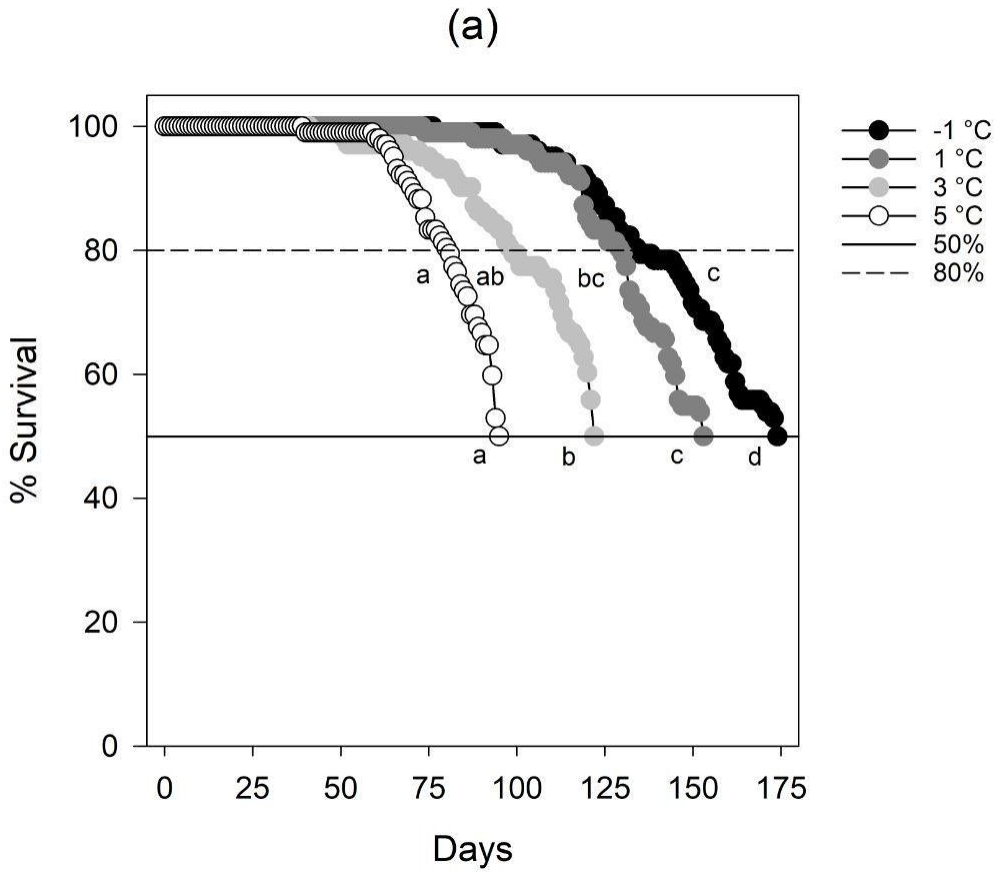

Fig. 1: Temperature-dependent survival of age-0 polar cod during simulated winter conditions in the laboratory. Experiments were run at -1, 1, 3 and 5 °C until 50% population mortality. Dashed and solid lines represent the point at which tank populations dropped to 80% or 50% survival, respectively. Data points represent temperature averages (n=3 tanks) and letters represent significant differences between temperature treatments.

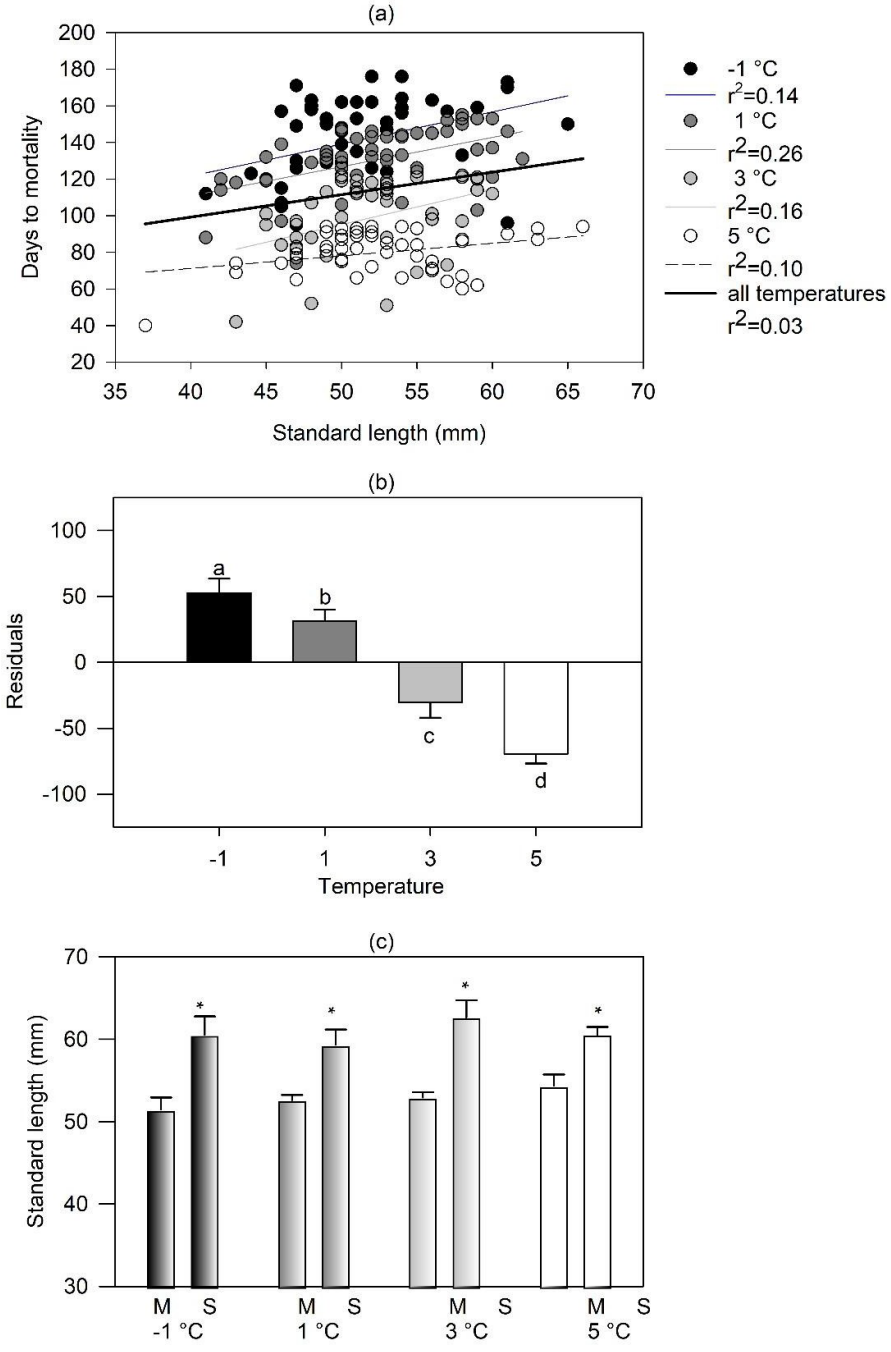

Fig. 2: The effect of temperature and length on age-0 polar cod survival time with (a) days to mortality only weakly affected by standard length with (b) size de-trended residuals showing a significant increase in starvation resistance at low temperatures compared to higher temperatures ($p<0.05$) and (c) fish that experienced mortality before 50% of the population (m) were significantly smaller than fish the survived (s) across all experimental temperatures ($p<0.05$).

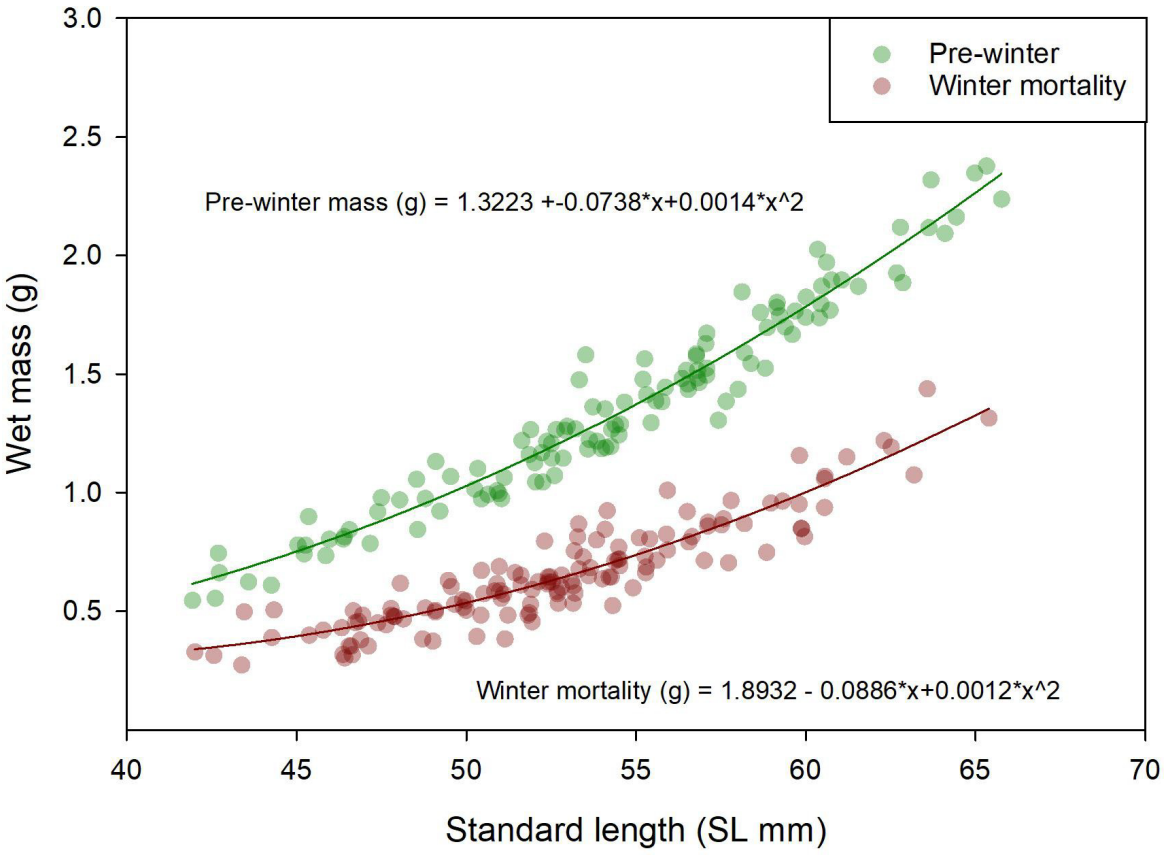

Fig. 3: Length-weight relationships for age-0 polar cod at the beginning of the experiment ('pre-winter') and at the time of mortality during the experiment ('winter mortality'). The winter mortality length-weight model is the theoretical lower weight threshold juvenile fish must maintain for survival during winter. Temperature-dependent growth loss (Fig. 4) was determined using the difference in weight at the time of mortality and length-based weight of the pre-winter model (See Methods).

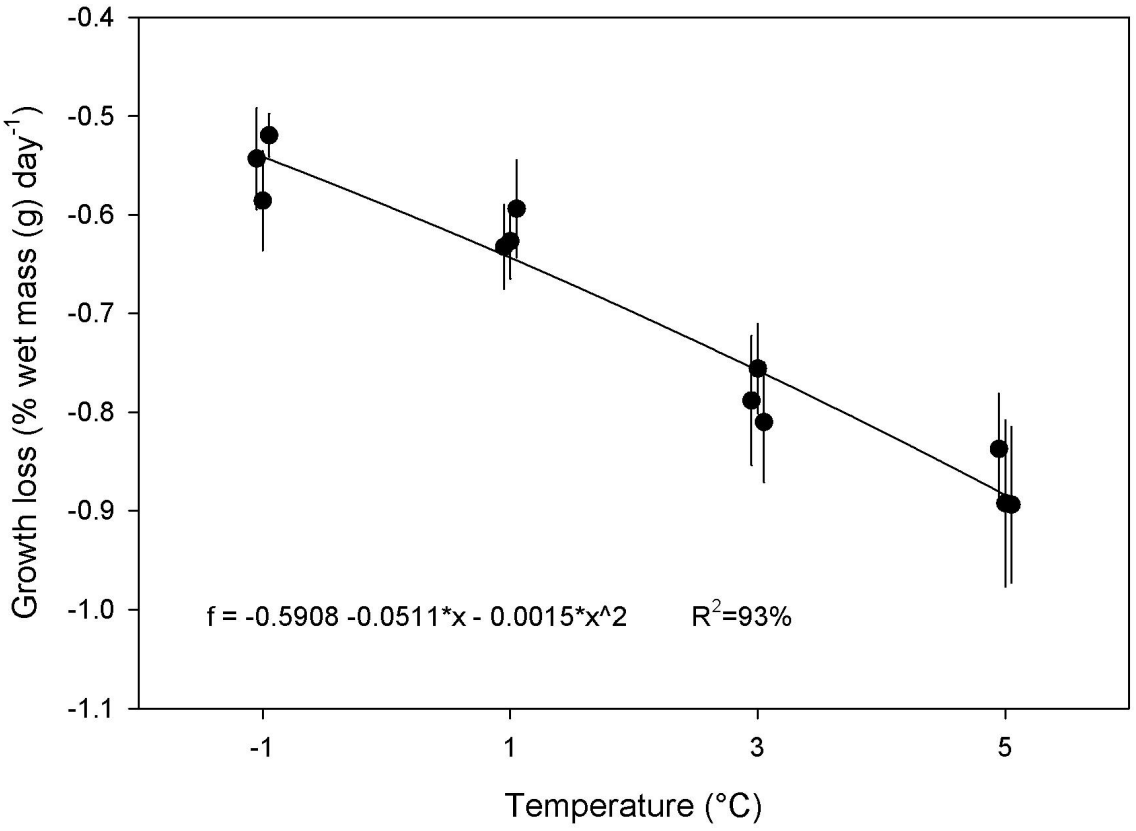

Fig. 4: Rate of temperature-dependent weight loss for age-0 juvenile polar cod during simulated temperature-dependent overwintering laboratory experiments. Experiments were run at -1, 1, 3 and 5 °C until 50% population mortality. Data are tank means (n=3 per temperature) of individual weight loss over time.

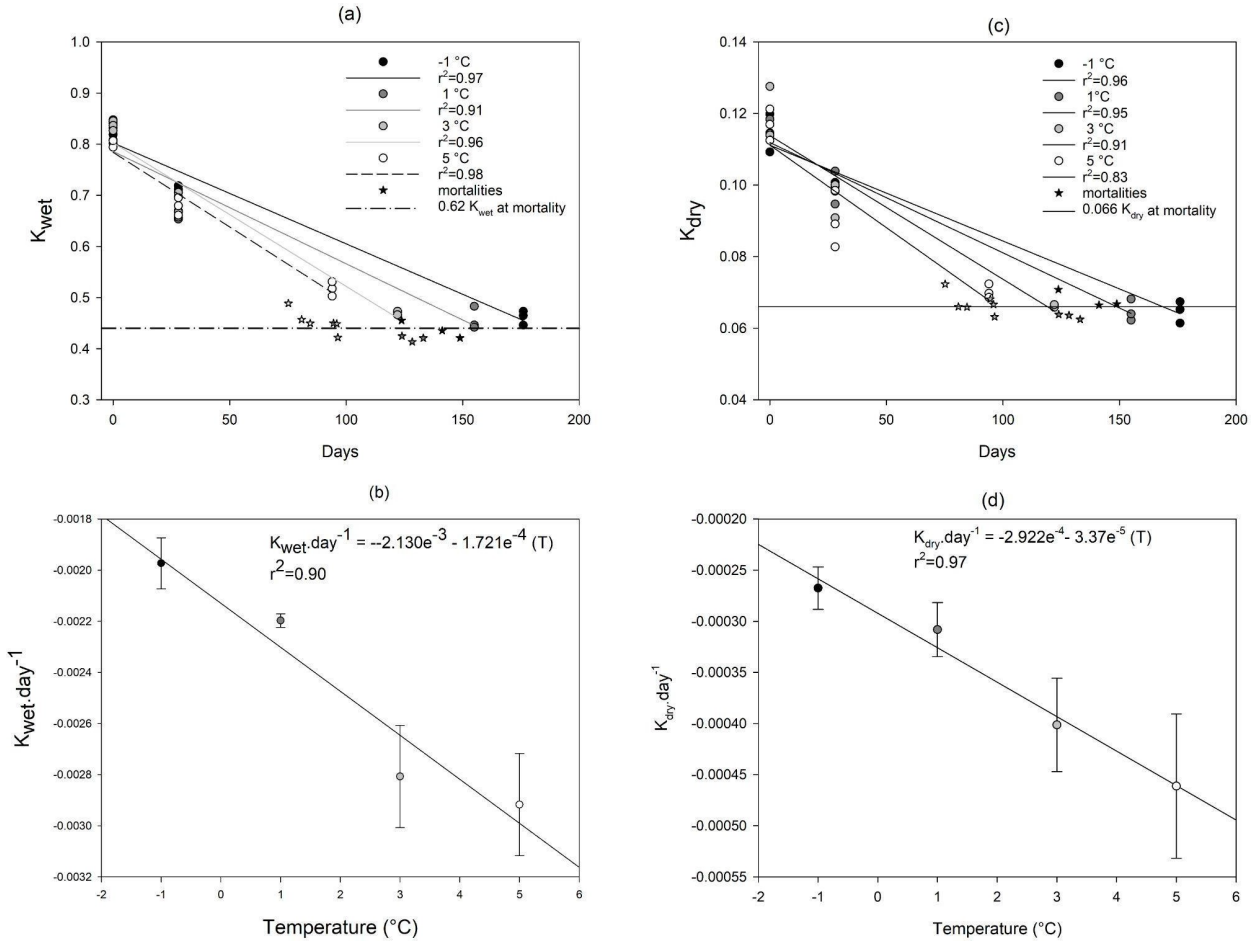

Fig. 5. Fulton's K condition factor per WWT shown (a) over the full overwintering experiment and (b) as a temperature-dependent rate of loss function. Fulton's K condition factor per DWT shown (c) over the full overwintering experiment and (d) as a temperature-dependent rate loss function. Data are the mean of 3 tank values (± 1 SE) for sampled fish (circles) and mortalities (stars) per temperature. Fish that died had an average Fulton's K_{wet} of 0.62 and Fulton's K_{dry} 0.066. Temperature dependent rate of loss functions are shown across four temperature treatments (-1, 1, 3, 5 °C).

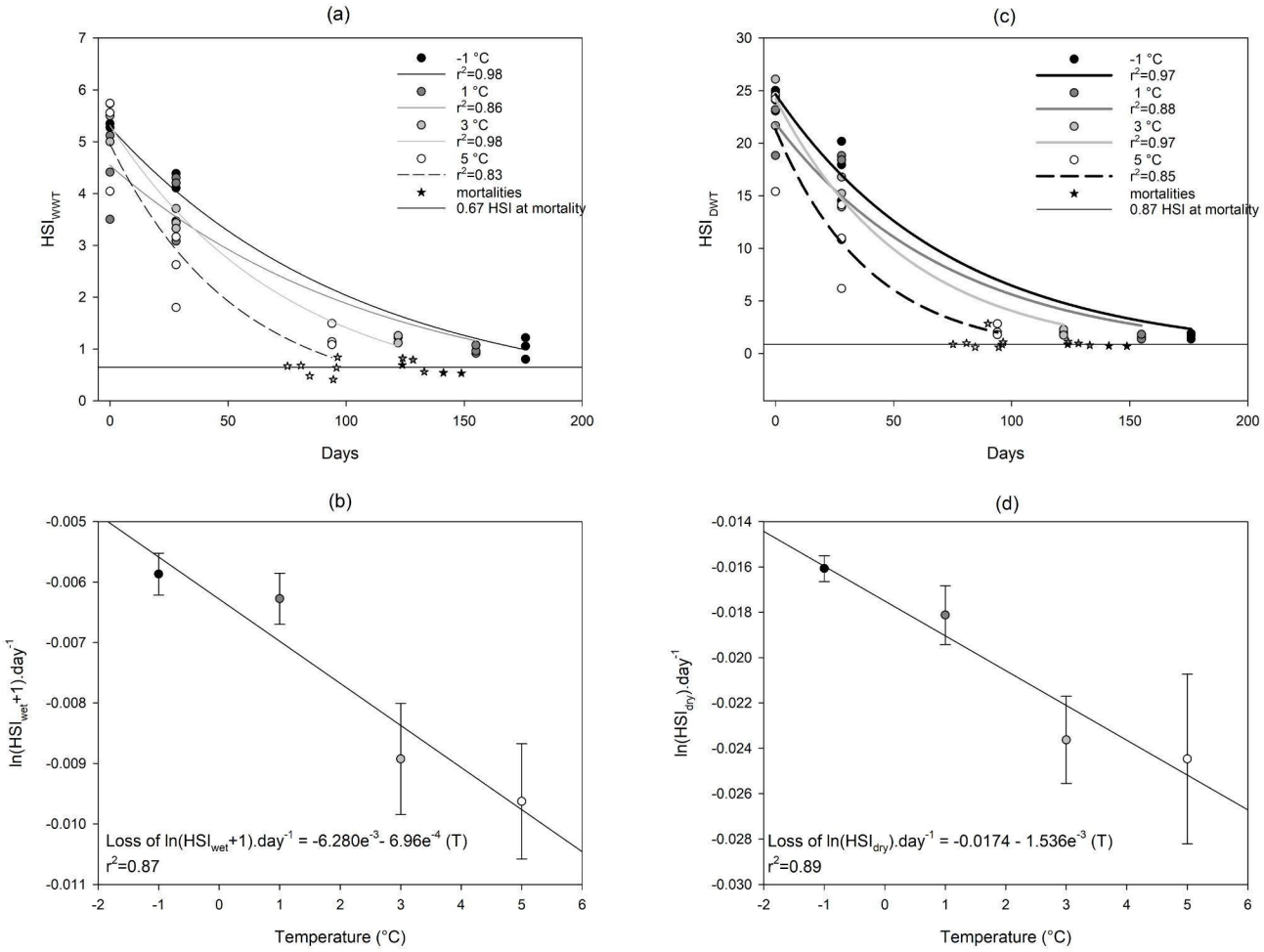

Fig. 6. Hepatosomatic index (HSI) per WWT shown (a) over the full overwintering experiment and (b) as a temperature-dependent rate of loss. HSI per DWT shown (c) over the full overwintering experiment and (d) as a temperature-dependent rate of loss. Data are the mean of 3 tank values (± 1 SE) for sampled fish (circles) and mortalities (stars) per temperature. Fish that died had an average HSI_{wet} of 0.67 and HSI_{dry} of 0.87. Temperature dependent rate of loss functions are shown across four temperature treatments (-1, 1, 3, 5 °C) for the natural log transformed HSI indices.

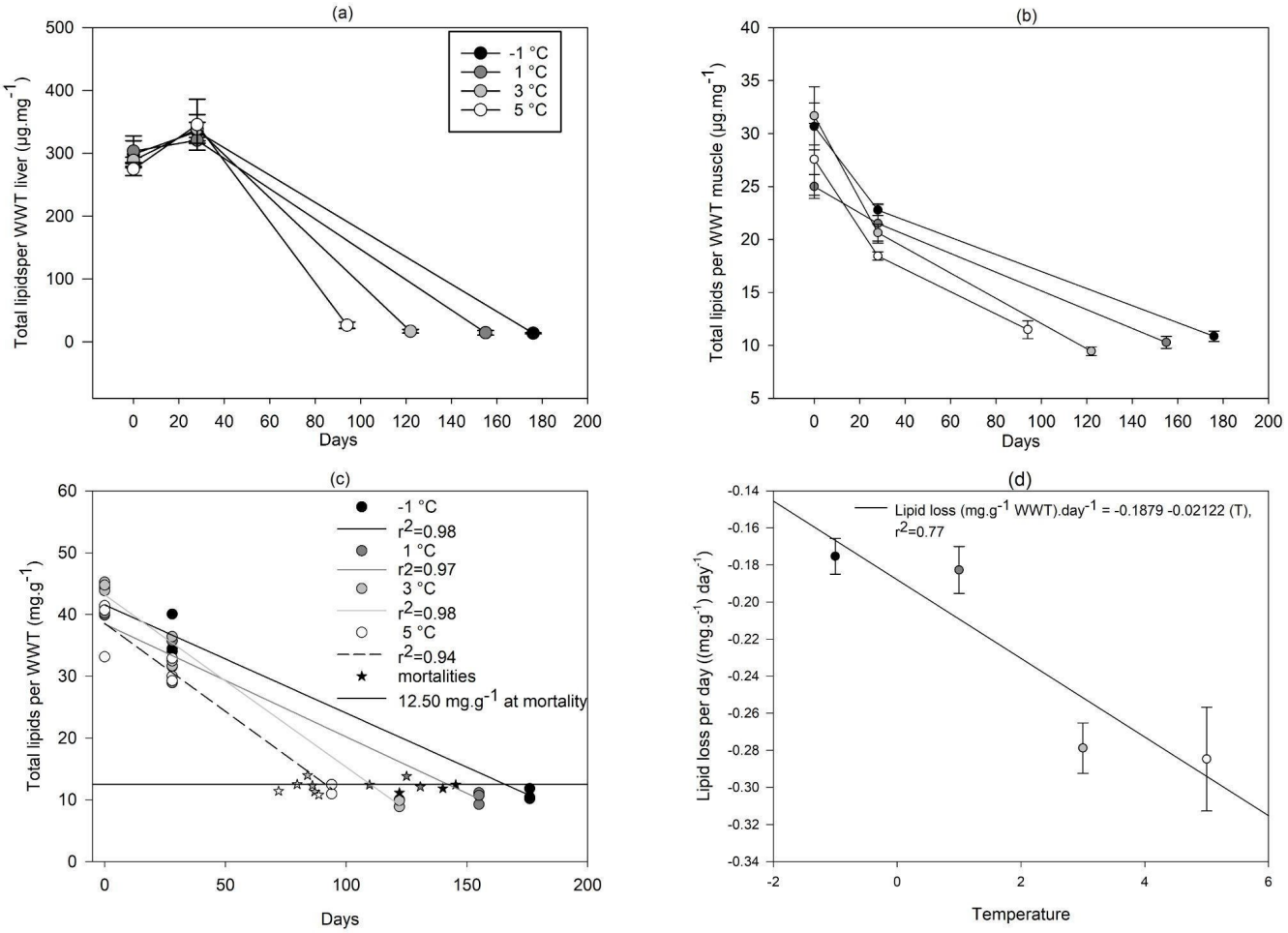

Fig. 7. Total lipids per WWT shown in (a) the liver, (b) muscle tissue and (C) estimated whole bodies of age-0 polar cod over the full overwintering experiment. Temperature dependent rate of lipid loss in whole fish (d) is shown across four temperature treatments (-1, 1, 3, 5 °C). Data are tanks means (n=3) for sampled fish (circles) and mortalities (stars) per temperature. Fish that died had an average whole body total lipid per WWT of 12.50 $mg.g^{-1}$.

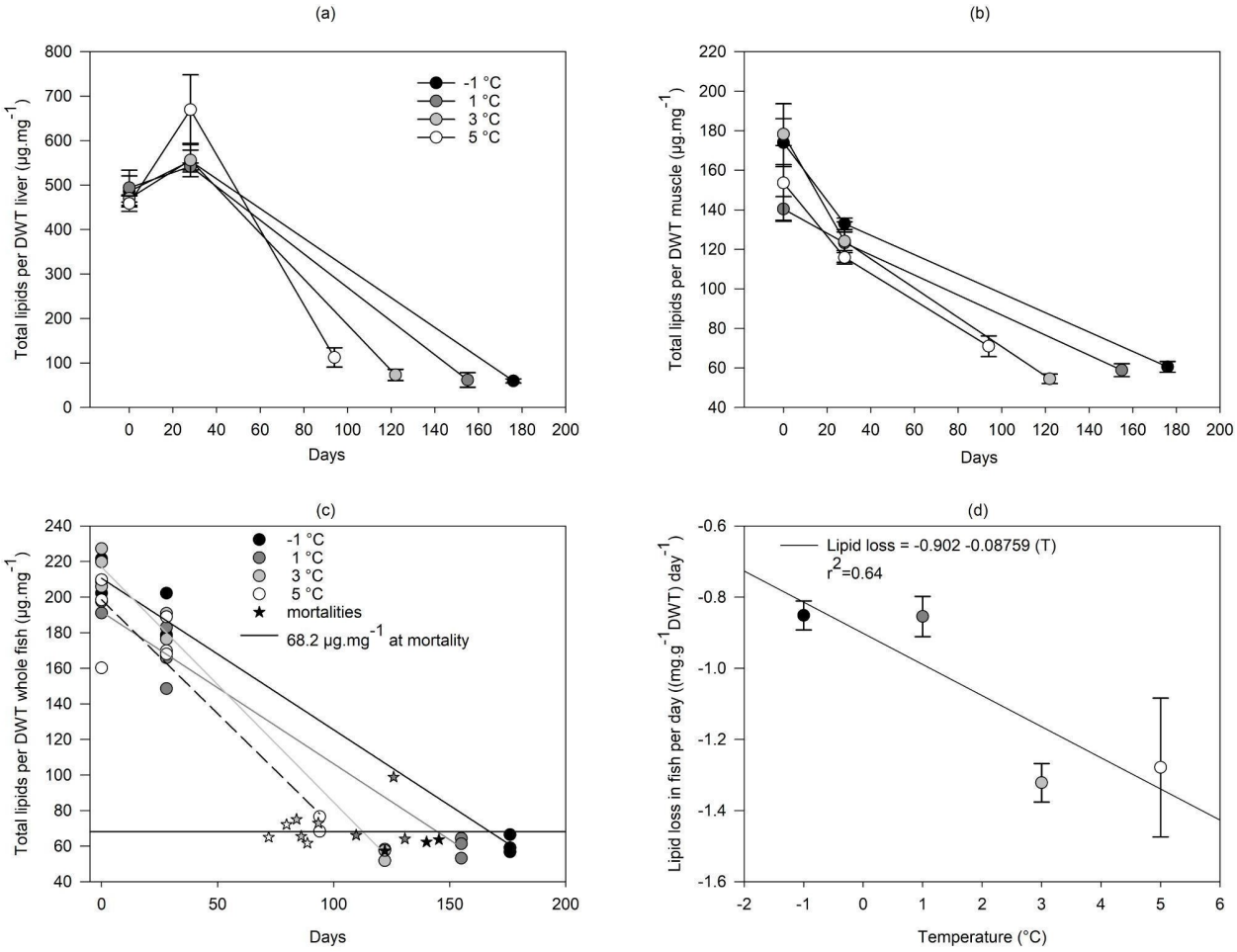

Fig. 8. Total lipids per DWT shown in (a) the liver, (b) muscle tissue and (C) estimated whole bodies of age-0 polar cod over the full overwintering experiment. Temperature-dependent rate of lipid loss in whole fish (d) is shown across four temperature treatments (-1, 1, 3, 5 °C). Data are tanks means (n=3) for sampled fish (circles) and mortalities (stars) per temperature. Fish that died had an average whole body total lipid per WWT of 68.2 $mg.g^{-1}$.

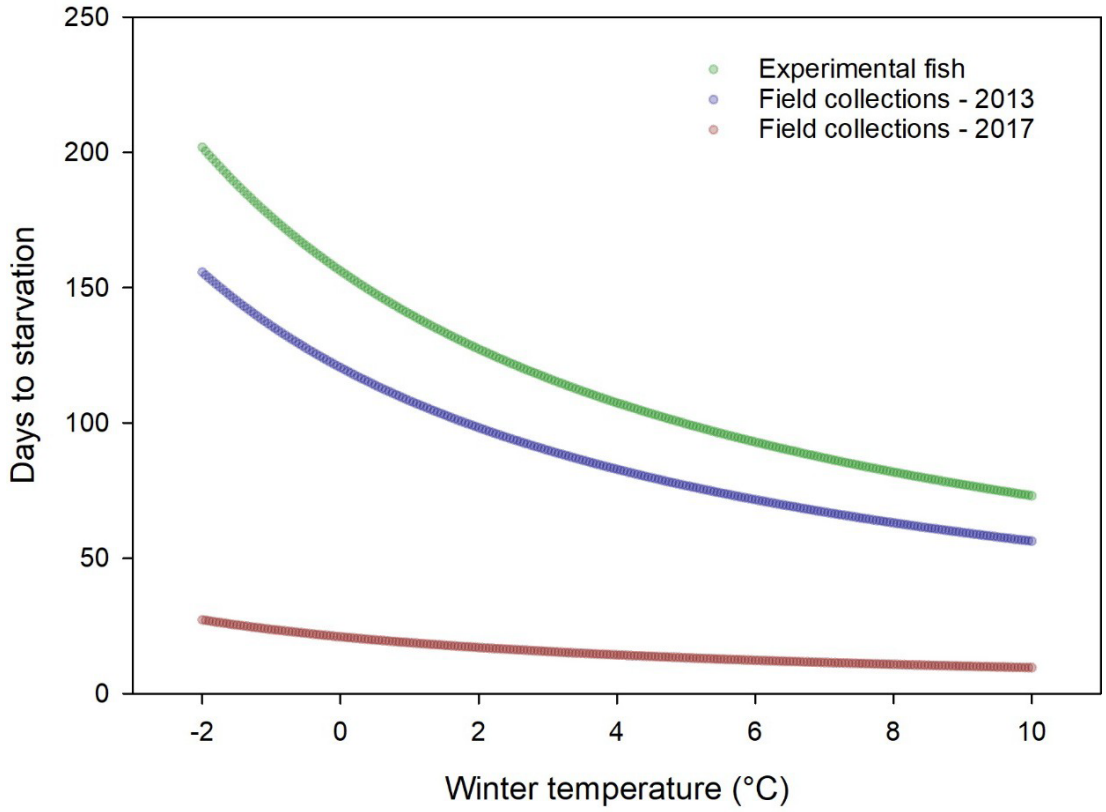

Fig. 9. Days to starvation based on the lab determined temperature-dependent lipid-loss model:

Lipid-loss (mg.g^{-1} WWT).day^{-1} = -0.1879 -0.02122 (T), r^2=0.77 (Fig. 7d).

Scenarios are shown for experimental fish, as well as polar cod from the central Chukchi Sea in a cold year (2013, Copeman et al. 2020) and a warm year (2017, Copeman et al. this report) to demonstrate variability in time to starvation for fish of different nutritional status over a wide range of temperatures. The mean lipid concentration values are given in Table 5 from fish sampled in the Central Chukchi Sea (68.25 - 70.74°N) with latitudinal region defined in Buckley and Whitehouse (2017)

Aune M, Raskhozheva E, Andrade H, Augustine S and others (2021) Distribution and ecology of polar cod (Boreogadus saida) in the eastern Barents Sea: A review of historical literature. Mar Environ Res:105262

Berge J, Daase M, Hobbs L, Falk-Petersen S, Darnis G, Søreide JE (2020a) Zooplankton in the Polar Night. In: Berge J, Johnsen G, Cohen JH (eds) POLAR NIGHT Marine Ecology: Life and Light in the Dead of Night. Springer International Publishing, Cham, p 113-159

Berge J, Johnsen G, Cohen JH (2020b) Introduction. In: Berge J, Johnsen G, Cohen JH (eds) POLAR NIGHT Marine Ecology: Life and Light in the Dead of Night. Springer International Publishing, Cham, p 1-15

Bouchard C, Fortier L (2008) Effects of polynyas on the hatching season, early growth and survival of polar cod *Boreogadus saida* in the Laptev Sea. Mar Ecol-Prog Ser 355:247-256

Boudreau SA, Shackell NL, Carson S, den Heyer CE (2017) Connectivity, persistence, and loss of high abundance areas of a recovering marine fish population in the Northwest Atlantic Ocean. Ecology and Evolution 7:9739-9749
Buckley TW, Whitehouse GA (2017) Variation in the diet of Arctic Cod (*Boreogadus saida*) in the Pacific Arctic and Bering Sea. Environ Biol Fishes 100:421-442
Byström P, Andersson J, Kiessling A, Eriksson LO (2006) Size and temperature dependent foraging capacities and metabolism: Consequences for winter starvation mortality in fish. Oikos 115:43-52
Chen L, DeVries AL, Cheng C-HC (1997) Convergent evolution of antifreeze glycoproteins in Antarctic notothenioid fish and Arctic cod. Proceedings of the National Academy of Sciences 94:3817-3822
Copeman L, Ryer C, Spencer M, Ottmar M and others (2018) Benthic enrichment by diatom-sourced lipid promotes growth and condition in juvenile Tanner crabs around Kodiak Island, Alaska. Mar Ecol Prog Ser 597:161-178
Copeman L, Spencer M, Heintz R, Vollenweider J and others (2020) Ontogenetic patterns in lipid and fatty acid biomarkers of juvenile polar cod (Boreogadus saida) and saffron cod (Eleginus gracilis) from across the Alaska Arctic. Polar Biol 43:1121-1140
Copeman LA, Parrish CC, Gregory RS, Wells JS (2008) Decreased lipid storage in juvenile Atlantic cod (*Gadus morhua*) during settlement in cold-water eelgrass habitat. Mar Biol 154:823-832
Copeman LA, Laurel BJ, Parrish CC (2013) Effect of temperature and tissue type on fatty acid signatures of two species of North Pacific juvenile gadids: a laboratory feeding study. J Exp Mar Biol Ecol 448:188-196
Copeman LA, Laurel BJ, Boswell KM, Sremba AL and others (2016) Ontogenetic and spatial variability in trophic biomarkers of juvenile saffron cod (*Eleginus gracilis*) from the Beaufort, Chukchi and Bering Seas. Polar Biol 39:1109-1126
Copeman LA, Laurel BJ, Spencer M, Sremba A (2017) Temperature impacts on lipid allocation among juvenile gadid species at the Pacific Arctic-Boreal interface: an experimental laboratory approach. Mar Ecol Prog Ser 566:183-198
Cusa M, Berge J, Varpe Ø (2019) Seasonal shifts in feeding patterns: Individual and population realized specialization in a high Arctic fish. Ecology and Evolution 9:11112-11121
David C, Lange B, Rabe B, Flores H (2015) Community structure of under-ice fauna in the Eurasian central Arctic Ocean in relation to environmental properties of sea-ice habitats. Mar Ecol-Prog Ser 522:15-32
David C, Lange B, Krumpen T, Schaafsma F, van Franeker JA, Flores H (2016) Under-ice distribution of polar cod Boreogadus saida in the central Arctic Ocean and their association with sea-ice habitat properties. Polar Biol 39:981-994
De Robertis A, Taylor K, Wilson CD, Farley EV (2016) Abundance and distribution of Arctic cod (*Boreogadus saida*) and other pelagic fishes over the U.S. Continental Shelf of the Northern Bering and Chukchi Seas. Deep-Sea Res II
Falk-Petersen S, Mayzaud P, Kattner G, Sargent J (2009) Lipids and life strategy of Arctic Calanus. Marine Biology Research 5:18-39
Farrell AP, Steffensen JF (2005) Fish physiology Vol. XXII: The physiology of polar fishes.
Fletcher G, Hew C, Davies P (2001) Antifreeze proteins of teleost fish. AnnuRevPhysiol 63:359-399
Flores H, Franeker JAv, Dorssen Mv, Meijboom A and others (2015) The Surface and Under-Ice Trawl (SUIT)
Froese R (2006) Cube law, condition factor and weight–length relationships: history, meta-analysis and recommendations. Journal of applied ichthyology 22:241-253
Geissinger EA, Gregory RS, Laurel BJ, Snelgrove PVR (2021) Food and initial size influence overwinter survival and condition of a juvenile marine fish (age-0 Atlantic cod). Can J Fish Aquat Sci 78:472-482
Geoffroy M, Majewski A, LeBlanc M, Gauthier S, Walkusz W, Reist JD, Fortier L (2016) Vertical segregation of age-0 and age-1+ polar cod (Boreogadus saida) over the annual cycle in the Canadian Beaufort Sea. Polar Biol 39:1023-1037

Geoffroy M, Priou P (2020) Fish Ecology During the Polar Night. In: Berge J, Johnsen G, Cohen JH (eds) POLAR NIGHT Marine Ecology: Life and Light in the Dead of Night. Springer International Publishing, Cham, p 181-216
Gotceitas V, Methven DA, Fraser S, Brown JA (1999) Effects of body size and food ration on over-winter survival and growth of age-0 Atlantic cod, Gadus morhua. Environ Biol Fishes 54:413-420
Guy CS, Brown ML (2007) Analysis and interpretation of freshwater fisheries data, Vol. American Fisheries Society
Hansen MJ, Boisclair D, Brandt SB, Hewett SW, Kitchell JF, Lucas MC, Ney JJ (1993) Applications of Bioenergetics Models to Fish Ecology and Management: Where Do We Go from Here? Transactions of the American Fisheries Society 122:1019-1030
Heermann L, Eriksson LO, Magnhagen C, Borcherding J (2009) Size-dependent energy storage and winter mortality of perch. Ecology of Freshwater Fish 18:560-571
Heintz RA, Vollenweider JJ (2010) Influence of size on the sources of energy consumed by overwintering walleye pollock (*Theragra chalcogramma*). J Exp Mar Biol Ecol 393:43-50
Heintz RA, Siddon EC, Farley EV, Napp JM (2013) Correlation between recruitment and fall condition of age-0 pollock (*Theragra chalcogramma*) from the eastern Bering Sea under varying climate conditions. Deep Sea Res Part II 94:150-156
Helser TE, Colman JR, Anderl DM, Kastelle CR (2017) Growth dynamics of saffron cod (Eleginus gracilis) and Arctic cod (*Boreogadus saida*) in the Northern Bering and Chukchi Seas. Deep-Sea Research Part Ii-Topical Studies in Oceanography 135:66-77
Henderson P, Holmes R, Bamber RN (1988) Size-selective overwintering mortality in the sand smelt, Atherina boyeri Risso, and its role in population regulation. J Fish Biol 33:221-233
Hop H, Gjosaeter H (2013) Polar cod (*Boreogadus saida*) and capelin (*Mallotus villosus*) as key species in marine food webs of the Arctic and the Barents Sea. Mar Biol Res 9:878-894
Hunt Jr GL, Coyle KO, Eisner LB, Farley EV and others (2011) Climate impacts on eastern Bering Sea foodwebs: a synthesis of new data and an assessment of the Oscillating Control Hypothesis. Ices J Mar Sci 68:1230-1243
Huntington HP, Danielson SL, Wiese FK, Baker M and others (2020) Evidence suggests potential transformation of the Pacific Arctic ecosystem is underway. Nat Clim Chang 10:342-348
Hurst TP (2007) Causes and consequences of winter mortality in fishes. J Fish Biol 71:315-345
Huserbråten MBO, Eriksen E, Gjøsæter H, Vikebø F (2019) Polar cod in jeopardy under the retreating Arctic sea ice. Communications Biology 2:407
Ivan LN, Höök TO, Post J (2015) Energy allocation strategies of young temperate fish: an eco-genetic modeling approach. Can J Fish Aquat Sci 72:1243-1258
Jonsson B, Linnansaari T, Cunjak RACA (2010) Patterns in apparent survival of Atlantic salmon (Salmo salar) parr in relation to variable ice conditions throughout winter. Can J Fish Aquat Sci 67:1744-1754
Kaartvedt S (2008) Photoperiod may constrain the effect of global warming in arctic marine systems. J Plankton Res 30:1203-1206
Kattner G, Hagen W, Lee RF, Campbell R and others (2007) Perspectives on marine zooplankton lipids. Can J Fish Aquat Sci 64:1628-1639
Kerr S (1971) Analysis of laboratory experiments on growth efficiency of fishes. Journal of the Fisheries Board of Canada 28:801-808
Koenker BL, Copeman LA, Laurel BJ (2018a) Impacts of temperature and food availability on the condition of larval Arctic cod (*Boreogadus saida*) and walleye pollock (*Gadus chalcogrammus*). Ices J Mar Sci 75:2370-2385
Koenker BL, Laurel BJ, Copeman LA, Ciannelli L, Robert HeD (2018b) Effects of temperature and food availability on the survival and growth of larval Arctic cod (*Boreogadus saida*) and walleye pollock (*Gadus chalcogrammus*). Ices J Mar Sci 75:2386-2402
Kohlbach D, Schaafsma F, Graeve M, Lebreton B and others (2017) Strong linkage of polar cod (Boreogadus saida) to sea ice algae-produced carbon: Evidence from stomach content, fatty acid and stable isotope analyses. Progress in Oceanography 152

Kooka K (2012) Life-history traits of walleye pollock, Theragra chalcogramma, in the northeastern Japan Sea during early to mid 1990s. Fish Res 113:35-44
Langbehn TJ, Varpe Ø (2017) Sea-ice loss boosts visual search: fish foraging and changing pelagic interactions in polar oceans. Global Change Biology 23:5318-5330
Laurel BJ, Gregory RS, Brown JA (2003) Predator distribution and habitat patch area determine predation rates on Age-0 juvenile cod Gadus spp. Mar Ecol-Prog Ser 251:245-254
Laurel BJ, Spencer M, Iseri P, Copeman LA (2016) Temperature-dependent growth and behavior of juvenile Arctic cod (*Boreogadus saida*) and co-occurring North Pacific gadids. Polar Biol 39:1127-1135
Laurel BJ, Copeman LA, Spencer M, Iseri P (2017) Temperature-dependent growth as a function of size and age in juvenile Arctic cod (Boreogadus saida). Ices J Mar Sci 74:1614-1621
Laurel BJ, Copeman LA, Spencer M, Iseri P, Handling editor: Dominique R (2018) Comparative effects of temperature on rates of development and survival of eggs and yolk-sac larvae of Arctic cod (Boreogadus saida) and walleye pollock (Gadus chalcogrammus). Ices J Mar Sci:fsy042-fsy042
Laurel J, Stoner AW, Ryer CH, Hurst TP, Abookire AA (2007) Comparative habitat associations in juvenile Pacific cod and other gadids using seines, baited cameras and laboratory techniques. J Exp Mar Biol Ecol 351:42-55
Leu E, Soreide JE, Hessen DO, Falk-Petersen S, Berge J (2011) Consequences of changing sea-ice cover for primary and secondary producers in the European Arctic shelf seas: Timing, quantity, and quality. Progress in Oceanography 90:18-32
Lough RG, O'Brien L (2012) Life-stage recruitment models for Atlantic cod (Gadus morhua) and haddock (Melanogrammus aeglefinus) on Georges Bank. Fish B-Noaa 110:123-140
Lu YH, Ludsin SA, Fanslow DL, Pothoven SA (2008) Comparison of three microquantity techniques for measuring total lipids in fish. Can J Fish Aquat Sci 65:2233-2241
Marsh JM, Mueter FJ (2020) Influences of temperature, predators, and competitors on polar cod (Boreogadus saida) at the southern margin of their distribution. Polar Biol 43:995-1014
Martin BT, Heintz R, Danner EM, Nisbet RM (2017) Integrating lipid storage into general representations of fish energetics. Journal of Animal Ecology 86:812-825
McCollum A, Bunnell D, Stein R (2003) Cold, Northern Winters: The Importance of Temperature to Overwinter Mortality of Age0 White Crappies. Transactions of The American Fisheries Society - TRANS AMER FISH SOC 132:977-987
Mogensen S, Post JR (2012) Energy allocation strategy modifies growth-survival trade-offs in juvenile fish across ecological and environmental gradients. Oecologia 168:923-933
Morley J, Buckel J, Lankford T, Rose K (2013) Relative contribution of spring- and summer-spawned bluefish cohorts to the adult population: effects of size-selective winter mortality, overwinter growth, and sampling bias. Can J Fish Aquat Sci 70:233-244
Mueter FJ, Bond NA, Ianelli JN, Hollowed AB (2011) Expected declines in recruitment of walleye pollock (*Theragra chalcogramma*) in the eastern Bering Sea under future climate change. Ices J Mar Sci 68:1284-1296
Munch S, Conover D (2002) Accounting for local physiological adaptation in bioenergetic models: Testing hypotheses for growth rate evolution by virtual transplant experiments. Canadian Journal of Fisheries and Aquatic Sciences - CAN J FISHERIES AQUAT SCI 59:393-403
Nash R, Valencia AH, Geffen A (2006) The origin of Fulton's condition factor - Setting the record straight. Fisheries 31:236-238
Pangle KL, Sutton TM, Kinnunen RE, Hoff MH (2004) Overwinter survival of juvenile lake herring in relation to body size, physiological condition, energy stores, and food ration. Transactions of the American Fisheries Society 133:1235-1246
Pörtner H-O, Farrell A (2008) ECOLOGY physiology and climate change. Science (New York, NY) 322:690-692
Post JR, Evans DO (1989) Size-dependent overwinter mortality of young-of-the-year yellow perch (Perca flavescens): laboratory, in situ enclosure, and field experiments. Can J Fish Aquat Sci 46:1958-1968

Shoup D, Wahl D (2011) Body Size, Food, and Temperature Affect Overwinter Survival of Age-0 Bluegills. Transactions of the American Fisheries Society 140:1298-1304
Siddon EC, Heintz RA, Mueter FJ (2013a) Conceptual model of energy allocation in walleye pollock (*Theragra chalcogramma*) from age-0 to age-1 in the southeastern Bering Sea. Deep Sea Res II 94:140-149
Siddon EC, Kristiansen T, Mueter FJ, Holsman KK, Heintz RA, Farley EV (2013b) Spatial Match-Mismatch between Juvenile Fish and Prey Provides a Mechanism for Recruitment Variability across Contrasting Climate Conditions in the Eastern Bering Sea. Plos One 8:13
Sogard SM (1997) Size-selective mortality in the juvenile stage of teleost fishes: A review. Bulletin of Marine Science 60:1129-1157
Sogard SM, Olla BL (2000) Endurance of simulated winter conditions by age-0 walleye pollock: effects of body size, water temperature and energy stores. J Fish Biol 56:1-21
Suthers IM (1998) Bigger? Fatter? Or is faster growth better? Considerations on condition in larval and juvenile coral-reef fish. Australian Journal of Ecology 23:265-273
Wagner H-J, Fröhlich E, Negishi K, Collin S (1998) The eyes of deep-sea fish II. Functional morphology of the retina. Progress in retinal and eye research 17:637-685
Wassmann P (2006) Structure and function of contemporary food webs on Arctic shelves: An introduction. Progress in Oceanography 71:123-128
Welch HE, Bergmann MA, Siferd TD, Martin KA and others (1992) Energy-flow through the marine ecosystem of the Lancaster Sound region, Arctic Canada. Arctic 45:343-357
Werner EE, Gilliam JF (1984) The Ontogenetic Niche and Species Interactions in Size-Structured Populations. Annual Review of Ecology and Systematics 15:393-425
Whitehouse GA, Aydin K, Essington TE, Hunt GL (2014) A trophic mass balance model of the eastern Chukchi Sea with comparisons to other high-latitude systems. Polar Biol 37:911-939

CHAPTER 9 - Variation in Nutritional Quality of Arctic Zooplankton and Fish

Objective 2: Quantify the distribution, abundance, and condition of pelagic marine fishes, in particular young-of-the-year Arctic gadids and other forage fishes

Johanna J Vollenweider[1], Ron Heintz[2], Brenda Norcross[3], Leandra Sousa[4], Alexei Pinchuk[3], Martin Robards[5], Robert Bradshaw[1]

[1] NOAA Fisheries, Alaska Fishery Science Center, Ted Stevens Marine Research Institute, Juneau, Alaska
[2] Sitka Sound Science Center, Sitka, Alaska
[3] University of Alaska Fairbanks, Fairbanks, Alaska
[4] North Slope Borough, Utqiagvik, Alaska
[5] Wildlife Conservation Society, Arctic Beringia Program, Fairbanks, Alaska

Abstract

One of the quintessential aims of marine science is predicting population productivity. In the newly ice-free areas of the Arctic, benchmark data are limited and traditional stock-assessment techniques cannot be used without knowledge of prior years of population fluctuations on which to build. Bioenergetics models are an ideal alternative tool because they integrate biotic and abiotic effects on organism function that can be extrapolated up to the population level. One of the fundamental inputs into bioenergetic models is the nutritional condition of organisms, which is virtually unquantified in waters of the U.S. Arctic. We measured the nutritional condition of the most abundant fish and zooplankton from seven surveys conducted between 2005 and 2019 across the Chukchi and western Beaufort Seas to maximize spatial and temporal variation. Condition indices included energy, lipid and protein content. We evaluated twenty-seven species of zooplankton from nine orders and forty-one species of fish from twelve families. Lipid was the most variable of the condition indices, differing by 35 times from the most lipid-rich fish species, Bering cisco (*Coregonus laurettae*), to the leanest fish, daubed shanny (*Leptoclinus maculatus*). Similarly, lipid was 28 times higher in the zooplankter *Calanus glacialis* than in *Argis lar.* Interspecific variation occurred within some families of fish and orders of zooplankton. For a given size fish, energy density of Pacific herring (*Clupea pallasii*), Pacific capelin (*Mallotus villosus*), Pacific sand lance (*Ammodytes personatus),* starry flounder (*Platichthys stellatus*), and to a lesser degree, saffron cod (*Eleginus gracilis*) collected during the late summer was lower in the Arctic than in the Gulf of Alaska, illustrating the bias introduced by using condition values from mismatched locations. Consequently, this catalog of fish and zooplankton condition should greatly improve the accuracy of bioenergetic modeling of a host of fish, seabird, and marine mammal populations in the U.S. Arctic. These results increase the capacity for prediction of Arctic species productivity and the Arctic ecosystem as a whole.

Keywords: energy density, lipid, protein, trophic ecology, Chukchi Sea, Beaufort Sea

Introduction

The Arctic is warming disproportionally faster than the rest of the globe from polar amplification and feedback processes associated with melting sea ice (Koenigk et al., 2020; NSIDC, 2020) and the newly, seasonal ice-free areas are gaining interest for transit, oil extraction, infrastructure development, and potential fisheries (Babin et al., 2020; Runge et al., 2020)). Managing the expanding user groups in the newly accessible areas requires a benchmark understanding of the biological communities that may be impacted as well as expectations for how the biological communities will be transformed by their changing habitat in the future. Recent shifts in marine biological community composition in the Arctic have occurred, presumably from changes in the marine environment such as reduced sea ice thickness, extent, and duration, warming ocean temperatures, increased freshwater input, increased storm activity, and variations in ocean currents and stratification (Wassmann et al., 2011).

Environmental forcing on Arctic marine biota is anticipated to be most pronounced in lower trophic levels that are tightly coupled with their environment. Zooplankton exemplify this because they are generally short-lived, limited in mobility, and have narrow physiological tolerances to temperature (Hays et al., 2005). These life history characteristics limit the potential for zooplankton to adapt in response to varying environmental conditions. Furthermore, observed and predicted changes to ocean stratification alter light levels, temperature gradients, and nutrient cycling, all of which are crucial components for plankton productivity (Carmack et al., 2004). Consequently, climate-driven environmental change has already changed zooplankton abundance, distribution, and timing of life-cycle events (Jonkers et al., 2019; Dam and Baumann, 2018; Chiba et al., 2015)).

Reorganization of zooplankton communities will influence community composition of secondary consumers such as fish. Larval and juvenile fish primarily consume zooplankton, and some fish species continue to be planktivores as adults (Gray et al., 2017, 2016; Whitehouse et al., 2017). Alterations in zooplankton community composition and timing of zooplankton production will have consequences for fish survival. Fish can contend with a changing prey base to some degree by relocating to more productive areas (Rose and Leggett, 1989). Similarly, fish move in response to habitat conditions such as temperature. Warming temperatures have facilitated northward range extensions of several fish species from sub-Arctic to Arctic regions (Hollowed et al., 2013, Rand and Logerwell, 2011; Mecklenburg et al., 2007). Alternate habitat is not always available, however, leaving adaptation as the only alternative for survival.

The ability for fish to adapt to changing environmental conditions is highly variable among species. Arctic fish residing in relatively steady-state conditions may be less capable of adaptation than southerly species, which routinely experience much greater swings in their surrounding temperatures, such as seasonal or daily changes. For example, Arctic cod (*Boreogadus saida*) range from the North Pole south to 57 °N in the Bering Sea and have narrow temperature tolerances compared to the eurythermal saffron cod (*Eleginus gracilis*) (Laurel et al., 2016), which range from 71 °N to 37 °N in the Pacific Ocean (Mecklenburg et al., 2016). Their different physiological tolerances have led to the prevailing hypothesis that saffron cod may potentially be more resilient to warming, while Arctic cod will likely struggle once temperatures exceed their threshold (Laurel et al., 2016; Reusser et al., 2013). The varying ability of fish species to adapt, move or perish in response to their changing environment and prey base will structure the abundance and distribution of Arctic fish.

Predicting trophic cascade effects on fishes, seabirds, and marine mammals from climate-induced changes in their prey is complex. The flow of energy is a primary component structuring food webs, and reductions in lipid-dense prey have caused declines of top-level predators in other ecosystems. In the North Sea and near Greenland, populations of lipidrich *Calanus* species were replaced by lower lipid zooplankter species, causing reduced body condition and fewer numbers of their sand eel (*Ammodytes marinus*) predators (Frederiksen et al, 2006). Similarly, low lipid diets correlated with impaired life-

history traits in a variety of seabird species throughout the world, including reduced productivity, slow growth, and reduced fledging fat reserves (Osterblom et al, 2008; Wanless et al, 2005; Romano, 2000). In the Gulf of Alaska, Steller sea lion (*Eumetopias jubatus*) population declines of 49% coincided with a major community reorganization in their prey base, from an abundance of lipid-rich forage fish to one dominated by lean groundfish (Fritz et al., 2005; Trites et al., 2003; Merrick et al., 1997). This phenomenon, coined the "junk food hypothesis," could potentially occur in the Arctic if the relatively high lipid, abundant forage fish, Arctic cod, were out-competed by a lower lipid prey such as saffron cod, reducing quality prey available for their predators.

There are several ways to assess the impacts of a changing prey base on predator health and survival. Laboratory feeding studies show direct impacts of prey quality, though results are restricted to single species that can be accommodated in captivity. A more comprehensive approach to evaluating the effect of a changing prey base is the use of bioenergetic food web models that can assess trophic shifts by computing the mass-balance of energy flow through entire ecosystems. Bioenergetic models rely on accurate quantification of prey condition parameters, which are currently sparse to nonexistent in the Arctic. Evaluations of the nutritional condition of Arctic zooplankton has been quantified for a relatively large number of species, however sampling is focused primarily in Norway and the Canadian-Atlantic (Falk-Petersen et al., 2009, 2000; Auel et al., 2002) and is nonexistent in the US Arctic. Arctic fish condition measurementsare extremely rare and are primarily limited to anadromous species such as Arctic char (*Salvelinus alpinus*) and broad whitefish (*Coregonus nasus*) or limited in geographic scope (Fechhelm et al., 2011; Lawson et al., 1998; Jorgensen et al., 1997; Hop et al., 1995).

Consequently, existing food web modeling efforts in the Chukchi and Beaufort Seas cite prey energetics as a significant data gap and relied on literature values of prey quality from disparate species, locations and sizes (Carroll et al. 2013; Bluhm and Gradinger, 2008; Welch et al., 1992). Using proxy species from other ecosystems is problematic as prey quality of zooplankton and fish is highly variable. Zooplankton species can vary widely in their lipid content, from lipid-rich *Calanus* copepods (>50% lipid of dry mass) to lipid-deplete gelatinous zooplankton (~10% lipid) (Syvaranta and Rautio, 2010; Clarke and Peck, 1991; Reinhardt and Van Vleet, 1986). Similarly, fish species can vary widely in their energetic content and other condition indices. Within an ecosystem, calorific content can vary 10-fold among some of the most abundant fish species (Vollenweider et al., 2011; Anthony et al. 2000) and by two-fold within a family (Tierney et al., 2002), underscoring the importance of using appropriate values of prey quality.

Our goal is to quantify the nutritional condition of the most abundant species of Arctic zooplankton and fish and to test the hypothesis that there is significant interspecific variation thereby conferring unequal quality of prey to their predators. We provide a comprehensive library of the nutritional condition of the most abundant Arctic zooplankton and fish species during the summer feeding season in the US Arctic. Specifically, we quantify the energy, lipid and protein content of Arctic zooplankton and fish species in the Chukchi Sea, western Beaufort Sea and the adjoining Elson Lagoon during the ice-free summer months. Our work fills a large data gap, providing accurate parameters for bioenergetic food web models in the US Arctic and consequently enhancing the predictive capacity for how the Arctic food web will reshuffle in the future.

Methods

Sample collections

Zooplankton and fish were collected from the US waters of the Chukchi Sea, the western Beaufort Sea, Elson Lagoon, and Kotzebue Sound during summer ice-free months (July - September) from 2005 to 2019 from eight different surveys (Figure 1). Sampling time and methods varied by project, which has the benefit of potentially detecting a broader range of species, and the detriment of an unbalanced study design (Table 1). Greater detail on net specifications and fishing methodologies adopted in these surveys

are described in Vollenweider et al. (2018), De Robertis et al. (2017), Pinchuk and Eisner (2017), Goddard et al. (2014), and Norcross et al. (2010). Macrozooplankton were targeted in four surveys (ACES, AFF, ArcticIERP, SHELFZ) with zooplankton nets and were picked opportunistically out of mid-water and bottom trawls from other surveys. Though the focus of this work was zooplankton, several abundant epibenthic invertebrates were collected opportunistically and analyzed for nutritional condition, including several shrimp and isopod species, and an Arctic basket star (*Gorgonocephalus arcticus*). Individual zooplankton and samples consisting of multiple individuals of a given species were blotted dry and frozen at sea. Fish were collected from each of the eight projects. Generally, five to fifteen fish of each species were retained from each haul/station and frozen at sea. Additional fish samples were obtained from subsistence collections made by rod and reel in Kotzebue, Alaska. At times small samples were obtained for species that were encountered infrequently, either because they were in low abundance or due to sampling method biases. Though sample sizes of one are relatively uninformative, they are presented here for several species to provide realistic values rather than borrowing from other species.

Laboratory processing

Zooplankton and fish samples were thawed and processed in the laboratory. Zooplankton were identified to the lowest taxonomic level possible using keys from northern latitudes (Vassilenko, 2009; Kozloff, 1987; Kathman, 1986). Total length (excluding antennae) was measured for most zooplankton except mysids and euphausiids which were measured from the rostrum to the end of the carapace. All lengths are reported to the nearest mm. Weights were measured to the nearest 0.01 g or 0.001 g when total mass < 0.01 g. Laboratory measurements of fish included total length (mm) for all species except the ammodytids, osmerids and salmonids which were measured for fork length (mm). Whole-body mass was measured to the nearest 0.01 g before stomach contents were removed.

In preparation for chemical analysis, individual zooplankton and small fish (< 0.5 g) were dried whole to a constant weight then homogenized, while large fish (≥ 0.5 g) were homogenized wet and an aliquot was dried to a constant weight. Drying occurred in either drying ovens set to 60 ºC or using a LECO Thermogravimetric Analyzer 601 or 701 at 135 ºC. For quality assurance assessment of percent moisture, a replicate sample was included with each batch of samples, not to exceed 1.5 standard deviation. In addition, two replicates of homogenate of Pacific herring (*Clupea pallasii*) from the Gulf of Alaska or Meat1546 from the National Institute of Standards and Technology (NIST) were dried with each group of samples, with percent moisture not to exceed 15% from target values. Dried samples were homogenized to a uniform consistency. When necessary, individual zooplankton and fish weighing less than 0.01 g dry were grouped together by haul to achieve enough mass for subsequent lipid analysis, while those weighing less than 0.04 g were grouped for bomb calorimetry. The moisture content of fish was calculated and used to calculate condition indices (energy density, lipid, and protein) on a wet-mass basis for direct applicability to bioenergetic models. Accurate wet weights of individual zooplankton were difficult to obtain, as water retained among appendages requires time and care in the field to delicately wick moisture from each organism prior to freezing. Therefore, zooplankton condition was presented on a dry mass basis and wet-mass values from the best-preserved specimens were estimated using moisture from individuals of the same species or similar species.

Chemical analysis

Energy density (ED; kJ/g dry mass) of zooplankton of sufficient mass and all fish was measured using bomb calorimetry. Dried homogenates of 30-70 mg or 70-200 mg were pressed into small or large pellets and combusted using a Parr 6725 semi-micro bomb calorimeter[3] using standard instrument operating

[3]Mention of trade names or commercial companies does not imply endorsement by the National Marine Fisheries Service, NOAA.

procedures from the instrument manual. Quality assurance samples included with each batch of samples were 1) duplicate benzoic acid standards, not to exceed 0.5 % coefficient of variance (CV) from each other or 0.5 % error from target values for large pellets (0.07 - 0.20 g dry) and 1.5 % CV and 2.0 % error for small (0.03 -0.07 g dry) pellets, 2) a sample replicate when sample mass permitted, not to exceed 1.5 standard deviation for both large and small pellets, and 3) a tissue reference sample of homogenized Pacific herring or walleye pollock (*Gadus chalcogrammus*) from the Gulf of Alaska (not to exceed 2.75 % or 3.0 % error for large and small pellets, respectively. Measured energy densities were converted to a wet-mass basis using moisture content. The total energy of individual zooplankton and fish (kJ) was calculated as energy density times the whole wet mass of the individual.

Lipid content of dried zooplankton and fish was measured using a sulfo-phospho-vanillin (SPV) colorimetric method (modified from Van Handel, 1985). Briefly, dry sample homogenates were placed in glass centrifuge tubes and 2 mL of 2:1 (v/v) chloroform/methanol was added to the tissue. Samples were sonicated for 30 minutes, diluted further to 1:10, and added to a 96-well plate in a fume hood. The plate was heated to 100 °C for 10 minutes, after which 20 µL of concentrated sulfuric acid was added to each well and heated for 10 more minutes before cooling to room temperature. Subsequently, 280 µL of SPV reagent (1.2 mg/ml vanillin and 80 % v/v phosphoric acid) was added to each well and the plate was vortexed at 500 rpm for 30 minutes. Light absorbance at a wavelength of 490 nm was measured through each sample and total lipid was calculated from a calibration curve. Quality assurance consisted of a Walleye Pollock tissue reference sample (percent lipid not to exceed 15 % from target values), a sample replicate (not to exceed 15 %), and a blank (not to exceed 0.3 % lipid). Percent lipid was converted from dry to wet mass basis using moisture content for use in bioenergetic models.

If more than 0.1 g of dried homogenate was available after completion of other analyses, protein content of fish samples was calculated from measured nitrogen values using a LECO[1] TruSpec CHN following methods in the instruction manual (LECO, 2007). Briefly, samples of approximately 0.1 g of dried homogenate were wrapped in foil and combusted at 950 °C. Expelled nitrogen was quantified and protein content was estimated by multiplying total nitrogen content by the Kjeldahl conversion factor of 6.25 to account for the nitrogen content of protein (AOAC, 1995). Prior to sample analysis, the LECO was calibrated with 1) ethylenediaminetetra-acetic acid (EDTA), 2) a standard reference material of Meat1546 that was not to exceed 6 % error from the target value, and 3) sucrose with zero nitrogen content. Quality assurance samples and their allowable thresholds included with every batch of 21 samples were 1) EDTA with < 1 % error from target protein value, 2) two atmospheric blanks not to exceed 0.1 % protein, and 3) one replicate of a sample varying less than 1.5 standard deviation.

Statistical analysis

Mean condition indices for zooplankton and fish were calculated across all collections for each species. Standard deviations were reported unless sample size was one. Species were ranked by condition indices and ranges of each index were calculated across all zooplankton and fish taxa and within family. Statistical comparisons among species of zooplankton and fish were evaluated using Analysis of Variance with natural log-transformed data to meet required assumptions for the test and a significant p-value of 0.05. Tukey's multiple comparison test was used to evaluate which pairwise comparisons were significantly different and values of Tukey's Honest Significant Difference (HSD) are reported. Relationships between fish length and energy density were evaluated for fourteen species of fish for which larger sample collections spanned multiple ages as inferred by their size ranges (Forster et al., 2018). Local weighted regression (LOWESS) curves with a smoothing span of one was fit to these relationships. As a discussion point, length-energy relationships of Pacific herring, Pacific capelin (*Mallotus villosus*), saffron cod, Pacific sand lance (*Ammodytes personatus)*, and starry flounder

(*Platichthys stellatus*) caught in the Arctic were compared to fishfrom the Gulf of Alaska (Vollenweider[4], Unpublished results) to evaluate regional variation.

Results

Body condition indices were measured for sixteen species of zooplankton from seven families and six orders. Ten species of opportunistically-collected epibenthic invertebrates were also analyzed, comprising five families and three orders. Lipid content was highly variable within the Calanoida and Gymnosomata orders, differinging by as much as 227 times amongst individual animals within the order Gymnosomata, the pteropods (0.09 – 19.7 % lipid wet mass; Figure 2). Mean lipid content also varied by species and was 19 times higher in *Calanus glacialis*, the most lipid-rich zooplankter (22.57 % lipid), than in *Parasagitta elegans*, the most lipid-poor species (0.81 %; Table 2). Interspecific variation in lipid content was less among the epibenthic invertebrates, with the most lipid-rich *Eualus macilentus* (6.02 % lipid) having 7.5 times as much lipid as the most lipid-poor *Argis dentata* (0.81 %). Within the decapods (shrimp) and euphausiids (krill), lipid content correlated highly with energy density (R^2 = 0.81 and 0.65, respectively), consequently, similar patterns occurred in energy content as in lipid (Table 2). Within the isopods, the correlation between lipid and energy density was considerably less strong (R^2 = 0.19).

Body condition indices were measured for forty-one species of fish from twelve families. Lipid content was highly variable among species, and was 35 times as great in Bering cisco (*Coregonus laurettae*) (25.71 % lipid), the most lipid-rich species, compared to daubed shanny (*Leptoclinus maculatus*), the most lipid-poor species (0.71 %). Bering cisco had twice as much lipid as the second most lipid-rich fish, Arctic cisco (11.50 %) while the majority of fish species analyzed for lipid content had <5 % lipid (Table 3).

Energy density of fish was positively correlated with lipid content (R^2 = 0.85), consequently similar patterns were observed between the two indices. The variability among fish species was less than for lipid content, however, with the most energy-rich species, Bering cisco, having 3.4 times greater energy density (11.01 kJ/g wet mass) than the most energy-deplete Alaska plaice (*Pleuronectes quadrituberculatus*) (3.27 kJ/g) (Table 3, Figure 3). Approximately half of the families had variation in energy density among species, including the salmonids, osmerids, gadids, and cottids (Figure 4). Within the salmonids, Bering cisco (11.01kJ/g) had 53% greater energy density than the other five species that were similarly low (4.98–7.59 kJ/g). Within the gadids, Arctic cod (4.66 kJ/g) had 16% higher energy density than saffron cod and walleye pollock that were similar (3.99–4.24 kJ/g) (Figure 4). Cottids ranged 42% amongst the most energy-rich hamecon (*Artediellus scaber*; 4.94 kJ/g) and energy-deplete species shorthorn sculpin (3.48 kJ/g). Within the osmerids, zoarcids and pleuronectids, there was no difference in energy density amongst species ($p > 0.05$). Species variability could not be assessed for stichaeids that had limited sample sizes.

Correlations between energy density and length could be evaluated for fourteen species that spanned relatively large size ranges with ample sample sizes. Four general patterns of energy accumulation with size were apparent. Pacific herring, Pacific capelin and Arctic cod gained relatively more energy with size initially, followed by a decrease (Figure 5). Both species of salmonids, humpback whitefish and least cisco, as well as Arctic flounder and Bering flounder, maintained consistent increases in energy density with size. Saffron cod and starry flounder reached an asymptotic energy densities at larger sizes. In contrast, the three cottid species decreased in energy density with size, though fourhorn may have a slight uptick at the largest sizes. Finally, energy density of slender eelblennies and Pacific sand lance were generally invariant with size.

[4] Vollenweider J, Unpublished data, 2020

Total energy content (kJ) of individual fish integrates size with energy density. Salmonids ranked as the top six species with the greatest energy content (1,161 – 10,027 kJ) and were the only species with individuals large enough to have greater than 1,000 total kJ (Figure 6). Due to their large size (20 - 163 g), multiple species of flatfishes moved higher in their ranking for total energy content than their rankings for energy density (Table 3). In particular, the Alaska plaice (*Pleuronectes quadrituberculatus*) which was the most energy-deplete species in terms of energy density, had the ninth greatest total energy content (496 kJ) though this observation is limited to a single fish. Within families, the ranking of species by total energy content differed from a ranking according to energy density. For example, on a gram-for-gram comparison, Arctic cod had 10% more energy than walleye pollock or 17% more energy than saffron cod.; When energy density is scaled up to total energy content of a whole fish, however, saffron cod (333 kJ) had ten times more total energy than the other gadids (33 kJ and 27 kJ for Arctic cod and walleye pollock, respectively) kJ) as the mass of an individual saffron cod was an order of magnitude greater than Arctic cod or walleye pollock sampled here (Figure 8.

Protein content was the least variable condition index measured, only ranging two-fold between the highest and lowest protein contents (Table 3). Salmonids were the top five species with the greatest protein content (18.15–19.30 %), whereas ribbed sculpin (9.55 %) had the least. Two-thirds of the species analyzed had protein contents higher than 15 %.

Discussion

This research has significantly expanded the library of body condition analyses of Arctic zooplankton and fish by enlarging the number of species analyzed as well as the spatial coverage to include the Chukchi and western Beaufort Seas. We highlight how size and location can have dramatic consequences on animal body condition and consequently the importance of using appropriate condition measures. We expound on the bioenergetics consequences of prey switching. Finally, we put forth this work as a foundational piece in supporting bioenergetics models to predict Arctic ecosystem communities in the future.

Of the zooplankton species previously reported from the Svalbard region off the coast of Norway and adjacent to Baffin Island, Canada (Mayzaud et al., 2016; Scott et al., 2000; Percy and Fife, 1981), species-specific lipid values generally fall within the ranges measured here. Euphausiids, however, had higher lipid in other regions than observed here, including the adjacent Bering Sea and more distant Arctic locations by Baffin Island and Svalbard (Harvey et al., 2012; Hopkins et al., 1978; Percy and Fife, 1981;). In contrast, energy densities of zooplankton measured in this study are consistently higher than those collected in the Norwegian Arctic near Svalbard (Westlawski 1994).

Changes in availability or timing of high quality zooplankton prey could have drastic effects on their zooplanktivore predators whose life cycle events are tightly paired to these events. For example, the time when juvenile fish such as Arctic Cod have exhausted their lipid sacs and begin their first feeding coincides with high spring zooplankton production, particularly lipid-rich calanoid copepods (Rand et al., 2013; Gray et al., 2016). Another example of a critical energetic event is in the summer when bowhead whales feed on ephemeral euphausiid aggregations caused from summer upwelling (Okkonen et al., 2011). Should these high quality prey resources be replaced with alternative prey, cascading effects could proliferate up the food chain. This phenomenon has been observed in the North Sea where warming ocean temperatures resulted in shifts from high lipid *Calanus finmarchicus* to a lower quality *Calanus helgolandicus*, causing reduced condition and abundance in their Sandeel (*Ammodytes marinus*) predators and subsequently declines in productivity of multiple species of seabirds feeding upon the Sandeels (Frederiksen et al., 2006). To evaluate bottom-up regulation of marine ecosystems as observed in the North Sea, accurate measures of zooplankton body condition are a foundational component.

Fish energy density variation of 267 % among the 41 evaluated species could potentially have large consequences for piscivorous predators. .. For example, for a seal to intake equal calories from a diet solely composed of Bering cisco, the most energy-rich fish, the seal would need to consume 3.4 times the biomass of Alaska plaice, the least energy-rich species. Bering cisco weigh approximately four times more than Alaska plaice meaning a seal would need to consume twelve Alaska plaice to equate to one Bering cisco. Similarly, eighty-seven shorthorn sculpin, the second-least energy-rich species, would be required to equate to one Bering cisco. These simple comparisons contrasting monospecific diets of prey of both extremely different quality and size show that consuming greater quantities of low-quality prey may not be possible. This has been demonstrated by Steller sea lions, which could not compensate for a low quality diet of walleye pollock by consuming sufficient biomass to maintain their body mass (Rosen and Trites, 2000). Furthermore, the comparison of monospecific diets is oversimplified as there are a host of additional complicating factors playing into predator foraging strategy, including abundance, distribution and timing of available prey species, as well as species-specific behavior of prey commensurate with particular feeding methods of predators, i.e., gulp feeding versus single fish selection (Petrov et al., 2020).

A more pertinent situation is that Arctic cod, which is relatively averse to warming temperatures, may be outcompeted in the Arctic by saffron cod which can tolerate warmer temperatures, or by invading temperate gadids such as walleye pollock (Laurel et al, 2016; Logerwell et al., 2015; Hollowed et al., 2013). With saffron cod as the dominant prey fish, predators would need to consume 17 % more biomass of it than of Arctic cod for equivalent ingested energy. However, saffron cod are significantly larger than Arctic cod, thus provide more energy per fish and consequently a single saffron cod provides the same the total energy as ten Arctic cod. If Arctic Cod are displaced by the juvenile walleye pollock caught in this study, a predator would need to consume 10 % more biomass of walleye pollock which equates to 1.2 individual pollock.. The different energy content of fish can have profound effects on their predators. Consider the grey seal (*Halichoerus grypus*), one of the few Arctic phocids whose energetic demands have been measured but inhabits the North Atlantic. Grey seals require 1,006 kJ/d for resting metabolism (Ronald et al. 1984).To meet daily energy requirements, a seal would need to consume 6 saffron cod, 33 Arctic cod, or 41 walleye pollock. In terms of biomass, this would equate to 287 g of saffron cod, 200 g of Arctic aod, or 245 g of walleye pollock. These discrepancies would be less pronounced for smaller phocids inhabiting the Chukchi Sea such as ringed seals (*Phoca hispida*), but significantly more pronounced for bearded seals (*Erignathus barbatus*) that can be twice as large as grey seals. This comparison has direct bearing for the Chukchi ecosystem as both phocids are known to consume all three gadid species (Crawford et al., 2015).

Predicting future changes in the biological community composition in the Arctic is considerably more complicated than comparisons of energy content. The comparison of gadids is complicated by different habitat preferences of the species. While Arctic cod and potentially walleye pollock have broader distributions across the Chukchi and Beaufort Seas, saffron cod prefer nearshore, shallow habitats (Vollenweider et al., 2018; De Robertis et al., 2017, Logerwell et al., 2015). Additionally, the most energy rich species were not highly abundant nor widespread. For example, Pacific herring was caught in relatively low abundance north of Norton Sound. Similarly, Pacific sand lance, Arctic staghorn sculpin, and rainbow smelt and anadromous species such as ciscos were caught more frequently in nearshore habitats than offshore (Vollenweider et al., 2018; De Robertis et al., 2017; Logerwell et al. 2015). Additional caveats of our energetic-based comparisons are the size and age of fish used for analysis. Though samples analyzed are probably relatively reflective of the most abundant size and ages of fish present, samples were derived from multiple studies with somewhat dissimilar sampling methods that would skew this, such as somewhat unbalanced sampling of pelagic versus benthic habitats and offshore versus nearshore. It is scenarios such as these in which spatially-explicit bioenergetic models can integrate prey quality, abundance, and distribution to predict biological community composition in the Arctic under future environmental scenarios.

There are some similarities and stark differences between the summertime energetics of the 41 Arctic species examined here compared to more southerly species in Alaska. In a similar study in the Gulf of Alaska (GOA), energy content was measured for 16 of the most abundant marine fish species, 5 of which also caught in this study study (Vollenweider et al. 2011). The average energy density of the fish species examined in these studies were very similar, ranging from 3.27–7.98 kJ/g wet mass in the Arctic versus 3.64–9.78 kJ/g in the GOA. In contrast, the range of average total energy of individual fish confounded by fish mass in the GOA was 14 times greater than Arctic fish (Arctic fish: 1–10,027 kJ; GOA: 30-30,624 kJ). This stark difference is due to the large size discrepancy of abundant fish between the two regions, with the Arctic comprised of many juveniles such as Arctic cod, walleye pollock, yellowfin sole, (Forster et al., 2018; De Robertis et al., 2017) as well as adult fish of diminutive size (Forster et al., 2020). Size and ontogenetic differences (Wuenschel et al., 2011; Post and Parkinson, 2001) of fishes illustrate the need for appropriate measures of energy content.

Five species of fish spanning large size ranges and sampled in relatively large numbers could be directly compared between the Arctic study and the GOA study. From the energy density-length relationships, energy accumulation with size was slower in the Arctic than in the GOA for both species of fish (Figure 6). Juvenile fish have rapid growth during significantly shorter summer growing seasons at high latitude which could tax their energy reserves relative to their southerly counterparts (Conover and Present, 1990). Though juveniles require large energy stores in the fall to sustain themselves during winter conditions with low food availability (Sewall et al., In Review; Sogard and Olla, 2000), Arctic fish in colder water may have significantly reduced metabolic rates and may therefore require less energy to sustain themselves through the winter (Bystrom et al 2006; Garvey et al., 2004). At higher latitudes fish are older at a given length, therefore lower energy content of mature fish may be associated with gonad development that commences earlier at higher latitudes in some species of fish (Garvey and Marschall, 2003). In addition, Pacific capelin may preferentially allocate energy to maturation and maximum gonad production over adult survival (Carscadden et al. 1997).

Foundation for bioenergetics modeling

Summer is an important feeding period in the Arctic as sea ice melts and habitat becomes seasonally available. Many species of seabirds and marine mammals migrate annually to the Arctic to feed during the ice-free season to take advantage of the high productivity. In the US Arctic, ocean currents transport large nutrient loads from the Bering Sea into the Chukchi Sea and then onto the Beaufort Sea Shelf through upwelling from the Arctic Basin (Tremblay et al., 2011; Danielson et al., 2017). The majority of the ~15,000 individuals of the Western Arctic stock of bowhead whales (*Balaena mysticetus*) migrates from the Bering Sea through the Chukchi and western Beaufort Seas each spring and fall to these feeding grounds (IWC 2018). Similarly, migration from the Bering Sea to the coast of the Chukchi Sea and to the eastern Beaufort Sea is performed annually by thousands of Beluga whales (*Delphinapterus leucas*) to calve and molt (Barber et al., 2001). Humpback (*Megaptera novaeangliae*), Fin (*Balaenoptera physalus*) and Minke whale (*Balaenoptera bonaerensis*) sightings are increasingly more common in the Chukchi Sea in the summer (Clarke et al., 2013). Millions of seabirds congregate in the Chukchi and Beaufort Seas to feed and breed during the summer (Kuletz et al., 2015; Smith, 2010). With such an immense seasonal influx of foraging animals to the Arctic, the quality of their zooplankton and fish prey in the summer is foundational to the region's food web. Understanding trophic linkages and predicting future ecosystem community composition under anticipated climatic changes can be evaluated using bioenergetic models with prey nutrition indices described here.

Though the summer period of Arctic productivity is generally the focal period of trophic analysis, winter may be of interest for non-migrating species that remain in the Arctic year- round. Winter prey quality descriptors of zooplankton and fish are nonexistent in the US Arctic due to substantial logistic constraints imposed by sea ice and perpetual darkness. Some zooplankton and fish, particularly those inhabiting pelagic habitats, undergo significant seasonal cycles in energy content in relation to their ontogenetic

development, food availability and maturation state (Vollenweider et al., 2011; Syvaranta and Rautio, 2010; Clarke and Peck, 1991; Hislop et al., 1991). Zooplankton in the water column also tend to fluctuate significantly likely due to high metabolic costs incurred in that habitat (Clarke and Peck, 1991; Syvaranta and Rautio, 2010; Falk-Petersen et al., 2009, 2000). This is especially true of pelagic species that rely most heavily on seasonal production. Ice algae has an important role in the phenology and energetics of some Arctic zooplankton species, and consequently, loss of sea ice will likely impact zooplankton condition and potentially survival of some species. Similar seasonal variation occurs in fish condition, generally with an increase in energy content during productive summer conditions, followed by a decrease in energy over winter when food is scarce and gonad development may concurrently take place in preparation for spawning (Paul and Paul, 1999; Robards et al., 1999). In the Gulf of Alaska, the most extreme seasonal energetic cycling occurs in Pacific Herring, for which energy density can nearly double from spring minima to fall maxima. Demersal species cycle less, likely due to a more steady-state conditions near the sea floor. To what degree the prey quality of Arctic zooplankton and fish species fluctuates seasonally warrants investigation.

Conclusions

This is the most thorough library of Arctic zooplankton and fish condition to date. Comparisons of prey quality illustrate that climate-induced changes in zooplankton and fish communities could result in a vastly different nutritional value of available prey for fish, seabirds and marine mammal predators. Specific effects on health and survival of upper-level trophic consumers can be ascertained using body condition of fish and zooplankton characterized here to parameterize bioenergetic models that take prey quality into account. These data provide critical prey quality indices that can be used in these models. As Arctic zooplankton and fish species have different energetic strategies than their congeners at lower latitudes, having location-specific condition values is critical for the accuracy of bioenergetic models. Inclusion of prey quality values in Arctic food webs will significantly enhance predictions and understanding of how the Arctic marine ecosystem will fare in the future.

Acknowledgements

A project of this size is not possible without the support of countless people! We thank our critical funding sources, including NPRB, BOEM, NSB, and the Wildlife Conservation Society/Arctic Beringia Program. People that proposed and secured funding for these projects include Ed Farley (NOAA), Franz Meuter (UAF), Kevin Boswell (FIU), Craig George (NSB) and Seth Danielson (UAF). Many, many people were critical in the collection of samples, notably Kris Cieciel (NOAA), Alex Andrews (NOAA), John Moran (NOAA), Wyatt Fournier (NOAA Affiliate), Scott Johnson (NOAA), John Thedinga (NOAA), and Alex Whiting (Native Village of Kotzebue). Ann Robertson, Mark Barton, and Brian Haggerty-Perrault led the collection and preservation of the nearshore samples. A fleet of boats and crewmen kept us safe and helped us achieve our goals, including the R/V Ocean Star, R/V Ukpik, and R/V Annika Marie. The people of Utqiagvik and Kotzebue were foundational in supporting nearshore project activities. An army of people in the laboratory provided biological processing and chemical analysis of the samples. Ann Robertson and Brian Haggerty-Perrault oversaw sample processing of the majority of fish, and large contributions were made by Matt Callahan, Kevin Heffern, Courtney Weiss, Corey Fugate, and Lawrence Schaufler.

References

AOAC (1995) Official methods of analysis, 16th edn. Association of Official Analytical Chemists, Arlington, Virginia.

Anthony JA, Roby DD, Turco KR (2000) Lipid content and energy density of forage fishes from the northern Gulf of Alaska. J Exper Mar Biol Ecol 248(1):53-78.

Auel H, Harjes M, da Rocha, R, Stubing D, Hagen W (2002) Lipid biomarkers indicate different ecological niches and trophic relationships of the Arctic hyperiid amphipods *Themisto abyssorum* and *T. libellula*. Pol Bio 25(5):374-383.

Babin J, Lasserre F, Pic P (2020) Arctic shipping and polar seaways. in: Maurice P (Ed.), Encyclopedia of Water: Science, Technology and Society. John Wiley & Sons, Inc. 13 p.

Barber DG, Saczuk E, Richard PR (2001) Examination of beluga-habitat relationships through the use of telemetry and a geographic information system. Arctgic 54(3):305-316.

Bluhm BA, Gradinger R (2008) Regional variability in food availability for Arctic marine mammals. Ecol App 18:S77-S96. 198 p.

Bystrom P, Kiessling A, Eriksson LO (2006) Size and temperature dependent foraging capacities and metabolism: consequences for winter starvation mortality in fish. Oikos 115:43-52.

Carmack EC, Macdonald RW, Jasper S (2004) Phytoplankton productivity on the Canadian Shelf of the Beaufort Sea. Mar Ecol Prog Ser 277:37-50.

Carscadden J, Nakashima BS, Frank KT (1997) Effects of fish length and temperature on the timing of peak spawning in capelin (Mallotus villosus). Can J Fish Aquat Sci 54(4):781-787.

Chiba S, Batten SD, Yoshiki T, Sasaki Y, Sasaoka K, Sugisaka H, Ichikawa T (2015) Temperature and zooplankton size structure: climate control and basin-scale comparions in the North Pacific. Ecol and Evol 5(4):968-978.

Clarke J, Stafford K, Moore SE, Rone B, Aerts L, Crance J (2013) Subacrctic cetaceans in the southern Chukchi Sea: evidence of recovery or response to a changing ecosystem. Oceanogr 26(4):136-149.

Clarke A, Peck LS (1991) The physiology of polar marine zooplankton. Polar Res 10(2):355-370.

Conover DO, Present TMC (1990) Countergradient variation in growth rate: compensation for length of the growing season among Atlantic silversides from different latitudes. Oecologia 83(3):316-324.

Crawford JA, Quakenbush LT, Citta JJ (2015) A comparison of ringed and bearded seal diet, condition and productivity between historical (1975-1984) and recent (2003-2012) periods in the Alaskan Bering and Chukchi Seas. Prog Oceanogr 136:133-150.

Dam HG, Baumann H (2018) Chapter 25. Climate change, zooplankton and fisheries. In: Climate Change Impacts on Fisheries and Aquaculture, a Global Analysis volume 1. (Eds.) BF Phillips, M Perez-Ramirez. Wiley Blackwell, Hoboken, NJ, pp. 851-874.

Danielson SL, Eisner L, Ladd C, Mordy C, Sousa L, Weingartner TJ (2017) A comparison between late summer 2012 and 2013 water masses, macronutrients, and phytoplankton standing crops in the northern Bering and Chukchi Seas. Deep Sea Res Part II 135:7-26.

De Robertis A, Taylor K, Wilson CD, Farley EV (2017) Abundance and distribution of Arctic cod (*Boreogadus saida*) and other pelagic fishes over the U.S. Continental Shelf of the Northern Bering and Chukchi Seas. Deep Sea Res Part II 1365:51-65.

Falk-Petersen S, Hagen W Kattner G, Clarke A, Sargent J (2000) Lipids, trophic relationships, and biodiversity in Arctic and Antarctic krill. Can J Fish Aquat Sci 57(S3):178-191.

Falk-Petersen S, Mayzaud P, Kattner G, Sargent JR (2009) Lipids and life strategy of Arctic *Calanus.* Mar Biol Res 5(1):18-39.

Fechhelm RG, Griffiths WB, Wilson WJ, Gallaway BJ, Bryan JD (2011) Intra- and interseasonal changes in the relative condition and proximate body composition of Broad Whitefish from the Prudhoe Bay region of Alaska. Trans Amer Fish Soc124(4):508-519.

Forster C, Norcross B, Meuter F (2020) Documenting growth parameters and age in Arctic fish species in the Chukchi and Beaufort Sea. Deep Sea Res II.

Forster C, Norcross B, Walker K, Frothingham A (2018) Fish life history characteristics: length, weight and age. In Vollenweider JJ, Heintz RA, Boswell KM, Norcross BL, Li C, Barton MB, Sousa L, Pinchuk A, Danielson S, George C (Eds.), Ecology of forage fishes in the Arctic nearshore. Final Report, North Slope Borough Shell Baseline Studies Program, pp. 258-310.

Frederiksen M, Edwards M, Richardson AJ, Halliday NC, Wanless S (2006) From plankton to top predators: bottom-up control of a marine food web across four trophic levels. J Animal Ecol 75:1259-1268.

Garvey JE, Marschall EA (2003) Understanding latitudinal trends in fish body size through models of optimal seasonal energy allocation. Can J Fish Aquat Sci 60:938-948..

Garvey JE, Ostrand KG, Wahl DH (2004) Energetics, predation, and ration affect size-dependent growth and mortality of fish during winter. Ecol 85:2860-2871

Goddard P, Lauth R, Armistead C (2014) Results of the 2012 Chukchi Sea bottom trawl survey of bottomfishes, crabs, and other demersal macrofauna. NOAA Tech Memo NMFS-AFSC-278, 123 p.

Gomez MD, Rosen DAS, Trites AW (2016) Net energy gained by northern fur seals (Callorhinus ursinus) is impacted more by diet quality than by diet diversity. Can J Zool 94:123-135.

Gray BP, Norcross BL, Beaudreau AH, Blanchard AL, Seitz AC (2017) Food habits of Arctic staghorn sculpin *(Gymnocanthus tricuspis*) and shorthorn sculpin (*Myoxocephalus scorpius*) in the northeastern Chukchi and western Beaufort Seas. Deep Sea Res Part II 135:111-123.

Gray BP, Norcross BL, Blanchard AL, Beaudreau, AH, Seitz AC (2016) Variability in the summer diets of juvenile polar cod (*Boreogadus saida*) in the northeastern Chukchi and western Beaufort Seas. Polar Biol 39(6):1069-1080.

Harvey HR, Pleuthner RL, Lessard EJ, Bernhardt MJ, Shaw CT (2012) Physical and biochemical properties of the euphausiids *Thysanoessa inermis*, *Thysanoessa raschii*, and *Thysanoessa longipes* in the eastern Bering Sea. Deep Sea Res Part II 65:173-183.

Hislop JRG, Harris MP, Smith JGM (1991) Variation in the calorific value and total energy content of the lesser sandeel (*Ammodytes marinus*) and other fish preyed on by seabirds. Journal Zool 224(3):501-517.

Hollowed AB, Planque B, Loeng H (2013) Potential movement of fish and shellfish stocks from the sub-Arctic to the Arctic Ocean. Fish Oceanogr 22(5):355-370.

Hop H, Graham M, Trudeau VL (1995) Spawning energetics of Arctic cod (Boreogadus saida) in relation to seasonal development of the ovary and plasma sex steroid levels. Can J Fish Aquat Sci 52:541-550.

Hopkins CCE, Falk-Petersen S, Tande K, Eilertsen HC (1978) A preliminary study of zooplankton sound scattering layers in Balsfjorden: structure, energetics, and migrations. Sarsia 63(4):255-264.

IWC (2018) https://iwc.int/home.

Jonkers L, Hillebrand H, Kucera M (2019) Global change drives modern plankton communities away from the pre-industrial state. Nature 570:372-375.

Jorgensen EH, Johansen SJS, Jobling M. 1997. Seasonal patterns of growth, lipid deposition and lipid depletion in anadromous Arctic charr. J Fish Biol 51:312-326.

Koenigk T, Key J, Vihma T (2020) Climate change in the Arctic. in: Kokhanovsky A, Tomasi C (Eds.), Physics and Chemistry of the Arctic Atmosphere. Spring Polar Sciences. Springer, Cham, pp. 673-705.

Kuletz KJ, Ferguson MC, Hurley B, Gall AE, Labunski EA, Morgan TC (2015) Seasonal spatial patterns in seabird and marine mammal distribution in the eastern Chukchi and western Beaufort Seas: identifying biologically important pelagic areas. Prog Oceanogr 136:175-200.

Laurel BJ, Spencer M, Iseri P, Copeman LA (2016) Temperature-dependent growth and behavior of juvenile Arctic cod (*Boreogadus saida*) and co-occurring North Pacific gadids. Polar Biol 39(6):1127-1135.

Lawson JW, Magalhaes AM, Miller EH (1998) Important prey species of marine vertebrate predators in the northwest Atlantic: proximate composition and energy density. Mar Ecol Progr Ser 164:13-20.

Kathman RD, Austin WC, Saltman JC, Fulton JD (1986) Identification manual to the Mysidacea and Euphausiacea of the northeast Pacific. Can Spec Pub of Fish and Aquat Sci 93:1-411.
Kozloff EN (1987).Marine Invertebrates of the Pacific Northwest. University of Washington Press. Seattle, WA.
Laurel BJ, Spencer M, Iseri P, Copeman LA (2016) Temperature-dependent growth and behavior of juvenile Arctic cod (*Boregadus saida*) and co-occurring North Pacific gadids. Polar Biol 39(6):1127-1135.
Leco (2007) TruSpec CHN/CHNS Carbon/Hydrogen/Nitrogen/Sulfur/Oxygen Determinators: Instruction manual. St. Joseph, MI.
Logerwell E, Busby M, Carothers C, Cotton S, Duffy-Anderson J, Farley E, Goddard P, Heintz R, Hollada B, Horne J, Johnson S, Lauth B, Moulton L, Neff D, Norcross B, Parker-Stetter S, Seigle J, Sformo T (2015) Fish communities across a spectrum of habitats in the western Beaufort Sea and Chukchi Sea. Progr Oceanogr 136:115-132.
Marsh JM, Mueter FJ, Iken K, Danielson S (2016) Ontogenetic, spatial and temporal variation in trophic level and diet of Chukchi Sea fishes. Deep-Sea Res. II, doi:10.1016/j.dsr2.2016.07.010.
Mayzaud P, Falk-Petersen S, Noyon M, Wold A, Boutoute M (2016) Lipid composition of the three co-existing Calanus species in the Arctic: impact of season, location and environment. Polar Biol 39(10):1819-1839.
Mecklenburg CW, Mecklenburg TA, Sheiko BA, Steinke D (2016) Pacific Arctic marine fishes. CAFF Monitoring Series Report No. 23. Conservation of Arctic Flora and Fauna, Akureyri, Iceland, 397 p.
Mecklenburg CW, Stein DL, Sheiko BA, Chernova NV, Mecklenburg TA, Holladay BA (2007) Russian-American long-term census of the Arctic: benthic fishes trawled in the Chukchi Sea and Bering Strait, August 2004. Northwestern Naturalist 88(3):168-187.
Miglavs I, Jobling M (1989) The effects of feeding regime on proximate body composition and patterns of energy deposition in juvenile Arctic charr, Salvelinus alpinus. J Fish Biol 35(1):1-11.
National Snow and Ice Data Center. http://nsidc.org/arcticseaicenews/. Accessed Feb 17, 2020.
Norcross BL, Holladay BA, Busby MS, Mier KL (2010) Demersal and larval fish assemblages in the Chukchi Sea. Deep-Sea Res. II 57(1-2):57-70.
Okkonen SR, Asjian CJ, Campbell RG, Clarke JT, More SE, Taylor KD (2011) Satellite observations of circulation features associated with a bowhead whale feeding 'hotspot' near Barrow, Alaska, Remote Sens Environ 115(8):2168-2174.
Osterblom H, Olsson O, Blenckner T, Furness RW (2008) Junk-food in marine ecosystems. Oikos 117:967-977.
Paul AJ, Paul JM (1999) Energy contents of whole body, ovaries, and ova from pre-spawning Pacific herring. Ak Fish Res Bull 6(1):29-34.
Percy JA, Fife FJ (1981) The biochemical composition and energy content of Arctic marine macrozooplankton. Arctic 307-313.
Petrov K, Spencer RJ, Malkiewicz N, Lewis J, Keitel C, Van Dyke JU (2020) Prey-switching does not protect a generalist turtle from bioenergetics consequences when its preferred food is scarce. BMC Ecol 20(11). https://doi.org/10.1186/s12898-020-00279-6.
Pinchuk AI, Eisner LB (2017) Spatial heterogeneity in zooplankton summer distribution in the eastern Chukchi Sea in 2012-2013 as a result of large-scale interactions of water masses. Deep Sea Res II 135:27-39.
Post JR, Parkinson EA (2001) Energy allocation strategy in young fish: allometry and survival. Ecol 82(4):1040-1051.
Rand KM, Logerwell EA (2011) The first demersal trawl survey of benthic fish and invertebrates in the Beaufort Sea since the late 1970s. Polar Biol 34(4):475-488.
Rand KM, Whitehouse A, Logerwell EA., Ahgeak E, Hibpshman R, Parker-Stetter S (2013) The diets of polar cod (*Boreogadus saida*) from August 2008 in the US Beaufort Sea. Polar Biol 36(6):907-912.

Reinhardt SB, Van Vleet ES (1986) Lipid composition of twenty-two species of Antarctic midwater zooplankton and fish. Mar Biol 91(2):14-159.
Reusser DA, Frazier ML, Loiselle RA, Lee H, Thorsteinson LK (2013) Chapter 5. Arctic climate change – a tale of two cods. In: Alaska Arctic Marine Fish Ecology Catalog. Ed LK Thorsteinson and MS Love. US Geological Survey Scientific Investigations Report 2016-5038, p. 559-677.
Robards MD, Anthony JA, Rose GA, Piatt JF (1999) Changes in proximate composition and somatic energy content for Pacific sand lance (Ammodytes hexapterus) from Kachemak Bay, Alaska relative to maturity and season. J Exper Mar Biol Ecol 242(2):245-258.
Romano MD, Roby DD, Piatt JF, Kitaysky A (2000) Effects of diet on growth and development of nestling seabirds. Exxon Valdez Oil Spill Restoration Project Final Report (Restoration Project 98163N). USGS Oregon Cooperative Fish and Wildlife Research Unit, Dept of Fisheries and Wildlife, Oregon State University, Corvallis, OR.
Ronald K, Keiver KM, Beamish FWH, Frank R (1984) Energy requirements for maintenance and faecal and urinary losses of the grey seal (*Halichoerus grypus*). Can J Zool 62(6):1101-1105.
Rose GA, Leggett WC (1989) Interactive effects of geophysically-forced sea temperatures and prey abundance on mesoscale coastal distributions of a marine predator, Atlantic Cod (*Gadus morhua*). Can J Fish Aquat Sci 46(11):1904-1913.
Rosen DA, Trites AW (2000) Pollock and the decline of Steller sea lions: testing the junk-food hypothesis. Can J Zool 78(7):1243-1250.
Runge CA, Daigle RM, Hausner VH (2020) Quantifying tourism booms and the increasing footprint in the Arctic with social media data. PLoS ONE 15(1): e0227189. https://doi.org/10.1371/journal.pone.0227189.
Scott CL, Kwasniewski S, Falk-Petersen S, & Sargent JR (2000) Lipids and life strategies of *Calanus finmarchicus, Calanus glacialis* and *Calanus hyperboreus* in late autumn, Kongsfjorden, Svalbard. Polar Biol 23(7):510-516.
Sewall F, Norcross B, Heintz R (In Review) Condition and performance of juvenile Pacific herring with different feeding histories. Mar Ecol Prog Ser.
Smith MA (2010) Arctic Marine Synthesis: Atlas of the Chukchi and Beaufort Seas. Audubon Alaska and Oceana, Anchorage.
Sogard SM, Olla BL (2000) Endurance of simulated winter conditions by age-0 walleye pollock: effects of body size, water temperature and energy stores. J Fish Biol 56:1-21.
Syvaranta J, Rautio M (2010) Zooplankton, lipids, and stable isotopes: importance of seasonal, latitudinal, and taxonomic differences. Can J Fish Aquat Sci 67(11):1721-1729.
Thedinga JF, Johnson SW, Neff AD, Hoffman CA, Maselko JM (2013) Nearshore fish assemblages of the Northeastern Chukchi Sea, Alaska. Arctic 66(3):257-268.
Tierney M, Hindell MA, Goldsworthy S (2002) Energy content of mesopelagic fish from Macquarie Island. Antarctic Sci 14(3):225-230.
Tremblay JE, Belanger S, Barber DG, Asplin M, Martin J, Darnis G, Fortier L, Gratton Y, Link H, Archambault P, Sallon A, Michel C, Williams WJ, Philipee B, Gosselin M (2011) Climate forcing multiplies biological productivity in the coastal Arctic Ocean. Geophys Res Lett 38:1-5.
Van Handel E (1985) Rapid determination of glycogen and sugars in mosquitoes. J am Mosq Control Assoc 299-301.
Vassilenko SV, Petryashov VV Eds. (2009) Illustrated Keys to Free-Living Invertebrates of Eurasian Arctic Seas and Adjacent Deep Waters, Vol 1. Alaska Sea Grant, University of Alaska Fairbanks.
Vollenweider JJ, Heintz RA, Boswell KM, Norcross BL, Li C, Barton MB, Sousa L, Pinchuk A, Danielson S, George C (2018) Ecology of forage fishes in the Arctic nearshore. Final Report, North Slope Borough Shell Baseline Studies Program, 480 p.
Vollenweider JJ, Heintz RA, Schaufler L, Bradshaw R (2011) Seasonal cycles in whole-body proximate composition and energy content of forage fish vary with water depth. Mar. Bio 158(2):413-427.
Wanless S, Harris HP, Redman P, Speakman JR (2005) Low energy values of a fish as a probably cause of a major seabird breeding failure in the North Sea. Mar Ecol Prog Ser 294:1-8.

Wassmann P, Duarte CM, Agusti S, Sejr MK (2011) Footprints of climate change in the Arctic marine ecosystem. Glob Change Biol 17:1235-1249.
Welch HE, Bergmann MA, Siferd TD, Martin KA, Curtis MF, Crawford RE, Conover RJ, Hop H (1992) Energy flow through the marine ecoysystem of the Lancaster Sound Region, Arctic Canada. Arctic 45(4):343-357.
Weslawski JM (1994) Diet of ringed seals (*Phoca hispida*) in a fjord of West Svalbard. Arctic 47(2):109-205.
Wuenschel MJ, Jugovish AR, Hare JA (2006) Estimating the energy density of fish: the importance of ontogeny. Trans Amer Fish Soc 135(2):379-385.

Figure 1. Station design of the projects from which samples were obtained, including The Arctic Coastal Ecosystem Survey (ACES), Arctic Lagoon Ecology of Forage Fishes in the Arctic Nearshore (AFF), ArcticEis, Arctic Integrated Research Project (IERP), Coastal Arctic Lagoons, Arctic Shelf Growth, Advection, Respiration and Deposition (ASGARD), Shelf Habitat and EcoLogy of Fish and Zooplankton (SHELFZ), and opportunistic samples from subsistence collections.

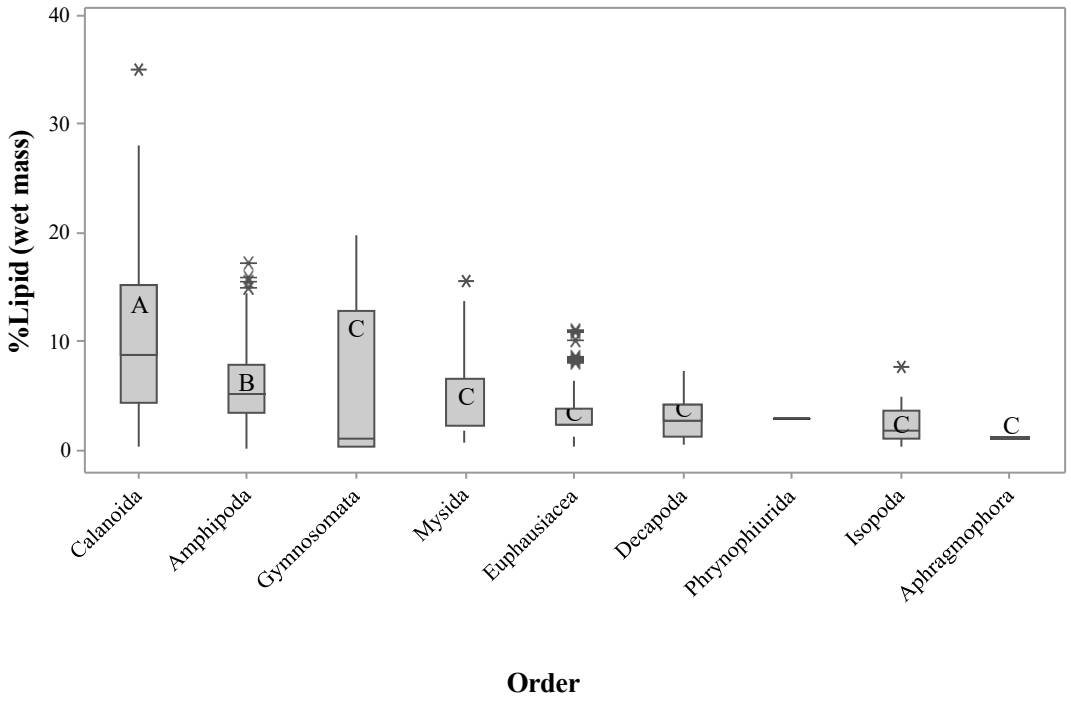

Figure 2. Lipid content (% wet mass) of zooplankton orders shown as boxplots, where the solid bars depict the interquartile range, the horizontal lines within the bars depict the median, vertical lines depict the range, and asterisks depict outliers. Like letters indicate statistical similarity.

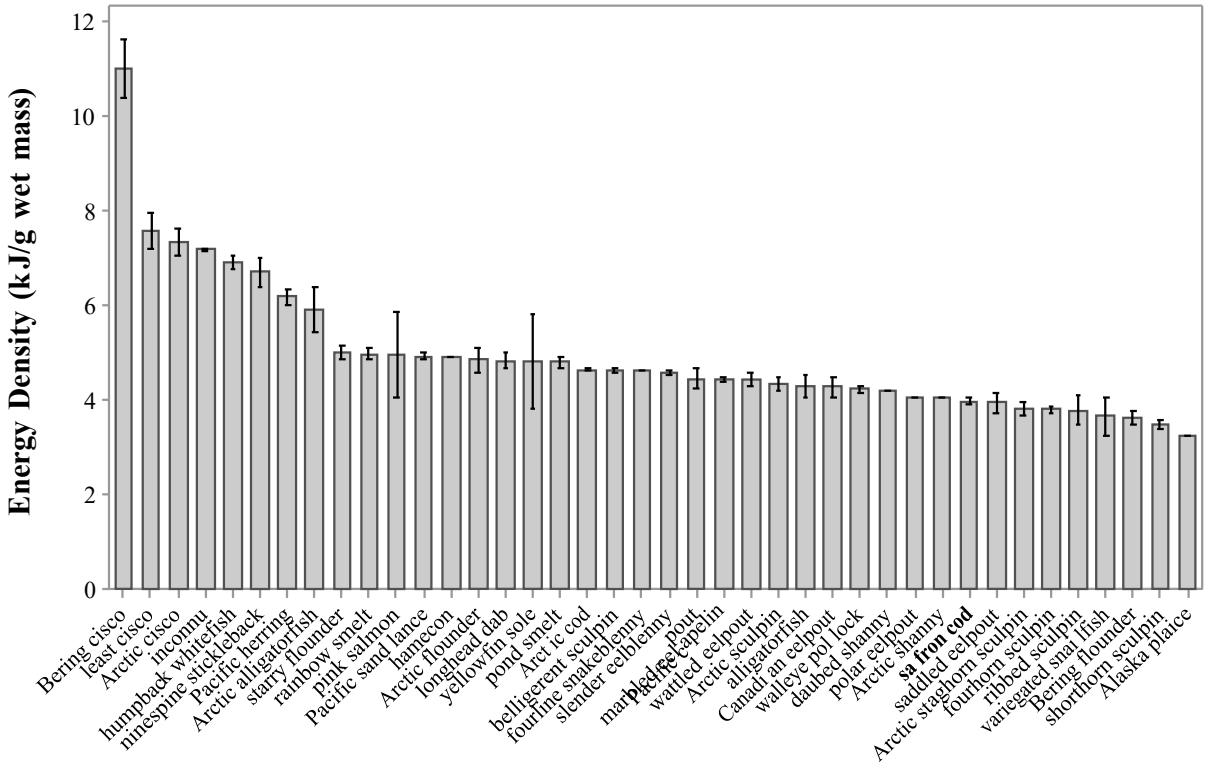

Figure 3. Mean energy density (kJ/g wet mass; ± standard error) of Arctic fish species. Lack of error bars indicates a sample size of one.

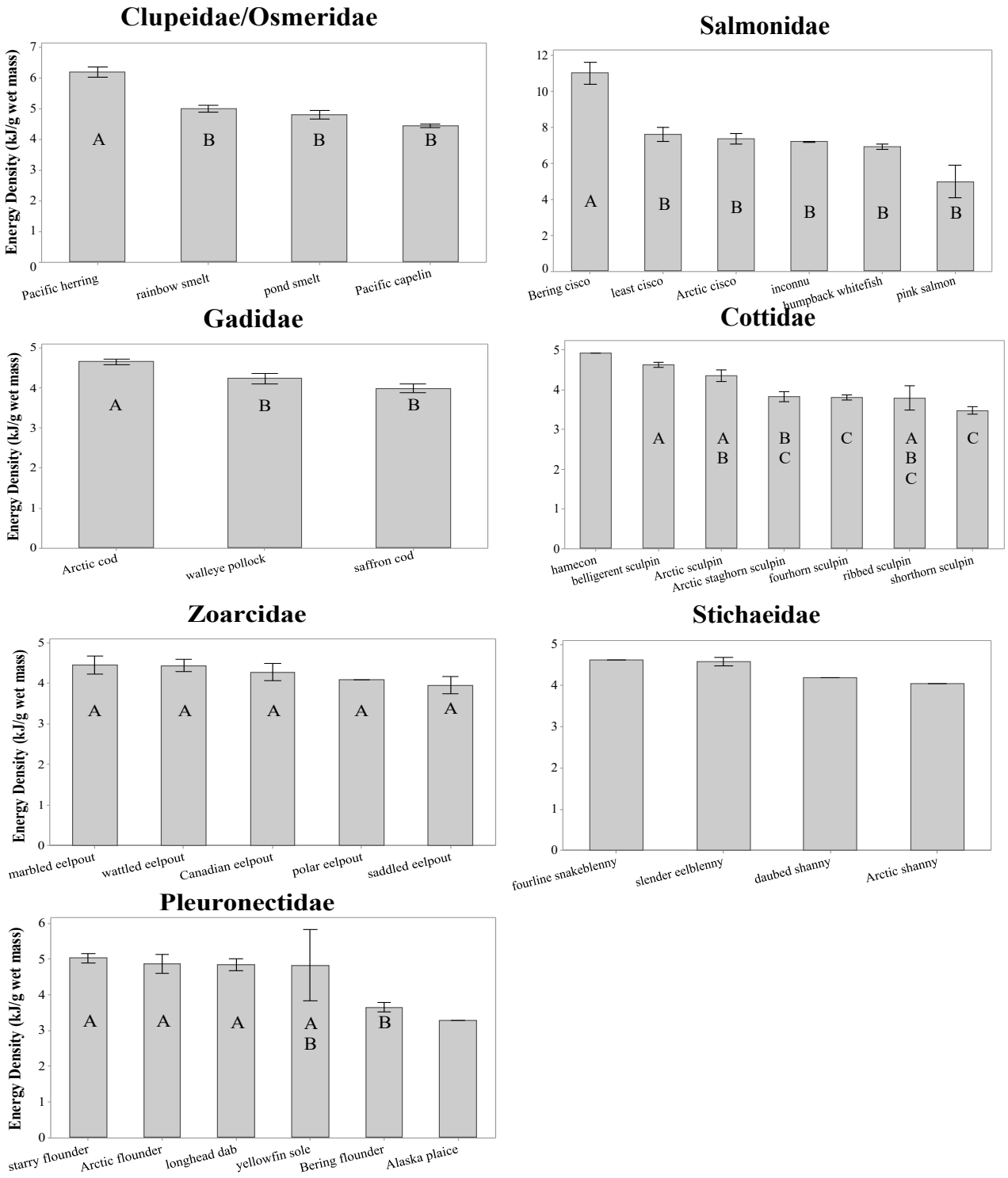

Figure 4. Mean energy density (kJ/g wet mass; ± standard error) of Arctic fish species by family. Like letters indicate statistical similarity. Lack of letters and error bars indicates a sample size of one.

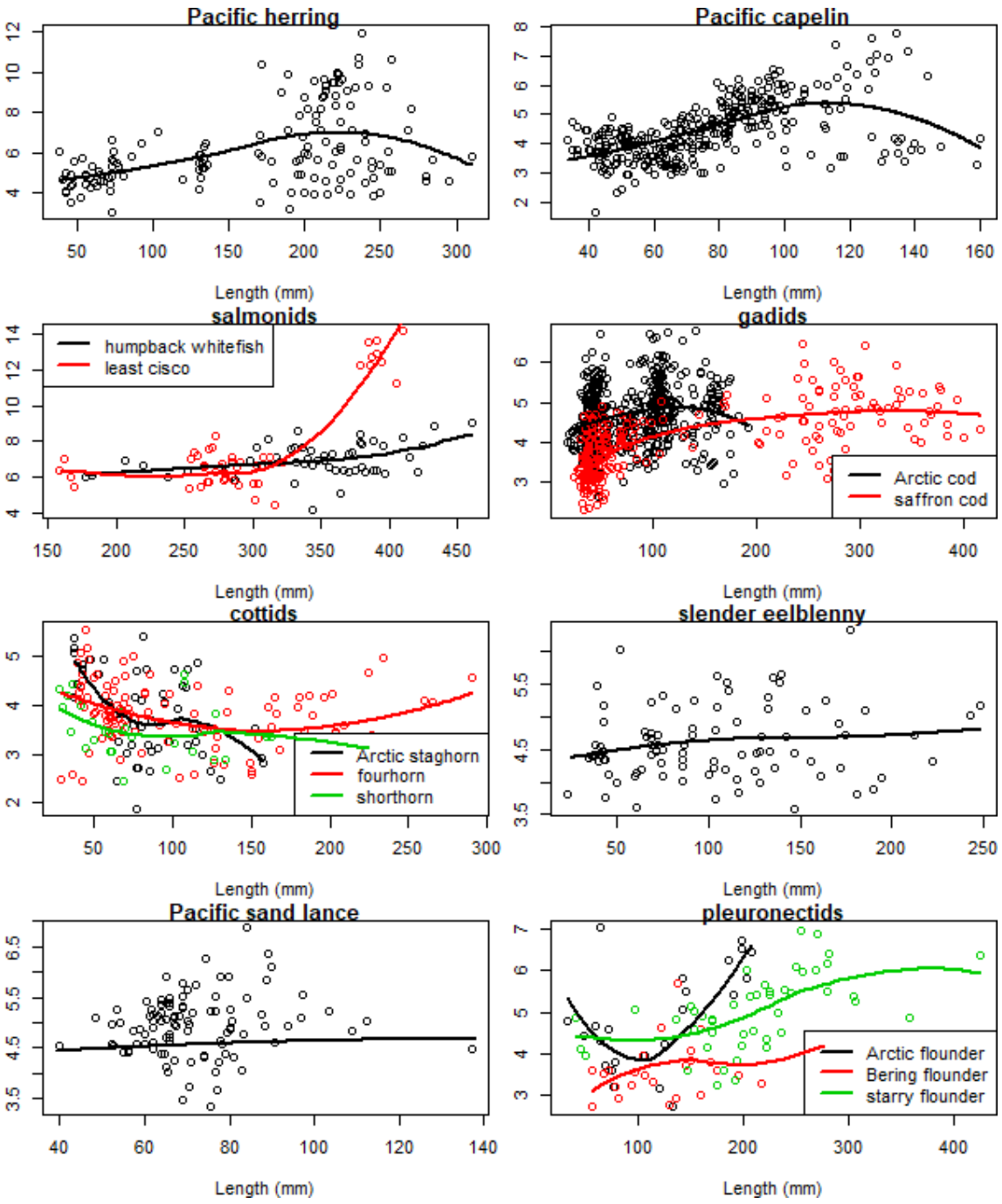

Figure 5. Length-energy density relationship of Arctic fish, where length is measured as fork length for Pacific herring, Pacific capelin, salmonids and Pacific sand lance and total length otherwise.

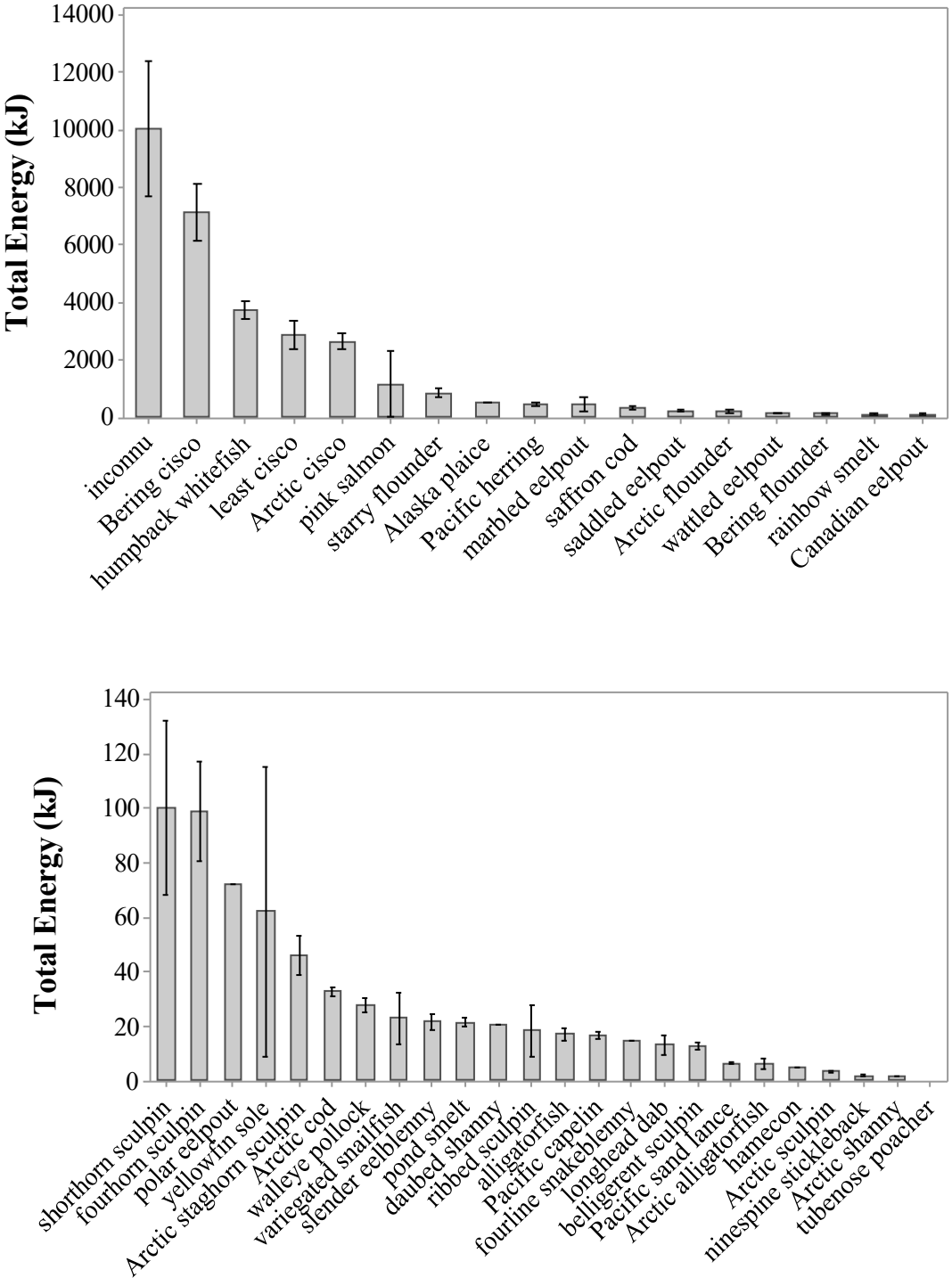

Figure 6. Average total energy content (kJ; ± standard error) of Arctic fish species. The top panel includes the species for which total energy exceeds 100 kJ while the bottom panel are those less than 100 kJ.

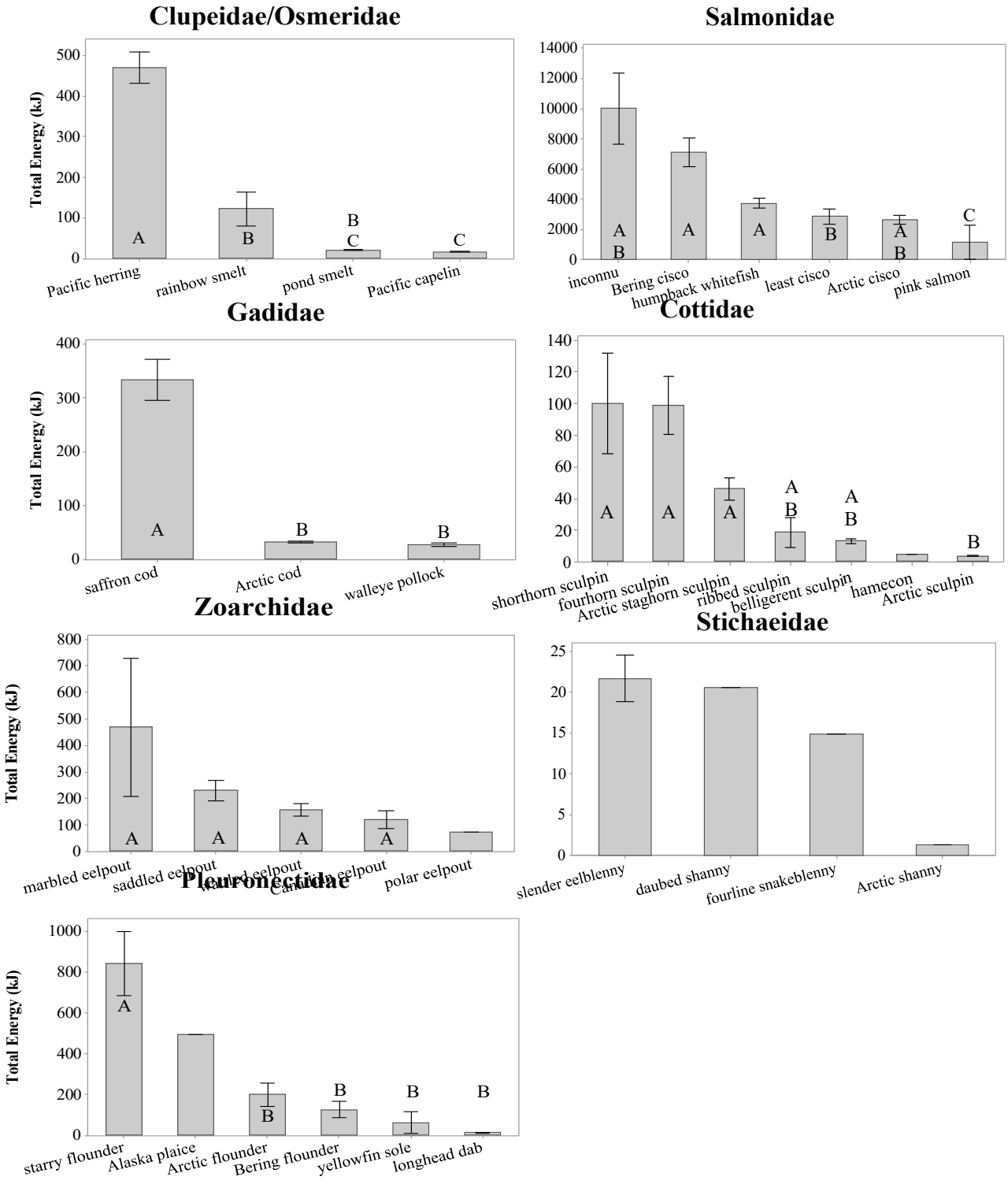

Figure 7. Average total energy content (kJ; ± standard error) of Arctic fish species. Like letters indicate statistical similarity. Lack of letters and error bars indicates a sample size of one.

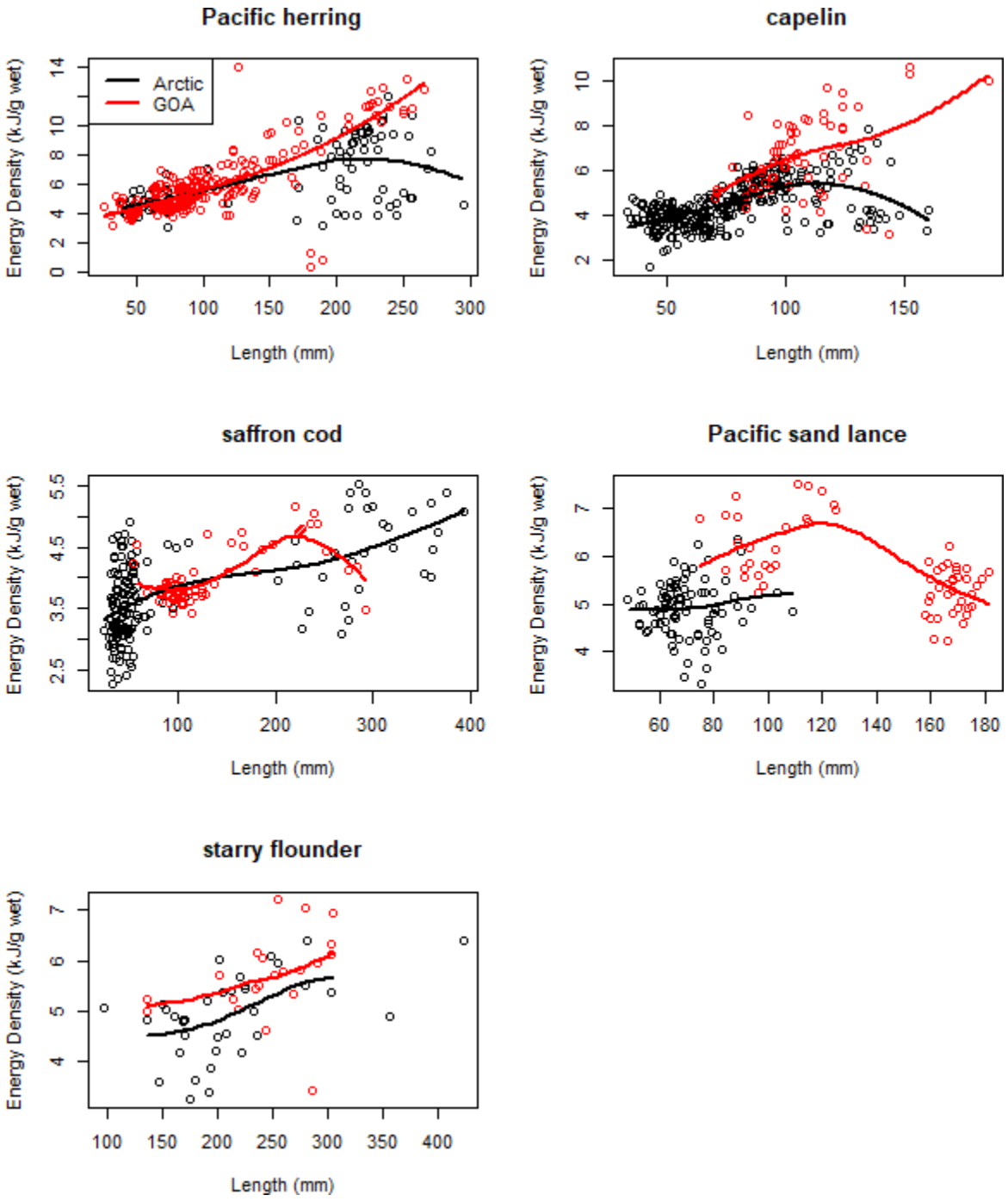

Figure 8. Length-energy density relationship of fish collected in the summer (July–September) from two Large Marine Ecosystems, the Arctic and the Gulf of Alaska.

Table 1. Survey details of the projects from which samples were obtained, including 1) The Arctic Coastal Ecosystem Survey (ACES), 2) Arctic Lagoon Ecology of Forage Fishes in the Arctic Nearshore (AFF), 3) ArcticEis, 4) Arctic Integrated Research Project (IERP) 5) Coastal Arctic Lagoons (ArcticLag), 6) Arctic Shelf Growth, Advection, Respiration and Deposition (ASGARD), 7) Shelf Habitat and EcoLogy of Fish and Zooplankton (SHELFZ), and 8) opportunistic samples from subsistence collections (Opp). Sample sizes (n) of zooplankton (Zoop) and Fish analyzed for prey quality are reported for each project.

Project	Years	Months	Zoop n	Fish n	Sampling Method
ACES	2005, 2007, 2012-2014	July-August	98	370	• 37 m variable mesh beach seine • 2.6 x 1.2 m otter trawl • 50 cm 333 µm mesh ring net
AFF	2015	July-September	220	684	• 37 m variable mesh beach seine • 5 x 3.5 m Aluette mid-water trawl • 4.7 m plumb staff beam trawl • 2.6 x 1.2 m otter trawl • 1^2 m 505 µm Tucker trawl • 50 cm 333 µm mesh ring net
ArcticEis	2012-2013	August-September	0	443	• 122 m CanTrawl 400/601 surface trawl • 6.1 x 6.1 m Marinovich mid-water trawl • 4.7 m plumb staff beam trawl • 34.1 m 83-112 Eastern otter trawl • 60 cm 505 µm bongo net
ArcticIERP	2015	August-September	81	291	• 122 m CanTrawl 400/601 surface trawl • 6.1 x 6.1 m Marinovich mid-water trawl • 60 cm 505 µm bongo net
ArcticLag	2016-2017	June-September	0	379	• variable mesh gillnet • fyke net • beach seine • rod and reel
ASGARD	2017-2018	June	0	17	• 4.7 m plumb staff beam trawl
SHELFZ	2013	August-September	54	146	• 5 x 3.5 m Aluette mid-water trawl • 6.1 x 6.1 m Aluette mid-water trawl • 4.7 m plumb staff beam trawl • 34.1 m 83-112 Eastern otter trawl • 37 m variable mesh beach seine • 1^2 m 505 µm Tucker trawl net
Opp	2011-2012	April, September, November	0	52	• rod and reel
		Total	453	2,382	

Table 2. Zooplankton and epibenthic invertebrage lipid content and energy density (ED) + standard error and sample size indicated in parentheses.

Phylum	Order	Family	Scientific name	Commo n name	Length (mm) Length type	Mass (g)	% Moisture (wet mass)	% Lipid (wet mass)	% Protein (wet mass)	Energy Density (kJ/g wet)	Total Energy (kJ/ind)
Arthropod a	Amphipod a	Hyperiidae	*Parathemist o sp.*	Hyperiid Amphipo d		0.006 (1)		4.17 (1)			
Arthropod a	Amphipod a	Hyperiidae	*Themisto libellula*	Hyperiid Amphipo d	19.41±4.0 0 TL (29)	0.11± 0.06 (30)	79.99±3.3 0 (29)	6.15±3.5 6 (29)		3.51±0. 28 (3)	0.47±0.2 9 (3)
Arthropod a	Amphipod a	Hyperiidae		Hyperiid Amphipo d	17.00 TL (1)	0.04±0.06 (3)	88.13 (1)	2.31±1.2 7 (3)			
Arthropod a	Amphipod a			Gammari d Amphipo d	21.64±7.8 1 TL (76)	0.28±0.32 (76)	73.59±6.7 9 (76)	6.32±4.1 6 (75)		4.94 (1)	0.19 (1)
Arthropod a	Calanoida	Calanidae	*Calanus glacialis*	Copepod		0.002±0.0003 (9)	73.33±0.6 4 (2)	22.57±6. 58 (9)			
Arthropod a	Calanoida	Calanidae	*Calanus hyperboreus*	Copepod		0.01±0.002 (2)	94.63 (1)	4.53±4.0 0 (3)			
Arthropod a	Calanoida	Calanidae	*Calanus marshallae* or *Calanus glacialis*	Copepod		0.005±0.007 (49)	99.20 (1)	9.90±5.8 9 (51)			
Arthropod a	Calanoida	Calanidae	*Neocalanus cristatus*	Copepod		0.006±0.002 (2)		6.67±5.9 4 (2)			
Arthropod a	Calanoida	Calanidae	*Neocalanus unid.*	Copepod		0.006±0.0002 (3)		2.96±1.3 8 (3)			

Arthropod a	Calanoida	Centropagida e	*Limnocalan us grimaldii*	Copepod		0.0003±0.000 1 (6)	84.08 (1)		3.99±0.5 4 (6)
Arthropod a	Decapoda	Crangonidae	*Argis dentata*	Arctic Argid	26.33±4.3 2 CL (6)	0.45±0.26 (6)	76.91±1.7 4 (6)		0.81±0.2 4 (6)

Table 2 continued.

Phylum	Order	Family	Scientific name	Comm on name	Length (mm) Length type	Mass (g)	% Moisture (wet mass)	% Lipid (wet mass)	% Protein (wet mass)	Energy Density (kJ/g wet)	Total Energy (kJ/ind)
Arthropo da	Decapod a	Crangonida e	*Argis lar*	Kuro Shrimp	57.78±6.02 CL (9)	5.30±1.7 7 (9)	75.32±1.72 (9)	2.57±1.2 4 (9)		4.63±0.5 3 (7)	24.77±8.44 (7)
Arthropo da	Decapod a	Crangonida e	*Sclerocran gon boreas*	Sculptu red Shrimp	61.00±1.83 CL (4)	6.45±0.7 5 (4)	76.42±2.10 (4)	0.85±0.2 0 (4)		3.87±0.4 5 (4)	24.92±3.84 (4)
Arthropo da	Decapod a	Hippolytid ae	*Eualus fabricii*	Arctic Eualid	28.50±1.00 CL (4)	0.52±0.1 0 (4)	72.87±0.49 (4)	2.82±0.3 9 (4)		5.06±0.0 8 (4)	2.61±0.55 (4)
Arthropo da	Decapod a	Hippolytid ae	*Eualus gaimardii*	Circum polar Eualid	31.92±5.95 CL (12)	0.67±0.3 5 (12)	74.32±2.00 (12)	3.41±1.4 7 (12)		5.17±0.5 9 (6)	4.61±2.12 (6)
Arthropo da	Decapod a	Hippolytid ae	*Eualus macilentus*	Greenla nd Shrimp	40.80±2.59 CL (5)	1.08±0.2 4 (5)	71.19±2.05 (5)	6.02±1.0 8 (5)		5.97±0.4 2 (5)	6.45±1.53 (5)
Arthropo da	Decapod a	Hippolytid ae	*Eualus sp.*	Eualid	39.00±1.00 CL (3)	1.16±0.2 3 (3)	75.43±0.59 (3)	5.03±1.2 2 (3)		5.10±0.1 2 (3)	5.94±1.26 (3)
Arthropo da	Decapod a	Pandalidae	*Pandalus goniurus*	Humpy Shrimp	37.00±1.41 CL (2)	0.89±0.0 8 (2)	74.81±2.73 (2)	2.96±0.3 4 (2)			

Arthropo da	Euphaus iacea	Euphausiid ae	*Thysanoess a inermis*	Krill			89.55 (1)	1.92 (1)		
Arthropo da	Euphaus iacea	Euphausiid ae	*Thysanoess a longipes*	Krill	11.00 CL (1)	0.01 (1)	80.54±6.32 (2)	2.26±0.3 9 (2)		
Arthropo da	Euphaus iacea	Euphausiid ae	*Thysanoess a raschii*	Krill	16.13±3.86 CL (40)	0.04±0.0 3 (40)	80.20±3.76 (52)	3.27±2.1 9 (46)	3.72±0.3 4 (11)	0.14±0.07 (11)
Arthropo da	Euphaus iacea	Euphausiid ae		Krill		0.03±0.0 3 (11)		4.72±3.7 2 (12)		

Table 2 continued.

Phylum	Order	Family	Scientific name	Commo n name	Length (mm) Length type	Mass (g)	% Moisture (wet mass)	% Lipid (wet mass)	% Protein (wet mass)	Energy Density (kJ/g wet)	Total Energy (kJ/ind)
Arthropo da	Euphausiac ea	Euphausiid ae		Krill Furcilia		0.007±0.00 6 (14)		1.45±2.1 1 (14)			
Arthropo da	Isopoda	Chaetiliida e	*Saduria entomon*	Isopod	57.25±25. 57 TL (24)	7.79±7.70 (27)	73.06±4. 35 (27)	2.74±1.7 6 (26)	11.02±1.4 0 (13)	6.67±2.2 7 (27)	57.92±66. 42 (27)
Arthropo da	Isopoda	Chaetiliida e	*Saduria sabini*	Isopod	87.00±4.3 4 TL (6)	13.59±2.95 (6)	74.70±2. 12 (6)	1.04±0.7 7 (4)	9.03±2.32 (2)	5.65±0.9 7 (6)	78.35±27. 82 (6)
Arthropo da	Mysida	Mysidae	*Mysis litoralis*	Mysid			73.78±5. 85 (3)	5.95±1.6 2 (3)			
Arthropo da	Mysida	Mysidae	*Mysis oculata*	Mysid	20.95±2.9 6 CL (21)	0.11±0.04 (21)	75.45±2. 50 (24)	6.41±2.9 8 (24)			
Arthropo da	Mysida	Mysidae	*Mysis relicta*	Mysid	17.29±1.5 0 CL (7)	0.06±0.01 (7)	74.08±5. 20 (16)	8.39±3.0 3 (16)			
Arthropo da	Mysida	Mysidae	*Neomysis rayii*	Mysid	29.61±3.5 6 CL (46)	0.27±0.09 (46)	78.11±1. 42 (52)	2.08±0.7 9 (47)	15.58±0.3 9 (6)	4.38±0.1 5 (5)	1.48±0.12 (5)
Arthropo da	Mysida	Mysidae	*Acanthomy sis sp.*	Mysid			78.51±4. 52 (8)	1.66±0.7 4 (8)			

Chaeto-gnatha	Aphragmo-phora	Sagittidae	*Parasagitta elegans*	Arrow Worm			94.31±0.14 (2)	1.15±0.06 (2)		
Chaeto-gnatha	Unknown	Unknown	*Unknown*	Arrow Worm		0.010±0.007 (12)		0.81±0.42 (12)		
Echino-dermata	Phryno-phiurida	Gorgono-cephalidae	*Gorgono-cephalus arcticus*	Arctic Basket Star	44.00 Disk (1)	878.69 (1)	56.65 (1)	2.82 (1)	2.87 (1)	2524.34 (1)
Mollusca	Gymno-somata	Clionidae	*Clione limacine*	Naked Sea Butterfly		0.02±0.01 (9)		5.70±7.66 (9)		

Table 3. Mean length (mm) measured as total length unless denoted by *, mass (g) and prey quality of Arctic fish species. Values indicate mean ± standard deviation.

Family	Scientific name	Common name	Total Length (mm)	Mass (g)	% Moisture (wet mass)	% Lipid (wet mass)	% Protein (wet mass)	Energy Density (kJ/g wet)	Total Energy (kJ/ind)
Clupeidae	*Clupea pallasii*	Pacific herring	169±74* (152)	67.0±56.6 (152)	74.32±5.12 (152)	8.27±6.51 (131)	16.58±2.48 (128)	6.19±1.97 (143)	470.10±467.58 (143)
Salmonidae	*Coregonus autumnalis*	Arctic cisco	312±18* (7)	356.9±84.3 (7)	70.62±2.06 (7)	11.50±3.77 (4)	18.92±0.72 (7)	7.34±0.75 (7)	2649.12±800.46 (7)
Salmonidae	*Coregonus laurettae*	Bering cisco	348±51* (23)	573.4±262.4 (23)	62.02±6.26 (23)	25.71±7.94 (20)	17.45±1.44 (23)	11.01±2.79 (21)	7127.19±4406.67 (21)
Salmonidae	*Coregonus sardinella*	least cisco	295±60* (50)	309.5±228.6 (50)	69.07±5.71 (50)	13.18±10.58 (38)	19.22±1.89 (50)	7.59±2.68 (47)	2866.48±3407.60 (47)
Salmonidae	*Coregonus pidschian*	humpback whitefish	337±59* (68)	495.1±259.5 (68)	70.34±2.66 (68)	9.37±3.92 (68)	18.97±1.17 (67)	6.92±0.93 (55)	3745.02±2327.48 (55)
Salmonidae	*Oncorhynchus gorbuscha*	pink salmon	233±246* (2)	283.8±398.0 (2)	74.90±1.21 (2)	1.81±2.17 (2)	19.30±0.94 (2)	4.98±1.27 (2)	1161.51±1623.47 (2)
Salmonidae	*Stenodus leucichthys*	sheefish	528±11* (2)	1395.0±473.8 (2)	71.13±0.43 (2)	8.81±0.01 (2)	18.15±0.22 (2)	7.20±0.05 (2)	10027.22±3345.72 (2)
Osmeridae	*Hypomesus olidus*	pond smelt	83±10* (25)	3.8±1.3 (25)	76.83±1.22 (25)	3.05±1.63 (25)	17.56±0.74 (25)	4.80±0.51 (15)	21.29±6.41 (15)
Osmeridae	*Mallotus villosus*	Pacific capelin	75±26* (370)	3.3±4.4 (370)	79.73±2.58	2.71±2.26 (139)	13.92±2.14	4.45±0.98 (330)	16.49±21.96 (330)

					(369)		(47)		
Osmeridae	*Osmerus mordax*	rainbow smelt	93±72* (22)	18.4±31.4 (22)	75.68±3.61 (22)	2.90±1.90 (10)	16.22±0.98 (12)	4.99±0.47 (17)	122.13±172.23 (17)
Gadidae	*Boreogadus saida*	Arctic cod	73±41 (602)	5.8±8.4 (602)	78.24±2.26 (601)	4.62±2.39 (382)	13.57±1.72 (118)	4.66±0.74 (505)	32.59±42.80 (505)

Table 3 continued.

Family	Scientific name	Common name	Total Length (mm)	Mass (g)	% Moisture (wet mass)	% Lipid (wet mass)	% Protein (wet mass)	Energy Density (kJ/g wet)	Total Energy (kJ/ind)
Gadidae	*Eleginus gracilis*	saffron cod	109±113 (329)	55.0±109.7 (329)	78.97±2.65 (329)	1.97±1.14 (228)	15.21±2.38 (86)	3.99±0.83 (240)	333.06±588.56 (240)
Gadidae	*Gadus chalcogramm us*	walleye pollock	97±17 (31)	6.4±3.3 (31)	80.22±1.18 (31)	3.60±1.14 (5)	15.30±1.22 (5)	4.24±0.37 (31)	27.40±14.68 (31)
Gasterosteid ae	*Pungitius pungitius*	ninespine sticklebac k	38±4 (2)	0.3±0.2 (2)	66.41±2.51 (2)	8.47 (1)		6.72±0.42 (2)	1.95±0.91 (2)
Cottidae	*Artediellus scaber*	hamecon	41 (1)	0.9 (1)	72.67 (1)	2.15 (1)		4.94 (1)	4.59 (1)
Cottidae	*Gymnocanth us tricuspis*	Arctic staghorn sculpin	86±30 (66)	14.1±15.0 (66)	78.44±3.24 (66)	1.73±0.67 (45)	11.58±1.67 (40)	3.83±0.88 (52)	45.96±50.79 (52)
Cottidae	*Megalocottus platycephalus*	belligerent sculpin	57±6 (18)	2.7±1.1 (18)	77.89±0.61 (18)	4.11±0.86 (10)	14.18±0.34 (17)	4.64±0.27 (17)	12.86±5.68 (17)
Cottidae	*Myoxocephal us quadricornis*	rourhorn sculpin	103±63 (131)	23.8±46.9 (131)	80.95±2.56 (130)	2.17±0.96 (62)	11.98±1.78 (54)	3.81±0.65 (114)	98.68±196.84 (114)
Cottidae	*Myoxocephal us scorpioides*	Arctic sculpin	38±6 (34)	0.6±0.3 (34)	81.08±3.93 (33)	2.23±0.94 (33)		4.36±0.67 (20)	3.39±1.30 (20)
Cottidae	*Myoxocephal us scorpius*	shorthorn sculpin	73±58 (46)	20.9±48.3 (46)	80.84±4.19 (46)	2.08±1.56 (38)	12.15±1.37 (24)	3.48±0.54 (31)	99.90±176.90 (31)

Cottidae	*Triglops pingelii*	ribbed sculpin	69±38 (8)	5.1±6.8 (8)	80.29±3.37 (8)	3.41±2.24 (4)	9.55±1.43 (4)	3.80±0.88 (8)	18.43±26.37 (8)

Table 3 continued.

Family	Scientific name	Common name	Total Length (mm)	Mass (g)	% Moisture (wet mass)	% Lipid (wet mass)	% Protein (wet mass)	Energy Density (kJ/g wet)	Total Energy (kJ/ind)
Agonidae	*Aspidophoroid es monopterygius*	alligatorfis h	91±55 (3)	2.7±2.3 (3)	50.90±29. 44 (3)	3.97±2.85 (3)	14.70±0.6 2 (2)	4.31±0.30 (2)	17.21±3.21 (2)
Agonidae	*Pallasina barbata*	tubenose poacher	34±7 (4)	0.1±0.03 (4)	47.81±26. 55 (4)	4.13±2.64 (4)			
Agonidae	*Ulcina olrikii*	Arctic alligatorfis h	53±12 (13)	0.9±0.6 (13)	63.11±6.1 3 (13)	4.39±2.46 (12)	18.01±2.4 7 (9)	5.93±1.08 (5)	6.12±4.49 (5)
Liparidae	*Liparis gibbus*	variegated Snailfish	67±31 (6)	6.2±8.3 (6)	78.64±3.1 6 (6)	1.96±1.25 (6)	11.38±2.2 8 (5)	3.67±0.87 (5)	23.01±20.89 (5)
Zoarcida e	*Lycodes polaris*	Canadian eelpout	157±59 (16)	29.7±42.6 (16)	77.57±3.6 1 (16)	1.87±0.98 (3)	16.31±1.1 8 (2)	4.28±0.85 (16)	119.63±139.31 (16)
Zoarcida e	*Lycodes raridens*	marbled eelpout	188±106 (7)	105.2±161 .9 (7)	78.33±1.8 8 (7)	4.34±2.28 (4)	13.93±0.0 7 (2)	4.46±0.58 (7)	468.41±687.82 (7)
Zoarcida e	*Lycodes mucos us*	saddled eelpout	201±4 (2)	57.5±9.8 (2)	76.67±0.0 6 (2)	1.63±0.65 (2)		3.96±0.31 (2)	229.05±56.80 (2)
Stichaeid ae	*Eumesogramm us praecisus*	fourline snakeblenn y	75 (1)	3.2 (1)	74.81 (1)	2.16 (1)	15.53 (1)	4.63 (1)	14.86 (1)
Stichaeid ae	*Leptoclinus maculatus*	daubed shanny	136 (1)	4.9 (1)	72.96 (1)	0.71 (1)	15.39 (1)	4.19 (1)	20.60 (1)

Stichaeid ae	*Lumpenus fabricii*	slender eelblenny	96±49 (143)	4.1±5.2 (143)	75.63±3.31 (143)	2.34±1.20 (98)	15.83±1.34 (78)	4.59±0.54 (97)	21.71±27.90 (97)

Table 3 continued.

Family	Scientific name	Common name	Total Length (mm)	Mass (g)	% Moisture (wet mass)	% Lipid (wet mass)	% Protein (wet mass)	Energy Density (kJ/g wet)	Total Energy (kJ/ind)
Stichaeidae	*Stichaeus punctatus*	Arctic shanny	29±6 (9)	0.2±0.1 (9)	65.23±6.27 (9)	1.74±0.93 (9)		4.05 (1)	1.31 (1)
Ammodytid ae	*Ammodytes hexapterus*	Arctic sand lance	73±15* (116)	1.4±1.0 (116)	76.73±1.67 (116)	4.41±1.49 (106)	15.86±1.74 (49)	4.94±0.60 (100)	6.41±5.13 (100)
Pleuronectid ae	*Hippoglossoides robustus*	Bering flounder	106±51 (70)	20.1±32.1 (70)	79.18±3.52 (70)	1.17±0.54 (64)	12.73±1.79 (50)	3.64±0.67 (25)	127.38±196.94 (25)
Pleuronectid ae	*Limanda aspera*	yellowfin sole	59±36 (23)	5.3±12.9 (23)	75.27±6.06 (23)	1.83±1.08 (23)	13.64±1.07 (3)	4.82±2.00 (4)	61.95±106.13 (4)
Pleuronectid ae	*Limanda proboscidea*	longhead dab	58±18 (28)	2.5±2.8 (28)	74.15±5.35 (28)	3.39±1.34 (27)	16.78±3.31 (11)	4.83±0.78 (21)	13.26±16.10 (21)
Pleuronectid ae	*Liopsetta glacialis*	Arctic flounder	114±62 (32)	35.5±44.9 (32)	73.14±6.23 (32)	4.65±3.05 (26)	17.89±2.33 (19)	4.86±1.25 (23)	201.32±273.69 (23)
Pleuronectid ae	*Platichthys stellatus*	starry flounder	213±67 (62)	162.9±161.9 (62)	75.98±2.73 (62)	4.62±2.92 (57)	16.30±1.25 (55)	5.02±0.88 (47)	842.66±1088.16 (47)

Pleuronectidae	*Pleuronectes quadrituberculatus*	Alaska plaice	232 (1)	151.7 (1)	81.29 (1)	1.2 (1)		3.27 (1)	495.65 (1)

CHAPTER 10 - Trade-offs among sampling designs for monitoring biodiversity and abundance of marine organisms in the Chukchi Sea

Objective 3: Combine results from previous Arctic surveys (Arctic EIS, Phase 1, BASIS) and planned surveys (Arctic IES Phase 2) to assess variability in pelagic and demersal fish ecology over time relative to ocean conditions.

Mueter, F.J.[1], Iken, K.[2], Cooper, D.[3], Grebmeier, J.[4], Hopcroft, R.[2], Kuletz, K.[5], Danielson, S.[2]

[1] College of Fisheries and Ocean Sciences, University of Alaska, Juneau, Alaska, USA
[2] College of Fisheries and Ocean Sciences, University of Alaska, Fairbanks, Alaska, USA
[3] Alaska Fisheries Science Center, NOAA Fisheries, Seattle, Washington, USA
[4] University of Maryland Center for Environmental Science, Chesapeake Biological Laboratory, Solomons, Maryland, USA
[5] US Fish and Wildlife Service, Anchorage, Alaska, USA

Abstract

Assessing and quantifying biodiversity at multiple levels is a key component of monitoring and understanding changes in marine ecosystems. Adequate monitoring is particularly challenging in remote, high-latitude regions such as the Chukchi Sea, an Arctic inflow shelf that is undergoing rapid environmental changes. Current monitoring efforts in the Chukchi Sea rely on opportunistic sampling in recognized 'hot spots' (the Distributed Biological Observatory, DBO) or dedicated, but typically short-term, monitoring programs. The relatively extensive sampling design used during Arctic Marine Biodiversity Observing Network (AMBON) surveys in the northeast Chukchi Sea in 2015 and 2017 and by the Arctic Integrated Ecosystem Survey (AIES) in 2017 provide an opportunity to evaluate the effectiveness of different sampling designs for quantifying biodiversity. We evaluated how common diversity measures and their uncertainty vary across a set of reduced survey designs that were pragmatic subsets of the stations sampled by the full AMBON and AIES designs. As a case study, we estimated the power to detect changes in diversity of the demersal fish community resulting from the expansion of new or rare species into the study region. A framework was developed to simulate changes from the 2017 baseline using temperature-dependent changes in the probability of occurrence of new or otherwise undetected species. Results suggest no apparent bias in diversity estimates for any of the reduced designs, including those with spatially restricted sampling such as the Distributed Biological Observatory (DBO), but substantial increases in uncertainty as sample sizes decrease. This high uncertainty contributed to the poor performance of most sampling designs in terms of detecting changes in the presence of relatively rare species from baseline conditions. Our study provides a general framework for evaluating alternative sampling designs in the context of monitoring biodiversity that can easily be adapted to other regions and communities and can be used to test a variety of hypotheses about the nature of possible changes.

Introduction

Monitoring trends in species occurrences and abundances is critical to the management and conservation of ecosystems and their components (Duffy *et al.*, 2013). Consequently, measures of biodiversity have been identified as key variables for monitoring ecosystems. Global monitoring efforts include terrestrial and marine biodiversity observing networks (BONs) that have been established in an effort to standardize biodiversity measurements through the development of Essential Biodiversity Variables (EBVs) (Proença *et al.*, 2017). Measures of diversity are relatively simple to interpret and are critical to ecosystem function, stability and productivity (Tilman *et al.*, 1994, 2012). However, monitoring biodiversity across multiple functional groups is costly, especially in remote marine regions like the Arctic (Iken *et al.*, 2019). Given

limited resources, there are clearly trade-offs among the extent of geographic coverage, sampling effort per site, the frequency of sampling, the number of functional groups monitored, and other costs associated with different sampling designs (Couvet *et al.*, 2011). While these trade-offs have been acknowledged, few studies have systematically evaluated trade-offs among sampling designs. Here we examine some of these trade-offs using data from the Arctic Marine Biodiversity Observing Network (Iken *et al.*, 2019).

The Arctic-Subarctic transition zone is characterized by rapid changes in ice conditions and ocean temperatures (Danielson *et al.*, 2020) with the potential to transform the Pacific Arctic ecosystem (Huntington *et al.*, 2020). These physical changes are associated with changing distributions of marine organisms from benthic macrofauna (Waga *et al.*, 2019) to fish (Stevenson and Lauth, 2019; Thorson *et al.*, 2019) and whales (Moore and Reeves, 2018). Projections based on an ensemble of species distribution models suggest increases in species richness and functional redundancy in the Chukchi Sea under continued warming as opportunistic subarctic species expand northward into the Arctic (Alabia *et al.*, 2020), a process that has been referred to as borealization (Carmack and Wassmann, 2006; Fossheim *et al.*, 2015). Thus, there is a need for continued monitoring in the Pacific Arctic to detect changes in biodiversity associated with changes in the abundances of common species as well as changes in the occurrence of rare species or of new, previously unrecorded species. Sampling effort in this region has been limited by logistical constraints and the high costs associated with remoteness and harsh environmental conditions, making it all the more important to optimize field sampling designs (Iken *et al.*, 2019).

A number of short-term field efforts have sampled the biological components of the Pacific Arctic in recent decades and two ongoing observational programs, AMBON and the Distributed Biological Observatory (DBO, Grebmeier *et al.*, 2019), continue to sample multiple trophic levels. Of these, the DBO reflects a minimal design focused on selected hot spots with three sampling transects in the Chukchi Sea, while AMBON includes two of these transects as part of a more extensive network of transects sampled in 2015 and 2017 (Fig. 1). In addition to these transect-based monitoring programs, gridded ecosystem surveys have been conducted in 2012 and 2013 (Mueter *et al.*, 2017), as well as in 2017 and 2019 during the Arctic Integrated Ecosystem Survey (AIES)[5]. The AMBON and AIES surveys conducted in 2017 (Fig. 1) overlapped in time and space, thereby providing an opportunity to assess the efficiency of different sampling designs for quantifying biodiversity at a regional scale that encompasses most of the US portion of the Chukchi Sea shelf.

Designing a biodiversity monitoring program requires a series of choices including the geographic extent of the study region, the target assemblages for monitoring, the sampling methodology (net sampling, visual surveys, acoustic surveys, environmental DNA, etc.), the frequency of sampling, the number of locations to sample (e.g. station density), the spatial arrangement of samples (random sampling, gridded survey, transects, etc) and many others. The AMBON program is part of a national effort to develop marine observing networks focusing on biodiversity (Duffy et al., 2013). The program samples multiple ecosystem components including microbes (eDNA), microalgal biomass (chlorophyll a); zooplankton (plankton net), meiobenthos and macrobenthos (van Veen grab), epibenthos and demersal fish (bottom trawl), as well as seabirds and marine mammals (visual observations) (Iken *et al.*, 2019). A long-term goal for the monitoring program is to serve as a change-detection array for biological resources in the region. Further borealization associated with the loss of sea ice and potential increases in northward advection through Bering Strait (Woodgate, 2018) are expected for this region, therefore detecting expansions of boreal species into the northern Chukchi Sea, or changes in abundance of key species, are important objectives. To meet these goals, the AMBON sampling design was a pragmatic choice that incorporates previous observational programs to extend existing time series (Iken *et al.*, 2019) and uses established methodologies for the selected target communities that are consistent with historical sampling efforts, while also adding new approaches such as eDNA to assess the microbial community.

[5] https://www.nprb.org/arctic-program

Our goal in this study was to assess the efficiency of different sampling designs and different amounts of sampling effort to quantify biodiversity for selected marine assemblages, using data from the 2017 AMBON and AIES surveys and simulated changes in diversity. Specific objectives were (1) to assess bias and uncertainty in three diversity measures estimated for 5 different assemblages from zooplankton to seabirds using a range of survey designs and station densities, and (2) to assess the sensitivity of these diversity measures to simulated changes in species diversity. The first objective aims to inform the choice of sampling design for ongoing and future monitoring programs in the Pacific Arctic to help identify an efficient sampling design for achieving biodiversity-related sampling goals, The second objective addresses our ability to detect changes in regional biodiversity associated with the ongoing borealization of Arctic communities. Finally, we hope that the approach presented here serves as a flexible template for assessing sampling designs for other biodiversity monitoring programs.

Methods

Study region

The shallow inflow shelf of the Chukchi Sea is strongly influenced by waters entering from the Bering Sea through Bering Strait, advecting heat, nutrients, and organisms from the Pacific to the Arctic (Coachman *et al.*, 1975; Hunt Jr *et al.*, 2016). The flow through Bering Strait transports about 0.8 Sv northward with stronger flow in the summer than in winter (Roach *et al.*, 1995; Woodgate *et al.*, 2006), but has increased over recent decades (Woodgate, 2018). The Bering Strait region and the Chukchi Sea are a transition zone between subarctic and arctic communities and as such are characterized by strong gradients in species composition, diversity, and abundance of fish and invertebrates (Stevenson and Lauth, 2012; Sigler *et al.*, 2017). The shallow Chukchi Sea shelf is characterized by high levels of primary production fueled by both advected and regenerated nutrients that support high standing stocks of zooplankton and a rich community of benthic invertebrates. The combination of advected zooplankton combined with high local production attract large numbers of seabirds and marine mammals that seasonally migrate to the Chukchi Sea to take advantage of abundant prey (Hunt *et al.*, 2013).

The Pacific water signature extends into the Northeast Chukchi Sea but varies in spatial extent from year to year. During summer, a frontal zone separates Pacific waters extending northward from Bering Strait from Arctic waters that typically consist of a bottom water mass from the previous winter and meltwater at the surface (Weingartner, 1997). The position of the front varies among year, resulting in interannual variations in the distribution of zooplankton and their predators (Day *et al.*, 2013).

For our analyses, we divided the study region into the central Chukchi Sea (CCS) and northern Chukchi Sea (NCS) at 71°N (Fig. 1). This division was selected for oceanographic, biological and pragmatic reasons. First, 71°N is the approximate location of the frontal zone between Pacific and Arctic water masses (Day *et al.*, 2013), although it's location is highly variable. Second, a biogeographic boundary near 71 °N separates northern Chukchi shelf (Arctic) communities from communities with stronger Pacific affinities (Day *et al.*, 2013; Pinchuk and Eisner, 2017; Sigler *et al.*, 2017). Finally, a division at 71 °N result in an approximate even distribution of stations between the CCS and NCS to facilitate comparisons of biodiversity.

Data collection

Data from two cruises conducted in 2017 were used in these analyses. The AMBON cruise occupied 81 stations in the central and northeast Chukchi Sea between August 6 and August 22, 2017, along a series of 6 cross shelf transects and two along-shelf transects (Fig. 1). Bottom depths at the sampling stations ranged from 15 m to 57 m with an average of 42 m. While the original AMBON design had five cross-shelf transects including the DBO3 and DBO4 lines (Iken *et al.*, 2019), a sixth transect was added opportunistically in 2017 to cover the previously under-sampled region between Cape Lisburne and Point Lay. At each station, water column properties were profiled using a CTD (Seabird SBE911), water samples were collected at discrete depths for nutrient, chlorophyll *a* and eDNA analyses; zooplankton

were collected using 150 µm and 305 µm plankton nets; surface sediment samples were collected for assessing surface chlorophyll, grain size and benthic infauna, and a plumb-staff beam trawl was deployed to collect demersal fish and epibenthic invertebrates. In addition, seabirds and marine mammals were assessed using visual sampling methods along the ship's track during daylight hours.

For these initial analyses, we focus on the demersal fish community to illustrate the simulation approach. Although both demersal fish and epibenthic invertebrates are benthic ecosystem components and are caught with the same gear, we considered them separately for this analysis following Iken et al. (2019). Demersal fish are generally more motile and have a strong association with water mass characteristics (Hunt *et al.*, 2013), while epifaunal invertebrates are more closely related to substrate characteristics (Bluhm *et al.*, 2009). Therefore, demersal fish are expected to respond more directly to changes in ice cover, temperature conditions and advection associated with climate change. The modified plumb-staff beam trawl (Abookire and Rose, 2005) effectively samples small demersal fish that characterize the Chukchi Sea benthic community (Norcross *et al.*, 2013; Kotwicki *et al.*, 2017) and had a 2.26 m opening and a 7-mm mesh net with a 4-mm cod end liner. Trawls were conducted for 2–5 min duration at approximately 1.5 knots, resulting in area swept estimates ranging from 113 to 1138 m^2 with an average of 507 m^2. Catches were sorted on board to the lowest taxonomic level possible at the species or genus level. Pelagic juvenile fishes (mostly gadids) were excluded from the analysis because they were likely collected in the water column while the trawl was retrieved. Trawl distance for area swept calculations was estimated by multiplying average trawling speed by the time the trawl was in contact with the bottom. Bottom contact was assessed based on depth recordings by a time-depth recorder (TDR, Star Oddi, Gardabaer, Iceland) attached to the net opening. Numerical abundance for all taxa were quantified for each haul as catch per unit effort (CPUE), where effort was computed as trawl distance multiplied by the estimated width of the net opening (= area swept).

The Arctic Integrated Ecosystem Survey sampled a total of 58 stations throughout the US portion of the Chukchi Sea between August 10 and September 26 with identical sampling gear and a similar sampling protocol, but using a gridded survey design. Of these sampling stations, 45 stations overlapped with the AMBON survey area and were included in this analysis (Fig. 1). Bottom depths at these stations ranged from 20 m to 58 m, comparable to the AMBON survey stations (15-57 m). Area swept estimates for CPUE calculations ranged from 128 m^2 to 1079 m^2 with an average of 602 m^2. As for the AMBON survey, catches were sorted on board to the lowest taxonomic level possible at the species or genus level and pelagic juveniles were excluded from the analysis.

Measuring diversity

Ecologists generally agree that the preferred measure of diversity in ecological applications should be Hill numbers (Ellison, 2010). Most commonly, Hill numbers of orders q = 0, 1 and 2 are used, corresponding to simple species richness, Shannon diversity and Simpson diversity, respectively (Chao *et al.*, 2014). Simple species richness disregards relative abundances, thereby emphasizing each species equally and effectively highlighting rare species in an assemblage. Because the focus in this study is on the possible northward expansion of species into the study region, which at least initially may occur at a low frequency, we highlight estimates of species richness to avoid an over-emphasis on small species with high numerical abundances. However, borealization may involve both an expansion of rare species as well as an expansion or a local increase of highly abundant species (Stevenson and Lauth, 2019), thus we also present Hill numbers of order q > 0, which measure the "effective" number of species. Specifically, we present Shannon diversity (q = 1), which can be interpreted as the equivalent number of "common" species, and Simpson diversity (q = 2), which corresponds to the equivalent number of the dominant species, as it discounts rare or less abundant species (Chao *et al.*, 2014).

It is well known that any measure of diversity strongly depends on sampling effort, therefore we standardize diversity to the same number of sampling units (number of hauls) for comparisons among regions and among different sampling designs. Effort also varied among hauls due to differences in area

swept. However, we found no relationship (linear or non-linear) between measures of diversity recorded in each haul and area swept ($p > 0.4$), therefore biodiversity metrics for each haul were assumed to provide standardized estimates of local species richness at a spatial scale of approximately 500 m^2. The occurrence or incidence of species at this local scale are then used to estimate biodiversity and its uncertainty at regional scales corresponding to the CCS, NCS and the total survey region (Fig. 1). Input data for the analyses therefore consists of a species by station matrix of occurrences with values of 1 if a species was present at a given station 0 otherwise. As a metric for comparison, we used occurrence-based measures evaluated within the rarefaction and extrapolation framework proposed by Colwell et al. (2012) and Chao et al. (2014), which interpolates diversity measures for cases where sample sizes are less than the observed number of samples (rarefaction) and extrapolates measures for sample sizes larger than the observed number of samples. Because the number of samples, and hence the expected number of species detected, differed among the sampling designs considered (see next section), all comparisons were based on the expected number of species caught in 30 hauls, with one haul sampled per station. Estimates were obtained by interpolating (rarefying) diversity if more than 30 stations were sampled and extrapolating to 30 stations if fewer stations were sampled. The number of samples used to standardize metrics for comparison (n=30) was selected to ensure that the number of stations sampled over the entire survey region under any given sampling design was no smaller than ~50% of the number used for standardization (minimum of n=14 for DBO). For estimating species richness, extrapolation is reliable for up to two times the number of samples, while higher-order indices can be reliably extrapolated to infinity (Chao *et al.*, 2014).

To assess spatial patterns in diversity and possible relationships between local species diversity and environmental characteristics, we used a generalized additive modeling approach. Samples from both the 2017 AMBON and 2017 AIES surveys were pooled for this analysis. First, we modeled local diversity metrics, for example species richness by haul, as a smooth function of latitude and longitude using a tensor product interaction between latitude and longitude (Wood, 2017). Predicted diversity over the survey region was then mapped to visually assess spatial patterns in diversity. Second, we modeled local diversity as additive smooth functions of temperature, salinity and Julian day to identify potential drivers of diversity. The GAM analyses and predictions were conducted using the *mgcv* package version 1.8.33 (Wood, 2017) in the R statistical programming language, version 4.0.3 (R Core Team, 2020).

Finally, we compare diversity accumulation curves based on Hill numbers between 2015 and 2017 using a reduced set of taxa that were identified to the same taxonomic level in both years. For each year, the full set of stations sampled in each year was included, rather than a common set of stations sampled in both years, to compare diversity at a given sample size.

Simulation framework to compare sampling designs

To assess the power of different sampling designs to detect changes in species diversity, we developed a simulation framework based on the existing gridded and transect-based designs. Specifically, we compared the relative performance of a range of sampling designs from the full AIES and AMBON 2017 designs to a minimal design based on the two DBO transects off Point Hope (DBO 3) and off Wainwright (DBO 4) (Fig. 2, Table 1). Alternative designs were based on the full gridded and transect-based designs and either reduced the number of transects without changing station density along transects or reduced the station density of the gridded design or along the 6 cross-shelf transects of the 'xShelf.6t' design (Table 1). We compared the performance of alternative sampling designs in two ways. Both approaches assume that the 2017 observed species occurrences provide a representative and unbiased estimate of the fish communities in the three regions considered. That is, they represent the "true" diversity against which reduced sampling designs or simulated changes in diversity are compared. To assess if the full survey designs provides an adequate assessment of diversity in the fish community, we constructed species accumulation curves separately for the two surveys and calculated asymptotic estimates for the three Hill numbers (the number of species or equivalent species that would be expected to be collected in a very large number of samples). In addition we assessed sample coverage, which is the fraction of the total

number of individuals in an assemblage that belong to species represented in the sample (Good, 1953; Good and Toulmin, 1956).

Our first approach to assessing the performance of different sampling designs simply asked: How does our perception of species richness and its uncertainty change under alternative sampling designs? Specifically, we were interested in comparing metrics between the two full designs (gridded vs transect-based), identifying potential biases of reduced designs relative to the full designs, and comparing uncertainty across designs. We estimated Hill numbers for each of the alternative designs, which were standardized to a sample size of 30 hauls using interpolation or extrapolation depending on the observed sample size, and constructed 95% confidence intervals for each estimate using a bootstrap approach (Chao *et al.*, 2014) as implemented in the iNEXT package version 2.0.20 (Hsieh *et al.*, 2016) in R version 4.0.3 (R Core Team, 2020).

The second approach assesses the performance of alternative sampling designs by quantifying their statistical power to detect simulated changes in species composition under selected scenarios. Our approach does not simulate "true" diversity but starts with species occurrences as estimated by the 2017 survey and assesses the performance of different designs by repeatedly simulating changes in species diversity from the 2017 baseline. Statistical power for a given sampling design was estimated by computing the fraction of simulations that correctly rejected the null hypothesis that diversity as quantified by Hill numbers were not significantly different from the 2017 baseline.

Scenarios for the simulations were developed under the assumption that ongoing and future reductions in sea ice, ocean warming, and advection are likely to result in the expansion of new or previously unsampled species (i.e. species not sampled in the 2017 surveys) into the northeast Chukchi Sea. Our analyses suggested that local diversity of the demersal fish community tends to decreases with bottom temperatures, therefore we simulated a temperature-dependent expansion of one or more Pacific-origin species into the northeast Chukchi Sea. Catches of these species were generated for each sampling design by randomly simulating their presence or absence based on station-specific probabilities of occurrence. The probability of a between one and five additional species being sampled in a given haul was scaled to the smoothed spatial pattern of the 2017 observed bottom temperatures, such that the probability of occurrence was highest at stations with the warmest temperatures and declined linearly with temperature to zero in areas with the coldest bottom temperatures (Fig. 3). For the base case, we assumed a mean probability of occurrence across the study region of 1%, implying that on average the species is "observed" at 1 in 100 stations. The assumed temperature dependent probabilities ranged from 0 at the coldest stations on the northern shelf to 2.25% at the warmest stations off Point Hope (Fig. 3). Simulations were repeated for different mean probabilities by multiplying the probabilities at each station by a value ranging from 1-10, hence the average probability of occurrence was 10% (maximum 22.5%) under the most extreme scenario. In addition, for each multiplier we simulated between one and five new species. The simulated occurrences of the new species were appended to the 2017 species-by-station matrix for computing changes in diversity relative to the 2017 baseline.

The power of different sampling designs to detect a resulting change in biodiversity due to the expansion of new species into the survey area was assessed for each combination of the number of new species and the multiplier for scaling the average probability of occurrence. We note that this is one possible and idealized scenario of change, and is unlikely to reflect true changes as the entire community composition is likely to change when environmental conditions change and as a result of increases in subarctic species. However, our goal was to compare the relative performance of different sampling designs in terms of their power to detect change rather than assessing absolute changes in diversity. As a sensitivity analyses we repeated the simulations using a latitudinal gradient in probability of occurrence, rather than a temperature-dependent gradient, as well as a constant probability of occurrence across the entire study area. For comparing sampling designs, we calculated the power to detect a change in diversity as the probability of concluding that a change of a given magnitude in each Hill number could be detected at a 95% or 99% confidence level. To simplify presentation of results, we show statistical power for different

scenarios (number of species, probability multiplier) by geographic region and by sampling design based on species richness (Hill number of order 0), temperature-dependent probabilities of occurrence, and a 95% significance level only. Results from other choices are discussed only if they may lead to different conclusions.

In addition to quantifying the power to detect changes in the probability of occurrence of relatively rare species, we assessed the power of alternative designs to detect changes in the individual abundances of two common species, Arctic cod and Arctic staghorn sculpin (Table 2). The same sampling designs were evaluated with respect to their power to detect differences in mean abundance across the entire study region or across either sub-region. We simulated changes in abundance ranging from a 50% decrease to a 50% increase in steps of 10% as follows: First, to estimate mean densities (fish per unit area) across the study region, we modeled the 2017 observed abundances using a generalized additive model with a negative binomial distribution to account for the large number of zeros and for apparent overdispersion in the data. Observed counts were used as the response variable and an offset was included to account for differences in effort (area swept) across hauls (base model). Changes in mean density under a given scenario (e.g. 10% increase) were then simulated by decreasing or increasing the overall mean density estimated by the base model and randomly drawing 'observed' counts at each station from the base model using the new mean and assuming that effort for each simulated haul was equal to the mean observed effort in 2017. This approach also assumes the same spatial pattern of distribution across simulations. Using the simulated data, mean densities by region (CCS and NCS) and overall were then estimated by fitting the same model to the simulated data, separately for each sampling design, i.e. only using the stations included in a given sampling design to fit the model. The estimated mean densities were then compared between each model that was fit to the simulated data and the mean density from the 2017 base model. The statistical power of each sampling design to detect changes in mean density was estimated over 1000 simulations by calculating the proportion of simulations that correctly rejected the null hypothesis of no change in mean density. All simulations were conducted in R version 4.0.3 (R Core Team, 2020).

Results

The demersal fish community in the Chukchi Sea had a relatively low number of taxa with 36 and 37 different taxa identified by the AMBON and AIES surveys, respectively, for a total of 43 unique fish taxa (Table 2) sampled across 125 stations (Fig. 1). Species diversity accumulated quickly with the higher-order Hill numbers approaching an asymptote at 40-60 stations sampled (Fig. 4), while species richness accumulated more slowly, especially at the scale of the entire study region. Due to spatial heterogeneity and a much higher species diversity in the CCS, this sub-region had a higher species richness for a given number of samples and accumulated species at a more rapid rate than when the number of samples was spread over a larger region (Fig. 4). The gridded AIES sampling design accumulated diversity more rapidly, particularly in the northern Chukchi Sea where the gridded stations encompass a somewhat broader geographic area, but the trade-off is a much broader confidence band around the point estimates for all three Hill numbers (Fig. 1).

Spatial patterns in species richness (Fig. 5), as well as the other diversity measures (not shown), show strong latitudinal and cross-shelf gradients in diversity. These gradients were significantly ($p < 0.001$) and positively related to temperature variability (Fig. 5); however, the smoothed spatial pattern and the temperature relationship explained only a small portion of the overall variability in species richness ($R^2 = 0.19$ and $R^2 = 0.12$, respectively). The spatial pattern primarily reflects higher species richness in warmer waters of Pacific origin, including both coastal waters that extend into the northeast Chukchi Sea and Bering shelf water.

Comparing sampling designs based on the 2017 data alone found no evidence of systematic biases as all but two of the 95% confidence intervals included the 2017 best estimates of diversity (Fig. 6). However, the trade-off between the number of stations sampled and uncertainty in diversity metrics is clearly

evident with the minimal DBO design resulting in a 95% confidence interval for the number of species expected to be caught in 30 hauls ranging from 28.4 to 44.6 species (mean = 36.5), corresponding to a coefficient of variation (CV) of 11.3%. While the DBO regions are known hotpots of high benthic productivity, the standard DBO stations do not observe fish at a higher rate than the survey overall or other reduced designs. In the northeast Chukchi Sea, the estimates of species richness and Shannon diversity expected in 30 hauls were lower than for any other design, but increased notably (and significantly, $p < 0.05$) in the 'DBO.plus' design, which extends the standard DBO line to include a larger cross-shelf gradient and estimated higher diversities than most other designs, although these differences were not significant ($p > 0.05$, Fig. 6). In the CCS, both the DBO and, in particular, the DBO.plus design estimated a higher diversity than other designs, suggesting that the DBO line is well placed to sample biodiversity in this region. We note, however, that estimating the number of species expected in 30 hauls involves considerable extrapolation beyond the number of observed stations (14 and 22 stations, respectively, Table 1), which accounts for the large uncertainty in the diversity estimates and poor performance in simulations.

The power of different sampling designs to detect changes in diversity resulting from simulated increases in up to 5 species was small under most scenarios and for most sampling designs (Fig. 7). Initial simulations were limited to increases in up to two species (approximately 5% of the observed number of species), but none of the sampling designs were able to detect a resulting change in diversity even at the highest level of probability of occurrence (mean probability = 10%, range 0-22.5%). Simulations were therefore extended to include increases in up to 5 species. The power of most sampling designs to detect changes within one of the sub-regions was less than 75% over the range of scenarios tested, with the exception of the full AMBON design (AMBON17) and the slightly reduced, 6-transect design (xShelf.6t). The opportunistic transect added to the orginal AMBON design in 2017, which was only included in these two designs, was critical to detecting changes in diversity within the CCS sub-region. The power to detect changes was generally highest when evaluating changes over the entire survey region, except for AMBON 15, which had a higher power to detect changes in the NCS under most scenarios due to the higher station density in the area. The full gridded survey was unable to detect changes within either of the sub-regions under any scenario, but performed similar to AMBON 15 when considering the entire survey area (Fig. 7).

Despite the poor power of most sampling designs to detect increases in diversity, comparison of the demersal fish communities between 2015 and 2017 showed substantially and significantly higher diversities over the survey region (Fig. 8) for all three diversity measures and for all sample sizes over 5. These differences were evident for diversity measures calculated over the entire area (Fig. 8) and for each sub-region (not shown).

Results from sensitivity analyses using a latitudinal gradient for the probability of occurrence of new species, or a uniform probability over the entire survey regions, showed very similar results and did not affect the relative rankings of different sampling designs in terms of their power to detect differences. The power to detect differences increased considerably when a lower (90%) or higher (99%) significance level was used for comparisons, but patterns across areas and sampling designs were identical. At a 99% significance level, only the full AMBON design detected changes under any scenario with a more than 75% probability.

Discussion and conclusions

The simulation framework presented here allows for an evaluation of sampling designs for the purposes of estimating changes in biodiversity of a community of interest. We focused on assessing the power to detect the expansion of new or previously rare species into an area using data from the Chukchi Sea and simulating changes from an observed baseline. This contrasts with approaches that use simulated data for the entire community based on an assumed species distribution model. An advantage of our approach is that it makes fewer assumptions about community structure and accounts for the observed spatial

heterogeneity in the region of interest in the comparisons. However, the approach requires more subjective choices about how species compositions may change. Here we assume that the addition of or increased probability of occurrence of rare species does not affect the relative species composition of the existing community, which may be the case initially but is clearly not realistic over longer time frames.

We found that a substantial change in the presence of rare species is required before recently employed sampling designs such as the transect-based AMBON design or the gridded AIES survey in the Chukchi Sea will detect the resulting changes in diversity based on Hill numbers. In contrast, most of the sampling designs had substantial power for detecting changes in abundance of common species, but not the resulting changes in diversity based on preliminary results. Thus, while the performance of such large-scale monitoring programs may be adequate for monitoring changes in relatively abundant species based on effort-adjusted catches, or in species composition based on multivariate analyses, they may not be very sensitive to changes in simple diversity measures such as species richness or other Hill numbers.

This study provides a general framework for evaluating alternative sampling designs in the context of monitoring biodiversity that can easily be adapted to other regions and communities. We are in the process of applying the framework to other communities sampled during AMBON, including zooplankton, benthic macrofauna, epibenthic invertebrates and seabirds. Relevant results and conclusions will be incorporated into this draft manuscript for comparing performance of sampling designs across multiple communities.

Acknowledgement

This work was funded through a National Ocean Partnership Program (NOPP Grant NA14NOS0120158) by the National Oceanographic and Atmospheric Administration (NOAA), the Bureau of Ocean Management and Shell Exploration & Production, under management of the Integrated Ocean Observing System (IOOS). Additional support was provided through the US Department of the Interior, Bureau of Ocean Energy Management Environmental Studies Program, Washington, DC, under Agreement Numbers M17PG00007 and M17AC00016.

References

Abookire, A. A., and Rose, C. S. 2005. Modifications to a plumb staff beam trawl for sampling uneven, complex habitats. Fisheries Research, 71: 247–254.

Alabia, I. D., Molinos, J. G., Saitoh, S.-I., Hirata, T., Hirawake, T., and Mueter, F. J. 2020. Multiple facets of marine biodiversity in the Pacific Arctic under future climate. Science of the Total Environment, 744: 140913. http://www.sciencedirect.com/science/article/pii/S0048969720344429.

Bluhm, B. A., Iken, K., Hardy, S. M., Sirenko, B. I., and Holladay, B. A. 2009. Community structure of epibenthic megafauna in the Chukchi Sea. Aquatic Biology, 7: 269–293.

Carmack, E., and Wassmann, P. 2006. Food webs and physical–biological coupling on pan-Arctic shelves: Unifying concepts and comprehensive perspectives. Progress in Oceanography, 71: 446–477. http://www.sciencedirect.com/science/article/pii/S0079661106001297.

Chao, A., Gotelli, N. J., Hsieh, T. C., Sander, E. L., Ma, K. H., Colwell, R. K., and Ellison, A. M. 2014. Rarefaction and extrapolation with Hill numbers: a framework for sampling and estimation in species diversity studies. Ecological Monographs, 84: 45–67. John Wiley & Sons, Ltd. https://doi.org/10.1890/13-0133.1

Coachman, L. K., Aagaard, K., and Tripp, R. B. 1975. Bering Strait: The Regional Physical Oceanography. University of Washington Press, Seattle. 175 pp.

Colwell, R. K., Chao, A., Gotelli, N. J., Lin, S.-Y., Mao, C. X., Chazdon, R. L., and Longino, J. T. 2012. Models and estimators linking individual-based and sample-based rarefaction, extrapolation and comparison of assemblages. Journal of Plant Ecology, 5: 3–21. https://doi.org/10.1093/jpe/rtr044

Couvet, D., Devictor, V., Jiguet, F., and Julliard, R. 2011. Scientific contributions of extensive biodiversity monitoring. Comptes Rendus Biologies, 334: 370–377. http://www.sciencedirect.com/science/article/pii/S1631069111000692.

Danielson, S. L., Ahkinga, O., Ashjian, C., Basyuk, E., Cooper, L. W., Eisner, L., Farley, E., *et al.* 2020. Manifestation and consequences of warming and altered heat fluxes over the Bering and Chukchi Sea continental shelves. Deep Sea Research Part II: Topical Studies in Oceanography, 177: 104781.
Day, R. H., Weingartner, T. J., Hopcroft, R. R., Aerts, L. A. M., Blanchard, A. L., Gall, A. E., Gallaway, B. J., *et al.* 2013. The offshore northeastern Chukchi Sea, Alaska: A complex high-latitude ecosystem. Continental Shelf Research, 67: 147–165.
Duffy, J. E., Amaral-Zettler, L. A., Fautin, D. G., Paulay, G., Rynearson, T. A., Sosik, H. M., and Stachowicz, J. J. 2013. Envisioning a Marine Biodiversity Observation Network. BioScience, 63: 350–361. https://doi.org/10.1525/bio.2013.63.5.8
Ellison, A. M. 2010. Partitioning diversity. Ecology, 91: 1962–1963.
Fossheim, M., Primicerio, R., Johannesen, E., Ingvaldsen, R. B., Aschan, M. M., and Dolgov, A. V. 2015. Recent warming leads to a rapid borealization of fish communities in the Arctic. Nature Climate Change, 5: 673–677.
Good, I. J. 1953. The population frequencies of species and the estimation of population parameters. Biometrika, 40: 237–264.
Good, I. J., and Toulmin, G. 1956. The number of new species, and the increase in population coverage, when a sample is increased. Biometrika, 43: 45–63.
Grebmeier, J. M., Moore, S. E., Cooper, L. W., and Frey, K. E. 2019. The Distributed Biological Observatory: A change detection array in the Pacific Arctic – An introduction. Deep Sea Research Part II: Topical Studies in Oceanography, 162: 1–7. http://www.sciencedirect.com/science/article/pii/S0967064519301699.
Hsieh, T. C., Ma, K. H., and Chao, A. 2016. iNEXT: an R package for rarefaction and extrapolation of species diversity (Hill numbers). Methods in Ecology and Evolution, 7: 1451–1456. John Wiley & Sons, Ltd. https://doi.org/10.1111/2041-210X.12613
Hunt, G. L., Blanchard, A. L., Boveng, P., Dalpadado, P., Drinkwater, K. F., Eisner, L., Hopcroft, R. R., *et al.* 2013. The Barents and Chukchi Seas: Comparison of two Arctic shelf ecosystems. Journal of Marine Systems, 109–110: 43–68.
Hunt Jr, G. L., Drinkwater, K. F., Arrigo, K., Berge, J., Daly, K. L., Danielson, S., Daase, M., *et al.* 2016. Advection in polar and sub-polar environments: Impacts on high latitude marine ecosystems. Progress in Oceanography, 149: 40–81. http://www.sciencedirect.com/science/article/pii/S0079661116302051.
Huntington, H. P., Danielson, S. L., Wiese, F. K., Baker, M., Boveng, P., Citta, J. J., De Robertis, A., *et al.* 2020. Evidence suggests potential transformation of the Pacific Arctic ecosystem is underway. Nature Climate Change, 10: 342–348. https://doi.org/10.1038/s41558-020-0695-2.
Iken, K., Mueter, F., Grebmeier, J. M., Cooper, L. W., Danielson, S. L., and Bluhm, B. A. 2019. Developing an observational design for epibenthos and fish assemblages in the Chukchi Sea. Deep-Sea Research Part II: Topical Studies in Oceanography, 162: 180–190.
Kotwicki, S., Lauth, R. R., Williams, K., and Goodman, S. E. 2017. Selectivity ratio: A useful tool for comparing size selectivity of multiple survey gears. Fisheries Research, 191: 76–86. http://www.sciencedirect.com/science/article/pii/S0165783617300498.
Moore, S. E., and Reeves, R. R. 2018. Tracking arctic marine mammal resilience in an era of rapid ecosystem alteration. PLoS Biology, 16: e2006708. Public Library of Science. https://doi.org/10.1371/journal.pbio.2006708
Mueter, F. J., Weems, J., Farley, E. V., and Sigler, M. F. 2017. Arctic Ecosystem Integrated Survey (Arctic Eis): Marine ecosystem dynamics in the rapidly changing Pacific Arctic Gateway.
Norcross, B. L., Raborn, S. W., Holladay, B. A., Gallaway, B. J., Crawford, S. T., Priest, J. T., Edenfield, L. E., *et al.* 2013. Northeastern Chukchi Sea demersal fishes and associated environmental characteristics, 2009–2010. Continental Shelf Research, 67: 77–95. http://www.sciencedirect.com/science/article/pii/S0278434313001635.
Pinchuk, A. I., and Eisner, L. B. 2017. Spatial heterogeneity in zooplankton summer distribution in the eastern Chukchi Sea in 2012-2013 as a result of large-scale interactions of water masses. Deep Sea

Research Part II: Topical Studies in Oceanography, 135: 27–39. https://doi.org/10.1016/j.dsr2.2016.11.003
Proença, V., Martin, L. J., Pereira, H. M., Fernandez, M., McRae, L., Belnap, J., Böhm, M., *et al.* 2017. Global biodiversity monitoring: From data sources to Essential Biodiversity Variables. Biological Conservation, 213: 256–263. http://www.sciencedirect.com/science/article/pii/S0006320716302786.
R Core Team. 2020. R: A language and environment for statistical computing. R Foundation for Statistical Computing, Vienna, Austria. http://www.r-project.org.
Roach, A. T., Aagaard, K., Pease, C. H., Salo, S. A., Weingartner, T., Pavlov, V., and Kulakov, M. 1995. Direct measurements of transportand water properties through the Bering Strait. Journal of geophysical Research, 100: 18443–18458.
Sigler, M. F., Mueter, F. J., Bluhm, B. A., Busby, M. S., Cokelet, E. D., Danielson, S. L., Robertis, A. De, *et al.* 2017. Late summer zoogeography of the northern Bering and Chukchi seas. Deep-Sea Research Part II: Topical Studies in Oceanography, 135: 168–189.
Stevenson, D. E., and Lauth, R. R. 2012. Latitudinal trends and temporal shifts in the catch composition of bottom trawls conducted on the eastern Bering Sea shelf. Deep Sea Research Part II: Topical Studies in Oceanography, 65–70: 251–259. http://www.sciencedirect.com/science/article/pii/S0967064512000355.
Stevenson, D. E., and Lauth, R. R. 2019. Bottom trawl surveys in the northern Bering Sea indicate recent shifts in the distribution of marine species. Polar Biology, 42: 407–421. https://doi.org/10.1007/s00300-018-2431-1
Thorson, J. T., Fossheim, M., Mueter, F. J., Olsen, E., Lauth, R. R., Primicerio, R., Husson, B., *et al.* 2019. Comparison of near-bottom fish densities show rapid community and population shifts in Bering and Barents seas. Department of Commerce, NOAA, http://www.arctic.noaa.gov/Report-Card
Tilman, D., Downing, J. A., and Wedin, D. A. 1994. Does diversity beget stability? Nature, 371: 113–114.
Tilman, D., Reich, P. B., and Isbell, F. 2012. Biodiversity impacts ecosystem productivity as much as resources, disturbance, or herbivory. Proceedings of the National Academy of Sciences of the United States of America, 109: 10394–10397. National Academy of Sciences. www.ncbi.nlm.nih.gov/pubmed/22689971
Waga, H., Hirawake, T., Fujiwara, A., Grebmeier, J. M. and Saitoh, S.-I. 2019. Impact of spatiotemporal variability in phytoplankton size structure on benthic macrofaunal distribution in the Pacific Arctic. Deep Sea Research Part II: Topical Studies in Oceanography, 162: 114-126. http://www.sciencedirect.com/science/article/pii/S0967064517302229
Weingartner, T. J. 1997. A review of the physical oceanography of the northeastern Chukchi Sea. *In* Fish Ecology in Arctic North America, pp. 40–59. Ed. by J. B. Reynolds. American Fisheries Society Symposium 19, Bethesda, Maryland.
Wood, S. N. 2017. Generalized Additive Models: An introduction with R. Chapman & Hall/CRC, Boca Raton, FL, USA. 476 pp.
Woodgate, R. A., Aagaard, K., and Weingartner, T. J. 2006. Interannual changes in the Bering Strait fluxes of volume, heat and freshwater between 1991 and 2004. Geophysical Research Letters, 33: L15609.
Woodgate, R. A. 2018. Increases in the Pacific inflow to the Arctic from 1990 to 2015, and insights into seasonal trends and driving mechanisms from year-round Bering Strait mooring data. Progress in Oceanography, 160: 124–154. http://www.sciencedirect.com/science/article/pii/S0079661117302215.

Table 1: Alternative survey designs considered for analyses and simulations, showing sample sizes (=number of hauls = number of stations sampled) by region and a rationale for including the design in the analysis.

Survey	Design	Stations			Rationale
		total	CCS	NCS	
AIES	fullGrid	45	17	28	gridded design for comparison with transect-based designs
	halfGrid	25	9	16	reduced gridded design to assess effects of sampling density
AMBON	AMBON17	81	41	40	extensive transect-based design including new transect in previously undersampled region
	AMBON15	69	29	40	original AMBON design to maximize overlap with previous sampling efforts (Iken et al. 2019)
	xShelf.6t	65	34	31	cross-shelf transect design that drops alongshore transects for improved sampling efficiency
	xShelf.4t	39	19	20	reduced effort cross-shelf transect design that maintains sampling density along transects
	DBO.plus	22	11	11	extended DBO design to better capture cross-shelf gradients from nearshore to offshore
	DBO	14	8	6	established DBO design
	xShelf67	44	24	20	reduced sampling density along fixed number of transects (~2/3 of 'xShelf.6t' stations)
	xShelf50	33	18	15	reduced sampling density along fixed number of transects (~1/2 of 'xShelf.6t' stations)
	xShelf33	24	13	11	reduced sampling density along fixed number of transects (~1/3 of 'xShelf.6t' stations)

Table 2: Species caught in the Chukchi Sea during the Arctic Integrated Ecosystem Survey (AIES) and the Arctic Marine Biodiversity Observing Network (AMBON) surveys in 2015 and the number of occurrences (number of stations at which a species was caught) for each species by survey.

Species caught in within overlapping region		Occurrences	
Scientific name	**Common name**	**AIES**	**AMBON**
Boreogadus saida	Arctic cod	40	70
Lumpenus fabricii	slender eelblenny	34	59
Gymnocanthus tricuspis	Arctic staghorn sculpin	32	52
Aspidophoroides olrikii	veteran poacher	21	51
Myoxocephalus scorpius	shorthorn sculpin	27	44
Liparis sp.	Liparis	23	46
Anisarchus medius	stout eelblenny	24	45
Artediellus scaber	hamecon	14	42
Hippoglossoides robustus	Bering flounder	20	36
Lycodes polaris	Canadian eelpout	14	33
Icelus spatula	spatulate sculpin	8	19
Podothecus sp.	poacher	3	23
Eleginus gracilis	saffron cod	10	14
Gymnelus hemifasciatus	halfbarred pout	11	13
Stichaeus punctatus	Arctic shanny	7	17
Triglops pingelii	ribbed sculpin	5	19
Leptoclinus maculatus	daubed shanny	10	13
Gymnelus viridis	fish doctor		16
Limanda aspera	yellowfin sole	3	11
Lycodes raridens	marbled eelpout	12	
Trichocottus brashnikovi	bullhorn sculpin	1	10
Gadus chalcogrammus	walleye pollock	9	1
Lycodes palearis	wattled eelpout	8	2
Ammodytes hexapterus	Arctic sandlance	4	5
Nautichthys pribilovius	eyeshade sculpin	9	
Aspidophoroides monopterygius	Alligatorfish	3	5
Eumesogrammus praecisus	fourline snakeblenny	2	6
Gadus macrocephalus	Pacific cod	7	
Lycodes mucosus	saddled eelpout	2	5
Limanda proboscidea	longhead dab	4	2
Chirolophis snyderi	bearded warbonnet	1	3
Hexagrammos stelleri	whitespotted greenling	2	2
Hypsagonus quadricornis	fourhorn poacher	2	2
Melletes papilio	butterfly sculpin		4
Myoxocephalus polyacanthocephalus	great sculpin	4	
Lycodes turneri	polar eelpout	3	
Myoxocephalus jaok	plain sculpin		3
Gymnocanthus pistilliger	threaded sculpin	2	

Limanda sakhalinensis	Sakhalin sole	1	1
Acantholumpenus mackayi	pighead prickleback		1
Enophrys diceraus			1
Enophrys lucasi	leister sculpin	1	
Pallasina barbata	tubenose poacher		1

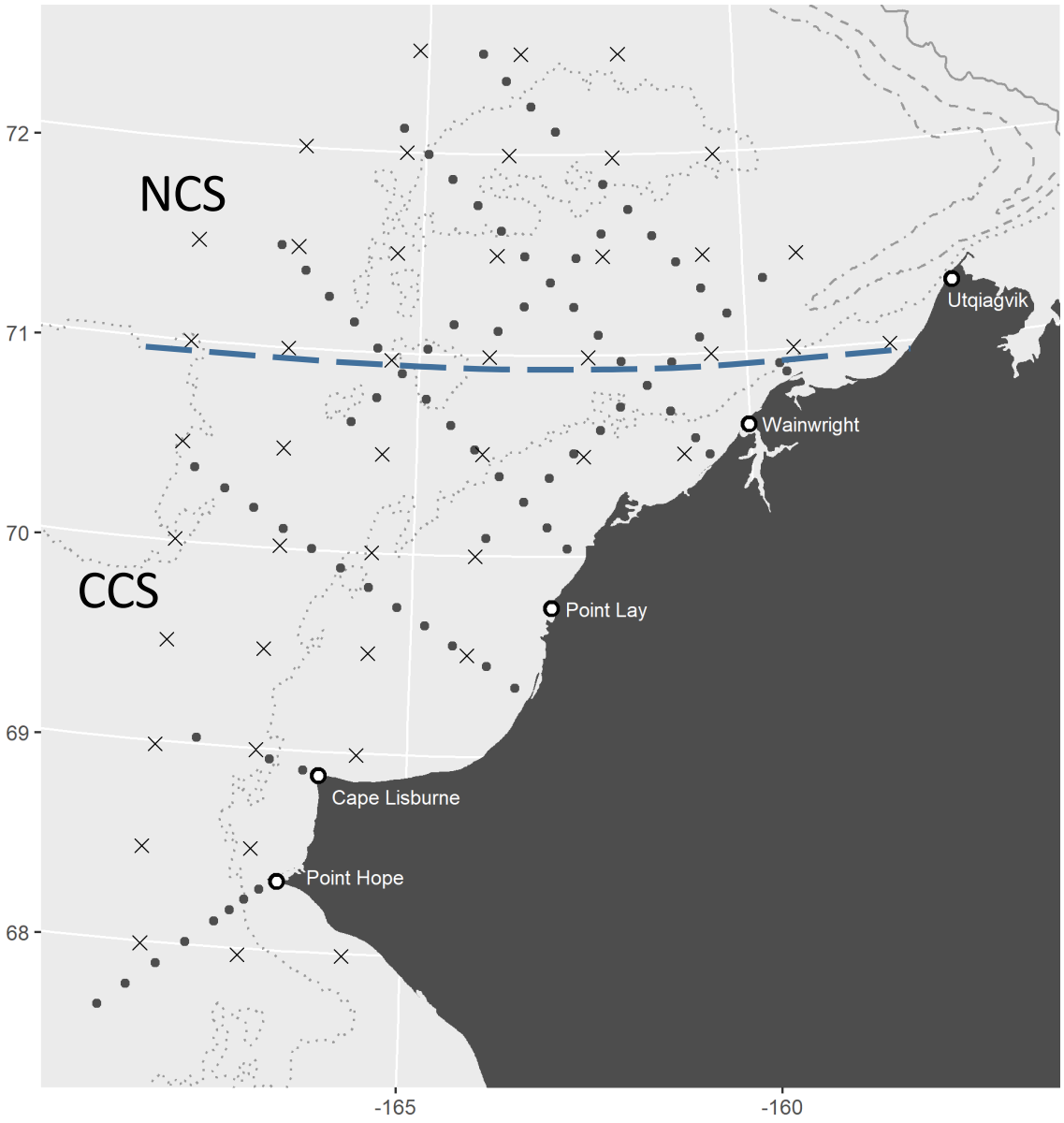

Figure 1: Stations sampled during the Arctic Marine Biodiversity Observing Network (AMBON) survey (filled circles along transects) and during the gridded Arctic Integrated Ecosystem Survey (AIES) in 2017. Heavy dashed line at 69.9 °N divides the central Chukchi Sea (CCS) and northern Chukchi Sea (NCS) subregions.

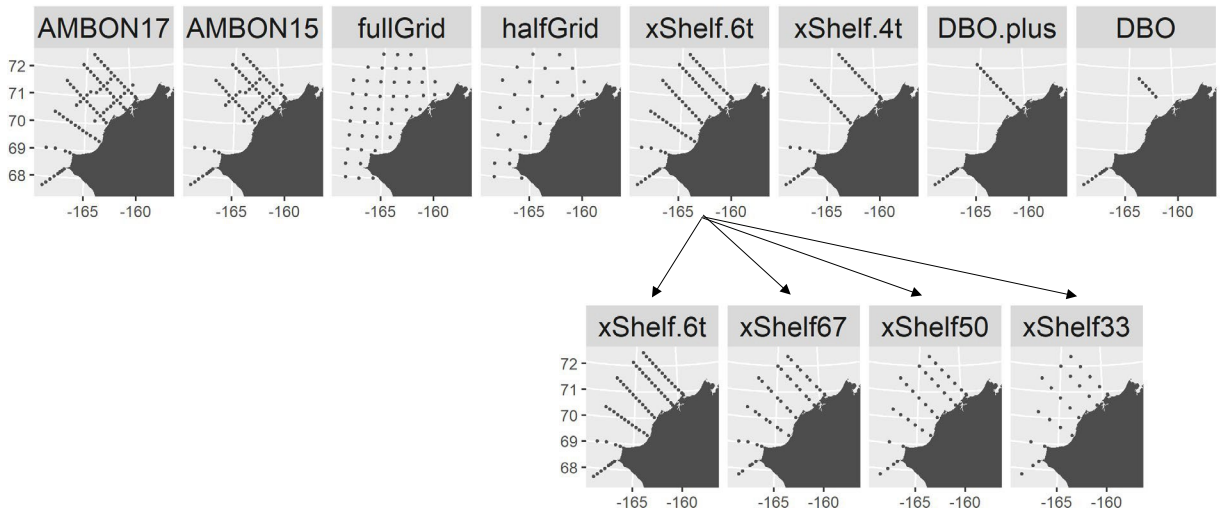

Figure 2: Alternative sampling designs considered in the analysis of their relative performance for quantifying and detecting changes in biodiversity of demersal fishes.

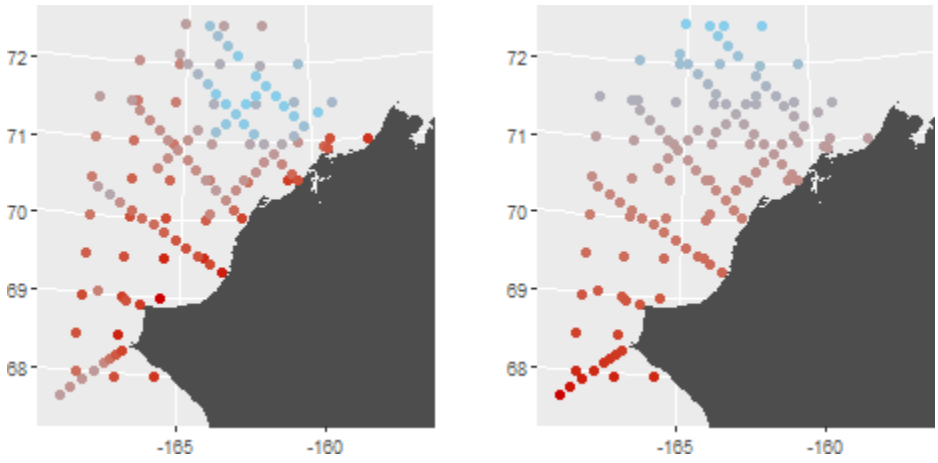

Figure 3: Temperature-dependent (left) and latitudinal gradients (right) in assumed probability of occurrence for simulating expansion of species into the northeast Chukchi Sea. Probabilities range from zero (blue) in the north to a maximum (red) in the south, scaled such that the mean across stations has a specified value.

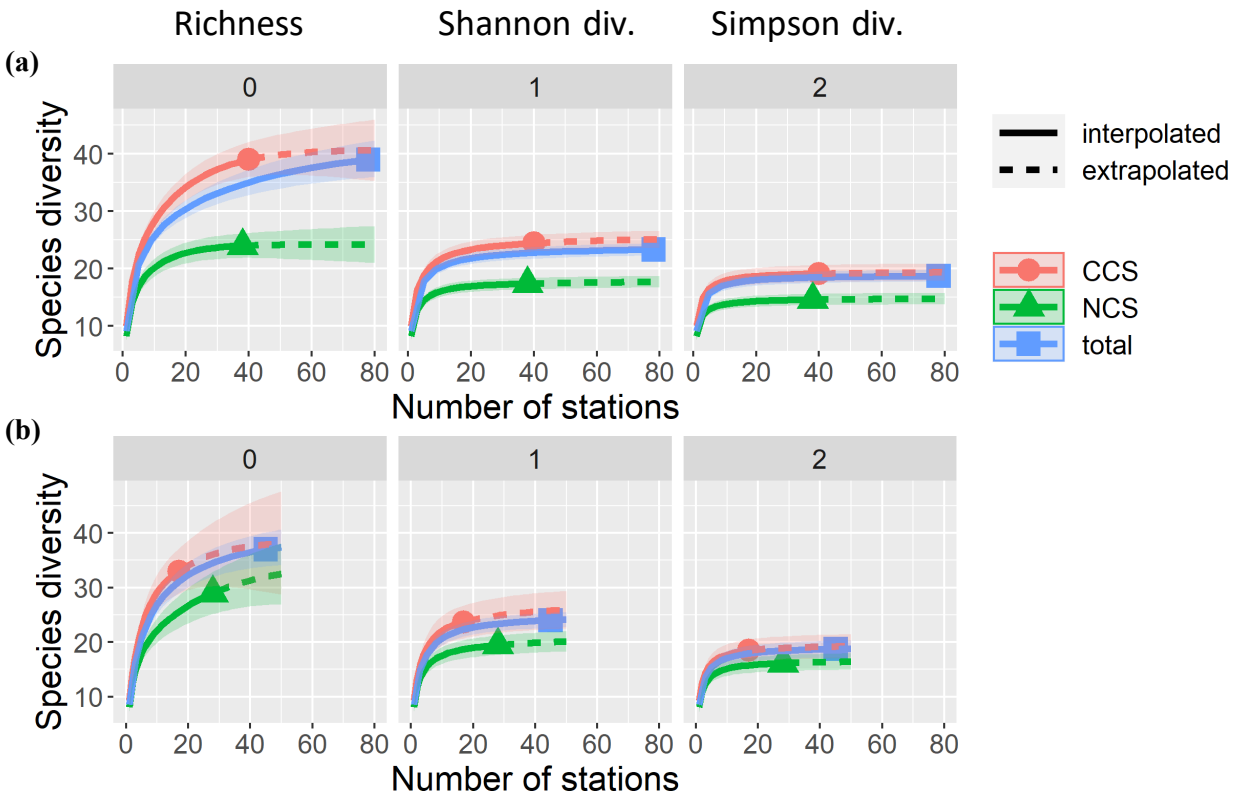

Figure 4: Diversity accumulation curves for three Hill numbers: species richness (q=0, left panels), Simpson diversity (q=1) and Shannon diversity (q=2) by geographic region (CCS = Central Chukchi Sea, NCS = Northern Chukchi Sea, total = total survey region). Diversity was estimated separately based on the 2017 AMBON survey (a) and based on the 2017 Arctic Integrated Ecosystem Survey (b). Symbols indicate estimated diversity for the observed number of stations; diversity is interpolated using a bootstrap approach for smaller sample sizes (solid lines) and extrapolated for larger sample sizes (dashed lines).

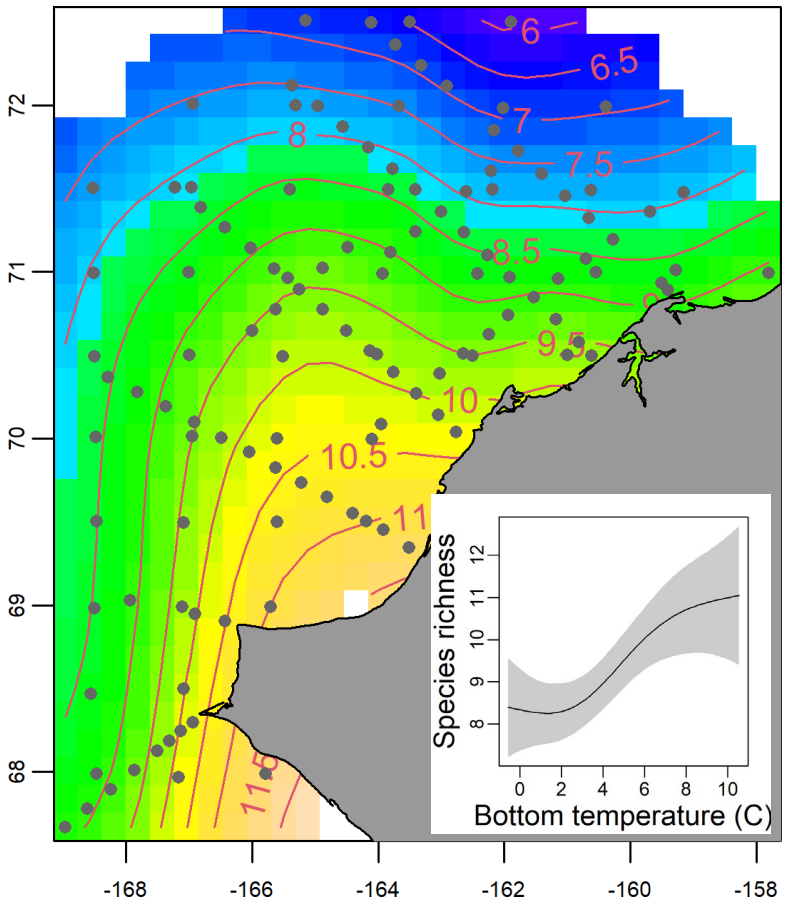

Figure 5: Spatial patterns of species richness estimated by fitting a smoothed surface to observed number of species by station using a tensor-product smoother. Inset shows estimated relationship between species richness and bottom temperature.

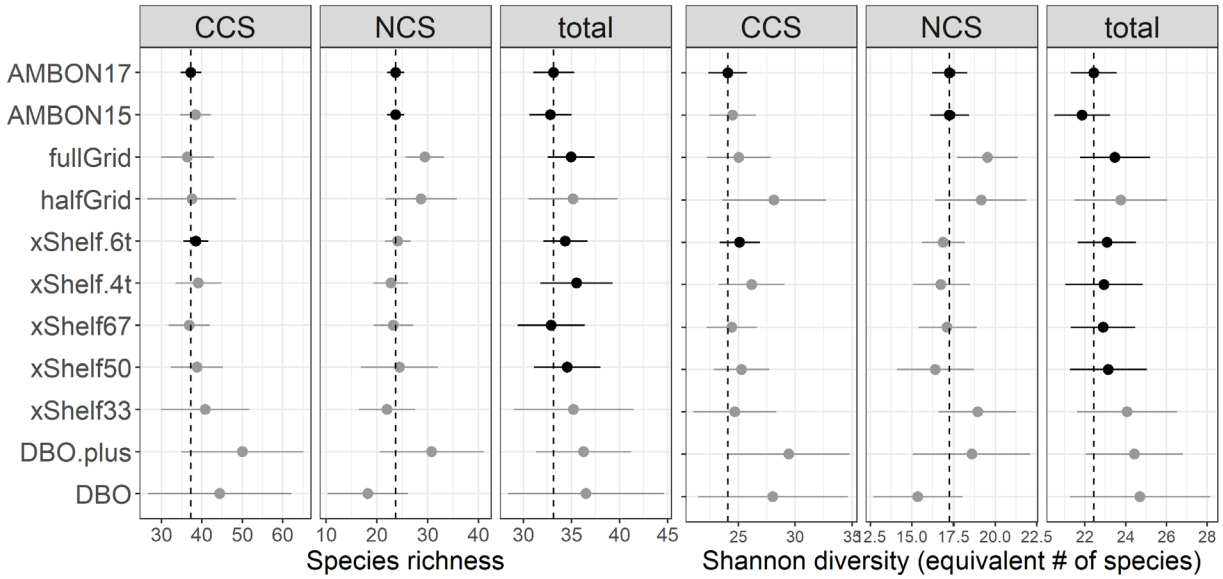

Figure 6: Comparison of species richness and Shannon diversity with 95% confidence intervals estimated from different sampling designs and standardized to the (equivalent) number of species expected to be caught in 30 hauls. Sample designs are based on subsets of the two full surveys ('AMBON17' and 'fullGrid') as shown in Fig. 2 and described in Table 1. Black dots denote interpolated estimates, while grey indicates extrapolation (< 30 stations sampled). Vertical bars show best estimates of diversity from the full AMBON 2017 survey (N = 81 stations).

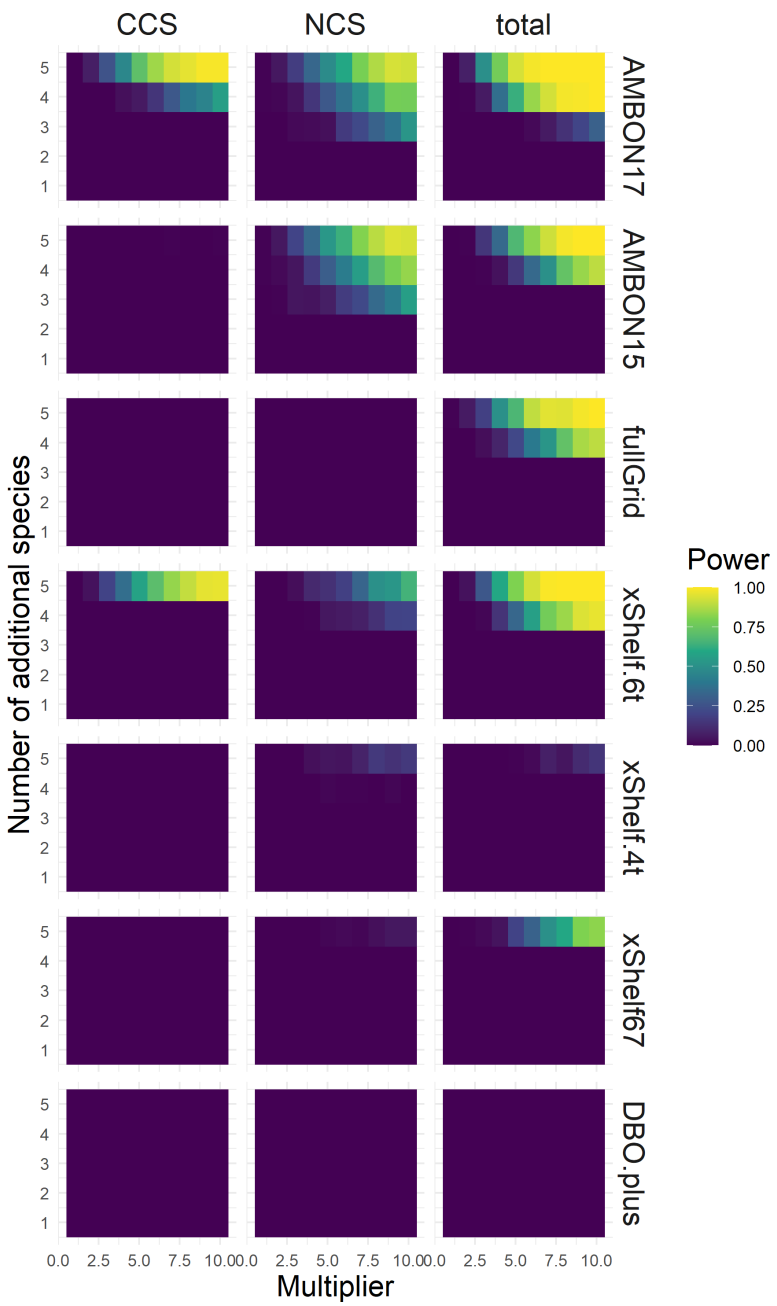

Figure 7: Estimated statistical power of different sampling designs for detecting a simulated increase in diversity due to temperature-dependent increases in the probability of occurrence of new or rare species within the survey area. Except for 'DBO.plus', designs whose power was less than 25% for all scenarios are not shown.

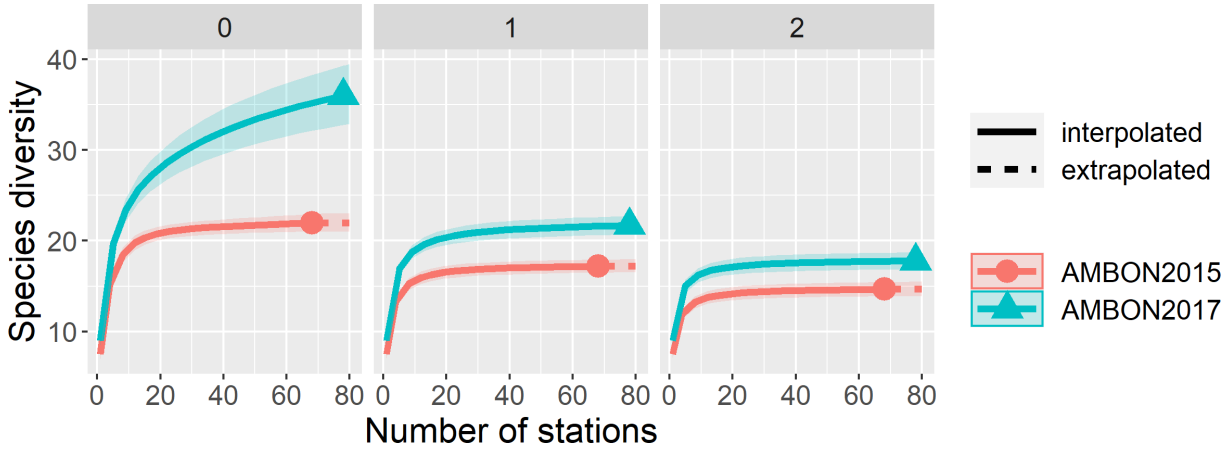

Figure 8: Diversity accumulation curves for three Hill numbers: species richness (q=0, left panels), Simpson diversity (q=1) and Shannon diversity (q=2) by year for 2015 and 2017 AMBON surveys. Diversity was estimated based on the full set of stations sampled in each year. Symbols indicate estimated diversity for the observed number of stations; diversity is interpolated using a bootstrap approach for smaller sample sizes (solid lines) and extrapolated for larger sample sizes (dashed lines).

CHAPTER 11 - Annual and spatial variation in the condition and lipid biomarkers of four juvenile gadid species from the Chukchi Sea during a recent period of dramatic warming (2012 to 2019).

Objective 3: Combine results from previous Arctic surveys (Arctic EIS, Phase 1, BASIS) and planned surveys (Arctic IES Phase 2) to assess variability in pelagic and demersal fish ecology over time relative to ocean conditions.

Louise Copeman, Carlissa Salant, Michelle Stowell, Mara Spencer, et al. (in preparation)

Abstract

The Arctic is undergoing dramatic environmental change with decreasing sea ice extent and increasing summer temperatures. The late summers of 2017 and 2019 on the Chukchi Sea were anomalously warm, nearly 4°C warmer than the previous 30-year average. Increased ocean temperatures are affecting North Pacific fish both via direct thermal effects on their physiology as well as through indirect changes to their diet quality. Here we describe the total lipids as well as fatty acid trophic markers in two Arctic juvenile gadids (polar cod, *Boreogadus saida* and saffron cod, *Eleginus gracilis*) as well as two invading boreal gadids (walleye pollock, *Gadus chalcogrammus* and Pacific cod, *Gadus macrocephalus*) collected on recent ecosystem surveys of the north Bering and Chukchi Seas. Allometric relationships between length and lipid storage revealed a unique high-lipid strategy in polar cod when compared to other Chukchi Sea congeners. Further, during 2017 both polar cod and saffron cod showed region-specific decreases in lipid storage compared to fish from 2013 and 2012, respectively. This reduction in total lipid, triacylglycerols, diatom- (16:1n-7/16:0) and *Calanus*-sourced fatty acids ($\sum C_{20}+C_{22}$) was particularly significant in polar cod collected over the Central Chukchi shelf in 2017. Age-0 juvenile gadids showed interspecific differences in the spatial distribution of high condition individuals, with polar cod having the highest lipid-based condition in the northern ice-associated regions of the Chukchi Sea. In 2019, polar cod were only abundant in the northern Chukchi Sea where they maintained higher region-specific lipid storage than in 2017. These data will be discussed in relation to the importance of lipids to overwintering survival in the Arctic. Data from laboratory experiments combined with evidence of declining lipid storage during warming events, may indicate that the southern and central Chukchi Sea are warming beyond the thermal limits of polar cod. If lower-fat fish such as walleye pollock or Pacific cod displace polar cod, Arctic predators will need to consume more fish to meet their energy requirements.

Introduction

There are four ecologically important species of gadids in Alaskan waters. These traditionally included the 'boreal gadids', walleye pollock (*Gadus chalcogrammus*) and Pacific cod (*Gadus macrocephalus*) in the Bering Sea and Gulf of Alaska and the 'Arctic gadids' saffron cod (*Eleginus gracilis*) and polar cod (*Boreogadus saida)* in the Chukchi and Beaufort Seas. Adult gadids occupy a range of habitats with polar cod and walleye pollock generally using pelagic and offshore habitats while saffron cod and Pacific cod are generally more demersal and often reside in both the nearshore and offshore regions, respectively (Laurel et al. 2007, Hurst et al. 2015, Logerwell et al. 2015). Conversely, pelagic habitats are important during the early life history stages of all four gadids where these cod species facilitate energetic transfer between zooplankton and upper trophic levels (Frost & Lowry 1981, Craig et al. 1982, Springer et al. 1996). Recent extreme warming and increased current flows from Bering Straits has resulted in the co-occurrence of all four juvenile gadids in pelagic waters of the South Eastern Chukchi Sea (SECS, Wildes et al., this report) with movement of boreal congeners as far north as the North Eastern Chukchi Sea (NECS) (Cooper et al., this report, Levine et al., this report).

In the last ten years, unprecedented warming of the Chukchi Sea (Danielson et al. 2020, Huntington et al.

2020) and record low sea ice in the Bering Sea (Stabeno & Bell 2019) have been noted. Concurrent with these oceanographic changes, Kimmel & Spear (Lower AIERP report) have measured a reduction in *Calanus glacialis* abundance throughout the Chukchi Sea with small copepods (i.e. *Pseudocalanus* spp.) increasing, particularly in the warm waters of the north Bering and SECS. In the most recent survey years (2017 & 2019), *C. glacialis* was an order of magnitude lower than in the previous decade (Kimmel & Spear). Small-bodied pelagic fish species are already well-recognized as being important biological indicators of climate-driven changes by way of direct temperature-dependent effects on their growth (Peck et al. 2013, Laurel et al. 2016) and lipid storage (Copeman et al. 2017). The direct effects of temperature on early survival and growth of gadids are now known to be dependent on ontogeny and also be species-specific ((Laurel et al. 2016, Laurel et al. 2017, Laurel et al. 2018)). However, the indirect effects of climate change on juvenile gadid survival and growth, such as through variable food quantity (Hurst et al. 2017, Koenker et al. 2018b) and quality (Copeman & Laurel 2010, Jonsson et al. 2013) are less well understood.

Previous studies in Alaska have shown that species-specific and ontogenetic differences in energy allocation should be considered when quantifying fish condition in cohorts of variable size individuals (Heintz et al. 2013, Martin et al. 2017, Copeman et al. 2020). This information will be vitally important in the Alaskan Arctic as temperatures continue to rise faster than in more southern regions (Renaud et al. 2015, Timmermans et al. 2017, Huntington et al. 2020). For many specialized Arctic species, temperatures throughout the SECS and CECS are already above or approaching their thermal limits (Pörtner & Farrell 2008, Laurel et al. 2017, Koenker et al. 2018a) with many species now projected to lose or gain habitat in future decades, depending on their thermal preferences (Frainer et al. 2017, Dahlke et al. 2018, Steiner et al. 2019) Logerwell et al. this report).

Measurement of lipids and fatty acids in juvenile fish provide temporally-integrated (weeks) information on both trophic relationships and energetic status (St John & Lund 1996, Copeman et al. 2008, Budge et al. 2012, Copeman et al. 2013). Trophic biomarkers such as fatty acids (FA) are produced at low trophic levels and are moved through the food web in a somewhat conservative manner, thus providing information about dietary origins when analyzed in consumers (Budge & Parrish 1998, Dalsgaard et al. 2003, Budge et al. 2006). Two specific fatty acid trophic markers are important in polar and upwelling food webs: diatom indicator fatty acids (16:1n-7/16:0) and long chain monounsaturated fatty acids (MUFA) indicative of calanoid copepod wax storage ($\sum C_{20+C22}$ MUFA) (Viso & Marty 1993, Lee et al. 2006, Kattner et al. 2007, Galloway & Winder 2015). Previous studies on polar cod and saffron cod have used these fatty acid trophic markers to show the degree of reliance on a diatom-*Calanus* sp. based food webs (Budge et al. 2008, Graham et al. 2014, Copeman et al. 2016, Kohlbach et al. 2017, Brewster et al. 2018, Dissen et al. 2018).

The goal of our study was to characterize size-dependent lipid allocation in four gadid species from the Alaskan Arctic in order to better understand spatial differences in fish condition as well as tissue lipids. Our approach was to 1) describe the species-specific relationships between length-weight and length-lipid storage using data from four survey years, 2) understand annual variation in gadid energetics by comparing region- and species-specific morphometric and lipid-based condition metrics, 3) use fatty acid trophic markers for diatoms (16:1n-7/16:0) and *Calanus*-sourced fatty acids ($\sum C_{20}+C_{22}$ MUFA) to explore interspecific and annual differences in fish food webs, 4) use lipid 'condition metrics' to explore annual and spatial variation in 'hot spots' for polar cod and walleye pollock across the Chukchi Sea, and 5) to discuss variable patterns in lipid storage in relation to overwintering survival on the Chukchi Sea shelf.

Methods

Field fish sampling and tissue collections

Juvenile gadids for this study were collected using a variety of gear types with methods with annual cruises, sample numbers, and gear types as shown in Table 1 and Figure 1 (Gunderson & Ellis 1986), De Robertis et al. (2016), (Marsh et al. 2017, Logerwell et al. 2018)). Collection methods, fish handling

techniques, and oceanographic temperatures for earlier years of saffron cod and polar cod sampling have previously been detailed as in Copeman et al. (2016) and (Copeman et al. 2020). Details on water column temperatures for 2017 and 2019 are detailed in Danielson et al. (AIERP final report).

Juvenile gadids from 2017 and 2019 surveys were sorted from the catch and were immediately placed on ice and frozen at < -20 °C within 6 hours of capture. Samples were stored at -80 °C in Juneau, AFSC-NOAA laboratories following the surveys and were later sorted and shipped frozen overnight from Alaska to the Marine Lipid Ecology Laboratory at the Hatfield Marine Science Center (HMSC) in Newport, OR, USA.

Samples from the 2019 survey were delayed in Juneau, AK and were not received in Newport until after the time that Covid 19 had closed our Newport, NOAA laboratories (February 2020). This delay was due to sampling of all juvenile gadids for species determination using genetic methods (Wildes et al., this report). All of our chemical analyses are based on fume hood work in laboratories so this significantly delayed our project and has made the Arctic IERP deadlines extremely difficult to manage. Newport laboratories have remained in phase "0", with only brief periods of phase "1" opening since our original closure in winter of 2020.

At the time of tissue sampling, standard length (SL, ± 0.1 mm) and wet weight (WWT, ± 0.0001 g) were recorded. During dissections, fish were washed with filtered seawater, blotted dry, stomachs and intestinal tracts were removed and heads were frozen for later annual incremental otolith analysis. All the remaining fish tissues, containing both muscle and liver, were re-weighed, placed in chloroform under nitrogen and frozen at -20 °C until lipid extraction, within 2 months of sampling.

Lipid extraction and analysis

All lipid analyses on field and laboratory collected fish were conducted at the Marine Lipids Ecology Laboratory at the HMSC in Newport, OR, USA. Tissues were homogenized in chloroform and methanol and total lipids were extracted according to Parrish (1987) using a modified Folch procedure (Folch et al. 1956).

Total lipids and lipid classes were determined using thin layer chromatography with flame ionization detection (TLC/FID) with a MARK V Iatroscan (Iatron Labratories, Tokyo, Japan) as described by Lu et al. (2008), Copeman et al. (2016) and Copeman et al. (2017). Extracts were spotted on duplicate silica-gel-coated Chromarods, and a three-stage development system was used to separate wax esters, triacylglycerols, free fatty acids, sterols and polar lipids. Polar lipid is mostly comprised of phospholipids with minor amounts of other acetone mobile polar lipids. The first rod development was in a chloroform: methanol: water solution (5:4:1 by volume) until the leading edge of the solvent phase reached 1 cm above the spotting origin. The rods were then developed in hexane: diethyl ether: formic acid solution (99:1:0.05) for 48 min, and finally rods were developed in a hexane: diethyl ether: formic acid solution (80:20:0.1) for 38 min. After each solvent development, rods were dried (5 min) and conditioned (5 min) in a constant humidity chamber (~32%) that was saturated with aqueous $CaCl_2$. Following the last development, rods were scanned using Peak Simple software (ver. 3.67, SRI Inc.) and the signal detected in millivolts was quantified with calibration curves using the following standards from Sigma (St Louis, MO, USA): palmitic acid (free fatty acids), cholesterol (sterols), L-alpha-phosphatidylcholine (polar lipids). Specialized standards were purified by column chromatography to use for triacylglycerols (from *Boreogadus saida* liver) following methods from Ohman (1997). Calibrated relationships between lipid class areas and standard lipid amounts (μg) had correlations with an r^2 >0.98 for all classes.

Following total lipid and lipid class analyses of fish tissues, samples were processed for fatty acid analyses. An internal standard (23:0 methyl ester) was added at approximately 10% of the total fatty acids

to all samples and total lipid extracts were derivatized into their fatty acid methyl esters (FAMEs) using sulphuric acid-catalyzed transesterification (Budge et al. 2006). Resulting FAMEs were analyzed on an HP 7890 GC FID equipped with an autosampler and a DB wax+ GC column (Agilent Technologies, Inc., U.S.A.). The column was 30 m in length, with an internal diameter of 0.25 mm and film thickness of 0.25 µm. The column temperature began at 65 °C and held this temperature for 0.5 min. Temperature was increased to 195 °C (40 °C min^{-1}), held for 15 min then increased again (2 °C min^{-1}) to a final temperature of 220 °C. Final temperature was held for 1 min. The carrier gas was hydrogen, flowing at a rate of 2 ml min^{-1}. Injector temperature was set at 250 °C and the detector temperature was constant at 250 °C. Peaks were identified using retention times based upon standards purchased from Supelco (37 component FAME, BAME, PUFA 1, PUFA 3) and in consultation with retention index maps performed under similar chromatographic conditions as our GC-FID (Wasta & Mjøs 2013). Column function was checked by comparing chromatographic peak areas to empirical response areas using a quantitative FA mixed standard, GLC 487 (NuCheck Prep). Chromatograms were integrated using Chem Station (version A.01.02, Agilent).

Data analysis of fish lipids

For each of the four juvenile gadid species, we examined length-weight and length-fatty acid (total fatty acids per animal, mg) relationships using a power function ($Y = a * X^b$) with an approximate value of *b* equal to 3 indicating isometric growth (Sigma plot 14.0).

Due to unequal spatial and temporal sampling and significant interactive effects of region and year on fish condition, we explored annual variability in fish condition separately for each species in a given region (one-way ANOVA). We divided the survey area into Southern (SECS), Central (CECS) and Northern (NECS) Chukchi Sea, areas of approximately equal latitudinal range as described in Buckley and Whitehouse (2017) (Fig. 1). We calculated one morphometric condition measurement, Fulton's condition index ($K = 100 * ((WWT, g) / (SL, cm)^3)$) and used multiple lipid-based condition indices: total lipid concentration per WWT ($mg.g^{-1}$), total fatty acid per WWT ($mg.g^{-1}$), % triacylglycerols (TAG), and finally the calanoid-specific fatty acid markers ($\sum C_{20} + C_{22}$) per WWT ($mg.g^{-1}$), an indicator of large lipid-rich copepods in juvenile fish diets.

Statistical differences among the fatty acid parameters of juvenile gadids were compared using individual FAs present at >1% in all samples as well as the percentage of bacterial FAs (∑odd and branched chains) and *Calanus* FAs ($\sum C_{20}+C_{22}$MUFA) using PRIMER v.7 (Primer-E) with a Permutational ANOVA, PERMANOVA add-on package. We were not able to perform tissue-specific fatty acid analyses, however, the inclusion of fatty acid concentration per WWT allowed us to determine FAs that were proportionally associated with higher total fatty acids in juvenile fish. Data (% total FA) was square-root transformed prior to analyses and were then used to calculate a triangular matrix of similarities (Bray-Curtis similarity) between each pair of samples. Non-metric multidimensional scaling (*n*MDS), an iterative process that uses ranks of similarities, was utilized to explore the effect of species and year of sampling on the FA composition of juvenile gadids ($p<0.05$).

To visually show region-specific differences in polar cod lipid composition from 2013, 2017 and 2019 we used bootstrap averages (60 per grouping, Primer v. 7) with 95% confidence intervals in metric multidimensional space. Distances between centroids of polar cod groups as a function of region and year of sampling were calculated in PCO space based on Bray-Curtis similarity matrix.

Empirical Bayesian kriging (Krivoruchko & Gribov 2019) was used to visualize spatial patterns in surface temperatures and lipid parameters by interpolating data from survey sample stations (ArcGIS Desktop 10.7). For symbology, interpolated data values were stretched along a color ramp using the standard deviations stretch type.

Results

Species-specific length-weight and length-lipid storage

The exponential regression coefficient *b*, for the relationship between length (mm) and WWT per fish (g) for all four species of juvenile gadids ranged between 2.85 and 3.22 (Fig. 2, 20-85 mm), indicating isometric growth. Analyses of log transformed length-weight relationships indicated that both length ($p<0.001$) and species (ANCOVA, species $F_{3,710}=49.62$, $p<0.001$) had a significant effect on the WWT of juvenile gadids. For a given length, Pacific cod and saffron cod were significantly heavier than walleye pollock and polar cod had the lowest weight-at-length for all gadid species (untransformed data, Fig. 2a & 2b, $p<0.05$).

The exponential coefficient *b* for the relationship between length (mm) and total fatty acids per fish (mg) ranged from a high of 3.85 in polar cod to a low of 2.19 in juvenile saffron cod, indicating allometric and alternative species-specific lipid allocation (Fig. 2c & 2d). Analyses of log transformed length-fatty acid data indicated that both length ($p<0.001$) and species (ANCOVA, species $F_{3,710}=53$, $p<0.001$) had a significant effect on the fatty acid storage (mg) in juvenile gadids. For a given length, polar cod had significantly higher fatty acid storage, followed by walleye pollock, Pacific cod and saffron cod had the lowest lipid storage of all gadids (untransformed data, Fig. 2d, $p<0.05$).

Region- and species-specific annual differences in condition

Due to variable catches, we were not able to analyzed all species across all regions and years for morphometric and lipid-based condition. Pacific cod, were only captured in 2017 and are discussed in detail in Cooper et al. (this report). Therefore, we have focused on annual differences within broad geographical regions for combinations where we obtained adequate samples.

Relative to lipid-based condition metrics, Fulton's K morphometric condition factor was fairly insensitive to annual changes in juvenile gadid condition (Fig. 3, 4 & 5). In the CECS we noted a significant decrease in all lipid-based condition factors from the earlier collections during a cold year (2013) to fish collected in 2017 (i.e. ANOVA %TAG $F_{1,63}=51.5$, $p<0.001$, Fig 3a). Further, a significant decline in calanoid copepod fatty acids was found in 2017, indicating that polar cod were storing less energy from large lipid-rich copepods than measured in 2013 (ANOVA $F_{1,75}=33.6$, $p<0.001$, Fig 3a).

In 2019, the distribution of polar cod retracted northward and fish were only available across all 3 survey years in the NECS. Comparison of the condition for polar cod in the NECS between 2013 and two contemporary warm years (2017 and 2019) showed that polar cod were generally in low lipid-based condition in 2017. During 2017, polar cod were abundant and caught throughout the whole latitudinal range of the Chukchi Sea (Levine et al. this report) but our data shows they were in poor lipid-based condition throughout much of the survey area. Lipid metrics for polar cod in 2019 were similar to those measured in an earlier cold year (2013), while fish were generally heavier at a given length in 2017 than in the other two years (ANOVA, $F_{2,195}=19.28$, $p<0.001$, Fig 3b). This could indicate that fish sampled in the late summer of 2017 were prioritizing growth over lipid storage (Fig 3b). Further, levels of calanoid copepod lipids in fish from the NECS were similar in 2013 and 2019 but were significantly lower in 2017 (ANOVA, $F_{2,200}=4.06$, $p<0.019$).

We were able to make annual comparisons of saffron cod condition between 2012 and 2017 in the SECS and the CECS, but relatively low abundances of this species in contemporary survey years (2017, 2019, Levine et al, this report) precluded other annual and spatial comparisons. We found significant region-specific declines in most lipid-based condition factors in saffron cod from both regions from 2012 to 2017 (Fig. 4). In the SECS, total lipids per WWT dropped more than 50% from 2012 (24.2 ± 2.3 mg.g^{-1}) to 2017 (9.6 ± 0.26 mg.g^{-1}, Fig 4a). This pattern was similar for the proportion of storage lipids, %TAG, as well as storage of total calanoid fatty acids (Fig. 4a). Trends of decreasing lipid-based condition metrics

in 2017 were also significant for saffron cod in the CECS but were less extreme than in the SECS (Fig 4b). We measured no change in Fulton's K morphometric condition for saffron cod in either region between years (i.e. CECS, ANOVA, $F_{1,63}=0.01$, $p=0.91$), despite dramatically declines in lipid-based condition (i.e. CECS, total lipid ANOVA, $F_{1,64}=16.39$, $p<0.001$).

Pollock from the SECS and CECS were analyzed in both contemporary warm years (2017 & 2019). In the SECS, pollock showed significantly higher Fulton's K in 2017 compared to 2019, while lipid-based condition metrics indicated an opposite trend with fish in 2019 having significantly higher total fatty acids per WWT and calanoid copepod storage lipids (Fig. 5a). In the CECS walleye pollock were in better lipid-based condition in 2019 for all lipid metrics, however, there was not significant difference in Fulton's K during the two contemporary sampling years (Fig 5b). In 2019, walleye pollock were also sampled in the NECS due to their range expansion further north (Wildes et al. and Levine et al. this report). However, our results indicate that pollock in the NECS were in poor morphometric and lipid-based condition compared to pollock in more southern areas of the Chukchi Sea (Fig 5b).

Species-specific differences in lipid composition

Across years and regions, polar cod had a unique lipid storage strategy compared to other Chukchi Sea gadids (Table 2, Fig. 2). Polar cod had twice the lipid concentration (total lipids per WWT, 20-35 $\mu g.mg^{-1}$) in their tissues compared to other juvenile gadids (Table 2). Elevated lipids in polar cod were typified by increased proportions of triacylglycerols (TAG, 27-57%) and very high monounsaturated fatty acids (MUFA, 38-50%, Table 2) relative to other species. MUFA in polar cod were likely accumulated from specialized predation on calanoid copepods, which in turn have high levels of the C_{20}+C_{22} MUFA originating from their unique seasonal wax ester storage. Polar cod had more than 5X the fatty acids per WWT originating from calanoid copepods (4 to 6.5 $mg.g^{-1}$) compared to all other gadid species (0.2 to 1.2 $mg.g^{-1}$, Table 2). The diatom indicator ratio (16:1n-7/16:0) was also elevated in polar cod tissues compared to other gadids. This gives further support to the theory that polar cod nutrition is highly dependent on specialized feeding in cold nutrient-rich waters that support diatom-*Calanus* based food webs. Both saffron cod and polar cod had relatively low diatom indicator fatty acids in warm contemporary years of sampling (2017, 2019), compared to fish from colder reference years (2012, 2013, Table 2).

Multivariate analyses of gadid lipid parameters from contemporary and historic years (Table 2, Fig. 6) illustrate the large relative variation in polar cod multivariate lipid composition compared to other species. Polar cod were spatially segregated due to their high lipid content (fatty acids per WWT) and their *Calanus*- and diatom-sourced lipid storage. Conversely, Pacific cod and saffron cod in 2017 were characterized by very low total fatty acids and elevated proportion levels of fatty acids indicative of membrane phospholipids rather than energy storage (22:6n-3, 18:0). It was evident that saffron cod and polar cod had a significant shift in their lipid composition from earlier cold years (2012, 2013) to warm conditions in 2017, with declining total and diatom sourced lipids (Fig. 6). Walleye pollock had an intermediate lipid storage level that was higher in 2019 than 2017. Pollock had relatively elevated proportions of fatty acids associated with flagellates (18:4n-3, 18:2n-6, phytoplankton marker as discussed in Nielsen et al, lower trophic AIERP report) compared to polar cod, which could indicate feeding on smaller copepods that are not as dependent on diatom production (Fig. 6). The largest species-specific variation in lipid composition was seen in polar cod. Investigation of the differences in polar cod multivariate lipid composition as a function of year and region (Fig. 7), showed the most extreme regional multivariate change in lipid composition in the CECS between 2013 and 2017. Less annual variation in the lipid composition of polar cod was measured annually in the NECS.

Hot-spots for juvenile gadid condition

Spatial trends for polar cod lipid-based condition (total fatty acids per WWT) reflected tissue levels of total *Calanus* copepod lipid storage, indicating the importance of *Calanus* lipids to juvenile polar cod

energetics (Fig. 8). In 2013 and 2017, polar cod had the highest fatty acid storage in the <5 ºC waters of the NECS, specifically surrounding Hanna Shoal, near the mouth of Barrow Canyon and in coastal regions off Icy Cape (Fig. 8). In southern waters with temperatures > 8 °C, polar cod had reduced abundance (Levine et al. this report), but also lower lipid-based condition and reduced *Calanus* lipid storage (Fig 8). In 2019, polar cod were still in high condition near the entrance to Barrow Canyon and in the ice-associated regions east of Hanna Shoal and north of Herald Shoal, but they had reduced lipid storage to the south of Hanna Shoal compared to 2013 and 2017.

In 2019, the regional distribution of polar cod and walleye pollock only overlapped at a few stations to the south and west of Hanna Shoal (Fig. 9), where polar cod were in high condition but walleye pollock were in relatively poor condition. Average surface water temperatures at polar cod stations in 2019 were 6.67 ± 0.16 °C while walleye pollock stations were 8.86 ± 0.8 °C. Polar cod lipids ranged between 14 and 34 $mg.g^{-1}$ throughout the Chukchi while walleye pollock ranged between 9 and 29 $mg.g^{-1}$. For walleye pollock, high condition patterns were also associated with *Calanus*-sourced lipid storage, but at a much lower absolute level of fatty acid storage. Walleye pollock generally had higher total fatty acids and *Calanus* indicators in the SECS.

Discussion

Lipids are the most variable component of juvenile fish energetic storage and their fluctuation in fish tissues have previously been linked to oscillations in overwinter survival and recruitment (Grant & Brown 1999, Heintz & Vollenweider 2010, Siddon et al. 2013). In highly seasonal environments, consumers must rapidly store lipids during times of high productivity to survival prolonged periods of low food availability (Hurst 2007, Copeman et al. 2016, Copeman et al. 2021). Lipids are the densest and therefore most efficient form of energy storage, providing at least two-thirds more energy per gram than proteins or carbohydrates (Parrish 2013). Examples of this polar lipid-rich energetic strategy are evidenced by the large wax ester-filled oil sacs of *Calanus* copepods or the triacylglycerol- enriched livers of cold water cod species (Kattner et al. 2007, Falk-Petersen et al. 2009, Copeman et al. 2017, Kohlbach et al. 2017, Renaud et al. 2018). As polar systems continue to warm, dramatic and complex changes to the structure, function and resulting energetic flow of Arctic marine food webs are likely to occur (Grebmeier 2012, Christiansen 2017). We present some of the first data on changes to juvenile gadid lipid storage and condition during a recent period of rapid warming across the Chukchi Sea.

Interspecific and intraspecific variation in the lipid and fatty acid biomarkers were evident in four co-occuring juvenile gadids. Specifically, we found significant species-specific difference in their length-weight and length-lipid relationships, with polar cod demonstrating a unique high lipid storage strategy. This points to the importance of ontogeny- and species-specific condition metrics for accessing the relative survival potential of field-collected juvenile fish (Suthers 1998, Martin et al. 2017). Secondly, we measured region-specific declines in Arctic gadid lipid storage during recent warming (2017) events compared to earlier cold survey years. However, the northward distributional shift of polar cod and the extremely low catches of saffron cod in 2019 limited our region-specific annual comparisons. In 2019, NECS polar cod maintained relatively high lipid storage compared to polar cod from other regions and years. Pacific cod had very low lipid storage compared to other gadids and in comparison to Pacific cod from more southern regions (discussed in Cooper et al., this AIERP report). Lipid storage in Walleye pollock was generally low, with fish in better condition in 2019 and in southern regions compared to the NECS.

Overwintering and summer lipid storage

Recent laboratory studies on the winter survival of juvenile polar cod (Copeman et al. this report) indicate that lipid content has an important bearing on survival potential. The magnitude of annual differences in lipid content of field collected polar cod from the CECS (2013: 34.7 ± 18.7 versus 2017: 16.0 ± 6.4) were particularly striking despite being similar in size (2013: 43.4 ± 3.9 versus 2017: 47.2 ± 10.3). Copeman et

al (this report) note that the lipid-loss models illustrate how winter thermal conditions are either highly important following summers that support fish in good condition (e.g., NECS 2013, 2019) or are potentially irrelevant when the preceding summer conditions result in a poor energetic state for age-0 juveniles e.g., 2017, 'dead fish swimming'. They also note that small changes in fall/winter temperature between -1 and 2°C have important implications for the survival of fish entering winter in a high energetic state. The importance of summer-fall prey availability and pre-winter condition are important processes regulating winter survival and thus recruitment of walleye Pollock (*Gadus chalcogramma*) in the Eastern Bering Sea (Hunt Jr et al. 2011, Mueter et al. 2011, Heintz et al. 2013). Regardless, the high prioritization for energy storage observed in small-bodied juvenile polar cod suggest there is high winter mortality risk in the Arctic and that this risk is more likely due to starvation than predation (Ivan et al. 2015).

The late summer/fall energetic storage of both Chukchi Sea Pacific cod and walleye pollock was low (2017 & 2019). Cooper et al. (this AIERP report) compared the length-weight and length-fatty acid residuals of Pacific cod captured in the Chukchi Sea to those from the Gulf of Alaska (2017). Pacific cod were significantly larger in August in the Gulf of Alaska than in September in the Chukchi Sea. Further, at a given length, Pacific cod from the Gulf of Alaska were heavier and had higher total fatty acids per WWT than fish from the Chukchi Sea. Similarly, walleye pollock from the Chukchi Sea contained very low lipids per WWT (~16 mg. g^{-1}) compared to pollock from both the south eastern Bering Sea (~34 mg. g^{-1}, calculated from Siddon et al. (2013)) and Gulf of Alaska (20-28 mg.g^{-1} , Heintz and Vollenweider (2010). Given the low lipid storage we found in both species of boreal gadids captured in the Chukchi Sea, it seems unlikely that these new invading juveniles can successfully overwinter in cold, low productivity Arctic winter environments found on the Chukchi Shelf.

Direct and indirect effects of warming

The direct effects of warming on juvenile fish vary with early life history stage (Rijnsdorp et al. 2009). Polar cod have the narrowest thermal tolerance during the egg (-1.5 to 3.0 ºC) and early larval (-1 to 5 ºC) stages that becomes much broader during the late pelagic juvenile stage (-1 to 11 ºC) (Laurel et al. 2017, Koenker et al. 2018b, Laurel et al. 2018). In recent years, the Chukchi Sea region has been generally ice-free for much of the spring-summer and has surface waters that in areas are already warming beyond the thermal limits of many early life history stages of polar cod (Laurel et al. 2017, Laurel et al. 2018, Danielson et al. 2020). Long term ecosystem surveys both in the Barents Sea and in the Canadian Arctic have reported decadal scale increases in size-at-age of juvenile polar cod (Bouchard et al. 2017, Dupont et al. 2020) concurrent with reductions in sea ice concentrations and earlier spring ice retreat. As a result, Bouchard et al. (2017) predicted that warming would cause a temporary increase in polar cod biomass but that with increased borealization of the Arctic, that polar cod would be replaced by less specialized subarctic fish. Laboratory studies on polar cod have shown that they hold an energetic advantage (higher lipid per WWT) over boreal cogeners only at temperatures < 5 ºC (Copeman et al. 2017). These laboratory data combined with evidence of declining lipid storage and abundance during warming events (> 8°C), may indicate that the SECS and CECS are currently warming beyond the thermal limits of polar cod.

Continued warming may have negative impacts on polar cod via changes in the quantity, quality and phenology of zooplankton production and thus the nutrition status of juvenile fish in the summer (Bouchard et al. 2017, Bouchard & Fortier 2020). Large Arctic zooplankton have elevated lipid storage that is dependent on both sympagic and open-water diatom lipid production, that is seasonally elevated in cold nutrient rich waters (Kattner et al. 2007, Kohlbach et al. 2017). Shifts in zooplankton dynamics during recent warming, such as increased abundance of small southern species concurrent with decreases in large Arctic zooplankton (e.g. *Calanus glacialis*), has likely resulted in lower zooplankton lipids available in the diet of juvenile Chukchi Sea fish (Kimmel et al. this AIERP). Previous studies have

found a higher degree of reliance of juvenile polar cod than saffron cod on calanoid-copepod lipids (Copeman et al. 2020). Here we measured large variability in polar cod lipid storage that was highly spatially associated with tissue storage of *Calanus*- and diatom-sourced fatty acid biomarkers (Fig. 6, 8, 9). We do not yet know what portion of the lipid storage in Chukchi Sea polar cod and Arctic zooplankton that originates from ice-algae (Graham et al. 2014, Wang et al. 2015) but it is likely lower than in other high Arctic ecosystems (Kohlbach et al. 2017).

Future work

Models that link polar cod lipid storage to oceanographic parameters, phytoplankton indicators as well as zooplankton abundance are still under development. Specifically, synthesis efforts should focus on 1) understanding spatial and annual links between temperature, phytoplankton quantity/quality and zooplankton abundance/lipids to understand observed changes in zooplankton quality and 2) combining newly generated species-specific Arctic zooplankton lipid values (Copeman et al. this IERP) with climate-driven changes in zooplankton species abundance (Kimmelet al. this IERP) to better forecast changing prey quality available to fish in a rapidly warming Chukchi Sea. Due to the high lipid storage strategy of polar cod relative to other Alaskan congers, it is likely that they are more sensitive to changes in prey quality and particularly to decreases in *Calanus*-sourced lipid storage.

Finally, in contrast to long-term ecosystem surveys available from the Canadian and Norwegian Arctic (Bouchard et al. 2017, Dupont et al. 2020), the pelagic Chukchi Sea is woefully under surveyed. Continued ecosystem monitoring of the Chukchi Sea shelf is needed to understand annual variability and forecast the abundances and nutritional condition of key-stone Arctic species. Increased annual replication would help us better understand climate mediated mechanisms that lead to observed changes in juvenile fish energetics and improve our ability to predict overwinter survival potential and resulting recruitment variability of polar cod in this rapidly warming ecosystem.

Table 1: Four species of juvenile gadids were collected over the Chukchi and northern Bering Sea from seven different Arctic surveys during 2012, 2013, 2017 and 2019. Below are samples sizes, gear types and filed collection citations as well as biochemical analyses performed to assess fish condition.

	Ecosystem Survey	Year	Age	Number of fish for lipid classes	Number of fish for fatty acids	Number of fish for morpho-metrics	Gear type	Region	Reference to collection methods
Polar cod	EIS	2013	0	38	67	66	Midwater/surface trawls	Chukchi Sea	(De Robertis et al. 2016, Copeman et al. 2020, Farley et al. 2020)
	SHELFZ	2013	1	35	68	68	Bottom/Midwater trawls	Chukchi Sea	(Gunderson & Ellis 1986, Logerwell et al. 2018)
	Arctic IERP	2017	0	112	112	110	Midwater/surface/ beam trawls	Chukchi Sea	(De Robertis et al. 2016, Logerwell et al. 2018, Copeman et al. 2020, Farley et al. 2020)
	Arctic IERP	2019	0	109	109	109	Midwater/surface trawls	Chukchi Sea	(De Robertis et al. 2016, Farley et al. 2020) (Levine et al. this final report)
Saffron cod	EIS	2012	0	48	48	48	Midwater/surface/ beam trawls	Chukchi Sea	(De Robertis et al. 2016, Copeman et al. 2020, Farley et al. 2020)
	EIS	2012	1	33	33	33	Midwater/surface	Chukchi Sea	(De Robertis et al. 2016, Copeman et al. 2020, Farley et al. 2020)
	AMBON	2017	0	37	37	36	IKMT/PSBTA	Chukchi Sea	
	Arctic IERP	2017	0	29	29	29	Midwater/surface/ beam trawls	Chukchi Sea	(De Robertis et al. 2016, Logerwell et al. 2018, Copeman et al. 2020, Farley et al. 2020)
	NBS	2017		30	30	30	Surface trawls	NBS	(Murphy et al. 2017, Farley et al. 2020)
Pacific cod	Arctic IERP	2017	0	117	117	117	Midwater/surface/ beam trawls	Chukchi Sea	(De Robertis et al. 2016, Logerwell et al. 2018, Copeman et al. 2020, Farley et al. 2020) (Cooper et al. this final report)
	NBS	2017	0	13	13	13	Surface trawls	NBS	(Murphy et al. 2017, Farley et al. 2020)

Walleye pollock	Arctic IERP	2017	0	47	47	47	Midwater/Surface trawls	Chukchi Sea	(De Robertis et al. 2016, Farley et al. 2020) (Levine et al. this final report)
	Arctic IERP	2019	0	111	111	111	Midwater/surface/ beam trawls	Chukchi Sea	(De Robertis et al. 2016, Logerwell et al. 2018, Copeman et al. 2020, Farley et al. 2020)

Table 2: Summary of lipid parameters for juvenile saffron cod (*Eleginus gracilis*), polar cod (*Boreogadus saida*), walleye pollock (*Gadus chalcogrammus*) and Pacific cod (*Gadus macrocephalus*) collected on ecosystem surveys during 2012, 2013, 2017 and 2019. Grey hi-lighted are for historical years representing a relatively normal 'cold' thermal phase of the Chukchi Sea, compared to the current 'warm' years (17 & 19).

Species	**Saffron**		**Polar cod**			**Walleye Pollock**		**Pacific cod**
Year	2012	2017	2013	2017	2019	2017	2019	2017
Age	0 &1	0	0 &1	0	0	0	0	0
Surface temperature °C	7.54 ± 0.26	7.02± 0.23	3.97 ± 0.16	5.49 ± 0.12	6.67 ± 0.16	5.64 ± 0.06	8.86 ± 0.075	6.02 ± 0.086
Standard length, mm	59.04 ± 2.36	58.08 ± 1.70	67.48 ± 2.30	43.55 ± 0.83	48.28 ± 0.89	58.45 ± 1.22	49.58 ± 0.98	67.04 ± 0.75
Sample size	81	96	73	112	109	47	111	130
Total lipids per WWT	17.33 ± 0.98	8.79 ± 0.21	34.44 ± 2.04	19.65 ± 0.95	30.21 ± 1.07	15.86 ± 0.94	17.27 ± 0.63	8.18 ± 0.12
%Triacylglycerols	12.74 ± 1.57	2.04 ± 0.44	57.34 ± 1.64	32.71 ± 2.04	27.79 ± 1.51	21.48 ± 2.05	17.43 ± 1.55	1.91 ± 0.28
% free fatty acids	27.64 ± 0.89	15.48 ± 0.86	14.71 ± 0.51	8.28 ± 0.24	15.96 ± 0.49	9.62 ± 0.34	21.94 ± 0.49	16.84 ± 0.56
% sterols	11.55 ± 0.46	12.87 ± 0.32	4.76 ± 0.17	6.69 ± 0.25	5.47 ± 0.2	7.49 ± 0.24	7.30 ± 0.28	12.90 ± 0.19
% Polar lipids	47.08 ± 1.23	69.61 ± 1.20	22.06 ± 1.17	52.33 ± 1.68	50.78 ± 1.11	61.41 ± 1.86	53.34 ± 1.24	68.35 ± 0.70
Sample size	81	96	137	112	109	47	111	128
Total FA per WWT	16.2 ± 0.7	7.4 ± 0.2	26.9 ± 0.9	18.2 ± 0.9	27.1 ± 1.0	12.0 ± 0.8	16.0 ± 0.7	7.0 ± 0.2
% 14:0	2.68 ± 0.10	1.32 ± 0.04	3.81 ± 0.11	2.83 ± 0.10	4.23 ± 0.12	2.68 ± 0.10	1.32 ± 0.04	1.13 ± 0.03
% 16:0	16.93 ± 0.25	17.72 ± 0.19	13.65 ± 0.18	14.40 ± 0.27	16.65 ± 0.24	16.93 ± 0.25	17.72 ± 0.19	17.52 ± 0.13
% 18:0	3.75 ± 0.13	4.53 ± 0.07	1.69 ± 0.04	2.08 ± 0.10	1.89 ± 0.07	3.75 ± 0.13	4.53 ± 0.07	3.96 ± 0.05
∑ % SFA	25.04 ± 0.43	24.62 ± 0.18	19.77 ± 0.23	19.93 ± 0.28	24.53 ± 0.24	24.70 ± 0.28	28.73 ± 0.25	23.45 ± 0.14
% 16:1 n-7	7.76 ± 0.48	2.74 ± 0.13	13.60 ± 0.43	8.53 ± 0.44	8.76 ± 0.33	4.24 ± 0.29	4.60 ± 0.23	2.26 ± 0.05
% 18:1 n-7	4.85 ± 0.24	3.60 ± 0.09	3.40 ± 0.10	2.89 ± 0.07	2.80 ± 0.04	3.41 ± 0.10	3.38 ± 0.08	3.85 ± 0.06
% 18:1 n-9	9.63 ± 0.17	7.22 ± 0.10	7.29 ± 0.12	6.43 ± 0.13	6.79 ± 0.15	8.65 ± 0.22	9.90 ± 0.16	7.35 ± 0.08
% 20:1 n-9	5.00 ± 0.30	1.38 ± 0.10	13.18 ± 0.35	11.00 ± 0.53	11.52 ± 0.44	3.21 ± 0.38	3.38 ± 0.19	1.47 ± 0.05
% 22:1 n-11	1.32 ± 0.13	0.57 ± 0.13	7.20 ± 0.22	5.37 ± 0.30	6.50 ± 0.37	1.36 ± 0.24	1.17 ± 0.11	0.50 ± 0.08
∑ % MUFA	32.68 ± 0.79	17.95 ± 0.30	50.15 ± 0.50	38.22 ± 1.11	41.96 ± 1.08	23.54 ± 1.03	25.24 ± 0.62	17.66 ± 0.20
% 20:4 n-6	1.03 ± 0.08	0.98 ± 0.05	0.20 ± 0.02	0.55 ± 0.02	0.24 ± 0.01	0.60 ± 0.03	0.55 ± 0.01	0.95 ± 0.2
% 20:5 n-3	13.21 ± 0.26	14.95 ± 0.25	11.90 ± 0.21	14.04 ± 0.27	10.65 ± 0.24	17.94 ± 0.31	14.75 ± 0.38	15.68 ± 0.2
% 22:6 n-3	19.99 ± 0.55	33.37 ± 0.44	11.60 ± 0.31	19.45 ± 0.74	15.09 ± 0.59	25.14 ± 0.93	22.48 ± .67	35.41 ± 0.36
∑ % PUFA	41.28 ± 0.66	56.45 ± 0.34	29.36 ± 0.44	41.13 ± 0.87	33.51 ± 0.93	51.13 ± 0.83	46.04 ± 0.53	58.14 ± 0.21
Diatom: 16:1n-7/16:0	0.48 ± 0.03	0.16 ± 0.00	1.03 ± 0.04	0.66 ± 0.04	0.55 ± 0.02	0.24 ± 0.02	0.23 ± 0.01	0.13 ± 0.00
Calanus ∑ % C20+C22 MUFA	7.49 ± 0.42	2.73 ± 0.21	23.65 ± 0.58	18.23 ± 0.88	20.50 ± 0.91	5.73 ± 0.68	5.28 ± 0.31	2.84 ± 0.12
Calanus ∑ mg/g C20+C22 MUFA	1.23 ± 0.09	0.21 ± 0.02	6.54 ± 0.30	3.99 ± 0.34	6.37 ± 0.46	0.80 ± 0.13	0.93 ± 0.09	0.20 ± 0.00

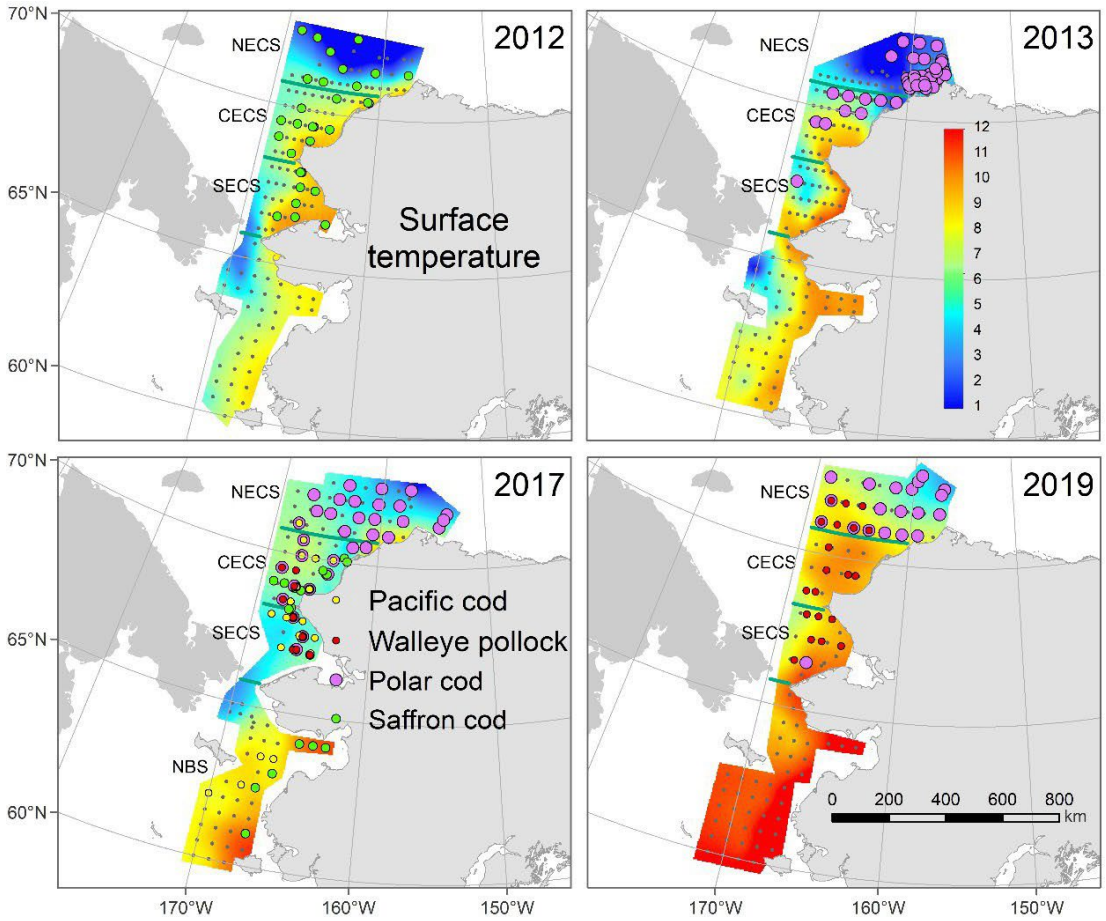

Fig. 1: Distribution of juvenile gadids collected on annual ecosystem surveys as detailed in Table 1. Species-specific stations are indicated for fish that were analyzed for detail condition and lipid biomarker analyses. Stations are plotted with surface temperature at the time of sampling to illustrate the dramatic warming in 2017 and 2019 compared with earlier sampling years.

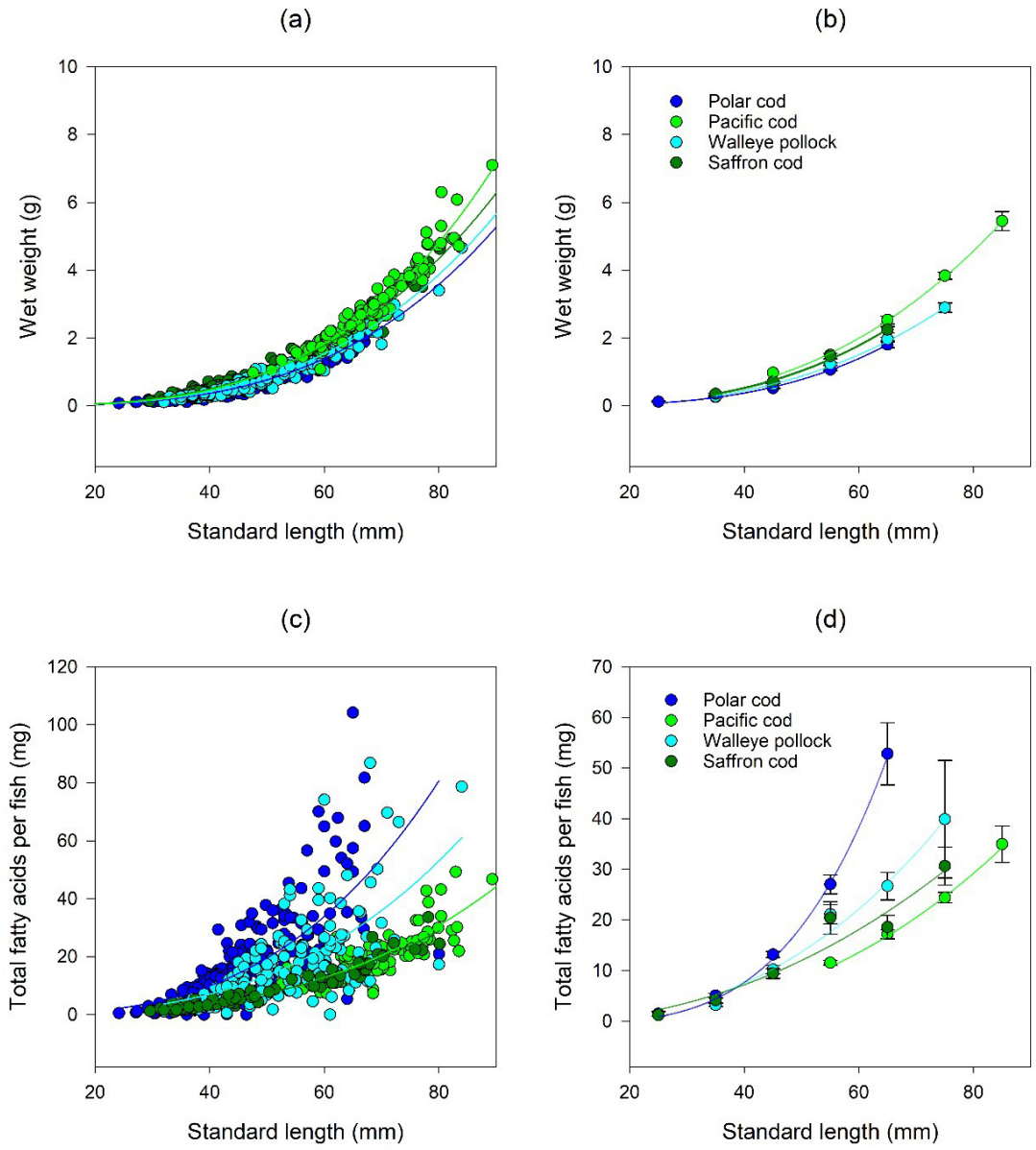

Fig. 2: Relationships between standard length (mm) and wet weight (WWT, g) as well as standard length (mm) and total fatty acids (mg per fish) for all age-0 juvenile Chukchi Sea gadids processed for lipid analyses (2012, 2013, 2017 and 2019). Data are shown for individual WWT (a), size binned WWT (b), individual total fatty acids (c) and size binned total fatty acids. Fish were binned into 10 mm increments to allow for visualization of the data.

Length-weight relationship on size binned data: Polar cod WWT (g) = 2.67E-006 SL(mm)$^{3.22}$, r^2 = 0.99, Pacific cod WWT (g) = 1.73E-005 SL (mm) $^{2.85}$, r^2=0.99, Walleye pollock lipids WWT (g) = 1.12E-005 SL (mm) $^{2.89}$, r^2 = 0.99, Saffron cod lipids WWT (g) = 9.7040E-006SL (mm)$^{2.96}$, r^2 = 0.91.

Length-total fatty acids relationship on size binned data: Polar cod lipid (mg) =5.41E-006 SL(mm)$^{3.85}$, r^2 = 0.99, Pacific cod (mg) = 0.0003 SL (mm) $^{2.61}$, r^2=0.99, Walleye pollock lipids (mg) = 0.0006 SL (mm) $^{2.58}$, r^2 = 0.99, Saffron cod lipids (mg) = 0.0024 SL (mm) $^{2.19}$, r^2 = 0.91

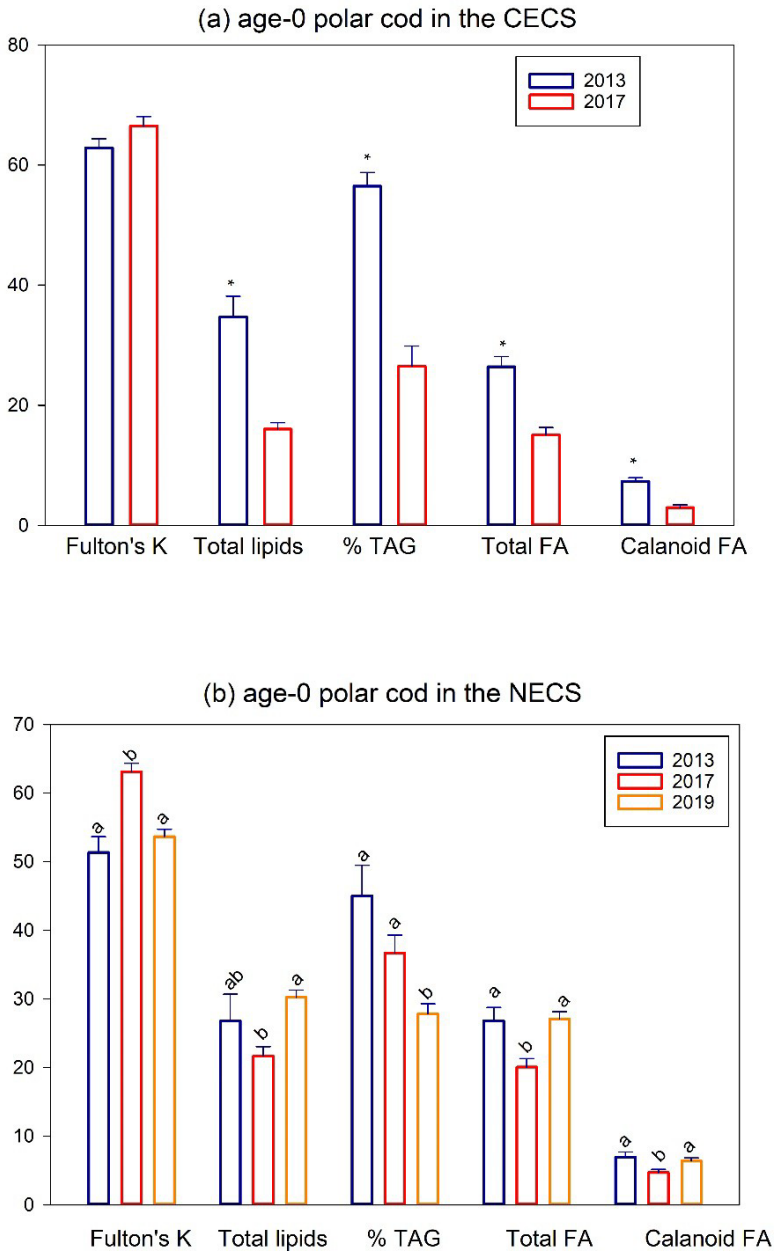

Fig. 3: Region-specific annual differences in condition metrics and lipid storage of age-0 polar cod in the Central Eastern Chukchi Sea (CECS) and the North Eastern Chukchi Sea (NECS). Fish were collected in one historical cold year (2013) and two current warm years (2017 and 2019). Polar cod were only captured in the NECS in 2019. Fulton's K (*100 percentage), total lipids (mg.g^{-1} WWT), triacylglycerols (% TAG), total fatty acids (mg.g^{-1} WWT), and total calanoid copepod fatty acid storage ($\sum C_{20}+C_{22}$ MUFA mg.g^{-1} WWT fish) are shown as mean ± SE by region-year. In the CECS * indicate significantly higher values in 2013 than 2017 while in 2019 different letters represent significant differences between years, ANOVA, $p<0.05$.

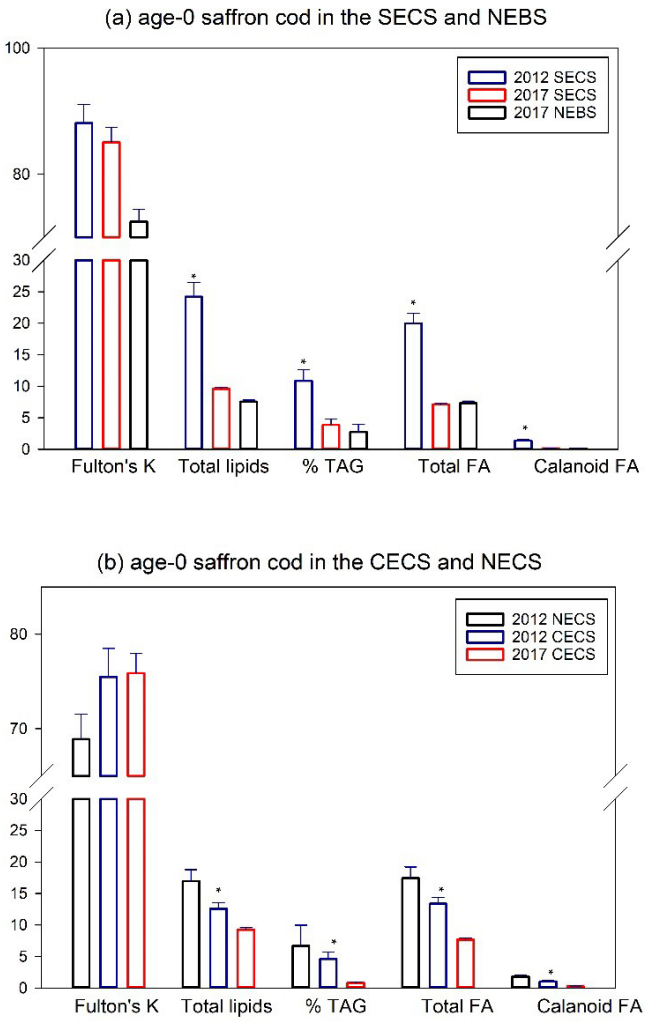

Fig. 4: Region-specific annual differences in condition metrics and lipid storage of age-0 saffron cod in the South Eastern Chukchi Sea (SECS) and the Central Eastern Chukchi Sea (CECS). Fish were collected in one historical cold year (2012) and one current warm year (2017). Saffron cod are shown for visual comparison only from the North Eastern Bering Sea (NEBS) in 2017 and the NECS in 2012. Fulton's K (*100 percentage), total lipids (mg.g^{-1} WWT), triacylglycerols (% TAG), total fatty acids (mg.g^{-1} WWT), and total calanoid copepod fatty acid storage ($\sum C_{20}$+C_{22} MUFA mg.g^{-1} WWT fish) are shown as mean ± SE by region-year. Statistical differences between 2012 and 2017 in the SECS and 2012 and 2017 in the CECS are indicated by an * with saffron cod having higher lipid indices in 2012 (cold) compared to 2017 (warm), ANOVA, $p<0.05$.

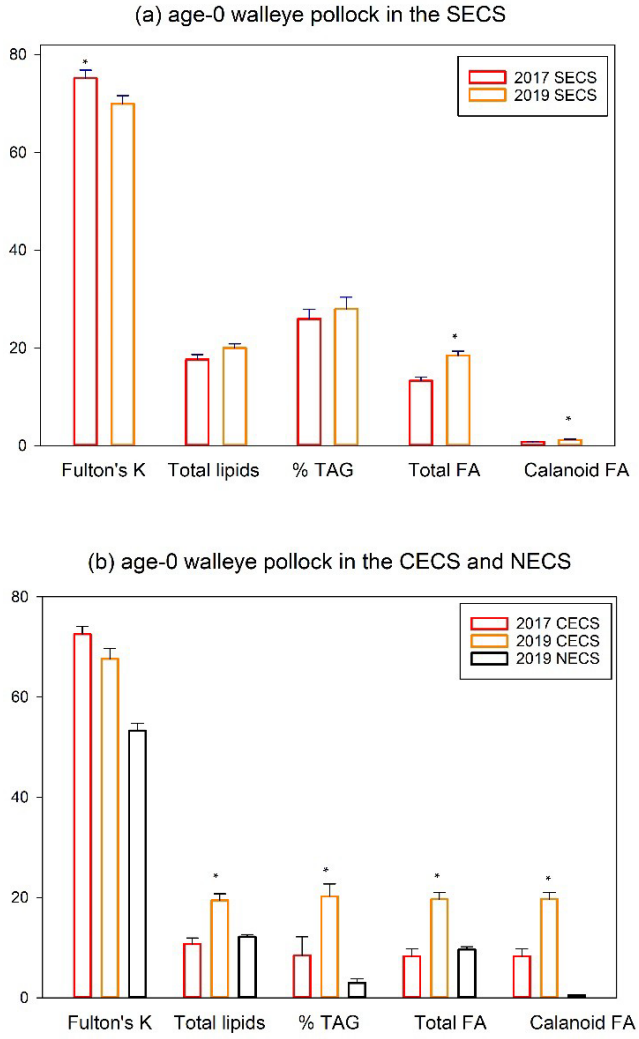

Fig. 5: Region-specific annual differences in condition metrics and lipid storage of age-0 walleye pollock cod in the South Eastern Chukchi Sea (SECS) and the Central Eastern Chukchi Sea (CECS). Fish were collected in two current warm year (2017 & 2019). Walleye pollock are also shown for visual comparison only from the NECS in 2019. Fulton's K (*100 percentage), total lipids (mg.g^{-1} WWT), triacylglycerols (% TAG), total fatty acids (mg.g^{-1} WWT), and total calanoid copepod fatty acid storage ($\sum C_{20}+C_{22}$ MUFA mg.g^{-1} WWT fish) are shown as mean ± SE by region-year. Statistical differences between 2017 and 2019 in the SECS and CECS are indicated by an * with walleye pollock having higher lipid indices in 2019 in the CECS than in 2017, ANOVA, $p<0.05$.

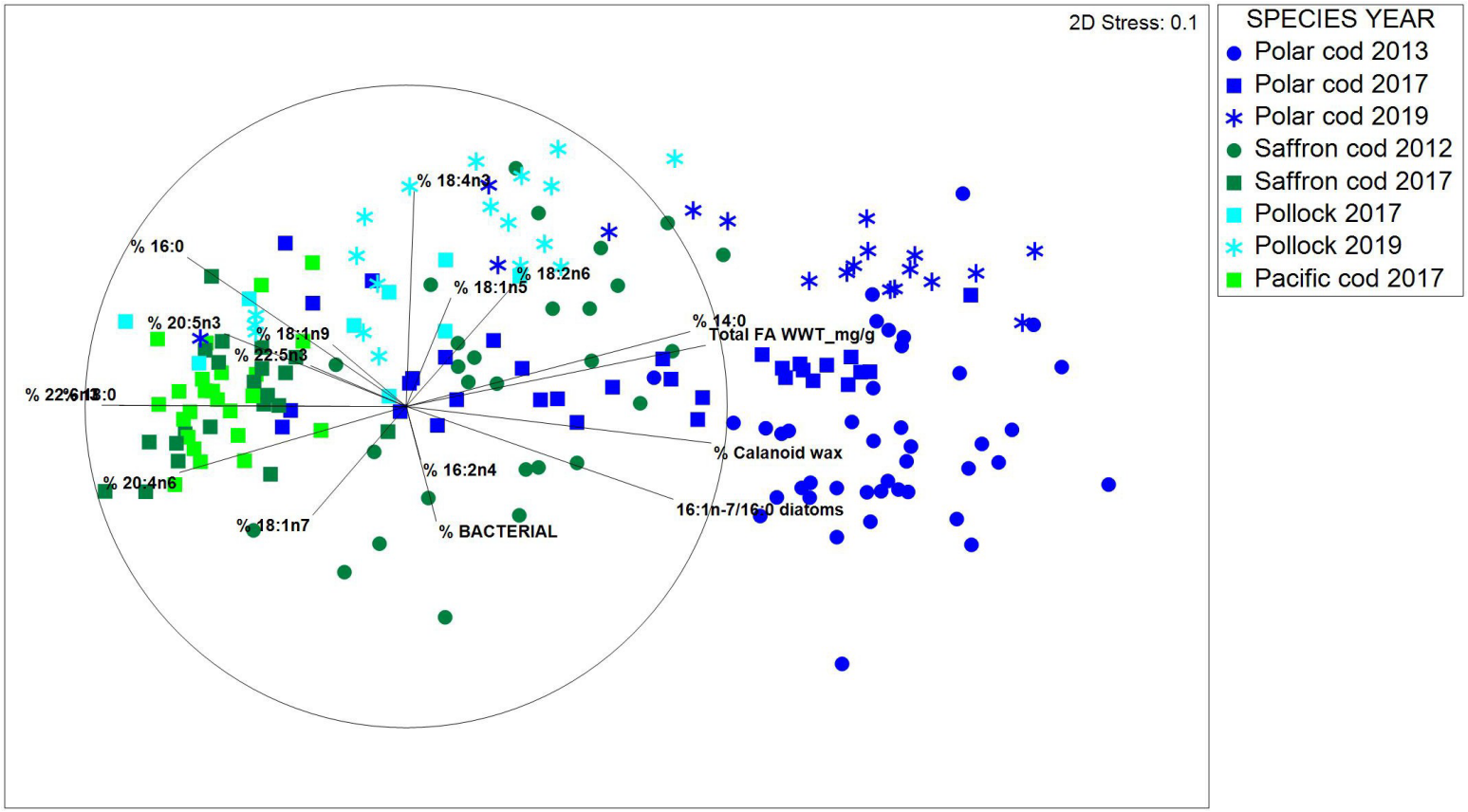

Fig 6: Nonmetric multidimensional scaling (*n*MDS) of the annual fatty acid composition of four species of juvenile gadids: saffron cod (*Eleginus gracilis*), polar cod (*Boreogadus saida*), Walleye pollock (*Gadus chalcogrammus*) and Pacific cod (*Gadus macrocephalus*) collected on ecosystem surveys during 2012, 2013, 2017 and 2019. Data points are annual station averages of ~ n=5 fish. Species and sampling as detailed in Table 1 & 2. Fatty acid vectors are shown for individual fatty acids >1% (Table 2) as well as total fatty acids per WWT (mg g−1), sum of calanoid-copepod fatty acids, bacterial fatty acids and a diatom indicator ratio. PERMANOVA for the effects of species and year showed a significant interactive effect Psuedo $F_{1,183}$=3.98, p=0.01 as illustrated by the larger annual change in polar cod lipids (2017 versus 2019) than measured for Walleye pollock over the same years.

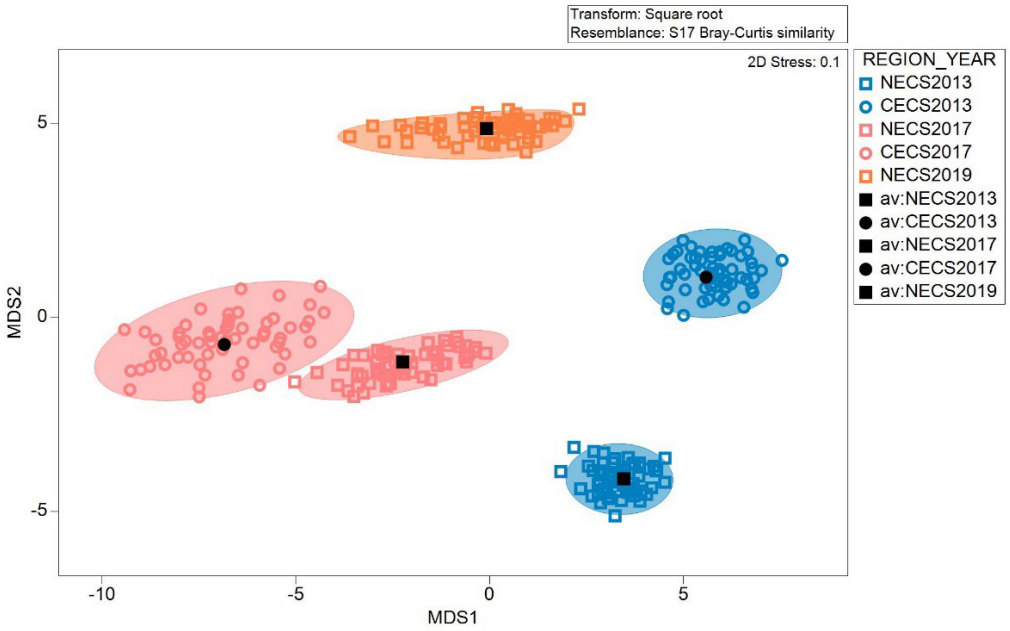

	CECS 2013	NECS 2013	CECS 2017	NECS 2017
CECS 2013	*	*	*	*
NECS 2013	6.3	*	*	*
CECS 2017	**11.3**	10.8	*	*
NECS 2017	7.5	7.0	4.9	*
NECS 2019	7.8	8.2	9.1	6.8

Fig 7: Bootstrap averages (60 per grouping) with 95% confidence intervals, and centroids of lipid distribution for polar cod illustrated by region and year. Data are shown in metric multidimensional space and the distance between centroids is given in table format. Of note is the large region-specific distance in polar cod lipids in the CECS between 2013 and 2017. Following 2017, polar cod were only captured in the NECS.

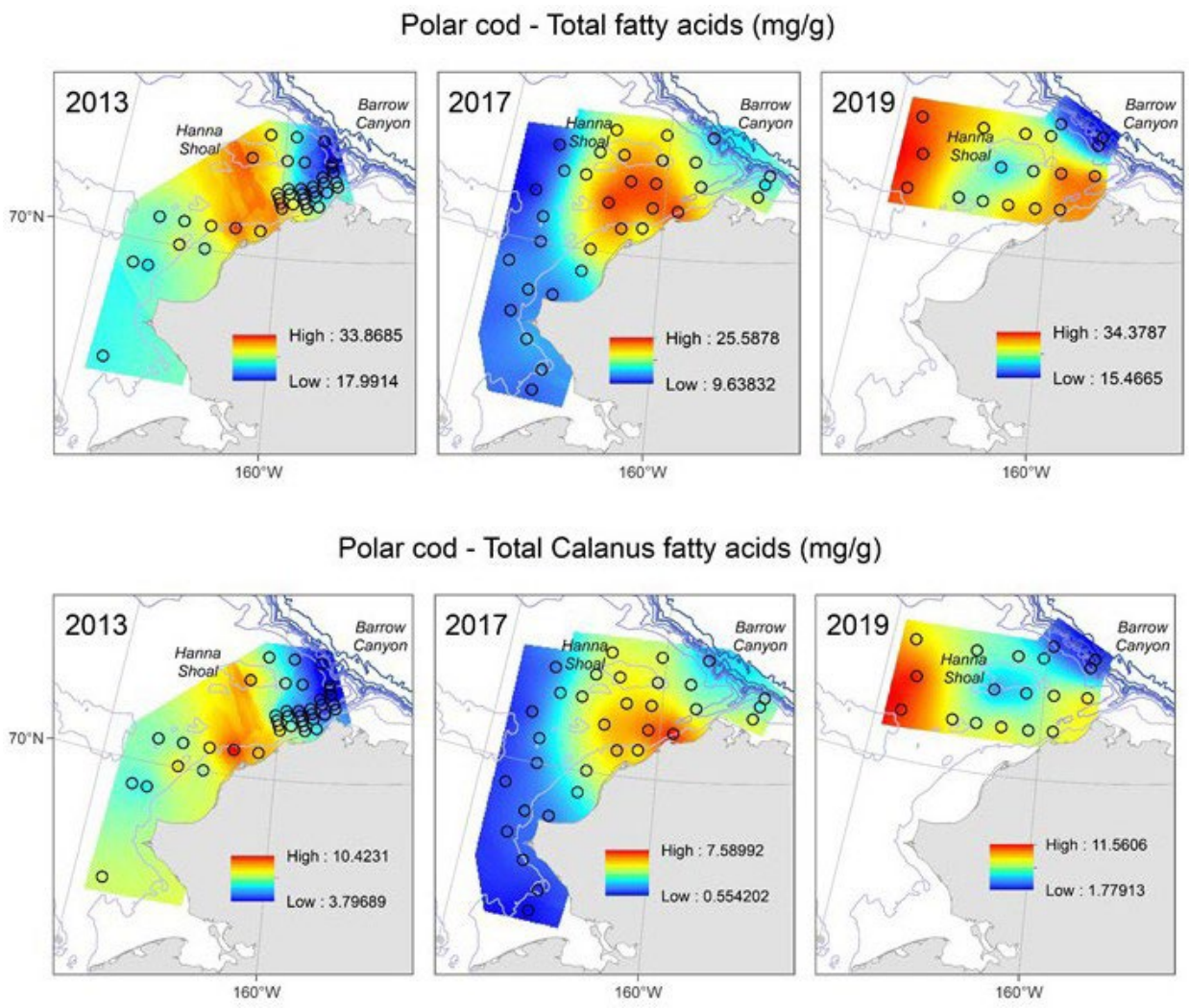

Fig 8: Annual spatial interpolation maps for 'hot spots' of a total fatty acids per WWT (mg.g^{-1}) and total *Calanus* fatty acid biomarkers $\sum C_{20}+C_{22}$ MUFA per WWT (mg. g^{-1}) in juvenile polar cod collected on Chukchi Sea Ecosystem surveys. Data sources and cruises details are as in table 1.

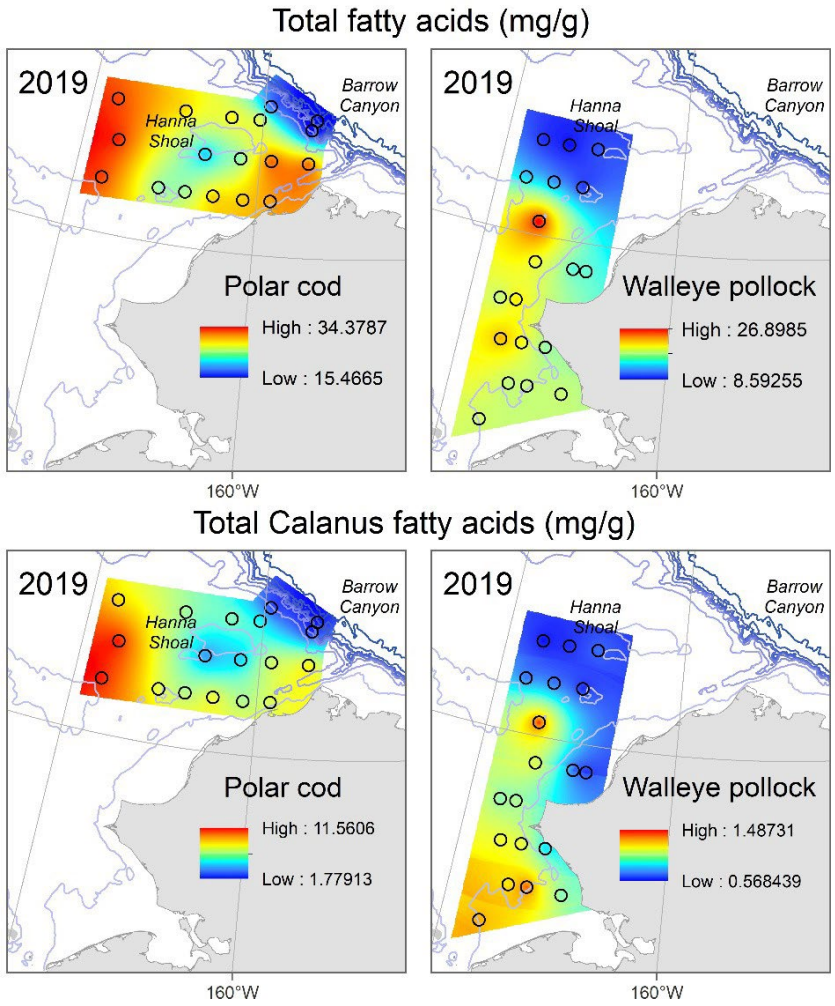

Fig 9: Species-specific spatial interpolation maps of 'hot spots' a total fatty acids per WWT ($mg.g^{-1}$) and total *Calanus* fatty acid biomarkers $\sum C_{20}+C_{22}$ MUFA per WWT ($mg.\ g^{-1}$) in juvenile polar cod and walleye pollock collected on Chukchi Sea Ecosystem surveys in 2019. Data sources and cruises details are as in table 1.

References

Bouchard C, Geoffroy M, LeBlanc M, Majewski A and others (2017) Climate warming enhances polar cod recruitment, at least transiently. Progress in Oceanography 156:121-129

Bouchard C, Fortier L (2020) The importance of Calanus glacialis for the feeding success of young polar cod: a circumpolar synthesis. Polar Biol 43:1095-1107

Brewster J, Giraldo C, Choy E, MacPhee S and others (2018) A comparison of the trophic ecology of Beaufort Sea Gadidae using fatty acids and stable isotopes. Polar Biol 41:149-162

Buckley TW, Whitehouse GA (2017) Variation in the diet of Arctic Cod (*Boreogadus saida*) in the Pacific Arctic and Bering Sea. Environ Biol Fishes 100:421-442

Budge SM, Parrish CC (1998) Lipid biogeochemistry of plankton, settling matter and sediments in Trinity Bay, Newfoundland. II. Fatty acids. Org Geochem 29:1547-1559

Budge SM, Iverson SJ, Koopman HN (2006) Studying trophic ecology in marine ecosystems using fatty acids: A primer on analysis and interpretation. Mar Mamm Sci 22:759-801

Budge SM, Wooller MJ, Springer AM, Iverson SJ, McRoy CP, Divoky GJ (2008) Tracing carbon flow in an arctic marine food web using fatty acid-stable isotope analysis. Oecologia 157:117-129

Budge SM, Penney SN, Lall SP (2012) Estimating diets of Atlantic salmon (*Salmo salar*) using fatty acid signature analyses; validation with controlled feeding studies. Can J Fish Aquat Sci 69:1033-1046

Christiansen JS (2017) No future for Euro-Arctic ocean fishes? Mar Ecol-Prog Ser 575:217-227

Copeman L, Spencer M, Heintz R, Vollenweider J and others (2020) Ontogenetic patterns in lipid and fatty acid biomarkers of juvenile polar cod (Boreogadus saida) and saffron cod (Eleginus gracilis) from across the Alaska Arctic. Polar Biol

Copeman LA, Parrish CC, Gregory RS, Wells JS (2008) Decreased lipid storage in juvenile Atlantic cod (*Gadus morhua*) during settlement in cold-water eelgrass habitat. Mar Biol 154:823-832

Copeman LA, Laurel BJ (2010) Experimental evidence of fatty acid limited growth and survival in Pacific cod larvae. Mar Ecol-Prog Ser 412:259-272

Copeman LA, Laurel BJ, Parrish CC (2013) Effect of temperature and tissue type on fatty acid signatures of two species of North Pacific juvenile gadids: a laboratory feeding study. J Exp Mar Biol Ecol 448:188-196

Copeman LA, Laurel BJ, Boswell KM, Sremba AL and others (2016) Ontogenetic and spatial variability in trophic biomarkers of juvenile saffron cod (Eleginus gracilis) from the Beaufort, Chukchi and Bering Seas. Polar Biol 39:1109-1126

Copeman LA, Laurel BJ, Spencer M, Sremba A (2017) Temperature impacts on lipid allocation among juvenile gadid species at the Pacific Arctic-Boreal interface: an experimental laboratory approach. Mar Ecol Prog Ser 566:183-198

Copeman LA, Ryer CH, Eisner LB, Nielsen JM, Spencer ML, Iseri PJ, Ottmar ML (2021) Decreased lipid storage in juvenile Bering Sea crabs (Chionoecetes spp.) in a warm (2014) compared to a cold (2012) year on the southeastern Bering Sea. Polar Biol 44:1883-1901

Craig PC, Griffiths WB, Haldorson L, McElderry H (1982) Ecological studies of Arctic cod (*Boreogadus saida*) in Beaufort Sea coastal waters, Alaska. Can J Fish Aquat Sci 39:395-406

Dahlke FT, Butzin M, Nahrgang J, Puvanendran V, Mortensen A, Pörtner H-O, Storch D (2018) Northern cod species face spawning habitat losses if global warming exceeds 1.5°C. Science Advances 4:eaas8821

Dalsgaard J, St John M, Kattner G, Muller-Navarra D, Hagen W (2003) Fatty acid trophic markers in the pelagic marine environment. Adv Mar Biol 46:225-340

Danielson SL, Ahkinga O, Ashjian C, Basyuk E and others (2020) Manifestation and consequences of warming and altered heat fluxes over the Bering and Chukchi Sea continental shelves. Deep Sea Research Part II: Topical Studies in Oceanography

De Robertis A, Taylor K, Wilson CD, Farley EV (2016) Abundance and distribution of Arctic cod (*Boreogadus saida*) and other pelagic fishes over the U.S. Continental Shelf of the Northern Bering and Chukchi Seas. Deep-Sea Res II

Dissen JN, Oliveira ACM, Horstmann L, Hardy SM (2018) Regional and temporal variation in fatty acid profiles of polar cod (*Boreogadus saida*) in Alaska. Polar Biol 41:2495-2510
Dupont N, Durant JM, Langangen Ø, Gjøsæter H, Stige LC (2020) Sea ice, temperature, and prey effects on annual variations in mean lengths of a key Arctic fish, Boreogadus saida, in the Barents Sea. Ices J Mar Sci 77:1796-1805
Falk-Petersen S, Mayzaud P, Kattner G, Sargent J (2009) Lipids and life strategy of Arctic Calanus. Marine Biology Research 5:18-39
Farley EV, Murphy JM, Cieciel K, Yasumiishi EM, Dunmall K, Sformo T, Rand P (2020) Response of Pink salmon to climate warming in the northern Bering Sea. Deep Sea Research Part II: Topical Studies in Oceanography 177:104830
Folch J, Less M, Sloane Stanley GH (1956) A simple method for the isolation and purification of total lipids from animal tissues. The Journal of Biological Chemistry 22:497-509
Frainer A, Primicerio R, Kortsch S, Aune M, Dolgov AV, Fossheim M, Aschan MM (2017) Climate-driven changes in functional biogeography of Arctic marine fish communities. Proceedings of the National Academy of Sciences 114:12202-12207
Frost KJ, Lowry LF (1981) Trophic importance of some marine gadids in Northern Alaska and their body-otolith size relationships. Fish B-Noaa 79:187-192
Galloway AWE, Winder M (2015) Partitioning the relative importance of phylogeny and environmental conditions on phytoplankton fatty acids. Plos One 10:23
Graham C, Oxtoby L, Wang SW, Budge SM, Wooller MJ (2014) Sourcing fatty acids to juvenile polar cod (*Boreogadus saida*) in the Beaufort Sea using compound-specific stable carbon isotope analyses. Polar Biol 37:697-705
Grant SM, Brown JA (1999) Variation in condition of coastal Newfoundland 0-group Atlantic cod (Gadus morhua): field and laboratory studies using simple condition indices. Marine Biology 133:611-620
Grebmeier JM (2012) Shifting Patterns of Life in the Pacific Arctic and Sub-Arctic Seas. Annu Rev Mar Sci 4:63-78
Gunderson DR, Ellis IE (1986) Development of a plumb staff beam trawl for sampling demersal fauna. . Fish Res 4:35-41
Heintz RA, Vollenweider JJ (2010) Influence of size on the sources of energy consumed by overwintering walleye pollock (*Theragra chalcogramma*). J Exp Mar Biol Ecol 393:43-50
Heintz RA, Siddon EC, Farley EV, Napp JM (2013) Correlation between recruitment and fall condition of age-0 pollock (*Theragra chalcogramma*) from the eastern Bering Sea under varying climate conditions. Deep Sea Res Part II 94:150-156
Hunt Jr GL, Coyle KO, Eisner LB, Farley EV and others (2011) Climate impacts on eastern Bering Sea foodwebs: a synthesis of new data and an assessment of the Oscillating Control Hypothesis. Ices J Mar Sci 68:1230-1243
Huntington HP, Danielson SL, Wiese FK, Baker M and others (2020) Evidence suggests potential transformation of the Pacific Arctic ecosystem is underway. Nat Clim Chang 10:342-348
Hurst TP (2007) Causes and consequences of winter mortality in fishes. J Fish Biol 71:315-345
Hurst TP, Cooper DW, Duffy-Anderson JT, Farley EV (2015) Contrasting coastal and shelf nursery habitats of Pacific cod in the southeastern Bering Sea. Ices J Mar Sci 72:515-527
Hurst TP, Laurel BJ, Hanneman E, Haines SA, Ottmar ML (2017) Elevated CO2 does not exacerbate nutritional stress in larvae of a Pacific flatfish. Fish Oceanogr 26:336-349
Ivan LN, Höök TO, Post J (2015) Energy allocation strategies of young temperate fish: an eco-genetic modeling approach. Can J Fish Aquat Sci 72:1243-1258
Jonsson B, Jonsson N, Finstad AG (2013) Effects of temperature and food quality on age and size at maturity in ectotherms: an experimental test with Atlantic salmon. Journal of Animal Ecology 82:201-210
Kattner G, Hagen W, Lee RF, Campbell R and others (2007) Perspectives on marine zooplankton lipids. Can J Fish Aquat Sci 64:1628-1639

Koenker BL, Copeman LA, Laurel BJ (2018a) Impacts of temperature and food availability on the condition of larval Arctic cod (*Boreogadus saida*) and walleye pollock (*Gadus chalcogrammus*). Ices J Mar Sci 75:2370-2385
Koenker BL, Laurel BJ, Copeman LA, Ciannelli L, Robert HeD (2018b) Effects of temperature and food availability on the survival and growth of larval Arctic cod (*Boreogadus saida*) and walleye pollock (*Gadus chalcogrammus*). Ices J Mar Sci 75:2386-2402
Kohlbach D, Schaafsma FL, Graeve M, Lebreton B and others (2017) Strong linkage of polar cod (*Boreogadus saida*) to sea ice algae-produced carbon: Evidence from stomach content, fatty acid and stable isotope analyses. Progress in Oceanography 152:62-74
Krivoruchko K, Gribov A (2019) Evaluation of empirical Bayesian kriging. Spatial Statistics 32:100368
Laurel BJ, Spencer M, Iseri P, Copeman LA (2016) Temperature-dependent growth and behavior of juvenile Arctic cod (*Boreogadus saida*) and co-occurring North Pacific gadids. Polar Biol 39:1127-1135
Laurel BJ, Copeman LA, Spencer M, Iseri P (2017) Temperature-dependent growth as a function of size and age in juvenile Arctic cod (Boreogadus saida). Ices J Mar Sci 74:1614-1621
Laurel BJ, Copeman LA, Spencer M, Iseri P, Handling editor: Dominique R (2018) Comparative effects of temperature on rates of development and survival of eggs and yolk-sac larvae of Arctic cod (Boreogadus saida) and walleye pollock (Gadus chalcogrammus). Ices J Mar Sci:fsy042-fsy042
Laurel J, Stoner AW, Ryer CH, Hurst TP, Abookire AA (2007) Comparative habitat associations in juvenile Pacific cod and other gadids using seines, baited cameras and laboratory techniques. J Exp Mar Biol Ecol 351:42-55
Lee RF, Hagen W, Kattner G (2006) Lipid storage in marine zooplankton. Mar Ecol Prog Ser 307:273-306
Logerwell E, Busby M, Carothers C, Cotton S and others (2015) Fish communities across a spectrum of habitats in the western Beaufort Sea and Chukchi Sea. Prog Oceanogr 136:115-132
Logerwell E, Rand K, Danielson S, Sousa L (2018) Environmental drivers of benthic fish distribution in and around Barrow Canyon in the northeastern Chukchi Sea and western Beaufort Sea. Deep Sea Research Part II: Topical Studies in Oceanography 152:170-181
Lu YH, Ludsin SA, Fanslow DL, Pothoven SA (2008) Comparison of three microquantity techniques for measuring total lipids in fish. Can J Fish Aquat Sci 65:2233-2241
Marsh JM, Mueter FJ, Iken K, Danielson S (2017) Ontogenetic, spatial and temporal variation in trophic level and diet of Chukchi Sea fishes. Deep-Sea Research Part Ii-Topical Studies in Oceanography 135:78-94
Martin BT, Heintz R, Danner EM, Nisbet RM (2017) Integrating lipid storage into general representations of fish energetics. Journal of Animal Ecology 86:812-825
Mueter FJ, Bond NA, Ianelli JN, Hollowed AB (2011) Expected declines in recruitment of walleye pollock (*Theragra chalcogramma*) in the eastern Bering Sea under future climate change. Ices J Mar Sci 68:1284-1296
Murphy JM, Howard KG, Gann JC, Cieciel KC, Templin WD, Guthrie III CM (2017) Juvenile Chinook salmon abundance in the northern Bering Sea: implications for future returns and fisheries in the Yukon River. Deep Sea Research Part II: Topical Studies in Oceanography 135:156-167
Ohman MD (1997) On the determination of zooplankton lipid content and the occurrence of gelatinous copepods. J Plankton Res 19:1235-1250
Parrish CC (1987) Separation of aquatic lipid classes by chromarod thin-layer chromatography with measurement by Iatroscan flame ionization detection. Can J Fish Aquat Sci 44:722-731
Parrish CC (2013) Lipids in Marine Ecosystems. ISRN Oceanography 2013:16
Peck MA, Reglero P, Takahashi M, Catalan IA (2013) Life cycle ecophysiology of small pelagic fish and climate-driven changes in populations. Progress in Oceanography 116:220-245
Pörtner H-O, Farrell A (2008) ECOLOGY physiology and climate change. Science (New York, NY) 322:690-692

Renaud P, Daase M, Banas N, Gabrielsen T and others (2018) Pelagic food-webs in a changing Arctic: a trait-based perspective suggests a mode of resilience. Ices J Mar Sci 75
Renaud PE, Sejr MK, Bluhm BA, Sirenko B, Ellingsen IH (2015) The future of Arctic benthos: Expansion, invasion, and biodiversity. Prog Oceanogr 139:244-257
Rijnsdorp AD, Peck MA, Engelhard GH, Möllmann C, Pinnegar JK (2009) Resolving the effect of climate change on fish populations. Ices J Mar Sci 66:1570-1583
Siddon EC, Heintz RA, Mueter FJ (2013) Conceptual model of energy allocation in walleye pollock (*Theragra chalcogramma*) from age-0 to age-1 in the southeastern Bering Sea. Deep Sea Res II 94:140-149
Springer AM, Piatt JF, VanVliet G (1996) Sea birds as proxies of marine habitats and food webs in the western Aleutian Arc. Fish Oceanogr 5:45-55
St John MA, Lund T (1996) Lipid biomarkers: Linking the utilization of frontal plankton biomass to enhanced condition of juvenile North Sea cod. Mar Ecol Prog Ser 131:75-85
Stabeno PJ, Bell SW (2019) Extreme Conditions in the Bering Sea (2017–2018): Record-Breaking Low Sea-Ice Extent. Geophysical Research Letters 46:8952-8959
Steiner NS, Cheung WWL, Cisneros-Montemayor AM, Drost H and others (2019) Impacts of the Changing Ocean-Sea Ice System on the Key Forage Fish Arctic Cod (Boreogadus Saida) and Subsistence Fisheries in the Western Canadian Arctic—Evaluating Linked Climate, Ecosystem and Economic (CEE) Models. Frontiers in Marine Science 6
Suthers IM (1998) Bigger? Fatter? Or is faster growth better? Considerations on condition in larval and juvenile coral-reef fish. Australian Journal of Ecology 23:265-273
Timmermans ML, Ladd C, Wood K (2017) Sea Surface Temperature [in Arctic Report Card 2017], . http://wwwarcticnoaagov/Report-Card
Viso AC, Marty JC (1993) Fatty-acids from 28 marine microalgae. Phytochemistry 34:1521-1533
Wang SW, Budge SM, Iken K, Gradinger RR, Springer AM, Wooller MJ (2015) Importance of sympagic production to Bering Sea zooplankton as revealed from fatty acid-carbon stable isotope analyses. Mar Ecol-Prog Ser 518:31-50
Wasta Z, Mjøs SA (2013) A database of chromatographic properties and mass spectra of fatty acid methyl esters from omega-3 products. Journal of Chromatography A 1299:94-102

CHAPTER 12 - Corrigendum: Species and size selectivity of two midwater trawls used in an acoustic survey of the Alaska Arctic

Objective 3: Combine results from previous Arctic surveys (Arctic EIS, Phase 1, BASIS) and planned surveys (Arctic IES Phase 2) to assess variability in pelagic and demersal fish ecology over time relative to ocean conditions.

Alex De Robertis, Kevin C. Taylor, Kresimir Williams, Christopher D. Wilson. in review. Corrigendum: species and size selectivity of two midwater trawls used in an acoustic survey of the Alaska Arctic. AIERP Special Issue

Here we describe a correction to estimates of the size and species selectivity of two survey trawls in De Robertis et al. (2017a). In that study, trawl selectivity was investigated by equipping a modified Marinovich survey trawl with recapture nets to estimate the degree to which organisms entering the trawl mouth escape during the capture process. On a subset of hauls, paired hauls with both the Marinovich and a larger Cantrawl trawl were conducted. The size and species selectivity of the nets was estimated by combining the catch data from both trawls in a statistical model. Escapement (E) from each section of the Marinovich was characterized as $SS = \frac{cc_{mmmmmm}}{ff_{mmmmmm}}$ where c_{mar} is the catch in the Marinovich recapture net in a given section of the net and f_{mar} is the fraction of the trawl surface area covered by the recapture nets in that section.

In De Robertis et al. 2017a, f_{mar} of 0.022 was used in the forward portion of the trawl, and 0.055 was used in the aft portion of the trawl. We have discovered that these values were incorrectly computed. The correct value of f_{mar} in the experimental configuration is 0.065 in the forward portion of the trawl, and 0.132 in the aft portion of the trawl. Here we summarize the impacts of this inadvertent error on the selectivity estimates reported in De Robertis et al. (2017a). We also examine the effects of this error on the abundance estimates of acoustic-trawl surveys conducted in the Chukchi Sea in 2012 and 2013 as these surveys applied these selectivity relationships in an effort to correct for the selectivity of the survey trawl (De Robertis et al. 2017b).

The proportion of mesh area covered by the recapture net in De Robertis et al. (2017a) was incorrect for two reasons. First, the size of the recapture net was miscommunicated, and the number of meshes covered by the recapture net was under-estimated. Second, the codend was not included in the trawl diagram, and the area of the net covered by the fine-mesh (2 by 3 mm) codend liner was misinterpreted. We thus incorrectly assumed that the liner was placed in the aft section of the net during they survey rather than lining a separate, undocumented codend. These errors were discovered by comparing the trawl with the net diagram. These errors could have been avoided by better documentation of the trawl and recapture nets, and verifying that the recapture nets and trawl matched the net plans as part of the experiment. Corrected diagrams of the trawl and recapture nets as used in the experiment (Figs. S1.1-1.2), and a protocol to estimate recapture net coverage in this and future studies (S2) are given as supplementary material.

The primary consequence of under-estimating f_{mar} by a factor of 3 in the forward section and 2.4 in the aft section is that escapement from the Marinovich trawl was over-estimated. Escapement from the Cantrawl was also over-estimated as this depends on the estimated abundance of fish in the volume sampled which depends on the estimated selectivity of the Marinovich (De Robertis et al. 2017a, their equation 9). The reductions in estimated escapement can be visualized by comparing the revised calculations (Table 1 and Figs S1.3-S1.7) with those in the original publication (their Table 2, Figs. 4-5 and 7-9).
Although the qualitative pattern of escapement from different sectors of the net is similar to that described by De Robertis et al. (2017a), the proportion of fish escaping though the meshes is smaller (Fig. S1.4). In

general, the corrected probability of retention in both nets is higher, but the slope of the curves remains similar (Figs. S1.5-7). The length at 50% retention (L_{50}), which is directly affected by the absolute value of escapement, increases when f_{mar} is corrected (compare Table 1 and De Robertis et al. (2017a), their Table 2). However, the slope of the curve defined by *SR*, which describes the difference in length at 75% and 25% retention (i.e. L_{75} - L_{25}), is less affected. For example, for Arctic cod, the most abundant species, L_{50} for the Marinovich shifts from 6.2 to 5.2 cm after correction, while *SR* is unchanged at 2.2 cm. In the case of the Cantrawl, L_{50} shifts from 5.6 to 5.3 cm, and *SR* is unchanged at 0.8 cm. Stated another way, the primary impact is that the probability of retention increased in both nets (i.e. L_{50} decreased). For example, the probability of retaining a 4 cm Arctic cod increased from 0.11 to 0.23 for the Marinovich after correction, and 0.01 to 0.02 for the Cantrawl. However, *SR* was unaffected in this case. Thus, although the corrected results indicate that the trawls are more likely to retain these small fishes than initially estimated, the relative differences between different sizes, species and trawls are less affected. We regret the error, and the corrected selectivity values and figures presented here should supersede those in the original publication.

The primary application of these selectivity relationships was to estimate selectivity-corrected species and size distributions from trawl catches for use in acoustic-trawl abundance surveys (De Robertis et al. 2017b). These survey estimates are a complex function of acoustic backscatter measurements, trawl catches, selectivity estimates, and the acoustic properties of the organisms. We re-computed the abundance estimates with the corrected selectivity estimates and find that as expected from prior sensitivity analyses (De Robertis et al. 2017b, their table 3), the effect on abundance estimates is relatively modest.

Total estimates for Arctic cod were within 0.7% of the previous estimates and those of other, less abundant species differed by at most 9.9% (Table 1). In addition, the reduced selectivity shifted size distributions towards larger sizes: mean length increased by up to 1.1% for Arctic and saffron cod, and by up to 7.9% for capelin and herring (Table 1). These differences are small because the acoustic-trawl estimates are sensitive to the relative change in escapement between species and size classes (i.e. changes in size and species composition) rather than the absolute changes in escapement. Thus, the impact of the error described above on the acoustic-trawl abundance estimates reported by De Robertis et al. (2017b) is modest, and does not appreciably alter the conclusions of that study. A revised data set with abundances computed with the corrected f_{mar} parameter is available for use in future studies (De Robertis, 2021).

Acknowledgements

This work was funded by the Alaska Fisheries Science Center, NOAA. This research builds on the Arctic EIS program and informs work relevant to the Arctic Integrated Ecosystem Research Program (IERP; http://www.nprb.org/arctic-program/). This manuscript is NPRB Publication ArcticIERP-37.

References

De Robertis, A. (2021), "De Robertis et al, 2017 - Chukchi shelf acoustic-trawl survey (corrected)", Mendeley Data, V1, doi: 10.17632/py3859yhnf.1 https://data.mendeley.com/datasets/py3859yhnf/1

De Robertis, A., Taylor, K., Williams, K., and Wilson, C. D. 2017a. Species and size selectivity of two midwater trawls used in an acoustic survey of the Alaska Arctic. Deep-Sea Research II, 135: 40-50. https://doi.org/10.1016/j.dsr2.2015.11.014

De Robertis, A., Taylor, K., Wilson, C., and Farley, E. 2017b. Abundance and Distribution of Arctic cod (*Boreogadus saida*) and other pelagic fishes over the U.S. continental shelf of the Northern Bering and Chukchi seas Deep-Sea Research II, 135: 51-65. https://doi.org/10.1016/j.dsr2.2015.11.014

Orr, J. W., Wildes, S., Kai, Y., Raring, N., Katugin, O., and Guyon, J. 2015. Systematics of North Pacific sand lances of the genus *Ammodytes* based on molecular and morphological evidence, with the description of a new species from Japan. Fishery Bulletin, 113: 129-156.

Table 1. Revised logistic selection curve parameters with bootstrapped confidence intervals. Methods are equivalent to those in De Robertis et al. (2017a) but with a correction for the degree of coverage of the recapture nets. L_{50} is the length in cm at 50% retention, and *SR* is the length in cm between 75 and 25% retention. Scientific names are follows: Arctic cod (*Boreogadus saida*), saffron cod (*Eleginus gracilis*), Arctic sand lance (*Ammodytes hexapterus*), Pacific capelin (*Mallotus villosus*). In the case of Arctic sand lance and capelin, some of the point estimates of L_{50} and SR fall outside of the 90% bootstrap confidence interval, which suggests that these values are affected by a small number of trawl hauls. Large values of SR imply little size selectivity across the observed size range. Note that *A. hexapterus* is referred to as Arctic sand lance (Orr et al., 2015), while this species was referred to as Pacific sand lance in De Robertis et al., 2017a,b.

Species Group	**Marin. L_{50} (cm) (90% CI)**	**Marin. *SR* (cm) (90% CI)**	**Can. L_{50} (cm) (90% CI)**	**Can. *SR* (cm) (90% CI)**
Arctic cod	5.2 (4.7,5.9)	2.2 (1.6, 3.1)	5.3 (4.1, 5.8)	0.8 (0.7, 1.0)
saffron cod	10.3 (8.3, 19.7)	6.1 (4.2, 14.2)	6.3 (-15.5, 24.4)	1.1 (-1.3, 3.3)
Arctic sand lance	11.1 (6.5, 18.9)	5.9 (2.1, 15.6)	257.2 (-64.3, 94.4)	77.5 (-19.7, 24.9)
capelin	-48.2 (-31.7, 45.7)	-88.8 (-56.3, 59.4)	6.2 (-4.3, 18.5)	1.0 (-12.2, 7.5)
other fishes	9.3 (8.2, 24.5)	5.2 (4.3, 15.7)	13.0 (9.1, 34.0)	2.9 (1.8, 9.0)
jellyfish	3.2 (-0.8, 3.8)	1.3 (0.1, 1.5)	89.4 (-437.6, 557.7)	52.6 (-283.8, 342.4)

CHAPTER 13 - Pacific cod or tikhookeanskaya treska (*Gadus macrocephalus*) in the Chukchi Sea during recent warm years: Distribution by life stage and age-0 diet and condition

Objective 3: Combine results from previous Arctic surveys (Arctic EIS, Phase 1, BASIS) and planned surveys (Arctic IES Phase 2) to assess variability in pelagic and demersal fish ecology over time relative to ocean conditions.

Daniel W. Cooper[a]., Kristin Cieciel[KC], Louise Copeman[a,LC], Pavel O. Emelin[PO], Elizabeth Logerwell[a], Nissa Ferm[a], Jesse Lamb[a], Robert Levine[RL], Kelia Axler[a], Rebecca A. Woodgate[RW], Lyle Britt[a], Robert Lauth[a], Benjamin Laurel[a], and Alexei M. Orlov[AO].

[a] Alaska Fisheries Science Center, NOAA, National Marine Fisheries Service
[KC] Alaska Regional Office, NOAA, National Marine Fisheries Service
[LC] Cooperative Institute for Marine Ecosystem and Resources Studies, University of Oregon
[PO] Russian Federal Research Institute of Fisheries and Oceanography, Moscow, Russia
[RW] University of Washington, Seattle, USA
[RL] School of Oceanography, University of Washington, Seattle, WA, USA
[AO] Shirshov Institute of Oceanology of the Russian Academy of Sciences, Moscow, Russia; Russian Federal Research Institute of Fisheries and Oceanography, Moscow, Russia; Severtsov Institute of Ecology and Evolution of the Russian Academy of Sciences, Moscow, Russia; Dagestan State University, Makhachkala, Russia; Tomsk State University, Tomsk, Russia; Caspian Institute of Biological Resources, Dagestan Federal Research Center of the Russian Academy of Sciences, Makhachkala, Russia

Abstract

Many fish species have moved poleward with ocean warming, and species distribution shifts can occur because of adult fish movement, or juveniles can recruit to new areas. In the Bering Sea, recent studies document a dramatic northward shift in the distribution of *Gadus macrocephalus* (Pacific cod in English and tikhookeanskaya treska in Russian) during a period of ocean warming, but it is unknown whether the current northward distribution shift continues into the Chukchi Sea. Here, we use catch data from multiple gear types to present larval, age-0, and older Pacific cod distributions from before (2010 and 2012) and during (2017, 2018, and 2019) recent Chukchi Sea warming events. We also report on the habitat, diet and condition of age-0 Pacific cod, which were present in the eastern Chukchi Sea in recent warm years (2017 and 2019), but were absent in a cold year (2012). We hypothesize that age-0 recruitment to the eastern Chukchi Sea is associated with recent warm temperatures and increased northward transport through the Bering Strait in the spring. Age-0 fish were present in both benthic and pelagic habitats and diets reflected prey resources at these capture locations. Age-1 Pacific cod were observed in the western Chukchi Sea in 2018 and 2019, indicating possible overwinter survival of age-0 fish, although there was little evidence that they survive and/or remain in the Chukchi Sea to age-2. Observed low lipid accumulation in age-0 Pacific cod from the Chukchi Sea suggests juvenile overwinter mortality may be relatively high compared to more boreal regions (e.g., Gulf of Alaska). Adult Pacific cod were also observed in the Chukchi Sea during 2018 and 2019. Although densities in the western Chukchi Sea were very low compared to the Bering Sea, the adults are the first known (to us) records from the Chukchi Sea. The increased presence of multiple age-classes of Pacific cod in the Chukchi Sea suggests poleward shifts in both nursery areas and adult summer habitat beyond the Bering Sea, but the quantity and quality (e.g., summer productivity and overwintering potential) of these habitats will require continued surveys.

Introduction

The ranges of many marine fish species have moved poleward in response to recent warming temperatures (Mueter and Litzow, 2008; Nye et al., 2009; Kotwicki and Lauth, 2013), which is impacting fisheries and ecosystems (Mueter and Litzow, 2008; Figueira and Booth, 2010; Hollowed et al. 2013). Distribution shifts caused by temperature often vary by ontogenetic stage (Morley et al., 2017; Barbeaux and Hollowed, 2018), because species may expand their range by multiple mechanisms, including movement of subadults and adults (Nye et al., 2009; Hill et al., 2016), or juveniles recruiting to new areas and remaining there as they grow (Rindorf and Lewy, 2006; Nye et al., 2009; Figueira and Booth, 2010).

Summer temperatures in the Bering and Chukchi seas (Figure 1) have increased in recent years (Stabeno and Bell, 2019; Danielson et al., 2020; Woodgate and Peralta-Ferriz, 2021). In the Bering Sea, sea-ice coverage during winter and spring causes an area of cold (<2 °C) bottom water known as the cold pool, which persists through the summer (Wyllie-Echeverria and Wooster, 1998; Stabeno et al., 2001). The annual spatial extent of the cold pool varies with annual sea-ice extent and can extend far into the southeastern Bering Sea in cold years, or be limited to areas of the northern Bering Sea in warm years (Overland et al., 2012; Stabeno et al., 2012). In recent decades, the Bering Sea has alternated between multi-year periods of cold and warm summer ocean bottom temperatures (Overland et al., 2012; Stabeno et al., 2012), including a cold period from 2007 through 2013, and a warm period which began in 2014 (Stabeno and Bell, 2019). The summer distribution of *Gadus macrocephalus* (Pacific cod in English or tikhookeanskaya treska in Russian, hereafter referred to as "cod") shifted northward in the eastern Bering Sea (EBS) during the recent warm period (Thompson, 2018; Stevenson and Lauth, 2019; Baker, 2021), likely in response to the spatial reduction of the cold pool in the EBS, and warmer summer bottom temperatures in the northern Bering Sea (NBS) (Stevenson and Lauth, 2019). Sub-adult and adult cod abundance increased by more than 900% in the NBS between 2010 and 2017 (Stevenson and Lauth, 2019). The size range of cod inhabiting the NBS has also changed: in 2010, the surveyed population was comprised of juvenile fish from 10 to about 35 cm fork length (FL), and also larger adults > 60 cm FL, with few fish in the intermediate size range. However, in 2017, there was a continuous length distribution of cod from juveniles through adults (Stevenson and Lauth, 2019). Temperatures of the Bering Sea inflow entering the Chukchi Sea during the summer have increased in recent years (Woodgate and Peralta-Ferriz, 2021), and temperatures on the Chukchi Sea shelf were historically high from 2014 – 2018 (Danielson et al., 2020). In 2017, cod densities in the NBS were elevated near the Bering Strait (Stevenson and Lauth, 2019), which is at the southern border of the Chukchi Sea (Figure 1), indicating that the population distribution may have continued into the unsampled southern Chukchi Sea. However, cod distribution and abundance have not been examined in the Chukchi Sea during the recent warm period, and the life stages and size distributions of any cod recently present in the Chukchi Sea are also unknown.

Juvenile cod have been documented in the Chukchi Sea (Barber et al., 1997; Mecklenburg et al., 2011, 2018; Logerwell et al., 2015) and Beaufort Sea (Andriashev, 1937; Rand and Logerwell, 2010), however relatively few records exist (Mecklenburg et al., 2011). In the Chukchi Sea, the largest reported cod were 33 cm (Logerwell et al., 2015), 31 cm (Barber et al., 1997), and 17.6 and 8.7 cm total length (TL) (Mecklenburg et al., 2011), which are below the smallest known size of maturity for cod in the EBS or Gulf of Alaska (Stark, 2007). Habitat of juvenile cod in the Chukchi Sea has not been examined. In the EBS, age-0 cod inhabit nearshore benthic habitat, or pelagic habitat in offshore deeper areas (Hurst et al., 2015). Because size and energetic storage are important factors contributing to the overwintering survival of juvenile marine fishes (Sogard, 1997; Hurst, 2007), it is unclear whether small boreal gadids such as cod can survive long periods of cold in low productivity habitats typical of the Chukchi Sea.

The juvenile cod observed in the Chukchi Sea may be sourced from larvae advected northward from the Bering Sea. Cod spawn in the EBS from March to mid-April (Neidetcher et al., 2014) and eggs likely

remain at their spawned location because they are demersal (Thomson, 1963; Fadeev, 2005). Larvae become more buoyant at hatch (Laurel et al. 2010) and are typically in surface waters where they have been reported in the EBS from April through June (Matarese et al., 2003) and in the western Bering Sea (WBS) in June (Bulatov, 1986). Ocean currents during the larval period may carry larvae from the NBS to the Chukchi Sea through the Bering Strait. Currents are measured by a mooring (A3) located just north of the Bering Strait (Figure 1), which provides hourly time series of ocean temperatures and northward transport through the Bering Strait (Woodgate, 2018).

The objectives of this study were to 1) investigate thermal and ocean transport conditions which could affect cod larvae transported between the NBS and Chukchi Sea; 2) describe cod distribution in the Chukchi Sea by life stage before (2010 and 2012) and during (2017, 2018, 2019) the recent period of warm summer ocean temperatures in the Chukchi Sea; and 3) understand the potential survival trajectories of age-0 cod in the Chukchi sea by comparing their habitat, size, diet and condition to juveniles collected farther south, in the Gulf of Alaska (GOA).

Methods

Bering Strait temperature and transport

Monthly averaged near-bottom temperatures in April through June from 1998 through 2019 measured at a subsurface mooring were used to investigate the thermal exposure of any cod larvae possibly in the Bering Strait during the larval period (Mooring A3 in Woodgate et al., 2015; Woodgate, 2018; Woodgate and Peralta-Ferriz, 2021). This mooring is located ~35 km north of the Bering Strait proper, at a point where water temperatures are considered to be a meaningful average of the water temperatures in the eastern and western sides of the Bering Strait (Woodgate, 2018). These measurements are made near bottom and represent the bottom layer (~30-40 m) of the water column. In April – June, sea surface temperatures are ~ 1 to 2 °C warmer than the near-bottom temperatures in the annual mean (Woodgate and Peralta-Ferriz, 2021; Woodgate, 2018, Figure 14). Thus, depending where they reside in the water column, larvae in April – June may be exposed to warmer (~1 to 2 °C) temperatures than considered here.

Estimates of water volume transport from the NBS to the Chukchi Sea during the larval period were obtained to investigate possible inter-annual differences in northward larval transport through the Bering Strait. Monthly-averaged northward transport estimates during April – June from 2000 – 2019 were calculated from the A3 mooring data (see Woodgate, 2018 for method), and an average transport value for April – June was calculated for each year.

Larval distributions

Larval cod were collected in the Bering Sea and southeastern Chukchi Sea during research cruises funded by the Arctic Integrated Ecosystem Research Program (AIERP) of the North Pacific Research Board (NPRB) in the spring and early summer months (April – June) of 2017 and 2018 using a paired 60-cm diameter bongo net (505-µm mesh) that was towed obliquely from the surface to 10 m off the bottom. Flowmeters attached to each net were used to quantify the volume filtered, allowing estimation of larval catch per unit effort (CPUE). CPUE for these larvae is reported as the number of larvae per 10 m^2 surface area calculated based on the maximum depth of the tow and volume filtered (Matarese et al., 2003). Samples were preserved at sea in 5% formalin buffered with sodium borate and seawater and identified to the lowest taxonomic level at the Plankton Sorting and Identification Center in Szczecin, Poland. Taxonomic verifications took place at the National Oceanic and Atmospheric Administration, Alaska Fisheries Science Center in Seattle, WA, USA. Conductivity, temperature, and depth (CTD) casts (Sea-Bird SBE 911 plus) were conducted immediately prior to net deployments to examine temperature (°C) across the study region. CTD-derived temperature measurements were averaged over the entire water

column (deepest CTD cast was ~60 m in Bering Strait in both years) and, for data visualization, the means were interpolated onto a 1 km × 1 km grid using local polynomial interpolation across longitude and latitude with the "stats" package in R (version 3.6.1; R Core Team 2020). These interpolated temperature measurements were then plotted with larval cod distributions (log(x+1)-transformed CPUE per 10 m^2) in June of 2017 and 2018.

Juvenile and adult distributions

Cod juveniles and adults were caught in several trawl types used for multi-species surveys in the eastern Chukchi Sea (ECS) and western Chukchi Sea (WCS) in cold years (2010 and 2012) and recent warm years (2017 – 2019; Table 1 and Figure 2).

Surface Trawl

A Nordic 264 Rope Trawl (NETS Systems) was deployed at nearshore stations during AIERP surveys in the ECS in 2017 and 2019 (Table 1, Figure 2). The rope trawl was 184 m long with non-uniform hexagonal mesh in the wings and body (maximum mesh size = 162 cm) and a 1.2 cm mesh liner in the codend. Tows were made at or near the surface for 30 minutes at 0.77 – 1.54 ms^{-1} (1.5 – 3 nautical miles $hour^{-1}$), and had typical trawl mouth openings of 20 m horizontally and 19 m vertically. All sampling was performed during daylight hours. CPUE was calculated as the number of fish divided by the surface area swept by the trawl. Surface area swept by the trawl was calculated as the width of the trawl opening multiplied by the distance fished. Distance fished was measured by Global Positioning System (GPS).

Midwater trawl

A modified-Marinovich midwater trawl (~34.5 m long, 12 m headrope, 6.4 to 1.8 cm mesh) with a 0.3 cm mesh codend liner was deployed during AIERP surveys in 2017 and 2019 in the ECS to conduct targeted midwater hauls (Table 1, Figure 2). Trawling location and depth were determined based on identification of strong scattering layers in shipboard acoustic data. CPUE of the midwater trawl was calculated as number of fish per trawl tow divided by the volume filtered by the trawl. Volume filtered was calculated as the trawl mouth opening multiplied by the distance fished. Distance fished was measured by GPS position. Net opening was measured using observation from a net sonar (Simrad FS70) placed on the headrope. For all hauls, the vertical net opening averaged 7.85 m (5.1 - 10.6 m range) and horizontal opening averaged 7.49 m (5 - 9.1 m range). Average headrope depth of midwater trawls was 32.1 m, ranging from 11.4 to 227.9 m, with an average ship speed during the tow of 1 – 1.5 m s^{-1}. Bottom depths of trawl locations ranged from 23 to 1130 m.

Small-mesh benthic trawl

A small-mesh benthic trawl was deployed in the ECS during the arctic ecosystem integrated survey (EIS) in 2012, and during AIERP surveys in 2017, and 2019 (Table 1, Figure 2). The trawl was a 3.05-m plumb staff beam trawl with a 7 mm mesh and 4 mm mesh codend liner (Gunderson and Ellis, 1986). In 2012, a tickler chain preceded the footrope (Gunderson and Ellis, 1986; Kotwicki et al., 2017). In 2017 and 2019, the tickler chain was removed, and the trawl was modified with a footrope of 10.2 cm rubber discs over a steel chain as in Abookire and Rose (2005). Mean trawl durations and ranges (minutes) were 2.9 (range = 2.8 – 7.4), 5.4 (range = 4.0 – 9.1), and 6.0 (range = 2.8 – 8.9) in 2012, 2017, and 2019, respectively. Targeted towing speed was 0.77 ms^{-1} (1.5 nautical miles $hour^{-1}$). CPUE was calculated as the number of cod in the trawl tow divided by the area swept by the trawl. Area swept by the trawl was the effective width of the trawl multiplied by the distance fished by the trawl. Effective trawl width of the trawl was assumed to be 2.26 m in 2012 (Gunderson and Ellis, 1986; Kotwicki et al., 2017), and 2.1 m in 2017 and 2019 (Abookire and Rose, 2005). Distance fished was measured as the distance between the

locations that the trawl began and stopped contact with the bottom. Bottom contact was determined by HOBO G acceleration data logger (Onset Corp.) placed in a waterproof steel housing and hung from the footrope in a manner forcing the data logger to pivot when it contacted the bottom. Time stamps from the acceleration data logger were used to match the start and conclusion of trawl bottom contact with location from GPS data.

Large-mesh benthic trawls

A large-mesh benthic trawl (DT 27.1/24.4 bottom trawl; Zakharov et al., 2013) was deployed in the WCS in 2010, 2018, and 2019 (Table 1, Figure 2). Trawl mesh was 8.0 cm in the wings and body, 6.0 cm in the intermediate, 3.0 cm in the codend, and the codend was equipped with a 10 mm mesh liner. Target trawl speed was ~1.5 ms^{-1} (3 nautical miles per hour) for a target duration of 30 minutes. CPUE was calculated as the number or weight of cod in the tow divided by the area swept by the trawl. Area swept by the trawl was calculated as the horizontal opening of the trawl (16.2 m) multiplied by the distance fished by the trawl. Distance fished was the distance between the locations that the trawl began and stopped contact with the bottom.

The large-mesh benthic trawl deployed in the ECS in 2012 (Table 1, Figure 2) as part of the Arctic EIS survey was an 83-112 Eastern Trawl (Stauffer, 2004). Deployment of the trawl in 2012 is described by Kotwicki et al. (2017). The trawl horizontal opening was approximately 17 m. Stretched mesh size was 10.2 cm in the wings and body, 8.9 cm in the intermediate and codend, and the codend was equipped with a 3.2 cm mesh liner. Target trawl speed was ~ 1.5 ms^{-1} (3 nautical miles per hour) for a target duration of 15 minutes. CPUE was calculated as the number of cod divided by the area swept of the trawl. Area swept was calculated as the distance fished multiplied by the width of the trawl opening. Width of the trawl opening was measured with acoustic net mensuration sensors (Marport Deep Sea Technologies, Inc.). Distance fished was measured as the distance between the locations that the trawl began and stopped contact with the bottom.

Gulf of Alaska small-mesh demersal seine

Age-0 juvenile cod were collected in August of 2017 during the annual summer nearshore seine survey on Kodiak Island to compare condition to those collected in the ECS in 2017. The GOA survey uses a 36 m demersal bag seine with 1 m wide seine wings at the ends expanding to 2.25 m in the middle. The mesh size was 13 mm within the wings and 5 mm in the bag-end. The seine wings were attached to 25 m ropes for deployment using a small boat and was set parallel to shore at a distance of 25 m away and then retrieved by two people standing on the shore, effectively sampling ~900 m^2 of bottom habitat (see more details in Laurel et al., 2007).

Trawl survey temperatures

Bottom temperatures were recorded at each station for the small- and large-mesh benthic trawls in the ECS using an SBE-39 (Seabird Scientific, Inc.) temperature sensor attached to the trawl headrope. Bottom temperatures in the WCS were recorded with either an SBE-19 or SBE-25 temperature sensor from CTD cast conducted at the trawl location. Gear temperatures for the surface and midwater trawls were measured with CTD casts taken with an SBE 911 plus. Near surface temperatures were used for the surface trawl, and temperatures averaged over the depth range between the trawl headrope and footrope at the targeted trawl depth were used for the midwater trawl. CTD casts were co-located with surface trawl tows; however, midwater trawl tows were opportunistic and temperatures were obtained from the nearest CTD cast (the same sampling grid as for the small-mesh benthic trawl each year; Figure 2).

Fish length and length-based age classification

In the surface, midwater, and small-mesh benthic trawls, cod were measured to the nearest millimeter at

sea. In 2017, TL was measured, and in 2019, one large fish was measured to FL, and the smaller fish were measured to standard length (SL). For comparison with laboratory data and other studies of age-0 fish, lengths of juveniles were converted to SL. To compare sizes of the juvenile cod with larger cod caught with the large-mesh trawls, lengths of juvenile fish were converted to FL. Lengths of juvenile fish were converted between length types using length data provided by Oregon State University, the AFSC's Auke Bay Laboratories and RACE Division's Midwater Assessment and Conservation Engineering program for fish within the same size range as the observed fish. The conversion factors were SL = TL(0.902) + 1.284 (based on 120 samples up to 110 mm in length) and SL = FL(0.952) - 0.663 (based on 11 samples up to 78 mm in length). Cod caught in both large-mesh benthic trawls were measured at sea to the nearest cm FL.

The length mode (49 – 103 mm FL) of small juveniles caught in the ECS in the small-mesh benthic, midwater, and surface trawls was similar to reported lengths of age-0 fish in the EBS during the summer (Hurst et al., 2012a; Hurst et al., 2015) and these fish will be referred to as age-0 for this study. The larger length mode of juveniles (100 – 230 mm FL) caught in the large-mesh benthic trawls in the ECS and WCS were smaller than age-1 fish in the Gulf of Alaska during the summer (150 – 250 mm TL; Laurel et al., 2016a); however they are assumed to be age-1 based on length mode analysis (they were larger than the mode of age-0 fish), and will be referred to as age-1 fish for this study. There was an overlap in the size ranges of the age-0 and age-1 fish (100 – 103 mm FL); however, the size range contained only 3% of the fish in this study. The larger cod (550 – 780 mm FL) caught in this study are greater than the size of 50% maturity for cod from the EBS and GOA (Stark, 2007) and are referred to as adults for this study.

Age-0 Diets

Diets of the age-0 cod caught in the ECS in 2017 were analyzed by capture trawl type (small-mesh benthic, midwater, and surface trawls) to investigate whether the age-0 cod captured in different parts of the water column used different prey resources. Sample sizes were 40 fish from 10 stations in the small-mesh benthic trawl, 28 fish from 6 stations in the midwater trawl, and 40 fish from 5 stations in the surface trawl. Fish were frozen at sea. Stomachs were dissected in the laboratory and stored in 10% formalin to fix stomach contents. Stomach contents were sorted to lowest practical taxonomic resolution and developmental stage (as appropriate) and weighed to the nearest 0.01 µg, and counted.

To determine prey importance in the age-0 cod diets, we used the percentage of the prey-specific index of relative importance (%PSIRI) (Brown et al., 2012). %PSIRI was calculated for age-0 cod collected in each type of trawl. %PSIRI is calculated using frequency of occurrence (FO), prey-specific count ($\%PN_i$), and prey-specific weight ($\%PW_i$), which were calculated using the following equations:
Frequency of occurrence (FO):

$$FO_i = \frac{n_i}{n},$$

Prey-specific count (%PN):

$$\%PNi = \sum_{j=1}^{n} \%N_{ij}/n_i.$$

Prey-specific weight ($\%PW_i$):

$$\%PW_i = \sum_{j=1}^{n} \%W_{ij}/n_i,$$

where $\%N_{ij}$ is the count (PN_i) and $\%W_{ij}$ is the weight (PW_i)) of prey category i in stomach sample j; n_i is the number of stomachs containing prey i, and n is the total number of stomachs.
The %PSIRI is then calculated:

$\%PSIRI_i = \frac{\%FO_i*(\%PN_i+\%PW_i)}{2}$.

%PSIRI was calculated for prey items at the lowest practical taxonomic resolution, and also for prey items grouped by the following prey habitat types: endobenthic, epibenthic, hyperbenthic, planktonic, or various. Each prey item was assigned a prey habitat type based on a literature search.

The symmetric niche overlap coefficient (Pianka, 1973), was calculated to determine whether there was niche overlap among the diets of cod caught in the different trawl types using the following equation:

$$O_{kl} = \frac{\sum_i^n p_{il} p_{ik}}{\sqrt{\sum_i^n p_{il}^2 \sum_i^n p_{ik}^2}}$$

where O_{kl} is the resource overlap index between capture trawl type k and l, and p_{il} is the proportion of resource i that is used by capture trawl type l.

This resource overlap index produces values from 0 to 1, where 0 indicates that no resources are shared and 1 indicates complete shared resource utilization between the cod collected in different trawl types. The capture trawl type by prey matrix was randomized 2000 times. For each randomization, the Pianka coefficient was calculated to create the null distribution. All data analysis was conducted using R statistical analysis software (R Core Team, 2020). The EcoSimR package was used to calculate the Pianka coefficient and determine if there was niche overlap among trawl types using a null model.

Age-0 Condition

One-hundred and seventeen age-0 cod collected in the ECS in 2017 and 30 age-0 fish from the annual August GOA beach seine survey in 2017 were saved for condition analyses. Fish from the four different gear types described above, small-mesh benthic (n=45), midwater (n=31), surface trawls (n=41) and the GOA beach seines (n=30) were frozen immediately at -20 ℃ and were maintained at -80 ℃ at the land-based laboratory. Samples were frozen and shipped overnight from Alaska to the Marine Lipid Ecology Laboratory at Oregon State University's Center for Marine Ecosystem and Resources Studies facility at the Hatfield Marine Science Center in Newport, OR, USA. Samples were stored at -80 ℃ and dissected within 6 months of capture. At the laboratory, all fish were measured to SL, (± 0.1 mm) and wet weight (WWT; ± 0.0001 g). All of the fish from the Chukchi Sea and 18 of the 30 fish from the GOA were used in the biochemical analysis. For these fish, intestinal tracts were removed and fish were washed with filtered seawater, blotted dry, and heads were removed for later otolith analysis. Fish were bisected along a dorsal ventral plane and half of the tissues were frozen for other analyses while half of the body tissues were placed in chloroform under nitrogen until extraction, within 1 month of sampling.

Cod tissues were homogenized in 2:1 chloroform:methanol according to Parrish (1987) using a modified Folch procedure (Folch et al., 1956). Lipid extracts were derivatized through acid transesterification using a Hilditch Reagent, H_2SO4 in MeOH as described in Budge et al. (2006). Fatty acid methyl esters (FAMEs) formed in the reaction were analyzed on an HP 7890 GC FID equipped with an autosampler and a DB wax+ GC column (Agilent Technologies, Inc.). The column length was 30 m with an internal diameter of 0.25 mm and a film thickness of 0.25 μm. The column temperature profile was as follows: 65 °C for 0.5 min, hold at 195 °C for 15 min after ramping at 40 °C min^{-1}, and hold at 220 °C for 1 min after ramping at 2 °C min^{-1}. The carrier gas was hydrogen, flowing at a rate of 2 ml. min^{-1}. Injector temperature was set at 250 °C and the detector temperature was constant at 250 °C. Peaks were identified using retention times based upon standards purchased from Supelco (BAME, PUFA 1, 37 component FAME, PUFA 3). Nu-Check Prep GLC 487 quantitative FA mixed standard was used to develop correction factors for individual FAs. Chromatograms were integrated using Chem Station (version A.01.02, Agilent). Total fatty acids were expressed in relation to fish WWT (g) to give an index of total acyl lipid storage.

Regressions between $\log_{10}$ (SL) and $\log_{10}$ (WWT) as well as $\log_{10}$ (SL) and fatty acid concentrations (mg/g) were run as indices of morphometric- and lipid-based condition, respectively. Residuals from these relationships were compared between the GOA and ECS using a two-sample t-test.

Results

Bering Strait temperature and transport

Monthly-averaged near-bottom water temperatures in the Bering Strait in April were consistently cold throughout the time series, ranging from -1.58 to -1.89 °C (Figure 3). Both temperature and inter-annual variability increased in May, although May near-bottom temperatures remained below 0 ˚C for all years except 2017 (Figure 3). Inter-annual temperature variability increased in June, with monthly averaged temperatures ranging from -0.83 to 2.95 °C. Any larvae transported northward though the Bering Strait in June 2012 would have been exposed to temperatures of ~ 0.5 – 1.5 °C (near bottom temperature of -0.5 °C + 1 – 2 °C warmer in the water column). June near-bottom temperatures from 2015 to 2019 were among the highest in the time series. Larvae in June would have been exposed to temperatures of ~ 4 – 5 °C in 2017 and ~2.3 – 3.3 °C in 2019.

Net northward transport from the NBS to the Chukchi Sea averaged over the larval period (April-June) has increased over the past two decades from ~ 0.7 Sv ($1Sv=10^6 m^3/s$) in 2000 to ~ 1.5 Sv in 2017, the record maximum (Figure 3).

Larval distributions and temperatures

Larvae were present in the NBS near the Bering Strait in 2017 and 2018 at sites with water temperatures which ranged from 2.6 to 3.7 °C and 2.1 to 6.0 °C on average in 2017 and 2018, respectively (Figure 4).

Age-0 cod in the ECS

Distribution and temperature

Age-0 cod ranging in length from 45 to 94 mm SL (49 – 103 mm FL) were caught in the surface, midwater, and small-mesh benthic trawls in 2017 and 2019 in the ECS (Figure 5). Age-0 cod were absent from the ECS in 2012; however, the only trawl type deployed in 2012 capable of catching small juveniles was the small-mesh benthic trawl. Detailed results are reported by trawl type.

In 2017, age-0 cod were present in the surface trawl catch at one station near Point Lay, and at several stations from the vicinity of Cape Lisburne to the southern end of the survey area (Figure 6). In 2019, age-0 cod were caught only at the most northerly surface trawl station, between Point Lay and Cape Lisburne. Surface temperatures where age-0 cod were present i
n the surface trawl ranged from 5.0 – 6.2 °C in 2017, and surface temperature was 9.3 °C at the one station with age-0 presence in 2019. In both years, age-0 cod were present at stations near the median temperatures of all available surface trawl stations (Figure 7). Bottom temperatures at stations where age-0 cod were caught in the surface trawl were slightly colder than surface temperatures (range = 4.1 – 5.6 °C) in 2017; however, bottom temperature was slightly warmer at the one station with age-0 presence in 2019 (Figure 7).

In 2017, age-0 cod were present in the midwater trawl catch at stations from offshore of Point Lay south to the vicinity of Point Hope (Figure 6). In 2019, the observed distribution of age-0 cod shifted north, with absences near Point Hope and Cape Lisburne, and presences north of Point Lay. Age-0 cod were present in the midwater trawl catch at stations with gear temperatures ranging from 4.6 – 6.7 °C and 2.3 –

10.0 °C in 2017 and 2019, respectively. Age-0 cod were almost exclusively caught in the midwater trawl at locations warmer than the median temperature of all midwater trawls (Figure 7). At stations with age-0 presence, bottom temperatures were colder than the midwater gear temperatures, however, generally by less than 1 °C (Figure 7).

In 2012, age-0 cod were absent at all 40 stations sampled with the small-mesh benthic trawl (Figure 8). In 2017, age-0 cod were present at 11 of 59 sampled stations, from offshore of Point Lay south to the southern edge of the sampling grid, including at 7 stations which had been sampled in 2012 (Figure 8). CPUEs at stations with fish presence in 2017 ranged from about 1350 – 46,000 age-0s km^{-2}. In 2019, age-0 cod were present at 4 of 49 sampled stations, at CPUEs ranging from about 1700 – 7,100 age-0s km^{-2} (Figure 8). Age-0 cod were present in bottom temperatures ranging from 2.5 to 5.9 °C and 4.4 to 9.5 °C in 2017 and 2019, respectively. Station bottom temperatures during the 2017 and 2019 surveys ranged from below 0 °C in the northern part of the survey area to near or exceeding 10 °C in the inshore and southern part of the survey grids each year (Figures 7 and 8). In the mooring data, June temperatures in the Bering Strait were colder in 2012 than in 2017 and 2019 (Figure 3), and summer bottom temperatures were colder in the northern and offshore stations in 2012 than in 2017 and 2019 (Figure 8). However, bottom temperatures at the southern and nearshore stations with age-0 cod presence in 2017 were generally warmer in 2012 than in 2017 (Figure 8), and the range of available bottom temperatures surveyed by the bottom trawl in 2012 included the temperature range where age-0 cod were present in 2012 and 2019 (Figure 7).

Age-0 catch rates by depth

Catch rates of age-0 cod by bottom depth varied by gear type in a similar pattern each year (Figure 9). The highest catch rates in the small-mesh benthic trawl were between 20 and 29 m and 30 to 39 m bottom depth in 2017 and 2019, respectively, and in both years, catch rates were lower at depths greater than 40 m. In contrast, the highest catch rates in the midwater trawl were at greater bottom depths; between 40 and 59 m in 2017, and between 40 and 49 m in 2019. Catch rates in the surface trawl were highest in the 20 – 29 m bottom depth range, however the surface trawl was fished only at nearshore station, and most surface trawls occurred over relatively shallow bottom depths.

Age-0 diet by gear type

Age-0 cod collected in all the surface, midwater, and small-mesh benthic trawls in 2017 consumed a variety of prey taxa (Table 2, Figure 10). Copepods were the most important (importance measured by % PSIRI) prey taxa for fish collected in all three gears (Figure 10), with benthic-caught fish primarily consuming the epibenthic calanoid copepod species *Eurytemora herdmandi* (PSIRI = 13.55%), while the surface- and midwater-caught fish primarily consumed various pelagic calanoid copepods (PSIRI = 70.54% and 26.40% for the surface and midwater trawls, respectively). The benthic-caught age-0 cod also consumed near equal percentages of a taxonomically-broad suite of prey items; including benthic prey taxa such as polychaetes, benthic amphipods, benthic decapods, and benthic cnidarians (anemones). The most important prey taxa for the pelagic-caught fish, after calanoid copepods, were decapods for the surface trawl-caught fish, and fish (unidentified Gadidae) and decapods for the midwater trawl-caught fish. The niche overlap indices for diets of age-0 cod caught in the benthic and pelagic trawls were low (benthic and midwater = 0.01, benthic and surface = 0.08), indicating little overlap in diets and somewhat higher overlap for the diets of the two pelagic trawls (surface and midwater = 0.2). Grouped by general habitat classifications, prey of the pelagic-caught fish were almost entirely pelagic or unknown, while the benthic-caught fish also consumed endo-, epi-, and hyper-benthic prey (Figure 10).

Age-0 Condition: ECS versus GOA

Two measures of condition, length-weight residuals and total fatty acid concentration, were compared between age-0 cod from the ECS and the nearshore GOA (Fig. 11). Age-0 cod from the GOA were longer and heavier than age-0 cod from the ECS even though they were collected in August compared to fish collected in September in the ECS. Fish from the GOA in August averaged ~80 mm SL and weighed 5 grams while fish from the ECS were ~67 mm SL and 3 grams. The residuals from the log-length and log-weight relationship demonstrated that fish from the GOA were heavier at a given length than fish from the ECS. Total fatty acids per WWT did not increase with length (r^2=0.02). The residuals from the length to total fatty acids relationship showed that fish from the GOA had a higher concentration of fatty acids per WWT at a given length than fish from the ECS ($p<0.001$). Both morphometric condition and that based on length-lipid concentration showed that fish from the GOA were in better condition at the end of the summer/fall than fish from the ECS.

Age-1 and adults

WCS distributions and temperatures

Cod were absent from the trawl sampling in the WCS in 2010 (Figure 12). Both age-1 juveniles and adults were present in the WCS in 2018 and 2019 (Figure 12). In both years, there was a length mode of juveniles (assumed to be age-1), from 130 – 180 and 100 – 230 mm FL in 2018 and 2019, respectively, and larger adult-sized fish, from 660 – 780 and 550 – 750 mm FL in 2018 and 2019, respectively (Figure 5). Although there were two juveniles larger than 180 mm FL in 2019, there was little evidence of a new length mode of fish greater than 180 mm FL in 2019, and these two fish are also assumed to be age-1. CPUEs of age-1 cod at stations where they were present ranged from 23 – 133 and 9 – 95 fish km^{-2} in 2018 and 2019, respectively. A total of five adult cod were caught in 2018 and four in 2019. Estimated densities of adult-sized fish, where they were present, ranged from 12 – 24 and 10 – 22 fish km^{-2} in 2018 and 2019, respectively. CPUEs by weight for the age-1 and adults combined at stations where they were present, and in units for comparison with previous reports in the Bering Sea were 0.004 – 1.54 and 0.0018 – 1.073 kg ha^{-1} in 2018 and 2019, respectively.

Bottom temperatures where cod were present ranged from 1.9 – 4.7 °C and 3.3 – 4.7 °C for age-1s and adults, respectively in 2018 (Figure 7), and from 1.4 – 4.9 °C and 0.4 – 4.9 °C for age-1s and adults, respectively in 2019 (Figure 7). Although 2010 was a year with cold temperatures in the Bering Strait in June (Figure 3), much of the sampled area in the southwestern Chukchi Sea in 2010 was within the bottom temperature range that contained cod in 2018 and 2019 (Figures 7 and 12).

ECS distributions and temperatures

Age-1 cod were present at three stations in 2012 in the large-mesh benthic trawl in the ECS (Figure 12). These age-1s ranged in size from 100 – 130 mm FL (Fig. 5), and CPUE from 44 – 106 fish km^{-2}. Adults were absent at all stations in the ECS in 2012.

Bottom temperatures where age-1 cod were present in 2012 in the large-mesh benthic trawl sampling ranged from 1.3 – 9.9 °C (Figure 7). Similar to 2010 in the WCS, 2012 was a year with cold June water temperature in the Bering Strait, (Figure 3); however, much of the sampled area in the shallow southeastern Chukchi Sea in 2012 was as warm as or warmer than areas with age-1 and adult presence in the WCS in 2018 and 2019 (Figures 7 and 12).

In addition to the age-0 cod caught in the midwater trawl (section 3.3.1), one much larger (64.7 cm FL) adult was caught using the midwater trawl during a tow that fished near the benthos at the southern end of the survey area in 2019 (Figure 6).

Discussion

Age-0 and adult cod were absent from the Chukchi Sea in the cold years and present in recent warm years of this study. One question is whether the observed increases in age-0 and adult cod are related to temperature and recent Arctic warming. We hypothesize that changes in annual springtime conditions at the Bering Strait and in the NBS are a possible reason for the observed increase in age-0 cod in the Chukchi Sea. In 2012, a cold year, larvae near the Bering Strait in June would have been exposed to cold (estimated ~0.5 to 1.5 °C) water. The growth of cod larvae is highly temperature-dependent and survival in the laboratory is reduced at 2 °C (Hurst et al., 2010). Unfed yolksac larvae can survive lower temperatures (e.g., 0 °C), but growth and development rates are very slow (Laurel et al., 2008) and hatch success is poor (Laurel and Rogers, 2020). It is therefore unlikely that eggs and larvae have historically occupied these Arctic regions where juveniles have recently been observed. We note that larvae were observed near the Bering Strait in June in warm years, which would have likely contributed to better larval survival and increased presence of age-0 fish in the Chukchi Sea in 2017 and 2019. Warm June temperatures at the Bering Strait also occurred in a previous year (2007) when age-0-sized cod were observed in the Chukchi Sea (Mecklenburg et al., 2011), and two years when age-1 fish observed in this study would have been larvae (age-1 fish observed in 2012 and 2019 would have been larvae in June of 2011 and 2018).

Warm temperatures in the NBS and Bering Strait during the larval period may also cause successful larval delivery to the Chukchi Sea by other mechanisms (or a combination of mechanisms), such as by shifting spawning northward in the Bering Sea, improving egg survival (Laurel and Rogers, 2020), or improving larval prey fields (Laurel et al. 2021). Increased ocean transport during the larval period from the NBS to the Chukchi Sea may also be a cause or partial cause of the age-0 cod observed in the Chukchi Sea in recent years, which would be similar to pollock (*Gadus chalcogrammus*), a pelagic boreal species that has been observed in the Chukchi Sea in recent years of high transport (Orlov et al., 2019, 2020, 2021; Levine et al., this issue; Antonov et al., this issue; Emelyanova et al., this issue).
Recent adult cod presence in the Chukchi Sea may also be related to warmer temperatures in the NBS and Bering Strait in the spring. Adult cod avoid the cold pool in the EBS (Kotwicki and Lauth, 2013), and the movement of adult cod into the NBS between 2010 and 2017 coincides with a reduction in the cold pool in the NBS (Stevenson and Lauth, 2019; Baker, 2021). Preliminary tagging data suggests that adult cod move from the EBS into the NBS after sea ice has retreated northward in the spring and summer (J. Nielsen, Kingfisher Marine Research, and S. McDermott, AFSC, personal communication, February 23, 2021). Based on these tagging data, it is possible that the early ice retreat in both 2018 and 2019 (Stabeno and Bell, 2019; Siddon et al., 2020) allowed the fish to reach the Bering Strait early enough in the year to continue northward into the Chukchi Sea by August.

Increased temperatures on the Chukchi Sea shelf in the summer are less likely to be the cause of the increased cod presence in recent years than temperatures in the NBS and Bering Strait. Annual summer water temperatures on the ECS shelf have increased since 2014 (Danielson et al., 2020); however, even in the earlier and colder years of this study (2010 and 2012), when age-0 and adult cod were absent, some of the sampled habitat was warm enough (based on observed presence in 2017 and 2019) to support cod. The entire water column of the relatively shallow southeastern Chukchi Sea warms in the summer due to both advection and wind mixing (Grebmeier et al., 2015; Woodgate et al., 2015), and the nearshore areas are in the Alaska Coastal Current, which is typically warmer than the rest of the shelf from June to at least October (Woodgate et al., 2010; Woodgate, 2018). Even in the cold years of this study, the Chukchi Sea appeared warm enough during the summer for age-0 and adult cod to be present.

Age-0 cod in the Chukchi Sea use both pelagic and demersal habitats, which is similar to their habitat use in the EBS (Hurst et al., 2015). Diet differences between age-0 fish in pelagic and benthic habitats imply that age-0 cod remain at a habitat type for, at minimum, a daily feeding cycle. In the EBS, age-0 cod are

pelagic over deeper water and benthic in nearshore shallower areas, which is possibly related to temperature; the juveniles occupy demersal habitat in inshore areas with relatively warm bottom temperatures, and occupy warmer pelagic habitat when they are over deep water with cold benthic habitat (Hurst et al., 2015). Age-0 habitat use in the Chukchi Sea fits the same general pattern, with the addition that some fish use the pelagic nearshore habitat. This may mean that, in addition to temperature, fish in nearshore areas may select their depth in the water column based on some other factor, such as localized prey fields, or salinity.

The absence of a length mode of juveniles in the ECS in 2019 larger than that observed in 2018 suggests that the age-1 cod in 2018 may not have survived to age-2. All previous reports of cod from the ECS have been of juvenile-sized fish (Barber et al., 1997; Mecklenburg et al., 2011, 2018; Logerwell et al., 2015). It seems that cod juveniles in the Chukchi Sea either suffer high mortality rates, or migrate to other areas prior to adulthood.

The juveniles in the Chukchi Sea may not be able to successfully grow and provision themselves well enough to survive to become adults. Condition (lipid densities and weight at length) was lower in the 2017 age-0 cod from the Chukchi Sea than those from the GOA. Lipid densities were also lower in the age-0 cod in this study than in co-occurring gadids in the Chukchi Sea in 2017 (Copeman et al., this issue). The age-0 cod in the Chukchi Sea in this study inhabited colder waters (2017, 2 – 6 °C) than age-0 cod during the summer in the EBS (~6 – 12 °C; Hurst et al. 2015; Hurst et al., 2018) and the Gulf of Alaska (~8 – 11 °C; Abookire et al., 2007; Laurel et al., 2016a). Further, summer temperatures in the Chukchi Sea are lower than those modeled for maximum growth (~11.0 to 11.5 °C) and maximum lipid accumulation (10 °C) in controlled laboratory growth experiments (Laurel et al., 2016b; Hurst et al., 2010; Hurst et al., 2012b; Copeman et al., 2017). Thus, temperatures during the summer in the Chukchi Sea may be too low for juvenile cod to achieve sufficient size or energetic thresholds to survive long, low-productive Arctic winters. Future monitoring of age-0 cod in the Chukchi Sea should include both growth and condition metrics.

The abundance of age-0 cod in the ECS is potentially high enough to be ecologically meaningful if they could survive to adulthood. Only small numbers of juveniles were caught with our small-mesh benthic trawl, but catch rates in the nearshore areas of the ECS were similar to catch rates in EBS nursery areas using a similar trawl (Hurst et al., 2015; Table 3); however, they were one order of magnitude lower than catch rates in GOA nursery areas in high-abundance years (Table 3). An abundance estimate based on our limited number of stations in 2017 should be viewed with caution, but it provides a general sense of the potential number of cod juveniles in the ECS in 2017. Benthic trawl catch rates in the ECS were highest from 67 °N to 69 °N inshore of 40 m bottom depth, an area of approximately 14,500 km^2. Mean catch rates here were approximately 12,000 fish per km^2. Assuming the trawl caught all of the fish in the towpath, and our sampling was representative of the area, mean density multiplied by area would equal approximately 174 million fish present in 2017 within the area from 67°N to 69 °N inshore of 40 m bottom depth. Alternatively, estimating abundance from the mean catch rates and area of the entire survey area south of 70 °N provides an estimate of approximately 150 million fish. Even if these estimates are high, there were tens of millions of age-0 cod in the ECS in 2017. If these or future age-0 cod survive to adulthood, and either remain in the Chukchi Sea or successfully migrate to other spawning areas, it would mean a northward expansion of cod nursery area habitat, which is one type of poleward distribution shift that has been documented in marine fish due to ocean warming (Rindorf and Lewy, 2006; Nye et al., 2009; Figueira and Booth, 2010).

Densities of adult and age-1 cod estimated in this study are very low compared to reports from the Bering Sea. CPUE by weight for combined age-1 and adult fish at stations where fish were present ranged from 0.0018 to 1.5 kg/ha in this study. Even in 2010, when cod were considered “almost completely absent” from the NBS, cod CPUE values at some stations were greater than 10 kg/ha, and CPUE values in the

EBS may be greater than 50 kg/ha (Stevenson and Lauth, 2019). These catch rate comparisons are between the DT 27.1/24.4 bottom trawl used in the WCS in this study, and the 83-112 trawl used in the NBS and EBS, however catchability differences seem unlikely to cause the much lower CPUE values observed in the WCS in this study. In the western Bering Sea (WBS), cod densities have been reported from surveys using the same large-mesh trawl as used in the WCS in this study (Shuntov et al., 2014). Cod densities in the WBS were summarized by statistical regions and depth range over the time period from 2006 through 2012. In regions and depth ranges where cod are present in the WBS, reported mean densities ranged from 235 to 7,631 kg ha-1, however these densities assumed that only 40% of fish encountering the trawl were retained by the trawl (Shuntov et al., 2014). To make these numbers comparable to the CPUE units used in this study (100% of fish retained), the values reported by Shuntov et al. (2014) were multiplied by 0.4. These converted mean CPUE values are 94 to 3,052 kg ha-1 and are much higher than even the peak CPUE values observed in the Chukchi Sea in this study.

Although estimated densities were low, the adult cod observed in the WCS (and the one adult caught in the ECS) in this study are among the first known (to us) adult Pacific cod caught in the Chukchi Sea. The only other is an adult Pacific cod caught in a subsistence fishing net near Point Hope, AK, in August 2020, and reported as a novel occurrence to the Alaska Arctic Observatory and Knowledge Hub (AAOKH; Donna Hauser, International Arctic Research Center, University of Alaska Fairbanks, personal communication, January 29, 2021). The lack of observed intermediate size ranges of fish between age-1 and adults makes it likely that there is not a self-recruiting cod population in the Chukchi Sea, and that the adults likely moved northward from the Bering Sea, similar to how adults moved into the NBS from the EBS (Stevenson and Lauth, 2019). Only one adult was caught in the ECS during this study, but it was caught when the pelagic midwater trawl was incidentally fished on the bottom while targeting a deep acoustic layer. It is possible that adults and larger juveniles were also present at other sampling stations in the ECS in the recent warm years of this study, but avoided the pelagic and small-mesh benthic sampling gear. Adult cod are primarily benthic (Fadeev, 2005; Nichol et al., 2007) and would not be available to the pelagic trawls, and could also likely avoid the small-mesh benthic trawl due to the small mouth opening and slow fishing speeds (Lauth et al., In prep). Therefore, the presence of larger juvenile and adult cod in the ECS is unknown and will remain unknown until the area is surveyed across a range of habitats with gear suited to their capture.

The data presented here show that multiple life stages of Pacific cod were present in the Chukchi Sea in recent warm years, which suggests that the species is expanding into the Chukchi Sea by both recruitment and adult movement. However, the true extent of this range expansion, its potential to persist into the future, and the ultimate fate of individuals that move into the Chukchi Sea, are still unknown. Monitoring surveys designed to estimate abundances and condition of multiple life stages are required to better understand this poleward distribution shift, and to assess its impacts to the ecosystem.

Acknowledgments

We thank Aleksey Somov (TINRO, Vladivostok, Russia) for first noticing the difference between juvenile saffron cod (*Eleginus gracilis*) and Pacific cod in our trawl catches during the 2017 Arctic IERP cruise. We also thank the captains, crews, and scientists aboard the RV *TINRO*, FV *Alaska Knight*, RV *Ocean Starr*, and RV *Professor Levanidov* for deploying the trawls and processing the catches. We thank James Orr and Duane Stevenson of the AFSC for visually confirming the identities of some Pacific cod voucher specimens, as well as Sharon Wildes and others at the AFSC for genetic confirmation of vouchered fish identification. We thank Brian Voss, Director of the NOAA Western Center Regional Library for locating several historical publications. We thank the Plankton Sorting and Identification Center in Szczecin, Poland, and the Alaska Fisheries Science Center ichthyoplankton team for their larval fish taxonomic expertise. We thank Carlissa Salant and Michelle Stowell at the Marine Lipid Ecology Lab in Newport, OR, for help with juvenile fish dissection and fatty acid analyses. This work is

contribution EcoFOCI-1001 to NOAA's Ecosystems and Fisheries-Oceanography Coordinated Investigations (EcoFOCI), and was funded by the North Pacific Research Board Arctic Integrated Research Program, and NOAA Essential Fish Habitat research funds. Funding for the Bering Strait mooring work is currently through NSF-OPP, (awards: PLR-1304052, 1758565), and Bering Strait mooring data and products are available at psc.apl.washington.edu/BeringStrait.html. The 2012 Arctic ecosystem integrated survey (EIS) was funded by the Bureau of Ocean Energy Management (BOEM), and the Coastal Impact Assistance Program (CIAP). Ingrid Spies and Duane Stevenson of the AFSC provided thoughtful reviews of previous versions of the MS and greatly improved the final version.

180011049
Yurk, H., Barrett-Lennard, L., Ford, J. and Matkin, C. (2002) Cultural transmission within maternal lineages vocal clans in resident killer whales in southern Alaska. *Animal Behaviour*, 63(6), pp.1103-1119.

Appendix

Table A. Results from independent samples t-test which compared different time and frequency parameters between the five described call types in the current study and Madrigal *et al* 2021.

T-Test Results Duration		**Difference**	**t-statistic**	**DF**	**P value**
	Flat	-0.06	-1.859	793	0.06
	Downsweep	0.09	1.74	281	0.08
	Upsweep	0.081	-0.368	178	0.71
	Modulated	-0.11	-1.22	104	p=0.22
	Single Modulated	-0.024	-0.398	77	p=0.0002
T-Test Results Start Freq		**Difference**	**t-statistic**	**DF**	**P value**
	Flat	-212.3	-11.19	793	<0.0001
	Downsweep	-506.04	-8.66	281	<0.0001
	Upsweep	-311.09	-5.19	178	<0.0001
	Modulated	-516.26	-7.94	104	<0.0001
	Single Modulated	-405.67	-4.83	77	p<0.0001
T-Test Results End Freq		**Difference**	**t-statistic**	**DF**	**P value**
	Flat	-176.92	-9.286	793	<0.0001
	Downsweep	-395.52	-10.35	281	<0.0001
	Upsweep	17.36	0.24	178	0.811
	Modulated	-427.26	-7.35	104	<0.0001
	Single Modulated	93.54	-2.98	77	p=0.004
T-Test Results Min Freq		**Difference**	**t-statistic**	**DF**	**P value**
	Flat	-124.4	-7.75	793	<0.0001
	Downsweep	-317.48	-8.83	281	<0.0001
	Upsweep	-185.91	-3.35	178	p=0.001
	Modulated	-402	-11.2	104	<0.0001
	Single Modulated	-278.33	-2.98	77	p=0.004
T-Test Results Max Freq		**Difference**	**t-statistic**	**DF**	**P value**
	Flat	-272.5	-13.5	793	<0.0001
	Downsweep	-479.62	-8.62	281	<0.0001
	Upsweep	-79.09	-1.085	178	p=.279
	Modulated	-397.35	-6.029	104	<0.0001
	Single Modulated	-347	-3.7	77	p=0.0004

T-Test Results Freq Med		Difference	t-statistic	DF	P value
	Flat	-177.32	-10.15	793	<0.0001
	Downsweep	-315.37	-7.74	281	<0.0001
	Upsweep	-85.82	-1.37	178	p=0.17
	Modulated	-441.52	-9.53	104	<0.0001
	Single Modulated	-420.33	-5.11	77	<0.0001

Chapter 3: Seasonal and geographic variation of marine mammals in the northern Bering Sea

Stafford, K.M., Danielson, S.L. *in preparation for submission to Polar Biology*

The Pacific Arctic Region (PAR), which includes the Bering Strait region, and Chukchi and Beaufort Seas, is a bellwether for climate change in the Arctic with sea ice extent and thickness decreasing and freshwater and heat content increasing. In 2017-2018, the PAR experienced extreme warming evidenced by high water temperatures and greatly reduced seasonal sea ice in the northern Bering and Chukchi Seas. The biological responses to these extreme physical changes are complex but may result in ecosystem shifts from primary productivity to upper trophic predators. To observe the response of upper trophic level species via changes in occurrence and/or distribution over both temporal and spatial scales, passive acoustic recorders were deployed on three ecosystem moorings in PAR hotspots: the northern Bering Sea off western St Lawrence Island, in the Chukchi Sea at Hanna Shoal, and on the shelf break of the western Beaufort Sea from 2017-18 (Figure 5).

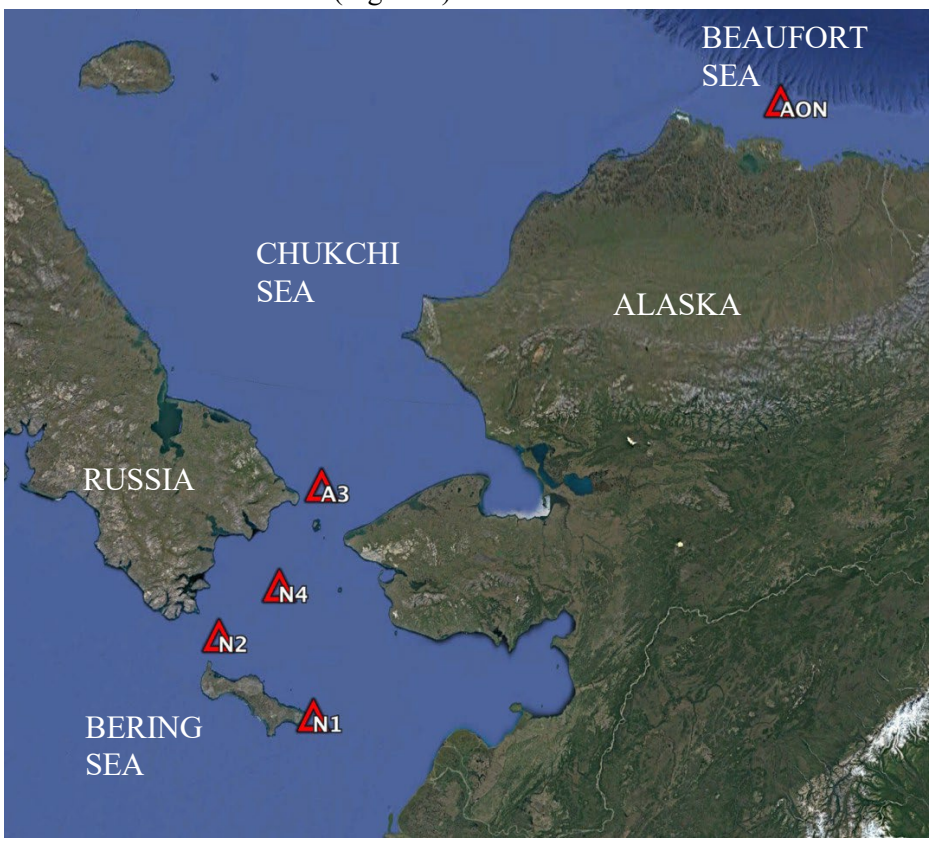

Figure 5. Map of the Pacific Arctic showing the locations of the five hydrophones used to examine the geographic variation in marine mammal occurrence.

To examine whether there were north-south or east-west changes in the presence of marine mammals, acoustic data from five biophysical moorings were used, including three from the ASGARD project (Table 1). Additional data were from a mooring just north of the Bering Strait (A3) and one from the

western Beaufort Sea (AON). Spectrograms of each acoustic data file were reviewed for the presence of marine mammals which resulted in time series of species presence by hour.

Mooring ID	Latitude	Longitude	Date range	Sample rate (Hz)	Duty cycle (min/hr)
N1	63 17.8	-168 25.7	8/1/17-6/28/18	16384	
N2	64 09.3	-171 31.6	6/8/17-7/7/18	16384	25/60
N4	65 55.7	-169 55.1	6/25/17-7/7/18	16384	25/60
A3	66 19.6	-168 57.6	7/14/17-7/7/18	16384	18/60
AON	71 24.0	-152 00	7/1/17-7/31/18	16384	5/60

The hydrophones in the Bering Sea (N1, N2, and N4) had the greatest seasonal occurrence of both subarctic and Arctic species. N2 and N4, in Anadyr Strait, showed that while subarctic and Arctic species had peak occurrences during different seasons, there was nevertheless extensive overlap in early winter of fin, humpback and bowhead whales. This overlap and overall community compositions decreased further north such that the only subarctic species detected in the Beaufort Sea was killer whales, which appear to have extended their distribution both northwards and eastwards into the Beaufort Sea (Willoughby et al. 2020; Stafford et al. 2022). The Arctic endemic species bowhead and beluga whales were each detected later in the fall and winter and earlier in the following spring along their migratory route in the Chukchi and Beaufort Seas.

Hypothesis 4 above seeks to understand whether there are north-south and east-west differences in marine mammal occurrence in the Bering Strait region. Although longer time series are required to understand how robust the patterns are, there is more acoustic diversity and longer acoustic seasonality of both subarctic and Arctic species to the west of St Lawrence Island than to the east and biodiversity decreases from south to north (Figure 6 and 7). Changes in sea ice extent and seasonality appear to be the most obvious drivers of the presence/absence of marine mammal species in the PAR (Figure 8). Understanding how these broad changes impact the smaller scale physical and lower trophic level biological environments that influence the phenology, residence time, and community composition of marine mammals, may shed light on whether an ecosystem transformation is underway in the Pacific Arctic and how robust the changes are. Given the recent proposal that 2017-2018 represented an ecosystem shift in the Pacific Arctic (Ballinger and Overland, 2022), the acoustic data presented here will be further explored in this context going forward.

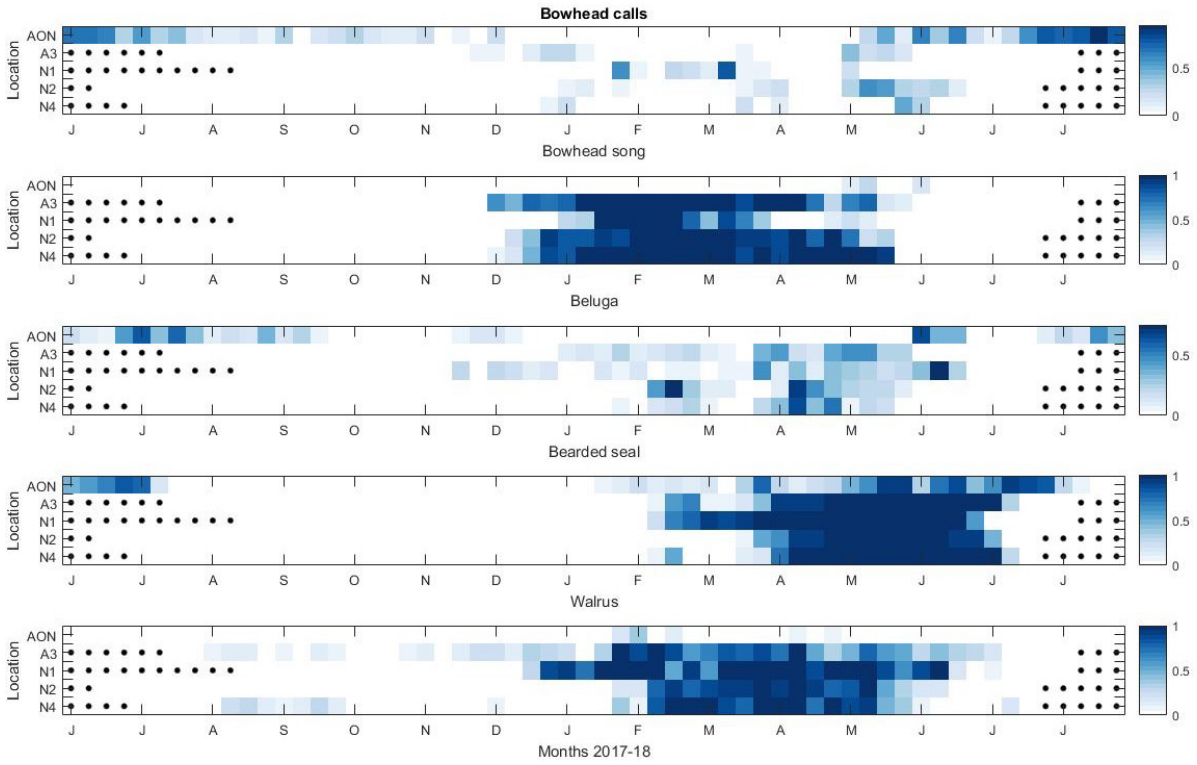

Figure 6. Seasonal occurrence of Arctic marine mammals from northern Bering Sea (N1, N2, N4) through the Bering Strait (A3) and into the Beaufort Sea (AON). Black dots indicate periods with no data.

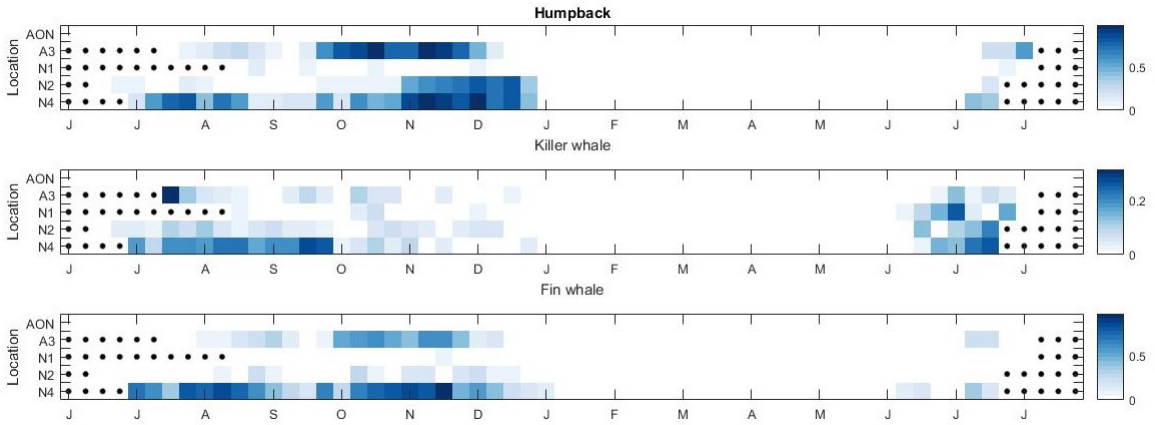

Figure 7. Seasonal occurrence of subarctic marine mammals from northern Bering Sea (N1, N2, N4) through the Bering Strait (A3) and into the Beaufort Sea (AON). Black dots indicate periods with no data.

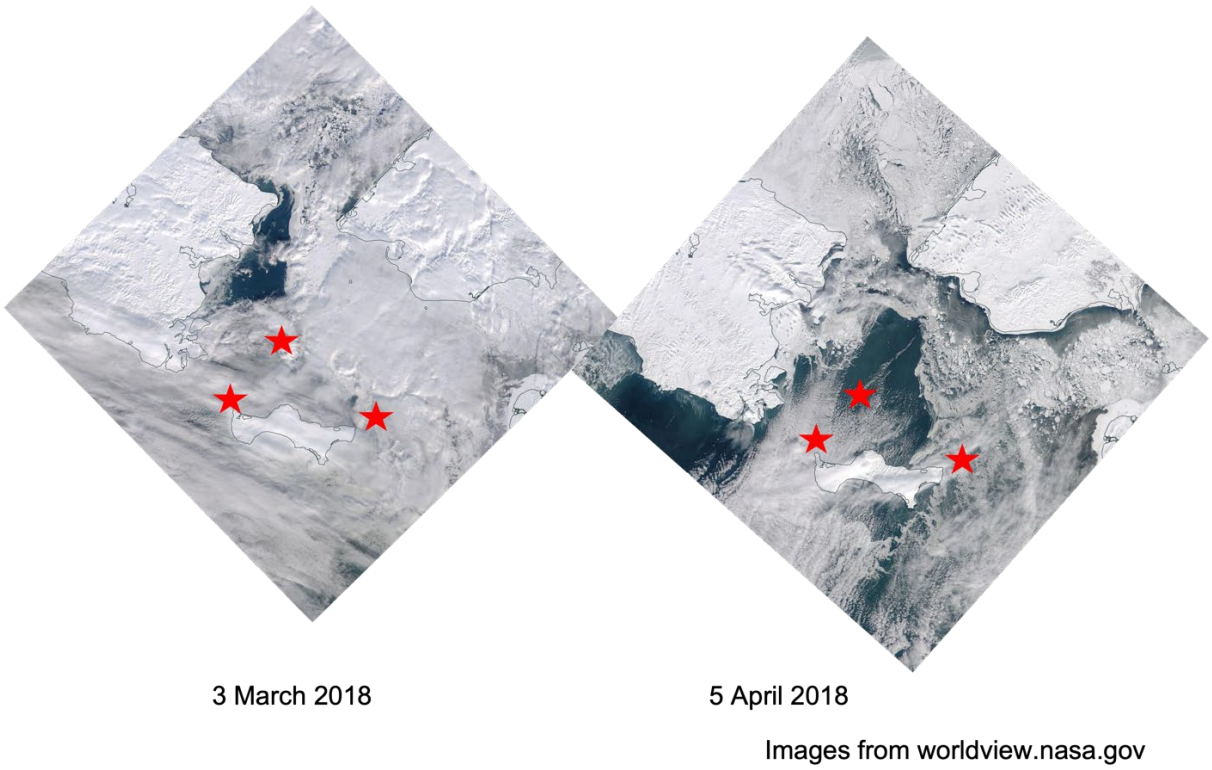

Figure 8. Sea ice coverage in the northern Bering Sea in March and April 2018 illustrating the greater extent of ice in the eastern region as compared to the west. Mooring locations from east to west are N1, N4, N2.

Chapter 4: Long-term marine mammal occurrence at the Chukchi Ecosystem Observatory

Stafford, K.M., Danielson, S.L., Escajeda, E. *in prep* Walrus and Bearded Seal Detections at the Chukchi Ecosystem Observatory 2016-2020

The Arctic as we know it is experiencing changes that range from invasions from subarctic species, changes in phenology of arctic species, and changes in Arctic food webs. The added pressure of increased economic ventures highlights the urgent need for long-term observations in the Arctic Ocean, including changes in biodiversity. Chukchi Ecosystem Observatory (CEO) was established in 2014 to provide year-round observations of core physical, chemical and biological processes in the Arctic. The CEO mooring is located in the biological "hotspot" located on the NE Chukchi Sea shelf near Hanna Shoal at 71°36N, 161°31.6W, where a thriving benthic community supports a major walrus foraging ground during summer and fall months. Beginning in 2015, a passive acoustic recorder was added to monitor the presence of vocal marine mammals and the overall Essential Ocean Variable of 'sound.'

The hydrophone package was programmed to record acoustic data from 10 Hz to 8 kHz on a 25% duty cycle (the first 15 min of every hour) for the duration of each year's deployment at the Chukchi Ecosystem Observatory (Figure 4 above). Upon recovery, the data were visually and aurally examined to determine the presence/absence of walrus and bearded seal vocalizations (Figure 9).

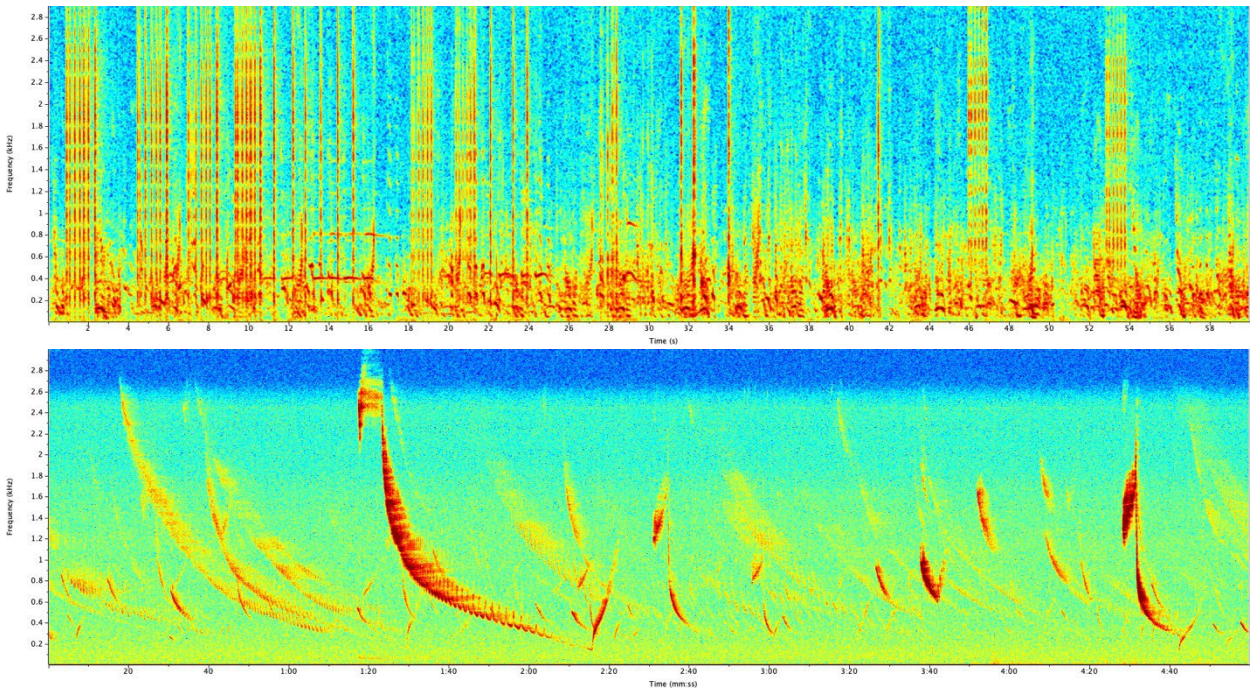

Figure 9. Spectrograms of characteristic signals produced by walrus (top panel) and bearded seals (bottom panel) used to detect the presence of each species. Note the different time axes.

Each of these species contribute significantly to the overall underwater soundscape at the CEO but at different times of the year (Figure 10). Walrus sounds started in late May, when sea ice concentration began to abruptly decrease and were heard continuously until early November annually. Walrus vocalizations ceased 1-3 weeks before sea ice began to form in autumn. In contrast, bearded seals were only seldom heard during the open water period, but their vocalizations were recorded 24h/day as soon as sea ice concentrations increased to over ~75% in early December. Bearded seal trills were heard through late June/early July and declined with sea ice concentration, except for 2019, when there was little or no ice at the CEO from late May to mid-June, when bearded seals were nevertheless recorded at very high levels. Although both walrus and bearded seals are Arctic endemic species that rely on sea ice for critical life history stages, and fill similar ecological niches, they clearly have different timing in their occupation of the CEO/Hanna Shoal region. This suggests that these Arctic pinnipeds may be partitioning this region of the Arctic based on the presence or absence of sea ice.

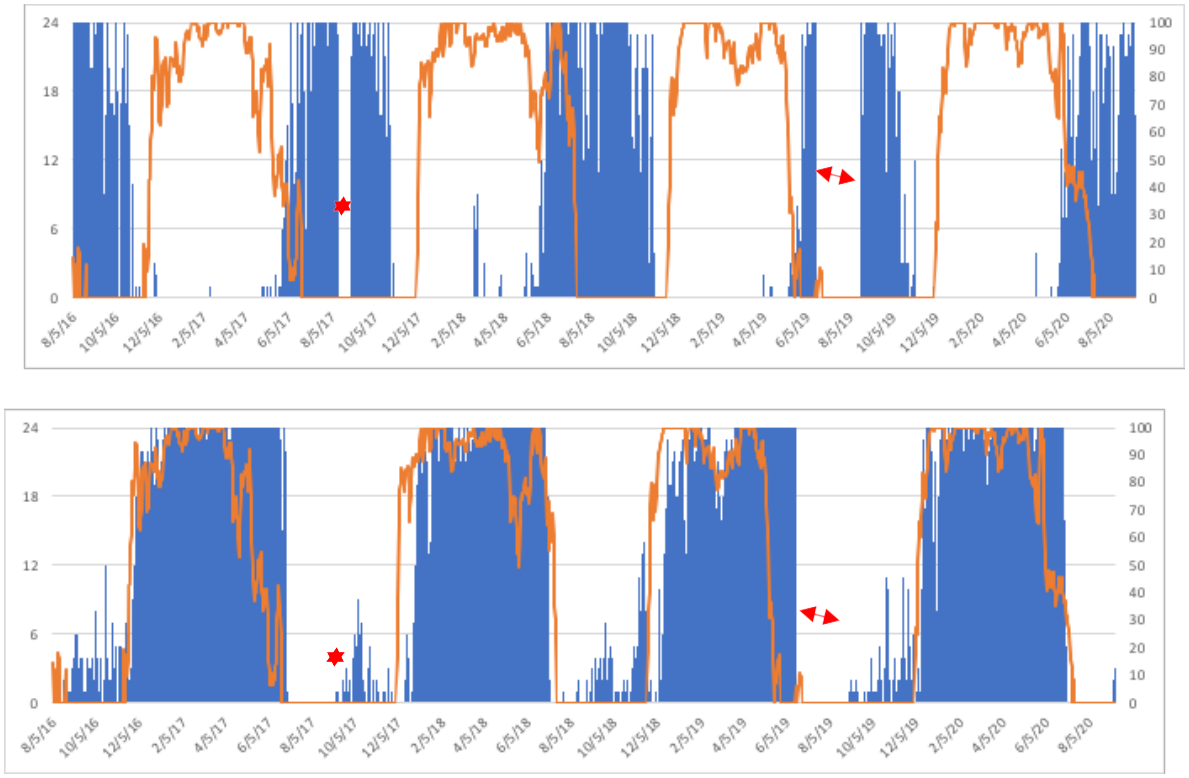

Figure 10. Acoustic detections of walrus (top panel) and bearded seals (bottom panel) with sea ice concentration (orange line) at the Chukchi Ecosystem Observatory from 2015-2020. Red star and arrows indicate missing data.

The presence of walrus at the CEO site was consistent from year to year; this species was heard from May until late October annually and likely reflects the migratory phenology of Pacific walrus. The modeled distribution of radio-tagged walrus which consistently showed walrus at the Hanna Shoal region from 2009-2011 (Jay et al. 2012). However, the high number of hours with detections in October is somewhat inconsistent with these earlier data and with the acoustic detections reported by Hannay et al. (2013). Clearly, walrus have changed their haulout behavior in the Chukchi Sea as the decline of sea ice has resulted in thousands of animals on shore of northwestern Alaska (Jay et al. 2012, 2017; Udevitz et al.,

2018; Fischbach et al. 2022). Jay et al. (2017) examined walrus haulout behavior on ice and found that walrus were less likely to be hauled out in windy conditions with cool air temperatures. Future work will include comparing the acoustic detections with wind speed and air temperature to determine if there are more acoustic detections due to animals being in the water.

Bearded seals appear to be year-round residents of the Chukchi Sea (Macintyre et al. 2013) however, they are only vocally active seasonally. Males produce elaborate trills (see Figure 9 above) to attract females and for male-male interactions. Bearded seal trill production is closely linked to their breeding season and the presence of sea ice on which they haul out, give birth and nurse young (Macintyre et al. 2015). During the open water season, bearded seals are present in the Chukchi Sea but produce many fewer sounds. Bearded seal trill seasonality closely matched the mean sea ice concentration at the CEO with the exception of spring 2019 when sea ice disappeared in early June but bearded seals continued to be heard until the hydrophone stopped recording in mid-June that year. The seasonality seen at the CEO from 2016-2020 is similar to that seen a decade prior (Hannay et al. 2013) when sea was more extensive in the region.

Chapter 5: Shipping noise in the Bering Strait region

Escajeda, E., Stafford, K.M., R. Woodgate, K.L. Laidre. *Under revision.* Quantifying the effect of ship noise on the acoustic environment of the Bering Strait. *Submitted to the Journal of the Acoustical Society of America.*

These data and analysis will form part of the PhD dissertation of Erica Escajeda at the University of Washington. This manuscript is currently under revision.

Abstract

The Bering Strait is the only conduit between the Pacific and the Arctic Oceans, making it an important location to study ship noise. We used *in situ* measurements to examine how ship noise impacts the Bering Strait soundscape during the open-water season (June–November) for 2013–2015, including quantifying ship source levels and modeling the extent of elevated sounds levels due to the presence of a ship. We also examined the relationship between ship source levels and vessel speed under varying wind conditions. Ships elevated ambient sound levels during the open-water season by ~6 dB on average, and moving vessels produce potentially harmful sound levels for marine mammals (≥120 dB re 1 μPa) out to ~0.9 km away, depending on the vessel type. We did not find significant relationships between vessel speed and source levels for the two major vessel types observed in the strait, cargo (n = 10) and tugboats (n = 19), indicating that other untested factors may influence vessel source levels in the area. Both wind and water speeds were significantly correlated to sound levels measured during the open-water season, indicating that environmental conditions need to be accounted for when examining ship noise in a shallow-water environment.

I. INTRODUCTION

Declining sea ice is opening the Arctic to increased ship activity, potentially impacting the acoustic habitat of marine mammals that inhibit Arctic waters (Moore *et al*., 2012; Halliday *et al*., 2017, 2021; Hauser *et al*., 2018). Known impacts of shipping on marine mammals include masking of important biological signals (Clark *et al*., 2009; Pine *et al*., 2018), increasing stress hormone levels (Rolland *et al*., 2012), and provoking avoidance behavior (Nowacek *et al*., 2007; Southall *et al*., 2007). Shipping in the Arctic is increasing (Eguíluz *et al.*, 2016), and the two major shipping routes—the Northwest Passage through the Canadian Arctic Archipelago, and the Northern Sea Route along the northern coast of the Russian Federation—are expected to see a sharp increase in trans-Arctic ship passages by 2050 (Stephenson *et al*., 2011, 2013; Smith and Stephenson, 2013). Both sea routes pass through the Bering Strait, making it an important region for studying the effects of ship noise on the underwater environment. In the present study, we set out to quantify the impact of ship noise on the soundscape of the Bering Strait region and evaluate the potential of vessel speed limits as a mitigation tool for managing ship noise.

The Bering Strait connects the Bering Sea to the south with the Chukchi Sea to the north (Fig. 1). The region is shallow (30-60 m), and relatively narrow, spanning only ~80 km at its narrowest point. The marine ecosystem of the Chukchi Sea is one of the richest in the world, home to dense aggregations of benthic invertebrates and swarms of lipid-rich zooplankton that attract marine mammals to the region (Grebmeier *et al*., 2006; Eisner *et al*., 2013; Ershova *et al*., 2015). Marine mammals endemic to the Arctic and commonly observed in the Chukchi Sea include bowhead whales *(Balaena mysticetus)*, belugas *(Delphinapterus leucas)*, walrus *(Odobenus rosmarus)*, bearded seals *(Erignathus barbatus)*, and ringed seals *(Pusa hispida)*, all of which are important subsistence species for the Chukchi, Iñupiaq, St. Lawrence Island Yupik, Siberian Yupik, and Yup'ik Peoples of the coastal Pacific Arctic (Huntington *et al*., 2015).

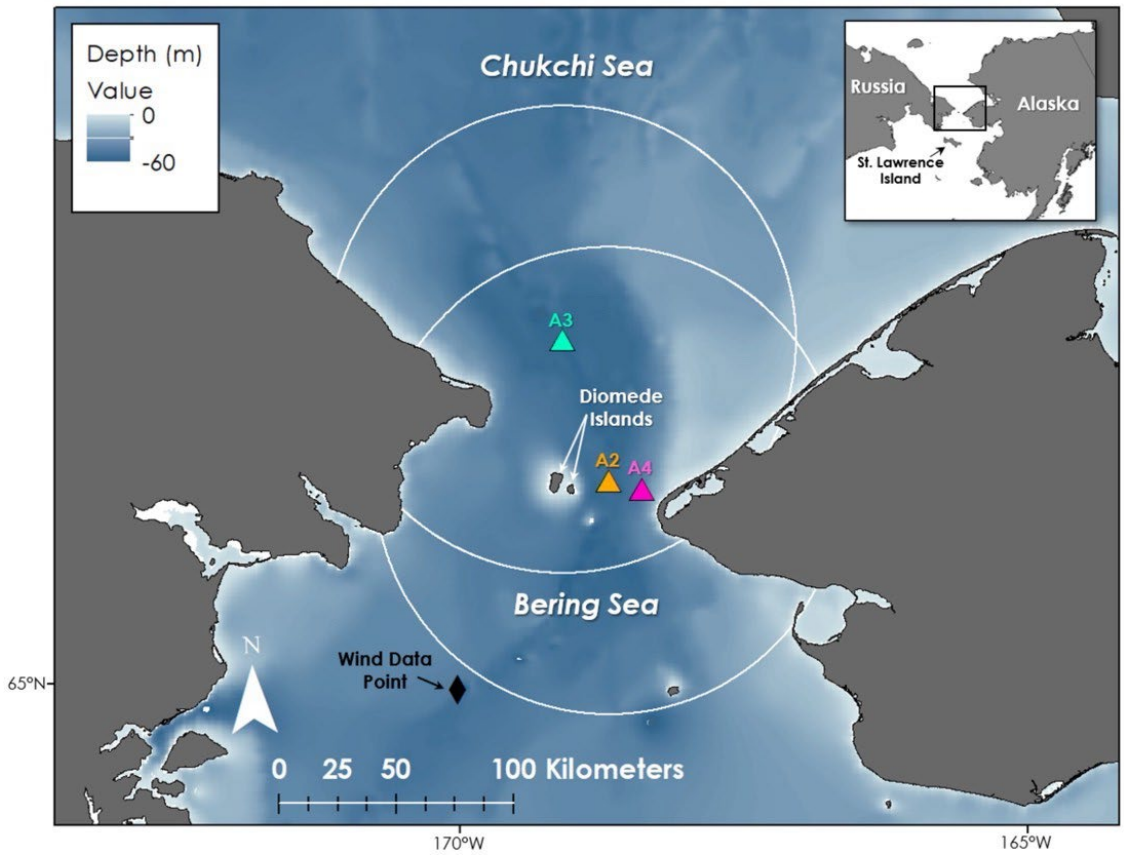

FIG. 1. Map of the Bering Strait study area with the three mooring locations—Sites A2 and A4 in the eastern channel of the strait, and Site A3 north of the strait. The nearest NCEP-NARR wind data point is located southwest of the strait (65°N, 170°W; Mesinger *et al*., 2006). The two white circles represent 100-km buffers around Sites A2 and A3, respectively, and were used for identifying ships within the Bering Strait region. Depth data are taken from the International Bathymetric Chart of the Arctic Ocean version 3.0 (500-m resolution; Jakobsson *et al*., 2012).

The seasonal ebb and flow of species into the Bering Strait region is driven by the melting of sea ice in the spring (~May), and formation of sea ice in the late fall and early winter (November–December; Frey *et al*., 2015; Serreze *et al*., 2016). When the sea ice disappears in the summer, subarctic baleen whales—namely gray whales *(Eschrichtius robustus)*, humpback whales *(Megaptera novaeangliae)*, fin whales *(Balaenoptera physalus)*, and minke whales *(B. acutorostrata)*—migrate northward into the Chukchi Sea to feed on seasonally abundant prey (Clarke *et al*., 2013; Woodgate *et al*., 2015; Brower *et al*., 2018; Escajeda *et al*., 2020). Marine mammals rely on sound as their primary sense (Richardson *et al*., 1995); consequently, the intrusion of ships into the Pacific Arctic presents a potential threat to the acoustic habitat of these animals.

Despite the looming threat of increased ship noise, there has been little work quantifying the impact of ship noise on ambient sound levels in the Bering Strait region. McKenna *et al*., (2021) examined the impact of ship noise on annual median sound pressure levels for third-octave frequency bands measured at a site west of St. Lawrence Island and found that noise measured from ships within 10 km of their hydrophone had little impact on year-round ambient levels (<1 dB difference between median sound levels with ships present and annual median sound levels for third-octave frequency bands between 100 and 1000 Hz). Instead, wind and sea ice were the most significant contributors to annual ambient sound levels (except for the 1000-Hz third octave band; McKenna *et al*., 2021). Most vessels are only able to transit the Arctic when its waters are ice-free (June-November), necessitating an examination of how ships affect ambient sound levels specifically during the open-water season.

In this study, we characterize the acoustic effects of shipping activity in the Bering Strait during the open-water season (June through November) for 2013–2015 using three moored hydrophones within the Bering Strain region. We expand upon previous work in the Pacific Arctic by Halliday *et al*. (2017, 2021) by examining the spatial impact of ship noise by modeling the "acoustic footprint" of ships, in addition to quantifying the impact of ship noise on ambient sound levels with a focus on frequency bands used by baleen whales (<1000 Hz; Southall *et al*., 2007; Moore *et al*., 2012). Lastly, we examine the relationship between ship source levels and vessel speed to evaluate speed limits as a means of reducing underwater ship noise. We take a similar approach to examining the relationship between vessel type and size. The results of our study could provide important information to managers and policymakers on the effectiveness of vessel speed limits in mitigating ship noise in the shallow-water environment of the Bering Strait.

II. METHODS

Acoustic Data Collection

We collected acoustic recordings from AURAL-M2 hydrophones (Autonomous Underwater Recorder for Acoustic Listening-Model 2; Multi-Électronique, Inc.) attached to three moorings positioned within the Bering Strait. Mooring site A2 was positioned in the center of the eastern channel and Site A4 on the east side of the eastern channel. Site A3 was positioned ~35 km north of the strait in the southern Chukchi Sea (Fig. 1). The mooring sites were originally established for measuring the physical properties of oceanic throughflow through the strait and have been collecting data for decades (Woodgate *et al*., 2015; Woodgate, 2018). The acoustic dataset we use here spans from July 2013 to December 2015. Hydrophone sensitivity was -155 dB re 1 V/µPa with a gain of 16 dB and a 16-bit recording resolution. Each hydrophone was positioned 4–8 m above the seafloor and sampled at 8192 Hz, with a 20-min (2013 and 2014) or 22-min (2015) duty cycle and varying deployment periods (Table I). All recordings were timed to start at the top of the hour.

We focused our analyses on recordings from June through November of each year since the Bering Strait is typically ice-free during this period (Serreze *et al*., 2016). Recordings were visualized in the *Ishmael* software program (2014 version; Mellinger, 2002) using a fast Fourier transform (FFT) size of 4096 samples with a Hamming window and spectrogram equalization enabled (time constant of 30 s). Hours with ship noise, as well as biotic sounds (e.g., whale calls) and instrument strumming (created by water rushing past the mooring) were identified by manually analyzing spectrograms of each recording. Marine mammals are sensitive to changes in frequency between third-octave bands, therefore summarizing sound amplitude using third-octave bands is useful for approximating sound level for a range of frequencies (Richardson *et al*., 1995). For reference, an octave is a range of frequencies where the highest frequency is twice the lower frequency, and for third-octaves, the upper limits is equal to the lower band frequency multiplied by the cube root of two. We calculated the root-mean-square (RMS) sound pressure levels integrated over third-octave frequency bands between 25–1000 Hz for each recording using *PAMGuide* software in *MATLAB* (FFT with a 1-s long Hann window and 50% overlap; Merchant *et al*., 2015). For the ship source level analysis, we took the RMS average for each minute, and for the ambient sound level analysis we took the RMS average of each individual recording (duty cycles; 2013 and 2014 = 1199 s; 2015 = 1399 s). We assumed that ambient sound levels recorded during the duty cycles were representative of the entire hour.

Effects of Wind and Water Speed on Ambient Sound Levels

To understand how ambient sound levels naturally vary during the study period, we examined the impact of wind and water speed on third-octave sound levels (25–1000 Hz) recorded by our hydrophones. Wind is an important contributor to ambient sound levels during the open-water season (Wenz, 1962; Hildebrand, 2009; Roth *et al*., 2012; Insley *et al*., 2017; McKenna *et al*., 2021), and thus, should be taken into consideration when quantifying the impact of ship noise since high winds can elevate background sound levels. The Bering Strait is also known to have high water speeds (Woodgate, 2018), which can lead to flow nosie and/or instrument strumming (McKenna *et al*., 2021) Consequently, it was important to consider how water speeds contribute to sound levels recorded by the hydrophone in each third-octave frequency band. Note that both flow noise and instrument strumming result from water flowing past the mooring, therefore they are not considered features of the broader acoustic environment.

To isolate the effect of wind and water speeds, we analyzed recordings with no ship noise, instrument strumming, or biotic sounds present. Data on wind speed and direction were taken from the National Centers for Environmental Predication (NCEP) North American Regional Reanalysis 2 (NARR) wind data product (grid size of ~32 km; Mesinger *et al*., 2006) calculated for the nearest grid point to the moorings (65°N, 170°W; Fig. 1). We calculated daily mean water speeds using hourly data measured at 30 m depth by Acoustic Doppler Current Profilers (ADCP) attached to each mooring. We examined the influence of daily mean wind and water speeds on daily median sound levels for third-octave bands between 25–1000 Hz using Spearman correlation tests in addition to linear regressions for each site all years combined

(e.g., 2013–2015 at Site A2). We used a significance threshold of 0.05 for all statistical tests, assuming that daily means for wind and water speeds were independent. All quantitative analyses were computed using the software package *R* (v. 4.1.0; R Core Team, 2021).

C. Characterizing Ship Activity & Estimating Ship Source Levels

We used Automatic Identification System (AIS) vessel tracking data to characterize the presence of ships throughout the open-water season (June–November) in the Bering Strait region, which we defined as within 100 km of the A2 and A3 moorings (see Fig. 1 for boundaries). We also noted whether any ships were present in May or December, however we did not examine the sound recordings for either month due to the abundance of vocalizing bearded seals and sea ice, which make isolating ship noise difficult. AIS data were obtained from the Nationwide Automatic Identification System (NAIS) dataset managed by the United States Coast Guard (https://marinecadastre.gov/ais/). The NAIS dataset is collected by land-based receivers every minute and includes vessel name (2015 only), status (2015 only), length, width, a unique Maritime Mobile Service Identity (MMSI) number, vessel type, latitude and longitude, speed over ground (knots), course over ground, and heading. The International Maritime Organization (IMO) only requires large vessels (>300 gross tonnage), passenger vessels, and large fishing vessels to carry AIS transmitters (IMO International Convention for the Safety of Life at Sea, 1974). Consequently, AIS is not a reliable tool for tracking the presence of small vessels (Hermannsen *et al*., 2019).

For quantifying ship noise and estimating ship source levels, we matched recordings with ship noise to concurrent AIS transmissions from ships that were within 100 km of the mooring. We refer to a recording that matched with the closest pass of a single, unique vessel by the mooring as a "ship event" (unique vessels were identified using their MMSI number). AIS transmissions for each ship event were visualized in *ArcMap* (v. 10.8; Environmental Systems Research Institute, ESRI, 2019) to ensure that the vessel was in a reasonable position to be heard by the hydrophone (i.e., not behind a landmass), and that the vessel was moving during the recording. We also eliminated any ship events with fewer than two AIS transmissions during the ~20/22-minute recording window, as well as ship events that had other sound sources present (e.g., whale calls, instrument strumming). We then eliminated duplicate ship events where the same vessel was detected at two mooring sites by selecting the recording from the closest hydrophone to the ship's track.

We calculated source levels (SL) for each ship event using the sonar equation (Urick, 1983), where SLs are estimated from received sound levels recorded by the receiver (i.e., the hydrophone) plus some transmission loss due to propagation. For the received levels, we used the RMS sound pressure level for the 250-Hz third-octave band for each minute of the ship event recording. The 250-Hz band likely captures peak sound levels for smaller vessels (Merchant *et al*., 2014), making it a good choice for quantifying ship sound levels. Additionally, sound levels at lower frequency bands (e.g., 63 and 125 Hz) tend to attenuate in shallow water, whereas sound

levels in the 250-Hz band do not (Merchant *et al*., 2014). We then estimated transmission loss using an empirical model that parameterizes transmission loss as geometric spreading plus some loss due to absorption. The model assumes that sound energy spreads spherically until it reaches an obstruction, assumed to be the seafloor or surface, after which it spreads cylindrically, resulting in the following equation (adapted from Richardson *et al*., 1995, p. 71):

$$SL = RL + 20\log_{10}(r_o) + 15\log_{10}\left(\frac{r}{r_o}\right) + \alpha r$$

where r is the slant distance from the ship to the hydrophone, r_o is the range at which spreading switches from the spherical to a form of cylindrical spreading, and α is an absorption coefficient. We estimated r_o as the difference between the sound source depth, assumed here as the draft of the ship, and water depth at the mooring site where the ship was recorded. We initially used a published value of 0.004 dB/km for the absorption coefficient (Francois and Garrison, 1982), however the published value underestimated propagation loss and resulted in a poor fit to our measured received levels (RL). Instead, we fitted an empirical absorption coefficient for all ship events combined using linear least squares regression. We then used the empirical absorption coefficient (α) along with normalized received levels from each ship event (i.e., $(RL_i – RL_{mean})/RL\sigma$) to calculate SL for each ship using a linear least squares regression (the resulting α is discussed in Section 3B).

D. Relationship Between Vessel Speed and Source Level

Previous research has shown that ship source levels increase with increasing vessel speed (Ross, 1976; McKenna *et al*., 2013; Cion *et al*., 2019; ZoBell *et al*., 2021) as well as vessel size (McKenna *et al*., 2013). The AIS data provided speed over ground, but a more relevant metric for quantifying vessel noise is speed through water (McKenna *et al*., 2012), which we calculated by subtracting the hourly mean water velocity from the reported speed over ground for each ship. Hourly mean water velocities (m/s) at ~12 m depth were taken from the ADCP data from the closes mooring to the ship. Northward water velocities during the 2013–2015 open-water seasons ranged from ~22–62 cm/s (~0.6–1.2 knots) and changed on the same timescale of the winds (hours to days; Woodgate, 2018). Prior work shows the flow field of the strait to be largely homogenous except for a coastal current on the Alaskan side (Woodgate *et al*., 2015). For vessel size, we used the vessel lengths (m) reported in the AIS data since we did not have gross tonnage data for 2013 and 2014.

We hypothesized that environmental factors, such as sea state, could affect engine power output at a given speed, and thus, vessel source levels. Therefore, we used wind speed as a proxy for sea state and divided the ships into categories based on daily wind speeds on the day of the ship event, arbitrarily defining “low-wind” ship events as transits that occurred on days with mean wind speeds <10 m/s, and “high-wind” events on days with mean wind speeds ≥10 m/s. Note that 10 m/s is the threshold between Beaufort sea states of 5 and 6 where large waves begin

to form, and that the prevailing northward current through the Bering Strait may be reversed to flow southwards by southward winds exceeding 10 m/s (Woodgate *et al*., 2005). We also included whether the ship was moving against the wind or with the wind as a predictor, using the mean course over ground (COG) during the ~20/22-minute recording window and daily mean wind velocities from the NCEP-NARR dataset. We classified a ship as moving "against" the wind if the ship's mean COG was within $\pm$45° of the wind's direction, and "with" the wind if its mean COG was within 180 $\pm$ 45° of the wind's direction (e.g., if a ship's COG = 23° and the wind direction as 175°, the ship would be classified as moving with the wind).

Following the suggestion of Mckenna *et al*., (2012), we examined the relationship between vessel speed and source levels for each vessel type separately. We used a separate general linear model with Gaussian errors for each vessel type to test for significant relationships between ship source levels and speed through water, vessel length, wind speed, wind speed category (i.e., "high wind" vs. "low wind"), and direction relative to the wind as a categorical variable ("against the wind" vs. "with the wind"). We confirmed normality of the ship source levels using a Shapiro-Wilks test and used the Akaike's information criterion with a correction for small sample size (AICc) to evaluate the model (Akaike, 1973). We then evaluated each variable separately using its significance term.

Comparison Between Vessel Noise and Ambient Sound Levels

We compared received sound levels when a single ship was present to ambient sound levels for the entire open-water season across all sites and years. We quantified both ambient and ship noise as third-octave sound pressure levels (SPL) averaged over the full duration of each recording (2013 and 2014 = averaged over 1199 s; 2015 = averaged over 1399 s), and then compared median ambient third-octave SPLs for all sites and years to median third-octave SPLs (McDonald *et al*., 2006; Insley *et al*., 2017), therefore we also examined median ambient and ship SPLs for days with wind speeds <10 knots (~5 m/s). Finally, we compared median sound levels for ambient vs. ship by vessel type.

Mapping the Acoustic Footprint of Ships

To estimate the acoustic footprint of a passing ship, we back-calculated received levels extending from the ship track using the estimated source level for the 250-Hz third-octave band and propagation loss as a function of range from the ship, *r* (see Section 2C for source level and propagation loss methods). We selected a ship from the six major vessel categories, including a cargo ship, military ship, research vessel, tanker, tugboat, and a ship in the "other" category, and mapped the areas where received levels were expected to exceed certain thresholds. The thresholds included: received levels $\geq$120 dB re 1 μPa, the behavioral disturbance threshold for marine mammals defined by the U.S. National Oceanic and Atmospheric Administration (NOAA, 2016); 110 dB re 1 μPa, which is the average ambient sound level on high-wind days in the Canadian Arctic found by Halliday *et al*., (2017); 105 dB re 1 μPa; and 100 dB re 1 μPa, the

level where some disturbance behavior has been observed in marine mammals (Southall *et al*., 2007). Transmission loss was estimated without consideration of interactions with the seafloor or elevated sound levels are likely overestimates (Farcas *et al*., 2016). We assumed that the vessels maintained a steady speed (and this we assume a steady sound source) over the length of the trackline segment.

III. RESULTS

We analyzed 36,274 recordings combined across the three sites and years. There were 2,998 recordings with ship noise, with 1,030 recordings at Site A2, 1029 at Site A3, and 939 recordings at Site A4. In total, there were 93 days with ship noise present in 2013, 103 days in 2014, and 131 days in 2015 (we refer to a day as a 24-hr period starting at 00:00 GMT). Most of the ships detected at Site A3 were also detected at Sites A2 and A4, and the AIS transmissions were closer to A2 and A4. Consequently, we focused our analyses only on Sites A2 and A4 (Fig. 1).

Effects of Wind and Water Speed on Ambient Sound Levels

The Spearman correlation test revealed significant correlations between daily mean water speeds and third-octave sound levels for all bands between 25–1000 Hz except the 250-Hz band (Spearman ρ range: ~0.2–0.9; Fig. 2A). Other bands had a non-significant correlation with water speed, and the sign, magnitude, and significance of the correlations differed by site (Fig. 2A). Correlations between water speed and low-frequency sound levels (third-octave bands <250 Hz) were positive, indicating that low-frequency sound levels increase with increasing water speed. In contrast, higher-frequency sound levels (>315 Hz) were negatively correlated with water speed (Fig. 2A), although those correlation values were small in magnitude (0 to -0.2). Conversely, sound levels for all bands were positively correlated with wind speed at both sites, with significant correlations for bands >80 Hz (Fig. 2B). Sound levels for bands ≥50 Hz increased with increasing daily mean wind speed at both mooring sites, indicating that background sound levels were higher on days with higher wind speeds. For example, there was a significant, positive relationship between daily mean wind speed and median sound pressure levels for the 250-Hz band for all three years at Site A2 pooled together (Fig. 3).

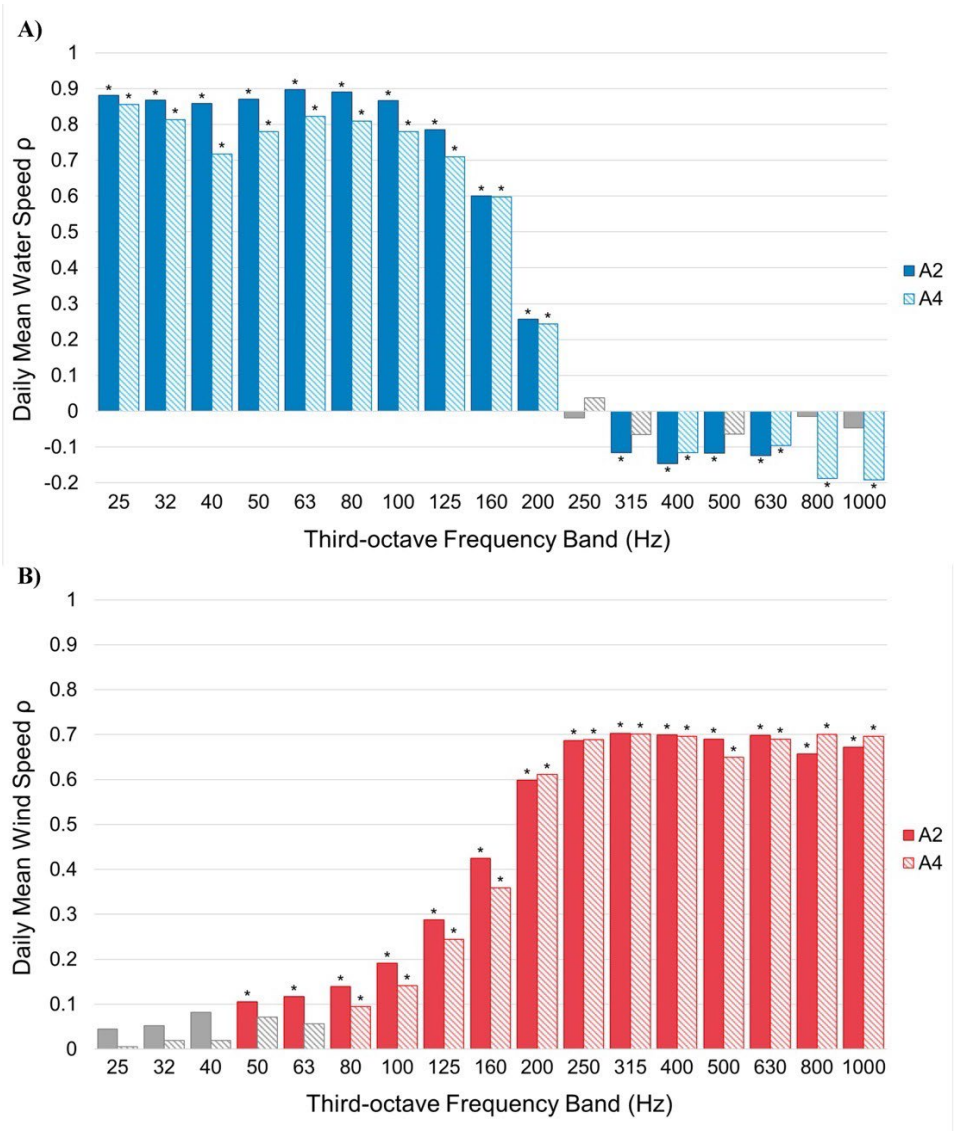

FIG. 2. Spearman ranked correlation coefficients (ρ) for correlation tests between (A) sound levels and water speeds and (B) sound levels and wind speeds. Daily median ambient third-octave sound levels (x-axis) were measured between June–November 2013–2015 at Sites A2 (darker colors) and A4 (lighter colors). Daily mean water speeds (ADCP data) were collected at 30 m depth, and daily mean wind speeds were taken from the NCEP-NARR dataset (Mesinger *et al*., 2006). Bars with an asterisk (*) indicate significant correlations ($p < 0.05$) and gray bars indicate non-significant correlations.

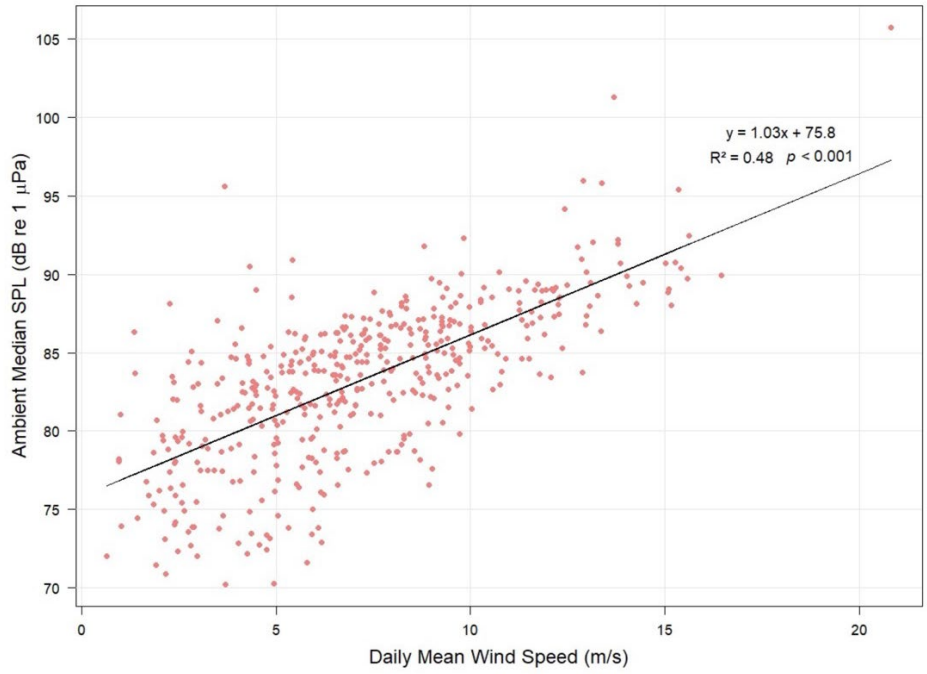

FIG. 3 . Median ambient sound pressure levels (SPL, dB re 1 μPa) measured for the 250-Hz third-octave band at Site A2 during the open-water season (June–November) 2013–2015 plotted as a function of daily mean wind speeds (NCEP-NARR data; Mesinger *et al*., 2006). Fitted values from the linear regression are plotted as a straight line (R^2 = 0.48) and show a significant positive relationship between the two variables ($p < 0.001$).

B. Ship Activity in the Bering Strait and Ship Source Levels

A total of 410 unique AIS-transmitting vessels entered the Bering Strait region from May to November 2013–2015. The highest number of unique passages occurred in 2013 with 154 vessels, compared to 122 vessels in 2014, and 134 vessels in 2015. Peak ship activity occurred in the months of July through September (Fig. 4), with the earliest ship transmission occurring in early May and the latest in mid-December. Two cargo ships and a military vessel traveled north of Site A3 on 4–6 May 2015, and the latest passage was made by a Russian icebreaker which transited northward through the western channel on 17 December 2015. A summary of the vessel types observed in the Bering Strait region can be found in Table II. Cargo ships were most common (n = 138 unique vessels, 33.7%), followed by tugboats (n = 85 vessels, 20.7%), and those in the "other" category (n = 75 vessels, 18.3%), which included research vessels, offshore supply vessels, and military/public vessels.

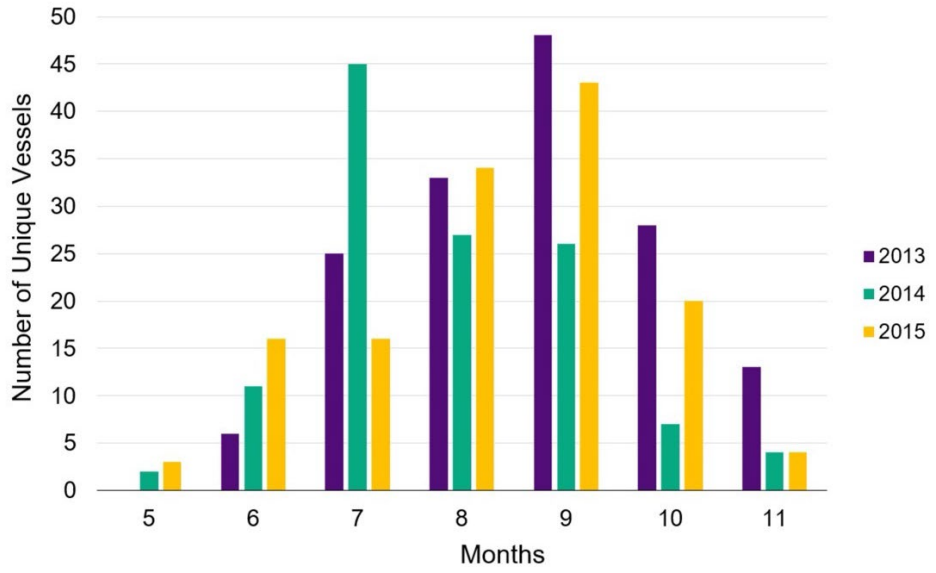

FIG. 4. Total counts of unique vessels that transited within 100 km of the Bering Strait region. Ships that had AIS transmissions within the merged 100-km buffers around Sites A2 and A3 counted as being within the Bering Strait (see Fig. 1). Note that the totals presented are likely underestimated since not all vessels are required to carry AIS transmitters.

A total of 63 recordings were matched with a single, unique vessel within 14 km of a mooring, and had no other sound sources present. The closest points of approach (CPA) for the ship events ranged from ~0.5 km to 13.9 km with an average of 4.4 km (standard deviation (SD): $\pm$ 2.8 km). Third-octave level received levels (dB re 1 μPa) at CPA for the 63 ship passages ranged from 61 to 123 dB re 1 μPa depending on the frequency band. We examined plots of received levels for the 250-Hz band as a function of range to the receiver when calculating the source levels for all 63 ship events and eliminated three ship events that had irregular patterns in their received level vs range plots (e.g., the received levels increased as the distance from the receiver increased). Estimation of source levels for vessels with CPAs > 10 km is likely unreliable, thus we also eliminated ships with CPA ranges > 10 km from the dataset. Source levels for the remaining ships (n = 57) were estimated using an absorption coefficient (α) of 1.46×10^{-7} dB/km (95% confidence interval: 8.56×10^{-8}, 2.07×10^{-7} dB/km) in a linear least squares regression model (R^2 = 0.62). See supplementary material at [URL will be inserted by AIP] for an example of the source level model fit. Source levels for remaining ship events ranged from 141 to 173 dB re 1 µPa at 1 m (source level ranges by vessel type are reported in Table III).

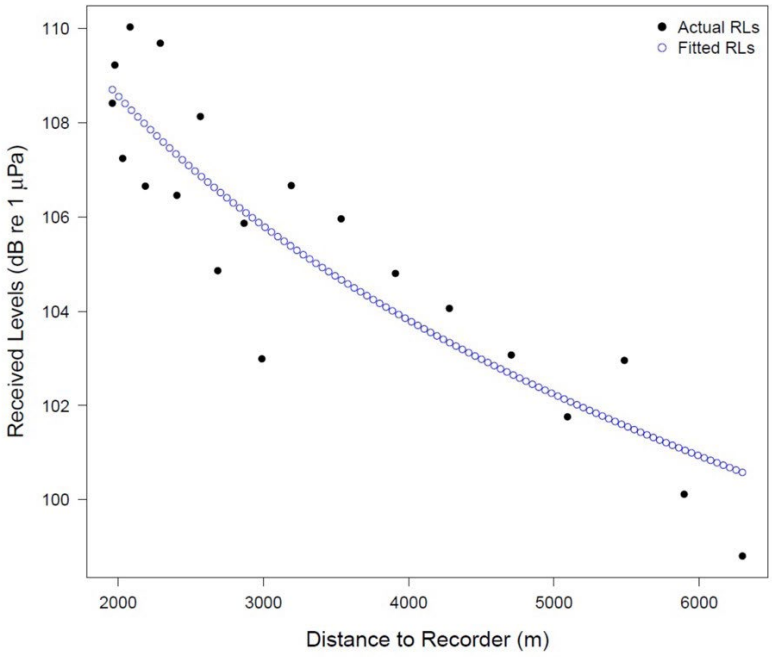

Supplemental FIG. S1. Example of the source level model fit for cargo ship #215000028. The hollow circles represent the fitted received levels (RLs) that were calculated using the estimated source level for the ship.

C. Vessel Speed and Source Levels

Speed through water for all vessel types combined (n = 63) ranged from 2.3 knots (tugboat) to 15.7 knots ("other" ship), with an average of 9.7 knots (SD: ± 3 knots). Cargo ships had the highest speeds on average with a mean of 12.4 knots (SD: ± 2.6 knots), while tugboats had the lowest speeds with a mean of 7.3 knots (SD: ± 2.2 knots; Table III).

We modeled the relationship between source level (SL) and various factors for cargo ships (n = 12) and tugboats (n = 19) since the two vessel types constituted the majority of ships that transited through the strait during the study period (Table II). We removed two cargo ships that had atypical lengths (≤70 m compared to > 120 m for the other vessels), reducing our cargo ship sample size to 10 vessels. All selected cargo ship events occurred on days with low wind speeds, thus we removed the wind speed category from the cargo ship model. The best cargo ship model according to the Akaike's information criterion score (AICc) was SL ~ WindSpeed, though the correlation of WindSpeed and SL was not significant (p = 0.08, R^2 = 0.33; Table IV). The best fit tugboat model according to the AICc score was SL ~ speed through water, however again the correlation between SL and speed through water was not significant (p = 0.42, R^2 = 0.04; Table IV).

Next, we separated the cargo ships and tugboats into length categories and wind speed categories (tugboats only). We defined "large" cargo ships as ships >200 m long (n = 8) and "small" cargo ships as <200 m long (n = 2). "Large" tugboats were tugs ≥30 m in length (n = 14), while "small" tugboats were <30 m long (n = 5). Insufficient sample sizes for small cargo ships (n = 2) and small tugboats (n = 5) precluded an examination of the relationship between ship source levels and speed through water for either category. We did not find a significant relationship between source levels and speed through water for large tugboats that transited on "low-wind" days (n = 10, R^2= 0.08, p = 0.44; Fig. 5), and whether the ship was traveling against or with the wind had a non-significant effect on source levels (p = 0.21, R^2 = 0.19). The model for large cargo ships that transited on "low-wind" days (n = 8) similarly produced non-significant results (p = 0.47), with a negative relationship between source levels and speed through water (R^2 = 0.09).

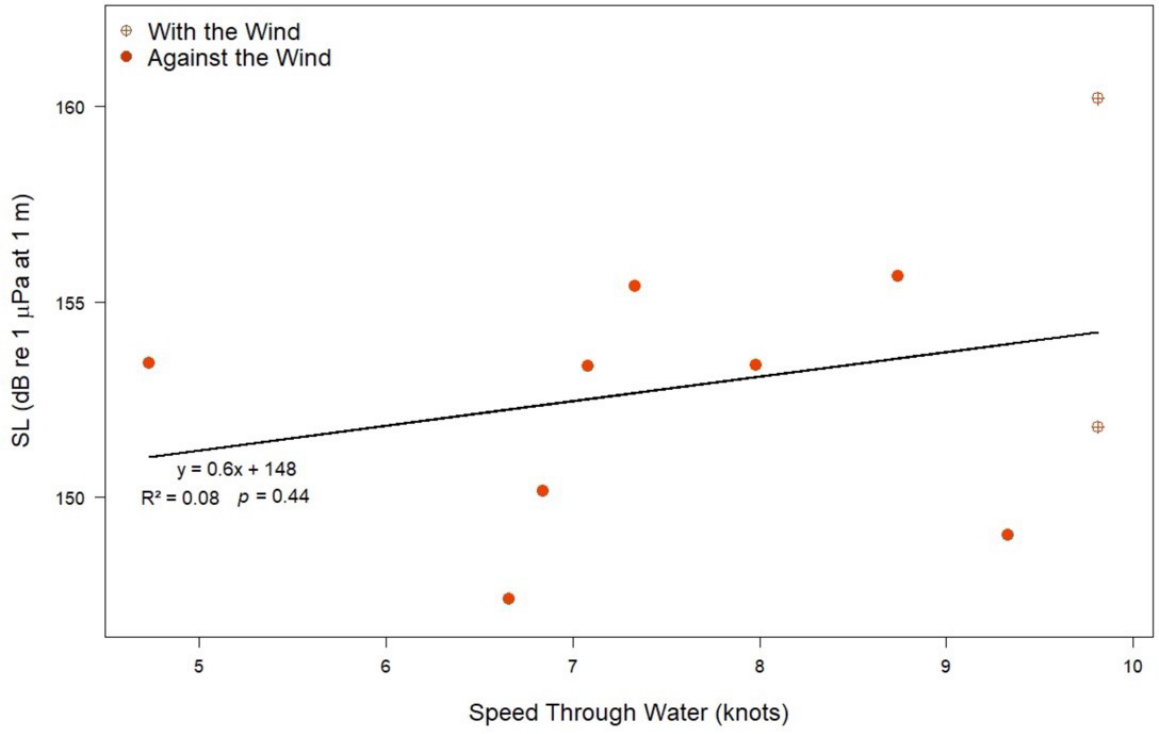

FIG. 5. Source levels (SL, dB re 1 µPa at 1 m) for large tugboats (>30 m long; n = 10) that transited on "low-wind" days (daily mean wind speed <10 m/s) plotted against speed through water (knots). Data points are symbolized by whether the vessel was traveling in the same direction as the wind ("With the Wind," hatched circles) or in the opposite direction ("Against the Wind," filled circles).

D. Comparison Between Vessel Noise and Ambient Sound Levels

Median sound levels when a ship was present were higher than ambient sound levels for third-octave frequency bands between 80–1000 Hz, with ships elevating sound levels by 3–9 dB above ambient (Fig. 6). The highest median received levels for both ambient and ship events were observed in the lower third-octave frequency bands (25–50 Hz; Fig. 6), potentially reflecting the influence of high water speeds (Section 3A; Fig. 2A). Median ambient sound levels on days with low wind speeds (<10 knots) were lower than those of the entire open-water season for third-octave frequency bands between 63–1000 Hz, though they were very similar to seasonal ambient levels for bands ≤50 Hz (Fig. 6A). To ensure that winds were not contributing to the difference between ship and ambient levels, we compared median sound levels when ships were present on low-wind days to ambient sound levels on low-wind days and found that ship levels were on average ~7 dB above ambient for frequency bands between 80–1000 Hz (Fig. 6A).

Since we found that lower frequency sound levels were correlated with water speeds, we examined ambient sound levels on days with low water speeds in comparison to ambient sound levels for the open-water season. We defined low water speeds as the first quartile of the daily mean water speeds measured at Sites A2 and A4 combined (27.6 cm/s), and pulled out ship events that occurred on days with mean water speeds below 27.5 cm/s (Fig. 6B). Median sound levels on days with ships present and low water speeds were still higher than ambient except for the 25-Hz band (mean difference = ~7 dB; Fig. 6B).

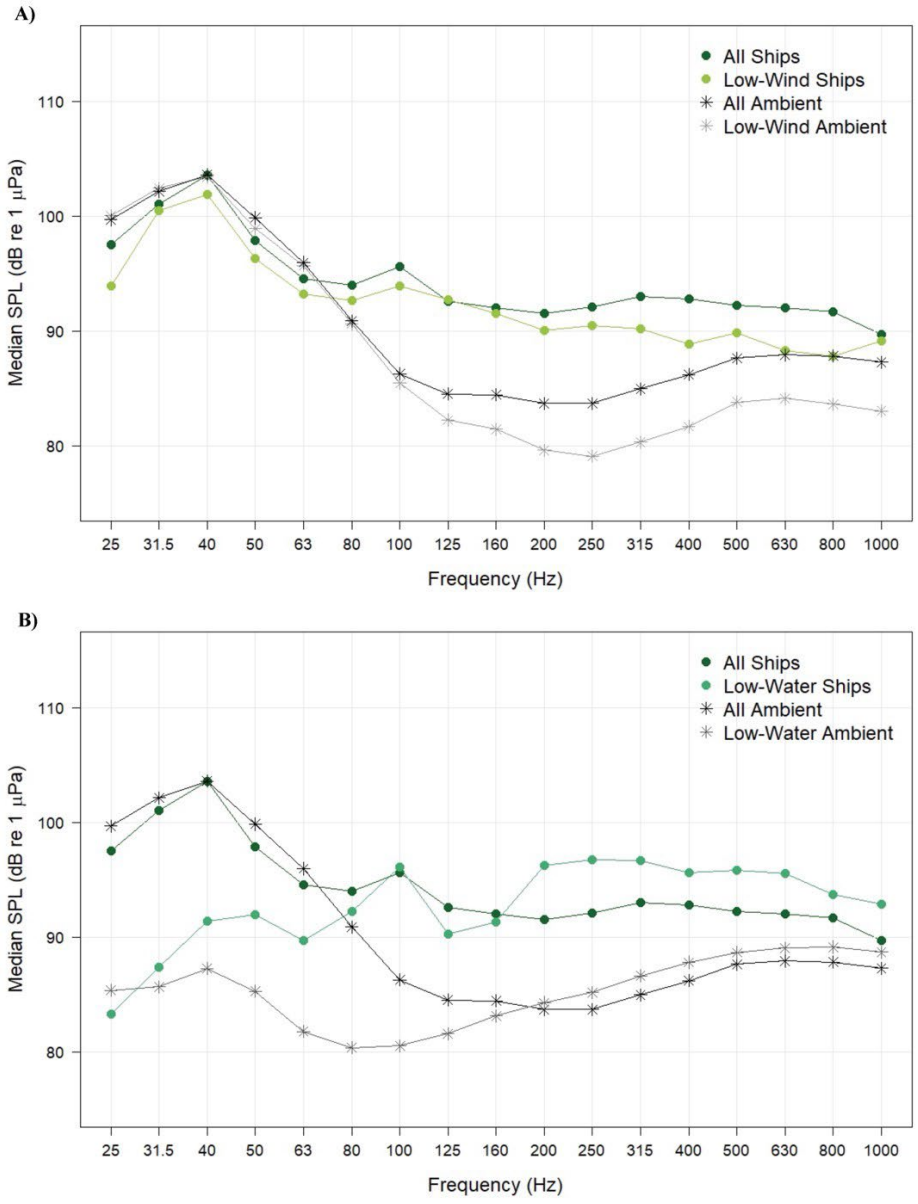

FIG. 6. Median sound pressure levels (SPL) measured across third-octave frequency bands (Hz) for ship events ("All Ships") plotted against ambient SPLs for the open-water season 2013–2015

("All Ambient"). Ambient SPLs for 2013–2015 at the two mooring sites were pooled and the median calculated for all ambient files ("All Ambient," n = 15,346 recordings; dark stars), and A) for days that had wind speeds <10 knots (~5 m/s; "Low-Wind Ambient," n = 3,925 recordings; light stars) and B) for days that had low water speeds (<27.6 cm/s; "Low-Water Ambient," n = 4,095 recordings). Median SPLs are plotted for all ships (n = 63 recordings; dark circles) and ship events on days with A) low wind speeds ("Low-wind Ships," n = 21 recordings; light circles), and B) low water speeds ("Low-Water Ships," n = 10 recordings). Note that the x-axes are not linear.

All vessel types had higher median sound levels than ambient for third-octave frequency bands ≥125 Hz (Fig. 7A). Only offshore supply vessels had higher median sound levels than ambient for bands ≥50 Hz and ≥63 Hz, respectively (Fig. 7A). The two military vessels had lower median sound levels than ambient for the lower frequency bands, likely because the ships transited on days with low wind and water speeds. Since lower frequency bands tend to be strongly correlated to water speeds (Section 3A; Fig. 2A), we plotted the median SPLs for ships vs. ambient for frequency bands 100–1000 Hz (Fig. 7B) and found that median sound levels with ships present were consistently higher than ambient, often by ≥10 dB. Except for low frequencies, ship noise exceeded ambient for the open-water season by >1 dB re 1μPa.

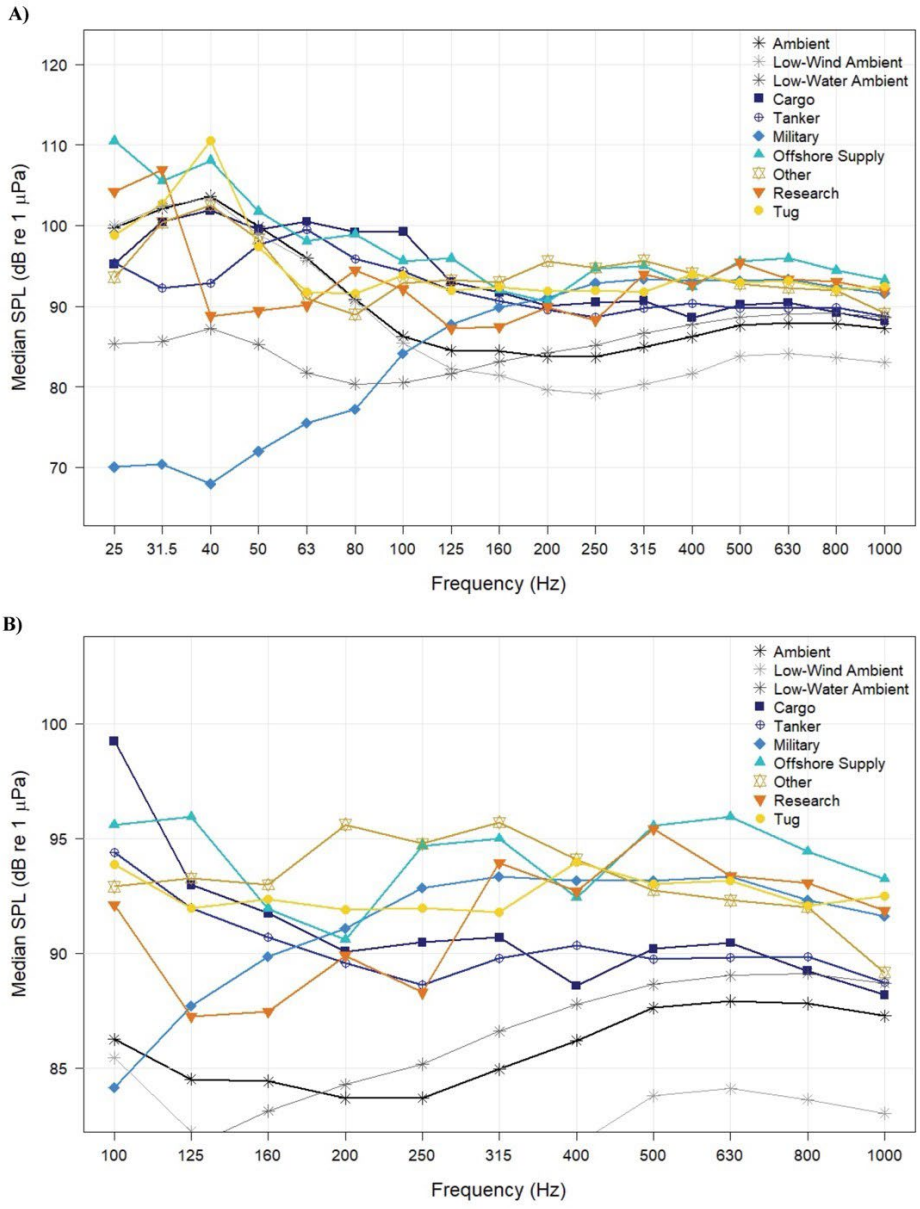

FIG. 7. Median ship sound pressure levels (SPL) measured at each third-octave frequency band (dB re 1 µPa) visualized by vessel type and plotted against median ambient SPLs for the open-water season (2013–2015) for (A) all third-octave frequency bands between 25–1000 Hz, and (B) bands between 100–1000 Hz. Note the difference in y-axis scale between the two plots. The plots include seven general vessel categories: cargo (n = 15), tanker (n = 4), military (n = 2), offshore supply (n = 3), other (n = 14), research (n = 3), and tug (n = 20). Ambient SPLs for days with low wind speeds <10 knots (~5 m/s; "Low-Wind Ambient") and low water speeds (<27.6 cm/s; "Low-Water Ambient") are included in the plot.

E. Acoustic Footprint of Ships

The modeled acoustic footprints varied in size across the six selected vessel types (Table V; Fig. 8). The loudest vessel, a military vessel (source level = 172 dB re 1 µPa at 1 m, 95% confidence interval: 171.5–173.4 dB re 1 µPa at 1 m), had the largest footprint with received levels exceeding 120 dB re 1 µPa out to ~0.9 km away from the vessel (Table V). Received levels around the quietest vessel, a ship in the "other" vessel class (source level = 141 dB re 1 µPa at 1 m, 95% confidence interval: 140.4–141.9 dB re 1 µPa at 1 m), only exceeded the 120-dB disturbance threshold (NOAA, 2016) out to 7 m. All six vessels produced modeled received levels that exceeded the 100-dB disturbance threshold (Southall *et al*., 2007), with radii ranging from ~0.2 km to 11 km around the vessel (Table V). We calculated the distance across the eastern channel of the Bering Strait as ~37 km from the eastern edge of Little Diomede Island to the Alaskan mainland (Fig. 1) and compared the widths of the acoustic footprint for each selected ship to this distance to estimate the spatial extent of elevated received levels. The loudest vessel (#367205050) was estimated to elevate received levels above the 120-dB disturbance threshold in ~5% of the eastern channel of the strait, while the remaining vessels elevated received levels above the 120-dB threshold in ≤2% of the eastern channel. In comparison, modeled received levels around the loudest vessel exceeded the 100-dB disturbance threshold in >50% of the eastern channel (Fig. 8).

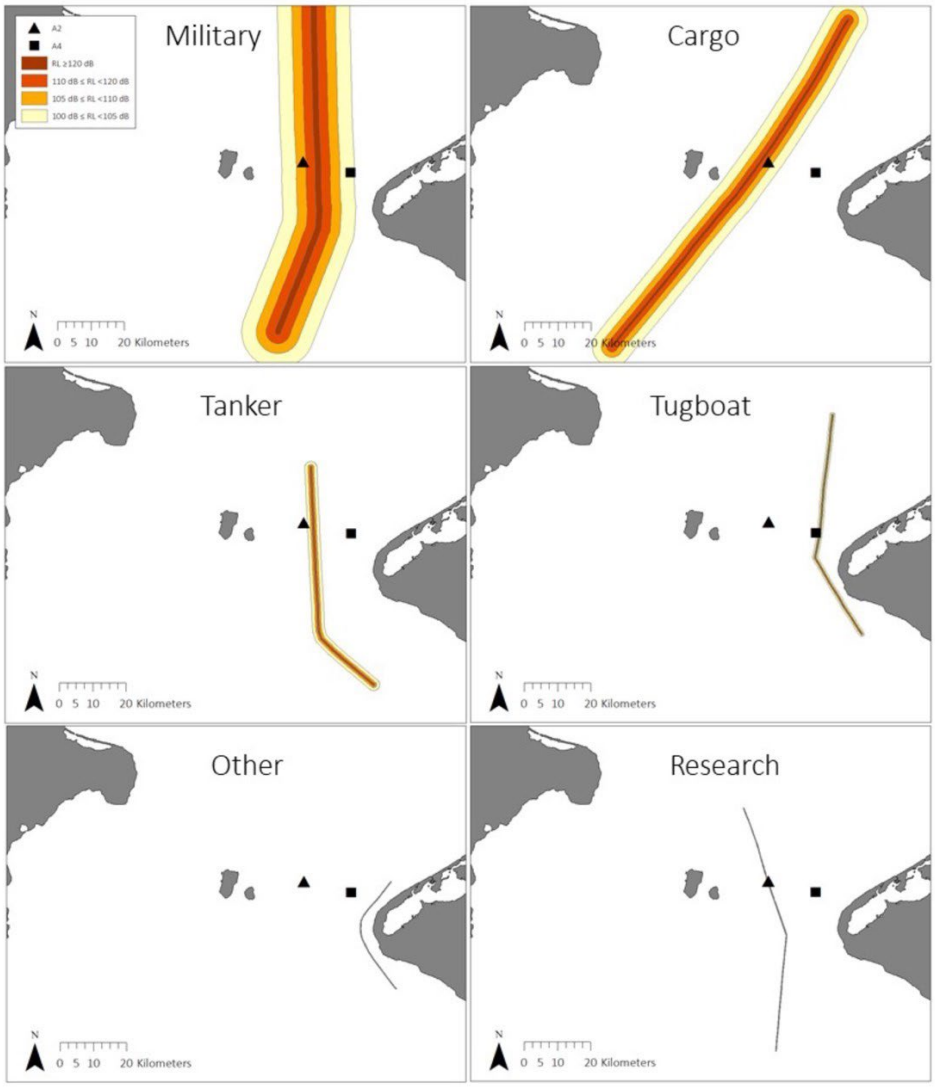

FIG. 8. Modeled acoustic footprint of ships selected from the major vessel types observed in the Bering Strait 2013–2015 (see Table II). The different colors represent the area where received sound levels are estimated to be within a certain radius around the ship's track.

IV. DISCUSSION

We set out to quantify how shop noise affects the soundscape of the Bering Strait region during the open-water season and found that ships elevate sound levels by ~6 dB on average for third-octave frequency bands >80 Hz, and an average of ~8 dB to ambient sound levels on days with low-wind speeds (Fig. 6). Moreover, how much sound a single ship contributed to ambient sound levels depended on vessel type. Offshore supply vessels had the highest sound levels above ambient while tankers and research vessels had the lowest (Figs. 7A and 7B). Similar to Halliday *et al*., (2017), we found that louder vessels affected larger areas than quieter vessels and the zones where received levels exceeded potentially harmful levels ranged from 7m to 10 km away from a ship's path (Table V; Fig. 8). Lastly, we did not find a significant relationship between vessel speed and source levels for cargo ships and tugboats, suggesting that vessel speed alone is not a good predictor of source levels for these two vessel types in our shallow study region. A larger sample size is needed to verify that reducing the speed of vessels will lead to lower noise levels in the Bering Strait.

Most of the ships detected in the Bering Strait during our study period were cargo ships and tugboats, reflecting an increasing trend in commercial shipping in the Arctic. The Bering Strait has served as a conduit for large vessels transiting to the Arctic from the Pacific since the late 1800s when commercial whaling vessels prowled its waters (Bockstoce, 1986). In the 20th century, most of the vessels in this region were small cargo ships, tugboats, tankers, and barges en route to support coastal Arctic communities in the Chukchi and Beaufort seas (AMSA, 2009). With increased industrial activity and resource extraction in the western Arctic, the number of cargo ships and tankers observed in the region increased steadily between the years of 2008 and 2013 (AMSA, 2009; Huntington *et al*., 2015). Along with cargo, ship activity related to tourism is expected to increase in the 21st century (AMSA, 2009). Only 6% of the AIS-transmitting vessels we observed in the Bering Strait region from 2013–2015 identified as pleasure crafts/passenger ships (Table II), however we anticipate that future studies of ship activity in the Bering Strait will observe more vessels of this type. (Note that more smaller ships may have been present during our study period but did not have AIS.)

Most of the ship transits through the strait occurred in the summer and early fall months (July–September; Fig. 4), similar to Eguíluz *et al*., (2016) and Halliday *et al*., (2021) who noted the highest numbers of Arctic transits in July–October. The peak in ship activity overlaps with the migrations of subarctic baleen whales through the strait (Clarke *et al*., 2013; Woodgate *et al*., 2015; Escajeda *et al*., 2020), increasing the probability of interactions between ships and whales. Though it was not the focus of the present study, we noted that October had the highest number of recording hours with both whales and ships present, followed by September and July. Ships transiting through the Bering Strait during the month of October should be aware of migrating whales in the region and slow down when whales are observed.

The source levels for various ship types calculated here are lower than previous studies. Veirs *et al*., (2016) estimated an average broadband source level of 175 ± 5 dB re 1 µPa at 1 m (20–40,000 Hz) for 206 unique cargo ships. For tugboats, they calculated a broadband source level of 175 ± 5 dB re 1 µPa at 1 m averaged over 85 unique vessels (20–40,000 Hz; Veirs *et al*., 2016). Both vessel types had a higher average speed over ground (14 knots) than the ships we examined (10 knots), and the authors did not calculated speed through water, which along with measuring broadband received sound levels over a wide frequency band (20–40,000 Hz) could have contributed to the difference in source level calculations. We found that sound levels in lower frequency bands were correlated to water speeds (Fig. 2A), indicating that flow noise impacts lower sound levels and could potentially bias broadband sound measurements. Additionally, Veirs *et al*., (2016) conducted their study in Haro Strait, a 200–300 m deep channel in British Columbia with likely different propagation conditions than the shallow Bering Strait.

Perhaps a more comparable study is that of Halliday *et al*., (2017) who calculated the source level for the Canadian icebreaker *CCGS Amundsen* using a shallow-water deployment near Sachs Harbor in the Canadian Arctic. The *CCGS Amundsen* is 98 m long and had an estimated broadband source level of 176 dB re 1 µPa at 1 m (63–20,000 Hz; Halliday *et al*., 2017). A similarly sized vessel in our dataset, a ship in the "other" vessel type class measuring 102 m long, had a source level of 169 dB re 1 µPa at 1 m (95% confidence interval: 168.4–170.2 dB re 1 µPa at 1 m). A review study by Chion *et al*., (2019) found that reported broadband source levels for various ship types differed as much as 30 dB, therefore it is not surprising to see a difference between source levels reported here and those from previous studies. A likely explanation for the difference in calculated source levels is in how each study calculated propagation loss. Most of the studies reviewed by Chion *et al*., (2019) were conducted in deep water, and thus, used spherical spreading for estimating transmission loss. Spherical spreading tends to overestimate transmission loss (Thilges *et al*., 2019), which may explain why previous calculations of source levels were much higher than those presented here.

It is likely that propagation loss in the Bering Strait is more complex than geometric spreading plus absorption loss, as we assumed. Sound propagation in shallow-water environments, such as the Bering Strait, can be complicated by interactions between sound waves, and the surface and seafloor. Absorption of sound by the seafloor and shifts in sound speeds due to varying water and sediment density can also contribute to propagation loss (Richardson *et al*., 1995; Farcas *et al.*, 2016). Such as interactions would result in a greater propagation loss than we estimated, and consequently, higher source levels. Future studies should employ the use of more complex propagation models, such as normal mode models (Richardson *et al*., 1995; Jensen *et al*., 2011; Wang *et al*., 2014) or parabolic equations (Halliday *et al*., 2021), for estimating transmission loss, pending the availability of accurate water column and sediment sound speed data for the Bering Strait.

Another key finding was that high water speed affected sound levels at lower frequencies, which has important implications for the frequency band used for quantifying ship noise. The

European Union currently recommends using the 63-Hz and 125-Hz third-octave band for measuring ship noise (Dekeling *et al*., 2014). However, both bands exhibited positive correlations to water speed (Fig. 2B), suggesting that sound levels for the 63-Hz and 125-Hz bands recorded by the hydrophone on days with strong currents may be artificially high. Our results corroborate the suggestion by Merchant *et al*., (2014) to use the 250-Hz band for quantifying ship noise when flow noise is a concern.

The acoustic footprints presented here likely represent a first approximation of ships' "zones of impact" for the Bering Strait region and show that ship noise potentially reduces the acoustic habitat available for communication among baleen whales. For instance, the area where sound levels exceeded 100 dB, a threshold where some disturbance to marine mammal behavior was observed by Southall *et al*., (2007), extended to ~6 km for the cargo ship and to ~11 km for the military ship we examined (Table V). Both distances exceed the communication for space of humpback whales, which is estimated to extend ~4 km (Dunlop, 2018). It is likely then that cargo and military ships could interrupt intraspecies communication for humpback whales, especially since they have been observed to cease calling when ships were present (Fournet *et al*., 2018). The impact of ship noise on the acoustic habitat of the Bering Strait is likely exacerbated by the presence of multiple ships. Here we estimated the impact of single ships on ambient sound levels, so quantifying the effects of multiple ships should be the focus of future inquiry.

Our result that ships raise sound levels 2–9 dB (mean: 6 dB) above ambient for third-octave frequency bands between 100 and 1000 Hz in the Bering Strait (Fig. 7B) is strikingly different from those of McKenna *et al*., (2021). McKenna *et al*., (2021) conducted a similar study using a single hydrophone west of St. Lawrence Island and found that median third-octave sound levels (100–1000 Hz) produced by ships traveling at >5 knots within 10 km of their recorder were <1 dB higher than annual median ambient sound levels. McKenna *et al*., (2021) also examined ship transits at a location in the Bering Strait during a 13-day period in October 2015, and found that ships elevated sound levels by 3–5 dB for third-octave frequency bands between 100–1000 Hz on days when wind speeds were less than ~5 m/s. For comparison, we conducted a similar analysis for three ships that transited on days with wind speeds ≤5 m/s in October 2013 and found that the ships contributed ~2–12 dB of sound to ambient third-octave sound levels for bands 100–500 Hz and were similar to ambient (within <1 dB) for bands 630–1000 Hz. A possible explanation for the disparity in results is that we compared ship sound levels to median ambient sound levels measured over the open-water season as opposed to median levels measured for the entire year. Additionally, the ships analyzed here were within a closer range of our hydrophones (<14 km) than the ships in the Bering Strait analyzed by McKenna *et al*., (2021) (15–40 km), which could have affected the amplitude of measured received levels.

Unlike previous studies (McKenna *et al*., 2013; Simard *et al*., 2016; Veirs *et al*., 2016; Chion *et al*, 2019; MacGillivray *et al*., 2019; ZoBell *et al*., 2021), we did not find a significant relationship between source level and speed through water. Note however the wide range of regression slopes found in previous studies: 0.4 to 6.6 dB per knot (Veirs *et al*., 2016; ZoBell *et al*.,

2021), which suggests that the relationship between source level and vessel speed likely differs depending on vessel type and environmental conditions. It may also depend on water depth since most of the previous efforts to quantify the relationship between vessel noise and speed were conducted in deep water (e.g., Haro Strait which ranges from 200–300 m depth; Veirs *et al*., 2016). Our results were unable to show that the positive relationship between vessel noise and speed holds for a shallow, coastal area, although our sample size was very small (n = 10). A greater sample size is necessary to test whether source level increases with speed for all vessel classes in the Bering Strait.

As the presence of ships continues to increase in the Bering Strait region, ship noise will become an ever-present threat to marine animals that rely on sound for critical life functions (Erbe and Farmer, 2000; Halliday *et al*., 2019, 2020). Previous management recommendations include limiting commercial ships to a specific route through the strait as well as encouraging vessel speed limits (Halliday *et al*., 2017, 2020). In late 2018, the IMO approved a joint proposal from the U.S. Coast Guard and Russian Federation for a two-way route for large ships in the western and eastern channel of the Bering Strait (IMO, 2017). The routing measures also include multiple "Areas to be Avoided," including the coastal region surrounding St. Lawrence Island, south of the Bering Strait. The routes are voluntary for vessels 400 gross tons and above, however a 2019 study by the Nuka Research and Planning Group found that compliance was high among large commercial vessels, including bulk carriers, tankers, and cargo ships (Fletcher *et al*., 2020).

Shipping routes through the Bering Strait region are a good first step to managing vessel traffic in this sensitive area, however they do not address the issue of ship noise. Though we did not find a significant relationship between vessel speed and source levels, results of previous studies (e.g., ZoBell *et al*., 2021) suggest that the reducing speed of ships could reduce noise levels. We also found that large vessels transiting the Bering Strait are already traveling at speeds around or below the 13-knot speed limit currently enforced in Glacier Bay National Park, Alaska (mean speed over ground = 10 ± 3 knots SD; Code of Federal Registrations [CFR] 36 CFR 13.65, 2001; Frankel and Gabriele 2017). Installing a voluntary speed limit through the strait is likely to have high compliance among ship operators given the fact that ships are already transiting at relatively slow speeds, and the fact that there is currently high compliance with Bering Strait routing measures (Fletcher *et al*., 2020). Decreasing the speed of vessels traveling the strait could have additional benefits such as of reducing the risk and lethality of vessel strikes for whales (Vanderlaan and Taggart, 2006) and lowering carbon emissions (Leaper, 2019). Therefore, voluntary speed limits should be pursued for the Bering Strait region.

Coordinated efforts among multiple governments and agencies are required to reduce the potential harm to marine organisms from the expansion of economic activity in the Arctic. It is also important to realize that noise pollution is just one impact of increased shipping in the Arctic. Ship strikes, oil spills (leaks or major accidents), introduction of invasive species, and disruption of marine mammal behavior such as feeding and migration (AMSA, 2009) will negatively affect sensitive species that are already facing challenges created by shifting habitat conditions brought on

by climate change (Laidre *et al*., 2008; Hauser *et al*., 2018; Halliday *et al*., 2020). The results presented here can serve as a baseline for measuring future impacts of shipping on the acoustic environment of the Bering Strait, however they are just a start. More research is needed to understand, anticipate, and mitigate the impacts of ships on the marine environment of the Pacific Arctic.

ACKNOWLEDGEMENTS

We are grateful for the guidance of Alexander Hornof, Dr. Peter Dahl, and Hanah Choice in developing the methods for this study. This study is based upon work supported by the National Science Foundation (NSF) Graduate Research Fellowship Program under grant number DGE-1256082. Any opinions, findings, and conclusions or recommendations expressed in this material are those of the author(s) and do not necessarily reflect the views of NSF. We also wish to thank the University of Washington School of Aquatic and Fishery Sciences for providing funding for the primary author. Additional funding for this study was provided to K. Stafford from the North Pacific Research Board Arctic IERP (A94-00), the Office of Naval Research Marine Mammals and Biology Program N000141712274, and the National Science Foundation Polar Programs ARC-1107106; and to R. Woodgate from the NSF Arctic Observing Network PLR-1304052 and 1758565. The Bering Strait mooring data can be found in the permanent archives of the U.S. National Centers for Environmental Information/National Oceanographic Data Center, (www.ncei.noaa.gov), and at: psc.apl.washington.edu/BeringStrait.html.

REFERENCES

Akaike, H. **(1973).** Information Theory and an Extension of the Maximum Likelihood Principle, in: Petrov, 8., Csaki, F. (Eds.), Second International Symposium on Information Theory. Akademiai Kiad6, Budapest, Hungary, pp. 267-281.

AMSA **(2009).** *Arctic marine shipping assessment* Arctic Council.

Bockstoce, J. R. **(1986).** *Whales, ice, and men: the history of whaling in the western Arctic,* University of Washington Press in association with the New Bedford Whaling Museum, Massachusetts, Seattle, Ist ed., 400 pages.

Brower, A. A., Clarke, J. T., and Ferguson, M. C. **(2018).** "Increased sightings of subArctic cetaceans in the eastern Chukchi Sea, 2008-2016: population recovery, response to climate change, or increased survey effort?" Polar Biol, **41,** 1033-1039. doi:10.1007/s00300-018-2257-x

Chion, C., Lagrois, D., and Dupras, J. **(2019).** "A meta-analysis to understand the variability in reported source levels of noise radiated by ships from opportunistic studies," Front. Mar. Sci., 6,714. doi:10.3389/fmars.2019.00714

Clark, C., Ellison, W., Southall, B., Hatch, L., Van Parijs, S., Frankel, A., and Ponirakis, D. **(2009).** "Acoustic masking in marine ecosystems: intuitions, analysis, and implication, "Mar. Ecol. Prog. Ser., **395,** 201-222. doi:10.3354/meps08402

Clarke, J., Stafford, K., Moore, S., Rone, B., Aerts, L., and Crance, J.
(2013). "Subarctic cetaceans in the southern Chukchi Sea: evidence of recovery or response to a changing ecosystem," Oceanography, **26,** 136-149. doi:10.5670/oceanog.2013.81

Dekeling, R., Tasker, M., Van Der Graaf, S., Ainslie, M., Andersson, M., Andre, M., Borsani, J., Brensing, K., Castellote, M., Cronin, D., Dalen, J., Folegot, T., Leaper, R., Pajala, J., Redman, P., Robinson, S., Sigray, P., Sutton, G., Thomsen, F., Werner, S., Wittekind, D. and Young, J. **(2014).** *Monitoring guidance for underwater noise in European seas: a guidance document within the common implementation strategy for the Marine Strategy Framework Directive. Part 11, Monitoring guidance specifications.,* European Commission. Joint Research Centre. Institute for Environment and Sustainability, Publications Office, LU. Retrieved from https://data.europa.eu/doi/10.2788/27158

Dunlop, R. A. **(2018).** "The communication space of humpback whale social sounds in wind-dominated noise," The Journal of the Acoustical Society of America, **144,** 540-551. doi:10.1121/1.5047744

Eguiluz, V. M., Fernandez-Gracia, J., Jrigoien, X., and Duarte, C. M. **(2016).** "A quantitative assessment of Arctic shipping in 2010-2014," Sci Rep, **6,** 30682. doi:10.1038/srep30682

Eisner, L., Hillgruber, N., Martinson, E., and Maselko, J. **(2013).** "Pelagic fish and zooplankton species assemblages **in** relation to water mass characteristics in the northern Bering and southeast Chukchi seas," Polar Biol, **36,** 87-113. doi:10. 1007/s00300-012-1241-0

Erbe, C., and Farmer, D. M. **(2000).** "Zones of impact around icebreakers affecting beluga whales in the Beaufort Sea," J. Acoust. Soc. Am., **108,** 1332.doi:10.1121/1.1288938 Ershova, E., Hopcroft, R., Kosobokova, K., Matsuno, K., Nelson, R. J., Yamaguchi, A., and Eisner, L. **(2015).** "Long-term changes in summer zooplankton communities of the western Chukchi Sea, 1945-2012," Oceanog, **28,** 100-115. doi:10.5670/oceanog.2015.60

Escajeda, E., Stafford, **K. M.,** Woodgate, R. A., and Laidre, K. L. **(2020).** "Variability in fin whale *(Balaenoptera physalus)* occurrence in the Bering Strait and southern Chukchi Sea in relation to environmental factors," Deep Sea Research Part II: Topical Studies in Oceanography, **177,** 104782. doi:10.1016/j.dsr2.2020.104782

Farcas, A., Thompson, P. **M.,** and Merchant, N. D. **(2016).** "Underwater noise modelling for environmental impact assessment," Environmental Impact Assessment Review, 57, 114-122.doi:10.1016/j.eiar.2015.11.012

Fletcher, S., Higman, B., Chartier, A., and Robertson, T. **(2020).** *Adherence to Bering Strait Vessel Routing Measures in 2019* Seldovia, AK: Nuka Research and Planning Group LLC, p. 39. Retrieved from https://www.pewtrusts.org/-/media/assets/2020/04/200131nukaberingstraitroutingstudy.pdf

Fournet, M., Matthews, L., Gabriele, C., Haver, S., Mellinger, D., and Klinck, H. **(2018).** "Humpback whales *Megaptera novaeangliae* alter calling behavior in response to natural sounds and vessel noise," Mar. Ecol. Prog. Ser., **607,** 251-268. doi: 10.3354/meps12784

Francois, R. E., and Garrison, G. R. **(1982).** "Sound absorption based on ocean measurements. Part II: Boric acid contribution and equation for total absorption," The Journal of the Acoustical Society of America, **72,** 1879-1890. doi:10.1121/1.388673

Frankel, A., and Gabriele, C. **(2017).** "Predicting the acoustic exposure of humpback whales from cruise and tour vessel noise in Glacier Bay, Alaska, under different management strategies," Endang. Species. Res., **34,** 397-415. doi:I 0.3354/esr00857

Frey, K. E., Moore, G. W. K., Cooper, L. W., and Grebmeier, J.M. **(2015).** "Divergent patterns of recent sea ice cover across the Bering, Chukchi, and Beaufort seas of the Pacific Arctic Region," Progress in Oceanography, **136,** 32-49. doi:10.1016/j.pocean.2015.05.009

Grebmeier, J.M., Cooper, L. W., Feder, H. M., and Sirenko, B. I. **(2006).** "Ecosystem dynamics of the Pacific-influenced Northern Bering and Chukchi Seas in the Amerasian Arctic," Progress in Oceanography, **71,** 331-361. doi:10.1016/j.pocean.2006.10.001

Halliday, W. D., Insley, S. J., Hilliard, R. C., de Jong, T., and Pine, M. K. **(2017).** "Potential impacts of shipping noise on marine mammals in the western Canadian Arctic," Marine Pollution Bulletin, **123,** 73-82. doi: 10.1016/j.marpolbul.2017.09.027

Halliday, W. D., Pine, M. K., Citta, J. J., Harwood, L., Hauser, D. D. W., Hilliard, R. C., Lea, E. V., et al. **(2021).** "Potential exposure of beluga and bowhead whales to underwater noise from ship traffic in the Beaufort and Chukchi Seas," Ocean & Coastal Management, **204,** 105473. doi: 10.10l6/j.ocecoaman.2020.105473

Halliday, W. D., Pine, M. K., and Insley, S. J. **(2020).** "Underwater noise and Arctic marine mammals: review and policy recommendations," Environ. Rev., **28,** 438-448. doi: 10.1139/er-2019-0033

Hauser, D. D. W., Laidre, K. L., and Stern, H. L. **(2018).** "Vulnerability of Arctic marine mammals to vessel traffic in the increasingly ice-free Northwest Passage and Northern Sea Route," Proc Natl Acad Sci USA, 115, 7617-7622. doi:10.1073/pnas.1803543115

Hermannsen, L., Mikkelsen, L., Tougaard, J., Beedholm, K., Johnson, M., and Madsen, P. T. (2019). "Recreational vessels without Automatic Identification System (AIS) dominate anthropogenic noise contributions to a shallow water soundscape," Sci Rep, 9, 15477. doi: 10.1038/s41598-019-5 l 222-9

Hildebrand, J. (2009). "Anthropogenic and natural sources of ambient noise in the ocean," Mar. Ecol. Prog. Ser., 395, 5-20. doi:10.3354/meps08353

Huntington, H.P., Daniel, R., Hartsig, A., Harun, K., Heiman, M., Meehan, R., Noongwook, G., et al. (2015). "Vessels, risks, and rules: Planning for safe shipping in Bering Strait," Marine Policy, 51, 119-127. doi:10.1016/j.mamol.2014.07.027

Insley, S. J., Halliday, W. D., and De Jong, T. (2017). "Seasonal patterns in ocean ambient noise near Sachs Harbour, Northwest Territories," ARCTIC, 70, 239. doi:10.14430/arctic4662

Jakobsson, M., Mayer, L., Coakley, B., Dowdeswell, J. A., Forbes, S., Fridman, B., Hodnesdal, H., et al. (2012a). "The International Bathymetric Chart of the Arctic Ocean (IBCAO) Version 3.0," Geophys. Res. Lett., 39, n/a-n/a. doi:10.1029/2012GL052219

Jakobsson, M., Mayer, L., Coakley, B., Dowdeswell, J. A., Forbes, S., Fridman, B., Hodnesdal, H., et al. (2012b). "The International Bathymetric Chart of the Arctic Ocean (IBCAO) Version 3.0: IBCAO VERSION 3.0," Geophys. Res. Lett., 39, n/a-n/a. doi:10.1029/2012GL052219

Jensen, F. B., Kuperman, W. A., Porter, M. B., and Schmidt, H. (2011). Computational Ocean Acoustics, Springer New York, New York, NY. doi:10.1007/978-1-4419-8678-8

Laidre, K. L., Stirling, I., Lowry, L. F., Wiig, 0., Heide-forgensen, M. P., and Ferguson, S. H. (2008). "Quantifying the sensitivity of arctic marine mammals to climate-induced habitat change," Ecological Applications, 18, S97-Sl 25. doi:10.1890/06-0546.1

Leaper, R. (2019). "The role of slower vessel speeds in reducing greenhouse gas emissions, underwater noise and collision risk to whales," Front. Mar. Sci., 6, 505. doi:10.3389/fmars.2019.00505

MacGillivray, A. 0., Li, Z., Hannay, D. E., Trounce, K. B., and Robinson, 0. M. (2019). "Slowing deep-sea commercial vessels reduces underwater radiated noise," The Journal of the Acoustical Society of America, 146, 340-351. doi:10.1121/1.5116140

McKenna, M. F., Ross, D., Wiggins, S. M., and Hildebrand, J. A. (2012). "Underwater radiated noise from modern commercial ships," The Journal of the Acoustical Society of America, 131, 92-103. doi:10.1121/1.3664100

McKenna, M. F., Southall, B. L., Chou, E., Robards, M., and Rosenbaum, H. C. (2021). "An integrated underwater soundscape analysis in the Bering Strait region," The Journal of the Acoustical Society of America, 150, 1883-1896. doi:10.1121/10.0006099

McKenna, M. F., Wiggins, S. M., and Hildebrand, J. A. (2013). "Relationship between container ship underwater noise levels and ship design, operational and oceanographic conditions," Sci Rep, 3, 1760. doi: 10.1038/srepO1760

Mellinger, D. (2002). Ishmael 1.0 User's Guide. NOAA Technical Memorandum OAR PMEL-120. http://www.pmel.noaa.gov/pubs/PDFImel12434/mell2434.pdf.

Merchant, N. D., Fristrup, K. M., Johnson, M. P., Tyack, P. L., Witt, M. J., Blonde!, P., and Parks, S. E. (2015). "Measuring acoustic habitats," (D. Hodgson, Ed.) Methods in Ecology and Evolution, 6, 257-265. doi:10.1111/2041-210X.12330

Merchant, N. D., Pirotta, E., Barton, T. R., and Thompson, P. M. (2014). "Monitoring ship noise to assess the impact of coastal developments on marine mammals," Marine Pollution Bulletin, 78, 85-95. doi:10.1016/j.marpolbul.2013.10.058

Mesinger, F., DiMego, G., Kalnay, E., Mitchell, K., Shafran, P. C., Ebisuzaki, W., Jovic, D., et al. (2006). "North American Regional Reanalysis," Bull. Amer. Meteor. Soc., 87, 343-360. doi:10. I I 75/BAMS-87-3-343

Moore, S. E., Reeves, R.R., Southall, B. L., Ragen, T. J., Suydam, R. S., and Clark, C. W. (2012). "A new framework for assessing the effects of anthropogenic sound on marine mammals in a rapidly changing Arctic," BioScience, 62, 289-295. doi:10.1525/bio.2012.62.3.10

National Marine Fisheries Service (2016). Technical guidance for assessing the effects of anthropogenic sound on marine mammal hearing: underwater acoustic thresholds for onset of permanent and temporary threshold shifts (NOAA Technical Memorandum No. NMFS-OPR-55).

Nowacek, D. P., Thorne, L. H., Johnston, D. W., and Tyack, P. L. (2007). "Responses of cetaceans to anthropogenic noise," Mammal Review, 37, 81- 115. doi:I 0.l I J J /j.1365-2907.2007.00104.x

Pine, M. K., Hannay, D. E., Insley, S. J., Halliday, W. D., and Juanes, F. (2018). "Assessing vessel slowdown for reducing auditory masking for marine mammals and fish of the western Canadian Arctic," Marine Pollution Bulletin, 135, 290-302. doi:10.1016/j.marpolbul.2018.07.03 l

R Core Team. (2021). R: A language and environment for statistical computing. R Foundation for Statistical Computing, Vienna, Austria. URL https://www.R-proiect.org/.

Richardson, W. J., Greene, Jr., C.R., Malme, C. I., and Thomson, D. H. (1995). Marine mammals and noise, Academic Press, San Diego California.

Rolland, R. M., Parks, S. E., Hunt, K. E., Castellote, M., Corkeron, P. J., Nowacek, D. P., Wasser, S. K., et al. (2012). "Evidence that ship noise increases stress in right whales," Proceedings of the Royal Society B: Biological Sciences, 279, 2363-2368.doi: l 0.1098/rspb.2011.2429

Romagosa, M., Perez-Jorge, S., Cascao, I., Mourino, H., Lehodey, P., Pereira, A., Marques, T. A., et al. (2021). "Food talk: 40-Hz fin whale calls are associated with prey biomass," Proc. R. Soc. B., 288, 20211156. doi: l 0.1098/rspb.202 I.I I 56

Ross, D. (1976). Mechanics of underwater noise, Pergamon, New York.

Serreze, M. C., Crawford, A. D., Stroeve, J.C., Barrett, A. P., and Woodgate, R. A. (2016). "Variability, trends, and predictability of seasonal sea ice retreat and advance in the Chukchi Sea," Journal of Geophysical Research: Oceans, 121, 7308-7325. doi:10.1002/2016JC011977

Simard, Y., Roy, N., Gervaise, C., and Giard, S. (2016). "Analysis and modeling of255 source levels of merchant ships from an acoustic observatory along St. Lawrence Seaway," The Journal of the Acoustical Society of America, 140, 2002-2018. doi:10.1121/1.4962557

Smith, L. C., and Stephenson, S. R. (2013). "New Trans-Arctic shipping routes navigable by midcentury," Proceedings of the National Academy of Sciences, 110, El 191-El 195. doi:10.1073/pnas.1214212 11 0

Southall, B. L., Bowles, A. E., Ellison, W. T., Finneran, J. J., Gentry, R. L., Greene, C. R., Kastak, D., et al. (2007). "Marine mammal noise exposure criteria: initial scientific recommendations," aquatic mammals, 33, 41 l-521. doi:10.1578/AM.33.4.2007.411

Stephenson, S. R., Smith, L. C., and Agnew, J. A. (2011). "Divergent long-term trajectories of human access to the Arctic," Nature Climate Change, 1, 156-160. doi:10.1038/nclimatel 120

Stephenson, S. R., Smith, L. C., Brigham, L. W., and Agnew, J. A. (2013). "Projected 21st-century changes to Arctic marine access," Climatic Change, 118, 885-899. doi: 10.1007/sl 0584-012-0685-0

Thilges, K., Potty, G., Freeman, S., Freeman, L., and Van Uffelen, L. (2019). "Measurements and models of acoustic transmission loss on two Hawaiian coral reefs," Acoustics Virtually Everywhere, 070005. Presented at the 179th Meeting of the Acoustical Society of America. doi:10.1121/2.0001336

Urick, R. J. (1983). Principles of underwater sound, McGraw-Hill, New York, 3rd ed., 423 pages.

Vanderlaan, A. S. M., and Taggart, C. T. (2007). "Vessel collisions with whales: the probability of lethal injury based on vessel speed," Marine Mammal Sci, 23, 144-156. doi:10.1111/j.1748-7692.2006.00098.x

Veirs, S., Veirs, V., and Wood, J. 0. (2016). "Ship noise extends to frequencies used for echolocation by endangered killer whales," PeerJ, 4, e1657. doi: 10.7717/peerj.1657

Wang, L. S., Heaney, K., Pangerc, T., Theobald, P., Robinson, S. P., and Ainslie, M. (2014). Review of underwater acoustic propagation models., Available: https://eprintspublications.npl.co.uk/6340/, (date last viewed: 27-Jan-22). Retrieved January 27, 2022, from https://eprintspublications.npl.co.uk/6340/

Wenz, G. M. (1962). "Acoustic ambient noise in the Ocean: spectra and sources," The Journal of the Acoustical Society of America, 34, 1936-1956. doi: I 0.1121/1.1909155

Woodgate, R. A. (2018). "Increases in the Pacific inflow to the Arctic from 1990 to 2015, and insights into seasonal trends and driving mechanisms from year-round Bering Strait mooring data," Progress in Oceanography, 160, 124-154. doi: 10.1016/j.pocean.2017.12.007

Woodgate, R. A., Aagaard, K., and Weingartner, T. J. (2005). "Monthly temperature, salinity, and transport variability of the Bering Strait through flow," Geophys. Res. Lett., 32, n/a- n/a. doi:10.1029/2004GL02 l 880

Woodgate, R., Stafford, K., and Prahl, F. (2015). "A synthesis of year-round interdisciplinary mooring measurements in the Bering Strait (I 990-2014) and the RUSALCA years (2004-2011)," Oceanography, 28, 46-67. doi:10.5670/oceanog.2015.57

ZoBell, V. M., Frasier, K. E., Morten, J. A., Hastings, S. P., Peavey Reeves, L. E., Wiggins, S. M., and Hildebrand, J. A. (2021). "Underwater noise mitigation in the Santa Barbara Channel through incentive-based vessel speed reduction," Sci Rep, 11, 18391. doi: 10.1038/s41598-021-96506-1

TABLES

TABLE 1. Hydrophone deployment data, including latitude and longitude (in decimal degrees) and recording settings. Dates are in the format 'yyyy-mm-dd.' Mooring names are from the Bering Strait mooring program (Woodgate *et al*., 2015).

Mooring	Deployment Year	Latitude N	Latitude W	Record Start Date	Record End Date	Hydrophone Depth (m)	Water Depth (m)	Sampling Rate (Hz)	Hourly Duty Cycle
A2	2013	65.78°	168.57°	2013-07-15	2014-07-01	48	54	8192	20 min
	2014	65.78°	168.57°	2014-07-10	2015-07-04	49	53	8192	20 min
	2015	65.78°	168.57°	2015-07-05	2016-07-08	49	54	8192	22 min
A3	2013	66.33°	168.97°	2013-07-15	2014-07-02	52	56	8192	20 min
	2014	66.33°	168.97°	2014-07-10	2015-07-02	50	56	8192	20 min
	2015	66.33°	168.97°	2015-07-05	2016-07-08	48	56	8192	22 min
A4	2013	65.75°	168.26°	2013-07-15	2014-07-02	42	47	8192	20 min
	2014	65.75°	168.25°	2014-07-10	2015-07-02	42	47	8192	20 min
	2015	65.75°	168.25°	2015-07-05	2016-07-08	41	47	8192	22 min

TABLE II. Total counts of vessels by type observed in the Bering Strait region during May–November for the years 2013–2015 according to the U.S. Coast Guard's Nationwide Automatic Identification System (NAIS) Automatic Identification System (AIS) data. Note that large vessels (>300 gross tonnage), passenger vessels, and large fishing vessels are required to carry AIS transmitters. Thus, the number of sailing and smaller vessels are likely to exceed these numbers.

Vessel Type	2013	2014	2015	Totals
Cargo	51	43	44	**138**
Tug Tow	27	23	35	**85**
Other	24	24	27	**75**
Tanker	21	12	10	**43**
NA	15	10	8	**33**
Passenger	7	6	6	**19**
Fishing	4	1	2	**7**
Pleasure Craft/Sailing	2	2	2	**6**
Military	3	1	0	**4**
Totals	**154**	**122**	**134**	**410**

TABLE III. Number of ship events (total $n = 57$) for each vessel type along with source level (SL) ranges, and mean speed through water (STW, knots) with the standard deviation in parentheses. A "ship event" is defined as a ship noise recording that matched with the closest passage of a single vessel.

Vessel Type	*n*	SL Range (dB re 1 µPa at 1 m)	Mean STW (knots)
Tug	19	147–160	7.3 (± 2.2)
Cargo	12	147–167	12.4 (± 2.6)
Other	12	141–169	9.6 (± 3.1)
Tanker	4	152–157	11 (± 1)
Research	3	141–156	10.5 (± 2.5)
Offshore Supply	3	152–165	9.9 (± 1.2)
Passenger/Pleasure	1	150	10.2
Military	2	146–172	12.3 (± 0.7)
Fishing	1	157	9.7

TABLE IV. Results of the linear regressions between a ship's source level measured at the 250-Hz third-octave band and its speed through water in knots ('STW'), length in meters ('VesselLength'), whether the vessel was traveling with or against the wind ('WindMatch'), the daily mean wind speed in m/s ('WindSpeed'), and the wind category ("low-wind" day vs a "high-wind" day, 'WindCat'). The Akaike's information criterion (AICc) score and R^2 for each model is listed along with the *p*-value for each variable ($p < 0.05$ is considered significant).

Cargo Ships ($n = 10$)				Tugs ($n = 19$)			
Variable	**AICc**	**R^2**	***p*-value**	**Variable**	**AICc**	**R^2**	***p*-value**
Full Model	90.7	0.44	*N/A*	Full Model	117.9	0.13	*N/A*
STW	65.7	0.09	0.40	STW	103.1	0.04	0.42
VesselLength	66	0.06	0.50	VesselLength	103.5	0.02	0.54
WindMatch	64.8	0.16	0.25	WindMatch	103.2	0.01	0.44
WindSpeed	62.6	0.33	0.08	WindSpeed	103.3	0.03	0.49
WindCat	*N/A*	*N/A*	*N/A*	WindCat	103.7	0.01	0.66

TABLE V. Source levels (SL) and potential areas of impact for selected vessels (identified by the MMSI number), given as the radius around the ship where sound levels are expected to exceed a disturbance threshold. The standard errors for the SL estimates are given in parentheses (dB re 1 µPa). Sound levels ≥ 120 dB re 1 µPa are hypothesized to have negative impacts on marine mammals while sound levels ≥ 100 dB re 1 µPa are thought to cause some behavioral disturbance (Southall *et al*., 2007).

Vessel Type	MMSI Number	SL (dB re 1 µPa at 1 m)	≥ 120 dB Area Radius (m)	≥ 100 dB Area Radius (m)
Cargo	215000028	167 (±0.5)	378	5,866
Military	367205050	172 (±0.5)	907	10,800
Research	431939000	141 (±0.4)	7	169
Tanker	210333000	157 (±0.5)	92	1806
Tug	366091888	152 (±0.6)	38	793
Other	366070091	141 (±0.4)	7	166

Chapter 6: Northward Range Expansion of Subarctic Upper Trophic Level Animals into the Pacific Arctic Region

Stafford, K.M.[1,2], E. Farley[3], M. Ferguson[4], K.J. Kuletz[5], R. Levine[6]. 2022. Northward Range Expansion of Subarctic Upper Trophic Level Animals into the Pacific Arctic Region. Oceanography 35(2). DOI: https://doi.org/10.5670/oceanog.2022.101

Abstract

In the Arctic, studies of the impacts of climate change in marine ecosystems have largely centered on endemic species, ecosystems, and the people who rely on them. Fewer studies have focused on the northward expansion of upper trophic level (UTL) subarctic species. We provide an overview of changes in the temporal and spatial distributions of subarctic fish, birds, and cetaceans, with a focus on the Pacific Arctic Region. Increasing water temperatures throughout the Arctic have increased 'thermal habitat' for subarctic fish species, resulting in northward shifts of species including walleye pollock and pink salmon. Ecosystem changes are altering the community composition and species richness of seabirds in the Arctic, as water temperatures change the available prey field which dictates the presence of planktivorous versus piscivorous seabird species. Finally, subarctic whales, among them killer and humpback whales, are arriving earlier, staying later, and moving consistently farther north, as evidenced by aerial survey and acoustic detections. Increasing ice-free habitat and changes in water mass distributions in the Arctic are changing the underlying prey structure, drawing UTL species northwards, by increasing spatial and temporal habitat for them. A large-scale shuffling of subarctic and Arctic communities is reorganizing high-latitude marine ecosystems.

INTRODUCTION

Poleward range expansion of plant and animal species is one clear indication of climate change. Such distribution shifts in the ocean may be driven by changes in temperature, nutrients or, as in the Arctic and Antarctic, sea ice extent. These atmospherically driven alterations are inextricably linked to changes in wind-driven mixing or circulation, which affects nutrient supply; greenhouse gases, which trap heat; and subsurface and deep ocean heat, which drives sea ice declines (Tamarin-Brodsky and Kaspi, 2017; Woodgate and Peralta-Ferriz, 2021). Under new climate regimes, species whose life history strategies allow them to rapidly adapt or expand into novel habitat, such as large, migratory generalist feeders, can become climate change "winners" (Kortsch et al., 2015; Moore and Reeves, 2018). Subsequent impacts on endemic ecosystems will depend on resource availability and competition among species. As the climate continues to warm, temperate regions are becoming "tropicalized" and Arctic regions are becoming "borealized," with subarctic species increasing in abundance and expanding their ranges northward (Fossheim et al., 2015; Alabia et al., 2018; Polyakov et al., 2020).

While climate change is altering the entire Arctic, not every region in the highly heterogeneous Arctic is equally affected (e.g., Moore et al., 2019; Polyakov et al., 2020; Mueter et al., 2021a). In the Atlantic, there are two wide, deep, high-latitude gateways to the Arctic: Davis Strait (300–900 km wide) and Fram Strait/Barents Sea (~450 km wide). The sole gateway to the Pacific Arctic is through the narrow Bering Strait (80 km), south of the broad, shallow Chukchi Sea shelf (**Figure 1**). Observed differences between the Atlantic and Pacific Arctic regions include a much greater increase in the open water season in the Barents Sea than in the Chukchi Sea, and differ- ences in water mass composition and advection of heat and nutrients, all of which shape ecosystem structure (Hunt et al., 2013; Oziel et al., 2017).

Numerous recent studies illustrate how changes in sea ice are potentially altering biological components of subarctic and Arctic marine ecosystems. Many of these studies focus on the impacts of climate change on Arctic endemic species (Laidre et al., 2008; Divoky et al., 2021), ecosystems (Post et al., 2013; Grebmeier and Maslowski, 2014; Pecuchet et al., 2020), and the people who rely on them (Huntington et al., 2016, 2020, 2021). In particular, the inclusion of upper trophic level (UTL) taxa in the suite of measurements collected by the Distributed Biological Observatory provides novel information on ecosystem dynamics at key locations across decadal time scales (Moore and Kuletz, 2019; Stafford et al., 2021). Several recent studies also highlight the role that UTL consumers such as marine fish, birds, and mammals can play as bellwethers of climate change, and how understanding their abundances, distributions, and diets can aid in tracking ecosystem-level biological responses to rapid change (e.g., Moore et al., 2014, 2019; Sydeman et al., 2021).

Here, we review recent information on northward range expansions of subarctic marine fish, seabirds, and mammals whose life histories have in some instances included limited seasonal occupation of the Arctic, with a focus on exemplar case studies from the Pacific Arctic Region. Our overarching goal here is to provide an updated overview of observed recent changes in the spatial and temporal distributions of subarctic marine fishes, seabirds, and marine mammals, and to explain related linkages among changes in biology, the atmosphere, the ocean, and the cryosphere.

MARINE FISHES

Marine fish species can rapidly track environmental change (Sorte et al., 2010; Pinsky et al., 2013). This is evident in the borealization of the Barents Sea in particular, where subarctic species including mackerel and Atlantic cod are expanding their ranges from the North Atlantic (Johannesen et al., 2012) while the distribution of Arctic species is retract- ing northward (Fossheim et al., 2015; Frainer et al., 2017). As the region continues to warm, the thermal habitat for boreal species has shifted farther into the Arctic (Eriksen et al., 2020), and

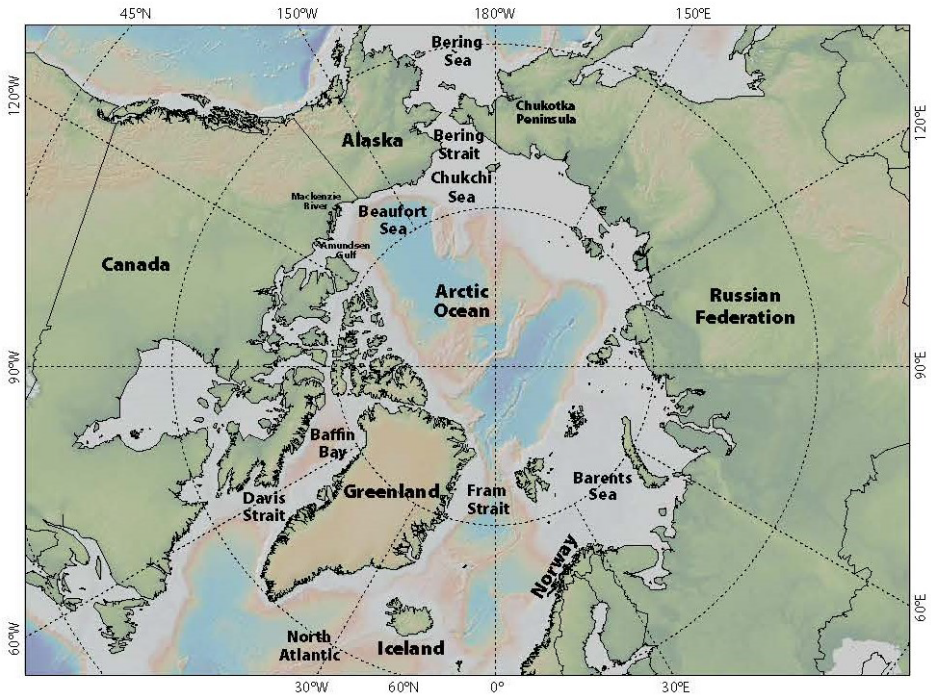

FIGURE 1. Map of the Arctic showing major gateways and waterways. Map made with GeoMapApp (http://www.geomapapp.org/; Ryan et al., 2009).

generalist boreal fishes are likely to outcompete the specialist diets of Arctic species (Kortsch et al., 2015).

Sigler et al. (2011) examined fish distribution records for the Pacific Arctic Region from the first decade of this century and found clear divisions in the distributions of planktivorous versus piscivorous species between the Bering Sea and the Chukchi and Beaufort Seas, as well as regional differences in taxa among bottom and surface fishes. Despite some evidence of northward migrations of subarctic species from the Bering Sea, these authors concluded that the persistence of the Bering Sea cold pool (Stabeno et al., 2001) would restrict range extensions of bottom fish such as walleye pollock, while pelagic species, such as pink salmon, might not be restricted by this thermal barrier (Sigler et al., 2011). However, given the retraction and possible collapse of the cold pool in recent years (Stabeno and Bell, 2019), more recent data suggest that these range extensions are long term (Grüss et al., 2021).

Walleye Pollock

Walleye pollock are widely distributed throughout the North Pacific, with known spawning grounds across the continental shelves from Japan to western Canada (Bailey et al., 1999). Cold bottom water in winter typically restricts the northward extent of the population. Adult pollock seasonally migrate northward and inshore in summer and then return to the outer shelf to avoid the cold pool (Kotwicki et al., 2005). A reduction in the size of the cold pool lessens the barrier for adult pollock to remain on the inner and northern shelf throughout the year, resulting in a northward shift during recent warm conditions (Stevenson and Lauth, 2019; Eisner et al., 2020; Grüss et al., 2021).

FIGURE 2. Historic and recent observations of walleye pollock distributions in the Bering and Chukchi Seas. Recent warming has led to a northward shift of the population in the Bering Sea (approximate distributions from Eisner et al., 2020), and surveys have reported large pollock populations in the east- ern (juvenile only; recent work of author Levine) and western (adult and juve- nile; Orlov et al., 2020) Chukchi Sea.

North of the Bering Strait, the summer forage fish community is dominated by small juvenile Arctic cod (De Robertis et al., 2017). Other common forage fishes in the region include capelin and Pacific herring, both of which are observed nearshore and largely in the southern Chukchi Sea. Juvenile pollock had previously been found in very low densities with few adults present (Wyllie-Echeverria, 1995; Mecklenburg et al., 2007; Rand and Logerwell, 2011; Goddard et al., 2014). Surveys during the recent period of extreme warming (2017–2020) indicate that while the distributions of the other pelagic forage fishes have not significantly changed, pollock abundance in the Pacific Arctic has substantially increased (**Figure 2**). In the eastern Chukchi Sea, juvenile pollock were widespread and highly abundant in 2017 and 2019 and found in comparable densities to Arctic species (Levine et al., 2021; recent work of author Levine). In the Russian sector, surveys in 2018 and 2019 found a significant increase in both juvenile and adult pollock north of the Chukotka Peninsula (Orlov et al., 2020). It is hypothesized that the recent increase in adult pollock in the northern Bering Sea serves as a source population for the larval and juvenile population observed in the Chukchi and Beaufort Seas (Levine et al., 2021) due to increased transport of Pacific water (Woodgate and Peralta-Ferriz, 2021) that advects juvenile fish northward.

Juvenile pollock growth rates exceed those of other gadid species under the warm conditions of the Arctic summer (Laurel et al., 2016), potentially allowing them to outcompete Arctic species; however, their hatch and survival rates are reduced under the seasonal freezing conditions (Laurel et al., 2018).

Thus, while the substantial increase in juvenile pollock in the Pacific Arctic suggests that environmental conditions now allow pollock to extend into the Chukchi Sea on a seasonal basis, their ability to establish permanent populations in the Arctic remains unknown.

Pink Salmon

Among salmonids, pink salmon are the most abundant species in the North Pacific Ocean (Ruggerone and Irvine, 2018) and have the broadest distribution in the Pacific Arctic Region. They occur from the large Yukon River to smaller coastal streams as far north as Point Barrow (Craig and Haldorson, 1986). Vagrants have also been found upstream in the Mackenzie River, extending east- ward across the Beaufort Sea toward Amundsen Gulf, and along the east coast of Greenland (Dunmall et al., 2013, 2018). Spawning pink salmon have also been documented along the Chukotka Peninsula coastline from the northern Bering Sea into the Chukchi Sea and as far west as the Kolyma River (Radchenko et al., 2018). While pink salmon abundance in northern regions of their range is still quite low in rela- tion to stocks farther south, there is evi- dence that the abundance of some north- ern stocks is increasing. For example, adult pink salmon have become more prevalent in subsistence catches in the high Arctic, particularly during even-numbered years (Dumnall et al., 2013, 2018). Furthermore, a survey during late summer 2007 found large numbers of juvenile pink salmon in the southern Chukchi Sea; these juveniles were larger and had higher energy content than juvenile pink salmon captured farther south (Moss et al., 2009). Consequently, adult pink salmon returns to the Beaufort Sea coast during 2008 were higher than in 2007 (Dunmall et al., 2013, 2018). It is still not clear whether the large catch of juvenile pink salmon in the Chukchi Sea in 2007 contributed to the higher returns in 2008. Conditions in both freshwater and marine environments are import- ant to the survival of pink salmon (Farley et al., 2020). In the northern extent of pink salmon distribution, cold river and stream temperatures in the fresh- water environment are believed to limit salmon production (Dunmall et al., 2016); however, continued warming of air and stream temperatures, and longer periods of ice-free conditions, may benefit salmon survival in this environment (Nielsen et al., 2013).

SEABIRDS

Seabirds link Arctic and subarctic marine and terrestrial ecosystems because they require land to nest and raise young, but forage in the ocean. Globally, pelagic seabird occurrences and distributions reflect the presence of the surface and subsurface zooplankton and forage fish upon which they feed (e.g., Sydeman et al., 2010). In the Pacific Arctic region, seabirds have been associated with underwater features and water mass characteristics that aggregate their prey (Gall et al., 2013; Kuletz et al., 2015). During chick rearing, seabirds must find sufficient high-quality prey within foraging distance of their nests, a distance that can vary from a dozen to hundreds of kilometers, depending on species and reproductive phase. When not breeding, many species are capable of long-distance migrations covering thousands of kilometers.

Sea ice cover in the Arctic affects seabird foraging, and extensive ice can restrict their access to prey. However, the marginal ice zone can provide a rich foraging opportunity (Hunt et al., 1996), as zooplankton and fish species often aggregate at ice edge habitats (Daase et al., 2021). Changes in sea ice extent and water temperature have resulted in changes in the available prey field for seabirds throughout the Arctic (Mallory et al., 2010; Frederiksen et al., 2013; Gall et al., 2017; Mueter et al., 2021a). For instance, in the North Atlantic, little auk wintering distribution expands and contracts with the distribution of their subarctic copepod prey, which is shifting northward (Amélineau et al., 2018). In the Pacific Arctic, low amounts of sea ice and warmer sea temperatures have been associated with low reproductive success and seabird die-offs, apparently due to low prey availability (Duffy-Anderson et al., 2019; Romano et al., 2020).

The timing of spring ice retreat in the Pacific Arctic has been shown to affect seabird distribution on the Bering Sea shelf, with contrasting patterns between birds that forage at the water's surface and species that are subsurface foragers (Hunt et al., 2018). Early spring sea ice retreat thus affects the spatial distributions of seabird species evident in summer and alters seabird communities. Ecosystem changes are clearly altering the community composition and species richness of seabirds in the Arctic (Descamps and Strøm, 2021; Mueter et al., 2021b).

Four decades of at-sea surveys (avail- able in the North Pacific Pelagic Seabird Database; Drew and Piatt, 2015) generally show that decreased sea ice cover and higher ocean temperatures during the first decade of this century favored planktivorous seabirds over piscivorous seabirds in the Chukchi Sea (Gall et al., 2017). With further warming, some species have shifted their overall distributions northward, likely in search of food (Kuletz et al., 2020).Will et al. (2020) concluded that conditions during the relatively warm years of 2016–2019 were detrimental to planktivorous auklets nesting in the northern Bering Sea. Because warmer ocean temperatures have been linked to the replacement of larger, lipid-rich zooplankton species with smaller, lipid-poor species (Eisner et al., 2013), ongoing changes in the Pacific Arctic may no longer favor planktivorous seabirds.

In the Bering Sea, subarctic sea- birds that appear to be expanding their post-breeding dispersal ranges north- ward include three species of Pacific albatrosses (Kuletz et al., 2014), northern fulmars (Renner et al., 2013), and ancient murrelets (Day et al., 2013). For all seabirds combined, there was a shift in distribution farther into the Pacific Arctic during the warm years of 2017–2019 compared to the previous decade (**Figure 3**). This northward shift included birds that breed in the Bering and Chukchi Seas (e.g., thick-billed murre), migrants that breed in the Southern Hemisphere but move to Alaska during their non-breeding season (e.g., short-tailed shearwater; Kuletz et al., 2020),

and Atlantic species that might have crossed the Canadian Arctic Archipelago (e.g., northern gannet; Day et al., 2013). Based on data from the eastern Chukchi Sea, seabirds that had been spatially correlated with prey communities during a relatively cool year (2015) were decoupled from the same communities in a warm year (2017), suggesting that these seabird communities did not adapt, at least in the short term, to a rapid change in conditions (Mueter et al., 2021b).

CETACEANS

Marine mammals have exhibited phenological and distributional changes throughout the Arctic. Endemic Arctic marine mammals spend their lives in the Arctic, often closely associated with sea ice. A number of subarctic species, particularly cetaceans, have become regular summer and autumn visitors to the Arctic, migrating into the region as sea ice melts in the spring or early summer and out of the region as the sea surface freezes in late autumn or early winter (Hamilton et al., 2021). As sea ice has declined in age, thickness, and extent throughout the Arctic, prey distributions have shifted and new migratory corridors have opened for subarctic marine mammal species (Buchholz et al., 2012; Berge et al., 2015; Storrie et al., 2018). These changes have expanded the temporal and spatial boundaries of habitat for cetaceans: they are now arriving in the Arctic earlier, staying later, and migrating farther north (Nieukirk et al., 2020; Ahonen et al., 2021).

Killer Whales

Killer whales are a globally distributed top predator with ecotypes that are distinguished by their phenotypes and preferred prey (de Bruyn et al., 2013). Killer whales are not a new species in the Arctic, as they have been documented there sporadically in summer months, feeding on a variety of marine mammal species (Stafford, 2019; LeFort et al., 2020). In the Arctic, killer whales avoid dense ice, and heavy multi-year sea ice once excluded them from most high Arctic regions during many months of the year. Though these whales still avoid heavy sea ice (Matthews et al., 2011), their increasing occurrence in the Arctic as sea ice declines in thickness and extent represents seasonal and geographic expansion. Recent (2010 to present) sighting and passive acoustic monitoring data provide evidence that this species is arriving in the Arctic earlier, departing later, and moving farther north in the eastern Canadian Arctic, and north and east in the Pacific Arctic (Higdon and Ferguson, 2009; S.H. Ferguson et al., 2010; Stafford, 2019; **Figure 4**). In the Pacific Arctic, passive acoustic monitoring has recently documented killer whales throughout the Chukchi Sea as far north as 75°N (recent work of author Stafford). This species has been heard in the Pacific Arctic as early as May and as late as October (Stafford, 2019). In both the Canadian and Pacific Arctic, the number of bowhead whales with killer whale scars has increased over time (Reinhart et al., 2013; George et al., 2017) as has evidence of depredation in bowhead whale carcasses (Willoughby et al., 2020). Matthews et al. (2019) posit that periodic ice entrapments of killer whales, which are usually fatal (Westdal et al., 2016), may slow their expansion into the Arctic, particularly as naive whales explore regions that can be ice choke points.

The northward range expansion, lon- ger seasonal presence, and higher num- bers of a top predator in the Arctic has the potential for top-down ecosystem reorganization and may represent the most immediate threat to Arctic endemic species (S.H. Ferguson et al., 2010). In the eastern Canadian Arctic, endemic narwhals, belugas, and bowhead whales

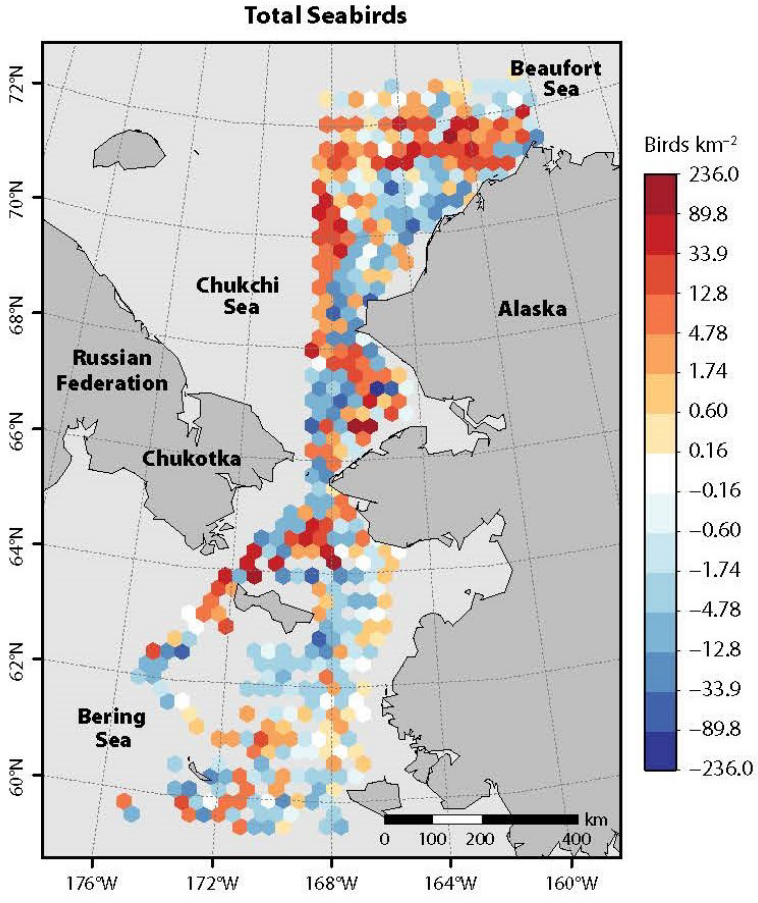

FIGURE 3. Distribution changes in the Pacific Arctic region for total seabird densities (birds km^{-2}) during 2017–2019 compared to the previous decade. Cells with increasing (orange) and decreasing (blue) densities during 2017– 2019 were based on mean densities of all observations within each 50 km grid cell. *Adapted from Kuletz et al. (2020)*

change their behavior in the presence of killer whales (reviewed in Matthews et al., 2020). Lefort et al. (2020) suggest that this species could have a significant negative impact on narwhal populations in the Canadian Arctic Archipelago.

Subarctic Baleen Whales

The historical occurrence of humpback, fin, and minke whales north of Bering Strait was documented by Soviet scientists, particularly near the Chukotka Peninsula, from June to October (summarized in Clarke et al., 2013). These species are regularly found in the Bering Sea during summer (M.C. Ferguson et al., 2015), and fin whales are present there year-round (Stafford et al., 2010). Evidence from visual (shipboard and aerial) and acoustic monitoring suggest that their use of the Pacific Arctic may be increasing (Clarke et al., 2013, 2020; Brower et al., 2018).

Four decades of aerial surveys (Clarke et al., 2020) provide the most extensive information on subarctic whales in the US Pacific Arctic. Fin whales first appear north of Bering Strait in the aerial survey database in 2008, humpback whales in 2009, and minke whales in 2011. All three subarctic baleen whales were sighted in every month from July through October, although most of the sightings through 2019 occurred from July through September (Clarke et al., 2020). Furthermore, fin and humpback whale calves have been observed in the region (Clarke et al., 2020). Aerial survey observers have commonly recorded all three species in close proximity to one another and to gray whales, particularly in Hope Basin, a benthic hotspot in the south central Chukchi Sea (Clarke et al., 2020). In 2019, the number of subarctic baleen whales detected per kilometer surveyed over Herald Shoal, which is ~145 km northwest of Point Lay, was 12.5 times greater than in any previous survey year. All three species have been documented feeding in the Pacific Arctic Region, and it is likely that the northward expansion of prey (krill and forage fish/or small schooling fish) distributions provided the whales' motivation to migrate to the Pacific Arctic (Clarke et al., 2020).

CONCLUDING THOUGHTS

What does the future hold for upper trophic level species and communities in the Arctic? It is clear across taxa that the effects of climate change are variable and dependent on the different ecological requirements of communities, feeding guilds, species, and age classes. There is no indication that climate change in the Arctic is going to decelerate any time soon. The habitat changes that have been seen in the past two decades will become the "new normal" (Thoman et al., 2020). There is clear evidence of temporal-spatial range expansion for many subarctic UTL species. Increasing ice-free habitat and changes in water mass distributions are altering the underlying prey structure and therefore attracting new UTL species, increasing habitat extent, and/or increasing the duration of residency in Arctic habitats. But for many subarctic species, annual sea ice cover, freezing temperatures, and months of darkness may still prevent them from becoming true Arctic residents. Pollock eggs and larvae are highly sensitive to cold temperatures, central place foraging seabirds need adequate nesting habitat within foraging distance of high prey abundance, and subarctic cetaceans can still be excluded from heavy ice as they risk injury to their dorsal fins and ice entrapment. To permanently expand northward, UTL species require the flexibility in physiology and behavior to adapt to ongoing habitat perturbations. If new species can adapt to year-round life in the Arctic, understanding the risks to Arctic endemic species from

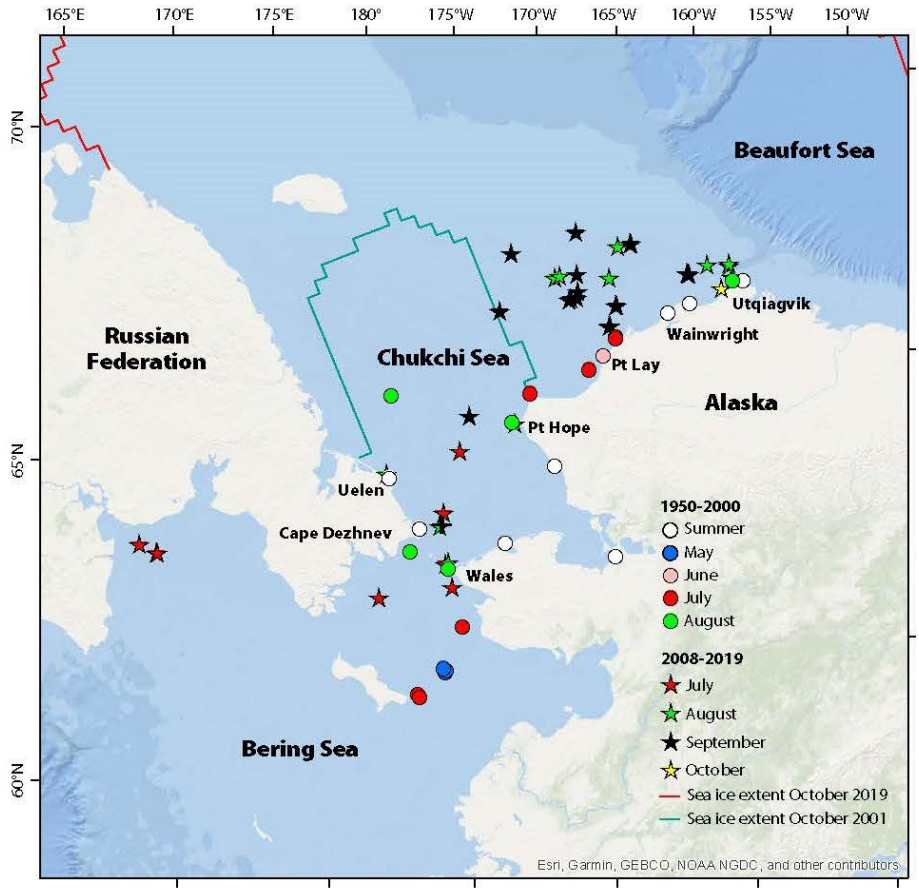

FIGURE 4. Killer whale sightings in the Pacific Arctic by month from 1950 to 2000 (circles) and 2008 to 2019 (stars). Sea ice extent is shown for October 2001 (blue line) and 2020 (red line). *Adapted from Stafford (2019)*

competition for prey, novel predators, and exposure to novel pathogens will be critical (e.g., Post et al., 2013; Kortsch et al., 2015; VanWormer et al., 2019). The evidence we summarize here indicates large-scale shuffling of subarctic and Arctic marine animal communities as high-latitude marine ecosystems undergo rapid reorganization.

REFERENCES

Ahonen, H., K.M. Stafford, C. Lydersen, C.L. Berchok, S.E. Moore, and K.M. Kovacs. 2021. Interannual variability in acoustic detection of blue and fin whale calls in the Northeast Atlantic High Arctic between 2008 and 2018. *Endangered Species Research* 45:209–224, https://doi.org/10.3354/esr01132.

Alabia, I.D., J.G. Molinos, S.-I. Saitoh, T. Hirawake, T. Hirata, and F.J. Mueter. 2018. Distribution shifts of marine taxa in the Pacific Arctic under contemporary climate changes. *Diversity and Distributions* 24(11):1,583–1,597, https://doi.org/10.1111/ddi.12788.

Amélineau, F., J. Fort, P.D. Mathewson, D.C. Speirs, N. Courbin, S. Perret, W.P. Porter, R.J. Wilson, and D. Grémillet. 2018. Energyscapes and prey fields shape a North Atlantic seabird wintering hotspot under climate change. *Royal Society Open Science* 5(1):171883, https://doi.org/10.1098/rsos.171883.

Bailey, K.M., T.J. Quinn, P. Bentzen, and W.S. Grant. 1999. Population structure and dynamics of walleye pollock, *Theragra chalcogramma*. *Advances in Marine Biology* 37:179–255, https://doi.org/10.1016/S0065-2881(08)60429-0.

Berge, J., K. Heggland, O.J. Lønne, F. Cottier, H. Hop, G.W. Gabrielsen, L. Nottestad, and O.A. Misund. 2015. First records of Atlantic mackerel (*Scomber scombrus*) from the Svalbard Archipelago, Norway, with possible explanations for the extension of its distribution. *Arctic* 68(1):54–61, https://doi.org/10.14430/arctic4455.

Brower, A.A, J.T. Clarke, and M.C. Ferguson. 2018. Increased sightings of subarctic cetaceans in the eastern Chukchi Sea, 2008–2016: Population recovery, response to climate change, or increased survey effort? *Polar Biology* 41:1,033–1,039, https://doi.org/10.1007/s00300-018-2257-x.

Buchholz, F., T. Werner, and C. Buchholz. 2012. First observation of krill spawning in the high Arctic Kongsfjorden, West Spitsbergen. *Polar Biology* 35:1,273–1,279, https://doi.org/10.1007/s00300-012-1186-3.

Clarke, J.T., K.M. Stafford, S.E. Moore, B. Rone, L. Aerts, and J. Crance. 2013. Subarctic cetaceans in the southern Chukchi Sea: Evidence of recovery or response to a changing ecosystem. *Oceanography* 26:136–149, https://doi.org/10.5670/oceanog.2013.81.

Clarke, J.T., A.A. Brower, M.C. Ferguson, A.L. Willoughby, and A.D. Rotrock. 2020. *Distribution and Relative Abundance of Marine Mammals in the Eastern Chukchi Sea, Eastern and Western Beaufort Sea, and Amundsen Gulf, 2019*. Annual Report, OCS Study BOEM 2020-027, 628 pp.

Craig, P., and L. Haldorson. 1986. Pacific salmon in the North American Arctic. *Arctic* 39:2–7, https://doi.org/10.14430/arctic2037.

Daase, M., J. Berge, J.E. Søreide, and S. Falk-Petersen. 2021. Ecology of Arctic pelagic communities. Pp. 219–259 in *Arctic Ecology*. D.N. Thomas, ed., Wiley, https://doi.org/10.1002/9781118846582.ch9.

Day, R.H., A.E. Gall, T.C. Morgan, J.R. Rose, J.H. Plissner, P.M. Sanzenbacher, J.D. Fenneman, K.J. Kuletz, and B.H Watts. 2013. Seabirds new to the eastern Chukchi and Beaufort Seas, Alaska: Response to a changing climate? *Western Birds* 44(3):174–182.

de Bruyn, P.J.N., C.A. Tosh, and A. Terauds. 2013. Killer whale ecotypes: Is there a global model? *Biological Reviews* 88:62–80, https://doi.org/10.1111/j.1469-185X.2012.00239.x.

De Robertis, A., K. Taylor, C.D. Wilson, and E.V. Farley. 2017. Abundance and distribution of Arctic cod (*Boreogadus saida*) and other pelagic fishes over the U.S. Continental Shelf of the Northern Bering and Chukchi Seas. *Deep Sea Research Part II* 135:51–65, https://doi.org/10.1016/j.dsr2.2016.03.002.

Descamps, S., and H. Strøm. 2021. As the Arctic becomes boreal: Ongoing shifts in a high-Arctic seabird community. *Ecology* 102(11):e03485, https://doi.org/10.1002/ecy.3485.

Divoky, G.J., E. Brown, and K.H. Elliott. 2021. Reduced seasonal sea ice and increased sea surface temperature change prey and foraging behaviour in an ice-obligate Arctic seabird, Mandt's Black Guillemot (*Cepphus grylle mandtii*). *Polar Biology* 44(4):701–715, https://doi.org/10.1007/s00300-021-02826-3.

Drew, G.S., and J.F. Piatt. 2015. North Pacific Pelagic Seabird Database (NPPSD): U.S. Geological Survey data release (ver. 3.0, February 2020), https://doi.org/10.3133/ofr20151123.

Duffy-Anderson, J.T., P. Stabeno, A.G. Andrews, K. Cieciel, A. Deary, E. Farley, C. Fugate, C. Harpold, R. Heintz, D. Kimmel, and others. 2019. Responses of the northern Bering Sea and southeastern Bering Sea pelagic ecosystems following record-breaking low winter sea ice. *Geophysical Research Letters* 46(1):9,833–9,842, https://doi.org/10.1029/2019GL083396.

Dunmall, K.M., J.D. Reist, E.C. Carmack, J.A. Babluk, M.P. Heide-Jørgensen, and M.F. Docker. 2013. Pacific salmon in the Arctic: Harbingers of change. Pp. 141–163 in *Responses of Arctic Marine Ecosystems to Climate Change*. F.J. Mueter, D.M.S. Dickson, H.P. Huntington, J.R. Irvine, E.A. Logerwell, S.A. MacLean, L.T. Quakenbush, and C. Rosa, eds, Alaska Sea Grant, University of Alaska Fairbanks, https://doi.org/10.4027/ramecc.2013.07.

Dunmall, K.M., N.J. Mochnacz, C.E. Zimmerman, C. Lean, and J.D. Reist. 2016. Using thermal limits to assess establishment of fish dispersing to high-latitude and high-elevation watersheds. *Canadian Journal of Fisheries and Aquatic Sciences* 73:1,750–1,758, https://doi.org/10.1139/cjfas-2016-0051.

Dunmall, K.M., D.G. McNicholl, and J.D. Reist. 2018. Community-based monitoring demonstrates increasing occurrences and abundances of Pacific salmon in the Canadian Arctic from 2000 to 2017. Pp. 87–90 in *North Pacific Anadromous Fish Commission Technical Report 11*.

Eisner, L., N. Hillgruber, E. Martinson, and J. Maselko. 2013. Pelagic fish and zooplankton species assemblages in relation to water mass characteristics in the northern Bering and southeast Chukchi Seas. *Polar Biology* 36(1):87–113, https://doi.org/10.1007/s00300-012-1241-0.

Eisner, L.B., Y.I. Zuenko, E.O. Basyuk, L.L. Britt, J.T. Duffy-Anderson, S. Kotwicki, C. Ladd, and W. Cheng. 2020. Environmental impacts on walleye pollock (*Gadus chalcogrammus*) distribution across the Bering Sea shelf. *Deep-Sea Research Part II* 181–182:104881, https://doi.org/10.1016/j.dsr2.2020.104881.

Eriksen, E., E. Bagøien, E. Strand, R. Primicerio, T. Prokhorova, A. Trofimov, and I. Prokopchuk. 2020. The record-warm Barents Sea and 0-Group fish response to abnormal conditions. *Frontiers in Marine Science* 7:338, https://doi.org/10.3389/fmars.2020.00338.

Farley, E.V. Jr., J.M. Murphy, K. Cieciel, E.M. Yasumiishi, K. Dunmall, T. Sformo, and P. Rand. 2020. Response of Pink salmon to climate warming in the northern Bering Sea. *Deep Sea Research Part II* 177:104839, https://doi.org/10.1016/j.dsr2.2020.104830.

Ferguson, M.C., J. Waite, C. Curtice, J.T. Clarke, and J. Harrison. 2015. Biologically important areas for cetaceans within US waters: Aleutian Islands and Bering Sea region. *Aquatic Mammals* 41(1):79–93, https://doi.org/10.1578/AM.41.1.2015.79.

Ferguson, S.H., J.W. Higdon, and E.G. Chmelnitsky. 2010. The rise of killer whales as a major Arctic predator. Pp. 117–136 in *A Little Less Arctic: Top Predators in the World's Largest Northern Inland Sea, Hudson Bay*. S.H. Ferguson, L.L. Loseto, and M.L. Mallory, eds, Springer, https://doi.org/10.1007/978-90-481-9121-5_6.

Fossheim, M., R. Primicerio, E. Johannesen, R.B. Ingvaldsen, M.M. Aschan, and A.V. Dolgov. 2015. Recent warming leads to a rapid borealization of fish communities in the Arctic. *Nature Climate Change* 5:673–678, https://doi.org/10.1038/nclimate2647.

Frainer, A., R. Primicerio, S. Kortsch, M. Aune, A.V. Dolgov, M. Fossheim, and M.M. Aschan. 2017. Climate-driven changes in functional biogeography of Arctic marine fish communities. *Proceedings of the National Academy of Sciences of the United States of America* 114(46):12,202–12,207, https://doi.org/10.1073/pnas.1706080114.

Frederiksen, M., T. Anker-Nilssen, G. Beaugrand, and S. Wanless. 2013. Climate, copepods and seabirds in the boreal northeast Atlantic—Current state and future outlook. *Global Change Biology* 19:364–372, https://doi.org/10.1111/gcb.12072.

Gall, A.E., R.H. Day, and T.J. Weingartner. 2013. Structure and variability of the marine-bird community in the northeastern Chukchi Sea. *Continental Shelf Research* 67:96–115, https://doi.org/10.1016/j.csr.2012.11.004.

Gall, A.E., T.C. Morgan, R.H. Day, and K.J. Kuletz. 2017. Ecological shift from piscivorous to planktivorous seabirds in the Chukchi Sea, 1975–2012. *Polar Biology* 40(1):61–78, https://doi.org/10.1007/s00300-016-1924-z.

George, J.C., G. Sheffield, D.J. Reed, B. Tudor, R. Stimmelmayr, B.T. Person, T. Sformo, and R. Suydam. 2017. Frequency of injuries from line entanglements, killer whales, and ship strikes on Bering-Chukchi-Beaufort Seas bowhead whales. *Arctic* 70(1):37–46, https://doi.org/10.14430/arctic4631.

Goddard, P., R. Lauth, and C. Armistead. 2014. *Results of the 2012 Chukchi Sea Bottom Trawl Survey of Bottomfishes, Crabs, and Other Demersal Macrofauna*. NOAA Technical Memorandum, NMFS-AFSC-278, 110 pp.

Grebmeier, J.M., and W. Maslowski, eds. 2014. *The Pacific Arctic Region*. Springer, Netherlands, https://doi.org/10.1007/978-94-017-8863-2.

Grüss, A., J.T. Thorson, C.C. Stawitz, J.C.P. Reum, S.K. Rohan, and C.L. Barnes. 2021. Synthesis of interannual variability in spatial demographic processes supports the strong influence of cold-pool extent on eastern Bering Sea walleye pollock (*Gadus chalcogrammus*). *Progress in Oceanography* 194:102569, https://doi.org/10.1016/j.pocean.2021.102569.

Hamilton, C.D., C. Lydersen, J. Aars, M. Biuw, A.N. Boltunov, E.W. Born, R. Dietz, L.P. Foklow, D.M. Glazov, T. Haug, and others. 2021. Marine mammal hotspots in the Greenland and Barents Seas. *Marine Ecology Progress Series* 659:3–28, https://doi.org/10.3354/meps13584.

Higdon, J.W., and S.H. Ferguson. 2009. Loss of Arctic sea ice causing punctuated change in sight- ings of killer whales (*Orcinus orca*) over the past century. *Ecological Applications* 19:1,365–1,375, https://doi.org/10.1890/07-1941.1.

Hunt, G.L. Jr., V. Bakken, and F. Mehlum. 1996. Marine birds in the marginal ice zone of the Barents Sea in late winter and spring. *Arctic* 49(1):53–61, https://doi.org/10.14430/arctic1183.

Hunt, G.L. Jr., A.L. Blanchard, P. Boveng, P. Dalpadado, K.F. Drinkwater, L. Eisner, R.R. Hopcroft, K.M. Kovacs, B.L. Norcross, P. Renaud, and others. 2013. The Barents and Chukchi Seas: Comparison of two Arctic shelf eco- systems. *Journal of Marine Systems* 109-110:43–68, https://doi.org/10.1016/j.jmarsys.2012.08.003.

Hunt, G.L. Jr., M. Renner, K.J. Kuletz, S. Salo, L. Eisner, P.H. Ressler, C. Ladd, and J.A. Santora. 2018. Timing of sea-ice-retreat affects the distribution of sea- birds and their prey in the southeastern Bering Sea. *Marine Ecology Progress Series* 593:209–230, https://doi.org/10.3354/meps12383.

Huntington, H.P., L.T. Quakenbush, and M. Nelson. 2016. Effects of changing sea ice on marine mam- mals and subsistence hunters in northern Alaska from traditional knowledge interviews. *Biology Letters* 12(8):20160198, https://doi.org/10.1098/ rsbl.2016.0198.

Huntington, H.P., S.L. Danielson, F.K. Wiese, M. Baker, P. Boveng, J.J. Citta, A. De Robertis, D.M.S. Dickson, E. Farley, J.C. George, and others. 2020. Evidence suggests potential transformation of the Pacific Arctic ecosystem is underway. *Nature Climate Change* 10:342–348, https://doi.org/10.1038/ s41558-020-0695-2.

Huntington, H.P., J. Raymond-Yakoubian, G. Noongwook, N. Naylor, C. Harris, Q. Harcharek, and B. Adams. 2021. "We Never Get Stuck": A col- laborative analysis of change and coastal commu- nity subsistence practices in the northern Bering and Chukchi Seas, Alaska. *Arctic* 74:113–126, https://doi.org/10.14430/arctic72446.

Johannesen, E., Å.S. Høines, A.V. Dolgov, and M. Fossheim. 2012. Demersal fish assemblages and spatial diversity patterns in the Arctic- Atlantic transition zone in the Barents Sea. *PLoS ONE* 7(4): e34924, https://doi.org/10.1371/journal. pone.0034924.

Kortsch, S., R. Primicerio, M. Fossheim, V. Dolgov, and M. Aschan. 2015. Climate change alters the struc- ture of Arctic marine food webs due to poleward shifts of boreal generalists. *Proceedings of the Royal Society B* 282(1814):20151546, https://doi.org/ 10.1098/rspb.2015.1546.

Kotwicki, S., T.W. Buckley, T. Honkalehto, and G. Walters. 2005. Variation in the distribution of walleye pollock (*Theragra chalcogramma*) with temperature and implications for seasonal migra- tion. *Fishery Bulletin* 103(4):574–587.

Kuletz, K.J., M. Renner, E.A. Labunski, and G.L. Hunt Jr. 2014. Changes in the distribution and abundance of albatrosses in the eastern Bering Sea: 1975– 2010. *Deep Sea Research Part II* 109:282–292, https://doi.org/10.1016/j.dsr2.2014.05.006.

Kuletz, K.J., M.C. Ferguson, B. Hurley, A.E. Gall, E.A. Labunski, and T.C. Morgan. 2015. Seasonal spatial patterns in seabird and marine mam- mal distribution in the eastern Chukchi and western Beaufort Seas: Identifying biolog- ically important pelagic areas. *Progress in Oceanography* 136:175–200, https://doi.org/ 10.1016/j.pocean.2015.05.012.

Kuletz, K., D. Cushing, and E. Labunski. 2020. Distributional shifts among seabird communi- ties of the northern Bering and Chukchi seas in response to ocean warming during 2017–2019. *Deep Sea Research Part II* 181–182:104913, https://doi.org/10.1016/j.dsr2.2020.104913.

Laidre, K.L., I. Stirling, L.F. Lowry, Ø. Wiig, M.P. Heide-Jørgensen, and S.H. Ferguson. 2008. Quantifying the sensitivity of Arctic marine mammals to climate-induced habitat change. *Ecological Applications* 18:S97–S125, https://doi.org/ 10.1890/06-0546.1.

Laurel, B.J., M. Spencer, P. Iseri, and L.A. Copeman. 2016. Temperature-dependent growth and behav- ior of juvenile Arctic cod (*Boreogadus saida*) and co-occurring North Pacific gadids. *Polar Biology* 39:1,127–1,135, https://doi.org/10.1007/s00300-015-1761-5.

Laurel, B.J., L.A. Copeman, M. Spencer, and P. Iseri. 2018. Comparative effects of temperature on rates of development and survival of eggs and yolk-sac larvae of Arctic cod (*Boreogadus saida*) and wall- eye pollock (*Gadus chalcogrammus*). *ICES Journal of Marine Science* 75:2,403–2,412, https://doi.org/10.1093/icesjms/fsy042.

Lefort, K.J., C.J. Garroway, and S.H. Ferguson. 2020. Killer whale abundance and predicted narwhal consumption in the Canadian Arctic. *Global Change Biology* 26:4,276–4,283, https://doi.org/10.1111/ gcb.15152.

Levine, R.M., A. De Robertis, D. Grünbaum, R. Woodgate, C.W. Mordy, F. Mueter, E. Cokelet, N. Lawrence-Slavas, and H. Tabisola. 2021. Autonomous vehicle surveys indicate that flow reversals retain juvenile fishes in a highly advec- tive high-latitude ecosystem. *Limnology and Oceanography* 66:1,139–1,154, https://doi.org/10.1002/lno.11671.

Mallory, M.L., A.J. Gaston, H.G. Gilchrist, G.J. Robertson, and B.M. Braune. 2010. Effects of climate change, altered sea-ice distribution and seasonal phenology on marine birds. Pp. 179–195 in *A Little Less Arctic: Top Predators in the World's Largest Northern Inland Sea, Hudson Bay*. S.H. Ferguson, ed., Springer, https://doi.org/10.1007/ 978-90-481-9121-5_9.

Matthews, C.J.D., S.P. Luque, S.D. Petersen, R.D. Andrews, and S.H. Ferguson. 2011. Satellite tracking of a killer whale (*Orcinus orca*) in the Eastern Canadian Arctic documents ice avoid- ance and rapid, long-distance movement into the North Atlantic. *Polar Biology* 34:1,091–1,096, https://doi.org/10.1007/s00300-010-0958-x.

Matthews, C.J.D., S.A. Raverty, D.P. Noren, L. Arragutainaq, and S.H. Ferguson. 2019. Ice entrapment mortality may slow expand- ing presence of Arctic killer whales. *Polar Biology* 42:639–644, https://doi.org/10.1007/ s00300-018-02447-3.

Matthews, C.J.D., G.A. Breed, B. LeBlanc, and S.H. Ferguson. 2020. Killer whale presence drives bowhead whale selection for sea ice in Arctic seascapes of fear. *Proceedings of the National Academy of Sciences of the United States of America* 117(12):6,590–6,598, https://doi.org/10.1073/pnas.1911761117.

Mecklenburg, C.W., D.L. Stein, B.A. Sheiko, N.V. Chernova, T.A. Mecklenburg, and B.A. Holladay. 2007. Russian-American Long-Term Census of the Arctic: Benthic fishes trawled in the Chukchi Sea and Bering Strait, August 2004. *Northwestern Naturalist* 88:168–187, https://doi.org/10.1898/1051-1733(2007)88[168:RLCOTA]2.0.CO;2.

Moore, S.E., E. Logerwell, L. Eisner, E.V. Farley Jr., L.A. Harwood, K. Kuletz, J. Lovvorn, J.R. Murphy, and L.T. Quakenbush. 2014. Marine fishes, birds and mammals as sentinels of ecosystem vari- ability and reorganization in the Pacific Arctic region. Pp. 337–392 in *The Pacific Arctic Region: Ecosystem Status and Trends in a Rapidly Changing Environment*. J.M. Grebmeier and W. Maslowski, eds, Springer, https://doi.org/10.1007/978-94-017-8863-2_11.

Moore S.E., and R.R. Reeves. 2018. Tracking arctic marine mammal resilience in an era of rapid eco- system alteration. *PLoS Biology* 16:e2006708, https://doi.org/10.1371/journal.pbio.2006708.

Moore, S.E., and K.J. Kuletz. 2019. Marine birds and mammals as ecosystem sentinels in and near Distributed Biological Observatory regions: An abbreviated review of published accounts and rec- ommendations for integration to ocean obser- vatories. *Deep-Sea Research Part II* 162:211–217, https://doi.org/10.1016/j.dsr2.2018.09.004.

Moore, S.E., T. Haug, G.A. Vikingsson, and G.B. Stenson. 2019. Baleen whale ecology in Arctic and subarctic seas in an era of rapid habitat alter- ation. *Progress in Oceanography* 176:102118, https://doi.org/10.1016/j.pocean.2019.05.010.

Moss, J.H., J.M. Murphy, E.V. Farley, L.B. Eisner, A.G. Andrews. 2009. Juvenile pink and chum salmon distribution, diet, and growth in the north- ern Bering and Chukchi Seas. *North Pacific Anadromous Fish Commission Bulletin* 5:191–196.

Mueter, F.J., B. Planque, G.L. Hunt, I.D. Alabia, T. Hirawake, L. Eisner, P. Dalpadado, M. Chierici, K.F. Drinkwater, N. Harada, and others. 2021a. Possible future scenarios in the gateways to the Arctic for subarctic and Arctic marine systems: Prey resources, food webs, fish, and fisheries. *ICES Journal of Marine Science* 78:3,017–3,045, https://doi.org/10.1093/icesjms/fsab122.

Mueter, F.J., K. Iken, L.W. Cooper, J.M. Grebmeier, K.J. Kuletz, R.R. Hopcroft, S.L. Danielson, R.E. Collins, and D.A. Cushing, 2021b. Changes in diversity and species composition across multiple assemblages in the northeast Chukchi Sea during two contrasting years are consistent with boreal- ization. *Oceanography* 34(2):38–51, https://doi.org/10.5670/oceanog.2021.213.

Nielsen, J.L., G.T. Ruggerone, and C.E. Zimmerman. 2013. Adaptive strategies and life history charac- teristics in a warming climate: Salmon in the Arctic? *Environmental Biology of Fishes* 96:1,187–1,226, https://doi.org/10.1007/s10641-012-0082-6.

Nieukirk, S.L., D.K. Mellinger, R.P. Dziak, H. Matsumoto, and H. Klinck. 2020. Multi-year occurrence of sei whale calls in North Atlantic polar waters. *The Journal of the Acoustical Society of America* 147:1,842–1,850, https://doi.org/10.1121/10.0000931.

Orlov, A.M., A.N. Benzik, E.V. Vedischeva, S.V. Gafitsky, K.M. Gorbatenko, S.V. Goryanina, V.L. Zubarevich, Q.V. Kodryan, M.A. Nosov, S.Yu. Orlova, and others. 2020. Fisheries research in the Chukchi Sea at the RV *Professor Levanidov* in August 2019: Some preliminary results. *Trudy VNIRO* 179:206–220, https://doi.org/10.36038/2307-3497-2020-179-206-225.

Oziel, L., G. Neukermans, M. Ardyna, C. Lancelot, J.L. Tison, P. Wassmann, J. Sirven, D. Ruiz-Pino, and J.-C. Gascard. 2017. Role for Atlantic inflows and sea ice loss on shifting phytoplankton blooms in the Barents Sea. *Journal of Geophysical Research*: *Oceans* 122:5,121–5,139, https://doi.org/10.1002/ 2016JC012582.

Pecuchet, L., M.-A. Blanchet, A. Frainer, B. Husson, L.L. Jørgensen, S. Kortsch, and R. Primicerio. 2020. Novel feeding interactions amplify the impact of species redistribution on an Arctic food web. *Global Change Biology* 26:4,894–4,906, https://doi.org/10.1111/gcb.15196.

Pinsky, M.L., B. Worm, M.J. Fogarty, J.L. Sarmiento, and S.A. Levin. 2013. Marine taxa track local cli- mate velocities. *Science* 341(6151):1,239–1,242, https://doi.org/10.1126/science.1239352.

Polyakov, I.V., M.B. Alkire, B.A. Bluhm, K.A. Brown, E.C. Carmack, M. Chierici, S.L. Danielson, I. Ellingsen, E.A. Ershova, K. Gårdfeldt, and others, 2020. Borealization of the Arctic Ocean in response to anomalous advection from sub- Arctic seas. *Frontiers in Marine Science* 7:491, https://doi.org/10.3389/fmars.2020.00491.
Post, E., U.S. Bhatt, C.M. Bitz, J.F. Brodie, T.L. Fulton, M. Hebblewhite, J. Kerby, S.J. Kutz, J. Stirling, and D.A. Walker. 2013. Ecological consequences of sea-ice decline. *Science* 341(6145): 519–524, https://doi.org/10.1126/science.1235225.
Radchenko, V.I., R.J. Beamish, W.R. Heard, O.S. Temnykh. 2018. Ocean ecology of pink salmon. Pp. 15–160 in *The Ocean Ecology of Pacific Salmon and Trout*. R.J. Beamish, ed., American Fisheries Society, Bethesda, Maryland, https://doi.org/10.47886/9781934874455.ch2.
Rand, K.M., and E.A. Logerwell. 2011. The first demer- sal trawl survey of benthic fish and invertebrates in the Beaufort Sea since the late 1970s. *Polar Biology* 34(4):475–488, https://doi.org/10.1007/ s00300-010-0900-2.
Reinhart, N.R., S.H. Ferguson, W.R. Koski, J.W. Higdon, B. Leblanc, O. Tervo, and P.D. Jepson. 2013. Occurrence of killer whale *Orcinus orca* rake marks on Eastern Canada-West Greenland bowhead whales *Balaena mysticetus*. *Polar Biology* 36:1,133–1,146, https://doi.org/10.1007/ s00300-013-1335-3.
Renner, M., J.K. Parrish, J.F. Piatt, K.J. Kuletz, A.E. Edwards, and G.L. Hunt Jr. 2013. Modeled distribution and abundance of a pelagic sea- bird reveal trends in relation to fisheries. *Marine Ecology Progress Series* 484:259–277, https://doi.org/10.3354/meps10347.
Romano, M., H.M. Renner, K.J. Kuletz, J.K. Parrish, T. Jones, H.K. Burgess, D.A. Cushing, and D. Causey. 2020. Die-offs and reproductive failure of murres in the Bering and Chukchi Seas in 2018. *Deep Sea Research Part II* 181–182, https://doi.org/ 10.1016/j.dsr2.2020.104877.
Ruggerone, G.T., and J.R. Irvine. 2018. Numbers and biomass of natural- and hatchery-origin pink salmon, chum salmon, and sockeye salmon in the North Pacific Ocean, 1925–2015. *Marine and Coastal Fisheries* 10:152–168, https://doi.org/ 10.1002/mcf2.10023.
Ryan, W.B.F., S.M. Carbotte, J. Coplan, S. O'Hara, A. Melkonian, R. Arko, R.A. Weissel, V. Ferrini, A. Goodwillie, F. Nitsche, and others. 2009. Global Multi-Resolution Topography (GMRT) synthesis data set. *Geochemistry, Geophysics, Geosystems* 10, Q03014, https://doi.org/10.1029/2008GC002332.
Sigler, M., M. Renner, S. Danielson, L. Eisner, R. Lauth, K. Kuletz, E. Logerwell, and G. Hunt. 2011. Fluxes, fins, and feathers: Relationships among the Bering, Chukchi, and Beaufort Seas in a time of climate change. *Oceanography* 24:250–265, https://doi.org/10.5670/oceanog.2011.77.
Sorte, C.J.B., S.L. Williams, and J.T. Carlton. 2010. Marine range shifts and species introductions: Comparative spread rates and community impacts. *Global Ecology and Biogeography* 19:303–316, https://doi.org/10.1111/j.1466-8238.2009.00519.x.
Stabeno, P.J., and S.W. Bell. 2019. Extreme conditions in the Bering Sea (2017–2018): Record-breaking low sea-ice extent. *Geophysical Research Letters* 46:8,952–8,959, https://doi.org/10.1029/2019GL083816.
Stabeno, P.J., N.A. Bond, N.B. Kachel, S.A. Salo, and J.D. Schumacher. 2001. On the temporal variability of the physical environment over the south-eastern Bering Sea. *Fisheries Oceanography* 10:81–98, https://doi.org/10.1046/j.1365-2419.2001.00157.x.
Stafford, K.M. 2019. Increasing detections of killer whales (*Orcinus orca*) in the Pacific Arctic. *Marine Mammal Science* 35:696–706, https://doi.org/10.1111/mms.12551.
Stafford, K.M., S.E. Moore, P.J. Stabeno, D.V. Holliday, J.M. Napp, and D.K. Mellinger. 2010. Biophysical ocean observation in the southeastern Bering Sea. *Geophysical Research Letters* 37:L02606, https://doi.org/10.1029/2009GL040724.
Stafford, K.M., J.J. Citta, S. Okkonen, and J. Zhang. 2021. Bowhead and beluga whale acoustic detections in the western Beaufort Sea 2008–2018. *PLoS ONE* 16(6):e0253929, https://doi.org/10.1371/journal.pone.0253929.
Stevenson, D.E., and R.R. Lauth. 2019. Bottom trawl surveys in the northern Bering Sea indicate recent shifts in the distribution of marine species. *Polar Biology* 42:407–421, https://doi.org/10.1007/s00300-018-2431-1.
Storrie, L., C. Lydersen, M. Andersen, R.B. Wynn, and K.M. Kovacs. 2018. Determining the species assemblage and habitat use of cetaceans in the Svalbard Archipelago, based on observations from 2002 to 2014. *Polar Research* 37, https://doi.org/10.1080/17518369.2018.1463065.
Sydeman, W., S.A. Thompson, J. Santora, M. Henry, K.H. Morgan, and S. Batten. 2010. Macro- ecology of plankton-seabird associations in the North Pacific Ocean. *Journal of Plankton Research* 32:1,697–1,713, https://doi.org/10.1093/plankt/fbq119.
Sydeman, W.J., S.A. Thompson, J.F. Piatt, S.G. Zador, and M.W. Dorn. 2021. Integrating seabird dietary and groundfish stock assessment data: Can puffins predict pollock spawning stock biomass in the North Pacific? *Fish and Fisheries* 23:213–226, https://doi.org/10.1111/faf.12611.
Tamarin-Brodsky, T., and Y. Kaspi. 2017. Enhanced poleward propagation of storms under cli- mate change. *Nature Geoscience* 10:908–914, https://doi.org/10.1038/s41561-017-0001-8.
Thoman, R.L., J. Richter-Menge, and M.L. Druckenmiller. 2020. Arctic Report Card 2020: Executive Summary, https://doi.org/10.25923/mn5p-t549.
VanWormer, E., J.A.K. Mazet, A. Hall, V.A. Gill, P.L. Boveng, J.M. London, T. Gelatt, B.S. Fadely, M.E. Lander, J. Sterling, and others. 2020. Viral emergence in marine mammals in the North Pacific may be linked to Arctic sea ice reduction. *Scientific Reports* 9:15569, https://doi.org/10.1038/s41598-019-51699-4.
Westdal, K.H., J.W. Higdon, and S.H. Ferguson. 2016. Review of killer whale (*Orcinus orca*) ice entrapments and ice-related mortality events in the Northern Hemisphere. *Polar Biology* 40:1,467–1,473, https://doi.org/10.1007/s00300-016-2019-6.
Will, A., A. Takahashi, J.-B. Thiebot, A. Martinez, E. Kitaiskaia, L. Britt, D. Nichol, J. Murphy, A. Dimond, S. Tsukamoto, and others. 2020. The breeding seabird community reveals that recent sea ice loss in the Pacific Arctic does not benefit piscivores and is detrimental to planktivores. *Deep-Sea Research Part II* 181–182:104902, https://doi.org/10.1016/j.dsr2.2020.104902.
Willoughby, A.L., M.C. Ferguson, R. Stimmelmayr, J.T. Clarke, and A.A. Brower. 2020. Bowhead whale (*Balaena mysticetus*) and killer whale (*Orcinus orca*) co-occurrence in the U.S. Pacific Arctic, 2009–2018: Evidence from bowhead whale carcasses. *Polar Biology* 43:1,669–1,697, https://doi.org/10.1007/s00300-020-02734-y.
Woodgate, R.A., and C. Peralta-Ferriz. 2021. Warming and freshening of the Pacific inflow to the Arctic from 1990–2019 implying dramatic shoaling in Pacific winter water ventilation of the Arctic water column. *Geophysical Research Letters* 48(9):e2021GL092528, https://doi.org/10.1029/2021GL092528.
Wyllie-Echeverria, T. 1995. Sea-ice conditions and the distribution of walleye pollock (*Theragra chalcogramma*) on the Bering and Chukchi Sea shelf. Pp. 131–136 in *Climate Change & Northern Fish Populations*. R.J. Beamish, ed., Canadian Special Publication of Fisheries and Aquatic Sciences, vol. 121, National Research Council of Canada, Ottawa.

ACKNOWLEDGMENTS

Support for this work was provided to KMS by NPRB grant A94-00 and ONR grants N000141712274 and N000142012413. D. Cushing kindly produced Figure 3. The scientific results and conclusions, as well as any views or opinions expressed herein, are those of the author(s) and do not necessarily reflect those of NOAA or the Department of Commerce or the US Fish and Wildlife Service. Reference to trade names does not imply endorsement by the National Marine Fisheries Service or NOAA.

AUTHORS

Kathleen M. Stafford (kate.stafford@oregonstate.edu) was Senior Principal Oceanographer, Applied Physics Laboratory, University of Washington, Seattle, WA, USA, and is now Associate Professor, Marine Mammal Institute, Oregon State University, Newport, OR, USA. **Edward V. Farley** is Program Manager, Alaska Fisheries Science Center, National Oceanographic and Atmospheric Administration (NOAA), Juneau, AK, USA. **Megan Ferguson** is Research Fisheries Biologist, Alaska Fisheries Science Center, NOAA, Seattle, WA, USA. **Kathy J. Kuletz** is Supervisory Wildlife Biologist, US Fish and Wildlife Service, Anchorage, AK, USA. **Robert Levine** is a graduate student in biological oceanography, School of Oceanography, University of Washington, Seattle, WA, USA.

ARTICLE CITATION

Stafford, K.M., E.V. Farley, M. Ferguson, K.J. Kuletz, and R. Levine. 2022. Northward range expansion of subarctic upper trophic level animals into the Pacific Arctic region. *Oceanography* 35(3–4):158–166, https://doi.org/10.5670/oceanog.2022.101.

COPYRIGHT & USAGE

Chapter 7: Evidence suggests potential transformation of the Pacific Arctic Ecosystem is underway

Huntington, H.P., S.L. Danielson, F.K. Wiese, M. Baker, P. Boveng, J.J. Citta, A. De Robertis, D.M. Dickson, E. Farley, J.C. George, K. Iken, D.G. Kimmel, K. Kuletz, C. Ladd, R. Levine, L. Quakenbush, P. Stabeno, K.M Stafford, D. Stockwell and C. Wilson, 2020. Evidence suggests potential transformation of the Pacific Arctic ecosystem is underway. *Nature Climate Change*, 10(4), pp.342-348

Abstract

The highly productive northern Bering and Chukchi marine shelf ecosystem has long been dominated by strong seasonality in sea ice and water temperatures. Extremely warm conditions from 2017 into 2019 – including loss of ice cover across portions of the region in all three winters – were a marked change even from other recent warm years. Biological indicators suggest this state change could alter ecosystem structure and function. Here we report observations of key physical drivers, biological responses, and consequences for humans, including subsistence hunting, commercial fishing, and industrial shipping.

We consider whether observed state changes are indicative of future norms, whether an ecosystem transformation is already underway, and if so, whether shifts are synchronously functional and system-wide, or reveal a slower cascade of changes from the physical environment through the food web to human society. Understanding of this observed process of ecosystem reorganization may shed light on transformations occurring elsewhere.

ARTICLES
https://doi.org/10.1038/s41558-020-0695-2
nature climate change

Evidence suggests potential transformation of the Pacific Arctic ecosystem is underway

Henry P. Huntington [1]✉, Seth L. Danielson[2], Francis K. Wiese[3], Matthew Baker[4], Peter Boveng[5], John J. Citta[6], Alex De Robertis [7], Danielle M. S. Dickson [4], Ed Farley[5], J. Craighead George[8], Katrin Iken[2], David G. Kimmel[5], Kathy Kuletz[9], Carol Ladd [10], Robert Levine [11], Lori Quakenbush[12], Phyllis Stabeno[10], Kathleen M. Stafford [11], Dean Stockwell[2] and Chris Wilson[13]

The highly productive northern Bering and Chukchi marine shelf ecosystem has long been dominated by strong seasonality in sea-ice and water temperatures. Extremely warm conditions from 2017 into 2019—including loss of ice cover across portions of the region in all three winters—were a marked change even from other recent warm years. Biological indicators suggest that this change of state could alter ecosystem structure and function. Here, we report observations of key physical drivers, biological responses and consequences for humans, including subsistence hunting, commercial fishing and industrial shipping. We consider whether observed state changes are indicative of future norms, whether an ecosystem transformation is already underway and, if so, whether shifts are synchronously functional and system wide or reveal a slower cascade of changes from the physical environment through the food web to human society. Understanding of this observed process of ecosystem reorganization may shed light on transformations occurring elsewhere.

The Pacific Arctic, which comprises the Chukchi and northern Bering seas (Fig. 1), is one of the world's most productive ocean ecosystems[1] and is characterized by high benthic biomass resulting from persistent, nutrient-rich flow through the Bering Strait[2], which fuels high primary production[3]. The region is home to millions of nesting and migratory seabirds in summer and autumn, with hotspots of foraging activity shared with marine mammals[4], supporting coastal Indigenous communities. The delivery of nutrients together with the extent and timing of the sea ice[5] are dominant environmental factors that structure this ecosystem. A freeze-up in autumn and winter eliminates large expanses of open water, causing whales, Pacific walruses (*Odobenus rosmarus divergens*), many seals and seabirds to migrate southwards into the Bering Sea and beyond[6]. The return of sunlight in spring heralds snow melt, growth of sea- ice algae, and a phytoplankton bloom that typically exceeds the consumption capabilities of pelagic consumers, resulting in carbon falling to the seabed and fuelling rich benthic communities[7,8]. Solar radiation and melting sea ice help stratify the upper water column, impeding the ability of winds to mix surface and subsurface waters. In summer, low-salinity surface waters near the pack ice remain cool relative to the shelf waters that are warmed by insolation. The Bering Sea cold pool (near-bottom shelf waters cooler than 2 °C, located south of the Bering Strait) has long served as a thermal barrier that prevents northwards migration of subarctic groundfish[9], which are major stocks for the southeastern Bering Sea's US $2 billion dollar fishery and account for about half of the seafood landings in the United States[10,11].

Recent changes in the Pacific Arctic marine ecosystem

Declining sea ice in this century has reduced surface albedo in spring and summer, accelerating oceanic heat uptake and causing earlier and more rapid sea-ice melt[12]. The pack ice and marginal ice zone has retreated north beyond the Chukchi shelf in recent summers, whereas warmer shelf waters delay sea-ice formation in autumn. Simultaneously, the flow of water northwards through the Bering Strait has increased, as has its temperature[2], so that it now delivers more heat, freshwater, nutrients and biota northwards into the Arctic[13]. Near-bottom water temperatures now exceed 0 °C for a larger portion of the year (Fig. 2).

The ramifications of these physical changes include more salmon in the Chukchi and Beaufort seas[14,15], walruses hauling-out on shore instead of sea ice in northwestern Alaska in late summer[16], an increase in the frequency and seasonal duration of killer whale (*Orcinus orca*) presence in the Chukchi Sea[17], an increase in planktivorous seabirds in the Chukchi Sea[18] and a northwards shift in the distribution of other seabird species[19,20]. For the Indigenous peoples of the region, spring marine mammal hunting opportunities that are dependent on the presence of sea ice have decreased and shifted in time[21], although the lack of sea ice has allowed additional whaling to occur in autumn and early winter in the northern Bering Sea[22].

And then came 2017

In 2017, physical conditions in the Pacific Arctic marine shelf ecosystem of the Chukchi and northern Bering seas described above showed signs of a sudden and dramatic shift relative to historical means and even to other recent unusually warm years. These physical changes seemingly precipitated several important ecological shifts, with consequences for the region's residents. On the basis of published material and unpublished data from the authors, many changes persisted in 2018 and even into 2019, suggesting that 2017

[1]Huntington Consulting, Eagle River, AK, USA. [2]University of Alaska Fairbanks, Fairbanks, AK, USA. [3]Stantec, Anchorage, AK, USA. [4]North Pacific Research Board, Anchorage, AK, USA. [5]Alaska Fisheries Science Center, NOAA, Seattle, WA, USA. [6]Alaska Department of Fish and Game, Juneau, AK, USA. [7]Alaska Fisheries Science Center, NOAA, Seattle, WA, USA. [8]North Slope Borough Department of Wildlife Management, Utqiaġvik, AK, USA. [9]US Fish and Wildlife Service, Anchorage, AK, USA. [10]Pacific Marine Environmental Laboratory, NOAA, Seattle, WA, USA. [11]University of Washington, Seattle, WA, USA. [12]Alaska Department of Fish and Game, Fairbanks, AK, USA. [13]Alaska Fisheries Science Center, NOAA, Seattle, WA, USA. ✉e-mail: henryphuntington@gmail.com

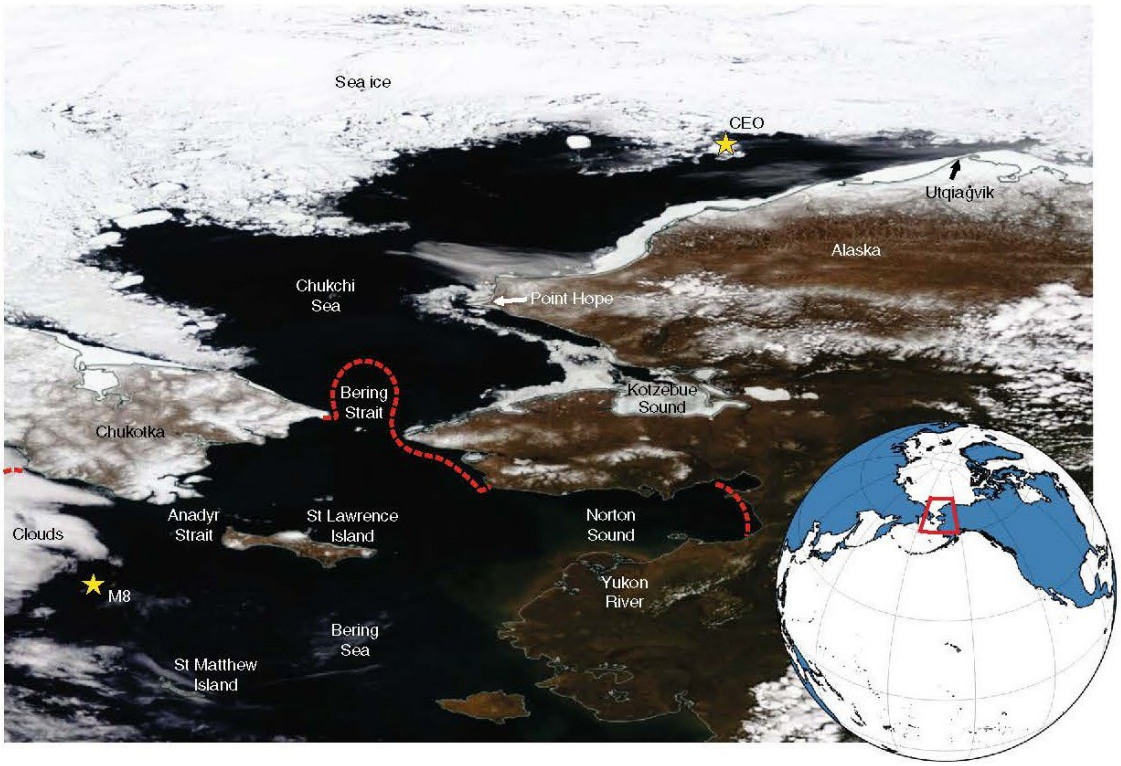

Fig. 1 | Sea-ice changes in recent years. A true-colour MODiS satellite image showing northern Bering and Chukchi sea-ice conditions on 2 June 2017. The red dotted lines denote the 1980–2010 ice-edge climatology for 2 June. Yellow stars denote locations of oceanographic moorings M8 and CEO. The inset locates the study region. Credit: NASA Worldview.

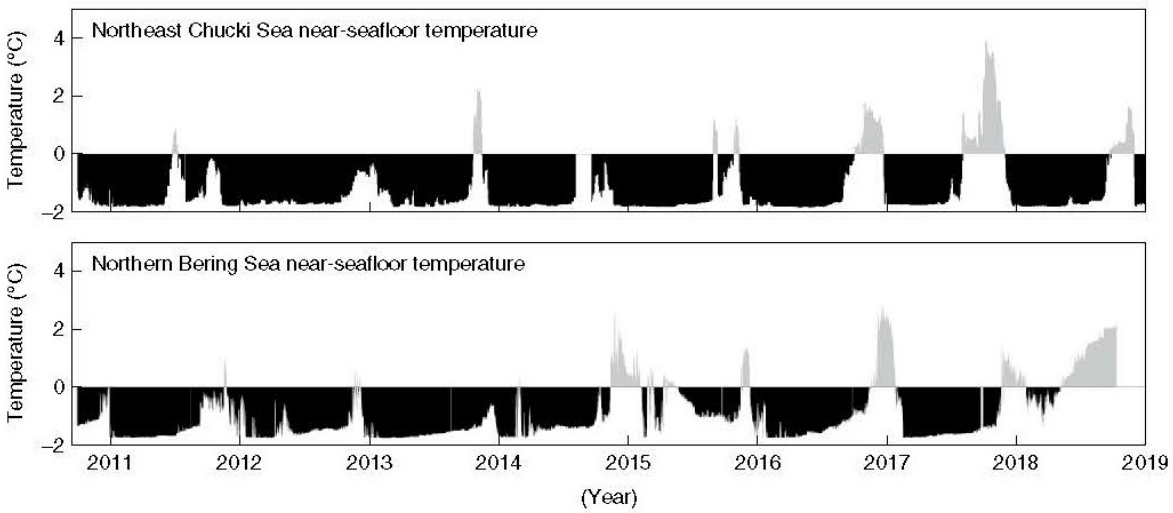

Fig. 2 | Near-bottom water temperatures. in past years, temperatures in important seafloor habitats remained below 0 °C for most of the year, whereas in recent years, an increasing number of months exhibited temperatures well above 0 °C. The mooring locations are indicated by gold stars on Fig. 1.

was not a passing oddity of brief consequence to social-ecological systems, but a sign of what is to come.

In early January 2017, the sea-ice edge had barely progressed south of the Bering Strait and for the entire winter its extent remained at least 2×10^5 km^2 below the long-term average. In June, ship-based observations found that the near-bottom ocean temperatures in the Bering Strait were nearly 4 °C, which are over 3 °C and four standard deviations warmer than the 1991–2016 June mean[2]. By June, the eastern Chukchi shelf was already mostly sea-ice free (Fig. 1). In early December 2017, the ice edge was over 1,000 km north of its climatological mean position near St Lawrence Island.

There was no sea ice in the Bering Strait in February 2018 and southerly winds forced a large ice retreat again in February 2019[23]. Waters in Norton Sound exceeded 10 °C before the end of June 2018 and the cold pool was again minimal by late summer.

Reduced ice cover and warmer seas probably impacted primary production by influencing thermal, light and stratification conditions. In the spring of 2018, the bloom was delayed in the southern Bering Sea due to a lack of freshwater input from melting sea ice, and chlorophyll concentrations were one-order-of-magnitude lower than usual; however, in the northern Bering Sea the ice-associated bloom was early and extensive[24]. Furthermore, the

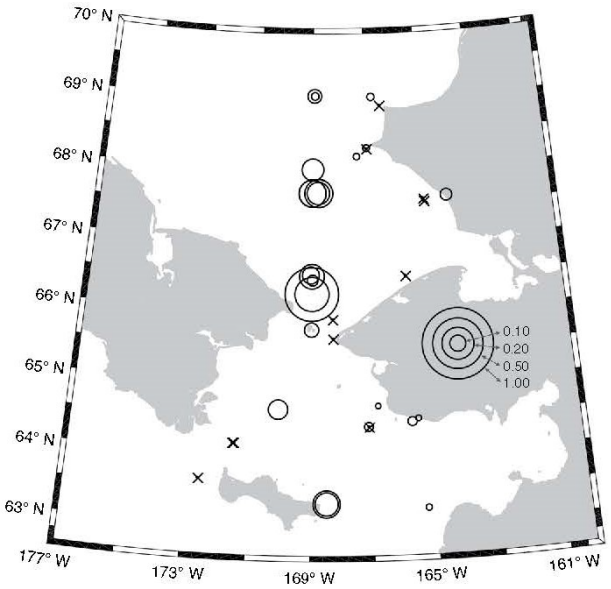

Fig. 3 | Seawater concentrations of domoic acid (nmol kg^{-1}), June 2017. Crosses indicate samples in which no toxins were detected.

detection of domoic acid in shipboard water samples (Fig. 3) and saxitoxin in a few stranded and harvested walruses from Bering Strait villages led to concern about harmful algal blooms and food safety from Indigenous residents, although analytical challenges make the impact difficult to determine[25].

Changes in species distributions had already been observed this century, but not to the extent observed in 2017. The copepods *Calanus glacialis/marshallae* were found that year to be remarkably low in abundance relative to 2012–2015 and multispecies epibenthic biomass in the southern Chukchi Sea also exhibited a pronounced decline relative to comparable collections in 2004, 2009, 2012 and 2015 (Fig. 4). By contrast, acoustic-trawl surveys indicated that age-zero Arctic cod abundance was dramatically higher in the Chukchi Sea in 2017 when compared with previous surveys: backscatter in the northern Chukchi Sea (67° N to 71.5° N) was 5.6 times greater than in 2013 and 16.3 times greater than in 2012 (Fig. 5), but the fish had low energy content. In surface trawl surveys in the northern Bering Sea, the catch per unit effort for juvenile pink salmon (*Oncorhyncus gorbuscha*) was two times greater during 2017 than previous years (Fig. 4); they return as adults in the following year, and during 2018 they returned to Norton Sound in much greater numbers than expected[26]. Adult walleye pollock (*Gadus chalcogramma*), Pacific cod (*Gadus macrocephalus*) and northern rock sole (*Lepidopsetta polyxystra*) biomass in bottom trawl surveys increased in the northeastern Bering Sea during 2017, probably due to northwards movement of these fishes in the absence of the Bering Sea cold pool[27].

In offshore waters, the total number of seabirds declined from 2012–2017 in the southern and northern Bering Sea, but densities were above the long-term mean in the Chukchi Sea during most of that period. The increase in the Chukchi Sea in 2015–2017 was primarily due to short-tailed shearwaters (*Ardenna tenuirostris*), which feed primarily on euphausiids, and less pronounced increases in piscivorous black-legged kittiwakes (*Rissa tridactyla*) and murres (*Uria* spp). By contrast, planktivorous auklets (*Aethia* sp.) had low densities in the Chukchi Sea in 2017 and 2018; however, their densities increased in the northern Bering Sea in those years[24]. Reproductive success was low for seabirds in the Bering Sea in 2017–2018 and there were mixed-species die offs there and in the Chukchi Sea[24,28], with dead birds emaciated. Notably, the numbers of murres and kittiwakes attending the large Chukchi Sea colony continued to increase[29] at a rate that suggested immigration of piscivorous nesting birds.

In the spring of 2017, bowhead whales, including females with calves, were seen near Utqiaġvik, Alaska, nearly a month earlier than usual and the Utqiaġvik whale hunt recorded the earliest known landing on 13 April. Four bowhead whales equipped with satellite transmitters all wintered (2017 to 2018) in the Chukchi instead of their usual wintering area south of Anadyr Strait in the Bering Sea[30] and a bowhead was recorded singing near Utqiaġvik on 11 January 2018, something that has never been recorded before at that time of year. In 2018 to 2019, the bowheads were again north of the Anadyr Strait in winter. Spotted seal (*Phoca largha*) pups in the spring of 2018 were found in poorer condition (less fat and lower mass/length) than in recent years, and almost no ribbon seals (*Histriophoca fasciata*) were seen during those same surveys, raising the spectre of a failure in the 2018 year class. In the spring and summer of 2018 and 2019, more than 280 bearded (*Erignathus barbatus*), ringed (*Pusa hispida*), spotted and unidentified seal carcasses (primarily young and many emaciated) were reported from beaches mostly in the northern Bering and southern Chukchi seas, nearly five times the annual average from 2014–2017, prompting the National Oceanic and Atmospheric Administration to declare an unusual mortality event[31].

Anomaly or transformation?

Changes in sea-ice extent, water temperature, currents, zooplankton abundance, animal distribution and health, hunting success and other aspects of the ecosystem are noteworthy in themselves, but such large-scale changes could conceivably occur without altering basic relationships among ecosystem components. The investigation of specific mechanisms underlying these changes were not part of the cited studies; however, it is known from other areas—including the southern Bering Sea—that the spring sea-ice break-up spurs a productive phytoplankton bloom and its timing, together with ocean temperatures, determines phytoplankton species composition, carbon export to the benthos and food quality for zooplankton[24]. Changes towards lower-lipid zooplankton reduces over-winter survival of fishes such as salmon and Arctic cod[32], even if they increase numerically in summer due to favourable thermal and oceanographic conditions. Lower zooplankton food quality and increased competition from predatory fish moving north from the Bering Sea might explain seabird and seal mortality.

The ecosystem-wide changes seen in 2017–2019 have the poten- tial to fundamentally reconfigure the Pacific Arctic marine food web. An altered physical environment characterized by warmer waters and a longer open-water season is allowing subarctic species to establish themselves in the Chukchi Sea; seasonally for now, but possibly year-round in the future. Subarctic invaders such as walleye pollock and Pacific cod could fundamentally transform interactions among pelagic species, benthic invertebrates, groundfish, seabirds and marine mammals by exerting strong predation pressure on forage fishes and benthic crab, worm and shrimp communities[10]. Predation pressure from these fishes adds top-down stresses to the bottom-up changes that are associated with altered temperature and primary and secondary productivity. Indigenous hunters may begin to find familiar species of fishes and marine mammals at unusual times of year or unfamiliar species during customary hunting and fishing periods[21].

An interdisciplinary look at the Pacific Arctic marine ecosystem as it changes may provide a rare opportunity to track ecosystem transformation in detail as it unfolds, rather than reconstructing details after the fact. The transformation of an ecosystem may reflect a cascade of sequential changes that take place over multiple

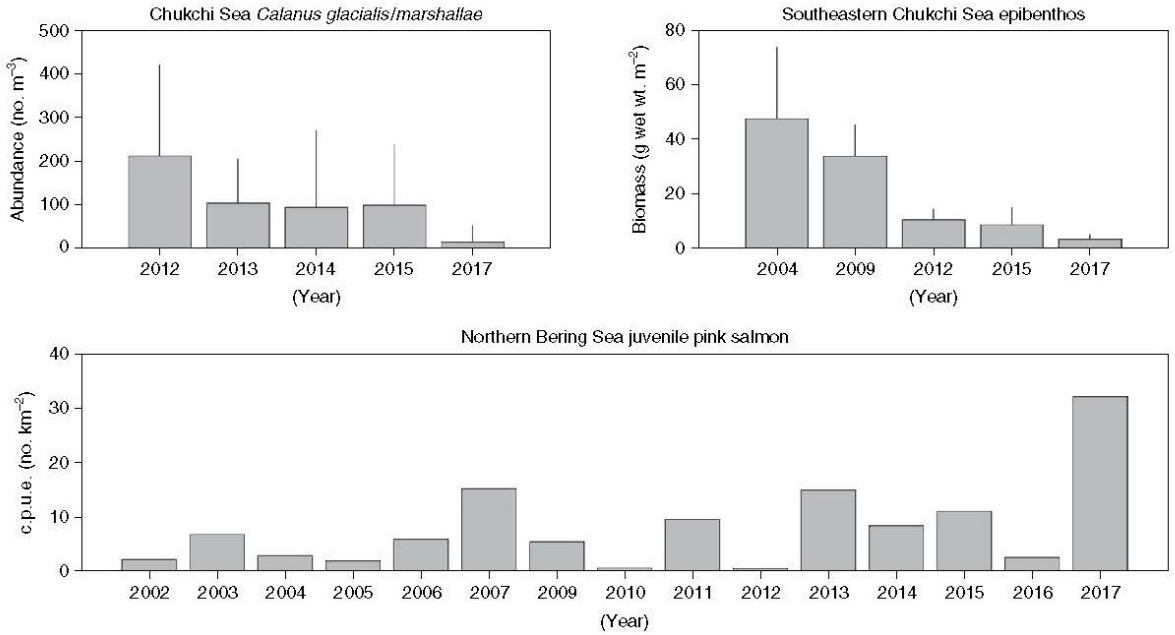

Fig. 4 | Biological changes in recent years. Observations show declines in *Calanus glacialis/marshallae* abundance (upper left) and epibenthic biomass (upper right) in 2017 relative to earlier years, and an increase in catch per unit effort (c.p.u.e.; bottom) for juvenile pink salmon. The upper two graphs show means and s.d. error bars.

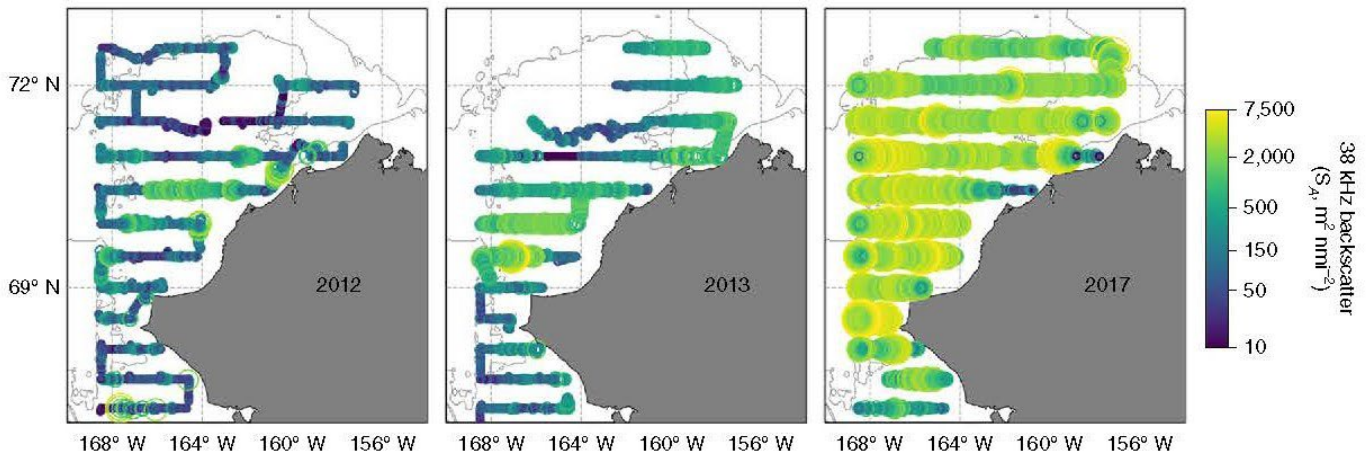

Fig. 5 | Change in Arctic cod abundance. Acoustic surveys indicate that the abundance of age-zero Arctic cod increased substantially in 2017 relative to 2012 and 2013. Trawl sampling indicated that Arctic cod dominated acoustic backscatter in this area in 2012 and 2013 (ref. [50]). This was also the case in 2017 where Arctic cod accounted for 95.4% of fish captured in 33 midwater trawl hauls. Measurements, s_A, are expressed as the nautical area backscattering coefficient[50] at 38 kHz.

years rather than a single shift or tipping point (for example, ref. [33]), although changes to individual ecosystem components may be sudden and dramatic; for example, because of positive feedbacks in the climate system (see ref. [12]), it is possible that 2017 marked the crossing of a threshold that precludes return to the system state that was common just a decade ago. We find that a closely coupled synergy between bottom-up and top-down factors (for example, ref. [34]) seems to best characterize this system's transition and the interactions among these multiple stressors have important implications for understanding any subsequent reorganization. The result would be the transformation of an Arctic marine ecosystem into one that is characterized by subarctic conditions, subarctic species and subarctic interactions (Box 1). The Chukchi Sea may soon resemble the east-central Bering Sea shelf in condition, structure and function, with annual sea ice, warmer bottom water temperatures and ecosystem productivity derived from forage fishes and pelagic zooplankton rather than the benthos. Changes in the historically strong benthic–pelagic coupling have already been observed in the southeastern Chukchi Sea, where overall epibenthic biomass declined by an order of magnitude from 2004 to 2017; the fact that the most abundant taxa were consistent over time may hint at overall changes in ecosystem productivity or pathways rather than specific habitat changes[35,36]. Yet this transformation is more complex than an ecosystem migrating north; for example, the Chukchi Sea would probably retain some characteristics that distinguish it from the Bering Sea shelf, due to higher latitude and downstream location relative to the Bering Strait nutrient supply. How these competing features will combine to create a new state of the Pacific Arctic ecosystem remains to be seen.

In addition to its regional importance, the pattern of change underway in the Pacific Arctic may eventually shed light on the progression of ecosystem transformation more generally[37], which manifests as large-scale alterations in the connections and interactions among species and among physical and biological processes.

Box 1 | Environmental changes and consequences for the ecosystem and humans

The figure shows the observed and potential future changes in the physical environment, and the following list highlights the observed and anticipated consequences for the biological and human components of the ecosystem:

- Altered timing and magnitude of spring-ice-associated phytoplankton and zooplankton blooms
- Higher frequency of toxic algae blooms
- Increased metabolic and respiration rates
- Seasonally altered distributions of fishes and marine mammals that associate with sea ice
- Seabird reproductive failures and die-offs
- Expansion of subarctic species distributions northwards

New predation pressure on Arctic pelagic and benthic communities

- Migration of commercial fish species away from the southeast Bering Sea
- Less stable ice and altered access to winter subsistence hunting grounds
- Altered seasonality for hunting
- New subsistence food sources
- New management decisions for commercial fishery oversight
- Increased vessel traffic in ice-free waters with associated increased risks of oil spills, marine mammal strikes and noise pollution
- Accelerated coastal erosion and delivery of terrestrial carbon to marine domain

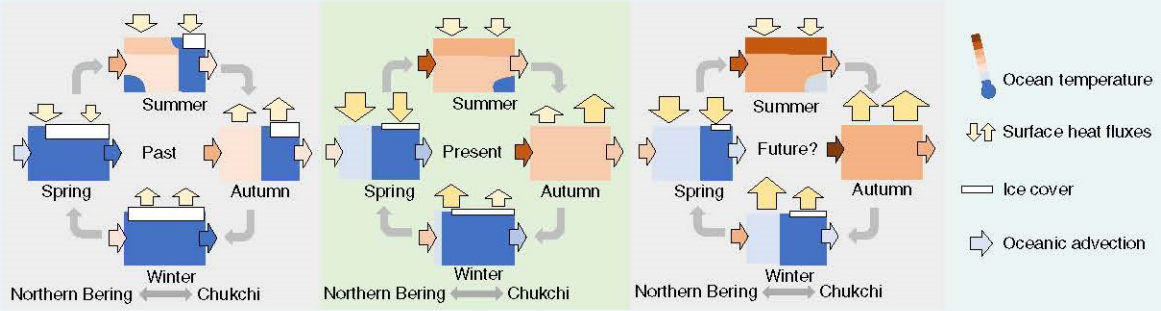

Environmental changes and related consequences. Observed and potential future changes in the physical environment (left and middle panels) in the Northern Bering and Chukchi shelf systems (that is, bottom-up forcing), along with observed and anticipated consequences for the biological and human components of the ecosystem (right panel).

Overpeck et al.[38] suggested the possibility of such a transformation resulting from the removal of perennial ice in the Arctic, although they focused on the before and after states of the system without describing the transformation in between. The pioneering work of Gunderson and Holling[39] recognized that transformation and reorganization are less predictable and less well understood than a simple shift from stability to instability.

What to expect next?

The expectation is for the sea-ice season to further shorten and sea-ice coverage to diminish[40]. Waters will become warmer and stay warm longer into autumn and winter. It is hard to predict how quickly these changes propagate through and persist in the system, and what additional sudden shifts may occur. It is likely, however, that there will be differences in the temporal and spatial scales over which physics and biology change[41]. Physical conditions that were once anomalous may become normal. The biological response will follow but may not carry over across years until species and behaviours that thrive in the new conditions are able to persist. Hunters and fishers will adjust to some degree but may find it necessary to switch the timing or targets of their efforts[42].

Specific trajectories of these changes and their implications for the Pacific Arctic ecosystem, including Indigenous coastal communities, are still unclear. To stay with or ahead of these system transformations rather than reacting to a new state some years from now, some critical unknowns (especially regarding ecosystem relationships) will require further attention and continued monitoring at multiple scales. As sea ice retreats earlier, will some species cling to existing fixed habitats (for example, depositional zones) and remain largely in place while others follow shifting habitats (such as the ice edge)? Will subarctic species be able to flourish and persist in the Chukchi Sea year-round, transforming the ecosystem into a locus of groundfish or pelagic predator abundance? Will increased industrial activity such as shipping combine with climate-driven ecosystem changes in ways that amplify the consequences of either alone[43]? How can coastal communities adjust and adapt quickly enough to retain cultural and nutritional security[44]?

Even in this age of information overload, it is how remarkable how scarce (and thus how valuable) the available data are for mak- ing statistically robust comparisons of today's conditions versus yesterdays; for example, quantifying changes in primary and secondary productivity cannot immediately follow the spring retreat of sea ice because previously the ice itself precluded ship-based measurements at locations and times now ice free. Across the study region, even 15 years of annually collected data is an unusually long time series, and for biological parameters most of these data are confined to summer months; hence, it is important to learn to distinguish surprises from completely new observations.

A cascade of effects through an ecosystem may include tipping points governed by positive feedbacks for individual components, making recovery to the previous structure and function ever less likely (for example, refs. [33,45]). Top-down changes such as increased predation may result from bottom-up changes, such as the removal of thermal barriers to the range expansion of predators. The experience so far in the Pacific Arctic by itself will not resolve these questions, but it does suggest that, with regards to cascades versus

tipping points or top-down versus bottom-up controls (for example, ref. [46]), ecosystem transformation may be a complex matter of 'both and' rather than a simple dichotomy of either/or.

These questions are more than a curiosity[47]. The well-being of coastal communities and the management of human activities in the region—including potential commercial fisheries—depend on reliable information and insight into what is likely to happen next. In Alaskan waters, industrial and research activities are planned in ways to reduce interference with Alaska Native subsistence harvests, and conscientious vessel operators communicate with communities and adjust their plans to avoid areas where hunters are active (for example, ref. [48]). Growing uncertainty about the timing of animal migrations and optimal harvest conditions increases the likelihood of conflict and concerns about food security. Coastal communities are likely to face difficult choices between capitalizing on increased economic opportunity and limiting industrial interference with subsistence activities.

The profound shift in ecosystem state and conditions suggest a new framework is needed to replace the paradigm that served well in recent decades. The Pacific Arctic marine ecosystem transforma- tion is not an isolated case. Social-ecological systems worldwide are facing similar pressures from changing physical conditions, with implications that are increasingly uncertain as transformation propagates through the food web and to human outcomes[49]. Long-term and multiscale data are necessary to detect, examine and respond to such changes. A better understanding of the nature of system transformation will help humans detect transformations earlier, perhaps in time for more effective response or adaptation, even if prevention may no longer be possible.

Online content

Any methods, additional references, Nature Research reporting summaries, source data, extended data, supplementary information, acknowledgements, peer review information; details of author contributions and competing interests; and statements of data and code availability are available at https://doi.org/10.1038/s41558-020-0695-2.

Received: 22 February 2019; Accepted: 8 January 2020;
Published online: 24 February 2020

References

1. Grebmeier, J. M., Cooper, L. W., Feder, H. W. & Sirenko, B. I. Ecosystem dynamics of the Pacific-influenced northern Bering and Chukchi seas in the Amerasian Arctic. *Prog. Oceanogr.* **71**, 331–361 (2006).
2. Woodgate, R. A. Increases in the pacific inflow to the Arctic from 1990 to 2015, and insights into seasonal trends and driving mechanisms from year-round Bering Strait mooring data. *Prog. Oceanogr.* **160**, 124–154 (2018).
3. Codispoti, L. A. et al. Synthesis of primary production in the arctic ocean. III. Nitrate and phosphate based estimates of net community production. *Prog. Oceanogr.* **110**, 126–150 (2013).
4. Kuletz, K. et al. Seasonal spatial patterns in seabird and marine mammal distribution in the eastern Chukchi and western Beaufort seas: identifying biologically important pelagic areas. *Prog. Oceanogr.* **136**, 175–200 (2015).
5. Cooper, L. W. et al. The relationship between sea ice break-up, water mass variation, chlorophyll biomass, and sedimentation in the northern Bering Sea. *Deep Sea Res. II* **65–70**, 141–162 (2012).
6. Smith, M. A., Goldman, M. S., Knight, E. J. & Warrenchuk, J. *Ecological Atlas of the Bering, Chukchi, and Beaufort Seas* 2nd edn (Audubon Alaska, 2018).
7. Grebmeier, J. M. et al. Ecosystem characteristics and processes facilitating persistent macrobenthic biomass hotspots and associated benthivory in the Pacific Arctic. *Prog. Oceanogr.* **136**, 92–114 (2015).
8. Moore, S. E., Stabeno, P. J., Grebmeier, J. M. & Okkonen, S. R. The Arctic marine pulses model: linking annual oceanographic processes to contiguous ecological domains in the pacific arctic. *Deep Sea Res. II* **152**, 8–21 (2018).
9. Stabeno, P. J. et al. Comparison of warm and cold years on the southeastern bering sea shelf and some implications for the ecosystem. *Deep Sea Res. II* **65**, 31–45 (2012).
10. Sigler, M. et al. Fluxes, fins, and feathers: relationships among the bering, chukchi, and beaufort seas in a time of climate change. *Oceanography* **24**, 250–265 (2011).
11. Haynie, A. C. & Pfeiffer, L. Climatic and economic drivers of the bering sea walleye pollock (*Theragra chalcogramma*) fishery: implications for the future. *Can. J. Fish. Aquat. Sci.* **70**, 841–853 (2013).
12. Stroeve, J. C. et al. The Arctic's rapidly shrinking sea ice cover: a research synthesis. *Clim. Change* **110**, 1005–1027 (2012).
13. Hunt, G. L. Jr et al. Advection in polar and sub-polar environments: impacts on high latitude marine ecosystems. *Prog. Oceanogr.* **149**, 40–81 (2016).
14. Dunmall, K. M., et al. in *Responses of Arctic Marine Ecosystems to Climate Change* (eds Mueter, F. J. et al.) 141–163 (Alaska Sea Grant, University of Alaska Fairbanks, 2013); https://doi.org/10.4027/ramecc.2013.07
15. Moore, S. E., et al. in *The Pacific Arctic Region: Ecosystem Status and Trends in a Rapidly Changing Environment* (eds J. M. Grebmeier, J. M. & Maslowski, W.) 337–392 (Springer, 2014); https://doi.org/10.1007/978-94-017-8863-2_2
16. Jay, C. V., Taylor, R. L., Fischbach, A. S., Udevitz, M. S. & Beatty, W. S. Walrus haul-out and in water activity levels relative to sea ice availability in the Chukchi Sea. *J. Mammal.* **98**, 386–396 (2017).
17. Stafford, K. M. Increasing detections of killer whales (Orcinus orca), in the Pacific Arctic. *Mar. Mammal. Sci.* **67**, 696–706 (2018).
18. Gall, A. E., Morgan, T. C., Day, R. H. & Kuletz, K. J. Ecological shift from piscivorous to planktivorous seabirds in the Chukchi Sea, 1975-2012. *Polar Biol.* **40**, 61–78 (2017).
19. Renner, M. et al. Modeled distribution and abundance of a pelagic seabird reveal trends in relation to fisheries. *Mar. Ecol. Prog. Ser.* **484**, 259–277 (2013).
20. Kuletz, K. J., Renner, M., Labunski, E. A. & Hunt, G. L. Changes in the distribution and abundance of albatrosses in the eastern Bering Sea: 1975–2010. *Deep Sea Res. II* **109**, 282–292 (2014).
21. Huntington, H. P., Quakenbush, L. T. & Nelson, M. Evaluating the effects of climate change on indigenous marine mammal hunting in northern and western alaska using traditional knowledge. *Front. Mar. Sci.* **4**, 319 (2017).
22. Noongwook, G., the Native Village of Gambell, the Native Village of Savoonga, H.P., Huntington, H. P. & George, J. C. Traditional knowledge of the bowhead whale (*Balaena mysticetus*) around St. Lawrence Island, Alaska. *Arctic* **60**, 47–54 (2007).
23. Stabeno, P. J. & Bell, S. W. Extreme conditions in the Bering Sea (2017-2018): record-breaking low sea-ice extent. *Geophys. Res. Lett.* **46**, 8952–8959 (2019).
24. Duffy-Anderson, J. T. et al. Response of the northern bering sea and southeastern bering sea pelagic ecosystems following record-breaking low winter sea ice. *Geophys. Res. Lett.* **46**, 9333–9842 (2019).
25. Lefebvre, K. A. et al. Prevalence of algal toxins in Alaskan marine mammals foraging in a changing Arctic and subarctic environment. *Harmful Algae* **55**, 13–24 (2016).
26. Brenner, R. E., Munro, A. R. & Larsen, S. J. (eds.) *Run Forecasts and Harvest Projections for 2019 Alaska Salmon Fisheries and Review of the 2018 Season* Special Publication no. 19-07 (Alaska Department of Fish and Game, 2019).
27. Stevenson, D. E. & Lauth, R. R. Bottom trawl surveys in the northern Bering Sea indicate recent shifts in the distribution of marine species. *Polar Biol.* **42**, 407–421 (2019).
28. Siddon, E. & Zador, S. *Ecosystem Considerations 2017: Status of the Eastern Bering Sea Marine Ecosystem* (Alaska Fisheries Science Center, National Marine Fisheries Service, NOAA, 2017); www.afsc.noaa.gov/REFM/Docs/2017/ecosysEBS.pdf
29. Dragoo, D. E., Renner, H. M. & Kaler, R. S. A. *Breeding Status and Population Trends of Seabirds in Alaska, 2018* Report AMNWR 2019/03 (US Fish and Wildlife Service, 2019).
30. Quakenbush, L. T. & Citta, J. J. *Satellite Tracking of Bowhead Whales: Habitat Use, Passive Acoustic, and Environmental Monitoring* (US Department of the Interior, 2019).
31. *2018–2019 Ice Seal Unusual Mortality Event in Alaska* (National Oceanic and Atmospheric Administration, 2019); https://www.fisheries.noaa.gov/alaska/marine-life-distress/2018-2019-ice-seal-unusual-mortality-event-alaska
32. Heintz, R. A., Siddon, E. C., Farley, E. V. & Napp, J. M. Correlation between recruitment and fall condition of age-0 pollock (*Theragra chalcogramma*) from the eastern bering sea under varying climate conditions. *Deep Sea Res. II* **94**, 150–156 (2013).
33. Wassman, P. & Lenton, T. M. Arctic tipping points in an earth system perspective. *Ambio* **41**, 1–9 (2012).
34. Lynam, C. P. et al. Trophic and environmental control in the North Sea. *Proc. Natl Acad Sci. USA* **114**, 1952–1957 (2017).
35. Grebmeier, J. M. et al. Time-series benthic community composition and biomass and associated environmental characteristics in the Chukchi Sea during the RUSALCA 2004–2012 program. *Oceanography* **28**, 116–133 (2015).
36. Iken, K. et al. Developing an observational design for epibenthos and fish assemblages in the Chukchi Sea. *Deep Sea Res. II* **162**, 180–190 (2019).
37. Scheffer, M. et al. Anticipating critical transitions. *Science* **338**, 344–348 (2012).
38. Overpeck, J. T. et al. Arctic system on trajectory to new state. *Eos* **86**, 309–313 (2005).

39. Gunderson, L. & Holling, C. S. *Panarchy: Understanding Transformations in Human and Natural Systems* (Island, 2001).
40. IPCC. *Climate Change 2014: Synthesis Report. Contribution of Working Groups I, II and III to the Fifth Assessment Report of the Intergovernmental Panel on Climate Change* (IPCC, 2014).
41. Huntington, H. P. et al. in *Ocean Sustainability in the 21st Century* (ed. Arico, S.) 109–126 (Cambridge University Press, 2015).
42. Huntington, H. P. et al. How small communities respond to environmental change: patterns from tropical to polar ecosystems. *Ecol. Soc.* **22**, 9 (2017).
43. Huntington, H. P. et al. Vessels, risks, and rules: planning for safe shipping in Bering Strait. *Mar. Policy* **51**, 119–127 (2015).
44. *Alaskan Inuit Food Security Conceptual Framework: How to Assess the Arctic from an Inuit Perspective* Technical Report (Inuit Circumpolar Council- Alaska, 2015).
45. Huggett, A. J. The concept and utility of ecological thresholds in biodiversity conservation. *Biol. Conserv.* **124**, 301–310 (2005).
46. Hunt, G. L. et al. Climate change and control of the southeastern Bering Sea pelagic ecosystem. *Deep Sea Res. II* **49**, 5821–5853 (2002).
47. Rocha, J., Yletyinen, J., Biggs, R., Blenckner, T. & Peterson Marine regime shifts: drivers and impacts on ecosystems services. *Philos. Trans. R.* Soc. B **370**, 20130273 (2015).
48. Konar, B., Frisch, L. & Moran, S. B. Development of best practices for scientific research vessel operations in a changing arctic: a case study for R/V *Sikuliaq*. *Mar. Policy* **86**, 182–189 (2017).
49. Rocha, J. C., Peterson, G. D. & Biggs, R. Regime shifts in the anthropocene: drivers, risks, and resilience. *PLoS ONE* **10**, e0134639 (2015).
50. De Robertis, A., Taylor, K., Wilson, C. & Farley, E. Abundance and distribution of arctic cod (*Boreogadus saida*) and other pelagic fishes over the U.S. continental shelf of the northern Bering and Chukchi seas. *Deep Sea Res. II* **135**, 51–65 (2017).
51. Maslanik, J. & Stroeve, J. *Near-Real-Time DMSP SSMIS Daily Polar Gridded Sea Ice Concentrations, Version 1* (National Snow and Ice Data Center, accessed 12 December 2018).

General Discussion

Environmental Setting

The Arctic IERP proposals were written in 2016, in the midst of the well-documented North Pacific Marine Heatwave (refs; Walsh et al, 2018). Although "the Blob" of warm water was first identified in the Gulf of Alaska (Freeland et al., 2014; Bond et al., 2015) and many dramatic examples of Gulf of Alaska ecosystem impacts were evident at that time and documented in the years since (Piatt et al., 2018, Suryan et al, 2021), anomalous warmth also extended across the Pacific Arctic at this time (Danielson et al., 2020). Little did we know, however, that the northern Bering and Chukchi seas were about to enter a period of unprecedented winter sea ice loss (Stabeno and Bell, 2018; Thoman et al., 2020) and equally as anomalous distribution shifts and changes in abundance of target commercial, non-commercial and subsistence harvest fishes and invertebrates as well as marine mammals (Huntington et al, 2020, Stevenson and Lauth, 2019).

In the Arctic, the main sources of naturally occurring sounds include waves, winds, sea ice, and marine mammals. There is a direct correlation between increasing wind speeds and increasing ambient sound levels over open water. Sound levels tend to be higher for the same wind speed in shallow waters, such as those found in much of the nearshore Arctic, including the northern Bering and southern Chukchi Seas, than in deep waters. With increasing open water, not only is noise from wind and waves increasing but noise from large ships such as tankers, tugs, and fishing vessels may be increasing as they take advantage of the increasing open water season in the Arctic. Vessel traffic through the Bering Strait increased 150% from 2008-2018 and the distance sailed in the Arctic Polar Code Area increased by 160% from 2013-2019 (PAME 2020). Vessels that passed through the Bering Strait from June to November in 2013-2015 included cargo ships, tankers, fishing vessels, research vessels, tugboats, passenger ships, and supply vessels. The sounds from these vessels are relatively low frequency (< 1000 Hz) and in the same frequency band used by many Arctic species including bowhead whales, walrus, bearded, ringed and ribbon seals.

Analysis of a nearly 100-year-long historical record (Danielson et al. 2020) shows that the Bering and Chukchi continental shelves exhibit different trends and multi-year intervals of warm and cold conditions – suggesting that while the Chukchi receives input from the Bering Sea it operates somewhat independently of the Bering's upstream heat inputs: more local processes dominate. Analyses show that the heat engines of both shelves accelerated over 2014-2018, with increased surface heat flux exchanges and increased lateral oceanic heat advection.

In retrospect, it appears that the Arctic IERP field years (2017-2019) encompassed the peak of the thermally anomalous conditions in this particular multi-year phase of regionally warm conditions; they are the only three years in the record with annual mean monthly temperature anomalies of greater than 1.5 °C (Figure 11). Given the likelihood of continued future warming, these years likely represent a preview of what may eventually be considered typical.

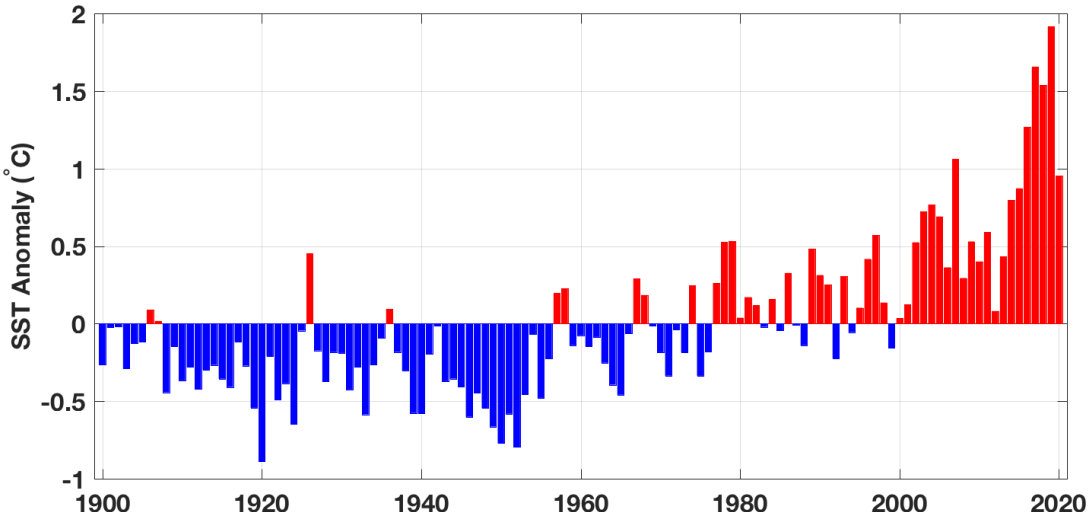

Figure 11. Sea surface temperature (SST) annual mean of all monthly anomalies over 1900-2020 from the Version 5 Extended Reconstructed SST dataset (ERSSTv5). Anomalies are computed relative to the full duration of this 1990-2020 time series. The integration region region for the data shown here extends across the whole of the Northern Bering and Chukchi Seas (60-75 °N, 180-155 °W).

The Over-arching Question

What regulates variations in carbon transfer pathways and how will the changing ice environment alter these pathways and ecosystem structure in the Pacific Arctic and how will a changing environment impact upper trophic level species and human use of the Arctic? Our observations and experiments revealed numerous insights into the character of the bottom-up forcing that helps maintain the Pacific Arctic shelf ecosystem, into how energy (carbon) is routed amongst the various marine system components from microbes to whales, and into how it may change in a warming climate. Temperature clearly stands out as a key factor in the regulation of energy consumption and trophic transfers, but temperature alone is far from the whole answer. The aggregate combination of species abundance and distributions and environmental setting (geomorphology of the Pacific Arctic shelves, large-scale pressure gradients driving mean flows, nutrient supply, strong seasonality in light, ice, winds) combined with the ability of the Pacific Arctic ecosystem to maintain its many services ultimately sets this ecosystem's unique biological character. While this character has never been static in nature, it appears to be crossing thresholds into states that have not previously been observed (Huntington et al., 2020; Ballinger and Overland, 2022). From a marine mammal standpoint, not only is changing sea ice altering habitat for both Arctic and subarctic species (Chapters 1-4), it is also potentially altering the soundscape. An example of this is increasing overlap in acoustically active species such as the subarctic humpback and Arctic bowhead whale (Figure 12).

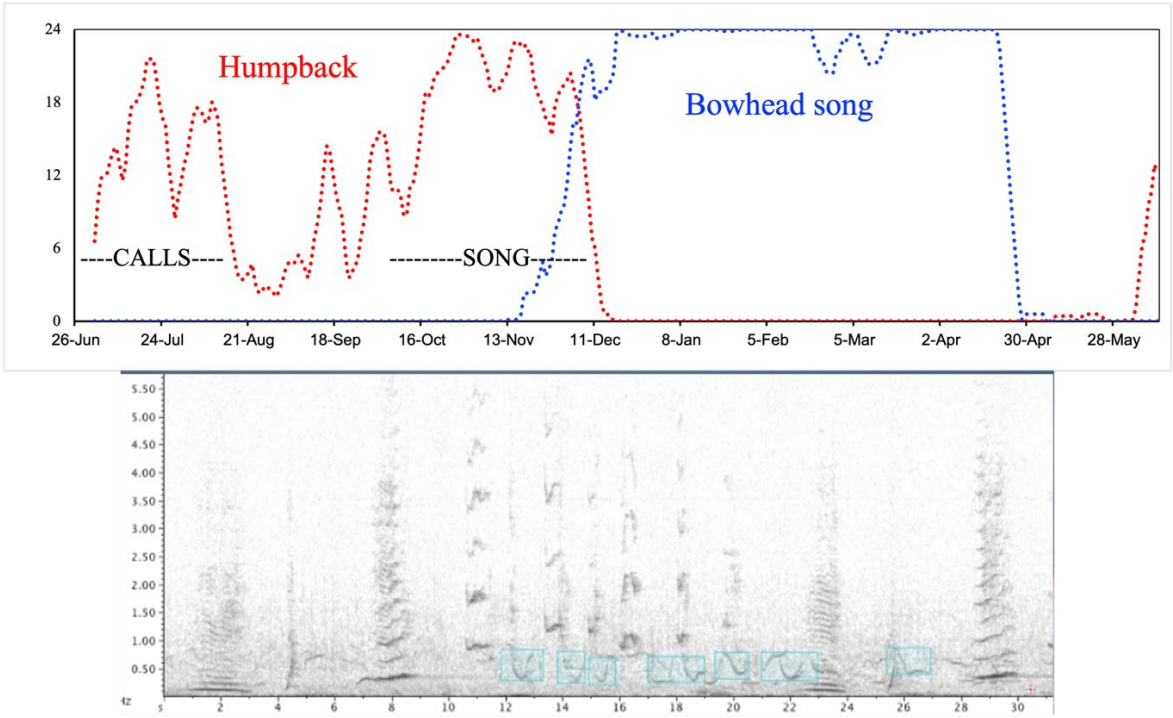

Figure 12. Seasonal occurrence of humpback and bowhead whale songs shows overlap in time and space in Anadyr Strait. In the spectrogram blue boxes highlight bowhead whale song notes in the midst of a humpback whale singing in late November 2017.

Extremely warm conditions from 2017 into 2019 – including loss of ice cover across portions of the region in all three winters – were a marked change even from other recent warm years and may represent a proxy for future decade "normal" conditions. Temperature-controlled respirometry experiments show that benthic oxygen consumption increases significantly (~30%) with warming temperatures and our mooring measurements showed an extended duration of time that the seafloor water temperatures remained 2-6 degrees above the freezing point during these recent warm years. Biological indicators, such as these temperature-dependent benthic respiration rates, suggest that thermal state change exhibits potential to alter ecosystem structure and function (Jones et al., 2021), but our measurements also show that the system exhibits resilient capacity to buffer some of the changes from a bottom-up perspective.

While the environmental alterations represent a bottom-up forcing, recent upper trophic level observations (Stevenson, D.E., Lauth, R.R., 2019; Huntington et. al. 2020, Chapter 7, Stafford et al. Chapter 6) suggest that top-down forcing of the ecosystem will also play a key, and possibly dominant, role in determining future changes to the overall character of the Pacific Arctic ecosystem. For example, the influx of sub-Arctic Pacific Cod and Walleye Pollock exhibit potential to impart a more substantive impact on the benthic community than changes in benthic productivity due to altered pelagic realm export. Sensitivity of the local upper trophic level populations to anthropogenic disturbance (e.g. shipping traffic, noise, see Chapter 5) and intra-species competition represent other potential vulnerabilities.

In aggregate, our results have helped both define and constrain our understanding of the conditions in which the future warmer Pacific Arctic ecosystem will exist. The examples summarized here, and many others in the published manuscripts cited and reprinted in this report, directly contribute to our understanding of how energy in the marine ecosystem is routed now, and how it may change as the

duration of sea ice cover continues to decline. The results of the ASGARD experiments will continue to be analyzed, synthesized, and published in coming years, each further revealing partial answers to the ASGARD and Arctic IERP over-arching question.

Application to Resource Management and Alaska Communities

Coastal Community Concerns

Food security is a paramount concern to residents of coastal communities that depend on a subsistence-based economy. Environmental conditions are changing rapidly, and hunters find themselves dealing with a multitude of factors that can degrade hunt success (Fall et al., 2013). For example, hunters report that their ability to forecast the weather is now at times diminished, fuel costs are high; ice conditions are different and less safe, and game can be less accessible. Hunters are concerned with the impact of vessel traffic on the behavior and location of marine mammals, bycatch from commercial fisheries, and increasing rates of coastal erosion that threaten the placement of entire villages.

Practical applications of our research will directly address issues, questions and concerns posed by coastal community members (e.g., Huntington et al, 2021). These include sea ice conditions and timing; whale, seal and walrus distributions with respect to vessel traffic noises; ramifications of changing climate conditions to the presence and success of marine mammals, clams, crabs, fish, and other animals; and toxic algae blooms that may impact whales and other marine mammals.

Our research allows us to provide scientific lenses through which we can help interpret the causes and consequences of environmental change. As communities continue to adapt – as they have done for millennia – information from scientific studies and scientific observations can help inform community decisions. Such decisions now commonly deal with the practical aspects of addressing climate change impacts to the environment or location availability of subsistence food resources.

Shifting Norms: Management Implications

Perhaps even sooner than many had anticipated, state and federal agencies are confronting resource management issues tied to loss of sea ice and northward-shifting distributions of sub-Arctic marine species. The incursion of Pollock and Pacific Cod into the Bering Strait region – and farther north – demand consideration and a careful assessment of new management actions. Considerations need to include biodiversity, ecosystem structure, and ecosystem function in relation to any potential fishery harvest levels. The recent (since the start of the Arctic IERP) increase of commercial fishing in the Chukchi Sea waters of the Russian Federation suggests that despite insufficient data from the US side of the convention line in the Chukchi Sea, there likely exists significant quantities of Pollock and Pacific Cod on the US side as well. In US waters, any potential fishing activities must consider the cultures and subsistence lifestyles of local indigenous communities, potential impacts of industrial activities (e.g. commercial fishing, oil and gas extraction), potential changes to regional ocean carrying capacity, and resilience of the arctic marine ecosystem (NRC, 2014). An ecosystem-based approach to fisheries management necessitates consideration of food security of the coastal Indigenous communities, their traditional subsistence hunting activities, and conservation of endangered marine mammal and seabird species.

With carbon (or sometimes nitrogen) as the basic currency with which we describe and quantify biological and biophysical interactions - including growth, respiration, energy conversion, energy movement, energy storage and intra-trophic transfers - we need to understand the rate at which carbon is consumed, converted, stored, buried, and relocated. Biophysical numerical models require as inputs sinking rates, growth rates and respiration rates for all important species or functional groups (Stock et al., 2013). As outputs, models predict primary productivity, secondary productivity and biomass. ASGARD data provide spatially explicit measures of the production and respiration rates for the dominant pelagic and benthic species,

along with more basic information about composition, biomass and abundance. Such data will prove critical for advancing spatially and temporally explicit models of ecosystem structure and applying them in appropriate and statistically robust to future scenario projections.

Directions for Future Research

Following a concentrated effort of field work, analysis and publication, further advancements in scientific understanding relies on testable hypotheses and experimental designs that probe the edges of our knowledge base and place our findings into a more complete ecological context. The process of analysis and interpretation of the Arctic IERP results is still ongoing, but a number of future research needs are already apparent. Below, we list a series of specific research directions that are applicable to the entire ASGARD suite of measurements but are targeted to marine mammal and underwater noise data that could further improve our ability to dig deeper into the ASGARD and Arctic IERP guiding questions and could provide management agencies with actionable guidance.

Below, we identify seven study focal areas that would, if addressed, lead to a fuller understanding of the Pacific Arctic ecosystem, its drivers, and future trajectory. All of the below listed studies would fill information gaps and/or needs that resource management agencies could apply to their task mandates.

Ecosystem Status and Change

1. Comparison of ASGARD data to more typical years

Our campaign existed across the two warmest years on record for the study region and are thus not well characteristic of typical conditions found in the first two decades of the 21st century. Repeated measurements in more "normal" years would allow us to better assess our warm phase June month shipboard measurements and year-round mooring measurements.

2. Applying ASGARD measurements to ecosystem models

The ASGARD project was designed in part to provide data useful for the parameterization and/or validation of numerical models. The need for such modeling efforts has not diminished and we now have significant amounts of data that can help bring model studies to a more advanced stage of operation.

3. Non-summer observations

The ASGARD expeditions in June provided valuable data outside of the more typical sampling months of July-September, but seasonal coverage in sampling remains heavily biased to summer and early fall months. Shipboard biological sampling in late fall, winter and early spring could provide data that are important to our understanding during the dark and cold portion of the year. Ecosystem ramification of multiple stressors in the Pacific Arctic Warming, ocean acidification, hypoxia, and increasing vessel traffic and other anthropogenic impacts present the likelihood of unanticipated outcomes due to the nature of nonlinear coupling between multiple stressors. Our ability to assess future ecosystem conditions in the study region depends on improvements in our understanding of how the system as a whole responds to such factors.

4. Management of vessel locations and speeds in the Pacific Arctic region

Increasing vessel traffic poses a risk to protected marine mammal and seabird species. Modeling that assesses potential dynamic and/or adaptive management approaches would improve conservation efforts and reduce the potential for conflict. This need applies year-round due to the different migration timings of the various species of interest, and the fact that vessels are now transiting through the Bering Strait region in all months.

5. Tracking of sub-Arctic species distribution, abundance, and biodiversity

Sub-Arctic species range distributions have been increasing northward in recent decades, and more recent indications show potential for displacement of endemic Arctic species as ranges over

6. Changing phenologies

As the ice, temperature and light conditions change, the timing of species presence, absence, match-mismatch timing with food resources, migration considerations and human interactions all should be assessed with respect to animal behaviors and environmental conditions.

7. Combined US and Russian sector studies

Many data collections end at the international dateline, but the ecosystem is not bound by national boundaries. Studies that bridge both the US and Russian Federation sectors of the Bering and Chukchi seas are needed to gain holistic understanding of the system.

Publications, Presentations, Outreach, and Collaborations

The full ASGARD *Publications* is given in Danielson et al. ASGARD Final Report. Here we include only cruise reports, the passive acoustic and marine mammal ASGARD publications to date, publications in preparation, and other publications that utilize ASGARD data or the participation of the ASGARD marine mammal PI.

Publications

1. Arctic IERP, 2021. Arctic Integrated Ecosystem Research Program Final Summary Brochure, NPRB, Anchorage, AK.
2. Baker, M.R., Farley, E.V., Ladd, C., Danielson, S.L., Stafford, K.M., Huntington, H.P. and Dickson, D.M., 2020. Integrated ecosystem research in the Pacific Arctic–understanding ecosystem processes, timing and change. Deep-Sea Res. II, 177 (2020), p. 104850, https://doi.org/10.1016/j.dsr2.2021.104950
3. Danielson, S., O. Ahkings, L. Edenfeld, L. Eisner, C. Forster, S. Hardy, S. Hartz, B. Holladay, R. Hopcroft, B. Jones, J. Krause, K. Kuletz, R. Lekanoff, M. Lomas, K. Lu, B. Norcross, S. O'Daly, J. Pretty, C. Pham, A. Poje, E. Roth, S. Seabrook, P. Shipton, B. Smith, C. Smoot, K. Stafford, D. Stockwell, A. Yamaguchi, and A. Zinkann, 2017. SKQ2017-09S ASGARD Cruise Report. Fairbanks, AK
4. Escajeda, E, Stafford KM, Laidre KL, Woodgate R. in prep Characterizing spatio-temporal patterns in the acoustic presence of subarctic baleen whales in the Bering Strait in relation to environmental factors
5. Escajeda, E, Stafford KM, Laidre KL, Woodgate R. *In revision.* Relationship between vessel speed and sound levels in the Bering Strait
6. Huntington, H.P., S.L. Danielson, F.K. Wiese, M. Baker, P. Boveng, J.J. Citta, A. De Robertis, D.M. Dickson, E. Farley, J.C. George, K. Iken, D.G. Kimmel, K. Kuletz, C. Ladd, R. Levine, L. Quakenbush, P. Stabeno, K.M Stafford, D. Stockwell and C. Wilson, 2020. Evidence suggests potential transformation of the Pacific Arctic ecosystem is underway. *Nature Climate Change*, 10(4), pp.342-348
7. Moore SE, Clarke JT, Okkonen SR, Gerbmeier JM, Berchok CL, Stafford KM. 2022. Changes in gray whale phenology and distribution related to prey variability and ocean biophysics in the northern Bering and eastern Chukchi seas. PLoSONE https://doi.org/10.1371/journal.pone.0265934
8. Stafford KM, Farley E, Ferguson M, Kuletz K, Levine R. 2022. Northward Range Expansion of Subarctic Upper Trophic Level Animals into the Pacific Arctic Region. Oceanography 35(2).
9. Stafford KM and Danielson S. *In prep*. Seasonal and geographic variation of marine mammals in the northern Bering Sea
10. Stafford, K.M., Danielson, S.L., Escajeda, E., in prep. Long-term marine mammal occurrence at the Chukchi Ecosystem Observatory

Research Cruise Collaborations: Participant Home Institutions

- BIGELOW LABS FOR OCEAN SCIENCE
- BOEM
- DAUPHIN ISLAND SEA LAB

- HOKKAIDO UNIVERSITY
- NATIVE VILLAGE OF DIOMEDE
- NOAA-PMEL
- NPRB
- OSU
- UAF
- USFWS
- UW

Data Sharing and Publication Collaborations: Home Institutions

Alaska Center for Climate Assessment and Policy
- Alaska Department of Fish and Game
- Amundsen Science
- Institute of Ocean Sciences, Fisheries and Oceans Canada (IOS-DFO) Canada
- College of Earth, Ocean and Atmospheric Science, Oregon State University
- Florida State University Coastal and Marine Laboratory
- Huntington Consulting
- International Arctic Research Center and College of Natural Science and Mathematics
- Japan Agency for Marine-Earth Science and Technology (JAMSTEC), Japan
- Native Village of Diomede
- NOAA, Alaska Fisheries Science Center, Auke Bay Lab
- NOAA, Alaska Fisheries Science Center, National Marine Fisheries Service
- NOAA, Pacific Marine Environmental Laboratory
- North Carolina State University
- North Slope Borough Department of Wildlife Management
- Russian Federal Research Institute of Fisheries and Oceanography, Pacific Branch of VINRO, TINRO, Vladivostok, Russia
- Stantec
- University of Toronto Mississauga, Mississauga, ON, Canada
- University of Manitoba, Winnipeg, Manitoba, Canada
- University of Maryland Center for Environmental Sciences, Chesapeake Biological Laboratory
- University of Washington, Applied Physics Laboratory
- University of Washington, Joint Institute for the Study of the Atmosphere and Ocean
- US Fish and Wildlife Service
- Woods Hole Oceanographic Institute

Sample Collections, Lab Analyses and Other Collaborations

(Including intra-Arctic IERP collaborations such as the NOAA-led Arctic EIS projects)
- Alaska Ocean Observing System (AOOS) (CEO program support)
- Alaska Sea Grant (UAF Nome Campus cruise support and community liaison support)
- Arctic Marine Biodiversity Observation Network (AMBON) (US Arctic biodiversity)
- Bering Strait Mooring Program (APL-UW) (monitoring of Bering Strait)
- Chukchi Ecosystem Observatory (CEO) (NE Chukchi Mooring Site)
- Distributed Biological Observatory (DBO) (Bering-Chukchi-Beaufort change detect array)

- UAF Museum of the North (underwater acoustic samples as part of the new bowhead whale skeleton exhibit)
- University of Washington, Applied Physics Laboratory (mooring platform)
- Woods Hole Oceanographic Institution and UAF (glider support)

National and International Symposia Collaborations

- 2016 – present (1-2 times per year). ASGARD representation at Distributed Biological Observatory (DBO) and the Pacific Arctic Group (PAG) collaboration meetings.
- February 2018. AGU/ALSO Ocean Sciences Meeting. Scientific session organization (with DBO and AMBON) and participation: "Linkages Between Environmental Drivers and Structure of Arctic Ecosystems". Session Abstract: Arctic ecosystems are adjusting to rapidly warming temperatures, sea ice loss and a myriad of other factors that are changing with time. Temperature-growth relations, altered seasonality, expanded and contracted range extents, and new trophic pathways may each affect biodiversity, population status of key species, and relations between humans and marine resources. As environmental change continues, can we anticipate how future Arctic ecosystems will compare to those of yesterday and today? Will the effects of a changing climate be the same across various Arctic regions? We welcome presentations from all regions of the Arctic examining rates, processes and mechanistic controls that impart structure on any aspect of the high-latitude marine ecosystem.
- February 2020. AGU/ALSO Ocean Sciences Meeting. Scientific session organization (with DBO and AMBON) and participation: "Ecosystem Structure in a Changing Arctic". Session Abstract: The rate of atmospheric warming in the Arctic is outpacing that of other regions, and is associated with sea ice loss, warming ocean temperatures, changes in the hydrological cycle, and impacted ecosystems. Temperature-growth relations, nutrient cycling dynamics, altered seasonality, changing freshwater balances, expanded and contracted species range extensions, and new trophic pathways may each affect biodiversity, the population status of key species, and relations between humans and marine resources. As environmental change continues, can we anticipate how future Arctic ecosystems will compare to those of the past and present? Will the effects of a changing climate be the same across various Arctic regions? Organizers welcome presentations from all regions of the Arctic examining the drivers, rates, processes, and mechanistic controls that impart structure on any aspect of the high-latitude marine ecosystem.
- February 2020. AGU/ALSO Ocean Sciences Meeting Town Hall organization (with AOOS, USARC and DBO) and participation: "Scientific Responses to an Ever Faster Changing Arctic: Making the Most of our Collective Research Efforts". With the U.S. Arctic experiencing such unprecedented, rapid change, the objective of this town hall was to provide an opportunity for the scientific community to informally discuss causality and linkages across results from recent field work and studies, including if a "new normal" for the Arctic can be determined and what this might look like. We would also like to see proposed actions developed for moving forward with coordinated research efforts, ideas for emerging research. And observing needs, and suggestion or how we can best oorganize ourselves to deliver the data and information products that northern communities, resource managers, industry, first responders, and other decision makers will need.
- December 2021. Acoustical Society of America biannual meeting: "Relationship between vessel speed and sounds levels in the Bering Strait." Abstract: Vessel speed limits have been proposed as a means of reducing underwater ship noise, however it is unclear how effective such a measure would be in the Bering Strait, a natural bottleneck for ships transiting into the Arctic from the Pacific Ocean. In this study, we examine how ship noise varies with vessel type and speed using Automatic Identification System (AIS) data collected from vessels traveling through the strait along with acoustic recordings from three moored hydrophones. We matched recordings with ship noise to individual vessels that passed within 100 km of each hydrophone in June through November 2013–2015. A total of 67 sound files were analyzed, with tug (n = 21) and cargo ships (n = 16) as the most common vessel type observed in our dataset. Sound levels for each vessel were calculated and compared as a function of vessel type and

speed. The results of our study could inform policymakers and managers on the effectiveness of vessel speed limits on reducing ship noise in a sensitive Arctic habitat.

- January 2021. Presentation in “Looking across borders: past, present and future US Russia collaboration in the Bering Sea” during a remote session associated with the Alaska Marine Science Symposium in January 2021.

Synopsis ASGARD project marine mammal studies

Why we did it

Sea ice is one of the defining characteristics of the Arctic Ocean, and while its timing and extent has already undergone significant human-induced changes, it is projected to further decline in the coming years. The ASGARD project was designed to better refine our knowledge of carbon and nutrient dynamics on the northern Bering and Chukchi sea continental shelves in the face of changing sea ice. The fundamental science question we addressed is: What regulates variations in carbon transfer pathways and how will the changing ice environment alter these pathways and ecosystem structure, including that of upper trophic animals, in the Pacific Arctic and beyond?

What we did

The ASGARD study consisted of ship-based and mooring-based studies that collected observations of: heat, salt, nutrients and plankton carried by ocean currents; phytoplankton primary productivity; zooplankton growth/reproduction, respiration and fecal pellet production rates; particle deposition rates from the water column to the seafloor; quality of organic matter deposited to the seafloor; benthic respiration and organic matter decomposition rates; abundance and biomass of benthic microbial and metazoan fauna; distribution of fishes at different life history stages; and underwater sound and seasonal distributions of marine mammals. We sailed to the northern Bering and southern Chukchi shelf in 2017 and 2018 on R/V Sikuliaq, occupying "process" stations at which experimental work was carried out, and "survey" stations at which we collected a reduced set of observations. Moorings were deployed in the water from June 2017 to August 2019.

What we learned and why it matters

Ample supplies of nutrients delivered to the Southern Chukchi Sea through Bering Strait fuel a high level of Chukchi shelf primary productivity during months in which water column light levels are sufficient to maintain phytoplankton blooms. Portions of the region likely exist in a near-perpetual state of patchy phytoplankton blooms from the spring ice retreat all the into the fall. Export fluxes to the benthos are large because large-celled diatoms sink rapidly to the shallow seafloor and because mesozooplankton often are unable to constrain the phytoplankton bloom by grazing. The benthic community carbon consumption and oxygen turnover rates are sensitive to the bottom water temperature and are species- specific. Arctic marine mammals occur more frequently to the west of Saint Lawrence Island than to the east and the overall biodiversity of vocal marine mammals is higher to the west. Further subarctic species were heard well into winter months at all locations. Together, these findings suggest that the future Pacific Arctic ecosystem will adjust in species composition and species abundance in a bottom-up response to environmental change. At the same time, range expansions of sub-Arctic predators into the Chukchi Sea will exert new top-down pressure on both the benthic and pelagic communities. Previously unobserved competition between Arctic and sub-Arctic species will also likely play a role in determining the eventual character of the Chukchi Sea ecosystem. Arctic marine mammals are critical to the food security and cultural and spiritual health of coastal Arctic communities and understanding changes in the timing and diversity of upper trophic bellwether species can be used to understand ecosystem-wide environmental changes.

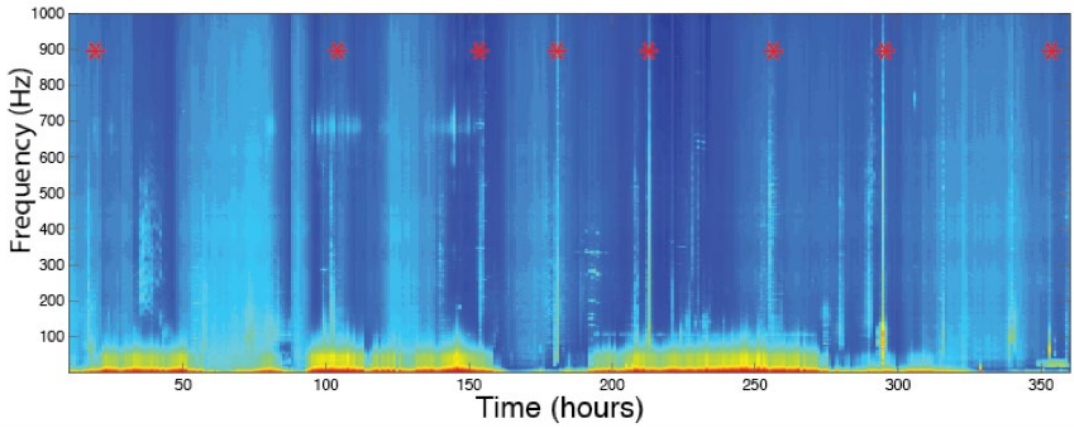

Long-term spectral average from mooring N4 in Anadyr Strait showing ship passages (*)

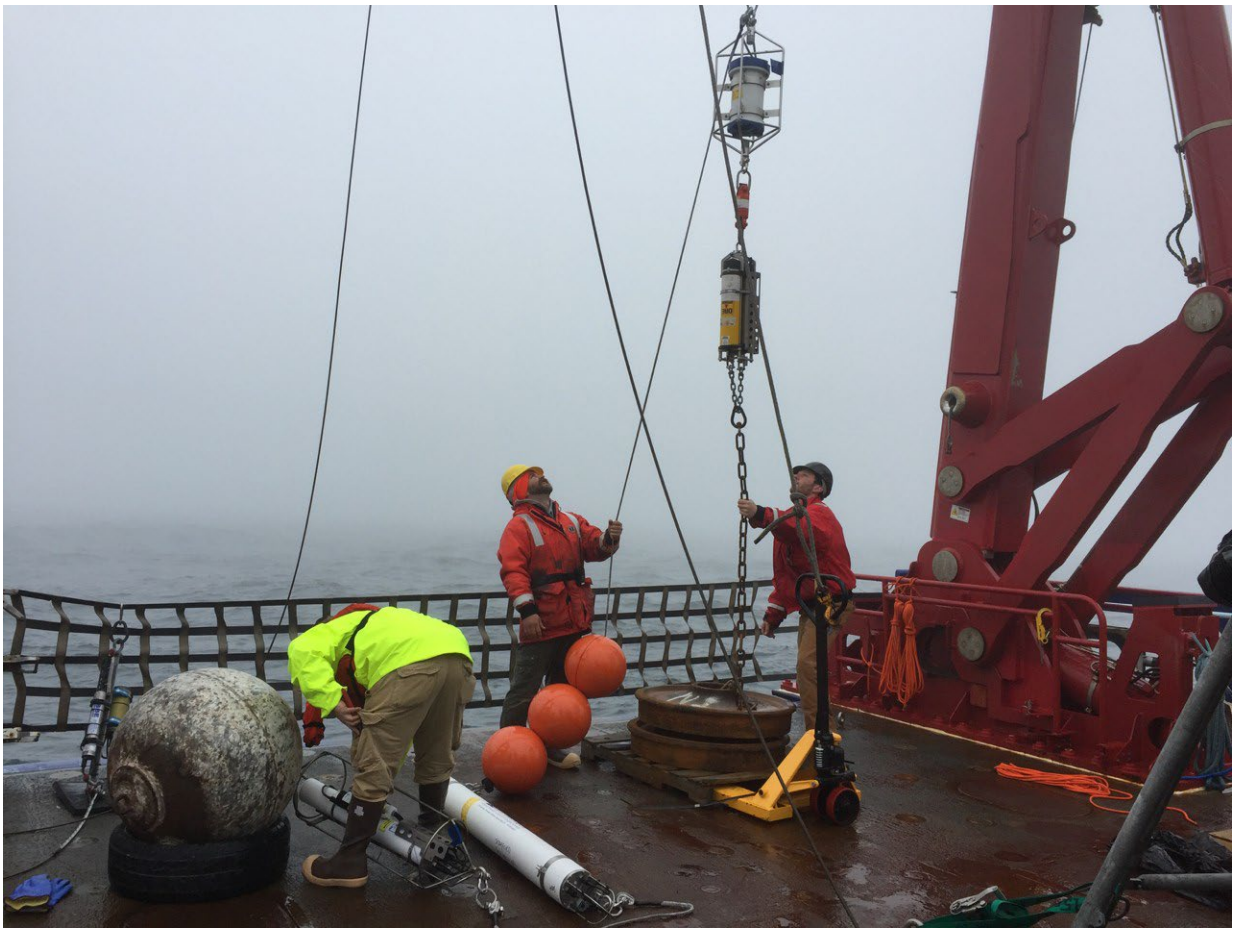

Mooring being deployed from the back deck of the Sikuliaq in June 2017

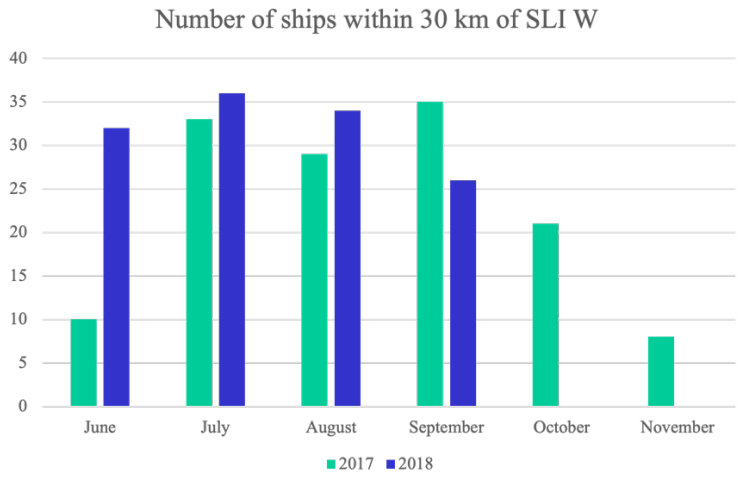

2017 June-November shipping

AIS ship tracks to the west of Saint Lawrence Island in 2017

References

Aagaard, K., T. J. Weingartner, S. L. Danielson, R. A. Woodgate, G. C. Johnson, and T. E. Whitledge. 2006. Some controls on flow and salinity in Bering Strait, Geophys. Res. Lett., 33, L19602, doi:10.1029/2006GL026612.

Ahonen, H., K.M. Stafford, C. Lydersen, C.L. Berchok, S.E. Moore, and K.M. Kovacs. 2021. Interannual variability in acoustic detection of blue and fin whale calls in the Northeast Atlantic High Arctic between 2008 and 2018. *Endangered Species Research* 45:209–24.

Alabia, I.D., J.G. Molinos, S.-I. Saitoh, T. Hirawake, T. Hirata, and F.J. Mueter. 2018. Distribution shifts of marine taxa in the Pacific Arctic under contemporary climate changes. *Diversity and Distributions* 24(11):1583–97.

Amélineau, F., J. Fort, P.D. Mathewson, D.C. Speirs, N. Courbin, S. Perret, W.P. Porter, et al. 2018. Energyscapes and prey fields shape a North Atlantic seabird wintering hotspot under climate change. *Royal Society Open Science* 5(1):1–4. doi:10.1098/rsos.171883.

Bailey, K.M., T.J. Quinn, P. Bentzen, and W.S. Grant. 1999. Population structure and dynamics of walleye pollock, *Theragra chalcogramma*. *Advances in Marine Biology* 37:179–255.

Ballinger, T. J., & Overland, J. E. 2022. The Alaskan Arctic regime shift since 2017: A harbinger of years to come? Polar Science, 100841. https://doi.org/10.1016/j.polar.2022.100841

Baumgartner MF, Stafford KM, Winsor P, Stascewich H, Fratantoni D. 2014. Glider based passive acoustic monitoring in the Arctic. Marine Technology Society Journal 48(5):40-51.

Baumgartner, M. F., and D. M. Fratantoni. 2008. Diel periodicity in both sei whale vocalization rates and the vertical migration of their copepod prey observed from ocean gliders. Limnology and Oceanography **53**:2197–2209.

Berge, J., K. Heggland, O.J. Lønne, F. Cottier, H. Hop, G.W. Gabrielsen, L. Nottestad, et al. 2015. First records of Atlantic mackerel (*Scomber scombrus*) from the Svalbard Archipelago, Norway, with possible explanations for the extension of its distribution. *Arctic* 68(1):54–61.

Berline L, Spitz YH, Ashjian CJ, Campbell RG, Maslowski W, Moore SE (2008) Euphausiid transport in the Western Arctic Ocean. Marine Ecology Progress Series 360:163-178

Brower, A.A, J.T. Clarke, and M.C. Ferguson. 2018. Increased sightings of subarctic cetaceans in the eastern Chukchi Sea, 2008–2016: population recovery, response to climate change, or increased survey effort? *Polar Biology* 41:1033–39.

Buchholz, F., T. Werner, and C. Buchholz. 2012. First observation of krill spawning in the high Arctic Kongsfjorden, West Spitsbergen. *Polar Biology* 35:1273–79.

Clark, C.W., W.T. Ellison, B.L. Southall, L. Hatch, S.M. Van Parijs, A. Frankel, and D. Ponirakis. 2009. Acoustic masking in marine ecosystems: intuitions, analysis and implication. Marine Ecology Progress Series 395, 201-222.

Clarke J, Stafford K, Moore SE, Rone B, Aerts L, Crance J. 2013. Subarctic Cetaceans in the Southern Chukchi Sea: Evidence of Recovery or Response to a Changing Ecosystem *Oceanography* 26(4):136–149.

Clarke J.T., K.M. Stafford, S.E. Moore, B. Rone, L. Aerts, and J. Crance. 2013. Subarctic cetaceans in the southern Chukchi Sea: evidence of recovery or response to a changing ecosystem. *Oceanography* 26:136–149.

Clarke, J.T., A.A. Brower, M.C. Ferguson, A.L. Willoughby, and A.D. Rotrock. 2020. Distribution and relative abundance of marine mammals in the Eastern Chukchi Sea, Eastern and Western Beaufort Sea, and Amundsen Gulf, 2019. Annual Report, OCS Study BOEM 2020-027.

Cooper, L.W. 2010. Bering Strait Environmental Observations: A scientific needs assessment. A Report to Scientific and Community Stakeholders. Available from **http://arctic.cbl.umces.edu**.

Craig, P., and L. Haldorson. 1986. Pacific salmon in the North American Arctic. *Arctic* 39:2–7.

Daase, M., J. Berge, J.E. Søreide, and S. Falk-Petersen. 2021. Ecology of Arctic Pelagic Communities. Chapter 9 in D.N. Thomas (ed.) Arctic Ecology. Wiley.

Day, R.H., A.E. Gall, T.C. Morgan, J.R. Rose, J.H. Plissner, P.M. Sanzenbacher, J.D. Fenneman, et al. 2013. Seabirds new to the eastern Chukchi and Beaufort Seas, Alaska: Response to a changing climate? *Western Birds* 44(3):174–82.

de Bruyn, P.J.N., C.A. Tosh, and A. Terauds. 2013. Killer whale ecotypes: Is there a global model? *Biological Reviews* 88:62–80.

De Robertis, A., K. Taylor, C.D. Wilson, and E.V.Farley. 2017. Abundance and distribution of Arctic cod (Boreogadus saida) and other pelagic fishes over the U.S. Continental Shelf of the Northern Bering and Chukchi Seas. *Deep Sea Research II* 135:51–65.

Delarue, J., B. Martin, D. Hannay, and C. L. Berchok. 2013. Acoustic Occurrence and Affiliation of Fin Whales Detected in the Northeastern Chukchi Sea, July to October 2007–10. Arctic **66**:159–172.

Descamps, S., and H. Strøm. 2021. As the Arctic Becomes boreal: ongoing shifts in a high-Arctic seabird community. *Ecology* 102(11): e03485.

Divoky, G.J., E. Brown, and K.H. Elliott. 2021. Reduced seasonal sea ice and increased sea surface temperature change prey and foraging behaviour in an ice-obligate Arctic seabird, Mandt's Black Guillemot (*Cepphus grylle mandtii*). *Polar Biology* 44(4):701–15.

Drew, G.S., and J.F. Piatt. 2015. North Pacific Pelagic Seabird Database (NPPSD): U.S. Geological Survey data release (ver. 3.0, February 2020), **https://doi.org/10.5066/F7WQ01T3**

Duffy-Anderson, J.T., P. Stabeno, A.G. Andrews, K. Cieciel, A. Deary, E. Farley, C. Fugate, et al., 2019. Responses of the northern Bering Sea and southeastern Bering Sea pelagic ecosystems following record-breaking low winter sea ice. *Geophysical Research Letters* 46(1):9833–42.

Dunmall, K.M., D.G. McNicholl, and J.D. Reist. 2018. Community-based monitoring demonstrates increasing occurrences and abundances of Pacific salmon in the Canadian Arctic from 2000 to 2017. *North Pacific Anadromous Fish Commission Technical Report* 11.

Dunmall, K.M., J.D. Reist, E.C. Carmack, J.A. Babluk, M.P. Heide-Jørgensen, M.P., and M.F. Docker. 2013. Pacific salmon in the Arctic: harbingers of change. In: Mueter, F. J., D.M.S. Dickson, H.P. Huntington, J.R. Irvine, E.A. Logerwell, S.A. MacLean, L.T. Quakenbush, C. Rosa, C. (Eds.), Responses of Arctic marine ecosystems to climate change. Alaska Sea Grant. University of Alaska Fairbanks, pp. 141–163.

Dunmall, K.M., N.J. Mochnacz, C.E. Zimmerman, C. Lean, and J.D. Reist. 2016. Using thermal limits to assess establishment of fish dispersing to high-latitude and high-elevation watersheds. *Canadian Journal of Fisheries and Aquatic Sciences* 73:1750–1758.

Eisner, L., N. Hillgruber, E. Martinson, and J. Maselko. 2013. Pelagic fish and zooplankton species assemblages in relation to water mass characteristics in the northern Bering and southeast Chukchi Seas. *Polar Biology* 36(1): 87–113.

Eisner, L., N. Hillgruber, E. Martinson, and J. Maselko. 2013. Pelagic fish and zooplankton species assemblages in relation to water mass characteristics in the northern Bering and southeast Chukchi seas. Polar Biology **36**:87–113.

Eisner, L.B., Y.I. Zuenko, E.O. Basyuk, L.L. Britt, J.T. Duffy-Anderson, S. Kotwicki, C. Ladd, and W. Cheng. 2020. Environmental impacts on walleye pollock (*Gadus chalcogrammus*) distribution across the Bering Sea shelf. *Deep-Sea Research II* 181–182:104881, doi:10.1016/j.dsr2.2020.104881.

Eriksen, E., E. Bagøien, E. Strand, R. Primicerio, T. Prokhorova, A. Trofimov, and I. Prokopchuk. 2020. The record-warm Barents Sea and 0-Group fish response to abnormal conditions. *Frontiers in Marine Science* 7:1–19, doi:10.3389/fmars.2020.00338.

Farley, E.V., Jr., J.M. Murphy, K. Cieciel, E.M. Yasumiishi, K. Dunmall, T. Sformo, and P. Rand. 2020. Response of Pink salmon to climate warming in the northern Bering Sea. *Deep Sea Research II* 177, 104839. doi:10.1016/j.dsr2.2020.104830

Ferguson, M.C., J. Waite, C. Curtice, J.T. Clarke, and J. Harrison. 2015. Biologically Important Areas for cetaceans within U.S. waters: Aleutian Islands and Bering Sea region. *Aquatic Mammals* 41(1):79-93.

Ferguson, S.H., J.W. Higdon, and E.G. Chmelnitsky. 2010. The Rise of Killer Whales as a Major Arctic Predator. In *A Little Less Arctic: Top Predators in the World's Largest Northern Inland Sea, Hudson Bay*, S.H. Ferguson, L.L. Loseto, and M.L. Mallory (Eds.), 117–36. Springer.

Fischbach, A. S., R. L. Taylor, and C. V. Jay. 2022. Regional walrus abundanceestimate in the United States Chukchi Sea in autumn. Journal of Wildlife Management e22256.https://doi.org/10.1002/jwmg.2225

Fossheim, M., R. Primicerio, E. Johannesen, R.B. Ingvaldsen, M.M. Aschan, and A.V. Dolgov. 2015. Recent warming leads to a rapid borealization of fish communities in the Arctic. *Nature Climate Change* 5:673–78.

Frainer, A., R. Primicerio, S. Kortsch, M. Aune, A.V. Dolgov, M. Fossheim, and M.M. Aschan. 2017. Climate-driven changes in functional biogeography of Arctic marine fish communities. *Proceedings of the National Academy of Sciences* 114(46):12202–12207.

Frederiksen, M., T.Anker-Nilssen, G. Beaugrand, and S. Wanless. 2013. Climate, copepods and seabirds in the boreal northeast Atlantic - current state and future outlook. *Global Change Biology* 19:364–72.

Gall, A.E., R.H. Day, and T.J. Weingartner. 2013. Structure and variability of the marine-bird community in the northeastern Chukchi Sea. *Continental Shelf Research* 67:96–115.

Gall, A.E., T.C. Morgan, R.H. Day, and K.J. Kuletz. 2017. Ecological shift from piscivorous to planktivorous seabirds in the Chukchi Sea, 1975–2012. *Polar Biology* 40(1):61–78.

George, J.C., G. Sheffield, D.J. Reed, B. Tudor, R. Stimmelmayr, B.T. Person, T. Sformo, and R. Suydam. 2017. Frequency of injuries from line entanglements, killer whales, and ship strikes on Bering-Chukchi-Beaufort Seas bowhead whales. *Arctic* 70(1):37–46.

Goddard, P., R. Lauth, and C. Armistead. 2014. Results of the 2012 Chukchi Sea bottom trawl survey of bottomfishes, crabs, and other demersal macrofauna. NOAA Technical Memorandum, NMFS-AFSC-278, 110 p.

Grebmeier, J. M. 2012. Shifting Patterns of Life in the Pacific Arctic and Sub-Arctic Seas. Annual Review of Marine Science **4**:63–78.

Grebmeier, J.M., and W. Maslowski (Eds.). 2014. The Pacific Arctic Region. Springer, Netherlands. doi:10.1007/978-94-017-8863-2

Grebmeier, J.M., J.E. Overland, S.E. Moore, E.V. Farley, E.C. Carmack, L.W. Cooper, K.E. Frey, J.H. Helle, F.A. McLaughlin, and S.L. McNutt. 2006b. A major ecosystem shift in the northern Bering Sea. Science 311:1461-1463.

Grebmeier, J.M., L.W. Cooper, H.M.Feder and B.I. Sirenko. 2006a. Ecosystem dynamics of the Pacific influenced northern Bering and Chukchi Seas in the Amerasian Arctic. Progress in Oceanography 71: 331-361.

Grüss, A., J.T. Thorson, C.C. Stawitz, J.C.P. Reum, S. K. Rohan, and C. L. Barnes. 2021. Synthesis of interannual variability in spatial demographic processes supports the strong influence of cold-pool extent on eastern Bering Sea walleye pollock (*Gadus chalcogrammus*). *Progress in Oceanography* 194:102569.

Hamilton, C.D., C. Lydersen, J. Aars, M. Biuw, A.N. Boltunov, E.W. Born, R. Dietz, et al., 2021. Marine mammal hotspots in the Greenland and Barents Seas. *Marine Ecology Progress Series* 659:3–28. doi:10.3354/meps13584.

Hannay, D. E., J. Delarue, X. Mouy, B. S. Martin, Del Leary, J. N. Oswald, and J. Vallarta. 2013. Marine mammal acoustic detections in the northeastern Chukchi Sea, September 2007–July 2011. Continental Shelf Research **67**:127–146.

Hatch, L. T., C. W. Clark, S. M. Van Parijs, A. S. Frankel, and D. W. Ponirakis. 2012. Quantifying Loss of Acoustic Communication Space for Right Whales in and around a U.S. National Marine Sanctuary. Conservation Biology **26**:983–994.

Higdon, J. W., and S.H. Ferguson. 2009. Loss of Arctic sea ice causing punctuated change in sightings of killer whales (*Orcinus orca*) over the past century. *Ecological Applications* 19:1365–75.

http://psc.apl.washington.edu/HLD/Bstrait/BeringSt**...**

Hunt, G., M. Renner, K. Kuletz, S. Salo, L. Eisner, P. Ressler, C. Ladd, et al. 2018. Timing of sea-ice-retreat affects the distribution of seabirds and their prey in the southeastern Bering Sea. *Marine Ecology Progress Series* 593:209-230**.**

Hunt, G.L. Jr., V. Bakken, and F. Mehlum. 1996. Marine birds in the marginal ice zone of the Barents Sea in late winter and wpring. *Arctic* 49(1):53-61.

Hunt, G.L., Jr., A.L. Blanchard, P. Boveng, P. Dalpadado, K.F. Drinkwater, L. Eisner, R.R. Hopcroft, et al., 2013. The Barents and Chukchi Seas: Comparison of two Arctic shelf ecosystems. *Journal of Marine Systems* 109-110:43–68.

Huntington, H. P., J. Raymond-Yakoubian, G. Noongwook, N. Naylor, C. Harris, Q. Harcharek, and B. Adams. 2021. "We Never Get Stuck" :A collaborative analysis of change and coastal community subsistence practices in the northern Bering and Chukchi Seas, Alaska. *Arctic* 74:113–126. doi:10.14430/arctic72446

Huntington, H.P., L.T. Quakenbush, and M. Nelson. 2016. Effects of changing sea ice on marine mammals and subsistence hunters in northern Alaska from traditional knowledge interviews. *Biology Letters* 12(8):20160198.

Huntington, H.P., S.L. Danielson, F.K. Wiese, M. Baker, P. Boveng, J.J. Citta, A. De Robertis, et al., 2020. Evidence suggests potential transformation of the Pacific Arctic ecosystem is underway. *Nature Climate Change* 1–11. doi:10.1038/s41558-020-0695-2.

Jay, C. V., A. S. Fischbach, and A. A. Kochnev. 2012. Walrus areas of use in the Chukchi Sea during sparse sea ice cover.Marine Ecology Progress Series 468:1–13.

Johannesen, E., Å.S. Høines, A.V Dolgov, and M. Fossheim. 2012. Demersal fish assemblages and spatial diversity patterns in the Arctic-Atlantic transition zone in the Barents Sea. *PLoS ONE*, 7(4) doi:10.1371/journal.pone.0034924.

Kortsch, S., R. Primicerio, M. Fossheim, V. Dolgov, and M. Aschan. 2015. Climate change alters the structure of arctic marine food webs due to poleward shifts of boreal generalists. *Proceedings of the Royal Society B*:282(1814):20151546.

Kotwicki, S., T.W. Buckley, T. Honkalehto, and G. Walters. 2005. Variation in the distribution of walleye pollock (*Theragra chalcogramma*) with temperature and implications for seasonal migration. *Fishery Bulletin* 103(4):574–587.

Kuletz, K., D. Cushing, and E. Labunski. 2020. Distributional shifts among seabird communities of the northern Bering and Chukchi seas in response to ocean warming during 2017–2019. *Deep Sea Research Part II* 181–182:104913.

Kuletz, K.J., M. Renner, E.A. Labunski, and G. L. Hunt Jr. 2014. Changes in the distribution and abundance of albatrosses in the eastern Bering Sea: 1975–2010. *Deep-Sea Research Part II* 109:282–92.

Kuletz, K.J., M.C. Ferguson, B. Hurley, A.E. Gall, E.A. Labunski, and T.C. Morgan. 2015. Seasonal spatial patterns in seabird and marine mammal distribution in the eastern Chukchi and western Beaufort seas: Identifying biologically important pelagic areas. *Progress in Oceanography* 136:175–200.

Laidre, K.L., I. Stirling, L.F. Lowry, Ø. Wiig, M.P. Heide-Jørgensen, and S.H. Ferguson. 2008. Quantifying the sensitivity of arctic marine mammals to climate-induced habitat change. *Ecological Applications* 18:S97–S125.

Laurel, B.J., L.A. Copeman, M. Spencer, and P. Iseri. 2017. Temperature-dependent growth as a function of size and age in juvenile Arctic cod (*Boreogadus saida*). *ICES Journal of Marine Science* 74:1614–1621.

Laurel, B.J., L.A. Copeman, M. Spencer, and P. Iseri. 2018. Comparative effects of temperature on rates of development and survival of eggs and yolk-sac larvae of Arctic cod (*Boreogadus saida*) and walleye pollock (*Gadus chalcogrammus*). *ICES Journal of Marine Science* 75:2403–2412.

Laurel, B.J., M. Spencer, P. Iseri, and L.A. Copeman. 2016. Temperature-dependent growth and behavior of juvenile Arctic cod (Boreogadus saida) and co-occurring North Pacific gadids. *Polar Biology* 39: 1127–1135.

Lefort, K.J., C.J. Garroway, and S.H. Ferguson. 2020. Killer whale abundance and predicted narwhal consumption in the Canadian Arctic. *Global Change Biology* 26:4276–83.

Levine, R.M., A. De Robertis, D. Grünbaum, R. Woodgate, C.W. Mordy, F. Mueter, E. Cokelet, et al. 2021. Autonomous vehicle surveys indicate that flow reversals retain juvenile fishes in a highly advective high-latitude ecosystem. *Limnology and Oceanography* 66:1139–1154.

Levine, R.M., A. De Robertis, D. Grünbaum, S. Wildes, E.V. Farley, P.K. Stabeno, and C.D. Wilson. *In review*. Climate-driven shifts in pelagic fish distributions in a rapidly changing Pacific Arctic. *Deep-Sea Research II*

Lowry, L.F., K.J. Frost, and J.J. Burns. 1980. Feeding of bearded seals in the Bering and Chukchi Seas and trophic interaction with pacific walruses. Arctic 33:330-342.

MacIntyre KQ, Stafford KM, Berchok CL, Boveng PL. (2013). Year-round acoustic detection of bearded seals (*Erignathus barbatus*) in the Beaufort Sea 2008-2010. Polar Biology 36(8):1161-1173.

MacIntyre KQ, Stafford KM, Conn PB, Laidre KL, Boveng PL (2015) The relationship between sea ice concentration and the spatiotemporal distribution of vocalizing bearded seals (*Erignathus barbatus*) in the Bering, Chukchi, and Beaufort Seas from 2008 to 2011. Prog Oceanogr 136:241–249

Mallory, M.L., A.J. Gaston, H.G. Gilchrist, G.J. Robertson, and B.M. Braune. 2010. Effects of climate change, altered sea-ice distribution and seasonal phenology on marine birds. In *A Little Less Arctic: Top*

Predators in the World's Largest Northern Inland Sea, Hudson Bay, S.H. Ferguson (Ed.), 179–95. Springer.

Matthews, C.J.D., G.A. Breed, B. LeBlanc, and S.H. Ferguson. 2020. Killer whale presence drives bowhead whale selection for sea ice in Arctic seascapes of fear. *Proceedings of the National Academy of Sciences* 117:1–9.

Matthews, C.J.D., S.A. Raverty, D.P. Noren, L. Arragutainaq, and S.H. Ferguson. 2019. Ice entrapment mortality may slow expanding presence of Arctic killer whales. *Polar Biology* 42:639–44.

Matthews, C.J.D., S.P. Luque, S.D. Petersen, R.D. Andrews, and S.H. Ferguson. 2011. Satellite tracking of a killer whale (*Orcinus orca*) in the Eastern Canadian Arctic documents ice avoidance and rapid, long-distance movement into the North Atlantic. *Polar Biology* 34:1091–96.

Mecklenburg, C.W., D.L. Stein, B.A. Sheiko, N.V. Chernova, T.A. Mecklenburg, and B.A. Holladay. 2007. Russian–American Long-Term Census of the Arctic: benthic fishes trawled in the Chukchi Sea and Bering Strait, August 2004. *Northwestern Naturalist* 88:168–187.

Milne, A. R., and J. H. Ganton. 1964. Ambient Noise under Arctic-Sea Ice. The Journal of the Acoustical Society of America **36**:855–863. Acoustical Society of America.

Moore SE, Clarke JT, Okkonen SR, Grebmeier JM, Berchok CL, Stafford KM (2022) Changes in gray whale phenology and distribution related to prey variability and ocean biophysics in the northern Bering and eastern Chukchi seas. PLoS ONE 17(4): e0265934.

Moore S.E., and R.R. Reeves. 2018. Tracking arctic marine mammal resilience in an era of rapid ecosystem alteration. PLOS Biology 16: e2006708.

Moore SE, Stafford KM, Melling H, Berchok C, Wiig O, Kovacs KM, Lydersen C, Richter-Menge J (2012) Comparing marine mammal acoustic habitats in Atlantic and Pacific sectors of the High Arctic: year-long records from Fram Strait and the Chukchi Plateau. Polar Biol 35:475–480.

Moore, S. E., E. Logerwell, L. Eisner, E. V. Farley, L. A. Harwood, K. Kuletz, J. Lovvorn, J. R. Murphy, and L.T. Quakenbush. 2014. Marine Fishes, Birds and Mammals as Sentinels of Ecosystem Variability and Reorganization in the Pacific Arctic Region. Pages 337–392 in *The Pacific Arctic Region: Ecosystem Status and Trends in a Rapidly Changing Environment*, Springer Netherlands, Dordrecht.

Moore, S.E., and K.J. Kuletz. 2019. Marine birds and mammals as ecosystem sentinels in and near Distributed Biological Observatory regions: An abbreviated review of published accounts and recommendations for integration to ocean observatories. *Deep-Sea Research Part II* 162:211–17.

Moore, S.E., E. Logerwell, L. Eisner, E.V. Farley Jr, L.A. Harwood, K. Kuletz, J. Lovvorn, et al. 2014. Marine fishes, birds and mammals as sentinels of ecosystem variability and reorganization in the Pacific Arctic region. In *The Pacific Arctic Region: Ecosystem Status and Trends in a Rapidly Changing Environment*, J.M. Grebmeier and W. Maslowski (Eds.), 337–92. Springer.

Moore, S.E., T. Haug, G.A. Vikingsson, and G. B. Stenson. 2019. Baleen whale ecology in arctic and subarctic seas in an era of rapid habitat alteration. *Progress in Oceanography* 176:102118. doi:10.1016/j.pocean.2019.05.010.

Moss, J.H., J.M., Murphy, E.V. Farley, L.B. Eisner, A.G. Andrews. 2009. Juvenile pink and chum salmon distribution, diet, and growth in the northern Bering and Chukchi seas. *North Pacific Anadromous Fish Commission Bulletin* 5:191–196.

Mueter, F.J., B. Planque, G.L. Hunt, I.D. Alabia, T. Hirawake, L. Eisner, P. Dalpadado, et al., 2021a. Possible future scenarios in the gateways to the Arctic for subarctic and Arctic marine systems: prey resources, food webs, fish, and fisheries. *ICES Journal of Marine Science* 78:3017-3045. doi:10.1093/icesjms/fsab122.

Mueter, F.J., K. Iken, L.W. Cooper, J.M. Grebmeier, K.J. Kuletz, R.R. Hopcroft, S.L. Danielson et al., 2021b. Changes in diversity and species composition across multiple assemblages in the northeast Chukchi Sea during two contrasting years are consistent with borealization. *Oceanography* 34(2):38-51.

Nielsen, J.L., G.T. Ruggerone, C.E. Zimmerman. 2013. Adaptive strategies and life history characteristics in a warming climate: salmon in the Arctic? *Environmental Biology of Fishes* 96:1187–1226.

Nieukirk, S.L., D.K. Mellinger, R.P. Dziak, H. Matsumoto, and H. Klinck. 2020. Multi-year occurrence of sei whale calls in North Atlantic polar waters. *The Journal of the Acoustical Society of America* 147:1842–50.

Orlov, A.M., A.N. Benzik, E.V. Vedishcheva, S.V. Gafitsky, K.M. Gorbatenko, S.V. Goryanina, V.L. Zubarevich, *et al.,* 2019. Fisheries research in the Chukchi Sea at the RV *Professor Levanidov* in August 2019: some preliminary results. *Trudy VNIRO*, 178:206–220,

Overland, J. E., J. Wang, R. S. Pickart, and M. Wang. 2014. Recent and Future Changes in the Meteorology of the Pacific Arctic. Pages 17–30 in *The Pacific Arctic Region: Ecosystem Status and Trends in a Rapidly Changing Environment*, Springer Netherlands, Dordrecht.

Overland, J.E. and P.J. Stabeno. 2004. Is the climate of the Bering Sea warming and affecting ecosystems? EOS, Transactions of the American Geophysical Union 82:309-316.

Oziel, L., G. Neukermans, M. Ardyna, C. Lancelot, J.L. Tison, P. Wassmann, J. Sirven, *et al.,* 2017. Role for Atlantic inflows and sea ice loss on shifting phytoplankton blooms in the Barents Sea. *Journal of Geophysical Research*: *Oceans* 122:5121–5139.

Pecuchet, L., M.-A. Blanchet, A. Frainer, B. Husson, L.L. Jørgensen, S. Kortsch, and R. Primicerio. 2020. Novel feeding interactions amplify the impact of species redistribution on an Arctic food web. *Global Change Biology* 26:4894–4906.

Pinsky, M.L., B. Worm, M.J. Fogarty, J.L. Sarmiento, and S.A. Levin. 2013. Marine taxa track local climate velocities. *Science* 341(6151):1239–42.

Polyakov, I.V., M.B. Alkire, B.A. Bluhm, K.A. Brown, E.C. Carmack, M. Chierici, S.L. Danielson, *et al.,* 2020. Borealization of the Arctic Ocean in response to anomalous advection from sub-arctic seas. *Frontiers in Marine Science* 7:1–32.

Post, E., U.S. Bhatt, C.M. Bitz, J.F., Brodie, T.L. Fulton, M. Hebblewhite, J. Kerby, *et al.,* 2013. Ecological consequences of sea-ice decline. *Science* 341(6145): 519–24.

Radchenko, V.I., R.J. Beamish, W.R. Heard, O.S. Temnykh. 2018. Ocean ecology of pink salmon. In: Beamish, R.J. (Ed.), The Ocean Ecology of Pacific Salmon and Trout. American Fisheries Society, Bethesda, pp. 15–160.

Rand, K.M., and E.A. Logerwell. 2011. The first demersal trawl survey of benthic fish and invertebrates in the Beaufort Sea since the late 1970s. *Polar Biology* 34(4):475–488.

Reeves, R. R. et al. 2013. Distribution of endemic cetaceans in relation to hydrocarbon development and commercial shipping in a warming Arctic. Marine Policy: 1–15.

Reinhart, N.R., S.H. Ferguson, W.R. Koski, J.W. Higdon, B. Leblanc, O. Tervo and P.D. Jepson. 2013. Occurrence of killer whale *Orcinus orca* rake marks on Eastern Canada-West Greenland bowhead whales *Balaena mysticetus*. *Polar Biology* 36:1133–1146.

Richardson, W. J., B. Würsig, and C. R. Greene. 1986. Reactions of bowhead whales, Balaena mysticetus, to seismic exploration in the Canadian Beaufort Sea. The Journal of the Acoustical Society of America **79**:1117–1128.

Rolland, R. M., S. E. Parks, K. E. Hunt, M. Castellote, P. J. Corkeron, D. P. Nowacek, S. K. Wasser, and S. D. Kraus. 2012. Evidence that ship noise increases stress in right whales. Proceedings of the Royal Society B: Biological Sciences **279**:2363–2368.

Romano, M., H.M. Renner, K.J. Kuletz, J.K. Parrish, T.Jones, H.K. Burgess, D.A. Cushing and D. Causey. 2020. Die-offs and reproductive failure of murres in the Bering and Chukchi Seas in 2018. *Deep Sea Research II* 181-182, doi:10.1016/j.dst2.2020.104877

Roth, E., J. Hildebrand, S. Wiggins, and D. Ross. 2012. Underwater ambient noise on the Chukchi Sea continental slope from 2006–2009. Journal of the Acoustical Society of America 131:104–110.

Ruggerone, G.T., and J.R. Irvine. 2018. Numbers and biomass of natural- and hatchery- origin pink salmon, chum salmon, and sockeye salmon in the North Pacific Ocean, 1925 – 2015. *Marine and Coastal Fisheries* 10:152–168.

Ryan, W. B. F., S.M. Carbotte, J. Coplan, S. O'Hara, A. Melkonian, R. Arko, R.A. Weissel, V. Ferrini, A. Goodwillie, F. Nitsche, J. Bonczkowski, and R. Zemsky. 2009. Global Multi-Resolution Topography (GMRT) synthesis data set, *Geochemistry, Geophysics, Geosystems* 10, Q03014, doi:**10.1029/2008GC002332**.

Sigler, M., M. Renner, S. Danielson, L. Eisner, R. Lauth, K. Kuletz, E. Logerwell, and G. Hunt. 2011. Fluxes, fins, and feathers: relationships among the Bering, Chukchi, and Beaufort Seas in a time of climate change. *Oceanography* 24: 250–65.

Sorte, C.J.B., S.L. Williams, and J.T. Carlton. 2010. Marine Range Shifts and Species Introductions: Comparative Spread Rates and Community Impacts. *Global Ecology and Biogeography* 19:303–16.

Stabeno, P.J., and S.W. Bell. 2019. Extreme conditions in the Bering Sea (2017-2018): Record-breaking low sea-ice extent. *Geophysical Research Letters* 46:8952–59. doi:10.1029/2019GL083816.

Stabeno, P.J., N.A. Bond, N.B. Kachel, S.A. Salo, and J.D. Schumacher. 2001. On the temporal variability of the physical environment over the south-eastern Bering Sea. *Fisheries Oceanography* 10:81–98.

Stafford KM, Okkonen SR, Clarke JT. 2013. Correlation of a strong Alaska Coastal Current with the presence of beluga whales (*Delphinapterus leucas*) near Barrow, Alaska. Marine Ecology Progress Series. 474:287-297.

Stafford, K. M., S. E. Moore, P. J. Stabeno, D. V. Holliday, J. M. Napp, and D. K. Mellinger. 2010. Biophysical Ocean Observation in the Southeastern Bering Sea, Geophys. Res. Lett., doi:10.1029/2009GL040724.

Stafford, K.M. 2019. Increasing detections of killer whales (*Orcinus orca*), In the Pacific Arctic. *Marine Mammal Science* 35:696–706.

Stafford, K.M., Citta, J.J., Moore, S.E., Daher, M.A. and George, J. 2009. Environmental correlates of blue and fin whale call detections in the North Pacific Ocean, 1997-2002. Marine Ecology Progress Series 395: 37-53.

Stafford, K.M., H. Melling, S.E. Moore, C.L. Berchok, E.K. Braen, A.M. Brewer, and B.M. Kimber. 2022.. Marine mammal and airgun detections on the Chukchi Plateau 2009-2020. *Journal of the Acoustical Society of America* 151:2521-2529.

Stafford, K.M., J.J. Citta, S. Okkonen, and J. Zhang. 2021. Bowhead and beluga whale acoustic detections in the western Beaufort Sea 2008– 2018. *PLoS ONE*, 1–16. doi:10.1371/journal.pone.0253929.

Stafford, K.M., Moore S.E., Spillane, M. and Wiggins, S. 2007. Gray whale calls recorded near Barrow, Alaska, throughout the Winter of 2003-04. Arctic 60:167-172.

Stevenson, D.E., R.R. Lauth. 2019. Bottom trawl surveys in the northern Bering Sea indicate recent shifts in the distribution of marine species. *Polar Biology* 42:407–421.

Storrie, L., C. Lydersen, M. Andersen, R.B. Wynn, and K.M. Kovacs. 2018. Determining the species assemblage and habitat use of cetaceans in the Svalbard Archipelago, based on observations from 2002 to 2014. *Polar Research* 37:1–22.

Stroeve, J. C., M. C. Serreze, M. M. Holland, J. E. Kay, J. Malanik, and A. P. Barrett. 2012. The Arctic's rapidly shrinking sea ice cover: a research synthesis. Climatic Change **110**:1005–1027.

Sydeman, W., S.A. Thompson, J. Santora, M. Henry, K.H. Morgan, and S. Batten. 2010. Macro-ecology of plankton–seabird associations in the North Pacific Ocean. *Journal of Plankton Research* 32:1697-1713.

Sydeman, W.J., S.A. Thompson, J.F. Piatt, S.G. Zador, and M.W. Dorn. 2021. Integrating seabird dietary and groundfish stock assessment data: Can puffins predict pollock spawning stock biomass in the North Pacific? *Fish and Fisheries* 23:213-226. doi:.1111/faf.12611.

Tamarin-Brodsky, T., and Y. Kaspi. 2017. Enhanced poleward propagation of storms under climate change. *Nature Geoscience* 10:908–14.

Thoman, R.L., J. Richter-Menge, and M.L. Druckenmiller. 2020. Arctic Report Card 2020: Executive Summary. doi: 10.25923/mn5p-t549

Thomson, J., and W. E. Rogers. 2014. Swell and sea in the emerging Arctic Ocean. Geophysical Research Letters.

Udevitz, M. S., C. V. Jay, R. L. Taylor, A. S. Fischbach, W. S. Beatty, and S. R. Noren. 2017. Forecasting consequences ofchanging sea ice availability for Pacific walruses. Ecosphere 8(11):e02014.

VanWormer, E., J.A.K. Mazet, A. Hall, V.A. Gill, P.L. Boveng, J.M. London, T. Gelatt, et al. 2020. Viral Emergence in Marine mammals in the North Pacific may be linked to Arctic sea ice reduction. *Scientific Reports* 1–12. doi:10.1038/s41598-019-51699-4.

Walsh, J.J. and 22 others. 1989. Carbon and nitrogen cycling within the Bering/Chukchi Seas: Source regions for organic matter effecting AOU demands of the Arctic Ocean, Progress in Oceanography 22,277-259.

Westdal, K.H., J.W. Higdon, and S.H. Ferguson. 2016. Review of killer whale (*Orcinus orca*) ice entrapments and ice-related mortality events in the Northern Hemisphere. *Polar Biology* 40:1467–73.

Will, A., A. Takahashi, J.-B. Thiebot, A. Martinez, E. Kitaiskaia, L. Britt, D. Nichol, et al. 2020. The breeding seabird community reveals that recent sea ice loss in the Pacific Arctic does not benefit piscivores and is detrimental to planktivores. *Deep-Sea Research Part II* 181-182:104902.

Willoughby, A.L., M.C. Ferguson, R. Stimmelmayr, J.T. Clarke, and A.A. Brower. 2020. Bowhead whale (*Balaena mysticetus*) and killer whale (*Orcinus orca*) co-occurrence in the U.S. Pacific Arctic, 2009–2018: Evidence from bowhead whale carcasses. *Polar Biology* 43:1669–97.

Woodgate R. A., K. Aagaard, T. J. Weingartner. 2005a. Monthly temperature, salinity, and transport variability of the Bering Strait through flow, Geophys. Res. Lett., 32, L04601, doi:10.1029/2004GL021880.

Woodgate R.A. 2013. Bering Strait Norseman II 2013 Mooring Cruise Report. Available from

Woodgate, R. A., and K. Aagaard. 2005b. Revising the Bering Strait freshwater flux into the Arctic Ocean, Geophys. Res. Lett., 32, L02602, doi:10.1029/2004GL021747.

Woodgate, R. A., K. Aagaard, and T. J. Weingartner. 2006. Interannual changes in the Bering Strait fluxes of volume, heat and freshwater between 1991 and 2004, Geophys. Res. Lett., 33, L15609, doi:10.1029/2006GL026931.

Woodgate, R. A., T. J. Weingartner, and R. Lindsay. 2012. Observed increases in Bering Strait oceanic fluxes from the Pacific to the Arctic from 2001 to 2011 and their impacts on the Arctic Ocean water column. Geophysical Research Letters **39**.

Woodgate, R.A., and C. Peralta-Ferriz. 2021. Warming and freshening of the Pacific inflow to the Arctic from 1990-2019 implying dramatic shoaling in Pacific winter water ventilation of the Arctic water column. *Geophysical Research Letters* 48:1–11. doi:10.1029/2021GL092528.

Wyllie-Echeverria, T. 1995. Sea-ice conditions and the distribution of walleye pollock (*Theragra chalcogramma*) on the Bering and Chukchi Sea shelf; Pp. 131–136. In R.J. Beamish, ed, Vol. 121. Canadian Special Publication of Fisheries and Aquatic Sciences

Appendix: ASGARD Project Data

Appendix A contains summaries of data types collected by the ASGARD marine project, methodologies, and their locations.

Table A1. ASGARD cruise marine mammal sightings.

Measurement Parameters	**Experiment Location / Instrument type**	**DOI**
Marine mammal sightings during 2017 cruise (location, date, time, species, number of animals)	Bridge observations	10.18739/A26T0GX06
Marine mammal sightings during 2018 cruise(location, date, time, species, number of animals)	Bridge observations	10.18739/A2NV99B09

Table A2. ASGARD mooring-based measurements.

Measurement Parameters	Instrument	Number of Locations
Water Speed and Direction, Temperature, Signal Strength	Teledyne-RDI 307 KHz ADCP	7 mooring sites*
Temperature, Conductivity, Salinity, Pressure, Chlorophyll *a* Fluorescence, PAR	SeaBird SBE-16+	3 mooring sites
Chlorophyll *a* Fluorescence, OBS, CDOM	Wetlabs Eco-Triplett	3 mooring sites*
Temperature, Conductivity, Salinity, Pressure	SeaBird SBE-37	7 mooring sites*
Sinking fluxes of particulate Mass, Carbon, Nitrogen, and Silica fluxes; Food quality of sinking particles	Hydrobios Sediment Trap	3 mooring sites*
NO3, NO2, NH4, SiO3, PO4	GreenEyes Water Sampler	2 mooring sites*
NO3	Satlantic SUNA V2	3 mooring sites*
Acoustic Backscatter at 38, 125, 200, and 455 KHz	ASL Acoustic Zooplankton Fish Profiler	1 mooring site*
Underwater Sound	AURAL	4 mooring sites*

* = one of the denoted sites includes the CEO mooring site near Hanna Shoal. CEO data are separately archived from the ASGARD data on the Axiom Research Workspace.

Arctic Integrated Ecosystem Research Program Final Report

Integrating marine mammal presence into ASGARD: Arctic Shelf Growth, Advection, Respiration and Deposition Rate Experiments

13 June 2022

K.M. Stafford

Table of Contents

Executive Summary

The ASGARD project

The Arctic Shelf Growth, Advection, Respiration and Deposition Rate Experiments projects (ASGARD; NPRB awards A91-99a, A91-00a, A94-00, A98-00a) proposed to address known information gaps that hinder a robustly comprehensive application of an ecosystem-based approach to resource management in the U.S. Pacific Arctic region. An ecosystem-based approach is needed to inform and guide policy-driven actions, but this approach requires synthesis of a detailed knowledge base that at the start of the Arctic IERP effort remained incomplete in three important ways. First, existing data were strongly biased to July through October although important ecosystem processes occur in spring, late fall and winter when access is difficult. Second, while we now understand the basic summer regional biogeography (Sigler et al., 2017), net community production (Codispoti et al., 2013), and drivers of species distributions for some taxonomic groups (Feder et al., 1994; Eisner et al. 2013; Blanchard, 2014; Grebmeier et al., 2015a; Ershova et al. 2015), we had scant information from any season about the fundamental chemical and biological rates that mediate carbon cycling and energy flows through the Northern Bering and Chukchi Sea ecosystem. Third, these knowledge gaps curtailed our ability to model the ecosystem, and our ability to make useful projections for management or policy decisions. Passive acoustic monitoring was added to the ASGARD effort to understand the impacts of changing Arctic on marine mammals and to better understand how drivers from physics to plankton to fish to upper trophic level predators are mediated. Thus, this project is not stand-alone but relies heavily on other ASGARD components (ASGARD; NPRB awards A91-99a, A91-00a, A94-00, A98-00a) to function. The present report draws strongly from the Danielson et al. final report as these projects were intimately linked. Herein we include relevant passages from that report but also focus on the passive acoustic data from ASGARD.

Accordingly, the hypotheses developed under the passive acoustic component of the ASGARD project were:

H-1. *The presence of sub-Arctic marine mammals will be driven by prey availability (fish, zooplankton) that is in turn driven by water mass characteristics*
H-2. *The relationship between ice cover and Arctic species migration from the Bering Sea into the Pacific Arctic can be quantitatively determined by comparing the onset of acoustic detection with ice advance (or formation) from, and retreat towards, the north (in the winter and spring, respectively).*
H-3. *Temperate marine mammal species will move progressively northwards as seasonal ice cover decreases and remain north of Bering Strait longer.*
H-4. *There will be differences in the species and seasonal occurrence of species between the eastern (eastern SLI and US Bering Strait) and western (Anadyr Strait and Russian Bering Strait) recordings. Data from the A3 climate site and the NE Chukchi Ecosystem Mooring site*

help establish if there are northern limits to sub-Arctic species and what the southern limits of Arctic species are.
H-5. *The number of ship passages through both sides of the Bering Strait will continue to increase over time*

Of the above hypotheses, most require much longer-term datasets than were available during the two years of data collection during the ASGARD project. They do, however, point towards the importance of future, long-term year-round data to determine interannual versus climatological changes in the environment. Hypotheses 1 and 4 can be addressed in the short-term from the ASGARD data however hypotheses 2,3 and 5 require longer term monitoring or data collection from extant locations. Data to support the testing of the latter hypotheses were obtained from long-term datasets north of Bering Strait, including the southern (site A3) and northeastern Chukchi Sea (CEO) as well as the western Beaufort Sea (AON).

Summary of Findings

Select key finds and descriptions of novel sample collections that target the proposed hypotheses and that are presented in the chapters of this report include the following highlights.

- Subarctic baleen whales are recorded in the northern Bering and southern Chukchi Seas from late spring into early winter and at times, overlap temporally and spatially with Arctic species • Killer whales are increasingly acoustically recorded in the Pacific Arctic
- Anadyr Strait is a marine mammal hotspot for many species of marine mammal, including both Arctic and subarctic species.
- Ship noise propagation in the Bering Strait region depends on ship size, speed, and ambient noise levels
- Bearded seals are commonly heard when sea ice concentration at the Chukchi Ecosystem Observatory is high. In contrast, walrus are heard at the same location when sea ice concentration is low
- Subarctic fish, birds and mammals are extending their ranges both spatially and temporally in the Pacific Arctic in response to environmental changes

Acknowledgements

We thank Captain Eric Piper, the crew of R/V Sikuliaq, Seward Marine Center shore support, and the Sikuliaq technical support team of Steven Hartz, Dan Nabor and Ethan Roth for their fantastic support throughout the program. Given the size and complexity of our experiments and especially our requirements of extensive climate-controlled incubation space, we believe that no other vessel would have been able to support such a wide array of activities and generate such across-the board successes in our field work.

We thank Bill Wiseman and the National Science Foundation for the addition of funded days at sea in 2017, and UAF's Alaska Sikuliaq Program for major support of ship days in 2017 and 2018. We thank Brendan Smith for accompanying us on the ASGARD cruises and providing photo documentation of our

work and we thank Danielle Dickson and Matt Baker for guidance and support of the project through all of its phases. We thank all of the Arctic IERP funders for sponsoring the program: the North Pacific Research Board (NPRB), the Collaborative Alaskan Arctic Studies Program (formerly the North Slope Borough/Shell Baseline Studies Program), the Bureau of Ocean Energy Management (BOEM), and the Office of Naval Research (ONR) Marine Mammals and Biology Program for funding the main ASGARD proposal and all associated linked studies and gap projects (grants A91-99a, A91-00a, A94-00, A98-00a, A96, A97, A99).

We acknowledge that our field work was conducted on the waters where traditional subsistence harvest activities have been conducted by Inupiaq, Siberian Yupik, and Yupik peoples, and we thank them for their continued stewardship. Out of the field, our research is also conducted at the University of Alaska Fairbanks Troth Yeddha' campus, on the customary homelands of the Lower Tanana Dene. Robert Suydam, Craig George and the Alaska Eskimo Whaling Commission provided valuable guidance for helping us avoid conflict with subsistence harvest activities. We thank Opik Ahkinga of Little Diomede for joining both research cruises and contributing as a valued member of the benthic team and for helping us better understand perspectives of the Bering Strait region residents.

Acronyms and Abbreviations

ACCAP	Alaska Center for Climate Assessment and Policy
ACW	Alaska Coastal Water
ADFG	Alaska Department of Fish and Game
AFSC	Alaska Fisheries Science Center
AGU	American Geophysical Union
AMBON	Alaska Marine Biodiversity Observation Network
Arctic IES	Arctic Integrated Ecosystem Survey
Arctic IERP	Arctic Integrated Ecosystem Research Program
AOOS	Alaska Ocean Observing System
ASGARD	Arctic Shelf Growth, Advection, Respiration and Deposition rate experiments project
ASLO	Association for the Sciences of Limnology and Oceanography
ASP	Amnesic Shellfish Poisoning
AURAL	Autonomous Underwater Recorder for Acoustic Listening
AW	Anadyr Water
BOEM	Bureau of Ocean Energy Management
CDOM	Colored Dissolved Organic Matterr
CEO	Chukchi Ecosystem Observatory
CFOS	College of Fisheries and Ocean Science
COAS	College of Earth, Ocean and Atmospheric Science
CPUE	Catch per unit effort
CTD	Conductivity-Temperature-Depth Instrument
DBO	Distributed Biological Observatory
DIC	Dissolved inorganic carbon
ECMWF	European Centre for Medium-Range Weather Forecast
EJ	Exajoules
ELHS	Early life history stages
ESV	Exact sequence variants
IARC	International Arctic Research Center
IARPC	U.S. Interagency Arctic Research Policy Committee
IOS-DFO	Institute of Ocean Sciences, Fisheries and Oceans Canada
ISHTAR	Inner Shelf Transfer and Recycling program
JAMSTEC	Japan Agency for Marine-Earth Science and Technology
K3S	Kitikmeot Sea Science Study (Canada)
LISST	Laser In-situ Scattering and Transmissometry Instrument
LME	Large marine ecosystem
NCP	Net Community Production

NMFS	National Marine Fisheries Service
nMDS	Nonmetric multidimensional scaling
NOAA	National Oceanographic and Atmospheric Administration
NPRB	North Pacific Research Board
NSB-DWM	North Slope Borough Department of Wildlife Management
NSF	National Science Foundation
OBS	Optical backscatter
OMIX	Ocean mixing project (Japan)
ONR	Office of Naval Research
OSU	Oregon State University
PACMARS	Pacific Marine Arctic Regional Synthesis
PAR	Photosynthetically Available Radiation
PI	Principal Investigator
PICES	North Pacific Marine Science Organization
PMEL	Pacific Marine Environmental Laboratory
POC	Particulate organic carbon
SEP	Weight-specific egg production
SKQ	Research Vessel Sikuliaq
SST	Sea surface temperature
TINRO	Russian Federal Research Institute of Fisheries and Oceanography
TPM	Total particulate matter
UAF	University of Alaska Fairbanks
UME	Unexplained mortality event
USARC	U.S. Arctic Research Commission
USFWS	U.S. Fish and Wildlife Service
UVP	Underwater Vision Profiler
UW	University of Washington
VNIRO	Russian Federal Research Institute of Fisheries and Oceanography
WHOI	Woods Hole Oceanographic Institute

Preamble

The Arctic Integrated Ecosystem Research Program

The Arctic Integrated Ecosystem Research Program (Arctic IERP, 2016-2021) was motivated by the rapid changes occurring in the waters of the northern Bering and Chukchi Seas. While much research has been done in the region, many important questions remain. As a cohesive research endeavor, the Arctic IERP was designed to address a single, overarching question:

How will reductions in Arctic sea ice and the associated changes in the physical environmental influence the flow of energy through the ecosystem in the Chukchi Sea?

The report you are reading now is one of five final reports from the fieldwork phase of the Arctic IERP (a synthesis phase was initiated in 2022 after the completion of the Arctic IERP field-based projects). This preamble provides a brief overview of the Arctic IERP, both to place each final report in the broader context of the whole program, and to encourage readers to examine the other final reports to learn more about the research that was done. More detailed information about the Arctic IERP can be found at https://www.nprb.org/arctic-program.

The spatial domain of interest for the Arctic IERP extended across the Chukchi Sea Large Marine Ecosystem (LME) as redefined by the Arctic Council's Protection of the Arctic Marine Environment (PAME) working group, and the northern Bering Sea (above 61.5° N) as it strongly influences dynamics in the Chukchi Sea from the upstream direction. The main focus has been on the greater Bering Strait region and the Chukchi Sea. The program included the Arctic Basin and Beaufort Sea insofar as processes in the Chukchi Sea are influenced by these adjacent areas.

Development of the Arctic IERP

Before any Arctic IERP research proposals were written, the NPRB administered an assessment program, the Pacific Marine Arctic Regional Synthesis (PACMARS; https://www.nprb.org/assets/uploads/files/Arctic/PacMARS_Final_Report_forweb.pdf), that applied $1.5M provided by Shell and ConocoPhillips to compile and synthesize existing information about the ecosystem and inform research priorities. This assessment included community meetings in 2013 in Savoonga, Gambell, Kotzebue, Nome, and Barrow (now Utqiaġvik), in which representatives from 17 communities between St. Lawrence Island in the Bering Sea and Barter Island in the Beaufort Sea participated. One major area of emphasis that emerged from these community meetings was concern about food security for the region's residents in light of the rapid environmental changes taking place. Results from the scientific assessment and input provided via the community meetings informed the creation of the Arctic IERP. The PACMARS report informed both the IERP Request for Proposals (https://www.nprb.org/arctic-program/request-for-proposals/) and the submitted proposals.

Following a proposal review process, the Arctic IERP formally began in 2016 with funding from the North Pacific Research Board (NPRB), the Collaborative Alaskan Arctic Studies Program (formerly the North Slope Borough/Shell Baseline Studies Program), the Bureau of Ocean Energy Management (BOEM), and the Office of Naval Research (ONR) Marine Mammals and Biology Program. Generous inkind support was contributed by the National Oceanic and Atmospheric Administration (NOAA), the University of Alaska Fairbanks (UAF), the U.S. Fish & Wildlife Service (USFWS), and the National Science Foundation (NSF). This coordinated program was developed in cooperation with the Interagency Arctic Research Policy Committee (IARPC) and the U.S. Arctic Research Commission.

The Research

The Arctic Integrated Ecosystem Research Program (IERP) invested approximately $18.6 million in studying marine processes in the northern Bering and Chukchi Seas in 2017-2021, beginning in the summer of 2017. The research was divided into three main, complementary projects. The Arctic Shelf Growth, Advection, Respiration, and Deposition Rate Experiments (ASGARD) project carried out research in late spring and early summer of 2017 and 2018 aboard R/V Sikuliaq. The Arctic Integrated Ecosystem Survey (Arctic IES) conducted fieldwork aboard R/V Ocean Starr in late summer and early fall 2017 and 2019. In addition to the vessel-based surveys, sub-surface moored sensors were deployed to gather biophysical information continuously from June 2017 to September 2019.

In addition to the vessel-based work, a team of Arctic residents and social scientists, including members from eight communities in the North Slope and Northwest Arctic Boroughs and the Bering Strait region, met several times during the project to assess and analyze Indigenous observations and experiences with various types of change occurring in the region from Savoonga to Utqiaġvik. This group also compiled an annotated bibliography of Traditional Knowledge or Indigenous Knowledge (available through the data portal described below), to help researchers from other components of the Arctic IERP find information relevant to their studies.

Prior to the commencement of fieldwork, meetings were held in the three hub communities of Nome, Kotzebue, and Utqiaġvik. Scientists from the Arctic IERP and NPRB staff met with community members from each region to discuss the research purpose and plans. Research plans were also shared and discussed at meetings of the Alaska Eskimo Whaling Commission (AEWC), the Indigenous Peoples Council for Marine Mammals (IPCoMM), and with the Tribal Councils of Gambell and Savoonga on St. Lawrence Island. One result of these meetings was a shift in timing of the ASGARD cruises from May until June as well as a shift in timing and survey regions for the Arctic IES cruises, to avoid conflicts with subsistence hunting activities during what is traditionally the time for walrus hunting. Another result was the creation of communication protocols to avoid conflicts by alerting coastal communities to the presence of research vessels and adjusting the ships' routes to avoid areas where hunting was taking place. These communication protocols included regular radio broadcasts and daily emails to community members throughout the research area.

Results from the research are published in a growing list of peer-review journal articles, as well as cruise reports that provide contemporary accounts of the cruises, and many social media postings that are available through the NPRB website. Data are publicly available as described below.

Collaborations

The NPRB collaborated and coordinated with several other U.S. agencies and organizations that fund Arctic marine research. NPRB staff worked closely with the U.S. Interagency Arctic Research Policy Committee (IARPC) and the U.S. Arctic Research Commission. As the Arctic IERP was developed, the NPRB secured commitments for collaboration from 22 existing research projects that were detailed in Appendix A of the request for proposals, and made connections with new projects as they were funded.

International researchers also collaborated with the Arctic IERP via the Pacific Arctic Group (PAG), the North Pacific Marine Science Organization (PICES), and the Intergovernmental Consultative Committee (US/Russia - bilateral) as well as collaborations developed by individual investigators. PAG participants, including researchers from Canada, China, Japan, Korea, Russia, and the United States, have coordinated their cruise plans to sample standard stations in the Chukchi and Beaufort Seas termed the Distributed Biological Observatory (DBO). The Arctic IERP contributed to this effort. US-Russian data sharing initiatives were hosted in San Diego in 2016 and Vladivostok in 2017 to promote collaboration and exchange and to facilitate collaboration and synthesis of data and trends of patterns observed in the US and Russian waters in the northern Bering and Chukchi seas (PICES Press, Volume 26, Issue 1). ICC collaborations and other connections also brought scientists from the Russian Federal Research Institute of Fisheries and Oceanography (VNIRO), the Russian Pacific Scientific Fisheries Research Center (TINRO), and Hokkaido University to the US to participate in the Arctic IES cruises and co-author results. This collaboration is expected to connect research interests within respective EEZs (Russia/US) of the Chukchi Sea.

COVID-19

While the fieldwork of the Arctic IERP was completed before the outbreak of COVID-19, the final meeting of researchers in November 2020 was changed from an in-person event to an online format. Other plans for in-person events, such as meetings in hub communities within the US Arctic region (Nome, Kotzebue, and Utqiaġvik), were cancelled. Laboratory work and some collaborations were postponed or cancelled due to COVID-related restrictions and concerns. The NPRB made supplemental funds available to assist researchers with unanticipated expenses due to the pandemic. The overall productivity of the Arctic IERP was likely not greatly reduced, due both to good fortune in the fieldwork being completed and to the collaborative relationships that had been built or strengthened during the program.

Data Portal

Axiom Data Science, Inc. provided data management support to the Arctic IERP throughout the field program. Axiom staff assisted the scientists in authoring metadata and publishing the datasets to public archives. The data collected by the Arctic IERP are publicly accessible at https://arcticierp.dataportal.nprb.org/

General Introduction

ASGARD Background & Scientific Rationale

As a changing climate and sea-ice retreat progressively expose the Chukchi Sea to a longer open water season, society will confront new resource management issues. These include the future of the cultures and subsistence lifestyles of local indigenous communities, potential impacts of industrial activities (e.g. commercial fishing, oil and gas extraction), potential changes to regional ocean carrying capacity, and resilience of the Arctic marine ecosystem (NRC, 2014).

An ecosystem-based approach is needed to inform and guide policy-driven actions but this approach requires synthesis of a detailed knowledge base that today remains incomplete in three important ways. First, existing data are strongly biased to July through October although important ecosystem processes occur in spring, late fall and winter when access is difficult. Second, while we now understand the basic summer regional biogeography (Sigler et al., submitted), net community production (Codispoti et al., 2013), and drivers of species distributions for some taxonomic groups (Feder et al., 1994; Eisner et al. 2013; Blanchard, 2014; Grebmeier et al., 2015a; Ershova et al. 2015), we have scant information from any season about the fundamental chemical and biological rates that mediate carbon cycling and energy flows through the ecosystem. Third, these knowledge gaps curtail our ability to model the ecosystem with even a basic level of confidence – and our ability to make useful projections upon which we can base management or policy decisions.

The ASGARD project addressed the above limitations by:

1. Coordinating and collaborating with other ongoing projects, including participating in ship-of opportunity sampling later in those years; and
2. Carrying out year-round biophysical mooring deployments.

With this approach, we gathered critically missing information required for modeling and follow-on synthesis activities, such as sought by Gibson and Spitz (2011) and Whitehouse et al. (2014). As shown in this report, some of these synthesis analyses have already been begun in the course of our initial publication efforts. Although the Arctic IERP program as a whole has advanced our understanding, the analyses that we might approach today include new questions that were not well appreciated just a few years ago when the program began.

The Arctic is experiencing rapid and extreme changes. The Pacific Arctic Region (PAR), which includes the Bering Strait region, and Chukchi and Beaufort Seas, is a bellwether for these changes with sea ice extent and thickness decreasing and freshwater and heat content increasing (i.e. Stroeve et al. 2012, Woodgate et al. 2012). The biological responses to these extreme physical changes are complex but may result in a shift in the northern Bering Sea and Bering Strait from an Arctic-type ecosystem to a subarctictype ecosystem (Grebmeier et al. 2006b, Grebmeier 2012). One way to monitor changes in, or impacts on, an ecosystem is to observe the response of a suite of upper trophic level species such as sea birds and marine mammals via changes in occurrence and/or distribution (Moore et al. 2014). For instance, the PAR ecosystem "reorganization," from benthic- to pelagic-based, might negatively impact marine mammal species that rely on sea ice for habitat (e.g. Ice seals, walrus, bowhead whales) and/or benthic infauna for food (e.g., walrus, gray whales, some ice seals) via a reduction in habitat and prey abundance (Grebmeier et al. 2006a). Other species, however, such as sub- Arctic "summer whales" may benefit from increased access to northern habitat and pelagic prey species (Moore and Huntington 2008, Clarke et al. 2013).

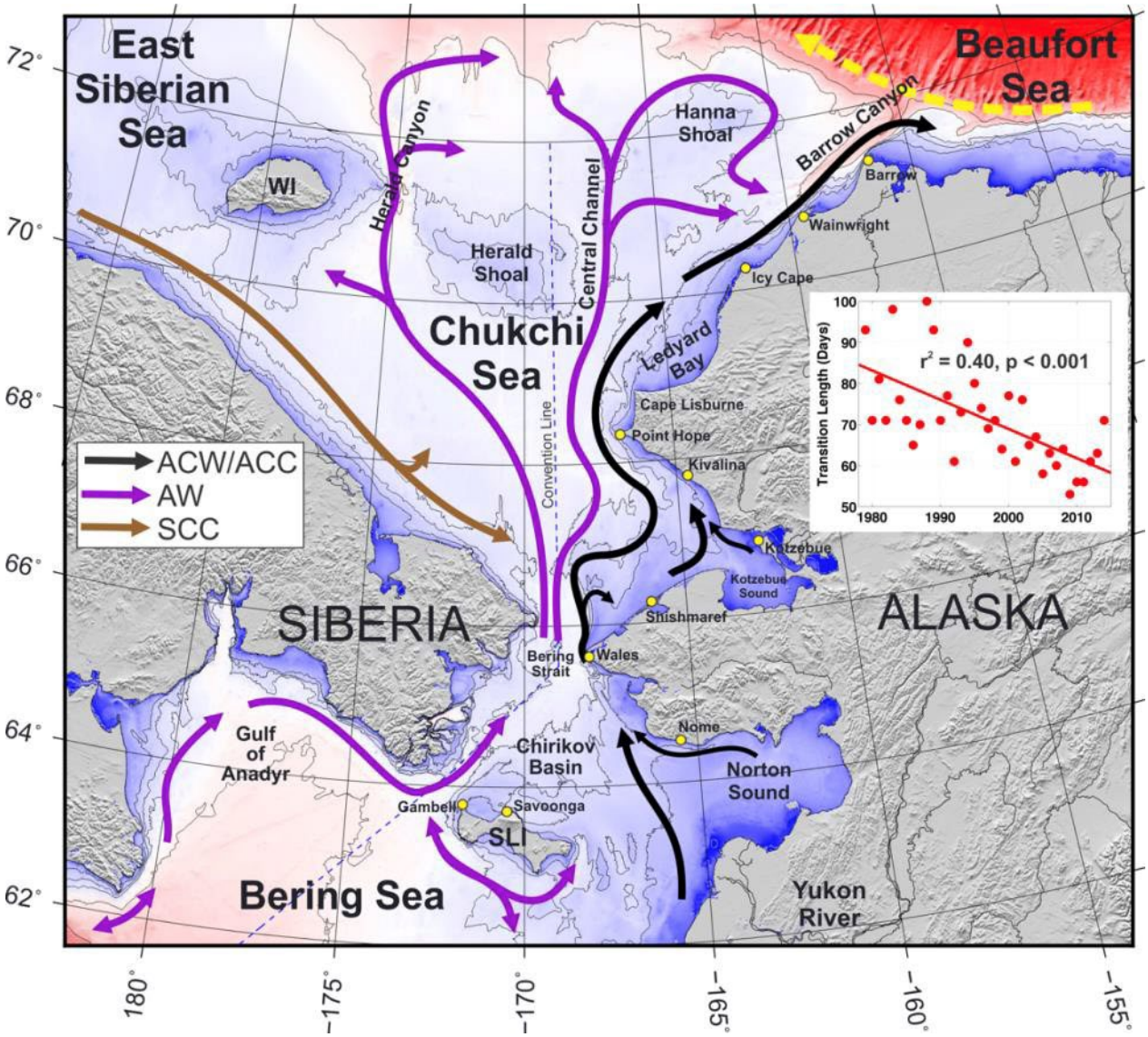

Figure 1. Map showing place names, persistent current systems, bathymetry (color shading). Inset: Decline in the regional duration of the annual spring sea-ice retreat, computed as the time between 80% and 20% ice cover (Map provided by Seth Danielson).

While the risk of potential competition for resources from sub-Arctic species expanding northwards is poorly understood (Clarke et al. 2013), integrating upper trophic level species with environmental data can provide insight into those environmental drivers result in increased competition. Further, assessment of impacts of increased human activities in the arctic (marine resource extraction and increased shipping) requires improved basic marine mammal population information (Reeves et al. 2013). Finally, there is concern among native Alaskans who live in the villages of the Arctic that environmental changes may result in changes in distribution of, and access to, species that are important for subsistence.

As the only oceanic gateway between the Pacific Ocean and the Arctic, the Bering Strait and Chukchi Sea are regions where climate change and changing anthropogenic utilization may have sizeable impacts on local marine fauna, and where changing fluxes of marine mammals to the Arctic can be confidently observed. The PAR is home seasonally to vocal Arctic species such as bowhead and beluga whales; bearded, ribbon and ringed seals; and walrus. Bowhead whales are currently listed as endangered species and walrus have been proposed for a "threatened" listing due to decreasing sea ice cover in the Arctic. In the summer, the northern Bering and Chukchi Seas provide habitat for fin, humpback, minke, gray and right whales (Clarke et al. 2013). Gray whales are regularly seen in the PAR and there have been recent sightings of humpback and fin whales north of the Bering Strait but relatively little is known of the northern limits of distribution for these "summer" whales.

The Bering Strait acts as a gateway for migration of animals between the Pacific Ocean and Bering Sea and the Pacific Arctic. The Bering Strait region is ice covered (i.e. those closed to marine mammals which need access to the surface to breathe) in the winter and "reopens" in the late spring, thereby influencing the migratory patterns of many marine mammal species (e.g., bowhead, beluga and gray whales, ice seals). Traditionally viewed as simply a route through which animals migrated, it is slowly becoming clear that marine mammals may spend significant portions of the summer and autumn in the PAR if prey is available there (Clarke et al. 2013; Lowry et al. 1980).

Flow from the Pacific advects nutrients and plankton into the Arctic Ocean, supporting very high levels of seasonal productivity that differ in the eastern and western PAR. The Bering Strait is the only source of Pacific inflow to the Arctic and has been the focus of ongoing research seeking to characterize circulation in the Arctic in light of global climate change (e.g., Aagaard al. 2006; Woodgate et al. 2005a, b; Woodgate et al. 2006, 2012). Pacific waters are a key source of nutrients for the Arctic Ocean (e.g.,
Walsh et al 1989), Therefore, in the PAR has important implications for Arctic biology, circulation, and the global freshwater budget (Woodgate et al. 2005b, 2006, 2012) and for the feeding success of marine mammals (Berline et al. 2008, Eisner et al. 2013). Differences in the physical oceanographic environment from east to west suggest that monitoring both sides of the PAR is critical to fully understanding changing ecosystem dynamics.

Changes in the timing and extent of annual sea ice influence the community ecosystem dynamics of this region. Ecosystem composition is affected directly via opening or closing of the strait and indirectly through the export of primary production to the shallow benthos (Grebmeier et al. 2006b). If the retreat of seasonal sea ice continues to shift the subarctic-Arctic temperature front, then community composition in the northern Bering and Chukchi Seas is likely to change, if not permanently, then seasonally (Overland and Stabeno 2004; Grebmeier et al. 2006a).
The PAR is home to native Alaskan and Russian communities that rely on marine mammals for subsistence. A recent workshop held in Nome, Alaska (Cooper 2010) identified the most pressing scientific questions to be addressed in the Bering Strait region from the perspective of local stakeholders (village inhabitants). Of highest priority for this group was increased monitoring of marine mammals, via visual and acoustic observations, because Arctic species and food security are integral to their nutritional cultural and spiritual subsistence.

As seasonal sea ice continues to diminish, ambient noise levels from shipping and seismic exploration will increase. As the Northern Sea Route and Northwest Passage become viable Pacific-Atlantic shipping routes, every ship along this route will pass through Bering Strait. The number of ships that used the Northern Sea Route increased dramatically from 4 in 2011 to 200 in 2013. This will lead to an inevitable increase in ambient noise levels at the low frequencies used by baleen whales, thereby decreasing the range over which they communicate and increasing the possibility of ship strikes (Clark et al. 2009; Hatch et al. 2012).

One means of assessing changes in marine ecosystems (the physical environment can be measured directly) is to examine the distribution of fauna that are directly influenced by such changes (Moore et al.
2014). As the top of short Arctic food webs, marine mammals can be considered sentinels of environmental change (Moore 2008; et al. 2014). Changes in cetacean abundance and distribution have been shown in conjunction with short and long time scale climate events in the north Pacific (Benson et al. 2002; Fiedler 2002; Croll et al. 2005) and Bering Sea (Stafford et al. 2010). Passive acoustic sampling is extremely robust, and can detect the presence of vocalizing marine mammals continuously (24 hours a day) in any weather conditions over weeks to months, over a distance of some 20-30 km and is a proven sampling method in waters offshore Alaska (Moore et al. 2006, 2012), including the Beaufort Sea and Chukchi Seas (Hannay et al. 2012, MacIntyre et al 2013; Stafford et al. 2007, 2013).

Species-specific characteristics of marine mammals vocalizations allow for unambiguous identifications based on acoustic signatures (Thomson and Richardson 1995). Therefore, acoustic monitoring can provide the ability to determine which species are present at a given time, and how species composition changes across seasons in the Bering and Chukchi Seas. For instance, gray whales, which have recently been regular summer visitors to the western Beaufort Sea, were detected

even in mid-winter in 2003-2004 by use of acoustic recordings (Stafford et al. 2007) and fin and humpback whales have been recorded in the Chukchi Sea (Delarue et al 2013; Hannay et al. 2013).

At present, the Arctic Ocean has relatively low ambient noise levels in winter due to ice cover that reduces wind waves (Milne and Ganton 1964; Roth et al. 2012) and in summer primarily due to the lack of commercial shipping, which has increased ambient noise levels significantly in other oceans (MacDonald et al. 2008). The reduction in seasonal sea ice and expansion of the open water season will change the seasonal ambient noise cycles of the Arctic. In late summer and fall, as the Northwest Passage and Northern Sea Route become viable Pacific-Atlantic shipping routes, every ship along this route will pass through Bering Strait resulting in increased ambient noise levels at the low frequencies used by baleen whales. In addition to anthropogenic increases in noise, the longer open water season and increasing storminess of Arctic regions (Overland et al. 2014; Thomson and Rogers 2014) will also lead to higher noise levels. Increases in ambient noise levels elsewhere have been shown to decrease the range over which marine mammals can receive signals, increase stress levels and change behavior (Richardson et al. 1986; Hatch et al. 2012; Rolland et al. 2012). While these reactions can be difficult to discern, longterm ambient noise data can be used to monitor ship passages, industrial exploration, and storms. Integration of acoustic detections of marine mammals is increasingly being used to understand correlations between habitat variables, prey, and marine animal presence. These include the use of generalized linear models, generalized additive models and time series analysis among others in order to determine what environmental factors most influence the presence of animals. In this manner, it may be possible to predict how the behavior of different species will change under changing environmental conditions (Baumgartner and Fratantoni 2008; Stafford et al. 2009, 2013; MacIntyre et al. 2015*;* Baumgartner et al, 2014).

In the shallow waters of the Chukchi and northern Bering Seas, low frequency acoustic signals from marine mammals (fin, bowhead, gray whales) are unlikely to transmit more than 20 km and higher frequency signals (from ice seals and beluga whales) will likely only be detected 5-10 km away. Therefore, the same signals will not be detected on multiple hydrophones. Each instrument will thus record signals local to the mooring area allowing comparison of the three proposed locations over the same time scales. When data from similar instruments deployed in Bering Strait and north of the Strait (Figure 1) are contributed, we will have coverage of all gateways between the Pacific and the Arctic Ocean. This will allow us to map migratory pathways and timing of the different species that use the Pacific Arctic.

By deploying acoustic recorders on biophysical oceanographic moorings, we can examine relationships between the physical and biological drivers in the PAR and quantify the animal fluxes in a manner that allows the investigation of seasonal and interannual change and understand the levels of underwater noise in the Arctic.

The ASGARD project is a coordinated ensemble of vessel- and mooring-based process studies consisting of physical, chemical, biological, and biogeochemical rate measurements that are designed to better constrain our understanding of carbon and nutrient dynamics of the northern Bering and Chukchi sea continental shelves.

Project Objectives

The ASGARD program was designed to address the NPRB Arctic Program's overarching questions outlined in their Request for Proposals: "How do physical, biological and ecological processes in the Chukchi Sea influence the distribution, life history, and interactions of species or species guilds critical to subsistence and ecosystem function? How might those processes change in the next fifty years?"

O-1: *Deploy hydrophones on 3 moorings in the northern Bering and Chukchi Sea.*

- Multi-electronique Aural M2 hydrophone packages were deployed on ASGARD moorings N1, N2 and N4 and were supplemented by data from a site north of Bering Strait (A3) and in the western Beaufort Sea (AON).

O-2*: Document the inter-seasonal and inter-annual presence of vocal marine mammals in the Pacific Arctic Region and compare of acoustic detections in the eastern, western, and central PAR.*

- Passive acoustic data from the ASGARD moorings as well as A3 and AON were analyzed for the presence of vocal marine mammals to determine geographic variability in the presence of different species.

O-3: *Integrate oceanographic drivers with acoustic detections to better understand how the physical environment influences the biological inhabitants of that environment*

- Deployment of hydrophones on biophysical moorings provides concurrent *in situ* data for comparing the physical environment with marine mammal presence. These analyses are ongoing.

O-*4:* *Collaborate with other ASGARD PIs to develop an integrated understanding of the ecosystem components of the Pacific Arctic Region from physical forcing through to upper trophic level consumers.*

- Meetings and collaborations with IERP colleagues resulted in two peer-reviewed publications (Huntington et al. 2020, Stafford et al. 2022) and on-going synergies for projects in the Pacific Arctic.

Approach

The ASGARD study consisted of ship-based and mooring-based studies designed to integrate with other proposed field, modeling, and human dimensions efforts. We selected the following focal measurements to help us address our main science question:

- Advective fluxes of physical, biotic and abiotic components of the water column
- Phytoplankton primary productivity
- Zooplankton growth/reproduction, respiration and fecal pellet production rates
- Particle deposition rates from the water column to the seafloor
- Quality of organic matter deposited to the seafloor
- Benthic respiration and organic matter decomposition rates
- Abundance and biomass of benthic microbial and metazoan fauna
- Distribution of fishes at different life history stages (NPRB Award A98-00a)
- Underwater sound and seasonal distributions of marine mammals (NPRB Award A94-00)

This report includes the overall goals of ASGARD with a specific focus on the inclusion of passive acoustic recording instrumentation on three of the ASGARD moorings and participation in the two research cruises. We sailed to the northern Bering and southern Chukchi shelf in 2017 and 2018 (Figure 2) on *R/V Sikuliaq*. In each year, working south to north, we first occupied ten "process" stations (yellow squares in Figure 2). As the ship visited the process stations, we paused to deploy and/or recover moorings (Figure 2) that recorded year-round time-series. Throughout the cruise we collected continuous underway navigational, ocean surface, ocean profile, and meteorological data and marine mammal observations (Figure 3) to provide additional environmental context for subsequent analyses.

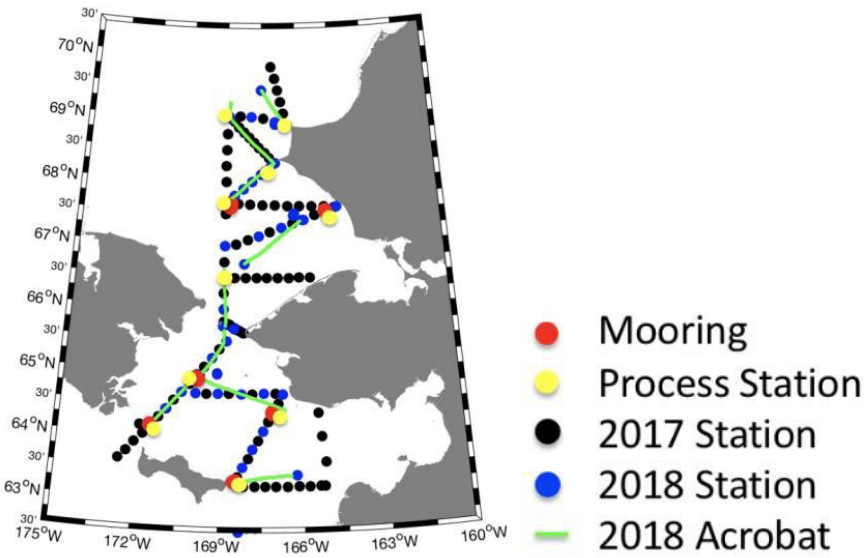

Figure 2. Location of field effort. Most 2018 stations (blue circles) were also occupied in 2017 (black circles). Some circles were shifted slightly on the map to reduce overlap.

The mooring array (Figure 2) consists of four biophysical moorings south of Bering Strait, two moorings in the southern Chukchi Sea plus the NPRB Long-Term Monitoring Program NE Chukchi Sea Ecosystem Mooring located on the southern flank of Hanna Shoal near Barrow Canyon. Together, these seven moorings allowed us to examine cross-shelf differences between the AW and ACW regimes and physical and biogeochemical changes imparted as the waters flow across the shelf into the Arctic. These instruments recorded year-round to reveal time histories of: nutrient and phytoplankton concentrations and fluxes; the bifurcation of flow to either side of St. Lawrence Island and the influence of regional winds on the upstream structure and partitioning of water masses feeding Bering Strait; conditions in Anadyr Strait, in the nexus of the most important zone at which subsurface nutrients are mixed to the surface as they arrive at Chirikov Basin and Bering Strait; AW and ACW properties and advection rates; phytoplankton blooms, sinking organic matter fluxes and their relationship to advective supply, light, ice thickness and the retreating ice edge; bottom sediment resuspension with respect to water and ice motion and ambient noise.

In addition, we aimed to contribute to the graduate educations of PhD students, including two students partially funded by the project and students not requiring financial support from ASGARD, but who participated in our cruises and collected data for use in their externally-supported research. We sought to strengthen existing and build new collaborations with national and international partners. We had cruise involvement of outreach specialists to help us communicate our science to targeted stakeholders and the public. We strengthened our ties to the coastal communities by participating in numerous co-management and other Alaskan Native Organization meetings, including Tribal Council consultations and the incorporation of a local observer on board our research cruises.

Field Expeditions

ASGARD field efforts (Figures 2 and 4) are documented in two detailed scientific cruise reports (Danielson et al., 2017; 2018) and one community observer report (Ahkinga, 2017) that are available at the NPRB Arctic IERP website https://www.nprb.org/arctic-program/about-theprogram/ The cruises took place in June 2017 and June 2018. We joined the Arctic EIS component of the IERP for final mooring recoveries in August 2019. Weather conditions and cruise timing allowed us to occupy more survey stations in 2017 than in 2018.

Emerging Stories

This report documents ASGARD project activities and results through the end of the initial phase of research and analysis (2016-2021). We were successful in collecting data that has been and will be applied to all of our focal objectives and hypotheses and as shown below, we addressed each from different vantage points. At the same time, we have only scratched the surface of the vast suite of potential results that the rich Arctic IERP dataset will yet reveal.

The *Results* section chapters document observations, and analyses that use data collected in the ASGARD field effort and were written in support of helping fill the three main information gaps identified in the ASGARD proposal (i.e., seasonal data gaps, rate measurements, and model parameterization/validation data) and guiding science question (i.e., ecosystem change in the face of diminishing sea ice). These chapters include graduate student dissertation chapters, and peer-reviewed journal articles (published and in preparation) that were written in support of the ASGARD project proposal and the Arctic IERP Integrated Work Plan (NPRB, 2016).

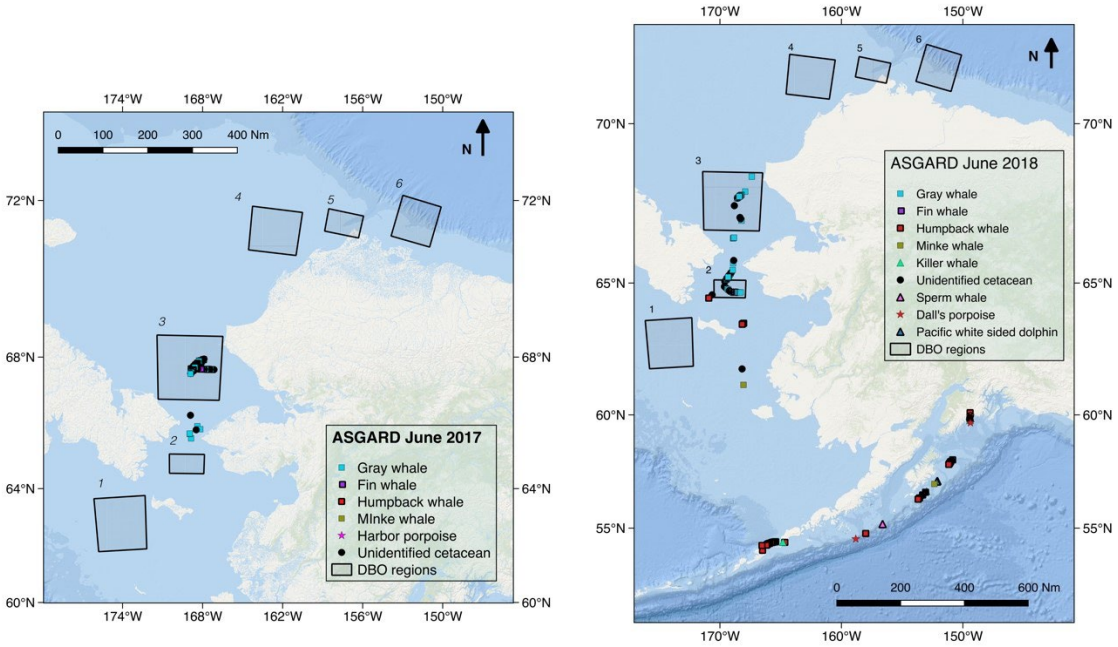

Figure 3. Left panel shows marine mammal sightings during the ASGARD 2017 cruise as well as Distributed Biological Observatory locations. Right panel shows sightings from the 2018 cruise.

Chapters are organized as follows. Chapters 1-4 concentrate on marine mammal occurrence and environmental conditions (physics and biology) and their temporal and spatial variability. Chapters 1-3 present information on the seasonal and spatial occurrence of marine mammals in the ASGARD study area and northwards and the interaction of these with environmental conditions. Chapter 4 examines the long-term changes in marine mammals at the Chukchi Ecosystem Observatory. Chapter 5 presents information on the underwater soundscape and ship noise contributions to the Bering Strait region. Chapter 6 is a review of changes in subarctic upper trophic level distributions. Chapter 7 (cited as Chapter 19 in the Danielson report) raises the question of whether this highly productive ecosystem could be in the midst of a significant ecological transformation.

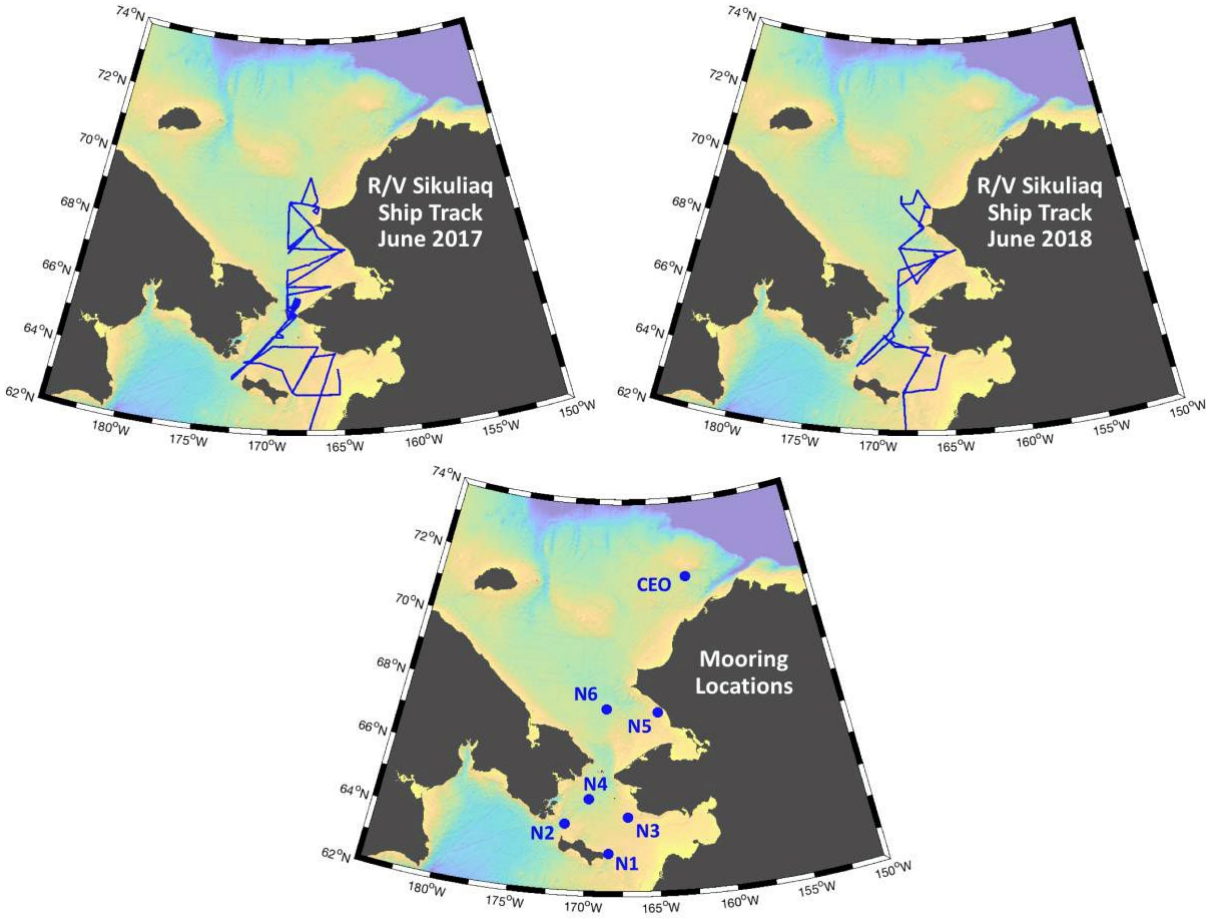

Figure 4. Vessel track lines (blue) for cruise SKQ2017-09S (June 2017, upper left), SKQ2018-13S (June 2018, upper right) and year-round mooring locations (blue circles, bottom). Identifying names for ASGARD moorings N1-N6 and the Chukchi Ecosystem Observatory (CEO) mooring cluster are labeled.

Results

The integration marine mammal presence into the ASGARD program using visual surveys on the two cruises and passive acoustic data on three of the 6 ASGARD-specific moorings as well as on the CEO (Fig 4) resulted in 3 peer-reviewed publications (Huntington et al. 2020, Moore et al. 2022, Stafford et al. 2022), an Honours thesis (Mottu 2022), PhD dissertation chapter (Escajeda et al. *in revision*), and additional in preparation collaborations (Stafford and Danielson and Stafford et al., in prep).

Chapter 1: Changes in gray whale phenology and distribution related to prey variability and ocean biophysics in the northern Bering and eastern Chukchi seas

Moore SE, Clarke JT, Okkonen SR, Grebmeier JM, Berchok CL, Stafford KM (2022) Changes in gray whale phenology and distribution related to prey variability and ocean biophysics in the northern Bering and eastern Chukchi seas. PLoS ONE 17(4): e0265934

Abstract

Changes in gray whale (*Eschrichtius robustus*) phenology and distribution are related to observed and hypothesized prey availability, bottom water temperature, salinity, sea ice persistence, integrated water column and sediment chlorophyll a, and patterns of wind-driven biophysical forcing in the northern Bering and eastern Chukchi seas. This portion of the Pacific Arctic includes four Distributed Biological Observatory (DBO) sampling regions. In the Bering Strait area, passive acoustic data showed marked declines in gray whale calling activity coincident with unprecedented wintertime sea ice loss there in 2017–2019, although some whales were seen there during DBO cruises in those years. In the northern Bering Sea, sightings during DBO cruises show changes in gray whale distribution coincident with a shrinking field of infaunal amphipods, with a significant decrease in prey abundance ($r = -0.314$, $p<0.05$) observed in the DBO 2 region over the 2010–2019 period. In the eastern Chukchi Sea, sightings during broad scale aerial surveys show that gray whale distribution is associated with localized areas of high infaunal crustacean abundance. Although infaunal crustacean prey abundance was unchanged in DBO regions 3, 4 and 5, a mid-decade shift in gray whale distribution corresponded to both: (i) a localized increase in infaunal prey abundance in DBO regions 4 and 5, and (ii) a correlation of whale relative abundance with wind patterns that can influence epi-benthic and pelagic prey availability. Specifically, in the northeastern Chukchi Sea, increased sighting rates (whales/km) associated with an ~110 km (60 nm) offshore shift in distribution was positively correlated with large scale and local wind patterns conducive to increased availability of krill. In the southern Chukchi Sea, gray whale distribution clustered in all years near an amphipod-krill 'hotspot' associated with a 50-60m deep trough. We discuss potential impacts of observed and inferred prey shifts on gray whale nutrition in the context of an ongoing unusual gray whale mortality event. To conclude, we use the conceptual Arctic Marine Pulses (AMP) model to frame hypotheses that may guide future research on whales in the Pacific Arctic marine ecosystem.

PLOS ONE

RESEARCH ARTICLE

Changes in gray whale phenology and distribution related to prey variability and ocean biophysics in the northern Bering and eastern Chukchi seas

Sue E. Moore[1]*, Janet T. Clarke[2], Stephen R. Okkonen[3], Jacqueline M. Grebmeier[4], Catherine L. Berchok[5], Kathleen M. Stafford [6¤]

1 Center for Ecosystem Sentinels, University of Washington, Seattle, WA, United States of America, **2** Cooperative Institute for Climate, Ocean and Ecosystem Studies, University of Washington, Seattle, WA, United States of America, **3** Institute of Marine Science, University of Alaska Fairbanks, Fairbanks, Alaska, United States of America, **4** Chesapeake Biological Laboratory, University of Maryland Center for Environmental Science, Solomons, MD, United States of America, **5** Marine Mammal Laboratory, Alaska Fisheries Science Center, NOAA, Seattle, WA, United States of America, **6** Applied Physics Laboratory, University of Washington, Seattle, WA, United States of America

¤ Current address: Marine Mammal Institute, Oregon State University, Newport, OR, United States of America
* moore4@uw.edu

OPEN ACCESS

Citation: Moore SE, Clarke JT, Okkonen SR, Grebmeier JM, Berchok CL, Stafford KM (2022) Changes in gray whale phenology and distribution related to prey variability and ocean biophysics in the northern Bering and eastern Chukchi seas. PLoS ONE 17(4): e0265934. https://doi.org/10.1371/journal.pone.0265934

Editor: Caroline Ummenhofer, Woods Hole Oceanographic Institution, UNITED STATES

Received: June 25, 2021

Accepted: March 10, 2022

Published: April 7, 2022

Peer Review History: PLOS recognizes the benefits of transparency in the peer review process; therefore, we enable the publication of all of the content of peer review and author responses alongside final, published articles. The editorial history of this article is available here: https://doi.org/10.1371/journal.pone.0265934

Data Availability Statement: Marine mammal sighting data from DBO research cruises are available here: arcticdata.io (doi:10.18739/

Abstract

Changes in gray whale (*Eschrichtius robustus*) phenology and distribution are related to observed and hypothesized prey availability, bottom water temperature, salinity, sea ice persistence, integrated water column and sediment chlorophyll *a*, and patterns of wind-driven biophysical forcing in the northern Bering and eastern Chukchi seas. This portion of the Pacific Arctic includes four Distributed Biological Observatory (DBO) sampling regions. In the Bering Strait area, passive acoustic data showed marked declines in gray whale calling activity coincident with unprecedented wintertime sea ice loss there in 2017–2019, although some whales were seen there during DBO cruises in those years. In the northern Bering Sea, sightings during DBO cruises show changes in gray whale distribution coincident with a shrinking field of infaunal amphipods, with a significant decrease in prey abundance ($r = -0.314$, $p<0.05$) observed in the DBO 2 region over the 2010–2019 period. In the eastern Chukchi Sea, sightings during broad scale aerial surveys show that gray whale distribution is associated with localized areas of high infaunal crustacean abundance. Although infaunal crustacean prey abundance was unchanged in DBO regions 3, 4 and 5, a mid-decade shift in gray whale distribution corresponded to both: (i) a localized increase in infaunal prey abundance in DBO regions 4 and 5, and (ii) a correlation of whale relative abundance with wind patterns that can influence epi-benthic and pelagic prey availability. Specifically, in the northeastern Chukchi Sea, increased sighting rates (whales/km) associated with an ~110 km (60 nm) offshore shift in distribution was positively correlated with large scale and local wind patterns conducive to increased availability of krill. In the southern Chukchi Sea, gray whale distribution clustered in all years near an amphipod-krill 'hotspot' associated with a 50-60m deep trough. We discuss potential impacts of observed and inferred prey shifts on

A26T0GX06). The ASAMM data are available here: https://www.fisheries.noaa.gov/resource/data/1979-2019-aerial-surveys-arctic-marine-mammals-historical-database PAM Data. Alaska Fisheries Science Center, 2021: AFSC/NMML: Acoustics long-term passive monitoring using moored autonomous recorders in the Bering, Chukchi, and Western Beaufort Seas, 2007-2012, https://www.fisheries.noaa.gov/inport/item/17343. Crustacean abundance and coincident environmental data are available on the DBO project page at the NSF Arctic Data Center archive, here: <https://arcticdata.io/catalog/portals/DBO/Data>. Note: When macrofaunal replicates were only 2-3 grabs/station (2016-2019) due to covid laboratory closures, the data sets will be available on the authors website until full processing of all replicates occurs (https://arctic.cbl.umces.edu). NCEP winds are available here: https://psl.noaa.gov/data/gridded/data.ncep.reanalysis.html. Bering Strait mooring data (including A3 transports) are available here: http://psc.apl.washington.edu/HLD/Bstrait/Data/BeringStraitDownloadregister.html; additional information on Bering Strait moorings here: http://psc.apl.washington.edu/HLD/Bstrait/bstrait.html.

Funding: Funding CB - PAM acoustic data: Interagency Agreement between BOEM and AFSC (ARCWEST IA# M12PG00021); grant from the Office of Naval Research, Marine Mammals and Biology Program (Award Number: N000141812792); internal-NOAA grant from the NOAA Fisheries, Office of Science and Technology Ocean Acoustics Program. JC - ASAMM visual data – Interagency Agreements between BOEM and AFSC including M07RG13260, M11PG00033, M16PG00013, and M17PG00031 KS -Marine Mammal DBO Watch visual data: National Science Foundation awards ARC-1107106) ARC-0855828, PLR-1603259, NPRB A94-00, ONR N00014-17-1-2274 JG - National Science Foundation Office of Polar Programs (awards OPP 1204082, 1702456 and 1917469) and National Oceanic and Atmospheric Administration Arctic Research Program (awards CINAR 22309.07 and 25984.02) SM & SO – no funding received for this study The funders had no role in study design, data collection and analysis, decision to publish, or preparation of the manuscript.

Competing interests: The authors have declared that no competing interests exist.

gray whale nutrition in the context of an ongoing unusual gray whale mortality event. To conclude, we use the conceptual Arctic Marine Pulses (AMP) model to frame hypotheses that may guide future research on whales in the Pacific Arctic marine ecosystem.

Introduction

Arctic and sub-arctic marine ecosystems are changing much faster than predicted [1]. Since the advent of satellite records in 1979, sea-ice areal extent has diminished by about 50% at the September minimum, with a roughly 75% year-round reduction in thickness of multi-year ice. This fundamental shift has not been linear in the Pacific Arctic region; rather, there were dramatic step-changes of sea-ice loss in late summer 2007 and 2012, and in winter 2017, 2018 and 2019 near Bering Strait [2]. Ocean temperatures have risen across the Arctic, driven both by increased solar insolation that is no longer reflected back into the atmosphere by sea ice and by transport of warm ocean water from the south into sub-arctic and arctic regions [3]. In the Pacific Arctic region, the loss of sea ice has been accompanied by ocean warming and freshening [4, 5], with 2014–2018 marking a period of increased ocean-atmosphere heat exchange coincident with unprecedented low ice cover [6]. The combination of sea-ice loss and warmer seawater has reset the clock on ecological processes in the Pacific Arctic [7], with the Bering Strait region described as in a state of transformation [8]. Compared to the late 1990s, primary production is initiated earlier in spring, with enormous blooms sometimes encountered under thin sea ice resulting in an overall 57% increase in net productivity [9]. Changes in primary productivity vary at regional and local scales, with production in the Chukchi Sea the highest in the Pacific Arctic region [10]. The biophysical impacts of reduced sea ice, increased ocean temperatures and primary production, combined with shifting atmospheric and ocean dynamics, can drive swift and fundamental changes near the base of marine food webs, the trophic level important to gray whales.

Gray whales are unique among mysticete whales in that they can suction sediment from the sea floor and effectively sieve out the infaunal prey on their short, coarse baleen leaving distinctive mud plumes at the surface (Fig 1A). Gray whales are also capable of efficiently feeding on epi-benthic prey swarms, pelagic zooplankton aggregations (Fig 1B), and even fish roe at the sea surface [11]. In the northern Bering and Chukchi seas, gray whales commonly feed on infaunal amphipods [12, 13], although epi-benthic and surface swarms of euphausiids (*Thysanoessa* spp.; hereafter, krill), eurisid amphipods (*Pontogeneia makarovi*), or cumaceans (*Diastylus glabra*) are sometimes the targeted prey [14, 15]. Reports on fine-scale feeding behavior at coastal study sites offshore Vancouver Island, Canada describe the ease with which gray whales can switch between various prey species based upon availability and sometimes size [16, 17]. While apex predators, such as marine mammals and birds, are now commonly recognized as ecosystem sentinels [18], gray whales were one of the first cetacean species so described. Specifically, evidence of connections between changes in gray whale phenology and distribution with shifts in their environment were summarized for six environmental factors, including oceanographic indices (i.e., Pacific Decadal Oscillation and El Nino Southern Oscillation), sea ice loss (N Bering) and thinning (W Beaufort), and shifts in infaunal and epi-benthic prey availability [19]. Taken together, these observations made a compelling case for gray whales as effective sentinels of ecosystem alteration in North Pacific and western Arctic ecosystems.

The Distributed Biological Observatory (DBO) was initiated in 2010 to provide standardized sampling to investigate biological responses to the rapid physical changes ongoing in the

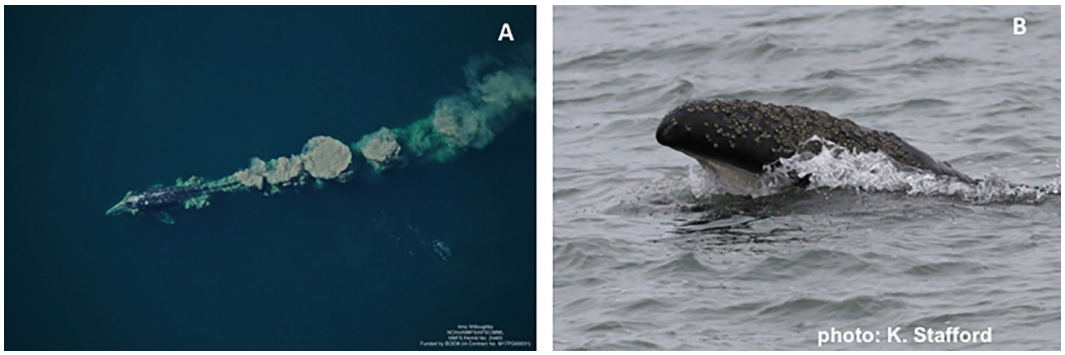

Fig 1. Gray whale feeding on infaunal amphipods, resulting in mud plumes (A), and a gray whale skim feeding on krill near Pt. Barrow, Alaska (B). Photo credits: A. Willoughby, NOAA/NMFS/AFSC/MML, NMFS permit number 20465, ASAMM project funded by BOEM via IA M17PG00031 (A); K. Stafford, co-author (B).

https://doi.org/10.1371/journal.pone.0265934.g001

Pacific Arctic marine ecosystem (Fig 2A) [20]. An opportunistic marine mammal watch was included in the standard DBO protocol to assess the capacity of marine mammal and other upper trophic level (UTL) species to act as sentinels of ecosystem variability and reorganization [21, 22]. Like fishes and seabirds, marine mammals rely on finding dense aggregations of prey to forage successfully. As a result, shifts in their ecology (i.e., phenology, distribution, and abundance) can signal changes in marine ecosystem trophic structure, which are in turn reflected physiologically by changes in diet and body condition [23]. In addition to sightings during DBO cruises, a robust program of marine mammal research has been conducted in the Pacific Arctic region, comprised of year-round Passive Acoustic Monitoring (PAM) of species-specific calls [24] and seasonal broad-scale Aerial Surveys of Arctic Marine Mammals (ASAMM) [25]. Changes in baleen whale phenology and seasonal distribution have been described based upon some of these data, with correlations to biophysical processes [26, 27] and details on prey availability included when possible [13, 28].

Here, we identify changes in gray whale phenology and seasonal distribution, based upon a compilation of information from the DBO, PAM, and ASAMM programs. We then relate

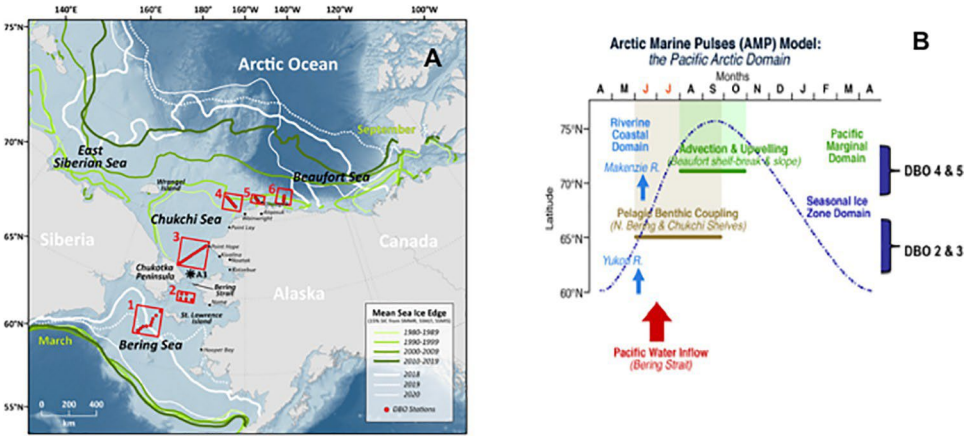

Fig 2. The Distributed Biological Observatory (DBO) and mean sea ice edge in the Pacific Arctic (A, revised from [10]), and a schematic of the conceptual Arctic Marine Pulses model (B, revised from [29]) depicting links among biophysical aspects of the Pacific Arctic marine ecosystem. The mean sea ice edge depicts the 15% concentration threshold using SMMR, SSM/I and SSMIS satellite data. All sea ice edge contours north (south) of Bering Strait represent September (March) conditions for three decadal periods (green) and annually for 2018, 2019 and 2020 (white).

https://doi.org/10.1371/journal.pone.0265934.g002

those shifts to changes in ocean biophysics that likely impact availability of their prey, including pelagic-benthic coupling, advection, ocean warming and freshening, and large and local-scale wind forcing. The conceptual Arctic Marine Pulses (AMP) model combines these biophysical factors into a regional framework (Fig 2B) [29]. We use the AMP model to contrast the advection and pelagic-benthic coupling drivers active in the Bering Strait region (DBO regions 2 & 3) to those factors combined with seasonal sea ice retention and wind-forcing dynamics in the northeastern Chukchi Sea (DBO regions 4 & 5) to investigate how these processes influence gray whale prey availability. Notably, the inclusion of long-term measures of infaunal crustacean abundance and species composition in DBO regions 2–5 provides direct evidence of, and fosters insights into, the impacts of shifting ocean biophysics on gray whale prey. The potential effects of observed and inferred prey alteration on gray whale nutrition are discussed in the context of an unusual mortality event that began in 2019 resulting in *ca*. 10-fold increase in annual number of stranded gray whales [30]. We close with suggested hypotheses that might guide future research on the ecology of gray and other baleen whales and enhance their capacity to act as sentinels of ongoing transformation of the Pacific Arctic marine ecosystem.

Methods

Gray whale passive acoustic and visual sampling

Our assessment of gray whale phenology, defined here as timing of arrival and departure from the Bering Strait region, is based on detection of their distinctive knock-like 'bongos' or 'Class 1 calls' [31]. Gray whale 'moans' or 'Class 3 calls' [31] were also included when detected with 'bongo' calls and when there were no accompanying humpback sounds with which they could be confused. Data were recorded on instruments deployed in or near DBO regions 2 and 3 (NM1 and PH1 on Fig 4A) from 2012–2019 as part of an extensive marine mammal PAM program [24]. Instruments were set to record on a duty cycle of 30% to extend battery life for a full year, with a sample rate of 16384 Hz for an effective bandwidth of 10–8192 Hz, which is sufficient to record all known gray whale signals [31]. Daily call detections were binned in 10-minute increments and normalized by recording effort, resulting in call histograms which depict the percent of calling activity/day, rather than an actual count of calls recorded. We examined histograms of gray whale calling activity at each site to identify phenological changes in annual pattern.

Our summary of gray whale distribution is based on sightings made during: (a) marine mammal watches on 22 DBO cruises (S1 Table), and (b) the broad scale ASAMM program conducted in the northeastern Chukchi Sea from 2009–2019 [25]. On DBO cruises, a visual watch for marine mammals was conducted during daylight hours when the ship was transiting between sampling or mooring stations, augmented by scans around the ship each hour when the ship was on station. An observer trained in marine mammal species identification used naked eye and handheld binoculars to scan a 120˚ arc forward of the ship (abeam, to +30˚ of the bow) out to the horizon. When two people were available to stand watch, the full 180˚ arc forward of the ship was scanned to the horizon. The watch stander was often assisted by other scientific party personnel and the ship's crew. The watch was curtailed when sea state exceeded Beaufort 05 (wind speed ~25kts, 12.8 m/s), or visibility was reduced to < 1km by precipitation or fog. Although DBO cruise tracks and ship speeds were similar among years, sighting rate (whales/km) could not be calculated due to variability in watch effort. Thus, while sightings from DBO cruises provide data on gray whale presence, especially in the Bering Strait region, these data are not included in statistical analyses.

During the ASAMM program, line-transect aerial surveys were conducted from July through September using twin engine aircraft outfitted with left- and right-side bubble windows. The study area encompassed the northeastern Chukchi Sea from 67˚N to 72˚N, and east of 169˚W, an area inclusive of DBO 3–5. Dedicated observers stationed at each window reported all marine mammal sightings and associated environmental conditions to a data recorder. Sightings of large whales were briefly circled over to confirm species identity, group size, behavior, and presence of calves. Surveys were conducted whenever weather conditions allowed (i.e., sea state ≀Beaufort 05; cloud ceiling consistently >335 m). Offshore transect lines were oriented perpendicular to the coastline to allow sampling across isobaths and prevailing currents, and to best assess marine mammal density gradients; a coastal transect was flown *ca*. 1-km offshore to better document nearshore habitat.

To examine changes in gray whale distribution in the context of environmental variability, ASAMM data were divided into three geographic areas for analysis: (1) the southern Chukchi Sea, referred to as the Hope Basin area and inclusive of DBO 3; and the northeastern Chukchi Sea, referred to as the (2) Wainwright and (3) Peard Bay areas, inclusive of DBO regions 4 and 5. Gray whale sighting rates were calculated for each area as the number of gray whales seen/offshore transect kilometer by month (July, August, September) and year (S2 Table). Effort and sightings on the coastal transect were not included in monthly SR analyses to avoid bias towards nearshore areas. All ASAMM data are publicly available at fisheries.noaa.gov/resource/data/1979-2019-aerial-surveys-arctic-marine-mammals-historical-database; databases used for analyses include versions 1979_2011_v3_36, 2012_2014_v0_28, 2015_2017_v22, and 2018_2019_v6.

Gray whale prey and environmental variability

Environmental factors relevant to the influence of pelagic-benthic coupling on gray whale infaunal prey were evaluated based upon a multi-decadal record of macrobenthos and sediment dynamics [32], with special focus on stations dominated by crustacean species at the start of the 2010–2019 time series [32, 33]. In brief, stations in DBO regions 2–5 were designed to sample sediments across localized areas of high benthic productivity and biomass. Stations in DBO regions 3, 4 and 5 were oriented along diagonal transects, while those in DBO 2 sampled along latitudinal transects. South of DBO 3, a series of stations (designated UTN, for University of Tennessee), were oriented roughly parallel to the International Date Line (IDL) from 66.5ºN to 68ºN latitude. Over the 2010–2019 period, small adjustments were made to sampling design in DBO regions 2 and 4. Specifically, In the DBO 2 region, the four original times series stations (UTBS) were augmented from 2016 onwards by the addition of three stations (BCL6c, DBO2.7, UTBS2A) to expand the spatial extent of sampling. In the DBO4 region, station placement was changed from six stations along a single transect line to six stations on three shorter transect lines (shown as DBO4 O, N, and n; Fig 5) to improve sampling the patchy distribution of benthic fauna in that area. At all stations, replicate sediment samples were collected using a 0.1 m^2 weighted van Veen grab. Sediments were sieved onboard through 1 mm mesh screens, with the retained macrofauna preserved with 10% buffered seawater and formalin for post-cruise taxonomic identification and analysis of abundance and wet weight biomass. The analysis of infaunal prey for gray whales focused only on the Class Crustacea, which is comprised primarily of amphipods, with a very minor (< 1%) inclusion of isopods and cumaceans. Additional details of sampling and analysis methods are provided in [32].

Gray whale infaunal crustacean prey were analyzed with attention to changes in species composition and abundance in response to trends in sea ice loss, ocean temperature, salinity, and measures of chlorophyll *a* both in the water column and in surface sediment. Spatial

interpolation was accomplished using geographical information system software [34]. Specifically, the Geostatistical Analyst Wizard Inverse Distance Weighting (IDW) tool in ESRI's ArcGIS Desktop v.10.8.1 was used with default settings to produce an interpolated surface map based on abundance of the class Crustacea per station for the years 2010 to 2019. Temporal patterns in crustacean abundance and Spearman's rho rank correlation analysis was used to determine correlations of crustacean abundance over time using JMP™ Pro 15.2.0 (www.jmp.com). Most macrofaunal data sets for the 2010–2019 period are available at the Arctic Data Center (ADC) DBO project page (https://arcticdata.io/catalog/portals/DBO/Data)), and the NOAA National Centers for Environmental Information (NCEI) website (https://www.ncei.noaa.gov/), although some replicate samples could not be included due to Covid limitations on laboratory work. To clarify data included this paper, a summary of crustacean abundance is listed by cruise number, station and date is provided supplemental S3 Table. Of note, the environmental data used for statistical analyses in relation to crustacean abundance listed in S3 Table are available at the aforementioned ADC and NCEI data archives for the associated cruises.

Environmental factors potentially indicative of the influence of advection and circulation on gray whale epi-benthic and pelagic prey availability were evaluated through application of an iterative correlation analysis (ICA) method [35, 36]. The ICA method is a supervised machine learning tool that uses, in the present case, a multiyear time series of gray whale SR derived from ASAMM data as a training set to identify a statistically similar interannual time series of either (i) a seasonally-averaged environmental factor (e.g. volume, heat, freshwater transports) measured at the 'climate mooring' north of Bering Strait [4; mooring A3], or (ii) local- to large-scale (Bering-Chukchi-Beaufort region) wind regimes derived from daily sea level wind products available at the National Centers for Environmental Prediction (NCEP)/National Center for Atmospheric Research [37]. For an environmental factor with time series information at a single location (e.g. transport at mooring A3), ICA identifies the seasonal start and end dates for which correlations between seasonally-averaged transports and gray whale SRs are statistically significant. For an environmental factor with time series information at multiple locations (e.g. NCEP winds), ICA identifies the seasonal start and end dates that maximize the ocean area north of the Bering Sea shelf break over which correlations between seasonally-averaged winds and gray whale SRs are statistically significant. Results for both single and multiple location ICA are summarized in the form of a heat map matrix that identifies the best-fit start and end dates from a range of candidate seasonal averaging periods.

Results

Changes in gray whale phenology and distribution

Acoustic detections. A change in gray whale acoustic activity was observed in the northern Bering Sea (DBO 2) where the period of calling activity extended from late May through November in 2012–2015, shortened to late May to mid-September in 2016, and followed by a near cessation of call detections in 2017–2019 (Fig 3A). In the southern Chukchi Sea (DBO 3), consistent calling activity extended from mid-June through October in 2012–2015. In 2017 call detections ended a month earlier (September), and there was a near cessation of calling activity throughout 2018–2019 (Fig 3B). These changes in calling activity suggest that gray whales departed DBO regions 2 and 3 earlier each year after 2016 and 2017, respectively.

Visual detections. Gray whales were seen during marine mammal watches on DBO cruises in all years (Fig 4A). Areas where gray whales were commonly seen included the northern Bering and southern Chukchi Seas, and waters offshore Wainwright and along the coast between Pt. Franklin and Pt. Barrow. While DBO cruise tracks were similar among years,

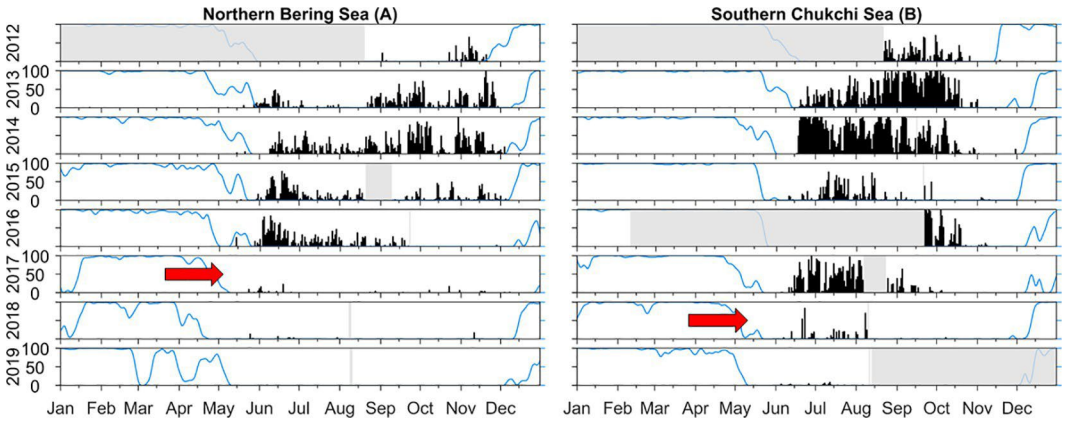

Fig 3. Gray whale annual calling activity in the northern Bering (A) and southern Chukchi (B) seas, 2012–2019. Black bars show gray whale calling activity, blue lines represent seasonal ice cover and grey shading indicate periods for which data are unavailable. Red arrows denote dramatic drop-off in calls coincident with 2017–2019 winter sea ice loss event. Hydrophone locations are shown in Fig 4 - DBO map.

https://doi.org/10.1371/journal.pone.0265934.g003

timing and platform operations varied, limiting inferences that can be drawn from these data for lack of SR calculations. Of note, however, is that gray whales were consistently seen in the northern area of DBO 2 and near the central and western-most sampling stations in DBO 3 (Fig 2A), as well as west of the International Date Line (IDL) in years that ships had access to those waters (2009, 2010, 2012). Also, in contrast to the PAM data, gray whales were seen in DBO regions 2 and 3 in 2017–2019 after the aforementioned loss of winter sea ice in those areas.

The ASAMM data provide the means to relate gray whale distribution to survey effort north of 67˚N and east of 169˚W in the Chukchi Sea. Over the eleven-year study period, there were 1,333 sightings of 2,358 gray whales from July through September, with most whales seen in south-central and northeastern Chukchi Sea waters (Fig 4B). Interannual variability in SR

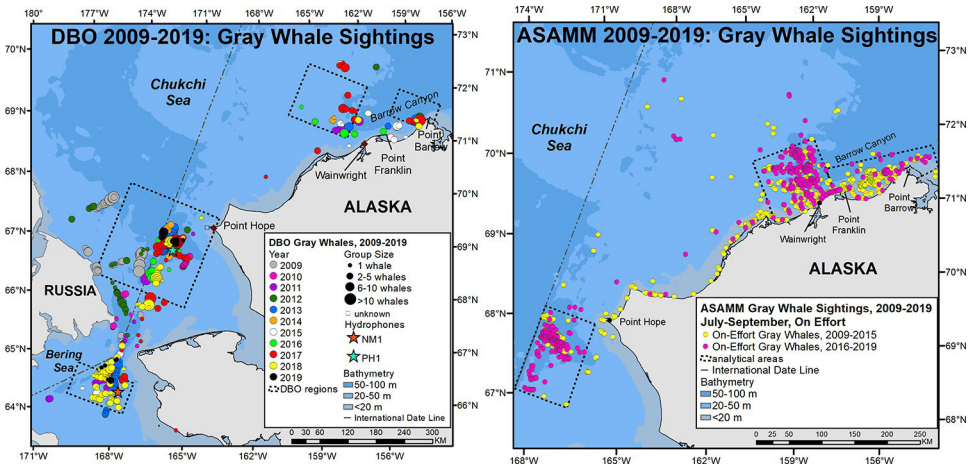

Fig 4. Gray whale distribution from sightings made during marine mammal watches on DBO cruises, and the broad scale Aerial Surveys of Arctic Marine Mammals (ASAMM) program, 2009–2019. Dashed lines depict boundaries of DBO regions and analytical areas, respectively. Gray whale sighting rates (SR = whales/km) in analytical areas were calculated solely from ASAMM data. ASAMM data are publicly available at fisheries.noaa.gov/resource/data/1979-2019-aerial-surveys-arctic-marine-mammals-historical-database. Databases used for maps include versions 1979_2011_v3_36, 2012_2014_v0_28, 2015_2017_v22, and 2018_2019_v6.

https://doi.org/10.1371/journal.pone.0265934.g004

Table 1. Annual ASAMM survey effort (km), number of gray whale sightings, number of whales seen and sighting rate (SR = whale/km), July-September, 2009–2019. Includes all sightings and effort on transect, including coastal and offshore transects, in ASAMM study area.

Year	Effort km	No. sightings	No. gray whales	SR (whales/ km)
2009	15,560	88	115	0.007
2010	16,089	52	74	0.005
2011	20,010	102	139	0.007
2012	21,077	124	221	0.011
2013	21,768	67	110	0.005
2014	19,032	164	291	0.015
2015	20,865	98	185	0.009
2016	21,381	161	366	0.017
2017	23,021	207	384	0.017
2018	15,589	167	311	0.020
2019	13,121	103	162	0.012
Total	207,513	1,333	2,358	0.011

https://doi.org/10.1371/journal.pone.0265934.t001

for the entire study area ranged from a high of 2 whales/100km in 2018 to a low of 0.5 whales/100km in 2010 (Table 1). In 2015, there was a *ca*. 110 km (60 nm) shift in gray whale distribution away from the coastal habitat between Pt. Franklin and Pt. Barrow to waters offshore Wainwright and near the head of Barrow Canyon. In the south-central Chukchi Sea, gray whale distribution clustered in a benthic trough 'hotspot' southwest of Pt. Hope in all years, with sightings extended further south after 2015. Since gray whales spend much of their time feeding while in the Chukchi Sea, these changes in distribution and associated shifts in SR were examined (i) with reference to observed changes in infaunal crustacean prey abundance and community composition from benthic sampling, and (ii) by correlation of sighting rates from ASAMM data with environmental factors associated with availability of epi-benthic and pelagic prey, as described in the next two sections.

Changes to infaunal crustacean abundance, community composition, and associated environmental factors

Our multi-decadal record of infaunal crustacean abundance provided the means to directly track changes to gray whale infaunal crustacean prey in productivity hotspots in the northern Bering and eastern Chukchi seas (Fig 5). The area of highest gray whale prey abundance is in the south-central Chukchi Sea, near the northernmost UTN and the western-most DBO3 stations and extends west of the International Date Line (IDL). Two smaller centers of prey abundance occur in DBO regions 4 and 5 in the northeastern Chukchi Sea. Conversely, the DBO 2 region, which used to encompass a well-documented gray whale prey hotspot in the northern Bering Sea, now is relatively 'cool' with only moderate measures of infaunal crustacean abundance.

The clearest change in gray whale prey during the 2010–2019 period was a significant decrease ($r = -0.314$, $p < 0.05$) in amphipod abundance in the DBO2 region (Table 2; Fig 6). Especially notable was the decline in crustacean abundance at the northwest sampling sites starting in 2015 and the nearly complete absence of crustacean prey at southwest sampling stations after 2012 (Fig 7). Of note, this decline in crustacean abundance represents a continuation for gray whale prey loss this region, which began in the late 1990s [32].

In the southern Chukchi Sea, comparatively small-bodied amphipod species from three families were found in the DBO 3 region, where gray whales are often seen feeding from both vessel and aircraft platforms. There was no significant trend in infaunal crustacean abundance

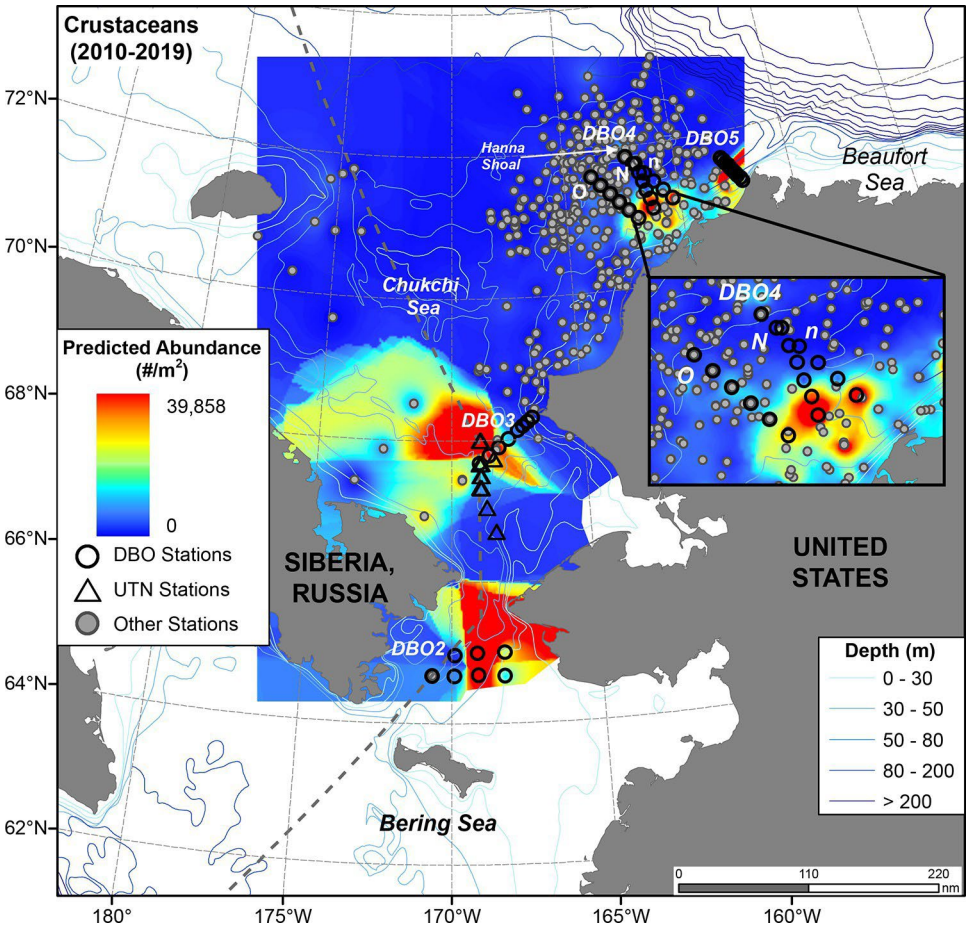

Fig 5. Distribution of infaunal crustacean abundance (#/m^2) at all stations where macrofauna were sampled during the period 2010–2019 in the northern Bering and eastern Chukchi seas. Key: open circles = DBO stations, open triangles = UTN stations, and closed gray circles = all remaining stations. Note that DBO4 has 3 transect links: O = original line 1, n = new line 1, and N = new line 2. The spatial interpolation map was made using the Geostatistical Analyst Wizard Inverse Distance Weighting (IDW) tool in ESRI's ArcGIS Desktop v.10.8.1 (ESRI 2020) with default settings. See S3 Table for DBO sampling site information and crustacean abundance data. The remainder of the all station crustacean abundance data are available at Arctic Data Center DBO data portal <https://arcticdata.io/catalog/portals/DBO/Data>.

https://doi.org/10.1371/journal.pone.0265934.g005

in this region, with the highest crustacean abundance consistently observed in the hotspot sampled by the UTN 7 and SEC 3 and 4 stations (Figs 6 and 7). Notably, although abundance remained stable over time, there was a shift in community composition, whereby the northernmost stations of the DBO 3 hotspot are now dominated by *Pontopoporeia femorata* (F. Pontoporeidae), which replaced the *Byblis* sp. (F. Ampelicidae) in the mid-2000s and has remained the dominant crustacean species since that time; meanwhile the small F. Isaeidae amphipods have remained second in abundance throughout the last decade.

In the northeastern Chukchi Sea, feeding gray whales were seen where both comparatively large infaunal amphipods (F. Pontoporeidae) and a variety of small infaunal crustacean species (F. Isaidae., F. Phoxochelidae) were found in a localized area along the eastern flank of Hanna Shoal in DBO 4 (Fig 5, Table 2). The infauna at all 6 stations in the time series were equitable in abundance (Fig 6), but there was notably higher amphipod abundance in 2016 and 2017 at the DBO 4.2N station (Fig 7) on the east flank of Hanna Shoal and close to the head of Barrow Canyon. In DBO 5, both the larger amphipods (F. Ampeliscidae) and smaller amphipods (F.

Table 2. Changes in infaunal crustacean community composition and abundance coincident with bottom water temperature and salinity, sea ice persistence (days from Sept-to Sept), and integrated water column and sediment chlorophyll in DBO regions 2–5 for the period 2010–2019.

	REGION			
Parameters	**DBO2**	**DBO3**	**DBO4**	**DBO5**
	2010–2019	2010–2019	2010–2019	2010–2019
Dominant crustacean families (by abundance)	Ampeliscidae, Isaeidae	Ampeliscidae, Isaeidae, Pontoporeidae	Isaeidae, Phoxocephalidae, Pontoporeidae	Ampeliscidae, Isaeidae, Phoxocephalidae, Leuconidae
Crustacean Abundance (no/m2)	5546 ± 6610	3588± 5477	3454 ± 4999	5400 ± 7528
	r = -0.314$^{\wr}$ (51)	r = -0.046, ns (134)	r = 0.065, ns, (51)	r = -0.022, ns (61)
Bottom water temperature (˚C)	1.98 ± 1.20	3.34 1.82	-0.57 ± 1.43	-0.41 ± 1.89
	r = +0.678$^{\wr\wr}$ (51)	**r = +0.377**$^{\wr\wr}$ (134)	**r = +0.616**$^{\wr\wr}$ (51)	r = -0.072, ns (61)
Bottom water salinity (psu)	32.56 ± 0.31	32.28 ± 0.51	32.44 ± 0.29	32.50 ± 0.85
	r = +0.367$^{\wr\wr}$ (51)	r = +0.113, ns (134)	**r = -0.502**$^{\wr\wr}$ (51)	r = +0.184, ns (61)
Sea ice persistence (days/year)	143 ± 28	172 ± 18	221 ± 32	260± 15
	r = -0.756$^{\wr\wr}$ (51)	**r = -0.725**$^{\wr\wr}$ (134)	**r = -0.896**$^{\wr\wr}$ (51)	**r = -0.634**$^{\wr\wr}$ (61)
Integrated water chlorophyll *a* (mg/m2)	66.73 ± 53.43	162 ± 183	106.80 ± 106.23	115.63 ± 129.64
	r = +0.370$^{\wr\wr}$ (51)	r = +0.131 (134)	**r = -0.296**$^{\wr}$ (51)	r = -0.056, ns (60)
Sediment chlorophyll *a* (mg/m2)	19.54 ± 7.24	20.55 ± 9.02	14.49 ± 7.80	13.65 ± 7.63
	r = +0.399$^{\wr\wr}$ (51)	r = -0.058, ns 134)	**r = +0.533**$^{\wr\wr}$ (51)	r = -0.117, ns, (56)

Values are average ± s.d. Key: **bold** is significant increase (+) or decrease (-) over the decade

$^{\wr}$**p<0.05**

$^{\wr\wr}$**p<0.01**; ns = not significant; (#) = number of stations, with sea ice persistence in number of days/year. Dominant species/family: Ampeliscidae (*Ampelisca macrocephala*, *A. birulai*, *Byblis* sp.), Isaeidae (*Protomedeia fasciata*, *Photis* sp.), Leuconidae (*Eudorella pacifica)*, Phoxocephalidae (*Grandifoxus* sp., *Heterophoxus* sp.), Pontoporeidae (*Pontoporeia femorata*).

https://doi.org/10.1371/journal.pone.0265934.t002

Isaeidae and F. Phoxocephalidae) and cumaceans (F. Leuconidae*)* were abundant along the narrow shelf nearshore (Table 2). Although there was no significant trend in infaunal crustacean abundance in the DBO 5 region (Fig 6), there was an indication of a local increase in abundance near the head of Barrow Canyon at the BarC 6 station in 2015 and especially in 2017 (Fig 7). Unfortunately, sea ice cover in 2018 precluded sampling the DBO5 stations and sorting of 2019 samples is in progress.

A summary of changes in environmental factors associated with the sampling of infaunal crustaceans provides context, but no simple answers, as to why there was a significant change in abundance only in the DBO 2 region (Table 2). Sea ice persistence has *decreased* in all DBO regions 2–5, while integrated water column chlorophyll increased only in the DBO2 region, suggesting an enhanced pelagic food supply in waters north of St. Lawrence Island. In contrast, seasonal variability in water mass nutrient content in the eastern Chukchi Sea (i.e., DBO 3–5) influences chlorophyll and productivity measurements over the open water season (see Frey et al, this volume). Notably, sediment chlorophyll increased only in DBO 2 and DBO 4. This suggests food supply to infaunal crustaceans has increased in those regions, making the *decline* of amphipods in DBO 2 unexpected and indicating that some combination of environmental factors is driving abundance. In reviewing those factors, we note that bottom water temperature has increased in all regions except DBO 5, accompanied by increased bottom water salinity in DBO 2 (Table 2). Bottom water salinity was variable across the DBO3 transect from nearshore to offshore stations, resulting in no trend. Bottom water became significantly fresher in DBO 4, likely due to increasing sea ice melt and perhaps freshwater pulses from the south. There was no change in bottom water salinity in DBO 5, likely due to the seasonal complexity of Barrow Canyon ocean dynamics.

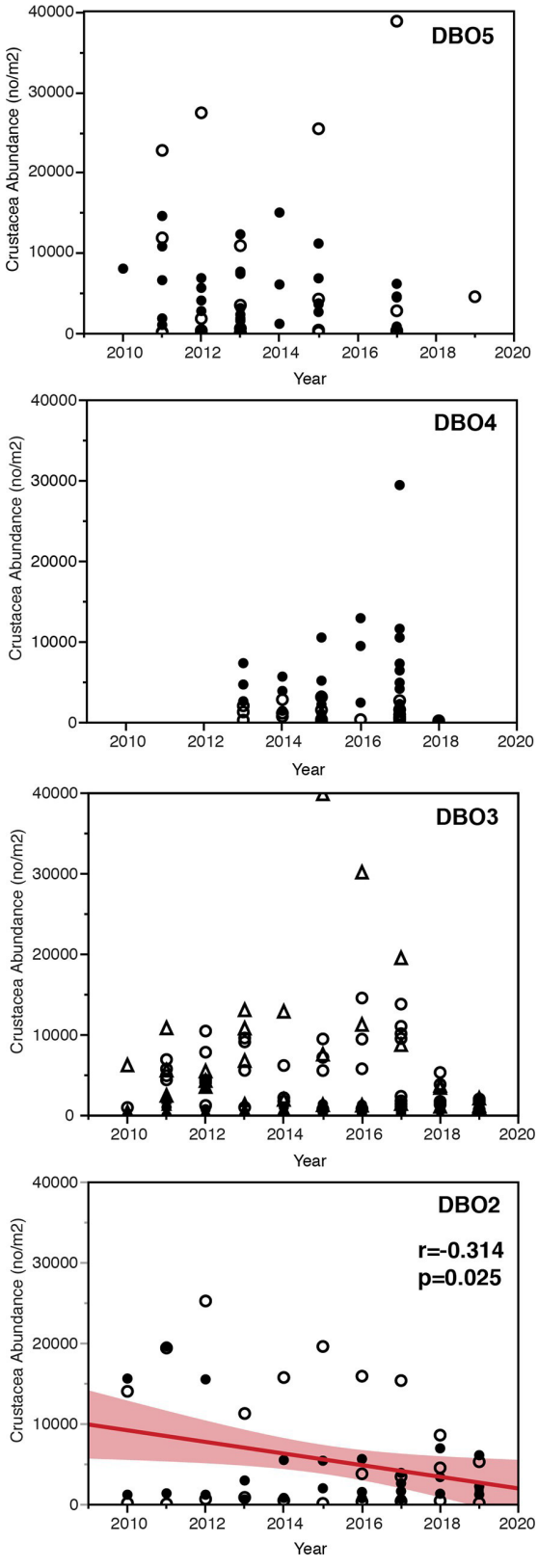
DBO5
DBO4
DBO3
DBO2
r=-0.314
p=0.025
Crustacea Abundance (no/m2)
Year
0
10000
20000
30000
40000
2010
2012
2014
2016
2018
2020

Fig 6. Macrofaunal crustacean abundance at time series stations over the 2010–2019 period in DBO regions 2–5 regions. A: DBO2 in the Northern Bering Sea (squares), with the red line indicating the linear fit using all the station data, with the confidence curves shaded red around the line and the correlation coefficient indicating the significant decline of crustacean abundance. B: DBO3 in the SE Chukchi Sea (triangles), C: DBO4 in the NE Chukchi Sea (circles), and D: DBO5 in Barrow Canyon (diamonds) had no significant trends in crustacean abundance over time, although there was spatial variation in values. Key: within each DBO region, the closed symbols = southern time series stations; open symbols = northern time series stations. This format provides a spatial perspective of station location for each DBO region, with reference to Fig 5.

https://doi.org/10.1371/journal.pone.0265934.g006

Environmental factors related to gray whale epi-benthic and pelagic prey availability

Since gray whales also feed on epi-benthic (e.g. mysids, cumaceans [11]) and pelagic (e.g. krill [14]) prey, integrative correlational analyses (ICA) were used to investigate drivers of Chukchi Sea circulation (regional wind forcing and transport through Bering Strait) that can alter prey availability and thereby influence whale distribution and sighting rates (SR). In the northeastern Chukchi Sea, interannual changes in gray whale monthly distribution and SR depict a shift in foraging away from the nearshore Peard Bay area (2009–2014) to offshore waters near the head of Barrow Canyon in the Wainwright area (2015–2019; Fig 8). The shift in distribution and SR is most evident for the month of July, with a near-abandonment of the Peard Bay area in August and September. To investigate this shift, combined annual July-August-September (JAS) SRs for Wainwright (W) and Peard Bay (PB; Fig 9A) were used to create a 2009–2019 time series of fractional SR, ($W_F = W_{JAS}/(W_{JAS} + PB_{JAS})$. This served as the ICA training set (Fig 9B) to identify periods of seasonally-averaged winds within the Bering-Chukchi-Beaufort domain that were significantly correlated ($r > 0.60$, $p<0.05$, $df = 9$) with the fractional SR. The ICA heatmap shows three loci, all with start dates in early June (Fig 9C), with averaging periods of: (i) ~21 days (end date late June; best fit indicated by diamond symbol), (ii) ~45 days (end date late July), and (iii) ~100 days (end date mid-September). The resulting wind regimes were similar for all three loci in that the action center is the region north of ~70˚ N and that statistically-significant variability primarily occurs with the E-W component of the wind field. These results suggest foraging conditions for epi-benthic and pelagic prey are relatively better in the Peard Bay area when late-spring and summer winds are easterly and persistent (warm color shading) over the northern Chukchi and southern Beaufort (Fig 9D). Conversely, gray whale foraging on epi-benthic or pelagic prey (e.g. krill) is likely better in the Wainwright area when late-spring and summer winds are weak, variable (cool color shading), or westerly (Fig 9E).

Interannual variability in gray whale monthly distribution and SR in the Hope Basin area depicts a more stable situation. Sightings were clustered around a quasi-stationary front associated with a bathymetric trough southwest of Pt. Hope, with a southern extension of sightings evident in the combined July distribution (Fig 10). Of note, there were very few gray whales seen in 2009–2013, likely due in part to limited survey effort in those years (S2 Table). Except for 2015, the combined annual JAS SR for gray whales in the Hope Basin area was consistently higher from 2014–2019 than for the years 2009–2013. Notably, an ICA for the Hope Basin area showed no clear relationship with winds over the Bering-Chukchi shelf region. Combined monthly SR showed intra and interannual variability, with peaks in July (2017 and 2019), August (2014 and 2017), and September (2014 and 2016) (Fig 11).

Interannual variations in gray whale SR in the Wainwright, Perd Bay and Hope Basin analytical areas were used as ICA training sets to identify time series of monthly-averaged transport at the A3 'climate' mooring site (see Fig 2A) north of Bering Strait. ICA results indicate that winter-to-early-spring volume, heat, and freshwater transports are positively correlated

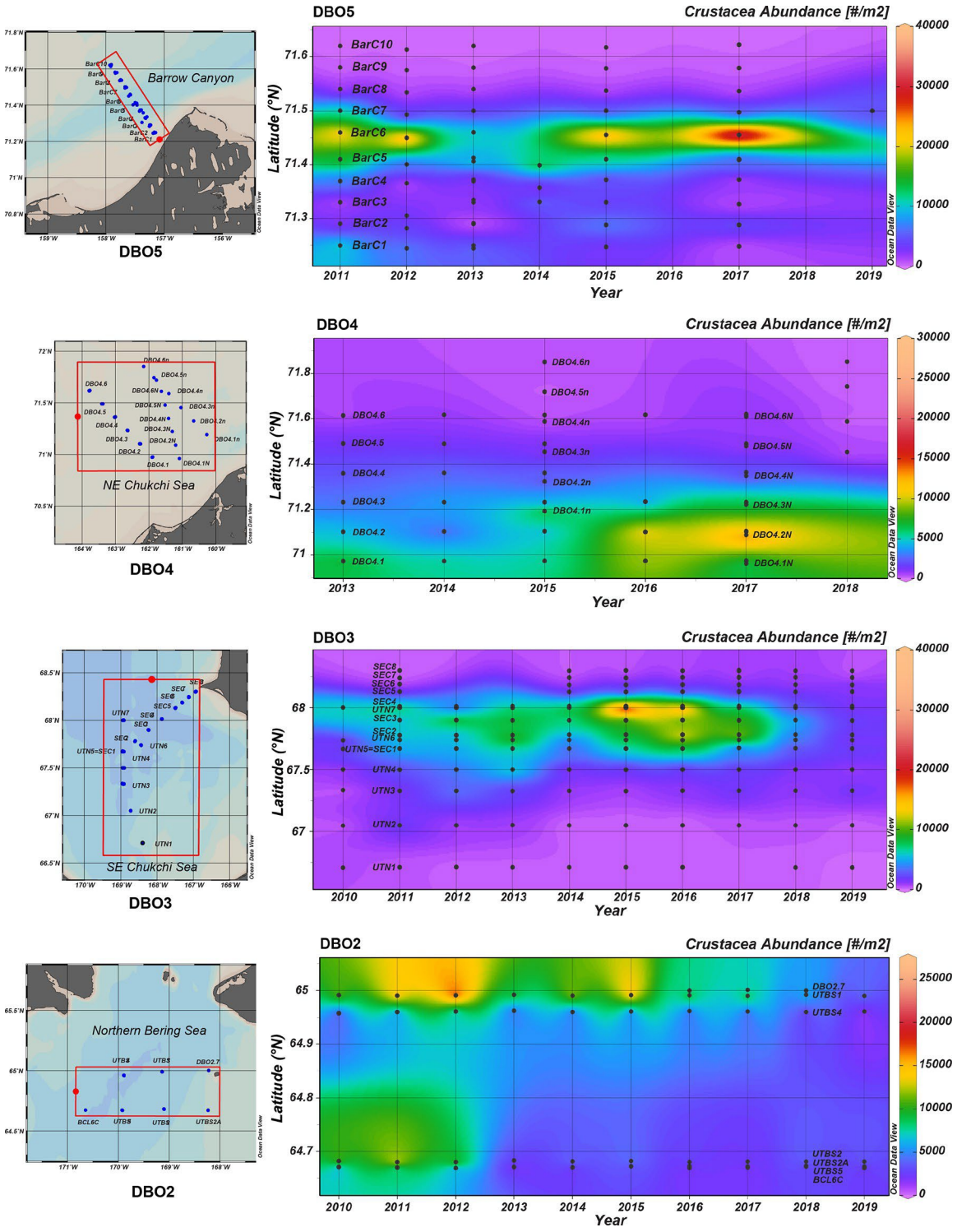

Fig 7. Time series of macrofaunal crustacean abundance at stations in DBO regions 2–5 over the 2010–2019 period. Figures are aligned from south to north over a latitudinal gradient with the red bounding boxes surrounding time series stations in each DBO region. The crustacea summary data plotted in this figure are provided in S3 Table and the Arctic Data Center DBO project page (https://arcticdata.io/catalog/portals/DBO/Data). All crustacean data in each DBO region were plotted using Ocean Data View software under a CC By license; see Methods for details of stations included in the visualization.

https://doi.org/10.1371/journal.pone.0265934.g007

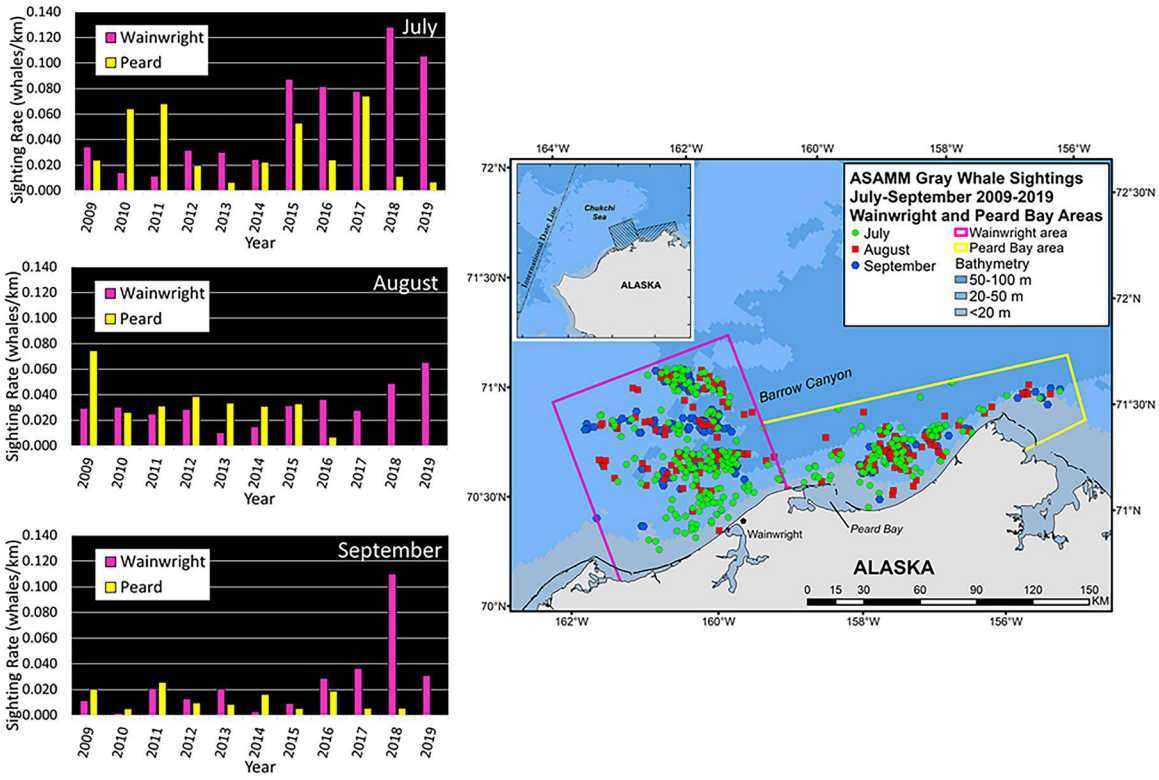

Fig 8. Interannual variability in gray whale monthly distribution and histogram of sighting rates (SR) for Wainwright and Peard Bay analytical areas in the northeastern Chukchi Sea, 2009–2019. Inset map shows the location of Wainwright and Peard Bay areas relative to the ASAMM study area. ASAMM data are publicly available at fisheries.noaa.gov/resource/data/1979-2019-aerial-surveys-arctic-marine-mammals-historical-database. Databases used for maps include versions 1979_2011_v3_36, 2012_2014_v0_28, 2015_2017_v22, and 2018_2019_v6.

https://doi.org/10.1371/journal.pone.0265934.g008

with the combined JAS SR in the Wainwright area and negatively correlated with combined JAS SR in the Peard Bay area (Table 3). In the Hope Basin area, interannual variations in August and September SR were negatively correlated with volume, heat, and freshwater transports. Notably, the negative correlations for the September SR were associated with 10-12-month time-averages of transport compared to the 1 to 4-month averages of transport found in other comparisons.

A summary of results relating variability in gray whale sighting rates (SR) to circulation drivers (A3 transport and winds), bathymetry, and likely whale prey highlights contrasts among the three analytical areas in the Chukchi Sea (Table 4). Notably, transport at A3 is correlated with gray whale SR in each of the regions, while a contrasting pattern of high and low SR can be correlated with alternate wind patterns only in the Peard Bay and Wainwright areas. In sum, bathymetry and transport appear to be drivers of gray whale pelagic prey in the Hope Basin area (inclusive of the DBO 3 region), while bathymetry, transport and wind forcing play a role in the northeastern Chukchi Sea (inclusive of DBO 4 and 5).

Discussion

Historical overview of gray whale ecology

Gray whale ecology in the northern Bering and Chukchi Seas has been the focus of intermittent research since the late 1960s, which provides a foundation upon which to interpret the

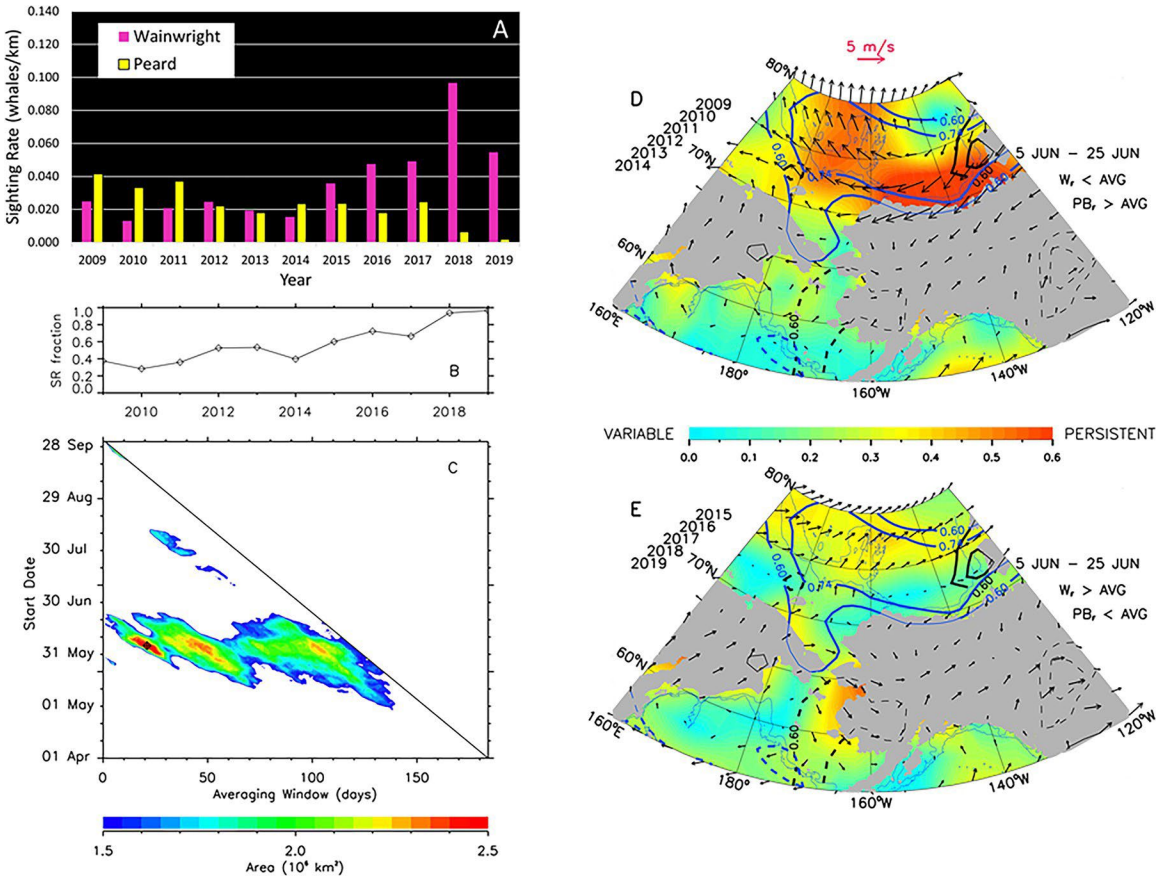

Fig 9. Relationship between gray whale sighting rates (SR) and wind forcing, including: Histogram of combined average July-August-September SR in the Wainwright and Peard Bay analytical areas (A); Wainwright area SR fraction (B); ICA heat map showing the area of the Bering-Chukchi-Beaufort ocean domain over which correlations between the SR fraction and time-averaged winds are statistically-significant ($r > 0.602$, $p<0.05$; $df = 9$, two-tailed test) (C); mean atmospheric circulation from 5 June to 25 June for years in which the Wainwright SR fraction was less than average and the Peard Bay SR fraction was greater than average (D); mean atmospheric circulation from 5 June to 25 June for years in which the Wainwright SR fraction was greater than average and the Peard Bay SR fraction was less than average (E). Mean wind vectors plotted at every 2nd ith grid point. Color shading indicates wind directional constancy, with correlations between SR fraction and U-component winds (blue contours) and V-component winds (black contours) statistically significant at $r = 0.60$ ($p < 0.05$) and 0.74 ($p < 0.01$).

https://doi.org/10.1371/journal.pone.0265934.g009

changes in their phenology and distribution reported here. For example, maps from Russian surveys from 1968–1982 show a near-continuous gray whale distribution along the Chukotka peninsula, with clustered aggregations of hundreds of whales in the coastal and central south-western Chukchi Sea [38]. Likewise, in a review of Russian research associated with commercial whaling, gray whales were reported as commonly seen feeding on benthic and epibenthic organisms in shallow waters along the Chukotka peninsula where prey concentrations were greater than 100 g/m^2, with distribution extending northwestward to the Eastern Siberian Sea and a very large aggregation (~2000 whales) encountered roughly 160 km offshore between 67˚40-68˚15'N and 169˚40'-172˚W during a 1980/81 expedition [12]. Stomach contents from whales taken in Mechigmensky Bay in 1980/81 contained roughly 122 benthic species [39], with various species of amphipods the most common in occurrence by percentage; e.g. *Pontoporeia femorata* (57.9%), *Ampelisca macrocephala* (53.9%), *Byblus longicornis* (51.3%) and *Lembos arcticus* (47.3%) Similarly, a satellite tracking study of 9 gray whales offshore Chukotka in late summer 2006 found that whales remained in shallow (< 30m) nearshore waters (< 5 km from coast) and were likely feeding on dense aggregations of amphipods [40].

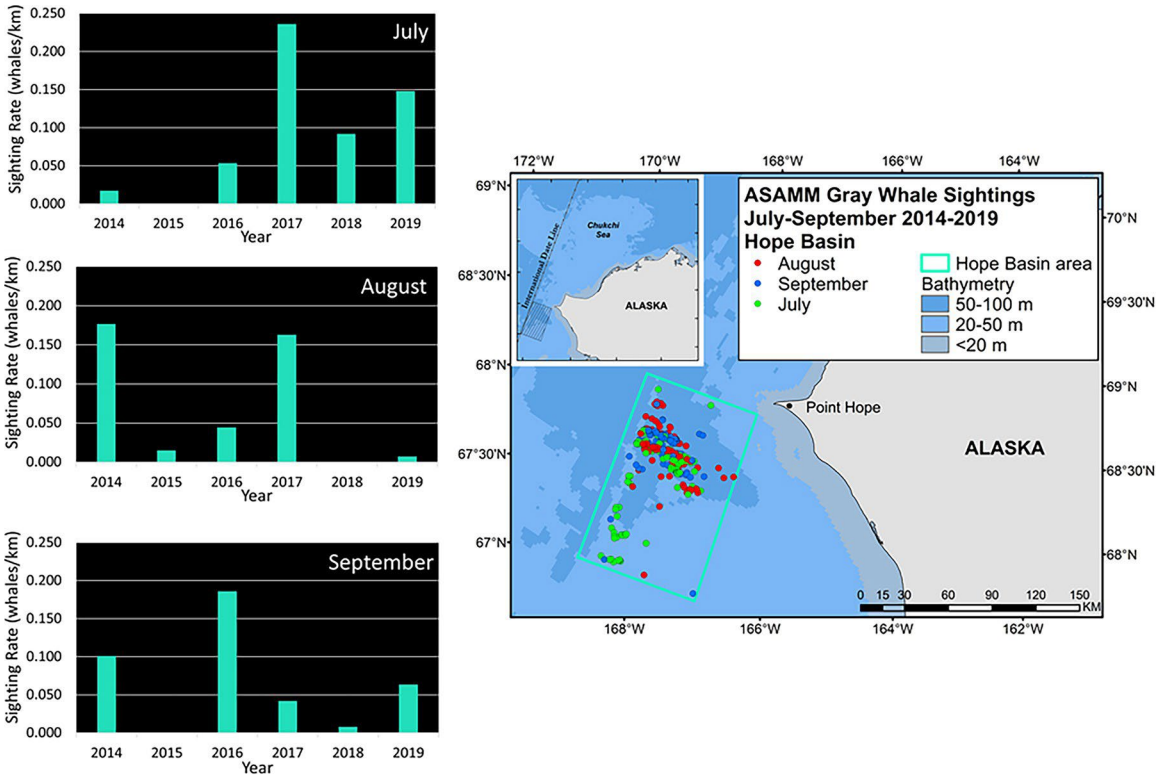

Fig 10. Interannual variability in gray whale monthly distribution and Sighting Rates (SR) for the Hope Basin area in the southern Chukchi Sea, 2014–2019. Inset map shows the location of the Hope Basin area relative to the ASAMM study area. ASAMM data are publicly available at fisheries.noaa.gov/resource/data/1979-2019-aerial-surveys-arctic-marine-mammals-historical-database. Databases used for maps include versions 2012_2014_v0_28, 2015_2017_v22, and 2018_2019_v6.

https://doi.org/10.1371/journal.pone.0265934.g010

While maps from 1975–1980 surveys offshore Alaska depict comparatively few gray whale sightings in the southeastern Chukchi Sea, there is a distinct distribution cluster in what is now called the DBO 3 'hotspot' area [41]. Conversely, the distribution of gray whales in the northern Bering Sea was extensive, with a dense cluster of sightings extending north from St. Lawrence Island through Bering Strait. This dense summertime distribution of gray whales in the DBO 2 area continued at least through the mid-1980s [42, 43], but by the early 2000s gray whale sightings were comparatively sparse and shifted northward following a shrinking pattern of amphipod distribution [44, 45]. In the northeastern Chukchi Sea, focal areas for gray whale distribution in the 1980s included coastal waters between Icy Cape and Pt. Barrow, with a cluster of sightings near Hanna Shoal northwest of Wainwright [42]. There are no year-round acoustic data for the Bering Strait region in 1980s, but gray whales were reported in the northern Bering and Chukchi Seas from May through at least mid-October, with some whales seen as late as December seemingly following the seasonal cycle of sea ice retreat and formation [12, 41].

Changes in gray whale phenology

Gray whale phenology, as described by patterns of calling activity in the Bering Strait region, suggests little change in late May arrival times from 2012–2016 in the northern Bering Sea (DBO 2), and through 2017 in the southern Chukchi Sea (DBO 3). Departure dates inferred from a drop in calling activity changed dramatically thereafter, shifting from November to

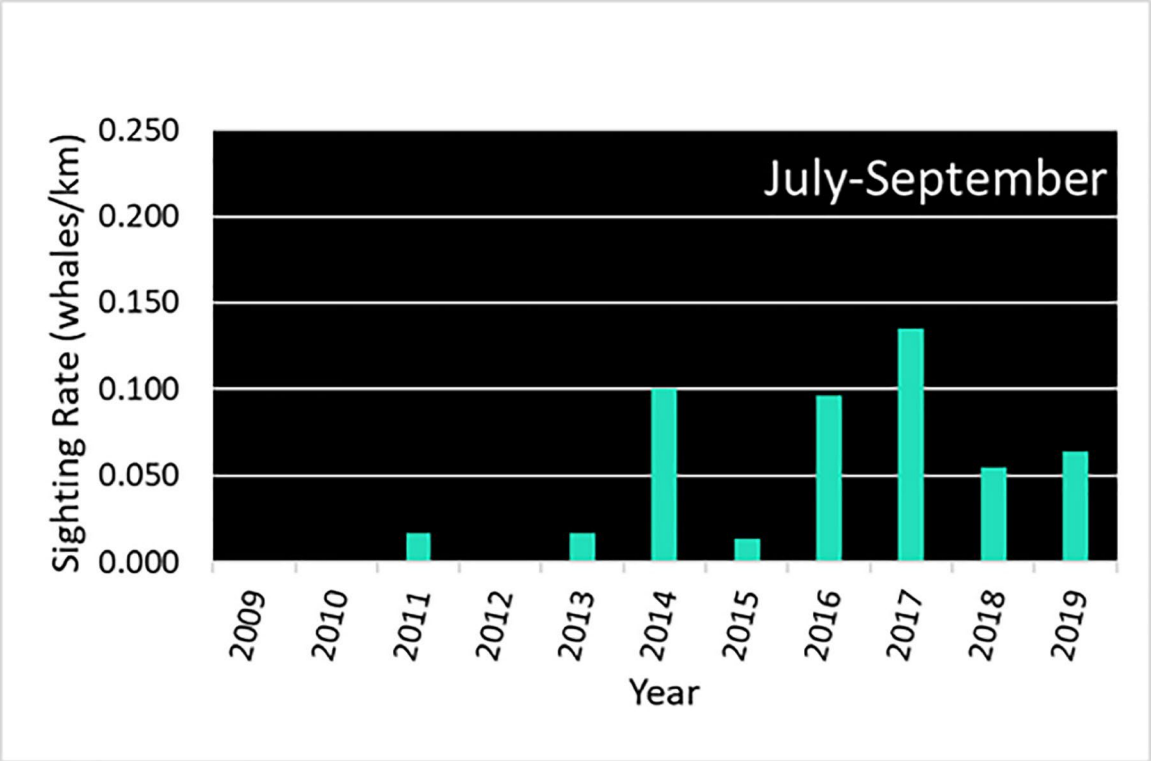

Fig 11. Gray whale combined July-August-September sighting rates (SR) in the Hope Basin area in the southern Chukchi Sea, 2009–2019. ASAMM data are publicly available at fisheries.noaa.gov/resource/data/1979-2019-aerial-surveys-arctic-marine-mammals-historical-database. Databases used for maps include versions 1979_2011_v3_36, 2012_2014_v0_28, 2015_2017_v22, and 2018_2019_v6.

https://doi.org/10.1371/journal.pone.0265934.g011

mid-September in 2016 (DBO 2) and from October to September in 2017 (DBO 3). This shift towards earlier departure dates and shorter residency periods culminated in a near-absence of calling activity in years 2017–2019 (DBO 2) and in 2018–2019 (DBO 3). This drop in calling activity in each region after 2017 and 2018 suggests that gray whales may have abandoned formerly prime foraging areas coincident with the anomalous 2017–2019 winter sea ice loss event [46]. Alternatively, because gray whale acoustic activity was based on detection of only two call types [31, Class 1 and 3], the drop in call detections could reflect changes in age-class composition or behaviors associated with those signals, rather than whale departure.

Table 3. Coefficients of linear correlation between 1 to 12- month time-averaged transport at mooring A3 (Woodgate 2018) and gray whale July-August-September (JAS) sighting rates (SR).

	Volume transport	Heat transport	Freshwater transport
Wainwright JAS SR (df = 9)	**0.799**, 3-month avg (Feb-Apr)	**0.932**, 3-month avg (Feb-Apr)	**0.829**, 3-month avg (Feb-Apr)
Peard Bay JAS SR (df = 9)	Not significant	**-0.766**, 1-month avg (Jan)	*-0.683*, 4-month avg Jan-Apr
Hope Basin Aug SR (df = 4)	*-0.880*, 1-month avg (Feb)	*-0.866*, 4-month avg (Jun-Sep, prior year)	*-0.871*, 1-month avg (Feb)
Hope Basin Sep SR (df = 4)	**-0.962**, 11-month avg	**-0.994**, 10-month avg	**-0.991**, 12-month avg
	Sep prior year -Jul	Nov prior year-Aug	Aug prior year-Jul

Correlations significant at $p < 0.01$ (bold); at *$p<0.05$ (italics)*.

https://doi.org/10.1371/journal.pone.0265934.t003

Table 4. Summary of bathymetry, gray whale prey and circulation drivers (transport and winds) used in iterative correlation analyses with Gray Whale (GW) Sighting Rates (SR) for three analytical areas in the northeastern Chukchi Sea.

Analytical Area	Bathymetry	Gray whale prey (see Table 2)	Transport @ A3 (see Table 3)	Winds over northern Chukchi Sea (see Figs 8, 9)
Peard Bay	Coastal shelf (20-40m deep)	Benthic species: amphipods cumaceans	**JAS GW SR**	**JAS GW SR**
	GW distributed along shore from Peard Bay to Point Barrow (Fig 4B)		negatively correlated with average winter transports	**High 2009–2014** Strong & persistent ENE winds in northern Chukchi in summer interrupt delivery of krill to head of Barrow Canyon, thereby making amphipods more accessible than krill
Wainwright	Offshore shelf	Benthic species:	**JAS GW SR**	**JAS GW SR**
	(40-50m deep)	amphipods, east flank of Hanna Shoal & near head of Barrow Canyon; increased abundance 2015–2017 (Fig 7)	positively correlated with average winter transports	**High 2015–2019**
	GW distribution clustered at the head of Barrow Canyon, NW of Wainwright (Fig 4B)	Pelagic & epi-benthic species: krill, possibly other spp.		Weak & variable winds in the northern Chukchi in summer promote the convergent delivery of krill to the head of Barrow Canyon
Hope Basin	Inflow shelf (~40m deep)	Benthic species: amphipods, in trough 'hotspot'	**August GW SR** negatively correlated with winter or preceding summer transports	ICA results not significant
	GW distribution localized over 50-60m trough SW of Point Hope; southward extension along central channel in 2014, 2018, 2017 (Fig 5B)	Pelagic & epi-benthic species: krill, at frontal system coincident with trough slope (Bluhm et al. 2007)	**September GW SR** negatively correlated with long-term average transports	

JAS = combined July-August-September SR.

https://doi.org/10.1371/journal.pone.0265934.t004

Sightings of gray whales in the Bering Strait region during DBO cruises conducted from July-October suggest that the abrupt changes in calling activity may indicate a modest (*ca*. 30–40 km) shift in distribution away from the recorder locations, rather than a substantial change in gray whale phenology. While propagation modeling has not been conducted at this site, evidence from modeling studies elsewhere in the Bering Sea [47] suggests that gray whale calls are not likely detected beyond a radius of about 35km (20nm). So, for example, a shift of whales northward to the remaining amphipod beds in DBO2 or westward toward the DBO 3 hotspot near the IDL could take them out of detection range of the recorder. However, because the clear truncation in gray whale calling activity coincided with anomalous wintertime sea ice loss event in 2017–2019, this potential shift in phenology and/or distribution is noteworthy. Future deployments of recorders near the remnant amphipod beds in DBO2, or the benthic trough hotspot in DBO3 could help resolve some of the uncertainty regarding shifts in gray whale phenology in the Bering Strait region.

Gray whale infaunal prey abundance, community composition, and environmental factors

Since 2010, the abundance of infaunal crustaceans that gray whales feed upon has significantly declined only in the DBO 2 region. This decline has been ongoing since the late 1980s [42, 43] leaving a reduced area of the northern Bering sea suitable for gray whale foraging. This change is concomitant with a shift in sediment quality due to faster currents, with the finer sediments required for tube building by *A*. *macrocephala* found only where current speed is reduced by land mass constriction south of Bering Strait [45]. Of note, the decline of infaunal crustaceans in DBO 2 is also coincident with an increase in polychaetes and bivalves [32, 33]. Collectively, these data suggest a physiological sensitivity of the dominant amphipods to warming

conditions in the DBO 2 region, with the potential to be outcompeted by organisms more tolerant of seawater changes and able to take advantage of increasing integrated and sediment chlorophyll carbon sources.

While there was no decline in infaunal crustacean abundance in DBO 3, a shift in dominant species was observed. Specifically, *Byblis* spp. (F. Ampeliscidae) was dominant from 1984–2004, but is now largely absent there, although it continues to be abundant in the DBO 5 region. The larger amphipod *Pontoporeia femorata* (F. Pontoporeidae) is now the dominant species in the northern portion of the DBO 3 hotspot, continuing to provide a benthic prey base for gray whales in the 'hotspot' area where they also appear to feed on advected krill [14]. Infaunal crustacean abundance in DBO regions 4 and 5 remained stable and without major changes in dominant fauna, at least through 2017.

Environmental factors and pelagic-benthic coupling

What has influenced the changes or stability of the infaunal crustacean communities across the DBO 2–5 sites? On the face of it, the lack of change to infaunal crustacean abundance in DBO regions 3, 4 and 5 seems inconsistent with a fundamental tenant of the pelagic-benthic coupling model whereby loss of sea ice results in reduced organic carbon from ice-associated algae dropping to the sea floor and thereby cutting food supply for benthic macrofaunal communities [48]. Yet, our observations show that surface sediment chlorophyll increased as sea ice persistence decreased in DBO regions 2 and 4 (Table 2). Notably the significant decrease in sea ice persistence was associated with a significant increase in integrated water column chlorophyll only in DBO 2, although satellite observations indicate increasing productivity north of Bering Strait. These observations support the idea that changes in the timing and magnitude of water column primary production play an important role in carbon transfer to the seafloor [32]. Previous studies indicated that primary production is highest in the northern Bering Sea (DBO 1–2) in April/May, with a production peak north of Bering Strait (DBO 3) in June followed by peak production in the northeastern Chukchi Sea (DBO 4–5) in July [49]. Recently, however, pelagic primary production north of Bering Strait has increased in June and July [9, 50], which may be mismatched with the arrival of zooplankton grazers thereby leaving phytoplankton production to fall to the seafloor and feed benthic macrofauna. This effect on pelagic-benthic coupling may be especially true in the DBO 3 hotspot where deposition is greatest [51]. However, recent sediment trap results indicate that the early season breakup of sea ice at the DBO2-4 sites resulted in shorter periods of chlorophyll and diatom fluxes, thus potentially reducing the biological pump [52], emphasizing the importance of advective carbon to sustain northern DBO sites.

Clearly other environmental factors, such as sea ice thinning [10], increase in ocean heat and freshwater in the Chukchi Sea [5, 6], and changing sediment grain size associated with variability in current speed [32, 33, 45] are also influencing benthic macrofauna community structure. Specifically, increased water temperatures in DBO regions 2–4 is likely affecting the distribution of benthic species, as has been reported for the northeastern Atlantic where *Ampelisca* spp. have extended their distribution northward with warming seawater [53]. Of note, DBO5 stations in Barrow Canyon do not show increased bottom water temperatures, likely due to its dynamic nature and the seasonally variable water masses reported there [54]. Finally, increasing bottom water salinity since 2019 in DBO2 is perhaps indicative of a stronger Anadyr water signal at depth that may also influence nutrient availability to surface waters by mixing upward of AW after storm events. By comparison, DBO4 in the NE Chukchi Sea shows a decrease in bottom water salinity and a decline in integrated chlorophyll a, likely a response to reduced brine production with declining sea ice and variable nutrient content.

Changes in gray whale distribution related to pelagic prey availability

Changes in gray whale distribution based on sightings were evident in the northeastern Chukchi Sea, and somewhat less so in the southern Chukchi Sea. Analyses of the ASAMM data show a mid-decade southwestward shift in distribution of roughly 110 km (60 nm), from coastal waters between Pt. Franklin and Pt. Barrow to waters offshore Wainwright. High gray whale sighting rates (SR) in the coastal Peard Bay area (2009–2014) were associated with strong and persistent easterly winds over the northern Beaufort-Chukchi region, while high SR in the Wainwright area (2015–2019) were associated with weak and variable winds that are conducive to krill remaining on the shelf over winter [28]. Winter-spring transports of volume, heat, and fresh water through Bering Strait were positively correlated with gray whale SR in the Wainwright area and negatively correlated with SR in the Peard Bay area (Table 4). This lagged relationship implies an advective timescale of ~4–6 months for biophysical signals to travel from Bering Strait to Barrow Canyon, which roughly comports with results from drifters traveling along that path in 90 days [55]. The heat signal, in particular, invites speculation that zooplankton development and survivability are enhanced in years with greater transport ultimately leading to improved summer foraging conditions near the head of Barrow Canyon. When krill remain on the northern Chukchi shelf, we postulate that they are subsequently aggregated via the convergence of northern Chukchi currents which promotes gray whale foraging near the head of Barrow Canyon. Although we have no confirmatory evidence (e.g., feces, stomach contents) that gray whales feed on krill in this area, they have been seen skim feeding on krill (Fig 1B) in association with foraging bowhead whales east of Pt. Barrow [28].

Changes in gray whale distribution in the southern Chukchi Sea were evaluated analytically using ASAMM data and, for waters south of 67˚ N, sightings during DBO cruises which provide qualitative information. Both data sources confirmed a strong and consistent aggregation of gray whales at a prey hotspot associated with a 50–60 m trough in the central Chukchi Sea. Furthermore, sightings during DBO cruises showed that this feeding hotspot extends across the international date line, with additional sighting of gray whales common along the Chukotka coast and associated with the western boundary of the central channel.

Implications for the Gray Whale Unusual Mortality Event (UME)

In 2019, a gray whale UME was declared when the number of dead animals found stranded on beaches along their migration route between Alaska and Mexico increased roughly ten-fold [30]. A similar UME occurred in 1999–2000 and the emaciated condition of some of the dead whales during both events suggested starvation or nutritional deficit as a likely cause [30, 56]. Notably, ship strikes, entanglement in fishing gear, and predation by killer whales (*Orcinus orca*) contributed to the death toll during both events, while mortalities due to disease and biotoxins could not be clearly identified [57].

Whether or not gray whales were nutritionally stressed due to a change or reduction in prey availability related to environmental forcing, and/or to increased competition for food resulting from their burgeoning population size, remains a pivotal question with regard to both UME events [58]. The 1999–2000 UME closely followed the powerful 1997–1998 El Niño, while the onset of the 2019 UME was subsequent to extreme ocean heat events in the North Pacific and Gulf of Alaska from 2014–2016 [59], as well as the aforementioned ocean warming and wintertime sea ice loss that persisted in the northern Bering and Chukchi Seas from 2017–2019. The latter event was contributory to a mass mortality of seabirds [45] and likely influenced an ice seal UME [60].

The record on infaunal crustacean communities presented here shows that while gray whale benthic prey abundance declined in the northern Bering Sea from 2010–2019, it remained stable in the Chukchi Sea. Specifically, a significant decrease in amphipod abundance was observed in the DBO 2 region of the northern Bering Sea, a decline that extends a trend that began in the mid-1980s [45]. Conversely, there was no decrease in infaunal crustacean prey abundance evident in DBO regions north of Bering Strait, although there was a shift from a smaller (*Byblis* spp) to a larger (*Pontoporeia* spp) dominant amphipod species in the DBO 3 region. Meanwhile, iterative correlational analyses support the hypothesis that, due to changes in wind-driven circulation, gray whales may be finding more opportunities to feed on krill near the head of Barrow Canyon in the northeastern Chukchi Sea.

While changes in gray whale prey, either among benthic infauna or between benthic and pelagic species, will have nutritional ramifications, it seems unlikely that a change in diet alone would result in a dramatic upsurge in mortality. In other words, from the perspective of gray whale prey abundance, our observations provide context but not causation for poor nutritional condition of gray whales that feed north of Bering Strait. Conversely, if a portion of the gray whale population exhibits feeding-site-fidelity to the northern Bering Sea, that could result in nutritional stress for those animals. Indeed, there is evidence at the local scale that biophysical events that impact gray whale prey availability can lead to changes in phenology, a reduction in feeding, and signs of poor body condition. This was the case in 2005 when late spring ocean conditions off the Oregon coast markedly decreased abundance of epi-benthic mysids leaving the small population of gray whales that feed there over summer with a nutritional deficit [61]. A subsequent study showed body condition of whales in these whales responded to upwelling conditions along the Oregon coast, with animals in 'good' condition following strong upwelling years (2013–2015) and in comparatively 'poor' condition following years of weak upwelling (2016–2018) [62].

The AMP model as a framework for future research

The Pacific Arctic marine ecosystem is in a state of transformation as it responds to amplified planetary warming [8]. In constructing the conceptual AMP model, we purposely imbedded mechanistic features such as transport through Bering Strait, pelagic-benthic coupling, advection, and upwelling as key drivers that influence biological outcomes in the region (Fig 2B) [29]. The challenge is to elucidate how these biophysical drivers interact in this productive inflow shelf system. Results from this and past studies suggests that this question may be best approached by investigating factors that (i) drive aspects of pelagic benthic coupling in the northern Bering and southern Chukchi Seas (DBO 2 and 3), and (ii) influence downstream advection, upwelling and ocean circulation dynamics in the northeastern Chukchi Sea (DBO 4 and 5). This type of approach was used to develop a mechanistic model for the persistence of benthic 'hotspots' in DBO regions 1–5, showing that those in regions 2, 3, and 5 rely on carbon supplied from upstream biological production, while those in regions 1 and 4 were supplied by local production [63]. As in past studies focused on macrofaunal biomass [32, 33], our observations of changes in infaunal crustacean prey abundance in DBO regions 2 and 3 suggest that the timing and magnitude of water column primary production, bottom water temperatures, bathymetric channeling, sediment grain size and the responses of other macrofaunal species may be as important as sea ice persistence in influencing pelagic-benthic coupling dynamics that lead to benthic community transitions.

The AMP conceptual model provides a rudimentary framework to guide future research aimed at elucidating changes in both benthic and pelagic realms of the Pacific Arctic. In the benthic realm, a focus on linking sea ice metrics [10] to biophysical data will provide a clearer

picture of their combined influence on productivity and community structure [33]. The addition of sediment trap data [52] can add additional detail to track pelagic-benthic coupling processes in the region. A key question for the Pacific Arctic region is: how important are krill as prey for upper trophic level predators? This requires investigating the more ephemeral prey aggregations in the epi-benthic and pelagic realm. The ICA results presented here suggests that the offshore shift of gray whale distribution after 2015 may have been influenced in part by the availability of krill in the northeastern Chukchi Sea. While this speculation builds on research focused on bowhead whale (*Balaena mysticetus*) foraging on krill in adjacent waters of the western Beaufort Sea [28], we have no direct evidence that gray whales are feeding on krill. Seabirds can also act as sentinels of krill availability, especially short tailed shearwaters (*Puffinus tenuirostris*) who feed on these advected prey in the northeaster Chukchi Sea more often now in the 1980s [64]. Using both marine mammal and bird species as ecosystem sentinels can alert researchers to changes in the pelagic realm across a broad range of space and time related to each species natural history [22] and we advocate for their continued inclusion in DBO and other ocean observatory protocols.

Supporting information

S1 Table. Summary of DBO cruises where a marine mammal watch was conducted.

(PDF)

S2 Table. Summary of survey effort, gray whale sighting and calculation of Sighting Rate (SR) from ASAMM 2009–2019.

(PDF)

S3 Table. Sampling details for crustacean abundance used in this paper.

(PDF)

Acknowledgments

We thank the captains and crews of the research vessels that provided safe operations and space for a marine mammal observer on the DBO research cruises. We appreciate the passive acoustic team from AFSC and CICOES who manually analyzed data from recorders on moorings in DBO2 and DBO3: Eric K. Braen, Stephanie L. Grassia, Eliza G. Ives, Daniel F. Woodrich, and Dana L. Wright. We thank the marine mammal observers, pilots, mechanics, programmers, flight followers, and organizations that enabled ASAMM surveys to be conducted safely and effectively, in particular Megan Ferguson, Amelia Brower, Amy Willoughby, NOAA Aircraft Operations Center, and Clearwater Air, Inc. The scientific results and conclusions, as well as any views or opinions expressed herein, are those of the author(s) and do not necessarily reflect those of NOAA or the Department of Commerce. Reference to trade names does not imply endorsement by the National Marine Fisheries Service or NOAA. JMG thanks past and current support staff at CBL for technical assistance, especially Stephanie Soques and Alicia Clark, and Alynne Bayard for GIS mapping and data analytics. Finally, we thank Dr. Karen Frey (Clark University) for providing Fig 2A, and Dr. Leigh Torres (OSU) and an anonymous reviewer for constructive comments that guided improvements to the final manuscript.

Author Contributions

Conceptualization: Sue E. Moore, Janet T. Clarke, Stephen R. Okkonen, Jacqueline M. Grebmeier.

Data curation: Janet T. Clarke, Jacqueline M. Grebmeier, Catherine L. Berchok, Kathleen M. Stafford.

Formal analysis: Janet T. Clarke, Stephen R. Okkonen, Jacqueline M. Grebmeier, Catherine L. Berchok, Kathleen M. Stafford.

Funding acquisition: Jacqueline M. Grebmeier, Catherine L. Berchok, Kathleen M. Stafford.

Project administration: Sue E. Moore.

Writing – original draft: Sue E. Moore, Janet T. Clarke, Stephen R. Okkonen, Jacqueline M. Grebmeier.

Writing – review & editing: Sue E. Moore, Janet T. Clarke, Stephen R. Okkonen, Jacqueline M. Grebmeier, Catherine L. Berchok, Kathleen M. Stafford.

References

1. Overland JE, Dunlea E, Box JE, Corell R, Forsius M, Kattsov V, et al. The urgency of Arctic change. Polar Sci. 2019 https://doi.org/10.1016/j.polar.2018.11.008.
2. Fetterer F, Knowles K, Meier WN, Savoie M, Windnagel AK. Sea Ice Index, Version 3. North Regional Sea Ice Monthly, updated daily. 2017 Boulder, Colorado USA. NSIDC: National Snow and Ice Data Center https://doi.org/10.7265/N5K072F8.
3. Polyakov IV, Aikire MB, Bluhm BA, Brown KA, Carmack EC, Chierichi M. Borealization of the Arctic Ocean in response to anomalous advection from sub-Arctic seas. Frontar Sci. 2020 7:491 https://doi.org/10.3389/fmars.2020.00491
4. Woodgate RA. Increases in the Pacific inflow to the Arctic from 1990 to 2015, and insights into seasonal trends and driving mechanisms from year-round Bering Strait mooring data. Prog Oceanogr. 2018 160:124–54.
5. Woodgate RA, Peralta-Ferriz C. Warming and freshening of the Pacific inflow to the Arctic from 1990–2019 implying dramatic shoaling in Pacific Winter Water ventilation of the Arctic water column. Geophy Res Lett. 2021 48, e2021GL092528. https://doi.org/10.1029/2021GL092528.
6. Danileson SL, Ahkinga O, Ashjian C, Basyuk E, Cooper LW, Eisner L, et al. Manifestation and consequences of warming and altered heat fluxes over the Bering and Chukchi Sea continental shelves. Deep-Sea Res II 2020 https://doi.org/10.1016/j.dsr2.2020.104781.
7. Duffy-Anderson JT, Stabeno P, Andrews AG, Kieciel K. et al. Responses of the northern Bering Sea and the southeast Bering sea pelagic ecosystems following record-breaking low winter sea ice. Geophys Res Lett. 2019 46 https://doi.org/10.1029/2019 GL083396.
8. Huntington HP, Danielson SL, Wiese FK, Baker M, Boveng P, Citta JJ. et al. Evidence suggests potential transformation of the Pacific Arctic ecosystem is underway. Nat Clim Chang. 2020 https://doi.org/10.1038/s41558-020=0695-2.
9. Lewis KM, van Kijken GL, Arrigo R. Changes in phytoplankton concentration now drive increased Arctic Ocean primary production. Science. 2020 369:198–202, https://doi.org/10.1126/science.aay8380PMID: 32647002
10. Frey KE, Comiso JC, Stock LV, Young LNC, Cooper LW, Grebmeier JM. A comprehenvice satellite-based assessment across the Pacific Arctic Distributed Biological Observatory shows wide-spread late-season sea surface warming and sea ice declines with variable influences on primary production. Plos ONE NOAA DBO Collection.
11. Nerini M. A review of gray whale feeding ecology. In: Jones ML, Swartz SL, Leatherwood S, editors. The Gray Whale *Eschrichtius robustus*. Florida: Academic Press; 1984. pp. 423–50. https://doi.org/10.1128/aem.47.2.421-423.1984 PMID: 6712212
12. Yablokov A, Bogoslovskaya LS. A review of Russian research on the biology and commercial whaling of the gray whale. In: Jones ML, Swartz SL, Leatherwood S, editors. The Gray Whale *Eschrichtius robustus*. Florida: Academic Press, 1984. pp.465–85.
13. Brower AA, Ferguson MC, Schonberg SV, Jewett SC, Clarke JT. Gray whale distribution relative to benthic invertebrate biomass and abundance: Northeastern Chukchi Sea 2009–2012. Deep-Sea Res II 2017 144: 156–174 http://dx.doi.org/10.1016/j.dsr2.2016.12.00.
14. Bluhm BA, Coyle KO, Konar K, Highsmith R. High gray whale relative abundances associated with an oceanographic front in the south-central Chukchi Sea. Deep-Sea Res II 2007 54 (23–26): 2919–33.

15. Kim SL, Oliver JS. Swarming benthic crustaceans in the Bering and Chukchi seas and their relation to geographic patterns in gray whale feeding. Can J Zool. 1989 67:1531–42.
16. Darling JD, Keogh IE, Streeves TE. Gray whale (*Eschrichtius robustus*) habitat utilization and prey species off Vancouver Island B.C. Mar Mamm Sci. 1998 14: 692–720.
17. Nelson TA, Duffus DA, Robertson C, Feyrer LJ. Spatial-temporal patterns in intra-annual gray whale foraging: Characterizing interactions between predators and prey in Clayquot Sound, British Columbia, Canada. Mar Mamm Sci. 2008 24(2): 356–70.
18. Hazen EI, Abrams B, Brodie S, Carroll G, Jacox MG, Savoca MC, et al. Marine top predators as climate and ecosystem sentinels. Front Ecol Environ. 2019 17 (10): 565–574, https://doi.org/10.1002/fee.2125
19. Moore SE. Marine mammals as ecosystem sentinels. 2008 J Mamm. 89(3) 534–40.
20. Grebmeier JM, Moore SE, Cooper LW, Frey KE. The Distributed Biological Observatory: a change detection array in the Pacific Arctic–an Introduction. Deep-Sea Res II 2019 162: 1–7.
21. Moore SE, Logerwell E, Eisner L, Farley EV Jr, Harwood LA, Kuletz K, et al. Marine fishes, birds and mammals as sentinels of ecosystem variability and reorganization in the Pacific Arctic region. In: Grebmeier JM, Maslowski W, editors. The Pacific Arctic Region-ecosystem status and trends in a rapidly changing environment. New York: Springer, 2014. pp.337–392.
22. Moore SE, Kuletz KJ. Marine birds and mammals as ecosystem sentinels in and near Distributed Biological Observatory regions: an abbreviated review of published accounts and recommendations for integration to ocean observatories. Deep-Sea Res II 2019 162: 211–217.
23. Moore SE. Climate change. In: Wursig B, Thewissen JGM, Kovacs KM, editors. Encyclopedia of Marine Mammals, 3rd Edition London: Elsevier Academic Press, 2018. pp.194–197.
24. Berchok CL, Wright DL, Braen EK, Grassia SL, Woodrich DF, Crance JL, et al. Seasonal occurrence of marine mammals at DBO regions 1–5. Plos ONE NOAA DBO Collection.
25. Clarke, JT, Brower, AA, Ferguson, MC, Willoughby, AL, Rothrock, AD. Distribution and Relative Abundance of Marine Mammals in the Eastern Chukchi Sea, Eastern and Western Beaufort Sea, and Amundsen Gulf, 2019. Annual Report, OCS Study BOEM 2020–027. 2020; Marine Mammal Laboratory, Alaska Fisheries Science Center, NMFS, NOAA, 7600 Sand Point Way NE, F/AKC3, Seattle, WA 98115–6349.
26. Moore SE, Haug T, Vikingsson GA, Stenson GB. Baleen whale ecology in Arctic and subarctic seas in an era of rapid habitat alteration. Prog Oceanogr. 2019 176:102–18. https://doi.org/10.1016/j.pocean.2019.05.010.
27. Moore SE. Is it 'boom times' for baleen whales in the Pacific Arctic region? Biol Lett. 2016 https://doi.org/10.1098/rsbl.2016.0251 PMID: 27601724
28. Ashjian CJ, Okkonen SR, Campbell RG, Alatalo P. Lingering Chukchi Sea sea ice and Chukchi Sea mean winds influence population age structure of euphausiids (krill) found in the bowhead whale feeding hotspot near Pt. Barrow. PLoS ONE 16(7): e0254418. https://doi.org/10.1371/journal.pone.0254418 PMID: 34252123
29. Moore SE, Stabeno PJ, Grebmeier JM, Okkonen SR. The Arctic Marine Pulses Model: linking annual oceanographic processes to contiguous ecological domains in the Pacific Arctic. Deep-Sea Res II 2018 152:8–21.
30. Christiansen F, Rodriguez-Gonzalez F, Martinez-Aguilar S, Urban J, Swartz S, Warick H, et al. Poor body condition associated with an unusual mortality event in gray whales. Mar Ecol Prog Ser. 2021 658 237–252 https://doi.org/10.3354/meps13585
31. Burnham R, Duffus D, Mouy X. Gray whale (*Eschrictius robustus*) call types recorded during migration off the west coast of Vancouver Island. Front Mar Sci. 2018 5:1–11. https://doi.org/10.3389/fmars.2018.00043 PMID: 29552559
32. Grebmeier JM, Frey KE, Cooper LW, Kedra M. Trends in benthic macrofaunal populations, seasonal sea ice persistence and bottom water temperatures in the Bering Strait region. Oceanogr. 2018 31(2) https://doi.org/10.5670/oceanog.2018.224.
33. Grebmeier JM, Cooper LW, Goethel CL, Frey KE. Time series macrobenthic populations and sediment dynamic trends in the Northern Bering and Chukchi Seas. Plos ONE NOAA DBO Collection
34. ESRI 2020. ArcGIS Desktop: Version 10.8.1 Redlands, CA: Environmental Systems Research Institute, Inc.
35. Okkonen SR, Ashjian CJ, Campbell RG, Alatalo P. The encoding of wind forcing into the Pacific-Arctic pressure head, Chukchi Sea ice retreat and late-summer Barrow Canyon water masses. Deep-Sea Res II 2019 162: 22–31 https://doi.org/10.1016/j.dsr2.2018.05.00
36. Okkonen S, Ashjian C, Campbell RG, Alatalo P. Diel vertical migration: a diagnostic for variability of wind forcing over the Beaufort and Chukchi Seas. Prog in Oceanogr. 2020 181, 2020102265 doi.org/10.1016/j.pocean.2020.102265.

37. Kalnay E, Kanamitsu M, Kistler R, Collins W, Deaven D, Gandin L, et al. 1996. The NCEP/NCAR 40-year reanalysis project. Bull Am Meteorol Soc. 1996 77: 437–70.

38. Berzin AA. Soviet studies of the distribution and numbers of the gray whale in the Bering and Chukchi seas, from 1968–1982. In: Jones ML, Swartz SL, Leatherwood S, editors. The Gray Whale *Eschrichtius robustus*. Florida: Academic Press; 1984. pp. 409–422.

39. Blokhin SA. Investigations of gray whales taken in the Chukchi coastal waters, USSR. In: Jones ML, Swartz SL, Leatherwood S, editors. The Gray Whale *Eschrichtius robustus*. Florida: Academic Press; 1984. pp. 487–510.

40. Heide-Jorgensen MP, Laidre KL, Litovka D, Jensen MV, Grebmeier JM, Sirenko BI. Identifying gray whale (*Eschrichtius robustus*) foraging grounds along the Chukotka Peninsula, Russia, using satellite telemetry. Polar Biol. 2012 35: 1035–1045 https://doi.org/10.1007/s00300-011-1151-6

41. Braham HW. Distribution and migration of gray whales in Alaska. In: Jones ML, Swartz SL, Leatherwood S, editors. The Gray Whale *Eschrichtius robustus*. Florida: Academic Press; 1984. pp. 249–266.

42. Moore SE, DeMaster DP, Dayton PK. Cetacean habitat selection in the Alaskan Arctic during summer and autumn. Arctic 2000 53(4): 432–447.

43. Coyle KO, Bluhm B, Konar B, Blanchard A, Highsmith RC. Amphipod prey of gray whales in the northern Bering Sea: comparison of biomass and distribution between 1980s and 2002–2003. Deep-Sea Res II. 2007 54: 2906–2918.

44. Moore SE, Grebmeier JM, Davies JR. Gray whale distribution relative to forage habitat in the northern Bering Sea: current conditions and retrospective summary. Can J Zoo. 2003 81: 734–742.

45. Kędra M, Grebmeier JM. Ecology of Arctic shelf and deep ocean benthos. In: Thomas DN, editor. Arctic Ecology. Wiley-Blackwell 2021 pp. 325–355.

46. Kuletz K, Cushing D, Labunski E. Distributional shifts among seabird communities of the Northern Bering and Chukchi seas in response to ocean warming during 2017–2019. Deep-Sea Res II. 2020 181–182, doi.org/10.1016/j.dsr2.2020.104913.

47. Baumgartner MF, Lysiak NSJ, Esche HC, Zerbini AN, Berchok CL, Clapham PJ. Associations between North Pacific right whales and their zooplanktonic prey in the southeastern Bering Sea. Mar Ecol Prog Ser 2013 490:267–284.

48. Grebmeier JM, Barry JP. The influence of oceanographic processes on pelagic–benthic coupling in polar regions: a benthic perspective. J Mar Syst. 1991 2: 495–518.

49. Hill V, Ardyna M, Lee SH, Varela DE. Decadal trends in phytoplankton production in the Pacific Arctic Region from 1950 to 2012. Deep-Sea Res II. 2018 152: 82–94, doi.org/101016/j.dsr2.201812.015.

50. Waga H, Hirawake T, Grebmeier JM. Recent changes in benthic macrofaunal community composition in relation to physical forcing in the Pacific Arctic. Polar Biol. 2020 43:285–294 https://doi.org/10.1007/s00300-020-02632-3.

51. Grebmeier JM, Bluhm BA, Cooper LW, Danielson SL, Arrigo KR, Blanchard AL, et al. Ecosystem characteristics and processes facilitating persistent microbenthic biomass hotspots and associated benthivory in the Pacific Arctic. Prog Oceanogr. 2015 136: 92–114, doi.org/10.1016/j.pocean.2015.05.006.

52. Laland C, Grebmeier JM, McDonnell A, Hopcroft RR, O'Daly S, Danielson S. Impact of a warm anomaly in the Pacific Arctic region derived from time-series export fluxes. Plos ONE 16(8): e0255837 https://doi.org/10.1371/journal.pone.0255837 PMID: 34398912

53. Dauvin J-C., Sampaio L., Rodrigues A.M., and Quintino V. 2021. Taxonomy and ecology of sympagic *Ampelisca* species (Crustacea, Amphipoda) from the Strait of Gibraltar to the Strait of Dover, North-Eastern Atlantic. Front Mar Sci 2021 https://doi.org/10.3389/fmars.2020.590273 PMID: 35004707

54. Pickart RS, Spall MA, Lin P, Bahr F, McRaven LT, Arrigo KR, et al. Physical controls on the macrofaunal benthic biomass in Barrow Canyon, Chukchi Sea. J Geophys Res Oceans. 2021 126, e2020JC017091 doi.org/10.1029/2020JC017091.

55. Stabeno P, Kachel N, Ladd C, Woodgate R. Flow patterns in the eastern Chukchi Sea. J Geophys Res Oceans. 2018 123 1177–1195 https://doi.org/10.1002/2017JC013135.

56. Moore SE, Urban J, Perryman WL, Gulland F, Perez-Cortes H, Wade PR, et al. Are gray whales hitting 'K' hard? Mar Mamm Sci. 2001 17(4): 954–958.

57. Stimmelmeyr r, Gulland FMD. Gray whale (*Eschrichtius robustus*) health and disease: review and future directions. Front Mar Sci. 2020 https://doi.org/10.3389/fmars.2020.588820

58. Stewart JD, Weller DW. Abundance of eastern north Pacific gray whales 2019–2020. NOAA-TM-NMFS-SWFSC-639 https://doi.org/10.25923/bmam-pe91.

59. Suryan RM, Arimitsu ML, Coletti HA, Hopcroft RR, Lindeberg MR, Barbeaux SJ, Batten SD, et al. Ecosystem response persists after prolonged marine heat waves. Nature Sci Rep. 2021 https://doi.org/10.1038/s41598-021-83818-5.

60. Boveng PL, Ziel HL, Mc Clintock BT, Cameron MF. Body condition of phocid seals during a period of rapid environmental. Change in the Bering Sea and Aleutian Islands, Alaska. Deep-Sea Res II. 2020 181–182 https://doi.org/10.1016/j.dsr2.2020.104904.

61. Newell CL, Cowles TJ. Unusual gray whale *Eschrichtius robustus* feeding in the summer of 2005 off the central Oregon Coast. Geophys Res Lett. 2006 33 https://doi.org/10.1029/2006gl027800 PMID: 19122778

62. Lemos LS, Burnett JD, Chandler TE, Sumich JL., Torres LG. Intra- and inter-annual variation in gray whale bod condition on a foraging ground. Ecosphere 2020 11(4): e03094 https://doi.org/10.1007/ ecs2.3094

63. Feng Z, Rubao J, Ashjian C, Zhang J, Campbell R, Grebmeier GM. Benthic hotspots on the northern Bering and Chukchi continental shelf: spatial variability in production regimes and environmental driv- ers. Prog Oceanogr. 2021 https://doi.org/10.1016/j.pocean.2020.102497.

64. Gall AE, Day RH, Weingartner TJ. Structure and variability of the marine-bird community in the north- eastern Chukchi Sea. Cont Shelf Res. 2013 67: 96–115 doi.org/10.1016/j.csr.2012.11.004.

Chapter 2: Acoustic Behaviour and Vocal Repertoire of Transient Killer Whales (*Orcinus orca*) in the Bering Strait and Southern Chukchi Sea

This chapter is the result of a Marine Biology Honours thesis of Abigail Mottu at St. Andrews University, Scotland. It will be revised and submitted as a peer-reviewed manuscript:

Mottu, A, Oswald JN, Wallace EE and Stafford KM. *in prep*. Acoustic detections of transient killer whales in the northern Bering and southern Chukchi Seas. Global Climate Change Biology

Abstract

In the Pacific Arctic, Killer whales (Orcinus orca) are historically classified as three genetically, morphologically, and acoustically distinct ecotypes: residents, offshores, and transients. Despite recent studies reporting an apparent increase in transient killer whale sightings in the Bering/Chukchi/Beaufort seas, there is still a lack of acoustic analysis of this phenomenon. Transient killer whale calls were recorded using passive acoustic data from three moored autonomous recorders in the Bering Strait and the southern Chukchi Sea from September 2009 to December 2018. An unsupervised neural network was used to categorize these calls into specific categories in order to generate a vocal repertoire of transients in this area. This identified 29 discrete, pulsed calls in the vocal repertoire of this transient population, which showed little apparent overlap with other described repertoires of transients. This study provides the first acoustic catalogue of transient killer whale calls in the Bering Strait and the southern Chukchi Sea.

180011049

1. Introduction

Many social animals have evolved complex vocal repertoires to facilitate a range of interactions, including, but not limited to, group cohesion, predator avoidance, and mating (Elie and Theunissen, 2016; Gall and Manser, 2017; Charlton et al., 2018). For example, the repertoire of Common Bottlenose Dolphins (*Tursiops truncatus*) consists of signature whistles in which an individual produces a distinctive whistle type that broadcasts the owner's identity (Janik and Sayigh, 2013). More broadly, vocal repertoires will typically vary interspecifically and can aid researchers in developing quantitative methodologies for studying these animals' location and behavioural attributes (Janik and Knörnschild, 2021). For marine mammals, understanding vocal repertoires is of particular importance because visual surveys can only detect a fraction of the animals present. This limited detection ability is because surveys are often constrained by bad weather, limited to daylight hours, and the overall sighting opportunities are solely when the animal(s) surfaces (Mellinger et al., 2007; Gillespie, 2019). Additionally, tagging methodologies are more expensive, short-lived (tags detach after roughly 25 days), and give information only on select individuals (Newman and Springer, 2008).

To combat these limitations, an increasing number of studies rely on Passive Acoustic Monitoring Methods (Mellinger et al., 2007). Recent technological advances have made Passive Acoustic Monitoring (PAM) a widely accessible, low-cost, and non-invasive way to understand species' spatiotemporal distribution and abundance since it capitalizes on distinct cetacean vocalizations used for different behaviours (Gillespie, 2019; Mellinger et al., 2007; Van Parijs et al., 2009; Hannay et al., 2013; Sousa-Lima et al., 2013). Some species, like killer whales (*Orcinus orca*), exhibit distinct, intraspecific vocalizations, which makes them an ideal candidate

180011049

for passive acoustic methodology (e.g. Deecke et al., 2010; Thomsen et al., 2001; Filatova et al., 2015; Emmons et al., 2021).

Killer whales are found in every ocean worldwide, making them the most widely distributed cetacean (Myers et al., 2021). Killer whales' overall success in occupying a range of ecological niches can be attributed to the intraspecific variation of hunting techniques derived from morphological and acoustic differences (de Bruyn et al., 2012). This intraspecific differentiation is not limited to geographically delineated areas but can also be found in sympatric populations. There are three described ecotypes of killer whales in the Pacific Arctic: residents, transients, and offshores. Despite inhabiting the same geographic region, these three ecotypes are all reproductively isolated from one another and differ in various ways (Hoelzel et al., 2007). Resident killer whales ascribe to a tight matrilineal social structure, are fish specialists, and display high site fidelity (home ranges < 200 km) (Deecke et al., 2010; Ford et al., 1998; Fearnbach et al., 2013). Transient killer whales feed primarily on marine mammals, have a much more fluid social structure than residents, in which it is more common to spread from their original pod, and have presumably large home ranges spanning from the Aleutian Islands to Barrow, Alaska (Ford et al., 1998; Baird and Whitehead, 2000; Clarke et al., 2013). Much less is known about offshore killer whales, but they are presumed to feed primarily on sharks and fish and spend time along the continental shelf (>15 km offshore) (Dahlheim et al., 2008). In addition to the differences in preferred prey, social structure, and geographic range, these three ecotypes all differ acoustically.

Sound is used by killer whales for foraging and social interactions, such as maintaining group cohesion (Madrigal et al., 2021; Ford and Fisher, 1983). Killer whales produce distinct sounds for different functions. These vocalizations can be placed into three discrete categories: whistles,

180011049

echolocation clicks, and pulsed calls (Ford, 1989; Barrett-Lennard et al., 1996; Riesch and Deecke, 2011; Deecke et al., 2005; Samarra et al., 2010; Filatova et al., 2012; Deecke et al., 2010; Ford and Fisher 1983; Filatova et al., 2015). Whistles are typically non-pulsed tonal sounds that are used for socializing, close-range interaction, and possibly food sharing (Ford, 1989; Riesch et al., 2006; Riesch and Deecke, 2011). Whistles produced by resident and transient killer whales differ in duration, end frequency, and maximum frequency (Thomsen et al., 2001; Riesch and Deecke, 2011). More recent studies have found that killer whales also produce high-frequency whistles ranging up to 75 kHz. It is still unclear the purpose of these ultrasonic whistles, but they have a higher degree of directionality and are presumed to be used for private communication (Samarra et al., 2010; Andriolo et al., 2015; Simonis et al., 2012). Echolocation clicks are short, broad-spectrum pulses of sound. These clicks are primarily used for hunting since they provide information to the individual emitting the signal about the target animal (Ford, 1989; Barrett-Lennard et al., 1996). Offshore and resident killer whales use echolocation clicks to forage, whereas transients rarely echolocate (Ford, 1989; Deecke et al., 2005). Pulsed calls (hereafter referred to as “calls”) are the most common form of killer whale vocalization. They are used for group recognition and behavioural coordination (Ford, 1989; Deecke et al., 2005). Calls vary in pitch across these three ecotypes in which offshores have the highest minimum frequency, followed by residents, then transients (Foote and Nystuen, 2008). In general, calls are highly stable and, in many studies, are further categorized into discrete call types (Sharpe et al., 2017; Ford and Fisher, 1983; Ford, 1991; Madrigal et al., 2021; Filatova et al., 2012; Deecke et al., 2010). Recently, multi-part calls, in which a singular call contains a high- and low-frequency component, have been described in resident and transient populations (Filatova et al., 2015; Madrigal et al., 2021). In residents, these are thought to aid in maintaining contact and

monitoring the position of individuals when pods are mixed (Filatova et al., 2015). This comparison of killer whale sounds across ecotypes illustrates that transients vocalize significantly less often than their counterparts. This finding has been attributed to ecotypes differences in preferred prey types. Since transient killer whales' preferred choice of prey are marine mammals, it is therefore suggested that they rarely vocalize to avoid prey eavesdropping (Deecke et al., 2005).

The distinct differences in killer whale vocalizations can be explained by the fact that they are socially learned behaviours. This creates dialects between ecotypes despite no geographical boundaries. (Ford 1991; Deecke et al., 2010; Yurk et al., 2002; Filatova et al., 2012). Evidence suggests even greater acoustic divergence within these ecotypes into subpopulations known as acoustic clans (Ford 1991). Acoustic clans are collections of pods that have shared call types between their group-specific repertoire. In residents, this acts as a reflection of maternal lineage (Ford, 1991; Yurk et al., 2002; Deecke et al., 2010; Miller and Bain, 2000). While it is much more thoroughly understood in residents, there is evidence that suggests that transients also exhibit clan structure (Ford and Ellis, 1999; Sautilus et al., 2005; Sharpe et al., 2017). A study on the genetics of killer whales in this area indicated the presence of three subpopulations of transients: West Coast transients, Gulf of Alaska transients, and AT1 transients (Barrett-Leonard, 2000). Further studies have demonstrated that beyond varying genetically, these populations exhibit different acoustic behaviours. Deecke (2003) explored calls from West Coast transients in which he described a repertoire difference between the California population, and the British Columbia and Southeast Alaska population. Sautilus *et al* (2005) described 14 discrete calls in the AT1 transient subpopulation and found no matches with neither the West Coast nor Gulf of Alaska transient subpopulations (Deecke et al., 2005). A more recent genetic analysis of

180011049

transients in the Gulf of Alaska population suggests that this described subpopulation can actually be divided into five further subpopulations (Parsons et al., 2013). Sharpe *et al* (2017) supported these findings, providing the first extensive catalogue of group-specific call types in the western Gulf of Alaska: Western Aleutian Islands; Pribilof Islands; Eastern and Central Aleutian Islands. The authors described 36 call categories in which only six were attributed to more than one region, suggesting that each region has its own repertoire of distinct call types and can in turn be deemed an acoustic clan (Ford, 1991).

Current stock assessments of transient killer whales group together the Gulf of Alaska, Aleutian Islands, and the Bering Sea populations together in one stock (Allen and Angliss, 2012). However, recent findings suggest that these should be considered subpopulations (Parsons et al., 2013; Sharpe et al., 2017). Madrigal *et al* (2021) was the first study to provide a repertoire in which they confirmed the presence of transient Killer Whales north of Pribilof Islands (off of Point Hope, Alaska), providing acoustic support for this subpopulation hypothesis. The acoustic catalogues outputted by Sharpe *et al* (2017) and Madrigal *et al* (2021) resulted in no exact matches, which could either be due to inconsistent methodologies or they could possibly indicate different subpopulations of transients in these two locations.

While Madrigal *et al* (2021) is the first and only study to analyze transient killer whale repertoires north of the Pribilof Islands, numerous studies suggest that there has been an increase in transient killer whale sightings in these more northern areas (Frost et al., 2012; Hannay et al., 2013; Clarke et al., 2013; Stafford, 2019). Frost *et al* (1992) reported an unusual number of killer whales in the southeastern Bering Sea in 1989 and 1990. Twenty years later, Clarke *et al* (2013) found six sightings of 37 whales just north of the Bering Strait region in the southern Chukchi Sea. Even more recently, Stafford (2019) found a marginally significant increase in killer whale

sightings in the fall months just north of the Bering Strait in the southern Chukchi Sea. All of these indicate that these sightings are presumably transient killer whales.

Over the past several decades, the Arctic has warmed at twice the global rate, which has a range of chemical, physical, and biological consequences, namely affecting sea ice extent (Grebmeier, 2012). The Bering Sea is one of the most productive marine ecosystems worldwide, with a host of climatic, biological, and oceanographic interactions (Woodgate, 2022). Recently, the Bering Sea has been deemed a "hotspot" for the effects of climate change (Sigler, 2010). The Bering Sea has been especially vulnerable to climate change because the region's productivity relies on the seasonal change of sea ice extent. For example, there is supposed to be roughly 500,000 km^2 of ice in April, which supports a wide range of trophic levels, acting as a platform for seals and serving as a space for primary production. In April of 2018, there was only 61,704 km^2 of sea ice, which is about 10% of the normal amount (Hansen, 2018). These observations were supported by Jones *et al* (2020), who found that sea ice conditions in the Bering Sea in 2018 were the lowest in the past 5500 years. A similar phenomenon has also been documented in the Chukchi Sea. In the Chukchi Sea, the open-water season now extends from mid-June to late November, an expansion of about 42 days over the past 30 years, indicating that sea ice in the region is becoming annual rather than perennial (Stafford, 2019). While negative for many species, Moore and Huntington (2008) ran a model to understand the resilience of different Arctic marine mammals when faced with sea ice loss and found that certain species, like the killer whale, are more adaptable to these changes and may be able to extend their range into more northern areas. This has been described in the Hudson Strait area, where an increase in killer whale sightings was suggested to be correlated with a decline in sea ice (Higdon and Ferguson, 2009). This also corresponds with the increase of sightings in the Bering Strait and the

Chukchi Sea, as noted above. A further change in oceanographic conditions has the potential to have a large effect on the ecosystem dynamics in these areas.

Through the Bering Strait, the Bering Sea acts as the only connection between the Pacific and the Arctic Ocean, making it the ideal study location (Woodgate, 2022; Hansen, 2018). The lack of detailed acoustic analysis in the Bering Strait and southern Chukchi Sea is partially due to; (a) a lack of dedicated effort until recently and (b) difficulties assessing this area. Long-term passive acoustic monitoring is a helpful tool that can monitor and assess killer whales without the need for a full-scale survey. However, for this methodology to be effective, a repertoire needs to be defined. While it is suggested the transient killer whales are expanding to these more northerly areas, due to the limited studies, the population that is exploiting this niche is not definitively known. As suggested by Sharpe *et al* (2017), transients may exhibit regional repertoires, and therefore analyses need to be carried out on a regional basis to figure out what population is moving to this region. This study aims to investigate the spatiotemporal distribution of transient Killer Whale calls in the Bering Strait and southern Chukchi Sea and characterize these calls into distinctive categories to describe a regional repertoire. Given the outcomes of the resilience model from Moore and Huntington (2008) and an increase in transient Killer Whale sightings in the Bering and Chukchi Seas, this study hypothesizes that the occurrence of calls will be greater in more recent years. Within this, this study hypothesizes that call occurrence varies by recorder location, year, and month. Like Madrigal *et al* 2021, this study also takes place partly in the Chukchi Sea, and therefore it is hypothesized to have similar call categories. Furthermore, this study hypothesizes that year, month, and recorder location will affect call type occurrence. This study will be the first to describe an acoustic catalogue of transients in the Bering Strait to increase our knowledge of the spatiotemporal distribution of killer whales in this highly

180011049

productive and changing area. The repertoire produced from his study will be able to be used as a baseline for future acoustic studies in this region.

2. Methods

2.1.Data Collection

Continuous passive acoustic data were collected from three moored autonomous underwater recorders (AURAL-M2 hydrophones, Autonomous Underwater Recorder for Acoustic Listening-Model 2, Multi-Électronique, Inc.; sensitivity of −154 dB re 1 V/µPa and 16-bit resolution) managed by the National Oceanic Atmospheric Association (NOAA) and the Applied Physics laboratory at the University of Washington (NOAA, 2022). These three moorings were positioned in different locations within the Bering Strait and southern Chukchi Sea: one in the centre of the Bering Strait on the east side of the Diomede Islands (A2), one in the centre of the eastern channel (A4), and a central strait location approximately 35 km north of the strait in the southern Chukchi Sea (A3) (Figure 1).

180011049

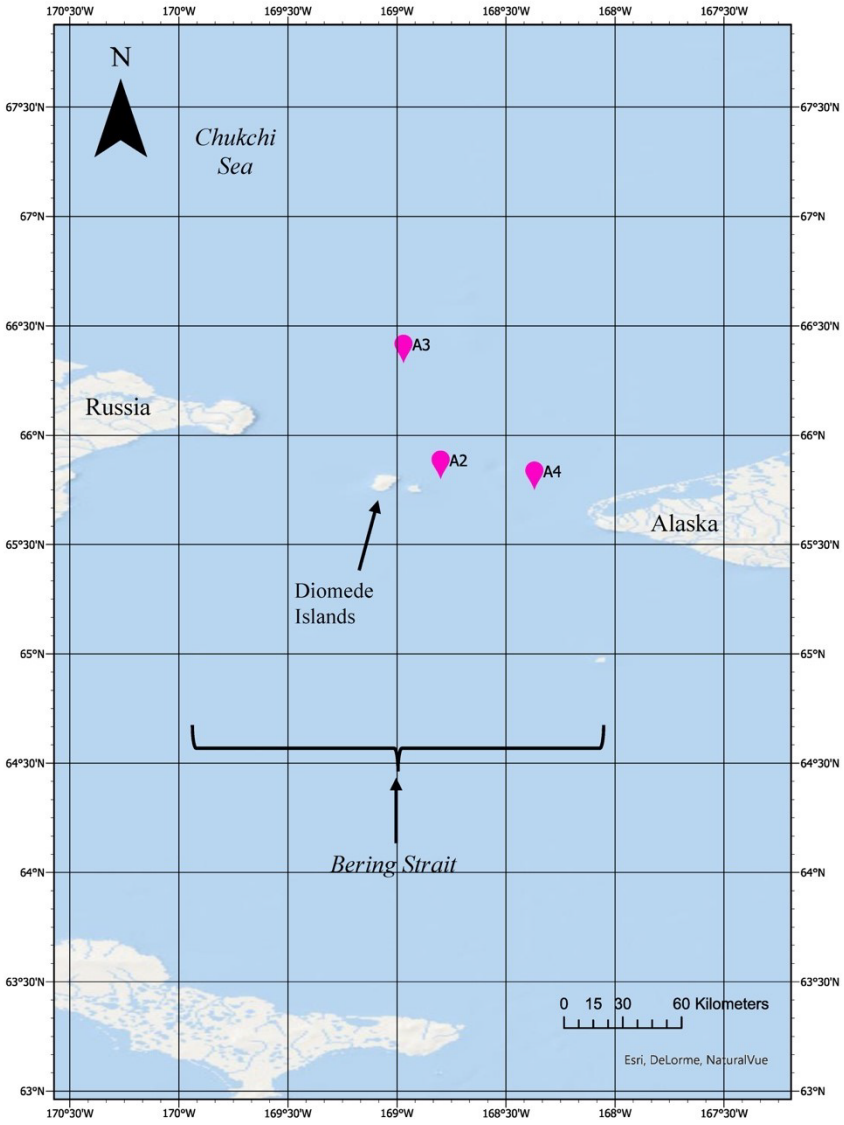

Figure 1. Map of the study region and the three moored autonomous recorders. The Diomede Islands are located roughly mid-strait in between the western and the eastern channel. A2: 65.8°N, 168.80°W; A3: 66.33°N, 168.97°W; A4: 65.75°N, 168.37°W. Scale bar of 60 km.

These hydrophones collected data from September 2009 through December 2018. While data was sampled at 8192 Hz or 16384 Hz, only files samples at 16384 Hz were used for further

180011049

analysis. Files sampled at 8192 Hz (2013, 2014, 2015) were disregarded since the spectrograms generated would not cover the typical range of killer whale calls (1-6 kHz) (Ford 1989; Samarra et al., 2016). This is because, in order to represent a sound accurately, samples taken need to be twice every wavelength. When sound is represented on a spectrogram, it appears as half the sample rate. So, recordings sampled at 8192 Hz would only generate spectrograms reaching 4 kHz and, therefore would potentially not provide an accurate representation of the range of killer whales.

2.2.Call Extraction

Recordings that were previously identified as transient killer whales were analyzed (NOAA, 2022). Acoustic recordings were aurally and visually inspected using the RAVEN 2.0.1 sound analysis program (Cornell Laboratory of Ornithology, NY) to examine spectrograms (512-point FFT, 16 kHz bandwidth, 10-second window). Calls were annotated and deemed either quality 1, 2, or 3. For a call to be considered quality 1 it must have been traceable, meaning it had to have a clear start and end, have little to no overlap of other calls or noise, have the majority of sidebands be visible, and was clearly audible. A sideband is how the pulse repetition rate of a call is displayed on a spectrogram. It appears as a series of harmonics bands that vary depending on the pulse repetition rate of the signal (Watkins, 1967). For a call to be deemed quality 2 it must have also been traceable meaning it must have had a distinguishable start and end, visible but not necessarily distinct sidebands, could have some overlap between other calls/noise, and be audible. Quality 3 calls were untraceable meaning that they did not have a clear start or end, overlapped with other calls/noise, and were only faintly audible. Due to the fact that quality 3 calls were, by definition, difficult to discern from other calls and background noise, they were

180011049

not included in any further analysis. The annotated quality 1 calls from RAVEN were then used for further analysis in PAMGuard 1.15 (Gillespie et al., 2008). The ROCCA (Real-time Odontocete Call Classification Algorithm) module in PAMGuard 1.15 was used to trace the lowest frequency component of quality 1 calls (Gillespie et al., 2008, Oswald and Oswald, 2013). Once a call contour was traced, ROCCA extracted the time and frequency points along with 56 additional variables that describe frequency (Oswald and Oswald, 2013; Oswald et al., 2021). Refer to Appendix A in Oswald and Oswald (2013) for more information regarding the details and meanings of the ROCCA output variables. For the purpose of this analysis, six of the variables that were measured by ROCCA were examined: (1) minimum frequency (Hz), (2) maximum frequency (Hz), (3) call duration (sec), (4) beginning frequency (Hz), (5) end frequency (Hz), (6) median frequency (Oswald et al. 2007, Oswald and Oswald, 2013). These variables were selected in accordance with similar studies so comparisons could be drawn accordingly (Madrigal et al., 2021).

2.3.Test of Interrater Reliability

An interrater reliability test was conducted to ensure the quality criteria assigned to the calls (1, 2, or 3) were defined well and consistently applied. The methodology for this was adapted from Riesch and Deecke (2011). A subset of 23 randomly chosen transient killer whale calls was used to confirm my initial classification of quality ratings. Spectrograms (512-point FFT, 16 kHz bandwidth, 10-second window) of transient killer whale calls were presented to four naïve observers. Out of the 23 chosen calls, eight calls were quality 1, eight were quality 2, and six were quality 3. All calls were printed on separate sheets of paper containing one spectrogram each (standardized 4-second window for each spectrogram shown) and presented in random

180011049

order. Observers were asked to divide the calls into three different quality categories based on defined criteria. A Kappa Statistic was used to test for interobserver reliability.

2.4.Call Type Categorization

Time-frequency call contours from ROCCA were organized into different call types using ARTwarp. ARTwarp is MATLAB-based software that uses an unsupervised adaptive resonance theory neural network and dynamic time-warping to group contours into categories (Deecke and Janik, 2006). Dynamic time warping is an algorithm that allows limited compression and/or expansion of the time axis to allow for maximum frequency overlap with the reference contour (Deecke and Janik, 2006). To be placed into a category, a call had to have a similarity index (vigilance parameter) of 81.24% to the reference contour. When a contour is undergoing categorization, it is compared to all the reference contours, and it is put in the first category that exceeds the similarity index, and then the reference contour is subsequently readjusted accordingly. A new reference contour is generated if the contour does not exceed the similarity index. It is these reference contours that make up the described call repertoire.

2.5.Call Type Comparison with Previous Literature

Madrigal *et al* (2021) created an acoustic catalogue of transient killer whale calls off of Point Hope, Alaska. The repertoire defined six main call types: multi-part, flat, upsweeps, downsweeps, modulated, and single modulated calls. Flat calls have a linear contour; Upsweeps have an ascending call contour with a lower start frequency than end frequency; Downsweeps have a descending call contour with a higher start frequency than end frequency; Modulated calls refer to calls that have more than one inflection point (i.e. at least two modulations; and Single modulated calls are calls that have only one inflection point (Madrigal et al., 2021). The current study only focused on pulsed calls, not multi-part; therefore, that call category was not used in

180011049

any further analysis. To see if similar categorization is possible in the Bering Strait and the Chukchi Sea, reference contours from ARTwarp were manually organized into the five described call types.

2.6.Statistical Analysis

Descriptive statistical metrics were analyzed using SPSS (IBM, 2017), in which call incidence by location, year, and the month was examined. To understand whether the occurrence of all calls varied with location, year, and time of year (month), a general linear model was used. *Recorder* and *Year* were both included as factors, and *Month* was included as a continuous variable. To combat the issue of the two locations recording at different times, the data was aggregated by month and then merged back into the main data file.

$$\text{full model} = calls \sim recorder + year + month$$

For a more thorough comparison, the years 2009, 2010, and 2012 specifically were analyzed since calls were detected in the same months across both recorders. The same model was used as described above, just with the filtered set of data.

Due to the high number of calls found in 2017 and 2018 at mooring A3, calls in these two years were compared. They were analyzed using a general linear model to see if there was a relationship between year and number of calls recorded.

$$\text{full model} = calls \sim year + month$$

A general linear model was also used to further understand whether specific call types occurred more commonly at a specific location and/or time (year and/or month). Call category refers to the outputs generated from ARTwarp. *Year* and *Recorder* were both included as factors and

180011049

Month as a continuous variable. Since the two recorders sometimes varied in what months and years data was recorded, the data was aggregated by month and then merged back into the main data file.

$$\text{full model} = callcategory \sim recorder + year + month$$

ANOVA tests were run to assess variable significance for all described linear models. Model analysis was performed using R 4.0.3 programming language with base and "dplyr" packages (R Core Team, 2020; Wickham et al., 2008).

Averages of the time and frequency parameters of flat, downsweep, upsweep, modulated, and single modulated calls were respectively extracted. These were used to compare against those described in Madrigal *et al* (2021). Independent sample T-tests were used to compare the six variables examined in this study with those reported in those of the call types reported in Madrigal *et al* (2021).

3. Results

A total of 107 hours from 353 audio files collected in 2009, 2010, 2012, 2017, and 2018 were processed (Table 1). 1670 calls were annotated in RAVEN and given a quality rating of 1 (n=600) or 2 (n=1070). A singular call was detected at recorder A4. Because this recorder had so few calls, it was not included in further analysis. The interrater reliability for the raters was found to be Kappa = 0.77 ($p < .0.001$), suggesting the definitions for calls were sufficient in describing quality. 600 high-quality (quality 1) calls were extracted in PAMGuard using the ROCCA module for further analysis.

180011049

Table 1. Summary of the location of recorders, the years, and months where and when files were recorded. The number of calls initially annotated in RAVEN (quality 1 and 2 calls) and the number of calls extracted (quality 1) in PAMGuard using ROCCA corresponds to each recorder by year and month. The one call extracted from the A4 recorder is listed; however, it was not used in subsequent analysis.

Mooring	Location	Year	Month	Number of Calls Annotated (RAVEN)	Number of Calls Extracted (PAMGuard)
A2	65.8°N, 168.80°W	2009	September	12	2
			October	8	1
		2010	August	1	0
			September	188	58
			November	15	0
		2012	September	31	8
			October	16	1
A3	66.33°N, 168.97°W	2009	September	4	0
			October	1	0
		2010	August	96	35
			September	57	13
			October	38	11
		2012	September	3	0
			October	16	5
		2017	September	221	96
			October	122	53
			November	51	42
		2018	June	49	12
			July	16	4
			August	21	6
			September	221	95
			October	36	7
			November	424	151
			December	22	0
A4	65.75°N, 168.37°W	2012	September	1	0
			Total	**1670**	**600**

3.1.Spatiotemporal distribution of all calls

The occurrence of killer whale calls at the two recorders was significantly dependent on month ($p<0.0005$) but not on recorder location ($p=1$) or year ($p=0.58$) ($F_{6,1662}=277.2$, $p<0.005$, adj $R^2=0.49$). Out of all 1669 calls, the most calls were annotated in the month of September (44.1%), followed by November (29.4%) (Figure 2). Even when separating call occurrence by the mooring, September had the most calls in both locations (A2: 85.2%; A3: 36.2%). When analyzing call occurrence during years where both moorings had recordings (2009, 2010, 2012) there were more calls are found at A2 (n=271) than A3 (n=215) (Figure 3). Within this subset,

180011049

year was a significant predictor of call occurrence ($F_{4,481}$=120.2, p<0.001, adj R^2=0.50). When analyzing call occurrence at mooring A3 in 2017 and 2018, more calls were recorded at the A3 mooring in 2018 (n=789) than in 2017 (n=394); however, this finding was not statistically significant ($F_{2,1180}$=592.5, p=0.181, adj R^2=0.50).

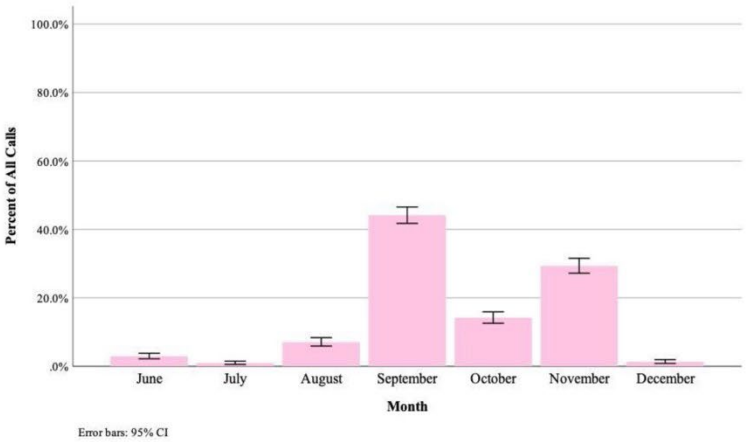

Figure 2. Percentage of overall call occurrence by month ± 2 standard error.

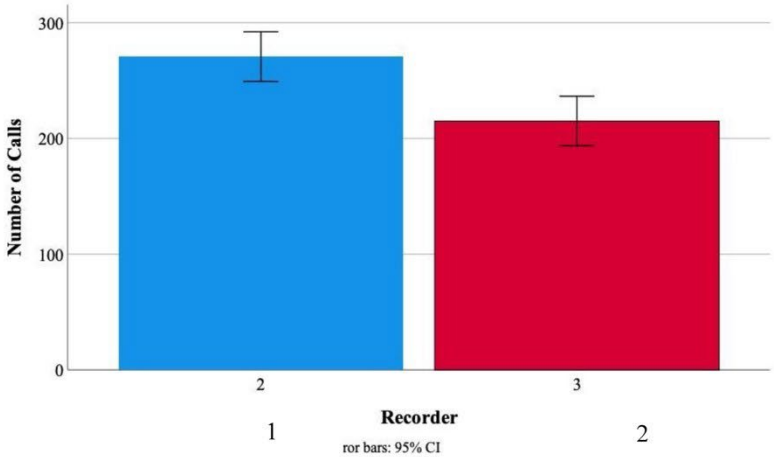

Figure 3. Total number of calls recorded at A2 mooring (blue) and A3 mooring (red) in 2009, 2010, and 2012 ± 2 standard error. $F_{4,481}$=120.2, p<0.001, adj R^2=0.50.

20

180011049

3.2. Categorizing Call Types

ARTwarp grouped the 600 traced calls into 29 types (Figure 4).

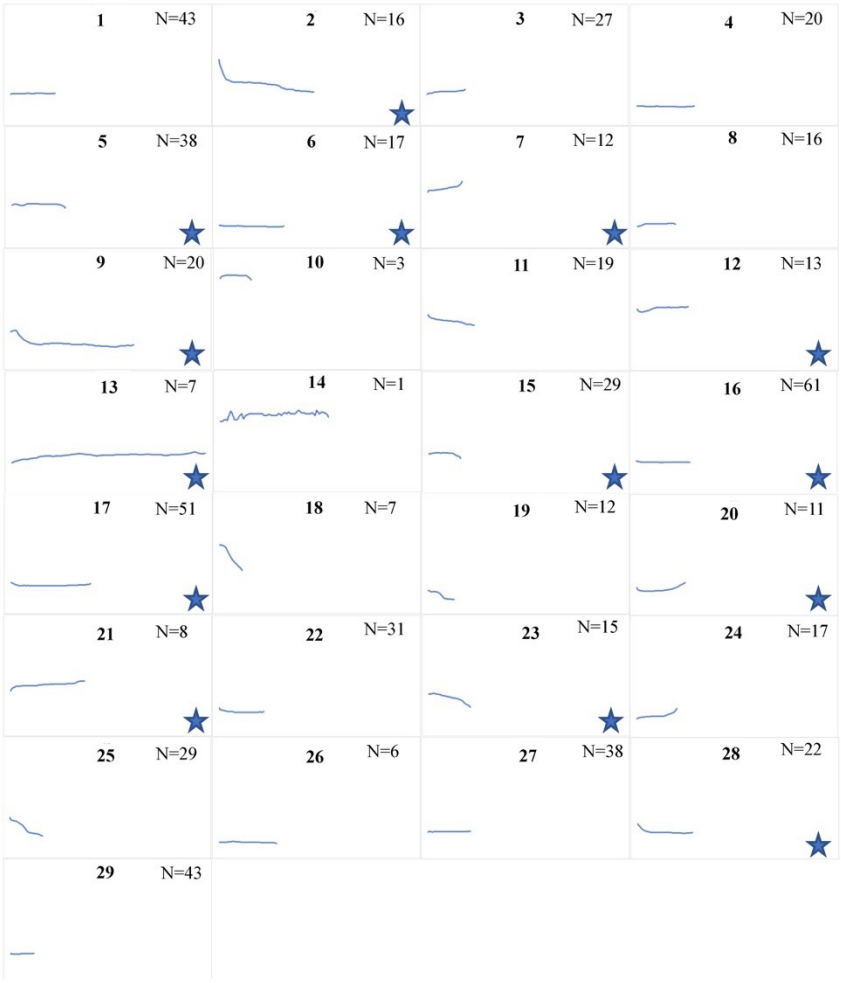

Figure 4. Reference contours of transient killer whale calls as outputted from ARTwarp. Time on the X-axis (0-19.6 seconds) and Frequency on the Y-axis (0-3600 Hz) are consistent for all plotted reference contours. N values refer to the number of calls that were sorted into each respective category. Stars indicate that call type was found at both A2 and A3 moorings.

All call types occurred at A3 whereas only call types 2, 5, 6, 7, 9, 12, 13, 15, 16, 17, 20, 21, 23, 28 occurred at A2 (Figure 4). Whether a certain call type is recorded is significantly

180011049

dependent on recorder location ($p<0.001$), month ($p<0.001$), and year ($p<0.001$) ($F_{6,593}=14.9$, $p<0.001$, adj $R^2=0.12$).

The four most common call types were 16 (n=61, 10.2% of calls), 17 (n=51, 8.5% of calls), 29 (n=43, 7.2% of calls), and 1 (n=43, 7.2% of calls) (Figure 5). Out of all calls found at recorder A2 (n=70), call 16 comprised 11.4% (n=8) and call 17 comprised 21.4% (n=15). Calls 1 and 29 were not detected at recorder A2. Out of all calls found at recorder A3 (n=530), call 16 made up 10% (n=53), call 17 made up 6.8% (n=36), call 1 made up 8.1% (n=43), and call 29 also made up 8.1% (n=43). Call 17 was the only one of these common calls recorded in every study year. Call 17 was recorded in September (n=28, 54.9% of all recordings of Call 17), October (n=5, 9.8%), and November (n=16, 31.3%). Call 16 was found in every study year except 2009. This call type was recorded in August (n=2, 3.2% of all recordings of Call 16), September (n=14, 22.9%), October (n=5, 8.2%), and November (n=40, 65.6%). Call 29 was found in 2010, 2017, and 2018. This call type was recorded in August (n=24, 55.8% of all recordings of call 29), September (n=15, 34.9%), and November (n=4, 9.3%). Call 1 was found in 2010, 2017, and 2018. This call type was recorded in September (n=6, 13.9% of all recordings of call type 1), October (n=5, 11.6%), and November (n=32, 74.4%).

180011049

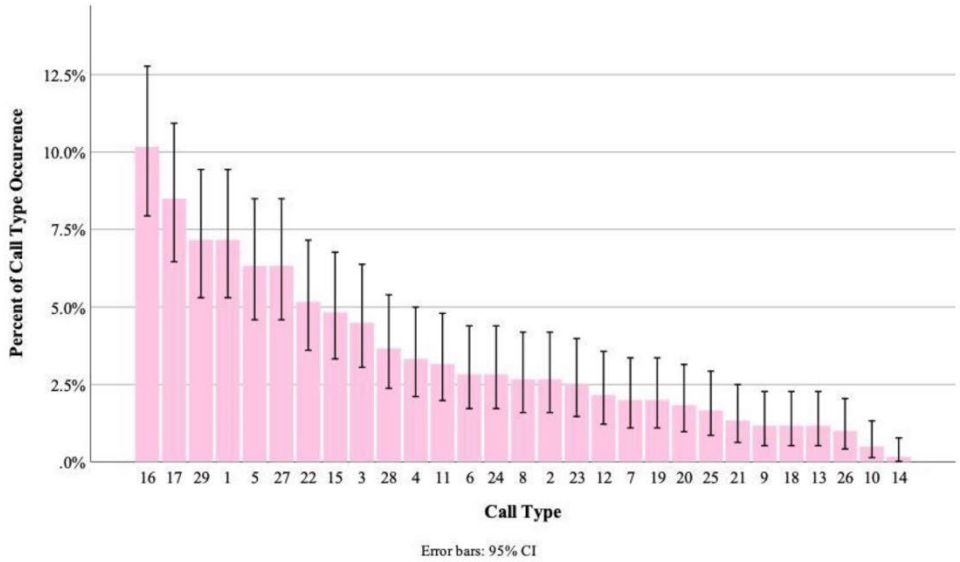

Figure 5. Percentage of overall call type occurrence ± 2 standard error. The x-axis is organized in ascending order from most common (Call 16, n=61, 10.2% of all calls) to least common (Call 14, n=1, 0.06% of all calls)

3.3.Call Types Comparison with Previous Literature

To compare the call structures of transient killer whales between the current study and Madrigal *et al* (2021), call types produced by ARTwarp were visually sorted into five broad call categories (flat, upsweep, downsweep, modulated, single modulated). Each broad category described contained several different ARTwarp reference contours that are referred to hereafter as subcategories. Table 2 shows the number of subcategories generated in the current study compared to Madrigal *et al* 2021.

180011049

Table 2. Comparison of the number of subcategories generated in the current study and those generated in Madrigal *et al* (2021).

	Current Study	Madrigal *et al* (2021)
Flat	9	6
Downsweep	6	4
Upsweep	8	6
Modulated	3	5
Single Modulation	3	2
Total	**29**	**23**

Similar to Madrigal *et al* (2021), flat calls were the most common call type described in the current study (n=310, 51.6%). However, the frequency parameters in the current study were different compared to Madrigal *et al* (2021) (Table 3). T-tests comparing the frequency and duration parameters of each call type between studies showed that most were significantly different from one another (Table 3). Upsweeps were similar to those described by Madrigal *et al* (2021), in which the only two significantly different variables were start frequency ($t(178)=-5.19$, $p<0.001$) and minimum frequency ($t(178)=-3.35$, $p<0.001$).

180011049

Table 3. Summary of variables measured in ROCCA (mean ± standard deviation). Rows in green correspond to measurements from Madrigal *et al* (2021). P-values from independent samples t-test are italicized and placed with respective call types.

Call Type	Duration (s)	Start Freq (Hz)	End Freq (Hz)	Maximum Freq (Hz)	Maximum Freq (Hz)	Freq Median (Hz)
Flat (n=310)	0.88 ± 0.55	940.30 ± 368.92	909.92 ± 362.53	790.4 ± 294.57	1057.55 ± 393.05	901.32 ± 325.56
Flat (n=485)	0.82 ± 0.36 *p=0.06*	728 ± 157 *p<0.01*	733 ± 169 *p<0.01*	666 ± 156 *p<0.01*	785 ± 166 *p<0.01*	724 ± 164 *p<0.01*
Downsweep (n=108)	0.86 ± 0.46	1365.04 ± 703.76	1014.52 ± 457.3	905.48 ± 436.23	1485.63 ± 667.88	1114.37 ± 495.99
Downsweep (n=175)	0.95 ± 0.40 *p=0.08*	859 ± 252 *p<0.01*	619 ± 170 *p<0.01*	588 ± 150 *p<0.01*	1006 ± 244 *p<0.01*	799 ± 167 *p<0.01*
Upsweep (n=88)	0.93 ± 0.57	1049.09 ± 536.35	1115.64 ± 606.11	898.91 ± 492.49	1257.09 ± 614.34	1043. 82 ± 538.28
Upsweep (n=92)	0.90 ± 0.52 *p=0.71*	738 ± 201 *p<0.01*	1133 ± 337 *p=0.81*	713 ± 196 *p<0.01*	1178 ± 326 *p=0.28*	958 ± 264 *p=0.17*
Modulated (n=46)	0.99 ± 0.58	1254.26 ± 471.15	1126.26 ± 291.54	976 ± 234.4	1464.35 ± 406.35	1228.52 ± 296.24
Modulated (n=60)	0.88 ± 0.34 *p=0.22*	738 ± 158 *p<0.01*	699 ± 298 *p<0.01*	574 ± 131 *p<0.01*	1067 ± 271 *p<0.01*	787 ± 178 *p<0.01*
Single Modulation (n=48)	0.69 ± 0.29	1142.67 ± 443.99	1067.33 ± 484.52	968 ± 412.95	1300 ± 483.04	1178.33 ± 427.17
Single Modulation (n=31)	0.45 ± 0.21 *p<0.01*	737 ± 178 *p<0.01*	789 ± 235 *p<0.01*	623 ± 168 *p<0.01*	953 ± 226 *p<0.01*	758 ± 201 *p<0.01*

In the current study, downsweeps were the most common call type at recorder A2 (n=26, 37.1%). Flat calls were the most common call type at recorder A3 (n=285, 53.8%). Flat calls were recorded in all years and months of the study. Downsweeps, upsweeps, and modulated calls were recorded every year except for 2009. The least recorded call type, single modulated calls, were recorded in 2009 (n=1), 2017 (n=13), and 2018 (n=34). All call types were recorded in September, October, and November at some point during the study period. Only flat, upsweeps, and single modulated calls were found in June or July.

180011049

4. Discussion

4.1.Call Occurrence

The first aim of this study was to use calls produced by transient killer whales to investigate their spatiotemporal distribution in the Bering Strait and the southern Chukchi Sea. The results presented here demonstrate that calls vary significantly by month but not necessarily by location or year. Aside from 2010, September contained the greatest number of calls in general and within each recorder location. These findings are consistent with sighting data of transient killer whales in the Chukchi Sea, where the highest number of detection days was also in September (Hannay et al., 2013).

In the current study, the location was hypothesized to have a significant effect on call occurrence because of the placement of recorders with respect to relative environmental factors. The Bering Strait is divided into two channels by the Diomede Islands, roughly mid-strait. The western channel is cold, salty, and comparatively more productive than the eastern channel, which tends to be warmer and contains fresher water (Escajeda et al., 2020). In terms of mooring location, A2 is located in the centre of the strait but on the eastern side of the channel, whereas A3 is located ~35 km north of the centre of the strait. Recorder A4 was located further into the eastern channel right in the Antarctic Coastal Current, which is known to be less productive and therefore, it was expected that there would be fewer calls at this location (Escajeda et al., 2020). It was also expected that the A2 mooring would have fewer calls because it is on the slightly less productive side of the channel than the A3 mooring, which had the potential of recording killer whales passing through both channels in the strait. Despite predicting that location would have a significant effect on call occurrence, it did not. A possible reason for this lack of significance could be attributed to the recorders' distance from one another. The recorders are approximately

180011049

57 km from one another, which is within the average maximum distance transients can travel in a straight line each day (95 km/day) (Parsons et al., 2013).

Despite year not being a significant variable in the model, it is worth noting the difference in the number of calls recorded in November in 2017 and 2018. Roughly eight times as many calls were recorded in November 2018 compared to November 2017. Additionally, when undergoing initial spectral analysis in RAVEN, 2018 contained numerous calls that were too messy (overlapping and background noise) to allow for further selection. Nonetheless, since transients do not vocalize often, these finding highlights that there may have been a greater number of transients in the area (Deecke et al., 2005). Further, it is likely that transient killer whale presence is still underrepresented in this region. They are likely underrepresented because of their calling behaviour (or lack thereof), the nature of duty-cycled recorders, and since there was no moored recorder in the western (more productive) channel in the Bering Strait if a transient travelled through this path, then any calls would not have been recorded (Deecke et al., 2005; Rand et al., 2022; Escajeda et al., 2020).

Even so, this study suggests that there is an apparent increase in transients in the Bering Strait and the southern Chukchi Sea in November. A possible explanation for this could be that 2018 had the lowest levels of sea ice concentration on record, meaning the longest ice-free season (Hansen, 2018; Jones et al., 2020). Transients have previously avoided these regions, except in the summer months, because of the heavy concentrations of sea ice posing a risk for ice entrapment and damage to their sizeable dorsal fine (Stafford et al., 2022; Ferguson et al., 2010). So, while transients were historically barred from months during the ‘freeze-up’ period in the Bering/Chukchi Seas, that is potentially no longer the case. The decline in sea ice is not unique to 2018. The Arctic is warming twice that of the global rate creating a range of cascading

180011049

ecological effects, with one of the biggest being a decline in sea ice (Grebmeier, 2012). While negative for many endemic Arctic species, transients are expected to benefit from this reduction in sea ice by exploiting these highly productive regions for longer periods of time (Moore and Huntington, 2008).

This idea has been supported by recent studies where there is a reported increase in transient killer whale sightings in the Bering, Chukchi, and Beaufort seas (Hannay et al., 2013; Clarke et al., 2013; Stafford, 2019). Killer whales moving to these more northerly areas affects ecological dynamics, specifically predator-prey relations. Many endemic Arctic marine mammal species are already quite limited in their ability to cope with the changing climate due to their narrow home ranges and reliance on sea ice for foraging or predator avoidance tactics (Moore and Huntington, 2008; Laidre et al., 2008; Ferguson et al., 2010). The combination of this heightened sensitivity to climate change and the increased presence of a mammal-eating killer whale puts these animals at risk. This phenomenon is more well understood in the Canadian Arctic, where it has been suggested that endemic Arctic species like the narwhals (*Monodon monoceros*), belugas (*Delphinapterus leucas*), and bowhead whales (*Balaena mysticetus*) all alter their behaviour in the presence of killer whales (Matthews et al., 2020). While the implications of killer whale expansion are less well understood in the Pacific Arctic, there is preliminary evidence to suggest that there damaging effects. For example, there is a suspected correlation between an increase in scars on Bowhead Whales in the Bering/Chukchi/Beaufort seas and an increase in killer whales in this area (George et al., 2017). Overall, even though this evidence suggests that transients are moving towards the Bering and Chukchi Seas, it does not explain what population of transients are undergoing this transition.

180011049

4.2.Regional Repertoire

The next objective of this study was to develop a call repertoire of transients in the Bering Strait and the southern Chukchi Sea. The population structure of transients in this area is not well understood, and therefore this call repertoire was then used to attempt to understand what population is found in the Bering Strait and the Chukchi Sea. To achieve this, the described call repertoire was used to examine whether there are similarities in calls between transients in different areas. The current study described a repertoire of 29 different call types. Results from the current study indicate that location, month, and year all influence the occurrence of a specific call type. Different clans of transients travelling through the Bering Strait at different times (yearly or monthly) and following different paths is a plausible explanation for why there is a significant difference in where and when a call type occurs. As suggested above, it is thought that the number of transients found in the Bering and Chukchi Seas is increasing (Hannay et al., 2013; Clarke et al., 2013; Stafford, 2019). Since the Bering Strait is the only connector between the Pacific and the Arctic Ocean, any transient killer whale wanting to move to these colder, more productive waters needs to travel through this passage. It is likely that if different clans of transients are travelling north, they are not all travelling at the same time. Since clans all produce distinct vocal dialects, different travel times and patterns could explain the significance of year, month, and recorder location on call type occurrence. A potential subpopulation moving through the Bering Strait is the Aleutian Islands transient population.

Preliminary satellite telemetry data suggest that it was the Aleutian Island transient population spotted near the edge of the Chukchi and Beaufort Seas (Hannay et al., 2013). However, studies have shown that even within the Aleutian Islands transient population, there are genetic and acoustic differences and, therefore, should be broken down into more

subpopulations (Parsons et al., 2013; Sharpe et al., 2017). This further subdivision of the Aleutian Island subpopulation supports the notion that it is multiple subpopulations travelling through the Bering Strait, which is why different call types are produced at different times and locations.

4.3.Methodological Discrepancies when Comparing to Previous Literature

Within the call categories from ARTwarp, five more broad call type categories were designated: downsweeps, flat, upsweeps, modulated, and single modulation. These categories were taken from Madrigal *et al* (2021), in which the authors defined a repertoire of 6 call categories with 36 subcategories, but since this included multi-part calls, for the purposes of this comparison Madrigal *et al* (2021) defined five call categories with 23 subcategories. The current study produced these five call categories, and the subcategories for this were the initial call categories as outputted in ARTwarp. In the current study, the most common call types were Flat calls and Downsweeps. Similarly, the most common call types in Madrigal *et al* (2021) were Flat calls and Downsweeps. Visual comparison and similar variables were chosen to analyze through ROCCA, which allowed for comparability of these transient repertoires; however, the actual classification methodology for determining call categories was quite different. In the study by Madrigal *et al* (2021), the first step of categorical assignment involved manual categorization into broad categories. Then, a hierarchical cluster in R was used to generate subcategories. Contrastingly, the first step of the category assignment in the current study used ARTwarp. Outputs were then manually sorted into the five call categories described by Madrigal *et al* (2021) to assess potential similarities.

Although the comparisons of these two studies yielded visual similarity, the statistical similarity was lacking. The only broad call type that had more statistical similarity than

180011049

difference was upsweeps (appendix). Despite a few different studies exploring the repertoires of transient killer whales, this study was only able to compare to Madrigal *et al* (2021) due to the type of frequency parameters extracted. Sautilus *et al* (2005) examined the vocal repertoire of the AT1 transient population using duration (ms), whistle component frequency (Hz) and frequency intervals between sidebands (Hz). Sharpe *et al* (2017) described the vocal repertoire of three subpopulations of transients within the Gulf of Alaska stock: Pribolif Island, Western Aleutian Island, and Eastern and Central Aleutian Islands. However, frequency parameters for described call types were not reported, and therefore there was a limited possibility to draw meaningful comparisons. Similarly, Deecke (2003) described a repertoire for West Coast transients, but frequency parameters were not definitively reported. This lack of standardized methodology raises the question as to whether some of these subpopulations actually have different repertoires or do these studies define repertoire differently. The lack of standardized methodology in defining Cetacea repertoires makes it difficult to both compare results from previous studies and add to existing data. Having a consistent methodology is of particular importance for this study to identify the population of transients travelling through the Bering Strait. It is difficult to discern both the origins and relevant differences of these transient killer whales without standardised methodology.

4.4.Conclusion

The current study examined transient killer whale call occurrence in the Bering and the southern Chukchi Sea to further understand the expected change in the spatiotemporal distribution of these animals. In addition, this study was the first to describe an acoustic repertoire for transients in the Bering Strait and the Chukchi Sea in an attempt to begin to understand their population structure. While the findings from this study do provide a solid

baseline, there are still many unknown elements. Despite an increase in survey effort in the Bering and Chukchi Seas regarding the northerly expansion of transient killer whales, the population structure of transients in this area is still not well described. The most straightforward way to begin to understand the population structure in this region is to develop a sound methodology for defining a vocal repertoire in this region. This methodology does not need but be novel but instead can adapt previously successful methods used in defining bird repertoires and apply similar principles to killer whale repertoires. For example, a study examining the effectiveness of the 'Coupon Collector' method as a way to define killer whale repertoires would allow for studies to take full advantage of the effective nature of passive acoustic monitoring. The 'Coupon Collector' method is a model of signal occurrence which has proven successful in providing an accurate indication of true repertoire size in certain bird species such as the northern mockingbird (*Mimus polyglottos*) (Kershenbaum et al., 2015). Once a standardized methodology is implemented, analyses conducted on passive acoustic recordings can be compared effectively and combined to yield more significant results. In addition, since subpopulations of killer whales also tend to vary genetically and morphologically, it is necessary to conduct intensive genetic analysis in photoID better to understand the population structure of transients in this area. With the Arctic warming rapidly, understanding the population structure of transients is necessary to understand the potential ecological implications in this region.

‘

180011049

References

Allen, B.M., and Angliss, R.P. (2012) Alaska Marine Mammal Stock Assessments, 2011. U.S. Department of Commerce, Seattle, WA. 288p Available online at: http://www.nmfs.noaa.gov/pr/pdfs/sars/ak2011.pdf.

Andriolo, A., Reis, S., Amorim, T., Sucunza, F., de Castro, F., Maia, Y., Zerbini, A., Bortolotto, G. and Dalla Rosa, L. (2015) Killer whale (*Orcinus orca*) whistles from the western South Atlantic Ocean include high frequency signals. *The Journal of the Acoustical Society of America*, 138(3), pp.1696-1701.

Baird, R.W. and Whitehead, H. (2000) Social organization of mammal-eating killer whales: group stability and dispersal patterns, *Canadian Journal of Zoology*, 78(12), pp. 2096–2105.

Barrett-Lennard, L. (2000) *Population structure and mating patterns of Killer Whales (Orcinus orca) as revealed by DNA analysis*. PhD. University of British Columbia.

Barrett-Lennard, L.G., Ford, J.K.B. and Heise, K.A. (1996) The mixed blessing of echolocation: differences in sonar use by fish-eating and mammal-eating killer whales, *Animal Behaviour*, 51(3), pp. 553–565.

Center for Conservation Bioacoustics. (2019). Raven Lite: Interactive Sound Analysis Software (Version 1.1.15) [Computer Software. Ithaca, NY: The Cornell Lab of Ornithology. Available from http://ravensoundsoftware.com/.

Charlton, B., Martin-Wintle, M., Owen, M., Zhang, H. and Swaisgood, R. (2018) Vocal behaviour predicts mating success in giant pandas. *Royal Society Open Science*, 5(10), p.181323.

Clarke, J., Stafford, K., Moore, S., Rone, B., Aerts, L. and Crance, J. (2013) Subarctic Cetaceans in the Southern Chukchi Sea: Evidence of Recovery or Response to a Changing Ecosystem. *Oceanography*, 26(4), pp. 136-149.

Dahlheim, M., Schulman-Janiger, A., Black, N., Ternullo, R., Ellifrit, D. and Balcomb III, K. (2008) Eastern temperate North Pacific offshore killer whales (*Orcinus orca*): Occurrence, movements, and insights into feeding ecology. *Marine Mammal Science*, 24(3), pp.719-729.

de Bruyn, P., Tosh, C. and Terauds, A. (2012) Killer whale ecotypes: Is there a Global Model? *Biological Reviews*, 88(1), pp.62-80.

Deecke, V. (2003) *The Vocal Behaviour of Transient Killer Whales (Orcinus orca): Communicating with Costly Calls*. PhD. University of St Andrews.

Deecke, V., Barrett-Lennard, L., Spong, P. and Ford, J. (2010) The structure of stereotyped calls reflects kinship and social affiliation in resident killer whales (*Orcinus orca*). *Naturwissenschaften*, 97(5), pp.513-518.

180011049

Deecke, V., Ford, J. and Slater, P. (2005) The vocal behaviour of mammal-eating killer whales: communicating with costly calls. *Animal Behaviour*, 69(2), pp.395-405.

Deecke, V., Ford, J. and Spong, P. (2000) Dialect change in resident killer whales: implications for vocal learning and cultural transmission. *Animal Behaviour*, 60(5), pp.629-638.

Deecke, V.B. and Janik, V.M. (2006) 'Automated categorization of bioacoustic signals: Avoiding perceptual pitfalls', *The Journal of the Acoustical Society of America*, 119(1), pp. 645–653.

Elie, J.E. and Theunissen, F.E. (2016) The vocal repertoire of the domesticated zebra finch: a data-driven approach to decipher the information-bearing acoustic features of communication signals, *Animal Cognition*, 19(2), pp. 285–315.

Emmons, C., Hanson, M. and Lammers, M. (2021) Passive acoustic monitoring reveals spatiotemporal segregation of two fish-eating killer whale Orcinus orca populations in proposed critical habitat, *Endangered Species Research*, 44, pp. 253–261.

Escajeda, E., Stafford, K., Woodgate, R. and Laidre, K. (2020). Variability in fin whale (*Balaenoptera physalus*) occurrence in the Bering Strait and southern Chukchi Sea in relation to environmental factors. *Deep Sea Research Part II: Topical Studies in Oceanography*, 177, p.104782.

Fearnbach, H., Durban, J., Ellifrit, D., Waite, J., Matkin, C., Lunsford, C., Peterson, M., Barlow, J. and Wade, P. (2013) Spatial and social connectivity of fish-eating "Resident" killer whales (*Orcinus orca*) in the northern North Pacific. *Marine Biology*, 161(2), pp.459-472.

Ferguson, S., Dueck, L., Loseto, L. and Luque, S. (2010) Bowhead whale *Balaena mysticetus* seasonal selection of sea ice. *Marine Ecology Progress Series*, 411, pp.285-297.

Filatova, O., Deecke, V., Ford, J., Matkin, C., Barrett-Lennard, L., Guzeev, M., Burdin, A. and Hoyt, E. (2012) Call diversity in the North Pacific killer whale populations: implications for dialect evolution and population history. *Animal Behaviour*, 83(3), pp.595-603.

Filatova, O., Miller, P., Yurk, H., Samarra, F., Hoyt, E., Ford, J., Matkin, C. and Barrett-Lennard, L. (2015) Killer whale call frequency is similar across the oceans, but varies across sympatric ecotypes. *The Journal of the Acoustical Society of America*, 138(1), pp.251-257.

Foote, A. and Nystuen, J. (2008) Variation in call pitch among killer whale ecotypes. *The Journal of the Acoustical Society of America*, 123(3), pp.1747-1752.

Ford, J. (1989) Acoustic behaviour of resident killer whales (*Orcinus orca*) off Vancouver Island, British Columbia. *Canadian Journal of Zoology*, 67(3), pp.727-745.

Ford, J. (1991) Vocal traditions among resident killer whales (*Orcinus orca*) in coastal waters of British Columbia. *Canadian Journal of Zoology*, 69(6), pp.1454-1483.

180011049

Ford, J., Ellis, G., Barrett-Lennard, L., Morton, A., Palm, R. and Balcomb III, K. (1998) Dietary specialization in two sympatric populations of killer whales (*Orcinus orca*) in coastal British Columbia and adjacent waters. *Canadian Journal of Zoology*, 76(8), pp.1456-1471.

Ford J.K.B, Stredulinsky, E.H., Ellis, G.M., Durban, J.W., and Pilkington, J.F. (2014) Offshore Killer Whales in Canadian Pacific Waters: Distribution, Seasonality, Foraging Ecology, Population Status and Potential for Recovery. DFO Can. Sci. Advis. Sec. Res. Doc. 2014/088. vii + 55 p.

Ford, J.K.B. and Ellis, G.M. (1999) *Transients: Mammal-hunting Killer Whales of British Columbia, Washington, and Southeastern Alaska*. UBC Press.

Ford, J.K.B. and Fisher, H (1983) 'Group-specific dialects of killer whales (*Orcinus orca*) in British Columbia', *Communication and behavior of whales,* 76, pp.129-161

Frost, K.J., Russell, R.B. and Lowry, L.F. (1992) Killer Whales, *Orcinus Orca*, in the Southeastern Bering Sea: Recent Sightings and Predation on Other Marine Mammals, *Marine Mammal Science*, 8(2), pp. 110–119.

George, J.C., G. Sheffield, D.J. Reed, B. Tudor, R. Stimmelmayr, B.T. Person, T. Sformo, and R. Suydam. (2017) Frequency of injuries from line entanglements, killer whales, and ship strikes on Bering-Chukchi-Beaufort Seas bowhead whales. *Arctic* 70(1), pp.37–46.

Gillespie, D.M., Gordon, J., McHugh, R., Mclaren, D., Mellinger, D., Redmond, P., Thode, A., Trinder, P. and Deng, X.Y. (2008) PAMGUARD: Semiautomated, open-source software for real-time acoustic detection and localization of cetaceans, *The Journal of the Acoustical Society of America*, 125.

Grebmeier, J. (2012) Shifting Patterns of Life in the Pacific Arctic and Sub-Arctic Seas. *Annual Review of Marine Science*, 4(1), pp.63-78.

Hannay, D., Delarue, J., Mouy, X., Martin, B., Leary, D., Oswald, J. and Vallarta, J. (2013) Marine mammal acoustic detections in the northeastern Chukchi Sea, September 2007–July 2011. *Continental Shelf Research*, 67, pp.127-146.

Hansen, K. (2018) Historic low sea ice in the Bering Sea, *NASA Earth Observatory*, 3 May.

Higdon, J. and Ferguson, S. (2009) Loss of Arctic Sea ice causing punctuated change in sightings of killer whales (*Orcinus orca*) over the past century. *Ecological Applications*, 19(5), pp.1365-1375.

Hoelzel, A., Hey, J., Dahlheim, M., Nicholson, C., Burkanov, V. and Black, N. (2007) Evolution of Population Structure in a Highly Social Top Predator, the Killer Whale. *Molecular Biology and Evolution*, 24(6), pp.1407-1415.

IBM Corp., 2017. *IBM SPSS Statistics for Windows*, Armonk, NY: IBM Corp. Available at: https://hadoop.apache.org.

180011049

Janik, V.M. and Knörnschild, M. (2021) 'Vocal production learning in mammals revisited', *Philosophical Transactions of the Royal Society B: Biological Sciences*, 376(1836), p. 20200244.

Janik, V.M. and Sayigh, L.S. (2013) 'Communication in bottlenose dolphins: 50 years of signature whistle research', *Journal of Comparative Physiology A*, 199(6), pp. 479–489.

Jones, M., Berkelhammer, M., Keller, K., Yoshimura, K. and Wooller, M. (2020) High sensitivity of Bering Sea winter sea ice to winter insolation and carbon dioxide over the last 5500 years. *Science Advances*, 6(36).

Kershenbaum, A., Freeberg, T. and Gammon, D. (2015) Estimating vocal repertoire size is like collecting coupons: A theoretical framework with heterogeneity in signal abundance. *Journal of Theoretical Biology*, 373, pp.1-11.

Laidre, K., Stirling, I., Lowry, L., Wiig, Ø., Heide-Jørgensen, M. and Ferguson, S. (2008) Quantifying The Sensitivity Of Arctic Marine Mammals To Climate-Induced Habitat Change. *Ecological Applications*, 18(sp2), pp.S97-S125.

Madrigal, B., Crance, J., Berchok, C. and Stimpert, A. (2021) Call repertoire and inferred ecotype presence of killer whales (*Orcinus orca*) recorded in the southeastern Chukchi Sea. *The Journal of the Acoustical Society of America*, 150(4), pp.A284-A284.

Matkin, C., Barett-Lennard, L., Yurk, H. and Ellifrit, D. (2007) Ecotypic variation and predatory behavior among killer whales (*Orcinus orca*) off the eastern Aleutian Islands, Alaska. *Fishery Bulletin- National Oceanic and Atmospheric Administration*, 105(1), pp.74-87

Matthews, C.J.D., Breed,G.A., LeBlanc, B., and Ferguson, S.H. 2020. Killer whale presence drives bowhead whale selection for sea ice in Arctic seascapes of fear. *Proceedings of the National Academy of Sciences of the United States of America,* 117(12):6, pp. 590–598

Mellinger, D., Stafford, K., Moore, S., Dziak, R. and Matsumoto, H. (2007) An Overview of Fixed Passive Acoustic Observation Methods for Cetaceans. *Oceanography*, 20(4), pp.36-45.

Miller, P.J.O. (2006) Diversity in sound pressure levels and estimated active space of resident killer whale vocalizations. *Journal of Comparative Physiology A*, 192(5), pp.449-459.

Miller, P.J.O. and Bain, D.E. (2000) 'Within-pod variation in the sound production of a pod of killer whales, Orcinus orca', *Animal Behaviour*, 60(5), pp. 617–628.

Moore, S. and Huntington, H. (2008) Arctic Marine Mammals and Climate Change: Impacts and Resilience. *Ecological Applications*, 18(sp2), pp.S157-S165.

Moore, S., Waite, J., Friday, N. and Honkalehto, T. (2002) Cetacean distribution and relative abundance on the central–eastern and the southeastern Bering Sea shelf with reference to oceanographic domains. *Progress in Oceanography*, 55(1-2), pp.249-261.

180011049

Myers, H., Olsen, D., Matkin, C., Horstmann, L. and Konar, B. (2021) Passive acoustic monitoring of killer whales (*Orcinus orca*) reveals year-round distribution and residency patterns in the Gulf of Alaska. *Scientific Reports*, 11(1).

Newman, K. and Springer, A.M. (2008) Nocturnal activity by mammal-eating killer whales at a predation hot spot in the Bering Sea, *Marine Mammal Science*, 121(3105).

NOAA OAR Pacific Marine Environmental Laboratory, National Marine Fisheries Service, NOS Office of National Marine Sanctuaries, and DOI NPS Natural Resource Stewardship and Science Directorate. (2022) NOAA Ocean Noise Reference Station Network Raw Passive Acoustic Data. NOAA National Centers for Environmental Information.

Oswald, J., Walmsley, S., Casey, C., Fregosi, S., Southall, B. and Janik, V. (2021) Species information in whistle frequency modulation patterns of common dolphins. *Philosophical Transactions of the Royal Society B: Biological Sciences*, 376(1836).

Oswald, J.N., and M. Oswald. 2013. ROCCA (Real-time Odontocete Call Classification Algorithm) User's Manual. Prepared for Naval Facilities Engineering Command Atlantic, Norfolk, Virginia under HDR Environmental, Operations and Construction, Inc Contract No. CON005-4394-009, Subproject 164744, Task Order 03, Agreement # 105067. Prepared by Bio-Waves, Inc., Encinitas, California.

Parsons, K., Durban, J., Burdin, A., Burkanov, V., Pitman, R., Barlow, J., Barrett-Lennard, L., LeDuc, R., Robertson, K., Matkin, C. and Wade, P. (2013) Geographic Patterns of Genetic Differentiation among Killer Whales in the Northern North Pacific. *Journal of Heredity*, 104(6), pp.737-754.

Rand, Z., Wood, J. and Oswald, J. (2022) Effects of duty cycles on passive acoustic monitoring of southern resident killer whale (*Orcinus orca*) occurrence and behavior. *The Journal of the Acoustical Society of America*, 151(3), pp.1651-1660.

Riesch, R. and Deecke, V. (2011) Whistle communication in mammal-eating killer whales (*Orcinus orca*): further evidence for acoustic divergence between ecotypes. *Behavioral Ecology and Sociobiology*, 65(7), pp.1377-1387.

Riesch, R., Ford, J. and Thomsen, F. (2006) Stability and group specificity of stereotyped whistles in resident killer whales, Orcinus orca, off British Columbia. *Animal Behaviour*, 71(1), pp.79-91.

R Core Team (2020). R: A language and environment for statistical computing. R Foundation for Statistical Computing, Vienna, Austria. URL https://www.R-project.org/.

Samarra, F., Deecke, V., Vinding, K., Rasmussen, M., Swift, R. and Miller, P. (2010) Killer whales (*Orcinus orca*) produce ultrasonic whistles. *The Journal of the Acoustical Society of America*, 128(5), pp.EL205-EL210.

180011049

Samarra, F.I.P., Deecke, V.B. and Miller, P.J.O. (2016) Low-frequency signals produced by Northeast Atlantic killer whales (*Orcinus orca*), *The Journal of the Acoustical Society of America*, 139(3), pp. 1149–1157.

Saulitis, E., Matkin, C. and Fay, F. (2005) Vocal repertoire and acoustic behavior of the isolated AT1 killer whale subpopulation in southern Alaska. *Canadian Journal of Zoology*, 83(8), pp.1015-1029.

Sharpe, D., Castellote, M., Wade, P. and Cornick, L. (2017) Call types of Bigg's killer whales (*Orcinus orca*) in western Alaska: using vocal dialects to assess population structure. *Bioacoustics*, 28(1), pp.74-99.

Sigler, M.F. (2010) How Does Climate Change Affect the Bering Sea Ecosystem?, *Eos, Transactions American Geophysical Union*, 91(48), p. 457.

Simonis, A., Baumann-Pickering, S., Oleson, E., Melcón, M., Gassmann, M., Wiggins, S. and Hildebrand, J. (2011) High-frequency modulated signals of killer whales (*Orcinus orca*) in the North Pacific. *The Journal of the Acoustical Society of America*, 130(4), pp.2322-2322.

Sousa-Lima, R., Norris, T., Oswald, J. and Fernandes, D. (2013) A Review and Inventory of Fixed Autonomous Recorders for Passive Acoustic Monitoring of Marine Mammals. *Aquatic Mammals*, 39(1), pp.23-53.

Stafford, K. (2019) Increasing detections of killer whales (*Orcinus orca*), in the Pacific Arctic. *Marine Mammal Science*, 35(2), pp.696-706.

Stafford, K., Farley, E., Ferguson, M., Kuletz, K. and Levine, R. (2022) Northward Range Expansion of Subarctic Upper Trophic Level Animals into the Pacific Arctic Region. *Oceanography*, 35(1).

Thomsen, F., Franck, D., and Ford, J.K.B. (2001) Characteristics of whistles from the acoustic repertoire of resident killer whales (*Orcinus orca*) off Vancouver Island, British Columbia, *The Journal of the Acoustical Society of America*, 109(3), pp. 1240–1246.

Watkins, W. (1968) *The Harmonic Interval: Fact or Artifact in Spectral Analysis of Pulse Trains,* Technical Report no 68-13, Pregamon Press, Oxford & New York.

Weiß, B., Symonds, H., Spong, P. and Ladich, F. (2007) Intra- and intergroup vocal behavior in resident killer whales,Orcinus orca. *The Journal of the Acoustical Society of America*, 122(6), pp.3710-3716.

Wickham, H., François, R., Henry, L., Müller, K. (2021) Dplyr: A Grammar of Data Manipulation. R package version 1.0.6. https://CRAN.R-project.org/package=dplyr

Woodgate, R., 2022. *Bering Strait: Pacific Gateway to the Arctic*. [online] Psc.apl.washington.edu. Available at: <http://psc.apl.washington.edu/HLD/Bstrait/bstrait.html>

The Chukchi Coastal Communities Component of the Arctic Integrated Ecosystem Research Program: Final Report

Henry P. Huntington, Huntington Consulting, Eagle River, Alaska

Julie Raymond-Yakoubian, Kawerak Inc., Nome, Alaska

And members of the Chukchi Coastal Communities team

November 30, 2021

Contents

Executive Summary

The well-being of Arctic communities is a vital part of U.S. Arctic policy. Understanding the relationships between coastal residents and the marine environment is an essential contribution to the effective management of Arctic marine resources and activities that affect those communities and resources. In the context of the Arctic Integrated Ecosystem Research Program (Arctic IERP), the Chukchi Coastal Communities component focused on Arctic Indigenous community understanding of and response to ecosystem changes being studied by other components of the Arctic IERP. We examined how ecosystem changes affect communities, and we made available to other Arctic IERP researchers an annotated bibliography of information that had already been documented from Arctic Indigenous coastal communities about ecosystem change in their region. Together, these efforts helped connect the overall work of the Arctic IERP with the interests and concerns of coastal communities in the region.

Our project explored the nature of human-environment relationships in the region by compiling what has already been documented about local, Traditional, and Indigenous knowledges of the Chukchi Sea ecosystem and the changes it is undergoing, and by examining collaboratively with a team of experienced coastal residents the responses of coastal communities to variability and change. Our findings illuminate how and why a changing ecosystem matters to coastal communities, and provide insights into the ways communities can respond effectively to changes that are beyond their control. The compilation of information and knowledge in the annotated bibliography provided information relevant to the overarching questions of the Arctic IERP and many of the specific questions that were addressed by the other projects that were funded. Our project addressed four specific questions:

- What are local people's perceptions of the natural physical and ecological drivers of changes in the availability of animals for subsistence harvest?
- What are the primary drivers (natural, social, cultural, economic) of shifts in subsistence use patterns?
- Have shifts in harvest patterns affected food security and, if so, how?
- How resilient are human communities to variability, anomalies, and shifts in the marine environment?

Our project's activities centered on meetings of the research team, including members of eight coastal communities. The communities involved were Savoonga, Diomede, Buckland, Kotzebue, Kivalina, Point Hope, Point Lay, and Utqiaġvik.

The Chukchi Coastal Communities component produced one scientific paper on its own, reporting the results of its research. This paper was published in the *Arctic* in June 2021. The main message of this paper is that traditional values and Indigenous leadership are essential for addressing the intertwined effects of social and environmental change in the region.

The PI of the Chukchi Coastal Communities component also led a group effort across the Arctic IERP that resulted in a paper published in *Nature Climate Change* in February 2020. The main message of this paper is that the northern Bering Sea-Chukchi Sea ecosystem is rapidly transforming.

Rapid environmental change, such as that found by the studies in the Arctic IERP, poses considerable challenges to resource management and to coastal community well-being. In terms of resource management, our findings show also that regional human activity causes environmental change in addition to larger processes such as a warming global climate. Resource management needs to take into account the combined effects of various forms of change and disturbance. Still, more work is needed to understand the complex interactions that create outcomes, especially in a time when widespread environmental change is happening even more rapidly than was expected when the Arctic IERP began.

For coastal communities, our findings reflect much of what their residents have already experienced. Sharing of information among the eight communities involved in our project was valuable in helping team members see the extent and type of change occurring throughout the region. Societal change cannot be separated from environmental change when it comes to community-level effects and responses. Key conclusions of the Chukchi Coastal Communities component are that traditional values remain essential to community well-being and that Indigenous leadership is necessary for responding to change in ways that will sustain overall community well-being (as defined by communities). An additional point is that equitable partnerships with scientists can help provide valuable information to communities as they determine how best to respond to change, and provide important information to the broader science community.

Preamble

The Arctic Integrated Ecosystem Research Program

The Arctic Integrated Ecosystem Research Program (Arctic IERP, 2016-2021) was motivated by the rapid changes occurring in the waters of the northern Bering and Chukchi Seas. While much research has been done in the region, many important questions remain. As a cohesive research endeavor, the Arctic IERP was designed to address a single, overarching question:

How will reductions in Arctic sea ice and the associated changes in the physical environmental influence the flow of energy through the ecosystem in the Chukchi Sea?

The report you are reading now is one of five final reports from the fieldwork phase of the Arctic IERP (a synthesis phase was initiated in 2022 after the completion of the Arctic IERP field-based projects). This preamble provides a brief overview of the Arctic IERP, both to place each final report in the broader context of the whole program, and to encourage readers to examine the other final reports to learn more about the research that was done. More detailed information about the Arctic IERP can be found at https://www.nprb.org/arctic-program.

The spatial domain of interest for the Arctic IERP extended across the Chukchi Sea Large Marine Ecosystem (LME) as redefined by the Arctic Council's Protection of the Arctic Marine Environment (PAME) working group, and the northern Bering Sea (above 61.5° N) as it strongly influences dynamics in the Chukchi Sea from the upstream direction. The main focus has been on the greater Bering Strait region and the Chukchi Sea. The program included the Arctic Basin and Beaufort Sea insofar as processes in the Chukchi Sea are influenced by these adjacent areas.

Development of the Arctic IERP

Before any Arctic IERP research proposals were written, the NPRB administered an assessment program, the Pacific Marine Arctic Regional Synthesis (PACMARS; https://www.nprb.org/assets/uploads/files/Arctic/PacMARS_Final_Report_forweb.pdf), that applied $1.5M provided by Shell and ConocoPhillips to compile and synthesize existing information about the ecosystem and inform research priorities. This assessment included community meetings in 2013 in Savoonga, Gambell, Kotzebue, Nome, and Barrow (now Utqiaġvik), in which representatives from 17 communities between St. Lawrence Island in the Bering Sea and Barter Island in the Beaufort Sea participated. One major area of emphasis that emerged from these community meetings was concern about food security for the region's residents in light of the rapid environmental changes taking place. Results from the scientific assessment and input provided via the community meetings informed the creation of the Arctic IERP. The PACMARS report informed both the IERP Request for Proposals (https://www.nprb.org/arctic-program/request-for-proposals/) and the submitted proposals.

Following a proposal review process, the Arctic IERP formally began in 2016 with funding from the North Pacific Research Board (NPRB), the Collaborative Alaskan Arctic Studies Program (formerly the North Slope Borough/Shell Baseline Studies Program), the Bureau of Ocean Energy Management (BOEM), and the Office of Naval Research (ONR) Marine Mammals and Biology Program. Generous in-kind support was contributed by the National Oceanic and Atmospheric Administration (NOAA), the University of Alaska Fairbanks (UAF), the U.S. Fish & Wildlife Service (USFWS), and the National

Science Foundation (NSF). This coordinated program was developed in cooperation with the Interagency Arctic Research Policy Committee (IARPC) and the U.S. Arctic Research Commission.

The Research

The Arctic Integrated Ecosystem Research Program (IERP) invested approximately $18.6 million in studying marine processes in the northern Bering and Chukchi Seas in 2017-2021, beginning in the summer of 2017. The research was divided into three main, complementary projects. The Arctic Shelf Growth, Advection, Respiration, and Deposition Rate Experiments (ASGARD) project carried out research in late spring and early summer of 2017 and 2018 aboard R/V *Sikuliaq*. The Arctic Integrated Ecosystem Survey (Arctic IES) conducted fieldwork aboard R/V *Ocean Starr* in late summer and early fall 2017 and 2019. In addition to the vessel-based surveys, sub-surface moored sensors were deployed to gather biophysical information continuously from June 2017 to September 2019 and autonomous platforms were brought to bear (e.g., gliders, saildrones, air-deployed profilers).

In addition to the vessel-based work, a team of Arctic residents and social scientists, including members from eight communities in the North Slope and Northwest Arctic Boroughs and the Bering Strait region, met several times during the project to assess and analyze Indigenous observations and experiences with various types of change occurring in the region from Savoonga to Utqiaġvik. This group also compiled an annotated bibliography of Traditional Knowledge or Indigenous Knowledge (available through the data portal described below), to help researchers from other components of the Arctic IERP find information relevant to their studies.

Prior to the commencement of fieldwork, meetings were held in the three hub communities of Nome, Kotzebue, and Utqiaġvik. Scientists from the Arctic IERP and NPRB staff met with community members from each region to discuss the research purpose and plans. Research plans were also shared and discussed at meetings of the Alaska Eskimo Whaling Commission (AEWC), the Indigenous Peoples Council for Marine Mammals (IPCoMM), and with the Tribal Councils of Gambell and Savoonga on St. Lawrence Island. One result of these meetings was a shift in timing of the ASGARD cruises from May until June as well as a shift in timing and survey regions for the Arctic IES cruises, to avoid conflicts with subsistence hunting activities during what is traditionally the time for walrus hunting. Another result was the creation of communication protocols to avoid conflicts by alerting coastal communities to the presence of research vessels and adjusting the ships' routes to avoid areas where hunting was taking place. These communication protocols included regular radio broadcasts and daily emails to community members throughout the research area.

Results from the research are published in a growing list of peer-review journal articles, as well as cruise reports that provide contemporary accounts of the cruises, and many social media postings that are available through the NPRB website. Data are publicly available as described below.

Collaborations

The NPRB collaborated and coordinated with several other U.S. agencies and organizations that fund Arctic marine research. NPRB staff worked closely with the U.S. Interagency Arctic Research Policy Committee (IARPC) and the U.S. Arctic Research Commission. As the Arctic IERP was developed, the

NPRB secured commitments for collaboration from 22 existing research projects that were detailed in Appendix A of the request for proposals, and made connections with new projects as they were funded.

International researchers also collaborated with the Arctic IERP via the Pacific Arctic Group (PAG), the North Pacific Marine Science Organization (PICES), and the Intergovernmental Consultative Committee (US/Russia - bilateral) as well as collaborations developed by individual investigators. PAG participants, including researchers from Canada, China, Japan, Korea, Russia, and the United States, have coordinated their cruise plans to sample standard stations in the Chukchi and Beaufort Seas termed the Distributed Biological Observatory (DBO). The Arctic IERP contributed to this effort. US-Russian data sharing initiatives were hosted in San Diego in 2016 and Vladivostok in 2017 to promote collaboration and exchange and to facilitate collaboration and synthesis of data and trends of patterns observed in the US and Russian waters in the northern Bering and Chukchi seas (PICES Press, Volume 26, Issue 1). ICC collaborations and other connections also brought scientists from the Russian Federal Research Institute of Fisheries and Oceanography (VNIRO), the Russian Pacific Scientific Fisheries Research Center (TINRO), and Hokkaido University to the US to participate in the Arctic IES cruises and co-author results. This collaboration is expected to connect research interests within respective EEZs (Russia/US) of the Chukchi Sea.

COVID-19

While the fieldwork of the Arctic IERP was completed before the outbreak of COVID-19, the final meeting of researchers in November 2020 was changed from an in-person event to an online format. Other plans for in-person events, such as meetings in hub communities within the US Arctic region (Nome, Kotzebue, and Utqiaġvik), were cancelled. Laboratory work and some collaborations were postponed or cancelled due to COVID-related restrictions and concerns. The NPRB made supplemental funds available to assist researchers with unanticipated expenses due to the pandemic. The overall productivity of the Arctic IERP was likely not greatly reduced, due both to good fortune in the fieldwork being completed and to the collaborative relationships that had been built or strengthened during the program.

Data Portal

Axiom Data Science, Inc. provided data management support to the Arctic IERP throughout the field program. Axiom staff assisted the scientists in authoring metadata and publishing the datasets to public archives. The data collected by the Arctic IERP are publicly accessible at https://arctic-ierp.dataportal.nprb.org/.

General Introduction

The well-being of Arctic communities is a vital part of U.S. Arctic policy (e.g., Obama 2013). Understanding the relationships between coastal residents and the marine environment is an essential contribution to the effective management of Arctic marine resources and activities that affect those communities and resources (e.g., BOEM 2014). In the context of the Arctic Integrated Ecosystem Research Program (Arctic IERP), the Chukchi Coastal Communities component focused on Arctic Indigenous community understanding of and response to ecosystem changes being studied by other components of the Arctic IERP. The intent was two-fold. First, we examined how ecosystem changes affect communities, especially in the context of other forms of change that they are experiencing at the same time, such as economic, cultural, and social changes. Second, we compiled and made available to other Arctic IERP researchers an annotated bibliography of information that had already been documented from Arctic Indigenous coastal communities about ecosystem change in their region, to make sure that information was considered along with instrumental and other scientific data. Together, these efforts helped connect the overall work of the Arctic IERP with the interests and concerns of coastal communities in the region.

Our project explored the nature of human-environment relationships in the region by compiling what has already been documented about local, Traditional, and Indigenous knowledges (LTK; NPRB 2005) of the Chukchi Sea ecosystem and the changes it is undergoing, and by examining collaboratively with a team of experienced coastal residents the responses of coastal communities to variability and change. Our findings illuminate how and why a changing ecosystem matters to coastal communities, and provide insights into the ways communities can respond effectively to changes that are beyond their control. The compilation of information and knowledge in the annotated bibliography provided information relevant to the overarching questions of the Arctic IERP and many of the specific questions that were addressed by the other projects that were funded. Our project addressed specific questions as follows:

What are local people's perceptions of the natural physical and ecological drivers of changes in the availability of animals for subsistence harvest?
We examined what has been documented already (e.g., ADF&G, N.D., Huntington et al. 1999, 2016, George et al. 2004, Braund 2013. Oceana and Kawerak 2014. B. Raymond-Yakoubian et al. 2014. J. Raymond-Yakoubian et al. 2014, Gadamus and Raymond-Yakoubian 2015a,b, Gadamus et al. 2015, the Northwest Arctic Borough subsistence mapping project, unpublished NSB work, Kawerak archives, UAF's Project Jukebox), emphasizing the region from St. Lawrence Island to Utqiaġvik. (The inclusion of St. Lawrence Island, in accordance with the Arctic RFP's scope, created an overlap with the five communities that were involved in the LTK component of the Bering Sea Project, of which Savoonga was the northernmost (Huntington et al. 2013a, b, c).) We additionally addressed specific questions or topics identified in collaboration with and via a survey of other Arctic Program PIs to better provide relevant information and create a foundation for collaborative analysis.

What are the primary drivers (natural, social, cultural, economic) of shifts in subsistence use patterns?
Have shifts in harvest patterns affected food security and, if so, how?
The review of existing information allowed us to address these questions. Of particular interest was a comparison with Bering Sea Project findings that indicated strong connections between communities and the ecosystem, in the sense of high subsistence production and powerful spiritual significance of the human-ecosystem relationship, but weak coupling in the sense that human activities and outcomes do not appear to respond rapidly and directly to environmental changes (Haynie and Huntington

2016). It is important to understand both the social system (culture, economics, policies, technology, regulations) and the ecosystem so as to understand how environmental change is moderated by the social system to produce effects and responses in coastal communities. While there was no doubt that environmental change affects coastal communities, the exact nature of the mechanisms of such change were not well understood. The concept of food security (Council of Canadian Academies 2014, ICC-Alaska 2014a, b, 2015) provided a useful framework for seeing the interplay of these factors.

How resilient are human communities to variability, anomalies, and shifts in the marine environment?
If coastal communities were unable to cope with variability, they could not have persisted as they have for decades, centuries, and millennia (e.g., Rainey 1947). Most research to date has examined the nature of changes in the environment (e.g., Cochran et al. 2013), rather than also considering the social system in which those environmental changes act (Haynie and Huntington 2016). We examined more carefully the mechanisms by which communities take advantage of favorable conditions and adjust to unfavorable ones. It is important to note in this context that change is not necessarily disadvantageous, although most assessments of change emphasize negative outcomes rather than new opportunities (cf. Noongwook et al. 2007, Huntington et al. 2017).

Our project's activities centered on meetings of the research team, including members of eight coastal communities. The communities involved were Savoonga, Diomede, Buckland, Kotzebue, Kivalina, Point Hope, Point Lay, and Utqiaġvik. The meetings were held in conjunction with the Arctic IERP's Principal Investigator (PI) meetings, in March 2017, March 2018, and January 2020. All of these were in Anchorage, Alaska. Project staff from Kawerak Inc. in Nome, Alaska, compiled an annotated bibliography of sources of LTK from the region, which was shared with all participants in the Arctic IERP.

The Chukchi Coastal Communities component produced one scientific paper on its own, reporting the results of its research. This paper was published in the *Arctic* in June 2021. The main message of this paper is that practicing traditional values and Indigenous leadership are essential for addressing the intertwined effects of social and environmental change in the region. This paper addresses all three of our research questions.

The PI of the Chukchi Coastal Communities component also led a group effort across the Arctic IERP that resulted in a paper published in *Nature Climate Change* in February 2020. The main message of this paper is that the northern Bering Sea-Chukchi Sea ecosystem is rapidly transforming. This paper went beyond the research questions addressed by our component of the Arctic IERP.

The accepted manuscripts are included as chapters of this final report. Publication details are provided in the appropriate section of this report.

Results of the Chukchi Coastal Communities component

This chapter presents the findings of the Chukchi Coastal Communities component, as reported in a paper published in Arctic *in June 2021. This chapter consists of the accepted manuscript for the paper. Note that the published manuscript was subject to copy editing and other changes. Full details of the publication can be found in the appropriate section of this report, below.*

"We never get stuck": a collaborative analysis of change and coastal community subsistence practices in the northern Bering and Chukchi Seas, Alaska

Authors
Henry P. Huntington, 23834 The Clearing Dr., Eagle River, AK 99577, USA; henryphuntington@gmail.com; ORCID 0000-0003-2308-8677 (Corresponding author)
Julie Raymond-Yakoubian, Kawerak Social Science Program, P.O. Box 924, Nome, AK 99762, USA; ORCID 0000-0002-3961-7660
George Noongwoook, Savoonga Whaling Captains Association, P.O. Box 81, Savoonga, AK 99769, USA
Noah Naylor, formerly with Northwest Arctic Borough, P.O. Box 1110, Kotzebue, AK 99752, USA; currently with Kikiktagruk Inupiat Corporation, P.O. Box 1050, Kotzebue, AK 99752, USA
Cyrus Harris, Maniilaq Association, P.O. Box 256, Kotzebue, AK 99752, USA
Qaiyaan Harcharek, formerly with North Slope Borough Department of Wildlife Management, P.O. Box 69, Utqiaġvik, AK 99723, USA
Billy Adams, North Slope Borough Department of Wildlife Management, P.O. Box 69, Utqiaġvik, AK 99723, USA

Abstract
The Indigenous communities of the northern Bering and Chukchi Sea are experiencing extensive social, economic, and technological change. The region's marine ecosystem is also characterized by a high degree of variability and by rapid change. Residents of eight coastal communities from Savoonga to Utqiaġvik were involved in the Chukchi Coastal Communities Project, which used the results of a literature review together with the experiences of the community participants to co-analyze what is known about societal and environmental change in the region and what the communities' experiences have been in responding to those changes. Some of the observed changes are transient in duration and effect, such as the passage of an individual ship, whereas others, such as the creation of the Red Dog Mine Port Site, persist and may force lasting changes by coastal residents. Some responses can use existing knowledge, for example hunting bowhead whales in fall as well as spring, whereas others may require learning and experimentation, such as harvesting new species such as the Hanasaki crab. Our findings show that the results of a change are more important than the source of the change. They also emphasize the continuing importance of traditional values and practices as well as attitudes conducive to persistence and innovation. Indigenous leadership is an essential component of continued resilience as the ecosystem continues to change. The resilient characteristics of coastal communities, and their ability to determine their own responses to change, need greater attention, to match the research effort directed at understanding the ecosystem.

Key Words:
Chukchi Sea, Bering Sea, Iñupiaq, St. Lawrence Island Yupik, subsistence, response

Introduction

Subsistence activities, which include traditional hunting, fishing, and gathering practices, provide vital cultural, nutritional, economic, social, and spiritual benefits to Indigenous residents of the northern Bering Sea and Chukchi Sea coast of western and northern Alaska (ICC-Alaska, 2015; Raymond-Yakoubian, 2019). In recent years, much attention has been given to the effects of climate change on subsistence and other aspects of Indigenous community life in Alaska and elsewhere (e.g., Fall et al., 2013; Gadamus, 2013; Pearce et al., 2015). At the same time, community members and researchers both recognize that subsistence practitioners have long dealt with considerable environmental variability on time scales from hours to decades (Kapsch et al., 2010; Huntington et al., 2013a). In addition to environmental considerations, subsistence practices have been affected by social, economic, regulatory, technological, and other forms of change (Kersey, 2011; Raymond-Yakoubian, 2013; Moerlein and Carothers, 2012; Huntington and Eerkes-Medrano, 2017). These societal shifts have affected both the demand for subsistence foods and the ability to procure those foods (Fall et al., 2013). For example, modern hunting equipment facilitates access but requires money for purchase, maintenance, and operation, which can limit participation for those with limited access to cash. While negative effects on subsistence get much attention and for good reason, the various changes communities have experienced have also had positive effects (e.g., Noongwook et al., 2007; Huntington et al., 2017a), in part due to the ability of communities to adjust where possible and to take advantage of opportunities.

That ability to adjust and to find and create opportunities is an essential attitude in an environment characterized by variability, as is the case for the northern Bering and Chukchi Sea marine ecosystem (e.g., Moore et al., 2018; Huntington et al., 2020). Weather and sea ice conditions can change within hours and can vary greatly from year to year. The harvest of marine mammals, seabirds, and fish in coastal communities also varies from year to year (e.g., Fall et al., 2013). If the Iñupiat and St. Lawrence Island Yupik of Alaska's western and northern coasts were unable to cope with that variability, their communities could not have persisted (e.g., Hovelsrud and Smit, 2010). This is not to say that such strategies are always effective. In both oral history and the archeological record, there is abundant evidence of the abandonment of settlements and shifts in subsistence patterns and technology (e.g., Mason and Gerlach, 1995). Nonetheless, the application of knowledge and skills to changing conditions, also described as adaptations to change, have been described in a number of papers. Thornton and Manasfi (2010), for example, define eight modes of adaptation, such as mobility and diversification. In addition, Walker and Salt (2012) describe societal characteristics or attitudes that promote adaptive responses, such as openness and diversity. Huntington et al. (2017a) examine how communities are able to respond to change, autonomously or in collaboration with others outside the community. Amid current concerns about the effects of climate change on the Arctic and its residents (e.g., Brinkman et al., 2016), the question of how coastal residents respond to change is ever more pertinent, deserving of detailed attention at the community level.

Our study started from the premise that much has already been documented about Indigenous observations of, experiences with, and responses to variability and change in this region. Rather than engage in another effort to interview community residents, we elected to engage community-identified experts in a co-analysis of the existing information. This approach is part of a shift in the role of community participants from providers of information to interpreters of information, and part of a wider movement towards meaningful collaborations, Indigenous leadership in research, and the co-production of knowledge, a paradigm emphasizing the need to work together from start to finish in research projects (Lemos and Morehouse, 2005; Bartlett et al., 2012; Meadow et al., 2015; Whyte, 2017; David-Chaves and Gavin, 2018; Peltier, 2018; Kirby et al., 2019). The aim of the study and of this paper therefore is not to generate or report new observations and basic information, but to take a new look at what is already on record, to better understand the meanings and implications of that existing information from the perspective of Indigenous communities.

Our project had two questions in mind. First, do different types of change manifest themselves in different ways, for example in the time scale on which they operate, and do they have demonstrable effects on subsistence outcomes? Climate change and other modes of change such as the effects of industrialization or commercial fishing are often regarded as a major influence on subsistence practices (e.g., Cochran et al., 2013; Brinkman et al., 2016). We seek evidence to support that oft-repeated assertion.

Second, what strategies are used by Iñupiaq and St. Lawrence Island Yupik residents of Alaska's northern Bering and Chukchi Sea coasts? If the strategies being used are likely to be effective in light of continued change to the ecosystem, it will be important to support the use of those strategies. If the strategies are unlikely to continue to be effective, it will be important to recognize their shortcomings and for coastal communities to develop alternatives. We conclude by considering the context in which environmental change affects the region's communities and its implications for the future well-being of those communities.

Figure 1: Map of the region showing the communities with experts on the project team.

The study area for this project extends from St. Lawrence Island in the northern Bering Sea to Utqiaġvik at the edge of the Chukchi and Beaufort Seas (Figure 1). There are over a dozen Alaska Native communities along the coast or close enough to the coast to use the marine environment for subsistence. Of these, we selected nine communities to be invited to join the project, based on their connections to the sea, their participation in previous collaborative research efforts of this type, and their willingness to take part. Eight were able to accept: Savoonga (2019 population est. 735; Alaska Department of Labor, 2020), Diomede (97), Buckland (509), Kotzebue (3,112), Kivalina (427), Point Hope (670), Point Lay (236), and Utqiaġvik (4,536; formerly known as Barrow). The participant chosen by the ninth community was unable to attend due to schedule conflicts and no substitute could be arranged. The communities are Iñupiaq and St. Lawrence Island Yupik, referred to collectively here as the "Chukchi coastal communities."

Methods

Our work (the Chukchi Coastal Communities Project) is part of the North Pacific Research Board's Arctic Integrated Ecosystem Research Program (Arctic IERP; http://www.nprb.org/arctic-program/about-the-program/). The Arctic IERP includes several projects spanning physical oceanography to social

science, in an effort to consider the Chukchi Sea ecosystem and the implications of the environmental changes taking place in the region. The scope of the Arctic IERP was shaped in part by previous efforts to engage coastal communities in the planning and conduct of Arctic research (Grebmeier, 2014). The Chukchi Coastal Communities Project examines the ways environmental changes affect the Iñupiaq and St. Lawrence Island Yupik communities along the Chukchi Sea coast of Alaska, and also seeks to make available their observations of change in order to contribute to the program's collective understanding of what is happening in the region's marine environment.

Recognizing that Alaska Native communities have been the subject of extensive research concerning subsistence and environmental change (among many other topics; see for example Cochran et al., 2013 and references therein; Raymond-Yakoubian and Raymond-Yakoubian 2017), the Chukchi Coastal Communities Project does not include primary research, such as interviews, in the communities. We instead conducted a literature review of publications relevant to Chukchi coastal communities and their role in the marine ecosystem. We found 248 publications, including articles in scientific journals, books, reports, and other materials. The review began with papers known to the project team and reviewing the reference lists of the publications already in the collection. We expanded through internet searches using keywords such as "Bering, Chukchi, Bering Strait, North Slope, Northwest Arctic, subsistence, indigenous, Alaska Native, hunting, climate change, adaptation, resilience," and other terms and combinations found in the works already in our collection. The bibliographic details of the publications and a short list of key points or topics for each one were compiled into a document which was archived in the Arctic IERP data collection. This material is summarized below and constitutes the starting point for our co-analysis discussions.

In parallel to the literature review, members of the eight participating communities along the coast were identified as experts and selected by the project leads in cooperation with Tribal and community leaders to take part in meetings to review and co-analyze what is known about societal and environmental change in the region and what these data tell us concerning the communities' experiences and well-being. By "co-analysis," we mean an effort to work together, not simply for academically trained researchers to ask questions of community experts and take notes, but for all involved to discuss observations and implications of changes, effects, and responses, based on each person's experiences and understanding.

The meeting discussions were organized around the topics mentioned in the Introduction. In March 2017, the project team met in Anchorage, Alaska, with 12 residents of the coastal communities (including two of the project leads) and two project leaders who live in the greater Anchorage area. In March 2018, the project team met again in Anchorage, this time with 11 residents of coastal communities (including two project leads and one project staff person) and the two project leaders from the Anchorage area. In both years, notes were taken of the discussions, circulated to participants for review and corrections, and archived as part of the Arctic IERP data collection.

The authors of this paper include the project leads as well as community experts who were interested in contributing to the paper, beyond the meeting discussions. The overall project lead (HPH) is a non-Indigenous scholar living near Anchorage, Alaska. Project co-leads include a non-Indigenous scholar living in the Anchorage area (JRY) and working for Kawerak, Inc., a regional non-profit based in Nome; an Iñupiaq from Kotzebue who at the time of the research was the planning and science director for the Northwest Arctic Borough (NN); and an Iñupiaq from Utqiaġvik who at the time of the research was a subsistence research specialist with the North Slope Borough Department of Wildlife Management (QH). The three remaining co-authors are a St. Lawrence Island Yupik whaling captain and local leader from Savoonga (GN), an Iñupiaq provider of social services in Kotzebue who grew up on the land away from the community (CH), and an Iñupiaq employee of the North Slope Borough Department of Wildlife Management from Utqiaġvik (BA). All six of the Indigenous co-authors are active and experienced subsistence practitioners with additional extensive experience as members of formal scientific research efforts.

Examples of Causes of Change, Effects on Subsistence Practices, and Responses to Change

The literature review provided numerous examples of changes that have occurred in Chukchi coastal communities and their surroundings over the past years and decades, as well as resulting effects on subsistence practices and outcomes, and a range of ways that individuals and communities have responded. These documented examples were complemented by observations of project team members during the co-analysis meetings. The list is not exhaustive. Instead, we have selected examples that community experts identified as representative of common experiences and trends, and that illustrate a range of factors driving those changes.

We found dozens of examples of effects on subsistence practices. Fewer studies documented clear changes in outcomes, such as reduced (or increased) harvest levels. The causes of effects on subsistence can be divided first into societal and environmental categories, and then further into subcategories. Environmental changes include changing weather, changing sea ice, changing abundance or distribution of harvested species, and the availability of new species to harvest. Societal changes include industrial activity such as shipping or offshore oil and gas activity, technological change, social or cultural change, economic change, and regulatory change. We considered both the short-term effects, lasting a season or less, and long-term effects, lasting for years or decades. A summary of examples of changes and effects is presented in Table 1.

In Table 2, we present examples of several categories of response and potential limits to the effectiveness of a given strategy. Broadly, the strategies fall into two categories: specific actions that can be taken, such as hunting bowhead whales in fall as well as spring, and general approaches that promote problem-solving and innovation, such as persistence and a willingness to experiment.

As noted earlier, the information in both tables was the foundation for our co-analysis discussions. The literature survey also provided an annotated bibliography for the use of Arctic IERP researchers and others interested in Chukchi coastal communities' observations of an experiences with change. This information could be used, for example, to compare findings from research cruises or remote sensing with local observations and understanding. Such efforts are separate from the purpose of this paper.

Table 1. Examples of changes experienced by Chukchi coastal communities and their short- and long-term effects on subsistence. These examples were documented in the literature included in our project bibliography and complemented by additional observations shared in our project meetings.

Examples of change	*Short-term (days to seasons) effects on subsistence*	*Long-term (years to decades) effects on subsistence*	*References*
More strong winds and storms Rapid break-up of ice leading to short duration of good hunting conditions Marine mammals migrating farther from some communities	Temporary poor hunting season	Reduced hunting opportunities	Ashjian et al., 2010; Hanson et al., 2013; Huntington et al., 1999, 2013a, 2017a; Oceana and Kawerak 2014; March 2017, 2018 discussions
Earlier break-up and later freeze up of sea ice	Earlier and later access for hunting from boats	More hunting opportunities from boats in Buckland, Utqiaġvik Fall whaling season in Savoonga	March 2017 discussions; Noongwook et al., 2007; Oceana and Kawerak 2014
Less reliable shorefast ice	Harder to find places to haul whales out for butchering	No bowhead whales taken in Kivalina since 1994	Huntington et al., 2017a; Slats et al., 2019
More rain in summer	Spoilage of drying meat and fish	Need to switch to other methods of preservation	Raymond-Yakoubian, 2013; Raymond-Yakoubian and Raymond-Yakoubian, 2015
Warmer weather	Flooding of ice cellars and loss of stored food	Thawing ice cellars and need to find other methods of preservation	Christie et al. 2018
Hanasaki crabs arriving near St. Lawrence Island Increased salmon near Utqiaġvik	Need to learn new skills, tastes	New source of food	Huntington et al., 2017b; Carothers et al., 2013
Increased commercial ship traffic	Marine mammals temporarily become wary and hard to approach	Change in marine mammal distribution and local abundance, e.g., near the Red Dog Mine Port Site, reduced hunting opportunities	Huntington et al., 1999, 2017a; Kawerak, 2013a
Shift from sled dogs to	In Emmonak, single-day hunting	Reduced harvests of ringed seals	Hall, 1971; Burch, 1985;

snowmachines for winter transport	trips become possible, resulting in a smaller use area	(*Pusa hispida*) and fish	Raymond-Yakoubian, 2013; Raymond-Yakoubian and Raymond-Yakoubian, 2015; Fienup-Riordan et al., 2013
Larger boats, more reliable motors, GPS navigation	Able to travel in worse conditions	Expansion of overall use areas	Raymond-Yakoubian et al., 2014; Huntington et al., 2017a
Arrests of Diomede residents for illegal trade in walrus ivory	Loss of hunters due to incarceration	Loss of hunting and skin boat making traditions as hunters avoid walrus hunting and skills are not passed on	March 2017 discussions
Imposition of bowhead quota by IWC	Changes in hunting patterns	Restriction on harvest, need to spend time lobbying for continued quota	Huntington, 1992; Noongwook, 2018
Schooling requirements	Loss of opportunities to participate in subsistence	Reduced transmission of subsistence skills and knowledge	Napoleon, 1996; March 2017, 2018 discussions; Raymond-Yakoubian, 2019
Greater participation in the wage economy	Shift to weekend hunting patterns to accommodate work schedule	Higher subsistence production in Utqiaġvik due to greater access to boats, snowmachines, etc	Kruse, 1991; Galginaitis, 2013
Reduced income, purchasing power	Embarrassment at lack of equipment, avoidance of subsistence activities	Reduced participation in subsistence activities	March 2017 discussions; Raymond-Yakoubian, 2019

Table 2: Response categories, examples, and what might constrain the effectiveness of the responses. These examples were documented in the literature included in our project bibliography and supplemented by additional observations shared in our project meetings.

Response	*Example*	*Limits on effectiveness*	*References*
Using different areas	Variation in use areas over time	If species remain available somewhere in range and the areas are available for use Added travel cost if new areas are farther away	Braund, 2010; Gadamus and Raymond-Yakoubian 2015a
	Moving from Diomede to Nome	If moving is an option, if hunting remains good in new area, if newcomers are allowed to hunt there	March 2017 discussions
Using different times	Fall whaling in Savoonga	If species remain available and conditions are suitable	Noongwook et al., 2007
Using different species	Variation in harvest composition from year to year	If at least some species remain abundant	Braund, 2010; Fall et al., 2013; Raymond-Yakoubian, 2013
Being prepared	Continual observation, readiness to take action when opportunity presents itself	If there are opportunities to seize	March 2017 discussions; Raymond-Yakoubian et al., 2014; Kawerak, 2013a, b; Huntington et al., 2017a
	Use of social media to share information about animal migrations	Access to social media, presence of animals	Christie et al., 2018
Being persistent	"We never get stuck"—not giving up, but continuing to look for ways to make things work	Until the obstacles are too great to overcome	March 2018 discussions
Using new species	Hanasaki crabs in Savoonga	If there are new species available, and if there are no regulatory barriers	Huntington et al., 2017b
Using new techniques and tools	Drones to scout for suitable ice, marine mammals	If techniques/tools are available and affordable, if the animals are still there; regulatory restrictions on some technologies	Schwing, 2016; Hughes, 2018; Raymond-Yakoubian et al., 2014; Woodford, 2019
Making new use of the harvest	Smoking salmon in Utqiaġvik	If there are options and the information needed	March 2018 discussions; Kersey,

		to employ those options	2011
Being willing to experiment	Hunting the first belugas (*Delphinapeterus leucas*) to pass Point Lay	As long as there are animals available; tolerance for risk	March 2017 discussions

Results of the Co-Analysis

Types and effects of change

Chukchi coastal communities face many types of change and disturbance, as illustrated in Table 1. Separating these by type—e.g., environmental vs. societal, or local vs. global—is less important than understanding the characteristics of each disturbance. For example, the duration of the disturbance marks the difference between a temporary problem, a seasonal problem, or a long-term problem. The passage of a single ship can disrupt marine mammal behavior for a day or two. The operation of the Red Dog Mine Port Site over many decades has caused a long-term shift in marine mammal distributions in the area. Similarly, a storm can keep hunters on shore for a few days. Poor spring weather or ice conditions can reduce harvests for a season. Declines in the reliability of shorefast ice has contributed to Kivalina not landing a bowhead whale (*Balaena mysticetus*) since the mid-1990s. Changes in ice break-up patterns have reduced the duration of good seal hunting conditions from weeks to days or even less.

The duration of a disturbance or alteration distinguishes variability from change. The Arctic environment has always been variable and hunters have had to adjust from day to day, season to season, and year to year. This is considered normal. The annual Pacific walrus (*Odobenus rosmarus divergens*) harvest on St. Lawrence Island varies greatly, due to weather and ice conditions as well as societal factors. The quote in the title of this paper—"We never get stuck"—is indicative of the expectation that community residents will have to find ways to make do, and that attitude is as important as skill in doing so.

More recently, the environment has also undergone persistent changes. Sea ice forms later and breaks up earlier and more rapidly, affecting marine mammal hunting patterns as well as fishing and crabbing through the ice. The loss of suitable hunting and fishing days has reduced opportunities. On the other hand, earlier break-up can create earlier access, as is the case for Buckland seal hunters, and a late freeze-up has created a new fall bowhead whaling season in Savoonga. More rain in summer makes it harder to dry fish and meat, complicating the task of preserving foods in traditional ways. Ice cellars, dug into permafrost to provide sub-freezing storage at no cost, are themselves threatened by thawing permafrost caused by warmer weather and other changes to soil conditions. Stronger and more frequent winds reduce the number of days suitable for boat travel, and larger boats cannot completely overcome this problem.

Shifts in the distribution and abundance of different species have also affected subsistence practices. The increased availability of salmon (*Oncorhyncus* spp.) in Utqiaġvik has created a new fishery and led people there to learn how to smoke salmon. The Hanasaki crab (*Paralithodes brevipes*) is a relatively new arrival in the waters off Savoonga, providing a new and valued source of food. In both cases, it appears that these changes are likely to persist.

As with environmental variability, short-term societal matters such as family health or a major construction project employing many local residents for a season are typically viewed as normal variability. Of greater note for the communities are long-term changes. Schooling requirements take up considerable time for children, reducing opportunities to participate in subsistence activities and learn the necessary skills and knowledge. Few schools make allowance for subsistence or provide in-school ways of learning from Elders. Replacing dog teams with snowmachines starting in the late 1960s reduced the demand and thus the harvest of seals and fish that were formerly used as dog food. Faster snowmachines

have had the counterintuitive effect of reducing the seal hunting area in some communities, because hunters can go out and back in a day rather than making extended camping trips to more distant locations.

The decades-long shift towards greater participation in the wage economy has raised incomes and thus the ability of some people to purchase equipment used for subsistence. Even those without jobs may benefit from relatives willing to share their gear. On the other hand, having a job can reduce the time available for hunting or the flexibility to go when conditions are good. Some employers in the region provide subsistence leave, above and beyond vacation days, but not all work can be put off in this way. The other side of this phenomenon is that people without the means to go hunting or fishing may be left out of subsistence activities. Their situation may be compounded by embarrassment that they have to walk to a harvesting area or use old equipment, so some individuals avoid potential social discomfort by staying home instead of trying to participate in subsistence.

Another persistent shift has been in the regulatory environment. The quota imposed since 1978 by the International Whaling Commission (IWC) for the bowhead whale hunt has, among other things, meant that leaders of the whaling community have had to spend considerable time traveling to meetings and other venues to defend their practices, taking them away from hunting and other responsibilities in the community. A major enforcement action in the early 1990s against illegal harvests of Pacific walrus tusks led to several hunters from the Bering Strait area being charged with this crime. One result was that the walrus harvest on Little Diomede declined sharply and has not recovered because some prominent hunters were jailed and as a consequence others were reluctant to hunt. The transmission of skills and knowledge to younger hunters was thus interrupted, creating an even more lasting effect.

Response strategies

Environmental changes in the Arctic attract a lot of scientific and media attention. Addressing the root causes of these changes, however, is a challenge. The causes are dispersed globally and include powerful economic interests as well as established patterns of energy-intensive human behavior. Some Arctic activists have taken up this cause, but it remains a major challenge.

Some societal influences on subsistence, on the other hand, are closer to home or have a clearer focal point. The effects of commercial shipping to Red Dog Mine or the North Slope oil fields can be raised with the companies involved. In the case of North Slope oil activities, one result has been a cooperative agreement between whalers and companies to improve communication and reduce or avoid ship traffic that interferes with whaling. Even the IWC quota for bowhead whales is at least set by a single international body that meets on a regular basis, so whalers know when and where to go to advocate for their way of life. Changing the schedules of local schools and employers has in general proved hard to do, but at least community members have access to the relevant decision makers. Adoption of new technology is up to the individual, subject to such considerations as affordability.

Whether the ultimate causes of change can be addressed or not, individual hunters can and do adjust in many ways to respond to change. Communities can pool their talents and resources to do so to an even greater extent. Hunting areas may shift and expand, both because animal distributions change and also because new technologies such as larger boats, more reliable engines, and GPS navigation allow for more efficient and safer travel, though going farther will take more time and fuel. Subsistence activities may also take place at different times, ranging from a shift of a few days or weeks if sea ice breaks up earlier, to Savoonga's creation of a fall whaling season. Harvest composition varies year to year (e.g., Bacon et al. 2009), and can also shift over time, in response to access, species availability, and other factors. Some changes, however, will require more than an individual or community can do alone. Collaboration and cooperation with those outside the community will be necessary, too. Such efforts can be as simple as Utqiaġvik harvesters learning from friends and relatives farther south how to smoke salmon, or as

complicated and difficult as persuading the U.S. government and the IWC to permit the harvest of other species of large whales. All of these strategies depend on having animals to harvest at some time and place within reach of the community.

In addition to changing activities, Chukchi coastal residents also recognize the importance of attitudes in creating effective responses to change. These characteristics do not simply exist, but are developed and encouraged within the communities of this study (and undoubtedly far beyond) as distinct skills to be practiced and refined. Harvesters have always been prepared for variable conditions, whether in recognizing signs of danger or being ready to act when opportunities arise. Being ready is not so much a response in itself as the foundation for any other response, from making use of the now-briefer seal hunting period after shorefast ice breaks up to using social media to share information from one community to the next about animal migrations. Persistence is similarly a necessary virtue, again as illustrated in the adage that "We never get stuck." Using new species, such as the Hanasaki crab, new tools, such as drones or satellite imagery for scouting sea ice conditions, or learning new ways to prepare and store foods are all part of a ceaseless search for what will work best at any given time. Here, too, there are ultimately limits to what can be accomplished, but not for lack of trying.

For all the attention to changes in the Chukchi marine ecosystem, widespread changes in subsistence outcomes are hard to identify. There are many relatively modest effects, as shown in the examples in Table 1, but the reduction of seal and fish harvests due to the replacement of dog teams with snowmachines is so far a much larger change than has been forced by environmental change in the region. One reason for the lack of apparent effects is range of responses used by subsistence harvesters, as shown in the examples in Table 2.

This is not to say that further changes will have similarly modest effects or that responses will continue to be effective. Coastal residents will remain innovative and committed to providing food for their communities. Modern technology will help in many ways, and remoteness and minimal competition for most of the marine resources of the region leaves the coastal communities considerable flexibility in what, when, and where to hunt. On the other hand, increased commercial shipping (AMSA, 2009) and industrial activities such as offshore oil and gas activity (Gautier et al., 2009; Holland-Bartels and Pierce, 2011) create another type of competition, not for species per se but for access to an undisturbed sea, even as they may provide more local income. Those lacking cash or equipment will have less ability to participate in subsistence, regardless of the abundance or accessibility of animals and plants. Regulatory restrictions could limit the ability of harvesters to adjust by not allowing the take of animals outside regulatory seasons even though the timing of animal presence and/or abundance have changed, taking species they have not harvested before, or by preventing them from making up for poor harvests of one species (e.g., bowhead whales) by increasing their take of another (e.g., caribou). Furthermore, the fixed infrastructure of today's communities limit hunters' and fishers' ability to always move to where the fish and animals are abundant or accessible.

Cataloguing the range of factors that influence Chukchi coastal communities and communities elsewhere is in itself of limited value in fostering resilience and adaptation to change. Community well-being will depend on many factors as well as the interplay among those factors, limiting the ability to predict or even to recognize which influences matter most. What is likely more important is the ability of communities to develop their own responses to change, on their own terms, and with support from and in cooperation with others when necessary and desired. The effects of environmental change on Chukchi coastal communities are not negligible but demonstrable, and play out under the influences of societal and other changes that mediate both the effects of those changes and the responses to them.

Discussion

Co-analysis and community perspectives

The movement towards collaborative research and the co-production of knowledge is in part a recognition of the rights of community residents to be more than study subjects (Smith 1999; Wilson 2008; Kovach 2009; Strega and Brown 2015). Involving Arctic peoples in all phases of a research project is worthwhile on its own merits, recognizing the full intellectual contributions made by everyone involved in such projects, and sharing the rewards of credit and income from the work of research. Scientifically, it is also reasonable to ask what is gained from a collaborative or co-productive approach as compared with other methods. In our study, the answer lies less in dramatic insights and more in the steady accumulation of additional ideas and perspectives.

The co-analysis emphasizes the importance of the results of change rather than the sources of change, when it comes to their effects on communities and the strategies used to address those changes. Whether marine mammal distribution has shifted because of vessel traffic or reduced sea ice, hunters still have to find ways to adjust. The ability to adjust is useful no matter the cause of change. Addressing the source of the change, by negotiating with a shipping company or advocating for one's community at the IWC, is also a form of adjustment, and doing so can give a sense of agency that reinforces the idea that one can affect the outcomes that matter. At the same time, changes that stem directly from a specific and identifiable human action, such as industrial activity or an oil spill, are also likely to produce a different reaction among those affected than would an event with unknown or natural causes, such as fluctuation in some animal populations. In the former case, stress is likely to be higher as individuals seek to blame those they see as responsible and realize the problem may have been preventable (e.g. Cunsolo Willox et al., 2013, 2015), whereas in the latter case, people may be better able to get on with adjusting to cope with what has changed (e.g., Himes-Cornell et al., 2018).

The co-analysis discussions emphasized the importance of attitude (e.g., Walker and Salt, 2012) as well as skill and knowledge, and the crucial role that traditional values and practices continue to play in successful subsistence outcomes. These are not new ideas in the literature on Arctic communities and change (e.g., Hovelsrud and Smit, 2010; Cochran et al., 2013; Ford et al., 2015; Huntington et al., 2017a), but they often receive less attention and emphasis than what is changing. The abilities, both learned and taught, to be ready and to carry on deserve more attention as effective elements of individual as well as collective (i.e., cultural) response to change, and greater recognition as traits essential to the well-being of remote communities in variable, changing, and challenging environments.

Together, these insights suggest a broader scope of inquiry and discussion, not limited to ecosystem studies or societal studies, but taking the community perspective as starting point, to address community needs and concerns (e.g., Huntington et al., 2019). Further documentation of how much is changing and how fast is useful only up to a point. Greater understanding of how people have already adapted to change and how those strategies can be fostered and supported in response to future change is a more useful contribution to supporting the well-being of region's coastal communities. More important still is a leading role for Tribal and community voices and leadership in deciding how they want to shape their own future (Raymond-Yakoubian and Daniel, 2018). Doing so is an opportunity for true collaboration between scientists and coastal residents and, ultimately, the local, regional, and national policy makers whose decisions will have a large influence on what happens next.

Theories of change and response

From an academic point of view, we can also consider the outcomes of the co-analysis discussions in light of existing theories of change and response, drawing for example from ecology and business management. The emphasis on the characteristics of disturbance, especially the role of duration, aligns with the ecological and social-ecological idea of pulse-press dynamics (e.g., Collins et al., 2011;

Ratajczak et al., 2017). Pulses are short-term disturbances that cause disruption but from which the system recovers to something close to its original state. Presses are long-term disturbances that led to long-term alterations in a system's structure and functioning. One poor hunting season may cause hardship and even loss, but communities and cultures have recovered from such events in the past. A change in sea ice conditions, however, may force marine mammal hunters to alter their practices, to the point of abandoning previous modes of hunting, as with Kivalina and bowhead whaling, or creating new modes of hunting, as for Savoonga and fall whaling.

Responses to change can be considered technical or adaptive, a concept taken from business management (e.g., Heifetz et al., 2009). Technical changes are those which apply a known solution to a problem, whereas adaptive changes are those that require developing a new solution, typically because the problem is of a nature not previously encountered. Technical changes may often be sufficient for pulse problems, since the basic nature of the system does not change, and in a system with high variability, subsistence harvesters have a number of alternatives to use if their primary methods are not sufficient in a given season. Under press-like changes, however, the system itself is likely to change, in turn sometimes—but not always—requiring the development of new knowledge, skills, and methods to achieve similar outcomes. Harvesting the Hanasaki crab may not be a major challenge, but it is still a new skill to learn. Using new tools such as drones, satellite imagery, and GPS require experimenting and the generation of new knowledge and skills. On the other hand, being ready to harvest when conditions are right has always been important, even if good conditions for some activities no longer last as long.

When discussing change and response to change, it is important not to overlook what should stay the same (Huntington et al., 2017a), as reflected in some entries in Table 2, such as being prepared, being persistent, and being willing to experiment. Sharing remains an essential component of social life in Indigenous communities and their hunting, fishing, and gathering practices (Raymond-Yakoubian, 2013). Hunters need to be mentally and physically prepared (Kawerak, 2013b). Respect for the animals is critical to the long-term well-being of hunter and hunted alike (Kawerak, 2013a; Raymond-Yakoubian and Raymond-Yakoubian, 2015; Gadamus and Raymond-Yakoubian, 2015b). Humility and cooperation are necessary for social cohesion. Effective response strategies exist not in isolation, but in a context of healthy interpersonal and human-animal and human-environment relationships (Hovelsrud and Smit, 2010). If that foundation is not solid, then dealing with change may become extremely difficult or impossible, no matter how extensive the resources one has available. With a solid foundation, by contrast, a great deal can be done even in the face of major environmental change. The ability of Savoonga's whalers to create a fall whaling season in the northern Bering Sea is but one example of what is possible through the synergy of Indigenous skill, knowledge, determination, and collaboration.

Our examples and findings are consistent with other studies of responses to change (e.g., Emery and Flora, 2006; Thornton and Manasfi, 2010; Walker and Salt, 2012), that humans draw on a wide range available resources to support an equally wide range of strategies of response. Our findings are also broadly consistent with other Arctic studies which have found that environmental and societal factors both have a large influence on community well-being, including subsistence practices (e.g., Hoveslrud and Smit, 2010; Pearce et al., 2010, 2015; Ford et al., 2015; Rasmussen et al., 2015; Hastrup, 2018; ICC Alaska, 2015), and that identifying demonstrable changes in community well-being (e.g., population trends) is difficult (Hamilton et al., 2016), perhaps due to the range of responses that provide a buffer against deleterious effects (Huntington et al., 2018).

Understanding the nature of changes, for example as pulse-press dynamics, and the types of responses those changes will require, such as technical and adaptive solutions, can help communities and their allies to focus their efforts and perhaps to make a more persuasive case when needed to convince others to change, too. Our co-analysis approach has emphasized the continuing importance of traditional values and practices, such as the attitude of never getting stuck, as well as the need for attention to the conditions within and outside communities that foster effective responses to change. Movement towards approaches

that use co-production of knowledge and are highly collaborative is a welcome step in this regard, especially if it can also lead towards collective action.

Acknowledgments

Our research was part of the North Pacific Research Board's Arctic Integrated Ecosystem Research Program. We are grateful to the NPRB for funding and to our colleagues in the Arctic IERP for their ideas and support. We thank the participants in the Chukchi Coastal Communities Project, our fellow team members, who contributed ideas and insights to this paper, including Lucinda Wieler and Niviaaluk Brandt, former project Research Assistants at Kawerak; Orville Ahkinga, Dora Ahkinga, Opik Ahkinga, and Frances Sistuq Ozenna from Diomede; Raymond Lee Jr. from Buckland; Millie Hawley from Kivalina; Steve Oomituk from Point Hope; Willard Neakok Jr. from Point Lay; and Michael Donovan from Utqiaġvik. We also thank the communities and researchers whose work is presented in the publications we reviewed, and for several colleagues who reviewed portions of this manuscript. Finally, we are grateful to Jeremy Davies for preparing the map in Figure 1, and to the reviewers for their constructive comments that led to a much better paper. This paper is Arctic IERP Publication #39.

References

Alaska Department of Labor. 2020. Alaska population estimates by borough, census area, city, and census designated place (CDP), 2010 to 2019. https://live.laborstats.alaska.gov/pop/

AMSA. 2009. Arctic marine shipping assessment. Copenhagen: Arctic Council.

Ashjian, C.J., Braund, S.R., Campbell, R.G., George, J.C., Kruse, J., Maslowski, W., Moore, S.E., et al. 2010. Climate variability, oceanography, bowhead whale distribution, and Iñupiat subsistence whaling near Barrow, Alaska. Arctic 63:179-194. https://doi.org/10.14430/arctic973

Bacon, J.J., Hepa, T.R., Brower, H.K. Jr., Pederson, M., Olemaun, T.P., George, J.C., and Corrigan, B.G. 2009. Estimates of subsistence harvest for villages on the North Slope of Alaska, 1994-2003. Barrow, Alaska: North Slope Borough, Department of Wildlife Management.

Bartlett, C., Marshall, M., and Marshall, A. 2012. Two-eyed seeing and other lessons learned within a co-learning journey of bringing together indigenous and mainstream knowledges and ways of knowing. Journal of Environmental Studies and Science 2:331-340. https://doi.org/10.1007/s13412-012-0086-8

Braund, S.R. & Associates. 2010. Subsistence mapping of Nuiqsut, Kaktovik, and Barrow. U.S. Department of the Interior, Minerals Management Service, Alaska OCS Region, Environmental Studies Program. MMC OCS Study Number 2009-003. Anchorage, Alaska.

Brinkman, T.J., Hansen, W.D., Chapin, F.S., Kofinas, G., BurnSilver, S., and Rupp, T.S. 2016. Arctic communities perceive climate impacts on access as a critical challenge to availability of subsistence resources. Climatic Change 139(3-4):413-427. https://doi.org/10.1007/s10584-016-1819-6

Burch, E.S. Jr. 1985. Subsistence production in Kivalina, Alaska: A twenty-year perspective. Technical Paper, 128. Juneau: Alaska Department of Fish and Game, Division of Subsistence.

Carothers, C., Cotton, S., and Moerlein, K. 2013. Subsistence use and knowledge of salmon in Barrow and Nuiqsut, Alaska. Final Report, March 2013. OCS Study BOEM 2013-0015. Fairbanks: University of Alaska.

Christie, K.S., Hollmen, T.E., Huntington, H.P., and Lovvorn, J.R. 2018. Structured decision analysis informed by traditional ecological knowledge as a tool to strengthen subsistence systems in a changing Arctic. Ecology and Society 23(4):42. https://doi.org/10.5751/ES-10596-230442

Cochran, P., Huntington, O.H., Pungowiyi, C., Tom, S., Chapin, F.S., Huntington, H.P., Maynard, N.G., and Trainor, S.F. 2013. Indigenous frameworks for observing and responding to climate change in Alaska. Climatic Change 120(3):557-567. https://doi.org/10.1007/s10584-013-0735-2

Collins, S.L., Carpenter, S.R., Swinton, S.M., Orenstein, D.E., Childers, D.L., Gragson, T.L., Grimm, N.B., Grove, J.M., Harlan, S.L., Kaye, J.P., and Knapp, A.K., 2011. An integrated conceptual

framework for long- term social–ecological research. Frontiers in Ecology and the Environment 9(6):351-357. https://doi.org/10.1890/100068
Cunsolo Willox, A., Harper, S.L., Edge, V.L., Landman, K., and Ford, J.D. 2013. The land enriches the soul: on climate and environmental change, affect, and emotional health and well-being in Rigolet, Nunatsiavut, Canada. Emotion, Space and Society 6:14-24. https://doi.org/10.1016/j.emospa.2011.08.005
Cunsolo Willox, A., Stephenson, E., Allen, J., Bourque, F., Drossos, A., Elgarøy, S., Kral, M.J., et al. 2015. Examining relationships between climate change and mental health in the Circumpolar North. Regional Environmental Change 15:169-182. https://doi.org/10.1007/s10113-014-0630-z
David-Chavez, M., and Gavin, M. 2018. A global assessment of Indigenous community engagement in climate research. Environmental Research Letters 13:123005. https://doi.org/10.1088/1748-9326/aaf300
Emery, M., and Flora, C. 2006. Spiraling-up: mapping community transformation with community capitals framework. Community Development 37:19-35. https://doi.org/10.1080/15575330609490152
Fall, J.A., Braem, N.M., Brown, C.L., Hutchinson-Scarbrough, L.B., Koster, D.S., and Krieg, T.M. 2013. Continuity and change in subsistence harvests in five Bering Sea communities: Akutan, Emmonak, Savoonga, St. Paul, and Togiak. Deep-Sea Research II 94:274-291. https://doi.org/10.1016/j.dsr2.2013.03.010
Fienup-Riordan, A., Brown, C., and Braem, N.M. 2013. The value of ethnography in times of change: the story of Emmonak. Deep-Sea Research II 94:301-311. https://doi.org/10.1016/j.dsr2.2013.04.005
Ford, J.D., McDowell, G., and Pearce, T. 2015. The adaptation challenge in the Arctic. Nature Climate Change 5:1046-1053. https://doi.org/10.1038/nclimate2723
Gadamus, L. 2013. Linkages between human health and ocean health: a participatory climate change vulnerability assessment for marine mammal harvesters. International Journal of Circumpolar Health 72. http://dx.doi.org/10.3402/ijch.v72i0.20715
Gadamus, L., and Raymond-Yakoubian, J. 2015a. Qualitative participatory mapping of seal and walrus harvest and habitat areas: documenting Indigenous knowledge, preserving local values, and discouraging map misuse. International Journal of Applied Geospatial Research (IJAGR), 6(1):76-93. https://doi.org/10.4018/ijagr.2015010105
Gadamus, L., and Raymond-Yakoubian, J. 2015b. A Bering Strait Indigenous framework for resource management: respectful seal and walrus hunting. Arctic Anthropology 52:87-101. https://doi.org/10.3368/aa.52.2.87
Galginaitis, M. 2013. Iñupiat fall whaling and climate change: observations from Cross Island. In: Mueter, F.J., Dickson, D.M.S., Huntington, H.P., Irvine, J.R., Logerwell, E.A., MacLean, S.A., Quakenbush, L.T., and Rosa, C., eds. Responses of Arctic marine ecosystems to climate change. Alaska Sea Grant, University of Alaska Fairbanks. pp. 181-199. https://doi.org/10.4027/ramecc.2013.09
Gautier, D.L., Bird, K.J., Charpentier, R.R., Grantz, A., Houseknecht, D.W., Klett, T.R., Moore, T.E., et al. 2009. Assessment of undiscovered oil and gas in the Arctic. Science 324:1175-1179. https://doi.org/10.1126/science.1169467
Grebmeier, J.M., ed. 2014. Pacific marine Arctic regional synthesis (PacMARS) community meetings during February-March 2013. Anchorage, Alaska: North Pacific Research Board.
Hall, E. 1971 The “iron dog” in northern Alaska. Anthropologica 13(1/2):237-254. https://doi.org/10.2307/25604852
Hamilton, L.C., Saito, K. Loring, P.A., Lammers, R.B., and Huntington, H.P. 2016. Climigration? Population and climate change in Arctic Alaska. Population and Environment 38:115-133. https://doi.org/10.1007/s11111-016-0259-6
Hansen, W.D., Brinkman, T.J., Leonawicz, M., Chapin III, F.S., and Kofinas, G.P. 2013. Changing daily wind speeds on Alaska’s North Slope: implications for rural hunting opportunities. Arctic 66:448-458. https://doi.org/10.14430/arctic4331
Hastrup, K. 2018. A history of climate change: Inughuit responses to changing ice conditions in North-West Greenland. Climatic Change 151:67-78. https://doi.org/10.1007/s10584-016-1628-y

Heifetz, R.A., Linsky, M., and Grashow, A. 2009. The practice of adaptive leadership. Brighton, Massachusetts: Harvard Business Press.
Himes-Cornell, A., Ormond, C., Hoelting, K., Ban, N.C., Koehn, J.Z., Allison, E.H., Larson, E.C., Monson, D.H., Huntington, H.P., and Okey, T.A. 2018. Factors affecting disaster preparedness, response, and recovery using the community capitals framework. Coastal Management 46:335-358. https://doi.org/10.1080/08920753.2018.1498709
Holland-Bartels, L., and Pierce, B., eds. 2011. An evaluation of the science needs to inform decisions on Outer Continental Shelf energy development in the Chukchi and Beaufort Seas, Alaska. U.S. Geological Survey Circular 1370. https://doi.org/10.3133/cir1370
Hovelsrud, G.K., and Smit, B., eds. 2010. Community adaptation and vulnerability in Arctic regions. London: Springer. https://doi.org/10.1007/978-90-481-9174-1
Hughes. Z. 2018. In doomed Alaska town, hunters turn to drones and caribou as sea ice melts. The Guardian, 2 March 2018. www.theguardian.com/environment/2018/mar/02/alaska-climate-change-indigenous-hunting
Huntington, H.P. 1992. Wildlife management and subsistence hunting in Alaska. London: Belhaven Press.
Huntington, H.P., and Eerkes-Medrano, L. 2017. Stakeholder perspectives. In: AMAP. Adaptation actions for a changing Arctic - perspectives from the Bering/Chukchi/Beaufort region. Oslo: Arctic Monitoring and Assessment Programme. p. 11-38.
Huntington, H.P., and the Communities of Buckland, Elim, Koyuk, Point Lay, and Shaktoolik. 1999. Traditional knowledge of the ecology of beluga whales (*Delpinapterus leucas*) in the eastern Chukchi and northern Bering seas, Alaska. Arctic 52(1):49-61. https://doi.org/10.14430/arctic909
Huntington, H.P., Noongwook, G., Bond, N.A., Benter, B., Snyder, J.A., and Zhang, J. 2013a. The influence of wind and ice on spring walrus hunting success on St. Lawrence Island, Alaska. Deep Sea Research II 94:312-322. https://doi.org/10.1016/j.dsr2.2013.03.016
Huntington, H.P., Ortiz, I., Noongwook, G., Fidel, M., Alessa, L., Kliskey, A., Childers, D., Morse, M., and Beaty, J. 2013b. Mapping human interaction with the Bering Sea ecosystem: comparing seasonal use areas, lifetime use areas, and "calorie-sheds". Deep-Sea Research II 94:292-300. https://doi.org/10.1016/j.dsr2.2013.03.015
Huntington, H.P., Daniel, R., Hartsig, A., Harun, K., Heiman, M., Meehan, R., Noongwook, G., et al. 2015. Vessels, risks, and rules: planning for safe shipping in Bering Strait. Marine Policy 51:119-127. https://doi.org/10.1016/j.marpol.2014.07.027
Huntington, H.P., Quakenbush, L.T., and Nelson, M. 2017a. Evaluating the effects of climate change on Indigenous marine mammal hunting in northern and western Alaska using traditional knowledge. Frontiers in Marine Science 4:319. https://doi.org/10.3389/fmars.2017.00319
Huntington H.P., Begossi, A., Gearheard, S.F., Kersey, B., Loring, P., Mustonen, T., Paudel, P.K., Silvano, R.A.M., and Vave, R. 2017b. How small communities respond to environmental change: patterns from tropical to polar ecosystems. Ecology and Society 22(3):9.
Huntington, H.P., Loring, P.A., Gannon, G., Gearheard, S., Gerlach, S.C., and Hamilton, L.C. 2018. Staying in place during times of change in Arctic Alaska: the implications of attachment, alternatives, and buffering. Regional Environmental Change 18(2):489-499. https://doi.org/10.1007/s10113-017-1221-6
Huntington, H.P., Carey, M., Apok, C., Forbes, B.C., Fox, S., Holm, L.K., Ivanova, A., Jaypoody, J., Noongwook, G., and Stammler, F. 2019. Climate change in context—putting people first in the Arctic. Regional Environmental Change 19(4):1217-1223. https://doi.org/10.1007/s10113-019-01478-8
Huntington, H.P., Danielson, S.L., Wiese, F.K., Baker, M., Boveng, P., Citta, J.J., De Robertis, A., Dickson, D., Farley, E., George, J.C., Iken, K., Kimmel, D.G., Kuletz, K., Ladd, C., Levine, R., Quakenbush, L., Stabeno, P., Stafford, K.M., Stockwell, D., and Wilson, C. 2020. Evidence suggests potential transformation of the Pacific Arctic Ecosystem is underway. Nature Climate Change 10:342-348. https://doi.org/10.1038/s41558-020-0695-2

ICC-Alaska. 2015. Alaskan Inuit food security conceptual framework: How to assess the Arctic from an Inuit perspective. Technical Report. Anchorage: Inuit Circumpolar Council-Alaska.
Kaiser, B.A., Azetsu-Scott, K., Burmeister, A. Falkenberg, L.J., Meire, L, Ravn-Jonsen, L., and Steiner, N. 2018. The Greenland shrimp (*Pandalus borealis*) fishery. In: AMAP. AMAP Assessment 2018: Arctic Ocean acidification. Tromsø, Norway: Arctic Monitoring and Assessment Programme. p. 101-128.
Kapsch, M.-L., Eicken, H., and Robards, M., 2010. Sea ice distribution and ice use by indigenous walrus hunters on St. Lawrence Island, Alaska. In: Krupnik, I., Aporta, C., Gearheard, S., Kielsen Holm, L., and Laidler, G., eds. SIKU – Arctic residents document sea ice and climate change. Berlin: Springer. pp. 115-144. https://doi.org/10.1007/978-90-481-8587-0_5
Kawerak. 2013a. Traditions of respect: Traditional knowledge from Kawerak's ice seal and walrus project. Nome: Kawerak Social Science Program.
Kawerak. 2013b. Seal and walrus hunting safety: Traditional knowledge from Kawerak's ice seal and walrus project. Nome: Kawerak Social Science Program.
Kersey, B. 2011. Enhancing household food security in times of environmental hazards. MSc thesis. University of East Anglia, Norwich, U.K.
Kirby, C., Harou, H., Whyte, K. Libarkin, J., Caldwell, C., and Edler, R. 2019. Ethical collaboration and the need for partnerships between Native American Tribes and climate science organizations. Gateways: International Journal of Community Research and Engagement 12(1):5894. https://doi.org/10.5130/ijcre.v12i1.5894
Kovach, M. 2009. Indigenous methodologies: characteristics, conversations, and contexts. Toronto: University of Toronto Press.
Kruse, J.A. 1991. Alaska Inupiat subsistence and wage employment patterns: Understanding individual choice. Human Organization 50(4):317-326. https://doi.org/10.17730/humo.50.4.c288gt2641286g71
Lemos, M.C., and Morehouse, B.J. 2005. The co-production of science and policy in integrated climate assessments. Global Environmental Change 15(1):57-68. https://doi.org/10.1016/j.gloenvcha.2004.09.004
Mason, O.K., and Gerlach, S.C. 1995. Chukchi hot spots, paleo-polynyas, and caribou crashes: climatic and ecological dimensions of North Alaska prehistory. Arctic Anthropology 32(1):101-130.
Meadow, A.M., Ferguson, D.B., Guido, Z., Horangic, A., and Owen, G. 2015. Moving toward the deliberate coproduction of climate science knowledge. Weather, Climate and Society 7:179-191. https://doi.org/10.1175/WCAS-D-14-00050.1
Moerlein, K. J., and Carothers, C. 2012. Total environment of change: impacts of climate change and social transitions on subsistence fisheries in northwest Alaska. Ecology and Society 17(1):10. http://dx.doi.org/10.5751/ES-04543-170110
Moore, S.E., Stabeno, P.J., Grebmeier, J.M., and Okkonen, S.R. 2018. The Arctic Marine Pulses Model: Linking annual oceanographic processes to contiguous ecological domains in the Pacific Arctic. Deep-Sea Research II 152:8-21. https://doi.org/10.1016/j.dsr2.2016.10.011
Napoleon, H. 1996. Yuuyaraq: the way of the human being. Fairbanks: Alaska Native Knowledge Network.
Noongwook, G. 2018. Perspective J: Hunting and co-management. In: AMAP. Adaptation actions for a changing Arctic - perspectives from the Bering/Chukchi/Beaufort region. Oslo: Arctic Monitoring and Assessment Programme. p. 26.
Noongwook, G., the Native Village of Savoonga, the Native Village of Gambell, Huntington, H.P., and George, J.C. 2007. Traditional knowledge of the bowhead whale (*Balaena mysticetus*) around St. Lawrence Island, Alaska. Arctic 60(1):47-54. https://doi.org/10.14430/arctic264
Oceana and Kawerak. 2014. Bering Strait marine life and subsistence use data synthesis. Juneau and Nome, Alaska: Oceana and Kawerak, Inc.

Pearce, T., Smit, B., Duerden, F., and Ford, J. 2010. Inuit vulnerability and adaptive capacity to climate change in Ulukhaktok, Northwest Territories, Canada. Polar Record 46(2):157-177. https://doi.org/10.1017/S0032247409008602

Pearce, T., Ford, J., Cunsolo Willox, A., and Smit, B. 2015. Inuit traditional ecological knowledge (TEK), subsistence hunting and adaptation to climate change in the Canadian Arctic. Arctic 68(2):233-245. https://doi.org/10.14430/arctic4475

Peltier, C. 2018 An application of two-eyed seeing: Indigenous research methods with participatory action research. International Journal of Qualitative Methods 17:1-12. https://doi.org/10.1177/1609406918812346

Pelto, P.J. 1973 The snowmobile revolution: technology and social change in the Arctic. Menlo Park, California: Cummings.

Rasmussen, R.O., Hovelsrud, G.K., and Gearheard, S. 2015. Community viability and adaption. In: Larsen, J.N., and Fondahl, G., eds. Arctic Human Development Report II: Regional Processes and Global Linkages. Copenhagen: Nordic Council of Ministers. pp 427-478.

Ratajczak, Z., D'Odorico, P., Collins, S.L., Bestelmeyer, B.T., Isbell, F.I. and Nippert, J.B., 2017. The interactive effects of press/pulse intensity and duration on regime shifts at multiple scales. Ecological Monographs 87(2):198-218. https://doi.org/10.1002/ecm.1249

Raymond-Yakoubian, J. 2013. "When the fish come, we go fishing'": Local ecological knowledge of non-salmon fish used for subsistence in the Bering Strait region. Final report to the U.S. Fish and Wildlife Service for Study 10-151. Nome, Alaska: Kawerak Social Science Program.

Raymond-Yakoubian, J. 2019. Salmon, cosmology, and identity in Elim, Alaska. PhD thesis. University of Alaska Fairbanks, Fairbanks, Alaska. https://scholarworks.alaska.edu/handle/11122/10531

Raymond-Yakoubian, J., and Daniel, R. 2018. An Indigenous approach to ocean planning and policy in the Bering Strait region of Alaska. Marine Policy 97:101-108. https://doi.org/10.1016/j.marpol.2018.08.028

Raymond-Yakoubian, B., and Raymond-Yakoubian, J. 2015. "Always taught not to waste": Traditional Knowledge and Norton Sound/Bering Strait Salmon Populations. 2015 Arctic-Yukon-Kuskokwim Sustainable Salmon Initiative Project 1333 Final Product. Nome, Alaska: Kawerak Social Science Program.

Raymond-Yakoubian, B., and Raymond-Yakoubian, J. 2017. Research processes and Indigenous communities in western Alaska: workshop report. Nome, Alaska: Kawerak Social Science Program. https://kawerak.org/wp-content/uploads/2018/04/Research-Processes-and-Indigenous-Communities-in-Western-Alaska-Workshop-Report.pdf

Raymond-Yakoubian, J., Khokhlov, Y., and Yarzutkina, A. 2014. Indigenous knowledge and use of Bering Strait region ocean currents. Final report to the National Park Service, Shared Beringian Heritage Program for Cooperative Agreement H99111100026. Nome, Alaska: Kawerak Social Science Program.

Schwing, E. 2016. Shishmaref man tracks sea ice conditions with drone. Juneau, Alaska: KTOO Public Media. www.ktoo.org/2016/03/14/shishmaref-man-tracks-sea-ice-conditions-with-drone/

Slats, R, Oliver, C., Bahnke, R., Bell, H., Miller, A., Pungowiyi, D., Merculief, J., Medadelook, N. Sr., Ivanoff, J., and Oxereok, C. 2019. Voices from the front lines of a changing Bering Sea: an Indigenous perspective for the 2019 Arctic Report Card. M.L. Druckenmiller, R. Daniel, and M. Johnson, eds. NOAA Arctic Report Card 2019. http://www.arctic.noaa.gov/Report-Card

Smith, L.T. 1999. Decolonizing methodologies: research and Indigenous Peoples. London: Zed Books.

Strega, S., and Brown, L., eds. 2015. Research as resistance: revisiting critical, Indigenous, and anti-oppressive approaches. 2nd Ed. Toronto: Canadian Scholar's Press.

Thornton, T.F., and Manasfi, N. 2010. Adaptation—genuine and spurious: demystifying adaptation processes in relation to climate change. Environment and Society: Advances in Research 1:132-155. https://doi.org/10.3167/ares.2010.010107

Walker, B., and Salt, D. 2012. Resilience practice: Building capacity to absorb disturbance and maintain function. Washington, DC: Island Press. https://doi.org/10.5822/978-1-61091-231-0
Whyte, K. 2017. Indigenous climate change studies: Indigenizing futures, decolonizing the Anthropocene. English Language Notes 55:1-2. https://doi.org/10.1215/00138282-55.1-2.153
Wilson, S. 2008 Research is ceremony: Indigenous research methods. Halifax: Fernwood Publishing.
Woodford, R. 2019. Drones and hunting. Alaska Fish and Wildlife News. April 2019. https://www.adfg.alaska.gov/index.cfm?adfg=wildlifenews.view_article&articles_id=908

Results of the Arctic IERP Group Effort

This chapter presents the findings of the Arctic IERP group effort (so named in order to distinguish it from the synthesis phase of the Arctic IERP, which is a separately funded part of the overall program to take place after the main research phase), as reported in a paper published in Nature Climate Change *in February 2020. This chapter consists of the accepted manuscript for the paper. Note that the published manuscript was subject to copy editing and other changes. Full details of the publication can be found in the appropriate section of this report, below.*

Evidence suggests potential transformation of the Pacific Arctic Ecosystem is underway

Authors & Affiliations:

Henry P. Huntington, Huntington Consulting, Eagle River, AK, 99577, USA
Seth L. Danielson, University of Alaska Fairbanks, Fairbanks, AK, USA
Francis K. Wiese, Stantec, Anchorage, AK, USA
Matthew Baker, North Pacific Research Board, Anchorage, AK, USA
Peter Boveng, NOAA-Alaska Fisheries Science Center, Seattle, WA, USA
John J. Citta, Alaska Department of Fish and Game, AK 99701, USA
Alex De Robertis, NOAA- Alaska Fisheries Science Center, Seattle, WA, USA
Danielle Dickson, North Pacific Research Board, Anchorage, AK, USA
Ed Farley, NOAA-Alaska Fisheries Science Center, Seattle, WA, USA
J. Craighead George, North Slope Borough Department of Wildlife Management, Utqiaġvik, AK, USA
Katrin Iken, University of Alaska Fairbanks, Fairbanks, AK, USA
David G. Kimmel, NOAA-Alaska Fisheries Science Center, Seattle, WA, USA
Kathy Kuletz, U.S. Fish and Wildlife Service, Anchorage, AK, USA
Carol Ladd, NOAA-Pacific Marine Environmental Laboratory, Seattle, WA, USA
Robert Levine, University of Washington, Seattle, WA, USA
Lori Quakenbush, Alaska Department of Fish and Game, Fairbanks, AK 99701, USA
Phyllis Stabeno, NOAA-Pacific Marine Environmental Laboratory, Seattle, WA, USA
Kathleen M. Stafford, University of Washington, Seattle, WA, USA
Dean Stockwell, University of Alaska Fairbanks, Fairbanks, AK, USA
Chris Wilson, NOAA-Alaska Fisheries Science Center (retired), Seattle, WA, USA

Abstract

The highly productive northern Bering and Chukchi marine shelf ecosystem has long been dominated by strong seasonality in sea ice and water temperatures. Extremely warm conditions from 2017 into 2019 - including loss of ice cover across portions of the region in all three winters - were a marked change even from other recent warm years. Biological indicators suggest this state change could alter ecosystem structure and function. Here we report observations of key physical drivers, biological responses, and consequences for humans, including subsistence hunting, commercial fishing, and industrial shipping. We consider whether observed state changes are indicative of future norms, whether an ecosystem transformation is already underway, and if so, whether shifts are synchronously functional and system-wide, or reveal a slower cascade of changes from the physical environment through the food web to human society. Understanding of this observed process of ecosystem reorganization may shed light on transformations occurring elsewhere.

[Main text]

The Pacific Arctic, composed of the Chukchi and northern Bering seas (Figure 1), is one of the world's most productive ocean ecosystems (1), characterized by high benthic biomass resulting from persistent, nutrient rich flow through the Bering Strait (2) that fuels high primary production (3). In summer and fall, the region is home to millions of nesting and migratory seabirds, with hotspots of foraging activity shared with marine mammals (4), supporting coastal Indigenous communities. The delivery of nutrients together with the extent and timing of sea ice (5) are dominant environmental factors structuring this ecosystem. Freeze-up in fall and winter eliminates large expanses of open water, causing whales, Pacific walrus (*Odobenus rosmarus divergens*), many seals, and seabirds to migrate southwards into the Bering Sea and beyond (6).

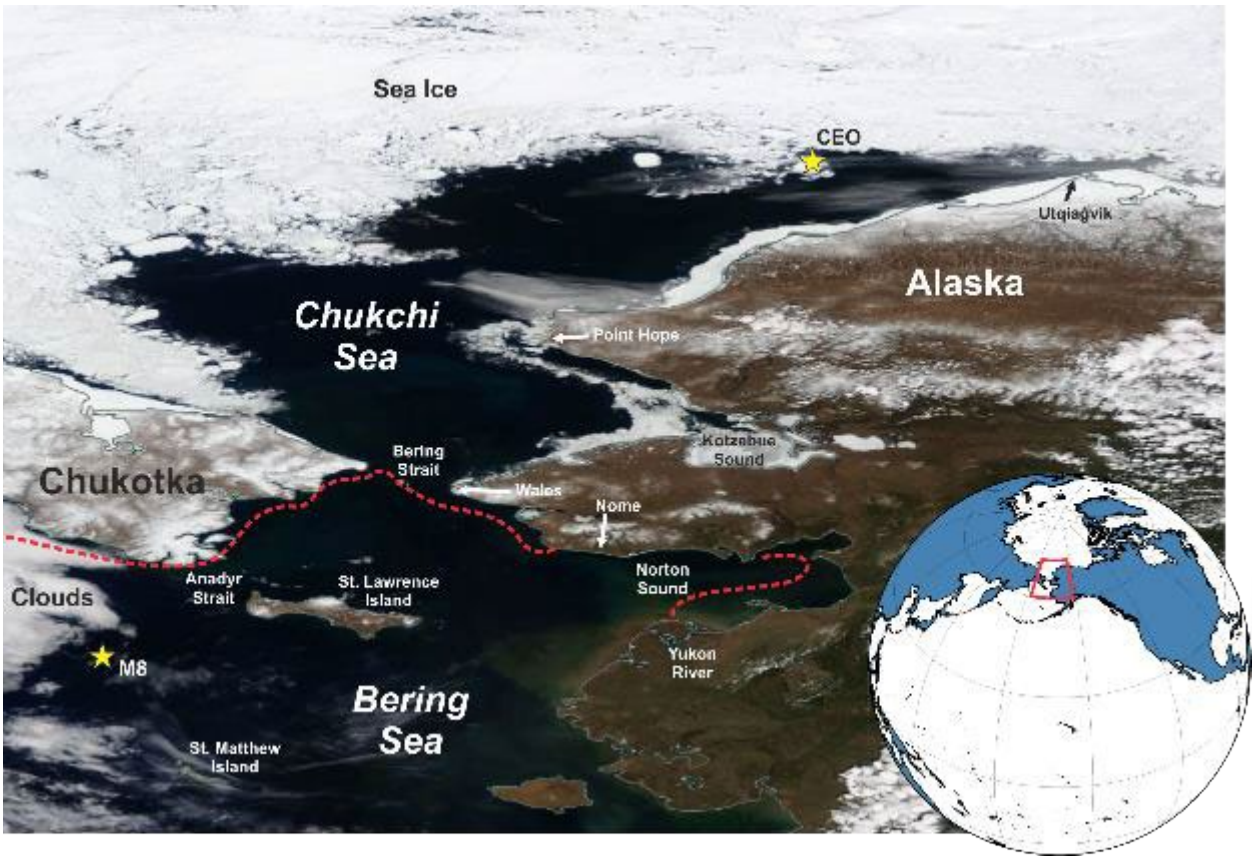

Figure 1. Sea ice changes in recent years. True-color MODIS satellite image showing northern Bering and Chukchi sea ice conditions on 2 June 2017. Red dotted lines denote the 1980-2010 ice edge climatology for June 2nd. Yellow stars denote locations of oceanographic moorings M8 and CEO. Inset locates the study region. Image from NASA Worldview.

In spring, the return of sunlight heralds snow melt, growth of sea ice algae, and a phytoplankton bloom that typically exceeds the consumption capabilities of pelagic consumers, resulting in carbon falling to the seabed, fueling rich benthic communities (7,8). Solar radiation and melting sea ice help stratify the upper water column, impeding the ability of winds to mix surface and subsurface waters. In summer, low-salinity surface waters near the pack ice remain cool relative to the shelf waters warmed by insolation. The Bering Sea cold pool, near-bottom shelf waters cooler than 2°C south of Bering Strait, has long served as a thermal barrier to northward migration of subarctic groundfish (9), which are major stocks for the southeastern Bering Sea's $2 billion fishery and account for about half the seafood landings in the United States (10,11).

Recent Changes in the Pacific Arctic Marine Ecosystem

Declining sea ice in this century has reduced surface albedo in spring and summer, accelerating oceanic heat uptake and causing earlier and more rapid sea ice melt (12). The pack ice and marginal ice zone has retreated north beyond the Chukchi shelf in recent summers, while warmer shelf waters delay sea ice formation in fall. Simultaneously, the northward flow of water through Bering Strait has increased, as has its temperature (2), so that it now delivers more heat, freshwater, nutrients, and biota northwards into the Arctic (13). Near-bottom water temperatures exceed 0°C for a larger portion of the year (Figure 2).

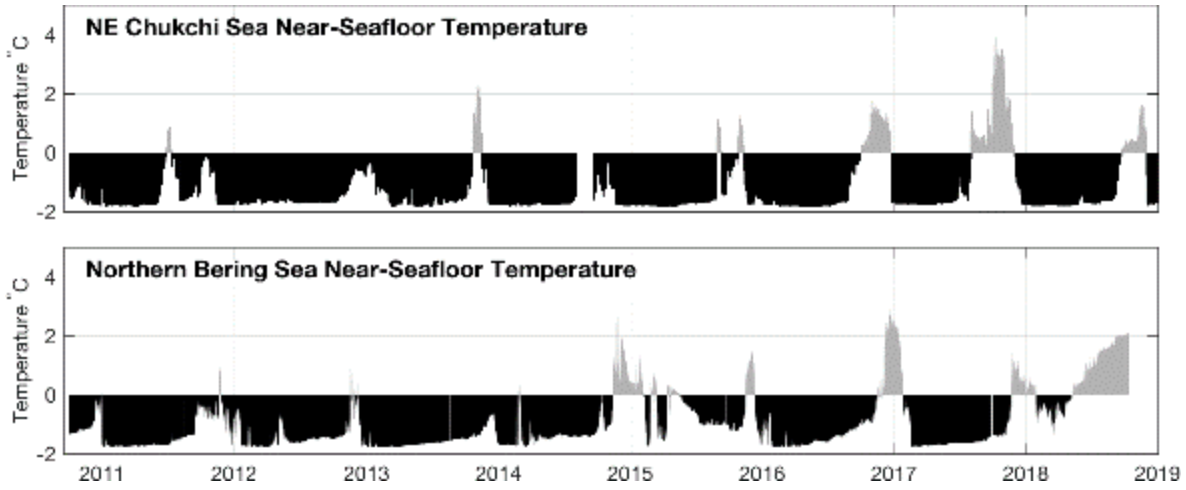

Figure 2. Near-bottom water temperatures. Previously, temperatures in important seafloor habitats remained below 0℃ for most of the year. In recent years, an increasing number of months exhibited temperatures well above 0℃. Mooring locations are indicated on Figure 1.

Ramifications of these physical changes have included more salmon in the Chukchi and Beaufort seas (14,15), walrus hauling out on shore in northwestern Alaska in late summer instead of on sea ice (16), an increase in the frequency and seasonal duration of killer whale (*Orcinus orca*) presence in the Chukchi Sea (17), an increase in planktivorous seabirds in the Chukchi Sea (18), and a northward shift in

the distribution of other seabird species (19,20). For the Indigenous peoples of the region, spring marine mammal hunting opportunities dependent on the presence of sea ice have decreased and shifted in time (21), although the lack of sea ice has allowed additional whaling to occur in fall and early winter in the northern Bering Sea (22).

And Then Came 2017

In 2017, physical conditions in the Pacific Arctic marine shelf ecosystem of the Chukchi and northern Bering seas described above showed signs of a sudden and dramatic shift relative to historical means and even to other recent unusually warm years. In turn, these physical changes seemingly precipitated several significant ecological shifts, with consequences for the region's residents. Based on published and unpublished data from the authors, many changes persisted in 2018 and even into 2019, suggesting that 2017 was not a passing oddity of brief consequence to social-ecological systems, but a sign of what is to come.

In early January 2017, the sea ice edge had barely progressed south of Bering Strait and for the entire winter its extent remained at least $2x10^5$ km^2 below the long-term average. In June, ship-based observations found near-bottom ocean temperatures in Bering Strait of nearly 4 °C, over 3°C and four standard deviations warmer than the 1991-2016 June mean (2). Indeed, by June, the eastern Chukchi shelf was already mostly sea ice-free (Figure 1). In early December 2017, the ice edge was over 1000 km north of its climatological mean position near St. Lawrence Island. There was no sea ice in the Bering Strait in February 2018 and southerly winds forced a large ice retreat again in February 2019 (23). Waters in Norton Sound exceeded 10°C before the end of June 2018 and the cold pool was again minimal by late summer.

Reduced ice cover and warmer seas likely impacted primary production by influencing thermal, light, and stratification conditions. In spring of 2018, in the southern Bering Sea, the bloom was delayed due to a lack of freshwater input from melting sea ice, and chlorophyll concentrations were an order of magnitude lower than usual; however in the northern Bering Sea the ice-associated bloom was early and extensive (24). In addition, the detection of domoic acid in shipboard water samples (Figure 3) and saxitoxin in a few stranded and harvested walruses from Bering Strait villages led to concern about harmful algal blooms and food safety from Indigenous residents, though analytical challenges make the impact difficult to determine (25).

Changes in species distributions had already been observed this century, but not to the extent observed in 2017. The copepods *Calanus glacialis/marshallae* in 2017 were found to be remarkably low in abundance relative to 2012-2015 (Figure 4). Multispecies epibenthic biomass in the southern Chukchi Sea also exhibited a pronounced decline relative to comparable collections in 2004, 2009, 2012, and 2015 (Figure 4). In contrast, acoustic-trawl surveys indicate that age-0 Arctic cod abundance was dramatically higher in the Chukchi Sea in 2017 compared with previous surveys: backscatter in the northern Chukchi Sea (67 N to 71.5 N) was 5.6 times greater than in 2013, and 16.3 times greater than in 2012 (Figure 5), but the fish had low energy content. Juvenile pink salmon (*Oncorhyncus gorbuscha*) catch per unit effort in surface trawl surveys in the northern Bering Sea was two times greater during 2017 than previous years (Figure 4). Juvenile pink salmon return as adults the following year, and the adult pink salmon return to Norton Sound was much stronger than expected during 2018 (27). Adult walleye pollock (*Gadus chalcogramma*), Pacific cod (*Gadus macrocephalus*), and northern rock sole (*Lepidopsetta polyxystra*) biomass in bottom trawl surveys increased in the northeastern Bering Sea during 2017, likely due to northward movement of these fishes in the absence of the Bering Sea cold pool (28).

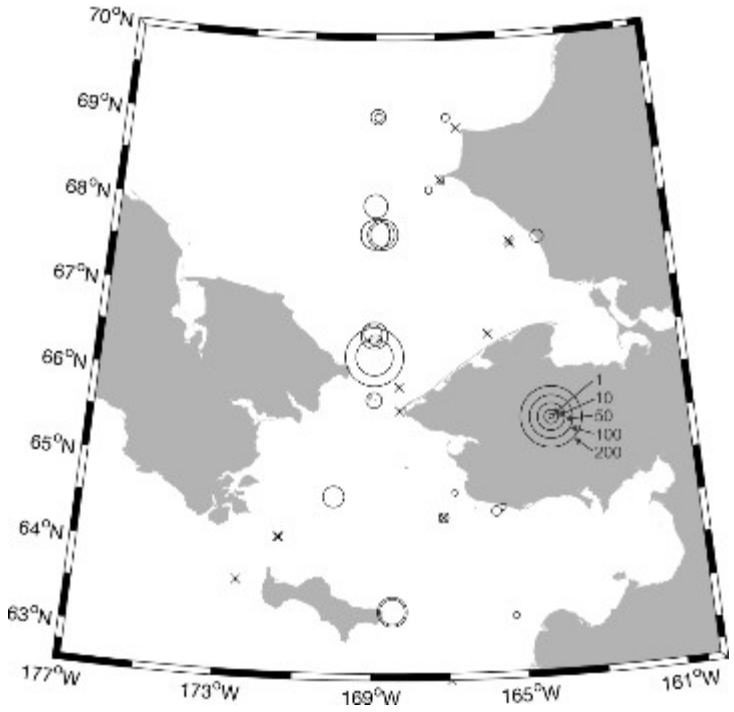

Figure 3. Seawater concentrations of domoic acid, June 2017. NTD = no toxin detected.

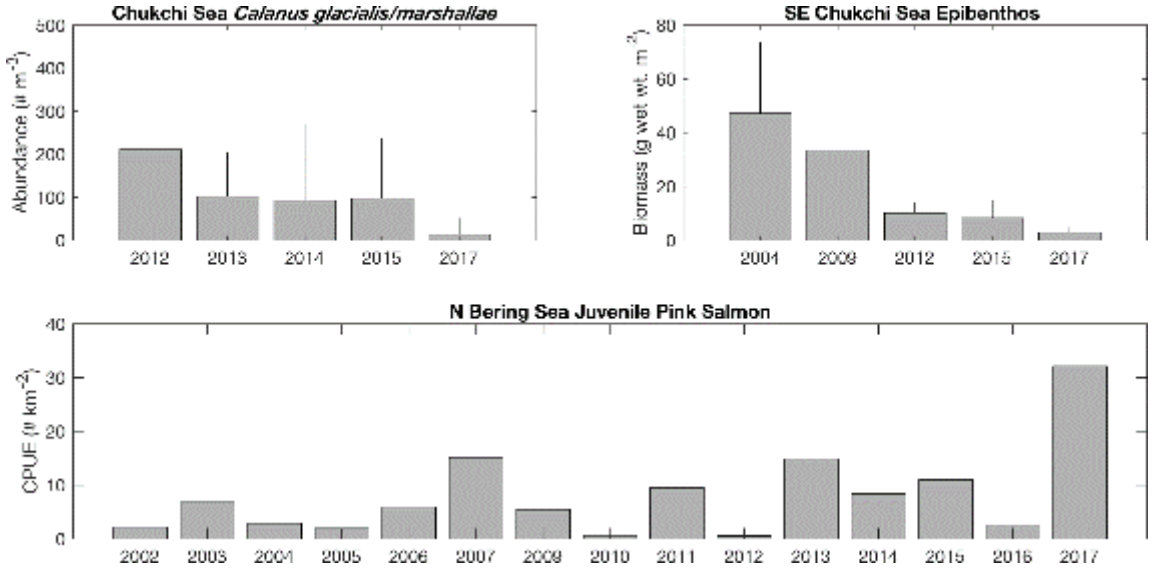

Figure 4. Biological changes in recent years. Observations show declines of Calanus glacialis/marshallae *abundance (upper left) and epibenthic biomass (upper right) in 2017 relative to prior years, and an*

increase in juvenile pink salmon catch per unit effort (CPUE) (bottom). The graphs in upper left and upper right show simple means and standard deviation error bars.

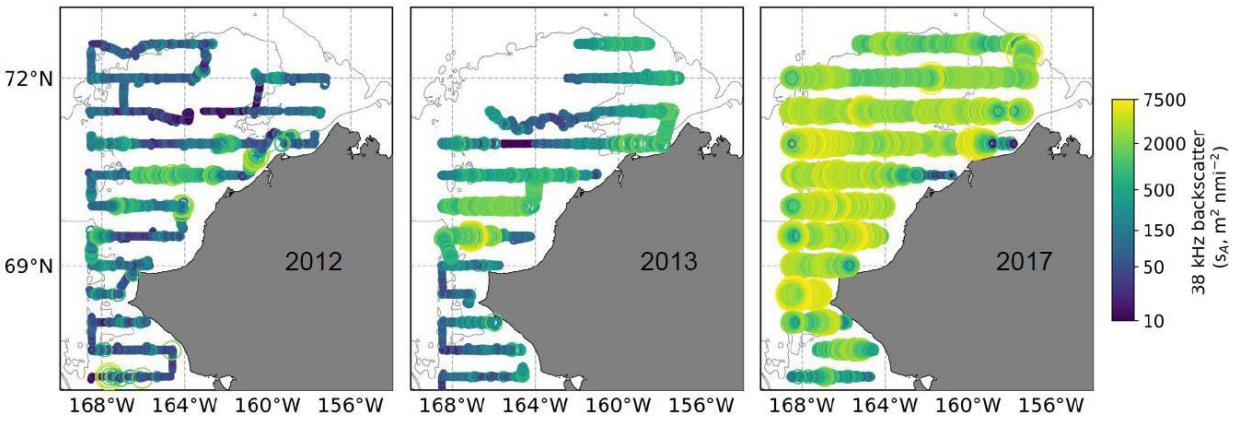

Figure 5. Arctic cod abundance change. Acoustic surveys indicate that the abundance of age-0 Arctic cod increased substantially in 2017 relative to 2012 and 2013. Trawl sampling indicated that Arctic cod dominated acoustic backscatter in this area in 2012 and 2013 (26). This was also the case in 2017: Arctic cod accounted for 95.4% of fish captured in 33 midwater trawl hauls.

In offshore waters, total seabirds declined from 2012-2017 in the southern and northern Bering Sea, but densities were above the long term mean in the Chukchi Sea during most of that period. The increase in the Chukchi Sea in 2015-2017 was primarily due to short-tailed shearwaters (*Ardenna tenuirostris*), which feed primarily on euphausiids, and less pronounced increases in piscivorous black-legged kittiwakes (*Rissa tridactyla*) and murres (*Uria* spp). In contrast, planktivorous auklets (*Aethia* sp.) had low densities in the Chukchi Sea in 2017 and 2018 but increased in the northern Bering Sea those years (24). Reproductive success was low for seabirds in the Bering Sea in 2017-2018, and there were mixed-species die offs there and in the Chukchi Sea (24,29;), with dead birds emaciated. Notably, numbers of murres and kittiwakes attending the large Chukchi Sea colony continued to increase (30) at a rate suggesting immigration of piscivorous nesting birds.

In the spring of 2017, bowhead whales, including females with calves, were seen near Utqiaġvik, Alaska, a month earlier than usual and the Utqiaġvik whale hunt recorded the earliest known landing, on 13 April. Four bowhead whales equipped with satellite transmitters all wintered (2017/18) in the Chukchi instead of their usual wintering area south of Anadyr Strait in the Bering Sea (31) and a bowhead was recorded singing near Utqiaġvik on 11 January 2018, something never recorded before at that time of year. In 2018/19, the bowheads were again north of Anadyr Strait in winter. Spotted seal (*Phoca largha*) pups in the spring of 2018 were found in poorer condition (less fat and lower mass/length) than in recent years, and almost no ribbon seals (*Histriophoca fasciata*) were seen during those same surveys, raising the specter of a failure in the 2018 year class. In the spring and summer of 2018 and 2019, more than 280 bearded (*Erignathus barbatus*), ringed (*Pusa hispida*), spotted, and unidentified seal carcasses, primarily young and many emaciated, were reported from beaches mostly of the northern Bering and southern Chukchi seas, nearly five times the annual average from 2014-2017, prompting the National Oceanic and Atmospheric Administration to declare an “unusual mortality event” (32).

Anomaly or Transformation?

Changes in sea ice extent, water temperature, currents, zooplankton abundance, animal distribution and health, hunting success, and other aspects of the ecosystem are noteworthy in themselves, but such large-scale changes could conceivably occur without altering basic relationships among ecosystem components. The investigation of specific mechanisms underlying these changes were not part of the cited studies, however it is known from other areas, including the southern Bering Sea, that the spring sea-ice break-up spurs a productive phytoplankton bloom, and its timing together with ocean temperatures determines phytoplankton species composition, carbon export to the benthos, and food quality for zooplankton (24). Changes towards lower-lipid zooplankton reduces over-winter survival of fishes such as salmon and Arctic cod (33), even if they increase numerically in summer due to favorable thermal and oceanographic conditions. Lower zooplankton food quality and increased competition from predatory fish moving north from the Bering Sea might explain seabird and seal mortality.

The ecosystem-wide changes seen in 2017-2019 have the potential to fundamentally reconfigure the Pacific Arctic marine food web. An altered physical environment characterized by warmer waters and a longer open-water season is allowing subarctic species to establish themselves in the Chukchi Sea; seasonally for now, but possibly year-round in the future. Subarctic invaders such as walleye pollock and Pacific cod could fundamentally transform interactions among pelagic species, benthic invertebrates, groundfish, seabirds, and marine mammals by exerting strong predation pressure on forage fishes and benthic crab, worm, and shrimp communities (10). Predation pressure from these fishes adds top-down stresses to the bottom-up changes associated with altered temperature and primary and secondary productivity. Indigenous hunters may begin to find familiar species of fishes and marine mammals at unusual times of year or unfamiliar species during customary hunting and fishing periods (21).

An interdisciplinary look at the Pacific Arctic marine ecosystem as it changes may provide a rare opportunity to track ecosystem transformation in detail as it unfolds, rather than reconstructing details after the fact. The transformation of an ecosystem may reflect a cascade of sequential changes that take place over multiple years rather than a single shift or tipping point (e.g., 34), though changes to individual ecosystem components may be sudden and dramatic. For example, because of positive feedbacks in the climate system (e.g., 12) it is possible that 2017 marked the crossing of a threshold that precludes return to the system state common just a decade ago. We find that a closely coupled synergy between bottom-up and top-down factors (e.g., 35) appear to best characterize this system's transition, and the interactions among these multiple stressors have important implications for understanding any subsequent reorganization.

The result would be the transformation of an Arctic marine ecosystem into one characterized by subarctic conditions, subarctic species, and subarctic interactions (Figure 6). The Chukchi Sea may soon resemble the east-central Bering Sea shelf in condition, structure, and function, with annual sea ice, warmer bottom water temperatures, and ecosystem productivity derived from forage fishes and pelagic zooplankton rather than the benthos. Changes in the historically strong benthic-pelagic coupling have already been observed in the southeastern Chukchi Sea, where overall epibenthic biomass declined by an order of magnitude from 2004 to 2017; the fact that the most abundant taxa were consistent over time may hint at overall changes in ecosystem productivity or pathways rather than specific habitat changes (36,37). Yet this transformation is more complex than an ecosystem migrating north. For example, the Chukchi Sea would likely retain some characteristics distinguishing it from the Bering Sea shelf, due to higher latitude and downstream location relative to the Bering Strait nutrient supply. How these competing features will combine to create a new state of the Pacific Arctic ecosystem remains to be seen.

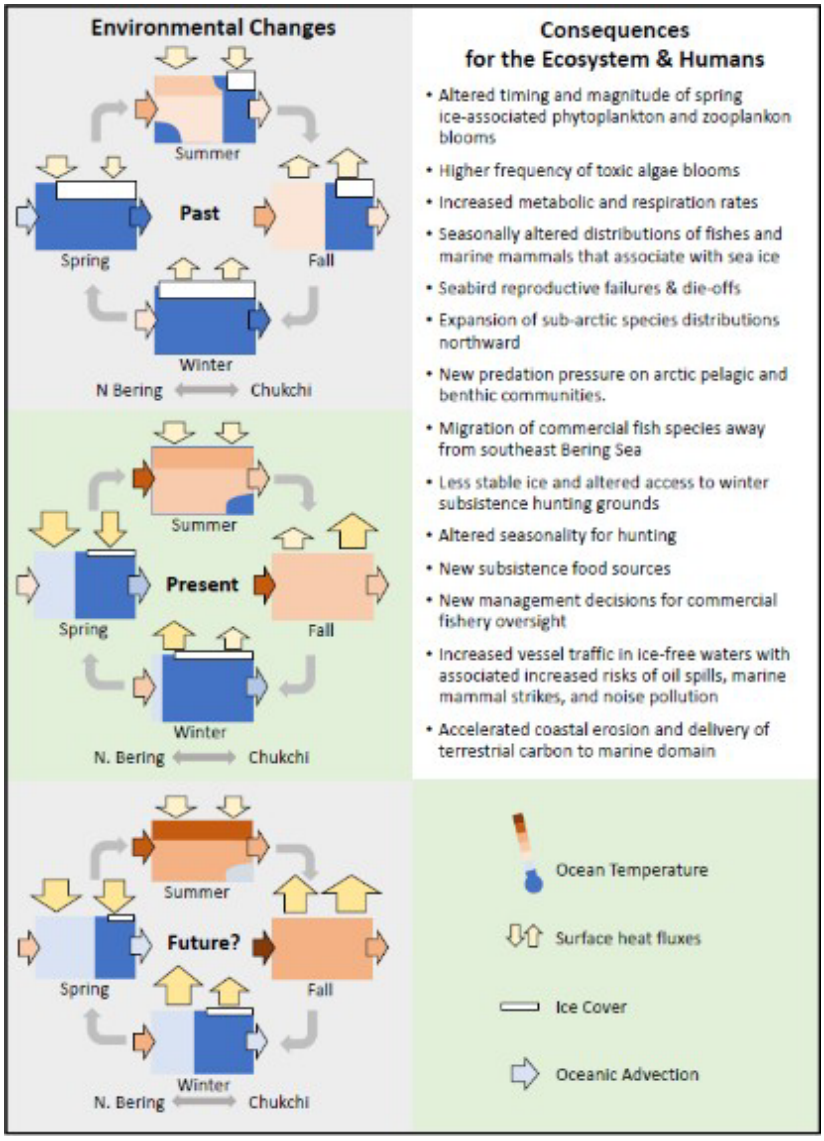

Figure 6. Environmental changes and related consequences. Observed and potential future changes in the physical environment (left panels) in the Northern Bering and Chukchi shelf systems (i.e., bottom-up forcing), along with observed and anticipated consequences for the biological and human components of the ecosystem (right panel).

In addition to its regional significance, the pattern of change underway in the Pacific Arctic may eventually shed light on the progression of ecosystem transformation more generally (38), which manifests as large-scale alterations in the connections and interactions among species and among physical and biological processes. Overpeck et al. (39) suggested the possibility of such a transformation resulting from the removal of perennial ice in the Arctic, though they focused on "before" and "after" states of the system without describing the transformation in between. The pioneering work of Gunderson and Holling (40) recognized that transformation and reorganization are less predictable and less well understood than a simple shift from stability to instability.

What To Expect Next?

The expectation is for the sea ice season to further shorten and sea ice coverage to diminish (41). Waters will become warmer and stay warm longer into fall and winter. How quickly these changes propagate through and persist in the system, and what additional sudden shifts may occur, are hard to predict. It is likely, however, that there will be differences in the temporal and spatial scales over which physics and biology change (42). Physical conditions that were once anomalous may become normal. The biological response will follow but may not carry over across years until species and behaviors that thrive in the new conditions are able to persist. Hunters and fishers will adjust to some degree but may find it necessary to switch the timing or targets of their efforts (43).

Specific trajectories of these changes and their implications for the Pacific Arctic ecosystem, including Indigenous coastal communities, are still unclear. To stay with or ahead of these system transformations rather than reacting to a new state some years from now, some critical unknowns, especially regarding ecosystem relationships, require further attention and continued monitoring at multiple scales. As sea ice retreats earlier, will some species cling to existing fixed habitats (e.g., depositional zones) and remain largely in place, while others follow shifting habitats (such as the ice edge)? Will subarctic species be able to flourish and persist in the Chukchi Sea year-round, transforming the ecosystem into a locus of groundfish or pelagic predator abundance? Will increased industrial activity such as shipping combine with climate-driven ecosystem changes in ways that amplify the consequences of either alone (44)? How can coastal communities adjust and adapt quickly enough to retain cultural and nutritional security (45)?

Even in this age of information overload, it is how remarkable how scarce (and thus how valuable) the available data are for making statistically robust comparisons of today's conditions versus yesterday's. For example, quantifying changes in primary and secondary productivity cannot immediately follow the spring retreat of sea ice because previously the ice itself precluded ship-based measurements at locations and times now ice-free. Across the study region, even 15 years of annually collected data is an unusually long time series, and for biological parameters most of these data are confined to summer months. Hence, it is important to learn to distinguish surprises from completely new observations.

A cascade of effects through an ecosystem may include tipping points governed by positive feedbacks for individual components, making recovery to the previous structure and function ever less likely (e.g., 34,46). Top-down changes such as increased predation may result from bottom-up changes such as the removal of thermal barriers to range expansion of predators. The experience to date in the Pacific Arctic by itself will not resolve these questions, but it does suggest that, with regard to cascades versus tipping points or top-down versus bottom-up controls (e.g., 47), ecosystem transformation may be a complex matter of "both and" rather than a simple dichotomy of "either/or."

These questions are more than a curiosity (48). The well-being of coastal communities and the management of human activities in the region, including potential commercial fisheries, depend on reliable information and insight into what is likely to happen next. In Alaska waters, industrial and research activities are planned in ways to reduce interference with Alaska Native subsistence harvests, and conscientious vessel operators communicate with communities and adjust their plans to avoid areas where hunters are active (e.g., 49). Growing uncertainty about the timing of animal migrations and optimal harvest conditions increases the likelihood of conflict and concerns about food security. Coastal communities are likely to face difficult choices between capitalizing on increased economic opportunity and limiting industrial interference with subsistence activities.

The profound shift in ecosystem state and conditions suggest a new framework is needed to replace the paradigm that served well in recent decades. The Pacific Arctic marine ecosystem

transformation is not an isolated case. Social-ecological systems worldwide are facing similar pressures from changing physical conditions, with implications that are increasingly uncertain as transformation propagates through the food web and to human outcomes (50). Long-term and multi-scale data are necessary to detect, examine, and respond to such changes. A better understanding of the nature of system transformation will help humans detect transformations earlier, perhaps in time for more effective response or adaptation, even if prevention may no longer be possible.

Data Availability

All data collected as a part of the North Pacific Research Board's Arctic Integrated Ecosystem Research Program (Arctic IERP) are being curated and preserved. Because the research is actively ongoing, the data are under program embargo through July 2021. At that time, all Arctic IERP data will be publicly released with a CC-0 license from the Research Workspace DataONE Member Node, and this paper will be cited in the DOI for those data, to create a formal link. In the interim, please contact the authors for access to Arctic IERP data.

In Figure 1, we acknowledge the use of imagery from the NASA Worldview application (https://worldview.earthdata.nasa.gov/), part of the NASA Earth Observing System Data and Information System (EOSDIS). Ice-edge marking is from Maslanik, J. and J. Stroeve. 1999. Near-Real-Time DMSP SSMIS Daily Polar Gridded Sea Ice Concentrations, Version 1, F17. Boulder, Colorado USA. NASA National Snow and Ice Data Center Distributed Active Archive Center. doi: https://doi.org/10.5067/U8C09DWVX9LM. Accessed 12-December-2018.

2015 epifauna data are available at https://doi.org/10.25921/b2g4-bs86.

Other data are available on request, pending curation and archiving as part of ongoing studies.

Corresponding Author

Henry P. Huntington is the corresponding author, to whom all requests for materials should be addressed.

Acknowledgments

- Much of the research reported here and preparation of the manuscript was conducted under the Arctic Integrated Ecosystem Research Program (Arctic IERP; http://www.nprb.org/arctic-program/). This manuscript is Publication Arctic IERP-014. Funding for the program was provided by North Pacific Research Board, the U.S. Bureau of Ocean Energy Management, the Collaborative Alaskan Arctic Studies Program (formerly the North Slope Borough/Shell Baseline Studies Program), and the U.S. Office of Naval Research Marine Mammals and Biology Program. Generous in-kind support was provided by the U.S. National Oceanic and Atmospheric Administration (NOAA; Alaska Fisheries Science Center and Pacific Marine Environmental Laboratory), University of Alaska Fairbanks, U.S. Fish & Wildlife Service, and the U.S. National Science Foundation. The findings and conclusions of this paper are those of the authors and not necessarily those of the agencies and organizations with which the authors are affiliated or which provided support.
- This manuscript is a contribution to the U.S. Marine Biodiversity Observation Network (MBON), the U.S. Integrated Ocean Observing System, and the Group on Earth Observations Biodiversity Observation Network (GEO BON). The work and publication were partially funded under the U.S. National Oceanographic Partnership Program (NOPP) through NOAA award # UAF NA14NOS0120158 Arctic Marine Biodiversity Observing Network (AMBON), with contributions from NOAA, the U.S. Bureau of Ocean Management (BOEM), Shell Exploration & Production under management of the Integrated Ocean Observing System (IOOS), as well as contributions of U.S. National Science Foundation (NSF) grant #1204082.

- We are grateful for the contributions of many colleagues to the research and writing of this paper, including Gay Sheffield.
- This paper is PMEL contribution # 4917.
- Collections of fish specimens were made under the auspices and terms of Scientific Research Permit numbers 2012-11, 2013-8, 2017-2 and 2019-7 issued by the NOAA's Alaska Regional Office and permit numbers CF-12-005, CF-13-016, CF-17-023, and CF-19-018 from Alaska's Department of Fish and Game.

Author Contribution Statement

HPH, SLD, FKW, EF, CL, and KS developed the idea and contributed to writing and editing the paper. MB, PB, JJC, ADR, DD, JCG, KI, DGK, KK, RL, LQ, PS, DS, and CW wrote sections of the paper and contributed to editing of the manuscript. All authors provided data and reviewed the final manuscript and approved it for submission and publication.

Competing Interests

The authors declare no competing interests.

References

1. Grebmeier, J. M., Cooper, L. W., Feder, H. W. & Sirenko, B. I. Ecosystem dynamics of the Pacific-influenced Northern Bering and Chukchi Seas in the Amerasian Arctic, *Prog. Oceanogr*. **71(2–4),** 331 – 361 (2006).
2. Woodgate, R. A. Increases in the Pacific inflow to the Arctic from 1990 to 2015, and insights into seasonal trends and driving mechanisms from year-round Bering Strait mooring data, *Progress in Oceanography* **160,** 124-154 (2018). doi:10.1016/j.pocean.2017.12.007
3. Codispoti, L. A., et al. Synthesis of primary production in the Arctic Ocean: III. Nitrate and phosphate based estimates of net community production. *Progress in Oceanography* **110**, 126-150 (2013).
4. Kuletz, K., et al. Seasonal spatial patterns in seabird and marine mammal distribution in the eastern Chukchi and western Beaufort Seas: Identifying biologically important pelagic areas. *Progress in Oceanography* **136,** 175-200 (2015).
5. Cooper, L. W., et al. The relationship between sea ice break-up, water mass variation, chlorophyll biomass, and sedimentation in the northern Bering Sea. *Deep Sea Research II* **65–70,** 141–162 (2012).
6. Smith, M. A., Goldman, M. S., Knight, E. J. & Warrenchuk, J. *Ecological Atlas of the Bering, Chukchi, and Beaufort Seas* 2nd edition. (Audubon Alaska, 2018.)
7. Grebmeier, J. M., et al. Ecosystem characteristics and processes facilitating persistent macrobenthic biomass hotspots and associated benthivory in the Pacific Arctic. *Progress in Oceanography* **136,** 92–114 (2015). http://dx.doi.org/10.1016/j.pocean.2015.05.006
8. Moore, S. E., Stabeno, P. J., Grebmeier, J. M. & Okkonen, S. R. The Arctic Marine Pulses Model: linking annual oceanographic processes to contiguous ecological domains in the Pacific Arctic. *Deep-Sea Research Part II* **152,** 8-21 (2018).
9. Stabeno, P. J., et al. Comparison of warm and cold years on the southeastern Bering Sea shelf and some implications for the ecosystem. *Deep Sea Research II* **65**, 31-45 (2012).
10. Sigler, M., et al. Fluxes, fins, and feathers: relationships among the Bering, Chukchi, and Beaufort seas in a time of climate change. *Oceanography* **24,** 250–265 (2011).
11. Haynie, A. C. & Pfeiffer, L. Climatic and economic drivers of the Bering Sea walleye pollock (*Theragra chalcogramma*) fishery: implications for the future. *Canadian Journal of Fisheries and Aquatic Sciences* **70,** 841–853 (2013).

12. Stroeve, J. C., et al. The Arctic's rapidly shrinking sea ice cover: a research synthesis. *Climatic Change* **110(3-4)**, 1005-1027 (2012).
13. Hunt Jr, G. L., et al. Advection in polar and sub-polar environments: Impacts on high latitude marine ecosystems. *Progress in Oceanography* **149**, 40-81 (2016).
14. Dunmall, K. M., et al. Pacific salmon in the Arctic: harbingers of change. In: F.J. Mueter, et al., eds. *Responses of Arctic Marine Ecosystems to Climate Change*. (Alaska Sea Grant, University of Alaska Fairbanks, 2013.) Doi:10.4027/ramecc.2013.07.
15. Moore, S. E., et al. Marine fishes, birds and mammals as sentinels of ecosystem variability and reorganization in the Pacific Arctic Region. In: J.M. Grebmeier & W. Maslowski, eds. *The Pacific Arctic Region: Ecosystem Status and Trends in a Rapidly Changing Environment*. p. 337-392. (Springer, 2014.) DOI 10.1007/978-94-017-8863-2_2.
16. Jay, C. V., Taylor, R. L., Fischbach, A. S., Udevitz, M. S. & Beatty, W. S. Walrus haul-out and in water activity levels relative to sea ice availability in the Chukchi Sea. *Journal of Mammalogy* **98,** 386-396 (2017). 10.1093/jmammal/gyw195.
17. Stafford, K. M. Increasing detections of killer whales (*Orcinus orca*), in the Pacific Arctic. *Marine Mammal Science* **67,** 116 (2018).
18. Gall, A. E., Morgan, T. C., Day, R. H. & Kuletz, K. J. Ecological shift from piscivorous to planktivorous seabirds in the Chukchi Sea, 1975-2012. *Polar Biology* **40,** 61-78 (2017). DOI 10.1007/s00300-016-1924-z.
19. Renner, M., et al. Modeled distribution and abundance of a pelagic seabird reveal trends in relation to fisheries. *Marine Ecology Progress Series* **484,** 259-277 (2013).
20. Kuletz, K. J., Renner, M., Labunski, E. A. & Hunt, G. L. Changes in the distribution and abundance of albatrosses in the eastern Bering Sea: 1975-2010. *Deep Sea Research II* **109,** 282-292 (2014).
21. Huntington, H. P., Quakenbush, L. T. & Nelson. M. Evaluating the effects of climate change on Indigenous marine mammal hunting in northern and western Alaska using traditional knowledge. *Front. Mar. Sci.* **4,** 40 (2017).
22. Noongwook, G., the Native Village of Gambell, the Native Village of Savoonga, H.P. Huntington, H. P. & George, J. C. Traditional knowledge of the bowhead whale (*Balaena mysticetus*) around St. Lawrence Island, Alaska. *Arctic* **60,** 47–54 (2007).
23. Stabeno, P. J. & Bell, S. W. Extreme conditions in the Bering Sea (2017–2018): record- breaking low sea- ice extent. *Geophysical Research Letters* **46** (2019). https://doi.org/10.1029/2019GL083816
24. Duffy-Anderson, J. T., et al. Response of the northern Bering Sea and southeastern Bering Sea pelagic ecosystems following record-breaking low winter sea ice. *Geophysical Research Letters* **46** (2019). https://doi.org/10.1029/2019GL083396
25. Lefebvre, K. A., et al. Prevalence of algal toxins in Alaskan marine mammals foraging in a changing arctic and subarctic environment. *Harmful Algae* **55,** 13–24 (2016). https://doi:dx.doi.org/10.1016/j.hal.2016.01.007
26. De Robertis, A., Taylor, K., Wilson, C. & Farley, E. Abundance and distribution of Arctic cod (*Boreogadus saida*) and other pelagic fishes over the U.S. continental shelf of the northern Bering and Chukchi Seas. *Deep-Sea Research II* **135,** 51-65 (2017).
27. Brenner, R. E., Munro, A. R. & Larsen, S. J., eds. *Run Forecasts and Harvest Projections for 2019 Alaska Salmon Fisheries and Review of the 2018 Season*. Special Publication No. 19-07. (Alaska Department of Fish and Game, 2019.)
28. Stevenson, D. E. & Lauth, R. R. Bottom trawl surveys in the northern Bering Sea indicate recent shifts in the distribution of marine species. *Polar Biology* **42**, 407-421 (2019). https://doi.org/10.1007/s003000-018-2431-1.
29. Siddon, E. & Zador, S. *Ecosystem Considerations 2017: Status of the Eastern Bering Sea Marine Ecosystem*. (Alaska Fisheries Science Center, National Marine Fisheries Service, NOAA, 2017.) Available at: www.afsc.noaa.gov/REFM/Docs/2017/ecosysEBS.pdf

30. Dragoo, D. E., H. M. Renner, and R. S. A. Kaler. Breeding status and population trends of seabirds in Alaska, 2018. U.S. Fish and Wildlife Service Report AMNWR 2019/03 (2019).
31. Quakenbush, L. T., & Citta, J. J. Satellite tracking of bowhead whales: habitat use, passive acoustic, and environmental monitoring. U.S. Dept. of the Interior, Bureau of Ocean Energy Management, Alaska Outer Continental Shelf Region, Anchorage, AK. *OCS Study BOEM* 2019-076 (2019).
32. NOAA. 2019. 2018-2019 ice seal unusual mortality event in Alaska. National Oceanic and Atmospheric Administration. https://www.fisheries.noaa.gov/alaska/marine-life-distress/2018-2019-ice- seal-unusual-mortality-event-alaska
33. Heintz, R. A., Siddon, E. C., Farley, E. V., & Napp, J. M. Correlation between recruitment and fall condition of age- 0 pollock (*Theragra chalcogramma*) from the eastern Bering Sea under varying climate conditions. *Deep Sea Research II* **94**, 150–156 (2013). https://doi.org/10.1016/j.dsr2.2013.04.006
34. Wassman, P. & Lenton, T. M. Arctic tipping points in an earth system perspective. *Ambio* **41(1),** 1-9 (2012). https://dx.doi.org/10.1007%2Fs13280-011-0230-9
35. Lynam, C. P., et al. Trophic and environmental control in the North Sea. *Proceedings of the National Academy of Sciences* 201621037 (2017). DOI: 10.1073/pnas.1621037114
36. Grebmeier, J. M., et al. Time-series benthic community composition and biomass and associated environmental characteristics in the Chukchi Sea during the RUSALCA 2004–2012 Program. *Oceanography* **28,** 116-133 (2015). http://dx.doi.org/10.5670/oceanog.2015.61
37. Iken, K., et al. Developing an observational design for epibenthos and fish assemblages in the Chukchi Sea. *Deep-Sea Research II* **162**, 180-190 (2019). https://doi.org/10.1016/j.dsr2.2018.11.005
38. Scheffer, M., et al. Anticipating critical transitions. *Science* **338,** 344-348 (2012). DOI: 10.1126/science.1225244
39. Overpeck, J. T., et al. Arctic system on trajectory to new state. *EOS* **86(34),** 309, 312-313 (2005).
40. Gunderson, L. & Holling, C. S., eds. 2001. *Panarchy: Understanding Transformations in Human and Natural Systems*. (Island Press, 2001.)
41. IPCC. *Climate Change 2014: Synthesis Report. Contribution of Working Groups I, II and III to the Fifth Assessment Report of the Intergovernmental Panel on Climate Change*. (IPCC, 2014.)
42. Huntington, H.P., et al. A new perspective on changing Arctic marine ecosystems: panarchy adaptive cycles in pan-Arctic spatial and temporal scales. In: S. Arico, ed. *Ocean Sustainability in the 21st Century*. p. 109-126. (Cambridge University Press, 2015.)
43. Huntington, H.P., et al. How small communities respond to environmental change: patterns from tropical to polar ecosystems. *Ecology and Society* 22(3), 9 (2017).
44. Huntington, H.P., et al. Vessels, risks, and rules: planning for safe shipping in Bering Strait. *Marine Policy* **51,** 119-127 (2015).
45. ICC-Alaska. Alaskan Inuit Food Security Conceptual Framework: How to Assess the Arctic from an Inuit Perspective. Technical Report. (Inuit Circumpolar Council-Alaska, 2015.)
46. Huggett, A. J. The concept and utility of ecological thresholds in biodiversity conservation. *Biological Conservation* **124,** 301-310 (2005).
47. Hunt, G. L., et al. Climate change and control of the southeastern Bering Sea pelagic ecosystem. *Deep Sea Research II* **49**, 5821–5853 (2002).
48. Rocha, J., Yletyinen, J., Biggs, R., Blenckner, T. & Peterson. Marine regime shifts: drivers and impacts on ecosystems services. *Philosophical Transactions of the Royal Society B* **370,** 20130273 (2015). https://doi.org/10.1098/rstb.2013.0273
49. Konar, B., Frisch, L. & Moran, S. B. Development of best practices for scientific research vessel operations in a changing Arctic: a case study for R/V Sikuliaq. *Marine Policy* **86,** 182-189 (2017).
50. Rocha, J. C., Peterson, G. D. & Biggs, R. Regime shifts in the Anthropocene: drivers, risks, and resilience. *PLoS ONE* **10(8),** e0134639 (2015). https://doi.org/10.1371/journal.pone.0134639

General Discussion

The main results of the Chukchi Coastal Communities component of the Arctic IERP have been presented in the chapter that consists of our manuscript accepted by *Arctic*. That chapter also includes a discussion of the results of our work, which we will not repeat here. Instead, this section will discuss the role of the Chukchi Coastal Communities component with regard to the Arctic IERP overall.

The Arctic IERP focused on changes to the marine ecosystem of the northern Bering and Chukchi Seas, Alaska. These changes were studied in various ways, from physical changes (sea ice, water temperature, etc.) to biological and ecological ones (energy flow through trophic levels, distribution and abundance of various species, occurrence of harmful algal blooms, etc.). Much of this research was carried out from research vessels operating in the region, with additional data gathered from instruments moored or deployed during the cruises and recovered later. Partly in the interest of avoiding interference with subsistence activities, much of the oceanographic work was conducted beyond core hunting and fishing areas of the coastal communities.

Basic patterns of change were evident and consistent throughout the region, as described by coastal residents. Ice formed later and melted earlier. Waters were warmer in summer than they had been in previous times. Fishes, seabirds, and marine mammals shifted their distribution, the timing of their migrations and movements, their behaviors, and their abundance. The meetings of the Chukchi Coastal Communities component team helped connect experiences and observations among the participating communities, again illustrating how widespread the changes were and how they affected all aspects of the ecosystem. The details documented by the ship-based research helped show how such changes extended throughout the study region. The convergence of information from different sources, as we saw in the Arctic IERP, has shown that changes are as extensive.

The main opportunities to share information between the ship-based teams and the coastal communities team came during the Arctic IERP PI meetings. The agendas for the meetings provided time for interactions between the two groups. Additional informal interactions occurred during breaks and outside the formal meeting. These interactions were effective in creating shared understanding. In addition, the Chukchi Coastal Communities team created an annotated bibliography of sources of LTK for the study region, which was made available to all other PIs. The Coastal Communities team also surveyed other PIs about their specific interests in what might be available from LTK. We are not aware, however, of how much these resources were used by the other PIs.

The Chukchi Coastal Communities component plan was designed based on experiences in the Bering Sea Project (2008-2013) and in light of a comparatively modest budget for community-based research within the Arctic IERP. Specifically, we decided not to pursue original research in coastal communities for two reasons. First, much research of this kind has already been done, and there is resistance from Alaska Native Tribes and communities to additional projects that appear to repeat what has already been done and which place additional demands on community residents to take part in gathering information. Second, the funds available to the Chukchi Coastal Communities component did not allow for extensive research in multiple communities, which would have limited the breadth of coastal community participation.

Accordingly, we decided instead to engage coastal community residents in analyzing the available information. This innovation served two purposes. First, we could involve several communities along the coast from Savoonga to Utqiaġvik. We had planned on nine communities, and in the end eight were able to participate. Second, the coastal residents would participate not simply as sources of information, but

also as analysts of that information. The movement towards co-production of knowledge, in which western-science trained researchers and community members work as partners throughout a project, involves among other things emphasizing equity among knowledge systems and team members to, in part, divest ourselves of hierarchical roles in research. Our approach attempted to provide for the full engagement of all participants in all aspects of the work.

Our initial results were promising. Team meetings in March 2017 and March 2018 generated a great deal of information and insight as well as enthusiasm among the participants. Both meetings were held in conjunction with PI meetings, helping to create a sense of belonging with the larger group. After that, unfortunately, other events intervened in our plans. The federal government shutdown in early 2019 forced us to cancel our plans for another team meeting that winter. The missed meeting robbed us of both momentum and continuity. Also during this period, some of the participating organizations in our project underwent personnel changes. In some cases, the individuals who took over the positions were willing to engage enthusiastically with the project. In other cases, less so. In January 2020, we held another team meeting, with a high degree of turnover from the previous ones, but still considerable enthusiasm for the effort overall.

Then COVID came, along with further personnel changes. COVID prevented additional in-person meetings for the duration of the project. While we were able to complete our major research paper, which addressed our hypotheses and fulfilled our commitments to the Arctic IERP, we were unable to take on additional work that we had hoped to do. For example, we had begun discussions with the larger PI group about a comparative analysis of the hazards that a changing environment poses for coastal communities. Without deep engagement and collaboration with coastal community members, however, such an undertaking was not possible. We tried virtual meetings, but found them unsatisfactory for this purpose. Additional personnel changes at one of the participating institutions, combined with the fact that the project was wrapping up, led to that region effectively dropping out of the project in mid-2020, though individuals continued to participate, including being co-authors of our *Arctic* paper.

We provide this history as context. The Chukchi Coastal Communities component of the Arctic IERP fulfilled its primary purpose. Engaging community members in analysis and interpretation of observations proved to be a valuable technique. The information already documented from coastal communities was a sufficient foundation for our work. What we missed, due in large part to the unexpected events noted in the previous two paragraphs, was further opportunity to interact with researchers from other components of the Arctic IERP. It is possible that those interactions may have led to additional collaborations. We are frustrated that circumstances prevented us from finding out where things may have gone.

Our experiences suggest a few considerations for future IERPs and also the synthesis phase of the Arctic IERP. First, as we also experienced on the Bering Sea Project, there is no substitute for repeatedly getting together when it comes to building relationships. Annual meetings were sufficient, but longer intervals made things more difficult. Making time during the meetings for a variety of interactions was also important. Time is always at a premium in PI meetings. Cross-cultural and cross-disciplinary relationships, on the other hand, need unstructured time to see where conversations and ideas will go. It is to the Arctic IERP's credit that the PI meetings included some time for exploratory conversations. Unfortunately, there was often insufficient time to see where those conversations would lead, especially in cases of challenging cross-cultural communications, and the inability to meet during the COVID era meant that conversations that had begun could not be continued. We are not sure what the solution is, but we do believe that the external disruptions to the PI meeting schedule exacerbated any communication problems during the Arctic IERP.

Second, collaboration needs to be an active process throughout a group effort. We provided the annotated bibliography of LTK sources, but this was insufficient on its own. It may be the case that the information from those sources simply was not pertinent to the interests and needs of the PIs from other components of the program. It is likely, however, that more intensive collaboration was required to develop specific research questions, identify relevant sources of information, interpret that information in light of the research questions, and present the findings of the joint effort. Because such collaborations often develop after the overall program is underway, it is difficult to budget for them at the start of a project. The synthesis phase of the Arctic IERP presents one option for pursuing such ideas, but it requires waiting for that phase to begin and also writing a separate proposal for the resources needed, both of which can sap momentum from a budding collaboration. Building time into the initial budget is another option, if the PIs are willing to forgo other tasks to leave the resources available and if program managers are willing to allow a portion of the budget to be flexible for these types of relationship building and collaboration.

Third, research and outreach are different activities. The Chukchi Coastal Communities component involved community members, but their time was committed to the role of researchers not community liaisons. The conflation of community-based research and community outreach is unfortunately widespread in the scientific world. Social science research is often conflated with community outreach as well. We appreciate that all researchers in the Arctic IERP had an obligation to contribute to outreach efforts, but such expectations need to be clearly communicated from the outset and budgeted accordingly. Strong community outreach takes as much time, effort, and preparation as other elements of the overall research enterprise. Expecting community members who participate in a program such as the Arctic IERP to take on this extra duty is unfair and also a poor substitute for properly supported outreach carried out by those with the appropriate connections, expertise, and experience.

Fourth, the benefits of participating in a program such as the Arctic IERP need to be made clear to communities from the beginning. In this case, ‘from the beginning’ means when conceptualizing and planning an IERP effort. This should involve including Tribal representatives and community members from the IERP area in the actual IERP planning efforts. It is not possible to create an IERP that meets the needs of multiple groups/communities/stakeholders without them being involved in the development of that IERP. It is also not possible to foster true and meaningful co-production of knowledge (if that is one of NPRB’s goals) without this early and ongoing involvement in questions such as: Is an IERP in X area needed? What are the topics or themes the IERP should focus on? Who will be involved in soliciting proposals (i.e., will there be, and what kind of, outreach to organizations that don’t conventionally submit proposals? What are the criteria for proposal review and who will be involved in reviewing proposals? etc., etc.). Contributing to the scientific enterprise is undoubtedly valuable, but may not be fully satisfactory to those concerned first and foremost with the well-being of their communities, and may not be sufficient motivation to engage fully and enthusiastically with a research program or project that communities have not been meaningfully involved in developing. Doing so will not happen as the result of a single community meeting, but will require extensive interaction, learning from experience, and a willingness to invest fully in community engagement and co-production.

Application to Resource Management and Alaska Communities

Rapid environmental change, such as that found by the studies in the Arctic IERP, poses considerable challenges to resource management and to coastal community well-being. In terms of resource management, our findings show also that regional human activity causes environmental change in addition to larger processes such as a warming global climate. For example, a regional increase in vessel traffic can affect the distribution of marine mammals on short and long time scales, depending on the duration of the disturbance. Although large-scale commercial fishing does not occur north of the Bering Strait at present, increased activity in the northern Bering Sea and experiences elsewhere have made many coastal community members wary of additional ecological and social changes if fisheries continue to move northwards. Resource management needs to take into account the combined effects of various forms of change and disturbance. At present, different forms of human activity tend to be managed separately. Fishing, shipping, and offshore petroleum development are managed in different ways by different agencies, albeit with efforts to consider cumulative effects. Still, more work is needed to understand the complex interactions that create outcomes, especially in a time when widespread environmental change is happening even more rapidly than was expected when the Arctic IERP began.

For coastal communities, our findings reflect and document much of what their residents have already experienced. Sharing of information among the eight communities involved in our project (in a way that is different from how information is typically shared) was valuable in contributing to team members' overall understanding of the extent and type of change occurring throughout the region. Thinking about the various forms of environmental change also helped illustrate how much is occurring in the region, a perspective that may not be apparent when focusing on one form of change or human activity at a time. Furthermore, societal change cannot be separated from environmental change when it comes to community-level effects and responses. Community leaders must pay attention to all the challenges facing their communities and must understand how those challenges interact with one another. Key conclusions of the Chukchi Coastal Communities component are that the practice of traditional values remains essential to community well-being and that Indigenous leadership is necessary for responding to change in ways that will sustain overall community well-being. An additional point is that equitable partnerships between communities and scientists can facilitate valuable two-way information exchange, including information that can be used by communities as they determine how best to respond to change.

Directions for Future Research

Our research has shown that more research is needed to understand the details of how coastal communities respond to change. Much work has been done to document the changes that are taking place, but far less has been done to understand the actions communities take in response and the degree to which those actions contribute to sustaining community well-being. Our paper in *Arctic* shows that there are a range of responses that communities are making, consistent with prior research. Still, understanding *what* is being done is not the same as understanding *how* and *why*. Such information can be valuable for other communities experiencing change, and also for those making decisions that affect community, region, and ecosystem well-being. Participation in research and management activities is time consuming and demanding, and those burdens are only increasing for coastal communities. Making the most of the effort expended will be important for sustaining their involvement and their ways of life.

As mentioned earlier, one potential research effort to consider is an appraisal of the various hazards coastal communities face from a changing environment. From greater storm exposure due to loss of sea ice to harmful algal blooms to shifting distributions of species harvested for subsistence, communities must weigh many demands on their time and attention. The various hazards also create different forms of risk, from loss of life and limb to infrastructure damage to changing harvests and diets. Comparing these hazards in terms of severity, urgency, and other factors is not a trivial undertaking. The comparison is also one that cannot be done by others on a community's behalf, but must fully involve the community from start to finish, from conceiving of the project and its scope to sharing the results in ways that do not cause additional harm through misunderstanding or stigmatization. Done well, such an effort could be valuable to community leaders as well as others whose work affects community well-being.

In addition to topics for future research, our project suggests an approach to be continued in future work. That is, the engagement of coastal community members in analysis and interpretation of information. This happened to some extent and largely incidentally in the Bering Sea Project, and by design to a far greater extent in the Chukchi Coastal Communities component of the Arctic IERP. We recommend using approaches like this to an even greater extent, extending also to sharing results in formats that are effective in reaching coastal community audiences and beyond. By this we do not mean outreach on behalf of the entire program, but specifically conceiving and generating products that present the findings of the project or projects for which community members have served as researchers. In other words, we recommend further progress towards the full and equitable engagement of community members in research that involves them, their communities, and their environment (i.e., their traditional lands and waters, as well as contemporary use areas, if those differ).

Publications, Presentations, and Collaborations

Publications

Huntington, H.P., S.L. Danielson, F.K.Wiese, M. Baker, P. Boveng, J.J. Citta, A. De Robertis, D.M.S. Dickson, E. Farley, J.C. George, K. Iken, D.G. Kimmel, K. Kuletz, C. Ladd, R. Levine, L. Quakenbush, P. Stabeno, K.M. Stafford, D. Stockwell, and C. Wilson. 2020. Evidence suggests potential transformation of the Pacific Arctic Ecosystem is underway. *Nature Climate Change* 10:342–348. https://doi.org/10.1038/s41558-020-0695-2

Huntington, H.P., J. Raymond-Yakoubian, G. Noongwook, N. Naylor, C. Harris, Q. Harcharek, and B. Adams. 2021. "We never get stuck": a collaborative analysis of change and coastal community subsistence practices in the northern Bering and Chukchi Seas, Alaska. *Arctic* 74(2):113-126. https://doi.org/10.14430/arctic72446

Presentations

Danielson, S., and H.P. Huntington. 2019. The Arctic Integrated Ecosystem Research Program: 2017 and 2018 conditions and consequences. Alaska Marine Science Symposium, Anchorage, Alaska.

Huntington, H.P. 2019. The Arctic Integrated Ecosystem Research Program. Northwest Arctic Borough Planning Commission, Kotzebue, Alaska.

Julie Raymond-Yakoubian provided regular updates on the Arctic IERP and the Chukchi Coastal Communities component to the Kawerak Board of Directors, Natural Resources Committee, and to the region's Tribes during the course of the project.

Data and Metadata

Huntington, H. 2021. Chukchi Coastal Communities meeting notes, Arctic Integrated Ecosystem Research Program, 2017-2019. Dataset. *link* 10.24431/rw1k59c

Huntington, H. 2021. Chukchi Coastal Communities literature survey, Arctic Integrated Ecosystem Research Program, 2017-2019. Dataset. *link* 10.24431/rw1k59b

Synopsis

"We never get stuck": How Chukchi Coastal Residents Are Dealing with Change

Why We Did It

Rapid changes are happening in the Arctic, including in Alaska's Indigenous coastal communities. The climate is warming, ecosystems are shifting, and cultures and societies are facing new and increasing stresses. At the same time, traditional values remain strong and vital. Our question is how coastal communities can remain resilient in the face of all that is happening.

Arctic communities have always had to respond to environmental variability. In contemporary times, they have also faced the long-term effects of colonization. The continued effects of colonization can be seen through the dominant society's policies and practices surrounding, for example, governance, education, and 'resource' management and access. These effects intersect with rapid warming of the ocean, air, and land. Community well-being depends on connection to and understanding of the environment and having the ability and authority to respond effectively to change. Our team of coastal community residents and researchers sought to understand more about these experiences and how communities can act to sustain their communities, cultures, and livelihoods.

What We Did

We formed a team of academically trained researchers and coastal community residents to analyze information together. We met several times during the course of the project to review what has already been documented, record additional observations, and look for patterns and lessons. Our approach fostered discussions among people from different coastal communities, leading to new insights and connections.

The study region and the communities that were involved in the Chukchi Coastal Communities component of the Arctic IERP. Map from our 2021 paper in Arctic.

What We Learned

For coastal community residents, the nature of the changes they are seeing and experiencing is more important than classifying them into different sources of disturbance. What matters is the effect of those changes on people's activities. Not surprisingly, long-term changes have long-term effects, and short-term changes have short-term effects. Coastal residents have responded to those changes in many ways, from shifting the timing and location of some food harvesting activities to harvesting new species. In addition to sovereignty in decision-making, coastal community team members emphasized the importance of one's attitudes toward change, especially a willingness to be flexible and innovative. The more power that Tribes and communities have to respond as they see fit, the more resilient they will be.

Seal hunters in the Chukchi Sea off of Kotzebue, Alaska, in November 2019. Formerly, the sea would have been frozen over by this time of year. Photo by Henry P. Huntington.

Why It Matters

Coastal communities are seeing many types of change in their waters, from loss of sea ice to harmful algal blooms. Understanding how those various changes may pose risks, and how those changes affect each other is important, as is determining how to respond effectively. Environmental changes are occurring along with extensive societal changes, too. None of these changes can be treated in isolation. Further research partnerships should consider best practices for equitable collaborations with communities, how best to share scientific information with partner communities, and how to assess and respond to the risks that are identified.

Acknowledgments

We thank the North Pacific Research Board for funding and support of the Chukchi Coastal Communities component of the Arctic Integrated Ecosystem Research Program. We thank the North Slope Borough for additional funding to support the participation of North Slope Borough and Northwest Arctic Borough team members throughout the project. We thank all who took part in our team meetings, including Lucinda Wieler and Niviaaluk Brandt, former project Research Assistants at Kawerak; Orville Ahkinga, Dora Ahkinga, Opik Ahkinga, and Frances Sistuq Ozenna from Diomede; Raymond Lee Jr. from Buckland; Noah Naylor, Cyrus Harris, Siikauraq Whiting, and John Chase from Kotzebue; Billy Lee from Shungnak; Millie Hawley and Alexis Hawley from Kivalina; Steve Oomituk from Point Hope; Willard Neakok Jr. from Point Lay; and Qaiyaan Harcharek, Billy Adams, Michael Donovan, Brower Frantz, Nicole Kanayurak, and Robert Suydam from Utqiaġvik. We also thank all participants in the Arctic IERP for engaging with the Chukchi Coastal Communities team to create a collaborative atmosphere for the program.

References

NB: These references do not include citations made only in the two manuscripts that form chapters of this report, as each of those chapters has its own reference section.

ADF&G. N.D. *Community Subsistence Information System*. Juneau: Alaska Department of Fish and Game, Division of Subsistence. https://www.adfg.alaska.gov/sb/CSIS/

BOEM. 2014. *Alaska Annual Studies Plan FY 2015*. Anchorage: Bureau of Ocean Energy Management, Alaska Outer Continental Shelf Region.

Braund, S.R & Associates. 2013. *COMIDA: Impact Monitoring for Offshore Subsistence Hunting, Wainwright and Point Lay, Alaska*. OSC Study BOEM 2013-211. Anchorage: Bureau of Ocean Energy Management, Alaska OCS Region.

Cochran, P., O.H. Huntington, C. Pungowiyi, S. Tom, F.S. Chapin III, H.P. Huntington, N.G. Maynard, and S.F. Trainor. 2013. Indigenous frameworks for observing and responding to climate change in Alaska. *Climatic Change* 120:557-567.

Council of Canadian Academies. 2014. *Aboriginal Food Security in Northern Canada: an Assessment of the State of Knowledge*. Ottawa: The Expert Panel on the State of Knowledge of Food Security in Northern Canada, Council of Canadian Academies. Xxxiii + 256p. [panel member]

Gadamus, L., and J. Raymond-Yakoubian. 2015a. Qualitative participatory mapping of seal and walrus harvest and habitat areas: Documenting indigenous knowledge, preserving local values, and discouraging misuse. *International Journal of Applied Geospatial Research* 6(1): 76-93.

Gadamus, L., and J. Raymond- Yakoubian. 2015b. A Bering Strait indigenous framework for resource management: respectful seal and walrus hunting. *Arctic Anthropology* 52(2): 87-101.

Gadamus, L., J. Raymond-Yakoubian, R. Ashenfelter, A. Ahmasuk, V. Metcalf, and G. Noongwook. 2015. Building an indigenous evidence-base for tribally-led habitat conservation policies. *Marine Policy* 62: 115-124.

George, J.C., H.P. Huntington, K. Brewster, H. Eicken, D.W. Norton, and R. Glenn. 2004. Observations on shorefast ice failures in Arctic Alaska and the responses of the Inupiat hunting community. *Arctic* 57(4): 363-374.

Haynie, A.C., and H.P. Huntington. 2016. Strong connections, loose coupling: the influence of the Bering Sea ecosystem on commercial fisheries and subsistence harvests in Alaska. *Ecology & Society* 21(4):6. https://doi.org/10.5751/ES-08729-210406

Huntington, H.P., and the Communities of Buckland, Elim, Koyuk, Point Lay, and Shaktoolik. 1999. Traditional knowledge of the ecology of beluga whales (*Delpinapterus leucas*) in the eastern Chukchi and northern Bering seas, Alaska. *Arctic* 52(1): 49-61.

Huntington, H.P., N.M. Braem, C.L. Brown, E. Hunn, T.M. Krieg, P. Lestenkof, G. Noongwook, J. Sepez, M.F. Sigler, F.K. Wiese, and P. Zavadil. 2013a. Local and traditional knowledge regarding the Bering Sea ecosystem: selected results from five indigenous communities. *Deep-Sea Research II* 94:323-332.

Huntington, H.P., I. Ortiz, G. Noongwook, M. Fidel, L. Alessa, A. Kliskey, D. Childers, M. Morse, and J. Beaty. 2013b. Mapping human interaction with the Bering Sea ecosystem: comparing seasonal use areas, lifetime use areas, and "calorie-sheds". *Deep-Sea Research II* 94:292-300.

Huntington, H.P., G. Noongwook, N.A. Bond, B. Benter, J.A. Snyder, and J. Zhang. 2013c. The influence of wind and ice on spring walrus hunting success on St. Lawrence Island, Alaska. *Deep-Sea Research II* 94:312-322.

Huntington, H.P., L.T. Quakenbush, and M. Nelson. 2016. Effects of changing sea ice on marine mammals and subsistence hunters in northern Alaska from traditional knowledge interviews. *Biology Letters* 12: 20160198. http://dx.doi.org/10.1098/rsbl.2016.0198.

Huntington, H.P., A. Begossi, S. Gearheard, B. Kersey, P. Loring, T. Mustonen, P.K. Paudel, R.A.M. Silvano, and R. Vave. 2017. Learning from doing: community-level hunting, fishing, and agricultural responses to rapid environmental change. *Ecology and Society* 22(3):9.

ICC-Alaska. 2014a. *Northwest Arctic Regional Food Security Workshop: How to Assess Food Security from an Inuit Perspective: Building a Conceptual Framework on How to Assess Food Security in the Alaskan Arctic*. Anchorage: Inuit Circumpolar Council-Alaska.

ICC-Alaska. 2014b. *Bering Strait Regional Food Security Workshop: How to Assess Food Security from an Inuit Perspective: Building a Conceptual Framework on How to Assess Food Security in the Alaskan Arctic*. Anchorage: Inuit Circumpolar Council-Alaska.

ICC-Alaska. 2015. *Alaskan Inuit food security conceptual framework: how to assess the Arctic from an Inuit perspective. Technical Report*. Anchorage: Inuit Circumpolar Council-Alaska.

Noongwook, G., the Native Village of Savoonga, the Native Village of Gambell, H.P. Huntington, and J.C. George. 2007. Traditional knowledge of the bowhead whale (*Balaena mysticetus*) around St. Lawrence Island, Alaska. *Arctic* 60(1):47-54.

NPRB (North Pacific Research Board). 2005. *North Pacific Research Board Science Plan*. North Pacific Research Board, Anchorage.

Obama, B. 2013. *National Strategy for the Arctic Region*. Washington, DC: The White House.

Oceana and Kawerak, Inc. 2014. *Bering Strait Marine Life and Subsistence Data Synthesis*. Jointly produced and distributed by Oceana and Kawerak, Inc. http://oceana.org/en/news-media/publications/reports/the-bering-strait-marine-life-and-subsistence-data-synthesis

Rainey, F.G. 1947. *The Whale Hunters of Tigara*. Anthropological Papers of the American Museum of Natural History, v. 41, pt. 2.

Raymond-Yakoubian, B., L. Kaplan, M. Topkok, and J. Raymond-Yakoubian. 2014. "The World has Changed": Iŋalit Traditional Knowledge of Walrus in the Bering Strait. Final report for North Pacific Research Board project 1013. Nome: Kawerak Social Science Program. Nome, Alaska.

Raymond-Yakoubian, J., Y. Khokhlov, and A. Yarzutkina. 2014. Indigenous Knowledge and Use of Bering Strait Region Ocean Currents. Final report to the National Park Service, Shared Beringian Heritage Program for Cooperative Agreement H99111100026. http://www.kawerak.org/forms/nr/OC%20report%20for%20web.pdf and http://www.kawerak.org/forms/nr/OceanCurrents%20book%20for%20web.pdf